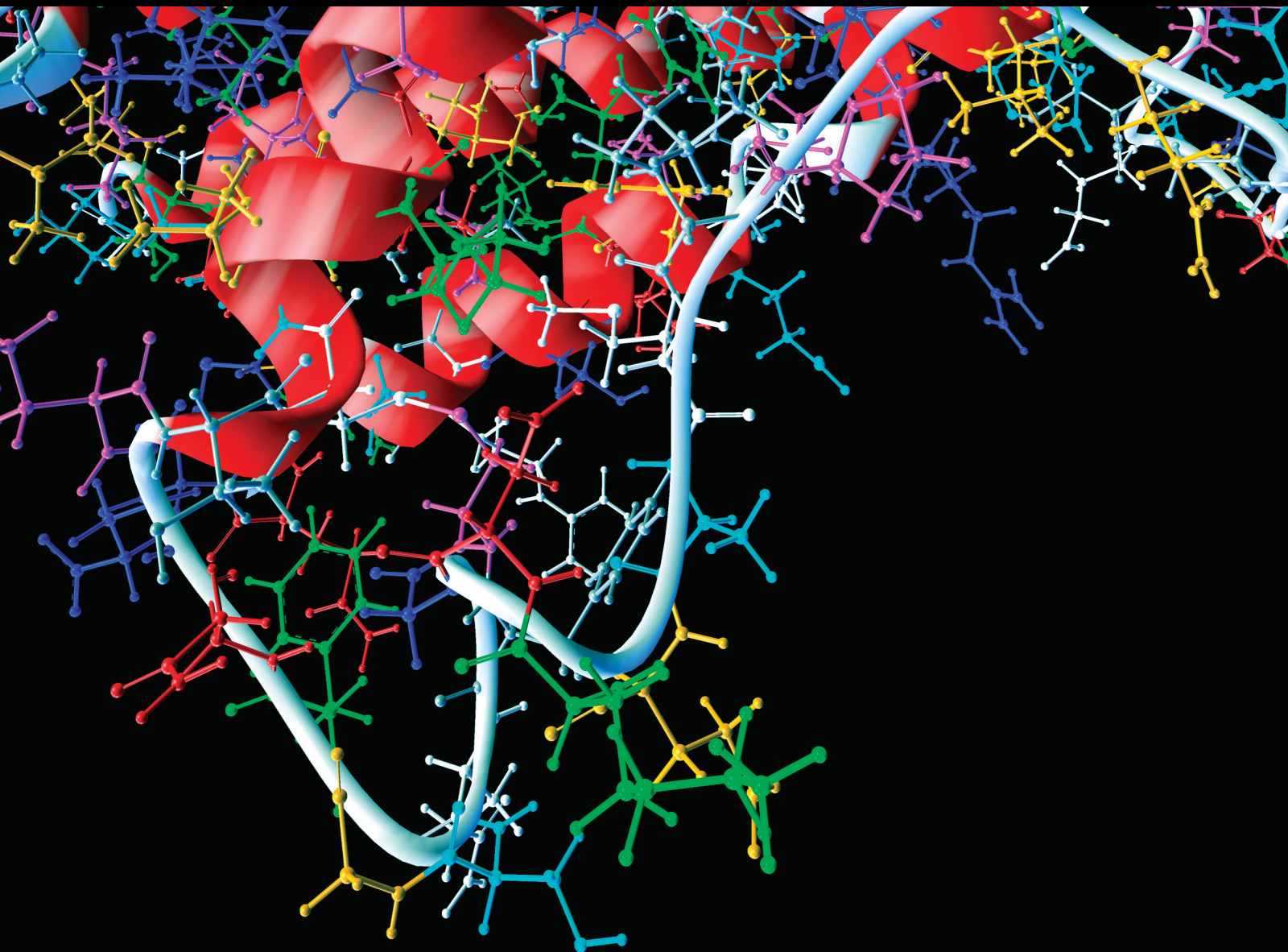


Computational and Mathematical Methods in Medicine

# Modeling, Analysis, and Simulations in Mathematical Biology

Lead Guest Editor: Naeem Jan

Guest Editors: László T. Kóczy and Lazim Abdullah





---

**Modeling, Analysis, and Simulations in  
Mathematical Biology**

Computational and Mathematical Methods in Medicine

---

**Modeling, Analysis, and Simulations in  
Mathematical Biology**

Lead Guest Editor: Naeem Jan

Guest Editors: László T. Kóczy and Lazim Abdullah






---

Copyright © 2023 Hindawi Limited. All rights reserved.

This is a special issue published in “Computational and Mathematical Methods in Medicine.” All articles are open access articles distributed under the Creative Commons Attribution License, which permits unrestricted use, distribution, and reproduction in any medium, provided the original work is properly cited.

## Associate Editors

Ahmed Albahri, Iraq  
Konstantin Blyuss , United Kingdom  
Chuangyin Dang, Hong Kong  
Farai Nyabadza , South Africa  
Kathiravan Srinivasan , India

## Academic Editors

Laith Abualigah , Jordan  
Yaser Ahangari Nanehkaran , China  
Mubashir Ahmad, Pakistan  
Sultan Ahmad , Saudi Arabia  
Akif Akgul , Turkey  
Karthick Alagar, India  
Shadab Alam, Saudi Arabia  
Raul Alcaraz , Spain  
Emil Alexov, USA  
Enrique Baca-Garcia , Spain  
Sweta Bhattacharya , India  
Junguo Bian, USA  
Elia Biganzoli , Italy  
Antonio Boccaccio, Italy  
Hans A. Braun , Germany  
Zhicheng Cao, China  
Guy Carrault, France  
Sadaruddin Chachar , Pakistan  
Prem Chapagain , USA  
Huiling Chen , China  
Mengxin Chen , China  
Haruna Chiroma, Saudi Arabia  
Watcharaporn Cholamjiak , Thailand  
Maria N. D.S. Cordeiro , Portugal  
Cristiana Corsi , Italy  
Qi Dai , China  
Nagarajan Deivanayagam Pillai, India  
Didier Delignières , France  
Thomas Desaive , Belgium  
David Diller , USA  
Qamar Din, Pakistan  
Irina Doytchinova, Bulgaria  
Sheng Du , China  
D. Easwaramoorthy , India

Esmaeil Ebrahimie , Australia  
Issam El Naqa , USA  
Ilias Elmouki , Morocco  
Angelo Facchiano , Italy  
Luca Faes , Italy  
Maria E. Fantacci , Italy  
Giancarlo Ferrigno , Italy  
Marc Thilo Figge , Germany  
Giulia Fiscon , Italy  
Bapan Ghosh , India  
Igor I. Goryanin, Japan  
Marko Gosak , Slovenia  
Damien Hall, Australia  
Abdulsattar Hamad, Iraq  
Khalid Hattaf , Morocco  
Tingjun Hou , China  
Seiya Imoto , Japan  
Martti Juhola , Finland  
Rajesh Kaluri , India  
Karthick Kanagarathinam, India  
Rafik Karaman , Palestinian Authority  
Chandan Karmakar , Australia  
Kwang Gi Kim , Republic of Korea  
Andrzej Kloczkowski, USA  
Andrei Korobeinikov , China  
Sakthidasan Sankaran Krishnan, India  
Rajesh Kumar, India  
Kuruva Lakshmana , India  
Peng Li , USA  
Chung-Min Liao , Taiwan  
Pinyi Lu , USA  
Reinoud Maex, United Kingdom  
Valeri Makarov , Spain  
Juan Pablo Martínez , Spain  
Richard J. Maude, Thailand  
Zahid Mehmood , Pakistan  
John Mitchell , United Kingdom  
Fazal Ijaz Muhammad , Republic of Korea  
Vishal Nayak , USA  
Tongguang Ni, China  
Michele Nichelatti, Italy  
Kazuhisa Nishizawa , Japan  
Bing Niu , China

Hyuntae Park , Japan  
Jovana Paunovic , Serbia  
Manuel F. G. Penedo , Spain  
Riccardo Pernice , Italy  
Kemal Polat , Turkey  
Alberto Policriti, Italy  
Giuseppe Pontrelli , Italy  
Jesús Poza , Spain  
Maciej Przybyłek , Poland  
Bhanwar Lal Puniya , USA  
Mihai V. Putz , Romania  
Suresh Rasappan, Oman  
Jose Joaquin Rieta , Spain  
Fathalla Rihan , United Arab Emirates  
Sidheswar Routray, India  
Sudipta Roy , India  
Jan Rychtar , USA  
Mario Sansone , Italy  
Murat Sari , Turkey  
Shahzad Sarwar, Saudi Arabia  
Kamal Shah, Saudi Arabia  
Bhisham Sharma , India  
Simon A. Sherman, USA  
Mingsong Shi, China  
Mohammed Shuaib , Malaysia  
Prabhishek Singh , India  
Neelakandan Subramani, India  
Junwei Sun, China  
Yung-Shin Sun , Taiwan  
Min Tang , China  
Hongxun Tao, China  
Alireza Tavakkoli , USA  
João M. Tavares , Portugal  
Jlenia Toppi , Italy  
Anna Tsantili-Kakoulidou , Greece  
Markos G. Tsipouras, North Macedonia  
Po-Hsiang Tsui , Taiwan  
Sathishkumar V E , Republic of Korea  
Durai Raj Vincent P M , India  
Gajendra Kumar Vishwakarma, India  
Liangjiang Wang, USA  
Ruisheng Wang , USA  
Zhouchao Wei, China  
Gabriel Wittum, Germany  
Xiang Wu, China

KI Yanover , Israel  
Xiaojun Yao , China  
Kaan Yetilmezsoy, Turkey  
Hiro Yoshida, USA  
Yuhai Zhao , China

# Contents

---

**Retracted: Evaluation of Football Teaching Quality Based on Big Data**

Computational and Mathematical Methods in Medicine

Retraction (1 page), Article ID 9782167, Volume 2023 (2023)

**Retracted: Online Education Satisfaction Assessment Based on Machine Learning Model in Wireless Network Environment**

Computational and Mathematical Methods in Medicine

Retraction (1 page), Article ID 9861049, Volume 2023 (2023)

**Retracted: Effectiveness Analysis of English Newspaper Reading Teaching Based on Deep Learning from the Perspective of Online and Offline Hybrid Teaching**

Computational and Mathematical Methods in Medicine

Retraction (1 page), Article ID 9817194, Volume 2023 (2023)

**Retracted: Research on Improving the Executive Ability of University Administrators Based on Deep Learning**

Computational and Mathematical Methods in Medicine

Retraction (1 page), Article ID 9803786, Volume 2023 (2023)

**Retracted: Innovating Pedagogical Practices for Handmade Courses in Preschool Education Using Artificial Intelligence**

Computational and Mathematical Methods in Medicine

Retraction (1 page), Article ID 9795637, Volume 2023 (2023)

**Retracted: The Use of Deep Learning Model for Effect Analysis of Conventional Friction Power Confinement**

Computational and Mathematical Methods in Medicine

Retraction (1 page), Article ID 9817901, Volume 2023 (2023)

**Retracted: The Feasibility Mechanism of Nerve Interventional Thrombectomy for Occlusion of Cranial Artery M1 and M2 Segments**

Computational and Mathematical Methods in Medicine

Retraction (1 page), Article ID 9789478, Volume 2023 (2023)

**Retracted: Text Feature Extraction for Public English Vocabulary Based on Wavelet Transform**

Computational and Mathematical Methods in Medicine

Retraction (1 page), Article ID 9754134, Volume 2023 (2023)

**Retracted: The Healing Effects of Piano Practice-Induced Hand Muscle Injury**

Computational and Mathematical Methods in Medicine

Retraction (1 page), Article ID 9894587, Volume 2023 (2023)

**Retracted: Evaluation and Analysis of Traditional Customary Law Based on the Perspective of Big Data**

Computational and Mathematical Methods in Medicine

Retraction (1 page), Article ID 9870242, Volume 2023 (2023)

**Retracted: Exploration of the Cultivation Path of Medical Students' Politico-Ideological and Humanistic Quality Based on Deep Learning**

Computational and Mathematical Methods in Medicine  
Retraction (1 page), Article ID 9851023, Volume 2023 (2023)

**Retracted: UAV Communication Network Modeling and Energy Consumption Optimization Based on Routing Algorithm**

Computational and Mathematical Methods in Medicine  
Retraction (1 page), Article ID 9845710, Volume 2023 (2023)

**Retracted: Contemporary Value Assessment of Marxist Ideology under the Context of Deep Learning**

Computational and Mathematical Methods in Medicine  
Retraction (1 page), Article ID 9828237, Volume 2023 (2023)

**Retracted: Integrated Design and Development of Intelligent Scenic Area Rural Tourism Information Service Based on Hybrid Cloud**

Computational and Mathematical Methods in Medicine  
Retraction (1 page), Article ID 9753697, Volume 2023 (2023)

**Retracted: Evaluation and Stratification for Chinese International Education Quality with Deep Learning Model**

Computational and Mathematical Methods in Medicine  
Retraction (1 page), Article ID 9840651, Volume 2023 (2023)

**Retracted: Design of Faster R-CNN-Based Fault Detection Method for Subway Vehicles**

Computational and Mathematical Methods in Medicine  
Retraction (1 page), Article ID 9839087, Volume 2023 (2023)

**Retracted: A Secure Private Cloud Storage Platform for English Education Resources Based on IoT Technology**

Computational and Mathematical Methods in Medicine  
Retraction (1 page), Article ID 9831726, Volume 2023 (2023)

**Retracted: Music Art Teaching Quality Evaluation System Based on Convolutional Neural Network**

Computational and Mathematical Methods in Medicine  
Retraction (1 page), Article ID 9827894, Volume 2023 (2023)

**Retracted: Effect of Sandplay Therapy on the Mental Health Level of College Students**

Computational and Mathematical Methods in Medicine  
Retraction (1 page), Article ID 9821086, Volume 2023 (2023)

**Retracted: Quality Assessment of Vocational Education Teaching Reform Based on Deep Learning**

Computational and Mathematical Methods in Medicine  
Retraction (1 page), Article ID 9813504, Volume 2023 (2023)



# Contents

---

**Retracted: Application of Sandplay Therapy in the Mental Health Education of Vocational College Students**

Computational and Mathematical Methods in Medicine  
Retraction (1 page), Article ID 9809561, Volume 2023 (2023)

**Retracted: Rural Planning Evaluation Based on Artificial Neural Network**

Computational and Mathematical Methods in Medicine  
Retraction (1 page), Article ID 9808930, Volume 2023 (2023)

**Retracted: Value and Application of Traditional Culture of Embedded Network Teaching Platform in Moral Education in Colleges and Universities**

Computational and Mathematical Methods in Medicine  
Retraction (1 page), Article ID 9785641, Volume 2023 (2023)

**Retracted: Monitoring Mycoplasma pneumoniae-Specific Antibody, C-Reactive Protein, and Procalcitonin Levels in Children with Mycoplasma Pneumonia Is Important**

Computational and Mathematical Methods in Medicine  
Retraction (1 page), Article ID 9781949, Volume 2023 (2023)

**Retracted: Design and Application of Legally Valid Payment Templates Based on Linking Contracts**

Computational and Mathematical Methods in Medicine  
Retraction (1 page), Article ID 9760952, Volume 2023 (2023)

**Retracted: Corpus-Driven Resource Recommendation Algorithm for English Online Autonomous Learning**

Computational and Mathematical Methods in Medicine  
Retraction (1 page), Article ID 9897439, Volume 2023 (2023)

**Retracted: Effect of Acupotomy Combined with Electroacupuncture Therapy on Finger Mobility and Pain Relief in Patients with Carpal Tunnel Syndrome**

Computational and Mathematical Methods in Medicine  
Retraction (1 page), Article ID 9874037, Volume 2023 (2023)

**Retracted: Analysis of Legal Attributes and Rights Attributes of Personal Information from the Perspective of Big Data**

Computational and Mathematical Methods in Medicine  
Retraction (1 page), Article ID 9872360, Volume 2023 (2023)

**Retracted: Application Effect Analysis of Clinical Nursing Pathway in the Care of Neonatal Hypoxic-Ischemic Encephalopathy**

Computational and Mathematical Methods in Medicine  
Retraction (1 page), Article ID 9872026, Volume 2023 (2023)

**Retracted: Construction Method of Industrial College in Vocational Colleges Based on Cluster Analysis Algorithm**

Computational and Mathematical Methods in Medicine  
Retraction (1 page), Article ID 9865146, Volume 2023 (2023)

**Retracted: miR-135a-5p Suppresses TBK1 and Activates NRF2/TXNIP Antioxidant Pathway in LPS-Driven ALI in Mice**





Computational and Mathematical Methods in Medicine  
Retraction (1 page), Article ID 9856268, Volume 2023 (2023)

**Retracted: Innovation of Ideological and Political Education Management of College Students Based on IOT Big Data Technology in a Wireless Network Environment**

Computational and Mathematical Methods in Medicine  
Retraction (1 page), Article ID 9853929, Volume 2023 (2023)


**Retracted: MicroRNA-424-5p Alleviates Isoflurane Anesthesia-Induced Neurotoxicity in Human Embryonic Stem Cell-Derived Neurons by Targeting FASN**

Computational and Mathematical Methods in Medicine  
Retraction (1 page), Article ID 9851824, Volume 2023 (2023)

Salma Kanwal , Yasmeen Farooq, Muhammad Kamran Siddiqui, Nazeran Idrees , Asima Razzaque , and Fikre Bogale Petros 


Research Article (13 pages), Article ID , ()

**Meta-analysis of Proton Pump Inhibitors in the Treatment of Pharyngeal Reflux Disease**

Xiulin Jin, Xufeng Zhou, Zongxian Fan, Yingchun Qin, and Junjie Zhan 


Research Article (9 pages), Article ID 9105814, Volume 2022 (2022)

**Diagnostic Values of Blood Urea Nitrogen (BUN), Creatinine (Cr), and the Ratio of BUN to Cr for Distinguishing Heart Failure from Asthma and Chronic Obstructive Pulmonary Disease**

Jingjing Zhang, Ling Zhou, and Yuezhan Zhang 


Research Article (7 pages), Article ID 4586458, Volume 2022 (2022)

**Effect of Perioperative Dexmedetomidine Anesthesia on Prognosis of Elderly Patients with Gastrointestinal Tumor Surgery**

Lijia Guo, Yufei Liu , and Meitan Wang


Research Article (11 pages), Article ID 7889372, Volume 2022 (2022)

**[Retracted] miR-135a-5p Suppresses TBK1 and Activates NRF2/TXNIP Antioxidant Pathway in LPS-Driven ALI in Mice**

Guotao Zou, Yiwen Zeng, Yingjuan Wang, and Yong Luo 

Research Article (11 pages), Article ID 9088727, Volume 2022 (2022)








**Efficacy and Safety of Vitamin D Adjuvant Therapy for Ulcerative Colitis: A Meta-Analysis**

Xinyi Guo, Changxing Liu, and Yahui Huang 

Research Article (9 pages), Article ID 6836942, Volume 2022 (2022)


## Contents

### **Application Value of the Diagnosis during Early Carcinoma of Upper Digestive Tract Based on Optical Enhanced Endoscopic Technique**

Yinghao Song , Yulei Qu , Lu Li , Mengxuan Xing , Baohui Jia , Yingjie Ma , and Yong Zhang 


Research Article (6 pages), Article ID 9587070, Volume 2022 (2022)

### **Teaching Analysis for Visual Communication Design with the Perspective of Digital Technology**

Qian Sun  and Yingjie Zhu


Research Article (10 pages), Article ID 2411811, Volume 2022 (2022)

### **Network Security Problems and Countermeasures of Hospital Information System after Going to the Cloud**

Shuming Gao 


Research Article (6 pages), Article ID 9725741, Volume 2022 (2022)

### **Effect Analysis of Degranulated Cell in Early Fertilization on FET Outcome and Offspring Safety with Data Mining**

Qingyang Li, Li Zhao, Liling Zhou, Rongju Liu, and Bo Chen 


Research Article (9 pages), Article ID 4955287, Volume 2022 (2022)

### **[Retracted] Design and Application of Legally Valid Payment Templates Based on Linking Contracts**

Yue Zhu 


Research Article (9 pages), Article ID 1331237, Volume 2022 (2022)

### **[Retracted] The Healing Effects of Piano Practice-Induced Hand Muscle Injury**

Hecheng Yu and Xiaoming Luo 


Research Article (6 pages), Article ID 1020504, Volume 2022 (2022)

### **[Retracted] Effectiveness Analysis of English Newspaper Reading Teaching Based on Deep Learning from the Perspective of Online and Offline Hybrid Teaching**

Zheng Zeng and Xi Wang 

Research Article (9 pages), Article ID 4065527, Volume 2022 (2022)

### **Evaluation of Application Effect of Self-Made Compression Cold Therapy in Postoperative Rehabilitation of Patients with Orthopedic Dyskinesia**

Xiaojuan Wan , Liping Ji, Min Zhao, Shixiang Zhu, and Meixiu Tang


Research Article (10 pages), Article ID 8222933, Volume 2022 (2022)

### **Detection of the Content of Two Coumarins, IM and ISOIM, and Their Mechanism of Action on Colitis Rats in Angelica albicans**

Juan Zhang , Leilei Dong, and Ying Pan


Research Article (8 pages), Article ID 5475559, Volume 2022 (2022)

**[Retracted] Effect of Acupotomy Combined with Electroacupuncture Therapy on Finger Mobility and Pain Relief in Patients with Carpal Tunnel Syndrome**

Jianfei Li, Yinqiao Kou , Suzhao Zhang, and Kaibing Wang


Research Article (6 pages), Article ID 2550875, Volume 2022 (2022)

**Application of Medical-Nursing-Assistance Integration Model Based on Theoretical Basis of Behavioral Psychology in Management of Children's ICU**

Yingying Jiang 


Research Article (13 pages), Article ID 1744357, Volume 2022 (2022)

**IGBT Fault Prediction Combining Terminal Characteristics and Artificial Intelligence Neural Network**

Cailin Li 



Research Article (10 pages), Article ID 7459354, Volume 2022 (2022)

**Mechanism of miR-760 Reversing Lung Cancer Immune Escape by Downregulating IDO1 and Eliminating Regulatory T Cells Based on Mathematical Biology**

Hong Ge, Lili Wang, Wenqiang Chen, and Lei Wang 


Research Article (13 pages), Article ID 2960773, Volume 2022 (2022)

**[Retracted] MicroRNA-424-5p Alleviates Isoflurane Anesthesia-Induced Neurotoxicity in Human Embryonic Stem Cell-Derived Neurons by Targeting FASN**

Xiaojiao Gu, Wei Yue, Mingyu Xiu, Quanyun Zhang , and Rufeng Xie 


Research Article (13 pages), Article ID 2517463, Volume 2022 (2022)

**The Application of Transcranial Electrical Stimulation in Sports Psychology**

Shuzhi Chang 



Research Article (11 pages), Article ID 1008346, Volume 2022 (2022)

**The Effect of PACS in Breast Tumor Diagnosis Based on Numerical Analysis**

Guijun Guo and Yi Chen 


Research Article (6 pages), Article ID 7259951, Volume 2022 (2022)

**The Potential of miR-370-3p and miR-495-3p Serving as Biomarkers for Sepsis-Associated Acute Kidney Injury**

Wenlu Ma , Xiaomei Miao, Fangfang Xia, Chao Ruan, Dan Tao , and Bing Li

Research Article (5 pages), Article ID 2439509, Volume 2022 (2022)

**Effect of Algoplague Hydrocolloid Dressing Combined with Nanosilver Antibacterial Gel under Predictive Nursing in the Treatment of Medical Device-Related Pressure Injury**

Chunxiu Li, Hongmei Chen, and Guanghui You 




Research Article (9 pages), Article ID 9756602, Volume 2022 (2022)

## Contents




### **Correlation between the Treg/Th17 Index and the Efficacy of PD-1 Monoclonal Antibody in Patients with Advanced Non-Small-Cell Lung Cancer Complicated with Chronic Obstructive Pulmonary Disease**

Xiaoyu Wang, Xinyuan She, Wei Gao, Xing Liu, and Bin Shi   
Research Article (11 pages), Article ID 2923998, Volume 2022 (2022)

### **Combined Effect of Smoking and Fatty Liver Disease on the Progression of Type 2 Diabetes: Insights from a Population-Based Cohort Study**

Tingting Zhang , Donghe Zhang, Jing Zeng, Yan Yang, Yi Fang , and Xuan Wang   
Research Article (8 pages), Article ID 1776875, Volume 2022 (2022)



### **Statistical Analysis of COVID-19 Data for Three Different Regions in the Kingdom of Saudi Arabia: Using a New Two-Parameter Statistical Model**

Ibrahim Al-Dayel , Mohammed N. Alshahrani, Ibrahim Elbatal, Naif Alotaibi , A. W. Shawki, and Mohammed Elgarhy   
Research Article (11 pages), Article ID 2066787, Volume 2022 (2022)

### **[Retracted] Design of Faster R-CNN-Based Fault Detection Method for Subway Vehicles**

Hanlin Ma  and Mingyang Yao   
Research Article (10 pages), Article ID 1400658, Volume 2022 (2022)


### **Influence of Three-Dimensional Visual Reconstruction Technology Combined with Virtual Surgical Planning of CTA Images on Precise Resection of Liver Cancer in Hepatobiliary Surgery**

Yuanyu Zhao, Ting Chen, Hui Wang, Qiang Xue, Wenyan Guo, Guoshan Ding, Junfeng Dong , and Junsong Ji   
Research Article (9 pages), Article ID 4376654, Volume 2022 (2022)


### **Meta-Analysis of Low Temperature Plasma Radiofrequency Ablation and CO<sub>2</sub> Laser Surgery on Early Glottic Laryngeal Carcinoma**

Cheng Wang , Ye Zhao , Changhu Li, Qiang Song, and Fuxing Wang  
Research Article (8 pages), Article ID 3417005, Volume 2022 (2022)


### **Biophilic Design as an Important Bridge for Sustainable Interaction between Humans and the Environment: Based on Practice in Chinese Healthcare Space**

Yang Zhao, Qinchuan Zhan , and Tiancheng Xu  
Research Article (14 pages), Article ID 8184534, Volume 2022 (2022)


### **[Retracted] The Feasibility Mechanism of Nerve Interventional Thrombectomy for Occlusion of Cranial Artery M1 and M2 Segments**

Xiang Fang, Taijian Liao, Junhui Chen, Juan Wu, and Biyu Xu   
Research Article (10 pages), Article ID 6350033, Volume 2022 (2022)

### **Observation on the Nursing Effect of the Whole Process in Patients with Severe Intracranial Hemorrhage**

Zhongwei Su, Wei Guo, Yun Luo, Yao Wang, and Yue Du   
Research Article (6 pages), Article ID 1546019, Volume 2022 (2022)

**Analysis of Soft Tissue Changes and Influencing Factors of Implant Absorption after Immediate Restoration of Anterior Teeth**

Guodong Peng , Xiaodong Sun, and Xiang Xu



Research Article (7 pages), Article ID 3759337, Volume 2022 (2022)

**Perinatal Outcomes and Related Risk Factors of Single vs Twin Pregnancy Complicated by Gestational Diabetes Mellitus: Meta-Analysis**

Xiaofang Zhu, Chan Huang, Li Wu , Yufeng Deng, Xuemei Lai, Huayan Gu, and Haiyan Zhang


Review Article (6 pages), Article ID 3557890, Volume 2022 (2022)

**[Retracted] Quality Assessment of Vocational Education Teaching Reform Based on Deep Learning**

Zai Ni  and Fei Wang 


Research Article (11 pages), Article ID 1499420, Volume 2022 (2022)

**Effect Analysis of Positive Molecular Therapy in Surgical Nursing Based on Data Transformation Analysis**

Yuan Liu , Sumei Wu, Guifen Wang, Xiaoxue Sun, Lei Liu, and Yaling Zhao

Research Article (10 pages), Article ID 3548854, Volume 2022 (2022)

**Q-Switched Laser Combined with Intense Pulsed Laser in the Treatment of Melasma Based on Reflection Confocal Microscope**

Jiali Xu and Yijing Pu 


Research Article (10 pages), Article ID 4413130, Volume 2022 (2022)

**Effects of Knee Debridement with Flurbiprofen on Knee Function, Inflammatory Levels, and Bone Metabolism Activity in Patients with Knee Osteoarthritis**

Tao Lin, Zemiao Liu , Wei Ji, and Peng Zhang



Research Article (6 pages), Article ID 8031360, Volume 2022 (2022)

**Enteral Nutrition: Based on the Combination of Nutrison Fibre and TPF-DM with A Marine Biological-Based Active Polysaccharide Preparation**

Qiuyue Tang and Yaqin Cheng 


Research Article (8 pages), Article ID 6213716, Volume 2022 (2022)

**Application Effect of Dexmedetomidine and Dezocine in Patients Undergoing Lung Cancer Surgery under General Anesthesia and Analysis of Their Roles in Recovery Time and Cognitive Function**

Jie Ding, Mengqi Zhu, Hu Lv, Jun Zhang , and Wei Chen 

Research Article (8 pages), Article ID 9889534, Volume 2022 (2022)


**Clinical Features of Acute Coronary Syndrome in Patients with Coronary Heart Disease and Its Correlation with Tumour Necrosis Factor in Cardiology**

Run Guo, Tingting Wu, Nan Zheng, Yanfang Wan, and Jun Wang 



Research Article (13 pages), Article ID 3439768, Volume 2022 (2022)

## Contents

**Correlation of Inpatients Suffering from Acute Acalculous Cholecystitis during ICU Treatment with Acute Physiology and Chronic Health Evaluation II Score, Duration of Ventilator Use, and Time on Total Parenteral Nutrition**

Yunfeng Zhang, Kaixian Wang, Yuhui Wang, and Yang Liu   
Research Article (6 pages), Article ID 3407997, Volume 2022 (2022)


**Effect of Predictive Nursing Combined with Early Drinking Water Therapy on Patients with Urinary Retention after Vaginal Delivery**

Gaiying Cui , Yong Zhang, Zhaoxia Liu, Xia Li, and Manting Sha   
Research Article (5 pages), Article ID 4204762, Volume 2022 (2022)


**[Retracted] Online Education Satisfaction Assessment Based on Machine Learning Model in Wireless Network Environment**

Jing Qin   
Research Article (11 pages), Article ID 7958932, Volume 2022 (2022)


**[Retracted] Application of Sandplay Therapy in the Mental Health Education of Vocational College Students**

Xiaojing Xu , Yanhua Zhang, and Libin Liu  
Research Article (5 pages), Article ID 6141326, Volume 2022 (2022)


**[Retracted] UAV Communication Network Modeling and Energy Consumption Optimization Based on Routing Algorithm**

Ran Zhuo , Shiqian Song, and Yejun Xu  
Research Article (10 pages), Article ID 4782850, Volume 2022 (2022)


**[Retracted] Evaluation of Football Teaching Quality Based on Big Data**

Yue Long and Wei Zhai   
Research Article (10 pages), Article ID 7174246, Volume 2022 (2022)


**[Retracted] Exploration of the Cultivation Path of Medical Students' Politico-Ideological and Humanistic Quality Based on Deep Learning**

Sainan Xue and Shuang Li   
Research Article (9 pages), Article ID 5766675, Volume 2022 (2022)


**Identification of Key Genes in Severe Burns by Using Weighted Gene Coexpression Network Analysis**

ZhiHui Guo , YuJiao Zhang, ZhiGuo Ming, ZhenMing Hao, and Peng Duan  
Research Article (12 pages), Article ID 5220403, Volume 2022 (2022)

**Imaging Diagnosis of Primary Liver Cancer Using Magnetic Resonance Dilated Weighted Imaging and the Treatment Effect of Sorafenib**


Bin Fan, Yunyi Zhang, and Shuai Guo   
Research Article (12 pages), Article ID 8586943, Volume 2022 (2022)

**[Retracted] Monitoring Mycoplasma pneumoniae-Specific Antibody, C-Reactive Protein, and Procalcitonin Levels in Children with Mycoplasma Pneumonia Is Important**

Xinying Cao 


Research Article (7 pages), Article ID 7976858, Volume 2022 (2022)

**Fetal and Neonatal Middle Cerebral Artery Hemodynamic Changes and Significance under Ultrasound Detection in Hypertensive Disorder Complicating Pregnancy Patients with Different Severities**

Pei Zhou, Yi Sun, Yongpan Tan, Yanru An, Xingxing Wang, and Lufang Wang 


Research Article (14 pages), Article ID 6110228, Volume 2022 (2022)

**MicroRNA-17-5p Protects against Propofol Anesthesia-Induced Neurotoxicity and Autophagy Impairment via Targeting BCL2L1**

Mingyu Xiu, Hengfei Luan, Xiaojiao Gu, Chuang Liu, and Deming Xu 


Research Article (11 pages), Article ID 6018037, Volume 2022 (2022)

**Clinical Usage of Different Doses of Cis-Atracurium in Intracranial Aneurysm Surgery and Its Effect on Motor-Evoked Potentials**

Zhongyuan Qiao and Rong Fan 


Research Article (12 pages), Article ID 5910019, Volume 2022 (2022)

**Pharmacokinetics of Veratramine and Jervine from Alcohol Extracts of Radix Veratri**

Song Wang, Jiali Cui, Gaoqiong Zhao, Hongbin Liu, and Jingkun Wang 



Research Article (13 pages), Article ID 8289548, Volume 2022 (2022)

**The Effect of Acceptance and Commitment Therapy on Psychological Nursing of Acute Cerebral Infarction with Insomnia, Anxiety, and Depression**

Xinyu Wang, Jie Chen, Yun-e Liu, and Yan Wu 


Research Article (8 pages), Article ID 8538656, Volume 2022 (2022)

**Prediction Model Construction for Ischemic Stroke Recurrence with BP Network and Multivariate Logistic Regression and Effect of Individualized Health Education**

Ting Lu  and Yun Wang 

Research Article (10 pages), Article ID 4284566, Volume 2022 (2022)

**Effect of Physical Exercise Intervention Based on Improved Neural Network on College Students' Mental Health**

Linlin Cai 

Research Article (9 pages), Article ID 4884109, Volume 2022 (2022)

**Prediction of Ischemic Stroke Recurrence Based on COX Proportional Risk Regression Model and Evaluation of the Effectiveness of Patient Intensive Care Interventions**

Yun Wang  and Ting Lu 

Research Article (9 pages), Article ID 8392854, Volume 2022 (2022)




# Contents

## **Stability Analysis of Geotechnical Landslide Based on GA-BP Neural Network Model**

Jin Xu  and Yanna Zhao


Research Article (10 pages), Article ID 3958985, Volume 2022 (2022)

## **Research on Forest Conversation Analysis Using Autoregressive Neural Network-Based Model**

Tianhao Ma, Yuchen She, and Junang Liu 


Research Article (7 pages), Article ID 3280928, Volume 2022 (2022)

## **The Modeling Analysis and Effect of CHI3L1 and CD31-Marked Microvessel Density in the Occurrence and Development of Cervical Squamous Cell Carcinoma**

Yanzi Qin  and Wenjun Zhao


Research Article (9 pages), Article ID 3516335, Volume 2022 (2022)

## **Efficacy of Digestive Endoscope Based on Artificial Intelligence System in Diagnosing Early Esophageal Carcinoma**

Zhentaο Zhao, Meng Li, Ping Liu, Jingfang Yu, and Hua Zhao 


Research Article (5 pages), Article ID 9018939, Volume 2022 (2022)

## **Influences of Magnetic Resonance Imaging Superresolution Algorithm-Based Transition Care on Prognosis of Children with Severe Viral Encephalitis**

Yan Wang, Yan Zhang, and Ling Su 

Research Article (9 pages), Article ID 5909922, Volume 2022 (2022)

## **[Retracted] Analysis of Legal Attributes and Rights Attributes of Personal Information from the Perspective of Big Data**

Jingzhong Yan 


Research Article (10 pages), Article ID 9731414, Volume 2022 (2022)

## **[Retracted] Integrated Design and Development of Intelligent Scenic Area Rural Tourism Information Service Based on Hybrid Cloud**

Hong Zhang  and Mingyang Li

Research Article (9 pages), Article ID 5316304, Volume 2022 (2022)

## **[Retracted] Application Effect Analysis of Clinical Nursing Pathway in the Care of Neonatal Hypoxic-Ischemic Encephalopathy**

Xiaoyu Zhang and Hai Wang 


Research Article (6 pages), Article ID 9379361, Volume 2022 (2022)

## **[Retracted] Contemporary Value Assessment of Marxist Ideology under the Context of Deep Learning**

Jian Sun 


Research Article (10 pages), Article ID 4654153, Volume 2022 (2022)

**[Retracted] Corpus-Driven Resource Recommendation Algorithm for English Online Autonomous Learning**

Ling Gu 


Research Article (10 pages), Article ID 9369258, Volume 2022 (2022)

**[Retracted] A Secure Private Cloud Storage Platform for English Education Resources Based on IoT Technology**

Wei Li  and Ying Guo


Research Article (12 pages), Article ID 8453470, Volume 2022 (2022)

**[Retracted] Evaluation and Analysis of Traditional Customary Law Based on the Perspective of Big Data**

Juanjuan Yang  and Tee Boon Chuan


Research Article (10 pages), Article ID 5088630, Volume 2022 (2022)

**Predictive Analysis of Hospital HIS System Usage Satisfaction Based on Machine Learning**

Yuhang Hu and Haotian Gan 

Research Article (11 pages), Article ID 1366407, Volume 2022 (2022)

**[Retracted] Construction Method of Industrial College in Vocational Colleges Based on Cluster Analysis Algorithm**

Xiaorong Liu 


Research Article (9 pages), Article ID 3278395, Volume 2022 (2022)

**Inception-LSTM Human Motion Recognition with Channel Attention Mechanism**

Yongtao Xu  and Liye Zhao 


Research Article (12 pages), Article ID 9173504, Volume 2022 (2022)

**[Retracted] Text Feature Extraction for Public English Vocabulary Based on Wavelet Transform**

Di Ye  and Xiaojing Shi


Research Article (10 pages), Article ID 7125242, Volume 2022 (2022)

**Effect of Painless Rehabilitation Nursing for Hip Replacement Patients**

Xiaona Zhao, Ru Bai, and Jing Yang 


Research Article (6 pages), Article ID 5164973, Volume 2022 (2022)

**[Retracted] Rural Planning Evaluation Based on Artificial Neural Network**

Yumei Liu  and Xuezhou Huang

Research Article (10 pages), Article ID 9746362, Volume 2022 (2022)


**[Retracted] Innovation of Ideological and Political Education Management of College Students Based on IOT Big Data Technology in a Wireless Network Environment**

Zheng Du 

Research Article (8 pages), Article ID 9585760, Volume 2022 (2022)


# Contents

## **Application of New Media in Student Management from the Perspective of Deep Learning and Evaluation and Analysis of Practical Effects**

Danjun Ji, Xuejiao Wang, and Tianyu Zhang 


Research Article (10 pages), Article ID 1765448, Volume 2022 (2022)

## **Immediate versus Delayed Implantation for Single-Tooth Restoration of Maxillary Anterior Teeth: A Comparative Analysis on Efficacy**

Zhimin Chen , Shuhuai Zhang, Jun Zhou, and Hongling Liang


Research Article (6 pages), Article ID 4490335, Volume 2022 (2022)

## **[Retracted] Research on Improving the Executive Ability of University Administrators Based on Deep Learning**

Chengyan Wei  and Shenxiang Wang


Research Article (10 pages), Article ID 6354801, Volume 2022 (2022)

## **[Retracted] Value and Application of Traditional Culture of Embedded Network Teaching Platform in Moral Education in Colleges and Universities**

Juanjuan Yang 


Research Article (13 pages), Article ID 2096583, Volume 2022 (2022)

## **Evaluation and Analysis of the Intervention Effect of Systematic Parent Training Based on Computational Intelligence on Child Autism**

Xuejin He, Yinzhen Yu, and Yanqiong Ouyang 


Research Article (9 pages), Article ID 7746374, Volume 2022 (2022)

## **Application of Neural Network Algorithm in Medical Artificial Intelligence Product Development**

Yineng Xiao 

Research Article (11 pages), Article ID 5413202, Volume 2022 (2022)

## **Design of Machine Learning Algorithm for Tourism Demand Prediction**

Nan Yu  and Jiaping Chen


Research Article (9 pages), Article ID 6352381, Volume 2022 (2022)

## **A Study on Mobile Resources for Language Education of Preschool Children Based on Wireless Network Technology in Artificial Intelligence Context**

QiuMing Li 

Research Article (10 pages), Article ID 6206394, Volume 2022 (2022)

## **[Retracted] The Use of Deep Learning Model for Effect Analysis of Conventional Friction Power Confinement**

Chuntong Liu, Xin Wang, and Zhenxin He 







Research Article (8 pages), Article ID 8733919, Volume 2022 (2022)

## **[Retracted] Effect of Sandplay Therapy on the Mental Health Level of College Students**

Gaoyong Li  and Xue Wu 


Research Article (4 pages), Article ID 3716849, Volume 2022 (2022)

**Ensemble Learning Framework with GLCM Texture Extraction for Early Detection of Lung Cancer on CT Images**

Sara A. Althubiti , Sanchita Paul , Rajanikanta Mohanty , Sachi Nandan Mohanty , Fayadh Alenezi , and Kemal Polat 

Research Article (14 pages), Article ID 2733965, Volume 2022 (2022)

**[Retracted] Music Art Teaching Quality Evaluation System Based on Convolutional Neural Network**

Fumei Xu and Yu Xia 


Research Article (9 pages), Article ID 8479940, Volume 2022 (2022)

**A Comparative Study of Text Genres in English-Chinese Translation Effects Based on Deep Learning LSTM**

Xiaoda Zhao  and Xiaoyan Jin

Research Article (9 pages), Article ID 7068406, Volume 2022 (2022)

**Application of Graphic Design with Computer Graphics and Image Processing: Taking Packaging Design of Agricultural Products as an Example**

Tianhe Xie, Rongyi Sun, Jiahao Zhang, Ruiqi Wang, and Jiashu Wang 


Research Article (10 pages), Article ID 6554371, Volume 2022 (2022)

**Analysis of the Impact Mechanism of Occupational Identity on Occupational Well-Being Based on Big Data**

Yuefen Wang  and Dianyuan Yang


Research Article (10 pages), Article ID 4870296, Volume 2022 (2022)

**Effect of Midwives' Application of Intelligent Delivery Room Management System on Delivery Outcome**

Xia Li, Ping Zhang, Yong Zhang, Gaiying Cui, and Hui Du 


Research Article (5 pages), Article ID 4912053, Volume 2022 (2022)

**Analysis of the Effect of Exercise Combined with Diet Intervention on Postoperative Quality of Life of Breast Cancer Patients**

Lihua Lu, Xiaofeng Chen, Ping Lu, Jianli Wu, Yunxia Chen, Tiantian Ren, Yiju Li , and Xiang Zhong


Research Article (5 pages), Article ID 4072832, Volume 2022 (2022)

**Efficacy and Safety Analysis of Phloroglucinol in Combination with Oxytocin for the Induction of Labor in Women with Term Premature Rupture of Membranes (PROM)**

Jiazheng Yu, Lili Chen, Xia Wang, and Xiangzhi Li 

Research Article (7 pages), Article ID 2617075, Volume 2022 (2022)

**[Retracted] Innovating Pedagogical Practices for Handmade Courses in Preschool Education Using Artificial Intelligence**


Jun Zhao and Na Wang 

Research Article (8 pages), Article ID 3585958, Volume 2022 (2022)

## Contents

---

**[Retracted] Evaluation and Stratification for Chinese International Education Quality with Deep Learning Model**

Min He 

Research Article (10 pages), Article ID 9627116, Volume 2022 (2022)

## Retraction

# Retracted: Evaluation of Football Teaching Quality Based on Big Data

### Computational and Mathematical Methods in Medicine

Received 17 October 2023; Accepted 17 October 2023; Published 18 October 2023

Copyright © 2023 Computational and Mathematical Methods in Medicine. This is an open access article distributed under the Creative Commons Attribution License, which permits unrestricted use, distribution, and reproduction in any medium, provided the original work is properly cited.

This article has been retracted by Hindawi following an investigation undertaken by the publisher [1]. This investigation has uncovered evidence of one or more of the following indicators of systematic manipulation of the publication process:

- (1) Discrepancies in scope
- (2) Discrepancies in the description of the research reported
- (3) Discrepancies between the availability of data and the research described
- (4) Inappropriate citations
- (5) Incoherent, meaningless and/or irrelevant content included in the article
- (6) Peer-review manipulation

The presence of these indicators undermines our confidence in the integrity of the article's content and we cannot, therefore, vouch for its reliability. Please note that this notice is intended solely to alert readers that the content of this article is unreliable. We have not investigated whether authors were aware of or involved in the systematic manipulation of the publication process.

In addition, our investigation has also shown that one or more of the following human-subject reporting requirements has not been met in this article: ethical approval by an Institutional Review Board (IRB) committee or equivalent, patient/participant consent to participate, and/or agreement to publish patient/participant details (where relevant).

Wiley and Hindawi regrets that the usual quality checks did not identify these issues before publication and have since put additional measures in place to safeguard research integrity.

We wish to credit our own Research Integrity and Research Publishing teams and anonymous and named external researchers and research integrity experts for contributing to this investigation.

The corresponding author, as the representative of all authors, has been given the opportunity to register their agreement or disagreement to this retraction. We have kept a record of any response received.

### References

- [1] Y. Long and W. Zhai, "Evaluation of Football Teaching Quality Based on Big Data," *Computational and Mathematical Methods in Medicine*, vol. 2022, Article ID 7174246, 10 pages, 2022.

## *Retraction*

# **Retracted: Online Education Satisfaction Assessment Based on Machine Learning Model in Wireless Network Environment**

### **Computational and Mathematical Methods in Medicine**

Received 17 October 2023; Accepted 17 October 2023; Published 18 October 2023

Copyright © 2023 Computational and Mathematical Methods in Medicine. This is an open access article distributed under the Creative Commons Attribution License, which permits unrestricted use, distribution, and reproduction in any medium, provided the original work is properly cited.

This article has been retracted by Hindawi following an investigation undertaken by the publisher [1]. This investigation has uncovered evidence of one or more of the following indicators of systematic manipulation of the publication process:

- (1) Discrepancies in scope
- (2) Discrepancies in the description of the research reported
- (3) Discrepancies between the availability of data and the research described
- (4) Inappropriate citations
- (5) Incoherent, meaningless and/or irrelevant content included in the article
- (6) Peer-review manipulation

The presence of these indicators undermines our confidence in the integrity of the article's content and we cannot, therefore, vouch for its reliability. Please note that this notice is intended solely to alert readers that the content of this article is unreliable. We have not investigated whether authors were aware of or involved in the systematic manipulation of the publication process.

Wiley and Hindawi regrets that the usual quality checks did not identify these issues before publication and have since put additional measures in place to safeguard research integrity.

We wish to credit our own Research Integrity and Research Publishing teams and anonymous and named external researchers and research integrity experts for contributing to this investigation.

The corresponding author, as the representative of all authors, has been given the opportunity to register their agreement or disagreement to this retraction. We have kept a record of any response received.

### **References**

- [1] J. Qin, "Online Education Satisfaction Assessment Based on Machine Learning Model in Wireless Network Environment," *Computational and Mathematical Methods in Medicine*, vol. 2022, Article ID 7958932, 11 pages, 2022.

## Retraction

# Retracted: Effectiveness Analysis of English Newspaper Reading Teaching Based on Deep Learning from the Perspective of Online and Offline Hybrid Teaching

### Computational and Mathematical Methods in Medicine

Received 17 October 2023; Accepted 17 October 2023; Published 18 October 2023

Copyright © 2023 Computational and Mathematical Methods in Medicine. This is an open access article distributed under the Creative Commons Attribution License, which permits unrestricted use, distribution, and reproduction in any medium, provided the original work is properly cited.

This article has been retracted by Hindawi following an investigation undertaken by the publisher [1]. This investigation has uncovered evidence of one or more of the following indicators of systematic manipulation of the publication process:

- (1) Discrepancies in scope
- (2) Discrepancies in the description of the research reported
- (3) Discrepancies between the availability of data and the research described
- (4) Inappropriate citations
- (5) Incoherent, meaningless and/or irrelevant content included in the article
- (6) Peer-review manipulation

The presence of these indicators undermines our confidence in the integrity of the article's content and we cannot, therefore, vouch for its reliability. Please note that this notice is intended solely to alert readers that the content of this article is unreliable. We have not investigated whether authors were aware of or involved in the systematic manipulation of the publication process.

In addition, our investigation has also shown that one or more of the following human-subject reporting requirements has not been met in this article: ethical approval by an Institutional Review Board (IRB) committee or equivalent, patient/participant consent to participate, and/or agreement to publish patient/participant details (where relevant).

Wiley and Hindawi regrets that the usual quality checks did not identify these issues before publication and have since put additional measures in place to safeguard research integrity.

We wish to credit our own Research Integrity and Research Publishing teams and anonymous and named external researchers and research integrity experts for contributing to this investigation.

The corresponding author, as the representative of all authors, has been given the opportunity to register their agreement or disagreement to this retraction. We have kept a record of any response received.

### References

- [1] Z. Zeng and X. Wang, "Effectiveness Analysis of English Newspaper Reading Teaching Based on Deep Learning from the Perspective of Online and Offline Hybrid Teaching," *Computational and Mathematical Methods in Medicine*, vol. 2022, Article ID 4065527, 9 pages, 2022.



## Retraction

# Retracted: Research on Improving the Executive Ability of University Administrators Based on Deep Learning

### Computational and Mathematical Methods in Medicine

Received 17 October 2023; Accepted 17 October 2023; Published 18 October 2023

Copyright © 2023 Computational and Mathematical Methods in Medicine. This is an open access article distributed under the Creative Commons Attribution License, which permits unrestricted use, distribution, and reproduction in any medium, provided the original work is properly cited.

This article has been retracted by Hindawi following an investigation undertaken by the publisher [1]. This investigation has uncovered evidence of one or more of the following indicators of systematic manipulation of the publication process:

- (1) Discrepancies in scope
- (2) Discrepancies in the description of the research reported
- (3) Discrepancies between the availability of data and the research described
- (4) Inappropriate citations
- (5) Incoherent, meaningless and/or irrelevant content included in the article
- (6) Peer-review manipulation

The presence of these indicators undermines our confidence in the integrity of the article's content and we cannot, therefore, vouch for its reliability. Please note that this notice is intended solely to alert readers that the content of this article is unreliable. We have not investigated whether authors were aware of or involved in the systematic manipulation of the publication process.

Wiley and Hindawi regrets that the usual quality checks did not identify these issues before publication and have since put additional measures in place to safeguard research integrity.

We wish to credit our own Research Integrity and Research Publishing teams and anonymous and named external researchers and research integrity experts for contributing to this investigation.

The corresponding author, as the representative of all authors, has been given the opportunity to register their agreement or disagreement to this retraction. We have kept a record of any response received.

### References

- [1] C. Wei and S. Wang, "Research on Improving the Executive Ability of University Administrators Based on Deep Learning," *Computational and Mathematical Methods in Medicine*, vol. 2022, Article ID 6354801, 10 pages, 2022.

## *Retraction*

# **Retracted: Innovating Pedagogical Practices for Handmade Courses in Preschool Education Using Artificial Intelligence**

### **Computational and Mathematical Methods in Medicine**

Received 17 October 2023; Accepted 17 October 2023; Published 18 October 2023

Copyright © 2023 Computational and Mathematical Methods in Medicine. This is an open access article distributed under the Creative Commons Attribution License, which permits unrestricted use, distribution, and reproduction in any medium, provided the original work is properly cited.

This article has been retracted by Hindawi following an investigation undertaken by the publisher [1]. This investigation has uncovered evidence of one or more of the following indicators of systematic manipulation of the publication process:

- (1) Discrepancies in scope
- (2) Discrepancies in the description of the research reported
- (3) Discrepancies between the availability of data and the research described
- (4) Inappropriate citations
- (5) Incoherent, meaningless and/or irrelevant content included in the article
- (6) Peer-review manipulation

The presence of these indicators undermines our confidence in the integrity of the article's content and we cannot, therefore, vouch for its reliability. Please note that this notice is intended solely to alert readers that the content of this article is unreliable. We have not investigated whether authors were aware of or involved in the systematic manipulation of the publication process.

Wiley and Hindawi regrets that the usual quality checks did not identify these issues before publication and have since put additional measures in place to safeguard research integrity.

We wish to credit our own Research Integrity and Research Publishing teams and anonymous and named external researchers and research integrity experts for contributing to this investigation.

The corresponding author, as the representative of all authors, has been given the opportunity to register their agreement or disagreement to this retraction. We have kept a record of any response received.

### **References**

- [1] J. Zhao and N. Wang, "Innovating Pedagogical Practices for Handmade Courses in Preschool Education Using Artificial Intelligence," *Computational and Mathematical Methods in Medicine*, vol. 2022, Article ID 3585958, 8 pages, 2022.

## Retraction

# Retracted: The Use of Deep Learning Model for Effect Analysis of Conventional Friction Power Confinement

### Computational and Mathematical Methods in Medicine

Received 19 September 2023; Accepted 19 September 2023; Published 20 September 2023

Copyright © 2023 Computational and Mathematical Methods in Medicine. This is an open access article distributed under the Creative Commons Attribution License, which permits unrestricted use, distribution, and reproduction in any medium, provided the original work is properly cited.

This article has been retracted by Hindawi following an investigation undertaken by the publisher [1]. This investigation has uncovered evidence of one or more of the following indicators of systematic manipulation of the publication process:

- (1) Discrepancies in scope
- (2) Discrepancies in the description of the research reported
- (3) Discrepancies between the availability of data and the research described
- (4) Inappropriate citations
- (5) Incoherent, meaningless and/or irrelevant content included in the article
- (6) Peer-review manipulation

The presence of these indicators undermines our confidence in the integrity of the article's content and we cannot, therefore, vouch for its reliability. Please note that this notice is intended solely to alert readers that the content of this article is unreliable. We have not investigated whether authors were aware of or involved in the systematic manipulation of the publication process.

Wiley and Hindawi regrets that the usual quality checks did not identify these issues before publication and have since put additional measures in place to safeguard research integrity.

We wish to credit our own Research Integrity and Research Publishing teams and anonymous and named external researchers and research integrity experts for contributing to this investigation.

The corresponding author, as the representative of all authors, has been given the opportunity to register their agreement or disagreement to this retraction. We have kept a record of any response received.

### References

- [1] C. Liu, X. Wang, and Z. He, "The Use of Deep Learning Model for Effect Analysis of Conventional Friction Power Confinement," *Computational and Mathematical Methods in Medicine*, vol. 2022, Article ID 8733919, 8 pages, 2022.

## Retraction

# Retracted: The Feasibility Mechanism of Nerve Interventional Thrombectomy for Occlusion of Cranial Artery M1 and M2 Segments

### Computational and Mathematical Methods in Medicine

Received 19 September 2023; Accepted 19 September 2023; Published 20 September 2023

Copyright © 2023 Computational and Mathematical Methods in Medicine. This is an open access article distributed under the Creative Commons Attribution License, which permits unrestricted use, distribution, and reproduction in any medium, provided the original work is properly cited.

This article has been retracted by Hindawi following an investigation undertaken by the publisher [1]. This investigation has uncovered evidence of one or more of the following indicators of systematic manipulation of the publication process:

- (1) Discrepancies in scope
- (2) Discrepancies in the description of the research reported
- (3) Discrepancies between the availability of data and the research described
- (4) Inappropriate citations
- (5) Incoherent, meaningless and/or irrelevant content included in the article
- (6) Peer-review manipulation

The presence of these indicators undermines our confidence in the integrity of the article's content and we cannot, therefore, vouch for its reliability. Please note that this notice is intended solely to alert readers that the content of this article is unreliable. We have not investigated whether authors were aware of or involved in the systematic manipulation of the publication process.

Wiley and Hindawi regrets that the usual quality checks did not identify these issues before publication and have since put additional measures in place to safeguard research integrity.

We wish to credit our own Research Integrity and Research Publishing teams and anonymous and named external researchers and research integrity experts for contributing to this investigation.

The corresponding author, as the representative of all authors, has been given the opportunity to register their agreement or disagreement to this retraction. We have kept a record of any response received.

### References

- [1] X. Fang, T. Liao, J. Chen, J. Wu, and B. Xu, "The Feasibility Mechanism of Nerve Interventional Thrombectomy for Occlusion of Cranial Artery M1 and M2 Segments," *Computational and Mathematical Methods in Medicine*, vol. 2022, Article ID 6350033, 10 pages, 2022.

## Retraction

# Retracted: Text Feature Extraction for Public English Vocabulary Based on Wavelet Transform

### Computational and Mathematical Methods in Medicine

Received 19 September 2023; Accepted 19 September 2023; Published 20 September 2023

Copyright © 2023 Computational and Mathematical Methods in Medicine. This is an open access article distributed under the Creative Commons Attribution License, which permits unrestricted use, distribution, and reproduction in any medium, provided the original work is properly cited.

This article has been retracted by Hindawi following an investigation undertaken by the publisher [1]. This investigation has uncovered evidence of one or more of the following indicators of systematic manipulation of the publication process:

- (1) Discrepancies in scope
- (2) Discrepancies in the description of the research reported
- (3) Discrepancies between the availability of data and the research described
- (4) Inappropriate citations
- (5) Incoherent, meaningless and/or irrelevant content included in the article
- (6) Peer-review manipulation

The presence of these indicators undermines our confidence in the integrity of the article's content and we cannot, therefore, vouch for its reliability. Please note that this notice is intended solely to alert readers that the content of this article is unreliable. We have not investigated whether authors were aware of or involved in the systematic manipulation of the publication process.

Wiley and Hindawi regrets that the usual quality checks did not identify these issues before publication and have since put additional measures in place to safeguard research integrity.

We wish to credit our own Research Integrity and Research Publishing teams and anonymous and named external researchers and research integrity experts for contributing to this investigation.

The corresponding author, as the representative of all authors, has been given the opportunity to register their agreement or disagreement to this retraction. We have kept a record of any response received.

### References

- [1] D. Ye and X. Shi, "Text Feature Extraction for Public English Vocabulary Based on Wavelet Transform," *Computational and Mathematical Methods in Medicine*, vol. 2022, Article ID 7125242, 10 pages, 2022.

## Retraction

# Retracted: The Healing Effects of Piano Practice-Induced Hand Muscle Injury

### Computational and Mathematical Methods in Medicine

Received 1 August 2023; Accepted 1 August 2023; Published 2 August 2023

Copyright © 2023 Computational and Mathematical Methods in Medicine. This is an open access article distributed under the Creative Commons Attribution License, which permits unrestricted use, distribution, and reproduction in any medium, provided the original work is properly cited.

This article has been retracted by Hindawi following an investigation undertaken by the publisher [1]. This investigation has uncovered evidence of one or more of the following indicators of systematic manipulation of the publication process:

- (1) Discrepancies in scope
- (2) Discrepancies in the description of the research reported
- (3) Discrepancies between the availability of data and the research described
- (4) Inappropriate citations
- (5) Incoherent, meaningless and/or irrelevant content included in the article
- (6) Peer-review manipulation

The presence of these indicators undermines our confidence in the integrity of the article's content and we cannot, therefore, vouch for its reliability. Please note that this notice is intended solely to alert readers that the content of this article is unreliable. We have not investigated whether authors were aware of or involved in the systematic manipulation of the publication process.

In addition, our investigation has also shown that one or more of the following human-subject reporting requirements has not been met in this article: ethical approval by an Institutional Review Board (IRB) committee or equivalent, patient/participant consent to participate, and/or agreement to publish patient/participant details (where relevant).

Wiley and Hindawi regrets that the usual quality checks did not identify these issues before publication and have

since put additional measures in place to safeguard research integrity.

We wish to credit our own Research Integrity and Research Publishing teams and anonymous and named external researchers and research integrity experts for contributing to this investigation.

The corresponding author, as the representative of all authors, has been given the opportunity to register their agreement or disagreement to this retraction. We have kept a record of any response received.

### References

- [1] H. Yu and X. Luo, "The Healing Effects of Piano Practice-Induced Hand Muscle Injury," *Computational and Mathematical Methods in Medicine*, vol. 2022, Article ID 1020504, 6 pages, 2022.

## Retraction

# Retracted: Evaluation and Analysis of Traditional Customary Law Based on the Perspective of Big Data

### Computational and Mathematical Methods in Medicine

Received 1 August 2023; Accepted 1 August 2023; Published 2 August 2023

Copyright © 2023 Computational and Mathematical Methods in Medicine. This is an open access article distributed under the Creative Commons Attribution License, which permits unrestricted use, distribution, and reproduction in any medium, provided the original work is properly cited.

This article has been retracted by Hindawi following an investigation undertaken by the publisher [1]. This investigation has uncovered evidence of one or more of the following indicators of systematic manipulation of the publication process:

- (1) Discrepancies in scope
- (2) Discrepancies in the description of the research reported
- (3) Discrepancies between the availability of data and the research described
- (4) Inappropriate citations
- (5) Incoherent, meaningless and/or irrelevant content included in the article
- (6) Peer-review manipulation

The presence of these indicators undermines our confidence in the integrity of the article's content and we cannot, therefore, vouch for its reliability. Please note that this notice is intended solely to alert readers that the content of this article is unreliable. We have not investigated whether authors were aware of or involved in the systematic manipulation of the publication process.

Wiley and Hindawi regrets that the usual quality checks did not identify these issues before publication and have since put additional measures in place to safeguard research integrity.

We wish to credit our own Research Integrity and Research Publishing teams and anonymous and named external researchers and research integrity experts for contributing to this investigation.

The corresponding author, as the representative of all authors, has been given the opportunity to register their agreement or disagreement to this retraction. We have kept a record of any response received.

### References

- [1] J. Yang and T. B. Chuan, "Evaluation and Analysis of Traditional Customary Law Based on the Perspective of Big Data," *Computational and Mathematical Methods in Medicine*, vol. 2022, Article ID 5088630, 10 pages, 2022.

## Retraction

# Retracted: Exploration of the Cultivation Path of Medical Students' Politico-Ideological and Humanistic Quality Based on Deep Learning

### Computational and Mathematical Methods in Medicine

Received 1 August 2023; Accepted 1 August 2023; Published 2 August 2023

Copyright © 2023 Computational and Mathematical Methods in Medicine. This is an open access article distributed under the Creative Commons Attribution License, which permits unrestricted use, distribution, and reproduction in any medium, provided the original work is properly cited.

This article has been retracted by Hindawi following an investigation undertaken by the publisher [1]. This investigation has uncovered evidence of one or more of the following indicators of systematic manipulation of the publication process:

- (1) Discrepancies in scope
- (2) Discrepancies in the description of the research reported
- (3) Discrepancies between the availability of data and the research described
- (4) Inappropriate citations
- (5) Incoherent, meaningless and/or irrelevant content included in the article
- (6) Peer-review manipulation

The presence of these indicators undermines our confidence in the integrity of the article's content and we cannot, therefore, vouch for its reliability. Please note that this notice is intended solely to alert readers that the content of this article is unreliable. We have not investigated whether authors were aware of or involved in the systematic manipulation of the publication process.

In addition, our investigation has also shown that one or more of the following human-subject reporting requirements has not been met in this article: ethical approval by an Institutional Review Board (IRB) committee or equivalent, patient/participant consent to participate, and/or agreement to publish patient/participant details (where relevant).

Wiley and Hindawi regrets that the usual quality checks did not identify these issues before publication and have since put additional measures in place to safeguard research integrity.

We wish to credit our own Research Integrity and Research Publishing teams and anonymous and named external researchers and research integrity experts for contributing to this investigation.

The corresponding author, as the representative of all authors, has been given the opportunity to register their agreement or disagreement to this retraction. We have kept a record of any response received.

### References

- [1] S. Xue and S. Li, "Exploration of the Cultivation Path of Medical Students' Politico-Ideological and Humanistic Quality Based on Deep Learning," *Computational and Mathematical Methods in Medicine*, vol. 2022, Article ID 5766675, 9 pages, 2022.



## Retraction

# Retracted: UAV Communication Network Modeling and Energy Consumption Optimization Based on Routing Algorithm

### Computational and Mathematical Methods in Medicine

Received 1 August 2023; Accepted 1 August 2023; Published 2 August 2023

Copyright © 2023 Computational and Mathematical Methods in Medicine. This is an open access article distributed under the Creative Commons Attribution License, which permits unrestricted use, distribution, and reproduction in any medium, provided the original work is properly cited.

This article has been retracted by Hindawi following an investigation undertaken by the publisher [1]. This investigation has uncovered evidence of one or more of the following indicators of systematic manipulation of the publication process:

- (1) Discrepancies in scope
- (2) Discrepancies in the description of the research reported
- (3) Discrepancies between the availability of data and the research described
- (4) Inappropriate citations
- (5) Incoherent, meaningless and/or irrelevant content included in the article
- (6) Peer-review manipulation

The presence of these indicators undermines our confidence in the integrity of the article's content and we cannot, therefore, vouch for its reliability. Please note that this notice is intended solely to alert readers that the content of this article is unreliable. We have not investigated whether authors were aware of or involved in the systematic manipulation of the publication process.

Wiley and Hindawi regrets that the usual quality checks did not identify these issues before publication and have since put additional measures in place to safeguard research integrity.

We wish to credit our own Research Integrity and Research Publishing teams and anonymous and named external researchers and research integrity experts for contributing to this investigation.

The corresponding author, as the representative of all authors, has been given the opportunity to register their agreement or disagreement to this retraction. We have kept a record of any response received.

### References

- [1] R. Zhuo, S. Song, and Y. Xu, "UAV Communication Network Modeling and Energy Consumption Optimization Based on Routing Algorithm," *Computational and Mathematical Methods in Medicine*, vol. 2022, Article ID 4782850, 10 pages, 2022.

## Retraction

# Retracted: Contemporary Value Assessment of Marxist Ideology under the Context of Deep Learning

### Computational and Mathematical Methods in Medicine

Received 1 August 2023; Accepted 1 August 2023; Published 2 August 2023

Copyright © 2023 Computational and Mathematical Methods in Medicine. This is an open access article distributed under the Creative Commons Attribution License, which permits unrestricted use, distribution, and reproduction in any medium, provided the original work is properly cited.

This article has been retracted by Hindawi following an investigation undertaken by the publisher [1]. This investigation has uncovered evidence of one or more of the following indicators of systematic manipulation of the publication process:

- (1) Discrepancies in scope
- (2) Discrepancies in the description of the research reported
- (3) Discrepancies between the availability of data and the research described
- (4) Inappropriate citations
- (5) Incoherent, meaningless and/or irrelevant content included in the article
- (6) Peer-review manipulation

The presence of these indicators undermines our confidence in the integrity of the article's content and we cannot, therefore, vouch for its reliability. Please note that this notice is intended solely to alert readers that the content of this article is unreliable. We have not investigated whether authors were aware of or involved in the systematic manipulation of the publication process.

Wiley and Hindawi regrets that the usual quality checks did not identify these issues before publication and have since put additional measures in place to safeguard research integrity.

We wish to credit our own Research Integrity and Research Publishing teams and anonymous and named external researchers and research integrity experts for contributing to this investigation.

The corresponding author, as the representative of all authors, has been given the opportunity to register their agreement or disagreement to this retraction. We have kept a record of any response received.

### References

- [1] J. Sun, "Contemporary Value Assessment of Marxist Ideology under the Context of Deep Learning," *Computational and Mathematical Methods in Medicine*, vol. 2022, Article ID 4654153, 10 pages, 2022.

## Retraction

# Retracted: Integrated Design and Development of Intelligent Scenic Area Rural Tourism Information Service Based on Hybrid Cloud

### Computational and Mathematical Methods in Medicine

Received 1 August 2023; Accepted 1 August 2023; Published 2 August 2023

Copyright © 2023 Computational and Mathematical Methods in Medicine. This is an open access article distributed under the Creative Commons Attribution License, which permits unrestricted use, distribution, and reproduction in any medium, provided the original work is properly cited.

This article has been retracted by Hindawi following an investigation undertaken by the publisher [1]. This investigation has uncovered evidence of one or more of the following indicators of systematic manipulation of the publication process:

- (1) Discrepancies in scope
- (2) Discrepancies in the description of the research reported
- (3) Discrepancies between the availability of data and the research described
- (4) Inappropriate citations
- (5) Incoherent, meaningless and/or irrelevant content included in the article
- (6) Peer-review manipulation

The presence of these indicators undermines our confidence in the integrity of the article's content and we cannot, therefore, vouch for its reliability. Please note that this notice is intended solely to alert readers that the content of this article is unreliable. We have not investigated whether authors were aware of or involved in the systematic manipulation of the publication process.

Wiley and Hindawi regrets that the usual quality checks did not identify these issues before publication and have since put additional measures in place to safeguard research integrity.

We wish to credit our own Research Integrity and Research Publishing teams and anonymous and named external researchers and research integrity experts for contributing to this investigation.

The corresponding author, as the representative of all authors, has been given the opportunity to register their agreement or disagreement to this retraction. We have kept a record of any response received.

### References

- [1] H. Zhang and M. Li, "Integrated Design and Development of Intelligent Scenic Area Rural Tourism Information Service Based on Hybrid Cloud," *Computational and Mathematical Methods in Medicine*, vol. 2022, Article ID 5316304, 9 pages, 2022.

## Retraction

# Retracted: Evaluation and Stratification for Chinese International Education Quality with Deep Learning Model

### Computational and Mathematical Methods in Medicine

Received 25 July 2023; Accepted 25 July 2023; Published 26 July 2023

Copyright © 2023 Computational and Mathematical Methods in Medicine. This is an open access article distributed under the Creative Commons Attribution License, which permits unrestricted use, distribution, and reproduction in any medium, provided the original work is properly cited.

This article has been retracted by Hindawi following an investigation undertaken by the publisher [1]. This investigation has uncovered evidence of one or more of the following indicators of systematic manipulation of the publication process:

- (1) Discrepancies in scope
- (2) Discrepancies in the description of the research reported
- (3) Discrepancies between the availability of data and the research described
- (4) Inappropriate citations
- (5) Incoherent, meaningless and/or irrelevant content included in the article
- (6) Peer-review manipulation

The presence of these indicators undermines our confidence in the integrity of the article's content and we cannot, therefore, vouch for its reliability. Please note that this notice is intended solely to alert readers that the content of this article is unreliable. We have not investigated whether authors were aware of or involved in the systematic manipulation of the publication process.

Wiley and Hindawi regrets that the usual quality checks did not identify these issues before publication and have since put additional measures in place to safeguard research integrity.

We wish to credit our own Research Integrity and Research Publishing teams and anonymous and named external researchers and research integrity experts for contributing to this investigation.

The corresponding author, as the representative of all authors, has been given the opportunity to register their agreement or disagreement to this retraction. We have kept a record of any response received.

### References

- [1] M. He, "Evaluation and Stratification for Chinese International Education Quality with Deep Learning Model," *Computational and Mathematical Methods in Medicine*, vol. 2022, Article ID 9627116, 10 pages, 2022.

## Retraction

# Retracted: Design of Faster R-CNN-Based Fault Detection Method for Subway Vehicles

### Computational and Mathematical Methods in Medicine

Received 25 July 2023; Accepted 25 July 2023; Published 26 July 2023

Copyright © 2023 Computational and Mathematical Methods in Medicine. This is an open access article distributed under the Creative Commons Attribution License, which permits unrestricted use, distribution, and reproduction in any medium, provided the original work is properly cited.

This article has been retracted by Hindawi following an investigation undertaken by the publisher [1]. This investigation has uncovered evidence of one or more of the following indicators of systematic manipulation of the publication process:

- (1) Discrepancies in scope
- (2) Discrepancies in the description of the research reported
- (3) Discrepancies between the availability of data and the research described
- (4) Inappropriate citations
- (5) Incoherent, meaningless and/or irrelevant content included in the article
- (6) Peer-review manipulation

The presence of these indicators undermines our confidence in the integrity of the article's content and we cannot, therefore, vouch for its reliability. Please note that this notice is intended solely to alert readers that the content of this article is unreliable. We have not investigated whether authors were aware of or involved in the systematic manipulation of the publication process.

Wiley and Hindawi regrets that the usual quality checks did not identify these issues before publication and have since put additional measures in place to safeguard research integrity.

We wish to credit our own Research Integrity and Research Publishing teams and anonymous and named external researchers and research integrity experts for contributing to this investigation.

The corresponding author, as the representative of all authors, has been given the opportunity to register their agreement or disagreement to this retraction. We have kept a record of any response received.

### References

- [1] H. Ma and M. Yao, "Design of Faster R-CNN-Based Fault Detection Method for Subway Vehicles," *Computational and Mathematical Methods in Medicine*, vol. 2022, Article ID 1400658, 10 pages, 2022.

## *Retraction*

# **Retracted: A Secure Private Cloud Storage Platform for English Education Resources Based on IoT Technology**

### **Computational and Mathematical Methods in Medicine**

Received 25 July 2023; Accepted 25 July 2023; Published 26 July 2023

Copyright © 2023 Computational and Mathematical Methods in Medicine. This is an open access article distributed under the Creative Commons Attribution License, which permits unrestricted use, distribution, and reproduction in any medium, provided the original work is properly cited.

This article has been retracted by Hindawi following an investigation undertaken by the publisher [1]. This investigation has uncovered evidence of one or more of the following indicators of systematic manipulation of the publication process:

- (1) Discrepancies in scope
- (2) Discrepancies in the description of the research reported
- (3) Discrepancies between the availability of data and the research described
- (4) Inappropriate citations
- (5) Incoherent, meaningless and/or irrelevant content included in the article
- (6) Peer-review manipulation

The presence of these indicators undermines our confidence in the integrity of the article's content and we cannot, therefore, vouch for its reliability. Please note that this notice is intended solely to alert readers that the content of this article is unreliable. We have not investigated whether authors were aware of or involved in the systematic manipulation of the publication process.

Wiley and Hindawi regrets that the usual quality checks did not identify these issues before publication and have since put additional measures in place to safeguard research integrity.

We wish to credit our own Research Integrity and Research Publishing teams and anonymous and named external researchers and research integrity experts for contributing to this investigation.

The corresponding author, as the representative of all authors, has been given the opportunity to register their agreement or disagreement to this retraction. We have kept a record of any response received.

### **References**

- [1] W. Li and Y. Guo, "A Secure Private Cloud Storage Platform for English Education Resources Based on IoT Technology," *Computational and Mathematical Methods in Medicine*, vol. 2022, Article ID 8453470, 12 pages, 2022.

## Retraction

# Retracted: Music Art Teaching Quality Evaluation System Based on Convolutional Neural Network

### Computational and Mathematical Methods in Medicine

Received 25 July 2023; Accepted 25 July 2023; Published 26 July 2023

Copyright © 2023 Computational and Mathematical Methods in Medicine. This is an open access article distributed under the Creative Commons Attribution License, which permits unrestricted use, distribution, and reproduction in any medium, provided the original work is properly cited.

This article has been retracted by Hindawi following an investigation undertaken by the publisher [1]. This investigation has uncovered evidence of one or more of the following indicators of systematic manipulation of the publication process:

- (1) Discrepancies in scope
- (2) Discrepancies in the description of the research reported
- (3) Discrepancies between the availability of data and the research described
- (4) Inappropriate citations
- (5) Incoherent, meaningless and/or irrelevant content included in the article
- (6) Peer-review manipulation

The presence of these indicators undermines our confidence in the integrity of the article's content and we cannot, therefore, vouch for its reliability. Please note that this notice is intended solely to alert readers that the content of this article is unreliable. We have not investigated whether authors were aware of or involved in the systematic manipulation of the publication process.

Wiley and Hindawi regrets that the usual quality checks did not identify these issues before publication and have since put additional measures in place to safeguard research integrity.

We wish to credit our own Research Integrity and Research Publishing teams and anonymous and named external researchers and research integrity experts for contributing to this investigation.

The corresponding author, as the representative of all authors, has been given the opportunity to register their agreement or disagreement to this retraction. We have kept a record of any response received.

### References

- [1] F. Xu and Y. Xia, "Music Art Teaching Quality Evaluation System Based on Convolutional Neural Network," *Computational and Mathematical Methods in Medicine*, vol. 2022, Article ID 8479940, 9 pages, 2022.

## *Retraction*

# **Retracted: Effect of Sandplay Therapy on the Mental Health Level of College Students**

### **Computational and Mathematical Methods in Medicine**

Received 25 July 2023; Accepted 25 July 2023; Published 26 July 2023

Copyright © 2023 Computational and Mathematical Methods in Medicine. This is an open access article distributed under the Creative Commons Attribution License, which permits unrestricted use, distribution, and reproduction in any medium, provided the original work is properly cited.

This article has been retracted by Hindawi following an investigation undertaken by the publisher [1]. This investigation has uncovered evidence of one or more of the following indicators of systematic manipulation of the publication process:

- (1) Discrepancies in scope
- (2) Discrepancies in the description of the research reported
- (3) Discrepancies between the availability of data and the research described
- (4) Inappropriate citations
- (5) Incoherent, meaningless and/or irrelevant content included in the article
- (6) Peer-review manipulation

The presence of these indicators undermines our confidence in the integrity of the article's content and we cannot, therefore, vouch for its reliability. Please note that this notice is intended solely to alert readers that the content of this article is unreliable. We have not investigated whether authors were aware of or involved in the systematic manipulation of the publication process.

In addition, our investigation has also shown that one or more of the following human-subject reporting requirements has not been met in this article: ethical approval by an Institutional Review Board (IRB) committee or equivalent, patient/participant consent to participate, and/or agreement to publish patient/participant details (where relevant).

Wiley and Hindawi regrets that the usual quality checks did not identify these issues before publication and have since put additional measures in place to safeguard research integrity.

We wish to credit our own Research Integrity and Research Publishing teams and anonymous and named external researchers and research integrity experts for contributing to this investigation.

The corresponding author, as the representative of all authors, has been given the opportunity to register their agreement or disagreement to this retraction. We have kept a record of any response received.

### **References**

- [1] G. Li and X. Wu, "Effect of Sandplay Therapy on the Mental Health Level of College Students," *Computational and Mathematical Methods in Medicine*, vol. 2022, Article ID 3716849, 4 pages, 2022.



## Retraction

# Retracted: Quality Assessment of Vocational Education Teaching Reform Based on Deep Learning

### Computational and Mathematical Methods in Medicine

Received 25 July 2023; Accepted 25 July 2023; Published 26 July 2023

Copyright © 2023 Computational and Mathematical Methods in Medicine. This is an open access article distributed under the Creative Commons Attribution License, which permits unrestricted use, distribution, and reproduction in any medium, provided the original work is properly cited.

This article has been retracted by Hindawi following an investigation undertaken by the publisher [1]. This investigation has uncovered evidence of one or more of the following indicators of systematic manipulation of the publication process:

- (1) Discrepancies in scope
- (2) Discrepancies in the description of the research reported
- (3) Discrepancies between the availability of data and the research described
- (4) Inappropriate citations
- (5) Incoherent, meaningless and/or irrelevant content included in the article
- (6) Peer-review manipulation

The presence of these indicators undermines our confidence in the integrity of the article's content and we cannot, therefore, vouch for its reliability. Please note that this notice is intended solely to alert readers that the content of this article is unreliable. We have not investigated whether authors were aware of or involved in the systematic manipulation of the publication process.

Wiley and Hindawi regrets that the usual quality checks did not identify these issues before publication and have since put additional measures in place to safeguard research integrity.

We wish to credit our own Research Integrity and Research Publishing teams and anonymous and named external researchers and research integrity experts for contributing to this investigation.

The corresponding author, as the representative of all authors, has been given the opportunity to register their agreement or disagreement to this retraction. We have kept a record of any response received.

### References

- [1] Z. Ni and F. Wang, "Quality Assessment of Vocational Education Teaching Reform Based on Deep Learning," *Computational and Mathematical Methods in Medicine*, vol. 2022, Article ID 1499420, 11 pages, 2022.

## Retraction

# Retracted: Application of Sandplay Therapy in the Mental Health Education of Vocational College Students

### Computational and Mathematical Methods in Medicine

Received 25 July 2023; Accepted 25 July 2023; Published 26 July 2023

Copyright © 2023 Computational and Mathematical Methods in Medicine. This is an open access article distributed under the Creative Commons Attribution License, which permits unrestricted use, distribution, and reproduction in any medium, provided the original work is properly cited.

This article has been retracted by Hindawi following an investigation undertaken by the publisher [1]. This investigation has uncovered evidence of one or more of the following indicators of systematic manipulation of the publication process:

- (1) Discrepancies in scope
- (2) Discrepancies in the description of the research reported
- (3) Discrepancies between the availability of data and the research described
- (4) Inappropriate citations
- (5) Incoherent, meaningless and/or irrelevant content included in the article
- (6) Peer-review manipulation

The presence of these indicators undermines our confidence in the integrity of the article's content and we cannot, therefore, vouch for its reliability. Please note that this notice is intended solely to alert readers that the content of this article is unreliable. We have not investigated whether authors were aware of or involved in the systematic manipulation of the publication process.

In addition, our investigation has also shown that one or more of the following human-subject reporting requirements has not been met in this article: ethical approval by an Institutional Review Board (IRB) committee or equivalent, patient/participant consent to participate, and/or agreement to publish patient/participant details (where relevant).

Wiley and Hindawi regrets that the usual quality checks did not identify these issues before publication and have since put additional measures in place to safeguard research integrity.

We wish to credit our own Research Integrity and Research Publishing teams and anonymous and named external researchers and research integrity experts for contributing to this investigation.

The corresponding author, as the representative of all authors, has been given the opportunity to register their agreement or disagreement to this retraction. We have kept a record of any response received.

### References

- [1] X. Xu, Y. Zhang, and L. Liu, "Application of Sandplay Therapy in the Mental Health Education of Vocational College Students," *Computational and Mathematical Methods in Medicine*, vol. 2022, Article ID 6141326, 5 pages, 2022.

## Retraction

# Retracted: Rural Planning Evaluation Based on Artificial Neural Network

### Computational and Mathematical Methods in Medicine

Received 25 July 2023; Accepted 25 July 2023; Published 26 July 2023

Copyright © 2023 Computational and Mathematical Methods in Medicine. This is an open access article distributed under the Creative Commons Attribution License, which permits unrestricted use, distribution, and reproduction in any medium, provided the original work is properly cited.

This article has been retracted by Hindawi following an investigation undertaken by the publisher [1]. This investigation has uncovered evidence of one or more of the following indicators of systematic manipulation of the publication process:

- (1) Discrepancies in scope
- (2) Discrepancies in the description of the research reported
- (3) Discrepancies between the availability of data and the research described
- (4) Inappropriate citations
- (5) Incoherent, meaningless and/or irrelevant content included in the article
- (6) Peer-review manipulation

The presence of these indicators undermines our confidence in the integrity of the article's content and we cannot, therefore, vouch for its reliability. Please note that this notice is intended solely to alert readers that the content of this article is unreliable. We have not investigated whether authors were aware of or involved in the systematic manipulation of the publication process.

Wiley and Hindawi regrets that the usual quality checks did not identify these issues before publication and have since put additional measures in place to safeguard research integrity.

We wish to credit our own Research Integrity and Research Publishing teams and anonymous and named external researchers and research integrity experts for contributing to this investigation.

The corresponding author, as the representative of all authors, has been given the opportunity to register their agreement or disagreement to this retraction. We have kept a record of any response received.

### References

- [1] Y. Liu and X. Huang, "Rural Planning Evaluation Based on Artificial Neural Network," *Computational and Mathematical Methods in Medicine*, vol. 2022, Article ID 9746362, 10 pages, 2022.

## Retraction

# Retracted: Value and Application of Traditional Culture of Embedded Network Teaching Platform in Moral Education in Colleges and Universities

### Computational and Mathematical Methods in Medicine

Received 25 July 2023; Accepted 25 July 2023; Published 26 July 2023

Copyright © 2023 Computational and Mathematical Methods in Medicine. This is an open access article distributed under the Creative Commons Attribution License, which permits unrestricted use, distribution, and reproduction in any medium, provided the original work is properly cited.

This article has been retracted by Hindawi following an investigation undertaken by the publisher [1]. This investigation has uncovered evidence of one or more of the following indicators of systematic manipulation of the publication process:

- (1) Discrepancies in scope
- (2) Discrepancies in the description of the research reported
- (3) Discrepancies between the availability of data and the research described
- (4) Inappropriate citations
- (5) Incoherent, meaningless and/or irrelevant content included in the article
- (6) Peer-review manipulation

The presence of these indicators undermines our confidence in the integrity of the article's content and we cannot, therefore, vouch for its reliability. Please note that this notice is intended solely to alert readers that the content of this article is unreliable. We have not investigated whether authors were aware of or involved in the systematic manipulation of the publication process.

Wiley and Hindawi regrets that the usual quality checks did not identify these issues before publication and have since put additional measures in place to safeguard research integrity.

We wish to credit our own Research Integrity and Research Publishing teams and anonymous and named

external researchers and research integrity experts for contributing to this investigation.

The corresponding author, as the representative of all authors, has been given the opportunity to register their agreement or disagreement to this retraction. We have kept a record of any response received.

### References

- [1] J. Yang, "Value and Application of Traditional Culture of Embedded Network Teaching Platform in Moral Education in Colleges and Universities," *Computational and Mathematical Methods in Medicine*, vol. 2022, Article ID 2096583, 13 pages, 2022.

## Retraction

# Retracted: Monitoring Mycoplasma pneumoniae-Specific Antibody, C-Reactive Protein, and Procalcitonin Levels in Children with Mycoplasma Pneumonia Is Important

### Computational and Mathematical Methods in Medicine

Received 25 July 2023; Accepted 25 July 2023; Published 26 July 2023

Copyright © 2023 Computational and Mathematical Methods in Medicine. This is an open access article distributed under the Creative Commons Attribution License, which permits unrestricted use, distribution, and reproduction in any medium, provided the original work is properly cited.

This article has been retracted by Hindawi following an investigation undertaken by the publisher [1]. This investigation has uncovered evidence of one or more of the following indicators of systematic manipulation of the publication process:

- (1) Discrepancies in scope
- (2) Discrepancies in the description of the research reported
- (3) Discrepancies between the availability of data and the research described
- (4) Inappropriate citations
- (5) Incoherent, meaningless and/or irrelevant content included in the article
- (6) Peer-review manipulation

The presence of these indicators undermines our confidence in the integrity of the article's content and we cannot, therefore, vouch for its reliability. Please note that this notice is intended solely to alert readers that the content of this article is unreliable. We have not investigated whether authors were aware of or involved in the systematic manipulation of the publication process.

In addition, our investigation has also shown that one or more of the following human-subject reporting requirements has not been met in this article: ethical approval by an Institutional Review Board (IRB) committee or equivalent, patient/participant consent to participate, and/or agreement to publish patient/participant details (where relevant).

Wiley and Hindawi regrets that the usual quality checks did not identify these issues before publication and have since put additional measures in place to safeguard research integrity.

We wish to credit our own Research Integrity and Research Publishing teams and anonymous and named external researchers and research integrity experts for contributing to this investigation.

The corresponding author, as the representative of all authors, has been given the opportunity to register their agreement or disagreement to this retraction. We have kept a record of any response received.

### References

- [1] X. Cao, "Monitoring Mycoplasma pneumoniae-Specific Antibody, C-Reactive Protein, and Procalcitonin Levels in Children with Mycoplasma Pneumonia Is Important," *Computational and Mathematical Methods in Medicine*, vol. 2022, Article ID 7976858, 7 pages, 2022.

## *Retraction*

# **Retracted: Design and Application of Legally Valid Payment Templates Based on Linking Contracts**

### **Computational and Mathematical Methods in Medicine**

Received 25 July 2023; Accepted 25 July 2023; Published 26 July 2023

Copyright © 2023 Computational and Mathematical Methods in Medicine. This is an open access article distributed under the Creative Commons Attribution License, which permits unrestricted use, distribution, and reproduction in any medium, provided the original work is properly cited.

This article has been retracted by Hindawi following an investigation undertaken by the publisher [1]. This investigation has uncovered evidence of one or more of the following indicators of systematic manipulation of the publication process:

- (1) Discrepancies in scope
- (2) Discrepancies in the description of the research reported
- (3) Discrepancies between the availability of data and the research described
- (4) Inappropriate citations
- (5) Incoherent, meaningless and/or irrelevant content included in the article
- (6) Peer-review manipulation

The presence of these indicators undermines our confidence in the integrity of the article's content and we cannot, therefore, vouch for its reliability. Please note that this notice is intended solely to alert readers that the content of this article is unreliable. We have not investigated whether authors were aware of or involved in the systematic manipulation of the publication process.

Wiley and Hindawi regrets that the usual quality checks did not identify these issues before publication and have since put additional measures in place to safeguard research integrity.

We wish to credit our own Research Integrity and Research Publishing teams and anonymous and named external researchers and research integrity experts for contributing to this investigation.

The corresponding author, as the representative of all authors, has been given the opportunity to register their agreement or disagreement to this retraction. We have kept a record of any response received.

### **References**

- [1] Y. Zhu, "Design and Application of Legally Valid Payment Templates Based on Linking Contracts," *Computational and Mathematical Methods in Medicine*, vol. 2022, Article ID 1331237, 9 pages, 2022.

## *Retraction*

# **Retracted: Corpus-Driven Resource Recommendation Algorithm for English Online Autonomous Learning**

### **Computational and Mathematical Methods in Medicine**

Received 25 July 2023; Accepted 25 July 2023; Published 26 July 2023

Copyright © 2023 Computational and Mathematical Methods in Medicine. This is an open access article distributed under the Creative Commons Attribution License, which permits unrestricted use, distribution, and reproduction in any medium, provided the original work is properly cited.

This article has been retracted by Hindawi following an investigation undertaken by the publisher [1]. This investigation has uncovered evidence of one or more of the following indicators of systematic manipulation of the publication process:

- (1) Discrepancies in scope
- (2) Discrepancies in the description of the research reported
- (3) Discrepancies between the availability of data and the research described
- (4) Inappropriate citations
- (5) Incoherent, meaningless and/or irrelevant content included in the article
- (6) Peer-review manipulation

The presence of these indicators undermines our confidence in the integrity of the article's content and we cannot, therefore, vouch for its reliability. Please note that this notice is intended solely to alert readers that the content of this article is unreliable. We have not investigated whether authors were aware of or involved in the systematic manipulation of the publication process.

Wiley and Hindawi regrets that the usual quality checks did not identify these issues before publication and have since put additional measures in place to safeguard research integrity.

We wish to credit our own Research Integrity and Research Publishing teams and anonymous and named external researchers and research integrity experts for contributing to this investigation.

The corresponding author, as the representative of all authors, has been given the opportunity to register their agreement or disagreement to this retraction. We have kept a record of any response received.

### **References**

- [1] L. Gu, "Corpus-Driven Resource Recommendation Algorithm for English Online Autonomous Learning," *Computational and Mathematical Methods in Medicine*, vol. 2022, Article ID 9369258, 10 pages, 2022.

## Retraction

# Retracted: Effect of Acupotomy Combined with Electroacupuncture Therapy on Finger Mobility and Pain Relief in Patients with Carpal Tunnel Syndrome

### Computational and Mathematical Methods in Medicine

Received 25 July 2023; Accepted 25 July 2023; Published 26 July 2023

Copyright © 2023 Computational and Mathematical Methods in Medicine. This is an open access article distributed under the Creative Commons Attribution License, which permits unrestricted use, distribution, and reproduction in any medium, provided the original work is properly cited.

This article has been retracted by Hindawi following an investigation undertaken by the publisher [1]. This investigation has uncovered evidence of one or more of the following indicators of systematic manipulation of the publication process:

- (1) Discrepancies in scope
- (2) Discrepancies in the description of the research reported
- (3) Discrepancies between the availability of data and the research described
- (4) Inappropriate citations
- (5) Incoherent, meaningless and/or irrelevant content included in the article
- (6) Peer-review manipulation

The presence of these indicators undermines our confidence in the integrity of the article's content and we cannot, therefore, vouch for its reliability. Please note that this notice is intended solely to alert readers that the content of this article is unreliable. We have not investigated whether authors were aware of or involved in the systematic manipulation of the publication process.

In addition, our investigation has also shown that one or more of the following human-subject reporting requirements has not been met in this article: ethical approval by an Institutional Review Board (IRB) committee or equivalent, patient/participant consent to participate, and/or agreement to publish patient/participant details (where relevant).

Wiley and Hindawi regrets that the usual quality checks did not identify these issues before publication and have since put additional measures in place to safeguard research integrity.

We wish to credit our own Research Integrity and Research Publishing teams and anonymous and named external researchers and research integrity experts for contributing to this investigation.

The corresponding author, as the representative of all authors, has been given the opportunity to register their agreement or disagreement to this retraction. We have kept a record of any response received.

### References

- [1] J. Li, Y. Kou, S. Zhang, and K. Wang, "Effect of Acupotomy Combined with Electroacupuncture Therapy on Finger Mobility and Pain Relief in Patients with Carpal Tunnel Syndrome," *Computational and Mathematical Methods in Medicine*, vol. 2022, Article ID 2550875, 6 pages, 2022.



## Retraction

# Retracted: Analysis of Legal Attributes and Rights Attributes of Personal Information from the Perspective of Big Data

### Computational and Mathematical Methods in Medicine

Received 25 July 2023; Accepted 25 July 2023; Published 26 July 2023

Copyright © 2023 Computational and Mathematical Methods in Medicine. This is an open access article distributed under the Creative Commons Attribution License, which permits unrestricted use, distribution, and reproduction in any medium, provided the original work is properly cited.

This article has been retracted by Hindawi following an investigation undertaken by the publisher [1]. This investigation has uncovered evidence of one or more of the following indicators of systematic manipulation of the publication process:

- (1) Discrepancies in scope
- (2) Discrepancies in the description of the research reported
- (3) Discrepancies between the availability of data and the research described
- (4) Inappropriate citations
- (5) Incoherent, meaningless and/or irrelevant content included in the article
- (6) Peer-review manipulation

The presence of these indicators undermines our confidence in the integrity of the article's content and we cannot, therefore, vouch for its reliability. Please note that this notice is intended solely to alert readers that the content of this article is unreliable. We have not investigated whether authors were aware of or involved in the systematic manipulation of the publication process.

In addition, our investigation has also shown that one or more of the following human-subject reporting requirements has not been met in this article: ethical approval by an Institutional Review Board (IRB) committee or equivalent, patient/participant consent to participate, and/or agreement to publish patient/participant details (where relevant).

Wiley and Hindawi regrets that the usual quality checks did not identify these issues before publication and have since put additional measures in place to safeguard research integrity.

We wish to credit our own Research Integrity and Research Publishing teams and anonymous and named external researchers and research integrity experts for contributing to this investigation.

The corresponding author, as the representative of all authors, has been given the opportunity to register their agreement or disagreement to this retraction. We have kept a record of any response received.

### References

- [1] J. Yan, "Analysis of Legal Attributes and Rights Attributes of Personal Information from the Perspective of Big Data," *Computational and Mathematical Methods in Medicine*, vol. 2022, Article ID 9731414, 10 pages, 2022.

## *Retraction*

# **Retracted: Application Effect Analysis of Clinical Nursing Pathway in the Care of Neonatal Hypoxic-Ischemic Encephalopathy**

### **Computational and Mathematical Methods in Medicine**

Received 25 July 2023; Accepted 25 July 2023; Published 26 July 2023

Copyright © 2023 Computational and Mathematical Methods in Medicine. This is an open access article distributed under the Creative Commons Attribution License, which permits unrestricted use, distribution, and reproduction in any medium, provided the original work is properly cited.

This article has been retracted by Hindawi following an investigation undertaken by the publisher [1]. This investigation has uncovered evidence of one or more of the following indicators of systematic manipulation of the publication process:

- (1) Discrepancies in scope
- (2) Discrepancies in the description of the research reported
- (3) Discrepancies between the availability of data and the research described
- (4) Inappropriate citations
- (5) Incoherent, meaningless and/or irrelevant content included in the article
- (6) Peer-review manipulation

The presence of these indicators undermines our confidence in the integrity of the article's content and we cannot, therefore, vouch for its reliability. Please note that this notice is intended solely to alert readers that the content of this article is unreliable. We have not investigated whether authors were aware of or involved in the systematic manipulation of the publication process.

Wiley and Hindawi regrets that the usual quality checks did not identify these issues before publication and have since put additional measures in place to safeguard research integrity.

We wish to credit our own Research Integrity and Research Publishing teams and anonymous and named external researchers and research integrity experts for contributing to this investigation.

The corresponding author, as the representative of all authors, has been given the opportunity to register their agreement or disagreement to this retraction. We have kept a record of any response received.

### **References**

- [1] X. Zhang and H. Wang, "Application Effect Analysis of Clinical Nursing Pathway in the Care of Neonatal Hypoxic-Ischemic Encephalopathy," *Computational and Mathematical Methods in Medicine*, vol. 2022, Article ID 9379361, 6 pages, 2022.

## Retraction

# Retracted: Construction Method of Industrial College in Vocational Colleges Based on Cluster Analysis Algorithm

### Computational and Mathematical Methods in Medicine

Received 25 July 2023; Accepted 25 July 2023; Published 26 July 2023

Copyright © 2023 Computational and Mathematical Methods in Medicine. This is an open access article distributed under the Creative Commons Attribution License, which permits unrestricted use, distribution, and reproduction in any medium, provided the original work is properly cited.

This article has been retracted by Hindawi following an investigation undertaken by the publisher [1]. This investigation has uncovered evidence of one or more of the following indicators of systematic manipulation of the publication process:

- (1) Discrepancies in scope
- (2) Discrepancies in the description of the research reported
- (3) Discrepancies between the availability of data and the research described
- (4) Inappropriate citations
- (5) Incoherent, meaningless and/or irrelevant content included in the article
- (6) Peer-review manipulation

The presence of these indicators undermines our confidence in the integrity of the article's content and we cannot, therefore, vouch for its reliability. Please note that this notice is intended solely to alert readers that the content of this article is unreliable. We have not investigated whether authors were aware of or involved in the systematic manipulation of the publication process.

In addition, our investigation has also shown that one or more of the following human-subject reporting requirements has not been met in this article: ethical approval by an Institutional Review Board (IRB) committee or equivalent, patient/participant consent to participate, and/or agreement to publish patient/participant details (where relevant).

Wiley and Hindawi regrets that the usual quality checks did not identify these issues before publication and have

since put additional measures in place to safeguard research integrity.

We wish to credit our own Research Integrity and Research Publishing teams and anonymous and named external researchers and research integrity experts for contributing to this investigation.

The corresponding author, as the representative of all authors, has been given the opportunity to register their agreement or disagreement to this retraction. We have kept a record of any response received.

### References

- [1] X. Liu, "Construction Method of Industrial College in Vocational Colleges Based on Cluster Analysis Algorithm," *Computational and Mathematical Methods in Medicine*, vol. 2022, Article ID 3278395, 9 pages, 2022.

## Retraction

# Retracted: miR-135a-5p Suppresses TBK1 and Activates NRF2/TXNIP Antioxidant Pathway in LPS-Driven ALI in Mice

### Computational and Mathematical Methods in Medicine

Received 25 July 2023; Accepted 25 July 2023; Published 26 July 2023

Copyright © 2023 Computational and Mathematical Methods in Medicine. This is an open access article distributed under the Creative Commons Attribution License, which permits unrestricted use, distribution, and reproduction in any medium, provided the original work is properly cited.

This article has been retracted by Hindawi following an investigation undertaken by the publisher [1]. This investigation has uncovered evidence of one or more of the following indicators of systematic manipulation of the publication process:

- (1) Discrepancies in scope
- (2) Discrepancies in the description of the research reported
- (3) Discrepancies between the availability of data and the research described
- (4) Inappropriate citations
- (5) Incoherent, meaningless and/or irrelevant content included in the article
- (6) Peer-review manipulation

The presence of these indicators undermines our confidence in the integrity of the article's content and we cannot, therefore, vouch for its reliability. Please note that this notice is intended solely to alert readers that the content of this article is unreliable. We have not investigated whether authors were aware of or involved in the systematic manipulation of the publication process.

Wiley and Hindawi regrets that the usual quality checks did not identify these issues before publication and have since put additional measures in place to safeguard research integrity.

We wish to credit our own Research Integrity and Research Publishing teams and anonymous and named external researchers and research integrity experts for contributing to this investigation.

The corresponding author, as the representative of all authors, has been given the opportunity to register their agreement or disagreement to this retraction. We have kept a record of any response received.

### References

- [1] G. Zou, Y. Zeng, Y. Wang, and Y. Luo, "miR-135a-5p Suppresses TBK1 and Activates NRF2/TXNIP Antioxidant Pathway in LPS-Driven ALI in Mice," *Computational and Mathematical Methods in Medicine*, vol. 2022, Article ID 9088727, 11 pages, 2022.

## Retraction

# Retracted: Innovation of Ideological and Political Education Management of College Students Based on IOT Big Data Technology in a Wireless Network Environment

### Computational and Mathematical Methods in Medicine

Received 25 July 2023; Accepted 25 July 2023; Published 26 July 2023

Copyright © 2023 Computational and Mathematical Methods in Medicine. This is an open access article distributed under the Creative Commons Attribution License, which permits unrestricted use, distribution, and reproduction in any medium, provided the original work is properly cited.

This article has been retracted by Hindawi following an investigation undertaken by the publisher [1]. This investigation has uncovered evidence of one or more of the following indicators of systematic manipulation of the publication process:

- (1) Discrepancies in scope
- (2) Discrepancies in the description of the research reported
- (3) Discrepancies between the availability of data and the research described
- (4) Inappropriate citations
- (5) Incoherent, meaningless and/or irrelevant content included in the article
- (6) Peer-review manipulation

The presence of these indicators undermines our confidence in the integrity of the article's content and we cannot, therefore, vouch for its reliability. Please note that this notice is intended solely to alert readers that the content of this article is unreliable. We have not investigated whether authors were aware of or involved in the systematic manipulation of the publication process.

In addition, our investigation has also shown that one or more of the following human-subject reporting requirements has not been met in this article: ethical approval by an Institutional Review Board (IRB) committee or equivalent, patient/participant consent to participate, and/or agreement to publish patient/participant details (where relevant).

Wiley and Hindawi regrets that the usual quality checks did not identify these issues before publication and have since put additional measures in place to safeguard research integrity.

We wish to credit our own Research Integrity and Research Publishing teams and anonymous and named external researchers and research integrity experts for contributing to this investigation.

The corresponding author, as the representative of all authors, has been given the opportunity to register their agreement or disagreement to this retraction. We have kept a record of any response received.

### References

- [1] Z. Du, "Innovation of Ideological and Political Education Management of College Students Based on IOT Big Data Technology in a Wireless Network Environment," *Computational and Mathematical Methods in Medicine*, vol. 2022, Article ID 9585760, 8 pages, 2022.

## Retraction

# Retracted: MicroRNA-424-5p Alleviates Isoflurane Anesthesia-Induced Neurotoxicity in Human Embryonic Stem Cell-Derived Neurons by Targeting FASN

### Computational and Mathematical Methods in Medicine

Received 25 July 2023; Accepted 25 July 2023; Published 26 July 2023

Copyright © 2023 Computational and Mathematical Methods in Medicine. This is an open access article distributed under the Creative Commons Attribution License, which permits unrestricted use, distribution, and reproduction in any medium, provided the original work is properly cited.

This article has been retracted by Hindawi following an investigation undertaken by the publisher [1]. This investigation has uncovered evidence of one or more of the following indicators of systematic manipulation of the publication process:

- (1) Discrepancies in scope
- (2) Discrepancies in the description of the research reported
- (3) Discrepancies between the availability of data and the research described
- (4) Inappropriate citations
- (5) Incoherent, meaningless and/or irrelevant content included in the article
- (6) Peer-review manipulation

The presence of these indicators undermines our confidence in the integrity of the article's content and we cannot, therefore, vouch for its reliability. Please note that this notice is intended solely to alert readers that the content of this article is unreliable. We have not investigated whether authors were aware of or involved in the systematic manipulation of the publication process.

Wiley and Hindawi regrets that the usual quality checks did not identify these issues before publication and have since put additional measures in place to safeguard research integrity.

We wish to credit our own Research Integrity and Research Publishing teams and anonymous and named

external researchers and research integrity experts for contributing to this investigation.

The corresponding author, as the representative of all authors, has been given the opportunity to register their agreement or disagreement to this retraction. We have kept a record of any response received.

### References

- [1] X. Gu, W. Yue, M. Xiu, Q. Zhang, and R. Xie, "MicroRNA-424-5p Alleviates Isoflurane Anesthesia-Induced Neurotoxicity in Human Embryonic Stem Cell-Derived Neurons by Targeting FASN," *Computational and Mathematical Methods in Medicine*, vol. 2022, Article ID 2517463, 13 pages, 2022.

## Research Article

# Study the Behavior of Drug Structures via Chemical Invariants Using TOPSIS and SAW

Salma Kanwal <sup>1</sup>, Yasmeen Farooq,<sup>1</sup> Muhammad Kamran Siddiqui,<sup>2</sup> Nazeran Idrees <sup>3</sup>,  
Asima Razzaque <sup>4</sup> and Fikre Bogale Petros <sup>5</sup>

<sup>1</sup>Department of Mathematics, Lahore College for Women University, Lahore, Pakistan

<sup>2</sup>Department of Mathematics, COMSATS University Islamabad, Lahore Campus, Pakistan

<sup>3</sup>Department of Mathematics, Government College University, Faisalabad, Pakistan

<sup>4</sup>Basic Science Department, Preparatory Year Deanship, King Faisal University, Al Ahsa, Saudi Arabia

<sup>5</sup>Department of Mathematics, Addis Ababa University, Addis Ababa, Ethiopia

Correspondence should be addressed to Fikre Bogale Petros; [fikre.bogale@aau.edu.et](mailto:fikre.bogale@aau.edu.et)

Received 15 May 2022; Revised 1 July 2022; Accepted 24 November 2022; Published 30 January 2023

Academic Editor: Naeem Jan

Copyright © 2023 Salma Kanwal et al. This is an open access article distributed under the Creative Commons Attribution License, which permits unrestricted use, distribution, and reproduction in any medium, provided the original work is properly cited.

Every year, various experiments emerge in which a strong link between topological chemical structures and their properties is found. These properties are numerous such as melting point, boiling point, and drug toxicity. Topological index is the functional tool to determine these properties. This research paper will analyze some of the molecular drug structures, i.e., hyaluronic acid-paclitaxel conjugates  $G_n$ , anticancer drug  $SP[n]$ , polyomino chain of  $n$ -cycle  $Z_n$ , triangular benzenoid  $T_n$ , and circumcoronene benzenoid series  $H_k$  using multicriteria decision-making techniques including TOPSIS and SAW. The topological indices used in this research paper include the Randić index for  $\alpha = 1, -1, 1/2$ , the augmented Zagreb index and the forgotten topological index.

## 1. Introduction

The introduction of mathematical “graph theory” to chemistry [1] has been playing a significant role. Chemical graph theory is a subset of graph theory that connects to chemical compounds and processes. Chemical graph theory depicts molecular structures as chemical graphs, with nodes and edges representing atoms and bonds. In cheminformatics, they depict chemical structures. The cornerstone for (quantitative) structure activity and structure property predictions—a key field of cheminformatics—is computable properties of graphs. These graphs can be reduced to descriptors or indices based on graph theory, which reflect the physical properties of molecules [2]. Topological indices are numerical values linked with chemical constitution that aim to link chemical structure to physical attributes, chemical reactivity, and biological activity. These distance-based graphical indices are commonly employed to build correlations between molecular graph structure and characteristics.

Chemical compounds’ physicochemical qualities and bioactivity can be predicted using topological indices [3]. Gao et al. [4] referred chemical and pharmaceutical processes to have advanced rapidly, resulting in the emergence of a slew of novel nanomaterials, crystals, and medications each year. The examination of these various chemicals necessitates a significant number of chemical experiments, which adds to researchers’ burden. According to Katritzky et al. [5], their experiments reveal a close link between topological molecule structures and their physical behaviors, chemical properties, and biological traits, such as melting point, boiling temperature, and drug toxicity. Any drug that is effective in the treatment of cancerous disease is known as an anticancer drug, also known as effective anticancer drug. Anticancer medications are divided into various categories, including alkylating agents, antimetabolites, natural compounds, and hormones. Additionally, there are a number of medications that do not fall into those classifications but have anticancer action and are thereby employed in the treatment of cancer.

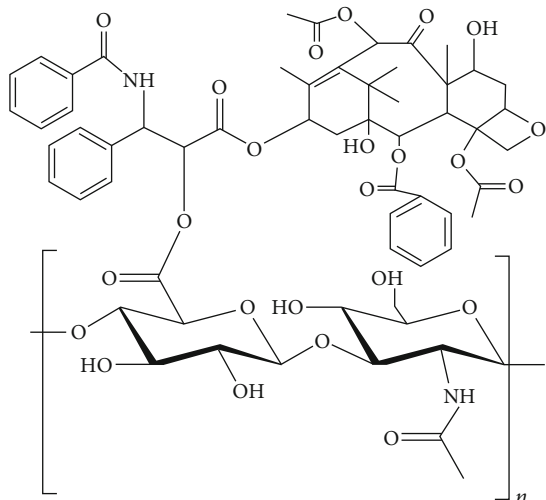


FIGURE 1: Molecular graph of HA-paclitaxel conjugates.

Chemotherapy is sometimes confused with the use of anti-cancer medications, whereas it refers to the use of chemical compounds to cure cancer in general. Using multicriteria decision-making techniques such as TOPSIS and SAW, this research looked at the behaviors of some drug structures such as anticancer drug SP[n]. This is the first research work to rank several drug structures with the help of certain MCDM techniques. TOPSIS is a ranking method that examines decision-making problems quantitatively and qualitatively. It provides the most accurate and timely solutions to our real-world problems than any other MCDM technique. Furthermore, the simplicity, logic, high processing efficiency, and capacity to quantify relative performance for each choice in a simple mathematical form are also advantages of this technique. On the other hand, one of the most basic and widely used weighted average approaches is the simple additive weighting method. This approach has the advantage of being a proportionate linear translation of the original data, which preserves the relative order of the variables. The SAW method demands normalizing the decision matrix to a scale that is comparable to all other ratings currently available.

## 2. Preliminaries

This research paper has considered finite graphs without loops and edges [6]. Let us consider a simple graph  $G(p, q)$  with vertex set  $V(G) = \{v'_1, v'_2, v'_3, \dots, v'_n\}$  and edge set  $E(G)$  with  $|V(G)| = q, |E(G)| = p$ . The number of edges connected to vertex  $p \in V(G)$  is called degree and is denoted by  $d_G(p)$ .

In 1975, the topological connectivity index  $RI(G)$  of a graph  $G$  defined as the sum of weights was proposed by Randić [7], i.e.,

$$RI(G) = \sum_{u'v' \in E(G)} \frac{1}{\sqrt{d_G(u')d_G(v')}}. \quad (1)$$

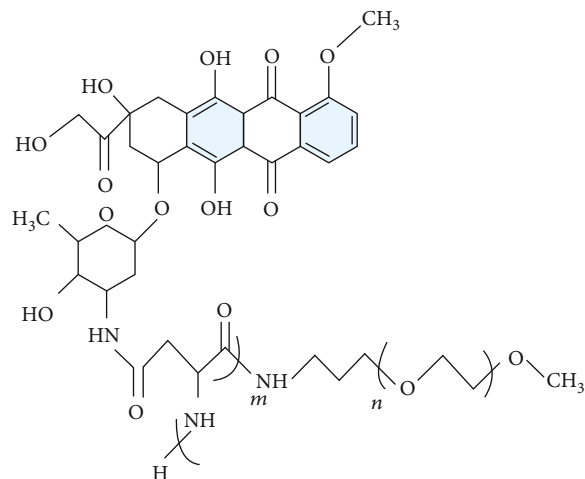
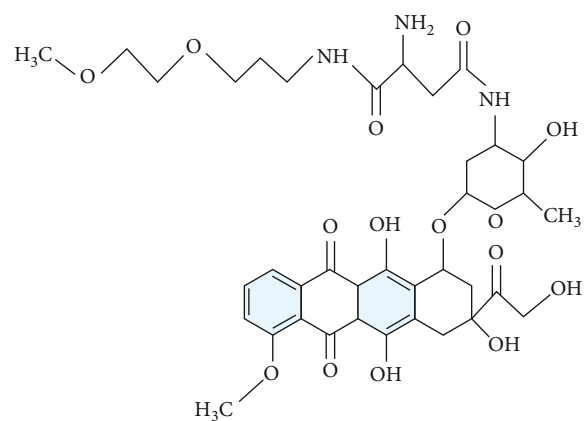


FIGURE 2: Chemical graph of SP[n].

FIGURE 3: Chemical graph of SP[n] for  $n = 1$ .

This index was originally known as the “branching index” or “molecular connectivity index,” and it was found to be useful in determining the level of branching. The Randić index is the name given to this parameter nowadays [8, 9]. Bollobás and Erdős [10] expanded this index in 1998 by substituting any real number for  $-1/2$  to produce the general Randić index  $RI_\alpha$ . Thus,

$$RI(G) = \sum_{u'v' \in E(G)} \left( d_G(u')d_G(v') \right)^\alpha. \quad (2)$$

Randić has demonstrated a link between the Randić index and a variety of physicochemical properties [11, 12]. Recently, Dvořák et al. [13] have shown if we have  $RI(G) \geq \text{rad}(G)/2$ , where  $\text{rad}(G)$  is the radius of  $G$ . The main point of their work was to introduce a new index,  $RI'(G)$ , which was defined as

$$RI'(G) = \sum_{u'v' \in E(G)} \frac{1}{\max \{d_G(u'), d_G(v')\}}. \quad (3)$$



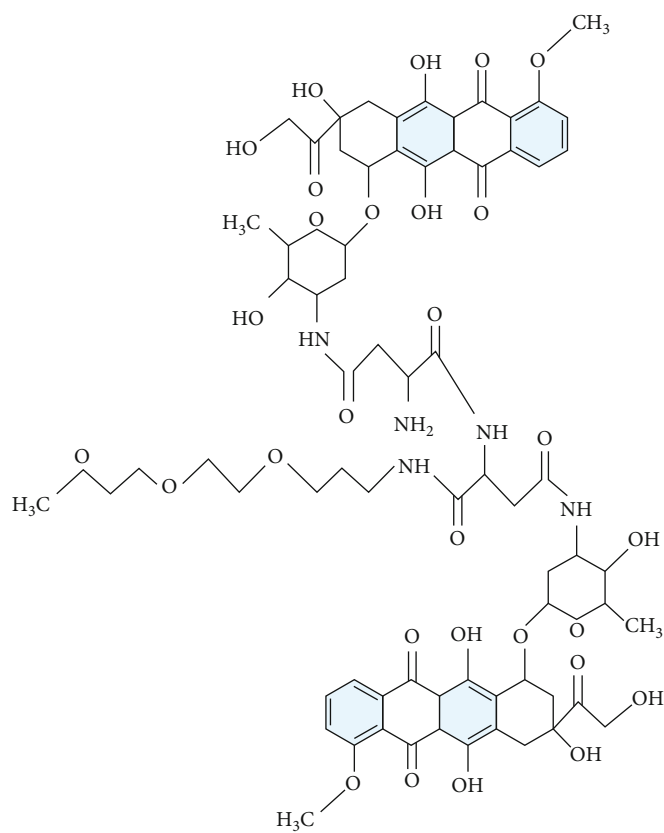


FIGURE 4: Chemical graph of  $SP[n]$  for  $n = 2$ .

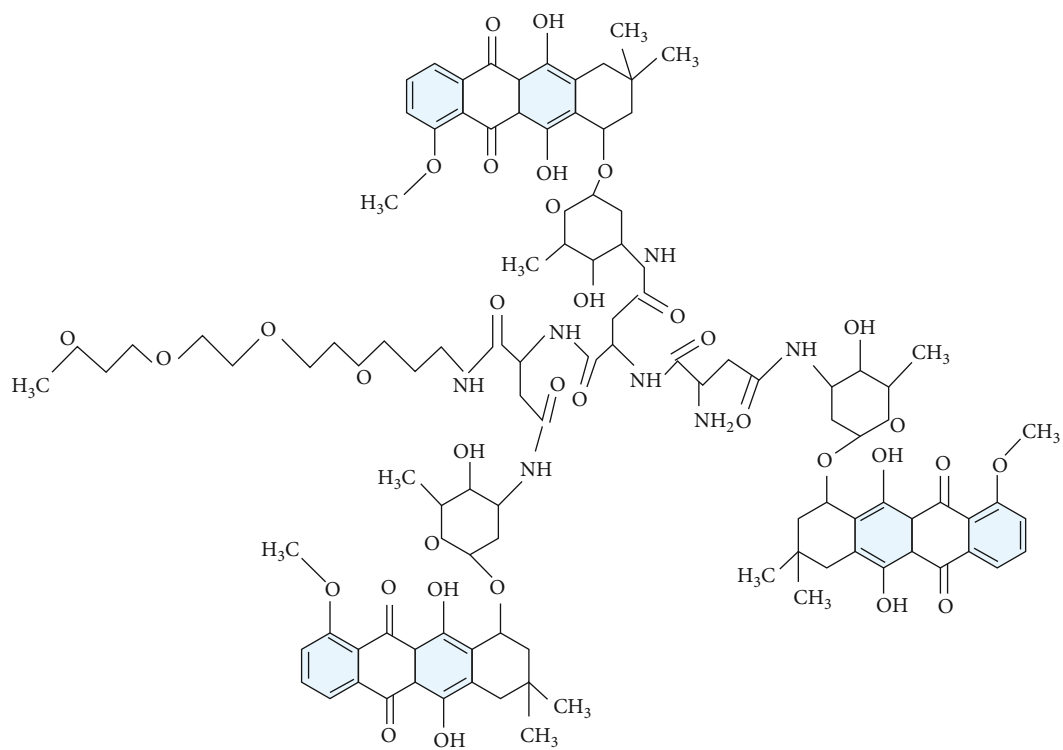


FIGURE 5: Chemical graph of  $SP[n]$  for  $n = 3$ .

Using this index, Cygan et al. [14] showed that, for any connected graph  $G$  of maximum degree at most four that is not a path with an even number of vertices,  $\chi(G) \geq \text{rad}(G)$ . Consequently, they resolve the conjecture  $\text{RI}(G) \geq \text{rad}(G) - 1$  specified by Zhang et al. [15]. They demonstrated that the inequality holds for all connected chemical graphs  $G$ ,  $\text{RI}'(G) \geq \text{rad}(G) - 1/2$  holds.

Furtula et al. [16] recently suggested the enhanced Zagreb index (AZI), a new topological measure based by the ABC index defined as

$$\text{AZI}(G) = \sum_{u'v' \in E(G)} \left( \frac{d(u') + d(v')}{d(u') + d(v') - 2} \right)^3, \quad (4)$$

whose predictive power exceeds that of the ABC index. He revealed that the AZI is a useful predictor of the heat of formation in heptanes and octanes [17]. It is possible to conclude that only this index passed the tests used in this investigation. As a result, when creating quantitative structure–property relationships, this index should be used [18]. Gao et al. [19] defined the forgotten topological index (or, F-index) which is stated as

$$\text{FI}(G) = \sum_{u'v' \in E(G)} \left( d(u')^2 + d(v')^2 \right). \quad (5)$$

De et al. [20] presented some basic properties of the forgotten topological index and demonstrated how this index can improve the Zagreb index's physical-chemical applicability.

### 3. Drug Structures

In this research paper, we consider several molecular structures of drugs along with their physiochemical properties, i.e., molecular weight, melting point, boiling point, complexity, and density. Disaccharide, its basic structure, has a high energy stability [21]. As a fast-developing platform for targeting CD44-overexpressing cells, HA is a promising cancer treatment [22]. HA works well as a drug transporter and a drug target. Increased water solubility and activity preservation are the great attributes of HA-PTX conjugates; more importantly, they could be applied as targeted drug delivery to boost antitumor efficacy [23]. Figure 1 depicts the structure of hyaluronic acid-paclitaxel conjugates.

The Dox-loaded micelle containing poly-(ethylene glycol)-poly(aspirate) PEG-PAsp block copolymer with chemically conjugated Dox (SP[n]) is depicted in Figure 2.

According to Nishiyama and Kataoka [24], it is a well-known smart polymer family that is used as an anthracycline anticancer antibiotic and is used to treat a variety of cancers. As a result, it possesses strong anticancer properties and is widely utilized in pharmaceuticals. The integer number  $n$  is the step of growth in this form of polymer, as seen in Figure 2.

When  $n = 1, 2, 3$  (see Figures 3–5, respectively).

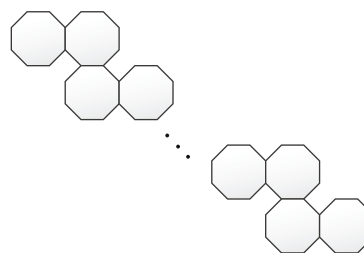


FIGURE 6: The zig-zag chain of 8-cycle  $Z_n$ .

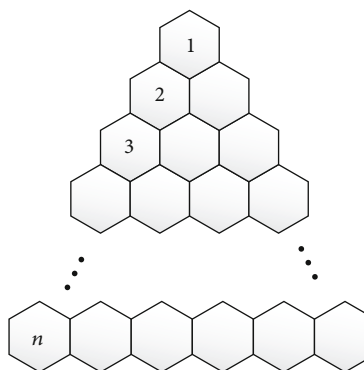


FIGURE 7: Molecular graph of triangular benzenoid  $T_n$ .

A polyomino system is a finite 2-connected plane system in which each internal face (also known as a cell) is enclosed by a one-length regular square [25, 26], which contains applications of polyomino systems to crystal physics. A polyomino chain is a polyomino system with a path as its inner dual graph (see Figure 6). It will be denoted by  $Z_n$ .

Now, look at the graph of triangular benzenoids  $T_n$ , where  $n$  is the number of hexagonal structures in the base graph. Figure 7 clearly shows that  $T_n$  has  $1/2n(n+1)$  hexagons [27]. It is crucial in pharmacy drug design and a variety of other applications.

We derive the circumcoronene series of benzenoid after generalizing benzene molecules [28]. Benzene is significant in chemistry because it aids in the production of aromatic compounds. The benzenoid series circumcoronene consists of several copies of benzene  $C_6$  on the perimeter (Figures 8 and 9). One family of benzenoid  $H_k$  that arises from the benzene molecule is the circumcoronene series. Coronene  $H_2$  or  $\text{Ca}(C_6)$ , the first term of the Capra-designed planar benzenoid series  $\text{Ca}_n(C_6)$ , is a well-known member of this family ( $C_6$ ).

### 4. Some Important Results

In this section, we emphasize on calculating the additive degree-based topological indices of the molecular graphs.

- (i) Additive degree-based topological invariants of conjugated Dox SP [n]

Let  $G$  be the graph of Dox-loaded micelle comprising PEG-PAsp block copolymer with chemically conjugated

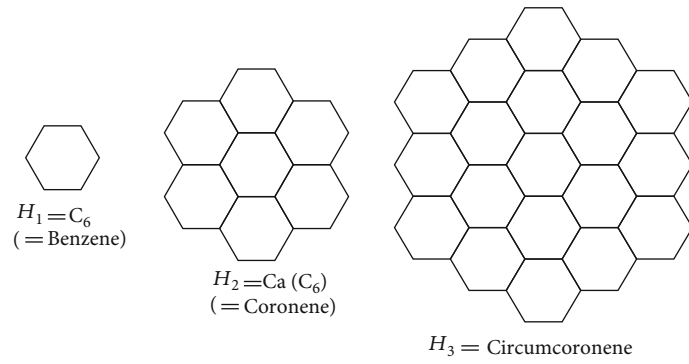


FIGURE 8: Renowned members of circumcoronene benzenoid series  $H_k$  for  $k \geq 1$ .

Dox (SP  $[n]$ ). Then, we have

$$\begin{aligned}
 R_1(G) &= 335n + 15, \\
 R_{-1}(G) &= 10.611n + 1.333, \\
 R_{1/2}(G) &= 131.6286n + 8.69677, \\
 AZ(G) &= 444 \cdot 8193n + 19.375, \\
 F(G) &= 744n + 34.
 \end{aligned}
 \tag{6}$$

From [6], the molecular graph of (SP  $[n]$ ) contains  $49n + 1$  vertices and  $54n + 5$  edges.

(ii) Additive degree-based topological invariants of hyaluronic acid-paclitaxel conjugates  $G_n$

Let  $G$  be graph of hyaluronic acid-paclitaxel conjugates  $G_n$ . Then, we have

$$\begin{aligned}
 R_1(G) &= 629n - 11, \\
 R_{-1}(G) &= 19.2278n - 0.0278, \\
 R_{1/2}(G) &= 243.1083n - 3.4494, \\
 AZ(G) &= 822.5972n - 11.3906, \\
 F(G) &= 1404n + 23.
 \end{aligned}
 \tag{7}$$

From [21], the molecular graph of ( $G_n$ ) contains  $87n$  vertices and  $96n$  edges.

(iii) Additive degree-based topological invariants of polyomino chain of  $n$ -cycle  $Z_n$

Let  $G$  be graph of polyomino chain of  $n$ -cycle  $Z_n$ . Then, we have

$$\begin{aligned}
 RI_1(G) &= 168n - 2, \\
 RI_{-1}(G) &= 5.2222n + 0.7778, \\
 RI_{1/2}(G) &= 67.5959n + 2, \\
 AZI(G) &= 251.125n + 9.2187, \\
 FI(G) &= 344n - 4.
 \end{aligned}
 \tag{8}$$

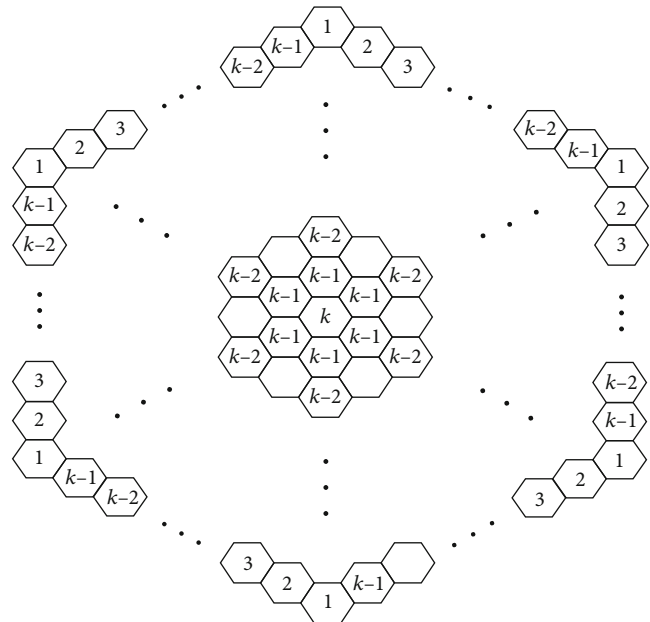


FIGURE 9: The molecular graph of  $H_k$  for  $k \geq 1$ .

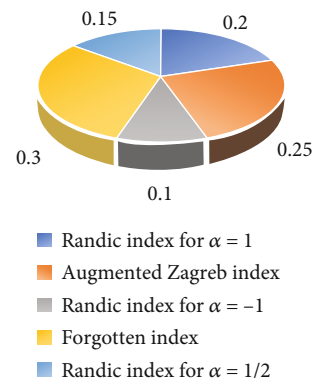


FIGURE 10: Allocation of weights

Some of the topological invariants named as  $I$  and  $V$  have taken from [29]; the molecular graph of ( $Z_n$ ) contains  $24n + 2$  vertices and  $28n + 2$  edges.

(iv) Additive degree-based topological invariants of circumcoronene series of benzenoid  $H_k, k \geq 1$

TABLE 1: Attributes and alternatives.

Alternative	Randić index ( $\alpha = 1$ )	Augmented Zagreb index	Randić index ( $\alpha = -1$ )	Forgotten topological index	Randić index ( $\alpha = 1/2$ )
Hyaluronic acid-paclitaxel conjugates $G_1$	618	811.2026	19.25	1381	239.6589
Anticancer drug SP[1]	350	464.1943	11.94	778	140.3254
Polyomino chain of $n$ -cycle $Z_2$	334	511.4687	11.22	684	137.1918
Circumcoronene benzenoid series $H_3$	546	749.7187	10.17	1173	196.7877
Triangular benzenoid $T_6$	564	718.4062	12.33	1116	212.2270

TABLE 2: Decision matrix  $D_{ij}$ .

Alternatives	$RI_1(G)$	$AZI(G)$	$RI_{-1}(G)$	$FI(G)$	$RI_{1/2}(G)$
$G_1$	618	811.2026	19.25	1381	239.6589
SP[1]	350	464.1943	11.94	778	140.3254
$Z_2$	334	511.4687	11.22	684	137.1918
$H_3$	546	749.7187	10.17	1173	196.7877
$T_6$	564	718.4062	12.33	1116	212.2270

TABLE 3: Normalized decision matrix  $H_{ij}$ .

Alternatives	$RI_1(G)$	$AZI(G)$	$RI_{-1}(G)$	$FI(G)$	$RI_{1/2}(G)$
$G_1$	0.2562	0.2492	0.2965	0.2568	0.2587
SP[1]	0.1451	0.1426	0.1839	0.1515	0.1515
$Z_2$	0.1284	0.1571	0.1728	0.1332	0.1481
$H_3$	0.2263	0.2303	0.1566	0.2285	0.2124
$T_6$	0.2338	0.2208	0.1899	0.2174	0.2291

TABLE 4: Weighted normalized decision matrix  $X_{ij}$ .

Alternatives	$RI_1(G)$	$AZI(G)$	$RI_{-1}(G)$	$FI(G)$	$RI_{1/2}(G)$
Weight $W_j$	<b>0.20</b>	<b>0.25</b>	<b>0.10</b>	<b>0.30</b>	<b>0.15</b>
$G_1$	0.0512	0.0623	0.0296	0.0770	0.0388
SP[1]	0.0290	0.0356	0.0184	0.0454	0.0227
$Z_2$	0.0276	0.0393	0.0172	0.0399	0.0222
$H_3$	0.0452	0.0575	0.0156	0.0628	0.0318
$T_6$	0.0467	0.0552	0.0189	0.0652	0.0343

Let  $G$  be graph of circumcoronene series of benzenoid  $H_k$ ,  $k \geq 1$ . Then, we have

$$\begin{aligned}
 RI_1(G) &= 81k^2 - 63k + 6, \\
 RI_{-1}(G) &= k^2 + 0.333k + 0.1667, \\
 RI_{1/2}(G) &= 27k^2 - 15.6061k + 0.60612, \\
 AZI(G) &= 102.5156k^2 - 74.8593k + 20.3437, \\
 FI(G) &= 162k^2 - 114k.
 \end{aligned} \tag{9}$$

From [29], the molecular graph of  $H_k$ ,  $k \geq 1$  contains  $6k^2 + 6k - 6$  vertices and  $9k^2 - 3k$  edges.

(v) Additive degree-based topological indices of triangular benzenoid  $T_n$

Let  $G$  be graph of triangular benzenoid  $T_n$ . Then, we have

$$\begin{aligned}
 RI_1(G) &= 9n^2 + 45n - 30, \\
 RI_{-1}(G) &= 0.25n^2 + 0.4167n + 0.8333, \\
 RI_{1/2}(G) &= 3.6742n^2 - 14.3257n - 6, \\
 AZI(G) &= 12n^2 + 56.3437n - 20.3437, \\
 FI(G) &= 19.5n^2 + 88.5n - 60.
 \end{aligned} \tag{10}$$

From [29], the molecular graph of  $T_n$  contains  $n^2 + 4n + 1$  vertices and  $((3/2)3/2n^2) + (9/2)$  edges.

The objectives of this paper are to give behavioral analysis of chemical structures of anticancer drug molecules using several topological indices, such as the Randić index and the augmented Zagreb index, as well as the forgotten topological index. We will also present a weighted evaluation of several topological indices in this research endeavor, as chemical

invariants aim to provide a less expensive and more efficient means for scientists and analysts to determine the physical and chemical features of anticancer medications. Two different decision-making techniques will be used to carry out this weighted evaluation. The Approach for Order Preference by Similarity to Ideal Solution (TOPSIS) will be the first technique. This weighted evaluation will be carried out for the ideal solution and the greatest distance from the worst solution. It also tries to use mathematics to assess the accuracy of molecular compound specifications. This method of multicriteria decision-making first appeared in the 1980s (MCDM).

(i) Allocation of weights: weights show how much of a drug structure should be taken into account. It is beneficial to have a drug structure with a wide range of physical and chemical properties. In that situation, we give them a lot more weight in comparison to the others and the others do as well (see Figure 10). The weight is allocated according the formula mentioned below

$$\sum_{j=1}^j W'_j = 1. \tag{11}$$

TABLE 5: Calculation of the positive ideal solution  $L^+$  and negative ideal solution  $L^-$ .

Alternatives	$RI_1(G)$	$AZI(G)$	$RI_{-1}(G)$	$FI(G)$	$RI_{1/2}(G)$
Properties	Molecular weight	Complexities	Density	Boiling point	Melting point
Weight $W_j$	<b>0.20</b>	<b>0.25</b>	<b>0.10</b>	<b>0.30</b>	<b>0.15</b>
$G_1$	0.0512	0.0623	0.0296	0.0770	0.0388
SP[1]	0.0290	0.0356	0.0184	0.0454	0.0227
$Z_2$	0.0276	0.0393	0.0172	0.0399	0.0222
$H_3$	0.0452	0.0575	0.0156	0.0628	0.0318
$T_6$	0.0467	0.0552	0.0189	0.0652	0.0343
$L^+$ (ideal best)	0.0276	0.0356	0.0156	0.0770	0.0222
$L^-$ (ideal worst)	0.0512	0.0623	0.0296	0.0399	0.0388

TABLE 6: Calculate the separation measures  $P_i^+$  and  $P_i^-$ .

Alternatives	$RI_1(G)$	$AZI(G)$	$RI_{-1}(G)$	$FI(G)$	$RI_{1/2}(G)$	$P_i^+$	$P_i^-$
$G_1$	0.0512	0.0623	0.0296	0.0770	0.0388	0.0416	0.0370
SP[1]	0.0290	0.0356	0.0184	0.0454	0.0227	0.0317	0.0402
$Z_2$	0.0276	0.0393	0.0172	0.0399	0.0222	0.0372	0.0369
$H_3$	0.0452	0.0575	0.0156	0.0628	0.0318	0.0309	0.0335
$T_6$	0.0467	0.0552	0.0189	0.0652	0.0343	0.0323	0.0290

- (ii) A drug's impact refers to whether it has a positive or negative impact. For example, which physiochemical feature is ideal best and which is ideal worst for our drug structure. The data values for a certain factor should be regarded as standard units
- (iii) Ideal best and ideal worst: we must first deal with the properties of our concerned drug structures and then correlate the abovementioned attributes with physical properties of every drug in order to determine the ideal best and ideal worst. The molecular weight, density, complexity, boiling point, and melting point are five common properties of drug structures. The solid density of pharmacological substances, from powder to tablet, is an important feature. It enables us to determine which chemicals will sink in a liquid. If the density of the substance is less than the density of the liquid in which it is immersed, it will flow [30]. As a result, low density is optimal for our pharmacological structures. The melting point is a fundamental physical feature that defines the transition in pharmaceutical sciences, chemical, and biological chemistry. In general, melting points with lower melting points are more likely to be absorbed than melting points with higher melting points. Another key attribute employed in the pharmaceutical industry is molecular weight. The degree of crystallinity of the polymer increased as the molecular weight of the polymer decreased [31]. The drug structures have a molecular weight of less than 1000 g/mol; hence, we use low molecu-

lar weight pharmaceuticals. The boiling point of a medicine is one of its most important characteristics [32]. It is for storing and carrying things. We have more storage for our pharmaceuticals if the boiling point is higher. Drug treatment complexity is acknowledged to be a risk factor for administration errors and nonadherence, resulting in increased healthcare expenses [33]

4.1. *TOPSIS*. Assume that each property is evaluated independently. Comparing the measure of similarity to the ideal alternative could be used to rate compromises [34]. From Table 1, there are  $m$  alternatives (drug structures) and  $n$  attributes (Randić indices, augmented Zagreb index, and forgotten topological index). In this regard, we attempt to set appropriate weights for the attributes in order to make the best decision and strike a balance between them [35].

*Step 1*. Selecting the important attributes and constituting the decision matrix based on  $m$  alternatives (drug structures) and  $n$  attributes (Randić indices, augmented Zagreb Index, and forgotten topological index) in Table 2:

$$D_{ij} = \begin{bmatrix} d_{11} & d_{12} & \cdots & d_{1n} \\ d_{21} & d_{22} & \cdots & d_{2n} \\ \vdots & \vdots & \vdots & \vdots \\ d_{n1} & d_{n2} & \cdots & d_{nn} \end{bmatrix}. \quad (12)$$

Now, we construct our decision matrix  $D_{ij}$ , that is

TABLE 7: Computation of relative closeness to the ideal solution  $O_i^*$ .

$P_i^+$	$P_i^-$	$O_i^*$
0.0416	0.0370	0.4706
0.0317	0.0402	0.5592
0.0372	0.0369	0.4975
0.0309	0.0335	0.5206
0.0323	0.0290	0.4730

TABLE 8: Rank the alternatives.

Alternatives	$O_i^*$	Rank
$G_1$	0.4706	5
SP[1]	0.5592	1
$Z_2$	0.4975	3
$H_3$	0.5206	2
$T_6$	0.4730	4

Step 2. Calculate the normalized decision matrix  $H_{ij}$  (Table 3). The normalized value  $r_{ij}$  of the  $i$ th alternate (drug structure) with respect to the  $j$ th attribute (topological indices).

$$H_{ij} = \begin{bmatrix} h_{11} & h_{12} & \cdots & h_{1n} \\ h_{21} & h_{22} & \cdots & h_{2n} \\ \vdots & \vdots & \vdots & \vdots \\ h_{n1} & h_{n2} & \cdots & h_{nn} \end{bmatrix}, \quad (13)$$

where  $H_{ij} = d_{ij} / \sqrt{\sum_{i=1}^m d_{ij}^2} \forall j = 1, 2, 3, \dots, n$  and  $i = 1, 2, 3, \dots, m$ .

Step 3. Calculate the weighted normalized decision matrix  $X_{ij}$  shown in Table 4.

The weighted normalized value is  $X_{ij} = W'_j \cdot h_{ij} \forall j = 1, 2, 3, \dots, n$ , where

$$\sum_{i=1}^j W'_j = 1. \quad (14)$$

Here, we allocate the highest-ranking topological descriptor highest weight.  $RI_{-1}(G)$  gives small values of their respective drug structures so that we assign lowest weight (0.10). Similarly,  $RI_{1/2}(G)$  has slightly different values from  $RI_{-1}(G)$  so we allocate it with little more weight (0.15). Next, if we notice  $RI_1(G)$ , the values for it are greater than  $RI_{1/2}(G)$  so we assign weight (0.20). Lastly, if we see  $FI(G)$ , that is richest in their values, we give a maximum weight (0.30) to it.

$$W'_j = 0.20, 0.25, 0.10, 0.30, 0.15. \quad (15)$$

TABLE 9: The decision matrix  $G_{ij}$ .

Alternatives	$R_1(G)$	AZ(G)	$R_{-1}(G)$	F(G)	$R_{1/2}(G)$
$G_1$	618	811.2026	19.25	1381	239.6589
SP[1]	350	464.1943	11.94	778	140.3254
$Z_2$	334	511.4687	11.22	684	137.1918
$H_3$	546	749.7187	10.17	1173	196.7877
$T_6$	564	718.4062	12.33	1116	212.2270
Best ( $g_j^+$ )	334	464.1943	10.17	1381	137.1918
Worst ( $g_j^-$ )	618	811.2026	19.25	684	239.6589

TABLE 10: Normalized decision matrix  $H_{ij}$ .

Alternatives	$R_1(G)$	AZ(G)	$R_{-1}(G)$	F(G)	$R_{1/2}(G)$
Weight $W_j$	<b>0.20</b>	<b>0.25</b>	<b>0.10</b>	<b>0.30</b>	<b>0.15</b>
$G_1$	0.540453	0.57223	0.528312	1	0.572446
SP[1]	0.954286	1	0.851759	0.56336	0.977669
$Z_2$	1	0.907571	0.906417	0.495293	1
$H_3$	0.611722	0.619158	1	0.849385	0.697156
$T_6$	0.592199	0.646145	0.824818	0.80811	0.646439

TABLE 11: Rank the alternatives.

Alternatives	$M_i$	Rank
$G_1$	0.689846	5
SP[1]	0.841691	1
$Z_2$	0.816123	2
$H_3$	0.736523	3
$T_6$	0.701856	4

We can calculate the normalized decision matrix using the formula given below.

$$X_{ij} = \begin{bmatrix} W'_1 h_{11} & W'_1 h_{11} & \cdots & W'_n h_{1n} \\ W'_1 h_{21} & W'_2 h_{22} & \cdots & W'_n h_{2n} \\ \vdots & \vdots & \vdots & \vdots \\ W'_1 h_{n1} & W'_2 h_{n2} & \cdots & W'_n h_{nn} \end{bmatrix}. \quad (16)$$

Step 4. Determine the positive ideal solution  $L^+$  and negative ideal solution  $L^-$  (Table 5).

To determine the distance between alternative  $i$  and the ideal alternative that is defined as

$$L^+ = \{x_i^+, \dots, x_j^+\} = (\max \text{ (or min) } X_{ij} | j \in J), \quad (17)$$

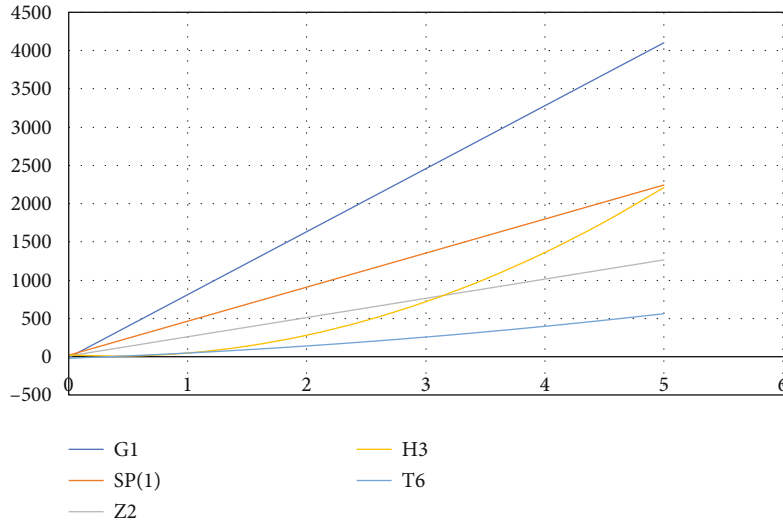


FIGURE 11: Comparison of alternatives using  $AZI(G)$ .

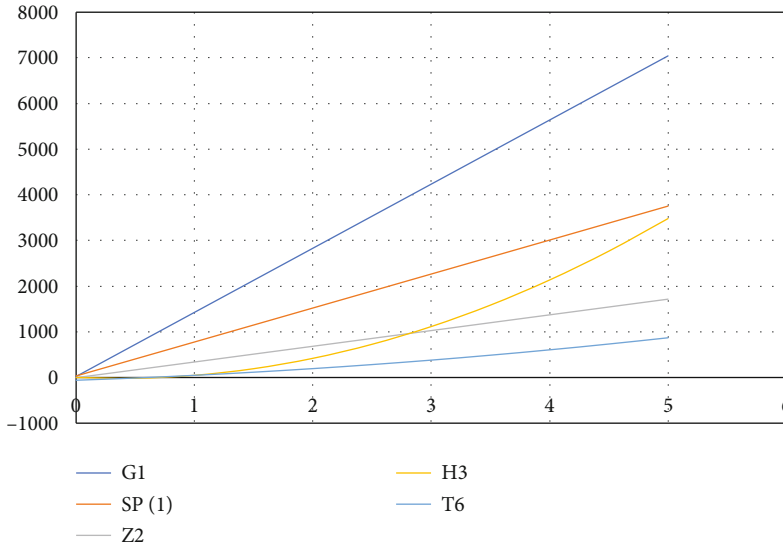


FIGURE 12: Comparison of alternatives using  $FI(G)$ .

and distance between alternative  $i$  and the minimum alternative that is defined as

$$L^- = \{x_i^-, \dots, x_j^-\} = (\min \text{ (or max) } X_{ij} | j \in J). \quad (18)$$

*Step 5.* Compute the separation measure, using the  $n$ -dimensional Euclidean distance in Table 6. The separation of each alternative from the ideal solution is given by

$$\begin{aligned} P_i^+ &= \sqrt{\sum_{j=1}^n (X_{ij} - L_j^+)^2}, \\ P_i^- &= \sqrt{\sum_{j=1}^n (X_{ij} - L_j^-)^2}. \end{aligned} \quad (19)$$

*Step 6.* Compute the relative closeness to the ideal solution (Table 7). The relative closeness of  $A_i$  with respect to  $A$  is defined as

$$O_i^* = \frac{P_i^-}{P_i^+ + P_i^-}, \quad (20)$$

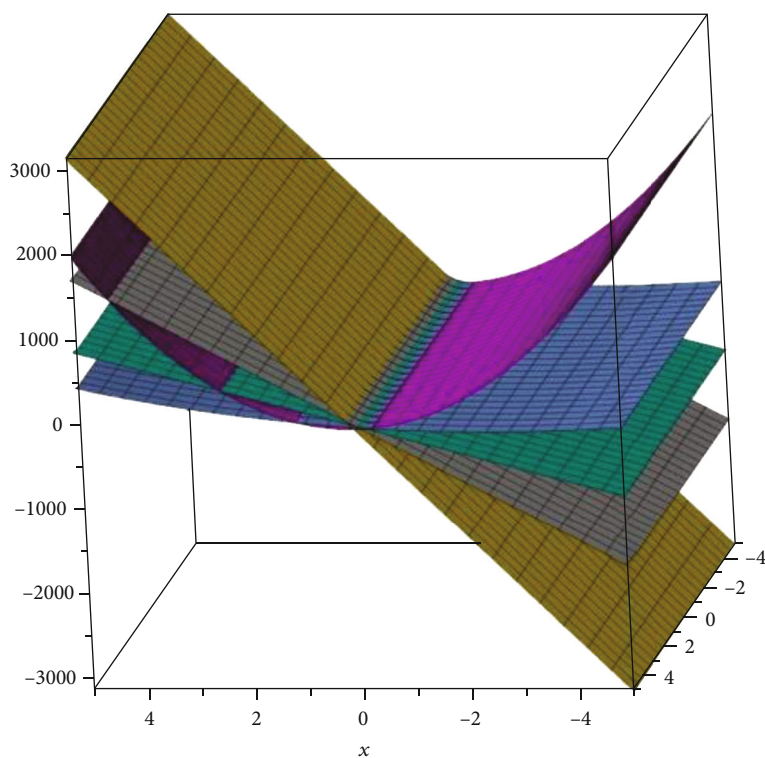
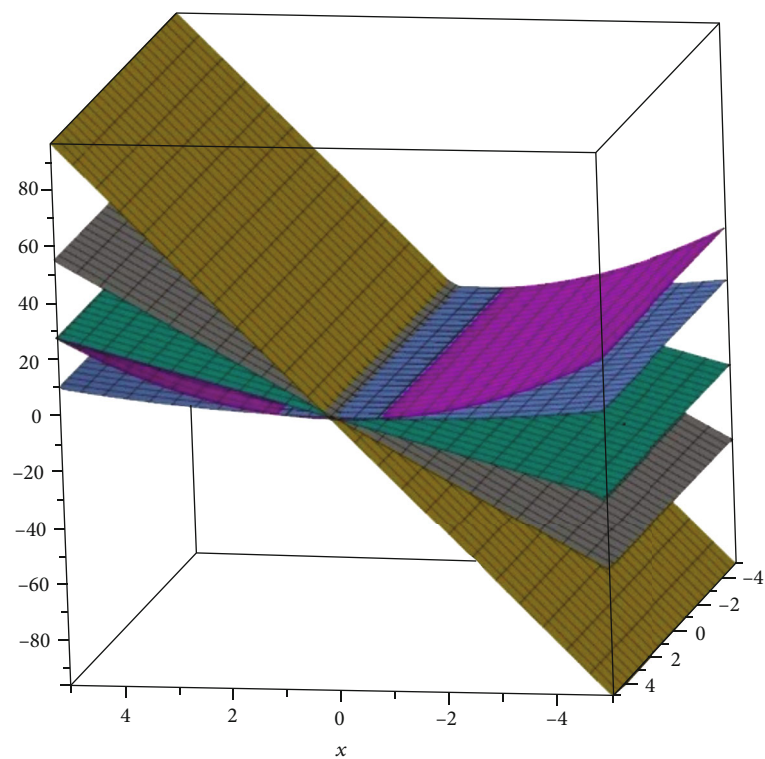
where  $0 < O_i^* < 1$ ,  $i = 1, 2, 3, \dots, n$ .

It is clear that  $O_i^* = 1$  if  $L_i = L^+$  and  $O_i^* = 0$  if  $L_i = L^-$ .

Therefore, a preferable option is the one that poses the value closer to 1.

*Step 7.* Rank the reference order based on the descending order of  $O_i^*$  in Table 8.

**4.2. SAW.** A multicriteria decision-making (MCDM) or multicriteria decision analysis method is the simple additive

FIGURE 13: Comparison of alternatives using  $RI_1(G)$ .FIGURE 14: Comparison of alternatives using  $RI_{-1}(G)$ .

weighting method (SAW), which is also known as weighted linear combination or scoring method [36]. This method is comprised on the weighted average. The weighted sum of the performance evaluations for every alternative among all

attributes is determined using the SAW method [37]. There are different  $m$  alternatives (drug structures) and  $n$  attributes (Randić indices, augmented Zagreb index, and forgotten topological index).



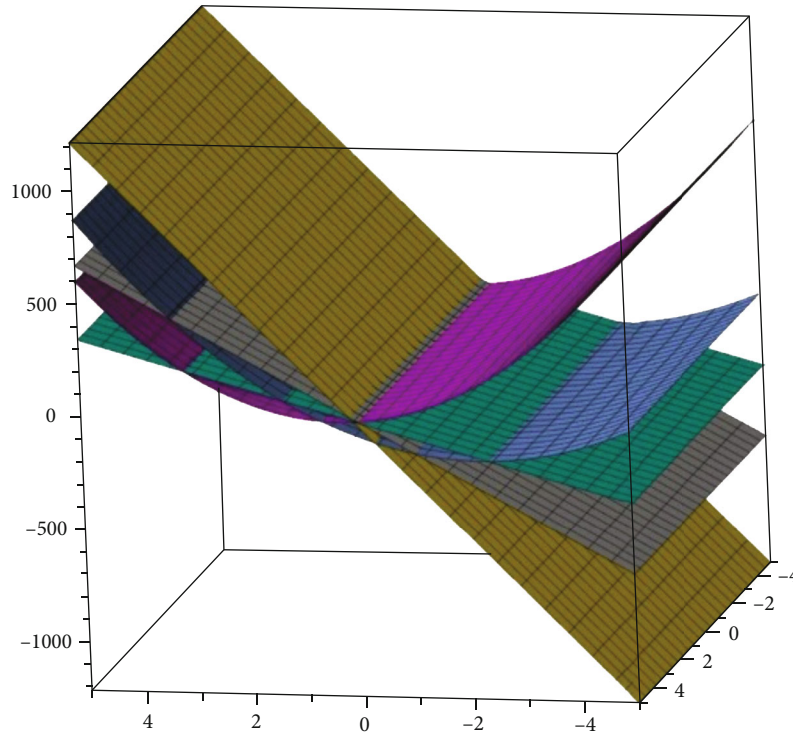


FIGURE 15: Comparison of alternatives using  $RI_{1/2}(G)$ .

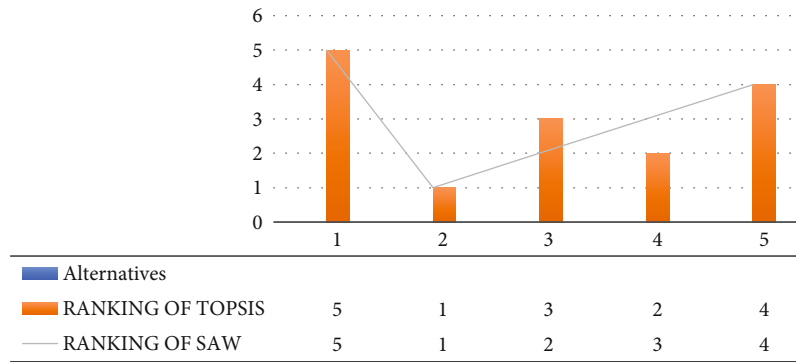


FIGURE 16: Ranking of TOPSIS and SAW.

The SAW method's compromise ranking algorithm consists of the following steps:

*Step 1.* Constitute the decision matrix of  $m$  alternatives and  $n$  attributes in Table 9.

$$G_{ij} = \begin{bmatrix} g_{11} & g_{12} & \cdots & g_{1n} \\ g_{21} & g_{22} & \cdots & g_{2n} \\ \vdots & \vdots & \vdots & \vdots \\ g_{n1} & g_{n2} & \cdots & g_{mn} \end{bmatrix}. \quad (21)$$

And determine the best  $g_j^+$  and worst  $g_j^-$  values of all the attributes  $j = 1, 2, 3, \dots, n$ .

*Step 2.* By using the abovementioned weighted criteria, we calculate the weights. Also, construct a normalized decision matrix  $H_{ij}$  according to the formula given below, where  $m$  is the alternatives and  $n$  is the attributes in Table 10.

$$h_{ij} = \frac{g_{ij}}{\max(g_{ij})}, \quad (22)$$

$$h_{ij} = \frac{\min(g_{ij})}{g_{ij}},$$

where  $i = 1, 2, 3, \dots, m$  and  $j = 1, 2, 3, \dots, n$ .

Step 3. Evaluate each alternative  $M_i$  by the following formula (Table 11):

$$M_i = \sum_{j=1}^n W_j h_{ij}, \quad (23)$$

where  $h_{ij}$  is the score of  $i$ th alternative with respect to the  $j$ th attribute and  $W_j$  is the weighted criteria of the attributes.

## 5. Graphical Interpretation of Drug Structures

The two-dimensional and three-dimensional graphical comparisons of the above results are depicted in Figures 11–15, respectively.

**5.1. Two-Dimensional Graphs.** In both the 2D plots of the drug structures along with the attributes, we have found that  $G_1$  gives us the highest value and  $T_6$  shows the smallest value.

**5.2. Three-Dimensional Graphs.** These 3D graphs are representing the behavior of the drug structures with attributes  $RI_1(G)$ ,  $RI_{-1}(G)$ , and  $RI_{1/2}(G)$ , respectively. Golden color is indicating  $G_1$  drug structure, grey is indicating SP[1], green is indicating  $Z_2$ , Niagara azure is indicating  $H_3$ , and purple is indicating  $T_6$  drug structures. In all the graphs, we have clearly seen that  $G_1$  gives us effective role as a drug structure in these plots.

## 6. Conclusion

Many drug studies reveal strong inner links between the medications' biological and pharmacological properties and their molecular structures. In this research article, using TOPSIS method, SP[1] is determined to be the most suitable drug structure as it has close distance to the ideal solution. The drug structures are thus ranked as  $H_3$ ,  $Z_2$ ,  $T_6$ , and lastly  $G_1$ , i.e.,  $H_3 > Z_2 > T_6 > G_1$ . On the other hand, using SAW, we have observed a slightly changed behavior of drugs as  $Z_2$  and  $H_3$  are ranked opposite in their behaviors. In the SAW method, SP[1] is determined to be the highest ranked drug structure. Other structures are ranked as  $Z_2 > H_3 > T_6 > G_1$ . Moreover, the results are plotted using the MS Excel and MAPLE in Figures 11–15, respectively. These theoretical results might be supportive to comprehend the topology of the aforementioned chemical drug structures. The histogram of the ranking is created through the MS Excel as shown in Figure 16. These theoretical results might be helpful to rank the drug structures via chemical invariants in the field of medicine, chemistry, drug discovery, and mathematical chemistry while evaluating these drugs in future.

## Data Availability

The data used to support this work are cited within the text as references.

## Conflicts of Interest

The authors declare that they have no conflicts of interest.

## Authors' Contributions

This work was equally contributed by all writers.

## Acknowledgments

This work was supported by the Deanship of Scientific Research, Vice Presidency for Graduate Studies and Scientific Research, King Faisal University, Saudi Arabia (Grant No. 2715).

## References

- [1] G. W. Milne, "Mathematics as a basis for chemistry," *Journal of Chemical Information and Computer Sciences*, vol. 37, no. 4, pp. 639–644, 1997.
- [2] N. Trinajstić, *Chemical Graph Theory*, CRC Press, Boca Raton, FL, 2nd edition, 1992.
- [3] O. Ivanciuc, T. Ivanciuc, and A. T. Balaban, "Vertex- and edge-weighted molecular graphs and derived structural descriptors," in *Topological Indices and Related Descriptors in QSAR and QSPR*, pp. 169–175, CRC Press, 1999.
- [4] W. Gao, W. Wang, and M. R. Farahani, "Topological indices study of molecular structure in anticancer drugs," *Journal of Chemistry*, vol. 2016, Article ID 3216327, 8 pages, 2016.
- [5] A. R. Katritzky, R. Jain, A. Lomaka, R. Petrukhin, U. Maran, and M. Karelson, "Perspective on the relationship between melting points and chemical structure," *Crystal Growth & Design*, vol. 1, no. 4, pp. 261–265, 2001.
- [6] Z. Shao, A. Jahanbani, and S. M. Sheikholeslami, "Multiplicative topological indices of molecular structure in anticancer drugs," *Polycyclic Aromatic Compounds*, vol. 42, no. 2, pp. 475–488, 2022.
- [7] M. Randić, "Characterization of molecular branching," *Journal of the American Chemical Society*, vol. 97, no. 23, pp. 6609–6615, 1975.
- [8] X. Zhang, A. Rauf, M. Ishtiaq, M. K. Siddiqui, and M. H. Muhammad, "On degree based topological properties of two carbon nanotubes," *Polycyclic Aromatic Compounds*, vol. 42, no. 3, pp. 866–884, 2022.
- [9] X. Zhang, M. K. Siddiqui, S. Javed, L. Sherin, F. Kausar, and M. H. Muhammad, "Physical analysis of heat for formation and entropy of ceria oxide using topological indices," *Combinatorial Chemistry & High Throughput Screening*, vol. 25, no. 3, pp. 441–450, 2022.
- [10] B. Bollobás and P. Erdős, "Graphs of extremal weights," *Ars Combinatoria*, vol. 50, pp. 225–233, 1998, <https://digitalcommons.memphis.edu/facpubs/4851>.
- [11] X. Li and Y. Shi, "A survey on the Randić index," *Match-Communications in Mathematical and Computer Chemistry*, vol. 59, no. 1, pp. 127–156, 2008.
- [12] P. Hansen and H. Mélot, "Variable neighborhood search for extremal graphs. 6. Analyzing bounds for the connectivity index," *Journal of Chemical Information and Computer Sciences*, vol. 43, no. 1, pp. 1–14, 2003.

- [13] Z. Dvořák, B. Lidický, and R. Škrekovski, "Randić index and the diameter of a graph," *European Journal of Combinatorics*, vol. 32, no. 3, pp. 434–442, 2011.
- [14] M. Cygan, M. Pilipczuk, and R. Škrekovski, "On the inequality between radius and Randić index for graphs," *Match-Communications in Mathematical and Computer Chemistry*, vol. 67, no. 2, pp. 451–465, 2012.
- [15] X. Zhang, X. Wu, S. Akhter, M. K. Jamil, J. B. Liu, and M. Farahani, "Edge-version atom-bond connectivity and geometric arithmetic indices of generalized bridge molecular graphs," *Symmetry*, vol. 10, no. 12, pp. 751–786, 2018.
- [16] B. Furtula, A. Graovac, and D. Vukičević, "Atom-bond connectivity index of trees," *Discrete Applied Mathematics*, vol. 157, no. 13, pp. 2828–2835, 2009.
- [17] X. Zhang, H. Jiang, J. B. Liu, and Z. Shao, "The cartesian product and join graphs on edge-version atom-bond connectivity and geometric arithmetic indices," *Molecules*, vol. 23, no. 7, p. 1731, 2018.
- [18] I. Gutman and J. Tošović, "Testing the quality of molecular structure descriptors. Vertex-degree-based topological indices," *Journal of the Serbian Chemical Society*, vol. 78, no. 6, pp. 805–810, 2013.
- [19] W. Gao, M. R. Farahani, and L. Shi, "Forgotten topological index of some drug structures," *Acta medica mediterranea*, vol. 32, no. 1, pp. 579–585, 2016.
- [20] N. De, S. M. A. Nayeem, and A. Pal, "F-index of some graph operations," *Discrete mathematics, algorithms and applications*, vol. 8, no. 2, article 1650025, 2016.
- [21] L. Zheng, Y. Wang, and W. Gao, "Topological indices of hyaluronic acid-paclitaxel conjugates' molecular structure in cancer treatment," *Open Chemistry*, vol. 17, no. 1, pp. 81–87, 2019.
- [22] A. Mráček, J. Varhaníková, M. Lehocký, L. Gřundělová, A. Pokopcová, and V. Velebný, "The influence of Hofmeister series ions on Hyaluronan swelling and viscosity," *Molecules*, vol. 13, no. 5, pp. 1025–1034, 2008.
- [23] F. Dosio, S. Arpicco, B. Stella, and E. Fattal, "Hyaluronic acid for anticancer drug and nucleic acid delivery," *Advanced Drug Delivery Reviews*, vol. 97, pp. 204–236, 2016.
- [24] N. Nishiyama and K. Kataoka, "Polymeric micelle drug carrier systems: PEG-PAsp (Dox) and second generation of micellar drugs," in *Polymer Drugs in the Clinical Stage*, Advances in Experimental Medicine and Biology, H. Maeda, A. Kabanov, K. Kataoka, and T. Okano, Eds., pp. 155–177, Springer, Boston, MA, 2004.
- [25] J. Rada, "The linear chain as an extremal value of VDB topological indices of polyomino chains," *Applied Mathematical Sciences*, vol. 8, pp. 5133–5143, 2014.
- [26] P. John, H. Sachs, and H. Zernitz, "Counting perfect matchings in polyominoes with an application to the dimer problem," *Applicaciones Mathematicae*, vol. 19, no. 3-4, pp. 465–477, 1987.
- [27] J. R. Dias, "Correlations and topology of triangular benzenoid hydrocarbons: a comparative study of two series representing the least and most stable benzenoid hydrocarbons," *Journal of Physical Organic Chemistry*, vol. 15, no. 2, pp. 94–102, 2002.
- [28] M. R. Farahani, "Computing edge-PI index and vertex-PI index of circumcoronene series of benzenoid Hk by use of cut method," *International Journal of Mathematical Modeling and Applied Computing*, vol. 1, no. 6, pp. 41–50, 2013.
- [29] M. Cancan, S. Mondal, N. De, and A. Pal, "Multiplicative degree based topological indices of some chemical structures in drug," *Proyecciones (Antofagasta)*, vol. 39, no. 5, pp. 1347–1364, 2020.
- [30] Q. Du, Y. Li, and L. Pan, "Wheelchair size and material application in human-machine system model," *Applied Mathematics and Nonlinear Sciences*, vol. 6, no. 2, pp. 7–18, 2021.
- [31] R. Bu, C. Qu, and Y. G. Sánchez, "Nonlinear mathematical modelling of bone damage and remodelling behaviour in human femur," *Applied Mathematics and Nonlinear Sciences*, vol. 6, no. 2, pp. 53–64, 2021.
- [32] M. Du, Y. Liu, and L. Li, "An empirical investigation of physical literacy-based adolescent health promotion," *Applied Mathematics and Nonlinear Sciences*, vol. 6, no. 2, pp. 133–146, 2021.
- [33] L. Sen, Z. Yang, Z. Caihong, and W. Chengliang, "A comprehensive evaluation of county economies in the Beijing-Tianjin-Hebei region based on entropy TOPSIS analysis," *Applied Mathematics and Nonlinear Sciences*, vol. 6, no. 2, pp. 499–516, 2021.
- [34] K. Naeem, M. Riaz, and F. Karaaslan, "A mathematical approach to medical diagnosis via Pythagorean fuzzy soft TOPSIS, VIKOR and generalized aggregation operators," *Complex & Intelligent Systems*, vol. 7, no. 5, pp. 2783–2795, 2021.
- [35] E. Roghanian and Z. Shakeri Kebria, "The combination of TOPSIS method and Dijkstra's algorithm in multi-attribute routing," *Scientia Iranica*, vol. 24, no. 5, pp. 2540–2549, 2017.
- [36] Ž. Stević, E. Durmić, M. Gajić, D. Pamučar, and A. Puška, "A novel multi-criteria decision-making model: interval rough SAW method for sustainable supplier selection," *Information*, vol. 10, no. 10, pp. 292–299, 2019.
- [37] Y. Irawan, "Decision support system for employee bonus determination with web-based simple additive weighting (SAW) method in PT. Mayatama Solusindo," *Journal of Applied Engineering and Technological Science (JAETS)*, vol. 2, no. 1, pp. 7–13, 2020.

## Research Article

# Meta-analysis of Proton Pump Inhibitors in the Treatment of Pharyngeal Reflux Disease

**Xiulin Jin, Xufeng Zhou, Zongxian Fan, Yingchun Qin, and Junjie Zhan** 

*Department of Otorhinolaryngology, First Affiliated Hospital of Jiamusi University, Jiamusi City, Heilongjiang Province, China*

Correspondence should be addressed to Junjie Zhan; zhanjunjie@jmsuf.com.cn

Received 27 May 2022; Revised 24 June 2022; Accepted 28 June 2022; Published 21 July 2022

Academic Editor: Naeem Jan

Copyright © 2022 Xiulin Jin et al. This is an open access article distributed under the Creative Commons Attribution License, which permits unrestricted use, distribution, and reproduction in any medium, provided the original work is properly cited.

The present study aimed to examine the safety and healing effects of proton pump inhibitors (PPIs) in people with laryngopharyngeal reflux disease (LPRD). To find all relevant studies published before April 1, 2022, we searched the PubMed, Embase, Web of Science, Clinical Trials, Cochrane Library, CNKI, and Wanfang databases. For SLE, we looked for all randomized controlled clinical trials related to PPIs versus placebo-controlled treatment of LPRD. Overall efficiency, reflux symptom index (RSI), reflux finding score (RFS), improvement in cough and hoarseness, and adverse reactions were compared using the Review Manager 5.3. Using the reflux symptom index (RSI) as an outcome indicator for efficacy assessment, the PPI group showed significant improvement compared with the placebo group [MD = 3.35, 95% CI (1.34, 5.37,  $P < 0.05$ )]. In terms of overall efficacy, the PPI group showed effectiveness, but its efficacy was not statistically significantly dissimilar from that of the placebo group [OR = 1.62, 95% CI (0.89, 2.95),  $P > 0.05$ ].

## 1. Introduction

Laryngopharyngeal reflux disease (LPRD) is a term used to describe a variety of symptoms and signs brought on by the reflux of stomach contents into the pharynx through the upper esophageal sphincter (UES) [1]. Due mostly to mucosal irritation that causes an inflammatory response and excessive mucus secretion, LPRD is currently regarded as one of the most prevalent chronic inflammatory disorders of the upper respiratory tract [2]. Clinical symptoms include foreign body sensation in the throat, persistent throat clearing, hoarseness, chronic cough, and laryngeal signs such as mucous membrane hyperplasia and hypertrophy in the posterior vocal fold area, diffuse congestion, and edema of the vocal folds [3]. In recent years, there has been a gradual increase in the number of patients with chronic, nonspecific throat discomfort associated with reflux seen in otolaryngology. Epidemiological surveys have found that the prevalence of LPRD in otolaryngology outpatients is 10% [4], European data show that the prevalence of LPRD is about 18.8% [5], while domestic surveys have found that the prevalence of LPRD is about 5% [6].

The etiology of LPRD is not well understood, and some studies have reported mechanisms associated with LPRD: direct contact between gastroesophageal reflux and the pharyngeal mucosa, acid stimulation of the vagus nerve, and lack of resistance of the pharyngeal mucosa to gastric acid compared to the esophageal mucosa [7, 8]. Small amounts of acid may not be sufficient to cause esophageal symptoms but may be sufficient to cause throat symptoms. Pharmacological intervention with PPIs, lifestyle changes, and dietary modification are now recommended as treatment strategies for LPRD [9]. PPIs are commonly used in the clinical empirical treatment of laryngopharyngeal reflux diseases. Inhibiting  $H^+ - K^+ - ATPase$  on gastric wall cells, decreasing gastric acid output, decreasing pepsin activity, and blocking the inflammatory response are the treatment methods used to lessen the direct throat damage [10]. However, the effectiveness of proton pump inhibitors in the treatment of laryngopharyngeal reflux disease has long been controversial. The efficacy and safety of PPIs in the treatment of patients with LPRD remain controversial, and further exploration of the efficacy and safety of PPIs in the treatment of LPRD is therefore warranted.

The efficacy and safety of PPIs are still controversial, and there is no standardized treatment protocol. Therefore, this meta-analysis aims to further investigate the therapeutic effects and safety of PPIs in LPRD.

The rest of the article is as follows: Section 2 defines the various methods. Section 3 evaluates the results. Section 4 discusses the discussion. Section 5 concludes the article.

## 2. Methods

**2.1. Literature Search Strategy.** The published literature on PPIs for the treatment of LPRD was located using a computer-based search of the PubMed, Embase, Web of Science, Clinical Trials, Cochrane Library, CNKI, and Wanfang databases. The search period was from the creation of the database until 1 April 2022. English and Chinese are the search languages. Search terms are as follows: “proton pumps antagonists” or “proton pumps inhibitors” or “histamine H2 antagonists” or rabeprazole or esomeprazole or pantoprazole or lansoprazole or omeprazole; laryngitis or pharyngitis or “laryngopharyngeal reflux”(LPR) or “gastro pharyngeal reflux”(GPR); “Randomized controlled trial” or “RCT.”

**2.2. Eligibility Criteria.** The following PICOS criteria were used to cover the studies.

**2.2.1. Participants of Various Types.** Adult patients aged >18 years with a diagnosis of LPRD-related disease were included in the study.

**2.2.2. Interventions.** The intervention was PPIs in the experimental group and placebo in the control group.

**2.2.3. Types of Result Measures.** The primary outcome measures covered the overall efficiency, reflux symptom index (RSI) [11], reflux finding score (RFS) [12], improvement in cough and hoarseness, and adverse reactions.

**2.2.4. Types of Studies.** Based on inclusion criteria for qualifying trials, full publications and data from randomised controlled studies of PPIs in patients with LPRD were obtained.

The literature was studied individually by two investigators, with the initial screening consisting of reading the abstracts and titles and saving the relevant material that met the inclusion criteria for rescreening.

**2.3. Information Extraction.** According to the proposed criteria, researchers independently extracted data and relevant information from the included literature and recorded the findings, which included the source of the literature (author, date of publication, and country), basic characteristics of the study population (sample size and age), and interventions (type of PPIs and duration of dose study). Researchers must evaluate one another, and if there is a disagreement, a third-party decision is required.

**2.4. Quality Assessment.** Use the Cochrane 5.1 manual’s risk of the bias assessment tool to assess the risk of bias in RCT studies [13]. The experimental PPI group was demonstrated to be beneficial overall; however, there was no statistically significant difference between them and the control group.

**2.5. Statistical Analysis.** A meta-analysis of the data was performed using Review Manager (RevMan) 5.3 software. The dichotomous variables (overall efficiency and adverse effects) were expressed as odds ratios, whereas the continuous variables (RSI, RFS, improvement of cough, and hoarseness) were reported as mean differences (OR). Both variables are described using a 95% confidence interval (CI). The included studies were tested for heterogeneity, and a fixed-effects model was used for meta-analysis if I<sup>2</sup> was <50%, and a random-effects model was used for meta-analysis if I<sup>2</sup> was ≥50%. Studies were considered to be statistically significant if  $P < 0.05$ . When the number of included studies was greater than or equal to 10, a funnel plot was used for publication bias analysis.

## 3. Results

**3.1. General Information on the Included Literature.** As shown in Figure 1, a total of 4168 relevant articles (72 from CNKI, 92 from Wanfang, 57 from CBM, 47 from Wipe, 88 from Cochrane, 2447 from PubMed, 1029 from Embase, and 336 from Web of Science) were identified according to the search strategy. Cochrane 88, PubMed 2447, Embase 1029, Web of science 336, computerized deduplication of 448 (72 in Chinese and 376 in English), exclusion of 3665 after reading the title abstracts, and further screening of 55 (30 in Chinese and 25 in English) might meet the inclusion criteria by reading the full text. A total of 14 randomized controlled trials that met the exclusion criteria were included.

**3.2. Basic Characteristics.** Fourteen randomized controlled trials included 815 patients with LPR, most diagnosed by laryngoscopy or esophageal pH monitoring, and the 14 studies were conducted in different parts of the world [14–27]. All 14 included papers gave baseline data for the experimental and control groups, which were similar and comparable between the two groups at baseline. Table 1 summarizes 14 studies with basic information.

**3.3. Quality Assessment.** Of the 14 included studies, one was a crossover controlled trial [21], and the rest were all randomized measured trials. 10 of the studies [14, 15, 17, 20, 22, 23, 25, 27] explicitly stated the method of generating the randomized sequence, and three studies [16, 24, 26] only suggested to randomize patients into experimental and control groups but did not state the method of generating the randomized sequence. The included studies were double-blinded except for the Chappity et al.’s [14] study which was single-blinded to the treatment group; 10 studies [15–20, 22, 23, 25, 26] explicitly gave allocation concealment schemes, and all trials did not selectively report outcomes; 3 studies [20, 22, 23] had missed visits, but the final data analysis excluded those who were missed and the number of people who fully performed the trial procedure for the quasi-analysis, and the remaining outcome data were reported in full (Figure 2).

### 3.4. Meta-analysis Results

**3.4.1. RSI Score.** Four studies [15, 17, 18, 22] reported a comparison of the improvement in pharyngeal RSI scores before

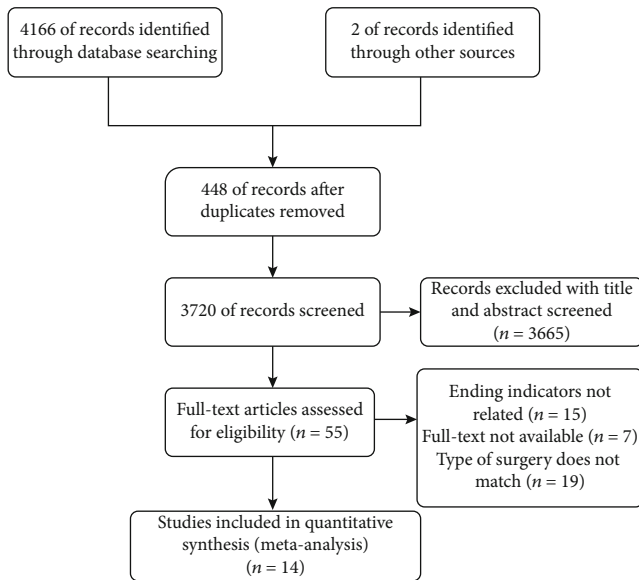


FIGURE 1: Flow chart of literature search and study selection.

and after treatment in patients with LPRD in the PPIs treatment group, with 132 cases in the experimental group and 105 cases in the control group, with the experimental group outperforming the control group in terms of improvement in RSI scores, with statistically significant differences [MD = 3.35, 95% CI (1.34, 5.37,  $P < 0.05$ )] (Figure 3).

**3.4.2. Overall Efficiency.** Ten studies [14, 16, 19, 26] compared the general effectiveness of PPI in patients with LPRD, with 329 cases in the experimental group and 271 in the control group. The outcomes demonstrated that the experimental group was successful; however, there was no statistically significant difference between the experimental group and the control group [OR = 1.62, 95% CI (0.89, 2.95),  $P > 0.05$ ] (Figure 4).

**3.4.3. RFS.** Four studies [15, 17, 18, 22] reported a comparison of PPI on pharyngeal RFS scores in patients with LPRD, with 112 cases in the experimental group and 105 cases in the control group, with no statistical difference in RFS scores [MD = 0.62, 95% CI (-1.28, 2.48),  $P > 0.05$ ] (Figure 5).

**3.4.4. Improvement of Cough and Hoarseness Symptoms.** Seven studies [15–18, 22, 24, 27] compared the improvement of PPI on cough in patients with LPRD, including 159 cases in the experimental group and 144 cases in the control group. There was no difference in the rate of relief of cough symptoms in patients with LPRD by PPI compared with the control group, and there was a strong placebo effect [SMD = -0.12, 95% CI (-1.44, 1.19),  $P > 0.05$ ] (Figure 6). Five studies [16–18, 22, 24] compared the improvement of hoarseness in patients with LPRD by PPI, with 129 cases in the treatment group and 119 cases in the control group, with no statistically significant difference between the two groups in terms of relief of hoarseness symptoms [SMD = -0.51, 95% CI (-1.36, 0.35),  $P > 0.05$ ] (Figure 7).

**3.4.5. Adverse Effects.** The results of the meta-analysis could not be combined due to inadequate reporting of data on adverse reactions in the included studies. We only performed descriptive analyses. 2 studies explored adverse reactions, and the results of Shaheen et al. [15] showed that no serious adverse drug reactions occurred during dosing and no patients withdrew from the study due to the safety of the drug. Vaezi et al. [20] showed that the experimental group experienced increased upper respiratory tract infections and discomfort with monitoring medical devices and gastrointestinal reactions compared to the control group; a higher proportion of patients in the experimental group experienced increased upper respiratory infections and discomfort and gastrointestinal reactions to monitoring equipment compared to the control group. There were no significant changes in weight, changes in vital signs, or relevant ECG parameters in either group, and there was a trend towards increased gastrin levels in the experimental group.

## 4. Discussion

Laryngopharyngeal reflux is a chronic inflammatory disease with no clear cause, which explains why it is so simple to misdiagnose given that its clinical symptoms are similar to those of many other laryngopharyngeal diseases. The RSI and RFS score scales are primarily used to screen patients for diseases by precisely assessing their clinical symptoms and indicators [28]. Changes in pepsin levels, gastric bubble size, and laryngopharyngeal reflux disease are somewhat correlated [29, 30]. A sore throat and hoarseness are relatively obvious symptoms of this disease. Symptoms such as persistent coughs, foreign bodies in the throat, and shortness of breath seriously impact patients' feature of life. Vocal cord edema is accompanied by glottis stenosis, mesangial hyperplasia, granulomas, diffuse congestion, and glottal stenosis. Laryngitis and pharyngitis can cause serious health problems, including chronic laryngitis and pharyngitis which negatively impact patients' physical and mental health if not treated promptly and effectively [31]. To promote a good prognosis and recovery for patients suffering from laryngopharyngeal reflux disease, rapid diagnosis and effective treatment are very important [32].

Proton pump inhibitors are commonly used in the clinical empirical treatment of laryngopharyngeal reflux diseases. It works by inhibiting  $H^+ - K^+ - ATPase$  on the gastric wall cells, reducing the excretion of gastric acid, reducing pepsin activity, and reducing inflammation, thereby reducing the effects of direct damage to the throat [33]. In clinical practice, many practitioners recommend the use of PPIs to improve symptoms associated with patients with LPRD and consider them to be effective. However, the effectiveness of proton pump inhibitors in the treatment of laryngopharyngeal reflux disease has long been controversial. In a study by Gatta et al. [34], there was no discernible improvement in reflux symptoms between PPIs and placebos. The reasonable use of PPI is a more successful treatment for GERD pharyngitis, according to a domestic meta-analysis conducted by Zhang et al. in 2012 [35], and this discrepancy in the results has significantly impacted

TABLE 1: Characteristics of individual studies included in the meta-analysis.

Study (year)	Country	Age (E/C)	Sample (E/C)	Interventions (E/C)	Follow-up (week)	Outcomes
Chappity et al. (2014) [14]	India	36.9	117/117	Omeprazole 20 mg (2 times/d)/lifestyle change treatment only	12	②
Shaheen et al. (2010) [15]	United States	49.5 ± 12/51.0 ± 11.6	22/18	Esomeprazole 40 mg (2 times/d)/placebo	12	①③④⑥
Fass et al. (2009) [16]	United States	63.25 ± 13.33/67.71 ± 9.47	24/17	Esomeprazole 20 mg (2 times/d)/placebo	12	②④⑤
Lam et al. (2010) [17]	China	46.29 ± 9.77/47.43 ± 8.66	42/40	Rabeprazole 20 mg (2 times/d)/placebo	12	①③④⑤
Reichel et al. (2008) [18]	United Kingdom	49 ± 13.9/47.6 ± 16	30/28	Esomeprazole 20 mg (2 times/d)/placebo	12	①③④⑤
Wo et al. (2005) [19]	United States	39/37	20/19	Pantoprazole 40 mg(1 time/d)/placebo	12	②
Vaezi et al. (2006) [20]	Australia	51.5 ± 15.2/50.5 ± 14.5	95/50	Esomeprazole 40 mg (2 times/d)/placebo	16	②⑥
Eherer et al. (2003) [21]	United States	48	10/10	Pantoprazole 40 mg (2 times/d)/placebo	12	②⑥
Steward et al. (2004) [22]	United States	45.8 ± 11.2/52.8 ± 11.5	21/21	Rabeprazole 20 mg (2 times/d)/placebo	8	①②③④⑤
El-Serag et al. (2001) [23]	United States	59/65	12/10	Lansoprazole 30 mg (2 times/d)/placebo	12	②
Noordzij et al. (2001) [24]	United States	51.7/45.3	15/15	Omeprazole 40 mg (2 times/d)/placebo	8	②④⑤
Ours et al. (1999) [25]	United States	54	8/9	Omeprazole 40 mg (2 times/d)/placebo	12	②
Langevin and Ngo (2001) [26]	Canada	53	14/16	Omeprazole 40 mg (2 times/d)/placebo	12	②
Rabeneck et al. (1999) [27]	Australia	54	8/7	Lansoprazole 30 mg (2 times/d)/placebo	12	④

① RSI score; ② overall effectiveness rate; ③ antitumor sign score; ④ relief of cough symptoms; ⑤ relief of hoarseness symptoms; ⑥ adverse effects rate.

	Random sequence generation (selection bias)	Allocation concealment (selection bias)	Blinding of participants and personnel (performance bias)	Blinding of outcome assessment (detection bias)	Incomplete outcome data (attrition bias)	Selective reporting (reporting bias)	Other bias
14.Chappity 2014	+	-	-	?	+	+	?
15.Shaheen 2010	+	+	+	+	+	+	?
16.Fass 2009	-	+	+	?	+	+	?
17.Lam 2010	+	+	+	+	+	+	?
18.Reichel 2008	+	+	+	+	+	+	?
19.Wo 2005	+	+	+	?	+	+	?
20.Vaezi 2006	+	+	+	?	+	+	?
21.Eherer 2003	+	-	+	+	+	+	?
22.Steward 2004	+	+	+	+	+	+	?
23.EL-Serag 2001	+	+	+	+	+	+	?
24.Noordzij 2001	-	-	+	?	+	+	?
25.Ours 1999	+	+	+	?	+	+	?
26.Langevin 2001	+	+	+	?	+	+	?
27.Havas 1999	+	+	+	?	+	+	?

FIGURE 2: Bias risk assessment results included RCT.

the marketing of this medication. Therefore, there is a need for a comprehensive evaluation of the efficacy of proton pump inhibitors in patients with laryngopharyngeal reflux disease through evidence-based medicine to provide a reliable evidence-based basis for the treatment of laryngopharyngeal reflux disease.

In the RSI score, the experimental PPI group was better than the control group in comparing the RSI score of throat symptom improvement, and the efficacy was statistically significant, and the difference between the two was statistically significant. The throat symptoms such as foreign body sensation in the throat and persistent throat clearing in the PPI treatment group improved significantly, which can be used as a reference to guide the clinical use of drugs. The mechanism of the improvement of throat symptom improvement by PPI is that PPI inhibits the H<sup>+</sup>-K-ATPase, which reduces gastric acid secretion and pepsin

activity, thereby reducing the direct damage to the throat. Five of the 13 randomized controlled trials that included 831 patients with LPRD in Wei, which used the RSI as an outcome indicator to assess the efficacy of PPI, showed significantly better improvement in RSI scores in the experimental group than in the placebo control group [36]. However, Liu et al. [37] included eight studies containing 370 patients in their 2016 meta-analysis, which showed a nonsignificant efficacy of the experimental group compared to the control group in terms of overall efficiency and improvement in cough symptoms in patients with LPRD. The difference in results compared to our study may be due to the relatively high quality of the included studies due to our inclusion of larger sample size and the development of strict inclusion and exclusion criteria. However, as the RSI does not cover all symptoms and should be used in conjunction with patient symptom improvement as an indicator of efficacy assessment, it is expected that subsequent studies will provide more objective indicators to evaluate the efficacy of PPI for LPRD.

In terms of overall effectiveness, the experimental PPI group was shown to be effective, but the difference with the control group was not statistically significant. We speculate that this may be due to the variability in lifestyle and diet of patients with LPRD. The expert consensus on LRPD states [38] that changing poor lifestyle and diet is the most basic treatment strategy, but the guidelines do not specify specific dietary interventions. Traditional dietary interventions suggest reducing the intake of some acidic foods such as caffeine, beer, and chocolate and using alkaline water, as well as changing lifestyle habits such as the traditional dietary interventions which include reducing the intake of acidic foods such as caffeine, beer, and chocolate and using alkaline water, as well as lifestyle changes such as smoking and alcohol cessation. While clinicians often give verbal advice on the importance of dietary modification in the treatment of LPRD, few studies provide detailed statistics on patient adherence. It is this wide variation in dietary habits that can affect the efficacy of PPI.

PPI did not show significant efficacy in improving RFS scores in adult LPRD patients. RFS is an eight-item grading scale, but it is subjective because the laryngologist who grades it is based on their experience. It has not been proven to be a reliable method for detecting reflux-induced laryngopharyngeal symptoms. Furthermore, because of a lack of standardization and clarification of nomenclature, there was a great deal of diversity in the interpretation of the larynx by both ENT and GI professionals [39].

In adults with LPRD, there is inadequate data to show that PPI has a meaningful benefit over placebo in reducing pharyngeal symptoms including cough and hoarseness. In their study, Lechien et al. noted that dietary changes and lifestyle modifications combined with the use of twice daily pantoprazole showed significant improvement in the symptoms of hoarseness caused by gastroesophageal reflux [40]. However, Johnson et al. applied acoustic parameters as an objective method to evaluate hoarseness and suggested that clinically cured patients (RSI <13 and RFS <7) showed no or little improvement in acoustic parameters and that their



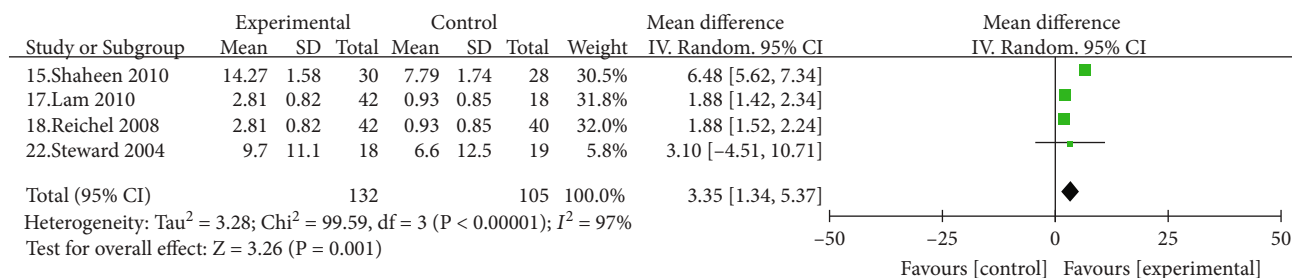


FIGURE 3: Comparison of reflux symptom index scores between the experimental group and the control group.

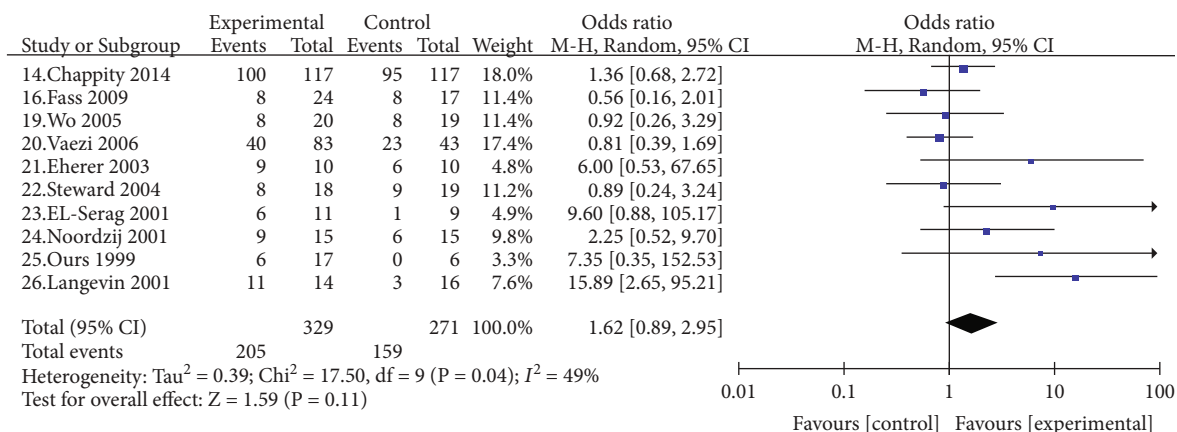


FIGURE 4: Comparison of the overall efficiency of the experimental group and the control group.

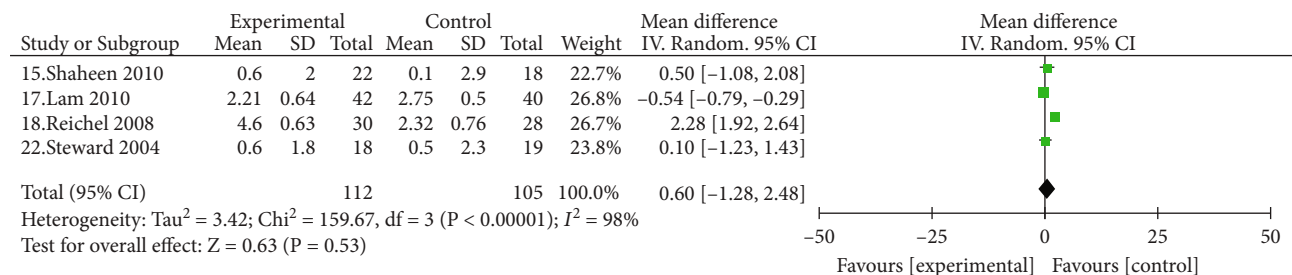


FIGURE 5: Comparison of reflux symptom scores between the experimental group and the control group.

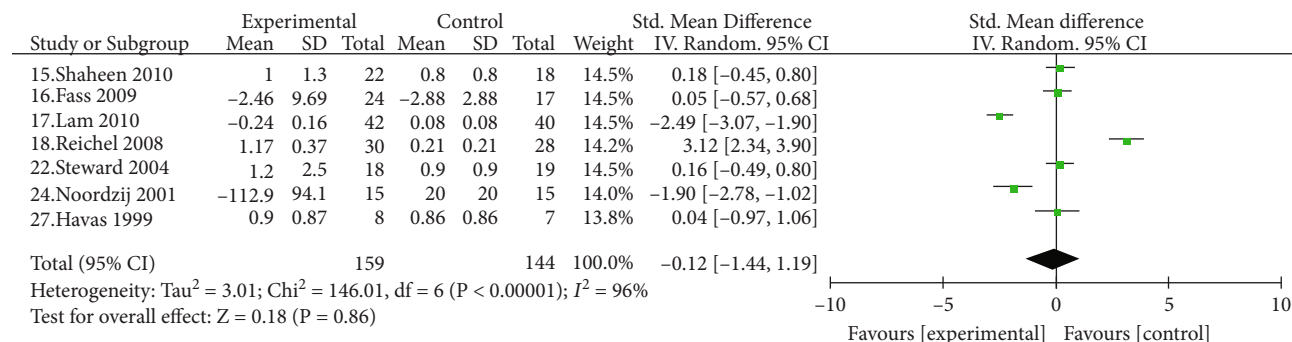


FIGURE 6: Comparison between the experimental group and the control group on the relief of cough symptoms in patients with pharyngeal reflux disease.

study could not confirm whether the significant improvement in voice quality was due to dietary modifications or to the therapeutic effect of PPIs [41]. In a study by Lechien

et al., it was noted that esophageal reflux was a cause of chronic cough in adults, that PPI treatment alone was ineffective and had a strong placebo effect, and that lifestyle

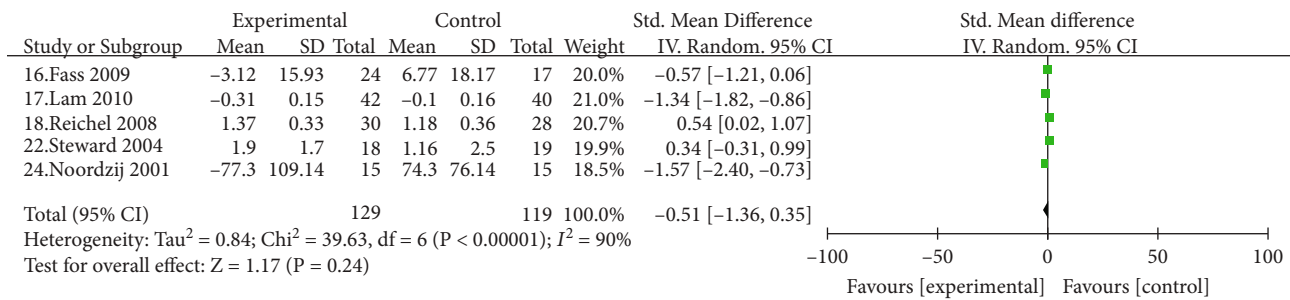


FIGURE 7: Comparison of the relief of hoarseness in patients with pharyngeal reflux disease between the experimental group and the control group.

modification combined with weight loss was beneficial for the improvement of cough symptoms [42]. The efficacy of PPI on cough and hoarseness remains controversial and may be related to the small number of studies included and the inadequate sample size, and it is expected that large sample size and multicenter randomized controlled clinical study will be available in the future to assess the efficacy of PPI on cough and hoarseness. The efficacy of PPI on cough and hoarseness is expected to be evaluated in future large sample size and multicenter randomized controlled studies.

After discontinuation of PPI, more than 90% of patients have a recurrence of symptoms and need to be treated with PPI again, while long-term PPI use has been associated with adverse effects such as reduced calcium and vitamin B12 absorption, increased risk of pulmonary infection, and cardiovascular events [43]. The data on adverse effects in our studies [15, 20] were inadequately reported, and more studies focusing on the safety of PPIs for LPRD are expected at a later stage.

Limitations of this paper are as follows:

- (i) The effectiveness of the drug was evaluated along with adverse drug reactions, but there are too few relevant data reported, so this study was not analyzed for comparison
- (ii) Although the criteria for determining efficacy were developed after reading the literature to reduce the heterogeneity of the data, there may be some risk of bias as the meta-analysis is a nonexperimental study, and it is not possible for all included study results to meet the effect indicators

In summary, PPIs were useful in alleviating throat symptoms in LPRD patients but were ineffective in reducing symptoms of cough and hoarseness. It is anticipated that more clinical trials will be conducted in the future to overcome the current limitations by utilizing large samples and multicenter randomized controlled trials with strict and uniform diagnostic and efficacy criteria to determine the true efficacy of PPI on LPRD. Nevertheless, this study still has some limitations, and these limitations will need to be addressed. It is expected that more clinical trials will be conducted in the future to overcome the current limitations, adopt large samples and multicenter randomized controlled trials, conduct rigorous and uni-

form diagnostic criteria and efficacy assessment to evaluate the true efficacy of PPIs on LPRD, avoid overdiagnosis and treatment, clarify the safety of the drugs, and reduce their side effects.

## 5. Conclusions

PPIs are effective in successful symptoms in patients with pharyngeal reflux disease and are recommended in the treatment strategy for patients with LPRD, possibly in combination with lifestyle alteration.

## Data Availability

Data to support the findings of this study is available on reasonable request from the corresponding author.

## Conflicts of Interest

The authors have no conflicts of interest to declare.

## Authors' Contributions

Xiulin Jin and Xufeng Zhou contributed equally to this work.

## References

- [1] M. Campagnolo, J. Priston, H. Thoen, T. Medeiros, and R. Assunção, "Laryngopharyngeal reflux: diagnosis, treatment, and latest research," *International Archives of Otorhinolaryngology*, vol. 18, no. 2, pp. 184–191, 2014.
- [2] R. Lechien, S. Saussez, and D. Karkos, "Laryngopharyngeal reflux disease: clinical presentation, diagnosis and therapeutic challenges in 2018," *Current Opinion in Otolaryngology & Head and Neck Surgery*, vol. 26, no. 6, pp. 392–402, 2018.
- [3] Chinese Journal of Otolaryngology, Head and Neck Surgery Editorial Committee, Pharyngology Group, Chinese Medical Association, Otolaryngology, Head and Neck Surgery Branch, "Expert consensus on the diagnosis and treatment of pharyngeal reflux disease (2015)," *Chinese Journal of Otolaryngology, Head and Neck Surgery*, vol. 51, no. 5, pp. 324–326, 2016.
- [4] R. Lechien, C. Finck, M. Khalife et al., "Change of signs, symptoms and voice quality evaluations throughout a 3- to 6-month empirical treatment for laryngopharyngeal reflux disease," *Clinical Otolaryngology*, vol. 43, no. 5, pp. 1273–1282, 2018.

- [5] N. Spantideas, E. Drosou, A. Bougea, and D. Assimakopoulos, "Laryngopharyngeal reflux disease in the Greek general population, prevalence and risk factors," *BMC Ear, Nose and Throat Disorders*, vol. 15, no. 1, p. 7, 2015.
- [6] M. Chen, Y. Li, L. Guo, T. Wang, and M. Lu, "Prevalence of laryngopharyngeal reflux disease in Fuzhou region of China," *Zhonghua er bi yan hou tou jing wai ke za zhi= Chinese Journal of Otorhinolaryngology Head and Neck Surgery*, vol. 51, no. 12, pp. 909–913, 2016.
- [7] K. Wong, G. Hanson, J. Waring, and G. Shaw, "ENT manifestations of gastroesophageal reflux," *The American Journal of Gastroenterology*, vol. 95, no. 1, pp. S15–S22, 2000.
- [8] R. Vardar, A. Varis, B. Bayrakci, S. Akyildiz, T. Kirazli, and S. Bor, "Relationship between history, laryngoscopy, and esophagogastroduodenoscopy for diagnosis of laryngopharyngeal reflux in patients with typical GERD," *European Archives of Oto-Rhino-Laryngology*, vol. 269, no. 1, pp. 187–191, 2012.
- [9] S. Ali, "Laryngopharyngeal reflux: diagnosis and treatment of a controversial disease," *Current Opinion in Allergy and Clinical Immunology*, vol. 8, no. 1, pp. 28–33, 2008.
- [10] H. Lu, J. He, D. Wei, S. Zhang, Y. Fang, and X. Yang, "Meta-analysis of proton pump inhibitors in the treatment of laryngopharyngeal reflux disease," *Chinese Otolaryngology Head and Neck Surgery Department*, vol. 25, pp. 150–156, 2018.
- [11] C. Belafsky, N. Postma, and A. Koufman, "Validity and reliability of the reflux symptom index (RSI)," *Journal of Voice*, vol. 16, no. 2, pp. 274–277, 2002.
- [12] C. Belafsky, N. Postma, and A. Koufman, "The validity and reliability of the reflux finding score (RFS)," *Laryngoscope*, vol. 111, no. 8, pp. 1313–1317, 2001.
- [13] S. Green and P. Higgins, "Preparing a Cochrane review," in *Cochrane Handbook for Systematic Reviews of Interventions*, pp. 11–30, John Wiley & Sons, 2008.
- [14] P. Chappity, R. Kumar, R. C. Deka, V. Chokkalingam, A. Saraya, and K. Sikka, "Proton pump inhibitors versus solitary lifestyle modification in management of laryngopharyngeal reflux and evaluating who is at risk: scenario in a developing country," *Clinical Medicine Insights: Ear, Nose and Throat*, vol. 7, article CMENT.S13799, 2014.
- [15] J. Shaheen, D. Crockett, D. Bright et al., "Randomised clinical trial: high-dose acid suppression for chronic cough – a double-blind, placebo-controlled study," *Alimentary Pharmacology & Therapeutics*, vol. 33, no. 2, pp. 225–234, 2011.
- [16] R. Fass, N. Noelck, M. R. Willis et al., "The effect of esomeprazole 20 mg twice daily on acoustic and perception parameters of the voice in laryngopharyngeal reflux," *Neurogastroenterology and Motility*, vol. 22, no. 2, p. 134, 2010.
- [17] K. Lam, L. Ng, K. Cheung et al., "Rabeprazole is effective in treating laryngopharyngeal reflux in a randomized placebo-controlled trial," *Clinical Gastroenterology and Hepatology*, vol. 8, no. 9, pp. 770–776, 2010.
- [18] O. Reichel, H. Dressel, K. Wiederänders, and W. J. Issing, "Double-blind, placebo-controlled trial with esomeprazole for symptoms and signs associated with laryngopharyngeal reflux," *Otolaryngology and Head and Neck Surgery*, vol. 139, no. 3, pp. 414–420, 2008.
- [19] J. M. Wo, J. Koopman, S. P. Harrell, K. Parker, W. Winstead, and E. Lentsch, "Double-blind, placebo-controlled trial with single-dose pantoprazole for laryngopharyngeal reflux," *The American Journal of Gastroenterology*, vol. 101, no. 9, pp. 1972–1978, 2006.
- [20] M. F. Vaezi, J. E. Richter, C. R. Stasney et al., "Treatment of chronic posterior laryngitis with esomeprazole," *The Laryngoscope*, vol. 116, no. 2, pp. 254–260, 2006.
- [21] A. J. Eherer, W. Habermann, H. F. Hammer, K. Kiesler, G. Friedrich, and G. J. Krejs, "Effect of pantoprazole on the course of reflux-associated laryngitis: a placebo-controlled double-blind crossover study," *Scandinavian Journal of Gastroenterology*, vol. 38, no. 5, pp. 462–467, 2003.
- [22] L. Steward, M. Wilson, H. Kelly et al., "Proton pump inhibitor therapy for chronic laryngo-pharyngitis: a randomized placebo-control trial," *Otolaryngology and Head and Neck Surgery*, vol. 131, no. 4, pp. 342–350, 2004.
- [23] H. B. El-Serag, P. Lee, A. Buchner, J. M. Inadomi, M. Gavin, and D. M. McCarthy, "Lansoprazole treatment of patients with chronic idiopathic laryngitis: a placebo-controlled trial," *The American Journal of Gastroenterology*, vol. 96, no. 4, pp. 979–983, 2001.
- [24] P. Noordzij, A. Khidr, A. Evans et al., "Evaluation of omeprazole in the treatment of reflux laryngitis: a prospective, placebo-controlled, randomized, double-blind study," *Laryngoscope*, vol. 111, no. 12, pp. 2147–2151, 2001.
- [25] M. Ours, S. Kavuru, J. Schilz, and J. E. Richter, "A prospective evaluation of esophageal testing and a double-blind, randomized study of omeprazole in a diagnostic and therapeutic algorithm for chronic cough," *The American Journal of Gastroenterology*, vol. 94, no. 11, pp. 3131–3138, 1999.
- [26] S. Langevin and H. Ngo, "GERD-induced ENT symptoms: a prospective placebo controlled study with omeprazole 40 mg a day," *Gastroenterology*, vol. 120, no. 5, p. A16, 2001.
- [27] L. Rabeneck, J. Soucek, K. Wristers et al., "A double-blind randomized placebo-controlled trial of proton pump inhibitor therapy," *The American journal of gastroenterology*, vol. 29, no. 1, pp. 243–246, 1999.
- [28] W. Zhang, Y. Cao, and B. Liu, "Correlation analysis of specific sensitivity of major symptoms and signs of laryngopharyngeal reflux disease," *Medical theory and practice*, vol. 31, pp. 1905–1907, 2018.
- [29] A. Jung, O. Kwon, J. Park et al., "Association between pepsin in the saliva and the subjective symptoms in patients with laryngopharyngeal reflux," *Journal of voice: official journal of the Voice Foundation*, vol. 33, no. 2, pp. 150–154, 2019.
- [30] Z. Sun, W. Wu, L. Li et al., "The correlation between gastric bubble size and laryngopharyngeal reflux pattern in patients with laryngopharyngeal reflux disease," *Zhonghua Yi Xue Za Zhi*, vol. 99, no. 44, pp. 3487–3493, 2019.
- [31] Z. Sun, "Analysis of diagnosis and treatment of laryngopharyngeal reflux disease," *Journal of Mathematical Medicine*, vol. 33, pp. 1363–1364, 2020.
- [32] L. Chen, H. Wu, W. Mei et al., "Dx-Ph correlation analysis between monitoring and proton pump inhibitor diagnostic tests in the diagnosis of laryngopharyngeal reflux diseases," *Chinese Journal of Otolaryngology-Head and Neck Surgery*, vol. 55, pp. 34–39, 2020.
- [33] P. Müller, A. Göksu, W. Fuchs, F. Schlüter, and B. Simon, "Initial potency of lansoprazole and omeprazole tablets on pentagastrin-stimulated gastric acid secretion—a placebo-controlled study in healthy volunteers," *Alimentary Pharmacology & Therapeutics*, vol. 14, no. 9, pp. 1225–1229, 2000.

- [34] L. Gatta, D. Vaira, G. Sorrenti, S. Zucchini, C. Sama, and N. Vakil, "Meta-analysis: the efficacy of proton pump inhibitors for laryngeal symptoms attributed to gastro-oesophageal reflux disease," *Alimentary Pharmacology & Therapeutics*, vol. 25, no. 4, pp. 385–392, 2007.
- [35] J. Zhang, G. Dong, S. Qiu, M. Ai, and J. Wang, "Meta-analysis of proton pump inhibitors in the treatment of gastroesophageal reflux pharyngitis," *Journal of Gastroenterology and Hepatology*, vol. 21, no. 9, pp. 834–840, 2012.
- [36] C. Wei, "A meta-analysis for the role of proton pump inhibitor therapy in patients with laryngopharyngeal reflux," *European Archives of Oto-Rhino-Laryngology*, vol. 273, no. 11, pp. 3795–3801, 2016.
- [37] C. Liu, H. Wang, and K. Liu, "Meta-analysis of the efficacy of proton pump inhibitors for the symptoms of laryngopharyngeal reflux," *Brazilian Journal of Medical and Biological Research*, vol. 49, no. 7, 2016.
- [38] R. Lechien, S. Saussez, A. Schindler et al., "Clinical outcomes of laryngopharyngeal reflux treatment: a systematic review and meta-analysis," *The Laryngoscope*, vol. 129, no. 5, pp. 1174–1187, 2019.
- [39] D. A. Johnson, G. L. Schechter, P. Katz, R. T. Sataloff, and D. O. Castell, "ENT and GI specialists interpretation of possible reflux laryngitis-coalition or confusion?," *Gastroenterology*, vol. 102, p. A91, 1992.
- [40] R. Lechien, K. Huet, M. Khalife et al., "Impact of laryngopharyngeal reflux on subjective and objective voice assessments: a prospective study," *Journal of Otolaryngology - Head & Neck Surgery*, vol. 45, no. 1, p. 59, 2016.
- [41] R. Lechien, V. Delvaux, K. Huet et al., "Phonetic approaches of laryngopharyngeal reflux disease: a prospective study," *Journal of Voice*, vol. 31, no. 1, pp. 119.e11–119.e20, 2017.
- [42] J. Kahrilas, W. Altman, B. Chang et al., "Chronic cough due to gastroesophageal reflux in adults: CHEST guideline and expert panel report," *Chest*, vol. 150, no. 6, pp. 1341–1360, 2016.
- [43] Y. Si, "Analysis of the therapeutic effect of proton pump inhibitors on gastroesophageal reflux pharyngitis," *Heilongjiang Medicine*, vol. 41, no. 6, pp. 523–524, 2017.

## Research Article

# Diagnostic Values of Blood Urea Nitrogen (BUN), Creatinine (Cr), and the Ratio of BUN to Cr for Distinguishing Heart Failure from Asthma and Chronic Obstructive Pulmonary Disease

Jingjing Zhang,<sup>1</sup> Ling Zhou,<sup>2</sup> and Yuezhan Zhang<sup>3</sup> 

<sup>1</sup>Department of Nephropathy, Lianyungang TCM Hospital Affiliated to Nanjing University of Chinese Medicine, Lianyungang, Jiangsu 222000, China

<sup>2</sup>Department of Emergency, Lianyungang TCM Hospital Affiliated to Nanjing University of Chinese Medicine, Lianyungang, Jiangsu 222000, China

<sup>3</sup>Department of Geriatrics, Lianyungang TCM Hospital Affiliated to Nanjing University of Chinese Medicine, Lianyungang, Jiangsu 222000, China

Correspondence should be addressed to Yuezhan Zhang; zhangyuezhan1979@njucm.edu.cn

Received 9 June 2022; Revised 7 July 2022; Accepted 11 July 2022; Published 21 July 2022

Academic Editor: Naeem Jan

Copyright © 2022 Jingjing Zhang et al. This is an open access article distributed under the Creative Commons Attribution License, which permits unrestricted use, distribution, and reproduction in any medium, provided the original work is properly cited.

**Background.** In clinical practise, it can be challenging to tell the difference between asthma and chronic obstructive pulmonary disease (COPD) and heart failure (HF), which share comparable dyspnea symptoms. We aimed to examine whether renal function indexes blood urea nitrogen (BUN), creatinine (Cr), and the ratio of BUN to Cr (BUN/Cr) can be used to distinguish HF from asthma and COPD. **Methods.** A total of 170 patients were admitted for dyspnea symptoms in this retrospective study. There are 69 patients with HF (HF group), 50 patients with asthma (asthma group), and 51 patients diagnosed with COPD (COPD group). The levels of BUN, Cr, and the ratio of BUN/Cr in the three groups were compared. Student's *t*-test or the one-way analysis of variance (ANOVA) test was used to compare means. Using the area under the receiver operating characteristic curve, model differentiation was evaluated (AUC). Z-test comparisons of AUC were carried out. **Results.** Compared with the asthma/COPD group (asthma group + COPD group) or the COPD group, the levels of BUN and Cr were raised in the HF group, while there was no significant difference of the BUN/Cr ratio. Compared with those in the asthma group, the levels of BUN, Cr, and BUN/Cr ratio were significantly increased in the HF group (all  $p < 0.05$ ), whereas no significant differences of BUN, Cr, and BUN/Cr ratio were found between asthma and COPD. The AUC in distinguishing HF from asthma/COPD were 0.736 and 0.751 for BUN and Cr, respectively, and no significant difference was observed between BUN and Cr. The cutoff values (specificity, sensitivity, and Youden index) in distinguishing between HF and asthma/COPD were 20.45 mg/dL (79.21%, 56.52%, and 0.357) for BUN and 0.782 mg/dL (72.28%, 68.12%, and 0.404) for Cr, respectively. **Conclusions.** BUN and Cr showed accurate and reliable diagnostic values which could be potential biomarkers for differentiating HF from asthma and/or COPD.

## 1. Introduction

Dyspnea, due to its high prevalence [1], was among the top ten principal reasons for adult presentation to the emergency department (ED) [2, 3]. There are a number of conditions that can lead to dyspnea, including heart failure (HF), asthma, and chronic obstructive pulmonary disease (COPD).

HF is a condition in which the heart cannot pump enough blood efficiently, while asthma and COPD are associated with chronic airway inflammation. A common sign of cardiopulmonary disease, dyspnea can range from moderate and short lived to severe and persistent. In clinical practise, it can be challenging to distinguish between HF, asthma, and COPD because they all have comparable dyspnea symptoms. At this

point, the right diagnostic laboratory tests may be beneficial to support a particular diagnosis and so play a vital role in justifying a more rapid evaluation and precise therapies.

Brain natriuretic peptide (BNP) [4, 5] and N-terminal pro-B-type natriuretic peptide (NT-proBNP) [6, 7], as recommended by guidelines, are valuable tools in distinguishing HF from asthma/COPD. However, this multitude of causes for the elevation of BNP or NT-proBNP, such as age and renal insufficiency, imposes limits on its diagnostic use for HF [4]. Furthermore, the measurement of BNP or NT-proBNP is expensive and increases the economic burden of patients. Thus, whether there are other common and cheap emergency blood tests that can help distinguish HF from asthma/COPD remains a challenging issue concerned by clinicians, when they encounter patients with dyspnea attack.

Aronson et al. [8] investigated 541 patients with decompensated HF and found that the blood urea nitrogen (BUN) and BUN/creatinine (BUN/Cr) ratio, but not serum Cr, remained related to mortality after adjusting for other risk factors during the follow-up period. Another study done by Filippatos et al. [9] came to a similar conclusion: after controlling for covariates, BUN, but not Cr, is a statistically significant predictor of mortality and the composite endpoint of death or heart failure hospitalization at 60 days after discharge. Georgiopoulou et al. [10] revealed that serum Cr in outpatients with HF was an adequate prognosticator of death or HF hospitalization and elevated BUN was associated with well all-cause and cardiovascular hospitalization rates and ED visits rates. Parrinello et al. [11] found that higher values of BUN in HF with a preserved ejection fraction was related to significantly increased all-cause mortality. Up to now, it remains uncertain whether these cheap and easy-to-obtain renal function indices (BUN, Cr, and BUN/Cr ratio) could differentiate HF from asthma/COPD preliminarily. To the best of our knowledge, there has not yet been a discussion on how to compare the diagnostic values of these renal function indicators to differentiate between HF and asthma/COPD. Our study may provide novel evidence for whether BUN, Cr, and BUN/Cr ratio could demonstrate accurate and reliable diagnostic values in distinguishing HF from asthma/COPD.

The paper's organization paragraph is as follows: the materials and methods is presented in Section 2. Section 3 discusses the experiments and results. Section 4 consists of the discussion section. Finally, in Section 5, the research work is concluded.

## 2. Materials and Methods

**2.1. Study Population.** A total of 170 patients with dyspnea attack admitted to Lianyungang TCM Hospital Affiliated to Nanjing University of Chinese Medicine were consecutively enrolled in this study between January 2018 and February 2021. The diagnoses of HF, asthma, and COPD were performed following the relevant guidelines [12–14]. All patients underwent echocardiography, pulmonary function test, electrocardiography, chest computed tomography, and BNP or NT-proBNP if necessary, except for cases with HF

or asthma/COPD confirmed by other hospitals recently. Finally, a total of 69 inpatients were diagnosed with HF (HF group) and the rest were inpatients with asthma or COPD (asthma group 50; COPD group 51). Inclusion criteria were adults  $\geq 30$  years old, at least symptoms presenting at the time of visit, and emergency renal function tests in the ED or on admission performed by all patients. Patients with comorbidities between HF, asthma, and COPD, patients who underwent renal function tests on the second day after admission, patients whose clinical data were incomplete, patients with gastrointestinal bleeding, kidney disease, thyroid disease, shock, trauma, pregnant women, and patients with other causes of dyspnea were all excluded. The study followed the *Declaration of Helsinki* and was approved by the ethics committee of Lianyungang TCM Hospital Affiliated to Nanjing University of Chinese Medicine.

**2.2. Clinical Data.** Medical records of patients admitted to Lianyungang TCM Hospital Affiliated to Nanjing University of Chinese Medicine were used to compile baseline data. The Hitachi7600 automatic biochemical analyzer was used to determine renal function variables (BUN and Cr). The BUN/Cr ratio was calculated and recorded (BUN: 1 mg/dL = 0.357 mmol/L, Cr: 1 mg/dL = 88.4  $\mu$ mol/L).

**2.3. Statistical Analysis.** Statistical analysis was performed using SPSS v19.0 (SPSS, Chicago, USA). Descriptive analysis of continuous variables was used to calculate the mean and standard deviation. Qualitative data were compared using the chi-squares test. Means were compared using Student's *t*-test or one-way analysis of variance (ANOVA) test for independent samples. Prognostic performance was tested by calculating receiver operating characteristic (ROC) curves and displayed in AUC. Comparison of AUC was performed using the *Z*-test of the software MedCalc v18.2.1 (MedCalc, Ostend, Belgium). From the ROC coordinates, the score value with the best Youden index (sensitivity + specificity - 1) was used to determine the cutoff value for the above scores.  $p < 0.05$  was considered statistically significant.

## 3. Results

**3.1. Patients' Characteristics.** A total of 69 inpatients diagnosed with HF (HF group) and 101 cases with asthma and COPD (asthma group 50; COPD group 51) were analyzed. The mean age of the study sample was  $73.12 \pm 12.12$  years. Among them, 103 (60.6%) were female and 67 (39.4%) were male. There were no significant differences of age or the rate of coronary heart disease (all  $p > 0.05$ ), except for the rates of gender, diabetes mellitus, and hypertension between HF and asthma/COPD (Table 1) and among three groups of HF, asthma, and COPD (Table 2). Renal function indices were the focus of the present study.

**3.2. BUN, Cr, and the BUN/Cr Ratio.** As shown in Table 1 and Figures 1(a)–1(c), the levels of BUN and Cr were boosted in the HF group compared with the asthma/COPD group (asthma group + COPD group) (all  $p < 0.05$ ), BUN and Cr levels were higher in the HF group compared to

TABLE 1: Comparison of the levels of different variables between two groups.

Variables	HF group ( $n = 69$ )	Asthma/COPD group ( $n = 101$ )	$p$ value
Age (years)	72.25 $\pm$ 14.54	73.71 $\pm$ 10.19	0.470
Gender (male/female)	40/29	27/74	<0001*
Hypertension (Y/N)	44/25	42/69	0.001*
Diabetes mellitus (Y/N)	23/46	16/85	0.008*
Coronary heart disease (Y/N)	22/47	22/79	0.140*
BUN (mg/dL)	24.41 $\pm$ 10.90	16.46 $\pm$ 5.58	<0.001
Cr (mg/dL)	0.98 $\pm$ 0.37	0.73 $\pm$ 0.23	<0.001
BUN/Cr ratio	25.66 $\pm$ 8.70	23.43 $\pm$ 7.97	0.087

Quantitative data were present as mean  $\pm$  standard deviations; Y: yes; N: no; HF: heart failure; COPD: chronic obstructive pulmonary disease; BUN: blood urea nitrogen; Cr: creatinine; BUN/Cr ratio: BUN to Cr ratio; \*Student's  $t$ -test or chi-squared test.

TABLE 2: Comparison of the levels of different variables among three groups.

Variables	HF group ( $n = 69$ )	Asthma group ( $n = 50$ )	COPD group ( $n = 51$ )	$p$ value
Age (years)	72.25 $\pm$ 14.54	72.08 $\pm$ 11.11	75.31 $\pm$ 9.02	0.304
Gender (male/female)	40/29	13/37	14/37	<0001*
Hypertension (Y/N)	44/25	24/26	17/34	0.004*
Diabetes mellitus (Y/N)	23/46	8/42	8/43	0.029*
Coronary heart disease (Y/N)	22/47	13/37	9/42	0.212*
BUN (mg/dL)	24.41 $\pm$ 10.90	15.82 $\pm$ 5.31	17.10 $\pm$ 5.82	<0.001
Cr (mg/dL)	0.98 $\pm$ 0.37	0.75 $\pm$ 0.24	0.71 $\pm$ 0.23	<0.001
BUN/Cr ratio	25.66 $\pm$ 8.70	21.86 $\pm$ 6.64	24.98 $\pm$ 8.87	0.039

Quantitative data were present as mean  $\pm$  standard deviations; Y: yes; N: no; HF: heart failure; COPD: chronic obstructive pulmonary disease; BUN: blood urea nitrogen; Cr: creatinine; BUN/Cr ratio: BUN to Cr ratio; \*ANOVA test or chi-squared test.

the COPD group following pairwise comparison of subgroup analysis, but the BUN/Cr ratio did not differ ( $p > 0.05$ ) (all  $p < 0.05$ ), while there was no difference in the BUN/Cr ratio ( $p > 0.05$ ) (T2, Figures 2(a)–2(c)); furthermore, the levels of BUN, Cr, and BUN/Cr ratio were promoted in the HF group compared with the asthma group (all  $p < 0.05$ ), whereas no differences of BUN, Cr, and BUN/Cr ratio were found between asthma and COPD (all  $p > 0.05$ ).

**3.3. Comparison of ROC Curves of BUN, Cr, and BUN/Cr Ratio in Distinguishing Different Groups.** The AUC (95% confidence interval (CI)) in distinguishing between HF and asthma/COPD were 0.736 (0.663 to 0.800) for BUN and 0.751 (0.679 to 0.814) for Cr (Figure 3). The cutoff values (specificity, sensitivity, and Youden index) in distinguishing between HF and Asthma/COPD were 20.45 mg/dL (79.21%, 56.52%, and 0.357, respectively) for BUN and 0.782 mg/dL (72.28%, 68.12%, and 0.404, respectively) for Cr. One result of subgroup analysis was that the AUC (95% (CI)) in distinguishing between HF and asthma were 0.760 (0.673 to 0.834) for BUN, 0.726 (0.636 to 0.804) for Cr, and 0.621 (0.528 to 0.708) for BUN/Cr ratio (Figure 4). The cutoff values (specificity, sensitivity, and Youden index) in distinguishing between HF and asthma were 19.86 mg/dL (82.00%, 59.42%, and 0.414, respectively) for BUN, 0.842 mg/dL

(76.00%, 62.32%, and 0.383, respectively) for Cr, and 21.26 (50.00%, 69.57%, and 0.196, respectively) for the BUN/Cr ratio. The other result of subgroup analysis was that the AUC (95% (CI)) in distinguishing between HF and COPD were 0.712 (0.622 to 0.791) for BUN and 0.776 (0.691 to 0.847) for Cr (Figure 5). The cutoff values (specificity, sensitivity, and Youden index) in distinguishing between HF and COPD were 20.45 mg/dL (76.47%, 56.52%, and 0.330, respectively) for BUN and 0.782 mg/dL (78.43%, 68.12%, and 0.466, respectively) for Cr.

## 4. Discussion

HF, asthma, and COPD are the most common and important differential diagnoses for dyspnea in older adults. Despite the three diseases' fundamentally different pathophysiology, their comparable clinical presentations make it challenging for clinicians to make a diagnosis and assess the severity of the underlying condition [6]. What is worse, overlapping clinical presentations (e.g., asthma and COPD) and comorbid diseases (e.g., HF and COPD) can conspire to confound accurate diagnosis and optimal therapy [15]. Thus, rapid evaluation and targeted diagnostic studies are of central importance for reducing mortality and disease burden [16].

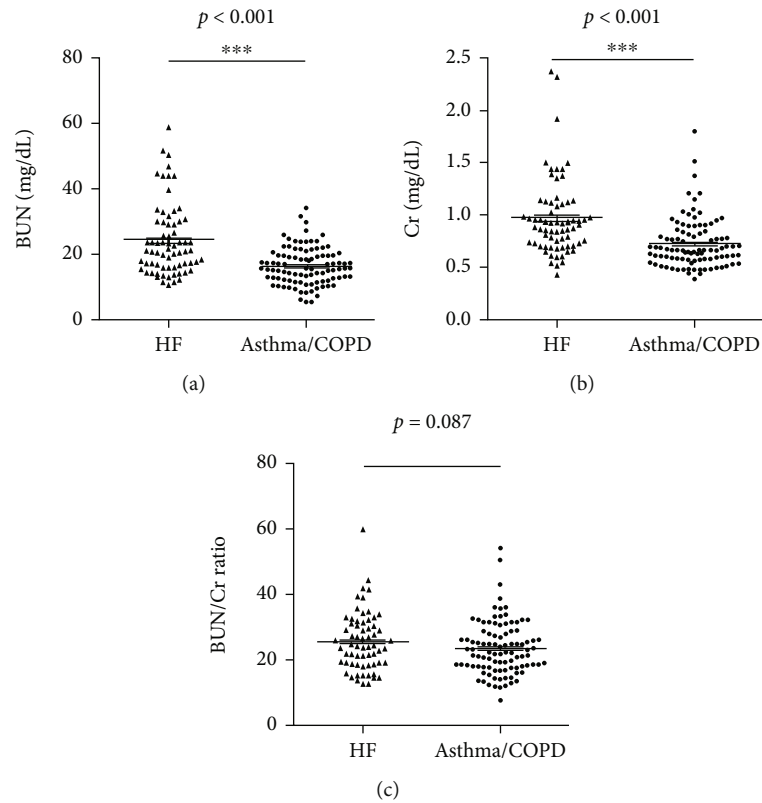


FIGURE 1: Comparison of BUN (a), Cr (b), and BUN/Cr ratio (c) between HF and asthma/COPD. HF: heart failure; COPD: chronic obstructive pulmonary disease; BUN: blood urea nitrogen; Cr: creatinine; BUN/Cr ratio: BUN to Cr ratio; \*\*\* $p < 0.001$ .

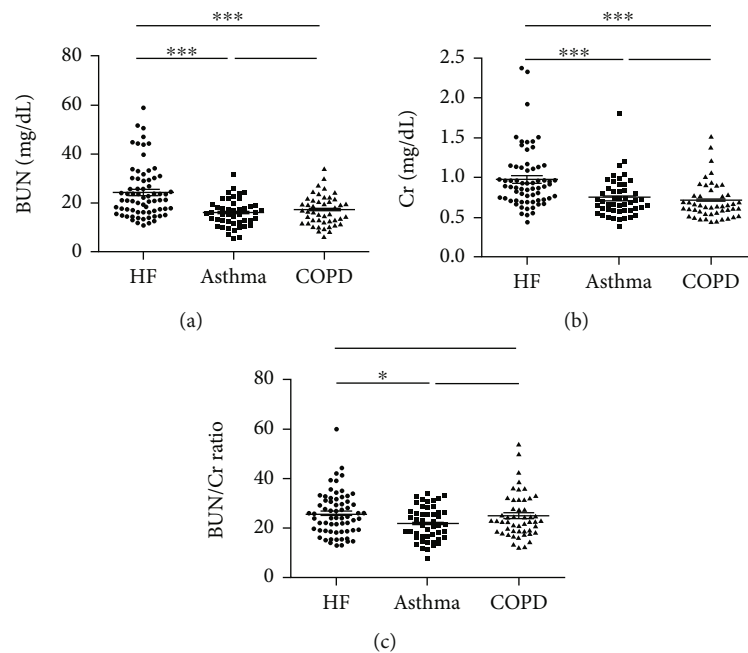


FIGURE 2: Comparison of BUN (a), Cr (b), and BUN/Cr ratio (c) among HF, asthma, and COPD. HF: heart failure; COPD: chronic obstructive pulmonary disease; BUN: blood urea nitrogen; Cr: creatinine; BUN/Cr ratio: BUN to Cr ratio; \* $p < 0.05$ , \*\*\* $p < 0.001$ .

In the present study, we have proved that BUN was raised in the HF group compared with the asthma/COPD group ( $p < 0.001$ ), suggesting that BUN could be used to dis-

tinguish between HF and asthma/COPD. Furthermore, after pairwise comparison of subgroup analysis, BUN was elevated in the HF group compared with the asthma or COPD



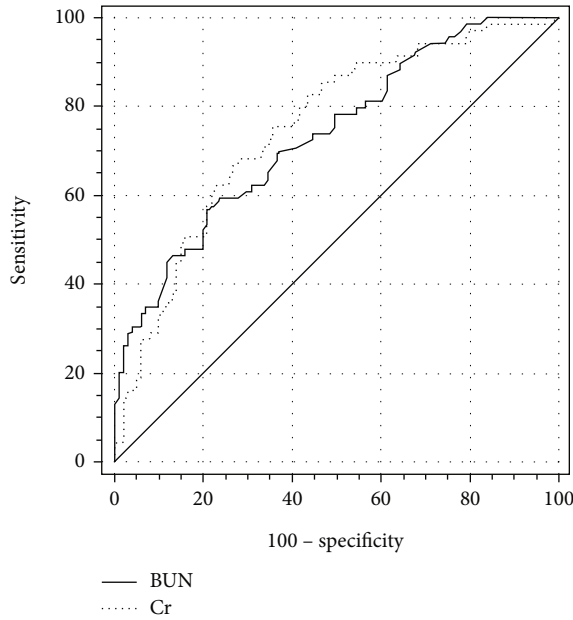


FIGURE 3: Comparison of ROC curves of BUN and Cr in distinguishing HF from asthma/COPD. HF: heart failure; COPD: chronic obstructive pulmonary disease; BUN: blood urea nitrogen; Cr: creatinine.

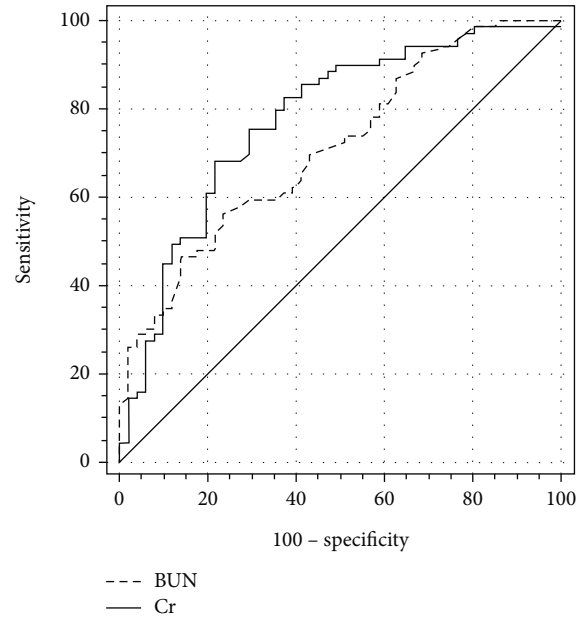


FIGURE 5: Comparison of ROC curves of BUN and Cr in distinguishing HF from COPD. HF: heart failure; COPD: chronic obstructive pulmonary disease; BUN: blood urea nitrogen; Cr: creatinine.

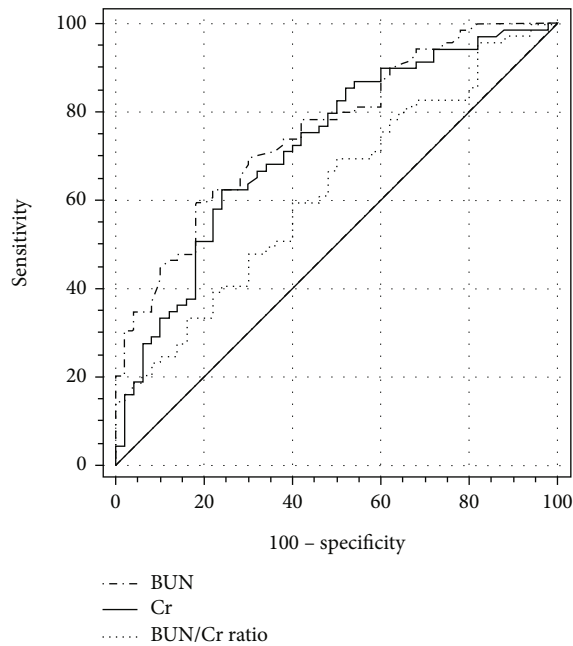


FIGURE 4: Comparison of ROC curves of BUN, Cr, and BUN/Cr ratio in distinguishing HF from asthma. HF: heart failure; BUN: blood urea nitrogen; Cr: creatinine; BUN/Cr ratio: blood urea nitrogen to creatinine ratio.

and COPD, indicating that BUN could not be used to distinguish them.

Next, Cr has also been found to show the same trend, suggesting that Cr could be applied to distinguish HF from asthma/COPD ( $p < 0.001$ ). Additionally, following pairwise comparison of the subgroup analysis, Cr could be used to similarly distinguish between HF and COPD as well as between HF and asthma (all  $p > 0.001$ ). However, Cr could not be applied to differentiate asthma from COPD ( $p > 0.05$ ).

Moreover, with respect to the BUN/Cr ratio, we proved that no significant difference was observed between HF and asthma/COPD, suggesting that the BUN/Cr ratio could not be used to distinguish HF from asthma/COPD ( $p > 0.05$ ). After pairwise comparison of subgroup analysis, the BUN/Cr ratio could not be used to distinguish between COPD and HF or asthma ( $p > 0.05$ ), similarly. However, the BUN/Cr ratio could be used to differentiate HF from asthma ( $p > 0.05$ ).

Finally, we also discovered that the AUC in distinguishing between HF and asthma/COPD were 0.736 for BUN and 0.751 for Cr and no significant difference was observed between BUN and Cr ( $Z = 0.389, p = 0.697$ ) (Figure 3). Subgroup analysis showed that the AUC in distinguishing between HF and asthma were 0.760 for BUN, 0.726 for Cr, and 0.621 for the BUN/Cr ratio and the only significant difference was observed between BUN and the BUN/Cr ratio (0.760 vs. 0.726,  $Z = 0.736, p = 0.462$ ; 0.760 vs. 0.621,  $Z = 3.063, p = 0.002$ ; and 0.726 vs. 0.621,  $Z = 1.299, p = 0.194$ ) (Figure 4). In other words, BUN could demonstrate better performance in distinguishing between HF and asthma than the BUN/Cr ratio. The other result of subgroup analysis was that the AUC in distinguishing between HF and COPD were

group (all  $p < 0.001$ ), suggesting that BUN could be used to distinguish not only between HF and asthma but also between HF and COPD, similarly. However, there was no significantly statistical difference of BUN between asthma

0.712 for BUN and 0.776 for Cr and no significant difference was observed between BUN and Cr ( $Z = 1.337$ ,  $p = 0.181$ ) (Figure 5).

We hypothesised that the causes of the aforementioned aberrant renal function indices in HF may be related to neurohormonal activation in addition to renal hypoperfusion brought on by abrupt hemodynamic changes during bouts of decompensation [8, 10, 17]. In addition, we have found that there were significant statistical differences of the rates of diabetes mellitus and hypertension in the HF group compared with the asthma and/or COPD group ( $p < 0.05$ ), suggesting that the common comorbidities (diabetes mellitus and hypertension) of HF could lead to the adverse effects on renal function [18]. Fedeli et al. [19] proved that renal dysfunction in COPD patients might be associated with systemic inflammation and malnutrition. Asthma kidney dysfunction may be caused by behavioural or biological variables such as inactivity and inflammation, according to research by Huang et al. The reason for the differences of renal function indices among HF, asthma, and COPD might be related to the abovementioned mechanisms.

We are aware of this study's shortcomings. First off, since this was a retroactive examination, a more exacting design was omitted. Second, from a single-center perspective, the sample size is small. Third, there is heterogeneity in the sample (e.g., different onset-to-admission intervals, different disease severity, and different comorbidity ratios). To validate findings, larger, more homogeneous samples from multicenter research are required.

## 5. Conclusion

BUN and Cr exerted accurate and reliable diagnostic value, suggesting that they were potential biomarkers for differentiating HF from asthma and/or COPD.

## Data Availability

All data generated or analyzed during this study are included in this published article.

## Ethical Approval

The present study was approved by the local ethics committee of Lianyungang TCM Hospital Affiliated to Nanjing University of Chinese Medicine.

## Conflicts of Interest

The authors declare that they have no conflicts of interest. The authors report no competing financial interests.

## Acknowledgments

This study was supported by the grants from the Health Commission of Lianyungang (no. ZD202002).

## References

- [1] M. B. Parshall, R. M. Schwartzstein, L. Adams et al., "An official American Thoracic Society statement: update on the mechanisms, assessment, and management of dyspnea," *American Journal of Respiratory and Critical Care Medicine*, vol. 185, no. 4, pp. 435–452, 2012.
- [2] A. Hutchinson, A. Pickering, P. Williams, J. M. Bland, and M. J. Johnson, "Breathlessness and presentation to the emergency department: a survey and clinical record review," *BMC Pulmonary Medicine*, vol. 17, no. 1, p. 53, 2017.
- [3] R. Niska, F. Bhuiya, and J. Xu, "National hospital ambulatory medical care survey: 2007 emergency department summary," *National Health Statistics Reports*, vol. 6, pp. 1–31, 2010.
- [4] P. Ray, S. Delorme, P. Jourdain, and C. Chenevier-Gobeaux, "Differential diagnosis of acute dyspnea: the value of B natriuretic peptides in the emergency department," *QJM: Monthly Journal of the Association of Physicians*, vol. 101, no. 11, pp. 831–843, 2008.
- [5] A. S. Maisel, P. Krishnaswamy, R. M. Nowak et al., "Rapid measurement of B-type natriuretic peptide in the emergency diagnosis of heart failure," *The New England Journal of Medicine*, vol. 347, no. 3, pp. 161–167, 2002.
- [6] D. Berliner, N. Schneider, T. Welte, and J. Bauersachs, "The differential diagnosis of dyspnea," *Deutsches Arzteblatt International*, vol. 113, no. 49, pp. 834–845, 2016.
- [7] A. A. Inamdar and A. C. Inamdar, "Heart failure: diagnosis, management and utilization," *Journal of Clinical Medicine*, vol. 5, no. 7, p. 62, 2016.
- [8] D. Aronson, M. A. Mittleman, and A. J. Burger, "Elevated blood urea nitrogen level as a predictor of mortality in patients admitted for decompensated heart failure," *The American Journal of Medicine*, vol. 116, no. 7, pp. 466–473, 2004.
- [9] G. Filippatos, J. Rossi, D. M. Lloyd-Jones et al., "Prognostic value of blood urea nitrogen in patients hospitalized with worsening heart failure: insights from the acute and chronic therapeutic impact of a vasopressin antagonist in chronic heart failure (ACTIV in CHF) study," *Journal of Cardiac Failure*, vol. 13, no. 5, pp. 360–364, 2007.
- [10] V. V. Georgiopoulou, W. H. W. Tang, G. Giamouzis et al., "Renal biomarkers and outcomes in outpatients with heart failure: the Atlanta cardiomyopathy consortium," *International Journal of Cardiology*, vol. 218, pp. 136–143, 2016.
- [11] G. Parrinello, D. Torres, S. Buscemi et al., "Right ventricular diameter predicts all-cause mortality in heart failure with preserved ejection fraction," *Internal and Emergency Medicine*, vol. 14, no. 7, pp. 1091–1100, 2019.
- [12] P. Ponikowski, A. A. Voors, S. D. Anker et al., "2016 ESC guidelines for the diagnosis and treatment of acute and chronic heart failure: the task force for the diagnosis and treatment of acute and chronic heart failure of the European Society of Cardiology (ESC) developed with the special contribution of the heart failure association (HFA) of the ESC," *European Heart Journal*, vol. 37, no. 27, pp. 2129–2200, 2016.
- [13] "Expert panel report 3 (EPR-3): guidelines for the diagnosis and management of asthma-summary report 2007," *The Journal of Allergy and Clinical Immunology*, vol. 120, no. 5, pp. S94–138, 2007.
- [14] D. Stolz, J. Barandun, H. Borer et al., "Diagnosis, prevention and treatment of stable COPD and acute exacerbations of COPD: the Swiss recommendations 2018," *Respiration*;

- International Review of Thoracic Diseases*, vol. 96, no. 4, pp. 382–398, 2018.
- [15] P. Pellicori, J. G. F. Cleland, and A. L. Clark, “Chronic obstructive pulmonary disease and heart failure: a breathless conspiracy,” *Heart Failure Clinics*, vol. 16, no. 1, pp. 33–44, 2020.
- [16] G. Güder and S. Störk, “COPD and heart failure: differential diagnosis and comorbidity,” *Herz*, vol. 44, no. 6, pp. 502–508, 2019.
- [17] A. Kazory, “Emergence of blood urea nitrogen as a biomarker of neurohormonal activation in heart failure,” *The American Journal of Cardiology*, vol. 106, no. 5, pp. 694–700, 2010.
- [18] R. T. Cole, A. Masoumi, F. Triposkiadis et al., “Renal dysfunction in heart failure,” *The Medical Clinics of North America*, vol. 96, no. 5, pp. 955–974, 2012.
- [19] U. Fedeli, A. de Giorgi, N. Gennaro et al., “Lung and kidney: a dangerous liaison? A population-based cohort study in COPD patients in Italy,” *International Journal of Chronic Obstructive Pulmonary Disease*, vol. 12, pp. 443–450, 2017.

## Research Article

# Effect of Perioperative Dexmedetomidine Anesthesia on Prognosis of Elderly Patients with Gastrointestinal Tumor Surgery

Lijia Guo,<sup>1</sup> Yufei Liu ,<sup>1</sup> and Meitan Wang<sup>2</sup>

<sup>1</sup>First Affiliated Hospital of Harbin Medical University, Harbin, 150000 Heilongjiang, China

<sup>2</sup>Harbin Children's Hospital, Harbin, 150000 Heilongjiang, China

Correspondence should be addressed to Yufei Liu; 201701330130@lzpcc.edu.cn

Received 19 May 2022; Revised 13 June 2022; Accepted 16 June 2022; Published 21 July 2022

Academic Editor: Naeem Jan

Copyright © 2022 Lijia Guo et al. This is an open access article distributed under the Creative Commons Attribution License, which permits unrestricted use, distribution, and reproduction in any medium, provided the original work is properly cited.

It was to investigate the influence of perioperative dexmedetomidine (DEX) anesthesia on the prognosis of elderly patients with gastrointestinal tumor (GIT) surgery. 90 patients who underwent laparoscopic radical gastrectomy for GIT were included. They were randomly divided into the experimental group (45 cases) with DEX+general anesthesia, and the control group (45 cases) with epidural anesthesia+general anesthesia. The indicators after surgery were compared between the two groups. The mean arterial pressure (MAP) was  $74.8 \pm 3.5$  mmHg and the heart rate (HR) was  $52.7 \pm 8.2$  beats/min<sup>-1</sup> in the experimental group, significantly lower than those of the control group ( $P < 0.05$ ). The Visual Analog Scale (VAS) scores of both groups decreased greatly associated to those before surgery ( $P < 0.05$ ). The levels of cortisol (COR) and immune adhesion inhibitor (FEIR) in the experimental group were significantly dissimilar from those in the control group ( $P < 0.05$ ). The tumor necrosis factor-alpha (TNF- $\alpha$ ) was  $96.4 \pm 21.8$  ng/L in the experimental group, observably lower than that in the control group ( $P < 0.05$ ). The postoperative diamine oxidase (DAO) and D-lactate (D-lac) were  $62.4 \pm 9.3$   $\mu$ mol/mL and  $33.8 \pm 7.2$  ng/L, respectively, in the experimental group, much lower than those in the control group ( $P < 0.05$ ). There were also significant differences in the initial recovery of bowel sounds, defecation, and total length of hospital stay (LOHS) between the groups ( $P < 0.05$ ). DEX anesthesia had ideal sedative and analgesic effects, improving the prognosis of patients during surgery, and shortening the LOHS. Thus, it deserved a clinical application value.

## 1. Introduction

With the development of modern society, the population is gradually showing an aging trend, and the proportion of elderly patients undergoing surgeries is increasing. When people become old, various organs in the body undergo degenerative changes gradually, the defense ability is weakened, and the metabolic efficiency of the body is also reduced [1]. Treatment measures such as surgery and anesthesia are likely to cause a defensive stress response in the elderly. In addition, the cardiovascular system of elderly patients is weak. When a stress response occurs, the body activates the hypothalamus-pituitary-adrenal axis, resulting in a large secretion of stress hormones, and eventually leading to serious adverse reactions [2]. With increasing age, the body is

gradually aging, and the probability of suffering from gastrointestinal tumor (GIT) increases. At present, the treatment of this disease is often surgery [3]. With the developing concept of fast recovery surgery, laparoscopic surgery has been promoted [4]. It has the advantages of high safety, less trauma to patients, easier postoperative recovery, and fewer complications. However, some researchers consider that carbon dioxide pneumoperitoneum is required during laparoscopic surgery, and carbon dioxide accumulates in the abdominal cavity for a long time, which may easily lead to an enlarged probability of postoperative pain of upper shoulder and abdomen in patients [5].

Some clinical studies have found that as the probability of pain after laparoscopic surgery increases, the probability of opioid use also increases. But the use of opioids will cause

many adverse reactions, such as mental dependence, nausea and vomiting, constipation, and respiratory depression [6]. Some studies also suggest that opioids can affect the normal proliferation of lymphocytes, resulting in a decrease in cytokine secretion [7]. It was shown that opioids can reduce human immunity to a certain extent [8] as well, especially elderly patients are more prone to such adverse reactions. Therefore, laparoscopic surgery has a certain negative impact on the perioperative safety of the elderly. Because the elasticity of blood vessels in the elderly is poor, and the stress response will induce insulin resistance, some elderly people will have a rise of blood sugar. This will further aggravate the damage to blood vessels and lead to increased cardiovascular and cerebrovascular risks in elderly patients [9]. The blood exhibits a hypercoagulable state in stress response, which makes an increased probability of thrombosis [10]. For the body of elderly patients with GIT has always been in a state of chronic consumption, coupled with the continuous differentiation of tumor cells destroying normal cells, the immune function of the body is weakened [11]. Laparoscopic surgery is performed under the tissues, which is prone to infection after surgery, leading to increased postoperative mortality in elderly patients [12]. Other clinical studies have exposed that the probability of postoperative tumor recurrence in patients with GIT is closely related to their own immunocompetence [13].

Epidural anesthesia has a good postoperative analgesic effect. It can inhibit the conduction of sympathetic nervous excitation and noxious stimulation, so that the application of opioids can be reduced. This anesthesia method can also advance immune function and reduce the probability of stress response effectively [14]. However, for elderly patients, this anesthesia method is inconvenient to operate, has a large impact on hemodynamic status, is easy to widen the block plane, and has many postoperative complications tough to control [15]. Dexmedetomidine (DEX) is one of the  $\alpha_2$  adrenergic receptor agonists with the effect of improving immune function, but its specific mechanism of action is not clear [16]. DEX can inhibit sympathetic nerve activity and adenylate cyclase and has good sedative and analgesic effects in clinical applications. It is conducive to maintaining hemodynamic stability without serious respiratory depression, so it is widely applied [17]. However, it also has some side effects. When the dose is enlarged, it may lead to adverse reactions such as xerostomia, bradycardia, and hypotension in patients [18]. Compared with epidural anesthesia, DEX anesthesia is easier to operate as it can be administered by intravenous infusion, with fewer postoperative complications that can be controlled easier.

Therefore, in this research, patients undergoing laparoscopic radical gastrectomy for GIT were selected. The patients were divided and given two different surgical anesthesia methods, respectively. Effect of DEX anesthesia on the prognosis of patients with GIT surgery was discussed, to further advance the therapeutic effect and provide reference for the clinical surgical treatment of GIT.

## 2. Research Methods

*2.1. Research Objects.* 90 patients who underwent laparoscopic radical gastrectomy for GIT in the First Affiliated

Hospital of Harbin Medical University from March 2020 to October 2021 were selected. These patients were randomly divided into the experimental group (45 cases) and the control group (45 cases). For patients in the former, DEX+general anesthesia was given, while epidural anesthesia+general anesthesia were given in the latter. There were 46 males and 34 females, aged 62-83 years old, with a mean age of  $68.5 \pm 3.8$  years old. They weighted 52-71 kg, with a mean weight of  $63.6 \pm 6.4$  kg. Inclusion criteria were as follows:

- (1) According to the standards of American Society of Anesthesiologists, the patients were in grade II or III
- (2) The patients had no history of other gastrointestinal surgery. Exclusion criteria were also enacted
- (3) Patients had severe cardiovascular, cerebrovascular, or respiratory diseases
- (4) Patients had severe liver and renal dysfunction
- (5) Patients suffered from endocrine and metabolic diseases
- (6) Patients had a history of mental illness
- (7) Patients got the second-degree atrioventricular block
- (8) Those were allergic to anesthetics
- (9) Those could not perform epidural puncture

*2.2. Anesthesia Methods.* Two hours before surgery, the patients in both groups were given with 375 mL of surgical energy drink orally. After being into the operating room, blood pressure, heart rate (HR), electrocardiogram, etc. were routinely monitored. During surgery, the goal-directed fluid therapy was performed according to the pulse pressure variation. The conventional general anesthesia induction was applied with sufentanil 0.4-0.5  $\mu\text{g}/\text{kg}$ , etomidate 0.2 mg/kg, and rocuronium bromide 0.6 mg/kg. Intravenous anesthesia was maintained, and propofol was pumped intravenously to the patient at 4-8 mg/kg/h, as well as remifentanyl at 0.05-0.2  $\mu\text{g}/\text{kg}/\text{min}$ . On the foundation of general anesthesia, patients in the experimental group were pumped with 1.0  $\mu\text{g}/\text{kg}$  DEX for 10 min before anesthesia induction; it was also pumped as 0.5  $\mu\text{g}/\text{kg}$  half an hour before the end of the surgery. The control group was given epidural anesthesia, for which the patients took the left lateral position. The puncture space was selected according to the surgical site, with the depth of the catheter was 3.5 cm. Before the anesthesia induction, 5 mL of 2% lidocaine was given. 5 min later, the effect of anesthesia was blocked and the level of anesthesia were tested. 5 mL of 0.2% ropivacaine was given through epidural space injection at the start of surgery, followed by regular administration for 50 min/time.

*2.3. Observation Indicators.* The mean arterial pressure (MAP) and HR of the two groups of patients were recorded before and after surgery, respectively; venous blood was collected before and after surgery to detect stress indicators. Serum norepinephrine (NE) concentration and serum

cortisol (COR) concentration were determined by enzyme-linked immunosorbent assay (ELISA). The rate of direct tumor erythrocyte rosette (DTER), an immune stress indicator, was detected; the determination method was expounded as follows. 0.1 mL of fresh serum from normal people and 0.1 mL of Ehrlich ascites cancer solution were mixed well and had a water bath at 37°C for 30 min. Normal saline was filled up, and the mixture was washed and then horizontally centrifugated (2000 rpm/min). After 5 min, 0.05 mL of erythrocyte suspension to be tested (washed 3 times,  $1 \times 10$  mL) was added to mix well; then, water bath was performed again at 37°C for 30 min. After taken out, it was added with 0.1 mL of normal saline and mixed well; afterwards, 0.05 mL of 0.25% glutaraldehyde was also added for mixing. After horizontal smear and Wright's staining, tumor cells became blue, erythrocytes were in red, and a tumor cell with 3 or more erythrocytes was denoted as a rosette. With 100 tumor cells, the DTER rate was calculated. The immune adhesion inhibitor (FEIR) was determined by Guo's method. The time of the first anal exhaust, time of first defecation, and the recovery time of bowel sounds, the time to get out of bed, the Visual Analog Scale (VAS) pain score, respiratory depression, nausea and vomiting, and the total length of hospital stay (LOHS) after surgery were recorded.

**2.4. Assessment of Cognitive Function.** Criteria for postoperative cognitive dysfunction (POCD) were as below. According to the developer's suggestions, if the object had less than 12 years of education, 1 point was added to the total score, so as to adjust for the influence of culture. A score below 26 indicated POCD [19]. For the timing of the test, it was tested 7 days after surgery.

**2.5. Detection of Inflammatory Factors.** The tumor necrosis factor- $\alpha$  (TNF- $\alpha$ ) and interleukin-6 (IL-6) were communal indicators of the degree of inflammation. D-lactate (D-lac) and diamine oxidase (DAO) were common indicators of intestinal permeability. Blood was drawn from the patients and centrifuged, then the supernatant was collected for testing. The contents of D-lac, DAO, TNF- $\alpha$ , and IL-6 in blood were determined strictly according to the instructions of the ELISA kit [20].

(1) D-lac determination: 40  $\mu$ L of sample for direct determination

Firstly, before D-lac was determined, the D-lac kit needed to be put at room temperature for about 40 min. To use the reagent, it was shaken or oscillated gently, so as to keep the concentration uniform.

Secondly, the standard substance was diluted. Five centrifuge tubes were marked as S1, S2, S3, S4, and S5, respectively. The standard substance stock solution (480  $\mu$ mol/mL) was diluted into 5 different concentrations using the standard substance diluent, which were in 15  $\mu$ mol/mL, 30  $\mu$ mol/mL, 60  $\mu$ mol/mL, 120  $\mu$ mol/mL, and 240  $\mu$ mol/mL, respectively.

Thirdly, sample loading was made. The sample well to be tested, the blank well, and the standard well were set accord-

ing to the relevant standards. The blank well could not be added with samples, biotin-labelled anti-D-lac antibody, and streptavidin-horseradish peroxidase (HRP); the remaining steps were the same. 40  $\mu$ L of samples was added to the sample wells to be tested; then, 10  $\mu$ L of anti-D-Lac antibodies and 50  $\mu$ L of streptavidin-HRP were added in turn. 50  $\mu$ L of different concentrations of standards was into the standard wells; because the biotin antibody had been integrated into the standards in advance, there was no need to add 50  $\mu$ L of streptavidin-HRP. When the samples were added, moving the wall of the wells should be avoided, and the samples were added to the bottom of the microplate reader. Gentle shaking was made to keep the reagent concentration uniform. After covered with sealing film, they were incubated at 37°C for 60 min.

Fourthly, the solution was confected in the following principles. The ratio of fresh medical double distilled water: concentrated washing solution was 30:1. It was shaken gently to keep the concentration uniform and then was put at room temperature for use.

Fifthly, washing. The sealing film was slowly peeled off, the liquid was discarded, and the remains was spin-dried. It was necessary to fill each well with the washing solution, and then placed for 30 seconds before discarding. It was repeated 5 times according to the above principles, and finally the ELISA plate was pat-dried with absorbent paper.

Sixthly, color development. 50  $\mu$ L of color developer A was added to each well in order; then, 50  $\mu$ L of color developer B was also added to each well. The plate was shaken gently to make the concentration of reagent uniform. The corresponding wells were placed at a temperature of 37°C and protected from light for the reaction for 10 min.

Seventhly, the reaction was terminated. As 50  $\mu$ L of terminating agent was added to each well, the reaction could be terminated (the color changed from blue at first to yellow.)

Eighthly, the optical density (OD) wanted to be measured at 450 nm of the microplate reader.

Ninthly, the sample content was calculated according to the prepared standard curve. The calculation equation was shown

$$y = a + bx + cx^{1.5} + dx^2 + ex^3. \quad (1)$$

Table 1 shows the D-lac concentrations of the standards, and Figure 1 shows the D-lac standard curve.

(2) DAO determination: 40  $\mu$ L was sampled for direct determination

Firstly, it was needed to put the DAO kit at room temperature for about 40 min before the determination of DAO. For using the reagent, it was shaken gently to make the reagent keep a uniform concentration.

Secondly, for dilution of standard substance, 5 centrifuge tubes were noticeable as S1, S2, S3, S4, and S5, respectively. The standard substance diluent was utilized to dilute the standard substance stock solution (480  $\mu$ mol/mL) into 5

TABLE 1: D-lac concentrations of the standards.

Concentrations ( $\mu\text{mol/mL}$ )	Measured OD	Absolute OD
0	0.119	0
15	0.404	0.285
30	0.671	0.552
60	1.105	0.986
120	1.677	1.558
240	2.334	2.215

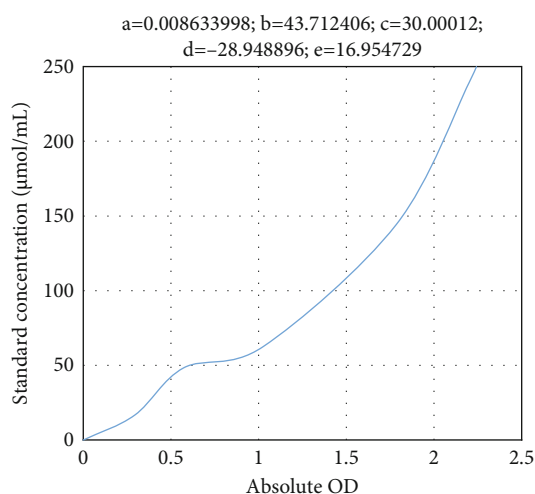


FIGURE 1: D-lac standard curve.

TABLE 2: DAO concentrations of the standards.

Concentrations ( $\mu\text{mol/mL}$ )	Measured OD	Absolute OD
0	0.105	0
15	0.284	0.178
30	0.484	0.378
60	0.850	0.744
120	1.359	1.254
240	1.929	1.823

different concentrations of 15, 30, 60, 120, and 240  $\mu\text{mol/mL}$ , respectively.

Thirdly, for sample loading, the following 3 wells were set depending on the relevant standards, which were the sample well to be tested, the blank well, and the standard well, respectively. Samples, biotin-labelled anti-DAO antibodies, and streptavidin-HRP could not be added into the blank well. 40  $\mu\text{L}$  of samples was added into the sample well to be tested, and 10  $\mu\text{L}$  of anti-DAO antibodies were added in sequence. The remaining steps were the same as above.

Table 2 shows the DAO concentrations of the standards, and Figure 2 shows the DAO standard curve.

- (3) Determination of TNF- $\alpha$ : 40  $\mu\text{L}$  of serum was taken directly for testing

$$a=0.029738246; b=89.563492; c=40.927834; \\ d=12.020001; e=27.126831$$

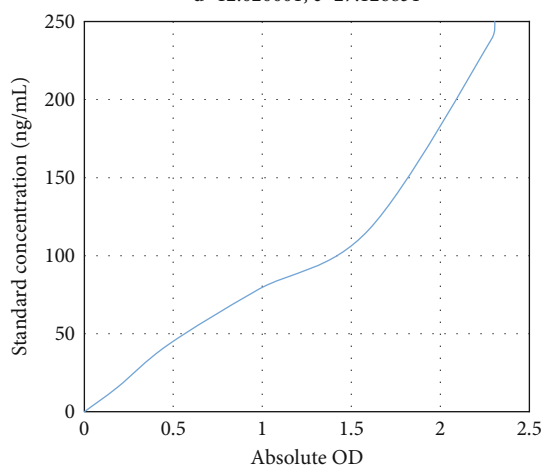


FIGURE 2: DAO standard curve.

Firstly, it was needed to put the TNF- $\alpha$  kit at room temperature for about 40 min before the determination. For the use of the reagent, it should be shaken gently for a uniform concentration.

Secondly, the dilutions of standard substance were made. With 5 centrifuge tubes marked as S2, S3, S4, S5, and S6, the standard substance stock solution (640  $\mu\text{mol/mL}$ ) was diluted with standard substance diluent into 5 different concentrations for use. These were in 30  $\mu\text{mol/mL}$ , 60  $\mu\text{mol/mL}$ , 120  $\mu\text{mol/mL}$ , 240  $\mu\text{mol/mL}$ , and 480  $\mu\text{mol/mL}$ , respectively.

Thirdly, for sample loading, the following 3 wells were set according to the relevant standards, namely, the sample well to be tested, the blank well, and the standard well. There was no sample, biotin-labelled anti-TNF- $\alpha$  antibody, and streptavidin-HRP was added into the blank well. 40  $\mu\text{L}$  of the sample was added to the sample well to be tested; then, 10  $\mu\text{L}$  of anti-TNF- $\alpha$  antibody was added in sequence. The rest of steps were the same as above.

Table 3 shows the TNF- $\alpha$  concentrations of the standards, and Figure 3 shows the TNF- $\alpha$  standard curve.

- (4) IL-6 assay: serum homogenate was taken directly for testing

Firstly, before the assay of IL-6, the IL-6 kit needed to be placed at room temperature for about 40 min. The reagent should be surprised or oscillated gently for an even concentration.

Secondly, the standard substance was diluted. Five centrifuge tubes were denoted as S2, S3, S4, S5, and S6, respectively. With standard substance diluent, the standard substance stock solution (640  $\mu\text{mol/mL}$ ) was diluted into 5 different concentrations of 20, 40, 80, 160, and 320  $\mu\text{mol/mL}$ , respectively.

Thirdly, 3 wells were set as the sample well to be tested, the blank well, and the standard well, respectively, for sample loading, according to relevant standards. The blank well could not be filled with samples, biotin-labelled anti-IL-6 antibody, or streptavidin-HRP. 40  $\mu\text{L}$  of the sample was

TABLE 3: TNF- $\alpha$  concentrations of the standards.

Concentrations (ng/L)	Measured OD	Absolute OD
0	0.056	0
30	0.337	0.281
60	0.571	0.515
120	0.971	0.915
240	1.594	1.538
480	2.586	2.530

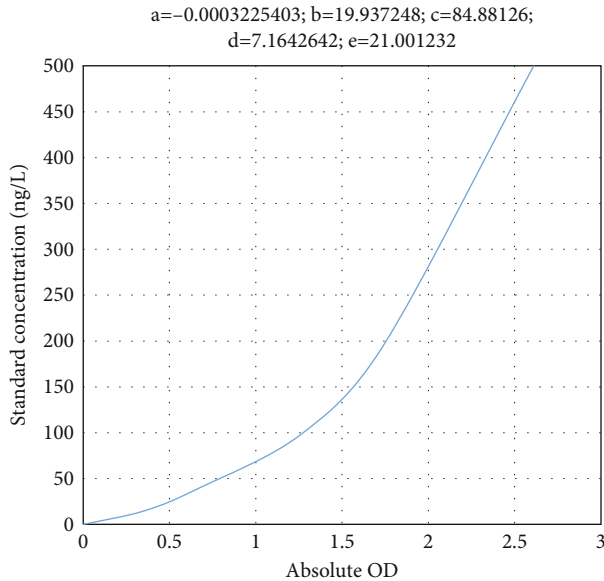


FIGURE 3: TNF- $\alpha$  standard curve.

TABLE 4: IL-6 concentrations of standards.

Concentrations (ng/L)	Measured OD	Absolute OD
0	0.060	0
30	0.376	0.316
60	0.656	0.596
120	1.109	1.049
240	1.822	1.762
480	2.933	2.873

added into the sample well to be tested, while 10  $\mu$ L of anti-IL-6 antibody was added in order. The rest of steps were the same as above.

Table 4 shows the IL-6 concentrations of standards, and Figure 4 shows the IL-6 standard curve.

**2.6. Handling of Special Cases.** The possible special circumstances during the experiment mainly comprised (severe) hypotension, (severe) bradycardia, and respiratory depression. HR and arterial blood pressure-based HR and blood pressure at rest 5 min after arterial puncture catheter placement were monitored. Bradycardia was defined as HR < 60 beats/min or less than the 20% of baseline value, and the treatment was a single intravenous injection of atropine

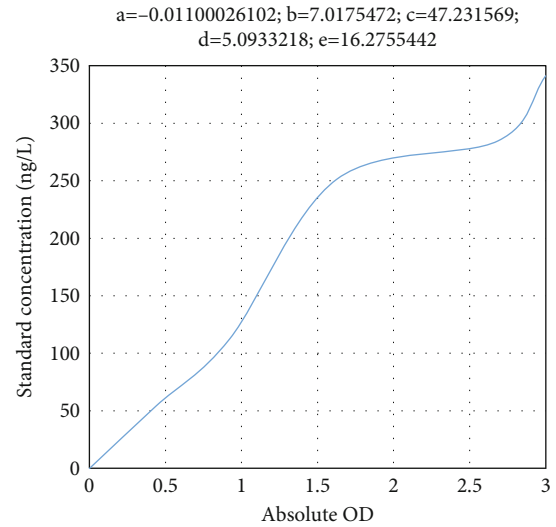


FIGURE 4: IL-6 standard curve.

0.1-0.3 mg. Plain bradycardia was defined as HR < 50 beats/min or lower than 30% of the baseline value. For the treatment measures, intravenous injection of atropine 0.3-0.5 mg was given. Intermittent intravenous injection of isoproterenol 2-10  $\mu$ g was given when there was no obvious effect, and this case was excluded. Hypotension was defined as a decrease in systolic blood pressure > 20% of the baseline. Severe hypotension was defined as a decrease in systolic blood pressure > 30% of the baseline. If blood pressure fluctuated continuously for over 2 min, vasoactive drugs were utilized or the dose of aesthetic drugs was adjusted. Respiratory depression was defined as pulse oxygen saturation (Sp O<sup>2</sup>)  $\leq$  90% under inhalation condition. In the event of respiratory depression, oxygen should be given through a mask timely, and artificial ventilation should be performed to assist respiration if necessary. If the above situation could not be better, the case was excluded from the experiment.

### 3. Statistical Methods

The statistical software SPSS 22.0 was used for processing in this research, and the measurement data were expressed as ( $\bar{x} \pm s$ ). When the data were in normal distribution and the alteration was homogeneous, the *t*-test was adopted for comparisons between the two groups, and the repeated-measurement analysis of variance was used for the comparisons among multiple groups. The enumeration data were expressed as the number of cases (%), while the unordered classification data were expressed by the  $\chi^2$  test.  $P < 0.05$  was considered the condition of a statistically significant difference.

### 4. Research Results

**4.1. The Detection Results of Hemodynamic Indicators.** The hemodynamic test results of the two groups of patients suggested that, compared with preoperative levels, the MAP and HR of both groups were decreased, but the control group



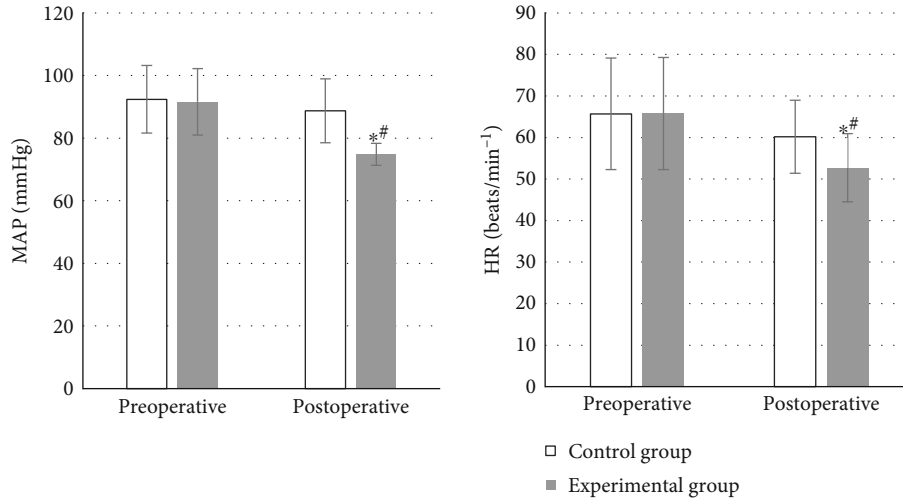


FIGURE 5: Comparison of hemodynamic indicators. Compared with preoperative level, the difference was considered statistically significant, \* $P < 0.05$ . The same compared to the control group, # $P < 0.05$ .

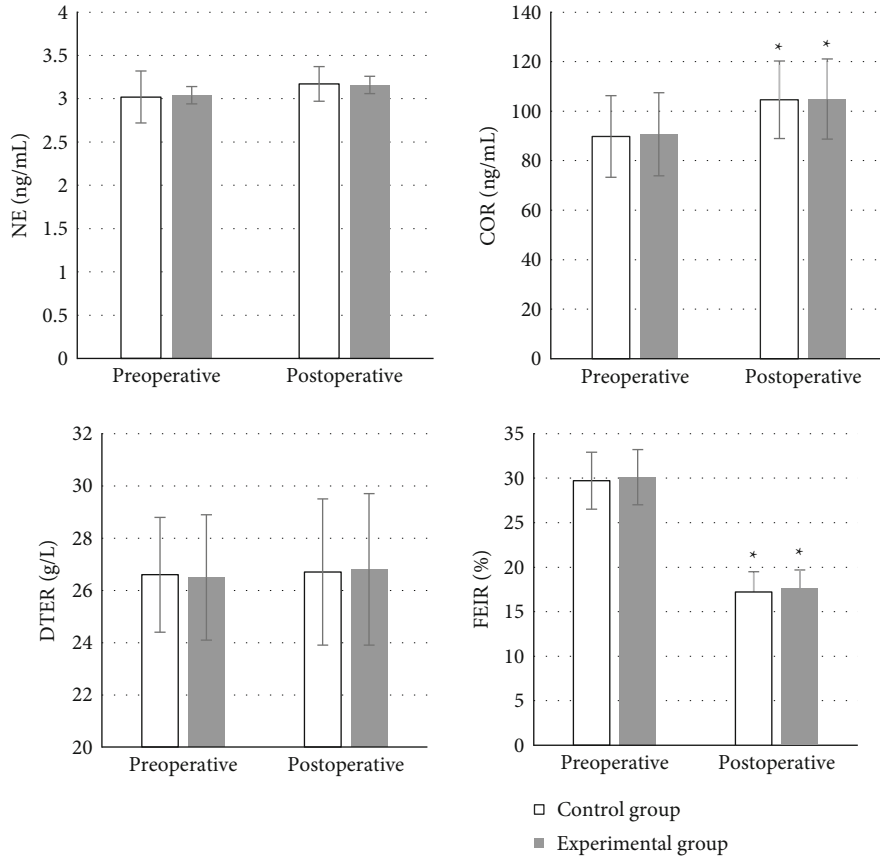


FIGURE 6: Comparison of immune indicators. Differences of statistical significance compared to preoperative levels, \* $P < 0.05$ . # $P < 0.05$  compared to the control group.

showed no significant change ( $P > 0.05$ ). The MAP  $74.8 \pm 3.5$  mmHg and HR  $52.7 \pm 8.2$  beats/min<sup>-1</sup> in the experimental group were remarkably lower compared with those before surgery and were also significantly lower than the  $88.7 \pm 10.2$  mmHg and  $60.2 \pm 8.8$  beats/min<sup>-1</sup> in the control

group. The differences above were all statistically significant ( $P < 0.05$ ), which could be observed in Figure 5.

4.2. Comparison of Perioperative Stress and Immune Indicators between the Two Groups. As the stress and

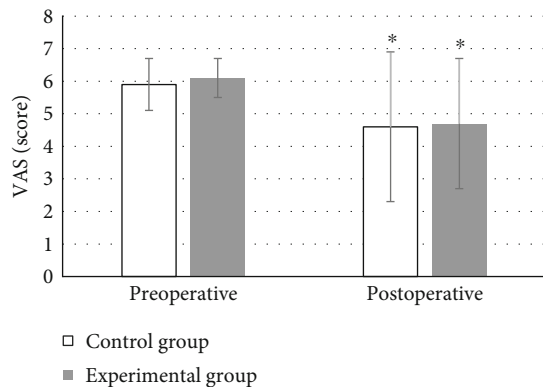


FIGURE 7: Comparison of VAS scores. The statistically significant difference in comparison with the preoperative levels and those in the control group, respectively, \* $P < 0.05$ , \* $P < 0.05$ .

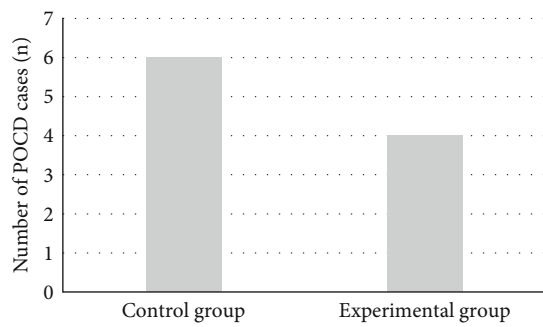


FIGURE 8: Comparison of occurrences of POCD.

immune indicators were detected, it was shown that the levels of NE and DTER in the two groups did not change much compared with preoperative levels, and the differences were not statistically significant ( $P > 0.05$ ). The COR was  $104.9 \pm 16.2$  ng/mL in the experimental group and  $104.6 \pm 15.7$  ng/mL in the control group, both of which observably increased compared to those before surgery with statistically significant differences ( $P < 0.05$ ). The FEIR was  $17.6 \pm 2.1\%$  in the experimental group and  $17.2 \pm 2.3\%$  in the control group were greatly lower than those before surgery, showing the differences of statistical significance ( $P < 0.05$ ). As presented in Figure 6, no significant difference was shown between the two groups ( $P > 0.05$ ).

**4.3. VAS Pain Scores.** Before surgery, there was not a significant difference in VAS scores between two groups ( $P > 0.05$ ). After surgery, the average VAS score of the experimental group was  $4.7 \pm 2$  and that of the control group was  $4.6 \pm 2.3$ , significantly lower than those before surgery with differences of statistical significance ( $P < 0.05$ ). No significant difference was between the groups ( $P > 0.05$ ), which could be discovered in Figure 7.

**4.4. Postoperative POCD Scores.** Postoperative POCD evaluation was performed on the patients. The results illustrated that POCD occurred in both groups, with 6 cases in the control group and 4 cases in the experimental group. Although

there were differences, which were not significant between groups ( $P > 0.05$ ). More details were displayed in Figure 8.

**4.5. Comparisons of IL-6 and TNF- $\alpha$  Levels in Serum before and after Surgery.** There was no significant difference in IL-6 before and after surgery in the experimental group ( $P > 0.05$ ). TNF- $\alpha$   $96.4 \pm 21.8$  ng/L was highly lower than that before surgery, and the difference was of statistical significance ( $P < 0.05$ ). Compared to the control group, postoperative TNF- $\alpha$   $115.3 \pm 24.6$  ng/L, the difference was also statistically significant ( $P < 0.05$ ) as presented in Figure 9.

Not a significant change was found in serum DAO and D-lac levels in the control group before and after surgery, without a difference of statistical significance ( $P > 0.05$ ). The postoperative DAO was  $62.4 \pm 9.3$   $\mu$ mol/mL, and D-lac was  $33.8 \pm 7.2$  ng/L in the experimental group, observably lower than the preoperative levels with statistically significant differences ( $P < 0.05$ ). In the control group, the postoperative DAO was  $72.7 \pm 15.2$   $\mu$ mol/mL and D-lac was  $38.2 \pm 6.4$  ng/L. The levels in the experimental group were considerably lower compared with those of the control, and the differences were proved to be statistically significant ( $P < 0.05$ ) in Figure 10.

**4.6. Other Indicators.** The time of the first anal exhaust, the time of first getting out of bed for activities, the postoperative respiratory depression, and postoperative MAP were not significantly different between groups ( $P > 0.05$ ). In the experimental group, the average postoperative recovery time of bowel sounds was  $2.8 \pm 0.7$  d, the average time of first defecation postoperatively was  $6.1 \pm 1.8$  d, the average LOHS was  $17.9 \pm 8.1$  d, and 2 cases had vomiting reaction. In the control group, the average recovery time of bowel sounds, the average time of first defecation, and the average LOHS postoperatively was  $3.9 \pm 1.2$  d,  $7.4 \pm 1.6$  d, and  $25.5 \pm 8.6$  d, respectively. There were 6 patients got vomiting in the control group. Each indicator was markedly higher compared to the experimental group, and the differences were thought of statistical significance ( $P < 0.05$ ) (Figure 11).

## 5. Discussion

GIT has developed into a common digestive tract tumor nowadays, which has a serious impact on the life and health of human beings, especially the elderly. Epidural anesthesia can inhibit sympathetic nerve conduction and sympathetic nerve excitation, thereby reducing the synthesis of catecholamines. Epidural anesthesia can also inhibit the hypothalamic-pituitary-adrenal axis pathway, reducing the secretion of COR and improving immune function [21]. DEX, as an adrenergic receptor agonist, has the effect of inhibiting sympathetic nerve activity and maintaining hemodynamic stability. It exerts its analgesic effect intraoperatively and can reduce the inhibition of breathing. Patients are easier to be awakened, and it also has the effect of improving immunity, reducing the dose of anesthetic drugs, and antichilling as well as diuretic effects. It is often used in the perioperative period of patients with radical mastectomy for malignant GIT and can improve the quality of prognosis

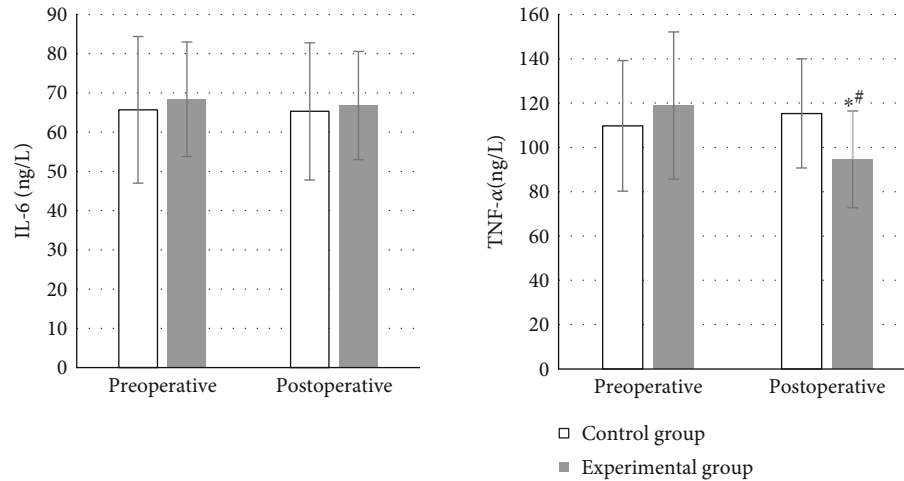


FIGURE 9: Comparison of serum TNF- $\alpha$  and IL-6 levels. Compared to the preoperative levels and the control group, \* and # marked the difference of statistical significance as  $P < 0.05$ , respectively.

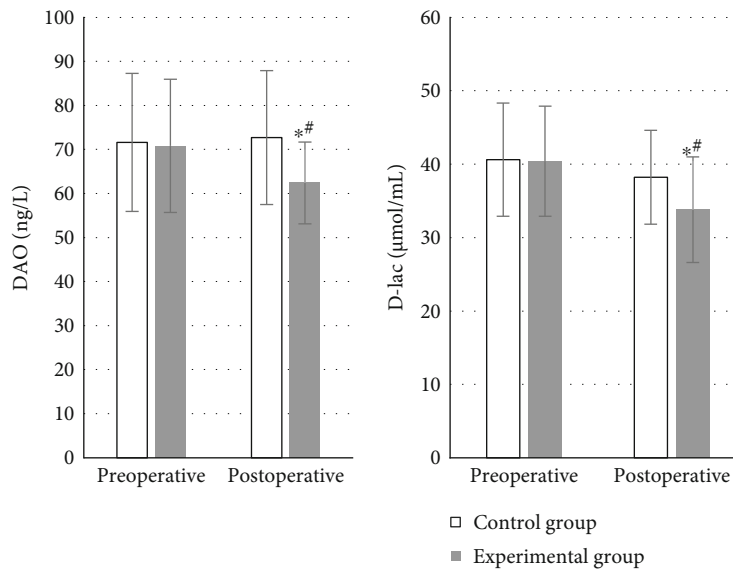


FIGURE 10: Comparison of serum DAO and D-lac levels. The differences were of statistical significance compared to preoperative levels and the control group, respectively, \* $P < 0.05$ , # $P < 0.05$ .

[22]. This work compared two anesthesia methods and analyzed the effect of DEX on the prognosis of elderly patients with GIT.

The results exposed that, compared with preoperative levels, MAP and HR in both groups decreased. The MAP of  $74.8 \pm 3.5$  mmHg and HR of  $52.7 \pm 8.2$  beats/min<sup>-1</sup> in the experimental group decreased dramatically compared with those preoperatively. MAP of  $88.7 \pm 10.2$  mmHg and HR of  $60.2 \pm 8.8$  beats/min<sup>-1</sup> in the control group were significantly lower compared to the experimental group with statistically significant differences ( $P < 0.05$ ). It was suggested that DEX had a stabilizing effect on hemodynamic situation and could inhibit the increase in HR and MAP effectively in patients undergoing extubating surgery. Similar previous study has shown that DEX can reduce the occur-

rence of agitation during the recovery period in patients with tonsillectomy after general anesthesia and has obvious sedative and analgesic effects [23]. After surgery, the average VAS score of the experimental group was  $4.7 \pm 2$  and that of the control group was  $4.6 \pm 2.3$ , which were significantly lower than those before surgery with differences of statistical significance ( $P < 0.05$ ). There was not a significant difference between the two groups ( $P > 0.05$ ). Two patients in the experimental group had vomiting reactions, while 6 patients in the control group had vomiting reactions. A study has also confirmed that DEX can reduce the stress response effectively, enhance immunity, and relieve postoperative pain and the incidence of adverse reactions in patients undergoing radical gastrectomy for gastric cancer [24]. This is consistent with the results of this work.

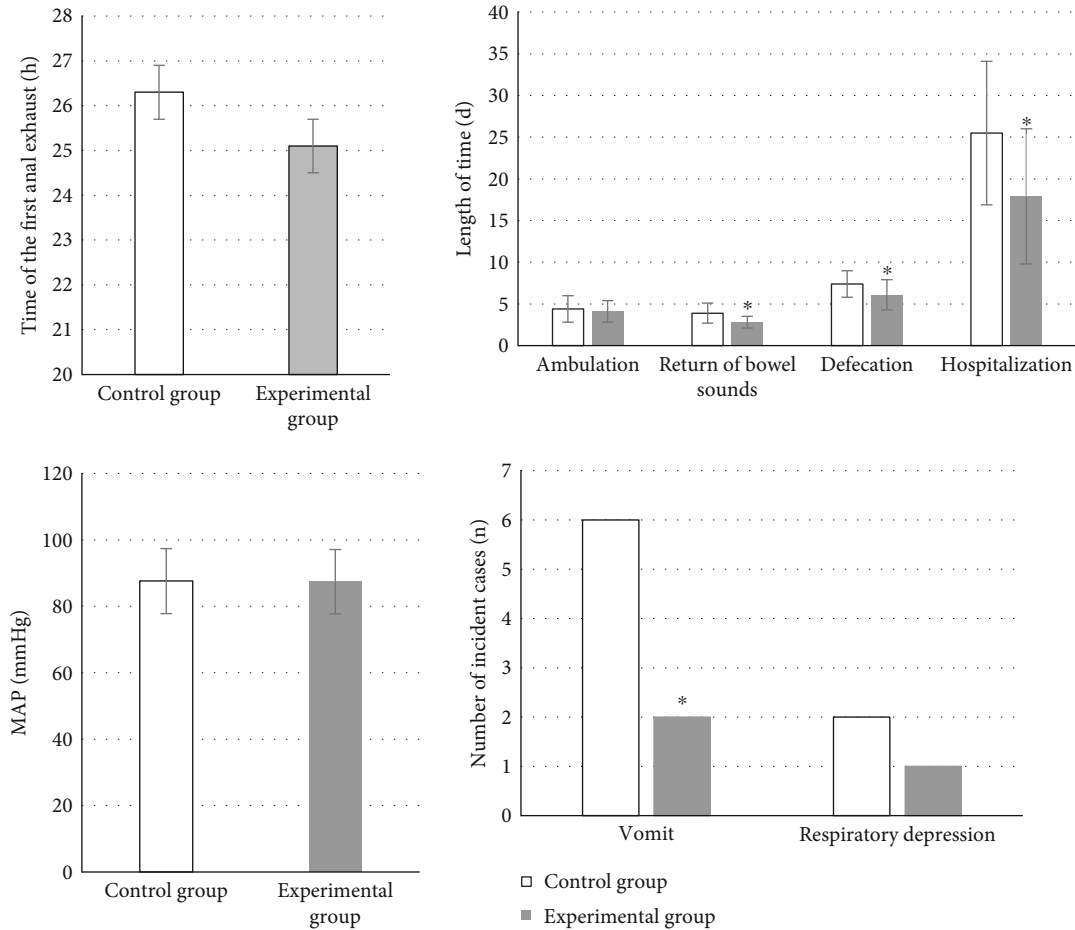


FIGURE 11: Comparisons of various indicators of postoperative gastrointestinal recovery.

COR can be utilized to reflect the degree of stress in the body [25], and FEIR is an indicator that reflects the adhesion function of red blood cells [26]. Surgical treatment will lead to a certain degree of weakened immune function and inhibit the immune adhesion of red blood cells, so the body's ability to remove tumor cells will also be weakened. It is necessary to reduce the adverse effects of laparoscopic gastrointestinal surgery on the immune function of elderly patients by changing anesthesia methods and anesthetic drugs. It is also necessary to enhance the immunity of patients and reduce the probability of recurrence. This work showed that the COR was  $104.9 \pm 16.2$  ng/mL and  $104.6 \pm 15.7$  ng/mL of the experimental and control groups, respectively, significantly increased compared with those before surgery. The FEIR of the experimental group was  $17.6 \pm 2.1\%$ , and the FEIR of the control group was  $17.2 \pm 2.3\%$ , both of which were notably lower than that before surgery with great difference statistically ( $P < 0.05$ ). Therefore, the application effect of DEX was better and it was worthy of promotion. At present, there is no unified standard for the optimal timing of POCD assessment. Generally, POCD can be divided into early, mid-term, and long-term cognitive changes. Within 1 week after surgery, it is the early POCD cognitive change, the mid-term cognitive change is within 3 months after surgery, and 1-2 years after surgery, it is the POCD

long-term cognitive change. Some study has shown that the possibility of patient death within 3 months after surgery can be predicted by early POCD assessment [27], so it is of great significance to evaluate the POCD of patients within 1 week after surgery. In this work, it was assessed 7 days after the surgery. POCD occurred in both groups, with 6 cases in the control group and 4 cases in the experimental group. Although there was a difference, it was not significant between the groups ( $P > 0.05$ ), perhaps because of the small sample size included. Thus, the effect of DEX could not be fully determined.

Studies have also proved that DEX can reduce systemic inflammatory response effectively in cases of elderly malignant GIT treated by laparoscopic surgery, which is conducive to the rapid recovery of patients after surgery [28]. This work demonstrated that the postoperative TNF- $\alpha$  of  $96.4 \pm 21.8$  ng/L in the experimental group was memorably lower than that before surgery, showing the difference of statistical significance ( $P < 0.05$ ). It was also statistically and greatly different from the postoperative TNF- $\alpha$  of  $115.3 \pm 24.6$  ng/L in the control group ( $P < 0.05$ ). It was suggested that DEX had an anti-inflammatory effect. A number of animal experiments have shown that DEX can significantly inhibit the excessive generation of inflammatory factors such as TNF- $\alpha$ , IL-1 $\beta$ , and IL-6 [29]. The postoperative DAO of

62.4 ± 9.3 μmol/mL and D-lac of 33.8 ± 7.2 ng/L were much lower than those before surgery in the experimental group, which were statistically different ( $P < 0.05$ ). Compared with the postoperative DAO of 72.7 ± 15.2 μmol/mL and D-lac of 38.2 ± 6.4 ng/L in the control group, those in the experimental group were statistically lower ( $P < 0.05$ ). Recent studies have suggested that stimulating vagal activity can play an important protective role in the intestinal barrier function damage triggered by inflammatory factors by regulating the cholinergic anti-inflammatory pathway [30]. In accumulation, not a significant difference was discovered in the time of the first anal exhaust, the first time to get out of bed, the occurrence of postoperative respiratory depression, and the postoperative MAP between two groups ( $P > 0.05$ ). The average recovery time of postoperative bowel sounds, the average time postoperative first defecation, and the average total LOHS was 2.8 ± 0.7 d, 6.1 ± 1.8 d, and 17.9 ± 8.1 d, respectively, in the experimental group. Those were 3.9 ± 1.2 d, 7.4 ± 1.6 d, and 25.5 ± 8.6 d, respectively, in the control group. Each indicator was remarkably and statistically higher than that of the experimental ( $P < 0.05$ ). Some study has also revealed that perioperative application of DEX can promote the recovery of gastrointestinal function and shorten the time of intestinal paralysis in patients with laparoscopic colorectal radical surgery [31]. It is consistent with the results of this work as well.

## 6. Conclusions

Through the comparison with epidural anesthesia, it was found that DEX anesthesia could improve postoperative stress response and immune function effectively and had ideal sedative and analgesic effects. It could also dismiss postoperative inflammatory response and reduce incidence of postoperative nausea and vomiting. Thus, the intestinal function of patients could be protected, and the LOHS of patients could also be shortened, which were beneficial to improve the prognosis of patients after surgery. It deserved a clinical application value. However, due to limited conditions, the included sample size was small, the study time was short, and some results showed no significant difference. The long-term prognosis of DEX anesthesia for patients with GIT surgery needed additional exploration. It illustrates that DEX can improve the intestinal permeability of patients and maintain the barrier function of the intestinal tract compared to epidural anesthesia.

## Data Availability

The data used to support the findings of this study are included within the article.

## Conflicts of Interest

The authors declare that they have no conflicts of interest to report regarding the present study.

## References

- [1] M. Kronfol, F. Jahr, M. Dozmorov et al., "DNA methylation and histone acetylation changes to cytochrome P450 2E1 regulation in normal aging and impact on rates of drug metabolism in the liver," *Geroscience*, vol. 42, no. 3, pp. 819–832, 2020.
- [2] S. A. Kundović, D. Rašić, L. Popović, M. Peraica, and K. Črnjar, "Oxidative stress under general intravenous and inhalation anaesthesia," *Arhiv za Higijenu Rada i Toksikologiju*, vol. 71, no. 3, pp. 169–177, 2020.
- [3] R. Shroff, E. Kennedy, M. Bachini et al., "Adjuvant therapy for resected biliary tract cancer: ASCO clinical practice guideline," *Journal of Clinical Oncology*, vol. 37, no. 12, pp. 1015–1027, 2019.
- [4] A. Agrusa, G. Di Buono, S. Buscemi, G. Cucinella, G. Romano, and G. Gulotta, "3D laparoscopic surgery: a prospective clinical trial," *Oncotarget*, vol. 9, no. 25, pp. 17325–17333, 2018.
- [5] F. Devick, B. S. Leise, S. Rao, and D. A. Hendrickson, "Evaluation of post-operative pain after active desufflation at completion of laparoscopy in mares undergoing ovariectomy," *The Canadian Veterinary Journal*, vol. 59, no. 3, pp. 261–266, 2018.
- [6] M. Imam, A. Kuo, S. Ghassabian, and M. T. Smith, "Progress in understanding mechanisms of opioid-induced gastrointestinal adverse effects and respiratory depression," *Neuropharmacology*, vol. 131, no. 1, pp. 238–255, 2018.
- [7] Y. Wu, Q. Xiong, S. Li, X. Yang, and F. Ge, "Integrated proteomic and transcriptomic analysis reveals long noncoding RNA HOX transcript antisense intergenic RNA (HOTAIR) promotes hepatocellular carcinoma cell proliferation by regulating opioid growth factor receptor (OGFr)," *Molecular & Cellular Proteomics*, vol. 17, no. 1, pp. 146–159, 2018.
- [8] R. Ackerman, K. Luddy, B. Icard, J. Piñeiro Fernández, R. A. Gatenby, and A. R. Muncey, "The effects of anesthetics and perioperative medications on immune function: a narrative review," *Anesthesia & Analgesia*, vol. 133, no. 3, pp. 676–689, 2021.
- [9] J. F. Scherrer, J. Salas, P. Lustman et al., "Combined effect of posttraumatic stress disorder and prescription opioid use on risk of cardiovascular disease," *European Journal of Preventive Cardiology*, vol. 27, no. 13, pp. 1412–1422, 2020.
- [10] M. A. Soliman, A. Khan, A. O. Aguirre et al., "Effectiveness and safety of continuous infusion regional anesthesia pumps for pain after thoracopelvic fusion surgery for persistent spinal pain syndrome," *World Neurosurgery*, vol. 154, no. 1, pp. e815–e821, 2021.
- [11] H. Hong, Q. Wang, J. Li, H. Liu, X. Meng, and H. Zhang, "Aging, cancer and immunity," *Journal of Cancer*, vol. 10, no. 13, pp. 3021–3027, 2019.
- [12] M. Sasaki, N. Miyoshi, S. Fujino et al., "The Geriatric Nutritional Risk Index predicts postoperative complications and prognosis in elderly patients with colorectal cancer after curative surgery," *Scientific Reports*, vol. 10, no. 1, pp. 1–9, 2020.
- [13] T. Tanaka, A. Teshigawara, J. Takei et al., "Rapid recurrence and anaplastic transformation of a pilocytic astrocytoma in an elderly patient: case report and review of the literature," *World Neurosurgery*, vol. 142, no. 1, pp. 441–449, 2020.
- [14] H. Xie, J. Zhou, W. du et al., "Impact of thoracic paravertebral block combined with general anesthesia on postoperative cognitive function and serum adiponectin levels in elderly patients undergoing lobectomy," *Videosurgery and Other Minimally Invasive Techniques*, vol. 14, no. 4, pp. 538–544, 2019.

- [15] S. Patel, R. Ackerman, D. Boulware, and M. A. Poch, "Epidural anesthesia may be associated with increased postoperative complications in the elderly population undergoing radical cystectomy: an analysis from the National Surgical Quality Improvement Project (NSQIP) database," *World Journal of Urology*, vol. 39, no. 2, pp. 433–441, 2021.
- [16] Y. Bai, H. He, P. Zhang, W. Liu, and L. Huang, "Effects of dexmedetomidine on immune function, renal function and inflammatory factors of patients undergoing percutaneous nephrolithotomy under general anesthesia," *Experimental and Therapeutic Medicine*, vol. 21, no. 4, pp. 1–9, 2021.
- [17] S. Lee, "Dexmedetomidine: present and future directions," *Korean Journal of Anesthesiology*, vol. 72, no. 4, pp. 323–330, 2019.
- [18] M. Daverio, F. Sperotto, L. Zanetto et al., "Dexmedetomidine for prolonged sedation in the PICU: a systematic review and meta-analysis," *Pediatric Critical Care Medicine*, vol. 21, no. 7, pp. e467–e474, 2020.
- [19] T. Pinto, L. Machado, T. Bulgacov et al., "Is the Montreal Cognitive Assessment (MoCA) screening superior to the Mini-Mental State Examination (MMSE) in the detection of mild cognitive impairment (MCI) and Alzheimer's disease (AD) in the elderly?," *International Psychogeriatrics*, vol. 31, no. 4, pp. 491–504, 2019.
- [20] S. Zhuang, J. Zhong, Y. Bian et al., "Rhein ameliorates lipopolysaccharide-induced intestinal barrier injury via modulation of Nrf2 and MAPKs," *Life Sciences*, vol. 216, no. 1, pp. 168–175, 2019.
- [21] V. Novak and J. Markovič, "Regional anaesthesia in thoracic and abdominal surgery," *Acta Clinica Croatica*, vol. 58, no. 1, p. 96, 2019.
- [22] A. Nair, M. Saifuddin, V. Naik, and B. K. Rayani, "Dexmedetomidine in cancer surgeries: present status and consequences with its use," *Indian Journal of Cancer*, vol. 57, no. 3, pp. 234–238, 2020.
- [23] H. Cho, Y. Yoon, H. Jin, and S. H. Hwang, "Efficacy of dexmedetomidine for perioperative morbidities in pediatric tonsillectomy: a metaanalysis," *The Laryngoscope*, vol. 128, no. 5, pp. E184–E193, 2018.
- [24] W. Zhai, L. Yang, P. Sun, Y. Li, J. Han, and G. Wang, "Effect of dexmedetomidine on hemodynamic changes and inflammatory responses in patients undergoing off-pump coronary-artery bypass grafting," *Experimental and Therapeutic Medicine*, vol. 20, no. 6, p. 1, 2020.
- [25] M. Wang, F. Wu, S. Xie, and L. Zhang, "Acute hypoxia and reoxygenation: effect on oxidative stress and hypoxia signal transduction in the juvenile yellow catfish (*Pelteobagrus fulvirdraco*)," *Aquaculture*, vol. 531, no. 1, article 735903, 2021.
- [26] W. Yang, X. Fan, X. du, Z. Wang, M. Wang, and N. Cao, "The value of inflammatory factors and red blood cell immune indices in predicting perinatal infection in hypertensive women after cesarean section," *American Journal of Translational Research*, vol. 13, no. 4, pp. 2990–2996, 2021.
- [27] J. Bai, P. Zhang, X. Liang, Z. Wu, J. Wang, and Y. Liang, "Association between dementia and mortality in the elderly patients undergoing hip fracture surgery: a meta-analysis," *Journal of Orthopaedic Surgery and Research*, vol. 13, no. 1, pp. 1–8, 2018.
- [28] Y. P. Qi, W. J. Ma, Y. Y. Cao et al., "Effect of dexmedetomidine on intestinal barrier in patients undergoing gastrointestinal surgery—a single-center randomized clinical trial," *Journal of Surgical Research*, vol. 277, no. 1, pp. 181–188, 2022.
- [29] H. Fang, H. F. Li, J. Y. Yan, M. Yang, and J. P. Zhang, "Dexmedetomidine-up-regulated microRNA-381 exerts anti-inflammatory effects in rats with cerebral ischaemic injury via the transcriptional factor IRF4," *Journal of Cellular and Molecular Medicine*, vol. 25, no. 4, pp. 2098–2109, 2021.
- [30] X. Li, X. You, C. Wang et al., "Bidirectional brain-gut-microbiota axis in increased intestinal permeability induced by central nervous system injury," *CNS Neuroscience & Therapeutics*, vol. 26, no. 8, pp. 783–790, 2020.
- [31] Y. Zhang, L. Jin, X. Zhou, Y. Liu, Y. Li, and L. Y. Wen, "Effect of dexmedetomidine on stress reactions and cellular immune function of patients in perioperative period following radial resection for rectal carcinoma," *Journal of Biological Regulators and Homeostatic Agents*, vol. 32, no. 1, pp. 139–145, 2018.

## Retraction

# Retracted: miR-135a-5p Suppresses TBK1 and Activates NRF2/TXNIP Antioxidant Pathway in LPS-Driven ALI in Mice

### Computational and Mathematical Methods in Medicine

Received 25 July 2023; Accepted 25 July 2023; Published 26 July 2023

Copyright © 2023 Computational and Mathematical Methods in Medicine. This is an open access article distributed under the Creative Commons Attribution License, which permits unrestricted use, distribution, and reproduction in any medium, provided the original work is properly cited.

This article has been retracted by Hindawi following an investigation undertaken by the publisher [1]. This investigation has uncovered evidence of one or more of the following indicators of systematic manipulation of the publication process:

- (1) Discrepancies in scope
- (2) Discrepancies in the description of the research reported
- (3) Discrepancies between the availability of data and the research described
- (4) Inappropriate citations
- (5) Incoherent, meaningless and/or irrelevant content included in the article
- (6) Peer-review manipulation

The presence of these indicators undermines our confidence in the integrity of the article's content and we cannot, therefore, vouch for its reliability. Please note that this notice is intended solely to alert readers that the content of this article is unreliable. We have not investigated whether authors were aware of or involved in the systematic manipulation of the publication process.

Wiley and Hindawi regrets that the usual quality checks did not identify these issues before publication and have since put additional measures in place to safeguard research integrity.

We wish to credit our own Research Integrity and Research Publishing teams and anonymous and named external researchers and research integrity experts for contributing to this investigation.

The corresponding author, as the representative of all authors, has been given the opportunity to register their agreement or disagreement to this retraction. We have kept a record of any response received.

### References

- [1] G. Zou, Y. Zeng, Y. Wang, and Y. Luo, "miR-135a-5p Suppresses TBK1 and Activates NRF2/TXNIP Antioxidant Pathway in LPS-Driven ALI in Mice," *Computational and Mathematical Methods in Medicine*, vol. 2022, Article ID 9088727, 11 pages, 2022.

## Research Article

# miR-135a-5p Suppresses TBK1 and Activates NRF2/TXNIP Antioxidant Pathway in LPS-Driven ALI in Mice

Guotao Zou,<sup>1</sup> Yiwen Zeng,<sup>1</sup> Yingjuan Wang,<sup>2</sup> and Yong Luo<sup>1</sup> 

<sup>1</sup>Department of Pediatrics, Yongchuan Hospital of Chongqing Medical University, 439 Xuanhua Road, Yongchuan District, Chongqing, China 402160

<sup>2</sup>Department of Emergency, Yongchuan Hospital of Chongqing Medical University, 439 Xuanhua Road, Yongchuan District, Chongqing, China 402160

Correspondence should be addressed to Yong Luo; rayonglou@163.com

Received 25 May 2022; Revised 28 June 2022; Accepted 1 July 2022; Published 20 July 2022

Academic Editor: Naeem Jan

Copyright © 2022 Guotao Zou et al. This is an open access article distributed under the Creative Commons Attribution License, which permits unrestricted use, distribution, and reproduction in any medium, provided the original work is properly cited.

**Objective.** Acute inflammation and oxidative stress are present in large numbers in patients with acute lung injury (ALI). This investigation probed miR-135a-5p/TBK1 axis within ALI together with its new therapeutic target. **Methods.** MLE-12 cultures were treated with lipopolysaccharide (LPS) and transfected with miR-135a-5p mimics or TBK1 vector. An ALI mouse model was also established. Analysis was done on the relationships between TBK1 and miR-135a-5p. Inflammatory components, SOD, MDA, and ROS content were all assessed. **Results.** Obvious inflammatory lesions were observed in lung tissues of ALI mice. Overexpression of miR-135a-5p or TBK1 knockdown remarkably decreased IL-1 $\beta$ , IL-6, and TNF- $\alpha$  serum concentrations and increased IL-10 level within lung tissues. Activated NRF2/TXNIP pathway and oxidative stress were additionally found within ALI murines, which were regulated by miR-135a-5p and TBK1. Further research revealed that miR-135a-5p negatively regulated TBK1 expression to mediate proinflammatory response and oxidative stress. **Conclusion.** miR-135a-5p targeted TBK1 to regulate inflammatory/oxidative stress responses in ALI. Such results might bring a new potential target for ALI treatment.

## 1. Introduction

Acute lung injury (ALI) is defined as a collection of acute hypoxemic respiratory failure accompanied with bilateral pulmonary infiltrations [1]. ALI can lead to a high morbidity up to 40% and has become a common and serious clinical syndrome in ICU department worldwide [2]. Despite recent advances in the treatment for ALI, the clinic outcomes and prognosis of ALI patients are rather poor [3]. Therefore, new treatments and novel therapeutic strategies for ALI are of great significance.

Acute lung injury (ALI) denotes a serious injury with an uncontrolled acute inflammatory response and activated oxidative stress, which ultimately leads to pulmonary endothelium and epithelial dysfunction [4]. The severity and development of the inflammatory response are thought to be related to the prognosis of ALI patients [5]. Meanwhile, a lot of data point to oxidative stress as a crucial factor in ALI development. Lipo-

polysaccharide- (LPS-) evoked ALI/ARDS model has been widely reported [6, 7]. A previous study revealed that Trillin attributed to the downregulation of MDA and inflammatory cytokines and the upregulation of CAT, SOD, GSH, and GSH-Px in ALI that were driven of LPS [8]. However, the underlying molecular mechanism for signaling pathways in inflammation and oxidative stress is still unclear.

Numerous studies have shown that microRNA (miR)-135a-5p is connected to autophagy and inflammatory response in a number of illnesses. According to a publication, miR-135a-5p overexpression or downregulation in atherosclerosis inhibits the ox-LDL-driven inflammatory response [9]. Another research indicated that miR-135a-5p inhibited oxidative stress/inflammatory response to restricted cerebral ischemia-reperfusion injury via regulating NR3C2 [10]. Similar result was also reported by Chen and Li in cerebral hypoxia/reoxygenation injury [11]. However, up to now, no studies focus parts played by miR-135a-5p within ALI.



miR-135a-5p's downstream target, TANK-binding kinase 1 (TBK1), plays a crucial part in numerous physiological pathways, including oxidative stress and inflammation [12]. According to a recent study, TBK1 is an endogenous inhibitor of RIPK1, and it also inhibits RIPK1-driven neuroinflammation and apoptosis during development and ageing [13]. However, in another study, Lin et al. revealed that overexpression of TBK1 activated NF- $\kappa$ B activity, as well as MAPKs and Akt signaling pathway in osteoclast differentiation [14]. These studies indicate that TBK1 plays dual roles in inflammation of different diseases or bioprocesses. However, how TBK1 influences ALI is inadequately illustrated.

The following paragraphs describe how the paper is organised: Section 2 presents the research materials and methods. The experiments and findings are covered in Section 3. The discussion portion is included in Section 4. The research project is completed in Section 5.

**1.1. Objective.** In the current study, we wanted to investigate the molecular mechanisms underlying the miR-135a-5p/TBK1 axis inside ALI. Our results demonstrated that in LPS-driven mouse ALI, miR-135a-5p controlled inflammation and oxidative stress by targeting TBK1 and activating the NRF2/TXNIP antioxidant pathway. Such present research might be available novel research and therapeutic targets for ALI.

## 2. Methods

**2.1. ALI Model Establishment and Animal Treatment.** Forty-eight C57BL/6 (6-8 weeks with 18~20 g) male mice (Beijing Vital River Laboratory Animal Technology™ Co., Ltd.) were kept within standard cages with 50-70% of humidity at  $24 \pm 1^\circ\text{C}$ . This study followed international guidelines for animal research projects and was accepted by the Animal Ethics Committee of YongChuan Hospital of ChongQing Medical University.

The establishment of ALI model was conducted as reported elsewhere [15]. In brief, mice were anesthetized with a 1 percent pentobarbital sodium, followed with a single intratracheal instillation dose of 0.05 mL *Escherichia coli* LPS (Sigma, Santa Clara, CA, USA) with dose of 5 mg/kg suspended in saline solution. The controls received the equal volume of saline solution.

For murine overexpression/inhibition of miR-135a-5p or TBK1, lentiviral plasmid-based miR-135a-5p mimic stable transfection was performed (Sigma-Aldrich, cat. no. MLMIR0048), as well as si-TBK1, pcDNA3.1-TBK1 (from GeneChem Corp., Shanghai, China, without sequence information), and corresponding NCs were injected into mice via tail vein ( $100 \mu\text{L}$ ,  $2 \times 10^7$  TU/mL). In all experiments, six animals were used in each group.

**2.2. Hematoxylin and Eosin (HE) Staining.** After the tests, the mice were slowly filled with an overdose of carbon dioxide gas before being put to death. The lung tissues were cut into three mm portions. After dehydrating the samples and fixing them in neutral formalin (10%), paraffin-embedded blocks were eventually produced. Briefly, the sections were

immersed in xylene and alcohol, following with the staining with hematoxylin and eosin. Finally, histopathology observation was conducted using an optical microscope.

**2.3. Cell Culture and Treatments.** MLE-12 cells (ATCC) were grown within RPMI-1640 (Sigma-Aldrich) augmented using 10% FBS, 100 IU/mL penicillin and 100  $\mu\text{g}/\text{mL}$  streptomycin (Sigma-Aldrich™) within an incubator ( $37^\circ\text{C}/5\% \text{CO}_2$ ). For *in vitro* model, cultures were exposed to 10  $\mu\text{g}/\text{mL}$  LPS.

Regarding cell transfection, this was performed using miR-135a-5p mimics, pcDNA3.1-TBK1, or the counterpart NCs (5 nM) through Lipofectamine® 3000 (Invitrogen™, Waltham, MA, USA) within serum-free Opti-MEM® medium.

**2.4. Western Blotting.** This was performed in order to detect TBK1, Nrf2, and TXNIP. In brief, all proteomic content was collected from lung tissue/MLE-12 cultures and quantitated through the Pierce™ BCA Protein Assay Kit® (Thermo Scientific™). Subsequently, 20  $\mu\text{g}$  proteomic aliquots underwent SDS-PAGE and were transported onto PVDF which were consequently placed into incubation together with primary antibody ( $4^\circ\text{C}$  overnight), and subsequent incubation with Goat Anti-Rabbit IgG H&L secondary antibody (ab96899, 1/1000) at  $37^\circ\text{C}$  for 45 min. Primary antibodies used were purchased from Abcam (USA): anti-TBK1 antibody (ab227182, 1/500), anti-Nrf2 antibody (ab92946, 1/1000), and anti-TXNIP antibody (ab188865, 1/1000). GAPDH served as internal/normalization control/reference.

**2.5. Quantitative RT-PCR Analysis.** miR-135a-5p/TBK1 transcriptomic expression within tissue samples/MLE-12 cells was detected. First, total RNA was extracted from lung tissues and MLE-12 cells using the TRIzol® (Sigma-Aldrich™) method, and quantification was carried out with a NanoDrop spectrophotometer (ND-1000, ThermoFisher Scientific). Subsequently, the conversion from RNA into cDNA was performed through TransScript® one-step gDNA removal and cDNA Synthesis SuperMix kit (Applied Biosystems). For the detection of miRNA, a miRcute miRNA qPCR detection kit (SYBR Green) on a 7900 HT Sequence Detection System was conducted in PCR reactions. For the quantification of mRNA, SYBR GREEN Master Mix® (Thermo Fisher Scientific, Inc.™) over the ABI 7500® platform (Applied Biosystems) was performed. The primary primers were used in PCRs: TBK1 forward 5'-GGAGCCGTCCAATGCGTAT-3', reverse 5'-GCCGTTCTCTCGGAGATGATTC-3'; miR-135a-5p forward 5'-AACCTGCTCGCAGTATTTGAG-3', reverse 5'-GCGGCAGTATGGCTTTTATTCC-3'; U6 forward 5'-ACTCCTGCCACTAGAGCTTGT-3', reverse 5'-CTCCGGGAACCAGCATTGTTA-3'; GAPDH forward 5'-AGGTCGGTGTGAACGGATTG-3', reverse 5'-GGGGTCGTTGATGGCAACA-3'. U6 and GAPDH served as the controls. mRNA expressions determined through  $2^{-\Delta\Delta\text{Ct}}$  methodology.

**2.6. Dual-Luciferase Reporter Assay.** Prediction for bonding sequence across miR-135a-5p/TBK1 was conducted on using Starbase (<http://starbase.sysu.edu.cn/>) and TargetScan

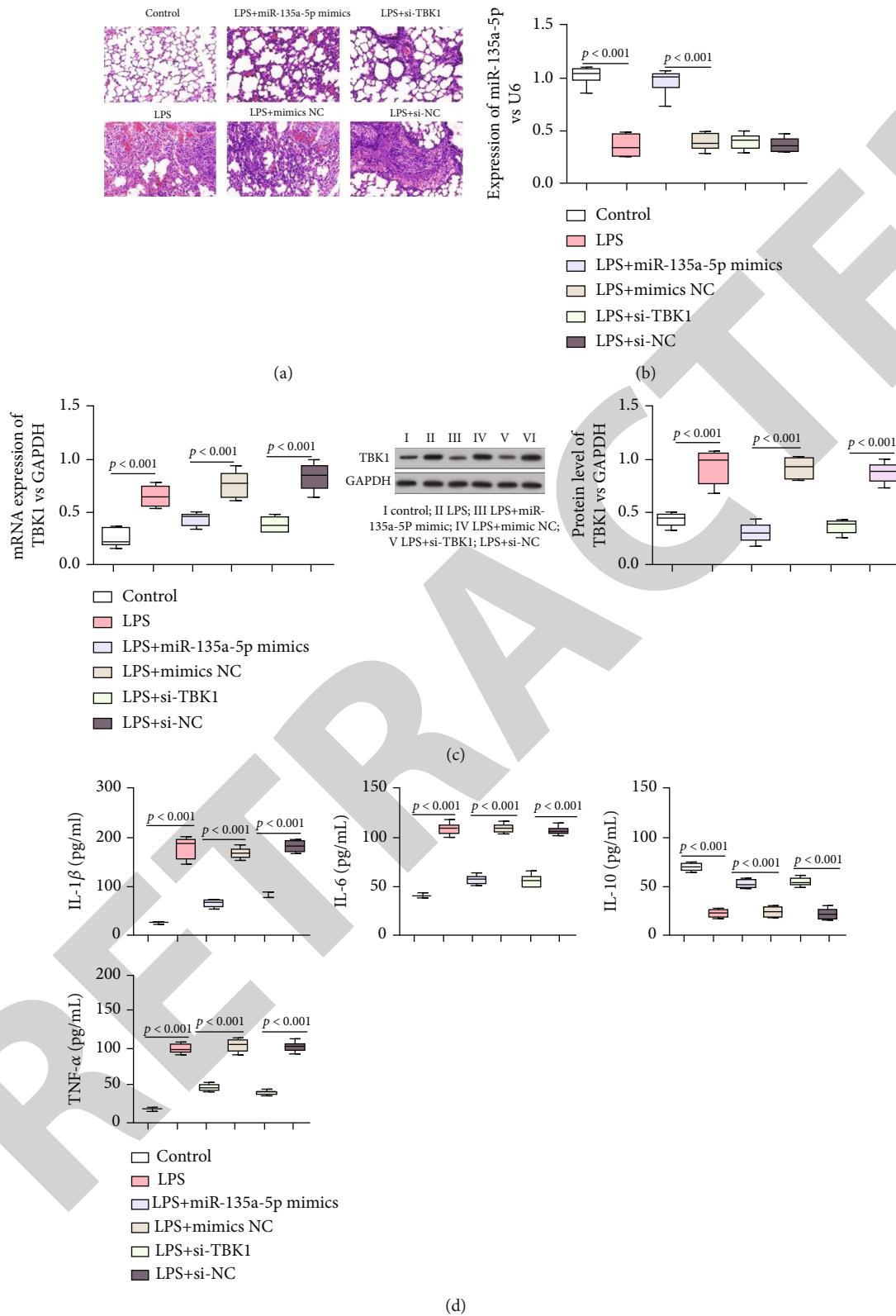


FIGURE 1: Overexpressed miR-135a-5p or inhibited TBK1 attenuates LPS-driven ALI and inflammatory response in mice. (a) Representative histopathological examination of mouse lung tissues by HE staining in LPS-driven group, LPS-driven group transfected with miR-135a-5p mimics, LPS-driven group transfected with si-TBK1, and corresponding NCs and the healthy controls. Scale bars: 25  $\mu$ m, magnified 400x,  $n = 6$  for each group. (b) Expression of miR-135a-5p by qRT-PCR. (c) mRNA of TBK1 was determined through RT-qPCR, and TBK1 proteomic content was evaluated using Western blotting. (d) IL-1 $\beta$ , IL-6, TNF- $\alpha$ , and IL-10 levels were determined through ELISA kits.  $P$  values were assessed through Student's  $t$  test.

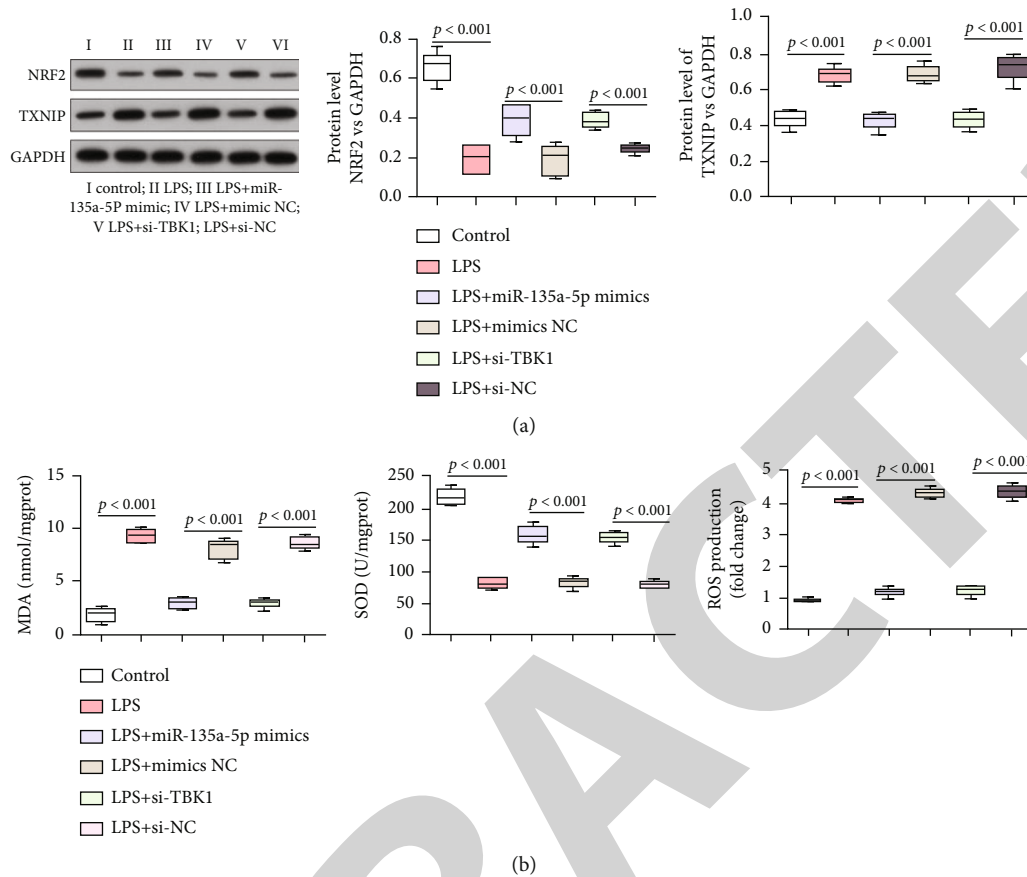


FIGURE 2: Overexpressed miR-135a-5p or inhibited TBK1 activated NRF2/TXNIP antioxidant pathway and suppresses oxidative stress. (a) NRF2/TXNIP proteomic levels were analyzed through western blotting. (b) MDA, ROS, and SOD of LPS-driven lung tissues were analyzed using ELISA kits. *P* values were assessed through Student's *t* test.

(<http://www.targetscan.org>); design of wild-type (WT) and mutant (MUT) fragments in TBK1 was performed accordingly. The WT and MUT of 3'-UTR of TBK1 sequences with/without the predicted binding responsive element for miR-135a-5p were amplified and subcloned to the p-MIR-report plasmid (Promega (Beijing) Biotech Co., Ltd. Beijing, China). Then, using Lipofectamine 3000, MLE-12 cells were cotransfected with miR-135a-5p vector (an inhibitor or mimic) and WT-TBK1 or MUT-TBK1 or NC vector (an inhibitor or mimic) (Invitrogen). MLE-12 cultures were extracted for detection using luciferase assay kits after two days of incubation (Promega™). Luciferase activities of cells was normalized using Renilla luciferase activities.

**2.7. Enzyme-Linked Immunosorbent Assay (ELISA).** Serum levels for IL-6, IL-1 $\beta$ , TNF- $\alpha$ , and IL-10 were measured by ELISA assay. Blood samples of the mice were collected and detected using corresponding commercial ELISA kits: IL-1 $\beta$ Kit (#MBS175967), IL-6 Kit (#MBS2023471), IL-10 Kit (#MBS2021945), and TNF- $\alpha$  (#MBS175787, all from MyBioSource).

**2.8. Measurement SOD, MDA, and ROS.** Expression of SOD, ROS, and MDA in tissues and MLE-12 cells was detected

using corresponding kits (Nanjing Jiancheng Bio-Technology™ Co., Ltd.) as instructed within manufacturer protocols.

**2.9. Statistical Analysis.** Continuous normally distributed datasets reflected mean  $\pm$  SD. Comparative analyses across two groups performed through Student's *t*-test. Overall, *P* < 0.05 was deemed to confer statistical significance. SPSS 18.0® and GraphPad 6.0 were used for the analysis.

### 3. Result

In this section, we define the overexpressed miR-135a-5p or inhibited TBK1 attenuates inflammation-based responses within mice and LPS-driven ALI, overexpression of miR-135a-5p or inhibition of TBK1 activated NRF2/TXNIP antioxidant pathway and suppresses oxidative stress, and miR-135a-5p negatively regulates TBK1 expression in detail.

**3.1. Overexpressed miR-135a-5p or Inhibited TBK1 Attenuates Inflammation-Based Responses within Mice and LPS-Driven ALI.** This investigation initially probed miR-135a-5p/TBK1 role/s within LPS-driven ALI and inflammation-based responses within mice. Representative

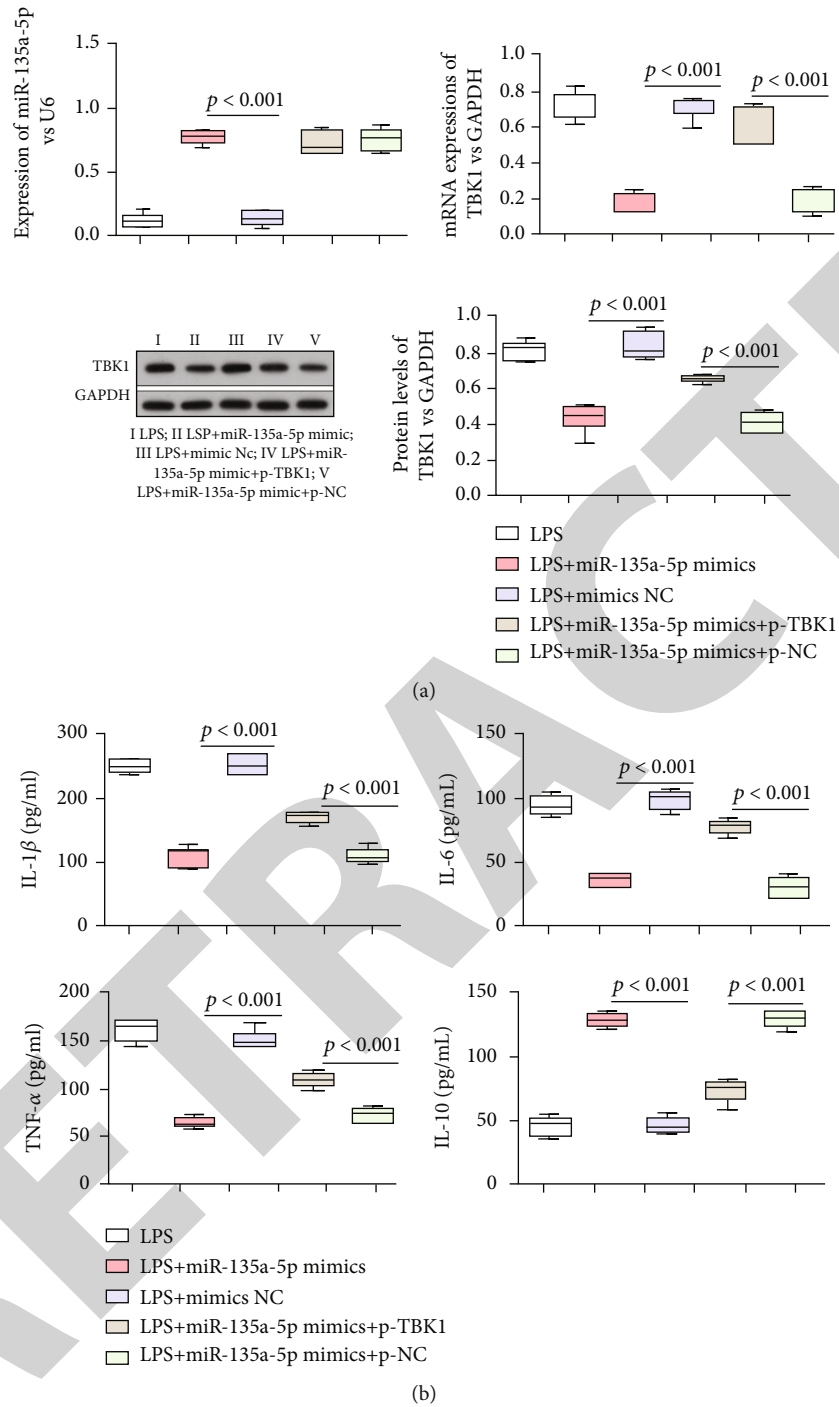


FIGURE 3: Continued.

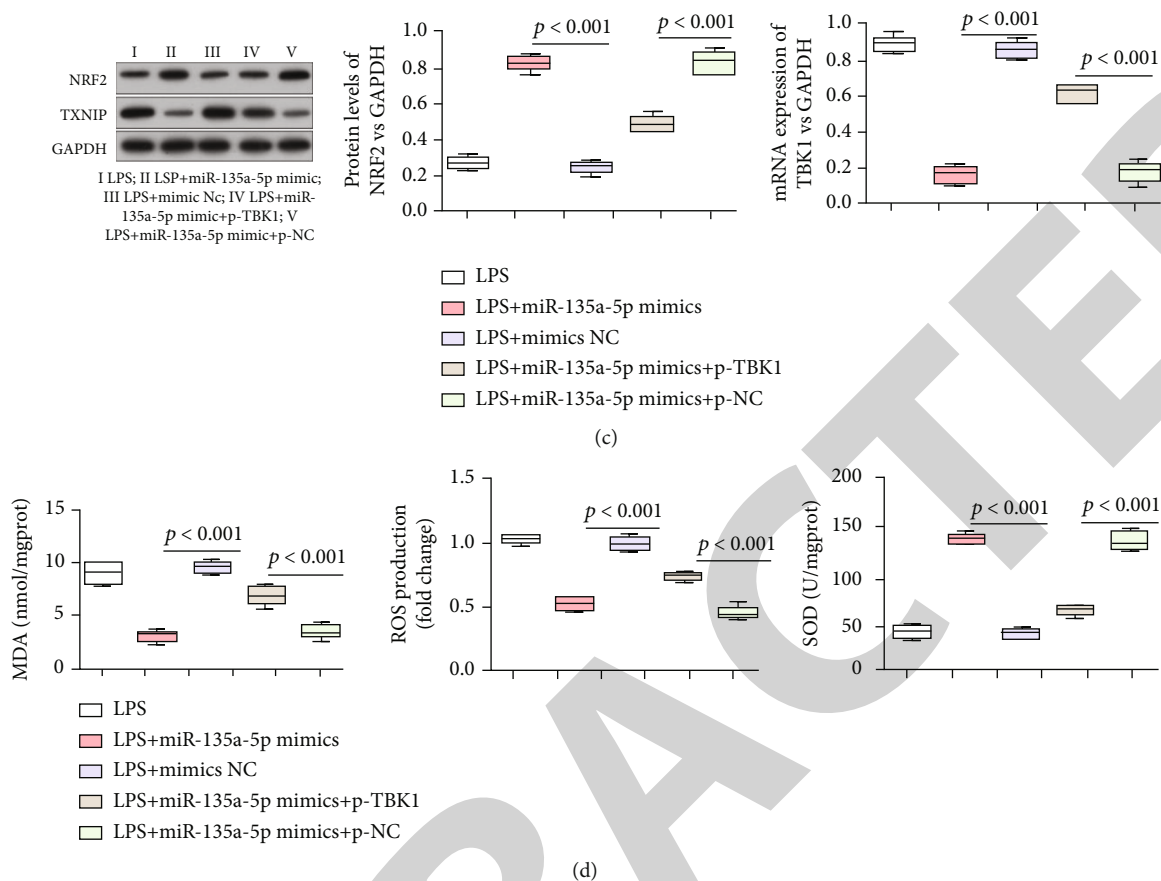


FIGURE 3: miR-135a-5p mediates inflammation and oxidative stress through regulating TBK1 in LPS-driven murine ALI. (a) mRNAs for miR-135a-5p and TBK1 were determined through RT-qPCR, and protein level for TBK1 was evaluated using Western blotting in lung tissues in LPS-driven group, LPS-driven group transfected with miR-135a-5p mimics, LPS-driven group transfected with miR-135a-5p mimics and pcDNA3.1-TBK1, and the corresponding NC controls. (b) Levels of IL-1 $\beta$ , IL-6, TNF- $\alpha$ , and IL-10 were determined using ELISA kits. (c) Protein levels of NRF2 and TXNIP were detected using Western blotting. (d) MDA, ROS, and SOD of LPS-driven lung tissues were analyzed using ELISA kits.  $P$  values were assessed through Student's  $t$  test.

images of lung tissue in each group was shown in Figure 1(a). Obvious inflammation in LPS-driven lung specimens was observed, which was alleviated by miR-135a-5p mimics or si-TBK1. RT-qPCR/Western blotting analyses revealed an around 2-fold increase in miR-135a-5p expression following miR-135a-5p mimic transfection, with an approximately 2- to 3-fold decrease of TBK1 expression by si-TBK1 transfection in LPS-driven lung tissues; additionally, miR-135a-5p mimics suppressed TBK1 expression (Figure 1(b)). ELISA results revealed both miR-135a-5p mimics and si-TBK1 inhibited serum level for TNF- $\alpha$ , IL-1 $\beta$ , and IL-6 though elevated expression of IL-10 (Figure 1(c)). Such revelations indicated overexpression of miR-135a-5p or inhibition of TBK1 attenuated ALI and inflammation.

**3.2. Overexpression of miR-135a-5p or Inhibition of TBK1 Activated NRF2/TXNIP Antioxidant Pathway and Suppresses Oxidative Stress.** This investigation additionally probed regulating mechanistic/s for miR-135a-5p and TBK1 for NRF2/TXNIP signal pathway as well as oxidative stress. Protein expression of NRF2 and TXNIP was detected in each group. The findings showed that in the lung tissues

of LPS-induced mice, TXNIP expression increased by about 3-fold whereas NRF2 expression decreased by around 4-fold. However, miR-135a-5p overexpression or inhibition of TBK1 increased NRF2 expression and decreased TXNIP expression (Figure 2(a)). We also noticed obvious elevation in MDA content and ROS generation and notable decline in SOD level in LPS-driven lung tissue. However, miR-135a-5p mimics or si-TBK1 remarkably inhibited the expression of MDA and ROS but enhanced SOD content (Figure 2(b)). These findings suggested overexpressed miR-135a-5p or inhibited TBK1 might activate NRF2/TXNIP antioxidant pathway and inhibit oxidative stress within LPS-driven ALI.

**3.3. miR-135a-5p Mediates Inflammation and Oxidative Stress through Regulating TBK1 within Murine LPS-Driven ALI.** Regulating mechanistic/s for miR-135a-5p within murine LPS-driven ALI inflammatory and oxidative stress responses were investigated. Dataset outcomes showed miR-135a-5p mimics aroused an approximately 3-fold reduction of TBK1, which was reversed by pcDNA3.1-TBK1 transfection in lung tissues (Figure 3(a)). Upregulated miR-135a-5p suppressed serum levels of

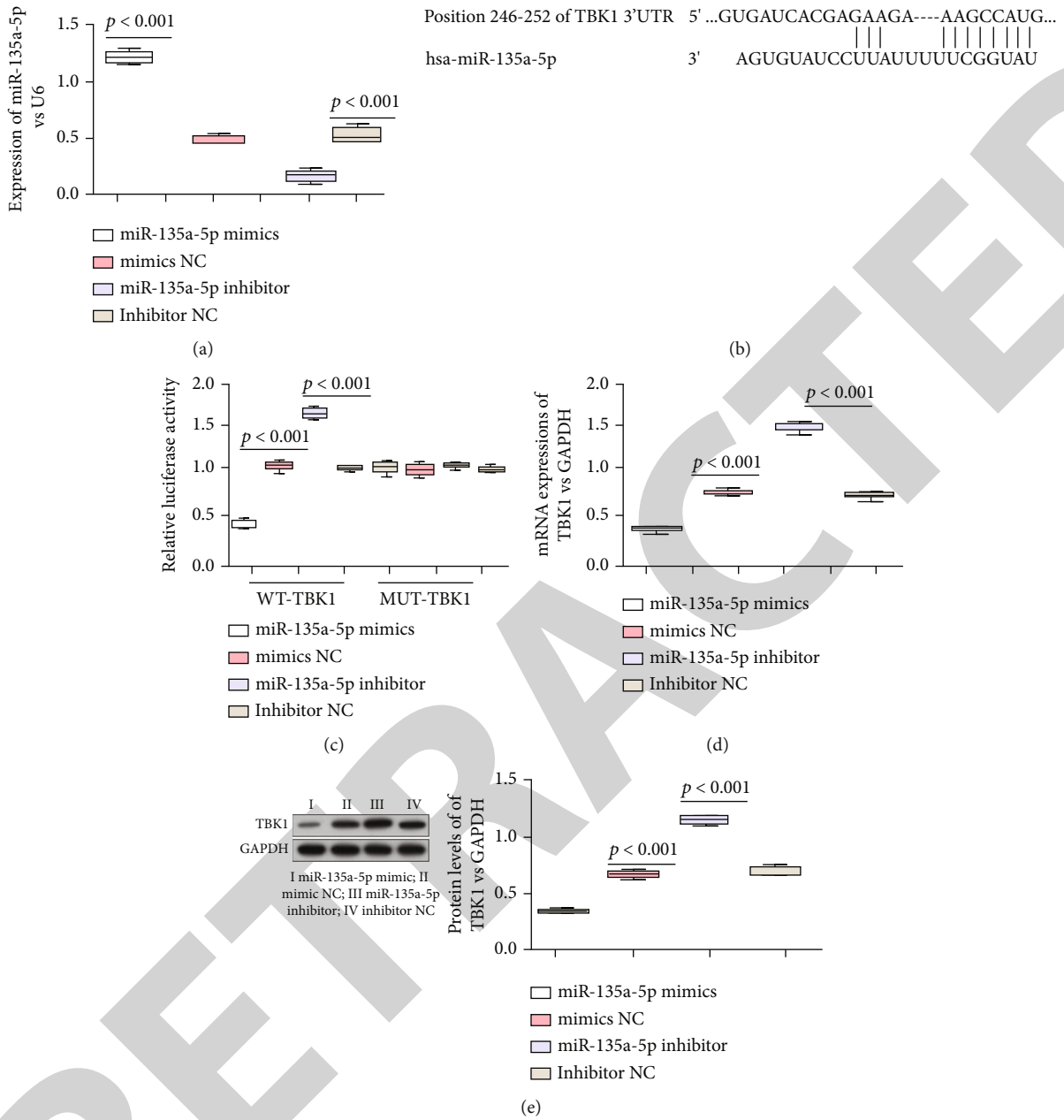


FIGURE 4: miR-135a-5p negatively regulates TBK1 expression. (a) miR-135a-5p transfected efficiency was analyzed using qRT-PCR. (b) Biding site between miR-135a-5p and TBK1 was predicted by Starbase (<http://starbase.sysu.edu.cn/>) and TargetScan (<http://www.Targetscan.org/>). (c) Targeting relationship between miR-135a-5p and TBK1 was analyzed by dual-luciferase reporter assay. (d, e) mRNA and protein levels of TBK1 were detected using qRT-PCR and Western blotting. *P* values were assessed through Student's *t* test.

proinflammatory factors but enhanced serum expression of anti-inflammatory interleukin, which was also rescued by upregulated pcDNA3.1-TBK1 (Figure 3(b)). Moreover, NRF2/TXNIP antioxidant pathway was activated by miR-135a-5p upregulation, reversing by overexpressed TBK1 (Figure 3(c)). Meanwhile, MDA content and ROS generation were inhibited, and the expression of SOD was enhanced by upregulated miR-135a-5p, rescued through overexpressed TBK1 in LPS-driven lung tissues (Figure 3(d)). The above results revealed miR-135a-5p-mediated inflammation and oxidative stress through regulating TBK1 in LPS-driven ALI in mice.

**3.4. miR-135a-5p Negatively Regulates TBK1 Expression.** In order to substantiate the regulation between TBK1/miR-135a-5p, MLE-12 mice cultures were used within this study. Firstly, the successful transfections of miR-135a-5p vector (inhibitor/mimics) were proven in MLE-12 cells (Figure 4(a)). Based on bioinformatics analysis, bonding location for miR-135a-5p/TBK1 was forecasted (Figure 4(b)). A dual-luciferase reporter test revealed that miR-135a-5p overexpression lowered the fluorescence intensity of TBK1-WT by a factor of 1.5 whereas miR-135a-5p knockdown increased it by about 3-fold. No obvious effects by miR-135a-5p upon TBK1-MUT were observed

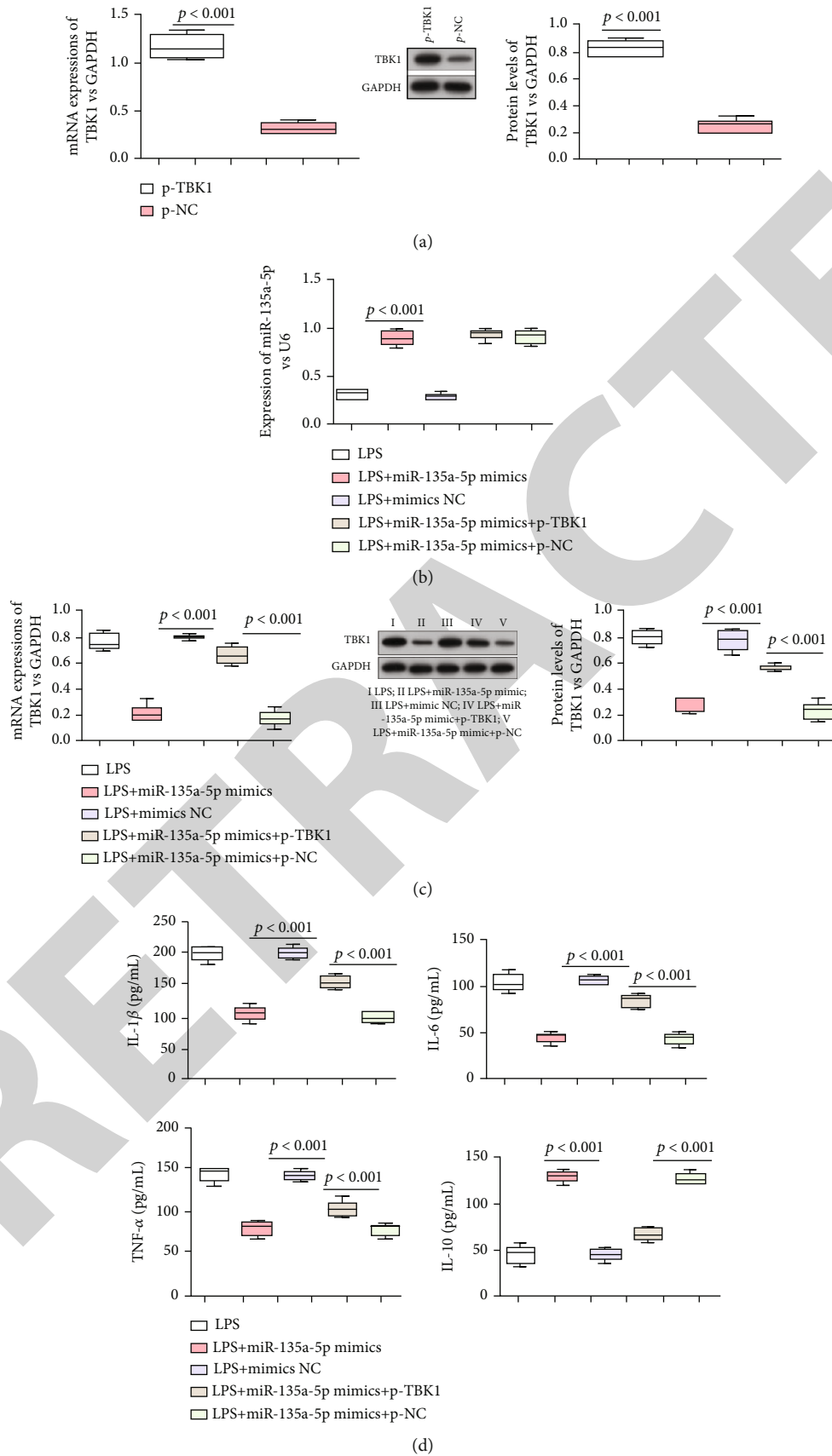


FIGURE 5: Continued.

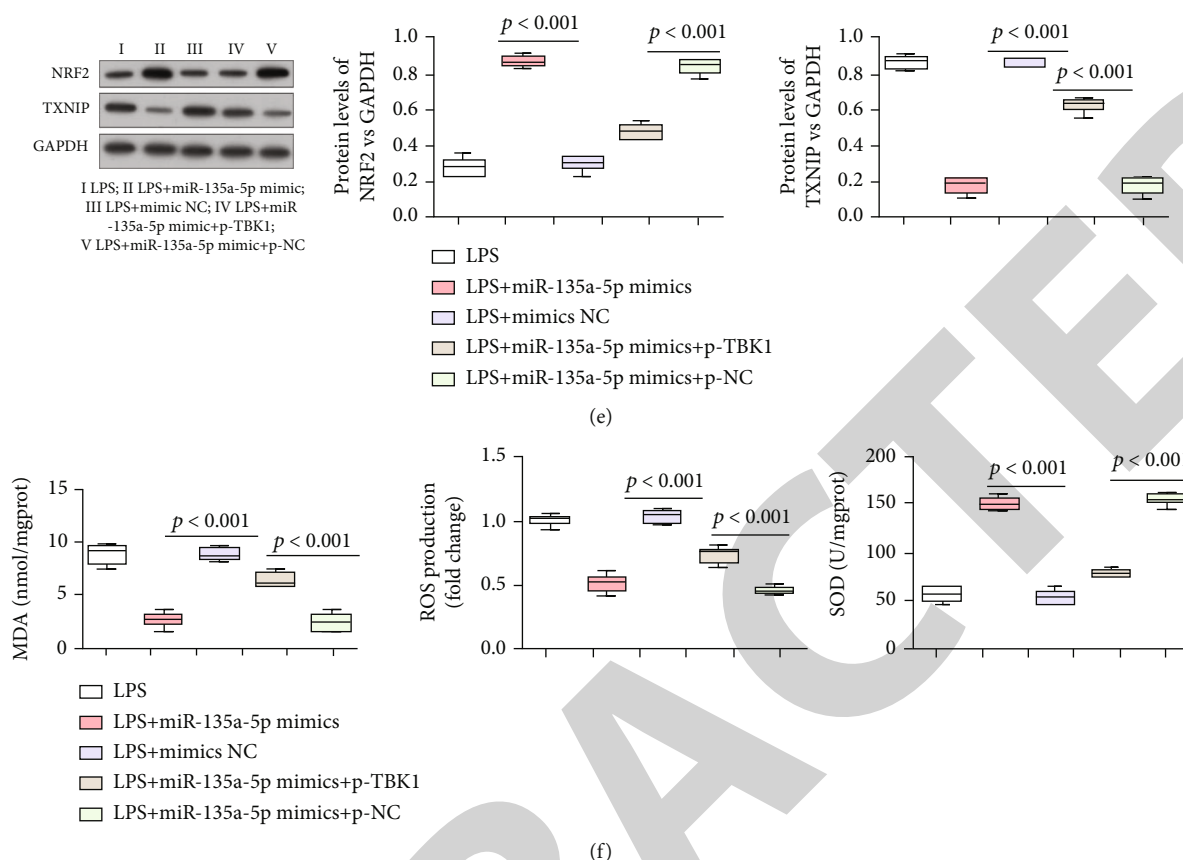


FIGURE 5: miR-135a-5p mediates inflammation and oxidative stress through regulating TBK1 in LPS-driven MLE-12 cells. (a) Transfection efficiency of TBK1 was confirmed using qRT-PCR. (b) Expression of miR-135a-5p by qRT-PCR. (c) mRNA and protein levels of TBK1 were detected using qRT-PCR or Western blotting in LPS-driven MLE-12 cells, LPS-driven MLE-12 cells transfected with miR-135a-5p mimics, LPS-driven MLE-12 cells transfected with miR-135a-5p mimics and pcDNA3.1-TBK1, and the corresponding NC controls. (d) Serum IL-1 $\beta$ , IL-6, TNF- $\alpha$ , and IL-10 were determined using ELISA kits. (e) Supernatant protein levels of NRF2 and TXNIP were detected using Western blotting. (f) Supernatant contents of MDA, ROS, and SOD were determined using ELISA kits. *P* values were assessed through Student's *t* test.

(Figure 4(c)). RT-qPCR analysis suggested negatively regulating miR-135a-5p influence upon TBK1, further verified in Western blotting analysis (Figures 4(d) and 4(e)). The result confirmed miR-135a-5p bound to TBK1 with negative regulation for TBK1 expression.

**3.5. miR-135a-5p Mediates Inflammation and Oxidative Stress through Regulating TBK1 within LPS-Driven MLE-12 Cultures.** Finally, molecular control by miR-135a-5p/TBK1 upon oxidative stress and inflammation-based responses within LPS-driven MLE-12 cultures was investigated. pcDNA3.1-TBK1 increased TBK1 expression by 4 times within MLE-12 cultures (Figure 5(a)). miR-135a-5p mimics suppressed TBK1 expression, which was rescued by cotransfection of pcDNA3.1-TBK1. Besides, overexpressed miR-135a-5p downregulated TNF- $\alpha$ , IL-6, and IL-1 $\beta$  and enhanced IL-10. Meanwhile, overexpressed TBK1 reversed the regulation of miR-135a-5p on inflammatory response (Figure 5(b)). It was also revealed that NRF2/TXNIP pathway was triggered by overexpressed miR-135a-5p, but was rescued by upregulated TBK1 (Figure 5(c)). Overexpression of miR-135a-5p decreased MDA and ROS expression while increasing SOD levels. Overexpression of TBK1 reversed this

effect. The results supported miR-135a-5p-mediated oxidative stress and inflammatory responses through regulating TBK1 within LPS-driven MLE-12 cells.

## 4. Discussion

ALI brings huge burden to the critically ill patients with high mortality and morbidity [16]. As we know, inflammation and oxidative stress have pivotal parts within ALI pathogenesis/development [17, 18]; nevertheless, the underlying mechanism remains uncertain. This *in vitro* and *in vivo* study investigated the regulating miR-135a-5p influence over LPS-driven ALI. Such findings demonstrate that miR-135a-5p mediates oxidative stress and inflammation through regulating TBK1 in LPS-driven ALI.

miR-135a-5p exhibits anti-inflammatory influence across multiple diseases. As reported, suppressing miR-135a-5p attenuated neuropathic pain by the inhibition of autophagy and inflammatory response in CCI rat model [19]. In addition, miR-135a-5p showed an inhibitory effect on the activation of NLRP3 inflammasome, causing a suppression for neuronal autophagy and ischemic brain injury. Overexpression of miR-135a-5p increased cell



proliferation but restrained cell apoptosis and the protein expressions associated with autophagy in neuronal cells [20]. Another study also found the suppression of miR-135a-5p/CXCL12/JAK-STAT signaling axis restrained inflammatory response and cell apoptosis in myocardial infarction, thereby alleviating myocardial injury [21]. However, no research illustrated the regulating parts played by miR-135a-5p within ALI. This study confirmed miR-135a-5p downregulation within ALI and that overexpressed miR-135a-5p could attenuate acute lung injury, inflammatory response as well as oxidative stress. Besides, miR-135a-5p mediated inflammation and oxidative stress through regulating TBK1 in lung injury.

TBK1 was reported to play anti-inflammatory roles in several studies. A recent research indicated TBK1 attenuated inflammation by phosphorylating and inducing the degradation of the IKK kinase NIK and negatively regulated NF- $\kappa$ B expression through AMPK pathway in controlling metabolism [22]. However, more studies suggested TBK1 might activate inflammatory pathways during inflammation. Ahmad et al. demonstrated that TBK1 and IKK $\epsilon$  were involved in the activation of IFN-inducing IFN-regulatory factor (IRF) transcription factors [23]. These inconsistent results indicated TBK1 might play a dual role in inflammatory response in different diseases. TBK1 is also found to be involved in affecting oxidative stress. Huh et al. reported TBK1 loss inhibited fasting-driven fatty acid oxidation in the liver [24]. Another study also revealed the inhibition of TBK1 alleviated lung injury, attenuated oxidative damage, and decreased expression of inflammatory factors in both mice and RAW264.7 mouse macrophages [25]. Nevertheless, the effect of TBK1 in acute lung injury has not been revealed in previous researches. This study illustrated that TBK1 inhibition not only suppressed inflammation and oxidative stress but also activated NRF2/TXNIP antioxidant pathway in lung injury.

## 5. Conclusion

In summary, our research revealed that overexpressed miR-135a-5p or inhibited TBK1 attenuated acute lung injury and inflammation, as well as activated NRF2/TXNIP antioxidant pathway and suppressed oxidative stress. Furthermore, we showed for the first time that miR-135a-5p reduced oxidative stress and inflammation by targeting TBK1 in MLE-12 cells. The findings could lead to the development of new treatment targets for acute lung injury in clinical settings.

## Data Availability

All data can be obtained from the manuscript or from request to the author.

## Conflicts of Interest

The authors declare no conflict of interest.

## References

- [1] E. R. Johnson and M. A. Matthay, "Acute lung injury: epidemiology, pathogenesis, and treatment," *Journal of Aerosol Medicine and Pulmonary Drug Delivery*, vol. 23, no. 4, pp. 243–252, 2010.
- [2] G. D. Rubenfeld and M. S. Herridge, "Epidemiology and outcomes of acute lung injury," *Chest*, vol. 131, no. 2, pp. 554–562, 2007.
- [3] Y. Butt, A. Kurdowska, and T. C. Allen, "Acute lung injury: a clinical and molecular review," *Archives of Pathology & Laboratory Medicine*, vol. 140, no. 4, pp. 345–350, 2016.
- [4] J. Lei, Y. Wei, P. Song et al., "Cordycepin inhibits LPS-induced acute lung injury by inhibiting inflammation and oxidative stress," *European Journal of Pharmacology*, vol. 818, pp. 110–114, 2018.
- [5] M. Bhatia, R. L. Zemans, and S. Jeyaseelan, "Role of chemokines in the pathogenesis of acute lung injury," *American Journal of Respiratory Cell and Molecular Biology*, vol. 46, no. 5, pp. 566–572, 2012.
- [6] H. Chen, C. Bai, and X. Wang, "The value of the lipopolysaccharide-induced acute lung injury model in respiratory medicine," *Respiratory Medicine*, vol. 4, no. 6, pp. 773–783, 2010.
- [7] Z. Dong and Y. Yuan, "Accelerated inflammation and oxidative stress induced by LPS in acute lung injury: inhibition by ST1926," *International Journal of Molecular Medicine*, vol. 41, no. 6, pp. 3405–3421, 2018.
- [8] W. Jiang, F. Luo, Q. Lu et al., "The protective effect of Trillin LPS-induced acute lung injury by the regulations of inflammation and oxidative state," *Chemico-Biological Interactions*, vol. 243, pp. 127–134, 2016.
- [9] X. Shao, Z. Liu, S. Liu, N. Lin, and Y. Deng, "Astragaloside IV alleviates atherosclerosis through targeting circ\_0000231/miR-135a-5p/CLIC4 axis in AS cell model in vitro," *Molecular and Cellular Biochemistry*, vol. 476, no. 4, pp. 1783–1795, 2021.
- [10] C. Wang and F. Hu, "Long noncoding RNA SOX2OT silencing alleviates cerebral ischemia-reperfusion injury via miR-135a-5p-mediated NR3C2 inhibition," *Brain Research Bulletin*, vol. 173, pp. 193–202, 2021.
- [11] H. Chen and X. Li, "LncRNA ROR is involved in cerebral hypoxia/reoxygenation-induced injury in PC12 cells via regulating miR-135a-5p/ROCK1/2," *American Journal of Translational Research*, vol. 11, no. 9, pp. 6145–6158, 2019.
- [12] T. Yu, Y. S. Yi, Y. Yang, J. Oh, D. Jeong, and J. Y. Cho, "The pivotal role of TBK1 in inflammatory responses mediated by macrophages," *Mediators of Inflammation*, vol. 2012, Article ID 979105, 2012.
- [13] D. Xu, T. Jin, H. Zhu et al., "TBK1 suppresses RIPK1-driven apoptosis and inflammation during development and in aging," *Cell*, vol. 174, no. 6, pp. 1477–1491.e19, 2018.
- [14] S. Lin, X. L. Zhao, and Z. Wang, "TANK-binding kinase 1 mediates osteoclast differentiation by regulating NF- $\kappa$ B, MAPK and Akt signaling pathways," *Immunology and Cell Biology*, vol. 99, no. 2, pp. 223–233, 2021.
- [15] R. F. Righetti, T. M. D. Santos, L. D. N. Camargo et al., "Protective effects of anti-IL17 on acute lung injury induced by LPS in mice," *Frontiers In Pharmacology*, vol. 9, pp. 1–15, 2018.
- [16] R. Herrero, G. Sanchez, and J. A. Lorente, "New insights into the mechanisms of pulmonary edema in acute lung injury," *Annals of Translational Medicine*, vol. 6, no. 2, pp. 17–32, 2018.

## Research Article

# Efficacy and Safety of Vitamin D Adjuvant Therapy for Ulcerative Colitis: A Meta-Analysis

Xinyi Guo,<sup>1</sup> Changxing Liu,<sup>1</sup> and Yahui Huang<sup>ID</sup><sup>2</sup>

<sup>1</sup>First School Clinical Medicine, Shaanxi University of Traditional Chinese Medicine, Xianyang 712046, China

<sup>2</sup>Xi'an Traditional Chinese Medicine Hospital, Xi'an 710016, China

Correspondence should be addressed to Yahui Huang; 220110122829@email.sntcm.edu.cn

Received 21 May 2022; Revised 12 June 2022; Accepted 15 June 2022; Published 20 July 2022

Academic Editor: Naeem Jan

Copyright © 2022 Xinyi Guo et al. This is an open access article distributed under the Creative Commons Attribution License, which permits unrestricted use, distribution, and reproduction in any medium, provided the original work is properly cited.

**Objective.** To examine the clinical efficacy and safety of Vitamin D in the treatment of ulcerative colitis in a systematic manner. **Methods.** RCT studies on Vitamin D in the treatment of ulcerative colitis were searched from CNKI, Wanfang Data, PubMed, Cochrane Library, and Web of Science databases. RevMan 5.4 software was used for analysis. **Results.** 10 articles were included, including 1077 patients. Meta-analysis results showed that when clinical efficacy was used as the outcome index, the clinical efficacy of the oral vitamin group was higher than that of the conventional treatment group (OR = 4.07, 95% CI 2.64-6.27), and the difference was statistically significant ( $Z = 6.38$ ,  $P < 0.00001$ ). When the Mayo risk score was used as the outcome index, the difference was statistically significant, indicating that oral Vitamin D significantly reduced the Mayo risk score (MD: -0.41, CI = (-0.47, -0.34),  $Z = 13.09$ ,  $P < 0.00001$ ). Using the intestinal mucosal barrier as the outcome index, the results showed that (1) the MDA group (MD = -0.75, 95% CI (-0.96~-0.53),  $P < 0.00001$ ), (2) the DAO group (MD = -1.17, 95% CI (-1.39-0.95),  $P < 0.00001$ ), and the Vitamin D group could effectively improve intestinal mucosal barrier function after sensitivity analysis (MD = -1.00, 95% CI (-1.08-0.92),  $P < 0.00001$ ). When inflammatory factors were used as outcome indicators, IL-6, TNF- $\alpha$ , and CRP groups had statistical significance (MD = -4.50, 95% CI (-5.13-3.87),  $P < 0.00001$ ; MD = -7.27, 95% CI (18.96-5.58),  $P < 0.00001$ ; and MD = -1.49, 95% CI (-1.76~-1.23),  $P < 0.00001$ , respectively). When the incidence of adverse reactions was used as the outcome indicator (OR = 0.73, 95% CI (0.34-1.32),  $P = 0.23$ ), there was no significant difference between the two groups. **Conclusion.** Vitamin D combined with mesalazine is effective in the treatment of ulcerative colitis, by improving the Mayo score and intestinal barrier function, and reducing inflammatory factors, with no significant safety difference. However, due to the quality of the included researches, more RCT researches needed to provide sufficient evidence to support clinical application. This study is registered with INPLASY 202250044.

## 1. Introduction

Ulcerative colitis (UC) is an inflammatory colonic disease with unknown etiology, characterized by continuous and diffuse colonic mucosal inflammation, commonly manifested as abdominal pain, mucus, pus, blood and stool, etc. [1]. This disease has the characteristics of long course, easy recurrence, and difficult to cure. About 20% of patients with chronic UC have the risk of developing colorectal cancer, and the number of UC cases in China is increasing at present [2]. Western medicine treatment mainly adopts protection and repair of intestinal mucosa, reduction of inflammatory factors, and prevention and treatment of

complications. Aminosalicic acid preparation is the most commonly used drug. If aminosalicic acid treatment effect is not good, glucocorticoids and immunosuppressants can be added [3].

Mesalazine is the most generally prescribed amino salicylic acid preparation for the treatment of UC, and it helps to protect the mucosa of the intestine. However, mesalazine alone has a low efficacy and a significant rate of side effects in some people [4]. As one of the sterols, Vitamin D is a recognized new immune factor, which exists in the form of 1, 25-hydroxyvitaminD3 (1,25-(OH) D3) in the human body and participates in various autoimmune regulations [5]. Relevant studies have shown that Vitamin D level is negatively

correlated with the risk of UC [6], but rigorous and standardized clinical evidence is still lacking. As a result, by examining domestic and international clinical randomized controlled studies on the treatment of UC, this research analyzed the efficacy of Vitamin D on UC and presented evidence-based evidence for the selection of UC treatment plans.

The paper is organized as follows: the data and methods are presented in Section 2. Section 3 discusses the experiments and results. Section 4 consists of the discussion, and finally, in Section 5, the research work is concluded.

## 2. Data and Methods

**2.1. Retrieval Strategy.** Figure 1 depicts the article screening procedure. PubMed, Cochrane Library, and Web of Science databases were searched for the “randomised controlled study” using terms like “inflammatory disease”, “Vitamin D”, “mesalazine”, and “Ulcerative colitis”, linked with “AND”/“OR” operators. Chinese search terms such as “ulcerative colitis”, “vitamin D”, “mesalazine”, and “clinical controlled trial” were searched in CKNI, and Wanfang databases.

### 2.2. Inclusion and Exclusion Criteria

**2.2.1. Literature Inclusion Criteria.** The literature should be a clinical randomized controlled study (RCT study).

**2.2.2. Intervention Measures.** Vitamin D and mesalazine were given orally to the treatment group, while mesalazine was given alone to the control group.

**2.2.3. Efficacy Evaluation Indicators.** Referring to Consensus on Diagnosis and Treatment of Ulcerative Colitis by Integrated Chinese and Western Medicine(2017) [7], clinical curative effect is the main indicator..

Secondary indicators are Mayo score, intestinal mucosal function (serum MDA and DAO), inflammatory factors (IL-6, CRP, and TNF- $\alpha$ ), and incidence of adverse reactions.

**2.2.4. Exclusion Criteria.** Animal studies, pharmacological studies, or literature with repeated discussions, reviews, and conference summaries and incomplete outcome indicators was excluded.

**2.3. Data Collection and Extraction.** According to the inclusion and exclusion criteria, the two researchers independently screen the title, abstract, and full text of the paper. If there is a dispute on the inclusion or exclusion of the research, all the research members participate in the discussion and make a decision together. Data were extracted from a uniform data extraction table, including first author, publication year, number of cases, sex, evaluation age, intervention, outcome measures, and randomization. A total of 10 RCT studies were included [8–17], with a total of 1077 patients. The basic characteristics are shown in Table 1.

**2.4. Quality Analysis of Included Literature.** The methodological quality of all included RCTs was evaluated using the risk bias assessment tool in the Cochrane Review Manual [18], including (1) whether to use random numbers or computer randomization, (2) whether to implement the

allocation hiding scheme, (3) whether blind method is used correctly, (4) data integrity, (5) selective outcome report, and (6) other sources of bias. The risk of bias from included studies is shown in Figure 2.

**2.5. Statistical Methods.** Meta-analysis was conducted using RevMan 5.4 software, and the main effect values were as follows: weighted standard deviation (WMD), standard mean difference (SMD), and 95% credibility interval (CI). If  $P > 0.05$  and  $I^2 \leq 50\%$ , the fixed effects model could be selected, indicating statistical homogeneity of subjects. On the contrary, if  $P < 0.05$  and  $I^2 > 50\%$ , it indicates that there is heterogeneity in the selected research object, and sensitivity analysis should be conducted step by step by eliminating all studies [19].

## 3. Results

### 3.1. Outcome Index Analysis

**3.1.1. Clinical Efficacy Indicators.** A total of 8 RCTswere included [8–13, 15, 16], including 393 patients in the treatment group and 396 patients in the control group. After the heterogeneity test ( $I^2 = 0\% < 50\%$ ) and Q test ( $P = 0.94 > 0.1$ ), indicating that there was no significant heterogeneity among the selected literatures, the fixed effects model was selected for meta-analysis: the clinical efficacy of the observation group was higher than that of the control group (OR = 4.07, 95% CI 2.64-6.27), and the difference was statistically significant ( $Z = 6.38, P < 0.00001$ ), as shown in Figure 3.

**3.1.2. The Mayo Score.** Four literatures [8–10, 13] were included to report the Mayo score, including 385 patients. Meta-analysis was performed to compare the improvement of the Mayo score between the oral vitamin D group and the control group. The MD value was used as the effect scale, and there was no statistical heterogeneity between studies ( $I^2 = 0\%, P = 0.82$ ).Our study reveals: (MD: -0.41, CI = [-0.47,-0.34],  $Z = 13.09, P < 0.00001$ ). The difference was statistically significant, indicating that oral vitamin D significantly reduced the Mayo score, as shown in Figure 4.

**3.1.3. Levels of Inflammatory Factors.** A total of 4 literatures [8, 12, 14, 17] measured the improvement of ulcerative colitis by the levels of inflammatory factors (IL-6, TNF- $\alpha$ , and CRP). Two literatures [8, 14] included IL-6 and TNF- $\alpha$  indicators, and 4 literatures [8, 12, 14, 17] included CRP indicators. Using the MD value as the effect scale, the subgroup analysis showed that the  $I^2$  of the three groups was all less than 50%, showing homogeneity. Using fixed effects model analysis, in the IL-6 group (MD = -4.50, 95% CI (-5.13-3.87),  $P < 0.00001$ ), TNF- $\alpha$  group (MD = -7.27, 95% CI (18.96-5.58),  $P < 0.00001$ ), and CRP group (MD = -1.49, 95% CI (-1.76~-1.23),  $P < 0.00001$ ), the differences in the three groups were statistically significant, suggesting that oral vitamin D can effectively reduce the levels of inflammatory factors, as shown in Figure 5.

**3.1.4. Intestinal Barrier Function.** Four of the included literatures [9, 11, 13, 14] used serum MDA or DAO indicators to describe intestinal barrier function, and MD was used as the

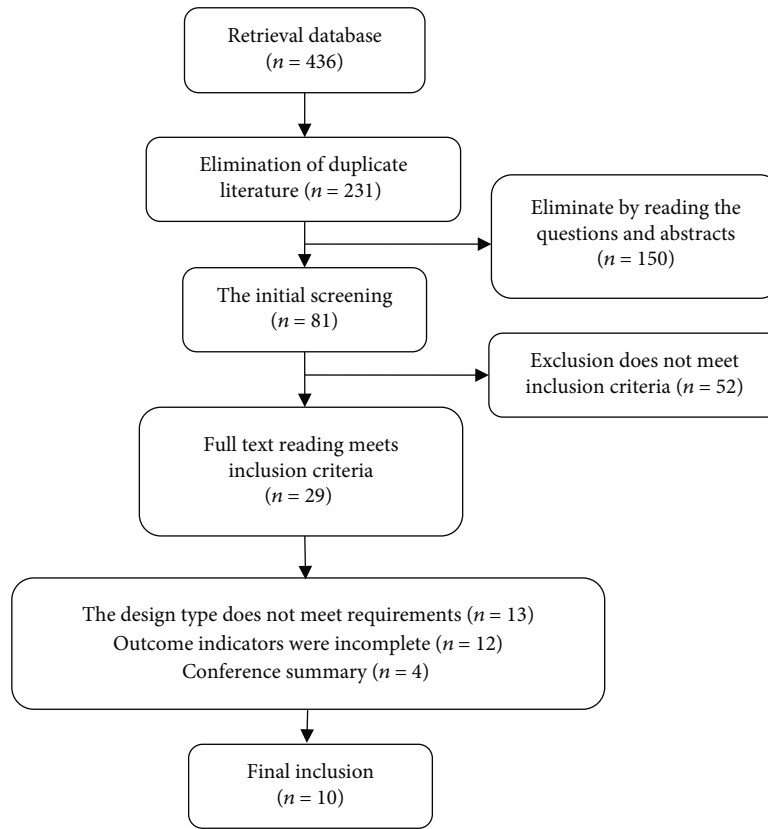


FIGURE 1: Specific process of literature screening.

TABLE 1: Baseline characterization of included literatures.

Author and year	Case load (T/C)	Gender (male/female)	Age (T/C, year)	Intervening measure	Time (w)	Outcome	Random method
Yu Xia 2020 [9]	60/60	61/59	38.4 ± 3.3 38.2 ± 3.1	C: mesalazine T: mesalazine+VD	8	①②④	—
Senyuan Zheng 2021 [10]	52/51	51/52	39.95 ± 6.5	C: mesalazine T: mesalazine+VD	8	①②	—
Haipeng Dou 2021 [11]	44/44	58/30	46.1 ± 10.7 44.7 ± 8.9	C: sulfasalazine T: sulfasalazine+VD	4	①③④⑧	Random number table
Ningning Yue 2020 [8]	40/40	38/44	41.30 ± 11.16 40.98 ± 10.94	C: mesalazine +placebo T: mesalazine+VD	8	①②⑤ ⑥⑦⑧	Computer stochastic method
Hongliang Gao 2021 [12]	57/59	59/57	40.2 ± 6.30 39.6 ± 6.90	C: mesalazine T: mesalazine+VD	24	①⑥⑨	—
Fenghui Chen 2018 [13]	40/42	44/38	42.30 ± 10.48 43.45 ± 12.5	C: mesalazine T: mesalazine+VD	6	①②③④	Random number table
Rong Yang 2017 [15]	40/40	51/39	41.19 ± 10.23 43.07 ± 11.87	C: mesalazine T: mesalazine+VD	12	①	—
Yang Jing 2019 [14]	99/99	104/94	41.38 ± 5.34 42.35 ± 5.09	C: mesalazine T: mesalazine+VD	4	④⑤⑥⑦	—
Shusheng Zhu 2015 [16]	60/60	60/60	34.6 ± 3.6	C: mesalazine T: mesalazine+VD	4	①⑧	—
Vahedi 2016 [17]	45/45	49/41	37.5 ± 9.0 35.0 ± 9.2	C: mesalazine+NS T: mesalazine+VD	6	⑥	Random number table

T: treatment group; C: control group. Clinical observation indicators: ①—effective rate, ②—Mayo risk score, ③—serum MDA, ④—serum DAO, ⑤—IL-6, ⑥—CRP, ⑦—TNF- $\alpha$ , and ⑧—incidence of adverse reactions.

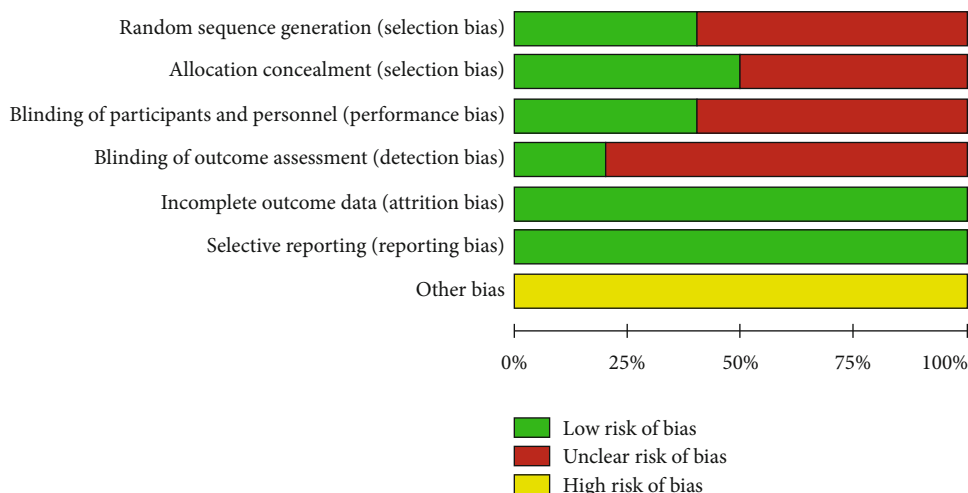


FIGURE 2: Risk of bias in the included literature for vitamin D treatment of UC.

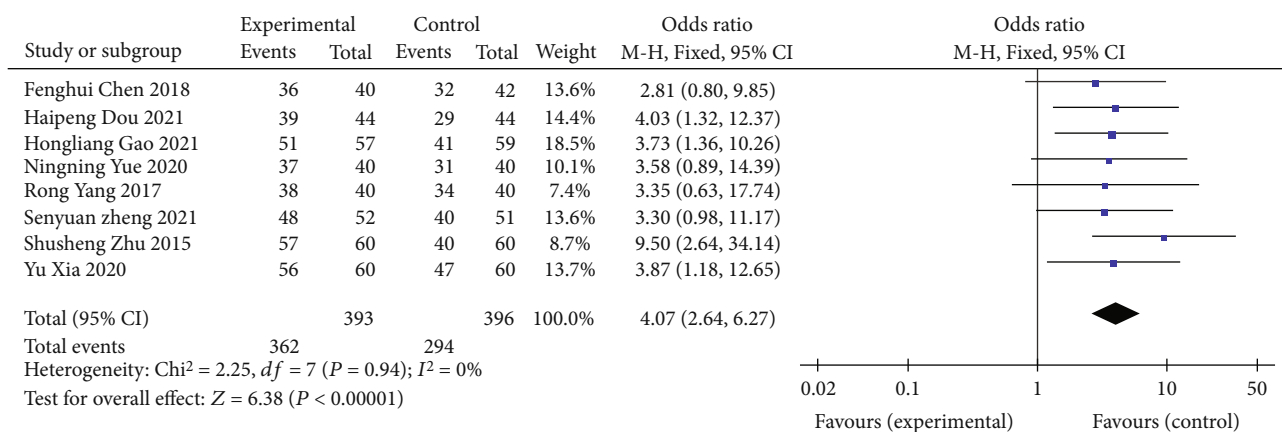


FIGURE 3: Forest map of clinical efficacy comparison.

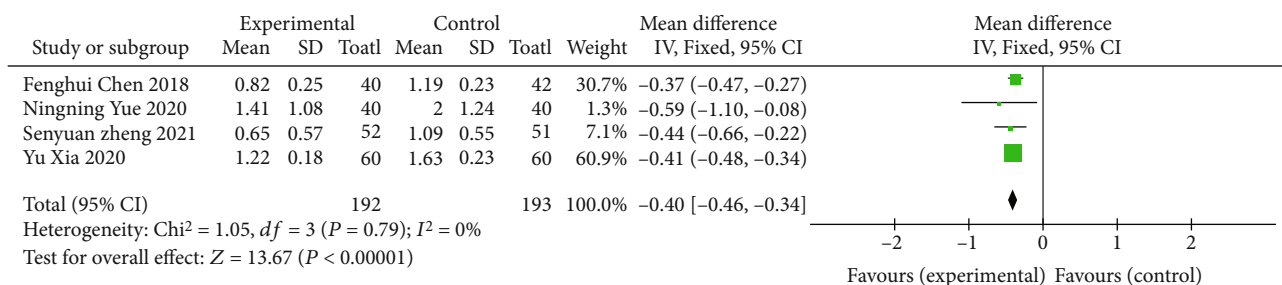


FIGURE 4: Forest map of Mayo score comparison.

effect scale. The results showed that the serum MDA group had homogeneity ( $I^2 = 0\%, P = 0.76$ ). The fixed effects model was used for analysis (MD = -0.75, 95% CI (-0.96~-0.53),  $P < 0.00001$ ), and the difference was statistically significant. Heterogeneity was observed in the serum DAO group ( $I^2 = 81\%, P = 0.001$ ), and the random effects model was used for analysis (MD = -1.17, 95% CI (-1.39-0.95),  $P < 0.00001$ ). The difference was statistically significant, as shown in Figure 6. Due to the heterogeneity of the 4 studies in the serum DAO group, the remaining 3 studies

show homogeneity ( $I^2 = 26\%, P = 0.26$ ) after sensitivity analysis and were analyzed using the fixed effects model (MD = -1.00, 95% CI (-1.08~-0.92),  $P < 0.00001$ ), as shown in Figure 7. The difference was statistically significant, suggesting that oral vitamin D improved the repair function of intestinal mucosa in both serum MDA and DAO indexes.

3.1.5. Incidence of Adverse Reactions. A total of 4 studies [8, 11, 12, 16] described the incidence of adverse events, and the heterogeneity test ( $I^2 = 30\% < 50\%, P = 0.23 > 0.1$ ) suggested

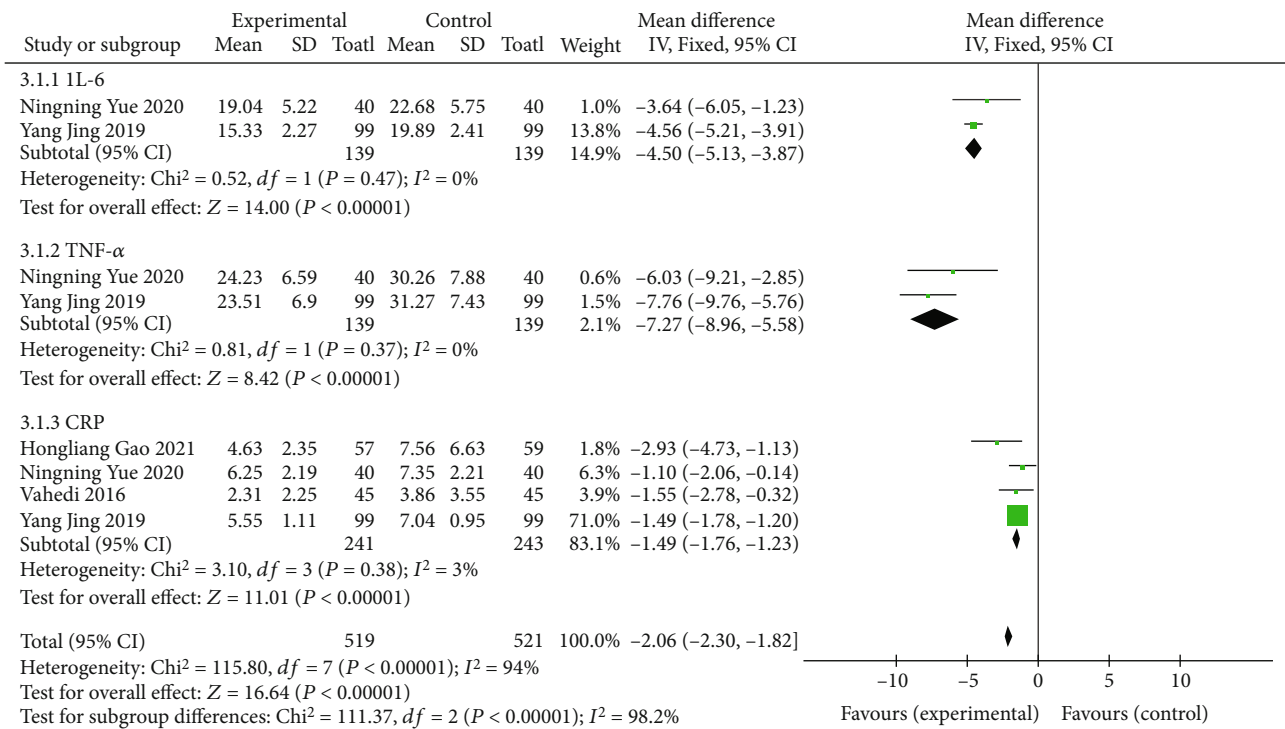


FIGURE 5: Forest map comparing inflammatory factors.

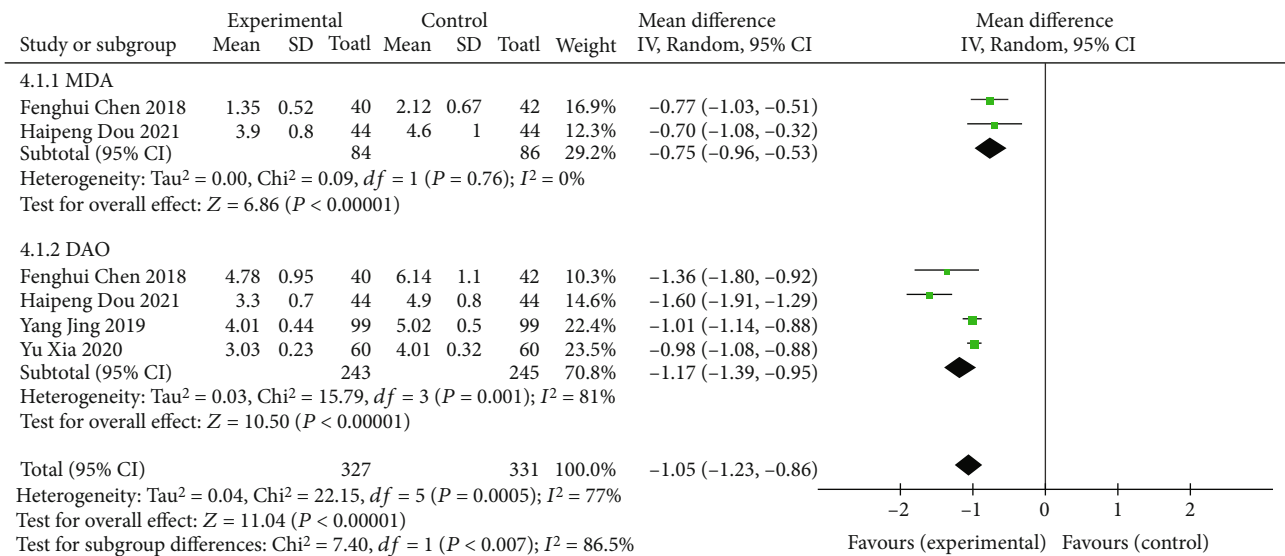


FIGURE 6: Forest map of intestinal barrier function comparison.

that there was no significant heterogeneity among the selected literatures, so the fixed effects model was selected for meta-analysis. There was no statistical significance between the two groups ( $\text{OR} = 0.73, 95\% \text{ CI } (0.34-1.32), P = 0.23$ ), as shown in Figure 8. It indicated that there was no significant difference in the incidence of adverse reactions between the oral mesalazine+vitamin D group and the single mesalazine group. However, more literatures may be required to be included in the future to further confirm the reliability of the results due to the small number of literatures included.

**3.2. Risk Analysis of Bias.** The funnel plot was drawn based on the influence of the included literature on the cure rate of UC, and the results showed that the circle was located around both sides of the midline, presenting an incomplete symmetrical distribution, suggesting a large possibility of publication bias in this study, as shown in Figure 9.

## 4. Discussion

**4.1. Mechanism of Vitamin D Adjuvant Treatment of UC.** Vitamin D is a fat-soluble steroid hormone that is mainly

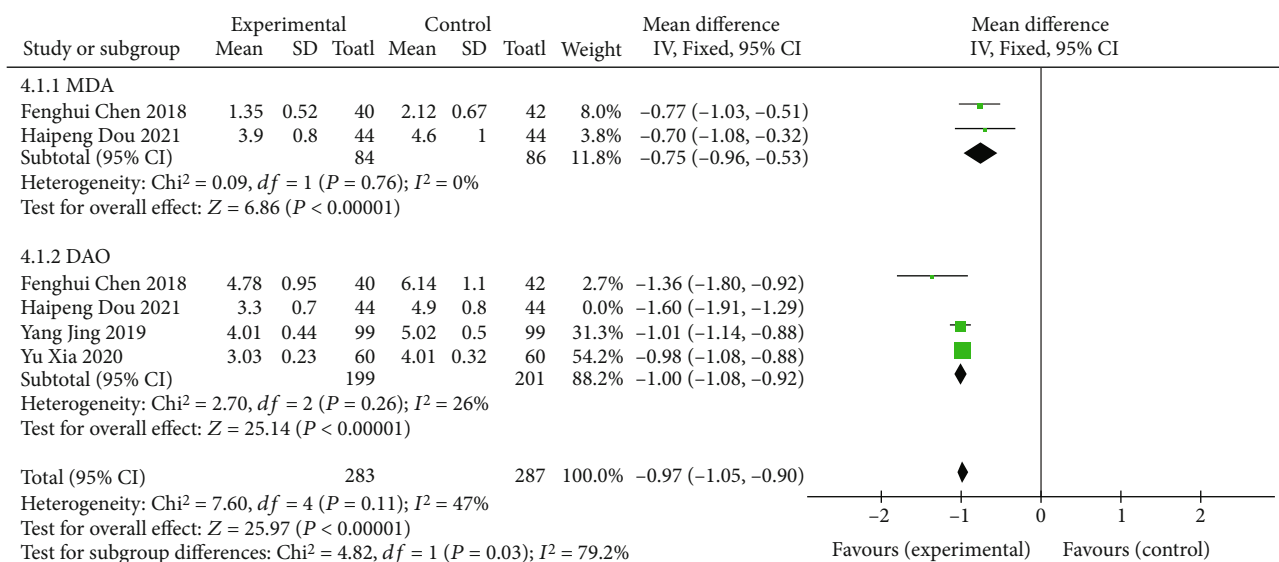


FIGURE 7: Sensitivity analysis of intestinal barrier function.

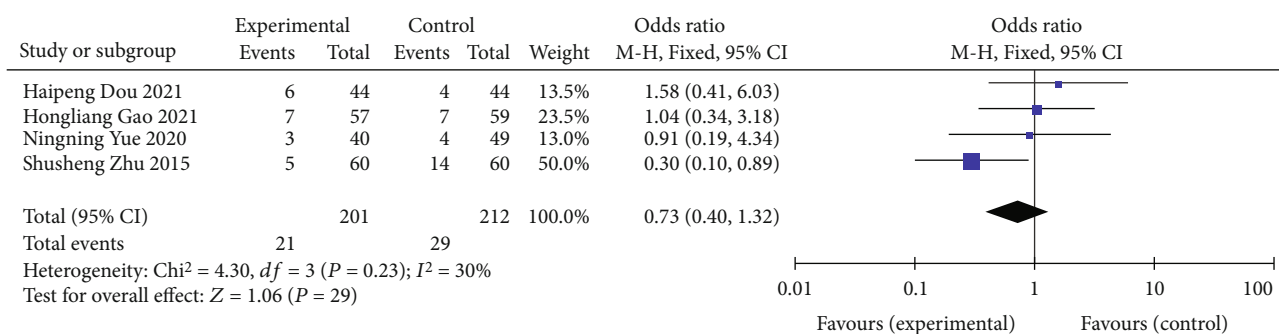


FIGURE 8: Forest plot comparing the incidence of adverse reactions.

present in the human body in two forms: plant-based vitamin D2 and animal-derived vitamin D3, both of which can be ingested through food [20]. Vitamin D is linked to biological processes such as regulating intestinal mucosal immunity and intestinal integrity, in addition to regulating calcium and phosphate metabolism and skeletal homeostasis [21]. Vitamin D insufficiency has thus been linked to immune-mediated illnesses, such as inflammatory bowel disease. Inflammatory response, intestinal microflora disorder, and mucosal barrier damage play an important role in the occurrence and development of ulcerative colitis, and vitamin D can induce and maintain UC remission through reducing inflammatory factors and promoting the repair of intestinal mucosal barrier [22, 23]. In previous systematic reviews, no study evaluated vitamin D as a supplement to adjuvant therapy for UC. In this study, through quantitative synthesis, it was found that compared with the control group, UC patients treated with vitamin D as adjuvant therapy had beneficial effects on the Mayo score, intestinal barrier function, IL-6, TNF- $\alpha$ , CRP, and other inflammatory factors. There was no significant difference in safety.

Vitamin D can reduce the levels of inflammatory factors. First, 1,25(OH) $_2$ D $_3$  combined with vitamin D receptor

(VDR) can induce the expression of anti-inflammatory factors in monocytes to reduce inflammatory factors [24]. Second, vitamin D can act directly on CD4 and T lymphocytes to enhance Th2 cell proliferation and differentiation while inhibiting Th1 cell proliferation in DC cells [25]. Vitamin D can upregulate mitogen-activated protein kinase phosphatase-1 and inhibit the activity of mitogen-activated protein kinase (MAPK) and reduce the production of TNF- $\alpha$  while decreasing IL-6 [26]. Multiple studies included in this study showed that vitamin D supplementation effectively reduced the levels of inflammatory factors (IL-6, TNF- $\alpha$ , and CRP) in patients with ulcerative colitis. The proposed inflammatory outcome index was consistent with Xue et al. [27]. Xue et al. collected biopsy samples from 103 patients with UC and found that vitamin D/vitamin D receptor (VDR) signaling has a protective effect on the onset or progression of inflammatory bowel disease (IBD) and proved that the activation of hypoxia-inducible factor 1 $\alpha$  (HIF-1 $\alpha$ ) is closely related to inflammatory factors. HIF-1 $\alpha$  inhibitors inhibit the expression of TNF- $\alpha$ , IL-6, and IL-17, thereby reducing the inflammatory response.

Furthermore, the most prominent pathogenesis of UC is mucosal barrier degradation, which can be separated into

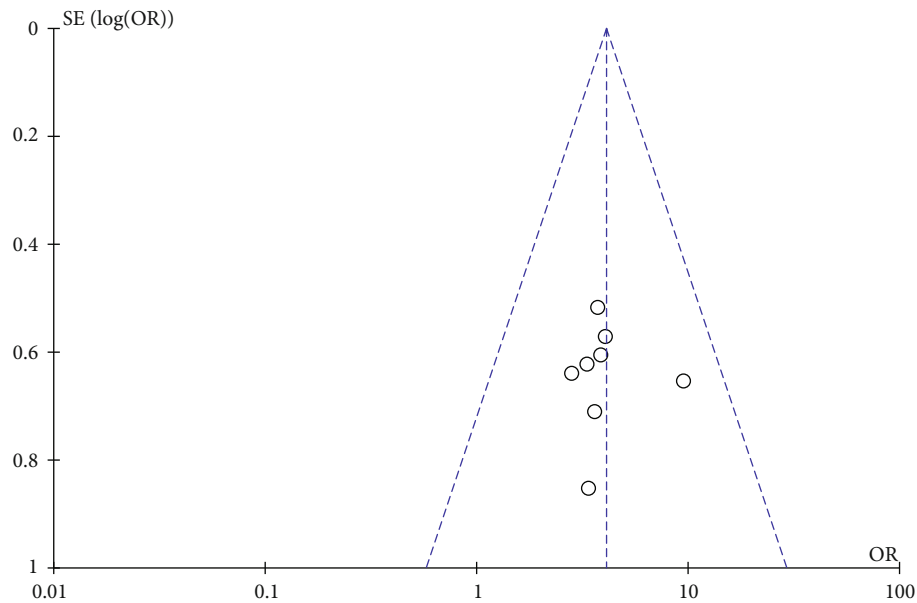


FIGURE 9: Funnel plot.

mechanical, immunological, chemical, and biological barriers. The four are self-contained and interact with one another, forming a massive defence system against foreign pathogenic pathogens [28]. Vitamin D enhances the connection between intestinal epithelial cells by promoting the expression of transmembrane proteins such as occludin and claudin and mucosal tight junction proteins such as zo-1, zo-2, and zo-3, thus constituting the mechanical barrier of intestinal mucosa [29, 30]. Based on mouse modeling, Wibowo et al. [31] gave different doses of vitamin D on the basis of blank control. By observing the intestinal brush-like margin component protein and the DAO level in peripheral blood under a microscope, it was concluded that vitamin D3 could activate the Wnt protein pathway, thus leading to cell differentiation and proliferation through stem cell signal transduction. Increase the proliferation of colonic mucosa cells to repair the colonic mucosa. Four of the literatures included in this study described intestinal barrier function by serum MDA or DAO indicators. After the mucosal cells of UC patients are damaged, DAO located in the mucous villi falls off and enters the blood and intestinal lumen [32]. When an inflammatory reaction occurs, a significant number of germs and endotoxins enter the bloodstream, and the body goes into survival mode, which inhibits SOD activity, weakens disproportionation reaction, and raises MDA levels as a lipid peroxide metabolic degradation product [33]. Therefore, DAO and MDA levels in peripheral blood are helpful to evaluate the degree of mucosal injury.

Recent studies have found that UC patients may be deficient in trace elements due to intestinal symptoms that lead to reduced nutrient intake and intestinal microbiota disorder, resulting in impaired mucosal barrier [34–36]. Vitamin D deficiency is more common [37]. Horta et al. [38] conducted a prospective study of 44 IBD patients living in Los Angeles (73% of whom had UC) and concluded that 75%

of the patients had varying degrees of vitamin D deficiency. Vitamin D can improve intestinal microflora imbalance, regulate immunity, and maintain the integrity of intestinal mucosal barrier, so it is recommended for the treatment or adjuvant treatment of UC. Therefore, this study adopted meta-analysis to analyze the efficacy and safety of vitamin D in the treatment of UC, providing evidence-based medical evidence for the clinical application of vitamin D.

**4.2. Research Limitations.** Studies on vitamin D adjuvant treatment of UC are still in the initial stage. Although meta-analysis showed that vitamin D can improve UC symptoms from repairing the intestinal mucosa and reducing inflammatory factors, there are still many deficiencies. In one thing, the sample size of the literatures included in this study was limited, which was consistent with the small number and low quality of the literatures. This may be because vitamin D has not been unified into the treatment standards in China. In one thing, In another thing, there were some differences in the measurement, usage, and course of vitamin D in the included literatures. In the future, more rigorous and prospective researches will be needed, such as collaboration between multiple centers.

## 5. Conclusion

Meta-analysis results show that, compared with the control group, vitamin D supplement is an effective intervention for UC. Vitamin D supplementation can increase intestinal mucosal repair factors and reduce inflammatory factors and Mayo risk score in UC patients. The results showed that there was no significant difference in the incidence of adverse events between the two methods, and it was a relatively safe adjuvant therapy. Moreover, vitamin D adjuvant therapy has the advantages of simplicity, effectiveness,



safety, and low price. However, due to the lack of corresponding multicenter and high-quality RCTs in China and the small number of foreign RCTs, the quality of evidence obtained is not high, and large-sample and high-quality RCTs are still needed to further verify its efficacy. To establish the therapeutic impact and quality of life, more randomised controlled trials with rigorous study design are required, and immune response of vitamin D supplementation in patients with ulcerative colitis and other related chronic complications should be further elucidated.

## Data Availability

The datasets used during the current study are available from the corresponding author on reasonable request.

## Conflicts of Interest

The authors declare that they have no conflict of interest.

## References

- [1] I. Ordás, L. Eckmann, M. Talamini, D. C. Baumgart, and W. J. Sandborn, "Ulcerative colitis," *The Lancet*, vol. 380, no. 9853, pp. 1606–1619, 2012.
- [2] X. Liang, F. Yin, and X. Zhang, "Consensus opinion on diagnosis and treatment of inflammatory bowel disease (2018, Beijing) part interpretation of ulcerative colitis," *Clinical Meta-Analysis*, vol. 33, no. 11, pp. 987–990, 2018.
- [3] S. M. Adams and P. H. Bornemann, "Ulcerative colitis," *American Family Physician*, vol. 87, no. 10, pp. 699–705, 2013.
- [4] K. Yagisawa, T. Kobayashi, R. Ozaki et al., "Randomized, crossover questionnaire survey of acceptabilities of controlled-release mesalazine tablets and granules in ulcerative colitis patients," *Intestinal Research*, vol. 17, no. 1, pp. 87–93, 2019.
- [5] M. T. Cantorna, "Vitamin D, multiple sclerosis and inflammatory bowel disease," *Archives of Biochemistry and Biophysics*, vol. 523, no. 1, pp. 103–106, 2012.
- [6] J. Fletcher, S. C. Cooper, S. Ghosh, and M. Hewison, "The role of vitamin D in inflammatory bowel disease: mechanism to management," *Nutrients*, vol. 11, no. 5, p. 1019, 2019.
- [7] J. Li and Y. Chen, "Consensus on diagnosis and treatment of ulcerative colitis with integrated Chinese and Western medicine (2017)," *Chinese Journal of Integrated Chinese and Western Medicine Digestion*, vol. 26, no. 2, 2018.
- [8] N. Yue and X. Chen, "Clinical efficacy of VitD combined with mesalazine in the treatment of mild and moderate ulcerative colitis," *Journal of Pharmaceutical Forum*, vol. 41, no. 12, pp. 50–53, 2020.
- [9] Y. Xia and H. Gao, "Effect of vitamin D3 combined with mesalazine on intestinal mucosal oxidative stress injury in patients with ulcerative colitis," *Gastroenterology*, vol. 25, no. 7, pp. 409–412, 2020.
- [10] S. Zheng, J. Li, and H. Gao, "Effects of vitamin D<sub>3</sub> combined with mesalazine on serum CCL11 and PTPRO expression in patients with mild and moderate ulcerative colitis," *Journal of Xinjiang Medical University*, vol. 44, no. 7, pp. 827–830, 2021.
- [11] D. Ha, D. Zhao, and X. Yao, "Clinical application of vitamin D combined with sulfasyridine in the treatment of ulcerative colitis," *Colorectal and Anal Surgery*, vol. 27, no. 1, pp. 35–39, 2021.
- [12] H. Gao and H. Zhou, "Efficacy of mesalazine combined with vitamin D<sub>3</sub> and probiotics in the treatment of ulcerative colitis in mild to moderate active stage," *Chinese Journal of Practical Diagnosis & Therapy*, vol. 34, no. 11, pp. 1169–1171, 2020.
- [13] F. Chen, X. Wang, and C. Fan, "Effects of vitamin D supplementation on oxidative and antioxidant imbalance, intestinal mucosal barrier and clinical prognosis in elderly patients with ulcerative colitis," *Shaanxi Medical Journal*, vol. 47, no. 12, pp. 1634–1637, 2018.
- [14] Y. Jin, Y. Q. Shi, J. Q. Zhang, and X. Y. Zhao, "Effects of exogenous vitamin D on intestinal mucosal barrier and inflammatory factors in patients with inflammatory bowel disease," *Gastroenterology*, vol. 24, no. 8, pp. 493–496, 2019.
- [15] R. Yang and X. Yang, "Effect of vitamin D on the recurrence of ulcerative colitis," *Colorectal and Anal Surgery*, vol. 23, no. 5, pp. 626–629, 2017.
- [16] S. Zhu, "Clinical efficacy of mesalazine combined with vitamin D in the treatment of inflammatory bowel disease," *Contemporary Medicine*, vol. 21, no. 31, pp. 143–144, 2015.
- [17] A. Sharifi, M. J. Hosseinzadeh-Attar, H. Vahedi, and S. Nedjat, "A randomized controlled trial on the effect of vitamin D3 on inflammation and cathelicidin gene expression in ulcerative colitis patients," *Saudi Journal of Gastroenterology*, vol. 22, no. 4, pp. 316–323, 2016.
- [18] O. Barcot, M. Boric, T. Poklepovic Pericic et al., "Risk of bias judgments for random sequence generation in Cochrane systematic reviews were frequently not in line with Cochrane Handbook," *BMC Medical Research Methodology*, vol. 19, no. 1, p. 170, 2019.
- [19] G. S. de Vasconcelos, A. Cini, G. Sbruzzi, and C. S. Lima, "Effects of proprioceptive training on the incidence of ankle sprain in athletes: systematic review and meta-analysis," *Clinical Rehabilitation*, vol. 32, no. 12, pp. 1581–1590, 2018.
- [20] C. Lamberg-Allardt, "Vitamin D in foods and as supplements," *Progress in Biophysics and Molecular Biology*, vol. 92, no. 1, pp. 33–38, 2006.
- [21] D. Bakke and J. Sun, "Ancient nuclear receptor VDR with new functions: microbiome and inflammation," *Inflammatory Bowel Diseases*, vol. 24, no. 6, pp. 1149–1154, 2018.
- [22] D. H. Kim, C. A. Meza, H. Clarke, J. S. Kim, and R. C. Hickner, "Vitamin D and endothelial function," *Nutrients*, vol. 12, no. 2, p. 575, 2020.
- [23] A. F. Gombart, N. Borregaard, and H. P. Koeffler, "Human cathelicidin antimicrobial peptide (CAMP) gene is a direct target of the vitamin D receptor and is strongly up-regulated in myeloid cells by 1,25-dihydroxyvitamin D<sub>3</sub>," *The FASEB Journal*, vol. 19, no. 9, pp. 1067–1077, 2005.
- [24] L. J. He, X. D. Zhu, Y. Wang, T. T. Guo, and D. Wang, "Dynamic expression of related inflammatory factors in serum and colon tissue of ulcerative colitis model rats with spleen and kidney Yang deficiency," *Chinese Journal of Traditional Chinese Medicine Information*, vol. 24, no. 1, pp. 59–62, 2017.
- [25] A. Boonstra, F. J. Barrat, C. Crain, V. L. Heath, H. F. J. Savelkoul, and A. O'Garra, "1 $\alpha$ ,25-Dihydroxyvitamin D<sub>3</sub> has a direct effect on naive CD4(+) T cells to enhance the development of Th2 cells," *Journal of Immunology*, vol. 167, no. 9, pp. 4974–4980, 2001.
- [26] Y. Zhu, B. D. Mahon, M. Froicu, and M. T. Cantorna, "Calcium and 1 $\alpha$ ,25-dihydroxyvitamin D<sub>3</sub> target the TNF-

- alpha pathway to suppress experimental inflammatory bowel disease,” *European Journal of Immunology*, vol. 35, no. 1, pp. 217–224, 2005.
- [27] G. Xue, R. Gao, Z. Liu et al., “Vitamin D/VDR signaling inhibits colitis by suppressing HIF-1 $\alpha$  activation in colonic epithelial cells,” *American Journal of Physiology. Gastrointestinal and Liver Physiology*, vol. 320, no. 5, pp. G837–g846, 2021.
- [28] J. Zhen and G. Huang, “Research progress in etiology and pathogenesis of ulcerative colitis,” *World Chinese Journal of Gastroenterology*, vol. 27, no. 4, pp. 245–251, 2019.
- [29] Y. Tan and C. Zheng, “Occludin and ZO-1 expression and clinical significance in ulcerative colitis,” *Modern Pharmaceutical & Clinical*, vol. 33, no. 7, pp. 1803–1808, 2018.
- [30] L. S. Poritz, L. R. Harris, A. A. Kelly, and W. A. Koltun, “Increase in the tight junction protein claudin-1 in intestinal inflammation,” *Digestive Diseases and Sciences*, vol. 56, no. 10, pp. 2802–2809, 2011.
- [31] S. Wibowo, K. Subandiyah, K. Handono, and S. Poeranto, “Role of vitamin D in Wnt pathway activation for colonic epithelial cell differentiation,” *Journal of Taibah University Medical Sciences*, vol. 16, no. 4, pp. 575–581, 2021.
- [32] G. Järnerot, M. Ström, A. Danielsson et al., “Allopurinol in addition to 5-aminosalicylic acid based drugs for the maintenance treatment of ulcerative colitis,” *Alimentary Pharmacology & Therapeutics*, vol. 14, no. 9, pp. 1159–1162, 2000.
- [33] Z. M. Song, F. Liu, Y. M. Chen, Y. J. Liu, X. D. Wang, and S. Y. du, “CTGF-mediated ERK signaling pathway influences the inflammatory factors and intestinal flora in ulcerative colitis,” *Biomedicine & Pharmacotherapy*, vol. 111, pp. 1429–1437, 2019.
- [34] D. Jayawardena and P. K. Dudeja, “Micronutrient deficiency in inflammatory bowel diseases: cause or effect?,” *Cellular and Molecular Gastroenterology and Hepatology*, vol. 9, no. 4, pp. 707–708, 2020.
- [35] F. K. Ghishan and P. R. Kiela, “Vitamins and minerals in inflammatory bowel disease,” *Gastroenterology Clinics of North America*, vol. 46, no. 4, pp. 797–808, 2017.
- [36] S. M. Karp and T. R. Koch, “Micronutrient supplements in inflammatory bowel disease,” *Disease-a-Month*, vol. 52, no. 5, pp. 211–220, 2006.
- [37] G. E. Mullin, “Micronutrients and inflammatory bowel disease,” *Nutrition in Clinical Practice*, vol. 27, no. 1, pp. 136–137, 2012.
- [38] G. Horta, S. Soto, and G. Labarca, “Vitamin D levels in patients with inflammatory bowel disease,” *Revista Médica de Chile*, vol. 149, no. 3, pp. 393–398, 2021.

## Research Article

# Application Value of the Diagnosis during Early Carcinoma of Upper Digestive Tract Based on Optical Enhanced Endoscopic Technique

Yinghao Song <sup>1</sup>, Yulei Qu <sup>1</sup>, Lu Li <sup>2</sup>, Mengxuan Xing <sup>3</sup>, Baohui Jia <sup>4</sup>, Yingjie Ma <sup>1</sup>  
and Yong Zhang <sup>2</sup>

<sup>1</sup>Department of Gastroenterology, People's Hospital of Henan University of Chinese Medicine, Henan University of Chinese Medicine, Zhengzhou, 450000 Henan Province, China

<sup>2</sup>Department of Gastroenterology, Zhengzhou Central Hospital Affiliated to Zhengzhou University, Zhengzhou University, Zhengzhou, 450000 Henan Province, China

<sup>3</sup>Xinxiang Medical University, Xinxiang, 453000 Henan Province, China

<sup>4</sup>Department of Critical Care Medicine, Fourth Affiliated Hospital of Nanchang University, Nanchang University, Nanchang, 330000 Jiangxi Province, China

Correspondence should be addressed to Yong Zhang; zhangyonglgz@163.com

Received 11 May 2022; Revised 20 June 2022; Accepted 24 June 2022; Published 19 July 2022

Academic Editor: Naeem Jan

Copyright © 2022 Yinghao Song et al. This is an open access article distributed under the Creative Commons Attribution License, which permits unrestricted use, distribution, and reproduction in any medium, provided the original work is properly cited.

**Objective.** The diagnostic value of optical enhanced endoscopy in early cancer of upper digestive tract was studied by comparing the disease accuracy, tumor type, invasion, and various surgical indicators between the two groups. **Methods.** 188 patients with early upper gastrointestinal cancer treated in our hospital from January 2020 to February 2021 were selected as the research objects. The patients were randomly divided into the observation group and control group with 94 cases in each group. **Results.** The accuracy of early detection of early carcinoma of upper digestive tract in the observation group was 94.68% and that in the control group was 76.60%. The accuracy of the observation group was significantly higher than that in the control group, with statistical significance ( $P < 0.05$ ). In the observation group, 36 cases of early gastric cancer, 28 cases of early esophageal cancer, and 30 cases of early colorectal cancer were detected; 25 cases of early gastric cancer, 19 cases of early esophageal cancer, and 28 cases of early colorectal cancer were detected; 26 cases of early carcinoma of upper digestive tract infiltration were detected; and 68 cases were not detected, and the detection rate was 27.66%, which was higher than 9.57% in the control group, and the difference was statistically significant ( $P < 0.05$ ). After different methods of treatment, no death occurred in all patients. Except for the operation time, the surgical indexes of the observation group were better than the control group, the difference was statistically significant ( $P < 0.05$ ). **Conclusion.** Optical enhanced endoscopic technique had obvious effect in the diagnosis of patients with early cancer of upper digestive tract, it was helpful to improve the clinical detection rate of early carcinoma of upper digestive tract and had certain diagnostic ability for the invasion depth of early cancer of high upper gastrointestinal tract, which was conducive to the detection of clinical invasion lesions and had high clinical promotion and application value.

## 1. Introduction

Upper gastrointestinal cancer is one of the most common malignant tumor diseases in clinical practice. According to relevant survey data, with the continuous change of people's lifestyle and dietary structure in recent years, the incidence

of upper digestive tract cancer is increasing year by year, which has caused serious impact on the life and health safety of residents [1, 2]. For a long time in the past, many scholars have studied the risk factors of upper gastrointestinal cancer, including smoking, drinking, eating habits, genetics, and infection, which are recognized as the risk factors of upper

gastrointestinal cancer [3, 4]. The cancers of the upper digestive tract mainly include gastric, esophageal, and duodenal cancers, which mainly refer to lesions confined to the mucosa or submucosa with or without lymph node metastasis [5]. In addition, due to the extremely insidious nature of upper gastrointestinal cancer in the early stage of its onset, patients generally have no significant clinical symptoms [6]. Therefore, the effective diagnosis of early carcinoma of upper digestive tract is particularly important, and it is also the focus of clinical attention. At present, the main method commonly used in clinical early digestive tract cancer is white light endoscopy, but white light endoscopy is prone to misdiagnosis and missed diagnosis. Optical enhanced endoscopy can make up for this deficiency. Optical enhanced endoscopy has a high detection rate for early digestive tract tumors, which is helpful to assist doctors in early treatment of patients [7, 8]. Optical enhanced endoscopy is a new type of electronic staining endoscopy. Its principle is to enhance the tumor surface structure and blood vessel shape through narrow-band imaging to achieve the observation effect of the tumor, so as to achieve the optical diagnosis of the tumor [9, 10]. The optical enhanced endoscopic technique has the characteristics of simple operation and high accuracy, which can magnify the observation of lesions, improve the conformity with pathological diagnosis, and evaluate the risk of lesions [11, 12].

In this study, 188 cases of early carcinoma of upper digestive tract in our hospital were selected to compare and analyze the application value of optical enhanced endoscopic technique and ordinary high-purity light endoscopy in the identification of upper digestive tract early cancer.

This study consists of four sections.

Section 2 shows the “materials and methods,” which introduces the basic information of the samples, the sampling methods, and the determination of key indicators.

Section 3 is the comparison results of the two groups. This section compares the two groups according to the three indicators (accuracy, types and infiltration of cancer, and surgical indexes) and obtains the comparison results.

Section 4 is the discussion, and the relevant results are discussed according to the data comparison in Section 3.

Section 5 is the conclusion. This section summarizes the research results of the full text, puts forward the value of this study, and points out the shortcomings of this study.

## 2. Materials and Methods

**2.1. General Information.** A total of 188 patients with early carcinoma of upper digestive tract admitted to our hospital from January 2020 to February 2021 were selected as the research objects.

Inclusion criteria are as follows: ① age  $\geq 18$  years old, ② the patient had developed the clinical features of early cancer, ③ knowing own illness, ④ the early carcinoma of upper digestive tract was confirmed by histologic biopsy, and ⑤ no relevant antitumor therapy was received before admission.

Exclusion criteria are as follows: ① pregnant women; ② serious diseases of the heart, liver, or kidney; ③ unable to communicate normally or combined with neurological dis-

eases; ④ complicated with other systemic malignancies; and ⑤ other unsuitable candidates.

They were divided into the observation group and control group, with 94 cases in each group. There was no significant difference in clinical data between the two groups, which was comparable ( $P > 0.05$ ). General information of the two groups is shown in Table 1.

### 2.2. Methods

**2.2.1. Endoscopy.** The control group was diagnosed by ordinary high-purity light endoscopy. The observation group underwent optical enhanced endoscopic technique, and the specific contents were as follows: 30 ml of 1.0% water suspension of dimethicone oil powder was taken orally 30 min before endoscopy, and dactronin hydrochloride gum slurry was given orally for pharyngeal anesthesia 10 min before examination [13]. The observation group was treated with general anesthesia, and then, the morphology, surface microstructure, boundary, and microvascular conditions of the lesions were observed. First, the depth and scope of the lesion were determined by the professional doctor using the optical enhanced endoscope, and the mark was made at the place 5 mm away from the edge of the lesion. Then, submucosal injection was performed on the outside of the mark to make the lesion bulge and separate from the original muscle layer of the patient. The mucosa and submucosa of the lesion were cut along all the mark points. Finally, the tissue at the lesion site was removed and the bleeding and perforation were treated. All endoscopic operations were completed independently by the same professional physician in our hospital.

**2.2.2. Pathological Diagnosis.** After the observation of the two groups, a part of the tissue was taken for biopsy, and the pathological biopsy tissue was placed in 10% formalin solution for fixation, and the pathological tissue sections were stained with HE [14]; pathological diagnosis was made by 2 experienced physicians from the Department of Pathology in our hospital. The pathological diagnostic criteria are as follows [15]:

- (1) Normal: the cytoplasm of mature squamous epithelial cells is rich and clear, and scattered lymphocytes and compressed nuclei are occasionally seen
- (2) Spinous layer thickening: normal squamous epithelial cells, but thickness  $\geq 0.5$  mm
- (3) Inflammation: the papilla of lamina propria grows to the upper third of the epithelium, and the proliferation of basal cells is greater than 15% of the total epithelial thickness. The epithelium was infiltrated by neutrophils or eosinophils. Lamina propria is densely infiltrated by mononuclear inflammatory cells or neutrophils
- (4) Basal cell hyperplasia: normal epithelium with thickening of basal region and thickness greater than 15% of total epithelial thickness. No extension or other abnormalities of the lamina propria papillae

TABLE 1: General information of the two groups.

Groups	Control group	Observation group	<i>P</i>
Cases	94	94	
Gender			
Male	45	48	>0.05
Female	49	46	
Age (average)	46.17 ± 11.25	46.56 ± 11.23	>0.05
Clinical manifestation			
Belching	24	20	>0.05
Abdominal distension	16	20	
Acid reflux	28	26	
Gasteremphraxis	26	28	
Inspection			
Gastrosocopy	46	49	>0.05
Enterosocopy	48	45	

TABLE 2: Results of accuracy.

Groups	Cases	Confirmed	Unconfirmed	Accuracy (%)
Control group	94	72	22	76.60
Observation group	94	89	5	94.68
$\chi^2$				25.741
<i>P</i>				<0.05

- (5) Atypical hyperplasia of squamous epithelium: abnormal nuclear atypia or loss of normal cell polarity and mild atypical hyperplasia involving the lower 1/3 of the epithelium. Moderate atypical hyperplasia involving the upper, middle, and lower epithelial layers, but not involving or infiltrating the whole layer, is called severe atypical hyperplasia

2.3. *Observational Index.* We observe the accuracy of disease, the types and infiltration of cancer, and various surgical indexes of the two groups.

- (1) Accuracy: number of confirmed cases, number of unconfirmed cases, and accuracy
- (2) Types and infiltration of cancer: the types of cancer were early gastric cancer, early esophageal cancer, and early colorectal cancer. The infiltration was divided into infiltration and noninfiltration, and the infiltration rate was calculated
- (3) Surgical indexes: duration of operation, amount of blood loss, length of hospital stay, and treatment cost

2.4. *Statistical Method.* SPSS 18.0 statistical software was used for analysis. Measurement data was expressed as  $x \pm s$ . The *t*-test was used for comparison between groups, and the count data was expressed as rate. The  $\chi^2$  test was used

for comparison between groups, and  $P < 0.05$  was considered statistically significant.

### 3. Results

This section is the comparison results of the two groups. This section compares the two groups according to the three indicators (accuracy, types and infiltration of cancer, and surgical indexes) and obtains the comparison results.

3.1. *Results of Accuracy.* The accuracy of early detection of early carcinoma of the upper digestive tract in the observation group was 94.68% and that of the control group was 76.60%. Results of accuracy are shown in Table 2.

The observation group was diagnosed through the optical enhanced endoscopic technique, and the detection results of the observation group is shown in Figure 1.

The observation group was diagnosed by ordinary high-purity light endoscopy, and the detection results of control group is shown in Figure 2.

3.2. *Results of Types and Infiltration of Cancer.* In the observation group, 36 cases of early gastric cancer, 28 cases of early esophageal cancer, and 30 cases of early colorectal cancer were detected. In the control group, 25 cases of early gastric cancer, 19 cases of early esophageal cancer, and 28 cases of early colorectal cancer were detected. In the observation group, 26 cases of early carcinoma of upper digestive tract infiltration were detected and 68 cases were not detected, and the detection rate was 27.66%. Results of types and infiltration of cancer are shown in Table 3.

3.3. *Results of Surgical Indexes.* After different methods of treatment, no death occurred in all patients. Except for the operation time, the observation group was higher than the control group. Results of surgical indexes are shown in Table 4.

### 4. Discussion

Cancer of the upper digestive tract has become one of the most important cancers in China. The incidence rate and mortality of cancer of the upper digestive tract are among the highest in China. In 2008, the incidence rate of gastric cancer and esophageal cancer in the national cancer registration areas was 26.58/100000 and 16.24/100000, respectively [16]. Early cancer of the digestive tract can be divided into several types, including esophagus, colorectal, and stomach [17]. Early screening of upper digestive tract cancer and early treatment of upper digestive tract cancer to the early stage or before the occurrence of cancer are extremely effective measures to reduce the incidence of upper digestive tract cancer and control the progress of upper digestive tract cancer [18]. Early esophageal cancer refers to the esophageal cancer in which the invasion depth of the focal area of the patient has reached the mucosal layer, but there is no lymphatic metastasis [19]. Early colorectal cancer refers to the infiltration depth of the patient's focal area to the corresponding mucosal layer or submucosa. Gastric early cancer is also the depth of the lesion reached the corresponding

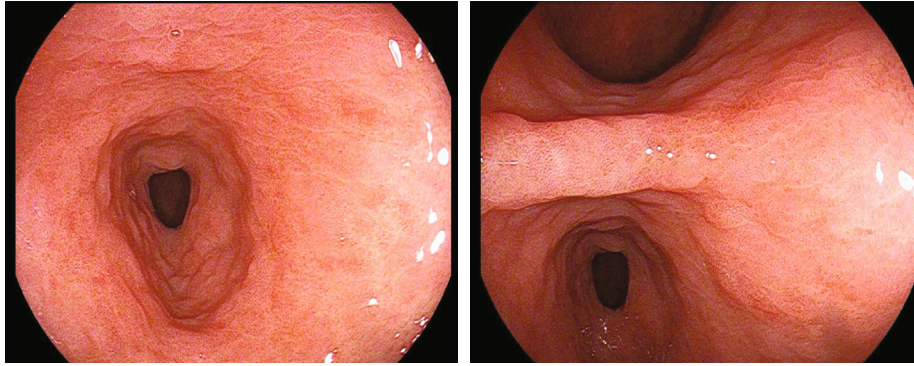


FIGURE 1: Detection results of the observation group.

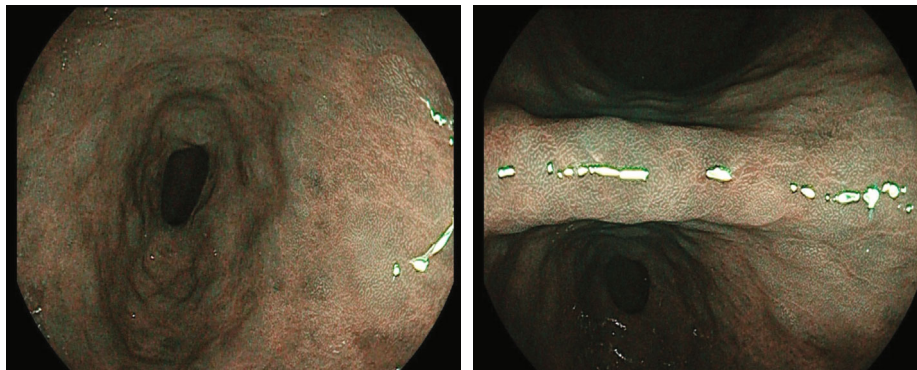


FIGURE 2: Detection results of the control group.

TABLE 3: Results of types and infiltration of cancer.

Groups	Cases	Types of cancer			Infiltration		Infiltration rate
		Early gastric cancer	Early esophageal cancer	Early colorectal cancer	Infiltration	Noninfiltration	
Control group	94	25	19	28	9	85	9.57%
Observation group	94	36	28	30	26	68	27.66%
$\chi^2$			5.624			4.816	
$P$			<0.05			<0.05	

TABLE 4: Results of surgical indexes.

Groups	Cases	Duration of surgery (min)	Amount of blood loss (ml)	Length of hospital stay (d)	Treatment cost (ten thousand yuan)
Control group	94	125.36 ± 13.25	125.22 ± 18.14	8.40 ± 2.36	2.15 ± 0.18
Observation group	94	80.15 ± 20.04	85.31 ± 12.30	4.18 ± 1.49	1.37 ± 0.11
$t$		8.038	14.325	18.142	55.634
$P$		<0.05	<0.05	<0.05	<0.05

mucosa or submucosa. Compared with white light endoscopy, the withdrawal time of optical enhanced endoscopy is similar, but under the influence of intestinal preparation, this is the advantage of optical enhanced endoscopy com-

pared with other electronic stained endoscopes [20, 21]. Among the above 3 types of cancer, only esophageal cancer was related to the presence or absence of lymphatic metastasis [22]. Under normal circumstances, early carcinoma of

upper digestive tract has no obvious clinical manifestations, and the external morphology of the lesions does not change significantly at the beginning of the disease. Patients often do not pay enough attention to it, which delays treatment time, and its diagnostic accuracy is also low in clinical practice. Upper digestive tract cancer screening enables more asymptomatic patients with upper digestive tract cancer to receive corresponding treatment as soon as possible, improves the current traditional cancer treatment mode, and advances the treatment of cancer before the deterioration of the disease, so as to improve the survival rate and quality of life of patients with upper digestive tract cancer [23, 24]. The optical enhanced endoscopic technique uses the concept of optical magnification to magnify it to 80~170 times, which is more direct than high-definition endoscopy [25]. Generally combined with electronic endoscopic staining and mucosal staining, the optical enhanced endoscopic technique can be used for close observation of the small vessels and structures on the mucosal surface of the digestive tract, and the lesions of the mucosa can be directly observed. This technique has a high sensitivity and recognition for intraepithelial neoplasia and gastric mucosal and intestinal metaplasia. Optical enhanced endoscopy has high diagnostic efficiency in real-time diagnosis and differentiation of pathological types of colorectal micropolyps and can reach the broad value of “discovery -retention” and “resection-discard” strategies of electronic staining endoscopy developed by ASGE for micropolyps [26]. The optical enhanced endoscopic technique uses the white light filter and filter calculation of the light source to obtain the narrow band spectrum, through the careful observation of the patient’s lesion fine structure and imaging [27, 28]. In addition, electronic endoscopic staining, amplification technology, and mucosal staining can be used to further determine the depth of infiltration of early esophageal cancer. Optical enhanced endoscopy has good interobserver consistency both with and without magnification [29].

The results of this study found that the accuracy of early detection of early carcinoma of the upper digestive tract in the observation group was 94.68% and that in the control group was 76.60%. 36 cases of early gastric cancer, 28 cases of early esophageal cancer, and 30 cases of early colorectal cancer were detected in the observation group. In the control group, 25 cases of early gastric cancer, 19 cases of early esophageal cancer, and 28 cases of early colorectal cancer were detected. In the observation group, 26 cases of early carcinoma of upper digestive tract infiltration were detected, and 68 cases were not detected, and the detection rate was 27.66%. After different methods of treatment, no death occurred in all patients.

## 5. Conclusion

The optical enhanced endoscopic technique had an obvious effect in the diagnosis of patients with early cancer of the upper digestive tract; it was helpful to improve the clinical detection rate of early carcinoma of upper digestive tract and had certain diagnostic ability for the invasion depth of

early cancer of high upper gastrointestinal tract, which was conducive to the detection of clinical invasion lesions, and had high clinical promotion and application value. However, the technology of optical enhanced endoscopy has high technical requirements for medical technicians. The operation team should be equipped with experienced doctors to reduce the false detection rate. At the same time, the diagnosis of early digestive tract cancer under optical contrast-enhanced endoscopy must be strictly combined with pathological diagnosis to get the correct diagnosis results.

## Data Availability

The data used to support the findings of this study are included within the article.

## Conflicts of Interest

The authors declare that they have no conflicts of interest.

## Acknowledgments

This work is supported by the Key Project of Science and Technology of Henan, No. 2018020795.

## References

- [1] Y. Chen, Y. Li, Y. Yin, and D. Zhang, “Application of cytoendoscopy in early carcinoma of upper digestive tract[J],” *Chinese Journal of Digestive Endoscopy*, vol. 35, no. 10, pp. 773–776, 2018.
- [2] D. Gerry, V. A. Fritsch, and E. J. Lentsch, “Spindle cell carcinoma of the upper aerodigestive tract,” *Annals of Otolaryngology & Laryngology*, vol. 123, no. 8, pp. 576–583, 2014.
- [3] M. Camorlinga-Ponce, L. Flores-Luna, E. Lazcano-Ponce et al., “Age and severity of mucosal lesions influence the performance of serologic markers in Helicobacter pylori-associated gastroduodenal pathologies,” *Cancer Epidemiology, Biomarkers & Prevention*, vol. 17, no. 9, pp. 2498–2504, 2008.
- [4] M. Gholipour, F. Islami, G. Roshandel et al., “Esophageal cancer in Golestan Province, Iran: a review of genetic susceptibility and environmental risk factors,” *Middle East Journal of Digestive Diseases*, vol. 8, no. 4, pp. 249–266, 2016.
- [5] E. Nure, F. Frongillo, M. C. Lirosi et al., “Incidence of upper aerodigestive tract cancer after liver transplantation for alcoholic cirrhosis: a 10-year experience in an Italian center,” *Transplantation Proceedings*, vol. 45, no. 7, pp. 2733–2735, 2013.
- [6] P. A. Suarez, K. Adler-Storthz, M. A. Luna, A. K. el-Naggar, F. W. Abdul-Karim, and J. G. Batsakis, “Papillary squamous cell carcinomas of the upper aerodigestive tract: a clinicopathologic and molecular study,” *Head & Neck*, vol. 22, no. 4, pp. 360–368, 2000.
- [7] F. Liu and T. Zhang, “Analysis of the effect and operation time of digestive endoscopy in the clinical diagnosis and treatment of early upper gastrointestinal cancer,” *Chinese Community Physician*, vol. 37, no. 29, pp. 38–39, 2021.
- [8] X. Yang, Z. Huang, and X. Ding, “Preliminary application of optical enhanced endoscopy in the diagnosis of laryngeal precancerous lesions and laryngeal carcinoma,” *Chinese*

- Otorhinolaryngology Head and neck surgery*, vol. 28, no. 2, pp. 67–70, 2021.
- [9] X. Cheng, M. Li, and C. Li, “Application of magnifying optical enhanced endoscopy in diagnosis and treatment of colorectal polyps,” *Chinese Journal of experimental diagnostics*, vol. 23, no. 3, pp. 436–439, 2019.
- [10] F. E. Johnson, K. S. Virgo, M. F. Clemente, M. H. Johnson, and R. C. Paniello, “How tumor stage affects surgeons’ surveillance strategies after surgery for carcinoma of the upper aerodigestive tract,” *Cancer*, vol. 82, no. 10, pp. 1932–1937, 1998.
- [11] Y. Zhuo, H. Kang, J. Qian, J. Chou, and H. Liu, “Progress in the application of blue laser imaging in the diagnosis of early carcinoma of upper digestive tract,” *Gastroenterology*, vol. 22, no. 6, pp. 377–380, 2017.
- [12] J. Ren and M. Niu, “Clinical value of digestive endoscopy in the diagnosis and treatment of early gastrointestinal cancer,” *Journal of Applied Clinical Medicine*, vol. 23, no. 5, pp. 106–108, 2019.
- [13] C. Muir and L. Weiland, “Upper aerodigestive tract cancers,” *Cancer*, vol. 75, no. S1, 1 Supplement, pp. 147–153, 1995.
- [14] C. Arens and M. Kraft, “Optical detection of cancer and precancerous lesions of the upper aerodigestive tract: methods for assessment of vertical extensions,” *Proceedings of SPIE*, vol. 8805, no. 2, pp. 363–366, 2013.
- [15] G. Wang, C. C. Abnet, Q. Shen et al., “Histological precursors of oesophageal squamous cell carcinoma: results from a 13 year prospective follow up study in a high risk population,” *Gut*, vol. 54, no. 2, pp. 187–192, 2005.
- [16] M. Zhou, H. Wang, J. Zhu et al., “Cause-specific mortality for 240 causes in China during 1990–2013: a systematic subnational analysis for the Global Burden of Disease Study 2013,” *The Lancet*, vol. 387, no. 10015, pp. 251–272, 2016.
- [17] T. Huang, G. Sun, B. Yan, K. Meng, and J. Yang, “Observation on the effect of standardized training of white light gastroscopy to improve the diagnostic level of early carcinoma of upper digestive tract,” *People’s Military Surgeon*, vol. 702, no. 5, pp. 444–446, 2018.
- [18] Q. Gao and J. Y. Fang, “early esophageal cancer screening in China,” *Best Practice & Research. Clinical Gastroenterology*, vol. 29, no. 6, pp. 885–893, 2015.
- [19] I. Kjær, T. Lindsted, C. Fröhlich et al., “Cetuximab resistance in squamous carcinomas of the upper aerodigestive tract is driven by receptor tyrosine kinase plasticity: potential for mAb mixtures,” *Molecular Cancer Therapeutics*, vol. 15, no. 7, pp. 1614–1626, 2016.
- [20] Q. Tan and C. Tang, “Review of endoscopic diagnosis of early gastrointestinal cancer,” *Medical Journal of West China*, vol. 28, no. 7, pp. 889–893, 2016.
- [21] R. M. Byers, G. L. Clayman, D. McGill et al., “Selective neck dissections for squamous carcinoma of the upper aerodigestive tract: patterns of regional failure,” *Head & Neck*, vol. 21, no. 6, pp. 499–505, 1999.
- [22] D. Landry and C. M. Glastonbury, “Squamous cell carcinoma of the upper aerodigestive tract,” *Radiologic Clinics of North America*, vol. 53, no. 1, pp. 81–97, 2015.
- [23] L. W. Solomon, K. R. Magliocca, C. Cohen, and S. Müller, “Retrospective analysis of nuclear protein in testis (NUT) midline carcinoma in the upper aerodigestive tract and mediastinum,” *Oral Surgery, Oral Medicine, Oral Pathology, Oral Radiology*, vol. 119, no. 2, pp. 213–220, 2015.
- [24] S. Nair, S. Datta, S. Thiagarajan, S. Chakrabarti, D. Nair, and P. Chaturvedi, “Squamous cell carcinoma of the upper aerodigestive tract in exclusive smokers, chewers, and those with no habits,” *Indian Journal of Cancer*, vol. 53, no. 4, pp. 538–541, 2016.
- [25] H. Zeng and Z. Zhang, “Diagnostic value of magnifying endoscopy combined with narrowband imaging in early carcinoma and precancerous lesions of upper digestive tract,” *Chinese Journal of Clinical Research*, vol. 29, no. 4, pp. 452–455, 2016.
- [26] Y. Yang, L. Wen, and R. Xu, “Clinical value of digestive endoscopy in the diagnosis and treatment of early carcinoma of upper digestive tract,” *Modern Digestion & Intervention*, vol. 22, no. 5, pp. 639–641, 2017.
- [27] P. Monnappa, G. Monnappa, and H. M. Kolakkadan, “Clinicopathologic profile of squamous cell carcinomas in resected specimens of upper aerodigestive tract: a retrospective study of 72 cases,” *IP Journal of Diagnostic Pathology and Oncology*, vol. 3, no. 4, pp. 263–267, 2020.
- [28] Y. Ji, “Study on the detection technology of optical properties of medical electronic endoscope,” *Automation & Instrumentation*, no. 5, pp. 224–226, 2017.
- [29] J. C. Fleming, Y. Al-Radhi, A. Kurian, and D. B. Mitchell, “Comparative study of flexible nasoendoscopic and rigid endoscopic examination for patients with upper aerodigestive tract symptoms,” *The Journal of Laryngology & Otology*, vol. 127, no. 10, pp. 1012–1016, 2013.



## Research Article

# Teaching Analysis for Visual Communication Design with the Perspective of Digital Technology

**Qian Sun**  and **Yingjie Zhu**

*Tangshan Normal University, Tangshan 063000, China*

Correspondence should be addressed to Qian Sun; [sunqian@tstc.edu.cn](mailto:sunqian@tstc.edu.cn)

Received 27 April 2022; Revised 24 May 2022; Accepted 27 May 2022; Published 19 July 2022

Academic Editor: Naeem Jan

Copyright © 2022 Qian Sun and Yingjie Zhu. This is an open access article distributed under the Creative Commons Attribution License, which permits unrestricted use, distribution, and reproduction in any medium, provided the original work is properly cited.

The turn of contemporary visual culture has led to the expansion of the connotation and scope of visual communication design (VCD) education, the generation of new artistic concepts and forms, and the great changes in the subject education system. VCD instruction now has an enhanced teaching environment and operational platform because of the rapid advancement of digital technology. Digital technology is expected to break through traditional learning methods in the future and will be more widely integrated into VCD courses. A topic that must be addressed and explored in the reform and growth of VCD education is how to build a fairer and more inclusive college art education subject system. Therefore, it is particularly important to design a complete VCD teaching evaluation system. In this paper, artificial intelligence technology is applied to the teaching quality evaluation (TQE) system, and a scientific and reliable TQE model is obtained. The main works of this paper are as follows: (1) analyze the background and significance of TQE research, and systematically expound the domestic and foreign research status of TQE, genetic algorithm, and neural network. (2) Using an adaptive mutation evolutionary method, this research builds a TQE system for the VCD course and produces a BPNN model. The adaptive mutation genetic algorithm's convergence speed is considerably faster than the regular genetic algorithms, the optimized neural network's performance is also superior, and the model has a faster convergence time and better prediction accuracy.

## 1. Introduction

With the continuous development of human science and culture, the fields involved in various disciplines continue to expand, and no discipline can exist and develop alone [1]. Influenced by today's diversified social forms, there is a closer connection between the design profession and social needs, especially the market economy society has brought new challenges to us when the VCD education has become diversified [2]. Today's society has entered the era of visual culture, which announces the decline of the centrality of language and print culture, and more importantly, a fundamental change in the way the public grasps the world: change from relying on personal experience and language to relying on vision, images, etc. When people communicate more visually, text-based models may not be able to adequately account for visual experience or visual literacy. Therefore, in the era of visual culture, the course teaching of VCD has

more important meaning. We can no longer understand design as a narrow concept, and VCD has gradually surpassed its original scope and moved to a wider and wider field [3]. Diversified visual concepts also imply that new VCD will break the boundaries of traditional design categories and make art design a carrier that can integrate multiple disciplines. Emerging digital technology has ushered in historic shifts in design production and manner. Designers can use digital technology to freely manipulate varied visual data and even generate characters that are not there in the computer, allowing them to change flat objects in their hands into three-dimensional shapes. And perform actions in the three-dimensional interface to make the design more lifelike [4, 5].

The digital revolution has revolutionized VCD from editing, typography, graphic processing, and illustration creation. Digital technology has revolutionized education with its advantages of rapidity, multidimensionality, and

convenient storage, broadening the scope of school education and the way students receive knowledge. Students majoring in VCD need to acquire a large number of advanced design concepts and popular ideas in the process of learning. In the past, students could only go to the library or bookstore to buy printed materials. When these materials are obtained, they may not be the latest information. Now, students themselves can access information from schools around the world by searching the database or through the Internet. The teaching environment has also undergone unprecedented changes. Students and teachers can establish a simulated teaching environment through digital technology, so that students in different regions can see the teaching content through the interaction provided in the simulated environment, so that in a short time gain knowledge. Information technology has changed the process and relationship of the interaction of system elements. High and new technologies have also brought about major changes in the responsibilities of teachers. It will no longer be based on dissemination of knowledge, but will focus on cultivating students to master the methods of information processing and the ability to analyze and solve problems [6–8]. Therefore, it has also become a necessary topic in this field to conduct a reasonable TQE in the teaching of VCD. In this context, this paper designs a teaching evaluation index system that conforms to the characteristics of the VCD course and introduces AI technology into teaching. TQE in the field of teaching, promoting the change of teaching evaluation methods and providing a basis for scientific and quantitative evaluation of VCD teaching quality, has great theoretical value and practical value.

The following is the paper's organisation paragraph: Section 2 discusses the associated work. The suggested work's approaches are examined in Section 3. The trials and results are discussed in Section 4. Finally, the research job is completed in Section 5.

## 2. Related Work

Vision and its applications are studied in VCD, which is also a major aspect of modern art design. The term "visual communication design" refers to a print art style that emerged in the middle of the nineteenth century in Europe and the United States as a continuation of the plane. During the World Design Conference in Tokyo, Japan in the 1960s, attendees discovered that vision and image had become autonomous techniques of communication in the media, and that they were becoming increasingly important. Graphic design, art design, stereoscopic picture design, and video design are all included in this scope. In today's fast-changing information society, the impact of various media is expanding, and the content of design performances can no longer include some new information communication channels [9]. These media are becoming increasingly important. As a result, VCD was born. As a design medium, the visual media of VCD expresses the time and the rich connotations of design in a way that conveys its message. A new area of design is being formed that is linked to and collaborative with other visual media as science and technology, as

well as the creation and use of product materials, continue to evolve. Visual communication is the use of vision as a medium to convey information, that is to say, as long as it is a design field associated with visual media, it should belong to the category of VCD [10]. In this sense, VCD is not only flat but also spatial and dynamic, which contains the trend of future design. Neither type of design can look at it from a graphic design perspective alone. VCD education moves from the classroom to the point-to-point learning between designers. As a new discipline, VCD has great particularity. Teaching and learning are not only done in a typical classroom setting; they are also done via the use of current educational tools, such as videoconferencing and online learning resources. The age of design necessitates that education in design follow suit [11]. Therefore, the TQE of VCD course is also extremely important. Many educators have spent a long time trying to figure out how to create and develop an objective and scientific TQE system. In this regard, countries such as the United Kingdom and the United States got a head start and built on their successes, advancing important ideas and approaches such as multiple intelligences theory, constructivism theory, and the Taylor evaluation model [12]. TQE has been classified into five stages since its inception in the second half of the nineteenth century, according to the features of each period: examination, test, description, reflection, and construction [13]. The initial teaching evaluation exists in the form of examinations, and the results are largely influenced by teachers' subjective judgments.

Since the birth of the concept of teaching evaluation, the development and needs of education have inspired many educators to continuously explore and improve and have also achieved some experience and results. For example, the book "Introduction to Psychological and Social Measurement" published by a famous American educator, the author expresses his thoughts and understanding of educational standardization and puts forward the relevant theoretical basis. This book marks the maturity of educational measurement [14]. Measurement methods such as "Bina-Simon Scale" and TCBE measurement compilation method were born and published one after another, which marked the further maturity of educational measurement [15]. Many scholars in the field of education have successively proposed various TQE models. Reference [16] uses the fuzzy algorithm to establish a quality evaluation system to improve the school's TQE. It can also conduct self-evaluation in stages according to the actual situation of students. Reference [17] used the analytic hierarchy process to quantitatively evaluate the teaching quality of colleges and universities and formed a corresponding evaluation system. Reference [18] constructed a set of teaching quality monitoring system based on the concept of "people-oriented, three-dimensional integration." "People-oriented" in the system mainly refers to teachers and students-oriented, while "three-dimensional" refers to schools, secondary colleges, teachers, etc. In order to improve the TQE, reference [19] uses the mathematical fuzzy analytic hierarchy process and adds a range of assessment methodologies. Reference [20] created a blended TQE model based on the implementation

process of the blended teaching paradigm. Useful outcomes have been obtained in practical applications. Because of the varying understanding and attention on teaching quality, there are some differences in the content and methods of assessment in various schools and institutions [21]. TQE approaches include expert evaluation, fuzzy comprehensive evaluation, neural network model method, and others, according to the available literature. These techniques have their unique evaluation characteristics [22]. Reference [23] uses BPNN and related theories to formulate the evaluation index system, constructs an effective computer graphics TQE model, and uses this model to evaluate the actual teaching situation of related courses. Reference [24] proposed an optimized BP algorithm, and the results after applying it to actual training show that the evaluation model established by this algorithm has fast convergence speed and high accuracy and has broad application prospects in teaching evaluation problems in higher education. Reference [25] combined AHP and neural network, combined the advantages of the two, added a screening process in the evaluation, and finally obtained the AHP-BPNN evaluation model. The PSO algorithm is combined with the neural network in reference [26], and the PSO algorithm is used to optimize the neural network and identify the globally optimal network parameters, resulting in a full TQE evaluation model.

### 3. Method

In this section, we define the principle of the BP neural network, adaptive mutation genetic algorithm steps, improved BP network model, and visual communication design teaching quality evaluation index system in detail.

**3.1. The Principle of BP Neural Network.** The forward transmission of information and the backward propagation of errors make up the BPNN. As soon as data is entered into the network, it begins to spread outward across the input layer of the network. To check whether this mistake fulfills the output result's criteria, the data is sent to the output layer after being processed and computed at each subsequent layer and propagated backwards through several layers of processing. If the fault is significant, it is sent back to the network, and the connection weight threshold between each unit is set at the same time. The neural network continues to propagate through these two phases once the output and conditions are met. Layers 1, 2, and 3 comprise the input, hidden, and output portions of a BPNN, as shown in Figure 1.

When using the BP method of learning, a forward propagation and a back propagation procedure are used in tandem. In a nutshell, the algorithm works like this:

- (1) The input vector is propagated in the reverse direction. To create the output vector, the input vector is first transported to the hidden layer through the input layer and then to the output layer. The weights of neural networks are not changed while they are sent. If the desired output is not met at the output layer, error back-propagation happens

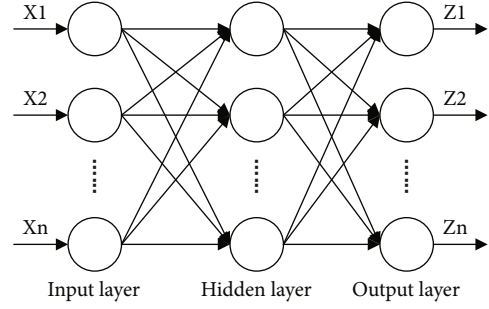


FIGURE 1: BP neural network structure diagram.

- (2) Error propagation is backwards. There are two layers of transmission: one between output and hidden layers, and one between hidden layers and input layers. During the error back-propagation stage, the neural network's weights are continually modified and rectified by the error feedback mechanism, and repeated iterations bring the network output to the intended output

The main idea of the BP learning algorithm is for  $q$  training samples,  $P_1, P_2, \dots, P_q$ , the corresponding output samples are  $T_1, T_2, \dots, T_q$ . The goal of learning is to correct the weights by making the error between the target vector  $T_1, T_2, \dots, T_q$  and the actual output  $A_1, A_2, \dots, A_q$ , so that the actual output  $A_i (i = 1, 2, \dots, q)$  approaches the expected value  $T_q$ , and the sum of squares of the network errors is minimized. The calculation steps of the BP algorithm are as follows.

- (1) Forward transmission of information; the output of the  $i$ th neuron in the hidden layer, as shown in the following formula

$$y_{h_i} = fh\left(wh_{ij}p_j + ah_i\right), i = 1, 2, \dots, m. \quad (1)$$

The output of the  $k$ th neuron in the output layer is shown in the following formula

$$y_{O_k} = fO\left(\sum_{i=1}^n wO_{ki}y_{h_i} + aO_k\right), k = 1, 2, \dots, n. \quad (2)$$

Define the error function, as shown in the following formula

$$E = \frac{1}{2} \sum_{k=1}^n \left(t_k - y_{O_k}\right)^2. \quad (3)$$

- (2) Use the gradient descent method to calculate the weight change and the back-propagation of the error. The weight change of the output layer is the

weight from the  $i$ th input to the  $k$ th output, as shown in the following formula

$$\Delta w_{O_{ki}} = -\mu \frac{\partial E}{\partial w_{O_{ki}}} = -\mu \frac{\partial E}{\partial y_{O_k}} \times \frac{\partial y_{O_k}}{\partial w_{O_{ki}}} = \mu \delta_{ki} y_{h_i}. \quad (4)$$

The hidden layer weight changes, for the weight from the  $j$ th input to the  $i$ th output, as shown in the following formula

$$\Delta w_{h_{ki}} = -\mu \frac{\partial E}{\partial w_{h_{ki}}} = -\mu \frac{\partial E}{\partial y_{O_k}} \times \frac{\partial y_{O_k}}{\partial w_{h_{ki}}} = \mu \delta_{ij} h_{ki}. \quad (5)$$

The weights and thresholds of each layer in the network should be changed, and the next training sample should be selected and fed into the input layer until all samples in the training set are learnt. If the result's error range falls within a certain range, the training may be repeated as many times as necessary to bring it into compliance. Training has been completed, so save the neural network for future use and stop.

### 3.2. Adaptive Mutation Genetic Algorithm Steps

- (1) Genetic algorithms do not directly look for possible answers in the process of addressing actual issues. It is instead encoded first, and encoding strategy has a significant impact on the genetic algorithm's ability to find the best global solution. Binary, sequence, real number, tree, out-of-order, and huge character set encoding are some of the most common genetic algorithm encoding techniques
- (2) There are a number of ways to determine the number of first solutions. For a global optimum solution to be discovered, a large beginning population is necessary. However, a larger starting population will need more fitness function computations, reducing the efficiency of the solution. As a result, there can be no extremes in terms of the size of the beginning population. Schaffer recommended a population size of between [20, 100]. A series of trials have shown that the least error, 0.2135, and the quickest convergence time occur when the starting population is 20. The starting population of 20 is used in this work
- (3) *Calculation of Fitness.* With an eye on improving fitness function, the genetic algorithm aims to find network weights and thresholds that minimize the network's total squared errors throughout all evolutionary generations. To that end, it adjusts network weights and thresholds in order to maximize fitness function. The learning error is shown in formula (6), and the fitness function is shown in formula (7).

$$E = \frac{\sum_{k=1}^n \sum_{j=1}^m (y_j^k - O_j^k)^2}{2}, \quad (6)$$

$$\text{Fit} = \frac{1}{E}, \quad (7)$$

where  $E$  is the learning error,  $n$  is the number of training samples,  $m$  is the number of output nodes, and  $y_j^k - O_j^k$  is the error of the  $k$ th sample relative to the  $j$ th output node.

- (4) *Genetic Operation.* Proportional selection, or replication, is the strategy used in this study. For each generation of people, the weight and threshold of the BP neural network are utilized to calculate the fitness value. Then, the entire fitness value is determined. An individual is more likely to be selected for further evaluation if their fitness values make up a larger proportion of their overall score. The formula for calculating the likelihood of selection is presented in the following equation below.

$$C(u_j) = \frac{f(u_j)}{\sum_{j=1}^P f(u_j)}, \quad (8)$$

where  $u_j$  represents an individual in the group,  $C(u_j)$  is the probability that  $u_j$  is selected,  $f(u_j)$  is the fitness value of individual  $u_j$ , and  $P$  is the population size.

In order to establish if a selected person may be passed down to future generations, it is required to compute the likelihood that the selected individual will be chosen. The calculation formula is shown in the following formula.

$$p(u_k) = \sum_{j=1}^k C(u_j), \quad (9)$$

where  $p(u_k)$  is the cumulative probability of individual  $u_k$ , then a new population of the next generation is obtained through genetic manipulation, the fitness value is judged, and the above steps are repeated until the population is stable.

It is the crossover operation in genetics that enables the creation of new people by exchanging a few genes. New gene structures are introduced more quickly in a population where the crossover probability is high, whereas the loss rate of previously discovered, highly effective gene structures are comparatively high in a population where the crossover probability is low. [0.6, 1.0] is the typical crossover probability range.

During the mutation process, some of the population's genes get mutated at a predefined pace. The adaptive mutation probability mutation operation is used in the model. There will be some undesirable shapes, but in general, the genetic algorithm's population will become more diverse as a result of the process of mutation, which retains some good mutations. As soon as possible, it leaves the local optimal situation, seeks for the optimal solution at the global level, and steers clear of any premature phenomena.

### 3.3. Improved BP Network Model

*3.3.1. AGA-BP Model.* The BPNN relies heavily on its starting weights and thresholds, which are provided at random.

Many researchers use new optimization strategies to enhance the neural network. Genomic algorithms, for example, are often used to enhance the neural network. As a result, the genetic algorithm may enhance the neural network based on gradient descent, which has a tendency to fall into a local minimum value and a sluggish convergence speed, by searching for the best solution in the whole space. The BPNN is improved using a genetic method that uses adaptive mutation. It is called the AGA-BPNN, and it has two parts: the BPNN and the AGA. The BPNN design process may be summarized as follows.

- (1) Multiple-layer feedforward neural networks only need two hidden layers for learning discontinuous functions. A hidden layer should be put up initially when creating a feedforward neural network with several layers. When the network's hidden layer nodes increase in number without improving performance, training expenses rise. As a consequence, this research attempts to use a hidden layer for the first time. This layer's number of nodes is governed by the input vector's size from the outside. A linear transfer function,  $f(x) = x$ , characterizes the input layer's transfer function in general. Trial and error is one method for determining the number of hidden layer nodes. It is possible to undertake experiments to determine the optimal number of hidden layers by increasing the number of hidden layers once a starting value has been determined. The number of hidden layer nodes may be calculated using the trial and error method employed in this study:

$$h = \sqrt{i + j} + b, \quad (10)$$

where  $h$  is the number of hidden layer nodes,  $i$  is the number of input layer nodes,  $j$  is the number of output layer nodes, and  $b$  is a constant between 1 and 10.

- (2) Obtain data samples and do data preprocessing to determine the number of samples. To a certain extent, greater numbers of experimental samples lead to more precise reactions, but at a certain point, the precision is fixed within a range and cannot be altered. As the network grows in size, the mapping connection becomes increasingly complicated. The entire number of network connection weights is often 5-10 times more than the total number of training samples
- (3) It is possible to choose the weights of the network in two different methods. As a first step, you may either choose a low beginning weight, or you can have both weights start at the same amount
- (4) Cycle training's weight loss is greatly influenced by the individual's pace of weight gain. Increasing the value will result in system instability, while decreasing it will result in an increased training time but a guaranteed error range

- (5) In order to terminate training, there are two options: one is to control over the error range, and the other is to achieve the maximum number of iterations possible. If one of the two prerequisites is met, the training can be halted. Typically, several networks are trained, and the best one is picked based on the research findings. The final AGA-BP algorithm model is shown in Figure 2

The AGA-BP algorithm model includes the flowchart of the BPNN and the adaptive mutation genetic algorithm. The optimal solution searched by the genetic algorithm is input into the BPNN as the initial weight and threshold of the network. Among them, the data flow of the model is as follows. AGA-BP algorithm model inputs begin with the BPNN portion. A neural network's topology, or the number of layers and neurons inside each layer, may be derived from the data acquired via the questionnaire. To find a solution that satisfies the stopping condition, that is, the optimal weight and threshold, the data information processing part begins with the genetic algorithm part of the adaptive mutation. Coding, fitness calculations, genetic operations, and other processes follow. It can lessen the time it takes to discover the best weights and thresholds to speed up network convergence. A better AGA-BP algorithm model is produced if the learning error of the sample or the number of iterations fulfills the conditions.

3.3.2. *EM-AGA-BP Model.* The entropy method, improved genetic algorithm, and neural network are combined to establish a TQE model, which is named EM-AGA-BP model. The adaptive mutation probability is adopted in the genetic operation process, which not only improves the speed of neural network convergence but also reduces the complexity of the training process. The model not only exerts the advantages of improved genetic algorithm global search and BPNN in nonlinear mapping but also reduces the influence of nonobjective factors. The main modeling steps of the TQE model are as follows:

- (1) By analyzing the existing problems of TQE, improving them, and establishing a more perfect and more suitable index system
- (2) TQE sample data should be gathered, and instructors' instructional qualities should be taken into consideration while selecting assessment indicators
- (3) BPNN parameters include learning rate, hidden layer number of neurons, maximum number of iterations, minimal error accuracy, transfer function, and training durations, and they need all be determined
- (4) Iterative training is performed until the algorithm is prompted to stop by using the evaluation model
- (5) Input the test samples for TQE to test whether the training effect of the EM-AGA-BP algorithm meets the requirements. If the prediction results meet the stopping requirements, go to the next step;

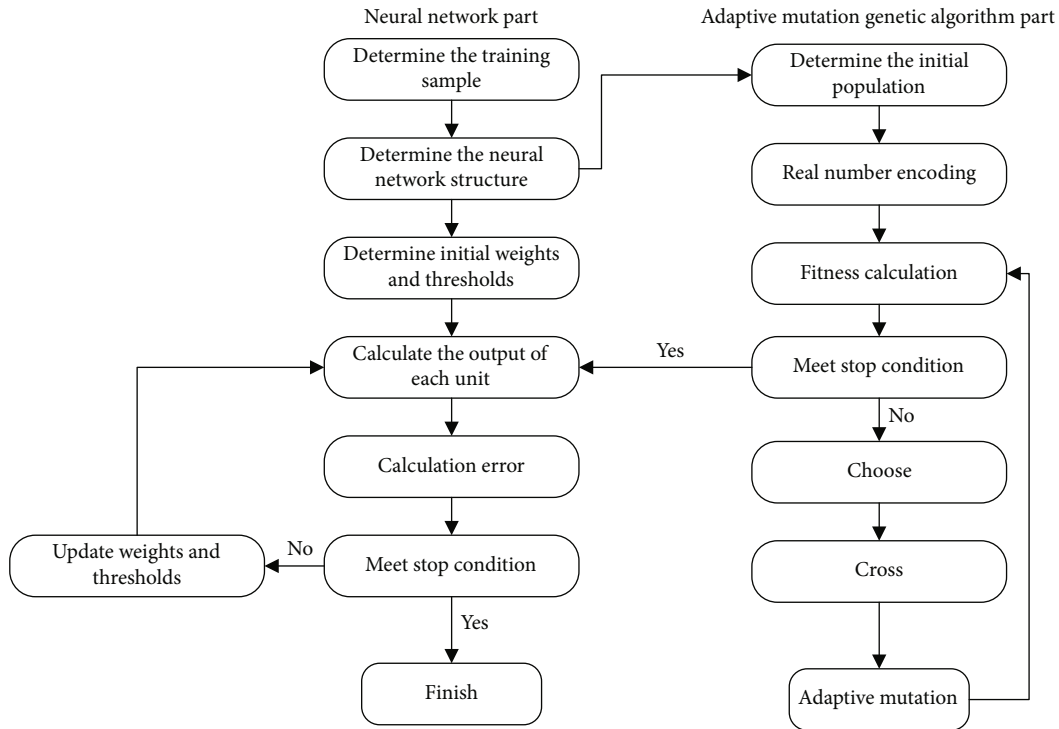


FIGURE 2: AGA-BP algorithm model.

otherwise, go back to the previous step and retrain the network, that is, go back to step (3).

- (6) Input the sample into the TQE model to get the TQE result

**3.4. Visual Communication Design Teaching Quality Evaluation Index System.** Different types of schools and courses have different characteristics and have different advantages and characteristics for the development of students. If the TQE system converges, it will make it difficult for the evaluation results to effectively and truly reflect on the essential level of teaching quality. All types of schools should strictly follow the standards and requirements for personnel training formulated by the national education policy and combine the actual situation of schools and courses to clarify their own school-running advantages and shortcomings and propose appropriate and reasonable scientific school-running goals and requirements. The consistency and similarity of the curriculum are transformed into the characteristics and differences of the curriculum. Schools need to update their own teaching models and methods in a timely manner according to the needs of the society. Individual growth, commonality, uniqueness, the common law of teaching, and the teaching characteristics of various types and degrees of school instructors should all be considered while building a TQE system. TQE standards are important at this time because they can assist prevent waste of educational resources and make efficient use of those that are available through a system that is diverse, reasonable, and unique. Survey results were used to identify and prioritize issues in current TQE systems and then used AI and other

nonlinear problem-solving methods to design a suitable TQE index system. It was determined that the previous TQE system was flawed, and a TQE model was developed based on an investigation into literature and the TQE index systems of other schools and institutions, which led to the improvement of the system. Table 1 illustrates the new TQE index scheme. Five levels of quality are assigned to the TQE findings as a consequence of the neural network's work: excellent, good, medium, and pass/fail.

## 4. Experiment and Analysis

In the experiment and analysis section, we discuss the data collection and preprocessing, determination of parameters, and testing the neural network model in depth.

**4.1. Data Collection and Preprocessing.** It is customary to conduct a questionnaire survey in order to gather data. An index system is developed, a questionnaire is created, and a return questionnaire is sent in this research, which incorporates relevant theory and practice of instructors' TQE. Multiple-choice and open-ended items are both included in the questionnaire we developed for this study. To take the TQE approach as an example, the first section of the course consists of multiple-choice questions. The TQE index system's five first-level indicators and sixteen second-level indicators are used to construct multiple-choice questions, with the most appropriate one chosen from various assessment levels for each index. It is required to provide numerical values to each choice after picking the most suited one, since this paper's questionnaire is quantitative in nature. The second section of the question is completely open-

TABLE 1: Visual communication design teaching quality evaluation index system.

First-level indicator	Secondary indicators	Label
Teacher quality	Educational goals are clear	X1
	Solid professional knowledge	X2
	Excellent teaching level	X3
Teaching attitude	Counseling patiently and actively	X4
	The teaching is conscientious and contagious	X5
	Rigorous attitude and excellence	X6
Teaching content	Concept theory is accurate and novel	X7
	Content-rich, attention-seeking exercise	X8
	Connect with reality and focus on skill training	X9
Teaching method	Expertise with depth and breadth	X10
	Good at inspiring, leading thinking	X11
	Variety of ways, appropriate citations	X12
Teaching effect	Teaching students according to their aptitude	X13
	Good basic knowledge	X14
	Improve self-learning ability and interest in learning	X15
	Improve comprehensive quality and innovation ability	X16

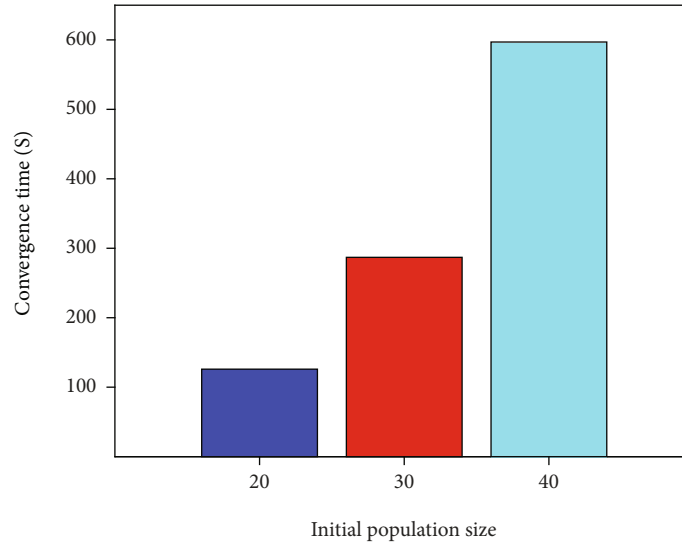


FIGURE 3: Comparison of convergence time for different population sizes.

ended. When it comes to calculating the overall questionnaire score, this section is not included. Students in a school's VCD program are the focus of a questionnaire survey. There were approximately 1,300 questionnaires distributed, 1,350 of which were retrieved, and 1,200 valid questionnaires were evaluated, totaling 1,200 pieces of valid data. [0, 100] was standardized to between [0, 1] according to the results of the aforementioned questionnaire. To maintain as much of the data's original meaning as possible, this study uses the maximum and minimum procedures, which are two of the most frequent normalizing techniques. The calculation of this method is shown in the following formula

$$X = \frac{S - S_{\min}}{S_{\max} - S_{\min}}, \quad (11)$$

where  $X$  is the normalized score, that is, the input value of the entropy method,  $S_{\min}$  is the minimum teaching quality score,  $S_{\max}$  is the maximum score, and  $S$  is the unprocessed score.

#### 4.2. Determination of Parameters

**4.2.1. Determination of Adaptive Genetic Algorithm Parameters.** The initial population size in this work is set at 20, 30, and 40 in accordance with the range of the initial population size, and experiments are carried out to acquire the population size training outcomes, in order to get a better initial population size, see it in Figures 3 and 4.

According to Figures 3 and 4, as can be observed, the convergence time is quickest, and the error is least when the starting population size is 20. Therefore, an initial population size of 20 is obtained. Set the crossover probability to

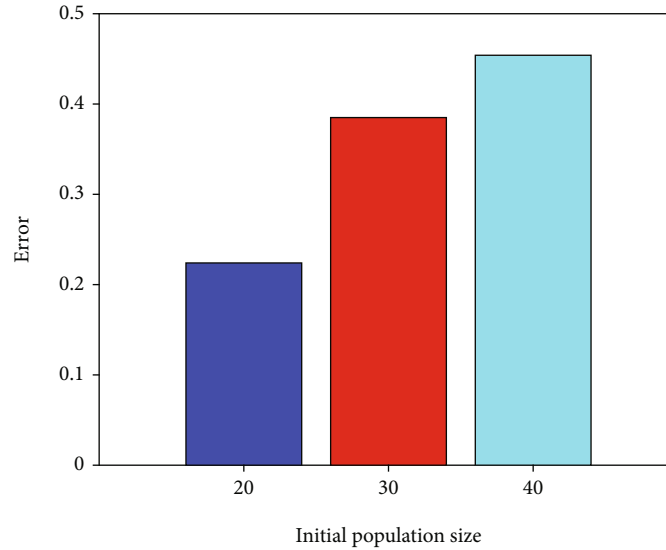


FIGURE 4: Comparison of error for different population sizes.

0.65. For the more complex solution space, the real number coding method can be used without decoding. It is thus necessary to utilize this coding strategy in order to code the possible solutions before applying BPNN weights and thresholds. The hidden layer threshold, the hidden layer weight, the hidden layer weight to the output layer, and the output layer threshold make up this system.

**4.2.2. Determination of BP Neural Network Parameters.** In practice, the most difficult tasks may be solved using a three-layer neural network. The number of layers may be raised in order to enhance the accuracy, but this will make the network more difficult. Increasing the number of neurons in the buried layer may help improve the mistake rate. From the perspective of structure realization, the method of adding hidden layer nodes is simpler than adding more hidden layers, and the training effect is easier to observe and adjust. In order to improve the network's accuracy and efficiency, this study employs the strategy of altering the number of hidden layer nodes. Using the TQE model of the study, the neural network is configured to have one hidden layer, a three-layer neural network.

The number of secondary indicators in the theoretical TQE system is 16; hence, the number of neurons in the input layer is determined to be 16. The number of neurons in the hidden layer may be determined using this method: multiple networks are created with 5 nodes in the hidden layer, and the number of nodes in each network's hidden layer is raised by 1 based on the empirical formula. Figure 5 shows the experimental outcomes. There are six hidden layers in the BPNN, and as can be seen, this yields the lowest error when there are six nodes buried under the surface. The number of neurons in the output layer is determined by the output target, which is the TQE result.

**4.3. Testing the Neural Network Model.** Since the indicators of the TQE system established in this paper are all positive indicators, the data translation step is omitted, and the entropy approach is used to calculate the weights of the

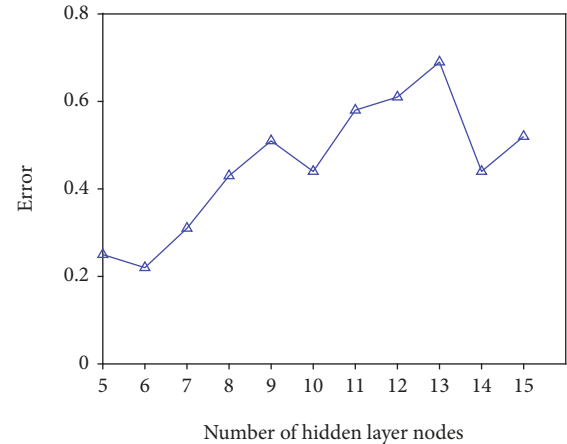


FIGURE 5: The number of hidden layer nodes and the corresponding error.

TQE indicators. The transfer function used in this paper's neural network output layer is an S-function, and its output is limited to (0 to 1), so the neural network output range is limited to (0 to 1) as a result (0,1). The range of the initial value of TQE determined by the entropy value method is (0,1), so data standardization is performed again. A total of 1200 groups of data were finally determined to participate in the experiment, of which 1000 groups were used for training the model so that the optimized BPNN structure could be obtained, and the remaining 200 groups of data were used for testing. The data of 16 secondary indicators as the input value of the network test, based on the entropy value technique, are contained in the 1-16 columns of each set of samples. The preliminary evaluation result is the output target of the network. After continuous learning, after obtaining an ideal model, input the score data of the TQE index of the 1001st~1200th group, and the neural network predicts and outputs the TQE results. Part of the experimental results is shown in Figure 6.



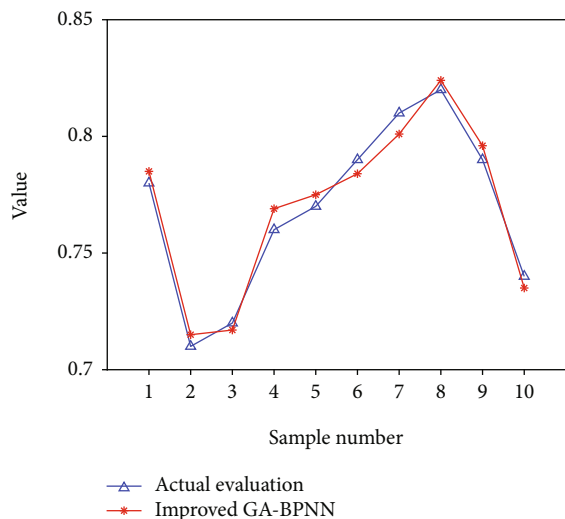


FIGURE 6: Experiment results of teaching quality evaluation model.

TABLE 2: Average evaluation accuracy of each network model.

Evaluation model	Prediction accuracy
BP neural network	85.37%
AGA-BP algorithm	90.76%
EM-AGA-BP algorithm	97.65%

The results of the final experiment are shown in Table 2. The BPNN model’s average evaluation accuracy for 200 sets of data is 85.37%, the AGA-BPNN model’s average evaluation accuracy is 90.76%, and the EM-AGA-BP algorithm’s average evaluation accuracy is 97.65%, an increase of 12.28% and 6.89%, respectively. It can be seen that the EM-AGA-BP algorithm has better evaluation results.

### 5. Conclusion

In the digital age, in order to achieve the expected purpose, the VCD course must improve the technological content and inject new connotations and characteristics of the times. The rapid development of digital technology provides an advanced teaching environment and operating platform for VCD teaching. Multimedia technology combines high integration, great interactivity, and a significant volume of data to give rich graphics, images, sounds, and text information. Multimedia technology is expected to fundamentally disrupt traditional learning methods in the future and become more widely integrated into VCD courses. Therefore, while inheriting the past cultural heritage and subject foundation, we must vigorously promote the integration of digital technology and curriculum reform, absorb high-tech achievements, improve teachers’ computer-aided teaching level, and extend the curriculum content to the level of intelligence and automation. As a result, developing a comprehensive VCD teaching assessment system is critical. In this study, AI is applied to the TQE system, resulting in a scientific and reliable TQE model. The main works of this paper are as

follows: (1) analyze the background and significance of TQE research, and systematically expound the domestic and foreign research status of TQE, genetic algorithm, and neural network. (2) According to the characteristics of the VCD course, this paper builds a TQE system for VCD that is more in line with the characteristics of the digital age. (3) The genetic algorithm and the BPNN model are combined to generate an adaptive mutation method that can be used to improve the initial threshold and weight of the BPNN model. The EM-AGA-BP algorithm is then created. An enhanced convergence time and better neural network performance have been shown by experimental data, which show that the EM-AGA-BP method outperforms classic genetic algorithms, and its convergence time and accuracy are better with the TQE model.

### Data Availability

The datasets used during the current study are available from the corresponding author on reasonable request.

### Conflicts of Interest

The authors declare that they have no conflicts of interest.

### Acknowledgments

This work was supported by Hebei Provincial Department of Education 2020-2021 Hebei Province Higher Education Teaching Reform Research and Practice Project (project number: 2020GJJG403) project name: Research on the “Four-dimensional entity” Talent Cultivation Innovation Model of Art Design Major under the New Culture Construction.

### References

- [1] C. Jones, “Interdisciplinary approach—advantages, disadvantages, and the future benefits of interdisciplinary studies,” *Essai*, vol. 7, no. 1, p. 26, 2010.
- [2] B. I. U. Dur, “Data visualization and infographics in visual communication design education at the age of information,” *Journal of arts and humanities*, vol. 3, no. 5, pp. 39–50, 2014.
- [3] J. P. H. Yeo, “An overview of research methods in visual communication design education,” *International Journal of Design Creativity and Innovation*, vol. 2, no. 1, pp. 51–62, 2014.
- [4] M. De Ree, G. Mantas, A. Radwan, S. Mumtaz, J. Rodriguez, and I. E. Otung, “Key management for beyond 5G mobile small cells: A survey,” *IEEE Access*, vol. 7, pp. 59200–59236, 2019.
- [5] M. Davis and J. Hunt, *Visual Communication Design: An Introduction to Design Concepts in Everyday Experience*, Bloomsbury Publishing, 2017.
- [6] C. M. Yang and T. F. Hsu, “New perspective on visual communication design education: an empirical study of applying narrative theory to graphic design courses,” *International Journal of Higher Education*, vol. 6, no. 2, pp. 188–198, 2017.
- [7] F. Adiloglu, “Visual communication: design studio education through working the process,” *Procedia-Social and Behavioral Sciences*, vol. 28, pp. 982–991, 2011.

- [8] B. Saris, "A review of engagement with creativity and creative design processes for visual communication design (VCD) learning in China," *International Journal of Art & Design Education*, vol. 39, no. 2, pp. 306–318, 2020.
- [9] P. Duan, Y. Jia, L. Liang, J. Rodriguez, K. M. S. Huq, and G. Li, "Space-reserved cooperative caching in 5G heterogeneous networks for industrial IoT," *IEEE Transactions on Industrial Informatics*, vol. 14, no. 6, pp. 2715–2724, 2018.
- [10] D. George, "From analysis to design: visual communication in the teaching of writing," *College Composition and Communication*, vol. 54, no. 1, pp. 11–39, 2002.
- [11] G. Christopher, "Gender, masculinities and life long learning," *International Journal of Lifelong Education*, vol. 32, no. 2, pp. 273–275, 2013.
- [12] W. X. Jiang and Y. Z. Zhong, "Research of teaching evaluation model based on ID3 decision making tree for polytechnic," *Journal of Applied Science and Engineering Innovation*, vol. 4, no. 3, pp. 95–98, 2017.
- [13] E. Lejonberg, E. Elstad, and K. A. Christophersen, "Teaching evaluation: antecedents of teachers' perceived usefulness of follow-up sessions and perceived stress related to the evaluation process," *Teachers and Teaching*, vol. 24, no. 3, pp. 281–296, 2018.
- [14] P. Spooren, D. Mortelmans, and J. Denekens, "Student evaluation of teaching quality in higher education: development of an instrument based on 10 Likert-scales," *Assessment & Evaluation in Higher Education*, vol. 32, no. 6, pp. 667–679, 2007.
- [15] X. H. Liu and C. Li, "Study on the measurement method of the content validity degree of papers based on the factor analysis," *International Journal of Social Scie-Nces in Universities*, vol. 2, no. 1, 2019.
- [16] Z. Xu, "Teaching practice of environmental art design specialty based on fuzzy algorithm," *Journal of Intelligent & Fuzzy Systems*, vol. Preprint, pp. 1–10, 2021.
- [17] J. F. Chen, H. N. Hsieh, and Q. H. Do, "Evaluating teaching performance based on fuzzy AHP and comprehensive evaluation approach," *Applied Soft Computing*, vol. 28, pp. 100–108, 2015.
- [18] M. H. Qin, H. X. Li, X. D. Zhang, and K. W. Cha, "Practitioner research," *Educational Research*, vol. 11, no. 1, pp. 83–87, 2007.
- [19] Q. W. Dong, S. M. Wang, F. J. Han, and R. D. Zhang, "Innovative research and practice of teachers' teaching quality evaluation under the guidance of 'innovation and entrepreneurship'," *Procedia Computer Science*, vol. 154, pp. 770–776, 2019.
- [20] Y. Gao, "Blended teaching strategies for art design major courses in colleges," *International Journal of Emerging Technologies in Learning (ijET)*, vol. 15, no. 24, pp. 145–158, 2020.
- [21] G. He, "Blended teaching mode of art course based on objective achievement scale," *International Journal of Emerging Technologies in Learning (ijET)*, vol. 15, no. 13, pp. 289–302, 2020.
- [22] K. Smimou and D. W. Dahl, "On the relationship between students' perceptions of teaching quality, methods of assessment, and satisfaction," *Journal of Education for Business*, vol. 87, no. 1, pp. 22–35, 2012.
- [23] L. Jiang and X. Wang, "Optimization of online teaching quality evaluation model based on hierarchical PSO-BP neural network," *Complexity*, vol. 2020, Article ID 6647683, 12 pages, 2020.
- [24] J. Cheng and Y. Xiong, "The quality evaluation of classroom teaching based on FOA-GRNN," *Procedia Computer Science*, vol. 107, pp. 355–360, 2017.
- [25] J. Li, Z. Zhou, J. Wu et al., "Decentralized on-demand energy supply for blockchain in internet of things: a microgrids approach," *IEEE transactions on computational social systems*, vol. 6, no. 6, pp. 1395–1406, 2019.
- [26] W. Duan, J. Gu, M. Wen, G. Zhang, Y. Ji, and S. Mumtaz, "Emerging technologies for 5G-IoV networks: applications, trends and opportunities," *IEEE Network*, vol. 34, no. 5, pp. 283–289, 2020.

## Research Article

# Network Security Problems and Countermeasures of Hospital Information System after Going to the Cloud

Shuming Gao 

Information Department, Pingdu People's Hospital, No. 112, Yangzhou Road, Pingdu, Shandong 266700, China

Correspondence should be addressed to Shuming Gao; gaoshuming@qust.edu.cn

Received 31 May 2022; Revised 22 June 2022; Accepted 25 June 2022; Published 18 July 2022

Academic Editor: Naeem Jan

Copyright © 2022 Shuming Gao. This is an open access article distributed under the Creative Commons Attribution License, which permits unrestricted use, distribution, and reproduction in any medium, provided the original work is properly cited.

In the current social context, information technology, network technology, and cloud computing have been widely used in all walks of life. The analysis of the specific application results of progressive technology shows that the use of technology has changed the working state of various industries and improved the work efficiency and quality of the industry. It should be noted that although the application of some technologies will bring many positive belongings, the potential risks brought by them cannot be ignored. As far as the hospital is concerned, the information system using cloud computing technology can make better use of the hospital's information data, but after the information system is on the cloud, new problems will appear in network security, resulting in the leakage of hospital patient information or research information. Based on this, in practice, it is necessary to analyze the network security problems after the hospital information system goes to the cloud and build and implement the corresponding strategies. The author analyzes and discusses the corresponding contents through work practice and combined with previous articles, in order to provide guidance and help for peers.

## 1. Introduction

Under the environment of the continuous development of network technology and the widespread use of mobile terminals, the application of network technology is becoming more and more common. According to the current data summary, the use of the Internet has changed the working state of all walks of life, solved many problems between information transmission and the connection of things, and achieved great changes in social life. It should be noted that the widespread use of the Internet brings not only the convenience of life and work but also some security issues, such as information leakage. Therefore, in the process of network application, it is of great significance to analyze and discuss related problems and emphasize the countermeasures to solve the problems [1–3]. Through the analysis of the current development of the hospital, the hospital information system stores, transmits, and utilizes a large amount of data, especially with the rise of Internet hospitals, and many hospitals begin to use cloud computing technol-

ogy. It greatly improves the patient's medical experience, but while the convenience of the hospital information system is brought by the cloud, new network security problems will also arise. Therefore, we analyze the network security problems after the hospital information system is connected to the cloud and provide countermeasures to solve the problem. The discussion has outstanding practical value.

## 2. Comparison of the Network Architecture before and after the Hospital Information System Goes to the Cloud

Comparing and analyzing the network structure of the hospital information system before and after going to the cloud have outstanding practical implication for a more specific analysis of the security network security difficulties after going to the cloud. The following is a comparative study of the information system of a tertiary hospital in China before and after the cloud.

*2.1. Original Network Architecture.* Figure 1 shows the original network architecture, and its basic operating mechanism is as follows:

- (1) The terminals in the hospital are divided into dissimilar VLANs, and the gateways are all on the core switch
- (2) Configure the NAT policy and port mapping of some terminals on the egress firewall. Only the external network segment and some servers that need to access the Internet can go to the Internet through the firewall
- (3) The egress firewall is also configured with an access control policy to block the traffic of known dangerous ports and restrict the server to only service ports that can pass through the firewall [4, 5]
- (4) Connect IPS intrusion prevention equipment in series between the egress firewall and the core switch to detect and block attacks
- (5) Configure ACL on the core switch to restrict the terminal in the hospital from accessing the management port of the network device and restrict the terminal from connecting to the service server through the remote desktop
- (6) Configure ACL on the server aggregation switch to restrict access to server file sharing ports
- (7) The server aggregation switch is connected to the IDS intrusion detection device to detect the interactive traffic between the server and the terminals in other areas and optimize and adjust the security policy of the equipment in each area according to the situation
- (8) Due to the limitations of the egress firewall NAT policy and port mapping, intranet terminals and most servers that are not within the scope of address translation and port mapping cannot interrelate with the Internet through the egress firewall

*2.2. Network Architecture after Going to the Cloud.* Figure 2 shows the cloud network architecture, and its operating mechanism is as follows:

- (1) The egress firewall has its own IPS function; so, the IPS device is removed
- (2) All office network segments in the hospital are configured with address translation. By configuring the access control policy, the original intranet terminal can only access the cloud server domain name through the DNS server equipped in the intranet, and the external network terminal can access the domain name except for the access control policy and blacklist. Other internet addresses and ports outside the restrictions

(3) The intranet DNS server only configures the mapping relationship between cloud service IP addresses and domain names [6]

(4) The security configuration rules of core switches and server aggregation switches are the same as before

*2.3. Comparative Analysis of Architecture.* Comparing the original structure and the cloud structure, there are the following differences:

- (1) After the cloud service is opened, the network architecture remains basically unchanged. The external network terminals, servers that need to access the Internet, and servers that need to be mapped to the outside still maintain the original security control policy, which is consistent with the experience before the cloud service goes online
- (2) Intranet terminals, DNS servers, and servers that were originally unable to access the Internet, after the cloud service goes online, set up address translation on the egress firewall, cooperate with the access control security policy, black, and white list functions, and can only access the necessary cloud server addresses and business port
- (3) The egress firewall has the IPS function, which is used to block external network attacks against the internal network, and the original IPS equipment is removed from the shelf
- (4) The security policy and blacklist configured on the egress firewall control the traffic interaction of dangerous ports between all internal terminals and external terminals
- (5) The egress firewall is changed from the original one to two, and the reliability of the egress device is enhanced through the hot backup function
- (6) The core switch and server aggregation switch keep the original port access control policy unchanged, still restrict the terminal's management of network devices, and limit the connection of remote desktop ports and file sharing ports
- (7) The security policy on the cloud server side is the responsibility of the relevant cloud operator, but its security information must be carefully checked

The paper arrangements are as follows: Section 2 discusses the network security problems and solutions after the hospital information system is migrated to the cloud. Section 3 analyzes the change the concept and pay attention to network security issues. Section 4 evaluates the building a network security system based on the actual needs of network security. Section 5 examines the emphasis on network security management. Section 6 concludes the article.

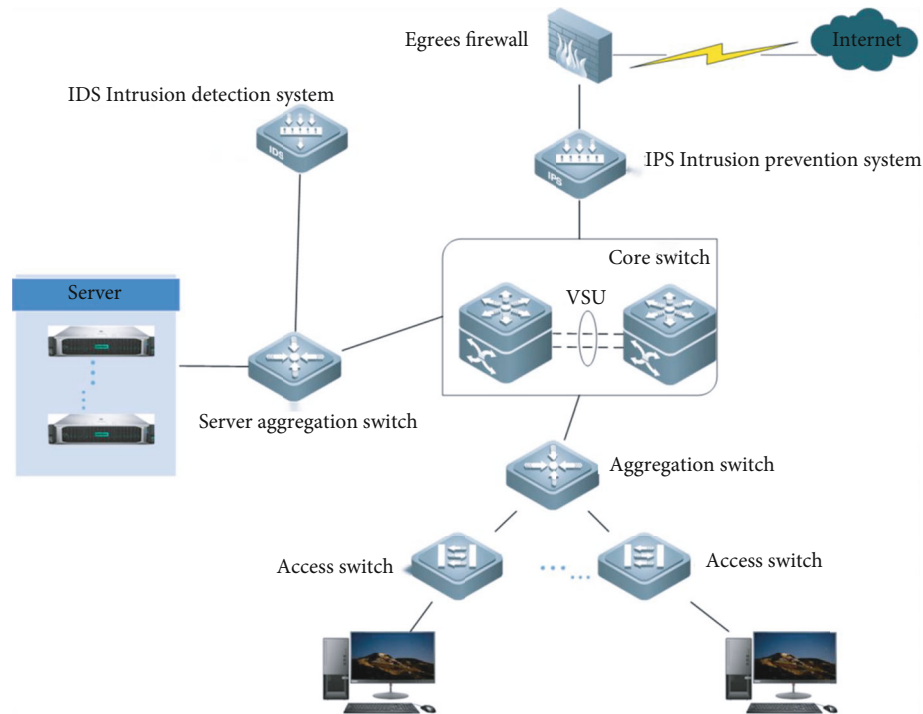


FIGURE 1: Original network architecture.

### 3. Network Security Problems and Solutions after the Hospital Information System Is Migrated to the Cloud

The main security problems after the hospital information system is migrated to the cloud are reflected in two aspects:

- (1) Information data leakage [7, 8]: the first problem after the hospital information system goes to the cloud is the leakage of information data. All hospital information is transmitted on the Internet. As far as hospital information and data are concerned, on the one hand, there is a large amount of patient information in the hospital. Once the data is leaked, it will lead to the disclosure of patient privacy, which is not good for the patient itself, and will also cause the patient to feel uncomfortable. The crisis of trust in the hospital is very unfavorable for alleviating the contradiction between doctors and patients. On the other hand, there is a large amount of disease research data in hospitals. If these data related to disease research are used properly, they will benefit society. If they are stolen by criminals or hostile elements, it is likely to cause social disasters and even endanger national security. So, the impact of a hospital research data breach is huge
- (2) Information data is lost or damaged [9, 10]: a large amount of information and data of a hospital has its value; so, the data of a hospital is one of the rare assets of a hospital. If the database resources are lost or the data resources are damaged and cannot be

recovered due to network problems, the related work of the hospital will be greatly affected, which is not conducive to the stable and sustainable development of the hospital's scientific research work and other work. Analyze and solve such problems. Faced with the security problems that exist after the hospital information system is migrated to the cloud, security protection measures should be deployed from the following aspects

### 4. Change the Concept and Pay Attention to Network Security Issues

Based on the analysis of practice, it can be seen that in the past hospital management practice, an important reason for the frequent occurrence of network security problems is that the hospital ignores the importance of network security in the process of using information systems; so, many work arrangements exist. There are omissions in cybersecurity [11–13]. Based on this, it is necessary to change cognition and pay attention to network security. As far as the current work practice is concerned, in order to change the perception of network security, the following work needs to be done:

- (1) Strengthen the discussion of network security issues and explain the practical value of network security. In the utilization practice of hospital information system, an significant reason why network security is neglected is that staff does not realize the value of network security. By making the staff aware of

Deployment architecture diagram

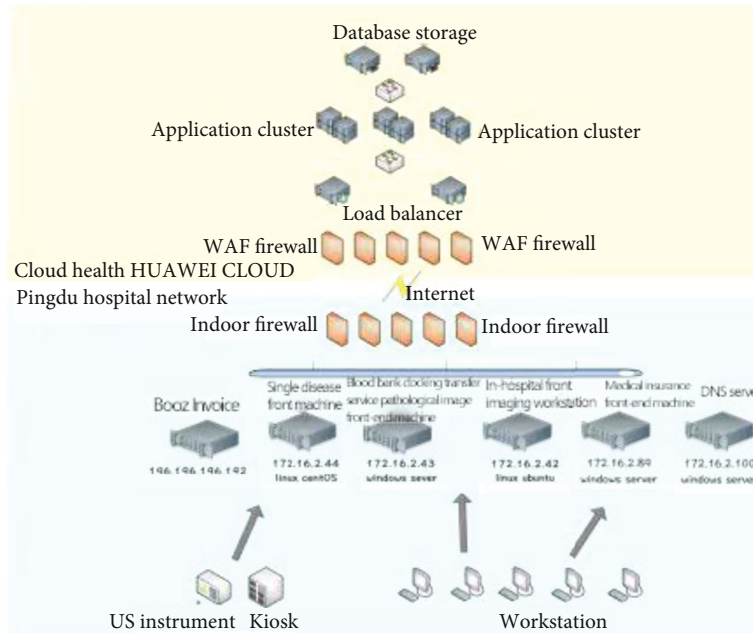


FIGURE 2: Cloud network architecture.

the value of network security through discussion, they will pay more attention to network security

- (2) Analyze the relevant elements of network security. In the practice of hospital network security, some staff is aware of the importance of network security, but they do not systematically recognize the influencing factors of network security; so, there is a one-sided phenomenon in the process of network security work organization and implementation. Based on this, in the organization and development of network security work, strengthen research and discussion and clarify the elements related to network security, so that the organization and development of network security work will be more targeted and effective. In short, through in-depth analysis to clarify the cognition of network security, this can provide theoretical guidance for the current hospital network security work

## 5. Building a Network Security System Based on the Actual Needs of Network Security

From the point of view of the network security after the hospital information system is migrated to the cloud, in order to truly prevent network security problems, it is necessary to formulate a security structure that has a protective effect on the hospital information system based on the current state of network security. As far as the construction of safety structure is concerned, the following contents need to be emphasized:

- (1) Basic investigation [14]: the so-called basic investigation mainly refers to the detailed investigation of the hospital information system. In the detailed investigation of the hospital information system, it is necessary to clarify the different data partitions of the information system, such as which databases exist in the information system and what is the specific application purpose of the database, which needs to be emphasized in the investigation. Because the application value of the database is obtained based on the investigation, it can provide a reference for the determination of the security level of the database within the information system
- (2) Determination of the security level of the information system [15]: under the guidance of basic survey data, the internal database of the information system and the use value of the data are analyzed, and the security level is evaluated. In this way, the security level evaluation result can provide a reference for the design and construction of the network security structure of the information system
- (3) Construction of network security structure based on security evaluation level [16]: based on the evaluation results, it can be seen that different data security levels have different requirements. Therefore, in the construction of the security structure, the multilayer protection structure is used as the security protection structure of the core database. Important databases, general databases, etc. can build a three-layer protection structure, or it is a two-layer protective structure

to protect it safely. To put it simply, based on the actual needs of network security, a targeted network security protection structure is constructed, so that the security protection effect of the hospital information system will be significantly improved

## 6. Emphasis on Network Security Management

The so-called management improvement refers to the use of management measures to avoid or stop the occurrence of network security problems. In terms of management strengthening, the main measures are as follows:

- (1) System improvement [17]: the implementation of specific safety management work needs to be supported by a sound system, so that the effectiveness and pertinence of the work implementation will be more prominent. As far as the current management of hospital information systems is strengthened, on the one hand, it is necessary to formulate a comprehensive responsibility system and clarify the responsibility for network security management. In this way, the implementation of management work will be more prominent. On the other hand, it is to instrument the supervision system, that is, to supervise the specific implementation of network security management work to confirm the actual effect of the work, so that network security problems can be effectively solved
- (2) Technological innovation [18]: the so-called technological innovation mainly refers to the use of advanced technology to reform the current network security management in the practice of network security management, so that the specific implementation of network security management will show more significant effects
- (3) Introduce an early warning mechanism in the process of network security management, which is, set up an alarm system in the network security structure and trigger the warning system when information leakage or other security problems occur, so that managers can timely discover network security loopholes and problem and deal with it. In this way, the adverse effects of network security issues in hospital information systems will be effectively dealt with [19, 20]

## 7. Conclusion

To sum up, the management of the hospital information system has a significant impact on the specific development of hospital work; so, it is necessary to strengthen the management of the hospital information system in practice. Based on the analysis of the current hospital practice, it can be seen that the hospital information system will face more significant network security problems after going to the cloud. Therefore, the article analyzes the performance and causes of the network security problems after the hospi-

tal information system goes to the cloud. At the same time, it discusses the countermeasures; the purpose is to guide practice.

## Data Availability

The dataset used in this paper are available from the corresponding author upon request.

## Conflicts of Interest

The author declares no conflicts of interest regarding this work.

## Funding

This paper received funding 13806424570.

## Acknowledgments

Gao Shuming is an Information System Project Manager Undergraduate mainly engaged in hospital informatization construction and management.

## References

- [1] Z. Wang, C. Wang, L. Hengwu, and H. Guo, "Analysis and countermeasure research of network security in smart campus environment," *Network Security Technology and Application*, vol. 12, pp. 80-81, 2021.
- [2] S. Fankui, "Common problems and solutions in meteorological information network security," *Nanfang Agricultural Machinery*, vol. 52, no. 23, pp. 141-143, 2021.
- [3] C. Xiang, "Wireless network security issues and countermeasures in the construction of smart campuses," *Industry and Technology Forum*, vol. 21, no. 1, pp. 222-223, 2022.
- [4] Y. Bo, F. Jiangfeng, and Z. Jinghua, "Problems and solutions of computer network security protection," *Digital Communication World*, vol. 12, pp. 125-127, 2021.
- [5] Q. Wang, "Discussion on computer network information security and encryption technology," *Science and Technology Innovation and Application*, vol. 11, no. 33, pp. 90-92+96, 2021.
- [6] J. Liujia, "Analysis of online catering food safety supervision problems and countermeasures," *China Market Supervision Research*, vol. 11, pp. 44-47, 2021.
- [7] L. Caiwen, "Research on the problems and countermeasures faced by college students' network security," *Caizhi*, vol. 32, pp. 134-136, 2021.
- [8] T. Wang, "Analysis of network security problems and countermeasures of Internet of Things wireless technology," *Network Security and Informatization*, vol. 11, pp. 27-30, 2021.
- [9] Z. Jiren, "Analysis of network information security problems and countermeasures based on e-government system," *China Science and Technology Information*, vol. 22, pp. 109-110, 2021.
- [10] Z. Yuan, "Problems and countermeasures of computer communication network security in public institutions," *China New Communication*, vol. 23, no. 21, pp. 21-22, 2021.
- [11] W. Zhong, L. Guangming, S. Guo, L. Qun, and J. Xianghong, "Discussion on computer network security and preventive

- countermeasures in the era of big data,” *Computer Knowledge and Technology*, vol. 17, no. 30, pp. 68-69, 2021.
- [12] A. Hamza, H. GharakheiliH, and V. Sivaraman, “IoT network security: requirements, threats, and countermeasures,” <http://arXiv:2008.09339v1>.
- [13] X. Liang and G. Jifu, “Analysis of the main problems and countermeasures facing hospital network information security in the new era,” *China New Communications*, vol. 23, no. 19, pp. 141-142, 2021.
- [14] Y. Liu and M. Cui, *Analysis of Influencing Factors and Countermeasures of Computer Network Security[C]/International Conference on Application of Intelligent Systems in Multi-Modal Information Analytics*, Springer, Cham, 2021.
- [15] Q. Li and S. Tian, “Environmental and social problems and countermeasures in transportation system under resource constraints,” *Complexity*, vol. 2020, 11 pages, 2020.
- [16] Y. Zhao, D. Chen, and J. Fan, “Sustainable development problems and countermeasures:a case study of the Qinghai-Tibet Plateau(QTP),” *Geography and Sustainability*, vol. 1, no. 4, pp. 275–283, 2020.
- [17] L. Jingang, “On the current situation, problems and countermeasures of rural social endowment insurance in China,” *Campus English*, vol. 21, p. 256, 2020.
- [18] Q. Dong, Z. Sui, and W. Zhan, “Problems and countermeasures in natural language processing evaluation,” <http://arxiv.2104.09712.2021>.
- [19] F. Yang, J. Zhang, W. Zheng, M. Huang, L. Zhang, and B. Zhang, “New problems and countermeasures in the prevention and control of COVID-19,” *Emergency and Critical Care Medicine*, vol. 1, no. 1, pp. 12-13, 2021.
- [20] W. A. N. G. Xianggang, L. I. Yanfang, Z. A. N. G. Fengzhi et al., “Disinfection technology for *Auricularia auricula* in bag cultivation:problems and countermeasures,” *Asian Agricultural Research*, vol. 12, no. 4, pp. 44–46, 2021.



## Research Article

# Effect Analysis of Degranulated Cell in Early Fertilization on FET Outcome and Offspring Safety with Data Mining

Qingyang Li, Li Zhao, Liling Zhou, Rongju Liu, and Bo Chen 

Center for Reproductive Medicine, Songshan Lake Central Hospital of Dongguan, Dongguan 523326, China

Correspondence should be addressed to Bo Chen; 201811111121697@stu.hubu.edu.cn

Received 26 May 2022; Revised 20 June 2022; Accepted 24 June 2022; Published 18 July 2022

Academic Editor: Naeem Jan

Copyright © 2022 Qingyang Li et al. This is an open access article distributed under the Creative Commons Attribution License, which permits unrestricted use, distribution, and reproduction in any medium, provided the original work is properly cited.

In vitro fertilization and embryo transfer is one type of assisted reproductive technology, although the technology is now more mature. Many factors, however, will have an impact on oocyte fertilization, embryo growth, pregnancy outcome, and child safety due to the journey from clinical to the laboratory. The influence of degranulated cells early in fertilization on frozen embryo transfer (FET) results is investigated in this study. This article analyzes 255 patients who underwent in vitro fertilization (IVF) and FET transplantation at the author's central unit from January 1, 2015, to June 30, 2021. Among them, IVF-assisted conception is the early degranulation of homologous oocyte fertilization. Correlation analysis is performed by observing the embryonic outcome of the early degranulation group and the overnight fertilization group and the clinical outcome after FET. Through data mining analysis, the results show that the polyfertilization rate and OPN rate for the early degranulation group are significantly higher than the overnight fertilization group (9.87% vs. 8.24% and 3.14% vs. 1.69%). In terms of normal fertilization rate, there is no significant difference between D3 high-quality embryo rate and D5 high-quality blastocyst rate (64.07% vs. 65.15%, 27.5% vs. 26.5%, and 15.97% vs. 17.35%). There is no significant difference in the complete recovery rate of embryos after thawing (93.24% vs. 93.46%), and the implantation rate, clinical pregnancy rate, abortion rate, and live birth rate are not significantly different between the two groups after FET. The offspring outcomes of singletons do not differ significantly between the two groups; however, twins born early degranulate have much greater rates of ultralow birth weight and ultrapreterm children than twins born overnight fertilization (14.29% vs. 0). Therefore, it can be concluded that degranulation of cells early in fertilization is a desirable method to prevent fertilization disorders. However, under the premise of ensuring that no fertilization disorder occurs, it is not appropriate to degranulate all the oocytes of the patient at the early stage of fertilization.

## 1. Introduction

People's ideas are becoming more open, living habits, eating habits, social environment, etc., have undergone great changes, and the incidence of infertility has also increased year by year. According to the World Health Organization, there are about 10%-20% of infertile couples in the world, the infertility rate in the United States is 10%-15%, the infertility rate in Europe is 20%, and the infertility rate in China is 17% [1]. It can be seen that infertility has become a common problem in countries all over the world. Due to the postponement of the age of marriage and childbearing in recent years, the incidence of infertility is increasing. The topic of human reproductive health has gotten a lot of press around

the world. Assisted reproductive technology (ART) has given infertile couples fresh hope since the world's first healthy test-tube baby was born. Assisted reproductive technology has now evolved into a full-fledged reproductive medicine system [2, 3]. After more than 30 years of development, IVF technology has been continuously improved and perfected, and its indications have expanded from infertility caused by fallopian tube obstruction in women to infertility caused by various factors in men and women. In 2007, the world's first IVF is conceived naturally and delivered smoothly, and IVF technology is considered to be a safe and effective method of infertility treatment [4, 5].

Many human reproductive problems are solved by assisted reproductive technology, but it also adds many

nonphysiological operations. Interventions in the reproductive process during the most critical and vulnerable period of life formation, i.e., fertilization and early embryonic development, will more or less affect the development of gametes and embryos. And it may be stably transmitted during cell lysis and embryonic development, thereby affecting the health of offspring and even the next generation [6, 7]. ART obtains more high-quality oocytes through controlled superovulation. These techniques interfere with the proliferation, fertilization, development, and differentiation processes of germ cells and can have adverse effects on the embryo and even the mother. As a result, there is also growing concern about the safety of ART. Research has found the incidence of preterm birth, low birth weight, and congenital malformations in offspring during ART pregnancy is increased. However, most scholars believe that this is related to the increased multiple pregnancy rate of ART and its own factors such as parents' age, body size, mental health, and disease, rather than the ART technology itself. Most studies have concluded that ART is safe, and ART offspring do not have an increased risk of adverse health compared with offspring born to natural pregnancies [8]. However, a growing number of studies have indicated that even when multiple births are ruled out, the poor health risk of singleton births in ART kids is still elevated. During routine in vitro fertilization operations, there are many factors that affect oocyte fertilization, embryonic developmental potential, and high-quality embryo rate. The ovulation induction program, semen optimization, sperm feeding time, sperm-oocyte cocubation time, culture environment, embryo exposure time in vitro, and degeneration timing all directly affect the outcome of IVF treatment [9].

Degeneration of cells during the early stages of fertilization is a typical treatment for preventing fertilization problems. The degenerated cells determine if the second polar body is expelled after 4-6 hours of fertilization and make a prompt decision on the fertilization condition. If fertilization fails, prompt intervention can result in clinical outcomes that are similar to those seen with standard ICSI [10]. However, the effect of degenerated cells in the early stage of fertilization on embryo quality and pregnancy outcome is still controversial, and the current studies mostly focus on freshly transplanted patients with cleavage-stage embryos.

The paper's organization paragraph is as follows: The related work is presented in Section 2. Section 3 analyzes the methods of the proposed work. Section 4 discusses the experiments and results. Section 5 consists of the discussion section. Finally, in Section 6, the research work is concluded.

## 2. Related Work

Literature [11] found that when immature oocytes and granulosa cells are cocultured, compared with the control group without granulosa cells, the former had a higher maturation rate, indicating that granulosa cells play a significant role in maturation for oocytes. Literature [12] proposed that granulosa cells are important in nutrition and information transmission to oocytes through many gap junctions and desmosomes, and oocytes also play a role in regulating the

differentiation and development of granulosa cells. Literature [13] proposed that in the process of oocyte development, the maturation of the nucleus and the maturation of the cytoplasm are not simultaneous. Nucleus maturation may precede cytoplasmic maturation in vitro, and nucleocytoplasmic maturation influences and promotes each other. The maturation process of the cytoplasm involves a series of complex physiological and biochemical changes, including gap junctions, migration and changes of cortical granules, mitochondrial rearrangement, and changes in the endoplasmic reticulum and Golgi apparatus. The comaturity of the two ensures that normal fertilization takes place. Literature [14] found that a better MII oocyte rate and fertilization rate can be obtained by controlling the degeneration time and the oocyte retrieval time to be more than 2.5 h. While the length of degeneration time did not affect embryo quality and pregnancy rate, the prolongation of preculture time may be related to the improvement of nuclear maturation. In the literature [15], it is believed that the degeneration time is more than 3 h, which is beneficial to improving fertilization rate and excellent embryo rate. They all found that too short incubation time is not conducive to oocyte maturation, thereby affecting the outcome of ICSI. The maturation of the oocyte nucleus and cytoplasm is asynchronous, and preculture before degeneration may aid in the maturation of the cytoplasm of MII oocytes. Reference [16] conducted a comparative study on the degeneration group 2-4 h after oocyte retrieval and the degeneration group immediately after oocyte retrieval. It is found that the former had a higher MII oocyte rate, fertilization rate, cleavage rate, and superior embryo rate. The MI oocyte rate and empty zona pellucida rate of the latter are significantly higher than those of the former, which confirmed the role of granulosa cells in promoting oocyte maturation in the preculture stage. Literature [17] studied the effect of degeneration time on the outcome of ICSI treatment. The results showed fertilization rate reached the highest when the time from oocyte retrieval to degeneration is about 3 hours. The oocyte retrieval to degeneration time is approximately 2 hours, and the implantation rate is at its maximum. Degeneration should be finished 2-3 hours after oocyte retrieval, based on fertilization and implantation rates. Their study also showed no correlation between degeneration time and MII oocyte maturity. This indicates that the period from oocyte retrieval to degeneration has no effect on nuclear maturation and does not affect meiosis. However, it may promote the maturation of the cytoplasm, thereby increasing the fertilization rate. This may be related to the secretion of certain factors, adhesion molecules, and other substances that promote oocyte maturation from granulosa cells. In ICSI, early degeneration may result in early interruption of granulosa cell-oocyte contact. Even when the nucleus is mature at this time, the maturation of the cytoplasm may be affected, various organelles function poorly, and the activation or inactivation of signaling molecules is limited. This affects subsequent meiotic resumption, prokaryotic fusion, and embryonic development.

Literature [18] found that the imperfect cortical response and zona pellucida response of immature oocytes may lead

to polyspermia. Literature [19] believes that the preincubation time of 1 h-3 h does not affect the outcome of ICSI. Degranulation time above 9 h may affect embryo quality due to oocyte aging, oxidative stress, and disturbance of Ca pump function. Literature [20] believed that the time from oocyte retrieval to degranulation is not related to the outcome of ICSI. This suggests that MII oocytes do not require further cytoplasmic maturation, and that granulosa cells are dispensable for oocyte survival, fertilization, and cleavage. Literature [21] believed that in the process of in vitro culture, with the extension of culture time, the levels of estradiol and progesterone in the culture medium gradually increased, and high concentrations of metabolites in the culture medium are not conducive to the development of oocytes and embryos. Reference [22] retrospectively analyzed 203 ICSI cycles and divided them into two groups according to the time from degranulation to ICSI injection. The results showed that the excellent embryo rate, implantation rate, and pregnancy rate of the short-term group are long-term group, but the fertilization rate had no statistical difference. It is believed that a better outcome may be obtained when ICSI is performed immediately after degranulation. Reference [23] believes that although degranulation may cause damage to the cell membrane, microinjection crosses the membrane barrier, and it is still recommended for skilled experimenters to perform microinjection immediately after degranulation.

### 3. Material and Method

**3.1. Research Object.** Patients who underwent IVF-assisted pregnancy and FET transplantation in our center from January 1, 2015, to June 30, 2021, are selected. The inclusion criteria are as follows: (1) Both parties have been infertile for 3 years or more or have not conceived after 2 treatments of artificial insemination. (2) The male sperm motility is at the critical value of IVF/ICSI or moderately oligospermia. (3) The number of oocytes retrieved is more than 10 pieces. In this study, patients' homologous oocytes are used for self-contrast.

**3.2. Superovulation and Oocyte Retrieval.** According to the patient's own situation, an individualized stimulation plan is formulated for the patient. The commonly used stimulation plans in our center are the standard long plan and the antagonist plan. The day of HCG is determined according to the monitoring of follicle development by B-ultrasound and the serological indicators of sex hormones, and oocyte retrieval is performed 35-37 hours after intramuscular injection of HCG. The obtained cumulus complexes are placed in a fertilization four-well plate, with 2-4 pieces per well, placed in a 37°C, 6% CO<sub>2</sub> incubator, and fertilized after 40 hours of HCG.

**3.3. Semen Processing and Fertilization.** The semen processing method employs double-layer density gradient centrifugation upstream. After the treatment, the uppermost layer of sperm is selected, and the concentration is adjusted to 4 - 8 \* 10<sup>6</sup>/ml. During fertilization, sperm is added away

from the cumulus complex, and the final concentration of fertilized sperm is about 5 \* 10<sup>4</sup>/ml. Only half of the total oocyte cumulus complexes are randomly picked for degranulation four hours after fertilization. A microscope is used to observe the discharge of the second polar body. If the fertilization rate is greater than 30%, the degranulated fertilized oocytes (early degranulation group) are transferred to fresh semen. The remaining nondegranulated cumulus complexes are subjected to overnight fertilization followed by degranulation (overnight fertilization group). Pronuclei are observed 19 hours after fertilization.

**3.4. Embryo Scoring.** Embryos are observed and recorded when cultured to D2, D3, D5, and D6. The scoring criteria for D3 embryos are as follows: (1) The blastomeres are uniform in size and less than 10% fragmented. (2) The blastomere is uniform in size, with 10-20% fragments. (3) The blastomere size is uneven, and the fragments are less than or equal to 20%. (4) Fragmentation is between 20% and 50%. (5) Fragmentation is greater than or equal to 50%. D3 high-quality embryos are the first grade of 7-9 cells that divide every 24 hours without multinucleation. Embryos above IV with D3 blastomeres ≥ 4 and dividing every 24 hours can be used for blastocyst culture. The blastocyst scoring criteria are scored according to Gardner's scoring method. High-quality blastocysts with no multinucleation at the cleavage stage and no C in the inner cell mass and trophoblast score are considered high-quality blastocysts.

**3.5. Transplant.** Frozen transplantation is based on the patient's own conditions to formulate a reasonable transplantation time, and transplantation is performed when the endometrium is greater than or equal to 8 mm. D3 embryos or D5/D6 blastocysts are thawed on the day of transfer and then transferred after 2-3 hours of culture. D3 14 days after the transfer and 12 days after the blastocyst transfer, the blood test for HCG is positive for biochemical pregnancy, and B-ultrasound is performed on the 28th to 35th day. If there is a gestational sac, it is a clinical pregnancy.

**3.6. Statistical Method.** For data mining and statistical analysis, the SPSS software is used. The chi-square test is used for embryonic developmental outcomes, namely, pregnancy outcomes, and the *T*-test is used for neonatal birth weight. *P* less than 0.05 considered the difference to be statistically significant.

## 4. Experiment Result

**4.1. Patient Information.** A total of 5230 oocytes were recovered from 255 patients in this trial, including 2452 in the early degranulation group and 2778 in the overnight fertilization group. In this paper, we include 255 patients because we observe and analyze easily. Among them, 169 patients underwent blastocyst culture, and the basic information of the patients is illustrated in Table 1.

**4.2. Comparison of Fertilization and Embryo Development Outcome.** The experimental data are shown in Table 2, and the visualization results are shown in Figure 1. This study

TABLE 1: Basic information of the patient.

Item	Information
Number	255
Woman's age	30.73 $\pm$ 4.5
Infertility years	4.50 $\pm$ 3.06
BMI	22.81 $\pm$ 3.41
AMH	6.06 $\pm$ 3.17
FSH	6.33 $\pm$ 1.38
LH	6.77 $\pm$ 4.3
Infertility factor	-
Fallopian tube factor	151
Endometriosis	4
Ovulation disorder	25
Oligospermia	53
Unknown reason	17
Old age	5

compares the fertilization and embryonic development outcomes of the two groups. 0PN is the embryo with 2 polar bodies observed on D1 but no pronucleus and cleavage on D2.

As can be seen from the data in the chart, the difference in the normal fertilization rate between the two groups is not significant, but the polyfertilization rate in the early degranulated cell group is higher than that in the overnight fertilization group. In addition, it is also found that the incidence of 0PN in the early degranulated cell group is significantly higher than that in the overnight fertilization group, and the difference in the rate of high-quality embryos between the two groups is not significant. The difference in the rate of D5 high-quality blastocysts among patients undergoing blastocyst culture is not significant, but the difference in the rate of D6 high-quality blastocysts is, and the early degranulation group is higher than the overnight group.

**4.3. Recovery Rate Comparison.** In this work, the recovery rate of the two groups is compared. The cleavage-stage embryos are all D3 embryos, and the number of thawed embryos includes embryos that are thawed for blastocyst culture. The experimental results are illustrated in Table 3.

The quality of the two groups of embryos is basically the same, and the difference in the complete recovery rate after thawing is not significant. In the thawed blastocysts, the blastocyst recovery rate in both groups is 100%.

**4.4. FET Outcome Comparison.** This study analyzes the results of FETs with transfers separated into three groups: early degranulation, overnight fertilization, and mixed transfers (early degranulation+overnight fertilization embryos). The results are illustrated in Table 4, and three groups are denoted as ED, OF, and MT in the table. Visualization results are demonstrated in Figure 2, TC is transplanted cycle, TE is transplanted embryo, ATE is an average transplanted embryo, PR is planting rate, CPR is clinical preg-

nancy rate, MR is miscarriage rate, and LBR is miscarriage rate.

The implantation rate, clinical pregnancy rate, and abortion rate of the three groups are not significantly different, as shown in the chart. However, the clinical pregnancy rate and live birth rate of the overnight fertilization group are lower than those of the other two groups, the live birth rate is significantly lower than that of the mixed transplantation group, and the miscarriage rate is also higher.

**4.5. Comparison of Birth Offspring.** This work compares the birth offspring of singletons and twins, and the experimental results are demonstrated in Tables 5 and 6.

Among singleton births, mean weight and gestational age did not differ significantly among the three groups. In the indicators of low body weight and very low body weight, preterm birth, and super preterm birth, there are no significant differences among the three groups. Among twins born, mean weight and mean gestational age are also not significantly different. However, in the indicators of ultra-low body weight and ultrapremature birth, the early degranulation group is higher and significantly higher than the overnight fertilization group. Among preterm infants, the early degranulation group remained high relative to the other two groups and is significantly higher than the mixed transplant group. None of the newborns are born with birth defects.

## 5. Discussion

To prevent fertilization failure, granulosa cells are removed around 4-6 hours after fertilization to avoid fertilization failure. However, while ensuring the fertilization rate, attention should also be paid to the low-temperature tolerance of embryos formed after early degranulation, that is, the survival after freezing and thawing. In addition, the live birth capacity of the embryos and the safety of the offspring should be determined.

This study examines embryonic development after early egg degranulation, postthaw pregnancy outcomes, and childbirths in depth. There is no significant difference in normal fertilization rate; however, the multipronucleus rate is much higher in the early degranulated cell group than in the overnight group. Fertilization is judged by the discharge of the second polar body after early degranulation, and the observation of the discharge of the second polar body indicates that the sperm has penetrated the oocyte, and a cortical reaction has occurred before degranulation [24]. Therefore, it is unlikely that multiple spermatozoa enter the oocyte, and the multipronucleus rate may not be caused by polyspermy. After the sperm penetrates the oocyte, the oocyte resumes second meiosis. Due to the active spindle and microtubule activities at this time [25, 26], it may be susceptible to external mechanical interference, resulting in abnormal meiosis and multiprocytic phenomenon. For oocytes that are immature at the time of early degranulation or had only one polar body, polypronuclei are observed on the second day. Whether the penetration of multiple spermatozoa is due to excessive suction at the time of early degranulation

TABLE 2: Comparison of embryonic developmental outcomes.

Item	Early degranulation	Overnight fertilization	<i>P</i>
2PN %	64.07 (1571/2452)	65.15 (1810/2778)	NS
≥3PN %	9.87 (242/2452)	8.24 (229/2778)	<0.05
0PN %	3.14 (77/2452)	1.69 (47/2778)	<0.001
D3 high-quality embryo rate	27.50 (432/1571)	26.52 (480/1810)	NS
D5 high-quality embryo rate	15.97 (176/1102)	17.35 (209/1204)	NS
D6 high-quality embryo rate	6.72 (74/1102)	4.65 (56/1204)	<0.05

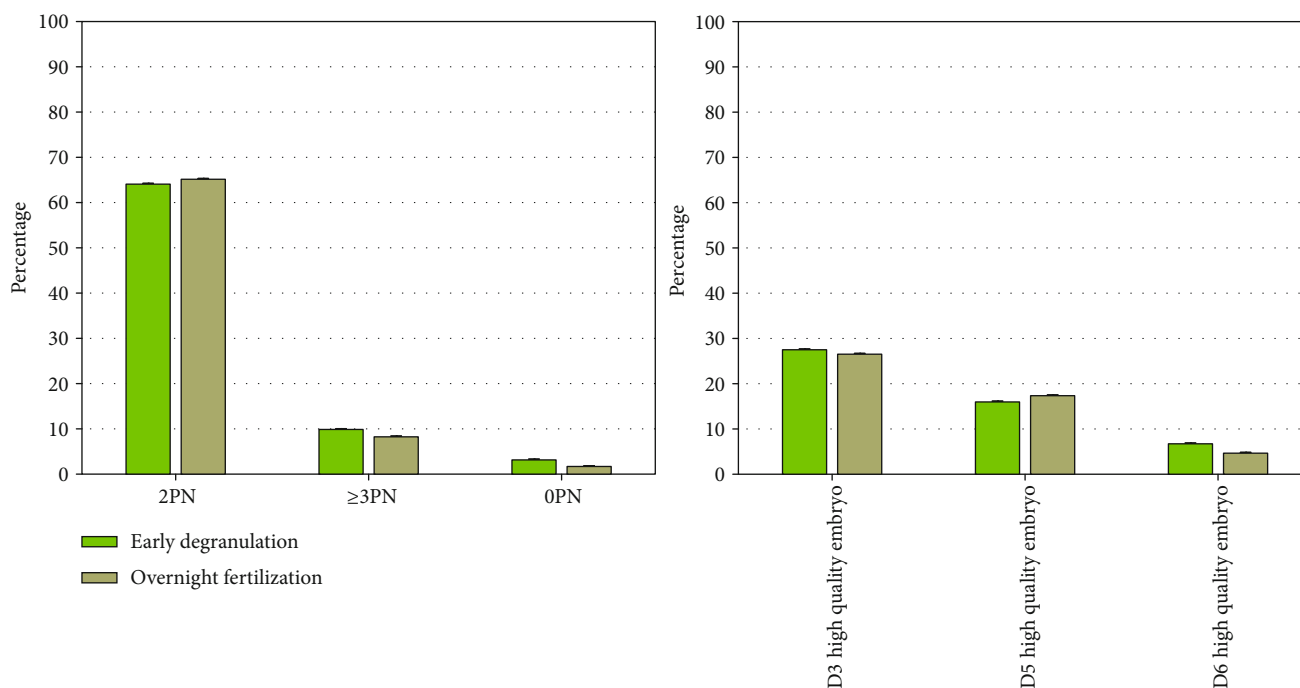


FIGURE 1: Comparison visualization of fertilization and embryo development outcome.

TABLE 3: Comparison of cleavage stage embryo recovery rate.

Item	Early degranulation	Overnight fertilization	<i>P</i>
Number of thawed embryos	222	260	-
Fragments ≤ 10%embryo ratio	95.05 (211/222)	93.85 (244/260)	NS
Complete recovery rate	93.24 (207/222)	93.46 (223/260)	NS

TABLE 4: Comparison of FET clinical outcome.

Item	ED	OF	MT	<i>P</i>
Age	31.07 ± 4.5	30.65 ± 4.8	30.38 ± 4.2	-
Transplanted cycle	116	136	110	-
Transplanted embryo	168	205	222	-
Average transplanted embryo	1.45	1.50	2.03	-
Planting rate	51.19 (86/168)	48.29 (99/205)	47.75 (106/222)	NS
Clinical pregnancy rate	66.38 (77/116)	59.55 (81/136)	67.27 (74/110)	NS
Miscarriage rate	20.78 (16/77)	22.22 (18/81)	12.16 (9/74)	NS
Live birth rate	52.57(61/116) <sup>a</sup>	46.32 (63/136) <sup>ab</sup>	59.09 (65/110) <sup>ac</sup>	<0.05

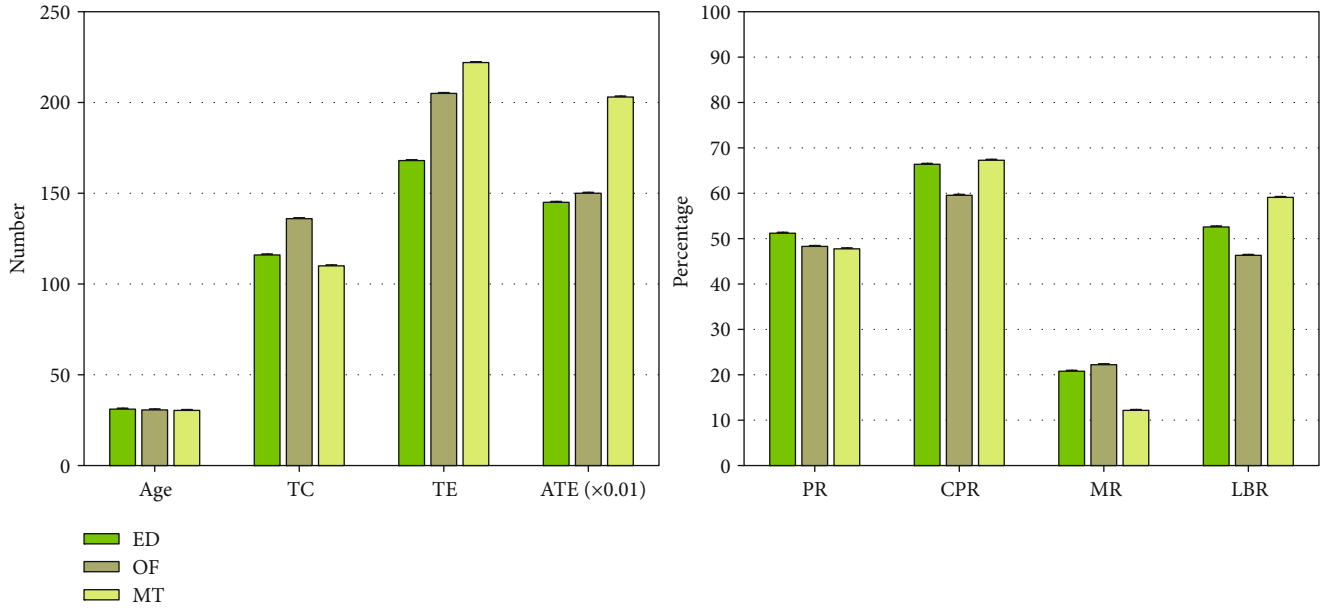


FIGURE 2: Comparison visualization of FET Outcome.

TABLE 5: Singleton birth comparison.

Item	ED	OF	MT	<i>P</i>
Birth	54	50	42	-
Average weight	3254.63 ± 500.16	3277.96 ± 497.54	3264.05 ± 507.86	NS
<1.50	0	2.0 (1/50)	0	NS
<2.50	3.70 (2/54)	2.0 (1/50)	7.14 (3/42)	NS
Average gestational age	38.53 ± 2.01	38.89 ± 1.76	38.43 ± 1.94	NS
<32 weeks	1.85 (1/54)	2.00 (1/50)	0	NS
<37 weeks	1.85 (1/54)	2.00 (1/50)	9.52 (4/42)	NS

TABLE 6: Twin birth comparison.

Item	ED	OF	MT	<i>P</i>
Birth	14	26	47	-
Average weight	2314.29 ± 536.16	2393.08 ± 338.29	2346.17 ± 499.52	NS
<1.5	14.29 (2/14) <sup>ac</sup>	0 <sup>bc</sup>	8.51 (4/47) <sup>c</sup>	<0.05
<2.5	57.14 (8/14)	53.85 (14/26)	59.57 (28/47)	NS
Average gestational age	35 ± 2.66	36.31 ± 1.67	35.78 ± 2.68	NS
<32 weeks	14.29 (2/14) <sup>ac</sup>	0 <sup>bc</sup>	8.51 (4/47) <sup>c</sup>	<0.05
<37 weeks	71.43 (10/14) <sup>ab</sup>	46.15 (12/26) <sup>b</sup>	34.04 (16/47) <sup>bc</sup>	<0.05

affects the zona pellucida response/cortical granule response has not yet been confirmed, or whether it inhibits second polar body expulsion. Embryos with multiple pronuclei should therefore be tested to determine the source of additional pronuclei.

In addition to the multipronucleus rate, the incidence of OPN is also significantly higher in the early degranulation group. After fertilization, the proximity of male and female pronuclei is dependent on the cytoskeletal network. And

two astral microtubules appear around both male and female nuclei, forming the poles of the first mitotic spindle, causing the appearance of the first mitotic spindle, and then the disappearance of the pronucleus and the beginning of the first cleavage [27, 28]. It is possible that more frequent blowing and suction activities during early degranulation interfere with the nucleus and cytoskeleton's management of the cell cycle, hastening the disappearance of the pronucleus and entry into the first mitosis. In conclusion,

abnormally fertilized embryos may be the result of more compact granulosa cells early in fertilization requiring stronger and more frequent aspiration. This reflects that early degranulation cells do not have an advantage for fertilization outcomes.

In terms of embryo development, there is no significant difference between the two groups in the D3 high-quality embryo rate and the D5 high-quality blastocyst rate. However, the high-quality blastocyst rate of D6 group is significantly higher than that of the overnight group, indicating that the embryos in the early degranulation group have more potential for continued development. However, the formation rate of D6 high-quality blastocysts is lower in both groups, and the euploidy rate and transfer success rate of D5 blastocysts are higher than those of D6 blastocysts, and the blastocysts formed by D5 are paid more attention [29]. At present, it is believed that the metabolites of sperm and granulosa cells in the fertilized fluid are not conducive to embryonic development, and the fertilized fluid should be transferred as soon as possible [21]. However, some studies have shown that the number of oocytes in the fertilization hole during fertilization has a greater impact on the accumulation of ammonium in the semen. Ammonium accumulation in more than 5 oocytes is significantly increased, whereas sperm concentration has no effect on ammonium accumulation [30]. However, there is no significant difference between the complete granulosa cell group and the partial excision group in the later stage of embryo development with fertilization holes of less than 5 oocytes, but more than 5 oocytes show an advantage in the partial excision group [31]. If the sperm concentration is higher at the time of fertilization, the number of dead sperm cells near the oocyte increases, thus affecting embryonic development. This explains why reducing sperm-oocyte incubation time in the presence of lower sperm concentration has no significant beneficial effect on embryo quality, whereas shortening sperm fertilization time in the presence of higher sperm concentration can explain the improved embryonic developmental capacity [32, 33]. Due to the type of fertilization vessel, oocyte density, short-term sperm-oocyte incubation time, and sperm concentration during fertilization in each center, there is no uniform standard [34]. Therefore, the impact of early degranulation cells on embryonic development is inconclusive.

After the embryos are frozen and thawed, the complete recovery rates of the two groups are basically the same. This indicates that the strength and number of blows and suction during early degranulation do not affect the low-temperature resistance of embryos with less fragmentation rate. Because transferring the best embryos gives the patient a higher chance of pregnancy, the transfer cases are divided into 3 groups. After transplantation, the implantation rate, clinical pregnancy rate, and yield rate of the three groups are not significantly different, and the live birth rate is significantly lower than that of the mixed transplantation group. The clinical outcome index of the early degranulation granule group is slightly better than that of the overnight group, but the difference is not significant, and its advantages are not clearly reflected. It may be because the sperm concentra-

tion of fertilization in this center is low ( $5 * 10^4/ml$ ), and some granulosa cells will be excised when picking oocytes. Furthermore, the volume of insemination fluid is  $750 \mu l$ , and 2 to 4 oocytes are placed, so that the density of granulosa cells is low. Therefore, the metabolites of sperm and granulosa cells (such as reactive oxygen species, E2, and progesterone [35, 36]) may not be sufficient to affect the late embryonic development and clinical outcomes of overnight fertilization. And the patients included in the study are younger (the average age is around 30 years old), and most of them are infertile due to fallopian factors. This means that the oocytes themselves are of good quality and are not affected by lower concentrations of sperm and granulosa cell metabolites. However, whether patients older than 35 years can benefit from early degranulation cells requires further study.

The mean birth weight and gestational age of the three groups of singleton infants are not statistically different. Furthermore, there are no significant changes in the indicators of overweight newborns, underweight infants, ultrapreterm births, and preterm births, demonstrating that early degranulation had no effect on singletons' perinatal outcome. There are no significant variations in mean birth weight, gestational age, or low birth weight between the three groups of twins born. However, among the ultralow birth weight infants, ultrapreterm infants, and preterm fetuses, the proportion of early degranulation is the highest. Among them, the preterm birth rate is as high as 71.43%, and the ultralow birth weight infants are also significantly higher than the overnight group. After excluding the factors of height and BMI, the results are still the same. One possible explanation for these findings may be that during degranulation early in fertilization, excessive repetitive mechanical stimulation may lead to epigenetic changes caused by DNA methylation and differential gene expression due to the compact granulosa cells encapsulated [37]. This has been associated with low birth weight in infants or preterm birth [38, 39]. However, in the mixed twins, although the origin of the two fetuses cannot be determined, their gestational age is better than that of the early degranulation group. There is no difference between the low birth weight infants and the early degranulation group, and there is no difference in the singleton birth index among the groups. Therefore, whether DNA methylation and epigenetic changes caused by degranulated cells at the early stage of fertilization are the main factors that aggravate the preterm birth of twins needs to be further proved. And the specific impact mechanism is still unclear, and further research is needed. However, there are many factors that affect preterm birth outcomes, such as cervical insufficiency, intrauterine infection, amniotic fluid volume, and pregnancy complications, and lifestyle also affects neonatal outcomes [39, 40], but we do not collect data on this. There is a case of monozygotic twins in the early degranulation group. It is also worth investigating whether the zona pellucida alters as a result of early degranulation. The low number of twin births in the early degranulation group is one of the study's shortcomings. In the later stage, more neonates born in the homologous oocyte early degranulation group should be included, and the pregnancy status during pregnancy should be tracked for further research.

## 6. Conclusion

Infertility has become a global reproductive health problem, and the prevalence of infertility has shown an increasing trend in recent years. The disease has become a global medical problem. Since 1978, with the birth of the first test-tube baby, human-assisted reproductive technology has become an important treatment method. Assisted reproductive technology is in the process of continuous improvement and development. In vitro fertilization-embryo transfer is a very common and effective assisted reproductive technology, but various factors can affect oocyte fertilization, embryo development, pregnancy outcome, and offspring safety. In this work, by observing the embryonic outcomes of the early degranulation group and the overnight fertilization group and the clinical outcomes after FET, we explore the impact of early degranulation cells on FET outcomes and offspring safety. The clinical outcome of embryos with early degranulation cells is similar to that of overnight fertilization, according to data mining analysis, and the clinical outcome is slightly better than that of embryos in the overnight fertilization group. The offspring outcomes of singletons are also not different from overnight fertilization groups, but the outcomes of twins are still unsatisfactory. Due to the small amount of data on offspring born in this paper, a more in-depth research is needed on the safety of newborns with early degranulation cells. Because the goal of any technological development should be to produce healthy progeny. As a result, it is not necessary to degranulate all of the patient's oocytes at the early stage of fertilization in order to ensure that no fertilization abnormality occurs.

## Data Availability

The datasets used during the current study are available from the corresponding author on reasonable request.

## Conflicts of Interest

The authors declare that they have no conflict of interest.

## Acknowledgments

This work was supported by the Dongguan Science and Technology of Social Development Program, Project No. 20211800900862.

## References

- [1] M. Amiri, Z. Sadeqi, M. H. Hoseinpoor, and A. Khosravi, "Marital satisfaction and its influencing factors in fertile and infertile women," *Journal of Family & Reproductive Health*, vol. 10, no. 3, pp. 139–145, 2016.
- [2] N. Venkatanarayanan and K. F. Walker, "Evidence around early induction of labor in women of advanced maternal age and those using assisted reproductive technology," *Best Practice & Research Clinical obstetrics & gynaecology*, vol. 77, pp. 42–52, 2021.
- [3] S. Pinto, D. F. Carrageta, M. G. Alves et al., "Sperm selection strategies and their impact on assisted reproductive technology outcomes," *Andrologia*, vol. 53, no. 2, article e13725, 2021.
- [4] S. Matsuzaki, Y. Nagase, T. Takiuchi et al., "Antenatal diagnosis of placenta accreta spectrum after in vitro fertilization-embryo transfer: a systematic review and meta-analysis," *Scientific Reports*, vol. 11, no. 1, pp. 1–12, 2021.
- [5] T. Lefebvre, T. Fréour, S. Ploteau, B. le Bizec, J. P. Antignac, and G. Cano-Sancho, "Associations between human internal chemical exposure to Persistent Organic Pollutants (POPs) and In Vitro Fertilization (IVF) outcomes: systematic review and evidence map of human epidemiological evidence," *Reproductive Toxicology*, vol. 105, pp. 184–197, 2021.
- [6] M. F. Heber and G. E. Ptak, "The effects of assisted reproduction technologies on metabolic health and disease," *Biology of Reproduction*, vol. 104, no. 4, pp. 734–744, 2021.
- [7] S. Furuya, K. Kubonoya, and T. Yamaguchi, "Incidence and risk factors for velamentous umbilical cord insertion in singleton pregnancies after assisted reproductive technology," *Journal of Obstetrics and Gynaecology Research*, vol. 47, no. 5, pp. 1772–1779, 2021.
- [8] R. D. Björvang, I. Hallberg, A. Pikki et al., "Follicular fluid and blood levels of persistent organic pollutants and reproductive outcomes among women undergoing assisted reproductive technologies," *Environmental Research*, vol. 208, p. 112626, 2022.
- [9] S. Epelboin, J. Labrosse, P. Fauque et al., "Endometriosis and assisted reproductive techniques independently related to mother-child morbidities: a French longitudinal national study," *Reproductive Biomedicine Online*, vol. 42, no. 3, pp. 627–633, 2021.
- [10] M. De Ree, G. Mantas, A. Radwan, S. Mumtaz, J. Rodriguez, and I. E. Otung, "Key management for beyond 5G mobile small cells: a survey," *IEEE Access*, vol. 7, pp. 59200–59236, 2019.
- [11] B. C. Vanderhyden and D. T. Armstrong, "Role of cumulus cells and serum on the in vitro maturation, fertilization, and subsequent development of rat oocytes," *Biology of Reproduction*, vol. 40, no. 4, pp. 720–728, 1989.
- [12] H. Shen, "Granulosa and oocyte development," *Journal of International Reproductive Health/Family Planning*, vol. 31, no. 5, pp. 344–347, 2012.
- [13] N. Ye, X. Dong, and D. Li, "The progress in apoptotic mechanism of ovarian granulosa cells involved in premature ovarian failure," *Journal of Capital Medical University*, vol. 3, pp. 379–383, 2014.
- [14] J. Y. P. Ho, M. J. Chen, Y. C. Yi, H. F. Guu, and E. S. C. Ho, "The effect of preincubation period of oocytes on nuclear maturity, fertilization rate, embryo quality, and pregnancy outcome in IVF and ICSI," *Journal of Assisted Reproduction and Genetics*, vol. 20, no. 9, pp. 358–364, 2003.
- [15] L. Rienzi, F. Ubaldi, R. Anniballo, G. Cerulo, and E. Greco, "Preincubation of human oocytes may improve fertilization and embryo quality after intracytoplasmic sperm injection," *Human Reproduction*, vol. 13, no. 4, pp. 1014–1019, 1998.
- [16] A. Isiklar, R. Mercan, B. Balaban, C. Alatas, S. Aksoy, and B. Urman, "Impact of oocyte pre-incubation time on fertilization, embryo quality and pregnancy rate after intracytoplasmic sperm injection," *Reproductive Biomedicine Online*, vol. 8, no. 6, pp. 682–686, 2004.



- [17] C. Patrat, A. Kaffel, L. Delaroche et al., "Optimal timing for oocyte denudation and intracytoplasmic sperm injection," *Obstetrics and Gynecology International*, vol. 2012, Article ID 403531, 7 pages, 2012.
- [18] H. Jin and Y. Sun, "Causes and mechanism of polyspermy," *Journal of Reproductive Medicine*, vol. 20, no. 2, pp. 90–92, 2011.
- [19] K. Yanagida, H. Yazawa, H. Katayose, K. Suzuki, K. Hoshi, and A. Sato, "Influence of oocyte preincubation time on fertilization after intracytoplasmic sperm injection," *Human Reproduction*, vol. 13, no. 8, pp. 2223–2226, 1998.
- [20] H. Van de Velde, A. De Vos, H. Joris, Z. P. Nagy, and A. C. Van Steirteghem, "Effect of timing of oocyte denudation and micro-injection on survival, fertilization and embryo quality after intracytoplasmic sperm injection," *Human Reproduction*, vol. 13, no. 11, pp. 3160–3164, 1998.
- [21] S. Kattera and C. Chen, "Short coincubation of gametes in vitro fertilization improves implantation and pregnancy rates: a prospective, randomized, controlled study," *Fertility and Sterility*, vol. 80, no. 4, pp. 1017–1021, 2003.
- [22] P. B. Cotti, C. Colasante, L. Perego, and L. De Lauretis, "Effect of early and late oocyte denudation on ICSI outcome," *Human Reproduction*, vol. 25, no. 20100600, p. 180, 2010.
- [23] L. Gong and W. Wang, "Inderbir Gill. The effect of different denuding time in ICSI to embryo quality and pregnant result," *Chinese Journal of Birth Health & Heredity*, vol. 19, no. 10, pp. 113–114, 2011.
- [24] Z. Machaty, A. R. Miller, and Z. Lu, "Degranulation activation at fertilization," *Oxygen Transport to Tissue XXXIII*, vol. 953, pp. 1–47, 2017.
- [25] L. Santella, N. Limatola, and J. T. Chun, "Cellular and molecular aspects of oocyte maturation and fertilization: a perspective from the actin cytoskeleton," *Zoological Letters*, vol. 6, no. 1, pp. 1–21, 2020.
- [26] N. H. Kim, "Cytoskeletal alteration of mammalian oocytes during meiotic maturation, fertilization and parthenogenesis," *Clinical and Experimental Reproductive Medicine*, vol. 22, no. 3, pp. 253–258, 1995.
- [27] H. Schatten and Q. Y. Sun, "Cytoskeletal functions, defects, and dysfunctions affecting human fertilization and embryo development," in *Human Reproduction: Updates and New Horizons*, John Wiley & Sons Inc, Hoboken, NJ, 2017.
- [28] Y. Terada, M. Tachibana, H. Hasegawa, T. Ugajin, N. Yaegashi, and K. Okamura, "Cytoskeletal dynamics during oocyte maturation and fertilization in primates with comparison to rodents," *Journal of Mammalian Ova Research*, vol. 25, no. 3, pp. 127–132, 2008.
- [29] Y. Li, J. Wang, T. Sun et al., "Pregnancy outcomes after day 5 versus day 6 blastocyst-stage embryo transfer: a systematic review and meta-analysis," *Journal of Obstetrics and Gynaecology Research*, vol. 46, no. 4, pp. 595–605, 2020.
- [30] R. Li, S. Ou, N. Ouyang et al., "Brief co-incubation of gametes benefits the outcomes of newborns," *Journal of Assisted Reproduction and Genetics*, vol. 35, no. 8, pp. 1537–1542, 2018.
- [31] S. Mumtaz, H. Lundqvist, K. M. S. Huq, J. Rodriguez, and A. Radwan, "Smart direct-LTE communication: an energy saving perspective," *Ad Hoc Networks*, vol. 13, pp. 296–311, 2014.
- [32] M. Lundqvist, U. Johansson, K. Milton, C. Westin, and N. Simberg, "Reducing the time of co-incubation of gametes in human in-vitro fertilization has no beneficial effects," *Reproductive Biomedicine Online*, vol. 3, no. 1, pp. 21–24, 2001.
- [33] V. Barraud-Lange, C. Sifer, K. Pocaté et al., "Short gamete co-incubation during in vitro fertilization decreases the fertilization rate and does not improve embryo quality: a prospective auto controlled study," *Journal of Assisted Reproduction and Genetics*, vol. 25, no. 7, pp. 305–310, 2008.
- [34] X. D. Zhang, J. X. Liu, W. W. Liu et al., "Time of insemination culture and outcomes of in vitro fertilization: a systematic review and meta-analysis," *Human Reproduction Update*, vol. 19, no. 6, pp. 685–695, 2013.
- [35] D. Enkhmaa, T. Kasai, and K. Hoshi, "Long-time exposure of mouse embryos to the sperm produces high levels of reactive oxygen species in culture medium and relates to poor embryo development," *Reproduction in Domestic Animals*, vol. 44, no. 4, pp. 634–637, 2009.
- [36] I. Y. Lebedeva, G. N. Singina, S. V. Uzbekova et al., "161 cumulus cell luteinization is enhanced during aging of bovine oocytes matured in vitro," *Reproduction, Fertility and Development*, vol. 30, no. 1, pp. 220–220, 2018.
- [37] L. Gordon, J. E. Joo, J. E. Powell et al., "Neonatal DNA methylation profile in human twins is specified by a complex interplay between intrauterine environmental and genetic factors, subject to tissue-specific influence," *Genome Research*, vol. 22, no. 8, pp. 1395–1406, 2012.
- [38] E. L. Niemitz and A. P. Feinberg, "Epigenetics and assisted reproductive technology: a call for investigation," *American Journal of Human Genetics*, vol. 74, no. 4, pp. 599–609, 2004.
- [39] L. A. Kondapalli and A. Perales-Puchalt, "Low birth weight: is it related to assisted reproductive technology or underlying infertility," *Fertility and Sterility*, vol. 99, no. 2, pp. 303–310, 2013.
- [40] S. D. McDonald, K. Murphy, J. Beyene, and A. Ohlsson, "Perinatal outcomes of singleton pregnancies achieved by in vitro fertilization: a systematic review and meta-analysis," *Journal of Obstetrics and Gynaecology Canada*, vol. 27, no. 5, pp. 449–459, 2005.

## Retraction

# Retracted: Design and Application of Legally Valid Payment Templates Based on Linking Contracts

### Computational and Mathematical Methods in Medicine

Received 25 July 2023; Accepted 25 July 2023; Published 26 July 2023

Copyright © 2023 Computational and Mathematical Methods in Medicine. This is an open access article distributed under the Creative Commons Attribution License, which permits unrestricted use, distribution, and reproduction in any medium, provided the original work is properly cited.

This article has been retracted by Hindawi following an investigation undertaken by the publisher [1]. This investigation has uncovered evidence of one or more of the following indicators of systematic manipulation of the publication process:

- (1) Discrepancies in scope
- (2) Discrepancies in the description of the research reported
- (3) Discrepancies between the availability of data and the research described
- (4) Inappropriate citations
- (5) Incoherent, meaningless and/or irrelevant content included in the article
- (6) Peer-review manipulation

The presence of these indicators undermines our confidence in the integrity of the article's content and we cannot, therefore, vouch for its reliability. Please note that this notice is intended solely to alert readers that the content of this article is unreliable. We have not investigated whether authors were aware of or involved in the systematic manipulation of the publication process.

Wiley and Hindawi regrets that the usual quality checks did not identify these issues before publication and have since put additional measures in place to safeguard research integrity.

We wish to credit our own Research Integrity and Research Publishing teams and anonymous and named external researchers and research integrity experts for contributing to this investigation.

The corresponding author, as the representative of all authors, has been given the opportunity to register their agreement or disagreement to this retraction. We have kept a record of any response received.

### References

- [1] Y. Zhu, "Design and Application of Legally Valid Payment Templates Based on Linking Contracts," *Computational and Mathematical Methods in Medicine*, vol. 2022, Article ID 1331237, 9 pages, 2022.

## Research Article

# Design and Application of Legally Valid Payment Templates Based on Linking Contracts

Yue Zhu 

School of Law, Tsinghua University, Beijing 100084, China

Correspondence should be addressed to Yue Zhu; [aeonis@tsinghua.edu.cn](mailto:aeonis@tsinghua.edu.cn)

Received 9 May 2022; Revised 29 May 2022; Accepted 2 June 2022; Published 18 July 2022

Academic Editor: Naeem Jan

Copyright © 2022 Yue Zhu. This is an open access article distributed under the Creative Commons Attribution License, which permits unrestricted use, distribution, and reproduction in any medium, provided the original work is properly cited.

Smart contracts are widely employed in many industries as a result of the high-quality development of science and economic technology, as well as the introduction of blockchain, which can automatically conduct retrieval, verification, and payment tasks. Smart contracts as an emerging topic, particularly the study of smart legal contracts, must remain forward-looking, and the smart contract sector cannot wait for the legal status of smart contracts to be resolved before advancing. The relative lag of the law becomes unavoidable due to the unassembled and unpredictable character of the law and thus its legislation. In this paper, we explore the incorporation of smart contracts into the scope of legal regulation, the construction of a series of systems for smart contracts, and the prognosis of smart contracts in terms of contract logic, arbitration process, and formal verification from the current law. Furthermore, a smart contract payment template based on semantic-aware graph neural networks is proposed to address the traditional smart contract vulnerability detection payment template method's low detection accuracy and high false alarm rate, as well as the neural network-based method's insufficient mining of bytecode-level smart contract features. Experiments comparing the method described in this research to comparable methods reveal that the strategy proposed in this study improves all types of indicators significantly.

## 1. Introduction

With the use and development of smart contracts, the form of smart contract clauses has become more complex and diverse, one of which is the smart contract payment linkage clause, which can connect numerous smart contracts and form various contractual interactive systems. Smart contracts, as a form of transaction, should still essentially belong to the category of contract law regulation. However, due to the characteristics of smart contracts, such as automatic execution, decentralized supervision and irrevocability, and the complexity and diversity of smart contract payment linkage clauses, smart contract payment linkage clauses bring great challenges to the regulation of contract law in terms of validity determination, post facto remedy, and prior regulation [1–3]. The question of how contract law should respond and regulate this is the subject of this paper.

The concept of a smart contract was first proposed by cryptographer Nick Szabo and is defined as “a set of digitally

defined promises, including an agreement on which the contracting parties can execute those promises.” Sabo’s working theory of smart contracts was not possible because computer programs could not actually trigger payments until the advent of blockchain technology, which allows smart contracts to enable real-world value exchange. The search popularity of linking contracts in Google is shown in Figure 1, which shows a sharp increase in recent years, indicating that this is a meaningful research direction [4–7]. Autonomy, self-sufficiency, and decentralization are three properties of blockchain-based smart contracts. Self-sufficiency indicates that the smart contract can generate its own revenue by offering services; autonomy means that the contract runs automatically once it is installed; decentralization means that it does not rely on a centralized server and runs automatically through network nodes [5].

International legal research on blockchain smart contracts has gone further than that in China, and there are preliminary explorations of the legal aspects of smart contracts

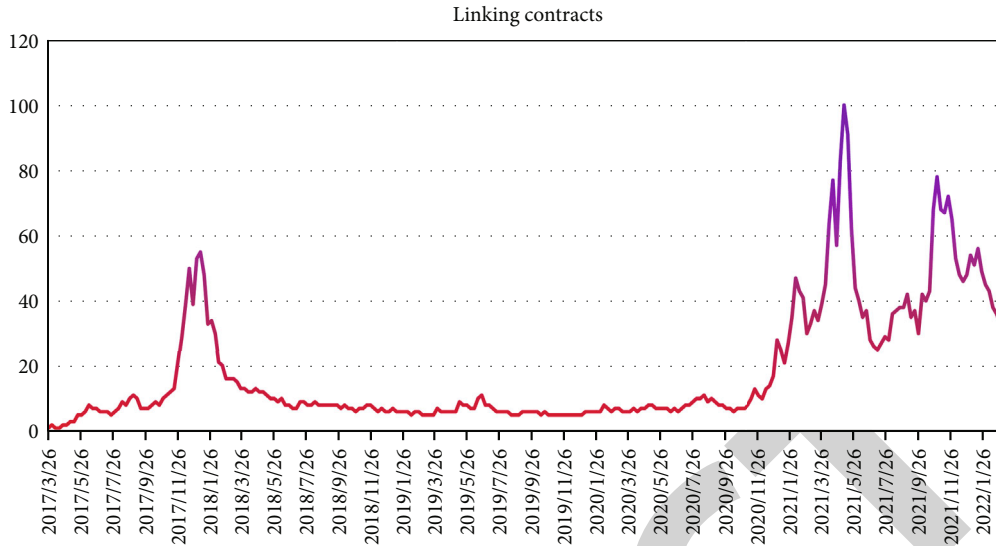


FIGURE 1: Linking contracts in Google search heat.

[8, 9]. These investigations focus on the legal properties of smart contracts and the relationship between smart contracts and existing contract law. As far as the legal attributes of smart contracts are concerned, there is a great deal of controversy among international scholars, mainly including the following views: self-help behavior. This view is that the self-execution feature of smart contracts indicates that they are an ex-ante self-help act, because they can be executed without judicial force. Max Reskin, J.D., of New York University, is a proponent of this view, citing the example of a smart car ignition device that prevents the car from being started if the owner fails to pay the bank loan on time, which was agreed upon at the time of the contract between the owner and the bank and the seller of the car. Apparently, the smart contract functions similarly to the car ignition. Escrow agent argument [10]: this view is that instead of calling it a smart contract, it should be called a “smart agent.” In a normal escrow agent arrangement, the parties to a transaction place the subject matter of the contract in the custody of a third party, who is entrusted with executing the contract once the parties have reached an agreement, because they do not trust each other. A smart contract acts as such a third party, with the parties placing blockchain assets in a contract that is automatically executed once the contract conditions are met. According to Nicolas Cornell, a smart contract is still a contract in the sense of contract law. According to the Restatement Second of the United States Law of Contracts, a contract is a promise or series of promises for which the law will provide relief in the event of a breach or which the law treats as an obligation enforceable by law. The self-executing function of a smart contract does not require legal compulsion, but it does not mean that a smart contract cannot be legally compelled either [11–13]. Therefore, in the opinion of these two professors, as long as a smart contract can change the rights and obligations between the parties according to their intention, it still belongs to a contract in the sense of contract law [14].

Although existing smart contract methods address the issue of low automation in traditional methods, they still have the following flaws: no semantic elements of smart contract bytecode are extracted, and the detection effect is poor. The graph neural network-based smart contract vulnerability detection payment template method focuses on the graph structure and ignores feature extraction of smart contract bytecode semantic features, instead focusing on the neural network’s learning of function invocation relationships, which results in the loss of a significant amount of semantic information in the nodes and makes it difficult to generate high-quality node representations (high-quality node representations can be used to measure node similarity and are also a prerequisite for accurate node classification). Some methods have less coverage on payment template types and are not well adapted for emerging vulnerabilities. In order to solve the above problems of smart contract vulnerability detection payment template methods, this paper proposes a semantic-aware graph neural network-based smart contract payment template method (L-GCN) for smart contracts in the actual deployment environment to solve the problem of low accuracy of vulnerability detection payment template methods with high false alarm rate and difficulty in covering complex smart contract function call relationships. The main advantages of the method are proposing a semantic extraction method based on smart contract bytecodes, applying the natural language processing method to the semantic extraction of smart contract bytecode instructions, using semantic vectors instead of low-dimensional vectors, and generating a higher quality node representation; using GCN’s high performance in processing non-Euclidean structure samples, merging semantic information for vulnerability detection payment templates, and improving node feature learning; the importance of semantic features for smart contract vulnerability detection payment templates is illustrated by experimental design.

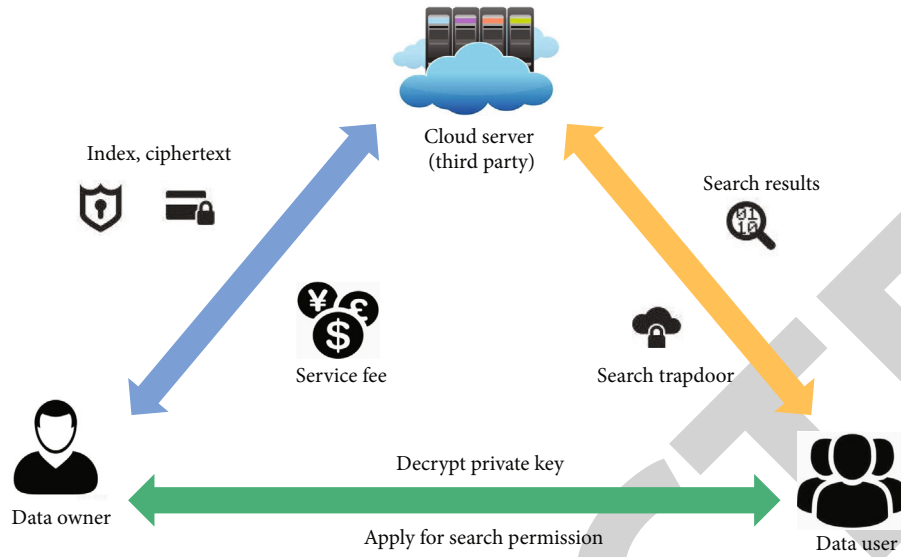


FIGURE 2: Cloud server-based ciphertext search solution.

The paper's organization paragraph is as follows. The related work is presented in Section 2. Section 3 analyzes the methodology of the proposed work. Section 4 discusses the experiments and results. Finally, in Section 5, the research work is concluded.

## 2. Related Work

**2.1. Third-Party Payment Encryption Scheme.** A ciphertext search system relying on a third party usually includes three subjects: the data owner, the user, and the cloud server, as shown in Figure 2. In the cloud server (third-party)-based ciphertext search scheme, the data owner encrypts the file using searchable encryption algorithm and at the same time extracts the keywords encrypted in the file and builds a secure index table and sends the file ciphertext and index together to the cloud server [15–17]. When a user needs to access a file containing a certain keyword, he sends the search credentials of the obtained keyword to the cloud server, which matches the search credentials with each file and finally returns the successfully matched file to the user. The user decrypts the ciphertext to obtain the desired file [18]. The server is honest and curious in the whole process, and the user needs to pay the service fee to the server before retrieving, and the server performs the search task honestly and returns the search results to the user. However, the search results returned by the server may be incorrect or may not be returned as required, and then, it is necessary for the authority to judge and arbitrate, even if the user is refunded the fee paid, but the whole process is complicated and long, which is unfair to the user, and this is the shortcoming of traditional ciphertext search based on third-party cloud servers [19]. This is also the drawback of traditional third-party cloud-based cipher search.

**2.2. Linking Contract-Based Payment Scheme.** Smart contracts can automatically perform retrieval, verification, and

payment functions. In this paper, we use smart contracts to solve the verification and fair payment problems in traditional ciphertext search. The smart contract-based ciphertext search and fair payment scheme contains five roles: data owner, server, user, and smart contract [20, 21]. As shown in Figure 3, the data owner can predefine the access policy in the ciphertext, and only when the user's attribute set satisfies the access policy can the decryption key be retrieved, resulting in the original ciphertext of the ciphertext validated by the smart contract search. Smart contracts have the ability to read and write stored files, send messages to users or servers, and deposit funds into the contract account on a temporary basis, temporarily deposit service fees in the contract account, temporarily deposit inquiry fees in the contract account, and smart contracts can verify the search results [22–23].

**2.3. The Legal Properties of Smart Contract Payments.** Smart contract payment linkage clause is not a concept in contract law, but refers to the contract clause that uses other smart contracts as the execution trigger, which can link the effectiveness and execution of multiple smart contracts. According to some scholars, smart contracts can be used to link many contracts into various kinds of contractual interactive network systems, which are called "linking contracts," and the smart contract payment linkage clause acts as such a linking node. Ethereum is the most widely used smart contract platform, and as an open-source platform, it can use the Turing-complete language, allowing users to write a variety of smart contract terms according to their needs. While the linguistic logic of the contract code makes smart contract payment linkage clauses seem similar to conditional contracts in contract law, in fact their application goes far beyond the meaning of conditional contracts. In the various contractual interactive systems formed by Ethereum, similarities can be found with many types of contracts governed by existing contract law, which may exist in the form of contract linkage, contract conjunctions, and other similar forms,

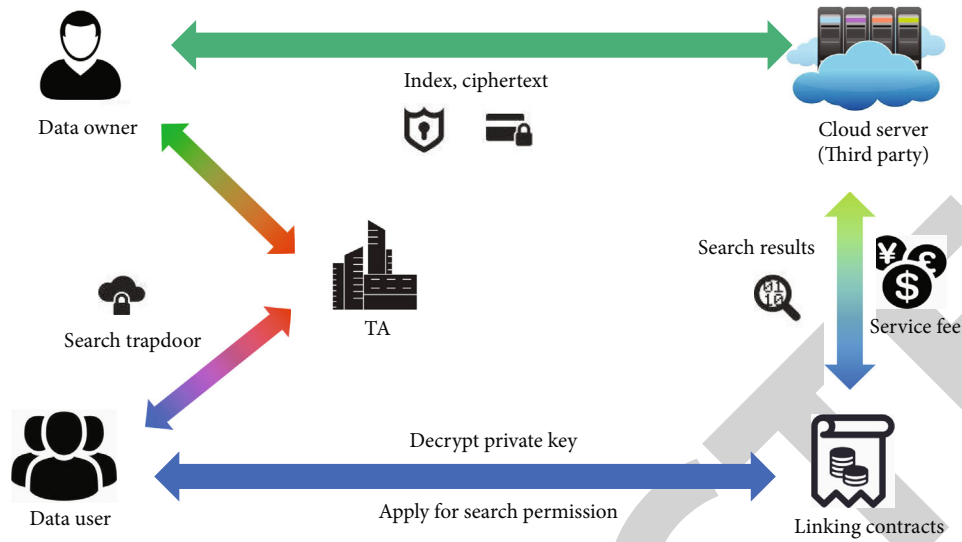


FIGURE 3: Framework diagram of smart contract-based ciphertext search and fair payment scheme.

in addition to being similar to contracts with conditional effect. A contract with conditional effect means that the parties agree on the corresponding conditions in the contract, and the occurrence or extinction of the contract effect is determined by the fulfillment or otherwise of the conditions.

The conditions attached to the contract here can be either a legal event or a legal act, so based on the definition of smart contract payment linkage clause in this paper, it seems to be concluded that all smart contract clauses with uncertain future contractual transaction behavior as a precondition are smart contract payment linkage clauses. However, in fact, many smart contracts are usually unilateral contracts deployed unilaterally by the user on the blockchain, and multiple smart contracts linked together may also express the same contractual relationship. For example, A and B agree to buy and sell, so A deploys smart contract A on the blockchain, agreeing that “if B pays the corresponding digital currency to this account, then the house corresponding to the digital asset under this account will be transferred to B,” and then, B writes smart contract B to confirm the payment of the corresponding digital currency to A. In this example, smart contract A is executed by smart contract B. Although it is in line with the characteristics of a contract with conditional effect, it is not a smart contract payment linkage clause, because the relationship between the two contracts is a sale and purchase contract according to the transaction purpose of the parties, and the condition predetermined by contract A is not a condition of a contract with conditional effect, but refers to the obligations under the sale and purchase contract. Therefore, the smart contract payment linkage clause in the form of a conditional contract must be manifested by the existence of two or more contractual relationships, and the precondition is a contractual act of uncertainty in the future.

### 3. Methodology

**3.1. Model Structure.** The method proposed in this paper is based on smart contract bytecode implementation. Because most smart contracts on Ethereum are written in bytecode, the method of collecting semantic information from bytecode and merging payment templates from graph neural networks is more suited to the smart contract operating environment. The overall framework of the method is shown in Figure 4.

The overall architecture of the method in this paper consists of four phases:

- (1) Smart contract bytecode generation phase: based on the smart contract source code in the public dataset, compiled according to the compiler version declared within the contract code to generate bytecode
- (2) Graph node feature generation phase: dividing nodes from the bytecode to generate CFG and inputting them into GCN for training to generate node features
- (3) Semantic feature generation phase: the word vector generated by extracting semantic information from the bytecode instructions within each node is input into the LSTM network for training to generate semantic features
- (4) Obtaining result stage: the vector representation of node features and semantic features are spliced and input into the fully connected layer, mapped to the sample tag space, and the final prediction results are obtained. The 4 parts are described in detail below

**3.2. Smart Contract Bytecode Generation.** Smart contracts run as bytecode when deployed on Ethereum, so it is more

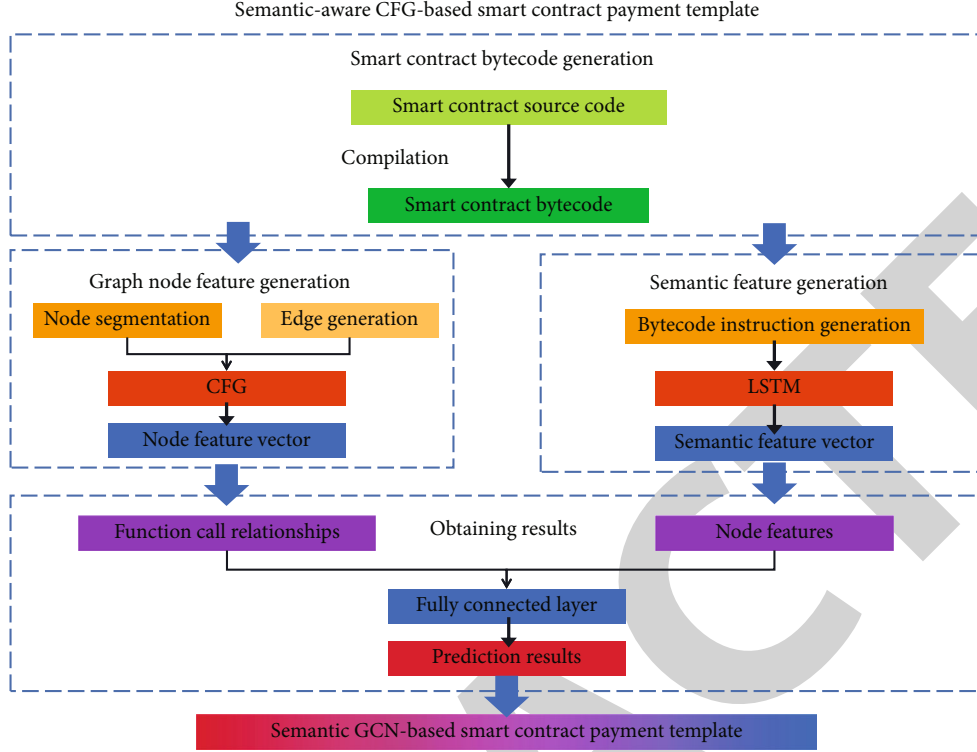


FIGURE 4: Model architecture.

practical to generate smart contract bytecode as the basis for vulnerability detection. However, the current public datasets of smart contracts are released in the form of source code, so the datasets need to be compiled to generate bytecode. Smart contract compiler versions are quite sophisticated, and different compiler versions are incompatible with one another, as well as the compiled bytecode. In this paper, we strictly follow the compiler version declared in the source code of each smart contract in the process of compilation to prevent the interference of the detection effect caused by the different bytecodes generated by different compiler versions.

**3.3. Graph Node Feature Extraction.** CFG contains smart contract structure information, which can represent the invocation relationship between functions. In this paper, the nodes are redivided based on smart contract bytecode instructions, which can make the function invocation relationships clearer and enable GCN to better learn control features from CFG. Programs can be converted into symbolic graph representations, and symbolic graph representations are able to preserve the semantic relationships between program elements. The value of various functions differs in the process of identifying smart contract vulnerabilities. This study uses function call relationships to redivide the nodes and builds CFGs from smart contract source code. Each smart contract generated CFG is represented by the nodes in the contract and the edges between the nodes, and the following describes how to obtain the nodes and edges, respectively. After compiling the source code in the dataset to generate bytecode, the bytecode is disassembled to generate bytecode instructions. After determining the function entry,

only the end instruction of the function needs to be found to divide a basic block according to the function. A summary of the instructions that represent the end of the basic block is shown in Table 1. Each node represents a basic block, and each basic block does not necessarily cover a complete function, because there are also instruction jumps within the function. A set is used to represent all the nodes in the CFG. After obtaining the nodes, the call relationship between nodes is considered as an edge, representing that the previous function may call the next function. Each node may call multiple nodes and may be called by multiple nodes. Use the set to represent the edges in  $E$  CFG,  $gg = (V; E)$ . After node division and edge construction, use  $G$  to represent the CFG. The CFG is fed into the GCN for training to obtain the features of the graph. For each layer of the neural network, it can be represented by the following nonlinear function.

$$H^{(l+1)} = f(H^{(l)}, \mathbf{A}), \quad (1)$$

where  $l$  denotes the number of network layers,  $H$  input layer and output layer, and  $f$  is the differentiable function of the neural network;  $\mathbf{A}$  is the adjacency matrix. The classification of the graph by GCN utilizes the feature information of the nodes themselves and the structure information of the graph, and the learning strategy is as follows.

$$\begin{aligned} \Gamma &= \Gamma_0 + \lambda \Gamma_{\text{reg}}, \\ \Gamma_{\text{reg}} &= f(\mathbf{X})^T \Delta f(\mathbf{X}), \end{aligned} \quad (2)$$

TABLE 1: Instructions representing the end of the basic block.

Command	Role
STOP	Stop
SELFDESTRUCT	Self-destruct
RETURN	Return
REVERT	Judgment
INVALID	Invalid
SUICIDE	Delete
JUMP	Jump
JUMPI	Jump

where  $F_0$  is the supervisory loss of the labeled nodes in the graph,  $F_{reg}$  is the loss introduced by the graph structure information,  $\lambda$  is the weight coefficient, and  $\mathbf{X}$  is the node feature vector matrix, with  $\Delta$  which represents the Laplace operator of the graph. The hierarchical propagation rule of the GCN model is as follows.

$$f(H^{(l+1)}, \mathbf{A}) = \sigma(\tilde{\mathbf{D}}^{-1/2} \tilde{\mathbf{A}} \tilde{\mathbf{D}}^{-1/2} H^{(l)} W^{(l)}), \quad (3)$$

where  $\tilde{\mathbf{A}} = \mathbf{A} + \mathbf{I}$ ,  $\mathbf{I}$  is the unit matrix,  $\mathbf{A}$  is the adjacency matrix added to the self-loop for aggregating the node's own information with all neighboring nodes,  $\mathbf{D}$  is the degree matrix of the  $\mathbf{A}$  matrix, and  $\sigma$  denotes the nonlinear activation such as linear rectification function functions.

**3.4. Node Semantic Information Extraction.** The CFG graph that is constructed contains graph structure information. The fundamental blocks of a smart contract are the nodes of the CFG graph, and each basic block consists of a set of instructions from which features must be extracted. Low-latency embedding based on manually selected features leads to a large amount of semantic information loss. Extracting these instructions as node features using natural language processing (NLP) models can maximize the preservation of semantic information. After obtaining the bytecode instructions of each node through node segmentation and bytecode disassembly, the bytecode instructions are treated as natural language processing. First, the instructions are divided into words according to the instructions; then, the sequences of words in the word set are used as word representations; finally, the instruction vector sequences are input into the LSTM network for training to obtain semantic representations, as show in Figure 5. Considering the temporal order and coherence between instruction information, using LSTM network can solve the gradient disappearance problem, learn the long-distance dependency between instructions, make the sequential nature between instructions fully reflected in the sequence, and preserve the semantic features to the maximum extent. LSTM uses gating mechanism, which consists of input gate, forgetting gate, and output gate as a module, formed by multiple modules with the same structure in series; when the instruction sequence sequentially passes through the LSTM network, the gate structures in these modules will be adjusted to the features

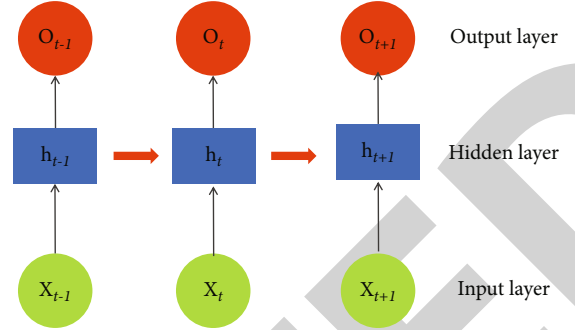


FIGURE 5: LSTM structure.

that need to be remembered and forgotten, thus obtaining the final generated semantic features with long-range dependencies. The specific formula of the gating mechanism is as follows.

$$\begin{aligned}
 \mathbf{f}_t &= \sigma(W_f \mathbf{x}_t + U_f \mathbf{h}_{t-1} + \mathbf{b}_f), \\
 \mathbf{i}_t &= \sigma(W_i \mathbf{x}_t + U_i \mathbf{h}_{t-1} + \mathbf{b}_i), \\
 \mathbf{o}_t &= \sigma(W_o \mathbf{x}_t + U_o \mathbf{h}_{t-1} + \mathbf{b}_o), \\
 \mathbf{c}_t &= \tan h(W_c \mathbf{x}_t + U_c \mathbf{h}_{t-1} + \mathbf{b}_c), \\
 \mathbf{c}_t &= \mathbf{f}_t \circ \mathbf{c}_{t-1} + \mathbf{i}_t \circ \mathbf{c}_t, \\
 \mathbf{h}_t &= \mathbf{o}_t \circ \tan h(\mathbf{c}_t),
 \end{aligned} \quad (4)$$

where  $\mathbf{x}_t$  and  $\mathbf{h}$  are the input and output vectors, respectively;  $\sigma$  denotes the sigmoid function;  $t$  is the time step value;  $W$  is the weight of the input;  $U$  is the weight of the cyclic output;  $\mathbf{h}_t$  is the output gate vector that controls what information the current internal state needs to output to the external state.

**3.5. Combining Features to Obtain Prediction Results.** After obtaining the node features and semantic information features, the two features are stitched together and input to the fully connected layer to combine the two features and map them to the sample labeling space. In order to reduce the isomorphism bias in the classification model, the output of the fully connected layer is obtained and input to the SoftMax layer for normalization.

$$\text{SoftMax}(g_i) = \frac{\exp(g_i)}{\sum_{z=1}^Z \exp(g_z)}, \quad (5)$$

where  $g_i$  is the output value of the  $i$ -th node;  $g_n$  is the number of output nodes;  $z$  by SoftMax function can transform the output into a probability distribution to accomplish the goal of prediction. Detection of no vulnerability for positive class samples, with vulnerability for negative class samples, by comparing with the label will have four cases, the four metrics are expressed as



$$\begin{aligned}
F_{\text{acc}} &= \frac{(n_{\text{TP}} + n_{\text{TN}})}{(n_{\text{TP}} + n_{\text{FN}} + n_{\text{FP}} + n_{\text{FN}})}, \\
F_{\text{pre}} &= \frac{n_{\text{TP}}}{(n_{\text{TP}} + n_{\text{FP}})}, \\
F_{\text{rec}} &= \frac{n_{\text{TP}}}{(n_{\text{TP}} + n_{\text{FN}})}, \\
F_1 &= 2 \cdot F_{\text{pre}} \cdot \frac{F_{\text{rec}}}{(F_{\text{pre}} + F_{\text{rec}})},
\end{aligned} \tag{6}$$

where  $F_{\text{acc}}$  is defined as accuracy,  $F_{\text{pre}}$  is precision,  $F_{\text{rec}}$  is recall, and  $F_1$  is the  $F1$  score.

## 4. Experiments and Results

In this section we define the dataset, experimental setup, and experimental results and analysis in detail.

**4.1. Dataset.** The SmartWild dataset was collected from real-world smart contracts with transactions that were repetitively screened for potentially vulnerable smart contracts, using real Ethereum contract addresses as the unique identifier. Because there are so many different versions of smart contract compilers and they are not all compatible, the bytecode output from source code compilation varies a lot, which can affect the experimental results. Many smart contracts written with older compiler versions are rarely used on Ether. This study leverages the dataset to better imitate the current smart contract situation by filtering out some smart contracts with too early compiler versions and bytecode repeated filtering for the remainder, ultimately using 21437 of them for tests. The SBcurated dataset consists of a part of real-world contracts with vulnerabilities and a part of hand-constructed contracts with vulnerabilities. Contracts: the smart contracts in this dataset are manually tagged with the location and class of vulnerabilities and can be used to evaluate the effectiveness of smart contract analysis tools in identifying vulnerabilities. The dataset has 136 samples. In this paper, we use the above two datasets for vulnerability detection in the experimental part and design comparative experiments to demonstrate the effective enhancement of semantic information for smart contract vulnerability detection and the ability to detect real-world smart contracts with vulnerabilities.

**4.2. Experimental Setup.** First, because the combination of Mythril and Slither provides both accuracy and efficiency, it was chosen to generate labels for the 21437 smart contracts in the SmartWild dataset. The number of training sets is 19437, and the number of testing sets is 2000 in this dataset, which is utilized for both training and testing. These smart contracts are detected using this paper’s method (LGCN), compared to Oyente, Smartcheck, and Manticore, three traditional detection tools, and a vulnerability detection method that uses only GCN networks without semantic features (referred to as GCN) for comparison. The evaluation metrics used are accuracy (accuracy), precision (precision), recall (recall), and  $F1$  score ( $F1$ ). The ability of this

TABLE 2: Performance comparison based on the SmartWild dataset.

Detection method	Accuracy (%)	Precision (%)	Recall rate (%)	$F1$ (%)
Manticore	36.57	31.90	86.32	46.58
Oyente	37.36	33.13	92.73	48.82
Smartcheck	39.72	32.53	81.01	31.09
GCN	68.05	67.42	88.73	76.62
L-GCN	81.40	79.23	92.79	85.48

paper’s method (L-GCN) to uncover real smart contract vulnerabilities versus classic Oyente, Smartcheck, Manticore, and GCN detection methods is then tested using 136 manually classified smart contracts from the SBcurated dataset. Since all contracts in this dataset are vulnerable, only the accuracy is compared.

**4.3. Experimental Results and Analysis.** The experimental results of the SmartWild dataset are analyzed, and Table 2 shows the results of the performance metrics of smart contract vulnerability detection using five methods on the SmartWild dataset of 21437 real smart contracts.

The experimental data in Table 2 reveals that the L-GCN suggested in this paper outperforms the other four approaches in all four metrics when compared to the other five methods. Among the 4 metrics, the L-GCN method has a large improvement in accuracy, precision, and  $F1$  score, but the difference in recall rate among the 5 methods is not large, indicating that all 5 methods focus more on the detection rate for smart contracts with vulnerabilities, while the lower precision metric indicates that the first 4 methods have a high false alarm rate along with a high detection rate, while the LGCN method has the highest recall rate value while improves the precision value, indicating that the method can effectively reduce the false alarm rate. Compared with the GCN method, all four metrics of the L-GCN method increased, indicating that adding semantic information can indeed improve vulnerability detection. It is worth mentioning that the Oyente method has a very high recall value, almost the same as the L-GCN method. The SmartWild dataset is tagged using a combination of smart contract vulnerability detection methods based on symbolic execution, which has some enhancement for the Oyente approach, which is also based on symbolic execution, according to the theory. This experimental result shows that adding semantic features can effectively improve smart contract vulnerability detection, and the smart contract vulnerability detection method proposed in this paper on semantic-aware graph neural network can achieve the goal of improving detection accuracy while reducing the false alarm rate.

Analysis of experimental results for the SBcurated dataset: Table 3 shows the accuracy of vulnerability detection and the number of smart contracts with vulnerabilities detected for 136 smart contracts in the SBcurated dataset using five methods.

The SBcurated dataset contains less data than the SmartWild dataset, but the smart contracts in it are manually

TABLE 3: SBcurated dataset accuracy.

Detection method	Accuracy (%)	Number of smart contracts containing vulnerabilities
Manticore	79.17	108
Oyente	80.88	110
Smartcheck	71.37	97
GCN	87.50	119
L-GCN	92.65	126

categorized and labelled with greater precision, demonstrating the usefulness of the detection methods. The remaining four methods were used to detect all of the samples. From the metrics in Table 3, the detection accuracy and the number of vulnerabilities contained in the semantic-aware smart contract vulnerability detection method (L-GCN) proposed in this paper are higher than those of the other four methods, but the improvement is not as obvious as that of the SmartWild dataset. It is speculated that the possible reason is that the samples in the SmartWild dataset all have vulnerabilities and are therefore all positive class samples, at which point the accuracy is effectively equivalent to the recall rate metric in Table 2. Comparing the recall metric in Table 2 with the accuracy in Table 3 also reveals that the five detection methods rank almost identically on these two metrics. This means that all five approaches have a high detection rate for susceptible contracts, and the detection impact improves as the number of vulnerable contracts in the sample grows larger; however, the L-GCN method suggested in this research still outperforms the other four ways. By counting the contracts with vulnerabilities detected, among all the contracts with vulnerabilities detected by the L-GCN method, there are four contracts with vulnerabilities that are not detected by the first four methods. This experiment shows that when detecting real smart contract vulnerabilities, the semantic-aware graph neural network-based smart contract vulnerability detection method proposed in this paper is more effective and can detect the contracts with vulnerabilities that other methods in the experiment failed to detect.

## 5. Conclusion

In this paper, we propose a fully automated smart contract vulnerability analysis method based on semantic-aware graph neural networks. Due to the unassembled and unpredictable nature of the law and therefore its legislation, the relative lag of the law becomes unavoidable. We combine the good processing ability of neural networks for graph structure with the extraction of semantic information by natural language processing methods and use both function call relationships and learning nodes' own bytecode features in the process of using payment templates and investigate the possibility of adding semantic information to neural networks for smart contracts, in comparison to existing methods. The possibility of adding semantic information to neural networks for intelligent contract vulnerability detection is explored. After extensive experiments, it is shown that

the semantic-aware graph neural network-based smart contract vulnerability detection method can effectively improve the detection accuracy and reduce the false alarm rate and has the ability to detect vulnerabilities in real smart contracts.

## Data Availability

The datasets used during the current study are available from the corresponding author on reasonable request.

## Conflicts of Interest

The author declares that he has no conflict of interest.

## References

- [1] J. Li, Z. Zhou, J. Wu et al., "Decentralized on-demand energy supply for blockchain in Internet of things: a microgrids approach," *IEEE transactions on computational social systems*, vol. 6, no. 6, pp. 1395–1406, 2019.
- [2] D. Jiang, F. Wang, Z. Lv et al., "QoE-aware efficient content distribution scheme for satellite-terrestrial networks," *IEEE Transactions on Mobile Computing*, p. 1, 2021.
- [3] J. Goldenfein and A. Leiter, "Legal engineering on the blockchain: 'smart contracts' as legal conduct," *Law and Critique*, vol. 29, no. 2, pp. 141–149, 2018.
- [4] G. Governatori, F. Idelberger, Z. Milosevic, R. Riveret, G. Sartor, and X. Xu, "On legal contracts, imperative and declarative smart contracts, and blockchain systems," *Artificial Intelligence and Law*, vol. 26, no. 4, pp. 377–409, 2018.
- [5] J. Akers and E. Seymour, "Instrumental exploitation: predatory property relations at city's end," *Geoforum*, vol. 91, pp. 127–140, 2018.
- [6] A. Gramzow, P. J. Batt, V. Afari-Sefa, M. Petrick, and R. Roothaert, "Linking smallholder vegetable producers to markets - a comparison of a vegetable producer group and a contract-farming arrangement in the Lushoto District of Tanzania," *Journal of Rural Studies*, vol. 63, pp. 168–179, 2018.
- [7] G. Exarchopoulos, P. Zhang, N. Pryce-Roberts, and M. Zhao, "Seafarers' welfare: a critical review of the related legal issues under the Maritime Labour Convention 2006," *Marine Policy*, vol. 93, pp. 62–70, 2018.
- [8] M. Manaa, M. T. Chimienti, M. M. Adachi et al., *Crypto-Assets: implications for financial stability, monetary policy, and payments and market infrastructures*, 2019.
- [9] V. Gatteschi, F. Lamberti, C. Demartini, C. Pranteda, and V. Santamaria, "Blockchain and smart contracts for insurance: is the technology mature enough?," *Future internet*, vol. 10, no. 2, p. 20, 2018.
- [10] Y. Ning, "Impact of quality performance ambiguity on contractor's opportunistic behaviors in person-to-organization projects: the mediating roles of contract design and application," *International Journal of Project Management*, vol. 36, no. 4, pp. 640–649, 2018.
- [11] C. McCarthy, "COVID-19 lessons can help limit future legal liability," *Campus Legal Advisor*, vol. 20, no. 12, pp. 4–5, 2020.
- [12] H. Y. Chong and A. Diamantopoulos, "Integrating advanced technologies to uphold security of payment: data flow diagram," *Automation in Construction*, vol. 114, p. 103158, 2020.

## Retraction

# Retracted: The Healing Effects of Piano Practice-Induced Hand Muscle Injury

### Computational and Mathematical Methods in Medicine

Received 1 August 2023; Accepted 1 August 2023; Published 2 August 2023

Copyright © 2023 Computational and Mathematical Methods in Medicine. This is an open access article distributed under the Creative Commons Attribution License, which permits unrestricted use, distribution, and reproduction in any medium, provided the original work is properly cited.

This article has been retracted by Hindawi following an investigation undertaken by the publisher [1]. This investigation has uncovered evidence of one or more of the following indicators of systematic manipulation of the publication process:

- (1) Discrepancies in scope
- (2) Discrepancies in the description of the research reported
- (3) Discrepancies between the availability of data and the research described
- (4) Inappropriate citations
- (5) Incoherent, meaningless and/or irrelevant content included in the article
- (6) Peer-review manipulation

The presence of these indicators undermines our confidence in the integrity of the article's content and we cannot, therefore, vouch for its reliability. Please note that this notice is intended solely to alert readers that the content of this article is unreliable. We have not investigated whether authors were aware of or involved in the systematic manipulation of the publication process.

In addition, our investigation has also shown that one or more of the following human-subject reporting requirements has not been met in this article: ethical approval by an Institutional Review Board (IRB) committee or equivalent, patient/participant consent to participate, and/or agreement to publish patient/participant details (where relevant).

Wiley and Hindawi regrets that the usual quality checks did not identify these issues before publication and have

since put additional measures in place to safeguard research integrity.

We wish to credit our own Research Integrity and Research Publishing teams and anonymous and named external researchers and research integrity experts for contributing to this investigation.

The corresponding author, as the representative of all authors, has been given the opportunity to register their agreement or disagreement to this retraction. We have kept a record of any response received.

### References

- [1] H. Yu and X. Luo, "The Healing Effects of Piano Practice-Induced Hand Muscle Injury," *Computational and Mathematical Methods in Medicine*, vol. 2022, Article ID 1020504, 6 pages, 2022.

## Research Article

# The Healing Effects of Piano Practice-Induced Hand Muscle Injury

Hecheng Yu<sup>1</sup> and Xiaoming Luo<sup>2</sup> 

<sup>1</sup>Department of Rehabilitation Medicine, Affiliated Tenth People's Hospital of Tongji University, Shanghai Tenth People's Hospital, China

<sup>2</sup>Department of Physical Therapy, Affiliated Yangzhi Rehabilitation Hospital of Tongji University, Shanghai Yangzhi Rehabilitation Hospital, China

Correspondence should be addressed to Xiaoming Luo; [xxiaomingluo@163.com](mailto:xxiaomingluo@163.com)

Received 19 May 2022; Revised 25 June 2022; Accepted 1 July 2022; Published 18 July 2022

Academic Editor: Naeem Jan

Copyright © 2022 Hecheng Yu and Xiaoming Luo. This is an open access article distributed under the Creative Commons Attribution License, which permits unrestricted use, distribution, and reproduction in any medium, provided the original work is properly cited.

**Background.** The muscles related to piano practice are mainly concentrated in the fingers and upper limbs, and the muscles related to other parts of the body are weak. Compared with other sports injuries, the injuries caused by piano practice are mainly chronic injuries caused by long-term strain of the upper limbs, and acute injuries rarely occur. The purpose of this study was to analyze the therapeutic effect of hand muscle injury caused by piano practice. **Method.** A total of 60 patients with hand muscle injury caused by piano practice admitted to our hospital from January 2019 to June 2020 were selected. According to the number random grouping method, they were randomly divided into two groups. There were 30 patients in the observation group, including 20 males and 10 females, aged 24-53 ( $39.51 \pm 7.01$ ) years old, and the course of disease was 1-5 ( $3.24 \pm 1.62$ ) months. In the control group, there were 30 patients, including 18 males and 12 females, aged 24-56 ( $39.62 \pm 7.17$ ) years old, and the course of disease was 1.5-5 ( $3.14 \pm 1.71$ ) months. If the observation group experienced excessive pain, the group took ibuprofen sustained-release capsules. On weekdays, exercise your fingers 2-3 times per day. After the intervention, the wrist joint function score of the observation group was higher than that before the intervention. **Results.** Before treatment, there was no significant difference in pain level scores between the two groups ( $P > 0.05$ ). After treatment, the limb pain score in the observation group was lower than that in the control group. The effective rate of hand tendon rehabilitation in the observation group was 93.33%. The effective rate of hand tendon rehabilitation in the control group was 70.00%. The comparison results showed that there was statistical significance ( $P < 0.05$ ). The score of the observation group was significantly higher than that of the control group, with statistically significant differences ( $P < 0.05$ ). **Conclusion.** Piano workouts can cause hand muscle difficulties, which can be alleviated by daily finger gymnastics. Daily finger exercises are simple and not limited by time and place. Piano practitioners can use the spare time of daily training and performance to exercise for a long time, so as to prevent or recover finger muscle damage caused by piano practice. It has the potential to help pianists avoid hand muscle injuries when practicing while also allowing music to reach its full potential.

## 1. Introduction

The upper limb muscles help us move our arms and hands under the command of our brain. Muscles can only exert force in one direction since they contract. Two muscles or two sets of muscles are required to move a bodily part in two directions, one to move it one way and the other to move it the other. Therefore, the movement of muscle has

the characteristics of unidirectional [1, 2]. Piano practice involves ten fingers, arms, shoulders, and neck muscles. It is an upper limb movement coordinated by many muscle groups [3]. To allow movement, the opposing muscle must relax and extend in response to the contraction of one muscle. If this does not occur, that is, if the opposing muscle stays tense—both muscles contract at the same time, which is known as cocontraction. Cocontraction is a movement-

inhibiting condition that can result in damage [4, 5]. Piano practice is a long-term, fast-paced upper limb movement. During piano practice, the upper limb muscles are in a high load contraction state for a long time [6]. Tense exercise causes muscle contraction for a long time, coupled with the irregularity of piano practice, which is the main source of muscle injury [7]. There are many factors that affect human muscle health: reasonable rest, adequate sleep, age growth, and scientific exercise and prevention [8]. This explains why some pianists can perform for years without incident before suffering an injury in their late thirties or forties. They are not playing any differently, but their bodies are less able to handle the stress. The finger flexor system, which is located in the top half of our lower arm around the elbow, controls the majority of finger movements [9, 10]. The interosseous muscle system is the second muscular system that regulates finger mobility. The interphalangeal muscles and the interosseous dorsal muscles are interosseous muscles that are dispersed across the palm [11]. Modern piano playing necessitates playing with the upper arm's gravity pull, with a focus on simple, sharp movements of the small muscles of the fingers and synchronised, relaxed motions of the upper body, shoulders, and arms [12, 13]. The muscle energy of the human body structure must be used to develop piano skills. It is simple to make training blunders and permanently injure human body muscles without this foundation [14]. The following are the results of 60 cases of hand muscle injury induced by piano practice that were collected and treated in this research. The specific chapter structure is shown in Figure 1.

## 2. Materials and Methods

**2.1. General Information.** A total of 60 patients with hand muscle injury caused by piano practice from January 2019 to June 2020 were selected and considered two research groups. The observation group included 20 males and 10 females, aged 24-53 ( $39.51 \pm 7.01$ ) years old, and the course of disease was 1-5 ( $3.24 \pm 1.62$ ) months. The control group included 18 males and 12 females, aged 24-56 ( $39.62 \pm 7.17$ ) years old, and the course of disease was 1.5-5 ( $3.14 \pm 1.71$ ) months. Details of the two groups are shown in Table 1.

In this study, we took the wrist and fingers as the whole research part. Because the muscle injury caused by piano practice has certain particularity, the inclusion criteria and exclusion criteria are formulated on the premise of diagnostic criteria.

- (1) Diagnostic criteria: according to the conscious symptoms of the wrist (positive for any of the acid, numbness, or tingling of the finger or wrist) and check the signs of the hand (positive for swelling or atrophy of the musculus magnus) [15], and the diagnosis was confirmed according to the relevant diagnostic criteria of practical neurological diseases and therapeutics [16]

- (2) Inclusion criteria: ① meeting the diagnostic criteria of hand muscle injury caused by piano practice; ② voluntary subjects signed informed consent; ③ oral medication or external application of traditional Chinese medicine in strict accordance with the doctor's advice; ④ cooperating with the collection of test results, compliance was good
- (3) Exclusion criteria: ① those who had taken oral analgesics or local physiotherapy before treatment to affect the efficacy evaluation; ② local skin rupture; ③ suffering from cervical spondylosis or other diseases that cause shoulder pain, such as intrashoulder joint fractures, tuberculosis, bone metastases, and other diseases that affected shoulder joint mobility; ④ acute phase with severe liver and kidney dysfunction, heart disease, endocrine disease, and other diseases

### 2.2. Methods

**2.2.1. Control Group.** The treatment method of the control group is to use drugs only to relieve pain; other methods of rehabilitation with fingers and wrists are not assisted. Among them, ibuprofen sustained-release capsules produced by Sino US joint venture Tianjin Shike Pharmaceutical Co., Ltd. were selected as the analgesic drugs: production batch number: National Pharmaceutical Standard H20013062, specification 0.4g, 1 capsule per time, taking it orally once in the morning and evening after meals, taking it with warm water after meals, and continuing treatment for 15 days. During this process, record the time from taking the medicine to pain relief, the degree of pain and the duration of pain, and the number of intermittent pain every day (including acid swelling and other finger and wrist discomfort).

**2.2.2. Observation Group.** In the observation group, the pain of the participants was first evaluated. If the pain was tolerable, they would not take drugs, and only use the finger exercise method proposed in this study. If the pain is too great, you can take ibuprofen sustained-release capsules to relieve the pain and continue to exercise your fingers 2-3 times a day for six months. Finger exercises include ① arm relaxation exercises, ② finger push-ups, and ③ wrist spring operation. Specific exercises related to the hands are shown in Figure 2.

- (1) Arm relaxation exercises: stand naturally with shoulders relaxed and falling. Then, bend elbows slightly and raise arms naturally to shoulder height. Hold for 2 or 3 seconds and let the whole arm fall into free fall. After practicing several times, alternate left and right hands to drop and lift. Then, make further adjustments to this exercise: slowly raising hands to head height. Hold for 2 or 3 seconds and then lower arms slowly and controllably. When reaching shoulder height, immediately relax and fall [17]. It should be noted that the relaxation should be carried out in an instant as much as possible and should not be gradually adjusted to a relaxed state. Let the slight

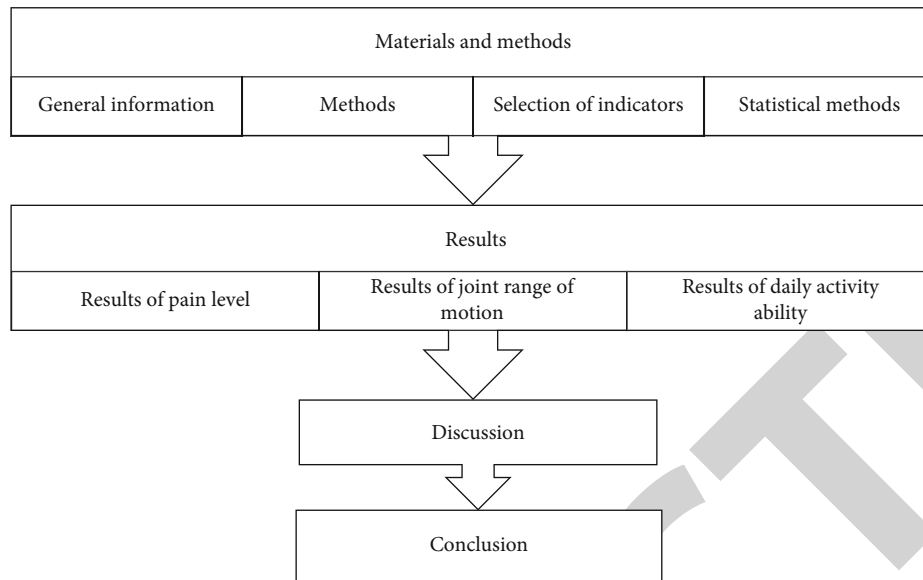


FIGURE 1: Structure of this study.

TABLE 1: General information.

Groups	Cases	Gender		Age	Course of disease (month)
		Males	Females		
Observation group	30	20	10	39.51 ± 7.01	3.24 ± 1.62
Control group	30	18	12	39.62 ± 7.17	3.14 ± 1.71

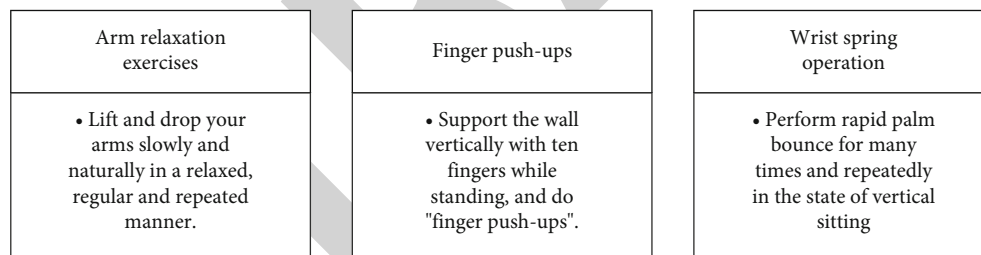


FIGURE 2: Main contents of finger motor rehabilitation.

tension control and the complete relaxation exercise combine to improve the ability of arm tightness adjustment

- (2) Finger push-ups: the training steps were as follows: stand upright, facing the wall, about two-thirds of the arm away from the wall; stand each finger separately on the wall, the palm joints protruding, the palms arched, the wrists slightly lower than the palm joints [18]. Then, slowly lean forward, bending elbows and letting weight pour into fingertips and toes to increase their support. After the weight pressure reached the appropriate level, stay for 2 or 3 seconds, slowly push away until the body was upright and return to its original state; let arms down and relaxed a little. Repeat this exercise
- (3) Wrist spring operation: sit with body upright, shoulders and arms relaxed, elbows bent to about 90 degrees

to play close to the body; relax the wrist and open the fingers naturally so that there was about an octave distance between the fingers, 2, 3, 4 fingers slightly raised in an arched hand shape. Then, keep the wrists and elbows of both hands at the original height, with the palm part facing the body direction, which was the upper part of the oblique after instant force, for a quick spring [19]. After that, relax completely and let hands fall naturally. This movement was just like the daily action of knocking on the door with the finger joints. Its force was mainly to bounce upwards. The three joints were used as the central fulcrum of the force to bounce, and the force was quickly concentrated and then relaxed instantly

2.3. Selection of Indicators. After 6 months of treatment, the pain degree, joint mobility, and daily activities of the two groups were compared.

- (1) The degree of pain: using NRS [20] (NRS is a scoring system for pain; the score range is 0-10 points, of which 0-3 points belong to mild pain, 4-7 points belong to moderate pain, and 8-10 points belong to severe pain) to assess the patient's shoulder pain, the scale used 0 to 10 points to represent different degrees of pain; 0 pointed to no pain, 10 pointed to unbearable severe pain, and the middle part indicated different degrees of pain, and it was evaluated once before and after treatment
- (2) Joint mobility: standard for measuring total active range of motion (TAM is a scoring system for evaluating the overall function of the palm advocated by the final results Committee of the American Society of Hand Surgery; TAM is the sum of the angles formed by the maximum flexion of the metacarpophalangeal joint, proximal and distal interphalangeal joints in the fist grip position minus the sum of the limited extension of these joints) [21]: excellent rehabilitation: TAM > 220; good recovery: TAM200~220; poor rehabilitation effect: TAM < 180
- (3) Ability to perform daily activities: both groups were assessed with the Daily Living Activity Scale (FIM, the main evaluation index of FIM is self-care activities, including the impact of walking and hand movement on life) [22]; there were 7 points for each item, a total of 42 points

**2.4. Statistical Methods.** Using SPSS 19.0 statistical software for data analysis, measurement data in line with the normal distribution were expressed as  $X \pm S$ . The comparison between groups was performed by  $t$ -test, statistical data were compared by using the  $\chi^2$  test, and  $P < 0.05$  meant the difference was statistically significant.

### 3. Results

This section follows the relevant standards proposed in the previous section, collates the two groups of data based on the three indicators: pain level, joint range of motion, and daily activity ability, and compares the results.

**3.1. Results of Pain Level.** There was no significant difference in pain level scores between the two groups ( $P > 0.05$ ) before treatment. The limb pain score in the observation group was lower than that of the control group after treatment. Results of pain level are shown in Table 2.

**3.2. Results of Joint Range of Motion.** The effective rate of hand tendon rehabilitation in the observation group was 93.33%. The effective rate of hand tendon rehabilitation in the control group was 70.00%, and the comparison results showed that there was statistical significance ( $P < 0.05$ ). Results of joint range of motion are shown in Table 3.

**3.3. Results of Daily Activity Ability.** There was no difference in daily living ability scores between the two groups ( $P > 0.05$ ), after treatment and before treatment. The scores of washing, wearing a jacket, going to the toilet, eating, bath-

ing, and wearing pants in both groups were all improved. Results of daily activity ability are shown in Table 4.

### 4. Discussion

Piano playing is a highly repetitive activity. The players sit for a long time, their upper limb muscles tense and contract during training and performance, and their wrists and fingers move fast, which brings great hidden dangers to the hand muscle injury of piano players [23]. Some scholars have done experiments to set the metronome at a quarter-note equal to 120 tempo, and the number of repetitions for playing a sixteenth-note one hour continuously is 28,800 times. It is only an hour, and with a little more effort, eight hours a day for more than twenty years, it can imagine how many times our fingers would repeat the work [24, 25]. Piano playing is another highly technical activity. It must be improved after thousands of times of practice. "Repetition" is unavoidable for every piano learner [26]. Highly repetitive performance is a prerequisite for the formation of performance sports injury. Piano skills training must be based on the body structure and muscle energy. Different trainees have their own characteristics in the hand muscle energy structure. They cannot be the same. Training should maximize strengths and avoid weaknesses. At the same time, when practicing the piano, the trainer should consider his own physical condition and avoid excessive exercise for a long time [27]. Modern piano playing requires the player to use hand muscles to coordinate the relaxed upper body and shoulder and arm muscles. How to find a way to relax the muscles while practicing and playing is a challenge that every piano practitioner needs to face [28]. In order to achieve natural, relaxed, and touching performance, players need to adopt macro comprehensive adjustment and micro detail control [29]. Macro comprehensive regulation requires piano players to pay attention to the prevention of hand muscle injury and pay attention to scientific rehabilitation methods after hand muscle injury. We should not blindly rely on drugs for pain relief. Drug pain relief has the characteristics of short term and temporary, so we cannot achieve the basic rehabilitation goals, nor can we keep a fluke mentality [30]. In the absence of external intervention, it is difficult to self-heal the hand muscle injury caused by piano training [31]. If it is not handled properly, it will not only affect the pianist's performance level but also have a great chance to leave sequelae such as finger joint deformation, tenosynovitis, and cervical spondylosis [32, 33]. Micro comprehensive adjustment requires piano players to formulate scientific and reasonable practice time and methods when preventing hand muscle injury. After hand muscle injury, go to the hospital for examination in time. With the help of doctors, formulate scientific health care plans and methods and reserve sufficient hand rest time. Pay attention to relaxing muscles while playing and training, and do scientific hand exercises between playing and training [34].

TABLE 2: Results of pain level.

Groups	Cases	Limb pain VAS		Wrist hand function VAS	
		Before	After	Before	After
Observation group	30	4.15 ± 1.28	2.01 ± 1.09	51.02 ± 17.61	73.06 ± 15.74
Control group	30	4.20 ± 1.34	3.52 ± 1.31	50.36 ± 16.22	70.05 ± 14.91

TABLE 3: Results of joint range of motion.

Groups	Cases	Excellent TAM	Good TAM	Poor TAM	Rate
Observation group	30	16	12	2	93.33
Control group	30	9	12	9	70.00

TABLE 4: Results of daily activity ability.

Groups	Time	Washing	Wearing a jacket	Going to the toilet	Eating	Bathing	Wearing pants	Total
Observation group	Before	3.18 ± 1.07	3.27 ± 1.09	3.17 ± 1.02	3.06 ± 1.04	3.09 ± 1.35	3.09 ± 1.48	19.08 ± 3.57
	After	6.38 ± 0.36	6.07 ± 0.65	6.23 ± 0.52	6.32 ± 0.63	6.78 ± 0.114	6.38 ± 0.23	35.23 ± 7.01
Control group	Before	3.01 ± 1.11	3.15 ± 1.21	3.23 ± 1.52	3.22 ± 1.01	3.26 ± 1.61	3.04 ± 1.71	18.23 ± 4.62
	After	5.64 ± 0.52	5.34 ± 0.33	5.60 ± 1.20	5.41 ± 1.256	5.33 ± 1.01	4.76 ± 1.01	30.45 ± 8.03

There was no significant difference in pain level scores between the two groups ( $P > 0.05$ ) before treatment, and the limb pain score in the observation group was lower than that of the control group after treatment. The effective rate of hand tendon rehabilitation in the observation group was 93.33%. The effective rate of hand tendon rehabilitation in the control group was 70.00%; the comparison results showed that there was statistical significance ( $P < 0.05$ ). Before treatment, there was no significant difference in daily living ability scores between the two groups ( $P > 0.05$ ). After treatment, the scores of washing, wearing a jacket, going to the toilet, eating, bathing, and wearing pants in both groups were all improved. However, the observation group's limb pain score was lower than the control group's, and the observation group's wrist hand function score was higher than the control group's.

## 5. Conclusion

Through the above research, we draw the following three conclusions:

- (1) Hand muscle injury is a common sports injury for piano players, which has the characteristics of high incidence and inevitability. The rehabilitation period of injury is long, which has a great impact on the life of piano practitioners
- (2) ① Arm relaxation exercises, ② finger push-ups, and ③ wrist spring operation: three kinds of body movements are of great help to the rehabilitation of piano players' muscle injuries

- (3) Daily finger exercises are simple and not limited by time and place. Piano practitioners can use the spare time of daily training and performance to exercise for a long time, so as to prevent or recover finger muscle damage caused by piano practice

## Data Availability

The data used to support the findings of this study are included within the article.

## Conflicts of Interest

This paper has no conflicts of interest.

## References

- [1] Y. Huang, "Basic principles of muscle recovery in sports training," *Boxing and fighting*, vol. 10, pp. 70–72, 2021.
- [2] Y. Ma, "How do muscles work?," *English Pictorial (high school edition)*, no. 8, p. 16, 2022.
- [3] Y. Cai, "Avoidance of hand muscle energy injury in piano skill training," *Huang Zhong (Journal of Wuhan Conservatory of music, China)*, no. 1, pp. 181–186, 2013.
- [4] S. Zhou and J. Yang, "Acute finger injury (I) – tendon and ligament," *Chinese general practice*, no. 11, pp. 900–901, 2006.
- [5] G. Pan, G. Wang, and B. Yin, "Application of finger micro coil MRI in the diagnosis of finger joint injury," *TCM bone setting*, vol. 30, no. 2, pp. 45–49, 2018.
- [6] Y. Geng, "Causes and countermeasures of sports injury during piano learning," *Northern music*, vol. 5, pp. 6–7, 2012.
- [7] H. Hao, "Research on piano playing skills," *Drama House*, vol. 5, pp. 57–58, 2018.



## Retraction

# Retracted: Effectiveness Analysis of English Newspaper Reading Teaching Based on Deep Learning from the Perspective of Online and Offline Hybrid Teaching

### Computational and Mathematical Methods in Medicine

Received 17 October 2023; Accepted 17 October 2023; Published 18 October 2023

Copyright © 2023 Computational and Mathematical Methods in Medicine. This is an open access article distributed under the Creative Commons Attribution License, which permits unrestricted use, distribution, and reproduction in any medium, provided the original work is properly cited.

This article has been retracted by Hindawi following an investigation undertaken by the publisher [1]. This investigation has uncovered evidence of one or more of the following indicators of systematic manipulation of the publication process:

- (1) Discrepancies in scope
- (2) Discrepancies in the description of the research reported
- (3) Discrepancies between the availability of data and the research described
- (4) Inappropriate citations
- (5) Incoherent, meaningless and/or irrelevant content included in the article
- (6) Peer-review manipulation

The presence of these indicators undermines our confidence in the integrity of the article's content and we cannot, therefore, vouch for its reliability. Please note that this notice is intended solely to alert readers that the content of this article is unreliable. We have not investigated whether authors were aware of or involved in the systematic manipulation of the publication process.

In addition, our investigation has also shown that one or more of the following human-subject reporting requirements has not been met in this article: ethical approval by an Institutional Review Board (IRB) committee or equivalent, patient/participant consent to participate, and/or agreement to publish patient/participant details (where relevant).

Wiley and Hindawi regrets that the usual quality checks did not identify these issues before publication and have since put additional measures in place to safeguard research integrity.

We wish to credit our own Research Integrity and Research Publishing teams and anonymous and named external researchers and research integrity experts for contributing to this investigation.

The corresponding author, as the representative of all authors, has been given the opportunity to register their agreement or disagreement to this retraction. We have kept a record of any response received.

### References

- [1] Z. Zeng and X. Wang, "Effectiveness Analysis of English Newspaper Reading Teaching Based on Deep Learning from the Perspective of Online and Offline Hybrid Teaching," *Computational and Mathematical Methods in Medicine*, vol. 2022, Article ID 4065527, 9 pages, 2022.

## Research Article

# Effectiveness Analysis of English Newspaper Reading Teaching Based on Deep Learning from the Perspective of Online and Offline Hybrid Teaching

Zheng Zeng and Xi Wang 

*School of Foreign Languages and International Education, Chengdu Technological University, Chengdu, 611730 Sichuan, China*

Correspondence should be addressed to Xi Wang; [wxi2@cdu.edu.cn](mailto:wxi2@cdu.edu.cn)

Received 19 April 2022; Revised 14 May 2022; Accepted 19 May 2022; Published 18 July 2022

Academic Editor: Naeem Jan

Copyright © 2022 Zheng Zeng and Xi Wang. This is an open access article distributed under the Creative Commons Attribution License, which permits unrestricted use, distribution, and reproduction in any medium, provided the original work is properly cited.

In recent years, China's higher education has developed rapidly, and the overall English proficiency of college students has improved significantly. In order to improve the English proficiency of students in higher education, English newspaper reading courses are offered, many of which are elective courses. Reading English newspapers in English can help college students improve their overall English proficiency and benefit them in their future lives. Reading English newspapers can improve students' English in many ways as part of college English teaching activities. For example, it helps students to accumulate common and authentic words and phrases, improve their English reading efficiency and level, and gain a broader perspective. This paper examines the role of English newspaper reading in college English teaching, proposes an effective analysis method of teaching English newspaper reading based on deep learning from the perspective of online and offline hybrid teaching, and tests the effectiveness of the model. Finally, the specific characteristics of English newspapers are combined to propose suggestions for improving the effectiveness of English teaching activities for college students.

## 1. Introduction

English reading teaching was first born in the United States in 1955. It mainly applies newspapers and other publications to school teaching. Its purpose is to improve students' reading ability and writing abilities [1]. At the same time, it can also help students understand and master relevant current affairs news and broaden their horizons. In China, English newspaper reading is mainly to enable English majors to improve their comprehensive ability, including improving the speed and level of reading English newspapers. At the same time, we should be familiar with and understand the writing characteristics of news articles in English-speaking countries such as the UK and the United States and be able to analyze and learn the ideas expressed in English newspapers and articles and some writing skills, so as to effectively improve the reading comprehension level of English majors [2]. In recent years, my country's higher education has developed rapidly, and the overall English level of college

students has been greatly improved. Schools in some big cities have higher and higher requirements for students' English ability and have set up English newspaper reading courses for this purpose, many of which take it as an elective course. English newspaper reading can lay an important foundation for improving the comprehensive English quality of college students, so that students can benefit a lot in their future life [3].

In college English teaching, the content of English reading not only embodies important humanistic value but also has far-reaching social significance. In order to improve the comprehensive English quality of college students, we must not only emphasize the utilitarian idea of English as a tool but also pay attention to the humanistic value behind English, so that college students can deeply realize that English learning can play a great role. It has a profound impact on the cultivation of its own humanistic quality [4]. Therefore, the goal of college English teaching at this stage should not be simply to take some exams but to fully

stimulate the interest and enthusiasm of learning English as a subject by reading English newspapers, so as to cultivate students' ability of independent learning and independent thinking [5]. At the same time, reading English newspapers and periodicals can also broaden students' horizons and better develop students' thinking ability and innovation abilities. After comparing English newspapers and periodicals with college school English textbooks, it can be found that English newspapers and periodicals have the advantages of internationalization, effectiveness, and practicability. Moreover, English newspapers and periodicals cover a wide range of contents, which can enable students to obtain relevant knowledge and information in various fields in the process of reading, help students understand the cultural background of different countries and regions, and enable students to more objectively understand the traditional culture and modern civilization of other countries and peoples [6]. On the other hand, to a certain extent, it can also deepen students' recognition of their own culture, which is conducive to the formation of students' correct outlook on life, and values, and lay a solid foundation for their future study, work, and life [7]. The significance and function of English newspaper reading are shown in Figure 1.

College English courses must include compulsory and elective courses. Students must take mandatory courses in order to learn fundamental English language information and develop basic English language aptitude. Simultaneously, in compulsory courses, we should promote active study habits and scientific and effective learning methods, and students should strengthen their cross-cultural communication skills [8]. Elective courses are to respect and meet the personalized characteristics of students because different students have differences in enrollment, employment, and personal interests. The content of elective courses is generally to further improve students' knowledge and skills in a small field, including English newspaper reading, English speech and debate, and primary English translation. According to relevant survey results, among college English elective courses, the most popular elective course for college students is English newspaper reading [9]. In college English teaching activities, the role of reading newspapers is very obvious. However, in the current college English teaching activities, teachers often overemphasize vocabulary, phrases, grammar, and other knowledge content in textbooks, while ignoring or not understanding the role of English newspaper reading in promoting students' English proficiency [10].

The following is a summary of the research: Section 2 contains the related work. Section 3 discusses the design of application model of the proposed work. In Section 4 contains the experiment and analysis of the proposed concepts. Finally, the conclusion brings the paper to a finish in Section 5.

## 2. Related Work

*2.1. Research Status of Online and Offline Hybrid Teaching.* The online and offline mixed teaching paradigm is based on constructivist learning theory and the application of modern information technology to achieve the development, integration, and exploitation of a variety of teaching

resources [11]. It is a revolutionary teaching approach that improves teaching efficiency and effectiveness by deeply integrating traditional offline classroom teaching content with online teaching, then maximizing the benefits of both online and traditional classroom teaching and fostering their complementarity [12]. During the practice of online and offline hybrid teaching mode, it embodies many functions, such as live recording and broadcasting, teaching interaction, teaching management, online teaching, and a course on-demand. It can effectively build a teaching platform and then organize online teaching to meet the learning needs of contemporary college students. Whether online or offline teaching, students are the main body of teaching and need to carry out various teaching activities centered on students. Therefore, students are participants in the mixed teaching mode [13]. The organization and development of teaching work should pay attention to providing students with learning support and guiding students to actively participate in the mixed teaching mode. Fully mobilize students' learning enthusiasm and initiative and promote teaching reform. The online and offline hybrid teaching mode not only organically combines the two classrooms and highlights the dominant position of students in learning but also reflects the leading role of teachers. It is a new direction of teaching reform and development in colleges and universities [14].

The characteristics of online and offline hybrid teaching are then discussed. To begin, online and offline hybrid teaching is defined as the synchronization of online and offline teaching formats in order to achieve an organic combination. Second, it must be clear that online teaching is not an auxiliary method of hybrid teaching, but the basis for the organization and implementation of teaching activities. Third, in the process of the reform of online and offline mixed teaching modes, a unified mode has not been formed [15]. However, the goal can be determined, which is to effectively improve the teaching effect and students' learning effect, and cultivate students' autonomous learning ability and good learning habits. In the process of curriculum integration teaching, we must clarify the nature of the curriculum. At present, not all the courses in colleges and universities are suitable for online and offline hybrid teaching. We should combine different courses and select the matching online teaching platform and teaching means [16]. Fourth, compared with traditional offline classroom teaching, the time and space of online and offline hybrid teaching modes are not limited, and teaching can be organized and carried out at any time or place. Therefore, the reform of online and offline mixed teaching mode is an inevitable method to break through the traditional teaching and also realizes the reconstruction of the traditional classroom. The concept of online and offline hybrid teaching is shown in Figure 2.

In fact, the online and offline mixed teaching mode reflects the most obvious characteristics, that is, it has changed the traditional teaching structure, and there are differences in the teaching structure between the online and offline mixed teaching mode and the traditional teaching [17]. Under the traditional classroom teaching mode, teachers usually assign preview tasks, and students generally

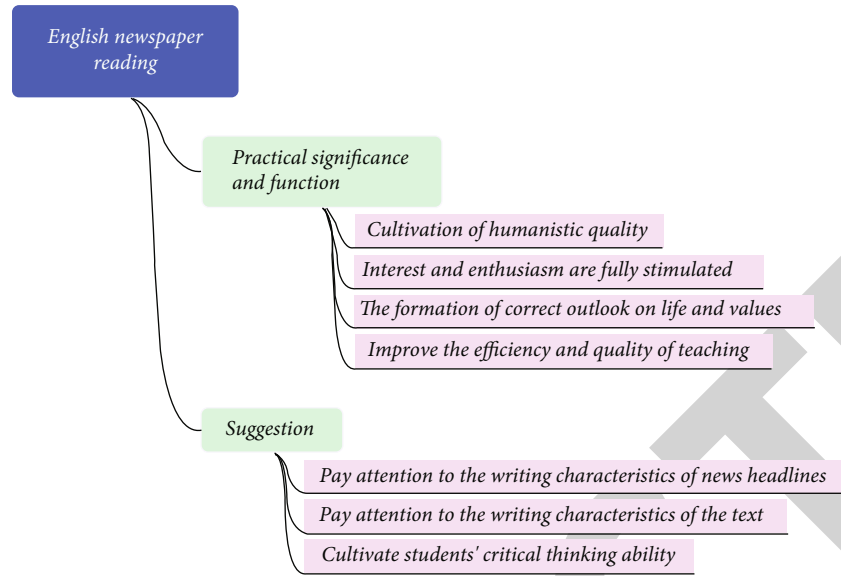


FIGURE 1: The significance and function of English newspaper reading.

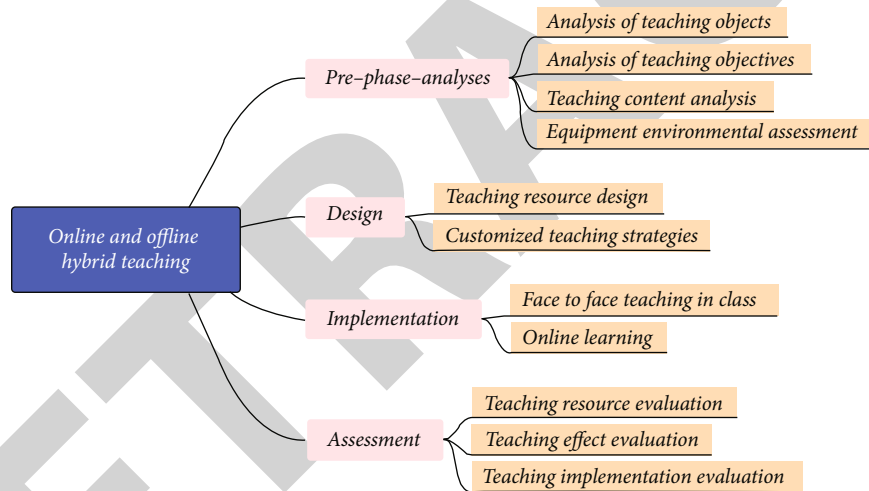


FIGURE 2: The concept of online and offline hybrid teaching.

understand knowledge before teaching. This preview usually lacks guidance, and even many students' preview knowledge content has nothing to do with classroom teaching. The online and offline hybrid teaching structure makes the limited classroom time more valuable. After students fully preview online, teachers do not need to waste a lot of time explaining the theoretical basis [18]. We can carry out in-depth discussions on the key and difficult knowledge, form a good classroom learning atmosphere, make full use of the limited teaching time, and promote the internalization and absorption of students' knowledge.

2.2. *Research Status of English Reading Teaching.* On the whole, domestic scholars have conducted in-depth research on English reading teaching based on the cultivation of core literacy. Although the literature has different expressions on the connotation of core literacy, most agree that focusing on core literacy is to emphasize that education should focus on

people all-around and sustainable development and give full play to the "educating" function of education. Many scholars agree that reading teaching plays an irreplaceable role in cultivating the four-dimensional core literacy of English subjects, but there are many problems in cultivating students' core literacy in college English reading teaching [19]. Domestic research did not begin till recently. The majority of the research focuses on the connotation, relevance, key characteristics, and realization requirements of core literacy [20], with a particular emphasis on the advanced experience at home and abroad in recent years. The research on the interactive relationship between core literacy and education and teaching is not deep enough, the attention to the heterogeneity of the interaction between core literacy and different disciplines is not high, there is a lack of systematic research on how to achieve the educational goal of core literacy training in curriculum teaching reform, and the research on integrating core literacy into English classroom teaching,

especially English Reading Teaching in college, is particularly rare. The five characteristics of English reading teaching are shown in Figure 3.

Most of the existing studies focus on the curriculum teaching practice itself from the perspective of teachers and rarely conduct in-depth research on learning subjects, teaching media, and external factors, especially the lack of relevant research on how students acquire core literacy [21]. Most of the existing studies are aimed at the teaching of reading in schools. There are few studies on how to guide students to read independently and cultivate students' core literacy after class [22]. As for how to cultivate the four-dimensional core literacy of English subjects in college English reading teaching, the existing research mainly focuses on cultivating students' thinking quality, and there are relatively few studies on the other three core literacy. Even in studies that focus on improving students' thinking skills, they tend to focus on abstract levels such as feasibility analysis, direction counseling, and strategy advice [23]. Whether they have guiding value is unknown. Therefore, looking for more practical strategies is worth further discussion. The existing research focuses on the theoretical analysis of reasons, current situation, and strategies and focuses on the experience sharing of fragmentation [24]. Although there are a small number of case studies, it has not formed a systematic and practical teaching model. Therefore, it is an important direction of future research to find an English reading classroom teaching model with universal guiding significance and based on the cultivation of students' core literacy [25]. The research on the effect of English reading teaching on the cultivation of students' core literacy is still in its infancy. Therefore, it is also an important topic of current research to construct a college English teaching evaluation system that not only conforms to the characteristics of China's education and education reform but also reflects the quality of students' core literacy training [26].

**2.3. Research Status of Deep Learning.** Deep learning belongs to machine learning and is a very important branch in the field of machine learning. Understanding the principle of machine learning will help us better understand deep learning. Machine learning is a branch of artificial intelligence. When people talk about artificial intelligence, they often cannot get around machine learning [27]. Obviously, machine learning studies how to make machines learn something independently like people. In short, it is to let the machine find some laws from a large number of sample data through algorithms and then identify new samples or make certain predictions for the future.

The goal of training the computer in supervised learning is for it to construct a one-to-one model from input to output. During training, each machine output will be compared to the right output that has been created ahead of time and changed accordingly [28]. For example, if we want the computer to recognise the photographs of various fruits, we must train it using a huge number of human annotated fruit images. Unsupervised learning has no guide, so there is only the process of inputting data, not the process of outputting comparison. The goal of the training machine is to analyze

the input data to obtain some knowledge of the data, which is typically represented by clustering. Reinforcement learning is a special kind of machine learning algorithm. In some applications, the machine needs to output a sequence of actions rather than a single result. An action excluded from the sequence is meaningless [29]. Only the sequence composed of these actions can achieve the given goal; that is, strategy is more important. Therefore, there is no best action during the execution of the machine. If the action can finally achieve the goal, that is, it is an integral part of a strategy; then, the action is good. In this case, the machine should be able to evaluate the quality of the strategy and get tips from the good action sequence learned before, so as to select the strategy with a higher success rate [30]. At present, there are many network frameworks based on the deep learning algorithms, but they are mostly based on the following four basic network frameworks.

In general, the emergence of deep learning has raised the status of machine learning to a new level, attracted extensive attention from people from all walks of life, and also led to the technological revolution in other fields. The rapid development of deep learning benefits not only from the rapid improvement of computer computing power but also from the contribution of past theories and algorithms. Although there are some limitations, such as the need for a large number of data training, good underlying hardware support, and long training time, its ability to deal with nonlinear problems and strong self-learning ability is unmatched by other algorithms.

### 3. Design of Application Model

**3.1. Classical Feature Extraction Network.** The region proposal network (RPN) region generation network utilised in the fast recurrent-convolutional neural network (R-CNN) develops the target proposal box for the location confidence problem and then approaches the target box using the boundary box regression method. The RPN network is used to judge whether the region corresponding to each point contains the required target. If so, the anchor box is used as an alternative box in the box regression and class regression layer for further correction and judgment. The method is to use a sliding window to select the region through the features to make the effective acceptance domain of the target larger and then further extract the features to perform the parallel operation of box and class in the full connection layer. Solve the problem of different scales under the same characteristics, and divide the width and height of the anchor frame by the coordinate difference to obtain a consistent prediction. The mathematical expression of the loss function is as follows:

$$\text{Loss} = \sum_i^N |t_*^i - W_*^T \Phi_S(A^i)|. \quad (1)$$

In order to minimize the loss, there is a need to be calculated with the following formula:

$$W_* = \operatorname{argmin}_{W_*} \sum_i^N |t_*^i - W_*^T \Phi_S(A^i)| + \lambda W_*. \quad (2)$$

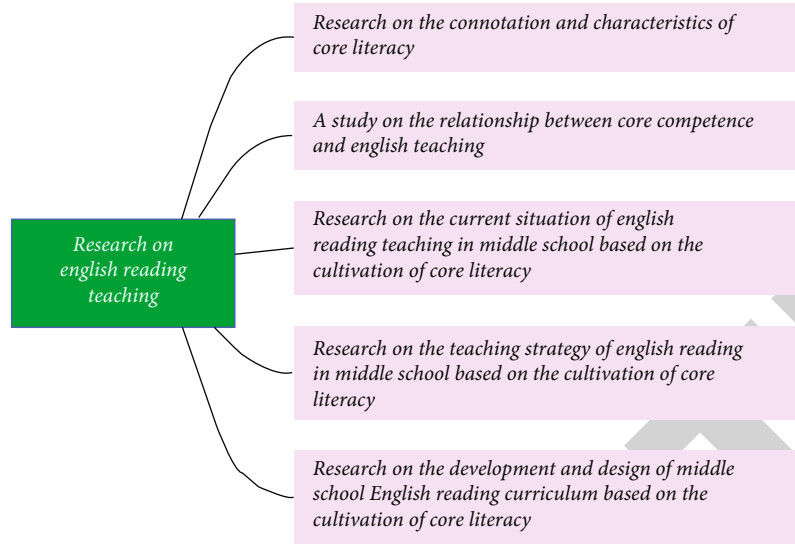


FIGURE 3: The five characteristics of English reading teaching.

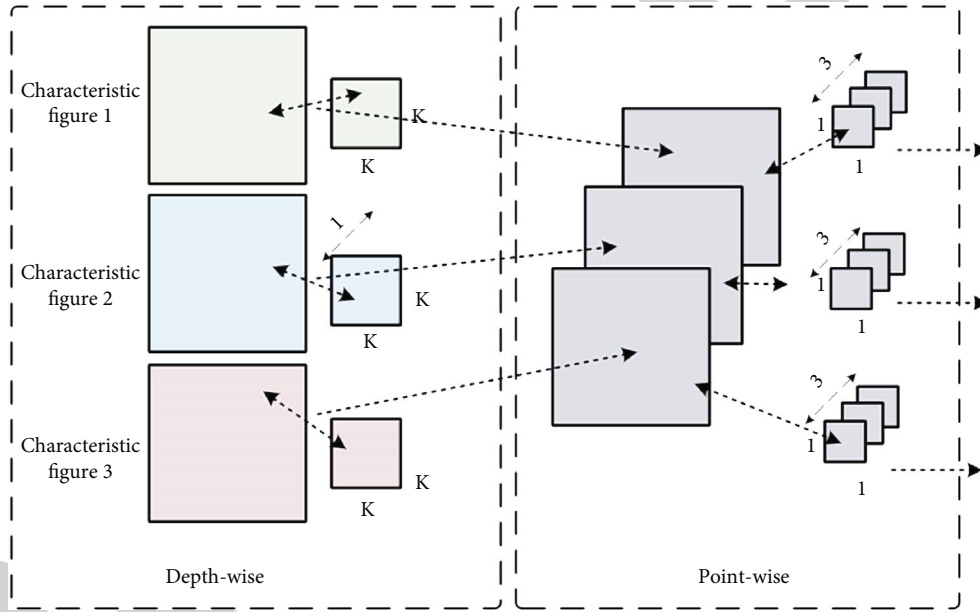


FIGURE 4: The schematic diagram of the classical feature extraction network.

$W_*$  can be obtained by applying gradient descent method or least square method. In order to prevent the over fitting phenomenon in the training process, the penalty factor is added to make the model tend to be stable. The difference between the anchor box and the confidence box is small, and the following expression is satisfied.

$$t_w = \log \frac{B_w^{gt}}{A_w} = \log \frac{B_w^{gt} + A_w - A_w}{A_w} = \log \left( 1 + \frac{B_w^{gt} - A_w}{A_w} \right). \quad (3)$$

When the threshold is introduced, because the overlap rate between the anchor frame and the confidence frame is high, it

can be regarded as an approximate linear transformation. Therefore, the desired region proposal frame can be obtained through the training of the model. While considering the use of IoU value to evaluate the distance between the prediction box and truth box, it is necessary to consider the problem that the gradient is zero and cannot be trained in the process of back-propagation when the IoU value is zero because the two boxes do not intersect. IoU can be expressed by the following formula:

$$IoU = \frac{|B^p \cap B^{gt}|}{|B^p \cup B^{gt}|}. \quad (4)$$

While considering the use of IoU value to evaluate the distance between the prediction box and truth box, it is necessary

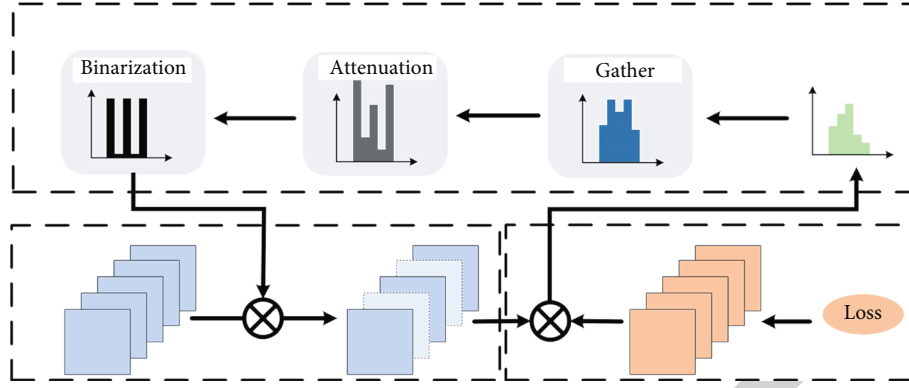


FIGURE 5: The network structure diagram.

TABLE 1: The survey of students' reading interest.

	Really like	Like	Neutral	Dislike
Before experiment	16.70%	26.70%	33.30%	23.30%
After experiment	30%	46.70%	13.30%	10%

to consider the problem that the gradient is zero and cannot be trained in the process of backpropagation when the IoU value is zero because the two boxes do not intersect. IoU can be expressed by the following formula. The schematic diagram of the classical feature extraction network is shown in Figure 4.

Specifically, the candidate target frame with the largest score is removed from the candidate queue and added to the second detection result queue, and then the other prediction frames in the candidate queue are compared with it. The frame with IOU greater than the threshold will be removed from the candidate queue; that is, the prediction frames with lower scores will be suppressed. Rep this process until the candidate box queue is empty and all candidate boxes in this cycle have been completed. The scores of prediction frames under different scales will be obtained in the next cycle due to the change in the anchor frame scale.

**3.2. Improved Depth Neural Network.** For real-time V detection, this chapter provides a closed center distance intersection and union ratio approach. The algorithm combines the standardized distance between the minimum closed box formed by the union of the prediction box and the target box and the center point of the target box and then integrates it into the boundary box regression calculation. The network structure diagram is shown in Figure 5.

The receptive field of deep convolution is large, so it contains more high-level semantic information. It is mainly used to detect large targets at this stage; that is, when the proportion of USV in the image is large, this stage will be dominant. Since each scale will be predicted according to the three preset anchor boxes, the corresponding center point positioning confidence loss can be expressed by the following formula:

$$\text{Loss}_{\text{coord}} = \lambda_{\text{coord}} \sum_{i=0}^{S^2} \sum_{j=0}^B \mathcal{L}_{ij}^{\text{obj}} [(x_i - \hat{x}_i)^2 + (y_i - \hat{y}_i)^2]. \quad (5)$$

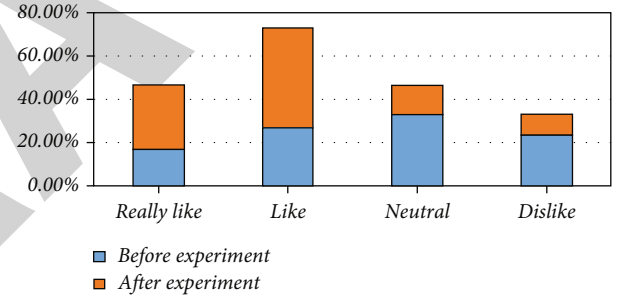


FIGURE 6: The survey of students' reading interest.

The prediction of the confidence of the prediction frame is constrained by the following formula:

$$\text{Loss}_{\text{conf}} = \sum_{i=0}^{S^2} \sum_{j=0}^B \mathcal{L}_{ij}^{\text{obj}} (C_i - \hat{C}_i)^2 + \lambda_{\text{noobj}} \sum_{i=0}^{S^2} \sum_{j=0}^B \mathcal{L}_{ij}^{\text{noobj}} (C_i - \hat{C}_i)^2. \quad (6)$$

That is, the network model is trained end-to-end including the confidence error of the object, the classification error of the prediction target category, and the positioning error of the prediction frame. In the process of backpropagation, the gradient will not decline or fail to reach the local optimal solution. The most direct result is that the expected training model is not obtained. Therefore, in order to make full use of the influence of loss function, some improvements are made according to the characteristics of the spatial target and prediction frame. The calculation formula of the intersection area is as follows:

$$\mathcal{F} = \left( \min(x_2, x_2^{gt}) - \max(x_1, x_1^{gt}) \right) \times \left( \min(y_2, y_2^{gt}) - \max(y_1, y_1^{gt}) \right). \quad (7)$$

TABLE 2: The self-assessment questionnaire for students' reading level.

	Very high	High	Neutral	Low
Before experiment	10%	23.30%	43.30%	23.30%
After experiment	20%	33.30%	36.70%	10%

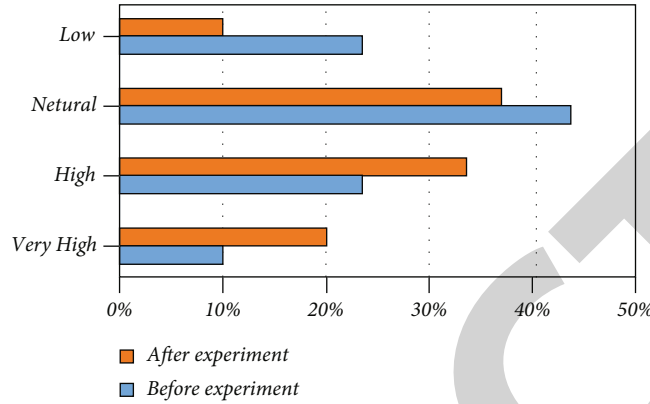


FIGURE 7: The self-assessment questionnaire for students' reading level.

The L1 loss can solve the gradient explosion problem caused by abnormally large loss value caused by outliers in the boundary box regression problem. That is, the introduction of L1 loss suppresses the influence of outliers and outliers. L1 loss is expressed as follows:

$$\text{Smooth}_{L_1}(x) = \begin{cases} 0.5x^2, & \text{if } |x| < 1, \\ |x| - 0.5, & \text{otherwise.} \end{cases} \quad (8)$$

For the loss, the binary cross-entropy is introduced to update the predicted mask.

$$L_{\text{mask}} = \text{BCE}(M, M_{gt}) = -(M_{gt} \cdot \log(M) + (1 - M_{gt}) \cdot \log(1 - M)). \quad (9)$$

In this way, by setting the proportion of each loss in the total loss, we can determine the branch of network key training.

#### 4. Experiments and Results

The author conducted a questionnaire survey, interview, and reading test to collect data and understand the students' reading levels and reading attitudes before the experiment. After adhering to the English newspaper teaching, in order to verify the auxiliary of English newspaper reading teaching to the development of students' reading ability, the authors conducted a series of investigations in the post-test stage. The questionnaire of the posttest survey is still conducted in an anonymous way, and the questionnaires are valid. The purpose of the questionnaire survey in the posttest is to investigate students' attitudes and feelings towards the implementation of newspaper reading. The authors compare and analyze the survey results of the same questions in the pretest questionnaire and the posttest questionnaire. The

survey of students' reading interests is shown in Table 1 and Figure 6.

The number of students interested in English reading has increased dramatically, with 30 percent and 46.70 percent of students indicating interest in English reading, respectively, a 33.30 percent increase over the total before the trial. The survey results show that during the experiment of English newspaper reading assisted reading teaching, most students' reading attitudes and emotions have changed positively, which proves that English newspaper reading can help students improve their reading interest. The self-assessment questionnaire for students' reading levels is shown in Table 2 and Figure 7.

It can be seen that before the experiment, only 33.30% of the students thought their reading level was high, but after the experiment, the number of students who thought their reading level was highly doubled, and the number of students who thought their reading level was high also increased by 10%, but there were still more students who thought their reading level was average, 36.70%. The survey results show that English newspaper reading, as an auxiliary reading, can make a considerable number of students increase their self-confidence, but the improvement of their level and the establishment of personal self-confidence are still subject to individual differences because it is a long and difficult process to greatly improve the self-awareness and reading level of all students. In other words, most students like the mixed learning effect evaluation index system, because the evaluation index system meets the needs of learners for the evaluation effect of English reading learning. The survey of students' weekly reading time is shown in Table 3 and Figure 8.

It can be seen that the students' reading time per week before the experiment is limited, and more than half of the students cannot guarantee even one hour per week. In the process of the experiment, the authors formulated a more detailed reading plan for students, which ensured the increase of



TABLE 3: The survey of students' weekly reading time.

	More than 2 hours	More than 1 hour	Within 1 hour	No reading
Before experiment	10%	23.30%	43.30%	23.30%
After experiment	20%	33.30%	36.70%	10%

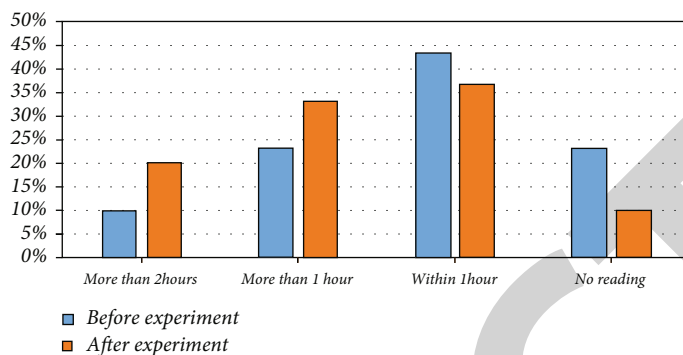


FIGURE 8: The survey of students' weekly reading time.

students' reading time as a whole, and gradually made it become students' reading habits. The survey results show that almost all students can have at least one hour of reading time per week. Maintaining such a stable reading time is very important for students to improve their reading ability, which also shows that the experiment helps students develop good reading habits. Through the comparison of the results of the two questionnaires before and after, the authors find that English newspaper reading has a significant positive impact on students' English learning habits, reading ability, and reading interest, so that students have a more positive learning emotional attitude and obtain more and more comprehensive schema accumulation, which fully reflects the views of theory and schema theory, and the teaching effect is worthy of affirmation.

## 5. Conclusion

This study proves that English newspaper reading plays an auxiliary role in English reading teaching and has a positive impact on the improvement of students' reading ability through theoretical research, actual newspaper reading teaching, and experimental analysis of the development of students' reading ability. Newspaper reading improves students' interest in learning English, which is reflected not only in reading newspapers but also in other English teaching time. The authors also feel that they are more confident in their English level, show a greater desire to improve their English learning performance, and have a great sense of achievement in the expansion of their vocabulary. To increase the amount of reading is to enrich various schemata in students' minds. Anyone with English teaching experience or English learning experience knows that reading is the cornerstone of cultivating writing ability. This paper analyzes and studies the role of English newspaper reading in college English teaching, puts forward an effective analysis method of English newspaper reading teaching based on deep learning from the perspective of online and offline

hybrid teaching, and verifies the effectiveness of the model through experiments.

In the process of English learning, there is no doubt about the importance of reading learning. As a result, our teachers should reflect on and investigate ways to improve their English reading teaching performance. Although this study demonstrates that English newspaper reading is beneficial to English reading instruction, it is apparent that the research has certain shortcomings. The authors hope that in the future teaching, we can also carry out empirical research on the auxiliary effect of English newspaper reading on English writing teaching, have the opportunity to exchange experience, and share achievements related to English newspaper reading teaching with teachers in other schools and further apply the research conclusions to practice for the benefit of students.

## Data Availability

The datasets used during the current study are available from the corresponding author on reasonable request.

## Conflicts of Interest

The authors declare that they have no conflict of interest.

## Acknowledgments

This work was supported by Chengdu University of Technology, research on construction of multidimensional teaching resources for online and offline hybrid courses of the glimpse of the Belt and Road under the background of integration of enterprises with vocational schools and universities (Project No. 20211103).

## Research Article

# Evaluation of Application Effect of Self-Made Compression Cold Therapy in Postoperative Rehabilitation of Patients with Orthopedic Dyskinesia

Xiaojuan Wan , Liping Ji, Min Zhao, Shixiang Zhu, and Meixiu Tang

*The People's Hospital of Rugao, Nantong, Jiangsu 226500, China*

Correspondence should be addressed to Xiaojuan Wan; [jsrgwxj252406@163.com](mailto:jsrgwxj252406@163.com)

Received 24 May 2022; Revised 20 June 2022; Accepted 23 June 2022; Published 18 July 2022

Academic Editor: Naeem Jan

Copyright © 2022 Xiaojuan Wan et al. This is an open access article distributed under the Creative Commons Attribution License, which permits unrestricted use, distribution, and reproduction in any medium, provided the original work is properly cited.

With the accelerated aging of the population, orthopedic injuries have become more collective. Among them, the incidence of ankle fractures remains high. Surgery is an effective way to treat ankle fractures by utilizing special surgical site, complex anatomical structure, and specific surgical methods. With surgical approach, it is easy for basis postoperative blood loss, pain, swelling, and other problems. After surgery, most patients suffer from symptoms of fear, increased pain sensitivity, and excessive irrational concerns about physical movement or activity. Compression cold therapy combines cold therapy with air pressure therapy to ease local exudation, constrict blood vessels, improve circulation, relieve pain, and control inflammation through the effects of low temperature and pressure. Application during the rehabilitation period can prevent joint swelling, reduce muscle soreness, and promote the functional recovery of limbs, which provides an effective guarantee for postoperative rehabilitation of patients with orthopedic dyskinesia. Based on this, it is very important to evaluate the application and effect of self-made compression cold therapy in postoperative rehabilitation of patients with orthopedic dyskinesia. This work proposes a one-dimensional deep convolutional neural network-based method; DenseNet for analyzing the rehabilitation effect of patients with orthopedic dyskinesia after ankle fracture surgery. The approach is to evaluate the rehabilitation effect of self-made compression cold therapy from the perspectives of feature reuse, attention mechanism, and feature decoupling. Experiments on the dataset show that the proposed neural network has better efficacy evaluation performance. The proposed systematic assessment based on the emerging deep learning network has great significance in healthcare domain, particularly in assessing applicability, side effects, and noninvasiveness of treatment methods.

## 1. Introduction

The ankle joint, also known as the talus calf joint, is one of the most important joints in the human body that plays an irreplaceable role in daily life and sports. The ankle joint connects the lower end of tibia and the lower end of the fibula. The talus constitutes the bony structure of the ankle joint. The lower end of the tibia and fibula shapes the articular surface of the talus. The medial malleolus articular surface, the lateral malleolus articular surface, the articular surface of the lower end of the tibia, and the posterior malleolus constitute the ankle point, which accommodates the talus joint head. The wider anterior part of the joint head enters the socket when the foot is dorsiflexed, and the joint

is stabilized. However, in plantar flexion, the narrower posterior part enters the socket, and the ankle joint loosens at this time and is prone to sprain. As overt from the anatomical structure of the ankle joint, the lateral malleolus is lower than the medial malleolus on the coronal plane, and the lateral malleolus is more posterior than the medial malleolus on the sagittal plane. This limits retroversion of the talus, so ankle injuries are most collective in the varus [1]. The stress area of the ankle joint is smaller than that of the knee and hip joint and is the weight-bearing joint closest to the ground [2–6].

Enhanced recovery after surgery (ERAS), which has been advocated in recent years, refers to the implementation of various proven and effective methods through the

perioperative period. It further reduces the traumatic stress of surgical patients, reduces the incidence of various complications, and achieves the purpose of reducing the mortality rate and shortening the length of hospital stay. This speeds up the patient's recovery, where effective analgesia and early postoperative mobilization are important elements of accelerated recovery. In the early stage of fracture injury, the body releases inflammatory response factors, proteases, and other substances, which increase the permeability of local blood vessels. This causes varying degrees of swelling and pain in the joints, and in severe cases, skin tension blisters, which affect the course of surgical treatment and increase the risk of infection. Postoperative swelling and pain are mostly related to surgical incision and intraoperative tissue damage. In severe cases, it will affect the functional exercise and rehabilitation process of the patient's joints. This prolongs the patient's bed rest time and increases the risk of lower extremity venous thrombosis and other complications. The ankle joint is an important joint for people's daily activities and walking. After the injury, normal life and work of the patients will be affected. If the treatment and rehabilitation are not warranted timely, it may also lead to long-term physical and psychological problems [7–11].

Cold therapy induces effects at the application site and spinal cord level through neural and vascular mechanisms, reducing the activation threshold of tissue nociceptors and the velocity of pain nerve signaling. Current research illustrations show that cold therapy reduces tissue blood flow, lowers the temperature of the superficial skin and subcutaneous tissue, slows cell metabolism, and inhibits cell activity [12]. A bone scan study found that 20 minutes of ice on one knee reduced arterial blood flow by 38% and soft tissue blood flow by 26% [13]. Bone resorption, which reflects changes in bone blood flow and metabolism, was reduced by 19%. The traditional ice treatment effect is not ideal, and there are disadvantages such as difficult temperature control, poor patient experience, and easy occurrence of frostbite. At room temperature, condensation droplets that form on the surface of the ice pack may contaminate the cut. The self-made pressure cold therapy device combines cold therapy with pressure therapy and has the advantages of soft material, large coverage area, stable temperature, and pressure, etc. At present, it has been widely used in the rehabilitation of soft tissue injury, joint replacement perioperative period, and fracture patients and has achieved good clinical results [14–17]. The recent approaches proposed in [18–20] may be helpful in predicting and evaluating the therapeutic effect and ensuring accurate decision making [21] in the realm of orthopedics.

Usually, surgery is advised to the patients suffering from kinesiophobia. Therefore, it becomes pertinent to evaluate the therapeutic effect of the self-compressed cold therapy device on patients after orthopedic surgery, which will help to formulate more appropriate rehabilitation measures. The neural network is the evolving machine learning method that can be rightly used in the systematic evaluation. This work utilizes neural networks in the medical domain and proposes a method for evaluating the therapeutic effect of self-made compression cold therapy on patients with dys-

kinesia. By comparing outcomes of the approach with the contemporary methods, it is revealed that the proposed 1D-DenseNet is more robust and accurate. Unlike other convolution neural networks, the approach of separable convolution is applied to the dense module. Moreover, to reduce feature map, an average pooling layer is used in the transition module. A comparatively promising information flow is obtained by escaping residual connections and utilizing fewer parameters. With 96.7% precision and 93.9% recall, an improved 3.2% precision was achieved. The approach recommended has great significance in physical and occupational therapy particularly in assessing applicability of treatment methods followed for cerebral palsy and joint contractures disorders.

The paper arrangements are as follows: Section 2 discusses the related work. Section 3 evaluates the various methods. Section 4 analyzes the experiment and discussion. Section 5 concludes the article.

## 2. Related Work

Leyes et al. [22] mentioned that the incidence of complications after ankle fracture is 5% to 40%, which may occur during conservative treatment and surgical treatment. It is stated in [23] that pain and swelling often occur in the early stage of injury, which causes inconvenience to patients' daily life and exercise, and also increases the medical burden on society. Vuurberg et al. [24] mentioned that the ankle joint is mostly wrapped by blood vessels and tendons. Affected by gravity and the immobilization of the affected limb, the venous and lymphatic drainage of the lower extremity is not smooth, and the blood supply is poor. These factors lead to severe soft tissue swelling after ankle fractures. Kadakia et al. [25] revealed that affected by the swelling and pain of the affected area, patients are prone to negative emotions such as tension and anxiety. Results of the study [26] proved about 18% of ankle sprains and up to 23% of ankle fractures will have distal syndesmotic injuries. If the fracture ends are not properly reduced or the joint injury is not clearly diagnosed, serious joint complications can develop over time with a high degree of ankle instability. Benedick et al. [27] mentioned that ankle fracture is an important risk factor for traumatic arthritis. Tension blisters are a common complication of orthopedic surgeons in the treatment of high-energy and low-energy breakages. Due to the lack of soft tissue coverage of the ankle joint and the bony prominence at the joint, tension blisters are prone to form around the fracture end. Commonly seen in the hours following acute injury, blisters are classified into two types: hyperemic and serous, depending on whether the epidermis is completely separated from the dermis [28].

Collins [29] believes that ice packs can constrict local blood vessels, slow down blood circulation, reduce the exudation and swelling of microcirculation and surrounding tissues, and thus achieve the purpose of reducing tissue metabolic rate. The low-temperature environment can also inhibit the inflammatory response and reduce the release of substances such as histamine. The use of cold therapy in the acute phase of fracture can maintain local low

temperature, reduce muscle tension, and slow down the conduction velocity of pain nerves, thereby exerting an effective analgesic effect. Lin et al. [30] applied cryotherapy in patients after calcaneal fracture surgery, which can effectively reduce the VAS score, and the infection rate is also greatly reduced. Park et al. [31] believe that in the treatment of limb swelling and pain before ankle fracture surgery, either evaporative coolant with ethanol as the main component or traditional ice packs can achieve good results. Winge et al. [32] are of the view that compression therapy can improve circulation, reduce limb swelling, and prevent it by compressing the circulation of limbs and tissues, promoting the return of blood and lymph, and accelerating the absorption of metabolites, inflammatory factors, and pain-causing factors in the blood. Clarkson et al. [33] mentioned that the use of arteriovenous pneumatic pump therapy after ankle fracture surgery can reduce the swelling of the affected area. Compression cold therapy devices combine cold therapy with air pressure therapy. It is treated according to the set time and temperature. In the acute stage of fracture, the effect of low temperature and pressure can reduce local exudation, constrict blood vessels, improve circulation, and achieve the purpose of relieving pain and controlling inflammation. Application during rehabilitation can prevent joint swelling, reduce muscle soreness, and promote functional recovery of limbs. At the same time, it can effectively avoid the occurrence of adverse events related to cold therapy and give patients a more comfortable experience. It has also been proved that continuous compression and cold therapy within 5 days after ankle arthroscopy can effectively control ankle swelling [34]. In the study [35], patients after total knee arthroplasty were treated with compression and cold therapy for 3 days, and the joint range of motion in the intervention group at discharge was greater than that in the control group.

The concept of dyskinesia is proposed in [36], for the treatment of chronic low back pain. Kinesophobia refers to persistent pain caused by physical activity, which makes the patient have an irrational excessive fear of physical activity, thereby increasing the patient's susceptibility to painful injuries, and even the risk of reinjury. Vlaeyen et al. [37] believe that patients with dyskinesia will show a stronger avoidance behavior to a certain behavior, so it is called the fear-avoidance model. Patients experience cognitive and behavioral changes due to fear of movement. Chung et al. [38] pointed out that fear-avoidance belief is one of the main factors leading to postoperative dysfunction in patients and even generalized pain. Francisco et al. [39] found that fear-avoidance performances may lead to loss of limb function and disability in patients.

### 3. Method

Deep learning (DL) is the emerging domain of machine learning deals with algorithms inspired by the structure and function of the human brain. In this study, a DL approach is utilized for analyzing the rehabilitation effect of patients with orthopedic dyskinesia. Details are presented in the following subsections.

*3.1. Basic Theory of CNN.* The convolutional neural network [40] first uses forward propagation to calculate the output value of the neural network and then updates the weights and biases of the neural network through back propagation. The neurons between adjacent layers in CNN are not fully connected but adopt a sparse connection. In addition to the advantages of traditional artificial neural networks, sparse connections in convolutional neural networks also have regularization effects. This increases the generalization ability of the network, avoids overfitting, and the sparse connection also reduces the number of parameters, reduces computational consumption, and enables the network to learn quickly. In addition, the convolutional neural network can directly use the original data as the input of the network, avoiding the tedious preprocessing operations on the original data and the need for prior knowledge. Generally speaking, a typical convolutional neural network mainly includes operations such as convolutional layers, pooling layers, and fully connected layers. The convolutional layer and the pooling layer cooperate with each other to extract features layer by layer and finally complete the classification through several full connections.

The function of the convolutional layer is to extract features based on the feature map output by the previous layer. The three most significant features of the convolutional layer are local perception, multikernel convolution, and parameter sharing. Each neuron only needs to perceive the local features in the image or feature map, and in the high layer of the network, the network will integrate the local information obtained by the low layer together to obtain a more global information. All neurons in the same layer of the convolutional neural network will share the same set of parameters, so the parameters in each neuron and its corresponding local receptive field will be regarded as a position-independent feature extraction method. If only one convolution kernel is included in the convolutional layer, such feature extraction is obviously insufficient. Therefore, each convolutional layer in the convolutional neural network will use multiple convolution kernels to learn more abundant features. More specifically, the essence of the convolution layer is to calculate a new feature map, and the process is to convolve the input feature map with a learnable convolution kernel. The convolution is to do the inner product of the local receptive field and the convolution kernel, that is, multiply each corresponding element one by one and then sum:

$$f_k^C = \sum_c \sum_{x,y} i_c(x,y) e_k(p,q). \quad (1)$$

In theory, the local perception and weight sharing mechanism of CNN reduces the complexity and number of parameters of the neural network to a certain extent. But it is still difficult to directly use all the features extracted by the convolution to train the classifier, because the dimension of the features is still very high, and it will lead to the occurrence of overfitting. In order to solve this problem, the pooling layer is used in the convolutional neural network to downsample the feature map, and the structures of different positions are aggregated and counted to achieve the purpose

of reducing the dimension of the feature map. In the compression of data, common pooling layers have two forms, namely, max pooling and average pooling. Max pooling selects the maximum value in the local receptive field as its output, while average pooling calculates the average value in the local receptive field as the output:

$$Z_k^C = g_p(F_k^C). \quad (2)$$

The convolution and pooling operations are both linear transformations, and the linear model is not expressive enough. It is feasible to operate only some linearly separable data. The activation function introduces nonlinear factors, which can divide the data into smooth curves. Approaching a smooth curve can handle various complex nonlinear data more easily, and the neural network also has better expressive ability and can better fit the objective function. Therefore, the activation function, as a decision function, helps to learn a complex model. Choosing an appropriate activation function can speed up the learning process:

$$T_k^C = g_a(F_k^C). \quad (3)$$

In a fully connected layer, all neurons between adjacent layers are fully connected. The number of input neurons in the fully connected layer is equal to the feature dimension extracted above, the number of output neurons is the same as the number of output categories, and the number of layers and neurons in the hidden layer are designed according to requirements. Furthermore, the output of a convolutional or pooling layer in a convolutional neural network is a multidimensional feature map. Before inputting these multidimensional feature maps to the fully connected layer, all elements of the feature map need to be flattened and concatenated into a one-dimensional vector, which can then be input to the fully connected layer for further computation.

In deep networks, the input data has been artificially normalized. With the step-by-step transmission of input data in each subsequent layer, the distribution of the input data in each subsequent layer will inevitably change, and the problem of internal covariance shift will occur. Batch normalization is used to solve related problems:

$$N_k^C = \frac{F_k^C - \mu_B}{\sqrt{\mu_B^2 + \varepsilon}}, \quad (4)$$

$$BN_k^C = \gamma N_k^C + \beta.$$

**3.2. Postoperative Rehabilitation Evaluation with 1D-DenseNet.** This paper recommends a deep convolutional neural network based on one-dimensional DenseNet for automatic feature extraction and classification of rehabilitation data. Figure 1 depicts the overall architecture of the proposed network. The proposed network structure is collected of three dense blocks and transition blocks in the interval. The input of the network is the patient's physiological data, and the network outputs the efficacy evaluation results.

**3.3. Dense Block.** Depending on the complexity of data, there might be multiple convolutional layers in a neural network. For instance, in AlexNet there are only 5 convolutional layers, in VGG there are 19 layers, while in ResNet there are more than 100 layers. In GoogLeNet, different sizes of convolution kernels are used in the inception module to calculate feature maps. A very significant trend in the field of convolutional neural networks is that the current network is becoming deeper and wider, that is, the number of layers stacked in the network is increasing, and the number of parallel layers is increasing. However, simply increasing the depth and width does not actually make much of a difference. It will also bring a large number of parameters to increase the computational burden and bring about problems such as gradient disappearance and gradient explosion. This makes the network very difficult to train and prone to overfitting, which is not applicable in practical applications. In some deep convolutional neural networks in recent years, some new connection methods have been proposed. Recently, a new connection method has been proposed in dense convolutional neural networks (DenseNet) and has shown outstanding results in the field of image recognition. It densely connects the feature maps in each dense module, that is, the output feature map of the previous layer in a module is used as the input of each subsequent layer, and the network becomes simplified by feature reuse. Therefore, this work introduces this connection method into the evaluation of postoperative curative effect of self-made compression cold therapy on orthopedic patients, so as to reduce the parameter consumption of neural network and realize a very simplified neural network method. Figure 2 shows the structure of a dense block. Figure 3 illustrates the structure of composite layer.

All feature maps densely connected within a dense module can be viewed as a global state. This not only brings feature reuse capability so that higher layers can directly use the feature maps of lower layers but also enables gradients to be passed more directly to lower layers during backpropagation. In the dense module, this paper selects a composite layer composed of multiple nonlinear operations and uses all the feature maps before this layer as input to calculate the output feature map of this layer. And set the growth rate hyperparameter to control the number of output feature maps of each layer. Although by controlling the growth rate, each composite layer produces only  $k$  output feature maps. However, the dimension of the input feature map is still very huge relative to the later layers, so a bottleneck structure composed of operations such as point-by-point convolution is used to control the upper limit of the input dimension. Weight sharing feature is also a feasible approach to reduce the number of trainable parameters and to improve the classification effect of neural network.

**3.4. Transition Module.** If all layers in the network are directly associated in a densely connected manner, the connections in the network will increase squarely. Such a connection pair has a very high consumption of computer memory/memory. If there are  $L$  layers in the network, there will be  $L(L+1)/2$  connections between layers. Therefore, the

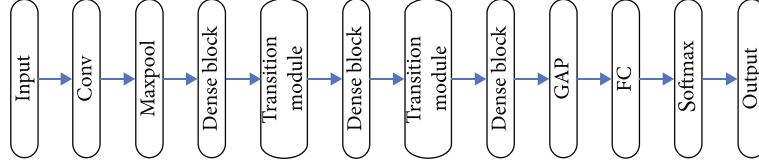


FIGURE 1: The structure of 1D-DenseNet.

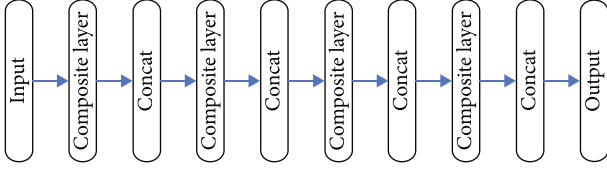


FIGURE 2: The structure of dense block.

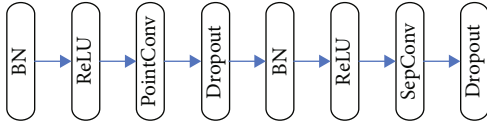


FIGURE 3: The structure of composite layer.

entire network is split into a way of stacking multiple dense modules, and transition modules are used for spacing between adjacent dense modules. In order to reduce the size of the feature map, the number of trainable network parameters need to be reduced. To improve classification effect, to reduce the training parameters, and to extract more global features, average pooling layer is used in the transition module. In addition, a lightweight interchannel attention mechanism from SENet is introduced into each transition module to achieve weighting between feature map channels. Through learning, the weights of more descriptive structures are increased and the weights of irrelevant features are reduced to ensure that more useful information can be sent to subsequent layers for further feature extraction. The structure of transition module is illustrated in Figure 4.

Specifically, this attention mechanism can be separated into two steps of compression and activation. In the first step, global average pooling is used to compress the information in the spatial dimension of the feature map into a channel description vector whose length is the same as the number of channels of the feature map. This can overcome the problem that the useful context information outside the receptive field cannot be utilized because the convolutional receptive field is too small.

**3.5. Separable Convolution.** Inspired by the construction of lightweight neural networks suggested in Xception and MobileNet [41], the concept of separating correlations between channels and spatial dimensions is utilized in feature maps. The paper announces the separable convolution (SepConv) structure combined with one-dimensional convolution and applies it to the proposed network. Separable convolution mainly separates ordinary convolution into two independent convolutions: channel-independent convo-

lution and pointwise convolution. Definition of pointwise convolution, channel-independent convolution and separable convolution:

$$\text{PointConv}(W, y)_{(i)} = \sum_{c=1}^C W_c \cdot y_{(i,c)},$$

$$\text{DepthConv}(W, y)_{(i)} = \sum_{k=-K}^K W_k * y_{(i,k)},$$

$$\text{SepConv}(W_p, W_d, y)_{(i)} = \text{DepthConv}_{(i)}(W_p, \text{DepthConv}_{(i)}(W_d, y)). \quad (5)$$

It has been proved that correlation between channels and spatial dimensions in the feature map can be completely decoupled [42]. Thus, separating ordinary convolutions can significantly reduce parameters and training time. By this way, the nonlinear ability of the network can be improved. Therefore, in the proposed method, the separable convolution is applied to the dense module instead of the ordinary convolution structure. Compared with the previous network using separable convolution, this method eliminates the residual connection and applies the dense connection method to make the information flow in the network more efficient while using a fewer parameters.

**3.6. Loss Function.** A common problem faced by deep learning models is class imbalance, where some classes have significantly more training samples while others have fewer samples. This usually makes the model tend to choose a large number of categories, but often categories with a small number of samples are more critical for research. The class imbalance problem has significant adverse effects on both convergence in training and generalization in testing. The current existing approaches to address this problem can be divided into two broad categories, namely, data-based methods and classifier-based methods.

In this paper, a classifier-based method is adopted, that is, a weighted cross-entropy loss (WCE) is used as the loss function of this neural network. It is a simple extension of the cross-entropy loss function:

$$\text{WCE}(p_t) = -\alpha_t \log(p_t). \quad (6)$$

**3.7. Network Details.** The one-dimensional DenseNet deep convolutional neural network proposed in the paper has a total of 44 layers, which can be mainly divided into three dense modules and spaced transition modules, and the number of layers in each dense module is the same. Feature maps

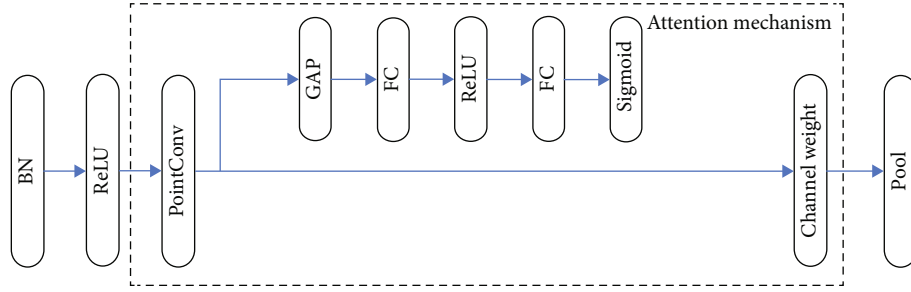


FIGURE 4: The structure of transition module.

TABLE 1: Detailed structure configuration.

Layer	Output size	Configuration
Conv	$1 \times 2500 \times 24$	Conv $1 \times 7$
Pool	$1 \times 1250 \times 24$	Maxpool $1 \times 3$
Dense block (1)	$1 \times 1250 \times 96$	Composite layer $k = 12$ SepConv $1 \times 3$ PointConv
Transition module (1)	$1 \times 625 \times 48$	Attention Avgpool $1 \times 2$
Dense block (2)	$1 \times 625 \times 120$	Composite layer $k = 12$ SepConv $1 \times 3$ PointConv
Transition module (2)	$1 \times 312 \times 60$	Attention Avgpool $1 \times 2$
Dense block (3)	$1 \times 312 \times 120$	Composite layer $k = 6$ SepConv $1 \times 3$
Classifier	$1 \times 1 \times 120$ 4	GAP FC

TABLE 2: Comparison between different methods.

Method	Precision	Recall
SVM	87.90	85.61
BP	91.20	88.71
1D-CNN	93.50	91.81
1D-DenseNet	96.70	93.91

before being fed into the first dense module, a large convolutional kernel of size 7 and stride 2 is used to extract low-level features from the input heart sound segments, and a 24-channel feature map is generated. Then, a max pooling of size 3 and stride 2 is used to reduce the size of the feature maps. In this neural network, each dense module contains 6 composite layers, and the growth rate  $k$  is set to 12. A smaller kernel is used in all separable convolutions of each dense module, the kernel size is set to 3, and the stride is set to 1. The transition modules of densely spaced modules mainly include pointwise convolution, attention mechanism, and an average pooling of size 2. After the last dense module, a global average pooling is used to convert the feature map

into a vector, and full connections and Softmax are used for final classification. See Table 1 for more detailed network structure details about the proposed 1D-DenseNet.

## 4. Experiment and Discussion

This study intends to evaluate efficacy of patients by conducting a comparative study. Details about the dataset and the results obtained from multiple perspectives are given as follows.

**4.1. Used Dataset.** This work uses a self-made dataset to evaluate the efficacy of self-made compression cold therapy in the treatment of dyskinesia in patients undergoing orthopedic surgery. This dataset contains a total of 35,938 samples, of which 23,959 samples are training sets and the remaining 11,979 samples are test sets. The input of each sample is the collected medical data, and the labels correspond to the efficacy grades, which are divided into four different effects. This work is a classification task, and the evaluation metrics used are precision and recall.

**4.2. Method Comparison.** To verify the correctness and effectiveness of the 1D-DenseNet network proposed in this work for evaluating the efficacy of patients, a comparative experiment was conducted. The compared methods include SVM, BP, and 1D-CNN, and the experimental results are shown in Table 2.

It is obvious that the method proposed in this work achieves the highest performance: 96.7% precision and 93.9% recall. Compared to the best strategy of 1D-CNN, 1D-DenseNet can obtain 3.2% precision improvement and 2.1% recall improvement. This verifies the validity and correctness of this work.

**4.3. Result of Dense Block.** As mentioned earlier, this work adopts the dense block strategy. To verify the effectiveness of using this strategy, this work conducts comparative experiments to compare the efficacy evaluation performance with and without dense block, respectively. The experimental results are illustrated in Figure 5.

It is obvious that the highest evaluation performance can be obtained using the dense block. Compared to not using this strategy, 2.1% precision improvement and 1.4% recall improvement can be obtained with a dense block. This verifies the correctness and reliability of the dense block strategy used in this work.

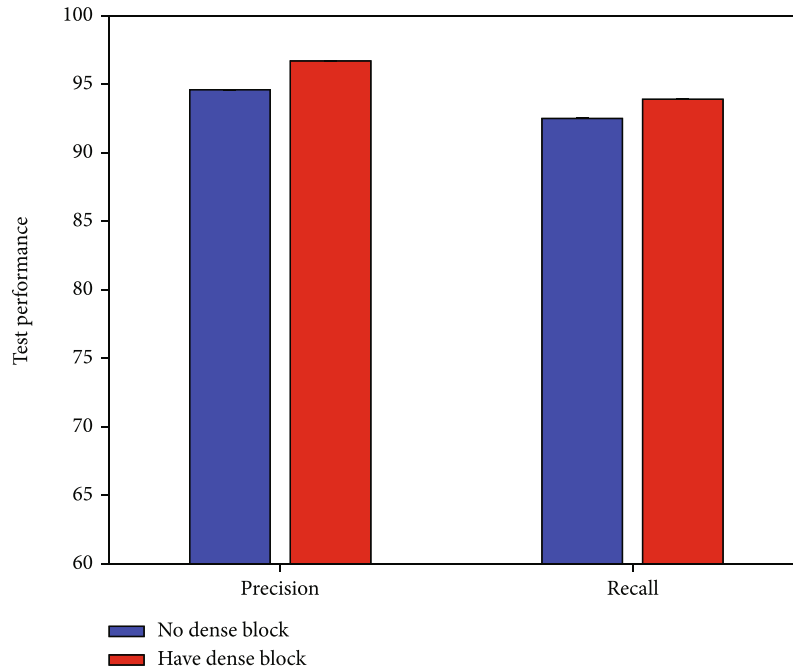


FIGURE 5: Result of dense block.

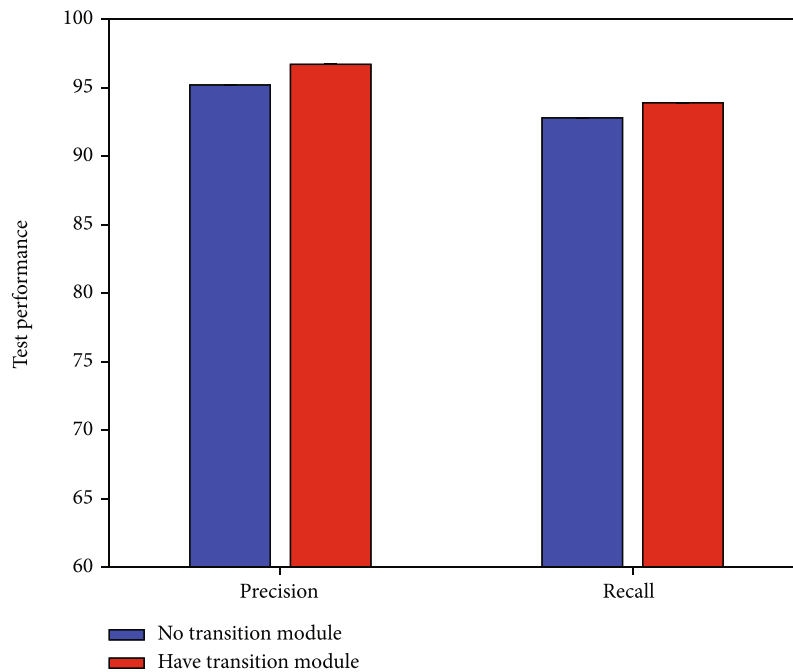


FIGURE 6: Result of transition module.

4.4. *Result of Transition Module.* As mentioned earlier, this work adopts the transition module strategy. To verify the effectiveness of using this strategy, this work conducts comparative experiments to compare the efficacy evaluation performance with and without transition module, respectively. The experimental results are illustrated in Figure 6.

It is obvious that the highest evaluation performance can be obtained using the transition module. Unlike other strat-

egies, 1.5% precision improvement and 1.1% recall improvement are achievable with the transition module. This verifies the correctness and reliability of the transition module strategy used in this work.

4.5. *Result of WCE Loss.* As mentioned earlier, this work adopts the WCE loss strategy. To verify the effectiveness of using this strategy, this work conducts comparative



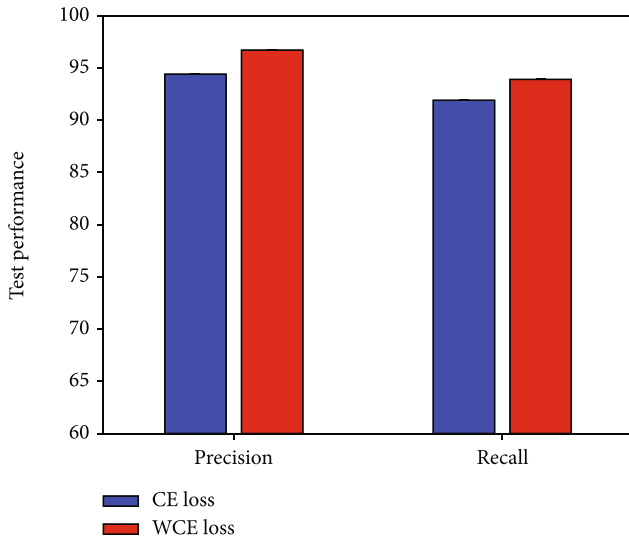


FIGURE 7: Result of WCE loss.

TABLE 3: Result of attention mechanism.

Method	Precision	Recall
No attention	94.9	92.7
Have attention	96.7	93.9

experiments to compare the efficacy evaluation performance with and without WCE loss, respectively. The experimental results are illustrated in Figure 7.

It is obvious that the highest evaluation performance can be obtained using the WCE loss. Compared to not using this strategy, 2.3% precision improvement and 2.0% recall improvement can be obtained with a WCE loss. This verifies the correctness and reliability of the WCE loss strategy used in this work.

**4.6. Result of Attention.** As mentioned earlier, this work adopts the attention strategy. To verify the effectiveness of using this strategy, this work conducts comparative experiments to compare the efficacy evaluation performance with and without attention, respectively. The experimental results are illustrated in Table 3.

It is obvious that the highest evaluation performance can be obtained using the attention mechanism. Encouraging results are obtained by comparing results of the proposed method with those which are without the attention mechanism. As a whole, 1.8% precision improvement and 1.2% recall improvement were obtained with the attention mechanism. This verifies the correctness and reliability of the attention mechanism used in this work.

## 5. Conclusion

Due to the particularity of structure and function, ankle fractures are the most common joint fractures in clinical practice. With the enrichment of leisure life and the development of social aging, the incidence rate has also

increased. Surgery is an effective way to treat ankle fractures. The existence of surgical incisions may main to tissue nerve damage, soft tissue swelling, and pain. If these problems cannot be solved in a timely and effective manner, various complications will occur. Most patients have postoperative kinesiophobia due to pain, and compression cold therapy can control refrigeration and reduce the possibility of tissue damage. Therefore, it is very important to evaluate the efficacy of self-made compression cold therapy on patients with dyskinesia after orthopedic surgery. This will help the medical staff to formulate the next treatment plan. This work proposes a one-dimensional deep convolutional neural network-based technique for analyzing the rehabilitation effect of patients with kinesiophobia after ankle fracture surgery. This work proposes a one-dimensional DenseNet-based network to evaluate the rehabilitation effect of self-made compression cold therapy on patients with orthopedic dyskinesia. In this paper, a deep convolutional neural network with low parameter consumption is constructed starting from the feature reuse of convolutional neural network, attention mechanism, correlation decomposition of feature map space, and channel dimension. Comprehensive and systematic experiments verify the correctness and efficiency of this work. In the future, we are determined to utilize the proposed approach in evaluating efficacy of the surgical treatment of knee arthroplasty, a rising resurfacing surgical technique.

## Data Availability

The datasets used during the current study are available from the corresponding author on reasonable request.

## Conflicts of Interest

The authors declare that they have no conflict of interest.

## Acknowledgments

This work was partially funded by the Nantong Municipal Health Commission (MB2020066).

## References

- [1] K. Venesky, L. Docherty, J. Dapena, and J. Schrader, "Prophylactic ankle braces and knee varus-valgus and internal-external rotation torque," *Journal of Athletic Training*, vol. 41, no. 3, pp. 239–244, 2006.
- [2] E. Caldemeyer, M. Brown, and K. Mulcahey, "Neuromuscular training for the prevention of ankle sprains in female athletes: a systematic review," *The Physician and Sportsmedicine*, vol. 48, no. 4, pp. 363–369, 2020.
- [3] M. Räisänen, T. Kulmala, J. Parkkari et al., "There is no relationship between lower extremity alignment during unilateral and bilateral drop jumps and the risk of knee or ankle injury: a prospective study," *Journal of orthopaedic & sports physical therapy*, vol. 50, no. 5, pp. 267–274, 2020.
- [4] W. Duan, J. Gu, M. Wen, G. Zhang, Y. Ji, and S. Mumtaz, "Emerging technologies for 5G-IoV networks: applications,

- trends and opportunities,” *IEEE Network*, vol. 34, no. 5, pp. 283–289, 2020.
- [5] N. Marshall, S. Valier, A. Yanda, and K. C. Lam, “The impact of a previous ankle injury on current health-related quality of life in college athletes,” *Journal of Sport Rehabilitation*, vol. 29, no. 1, pp. 43–50, 2020.
  - [6] Z. Tian, H. Zhang, and C. Shang, “Farrerol ameliorate adjuvant-induced ankle injury via alteration of PPAR- $\gamma$  signal pathway,” *Journal of Food Biochemistry*, vol. 45, no. 5, article e13585, 2021.
  - [7] B. Pomeranz and J. Bartolotta, “Pediatric ankle injuries: utilizing the Dias-Tachdjian classification,” *Skeletal Radiology*, vol. 49, no. 4, pp. 521–530, 2020.
  - [8] C. Clark and H. Clacher, “Lower-limb motor-performance asymmetries in English community-level female field hockey players: implications for knee and ankle injury prevention,” *Physical Therapy in Sport*, vol. 43, pp. 43–51, 2020.
  - [9] J. Seo, H. Yang, W. Shim, H. Cho, and Y. C. Park, “Marginal impaction associated with posterior malleolar fracture in rotational ankle injury,” *Injury*, vol. 53, no. 2, pp. 756–761, 2022.
  - [10] H. Miller, L. Fawcett, and A. Rushton, “Does gender and ankle injury history affect weightbearing dorsiflexion in elite artistic gymnasts,” *Physical Therapy in Sport*, vol. 42, pp. 46–52, 2020.
  - [11] V. Borra, C. Berry, D. Zideman, E. Singletary, and E. de Buck, “Compression wrapping for acute closed extremity joint injuries: a systematic review,” *Journal of Athletic Training*, vol. 55, no. 8, pp. 789–800, 2020.
  - [12] E. White and D. Wells, “Cold-water immersion and other forms of cryotherapy: physiological changes potentially affecting recovery from high-intensity exercise,” *Extreme Physiology & Medicine*, vol. 2, no. 1, pp. 1–11, 2013.
  - [13] F. Nadler, K. Weingand, and J. Kruse, “The physiologic basis and clinical applications of cryotherapy and thermotherapy for the pain practitioner,” *Pain Physician*, vol. 7, no. 3, pp. 395–399, 2004.
  - [14] J. Alexander, J. Selfe, O. Greenhalgh, and D. Rhodes, “Cryotherapy and compression in sports injury management: a scoping review,” *International Journal of Therapy and Rehabilitation*, vol. 28, no. 10, pp. 1–19, 2021.
  - [15] H. Yang, X. Gong, and M. Zhu, “Case series of acute ankle sprain treated by fumigation and external application of Chinese medicine,” *Global Journal of Medicine*, vol. 1, no. 1, pp. 30–33, 2020.
  - [16] D. Javorac, V. Stajer, L. Ratgeber et al., “Hydrotherapy with hydrogen-rich water compared with RICE protocol following acute ankle sprain in professional athletes: a randomized non-inferiority pilot trial,” *Research in Sports Medicine*, vol. 29, no. 6, pp. 517–525, 2021.
  - [17] J. Tittley, J. Hébert, and S. Roy, “Should ice application be replaced with neurocryostimulation for the treatment of acute lateral ankle sprains? A randomized clinical trial,” *Journal of Foot and Ankle Research*, vol. 13, no. 1, pp. 1–11, 2020.
  - [18] R. Ali, M. Afzal, M. Hussain et al., “Multimodal hybrid reasoning methodology for personalized wellbeing services,” *Computers in Biology and Medicine*, vol. 69, pp. 10–28, 2016.
  - [19] R. Ali, J. Hussain, H. Siddiqi, M. Hussain, and S. Lee, “H2RM: a hybrid rough set reasoning model for prediction and management of diabetes mellitus,” *Sensors*, vol. 15, no. 7, pp. 15921–15951, 2015.
  - [20] R. Ali, H. Siddiqi, M. Idris, H. Kang, and S. Lee, “Prediction of diabetes mellitus based on boosting ensemble modeling,” in *International conference on ubiquitous computing and ambient intelligence*, pp. 25–28, 2014.
  - [21] R. Ali, M. Afzal, M. Sadiq et al., “Knowledge-based reasoning and recommendation framework for intelligent decision making,” *Expert Systems*, vol. 35, no. 2, article e12242, 2018.
  - [22] M. Leyes, R. Torres, and P. Guillén, “Complications of open reduction and internal fixation of ankle fractures,” *Foot and Ankle Clinics*, vol. 8, no. 1, pp. 131–147, 2003.
  - [23] A. Gribble, M. Bleakley, M. Caulfield et al., “Evidence review for the 2016 International Ankle Consortium consensus statement on the prevalence, impact and long-term consequences of lateral ankle sprains,” *British Journal of Sports Medicine*, vol. 50, no. 24, pp. 1496–1505, 2016.
  - [24] G. Vuurberg, A. Hoorntje, M. Wink et al., “Diagnosis, treatment and prevention of ankle sprains: update of an evidence-based clinical guideline,” *British Journal of Sports Medicine*, vol. 52, no. 15, pp. 956–956, 2018.
  - [25] J. Kadakia, M. Ahearn, M. Schwartz, S. Tenenbaum, and J. Bariteau, “Ankle fractures in the elderly: risks and management challenges,” *Orthopedic Research and Reviews*, vol. - Volume 9, pp. 45–50, 2017.
  - [26] P. Gerber, N. Williams, R. Scoville, R. A. Arciero, and D. C. Taylor, “Persistent disability associated with ankle sprains: a prospective examination of an athletic population,” *Foot & Ankle International*, vol. 19, no. 10, pp. 653–660, 1998.
  - [27] A. Benedick, A. Audet, and A. Vallier, “The effect of obesity on post-operative complications and functional outcomes after surgical treatment of torsional ankle fracture: a matched cohort study,” *Injury*, vol. 51, no. 8, pp. 1893–1898, 2020.
  - [28] G. Quevedo, S. Siles, R. Tomba, I. T. Mariño, M. F. B. Bardaji, and F. V. Pareja, “Blisters in ankle fractures: a retrospective cohort study,” *The Journal of Foot and Ankle Surgery*, vol. 56, no. 4, pp. 740–743, 2017.
  - [29] C. Collins, “Is ice right? Does cryotherapy improve outcome for acute soft tissue injury,” *Emergency Medicine Journal*, vol. 25, no. 2, pp. 65–68, 2008.
  - [30] S. Lin, J. Xie, X. Yao, Z. Dai, and W. Wu, “The use of cryotherapy for the prevention of wound complications in the treatment of calcaneal fractures,” *The Journal of Foot and Ankle Surgery*, vol. 57, no. 3, pp. 436–439, 2018.
  - [31] H. Park, H. Song, J. Kim, S. H. Kang, A. S. Chang, and H. J. Kim, “Comparison of the use of evaporative coolants and ice packs for the management of preoperative edema and pain in ankle fractures: a prospective randomized controlled trial,” *Archives of Orthopaedic and Trauma Surgery*, vol. 139, no. 10, pp. 1399–1405, 2019.
  - [32] R. Winge, L. Bayer, H. Gottlieb, and C. Ryge, “Compression therapy after ankle fracture surgery: a systematic review,” *European Journal of Trauma and Emergency Surgery*, vol. 43, no. 4, pp. 451–459, 2017.
  - [33] R. Clarkson, S. Mahmoud, A. Rangan, W. Eardley, and P. Baker, “The use of foot pumps compression devices in the perioperative management of ankle fractures: systematic review of the current literature,” *The Foot*, vol. 31, pp. 61–66, 2017.
  - [34] J. Sultan, T. Zhing, J. Morris, N. Kurdy, and C. McCollum, “Compression stockings in the management of fractures of the ankle: a randomised controlled trial,” *The Bone & Joint Journal*, vol. 96-B, no. 8, pp. 1062–1069, 2014.
  - [35] B. Kullenberg, S. Ylipää, K. Söderlund, and S. Resch, “Postoperative cryotherapy after total knee arthroplasty,” *The Journal of Arthroplasty*, vol. 21, no. 8, pp. 1175–1179, 2006.

- [36] H. Kori, P. Miller, and D. Todd, "Kinesiophobia: a new view of chronic pain behavior," *Pain Management*, vol. 3, pp. 35–43, 1990.
- [37] W. Vlaeyen, M. Kole, G. Boeren, and H. Van Eek, "Fear of movement/(re) injury in chronic low back pain and its relation to behavioral performance," *Pain*, vol. 62, no. 3, pp. 363–372, 1995.
- [38] J. Chung, G. Hur, and H. Lee, "A study of the relationship among fear-avoidance beliefs, pain and disability index in patients with low back pain," *Journal of Exercise Rehabilitation*, vol. 9, no. 6, pp. 532–535, 2013.
- [39] K. Francisco, A. Victor, C. Alejandra et al., "Fear avoidance beliefs do not influence disability and quality of life in Spanish elderly subjects with low back pain," *Spine*, vol. 32, no. 19, pp. 2133–2138, 2007.
- [40] L. Alzubaidi, J. Zhang, J. Humaidi et al., "Review of deep learning: concepts, CNN architectures, challenges, applications, future directions," *Journal of Big Data*, vol. 8, no. 1, pp. 1–74, 2021.
- [41] S. Seo, C. Kim, H. Kim, K. Mo, and P. Kang, "Comparative study of deep learning-based sentiment classification," *IEEE Access*, vol. 8, pp. 6861–6875, 2020.
- [42] J. Tang, M. Liu, N. Jiang, W. Yu, and C. Yang, "Spatial and channel dimensions attention feature transfer for better convolutional neural networks," in *2021 IEEE International Symposium on Circuits and Systems (ISCAS)*, pp. 1–5, 2021.

## Research Article

# Detection of the Content of Two Coumarins, IM and ISOIM, and Their Mechanism of Action on Colitis Rats in *Angelica albicans*

Juan Zhang , Leilei Dong, and Ying Pan

Department of Pharmacy, Third Hospital of Hebei Medical University, Shijiazhuang, 050000 Hebei, China

Correspondence should be addressed to Juan Zhang; xiaojuaner@hebmh.edu.cn

Received 5 May 2022; Revised 30 May 2022; Accepted 17 June 2022; Published 16 July 2022

Academic Editor: Naeem Jan

Copyright © 2022 Juan Zhang et al. This is an open access article distributed under the Creative Commons Attribution License, which permits unrestricted use, distribution, and reproduction in any medium, provided the original work is properly cited.

*Angelica albicans* is being used in the cure of different, respiratory, neuromuscular, and cutaneous diseases in traditional eastern medicine. The pharmacokinetic (PK) characteristics of imperatorin (IM) and isoimperatorin (ISOIM), the main effective components in *Angelica albicans*, were investigated. The rapid, subtle, and measuring the PKs of a drug, a validated UPLC/MS/MS methodology was designed for a total of 2 furanocoumarins in 2,4,6-trinitrobenzene sulfonic acid-stimulated and untreated mice. After that, blood samples were obtained. *Angelica albicans* (0.5 and 1.0 g/kg) was given orally, taken regularly from the tail vein. The time it takes for colitis rats to achieve their maximal concentration ( $T_{max}$ ) imperatorin and isoimperatorin was considerably postponed. In comparison to normal rats, all furanocoumarins had lesser peak plasma concentrations ( $C_{max}$ ) and higher represent residence durations. The area below the  $C_{max}$  time-curve or clearance half-life did not differ significantly. In normal rats, all two furanocoumarins attained maximal plasma levels between 40 and 75 minutes, demonstrating fast oral absorption. The periods to attain  $T_{max}$  of the two furanocoumarins, on the other hand, were shorter than in earlier studies. Therefore, colitis-linked alterations in the drug-absorption stage may result in a late  $T_{max}$  and lowered  $C_{max}$ , which have no effect on its clearance in half-life. Hence, conclusively, as a result, more consideration should be given to the prescription and administration of *Angelica albicans* in colitis individuals, and more research is needed to determine whether the changed PK profile was clinically meaningful for medicinal dose.

## 1. Introduction

*Angelica albicans* is a valuable medicinal herb with a higher vitamin and mineral content that is widely utilized in food and supplements, as well as a natural herb [1]. Marsh tea with communal tansy was utilized as organic pest repellents. *Angelica albicans* has also been demonstrated to have antimicrobial, anti-inflammation, -asthma, -hypertensive, and -cancer activities in recent pharmacological research [2]. In longer-term clinical findings of colitis individuals, *Angelica albicans* alleviated the edema and atrophic patches of the colonic mucous membrane. *Angelica albicans* has been linked to the discovery of more than 70 coumarins. Furanocoumarins, such as imperatorin (IM) and isoimperatorin (ISOIM), are among the most active components of *Angelica albicans* [3]. They have a slew of biological features. IM and ISOIM have anticon-

vulsant, -hypertensive, vasodilator, -inflammatory, -spasmodic, and -cancer properties. The pharmacokinetics (PKs) of the two furanocoumarins in *Angelica albicans* must be assessed in a variety of disease conditions to provide more evidence about their effectiveness and also to truly comprehend the pharmacological underpinnings of their activities [4].

A recent study showed the adipogenic transcription factor peroxisome proliferator-activated receptor (PPAR), as well as the CCAAT enhancer-binding protein (C/EBP), was greatly boosted in mRNA and protein expression by ISOIM. Following isoimperatorin therapy, mRNA development of downriver adipogenesis-linked genomes sterol regulating element-binding transcription factor 1c, fatty-acid synthase, adiponectin, and so on, is grown dramatically. In 3T3-L1 cells, ISOIM enhanced adipogenesis and vastly enhanced lipid formation in a dose-dependent way. ISOIM

increased insulin signalling pathway stimulation by phosphorylating Akt, which is required for PPAR and C/EBP expression and transcription factors. Increased production of the genes FAS, DGAT2, and adiponectin, which are involved in 3 T3-L1 adipocyte development, may have resulted as a result of this [5]. Furthermore, through stimulating G protein-linked bile acid receptors 1 in mice, dietary furocoumarin IM, ISOIM isomer, promotes glucagon-based peptide production, lowering blood glucose [6]. Lipodystrophic individuals also have a triglyceride storage shortage in adipose tissue, which leads to ectopic lipid accumulation and severe insulin resistance [7, 8]. Furthermore, increased fatty capacity storage in adipose tissue paired with slower fat mobilization promotes fat mass growth may be the most efficient approach to store lipids in safe compartments [8]. In their study, they identified that the underlying mode of action through ISOIM which controls the diversity of 3 T3-L1 adipocytes is followed by the accretion of lipids. This research study can subsidize the growth of new medicines which can be used for the management of diabetes and other disorders.

*Angelica albicans* PK investigations in rats have been studied using a variety of analytical methodologies. Gas chromatography is used for measurement in rat plasma of IM [9]. Two ultrahigher-performance liquid methods based on mass spectroscopy (UPLC/MS/MS) by lesser quantification limits (LLOQ) of 5 ng/mL, run lengths of more than 20 minutes, or the need for big plasma samples were also factors. In rats, it was used to investigate the PKs of coumarins produced from herbal remedies [10].

Nonetheless, more sensitive, fast, and particular analytical techniques for instantaneous measurement of target analytes are still needed in PK research. As a result, a sensitivity UPLC/MS/MS technique for the detection of IM as well as ISOIM in rat plasma was developed and validated in this work. Functional and structural changes in the gastrointestinal system, such as lumen pH, flexibility, diarrhoea, and ulcer, can modify the PK profile of active substances administered orally [11]. We investigated whether the PK profiles of herbal therapies are altered in rats with experimentally-stimulated colitis because they are frequently administered orally.

The following is a summary of the research: Section 2 contains the methodology of the proposed work. Section 3 discusses the experiment and results. Finally, the conclusion brings the paper to a finish in Section 4.

## 2. Methodology

ChemFaces (Wuhan, China; Figure 1) provided IM and ISOIM. Sigma-Aldrich provided warfarin as a formic acid, IS, followed via 2,4,6-trinitrobenzene sulfonic acid (TNBS). "MS-grade" water and acetonitrile were used for MS research and plasma production. Raw *Angelica albicans* materials were attained. An ethanolic of *Angelica albicans*, a lyophilized brownish powder, was produced. *Angelica albicans* contained 6.67 and 2.34 mg/g extract of IM and ISOIM, respectively [12].

**2.1. UPLC-MS/MS Study and Technique Corroboration.** The  $C_{\max}$  of two furanocoumarins is measured by employing a Thermo Q-Exactive equipped with an UltiMate 3000. A

Hypersil GOLD column and a gradient method were used for the chromatography-based separation. By a 0.3 mL per minute flow rate, gradient elution is designed. Positive-ion mode, as well as a parallel reaction monitoring (PRM) approach, was used in the MS/MS study [13]. To obtain optimum sensitivity and selectivity with the PRM approach, the spray voltage, capillary temperature, sheath-, auxiliary-gaseous pressure, and resolution were set. Table 1 shows the normalised collision energy for each analyte. Each plasma specimen was chemical degradation with acetonitrile containing IS, vortexed strongly for 5 minutes, and centrifuged to clean the plasma [14]. An aliquot of the filtered supernatant was then fed to the UPLC/MS/MS equipment. The linearity, selectivity, accuracy, precision, retrieval, matrix impacts, and durability of the approach model were all validated. For process corroboration, quality control specimens ( $n = 6$ ) were used at 3 concentrations [15].

**2.2. Animal Study.** The China Animal Ethical centre approved for rats. Male Sprague-Dawley rats weighing 245–260 g were procured and acclimated for seven days in conventional laboratory settings by permitted access to food and water [15]. Thus, experimental colitis is produced by TNBS below isoflurane anaesthesia. The rats were starved for 24 hours before being infected with colitis. The rats are provided with one rectal dosage of TNBS over a pharmaceutical-grade polyurethane catheter in descending colon 8 cm from anus sphincter while under isoflurane anaesthesia [16]. To prevent intracolonic TNBS leaking, the rats are held in a supine Trendelenburg location for 3 minutes after gradually administering the TNBS over 1 minute. On day five of TNBS/50 percent ethanol therapy, normal rats were given 50 percent ethanol rather than TNBS, as well as the animals are employed in the PK investigation [17]. To prevent interfering with the colitis induction, no pain killers were given before the PK research. Normal and induced-colitis animals are randomly assigned to 1 of 4 groups: group 1, *Angelica albicans* 0.5 gram per kg in normal mice; group two, *Angelica albicans* 1 g per kg in normal rats; group three, *Angelica albicans* 0.5 gram per kg in stimulated-colitis mice; group four, *Angelica albicans* 1 g per kg in induced-colitis rats [18]. *Angelica albicans* was made with distilled water and given orally as a continuous gavage. Without anaesthesia, blood specimens are taken from the tail vein at regular intervals for 480 minutes. Blood specimens are centrifuged to extract the plasma, which was then kept at 80°C before usage.

**2.3. Data Study.** All of the data is given as a mean with standard deviation. The programme PK Solver was used to perform a noncompartmental PK study on the time concentration data of two furanocoumarins. Analysis of variance is utilized in comparison with PK constraints among normal and TNBS-treated rats.  $p$  values lesser than 0.05 are measured statistically important [19].

## 3. Results

**3.1. Examination and Method Validation of UPLC/MS/MS**

**3.1.1. Selectivity.** No endogenous intervention in peaking areas of IM at 4.51 min and ISOIM at 5.04 min or a standard

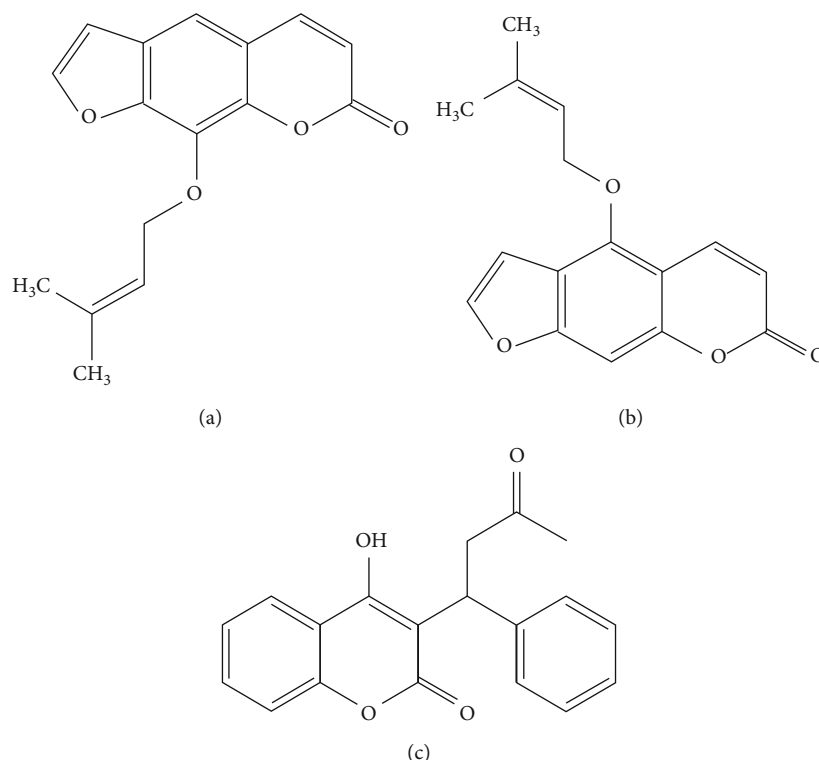


FIGURE 1: Chemical assemblies of (a) IM, (b) ISOIM, and (c) warfarin (internal standard: IS).

TABLE 1: The concept and data on PRM features.

Components	Formula	Precursor ion $[M + H]^+$		Synthesis	Normalized collision energy
		Estimated	Measured		
IM	$C_{16}H_{14}O_4$	281.096	281.095	213.033	20
ISOIM	$C_{16}H_{14}O_4$	281.096	281.096	213.033	20
Warfarin (IS)	$C_{19}H_{16}O_4$	319.112	319.252	261.069	50

solution in blank plasma with/without solutes and reliable plasma specimens underneath a founded UPLC/MS/MS analytical conditions [20] (Figure 2). The figure shows the 203.03345 from 287.09088, 203.03336 from 271.09573, 203.03336 from 271.09573, and most 163.03865 from 309.25220, respectively, were the most numerous and steady result ions of IM and ISOIM (Figure 3). Imperatorin, isoimperatorin, and warfarin (IS) were chosen from 287.09 to 203.03, 271.09 to 203.03, and 309.25 to 163.03.

Their standard curve was linear ( $r > 0.9994$ ), so all analytes by the signal-to-noise ratio of 20 had a lower bound of quantitation (LLOQs) of 1.0 ng per mL (Table 2).

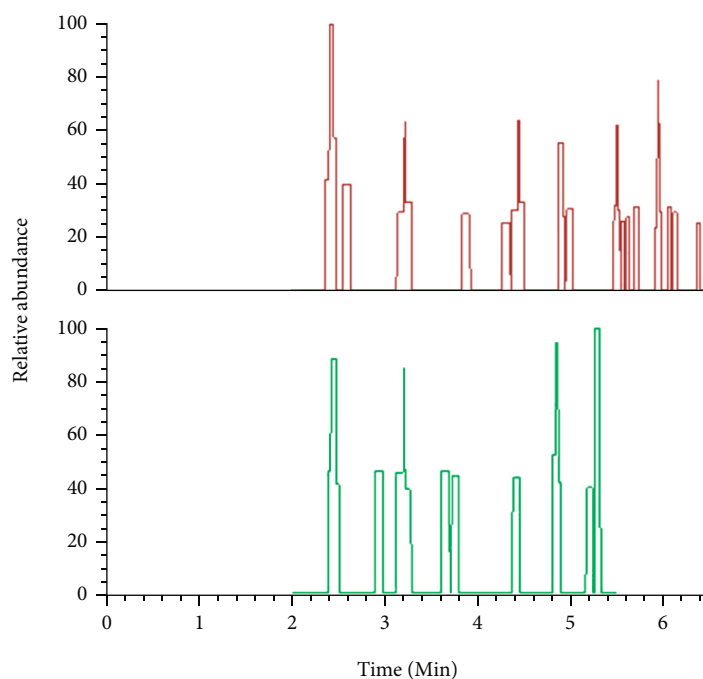
**3.2. Accuracy.** An intra- and interday correctness was reviewed in examinations of specimens for three concentrations of two furanocoumarins on the same day, three different days. All analytes on these day accurateness and precision were 6.9–6.8% and 1.3 percent to -9.4 percent (Table 3).

Table 4 shows an analytes removal efficiency, matrix impacts followed by stabilization in rat plasma. The target analytes were recovered at a rate ranging from 70.3 percent

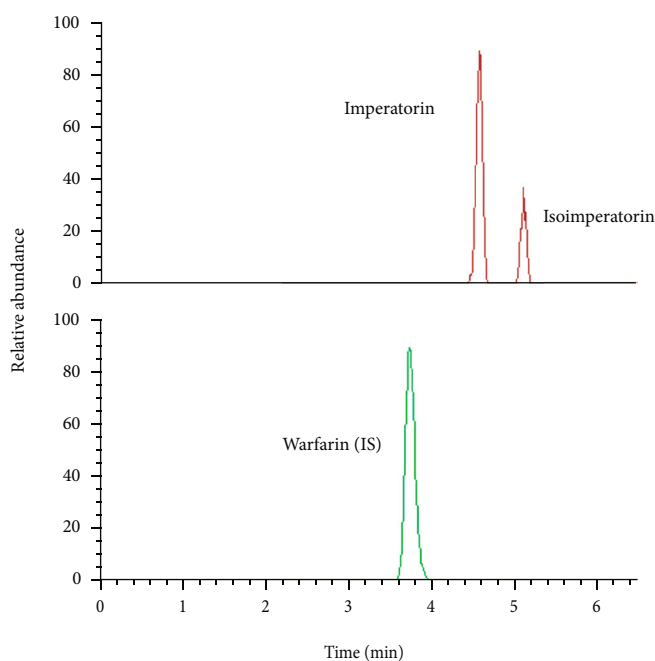
to 97 percent utilising liquid-liquid extraction. The removal efficiencies of acetonitrile, which was used for specimen preparation, were good, and all analytes were recovered reliably and consistently at all concentrations. There was no discernible matrix impact, and the matrix impacts ranged from 85% to 100%. During the specimen storage and processing methods, the target analytes' durability was assessed independently. All target solutes in rat plasma are durable below our simulated circumstances, with stability ranging from 94 percent to 101 percent.

The goal of this research was to create a simple, precise analytical approach for studying the PKs of IM and ISOIM. Due to a decline in blood volume caused by blood loss, the volume of blood serum specimens acquired and continued assembly in the body can modify PK parameters in PK experiments. In comparison to previously described approaches, this projected technique utilizes lesser plasma and required quicker run periods.

In comparison to the approach, the target analytes' sensitivities were increased by over fourfold. In conclusion, we devised a more sensitive, quick, and particular UPLC/MS/MS study, as



(a) Plasma blank



(b) Spiked blank plasma in LLOQ

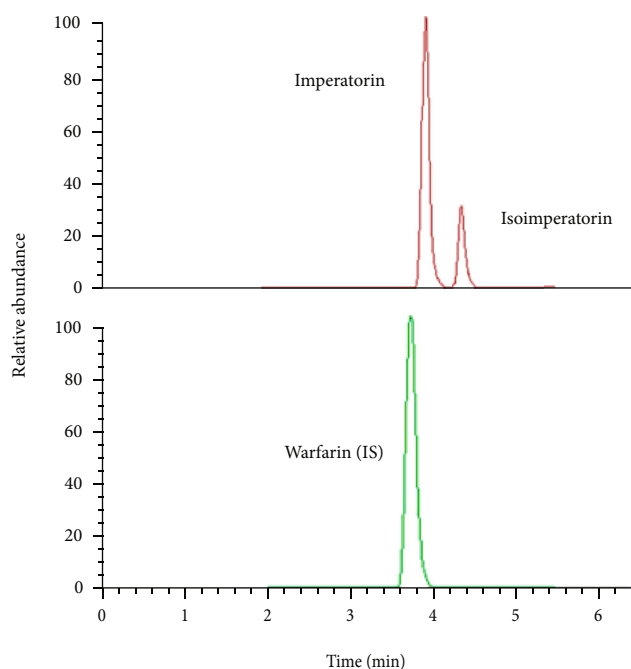
(c) Plasma sample after oral administration of *Angelica albicans*

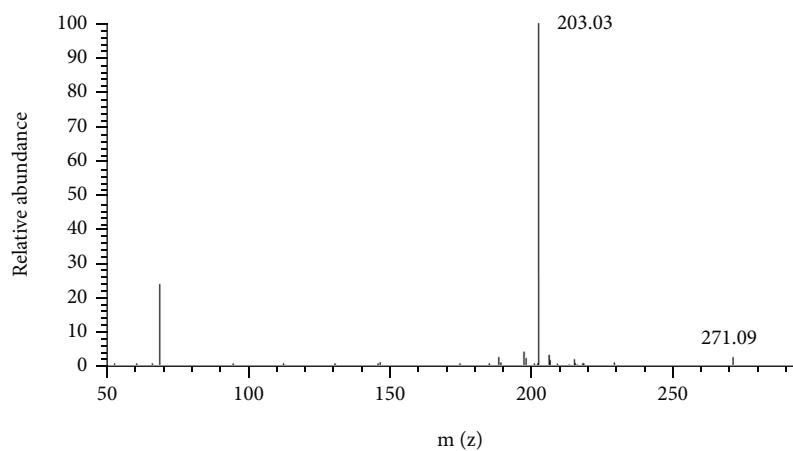
FIGURE 2: (a–c) PRM chromatogram of the analytes and plasma internal standard (IS).

well as a modest specimen preparation procedure, for the real-time measurement of two furanocoumarins in rats [21].

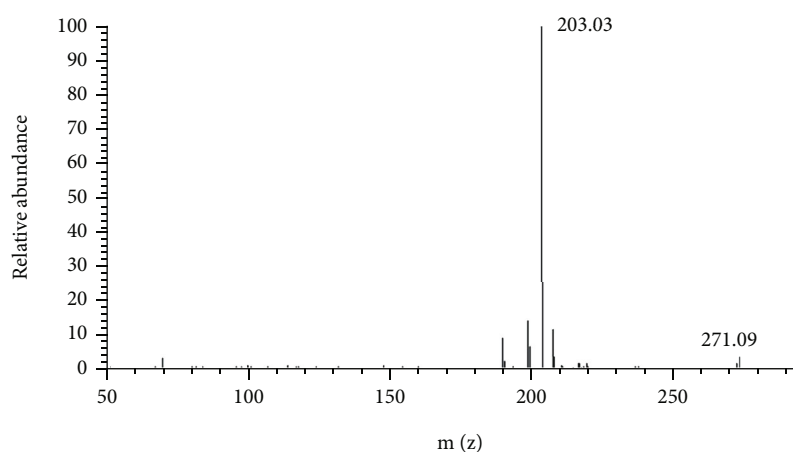
### 3.3. Uses

**3.3.1. Induction of Experimental Colitis.** Within three to seven days after rectal treatment of TNBS, rats develop acute inflammatory and substantial disruption to an intestinal barricade [22]. Ethanol breaks down the mucosa bar-

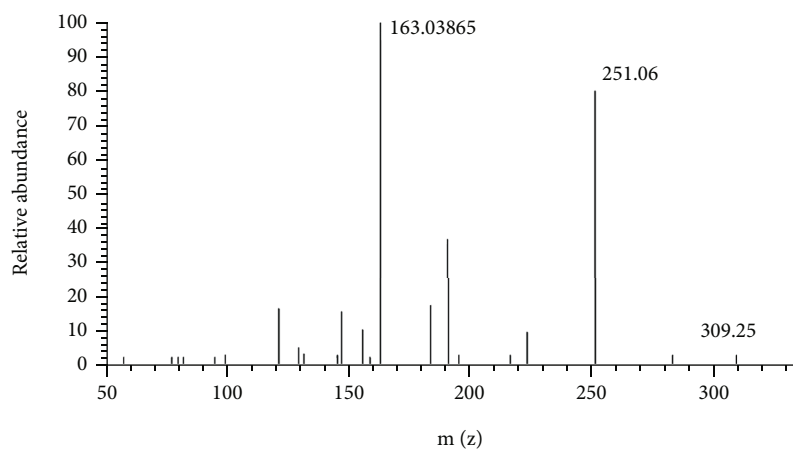
rier, and TNBS haptizes autologous colonies as well as bacterial receptors via the human immune system. The induced-colitis rats in groups 3 and 4 had bloody stools and lost 12.5% and 13.2% of their body weight, respectively. TNBS induced severe ulceration at the instillation area as well as a considerable rise in colon weight, according to necropsy Figure 4. TNBS-treated rats were utilized to see how colitis affects the PKs of furanocoumarins in *Angelica albicans*.



(a) Imperatorin



(b) Isoimperatorin



(c) Warfarin (IS)

FIGURE 3: (a-c) Mass spectroscopy of the analytes and IS.

TABLE 2: Calibration and linearity curves of IM and ISOIM.

Constituent	Range (ng/ML)	Equation of linear regression	Correlation coefficient	LLOQ (ng/mL)
IM	1-200	$Y = 0.08x + 0.013$	0.99	1
ISOIM	1-200	$Y = 0.04x + 0.025$	0.99	1



TABLE 3: Precision and accuracy of IM and ISOIM in rat plasma.

Constituents	Conc. nominal (ng/mL)	Intraday			Interday		
		Estimated conc. (ng/mL)	RE (%)	RSD (%)	Estimated conc. (ng/mL)	RE (%)	RSD (%)
IM	2	1.90	-6.90	8.30	1.90	-4.90	8.70
	50	49.40	-2.20	3.90	49.90	-0.50	4.50
	150	149.10	-0.60	3.80	151.70	1.20	3.10
ISOIM	2	1.90	-5.10	07	02	-4.10	4.40
	50	50.30	01	3.60	48.60	-5.60	2.80
	150	150.20	0.10	1.90	151.40	0.90	1.80

TABLE 4: Extraction recovery, matrix impacts, and stability of IM and ISOIM in rat plasma.

Constituents	Conc. nominal (ng/mL)	Recovery rate in %	Matrix (%)	Durability (%)		
				Free-thaw cycles	At -70 °C for 30 days	At room $T$ for 24 hrs
IM	2	84.9	91	97	99	97
	50	83.4	92	100	101	100
	150	79.8	85	101	94	101
ISOIM	2	85.3	94	101	98	95
	50	75.6	96	98	98	100
	150	70.3	94	95	97	97

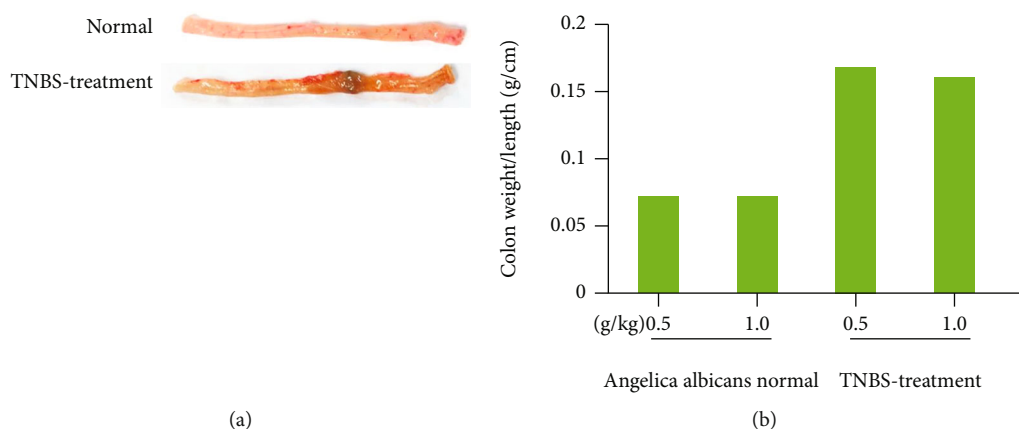


FIGURE 4: TNBS-stimulated experiment-based colitis in rats. (a) Macroscopic presence of normal and injured colon and (b) mass of explanted colon.

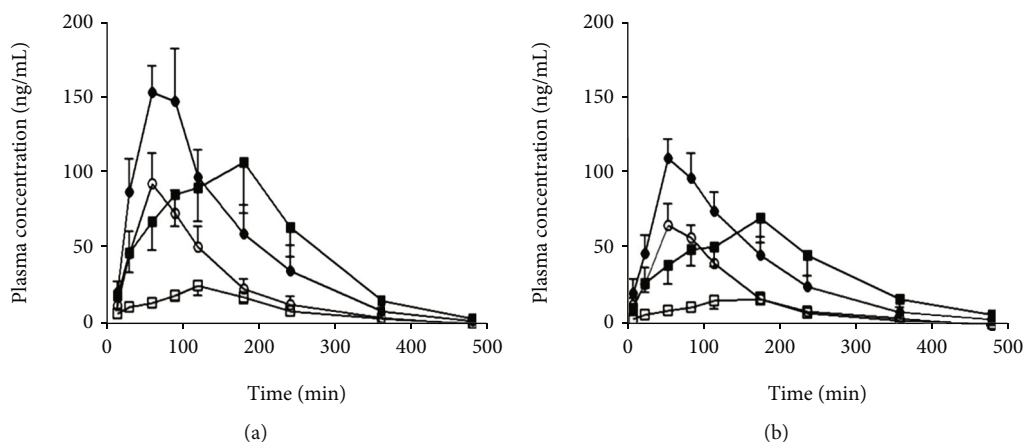
FIGURE 5:  $C_{\max}$ -time curves of (a) IM and (b) ISOIM after oral administration of Angelica albicans.

TABLE 5: Pharmacokinetic properties of IM and ISOIM after oral administration of *Angelica albicans* to normal and experimental-based TNBS-treated rat.

Properties	Normal rat		TNBS-treated rat	
	0.5 g/kg	1 g/kg	0.5 g/kg	1 g/kg
IM	59	61	65	56
$t_{1/2}$ (min)	54	72	113	127
$T_{\max}$ (min)	94	201	27	118
$C_{\max}$ (ng/mL)	11860	23889	5196	24845
$AUC_{0 \rightarrow \infty}$	121	127	172	187
MRT (min)				
ISOIM	63	78	88	68
$t_{1/2}$ (min)	72	67	120	144
$T_{\max}$ (min)	72	128	21	71
$C_{\max}$ (ng/mL)	9445	17778	4197	17881
$AUC_{0 \rightarrow \infty}$	143	145	204	225
MRT (min)				

$t_{1/2}$  denotes half-life,  $T_{\max}$  represents time to attain peak concentration,  $C_{\max}$  signifies plasma concentration peak,  $\rightarrow AUC_{0 \rightarrow \infty}$  is the area in plasma concentration, MRT means mean residence time,  $*p < 0.05$  represents comparison of dosage treated normal rats.

3.3.2. *PKs of Angelica albicans in Untreated and Colitis-Treated Rats.* After orally administered *Angelica albicans*, Figure 5 depicts the mean  $C_{\max}$ -time curves of IM and ISOIM, and Table 5 recapitulates their important PK properties. The  $T_{\max}$  of the two furanocoumarins varied depending on the dose of *Angelica albicans* delivered (0.5 or 1 gram per kg) in both normal and TNBS-used mice [23]. Oral IM and ISOIM PK investigations in normal, as well as treated-colitis rats ( $n = 6$ ), were effective, and two furanocoumarins are verified as biologically available active ingredients of *Angelica albicans*.

All two furanocoumarins reached maximum plasma levels in normal rats between 40 and 75 minutes, indicating rapid oral absorption. The periods to attain maximal concentration ( $T_{\max}$ ) of the two furanocoumarins, on the other hand, were shorter than in earlier studies. The PK profile of one component and the *Angelica albicans* extract after oral administration may differ due to administration composition. In this investigation, the *Angelica albicans* dosages are 4.5 and 9.0 times lesser than those utilized in another study. Extra dosages have been demonstrated to impact PK parameters during the absorption phases in PK studies. The variation in  $T_{\max}$ , in this case, could be attributable to variances in the quantity of furanocoumarin as well as nonfuranocoumarin constituents are the consequence of an *Angelica albicans* manufacturing process and the test substance dose. The  $T_{\max}$  of IM and ISOIM was significantly delayed in colitis rats, ranging from 113 to 144 minutes. The  $C_{\max}$  of IM and ISOIM dropped dramatically to around 50% after *Angelica albicans* injection. The MRT of IM and ISOIM, on the other hand, was increased by 40% to 65% ( $p < 0.05$ ). Comparing normal and colitis-induced rats, the area underneath the  $C_{\max}$ -time curve, as well as the exclusion  $t_{1/2}$  of the

two furanocoumarins, are not substantially diverse. The delayed  $T_{\max}$  and lowered  $C_{\max}$  in colitis-induced rats could be affected during the medication absorption period.

## 4. Conclusion

In PK rat research, a quick, sensitive UPLC/MS/MS technique for its purpose of two furanocoumarins was identified and utilized to investigate the impact of colitis. The effects of colitis on the pace and degree of oral absorption of key bioactive components following *Angelica albicans* administration were initially observed; however, the processes are unknown. As a result, more consideration should be given to the prescription and administration of *Angelica albicans* in colitis individuals, and more research is needed to determine whether the changed PK profile was clinically meaningful for medicinal dose. Modifications in physiological milieu associated with gastrointestinal tract illnesses, such as colitis, might impact intestinal absorption when therapeutic drugs are administered orally, resulting in therapeutic failure or harmful consequences. Dyspepsia, intestinal hypomotility, and late gastric emptying were all symptoms of colitis, as are structural alterations caused by inflammation infiltrates, tissue edema, and ulceration. Dyspeptic symptoms and gastroparesis, which result in lessened and deferred stomach emptying, are common in colitis individuals, and late gastric emptying can affect PK characteristics of oral medications including  $T_{\max}$  and  $C_{\max}$ . In rats with TNBS-induced colitis, a neurological pathway connecting pelvic afferent nerve hyperactivity prevented stomach emptying from causing an increase in intestinal transit. Furthermore, colitis-induced changes in CYP expression and decreased metabolic activity may have an impact on the plasma levels of CYP-metabolized medicines. A study discovered that in TNBS-treated rats, the levels and activity are reduced. IM and ISOIM are converted by liver microsomes into xanthotoxol and heraclenin, through demethylation, oxidation, and so on, and these metabolites have been found in rat plasma, bile, and urine. Without  $AUC_{0 \rightarrow \infty}$ , TNBS-treated colitis caused a reduction in  $C_{\max}$  as well as an interruption in  $T_{\max}$ , suggesting reduced oral absorption of the two furanocoumarins in the current investigation. In pathophysiological settings, an additional mode of study of aspects governing their oral absorption, such as below the conditions indicated above, was required.

## Data Availability

The data used to support the findings of this study can be obtained from the corresponding author upon reasonable request.

## Ethical Approval

The Ethics Committee of the Third Hospital of Hebei Medical University has reviewed and approved this study.

## Conflicts of Interest

The authors declare no conflicts of interest.

## Acknowledgments

This work was supported by department of drug analysis, Hebei Medical University.

## References

- [1] H. Nasri, A. Baradaran, H. Shirzad, and M. Rafeian-Kopaei, "New concepts in nutraceuticals as alternative for pharmaceuticals," *International Journal of Preventive Medicine*, vol. 5, no. 12, pp. 1487–1499, 2014.
- [2] R. I. Korpinen, A. L. Välimaa, J. Liimatainen, and S. Kunas, "Essential oils and supercritical CO<sub>2</sub> extracts of Arctic *Angelica (Angelica archangelica L.)*, marsh Labrador tea (*Rhododendron tomentosum*) and common tansy (*Tanacetum vulgare*)—chemical compositions and antimicrobial activities," *Molecules*, vol. 26, no. 23, p. 7121, 2021.
- [3] D. Kumar, Z. A. Bhat, V. Kumar, and M. Y. Shah, "Coumarins from *Angelica archangelica* Linn. and their effects on anxiety-like behavior," *Progress in Neuro-Psychopharmacology and Biological Psychiatry*, vol. 40, pp. 180–186, 2013.
- [4] L. N. Chan and G. D. Anderson, "Pharmacokinetic and pharmacodynamic drug interactions with ethanol (alcohol)," *Clinical Pharmacokinetics*, vol. 53, no. 12, pp. 1115–1136, 2014.
- [5] T. Jiang, X. Shi, Z. Yan, X. Wang, and S. Gun, "Isoimperatorin enhances 3T3-L1 preadipocyte differentiation by regulating PPAR $\gamma$  and C/EBP $\alpha$  through the Akt signaling pathway," *Experimental and Therapeutic Medicine*, vol. 18, no. 3, pp. 2160–2166, 2019.
- [6] L. Y. Wang, K. C. Cheng, Y. Li, C. S. Niu, J. T. Cheng, and H. S. Niu, "The dietary furocoumarin imperatorin increases plasma GLP-1 levels in type 1-like diabetic rats," *Nutrients*, vol. 9, no. 11, p. 1192, 2017.
- [7] V. T. Samuel, K. F. Petersen, and G. I. Shulman, "Lipid-induced insulin resistance: unravelling the mechanism," *The Lancet*, vol. 375, no. 9733, pp. 2267–2277, 2010.
- [8] S. Virtue and A. V. Puig, "Molecular enzymology of carnitine transfer and transport," *Biochimica et Biophysica Acta (BBA) - Protein Structure and Molecular Enzymology*, vol. 1801, no. 3, pp. 338–349, 2001.
- [9] G. Zhao, C. Peng, W. Du, and S. Wang, "Pharmacokinetic study of eight coumarins of *Radix Angelicae Dahuricae* in rats by gas chromatography-mass spectrometry," *Fitoterapia*, vol. 89, pp. 250–256, 2013.
- [10] A. G. Frenich, J. L. M. Vidal, R. Romero-González, and M. del Mar Aguilera-Luiz, "Simple and high-throughput method for the multimycotoxin analysis in cereals and related foods by ultra-high performance liquid chromatography/tandem mass spectrometry," *Food Chemistry*, vol. 117, no. 4, pp. 705–712, 2009.
- [11] P. Panuwet, R. E. Hunter Jr., P. E. D'Souza et al., "Biological matrix effects in quantitative tandem mass spectrometry-based analytical methods: advancing biomonitoring," *Critical Reviews in Analytical Chemistry*, vol. 46, no. 2, pp. 93–105, 2016.
- [12] J. Widelski, M. Popova, K. Graikou, K. Glowniak, and I. Chinou, "Coumarins from *Angelica lucida* L.-antibacterial activities," *Molecules*, vol. 14, no. 8, pp. 2729–2734, 2009.
- [13] C. Fu, M. Liu, Y. Li et al., "UPLC-Q-exactive orbitrap MS analysis for identification of lipophilic components in citri sarcodactylis fructus from different origins in China using supercritical CO<sub>2</sub> fluid extraction method," *ACS Omega*, vol. 5, no. 19, pp. 11013–11023, 2020.
- [14] L. F. Gamon, C. Guo, J. He, P. Häggglund, C. L. Hawkins, and M. J. Davies, "Absolute quantitative analysis of intact and oxidized amino acids by LC-MS without prior derivatization," *Redox Biology*, vol. 36, article 101586, 2020.
- [15] C. Douny, A. Tihon, P. Bayonnet et al., "Validation of the analytical procedure for the determination of malondialdehyde and three other aldehydes in vegetable oil using liquid chromatography coupled to tandem mass spectrometry (LC-MS/MS) and application to linseed oil," *Food Analytical Methods*, vol. 8, no. 6, pp. 1425–1435, 2015.
- [16] E. Antoniou, G. A. Margonis, A. Angelou et al., "The TNBS-induced colitis animal model: an overview," *Annals of medicine and surgery*, vol. 11, pp. 9–15, 2016.
- [17] M. El-Salhy, K. Umezawa, O. H. Gilja, J. G. Hatlebakk, D. Gundersen, and T. Hausken, "Amelioration of severe TNBS induced colitis by novel AP-1 and NF- $\kappa$ B inhibitors in rats," *The scientific world journal*, vol. 2014, Article ID 813804, 8 pages, 2014.
- [18] F. Algieri, A. Rodriguez-Nogales, T. Vezza et al., "Anti-inflammatory activity of hydroalcoholic extracts of *Lavandula dentata* L. and *Lavandula stoechas* L.," *Journal of Ethnopharmacology*, vol. 190, pp. 142–158, 2016.
- [19] A. Schipani, H. Pertinez, R. Mlota et al., "A simultaneous population pharmacokinetic analysis of rifampicin in Malawian adults and children," *British Journal of Clinical Pharmacology*, vol. 81, no. 4, pp. 679–687, 2016.
- [20] W. Xiong, L. Wang, H. Zhang et al., "Quantitation of apremilast in beagle dogs plasma by UPLC-MS-MS and its application to pharmacokinetic studies," *Journal of Analytical Methods in Chemistry*, vol. 2021, 7 pages, 2021.
- [21] B. C. Nelson, K. Putzbach, K. E. Sharpless, and L. C. Sander, "Mass spectrometric determination of the predominant adrenergic protoalkaloids in bitter orange (*Citrus aurantium*)," *Journal of Agricultural and Food Chemistry*, vol. 55, no. 24, pp. 9769–9775, 2007.
- [22] S. S. Sadar, N. S. Vyawahare, and S. L. Bodhankar, "Ferulic acid ameliorates TNBS-induced ulcerative colitis through modulation of cytokines, oxidative stress, iNOs, COX-2, and apoptosis in laboratory rats," *EXCLI Journal*, vol. 15, pp. 482–499, 2016.
- [23] W. Li, J. Guo, Y. Tang et al., "Pharmacokinetic comparison of ferulic acid in normal and blood deficiency rats after oral administration of *Angelica sinensis*, *Ligusticum chuanxiong* and their combination," *International Journal of Molecular Sciences*, vol. 13, no. 3, pp. 3583–3597, 2012.

## Retraction

# Retracted: Effect of Acupotomy Combined with Electroacupuncture Therapy on Finger Mobility and Pain Relief in Patients with Carpal Tunnel Syndrome

### Computational and Mathematical Methods in Medicine

Received 25 July 2023; Accepted 25 July 2023; Published 26 July 2023

Copyright © 2023 Computational and Mathematical Methods in Medicine. This is an open access article distributed under the Creative Commons Attribution License, which permits unrestricted use, distribution, and reproduction in any medium, provided the original work is properly cited.

This article has been retracted by Hindawi following an investigation undertaken by the publisher [1]. This investigation has uncovered evidence of one or more of the following indicators of systematic manipulation of the publication process:

- (1) Discrepancies in scope
- (2) Discrepancies in the description of the research reported
- (3) Discrepancies between the availability of data and the research described
- (4) Inappropriate citations
- (5) Incoherent, meaningless and/or irrelevant content included in the article
- (6) Peer-review manipulation

The presence of these indicators undermines our confidence in the integrity of the article's content and we cannot, therefore, vouch for its reliability. Please note that this notice is intended solely to alert readers that the content of this article is unreliable. We have not investigated whether authors were aware of or involved in the systematic manipulation of the publication process.

In addition, our investigation has also shown that one or more of the following human-subject reporting requirements has not been met in this article: ethical approval by an Institutional Review Board (IRB) committee or equivalent, patient/participant consent to participate, and/or agreement to publish patient/participant details (where relevant).

Wiley and Hindawi regrets that the usual quality checks did not identify these issues before publication and have since put additional measures in place to safeguard research integrity.

We wish to credit our own Research Integrity and Research Publishing teams and anonymous and named external researchers and research integrity experts for contributing to this investigation.

The corresponding author, as the representative of all authors, has been given the opportunity to register their agreement or disagreement to this retraction. We have kept a record of any response received.

### References

- [1] J. Li, Y. Kou, S. Zhang, and K. Wang, "Effect of Acupotomy Combined with Electroacupuncture Therapy on Finger Mobility and Pain Relief in Patients with Carpal Tunnel Syndrome," *Computational and Mathematical Methods in Medicine*, vol. 2022, Article ID 2550875, 6 pages, 2022.

## Research Article

# Effect of Acupotomy Combined with Electroacupuncture Therapy on Finger Mobility and Pain Relief in Patients with Carpal Tunnel Syndrome

Jianfei Li, Yinqiao Kou , Suzhao Zhang, and Kaibing Wang

Department of Acupuncture and Moxibustion Rehabilitation, Hebei Provincial Hospital of Traditional Chinese Medicine, Shijiazhuang, 050011 Hebei, China

Correspondence should be addressed to Yinqiao Kou; [kouyinqiao@hbszyy.org.cn](mailto:kouyinqiao@hbszyy.org.cn)

Received 26 May 2022; Revised 24 June 2022; Accepted 28 June 2022; Published 14 July 2022

Academic Editor: Naeem Jan

Copyright © 2022 Jianfei Li et al. This is an open access article distributed under the Creative Commons Attribution License, which permits unrestricted use, distribution, and reproduction in any medium, provided the original work is properly cited.

**Objective.** To explore the effect of acupotomy in combination with electroacupuncture therapy on the finger mobility and pain relief in patients who had carpal tunnel syndrome (CTS). **Methods.** The clinical data of 60 CTS patients in our hospital from November 2020 to November 2021 received retrospective analysis. With 30 cases in each group, they were randomly divided into the treatment group and the control group. The control group underwent hot compress, oral medication, and local injection during hospitalization, while the treatment group received acupotomy and electroacupuncture therapy on top of the above treatments, and the clinical effects, finger mobility, and pain relief were compared between both groups. **Results.** The clinical indexes in the treatment group after treatment were remarkably better than those in the control group ( $P < 0.05$ ), with the remarkably higher number of cured cases in the treatment group ( $P < 0.05$ ). After treatment, the treatment group had remarkably higher mean total active motion (TAM) and score of the 36-item short form (SF-36) health survey and a remarkably lower mean score of visual analog scale (VAS) than those in the control group ( $P < 0.001$ ). **Conclusion.** The quality of life and finger mobility of CTS sufferers can be improved with acupotomy in conjunction with electroacupuncture therapy. In-depth research will help build better procedures for these patients because this approach lessens the discomfort and shortens the symptom duration in CTS sufferers.

## 1. Introduction

Carpal tunnel syndrome (CTS) is a peripheral nerve entrapment disease in the upper extremity that occurs when median nerve is injured and compressed in the narrow space of carpal tunnel [1], which is most often diagnosed in women and has a growing trend in prevalence rate in recent years. CTS patients show abnormal sensations in the hands and wrists, the typical symptoms of pain, numbness and abnormal sensation in the radial three fingers, and muscle weakness in severe cases which results in a series of syndromes such as motor dysfunction, bringing about serious psychological burden to patients and declining the quality of life [2, 3]. Clinically preferable treatments for mild to moderate CTS include wrist splinting, therapeutic ultrasonography, and oral medicines. However, these treatments have short-term sustained efficacy and patients

are susceptible to recurrence [4]. Surgical treatments have some efficacy but also bring about complications such as post-operative pain and weakness. As a result, safe and effective nonsurgical methods have great implications for the treatment of CTS [5].

Acupotomy is a modern treatment technique developed with the advancement of medical technology, which combines the features of the acupuncture needle from traditional Chinese medicine and the scalpel from Western medicine in order to better relieve the pathological state of the tissues and restore the dynamic balance of the affected areas. A study [6] has found that acupotomy can effectively reduce pain and greatly shorten the treatment time. A study [7] has confirmed that electroacupuncture has obvious advantages in the treatment of CTS. On the one hand, acupuncture can successfully increase blood flow to the wrist of patients and reduce adhesion

and inflammatory responses in the surrounding tissues; on the other hand, acupuncture relieves spasm, edema, and discomfort by dredging qi and blood in nearby veins. Current research on acupotomy combined with electroacupuncture as a conservative treatment for CTS is still very limited. Therefore, this study further confirms the effect of combined therapy on the finger mobility and pain relief in CTS patients by a comparative study, aiming to search for more evidence for the treatment of this disease.

The paper's organization paragraph is as follows: the research materials and methods is presented in Section 2. Section 3 discusses the experiments and results. Finally, in Section 4, the research work is concluded.

## 2. Materials and Methods

In this section, we define the general data, inclusion and exclusion criteria, methods, observational indexes, and statistical disposal in detail.

*2.1. General Data.* 60 CTS patients chosen from our hospital from November 2020 to November 2021 received retrospective analysis, which was in line with the Declaration of Helsinki (2013) [8]. With 30 cases in each group, the patients were randomly divided into the treatment group and the control group. There were no remarkable differences in clinical data such as age, course of disease, and previous treatments between the two groups ( $P > 0.05$ ), as shown in Table 1.

*2.2. Inclusion and Exclusion Criteria.* Inclusion criteria are as follows. (1) The patients displayed typical CTS symptoms such as sensory loss and numbness in the area of the median nerve distribution, hypoesthesia, and thenar muscle atrophy that were discovered during physical examinations, as well as positive results from the Phalen or Tinel tests; (2) the patients were aged between 18 and 70, with no gender limitations; and (3) the patients had the median nerve motor latency of  $\geq 4.5$  ms and the sensory nerve conduction velocity of  $< 40$  m/s by nerve electrophysiological examination.

Exclusion criteria are as follows: (1) patients with cervical spondylotic radiculopathy or polyneuritis; (2) patients with infections, severe cardiovascular and cerebrovascular diseases, or liver and kidney diseases; and (3) patients with other diseases that cannot be treated with acupotomy or electroacupuncture.

*2.3. Method.* The control group underwent hot compress, oral medication, and local injection, with the specific steps as follows. For two weeks, the patients received heat compress therapy on their carpometacarpal side five times each week for 20 minutes each session. Oral mecobalamin (manufacturer: Eisai China Inc.; NMPA Approval No. H20143107; specification: 0.5 mg \* 10 tablets \* 2 plates/box) was administrated with 0.5 mg each time, with 3 times a day for 2 weeks. The midpoint of the proximal transverse carpal ligament in patients was given local injection of 3 mg of dexamethasone (manufacturer: Guangzhou Baiyunshan Tianxin Pharmaceutical Co., Ltd.; NMPA Approval No. H44022091; specification: 5 mg : 1 ml \* 10 piece) and 3 ml of normal saline, once a week for 2 times.

Based on the therapies received by the control group, the treatment group added acupotomy and electroacupuncture,

with the specific stages being as follows. The entry point was chosen among the midpoint of the proximal transverse carpal ligament, the flexor carpi radialis muscle tendon, and the palmaris longus tendon, and 0.5 ml of lidocaine (manufacturer: Jinling Pharmaceutical Co., Ltd. Nanjing Jinling Pharmaceutical Factory; NMPA Approval No. H20054551; specification: 5 ml : 40 mg) was used for skin anesthesia. The acupotomy was performed with the blade parallel to the path of the tendon and perpendicular to the wrist before switching to a gradual piercing motion toward the distal limb and fingers. At the same time, the patients were asked how they felt about the acupotomy, adjusting the stabbing direction slightly when obvious pain or sense of electric shock occurred. Looking for the sense of loosening when the acupotomy was walking under the transverse carpal ligament, the treatment was terminated after 2-3 times of loosening. Bandaging was done after removing the acupotomy and pressing the pinhole with a sterile cotton pellet for 30 s, and the patients were told to keep the pinhole dry for 24 h. Daling and Jingqu acupoints on the affected side were located according to the acupuncture methods from traditional Chinese medicine and punctured into 3-cun acupuncture needles which were connected to an electro-acupuncture apparatus (manufacturer: Jinan Qiansi Biotechnology Co., Ltd.; model: G6805-II) for treatment, with 20 min each time, once every other day, and three times a week. The continuous waves and intensity were appropriate for the patients to feel weird but no pain.

*2.4. Observation Indexes.* Clinical indexes are as follows. The time from treatment to pain relief, numbness relief, and the distension sensation scores were recorded for both groups, with the marking criteria as follows. The affected part with obvious distension sensation, tension blisters, and a central height of  $> 1$  cm was degree 3 (points); the affected part with increased tension compared to normal skin, clear skin lines, no tension blisters, and a central height of 0.5-1 cm was degree 2 (points); the affected part with mild distension sensation, clear skin lines, and a central height of  $< 0.5$  cm was degree 1 (points); skin with no distension sensation, clear lines, and normal elasticity was degree 0 (points).

Evaluation of efficacy is as follows. (1) Cured: after treatment, the clinical symptoms and signs disappeared, and the wrist and fingers moved freely, with negative result of the carpal flexion and extension test or the Tinel test. (2) Improved: when compared to prior therapy, the clinical symptoms and indicators significantly improved. However, the Tinel test or carpal flexion and extension test revealed positive results, and the wrist was weak after effort. (3) Ineffective: there was no improvement in the clinical signs after treatment, with positive result of the carpal flexion and extension test or the Tinel test.

Mobility of fingers is as follows. The total active motion (TAM) of fingers after treatment was evaluated in both groups with reference to the trial criteria for upper limb function assessment of the Hand Surgery Society of Chinese Medical Association [9]. TAM = active flexion [metacarpophalangeal (MP) + proximal interphalangeal (PIP) + distal interphalangeal (DIP)] - extension deficit (MP + PIP + DIP). Joints extended to  $0^\circ$  were straight, excluding the overstretched part.

TABLE 1: Comparison of clinical data.

Items	Treatment group ( $n = 30$ )	Control group ( $n = 30$ )	$X^2/t$	$P$
Gender			0.278	0.598
Male/female	13/17	11/19		
Mean age (mean $\pm$ SD, years)	44.90 $\pm$ 15.88	45.90 $\pm$ 15.99	0.243	0.809
BMI (mean $\pm$ SD, kg/m <sup>2</sup> )	19.87 $\pm$ 0.92	20.14 $\pm$ 0.84	1.187	0.240
Course of disease (mean $\pm$ SD, months)	2.10 $\pm$ 0.88	1.93 $\pm$ 0.83	0.770	0.445
Previous treatments				
Wrist immobilization brace	20 (66.67)	21 (70.00)	0.077	0.781
Therapeutic ultrasound	3 (10.00)	4 (13.33)	0.162	0.688
Topical corticosteroid injection	5 (16.67)	2 (6.67)	1.241	0.265
Low-level laser therapy	2 (6.67)	3 (7.14)	0.218	0.640
Education levels				
Junior college and above	6 (20.00)	4 (13.33)	0.480	0.488
High school	4 (13.33)	3 (10.00)	0.162	0.688
Middle school	11 (36.67)	14 (33.33)	0.617	0.432
Primary school	6 (20.00)	4 (13.33)	0.480	0.488
Illiteracy	3 (10.00)	5 (16.67)	0.577	0.448
Residence ( $n$ (%))			0.067	0.795
Urban area	14 (46.67)	13 (43.33)		
Rural area	16 (53.33)	17 (56.67)		

TABLE 2: Comparison of clinical indexes (mean  $\pm$  SD).

Groups	$n$	Time from treatment to pain relief (d)	Time of numbness relief (d)	Distension sensation scores (points)
Treatment group	30	5.97 $\pm$ 1.450	5.90 $\pm$ 2.01	1.10 $\pm$ 0.92
Control group	30	9.50 $\pm$ 1.590	7.30 $\pm$ 1.86	2.03 $\pm$ 0.72
$t$		8.985	2.800	4.360
$P$		<0.001	<0.050	<0.050

Relief of pain is as follows. The improvement in pain of patients after treatment was assessed by the visual analog scale (VAS) [10], which needed to prepare a 10 cm graduated line with 0 on the left side as “no pain” and 10 on the right side as “the worst pain.” The physicians rated specific pain scores according to the positions marked by patients on the line.

Quality of life is as follows. The living quality after treatment was assessed by the 36-item short form (SF-36) health survey [11], which consisted of eight parts and was scored out of 100, with a higher total score indicating a better quality of life.

**2.5. Statistical Disposal.** In this work, GraphPad Prism 7 and SPSS 26.0 were used to process the data (GraphPad Software, San Diego, USA) for picture drawing. Count data were tested by  $X^2$  test and represented as  $n$  (%), and measurement data were  $t$  test and  $\bar{x} \pm s$ . The differences were statistically remarkable when  $P < 0.05$ .

### 3. Results

**3.1. Comparison of Clinical Indexes.** The clinical indexes in the treatment group after treatment were remarkably better

than those in the control group ( $P < 0.05$ ), as detailed in Table 2.

**3.2. Comparison of Clinical Efficacy.** The results indicated that the treatment group had a remarkable higher number of cured cases than the control group ( $P < 0.05$ ), with no remarkable difference in the numbers of improved and ineffective cases of both groups ( $P > 0.05$ ), which was detailed in Table 3.

**3.3. Comparison of Mobility of Fingers.** After treatment, the mean TAM in the treatment group was remarkably higher than that in the control group ( $P < 0.001$ ), which was detailed in Figure 1.

**3.4. Comparison of Pain Relief.** The VAS score after treatment in the treatment group was remarkably lower than that in the control group ( $P < 0.001$ ), which was detailed in Figure 2.

**3.5. Comparison of Quality of Life.** After treatment, the mean SF-36 score in the treatment group was remarkably higher than that in the control group ( $P < 0.001$ ), as detailed in Figure 3.

TABLE 3: Comparison of clinical efficacy ( $n$  (%)).

Groups	$n$	Cured	Improved	Ineffective
Treatment group	30	17 (56.67)	11 (36.67)	2 (6.67)
Control group	30	9 (30.00)	14 (46.67)	7 (23.33)
$\chi^2$		4.344	0.617	3.268
$P$		<0.050	0.432	0.071

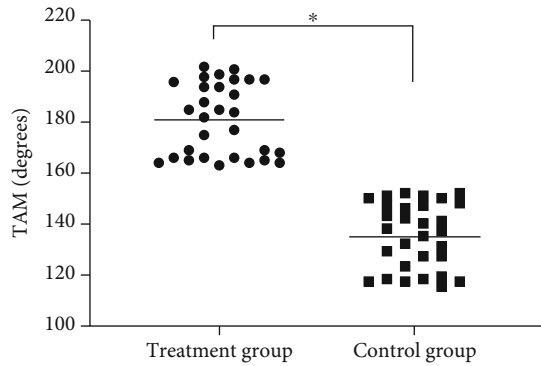


FIGURE 1: Comparison of mobility of fingers after treatment (mean  $\pm$  SD). Notes: the transverse axis was the treatment group and the control group, and the longitudinal axis was the TAM (degrees). The mean TAM in the treatment group and the control group was  $181.03 \pm 14.22$  degrees and  $135.33 \pm 12.92$  degrees, respectively. \* suggested remarkable differences in terms of the mean TAM between both groups ( $t = 13.028$ ,  $P < 0.001$ ).

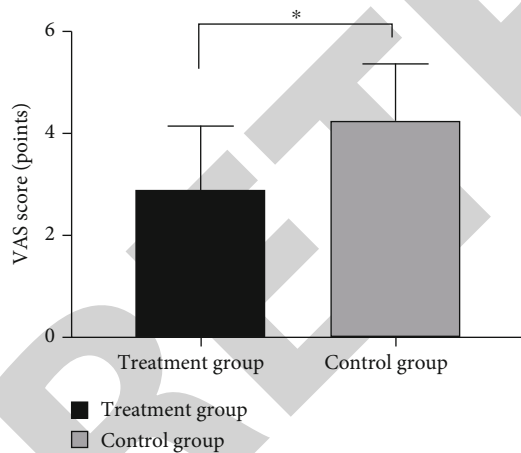


FIGURE 2: Comparison of pain relief (mean  $\pm$  SD). Notes: the transverse axis was the treatment group and the control group, and the longitudinal axis was the VAS score (points). The VAS scores in the treatment group and the control group were  $2.90 \pm 1.27$  points and  $4.27 \pm 1.14$  points, respectively. \* suggested remarkable differences in terms of VAS scores between both groups ( $t = 4.397$ ,  $P < 0.001$ ).

#### 4. Discussion

CTS is a common peripheral nerve entrapment disease in clinic [12], whose pathological manifestations are chronic inflammatory edema and thickening of transverse carpal ligament, compression and degeneration of median nerve, and adhesion of

the peripheral tissues [13]. The median nerve, which is composed of the anterior rami of the spinal nerve  $C_6-T_1$ , descends between the flexor digitorum superficialis and flexor digitorum profundus into the wrist and crosses the carpal tunnel to reach the palm of the hand on the deep side, distributing over the partial skin of the palm and dorsal parts of the index, middle, and the ring fingers [14, 15]. CTS mostly occurs in manual workers, but with the popularization of computers in recent years, its incidence has increased dramatically.

Pain and numbness are the most frequent clinical symptoms in patients with CTS [16] whose current treatments are mainly conservative therapies that are ineffective and time-consuming and the appropriate treatments remain unclear. Some scholars [17] believe that when the median nerve is compressed, the nerve blood circulation will be affected, resulting in ischemic edema and congestion, leading to nutritional impairment and subsequent nerve atrophy which induces the development of CTS. CTS belongs to the category of flaccidity syndrome and tendon injury in traditional Chinese medicine. *Suwen-Yinyang Yingxiang Dalun* (*The Great Treatise on Yin and Yang's reflection of signs*) says that "blockage of qi brings about pains, injury of form leads to swelling." CTS is mostly caused by the lack of healthy energy in the body and weiqi's insecurity of defense, which induces the invasion of wind pathogen [18]. Acupuncture and moxibustion at acupoints can dredge the meridians and collaterals and induce diuresis to alleviate edema and pain, thereby reducing the volume of carpal tunnel contents and alleviating the compression of median nerve. Animal experiments have also fully confirmed [19] that the stimulation of acupuncture and moxibustion can promote the regeneration of peripheral nerves. In addition, acupotomy can release the nerve compression with remarkable efficacy while avoiding incisions on patients. It provides the possibility of recovery of the median nerve by loosening the transverse carpal ligament, releasing the pressure on the carpal tunnel and the nerve compression, which serves to alleviate muscle tension and reduce wrist pain, as confirmed in a study by Chen et al. [20].

The study was conducted using a randomized controlled trial, drawing on previous treatment experience. Patients in the control group was treated with hot compress, oral medication, and local injection during hospitalization, while the treatment group received acupotomy and electroacupuncture therapy on top of the above treatments. In terms of clinical effects, the treatment group after treatment had a remarkably higher cure rate than the control group ( $P < 0.05$ ), probably because acupotomy reduced the compression on median nerve in the carpal tunnel by cutting and loosening the transverse carpal ligament, addressing the cause of the disease at its source [21]. Some scholars believe that [22, 23] the acupotomy treatment of CTS improves blood circulation, accelerates metabolism, and better repairs muscle ligament injury. Electroacupuncture promotes the repair of median nerve and the recovery of wrist function and can also dredge local meridian qi [24]. In contrast, although the treatment plan of hot compress, oral medication, and local injection can reduce the clinical symptoms to a certain extent, the sustained efficacy is short and the disease are easy to relapse [25]. In terms of pain alleviation and finger mobility, the treatment group did better



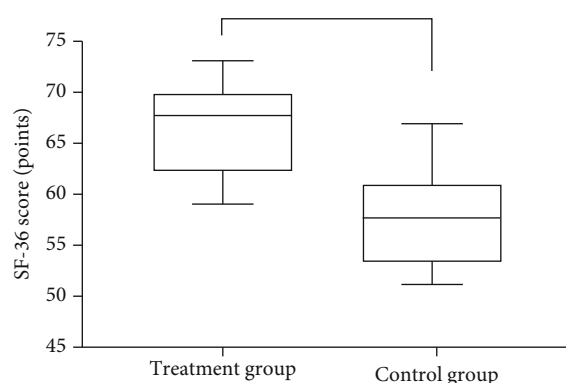


FIGURE 3: Comparison of SF-36 score (mean  $\pm$  SD). Notes: the transverse axis was the treatment group and the control group, and the longitudinal axis was the SF-36 score (points). The mean SF-36 scores in the treatment group and the control group were  $66.47 \pm 4.51$  points and  $57.77 \pm 4.84$  points, respectively. \* suggested remarkable differences in terms of the mean SF-36 scores between both groups after treatment ( $t = 7.203$ ,  $P < 0.001$ ).

than the control group, indicating that acupotomy combined with electroacupuncture therapy can promote the finger mobility and relieve the pain efficaciously, so as to achieve the purpose of treating peripheral nerve injuries and restoring their function.

In conclusion, acupotomy combined with electroacupuncture therapy has a high clinical application value in the treatment of CTS. This combination can increase finger mobility, reduce discomfort, and enhance quality of life. Further research will support the development of a better regimen. Limited by the research conditions, the study has a small sample size and a short follow-up course, of which the expansion is required to further validate the effectiveness of study in the future.

## Data Availability

Data to support the findings of this study is available on reasonable request from the corresponding author.

## Conflicts of Interest

The authors do not have conflicts of interest to declare.

## References

- [1] L. L. Yuan, M. Yang, W. D. Xu et al., "Clinical observation of arthroscopic single channel treatment of carpal tunnel syndrome with self-made instruments," *Zhongguo Gu Shang*, vol. 34, pp. 1120–1125, 2021.
- [2] E. Lauren, E. Samuel, and M. Nataliya, "Development of carpal tunnel syndrome in association with checkpoint inhibitors," *Journal of Oncology Pharmacy Practice*, vol. 27, no. 3, pp. 764–765, 2021.
- [3] B. E. Shields Lisa and G. Iyer Vasudeva, "Acute carpal tunnel syndrome: Clinical, electromyographic, and ultrasound features in 25 patients," *Clinical Neurology and Neurosurgery*, vol. 210, p. 106984, 2021.
- [4] S. I. Kamel, B. Freid, C. Pomeranz, E. J. Halpern, and L. N. I. Nazarian, "Minimally invasive ultrasound-guided carpal tunnel release improves long-term clinical outcomes in carpal tunnel syndrome," *American Journal of Roentgenology*, vol. 217, no. 2, pp. 460–468, 2021.
- [5] P. C. Hsu, J. W. Chiu, Y. C. Yang, and M. J. Jeng, "Carpal tunnel syndrome in autoimmune rheumatic diseases and inflammatory bowel diseases: retrospective population cohort study," *American Journal of Physical Medicine & Rehabilitation*, vol. 100, pp. 760–765, 2021.
- [6] T. Y. Li, S. R. Chen, Y. P. Shen et al., "Long-term outcome after perineural injection with 5% dextrose for carpal tunnel syndrome: a retrospective follow-up study," *Rheumatology (Oxford)*, vol. 60, no. 2, pp. 881–887, 2021.
- [7] A. W. Ng, J. F. Griffith, C. Tsoi et al., "Ultrasonography findings of the carpal tunnel after endoscopic carpal tunnel release for carpal tunnel syndrome," *Korean Journal of Radiology*, vol. 22, no. 7, pp. 1132–1141, 2021.
- [8] World Medical Association, "World Medical Association Declaration of Helsinki: ethical principles for medical research involving human subjects," *Journal of the American Medical Association*, vol. 310, no. 20, pp. 2191–2194, 2013.
- [9] Q. Zhou, Y. Shen, X. Sun, Z. Qiu, Y. Jia, and S. Li, "Acupotomy for patients with carpal tunnel syndrome: a systematic review protocol," *Medicine (Baltimore)*, vol. 98, no. 51, article e18336, 2019.
- [10] H. R. Mutneja, A. Bhurwal, B. M. Attar et al., "Efficacy and safety of primary needle-knife fistulotomy in biliary cannulation: a systematic review and meta-analysis," *European Journal of Gastroenterology & Hepatology*, vol. 33, no. 1S, pp. e71–e77, 2021.
- [11] J. Zhu, Z. Zheng, Y. Liu et al., "The effects of small-needle-knife therapy on pain and mobility from knee osteoarthritis: a pilot randomized-controlled study," *Clinical Rehabilitation*, vol. 34, no. 12, pp. 1497–1505, 2020.
- [12] Z. Chen, S. Wei, W. Xu et al., "Adoption of a new gait system to evaluate the clinical effects of minimally invasive needle-knife scope therapy for the treatment of rheumatoid arthritis of the knee joint," *Annals of Palliative Medicine*, vol. 9, no. 5, pp. 3340–3349, 2020.
- [13] K. Hiramatsu, T. Naito, Y. Akazawa et al., "Bipolar-current needle-knife with a water jet function (Jet B-knife) shortens the procedure time of endoscopic submucosal dissection for colorectal tumors," *Surgical Endoscopy*, vol. 35, no. 7, pp. 3600–3606, 2021.
- [14] Y. You, M. Cai, J. Lin et al., "Efficacy of needle-knife combined with etanercept treatment regarding disease activity and hip joint function in ankylosing spondylitis patients with hip joint involvement: a randomized controlled study," *Medicine (Baltimore)*, vol. 99, no. 19, article e20019, 2020.
- [15] S. I. Jang, D. U. Kim, J. H. Cho et al., "Primary needle-knife fistulotomy versus conventional cannulation method in a high-risk cohort of post-endoscopic retrograde cholangiopancreatography pancreatitis," *Official journal of the American College of Gastroenterology | ACG*, vol. 115, pp. 616–624, 2020.
- [16] Z. Vincent, "Blunt bile duct isolation during needle-knife pre-cut for difficult biliary access," *Gastrointestinal Endoscopy*, vol. 91, no. 1, pp. 198–199, 2020.
- [17] H. Hasanabadi, M. H. Jokar, and A. Iranmanesh, "Acupuncture for carpal tunnel syndrome: a randomized controlled trial studying changes in clinical symptoms and electrodiagnostic

## Research Article

# Application of Medical-Nursing-Assistance Integration Model Based on Theoretical Basis of Behavioral Psychology in Management of Children's ICU

Yingying Jiang 

*Surgical Intensive Care Unit, Children's Hospital Affiliated to Zhejiang University School of Medicine, Hangzhou, 310000 Zhejiang Province, China*

Correspondence should be addressed to Yingying Jiang; 14055102210014@hainanu.edu.cn

Received 14 May 2022; Revised 5 June 2022; Accepted 10 June 2022; Published 14 July 2022

Academic Editor: Naeem Jan

Copyright © 2022 Yingying Jiang. This is an open access article distributed under the Creative Commons Attribution License, which permits unrestricted use, distribution, and reproduction in any medium, provided the original work is properly cited.

The children's intensive care unit is a closed management area with limited visiting time and no accompanying persons. It fails to systematically reflect and summarize the opinions and needs of the families of the children. The more critically ill the family members are, the higher the requirements for medical care. Good relationship between doctors, nurses, assistant, and patients can promote the rehabilitation of children's diseases and achieve the advanced medical model level of "seamless management and no loopholes." In order to aid the complete intensive care process, it is vital to understand children's psychological and physical development based on children's behavioral psychology when the medical-nursing-assistance (MNA) integration model is used in the children's intensive care unit. Therefore, this paper has completed the following tasks: (1) the development status of the domestic and foreign MNA integration model in the quality management of children's intensive care units is introduced, and the MNA integration model based on the theoretical basis of behavioral psychology is proposed for the following article in children's intensive care. The effect evaluation system of room management provides a theoretical basis. (2) The principle of BP neural network is introduced, and the effect evaluation model of the integrated mode of MNA based on BPNN in the management of children's intensive care unit is constructed. (3) The relevant data collected are used to form an available data set for the model accuracy test. The experimental results show that, after the research in this paper, the BPNN model proposed in this paper is introduced into the MNA integration model to evaluate the effect of the management of children's intensive care units which is practical and effective.

## 1. Introduction

The children's ICU is a specific area equipped with a sufficient number of staff who have received special training and master the basic concepts, basic knowledge, and basic operating skills of critical medicine, including physicians, inspection technicians, nurses, and life assistants. Equipped with professional and technically necessary monitoring and treatment equipment to centralize the management, rescue, treatment, nursing, and rehabilitation of critically ill children, the purpose is to improve the rescue success rate of critically ill children and reduce mortality [1, 2]. The traditional medical model is the division of medical, nursing, and single-handling channels. The work is not completely

connected, and there are loopholes and gaps. Real-time medical orders and auxiliary inspections are not implemented in a timely manner. The effect of medical order processing is not good.

It has drawbacks in the overall operation and management of children's ICU and cannot meet the management needs of children's ICU in comprehensive large hospitals, which has caused widespread concern in the medical community [3]. The requirements for treatment, nursing, and living needs of children's ICU work are higher than those of ordinary wards. Especially in the process of medical, nursing, and assistant shifts, it involves a wide range of areas. For example, children's ICU needs to understand children's psychological and physical development according to children's

behavioral psychology during the medical and nursing process. Because children are in the primary development and growth stage of life, they are different from adults in behavior and psychology, so the medical and nursing processes are also different. Only a further understanding of children's psychology and behavior can contribute to the entire intensive care process [4]. Therefore, in the process of work, doctors, nurses, and life assistants need to be in close contact. The integration of MNA does not simply mean that doctors, nurses, and assistants work together, but a process of co-working in which the staff are independent, work division and cooperation, share information, help each other, promote each other, and share responsibilities; the patient's diagnosis and treatment, health education, and rehabilitation programs are jointly formulated by doctors, nurses, and patients after thorough communication. The integrated clinical nursing model of MNA builds a bridge between doctors, nurses, and life assistants, making the communication and cooperation between doctors, nurses, and assistants faster and more efficient. MNA are gradually subordinated to the implementation of active communication, mutual cooperation, and codominant transformation of medical and nursing staff. The integrated clinical nursing model of MNA is conducive to the formation of a positive cooperative attitude and promotes the increase of cooperative behaviors of MNA. At the same time, this mode makes the communication channels and methods between doctors, nurses, and assistants more smooth and effective and can quickly realize the exchange and information sharing of patient-related information, so that both doctors and nurses can more comprehensively understand the needs of patients and clearly understand the needs of patients. Changes in the condition are conducive to both medical and nursing parties to make correct decisions on clinical medical treatment and clinical nursing rehabilitation, thereby improving the overall quality of medical and nursing services. Studies have confirmed that the cooperative behavior of doctors, nurses, and assistants is an important factor that directly affects the quality of medical care, the relationship between doctors and nurses, patient health outcomes, and patient satisfaction [5–7].

MNA's integrated clinical nursing model requires nurses and assistants to incorporate the idea of doctor and patient participation in clinical nursing work such as nursing procedures and health education in order to achieve complementarity of specialised knowledge and professional skills among doctors, nurses, and assistants, as well as patients and caregivers, in order to obtain consistent and standardised scientific rehabilitation guidance and assistance from various perspectives. Some studies have proposed that positive medical-nursing cooperation is beneficial to changing the stereotyped image of patients and their families that nurses are subordinate to doctors. Patients and their families should give nurses enough trust and respect, which is an effective measure to improve the relationship between nurses and patients and the quality of nursing [8]. It is an inevitable trend to explore the integrated mode of medicine, nursing, and assistance. Doctors, nurses, and assistants all share the goal of providing a safe treatment environment and high-quality services to patients. The integrated model creates a

positive relationship between nurses and patients, as well as between doctors and nurses. This study uses the integrated mode of MNA in the medical and nursing management of children's ICU to improve the safety of Chinese medicine prescriptions, the timely implementation of auxiliary inspections, and the timely follow-up of inspection reports. It can also improve nursing quality and safety, patient handover safety, infusion safety, and equipment management safety and improve the satisfaction of doctors, nurses, and assistants, with good results.

The following is the paragraph that organises the paper: the related work is found in Section 2. In Section 3, the methodologies used in the proposed work are examined. Section 4 discusses the experiments and their outcomes. Finally, in Section 5, the research task is accomplished.

## 2. Related Work

With the transformation of the medical model to "biological-psychological-social medicine," the traditional "dominant-subordinate" doctor-nurse relationship can no longer meet the needs of clinical work [9]. Under the background of the adjustment of medical relationship, "integration of medical and nursing," as an advanced medical and nursing work mode, is widely carried out in various clinical departments and has achieved remarkable results. The integration of medical and nursing is essentially a localized concept, which is called "medical-nursing cooperation" internationally [10]. Since the concept of medical and nursing integration was put forward, its connotation has been continuously enriched and developed. Initially, some researchers believed that medical-nursing cooperation is essentially an interdisciplinary exchange, the core of which is that both nursing and nursing parties must participate in the entire process of patient assessment, decision-making, clinical goal formulation, and problem solving and share responsibilities [11]. In the 1950s, the UK and other European countries took the lead in implementing advanced nurse nursing activities and gradually formed a nursing model combining nurse and doctor services, which was conducive to the recovery of patients. Under this model, a benign teamwork model with reasonable division of labor, clear responsibilities, information sharing, close contact, and mutual cooperation has been formed between doctors and nurses. It is of positive significance to effectively improve the preoperative and postoperative anxiety and other emotions of patients, improve the patient's self-care ability, and improve the quality of life of patients [12]. This new model of healthcare cooperation is defined by the American Nursing Association as "a novel and trustworthy way of cooperation among healthcare workers that safeguards both sides' interests while attaining mutual goals." But so far, many scholars have not formed a unified concept of the medical-nursing integration work mode, but they all include some common points. First of all, the medical-nursing integration work mode should be based on the mutual equality, respect, and trust of medical and nursing. On the premise of recognizing each other's professional knowledge and ability, through mutual communication

and coordination, the specific method of participating in clinical decision-making by both medical and nursing parties is adopted, and there is shared responsibility for providing medical care to patients [13]. The medical-nursing integration work mode focuses on the joint participation and cooperation of both medical and nursing parties, mutual exchange of medical treatment and nursing, and joint provision of medical and nursing services for patients. Studies have shown that, compared with the traditional nursing mode in which both medical and nursing parties work separately, the integration of medical and nursing as an emerging work mode has greater advantages in improving the quality of medical and nursing services [14]. In the 1990s, reference [15] put forward four necessary conditions for medical cooperation, namely, ability, confidence, commitment, mutual respect, and trust. In 2003, the American Nursing Association (ANA) clearly defined healthcare cooperation as a process of trust-based and reliable cooperation between healthcare workers. At present, there is no consensus on the exact concept of medical and nursing integration. Although the views of various scholars include some common elements, their views are not exactly the same. Nevertheless, under the guidance of the medical-nursing integration model, the nursing quality of each clinical department has been significantly improved [16].

Reference [17] applied the medical-nursing integration model to the thyroid surgery clinic and established a collaborative group composed of specialist physicians and responsible nurses. And the medical staff are grouped according to their professional titles and ages, and each performs its own duties to ensure that patients are seamlessly connected in each diagnosis and treatment process. The study concluded that the medical-nursing integration model can effectively reduce the waiting time of outpatients and improve the service experience of medical staff. In 2013, the emergency department of a university-affiliated hospital introduced a medical-nursing integrated emergency patient-hospital process management model, which effectively solved the problems of low efficiency of emergency ward management and low efficiency of human-hospital contact. The work efficiency and satisfaction of front-line medical staff in the emergency department have been significantly improved [18]. As a result, this study uses a prospective research technique to assess the importance of routine nursing and integrated nursing care for patients, in order to create a more solid foundation for improving patient clinical nursing. The medical-nursing integration work paradigm has been widely utilised in the field of nursing to guide clinical nursing, nursing management, nursing research, and nursing education, with impressive outcomes. Reference [19] research shows that the integration of medical and nursing can improve the cooperation degree of medical and nursing work, the awareness rate of health education, and patient satisfaction. The research of reference [20] shows that the integrated medical and nursing work mode realizes the seamless connection between the transfer and handover departments, ensures the safety of patients, and improves the work efficiency. Reference [21] believes that the integration of medical and nursing has broadened the specialist

knowledge of surgical nurses, improved the initiative and predictability of surgical cooperation, and is an effective method to improve the clinical practice ability of orthopaedic surgery specialist nurses. A university-affiliated hospital has successively carried out research on the medical-nursing integration cooperation model and believes that the medical-nursing integration work mode has achieved relatively good results in many aspects such as the synergy of the medical-nursing cooperation group, the improvement of the scientific research level of medical care, and the post-operative stress response of patients which have achieved relatively good results [22]

### 3. Method

#### 3.1. Principle of BP Neural Network

*3.1.1. The Concept of BP Neural Network.* The artificial neural network (ANN) is a computer information processing technique that can mimic the human brain. It is a frequently used machine learning algorithm with a lot of capability. In the ANN system, BPNN is a brilliant pearl. It mainly has the following characteristics:

- (1) Self-adaptation and self-learning: self-adaptive means that its own characteristics can adapt to changes in the environment and change accordingly. When the external environment changes, input new sample data into the neural network model for training, the model will automatically adjust the influencing parameters and mapping relationships during the training process, so that different input data can produce a desired output value within a specific range. Therefore, the neural network has stronger flexibility and adaptability than the expert system that uses a fixed model for calculation and is more similar to the operation law of the human brain
- (2) Nonlinearity problems in the real world are complex and nonlinear, and the human brain is also a nonlinear signal processing organization. Activating or inhibiting artificial neurons is essentially a nonlinear problem between processing data. The neural network reflects the data in the training samples to the connection weights to ensure that there is a nonlinear mapping relationship
- (3) The fault-tolerant BPNN has a wide distribution of nodes in the data storage process. When the input information is partially damaged, although the operating efficiency of the ANN will be moderately weakened, it will not lead to huge deviations in the operating results. This is very important in evaluation applications, because we often cannot be sure that every reference sample is absolutely correct
- (4) Computational parallelism and storage distribution inherent parallelism of BPNN enable each neuron to receive the input data accurately at the same time and then perform independent operation processing

on the data and obtain the corresponding output result. Neurons in the same layer can perform operations at the same time and then output the results to the next layer for calculation processing through the transfer function. Therefore, the parallel computing of neural network can give full play to its advantages and improve the operation efficiency

**3.1.2. Structure of BP Neural Network.** The data processing function of BPNN is closely related to the activity of neurons, how the neurons are connected, the size of the weights of the connections between neurons, and the maximum acceptance value of neurons.

- (1) Artificial neuron model: the neuron is the smallest unit of neural network, and its specific structure is shown in Figure 1, where  $x_i (i = 1, 2, \dots, m)$  is the input value of the neuron,  $w_i (i = 1, 2, \dots, m)$  represents the connection weight between the upper and lower levels of neurons, and  $p = w_i$  is the threshold of each layer node; if  $x_0 = 1$  is also regarded as the input value of the neuron, at this time,  $w_0$  is a special connection weight value,  $f$  is the transfer function, and  $y$  is the neuron output value; there are

$$y = f\left(\sum_{i=1}^m x_i w_i + p\right) \quad (1)$$

- (2) Hierarchical composition of BPNN

BPNN consists of an input layer, a hidden layer, and an output layer. The hidden layer may be from 1 to  $n$  layers, and the number of layers is mainly related to the complexity of the data to be processed. Figure 2 shows a neural network with a double hidden layer structure. There are nodes at both ends of the three levels, and the connection weights between nodes are connected, and different nodes correspond to different thresholds. When there is a signal input, the input signal is first transmitted to the input layer and then passes through each hidden layer and output layer in turn, and finally, the result is obtained.

- (3) Transfer function

The basic function of the transfer function of the BPNN is to activate the input and transform it into the output through the transformation of the transfer function. The transfer function must be differentiable from a mathematical point of view, otherwise it is meaningless. In the initial design of the model, the BPNN generally uses the sigmoid function as the transfer function of the hidden layer and the linear function as the transfer function of the output layer. At the same time, the sigmoid function can be divided into Log form and Tan form, which are selected according to whether the output value is negative. The specific form of the above transfer function is as follows:

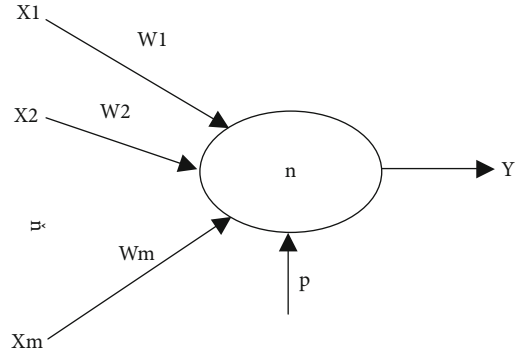


FIGURE 1: Neuron structure diagram.

Linear function

$$A = f(Wx + p) = Wx + p. \quad (2)$$

Log-sigmoid function

$$f(x) = \frac{1}{1 + e^{-x}}. \quad (3)$$

Tan-sigmoid function

$$f(x) = \frac{1 - e^{-2x}}{1 + e^{-2x}}. \quad (4)$$

**3.1.3. The Calculation Principle of BP Neural Network.** BPNN is a self-correcting learning method. In the self-correction learning, each training sample corresponds to a learning signal, and many different learning signals jointly affect the output value. The network system regards the learning signal as the expected output. After the model is trained, the error between the expected output value and the actual output value will be obtained, and then, the network weights will be corrected many times according to the specific situation of the error. Through repeated self-learning and adjustment of the error, the model makes the error reach the preset local minimum value. At this time, the entire network forms a complete closed system. The size of the error can be measured by the mean square error between the output value of the output node and the expected value, thus forming a dependent variable with the input value as the independent variable, the connection weight as the correction coefficient, and the output value, by judging the size of the error. It is a function to evaluate the performance of the network, and the self-learning training of the network is transformed into the problem that the solution error falls into a minimum value.

The basic process of BPNN consists of two parts: forward propagation of learning signals and feedback propagation of output results. That is, the input value is processed layer by layer from the input layer, gradually approaching the output layer; the connection weights and node thresholds are corrected from the output layer.

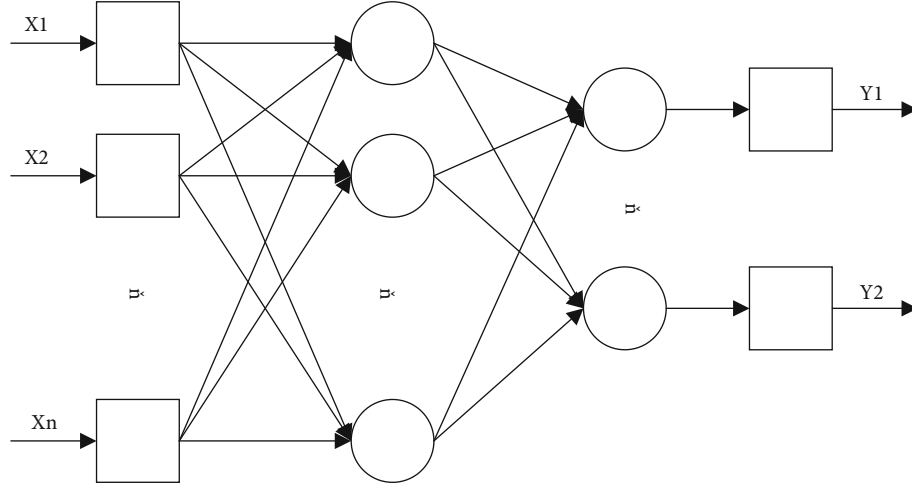


FIGURE 2: BP model structure diagram.

(1) The forward propagation process of the signal. Input value at hidden layer node:

$$\text{net}_i = \sum_{j=1}^M w_{ij}x_j + \theta \quad (5)$$

Output value at hidden layer node  $i$

$$y_i = \Phi(\text{net}_i) = \Phi\left(\sum_{j=1}^M w_{ij}x_j + \theta_i\right). \quad (6)$$

The input value at node  $k$  of the output layer

$$\text{net}_k = \sum_{i=1}^l w_{ki}x_i + a_k = \sum_{i=1}^q w_{ki}\Phi\left(\sum_{j=1}^M w_{ij}x_j + \theta_i\right) + a_k. \quad (7)$$

Input value at node  $k$  of the output layer

$$\begin{aligned} O_k &= \varphi(\text{net}_k) = \varphi\left(\sum_{i=1}^q w_{ki}x_i + a_k\right) \\ &= \varphi\left[\sum_{i=1}^q w_{ki}\Phi\left(\sum_{j=1}^M w_{ij}x_j + \theta_i\right) + a_k\right]. \end{aligned} \quad (8)$$

(2) Error feedback propagation process: in error feedback propagation, first obtain the output result of the hidden layer in the output layer and then perform error analysis on the result; if the error is not within the expected range, adjust the output layer, hidden layer, and input weights and node thresholds between the layers; take the output results as input values; run toward the input layer; repeat the training for many times until the output results of the

output layer are within the expected range; and then, end the operation. One-sample error function  $E_p$

$$E_p = \frac{1}{2} \sum_{k=1}^L (T_k - O_k)^2 \quad (9)$$

The multisample error criterion function  $E$

$$E = \frac{1}{2} \sum_{p=1}^P \sum_{k=1}^L (T_k^p - O_k^p)^2. \quad (10)$$

The following four formulas are the correction amount of the output layer weight  $\Delta w_{ki}$ , the correction amount of the hidden layer weight value  $\Delta w_{ij}$ , the correction amount of the output layer threshold value  $\Delta a_k$ , and the correction amount of the hidden layer threshold value  $\Delta \theta_i$ . All of them are obtained by modifying the connection weights and node thresholds by the gradient descent method.

The formula for adjusting the weights of the output layer is as follows:

$$\Delta w_{ki} = -\mu \frac{\partial E}{\partial w_{ki}} = -\mu \frac{\partial E}{\partial y_i} \frac{\partial O_k}{\partial \text{net}_k} \frac{\partial \text{net}_k}{\partial w_{ki}}. \quad (11)$$

The formula for adjusting the weights of the hidden layer is as follows:

$$\Delta w_{ij} = -\mu \frac{\partial E}{\partial w_{ij}} = -\mu \frac{\partial E}{\partial y_i} \frac{\partial y_i}{\partial \text{net}_i} \frac{\partial \text{net}_i}{\partial w_{ij}}. \quad (12)$$

The formula for adjusting the threshold of the output layer is as follows:

$$\Delta a_k = -\mu \frac{\partial E}{\partial a_k} = -\mu \frac{\partial E}{\partial O_k} \frac{\partial O_k}{\partial \text{net}_k} \frac{\partial \text{net}_k}{\partial a_k}. \quad (13)$$

The formula for adjusting the threshold of the hidden

layer is as follows:

$$\Delta\theta_i = -\mu \frac{\partial E}{\partial \theta_i} = -\mu \frac{\partial E}{\partial y_i} \frac{\partial y_i}{\partial \text{net}_i} \frac{\partial \text{net}_i}{\partial \theta_i}. \quad (14)$$

**3.2. Determination of Network Parameters.** The BPNN needs a large amount of prior data as support, and the calculation amount in the operation process is very huge. The Matlab scientific computing software launched by American Math-Works has powerful matrix computing capabilities, which greatly shortens the network training time. Using the neural network toolbox in Matlab can bring great convenience to users and related researchers. Users can directly call the functions in the toolbox to build a fully functional BPNN model. The neural network model in the Matlab toolbox mainly designs the input layer, the hidden layer, the output layer, the number of nodes in each layer, the connection weights and node thresholds, and the transfer function.

**3.2.1. Design of Input Layer and Output Layer.** The selection of the number of nodes in the input layer and the output layer is determined by the actual situation. If the sample data is more complex, the more nodes are required to process the data. The number of nodes in the input layer is equal to the training dimension of the sample data, which can be the initial dimension or the dimension of the feature variable: the number of nodes in the output layer varies according to the network. In the classification network, select the number of categories, and in the simulation, select the output space dimension in the fit function in the fit network.

**3.2.2. Design of Hidden Layer.** The design of the hidden layer mainly includes the design of the number of hidden layers and the number of nodes related to it.

(1) *Design the Number of Hidden Layers.* In the 1980s, Nielsen proved that a BPNN model with a single hidden layer can make a continuous function in any closed interval infinitely close to a regression value. Because a 3-layer BP design network with a single hidden layer is enough to complete any multidimensional mapping, double hidden layers are only needed to ensure the continuity of model learning when the function is discontinuous, so the neural network is mostly a single hidden layer or double hidden layers.

(2) *Design the Number of Hidden Layer Nodes.* The operation of the neural network is closely related to the number of hidden layer nodes. If there are not enough hidden layer nodes, the available mapping information will be insufficient, the error will be large, the fault tolerance rate will be low, and the sample recognition ability without self-learning will be weak, and it will be difficult to effectively complete the training; but if the number of hidden layer nodes is too large, it will be difficult to effectively complete the training. The structure of the neural network is complex, the number of iterations is increased, the operation efficiency is reduced, and the nonsalient content in the sample is input, which weakens the generalization ability. The generalization ability of ANN refers to the ability of neural net-

work model to obtain correct output when inputting new data other than its training samples after completing multiple complete trainings. At present, the number of hidden layer nodes is often determined according to the personal experience of the model designer. Generally speaking, it is closely related to the number of input and output layer nodes, and the following formulas are usually used to determine the number of hidden layer nodes:

$$I = \sqrt{m + n} + b, \quad (15)$$

where  $b$  is a constant value between 1 and 10,  $n$  is the number of nodes in the input layer,  $I$  is the number of nodes in the hidden layer, and  $m$  is the number of nodes in the output layer.

**3.2.3. Selection of BP Artificial Neural Network Algorithm.** The BPNN has the advantages of simple operation, large scale of parallel processing data, less time-consuming, and high efficiency, making the BP algorithm one of the most widely used, stable, and perfect training algorithms at present. It essentially approximates the error of the output result to the extreme value of the expected range. However, when dealing with nonlinear issues, the gradient descent approach requires frequent modification of the connection weights and thresholds, which can result in a long training time, low learning efficiency, slow convergence speed, and an easy fall into the problem of local minimum range. Due to the above problems, the BP algorithm needs to be improved, and the commonly used methods are as follows:

- (1) Trainingdm additional momentum method: the additional momentum method makes the network consider both the effect of the error change and the influence of the error itself when modifying the connection weights. In the case where the additional momentum method is not used, the output value of the neural network may fall into the local minimum value, and after using the additional momentum method, the output value can skip these local values. This method uses the feedback propagation method to add a weight change value in the process to each old weight value to obtain a new weight value and repeat the training for many times to calculate the weight value change to achieve the minimum error and adjust the threshold which is the same as the above process
- (2) Trainingdx adaptive learning method: for a special and ambiguous problem, it is not easy to choose an appropriate learning rate. It is generally obtained through experience or experiments, and after starting training, the optimal learning rate will follow the training and changes with the progress. The network will fluctuate, and the output curve will oscillate if the learning rate is too high; if the learning rate is too low, the network will increase the training time, resulting in an increase in the number of convergence times and a slower network convergence

rate, even if the network is stable. Therefore, it is hoped that by automatically adjusting the learning rate during the training process, the training efficiency can be kept the highest when the network is stable. The specific method of adjusting the learning rate is as follows: check the relationship between the connection weight and the error function at first. If the performance of the error function is reduced, it means that the learning rate is low and can be appropriately increased; if the performance of the error function is not reduced, it is improved; then, the learning rate should be reduced

- (3) Elastic algorithm: in the traditional BP algorithm, the activation function usually adopts the sigmoid function, which is characterized by the ability to convert any input value into an output value within a limited range. However, when the input value tends to infinity, the derivative will approach 0; that is, the gradient value will approach 0, and the network will stop modifying the weights. The elastic algorithm can effectively solve this problem. It only considers the positive and negative of the partial derivative, regardless of its specific value. The degree of weight update is determined by a predetermined independent value, and the direction of weight correction is determined by the sign of the partial derivative. In the process of two consecutive iterative derivations, if the sign of the partial derivative of the error function with respect to a certain weight does not change, the independent value will be increased. If the partial derivative changes, decrease the independent value. When the sign of the partial derivative remains the same in the continuous multiple iterations, it indicates that the direction of error correction is correct, and the workload of weight correction should be increased to improve the working efficiency of the neural network. Therefore, the elastic algorithm can significantly improve the speed and the convergence of the BP network

*3.3. Evaluation Indicators for the Integration of Medicine, Nursing, and Assistance.* Before constructing the evaluation indicators, the practical application of the medical-nursing-assistance integration model is introduced.

- (1) Before the implementation of the medical-nursing-assistance integrated model, the children's intensive care unit's morning shift mode is as follows: when the children's intensive care unit was handed over in the morning before the medical-nursing-assistance integrated model was implemented, the nursing work was the main content of the shift, and the doctor did not supplement it; instead, the doctor listened to the shift, focusing on the special situation of children at night, reviewing the imaging results and test results, and reviewing the medical history. Nurses get together to discuss the work of nursing. The doctors and nurses stagger the beds

and rounds to avoid mutual interference, and then, the doctor issues a doctor's order, and the nurse immediately goes to process, execute the doctor's order, implement auxiliary examinations, and check abnormal examination reports. Nurses take over the shift in groups and pick up the beds, infusions, instruments, and equipment under their control. Life assistants assist nurses in daily care and receive visits from family members of children. Doctors, nurses, and assistants complete their duties within their respective responsibilities and conduct monthly self-examinations and quarterly inspections to evaluate the implementation of the core system of patient safety and nursing, supervision, and evaluation of the implementation of the nurse bed responsibility system and service satisfaction surveys

- (2) After the implementation of the integrated medical-nursing-assistance model, the shift mode of the children's intensive care unit: the nursing shift is the main priority, and the doctor on duty supplements the new admission, rescue, and abnormal reports of the children at night. Remind nurses what to focus on. Head nurses and department directors follow up on shifts involving patient safety, ward safety, and the opinions of patients' families to make rectifications. Medical assistants take part in discussions about complex situations, study documentation and materials, thoroughly analyze cases, and discuss any bottlenecks that arise. Conduct ward rounds for critically ill patients together, urge doctors and nurses to stay focused on their jobs, collaborate with medical care for multidisciplinary and critically sick patients, and put treatment and nursing measures in place. We should timely and correctly implement the emergency medical orders, implement the treatment plan as soon as possible, and feedback and track the treatment effect. For emergency auxiliary examination at the bedside, the nurse in charge of the bed assists the doctor to prepare medicines and supplies. Before going out, clean the respiratory tract; carry oxygen bags, first aid kits, warm appliances, and bed rails; and notify the transportation center to wait in the elevator. At the bedside, the mobile phone mobile core system can be used to check the inspection report in time and quickly, follow up the treatment of critical values, take special inspection results such as multi-drug-resistant bacteria, and take timely intervention measures, through joint participation in the discovery of nursing quality and safety, infusion safety, equipment safety hazards, the accuracy of infusion balance, pipeline medication arrangements, and equipment operation failure handling and other series of management. Everyone works together and participates in a working model that is both independent implementation and mutual cooperation. A small summary of daily shifts is posted on WeChat to facilitate the knowledge of all staff, regular medical-nursing-assistance communication meetings are held, family members are consulted in a timely manner, and the effect of the implementation of the



TABLE 1: Evaluation indicators for the integration of medicine, nursing, and assistance.

Index	Label
Execute medical orders in a timely manner	I1
Auxiliary inspections are implemented in a timely manner	I2
The doctor's order is very effective	I3
Follow-up of inspection reports in a timely manner	I4
Bed unit environmental safety	I5
Comprehensive patient handover	I6
Infusion balance is correct	I7
Instrument and equipment safety	I8
Patient satisfied with doctor	I9
Patient satisfied with nurse	I10
Patient satisfied with life assistant	I11

TABLE 2: Initial parameter settings.

Network parameters	Value or setting
Number of iterations	1500
Learning rate	0.15
Learning target	0.00005
Learning function	Trainlm
Hidden layer transfer function	Logsig
Number of hidden layer nodes	5

integrated medical-nursing assistance model is summarized. The nurses' bed management responsibility system implements supervision and evaluation and service satisfaction survey

- (3) Indicators of observation and evaluation criteria are compared. The scale uses the patient safety and nursing core system implementation evaluation form to compare the number of defective cases of untimely execution of real-time doctor orders, untimely implementation of auxiliary inspections, poor doctor order processing, and untimely follow-up of inspection reports in children's intensive care units before and after the implementation of the medical-nursing-assistance integration model. Compared with the results of nursing projects, the quality of the bed unit was unsafe, the patient handover was incomplete, the infusion volume was incorrect, and the safety indicators of equipment were implemented. Investigate the satisfaction of doctors, nurses, and assistance services, and summarize the hospitalization and discharge feedback messages of the patient's family members

An evaluation method for the application effect of the integrated medical-nursing-assistance model based on the theoretical basis of behavioral psychology in the administration of children's critical care units was established based on the preceding descriptions, as shown in Table 1. The output is divided into three levels according to the input metrics.

## 4. Experiment and Analysis

### 4.1. Data Sources and Pretraining Processing

- (1) This study selects the data collected by a tertiary hospital from January 2016 to December 2017 in the implementation of the integrated medical-nursing-assistance model in the children's intensive care unit. The management of doctor's order processing effect, inspection report follow-up, bed unit environment safety, patient handover safety, infusion safety, and equipment safety management, using noncontemporaneous control, by comparing the integration before implementation (January 2014-December 2015) and implementation afterwards (January 2016-December 2017), the children's intensive care unit managed the safety of traditional Chinese medicine orders, the quality and safety of nursing, and the satisfaction of doctors, nurses, and assistants. 300 sets of data before and after implementation were obtained, respectively. Among them, 275 samples are used as the training samples of the neural network model, and 25 samples are used as the test samples of the neural network model
- (2) Usually, the input and output data of the neural network should be between 0 and 1. Since the model constructed in this paper does not meet such requirements, it is necessary to normalize the sample data before inputting it into the model. In this paper, the maximum and minimum method is used for normalization processing:

$$y = \frac{x - x_{\min}}{x_{\max} - x_{\min}}, \quad (16)$$

where  $x$  is the sample data outside the interval  $[0, 1]$ ,  $x_{\min}$  is the minimum number in the data sequence,  $x_{\max}$  is the maximum number in the sequence, and  $y$  is the normalized value of the sample data  $x$

### 4.2. Preliminary Training of the Model

**4.2.1. Model Construction Ideas.** First, use all the information of the training samples, including the feature information of the training samples, to train the neural network. After the network adaptive learning is completed, input the features of the test samples to the trained network. The trained network will automatically analyze and predict and give the prediction of the effect level of the test sample predicted by the neural network model and compare it with the actual evaluation level of the corresponding test sample to judge the feasibility of the model.

**4.2.2. Initial Parameter Setting.** The model is initially established by using the `newff` command in Matlab, and the initial parameter configuration of the network is set by default. The specific settings are shown in Table 2.

After the initial operation, it is found that the network output error of the model reaches the expected error range

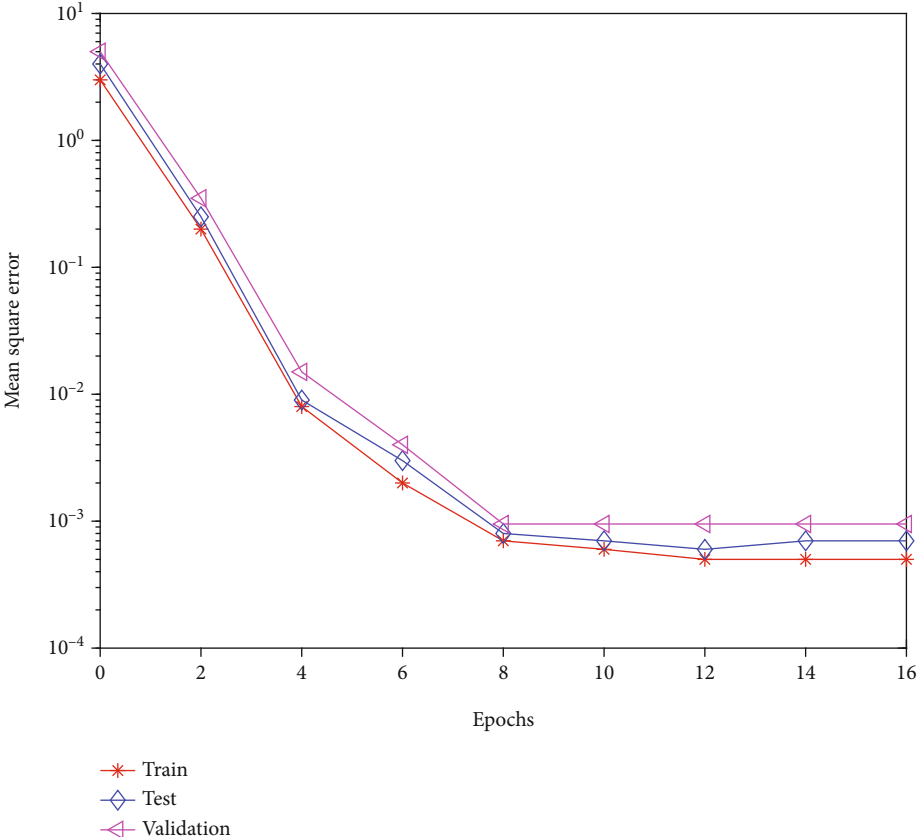


FIGURE 3: Error change graph.

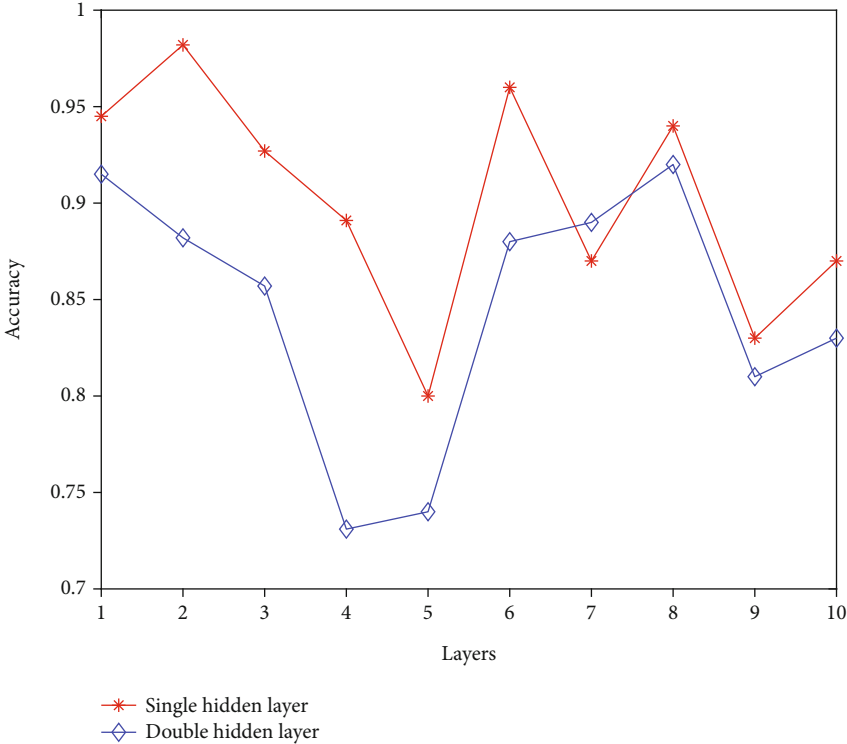


FIGURE 4: Test results when the number of hidden layers is different.

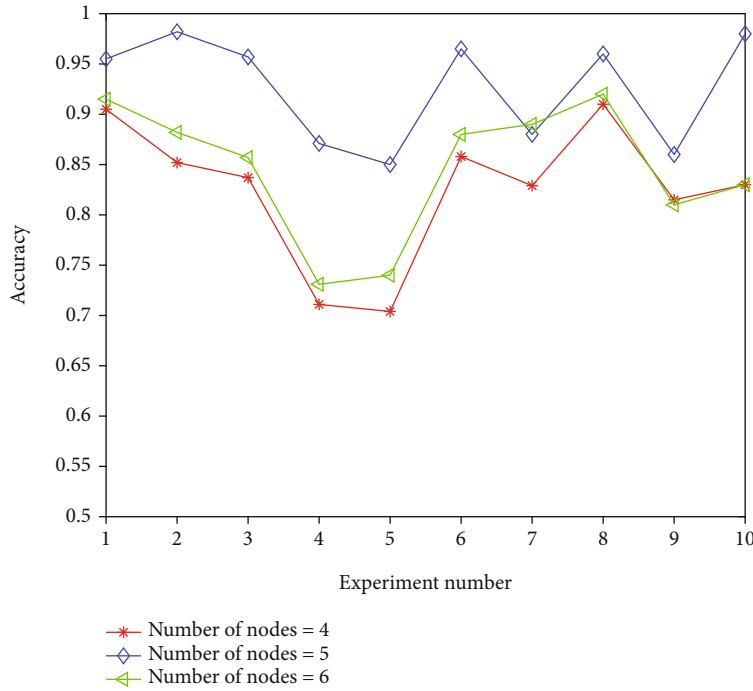


FIGURE 5: Test results of nodes in different hidden layers.

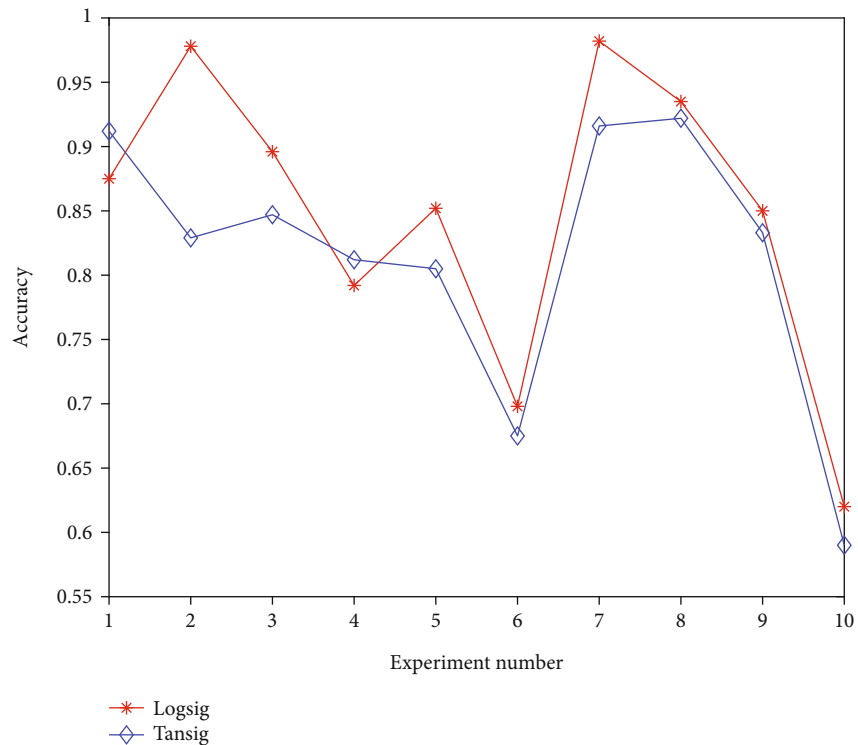


FIGURE 6: Different transfer function test results.

after 16 iterations, the time consumption is very short, and the error is also small, which shows that the network learning state is good.

4.2.3. *Model Test.* The test of the model mainly starts from two aspects, the validity test and the accuracy test. As the name

suggests, the validity test is to test the rationality of the model, such as whether the network convergence is reasonable and whether the model results are reliable, and the accuracy test is the correctness of the model, often measured by the error rate. The program's operating process can be used to reflect the validity test. The neural network's performance is poor

TABLE 3: Optimizing model run results.

Number	1	2	3	4	5	6	7	8	9	10
Accuracy	0.92	0.95	0.96	0.97	0.93	0.98	0.98	0.95	0.96	0.95

when it runs slowly, has too many iterations, or has a big mean square error. As can be seen from the figure below, the indicators of the model established in this paper are relatively reasonable after the initial training. After 16 iterations of the model, the network output error reaches the expected error range, and the error value is 0.001625 within the effective range. The change process diagram is shown in Figure 3.

The accuracy test is mainly to test the gap between the input value of the neural network and the expected value, that is, the actual value of the test sample. The smaller the gap, the higher the accuracy. It is usually expressed by error or error rate, which is more suitable for the effect analysis of a single sample; you can also average multiple samples. Because this paper uses multiple samples to test the performance of the network, there is an error value for each sample data. We want the error rate to be as low as feasible; hence, this study uses a correct rate to assess the developed model's accuracy. It is the ratio of the number of times that the error rate between the actual value and the predicted value is within 10% of all the calculation results in the 275 training samples.

**4.3. Optimization of the Model.** Many parameters in the BPNN components, such as the number of hidden layers and their nodes, the selection of transfer functions, and the selection of training functions, will affect the final training results of the neural network. However, the specific selection of these parameters has not yet been accurately guided by the academic community, and more judgments are made through experience. Therefore, in order to ensure the accuracy and effectiveness of the neural network model, this paper decides that when the model is first constructed, the parameters that need to be determined are selected from the default parameters of the system, and then, the parameters of the model are adjusted one by one by controlling the parameter variables so as to finally determine a stable network model. The specific optimization process is as follows.

**4.3.1. Optimization of the Number of Hidden Layers.** In this paper, a hidden layer is used in the initial training above, and a hidden layer is added below for training and result comparison. It can be seen from the test results that the accuracy of a single hidden layer is higher than that of a double hidden layer, so we do a more in-depth test on the basis of a single hidden layer. The test results are shown in Figure 4.

**4.3.2. Optimization of the Number of Hidden Layer Nodes.** In this paper, 5 hidden layers are used in the initial training of the model, and integers around 5 are used as the number of hidden layers for testing. The test results are shown in Figure 5.

The data shows that when the number of hidden layer nodes is 5, the correct rate is high, so 5 is still selected as the number of hidden layer nodes.

**4.3.3. Optimization of Transfer Function.** The commonly used transfer functions are logsig and tansig. The selection of transfer function has a great influence on the prediction result. The two transfer functions are tested, as shown in Figure 6.

The tabular data shows that the correct rate of the logsig function is higher, and the results of each correct rate are relatively stable, and the logsig function is still selected.

**4.4. Analysis of Test Results.** After combining the above model optimization, it is finally determined that the model has a single hidden layer structure with 5 hidden layer nodes, the transfer function selects logsig, and the training function selects trainlm. The running results of the optimized model are shown in Table 3.

It can be seen from the above table that the trained neural network can correctly predict the effect evaluation level, and the error is very low, which is a very significant level. At the same time, for the processing and analysis of 275 samples, the average time of BPNN is less than 2s. The whole process is very convenient and much faster than the manual evaluation of evaluators. Applying performance evaluation is practical and remarkably efficient.

## 5. Conclusion

After the implementation of the medical-nursing-assistance integration model, the number of defects in the execution of real-time doctor's orders, the implementation of auxiliary inspections, the processing of doctor's orders, and the untimely follow-up of inspection reports in the children's intensive care unit decreased. Before the implementation of the integrated medical-nursing-assistance model, the children's intensive care unit mainly focused on the nursing work when the shift was handed over. The doctor did not supplement or provided little supplement, but after listening to the handover, the doctor focused on the special situation of the children at night. At this time, the content of the discussion is obviously related to the nursing shift, that is, the lack of a harmonious way and atmosphere of communication. The medical staff could not solve the problems encountered together. In order to avoid mutual interference, the doctors and nurses staggered the ward rounds, and then, the doctor issued a medical order without communicating the urgent needs to be dealt with in a timely manner. Irregular usage, inconsistent charging codes, etc. failed to communicate and urge improvement in a timely manner. There was a lack of effective communication in the real-time execution of medical orders and the safety of medical order execution. After the implementation of the integrated

model of medical care and assistance, personnel supervision was strengthened and then improved. Working together can effectively prevent the occurrence of medical accidents and ensure patient safety. Improving and strengthening management and other countermeasures can effectively improve the quality of doctor's order execution and improve nursing quality and nursing safety. After running-in, communication, and implementation of the integrated model of medical and nursing assistance, the patient safety and nursing core system implementation evaluation is carried out through inspection, and real-time doctor's order execution and auxiliary inspection are displayed. The number of defects caused by untimely implementation, treatment of doctor's orders, and untimely follow-up of inspection reports is significantly lower than before the implementation. Therefore, this paper has completed the following work: (1) introduced the current state of the domestic and international medical-nursing-assistance integration model in the quality management of children's intensive care units and proposed a medical-nursing-assistance integrated model in children's intensive care units based on the theoretical foundation of behavioral psychology. The effect evaluation system of intensive care unit management provides a theoretical basis. (2) The principle of BPNN is introduced, and the effect evaluation model of the integrated mode of medical care and assistance based on BPNN in the management of children's intensive care unit is constructed. (3) The relevant data collected are used to form an available data set for the model accuracy test. The experimental results suggest that the BPNN model described in this study is realistic and effective when it is integrated into the medical-nursing-assistance integration model to evaluate the effect of the management of children's critical care units following the research in this paper.

### Data Availability

The data sets used during the current study are available from the corresponding author on reasonable request.

### Conflicts of Interest

The author declares that he has no conflict of interest.

### References

- [1] S. Mumtaz, H. Lundqvist, K. M. S. Huq, J. Rodriguez, and A. Radwan, "Smart Direct-LTE communication: An energy saving perspective," *Ad Hoc Networks*, vol. 13, pp. 296–311, 2014.
- [2] D. Stayer and J. S. Lockhart, "Living with dying in the pediatric intensive care unit: a nursing perspective," *American Journal of Critical Care*, vol. 25, no. 4, pp. 350–356, 2016.
- [3] V. L. Montgomery, "Effect of fatigue, workload, and environment on patient safety in the pediatric intensive care unit," *Pediatric Critical Care Medicine*, vol. 8, Supplement, pp. S11–S16, 2007.
- [4] J. E. Rennick, G. Dougherty, C. Chambers et al., "Children's psychological and behavioral responses following pediatric intensive care unit hospitalization: the caring intensively study," *BMC Pediatrics*, vol. 14, no. 1, pp. 1–11, 2014.
- [5] M. Heyeres, J. McCalman, K. Tsey, and I. Kinchin, "The complexity of health service integration: a review of reviews," *Frontiers in Public Health*, vol. 4, p. 223, 2016.
- [6] R. M. Gyasi, K. Abass, S. Adu-Gyamfi, B. T. Accam, and V. M. Nyamadi, "The capabilities of nurses for complementary and traditional medicine integration in Africa," *The Journal of Alternative and Complementary Medicine*, vol. 24, no. 3, pp. 282–290, 2018.
- [7] Y. J. Wang, "Research on the effect of the application of medical-nursing-assistance unaccompanied model in clinical nursing," *Diet Health*, vol. 15, pp. 192–193, 2021.
- [8] Q. L. Ye, "Application of medical-nursing-assistance integration model in quality management of morning shift in children's intensive care unit," *Chinese General Practice Nursing*, vol. 19, no. 32, pp. 4598–4600, 2021.
- [9] P. Duan, Y. Jia, L. Liang, J. Rodriguez, K. M. S. Huq, and G. Li, "Space-reserved cooperative caching in 5G heterogeneous networks for industrial IoT," *IEEE Transactions on Industrial Informatics*, vol. 14, no. 6, pp. 2715–2724, 2018.
- [10] Y. Doyle, J. Keen, and A. Bull, "Role of private sector in United Kingdom healthcare system commentary: cooperation should be based on what the public wants and needs from its healthcare system," *BMJ*, vol. 321, no. 7260, pp. 563–565, 2000.
- [11] E. Eatwell and A. Swierczyna, "Emerging voluntary cooperation between European healthcare systems: are we facing a new future?," *Medicine Access@ Point of Care*, vol. 3, 2019.
- [12] B. D. Pedersen, I. K. Poulsen, C. V. Ringsted, and T. V. Schroeder, "Interprofessional communication and cooperation training in ward rounds for medical and nursing students: a pilot project," *Ugeskrift for Laeger*, vol. 168, no. 25, pp. 2449–2451, 2006.
- [13] A. S. Bashatah, K. A. Al-Ahmary, M. Al Arifi et al., "Interprofessional cooperation: an interventional study among Saudi healthcare teaching staff at King Saud University," *Journal of Multidisciplinary Healthcare*, vol. 13, pp. 1537–1544, 2020.
- [14] M. C. Beuscart-Zépher, S. Pelayo, F. Anceaux, J. J. Meaux, M. Degroisse, and P. Degoulet, "Impact of CPOE on doctor-nurse cooperation for the medication ordering and administration process," *International Journal of Medical Informatics*, vol. 74, no. 7–8, pp. 629–641, 2005.
- [15] Z. H. Tan, "Application of doctors, nurses and assistant nurse integration services in unattended ward nursing management," *Nursing Practice and Research*, vol. 15, no. 6, pp. 116–118, 2018.
- [16] S. Tastan, G. C. F. Linch, G. M. Keenan et al., "Evidence for the existing American Nurses Association-recognized standardized nursing terminologies: a systematic review," *International Journal of Nursing Studies*, vol. 51, no. 8, pp. 1160–1170, 2014.
- [17] Y. Yang, Y. Zhang, L. Dai, J. Li, S. Mumtaz, and J. Rodriguez, "Transmission Capacity Analysis of Relay-Assisted Device-to-Device Overlay/Underlay Communication," *IEEE Transactions on Industrial Informatics*, vol. 13, no. 1, pp. 380–389, 2017.
- [18] Y. Feng, "Research on the application of the integrated service model of medical care and assistance in the nursing management of unaccompanied wards," *Diet Health*, vol. 6, no. 21, p. 119, 2019.
- [19] X. He, "Application of medical-nursing-assistance integrated service model in neurology ward," *Modern Nurse*, vol. 25, no. 3, pp. 176–179, 2018.

- [20] J. Li, Z. Zhou, J. Wu et al., “Decentralized on-demand energy supply for blockchain in Internet of Things: a microgrids approach,” *IEEE transactions on computational social systems*, vol. 6, no. 6, pp. 1395–1406, 2019.
- [21] W. Duan, J. Gu, M. Wen, G. Zhang, Y. Ji, and S. Mumtaz, “Emerging technologies for 5G-IoV networks: applications, trends and opportunities,” *IEEE Network*, vol. 34, no. 5, pp. 283–289, 2020.
- [22] M. De Ree, G. Mantas, A. Radwan, S. Mumtaz, J. Rodriguez, and I. E. Otung, “Key management for beyond 5G mobile small cells: A survey,” *IEEE Access*, vol. 7, pp. 59200–59236, 2019.

## Research Article

# IGBT Fault Prediction Combining Terminal Characteristics and Artificial Intelligence Neural Network

Cailin Li <sup>1,2</sup>

<sup>1</sup>*School of Architecture and Transportation Engineering, Guilin University of Electronic Technology, Guangxi, China*

<sup>2</sup>*Guangxi Key Laboratory of Manufacturing System & Advanced Manufacturing Technology, School of Mechanical and Electrical Engineering, Guilin University of Electronic Technology, China*

Correspondence should be addressed to Cailin Li; [leecailin@guet.edu.cn](mailto:leecailin@guet.edu.cn)

Received 8 April 2022; Revised 27 April 2022; Accepted 30 April 2022; Published 14 July 2022

Academic Editor: Naeem Jan

Copyright © 2022 Cailin Li. This is an open access article distributed under the Creative Commons Attribution License, which permits unrestricted use, distribution, and reproduction in any medium, provided the original work is properly cited.

The insulated gate bipolar transistor (IGBT) is widely utilized in the transportation, power, and energy domains because of its high input impedance and minimal on-voltage drop. IGBTs are frequently used in industrial applications for lengthy periods of time, collecting fatigue damage and eventually aging and failing, which can result in system shutdown and financial losses in severe circumstances. As a result, a study into the IGBT's reliability is extremely important. Fault prediction technology, which is an important aspect of reliability research, may analyze device state through changes in terminal parameters, anticipate aging trends, and issue early warnings at thresholds to avoid significant safety issues caused by IGBT aging failures. Therefore, the appropriate end parameters are selected as aging characteristic parameters, and fault prediction is performed. Therefore, this paper has carried out research on the IGBT fault prediction technology that integrates the terminal characteristics and artificial intelligence neural network. The main research contents include the following: (1) this paper starts from the basic principle of IGBT and the structure of its device and analyzes its failure mode on the failure of IGBT. The characteristic parameter of collector-emitter turn-off peak voltage value is selected for IGBT fault prediction, and the aging data of NASA PCoE Research Center is used to verify that the characteristic parameter can be used for fault prediction. (2) In view of the shortcomings of traditional fault forecasting methods, this paper proposes to use deep learning time series forecasting methods for fault forecasting. The LSTM is theoretically analyzed, and the prediction network is built. The experimental results show that the LSTM network model can improve the accuracy of IGBT fault prediction, with fewer parameters and higher prediction efficiency.

## 1. Introduction

As the most important component in a power electronic system, IGBT is the first-choice module for power semiconductor devices. IGBT was invented in 1982. Although it is a very new type of power semiconductor device, it is still developing and improving. From the point of view of power consumption, when the rated current of the IGBT is 75 A and the rated voltage is 600 V, the rated power of the first generation IGBT is 100 watts, and now, it is less than 30 watts. At present, the maximum collector current of the IGBT has been more than 3500 A [1]. From the point of view of the manufacturing process, the current IGBT process is already less than 1 micron. At the same time, the gate trenching

technology is adopted in the fourth-generation products, and the size of the chip is also reduced by 80% compared with the previous generation [2]. With the continuous improvement and optimization of the performance and volume of IGBTs, it is reasonable to seize most of the power electronic equipment market. Its superior performance and low power consumption are powerful tools to promote the development of the new energy era. At present, the application prospect is very broad, and it is an indispensable part of many fields such as rail transit, household appliances, infrastructure, and new energy vehicles. For example, in the "heart" of the train, the traction converter uses IGBT modules [3]. The above are all civil fields. For other fields such as aerospace equipment, IGBT also plays a key role. It can

be said that the status of IGBTs for power electronic systems is not lower than that of CPUs for computer systems. IGBT modules, on the other hand, have a very high internal resistance under high pressure or high temperature, are prone to high conduction loss, and are not very resistant to high impact force, so they are used in harsh production environments, or after long-term use, they will gradually age or even fail, causing the equipment to stop running, and even the entire power system to be paralysed, causing serious economic losses and even threatening human life [4]. According to the statistics of the British Wind Energy Agency, before 2009, more than 700 wind turbines were burned in the world, many of which were caused by the failure of IGBTs. The reliability of IGBTs plays an important role in the smooth operation of power electronic systems, so it is very meaningful to study the causes of IGBT failures and fault prediction [5]. Before IGBT failure prediction, it is necessary to first study the cause of IGBT failure, that is, the failure mechanism of IGBT. After understanding the changing trend of the degradation parameters before the IGBT fails, measure these parameters. When the parameters are found to be abnormal or about to reach the alarm threshold, it means that the device may fail, so that it can be repaired or replaced in time to avoid more serious accidents [6]. Not only that, while avoiding equipment failure, it can also automate maintenance and repair, redundant copy replacement, etc., which improves the efficiency and cost of operation management and reduces the burden of manual maintenance. In this context, in order to reduce the heavy losses caused by the shutdown of the power system due to IGBT failure during the operation of power electronic equipment and improve the stability of the power system operation, countries around the world are actively carrying out IGBT fault prediction research [7]. The direction of its fault research can be roughly divided into two types: one is based on the machine model and probability model of IGBT, the focus of the research is mainly on the characteristics and materials of the device itself, and the fault prediction model is obtained through statistical analysis of a large number of aging experimental data. The other is an intelligent algorithm prediction model driven by IGBT data. The focus of the research is on the data drive of degradation parameters. Consider using intelligent algorithms such as popular neural networks to build fault prediction models [8]. In today's intelligent world, the rapid development of ANN has ushered in a data-driven era. Finding the relationship between features and targets through data is the mainstream direction of the current social forecasting development. In this paper, the terminal characteristics and neural network are combined to predict the fault of IGBT, because the neural network has incomparable advantages in dealing with nonlinear problems. It provides a good solution for data prediction of nonlinear, time-varying, strongly constrained, large-lag processes.

The following is the paper's organization paragraph: In Section 2, the related work is provided. The suggested work's methods are examined in Section 3. The experiments and results are discussed in Section 4. Finally, the research job is completed in Section 5.

## 2. Related Word

Abroad, Reference [9] proposes a physical model for life estimation of standard power modules. The proposed model can physically explain the dependence of life on various characteristics of the temperature profile, such as frequency, maximum, and minimum temperature. The model uses the Clech method to simulate the stress-strain solder response under cyclic thermal loading and uses a solder deformation mechanism diagram to describe the dominant failure mechanism under stress-temperature circumstances. Reference [10] studied the fundamental frequency thermal cycle and proposed a life estimation method for modular multilevel converter submodules based on the combination of finite element analysis and physical life model. This method provides a more in-depth physical description of the failure mechanism and takes into account the thermal coupling between chips, making life calculations more accurate. Reference [11] obtained the thermomechanical stress distribution around the IGBT defect through finite element analysis, gave a life model combined with the performance of the solder layer, and then verified the model through power cycling experiments and microscale CT scanning. Reference [12] demonstrated the influence of solder joint thickness on the service life of power semiconductor IGBT, and based on this, the optimization problem of solder layer thickness was studied. In China, Reference [13] considers the failure position of the solder layer and the feedback effect of thermal characteristics caused by fatigue, establishes a multiphysics coupling simulation of IGBT, uses an update strategy based on the Caer thermal network model, and establishes a method that takes into account the cumulative effect of solder layer fatigue. The IGBT life prediction model of the wind turbine converter is finally evaluated. The analytical life model of IGBT mainly describes the relationship between load current, current frequency, average temperature, temperature fluctuation value, temperature rise rate, and other factors and the number of failures, that is, life. At present, the life model provided by device manufacturers is mainly based on the average temperature. In the relationship between the temperature fluctuation value and the number of failures, the number of failures is obtained by power cycle or temperature cycle experiments. Reference [14] established the finite element model of the IGBT model SKM50GB12T4, considering the influence of the power cycle load temperature level on the fatigue life of the solder layer of the device, improved the Coffin-Manson model, and applied the improved model to the IGBT life prediction. In China, by analyzing the failure mechanism of IGBT, Reference [15] designed a power cycle experiment and formulated an experimental plan, used the Weibull distribution to obtain the parameters of the device life model, and then established the Coffin-Manson-Arrhenius life model. The model has higher accuracy, and the effect of junction temperature is more in line with the actual situation. The fault prediction approach based on terminal characteristics compares characteristic parameters in the actual operating state with known aging characteristic parameters of the device, judges the current operating



condition, and predicts future parameter trend curves. When the specified aging threshold is reached, the aging IGBT can be maintained, repaired, or replaced in time. The core of this method is to extract and transform historical data and use some intelligent algorithms to estimate the trend of the device's future operating state. Its key technologies include aging feature parameter extraction and prediction algorithm design, and mainstream algorithms include regression algorithms in numerical algorithms, filtering algorithms, and artificial neural networks (ANNs) in machine learning.

Abroad, a research group from Cranfield University used the collector-emitter voltage  $V_{CE}$  of IGBT as a characteristic parameter, established a random degradation model based on probability distribution, and studied the effects of the gamma distribution, exponential distribution, Poisson distribution, and combined distribution models on IGBTs. The accuracy of life prediction is improved, and the failure model based on a time-delay neural network (TDNN) is used to improve the prediction accuracy. Compared with the method based on the stochastic model, the error of the prediction method based on TDNN is less than 4% [16–18]. Reference [19] studied the fault prediction framework of IGBT. The framework uses the Mahalanobis distance method for abnormality monitoring. After monitoring the abnormality, the particle filter (PF) method is used to predict the fault time, and the collector-emitter saturation voltage is selected. Decreasing  $V_{CE(ON)}$  is an aging characteristic parameter, and its value increases by 20% as the failure threshold. The prediction error of the research and analysis algorithm is 20%. Reference [20] studied a fault prediction method based on a neural network and adaptive neurofuzzy inference system and used it to predict the degradation of IGBT devices, using the IGBT collector-emitter voltage degradation life data in the NASA Research Center database to compare the proposed method. For verification, the prediction errors of the two methods are 19% and 31%, respectively. The fault prediction method based on end characteristics does not require the mathematical model and physical model of the object and estimates the future operation trend of the object based on the condition monitoring data, thus avoiding the shortcomings of the model-based fault prediction method, but in practical engineering applications, some historical data are difficult to obtain or expensive to obtain, and the obtained data also has certain uncertainty and incompleteness, which increases the difficulty of the method based on end characteristics [21, 22]. Moreover, the traditional prediction algorithms used in some literature cannot make full use of the historical information of the data, resulting in inaccurate prediction and low precision. Therefore, how to effectively use the time-series information of the data is also an important point. There are many classifications of intelligent algorithms in fault prediction based on terminal characteristics, especially in the field of machine learning led by neural networks, which have unparalleled advantages in solving nonlinear problems, and some of them also have good solutions to time series problems, and more importantly, it is more in

line with the current trend of rapid development of big data technology.

### 3. Method

**3.1. IGBT Aging Characteristic Parameter Selection.** The aging failure or failure of IGBT will lead to changes in its physical and chemical properties; that is to say, the aging failure problem of IGBT will be manifested in its terminal parameters to a certain extent. Therefore, on the basis of studying the failure mechanism of IGBT, the terminal parameters that best represent its health state can be selected as the aging characteristic parameters and combined with some intelligent algorithms to predict the failure. This section will list the key terminal parameters of IGBT and analyze the changes in their values with aging and finally select appropriate parameters as aging characteristic parameters. The terminal parameters of IGBT devices mainly include gate turn-on threshold voltage, module thermal resistance value, collector-emitter saturation voltage value, and collector-emitter turn-off peak voltage value. Each eigenvalue is analyzed below.

**3.1.1. Gate Turn-On Threshold Voltage.** The gate turn-on threshold voltage is the minimum voltage value for the IGBT to ensure that the device can be turned on. As the IGBT gradually degrades and fails, the material layer at its gate will gradually degrade, resulting in a larger turn-on voltage during the turn-on process. This indicates that the gate turn-on threshold voltage gradually increases during the IGBT degradation process, which can be used as a characteristic parameter for fault prediction. However, the gate voltage in a normal application environment is controlled by a steady source circuit signal, and it is difficult to effectively detect the gradually changing minimum turn-on threshold voltage.

**3.1.2. Module Thermal Resistance Value.** Since the IGBT works in a high-temperature and high-pressure environment for a long time, its degradation effect is very obvious, resulting in expansion cracks in the device material layer, which increases the thermal resistance value of the module and the junction temperature value of the module, further accelerating the degradation of the device. For the detection of junction temperature and thermal resistance, it is currently necessary to go deep into the device for measurement, which can still be achieved in the experimental environment, but it is difficult to effectively measure the IGBT device in normal use, which is not conducive to using this characteristic parameter for IGBT fault prediction.

**3.1.3. Collector-Emitter Saturation Voltage Value.** The IGBT is in the off-and-on state for a long time, and its ideal equivalent principle can be compared to a lossless on-off switch. However, in practical applications, there will be internal on-off resistance. This results in a voltage drop between collector and emitter. Some literature studies have shown that the voltage between the collector and the emitter is not constant, but changes with the degradation of the IGBT. During the degradation process, the collector-emitter saturation

voltage value is gradually rising, so it can be a characteristic parameter for IGBT fault prediction.

*3.1.4. Collector-Emitter Turn-Off Peak Voltage Value.* During the IGBT turn-off process, due to the existence of the parasitic transistor, the transistor generates a transient voltage, and this voltage and the IGBT collector-emitter voltage work together to generate an instantaneous peak voltage. At the moment of a turn-off, the  $V_{CE}$  of the IGBT will have a high peak value, the turn-off current will drop rapidly, and the turn-off voltage will rise rapidly. When the voltage rises, there will be a voltage value exceeding the normal voltage, and there will be a protruding peak in the waveform. The existence of this overvoltage will cause stress shock to the device, so it is very necessary to analyze the voltage value. Analysis of laboratory aging data shows that when the IGBT degradation changes, the instantaneous peak voltage of its turn-off is gradually decreasing, so this parameter can be used to predict IGBT faults.

Through the comparison of experimental data, the collector-emitter turn-off peak voltage value shows a downward trend in the process of IGBT degradation, and the effect is obvious, while the collector-emitter saturation voltage value has no obvious upward trend in this data set. From the previous theoretical analysis and degradation experimental data, it is shown that the collector-emitter turn-off peak voltage value can be well used as the characteristic parameter of IGBT fault prediction. This paper will select this characteristic parameter and use this data set to study the IGBT fault prediction algorithm. Write a Python program to extract the peak voltage value of each group of data and obtain a total of 540 groups of peak voltage values.

*3.2. Time Series Forecasting Methods.* The purpose of failure prediction is to find out the failure of the device in advance so that the staff can deal with it in time and reduce the loss of system operation. The traditional IGBT fault prediction method is to use mathematical statistics to mathematically model the IGBT degradation parameters, but this method fails to make full use of the data time series information, and the model is difficult to apply to complex production and life. Machine learning algorithms and BP neural network algorithms have significantly improved prediction accuracy. However, the IGBT failure process gradually degrades with time. Therefore, this paper focuses on the application of deep learning time series prediction algorithms in IGBT fault prediction. The time series forecasting method developed earlier, there are many forecasting methods, and the application is also very wide. The traditional time series forecasting method is developed from the mathematical statistics theory, and now, there are many branches of forecasting methods. The nature of prediction can be divided into quantitative analysis method and qualitative analysis method, and many subsequent prediction methods are also evolved on the basis of this method. The regression methods such as univariate linear regression evolved from the causal prediction method to determine the relationship between data samples by means of data processing. In the process of modeling regression, this method

does not make full use of the contextual relationship of the data sequence, and it is difficult for the regression model to make effective predictions on future data. The moving average method evolved from the trend forecasting method uses time-series historical information for forecasting. The moving average method mainly seeks the average value of a historical time series for a stationary time series to predict the data. The weighted moving method is an improvement and improvement of the moving average method. It mainly weights the historical information, assigns different weights to different historical information, and then predicts the future data. The moving average method has good prediction accuracy for stable series, but it is difficult to apply effectively to nonstationary series. The weighted movement method needs to retain the information of the entire historical sequence when forecasting, and its forecasting efficiency is greatly reduced in the face of the huge amount of data forecasting.

With the continuous progress of science and technology in recent years, AI has developed rapidly. The model function fitting ability of AI algorithms is much higher than that of traditional modeling methods.

*3.2.1. Decision Tree.* It is a method of using information gain to predict or classify data, and its commonly used forms are decision trees such as ID3 and C4.5. This method realizes the decision-making model through continuous attribute judgment and decision-making and achieves the application purpose. However, when constructing the model, the decision tree ignores the relationship between attributes and features, and it is more prone to decision bias for data with unbalanced samples.

*3.2.2. Bayesian Network.* It is a directed acyclic graph model, which represents a set of conditional probabilities, and can also be regarded as a nonlinear extension of a Markov chain. The advantage of this network is that the attribute variables can be connected to make inferences and predictions; the disadvantage is that the training of the network structure is more complicated, and it is not easy to train the model application.

*3.2.3. Support Vector Machine (SVM).* SVM is used on various occasions due to its extremely robust performance. It works by efficiently dividing the data by finding the hyperplane with the largest spacing of the data. Support vector regression is to make all the data of a set have the closest distance to the plane, so as to achieve the purpose of data prediction. However, this method cannot fully utilize the historical information of time series.

*3.2.4. Neural Network.* Due to the strong function fitting ability of neural networks and model construction through learning and training, the application of neural networks has developed rapidly in recent years. Now, the neural network has developed many branches, including back propagation neural network (BPNN), recurrent neural network (RNN), and convolutional neural network (CNN), which are the development and application neural networks. BPNN can fit any nonlinear function, and its prediction model has a strong expressive ability. Due to the influence

of its own structure, the RNN has a more obvious solution to dealing with time series problems, such as speech recognition and machine translation. Recent studies have shown that CNN can also perform time series prediction. The method is to use the network to make predictions on the time series data by constructing spatial data information from the sample data time series. To sum up, the time series forecasting method is developing in the direction of AI. Among them, the neural network has been paid more and more attention by scholars and research institutions from all walks of life due to its strong model construction and expression ability.

### 3.3. Deep Learning-Related Technologies

**3.3.1. Deep Learning Concepts.** The performance and generalization ability of the shallow network model is limited. In order to improve the performance of the model, the artificial neural network (ANN) has been improved and extended. The multilayer and various neural networks are connected and combined, and the training optimization algorithm is improved to construct a network model belonging to the deep neural network (DNN) model. Compared with the shallow network, the improved multilayer network has greatly improved the ability to solve complex problems. Due to the different structures of the neural network, the deep learning neural network includes the following three network structures:

(1) *DNN Network Is Composed of Multilayer Neural Networks.* Compared with the BPNN, it has more layers in general. The complexity of the network model is improved by increasing the number of hidden layers of the network, which is mainly used to solve application problems such as nonlinearity or linearity.

(2) *CNN Is Different from the Fully Connected Network.* It belongs to the partially connected network model. Network layers are connected by convolution kernel operations. This kind of network mainly performs feature processing on images through convolution operations and is mainly used in image processing.

(3) *RNN Is a Network with a Feedback Connection.* Due to the special structure of the network itself, the network has an excellent effect in dealing with time series problems, mainly used for speech recognition and time series prediction. RNN has developed rapidly in recent years, and a variety of improved RNN structures have been formed, such as the Long Short-Term Memory Network (LSTM) structure and GRU structure. In the application, in order to improve the use effect, most of them use a combination of various network structures to improve the performance of the model. In this paper, RNN such as LSTM is used in the study of IGBT fault prediction. And use the combined network model to improve the prediction network, and finally explore the best prediction network, model.

**3.3.2. Loss Function.** Compared with the actual value, the predicted value obtained by the neural network model will

have a certain error. During the model training process, we always hope that the error value can gradually become smaller. The function that measures the error distance between the predicted value and the true value is called the loss function. The loss function is used to update the weights during training so that the loss function is gradually reduced and the model parameters are continuously optimized. The selection of the loss function is related to the occasion to be applied. Common loss functions include cross-entropy, maximum likelihood error, maximum a posteriori probability, and mean square error. This paper studies the IGBT fault prediction problem, and the prediction problem belongs to the regression problem. Formula (1) shows the expression of the mean square error loss function:

$$L_{(\sigma)} = \frac{1}{n} \sum_{i=1}^n (y^i - y_{\sigma}(x^i))^2, \quad (1)$$

where  $L_{(\sigma)}$  represents the error between the real value and the predicted value, that is, the loss function;  $n$  is the number of training samples;  $y^i$  represents the real value;  $\sigma$  is the parameter variable of the network; and  $y_{\sigma}(x^i)$  represents the predicted value of the network model. The larger the value of  $L$ , the greater the deviation between the predicted value of the network model and the true value. The process of deep learning network training is to continuously fit the prediction function model by continuously reducing the loss function value.

### 3.4. IGBT Fault Prediction Based on LSTM

**3.4.1. LSTM Network.** Due to the existence of the cyclic structure of the RNN network introduced above, when using the chain derivation rule for gradient descent, it is very likely that the gradient disappears or the gradient explodes. Therefore, the long-term dependence of the RNN network makes it difficult to apply for a long-time sequence. In order to solve the impact of a long-term dependence on RNN, the long-short-term memory network LSTM came into being. LSTM is a special loop structure that learns information in network parameters through the control of three gate structures. The LSTM structure has three "gates," namely, the input gate, forget gate, and output gate. The calculation method of the LSTM unit is shown in the following formulas:

$$\begin{aligned} f_t &= \mu(W_f^T \times h_{t-1} + U_f^T \times x_t + d_f), \\ i_t &= \mu(W_i^T \times h_{t-1} + U_i^T \times x_t + d_i), \\ C'_t &= \tanh(W_C^T \times h_{t-1} + U_C^T \times x_t + d_C), \\ O_t &= \mu(W_O^T \times h_{t-1} + U_O^T \times x_t + d_O), \end{aligned} \quad (2)$$

where  $W$  and  $U$  represent the weight parameters of the corresponding gate structure.

**3.4.2. LSTM Prediction Network Design.** From the analysis of the LSTM network structure in the previous chapters, we can see that the special structure of the LSTM network

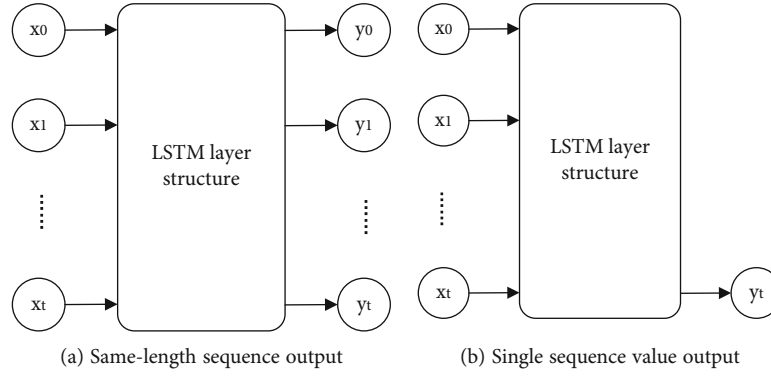


FIGURE 1: LSTM network output method.

makes it possible to solve time series problems. The special gate structure of LSTM can store input information of longer time series and prevent the problem of gradient disappearance. The advantages of LSTM are as follows:

- (1) It solves the long-term dependence problem of RNN, enabling it to learn information from long time series
- (2) LSTM network has strong data fitting ability, and its robustness and versatility are strong
- (3) The network parameters of the recurrent layer are shared, and their parameters do not increase with the length of the time series. Due to the special structure of LSTM and its advantages for time series processing, the LSTM network can be used for IGBT fault prediction tasks. Next, a prediction network will be designed step by step for the IGBT fault prediction problem

(1) *The Input and Output of the Network.* The input of the LSTM network is time-series data, and its sequence length can be set to  $T$ . For the network output part, LSTM has two output forms: one is that the input time series  $X_T$  is processed by the network to output the same length of time series data  $Y_T$ ; the other is that the output contains only one output result value. The input and output of its single-layer LSTM network are shown in Figure 1.

Here,  $X_T$  represents a certain sample sequence;  $Y_T$  represents the output result sequence, and the following formulas can be used.

$$\begin{aligned} X_T &= [x_0, x_1, \dots, x_t], \\ Y_T &= [y_0, y_1, \dots, y_t]. \end{aligned} \quad (3)$$

Figure 1 shows the two output modes of the LSTM network, which are used in the combination of multi-layer LSTM networks (Figure 1(a)) to pass the time series backward. Figure 1(b) can be used to get the results when doing the output of a single-layer network or the last layer of a multilayer network.

(2) *Selection of Activation Function.* Sigmoid and tanh activation functions have gradient disappearance in the value range, so the IGBT fault prediction network in this paper will use the Leaky ReLU activation function with better performance to reduce the possibility of gradient disappearance in a recurrent network.

(3) *Hidden Layer Design.* The number of hidden layers and nodes in the hidden layer has an important influence on the output results of the prediction network. The increase in the number of layers and nodes will make the network model more complex and deeper, which will help improve the data fitting ability but is not conducive to network training. There is no specific theoretical basis for the design of the hidden layer, and it is generally set according to an empirical formula. When setting, you can refer to the empirical formula such as

$$h = \sqrt{m + n} + b, \quad (4)$$

where  $h$  is the number of hidden layer nodes,  $m$  is the number of input layer nodes,  $n$  is the number of output layer nodes, and  $b$  is a constant value of about 10.

(4) *Loss Function.* This paper studies the problem of IGBT fault prediction, so the mean square error is chosen as the loss function of the network.

(5) *Prevent Overfitting Method.* Overfitting means that the trained network model performs well in the training set, but the performance in the test set is poor, making it difficult to apply in practice. Since the network model has many parameters and is prone to overfitting, it is necessary to optimize the model by limiting overfitting. Commonly used methods to limit overfitting include  $L_1$  and  $L_2$  regularization, both of which are optimized by “penalizing” weight parameters. Formulas (5) and (6) show the calculation methods of these two regularization methods:

$$L_1 = L(\sigma_n) + \lambda \sum_i^n |\sigma_i|, \quad (5)$$

$$L_2 = L_{(\sigma_n)} + \lambda \sum_i^n \sigma_i^2, \quad (6)$$

where  $L_{(\sigma_n)}$  represents the loss function and  $\lambda$  represents the regularization coefficient, which is generally set to 0.5. Since  $L_1$  regularization produces sparse solutions, this paper uses the  $L_2$  regularization method to prevent overfitting when designing an IGBT fault prediction network.

In this paper, the IGBT fault prediction network will use the above design method to design the prediction network and explore the best IGBT fault prediction network model by changing the LSTM network with different hidden layers, different nodes, and different time series lengths.

**3.5. Predictive Evaluation Indicators.** In order to facilitate the comparison of the prediction effect of the prediction method network, it is necessary to quantify the prediction results to measure the quality of the prediction results of the network model. Evaluation indicators need to be appropriately selected according to actual problems. The IGBT fault prediction problem studied in this paper belongs to regression analysis, so the regression prediction index can be used to evaluate the model effect. In this paper, the following two regression prediction evaluations are finally selected.

**3.5.1. Mean Absolute Error (MAE).** MAE reflects the mean absolute difference between the predicted value and the true value, and its calculation formula is shown in

$$\text{MAE} = \frac{1}{n} \sum_{i=1}^n |y - \hat{y}|, \quad (7)$$

where  $y$  represents the real value,  $\hat{y}$  represents the predicted value, and  $n$  represents the number of predicted samples.

**3.5.2. Root Mean Square Error (RMSE).** The definition of RMSE is shown in

$$\text{RMSE} = \sqrt{\frac{1}{n} \sum_{i=1}^n (y - \hat{y})^2}, \quad (8)$$

where  $y$  represents the real value,  $\hat{y}$  represents the predicted value, and  $n$  represents the number of predicted samples.

## 4. Experiment and Analysis

**4.1. Data Normalization.** For network training, data samples are essential. The dimensions of the samples in the original data are different, and the value ranges are inconsistent, which could lead to bias in the network prediction outputs due to the values of different attribute values in the network training. The network is likely to ignore a little value, impacting network training, and prediction accuracy. The scaling of data so that it falls inside a tiny defined interval is known as data normalization. Standardizing the data reduces the impact of varied dimensions and values on network training, improves prediction accuracy, and places the

data in the gradient-sensitive part of the activation function, which speeds up network training. In this paper, the following normalization methods are used for data normalization in fault prediction data processing, and its data is normalized to between [0, 1] according to the most typical normalization range.

$$\delta_i = \frac{x_i - X.\text{Min}}{X.\text{Max} - X.\text{Min}}, \quad (9)$$

$$\hat{x}_i = \frac{\delta_i}{\text{Max} - \text{Min}} + \text{Min},$$

where  $x_i$  represents the sample value,  $X.\text{Min}$  represents the minimum value in the sample,  $X.\text{Max}$  represents the maximum value in the sample,  $\text{Min}$  represents the minimum value of the specified scaling,  $\text{Max}$  represents the maximum value of the specified scaling, and  $\hat{x}_i$  represents the value after normalization.

**4.2. Sliding Time Window Samples.** Failure prediction methods have been described in previous chapters, and LSTM networks are capable of processing time series data. The input data of the LSTM network are time-series samples, so it is necessary to construct time series samples when training the network and predicting the output. The NASA PCoE dataset used in this paper to study IGBT fault prediction contains 540 collector-emitter turn-off spike voltage values. Because spike voltage values are discrete data values, autocorrelation time series data samples for input to the LSTM network must be created. The sliding time window method is used in this paper to create data samples for network training. The sliding time window method moves on the data value using the supplied input sequence length as the size of the sliding window, uses the value following the window sequence as the sample label value, and generates data samples for training while sliding. The process of the sliding window method is shown in Figure 2.

Among them, the Figure 2 shows the construction process of time series data samples with a sequence length of 5 by the sliding window method. For example,  $[[x0, x1, x2, x3, x4], [x5]]$  represents a time series sample constructed by the sliding window method, and  $[x5]$  represents the sample label value. This paper uses the sliding window method when constructing time-series samples and uses the previous time series values to predict the next sample point. First, write a Python program to normalize the 540 values of NASA PCoE data using the data normalization method in the previous section, and write a function program for constructing time series samples in Python to construct time series lengths sample sets of 5, 10, 15, 20, and 25, and use 80% of the time series samples for training and 20% for testing.

**4.3. LSTM Network Experimental Results and Analysis.** This section conducts IGBT fault prediction experiments based on the LSTM network. Set different time series lengths, different network layers, and different hidden layer nodes to explore the best fault prediction model of LSTM. In the LSTM network experiment, the learning rate is set to

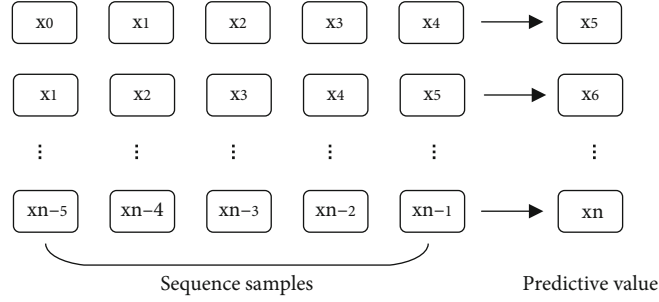


FIGURE 2: Sliding window method.

TABLE 1: Normalized RMSE for different number of nodes in a single-layer LSTM.

Number of nodes	5	10	15	20	25
30	0.0113	0.0113	0.0138	0.0118	0.0106
40	0.0125	0.0104	0.0118	0.0103	0.0107
50	0.0119	0.0104	0.0103	0.0108	0.0107

0.001; the LSTM network layer is set to 1 and 2 layers; the hidden nodes of each layer are set to 30, 40, and 50 nodes according to the empirical formula, and the time series length is set to 5, 10, 15, 20, and 25; batch size is set to 10; adjust each parameter and the number of model iterations to make the model converge to the best. The first 80% of the constructed sample set is utilized for dry training, while the remaining 20% is used for dry testing. Keras is a Python library of deep learning techniques that improves and simplifies TensorFlow. In this paper, Keras and Python are used to create programmer algorithms based on network architecture and to conduct prediction effect experiments. On the IGBT fault curve, LSTM network prediction is conducted using the above parameter settings. To explore the influence of different network depths, nodes, and time series lengths on the prediction results, the single-layer LSTM, 30-node, 40-node, and 50-node network fault prediction experiments are now performed. The experimental results are shown in Table 1 and Figures 3 and 4.

Table 1 and Figures 3 and 4, show the error results of 30, 40, and 50 nodes of a single-layer LSTM network. The normalization (RMSE) in the table represents the root mean square error value of the data value after normalization, 5, 10, 15, 20, 25 indicates the set time series length.

At the same time, this paper also adds a two-layer LSTM network to explore the fault prediction results, as shown in Table 2 and Figures 5 and 6.

Table 2 and Figures 5 and 6 show the error result values of nodes 30, 40, and 50 of the two-layer LSTM network. The normalization (RMSE) in the table represents the root mean square error value of the data values after normalization; 5, 10, 15, 20, and 25 represent the set time series length. When the LSTM network experiment is deepened again, the adjustment parameters cannot converge the model, and the network that is too deep cannot learn the sample data. Therefore, in the above network experiment results, a network model that can predict IGBT faults better is found.

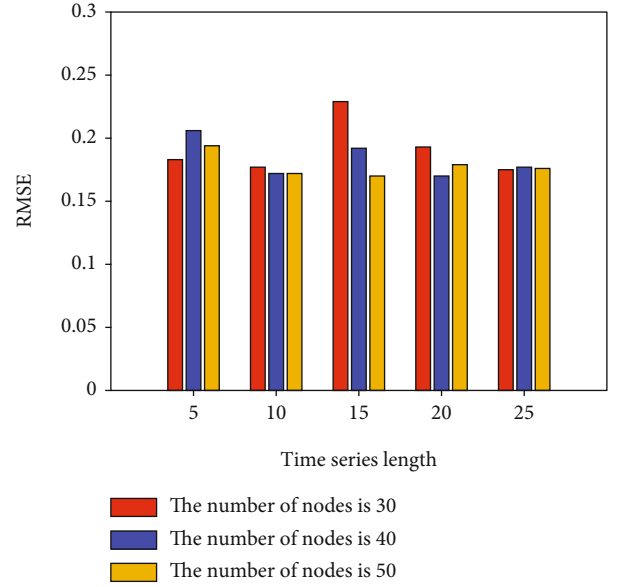


FIGURE 3: RMSE for different number of nodes in a single-layer LSTM.

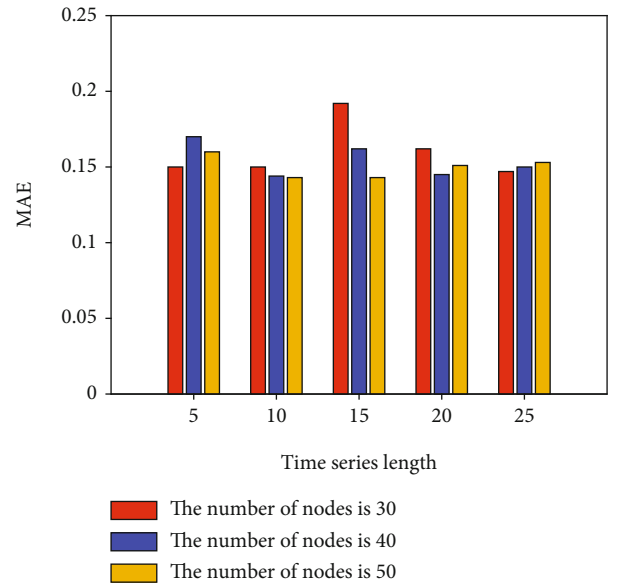


FIGURE 4: MAE for different number of nodes in a single-layer LSTM.

TABLE 2: Normalized RMSE for different number of nodes in a two-layer LSTM.

Number of nodes	5	10	15	20	25
30	0.0113	0.0162	0.0109	0.0110	0.0113
40	0.0135	0.0153	0.0106	0.0111	0.0104
50	0.0127	0.0138	0.0107	0.0103	0.0178

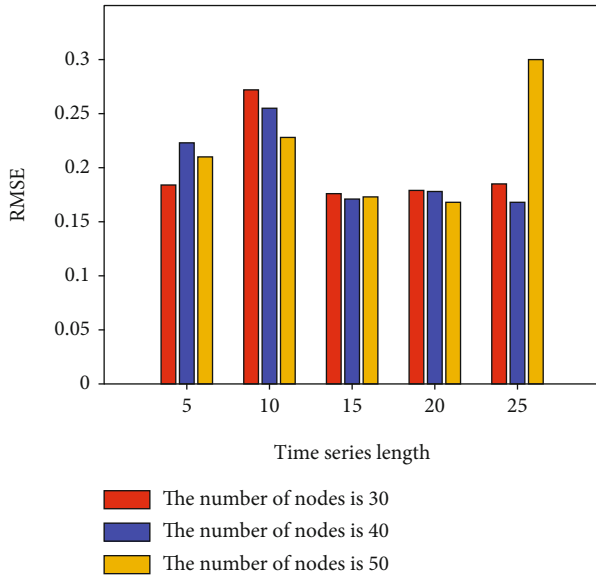


FIGURE 5: RMSE for different number of nodes in a two-layer LSTM.

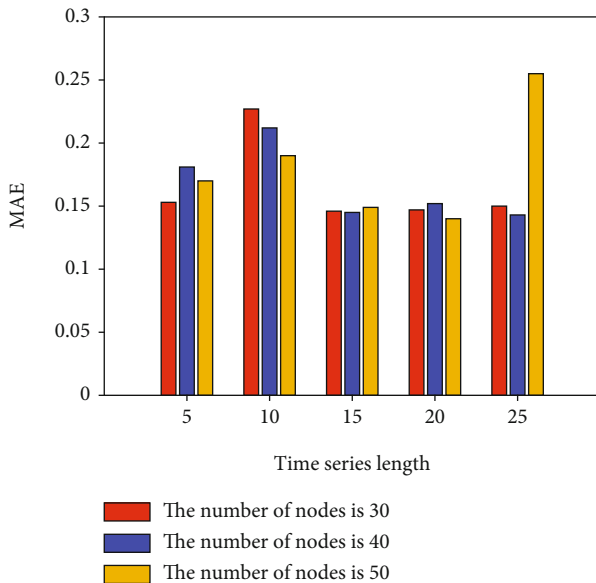


FIGURE 6: MAE for different number of nodes in a two-layer LSTM.

The preceding experimental findings show that correctly expanding the length of the time series can increase the network model's prediction accuracy. When the time series is changed from 5 to 20, for example, the MAE decreases. Similar to single-layer LSTM, when the number of LSTM net-

work layers is raised, the MAE and RMSE in 15 and 20-time series have lower error values, and the prediction model's accuracy improves. After the above experimental results, it is found that when the network parameters are set to the LSTM layer number of 2, 50 nodes, and the time series of 20, the RMSE and MAE error values for IGBT fault prediction are the smallest.

## 5. Conclusion

With the advancement of science and technology, the use of power electronic gadgets has increased dramatically. IGBTs are being used with increasingly powerful system equipment. Furthermore, IGBT devices offer numerous advantages, resulting in an increase in the use of IGBTs and an increase in the number of applications. However, due to the hostile working environment and high working intensity of the IGBT during usage, the IGBT suffers significant fatigue damage, increasing the likelihood of failure. The majority of traditional IGBT fault prediction research relies on fault characteristic parameters for mathematical statistics or uses machine learning methods to construct prediction models. These models fail to make full use of the historical damage information in the process of IGBT degradation over time, and the prediction accuracy is not high. It is difficult to combine with practical application. This article has read a large number of IGBT fault research papers and deep learning algorithm prediction data and has a deep understanding of the current IGBT fault prediction. In this paper, a fusion of terminal characteristics and a deep learning time series prediction algorithm is proposed to predict the fault of IGBT, and the fault prediction network is designed according to the theoretical analysis and experimental results, and the optimal IGBT fault prediction LSTM network model is finally obtained. The main research work in this paper is as follows: (1) This paper starts from the basic principle of IGBT and the structure of its device and analyzes its failure mode on the failure of IGBT. The characteristic parameter of collector-emitter turn-off peak voltage value is selected for IGBT fault prediction, and the aging data of NASA PCoE Research Center is used to verify that the characteristic parameter can be used for fault prediction. (2) In view of the shortcomings of traditional fault forecasting methods, this paper proposes to use deep learning time series forecasting methods for fault forecasting. The prediction network is developed once the LSTM is theoretically studied. The experimental results suggest that using the LSTM network model, which has fewer parameters and a greater prediction efficiency, can increase the accuracy of IGBT failure prediction.

## Data Availability

The datasets used during the current study are available from the corresponding author on reasonable request.

## Conflicts of Interest

The author declares that he has no conflict of interest.

## Acknowledgments

The research is supported by the Guangxi Key Laboratory of Manufacturing System & Advanced Manufacturing Technology (Grant No. 19-050-44-007Z).

## References

- [1] P. Duan, Y. Jia, L. Liang, J. Rodriguez, K. M. Saidul Huq, and G. Li, "Space-reserved cooperative caching in 5G heterogeneous networks for industrial IoT," *IEEE Transactions on Industrial Informatics*, vol. 14, no. 6, pp. 2715–2724, 2018.
- [2] J. M. Thebaud, E. Woirgard, C. Zardini, S. Azzopardi, O. Briat, and J. Vinassa, "Strategy for designing accelerated aging tests to evaluate IGBT power modules lifetime in real operation mode," *IEEE Transactions on Components & Packaging Technologies*, vol. 26, no. 2, pp. 429–438, 2003.
- [3] B. Tian, W. Qiao, Z. Wang, T. Gachovska, and J. L. Hudgins, "Monitoring IGBT's health condition via junction temperature variations," in *2014 IEEE Applied Power Electronics Conference and Exposition-APEC 2014*, pp. 2550–2555, Fort Worth, TX, USA, 2014.
- [4] T. D. Batzel and D. C. Swanson, "Prognostic health management of aircraft power generators," *IEEE Transactions on Aerospace & Electronic Systems*, vol. 45, no. 2, pp. 473–482, 2009.
- [5] R. C. Taylor, "An overview of the Hadoop/MapReduce/HBase framework and its current applications in bioinformatics," *BMC Bioinformatics*, vol. 11, no. S12, p. S1, 2010.
- [6] M. De Ree, G. Mantas, A. Radwan, S. Mumtaz, J. Rodriguez, and I. E. Otung, "Key management for beyond 5G mobile small cells: A survey," *IEEE Access*, vol. 7, pp. 59200–59236, 2019.
- [7] H. Sumida and A. Hirabayashi, "The substrate bias effect on the static and dynamic characteristics of the lateral IGBT on the thin SOI film," *IEICE Transactions on Electronics*, vol. 779, pp. 1464–1471, 1994.
- [8] S. Mumtaz, H. Lundqvist, K. Z. Saidul Huq, J. Rodriguez, and A. Radwan, "Smart Direct-LTE communication: An energy saving perspective," *Ad Hoc Networks*, vol. 13, pp. 296–311, 2014.
- [9] N. Patil, J. Celaya, D. Das, K. Goebel, and M. Pecht, "Precursor parameter identification for insulated gate bipolar transistor (IGBT) prognostics," *IEEE Transactions on Reliability*, vol. 58, no. 2, pp. 271–276, 2009.
- [10] P. Baraldi, F. Cadini, F. Mangili, and E. Zio, "Model-based and data-driven prognostics under different available information," *Probabilistic Engineering Mechanics*, vol. 32, no. 4, pp. 66–79, 2013.
- [11] B. Hu, S. Konaklieva, S. Kourra, S. A. Williams, L. Ran, and W. Lai, "Long term reliability evaluation of power modules with low amplitude thermomechanical stresses and initial defects," *IEEE Journal of Emerging and Selected Topics in Power Electronics*, vol. 9, no. 1, pp. 602–615, 2021.
- [12] R. Elakkiya, G. Kavithaa, V. Samavatian et al., "Reliability enhancement of a power semiconductor with optimized solder layer thickness," *IEEE Transactions on Power Electronics*, vol. 35, no. 6, pp. 6397–6404, 2019.
- [13] M. Y. Chen, Y. G. Chen, B. Gao, W. Lai, T. Huang, and S. Y. Xu, "Lifetime evaluation of IGBT module considering fatigue accumulation of solder layers," *Proceedings of the CSEE*, vol. 38, no. 20, pp. 6053–6061, 2018.
- [14] L. Rabiner and B. Juang, "An introduction to hidden Markov models," *Current Protocols in Bioinformatics*, vol. 3, pp. 4–16, 2007.
- [15] W. Lai, Y. Chenm, L. Ran, X. M. Wang, and S. Y. Xu, "IGBT lifetime model based on aging experiment," *Transactions of China Electrotechnical Society*, vol. 31, no. 24, pp. 173–180, 2016.
- [16] A. Alghassi, S. Perinpanayagam, and M. Samie, "Stochastic RUL calculation enhanced with TDNN-based IGBT failure modeling," *IEEE Transactions on Reliability*, vol. 65, no. 2, pp. 558–573, 2016.
- [17] T. Sreenuch, A. Alghassi, S. Perinpanayagam, and Y. Xie, "Probabilistic Monte-Carlo method for modelling and prediction of electronics component life," *Development*, vol. 5, no. 1, p. 104, 2014.
- [18] A. Alghassi, S. Perinpanayagam, M. Samie, and T. Sreenuch, "Computationally efficient, real-time, and embeddable prognostic techniques for power electronics," *IEEE Transactions on Power Electronics*, vol. 30, no. 5, pp. 2623–2634, 2015.
- [19] N. Patil, D. Das, and M. Pecht, "A prognostic approach for non-punch through and field stop IGBTs," *Microelectronics Reliability*, vol. 52, no. 3, pp. 482–488, 2012.
- [20] D. K. Ghose, S. S. Panda, and P. C. Swain, "Prediction of water table depth in western region, Orissa using BPNN and RBFN neural networks," *Journal of Hydrology*, vol. 394, pp. 296–304, 2010.
- [21] J. Li, Z. Zhou, J. Wu et al., "Decentralized on-demand energy supply for blockchain in internet of things: a microgrids approach," *IEEE transactions on computational social systems*, vol. 6, no. 6, pp. 1395–1406, 2019.
- [22] W. Duan, J. Gu, M. Wen, G. Zhang, Y. Ji, and S. Mumtaz, "Emerging technologies for 5G-IoV networks: applications, trends and opportunities," *IEEE Network*, vol. 34, no. 5, pp. 283–289, 2020.



## Research Article

# Mechanism of miR-760 Reversing Lung Cancer Immune Escape by Downregulating IDO1 and Eliminating Regulatory T Cells Based on Mathematical Biology

Hong Ge,<sup>1</sup> Lili Wang,<sup>2</sup> Wenqiang Chen,<sup>3</sup> and Lei Wang<sup>4</sup> 

<sup>1</sup>Pulmonary and Critical Care Medicine, Zibo Central Hospital of Shandong Province, Zibo, 255000 Shandong, China

<sup>2</sup>Pneumology Department, Chengwu Hospital, Chengwu, China

<sup>3</sup>Laboratory Medicine, Zibo Zhoucun People's Hospital, Zibo, 255300 Shandong, China

<sup>4</sup>Department of Oncology, Chengyang District People's Hospital, Qingdao, 266100 Shandong, China

Correspondence should be addressed to Lei Wang; [wanglei@qdcyyy.org.cn](mailto:wanglei@qdcyyy.org.cn)

Received 25 May 2022; Revised 16 June 2022; Accepted 20 June 2022; Published 14 July 2022

Academic Editor: Naeem Jan

Copyright © 2022 Hong Ge et al. This is an open access article distributed under the Creative Commons Attribution License, which permits unrestricted use, distribution, and reproduction in any medium, provided the original work is properly cited.

In cancer biology, mathematical models have become indispensable. They are useful for gaining a mechanistic grasp of cancer's dynamic processes. In cancer research, mathematical modelling approaches are becoming more common. The complexity of cancer is well suited to quantitative approaches as it provides challenges and opportunities for new developments (Altrock et al., 2015). *Background.* MicroRNA-760 (miR-760), as an early discovered tumor suppressor gene, is poorly expressed in lung cancer (LC). Indoleamine 2,3-dioxygenase 1 (IDO1), as an important regulator of T cell function, is active in immune tolerance. We discovered that miR-760 has a targeted relationship with IDO1, but the regulatory mechanism between miR-760 and IDO1 is still unclear. *Method.* The miR-760 and IDO1 levels in NSCLC were tested via real-time quantitative polymerase chain reaction (qRT-PCR) and western blotting (WB). Cell growth was tested by CCK8, and NSCLC cell migration and invasion were analyzed through Transwell analysis. The binding conditions and target gene of miR-451 in NSCLC cells were determined via double luciferase reporter gene. The CD8+ T and CD4+ T cell ratio in CD45+ cells was assessed by flow cytometry. *Results.* qRT-PCR revealed that miR-760 was low-expressed and IDO2 was highly expressed in LC. miR-760 mimics suppressed cell growth, invasiveness, and migration. We also observed that miR-760 could downregulate the IDO1 protein level. Significantly, we revealed that miR-760 could inhibit CD8+ T cell apoptosis by controlling IDO1 enzyme function. *Conclusion.* Our findings show that miR-760 inhibits CD8+ T cell responses in LC through regulating IDO1, laying the groundwork for the development of novel vaccination therapies for the treatment of LC.

## 1. Introduction

Lung carcinoma (LC) is the most common type of cancer in people worldwide [1]. According to statistics [2], around one million new patients are admitted each year. Small cell lung carcinoma (SCLC) and non-small-cell lung carcinoma (NSCLC) are the two types of LC, with the latter accounting for approximately 85% of cases. Despite the development of numerous therapeutic options, the long-term viability of LC patients is still quite low. The prognosis of advanced or metastatic LC patients is rather poor [3]. Therefore, it is very crucial to understand the pathogenesis of LC for developing new therapeutic targets.

MicroRNA (miR) is an endogenous small noncoding RNA, 20-25 nucleotides long [4–6]. miR can control cell viability, growth, differentiation, migration, invasiveness, and metastasis through the binding of 3'-untranslated regions (UTR) of some targeted genes [7–9]. Currently, studies have shown that [10] more than 30% of human genes can be controlled by miR. Moreover, more and more studies have confirmed that [11, 12] miR affects the development and progress of various tumors through downstream target genes. miR-760 is located on human chr1 chromosome. miR-760 directly affects human carcinoma processes (such as tumorigenesis, migrations, and metastases) and regulates

various tumor progression [13–15]. miR-760's mechanism in LC is still vague.

Indoleamine 2,3-dioxygenase 1 (IDO1) is a rate-limiting enzyme in tryptophan catabolism and suppresses T-lymphocytes and other immune cells [16]. Evidence showed that IDO-1 not only participates in the immune escape process of lung cancer but also contributes to the safety of the pretumor area [17]. In addition, studies have shown [18] that IDO-1 can induce immunosuppression and promote tumor progression in LC animal models. We first predicted miR-760's potential targeted genes online and concluded that miR-760 and IDO1 had a targeted binding connection. This suggested that miR-760 might affect the immune regulation of LC by targeting IDO1. Therefore, this research seeks miR-760's potential mechanism in LC, providing a new direction for clinical targeted therapy and drug development.

The arrangements of this paper are as follows: Section 2 discusses the materials and methods. Section 3 examines a result and experiments. Section 4 analyzes a discussion. Section 5 concludes the article.

## 2. Methods and Materials

**2.1. Clinical Data.** From January 2014 to January 2016, fifty-two NSCLC cases in our hospital were selected, and their tumor and surrounding tissues were collected. The tissues were transited in liquefied nitrogen and conserved at  $-80^{\circ}\text{C}$  for later use and unified testing. In this research, all participants had not received antitumor treatment before. Informed consent forms were obtained, and the research was ratified by the Medical Ethics Committee. This study was based on Declaration of Helsinki [19].

**2.2. Cell Culture.** Human LC cells (A549, H1975, and H1299) and bronchus epithelial cell strain HBE were from American Type Culture Collection (ATCC, Shanghai, China). The purchased cell strains were cultivated in RPMI 1640 medium comprising 10% FBS, 100 IU/ml penicillin and 100  $\mu\text{g}/\text{ml}$  streptomycin at 5%  $\text{CO}_2$  and  $37^{\circ}\text{C}$  (Invitrogen, Carlsbad, CA, the United States).

**2.3. Cell Transfection [20].** The miR-760 mimics (miR-760-mimics), miR-760 inhibitor (miR-760-inhibit), and nonspecific control miRNA (mimics-NC/inhibit-NC) were provided by Riobio (Guangzhou, China). IDO2 sequence length was selected and pcDNA-3.1 was used as the vector. Overexpression vector of IDO2 (pcDNA-IDO2) was constructed and blank vector was used as control (pcDNA-NC) for transient transfection. Lipofectamine 2000 (Invitrogen, Carlsbad, CA) was used to inoculate cells onto six-hole culture plates. The precursor sequences of miR-760 and miR-NC (negative control) were introduced into the pLV-THM lentivirus vector to create a nude mouse tumor allogeneic model. Cotransfection of HeK-293T cells with pSPAX2, pMD2.G, and LipoFilter reagent resulted in the packaging of the recombinant lentivirus. The supernatant liquid with lentivirus particles was obtained after transfection for 48 h and 72 h and filtered and centrifuged at high speed to concen-

trate the recombinant lentivirus. In the presence of 5  $\mu\text{g}/\text{ml}$  polypropylene, lentivirus with MOI of about 5 was transduced into A549 cells. The supernatant was removed and replaced by fresh complete medium 24 h later. The infection efficiency was verified through RT-PCR after infection for 96 h. Cells were chosen with 2  $\mu\text{g}/\text{ml}$  puromycin for two weeks.

**2.4. qRT-PCR [21].** The general RNA was obtained from collected tissues and cells with TRIzol (Invitrogen, the United States) agent. General RNA of each specimen was transcribed into first strand cDNA via PrimeScript™ RT Master Mix kit (TaKaRa, Tokyo, Japan). The SYBR Premix Ex Taq™ and ABI Prism 7500 detecting systems were conducted to real-time PCR, and the reaction system and reaction conditions were configured in accordance with the manufacturer's specifications.  $2^{-\Delta\Delta\text{Ct}}$  was applied to analyze data and data processing [19]. The following are the primers: miR-760 upstream primer 5'-CGAGCGCTCTGGGTCTG-3' and downstream primer 5'-CAGTGCAGGGTCCGAGGT-3', U6 upstream primer 5'-GCGTCGTGAAGCGTTC-3' and downstream primer 5'-GTGCAGGGTCCGAGGT-3', and IDO1 upstream primer 5'-AGGATGCGTGACTTTGTG-3' and downstream primer 5'-GATCTACTATTGCGAGGTG-3'. GAPDH was the inner reference of mRNA and U6 was for miR.

**2.5. WB Experiment.** The logarithmic growth phase cells were collected, and the cell concentration was adjusted to  $5 \times 10^5/\text{ml}$  and inoculated in a 6-hole plate overnight at  $37^{\circ}\text{C}$ , 5%  $\text{CO}_2$  incubator; then, the culture solution was discarded and dihydrotanshinone I solution was added dropwise with different concentrations; 100  $\mu\text{l}$  of culture medium was set as a blank control group and cultivated at  $37^{\circ}\text{C}$ , 5%  $\text{CO}_2$ . It was rinsed 3 times in PBS solution, and cells were put in an EP tube, and RIPA lysate was added dropwise, 30 min later centrifuged for 15 min at 12000 r/min. The supernatant was obtained and transferred to a new EP tube. The OD value was tested via a microplate reader at a wavelength of 490 nm for protein quantitative analysis. The wet transfer method was used to transfer the protein to the nitrocellulose membrane, and 5% skim milk was added dropwise and blocked for 60 min; GAPDH was the internal reference protein, and the primary antibody was added dropwise, with a dilution ratio of 1:1000, and cultivated at  $4^{\circ}\text{C}$ . Subsequently, it was cleaned by PBS solution 3 times, and the corresponding secondary antibody was added dropwise, with a dilution ratio of 1:5000, and then sealed for 1 h. It was performed in accordance with the instructions of the ECL chemiluminescence detection kit, and a gel imaging analysis system was used to analyze the bands and determine the OD value of each band.

**2.6. Detection of Cell Proliferating.** Cell growth was tested via cell counting kit 8 (CCK-8). The brief description was as follows: the transfected cells were inoculated in 96-hole plate at  $4 \times 10^3$  cells per hole and cultivated for 24 h, 48 h, 72 h, or 96 h. CCK-8 solution (Keygen Biotech, Nanjing, China) was put in. Then, cells were cultivated at  $37^{\circ}\text{C}$  for 60 min.

The absorbance was tested at 450 nm via a spectrophotometer. Data represented three independent tests conducted in triplicate.

**2.7. Transwell Experiment.** Transwell test was employed to test cell invasiveness and migration. Matrigel (BD Biosciences, USA) was precoated in Transwell's upper chamber during invasion, but not in the upper chamber during migration. The exact procedure was as follows: the transfected cells were suspended in single cell suspension in serum-free culture media at a density of  $5 \times 10^4$  cells/ml in the upper chamber. A total of medium (500  $\mu$ l) comprising 10% FBS was put in the lower chamber. All Transwell chambers were placed 25 h at 37°C and 5% CO<sub>2</sub>. Invasive cells were immobilized with 4% formaldehyde and dyed with 0.1% crystal violet. Invading cells were counted under an optical microscope (Nikon, Tokyo, Japan).

**2.8. Immunofluorescence Staining [22].** The tissue slices of nude mice with LC were obtained, dried at 60°C for 1 h, dewaxed with xylene, and rehydrated with ethanol fractionation. The antigen repair was processed with citrate buffer (pH 6.0), autoclaved and sterilized at 121°C, cleaned by PBS, and sealed 30 min with goat serum at room temperature. Then, the rat anti-mouse IDO1 and rabbit anti-mouse CD8+ antibodies were added, respectively, and kept at 4°C for one night. The slides were rinsed with PBS, and the goat anti-rabbit and anti-rat IgG second antibodies were added, respectively, and placed at ambient temperature in the dark for 2 h. The fluorescence staining was observed under laser scanning confocal microscope.

**2.9. Immunohistochemical Staining [23].** The tissue slices of nude mice with LC were obtained, dried 1 h at 60°C, dewaxed with xylene, and rehydrated with ethanol fractionation. The antigen repair was processed with citrate buffer (pH 6.0), autoclaved and sterilized at 121°C, washed with PBS, and sealed with goat serum (Boster, Wuhan) at ambient temperature for 30 min. The slices were cultivated with IDO1 and CD8+ antibodies at 4°C overnight or TUNEL apoptosis assay colorimetric kit (Beyotime, Shanghai, China) at 37°C for 60 min. Then, it was washed by PBS and sliced. Polink-1 HRP DAB and one-step polymer detecting systems were used to incubate at ambient temperature for 20 min. Lastly, the slides were counterstained with hematoxylin. The positive staining cells were counted in five stochastically selected regions, and the average of positive staining cells in each region was calculated. Image-Pro Plus 6.0 was used to quantitatively analyze the staining of IDO1, CD8+, and TUNEL (apoptotic markers).

**2.10. Isolation and Culture of White Blood Cells.** Human white blood cells were obtained by separating peripheral blood. The test tubes of ethylenediaminetetraacetic acid were used for subpackaging and analysis. At room temperature, it was centrifuged at  $500 \times g$  for 10 min and the supernatant was discarded. The volume of ACK lysis buffer solution (10 times) was added. It was then lightly swirled for 5 min and centrifuged ( $500 \times g$ , 10 min), and the supernatant was discarded. The procedure was repeated until all erythrocytes

were completely removed. Finally, leukocytes were collected. Under the condition of RPMI 1640 with 10% FBS, the cells were regulated to  $4 \times 10^6$  cells/ml. The miR-760-mimics or the control group was transfected into A549 and H1299 cells at 30 ng/ml IFN- $\gamma$ , respectively (GenScript, China). IFN- $\gamma$  was treated for 24 h and used as conditioned medium (CM). Then, we collected the supernatant after cell culture. The leukocytes (100  $\mu$ l) were inoculated into the 96-well plate, and then, different CM (100  $\mu$ l) was put in the 96-hole plate and cultivated for 48 h.

**2.11. Analysis of Flow Cytometry.** The leukocytes cultured in different CM for 48 hours were collected, resuspended with PBS, and dyed 15 min with FITC anti-human CD8+ in the dark at 4°C. Cells were centrifuged and suspended in binding buffer. The annexin V-APC/7-AAD double dyeing was performed with annexin V-APC/7-AAD apoptosis kit, and the staining method was carried out based on the kit instructions. In addition, tumor tissues of mice were separated by using the Tumor Dissociation Kit and then adjusted to single cell suspension. The single cell suspension was stimulated with BD white blood cell activation mixture (No. 550583) for 5 h. The tumor cells were dyed for 0.5 h with the Zombie Yellow™ Fixable Viability Kit. Then, the cells were dyed with CD45, CD4, and CD8+ for 0.5 h. After immobilization and permeabilization, the cells were fluorescently dyed with Foxp3. Cytex Aurora flow cytometer and FlowJo were used. The apoptosis was tested via annexin V-FITC apoptotic kit (BD Biosciences, Erembodegem, Belgium). Cells were obtained, rinsed twice through cold PBS, and resuspended in annexin V binding buffer. After that, they were dyed 15 min through fluorescein isothiocyanate (FITC) and propidium iodide (PI) at 4°C.

**2.12. Double Luciferase Report.** The bioinformatics analysis tools were applied (TargetScan ([http://www.targetscan.org/vert\\_72/](http://www.targetscan.org/vert_72/)) and miRDB (<http://mirdb.org/>)). The luciferase pmirGLO reporter vector was performed for constructing IDO1-wild type 3'-UTR (IDO1-wt) and IDO1 mutant 3'-UTR (IDO1-mut). Cells were inoculated into a 12-hole plate at  $1 \times 10^5$  per hole, cultivated for one night, and cotransfected with 100 nmol of miR-760-mimics or control group plus 100 ng of pmirGLO-30-UTR. The UTR plasmid of Lipofectamine 3000 (Invitrogen) was used for 48 h. The luciferase activity was tested via a dual-luciferase reporter (Promega Corporation, Madison, WI, the United States).

**2.13. Statistical Analysis.** The required pictures were drawn and data were assessed via GraphPad 8. The measuring data were marked as mean number  $\pm$  standard deviation (mean  $\pm$  SD) and compared through independent sample *t* test. The counting data were shown as percentage (%) and tested by chi-squared test, represented as  $\chi^2$ . One-way analysis of variance was employed for multigroup comparison, marked by F. LSD-t test was applied for pairwise comparison afterward. Multiple time points were analyzed by repeated measures analysis of variance and marked by F. Bonferroni was used for back testing. The correlation of miR with mRNA in patients' tumor tissues was analyzed. The

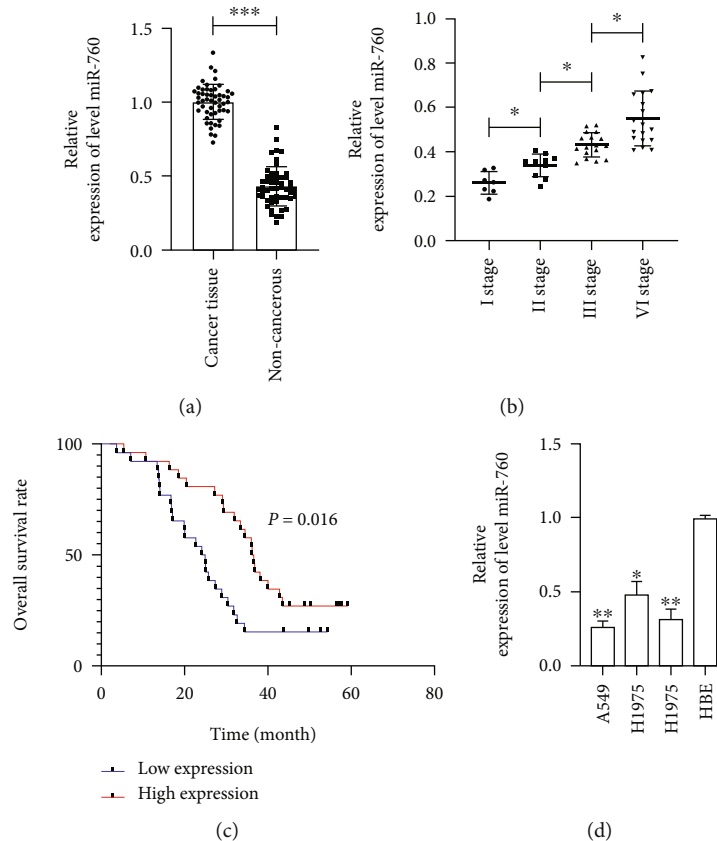


FIGURE 1: miR-760 level and prognosis in NSCLC patients. (a) The miR-760 level in NSCLC patients is tested via qRT-PCR. (b) The miR-760 level in different stages of NSCLC patients is tested via qRT-PCR. (c) The total survival of patients in miR-760 high and low expression groups is assessed via K-M survival. (d) The miR-760 level in LC cell lines is tested via qRT-PCR. \* $P < 0.05$ , \*\* $P < 0.01$ , and \*\*\* $P < 0.001$ .

relationship of miR-760 with survival was analyzed by K-M test ( $P < 0.05$ ).

### 3. Results

**3.1. miR-760 Was Reduced in NSCLC Patients with Unfavourable Prognosis.** The miR-760 in NSCLC patients was first tested by qRT-PCR. The results manifested that the miR-760 in the tumor tissues of NSCLC patients was downregulated compared with the adjacent tissues (Figure 1(a)). Further analysis denoted that reduced miR-760 level was bound up with the tumor stage of NSCLC (Figure 1(b)). Furthermore, patients were separated into high and low expression groups on the basis of miR-760's median value [24, 25]. miR-760 was discovered to be unrelated to age, gender, tumor size, or differentiation, although it was related to TNM stage and lymphatic metastasis (Table 1). In addition, we followed up with the patients. By January 2019, all patients had been followed up on, and no follow-ups had been missed. It was observed that the total survival time of low-expressed miR-760 patients was obviously lower than that of those with high expression (Figure 1(c)). Therefore, miR-760 was a latent prognostic index for NSCLC patients. qRT-PCR detection manifested that the miR-760 in LC cell strains also showed a downward trend

(Figure 1(d)). This indicated that miR-760 might affect the development and progress of LC.

**3.2. miR-760 Affects LC Development and Progression.** To ascertain miR-760's mechanism in LC, we carried out cell experiments in vitro. At first, we established miR-760-mimics and miR-760-inhibit vectors, respectively, and transfected them into A549 and H1299 cells. It turned out that the miR-760 enhanced after transfection of miR-760-mimics, but it reduced obviously after transfection of miR-760-inhibit (Figure 2(a)). Then, we tested the growth, invasiveness, migration, and apoptosis of cells transfected with miR-760-mimics and miR-760-inhibit by CCK-8, Transwell, and FACS, respectively. CCK-8 test revealed that the proliferation of cells transfected with miR-760-mimics was obviously inhibited compared with the control group, while the growth of cells with miR-760-inhibit was obviously enhanced (Figure 2(b)). Transwell experiment also denoted that cell invasion and migration after transfection of miR-760-mimics reduced obviously compared with the control group, while those after transfection of miR-760-inhibit enhanced obviously (Figures 2(c) and 2(d)). In addition, FACS experiments also showed that apoptosis was induced after transfection with miR-760-mimics, while the apoptosis rate reduced after transfection with miR-760-mimics (Figure 2(e)). These experiments confirmed that miR-760

TABLE 1: Relationship between miR-760 and clinical data of patients.

Factors		miR-760 relative level		P value
		Low expression ( $n = 26$ )	High expression ( $n = 26$ )	
Gender	Male ( $n = 28$ )	13	15	0.578
	Female ( $n = 24$ )	13	11	
Age	$\geq 60$ years old ( $n = 21$ )	9	12	0.397
	$< 60$ years old ( $n = 31$ )	17	14	
Tumor size	$\geq 5$ cm ( $n = 27$ )	12	15	0.405
	$< 5$ cm ( $n = 25$ )	14	11	
Differentiation	Poorly differentiated ( $n = 18$ )	10	8	0.560
	Middle+well differentiated ( $n = 34$ )	16	18	
Lymphatic metastasis	Metastasis ( $n = 15$ )	11	4	0.032*
	Nonmetastasis ( $n = 37$ )	15	22	
TNM staging	I+II ( $n = 35$ )	14	21	0.039*
	III+IV ( $n = 17$ )	12	5	

Note: \* means  $P < 0.05$ , and there were differences between groups.

affected the occurrence of LC and it was a latent therapeutic target in clinic.

**3.3. There Was a Targeted Relationship of miR-760 with IDO1.** miR regulated downstream target genes to take part in tumor development. We concluded that there was a targeted connection of IDO1 with miR-760 through online prediction analysis. At first, we tested the IDO1 mRNA and protein in LC cell strains after transfection of miR-760-mimics and miR-760-inhibit by qRT-PCR and WB. It manifested a significant regulatory effect (Figures 3(a) and 3(b)). Then, we further detected the IDO1 in tumor tissues of NSCLC patients. The findings signified that the IDO1 in tumor tissues of NSCLC patients increased obviously (Figure 3(c)). Correlation analysis concluded that miR-760 was positively correlated with the IDO1 relative expression in tumor tissues of NSCLC patients (Figure 3(d)). There was a targeted regulatory relationship of miR-760 with IDO1. Then, the double luciferase reporter revealed that miR-760-mimics suppressed IDO1-wt fluorescence activity, while miR-760-inhibit upregulated the fluorescence activity of IDO1 (Figures 3(e)–3(g)). It could be concluded that miR-760 and IDO1 were targetly related.

**3.4. Upregulating miR-760 Could Reverse LC Cell Growth and Metastasis Induced by Overexpression of IDO1.** miR-760 was tested in rescue experiments to see if it had a role in LC cell growth and progression through regulating

IDO1. The following were our initial findings. A549 and H1299 cells were transfected with pcDNA-IDO1, which promoted LC cell proliferation, invasiveness, and migration while suppressing apoptosis. However, the above effects were reversed after miR-760-mimics and pcDNA-IDO1 cotransfection; that is, cell growth, invasiveness, and migration were obviously accelerated, and apoptosis was promoted. So, miR-760 could regulate IDO1 to take part in LC development (Figure 4).

**3.5. IFN- $\gamma$  Improved the Survival of CD8+ T Cells by Inhibiting miR-760 and Upregulating IDO1.** Early studies have shown that IFN- $\gamma$  can upregulate IDO1 in LC cells. Moreover, IDO1 also affects tumor immunity. Tumor occurrence and development are influenced by the tumor immunological microenvironment. Treg cells, a type of lymphocyte subgroup with immune regulation function, keep the immune system in check and prevent illnesses, particularly by boosting tumor progression and helping tumor escape. Therefore, we have speculated that miR-760/IDO1 axis may also play an immunomodulatory role in LC. First, we analyzed the effect of miR-760 upregulation on the CD8+ T level and found that the number of CD8+ T cells in the miR-760-mimic group increased. Then, we transfected miR-760-mimics or control group into A549 and H1299 cells at 30 ng/ml IFN- $\gamma$ . By detecting the apoptosis ratio of CD8+ T cells, FACS revealed that compared with NC group without IFN- $\gamma$  treatment, the percentage of apoptotic CD8+ T cells treated with control

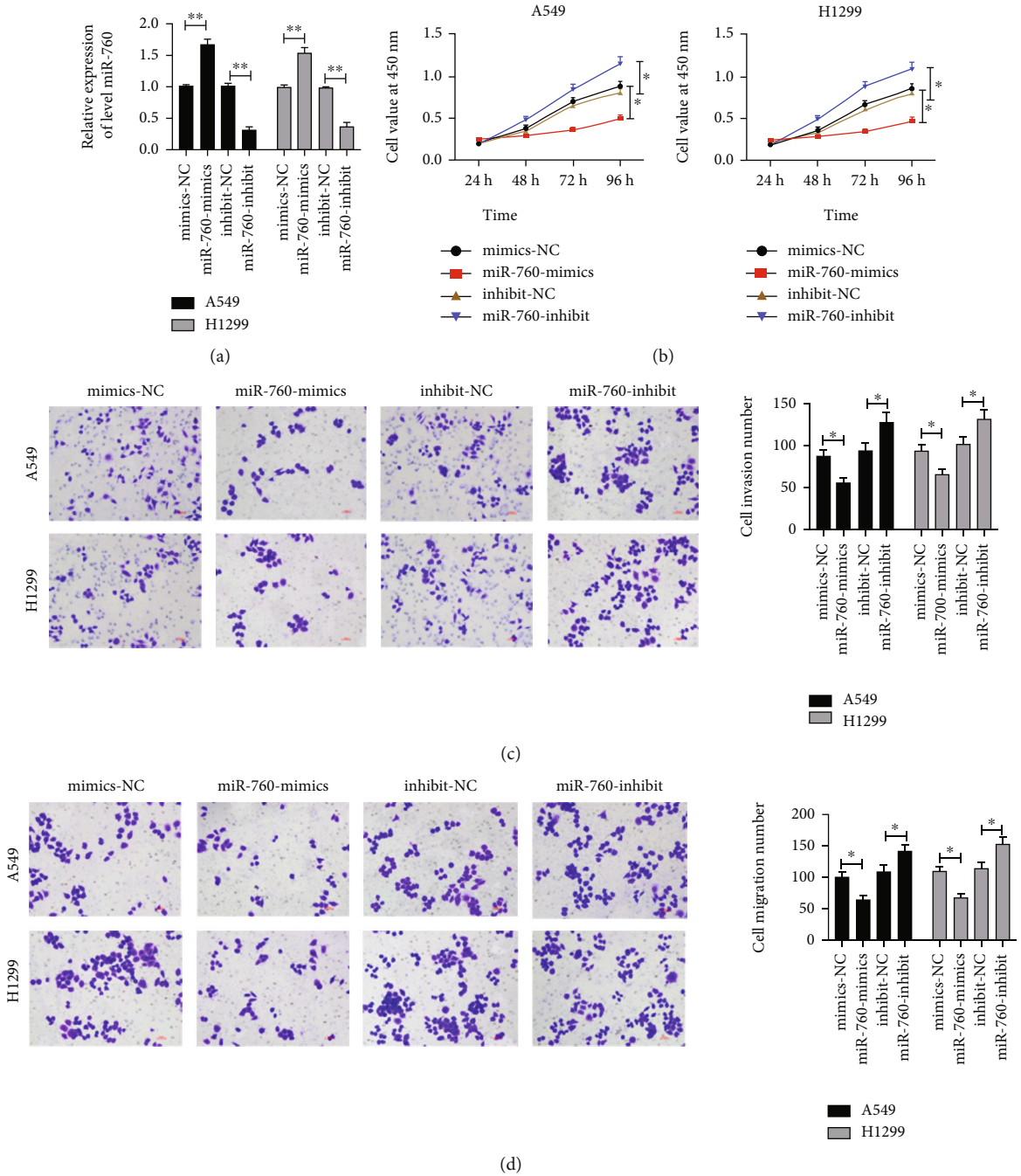
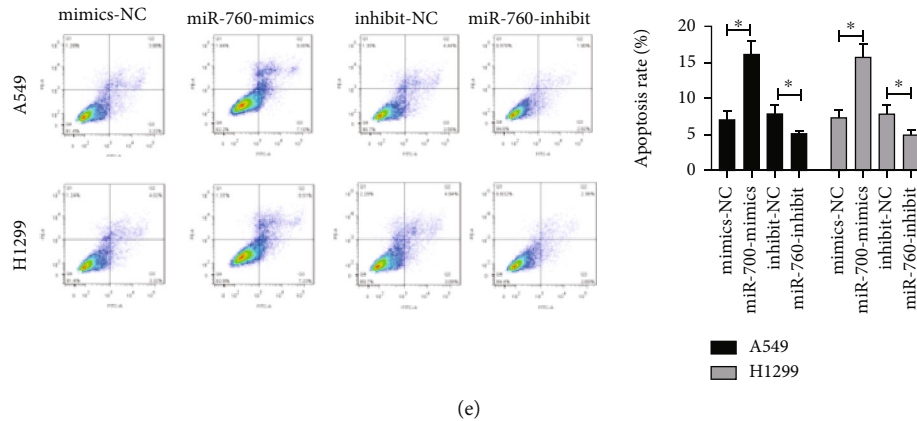


FIGURE 2: Continued.



(e)

FIGURE 2: miR-760's effect on LC cell growth and development. (a) The miR-760 level in LC cells after transfection of miR-760-mimics and miR-760-inhibit is tested via qRT-PCR. (b) LC cell proliferation after transfection of miR-760-mimics and miR-760-inhibit is tested via CCK-8. (c and d) The number of LC cells invasion and migration after transfection of miR-760-mimics and miR-760-inhibit is assessed via Transwell test. (e) The apoptosis rate of LC cells after transfection of miR-760-mimics and miR-760-inhibit is assessed via FACS test. \* $P < 0.05$  and \*\* $P < 0.01$ .

group and IFN- $\gamma$  increased. However, compared with the NC group, the percentage of apoptotic CD8+ T cells in miR-760-mimics group was relatively lower, which indicated that miR-760 heightened the survival rate of CD8+ T cells (Figures 5(a) and 5(b)), suggesting that miR-760 could mediate IDO1 to regulate CD8+ T cell apoptosis.

**3.6. miR-760 Mediated IDO1 to Inhibit CD8+ T Cell Reaction in Tumor Tissues of Nude Mouse.** To further evaluate the regulatory effect of the miR-760/IDO1 axis on CD8+ T apoptosis, we created an in vivo model. To observe tumor formation, nude mice were injected subcutaneously with lentivirus transfected and stably expressed pLV-THM-miR-760 or pLV-THM-miR-NC A549 cells. The findings manifested that the tumor volume of nude mice in pLV-THM-miR-760 group gradually decreased compared with pLV-THM-miR-NC group with the increase of time. The nude mice were killed and the quality of tumor tissue was compared after 28 days. It was also found that the quality of tumor tissue in pLV-THM-miR-760 group was obviously lower than that in pLV-THM-miR-NC group. What is more, qRT-PCR and WB denoted that the miR-760 level of nude mice tissue increased in pLV-THM-miR-760 group, while the IDO1 mRNA and protein level decreased. Furthermore, we further explored through IHC technology and found that after pLV-THM-miR-760 intervention, the number of IDO1+ cells was lower than that in pLV-THM-miR-NC group, and that of CD8+ T cells in tumor tissues after pLV-THM-miR-760 intervention was obviously higher than that in the pLV-THM-miR-NC group. Immunofluorescence staining found that IDO1 was localized in cytoplasm, mainly in tumors. CD8+ was localized on lymphocyte membrane, and CD8+ in cells was observed. The results of IDO1 staining were consistent with IHC. At this point, we proved that miR-760 could promote CD8+ T cell apoptosis by downregulating IDO1, thus inhibiting the immune escape of cells (Figure 6).

## 4. Discussion

LC is one of the main reasons of carcinoma death, and there is no good treatment plan at present [26, 27]. In our research, we experimentally confirmed that miR-760 was low expressed in LC and it promoted CD8+ cell apoptosis by regulating IDO1. It provides a potential theoretical foundation for the development of new immunization therapy in treating LC.

miR is a short-chain noncoding RNA. Research has manifested that miR is relevant to LC development and progression [28]. miR-760 is a familiar tumor suppressor gene with low expression in esophageal cancer [29], ovarian cancer [30], and liver cancer [31]. miR-760's mechanism in LC was not reported. Therefore, this research was devised to analyze the related mechanisms of miR-760 in LC. We first analyzed the miR-760 in tumor tissues of NSCLC patients. And we concluded that the miR-760 in tumor tissues of NSCLC patients and LC cell strains decreased obviously. Further analysis revealed that the miR-760 reduced gradually with the increase of TNM stage, which uncovered that miR-760 might be related to the occurrence of LC. Besides, we analyzed the connection of miR-760 with clinical data and discovered that the incidence of high TNM stage and lymphatic metastasis increased in low-expressed miR-760 patients. K-M survival analysis revealed that the overall survival rate of patients with low expression of miR-760 reduced. These studies proved that miR-760 was a latent prognostic index of NSCLC.

In clinic, encouraging apoptosis and slowing tumor development are significant techniques for treating tumors [31]. The LC cell lines transfected with miR-760-mimics and miR-760-inhibit were created to evaluate miR-760's influence on LC cell development and progression. We discovered that upregulation of miR-760 inhibited cell growth, invasion, and migration, as well as induced apoptosis, in experiments. However, when miR-760 was

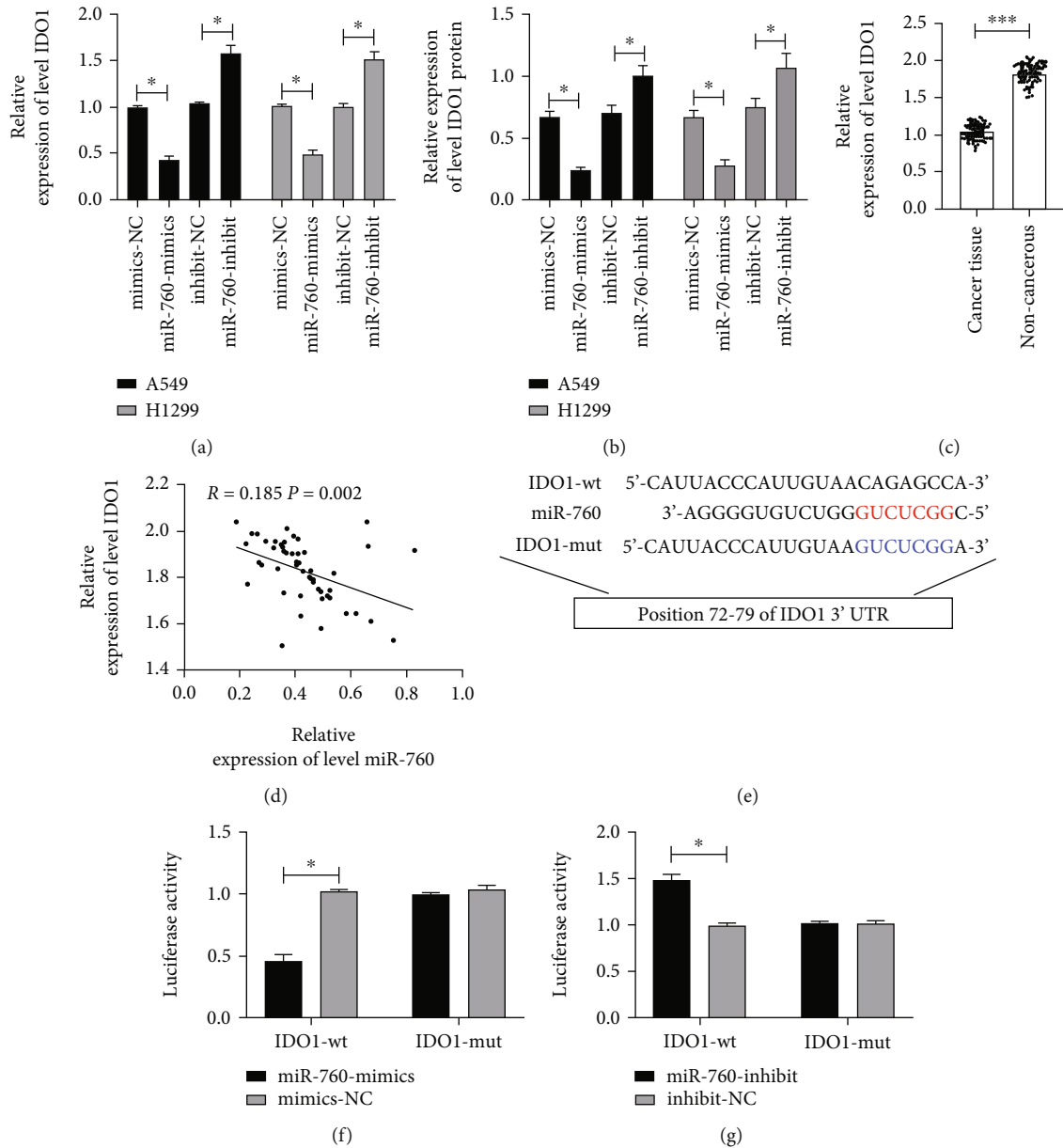


FIGURE 3: miR-760 could target IDO1. (a) The IDO1 mRNA level in cells transfected with miR-760-mimics/miR-760-inhibit is tested via qRT-PCR. (b) The IDO1 protein level in cells transfected with miR-760-mimics/miR-760-inhibit is tested via WB. (c) The IDO1 level in tumor tissues of NSCLC patients is tested via qRT-PCR. (d) The correlation between IDO1 and miR-760 in tumor tissues of NSCLC patients is assessed via Pearson test. (e) Binding and mutation sites of miR-760 and IDO1. (f and g) Dual-luciferase reporter confirmed that miR-760 had target correlation with IDO1. \* $P < 0.05$  and \*\*\* $P < 0.001$ .

inhibited, the above results were reversed, indicating that miR-760 was involved in cell development and progression and could be a therapeutic target. To better seek the potential mechanisms of miR-760, we conducted online prediction site analysis and discovered that there might be a targeting relationship between IDO1 and miR-760. IDO1 is an immunomodulatory enzyme, which can induce apoptosis/dysfunction of effector T cells and produce immunosuppressive regulatory T cells [32]. To verify their regulatory relationship, we tested the IDO mRNA and protein relative expressions in cells transfected with miR-

760-mimics and miR-760-inhibit via qRT-PCR and WB experiments, respectively. The findings showed that the IDO mRNA and protein in cells was regulated after over-expression or inhibition of miR-760. We speculated that there might be a targeting relationship between IDO1 and miR-760. Then, we verified our hypothesis by double luciferase report. In addition, we also confirmed that IDO1 was highly expressed in tumor tissues of NSCLC patients and negatively correlated with miR-760, which also verified our results from the side. Furthermore, the cell experiments denoted that cell growth, invasiveness, and



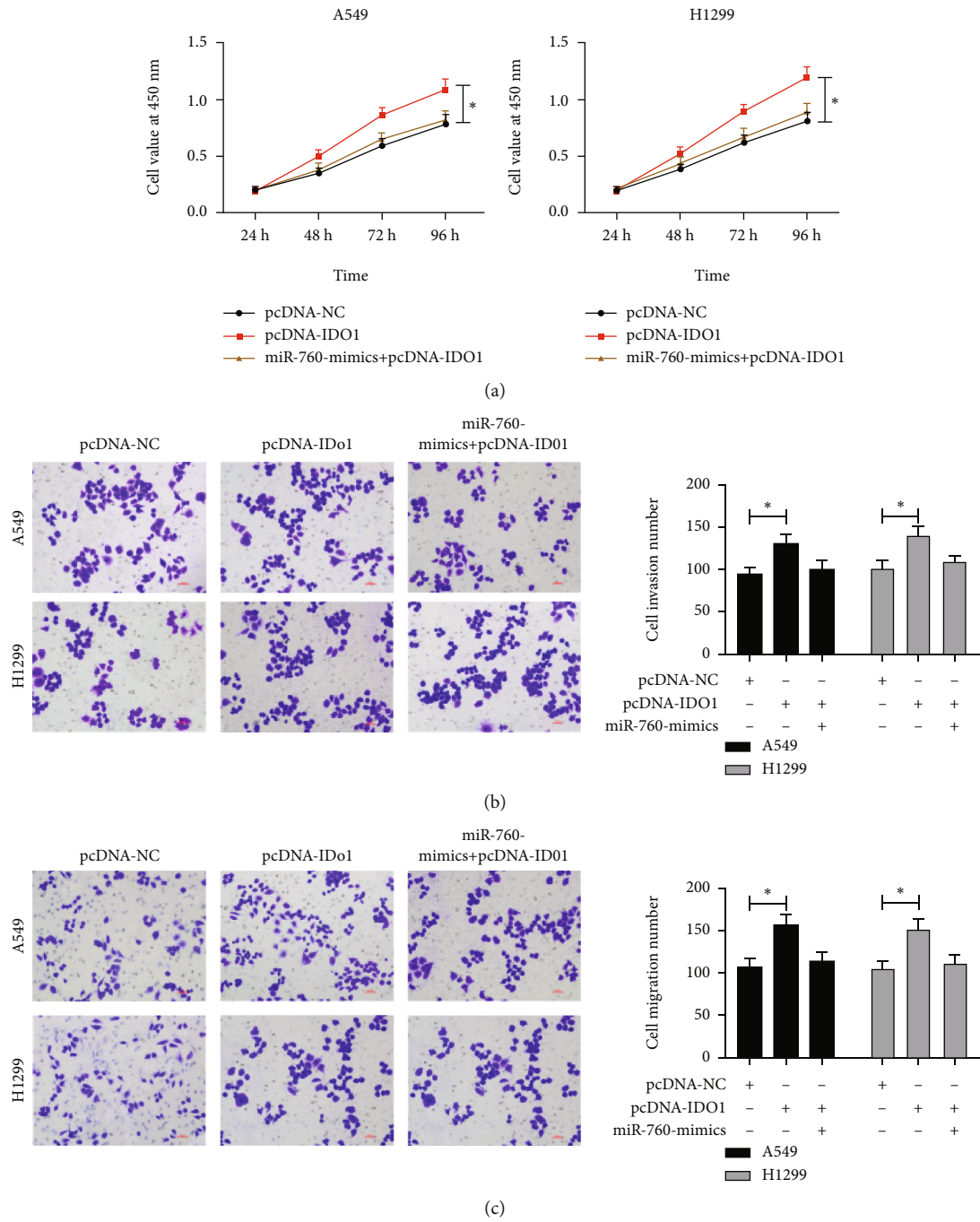


FIGURE 4: Continued.

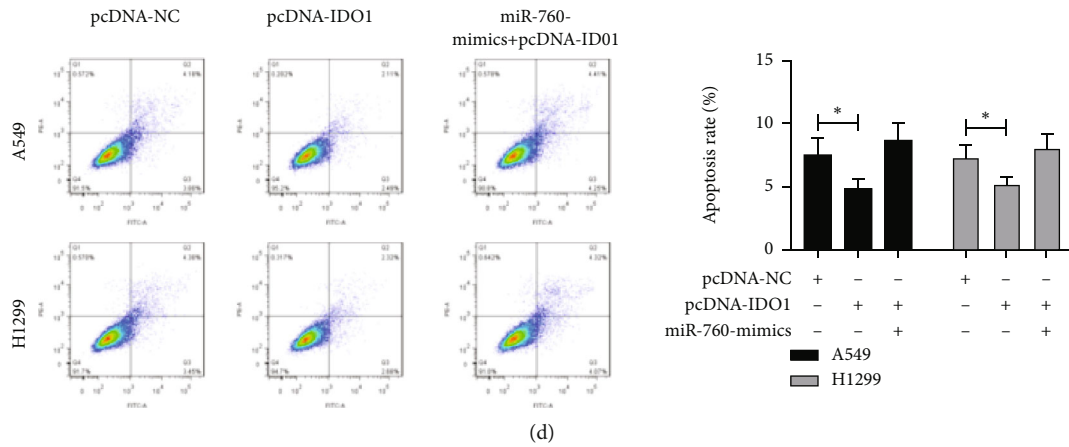


FIGURE 4: miR-760 targeted IDO1 to inhibit LC cell growth. (a) Cell proliferation after cotransfection of miR-760-mimics and pcDNA-IDO1 is tested via CCK-8 experiment. (b and c) Cell invasion and migration after cotransfection of miR-760-mimics and pcDNA-IDO1 are assessed via Transwell test. (d) The apoptosis rate after cotransfection of miR-760-mimics and pcDNA-IDO1 is tested via FACS. \* $P < 0.05$ .

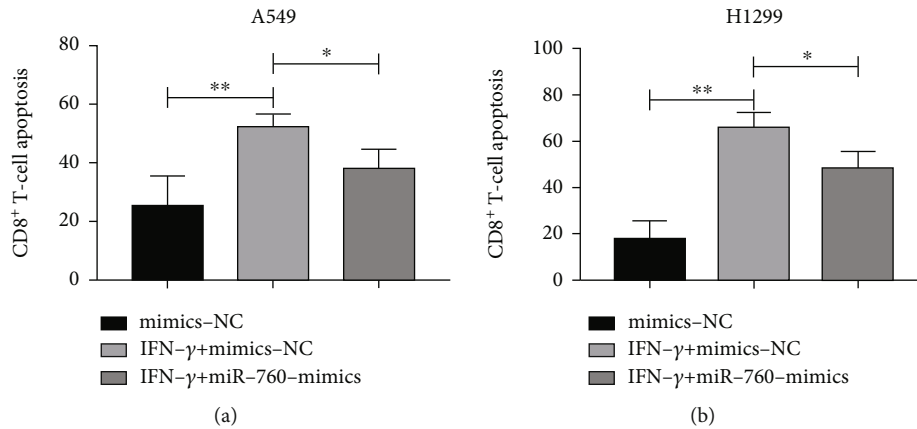


FIGURE 5: IFN- $\gamma$  improved CD8+ T cell survival by regulating miR-760/IDO1 axis. (a) CD8+ T cell survival after A549 cell coculture. (b) CD8+ T cell survival after H1299 cell coculture. \* $P < 0.05$  and \*\* $P < 0.01$ .

migration were enhanced after transfection of pcDNA-IDO1, and the decrease of apoptosis rate was saved after miR-760-mimics cotransfection. All these experiments indicated that miR-760 participated in the development of LC by regulating IDO1.

Research has shown that the functional inactivation of tumor-reactive T cells may be an important mechanism to escape tumor immunity [33]. Early studies have shown that [34] IDO1 can promote tumor immune escape. IFN- $\gamma$  is a crucial cytokine produced by activated T cells, natural killer cells (NK), and NK T cells in tumor micro-environment, and it exerts vital effects in coordination process [35, 36]. In addition, early studies have shown that [37, 38] IFN- $\gamma$  can activate IDO1, which can promote CD8+ cell apoptosis and realize immune escape. In order to explore whether miR-760 can regulate IDO1 to participate in tumor immune response, 30 ng/ml of IFN- $\gamma$  was cocultured with LC cells transfected with miR-760-mimics. It manifested that the apoptosis rate of CD8+ cells in LC increased obviously in the IFN- $\gamma$ +mimics-NC

group, but the apoptosis of CD8+ cells was inhibited after coculture, suggesting that upregulating miR-760 suppressed CD8+ cell apoptosis by inhibiting IDO1, thus inhibiting tumor immune escape.

To further understand the mechanism of miR-760 in LC, we created an in vivo model. It was discovered that miR-760 grew significantly in tumors of naked mice, indicating that the in vivo model had been successfully developed. Further detection of tumor volume and mass in nude mice manifested that the tumor volume and mass were significantly inhibited in pLV-THM-miR-760 group compared with the control group. Furthermore, the IDO1 mRNA and protein relative in tumor tissues was also significantly inhibited.

Nevertheless, there are still some shortcomings in this research. First of all, IDO1 can induce apoptosis/dysfunction of T cells by catalyzing tryptophan degradation to kynurenine. Unfortunately, these two indicators were not detected in this study. Secondly, we did not test the IDO1 protein in tumor tissues of NSCLC patients in this research. Early

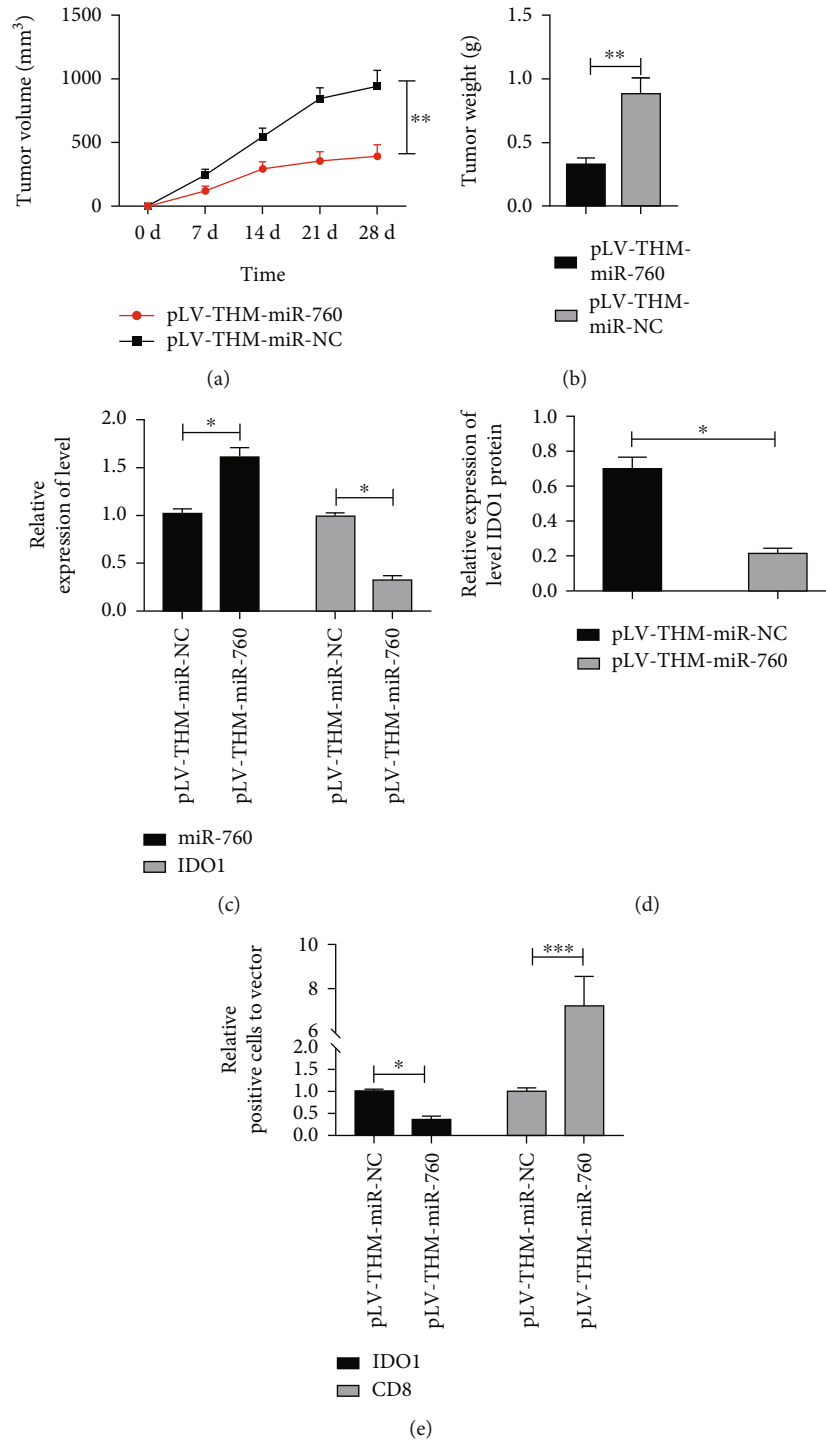


FIGURE 6: Upregulating miR-760 inhibited CD8+ T cells in tumor through IDO1. (a) Changes of tumor volume within 28 days of the tumorigenesis experiment. (b) Comparison of tumor mass in nude mice killed at 28 days. (c) The miR-760 and IDO1 levels in tumor tissues of nude mice are tested via qRT-PCR. (d) The IDO1 protein level in tumor tissues of nude mice is tested via WB. (e) Immunohistochemical staining of IDO1 and CD8+ in tumor tissue sections of nude mice in pLV-THM-miR-760 or pLV-THM-miR-NC group. \* $P < 0.05$  and \*\*\* $P < 0.001$ .

researches have revealed that IDO1 protein is highly expressed in colon cancer, but there is no difference in IDO1 mRNA level between colon cancer and normal tissues. For this reason, we will conduct more basic experiments to continuously enrich our conclusions.

## 5. Conclusion

Evidence showed that IDO-1 not only participates in the immune escape process of lung cancer but also contributes to the safety of the pretumor area. In addition, studies have

shown that IDO-1 can induce immunosuppression and promote tumor progression in LC animal models. Overall, upregulating miR-760 can inhibit the apoptosis-promoting effect of IDO1 on CD8+, thus inhibiting tumor immune escape, which is a latent strategy for treatment and new drug development.

### Data Availability

The datasets used and/or analyzed during the current study are available from the corresponding author on reasonable request.

### Ethical Approval

The research was ratified by the Ethics Committee of Zibo Central Hospital of Shandong Province, China.

### Consent

Signed written informed consents were obtained from patients and/or guardians.

### Conflicts of Interest

The authors declare that they have no competing interests.

### Authors' Contributions

HG designed the study and drafted the manuscript. LW and WC were responsible for the collection and analysis of the experimental data. This suggested that miR-760 might affect the immune regulation of LC by targeting IDO1. Therefore, this research seeks miR-760's potential mechanism in LC, providing a new direction for clinical targeted therapy and drug development. JJ revised the manuscript critically for important intellectual content. All authors read and approved the final manuscript. Hong Ge and Lili Wang contributed equally to this work.

### References

- [1] R. D. Neal, F. Sun, J. D. Emery, and M. E. Callister, "Lung cancer," *BMJ*, vol. 365, article l1725, 2019.
- [2] F. Bray, J. Ferlay, I. Soerjomataram, R. L. Siegel, L. A. Torre, and A. Jemal, "Global cancer statistics 2018: GLOBOCAN estimates of incidence and mortality worldwide for 36 cancers in 185 countries," *CA: a Cancer Journal for Clinicians*, vol. 68, no. 6, pp. 394–424, 2018.
- [3] G. A. Woodard, K. D. Jones, and D. M. Jablons, "Lung cancer staging and prognosis," *Cancer Treatment and Research*, vol. 170, pp. 47–75, 2016.
- [4] T. X. Lu and M. E. Rothenberg, "MicroRNA," *The Journal of Allergy and Clinical Immunology*, vol. 141, no. 4, pp. 1202–1207, 2018.
- [5] A. Creugny, A. Fender, and S. Pfeffer, "Regulation of primary microRNA processing," *FEBS Letters*, vol. 592, no. 12, pp. 1980–1996, 2018.
- [6] Y. Ma, "The challenge of microRNA as a biomarker of epilepsy," *Current Neuropharmacology*, vol. 16, no. 1, pp. 37–42, 2018.
- [7] Z. F. Zhang, G. R. Li, C. N. Cao, Q. Xu, G. D. Wang, and X. F. Jiang, "MicroRNA-1294 targets HOXA9 and has a tumor suppressive role in osteosarcoma," *European Review for Medical and Pharmacological Sciences*, vol. 22, no. 24, pp. 8582–8588, 2018.
- [8] J. Cui, G. Pan, Q. He, L. Yin, R. Guo, and H. Bi, "MicroRNA-545 targets ZEB2 to inhibit the development of non-small cell lung cancer by inactivating Wnt/ $\beta$ -catenin pathway," *Oncology Letters*, vol. 18, no. 3, pp. 2931–2938, 2019.
- [9] H. Zhang, Z. Feng, R. Huang, Z. Xia, G. Xiang, and J. Zhang, "MicroRNA-449 suppresses proliferation of hepatoma cell lines through blockade lipid metabolic pathway related to SIRT1," *International Journal of Oncology*, vol. 45, no. 5, pp. 2143–2152, 2014.
- [10] M. Dragomir, A. C. P. Mafra, S. M. G. Dias, C. Vasilescu, and G. A. Calin, "Using microRNA networks to understand cancer," *International Journal of Molecular Sciences*, vol. 19, no. 7, p. 1871, 2018.
- [11] J. Xu, X. Pan, and Z. Hu, "MiR-502 mediates esophageal cancer cell TE1 proliferation by promoting AKT phosphorylation," *Biochemical and Biophysical Research Communications*, vol. 501, no. 1, pp. 119–123, 2018.
- [12] H. Fan, X. Liu, W. W. Zheng, Z. H. Zhuang, and C. D. Wang, "MiR-150 alleviates EMT and cell invasion of colorectal cancer through targeting Gli1," *European Review for Medical and Pharmacological Sciences*, vol. 21, no. 21, pp. 4853–4859, 2017.
- [13] X. Zhang, L. Wang, Y. Liu, W. Huang, and D. Cheng, "MiR-760 enhances TRAIL sensitivity in non-small cell lung cancer via targeting the protein FOXA1," *Biomedicine & Pharmacotherapy*, vol. 99, pp. 523–529, 2018.
- [14] L. Cao, Y. Liu, D. Wang et al., "MiR-760 suppresses human colorectal cancer growth by targeting BATF3/AP-1/cyclinD1 signaling," *Journal of Experimental & Clinical Cancer Research*, vol. 37, no. 1, p. 83, 2018.
- [15] C. Yan, W. Zhang, X. Shi, J. Zheng, X. Jin, and J. Huo, "MiR-760 suppresses non-small cell lung cancer proliferation and metastasis by targeting ROS1," *Environmental Science and Pollution Research International*, vol. 25, no. 19, pp. 18385–18391, 2018.
- [16] L. Zhai, E. Ladomersky, A. Lenzen et al., "IDO1 in cancer: a Gemini of immune checkpoints," *Cellular & Molecular Immunology*, vol. 15, no. 5, pp. 447–457, 2018.
- [17] M. H. Mazdarani, M. Jafarikia, and F. Nemati, "Investigation of indolamine 2, 3 dioxygenase (IDO-1) gene expression by real-time PCR among patients with lung cancer," *Journal of Cellular Physiology*, vol. 234, no. 8, pp. 13781–13787, 2019.
- [18] W. Yamasuge, Y. Yamamoto, H. Fujigaki et al., "Indoleamine 2,3-dioxygenase 2 depletion suppresses tumor growth in a mouse model of Lewis lung carcinoma," *Cancer Science*, vol. 110, no. 10, pp. 3061–3067, 2019.
- [19] "Issue information-Declaration of Helsinki," *Journal of Bone and Mineral Research*, vol. 33, no. 11, 2018.
- [20] A. S. Pal, A. Agredo, and A. L. Kasinski, "Abstract 3142: aberrantly expressed microRNAs drive the development of acquired erlotinib resistance in non-small cell lung cancer," *Cancer Research*, vol. 77, no. 13, pp. 3142–3142, 2017.
- [21] N. Sadeghiyeh, N. Sehati, B. Mansoori et al., "MicroRNA-145 replacement effect on growth and migration inhibition in lung cancer cell line," *Biomedicine & Pharmacotherapy*, vol. 111, no. 23, pp. 460–467, 2019.
- [22] E. Zernickel, A. Sak, A. Riaz, D. Klein, M. Groneberg, and M. Stuschke, "Targeting of BRM sensitizes BRG1 mutant lung cancer cell lines to radiotherapy," *Molecular Cancer Therapeutics*, vol. 18, no. 3, pp. 656–666, 2019.

- [23] M. Noi, K. I. Mukaisho, S. Yoshida et al., “ERK phosphorylation functions in invadopodia formation in tongue cancer cells in a novel silicate fibre-based 3D cell culture system,” *Journal of Oral Science*, vol. 10, no. 4, pp. 1–10, 2018.
- [24] K. J. Livak and T. D. Schmittgen, “Analysis of relative gene expression data using real-time quantitative PCR and the  $2^{-\Delta\Delta CT}$  method,” *Methods*, vol. 25, no. 4, pp. 402–408, 2001.
- [25] C. J. A. MacArthur and D. Sun, “Guidelines for the ethical review of laboratory animal welfare People’s Republic of China National Standard GB/T 35892-2018,” *Animal Models and Experimental Medicine*, vol. 3, no. 1, pp. 103–113, 2020.
- [26] N. Duma, R. Santana-Davila, and J. R. Molina, “Non-small cell lung cancer: epidemiology, screening, diagnosis, and treatment,” *Mayo Clinic Proceedings*, vol. 94, no. 8, pp. 1623–1640, 2019.
- [27] N. Bushati and S. M. Cohen, “MicroRNA functions,” *Annual Review of Cell and Developmental Biology*, vol. 23, no. 1, pp. 175–205, 2007.
- [28] X. Yang, C. Zhang, H. Tie, J. Luo, Y. Wang, and Q. Wu, “miR-760 exerts an antioncogenic effect in esophageal squamous cell carcinoma by negatively driving fat metabolism via targeting c-Myc,” *Journal of Cellular Biochemistry*, vol. 121, no. 4, pp. 2950–2961, 2020.
- [29] Y. Liao, Y. Deng, J. Liu et al., “MiR-760 overexpression promotes proliferation in ovarian cancer by downregulation of PHLPP2 expression,” *Gynecologic Oncology*, vol. 143, no. 3, pp. 655–663, 2016.
- [30] L. Yin, T. Sun, and R. Liu, “NACC-1 regulates hepatocellular carcinoma cell malignancy and is targeted by miR-760,” *Acta Biochim Biophys Sin (Shanghai)*, vol. 52, no. 3, pp. 302–309, 2020.
- [31] A. Singh, P. Trivedi, and N. K. Jain, “Advances in siRNA delivery in cancer therapy,” *Artificial cells, Nanomedicine, and Biotechnology*, vol. 46, no. 2, pp. 274–283, 2018.
- [32] F. Li, R. Zhang, S. Li, and J. Liu, “IDO1: an important immunotherapy target in cancer treatment,” *International Immunopharmacology*, vol. 47, pp. 70–77, 2017.
- [33] B. V. Kumar, T. J. Connors, and D. L. Farber, “Human T cell development, localization, and function throughout life,” *Immunity*, vol. 48, no. 2, pp. 202–213, 2018.
- [34] G. C. Prendergast, W. J. Malachowski, A. Mondal, P. Scherle, and A. J. Muller, “Indoleamine 2,3-dioxygenase and its therapeutic inhibition in cancer,” *International Review of Cell and Molecular Biology*, vol. 336, pp. 175–203, 2018.
- [35] A. Murthy, S. A. Gerber, C. J. Koch, and E. M. Lord, “Intratumoral hypoxia reduces IFN- $\gamma$ -mediated immunity and MHC class I induction in a preclinical tumor model,” *Immunohorizons*, vol. 3, no. 4, pp. 149–160, 2019.
- [36] J. D. Burke and H. A. Young, “IFN- $\gamma$ : a cytokine at the right time, is in the right place,” *Seminars in Immunology*, vol. 43, p. 101280, 2019.
- [37] T. A. Triplett, K. C. Garrison, N. Marshall et al., “Reversal of indoleamine 2,3-dioxygenase-mediated cancer immune suppression by systemic kynurenine depletion with a therapeutic enzyme,” *Nature Biotechnology*, vol. 36, no. 8, pp. 758–764, 2018.
- [38] Z. T. Xue, H. O. Sjogren, L. G. Salford, and B. Widegren, “An epigenetic mechanism for high, synergistic expression of indoleamine 2,3-dioxygenase 1 (IDO1) by combined treatment with zebularine and IFN- $\gamma$ : potential therapeutic use in autoimmune diseases,” *Molecular Immunology*, vol. 51, no. 2, pp. 101–111, 2012.

## Retraction

# Retracted: MicroRNA-424-5p Alleviates Isoflurane Anesthesia-Induced Neurotoxicity in Human Embryonic Stem Cell-Derived Neurons by Targeting FASN

### Computational and Mathematical Methods in Medicine

Received 25 July 2023; Accepted 25 July 2023; Published 26 July 2023

Copyright © 2023 Computational and Mathematical Methods in Medicine. This is an open access article distributed under the Creative Commons Attribution License, which permits unrestricted use, distribution, and reproduction in any medium, provided the original work is properly cited.

This article has been retracted by Hindawi following an investigation undertaken by the publisher [1]. This investigation has uncovered evidence of one or more of the following indicators of systematic manipulation of the publication process:

- (1) Discrepancies in scope
- (2) Discrepancies in the description of the research reported
- (3) Discrepancies between the availability of data and the research described
- (4) Inappropriate citations
- (5) Incoherent, meaningless and/or irrelevant content included in the article
- (6) Peer-review manipulation

The presence of these indicators undermines our confidence in the integrity of the article's content and we cannot, therefore, vouch for its reliability. Please note that this notice is intended solely to alert readers that the content of this article is unreliable. We have not investigated whether authors were aware of or involved in the systematic manipulation of the publication process.

Wiley and Hindawi regrets that the usual quality checks did not identify these issues before publication and have since put additional measures in place to safeguard research integrity.

We wish to credit our own Research Integrity and Research Publishing teams and anonymous and named

external researchers and research integrity experts for contributing to this investigation.



The corresponding author, as the representative of all authors, has been given the opportunity to register their agreement or disagreement to this retraction. We have kept a record of any response received.

### References

- [1] X. Gu, W. Yue, M. Xiu, Q. Zhang, and R. Xie, "MicroRNA-424-5p Alleviates Isoflurane Anesthesia-Induced Neurotoxicity in Human Embryonic Stem Cell-Derived Neurons by Targeting FASN," *Computational and Mathematical Methods in Medicine*, vol. 2022, Article ID 2517463, 13 pages, 2022.

## Research Article

# MicroRNA-424-5p Alleviates Isoflurane Anesthesia-Induced Neurotoxicity in Human Embryonic Stem Cell-Derived Neurons by Targeting FASN

Xiaojiao Gu,<sup>1</sup> Wei Yue,<sup>2</sup> Mingyu Xiu,<sup>1</sup> Quanyun Zhang <sup>3</sup>, and Rufeng Xie <sup>2</sup>

<sup>1</sup>Department of Anesthesiology, The First People's Hospital of Lianyungang, Lianyungang 222000, China

<sup>2</sup>Department of Anesthesiology, Women's Hospital of Nanjing Medical University, Nanjing Maternity and Child Health Care Hospital, No. 123, Tianfeixiang, Mochou Road, Nanjing 210004, China

<sup>3</sup>Department of Pain Medical Center, Lianyungang Second People's Hospital, Lianyungang, 222000 Jiangsu, China

Correspondence should be addressed to Quanyun Zhang; zhangquanyun2006@163.com and Rufeng Xie; rufengxie@yeah.net

Received 16 May 2022; Revised 19 June 2022; Accepted 23 June 2022; Published 13 July 2022

Academic Editor: Naeem Jan

Copyright © 2022 Xiaojiao Gu et al. This is an open access article distributed under the Creative Commons Attribution License, which permits unrestricted use, distribution, and reproduction in any medium, provided the original work is properly cited.

Isoflurane (ISO) is a type of anesthetic that might cause neurotoxicity in children. Although miR-424-5p is considerably downregulated in ISO-treated rat brain samples, its physiological role in ISO-induced neuronal injury in human embryonic stem cell-derived neurons remains unknown (hESC-derived neurons). miR-424-5p expression and fatty acid synthase (FASN) in ISO-treated hESC-derived neurons were tested via qRT-PCR. The amount of protein for Bax, Cleaved-caspase-8, Bcl-2, and FASN was investigated through western blot analysis. The viability and apoptosis of hESC-derived neurons were estimated through cell counting kit-8 assessment and TUNEL assay, accordingly. Superoxide dismutase, glutathione, and malondialdehyde levels were discovered via corresponding kits. The contents of inflammatory factors including interleukin-6 and tumor necrosis factor- $\alpha$  were examined by enzyme-linked immunosorbent assays. The combination between FASN and miR-424-5p was resolute via dual-luciferase reporter assessment. After exposure to ISO, induced neurotoxicity and a decreased miR-424-5p production were identified in hESC-derived neurons. Upregulation of miR-424-5p repressed ISO-induced apoptosis and mitigated ISO-induced inflammatory response and oxidative stress *in vitro*. FASN expression levels were reduced by elevation of miR-424-5p and upregulated after ISO treatment. Mechanically, FASN was directly targeted by miR-424-5p in hESC-derived neurons. Of note, the miR-424-5p elevation-suppressed neuronal apoptosis, inflammatory response, and oxidative stress were countered by upregulation of FASN.

## 1. Introduction

Plenty of newborns and pregnant women require anesthesia for diagnostic or operative targets [1, 2]. Due to the frequent use of anesthesia-related medicines, the challenges induced by anesthesia increase year by year [3]. Notably, the negative effects of prolonged or excessive exposure to anesthetics on the central nervous system, especially on memory and learning in children and infants, have been broadly represented [4, 5]. Isoflurane (ISO), as one of the most used inhalation anesthetics, simply crosses the placental barrier and decreases the

regeneration of neuronal stem cells and inhibits the proliferation, sustenance, and development of human neural progenitor cells at clinically relevant concentrations [6–8]. In recent years, ISO-induced neuronal damage in the developing brain has received more and more attentions [9]. Animal studies have shown that ISO treatment leads to neuronal apoptosis, thus resulting in long-term cognitive dysfunction of rats [10]. These investigations illuminate that ISO can demonstrate potential toxic influences on neuronal progression. Anesthesia-associated neuronal apoptosis is one of the important mechanisms in anesthesia-induced nerve injury

[11]. However, the mechanisms responsible for ISO-induced neuronal apoptosis and neural toxicity have not been completely clarified.

MicroRNAs, as a variety of small noncoding RNA molecules with 18 to 25 nucleotides, reduce mRNAs stability through adhering to the compatible pattern on the 3'-untranslated region (3'-UTR) of related mRNAs [12]. miRNAs are reported to functionally modulate plenty of biological procedures, including neuron differentiation, proliferation, and neuronal inflammation in both animals and humans [13]. It has been proved that miRNAs are implicated in the regulation of neurodegenerative disorders like spinal cord injury [14], Parkinson's disease [15], Alzheimer's disease [16], and subarachnoid hemorrhage [17]. In addition, numerous miRNAs are reported to control anesthesia-induced cognitive impairment. Downregulation of miR-106a alleviates the cognition-related impairments of mice subjected to ISO treatment [18]. miR-124 is confirmed to protect against sevoflurane-induced cognitive dysfunction via targeting the Capn4/NF- $\kappa$ B signaling [19]. Recently, miRNAs have presented potential influence on the regulation of neuronal injury induced by ISO. miR-142-5p depletion alleviates ISO-inhibited neuron viability and mitigated ISO-stimulated neuron apoptosis [20]. Upregulation of miR-133b attenuates ISO exposure-induced apoptosis of hippocampal neurons [21]. Oxidative stress and neuroinflammation are crucial pathological procedures in neurological diseases [22]. Recent documents have manifested that oxidative stress and inflammatory response exert essential functions in ISO-induced neurons or rat models [23, 24]. Researchers found that dysregulated levels of oxidative stress indicators comprising superoxide dismutase (SOD), catalase (CAT), glutathione (GSH), malondialdehyde (MDA), and lactate dehydrogenase (LDH) may give rise to high risks of neuronal apoptosis in rats with Alzheimer's disease [25]. Additionally, ISO exposure results in the elevation of interleukin-1 $\beta$  (IL-1 $\beta$ ), tumor necrosis factor- $\alpha$  (TNF- $\alpha$ ), and interleukin-6 (IL-6) levels in hippocampal tissues of rats [26]. According to a previous report, miR-424-5p was verified to implicate in the modulation of neuronal apoptosis in ischemic stroke [27]. Furthermore, miR-424-5p displayed substantially decreased expression in ISO-treated rat brain samples [28].

The miR-424-5p influence on ISO-induced neurotoxicity of human embryonic stem cell-derived neurons (hESC-derived neurons) was the focus of this present exploration. It was speculated that miR-424-5p may alleviate ISO-induced neuron damage by suppression of oxidative stress and inflammatory response, which may present valuable therapeutic targets for treating ISO-induced neurotoxicity.

In vitro investigations have only confirmed the protective impact of miR-424-5p in ISO-treated hESC-derived neurons; in vivo assays are needed to confirm whether miR-424-5p has protective activity in ISO-treated animals. Second, because biological mechanisms are complicated, certain putative signaling pathways related with miR-424-5p in ISO-treated hESC-derived neurons should be investigated further.

The arrangements of the paper are as follows: Section 2 discusses the methods and materials. Section 3 analyzes the

result, and Section 4 evaluates the results. Section 5 concludes the article.

## 2. Methods and Materials

*2.1. Neural Differentiation of Human Embryonic Stem Cells.* The human embryonic stem cell (hESC) line, human WA01 (H1) cell, was donated by WiCell (WiCell Research Institute, USA). The procedure for propagating and differentiating hESCs into neurons was based on previously published publications [29, 30], with minor modifications. During the night hours, mouse embryonic fibroblasts (MEFs) treated with mitomycin-C (AbMole, Shanghai, China) were plated in a plate with 6 wells precoated with 0.1 percent gelatin (Huijia Biotechnology, China) as a feeder layer.

HESCs were seeded in the plates containing 6 wells, and the conditions for cell culture were 5% CO<sub>2</sub> and 37°C. To culture hESCs, stem cell propagation medium containing Dulbecco's modified Eagle's medium (DMEM; D6429, Sigma-Aldrich, St. Louis, USA) supplied by 10% fetal bovine serum (FBS; Sigma-Aldrich) and 1% penicillin streptomycin (Sigma Aldrich) was utilized. Cell passage was conducted upon the confluence which was up to 75% to 95%. The generation of neural progenitor cells (NPCs) was achieved through treating hESCs with neural progenitor milieu having DMEM/F12 (Sigma Aldrich) added with 20% knock-out serum (Sigma Aldrich), 1% penicillin-streptomycin (Sigma Aldrich), 1 mM L-glutamine (Sigma Aldrich), 0.1 mM  $\beta$ -mercaptoethanol (Sigma Aldrich), and 1% nonessential amino acids (Sigma Aldrich) for 7 days. Subsequently, 5 ng/ml human recombinant basic fibroblast growth factor (bFGF, Sigma Aldrich) and the neuronal induction milieu including neural progenitor medium plus 1 mg/ml heparin (Sigma Aldrich) although without L-glutamine were employed to treat NPCs for 14 days. HESC-derived neurons were generated by collecting the rosettes from NPC cultivation and replated the rosettes in gelatin-coated plates containing 6 wells in a neuronal induction milieu with N2/B27 neural supplements (Sigma Aldrich) for ten to eighteen days.

*2.2. ISO-Induced Neurotoxicity in hESC-Derived Neurons.* ISO (Merck Millipore, USA) was used to concept ISO-induced cell model in vitro in this study. As illustrated in previous studies, hESC-derived neurons were processed with numerous quantities of ISO (0, 0.25%, 0.50%, 0.75%, 1.00%, 1.25%, and 1.50%) plus O<sub>2</sub> (21%) and CO<sub>2</sub> (5%) for 12 hours or similar quantity of ISO (1.00%) with O<sub>2</sub> (21%) and CO<sub>2</sub> (5%) for 0, 6, 12, 24, and 48 h [31, 32]. Briefly, hESC-derived neurons in 1.5 ml of cell culture medium with a density of  $1 \times 10^6$  were incubated in a plate containing 6 wells at 37°C. An anesthesia machine was used to deliver different concentrations of ISO with O<sub>2</sub> (21%) and CO<sub>2</sub> (5%) enclosed in a locked plastic container, in the incubator. The delivered concentrations of ISO, O<sub>2</sub>, and CO<sub>2</sub> were continuously monitored by a Datex infrared gas analyzer (Puritan-Bennett, Tewksbury, USA).

*2.3. Cell Transfection.* miR-424-5p mimics were used for miR-424-5p overexpression while pcDNA3.1/FASN was



used to elevate FASN expression. Genepharma (Shanghai, China) provided the miR-424-5p mimics, pcDNA3.1/FASN, and the related respective negative control (NC) mimics and empty pcDNA3.1. The abovementioned oligonucleotides were transfected into hESC-derived neurons treated with or without ISO using Lipofectamine 2000 (Invitrogen, USA). Neurons transfected with random sequences of oligonucleotides by Lipofectamine 2000 served as the negative controls. Twenty-four hours later, the transfected samples were collected for the follow-up experiments.

**2.4. Quantitative Real-Time Polymerase Chain Reaction (qRT-PCR).** The qRT-PCR was executed as the method demonstrated in the last report [33]. Total RNA of hESC-derived neurons was extracted through TRIzol reagent (Invitrogen, USA) as instructed by the product manuals. The reverse transcription kit (QIAGEN, Germany) was applied for the reverse transcription of total RNA into complementary DNA (cDNA). The qRT-PCR was working to assess the quantities of miRNAs or mRNAs via the SYBR Green Master Mix (Vazyme Biotech Co., Ltd, China). The thermal cycling conditions for qRT-PCR was  $95^{\circ}\text{C} \times 5 \text{ min}$ , 40 cycles of  $95^{\circ}\text{C} \times 30 \text{ s}$ ,  $60^{\circ}\text{C} \times 30 \text{ s}$ , and  $72^{\circ}\text{C} \times 1 \text{ min}$ . The PCR primers are shown as follows: miR-424-5p forward: 5'-GCCAGCAGCAATTCATGT-3', reverse: 5'-TATGGT TTTGACGACTGTGTGAT-3'; FASN forward: 5'-CAAC CTCTCCCAGGTATGC-3', reverse: 5'-TGCTGATGATG GACTCCAG-3'; glyceraldehyde-3-phosphate dehydrogenase (GAPDH) forward, 5'-TGCACCACCAACTGCTTAG C-3', reverse: 5'-GGCATGGACTGTGGTCATGAG-3'; U6 forward: 5'-CCCCTGGATCTTATCAGGCTC-', reverse: 5'-GCCATCTCCCCGGACAAAG-3'. GAPDH served as internal reference for mRNA while U6 functioned as internal reference for miRNA. The StepOnePlus™ software (Thermo Fisher Scientific, USA) was employed for analyzing the miRNA or mRNA expression which were then evaluated by the  $2^{-\Delta\Delta\text{Ct}}$  approach [34].

**2.5. Western Blot Analysis.** RIPA buffer (V900854, Merck & Co Inc, USA) was employed for extracting the entire protein samples from hESC-derived neurons for half an hour. The collected lysates centrifuged at  $12,000 \times g$  for 15 minutes yielded 35 micrograms of protein which was divided through 10% sodium dodecyl sulfate-polyacrylamide gel electrophoresis (SDS-PAGE; KL81205-30, KLANG, Shanghai, China), followed by being moved to 0.22  $\mu\text{m}$  polyvinylidene difluoride (PVDF) membranes (3010040001, Merck & Co Inc) for 2 h. After being blocked with 5% nonfat milk in Tris-buffered saline plus 0.02% Tween-20 (TBST) at  $37^{\circ}\text{C}$  for 1.5 hours, incubation of membranes was done with the primary antibodies versus Bax (1/1000, #5023, CST), Cleaved-caspase-8 (1/1000, #9496, CST), Bcl-2 (1/1000, #15071, CST), FASN (1/1000, #3180, CST), and GAPDH (1/1000, #2118, CST) during the night hours in a  $4^{\circ}\text{C}$  refrigerator. After that, membranes were treated for one hour at  $37^{\circ}\text{C}$  by horseradish peroxidase-conjugated (HRP) secondary antibodies. The enhanced chemiluminescence (ECL) system (RPN2108, Cytiva, Shanghai, China) was used for

the observation of all protein bands that were normalized to GAPDH and quantified by ImageJ software (NIH, Bethesda, USA) [35].

**2.6. Cell Counting Kit-8 (CCK-8) Assay.** The hESC-derived neuron survival was examined through CCK-8 assessment as instructed by the manufacturer. After inoculating hESC-derived neurons ( $5 \times 10^3$  cells/well) into the plates containing 96 wells, the transfected cells were processed with or without ISO and then cultured by 10  $\mu\text{l}$  of CCK-8 solution (CK04, SciencBio, Beijing, China) at  $37^{\circ}\text{C}$  for another 4 h. Microplate reader (Bio-Rad, USA) was adopted for determining the optical density (OD) at 450 nm.

**2.7. Terminal Deoxynucleotidyl Transferase dUTP Nick End Labeling (TUNEL) Staining.** As per the instructions of the in situ cell death detection kit (Roche, Basel, Switzerland), DNA fragmentation was detected and TUNEL staining assessment was performed. In brief, hESC-derived neurons with a density of  $1 \times 10^5$  cells in each well were placed in a plate containing 6 wells. 24 hours later, the cultivated neurons were washed with cold PBS, fixed by 4% paraformaldehyde, and were permeated with 0.25% Triton X-100, respectively. Then, TUNEL reaction buffer was adopted to process the neuron samples for 01 hour and 4',6-diamidino-2-phenylindole (DAPI) solution (Invitrogen) was utilized to counterstain all nuclei. Observation of the positive apoptotic neurons was achieved by using a microscope.

**2.8. Enzyme-Linked Immunosorbent Assay (ELISA).** According to instructions of IL-6 kit (Y-S Biotechnology, Shanghai, China) and TNF- $\alpha$  kit (Has Biotech, Shenzhen, China), the contents of TNF- $\alpha$  and IL-6 were estimated via ELISA. In brief, hESC-derived neurons were inserted with NC mimics, miR-424-5p mimics, or miR-424-5p mimics+FASN and were then treated with 1.00% of ISO for 12 h. After being washed by PBST (Sigma, USA), the collected supernatants were added into the plates containing 96 wells which were coated with primary antibodies and cultivated at  $37^{\circ}\text{C}$  for 2 h. Subsequently, HRP-conjugated secondary antibodies were put into plates and further cultured for 1 hour at  $37^{\circ}\text{C}$ . After adding 2 mol/l sulfuric acid solution to each well to stop the reaction, an ELISA reader (Sigma) was instantly used for the observation of the absorbance at 570 nm.

**2.9. Measurement of Superoxide Dismutase (SOD) Activity and Decreased Glutathione (GSH) and Malondialdehyde (MDA) Quantity.** Transfected hESC-derived neurons were accumulated and the SOD, GSH, and MDA quantities were examined with SOD assay kit (KTB1030-1, Abbkine, China), GSH assessment kit (KTB1600-2, Abbkine, China), and MDA assessment kit (KTB1050-2, Abbkine, China) as instructed by the manufacturer's protocols.

**2.10. Dual-Luciferase Reporter Assay.** The mutant (Mut) 3'-UTR and wild-type (WT) sequences of FASN were intensified and placed in luciferase reporter pmirGLO (Promega, US) to construct FASN-Wt and FASN-Mut vectors. Lipofectamine 2000 (Promega, US) was used for the cotransfection of FASN-Wt or FASN-Mut with miR-424-5p mimics or NC

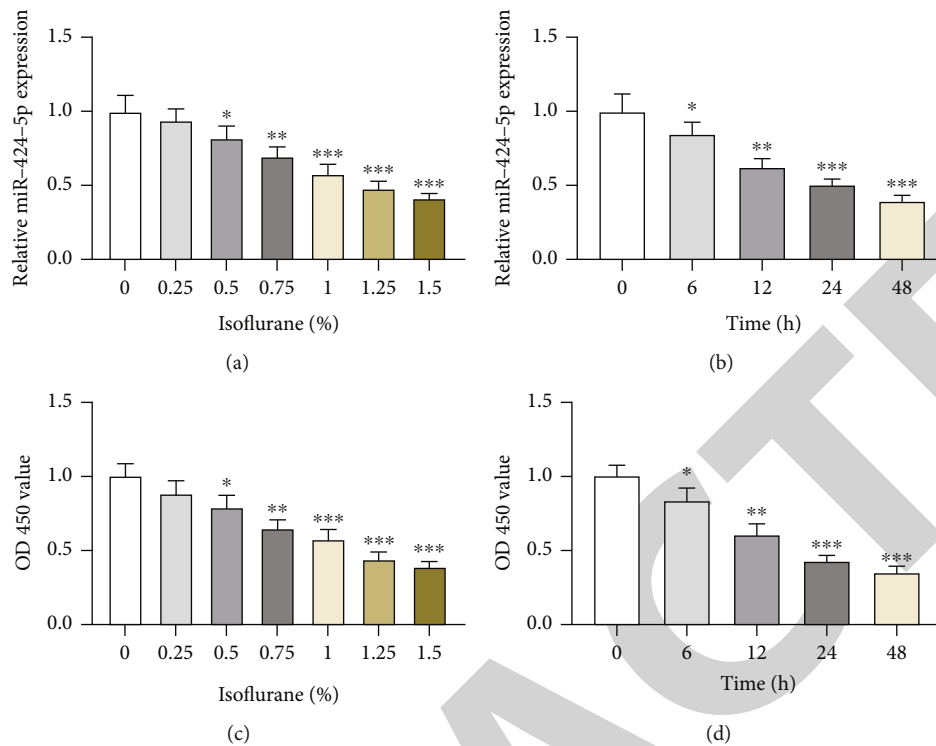


FIGURE 1: ISO induces neurotoxicity and downregulation of miR-424-5p. (a) miR-424-5p expression in hESC-derived neurons after treatment with increased ISO quantities for 12 hours was examined by qRT-PCR. (b) miR-424-5p expression in hESC-derived neurons was administered with 1.00% of ISO for various times (0, 6, 12, 24, and 48 h) by qRT-PCR. (c) After treatment of hESC-derived neurons with increased doses of ISO for 12 h, CCK-8 was performed to determine cell survival. (d) The viability of hESC-derived neurons was detected after treatment with 1.00% of ISO for 0, 6, 12, 24, and 48 h by CCK-8 assay. \* $p < 0.05$ , \*\* $p < 0.01$ , and \*\*\* $p < 0.001$ .

mimics in hESC-derived neurons. After 48 h, the luciferase activities of transfected hESC-derived neurons were examined by employing a luciferase detection kit (K801-200; Bio-Vision Milpitas, USA).

**2.11. Statistical Analysis.** GraphPad Prism computer program, version 7.0 (San Diego, US), was applied to for carrying out the statistics. Biorepeats were run in triplicate, and the obtained experimental outcomes are demonstrated as mean  $\pm$  standard deviation. For comparing the 02 groups, unpaired two-tailed Student's  $t$  test was employed. Discrepancies between various groups were scrutinized by 1-way ANOVA accompanied by Tukey's post hoc analysis. Significance was denoted as  $p$  value lower than 0.05.

### 3. Results

**3.1. ISO Induces Neurotoxicity and Downregulation of miR-424-5p.** miR-424-5p is validated for being decreased in ISO-treated rat brain samples. To ascertain miR-424-5p expression in ISO-treated hESC-derived neurons, qRT-PCR was conducted, and the results illustrated that after treating hESC-derived neurons by different doses of ISO (0, 0.25%, 0.50%, 0.75%, 1.00%, 1.25%, and 1.50%) for 12 h, miR-424-5p expression displayed a significant downward trend (Figure 1(a)). Subsequently, miR-424-5p expression was tested in hESC-derived neurons treated with 1.00%

of ISO for 0, 6, 12, 24, and 48 h. Furthermore, miR-424-5p expression was time-dependently suppressed by 1.00% of ISO (Figure 1(b)). The effects of various ISO concentrations (0, 0.25 percent, 0.50 percent, 0.75 percent, 1.00 percent, 1.25 percent, and 1.50 percent) on the survival of hESC-derived neurons were then investigated. CCK-8 analysis revealed that ISO decreased the survival of hESC-derived neurons in a dose-dependent manner, demonstrating that ISO stimulation caused neurotoxicity in hESC-derived neurons (Figure 1(c)). Similarly, the survival of hESC-derived neurons was decreased as time passed after 1.00 percent ISO treatment, and in the subsequent studies, 1.00 percent ISO was used to grow the hESC-derived neurons for 24 hours (Figure 1(d)). Finally, ISO produced neurotoxicity in hESC-derived neurons, and ISO stimulation decreased miR-424-5p expression in a dose- and time-dependent manner.

**3.2. miR-424-5p Overexpression Inhibits ISO-Induced Cell Apoptosis.** To probe the physiological role of miR-424-5p in ISO-mediated apoptosis of hESC-derived neurons, miR-424-5p transfection with NC mimics was executed. As displayed in Figure 2(a), compared with hESC-derived neurons transfected with NC mimics, miR-424-5p production was significantly elevated following miR-424-5p mimic transfection. Importantly, ISO notably decreased miR-424-5p production in hESC-derived neurons, while this effect was

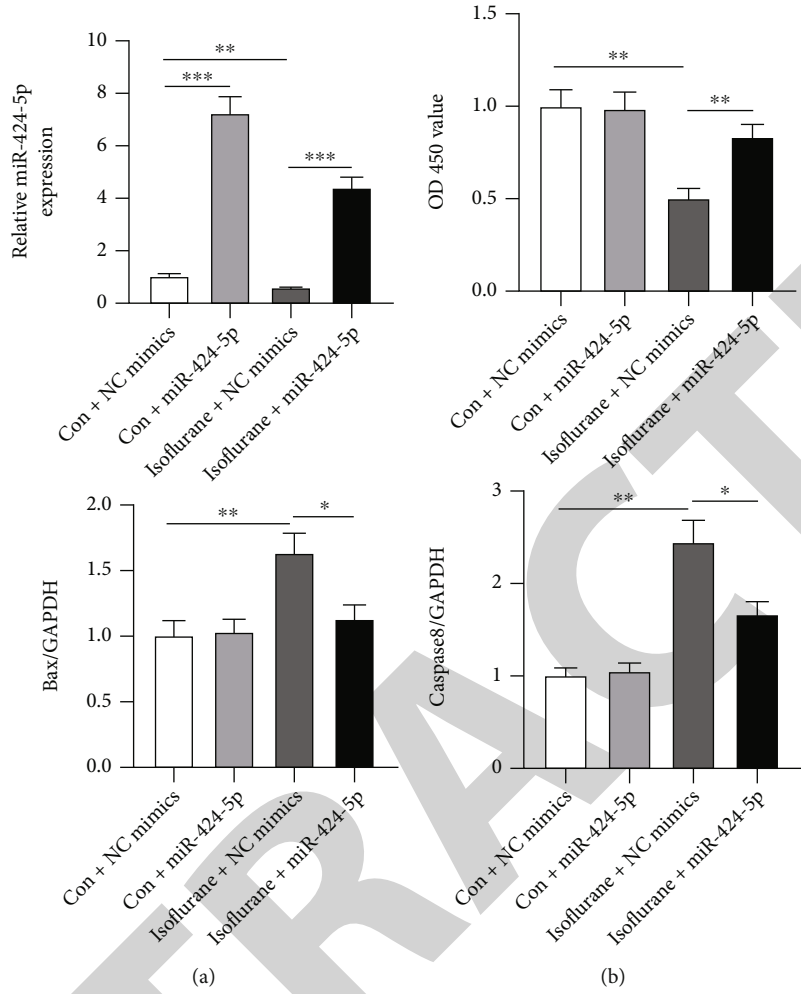
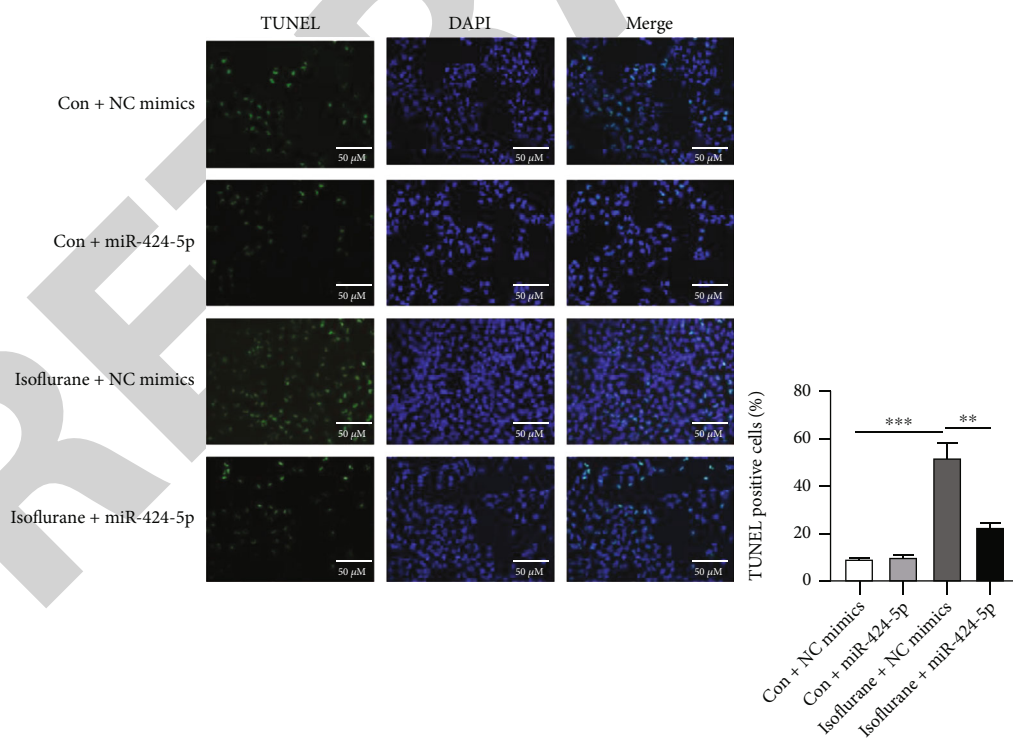
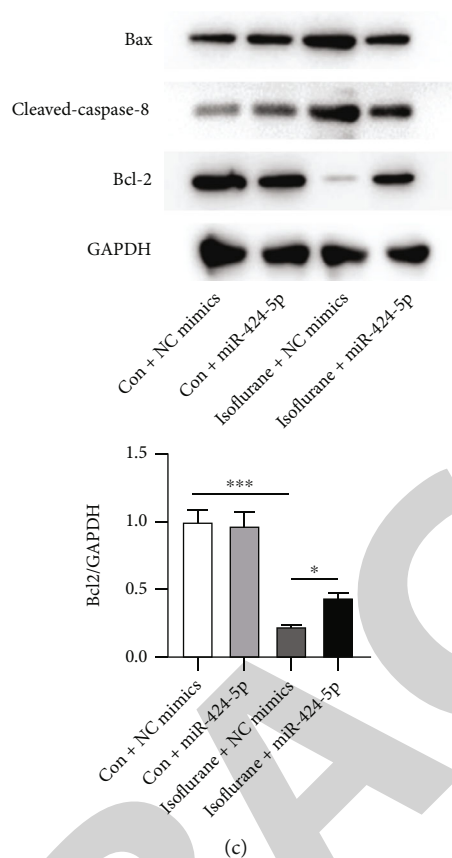


FIGURE 2: Continued.



(d)

FIGURE 2: miR-424-5p overexpression inhibits ISO-induced cell apoptosis. HESC-derived neurons were treated with or without 1.00% of ISO for 24 h and divided into four groups: Con+NC mimics, Con+miR-424-5p, Isoflurane+NC mimics, and Isoflurane+miR-424-5p. (a) miR-424-5p overexpression in hESC-derived neurons. (b) The viability of hESC-derived neurons was detected via CCK-8 assay. (c) Apoptosis proteins (Bax, Bcl-2, and Cleaved-caspase-8) by western blot assessment. (d) The impacts of miR-424-5p elevation on ISO-mediated apoptosis of hESC-derived neurons was detected by TUNEL assessment. \* $p < 0.05$ , \*\* $p < 0.01$ , and \*\*\* $p < 0.001$ .

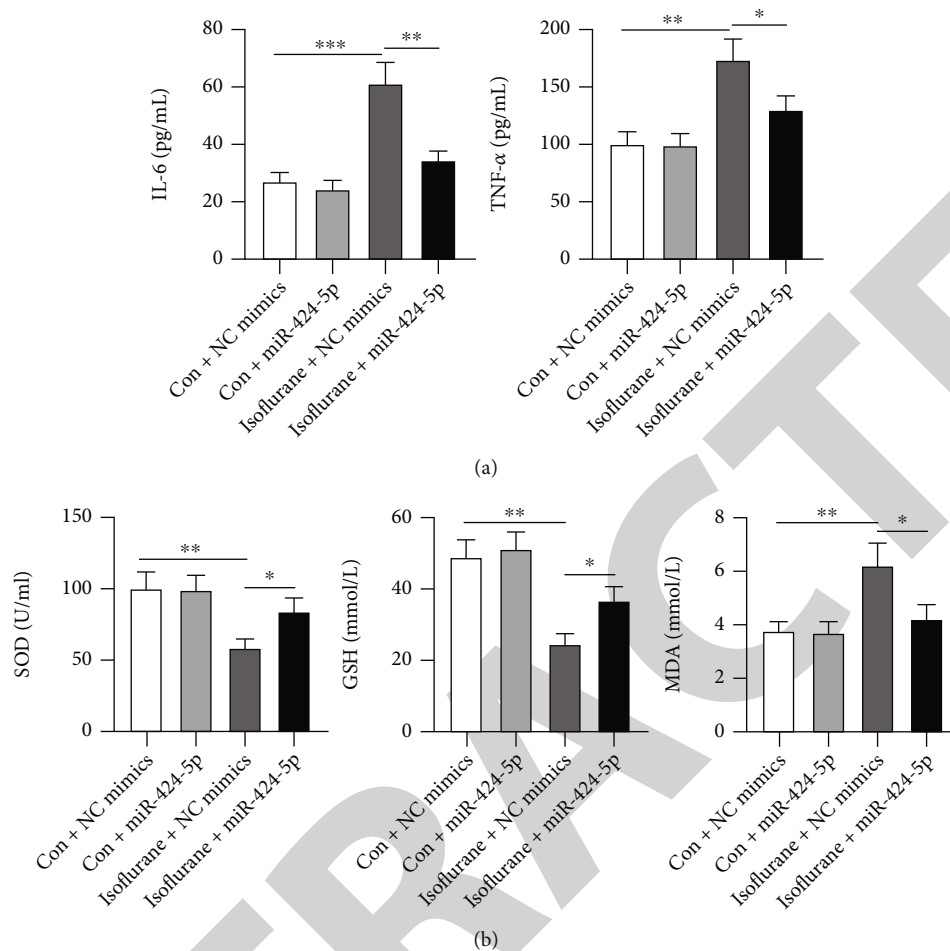


FIGURE 3: miR-424-5p upregulation alleviates ISO-induced inflammatory response and oxidative stress. After treating the hESC-derived neurons with or without 1.00% of ISO for 24 h, the follow-up experiments were conducted. (a) ELISA was employed for the evaluation of IL-6 and TNF- $\alpha$  levels after transfection of NC mimics or miR-424-5p mimics. (b) The levels of SOD, GSH, and MDA in hESC-derived neurons after transfection were evaluated through the relative kits. \* $p < 0.05$ , \*\* $p < 0.01$ , and \*\*\* $p < 0.001$ .

altered by miR-424-5p mimics. Afterwards, viability of hESC-derived neurons was tested by performing CCK-8 assay. Results manifested that miR-424-5p-augmented production countered the suppressed viability of ISO-stimulated hESC-derived neurons (Figure 2(b)). In subsequent assays, the proteins (Bax, Cleaved-caspase-8, and Bcl-2) associated with cell apoptosis were appraised through western blot assessment. It was discovered that protein amount of Bax and Cleaved-caspase-8 enhanced by ISO were reduced by upregulated miR-424-5p. However, transfection of miR-424-5p mimics rescued the suppression of ISO treatment on Bcl-2 protein level (Figure 2(c)). TUNEL assay further illuminated that ISO stimulation-induced promotion on cell apoptosis was suppressed via overexpressed miR-424-5p (Figure 2(d)). Thus, it was concluded that ISO-induced cell apoptosis was inhibited through miR-424-5p elevation.

**3.3. miR-424-5p Upregulation Alleviates ISO-Induced Inflammatory Response and Oxidative Stress.** miR-424-5p has been illuminated for the inhibition of inflammatory

response and regulate oxidative stress [36, 37]. Therefore, it was aimed at investigating whether miR-424-5p suppresses inflammatory reactions and modulates oxidative stress in ISO-induced hESC-derived neurons. ELISA was implemented for examining the quantities of inflammatory mediators (IL-1 and TNF- $\alpha$ ). The experimental data illuminated that ISO treatment-mediated promotion on the TNF- $\alpha$  and IL-6 levels was partially abolished by miR-424-5p upregulation (Figure 3(a)). Subsequently, the influence of miR-424-5p mimics on oxidative stress in hESC-derived neurons was examined. It was observed that ISO treatment decreased the amount of GSH and SOD while it enhanced the MDA level. Nonetheless, these impacts were altered by upregulation of miR-424-5p (Figure 3(b)). Achieved observations demonstrate that overexpressed miR-424-5p ameliorated inflammatory response and oxidative stress induced by ISO in hESC-derived neurons.

**3.4. miR-424-5p Targets FASN in hESC-Derived Neurons.** Seven potential downstream targets (PAPPA, FASN,

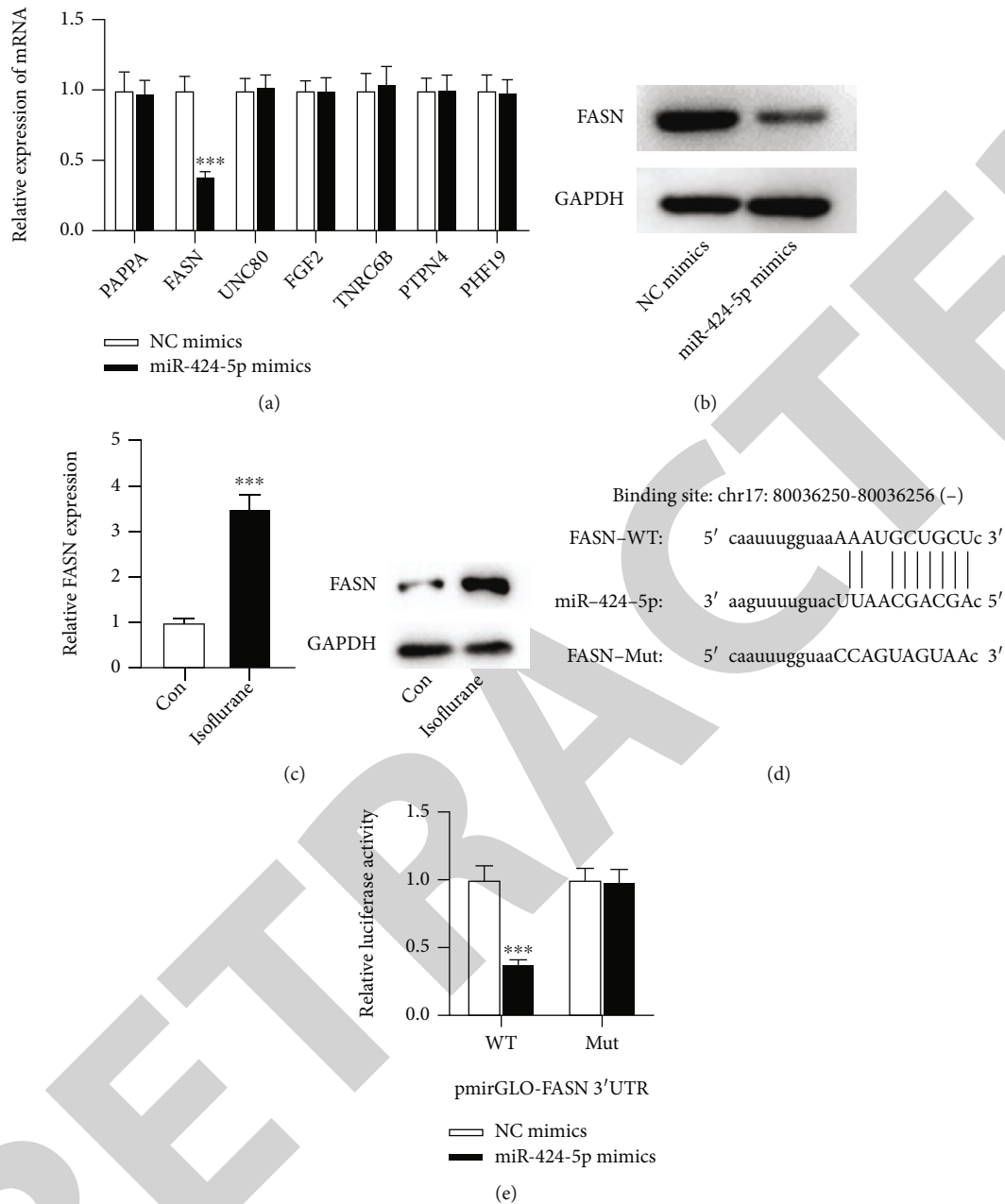
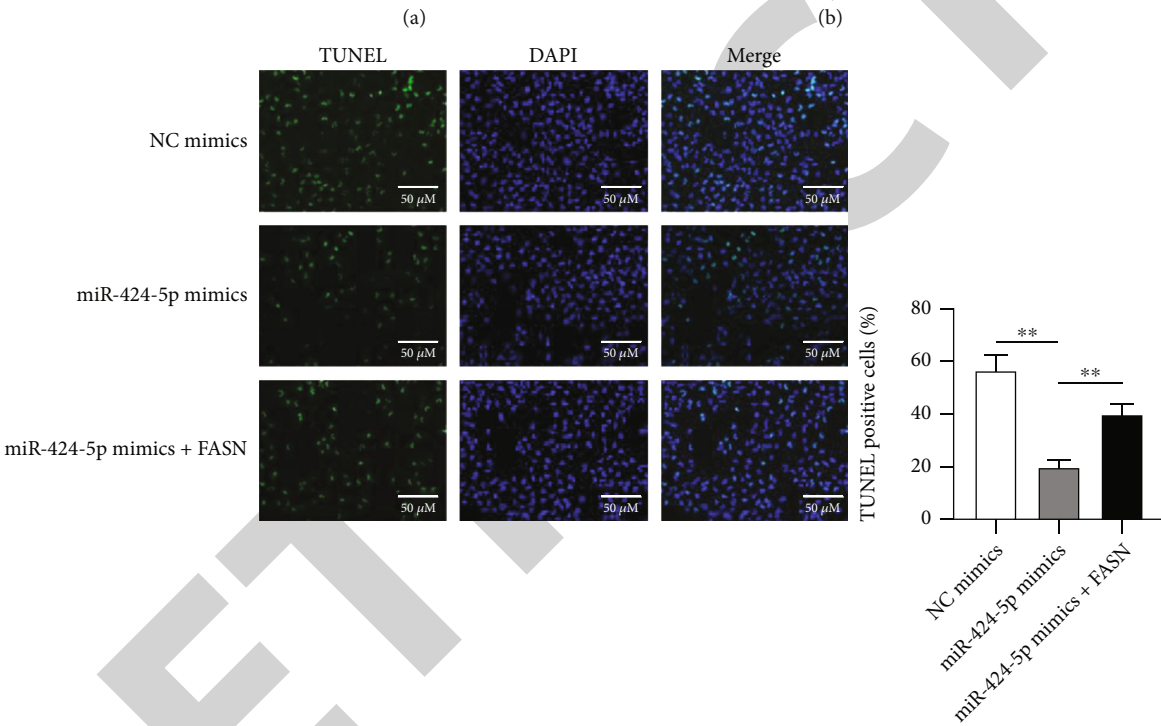
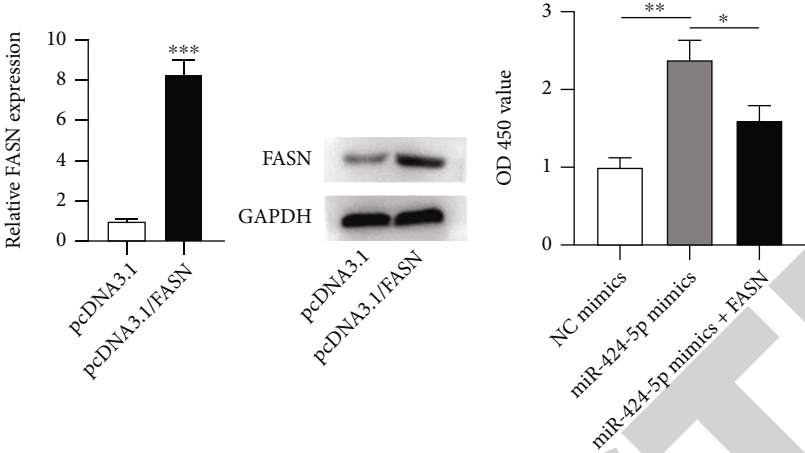


FIGURE 4: miR-424-5p targets FASN in hESC-derived neurons. (a) The effect of miR-424-5p mimics on mRNA levels of PAPPA, FASN, UNC80, FGF2, TNRC6B, PTPN4, and PHF19 through qRT-PCR. (b) The protein quantity of FASN in transfected hESC-derived neurons by western blot. (c) Protein and mRNA quantity for FASN in hESC-derived neurons processed with or without 1.00% of ISO for 24 h was ascertained through qRT-PCR and western blot, accordingly. (d) The position of binding among miR-424-5p and FASN predicted from StarBase. (e) Luciferase activity of FASN-Wt or FASN-Mut in hESC-derived neurons inserted with NC mimics or miR-424-5p mimics was assessed through the luciferase reporter assessment. \*\*\* $p < 0.001$ .

UNC80, FGF2, TNRC6B, PTPN4, and PHF19) that may have binding sequences with miR-424-5p were identified using bioinformatics analysis utilising the miRDB website with the screening condition of target score = 100. Only FASN mRNA expression was downregulated in hESC-derived neurons after the insertion of miR-424-5p mimics, according to qRT-PCR analysis, while the other mRNAs showed no significant change when miR-424-5p production was raised (Figure 4(a)). As a result, it was postulated

that miR-424-5p could target FASN. The level of protein for FASN was investigated using a western blot to confirm this theory. As a result, FASN protein level was notably reduced in hESC-derived neurons after miR-424-5p mimics transfection (Figure 4(b)). Protein and mRNA of FASN which presented the increased levels were also observed in ISO-treated hESC-derived neurons (Figure 4(c)). According to StarBase, miR-424-5p was estimated to have a site of binding for FASN (Figure 4(d)). To prove the combination



(c)  
FIGURE 5: Continued.

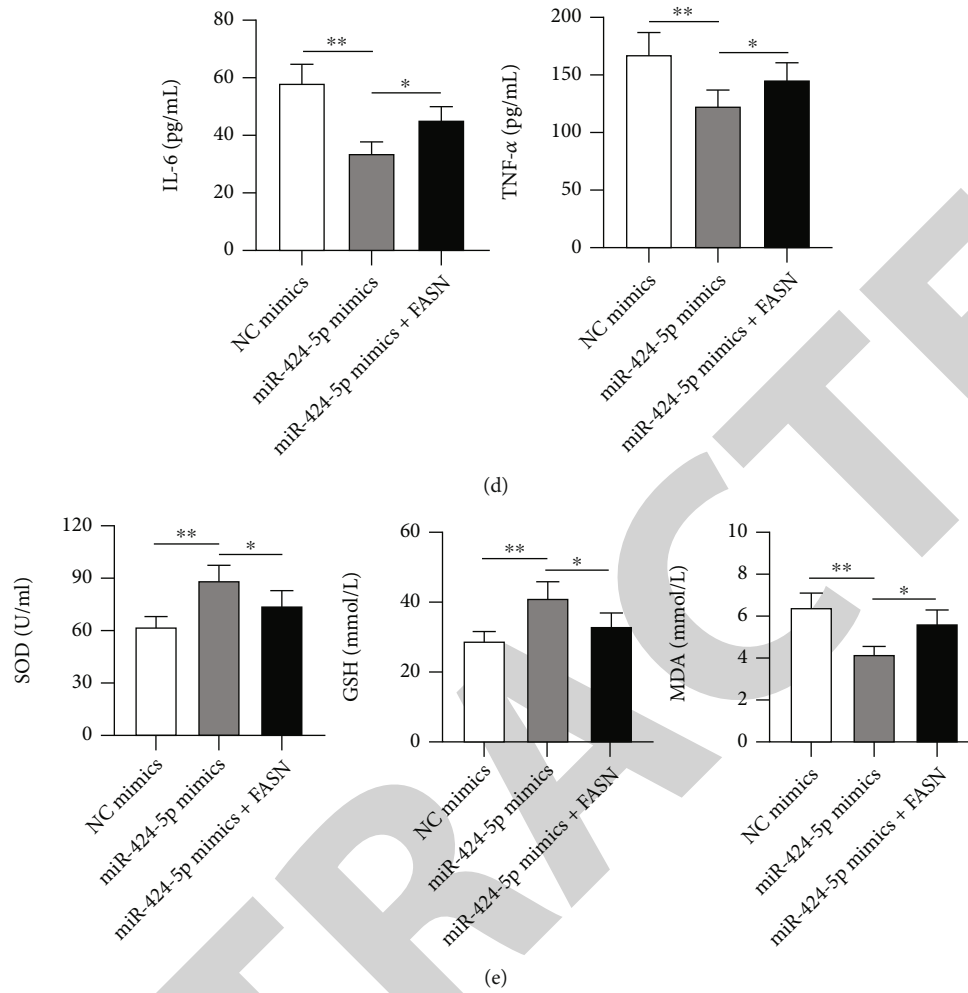


FIGURE 5: Upregulation of miR-424-5p attenuates neuron apoptosis, inflammatory response, and oxidative stress by targeting FASN. After hESC-derived neurons were subjected to 1.00% of ISO for 24 h, the following rescue assays were performed. (a) Overexpression efficacy of FASN. (b) The viability of hESC-derived neurons was detected via CCK-8 assay in NC mimic, miR-424-5p mimic, and miR-424-5p+FASN groups. (c) TUNEL assay was implemented to appraise apoptosis in the abovementioned groups. (d) ELISA was used for the assessment of IL-6 and TNF- $\alpha$  levels after transfection of NC mimics, miR-424-5p mimics, or miR-424-5p+FASN. (e) Indicated plasmids were transfected into hESC-derived neurons to test the activities of SOD, GSH, and MDA. \* $p < 0.05$ , \*\* $p < 0.01$ , and \*\*\* $p < 0.001$ .

between FASN and miR-424-5p further, luciferase reporter assessment was applied. miR-424-5p mimics substantially decreased luciferase activity of FASN-Wt, although no notable change was observed in the FASN-Mut group (Figure 4(e)). Here, it was determined that FASN was directed targeted by miR-424-5p in hESC-derived neurons.

**3.5. Elevation of miR-424-5p Attenuates Neuron Apoptosis, Inflammatory Response, and Oxidative Stress by Targeting FASN.** Several restoration studies in ISO-stimulated hESC-derived neurons were carried out to investigate the impact of the miR-424-5p/FASN axis on neuronal apoptosis, inflammatory response, and oxidative stress. Transfecting pcDNA3.1/FASN into ISO-treated hESC-derived neurons increased FASN protein and mRNA expression (Figure 5(a)). The CCK-8 experiment revealed that increasing FASN inhibited miR-424-5p-overexpressing hESC-derived neurons from proliferating (Figure 5(b)). Furthermore, FASN overexpression

reversed the inhibition of apoptosis in ISO-treated hESC-derived neurons caused by miR-424-5p mimics (Figure 5(c)). Overexpressed FASN also saved the inhibitive property of miR-424-5p elevation on IL-6 and TNF- $\alpha$  level (Figure 5(d)). Furthermore, as presented in Figure 5(e), elevation of FASN reversed the promotive impacts of miR-424-5p mimics on SOD and GSH quantities, while reversing the inhibitive effect of miR-424-5p upregulation on the MDA levels. Achieved findings ascertained that miR-424-5p elevation alleviated neuron apoptosis, inflammatory response, and oxidative stress in ISO-stimulated hESC-derived neurons by suppression of FASN.

#### 4. Discussion

To date, a large portion of infants and children require anesthesia surgery during treatment procedures, which may affect neuronal function and development of brains [38]. In



addition, approximately 30% of adults aged 65 or older receive some form of anesthesia each year in developed countries, but inhalation of anesthetics influences the neuropathogenesis of patients to a great extent [39, 40]. miRNAs have been validated to be involved in anesthesia-mediated neurotoxicity [41]. hESC-derived neurons are broadly employed for constructing anesthetic-induced models in vitro [42]. Therefore, the task and molecular strategy of miR-424-5p on anesthesia-induced neurotoxicity by constructing ISO-induced hESC-derived neurons in vitro were investigated.

A growing number of studies have shown that miRNAs are linked to anesthesia-induced neurotoxicity [43]. According to a recent study, miR-424-5p is implicated in ropivacaine-mediated cell growth, and silencing miR-424-5p counteracts ropivacaine-induced cell development and promotes cell death [44]. It is worth noting that miR-424-5p has been shown to have low expression in ISO-treated rat brain tissues [28]. This study consistently found downregulated expression of miR-424-5p in ISO-stimulated hESC-derived neurons. Moreover, it was also found that ISO treatment led to the repressed neuron viability and elevated neuron apoptosis presented by the higher number of TUNEL positive cells and enhanced Bax and Cleaved-caspase-8 protein levels and also the weakened Bcl-2 protein production, but miR-424-5p overexpression partially eliminated these effects. It was identified that oxidative stress and neuroinflammation are vital pathological procedures in neurological diseases [45]. The miR-424-5p effect on oxidative stress and inflammation response has been detected in lipopolysaccharide-induced acute lung injuries that miR-424-5p hinders LPS-driven injuries through decreasing the levels of LDH, ROS, MDA, TNF- $\alpha$ , IL-1 $\beta$ , and IL-1 $\beta$  [37]. Here, the miR-424-5p effect on oxidative stress and inflammation response in ISO-treated hESC-derived neurons is discovered. Results illustrated that elevation of miR-424-5p repressed the TNF- $\alpha$  and IL-6 in ISO-treated hESC-derived neurons. Similarly, overexpressed miR-424-5p altered the levels of oxidative stress markers shown as an enhancement in GSH and SOD levels and reduced levels of MDA in ISO-treated hESC-derived neurons. The findings illuminated that upregulation of miR-424-5p inhibited ISO-induced inflammation response and oxidative stress in hESC-derived neurons.

Although new evidence suggests that miR-424-5p plays a regulatory role in a variety of physiopathological processes, the exact biological mechanism by which it works in ISO-induced hESC-derived neurons is unknown. Understanding how miR-424-5p genes affect ISO-induced hESC-derived neurons requires determining which miR-424-5p genes should be targeted. In this study, through searching online website miRDB, fatty acid synthase (FASN), which presented downregulated production in hESC-derived neurons by the transfection of miR-424-5p mimics, was predicated to be the downstream target of miR-424-5p. FASN, as a central lipogenic enzyme that produces free fatty acids, was determined to interact momentarily with protrudin [46]. It has been reported that FASN is involved in the myelination and remyelination in the central nervous system [47]; however, almost nothing is understood regarding its molecular

processes in anesthesia-induced neurotoxicity. In this investigation, by performing dual-luciferase reporter assay, FASN was validated to be directly targeted by miR-424-5p. In addition, it was found that the production of FASN at levels of mRNA and protein in hESC-derived neurons after ISO treatment was upregulated. Importantly, it was discovered that miR-424-5p overexpression-triggered repression on inflammation response and oxidative stress was partially abrogated by upregulation of FASN.

Briefly, the findings of the current analysis designated that miR-424-5p alleviates ISO anesthesia-driven neurological damage in hESC-derived neurons by suppression of apoptosis, inflammation response, and oxidative stress via downregulating FASN. As far as we know, this is the unprecedented research for probing into the purpose of miR-424-5p/axis in ISO-induced neurotoxicity in hESC-derived neurons, which may deliver implications for the treatment ISO-induced neurotoxicity. However, there are some limitations in this research. First, the protective effect of miR-424-5p in ISO-treated hESC-derived neurons was just validated in in vitro experiments, and in vivo assays are necessary to further verify if miR-424-5p exhibits the protective activity in ISO-treated animals. Second, due to the complexity of biological mechanisms, some potential signaling pathways associated with miR-424-5p in ISO-treated hESC-derived neurons deserve further exploration.

## 5. Conclusion

miR-424-5p alleviates ISO-induced neurotoxicity, inflammatory response, and oxidative stress in hESC-derived neurons by downregulating FASN.

## Data Availability

Data will be provided upon request to the authors.

## Conflicts of Interest

The authors declare that they have no conflicts of interest.

## Authors' Contributions

Xiaojiao Gu and Wei Yue contributed equally to this work.

## Acknowledgments

The authors appreciate all the participants providing supports for this study.

## References

- [1] M. McCann and S. Soriano, "Progress in anesthesia and management of the newborn surgical patient," *Seminars in Pediatric Surgery*, vol. 23, no. 5, pp. 244–248, 2014.
- [2] R. N. Mhuireachtaigh and D. A. O'Gorman, "Anesthesia in pregnant patients for nonobstetric surgery," *Journal of Clinical Anesthesia*, vol. 18, no. 1, pp. 60–66, 2006.
- [3] D. Wadlund, "Local anesthetic systemic toxicity," *AORN Journal*, vol. 106, no. 5, pp. 367–377, 2017.

- [4] S. Song, X. W. Meng, Z. Y. Xia et al., "Cognitive impairment and transcriptomic profile in hippocampus of young mice after multiple neonatal exposures to sevoflurane," *Aging*, vol. 11, no. 19, pp. 8386–8417, 2019.
- [5] Y. Dong, W. Hong, Z. Tang, Y. Gao, X. Wu, and H. Liu, "Sevoflurane leads to learning and memory dysfunction via breaking the balance of tPA/PAI-1," *Neurochemistry International*, vol. 139, p. 104789, 2020.
- [6] J. Culley, J. D. Boyd, A. Palanisamy et al., "Isoflurane decreases self-renewal capacity of rat cultured neural stem cells," *Anesthesiology*, vol. 115, no. 4, pp. 754–763, 2011.
- [7] X. Zhao, Z. Yang, G. Liang et al., "Dual effects of isoflurane on proliferation, differentiation, and survival in human neuroprogenitor cells," *Anesthesiology*, vol. 118, no. 3, pp. 537–549, 2013.
- [8] A. Ronca, R. Abel, and J. Alberts, "Maternal anesthesia via isoflurane or ether differentially affects pre-and postnatal behavior in rat offspring," *Developmental Psychobiology*, vol. 49, no. 7, pp. 675–684, 2007.
- [9] X. Yi, Y. Cai, and W. Li, "Isoflurane damages the developing brain of mice and induces subsequent learning and memory deficits through FASL-FAS signaling," *BioMed Research International*, vol. 2015, Article ID 315872, 2015.
- [10] S. Johnson, C. Young, and J. Olney, "Isoflurane-induced neuroapoptosis in the developing brain of nonhypoglycemic mice," *Journal of Neurosurgical Anesthesiology*, vol. 20, no. 1, pp. 21–28, 2008.
- [11] L. Wang, M. Zheng, S. Wu, and Z. Niu, "MicroRNA-188-3p is involved in sevoflurane anesthesia-induced neuroapoptosis by targeting MDM2," *Molecular Medicine Reports*, vol. 17, no. 3, pp. 4229–4236, 2018.
- [12] J. Liu, Z. Chen, J. Xiang, and X. Gu, "MicroRNA-155 acts as a tumor suppressor in colorectal cancer by targeting CTHRC1 in *in vitro*," *Oncology Letters*, vol. 15, no. 4, pp. 5561–5568, 2018.
- [13] D. Chen, S. Hu, Z. Wu, J. Liu, and S. Li, "The role of MiR-132 in regulating neural stem cell proliferation, differentiation and neuronal maturation," *Cellular Physiology and Biochemistry*, vol. 47, no. 6, pp. 2319–2330, 2018.
- [14] J. Huang, Y. Xu, X. M. Yin, and F. Y. Lin, "Exosomes derived from miR-126-modified MSCs promote angiogenesis and neurogenesis and attenuate apoptosis after spinal cord injury in rats," *Neuroscience*, vol. 424, pp. 133–145, 2020.
- [15] Y. Su, M. F. Deng, W. Xiong et al., "MicroRNA-26a/death-associated protein kinase 1 signaling induces synucleinopathy and dopaminergic neuron degeneration in Parkinson's disease," *Biological Psychiatry*, vol. 85, no. 9, pp. 769–781, 2019.
- [16] X. Wang, D. Liu, H. Z. Huang et al., "A novel microRNA-124/PTPN1 signal pathway mediates synaptic and memory deficits in Alzheimer's disease," *Biological Psychiatry*, vol. 83, no. 5, pp. 395–405, 2018.
- [17] N. Lai, D. Wu, T. Liang et al., "Systemic exosomal miR-193b-3p delivery attenuates neuroinflammation in early brain injury after subarachnoid hemorrhage in mice," *Journal of Neuroinflammation*, vol. 17, no. 1, p. 74, 2020.
- [18] N. Zhang, W. Ye, T. Wang, H. Wen, and L. Yao, "Up-regulation of miR-106a targets LIMK1 and contributes to cognitive impairment induced by isoflurane anesthesia in mice," *Genes Genomics*, vol. 42, no. 4, pp. 405–412, 2020.
- [19] Z. Zhao, L. Ma, Y. Li et al., "MiR-124 protects against cognitive dysfunction induced by sevoflurane anesthesia in vivo and in vitro through targeting calpain small subunit 1 via NF- $\kappa$ B signaling pathway," *Advances in Clinical and Experimental Medicine*, vol. 30, no. 7, pp. 701–709, 2021.
- [20] C. Xie, H. Wang, Y. Zhang, and Y. Wei, "Neuroprotective effects of miR-142-5p downregulation against isoflurane-induced neurological impairment," *Diagnostic Pathology*, vol. 15, no. 1, p. 70, 2020.
- [21] Y. Zhang, J. Liu, C. Xie, and P. Wu, "Overexpression of miR-133b protects against isoflurane-induced learning and memory impairment," *Experimental and Therapeutic Medicine*, vol. 22, no. 5, p. 1207, 2021.
- [22] H. Chen, Y. He, S. Chen, S. Qi, and J. Shen, "Therapeutic targets of oxidative/nitrosative stress and neuroinflammation in ischemic stroke: applications for natural product efficacy with omics and systemic biology," *Pharmacological Research*, vol. 158, p. 104877, 2020.
- [23] D. Shao, Z. Wu, S. Bai, G. Fu, and Z. Zou, "The function of miRNA-153 against isoflurane-induced neurotoxicity via Nrf2/ARE cytoprotection," *Molecular Medicine Reports*, vol. 19, no. 5, pp. 4001–4010, 2019.
- [24] W. Hu, E. Yang, J. Ye, W. Han, and Z. L. du, "Resveratrol protects neuronal cells from isoflurane-induced inflammation and oxidative stress-associated death by attenuating apoptosis via Akt/p38 MAPK signaling," *Experimental and Therapeutic Medicine*, vol. 15, no. 2, pp. 1568–1573, 2018.
- [25] Q. Wang, X. Ge, J. Zhang, and L. Chen, "Effect of lncRNA WT1-AS regulating WT1 on oxidative stress injury and apoptosis of neurons in Alzheimer's disease via inhibition of the miR-375/SIX4 axis," *Aging (Albany NY)*, vol. 12, no. 23, pp. 23974–23995, 2020.
- [26] M. Wang, H. Liu, L. Xu, M. Li, and M. Zhao, "The protective effect of notoginsenoside R1 on isoflurane-induced neurological impairment in the rats via regulating miR-29a expression and neuroinflammation," *Neuroimmunomodulation*, vol. 29, no. 1, pp. 70–76, 2022.
- [27] Y. Xiang, Y. Zhang, Y. Xia, H. Zhao, A. Liu, and Y. Chen, "LncRNA MEG3 targeting miR-424-5p via MAPK signaling pathway mediates neuronal apoptosis in ischemic stroke," *Aging*, vol. 12, no. 4, pp. 3156–3174, 2020.
- [28] Y. Chen, Z. Zhou, and Y. Wang, "Prediction and analysis of weighted genes in isoflurane induced general anesthesia based on network analysis," *The International Journal of Neuroscience*, vol. 130, no. 6, pp. 610–620, 2020.
- [29] S. Zhang, M. Wernig, I. D. Duncan, O. Brüstle, and J. A. Thomson, "In vitro differentiation of transplantable neural precursors from human embryonic stem cells," *Nature Biotechnology*, vol. 19, no. 12, pp. 1129–1133, 2001.
- [30] J. Itskovitz-Eldor, M. Schuldiner, D. Karsenti et al., "Differentiation of human embryonic stem cells into embryoid bodies compromising the three embryonic germ layers," *Molecular Medicine*, vol. 6, no. 2, pp. 88–95, 2000.
- [31] Z. Xie, D. J. Culley, Y. Dong et al., "The common inhalation anesthetic isoflurane induces caspase activation and increases amyloid beta-protein level in vivo," *Annals of Neurology*, vol. 64, no. 6, pp. 618–627, 2008.
- [32] B. Zhang, Y. Dong, G. Zhang et al., "The inhalation anesthetic desflurane induces caspase activation and increases amyloid beta-protein levels under hypoxic conditions," *The Journal of Biological Chemistry*, vol. 283, no. 18, pp. 11866–11875, 2008.
- [33] J. Liu, Z. Gu, Y. Tang, J. Hao, C. Zhang, and X. Yang, "Tumour-suppressive microRNA-424-5p directly targets

## Research Article

# The Application of Transcranial Electrical Stimulation in Sports Psychology

Shuzhi Chang <sup>1,2</sup>

<sup>1</sup>Teaching Laboratory and Training Center, Tianjin University of Sport, Tianjin 301617, China

<sup>2</sup>Key Laboratory of Competitive Psychological and Physiological Regulation of General Administration of Sport, Tianjin University of Sport, Tianjin 301617, China

Correspondence should be addressed to Shuzhi Chang; zhizi@tj.us.edu.cn

Received 2 June 2022; Revised 24 June 2022; Accepted 27 June 2022; Published 13 July 2022

Academic Editor: Naeem Jan

Copyright © 2022 Shuzhi Chang. This is an open access article distributed under the Creative Commons Attribution License, which permits unrestricted use, distribution, and reproduction in any medium, provided the original work is properly cited.

The problem of sports psychological fatigue has become one of the focal points of common concern among scholars at home and abroad. Athletes will face many problems and challenges in competition or training, and if they are not handled properly, they will have negative experiences, which will affect the training benefits and develop psychological fatigue. Transcranial electrical stimulation (TES), which contains transcranial direct current stimulation, transcranial alternating current stimulation, and transcranial random noise stimulation, is a noninvasive brain stimulation method. By applying specific patterns of low-intensity electrical currents to specific brain regions through electrodes of different sizes, it modulates cortical neural activity and/or excitability and enhances the connections between the brain and nerves and muscles to achieve improved motor performance. TES technology is currently making the transition from laboratory research to applied research in sports science. In this paper, we first describe the neural mechanisms of TES action on the cerebral cortex, including five aspects of body balance, endurance performance, exercise fatigue, muscle strength, and motor learning ability; then, we review the relevant studies on the application of TES in functional connectivity of brain networks and explore the importance of this field for TES to improve athletic performance. This research provides a machine learning-based and transcranial electrical stimulation model for the locomotor psychological fatigue problem in rock climbers since rock climbing is a sport that places great demands on athletes' psychological quality. The research on the factors influencing the psychological fatigue of climbers and the intervention measures is beneficial to the early diagnosis and the prevention and intervention of it.

## 1. Introduction

In modern high water competitive sports, the physical and technical and tactical abilities of the participating athletes are getting closer and closer, and the stable psychological quality becomes an important factor to achieve the victory of the competition, especially the climbing sports competition has a greater consumption of the athletes' psychological energy; if the athletes do not have good psychological quality, even if they have strong physical quality, technical, and tactical ability, it is difficult to achieve excellent sports performance. As the American scholar Grubaugh pointed out for junior athletes, 80% is biomechanical factors, 20% is psychological factors, senior athletes are the opposite, 80% is psychological factors, and 20% is biomechanical factors.

Therefore, in the process of physical and technical and tactical training for rock climbers, it is crucial to strengthen the psychological quality training of athletes.

In rock climbing sport characteristics and climbing psychological training, climbing site, and the sport form of special, climbing site mainly rock cliff face fissure rock face boulder and artificial rock wall, etc., the rock face mostly has a certain elevation angle and pitch angle, and the shape of the rock wall and rock point of the shape of a thousand changes, thus forming the form of rock-climbing sport diversity unconventional work at height and the complexity of technical operations and other characteristics [1–3]. Figure 1 depicts the diagram for using rock climbing to enhance psychological quality. A set of difficult and beautiful sports, rock climbing is demanding and risky. Its core traits

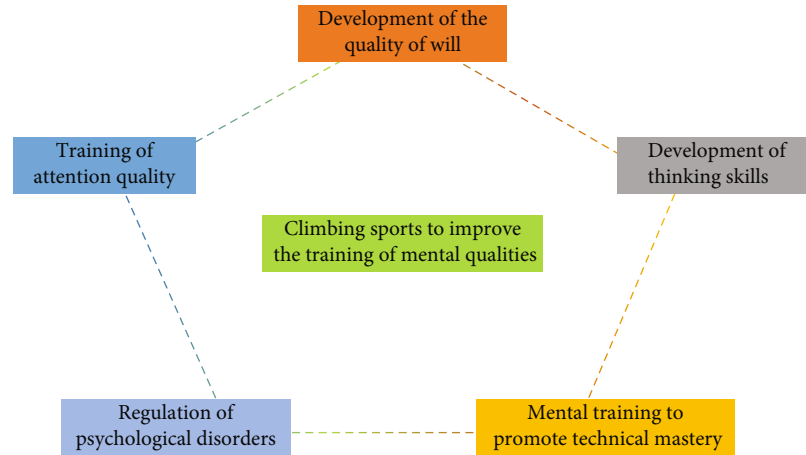


FIGURE 1: Rock climbing to enhance the psychological quality of the schematic diagram.

can be summed up as dangerous, difficult, and beautiful. The angle and shape of the rock wall, the difficulty of the climbing route, the size and shape of the pivot points, and the ever-changing weather are all huge obstacles to climbing; so, athletes are required to have strong resilience and adjust their physical and mental state to better complete the competition. If you make a mistake, you may have the danger of slipping and falling, and you are prone to casualties. Rock-climbing psychological training refers to the process of rock-climbing training, purposely and systematically exerts influence on the psychological process and personality psychological characteristics of athletes, and through special methods and means to make athletes learn to regulate and control their own psychological state, and then regulates and controls their own climbing behavior process due to the specificity of the rock-climbing site the variability of the wall pivot points the diversity of equipment preparation the complexity of technical actions, and it can promote the perfection of athletes' psychological process, form good personality and psychological characteristics compatible with rock climbing, obtain a high level of psychological energy reserves, enable athletes to adapt to the thrilling climbing activities, and lay a good psychological foundation for the victory of the climbing competition. The climbing competition is carried out under the condition of independent combat without guidance, and in the application of techniques and tactics in the process of the competition, the athletes should make timely self-adjustment according to the difficulty angle of the line pivot point and personal advantages and disadvantages of the competition. Good psychological quality makes athletes confident of victory, energetic, vigorous, muscular strength, and increased resilience, so that they can give full play to their existing skills and tactics, and even play beyond the level of psychological training is generally divided into psychological training and psychological training in preparation for specific competitions. General psychological training aims to improve the psychological factors of athletes related to special sports and is also called long-term psychological training because it can be arranged throughout the training process. Psychological training in preparation for specific competitions is

mainly for the specific competition and psychological preparation, generally in the two or three months before the competition to start practicing, and continues until the competition period pregame special psychological training aims to enable athletes to master and use the method of self-regulation of mental state in a relatively short period of time, in order to form the best competitive state [4–6].

Human motor control ability is one of the important motor abilities of the human body. Motor control not only affects the athletes' performance but also has a significant impact on the quality of life of healthy people in general, especially the elderly and patients with motor control deficits. Previous approaches to improve motor control in humans have focused on enhancing motor control through interventional training to modify the function of the skeletal muscle system. However, the nervous system plays a very important role in the process of motor control. In recent years, research on motor control has focused more on the effects of neurological interventions on human motor control [7]. Transcranial electrical stimulation (TES) is a noninvasive transcranial electrical stimulation technique that generates a weak current (1 to 2 mA) in the superficial layers of the skull through paired electrodes placed on the scalp, which affects neural activity in the cerebral cortex and alters brain function to promote motor performance in humans. The main transcranial electrical stimulation techniques used today are transcranial direct current stimulation (tDCS), transcranial alternating current stimulation (tACS), and transcranial random noise stimulation (TRS). These electrical stimulation techniques can be used to achieve different stimulation effects by changing the position of electrodes, the intensity of current, the duration of stimulation, and the frequency of stimulation. As a noninvasive and safe brain stimulation technique, TES has been gradually announced into sports science applications from the treatment of neurological or psychiatric disorders. In this paper, we focus on the research and application of TES in improving sports mental performance, especially in rock climbing. A machine learning algorithm-based transcranial electrical stimulation in sports psychology is proposed for applications including improving mental balance, enhancing

mental endurance performance and/or relieving exercise fatigue, improving muscle strength, and enhancing sports psychological learning ability, which provides theoretical references for better understanding and application of TES techniques. The effectiveness of the proposed method was demonstrated in relevant experiments [8].

The usefulness of transcranial electrical stimulation in enhancing psychomotor balance, psychomotor endurance performance, psychomotor strength, and decreasing motor fatigue is further examined in this paper.

The arrangements of the paper are as follows: Section 2 discusses the related work. Section 3 examines the various methods. Section 4 analyzes the experiments and results. Section 5 concludes the article.

## 2. Related Work

*2.1. Transcranial Electrical Stimulation and Sports.* Currently, TES is more frequently used in the rehabilitation of patients with neurological impairment or psychiatric disorders and has good belongings on the recovery of brain injury, mood regulation, and improvement of cognitive function. In recent years, some researchers have gradually applied TES to the field of sports science to improve human muscle coordination in sports and enhance human sports performance by increasing the connection between the brain and nerves and muscles, such as improving body balance, enhancing endurance performance, relieving sports fatigue, and improving muscle strength and motor learning ability. Improve body balance ability is one of the main physical qualities of humans, which refers to the ability to maintain body posture even during exercise or under external forces, and it is related to body structure, muscle coordination, and the regulation of brain tissue involved in balance [9–12]. It was found that 1 mA tDCS anodal stimulation of the motor cortex of healthy elderly people for 20 min per day resulted in improved gait and dynamic balance after 5 d of continuous intervention and was maintained for 1 week. Stimulation of the sensorimotor area of healthy adults with high precision tDCS for 20 min better the static balance ability of the subjects. Body balance is one of the basic abilities that athletes possess, especially in nonperiodic events, and directly affects the performance of athletes' skills and physical abilities, etc. Whether tDCS can improve dynamic and static balance in elite athletes needs further study. Enhance endurance performance and/or relieve exercise and fatigue. Endurance is the body's ability to perform muscle activity for long periods of time and is the basis for improving qualities such as speed and strength. The goodness of endurance directly affects human athletic performance. Currently, some studies have investigated whether tDCS intervention in the cerebral cortex has a positive effect on neurological and muscular fatigue recovery [13].

The exact neurophysiological mechanisms of transcranial direct current action can be divided into the following mainstream views: altering cortical excitability, increasing synaptic plasticity, altering local cerebral blood flow, and regulating local cortical and brain network connections. Changing cortical excitability is as follows: tDCS changes

the excitability of the brain by stimulating the membrane potential of neurons, causing depolarization of the anode to lower the threshold of action potential generation, and increasing the excitability of the anodal cortex; [14–16]. Increase synaptic plasticity is as follows: tDCS performs sub-threshold stimulation of the resting membrane potential of neurons, which induces the expression of N-methyl aspartate receptors and the release of  $\gamma$ -aminobutyric acid, while NMDA is involved in synapse formation, increasing synaptic plasticity, which in turn produces long-duration inhibitory or enhancing effects. Alteration of local cerebral blood flow is as follows: when the tDCS anode acts on the dorsolateral prefrontal cortex, it increases cerebral blood flow in the stimulated area and decreases cerebral blood flow under the cathode, which is highly correlated with the MEP amplitude at the stimulation location. Modulation of local cortical and brain network connectivity is as follows: EEG and functional magnetic resonance imaging studies revealed that anodal tDCS stimulation of area M1 significantly increased functional connectivity in the premotor, motor, and sensorimotor areas within the stimulated hemisphere and induced changes in connectivity between the left and right hemispheres, further corroborating that tDCS induces functional brain connectivity. tACS stimulation is dependent on the stimulation. The mechanisms of tACS action can be classified as follows: exogenous oscillations induce endogenous oscillations in the brain, affecting synaptic plasticity to regulate brain function. When tACS acts on the brain, part of the current reaches the cerebral cortex and changes the membrane potential of dendrites or axons in an oscillatory manner, making it possible for neurons to develop action potentials. When the frequency of tACS is the same as the endogenous frequency, resonance occurs, causing excitation of neurons in the brain; when tACS is stimulated at a higher frequency, it can trigger neuronal oscillations in a wider frequency range. Stimulation at specific frequencies can also drive oscillatory frequencies within the brain and induce synchronous oscillations in neurons with rhythms imposed by tACS on specific cortices. tACS modulates brain function by affecting synaptic plasticity. When tACS causes presynaptic action potentials to precede postsynaptic action potentials, it produces long-lasting excitation of brain function, and when it causes postsynaptic potentials to precede presynaptic potentials, it causes long-lasting inhibition of brain function, a phenomenon that has been confirmed by many studies.

*2.2. Psychological Analysis of Rock Climbing.* Rock climbing is a kind of mountaineering sport, which fully exploits the human body's climbing potential, and the climber relies on the coordination of hands, feet, waist, and muscle functions and uses gouging, grasping, bracing, and other means to operate the body upward. Both man-made and natural rock walls can be climbed, with man-made rock walls having the most participants. According to the psychological requirements of rock climbing, climbers must perform well in specialized psychological quality training to improve their capacity for psychological adjustment and obstacle surmounting [17–19]. The sport of rock

climbing demands exceptional physical, intellectual, and psychological qualities.

Rock climbing is a sport with long time, high density, and large volume of transportation. The process of rock climbing puts forward extremely high requirements on athletes' physical ability, and athletes need strong physical ability, intelligence, and good psychological quality to complete a complete climb. In the process of rock climbing, the athletes' psychological ability is extremely important. In the process of rock climbing, due to the rapid consumption of physical energy, it often causes a rapid decline in the athletes' functional reserve and central nervous fatigue, which leads to a series of bad emotions such as inattention, irritability, and decrease in the level of will. If these bad emotions deteriorate further, it will cause the athletes to move slowly, have stiff muscles, and panic in their hands and feet. These bad emotions, if further worsened, will cause the athletes to move slowly, muscle stiffness, and hands and feet panic, affecting the completion of rock climbing. In serious cases, it will lead to sports injury or even danger. Therefore, the special psychological training for rock climbers is extremely important, through effective psychological training, so that athletes can effectively psychologically regulate themselves in the process of rock climbing and help them maintain emotional stability [20, 21]. We know that rock climbing has a certain degree of danger, and the psychology of fear in the procedure of rock climbing is caused by a variety of reasons. One of the most important factors is the climber's understanding of the degree of obstacles and the climber's level of trust in protective events and protection personnel. To train and improve climbers to overcome psychological barriers, it is necessary to find the cause and prescribe the right remedy: first, to make climbers fully understand the degree of difficulty of this climb and some related knowledge and second, to make climbers do good communication with staff to enhance their trust in protection workers and safety measures.

Concentration training is extremely important for rock climbers. Only by concentrating on one goal can the climber not be disturbed by the external environment and internal factors during the climbing process, not be distracted during the climbing, and reach the summit successfully. The concentration of attention training generally has two forms: one is the muzzle training method: the so-called muzzle training refers to the trainer in the usual training by issuing some volume weak, just can barely hear the sound, and let the trainee to complete the task, and such a weak voice muzzle needs athletes to focus on a high degree of attention to complete. Second is the stopwatch training method [22]. The so-called stopwatch training is to allow athletes to focus on the rotation of the stopwatch, record the time of each attentiveness, in the training time lengthened one by one, until the end of inattention, and then repeat the training in accordance with this time standard. Training regulates arousal level in rock climbing; there are two kinds of training to regulate arousal level in rock climbing: one is to increase the arousal level of AH, and the other is to decrease, the arousal level of sex. Arousal level refers to the physiological activation of the muscles in different degrees and states,

and the state of arousal level is directly related to the level of athletes. The human body can change and maintain the excitability of the brain's nervous system through arousal and use this state of arousal to maintain a high level of concentration and provide conscious energy to the muscles. In general, in sports that are mainly speed and strength-based, a higher level of arousal is required, while in sports that are mainly regulated by small muscle groups and have complex tasks. Exercise classes that require coordinated coordination require a lower level of arousal [23].

The so-called representational training refers to the training to promote the athletes to improve their climbing skills and technical level of play; in the representational training, coaches can make the athletes form the representational movement in the brain consciousness through verbal explanation, video images, video materials, and other means, so that the athletes can train through the full imagination. The main purpose of representational training is to allow athletes to train in actual combat before. In addition, representational movement also includes the reproduction of previously learned technical movements after training, through the recollection and reproduction of movements in the brain, the wrong movements can be corrected, and the correct movements can be consolidated. In the process of representational training, athletes can categorize and organize the decomposed movements one by one in their mind and make corrections and improvements, so that they can complete the whole climbing process independently in their own mind. Representation training not only makes the athletes get twice the result with half the effort in the climbing process but also increases the information reserve and develops their intelligence.

### 3. Methods

*3.1. Model Architecture.* Decoding and analyzing the event-related desynchronization/event-related synchronization generated by the conceptual activity of rock climbing to determine the user's motor intention and brain state are the basis for the implementation of a brain-machine interface based on the psychology of rock-climbing. Users gain the ability to actively regulate their sensorimotor rhythms to give control commands in the psychological brain-machine interface based on rock climbing. The modulation patterns induced by psychomotor rhythms in the brain can be used as control input signals for the BCI, and through learning and training, climbers can autonomously generate the corresponding EEG patterns. The model structure diagram of the psycho-brain-computer interface for rock climbing is shown in Figure 2. The system is similar to other brain-computer interface systems and is generally composed of the following parts: signal acquisition part, signal preprocessing, feature extraction, pattern classification, and output module. Signal acquisition part is as follows: the main role is to record the EEG signals that the subjects go through the psychological experiment paradigm of rock-climbing exercise and thus generate. Signal preprocessing is as follows: the preprocessing stage is mainly to remove the noise from the EEG signal, usually using a band-pass filter, and to

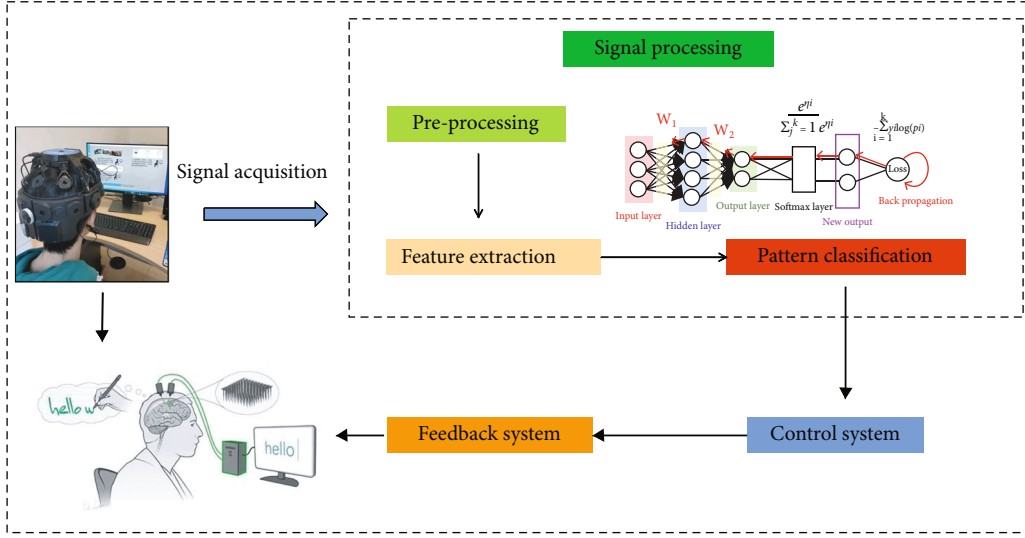


FIGURE 2: Model structure.

remove the electrooculography and motion artifacts using various methods as needed. Feature extraction is as follows: since the EEG signals of climbers during the mental activity of rock-climbing sports are mixed with those generated by other neural activities and are overwhelmed by a large amount of spontaneous EEG, the feature signals related to the mental activity of rock-climbing sports need to be extracted from these mixed EEG signals by reducing the dimensionality of the EEG signals so as to extract the relevant features. Pattern classification is as follows: the extracted to feature information is analyzed and judged, so that these features can be decoded into various instructions or parsed into the user's intention of rock-climbing sports psychology. Output module includes two parts: control system and feedback system. There are some brain-machine interfaces based on rock-climbing psychology aiming at helping paralyzed climbers to perform some daily activities, and then the extracted feature information will be decoded into various control commands to control external devices, such as robots, wheelchairs, and mice. There are also some brain-machine interfaces based on the psychology of rock climbing, whose purpose is to help climbers with neurological damage to carry out neural pathway rehabilitation or healthy climbers to improve their athletic ability through the psychological training of rock-climbing, without controlling external devices, and then the decoded commands will be analyzed and returned to the climbers through the feedback system.

**3.2. Preprocessing.** In this paper, after the EEG data are acquired, the calculation of subject-specific band  $r^2$  is performed in the preprocessing stage for the determination of the subject's band-pass filter.  $r^2$  is calculated as follows.

$$r^2 = \left( \frac{\sqrt{N_1 N_2} \text{MEAN}(P_1) - \text{MEAN}(P_2)}{N_1 + N_2} \text{STD}(P_1 \cup P_2) \right)^2. \quad (1)$$

In the equation,  $N_1$  and  $N_2$  are the number of tasks included in the EEG data, respectively,  $N_1$  represents the number of trails for the left-hand motor imagery task, and  $N_2$  represents the number of trails for the right-hand motor imagery task.  $P_1$  and  $P_2$  are the power spectra of the EEG data for the motor imagery task,  $P_1$  represents the power spectrum of the left-hand motor imagery EEG data, and  $P_2$  represents the power spectrum of the right-hand motor imagery EEG data. The larger the value of  $r^2$ , the greater the energy difference between the EEG data of left- and right-handed motor imagery tasks in that frequency band. According to the value of  $r^2$ , a suitable band-pass filtering band is selected to perform specific band-pass filtering on the motor imagery EEG data, followed by CSP feature extraction and LDA pattern classification.

**3.3. Feature Extraction.** The flow of signal data feature extraction is shown in Figure 3. For the together EEG signals, there are three main features: time domain features, frequency domain features, and spatial domain features, and we need to choose the corresponding feature extraction methods for dissimilar features. For example, spatial domain features are usually extracted by choosing spatial domain filters—Common Spatial Pattern (CSP), while frequency domain features are generally extracted by power spectrum analysis and some other wavelets transform, sample entropy method, etc. Each of these methods has its own advantages and disadvantages, as shown in Table 1.

In this study, the purpose is to extract the two characteristic signals of left-handed motion and right-handed motion generated by the user's motion imagination, and using the CSP algorithm is more in line with our requirements. The CSP algorithm is to calculate all channels, and we know that the variance represents the energy, due to the phenomenon of ERD/ERS generated by motion imagination, and it is easier to use the CSP algorithm. Because of the ERD/ERS phenomenon, it is easier to extract the features with the greatest difference in energy to classify the motor imagery intention.

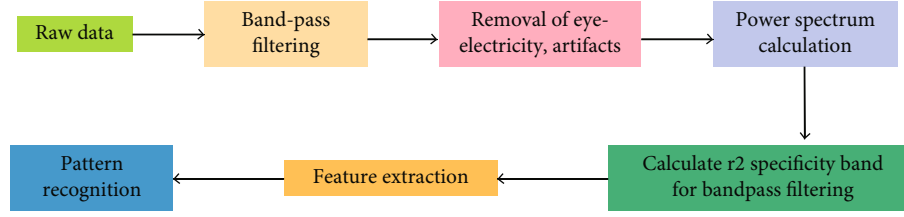


FIGURE 3: Signal data feature extraction process.

TABLE 1: Advantages and disadvantages of different feature extraction methods.

Feature extraction method	Advantages	Disadvantages
Power spectrum analysis method	Simple algorithm, easy to operate	Low resolution, inability to display brain telecommunication nonlinear information of the number
Wavelet transform	Multiple resolutions for more detailed characterize the signal	Inflexible algorithm
Sample entropy method	Stable algorithm, low computational effort	Cannot express the time-frequency characteristics of the signal
Common spatial pattern method	Good performance in feature extraction for binary classification	Requires multiple leads for analysis and is susceptible to noise interference

**3.4. CSP Algorithm.** The CSP algorithm is a feature extraction algorithm for two arrangement tasks. The computational procedure of the CSP algorithm is as follows: assume that  $X_1$  and  $X_2$  are the matrices of the single evoked EEG signals under the same experimental conditions of the left and right handed two motor imagery responsibilities, respectively, and the matrix dimension  $N \times T$ ,  $N$  is the number of channels of EEG signals, and  $T$  is the number of sampling points of EEG signals, as the number of channels of EEG signals commonly used is 8 conductors, 16 conductors, 32 conductors, 64 conductors, and 128 conductors.  $N$  must be less than  $T$  to satisfy the condition of calculating the covariance matrix. Specify that  $Y_1$  and  $Y_2$  are two types of tasks for left-handed motion and right-handed motion, and  $X_1$  and  $X_2$  are represented as follows, respectively, when noise interference is ignored.

$$X_1 = [A_1 A_m] \begin{bmatrix} Y_1 \\ Y_M \end{bmatrix}, X_2 = [A_2 A_m] \begin{bmatrix} Y_2 \\ Y_M \end{bmatrix}. \quad (2)$$

Assume that the source signals of the two tasks,  $Y_1$  for left-handed motion and  $Y_2$  for right-handed motion, are linearly independent of each other,  $Y_u$  represents the common source signal possessed by these two tasks,  $Y_1$  consisting of  $m_1$  sources and  $Y_2$  consisting of  $m_2$  sources, then  $A_1$  consists of  $m_1$  covariance patterns associated with  $X_1$ ,  $A_2$  consists of  $m_2$  covariance patterns associated with  $X_2$ . The purpose of the CSP algorithm is to design a spatial filter parameter to obtain the best projection matrix  $W$ . The EEG signals are passed through this spatial filter to obtain new signals where one has the largest variance, the other has the smallest variance, and then the two types of signals are classified by a

classification algorithm. Calculate the covariance matrix of  $X_1$  and  $X_2$ , respectively.

$$R_1 = \frac{X_1 X_1^T}{\text{tr}(X_1 X_1^T)}, \quad (3)$$

$$R_2 = \frac{X_2 X_2^T}{\text{tr}(X_2 X_2^T)},$$

$r$  denotes the trace of the matrix, which is the sum of the diagonal elements of the matrix  $X_1 X_1^T$ . Here,  $R_1$  and  $R_2$  are the covariance matrices for a single trial, and then the respective average covariance matrices  $\bar{R}_1$  and  $\bar{R}_2$  are calculated based on the total number of trials for each of the left- and right-hand tasks, denoted as  $n_1$  and  $n_2$ :

$$\bar{R}_1 = \frac{1}{n_1} \sum_{i=1}^{n_1} R_{1i}, \quad (4)$$

$$\bar{R}_2 = \frac{1}{n_2} \sum_{i=1}^{n_2} R_{2i}.$$

Calculate the mixed-space covariance matrix  $R$ .

$$R = \bar{R}_1 + \bar{R}_2. \quad (5)$$

Since the obtained mixed-space covariance matrix  $R$  is a positive definite matrix, the eigenvalue decomposition of the obtained mixed-space covariance matrix  $R$  is performed according to the singular value theorem as follows.

$$R = U \Lambda U^T. \quad (6)$$



$\lambda$  denotes the diagonal matrix composed of eigenvalues arranged in descending order, and  $U$  denotes the matrix composed of eigenvectors corresponding to the decomposed eigenvalues, resulting in the whitening transformation matrix  $P$ .

$$P = \frac{1}{\sqrt{\lambda U^T}}. \quad (7)$$

For the formal experimental data, to avoid transient abrupt changes in the EEG signal caused by body movements, its variance is calculated and normalized for the eigensignal obtained through the spatial filter, and then the eigenvectors are extracted as follows.

$$\begin{cases} Z_i = WX_i, \\ f_i = \frac{\text{var}(Z_i)}{\sum \text{var}(Z_i)}. \end{cases} \quad (8)$$

**3.5. Pattern Classification.** To interpret the subject's motor imagery intention and to differentiate the brain activity caused by left-handed and right-handed motor imagery activities, the recovered features from the EEG signal must be sent to a classifier for pattern classification after the signal has been retrieved. The algorithms used to categorize the extracted features into patterns are both linear and nonlinear, and the linear algorithms include linear discriminant classifiers and linear classifiers of Marxian distance, among others. Based on the above mentioned and the characteristics of motor imagery EEG signals.

LDA is an effective feature extraction method that can classify data and compress the feature space dimension. This section introduces the basic principle of LDA starting from the simpler class II LDA. First assume that there are  $m$  samples in the dataset, denoted as

$$D = \{(x_1, y_1), (x_2, y_2), \dots, (x_m, y_m)\}, \quad (9)$$

where  $x$  is an  $n$ -dimensional vector and  $y_i \in \{0, 1\}$ . We define  $N_j (j \in \{0, 1\})$  as the number of samples of the  $j$ -th class and  $X_j (j \in \{0, 1\})$  as the set of samples of the  $j$ -th class, and then the mean vector of samples of the  $j$ -th class can be expressed as

$$\mu_j = \frac{1}{N_j} \sum_{x \in X_j} x, j \in \{0, 1\}. \quad (10)$$

The covariance matrix of the  $j$ -th class of samples can be expressed as

$$\Sigma_j = \sum_{x \in X_j} (x - \mu_j)(x - \mu_j)^T, j \in \{0, 1\}. \quad (11)$$

The projection vector is denoted by  $w$ . Then, any sample  $x$  becomes  $w^T x_i$  after projection. As mentioned above, the purpose of the LDA algorithm is to make the distance

TABLE 2: Experimental parameter setting.

Parameter name	Parameter value
Initial learning rate	0.002
Optimizer	Adam
Initial momentum	0.5
Batch size	30
Maximum number of training sessions	40

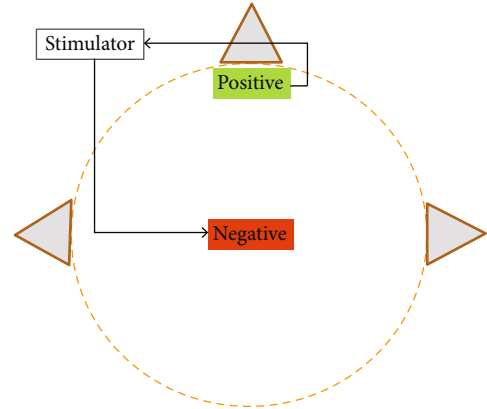


FIGURE 4: Stimulation electrode location map.

between similar data as small as possible, and the distance between different classes of data as large as possible.

$$G_1 = w^T \Sigma_0 w + w^T \Sigma_1 w. \quad (12)$$

The distance between samples of different categories is expressed as the square of the second parametric number, as follows:

$$G_2 = w^T \mu_0 - w^T \mu_1^2. \quad (13)$$

In summary, the optimization objective of the LDA algorithm is

$$\begin{aligned} w^* &= \arg \max_w \frac{G_2}{G_1} = \frac{w^T \mu_0 - w^T \mu_1^2}{w^T \Sigma_0 w + w^T \Sigma_1 w} \\ &= \frac{w^T (\mu_0 - \mu_1)(\mu_0 - \mu_1)^T w}{w^T (\Sigma_0 + \Sigma_1) w}. \end{aligned} \quad (14)$$

## 4. Experiments and Results

In this section, it discusses the various experimental setups and define the transcranial electrical stimulation. They analyze the experimental results.

**4.1. Experimental Setup.** This chapter investigates the effects of transcranial electrical stimulation on motor imagery task ability based on the motor imagery brain-machine interface. In the ERD/ERS data, changes in classification accuracy before and after transcranial electrical stimulation were analyzed separately to investigate the electrophysiological effects

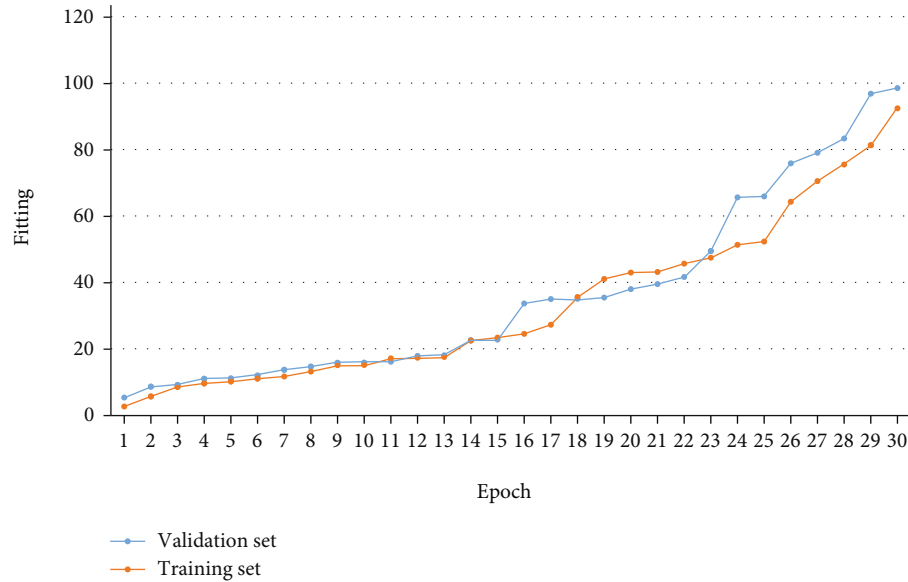


FIGURE 5: Schematic diagram of the performance improvement of the training process.

of transcranial electrical stimulation on motor imagery. This experiment was a single-blind experiment, subjects were required to perform a total of four experiments, and the sequence of stimulation and control experiments was randomly arranged by the main subjects. To avoid the after-effects of transcranial electrical stimulation, the time interval between each group of stimulation and control experiments was ensured to be at least 24 hours.

Ten rock climbers (age range 23-25 years, mean age  $24.4 \pm 0.44$  years) were recruited for this experiment, and all participants were active climbers and received monetary compensation. During the experiment, subjects would receive a total of four MI task experiments and three transcranial electrical stimulations. The subjects first underwent the first MI task experiment to determine the baseline level of each outcome for comparison and analysis with the subsequent experiments, followed by three randomized transcranial electrical stimulation sessions with corresponding MI task experiments and EEG recordings. The duration of the after-effects of transcranial direct current stimulation is not more than 10 min, and the duration of the after-effects of transcranial alternating current stimulation has not been systematically studied, but the duration of the after-effects of 10 Hz, 1 mA alternating current stimulation, is 30 min; so, the interval between each stimulation is guaranteed to be more than 24h to avoid the after-effects from affecting the results of the subsequent experiments. The experimental parameters are set as shown in Table 2.

#### 4.2. Transcranial Electrical Stimulation

- (1) Electrical stimulation equipment: publicly available transcranial electrical stimulation equipment. It is capable of three stimulation modes tACS, and pseudostimulation

- (2) Stimulation intensity: (a) tDCS: all subjects uniformly use 1 mA current intensity, and the stimulating electrodes use  $5 \times 7$  cm saline soaked sponge electrodes. (b) tACS: The stimulation intensity was determined according to the subject's stimulation threshold specificity as described, and the stimulation electrode was a  $5 \times 7$  cm saline-soaked sponge electrode
- (3) Stimulation position: the electrode placement was as shown in Figure 4, with the anode placed at the location of the motor sensory M1 area and the cathode electrode located at the forehead area
- (4) Stimulation frequency: 10 Hz (mean of  $\mu$  rhythm) was used to stimulate the subjects during the tACS experiment. (5) Stimulation time: for both tACS and tDCS, a current stimulation lasting 10 min was applied to the subjects

After the raw EEG data were collected and pre-processed, the LDA algorithm was used to calculate the classification accuracy of the EEG data for the two motor imagery tasks, as well as to calculate the power spectrum of the EEG data in the prestimulation and poststimulation phases to observe the changes in ERD/ERS, respectively. The diagram of the training process performance improvement is shown in Figure 5.

**4.3. Experimental Results.** For motor mental classification accuracy, this paper used one-way frequent measures ANOVA to test the significance of the classification accuracy of subjects' motor imagery before and after different experimental conditions.  $p < 0.05$  was considered to be a significant difference. Among the ten subjects, one subject's data was eliminated for excessive noise, and the EEG data of the remaining nine subjects were finally used for the analysis.

TABLE 3: Accuracy of subjects' psychological recovery from rock climbing exercise.

	Before stimulation	After pseudoarousal	After tACS	After tDCS
Subject 1	91.25	93.21	98.75	96.88
Subject 2	83.83	85.84	92.50	97.50
Subject 3	74.68	76.25	86.25	80.00
Subject 4	85.00	85.00	89.74	90.06
Subject 5	82.49	85.00	80.00	86.25
Subject 6	77.50	78.64	85.05	82.68
Subject 7	77.61	71.25	81.27	87.49
Subject 8	77.49	77.50	75.11	81.27
Subject 9	88.77	91.28	94.93	96.31
Mean $\pm$ standard deviation	82.07 $\pm$ 5.67	82.66 $\pm$ 7.25	87.07 $\pm$ 7.63	88.71 $\pm$ 6.88

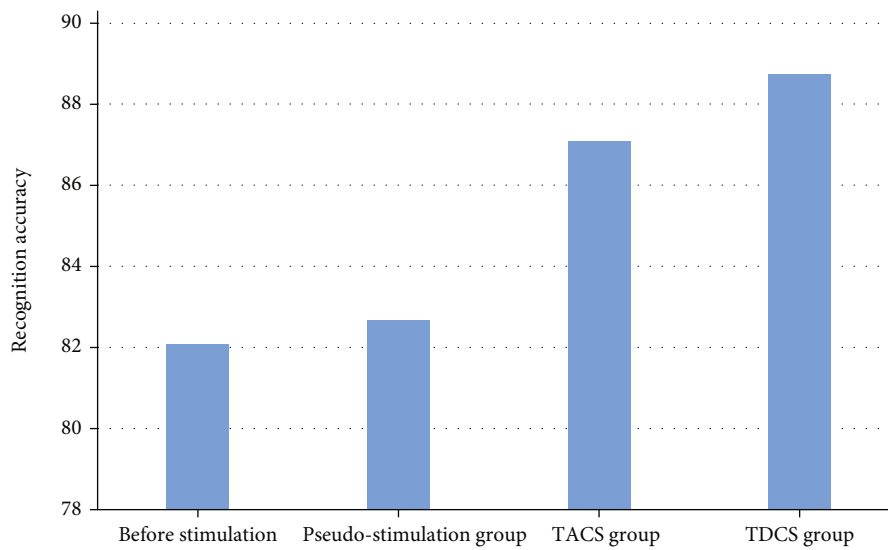


FIGURE 6: Average accuracy of task classification.

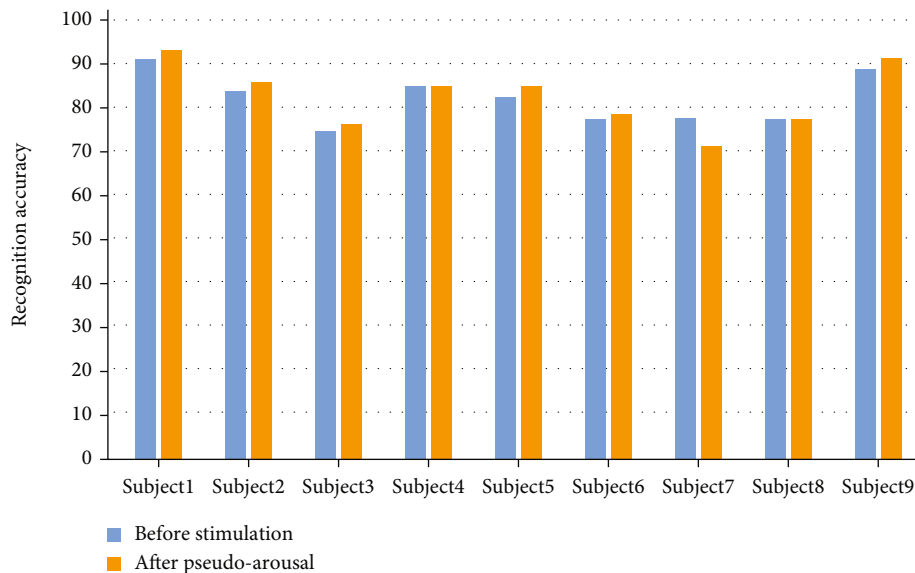


FIGURE 7: Accuracy of mental recovery in rock climbing sports without transcranial electrical stimulation.

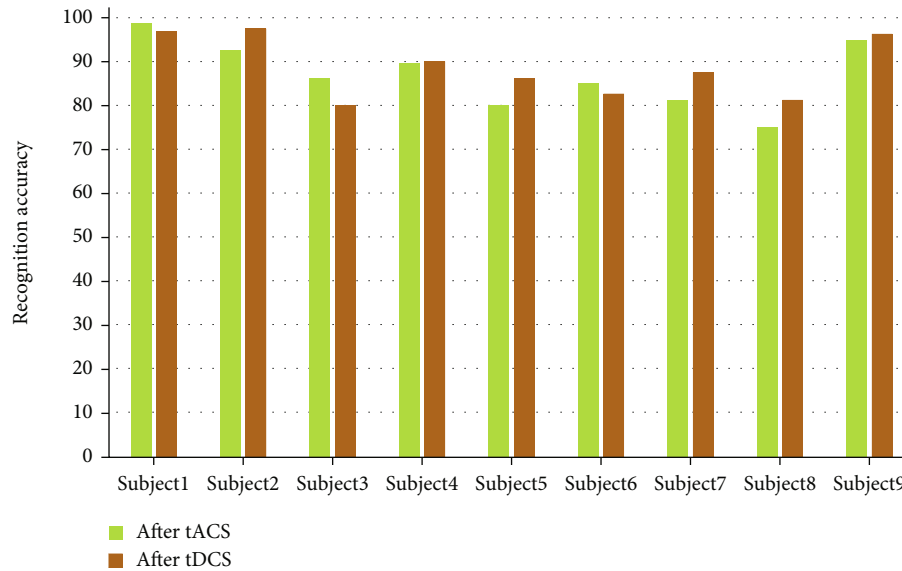


FIGURE 8: Accuracy of psychological recovery in rock climbing with transcranial electrical stimulation.

The accuracy of subjects' psychological recovery during rock climbing exercise is shown in Table 3.

The average accuracy of task classification is shown in Figure 6. A one-way repeated measures ANOVA was performed on the four experimental groups,  $F(3, 24) = 10.436$ ,  $p < 0.05$ , indicating a significant main effect. The following results were obtained from a two-by-two comparison of the four experimental groups: tACS group compared to tDCS compared to the prestimulus group experiment,  $p_1 = 0.08 > 0.05$  and  $p_2 = 0.002 < 0.05$ , respectively, and tACS group compared to tDCS compared to the pseudostimulus group experiment,  $p_3 = 0.193 > 0.05$  and  $p_4 = 0.02 < 0.05$ , respectively. From the classification accuracy of the MI task in the four groups, it can be seen that the accuracy of the subjects after the tDCS inspiration was significantly improved compared to the prestimulation and pseudostimulation groups, and the accuracy of the subjects after the tACS stimulation was better quality compared to the prestimulation and pseudostimulation groups but was not significant. In terms of the overall level of accuracy improvement, tDCS was more effective in improving classification accuracy than the tACS group.

The visualization results of the accuracy of mental recovery in rock climbing without and with transcranial electrical stimulation are shown in Figures 7 and 8, respectively. From the individual subjects' point of view, the accuracy of motor imagery was effectively improved in all nine subjects after tDCS stimulation. For tACS, subjects 5 and 8 showed a decrease in accuracy after tACS compared to the prestimulation period, and subjects 1, 3, and 6 showed a better increase in accuracy after tACS than they did after tDCS. Among all the subjects in the experimental group, the highest accuracy rate was that of subject 1 after tACS inspiration, with an accuracy rate of 98.75%. Among all subjects in the experimental group, the lowest accuracy rate was for subject 8 after tACS stimulation, with an accuracy rate of 75.11%.

## 5. Conclusion

Rock climbing requires climbers to have good psychological quality, and these psychological qualities include the ability to overcome anxiety, fear, and obstacles, but also includes the level of the athlete's will, the degree of concentration, etc. The psychological training of climbers should be targeted according to the specific characteristics of each athlete to improve their psychological mechanisms through training.

The brain controls most of the human learning and movement. Although sports training focuses on physical performance and motor abilities, its fundamental nature still depends on the cerebral cortex to create neural connections that help the nervous system better govern muscles. There is a transcranial electrical stimulation's efficiency in enhancing human motor performance. This paper further analyzes the effectiveness of transcranial electrical stimulation in improving psychomotor balance, psychomotor endurance performance, and psychomotor strength and reducing motor fatigue.

## Data Availability

The datasets used during the current study are available from the corresponding author on reasonable request.

## Conflicts of Interest

The author declares that he has no conflict of interest.

## Acknowledgments

This work was supported by the Scientific Research Plan Project of Tianjin Municipal Education Commission (Project Number: 2018KJ234).

## References

- [1] S. Ding, S. Qu, Y. Xi, and S. Wan, "A long video caption generation algorithm for big video data retrieval," *Future Generation Computer Systems*, vol. 93, pp. 583–595, 2019.
- [2] Z. Gao, Y. Li, and S. Wan, "Exploring deep learning for view-based 3D model retrieval," *ACM transactions on multimedia computing, communications, and applications (TOMM)*, vol. 16, no. 1, pp. 1–21, 2020.
- [3] Z. Gao, H. Xue, and S. Wan, "Multiple discrimination and pairwise CNN for view-based 3D object retrieval," *Neural Networks*, vol. 125, pp. 290–302, 2020.
- [4] S. Ding, S. Qu, Y. Xi, and S. Wan, "Stimulus-driven and concept-driven analysis for image caption generation," *Neuro-computing*, vol. 398, pp. 520–530, 2020.
- [5] J. Pei, Z. Yu, J. Li, M. Jan, and K. Lakshmana, "TKAGFL: a federated communication framework under data heterogeneity," *IEEE Transactions on Network Science and Engineering*, 2022.
- [6] I. Evans, S. Palmisano, and J. Croft, "Effect of ambient lighting on frequency dependence in transcranial electrical stimulation-induced phosphenes," *Scientific Reports*, vol. 12, no. 1, pp. 1–9, 2022.
- [7] S. Sharma and N. Vandana, "Osteopathic uterus manipulation and cranial stimulation influence on anterior uterocervical angle in primary dysmenorrhea: a randomized controlled trial protocol," *Journal of Positive School Psychology*, vol. 6, no. 2, pp. 5451–5455, 2022.
- [8] E. Ghanbari, P. Asgari, and N. Seraj-Khorrami, "Effectiveness of transcranial direct current stimulation on cravings in overweight individuals," *International Journal of Body, Mind and Culture*, vol. 9, no. 2, 2022.
- [9] R. Mohammadi, H. Javanmard, A. Alipour, and H. Zare, "Effects of mindful breath awareness and muscle relaxation and transcranial electrical stimulation techniques on improving blood pressure status in patients with type 2 diabetes," *Explore*, vol. 18, no. 2, pp. 200–204, 2022.
- [10] I. Pozdniakov, "Transcranial electrical stimulation: possibilities and limitations," *The Russian Journal of Cognitive Science*, vol. 5, no. 3, 2018.
- [11] A. Indahlastari, A. Albizu, A. O'Shea et al., "Modeling transcranial electrical stimulation in the aging brain," *Brain Stimulation*, vol. 13, no. 3, pp. 664–674, 2020.
- [12] H. Mehrsafari, S. Rosa, M. Zadeh, and P. Gazerani, "A feasibility study of application and potential effects of a single session transcranial direct current stimulation (tDCS) on competitive anxiety, mood state, salivary levels of cortisol and alpha amylase in elite athletes under a real-world competition," *Physiology & Behavior*, vol. 227, p. 113173, 2020.
- [13] M. Majdi, M. Bakhtiyari, R. Rostami, A. M. Arani, and M. Saberi, "Effect of repetitive transcranial magnetic stimulation on meta-worry and neuropsychological functions among patients with depression," *Iranian Red Crescent Medical Journal*, vol. 23, no. 2, 2021.
- [14] I. Diéguez-Pérez and R. Leirós-Rodríguez, "Effectiveness of different application parameters of neuromuscular electrical stimulation for the treatment of dysphagia after a stroke: a systematic Review," *Journal of Clinical Medicine*, vol. 9, no. 8, p. 2618, 2020.
- [15] H. Ekhtiari, P. Ghobadi-Azbari, A. Thielscher et al., "A checklist for assessing the methodological quality of concurrent tES-fMRI studies (ContES checklist): a consensus study and statement," *Nature Protocols*, vol. 17, no. 3, pp. 596–617, 2022.
- [16] R. Nayak and K. Banik, "Current innovations in peripheral nerve stimulation," *Pain Research and Treatment*, vol. 2018, Article ID 9091216, 5 pages, 2018.
- [17] M. Kamali, M. Kazemiha, B. Keshtkarhesamabadi et al., "Simultaneous transcranial and transcutaneous spinal direct current stimulation to enhance athletic performance outcome in experienced boxers," *Scientific Reports*, vol. 11, no. 1, pp. 1–10, 2021.
- [18] X. Sun, X. Dong, Q. Yuan et al., "Effects of transcranial direct current stimulation on patients with post-stroke fatigue: a study protocol for a double-blind randomized controlled trial," *Trials*, vol. 23, no. 1, pp. 1–10, 2022.
- [19] F. Nieuwhof, I. Toni, G. Buijink, A. F. van Rootselaar, B. P. C. van de Warrenburg, and R. C. Helmich, "Phase-locked transcranial electrical brain stimulation for tremor suppression in dystonic tremor syndromes," *Clinical Neurophysiology*, 2022.
- [20] V. Schöffl, C. Lutter, K. Woollings, and I. Schöffl, "Pediatric and adolescent injury in rock climbing," *Research in Sports Medicine*, vol. 26, supplement 1, pp. 91–113, 2018.
- [21] M. Boggess, R. Harrison, and G. Bishop, "Impacts of rock climbing on cliff vegetation: a methods review and best practices," *Applied Vegetation Science*, vol. 24, no. 2, article e12583, 2021.
- [22] E. A. Rogers, M. E. Carney, S. H. Yeon, T. R. Clites, D. Solav, and H. M. Herr, "An ankle-foot prosthesis for rock climbing augmentation," *IEEE Transactions on Neural Systems and Rehabilitation Engineering*, vol. 29, pp. 41–51, 2021.
- [23] Y. Zheng and H. Ke, "The adoption of scale space hierarchical cluster analysis algorithm in the classification of rock-climbing teaching evaluation system," *Journal of Ambient Intelligence and Humanized Computing*, pp. 1–9, 2020.

## Research Article

# The Effect of PACS in Breast Tumor Diagnosis Based on Numerical Analysis

Guijun Guo and Yi Chen 

Chongqing Red Cross Hospital (People's Hospital of Jiangbei District) Department of Radiology, Chongqing 400020, China

Correspondence should be addressed to Yi Chen; [chenyi19@zqshszhyy.wecom.work](mailto:chenyi19@zqshszhyy.wecom.work)

Received 16 May 2022; Revised 8 June 2022; Accepted 11 June 2022; Published 13 July 2022

Academic Editor: Naeem Jan

Copyright © 2022 Guijun Guo and Yi Chen. This is an open access article distributed under the Creative Commons Attribution License, which permits unrestricted use, distribution, and reproduction in any medium, provided the original work is properly cited.

The incidence and mortality rates are increasing year by year, and the incidence of the disease is gradually becoming younger. The purpose of this study was to investigate the clinical diagnostic value of PACS in breast tumor patients. *Methods.* 20 patients with breast tumor diagnosed by PACS were selected for the study, and the diagnosis was confirmed by pathological puncture or surgery. *Results.* The detection rates of breast tumor by MRI and CT were 94.44% and 96.67%, the sensitivities were 18.82% breast tumor and 96.67%, and the specificities were 53.84% and 54.54%, with no statistically significant difference ( $P > 0.05$ ). There was no statistically significant difference in the detection rate of invasive lobular carcinoma (LDC) and PACS ( $P > 0.05$ ). *Conclusion.* PACS has a greater detection rate for breast tumor and offers some diagnostic usefulness in diagnosing malignant breast tumor. The detection rate of breast tumors can be increased by selecting the most appropriate diagnostic tool for the patient's current circumstances.

## 1. Introduction

The incidence and mortality rates are increasing year by year, and the incidence of the disease is gradually becoming younger [1–3]. In recent years, it has been found that the clinical outcome and prognosis of breast tumor are closely related to different molecular subtypes [4]. In clinical practice, the early identification of molecular subtypes [5].

Breast cancer is a malignant tumor that is genetically heterogeneous. There are some disparities in prognosis due to the varied biological behaviours of different molecular subtypes of breast tumor, which has been a hot issue of research both at home and abroad in recent years [6]. Many studies [7] have shown that the clinicopathological characteristics and prognosis of different molecular subtypes of breast tumor are significantly different. Molecular biology studies have confirmed the role of ER, PR, and HER-2 in the development of breast tumors, making them one of the most important reference indicators for assessing the biological behaviour of cancer cells and developing treatment plans [8]. The molecular pathology of luminal B breast tumor is characterized by ER-positive or/and PR-positive and HER-

2 positive or negative but  $Ki-67 > 14\%$  [9], and endocrine therapy is effective, while molecularly targeted therapy is feasible due to partial positive HER-2 expression. HER-2 overexpression type is effective for molecular targeted therapy but is prone to metastasis, high recurrence rate, and poor prognosis [10].

The triple negative type is resistant to both endocrine and molecular targeted therapy but is very aggressive and prone to metastasis and has the worst prognosis of all molecular subtypes. Early identification of diverse genetic subtypes of breast carcinoma is therefore critical in clinical practice for early and specific clinical treatment and prognosis [11, 12]. Results from prospective screening trials in European populations have shown that DBT as a stand-alone diagnosis or as an adjunct to digital mammography (DM) increases cancer detection rates by approximately 30% compared to DM alone [13]. The aim of this paper is to analyze the value of combining DM and DBT in the diagnosis of molecular subtypes of breast tumor and to provide a basis for more targeted clinical treatment planning [14].

The paper's organization paragraph is as follows: the related work is presented in Section 2. Section 3 analyzes

the materials and methods of the proposed work. Section 4 discusses the experiments and results. Section 5 consists of the discussion; finally, in Section 6, the research work is concluded.

## 2. Related Work

Currently, the diagnosis of molecular subtypes of breast tumor is mainly based on surgical or puncture biopsy immunohistochemistry, which is the gold standard for the detection of ER, PR, HER-2, and Ki-67 expression, and the reliability of its tests also depends on the handling of the tissue, which may sometimes lead to false positives and false negatives [15]. Therefore, predicting the molecular subtype of breast tumor by imaging signs can further improve the reliability of preoperative treatment strategies, which is of great value for the precise treatment of breast tumor and improving the prognosis. With the development of imaging technology in recent years, DBT technology has played an important role in the diagnosis of breast tumor. DBT can clearly show the morphology, margins, and relationship with surrounding tissues of the lesion [16]. A simple lump is the most common and direct manifestation of breast tumor, and the results of this paper show that the majority of breast tumors present as simple lumps, with the main molecular subtype being luminal A. Burrs are a characteristic feature of invasive breast tumor, and their formation may be related to tumor pulling on the normal Cooper ligament or tumor cells infiltrating the surrounding tissue [17]. [18] found that 71% of burr masses in 317 breast tumor patients in DM were luminal A. Luminal A was 10.3 times more likely to show burr-like masses on radiographs than other subtypes, so luminal A correlated with burr-like mass margins. [19] found that burrs on the margins of the mass were 3.77 times more likely to be luminal A than those without burrs, and that burrs did not correlate significantly with luminal B. This means that burrs are strongly associated with luminal A breast tumor. In this paper, the predominance of masses with burrs on the margins in luminal A is generally consistent with the results of the literature, and DBT is of great value in showing the boundaries of masses, especially malignant masses with burrs. DBT was shown to be able to see roughly 77 percent of the boundaries of a displayable mass in [20], whereas DM could only see about 53 percent of the boundaries.

In the study by [18], HER-2 types were most frequently seen as masses with calcification, followed by calcification alone, which is consistent with the results of this paper. [19] reported that breast tumors with HER-2 expression or amplification in molecular subtypes are more aggressive and difficult to treat, and malignant calcifications are more likely to develop in patients with HER-2 expression or amplification breast tumor. However, it has also been shown [20] that the presence of malignant calcification in breast tumor is not only associated with HER-2 expression or amplification but may also be related to other factors such as hormonal expression status. The results of this paper show that calcification is mainly seen in HER-2 expressing types and that DM combined with DBT does not improve

the detection of calcification. However, it has also been reported that due to the abundance of glands in the breast, micro calcifications may be masked and DBT may reduce the interference of overlapping glands and improve the detection of calcifications.

In summary, the results of this paper suggest that DM combined with DBT is predictive of molecular subtypes of breast tumor and that certain imaging signs may be useful for preoperative individualization of treatment strategies and prognostic assessment.

## 3. Materials and Methods

*3.1. General Information.* Patients with breast tumor attending our hospital were selected. A total of 20 patients with 15 lesions were included in the analysis, all were female, aged 33-75 years, with a mean age of  $52.6 \pm 10.3$  years. Inclusion criteria are as follows: (1) patients with breast tumor confirmed by puncture biopsy or surgical pathology and (2) mammography and DBT were performed before biopsy or surgery. Exclusion criteria are as follows: the quality of the images did not meet the diagnostic requirements. This work was approved by our hospital.

*3.2. Inspection Methods.* The Siemens Mammomat Inspiration completely digital mammography equipment is used to perform mammography in the craniocaudal (CC) and mediolateral oblique (MLO) orientations. In each case, a single DM position is obtained, followed by an automatic DBT scan under the same compression conditions, in which the X-ray bulb is rotated over the breast and the breast is scanned from  $-25^\circ$  to  $25^\circ$ , with automatic exposure every  $2^\circ$  of rotation, to obtain multiple low-dose X-ray images at different angles. The glandular thickness of the compressed breast determines the number of layers.

*3.3. Image Analysis.* The films were independently reviewed by two breast diagnosticians with associate or higher titles, and a consensus was reached after consultation. Breast tumor is described and evaluated on digital X-rays using the American College of Radiology's Breast Imaging Reports and Data (BI-RADS) standard, which assesses the different imaging presentations of breast tumor, including masses, calcifications, masses with calcifications, and structural distortions.

## 4. Results

*4.1. General Comparison.* A total of 20 lesions were found in 15 breast tumor patients, of which 13 (35.5%) were luminal A. Radiographs showed 13 (54.3%) simple masses and 7 (23.7%) masses with calcification. The difference in the percentage of different molecular subtypes was statistically significant ( $P < 0.05$ ), as shown in Table 1. Simple masses were the most common among the molecular subtypes, especially luminal A. The percentage of calcification alone was higher in the HER-2 overexpressing type, with 35 cases of calcification alone and 20 cases of HER-2 overexpressing type (57%), a statistically significant difference compared with the other three types ( $P < 0.05$ ). The margins of the

TABLE 1: Comparison of different molecular subtypes of X-ray lesion types.

Mass margin	Luminal type A	Luminal type B	HER-2 overexpression	Three yin types	$\chi^2$	$P$
Simple mass	5	7	9	4	1.247	<0.001
Mass with calcification	6	3	4	3		
Simple calcification	7	2	1	0		
Structural distortion	1	9	2	0		

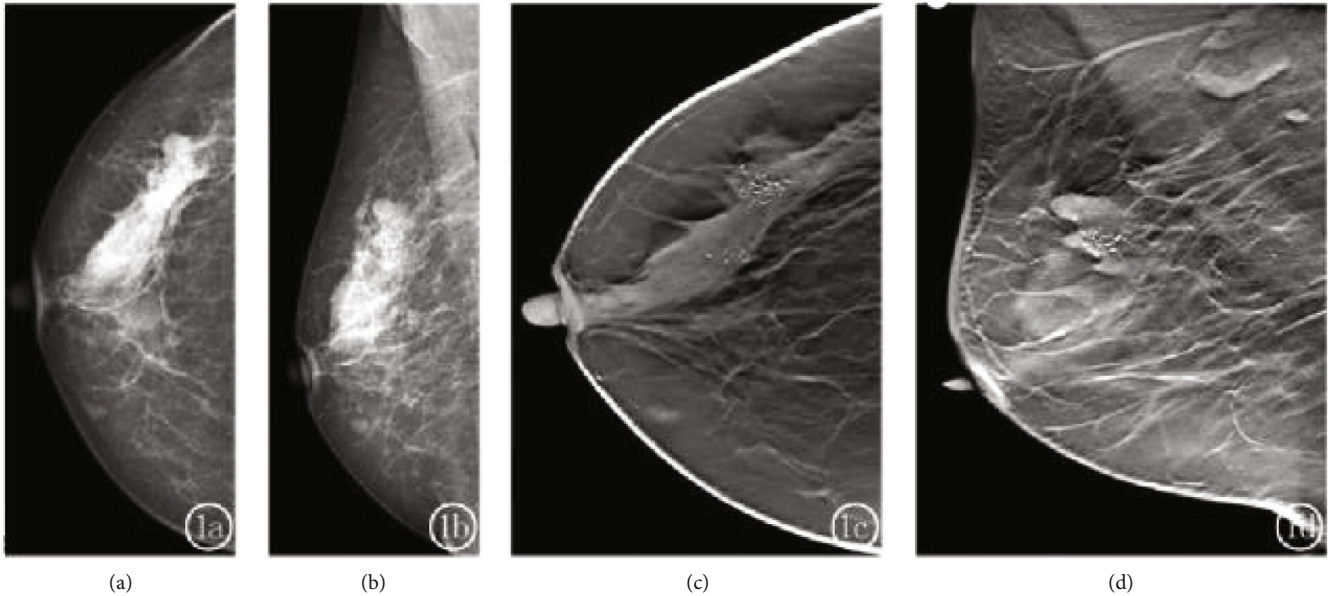


FIGURE 1: Female, 63 years old. Luminal type B invasive ductal carcinoma.

masses were classified as clear, blurred, microlobulated, and burr-like (Figures 1–3), and the difference in the percentage of different molecular subtypes was statistically significant ( $P < 0.05$ ), as shown in Table 2. The difference in the percentage of masses with clear margins was higher in the triple-negative type; the difference in the percentage of masses with indistinct margins was not statistically significant among the subtypes. The difference between PACS combined with DBT was statistically significant ( $P < 0.05$ ), especially for masses with burr-like margins, as shown in Table 3 and Figures 1–3 showing specific examples.

Figures 1(a) and 1(b) are mammograms showing disorganisation of the external superior structures of the right breast with localised nodular changes. Figures 1(c) and 1(d) are mammograms of the breast.

The tomosynthesis shows a well-defined mass with segmental distribution of polymorphic calcifications. Triple negative invasive ductal carcinoma.

Figures 3(a) and 3(b) are mammograms showing a right supratentorial nodule with poorly defined margins. Figures 3(c) and 3(d) are tomosynthesis images of the mammary gland showing small nodules with well-defined margins and burrs. The nodules have well-defined margins with burrs and clearer signs of malignancy.

**4.2. Comparison of Clinical Features.** Benign breast tumors: MRI pattern is round, oval, or lobulated; uniform density; smooth, sharp margins; surrounding tissue shows halo signs,

compression pushing; CT shows irregular or oval shape; well-defined borders; lobulated masses with burrs; tumor is denser than the gland on plain scan, but more clearly outlined on enhanced scan. Breast tumor: MRI is lobulated, nodular, or irregular; uneven density, infiltrative margins, burrs, surrounding invasion, irregular edematous bands, irregular margins; CT shows a confined lamellar lesion in the breast with no obvious mass shadow, higher density than the surrounding gland, unclear borders, significant calcification; infiltrative patients show flattened dense areas throughout the gland, with pinpoint edges of varying length.

The detection rate of breast tumor by MRI and CT was 95.21% and 96.37%, sensitivity was 98.74% and 98.21%, and specificity was 52.34% and 54.23%, with no statistically significant difference ( $P > 0.05$ ); see Tables 4 and 5.

There was no statistically significant difference between CT and MR in the detection rates of LDC and IDC ( $P > 0.05$ ); see Table 6.

## 5. Discussion

PACS is an important adjunct to the early diagnosis of breast tumor in clinical practice, as it can provide multisequence, multiparameter, multidirectional imaging with high soft tissue resolution and can effectively differentiate between benign and malignant tumors. In this study, 90 of the 98 patients with PACS-diagnosed breast tumors were ultimately diagnosed as breast tumors after pathological



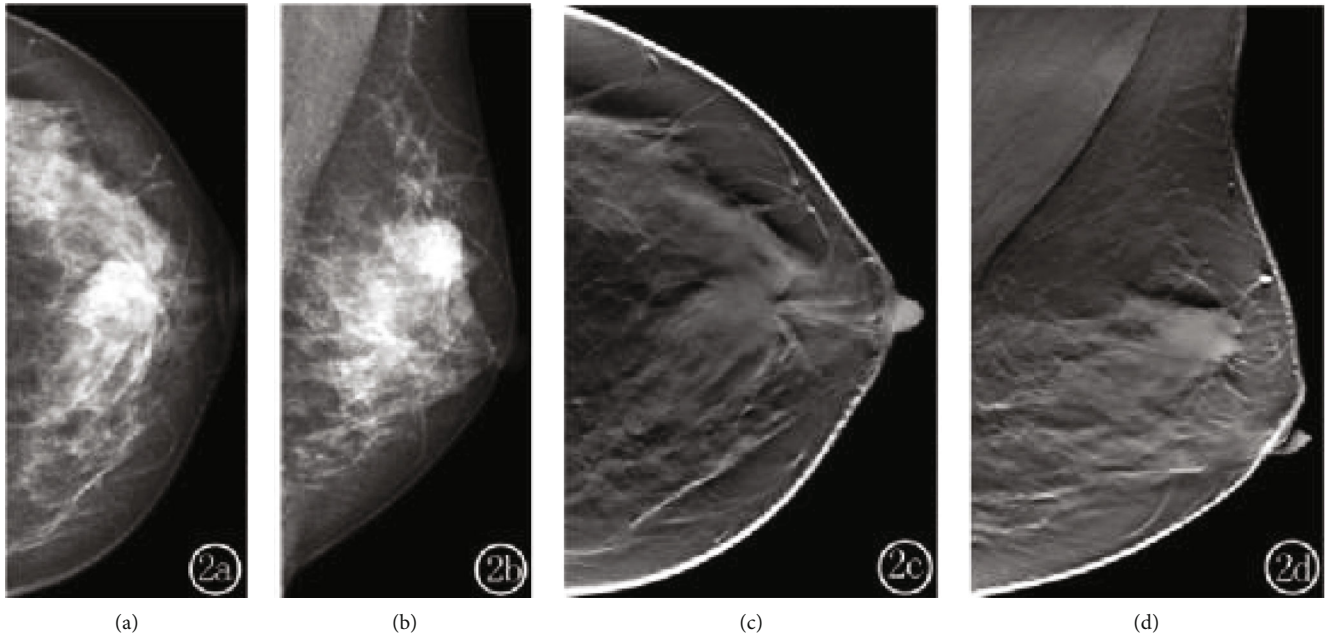


FIGURE 2: (a) and (b) are mammograms. The mammogram shows an upper middle breast mass with poorly defined margins. (c) and (d) are tomosynthesis images of the breast showing radiolucent burrs around the mass with clear signs of malignancy.

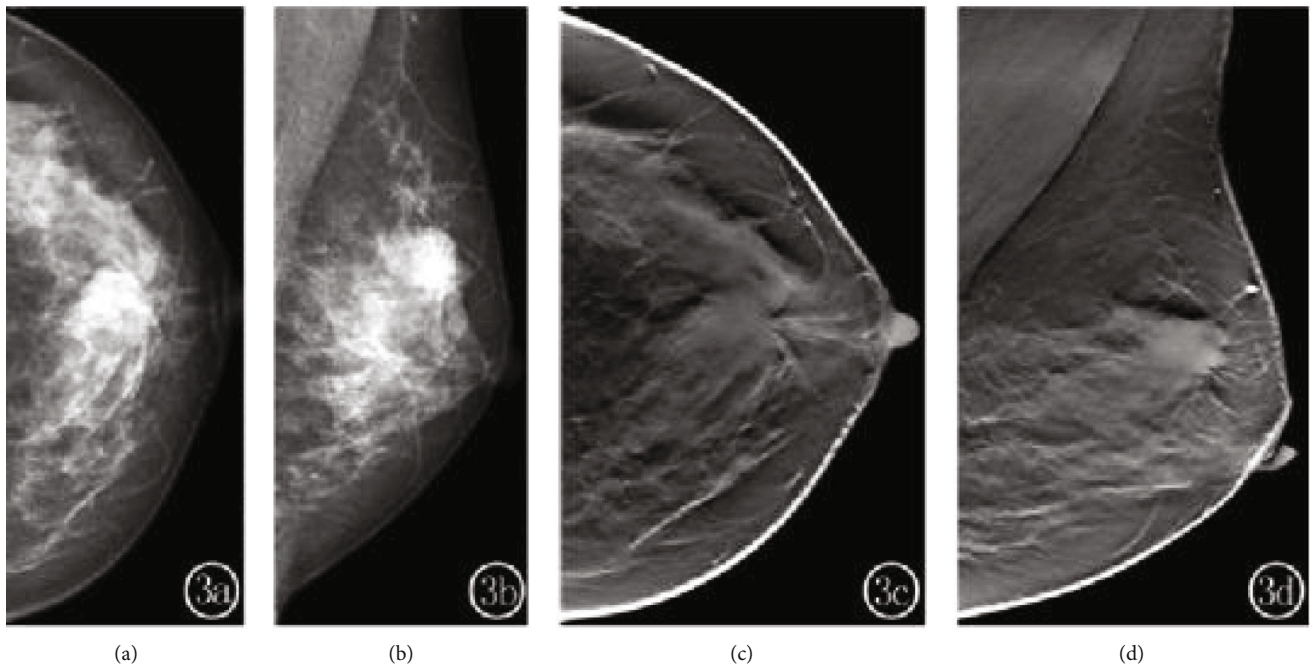


FIGURE 3: Female, 68 years old. Luminal type A invasive ductal carcinoma.

TABLE 2: Comparison of the margins of the masses on X-rays with different molecular typing.

Mass margin	Luminal type A	Luminal type B	HER-2 overexpression	Three yin types	$\chi^2$	$P$
Clear edge	6	7	0	2	5.257	<0.001
Edge blur	1	2	4	9		
Differential leaf	3	1	5	2		
Skin needling	3	2	3	2		

TABLE 3: Comparison of DM and DM combined with DBT image features.

		DM	DM+DBT	$\chi^2$	$P$
Lesion type	Simple mass	6	3	1.124	<0.001
	Mass with calcification	2	5	2.024	0.002
	Simple calcification	1	3	0.270	0.541
	Clear edge	2	2	2.234	0.039
Mass margin	Edge blur	2	5	5.471	<0.001
	Differential leaf	1	3	3.958	0.001
	Prickly	4	1	1.587	0.001

TABLE 4: Comparison of MRI and CT diagnostic findings with pathological procedures (cases).

Surgical pathology	MRI		Total
	Positive	Negative	
Positive	4	6	10
Negative	1	7	8
98 total	5	3	8

Surgical pathology	CT		Total
	Positive	Negative	
Positive	5	5	11
Negative	2	6	8
98 total	7	1	8

TABLE 5: Value of MRI and CT in breast tumor (%).

Inspection method	Detection rate	Sensitivity	Specificity
MRI	95.210	98.740	52.340
CT	96.370	98.210	54.240
$\chi^2$ value	0.101	10123	0.114
$P$ value	0.785	0.814	0.797

TABLE 6: MRI and CT in different types of breast tumor (%).

Inspection method	Detection rate	Pathological type		
		DCLS	LDC	IDC
MRI	92.24	85.74	100	100
CT	95.37	100	95.710	96.210

histological investigation or surgery, while the remaining eight cases were benign tumors.

Most breast tumors appear as irregular low-signal masses at T1W1, while at T2W1, they appear as enhanced signals. The signal characteristics of the tumor are related to the internal composition of the tumor; the more collagen fibres the cells have, the more water they contain and the more pronounced their signal. Mucinous adenocarcinoma shows high signal due to the large amount of mucus and low signal due to calcification and collagen degeneration in the hard interstitium. Because the tumor tissue is not clearly distinguished from the lesion tissue due to congestion, oedema, and surrounding infiltration, oedematous bands

with stellate borders might be seen. In cases of tumor invasion of the Cooper Tropic or skin, local indentation, or thickening of the skin, involvement of the nipple and milk ducts may be observed. The pectoralis major muscle and fascia may be involved when the tumor is more advanced. However, PACS has its limitations and is not good at detecting significant calcification in the lesion.

PACS has an important application in tumor diagnosis because of its high spatial and density resolution. In this study, the tumor density was slightly higher than that of the gland on PACS plain scan, and the PACS values were more variable on enhanced scan, which is consistent with previous studies, due to the abnormal metabolism of breast tumor, the varying degree of development, and the high iodine uptake by tumor cells [21].

The irregular shape of the tumor, with infiltrative growth and raised burr margins, often associated with lobular hyperplasia or dense mammary glands, makes it difficult to distinguish the mass from normal tissue and hyperplastic glands, which is also a major factor in misdiagnosis on CT. In this study, the diagnostic accuracy, sensitivity, and specificity of CT for breast tumor were 96.67%, 96.67%, and 54.54%, with five cases being misdiagnosed, and the misdiagnosis rate was slightly higher than that of PACS. In the remaining two cases, the extent of enhancement may be lower than the actual extent of cancer due to the strong dependence of cancer enhancement on tumor vascularity. In the present study, the detection rate of DCIS was statistically higher on CT than on MRI ( $P < 0.05$ ), while the detection rates of LDC and IDC on PACS were not statistically different ( $P > 0.05$ ).

DCIS is a malignant proliferation of epithelial cells in the ductal system of the breast, which is characterized microscopically by a poorly defined peribasal stromal infiltration.

## 6. Conclusions

However, PACS is not suitable for patients with metal prosthesis, pacemakers, obesity, and claustrophobia, while CT requires a certain amount of X-ray irradiation and may cause radiation damage. Furthermore, certain patients who are allergic to contrast chemicals are not candidates for PACS; thus, the clinical practice can select the most appropriate examination approach based on the patient's current circumstances in order to increase the lesion's detection rate. The accuracy and sensitivity of the test can also be improved by combining the tests.

## Data Availability

The dataset used in this paper are available from the corresponding author upon request.

## Conflicts of Interest

The authors declared that they have no conflicts of interest regarding this work.

## References

- [1] D. Fuster, J. Duch, P. Paredes et al., “Preoperative staging of large primary breast cancer with [18F]fluorodeoxyglucose positron emission tomography/computed tomography compared with conventional imaging procedures,” *Journal of Clinical Oncology*, vol. 26, no. 29, pp. 4746–4751, 2008.
- [2] M. Pennant, Y. Takwoingi, L. Pennant et al., “A systematic review of positron emission tomography (PET) and positron emission tomography/computed tomography (PET/CT) for the diagnosis of breast cancer recurrence,” *Health Technology Assessment*, vol. 14, no. 50, pp. 1–103, 2010.
- [3] J. L. Alberini, F. Lerebours, M. Wartski et al., “18F-fluorodeoxyglucose positron emission tomography/computed tomography (FDG-PET/CT) imaging in the staging and prognosis of inflammatory breast cancer,” *Cancer: Interdisciplinary International Journal of the American Cancer Society*, vol. 115, no. 21, pp. 5038–5047, 2009.
- [4] R. Tang, M. Saksena, S. B. Coopey et al., “Intraoperative micro-computed tomography (micro-CT): a novel method for determination of primary tumour dimensions in breast cancer specimens,” *The British Journal of Radiology*, vol. 89, no. 1058, article 20150581, 2016.
- [5] W. Siggelkow, M. Zimny, A. Faridi, K. Petzold, U. Buell, and W. Rath, “The value of positron emission tomography in the follow-up for breast cancer,” *Anticancer Research*, vol. 23, no. 2C, pp. 1859–1867, 2003.
- [6] K. Michielsen, R. Dresen, R. Vanslebrouck et al., “Diagnostic value of whole body diffusion-weighted MRI compared to computed tomography for pre-operative assessment of patients suspected for ovarian cancer,” *European Journal of Cancer*, vol. 83, pp. 88–98, 2017.
- [7] T. Uematsu, S. Yuen, M. Kasami, and Y. Uchida, “Comparison of magnetic resonance imaging, multidetector row computed tomography, ultrasonography, and mammography for tumor extension of breast tumor,” *Breast tumor research and treatment*, vol. 112, no. 3, pp. 461–474, 2008.
- [8] Z. H. A. N. G. Zhengwan, Z. H. A. N. G. Chunjong, L. I. Hongbing, and X. I. E. Tao, “Multipath transmission selection algorithm based on immune connectivity model,” *Journal of Computer Applications*, vol. 40, no. 12, p. 3571, 2020.
- [9] F. Valdora, N. Houssami, F. Rossi, M. Calabrese, and A. S. Tagliafico, “Rapid review: radiomics and breast tumor,” *Breast tumor research and treatment*, vol. 169, no. 2, pp. 217–229, 2018.
- [10] Z. Yang, Y. Sun, J. Xue et al., “Can positron emission tomography/computed tomography with the dual tracers fluorine-18 fluoroestradiol and fluorodeoxyglucose predict neoadjuvant chemotherapy response of breast tumor?—A pilot study,” *PLoS One*, vol. 8, no. 10, article e78192, 2013.
- [11] G. V. Walker, N. Niikura, W. Yang et al., “Pretreatment staging positron emission tomography/computed tomography in patients with inflammatory breast cancer influences radiation treatment field designs,” *Physics*, vol. 83, no. 5, pp. 1381–1386, 2012.
- [12] Y. L. Gu, S. M. Pan, J. Ren, Z. X. Yang, and G. Q. Jiang, “Role of magnetic resonance imaging in detection of pathologic complete remission in breast tumor patients treated with neoadjuvant chemotherapy: a meta-analysis,” *Clinical breast tumor*, vol. 17, no. 4, pp. 245–255, 2017.
- [13] B. B. Koolen, M. J. T. Vrancken Peeters, T. S. Aukema et al., “18F-FDG PET/CT as a staging procedure in primary stage II and III breast tumor: comparison with conventional imaging techniques,” *Breast Tumor Research and Treatment*, vol. 131, no. 1, pp. 117–126, 2012.
- [14] T. Komori, I. Narabayashi, K. Matsumura et al., “2-[Fluorine-18]-fluoro-2-deoxy-D-glucose positron emission tomography/computed tomography versus whole-body diffusion-weighted MRI for detection of malignant lesions: initial experience,” *Annals of Nuclear Medicine*, vol. 21, no. 4, pp. 209–215, 2007.
- [15] J. Morawitz, N. M. Bruckmann, F. Dietzel et al., “Comparison of nodal staging between CT, MRI, and [18F]-FDG PET/MRI in patients with newly diagnosed breast cancer,” *European Journal of Nuclear Medicine and Molecular Imaging*, vol. 49, no. 3, pp. 992–1001, 2022.
- [16] D. A. Podoloff, R. H. Advani, C. Allred et al., “NCCN task force report: positron emission tomography (PET)/computed tomography (CT) scanning in cancer,” *Journal of the National Comprehensive Cancer Network*, vol. 5, no. S1, p. S-1, 2007.
- [17] N. C. Hodgson and K. Y. Gulenchyn, “Is there a role for positron emission tomography in breast cancer staging?,” *Journal of Clinical Oncology*, vol. 26, no. 5, pp. 712–720, 2008.
- [18] F. Puglisi, A. Follador, A. M. Minisini et al., “Baseline staging tests after a new diagnosis of breast cancer: further evidence of their limited indications,” *Annals of Oncology*, vol. 16, no. 2, pp. 263–266, 2005.
- [19] S. Y. Choi, Y. W. Chang, H. J. Park, H. J. Kim, S. S. Hong, and D. Y. Seo, “Correlation of the apparent diffusion coefficient values on diffusion-weighted imaging with prognostic factors for breast cancer,” *The British Journal of Radiology*, vol. 85, no. 1016, pp. e474–e479, 2012.
- [20] S. Mahner, S. Schirmacher, W. Brenner et al., “Comparison between positron emission tomography using 2-[fluorine-18]fluoro-2-deoxy-D-glucose, conventional imaging and computed tomography for staging of breast cancer,” *Annals of Oncology*, vol. 19, no. 7, pp. 1249–1254, 2008.
- [21] M. Akin, S. Orguc, F. Aras, and A. R. Kandiloglu, “Molecular subtypes of invasive breast cancer: correlation between PET/computed tomography and MRI findings,” *Nuclear Medicine Communications*, vol. 41, no. 8, pp. 810–816, 2020.

## Research Article

# The Potential of miR-370-3p and miR-495-3p Serving as Biomarkers for Sepsis-Associated Acute Kidney Injury

Wenlu Ma , Xiaomei Miao, Fangfang Xia, Chao Ruan, Dan Tao , and Bing Li

Department of Nephrology, SINOPHARM North Hospital, Baotou, 014030 Inner Mongolia, China

Correspondence should be addressed to Wenlu Ma; [mawenlu@gybfyy.org.cn](mailto:mawenlu@gybfyy.org.cn)

Received 25 May 2022; Revised 24 June 2022; Accepted 27 June 2022; Published 11 July 2022

Academic Editor: Naeem Jan

Copyright © 2022 Wenlu Ma et al. This is an open access article distributed under the Creative Commons Attribution License, which permits unrestricted use, distribution, and reproduction in any medium, provided the original work is properly cited.

**Objective.** This study is aimed at evaluating the miR-370-3p and miR-495-3p expression in the urine of patients with sepsis-associated acute kidney injury (SA-AKI) and exploring its diagnosis value in for SA-AKI. **Methods.** 184 sepsis invalids were collected and divided two groups (non-AKI group or AKI group) according to whether they had acute kidney injury. RT-qPCR was utilized to measure miR-370-3p and miR-495-3p expressions. ROC curve was performed to evaluate the diagnostic value of miR-370-3p and miR-495-3p for SA-AKI. Patients diagnosed with SA-AKI were followed up for 28 days to record survival time. The prognostic performance of miR-370-3p and miR-495-3p for SA-AKI was evaluated by survival curves. **Results.** Compared with non-AKI invalids, miR-370-3p and miR-495-3p expressions were obviously lower in the urine of AKI invalids. miR-370-3p and miR-495-3p expressions were markedly negatively correlated with biomarkers of renal injury. Furthermore, the area under the curve (AUC) of miR-370-3p and miR-495-3p for diagnosing sepsis SA-AKI was 0.896 and 0.814, respectively. The higher 28 days-survival rate was observed in patients with high miR-370-3p and miR-495-3p expressions. **Conclusions.** A novel biomarker for the early diagnosis of SA-AKI may be miR-370-3p and miR-495-3p, which was clearly reduced in the urine of SA-AKI patients.

## 1. Introduction

Sepsis is a life-threatening organ dysfunction resulting from a dysregulation of the body's response to infection [1]. The incidence of sepsis and death rates remain high despite advances in anti-infective treatment and basic life support. One of the most common organs injured in sepsis is the kidney, resulting in sepsis-associated acute kidney injury (SA-AKI) [2]. AKI can occur in 30% to 50% of patients with sepsis in the intensive care unit, which is significantly higher than AKI caused by other causes [3]. In a US study including 192,980 patients with sepsis, 22% of patients with sepsis progressed to AKI, with a 38.2% mortality rate [4]. A multicenter prospective study with 1255 patients found that the incidence of AKI in the ICU was 31.6%, with sepsis accounting for 44.9% of patients [5]. Early diagnosis and timely intervention can improve the prognosis of invalids with SA-AKI [2]. KDIGO defines the diagnosis of SA-AKI more finely, relying on increased serum creatinine or decreased urine output, both of which have their limitations. Because

kidney function is highly compensatory, even if one kidney is damaged, the change in serum creatinine level does not fluctuate much. The measurement of urine volume is strongly influenced by the subjectivity of the tester. In order to detect the occurrence of SA-AKI, it is necessary to investigate additional early and efficient biomarkers. However, these markers are currently not used in clinical therapy. Various novel markers may be useful for the early detection of SA-AKI in sepsis.

Noncoding RNAs called miRNAs, which have 21–25 nucleotides, recognise particular target mRNAs and control gene expression. miRNA is crucial in a number of pathogenic processes and can be involved in controlling cell growth, differentiation, metabolism, apoptosis, and other processes [6]. Various miRNAs are involved in the occurrence and development of SA-AKI through different mechanisms such as oxidative stress, inflammatory response, and mitochondrial autophagy [7, 8]. In SA-AKI patient sera, miR-22-3p expression was decreased and was inversely associated with the levels of renal damage markers. miR-22-3p

TABLE 1: Patient clinical information.

Items	Non-AKI ( $n = 49$ )	AKI ( $n = 39$ )	$P$
Age (years)	51.23 $\pm$ 9.76	49.77 $\pm$ 9.960	0.318
Gender (male/female)	56/40	48/40	0.605
BMI (kg/m <sup>2</sup> )	20.87 $\pm$ 2.41	21.08 $\pm$ 2.290	0.543
Hypertension	21	17	0.669
Diabetes mellitus	10	12	0.501
Cardiovascular disease	7	4	0.433
CRP (ng/mL)	65.27 $\pm$ 24.860	83.92 $\pm$ 31.630	0.001
PCT (ng/mL)	3.94 $\pm$ 0.990	3.47 $\pm$ 1.570	0.014
WBC ( $\times 10^9/L$ )	14.86 $\pm$ 6.390	15.77 $\pm$ 8.270	0.403
eGRF (mL/min per 1.73 m <sup>2</sup> )	61.76 $\pm$ 14.540	49.91 $\pm$ 18.570	<0.001
Scr ( $\mu M$ )	94.39 $\pm$ 27.020	151.79 $\pm$ 28.050	<0.001
Cys-C (mg/L)	0.58 $\pm$ 0.090	2.10 $\pm$ 0.460	<0.001
NGAL (ng/mL)	53.36 $\pm$ 15.110	80.38 $\pm$ 17.980	<0.001
KIM-1 (ng/mL)	4.55 $\pm$ 0.460	21.81 $\pm$ 5.550	<0.001

TABLE 2: Primer sequences.

Items	Primer sequences (5'-3')
miR-370-3p	F:GCCTGCTGGGGTGGAACTGGT R:CTCAACTGGTGTCTGGGA
miR-495-3p	F: AAACAAACATGGTGCA R: GAGCAGGCTGGAGAA
$\beta$ -Actin	F:GCACCACACCTTCTACAATG R:TGCTTGCTGATCCACATCTG

was also useful for diagnosing SA-AKI in patients [9]. There are, however, not many research on the connection between miRNAs and SA-AKI. There are, however, not many miRNAs currently available for the diagnosis of AKI, and there have not been many investigations on the connection between miRNA and SA-AKI. Therefore, more investigation into novel biomarkers for SA-AKI diagnosis and prognosis is required. This study mainly investigated the value of miR-370-3p and miR-495-3p in the noninvasive diagnosis of SA-AKI.

The remaining of this manuscript was arranged as the following: part 2 introduced the basic theory of materials and methods. The third part verified the proposed method through experiments and analyzes the experimental results. Part 4 was conclusion.

## 2. Material and Methods

In this study, 184 sepsis patients were divided two group according to whether they had acute kidney injury, including non-AKI and AKI group. The criteria for defining AKI were as described by Zhang et al. [9]. The patients were excluded in case they (1) aged  $\geq 18$  years without other major comorbidities and (2) consent to include their own clinical information in this study. Exclusion criteria: (1)

patients have other causes of acute kidney injury, including obstruction of the urinary tract system, glomerular necrosis, glomerulonephritis, and nephrovascular disease; (2) myolysis and amputation; and (3) kidney transplantation. The fundamental statistics and clinical details of the patients were summarized in Table 1. On the first day of admission, clinical records for patients are questioned. The experimental project was disclosed to the patients.

**2.1. Sample Collection.** Urine was collected from non-AKI and AKI patients. The specimen was centrifuged at 3000 r/min to obtain the supernatant. Scr and Cys-C concentrations were detected by AU5800 machine (Beckman, USA). NGAL and KIM-1 concentrations were measured via ELISA kits (Absin, China).

**2.2. RT-qPCR.** Total RNA was extracted by Trizol (Absin, China). The RNA of qualified purity was reverse transcribed to cDNA. The real-time PCR reaction was performed using a 7500 PCR instrument (ABI, USA) and SYBR Green kit (Takara, Japan). The primers were designed and synthesized by Tingske Biotech (Table 2).

**2.3. Follow-Up.** Patients diagnosed with SA-AKI need to be followed up for 28 days to record survival and time to death for use in survival curve plotting.

**2.4. Statistical Analysis.** The SPSS 23.0 software was utilized.  $T$ -test or Chi square test was utilized to compare difference between groups.  $P < 0.05$  meant significantly difference. ROC curve was established for measuring the diagnostic value of miR-370-3p and miR-495-3p for SA-AKI. Prediction of SA-AKI prognosis by miR-370-3p and miR-495-3p expression levels was constructed by survival curves.

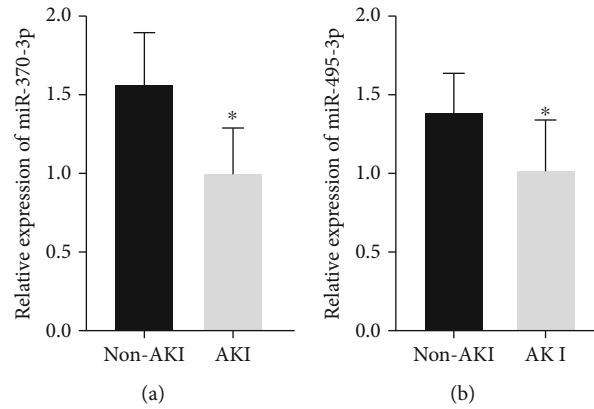


FIGURE 1: Urinary miR-370-3p (a) and miR-495-3p (b) expressions were measured by RT-qPCR for sepsis AKI.

TABLE 3: Correlation between miR-370-3p, miR-495-3p, and SA-AKI biomarkers.

Items	miR-370-3p		miR-495-3p	
	<i>r</i> value	<i>P</i> value	<i>r</i> value	<i>P</i> value
Scr ( $\mu$ M)	-0.661	0.001	-0.564	0.001
Cys-C (mg/L)	-0.615	0.001	-0.478	0.001
NGAL (ng/mL)	-0.714	0.001	-0.596	0.001
KIM-1 (ng/mL)	-0.623	0.001	-0.514	0.001

### 3. Results

**3.1. Patient Clinical Information.** Table 1 displayed the clinical data of the patients. CRP, Scr, Cys-C, NGAL, and KIM-1 were clearly higher in the AKI group compared to non-AKI patients. By comparison with non-AKI patients, PCT was markedly increased in AKI group. There was no difference between the two groups at other indicators.

miR-370-3p and miR-495-3p were lower expressed in SA-AKI patients.

As shown in Figure 1(a), miR-370-3p expression was markedly declined in AKI invalids. In addition, miR-495-3p expression was also markedly declined in sepsis AKI invalids (Figure 1(b)).

**3.2. Relationship between miR-370-3p, miR-495-3p Expression, and Biomarkers of SA-AKI.** Urinary miR-370-3p was significantly correlated negatively with Scr, Cys-C, NGAL, and KIM-1, according to Pearson correlation analysis (Table 3). Similar to the above results, miR-495-3p also showed a significant negative correlation with Scr, Cys-C, NGAL, and KIM-1 (Table 3).

**3.3. Diagnostic Performance of miR-370-3p and miR-495-3p for SA-AKI.** ROC curve was established for measuring the diagnostic value of miR-370-3p and miR-495-3p for SA-AKI. The area under the curve (AUC) of miR-370-3p for diagnosing sepsis AKI was 0.896 (Figure 2(a)). The AUC of miR-495-3p for diagnosing SA-AKI was 0.814 (Figure 2(b)).

**3.4. Prediction of SA-AKI Prognosis by miR-370-3p and miR-495-3p Expression Levels.** Survival curves were constructed

to evaluate association between miR-370-3p, miR-495-3p, and patients' 28-day survival. The 28-day survival rate of invalids with high expression of miR-370-3p was obviously higher in contrast to those with lower miR-370-3p expression (Figure 3(a)). Patients with high miR-495-3p expression had significantly higher 28 days-survival rates in contrast to those with low miR-495-3p expression (Figure 3(b)).

### 4. Discussion

A frequent and serious illness known as AKI occurs when kidney function rapidly declines for a variety of reasons. It is a typical critical sickness affecting a number of organs and systems. Acute onset and a significant inflammatory response are the hallmarks of SA-AKI [2]. Patients with SA-AKI have markedly elevated serum creatinine, abnormal liver function, coagulation abnormalities, increased inflammatory markers, hyperuricemia, hyperglycemia, and hyperlactatemia [10], and most patients require hemodynamic support and mechanical ventilation [11]. SA-AKI has a poor clinical prognosis, and the in-hospital mortality rate was approximately 30-50% [12].

The primary diagnostic tool for SA-AKI and an indicator of its severity is currently serum creatinine [13]. However, there are several drawbacks to using serum creatinine as an early SA-AKI diagnosis. First, exogenous creatinine and endogenous creatinine make up creatinine. Consumption of meat-based foods has a direct impact on exogenous creatinine, but endogenous creatinine is influenced by factors such as age, gender, race, exercise, weight, muscle content, and the body's inflammatory response [14]. Second, the kidney is powerful in compensation, and it can maintain the normal value of serum creatinine level even when the unilateral kidney function is functioning [3], and the serum creatinine can be maintained in the normal range in early and mild kidney injury [13]. In addition, urine volume is insensitive to the diagnosis of acute kidney injury and cannot be easily measured outside of the monitoring room. The measurement of urine volume is susceptible to subjective influence. The measurement of urine volume is subjective. Therefore, there is a clinical need for more effective early diagnosis of SA-AKI. Khawaja et al. measured early plasma NGAL concentration in 48 septic patients and found

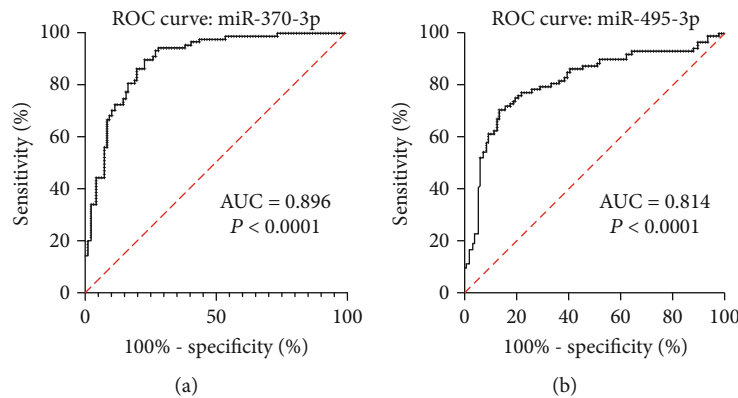


FIGURE 2: ROC curve analysis of urinary miR-370-3p (a) and miR-495-3p (b) for SA-AKI.

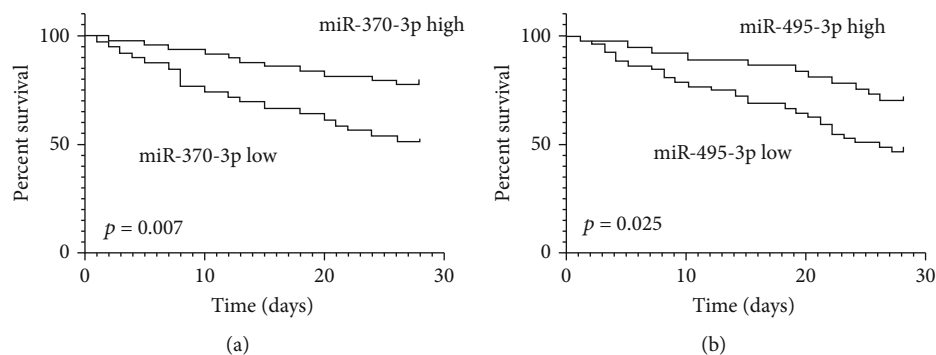


FIGURE 3: Kaplan-Meier survival analysis of 28 d survival rate according to urinary miR-370-3p (a) and miR-495-3p (b) levels.

that early NGAL concentration could effectively predict AKI, with AUC of 0.82, sensitivity of 70.8%, and specificity of 90.9%, and NGAL concentration was positively correlated with ICU stay [15].

miRNAs are evolutionarily highly conserved and can regulate gene expression, participating in a variety of pathological and physiological processes [16]. Urine specimens are readily available, and a variety of miRNAs can be detected in urine [17]. miRNAs may reflect the extent of renal tissue damage [18, 19]. The mechanism of miRNA action in SA-AKI has not been elucidated and may contribute to the development of SA-AKI in sepsis patients through ischemia-reperfusion injury, inflammatory mediator release, oxidative stress, and mitochondrial damage. miR-370-3p was lower expressed in SA-AKI patients, and miR-370-3p overexpression could inhibit SA-AKI via targeting MYD88 [20]. miR-495-3p was reported to be regulated by SNHG14 to alleviate SA-AKI and lower expressed in SA-AKI patients [21]. In the current investigation, sepsis AKI patients' urine miR-370-3p and miR-495-3p expression levels were significantly lower than those of non-AKI patients. These findings showed that miR-370-3p and miR-495-3p may serve as novel biomarkers for SA-AKI.

Next, we further explored the association of miR-370-3p and miR-495-3p with known AKI biomarkers. Pearson correlation analysis demonstrated miR-370-3p and miR-495-3p were markedly negatively correlated with AKI biomarkers. In addition, ROC curve was established for measuring diag-

nostic value of miR-370-3p and miR-495-3p for SA-AKI. The AUC of miR-370-3p and miR-495-3p for diagnosing sepsis SA-AKI was 0.896 and 0.814, respectively. These results demonstrated miR-370-3p and miR-495-3p were useful for the diagnosis of SA-AKI. The 28-day survival rate of invalids with high expression of miR-370-3p was obviously higher in contrast to those with lower miR-370-3p expression. Patients with high miR-495-3p expression had significantly higher 28 days-survival rates in contrast to those with low miR-495-3p expression.

In conclusion, the current investigation showed that miR-370-3p and miR-495-3p in the urine were involved in the diagnosis of SA-AKI, and the procedure is quick, easy, safe, and noninvasive. However, there are few studies on miR-370-3p and miR-495-3p and AKI, especially SA-AKI. The role of miR-370-3p and miR-495-3p in SA-AKI needs to be confirmed by further studies.

## Data Availability

Data to support the findings of this study is available on reasonable request from the corresponding author.

## Conflicts of Interest

The authors have no conflicts of interest to declare.

## References

- [1] J. Rello, F. Valenzuela-Sánchez, M. Ruiz-Rodríguez, and S. Moyano, “Sepsis: a review of advances in management,” *Advances in Therapy*, vol. 34, no. 11, pp. 2393–2411, 2017.
- [2] J. T. Poston and J. L. Koyner, “Sepsis associated acute kidney injury,” *BMJ*, vol. 364, article k4891, 2019.
- [3] M. G. Mercado, D. K. Smith, and E. L. Guard, “Acute kidney injury: diagnosis and management,” *American Family Physician*, vol. 100, no. 11, pp. 687–694, 2019.
- [4] I. Keir and J. A. Kellum, “Acute kidney injury in severe sepsis: pathophysiology, diagnosis, and treatment recommendations,” *Journal of Veterinary Emergency and Critical Care (San Antonio, Tex.)*, vol. 25, no. 2, pp. 200–209, 2015.
- [5] Y. J. Jiang, X. M. Xi, H. M. Jia et al., “Risk factors, clinical features and outcome of new-onset acute kidney injury among critically ill patients: a database analysis based on prospective cohort study,” *BMC Nephrology*, vol. 22, no. 1, p. 289, 2021.
- [6] Z. Liu, D. Yang, J. Gao et al., “Discovery and validation of miR-452 as an effective biomarker for acute kidney injury in sepsis,” *Theranostics*, vol. 10, no. 26, pp. 11963–11975, 2020.
- [7] Z. Sang, S. Dong, P. Zhang, and Y. Wei, “miR-214 ameliorates sepsis-induced acute kidney injury via PTEN/AKT/mTOR-regulated autophagy,” *Molecular Medicine Reports*, vol. 24, no. 4, 2021.
- [8] X. Li, L. Yao, X. Zeng et al., “miR-30c-5p alleviated pyroptosis during sepsis-induced acute kidney injury via targeting TXNIP,” *Inflammation*, vol. 44, no. 1, pp. 217–228, 2021.
- [9] H. Zhang, L. Che, Y. Wang et al., “Deregulated microRNA-22-3p in patients with sepsis-induced acute kidney injury serves as a new biomarker to predict disease occurrence and 28-day survival outcomes,” *International Urology and Nephrology*, vol. 53, no. 10, pp. 2107–2116, 2021.
- [10] S. Ma, R. G. Evans, N. Iguchi et al., “Sepsis-induced acute kidney injury: a disease of the microcirculation,” *Microcirculation*, vol. 26, no. 2, article e12483, 2019.
- [11] J. A. Kellum, X. Wen, M. P. de Caestecker, and N. A. Hukriede, “Sepsis-associated acute kidney injury: a problem deserving of new solutions,” *Nephron*, vol. 143, no. 3, pp. 174–178, 2019.
- [12] K. Yoshimoto, Y. Komaru, M. Iwagami, and K. Doi, “Acute kidney injury in sepsis: evidence from Asia,” *Seminars in Nephrology*, vol. 40, no. 5, pp. 489–497, 2020.
- [13] S. Peerapornratana, C. L. Manrique-Caballero, H. Gómez, and J. A. Kellum, “Acute kidney injury from sepsis: current concepts, epidemiology, pathophysiology, prevention and treatment,” *Kidney International*, vol. 96, no. 5, pp. 1083–1099, 2019.
- [14] T. Guinovart, D. Hernández-Alonso, L. Adriaenssens et al., “Recognition and sensing of creatinine,” *Angewandte Chemie (International Ed. in English)*, vol. 55, no. 7, pp. 2435–2440, 2016.
- [15] S. Khawaja, L. Jafri, I. Siddiqui, M. Hashmi, and F. Ghani, “The utility of neutrophil gelatinase-associated lipocalin (NGAL) as a marker of acute kidney injury (AKI) in critically ill patients,” *Biomarker Research*, vol. 7, no. 1, p. 4, 2019.
- [16] J. R. Iacona and C. S. Lutz, “miR-146a-5p: expression, regulation, and functions in cancer,” *Wiley Interdiscip Rev RNA*, vol. 10, no. 4, article e1533, 2019.
- [17] L. Wei, C. Cao, X. Ma, X. Wang, M. Wang, and P. Zhang, “Elevated serum and urine MiR-429 contributes to the progression of gestational diabetes mellitus,” *Clinical Laboratory*, vol. 67, 2021.
- [18] J. Y. Cao, B. Wang, T. T. Tang et al., “Exosomal miR-125b-5p deriving from mesenchymal stem cells promotes tubular repair by suppression of p53 in ischemic acute kidney injury,” *Theranostics*, vol. 11, no. 11, pp. 5248–5266, 2021.
- [19] N. Putkonen, A. Laiho, D. Ethell et al., “Urine microRNA profiling displays miR-125a dysregulation in children with fragile X syndrome,” *Cell*, vol. 9, no. 2, p. 289, 2020.
- [20] Y. Zhou, M. Qing, and M. Xu, “Circ-BNIP3L knockdown alleviates LPS-induced renal tubular epithelial cell injury during sepsis-associated acute kidney injury by miR-370-3p/MYD88 axis,” *Journal of Bioenergetics and Biomembranes*, vol. 53, no. 6, pp. 665–677, 2021.
- [21] N. Yang, H. Wang, L. Zhang et al., “Long non-coding RNA SNHG14 aggravates LPS-induced acute kidney injury through regulating miR-495-3p/HIPK1,” *Acta Biochimica et Biophysica Sinica Shanghai*, vol. 53, no. 6, pp. 719–728, 2021.



## Research Article

# Effect of Algoplaque Hydrocolloid Dressing Combined with Nanosilver Antibacterial Gel under Predictive Nursing in the Treatment of Medical Device-Related Pressure Injury

Chunxiu Li,<sup>1</sup> Hongmei Chen,<sup>2</sup> and Guanghui You <sup>3</sup>

<sup>1</sup>Department of Neurosurgery, Chongqing Qijiang District People's Hospital, Chongqing 401420, China

<sup>2</sup>Department of Endocrinology, Chongqing Qijiang District People's Hospital, Chongqing 401420, China

<sup>3</sup>Department of Gastroenterology, Chongqing Qijiang District People's Hospital, Chongqing 401420, China

Correspondence should be addressed to Guanghui You; 763540945@qq.com

Received 25 April 2022; Revised 27 May 2022; Accepted 30 May 2022; Published 11 July 2022

Academic Editor: Naeem Jan

Copyright © 2022 Chunxiu Li et al. This is an open access article distributed under the Creative Commons Attribution License, which permits unrestricted use, distribution, and reproduction in any medium, provided the original work is properly cited.

It was aimed at the clinical value of predictive nursing and Algoplaque hydrocolloid dressing (AHD) combined with nanosilver antibacterial gel in treating medical device-related pressure injury (MDRPI). 100 patients, who underwent surgery in Chongqing Qijiang District People's Hospital from February 2019 to February 2020, were selected as the research objects and were randomly divided into the experimental group (50 cases) and the control group (50 cases). For the characterization test, a nanosilver antibacterial gel was created first. Patients in both groups received predictive nursing, but those in the experimental group received AHD and nanosilver antibacterial gel, and those in the control group received gauzes. MDRPI incidence, pressed skin injury severity, comfort level, clothing changes, nursing satisfaction, and other factors were all compared. The particle size of the nanosilver gel was 45-85 nm, with a relatively homogeneous distribution with the medium size, according to the findings. The incidence of MDRPI in the experimental group was lower than that in the control group significantly (6% vs. 30%,  $P < 0.05$ ). The degree of injury of pressured skin in the experimental group was milder than that in the control group ( $P < 0.05$ ), the degree of comfort and nursing satisfaction was higher in the experimental group than in the control group ( $P < 0.05$ ), and dressing change count was lower than that in the control group ( $P < 0.05$ ). In the treatment of MDRPI, predictive nursing and AHD using nanosilver antibacterial gel showed high clinical application value.

## 1. Introduction

Various complex medical technologies emerge and are widely used in clinical practice as medical technology continues to develop and progress. Medical device-related pressure injury (MDRPI) occurs when modern medical equipment are employed in clinical settings [1, 2]. With the deepening researches, the relevant theories of MDRPI are accepted and recognized clinically. Clinical studies have shown that the appearance of skin injury caused by medical devices is generally the same as that of medical devices, and the most common injury sites include the head, face, neck, and limbs [3]. In recent years, most of the reports on MDRPI are reported in the intensive care unit (ICU), of which 1/3 of the skin injury is caused by medical devices. MDRPI often

results in adverse complications such as infection, which influence the prognosis and postrecovery greatly [4–6]. At present, domestic researches mostly focus on MDRPI caused by a certain type and a certain factor, suggesting a lack of prospective and multicenter research [7].

Predictive nursing is guided by holistic nursing, with prevention first and then treatment. In its clinical application, it has shown significant curative effect in preventing and controlling complications [8, 9]. Some scholars have applied the predictive nursing to cardiopulmonary bypass surgery, which turns passive work into active work, shortening the operation time and reducing the incidence of complications effectively [10]. In addition, predictive nursing is carried out for preventive care on the grounds of the patient's condition, so that human resources are optimally

prepared before the condition changes, thus highly improving the quality of nursing [11]. All in all, predictive nursing is an effective way to promote the effectiveness, standardization, and refinement of nursing. It can not only greatly prevent nursing defects but also improve the preventability and controllability of nursing, having a high clinical application value [12].

Relevant clinical studies have shown that the incidence and severity of MDRPI in patients using Algoplaque hydrocolloid dressing (AHD) are significantly higher than those in control patients [13]. That may be because the AHD is a semipermeable hydrogel dressing that can adhere to the skin surface, absorb exudate 30 times of its own mass, and swell to form a mild and moist gel filling layer. As a result, the direct stimulation of moisture to the skin is decreased, and the stressed skin is protected. On the other hand, it can successfully increase blood circulation in the pressurized skin and relieve congestion in the patient's pressurized area. AHD has a certain thickness with a smooth and soft surface, which can effectively buffer the pressure and other damage to the skin, so as to prevent and reduce the pressure injury of the patient's skin [14]. In clinical treatment, the long-term use of medical devices will cause patients to experience adverse symptoms such as skin ulceration and itching. AHD can be gently and safely stucked on the skin, protecting the local skin and relieving the discomfort of the patient effectively [15]. With the advancement of science and the rapid development of nanotechnology over time, nanosilver has emerged and has shown more advantages apart from the effect of silver itself [16]. Nanosilver gel is a gel made of nanosilver, and it is mostly used in wounds. The unique physical features of gel will allow nanosilver to work continuously and efficiently limit bacterial growth and proliferation. It can also cause bacterial proteins to denaturize, which aids in sterilisation [17].

Under the predictive nursing, the effect of AHD combined with nanosilver antibacterial gel was discussed in the treatment of MDRPI. This work was aimed at laying a foundation for promoting the compliance of patients and improving the treatment outcomes.

The paper's organization paragraph is as follows: the materials and methods is presented in section 2. Section 3 discusses the experiments and results. Section 4 consists of the conclusion section of the proposed work. Finally, in Section 5, the research work is concluded.

## 2. Materials and Methods

**2.1. Research Objects.** The research subjects were 100 patients who underwent surgery at Chongqing Qijiang District People's Hospital between February 2019 and February 2020. There were 55 male patients and 45 female patients, with an average age of  $42.3 \pm 10.3$  years old. The patients were randomly divided into the experimental group with 50 cases and the control group with 50 cases as well. Inclusion criteria were as follows. The age of patients should be  $\geq 12$  years old. There was no pressure ulcer or skin injury or scar tissue prior to surgery or the use of medical equipment. The surgery was the first surgery during hospitaliza-

tion, and the estimated operation time was  $\geq 2$  hours. The criteria for exclusion are stated below. During the procedure, the patients were given either local infiltration an aesthetic or nerve block anesthesia. The patients had severe skin disorders or conditions that interfered with skin observation. If the surgery was an emergency surgery, the patient was also excluded. All the patients signed informed consents, and all studies here conformed to the medical ethics.

**2.2. Preparation Method of Nanosilver Mixture Solution.** 400 mg of silver nitrate was added to 1 L of distilled water or ultrapure water, and the mixture was stirred well. Under magnetic stirring (1600 r/min), 300 mg of povidone K-30 or 300 mg of poloxamer 407 was added. After stirring evenly, 300 mg of trisodium citrate was also added. Then, the ultraviolet lamp was turned on. With the reaction under the irradiation of the ultraviolet lamp and magnetic stirring for 4-5 hours, the nanosilver mixture could be obtained. The obtained liquid was centrifuged, and then, the supernatant was discarded. The remains were diluted with distilled water or ultrapure water and then were centrifuged again, and these steps were repeated twice. Finally, the nanosilver precipitate obtained after centrifugation was dried, and an appropriate amount of nanosilver solution was weighed to prepare a 240  $\mu\text{g}/\text{mL}$  nanosilver stock solution.

Characterization test of the nanosilver solution was performed. In the scanning electron microscope (SEM) experiment, 1-2 drops of sample solution were added dropwise to a clean glass slide and dried in a constant temperature oven at  $50^\circ\text{C}$ , and then, the surface was gold-plated. The microstructure of the nanosilver solution was observed on an ultra-high-resolution field emission SEM. The main parameters selected were 10 KV high pressure, high vacuum mode, and secondary electron mode. In X-ray powder diffraction experiment, the nanosilver powder obtained by drying was used, the scanning angle was  $10^\circ\text{-}90^\circ$ , and the Cu target was taken as the X-ray generating device.

**2.3. Preparation of Nanosilver Antibacterial Gel.** 15 mL of distilled water was added into a 50 mL beaker and 200  $\mu\text{L}$  of glacial acetic acid, and then, 2,000  $\mu\text{L}$  of the prepared nanosilver solution was added to the distilled water in turn. 600  $\mu\text{L}$  of glycerol was also added and stirred until it was completely dissolved. After that, 0.42 g of chitosan was added, stirred evenly, and left overnight. The mixture was fully swelled, and the air bubbles were removed. Finally, 2 mL of sodium bicarbonate solution with a concentration of 1 mol/L was added dropwise into the beaker. Distilled water was added dropwise after stirring evenly to prepare a 20 mL of sol system, which was allowed to stand for a few days to form a gel.

Characterization of the nanosilver gel was also performed. An appropriate amount of the prepared chitosan wet gel was put into a desiccator for drying at room temperature. When the weight of the gel no longer changed, a small amount of dry gel sample was taken out and pulled apart; then, the surface was gold-plated. The microstructure of the gel section was observed on the ultra-high-resolution field emission SEM. The selected parameters included the

TABLE 1: Evaluation criteria for the degree of injury in the pressured area.

Degree of injury	Symptom description
Mild	The skin of the pressure area was sore, slightly painful, and without induration; the symptoms were relieved after the pressure was relieved.
Moderate	Redness, swelling, and induration occurred in the skin at the pressured area, with obvious pain after touching and no relief after the pressure was relieved.
Severe	Skin damage and ulceration appeared in the area of pressure.

TABLE 2: Evaluation criteria for comfort level of patients.

Comfort levels	Symptom description
Comfortable	No discomfort in the pressured area
Less comfortable	Slight discomfort in the pressured area
General	Pain after pressure
Uncomfortable	Severe pressured pain

high pressure of 10 KV, high vacuum mode, and secondary electron mode, and the magnification was 5000 times.

*2.4. Nursing Methods.* Patients in both groups were treated with the predictive nursing, as the specific methods were described as follows.

To begin, the patients are seen and assessed before to surgery. The circulating or scrub nurse did a preoperative visit and assessment the day before the surgery after receiving news of the surgery. The medical records of the patient, as well as numerous examination indicators, were thoroughly checked, and anomalous indicators were noted. The nurse learned about the patient's medical history, described the intraoperative precautions, and assessed the patient's skin condition. Second, there are critical point shifts. The circulating or scrub nurse fed the collected abnormal conditions back to the on-duty nurses timely, and the key points could be highlighted at the morning shift. Thus, the medical staff would pay more attention to the abnormal conditions. Third is the reevaluation on the day of the surgery. On the day of the surgery, reevaluation was carried out according to the results of the skin evaluation of the preoperative visit, especially the abnormal parts needed to be paid more attention. Fourthly, the operation time was estimated according to the anesthesia method, surgical position, surgical method, and intraoperative external force. Then, a comprehensive evaluation was made, and corresponding surgical measures were taken. Fifthly, the corresponding nurse mode should be adopted depending on the patient's own diseases. For example, the blood circulation of the peripheral end of the foot of the diabetic patient was not good. It is also important to keep the foot warm while doing postural nursing. Sixth, to avoid alterations in the microenvironment around the skin, the surrounding skin was kept clean and dry. Seventhly, the use of medical devices should be reduced, and the prevention should be strengthened during surgery. With the surgical plan for the patient, the number of medical equipment used should be reduced as much as possible without affecting the

TABLE 3: General data of patients in the two groups.

Items	Experimental group (50 cases)	Control group (50 cases)	<i>P</i>
Gender			
Male	26	31	0.51
Female	24	19	0.48
Age			
Departments	33 ± 11.3	36 ± 9.96	1.10
Otorhinolaryngology	05	06	1.20
Thoracic surgery	07	09	1.11
Neurosurgery	11	08	0.88
Obstetrics	04	06	0.93
Orthopedics	23	21	0.64
Injury areas			
Face	08	11	1.13
Nose	09	10	1.06
Ears	12	11	1.33
Chests	16	14	0.97
Upper arms	03	04	0.68
Knees	02	01	0.72
Surgical positions			
Supine position	19	17	0.81
Prone position	17	18	0.92
Lateral position	14	15	0.77
Anesthesia			
General anesthesia	26	30	0.55
Intraspinal anesthesia	24	20	0.63

curative effect. Eighthly, the key observations were implemented on key parts. Before the surgery, the skin of the pressured area was checked again, especially the skin pressured by the medical devices. The parts with higher risk were marked and focused on with close observation intraoperatively. Ninthly, awareness of prevention should be raised and continuing education should be strengthened.

Apart from the above-mentioned nursing measures, the patients in the experimental group used AHD and nanosilver gel to protect the key parts, especially the areas would be pressured by medical devices. The medical equipment could then be worn after that. Gauze was used to cover the important sections for protection in the control group.

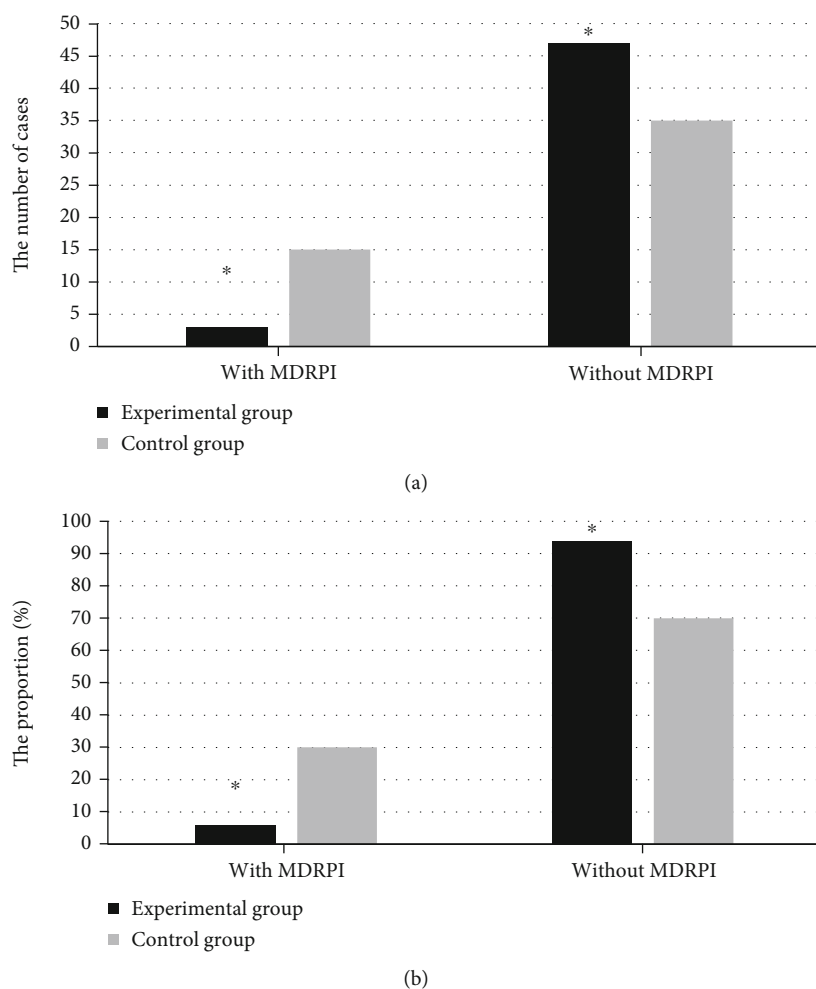


FIGURE 1: Comparison of the incidence of MDRPI between the two groups. Note:  $*P < 0.05$  was obtained compared with the data of the control group.

**2.5. Observation Indicators.** The incidence of MDRPI, the degree of injury to the pressured area, comfort level, nursing satisfaction, and more indicators were statistically analyzed between the two groups. The specific evaluation criteria for the degree of injury and comfort level are shown in Tables 1 and 2, respectively.

**2.6. Statistical Analysis.** All data analyses were completed by SPSS19.0 software. The measurement data were expressed as mean  $\pm$  standard deviation, and the test method was the independent sample  $t$  test. The enumeration data were expressed as frequencies, and the comparison between groups was done by chi-square test.  $P < 0.05$  meant the difference was statistically significant.

### 3. Results

**3.1. General Information of Patients.** The general data of patients in the two groups are shown in Table 3. The experimental group included 26 male cases and 24 female cases, having an average age of  $33 \pm 11.3$  years old. In the control group, there were 31 male patients and 19 female patients, and the average age of the patients was  $36 \pm 9.96$  years old.

No significant difference was discovered in the general data such as gender, age, department, and surgical position between the two groups, which showed the comparability.

**3.2. Comparison of the Incidence of MDRPI between the Two Groups.** The incidence of MDRPI was compared between the two groups, and the comparison results are shown in Figure 1. There were 3 patients with MDRPI in the experimental group (6%) and 47 patients without MDRPI (94%). MDRPI was found in 15 cases (30%) in the control group, but MDRPI was not found in the remaining 35 cases (70%). The differences between groups were of statistical significance ( $P < 0.05$ ).

**3.3. Comparison of the Degree of Skin Injury in the Two Groups.** The comparison results of the degree of skin injury in the two groups of patients are shown in Figure 2. 1 (2%), 1 (2%), and 1 (2%) patient got mild, moderate, and severe skin injury, respectively, in the experimental group. In the control group, there were 4 (8%), 8 (16%), and 3 (6%) patients had mild, moderate, and severe skin injury, respectively. The differences between the groups were deemed statistically significant by the researchers ( $P < 0.05$ ).

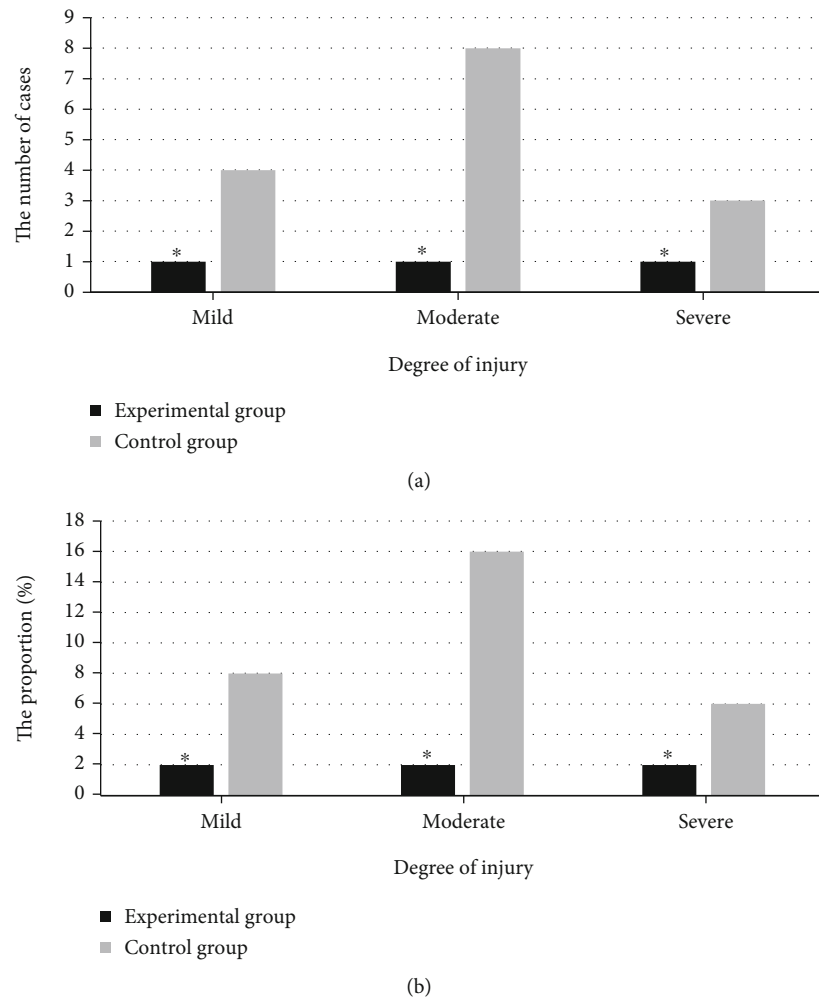


FIGURE 2: Comparison of the degree of skin injury in patients in the two groups. Note: \* $P < 0.05$ , compared with those of the control group.

**3.4. Comparison of Comfort Level and Dressing Changes between the Two Groups.** The comfort level and dressing changes of patients were compared between two groups, as shown in Figure 3. In the experimental group, the number of patients whose comfort levels were comfortable, less comfortable, general, and uncomfortable was 45 (90%), 2 (4%), 2 (4%), and 1 (2%), respectively. The number of patients in the control group whose comfort level was comfortable, less comfortable, average, and uncomfortable was counted to be 12 (24%), 15 (30%), 15 (30%), and 8 (16%), respectively. The differences between groups were also statistically significant ( $P < 0.05$ ). The number of dressing changes in the experimental group was  $0.5 \pm 0.08$  times, and that in the control group was  $4.4 \pm 0.22$  times, showing a statistically significant difference as  $P < 0.05$ .

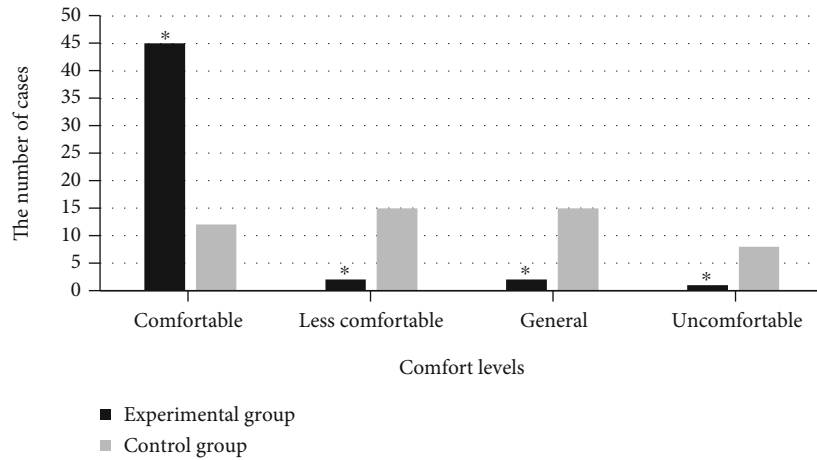
**3.5. Comparison of Nursing Satisfaction of Patients in the Two Groups.** The comparison of nursing satisfaction between the two groups is shown in Figure 4. It was found that, in the experimental group, the number of patients whose nursing satisfaction was satisfied, less satisfied, and unsatisfied was counted as 36, 12, and 2, respectively. The total satisfied rate for nursing was 72% in the experimental

group. There were 11 satisfied patients, 15 less satisfied patients, and 24 unsatisfied patients in the control group, and the total satisfied rate was 22%. With the comparison between two groups, the nursing satisfaction of the experimental group was higher than that of the control group significantly ( $P < 0.05$ ).

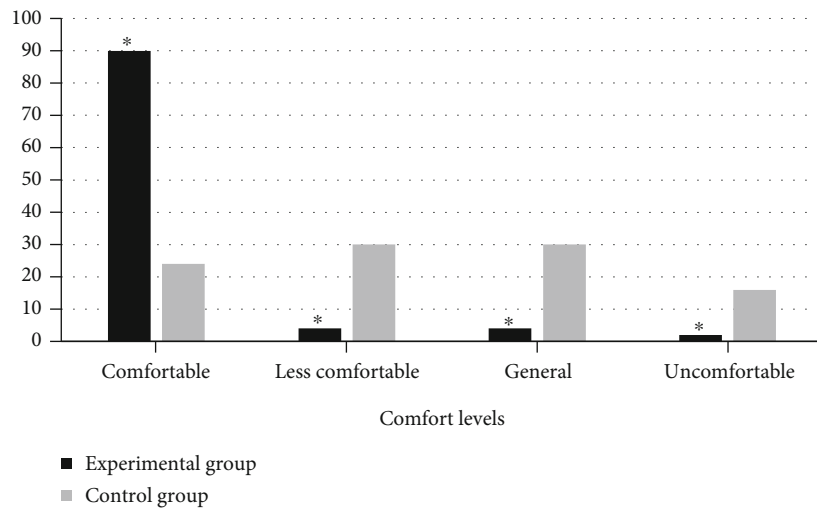
**3.6. SEM Results of Nanosilver Antibacterial Gel.** The SEM results of nanosilver are shown in Figure 5. The particle size of the nanosilver antibacterial gel prepared in this research was 45–85 nm, and the particle size was medium and distributed uniformly. It not only avoided the reduction of antibacterial activity due to excessive particle size but also avoided increased cytotoxicity for the too small particle size. Besides, it could also be observed that the nanosilver particles were wrapped by polymer materials.

## 4. Discussion

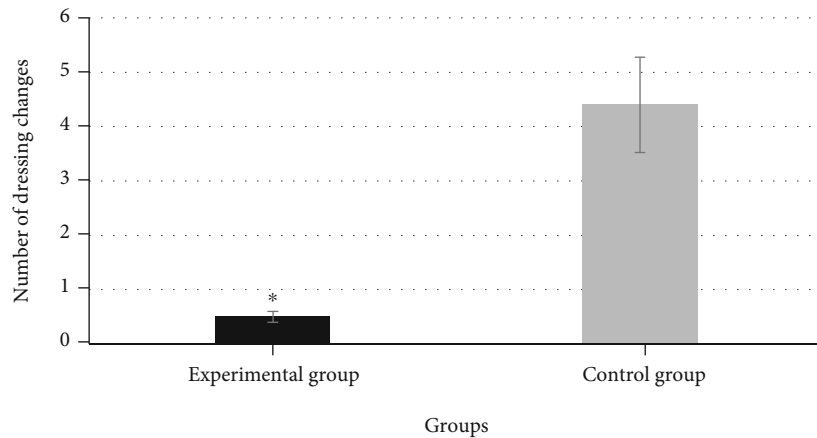
Clinical studies have indicated that MDRPI can be induced by a range of factors, including the material qualities of the device, difficulty helping or immobilising the patient's body, or persistent pressure release in the same location [18].



(a)



(b)



(c)

FIGURE 3: The comfort level and number of dressing changes of patients in the two groups. Note:  $*P < 0.05$ , which were compared with those in the control group.

Patients' comfort levels will be substantially impacted with the onset of MDRPI, leading in decreased compliance and, as a result, treatment. If no appropriate therapy is given after the emergence of MDRPI, it can lead to infection and inflam-

mation, which can have a negative impact on the disease's prognosis and treatment. Clinical research data suggest that MDRPI accounts for 34.5% of all pressure injuries, so its incidence is quite high [19]. If effective preventive intervention

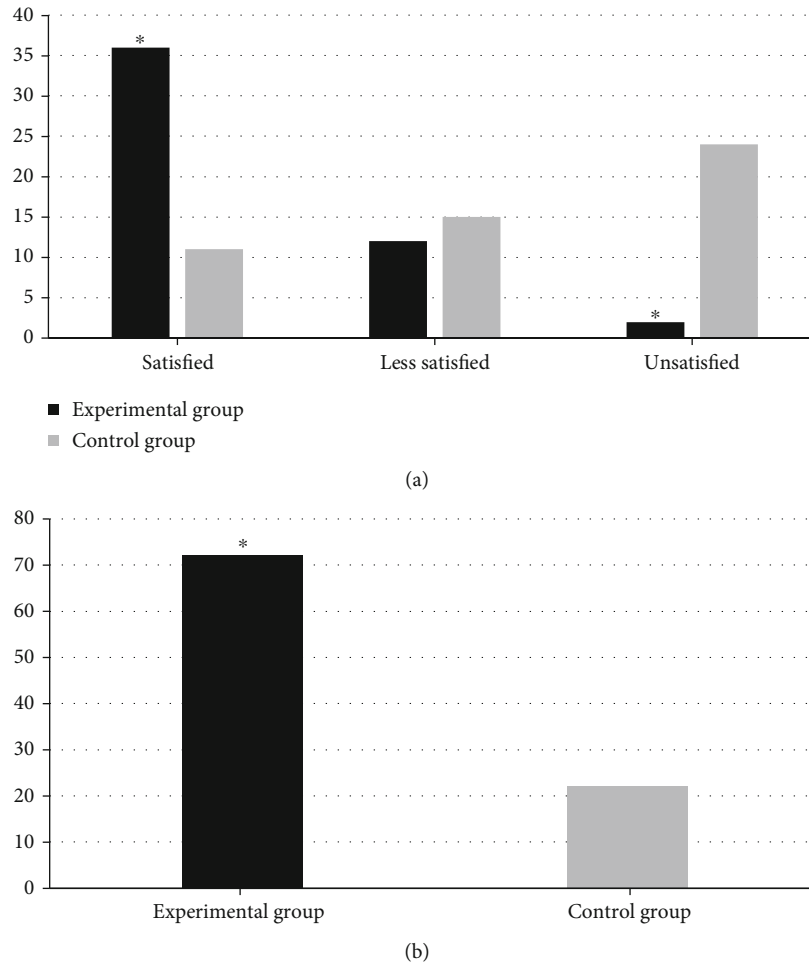


FIGURE 4: Comparison of nursing satisfaction of patients between two groups. Note: \* $P < 0.05$  compared with those of the control group.

measures can be taken, it is of great significance to improve the curative effect, reduce the pain, and improve the compliance of patients.

The predictive nursing is also called advanced nursing, which refers to the nursing staff analyze and predict the specific situation of the patient as well as possible nursing problems before and during the nursing process, utilizing nursing knowledge. Thereby, the nursing focuses can be determined, and the preventive measures can be taken in advance to minimize the pain and accidents of patients. It is a nursing method change from passive to active [20–22]. Compared with traditional nursing methods, predictive nursing is more systematic, comprehensive, and individualized and has more advantages [23]. Some scholars have applied predictive nursing to the transfer nursing of emergency patients and patients with severe traumatic brain injury, which has greatly shortened the transfer time, reduced the incidence of transfer accidents, and improved nursing safety [24].

One of the most widely utilized clinical approaches for treating and preventing pressure injuries is AHD. Traditionally, materials such as gauze were used to treat antipressure skin injuries [25]. Gauze has been shown in clinical investigations to have flaws like hygroscopicity, poor air permeabil-

ity, and easy displacement, all of which contribute to a poor fit between the skin and the medical device. The local skin is prone to fibrous impressions and even problems such as flush and erosion with long-term gauze use. In addition, due to the hygroscopicity of gauze, it increases the irritation of the patient's skin for moisture, so that it is often necessary to replace the gauze every 1-2 days. The workload of the nursing staff is increased, but also, damage would be caused to the skin by pulling the gauze repeatedly [26]. In comparison, the AHD can be safely attached to the skin, and it has good self-adhesiveness. It can protect the skin and absorb exudates effectively; meanwhile, its softness, a certain thickness, and other advantages can make it reduce and relieve pressure effectively [27]. Nanosilver gel is a kind of skin gel commonly used in clinical practice. Compared with other external drugs, nanosilver gel can reduce exudation obviously, improve wound healing rate, and shorten wound healing time. Thereby, the formation of scars is also reduced, improving the quality of healing [28, 29]. Some scholars have used nanosilver antibacterial gel combined with AHD in the treatment of unstageable pressure ulcers, and a higher cured rate was achieved than using AHD alone [30]. In general, nanosilver antibacterial gel has a high clinical application value in the treatment of skin wounds.

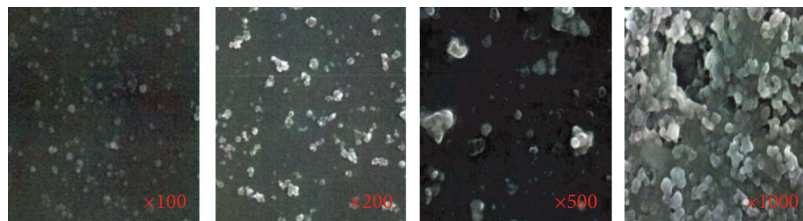


FIGURE 5: SEM results of nanosilver antibacterial gel.

In this research, 100 patients were chosen as the research objects, as they were subjected to surgery in Chongqing Qijiang District People's Hospital from February 2019 to February 2020. All these patients were cared for with the predictive nursing after surgery. Nanosilver antibacterial gel was also prepared independently and was characterized by SEM. During the nursing procedure, the experimental group's patients were treated with AHD mixed with nanosilver antibacterial gel as pressed skin dressings, whereas the control group's patients were treated with gauzes. Afterwards, the incidence of MDRPI, the degree of skin injury, comfort level, nursing satisfaction, and more indicators were compared between the two groups. It was proved from the results that the nanosilver antibacterial gel prepared had uniform and moderate particle size with good quality. The incidence of MDRPI in the experimental group was remarkably lower, the degree of skin injury was slighter, and the comfort level and nursing satisfaction were higher significantly.

## 5. Conclusion

The nursing impact of nanosilver antibacterial gel mixed with AHD on pressed skin in the predictive nursing mode was investigated in this study. All the incidence of MDRPI, the degree of injury, comfort level, and nursing satisfaction were improved notably. MDRPI incidence, pressed skin injury severity, comfort level, clothing changes, nursing satisfaction, and other factors were all compared. The nanosilver antibacterial gel created had a homogeneous particle size, moderate particle size, and good quality, according to the findings. It was suggested that the combination of predictive nursing, AHD, and nanosilver antibacterial gel had a high clinical application value in the treatment of MDRPI.

## Data Availability

All data, models, and code generated or used during the study appear in the submitted article.

## Conflicts of Interest

The authors declare that they have no conflicts of interest.

## Authors' Contributions

Chunxiu Li and Hongmei Chen contributed equally to this work as co-first authors.

## References

- [1] A. Grigatti and A. Gefen, "What makes a hydrogel-based dressing advantageous for the prevention of medical device-related pressure ulcers," *International Wound Journal*, vol. 19, no. 3, pp. 515–530, 2022.
- [2] A. Lustig, R. Margi, A. Orlov, D. Orlova, L. Azaria, and A. Gefen, "The mechanobiology theory of the development of medical device-related pressure ulcers revealed through a cell-scale computational modeling framework," *Biomechanics and Modeling in Mechanobiology*, vol. 20, no. 3, pp. 851–860, 2021.
- [3] A. Grigatti and A. Gefen, "The biomechanical efficacy of a hydrogel-based dressing in preventing facial medical device-related pressure ulcers," *International Wound Journal*, 2021.
- [4] R. Margi and A. Gefen, "Evaluation of facial tissue stresses under medical devices post application of a cyanoacrylate liquid skin protectant: an integrated experimental-computational study," *International Wound Journal*, vol. 19, no. 3, pp. 615–632, 2022.
- [5] R. Méndez Rojano, S. Mendez, and F. Nicoud, "Introducing the pro-coagulant contact system in the numerical assessment of device-related thrombosis," *Biomechanics and Modeling in Mechanobiology*, vol. 17, no. 3, pp. 815–826, 2018.
- [6] G. Amrani and A. Gefen, "Which endotracheal tube location minimises the device-related pressure ulcer risk: the centre or a corner of the mouth?," *International Wound Journal*, vol. 17, no. 2, pp. 268–276, 2020.
- [7] L. Peko Cohen, Z. Ovadia-Blechman, O. Hoffer, and A. Gefen, "Dressings cut to shape alleviate facial tissue loads while using an oxygen mask," *International Wound Journal*, vol. 16, no. 3, pp. 813–826, 2019.
- [8] A. Gefen, "The bioengineering theory of the key modes of action of a cyanoacrylate liquid skin protectant," *International Wound Journal*, vol. 17, no. 5, pp. 1396–1404, 2020.
- [9] A. Kilic, "Artificial intelligence and machine learning in cardiovascular health care," *The Annals of Thoracic Surgery*, vol. 109, no. 5, pp. 1323–1329, 2020.
- [10] A. Meyer, D. Zverinski, B. Pfahringer et al., "Machine learning for real-time prediction of complications in critical care: a retrospective study," *The Lancet Respiratory Medicine*, vol. 6, no. 12, pp. 905–914, 2018.
- [11] J. Q. Sheng, P. J. Hu, X. Liu, T. S. Huang, and Y. H. Chen, "Predictive analytics for care and management of Patients with acute diseases: deep learning-based method to predict crucial complication phenotypes," *Journal of Medical Internet Research*, vol. 23, no. 2, 2021.
- [12] X. Chen, Y. Lao, Y. Zhang, L. Qiao, and Y. Zhuang, "Risk predictive models for delirium in the intensive care unit: a systematic review and meta-analysis," *Annals of Palliative Medicine*, vol. 10, no. 2, p. 1467, 2020.



- [13] S. Eggmann, M. L. Verra, V. Stefanicki et al., “Predictive validity of the Chelsea critical care physical assessment tool (CPAx) in critically ill, mechanically ventilated adults: a prospective clinimetric study,” *Disability and Rehabilitation*, vol. 7, pp. 1–6, 2022, Epub ahead of print.
- [14] D. J. Rubin and A. A. Shah, “Predicting and preventing acute care re-utilization by patients with diabetes,” *Current Diabetes Reports*, vol. 21, no. 9, p. 34, 2021.
- [15] F. F. Dibra, A. J. Silverberg, T. Vasilopoulos, C. F. Gray, H. K. Parvataneni, and H. A. Prieto, “Arthroplasty care redesign impacts the predictive accuracy of the risk assessment and prediction tool,” *The Journal of Arthroplasty*, vol. 34, no. 11, pp. 2549–2554, 2019.
- [16] B. E. Belsher, D. J. Smolenski, L. D. Pruitt et al., “Prediction models for suicide attempts and deaths: a systematic review and simulation,” *JAMA Psychiatry*, vol. 76, no. 6, pp. 642–651, 2019.
- [17] J. Cho, K. Place, R. Salstrand et al., “Developing a predictive tool for hospital discharge disposition of patients poststroke with 30-day readmission validation,” *Stroke Research and Treatment*, vol. 2021, 9 pages, 2021.
- [18] P. Iyer and A. Shukla, “Partial paternity does not always select for female-biased care,” *Evolution*, vol. 75, no. 11, pp. 2672–2684, 2021.
- [19] K. Giannakou, *Prediction of pre-eclampsia. Obstetric Medicine*, vol. 14, no. 4, pp. 220–224, 2021.
- [20] T. Deshmukh, A. Varma, S. Damke, and R. Meshram, “Predictive efficacy of pediatric logistic organ dysfunction-2 score in pediatric intensive care unit of rural hospital,” *Indian Journal of Critical Care Medicine: Peer-reviewed, Official Publication of Indian Society of Critical Care Medicine*, vol. 24, no. 8, pp. 701–704, 2020.
- [21] M. Liu, J. Liu, E. K. Weitzel, and P. G. Chen, “The predictive utility of the 22-item sino-nasal outcome test (SNOT-22): a scoping review,” *International forum of allergy & rhinology*, vol. 12, no. 1, pp. 83–102, 2022.
- [22] J. S. Martin, E. J. Ringen, P. Duda, and A. V. Jaeggi, “Harsh environments promote alloparental care across human societies,” *Proceedings of the Royal Society B*, vol. 287, no. 1933, p. 20200758, 2020.
- [23] R. Joshi, Z. Peng, X. Long, L. Feijs, P. Andriessen, and C. Van Pul, “Predictive monitoring of critical cardiorespiratory alarms in neonates under intensive care,” *IEEE Journal of Translational Engineering in Health and Medicine*, vol. 7, no. 7, pp. 1–10, 2019.
- [24] E. S. Rosenthal, “Seizures, status epilepticus, and continuous EEG in the intensive care unit,” *Continuum (Minneapolis)*, vol. 27, no. 5, pp. 1321–1343, 2021.
- [25] J. O. Gjengstø Hunderi, K. C. Lødrup Carlsen, L. B. Rolfsjord, K. H. Carlsen, P. Mowinckel, and H. O. Skjerven, “Parental severity assessment predicts supportive care in infant bronchiolitis,” *Acta Paediatrica*, vol. 108, no. 1, pp. 131–137, 2019.
- [26] K. Palla, S. L. Hyland, K. Posner et al., “Intraoperative prediction of postanaesthesia care unit hypotension,” *British Journal of Anaesthesia*, vol. S0007-0912, no. 21, pp. 00758–00763, 2022.
- [27] E. P. Rotar, J. P. Beller, M. E. Smolkin et al., “Prediction of prolonged intensive care unit length of stay following cardiac surgery,” *Seminars in Thoracic and Cardiovascular Surgery*, vol. 34, no. 1, pp. 172–179, 2022.
- [28] B. Roy, T. Stepišnik, Pooled Resource Open-Access ALS Clinical Trials Consortium, C. Vens, and S. Džeroski, “Survival analysis with semi-supervised predictive clustering trees,” *Computers in biology and medicine*, vol. 141, p. 105001, 2022.
- [29] J. L. Fernández-Martínez, Z. Fernández-Muñiz, A. Cernea, and A. Kloczkowski, “Predictive mathematical models of the short-term and long-term growth of the COVID-19 pandemic,” *Computational and Mathematical Methods in Medicine*, vol. 2021, 14 pages, 2021.
- [30] J. Op den Buijs, M. Pijl, and A. Landgraf, “Predictive modeling of 30-day emergency hospital transport of German patients using a personal emergency response: retrospective study and comparison with the United States,” *Inform*, vol. 9, no. 3, 2021.

## Research Article

# Correlation between the Treg/Th17 Index and the Efficacy of PD-1 Monoclonal Antibody in Patients with Advanced Non-Small-Cell Lung Cancer Complicated with Chronic Obstructive Pulmonary Disease

Xiaoyu Wang,<sup>1</sup> Xinyuan She,<sup>2</sup> Wei Gao,<sup>1</sup> Xing Liu,<sup>1</sup> and Bin Shi<sup>1</sup> 

<sup>1</sup>Department of Respiratory Medicine, The Affiliated Suqian Hospital of Xuzhou Medical University, Suqian, 223800 Jiangsu, China

<sup>2</sup>Department of Pathology, The Affiliated Suqian Hospital of Xuzhou Medical University, Suqian, 223800 Jiangsu, China

Correspondence should be addressed to Bin Shi; 142791032@st.usst.edu.cn

Received 28 April 2022; Revised 24 May 2022; Accepted 27 May 2022; Published 9 July 2022

Academic Editor: Naeem Jan

Copyright © 2022 Xiaoyu Wang et al. This is an open access article distributed under the Creative Commons Attribution License, which permits unrestricted use, distribution, and reproduction in any medium, provided the original work is properly cited.

**Objective.** It was to explore the correlation between regulatory T cells (Treg)/T helper cell 17 (Th17) and the efficacy of receiving a programmed death protein-1 (PD-1) monoclonal antibody (mAb) in patients with advanced non-small-cell lung cancer (NSCLC) complicated with chronic obstructive pulmonary disease (COPD). **Methods.** The research subjects were 82 patients who were clinically evaluated and treated in the Respiratory Department of Suqian Hospital connected with Xuzhou Medical University from January to December 2021. All of the patients were given PD-1 immunotherapy, and 50 healthy people were chosen as the control group. Classification was carried out according to tumor type and tumor stage. The levels of Th17 and Treg/Th17 in the peripheral blood of patients with different tumor-node-metastasis (TNM) stages and different types were compared, and the immune function, lung function (forced expiratory volume in one second/forced vital capacity (FEV1%/FVC), FEV1%, and FVC), and changes in inflammatory factors were compared before and after treatment. The levels of interleukin (IL)-17, IL-6, tumor necrosis factor (TNF)- $\alpha$ , and transforming growth factor (TGF)- $\beta$  were compared between the two groups. The correlation between Th17 cells and Treg cells in the peripheral blood of patients with NSCLC complicated with COPD was analyzed. **Results.** After treatment, the levels of IL-17, IL-6, TNF- $\alpha$ , and TGF- $\beta$  in patients with NSCLC combined with COPD were notably superior to those in the control group ( $P < 0.05$ ). The immune function and lung function of the patients were improved after treatment. There were 43 cases of squamous cell carcinoma, 30 cases of adenocarcinoma, and 9 cases of large cell carcinoma. The proportion of Th17 cells to CD4+ T cells in the blood of the three types of patients and the proportion of CD4+CD25<sup>Hi</sup>CD127<sup>Lo</sup> regulatory T cells to CD4+ lymphocyte cells in Treg cells showed no considerable difference among the different case types ( $P > 0.05$ ). No considerable difference was indicated in Treg/Th17 in peripheral blood between stage IIIB and stage IV lung cancer patients ( $P > 0.05$ ). A positive linear correlation was revealed between Th17 cells and Treg cells in the peripheral blood of patients with NSCLC combined with COPD,  $R = 0.26$ ,  $P = 0.039$ . **Conclusion.** Treg and Th17 cells were shown to be much higher in lung cancer patients with COPD, which could lead to immunosuppression and tumor growth. PD-1 therapy for NSCLC has demonstrated efficacy and can improve patients' immunological state while being extremely safe.

## 1. Introduction

Lung cancer is a respiratory malignancy with high morbidity and mortality worldwide. Eighty-five percent of lung cancer patients have non-small-cell lung cancer (NSCLC), most of whom are diagnosed at an advanced stage. In 2016, 162,510 people died of lung cancer in the United States.

Lung cancer has also become the cause of death of malignant tumors in China, and its morbidity and mortality are also increasing [1, 2]. At the individual level, there are several reasons for the disease, including smoking, environmental pollution, and occupational exposure. The patient can experience dyspnea, weight loss, hemoptysis, loss of appetite, and other symptoms. The patient will have severe mental pain,

depression, anxiety, and fear, and the patient's quality of life will be greatly reduced. The main cause of lung cancer is smoking [3, 4]. Chronic obstructive pulmonary disease (COPD) is a common respiratory condition among the elderly that is linked to lung cancer incidence and patient symptom reports. COPD is becoming more common as economic development, and people's living standards increase at a rapid pace. According to the World Health Organization (WHO) survey, the mortality rate of COPD occupies fourth place in the time, and the prevalence in the elderly in China is roughly in the range of 6.5-8.5%, with a high patient rate of ten. Male COPD patients with moderate or heavy smoking and female COPD patients with smoking and occupation are also at high risk of lung cancer. Most elderly COPD patients with lung cancer have advanced cancer when diagnosed, and some patients cannot tolerate chemotherapy due to ventilatory dysfunction and pulmonary disease [5, 6]. COPD is an independent risk factor for lung cancer, and the incidence in lung cancer patients with COPD is five times higher than that in smokers with normal lung function [7-9]. Symptoms of many patients include dyspnea, cough, and sputum, which seriously affect patients' lives, and these symptoms also bring great trouble to patients' breathing [10-13].

Patients with NSCLC combined with COPD have ventilation disorders and poor lung functional reserve, and some patients are likely to lose the opportunity for surgery and chemotherapy due to delayed diagnosis, which requires many new forms of research and application in the treatment of NSCLC [14]. In addition to surgery, chemotherapy, radiotherapy, and targeted therapy, the treatment of NSCLC also includes immunotherapy. In recent years, immunotarget inhibitors have emerged as a new approach for NSCLC treatment [15, 16]. Conventional drugs for the treatment of lung cancer generally act directly on tumor cells to kill them. Immunosuppressants mainly block the inhibition and mutual ligand expressed on T cells to block the pathway at the immune checkpoint in the tumor microenvironment to stimulate the function of tumor-specific T cells [17, 18]. Endogenous antitumor immunity was enhanced, and antitumor ability was enhanced. PD-1 and programmed death-ligand 1 (PD-L1) inhibitors are used in the second-line treatment of NSCLC, and studies have shown that these inhibitors can be used as second-line treatments for advanced NSCLC [19, 20]. However, there are still some disadvantages; the side effects of drugs still exist, and the cure rate is only 18%, so it is particularly important to know which patients can benefit from immunotherapy [21]. Helper T cell 17 (Th17) is a subpopulation of CD4+ T lymphocytes other than Th1 and Th2 that are capable of independent regulation and differentiation mechanisms. Th17 cells are a new leukocyte differentiation antigen CD4 helper T cell subgroup that secretes IL-17 and plays a certain role in the process of tumor cases, infectious diseases, and autoimmune diseases [22]. Different from helper T cells, Treg cells play an inhibitory role in antitumor immunity, are responsible for the negative regulation of collective immune function, and can induce an immune response

by inhibiting antitumor activity in the body. Under normal circumstances, Treg and Th17 cells maintain a balance. During differentiation, Treg and Th17 cells fight against each other. If cell differentiation of the inflammatory molecule Th17 is enhanced, Treg/Th17 imbalance will be caused, and the autoimmune system will be damaged, resulting in transplant rejection. Proinflammatory Th17 cells and anti-inflammatory Tregs work together to keep the body in balance, which is important for immune stability. An aberrant immune response results from the formation of an inflammatory response, and variations in Treg cell expression/Th17 cells alter the airway response. In recent years, it has become a hot topic to fully and deeply understand the differentiation and regulation mechanism of Treg and Th17 cells and to search for the role of these two cells in the development of related diseases. An imbalance between Treg and Th17 cells exists in autoimmune diseases and plays an important role in the immune response of cells. Treg and Th17 imbalance is closely related to the development and treatment of malignant tumors [23, 24]. In-depth study of Treg and Th17 indicators in advanced NSCLC patients could provide new methods for new anti-inflammatory analysis and immunotherapy, as well as new strategies for tumor treatment.

With the rapid development of biotechnology, the immune system has become increasingly recognized by people, and the use of immunotherapy for tumors has become a new form. In clinical application, the comprehensive tumor treatment system also occupies an important position, but the side effects after treatment have not been eliminated. It is also necessary to study Treg/Th17 and (PD-1) monoclonal antibody (mAb) in the treatment of NSCLC complicated with COPD. Based on this, qualified patients with advanced NSCLC were included to explore the efficacy of the Treg/Th17 index and (PD-1) mAb in the treatment of NSCLC, hoping to improve the recognition rate of patients with early lesions and provide a basis for screening and prediction of clinical immunotherapy.

The paper's organization paragraph is as follows: The materials and methods is presented in Section 2. Section 3 analyzes the results and discussion of the proposed work. Section 4 discusses the discussion of the paper. Finally, in Section 5, the research work is concluded.

## 2. Materials and Methods

*2.1. The Research Objects.* A total of 82 patients clinically diagnosed and treated in the Respiratory Department of Suqian Hospital affiliated with Xuzhou Medical University from 2021 January to December 2021 were selected as the research subjects. All patients received PD-1 immunotherapy for advanced NSCLC, and their clinical data were retrospectively analyzed. There were 17 females and 65 males, ranging in age from 45 to 72 years, with an average age of  $54.62 \pm 9.31$  years. This experiment was approved by the ethics committee of Suqian Hospital affiliated with Xuzhou Medical University, and all patients and their families gave informed consent.

### 2.1.1. Inclusion Criteria

- (i) Long-term patients in our hospital
- (ii) Detailed information of inpatients (including age, sex, previous medication history, and disease history)
- (iii) Patients diagnosed with advanced NSCLC complicated with COPD by histological and imaging examinations, while disease progression cannot be tolerated after the failure of standard treatment, such as chemotherapy, targeted therapy, and immunotherapy other than targeting PD-1/PD-L1
- (iv) Patients with no other mental diseases
- (v) Patients with good understanding and communication skills
- (vi) Advanced NSCLC patients without other treatment
- (vii) Patients with measurable lesions that met the *Response Evaluation Criteria in Solid Tumors 1.1* (RECIST 1.1)

### 2.1.2. Exclusion Criteria

- (i) Patients who did not agree to participate in this research
- (ii) Incomplete case data
- (iii) Patients with long-term use of hormones or hematopoietic factors
- (iv) Patients with acute or chronic inflammation (human immunodeficiency virus and hepatitis)
- (v) Patients suffering from mental illness
- (vi) Patients with previous or existing autoimmune disorders
- (vii) Patients with pulmonary interstitial lesions

**2.2. The Research Methods.** All patients immunized with mAb to PD-1 underwent routine blood and biochemical tests one week before treatment and were divided into sintilimAb, toripalimAb, pembrolizumAb, and nivolumAb groups according to the type of PD-1 mAb.

SintilimAb treatment: a 3-week cycle of 200 mg drops of vein injection

ToripalimAb treatment: a 2-week cycle of 3 mg/kg drops of vein injection

PembrolizumAb: a 3-week cycle of 2 mg/kg drops of vein injection

NivolumAb: a 2-week cycle of 3 mg/kg drops of vein injection

Patients were divided into first-line, second-line, and  $\geq$  third-line groups according to the number of lines received by PD-1 mAb. Patients were rolled into two groups regarding whether they smoked. Patients were rolled into two

groups regarding whether there were immune-related adverse reactions.

According to tumor types, patients were classified into large cell carcinoma, adenocarcinoma, and squamous cell carcinoma groups. The tumor was stage IIIB or IV.

**2.3. Experimental Reagents and Instruments.** Flow cytometry was purchased from American BD, and the analysis software was *Div*a. 2IL-17A-APC antibody, antihuman Foxp3-PE antibody, film-breaking agent, and staining agent were purchased from the American eBioscience. APC-labeled mouse antihuman CD25, RPMI-1640 medium, hemolysin, and IL-17 mAb reagent were purchased from BD, USA. Ionomycin and phorbol 12-myristate 13-acetate (PMA) were purchased from the Sigma, USA. The 1% paraformaldehyde and lymphocyte isolate (Ficoll isolate) were purchased from Huajing Biotechnology. A medical centrifuge (KDC-1044) was purchased from USTC Innovation Co., Ltd. A waterproof constant temperature incubator (GSP-9050MBE) was purchased from Shanghai Boxun Industrial Co., Ltd. Medical Equipment Factory. A thermostatic oscillator was purchased from Shanghai Yuejin Medical Device Co., Ltd. A microplate reader was purchased from Tecan Austria.

**2.4. Th17 and Treg Cells Detected by Flow Cytometry.** Flow cytometry detection of Th17 cells referred to the detection of peripheral blood mononuclear cells, including monocytes and lymphocytes. Fifty healthy subjects and lung cancer patients were selected to take 5 mL venous blood and 2 mL separated serum at  $-20^{\circ}\text{C}$  in the morning for use in an enzyme-linked immunosorbent assay (ELISA). Then, 3 mL was used for ethylenediaminetetraacetic acid (EDTA) anticoagulation. Two milliliters of peripheral anticoagulant blood was collected from lung cancer patients, diluted with phosphate-buffered saline (PBS) buffer of the same amount, and then mixed gently. The centrifuge tube was filled with ten milliliters of lymphocyte separation solution, and then PBS-diluted peripheral blood was deposited onto the liquid surface of the lymphocyte separation solution. It was ensured that there was a clear interface between the liquid level, and after centrifugation for 20 min at 2,000 r/min and stratification, the lower layer was displayed for red blood cells and neutrophils, the upper layer was displayed for plasma and platelets, and the intermediate layer was a cloud of mononuclear cells. The cloud layer was slowly inhaled in another 15-mL centrifuge tube, and then five times the PBS buffer was added. After mixing, centrifugation was conducted for 10 min at 1,000 r/min, and the obtained precipitate was mononuclear cells, which were counted under the microscope, and the cell density was adjusted to  $2 \times 10^6$  per mL.

One millimeter of lymphoid tissue was added to 1 mL Roswell Park Memorial Institute (RPMI1640) medium and filtered through a 200-mesh steel mesh. The cell density was adjusted to  $1 \times 10^6/\text{mL}$ , and then the final concentration of phorbol ester was added to 100 ng/mL, the final concentration of ionomycin was added to 1 mg/L, and the final concentration of monomycin was added to 2 mL/L. The cells

were placed in an incubator with 5% CO<sub>2</sub> at 37°C and stimulated for 6 hours.

Intracellular antibody labeling was performed as follows. The stimulated cells were fixed with 1% paraformaldehyde for 15 minutes, washed with PBS, and centrifuged for 5 min at 1,500 r/min, and the supernatant was removed. Then, phycoerythrin (PE)-labeled mouse antihuman CD8 antibody and rat antihuman CD3 antibody labeled with fluorescein isothiocyanate (FITC) were added, incubated at room temperature for 20 min in the dark, washed again with PBS, and centrifuged for 5 min at 1,500 r/min, and then the supernatant was discarded. Then, 200  $\mu$ L of film breaker was added, incubated at room temperature for 20 min in the dark, centrifuged, added to APC-labeled mouse antihuman IL-17 antibody, incubated for 20 min, washed with PBS, and centrifuged for 5 min at 1,500 r/min. Then, the supernatant was superfluous. Then, 300  $\mu$ L PBS was added to suspend the cells. The cells were transferred to a special flow cytometer tube, away from light standby, for analysis.

**2.5. Flow Cytometry Detection of the Proportion of CD4<sup>+</sup>CD25<sup>Hi</sup>CD127<sup>Lo</sup> Regulatory T Cells in CD4+ Lymphocytes.** One hundred microliters of anticoagulant whole blood from patients in observation group and healthy controls was added to the flow tube. Antibodies against CD4-FITC, CD25-APC, and CD25-APC were added to each detection tube according to the operation steps and then mixed and incubated at room temperature for 20 min. Two milliliters of hemolysin was added, fully mixed, and then incubated at room temperature for 10 minutes. After the red blood cells were fully lysed, PBS was added to each tube twice for washing. The lysed red blood cells were obtained by centrifugation for 5 min at 1,500 r/min. In the detection before the machine, 200  $\mu$ L PBS was added to each tube for blending. Then, *CellQuest* was used to analyze the results, and the percentage of CD4<sup>+</sup>CD25<sup>Hi</sup>CD127<sup>Lo</sup> regulatory T cells in CD4+ lymphocyte cells in Treg cells was expressed.

**2.6. Serum IL-17 Concentration Detected by ELISA.** The concentration of IL-17 in serum was detected by a double-antibody sandwich. First, all reagents were restored to room temperature. Fifty milliliters of concentrated IL-17 solution was prepared, and 950 mL of double distilled water was added to it and fully mixed for later use. Then, 5 mL of IL-7 analysis buffer stock was added to 95 mL of double steam water and mixed well. For antibody preparation, 60  $\mu$ L of IL-17 enzyme antibody was added to 5.94 mL of dilution analysis buffer for later use. Then, 11.94 mL of the prepared solution was added to 60  $\mu$ L of streptavidin-HRP, which was prepared half an hour before the addition. The standard il-17 solution was then prepared, and 400  $\mu$ L of double distilled water was added to the il-17 powder to resuscitate to prepare a standard il-17 concentrate of 200 pg/mL. Seven tubes were labeled as 1-7, and 225  $\mu$ L dilution analysis buffer was added to them. A standard concentrate of 200 pg/mL RGF- $\beta$ 1 (225  $\mu$ L) was added to tube no. 1 and mixed. Standard curves with concentrations of 100, 50, 25, 12.5, 6.3, 3.1, and 1.6 pg/mL were successively prepared, and diluted analytical buffer was selected as a blank.

The specific operation steps are as follows. First, the 96-well plate was washed twice with buffer solution on the automatic plate washing machine and then dried. Seven standard series solutions were added to the wells, and 50  $\mu$ L of analysis buffer was added to the other wells. Then, 50  $\mu$ L of enzyme antibody was added to each well, shaken, incubated for 2 h at 100 r/min, and then washed 4 times. After drying, 100  $\mu$ L of streptavidin-HRP was added, incubated for 1 h by shaking for 100 r/min, washed, and dried again. Then, 100  $\mu$ L chromogenic agent was added to each well and incubated for 10 min at room temperature. Finally, 100  $\mu$ L stop solution was added. After mixing, the optical density was determined at 450 nm using a microplate reader to calculate the concentration of IL-1. IL-6 was determined using the same method.

**2.7. Serum TGF- $\beta$  Concentration Detected by ELISA.** TGF- $\beta$  concentrations in serum were also measured using a double-antibody sandwich ELISA. All reagents were first brought to room temperature. Fifty milliliters of TGF- $\beta$  concentrate were made, and 950 milliliters of double-steamed water were added and thoroughly mixed before being used. Then, 5 mL of TGF- $\beta$  analysis buffer stock was added to 95 mL of double-steamed water and mixed well. For antibody preparation, 120  $\mu$ L TGF- $\beta$  enzyme antibody was added to 11.88 mL dilution breakdown buffer for later use. Then, 11.88 mL streptavidin-HRP was added to 120  $\mu$ L streptavidin-HRP, and the solution was organized half an hour before the addition. Then, a TGF- $\beta$  standard solution was prepared, 400  $\mu$ L double steam water was added to the TGF- $\beta$  powder, and 4,000 pg/mL TGF- $\beta$  standard ponder was prepared after resurgence. Seven tubes were labeled as 1-7, and 225  $\mu$ L dilution analysis buffer was added to them. A standard solution of 2,000 pg/mL was prepared by adding 225  $\mu$ L of 4,000 pg/mL RGF- $\beta$ 1 standard concentrate into a no. 1 tube. Then, it was added to a no. 2 tube, mixed evenly, and successively used to prepare standard curves with concentrations of 2,000, 1,000, 500, 250, 125, 63, and 31 pg/mL. Dilution analysis buffer was selected as a blank.

First, the sample was pretreated. The sample was diluted at a ratio of 1 : 10. 180  $\mu$ L dilution analysis buffer was added to 20  $\mu$ L sample, and 20  $\mu$ L 1N hydrochloric acid solution was added, mixed. After incubation for 1 h, the sample was neutralized with 20  $\mu$ L of 1N NaOH in a 96-well plate. The plate was washed twice with buffer solution on an automatic plate washing machine and then patted dry. The wells were filled with seven standard series solutions, and the rest went into the analysis buffer. Then, 60  $\mu$ L analytical buffer solution was added to each well, and 40  $\mu$ L pretreated samples were added in turn, shaken, and incubated at 100 r/min for 2 h. The automatic plate washing machine was employed to wash it 5 times, patted dry, added to 100  $\mu$ L of enzyme antibody, shaken again for 100 r/min, incubated for 1 h, washed 5 times, and patted dry again. Streptavidin-HRP (100  $\mu$ L) was added to each well, shaken, incubated at 100 r/min for 1 h, washed 5 times, and patted dry again. Then, 100  $\mu$ L chromogenic agent was added to each well and incubated at room temperature for 30 minutes. Then, 100  $\mu$ L stop solution was added and mixed well. A

microplate reader was employed to determine the optical density at 450 nm, and the concentration of TGF- $\beta$  was calculated. The same method was used to determine TGF- $\alpha$ .

**2.8. Statistical Methods.** Excel 2007 and SPSS 25.0 (SPSS Inc., Chicago, IL, USA) were used to input the collected data for statistical analysis. Analysis of variance was adopted to compare the correlation between Th17 cells and Treg cells. *Cell-Quest* was employed to analyze the results, and Th17 cells were expressed as a percentage. The mean  $\pm$  standard deviation ( $\bar{x} \pm s$ ) was used to represent the measurement data conforming to a normal distribution. ANOVA was used to represent Th17 cells and Treg cells among lung cancer groups with different stages and types, and frequency and frequency (%) were used to represent the nonconforming count data. The correlation between Th17 cells and Treg cells was analyzed by Pearson correlation analysis. The counting data were tested by  $\chi^2$ . The difference was substantial at  $P < 0.05$ .

### 3. Results and Discussion

**3.1. General Information.** Among the 82 patients selected, 65 were male, accounting for 79.27%, and 17 were female, accounting for 20.73% (Table 1). There were 31 patients in stage IIIB, accounting for 37.80%, and 51 patients in stage IV, accounting for 62.20%. There were three tumor types, including 43 cases of squamous carcinoma (52.44%), 30 cases of adenocarcinoma (36.59%), and 9 cases of large cell carcinoma (10.98%). The 52 cases of smoking patients accounted for 63.41% higher than that of nonsmoking patients. There were 25 cases with immunotoxic reactions (30.49%) and 57 cases without immunotoxic reactions (69.51%).

**3.2. Ratio of Th17 Cells in Peripheral Blood.** Eighty-two patients with NSCLC combined with COPD were the observation group, and normal healthy people were the control group. Figure 1 shows that the proportion of Th17 cells in the peripheral blood of patients in observation group was notably superior to that in the controls ( $P < 0.01$ ). Treg/Th17 in the peripheral blood of patients decreased remarkably versus controls ( $P < 0.05$ ).

**3.3. Comparison of Th17 and Treg/Th17 Cells of Patients with Different Case Types.** Among the 82 subjects, there were 43 cases of squamous cell carcinoma, 30 cases of adenocarcinoma, and 9 cases of large cell carcinoma (Figure 2). There was no considerable difference among different case types in the proportion of Th17 cells in CD4+ T cells in the blood of the three types of patients and the proportion of CD4+ CD25<sup>Hi</sup>CD127<sup>Lo</sup> regulatory T cells in CD4+ lymphocyte cells of Treg cells ( $P > 0.05$ ).

**3.4. Comparison of Peripheral Blood Th17 and Treg/Th17 in Patients with Different TNM Stages.** There was no considerable difference in the proportion of Th17 cells to CD4+ T cells in the peripheral blood of patients with stage IIIB and stage IV lung cancer (Figure 3), and there was no great difference in the proportion of CD4+ CD25<sup>Hi</sup>CD127<sup>Lo</sup> regulatory T cells to CD4+ lymphocyte cells in Treg cells

TABLE 1: General clinical characteristics of the patients.

	Total	Proportion	<i>P</i>
Gender	82	100%	0.812
Female	17	20.730	
Male	65	79.270	
Tumor staging			0.531
IIIB	31	37.800	
IV	51	62.200	
Tumor types			0.624
Adenocarcinoma	30	36.590	
Squamous cell carcinomas	43	52.440	
Large cell carcinoma	9	10.980	
Smoking			0.063
No	30	36.590	
Yes	52	63.410	
Immune toxicity and side effects			0.008
No	57	69.510	
Yes	25	30.490	

( $P > 0.05$ ). There was no considerable difference in Treg/Th17 in peripheral blood between stage IIIB and stage IV lung cancer patients ( $P > 0.05$ ).

**3.5. Correlation Analysis of Th17 Cells and Treg Cells of Lung Cancer Patients with COPD.** The correlation between Th17 cells and Treg cells in the peripheral blood of patients with NSCLC complicated with COPD was analyzed. The results are shown in Figure 4, showing a positive linear correlation between the two,  $R = 0.26$  and  $P = 0.039$ .

**3.6. Comparison of Immune Function before and after Treatment.** In Figure 5, CD4+ and CD4+/CD8+ were notably superior to before treatment, while CD8+ was greatly inferior to before treatment. The cellular immune indexes of patients before and after treatment were compared, and the difference was substantial ( $P < 0.05$ ).

**3.7. Pulmonary Function Changes before and after Radiotherapy.** The FEV1%/FVC, FEV1%, and FVC of patients before and after chemotherapy were compared and analyzed (Figure 6), and the difference was substantial one month after radiotherapy compared with that before radiotherapy ( $P < 0.05$ ). There was no considerable difference in FEV1%/FVC of patients two weeks after radiotherapy compared with that before radiotherapy ( $P > 0.05$ ), but there were considerable differences in FEV1% and FEV ( $P < 0.05$ ). After receiving radiotherapy, the lung function of patients showed varying degrees of change, with some changes in lung function, and some indexes had considerable differences relative to those before radiotherapy ( $P < 0.05$ ).

**3.8. Comparison of MVV/MEF before and after Radiotherapy.** In Figure 7, MVV and MEF were changed after two weeks and one month of treatment compared with those before treatment, and pulmonary function improved remarkably ( $P < 0.05$ ).

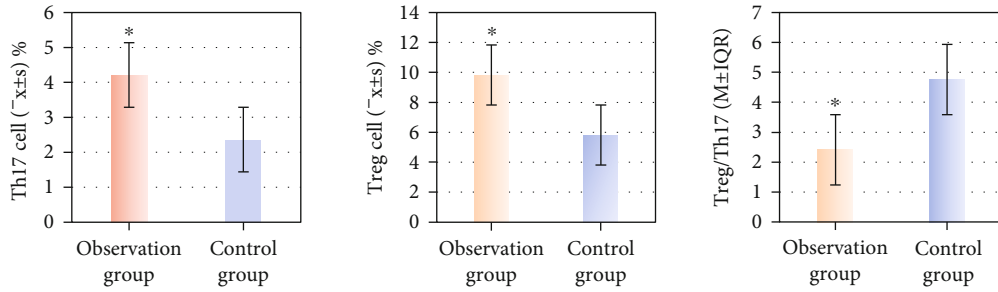


FIGURE 1: Comparison results of peripheral blood cells between the two groups. (\* indicates considerable difference,  $P < 0.05$ ).

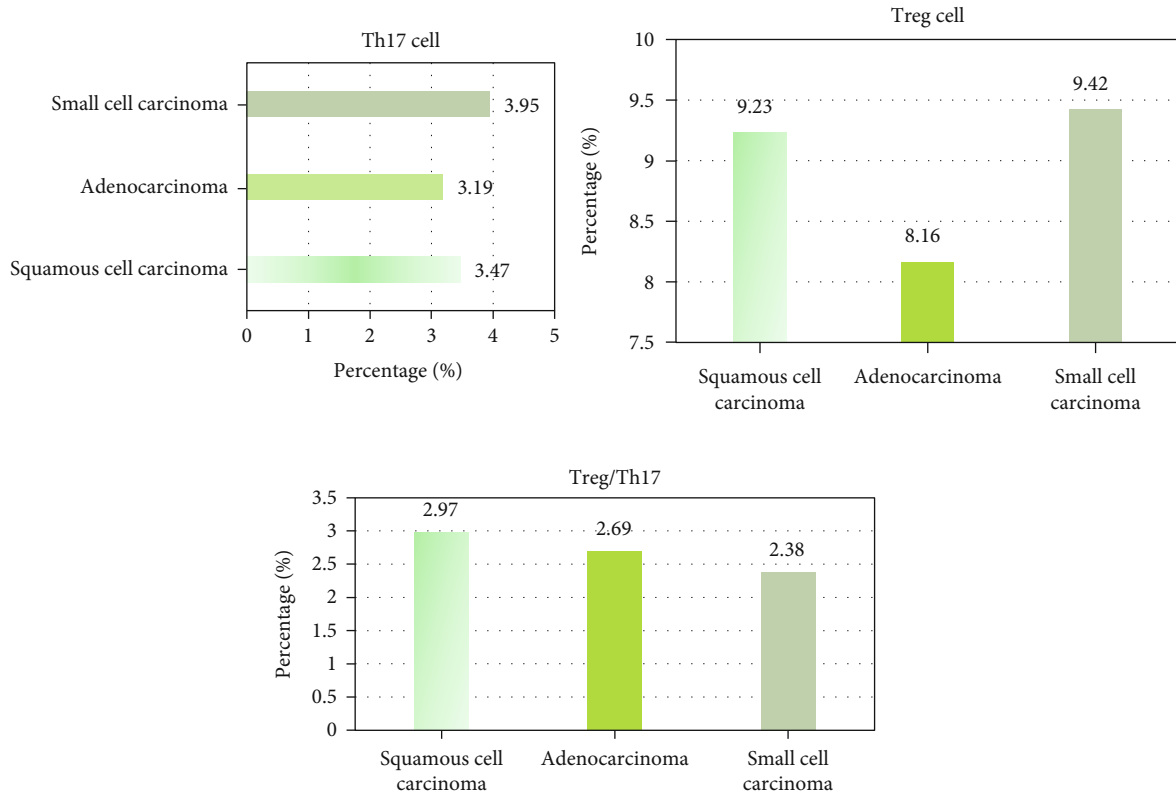


FIGURE 2: Comparison of Th17 and Treg/Th17 cell proportions of patients with different case types.

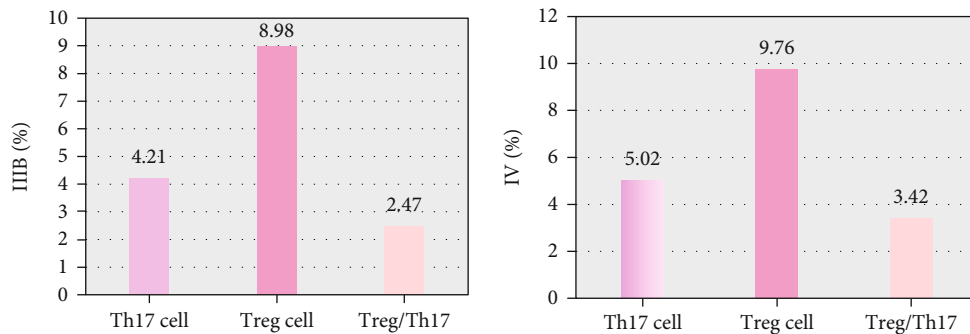


FIGURE 3: Comparison of Th17 and Treg/Th17 cell proportions of patients with different TNM types.

3.9. Comparison of the Peripheral Blood Cytokines IL-17, IL-6, TNF- $\alpha$ , and TGF- $\beta$ . The levels of IL-17, IL-6, TNF- $\alpha$ , and TGF- $\beta$  in the peripheral blood of lung cancer patients in

observation group and control group were compared (Figure 8), and those in lung cancer patients with COPD were notably superior to those in control group ( $P < 0.05$ ).

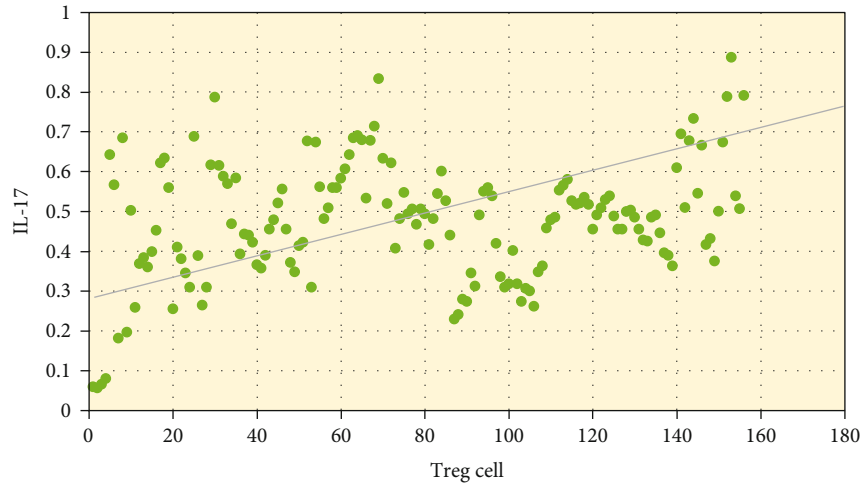


FIGURE 4: Correlation between peripheral blood Th17 cells and Treg cells.

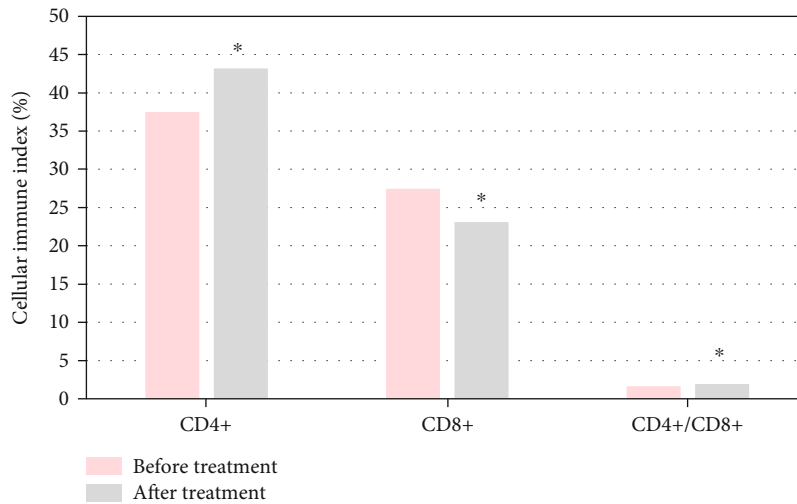


FIGURE 5: Comparison of immune function before and after treatment. (\* indicates a substantial difference vs. before treatment,  $P < 0.05$ ).

#### 4. Discussion

COPD is a widespread respiratory disease with a high mortality rate, affecting more than 5% of the world’s population. Cough and sputum are the most common clinical symptoms of COPD and lung cancer, and misdiagnosis and missed diagnoses are common during the diagnosis and treatment process [25]. Immunosuppressants have been applied to treat NSCLC and have brought some benefits to patients. Clinically, the lung function and immune function of patients with NSCLC complicated with COPD will decline to varying degrees, as will their immunity [26, 27]. Clinical data showed that patients with NSCLC complicated with COPD had different degrees of decline in lung function after receiving radiotherapy, and patients received different doses of radiotherapy. In this study, patients with advanced NSCLC complicated with COPD were treated with PD-1 and Treg/Th17 cells. Comparative investigation of the results of patients before and after radiotherapy showed that

the lung function of various patients showed different degrees of change after radiotherapy. The change in lung function was more dramatic than the change before treatment, and some lung function indicators were significantly different from those before radiotherapy, with statistical significance ( $P < 0.05$ ). In many studies of COPD, FEV1%/FEV and FEV1% are the primary evaluation indexes. Studies have shown that the diagnostic rate of the lung function index of FEV1%/FVC, FEV1%, and FVC is more than 95%. There was a large difference in the therapeutic effect of NSCLC between smokers and nonsmokers. Smokers had a higher mutation load, and the response to immune target inhibitors was also enhanced. PD-1 has a poor therapeutic effect on smokers, which also shows that smoking history can be an effective predictor [28, 29].

Immunotherapy for NSCLC has taken a new turn with the introduction of immunosuppressive medicines. These medications have few side effects, are well tolerated, and are frequently utilized in the treatment of tumors. In this



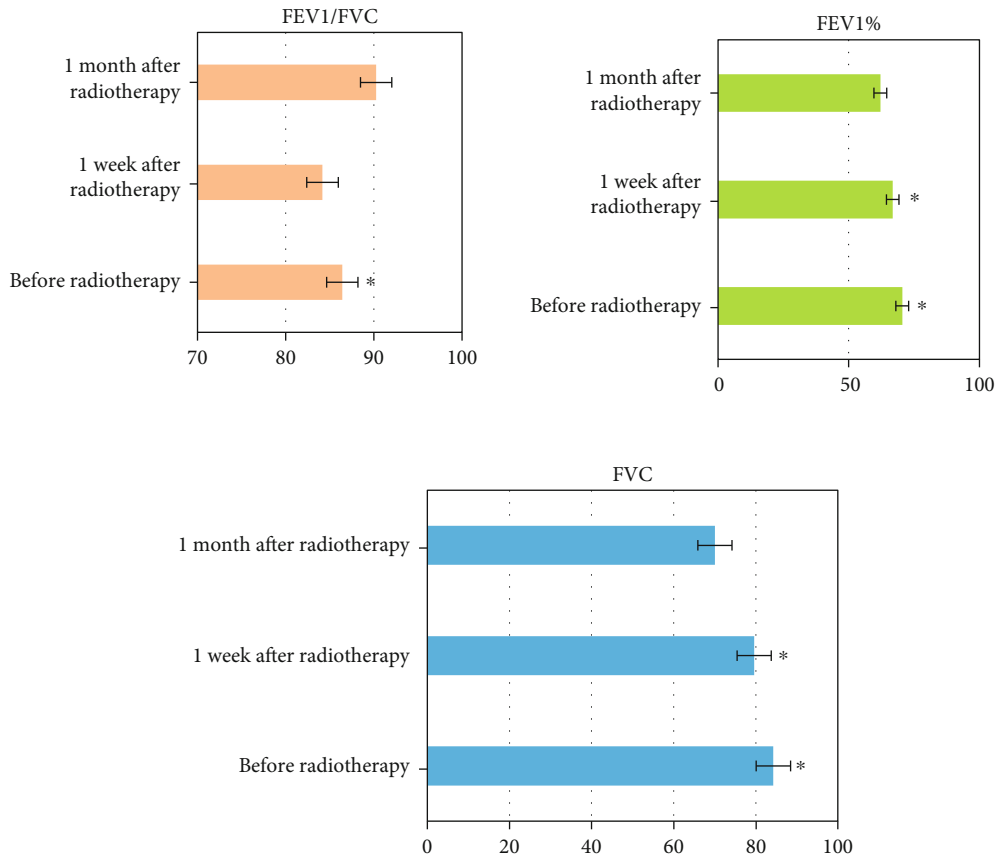


FIGURE 6: Comparison of FEV1%/FVC, FEV1%, and FVC before and after chemotherapy. (\* indicates a substantial difference vs. before radiotherapy,  $P < 0.05$ ).

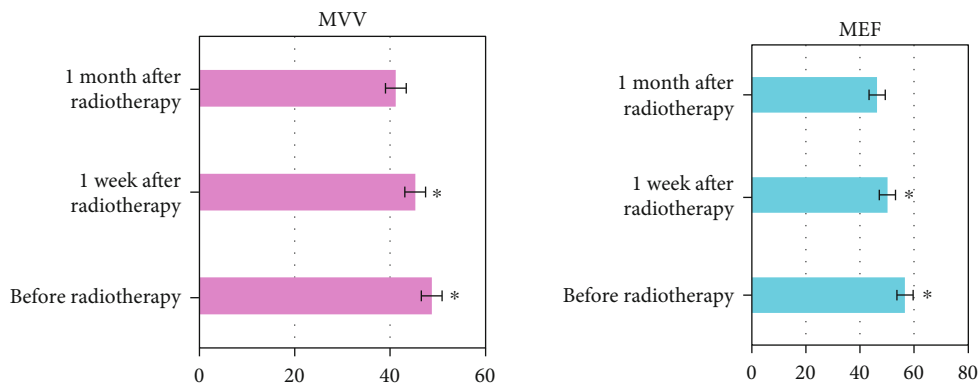


FIGURE 7: Comparison of MVV and MEF before and after chemotherapy. (\* indicates a substantial difference vs. before radiotherapy,  $P < 0.05$ ).

study, a PD-1 mAb was used to treat NSCLC patients. CD4+ and CD4+/CD8+ were remarkably higher after treatment than before, while CD8+ was greatly inferior to before. The cellular immune indexes of patients before and after treatment were compared with those before treatment, and the difference was substantial ( $P < 0.05$ ), indicating that PD-1 can improve the immune function of patients with NSCLC and has high clinical application value. This is consistent with many studies. PD-1 expression is one of the most widely used clinical markers for immunotherapy prediction,

and the expression of PD-1 in solid tumor tissues monitored by histochemistry is associated with poor prognosis of gastric cancer, liver cancer, and cell carcinoma. Data suggest that patients with advanced NSCLC with high PD-1 expression respond better to pembrolizumAb treatment [30]. PD-1 mAb is effective in tumor immune escape due to its role in promoting tumor T cell apoptosis in both an independent and dependent manner. By altering the surrounding environment, cancer cells promote immune evasion, multiplication, and survival. PD-1 therapy's main goal is to stimulate T

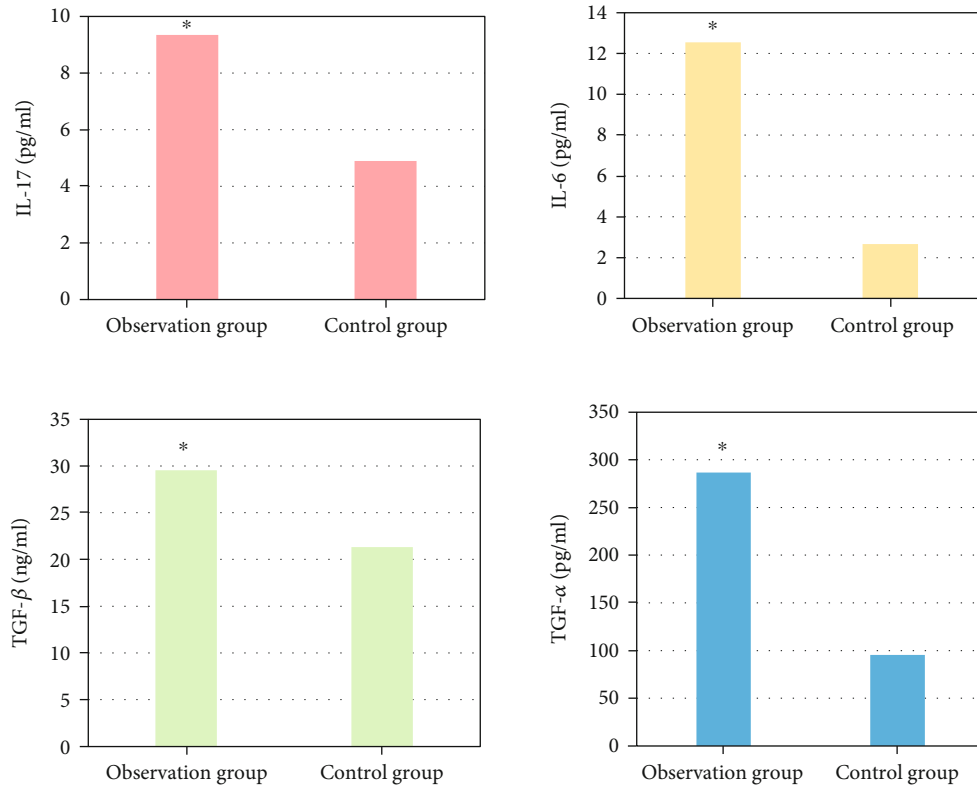


FIGURE 8: Comparison of the cytokines IL-17, IL-6, TGF- $\beta$ , and TGF- $\alpha$  in peripheral blood. (\* indicates a substantial difference vs. before treatment,  $P < 0.05$ ).

lymphocytes in the tumor microenvironment in order to establish tumor resistance [31, 32]. Gauvain et al. [33] looked at patients with NSCLC brain metastases who were given nivolumAb and found that the intracerebral control rate was 51%, indicating some safety. The level of Th17 cells increases to varying degrees in a variety of solid tumor tissues. In cancer diseases, the higher the TNM stage, the more obvious the increase in the level of Th17 cells. Th17 cells can secrete IFN- $\gamma$  to a certain extent, which can play an antitumor role. Studies have shown that TGF- $\beta$  can inhibit Th17 production and induce Treg cell formation in ovarian cancer cells. Th17 cells in tumor patients were greatly inferior to those in normal subjects, indicating immunosuppression in the tumor microenvironment. When the Treg level increases, antitumor immunity is suppressed, resulting in an imbalance in the Th17/Treg status in tumor patients [34]. Li et al. [35] discussed the relationship between TregFoxP3(+) and Th17 cells and the occurrence of lung cancer and showed that the ratio of TregFoxP3(+), Th17 and TregFoxP3(+)/Th17 in the peripheral blood of NSCLC patients was higher than that of healthy controls ( $P < 0.05$ ). The proportion of Th17 cells in NSCLC patients was positively correlated with the proportion of TregFoxP3(+) ( $r = 0.81$ ,  $P < 0.05$ ). In this study, the same results were obtained, and there was a positive linear correlation between Th17 cells and Treg cells in the peripheral blood of patients with NSCLC combined with COPD by Treg/Th17 ratio analysis after treatment in NSCLC patients,  $R = 0.26$ ,  $P = 0.039$ . TGF- $\beta$ , IL-17,

and IL-6 levels were higher in NSCLC patients than controls. Patients with stage IIIB and IV disease showed significant improvement in lung function after PD-1 immunotherapy. It was concluded that the Treg/Th17 ratio was related to the stage of NSCLC, but there was no considerable difference between TNN stages in this study, and both stage IIIB and stage IV were probably advanced, so the difference was not significant. The patients' immunological indices improved after treatment. This also suggests that PD-1 immunotherapy influences the immune status of patients with advanced NSCLC.

## 5. Conclusions

The efficacy of Treg/Th17 and PD-1 monoclonal antibodies in the treatment of NSCLC in patients with NSCLC complicated with COPD was investigated. Treg and Th17 cells were remarkably higher, which may lead to immunosuppression and promote tumor formation in COPD patients with NSCLC. PD-1 treatment of NSCLC has clear efficacy and can improve the immune status of patients with high safety. The cytokine modulation of Treg and Th17 cells may be linked to the Treg/Th17 ratio imbalance in lung cancer patients. Furthermore, follow-up research can conduct in-depth studies on the imbalance of the Treg/Th17 ratio in the hopes of clarifying the relationship between many components in this process and providing more accurate data support for tumor cure.

## Data Availability

The data used to support the findings of this study are available from the corresponding author upon request.

## Conflicts of Interest

The authors declare that they have no conflicts of interest.

## References

- [1] R. L. Siegel, K. D. Miller, and A. Jemal, "Cancer statistics, 2016," *CA: a Cancer Journal for Clinicians*, vol. 66, no. 1, pp. 7–30, 2016.
- [2] R. Luengo-Fernandez, J. Leal, A. Gray, and R. Sullivan, "Economic burden of cancer across the European Union: a population-based cost analysis," *The Lancet Oncology*, vol. 14, no. 12, pp. 1165–1174, 2013.
- [3] J. C. Soria, Y. Ohe, J. Vansteenkiste et al., "Osimertinib in untreated EGFR-mutated advanced non-small-cell lung cancer," *The New England Journal of Medicine*, vol. 378, no. 2, pp. 113–125, 2018.
- [4] M. Nakao, H. Muramatsu, Y. Kagawa et al., "Immunological status may predict response to nivolumab in non-small cell lung cancer without driver mutations," *Anticancer Research*, vol. 37, no. 7, pp. 3781–3786, 2017.
- [5] E. Bagdonas, J. Raudoniute, I. Bruzauskaite, and R. Aldonyte, "Novel aspects of pathogenesis and regeneration mechanisms in COPD," *International Journal of Chronic Obstructive Pulmonary Disease*, vol. 10, pp. 995–1013, 2015.
- [6] N. A. Negewo, P. G. Gibson, and V. M. McDonald, "COPD and its comorbidities: impact, measurement and mechanisms," *Respirology*, vol. 20, no. 8, pp. 1160–1171, 2015.
- [7] M. C. Smith and J. P. Wrobel, "Epidemiology and clinical impact of major comorbidities in patients with COPD," *International Journal of Chronic Obstructive Pulmonary Disease*, vol. 9, pp. 871–888, 2014.
- [8] R. Gloeckl, B. Marinov, and F. Pitta, "Practical recommendations for exercise training in patients with COPD," *European Respiratory Review*, vol. 22, no. 128, pp. 178–186, 2013.
- [9] W. S. D. Tan, H. M. Shen, and W. S. F. Wong, "Dysregulated autophagy in COPD: a pathogenic process to be deciphered," *Pharmacological Research*, vol. 144, pp. 1–7, 2019.
- [10] S. P. Duffy and G. J. Criner, "Chronic obstructive pulmonary disease," *The Medical Clinics of North America*, vol. 103, no. 3, pp. 453–461, 2019.
- [11] P. Jones, M. Miravittles, T. van der Molen, and K. Kulich, "Beyond FEV<sub>1</sub> in COPD: a review of patient-reported outcomes and their measurement," *International Journal of Chronic Obstructive Pulmonary Disease*, vol. 7, pp. 697–709, 2012.
- [12] M. Vitacca and M. Paneroni, "Rehabilitation of patients with coexisting COPD and heart failure," *COPD: Journal of Chronic Obstructive Pulmonary Disease*, vol. 15, no. 3, pp. 231–237, 2018.
- [13] B. M. Thomashow, D. M. Mannino, R. Tal-Singer, and J. D. Crapo, "A rapidly changing understanding of COPD: World COPD Day from the COPD Foundation," *American Journal of Physiology. Lung Cellular and Molecular Physiology*, vol. 321, no. 5, pp. L983–L987, 2021.
- [14] S. Bins, E. A. Basak, S. el Bouazzaoui et al., "Association between single-nucleotide polymorphisms and adverse events in nivolumab-treated non-small cell lung cancer patients," *British Journal of Cancer*, vol. 118, no. 10, pp. 1296–1301, 2018.
- [15] S. Jonna and D. S. Subramaniam, "Molecular diagnostics and targeted therapies in non-small cell lung cancer (NSCLC): an update," *Discovery Medicine*, vol. 27, no. 148, pp. 167–170, 2019.
- [16] S. S. Lee and Y. K. Cheah, "The interplay between microRNAs and cellular components of tumour microenvironment (TME) on non-small-cell lung cancer (NSCLC) progression," *Journal of Immunology Research*, vol. 2019, Article ID 3046379, 2019.
- [17] E. N. Imyanitov, A. G. Iyevleva, and E. V. Levchenko, "Molecular testing and targeted therapy for non-small cell lung cancer: current status and perspectives," *Critical Reviews in Oncology/Hematology*, vol. 157, article 103194, 2021.
- [18] Y. K. Chae, S. Chang, T. Ko et al., "Epithelial-mesenchymal transition (EMT) signature is inversely associated with T-cell infiltration in non-small cell lung cancer (NSCLC)," *Scientific Reports*, vol. 8, no. 1, p. 2918, 2018.
- [19] D. Saraggi, F. Galuppini, A. Remo et al., "PD-L1 overexpression in ampulla of Vater carcinoma and its pre-invasive lesions," *Histopathology*, vol. 71, no. 3, pp. 470–474, 2017.
- [20] P. Fessas, H. Lee, S. Ikemizu, and T. Janowitz, "A molecular and preclinical comparison of the PD-1-targeted T-cell checkpoint inhibitors nivolumab and pembrolizumab," *Seminars in Oncology*, vol. 44, no. 2, pp. 136–140, 2017.
- [21] N. A. Pennell, M. E. Arcila, D. R. Gandara, and H. West, "Biomarker testing for patients with advanced non-small cell lung cancer: real-world issues and tough choices," *American Society of Clinical Oncology Educational Book*, vol. 39, pp. 531–542, 2019.
- [22] L. La Fleur, J. Botling, F. He et al., "Targeting MARCO and IL37R on immunosuppressive macrophages in lung cancer blocks regulatory T cells and supports cytotoxic lymphocyte function," *Cancer Research*, vol. 81, no. 4, pp. 956–967, 2021.
- [23] J. C. Liu, S. Narva, K. Zhou, and W. Zhang, "A review on the antitumor activity of various nitrogenous-based heterocyclic compounds as NSCLC inhibitors," *Mini Reviews in Medicinal Chemistry*, vol. 19, no. 18, pp. 1517–1530, 2019.
- [24] A. Nambirajan, V. Singh, N. Bhardwaj, S. Mittal, S. Kumar, and D. Jain, "SMARCA4/BRG1-deficient non-small cell lung carcinomas: a case series and review of the literature," *Archives of Pathology & Laboratory Medicine*, vol. 145, no. 1, pp. 90–98, 2021.
- [25] E. Redin, I. Garmendia, T. Lozano et al., "SRC family kinase (SFK) inhibitor dasatinib improves the antitumor activity of anti-PD-1 in NSCLC models by inhibiting Treg cell conversion and proliferation," *Journal for Immunotherapy of Cancer*, vol. 9, no. 3, article e001496, 2021.
- [26] H. Van Damme, B. Dombrecht, M. Kiss et al., "Therapeutic depletion of CCR8+tumor-infiltrating regulatory T cells elicits antitumor immunity and synergizes with anti-PD-1 therapy," *Journal for Immunotherapy of Cancer*, vol. 9, no. 2, article e001749, 2021.
- [27] N. Shi, D. Feng, Y. Gu, C. Zheng, and M. Miao, "TUSC8 enhances cisplatin sensitivity of NSCLC cells through regulating VEGFA," *Journal of BUON*, vol. 26, no. 2, pp. 336–344, 2021.

- [28] H. Borghaei, L. Paz-Ares, L. Horn et al., “Nivolumab versus docetaxel in advanced nonsquamous non-small-cell lung cancer,” *The New England Journal of Medicine*, vol. 373, no. 17, pp. 1627–1639, 2015.
- [29] M. Reck, D. Rodríguez-Abreu, A. G. Robinson et al., “Pembrolizumab versus chemotherapy for PD-L1-positive non-small-cell lung cancer,” *New England Journal of Medicine*, vol. 375, no. 19, pp. 1823–1833, 2016.
- [30] M. Muller, R. D. Schouten, C. J. De Gooijer, and P. Baas, “Pembrolizumab for the treatment of non-small cell lung cancer,” *Expert Review of Anticancer Therapy*, vol. 17, no. 5, pp. 399–409, 2017.
- [31] J. Bellmunt, T. Powles, and N. J. Vogeizang, “A review on the evolution of PD-1/PD-L1 immunotherapy for bladder cancer: the future is now,” *Cancer Treatment Reviews*, vol. 54, no. 27, pp. 58–67, 2017.
- [32] V. Prasad and V. Kaestner, “Nivolumab and pembrolizumab: monoclonal antibodies against programmed cell death-1 (PD-1) that are interchangeable,” *Seminars in Oncology*, vol. 44, no. 2, pp. 132–135, 2017.
- [33] C. Gauvain, E. Vauléon, C. Chouaid et al., “Intracerebral efficacy and tolerance of nivolumab in non-small-cell lung cancer patients with brain metastases,” *Lung Cancer*, vol. 116, no. 15, pp. 62–66, 2018.
- [34] M.-C. Duan, X.-N. Zhong, G.-N. Liu, and J.-R. Wei, “The Treg/Th17 paradigm in lung cancer,” *Journal of Immunology Research*, vol. 2014, Article ID 730380, 2014.
- [35] S. Li, Y. Li, X. Qu, X. Liu, and J. Liang, “Detection and significance of TregFoxP3(+) and Th17 cells in peripheral blood of non-small cell lung cancer patients,” *Archives of Medical Science*, vol. 10, no. 2, pp. 232–239, 2014.

## Research Article

# Combined Effect of Smoking and Fatty Liver Disease on the Progression of Type 2 Diabetes: Insights from a Population-Based Cohort Study

Tingting Zhang <sup>1</sup>, Donghe Zhang,<sup>2</sup> Jing Zeng,<sup>1</sup> Yan Yang,<sup>1</sup> Yi Fang <sup>1</sup> and Xuan Wang <sup>1</sup>

<sup>1</sup>Department of Endocrinology, The Fifth Medical Center of Chinese PLA Hospital, Beijing, China

<sup>2</sup>Department of Day Clinic, The Fifth Medical Center of Chinese PLA Hospital, Beijing, China

Correspondence should be addressed to Yi Fang; [fangyi5zhongxin@163.com](mailto:fangyi5zhongxin@163.com) and Xuan Wang; [endocrine@163.com](mailto:endocrine@163.com)

Tingting Zhang and Donghe Zhang contributed equally to this work.

Received 5 May 2022; Revised 26 May 2022; Accepted 30 May 2022; Published 9 July 2022

Academic Editor: Naeem Jan

Copyright © 2022 Tingting Zhang et al. This is an open access article distributed under the Creative Commons Attribution License, which permits unrestricted use, distribution, and reproduction in any medium, provided the original work is properly cited.

**Objectives.** Fatty liver disease (FLD) is strongly linked to the occurrence of type 2 diabetes mellitus (T2DM). Insulin resistance (IR) is linked to smoking. Our study's purpose was to see how smoking and fatty liver accompanied affected the development of T2DM in the past. **Materials and Methods.** We collected data from 15,464 Japanese adults aged 18 to 79 years who took part in the NAGALA research, and our team utilized a Cox proportion risk model to look at the combination effect of FLD and smoking status on the incidence of T2DM. Participants were separated into three categories: nonsmokers, ex-smokers, and current smokers. An abdominal ultrasound was used to diagnose FLD. **Results.** 384 subjects had T2DM after a median follow-up of 5.4 years. In comparison to the other groups, current FLD smokers had a greater chance of developing T2DM. Ex-smokers and present FLD smokers, on the other hand, had no significant difference in their likelihood of acquiring T2DM. When compared to ex-smokers and nonsmokers without FLD, current smokers with FLD had a considerably greater chance of acquiring T2DM. Furthermore, the risk of T2DM among nonsmokers, ex-smokers with FLD, and current smokers without FLD was not statistically significant. **Conclusions.** In order to prevent the progression of T2DM, we should recognize that smoking status may vary in FLD.

## 1. Introduction

As one of the most rapidly growing chronic diseases nowadays, early intervention for diabetes is of great interest. The International Diabetes Federation reports that in 2019, the global prevalence of diabetes is 9.3% among adults aged 20-79 years (an astonishing 463 million people), and this number is anticipated to attain 700 million by 2045 [1]. Individuals, society, and the nation all bear a significant financial burden due to type 2 diabetes mellitus (T2DM) and its sequelae. Unhealthy eating habits, obesity, and a sedentary life style are all key risk factors for type 2 diabetes [2, 3]. Therefore, it is important to prevent and treat T2DM. Fatty liver disease (FLD), is tightly related to IR in the body. Cur-

rently, it is considered one of the main reasons of ectopic fat cumulation [4, 5] and has been reported as a vital risky factor for the developmental process of T2DM [5].

As a major issue of social and human health, smoking itself now affects about 1.1 billion people worldwide [6]. Based on four main aspects of pathological mechanisms, increased abdomen fat cumulation, elevated sympathetic activity, chronic pancreatic cell inflammation, and straight toxic impairment to pancreas cells, smoker develops abnormal glucose metabolism and even promotes the development of diabetes [7, 8]. In patients who were diagnosed with diabetes, studies also have found that smoking causes inflammation and vascular endothelial dysfunction, which in turn increases the risks of micro blood vessel and major

vessel illnesses in diabetic's sufferers [7, 9]. Cotinine-validated current smoking and self-reported current smoking have both been associated to nonalcoholic fatty liver disease (NAFLD) [10]. As a result, depending on background variables like FLD, the effect of smoking status on T2DM may differ. However, no prior research has looked at the combined impact of FLD and smoking status on the development of T2DM.

The influence of smoking status on the incidence of incident T2DM in people with and without FLD was investigated in the present study. The findings of this study could help doctors better understand how to counsel people about quitting smoking based on their unique circumstances, such as the presence of FLD.

The structure of this article is organized as follows. The materials and methods is presented in Section 2. The statistical analysis is explained in Section 3. The experimental results is presented in Section 4. Section 5 consists of the discussion section. Finally, Section 6 summarizes the paper's main points.

## 2. Materials and Methods

*2.1. Data Source.* Our team acquired data from the publicly available "DRYAD" database (<https://datadryad.org/>). Data can be obtained from the following article: ectopic fat obesity presents the greatest risk for incident T2DM: a population-based longitudinal study [5] (data set: 10.5061/dryad.8q0p192).

*2.2. Study Design and Participants.* This research was on the foundation of the accessible data from the NAGALA study. From 2004 to 2015, it was a longitudinal research at Murakami Memorial Hospital's Medical Health Checkup Center (Gifu, Japan). The NAGALA research was discussed in depth in the original article. In total, 20,944 individuals were recruited for this study between 2004 and 2015, and all participated in a physical examination program and completed at least two exams.

Finally, exclusion criteria were used to select 15,464 individuals for data analysis. (1) People who were already on medication at the time of the baseline detection ( $n = 2321$ ), (2) sufferers with abnormal glucose metabolism (T2DM  $n = 323$  or impaired fasting glucose (IFG)  $n = 808$ ), (3) people who drink heavily ( $n = 739$ ), (4) patients with a diagnosis of chronic viral hepatitis (like hepatitis B or hepatitis C ( $n = 416$ )), (5) patients with missing covariate data, such as height, exercise, alcohol intake, or abdomen ultrasound ( $n = 863$ ), and (6) patients with inaccurate data on waist circumference (WC) ( $n = 2$ ). The investigation was done by Okamura et al. [5]. According to their description, the study was accepted by Murakami Memorial Hospital's ethics committee, and each participant gave their informed permission.

*2.3. Measurements and Data Collection.* All participants completed a standardized self-administered questionnaire to acquire medical information and life style variables, such as alcohol use, smoking status, and physical activity. Experienced nurses performed anthropometric measurements of

participants such as weight, height, WC, and blood pressure. Body mass index (BMI) was computed via normal formula (weight/height squared ( $\text{kg}/\text{m}^2$ )). Fasting blood specimens were harvested and completed for measurements and analyses of biochemical indicators and other relevant indicators. These include total cholesterol, triglycerides, LDL-C, HDL-C, fasting blood glucose (FPG), and glycated hemoglobin (HbA1c).

*2.4. Definition of FLD.* Abdominal ultrasound was performed by a trained technician, and then, the gastroenterologist examined the ultrasound images without reference to other personal data of the subject. The diagnosis of FLD on ultrasound images is based on four criteria: vascular blurring, deep attenuation, liver and kidney sonography, and liver brightness [11].

*2.5. Definition of T2DM.* The diagnosis of T2DM in this study was on the foundation of  $\geq 1$  standards below that have been validated: FBG  $\geq 7.0$  mmol/L, HbA1c  $\geq 6.5\%$ , self-reported diabetic disease, or already treated for diabetes treatment [12].

Information on the smoking history of the study population was clarified by chart review and direct interviews with patients. The included study population was informed by a study information letter and then interviewed by telephone. From this interview and medical records, the study population was further divided into "nonsmokers" or "ex-smokers" and "current smokers."

## 3. Statistical Analysis

All analysis was completed via R Statistical Software (<http://www.r-project.org/>), and  $P < 0.05$  had significance on statistics. In addition, continuous variates are presented as average  $\pm$  SD, and categorical variates are presented as percentages (%).

Based on the presence of FLD and current smoking status, the participants were divided into six groups in our study and compared the differences between groups. The Kaplan-Meier technique was also utilized to provide a graphic representation of time to incident T2DM throughout follow-up, as well as the log-rank test to determine the importance of diversities between the six groups. Multivariable Cox regressive models were used to determine hazard ratios (HRs) and 95 percent confidence intervals (95 percent CI) for incident T2DM due to the presence of censored cases and the follow-up time being inconsistent. Models were provided that were both nonadjusted and multivariate adjusted. Confounding factors were defined as variables that altered the original regressive coefficients by more than 10%. Gender, age, BMI, alcohol consumption, fatty liver, SBP, triglycerides, HDL-C, FPG, and HbA1c were all adjusted in this study. Cox regression was used to test for trend by using the median value of six groups as categorical variables in the models. The stratified Cox regressive models were utilized to perform the subgroup analysis.

TABLE 1: The Characteristic of participants in the NAGALA study, 2004–2015.

	Total	Nonsmoker	Ex-smoker	Current smoker
FLD- ( <i>n</i> )	12723	7805	2226	2692
Sex, <i>n</i> (%)				
Women	6548 (51.5)	5709 (73.1)	416 (18.7)	423 (15.7)
Age (year)	43.5 ± 9.0	42.9 ± 8.7	45.2 ± 9.7	43.6 ± 9.0
Body weight (kg)	72.3 ± 11.2	70.5 ± 12.0	72.8 ± 9.5	74.7 ± 11.1
Body mass index (kg/m <sup>2</sup> )	21.4 ± 2.6	21.0 ± 2.6	22.1 ± 2.4	21.9 ± 2.7
Waist circumference (cm)	74.4 ± 8.0	72.6 ± 7.7	77.6 ± 7.3	77.0 ± 7.7
SBP (mm Hg)	112.5 ± 14.2	111.0 ± 14.1	116.4 ± 14.2	113.8 ± 14.0
DBP (mm Hg)	70.2 ± 10.0	68.9 ± 9.8	73.2 ± 10.0	71.3 ± 9.9
Exercise type, <i>n</i> (%)				
Irregular exercise	10415 (81.9)	6413 (82.2)	1699 (76.3)	2303 (85.5)
Regular exercise	2308 (18.1)	1392 (17.8)	527 (23.7)	389 (14.5)
HDL cholesterol (mmol/L)	1.5 ± 0.4	1.6 ± 0.4	1.5 ± 0.4	1.3 ± 0.4
Total cholesterol (mmol/L)	5.1 ± 0.8	5.1 ± 0.9	5.1 ± 0.8	5.0 ± 0.8
Triglycerides (mmol/L)	0.8 ± 0.5	0.7 ± 0.4	0.9 ± 0.6	1.0 ± 0.7
Fasting plasma glucose (mmol/L)	5.1 ± 0.4	5.0 ± 0.4	5.2 ± 0.4	5.2 ± 0.4
HbA1C (%)	5.1 ± 0.3	5.2 ± 0.3	5.1 ± 0.3	5.1 ± 0.3
Alcohol consume type, <i>n</i> (%)				
None or minimal alcohol consumer	9717 (76.4)	6838 (87.6)	1332 (59.8)	1547 (57.5)
Light alcohol consumer	1472 (11.6)	599 (7.7)	411 (18.5)	462 (17.2)
Moderate alcohol consumer	1110 (8.7)	295 (3.8)	347 (15.6)	468 (17.4)
Heavy alcohol consumer	424 (3.3)	73 (0.9)	136 (6.1)	215 (8)
ALT (IU/L)	15.0 (12.0, 20.0)	14.0 (11.0, 19.0)	17.0 (14.0, 22.0)	17.0 (13.0, 23.0)
AST (IU/L)	17.0 (14.0, 20.0)	16.0 (14.0, 20.0)	18.0 (14.0, 22.0)	17.0 (14.0, 20.0)
GGT (IU/L)	14.0 (11.0, 20.0)	13.0 (10.0, 16.0)	17.0 (13.0, 24.0)	17.0 (13.0, 24.0)
FLD+ ( <i>n</i> )	2741	1226	726	789
Sex, <i>n</i> (%)				
Women	486 (17.7)	430 (35.1)	25 (3.4)	31 (3.9)
Age (year)	44.8 ± 8.3	44.4 ± 8.4	46.4 ± 8.7	44.0 ± 7.6
Body weight	72.3 ± 11.2	70.5 ± 12.0	72.8 ± 9.5	74.7 ± 11.1
Body mass index (kg/m <sup>2</sup> )	25.5 ± 3.1	25.5 ± 3.3	25.2 ± 2.7	25.7 ± 3.2
Waist circumference (cm)	86.1 ± 7.7	85.3 ± 8.2	86.2 ± 6.6	87.2 ± 7.8
SBP (mm Hg)	123.8 ± 14.8	124.5 ± 15.2	124.6 ± 14.4	121.9 ± 14.4
DBP (mm Hg)	78.1 ± 10.2	78.2 ± 10.3	79.2 ± 10.1	77.0 ± 10.0
Exercise type, <i>n</i> (%)				
Irregular exercise	2340 (85.4)	1046 (85.3)	605 (83.3)	689 (87.3)
Regular exercise	401 (14.6)	180 (14.7)	121 (16.7)	100 (12.7)
HDL cholesterol (mmol/L)	1.2 ± 0.3	1.3 ± 0.3	1.2 ± 0.3	1.1 ± 0.3
Total cholesterol (mmol/L)	5.4 ± 0.9	5.4 ± 0.9	5.4 ± 0.8	5.5 ± 0.9
Triglycerides (mmol/L)	1.5 ± 0.8	1.3 ± 0.8	1.5 ± 0.9	1.6 ± 0.9
Fasting plasma glucose (mmol/L)	5.4 ± 0.4	5.4 ± 0.4	5.4 ± 0.4	5.4 ± 0.3
HbA1C (%)	5.3 ± 0.3	5.3 ± 0.3	5.3 ± 0.3	5.3 ± 0.3
Alcohol consume type, <i>n</i> (%)				
None or minimal alcohol consumer	2088 (76.2)	1069 (87.2)	480 (66.1)	539 (68.3)
Light alcohol consumer	286 (10.4)	82 (6.7)	104 (14.3)	100 (12.7)
Moderate alcohol consumer	250 (9.1)	55 (4.5)	101 (13.9)	94 (11.9)

TABLE 1: Continued.

	Total	Nonsmoker	Ex-smoker	Current smoker
Heavy alcohol consumer	117 (4.3)	20 (1.6)	41 (5.6)	56 (7.1)
ALT (IU/L)	27.0 (20.0, 39.0)	25.0 (19.0, 36.8)	28.5 (22.0, 41.0)	28.0 (21.0, 40.0)
AST (IU/L)	21.0 (17.0, 26.0)	20.0 (17.0, 26.0)	21.0 (17.0, 27.0)	20.0 (16.0, 25.0)
GGT (IU/L)	23.0 (17.0, 35.0)	21.0 (15.0, 30.8)	25.0 (19.0, 37.0)	25.0 (19.0, 38.0)

Data are expressed as the number (%) of subjects or mean (SD). ALT: alanine transaminase; AST: aspartate transaminase; DBP: diastolic blood pressure; FLD: fatty liver disease; GGT: gamma-glutamyl transferase; HDL: high-density lipoprotein; SBP: systolic blood pressure.

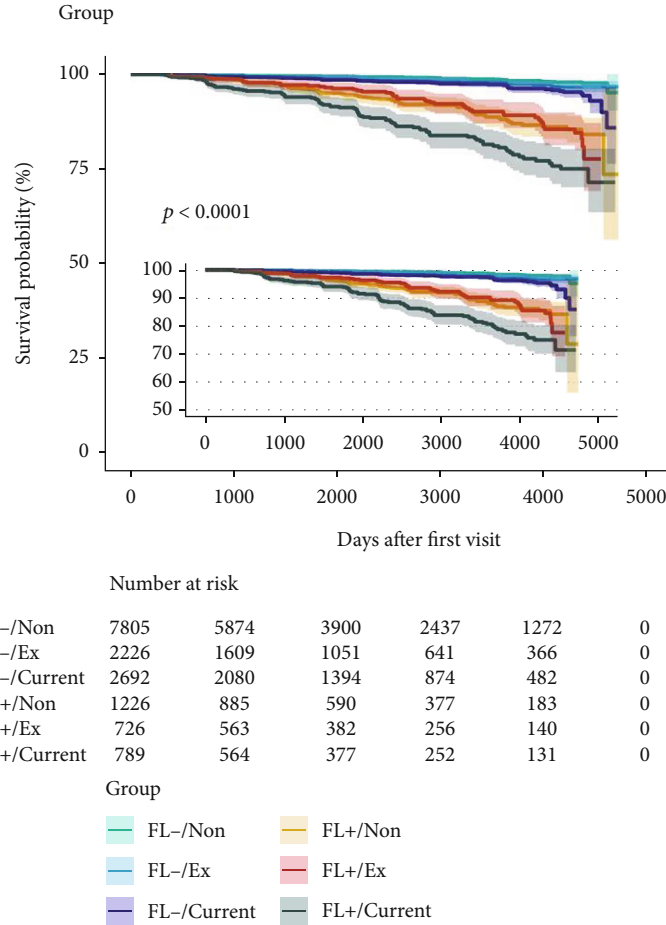


FIGURE 1: The Kaplan-Meier analysis of incident type 2 diabetes in the NAGALA study, 2004–2015.

## 4. Results

**4.1. Baseline Features of Participants.** At a median follow-up of 5.4 years, 373 of the 15,464 subjects had T2DM. The average age of the entire participants was  $43.71 \pm 8.90$  years, and 54.5% of the study population was male. All baseline information is shown in Table 1.

The proportions of nonsmoker, ex-smoker, and current smoker were 58.4% (9031), 19.1% (2952), and 22.5% (3481), respectively. We categorized six groups based on FLD status (with/without) and current smoking status, as well as the differences in baseline features between the six groups. The proportions (number) of nonsmoker, ex-

smoker, and current smoker without FLD were 61.3% (7805), 17.5% (2226), and 21.2% (2692), respectively, and that of nonsmoker, ex-smoker, and current smoker with FLD were 44.7% (1226), 26.5% (726), and 28.8% (789), respectively. Patients with FLD were much heavier than those without the disease. Furthermore, in patients with FLD, WC was significantly higher than in patients without FLD. Nonsmokers, ex-smokers, and current smokers had higher fasting glucose levels and lower HbA1C levels (Table 1).

At a median follow-up of 5.4 years, 373 participants had T2DM. The cumulative incidence of 4000-day T2DM was 11.9%, 6.9%, and 6.4% in nonsmokers, ex-smokers, and



TABLE 2: Univariate analysis for incident type 2 diabetes in the NAGALA study, 2004–2015.

	HR (95% CI)	<i>P</i> (Wald's test)	<i>P</i> (LR-test)
Sex: men vs. women	2.52 (1.98, 3.21)	< 0.001	< 0.001
Age (year)	1.06 (1.04, 1.07)	< 0.001	< 0.001
Fatty liver: yes vs. no	7.02 (5.70, 8.63)	< 0.001	< 0.001
Body mass index (kg/m <sup>2</sup> )	1.24 (1.22, 1.27)	< 0.001	< 0.001
Waist circumference (cm)	1.09 (1.08, 1.10)	< 0.001	< 0.001
ALT (mmol/L)	1.01(1.01, 1.01)	< 0.001	< 0.001
AST (mmol/L)	1.01 (1.01, 1.01)	< 0.001	< 0.001
GGT (mmol/L)	1.01 (1.01, 1.01)	< 0.001	< 0.001
HDL-C (mmol/L)	0.15 (0.11, 0.20)	< 0.001	< 0.001
TC (mmol/L)	1.49 (1.34, 1.66)	< 0.001	< 0.001
TG (mmol/L)	1.80 (1.68, 1.92)	< 0.001	< 0.001
HBA1C (%)	54.30 (39.51, 74.62)	< 0.001	< 0.001
Exercise : regular vs. irregular	0.76 (0.56, 1.02)	0.064	0.056
Alcohol consumption (%) ref. = 1			0.001
Light	0.90 (0.65, 1.26)	0.551	
Moderate	1.15 (0.82, 1.62)	0.424	
Heavy	2.24 (1.54, 3.27)	< 0.001	
Smoking status (%) ref. = 1			< 0.001
Ex-smoker	1.66 (1.26, 2.18)	< 0.001	
Current-smoker	2.58 (2.06, 3.24)	< 0.001	
FBG (mmol/L)	25.38 (18.71, 34.42)	< 0.001	< 0.001
SBP (mm Hg)	1.03 (1.03, 1.04)	< 0.001	< 0.001
DBP (mm Hg)	1.05 (1.04, 1.06)	< 0.001	< 0.001

BMI: body mass index; WC: waist circumference; HDL-C: high-density lipoprotein cholesterol; TC: total cholesterol; TG: triglyceride; FPG: fasting plasma glucose; SBP: systolic blood pressure; DBP: diastolic blood pressure; T2DM: type 2 diabetes mellitus; CI: confidence interval; HR: hazard ratio.

current smokers without FLD, respectively (Figure 1). Compared with nonsmoker, ex-smoker displayed a remarkable risk for incident T2DM (HR 1.66, 95% CI 1.26 to 2.18,  $P < 0.001$ ), and current smoker displayed a remarkable risk as well (HR 2.58, 95% CI 2.06 to 3.24,  $P < 0.001$ ). FLD displayed a remarkable risk as well (HR 7.02, 95% CI 5.7 to 8.63,  $P < 0.001$ ) (Table 2).

To examine the six groups' risk of developing T2DM, we employed Cox proportion risk models (univariable and multivariable Cox proportion risk models). The effect sizes (HR) and 95% CI intervals are listed in Table 3. Current smokers without FLD had a significantly higher risk of incident T2DM in gender- and age-adjusted Cox-hazard regression analysis (HR, 2.16; 95% CI, 1.45 to 3.22); in the fully adjusted model, Cox-hazard regression analysis, current smoker without FLD significantly increased risk for incident T2DM (HR, 1.78; 95% CI, 1.18 to 2.68) (Table 3). In gender- and age-adjusted Cox-hazard regression analysis, nonsmoker with FLD significantly increased risk for incident T2DM (HR, 7.44; 95% CI, 5.29 to 10.52); in the fully adjusted model, Cox-hazard regressive analyses, nonsmoker with FLD significantly increased risk for incident T2DM (HR, 2.02; 95% CI, 1.38 to 2.95) (Table 3). In gender- and age-adjusted Cox-hazard regressive analyses, current smoker with FLD remarkably elevated risk for incident T2DM (HR, 13.39; 95% CI, 9.19 to 19.5). In the fully adjusted model,

Cox-hazard regressive analyses, current smoker with FLD significantly increased risk for incident T2DM (HR, 3.63; 95% CI, 2.41 to 5.48) (Table 3).

Figure 2 depicts the findings of HRs for each of the six groups on incident T2DM. Nonsmokers without FLD and ex-smokers without FLD had a reduced incidence of incident T2DM than the other categories. The nonsmoker group with FLD and the ex-smoker group with FLD, on the other hand, had a substantially greater risk of incident T2DM than the nonsmoker group without FLD and the ex-smoker group without FLD, respectively. Current smokers with FLD exhibited a considerably elevated risk when compared to the other groups. Current smokers with no FLD had a remarkably elevated risk of having T2DM than ex-smokers without FLD and nonsmokers with no FLD (vs. none HR 1.78, 95 percent CI 1.18 to 2.68,  $P = 0.006$ ; vs. ex-smoker, HR 1.75, 95 percent CI 1.1 to 2.79,  $p = 0.018$ ), but no evident diversity existed in the risk for developing T2DM between nonsmoker and ex-smoker with FLD (vs. HR 0.88, 95% CI 0.6 to 1.28,  $P = 0.495$ ).

## 5. Discussion

In a cohort of 15464 Japanese people who were followed for a mean of 5.4 years, we looked at the risk of incident T2DM in relation to both the existence of FLD and the status of

TABLE 3: Association between FL with smoking statuses and incident type 2 diabetes in the NAGALA study, 2004–2015.

Exposure	Nonadjusted		Adjust I		Adjust II	
	HR (95% CI)	P value	HR (95% CI)	P value	HR (95% CI)	P value
Smoking status						
FL-/none	1 (reference)		1 (ref)		1 (ref)	
FL-/ex	1.50 (0.96, 2.35)	0.074	1.23 (0.76, 2)	0.401	1.01 (0.62, 1.66)	0.956
FL-/current	2.37 (1.66, 3.37)	<0.001	2.16 (1.45, 3.22)	<0.001	1.78 (1.18, 2.68)	0.006
FL+/none	7.94 (5.73, 11.02)	<0.001	7.44 (5.26, 10.52)	<0.001	2.02 (1.38, 2.95)	<0.001
FL+/ex	7.83 (5.42, 11.31)	<0.001	6.21 (4.05, 9.51)	<0.001	1.77 (1.13, 2.77)	0.013
FL+/current	14.30 (10.44, 19.6)	<0.001	13.39 (9.19, 19.5)	<0.001	3.63 (2.41, 5.48)	<0.001
P for trend	<0.001		<0.001		<0.001	

Notes: data presented are HR (95% CI); Adjust I model adjust for age and gender; Adjust II model adjust for Adjust I+BMI, SBP, DBP, WC, ALT, AST, GGT, and HDL-C+TC+TG+HBA1C+FBG. Abbreviation: FL: fatty liver.

1:FL-/Non 66/7805 (0.8%)					
2 vs 1 1.01 (0.62–1.66) P = 0.956	2:FL-/Ex 27/2226 (1.2%)				
3 vs 1 1.78 (1.18–2.68) P = 0.006	3 vs 2 1.75 (1.1–2.79) P = 0.018	3:FL-/Current 57/2692 (2.1%)			
4 vs 1 2.02 (1.38–2.95) P < 0.001	4 vs 2 1.99 (1.23–3.22) P = 0.005	4 vs 3 1.14 (0.77–1.67) P = 0.519	4:FL+/Non 79/1226 (6.4%)		
5 vs 1 1.77 (1.13–2.77) P = 0.013	5 vs 2 1.74 (1.07–2.85) P = 0.027	5 vs 3 1. (0.66–1.49) P = 0.981	5 vs 4 0.88 (0.6–1.28) P = 0.495	5:FL+/Ex 50/726 (6.9%)	
6 vs 1 3.63 (2.41–5.48) P < 0.001	6 vs 2 3.58 (2.26–5.08) P < 0.001	6 vs 3 2.04 (1.43–2.93) P < 0.001	6 vs 4 1.8 (1.3–2.49) P < 0.01	6 vs 5 2.05 (1.44–2.92) P < 0.01	6:FL+/Current 94/789 (11.9%)

FIGURE 2: HRs and 95% CIs for incident type 2 diabetes. The numbers below each group indicate the number of participants who developed type 2 diabetes/participants classified in each group (percentage). The HRs and 95% CIs were calculated adjusting for sex, age, body mass index, waist circumference, exercise, fasting plasma glucose, hemoglobin A1c, SBP, DBP, total cholesterol, triglycerides, HDL cholesterol, and alanine transaminase at baseline. FL: fatty liver; non-: none.

smoking. Many prior cross-section researches and longitudinal researchers have found that smoking is a risky factor for T2DM, with the great risk being about as 30% to 40% among current smokers vs. nonsmokers [7–9, 13]. We discovered that our sample with FLD had a greater rate of current smoking (28.8%) than those without FLD (21.2%). This indicates that primary and/or secondary preventative smoking cessation recommendations are not being followed to their full potential in this high-risk cohort. Meanwhile, we discovered that never smokers and ex-smokers without FLD were less likely to develop incident T2DM than never smokers and ex-smokers with FLD; but nonsmokers and ex-smokers with FLD had a greater risk of having incident T2DM than never smokers and ex-smokers without FLD.

On the other hand, the risk of current smoker even with no FLD was greater, compared with that nonsmoker and ex-smoker with no FLD. In addition, our team has unveiled that the risk of incident T2DM in current smokers with FLD was the greatest among the six groups.

Many researchers have found that self-reported previous smoking does not elevate the risk of developing diabetes. Moreover, there are contradictory views as to whether previous smoking is related to an elevated risk of having diabetes [14–16]. The current study suggests that in the early phases of smoking quitting, accompanied by weight gain, particularly abdominal fat, patients may develop IGT, insulin resistance, and even diabetes. However, as the length of smoking cessation extended, it was discovered that stopping smoking

was closely linked to a reduction in the risk of diabetes illness in this group [14]. As a result of the findings of this study, the function of smoking in IR, glycemic control, and diabetic development may be reversible. Through our study, we found no remarkable diversity between the prevalence of diabetes in the ex-smoker and never smoker groups for the population without FLD, suggesting the importance of timely smoking cessation in the absence of fatty liver to delay the onset of diabetes. Compared to the current smoking group, the ex-smoking group focused on adjusting poor lifestyle and improving various metabolic syndrome-related factors, like controlling blood pressure and lipid and glucose (GLU) levels, which may have played a balancing role in the relationship between smoking and diabetes prevalence. Given the persistently high prevalence of smoking and our report above, assessment of tobacco use and counseling or treatment to help quit smoking should be considered necessary for the development of T2DM, as recommended by the guidelines.

One of the greatest strengths of our study, it is a longitudinal study based on a relatively large Asian population. The combined effect of smoking status and fatty liver on T2DM was focused on, which is an important clinical guideline for preventing the development of diabetes from a lifestyle perspective. In addition, the same standardized diagnostic criteria were used for the diagnoses of fatty liver in the study, and a standardized questionnaire for life style factors was used.

However, there are certain faults in this paper. An abdominal ultrasound was used to confirm the diagnosis of FLD. Ultrasound, unlike liver biopsies, may not be accurate. Second, because our team failed to conduct an oral GLU tolerance assay at the time of diabetes diagnosis, the occurrence of T2DM may not be adequately estimated. Third, we did not record the amount of smoking and duration of smoking in self-reported current smokers (smoking/day). Fourth, the ability to detect the effects of diverse degrees of physical activities on the body's GLU metabolic homeostasis and ectopical adiposity is insufficient. In the future, if we can adequately assess the intensities and frequencies of exercises, analyses with more accuracy can be performed. Fifth, we could not assess the incidence of passive smoking on diabetes in this study because passive smoking was not documented and we could not assess the incidence of passive smoking in this study. Finally, we did not have detailed data on the types of drugs. If our team acquired those information, a subanalysis of the excluded patients might offer novel enlightenment.

## 6. Conclusion

Holistically, among the six groups, current FLD smokers had the greatest risk of developing T2DM. In addition, never smoking was related to a lower risk of T2DM in sufferers without FLD, but not in sufferers with FLD. Ex-smokers had a reduced incidence of T2DM than current smokers in patients with FLD. Clinicians must be worried about the presence of FLD and the patient's smoking status in order to prevent the development of T2DM and should advise smoking cessation.

## Data Availability

The data used to support the findings of this study are available from the corresponding author upon request.

## Conflicts of Interest

The authors declare that they have no conflict of interest.

## Authors' Contributions

Tingting Zhang and Donghe Zhang contributed equally to this work. Each author either made substantial contributions to the conception or design of the work. All authors have read and approved the final manuscript.

## References

- [1] I. D. Federation, "IDF diabetes atlas-diabetes is rising worldwide... And is set to rise even further," *Mar*, vol. 21, article 2020, 2019.
- [2] A. P. Hills, R. Arena, K. Khunti et al., "Epidemiology and determinants of type 2 diabetes in South Asia," *The Lancet Diabetes and Endocrinology*, vol. 6, no. 12, pp. 966–978, 2018.
- [3] Y. Zheng, S. Ley, and F. Hu, "Global aetiology and epidemiology of type 2 diabetes mellitus and its complications," *Nature Reviews. Endocrinology*, vol. 14, no. 2, pp. 88–98, 2018.
- [4] C. D. Byrne and G. Targher, "Ectopic fat, insulin resistance, and nonalcoholic fatty liver disease," *Arteriosclerosis, Thrombosis, and Vascular Biology*, vol. 34, no. 6, pp. 1155–1161, 2014.
- [5] T. Okamura, Y. Hashimoto, M. Hamaguchi, A. Obora, T. Kojima, and M. Fukui, "Ectopic fat obesity presents the greatest risk for incident type 2 diabetes: a population-based longitudinal study," *International Journal of Obesity*, vol. 43, no. 1, pp. 139–148, 2019.
- [6] A. Miranda-Filho, M. Piñeros, and F. Bray, "The descriptive epidemiology of lung cancer and tobacco control: a global overview 2018," *Salud Publica De Mexico*, vol. 61, no. 3, pp. 219–229, 2019.
- [7] S. A. Chang, "Smoking and type 2 diabetes mellitus," *Diabetes & Metabolism Journal*, vol. 36, no. 6, pp. 399–403, 2012.
- [8] S. Akter, A. Goto, and T. Mizoue, "Smoking and the risk of type 2 diabetes in Japan: a systematic review and meta-analysis," *Journal of Epidemiology*, vol. 27, no. 12, pp. 553–561, 2017.
- [9] US Department of Health and Human Services, *The Health Consequences Of Smoking—50 Years Of Progress: A Report of the Surgeon General*, Department of Health and Human Services, Centers for Disease Control and Prevention, National Center for Chronic Disease Prevention and Health Promotion, Office on Smoking and Health, Atlanta, U.S, 2014.
- [10] N. H. Kim, Y. S. Jung, H. P. Hong et al., "Association between cotinine-verified smoking status and risk of nonalcoholic fatty liver disease," *Liver International*, vol. 38, no. 8, pp. 1487–1494, 2018.
- [11] M. Hamaguchi, T. Kojima, Y. Itoh et al., "The severity of ultrasonographic findings in nonalcoholic fatty liver disease reflects the metabolic syndrome and visceral fat accumulation," *The American Journal of Gastroenterology*, vol. 102, no. 12, pp. 2708–2715, 2007.

- [12] Diabetes, DOF, "American Diabetes Association. Diagnosis and classification of diabetes mellitus," *Diabetes Care*, vol. 34, pp. S62–S69, 2009.
- [13] B. Eliasson, "Cigarette smoking and diabetes," *Progress in Cardiovascular Diseases*, vol. 45, no. 5, pp. 405–413, 2003.
- [14] C. Willi, P. Bodenmann, W. A. Ghali, P. D. Faris, and J. Cornuz, "Active smoking and the risk of type 2 diabetes," *Journal of the American Medical Association*, vol. 298, no. 22, pp. 2654–2664, 2007.
- [15] S. G. Wannamethee, A. G. Shaper, and I. J. Perry, "Smoking as a modifiable risk factor for type 2 diabetes in middle-aged men," *Diabetes Care*, vol. 24, no. 9, pp. 1590–1595, 2001.
- [16] F. Beziaud, J. M. Halimi, P. Lecomte, S. Vol, and J. Tichet, "Cigarette smoking and diabetes mellitus," *Diabetes & Metabolism*, vol. 30, no. 2, pp. 161–166, 2004.

## Research Article

# Statistical Analysis of COVID-19 Data for Three Different Regions in the Kingdom of Saudi Arabia: Using a New Two-Parameter Statistical Model

Ibrahim Al-Dayel <sup>1</sup>, Mohammed N. Alshahrani,<sup>2</sup> Ibrahim Elbatal,<sup>1</sup> Naif Alotaibi <sup>1</sup>,  
A. W. Shawki,<sup>3</sup> and Mohammed Elgarhy <sup>4</sup>

<sup>1</sup>Department of Mathematics and Statistics, College of Science, Imam Mohammad Ibn Saud Islamic University (IMSIU), Riyadh 11432, Saudi Arabia

<sup>2</sup>Department of Mathematics, College of Science, Alkharj, Prince Sattam University, Saudi Arabia

<sup>3</sup>Central Agency for Public Mobilization & Statistics (CAPMAS), Cairo, Egypt

<sup>4</sup>The Higher Institute of Commercial Sciences, Al Mahalla Al Kubra, Algalbia 31951, Egypt

Correspondence should be addressed to Mohammed Elgarhy; [m\\_elgarhy85@sva.edu.eg](mailto:m_elgarhy85@sva.edu.eg)

Received 15 May 2022; Revised 17 June 2022; Accepted 23 June 2022; Published 9 July 2022

Academic Editor: Naeem Jan

Copyright © 2022 Ibrahim Al-Dayel et al. This is an open access article distributed under the Creative Commons Attribution License, which permits unrestricted use, distribution, and reproduction in any medium, provided the original work is properly cited.

Since December 2019, the COVID-19 outbreak has touched every area of everyday life and caused immense destruction to the planet. More than 150 nations have been affected by the coronavirus outbreak. Many academics have attempted to create a statistical model that may be used to interpret the COVID-19 data. This article extends to probability theory by developing a unique two-parameter statistical distribution called the half-logistic inverse moment exponential (HLIMExp). Advanced mathematical characterizations of the suggested distribution have explicit formulations. The maximum likelihood estimation approach is used to provide estimates for unknown model parameters. A complete simulation study is carried out to evaluate the performance of these estimations. Three separate sets of COVID-19 data from Al Bahah, Al Madinah Al Munawarah, and Riyadh are utilized to test the HLIMExp model's applicability. The HLIMExp model is compared to several other well-known distributions. Using several analytical criteria, the results show that the HLIMExp distribution produces promising outcomes in terms of flexibility.

## 1. Introduction

In recent years, many various of statisticians have been attracted by create new families of distributions for example; exponentiated generalized-G in [1], logarithmic-X family of distributions [2], sine-G in [3], odd Perks-G in [4], odd Lindley-G in [5], truncated Cauchy power-G in [6], truncated Cauchy power Weibull-G-G in [7], Topp-Leone-G in [8], odd Nadarajah-Haghighi-G in [9], the Marshall-Olkin alpha power-G in [10], T-X generator studied in [11], type I half-logistic Burr X-G in [12], KM transformation family in [13], (DUS) transformation family in [14], arcsine exponentiated-X family in [15], Marshall-Olkin odd Burr III-G family in [16], among others.

Reference [17] investigates the half-logistic-G (HL-G) family, a novel family of continuous distributions with an additional shape parameter  $\theta > 0$ . The HL-G cumulative distribution function (cdf) is supplied via

$$F(z; \theta, \omega) = \frac{1 - [1 - G(z; \omega)]^\theta}{1 + [1 - G(z; \omega)]^\theta}, \quad z \in R, \theta > 0. \quad (1)$$

The HL-G family's density function (pdf) is described as

$$f(z; \theta, \omega) = \frac{2\theta g(z; \omega)[1 - G(z; \omega)]^{\theta-1}}{[1 + [1 - G(z; \omega)]^\theta]^2}, \quad z \in R, \theta > 0, \quad (2)$$

TABLE 1: Numerical values of Mos for the HLIMExp model for  $\beta = 3$  different values of parameter  $\theta$ .

$\theta$	$E(Z)$	$E(Z^2)$	$E(Z^3)$	$E(Z^4)$	$H$	$\sigma^2$	SK	KU	CV
4	0.452	9.951	1.702	0.290	1.006	6.582	2.992	1.709	1.192
4.5	0.425	8.335	1.513	0.227	1.052	4.469	2.341	1.486	1.122
5	0.404	7.293	1.370	0.186	1.092	3.275	1.915	1.322	1.066
5.5	0.387	6.568	1.256	0.156	1.130	2.531	1.616	1.197	1.020
6	0.372	6.036	1.163	0.134	1.164	2.034	1.398	1.098	0.982
6.5	0.360	5.630	1.086	0.117	1.195	1.684	1.231	1.018	0.949
7	0.349	5.310	1.019	0.103	1.224	1.427	1.101	0.952	0.921
7.5	0.340	5.052	0.961	0.093	1.251	1.232	0.996	0.896	0.896
8	0.331	4.840	0.910	0.084	1.276	1.080	0.910	0.848	0.874
8.5	0.324	4.662	0.865	0.077	1.300	0.959	0.839	0.807	0.855

respectively. A random variable (R.v) $Z$ has pdf (2) which would be specified as $Z \sim HL - G(z; \omega)$ .

Reference [18] presented the moment exponential (MExp) model by allocating weight to the exponential (Exp) model. They established that the MExp distribution is more adaptable than the Exp model. The cdf and pdf files are available.

$$G(t; \beta) = 1 - \left(1 + \frac{t}{\beta}\right) e^{-(t/\beta)}, \quad t > 0, \quad (3)$$

$$g(t, \beta) = \frac{t}{\beta^2} e^{-(t/\beta)}, \quad t > 0, \quad (4)$$

respectively, where  $\beta > 0$  is a scale parameter.

The inverse MExp (IMExp) distribution was presented in reference [19], and it is produced by utilizing the R.v  $Z = 1/T$ , where  $T$  is as follows (4). The cdf and pdf files in the IMExp distribution are specified as

$$G(z; \beta) = \left(1 + \frac{\beta}{z}\right) e^{-(\beta/z)}, \quad z > 0, \quad \beta > 0, \quad (5)$$

$$g(z; \beta) = \frac{\beta^2}{z^3} e^{-(\beta/z)}, \quad z > 0, \quad \beta > 0.$$

In this research, we propose an extension of the IMExp model, which is built using the HL-G family and the IMExp model, known as the half-logistic inverse moment exponential (HLIMExp) distribution.

The aim goal of this article can be considered in the following items:

- (i) To introduce a new two-parameter lifetime model which is called the HLIMExp
- (ii) The new model is very flexible, and the pdf can take different shapes such as unimodal, right skewness, and heavy tail. Also, the hrf can be increasing, upside-down, and J-shaped
- (iii) Many numerical values of the moments are calculated in Table 1. And we can note from it that (a)

TABLE 2: MLEs,  $\Omega_1$ s,  $\Omega_2$ ,  $\Omega_3$ , and  $\Omega_4$  of the HLIMExp model for  $\beta = 0.5$  and  $\theta = 0.5$ .

$n$	MLEs	$\Omega_1$		90%		95%		$\Omega_4$
		$\Omega_1$	$\Omega_2$	$\Omega_3$	$\Omega_4$	$\Omega_2$	$\Omega_3$	
30	0.582	0.042	0.360	0.805	0.445	0.317	0.847	0.530
	0.571	0.037	0.309	0.833	0.523	0.259	0.883	0.624
50	0.548	0.009	0.381	0.715	0.334	0.349	0.747	0.398
	0.593	0.025	0.366	0.819	0.453	0.323	0.862	0.539
100	0.550	0.005	0.419	0.680	0.261	0.394	0.705	0.311
	0.528	0.009	0.373	0.684	0.311	0.343	0.714	0.371
300	0.511	0.003	0.426	0.596	0.170	0.410	0.612	0.202
	0.496	0.005	0.391	0.601	0.211	0.371	0.621	0.251
400	0.510	0.001	0.461	0.559	0.098	0.452	0.568	0.116
	0.525	0.003	0.460	0.589	0.129	0.448	0.602	0.154
500	0.511	0.001	0.473	0.548	0.076	0.465	0.556	0.090
	0.522	0.002	0.472	0.571	0.099	0.462	0.581	0.119

when  $\beta = 3$  and  $\theta$  is increasing, then the numerical values of  $E(Z), E(Z^2), E(Z^3), E(Z^4)$ , variance ( $\sigma^2$ ), skewness (SK), and kurtosis (KU) are decreasing but the numerical values of harmonic mean ( $H$ ) are increasing

- (iv) The simulation study is carried out to assess the behavior of parameters, and the numerical results are mentioned in Tables 2–5. From these tables, we can note that when the value of  $n$  is increased, the value of  $\Omega_1$  and  $\Omega_4$  is decreased
- (v) Three separate sets of COVID-19 data from Al Bahah, Al Madinah Al Munawarah, and Riyadh are utilized to test the HLIMExp model’s applicability. The HLIMExp model is compared to several other well-known distributions. Using several analytical criteria, the results show that the HLIMExp distribution produces promising outcomes in terms of flexibility

The following is an outline of the remainder of this article: Section 2 discusses the construction of the HLIMExp

TABLE 3: MLEs,  $\Omega_1$ ,  $\Omega_2$ ,  $\Omega_3$ , and  $\Omega_4$  of HLIMExp model for  $\beta = 0.5$  and  $\theta = 0.8$ .

$n$	MLEs	$\Omega_1$	90%			95%		
			$\Omega_2$	$\Omega_3$	$\Omega_4$	$\Omega_2$	$\Omega_3$	$\Omega_4$
30	0.504	0.014	0.317	0.691	0.374	0.281	0.727	0.446
	0.955	0.194	0.460	1.450	0.990	0.365	1.545	1.179
50	0.523	0.013	0.365	0.682	0.316	0.335	0.712	0.377
	0.955	0.063	0.562	1.348	0.786	0.487	1.423	0.936
100	0.524	0.006	0.401	0.647	0.245	0.378	0.670	0.292
	0.864	0.021	0.592	1.137	0.545	0.540	1.189	0.649
300	0.512	0.003	0.428	0.597	0.169	0.411	0.613	0.202
	0.840	0.011	0.652	1.028	0.376	0.615	1.064	0.448
400	0.504	0.001	0.456	0.552	0.096	0.447	0.561	0.114
	0.794	0.003	0.691	0.897	0.205	0.672	0.916	0.245
500	0.503	0.000	0.466	0.540	0.074	0.459	0.547	0.088
	0.814	0.003	0.732	0.896	0.163	0.717	0.911	0.195

TABLE 4: MLEs,  $\Omega_1$ ,  $\Omega_2$ ,  $\Omega_3$ , and  $\Omega_4$  of HLIMExp model for  $\beta = 0.5$  and  $\theta = 1.2$ .

$n$	MLEs	$\Omega_1$	90%			95%		
			$\Omega_2$	$\Omega_3$	$\Omega_4$	$\Omega_2$	$\Omega_3$	$\Omega_4$
30	0.519	0.006	0.355	0.683	0.329	0.323	0.715	0.392
	1.519	0.337	0.742	2.295	1.554	0.593	2.444	1.851
50	0.488	0.007	0.370	0.607	0.237	0.347	0.629	0.282
	1.122	0.033	0.683	1.562	0.879	0.599	1.646	1.047
100	0.507	0.005	0.420	0.595	0.175	0.403	0.612	0.209
	1.240	0.083	0.900	1.579	0.679	0.835	1.644	0.809
300	0.508	0.001	0.446	0.570	0.124	0.434	0.582	0.148
	1.244	0.032	1.002	1.485	0.484	0.955	1.532	0.576
400	0.502	0.001	0.452	0.551	0.100	0.442	0.561	0.119
	1.207	0.011	1.016	1.399	0.384	0.979	1.436	0.457
500	0.491	0.001	0.449	0.533	0.084	0.441	0.542	0.101
	1.176	0.011	1.014	1.339	0.325	0.982	1.370	0.388

model. Section 3 calculates the basic properties of the distribution, including the linear representation of HLIMExp pdf, order statistics, moments, moment generating function, and conditional moment. In contrast, Section 4 discusses parameter estimation using the maximum likelihood (ML) estimation method. Section 5 employs Monte Carlo simulation techniques. In Section 6, we investigated the potentiality of the HLIMExp using three different metrics of goodness of fit such as the Akaike Information Criterion (IC) ( $\mathfrak{B}1$ ), Consistent AIC ( $\mathfrak{B}2$ ), Bayesian IC ( $\mathfrak{B}3$ ), Hannan-Quinn IC ( $\mathfrak{B}4$ ), Kolmogorov-Smirnov ( $\mathfrak{B}5$ ) test, and  $p$  value ( $\mathfrak{B}6$ ). Finally, Section 7 mentions the conclusion.

## 2. The New Two-Parameter Statistical Model

A nonnegative R.v  $Z$  with the HLIMExp model is constructed by putting (5) and (6) in (1) and (2), respectively; we should

get cdf and pdf.

$$F(z; \beta, \theta) = \frac{1 - [1 - (1 + (\beta/z))e^{-(\beta/z)}]^\theta}{1 + [1 - (1 + (\beta/z))e^{-(\beta/z)}]^\theta}, \quad z > 0, \beta, \theta > 0. \tag{6}$$

$$f(z; \beta, \theta) = \frac{2\theta(\beta^2/z^3)e^{-(\beta/z)}[1 - (1 + (\beta/z))e^{-(\beta/z)}]^{2\theta-1}}{[1 + [1 - (1 + (\beta/z))e^{-(\beta/z)}]^\theta]^2}, \quad z > 0, \theta > 0. \tag{7}$$

The survival function (sf) is provided by

$$\bar{F}(z; \beta, \theta) = \frac{2[1 - (1 + (\beta/z))e^{-(\beta/z)}]^\theta}{1 + [1 - (1 + (\beta/z))e^{-(\beta/z)}]^\theta}, \quad z > 0, \beta, \theta > 0. \tag{8}$$

The hrf or failure rate and reversed hrf for the HLIMExp are calculated as follows:

$$h(z; \beta, \theta) = \frac{\theta(\beta^2/z^3)e^{-(\beta/z)}}{[1 - (1 + (\beta/z))e^{-(\beta/z)}][1 + [1 - (1 + (\beta/z))e^{-(\beta/z)}]^\theta]},$$

$$\tau(z; \beta, \theta) = \frac{2\theta(\beta^2/z^3)e^{-(\beta/z)}[1 - (1 + (\beta/z))e^{-(\beta/z)}]^{2\theta-1}}{1 - [1 - (1 + (\beta/z))e^{-(\beta/z)}]^{2\theta}}. \tag{9}$$

Different shapes of the pdf and hrf of HLIMExp with different parameter values are mentioned in Figures 1 and 2.

## 3. Statistical Properties

We discussed certain HLIMExp distribution features in this part, including linear representation of HLIMExp pdf, moments (Mo), the harmonic mean ( $H$ ), moment generating function (MoGF), and conditional moment (CoMo).

**3.1. Linear Representation.** A linear form of the pdf and cdf is offered in this part to introduce statistical properties of the HLIMExp distribution. Using the following binomial expansion,

$$(1 + z)^{-m} = \sum_{i=0}^{\infty} (-1)^i \binom{m+i-1}{i} z^i, \tag{10}$$

where  $|z| < 1$  and  $b$  is a positive real noninteger. By applying (10) in the next term, we get

$$\left[1 + \left[1 - \left(1 + \frac{\beta}{z}\right)e^{-(\beta/z)}\right]^\theta\right]^{-2}$$

$$= \sum_{i=0}^{\infty} (-1)^i (i+1) \left[1 - \left(1 + \frac{\beta}{z}\right)e^{-(\beta/z)}\right]^{2i}. \tag{11}$$

TABLE 5: MLEs,  $\Omega_1$ ,  $\Omega_2$ ,  $\Omega_3$ , and  $\Omega_4$  of HLIMExp model for  $\beta = 1.5$  and  $\theta = 1.2$ .

$n$	MLEs	$\Omega_1$	90%			95%		
			$\Omega_2$	$\Omega_3$	$\Omega_4$	$\Omega_2$	$\Omega_3$	$\Omega_4$
30	1.687	0.277	1.010	2.363	1.353	0.881	2.492	1.612
	1.239	0.043	0.853	1.626	0.773	0.779	1.700	0.921
50	1.526	0.045	1.070	1.982	0.912	0.983	2.070	1.087
	1.225	0.014	0.909	1.501	0.592	0.852	1.557	0.706
100	1.529	0.032	1.206	1.852	0.646	1.144	1.914	0.770
	1.218	0.012	0.999	1.418	0.419	0.959	1.458	0.499
300	1.556	0.014	1.366	1.747	0.381	1.330	1.783	0.454
	1.215	0.006	1.121	1.369	0.249	1.097	1.393	0.297
400	1.513	0.005	1.354	1.672	0.318	1.323	1.702	0.379
	1.198	0.003	1.094	1.302	0.208	1.074	1.321	0.248
500	1.545	0.011	1.399	1.691	0.292	1.372	1.719	0.348
	1.201	0.001	1.131	1.321	0.189	1.113	1.339	0.225

Inserting the previous equation in (7), we have

$$f(z; \beta, \theta) = 2\theta\beta^2 \sum_{i=0}^{\infty} (-1)^i (i+1) z^{-3} e^{-(\beta/z)} \cdot \left[ 1 - \left( 1 + \frac{\beta}{z} \right) e^{-(\beta/z)} \right]^{\theta(i+1)-1}. \quad (12)$$

Again, applying the general binomial theorem, we get

$$\begin{aligned} & \left[ 1 - \left( 1 + \frac{\beta}{z} \right) e^{-(\beta/z)} \right]^{\theta(i+1)-1} \\ &= \sum_{j=0}^{\infty} (-1)^j \binom{\theta(i+1)-1}{j} \left( 1 + \frac{\beta}{z} \right)^j e^{-(j\beta/z)}. \end{aligned} \quad (13)$$

Inserting the previous equation in (7), we have

$$f(z; \beta, \theta) = 2\theta\beta^2 \sum_{i,j=0}^{\infty} (-1)^{i+j} (i+1) \binom{\theta(i+1)-1}{j} \cdot z^{-3} e^{-(\beta(j+1)/z)} \left( 1 + \frac{\beta}{z} \right)^j. \quad (14)$$

Again, using the binomial expansion, we get

$$f(z; \beta, \theta) = \sum_{k=0}^{\infty} \mathbb{S}_k z^{-k-3} e^{-(\beta(j+1)/z)}, \quad (15)$$

where

$$\mathbb{S}_k = 2\theta\beta^{k+2} \sum_{i,j=0}^{\infty} (-1)^{i+j} (i+1) \binom{j}{k} \binom{\theta(i+1)-1}{j}. \quad (16)$$

3.2. *Moments.* The  $r^{\text{th}}$  Mos of the HLIMExp distribution are

discussed in this subsection. Moments are essential in any statistical study, but especially in applications, it can be used to investigate the main properties and qualities of a distribution (e.g., tendency, dispersion, skewness, and kurtosis). The  $r^{\text{th}}$  Mo of  $Z$  denoted by  $\mu_r$ , may be calculated using (8).

$$\mu_r = E(Z^r) = \sum_{k=0}^{\infty} \mathbb{S}_k \int_0^{\infty} z^{r-k-3} e^{-(\beta(j+1)/z)} dz, \quad (17)$$

then,

$$\mu_r = \sum_{k=0}^{\infty} \mathbb{S}_k (\beta(j+1))^{-r-k-2} \Gamma(k+r+2). \quad (18)$$

The  $r^{\text{th}}$  inverse Mo of  $Z$  denoted by  $\mu_r$ , may be calculated using (8).

$$\mu_{r-1} = E(Z^{-r}) = \sum_{k=0}^{\infty} \mathbb{S}_k \int_0^{\infty} z^{r-k-3} e^{-(\beta(j+1)/z)} dz, \quad (19)$$

then,

$$\mu_{r-1} = \sum_{k=0}^{\infty} \mathbb{S}_k (\beta(j+1))^{r-k-2} \Gamma(k-r+2). \quad (20)$$

The harmonic mean of  $Z$  is given by

$$H = E\left(\frac{1}{Z}\right) = \sum_{k=0}^{\infty} \mathbb{S}_k \int_0^{\infty} z^{-k-4} e^{-(\beta(j+1)/z)} dz, \quad (21)$$

then,

$$\mu_r = \sum_{k=0}^{\infty} \mathbb{S}_k (\beta(j+1))^{-k-3} \Gamma(r+3). \quad (22)$$

MoGFs are useful for several reasons, one of which is their application to analysis of sums of random variables. The MoGF of  $ZM_z(t)$  is deduced from (7) as

$$M_z(t) = \sum_{r=0}^{\infty} \frac{t^r}{r!} \mu_r' = \sum_{r=0}^{\infty} \sum_{k=0}^{\infty} \frac{\mathbb{S}_k t^r \Gamma(k-r+2) (\beta(j+1))^{r-k-2}}{r!}. \quad (23)$$

Numerical values for specific values of parameters of the first four ordinary Mos,  $E(Z)$ ,  $E(Z^2)$ ,  $E(Z^3)$ ,  $E(Z^4)$ , variance ( $\sigma^2$ ), skewness (SK), and kurtosis (KU) of the HLIMExp model are reported in Table 1.

3.3. *The Conditional Moment.* For empirical intents, the shapes of various distributions, such as income quantiles and Lorenz and Bonferroni curves, can be usefully described by the first incomplete moment, which plays a major role in evaluating inequality. These curves have a variety of applications in economics, reliability, demographics, insurance, and medical. Let  $Z$  denote a R.v with the pdf given in (7). The  $s^{\text{th}}$



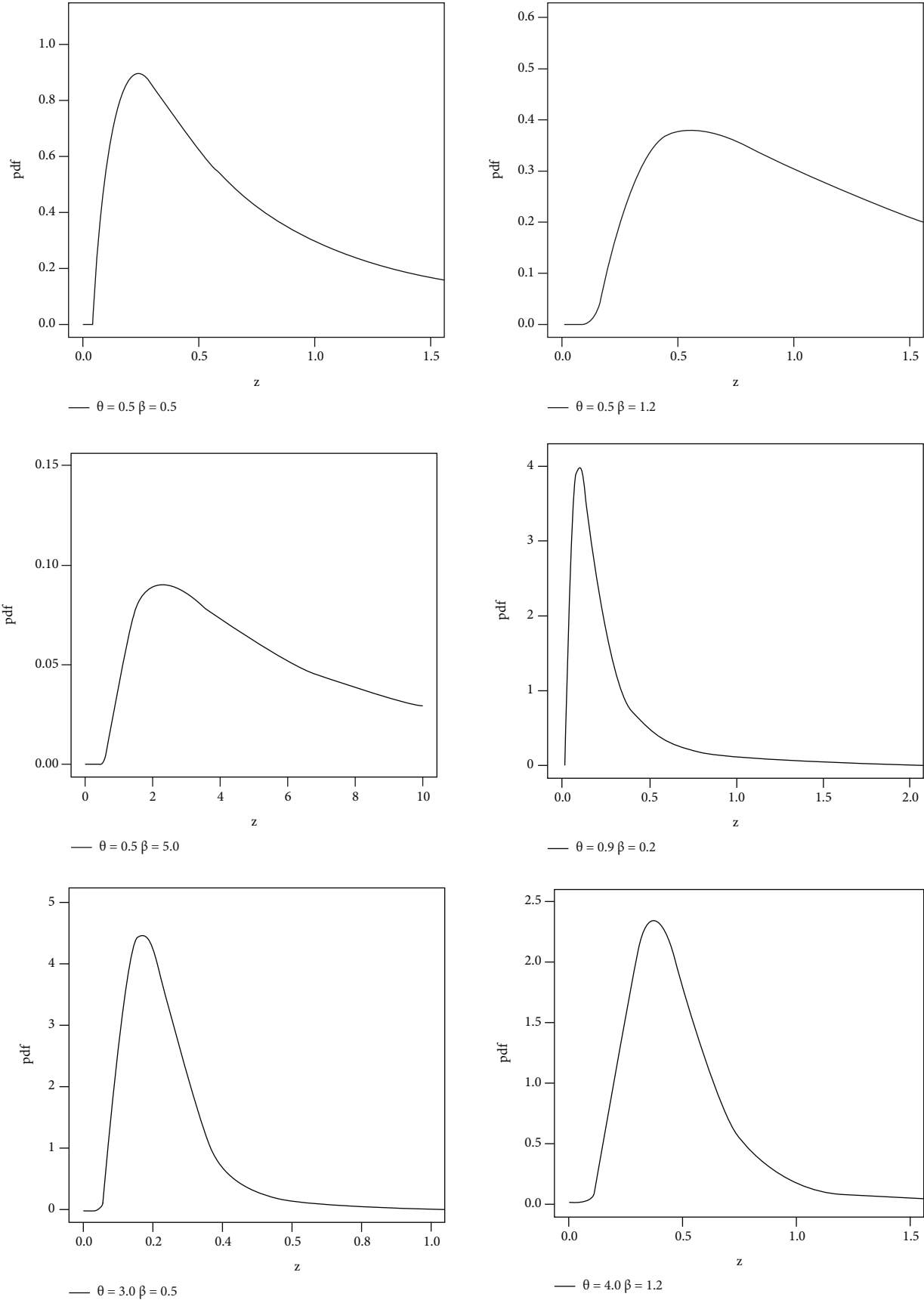


FIGURE 1: Different shapes of pdf for the HLIMExp model.

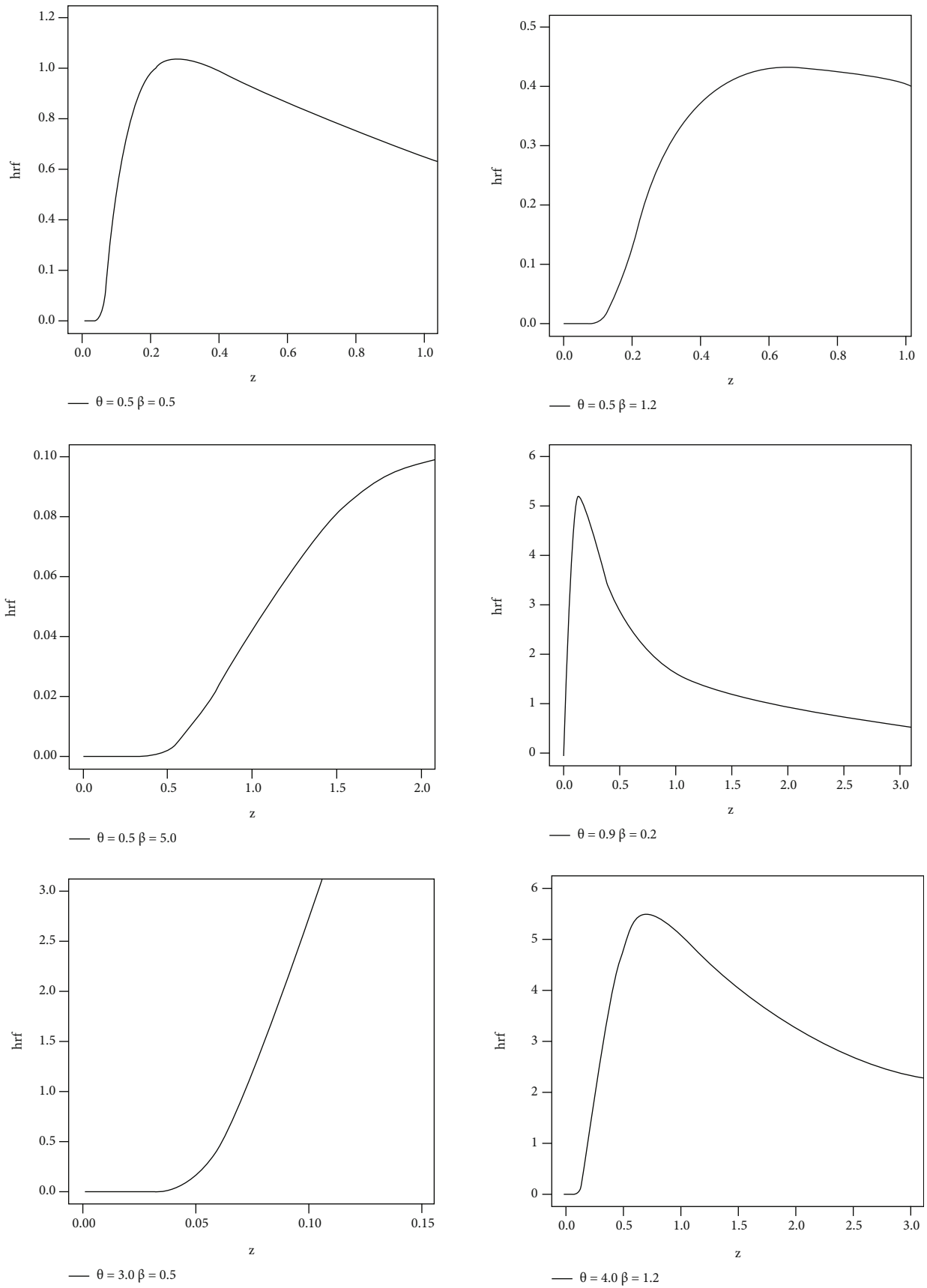


FIGURE 2: Different shapes of hrf for the HLIMExp model.

upper incomplete Mo say  $\eta_s(t)$  could be expressed with

$$\begin{aligned} \eta_s(t) &= \int_t^\infty z^s f(z; \beta, \theta) dz = \sum_{k=0}^\infty \mathbb{S}_k \int_t^\infty z^{s-k-3} e^{-(\beta(j+1)/z)} dz \\ &= \sum_{k=0}^\infty \mathbb{S}_k (\beta(j+1))^{s-k-2} \Gamma\left(k-s+2, \frac{\beta(j+1)}{t}\right). \end{aligned} \tag{24}$$

Similarly, the  $s^{\text{th}}$  lower incomplete Mo function is provided through

$$\begin{aligned} \phi_s(t) &= \int_0^t z^s f(z; \beta, \theta) dz = \sum_{k=0}^\infty \mathbb{S}_k \int_0^t z^{s-k-3} e^{-(\beta(j+1)/z)} dz \\ &= \sum_{k=0}^\infty \mathbb{S}_k (\beta(j+1))^{s-k-2} \gamma\left(k-s+2, \frac{\beta(j+1)}{t}\right). \end{aligned} \tag{25}$$

#### 4. Method of Maximum Likelihood

Let  $z_1, z_2, \dots, z_n$  be a random sample of size  $n$  from the HLI-MExp model with two parameters  $\beta$  and  $\theta$ ; the log-likelihood function is

$$\begin{aligned} L &= n \ln(2\theta) - 2n \ln \beta - 3 \sum_{i=1}^n z_i - \sum_{i=1}^n \frac{\beta}{z_i} \\ &+ (\theta - 1) \sum_{i=1}^n \log[G_i] - 2 \sum_{i=1}^n \log\left[1 + [G_i]^\theta\right]. \end{aligned} \tag{26}$$

For calculation MLE estimation, we need partial derivatives of  $L(Z | \beta, \theta)$  by parameters

$$\begin{aligned} \frac{\partial \log L}{\partial \beta} &= \frac{-2n}{\beta} - \sum_{i=1}^n \frac{1}{z_i} + (\theta - 1) \sum_{i=1}^n \frac{V_i}{G_i} - 2 \sum_{i=1}^n \frac{\theta V_i [G_i]^{\theta-1}}{[1 + [G_i]^\theta]}, \\ \frac{\partial \log L}{\partial \theta} &= \frac{n}{\theta} + \sum_{i=1}^n \log[G_i] - 2 \sum_{i=1}^n \frac{(G_i)^\theta \ln[G_i]}{1 + [G_i]^\theta}, \end{aligned} \tag{27}$$

where  $G_i = 1 - (1 + (\beta/z_i))e^{-(\beta/z_i)}$  and  $V_i = \partial G_i / \partial \beta = (\beta / (z_i)^2) e^{-(\beta/z_i)}$ . As result, estimations of the parameters can be found  $\hat{\beta}_{MLE}$  and  $\hat{\theta}_{MLE}$  the solution of the two equations  $\partial L / \partial \beta = 0$  and  $\partial L / \partial \theta = 0$  by using software Mathematica (9).

#### 5. Simulation Results

A simulation result is included in this section to analyze the behavior of estimators in the presence of complete samples by using the Newton-Raphson iteration method and by using Mathematica (8) software. Mean square errors ( $\Omega 1$ ), lower and upper bound ( $\Omega 2$  and  $\Omega 3$ ) of confidence interval (CI), and average length ( $\Omega 4$ ) of 90% and 95% are computed using Mathematica 9. The accompanying algorithm is constructed in the next part:

TABLE 6: Al Bahah, Al Madinah Al Munawarah, and Riyadh Regions, coronavirus cases (COVID-19).

Year	Month	Coronavirus cases by regions			
		Al Bahah	Al Madinah	Al Munawarah	Riyadh
2021	Jan	85		281	1994
2021	Feb	213		273	4524
2021	Mar	78		475	5612
2021	Apr	227		1001	12038
2021	May	409		2266	10458
2021	Jun	541		2167	7593
2021	Jul	772		1860	8747
2021	Aug	292		1050	3856
2021	Sep	32		193	760
2021	Oct	7		89	549
2021	Nov	6		73	401
2021	Dec	55		341	2541
2022	Jan	1430		8607	44169
2022	Feb	644		2477	19641
2022	Mar	77		460	1612
2022	Apr	49		423	691
2022	May	22		163	170

TABLE 7: Some descriptive analysis of the data.

	Al Bahah	Al Madinah	Al Munawarah	Riyadh
$N$	17		17	17
Mean	290.529		1305.824	7373.882
Median	85		460	3856
Skewness	1.982		3.108	2.756
Kurtosis	4.327		10.927	8.65
Range	1424		8534	43999
Min	6		73	170
Max	1430		8607	44169
Sum	4939		22199	125356

- (i) 5000 RS of size  $n = 30, 50, 100, 300, 400,$  and  $500$  are generated from the HLIMExp model
- (ii) The parameters' exact values are chosen
- (iii) The ML estimates (MLEs),  $\Omega 1s, \Omega 2, \Omega 3,$  and  $\Omega 4$  for selected values of parameters are computed
- (iv) Tables 2–5 provide the numerical outputs based on the entire data set

#### 6. Applications

This section concerned with three important real data sets. The data called Saudi Arabia Coronavirus cases (COVID-19) situation in Al Bahah, Al Madinah Al Munawarah and Riyadh regions from January 2022 to May 2022.

TABLE 8: Numerical values of MLEs, SEs,  $\mathfrak{B}_1$ ,  $\mathfrak{B}_2$ ,  $\mathfrak{B}_3$ ,  $\mathfrak{B}_4$ ,  $\mathfrak{B}_5$ , and  $\mathfrak{B}_6$  tests for the first data set.

Distributions	MLE and SE				$\mathfrak{B}_1$	$\mathfrak{B}_2$	$\mathfrak{B}_3$	$\mathfrak{B}_4$	$\mathfrak{B}_5$	$\mathfrak{B}_6$
	$\alpha$	$\beta$	$\theta$	$\lambda$						
HLIMExp		24.214 (9.688)	0.336 (0.081)		231.459	232.317	229.92	231.625	0.167	0.732
TIITOLIR	6.626 (1.828)	0.196 (0.051)			236.208	237.065	234.669	236.373	0.244	0.265
HLOIR	8.739 (2.643)	0.272 (0.059)			233.253	234.11	231.714	233.419	0.204	0.48
W-Li	0.088 (0.078)	0.004 (0.001)			232.468	233.326	230.929	232.634	0.275	0.153
BT-Li	0.010 (0.017)	0.320 (0.568)	0.359 (0.138)	0.383 (1.139)	232.376	235.709	229.297	232.707	0.181	0.631
TMW	0.230 (0.140)	0.00000001 (0.00002)	0.0027 (0.0011)	0.481 (0.496)	235.812	241.267	231.965	236.226	0.243	0.27
ILBE	70.429 (12.078)				263.621	263.888	262.851	263.704	0.427	0.004109
LBE	145.265 (24.913)				247.564	247.831	246.794	247.647	0.321	0.06

TABLE 9: Numerical values of MLEs, SEs,  $\mathfrak{B}_1$ ,  $\mathfrak{B}_2$ ,  $\mathfrak{B}_3$ ,  $\mathfrak{B}_4$ ,  $\mathfrak{B}_5$ , and  $\mathfrak{B}_6$  tests for the second data set.

Distributions	MLE and SE				$\mathfrak{B}_1$	$\mathfrak{B}_2$	$\mathfrak{B}_3$	$\mathfrak{B}_4$	$\mathfrak{B}_5$	$\mathfrak{B}_6$
	$\alpha$	$\beta$	$\theta$	$\lambda$						
HLIMExp		292.561 (103.158)	0.520 (0.138)		276.46	277.317	274.921	276.626	0.118	0.972
TIITOLIR	89.906 (20.808)	0.311 (0.085)			278.671	279.528	277.132	278.837	0.163	0.755
HLOIR	114.890 (29.837)	0.412 (0.095)			277.112	277.969	275.573	277.278	0.125	0.954
W-Li	0.053 (0.075)	0.0008 (0.0002)			282.778	283.635	281.239	282.943	0.288	0.119
BT-Li	0.001 (0.002)	0.496 (0.726)	0.478 (0.225)	0.663 (1.037)	284.572	287.905	281.494	284.903	0.358	0.026
TMW	0.519 (0.400)	0.00000004 (0.00002)	0.0006 (0.0002)	0.669 (0.376)	286.033	291.488	282.185	286.447	0.239	0.286
ILBE	596.909 (102.369)				284.757	285.023	283.987	284.84	0.291	0.112
LBE	652.912 (111.973)				294.272	294.539	293.503	294.355	0.272	0.16

The three data sets were obtained from the following electronic address: <https://datasource.kapsarc.org/explore/dataset/saudi-arabia-coronavirus-disease-COVID-19-situation/>. The data sets are reported in Table 6. The descriptive analysis of the three data sets is reported in Table 7.

Here, in this section, the three data sets mentioned below are examined to demonstrate how the HLIMExp distribution outperforms alternative models, comparing

the new model to some models, namely, type II Topp-Leone inverse Rayleigh (TIITOLIR) distribution by [20], half-logistic inverse Rayleigh (HLOIR) distribution by [21], beta transmuted Lindley (BTLi) distribution by [22], the transmuted modified Weibull (TMW) distribution by [23], and the weighted Lindley (W-Li) distribution by [24]. We calculate the model parameters' MLEs and standard errors (SEs). To evaluate distribution

TABLE 10: Numerical values of MLEs, SEs,  $\mathfrak{B}_1$ ,  $\mathfrak{B}_2$ ,  $\mathfrak{B}_3$ ,  $\mathfrak{B}_4$ ,  $\mathfrak{B}_5$ , and  $\mathfrak{B}_6$  tests for the third data set.

Distributions	$\alpha$	MLE and SE		$\lambda$	$\mathfrak{B}_1$	$\mathfrak{B}_2$	$\mathfrak{B}_3$	$\mathfrak{B}_4$	$\mathfrak{B}_5$	$\mathfrak{B}_6$
		$\beta$	$\theta$							
HLIMExp		822.893 (320.841)	0.377 (0.093)		339.578	340.435	338.039	339.744	0.158	0.788
TIITOLIR	224.204 (59.549)	0.218 (0.058)			344.149	345.006	342.61	344.314	0.216	0.407
HLOIR	292.158 (84.846)	0.299 (0.065)			341.443	342.3	339.904	341.609	0.178	0.653
W-Li	0.020 (0.041)	0.0001 (0.00003)			341.224	342.082	339.685	341.39	0.2	0.506
BT-Li	0.00032 (0.00007)	0.859 (0.103)	1.157 (0.337)	0.229 (0.385)	365.36	368.694	362.282	365.692	0.319	0.064
TMW	0.302 (0.177)	0.00000027 (0.00008)	0.0001 (0.00004)	0.619 (0.425)	345.244	350.698	341.396	345.658	0.179	0.648
ILBE	2175 (372.994)				363.338	363.605	362.569	363.421	0.419	0.0051
LBE	3687 (632.305)				356.487	356.753	355.717	356.569	0.281	0.1360

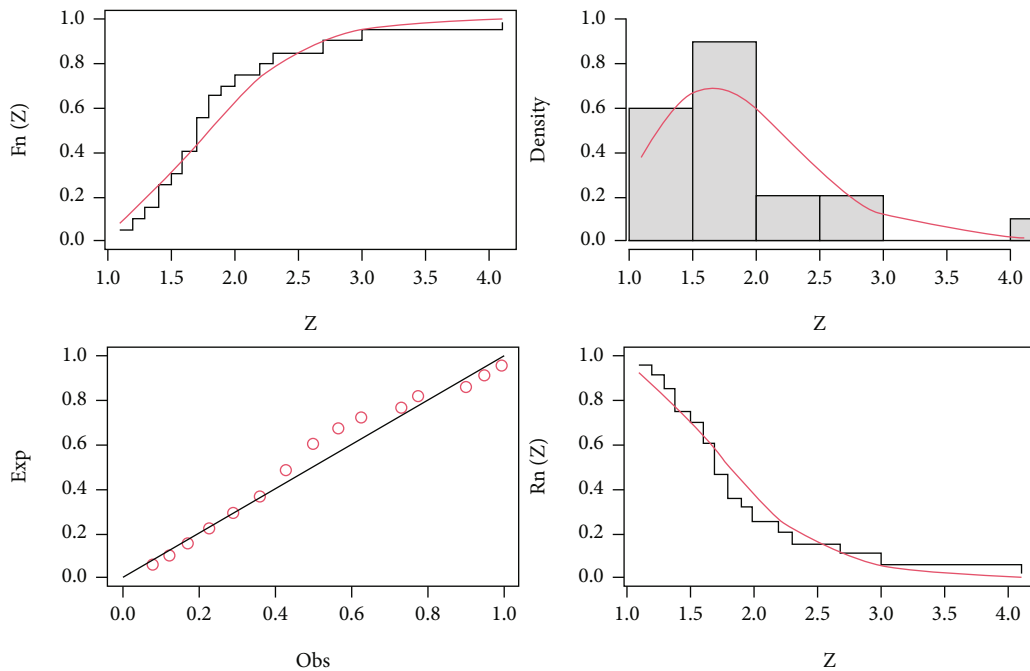


FIGURE 3: The fitted cdf, pdf, and pp plots and fitted sf of the HLIMExp model for the first data.

models, we use criteria such as the  $\mathfrak{B}_1$ ,  $\mathfrak{B}_2$ ,  $\mathfrak{B}_3$ ,  $\mathfrak{B}_4$ ,  $\mathfrak{B}_5$ , and  $\mathfrak{B}_6$  tests. In contrast, the wider distribution relates to smaller  $\mathfrak{B}_1$ ,  $\mathfrak{B}_2$ ,  $\mathfrak{B}_3$ ,  $\mathfrak{B}_4$ , and  $\mathfrak{B}_5$  and the highest value of  $\mathfrak{B}_6$ . The MLEs of the eight fitted models and their SEs and the numerical values of  $\mathfrak{B}_1$ ,  $\mathfrak{B}_2$ ,  $\mathfrak{B}_3$ ,  $\mathfrak{B}_4$ ,  $\mathfrak{B}_5$ , and  $\mathfrak{B}_6$  for the three data sets are presented in Tables 8–10. We find that the HLIMExp distribution with two parameters provides a better fit than

seven models. It has the smallest values of  $\mathfrak{B}_1$ ,  $\mathfrak{B}_2$ ,  $\mathfrak{B}_3$ ,  $\mathfrak{B}_4$ , and  $\mathfrak{B}_5$  and the greatest value of  $\mathfrak{B}_6$  among those considered here. Moreover, the plots of empirical cdf, empirical pdf, and PP plots of our competitive model for the three data sets are displayed in Figures 3–5, respectively. The HLIMExp model clearly gives the best overall fit and so may be picked as the most appropriate model for explaining data.

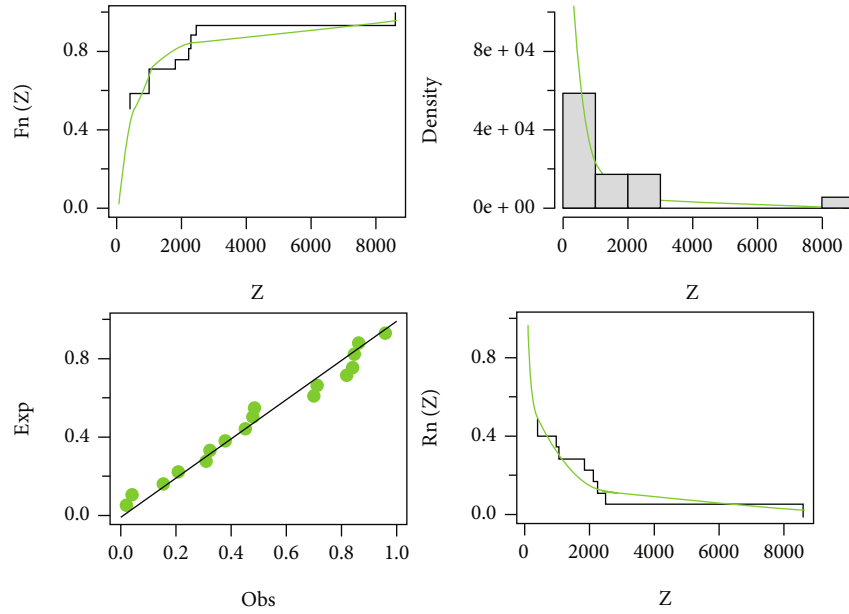


FIGURE 4: The fitted cdf, pdf, and pp plots and fitted sf of the HLIMExp model for the second data.

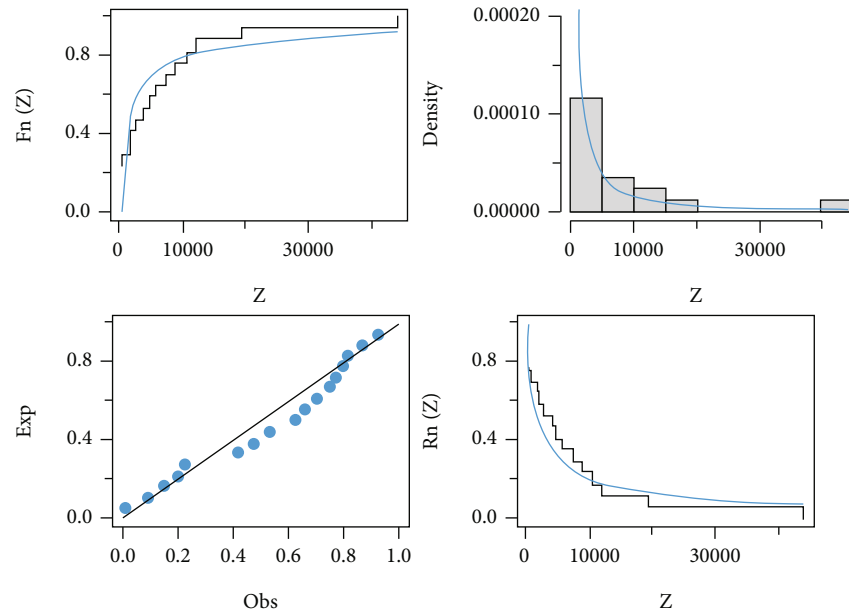


FIGURE 5: The fitted cdf, pdf, and pp plots and fitted sf of the HLIMExp model for the third data.

### 7. Conclusion

We propose a novel two-parameter distribution called the half-logistic inverted moment exponential distribution in this research. HLIMExp’s pdf may be written as a linear combination of IMExp densities. We compute explicit formulas for several of its statistical features, such as HLIMExp pdf linear representation, OS, Moms, MoGF, and CoMo. The greatest likelihood estimate is investigated. The accuracy and performance of estimations are evaluated using simulation results. Three separate sets of COVID-19 data from Al Bahah, Al Madinah Al Munawarah, and Riyadh are utilized

to test the HLIMExp model’s applicability. The HLIMExp model is compared to several other well-known distributions. Using several analytical criteria, the results show that the HLIMExp distribution produces promising outcomes in terms of flexibility. In the future works, we can use the new suggested model in many works such as (a) using it to study the statistical inference of the suggested model under different censored schemes, (b) using it to study the statistical inference of the suggested model under different ranked set sampling, (c) accelerated lifetime test can be studied for the new model, and (d) the statistical inference of stress strength model for the new suggested model can be studied.

## Data Availability

All data are mentioned in this article.

## Conflicts of Interest

The authors declare no conflict of interest.

## Acknowledgments

This research was supported by the Deanship of Scientific Research, Imam Mohammad Ibn Saud Islamic University (IMSIU), Saudi Arabia, Grant No. 21-13-18-034.

## References

- [1] G. M. Cordeiro, E. M. Ortega, and D. C. Da Cunha, "The exponentiated generalized class of distributions," *Journal of Data Science*, vol. 11, no. 1, pp. 1–27, 2013.
- [2] M. Liu, S. K. Ilyas, S. K. Khosa et al., "A flexible reduced logarithmic-X family of distributions with biomedical analysis," *Computational and Mathematical Methods in Medicine*, vol. 2020, Article ID 4373595, 15 pages, 2020.
- [3] D. Kumar, U. Singh, and S. K. Singh, "A new distribution using sine function- its application to bladder cancer patients data," *Journal of Statistics Applications & Probability*, vol. 4, no. 3, pp. 417–427, 2015.
- [4] I. Elbatal, N. Alotaibi, E. M. Almetwally, S. A. Alyami, and M. Elgarhy, "On odd perks-G class of distributions: properties, regression model, discretization, Bayesian and non-Bayesian estimation, and applications," *Symmetry*, vol. 14, no. 5, p. 883, 2022.
- [5] F. Gomes, A. Percontini, E. de Brito, M. Ramos, R. Venancio, and G. Cordeiro, "The odd Lindley- G family of distributions," *Austrian Journal of Statistics.*, vol. 46, no. 1, pp. 65–87, 2017.
- [6] M. A. Aldahlan, F. Jamal, C. Chesneau, M. Elgarhy, and I. Elbatal, "The truncated Cauchy power family of distributions with inference and applications," *Entropy*, vol. 22, no. 3, p. 346, 2020.
- [7] N. Alotaibi, I. Elbatal, E. M. Almetwally, S. A. Alyami, A. S. Al-Moisheer, and M. Elgarhy, "Truncated Cauchy power Weibull-G class of distributions: Bayesian and non-Bayesian inference modelling for COVID-19 and carbon fiber data," *Mathematics*, vol. 10, no. 9, p. 1565, 2022.
- [8] A. Al-Shomrani, O. Arif, A. Shawky, S. Hanif, and M. Q. Shahbaz, "Topp-Leone family of distributions: some properties and application," *Pakistan Journal of Statistics & Operation Research*, vol. 12, no. 3, pp. 443–451, 2016.
- [9] A. Nascimento, K. F. Silva, G. M. Cordeiro, M. Alizadeh, H. M. Yousof, and G. G. Hamedani, "The odd Nadarajah-Haghighi family of distributions: properties and applications," *Studia Scientiarum Mathematicarum Hungarica*, vol. 56, no. 2, pp. 185–210, 2019.
- [10] M. Nassar, D. Kumar, S. Dey, G. M. Cordeiro, and A. Z. Afify, "The Marshall-Olkin alpha power family of distributions with applications," *Journal of Computational and Applied Mathematics*, vol. 351, pp. 41–53, 2019.
- [11] A. Alzaatreh, C. Lee, and F. Famoye, "A new method for generating families of continuous distributions," *Metron*, vol. 71, no. 1, pp. 63–79, 2013.
- [12] A. Algarni, A. M. Almarashi, I. Elbatal et al., "Type I half logistic Burr X-G family: properties, Bayesian, and non-Bayesian estimation under censored samples and applications to COVID-19 data," *Mathematical Problems in Engineering*, vol. 2021, Article ID 5461130, 21 pages, 2021.
- [13] P. Kavya and M. Manoharan, "Some parsimonious models for lifetimes and applications," *Journal of Statistical Computation and Simulation*, vol. 91, no. 18, pp. 3693–3708, 2021.
- [14] D. Kumar, U. Singh, and S. K. Singh, "A method of proposing new distribution and its application to bladder cancer patients data," *Journal of Statistics Applications and Probability Letters*, vol. 2, no. 3, pp. 235–245, 2015.
- [15] W. He, Z. Ahmad, A. Z. Afify, and H. Goual, "The arcsine exponentiated-X family: validation and insurance application," *Complexity*, vol. 2020, Article ID 8394815, 18 pages, 2020.
- [16] A. Z. Afify, G. M. Cordeiro, N. A. Ibrahim, F. Jamal, M. Elgarhy, and M. A. Nasir, "The Marshall-Olkin odd Burr III-G family: theory, estimation, and engineering applications," *IEEE Access*, vol. 9, pp. 4376–4387, 2021.
- [17] G. M. Cordeiro, M. Alizadeh, M. Diniz, and R. Pedro, "The type I half-logistic family of distributions," *Journal of Statistical Computation and Simulation*, vol. 86, no. 4, pp. 707–728, 2016.
- [18] T. Dara and M. Ahmad, *Recent advances in moment distributions and their hazard rate*, [Ph.D. thesis], National College of Business Administration and Economics, Lahore, Pakistan, 2012.
- [19] W. Almutiry, "Inverted length-biased exponential model: statistical inference and modeling," *Journal of Mathematics*, vol. 2021, Article ID 1980480, 8 pages, 2021.
- [20] H. F. Mohammed and N. Yahia, "On type II Topp Leone inverse Rayleigh distribution," *Applied Mathematical Sciences*, vol. 13, no. 13, pp. 607–615, 2019.
- [21] M. Almarashi, M. M. Badr, M. Elgarhy, F. Jamal, and C. Chesneau, "Statistical inference of the half-logistic inverse Rayleigh distribution," *Entropy*, vol. 22, no. 4, p. 449, 2020.
- [22] A. Z. Afify, H. M. Yousof, and S. Nadarajah, "The beta transmuted-H family for lifetime data," *Statistics and its Interface*, vol. 10, no. 3, 2017.
- [23] M. S. Khan, R. King, and I. L. Hudson, "Transmuted modified Weibull distribution: properties and application," *European Journal of Pure and Applied Mathematics*, vol. 11, no. 2, pp. 362–374, 2018.
- [24] M. E. Ghitany, F. Alqallaf, D. K. Al-Mutairi, and H. A. Husain, "A two-parameter weighted Lindley distribution and its applications to survival data," *Mathematics and Computers in Simulation*, vol. 81, no. 6, pp. 1190–1201, 2011.

## Retraction

# Retracted: Design of Faster R-CNN-Based Fault Detection Method for Subway Vehicles

### Computational and Mathematical Methods in Medicine

Received 25 July 2023; Accepted 25 July 2023; Published 26 July 2023

Copyright © 2023 Computational and Mathematical Methods in Medicine. This is an open access article distributed under the Creative Commons Attribution License, which permits unrestricted use, distribution, and reproduction in any medium, provided the original work is properly cited.

This article has been retracted by Hindawi following an investigation undertaken by the publisher [1]. This investigation has uncovered evidence of one or more of the following indicators of systematic manipulation of the publication process:

- (1) Discrepancies in scope
- (2) Discrepancies in the description of the research reported
- (3) Discrepancies between the availability of data and the research described
- (4) Inappropriate citations
- (5) Incoherent, meaningless and/or irrelevant content included in the article
- (6) Peer-review manipulation

The presence of these indicators undermines our confidence in the integrity of the article's content and we cannot, therefore, vouch for its reliability. Please note that this notice is intended solely to alert readers that the content of this article is unreliable. We have not investigated whether authors were aware of or involved in the systematic manipulation of the publication process.

Wiley and Hindawi regrets that the usual quality checks did not identify these issues before publication and have since put additional measures in place to safeguard research integrity.

We wish to credit our own Research Integrity and Research Publishing teams and anonymous and named external researchers and research integrity experts for contributing to this investigation.

The corresponding author, as the representative of all authors, has been given the opportunity to register their agreement or disagreement to this retraction. We have kept a record of any response received.

### References

- [1] H. Ma and M. Yao, "Design of Faster R-CNN-Based Fault Detection Method for Subway Vehicles," *Computational and Mathematical Methods in Medicine*, vol. 2022, Article ID 1400658, 10 pages, 2022.



## Research Article

# Design of Faster R-CNN-Based Fault Detection Method for Subway Vehicles

Hanlin Ma <sup>1</sup> and Mingyang Yao <sup>2</sup>

<sup>1</sup>School of Power Technology, Liuzhou Railway Vocational Technical College, Liuzhou Guangxi 545616, China

<sup>2</sup>School of Automatic Control, Liuzhou Railway Vocational Technical College, Liuzhou Guangxi 545616, China

Correspondence should be addressed to Mingyang Yao; [v31414021@stu.ahu.edu.cn](mailto:v31414021@stu.ahu.edu.cn)

Received 21 April 2022; Revised 21 May 2022; Accepted 24 May 2022; Published 8 July 2022

Academic Editor: Naeem Jan

Copyright © 2022 Hanlin Ma and Mingyang Yao. This is an open access article distributed under the Creative Commons Attribution License, which permits unrestricted use, distribution, and reproduction in any medium, provided the original work is properly cited.

A substantial amount of maintenance and fault data is not properly utilized in the daily maintenance of pantographs in urban metro cars. Pantograph fault analysis can begin with three factors: the external environment, internal flaws, and joint behavior. Based on the analysis of pantograph fault types, corresponding measures are proposed in terms of pantograph fault handling and maintenance strategies, in order to provide safety guarantee for the safe and effective realization of rail transit vehicle speed-up and also provide reference for the maintenance and overhaul of pantographs. For the problem of planned maintenance no longer meeting current pantograph maintenance requirements, a defect diagnosis system based on a combination of faster R-CNN neural networks is presented. The pantograph image features are extracted by introducing an alternative to the original feature extraction module that can extract deep-level image features and achieve feature reuse, and the data transformation operations such as image rotation and enhancement are used to expand the sample set in the experiment to enhance the detection effect. The simulation results demonstrate that the diagnosis procedure is quick and accurate.

## 1. Introduction

The development of society and urbanization construction continues to deepen and improve people's material living standards, so that they improve the requirements for quality of life. In addition, the progress of society has led to the development of China's transportation industry, such as the development of China's metro rail transportation field is in a better situation, and the station has a high flow of people. In this development context, to create a safe travel environment for the public, for metro transportation operations, it is necessary to focus on the operation, monitoring, and maintenance management of station equipment, timely understanding of equipment safety conditions, the discovery of faults, and effective handling of problems, to ensure the safe operation of metro transportation [1–3]. With the continuous progress of rail transportation technology in China, the development of rail transportation operating vehicles from steam locomotives to internal combustion locomotives and

electric locomotive traction is particularly notable. Electrified railroads occupy a large part of China's rail traffic mileage, for the routine and troubleshooting of rail vehicles which are particularly important. In the existing electrified railroad operation lines, according to the statistics of various accidents in the past years, the vehicle equipment failures caused by pantographs account for a relatively large proportion. Pantograph is an important part of the vehicle but also is in direct contact with the contact network part, in the vehicle high-speed travel by wear and tear, and has a high probability of failure [4–6]. Rail vehicle power supply and operation disruptions have a significant impact on line transportation order and are a major issue for rail cars. As a result, understanding and treating common pantograph failure is critical for the safe and reliable operation of rail transit. The subway fault diagnosis system is shown in Figure 1.

China's environmental monitoring equipment industry started late, environmental monitoring equipment is mostly produced by small and medium-sized enterprises, and

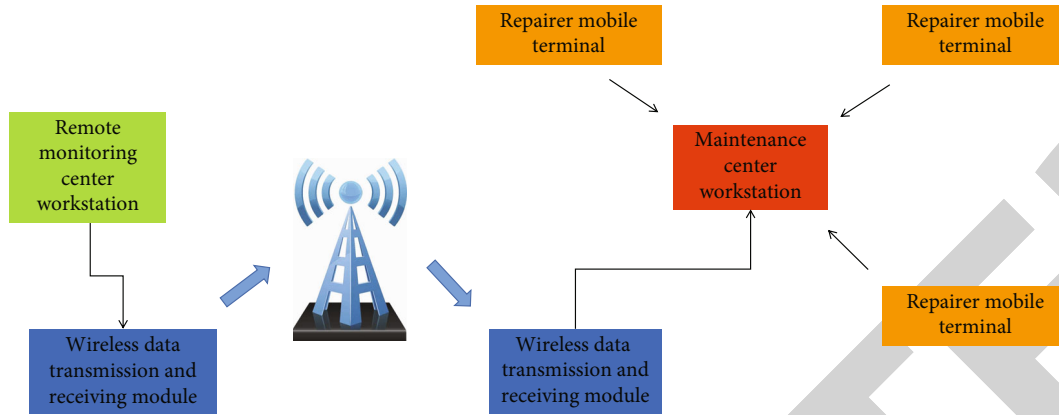


FIGURE 1: Subway fault diagnosis system.

products are basically concentrated in the low-grade environmental monitoring equipment, still far from being able to meet the needs of the development of China's environmental monitoring work, mainly in terms of poor product quality, short service life, unstable performance, and high failure, which leads to low frequency of environmental monitoring, sampling errors, and inaccurate monitoring data can not. This leads to low frequency of environmental monitoring, large sampling errors, and inaccurate monitoring data and cannot reflect the environmental quality in a timely manner. Therefore, it is of great significance to strengthen the equipment fault monitoring to ensure the normal operation of the equipment and improve the safety and reliability of the equipment [7, 8]. Currently, equipment defect detection research is mostly focused on the analysis of infrared thermal pictures of equipment. The maximum temperature value around the equipment is calculated in the detection of thermal faults in power equipment by identifying the power equipment in the thermal image based on the shape characteristics of the equipment, the diagnosis is made after correcting for various influencing factors, and satisfactory results are achieved. It is also possible to achieve high detection accuracy and robustness in the detection of thermal faults in power equipment by comparing the results obtained from the temperature information in the alignment area of the infrared image with each other. Due to the influence of environmental temperature and other factors on infrared thermal images, these methods still have great limitations. With the wide application of deep learning in the field of target detection, faster R-CNN algorithm, as one of the classical algorithms in this field, has high recognition accuracy and fast detection speed and has been widely used in vehicle detection, static aircraft detection, commodity image detection, etc. [9].

In this paper, we propose a faster R-CNN-based fault detection and recognition method for environmental monitoring equipment, which applies faster R-CNN to the fault detection of environmental monitoring equipment. Then, through the equipment fault online detection system, we can realize online real-time monitoring, so that we can get the information whether the equipment has a fault in time and effectively and notify the relevant staff [10, 11]. This

paper mainly verifies the feasibility of deep learning in environmental monitoring equipment fault identification from three aspects: equipment switches status identification, equipment indicator abnormality identification, and equipment display abnormal data identification, which effectively solves the problem of fault detection of environmental monitoring equipment, saves human and material resources, and further realizes the automatic detection of equipment. For the problem of low detection accuracy in the case of small contact network pantograph fault image samples, a dense convolutional neural network model is introduced as the feature extraction network of the faster R-CNN model for pantograph fault detection. The fused multilevel target features are extracted to improve the recognition capability of the model, and the sample set is expanded by using data transformations such as image rotation and enhancement to further improve the detection performance of the model. Through the experimental detection of the collected contact network pantograph images, the faster R-CNN model with a backbone network achieves good detection results in terms of both detection accuracy and speed.

The following is the paper's organization paragraph: Section 2 discusses the overall research related work. The method of the proposed concepts of this paper is examined in Section 3. The calculation example is discussed in Section 4. Finally, the research job is completed in Section 5.

## 2. Related Work

**2.1. Intelligent Detection of Subway Faults.** Research on fault detection and intelligent diagnosis system of metro electromechanical equipment and monitoring function are as follows: dynamic image display function. Dynamic image display function, the fault detection and intelligent diagnosis of subway electromechanical equipment work, can fully display the operation of the equipment [12–14]. During the actual work of the staff, use the system operation to analyze the data information of the equipment work as well as the operation safety, use the mouse to link to the property bar of the equipment, find the operation work information of the equipment, and set the corresponding authority. Alarm function is as follows: when problems occur during the

operation of electromechanical equipment in the system, the intelligent diagnosis system can give priority to the alarm processing of faults, display the faults visually and comprehensively in the human-machine interface, and take effective measures to solve the actual problems by combining the severity of the problems. Control function is as follows: the control function of electromechanical equipment. Through the intelligent diagnosis system, the fault personnel can directly log into the metro station control system and use the system's assigned authority to effectively control the electromechanical equipment. The functions of electromechanical equipment are group control function, control function of single machine equipment, and enthalpy control function. Mode of control [15, 16]: combined with the actual application of electromechanical equipment in demand, the staff selects the appropriate mode to set each parameter of the system, selects the appropriate parameters, and controls in this mode. For example, in the case of BAS modal control, the staff can optimize the parameters according to their own needs and set the correct parameter values, which can ensure the optimal operation of different modes. Display function: metro electromechanical devices and equipment, in the fault detection phase, the system can be displayed in the interface using human-computer interaction technology [17]. This enables staff to grasp the dynamic operation effect and parameters of each device, use the interface to present operating data, judge the device's performance in a timely manner, identify safety threats, offer relevant control instructions in a timely manner, and apply effective methods to solve.

The subway fault handling process is shown in Figure 2. There is the fault detection logical architecture scheme of the subway electromechanical equipment, fault monitoring and intelligent diagnosis system, manipulation, and maintenance of electromechanical devices through intelligent means, and the entire system framework covers data acquisition system, diagnosis system, transmission system, decision-making system, and various parts of the application layer. The above-mentioned parts are also the main elements of the system logical architecture, and attention should be paid to the need to cover during the design of the program. Data acquisition system designs program data acquisition layer, detecting the main sections of the equipment using the actual operational condition of electromechanical equipment and the acquisition of fault information, rather than equipment running speed, temperature, and vibration, etc. At the same time, for each intelligent equipment, screen doors, subway elevators, and other equipment, intelligent detection objectives can be achieved, through the interface of data, can directly obtain the detection data, through the sensing equipment to control the temperature during the operation of the equipment and vibration information, and can ensure the real-time information collection [18]. The data analysis system is designed to obtain data and information during the operation of the system, to analyze it in-depth, to build algorithms for data analysis and a database of fault information, to facilitate the accurate acquisition of fault characteristics and signals, and to analyze the causes of faults and future development directions. The data analysis system can also

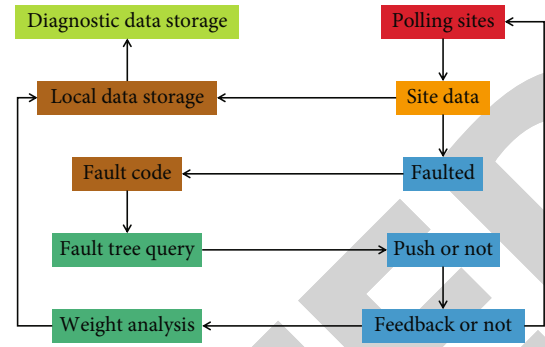


FIGURE 2: Subway fault handling process.

effectively analyze the spectrum of equipment vibration time, accurately determine the existing problems, and complete the intelligent diagnosis and processing of electromechanical devices. The data transmission system uses network technology to achieve equipment diagnosis and fault analysis, the field data transmission to the subway station, and maintenance management office, facilitating the timely transmission of effective information to the staff, as equipment and system operation, the implementation of management work. At the same time, standardized and open network protocols are set for data transmission to facilitate timely access to data information by staff [19–21].

**2.2. Subway Fault Intelligent Diagnosis.** The function of the decision evaluation system is to store the expert system for the maintenance of metro devices, to accurately evaluate the state of the equipment, historical data, and maintenance information, to make a comprehensive judgment on the operation of the equipment, to assess the future development situation, to reduce the difficulty of the maintenance work for the staff, and to do early warning work. At the same time, it is also able to combine the actual operation of the set, optimize the plan of maintenance, and strengthen the maintenance efficiency of electromechanical equipment. Application system functions as follows: providing a large amount of maintenance information and technical support, providing effective information for electromechanical equipment maintenance work, using the interface of human-computer interaction, and showing equipment operation data and information. The data and information of equipment operation, various resources, and maintenance data are recorded, accurately counted, queried, stored, and processed in a timely manner. In addition, it can also provide data information printing services for practical applications based on specific work requirements [22].

The structure design of fault detection and intelligent diagnosis system of metro electromechanical equipment is divided into a three-level detection and two-level management structural framework based on the above logical system design and combined with the specific functional requirements of the system. The main content covers the line maintenance center system, the maintenance of the working area of the accumulation equipment, and the three-level detection of the equipment. The hierarchical management and data transmission of the system can be

realized by using network information technology and software platform, and through the framework mode of hierarchical distribution, this structure is more flexible in deployment and easy to expand. In addition, the application of Web technology reduces the difficulty of staff work, timely access to fault detection, and intelligent diagnosis of data information. Line maintenance of the central system, set in the subway line vehicle section of the maintenance center location, the use of network data transmission and information management methods, intelligent processing of data information in operation, combined with data implementation equipment management, and detection of information in the whole line, can determine the fault for the future development trend, to achieve the alarm function of the fault, to create favorable conditions for the work of the staff, accurate find the cause and location of the fault, the location, fault characteristics, and other information, transported to the system's database center, and can achieve the goal of information-based maintenance of equipment. The electrical and mechanical work area system combines the actual operation needs of the subway, and based on past experience, the system treats four to six stations as intervals and installs electrical work areas at each interval point to facilitate maintenance and management in conjunction with the actual situation and to determine the factors that produce faulty equipment. In addition, the fault personnel is able to operate the faulty equipment and obtain the operation information and data of the accumulated equipment inside the work area and associate it with the printer to realize the printing and maintenance of information [23].

### 3. Methods

**3.1. Analysis of Faults.** There are many different types of pantograph structures, which can be classified as pop-up and inflatable based on their transmission methods, single-arm and double-arm based on their arm shapes, high-speed and normal-speed based on their usage speeds, and single pantograph and double pantograph based on the number of pantograph frames. Single-arm pantographs are currently the most common on China's rail vehicles. Pantograph is mainly composed of bow head, frame, chassis, and driving mechanism. The chassis support frame is installed in the upper part of the vehicle through the insulator, and the support frame supports the pantograph head by lifting the bow spring. From the structural point of view, the whole frame is composed of 2 four-bar mechanisms, and the drive mechanism is installed in the lower arm of the frame to realize the up-and-down movement of the pantograph. When the pantograph head is in operation, the height of the contact network varies, and the head's basic level must be maintained as the pantograph moves. If the pantograph head cannot maintain horizontal movement, the contact surface between the contact wire and the slide plate cannot be continuous, which may cause the pantograph head to wear out and lead to the contact wire going offline. Figure 3 shows the structure of single arm pantograph.

Here are the following parts of the pantograph: (1) carbon slide plate, (2) bracket, (3) balance bar, (4) upper frame,

(5) hinge seat, (6) lower arm bar, (7) sector plate, (8) buffer valve, (9) drive cylinder, (10) piston, (11) lowering bow spring, (12) link insulator, (13) slip ring, (14) link rod, (15) support insulator, (16) raising bow spring, (17) bottom frame, and (18) push rod. After the pantograph of a subway rail vehicle is raised and meets the overhead contact network, current is obtained from the contact network and transmitted to the vehicle electrical system. The current flows from the contact network to the head of the bow and flows into the bottom frame through the upper arm bar and lower arm bar in turn and finally enters the vehicle electrical system through the connecting plate and roof bus. When raising the bow, start the air compressor, when the rated working air pressure of the pantograph is reached, press the button to raise the bow, the compressed air enters the air spring from the solenoid valve and control box, the pneumatic equipment pushes the wire rope to drive the movement of the lower arm bar and holds up the upper arm bar of the pantograph, and the bow head moves smoothly to the height of the contact network to complete the raising of the bow. When lowering the bow, the pantograph falls smoothly to the rubber stop on the bottom frame with the help of gravity, and the hydraulic damper after the pantograph control box releases the compressed air in the air spring. According to the summary analysis of the daily maintenance records of this type of pantograph, combined with the failure mode of single-arm pneumatic pantograph and its mechanism analysis, the failure forms of pantograph can be summarized into five types of pantographs: pantograph cannot be raised, status display mismatch, bow network arc pulling, pantograph parts damage, and pantograph cannot respond.

**3.2. Model Structure.** The faster R-CNN model consists of two modules: the candidate region proposal network (RPN) and the fast R-CNN detection module. It can be subdivided into four parts: the first part is the convolutional neural network, which is mainly used to extract the features of the input pantograph images, the VGG16 network is used, and the feature map is the extracted pantograph image features; the second part is the region proposal network (RPN), which is mainly used to generate the candidate regions and initially. The third part is the region of interest pooling (RoI pooling), which is used to convert the input candidate regions of different sizes into fixed sizes and output them as vectors of the same length; the fourth part is the classification and border regression, which is used to output the pantograph state classes to which the candidate regions belong and the exact positions of the candidate regions in the original image. The fourth part is classification and border regression, which is used to output the pantograph state category to which the candidate region belongs and the exact position of the candidate region in the original image. The proposed model architecture is shown in Figure 4.

**3.3. Pretrained Convolutional Neural Network Models.** Pre-trained models are models created by previous authors to solve similar problems. Using pretrained models can save a

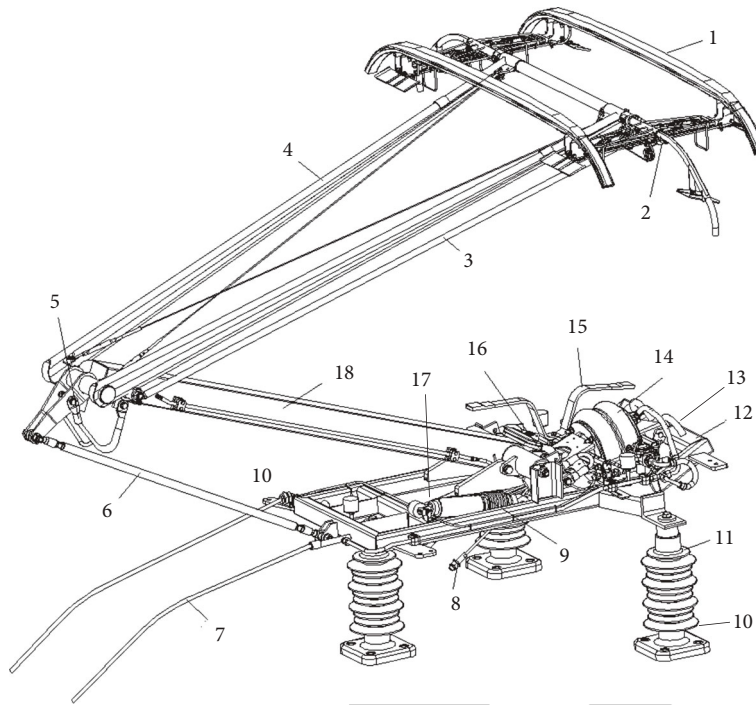


FIGURE 3: Pantograph schematic.

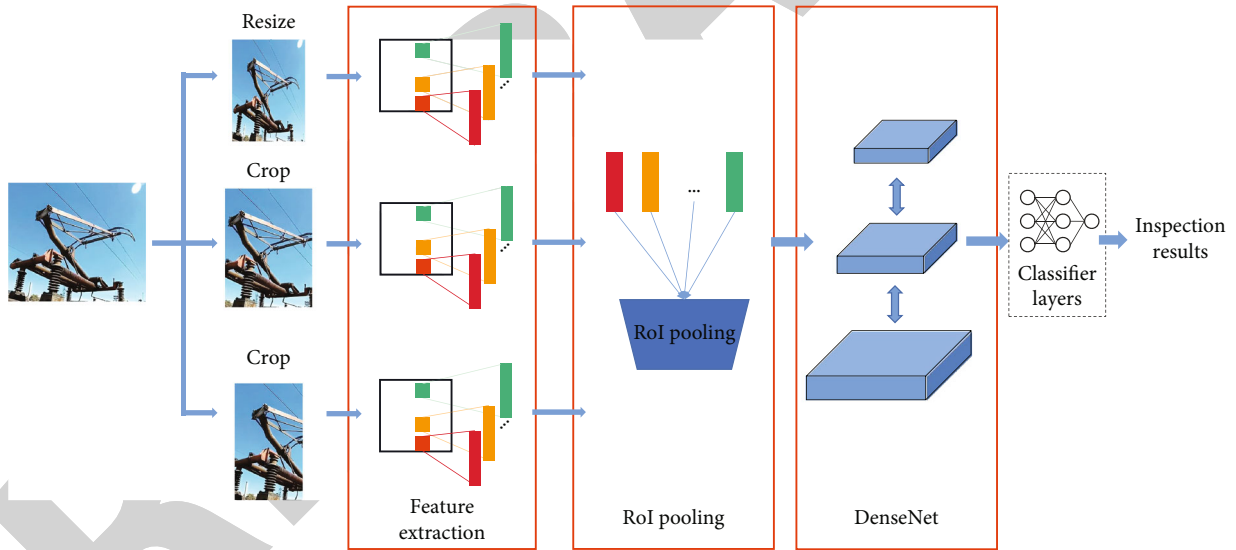


FIGURE 4: Model architecture.

lot of time by not having to train a new model from scratch. Varied convolutional neural network models, on the other hand, can have different effects on detection speed, accuracy, and other factors. The authors of the original faster R-CNN paper extract picture features using the Ziller and Fergus network model and the visual geometry group network model as the backbone network of faster R-CNN. Among them, ZFNet mainly adjusts the parameters of AlexNet by reducing the convolutional kernel and step size so that the network can extract more detailed features and thus improve the performance of the network; while in VGGNet, the convolutional layers all use the same convolutional parameters,

the pooling layers all use the same pooling parameters, and its network consists of several  $3 \times 3$  convolutional layers and  $2 \times 2$  pooling layers stacked repeatedly. The network structure is simple, but uses more parameters, has a higher memory occupation, and requires more computational resources.

**3.4. RPN Network.** In training the RPN network, the above pretrained network model is directly used to initialize the RPN, and the pantograph feature maps extracted by the pretrained network model are input to the RPN network. The RPN network generates region proposals on the feature

maps using sliding windows of different sizes and dimensions, and then the region proposals are input to the classification layer and the regression layer, respectively. In the classification layer, a normalization function (Softmax) is used for target detection to determine whether the proposed region contains a pantograph target, while the regression layer is used to calculate the offset of the proposed region bounding box regression, which is used to adjust the anchor points to obtain an accurate target candidate region. The RPN network uses a multitask loss function to calculate the loss, including classification loss and border regression loss, and the formula is defined as

$$L(\{P_i\}, \{t_i\}) = \frac{1}{N_{\text{cls}}} \sum_i L_{\text{cls}}(P_i, P_i^*) + \lambda \frac{1}{N_{\text{reg}}} \sum_i P_i^* L_{\text{reg}}(t_i, t_i^*), \quad (1)$$

where  $i$  is the index of anchors in small batch training,  $P_i$  denotes the probability that an anchor is a target,  $P_i^*$  denotes the presence or absence of a target for the anchor (1 for the presence of a target, 0 for the absence),  $t_i$  denotes the 4 parameterized coordinate vector of the predicted bounding box,  $t_i^*$  denotes the coordinate vector of the labeled bounding box,  $N_{\text{cls}}$  denotes the batch size (generally taken as 256),  $N_{\text{reg}}$  denotes the number of anchors,  $\lambda$  is the balance parameter and is set to 10 by default; the outputs of classification and regression layers consist of  $\{P_i\}$ ,  $\{t_i\}$ , respectively,  $L_{\text{cls}}$  is the classification loss, which denotes the logarithmic loss of two classes (target and nontarget), and  $L_{\text{reg}}$  is the regression loss, defined as

$$L_{\text{reg}}(t_i, t_i^*) = R(t_i - t_i^*) = \begin{cases} 0.5(t_i - t_i^*)^2 & \text{if } |x| < 1. \\ |t_i - t_i^*| - 0.5 & \text{otherwise} \end{cases} \quad (2)$$

**3.5. Fast R-CNN.** The fast R-CNN module consists of two parts: ROI pooling and classification regression; in faster R-CNN, the input of fast R-CNN module is the candidate regions output by RPN network. Features protect the complete structure and original shape information of the input image. Each feature vector is then fed into multiple fully connected layers behind and finally output by two subconnected layers of the same level, the classification layer and the regression layer, similar to the output of RPN networks, except that the output of the classification layer is the probability value of the candidate region belonging to each category, and the output. The loss function used in the fast recurrent-convolutional neural network (R-CNN) module is similar to that of the RPN module, except that the binary classification is changed to multiclassification, and only the regression loss of the candidate regions predicted to be labeled classes is considered. The DenseNet model borrows the idea of the RPN model, which also connects the features of the front layer of the network to the back layer, but unlike ResNet, it adopts a new network structure, in which the core

idea of the ResNet model is to establish a ‘‘short-circuit connection’’ between the front layer and the back layer, using the connection method of element-level summation, whereas DenseNet establishes a dense connection between all the preceding layers and the following layers, in which the input of each layer of the network is the concatenation of the output of all the preceding layers within a module. This difference can also be visualized from the transfer functions of the two network structures: The transfer function of the ResNet network is

$$x_l = H_l(x_{l-1}) + x_{l-1}. \quad (3)$$

The transfer function of the DenseNet network is

$$x_l = H_l([x_0, x_1, \dots, x_{l-1}]). \quad (4)$$

The dense connection has many advantages, it can directly parallelize the features from different layers to achieve feature reuse, which is more conducive to information transfer, and it can mitigate the gradient disappearance during back propagation and reduce the problem of easy overfitting due to the small sample size of the network training. The schematic diagram of the densely connected network is shown in Figure 5.

**3.6. Data Preprocessing.** Since the collected pantograph initial state data involve many parameter variables, this paper selects the principal element analysis method to reduce its dimensionality. The principal element analysis (PCA) method is a transformation method that reflects multiple relevant variables with relatively few feature variables but carrying enough information. On the premise of ensuring the correct diagnosis rate, redundancy and noise are eliminated, and then the dimensionality reduction of the original feature data variables is realized to reduce the diagnosis time consuming and improve the diagnosis efficiency. The calculation process is as follows:

- (1) Construct the original variable matrix  $X_0 \in R$ . the rows  $x_i$  of the matrix correspond to the original data samples, and the columns  $x_j$  of the matrix correspond to the different measured. Since the different magnitudes of the initial data can lead to serious dispersion of the variable results, the observation samples need to be standardized
- (2) The covariance solution of the processed matrix  $X_0$  is performed, i.e., the calculation of the correlation coefficient matrix  $R$ ; that is,

$$r_{jk} = \frac{\sum_{k=1}^n (x_{ki} - x_i)(x_{kj} - x_j)}{\sqrt{\sum_{k=1}^n (x_{ki} - x_i)^2 \sum_{k=1}^n (x_{kj} - x_j)^2}}. \quad (5)$$

- (3) Solve the covariance matrix to obtain the eigenvalue eigenvectors. Calculate the value of the eigenequation

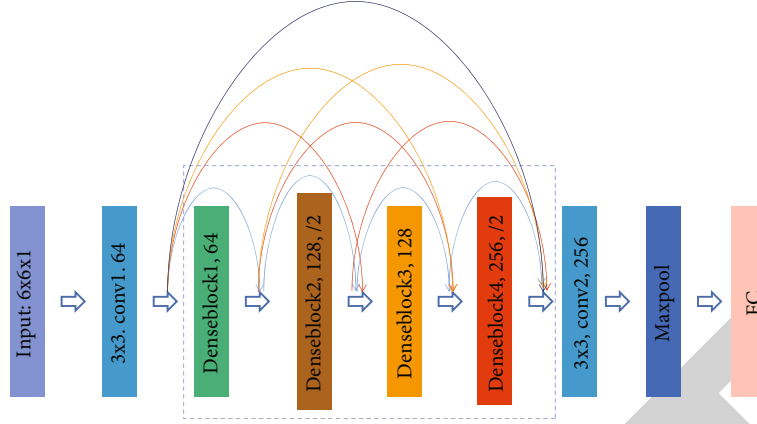


FIGURE 5: Schematic diagram of densely connected network.

$|\lambda I - R| = 0$  and order the eigenvalues sought, from largest to smallest, noted as  $\lambda_1 \geq \lambda_2 \geq \dots \geq \lambda_m \geq 0$ , corresponding to the eigenvectors  $I_1, I_2, \dots, I_m$

- (4) The feature vectors are transformed into principal elements, and the contribution rate and cumulative contribution rate of the principal elements are calculated:

$$T_j = I_1 X_1 + I_2 X_2 + \dots + I_m X_m, \quad (6)$$

where  $T_j$  is the  $j$ -th principal element, representing the projection of matrix  $X$  on the corresponding principal element feature vector, and the larger the corresponding coverage, the longer its projection length will be. If the principal element  $T_j$  decreases, then  $I_1$  is the direction that covers the widest degree of information.

- (5) Calculate the cumulative contribution rate  $\alpha$

$$\begin{aligned} T_j &= \frac{\lambda_j}{\sum_{j=1}^p \lambda_j} \times 100\%, \\ \alpha &= \frac{\sum_{s=1}^i \lambda_s}{\sum_{j=1}^p \lambda_k} \times 100\%. \end{aligned} \quad (7)$$

## 4. Experiments and Results

**4.1. Data Set.** The pantograph image data for this experiment mainly came from the pantograph images collected by the contact network suspension state detection and monitoring device (4C device), and the samples were divided into three categories by analyzing the pantograph morphology in the images: the first category was normal pantographs, the second category was bent pantographs, and the third category was broken pantographs.

**3.2 Data set processing.** This experiment got a total of 3563 contact network photos taken by the 4C device. After choosing and eliminating the blurred and pantograph-free samples from the 3563 contact network

TABLE 1: Data information.

Sample	Datasets	zcdx	xbdx	dkdx
Dataset 1	Total number	856	206	223
	Training set	599	144	156
	Test set	257	62	67
Dataset 2	Total number	5992	1442	1561
	Training set	4194	1099	1093
	Test set	1798	433	468

images received from 4C equipment, 1672 good samples were obtained. The database details are shown in Table 1. To increase the diversity of samples and improve the accuracy of pantograph identification and fault detection, this paper expands the sample set by rotating the original images clockwise by  $30^\circ$ ,  $60^\circ$ , and  $90^\circ$ , enhancing the brightness to 1.2 times, attenuating it to 0.8 times, and adding pepper noise with a density of 0.01 and other six data transformation operations. A total of  $1672 \times 7 = 11704$  samples of the data set were obtained after processing. Considering that the actual detection process does not require too high a resolution, and that the pretrained models used in this paper were all trained on the PASCALVOC dataset; the resolution of the image aspect was scaled by 10 times each for the compression process, and the compressed image aspect was between 300 and 600 pixels. Then, all samples in the dataset were labeled using the LabelImg standard tool. The category labels of normal pantograph, bending deformation pantograph, and broken pantograph are labeled as "zcdx," "xbdX," and "dkdx," respectively. Then, the samples of the data set were randomly divided into training and test sets in the ratio of 7:3, where data set 1 is the original data sample; data set 2 is the data sample after adding the data transformation process.

**4.2. Experimental Setup.** This experiment is conducted under Windows 10 Home Edition operating system, based on Intel(R) Core (TM) i5-8300H CPU2, 3GHz (8GByte running memory), and NVIDIA GeForce GTX1050Ti GPU (4GByte running video memory) hardware device to build

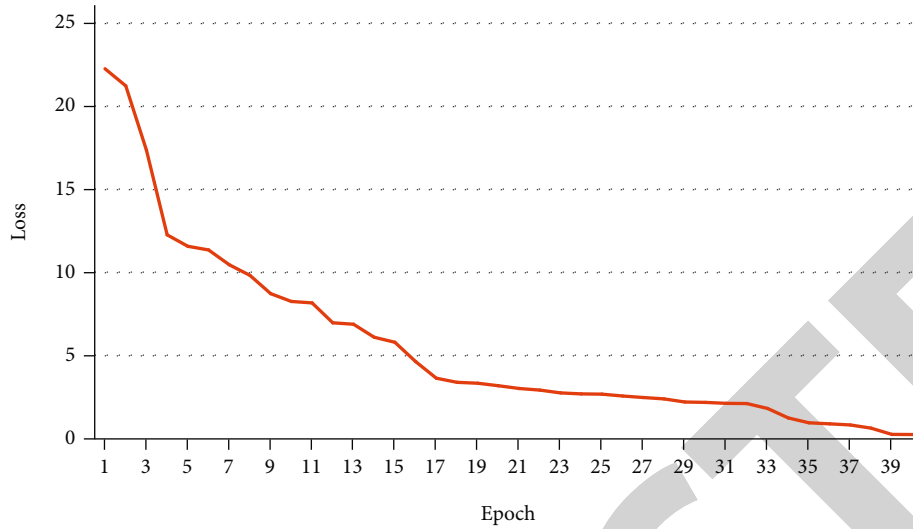


FIGURE 6: Schematic diagram of loss reduction during training.

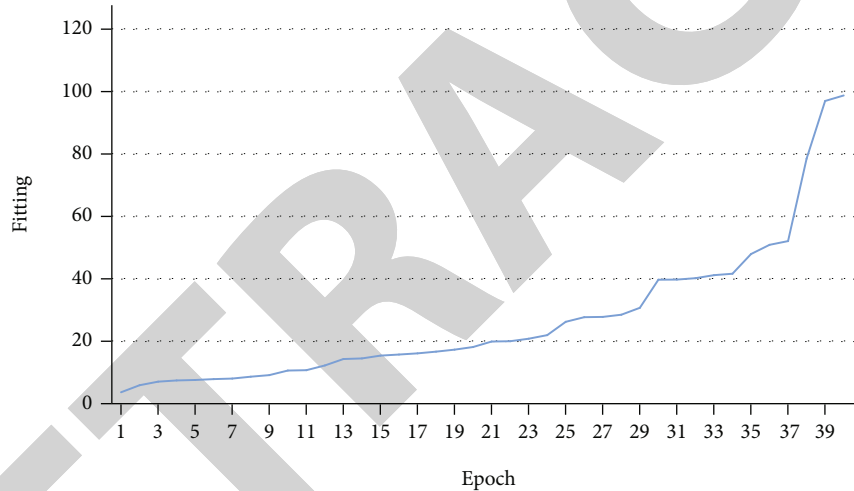


FIGURE 7: Training process performance improvement schematic.

Google TensorFlow graph (TensorFlow) deep learning framework, using the Python programming language, using the faster R-CNN architecture to implement the training of network models, using the divided dataset as training samples, and using VGG16, ResNet101, and DenseNet121 as the backbone network of the faster R-CNN in turn to train the pretrained. The training of the contact network pantograph identification and fault detection network model is accomplished using the faster R-CNN model. In this paper, the end-to-end training method is used to share convolutional features, and the stochastic gradient descent (SGD) algorithm is used to optimize the model, with the maximum number of iterations set to 40,000, the initial learning rate set to 0.001, the momentum factor set to 0.9, and the learning rate adjusted to 0.0001 when the number of iterations reaches 20,000.0001; meanwhile, output its average loss every 1000 times and stop training when the loss function converges, and the number of iterations reaches 40,000, using VGG16, ResNet101, and DenseNet121 as the back-

bone network to train the faster R-CNN model. After training, the trained model parameters are saved, and the model effect is further validated using the divided test set, preserving the four sample target classes with confidence levels larger than 0.5. Figure 6 depicts the loss degradation during training, while Figure 7 depicts the improvement in performance.

**4.3. Experimental Results.** The metrics for measuring the goodness of the model in this research are average precision (AP) and mean accuracy (mAP), where AP is calculated based on the precision rate  $P$  and recall rate  $R$ , if the classification results are represented as in Table 2.

In this paper, the same computer is used for training and testing of all samples. In order to improve the accuracy of model recognition, multiple data transformations are used to expand the sample set, and different network models are used as the backbone network of the faster R-CNN model, while mAP is cited to visually compare the recognition accuracy of each network model, combined with the recognition



TABLE 2: Classification information.

Real situation	Predicted results	
	Positive example	Counterexamples
Positive example	TP (true example)	FN (false counter example)
Counter example	FP (false positive example)	TN (true counterexample)

TABLE 3: Performance comparison.

Model	xbdx	dkdx	zcdx	Time	mAP
Faster + VGG16	91.30	86.30	88.40	0.23	88.67
Faster + ResNet101	95.30	90.50	94.30	0.33	93.37
Faster + DenseNet121	96.10	92.90	96.30	0.20	95.10

speed, to select the best applicable contact network pantograph fault detection. The network models are selected as the best network models for pantograph fault detection. 4. 1 Comparison of recognition results of three network models. The faster R-CNN models with VGG16, ResNet101, and DenseNet121 as the backbone networks are trained using the training set of the original dataset1 in turn, and the training methods in Section 3.3 are used for all training methods. The resulting models were then evaluated against the test set of datasets 1, and the AP values of each category were produced based on each model's detection outcomes and combined with the detection speed as a criterion for rating the models' goodness. The detection results of the three network models in pantograph faults are shown in Table 3, where the detection time is the average time of detection of all test samples in dataset 1.

From the detection results in Table 3, it can be seen that the faster R-CNN model based on DenseNet121 achieves an AP value of more than 92% for all types of pantograph states with only the original data set, which is more than 5% higher than VGG16 and about 1% higher than ResNet101, and in the detection of pantograph disconnection and bending faults, the DenseNet121 network is 2% higher than the ResNet101 network because DenseNet is able to extract deeper pantograph image features and has good overfitting resistance even in the case of small pantograph fault sample size. The detection speed is also faster than that of the ResNet101 network because the DenseNet network uses directly connected pantograph image features from different network layers in parallel, and each layer needs to learn fewer parameters; so, the detection speed of the DenseNet network is faster when the network layers are comparable.

## 5. Conclusion

By using the DenseNet network as a feature extraction network for the faster R-CNN model, which can extract deep-level image features and accomplish feature reuse, deep-level pantograph image features may be exploited, and the subway fault detection effect improved. The detection model is evaluated using pantograph images under various conditions such as multiple pantographs, in-tunnel and at night,

and compared with the original model and the detection results based on the ResNet network model. The simulation results show that the method presented in this paper is more effective in pantograph fault detection, with a mean average accuracy of more than 4% higher than the original detection model, and a mean average accuracy of more than 98% after adding expanded samples, effectively addressing the problem of low detection accuracy in the case of fewer pantograph fault samples. In this paper, only the pantograph positioning and the detection of two obvious faults of broken wire and bending are realized, and further research on the detection of other pantograph faults will be conducted on this basis in the next step.

## Data Availability

The datasets used during the current study are available from the corresponding author on reasonable request.

## Conflicts of Interest

The authors declare that they have no conflict of interest.

## Acknowledgments

This work was supported by "Research on Fault Diagnosis and Prediction of Traction Inverter Based on Feature Fusion," the Project of Improving the Basic Scientific Research Ability of Young Teachers in Guangxi Universities (2022KY1415) and "Research on Predictive Control of The BAS System of Subway Based on Load Calculation," the Project of Improving the Basic Scientific Research Ability of Young Teachers in Guangxi Universities (2022KY1410).

## References

- [1] W. Wang, Y. Feng, Y. Shi, M. Cheng, W. Hua, and Z. Wang, "Fault-tolerant control of primary permanent-magnet linear motors with single phase current sensor for subway applications," *IEEE Transactions on Power Electronics*, vol. 34, no. 11, pp. 10546–10556, 2019.
- [2] G. Liu and Z. Hou, "Cooperative adaptive iterative learning fault-tolerant control scheme for multiple subway trains," *IEEE Transactions on Cybernetics*, vol. 52, no. 2, pp. 1098–1111, 2020.
- [3] J. Loy-Benitez, Q. Li, K. J. Nam, and C. K. Yoo, "Sustainable subway indoor air quality monitoring and fault-tolerant ventilation control using a sparse autoencoder-driven sensor self-validation," *Sustainable Cities and Society*, vol. 52, p. 101847, 2020.
- [4] H. Wang and Z. Hou, "Model-free adaptive fault-tolerant control for subway trains with speed and traction/braking force

## Research Article

# Influence of Three-Dimensional Visual Reconstruction Technology Combined with Virtual Surgical Planning of CTA Images on Precise Resection of Liver Cancer in Hepatobiliary Surgery

Yuanyu Zhao,<sup>1</sup> Ting Chen,<sup>2</sup> Hui Wang,<sup>2</sup> Qiang Xue,<sup>3</sup> Wenyuan Guo,<sup>1</sup> Guoshan Ding,<sup>1</sup> Junfeng Dong ,<sup>1</sup> and Junsong Ji <sup>1</sup>

<sup>1</sup>Department of Liver Surgery, Changzheng Hospital, Naval Medical University, Shanghai 200003, China

<sup>2</sup>Department of General Surgery, Shanghai Jing'an District Zhabei Central Hospital, Shanghai 200070, China

<sup>3</sup>Department of Neurosurgery, Eastern Hepatobiliary Surgery Hospital, Navy Medical University, Shanghai 200082, China

Correspondence should be addressed to Junfeng Dong; isher0214@126.com and Junsong Ji; jijunsong@smmu.edu.cn

Yuanyu Zhao, Ting Chen, and Hui Wang contributed equally to this work.

Received 24 April 2022; Revised 16 May 2022; Accepted 19 May 2022; Published 7 July 2022

Academic Editor: Naeem Jan

Copyright © 2022 Yuanyu Zhao et al. This is an open access article distributed under the Creative Commons Attribution License, which permits unrestricted use, distribution, and reproduction in any medium, provided the original work is properly cited.

Hepatobiliary malignancies, such as hepatocellular carcinoma (HCC) and biliary tract cancers, namely, gallbladder carcinoma and cholangiocarcinoma, are linked to a high rate of morbidity and mortality, depending on the phase of the disease. The intricate hepatobiliary anatomy and the need for accurate preoperative management, especially in patients with advanced liver disease, make these tumors difficult to treat. Surgical resection is a notable therapy for hepatobiliary cancers. Unnecessary or excessive liver excision influences patient rehabilitation, normal liver function, and postoperative complications. Hepatobiliary operations must therefore include accurate liver removal. The present advancements in imaging technology are aimed at improving the diagnostic efficacy of liver injury even more. Three-dimensional visual reconstruction is becoming more important in the diagnosis as well as treatment of a variety of disorders. In this paper, we proposed a novel three-dimensional visual reconstruction technology using enhanced nonuniform rational basis spline (ENURBS) combined with virtual surgical planning of Computed Tomography Angiography (CTA) images for precise liver cancer resection. The purpose of this project is to rebuild 2D CTA scan images of liver cancer into a 3D reconstructed model for efficient visualization and diagnosis of liver cancer and to prepare an effective preoperative surgical plan for precise liver excision based on a 3D recreated liver model. This method's performance is compared to that of 2D planning in terms of accuracy and time taken to complete the plan. It is concluded that our proposed technique outperforms the planning technique based on 2D images.

## 1. Introduction

One of the most dangerous diseases is liver cancer, often known as hepatic cancer. Hepatitis B and C viruses, fatty liver illness, drug-related cirrhosis, glowing, fatness, diabetes, iron overburden, and different dietary hazards are all prominent causes of HC. Liver cancer is the most common reason for cancerous deaths worldwide and the 5<sup>th</sup> most prevalent in the US, and it is one of the top 5 dangerous malignancies

to experience a yearly proportion increase in occurrences [1]. HCC has been the most prevalent kind of liver cancer, responsible for roughly 80% of all occurrences [2]. Nearly 78 percent of the 600,000 instances of HCC are noted worldwide in Asian countries. Chronic hepatitis B virus disease is the major source of HCC in Eastern Asia.

In the complete medication of liver disease, surgical resection (removal of the cancerous segment in the organ) remains supreme. It has the potential to cure patients with

better efficiency and to extend the overall survival duration of those who undergo surgery. Liver resection is a significant, life-threatening procedure that should only be performed by surgeons with extensive experience. The major concern for surgeons is the selection of the correct tumor segment for liver resection from the 2D medical images such as CT, MRI, CTA, and X-ray because of the complexities in the analysis of hepatobiliary anatomy. Computed Tomography Angiography (CTA) is an imaging technique that combines injection of contrast material into the blood vessel with a CT scanner to produce cross-sectional pictures of soft tissue, skeletal anatomy, and vascular frames. 3D images reduce the complexities in the analysis of hepatic anatomy.

Doctors previously used their personal knowledge to transform 2D scan images into an abstract 3D model. Nonetheless, the reconstruction conclusion may be incorrect and inconsistent due to the limitations and ambiguities of their experience [7]. As a result, utilizing computer-aided software or mathematical models to digitally reconstruct 3D images from 2D photographs could be a viable solution to the aforementioned dilemma. Three-dimensional visual reconstruction (3DVR) is becoming more and more important in the analysis and cure of liver illnesses [8]. Although 3D rebuilt or 3D printing technology designs may visually represent intrahepatic blood vessel changes, they also include an efficient and comfortable approach for liver volume estimation, virtual simulation operation, and operative guidance [9]. 3D viewing includes extraction of features and 3D reconstruction of CT/MRI/CTA images utilizing modern computing techniques. It is a method of seeing, describing, and evaluating 3D anatomy and morphological properties of organs in order to make more intuitive, realistic, and reliable medical decisions [10].

When surgical treatments are preceded by proper planning, the results are usually better. Proper planning of liver resection which includes the examination of precise tumor segment that must be excised is required because unnecessary liver resection has an impact on patient recovery, surgical complications, and liver function [11]. To provide optimal treatment, it is critical to visualize the lesion to be treated directly or indirectly from the 3D reconstructed image. Virtual surgical planning (VSP) is quickly becoming a standard of care for even the most complex surgeries [12].

In this research, we proposed a new enhanced three-dimensional visual reconstruction technology-enhanced non-uniform rational basis spline (ENURBS) combined with virtual surgical planning of CTA images on precise resection of liver cancer in hepatobiliary surgery. The first focus of this work is to reconstruct the 2D CTA images of liver cancer into 3D reconstructed model using the ENURBS algorithm for efficient visualization and diagnosis of liver cancer. The second goal is to plan the surgical methods using VSP based on the 3D reconstructed liver model for precise liver resection. The performance of this approach is compared with that of 2D images.

The further organizations of the research paper are shown below. Section 2 shows the problem statement. Section 3 provides the flow of the proposed work. Performance evaluation is given in Section 4. Finally, Section 5 gives the conclusion of the proposed paper.

## 2. Problem Statement

Liver disease is a major risk to human life, so it was among the most internal cancers in the world, as well as one of the principal factors of cancer-related death. Hence, efficient diagnosis and proper treatment are the major concerns in curing the patients. Diagnosis using 2D CTA images of the liver is very complicated and time-consuming for surgeons because of the complex hepatic structure. So there is a need for modern imaging techniques. One such technique is a 3D visual reconstruction from 2D images which provides a clear visualization of liver anatomy and improves the surgeon's knowledge. Surgical resection is the prominent treatment for preventing the further dispersal of liver tumors and curing the patients. Choosing an optimal approach for liver resection is a critical task before treatment because unnecessary liver resection has an impact on patient recovery and normal liver function. Hence, advanced preoperative surgical planning before surgical intervention is required for removing precise liver tumor segments and improving the efficiency of treatment. By considering these factors, we proposed three-dimensional visual reconstruction technology combined with virtual surgical planning of CTA images on precise resection of liver cancer in hepatobiliary surgery.

## 3. Proposed Work

In this section, we define the dataset, image processing, 3D reconstruction-virtual surgical planning, ENURBS algorithm, 3D reconstruction of the hepatic centerline, 3D reconstruction of the hepatic cross section, 3D reconstruction of the hepatic surface, and planning of surgical methods in detail.

Accurate liver resection is very significant for a better outcome in curing patients with liver cancer. Three-dimensional visual reconstruction technology combined with virtual surgical planning is used in this work. The 2D CTA images of liver cancer are preprocessed at first. Then, the images are reconstructed into a 3D image using ENURBS for efficient visualization and diagnosis of liver cancer. Finally, planning of the surgical methods based on the 3D reconstructed liver model for precise liver resection is performed using VSP. The flow of the proposed work is shown in Figure 1 and explained in this section.

*3.1. Dataset.* In our study, we used the clinical dataset that was prescribed in [6]. The dataset consists of six CTA volumes of the abdomen imaged at the portal venous region, among which two volumes are pathologic. Every dataset volume is made up of a sequence of 2D CT layers with a quality of  $512 * 512$  axial planes as well as a width of 0.5–2 mm. Every volume has a different quantity, ranging between 212 and 395.

*3.2. Image Preprocessing.* Noise removal and node and segment labeling are included in the image preprocessing of 2D CTA liver images. The presence of noise in an image can reduce image quality, further complicating the image processing process [13]. As a result, to increase image quality,

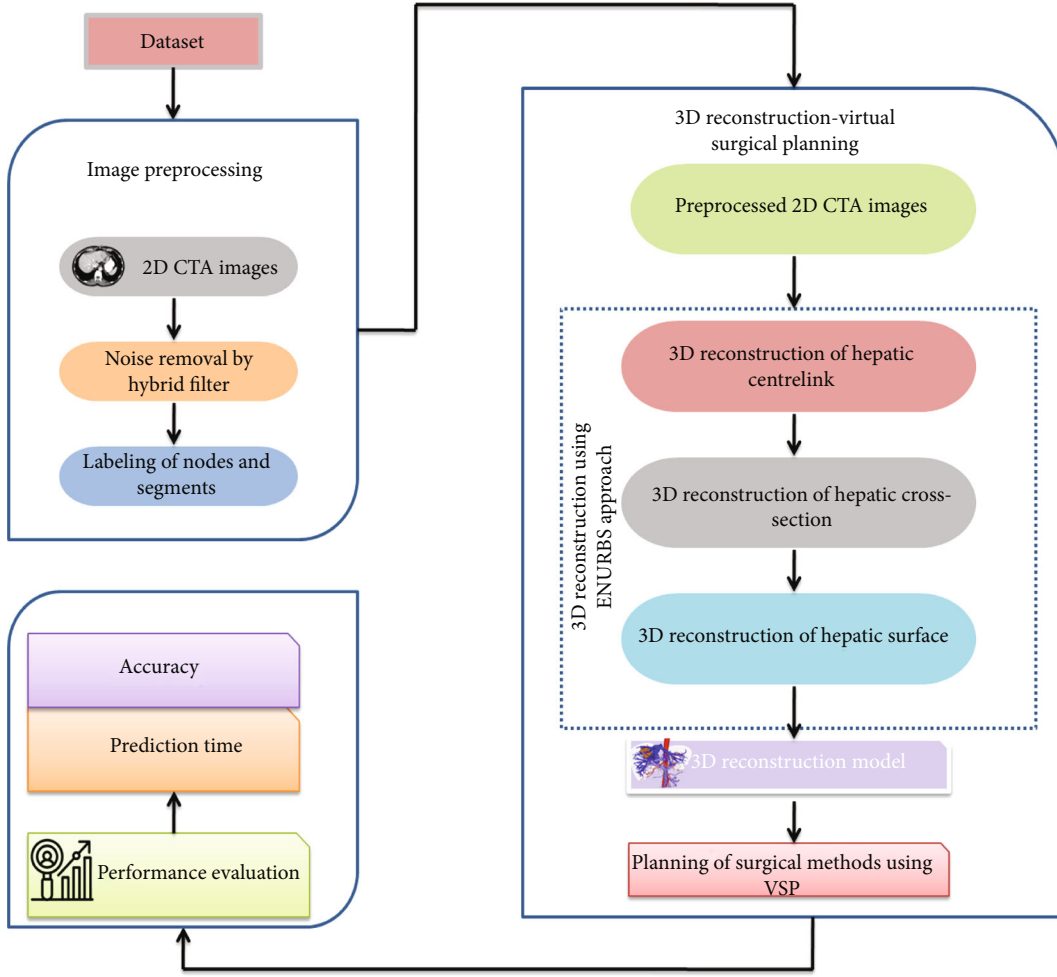


FIGURE 1: Detailed flow of the proposed work.

undesirable noises must be removed. A hybrid median filter was employed to remove noises such as impulsive and Gaussian disturbances. With the use of the Gaussian distribution, Gaussian smoothing is accomplished in conjunction with a median filter. The median filter uses the Gaussian distribution and medians to remove noisy pixels or noise without affecting edges or minute details. Each component of the image is recreated using the preprocessed photo elements [14]. The final stage is to improve image quality to obtain a high-quality image for future diagnostics and processing [15].

The Gaussian distribution  $R_{(b)}(A)$  is determined by

$$R_{(b)}(A) = \frac{1}{\sigma\sqrt{2\pi}} e^{-\frac{(A-\mu)^2}{2\sigma^2}}, \quad (1)$$

where  $\mu$  is the mean and  $\sigma$  denotes the standard deviation.

The median of the image pixels is  $y[m, n]$  by

$$y[m, n] = \text{median}_{(u,v) \in k_{xy}} \{g(u,v)\}, \quad (2)$$

where  $k_{xy}$  are the coordinate sets centered at the point  $(x, y)$ .

2D liver borders are eliminated employing a fast marching level set technique on the CTA abdominal picture by characterizing liver borders as the reproducing front final location. The vascular centerline is determined using a sub-voxel precise skeletonization method. The centerline can be computed as the cheapest path between an ending point and a beginning point by performing a gradient descent over the fast marching distance map.

Given a 2D image of the skeleton of a liver structure, nodes (that is, branching points) and segments were discovered and labeled on each projection using the binary image's connection matrix. An eight-connectivity seed-fill technique was used to find connected pixels. The seed-fill technique began with a center point and explored its neighbors iteratively to find related facts [16]. Labels may propagate differently depending on the projection. The insertion points for liver removal are used to verify label correspondence. These points were marked to ensure that they were consistent among forecasts. The Euclidean distance was used to match an insertion point to a node. Only nodes with the same initialization point were kept.

TABLE 1: 3D visualization classification of HCC.

Classification description	Surgical methods
Type I: lesions are identified in the parenchyma of liver segments V and VIII or both segments and are distinguished by their closeness to, or even direct violation of, the next portal vein. They do not cling to the right hepatic vein trunk or compress it	Excision of liver segments V and VIII $\pm$ partial intervention of segment IV
Type II: lesions are located in the parenchyma of hepatic segments IVa and IVb or both segments and are distinguished by their proximity to, or even direct violation of, the left hepatic vein branch. Furthermore, it does not attach to or compress the trunk of the left hepatic vein	Excision of liver segments IVa and IVb or left hepatectomy
Type III: most of the liver parenchyma in segments IV, V, and VIII is occupied by the lesions, which is characterized by a wide and deep invasion of the parenchyma, as well as proximity to the main hepatic vein	Central bisectionectomy (removal of segments IV, V, and VIII $\pm$ I)
Type IV: most liver parenchyma in segments IV, V, and VIII is occupied by lesions, which is distinguished by its closeness to, or direct violation of, the left/right portal vein branch or the left/right hepatic vein.	Excision of segment IV, V, VI, VII, and VIII removal reduced right trisectionectomy or reduced left trisectionectomy Associating liver partition and portal vein ligation for staged hepatectomy (ALPPS)
Type V: the superficial liver parenchyma of segments IV, V, and VIII is occupied by this form of liver tumor. Neither the portal branch nor the hepatic vein is near the lesions	Hepatectomy with a negative margin

As a result, node labels and branching across projections were guaranteed to match.

**3.3. 3D Reconstruction-Virtual Surgical Planning.** The proposed technique involves reconstruction of the 3D image from the 2D CTA image using the ENURBS 3D approach and planning of the surgical methods based on the 3D reconstructed liver model for precise liver resection using VSP.

**3.4. ENURBS Algorithm.** The major steps involved in our proposed algorithm are as follows:

- (i) 3D reconstruction of the hepatic centerline
- (ii) 3D reconstruction of the hepatic cross section
- (iii) 3D reconstruction of the hepatic surface

Using this algorithm, a 3D reconstructed CTA liver image will be generated from the preprocessed 2D CTA image.

**3.5. 3D Reconstruction of the Hepatic Centerline.** A 3D vascular centerline was created by intersecting surfaces defined by comparable liver segments. The segment correspondences between two projection planes  $P_n$  and  $P_m$  were estimated. Let the pair of transformed liver centerlines be  $X_n$  and  $X_m$  and their corresponding focal points be  $F_n$  and  $F_m$ . The surfaces  $R_n$  and  $R_m$  representing the projection beams for  $X_n$  and  $X_m$  were produced by connecting the centerlines

and focal points. The issue of identifying the 3D centerline ( $C$ ) in the curves  $X_n$  and  $X_m$  can be mitigated to the identification of the intersection line of the 2 surfaces  $R_n$  and  $R_m$ , as given in

$$C = R_m \cap R_n. \quad (3)$$

$R_n$  and  $R_m$  were triangulated surfaces, and the fast mutual triangle intersection testing was used to calculate their intersection. If two triangles meet, they lap over at the intersection line of their various planes, according to this analysis. In a nutshell, the test determines the signed range between a triangle's three vertices in the plane comprising another triangle. The two triangles do not intersect if all of the distances have the same sign. Otherwise, they may meet, reducing the problem to a two-segment overlap test on the junction line. The algorithm determines whether scalar gaps within each triangle have an intersecting path; if they do, the intersecting line segment that would be the two separate places is determined [17]. Construction difficulties can develop whenever the triangles are mostly coplanar or even when one border is approximately coplanar to another triangle. To handle such scenarios, a tolerance valuation for the ranges between vertices of two triangles has been determined by noticing the greatest 3D Euclidean distance with both relating sights attained experimentally; that is, if a tip is fairly similar to the plane of other triangles, it is taken into account to be on the plane. The crossings between 2 triangulated



FIGURE 2: 3D reconstructed liver model.

fields produced an organized number of attributes, which were linked to form a 3D midline.

**3.6. 3D Reconstruction of the Hepatic Cross Section.** The 3D cross sections were produced by keeping the 3D generated centerline as the base. The collection of accessible projection lines, their mutual alignment, and their direction concerning the liver section of interest affect the precision of the liver contour in 3D reconstruction from CTA. In CTA images, there are few  $N$  projection planes. Based on these findings, a 3D cross section was built in two stages: initially, an estimate was employed to deal with a limited set of projections, and then, the original cross section was localized in line with 2D liver borders.

At equidistant places “ $a$ ” along a 3D rebuilt centerline curve, cross-sectional planes were formed in 3D space. With a 3D point  $(x_a, y_a, z_a)$  on  $C$ , a cross-sectional plane  $R_a$  was determined with the help of tangential vector  $\widehat{m}_{R_a}$  of  $C$  at  $(x_a, y_a, z_a)$ . The 2D image point  $(u_{a,m}, v_{a,m})$  is the point of projection  $(x_a, y_a, z_a)$  on the projection plane  $P_m$ . The diameter vector which is orthogonal to the direction of the 2D liver centerline at  $(u_{a,m}, v_{a,m})$  was  $D_{a,m}$ . The magnification factor (M.F), which was derived using equation (4), was then applied to expand this vector.

$$\text{M.F} = \frac{(x_a, y_a, z_a)}{D(F_m, (u_{a,m}, v_{a,m}))}. \quad (4)$$

The diameter vector was not always orthogonal to  $C$  at  $(x_a, y_a, z_a)$ . Hence, the expanded diameter  $D_{a,m}^N$  is imposed on the plane of the cross-sectional plane at  $(x_a, y_a, z_a)$ . A liver contour was developed as a circle at this point, with a diameter equal to the average length of rebuilt diameter vectors  $D'_{a,m}$  given in

$$D'_{a,m} = D_{a,m}^N - (D_{a,m}^N \cdot \widehat{m}_{R_a}) \widehat{m}_{R_a}. \quad (5)$$

To parametrize a liver contour, the nonuniform rational basis spline (NURBS) mechanism was applied. The creation

of a flexible and versatile cross-section modeling utilizing NURBS parameterization, which can express simple curves like circles as well as more complex free-form curves, is performed. The determination of liver contour is given in

$$\gamma_a(u) = \sum_{i=0}^m B_{i,p}(u) Q_i u \in [0, 1], \quad (6)$$

where  $n + 1$  represents the total number of used control points, “ $Q_i$ ” denotes the control points,  $p$  is the curve’s degree, and  $B_{i,p}(u)$  is a function defined on the knot vector of the  $i^{\text{th}}$  control points and  $p^{\text{th}}$  degree, which is dependent on a rational basis.

The circular contour  $\gamma_a(u)$  was first sampled evenly along its path, and the curve’s order was three. The control points were uniformly dispersed along their length. The curve’s shape was then tweaked as follows. A pair of 3D axial points used for the description of the 3D liver cross section at  $(x_a, y_a, z_a)$  is generated for each plane by equation (5). Let  $N$  represent the overall planes of projection. Then,  $Q_a = 2N$  points which denote the 3D liver cross sections of the liver were produced.

For the liver contour  $\gamma_a(u)$ , 3D points  $Q_a$  were tagged as interpolatory control points. The Euclidean distances were calculated from the control points  $\gamma_a(u)$  for each  $Q_a$ . Every point  $Q_a$  replaced its nearest point. The multiplicity of a point’s knot value was enhanced to attain interpolation. A knot value was inserted continuously till its multiplicity attains the curve’s degree. Noninterpolatory control points were designated on the remaining control points.

**3.7. 3D Reconstruction of the Hepatic Surface.** To construct the 3D surface of a liver scan traversing through a collection of liver contours, a technique known as lofting or skinning can be used. The new control points  $s$  of the lofted vessel surface were obtained by interpolating over the control points in each liver contour. Some attention was made to maintain liver surface continuity before interpolation over contours. To ensure that the liver surface did not flip or twist, control points were sorted according to their angles on the plane and in the same direction (clockwise). Furthermore, every starting control point of contours established a continuous curve; without this precaution, torsion regions in the liver surface would appear according to the curve discontinuities [18].

The curves also had to be suitable, which means that they should have the identical number of control points and degrees; also, they should be described on the identical knot vector. Knot vectors were merged, degrees were raised to their peak value, and knots were placed by which all contours will have identical knot vector and control points. These steps are conducted for ensuring compatibility. This procedure did not affect the structure of the liver outlines.

The knot vector “ $V$ ” was estimated, and it is applied to interpolate degree- $q$  curves  $\gamma_i(v)$  through the control

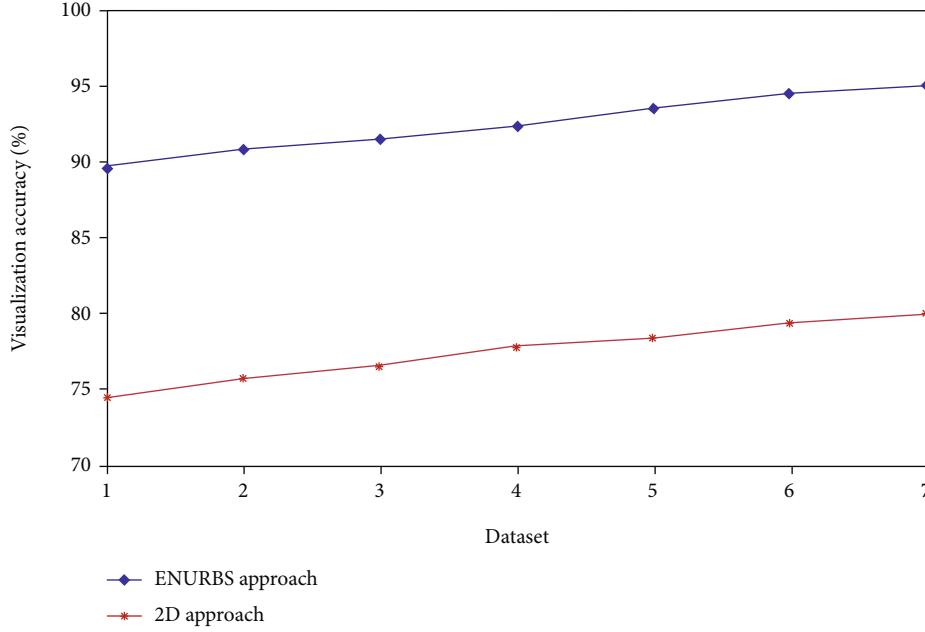


FIGURE 3: Accuracy of the 3D reconstructed model.

TABLE 2: Comparative analysis of the performance of 3D and 2D approaches.

Approaches	Average time for completing the plan (s)	Accuracy of the plan (%)
Surgical planning based on 2D images	86	65
ENURBS-VSP technique (proposed)	70	85

points by

$$\gamma_i(v) = \sum_{j=0}^n B_{j,p}(v)P_j. \quad (7)$$

As a result, equation (8) interpolated  $Q_i$  at different  $v$  values.

$$G(u, v) = \sum_i^m \sum_j^n B_{i,p}(u)B_{j,q}(v)P_{i,j}. \quad (8)$$

These newly discovered control points are the lofted surface that is the hepatic surface and control points specified across the knot vectors  $U$  and  $V$ . As shown in equation (8), 3D liver surfaces were recreated using the lofting technique.

By integrating the results of the above three steps, a 3D reconstructed liver image was obtained. The liver cross-sectional areas of the resultant 3D reconstructed segment were computed using Stokes theorem for determining the area of a planar polygon. On a liver cross-sectional curve, parametric points  $p_i$  given by equation (9) were generated using a uniform distribution.

$$\{p_i = (u_i, v_i)\}, \quad i = 0, \dots, n. \quad (9)$$

The area  $A$  contained by the curve was calculated by

$$A = \frac{1}{2} \sum_{i=0}^m (u_i V_{(i+1)} - u_{(i+1)} V_i). \quad (10)$$

**3.8. Planning of Surgical Methods.** Virtual surgical planning is used to plan liver resections, which includes detecting precise tumor portions that must be removed for effective treatment (VSP). VSP is a preoperative planning approach that involves visualizing a surgical procedure in a computer or virtual environment and developing a realistic plan using 3D reconstructed models. The steps in VSP are as follows.

Once the 3D reconstructed liver image is obtained, a VSP meeting with a biomedical engineer or a 3D designer and the surgical team is held online. 3D models are further expanded to produce cutting guides and the custom plate based on surgical needs for resection (e.g., clear margins from tumors and viable tissue in osteonecrosis) and reconstruction (e.g., number of segments following osteotomies). Before surgery, the stereolithographic recipient and donor models, liver cutting guides, fixation guide, and virtual reconstructed liver model are 3D printed, tested, and changed as needed. The final models are 3D printed and sterilised before the surgery. If a custom-made titanium plate is possible, it is built and sent along with the printed model; if not, a reconstruction plate is installed.

The following parameters are considered in 3D visualization in VSP:

- (i) Examination of lesions in the hepatic region of the 3D model based on the attributes such as shape, size, and location of lesions and the study of the structural connection between lesions and intrahepatic arteries

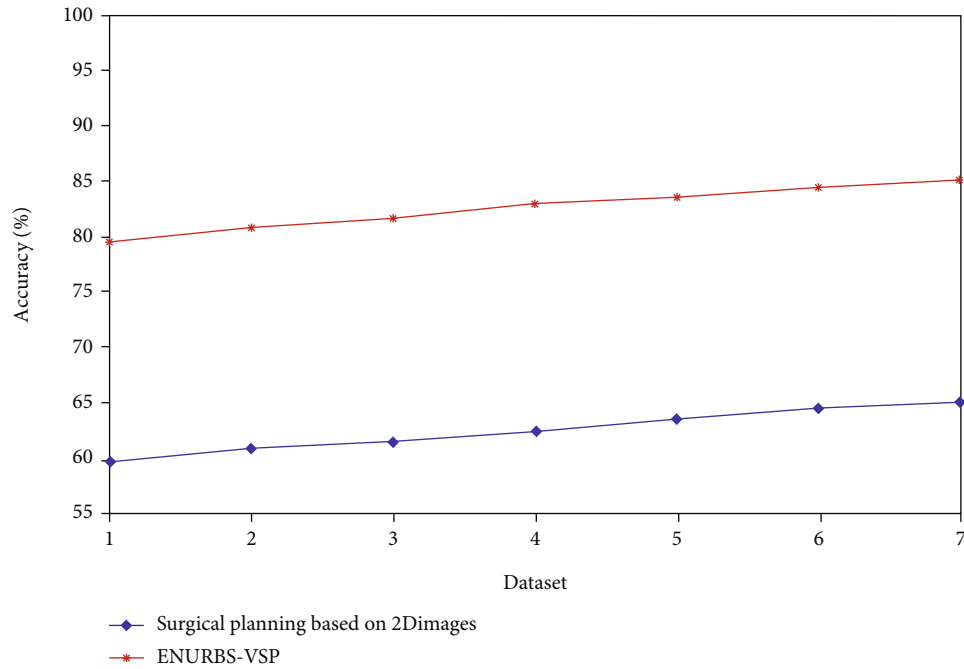


FIGURE 4: Accuracy of surgical planning techniques.

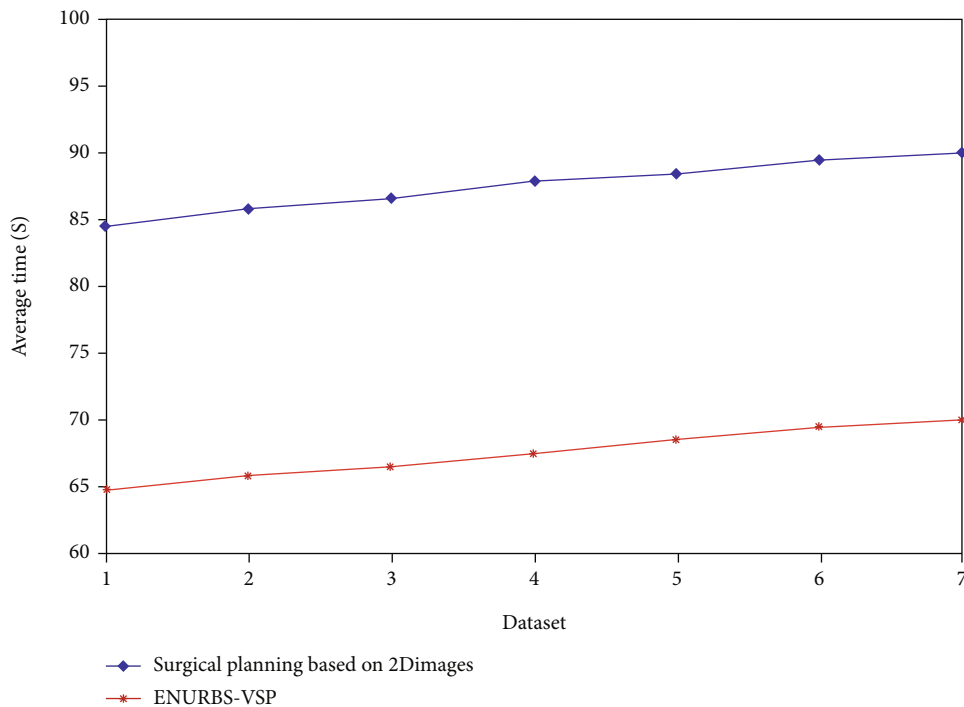


FIGURE 5: Average time taken to finish the plan by different techniques.

- (ii) Morphological analysis of the arterial system in the hepatic area
- (iii) Detection of the venous system of the liver
- (iv) Structural examination of the portal venous segment of the liver
- (v) Liver segmentation and calculation of liver volume. To segment and compute the liver volume, the structural relationship of blood flow in portal veins is used. In the meantime, the volume of drainage area in any branch of the portal vein branch is determined. Volume predictions are also required



for significant liver resections and living liver donations. Initially, the 3D classification method shown in Table 1 is according to [4]. This aids surgeons in assessing the liver parts for resection in VSP. The optimal plane of virtual resection is estimated depending on the location of the tumor and the spatial relationship and distance between the intrahepatic vascular system and the region of the tumor. The volume of the functional liver that remains is determined using simulation surgery. In the meantime, the postoperative integrity of drainage and blood supply of hepatic veins in each hepatic segment retained should be ensured

#### 4. Results and Discussion

3D reconstruction of the 2D CTA liver image taken from the dataset was performed using the ENURBS algorithm, and then, preoperative planning of the surgical method was done using VSP. This section deals with the simulation results and their detailed explanation. The influence of our approach on liver resection was evaluated based on the performance metrics such as accuracy and prediction time. Simulation graphs were obtained using MATLAB. Figure 2 shows the sample of a 3D reconstructed liver tumor model of a 2D CTA image considered from the dataset.

From Figure 3, it is shown that the accuracy of visualizing the precise tumor segment from the 3D reconstructed liver model using ENURBS is higher than that of 2D CTA images. Figure 1 shows that surgeons can more precisely visualize the tumor section from the 3D reconstructed model than from 2D images. Our findings suggest that 3D reconstruction increases clinicians' ability to create the best surgical strategy.

Comparative analysis of the performance of the surgical planning methods based on 2D images and our proposed method is shown in Table 2. Figure 4 shows the accuracy of the surgical plans generated by the above-mentioned two approaches. The proposed ENURBS-VSP method generates the surgical plan for liver resection with higher accuracy compared to that generated based on 2D scan reports. Figure 5 depicts that the time taken to complete the overall surgical plan using the proposed VSP technique was significantly lesser compared to that taken by the 2D planning method. Hence, it is concluded from the simulation results that 3DVR using the ENURBS approach integrated with VSP can provide a proper and accurate preoperative plan before surgical liver intervention in a short period. Using this plan, the excision of a precise tumor segment from the whole liver organ can be achieved. So patients with liver cancer can effectively be treated.

#### 5. Conclusions

Liver cancer is one of the most significant fatal malignancies all over the world. Surgical intervention is the prominent treatment for curing liver cancer. The advancements in digital intelligent screening and treatment technologies have promoted the efficiency of liver surgery. In this paper, we

combined 3D visual reconstruction of CTA liver images using the ENURBS 3DVR technique with virtual surgical planning in liver cancer resection. The goal of this research is to use precise removal of liver tumor segments to cure patients more quickly and reduce operation time. According to the simulation results, 3DVR with ENURBS paired with VSP can provide a proper and accurate preoperative plan before surgical liver intervention in a short amount of time. With this plan, a specific tumor part can be excised from the complete liver organ. Hence, people with liver cancer can be treated efficiently. In the future, this study must be extended to a larger dataset. In addition, extensive postoperative investigations on the patient's health and liver functionality must be conducted.

#### Data Availability

The analyzed datasets generated during the study are available from the corresponding author upon request.

#### Conflicts of Interest

The authors declare that they have no conflicts of interest.

#### Authors' Contributions

Yuanyu Zhao, Ting Chen, Hui Wang contributed equally and are all co-first authors for this work.

#### References

- [1] D. Anwanwan, S. K. Singh, S. Singh, V. Saikam, and R. Singh, "Challenges in liver cancer and possible treatment approaches," *Cancer*, vol. 1873, no. 1, article 188314, 2020.
- [2] S. Naeem, A. Ali, S. Qadri et al., "Machine-learning based hybrid-feature analysis for liver cancer classification using fused (MR and CT) images," *Applied Sciences*, vol. 10, no. 9, p. 3134, 2020.
- [3] F. Galassi, M. Alkhalil, R. Lee et al., "3D reconstruction of coronary arteries from 2D angiographic projections using non-uniform rational basis splines (NURBS) for accurate modeling of coronary stenoses," *PLoS One*, vol. 13, no. 1, article e0190650, 2018.
- [4] C. Fang, J. An, A. Bruno et al., "Consensus recommendations of three-dimensional visualization for diagnosis and management of liver diseases," *Hepatology International*, vol. 14, no. 4, pp. 437–453, 2020.
- [5] M. L. Barr, C. S. Haveles, K. S. Rezzadeh et al., "Virtual surgical planning for mandibular reconstruction with the fibula free flap," *Annals of Plastic Surgery*, vol. 84, no. 1, pp. 117–122, 2020.
- [6] Y. Z. Zeng, Y. Q. Zhao, S. H. Liao, M. Liao, Y. Chen, and X. Y. Liu, "Liver vessel segmentation based on centerline constraint and intensity model," *Biomedical Signal Processing and Control*, vol. 45, pp. 192–201, 2018.
- [7] C. T. Yeo, A. MacDonald, T. Ungi et al., "Utility of 3D reconstruction of 2D liver computed tomography/magnetic resonance images as a surgical planning tool for residents in liver resection surgery," *Journal of Surgical Education*, vol. 75, no. 3, pp. 792–797, 2018.

- [8] W. Cai, Y. Fan, H. Hu, N. Xiang, C. Fang, and F. Jia, "Postoperative liver volume was accurately predicted by a medical image three dimensional visualization system in hepatectomy for liver cancer," *Surgical Oncology*, vol. 26, no. 2, pp. 188–194, 2017.
- [9] K. Tomiyama, A. Ghazi, and R. Hernandez-Alejandro, "Looking beyond the horizon: patient-specific rehearsals for complex liver surgeries with 3D printed model," *Annals of Surgery*, vol. 273, no. 1, pp. e28–e30, 2021.
- [10] C. H. Fang, P. Zhang, W. P. Zhou et al., "Efficacy of three-dimensional visualization technology in the precision diagnosis and treatment for primary liver cancer: a retrospective multicenter study of 1 665 cases in China," *Zhonghua wai ke za zhi [Chinese Journal of Surgery]*, vol. 58, no. 5, pp. 375–382, 2020.
- [11] V. Chheang, P. Saalfeld, F. Joeres et al., "A collaborative virtual reality environment for liver surgery planning," *Computers & Graphics*, vol. 99, pp. 234–246, 2021.
- [12] Y. Oshiro and N. Ohkohchi, "Three-dimensional liver surgery simulation: computer-assisted surgical planning with three-dimensional simulation software and three-dimensional printing," *Tissue Engineering Part A*, vol. 23, no. 11-12, pp. 474–480, 2017.
- [13] C. Boedecker, F. Huettl, P. Saalfeld et al., "Using virtual 3D-models in surgical planning: workflow of an immersive virtual reality application in liver surgery," *Langenbeck's Archives of Surgery*, vol. 406, no. 3, pp. 911–915, 2021.
- [14] J. Fletcher and D. Miskovic, "Digital and 3D printed models for surgical planning," in *Digital Surgery*, pp. 95–110, Springer, Cham, 2021.
- [15] W. Sheng, C. Yuan, L. Wu, J. Yan, J. Ge, and J. Lei, "Clinical application of a three-dimensional reconstruction technique for complex liver cancer resection," *Surgical Endoscopy*, pp. 1–8, 2021.
- [16] G. Quero, A. Lapergola, L. Soler et al., "Virtual and augmented reality in oncologic liver surgery," *Surgical Oncology Clinics*, vol. 28, no. 1, pp. 31–44, 2019.
- [17] K. Lin, Y. Zeng, L. I. Yuntong, S. Luo, J. Zeng, and J. Liu, "Application value of 3D reconstruction virtual surgery planning in the surgical treatment of hilar cholangiocarcinoma," *Chinese Journal of Digestive Surgery*, vol. 17, no. 4, pp. 383–388, 2018.
- [18] W. Zhang, W. Zhu, J. Yang et al., "Augmented reality navigation for stereoscopic laparoscopic anatomical hepatectomy of primary liver cancer: preliminary experience," *Frontiers in Oncology*, vol. 11, p. 996, 2021.
- [19] F. Huettl, P. Saalfeld, C. Hansen et al., "Virtual reality and 3D printing improve preoperative visualization of 3D liver reconstructions—results from a preclinical comparison of presentation modalities and user's preference," *Annals of Translational Medicine*, vol. 9, no. 13, p. 1074, 2021.
- [20] Z. K. Ni, D. Lin, Z. Q. Wang et al., "Precision liver resection: three-dimensional reconstruction combined with fluorescence laparoscopic imaging," *Surgical Innovation*, vol. 28, no. 1, pp. 71–78, 2021.
- [21] S. Irtan, E. Hervieux, H. Boutroux et al., "Preoperative 3D reconstruction images for paediatric tumours: advantages and drawbacks," *Pediatric Blood & Cancer*, vol. 68, no. 1, article e28670, 2021.

## Research Article

# Meta-Analysis of Low Temperature Plasma Radiofrequency Ablation and CO<sub>2</sub> Laser Surgery on Early Glottic Laryngeal Carcinoma

Cheng Wang <sup>1,2</sup>, Ye Zhao <sup>1,3</sup>, Changhu Li,<sup>2</sup> Qiang Song,<sup>2</sup> and Fuxing Wang<sup>2</sup>

<sup>1</sup>Krirk University, Thailand

<sup>2</sup>Tianjin Liyuan Medical Technology Co., Ltd., China

<sup>3</sup>Shandong University of Traditional Chinese Medicine, China

Correspondence should be addressed to Cheng Wang; wang\_cheng@leadrun.net

Received 9 May 2022; Revised 18 June 2022; Accepted 21 June 2022; Published 6 July 2022

Academic Editor: Naeem Jan

Copyright © 2022 Cheng Wang et al. This is an open access article distributed under the Creative Commons Attribution License, which permits unrestricted use, distribution, and reproduction in any medium, provided the original work is properly cited.

**Objective.** Meta-analysis is used to analyze the treatment of early glottic laryngeal carcinoma by cryogenic plasma radiofrequency ablation combined with CO<sub>2</sub> laser surgery. **Methods.** Retrieval of PubMed, Embase, Medline, VIP, Wanfang, and CNKI databases using a computer. The retrieval period is from the creation of the database until August 31, 2021. References to the included literature were also searched at the same time. According to the inclusion and exclusion criteria, literatures are screened independently, relevant data were extracted, and meta-analysis was conducted. **Results.** Recurrence rates are reported in seven literatures. In interstudy heterogeneity test:  $P = 0.624$ ,  $I^2 = 0\%$ , fixed effect model analysis shows that there is no significant difference in recurrence rate between low temperature plasma radiofrequency ablation and CO<sub>2</sub> laser ablation (OR = 0.80, 95% CI (0.35, 1.29),  $P = 0.371$ ). Intraoperative blood loss is reported in 5 literatures, and heterogeneity test of each study is as follows:  $P = 0.03$ ,  $I^2 = 67\%$ . Low temperature plasma radiofrequency ablation results in more intraoperative blood loss than CO<sub>2</sub> laser ablation (SMD = -0.71, 95% CI (0.08, 0.82),  $P = 0.01$ ). There are five reports on postoperative pain in two treatments:  $P = 0.04$ ,  $I^2 = 64\%$ . There is no significant difference in postoperative pain between low temperature plasma radiofrequency ablation and CO<sub>2</sub> laser ablation (SMD = -0.21, 95% CI (-0.44, 0.10),  $P = 0.134$ ). Operative time is reported in nine articles:  $P < 0.01$ ,  $I^2 = 95\%$ . The operative time of low temperature plasma radiofrequency ablation is significantly shorter than CO<sub>2</sub> laser ablation (SMD = -2.38, 95% CI (-3.91, -1.62),  $P < 0.01$ ). There are two reports on postoperative mucosal recovery:  $P = 0.328$ ,  $I^2 = 2\%$ . Low temperature plasma radiofrequency ablation was significantly better than CO<sub>2</sub> laser ablation in postoperative mucosal recovery (OR = 5.49, 95% CI (2.36, 10.18),  $P < 0.01$ ). **Conclusion.** Low temperature plasma radiofrequency ablation is superior to CO<sub>2</sub> laser surgery in the treatment of early glottic laryngeal carcinoma in terms of operative time and postoperative mucosal recovery. Low-temperature plasma radiofrequency ablation, on the other hand, results in higher intraoperative blood loss, with no discernible difference in recurrence rate or postoperative pain severity between the two treatments.

## 1. Introduction

Laryngeal cancer is a common tumor in otorhinolaryngology, accounting for 1%~5% of all malignant tumors. The total incidence of laryngeal cancer is about 2.04/100 000, among which the incidence of male is higher than that of female. In the early stage of the disease, patients will have

clinical manifestations of hoarseness. At the same time, it is difficult to be found in clinical practice because blood and lymphatic metastasis are rare in the early stage [1]. Laryngeal cancer is associated with a variety of factors, including age, smoking, alcohol consumption, environmental pollution, family history, and glutathione S-transferase M1 gene deletion. Therefore, for the prevention and

treatment of early glottic laryngeal cancer, it is particularly important to ensure that you do not smoke, drink, eat hot and spicy food, and have regular physical examination [2, 3]. The early glottic carcinoma in clinic mainly invades the glottic tissue of the larynx. Clinically, glottic laryngeal carcinoma can be divided into three stages: Tis stage, T1a stage, and T1b stage, and a small number of lesions are limited to T2 stage [4, 5]. Because of the large trauma area of open surgery, and some patients need to take endotracheal intubation for a long time to maintain treatment, and the body tolerance is poor, the clinical promotion of open surgery is greatly limited by the difference of patients' physical quality [6–8]. The main aim of laryngeal cancer treatment is to completely remove the tumor tissue and preserve laryngeal function as much as possible. CO<sub>2</sub> laser has been applied in laryngeal microsurgery for glottic laryngeal carcinoma since 1970s. Plasma radiofrequency ablation is a new minimally invasive surgical method. These two surgical methods have been applied in microsurgery of otorhinolaryngology [9]. It is difficult to ensure the safety edge because to its wide knife head and limited operation in the throat; thus, it cannot cut as accurately as a CO<sub>2</sub> laser. Despite the fact that several studies have validated the usefulness of the two minimally invasive procedures, there is still debate about their efficacy [10]. The significance of this meta-analysis is to obtain the analysis results by comparing various outcome indicators of the two surgical methods through large-scale evidence-based medical data, to provide evidence-based medical evidence for clinicians to choose appropriate surgical methods according to the characteristics of patients with early glottic laryngeal carcinoma.

The main body of this study is as follows:

Section 1-Data and Methods: this section first introduces the literature retrieval methods used in this study; then, based on the purpose of the study, the inclusion and exclusion criteria of the literature are set, and the quality of the literature is evaluated; finally, the relevant data are extracted, and the statistical methods used in this study are described

Section 2-Results is as follows: this section evaluates the quality of the included literature based on the screening results of the literature and finally obtains the results of the meta-analysis

Section 3-Discussion: based on the results of the meta-analysis in Section 2, this section discusses the relevant issues

Section 4-Conclusion: final conclusion of this study

## 2. Data and Methods

**2.1. Retrieval Methods.** Two evaluators search for published domestic and foreign controlled trials. There is a computer retrieval of PubMed, Embase, Medline, VIP, Wanfang, and CNKI databases. The retrieval period is from database construction to August 31, 2021. If the outcome data report is not available or the original data is missing, send a note to the author requesting the data and including as much of the needed literature as feasible.

**2.2. Literature Inclusion and Exclusion Criteria.** In accordance with PRISMA (Preferred Reporting Items for Systematic Reviews and Meta-Analyses) principle, 2 evaluators independently screen, include, and exclude literatures for multiple times by reading the key words, abstract, and full text of literatures in detail.

Inclusion criteria were as follows: ① the patients are confirmed to have primary early laryngeal carcinoma or precancerous lesion by pathologic and cytological examination, and none of them undergo surgery or radiotherapy, ② clinical and radiographic examinations reveal no distant metastases or lymph node metastasis, and ③ the types of studies include randomized controlled trials and retrospective studies.

Exclusion criteria were as follows: ① raw data reports are incomplete, and authors cannot be contacted, ② duplicate studies with incomplete data, or multiple studies from the same center with duplicate data, the most recent study will prevail, and ③ investigate the efficacy of single treatment such as low-temperature plasma radiofrequency ablation of glottic carcinoma under supported laryngoscope or CO<sub>2</sub> laser glottic carcinoma resection.

**2.3. Literature Quality Evaluation.** The included literatures are evaluated by two reviewers according to the Cochrane risk assessment criteria for bias (2016 edition. It is one of the most common bias risk assessment tools in the field of evidence-based medicine. It is mainly applicable to randomized controlled trials (RCTs)). The evaluation includes the following: ① whether a randomized controlled study, ② whether there is a distribution plan, ③ whether to perform blinding, ④ integrity of resulting data, and ⑤ other bias [11].

**2.4. Data Extraction.** Two evaluators independently screen the literature in the search results to determine potential relevance. If both parties fail to form a unified understanding, a third party can be invited to participate in the discussion to help make a decision. Literature screening is as follows: first, read the title and abstract of the literature for preliminary screening. Then, follow the established inclusion criteria and exclusion criteria to screen the literature and finally obtain the literature that meets the research objectives.

**2.5. Statistical Method.** Meta-analysis is performed using Review Manager5.3 software provided by the Cochrane collaboration for data synthesis, and the test level is  $\alpha = 0.05$ . OR (odds ratio) is used for combined analysis for counting data. If the measurement tools are the same, MD (weighted mean difference) is used for continuous data analysis. SMD (standard mean difference) is used for analysis if the measurement tools are different, and 95% confidence intervals (CI) are calculated for all analyses.  $\chi^2$  test is used to analyze heterogeneity. In Q test and  $I^2$  test,  $P > 0.1$  and  $I^2 < 50\%$  are regarded as homogeneity, and fixed effect model is used to analyze heterogeneity [12].  $P < 0.05$  is considered statistically significant. The sensitivity analysis method is one by one elimination.

TABLE 1: Basic information of included literature.

Included in the study	Published year	Interventions	Sample size	Gender (male/female)	Age	Observation target
Semmler et al. [13]	2011	Radio frequency group	93	79/14	60.33 ± 1.25	①, ③, ④
		Laser group	93	77/16	62.19 ± 10.13	
Liu Jianyong et al. [14]	2014	Radio frequency group	42	35/7	63.33 ± 10.88	①, ②, ③, ④
		Laser group	42	32/10	65.40 ± 10.14	
Shuang et al.[15]	2015	Radio frequency group	37	26/11	56.79 ± 9.91	②, ③
		Laser group	37	27/10	57.15 ± 10.52	
Mourad et al. [16]	2016	Radio frequency group	30	21/9	51.44 ± 8.76	②, ③, ⑤
		Laser group	30	23/7	54.23 ± 7.21	
Jun et al. [17]	2017	Radio frequency group	47	39/8	58.15 ± 8.41	①, ③, ④
		Laser group	46	36/10	57.29 ± 9.08	
Jinhui and Chengyu [18]	2018	Radio frequency group	64	51/13	55.26 ± 2.45	①, ②, ③, ④
		Laser group	64	50/14	56.79 ± 4.51	
Yuke et al. [19]	2019	Radio frequency group	52	40/12	61.19 ± 6.54	①, ③, ④
		Laser group	52	38/14	62.37 ± 6.76	
Yong et al. [20]	2020	Radio frequency group	48	37/11	60.04 ± 6.99	①, ②, ③
		Laser group	47	40/7	59.63 ± 4.58	
Bin et al. [21]	2021	Radio frequency group	33	24/9	58.33 ± 9.36	①, ③, ⑤
		Laser group	33	23/10	59.17 ± 8.64	

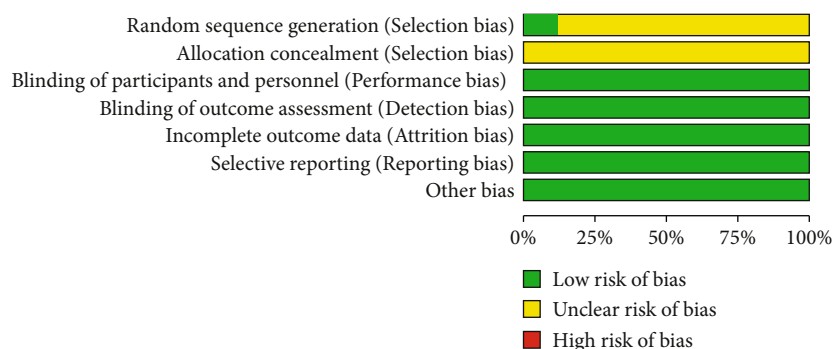


FIGURE 1: Bias risk analysis.

TABLE 2: Quality evaluation of RCS included literature.

Included in the study	Grouping method	Report lost to follow-up	Blind method	Diagnostic criteria	Baseline	Confounding factor control	Total score
Liu Jianyong et al.	No specific description	No lost to follow-up	Not mentioned	The “gold standard” diagnosis	Well described, well balanced	Appropriate	9
Jun et al.	No specific description	No lost to follow-up	Not mentioned	The “gold standard” diagnosis	Well described, well balanced	Appropriate	9
Yuke et al.	No specific description	Reported lost to follow-up and the rate of lost to follow-up <10%	Not mentioned	Not described	Well described, well balanced	Appropriate	8

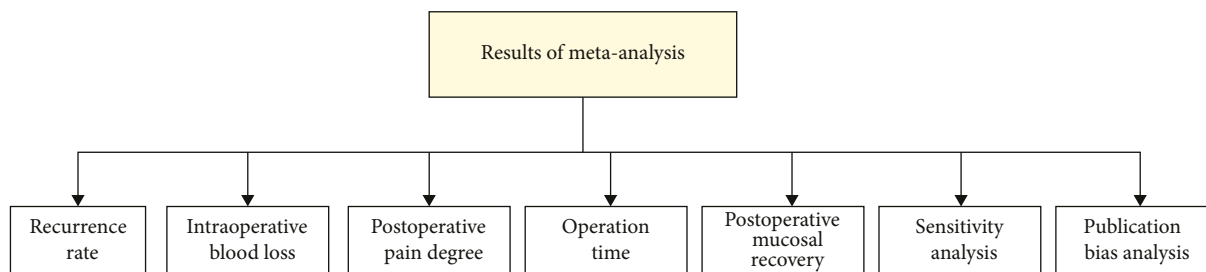


FIGURE 2: Results of meta-analysis.

TABLE 3: Results of meta-analysis on recurrence rate.

Study or subgroup	Radio frequency group		Laser group		Weight	Odds ratio, <i>M-H</i> , fixed, 95% CI
	Events	Total	Events	Total		
Semmler et al.	12	93	11	93	36.24%	0.74 [0.21, 2.06]
Liu Jianyong et al.	1	42	3	42	9.21%	0.13 [0.03, 2.87]
Jun et al.	2	47	1	46	1.67%	4.98 [0.23, 1113.13]
Jinhui and Chengyu	7	64	5	64	17.35%	1.784 [0.36, 4.56]
Yuke et al.	2	52	5	52	5.29%	0.36 [0.08, 2.08]
Yong et al.	2	48	3	47	5.12%	0.53 [0.08, 6.14]
Bin et al.	1	33	0	33	25.12%	0.754 [0.42, 1.89]
Total (95% CI)		379		377	100.00%	0.80 [0.35, 1.29]
Total events	27		28			

Heterogeneity:  $\chi^2 = 4.82$ ,  $df = 7$  ( $P = 0.624$ );  $I^2 = 0\%$ . Test for overall effect:  $Z = 0.88$  ( $P = 0.371$ ).

TABLE 4: Meta-analysis results of intraoperative blood loss.

Study or subgroup	Radio frequency group		Laser group		Weight	Odds ratio, <i>M-H</i> , fixed, 95% CI
	Mean $\pm$ SD	Total	Mean $\pm$ SD	Total		
Liu Jianyong et al.	10.28 $\pm$ 2.62	42	10.67 $\pm$ 2.34	42	22.17%	-0.98 [-0.34, 0.31]
Shuang et al.	11.33 $\pm$ 2.45	37	10.42 $\pm$ 6.87	37	18.09%	0.24 [-0.23, 0.65]
Mourad et al.	10.27 $\pm$ 2.37	30	8.52 $\pm$ 2.17	30	23.11%	0.87 [0.24, 1.35]
Jinhui and Chengyu	10.30 $\pm$ 2.39	64	8.97 $\pm$ 2.36	64	17.09%	0.64 [0.92, 1.22]
Yong et al.	10.32 $\pm$ 0.79	48	9.37 $\pm$ 0.45	47	19.54%	0.67 [0.28, 1.35]
Total (95% CI)		221		220	100.00%	0.43 [0.08, 0.82]

Heterogeneity:  $\tau^2 = 0.09$ ;  $\chi^2 = 11.37$ ,  $df = 5$  ( $P = 0.03$ );  $I^2 = 67\%$ . Test for overall effect:  $Z = 2.49$  ( $P = 0.01$ ).

TABLE 5: Results of meta-analysis of postoperative pain degree.

Study or subgroup	Radio frequency group		Laser group		Weight	Odds ratio, <i>M-H</i> , fixed, 95% CI
	Mean $\pm$ SD	Total	Mean $\pm$ SD	Total		
Semmler et al.	2.78 $\pm$ 0.37	93	2.88 $\pm$ 0.98	93	19.89%	-0.07 [-0.35, 0.26]
Liu Jianyong et al.	2.76 $\pm$ 1.08	42	2.90 $\pm$ 0.25	42	17.98%	-0.31 [-0.65, 0.09]
Jun et al.	2.67 $\pm$ 0.98	47	3.09 $\pm$ 1.12	46	13.12%	-0.32 [-0.76, 0.29]
Jinhui and Chengyu	2.86 $\pm$ 0.14	64	2.77 $\pm$ 0.55	64	15.09%	0.16 [-0.45, 0.65]
Yuke et al.	2.84 $\pm$ 0.63	52	3.18 $\pm$ 0.47	52	33.92%	-0.75 [-1.25, -3.08]
Total (95% CI)		298		297	100.00%	0.16 [-0.44, 0.10]

Heterogeneity:  $\tau^2 = 0.07$ ;  $\chi^2 = 13.25$ ,  $df = 5$  ( $P = 0.04$ );  $I^2 = 64\%$ . Test for overall effect:  $Z = 1.38$  ( $P = 0.134$ ).

TABLE 6: Results of meta-analysis of operation time.

Study or subgroup	Radio frequency group		Laser group		Weight	Odds ratio, <i>M-H</i> , fixed, 95% CI
	Mean ± SD	Total	Mean ± SD	Total		
Semmler et al.	1.25 ± 0.44	93	1.08 ± 0.29	93	11.23%	-2.09 [-2.33, -1.79]
Liu Jianyong et al.	2.69 ± 0.15	42	1.82 ± 0.39	42	10.32%	-2.87 [-2.98, -1.09]
Shuang et al.	1.04 ± 0.16	37	1.23 ± 0.17	37	3.89%	-3.44 [-4.09, -2.41]
Mourad et al.	1.09 ± 0.39	30	1.46 ± 0.18	30	10.08%	22.87 [16.43, 0.81]
Jun et al.	2.63 ± 0.34	47	3.94 ± 0.58	46	10.67%	-1.82 [-0.24, -1.79]
Jinhui and Chengyu	5.61 ± 0.28	64	4.76 ± 0.33	64	10.59%	-1.23 [-0.24, -1.79]
Yuke et al.	2.65 ± 0.18	52	3.58 ± 0.54	52	10.49%	-1.82 [-2.44, -1.79]
Yong et al.	4.81 ± 0.18	48	5.76 ± 0.34	47	11.34%	-1.86 [-1.53, -3.10]
Bin et al.	21.32 ± 3.05	33	22.14 ± 3.78	33	21.39%	-4.76 [-5.09, -4.01]
Total (95% CI)		446		444	100.00%	-2.06 [-3.91, -1.62]

Heterogeneity:  $\tau^2 = 2.78$ ;  $\chi^2 = 225.98$ ,  $df = 9$  ( $P < 0.01$ );  $I^2 = 95\%$ . Test for overall effect:  $Z = 5.72$  ( $P \leq 0.01$ ).

TABLE 7: Results of meta-analysis of postoperative mucosal recovery.

Study or subgroup	Radio frequency group		Laser group		Weight	Odds ratio, <i>M-H</i> , fixed, 95% CI
	Events	Total	Events	Total		
Mourad et al.	24	30	16	30	74.38%	4.35 [2.09, 9.02]
Bin et al.	27	33	19	33	25.62%	25.18 [2.31, 23.09]
Total (95% CI)		63		63	100.00%	5.49 [2.36, 10.18]
Total events	51		35			

Heterogeneity:  $\chi^2 = 2.09$ ,  $df = 2$  ( $P = 0.328$ );  $I^2 = 2\%$ . Test for overall effect:  $Z = 5.19$  ( $P < 0.01$ ).

### 3. Results

This section evaluates the quality of the included literature based on the screening results of the literature and finally obtains the results of the meta-analysis.

**3.1. Results of Literature Screening and the Basic Information of Included Studies.** A total of 47 relevant literatures were retrieved using the above retrieval methods, comprising 35 Chinese literatures and 12 international literatures. After reading the full texts, 9 articles were included according to the criteria.

Gender and age differences between the observation and control groups are not statistically significant ( $P > 0.05$ ). Outcome indicators included the following: ① recurrence rate, ② intraoperative blood loss, ③ operation time, ④ postoperative pain degree, and ⑤ postoperative mucosal recovery. Basic information of included literature is shown in Table 1.

**3.2. Methodological Quality Evaluation of Included Studies.** The included literature includes 6 RCTS and 3 RCS. Among the 9 RCTS, 1 is double-blind, and 1 is single-blind. The truncated data of 1 of all the studies are incomplete, but the reasons could be explained. The quality of the included literature meets the requirements of this study in conclusion. Bias risk analysis is shown in Figure 1.

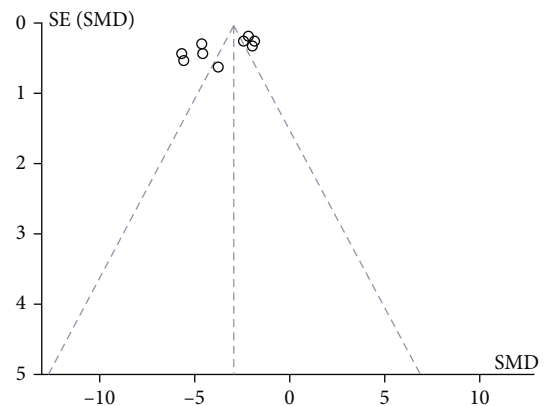


FIGURE 3: Funnel plot of operation time.

The total score of 3 RCS scores was  $\geq 7$  points, see Table 2 for the quality evaluation of RCS documents.

**3.3. Results of Meta-Analysis.** Combined with the clinical indicators concerned about the treatment of early glottic laryngeal cancer, this study obtained the research results on the following seven indicators (Figure 2): ① recurrence rate, ② intraoperative blood loss, ③ postoperative pain degree, ④ operation time, ⑤ postoperative mucosal recovery, ⑥ sensitivity analysis, and ⑦ publication bias analysis.

**3.4. Recurrence Rate.** Recurrence rates are reported in seven literatures. In interstudy heterogeneity test:  $P = 0.624$ ,  $I^2 = 0\%$ , fixed effect model analysis shows that there is no significant difference in recurrence rate between low temperature plasma radiofrequency ablation and CO<sub>2</sub> laser ablation (OR = 0.80, 95% CI (0.35, 1.29),  $P = 0.371$ ). Results of meta-analysis on recurrence rate are shown in Table 3.

**3.5. Blood Loss in Intraoperative.** Intraoperative blood loss is reported in 5 literatures, and heterogeneity test of each study is as follows:  $P = 0.03$ ,  $I^2 = 67\%$ . Low temperature plasma radiofrequency ablation results in more intraoperative blood loss than CO<sub>2</sub> laser ablation (SMD = -0.71, 95% CI (0.08, 0.82),  $P = 0.01$ ). Meta-analysis results of intraoperative blood loss are shown in Table 4.

**3.6. Postoperative Pain Degree.** There are five reports on postoperative pain in two treatments:  $P = 0.04$ ,  $I^2 = 64\%$ . Between low temperature plasma radiofrequency ablation and CO<sub>2</sub> laser ablation (SMD = -0.21, 95% CI (-0.44, 0.10),  $P = 0.134$ ) has no significant difference in postoperative pain (Table 5).

**3.7. Operation Time.** Operative time is reported in nine articles:  $P < 0.01$ ,  $I^2 = 95\%$ . The operative time of low temperature plasma radiofrequency ablation is significantly shorter than CO<sub>2</sub> laser ablation (SMD = -2.38, 95% CI (-3.91, -1.62),  $P < 0.01$ ) (Table 6).

**3.8. Postoperative Mucosal Recovery.** There are two reports on postoperative mucosal recovery:  $P = 0.328$ ,  $I^2 = 2\%$ . Low temperature plasma radiofrequency ablation was significantly better than CO<sub>2</sub> laser ablation in postoperative mucosal recovery (OR = 5.49, 95% CI (2.36, 10.18),  $P < 0.01$ ), see Table 7 for the above analysis results:

**3.9. Sensitivity Analysis.** In meta-analysis of operative time and postoperative vocal quality, there is no significant difference in the combined results before and after elimination.  $I^2$  is still greater than 50% ( $I^2 = 69\%$ ) when the study of Shuang et al. is excluded, but the combined results of META analysis showed significant differences (SMD = 0.38, 95% CI (0.17, 0.28),  $P = 0.01$ ). In the meta-analysis of postoperative pain,  $I^2$  decreases to 17% after removing the study of Yuke et al., and the combined results of meta-analysis still show no difference.

**3.10. Publication Bias Analysis.** Figure 3 shows a funnel plot of the operative time and recurrence rate for cryogenic plasma radiofrequency ablation and CO<sub>2</sub> laser excision for early glottic laryngeal cancer and Figure 4.

## 4. Discussion

Patients with early glottic laryngeal cancer have no obvious clinical signs and are accompanied by adverse symptoms. Early treatment is often ignored. For early glottic laryngeal carcinoma, if timely diagnosis and surgical intervention, the prognosis is better [22]. Open surgery, on the other hand, has a big wound area, poor tolerance, slow postopera-

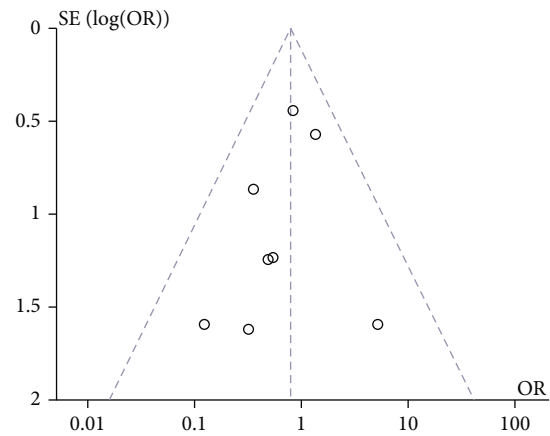


FIGURE 4: Funnel plot of recurrence rate.

tive recovery, and a wide range of resection, and postoperative breathing, swallowing, and vocalization functions are frequently impacted to variable degrees, lowering quality of life [23]. Therefore, it is difficult to popularize the pioneering operation in the treatment of patients with early glottic laryngeal cancer [24]. CO<sub>2</sub> laser is a kind of gas molecular laser that can be continuously emitted by invisible light and far infrared spectrum. The tissue is vaporized instantly after contacting the high energy laser beam. It has the advantages of accurate target and rapid treatment [25, 26]. However, the linear beam of CO<sub>2</sub> laser may increase the risk of postoperative recurrence due to the obscuring of visual field caused by poor exposure during surgery. Compared with CO<sub>2</sub> laser, plasma is a new surgical method for early glottic laryngeal carcinoma with a shorter time. In addition, the plasma cutter head used in plasma radiofrequency ablation has the functions of ablation, cutting, and hemostasis. The operation is convenient, and the plasma knife head can be bent to a narrow space and cut off the lesion that is difficult to be handled by ordinary surgery [27, 28]. The basic frequency perturbation, amplitude perturbation, and harmonic noise ratio are used in a meta-analysis of postoperative vocal quality indicators to reflect the postoperative voice quality of patients. The fundamental frequency perturbation reflects the roughness of the sound, the amplitude perturbation reflects the hoarseness of the sound, and the harmonic noise ratio is related to the sound quality [29].

## 5. Conclusion

In conclusion, low temperature plasma radiofrequency ablation is superior to CO<sub>2</sub> laser surgery in the treatment of early glottic laryngeal carcinoma in terms of operative time and postoperative mucosal recovery. In terms of postoperative pain, plasma radiofrequency ablation was less painful than CO<sub>2</sub> laser, and the subjective and objective voice function recovered better. However, low temperature plasma radiofrequency ablation has more intraoperative blood loss, and there is no significant difference in recurrence rate and postoperative pain degree between the two treatments. In a comprehensive comparison, low-temperature plasma radiofrequency ablation for early



glottic laryngeal cancer has the advantages of convenient operation, hemostasis, fast wound healing, and little damage to the surrounding tissues, which has the value of clinical promotion.

### Data Availability

The data used to support the findings of this study are included within the article.

### Conflicts of Interest

The authors declare that there are no conflicts of interest regarding the publication of this paper.

### References

- [1] D. Testa, G. Guerra, G. Conzo et al., "Glottic-subglottic adenoid cystic carcinoma. A case report and review of the literature[J]," *BMC Surgery*, vol. 13, no. 2, pp. 1–5, 2013.
- [2] Z. Chunhong, L. Yujie, Y. Min et al., "Comparison of CO2 laser and plasma radiofrequency ablation in the treatment of early glottic laryngeal carcinoma," *Journal of Audiology and Speech Disorders*, vol. 000, no. 3, pp. 307–309, 2015.
- [3] X. Hua, Z. Haiping, and L. Le, "Comparison between radiofrequency ablation combined with chemotherapy and surgery combined with chemotherapy in the treatment of glottic laryngeal carcinoma[J]," *China Medical Guide*, vol. 13, no. 20, pp. 100–102,114, 2016.
- [4] W. Yong and L. Jianfeng, "To explore the clinical effect of carbon dioxide laser therapy on early glottic laryngeal cancer [J]," *Chinese Medical Abstracts (otorhinolaryngology)*, vol. 36, no. 6, pp. 103–105, 2021.
- [5] J. Xiaoling, "Effect of plasma ablation assisted by supporting laryngoscope and endoscope on postoperative rehabilitation and voice function of patients with early glottic laryngeal cancer [J]," *Medical theory and practice*, vol. 35, no. 9, pp. 1503–1505, 2022.
- [6] G. Peng and L. Xiongwei, "Effect of low temperature plasma radiofrequency ablation on early glottic laryngeal carcinoma [J]," *Journal of Practical Cancer*, vol. 6, pp. 902–904, 2018.
- [7] D. Fei, C. Yi, C. Yanchen, and Z. Huiwen, "Clinical effect of carbon dioxide laser treatment of early glottic laryngeal carcinoma under support laryngoscope [J]," *Chinese contemporary medicine*, vol. 28, no. 24, pp. 167–169, 2021.
- [8] L. V. Meijuan, L. Yixing, and Y. Gendong, "Treatment of glottic laryngeal carcinoma by low temperature plasma radiofrequency ablation under microsupport laryngoscope [J]," *Zhejiang trauma surgery*, vol. 27, no. 1, pp. 127–129, 2022.
- [9] P. F. Nguyen-Tan, Q. T. Le, J. M. Quivey et al., "Treatment results and prognostic factors of advanced T3–4 laryngeal carcinoma: the University of California, San Francisco (UCSF) and Stanford University Hospital (SUH) experience[J]," *International Journal of Radiation Oncology • Biology • Physics*, vol. 5, pp. 1172–1180, 2001.
- [10] L. Quansheng, H. Yiyang, L. Wang, W. Jiang, and L. Hongwei, "Effect of transoral CO<sub>2</sub> laser, partial laryngectomy and low temperature plasma radiofrequency ablation on glottic laryngeal carcinoma [J]," *Chinese Oncology Clinic and Rehabilitation*, vol. 27, no. 11, pp. 1332–1335, 2020.
- [11] T. Huiling and G. Jialiang, "Research progress in minimally invasive treatment of early glottic laryngeal carcinoma[J]," *Cancer Progress*, vol. 19, no. 11, pp. 2551–2554, 2021.
- [12] H. Juntao, C. Lixin, W. Linrong, Y. Ting, and S. Yi, "Meta-analysis of the efficacy of cryogenic plasma radiofrequency ablation and carbon dioxide laser in the treatment of early glottic laryngeal carcinoma [J]," *Chinese Journal of Cancer Prevention and Treatment*, vol. 28, no. 11, pp. 864–870, 2021.
- [13] M. Semmler, T. Keck, R. Reiter, and P. M. Gruen, "Endolaryngeal posterior mucosal flap for surgical repair of posterior glottic stenosis," *Auris Nasus Larynx*, vol. 38, no. 5, pp. 608–611, 2011.
- [14] L. Jianyong, L. Jianbin, L. Menglin, X. Yue, Y. Qi, and Y. Yifang, "Clinical effect of low temperature plasma radiofrequency ablation on early glottic laryngeal carcinoma[J]," *Chinese Journal of Integrated Traditional and Western Medicine Otolaryngology*, vol. 22, no. 4, pp. 305–306, 2014.
- [15] S. Yu, L. Chao, H. Yongwang, and W. Shuang, "Comparison of cryogenic plasma radiofrequency ablation and CO2 laser in the treatment of early glottic laryngeal carcinoma[J]," *Journal of Audiology and Speech Disorders*, vol. 23, no. 4, pp. 372–376, 2015.
- [16] M. Mourad, A. Dezube, E. Moshier, and E. Shin, "Geographic trends in management of early-stage laryngeal cancer," *Laryngoscope*, vol. 126, no. 4, pp. 880–884, 2016.
- [17] D. Jun, H. De, and C. Zhibin, "Clinical observation of CO2 laser combined with cryogenic plasma radiofrequency ablation in the treatment of early glottic laryngeal carcinoma with pre-involvement[J]," *Chinese Oncology Clinic and Rehabilitation*, vol. 24, no. 6, pp. 670–672, 2017.
- [18] Z. Jinhui and W. Chengyu, "Effects of CO2 laser and plasma radiofrequency ablation on surgical indicators, pain and recurrence of early glottic laryngeal carcinoma [J]," *Chinese General Practice*, vol. 1, pp. 200–202, 2018.
- [19] D. Yuke, L. Yujie, and H. Wei, "Effects of CO2 laser combined with plasma radiofrequency ablation on cytokine levels in early glottic laryngeal carcinoma[J]," *Chinese Journal of Modern Medicine*, vol. 29, no. 6, pp. 69–72, 2019.
- [20] T. Yong, J. Yuzi, M. Jiqing et al., "The prognostic value of low temperature plasma radiofrequency ablation,CO2 laser and laryngeal dehiscence in the treatment of early glottic laryngeal carcinoma in the elderly by serum thymidine kinase 1[J]," *Journal of Practical Cancer*, vol. 35, no. 4, pp. 570–574, 2020.
- [21] H. Bin, H. Weiping, Y. Zhongpu, and L. Yonggang, "Effect and influencing factors of low temperature plasma radiofrequency ablation in the treatment of early glottic laryngeal carcinoma [J]," *Cancer Progress*, vol. 19, no. 13, pp. 1345–1348, 2021.
- [22] T. Furusaka, Y. Susaki, T. Saito, Y. Katsura, and M. Ikeda, "Long-term follow-up and salvage surgery in patients with T2N0M0 squamous cell carcinoma of the glottic larynx following concurrent chemoradiation therapy with cisplatin and 5-fluorouracil for laryngeal preservation," *Acta Oto-Laryngologica*, vol. 133, no. 1, pp. 91–98, 2013.
- [23] C. Jianli and Z. Zhiqiang, "Effects of cryogenic plasma radiofrequency ablation on VAS score and complications of early glottic laryngeal carcinoma [J]," *Modern Digestion & Intervention*, vol. 2, pp. 71–72, 2019.
- [24] Z. Min and L. Yujun, "Research progress in the treatment of early glottic laryngeal carcinoma [J]," *Journal of practical cardiovascular diseases*, vol. 29, no. S2, pp. 87–91, 2021.

- [25] Y. Jiaming, Y. Xufen, and Z. Yali, "Discussion on CO under microsupport laryngoscope\_ clinical effect of laser therapy on early glottic laryngeal carcinoma [J]," *Yunnan medicine*, vol. 43, no. 2, pp. 50-51, 2022.
- [26] L. Ming, "CO2 laser therapy for suprglottic laryngeal carcinoma [J]," *Journal of Otolaryngology, Shandong University*, vol. 32, no. 6, pp. 4-7, 2018.
- [27] L. Dasong, F. Yongjun, Z. Chunrong, and W. Mingjing, "Comparative analysis of the efficacy of endoscopic low temperature plasma radiofrequency ablation and conventional laryngeal dehyis in the treatment of early glottic laryngeal carcinoma[J]," *Journal of Clinical Pathology*, vol. 36, no. 12, pp. 1975-1980, 2016.
- [28] L. Weixing, C. Gui, S. Lijuan, L. Wenjing, and Z. Xiaowen, "Plasma radiofrequency ablation and Co\_ effect of laser surgery on pain and recurrence in patients with early glottic laryngeal cancer [J]," *Chinese Journal of modern medicine*, vol. 24, no. 1, pp. 74-76, 2022.
- [29] L. Weixing, C. Gui, S. Lijuan et al., "Metaanalysis of cryogenic plasma radiofrequency ablation and CO 2 laser therapy for early glottic laryngeal carcinoma [J]," *Chinese Journal of Bio-medical Engineering*, vol. 1, pp. 15-20, 2020.

## Research Article

# Biophilic Design as an Important Bridge for Sustainable Interaction between Humans and the Environment: Based on Practice in Chinese Healthcare Space

Yang Zhao,<sup>1</sup> Qinchuan Zhan ,<sup>1</sup> and Tiancheng Xu<sup>2</sup>

<sup>1</sup>College of Art and Design, Shaanxi University of Science & Technology, Xi'an, China

<sup>2</sup>Key Laboratory of Acupuncture and Medicine Research of Ministry of Education, Nanjing University of Chinese Medicine, Nanjing, China

Correspondence should be addressed to Qinchuan Zhan; zhanqinchuan@sust.edu.cn

Received 11 May 2022; Revised 1 June 2022; Accepted 8 June 2022; Published 6 July 2022

Academic Editor: Naeem Jan

Copyright © 2022 Yang Zhao et al. This is an open access article distributed under the Creative Commons Attribution License, which permits unrestricted use, distribution, and reproduction in any medium, provided the original work is properly cited.

Since the COVID-19 epidemic, there has been an increased need for well-being and sustainable development, making biophilic design in hospital environments even more significant. However, after investigation, it was found that in many countries including China, the biophilic design of some hospitals is seriously absent, while other parts have the integration of biophilic design, but the standardization and recognition are not high. By restoring the interaction between buildings and nature, biophilic design improves the quality of environments and the health of users. The basic theoretical framework of environmental psychology is followed in this research. The health promotion mechanism, applicable natural features, and relative health advantages of hospital space and environment biophilic design are first investigated. Furthermore, according to the current status of biophilic design applications in the 12 hospitals that have the closest interaction between people and the environment. Combined with the professional and functional requirements of the healthcare spaces and the users' special demands, we propose appropriate update design methods. The goal of this study was to present ideas for healthy and efficient space environment design and to inspire sustainable environmental design for future healthcare environments.

## 1. Introduction

The normalization and recurrence of the COVID-19 have made the development of the healthcare spaces to become a global concern. In addition to balancing hygiene, efficiency, and equity, the design of healthcare spaces needs to be more integrated with the concept of sustainability, thus serving the health of all humanity in the context of the carbon neutral era [1]. As the number of hospital building projects grows, health administrators are progressively adopting green initiatives and ecologically friendly techniques. According to the federal Office of the Environment Executive (OFEE), "Sustainable hospitals can be defined as the practice of designing, constructing, operating, maintaining, and removing buildings in ways that conserve natural resources and reduce pollution [2]." The healthcare spaces have become one of the most visible venues for the green

building movement as a result of concerns about hospitals' environmental implications. In the realm of architecture and design, there has been an increasing interest in the influence of nature on people in buildings [3, 4]. Biophilic design, which is strongly related to people's emotional experiences, is thought to play a significant role in this loop [5]. As an environmental design philosophy that promotes public health through the healing effects of nature, biophilic design interprets the relationship between nature, space environment, and human health from the perspectives of biology and psychology [6]. In the past decade, there has been a substantial increase in research related to biophilic design published by scholars from various countries [7], with applications ranging from interior design and architectural design to parks, streetscapes, schools, and urban design [8, 9]. Simultaneously, a group of researchers is looking into how the use of biophilic design in buildings and interior spaces

improves patients' health and well-being [10]. Depression and mental health disorders are the main cause of disability globally, according to the World Health Organization, and because people spend 90% of their time in buildings [11], environmental design poses both difficulty and opportunity for designers [12].

In the context of COVID-19, people are forced to stay indoors in closed environments for extended periods, leading to heightened anxiety about the indoor environment and an urgent need to create medical spaces that promote emotional and physical well-being [13]. As a central place for the restoration of human health, hospitals are also working to create health-friendly spatial environments through the power of nature [14]. The main participants in medical activities, such as nurses and patients, are in a special state of intense concentration and are relatively fragile and sensitive [15]. The quality of the healthcare spaces' spatial environment is directly related to the effectiveness of medical treatment. And the natural attributes that biophilic design can give to the healthcare space's spatial environment and the health benefits it can create are highly compatible with the functions of the hospital and the demands of its users [16]. The existing literature suggested the various psychological and cognitive benefits of biophilic design, such as helped to have a positive impact on the patient's physiology and psychology [10], reduced negative emotions such as panic and anxiety [17], stimulated the patient's body's potential and promoting a return to health [16], reduced staff stress and fatigue [18], improved productivity, increased security in the environment [19], and negative associations with mortality [20].

To achieve restorative environmental design, real sustainability in healthcare environments should integrate low environmental impact design with biophilic design [21]. However, there is a lack of consistency in current research and practice in this area. Several issues with biophilic design have been observed in existing healthcare environments in China, according to the author's research. Natural resources are undervalued and in short supply. And some hospitals that use natural elements blindly copy them without appropriate selection and application according to the specific situation, lacking a systematic design theory to guide them, and ignoring the positive influence natural spaces bring to people. To seek the direction of sustainable design of healthcare spaces, as the starting point of creating a healthy environment for people, this research analyzes the application mode and existing problems of 12 healthcare spaces in China from the perspective of biophilic design and proposes suitable design solutions. Furthermore, given the size of the reaction to COVID-19 and its impact on health systems and the economy, constructive research action is crucial to reducing future health system restrictions and ensuring high-quality, accessible, and sustainable services [22].

The research is organized as follows: the introduction is presented in Section 1. Section 2 analyzes the materials and methods of the proposed work. Section 3 discusses the literature review. In Section 4, case study on biophilic design of healthcare spaces in China was explored in depth. In Section 5, the proposed methods are compared with previous con-

cepts and made the results. Finally, in Section 6, the research work is concluded.

## 2. Materials and Methods

This paper conducted a literature analysis and a case study to establish the spatial design characteristics of healthcare settings using the biophilic design principle. The following is a detailed description of the research method and scope: we first outlined the positive effects of nature on human health, as well as the concept, elements, and patterns of biophilic design, based on the literature review. Second, to integrate and classify similar or flawed items in the biophilic design model in Chinese healthcare spaces from the case study results through field research and structured interviews to identify the characteristics and problems. Third, the transformed medical space environment was designed using software, including the 2021 edition of SketchUp, Lumion10 version, Enscape3.0 version, and AutoCAD2020. SketchUp is a 3D modeling software used in the interior design industry. Lumion is a real-time 3D visualization tool that covers areas including architecture, planning, and design. Enscape3.0 is used to render models. AutoCAD2020, or computer-aided design, uses computers and their graphics equipment to help designers with their design work. In the practical session, we used the concept of biophilic design to carry out an initial evaluation and update of a selected healthcare space environment.

## 3. Literature Review

*3.1. Natural Elements and Human Health.* Nature's therapeutic effect on physical and mental health has long been discussed. There are numerous direct and indirect relationships between human health and nature. Nature connectedness, in addition to meeting basic human requirements (such as food and natural resource availability), heals or mitigates the majority of ailments and can be considered a health resource (which keeps people healthy) [23]. The earliest site of physical healing by nature was the Sanctuary of Asklepios at Epidaurus, on a hill with fresh air and lush views was a rehabilitation centre in ancient Greece in classical times [24]. Professor Clair Cooper Marcus pointed out in her book *Healing Gardens: Therapeutic benefits and design recommendations*: "90% of garden users experience a positive change in their mood after taking a rest outside [25]." Ester M Sternberg wrote in her book *Healing Spaces: the science of place and well-being*: "When you see a scene that everyone likes, such as a beautiful view, sunset, woods, dormant nerve cells will become active." Your mind is buzzing like a morphine addict. Both authors agreed that being in or observing a natural environment caused positive changes in the mind and body. As a source of healing and source of inspiration, nature plays an important role in the identity of people and the development of its sense of place.

The development of modern science and technology and the process of industrialization have brought about the transformation of human's view of nature to mechanistic, and the integrity and systematicness of nature have been

broken in human cognition, which has led to essential changes in the relationship between human and nature. “The epidemic has made us understand that human health is inextricably linked to the health of natural ecosystems,” experts from the World Wide Fund for Nature (WWF) said. Human activities such as excessive and unnecessary production are primarily to blame for the calamities we have witnessed. We need to reverse this vicious cycle and protect and restore healthy ecosystems that thrive [26].

**3.2. Biophilic Design.** The international practice of biophilic design has a significant geographical dimension due to many factors such as regional development and socio-economic levels and culture. The 2006 conference in Rhode Island, USA, was the beginning of the formal introduction of biophilia into the field of environmental design, exploring the value and implementation strategies of its integration in cities and buildings [8]. In 2008, with the publication of *Biophilic Design: The Theory, Science, and Practice of Bringing Buildings to Life*, the term “biophilic design” was officially named and established. Biophilic design is about learning from nature and creating artificial environments that support and revive human biophilic nature by recreating, using, modeling, and extracting nature [27]. Kellert et al. proposed four basic principles for biophilic design in the same year: first, the importance of repeated and continuous engagement with nature; second, a focus on human adaptation to the natural world; third, encouraging emotional attachment to specific environments and places; fourth, promoting positive interaction between people and nature, encouraging an expanded sense of relationship and responsibility between human and natural communities; fifth, encouraging mutually reinforcing, interconnected and integrated architectural solutions [28]. William Browning proposed 14 biophilic design patterns in 2014 (Browning, Ryan, and Clancy 2014) in Table 1, and Stephen Kellett and Elizabeth Calabrese proposed 24 biophilic design strategies in 2015 [29] in Table 2. A comparative analysis of the two reveals that the design approach develops in three ways: the use of real natural elements, the abstraction and extraction of natural elements or characteristics, and the deduction and transformation of the relationship between man and nature. William Browning categorizes the first two components in terms of their homogeneity, reflecting a more simplified result, and adds to the third two features of “mystery” and “adventure.” By now, biophilic design has become a mainstream design approach in the field of architecture, widely accepted and used, and even included in the measurement criteria for evaluating the built environment. Biophilic design is not simply the transplantation of any natural elements into the spatial environment, but the translation of selected natural elements that have a positive effect on humans into concrete or abstract design language is based on the expansion of the connotation of natural elements, and their integration into each other and their application to the spatial environment in an effective way.

In conclusion, the biophilic design of buildings and urban environments abroad started early and has taken shape. To some extent, economically developed cities have

launched biophilic design study and practice, demonstrating that biophilic design has become a significant trend in urban design. Although China’s urban buildings are gradually adopting concepts like green ecology and sustainable development, many of the related designs still fall short of biophilic. This demonstrates that China is still systematically applying biophilic theories, models, and procedures. Many of the existing successful schemes are from Western countries. It is critical to learn from international advanced thoughts and experiences and investigate biophilic design methodologies that are appropriate for China’s unique circumstances.

**3.3. Biophilic Design in Healthcare Spaces.** Ulrich conducted some of the earliest research into the application of biophilic design in healthcare spaces in the 1980s. His research found that patients in rooms overlooking green areas had shorter postoperative hospital stays and used less pain medication than patients in similar rooms but overlooking the built environment [31]. Following international investigations, it was shown that 95% of patients and families that were exposed to nature had lower stress levels, more positive attitudes, and improved coping skills [32]. Biederman and Vessel suggested that plants in healthcare spaces and roof gardens could reduce patients’ pain, anxiety in therapeutic psychology in 2006 [33]. Eisen et al. conducted a study of art preferences among pediatric inpatients, which showed that children of different ages and genders did not differ much in their choice of artwork. They preferred nature art to abstract art, with nearly 75% preferring nature art (forests with lakes and deer) or impressionistic nature scenes (beaches with waves) [17].

Natural materials can improve patients’ perceptions of their surroundings and their recovery from disease. This is because natural materials improve optical effects (by absorbing more light than they reflect) and have a favorable impact on olfactory comfort (through essential oils), creativity, overall health, and the immune system [34]. The famous German geographer and explorer Alexander von Humboldt emphasized the role of gardens in healing, suggesting that design should be integrated with nature, thus enhancing the quality of the existing environment [35]. The Sir Robert Ogden Macmillan Cancer Centre’s chemotherapy space was created in the shape of a long cobblestone in response to patients’ photosensitive and olfactory drug reactions, providing a long and soothing view of the patient’s dizziness [36]. In 2020, Dushkova and Maria’s biophilic-inspired “restorative healthcare environment design extends the focus from the outdoor landscape to the indoor architectural space.” Extensive experimental data showed that biophilic design in terms of natural light, greenery, green windows, outlook spaces, natural sounds, aromas, water features, real marine life, visual comfort, and a sense of personal control can all have a positive effect on promoting positive emotions and accelerating recovery [23]. Healthcare spaces are the core place for rehabilitation, and the study of the biophilic design of medical space environments has positive significance for improving the health of patients. The biophilic design research system of medical space is not yet perfect,

TABLE 1: The biophilic design methods from William Browning in 2014 [30].

Classification of design methods	Design elements
Apply natural elements	(1) Visual connections; (2) nonvisual connections; (3) irregular sensory stimuli; (4) heat and air currents; (5) water; (6) dynamic diffuse light; (7) natural systems
Simulation of natural analogs	(8) natural forms; (9) natural materials; (10) complexity and order
Construct the relationship between human and nature	(11) Prospect; (12) refuge; (13) mystery; (14) adventure

TABLE 2: The biophilic design methods from Stephen Kellert in 2015 [29].

Classification of design methods	Design elements
Direct nature experience	(1) light; (2) air; (3) water; (4) plants; (5) animals; (6) weather; (7) natural systems; (8) fire
Indirect nature experience	(9) natural patterns; (10) natural materials; (11) natural colors; (12) simulated natural light and natural ventilation; (13) natural shapes or forms; (14) natural associations; (15) information richness; (16) change of time; (17) natural geometry; (18) bionics
The experience of space and place	(19) foresight-shelter; (20) organize complexity; (21) integration; (22) transitional spaces; (23) mobility and wayfinding; (24) emotional connection of place

and the norms and methods for the application of natural elements need to be further optimized in practice.

#### 4. Case Study on Biophilic Design of Healthcare Spaces in China

Some hospitals in China were chosen for field research on the healthcare sector's spatial environment. The variety of hospital kinds was rather extensive, covering practically every aspect of medicine. Biophilic design applications were examined in some nodes with high foot traffic in hospital public spaces using field surveys and structured interviews. The aim was to identify the deficiencies and shortcomings of current healthcare institutions, propose corresponding solutions, and identify the characteristics of the biophilic design model for healthcare spaces. Table 3 shows the basic information of 12 national hospitals with a floor area of 50,000 square meters or more.

Based on the selection of hospitals, the nodes with the high pedestrian flow in the hospital environment were selected, and seven nodes in the medical space, namely, the lobby reception, registration, and payment, waiting area, corridor, CT room, inpatient ward, and hospital lift, were extracted for study. The details of each node are shown in the following Table 4.

Through field research in a number of the above hospitals, it is possible to summarise the current biophilic design issues within the healthcare environment: the first is that the natural element is not valued and is severely lacking. Second, some hospitals that use natural elements blindly copy them without appropriate selection and application according to the specific situation, lacking a systematic design theory to guide them, and ignoring the positive influence natural spaces bring to people. Finally, the design approach's simplicity within some healthcare environments does not allow for efficient, rapid, and sustained action on human physiology. In terms of validity, the integration of individual natural elements into the hospital's spatial environment is

isolated and stagnant, and the elements are not sufficiently appealing to people. In some healthcare environments where the principles of biophilic design are applied, it can be seen that such spaces not only relieve physical fatigue and reduce depression but also stimulate good moods and make patients cooperate with the examination and treatment.

The characteristics of biophilic design patterns in healthcare environments given in the literature and case studies were used to create 27 survey items in three patterns. To enhance respondents' comprehension, the questionnaire included photos of each scenario as well as the effect of applying the features. There were 240 responses, with a significant proportion of men (55%) and those aged 41 or older (41%) and patients (57.5%). The overall characteristics of survey respondents are shown in Table 5.

The importance of biophilic design patterns in healthcare spaces are shown in Table 6. The overall mean of the importance assessment was 4.08, which represents a consensus among the respondents on the importance of biophilic design. The importance of biophilic design patterns above the total mean was highest for "experience mode of natural sense of space" (4.24), followed by "direct nature experience mode" (4.09), and "indirect nature experience mode" (3.83).

As for the mean of importance by item, the highest was "create a relatively inward-looking space environment that resembles a cave in nature, with a long-distance open view in the foreground, and a sense of wrapping from overhead, behind, and on both sides, such as entrances with overhangs and colonnades balconies, sofa seats, etc." (4.58), followed by "real plants or specimens, green roofs, green walls" (4.55), and "the natural building or decorative materials such as wood, stone, wool, cotton and leather, bamboo, rattan" (4.47). And each element of the biophilic design pattern brings different physiological, psychological, and perceived benefits to the user. From the results of the public's assessment of the importance of the elements of biophilic design patterns, it can be concluded that they need small spaces that

TABLE 3: General information of healthcare spaces in China was studied in the case.

The name of the hospital institution	Geographical location	Total area (m <sup>2</sup> )	Nature
Nanjing University of Chinese Medicine	Nanjing, China	55000	National General Hospital
Jiangsu Dental Hospital	Suzhou, China	63000	National Specialist Hospital
Jiangsu Province Hospital	Nanjing, China	20000	National General Hospital
Jiangsu Provincial Hospital of Medicine	Nanjing, China	49000	National General Hospital
Nanjing Children's Hospital	Nanjing, China	112500	National General Children's Hospital
Nanjing Maternity and Child Healthcare Hospital	Nanjing, China	20200	National General Hospital
Nanjing Brain Hospital	Nanjing, China	66000	National Specialist Hospital
Nanjing Medical University Affiliated Eye Hospital	Nanjing, China	20000	National Specialist Hospital
Jiangsu Province Reproductive Centre	Nanjing, China	33110	National Specialist Hospital
Xi'an Children's Hospital	Xi'an, China	75000	National General Hospital
Jinwan Hospital	Zhuhai, China	62000	National General Hospital
Zhongshan Hospital	Shanghai, China	96000	National General Hospital

can provide shelter and lookout and prefer direct natural elements. When planning the design of the medical space in the future, the biophilic design pattern characteristics of the healthcare spaces that are relatively important in the analysis results should be considered.

## 5. Results

This chapter will present appropriate design strategies for the problems found in the biophilic design of healthcare spaces in the research.

*5.1. The Overall Design Idea of Transformation.* The outpatient hall and other locations guidance systems of some hospitals such as Jiangsu Provincial Hospital are relatively single, the overall color is single, the use of natural elements is less and stiff, and the introduction of natural light is limited. In response to the above problems, further skylights can be added in the outpatient halls and corridors to introduce natural light into the indoor space, which can not only relieve the pressure of patients but also save electricity and reflect the concept of sustainable development. Second, the use of floor-to-ceiling windows in the waiting room should be raised in an appropriate amount to increase the gentle combination of indoor and outdoor spaces, so that patients waiting can enjoy the view of the outdoors from the comfort of their own home (especially by making good use of the landscape resources of the adjacent mountains). Third, indirect natural elements are incorporated into the stylistic design by reducing the use of arrow-like directional signs and using green, blue, yellow, or faceted signs to guide and divide spaces. In the Kaiyi Hospital's hall design, designers have shaped the hospital hall into a well-lit and ventilated atrium. The lounge area in the hall is arranged to look like a living room, with sunlight illuminating the whole hall through the skylight on the roof, and with indoor greenery, trying to create a homely atmosphere and a warm resting space for doctors and patients. In the lobby, the supporting beams are used as a base combined with the top lighting to create a decorative design in the shape of a ginkgo tree, which symbolizes strength, hope, and resilience. At the same

time, its color reflects the representative color of Jiaxing, namely, the Ginkgo Avenue on Swan Lake Road in autumn, incorporating local cultural elements into a modern large general hospital. These qualities were distilled into an abstract design language by the designers and used in the hospital interior design (Figure 1).

### *5.2. The Partial Transformation of the Consultation Room.*

The overall spaces of the waiting area in some hospitals are relatively closed, mostly in a room with glass on one side, which lacks communication with the outdoor environment and has a relatively depressing atmosphere, which is unfavorable for both doctors and patients. To address the aforementioned difficulties, a small patio-style garden can be added to the waiting area, introducing natural light through the patio and floor-to-ceiling windows so that patients can enjoy the external beauty even when they are inside. The two-story cedar shingle walls and windows of various offices look out over the space, which is filled with plants, the majority of which are medicinal species. Second, the paths leading to the two seats at either end are unusual water features made of concrete stepping stones set in moss [2]. Multimedia equipment is added to the wall facing the waiting patients, decorated with geometric patterns of the golden ratio. Finally, add several cave-like lounge sofas and play soft music containing natural elements such as the sound of water and birdsong, which can help to alleviate the fatigue of people and relieve the patient's anxiety (Figure 2).

### *5.3. Renovation of the Functional Examination Unit.*

The CT room is undecorated, and the white walls and cold machines can put patients in a depressing and frightening mood, especially as the examinations often allow only the patient to be alone, while examinations such as fMRI take 30 minutes or more. To address these concerns, the walls can be painted in a natural-elements design, and vegetation can be put to the room to help the patient relax. Since the patient is in a lying position during the examination, the eyes are focused on the top, natural patterns such as the sky or woods can be added to the ceiling, while natural sounds such as fountains, streams, waves, birdsong, and rain can be added to

TABLE 4: Characteristics of biophilic design elements and patterns in healthcare spaces of China.



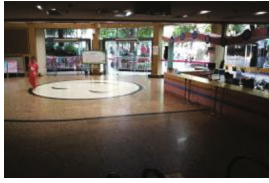

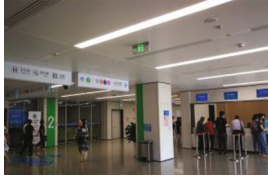




	Research status		
Situation picture			
Name	Nanjing University of Chinese Medicine	Nanjing Brain Hospital	Nanjing Children's Hospital
Node		Lobby reception	
Behavior		Enter the lobby to look for the department, waiting	
Mood	Peaceful	Depression	Boredom
Biophilic design applications	Accelerate smooth recovery of physiological features using real plant elements in the direct nature experience model.	Lacking	Large glazed windows extend the view of the natural landscape outside the house and also help to increase the light inside the house.
Problem	Lack of organic interaction between clusters.	Lack of interactive design in the lobby and lack of natural elements.	Lack of a clear signage system to avoid confusion and congestion.
Situation picture			
Name	Jiangsu Dental Hospital	Jiangsu Province Hospital	Nanjing Children's Hospital
Node		Registration and payment	
Behavior		Waiting inline	
Mood	Dull	Boredom	Tension
Biophilic design applications	Lacking	The use of natural colors such as green and wood gives a fresh, vibrant feel, and effectively divides the space.	Lacking
Problem	The overall color is metallic, cold, and monochrome.	Insufficient shade and proper privacy space.	Lack of natural elements.
Situation picture			
Name	Jiangsu Dental Hospital	Jiangsu Province Hospital	Jiangsu Province Reproductive Centre
Node		Waiting area	
Behavior		Waiting, consulting	
Mood	Depression	Peaceful	Somber
Biophilic design applications	Lacking	Both the walls and the seats are in carpenter's colors can be used to recreate the feeling of the forest and the plants.	Skylight for increased natural light.
Problem	The waiting area has no windows, and the lighting is weak, creating an overall dim atmosphere.	Lack of interactive elements.	The decorative dividing lines on the walls are crossed series a straight line, giving a serious and discreet impression.



TABLE 4: Continued.


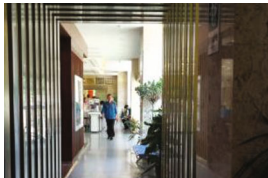







	Research status		
Situation picture			
Name	Jiangsu Province Hospital	Jiangsu Province Reproductive Centre	Jiangsu Dental Hospital
Node		Corridor	
Behavior		Walking, searching, resting	
Mood	Pleasant	Comfortable	Boring
Biophilic design applications	A large aquarium with a variety of aquatic animals, where the creatures swim to add life and vitality.	The use of bamboo and greenery to create shade, large windows to increase natural light.	A considerable amount of sky blue has been used to help create an overall bright and vibrant interior.
Problem	The single form of interaction.	Lack of multisensory indirect natural elements.	Lack of multisensory indirect natural elements.
Situation picture			
Name	Xi'an Children's Hospital	Jiangsu Province Hospital	Jinwan Hospital
Node		CT room	
Behavior		Body checking	
Mood	Funny	Tension	Comfortable
Biophilic design applications	The cartoonish design of the forest elements on the base and around the treatment equipment and the house makes it more accessible and enjoyable for children.	Lacking	Natural light, warm walls, outdoor greenery, and landscape paintings create a warm and welcoming atmosphere.
Problem	Raw use of natural elements.	Lack of biophilic design.	The lighting setup is a little complicated.
Situation picture			
Name	Nanjing Medical University Affiliated Eye Hospital	Xi'an Children's Hospital	Nanjing Maternity and Child Healthcare Hospital
Node		Inpatient Ward	
Behavior		Hospitalization, visiting patients	
Mood	Torment	Lively	Comfortable
Biophilic design applications	Lacking	Natural elements such as animals and ocean glaciers set the mood, tension-relieving colors such as pink and blue.	The use of natural, warm colors creates a warm and inviting atmosphere.
Problem	The large areas of cold white and the hard iron chairs on the walls tend to bring depression to people recovering from hospitalization.	Lack of multisensory direct and indirect natural elements.	Lack of multisensory direct and indirect natural elements.

TABLE 4: Continued.

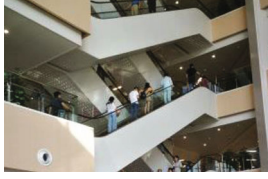
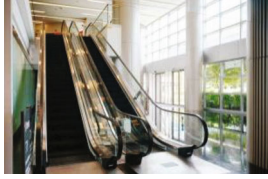

	Research status		
Situation picture			
Name	Xi'an Children's Hospital	Zhongshan Hospital	Nanjing Brain Hospital
Node		Hospital lift	
Behavior		Walking, looking	
Mood	Boring	Peaceful	Boring
Biophilic design applications	Lacking	The large floor-to-ceiling windows not far from the lift bring in a lot of natural light into the medical space and help communication between the inner and outer spaces.	Lacking
Problem	Crowded surroundings monochromatic colors single layout.	Lack of multisensory direct and indirect natural elements.	Cold lifts and empty grounds give a dead feeling and are not conducive to healing.

TABLE 5: General characteristics of survey respondents.

Category	Item	N	%
Gender	Male	132	55
	Female	108	45
	Total	240	100
Age	Age 25-30	73	30
	Age 31-40	69	29
	Age 41 or older	98	41
	Total	240	100
Identity	Patient	137	57.5
	Hospital staff	58	24.2
	Others	45	18.3
	Total	240	100

soothe the patient through a combination of audio and visual stimulation [37].

**5.4. Ward Transformation.** The overall color palette of the ward space is predominantly white, lacking color variation and plants, while the furniture and cabinets are mostly made of metal and plastic, lacking a sense of intimacy. The beds in the multiperson ward are separated from each other only by bed curtains and lack personal space. To address these concerns, natural elements can be used to beautify the wards by including appropriate plants and animals, such as green buckets and goldfish. Create a unique natural element in the landscape by forming the walls in the shape of a natural environment, such as a beehive, and then adding suitable plants to the individual units. Second, instead of bed curtains, screens with pulleys can be used. Screens of rigid material are more capable of dividing space than fabric bedroom curtains, and the pulleys ensure that the flow of space

is unobstructed [28]. The ward unit adopts a zigzag plane, and green platforms are arranged in the recesses in the plane so that there is a natural landscape outside each window. Combined with the external multilevel healing garden, patients on each floor have the opportunity to have direct contact with nature and use the “direct experience mode” with nature in the biophilic design to enhance the healing properties of the interior space. In addition, through the overall consideration of the window size and the location of the hospital bed, the window ventilation only serves the nearby patients, reducing the risk of mutual infection. The windows also feature removable louvers to maximize daylight and minimize glare, shielding patients from low-angle sunlight in the morning and evening. And a forward-facing eave can be added to the window to give the patient a sense of perspective (Figure 3).

**5.5. Garden Renovation.** The survey found that some Chinese hospitals did not realize the role of healing gardens, several healing garden space is less functional, the configuration of plants and so on is relatively single, and the landscape modes are not sparse and dense. First, a multifaceted composite landscape system can be introduced into the garden, such as different scales and types of nonirritating odor plants, to create spatial places with different experiential sensations and to increase complexity and connectivity. The use of plants and geometric cuts and microtopographical enclosures creates a private and secluded place that adds a sense of mystery and provides a sense of refuge for patients [38]. Tree-shrouded paths lead people's eyes to distant views and landmarks, giving depth and coherence to the space of this journey. This atmosphere allows people to control their emotions and restore their focus by providing a momentary getaway, a sense of “distance.” Then there is the introduction of water features, which are classified as either dynamic or

TABLE 6: Importance of biophilic design patterns in healthcare spaces.

Biophilic design pattern	Associated natural elements	Biophilic design pattern characteristics	Impact on users			Mean of importance
			(a)	(b)	(c)	
Direct nature experience mode	Plant	Real plants or specimens, green roofs, green walls.	●	●	●	4.55
		Dedicated, safe, and effective space for animal-assisted therapy.	●	●	●	3.94
	Animal	The hospital waiting for the hall, restaurant, and other spaces are equipped with aquariums with a variety of aquatic animals.	●	●	●	4.13
		Introduce natural light indoors by setting up roof gardens, sunken gardens, corridors with windows and skylights, offices, lounges, wards, etc.	●			4.26
	Water	Water bodies, fountains, constructed wetlands, small waterfalls, water sound.	●	●	●	4.11
		Air	Natural ventilation.	●	●	
	Weather	Through the interface design of transition spaces such as building doors and windows, skylights, balconies, corridors, etc., people can know the weather conditions.	●	●	●	4.25
		Fire	A fireplace or a fire that simulates the light’s color, motion, and temperature.	●		
	Natural systems	The holistic nature is composed of plants, animals, water bodies, soil, rocks, etc., including topography, vegetation landscapes, and ecosystems.		●		4.23
		Natural images	Natural images are represented by photographs, paintings, sculptures, murals, videos, computer simulations, and other means.	●	●	
	Natural sound	Play soft natural sounds of fountains, streams, waves, waterfalls, rain, wind, birdsong, and more.	●	●	●	3.43
		Natural materials	The natural building or decorative materials such as wood, stone, wool, cotton and leather, bamboo, and rattan.		●	●
	Natural color	Natural pastel shades of soil, rocks, plants, etc., avoiding strongly artificial, contrasting, and vibrating colors.		●	●	4.45
		Simulate light and air	Simulation of natural spectral and dynamic properties and natural ventilation.	●	●	●
Indirect nature experience mode	Natural form	Extraction of natural forms, such as plant patterns such as flowers and trees; animal forms such as shells and honeycombs.	●	●	●	3.54
		Abstraction and symbolization of natural forms.		●		3.65
	Informative	Rich environmental information can activate the perception of the environment by various senses, such as vision, touch, and smell.	●	●	●	3.43
	Change of time	Visualization and characterization of changes over time, such as aging of materials and oxidation of metals.		●		4.38
	Natural geometry	The use of natural geometry, such as fractals, golden ratio, golden spiral, Fibonacci sequence, and dynamic symmetry.	●	●	●	3.54
Integration		Numerous unique elements come together into a unified whole, including continuous spatial relationships, clear boundaries, functional, or formal focal points.		●		3.43
Experience mode of natural sense of space	Bionics	Imitation of nature to optimize performance, not simple morphological replication.		●		3.41
		Create a relatively inward-looking space environment that resembles a cave in nature, with a long-distance open view in the foreground, and a sense of wrapping from overhead, behind, and on both sides, such as entrances with overhangs and colonnades balconies and sofa seats.	●	●	●	4.58
	Mobile wayfinding	Clear paths and exits and guidance systems ensure autonomous movement of the individual.		●		4.36
Transition space	Clear boundaries and connectors to ensure an individual’s sense of domain and control.		●		3.80	

TABLE 6: Continued.

Biophilic design pattern	Associated natural elements	Biophilic design pattern characteristics	Impact on users			Mean of importance
			(a)	(b)	(c)	
	Place emotional connection	Establish a connection between the individual and the local geography, history, culture, or ecological environment to enhance a sense of belonging and identity.	●	●	●	4.41
	Mystery	On the premise of ensuring safety and control, set up winding paths, or use plants to partially cover the building, blur some sensory information, and stimulate people’s curiosity for further exploration.		●	●	3.94
	Order and complexity	Introduce a landscape system with multiple elements; adopt a hierarchical spatial structure; moderately use fractal patterns in nature; repeat motifs.	●	●	●	3.65

(a) represents physiological benefits, (b) representing psychological benefits, and (c) representing perceived benefits.

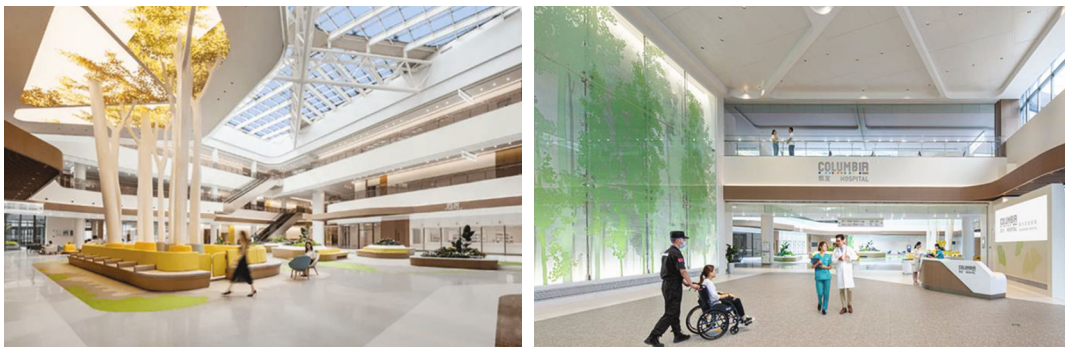


FIGURE 1: Kaiyi Hospital’s Hall biophilic design update renderings.

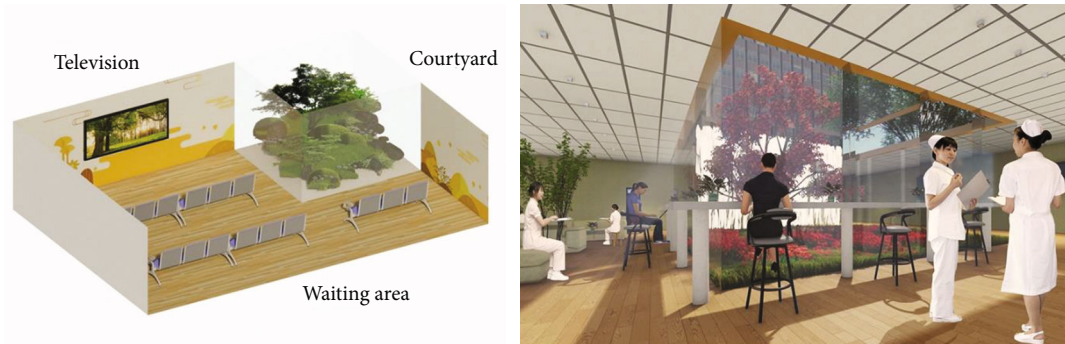


FIGURE 2: Rendering of the updated biological design of the waiting area.

static depending on their qualities. Dynamic water features such as cascading water and streams can create a natural and dynamic water ecology and bring vitality to patients. Landscapes such as water mists and fogs can increase the humidity of the air in the hospital environment and create a microclimate of comfortable spaces. Patients can interact with the water features to create a pleasant emotional experience. Third, the introduction of animal therapy, the inclusion of animal elements, can promote interaction between people and nature and increase the emotional connection of the place. The interaction and play of patients with animals can increase patients’ sense of belonging to the hospital

space, which in turn relieves patients’ physical exhaustion and pain (Figure 4).

## 6. Conclusions and Discussion

To achieve true sustainability in healthcare facilities, low environmental impact design should be combined with biophilic design (or positive environmental impact design), resulting in what is known as a restorative environmental design [28]. Biophilic design is based on the biophilic nature of human beings. It is a space-environment design concept that can boost human health, cognition, and productivity.

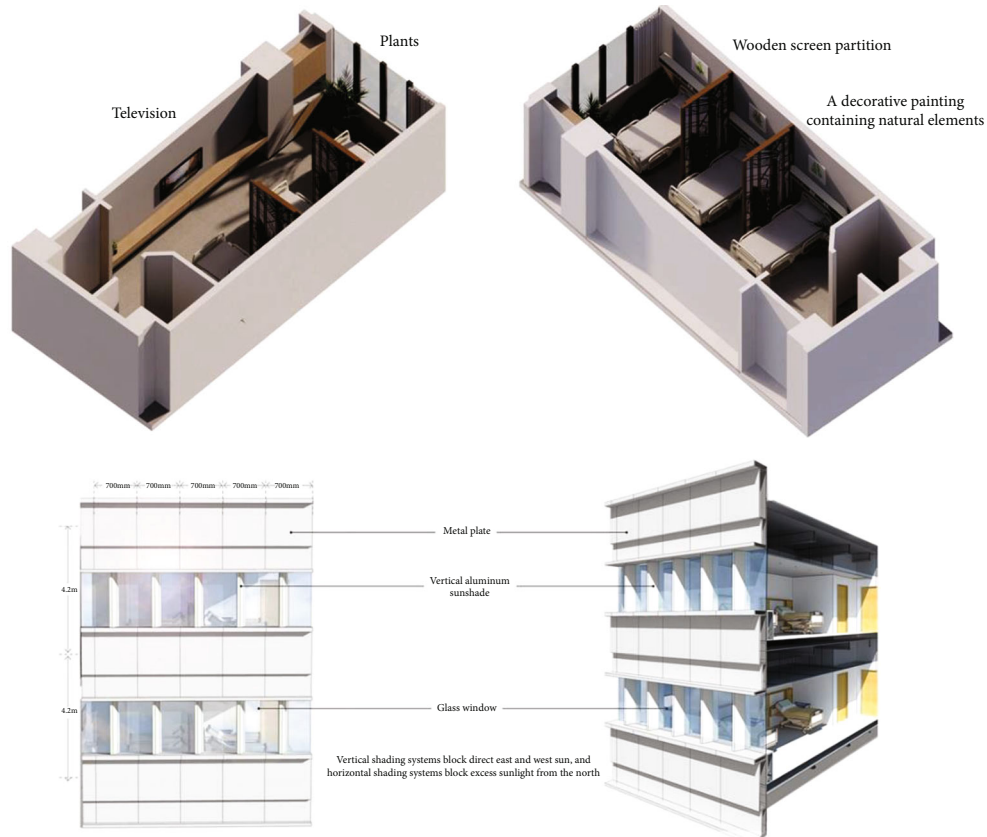


FIGURE 3: Ward biophilic design update renderings.



FIGURE 4: Healing garden biophilic design update renderings.

The biophilic design idea highlights the relationship between nature, space environment, and human health from a biological aspect and can drive the long-term development of the healthcare spaces environment. To ensure safety and standardization, natural elements suitable for the healthcare spaces environment should be picked, and then prudent and effective design approaches should be used, all while not interfering with medical activities and completely addressing the demands of patients. The idea is to continuously stimulate the human body using a variety of sensory inputs like vision, hearing, touch, and smell. People’s biophilia is stimulated, and doctors’ and patients’ health is enhanced, by leading the human body to create a response to natural com-

ponents. This is a paradigm aimed at reestablishing a harmonious balance between humans and nature in the building environment. Biophilic design, within this concept, may represent the missing piece in sustainable design, which is still related to an understanding of nature as an ethical value rather than a physiologically determined condition.

To ensure the correct biophilic design of the healthcare space environment, to ensure the safety of patients’ lives, and to avoid additional physical and psychological harm to patients during the treatment process, the biophilic design process must carefully select natural elements and use highly controlled design methods to avoid the possible increased risk of infection and physiological burden of natural

elements. Based on the existing theoretical framework of biophilic design, this study analyzes the existing problems, health promotion mechanism, and specific associated health benefits of biophilic design through field investigations in 12 healthcare spaces in China. Then combined with the professional requirements of hospital functions and the special needs of users, the following three points of biophilic design are proposed:

*6.1. Optimize the Interaction Mode between Direct or Indirect Natural Elements and People.* In traditional medical spaces, natural elements such as greenery and animals are used for aesthetic and even Feng Shui reasons. In most of the hospitals and clinics we studied, greenery was used only as a landscape, at best for the short-term value of “removing formaldehyde” [39], but not for its value in optimizing the flow of care or even for its medical value [40]. Natural elements such as plants and natural light can themselves create order and hierarchy. The placement of plants in our design corresponds to, and even merges with, the flow design of medical appointments, serving as a good segregation and guide. And this is just the beginning of its job. The plants themselves can become the focus of attention for patients and doctors, especially in information-heavy waiting and registration areas, and the interplay of information screens and varied signage with the plant arrangement can serve to reduce anxiety among patients [41]. The introduction of animals is a bold design, but we were fortunate to see more than one site in the hospitals we researched that had adopted this element, such as the ornamental fish pond provided in the outpatient halls of the Jiangsu Provincial Hospital of Traditional Chinese Medicine. This design enhances the cognitive and reactive abilities of patients through the interaction of animals with them. Especially for dentistry, a department that causes more direct pain, the active character of the fish has a relaxing effect on patients [42]. Animals are especially important in the medical value of human interaction because their natural curiosity helps to provide additional healing space for parents with children, whose increased attention to animals reduces their attention to other things around them, such as crying children and anxious patients.

In addition, the use of indirect natural elements such as natural colors (e.g., soft colors such as green, blue, and yellow), natural materials (e.g., wood, stone, and bamboo), simulated light and air, natural geometry (fractals, golden ratio, golden spiral, etc.), natural associations (abstraction and symbolization of natural forms), and natural images (multimedia natural landscapes) in interior spaces also need to be based on the needs of the patient’s healthcare experience. And to systematically examine the volume of consultations and the geographical distribution of specialties in the renovated premises, to improve the health of the staff in three directions: mental cognition, psycho-emotional, and physiological functions.

*6.2. Increase the Emotional Connection of the Place and Provide an Interactive Place for Shelter and Lookout.* Following extensive fieldwork, the research identified a lack of natural spatial experience models in healthcare settings.

Hospitals are stressful places where both staff and patients want some private sanctuary to relieve their emotions. The advantage of the natural space experience model is that it is easier to create an immersive experience of nature by creating a spatial organization in an artificial environment that resembles that which exists in nature. Relevant natural elements include a sense of shelter and watchfulness, order and complexity, mystery, and contrast. In the actual design process, real natural objects, natural analogs, and products are often used to assist in creating a sense of natural space. This model not only helps to alleviate mental fatigue caused by continuous and intense work but it also promotes refocusing and intelligent recovery; it also helps to increase health care staff motivation, willingness to communicate with patients, and overall work effectiveness, all of which have a positive impact on patient recovery.

For example, healing gardens can provide a temporary sanctuary with a degree of privacy, offering a place to escape for patients who have been in a group living space. Create a relatively inward-looking space environment that resembles a cave in nature, with a long-distance open view in the foreground, and a sense of wrapping from overhead, behind, and on both sides, such as entrances with overhangs and colonnades balconies, sofa seats, etc., and it can increase patient’s emotional attachment. Emotional attachment is a person’s high identification with the environment, which helps patients to develop a series of positive emotions, such as relaxation, willingness to integrate into the treatment environment, and more confidence in the treatment plan.

*6.3. Realize Systematic Compounding with Real and Diverse Designs.* In terms of achieving effectiveness in the biophilic design of healthcare spaces, research has shown that real natural objects can have a more positive effect than simulated natural analogs, and that overly distorted natural analogs can cause boredom and resentment [28]. The combined health advantages of using several natural components in a systematic way are more important and conducive to the production of a sense of natural space and environment than the benefits of using individual natural elements alone [21]. The multisensory complex stimulation of the human body by natural elements is more attractive than the stimulation of a single sense. Elements of nature that attract active participation and physical activity are more influential than those that only allow for static appreciation of dwelling [43].

Considering the complexity of the spatial environment of the hospital and the specificity of the personnel, to enhance the effectiveness of the design: first, it should try to objectively and realistically display the diversified natural elements more understandably, moderately highlight the dynamic changes and attractiveness of the natural elements, and thus enhance the participation of the personnel; second, the biophilic design of each spatial interface is compounded. Patients are often supine when receiving treatment and resting, so the design should focus on the roof interface, which is often overlooked but has a high frequency of patient sighting; third, when it is difficult to make a direct connection between the imaging centre and the real exterior natural world due to the spatial limits imposed by the functional

requirements of healthcare, reference can be made to the indirect natural experience model by systematically using natural materials such as logs to awaken tactile perception, electronic media, and virtual reality technology to reshape the audiovisual experience, and natural scents to activate the olfactory memory, creating a comprehensive fake natural experience.

Millions of people's health had improved significantly before the COVID-19 epidemic. However, additional work is needed to completely eradicate a variety of diseases and treat a variety of persistent new health challenges. Biophilic design is one of the efforts that need to be implemented, a concept that is difficult to implement in many developing countries and regions due to economic factors and research limitations. In line with the general trend of human evolutionary progress, the biophilic design is founded on genuine life impulses and survival laws. Biophilic design can contribute to the health promotion of hospital spaces and is in line with the requirements of sustainable development. With the development of mankind's understanding of the relationship between humans and nature, the natural elements with health-promoting potential can be further expanded in the future through more extensive and scientific empirical research, and their health-promoting effects on specific people in specific hospital spatial environments can be explored in a targeted manner, providing a more adequate theoretical basis and empirical guidance for the future biophilic design of hospital spatial environments.

### Data Availability

The datasets used during the current study are available from the corresponding author on reasonable request.

### Conflicts of Interest

The authors declare that they have no conflict of interest.

### Authors' Contributions

Q.C.Z. did the software and writing—original draft preparation. T.C.X. did the investigation. Y.Z. did the writing—review, and editing. All authors have read and agreed to the published version of the manuscript.

### Acknowledgments

This work was supported by the National Social Science Foundation of China, grant number 21BG107.

### References

- [1] M. Golbazi and C. B. Aktas, "Analysis of credits earned by LEED healthcare certified facilities," *Procedia Engineering*, vol. 145, pp. 203–210, 2016.
- [2] A. Balabel and M. Alwetaishi, "Toward sustainable healthcare facilities: an initiative for development of "Mostadam-HCF" rating system in Saudi Arabia," *Sustainability (Switzerland)*, vol. 13, no. 12, p. 6742, 2021.
- [3] A. Coburn, O. Kardan, H. Kotabe et al., "Psychological responses to natural patterns in architecture," *Journal of Environmental Psychology*, vol. 62, pp. 133–145, 2019.
- [4] J. Heerwagen and B. Hase, "Building biophilia: connecting people to nature in building design," *Environmental Design and Construction*, vol. 3, pp. 30–36, 2001.
- [5] K. Gillis and B. Gatersleben, "A review of psychological literature on the health and wellbeing benefits of biophilic design," *Buildings*, vol. 5, no. 3, pp. 948–963, 2015.
- [6] C. O. Ryan, W. D. Browning, J. O. Clancy, S. L. Andrews, and N. B. Kallianpurkar, "Biophilic design patterns: emerging nature-based parameters for health and well-being in the built environment," *Archnet-IJAR*, vol. 8, no. 2, pp. 62–76, 2014.
- [7] G. Barbiero and R. Berto, "Biophilia as evolutionary adaptation: an onto- and phylogenetic framework for biophilic design," *Frontiers in Psychology*, vol. 12, 2021.
- [8] P. Downton, D. Jones, J. Zeunert, and P. Roös, "Biophilic design applications: putting theory and patterns into built environment practice," *KnE Engineering*, vol. 2, no. 2, p. 59, 2017.
- [9] T. Peters and K. D'Penna, "Biophilic design for restorative university learning environments: a critical review of literature and design recommendations," *Sustainability (Switzerland)*, vol. 12, no. 17, p. 7064, 2020.
- [10] J. Hinds and P. Sparks, "The affective quality of human-natural environment relationships," *Evolutionary Psychology*, vol. 9, no. 3, pp. 451–469, 2011.
- [11] N. E. Klepeis, W. C. Nelson, W. R. Ott et al., "The National Human Activity Pattern Survey (NHAPS): a resource for assessing exposure to environmental pollutants," *Journal of Exposure Analysis and Environmental Epidemiology*, vol. 11, no. 3, pp. 231–252, 2001.
- [12] M. S. Berry, M. A. Repke, A. L. Metcalf, and K. E. Jordan, "Promoting healthy decision-making via natural environment exposure: initial evidence and future directions," *Frontiers in Psychology*, vol. 11, pp. 1–6, 2020.
- [13] P. Cui, J. Zhang, and T. T. Li, "Research on acoustic environment in the building of nursing homes based on sound preference of the elderly people: a case study in Harbin, China," *Frontiers in Psychology*, vol. 12, pp. 1–16, 2021.
- [14] T. Izutsu, A. Tsutsumi, H. Minas, G. Thornicroft, V. Patel, and A. Ito, "Mental health and wellbeing in the sustainable development goals," *The Lancet Psychiatry*, vol. 2, no. 12, pp. 1052–1054, 2015.
- [15] R. Cronk and J. Bartram, "Environmental conditions in health care facilities in low- and middle-income countries: coverage and inequalities," *International Journal of Hygiene and Environmental Health*, vol. 221, no. 3, pp. 409–422, 2018.
- [16] S. Totaforti, "Applying the benefits of biophilic theory to hospital design," *City, Territory and Architecture*, vol. 5, no. 1, pp. 1–9, 2018.
- [17] S. L. Eisen, R. S. Ulrich, M. M. Shepley, J. W. Varni, and S. Sherman, "The stress-reducing effects of art in pediatric health care: art preferences of healthy children and hospitalized children," *Journal of Child Health Care*, vol. 12, no. 3, pp. 173–190, 2008.
- [18] L. Tyrväinen, A. Ojala, K. Korpela, T. Lanki, Y. Tsunetsugu, and T. Kagawa, "The influence of urban green environments on stress relief measures: a field experiment," *Journal of Environmental Psychology*, vol. 38, pp. 1–9, 2014.

- [19] F. E. Kuo, M. Bacaicoa, and W. C. Sullivan, "Transforming inner-city landscapes: trees, sense of safety, and preference," *Environment and behavior*, vol. 30, no. 1, pp. 28–59, 1998.
- [20] P. James, J. E. Hart, R. F. Banay, and F. Laden, "Exposure to greenness and mortality in a nationwide prospective cohort study of women," *Environmental Health Perspectives*, vol. 124, no. 9, pp. 1344–1352, 2016.
- [21] B. Bolten and G. Barbiero, "Biophilic design: how to enhance physical and psychological health and wellbeing in our built environments," *Visions for Sustainability*, vol. 2020, no. 13, pp. 11–16, 2020.
- [22] S. J. Alsunaidi, A. M. Almuhaideb, N. M. Ibrahim et al., "Applications of big data analytics to control COVID-19 pandemic," *Sensors*, vol. 21, no. 7, p. 2282, 2021.
- [23] D. Dushkova and M. Ignatieva, "New trends in urban environmental health research: from geography of diseases to therapeutic landscapes and healing gardens," *Geography, Environment, Sustainability*, vol. 13, no. 1, pp. 159–171, 2020.
- [24] J. Maas, R. A. Verheij, S. De Vries, P. Spreeuwenberg, F. G. Schellevis, and P. P. Groenewegen, "Morbidity is related to a green living environment," *Journal of Epidemiology and Community Health*, vol. 63, no. 12, pp. 967–973, 2009.
- [25] C. C. Marcus and M. Barnes, *Healing Gardens: Therapeutic Benefits and Design Recommendations (Wiley Series in Healthcare and Senior Living Design)*, John Wiley & Sons, 1999.
- [26] H. Kopnina, "Animal cards, supermarket stunts, and the world wide fund for nature: exploring the educational value of a business-environmental non-governmental organization partnership for sustainable consumption," *Journal of Consumer Culture*, vol. 16, no. 3, pp. 926–947, 2016.
- [27] M. Mehaffy, "Biophilic design: the theory, science, and practice of bringing buildings to," *Life*, vol. 165, 2012.
- [28] S. R. Kellert, J. Heerwagen, and M. Mador, *Biophilic Design: The Theory, Science and Practice of Bringing Buildings to Life*, 2011.
- [29] S. R. Kellert, *Nature by Design: The Practice of Biophilic Design*, Yale University Press, Yale, 2015.
- [30] W. Browning, C. Ryan, and J. Clancy, "14 patterns of biophilic design," *Terrapin Bright Green, LLC*, vol. 14, pp. 9–11, 2014.
- [31] R. S. Ulrich, "View through a window may influence recovery from surgery," *Science*, vol. 224, no. 4647, pp. 420–421, 1984.
- [32] J. Söderlund and P. Newman, "Improving mental health in prisons through biophilic design," *Prison Journal*, vol. 97, no. 6, pp. 750–772, 2017.
- [33] I. Biederman and E. Vessel, "Perceptual pleasure and the brain," *American Scientist*, vol. 94, no. 3, pp. 247–253, 2006.
- [34] Y. Tsunetsugu, J. Lee, B. J. Park, L. Tyrväinen, T. Kagawa, and Y. Miyazaki, "Physiological and psychological effects of viewing urban forest landscapes assessed by multiple measurements," *Landscape and Urban Planning*, vol. 113, pp. 90–93, 2013.
- [35] C. B. Valenčius, "Chapter 1: histories of medical geography," *Medical History*, vol. 44, no. S20, pp. 3–28, 2000.
- [36] T. T. A. T. T. Peters, "Design for health : sustainable approaches to therapeutic architecture LK," 2017, <https://Virginiatech.on.Worldcat.Org/Oclc/982451708>.
- [37] M. M. Shepley, R. P. Gerbi, A. E. Watson, S. Imgrund, and R. Sangha-Zadeh, "The impact of daylight and views on ICU patients and staff," *Health Environments Research and Design Journal*, vol. 5, no. 2, pp. 46–60, 2012.
- [38] D. M. Alotaibi, M. Akrami, M. Dibaj, and A. A. Javadi, "Smart energy solution for an optimised sustainable hospital in the green city of NEOM," *Sustainable Energy Technologies and Assessments*, vol. 35, pp. 32–40, 2019.
- [39] S. Panyametheekul, T. Rattanapun, J. Morris, and M. Ongwandee, "Foliage houseplant responses to low formaldehyde levels," *Building and Environment*, vol. 147, pp. 67–76, 2019.
- [40] W. Zhang, H. Liu, Z. Li, and H. Liu, "Synergistic effects of edible plants with light environment on the emotion and sleep of humans in long-duration isolated environment," *Life Sciences in Space Research*, vol. 24, pp. 42–49, 2020.
- [41] M. Akram, M. Daniyal, N. Munir, E. Mohiuddin, and S. Sultana, "Medicinal plants combating against insomnia," *Journal of Nervous and Mental Disease*, vol. 207, no. 11, pp. 927–935, 2019.
- [42] D. S. Ling, M. Kelly, and A. Diamond, *Human-animal interaction and the development of executive functions*, The Social Neuroscience of Human-Animal Interaction, 2016.
- [43] M. Mollazadeh and Y. Zhu, "Application of virtual environments for biophilic design: a critical review," *Buildings*, vol. 11, no. 4, p. 148, 2021.



## Retraction

# Retracted: The Feasibility Mechanism of Nerve Interventional Thrombectomy for Occlusion of Cranial Artery M1 and M2 Segments

### Computational and Mathematical Methods in Medicine

Received 19 September 2023; Accepted 19 September 2023; Published 20 September 2023

Copyright © 2023 Computational and Mathematical Methods in Medicine. This is an open access article distributed under the Creative Commons Attribution License, which permits unrestricted use, distribution, and reproduction in any medium, provided the original work is properly cited.

This article has been retracted by Hindawi following an investigation undertaken by the publisher [1]. This investigation has uncovered evidence of one or more of the following indicators of systematic manipulation of the publication process:

- (1) Discrepancies in scope
- (2) Discrepancies in the description of the research reported
- (3) Discrepancies between the availability of data and the research described
- (4) Inappropriate citations
- (5) Incoherent, meaningless and/or irrelevant content included in the article
- (6) Peer-review manipulation

The presence of these indicators undermines our confidence in the integrity of the article's content and we cannot, therefore, vouch for its reliability. Please note that this notice is intended solely to alert readers that the content of this article is unreliable. We have not investigated whether authors were aware of or involved in the systematic manipulation of the publication process.

Wiley and Hindawi regrets that the usual quality checks did not identify these issues before publication and have since put additional measures in place to safeguard research integrity.

We wish to credit our own Research Integrity and Research Publishing teams and anonymous and named external researchers and research integrity experts for contributing to this investigation.

The corresponding author, as the representative of all authors, has been given the opportunity to register their agreement or disagreement to this retraction. We have kept a record of any response received.

### References

- [1] X. Fang, T. Liao, J. Chen, J. Wu, and B. Xu, "The Feasibility Mechanism of Nerve Interventional Thrombectomy for Occlusion of Cranial Artery M1 and M2 Segments," *Computational and Mathematical Methods in Medicine*, vol. 2022, Article ID 6350033, 10 pages, 2022.

## Research Article

# The Feasibility Mechanism of Nerve Interventional Thrombectomy for Occlusion of Cranial Artery M1 and M2 Segments

Xiang Fang, Taijian Liao, Junhui Chen, Juan Wu, and Biyu Xu 

Division 1 Department of Neurology, Nanping First Hospital, Nanping, 353000 Fujian Province, China

Correspondence should be addressed to Biyu Xu; [baoxiagu356706@163.com](mailto:baoxiagu356706@163.com)

Received 8 May 2022; Revised 29 May 2022; Accepted 1 June 2022; Published 6 July 2022

Academic Editor: Naeem Jan

Copyright © 2022 Xiang Fang et al. This is an open access article distributed under the Creative Commons Attribution License, which permits unrestricted use, distribution, and reproduction in any medium, provided the original work is properly cited.

This study was aimed at exploring the feasibility and clinical efficacy of nerve interventional thrombectomy (NIT) to treat occlusion of cranial artery M1 and M2 segments. 80 patients were selected and rolled into a control group (intravenous thrombolysis) and an experimental group (NIT). Patients' vascular recanalization rates following therapy were compared, and the National Institutes of Health Stroke Scale (NIHSS) was used to measure neurological function. The improvement in hemodynamics and the occurrence of adverse responses were compared. The results showed that the experimental group's recanalization rate was up to 74.23%, which was significantly greater than the control group's ( $P < 0.05$ ). One week after treatment, the neurological function scores in both groups decreased, and the score in the experimental group was only 15.23, which was much lower than that in the control group ( $P < 0.05$ ). The peak systolic flow rates of the basilar artery, internal carotid artery, and common carotid artery in the experimental group were 132 cm/s, 147 cm/s, and 114 cm/s, respectively, which were lower greatly than those in the control group ( $P < 0.05$ ). There was no significant difference in incidence of adverse reactions between the two groups ( $P > 0.05$ ). In summary, NIT showed a significant therapeutic effect on cranial artery occlusion of M1 and M2 segments, can dredge the occluded blood vessels, and effectively improve the neurological deficits of patients, showing reliable feasibility.

## 1. Introduction

The middle cerebral artery (MCA) is usually divided into five segments on the image: M1 (horizontal), M2 (circumflex), M3 (lateral sulcus), M4 (bifurcation), and M5 segment (angular gyrus artery) [1, 2]. The MCA serves as the main blood vessel, and the ischemic stroke caused by the MCA occlusion is much higher than that caused by other blood vessel occlusion [3, 4]. Stroke is a common ischemic encephalopathy; the clinical manifestations are mainly blindness, contralateral hemiplegia, sensory disturbance, hemianopia, etc., often accompanied by coma and poor prognosis [5, 6]. With the intensification of population aging and changes in dietary work and rest, the incidence of stroke is increasing year by year and tends to be younger, becoming the leading cause of adult death and disability in China [7–9]. Investigations and studies have pointed out that cardiovascular and

cerebrovascular mortality rate in China is 271.8 per 100,000, of which in patients with stroke, about 70% are caused by acute occlusion of cerebral arteries [10]. Moreover, in patients with ischemic stroke, 9%-38% are caused by acute occlusion of the M2 segment of the middle cerebral artery, which accounts for 16%-41% of all infarcts in the middle cerebral artery region [11, 12].

Thrombolysis is currently the most commonly recommended clinical treatment for patients with acute cerebral infarction. Intravenous thrombolysis and transarterial thrombolysis are two common types of thrombolysis. However, due to the various methods and timings of thrombolysis, there are some variances in thrombolysis efficacy [13–15]. Compared with intravenous thrombolysis, nerve interventional thrombectomy (NIT) has the advantages of higher postoperative recanalization rate, fewer systemic side effects, lower risk of bleeding, and lower incidence of

postoperative adverse reactions [16]. Interventional therapy entails inserting guide wires, catheters, and other instruments into the lesion and performing local procedures to achieve the goal of exact treatment [17].

In conclusion, stroke tends to strike younger people, the prognosis is bad, and the side effects of NIT are minor. As a result, in order to provide an effective reference for the therapeutic treatment of stroke patients, this study investigated the feasibility and clinical effects of NIT in the treatment of cranial artery occlusions produced by occlusions of M1 and M2 segments.

The paper's organization paragraph is as follows: the materials and methods are presented in Section 2. Section 3 discusses the experiments and results. Section 4 analyzes the discussion of the proposed work. Finally, in Section 5, the research work is concluded.

## 2. Materials and Methods

**2.1. Research Objects.** A total of 80 patients with acute cerebral infarction admitted to Nanping First Hospital from January 2016 to December 2020 were selected and divided into a control group (intravenous thrombolysis) and an experimental group (NIT) according to different treatment methods. In the control group ( $n = 40$ ), there were 22 males and 18 females, they aged 41~70 years old (with an average of  $60.35 \pm 1.78$  years old), the time from onset to admission was 3~5 hours (with an average of  $2.03 \pm 1.02$  hours). There were 23 males and 17 females in the experimental group ( $n = 40$ ), with ages ranging from 40 to 72 (with an average of  $61.24 \pm 1.42$  years old), and the time from onset to admission was 2 to 5 hours (with an average of  $2.31 \pm 1.05$  hours). The basic clinical data of patients were collected. The Medical Ethics Committee of Nanping First Hospital approved and supported this experimental study. All of the subjects gave written informed consents and chose to take part in the study.

Inclusion criteria were given as follows: patients who met the diagnostic criteria for cerebral infarction in the *Chinese Guidelines for the Diagnosis and Treatment of Acute Ischemic Stroke 2018* [18], patients with occlusion of the M1 and M2 segments of the MCA for the first time, and patients with MCA in occlusion of M1 and M2 segments diagnosed by computed tomographic angiography (CTA) and (or) magnetic resonance angiography (MRA). The exclusion criteria were given as follows: patients combined with liver and kidney failure and coagulation dysfunction, patients with history of medication such as aspirin or heparin, patients combined with bleeding diseases such as intracranial hemorrhage and peptic ulcer bleeding, and patients with mental illness.

**2.2. Thrombolytic Therapy.** The alteplase (rt-PA) was applied for intravenous thrombolysis, the dosage should be calculated according to the weight of the patient, and the maximum dosage was  $\leq 90$  mg. 0.9 mg per kilogram was mixed into 100 mL of 0.9 sodium chloride solution, 10% was injected by intravenous bolus within 1 minute, and the

remaining drug would be administered by intravenous drip for 1 hour.

The cranial CT, MRI, and other examinations were performed on the patient before treatment to clarify the internal conditions of the cerebral infarction. After entering the operating room, the patient underwent local anesthesia, and a whole brain digital subtraction angiography (DSA) examination with Seldinger femoral artery puncture was performed to understand the blood circulation status of the patient's brain. If the blood vessel was still occluded or there was vascular stenosis after dredging, 6F guiding could be inserted under the guidance of the guide wire. The angiography showed the diseased blood vessel site, and then, the micro-guide wire was placed. The microcatheter was placed at the embolization position, and its tip reached the distal end of the embolized blood vessel. After the positioning was accurate, Solitaire AB (4 or 6 mm  $\times$  20 mm) should be sent to the diseased blood vessel and the stent should be released until the angiography was performed again to observe the occlusion of the blood vessel and the blood flow was in good condition. After the catheter sheath was retained for 6 hours and then removed, the local routine compression hemostasis treatment was performed, and a bandage was used to compress the patient's myocardial infarction thrombolytic therapy (TIMI) blood flow classification.

**2.3. Evaluation Standard.** The postoperative vascular recanalization rate of patients in the control group and the experimental group was compared. It could be divided into three levels according to the degree of patency: complete recanalization, partial recanalization, and nonvascular recanalization (as shown in Figure 1). The vascular recanalization rate calculation equation was as follows:

$$\text{Vascular recanalization rate (\%)} = \frac{\text{CRC} + \text{PRC}}{\text{total number of cases}} \times 100\%. \quad (1)$$

In the above equation, CRC represented the number of complete recirculation cases, and PRC represented the number of partial recirculation cases.

Before treatment and 1 week after treatment, the neurological function of patients was scored using the National Institutes of Health Stroke Scale (NIHSS) [19]. According to the percentage decrease of NIHSS score before and after treatment, it can be divided into 4 situations: cured, markedly effective, effective, and ineffective, as shown in Figure 2. The equation for calculating TRT was as follows:

$$\text{TRT} = \text{recovery rate} + \text{apparent efficiency} + \text{efficient}. \quad (2)$$

The hemodynamic improvement of the two groups of patients before and 6 months after the surgery was compared, and the transcranial Doppler blood analysis instrument (Doppler XTCD detector from DWL, Germany) was used for examination, including basilar artery peak systolic flow rate, internal carotid artery peak systolic flow rate, and common carotid artery peak systolic flow rate.

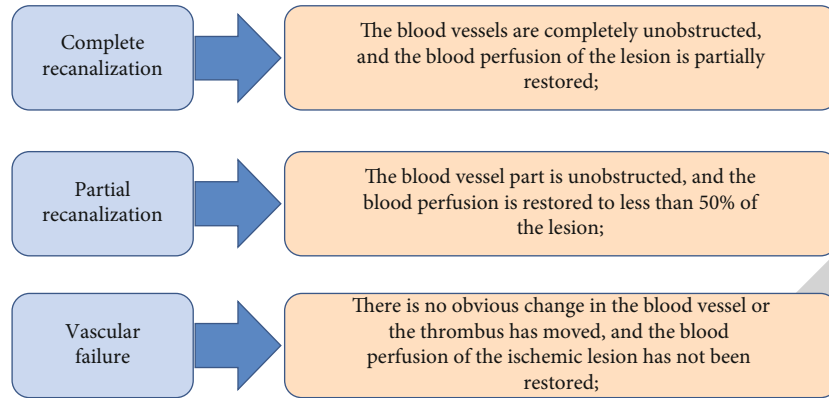


FIGURE 1: Postoperative vascular recanalization rate.

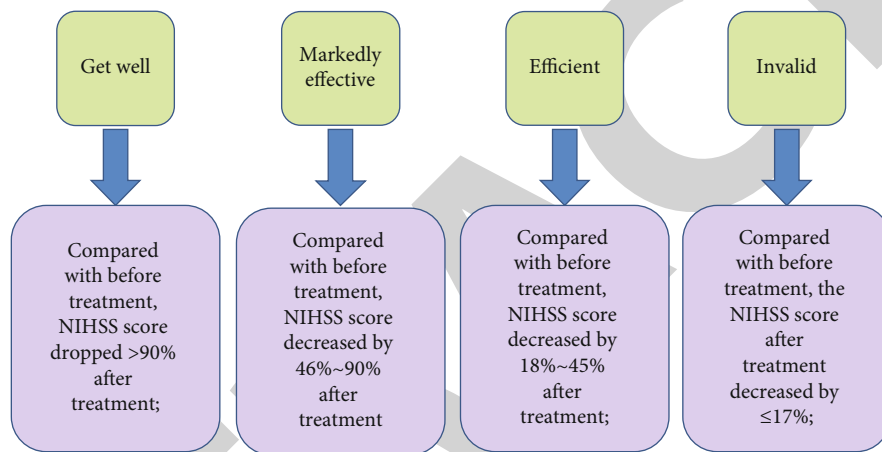


FIGURE 2: Percentage reduction of NIHSS score before and after treatment.

The patients were followed up for half a year, and the occurrence of adverse reactions (lowering blood pressure, headache, arrhythmia, etc.) of patients was compared in the control group and the experimental group.

2.4. *Statistical Analysis.* In this study, the SPSS 13.0 software was adopted to process the data. Measurement data conforming to normal distribution and homogeneity of variance were represented by  $(\bar{x} \pm s)$ , and the independent sample mean *t* test was used for comparison between groups. The count data was represented by rate, and the  $\chi^2$  test was used for comparison between groups.  $P < 0.05$  meant the difference was statistically significant.

### 3. Results

3.1. *General Data of Patients.* A total of 80 patients were chosen for the study, and they were divided into two groups based on the treatment methods used: a control group and an experimental group. The following statistics were used to compare the two groups of patients (gender, average age, and average time from onset to hospital admission) (as shown in Figure 3 below), and there was no statistical difference between the two ( $P > 0.05$ ).

Case 1 was a 51-year-old female patient who was admitted to the hospital due to fainting once, headache, and dizziness for several months. Recently, her symptoms worsened and she could not stand. After standing, she developed dizziness and severe vomiting. The symptoms of antiplatelet and lipid-lowering treatments did not improve. In addition, she had a history of hypertension for many years. The physical examination showed a blood pressure of 140/80 mmHg, clear mind, clear speech, no abnormalities in cranial nerves, muscle strength of limbs 5, normal feeling, and bilateral pathological signs. Figure 4 was an image of the patient. The magnetic resonance angiography (MRA) showed that the left MCA was blocked, digital subtraction angiography (DSA) showed the occlusion of the M1 segment of the left MCA, the anterior cerebral artery was compensated by the pial branch, and the posterior circulation was uncompensated.

Case 2 was a 68-year-old female patient who was admitted to the hospital due to unconsciousness, aphasia, and right hemiplegia for 4 hours and 30 minutes. The patient suffered from the history of diabetes. The patient was admitted to the hospital with impaired consciousness, complete aphasia, and level 0 muscle strength of the right limb. Head CT showed no infarct lesions. Figure 5 was the imaging of patient. MRA showed that the M2 segment of the left

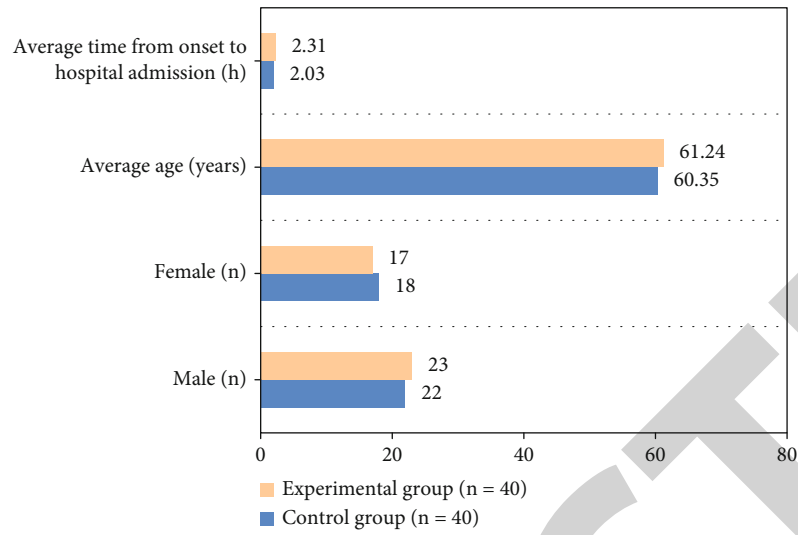


FIGURE 3: General statistics of patients.

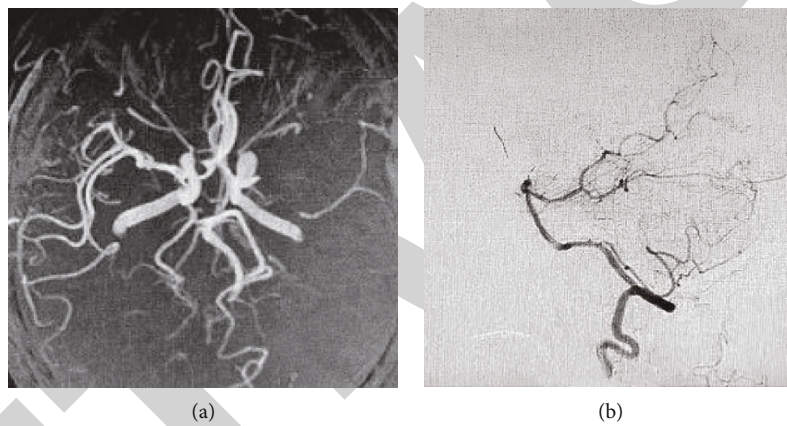


FIGURE 4: An image for occlusion of the M1 segment of the MCA in a 51-year-old female patient. (a) Show an MRA image. (b) Shows a DSA image.

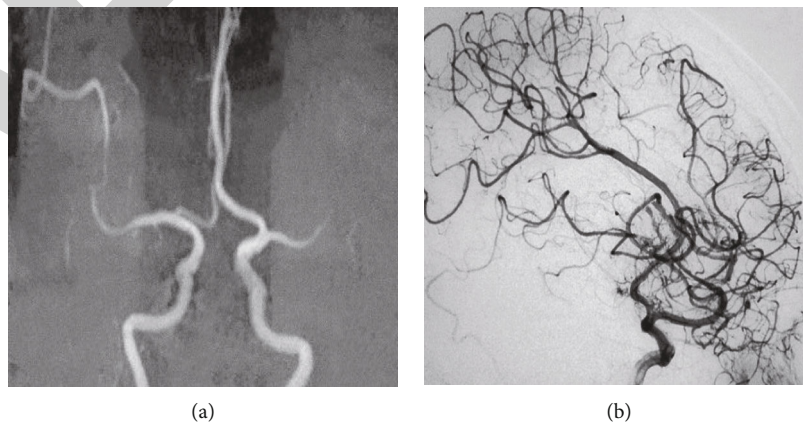
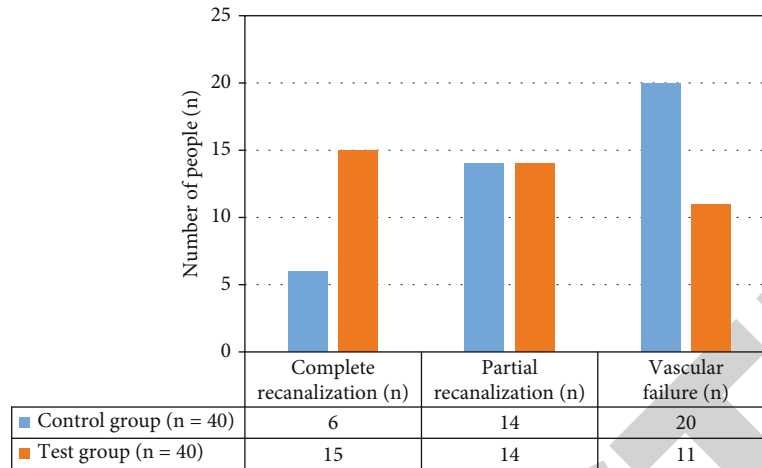
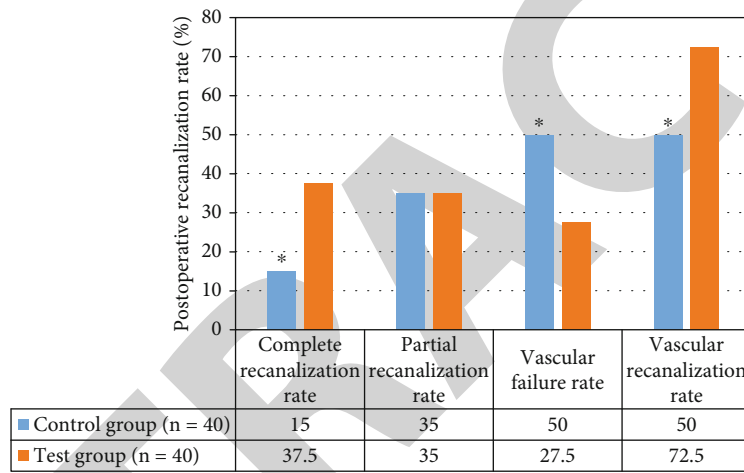


FIGURE 5: The occlusion image of the M2 segment of the MCA in a 63-year-old female patient. (a) Shows the MRA image, and (b) shows the DSA image.



(a)



(b)

FIGURE 6: Comparison on postoperative vascular recanalization rate between the two groups. (a) Shows the statistics of the number of vascular recanalization. (b) Shows the comparison of vascular recanalization rate. Note: \* indicated that the difference was statistically significant compared to the experimental group ( $P < 0.05$ ).

MCA was not developed, and DSA showed that the M2 segment of the left MCA was not developed.

**3.2. Comparison of Postoperative Vascular Recanalization Rate between the Two Groups.** Figure 6(a) shows the findings of the study, which calculated the number of postoperative recanalization in the two groups of patients. Total recanalization, partial recanalization, and nonvascular recanalization were 6, 14, and 20 in the control group, respectively; and those in the experimental group were 15 people, 14 people, and 11 people, respectively. Based on the number of postoperative vascular recanalization, the postoperative vascular recanalization rate of the two groups of patients was calculated (as shown in Figure 6(b)), which was 72.5% in the experimental group and 50% in the control group. It suggested that the therapeutic effect of NIT was significantly higher than that of intravenous thrombolysis, and the difference was statistically significant ( $P < 0.05$ ).

Figure 7 depicts the NIT treatment and postoperative vascular patency of patients in Cases 1 and 2, with Figures 7(a) and 7(c) depicting intraoperative angiography and Figures 7(b) and 7(d) depicting postoperative angiograms. The blood vessels at the occlusion were well recanalized, and the cortex was compensated for blood supply via the anterior cerebral artery.

**3.3. Comparison of Therapeutic Effect between Two Groups of Patients.** To study the therapeutic effect of the two groups of patients, the number of cured, markedly effective, effective, and ineffective patients was counted. The numbers of patients with cured, markedly effective, effective, and ineffective effect were 5, 10, 16, and 9, respectively, in the control group, and 9, 15, 10, and 6, respectively, in the experimental group. Based on the statistical results, the total effective rate of the two groups of patients was calculated. The total effective rate in the control group was 77.5 percent, while it was 85 percent in the experimental group, so the difference was

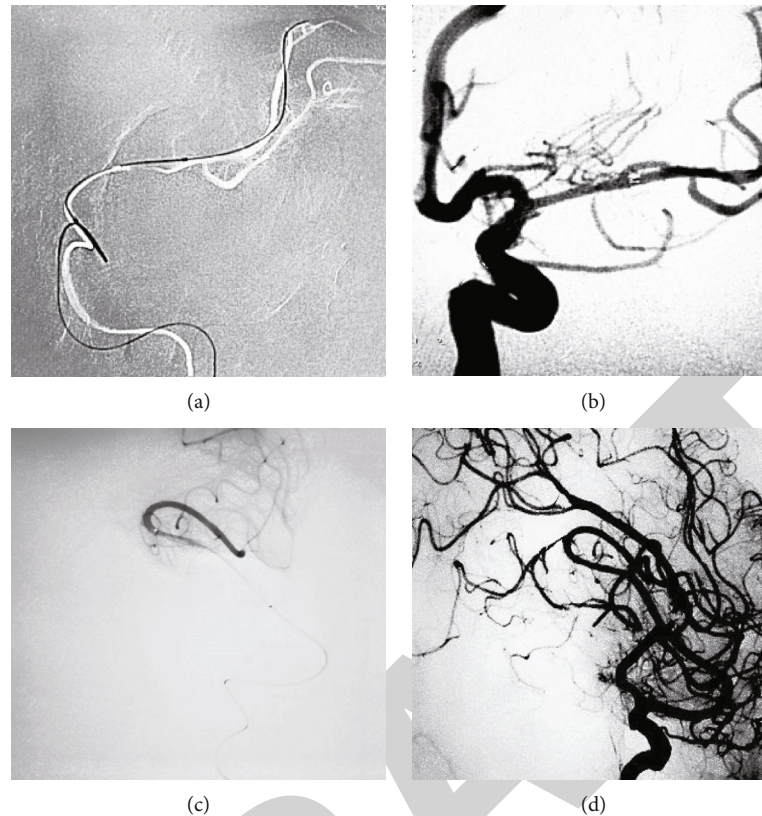


FIGURE 7: NIT treatment and postoperative vascular patency of Case 1 and Case 2. (a, c) Show the intraoperative angiography of NIT treatment. (b, d) Show the postoperative angiography.

not significant and statistically insignificant ( $P > 0.05$ ). The specific details are shown in Figure 8.

**3.4. Comparison of NIHSS Scores between the Two Groups before and after Surgery.** Figure 9 illustrated the comparison on NIHSS scores between two groups of patients before and after surgery. The average preoperative NIHSS scores of the experimental group and the control group were 22.89 points and 23.16 points, respectively, and the difference between the two was not statistically significant ( $P > 0.05$ ). One week after the surgery, the average NIHSS scores of the control group and the experimental group were 18.74 points and 15.36 points, which were significantly lower than those before the surgery; and the average NIHSS scores of the experimental group after the surgery were significantly lower than those of the control group, showing statistically obvious difference ( $P < 0.05$ ).

**3.5. Comparison of Hemodynamic Improvement between the Two Groups of Patients.** Figure 10 shows the difference in hemodynamic improvement between the two patient groups. There was no significant difference in hemodynamic indicators between the two groups of patients before therapy (basilar artery peak systolic flow rate, internal carotid artery peak systolic flow rate, and common carotid artery peak systolic flow rate) ( $P > 0.05$ ). After treatment, the relevant indicators of the two groups of patients were greatly reduced, and the difference before and after treatment was statistically

obvious ( $P < 0.05$ ). Among them, the basilar artery peak systolic flow rate, internal carotid artery peak systolic flow rate, and common carotid artery peak systolic flow rate after treatment in the experimental group were 132 cm/s, 147 cm/s, and 114 cm/s, respectively; all were lower than those in the control group, and the differences were statistically observable ( $P < 0.05$ ).

**3.6. Comparison of Adverse Reactions between the Two Groups of Patients.** The incidence of adverse reactions following surgery in the two groups of patients was counted in this study, and the results are presented in Figure 11. In the control group, 4 patients had adverse reactions, and the incidence of adverse reactions was 10%. In the experimental group, 3 patients had postoperative adverse reactions, and the incidence of adverse reactions was 7.5%, which was significantly lower than that of the control group, and there were statistically significant differences ( $P < 0.05$ ).

## 4. Discussion

At present, conventional thrombolytic drugs combined with intravenous thrombolysis is a common treatment method for the treatment of ischemic cerebrovascular diseases in China. The method is relatively mature, and there are a large number of clinical trials to prove its safety and effectiveness, and the operation is simple. However, the rate of vascular recanalization after treatment is low, and there is a risk of

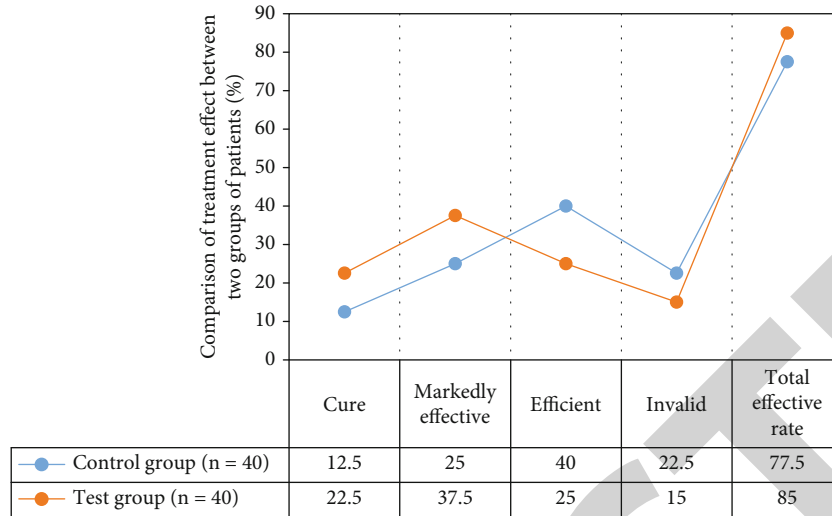


FIGURE 8: Comparison of therapeutic effect between two groups of patients.

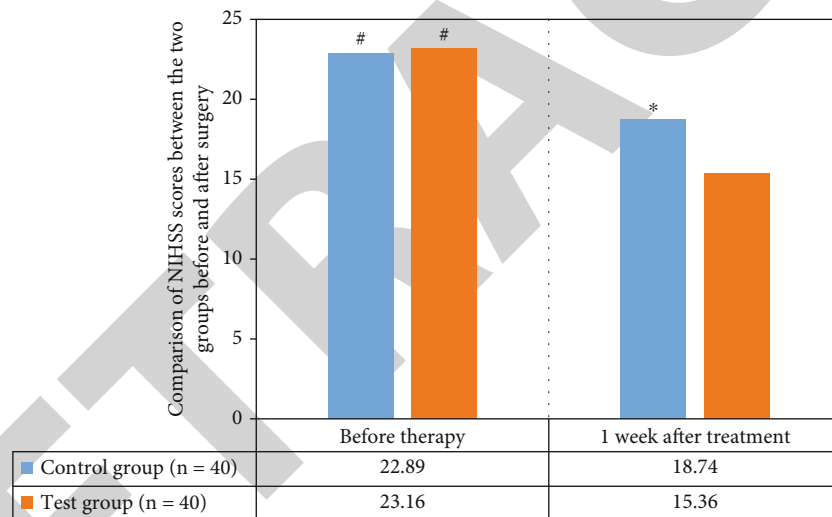


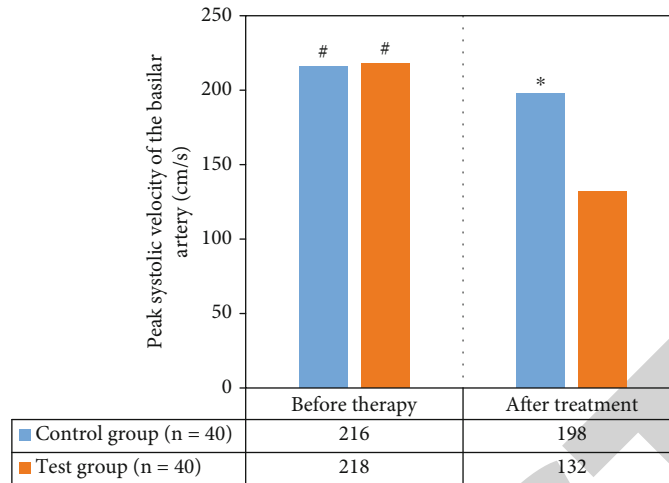
FIGURE 9: Comparison of NIHSS scores between the two groups of patients before and after surgery. Note: # indicated that the difference was statistically significant compared with the postoperative; \* indicated that the difference was statistically significant compared to the experimental group ( $P < 0.05$ ).

bleeding, which can fulfil the clinical treatment demands of patients [20–22]. With the advancement of medical imaging technology in recent years, NIT technology has become increasingly popular in clinical settings. Chen et al. [23] pointed out that NIT treatment can effectively reduce the secondary damage of neurons, thereby promoting the recovery of nerve function. The results of this study showed that the experimental group of patients treated with NIT had a 22.5% higher vascular recanalization rate than the control group of patients treated with intravenous thrombolysis, and the difference was statistically significant ( $P < 0.05$ ). This progress verifies the feasibility of NIT in the treatment of cranial artery M1 and M2 occlusion. Based on the results of NIHSS score statistics before and after the operation, the study calculated the total effective rate of the two groups of

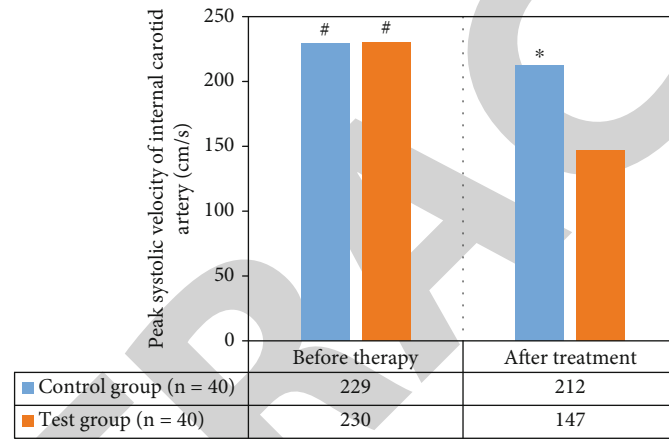
patients, which was 77.5% and 85% in the control group and experimental group, respectively, so there was little difference between the two and no statistical significance ( $P > 0.05$ ). But one week after the surgery, the average scores of NIHSS of the control group and the experimental group were 18.74 points and 15.36 points, respectively, which were significantly lower than those before the surgery. The average score of NIHSS after operation in the experimental group was significantly lower than that in the control group, and the difference was statistically significant ( $P < 0.05$ ). In addition, NIT can effectively improve the neurocognitive function of patients with cranial artery M1 and M2 occlusion, which is similar to the results of Zhao et al. [24].

According to Huang et al. [25], neurointerventional therapy uses the flexibility of blood vessels to raise the inner

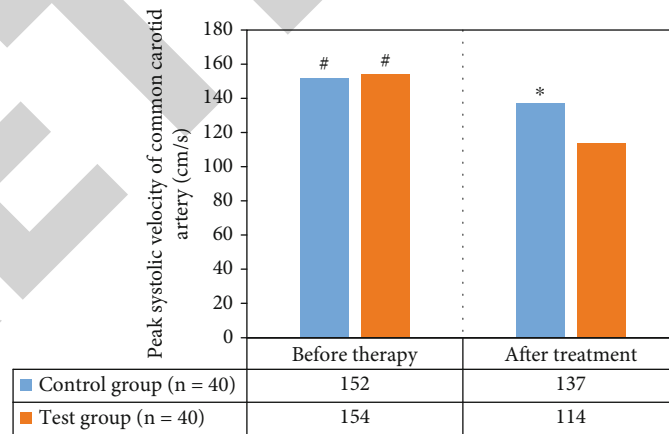




(a)



(b)



(c)

FIGURE 10: Comparison of hemodynamic improvement between the two groups of patients. (a) Shows the basilar artery peak systolic flow rate; (b) shows the internal carotid artery peak systolic flow rate; (c) shows the common carotid artery peak systolic flow rate. Note: # indicated that the difference was statistically significant compared with the postoperative; \* indicated that the difference was statistically significant compared to the experimental group ( $P < 0.05$ ).

diameter of blood vessels, and it can fundamentally solve the problem of patients with vascular stenosis when compared to pure medication thrombolytic therapy. Hemodynamic-related indicators (basilar artery, internal carotid artery,

and common carotid artery peak systolic flow rate) can effectively evaluate the problem of vascular stenosis; and the narrower the diameter of the blood vessel, the faster the blood flow rate [26, 27]. Therefore, the hemodynamic

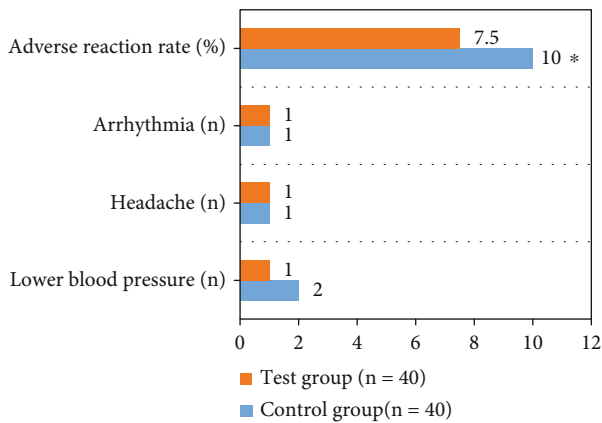


FIGURE 11: Comparison of adverse reactions between the two groups of patients. Note: \* indicated that the difference was statistically significant compared to the experimental group ( $P < 0.05$ ).

indicators of the two groups of patients were compared before and after treatment. The results showed that the difference between the two groups before treatment was not statistically significant ( $P > 0.05$ ). After treatment, the relevant indicators of the two groups of patients were significantly reduced, which was statistically significant compared with the difference before treatment ( $P < 0.05$ ). After treatment, the basic artery peak systolic flow rate, internal carotid artery peak systolic flow rate, and common carotid artery peak systolic flow rate of the experimental group were 132 cm/s, 147 cm/s, and 114 cm/s, respectively, which were significantly lower than those of the control group, showing statistically great differences ( $P < 0.05$ ). It shows that NIT treatment can effectively improve the vascular stenosis in patients. Finally, the research studies the occurrence of adverse reactions (lowering blood pressure, headache, and arrhythmia) in the two groups of patients after surgery. Among them, 4 patients in the control group had adverse reactions, and the incidence of adverse reactions was 10%, while in the experimental group, 3 patients had adverse reactions after the operation, and the incidence of adverse reactions was 7.5%, which was significantly lower than that of the control group ( $P < 0.05$ ). It shows that NIT treatment is not only effective but also safe and can effectively improve the prognosis of patients with cranial artery caused by M1 and M2 occlusion.

## 5. Conclusion

The practicality and clinical efficacy of NIT in the treatment of cranial artery M1 and M2 segment occlusion were investigated in this study, and it was compared to intravenous thrombolysis. The results showed that NIT had a significant therapeutic effect on cranial artery M1 and M2 occlusion, can dredge the occlusion vessels, and effectively improve the neurological deficits and prognosis of patients. The vascular recanalization rates of patients after treatment were compared, and the neurological function score was assessed by the National Institutes of Health Stroke Scale (NIHSS). It

had a high level of safety and effectiveness, as well as a high degree of feasibility. This study, on the other hand, had a limited sample size, a lack of overall representativeness, and a short follow-up period. In general, this study provided an effective reference for the clinical treatment of patients with cranial artery caused by M1 and M2 occlusion.

## Data Availability

All data, models, and code generated or used during the study appear in the submitted article.

## Additional Points

*Industry Contributions.* (1) In this work, it was proved by experiments that the therapeutic efficiency of nerve interventional thrombectomy was comparable to that of intravenous thrombolysis. For patients with late admission and severe symptoms, intravenous thrombolysis was more risky, and nerve interventional thrombectomy was a safer and more suitable option. (2) The vascular recanalization rate of intravenous thrombolysis was higher than that of intravenous thrombolysis, which could effectively improve the neurocognitive function of patients with cranial artery M1 and M2 occlusion and could fundamentally solve the vascular stenosis in patients. (3) Nerve interventional thrombectomy was effective and safe, with low incidence of postoperative complications and can effectively improve the prognosis of patients with cranial arteries caused by M1 and M2 occlusion. (4) This work explored the important value of intravenous thrombolysis in the treatment of cerebral artery occlusion. Intravenous thrombolysis was not only one of the alternative treatment options for intravenous thrombolysis but also a rescue option for patients with contraindications to intravenous thrombolysis. (5) This work provided a sustainable reference for the clinical treatment of cerebral artery occlusion caused by acute cerebral infarction and other cerebrovascular diseases.

## Ethical Approval

This experimental study was approved by the Medical Ethics Committee of Nanping First Hospital (authorization number: 2015845).

## Consent

Written informed consent was obtained from the individual for the publication of any potentially identifiable images or data included in this article with trial registration number 2020121401. All participants signed the written informed consents and voluntarily participated in this experimental study.

## Conflicts of Interest

The authors declare that they have no conflicts of interest.

## Research Article

# Observation on the Nursing Effect of the Whole Process in Patients with Severe Intracranial Hemorrhage

Zhongwei Su, Wei Guo, Yun Luo, Yao Wang, and Yue Du 

Emergency Department, Beijing Tiantan Hospital, Capital Medical University, Beijing, China

Correspondence should be addressed to Yue Du; [suzw111@163.com](mailto:suzw111@163.com)

Received 14 April 2022; Revised 17 June 2022; Accepted 20 June 2022; Published 4 July 2022

Academic Editor: Naeem Jan

Copyright © 2022 Zhongwei Su et al. This is an open access article distributed under the Creative Commons Attribution License, which permits unrestricted use, distribution, and reproduction in any medium, provided the original work is properly cited.

**Objective.** The goal of this study was to look at the clinical impact of the entire process of nursing care for patients with severe cerebral hemorrhage. **Method.** From January 2018 to December 2019, the clinical data of 160 patients with severe cerebral hemorrhage who were hospitalized to our hospital were reviewed retrospectively. They were separated into two groups based on their admission: routine and complete procedure. The routine group used routine emergency care, the whole process group was provided first aid care with whole process nursing. The diagnosis and treatment time, the success rate of emergency care, the incidence of adverse events, and the complaint rate were compared between the two groups. **Results.** The treatment time, emergency examination time, and preoperative rescue time of emergency patients in the whole process group were significantly shorter than those in the conventional group, with statistically significant differences (all  $P < 0.05$ ). The rescue success rate of emergency patients in the whole process group was 95.00% (76/80), and the rescue success rate of emergency patients in the routine group was 83.75% (67/80); the difference was statistically significant ( $\chi^2 = 4.378$ ,  $P = 0.034$ ). The complaint rate of emergency patients in the whole process group was 2.50% (2/80), while that in the routine group was 8.75% (7/80), with statistically significant difference ( $\chi^2 = 4.732$ ,  $P = 0.024$ ). The incidence of total nursing adverse events was 6.25% (5/80) in the whole process group and 17.50% (14/80) in the routine group; the difference was statistically significant ( $\chi^2 = 5.011$ ,  $P = 0.027$ ). **Conclusion.** The implementation of whole process nursing care for patients with severe intracranial hemorrhage can shorten the time-consuming first aid for patients with intracranial hemorrhage. And it also can improve the rescue success rate of patients and reduce the incidence of adverse events and complaints, which represents a significant clinical application effect.

## 1. Introduction

Intracranial hemorrhage is a very common disease in clinical neurosurgery. Intracranial hemorrhage is one of the symptoms of “stroke” in traditional Chinese medicine, and most patients had hypertension or cerebrovascular malformation [1–3]. Intracranial hemorrhage is a hemorrhage caused by nontraumatic rupture of blood vessels in the brain parenchyma. The blood clot caused by hemorrhage leads to edema at the bleeding site and compression of cerebral nerves, and the gradual increase in cranial pressure leads to a series of clinical symptoms [4, 5]. Among them, intracranial hemorrhage caused by hypertension is very common. Its early manifestations are vomiting, impaired movement, and difficult walking. The main clinical manifestations are headache, nausea, drowsiness, and so on, and severe diseases such as

hemiplegia and speech disorder may occur, even endangering the life of the patients, which has a certain impact on the prognosis of the patients’ quality of life [6, 7]. The therapeutic effect of patients with intracranial hemorrhage is closely related to the timeliness of treatment. Due to the lack of early warning of intracranial hemorrhage, people often ignore the importance of the harm of intracranial hemorrhage. In addition, the rapid onset, deterioration, and impact on the body of intracranial hemorrhage are closely related to the time when patients are treated [8, 9]. The recognition of the status of rehabilitation nursing for patients with intracranial hemorrhage is considered “three points of treatment and seven points of nursing” in the medical industry, which shows the importance of efficient nursing for the rehabilitation of patients with intracranial hemorrhage. For patients with severe intracranial hemorrhage, a set of reasonable care

TABLE 1: Comparative results of clinical data.

Groups	Cases	Age	GLS	Intracranial hemorrhage (ml)	Time in ICU (h)	Chronic lung disease (cases)	Operation (cases)
Routine group	80	40.15 ± 5.26	7.15 ± 1.03	32.88 ± 5.03	9.15 ± 2.05	58	67
Whole process group	80	40.23 ± 5.47	7.05 ± 1.21	33.51 ± 3.82	9.39 ± 1.92	60	70
$t$		0.32	0.23	-0.091	-0.35	0.0091	0.093
$P$		0.7446	0.852	0.7105	0.7216	0.9204	0.7582

should be given early. Intervention measures are urgent. Patients with intracranial hemorrhage have brought great difficulties and challenges to medical staff in the process of treatment and nursing due to their difficult actions, vague speech, and ambiguous language [10]. Whole process nursing is a continuous, full-process, efficient, and zero-distance nursing care method implemented by medical staff to patients. In order to improve the rescue level of critical patients, the whole process nursing was applied in the treatment of patients with severe intracranial hemorrhage in this study, and the effect was good. It is reported as follows.

The paper is organized as follows: the materials and methods are presented in Section 2. Section 3 discusses the experiments and results. Section 4 is discussed in combination with the relevant data analysis of this study. Finally, the research work is concluded; it points out the specific sharing made by this research and the future development direction of this field.

## 2. Materials and Methods

**2.1. Normal Information.** The clinical data of 160 patients with severe intracranial hemorrhage admitted to our hospital from January 2018 to December 2019 were retrospectively analyzed. They were divided into the routine group (January-December 2018) and the whole process group (January-December 2019) according to their admission sequence, with 80 patients in each group. There were 56 males and 24 females in the whole process group. The average age was  $40.23 \pm 5.47$  years old; the AIS-ISS injury score ranged from 16 to 50 points, with an average score of  $30.52 \pm 3.63$ . There were 58 males and 22 females in the routine group. The average age was  $40.15 \pm 5.26$  years old; the AIS-ISS injury score ranged from 16 to 50 points, with an average score of  $31.24 \pm 3.81$ . There was no statistically significant difference in general data between the two groups ( $P > 0.05$ ), which was comparable. Comparative results of clinical data are shown in Table 1.

According to the purpose of the study and the relevant research results of previous scholars, the enrollment criteria and exclusion criteria formulated in this study are as follows:

Enrollment criteria were as follows:

- (1) Hypertension led to severe intracranial hemorrhage
- (2) Intracranial hemorrhage was confirmed by imaging examination

- (3) The patients and their families knew and agreed to participate in this study voluntarily

Exclusion criteria were as follows:

- (1) Severe intracranial hemorrhage caused by other reasons (including congenital cerebral vascular malformation and severe intracranial hemorrhage caused by trauma)
- (2) Severe functional insufficiency of other organs
- (3) Patients who had died prior to medical consultation
- (4) A history of severe cardiopulmonary dysfunction
- (5) Cognitive, intellectual, and mental disorders
- (6) A history of physical disability or dysfunction
- (7) Patients who gave up treatment on their own during rescue
- (8) Incomplete data

### 2.2. Methods

**2.2.1. Routine Group.** Conventional emergency care was adopted, and emergency rescue was carried out according to the rescue procedures of ventilation → dilatation → cardiac pump → control of bleeding → operation [11]. Specifically, it was to keep the airway unobstructed and fully inhale oxygen, establish a venous channel for blood transfusion or infusion as soon as possible, test the heart function to restore the cardiac blood function, and control the bleeding and operate as soon as possible. The nursing staff should perform routine examinations and rescues of patients as directed by the doctor, improve preoperative preparation, monitor the physical symptoms of patients with severe cerebral bleeding, and establish venous access as quickly as feasible during the implementation of rescue. And they cooperated with doctors to carry out targeted multiple examinations (such as chest puncture and abdominal puncture) to prevent traumatic shock. After admission, paramedics assisted necessary examination and followed up routine nursing staff after emergency surgery evaluated the injury.

**2.2.2. Whole Process Group.** Carry out emergency care with whole process care.

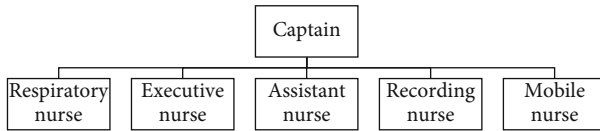


FIGURE 1: The staffing of the whole process nursing team.

(1) *Setting up a Whole Process Nursing Team.* The whole process nursing team first set up a captain, who was the chief commander in the entire emergency care nursing process; one respiratory nurse was on hand to help respiratory doctors in carrying out medical orders; an executive/circulatory nurse assisted the doctor in managing the patient’s respiratory and circulatory system. There was one assistant nurse, who cooperated with the doctor to operate instruments and equipment and was responsible for drug delivery, blood sample collection, and other auxiliary examinations. There was one recording nurse, who was responsible for recording basic patient information, rescue records, doctor’s orders, and changes in the patient’s condition and responsible for outreach work, timely communication with the laboratory, imaging department, and so on, to ensure full cooperation in emergency care. At the same time, prepare a mobile nurse to cooperate with other posts at any time. The management team provided whole process care throughout the first aid care process. The staffing of the whole process nursing team is shown in Figure 1.

(2) *The Whole Process Nursing Service System.* The whole process nursing service system includes the whole process of service consciousness, the whole process of management, the whole process of professional technology, the whole process of first aid, and the whole process of medical cooperation (Figure 2).

(1) The whole process of service consciousness

Organize the study of humanized nursing service concept regularly, change the passive service into active service, and emphasize the importance of active service in the rescue of severe intracranial hemorrhage.

(2) The whole process of management

The management team shall refine the routine rescue procedures and formulate the emergency plan for severe intracranial hemorrhage, and the team leader shall evaluate the implementation rules of detection to ensure the implementation of the rescue procedures.

(3) The whole process of professional technology

Hire nursing staff with rich rescue experience to give regular special lectures to strengthen the professional ability of the nursing team.

(4) The whole process of first aid

Select nurses with strong professional competence for consultation, and the attending nurses assist in the judgment

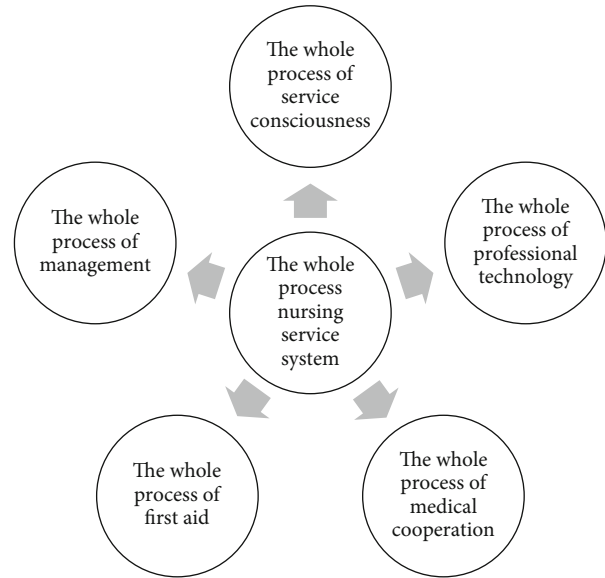


FIGURE 2: The whole process nursing service system.

of illness. Once confirmed as severe intracranial hemorrhage, immediately start the whole process of nursing and the completion of emergency care nursing task.

(5) The whole process of medical cooperation

The comprehensive treatment mode was adopted for rescue nursing.

The principle of rescue first and payment later was to assist them to go through the admission procedures, and at the same time, nurses cooperated with the doctors to give first aid. This principle not only saves valuable rescue time, improves the treatment effect, and simplifies the process of patients before admission but also improves the satisfaction of patients’ family members.

(1) Respiratory care [12]

The suction nurse assisted in cleaning up foreign bodies in the patient’s mouth, who was ready to attract and suck sputum at any time, keep the airway open, and closely monitor the patient’s breathing state to ensure that the airway was open.

(2) Circular care [13]

Circulation nurses assisted in establishing venous access, correcting electrolyte acid-base balance disorder, maintaining circulating blood volume in the trauma area, and preventing cardiac arrest, hemorrhagic shock, and so on.

(3) Condition observation [14, 15]

The team leader closely monitored the patient’s condition while managing the rescue scene, focusing on the patient’s state of consciousness. In addition, the implementation of the doctor’s advice should be checked in a timely manner to prevent errors made by the nursing staff due to

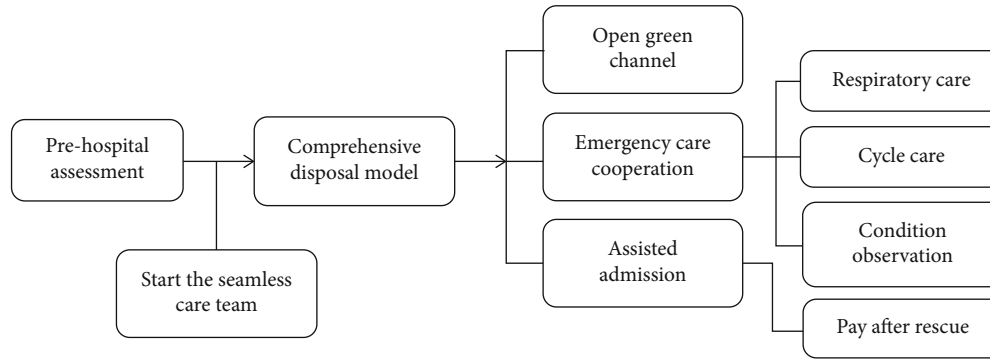


FIGURE 3: Flowchart of the whole process nursing.

TABLE 2: Comparison of diagnosis and treatment time.

Groups	Cases	Treatment time	Emergency examination time	Preoperative rescue time
Routine group	80	41.34 ± 4.35	32.09 ± 4.52	71.25 ± 8.13
Whole process group	80	35.75 ± 3.30	21.30 ± 3.05	53.24 ± 5.66
<i>t</i>		8.956	18.525	15.912
<i>P</i>		<0.001	<0.001	<0.001

stress. At the same time, mobile nurses are on standby to increase the links or posts in need of help, so as to improve the timeliness of work. The flowchart of the whole process nursing is shown in Figure 3.

### 2.3. Observation Target

#### (1) Time indicators for diagnosis and treatment

This includes patient reception time, emergency examination time, and preoperative rescue time. Attendance time referred to the time from the time the medical staff receives the distress call to the time they arrive at the rescue scene. The time of emergency assessment was defined as the sum of the time spent on routine blood tests, coagulation function, blood matching, virus antibody testing, and imaging testing, among other things. Preoperative rescue time referred to the time from the patient's admission to the emergency operating room.

#### (2) Success rate of emergency care

If the patient's vital signs remained stable and the patient was safely transferred to the relevant department, the rescue was a success. Rescue success rate (%) = number of successful rescue/total number of people × 100%.

#### (3) Adverse event incidence and complaint rate

Adverse events mainly included pipe shedding, incorrect execution of medical advice, incomplete drug preparation, accidental injury, and so on.

**2.4. Statistical Analysis.** Using SPSS 21.0 statistical software, measurement data was expressed as  $x \pm s$ , and the *t*-test was used; the count data was expressed as a percentage and as a

TABLE 3: Comparison of the rescue success rate.

Groups	Cases	Rescue success	Rate
Routine group	80	67	83.75%
Whole process group	80	76	95.00%
$\chi^2$			4.378
<i>P</i>			0.034

TABLE 4: Comparison of the incidence of nursing adverse events and complaint rate.

Groups	Cases	Complaint rate	Incidence of nursing adverse events
Routine group	80	8.75%	17.50%
Whole process group	80	2.50%	6.25%
$\chi^2$		4.732	5.011
<i>P</i>		0.024	0.027

frequency. The theoretical frequency  $\geq 0$  and  $\leq 5$  count data between groups were corrected and tested. If the theoretical frequency was greater than 5, the count data between groups would be tested by  $\chi^2$ .  $P < 0.05$  or  $P < 0.01$  indicated that the difference was statistically significant.

## 3. Results

In this section, comparison of diagnosis and treatment time between the two groups, comparison of the rescue success rate between the two groups, and comparison of the incidence of nursing adverse events and complaint rate between the two groups were discussed in detail.

**3.1. Comparison of Diagnosis and Treatment Time between the Two Groups.** The treatment time, emergency examination time, and preoperative rescue time of emergency patients in the whole process group were significantly shorter than those in the conventional group, with statistically significant differences (all  $P < 0.05$ ). Comparison of diagnosis and treatment time is shown in Table 2.

**3.2. Comparison of the Rescue Success Rate between the Two Groups.** The rescue success rate of emergency patients in the whole process group was 95.00% (76/80), and the rescue success rate of emergency patients in the routine group was 83.75% (67/80); the difference was statistically significant ( $\chi^2 = 4.378$ ,  $P = 0.034$ ). Comparison of the rescue success rate is shown in Table 3.

**3.3. Comparison of the Incidence of Nursing Adverse Events and Complaint Rate between the Two Groups.** The complaint rate of emergency patients in the whole process group was 2.50% (2/80), while that in the routine group was 8.75% (7/80), with statistically significant difference ( $\chi^2 = 4.732$ ,  $P = 0.024$ ). The incidence of total nursing adverse events was 6.25% (5/80) in the whole process group and 17.50% (14/80) in the routine group; the difference was statistically significant ( $\chi^2 = 5.011$ ,  $P = 0.027$ ). Comparison of the incidence of nursing adverse events and complaint rate is shown in Table 4.

## 4. Discussion

Intracranial hemorrhage is a common neurological disease, characterized by acute onset, rapid progression, poor prognosis, and high mortality, which seriously threatens the health and life safety of patients. Craniotomy and targeted minimally invasive bloodletting to reduce intracranial pressure are widely used in patients with severe intracranial hemorrhage [16]. The success of brain resuscitation in patients with severe intracranial hemorrhage, whether there is rebleeding in the brain and whether there are nosocomial-acquired lower respiratory tract infections and other related serious complications, is the key to successful treatment, increased survival rate, and reduced mortality [17, 18]. It can be seen that patients with severe intracranial hemorrhage not only depend on the doctor's diagnosis and treatment strategy but also are closely related to the correct nursing intervention measures [19–21]. The whole process of nursing for patients with severe intracranial hemorrhage in the rescue of the clinical effect reduces complications, and the prevention of rebleeding has obvious effects [22–24].

The findings showed that the whole process group's treatment time, emergency examination time, and preoperative rescue time were much shorter than the traditional group's, with statistically significant differences (all  $P < 0.05$ ). The rescue success rate of emergency patients in the whole process group was 95.00% (76/80), and the rescue success rate of emergency patients in the routine group was 83.75% (67/80); the difference was statistically significant ( $\chi^2 = 4.378$ ,  $P = 0.034$ ). The complaint rate of emergency patients in the whole process group was 2.50% (2/80), while

that in the routine group was 8.75% (7/80), with statistically significant difference ( $\chi^2 = 4.732$ ,  $P = 0.024$ ). The incidence of total nursing adverse events was 6.25% (5/80) in the whole process group and 17.50% (14/80) in the routine group; the difference was statistically significant ( $\chi^2 = 5.011$ ,  $P = 0.027$ ).

## 5. Conclusion

To summarize, implementing whole process nursing for patients with severe intracranial hemorrhage can reduce the time it takes for patients to receive first aid, increase the success rate of rescue, decrease the incidence of adverse events and complaints, and have a significant clinical application effect. However, due to the rapid onset of severe intracranial hemorrhage and high degree of harm, how to appease the emotion of the patient's family members in the rescue process is also one of the contents of modern nursing. Patients need long-term continuous care and regular examination after discharge. How to prevent the recurrence of intracranial hemorrhage, slow down the complications and sequelae caused by intracranial hemorrhage, and speed up the rehabilitation process have provided new challenges for patients' families and medical staff.

## Data Availability

The datasets used during the present study are available from the corresponding author upon reasonable request.

## Conflicts of Interest

The authors declare that there are no conflicts of interest regarding the publication of this paper.

## References

- [1] X. Feng, T. Zhao, J. Liu, and C. Zhou, "Cerebral venous sinus thrombosis with cerebral hemorrhage presenting with status epilepticus in early pregnancy," *Clinical Laboratory*, vol. 64, pp. 611–614, 2018.
- [2] S. Kaya, L. D. Cingz, N. Uzunolu, C. Kizmazoğlu, H. Aydin, and N. Yüceer, "Predictors of mortality in patients with surgically treated spontaneous intracranial hemorrhage," *Turkish Journal of Neurology*, vol. 25, no. 4, pp. 214–217, 2019.
- [3] P. G. Kranz, M. D. Malinzak, and T. J. Amrhein, "Approach to imaging in patients with spontaneous intracranial hemorrhage," *Neuroimaging Clinics of North America*, vol. 28, no. 3, pp. 353–374, 2018.
- [4] W. Y. Huang, J. L. Saver, Y. L. Wu, C. J. Lin, M. Lee, and B. Ovbiagele, "Frequency of intracranial hemorrhage with low-dose aspirin in individuals without symptomatic cardiovascular disease: a systematic review and meta-analysis," *JAMA Neurology*, vol. 76, no. 8, pp. 906–914, 2019.
- [5] A. B. Wang and H. Zhang, "Efficacy of microsurgery for patients with cerebral hemorrhage secondary to gestational hypertension," *Medicine*, vol. 98, no. 42, p. e17558, 2019.
- [6] M. Shahreyar, T. Bob-Manuel, R. N. Khouzam et al., "Trends, predictors and outcomes of ischemic stroke and intracranial hemorrhage in patients with a left ventricular assist device," *Annals of Translational Medicine*, vol. 6, no. 1, pp. 5–5, 2018.

- [7] S. N. Yanishevsky, "Intracranial hemorrhage in patients taking oral anticoagulants. Current possibilities for therapy," *Psychosomatics*, vol. 11, no. 3S, pp. 82–88, 2019.
- [8] M. A. Nestor and B. Boling, "Reversing direct oral anticoagulants in acute intracranial hemorrhage," *Critical Care Nurse*, vol. 39, no. 3, pp. e1–e8, 2019.
- [9] D. L. Yuan, Y. H. Zhao, H. T. Deng, and L. L. Xu, "Application of self-made vacuum sealing drainage device in postoperative fixation and drainage of abdominal pedicled flaps in 8 patients with deep burns of upper limbs," *Chinese Journal of Burns*, vol. 35, no. 8, pp. 611–613, 2019.
- [10] H. C. Diener and G. J. Hankey, "Primary and secondary prevention of ischemic stroke and cerebral hemorrhage," *Journal of the American College of Cardiology*, vol. 75, no. 15, pp. 1804–1818, 2020.
- [11] A. V. Bocharov and D. V. Sidorov, "The bleeding safety of ticagrelor in patients with ST-elevation acute coronary syndrome treated with fibrinolytic therapy," *Kardiologiia*, vol. 60, no. 6, pp. 92–95, 2020.
- [12] L. Bjermer, Z. Diamant, and V. Backer, "Clinical and daily respiratory care and clinical trials within the COVID-19 era," *European Clinical Respiratory Journal*, vol. 7, no. 1, article 1766817, 2020.
- [13] Y. Han, "Observation on the clinical effect of cluster nursing on the incidence of lower extremity deep venous thrombosis in cerebral hemorrhage patients," *Journal of Hunan University of Chinese Medicine*, vol. A01, pp. 578–579, 2018.
- [14] X. Zhou, "Observation on the effect of clinical nursing pathway in nursing of patients with cervical hemorrhage," *Chinese Journal of Continuing Medical Education*, vol. 10, no. 26, pp. 192–194, 2018.
- [15] Y. M. Khorchid and M. Malkoff, "Intracranial hemorrhage focused on cancer and hemato-oncologic patients," in *Oncologic Critical Care*, pp. 381–394, Springer, Cham, 2020.
- [16] W. J. Lee, M. K. Kim, and Y. C. Lim, "Clinical analysis of young adult patients with ruptured intracranial aneurysms: a single-center study of 113 consecutive patients," *Journal of Cerebrovascular and Endovascular Neurosurgery*, vol. 22, no. 3, pp. 127–133, 2020.
- [17] F. Cao, "The effect analysis and nursing inquiry of conservative treatment of hypertensive cerebral hemorrhage," *Journal of Clinical Examination (Electronic Version)*, vol. 8, no. 3, pp. 122–123, 2019.
- [18] H. Bae, J. Y. Park, S. Kang, U. Yun, S. W. Ha, and S. M. Kim, "Simultaneous nonaneurysmal subarachnoid hemorrhage and acute cerebral infarction in a patient with intracranial atherosclerosis," *Journal of the Korean Neurological Association*, vol. 37, no. 4, pp. 429–431, 2019.
- [19] Y. Long, S. Guo, and Z. Zou, "Effects of enteral nutrition support combined with individualized nutrition nursing on the rehabilitation effect of patients with primary cerebral hemorrhage," *Guizhou Medicine*, vol. 44, no. 4, pp. 659–660, 2020.
- [20] Y. Liu and Y. He, "Observation on the effect of postoperative analgesia and sedation nursing intervention in patients with cerebral hemorrhage," *Journal of Xinxiang Medical College*, vol. 36, no. 3, pp. 288–290, 2019.
- [21] P. Liu, "Observation on effect of rehabilitation nursing intervention on promoting motor function recovery of cerebral hemorrhage hemiplegia patients," *Journal of Hunan University of Chinese Medicine*, vol. A01, pp. 1089–1090, 2018.
- [22] Q. Chen, "Effect of comprehensive nursing intervention on premature infants with intracranial hemorrhage," *Contemporary Nurses*, vol. 27, no. 8, pp. 61–63, 2020.
- [23] C. Fang and J. Cheng, "Emergency nursing methods and effects of intracranial hemorrhage," *Chinese and Foreign Women's Health Research*, vol. 4, pp. 137–157, 2019.
- [24] Y. Yan, "Analysis of the effect of comprehensive nursing intervention in the nursing of patients with intracranial pressure monitoring after operation of cerebral trauma and intracranial hemorrhage," *Chinese Community Physician*, vol. 34, no. 11, pp. 160–161, 2018.



## Research Article

# Analysis of Soft Tissue Changes and Influencing Factors of Implant Absorption after Immediate Restoration of Anterior Teeth

Guodong Peng <sup>1</sup>, Xiaodong Sun,<sup>2</sup> and Xiang Xu<sup>2</sup>

<sup>1</sup>Department of Stomatology, The First People's Hospital of Jingzhou, Jingzhou, Hubei 434000, China

<sup>2</sup>Department of Stomatology, Yichang Central People's Hospital, Yichang, Hubei 443003, China

Correspondence should be addressed to Guodong Peng; pengguodong1008@sina.com

Received 18 May 2022; Revised 16 June 2022; Accepted 20 June 2022; Published 4 July 2022

Academic Editor: Naeem Jan

Copyright © 2022 Guodong Peng et al. This is an open access article distributed under the Creative Commons Attribution License, which permits unrestricted use, distribution, and reproduction in any medium, provided the original work is properly cited.

**Objective.** Using a digital model, evaluate the changes in the soft tissue following rapid restoration of anterior teeth and analyze the factors impacting implant absorption. **Methods.** A retrospective analysis was performed on 84 patients who received immediate implant restoration for a single anterior tooth in the department of Stomatology of our hospital from April 2020 to August 2021. According to different surgical methods, they were divided into the study group ( $n = 42$ ) and control group ( $n = 42$ ). Immediate implant repair was given to the research group, while delayed implant restoration was given to the control group. The influence of the two surgical techniques on the alterations of soft tissues around implants was studied using a 3Shape oral scan and a digital model before and 1, 3, and 5 months after the operation, respectively. Patients in the study group were divided into the excellent group ( $n = 26$ ) and poor group ( $n = 16$ ) according to the test results of implant bone absorption, and the risk factors of poor implant absorption after immediate restoration of anterior teeth were analyzed by univariate and multivariate analyses. **Results.** The levels of 1 mm and 3 mm below the gum mucosa margin in the two groups increased gradually with the time, and the gingival level and soft tissue thickness at the lip of the baseline implant also increased gradually. However, the changes of soft tissue in the study group were better than those in the control group at 3 and 6 months after surgery ( $P < 0.05$ ). The PES score was significantly improved in both groups after treatment, and the aesthetic score was higher in the study group than in the control group ( $P < 0.05$ ). Univariate and binary logistic multifactor regression showed that smoking and poor implant health were the related factors affecting implant absorption ( $P < 0.05$ ). **Conclusion.** Immediate anterior tooth implantation and pharyngeal implant restoration can better restore the soft tissue and aesthetic degree of patients, but immediate implant restoration can more effectively restore the soft tissue, and controlling smoking and keeping clean around the implant after surgery is conducive to implant absorption.

## 1. Introduction

Oral implant repair is the main method for the treatment of dentition defect and dentition loss. For patients with dentition loss in the aesthetic area of front teeth, traditional implant treatment will increase the repair time of missing teeth due to the prolonged operation time, which will have varying degrees of impact on the quality of life and emotion of patients [1]. With the advancement of medical technology, immediate anterior tooth implant repair has become

more extensively used in clinical practice to obtain better aesthetic results by reducing the time it takes for missing teeth to recover [2]. However, immediate implantation still has some limitations. Some studies have pointed out that the potential keratinized mucosa defect in the surgical area will reduce the initial stability of the implant, and the surface soft tissue morphology of the alveolar bone will also change with tooth extraction [3, 4]. Therefore, the evaluation of soft tissue morphology has always been a difficult problem in clinical practice. Some scholars used plaster model to

measure and evaluate oral soft tissue before, but the results produced errors due to the shrinkage and expansion of model materials [5]. However, because the continuous development of three-dimensional image technology provides a technical basis for soft tissue evaluation, this study created a digital model to observe the impact of different anterior tooth restoration implant methods on patient soft tissue changes and then used a multifactor analysis to identify risk factors for poor implant absorption after surgery. To provide a more effective treatment for patients with dentition defect in the aesthetic area of anterior teeth and lay a theoretical foundation for improving prognosis, it will be reported as follows [6].

The arrangements of this paper are as follows: Section 1 discusses the general information and methods. Section 2 examines an experimental result. Section 3 concludes the article with discussion.

## 2. General Information and Methods

**2.1. General Information.** A retrospective analysis was performed on 84 patients who underwent immediate implant restoration of the single anterior tooth in stomatology Department of our hospital from April 2020 to August 2021. According to different surgical methods, they were divided into the study group ( $n=42$ ) and control group ( $n=42$ ). The comparison of baseline data between the two groups was shown in Table 1, with no significant difference ( $P>0.05$ ). In addition, patients in the study group were divided into the excellent group ( $n=26$ ) and poor group ( $n=16$ ) according to the test results of bone absorption of implants. Before surgery, all patients in the study completed an informed consent form, and the general information and clinical data gathered in this study were kept private and not utilized for any other reason.

Inclusion criteria are as follows: (1) patients did not have inflammation at the root tip, (2) the patient had a healthy gingiva and stable occlusal relationship, (3) no contraindications of other dental implants, and (4) signed informed consent.

Exclusion criteria are as follows: (1) patients with mental diseases cannot cooperate with the study, (2) unclear clinical imaging data, (3) patients with poor treatment compliance, which influenced the study results, and (4) combined with autoimmune dysfunction.

### 2.2. Methods

**2.2.1. Treatment Methods.** Before treatment, both groups were given the same routine treatment such as periodontal cleaning and local anesthesia during the operation.

In the study group, immediate implant restoration was performed. After anesthesia took effect, the mucosa was cut along the extraction socket and the gingival was peeled off, and the edge of the extraction socket was fully exposed. According to the breadth of the tooth neck and the length of the root, the extraction socket was adequately extended. The autologous bone hole was collected at the standby hole when the implant's cervical margin reached 2 mm below

the alveolar crest, and then, the bio-OSS shares were used for bone grafting and the Bio-Gide film was coated. The screw hole in the upper segment of the implant was screwed, and the mucosa was sutured, and the gauze was occluded for 30 minutes after surgery, as shown in Figure 1.

In the control group, a trapezoidal incision was made at 3 mm of the alveolar crest on the labial side about 5 weeks after tooth extraction, and transverse incision was made on the alveolar crest. Other steps were the same as those in the study group.

Both groups were inserted 2 weeks after surgery and followed up for 6 months.

**2.2.2. Data Acquisition and Digital Model Establishment.** A professional physician performed preoperative and postoperative oral scans on the maxillary denture and labial gingival soft tissue to obtain digital impression modulus data (Figure 2), which will be entered into Geomagic Studio. The apical points with obvious features in the two models to be registered were selected, and the alignment function was performed, and the fitting alignment function was used for correction (Figure 3). The superimposed two models were analyzed by analytical function analysis, and the soft tissues around implants were labeled by 15-stage chromatography (Figure 4).

**2.2.3. 3D Reconstruction of Soft Tissue Morphology and 3D Morphological Measurement and Analysis.** The preoperative scan model was superposed with the postoperative scan model, and the critical value MAX was set to 2.45 mm in the software, and the nominal values (MIX/MAX) were  $\pm 0.123$  mm, respectively. When the change exceeded 0.123 mm, the color other than green would be displayed, so the aligned part was green and the soft tissue contour changed to blue in the model. And the darker the color, the higher the degree of change (Figure 4). Chromatography shows implant surrounding soft tissue changes (Figure 5) and keeps the green parts out the blue part and changes in the area of the surface of the two local choice of 6 months after surface and reverse flip; flip was observed before and after an internal space between two surfaces (Figure 6), the filled function for filling out this space so as to form a closed space. The reconstructed 3D model is the changes of soft tissues around the implant (Figure 7).

Professional surveyors will measure the superimposed model. The "Boolean Operation" function in the software will be used to integrate the superimposed model (Figure 8). Import the integrated model into Geomagic Qualify for section creation. The changes of 1 mm (RW1) and 3 mm (RW3) below the gingival mucosa margin were measured in the cross-sectional view again. The level of the baseline implant lip gingival (ML) was measured at the lip gingival apex of the preoperative end point, and the mean thickness of the soft tissue contour was measured ( $D$ ).

**2.2.4. Aesthetic Evaluation of Pink in Planting Area (PES).** The evaluation scale mainly contains 7 items, including gingival color, texture, shape, alveolar ridge defect, gingival margin level, middle gingival papillary filling, and proximal

TABLE 1: Comparison of baseline data.

	Study group ( $n = 42$ )	Control group ( $n = 42$ )	$t/x^2$	$P$
Age	$35.23 \pm 6.32$	$35.61 \pm 6.29$	-0.276	0.783
Gender			0.198	0.657
Man	26 (61.90%)	24 (57.14%)		
Woman	16 (38.10%)	18 (42.86%)		
BMI ( $\text{kg}/\text{m}^2$ )	$23.32 \pm 2.14$	$23.21 \pm 2.16$	0.234	0.815
Tooth loss time (week)	$5.58 \pm 2.35$	$5.47 \pm 2.42$	0.211	0.833

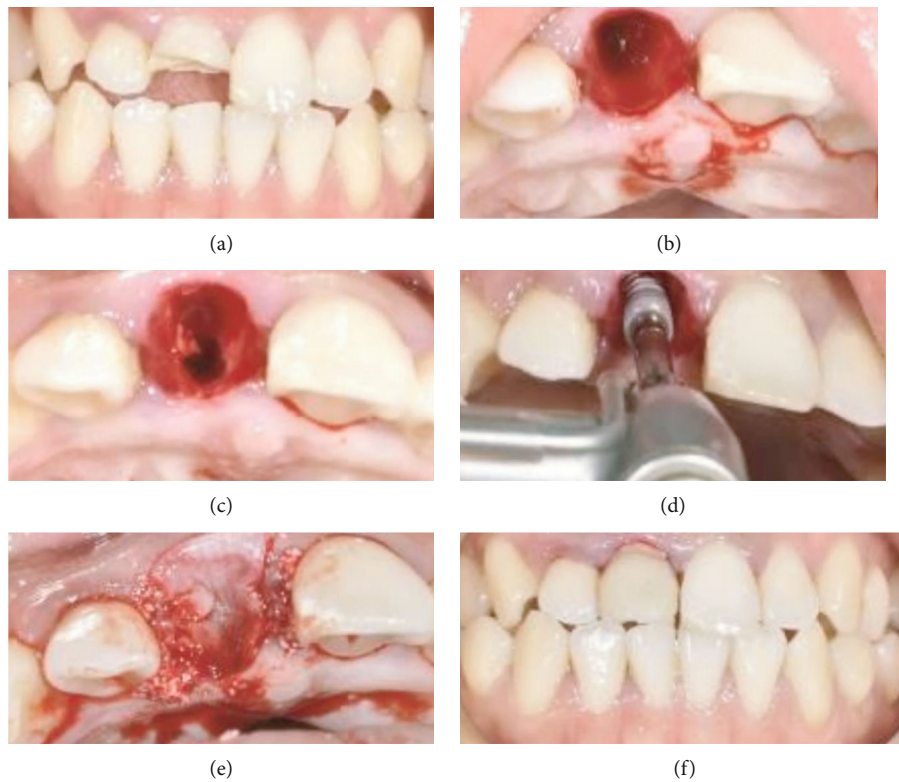


FIGURE 1: Immediate implant repair map. (a) The preoperative positive image. (b) After tooth extraction. (c) The backup cave map. (d) The implant. (e) Bone meal implanted and coated. (f) The postoperative positive view.



FIGURE 2: Oral scan models at different time points.

middle gingival papillary filling. The score range is 0 to 14, and the lower the score is, the lower the aesthetic degree of the patient is.

2.2.5. *Evaluation of Implant Bone Absorption.* The team completed in implant surgery and postoperative patients with six months for X-ray, stabilizing the tooth slice of film-

ing process, and using image processing software for processing; after filming in a more accurate to evaluate implant absorption degree, the implant length is measured in the X line and compared the magnification (the length of the X-ray showed that planting-actual implant length), and the height of marginal alveolar bone was measured and bone resorption was evaluated. Those with bone

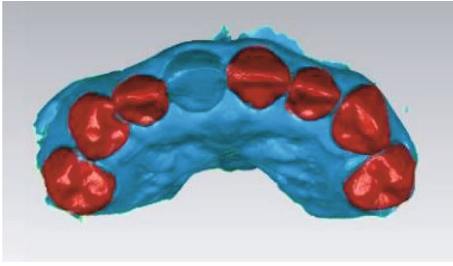


FIGURE 3: Note: the red area is the artificial overlap of similar surfaces of other teeth.

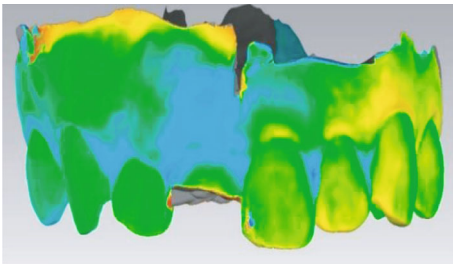


FIGURE 4: The overlap of preoperative and postoperative models and the change of soft tissue on the labial side at the implantation site by chromatography, in which the light blue area is the soft tissue collapse.

resorption less than 1.5 mm were included in the excellent group, and those with bone resorption  $\geq 1.5$  mm were included in the poor group. The factors affecting bone resorption were analyzed by a single factor and multiple factors.

**2.3. Statistical Treatment.** The study data were put into SPSS 22.0 for statistical processing. If the measurement data followed normal distribution and homogeneity of variance, they were expressed as mean  $\pm$  standard deviation. The independent sample *T* test was used to assess intergroup differences, while the paired *T* test was used to test intragroup comparisons. Counting data were represented by (%), and the differences between groups were tested by  $\chi^2$  test. Repeated measurement analysis and parallel spherical test were used for measurements at different time points. Univariate and multivariate analyses of factors affecting bone resorption of implants were done. All the above data were at  $P < 0.05$ , and the differences among the data were statistically significant.

### 3. Results

**3.1. Postoperative Soft Tissue Changes in Each Group.** The results showed that the levels of 1 mm and 3 mm below the gum mucosal margin in the two groups gradually increased over time after surgery, and the gingival level and soft tissue thickness at the lip of the baseline implant also gradually increased. However, the changes of soft tissue in the study

group were better than those in the control group at 3 and 6 months after surgery ( $P < 0.05$ ), as shown in Table 2.

**3.2. Postoperative PES Score Changes in Each Group.** PES scores of patients in both groups were significantly improved after treatment, and the aesthetic score of the study group was higher than that of the control group ( $P < 0.05$ ), as shown in Table 3.

**3.3. Univariate and Multivariate Analyses of Factors Affecting Bone Resorption of Implants.** Univariate and binary logistic multifactor regression showed that smoking and poor implant health were the related factors affecting implant absorption ( $P < 0.05$ ), as shown in Table 4 and Figure 9.

### 4. Discussion

As a treatment method for repairing the aesthetic area of the anterior teeth, immediate implant restoration of anterior teeth can better evaluate the clinical efficacy of this method for patients with tooth loss by observing the soft tissue changes after restoration [7]. In the past, worried models were commonly used in clinical practice to evaluate soft tissue changes, but this method was vulnerable to the influence of model materials and mould taking procedures, and the gypsum model measurement method was too solitary, leading in low accuracy of results [8]. With the continuous development of digital information technology, some scholars have pointed out that digital light scanning can be used to achieve multiangle measurement of the surrounding soft tissues of implants, so as to assist doctors to more accurately assess the prognosis of patients and provide corresponding treatment plans [9]. But at this stage on this technology is applied to the soft tissue changes after immediate implant prosthesis research is relatively small, therefore, this study through the line to our hospital were retrospectively analyzed to dental implant prosthesis of the 84 patients, compare the different repair methods on the influence of the soft tissue changes, and further analyze the related factors influencing the postoperative implant absorption, to provide clinical treatment basis for improving the clinical treatment of patients with anterior tooth loss.

The study's findings revealed that at 3 and 6 months following surgery, the level of 1 mm and 3 mm below the gingival mucosal margin, the level of baseline labial implants, and the thickness of soft tissue in the study group were higher than those in the control group ( $P < 0.05$ ). By reviewing relevant literature and combining the results of this study, the author believed that, when making an immediate implant prosthesis because patients with tooth extraction socket are not yet healed, more effective orientation for judgment of alveolar socket must be done, so it is easier to implant into the ideal anatomical location, and more joint biomechanics, and immediate implant prosthesis can effectively shorten the patient's growing cycle, and reduce the missing tooth bone mass loss. It also plays a role in improving the quality of life [10]. Simultaneously, the changes in soft tissue generated by rapid implant repair could be caused by the restoration of

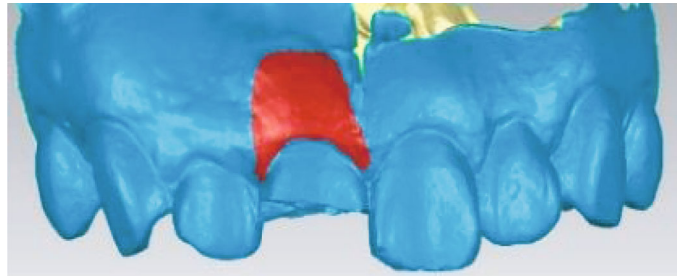


FIGURE 5: The changes of soft tissue at the implant site manually marked after 3D reconstruction.

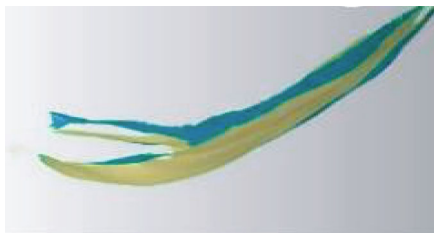


FIGURE 6: The flipped postoperative image, showing a gap between the two surfaces.

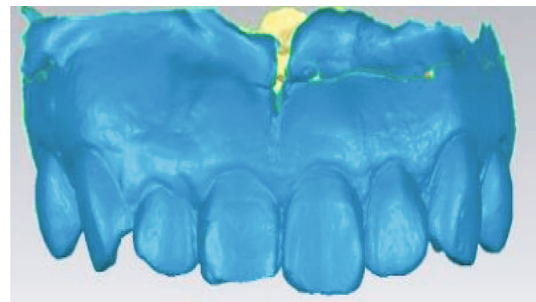


FIGURE 8: The integration of preoperative and postoperative linear measurements as a whole.

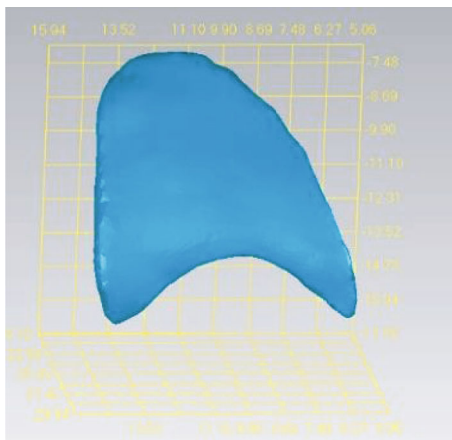


FIGURE 7: The three-dimensional morphology of soft tissue after reconstruction.

the alveolar bone beneath the implant, leading in a change in alveolar crest size and then the retraction of the peripheral mucosa around the implant. In addition, studies have confirmed that there are many clinical factors that can cause the retraction of the peripheral mucosa. Based on this, some scholars have proposed that immediate implant repair can reduce postoperative mucosal edge retraction by reducing the degree of flap flap or avoiding flap flap [11, 12]. In addition, PES was used to compare the aesthetic degree of the two groups of patients after surgery. PES score of the study group was significantly higher than that of the control group ( $P < 0.05$ ), which further demonstrated that immediate implant repair could not only promote the recovery of

periodontal soft tissue but also enhance the aesthetic degree after surgery.

In addition, the risk factors causing poor implant absorption were analyzed in this study, and the results showed that postoperative smoking and poor implant health were independent risk factors affecting implant absorption ( $P < 0.05$ ). Smoking is one of the factors causing poor implant absorption after surgery, which may be related to smoking inhibiting epithelial tissue generation and slowing down wound healing [13]. As a result, it is recommended that patients discontinue smoking prior to surgery and then reduce or quit smoking afterward, in order to ensure the greatest surgical outcomes and prognosis. In addition there are a large number of studies confirm that poor oral health situation is one of the important reasons influence a variety of oral disease, postoperative patients with immediate implant prosthesis implants with poor absorption also has close ties, and this study also showed that patients with poor oral health is another risk factor for postoperative implant absorption is poor, in line with previous studies [14, 15]. Therefore, it is recommended that patients keep their oral cavity clean after surgery, brush their teeth regularly to reduce and inhibit the formation of dental plaque, and improve the success rate of treatment and the effect of implant repair. Although this study has achieved some clinical results, due to the small sample size, the rigor of the results needs to be further supported by more scholars.

Finally, rapid implant restoration of anterior teeth can help the soft tissue around the implant recover more quickly and improve the overall aesthetic appearance. Meanwhile,

TABLE 2: Postoperative soft tissue changes.

Group	Number		1 months after surgery	3 months after surgery	6 months after surgery	F	P
Study group	42	RW1 (mm)	0.14 ± 0.07	0.23 ± 0.12*	0.28 ± 0.08* <sup>#</sup>	2.214	0.023
		RW3 (mm)	0.21 ± 0.11	0.32 ± 0.19*	0.39 ± 0.13* <sup>#</sup>	3.342	0.038
		D (mm)	0.31 ± 0.11	0.52 ± 0.13*	0.61 ± 0.16* <sup>#</sup>	5.562	<0.001
		ML (mm)	0.22 ± 0.11	0.32 ± 0.18*	0.41 ± 0.14* <sup>#</sup>	3.267	0.026
Control group	42	RW1 (mm)	0.13 ± 0.08	0.22 ± 0.13*	0.26 ± 0.09* <sup>#</sup>	2.042	0.032
		RW3 (mm)	0.20 ± 0.12	0.30 ± 0.16* <sup>&amp;</sup>	0.35 ± 0.15* <sup>#&amp;</sup>	3.283	0.041
		D (mm)	0.28 ± 0.09	0.45 ± 0.14* <sup>&amp;</sup>	0.52 ± 0.15* <sup>#&amp;</sup>	4.983	<0.001
		ML (mm)	0.21 ± 0.06	0.27 ± 0.14* <sup>&amp;</sup>	0.35 ± 0.13* <sup>#&amp;</sup>	3.163	0.032

Note: \* compared with 1 month after surgery, \* $P < 0.05$ , <sup>#</sup> compared with 3 months after surgery, <sup>#</sup> $P < 0.05$ ; and <sup>&</sup> compared with the study group, <sup>&</sup> $P < 0.05$ .

TABLE 3: Aesthetic score changes after surgery.

Group	Number	Preoperative	6 months after surgery	t	P
Study group	42	6.63 ± 2.14	11.27 ± 2.31	-9.550	<0.001
Control group	42	6.52 ± 2.05	10.04 ± 2.16	-7.660	<0.001
t		0.241	2.521		
P		0.810	0.014		

TABLE 4: Univariate analysis.

	Good group (n = 26)	Bad group (n = 16)	t/ $\chi^2$	P
Age	36.23 ± 5.61	36.46 ± 5.66	-0.129	0.898
Gender			1.553	0.213
Man	18 (69.23%)	8 (50.00%)		
Woman	8 (30.77%)	8 (50.00%)		
BMI (kg/m <sup>2</sup> )	23.32 ± 2.10	23.21 ± 2.05	0.166	0.869
Smoking			17.374	<0.001
Y	3 (11.54%)	12 (75.00%)		
N	23 (88.46%)	4 (25.00%)		
Local health of implantation			4.423	<0.001
Cleaning	21 (80.77%)	5 (31.25%)		
Food residue	4 (15.38%)	5 (31.25%)		
Dental calculus	1 (3.85%)	6 (37.50%)		

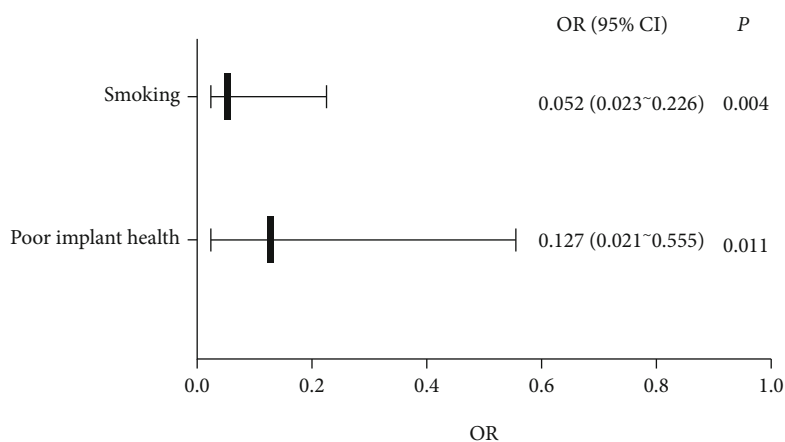


FIGURE 9: Multivariate analysis.

reducing the frequency of smoking and maintaining clean oral hygiene after surgery can promote the implant restoration effect and clinical efficacy, improve the implant absorption degree, and further improve the prognosis.

## Data Availability

The datasets used in this paper are available from the corresponding author upon request.

## Conflicts of Interest

The authors declared that they have no conflicts of interest regarding this work.

## References

- [1] W. Zhang and P. C. Yelick, "Tooth repair and regeneration: potential of dental stem cells," *Trends in Molecular Medicine*, vol. 27, no. 5, pp. 501–511, 2021.
- [2] X. Zhang, M. Wang, and A. Mo, "An alternative method for immediate implant-supported restoration of anterior teeth assisted by fully guided templates: a clinical study," *The Journal of Prosthetic Dentistry*, vol. 126, no. 5, pp. 636–645, 2021.
- [3] K. W. Slagter, G. M. Raghoobar, D. F. M. Hentenaar, A. Vissink, and H. J. A. Meijer, "Immediate placement of single implants with or without immediate provisionalization in the maxillary aesthetic region: a 5-year comparative study," *Journal of Clinical Periodontology*, vol. 48, no. 2, pp. 272–283, 2021.
- [4] Z. Yao, B. Jia, S. Lin, and J. Shao, "Effect of Straumann implant on crown appearance in immediate implant restoration of maxillary anterior teeth," *Nan Fang Yi Ke Da Xue Xue Bao*, vol. 40, no. 9, pp. 1365–1368, 2020.
- [5] E. Ruales-Carrera, P. Pauletto, K. Apaza-Bedoya, C. A. M. Volpato, M. Özcan, and C. A. M. Benfatti, "Peri-implant tissue management after immediate implant placement using a customized healing abutment," *Journal of Esthetic and Restorative Dentistry*, vol. 31, no. 6, pp. 533–541, 2019.
- [6] S. J. Yan, C. Zhou, J. Liu et al., "Clinical evaluation of the socket-shield technique for immediate implantation in the maxillary anterior region," *Hua Xi Kou Qiang Yi Xue Za Zhi*, vol. 37, no. 6, pp. 615–620, 2019.
- [7] K. C. Oh, J. Paik, and J. H. Kim, "Esthetic rehabilitation of maxillary anterior teeth, including an immediate provisionalization with an implant-supported fixed dental prosthesis," *Journal of Clinical Medicine*, vol. 8, no. 4, p. 428, 2019.
- [8] L. G. Ladino and D. Rosselli, "Use of extracted anterior teeth as provisional restorations and surgical guide for immediate multiple implant placement: a clinical case report," *Journal of Esthetic and Restorative Dentistry*, vol. 31, no. 3, pp. 209–212, 2019.
- [9] L. Shapira, B. P. Levin, and A. Stabholz, "Long-term esthetic complications associated with anterior implant-supported restorations," *The Compendium of Continuing Education in Dentistry*, vol. 42, no. 7, pp. 358–363, 2021.
- [10] X. X. Zhang, X. Y. Wu, T. Xia et al., "Evaluation of immediate implant in patients with limited buccal bone wall dehiscence in single upper anterior tooth," *Zhonghua Kou Qiang Yi Xue Za Zhi*, vol. 55, no. 11, pp. 831–837, 2020.
- [11] L. Sun, M. M. Yang, J. M. Zhao, X. Zhang, and Z. Qu, "Analysis of the hard and soft tissue following immediate and early implant placement in the anterior area of maxilla," *Zhonghua Kou Qiang Yi Xue Za Zhi*, vol. 55, no. 11, pp. 857–863, 2020.
- [12] J. Babiker, N. H. K. Affendi, M. Y. P. M. Yusof, and S. J. Chu, "Qualitative and quantitative assessments of alveolar bone dimension and its correlation with tooth angulation in the anterior maxilla for immediate implant placement," *The Journal of Contemporary Dental Practice*, vol. 22, no. 11, pp. 1237–1242, 2021.
- [13] I. Gamborena, Y. Sasaki, and M. B. Blatz, "Predictable immediate implant placement and restoration in the esthetic zone," *Journal of Esthetic and Restorative Dentistry*, vol. 33, no. 1, pp. 158–172, 2021.
- [14] Y. Xie, L. Jiang, J. He, C. F. Deng, and B. H. Zhao, "Comparison of short-term clinical effect and assessment of influential factors around single-tooth in the aesthetic area: immediate implant placement versus delayed implant placement," *Shanghai Journal of Stomatology*, vol. 28, no. 2, pp. 148–153, 2019.
- [15] O. González-Martín, E. Lee, A. Weisgold, M. Veltri, and H. Su, "Contour management of implant restorations for optimal emergence profiles: guidelines for immediate and delayed provisional restorations," *The International Journal of Periodontics & Restorative Dentistry*, vol. 40, no. 1, pp. 61–70, 2020.

## Review Article

# Perinatal Outcomes and Related Risk Factors of Single vs Twin Pregnancy Complicated by Gestational Diabetes Mellitus: Meta-Analysis

Xiaofang Zhu, Chan Huang, Li Wu , Yufeng Deng, Xuemei Lai, Huayan Gu, and Haiyan Zhang

Department of Obstetrics and Gynecology, Women and Children's Hospital of Chongqing Medical University, Chongqing 401147, China

Correspondence should be addressed to Li Wu; [chqw136@163.com](mailto:chqw136@163.com)

Received 16 May 2022; Revised 17 June 2022; Accepted 20 June 2022; Published 4 July 2022

Academic Editor: Naeem Jan

Copyright © 2022 Xiaofang Zhu et al. This is an open access article distributed under the Creative Commons Attribution License, which permits unrestricted use, distribution, and reproduction in any medium, provided the original work is properly cited.

**Objective.** Perinatal outcomes and related risk factors of single vs twin pregnancy complicated with gestational diabetes mellitus (GDM) were clarified, providing evidence for developing preventive measures. **Methods.** The Chinese National Knowledge Infrastructure (CNKI), China Biology Medicine (CBM), CQVIP, Wanfang, and PubMed databases were searched for published research on the perinatal outcomes and risk factors of single and twin pregnancy complicated by GDM from 2000 to 2021. The quality of the included literature was evaluated according to the Newcastle-Ottawa Scale (NOS). Meta-analysis of the included literature was conducted using RevMan5.3 software. **Results.** Relative to a single pregnancy group, infertility, gestational weight gain, and family history of diabetes presented statistical significance in the twin pregnancy group ( $P < 0.05$ ); gestational age at delivery, cesarean section, preterm birth  $< 37$  weeks, and preeclampsia presented statistical significance in the twin pregnancy group ( $P < 0.05$ ); and neonatal birth weight, small for gestational age (SGA), neonatal asphyxia, neonatal hypoglycemia, neonatal respiratory distress syndrome (NRDS), neonatal hyperbilirubinemia, and neonatal death presented statistical significance in the twin pregnancy group ( $P < 0.05$ ). **Conclusion.** Infertility, prenatal weight gain, and diabetes in the family are all risk factors for postpartum impaired glucose metabolism in pregnant women with GDM who are carrying twins. The gestational age at delivery, cesarean section, preterm birth  $< 37$  weeks, and preeclampsia of twin pregnant women with diabetes will affect the perinatal status of twin pregnant women. Neonatal birth weight, SGA, neonatal asphyxia, neonatal hypoglycemia, NRDS, neonatal hyperbilirubinemia, neonatal death, etc. should be paid special attention in the perinatal process.

## 1. Introduction

Gestational diabetes mellitus (GDM) is the most common metabolic disease in pregnancy, and its incidence is increasing globally due to elevated obesity in women of childbearing age, elderly parturient women, and assisted reproductive technologies. Incidence of GDM in twin pregnancy presents elevation relative to single pregnancy, and twin pregnancy is an independent risk factor for GDM occurrence [1, 2].

Preterm birth, infection, macrosomia, polyhydramnios, postpartum hemorrhage, newborn hypoglycemia, neonatal respiratory distress syndrome (NRDS), neonatal hypercholesterolemia, and other perinatal problems have all been

linked to GDM in single pregnancies [3]. There are different opinions at home and abroad about whether GDM will increase the adverse pregnancy outcome of twin pregnancy. The related risk factors and early prediction research of GDM also focus on single pregnancy, and reports on twin pregnancy are rare. Understanding the perinatal outcomes and risk factors of GDM, as well as GDM prevention, early diagnosis, and early treatment, is critical for enhancing the quality of life of pregnant and lying-in women, as well as perinatal infants.

The following is the paper's organization paragraph: in Section 2, the materials and methods is provided. The experiments and results are discussed in Section 3. Section 4



consists of the discussion; finally, the research job is completed in Section 5.

## 2. Materials and Methods

In this section, we defined the data source, literature inclusion criteria, literature exclusion criteria, literature screening and data extraction, quality evaluation, and statistical analysis in detail.

**2.1. Data Source.** The China National Knowledge Infrastructure (CNKI), China Biology Medicine (CBM), CQVIP, Wanfang, and PubMed databases were retrieved, combined with literature tracing and manual retrieval using the combination of subject headings and keywords. The literatures published on the risk factors of GDM in Chinese women from January 2000 to December 2021 were collected. The literature retrieval terms were as follows: “single vs twin pregnancies,” “gestational diabetes mellitus,” “risk factors,” “perinatal outcomes,” and “case-control study.”

### 2.2. Literature Inclusion Criteria

- (1) A case-control study
- (2) Clinically confirmed GDM cases in a case group
- (3) OR value and its 95% CI being provided or possibly being obtained indirectly by calculation
- (4) For the report of the same population, a recently published literature being chosen

### 2.3. Literature Exclusion Criteria

- (1) The study did not set up a control group
- (2) The diagnostic criteria for GDM were not mentioned or were not clear
- (3) The unavailable literatures were published repeatedly, with poor quality and incomplete data

**2.4. Literature Screening and Data Extraction.** Two researchers screened the literature and extracted data according to the inclusion and exclusion criteria, respectively, and crosschecked to exclude bias. If there was any disagreement, two researchers discussed it first and negotiated with a third party to resolve it if necessary. The literature data were extracted using Excel, including key elements of literature quality evaluation (title, author, publication time, and sample size), exposure factors (included when there were  $\geq 3$  literature reports), and outcome measurement data.

**2.5. Quality Evaluation.** Two researchers evaluated the quality of the included literature according to the Newcastle-Ottawa Scale (NOS), which included 3 dimensions and 8 items in total, with a full score of 9 points. A total score of  $\leq 4$  was considered low quality, 5–6 was considered moderate quality, and  $\geq 7$  was considered high quality. If there was a disagreement in the evaluation results, two researchers discussed it first and negotiated with a third party to resolve it if necessary.

**2.6. Statistical Analysis.** Meta-analysis was conducted using RevMan5.3 software. Results were expressed as odds ratio (OR) with 95% confidence intervals (95% CI). The  $\chi^2$  test evaluated the heterogeneity of the included literature (the test level was  $\alpha = 0.05$ ), and the size of the heterogeneity was evaluated according to the  $I^2$  value. When  $P > 0.05$  and  $I^2 \leq 50\%$ , it indicated that the heterogeneity of the results in each study presented no statistical significance and a fixed-effects model (FEM) was used for meta-analysis; when  $P \leq 0.05$  and  $I^2 > 50\%$ , it indicated that the study results presented statistical significance; a random-effects model (REM) was used for meta-analysis after excluding clinical heterogeneity. Sensitivity analysis determined whether the combined results of exposure factors were stable.

## 3. Results

**3.1. Literature Screening Process and Results.** EndNote X9 was utilized to reduplicate a total of 1725 linked literatures found through retrieval. After preliminary screening by reading the title and abstract and rescreening by reading the full text, 11 studies were finally included, with a total of 383752 subjects, including 376563 cases in the single pregnancy group (control group) and 7189 cases in the twin pregnancy group (experimental group) (Figure 1).

**3.2. General Characteristics and Quality Evaluation of Included Literature.** A total of 11 case-control reports were included in this study, and the NOS score was 5 for 1 literature, 6 for 5 literatures, 7 for 3 literatures, and 8 for only 2 literatures (Table 1).

### 3.3. Meta-Analysis Results

**3.3.1. Analysis of Related Risk Factors.** Family history of diabetes and pre-BMI presented no difference in the heterogeneity test ( $P > 0.1$  or  $I^2 < 50\%$ ), and FEM was used for analysis; other risk factors presented statistical significance in the heterogeneity test ( $P \leq 0.1$  or  $I^2 > 50\%$ ), and REM was used for analysis. Relative to the single pregnancy group, infertility, gestational weight gain, and family history of diabetes presented statistical significance in the twin pregnancy group ( $P < 0.05$ ), indicating that infertility, gestational weight gain, and family history of diabetes are risk factors for twin pregnant women with GDM. Age and pre-BMI presented no difference after combination (Table 2).

**3.3.2. Analysis of Perinatal Outcomes of Pregnant Women.** Perinatal outcome indicators of gestational age at delivery, cesarean section, preterm birth  $< 37$  weeks, gestational hypertension, and preeclampsia presented statistical significance in the heterogeneity test ( $P \leq 0.1$  or  $I^2 > 50\%$ ), and REM was used for analysis. Relative to the single pregnancy group, gestational age at delivery, cesarean section, preterm birth  $< 37$  weeks, and preeclampsia presented statistical significance ( $P < 0.05$ ), indicating that gestational age at delivery, cesarean section, preterm birth  $< 37$  weeks, preeclampsia, and gestational diabetes mellitus are important indicators of perinatal outcomes in twin pregnant women

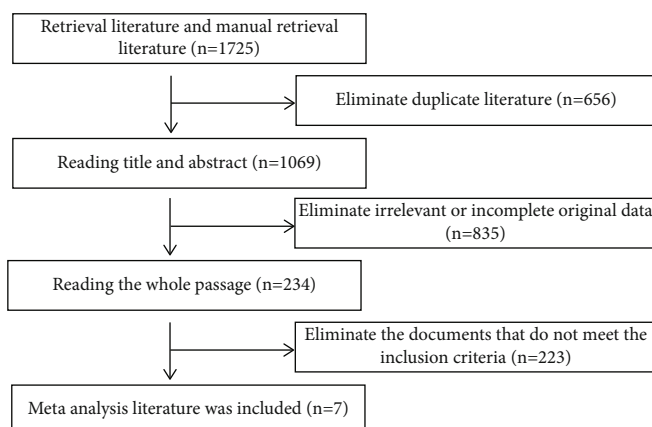


FIGURE 1: Flowchart of literature screening.

TABLE 1: Literature quality evaluation.

Author	Year	Groups		NOS score
		Single pregnancy group	Twin pregnancy group	
Buhling et al., [4]	2003	178	89	6
Jung et al., [5]	2015	3435	143	6
Lai et al., [6]	2012	327198	5552	5
Rauh-Hain et al., [7]	2009	22503	553	7
Akiba et al., [8]	2019	451	20	8
Morikawa et al., [9]	2015	3667	110	6
Ashwal et al., [10]	2021	1893	180	7
González González et al., [11]	2014	39	39	6
Guillén-Sacoto et al., [12]	2018	240	120	7
Hiersch et al., [13]	2018	16,731	326	8
Weiner et al., [14]	2018	228	57	6

TABLE 2: The related risk factors.

Exposure factors	Number of literatures	$I^2$ (%)	Heterogeneity test		OR (95% CI)	$P$
			$P$	Effect model		
Age	10	93	<0.00001	REM	0.46 [-0.42, 1.33]	0.31
Infertility	8	95	<0.00001	REM	1.94 [1.03, 3.67]	0.04
Gestational weight gain	4	96	<0.00001	REM	3.80 [1.08, 6.52]	0.006
Family history of diabetes	5	52	0.08	FEM	1.31 [1.19, 1.44]	<0.00001
Pre-BMI	9	20	0.26	FEM	-0.09 [-0.30, 0.11]	0.37

with GDM. Gestational hypertension presented no difference after combination (Table 3).

3.3.3. *Analysis of Perinatal Outcomes of Neonates.* Perinatal outcome indicators of neonatal SAG, neonatal hypoglycemia, neonatal hyperbilirubinemia, and neonatal death presented no difference in the heterogeneity test ( $P > 0.1$  or  $I^2 < 50\%$ ); FEM was used for analysis; neonatal birth weight, large for gestational age (LGA), neonatal asphyxia, and NRDS ( $P \leq 0.1$  or  $I^2 > 50\%$ ) presented statistical significance

in the heterogeneity test; REM was used for analysis. Relative to the single pregnancy group, neonatal birth weight, SGA, neonatal asphyxia, neonatal hypoglycemia, NDS, neonatal hyperbilirubinemia, and neonatal death presented statistical significance ( $P < 0.05$ ). LGA presented no difference after combination (Table 4).

3.3.4. *Analysis of Publication Bias.* The funnel plots were essentially symmetrical, according to the literature included in the meta-analysis (Figure 2), suggesting that the meta-analysis results are less likely to have publication bias.

TABLE 3: Perinatal outcomes of pregnant women.

Perinatal outcome indicators	Number of literatures	$I^2$ (%)	Heterogeneity test		OR (95% CI)	$P$
			$P$	Effect model		
Gestational age at delivery	6	98	<0.00001	REM	-3.37 [-3.77, -2.97]	<0.00001
Cesarean section	5	99	<0.00001	REM	4.79 [1.68, 13.67]	0.003
Preterm birth < 37 weeks	5	92	<0.00001	REM	13.47 [5.67, 32.02]	<0.00001
Gestational hypertension	5	71	0.008	REM	0.98 [0.27, 3.53]	0.98
Preeclampsia	3	72	0.03	REM	2.46 [1.48, 4.08]	0.0005

TABLE 4: Perinatal outcomes of neonates.

Perinatal outcome indicators	Number of literatures	$I^2$ (%)	Heterogeneity test		OR (95% CI)	$P$
			$P$	Effect model		
Neonatal birth weight	4	61	0.050	REM	-1306.550 [-1403.690, -1209.41]	<0.00001
SAG	4	0	0.760	FEM	2.24 [1.78, 2.82]	<0.00001
LAG	4	87	<0.0001	REM	1.30 [0.53, 3.17]	0.57
Neonatal asphyxia	3	98	<0.00001	REM	5.08 [1.29, 20.06]	0.02
Neonatal hypoglycemia	3	41	0.180	FEM	2.86 [2.18, 3.75]	<0.00001
NRDS	2	94	<0.0001	REM	25.94 [5.42, 124.24]	<0.0001
Neonatal hyperbilirubinemia	2	0	0.780	FEM	5.41 [2.80, 10.45]	<0.00001
Neonatal death	3	0	0.400	FEM	5.33 [4.59, 6.19]	<0.00001

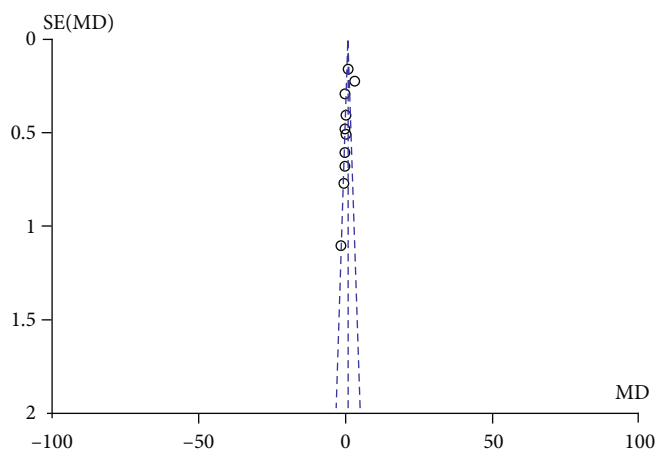


FIGURE 2: Funnel plots.

## 4. Discussion

**4.1. Analysis of Risk Factors for GDM in Twin Pregnancy.** At present, domestic and foreign studies generally believe that GDM may be the result of the combined effect of genetic factors and social environmental factors. Though academics at home and abroad have done a lot of research on the risk factors for GDM and have achieved a lot of new discoveries and understandings, earlier publications' results aren't always consistent [15]. Currently identified risk factors are race, advanced pregnancy, prolificacy, family history of diabetes, obstetric history, and overweight. Herein, meta-analysis systematically evaluated the risk factors of GDM by synthesizing the epidemiological research results on the risk factors

of GDM in Chinese women in the past 21 years. The study analyzed 11 Chinese and English literatures, and the results demonstrated that infertility, gestational weight gain, and family history of diabetes were the risk factors for postpartum abnormal glucose metabolism in twin pregnant women complicated with GDM. According to one study, prepregnancy overweight or obesity is an independent risk factor for GDM [16], which could be linked to obese people's increased insulin resistance and decreased glucose tolerance. Controlling prepregnancy obesity is a critical step in preventing GDM. Young et al. have revealed that among those with abnormal OGTT during pregnancy, the risk of postpartum diabetes in obese prepregnancy was 22.4 times that of normal weight [17]. Thus, pregnant women with a family

history of diabetes should have a reasonable diet and controlling prepregnancy obesity and gestational weight gain is a crucial measure to prevent GDM occurrence. Pregnant women with prepregnancy obesity should be more monitored, prenatal examinations should be carried out on time, and GDM should be detected and diagnosed early, so as to reduce the risk of maternal and infant complications.

Analysis of perinatal outcomes in twin pregnancies with GDM: twin pregnancy has been linked to a higher risk of caesarean delivery, GDM, preeclampsia, and preterm birth, but the extent to which GDM enhances the maternal and fetal risk associated with twin pregnancy is unknown. At present, there is no unified conclusion in domestic and foreign studies. Xiao et al. retrospectively analyzed 197 twin pregnancies and believed that GDM did not increase the adverse perinatal outcome of twin pregnancy [18]; Li et al. retrospectively analyzed the clinical data of 329 dichorionic twin pregnancies and concluded that GDM did not increase the adverse perinatal outcomes of dichorionic twin pregnancy [19]. Australian scholars Ooi and Wong retrospectively analyzed the perinatal outcomes of 410 twin pregnancies, of which 99 were diagnosed with GDM, and discovered that twin pregnancies with GDM were more prone to the occurrence of preterm birth, gestational hypertension, and preeclampsia. The incidence of neonatal intensive care unit (NICU) admission and perinatal mortality presented elevation, concluding that twin pregnancies with GDM are a high-risk group with a high incidence of adverse pregnancy outcomes [20]. The meta-analysis of McGrath et al. in 2017 concluded that gestational age and incidence of LGA and SGA presented no difference between GDM twins and non-GDM twins. Twins with GDM has no association with RDS, hypoglycemia, and 5 min Apgar score < 7 points, whereas twin neonates with GDM had a higher chance of being admitted to NICU [21]. Australian scholars Sheehan et al. studied 194 twin pregnancies, of which 39 were complicated with GDM, and believed that in addition to neonatal hypoglycemia, GDM did not increase other adverse perinatal outcomes of twin pregnancy [22]. Hirsch et al. conducted a retrospective cohort study analysis [23]. The research subjects included twin and single live births in Canada from 2012 to 2016. A total of 270843 cases were included, including 266942 single cases, among which 16731 cases were complicated with GDM, with single GDM incidence of 6.3%, and 3901 twin cases, among which 326 cases were complicated with GDM, with twin GDM incidence of 8.3%. No matter in single or twin pregnancy, GDM was related to cesarean section delivery, preterm birth < 37 weeks, and preterm birth < 34 weeks. GDM can raise the risk of gestational hypertension and preeclampsia in a single pregnancy, but not in a twin pregnancy. In terms of neonatal pregnancy outcomes, the rates of neonatal NICU hospitalization, RDS, and hypoglycemia were higher in single GDM but not in twin GDM and the incidence of LGA and neonatal jaundice was higher in single GDM but not in twin GDM. Collectively, relative to single pregnancy, twin GDM has no association with hypertensive disorders complicated with pregnancy and certain neonatal diseases. Nonetheless, the research still highlighted that GDM has

association with several adverse pregnancy outcomes in twin pregnancy, including increased cesarean delivery and preterm birth rates and impaired twin fetal growth and development. Herein, relative to the single pregnancy group, five perinatal outcome indicators of gestational age at delivery, cesarean section, preterm birth < 37 weeks, and preeclampsia presented statistical significance in the twin pregnancy group ( $P < 0.05$ ). The analysis of neonatal perinatal outcomes demonstrated that, relative to single pregnancy group, eight perinatal outcome indicators of neonatal birth weight, SGA, neonatal asphyxia, neonatal hypoglycemia, NRDS, neonatal hyperbilirubinemia, and neonatal death presented statistical significance in the twin pregnancy group ( $P < 0.05$ ), suggesting that neonatal birth weight, SGA, neonatal asphyxia, neonatal hypoglycemia, NRDS, neonatal hyperbilirubinemia, and neonatal death are vital indicators for neonatal perinatal outcomes of twin pregnancy complicated by diabetes. LGA presented no difference after combination.

The results of this research are also limited by multiple factors:

- (1) The number of included literatures is small, and the sample content of each literature varies greatly
- (2) GDM screening methods and diagnostic criteria used in different literatures are different. However, due to the small number of included literatures, this study did not conduct a stratified analysis of risk factors generated from various diagnostic criteria, which may have influenced the accuracy of the results
- (3) Meta-analysis itself is a secondary analysis, and there is publication bias, positioning bias, citation bias, etc. The authenticity and validity of its analysis results also largely depend on the quality of original literatures

## 5. Conclusion

In conclusion, infertility, gestational weight gain, and family history of diabetes are risk factors for postpartum abnormal glucose metabolism in twin pregnant women with GDM and these factors are both independent and mutually influencing. To avoid and limit the occurrence and development of postpartum abnormal glucose metabolism in pregnant women with GDM, clinical medical staff should focus on the prevention and regulation of these factors. Moreover, gestational age at delivery, cesarean section, preterm birth < 37 weeks, and preeclampsia of twin pregnant women complicated by diabetes will affect the perinatal status of twin pregnant women. Neonatal birth weight, SGA, neonatal asphyxia, neonatal hypoglycemia, NRDS, neonatal hyperbilirubinemia, neonatal death, etc. should be paid special attention in the perinatal process.

## Data Availability

Data appear in the submitted manuscript.

## Conflicts of Interest

All authors confirmed that there are no competing interests in this study.

## Acknowledgments

This work was supported by the 2020 Scientific Research Plan of Yuzhong District (grant number: 20200159).

## References

- [1] R. Retnakaran and B. R. Shah, "Impact of twin gestation and fetal sex on maternal risk of diabetes during and after pregnancy," *Diabetes Care*, vol. 39, no. 8, pp. e110–e111, 2016.
- [2] A. Weissman and A. Drugan, "Glucose tolerance in singleton, twin and triplet pregnancies," *Journal of Perinatal Medicine*, vol. 44, no. 8, pp. 893–897, 2016.
- [3] J. Dillon, C. J. Mitchell, T. Ellett, A. Siegel, A. E. Denoble, and S. K. Dotters-Katz, "Pregnancy outcomes among women with class III obesity with pre-diabetic early hemoglobin A1C," *American Journal of Perinatology*, vol. 39, no. 3, pp. 238–242, 2022.
- [4] K. Buhling, W. Henrich, E. Starr et al., "Risk for gestational diabetes and hypertension for women with twin pregnancy compared to singleton pregnancy," *Archives of Gynecology and Obstetrics*, vol. 269, no. 1, pp. 33–36, 2003.
- [5] Y. J. Jung, J. Y. Kwon, H. Y. Cho, Y. W. Park, and Y. H. Kim, "Comparison of the performance of screening test for gestational diabetes in singleton versus twin pregnancies," *Science*, vol. 58, no. 6, p. 439, 2015.
- [6] F. Y. Lai, J. A. Johnson, D. Dover, and P. Kaul, "Outcomes of singleton and twin pregnancies complicated by pre-existing diabetes and gestational diabetes: a population-based study in Alberta, Canada, 2005–11," *Journal of Diabetes*, vol. 8, no. 1, pp. 45–55, 2016.
- [7] J. A. Rauh-Hain, S. Rana, H. Tamez et al., "Risk for developing gestational diabetes in women with twin pregnancies," *The Journal of Maternal-Fetal & Neonatal Medicine*, vol. 22, no. 4, pp. 293–299, 2009.
- [8] Y. Akiba, K. Miyakoshi, S. Ikenoue et al., "Glycemic and metabolic features in gestational diabetes: singleton versus twin pregnancies," *Endocrine Journal*, vol. 66, no. 7, pp. 647–651, 2019.
- [9] M. Morikawa, T. Yamada, R. Akaishi et al., "Prevalence of hyperglycaemia in singleton versus twin pregnancy," *Diabetes/Metabolism Research & Reviews*, vol. 31, no. 2, pp. 198–203, 2015.
- [10] E. Ashwal, H. Berger, L. Hirsch et al., "Gestational diabetes and fetal growth in twin compared with singleton pregnancies," *American Journal of Obstetrics and Gynecology*, vol. 225, no. 4, pp. 420.e1–420.e13, 2021.
- [11] N. L. González González, E. González Dávila, M. Goya et al., "Twin pregnancy among women with pregestational type 1 or type 2 diabetes mellitus," *International Journal of Gynaecology & Obstetrics the Official Organ of the International Federation of Gynaecology & Obstetrics*, vol. 126, no. 1, pp. 83–87, 2014.
- [12] M. A. Guillén-Sacoto, B. Barquiel, N. Hillman, M. Á. Burgos, and L. Herranz, "Diabetes mellitus gestacional: control glucémico durante el embarazo y su relación con los resultados neonatales en embarazos gemelares y de feto único," *Endocrinología Diabetes Y Nutrición*, vol. 65, no. 6, pp. 319–327, 2018.
- [13] L. Hirsch, H. Berger, R. Okby et al., "Incidence and risk factors for gestational diabetes mellitus in twin versus singleton pregnancies," *Archives of Gynecology & Obstetrics*, vol. 298, no. 3, pp. 579–587, 2018.
- [14] E. Weiner, E. Barber, O. Feldstein et al., "The placental component and neonatal outcome in singleton vs. twin pregnancies complicated by gestational diabetes mellitus," *Placenta*, vol. 63, pp. 39–44, 2018.
- [15] A. M. Borissov, B. Trifonova, L. Dakovska, E. Michaylova, and M. Vukov, "Age, obesity, family history, previous gestational diabetes are major risk factors for hyperglycemia in pregnant Bulgarian women," *European Journal of Preventive Medicine*, vol. 9, no. 2, p. 39, 2021.
- [16] J. Pirkola, A. Pouta, A. Bloigu et al., "Prepregnancy overweight and gestational diabetes as determinants of subsequent diabetes and hypertension after 20-year follow-up," *The Journal of Clinical Endocrinology and Metabolism*, vol. 95, no. 2, pp. 772–778, 2010.
- [17] C. Young, T. J. Kuehl, P. J. Sulak, and S. R. Allen, "Gestational diabetes screening in subsequent pregnancies of previously healthy patients," *American Journal of Obstetrics and Gynecology*, vol. 182, no. 5, pp. 1024–1026, 2000.
- [18] H. Y. Xiao, J. Yu, Y. Liu et al., "Gestational diabetes does not increase the risk of adverse perinatal outcome of twin pregnancy," *Chinese Journal of Perinatal Medicine*, vol. 19, no. 5, pp. 345–349, 2016.
- [19] Z. Y. Li, P. P. Liu, C. X. Zhu, H. T. Chen, and Z. L. Wang, "Effect of gestational diabetes mellitus on perinatal outcome of double chorionic twins," *Journal of Sun Yat Sen University: Medical Science Edition*, vol. 37, no. 5, p. 5, 2016.
- [20] S. Ooi and V. W. Wong, "Twin pregnancy with gestational diabetes mellitus: a double whammy?," *Diabetes Care*, vol. 41, no. 2, pp. e15–e16, 2018.
- [21] R. T. McGrath, S. L. Hocking, E. S. Scott, S. K. Seeho, G. R. Fulcher, and S. J. Glasstras, "Outcomes of twin pregnancies complicated by gestational diabetes: a meta-analysis of observational studies," *Journal of Perinatology*, vol. 37, no. 4, pp. 360–368, 2017.
- [22] A. Sheehan, M. P. Umstad, S. Cole, and T. J. Cade, "Does gestational diabetes cause additional risk in twin pregnancy?," *Twin Research and Human Genetics*, vol. 22, no. 1, pp. 62–69, 2019.
- [23] L. Hirsch, H. Berger, R. Okby et al., "Gestational diabetes mellitus is associated with adverse outcomes in twin pregnancies," *American Journal of Obstetrics and Gynecology*, vol. 220, no. 1, p. 102.e1, 2019.

## Retraction

# Retracted: Quality Assessment of Vocational Education Teaching Reform Based on Deep Learning

### Computational and Mathematical Methods in Medicine

Received 25 July 2023; Accepted 25 July 2023; Published 26 July 2023

Copyright © 2023 Computational and Mathematical Methods in Medicine. This is an open access article distributed under the Creative Commons Attribution License, which permits unrestricted use, distribution, and reproduction in any medium, provided the original work is properly cited.

This article has been retracted by Hindawi following an investigation undertaken by the publisher [1]. This investigation has uncovered evidence of one or more of the following indicators of systematic manipulation of the publication process:

- (1) Discrepancies in scope
- (2) Discrepancies in the description of the research reported
- (3) Discrepancies between the availability of data and the research described
- (4) Inappropriate citations
- (5) Incoherent, meaningless and/or irrelevant content included in the article
- (6) Peer-review manipulation

The presence of these indicators undermines our confidence in the integrity of the article's content and we cannot, therefore, vouch for its reliability. Please note that this notice is intended solely to alert readers that the content of this article is unreliable. We have not investigated whether authors were aware of or involved in the systematic manipulation of the publication process.

Wiley and Hindawi regrets that the usual quality checks did not identify these issues before publication and have since put additional measures in place to safeguard research integrity.

We wish to credit our own Research Integrity and Research Publishing teams and anonymous and named external researchers and research integrity experts for contributing to this investigation.

The corresponding author, as the representative of all authors, has been given the opportunity to register their agreement or disagreement to this retraction. We have kept a record of any response received.

### References

- [1] Z. Ni and F. Wang, "Quality Assessment of Vocational Education Teaching Reform Based on Deep Learning," *Computational and Mathematical Methods in Medicine*, vol. 2022, Article ID 1499420, 11 pages, 2022.

## Research Article

# Quality Assessment of Vocational Education Teaching Reform Based on Deep Learning

Zai Ni <sup>1</sup> and Fei Wang <sup>2</sup>

<sup>1</sup>Dean's Office, Hangzhou Vocational and Technical College, Hangzhou Zhejiang 310018, China

<sup>2</sup>Human Resources Office, Hangzhou Vocational and Technical College, Hangzhou Zhejiang 310018, China

Correspondence should be addressed to Fei Wang; 2004010037@hzvtc.edu.cn

Received 25 April 2022; Revised 18 May 2022; Accepted 23 May 2022; Published 1 July 2022

Academic Editor: Naeem Jan

Copyright © 2022 Zai Ni and Fei Wang. This is an open access article distributed under the Creative Commons Attribution License, which permits unrestricted use, distribution, and reproduction in any medium, provided the original work is properly cited.

In my country, vocational training is an important part of the educational system. In my country's vocational education system, there is currently a conscious focus on reform and innovation. It is critical to undertake a thorough assessment of teaching quality in vocational education in order to improve teaching quality. Artificial intelligence technology, particularly deep learning technology, can successfully handle this challenge because of the various and complicated aspects involved in the assessment of teaching quality. This article thus provides an evaluation approach for the quality of vocational education that is based on a thorough investigation. Finally, research has demonstrated that this approach is capable of objectively and fairly evaluating a teacher's teaching quality, increasing a teacher's teaching passion, improving a teacher's teaching quality, and nurturing extraordinary abilities.

## 1. Introduction

Vocational education is an educational activity implemented in order to enable learners to master professional knowledge, acquire professional skills, and form good professional ethics, so as to serve social production [1]. Therefore, vocational education is inextricably linked with the economic development of a country and a nation. With the continuous development and transformation of the economy, the connotation and types of vocational education also change and evolve. Vocational education is an important part of national education and an important source of support for social labor. Vocational colleges are the main body of vocational education, and the rational construction of the teaching system is the core of improving the quality of all schools. As the most direct way to achieve teaching goals and ensure teaching quality, the development of vocational education teaching activities is the most critical link in vocational education. Therefore, teaching innovation is the key to the successful reform of

vocational education to adapt to the new economic normal and provide high-quality human capital for the new economy [2]. It was previously said by our nation's education minister that the most important job of vocational education in the future would be to increase the quality of education; this is done by enhancing teaching quality, which is done by conducting effective teaching evaluations.

The quality of vocational schools will be directly related to the development of vocational education in our country. The school's direction, educational quality, and the impact of educational reform are all determined by the quality and level of the school's teaching staff. To establish a high-quality teacher team, first of all, teachers should have a comprehensive understanding and correct evaluation. This can not only encourage teachers to improve their own quality consciousness, make them understand their own achievements and deficiencies, consciously regulate their own behavior, continuously improve and perfect their previous work, and move towards higher goals, but, at the same time, it can also promote the school leaders' awareness of the

problems and importance of improving teachers' quality and teaching level enables the school to take effective measures to strengthen the construction of the teaching staff in a more targeted and planned manner. Classroom teaching is the main way for schools to achieve educational goals. From the perspective of school management, in order for school leaders and managers to have a thorough understanding of the school's teaching work and to enhance the quality of teaching, it is necessary to evaluate the quality of teachers' classroom instruction [3]. The level of teaching work has a great influence on the level of talents trained, so the evaluation of school teaching work level has become an important content of teaching management. School teaching quality assessment is a quite complicated procedure.

Teachers and students have a complicated connection in the classroom, and a variety of variables influence how well a lesson is taught. How can a scientific and acceptable teaching quality assessment system be established such that it can objectively and fairly evaluate the teaching of teachers? Quality is a very important topic. Since the birth of the concept of artificial intelligence, it has continued to develop with the transformation of computers. Artificial intelligence has mainly experienced the reasoning period in the 1960s, the knowledge period in the 1970s, and the machine learning period that started in the 1980s and continues to this day. Connectionism, statistical learning, and deep learning were the three stages of machine learning, and deep learning is currently at a stage of rapid development. Deep learning is based on neural networks for supervised or unsupervised feature learning, representation, classification, and pattern recognition through multilevel nonlinear information processing and abstraction. Unfortunately, the integration of teaching quality assessment and deep learning technology is still relatively limited. Based on this background, this paper proposes a teaching quality evaluation method for vocational education based on deep learning. Using the advantages of neural network to solve nonlinear problems, an improved method of BP algorithm and simulated annealing method is proposed [4]. On this basis, the network structure, learning parameters, and learning algorithm of the teaching quality assessment model are determined. It has realized the efficient, network, and intelligent evaluation of teaching quality [5].

The paper arrangements are as follows: Section 2 describes the related work; Section 3 defines the methods of the proposed work. Section 4 discusses the experiment and results. In Section 5, the article comes to a close.

## 2. Related Work

Most of my country's research on vocational education reform is currently at the macro level; that is, it primarily emphasizes the importance of vocational education adapting to the new normal and reform ideas at the broadest, most specific levels. In recent years, the United States, France, Australia, Germany, and other nations have emphasized action-oriented teaching, multidisciplinary program with vocational elements, situational teaching, and "self-paced" learning in their reforms of vocational educa-

tion teaching methods. For the vocational education teaching system, many countries have put the reform emphasis on the credit transfer system, the unit system, and the mutual recognition system of learning and work experience, the main purpose of which is to establish a flexible vocational education teaching system. From the 1970s to the 1980s, the German vocational education circle has attached great importance to the action orientation in teaching activities. In order to promote the more extensive and effective development of action-oriented teaching activities, Germany has implemented a series of teaching reform pilot projects related to vocational preparation education and vocational education [6]. The development of modern apprenticeship based on traditional apprenticeship is one of the important goals of British vocational education and training reform. The so-called British modern apprenticeship system can also be understood as a combination of school education and enterprise training. Finally, the comprehensive ability is improved [7].

The field of educational assessment is both old and new. It started early in the United States, Britain, Germany, and other countries. Since the end of the 19th century, it has been regarded as an independent branch subject and has gradually developed into a scientific direction. Teaching quality assessment may be accomplished via a variety of means. The commonly used evaluation methods are as follows: the existing teaching quality evaluation work is divided into two parts; one is to determine the content in the evaluation system, and the other is to classify the teaching quality according to the content score [8, 9]. It is decided what will be included in the assessment of the quality of the instruction being provided to students. It is difficult to designate a specific course, a specific learning stage, to a specific course when constructing the content of the teaching level assessment system since learning and development are ongoing processes and the learning and growing environment is various. The teacher's involvement is measured by focusing on the evaluative content of the teaching process rather than on course performance or teaching impact as the primary indication. With regard to educational processes, it is difficult to compare the teaching of different disciplines and courses of diverse type, as well as various linkages and teaching objects, because of the many factors involved. As a result, only those criteria that directly indicate the teaching level and have similar construction in the assessment system should be included. Based on the current system of evaluating teaching levels, the development of indicators is focused on the following aspects: teaching attitude, teaching material, teaching ability, teaching technique, teaching and educating people, and the teaching impact [10]. In the current teaching quality evaluation method, in order to form a total evaluation of teaching quality, it is necessary to organize students to evaluate and score the above six indicators and obtain the quality grade coefficient of each evaluation content according to a reasonable procedure and scoring method. Obviously, the grading of the total index is a classification problem. For large and complex evaluation systems, there are many evaluation indexes, the grading criteria are complex, and it is



difficult to use an analytical expression to give an appropriate mathematical model, which is mostly a nonlinear classification problem [11].

Deep learning is now experiencing a surge. Neural networks are the foundation of deep learning. Artificial neural network research has gradually recovered since the 1980s, resulting in a research climax around the world. Worldwide, scientists and entrepreneurs are organizing and implementing related scientific research projects, such as the DARPA program in the United States, the HFSP program in Japan, the “Eureka” program in France, the “European Defense” program in Germany, and the “High-Tech Development” program in Russia [12, 13]. In my country, since the annual academic conference of neural network was held in 1990, artificial neural network has also become a major research hotspot in my country, and research work has been carried out in universities and research institutes. Artificial neural network is a fast-growing interdisciplinary subject, a new type of intelligent information processing system developed by learning from biological neural network. Because its structure “imitation” the biological nervous system of the human brain, it also has some kind of intelligence in function features [14]. It is similar to the method of repeated learning in the human brain, first giving a series of samples, learning, and training, so as to generate patterns that distinguish different characteristics between various samples. The sample set should be as representative as possible. In order to accurately fit various sample data, the system finally obtains potential patterns through hundreds or even thousands of training and learning times. When it encounters new sample data, the system automatically makes predictions and classifications based on the training results [15]. The unique information processing and distinctive solution capabilities of neural networks have garnered considerable interest in recent years, indicating a wide range of potential applications. For example, neural network technology has showed a remarkable ability to recognize and categorize patterns, as well as to filter out noise and anticipate future events. Unlike many older approaches, it can process almost any form of data [16]. Data that is complicated and has unknown patterns may be discovered via continual learning. The conventional analytical procedure and the challenge of picking a suitable model function form are both solved by the neural network technique. Modeling and analysis benefit greatly from the inherent nonlinearity of the process, which does not need identifying the specific nonlinear connection at hand [17]. At present, in foreign financial circles, there have been some successful examples of neural networks used in mortgage risk assessment and credit insurance analysis. These successful examples provide a new method for us to study evaluation or evaluation problems in the field of education and new ideas [18].

### 3. Method

In this section, we discuss the neural network theory, BP artificial neural network, and teaching quality evaluation model based on neural network in depth.

#### 3.1. Neural Network Theory

**3.1.1. Neural Network Basics.** An adaptive nonlinear dynamic system is formed by a large number of neurons coupled together in an ANN. Neurons are the basic units that make up a brain network. A neuron is the smallest computational unit in a neural network. It is generally a multi-input/single-output nonlinear device. Its action is very simple. It only multiplies the input vector with the weight vector and then undergoes a transformation to obtain the output value. This output is then passed down through the interconnections of the network and becomes the input to many neurons. Neurons may be abstracted into a simple mathematical model, as illustrated in Figure 1, based on their features and functions.

In the figure,  $x_1, x_2, \dots, x_n$  are the input of neurons;  $\omega_{i1}, \omega_{i2}, \dots, \omega_{in}$  are the weight coefficients of  $i$  neuron with  $x_1, x_2, \dots, x_n$ , respectively;  $Y_i$  is the output of the neuron  $i$ ;  $f$  is called the transfer function or the excitation function, which determines the output of the  $i$  neuron when the costimulation of the input  $x_1, x_2, \dots, x_n$  reaches the threshold value. Its input-output relationship can be described as

$$I_i = \sum_{j=1}^n \omega_{ij} x_j - \theta_i. \quad (1)$$

Sometimes, for the sake of convenience,  $\theta_i$  is often regarded as the weight corresponding to the input quantity  $x_{i0}$  that is always equal to 1, which is recorded as

$$I_i = \sum_{j=1}^n \omega_{ij} x_j, \quad (2)$$

where  $\omega_{i0} = -\theta_i; x_{i0} = 1$ .

**3.1.2. Activation Function.** The neuron should deliver the correct output after getting input from the network. Each neuron has a threshold that is based on biological neuron characteristics. When the input signal’s cumulative effect exceeds a threshold value, neurons are said to be stimulated; otherwise, they should be in an inhibitory state. In order to make the system have a wider applicability, it is hoped that the artificial neuron has a more general transformation function. This is utilized to accomplish the modification of the network input that the neuron receives. Activation functions are also known as the excitation functions, and they may be expressed as either a linear or nonlinear slope function, a threshold, or S shape.

The interpretation function is also referred to as the step function. To test if the neuron’s network input exceeds a predetermined threshold, the activation function is utilized. The simplest fundamental activation function is the linear function, which serves as an adequate linear amplification of the network input received by the neuron. Its general form is

$$f(x) = kx, \quad (3)$$

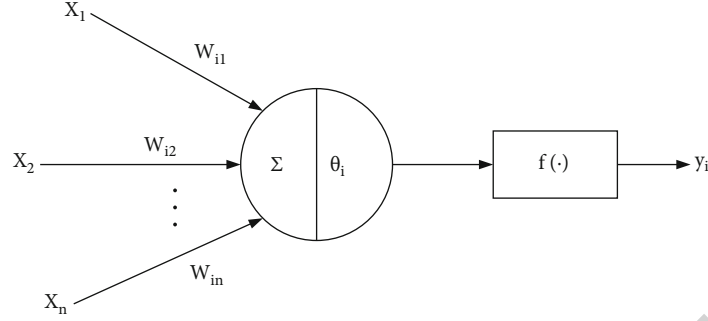


FIGURE 1: Artificial neuron model.

where the magnification factor,  $k$ , and the displacement factor,  $c$ , are both constants in mathematical expressions.

*Nonlinear slope function:* the linear function is very simple, but its linearity greatly degrades the performance of the network, and it even degrades the function of a multilevel network to that of a single-level network. As a result, nonlinear activation functions in artificial neural networks are required.

$$f(x) = \begin{cases} 1 & x \geq x_0, \\ ax + b & x_1 \leq x \leq x_0, \\ 0 & x \leq x_0. \end{cases} \quad (4)$$

*S-shaped transfer function:* it is usually a monotonically differentiable function with continuous values in  $(0, 1)$  or  $(-1, 1)$  and is usually represented by a logarithmic or tangent type of S-shaped curve.

**3.1.3. Neural Networks.** In an artificial neural network, a specific topological structure connects a large number of neurons in a large-scale parallel manner. A neuron is a single processing unit that is incapable of performing complex operations. Only a neural network with a vast number of neurons is capable of processing and storing complicated data and exhibiting a variety of superior properties. Therefore, the choice of connection scheme is the main problem in designing neural network systems. First and final levels of a computer's processing unit are known as "input" and "output," respectively; additional layers are referred to as "hidden." The number of processing units in each layer is also a matter of choice. In some networks, each processing unit of the current layer gets an input signal from the previous layer, and its output is passed to the processing unit of the next layer. Some networks allow communication between processing units between layers, and the feedback structure also needs to allow the processing units of the previous layer to accept the output of the processing units of the next layer. The feedback neural network model and the forward neural network model may be distinguished based on the architecture of the neural network. Neural network models now fall into the following categories.

There are many different types of feed-forward networks, but the most popular is the error backpropagation (BP) neural network. A multilayer mapping neural network

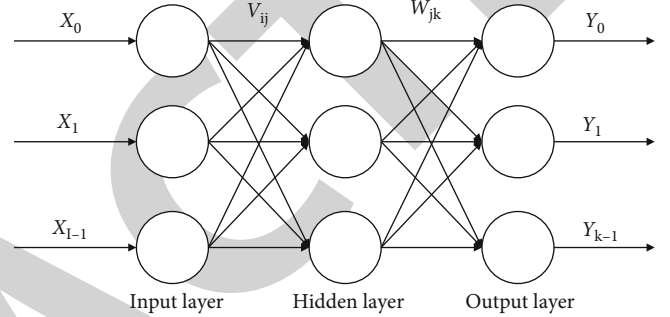


FIGURE 2: Schematic diagram of three-layer BP neural network structure.

TABLE 1: Evaluation indicator table.

Indicator category	Label
Rigorous lesson preparation	$X_1$
Homework correction, tutoring students	$X_2$
Systemicity of content	$X_3$
Clearly express complex issues	$X_4$
Heuristic, auxiliary teaching methods	$X_5$
Key points, difficult points to deal with	$X_6$
Motivate students' enthusiasm	$X_7$
Teaching students according to their aptitude	$X_8$
Focus on inspiration	$X_9$
Focus on communicating and interacting with students	$X_{10}$
Whether the student's requirements are strict and fair	$X_{11}$
Student ability improvement	$X_{12}$

that uses the lowest mean square error learning strategy is one of the most widely utilized neural network models presently. In addition to being the neural network model in use in this article, it is widely utilized in voice synthesis, control, recognition, and teacher training. The other neural network models are Hopfield network, Kohonen network, and neural network with radial basis function.

**3.1.4. Training of Artificial Neural Network.** Artificial neural networks' capacity to learn is by far its most appealing characteristic. The renowned learning theorem of artificial neural

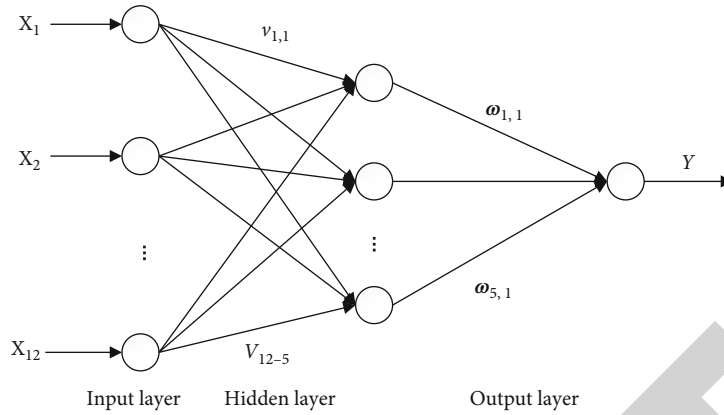


FIGURE 3: BP neural network model for teaching quality assessment.

networks was developed in 1962 by a group of researchers. An artificial neural network's training is the first step in the learning process. The term "training" refers to the act of adjusting the connection weights between neurons in the artificial neural network during the process of entering a sample set of sample vectors into the network. With a weight matrix, a sample set's connotation may be saved as the network takes input. It can give an appropriate output. From the perspective of advanced forms of learning, one is tutored learning and the other is tutorless learning, and the former seems to be more common. Whether students go to school to receive education from teachers or study by themselves, they all belong to tutored learning. There are still many times. People are constantly summarizing and learning through some practical experience; maybe, these should be regarded as unsupervised learning.

Learning with a mentor corresponds to training with a mentor. In this training, the user is required to give the corresponding ideal output vector at the same time as the input vector. Therefore, the network trained by this training method implements a heterogeneous mapping, and the input vector and its corresponding output vector form a "training pair." Among the tutored training algorithms, the most important and widely used is the Delta rule. Its form is

$$\omega_{ij}(t + 1) = \omega_{ij}(t) + \alpha(y_i - o_j(t))o_i(t), \quad (5)$$

where  $\omega_{ij}(t + 1)$  and  $\omega_{ij}(t)$  represent the weights of the connection between neurons  $AN_i$  to  $AN_j$ ; at time  $t + 1$  and time  $t$ , respectively,  $o_j(t)$  and  $o_i(t)$  are these two neurons. The output of the unit at time  $t$ ,  $y_i$ , is the ideal output of the neuron  $AN_j$ ;  $\alpha$  is the given learning rate.

**3.2. BP Artificial Neural Network.** The error backpropagation method is often used to refer to a multilayer forward neural network (BP algorithm). By reintroducing the error backpropagation method for forward neural networks in parallel distributed processing research in 1986, Rumelhart and McClelland addressed the multilayer forward neural network's learning difficulty and made it applicable in other industries. For practical applications of artificial neural net-

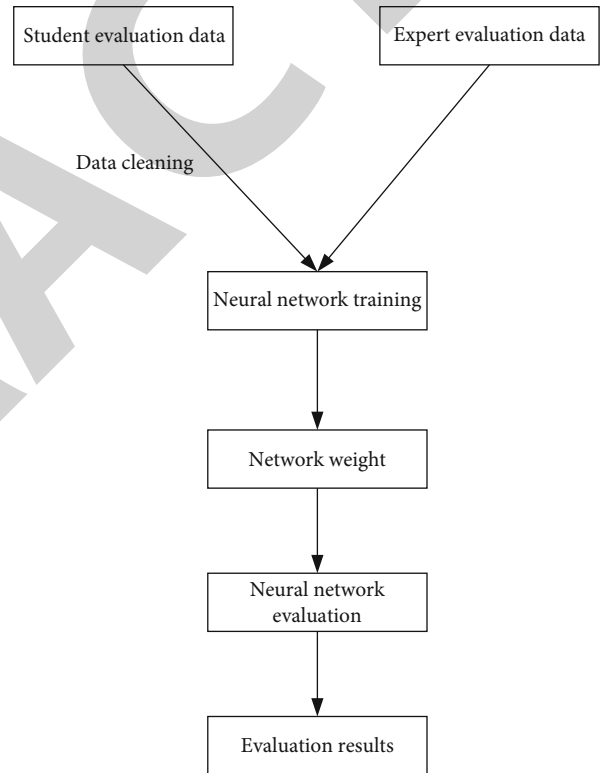


FIGURE 4: System implementation process.

works, BP networks and their variations, which are the heart of the forward network, are widely used. This is also the most fundamental aspect of artificial neural networks. Nearly 90% of neural network applications are based on the BP algorithm, according to data.

**3.2.1. BP Network Structure.** The BP neural network is a three- or more-layered hierarchical neural network. All three layers are included inside this structure. Because the layers are only partially interconnected, neurons in one layer are not related to those in the next. To implement the BP

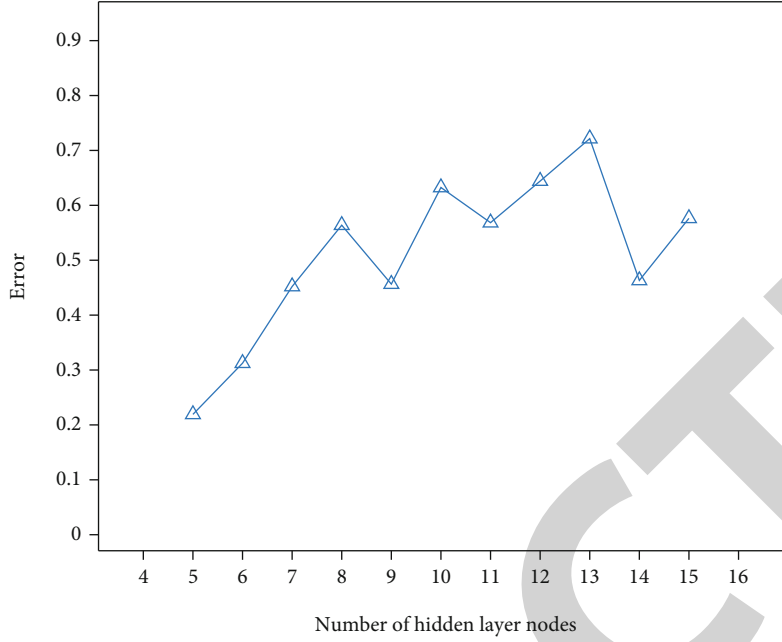


FIGURE 5: The number of nodes in the hidden layer of the network and the error.

algorithm, a three-layer BP network with one hidden layer is shown in Figure 2.

In Figure 2, it is assumed that the number of units of the input layer, hidden layer, and output layer is  $I$ ,  $J$ , and  $K$ , respectively; the input is  $(x_0, x_1, x_2, \dots, x_{i+1})$ ; the hidden layer output is  $(h_0, h_1, h_2, \dots, h_{k-1})$ , the actual output of the network is  $(y_0, y_1, y_2, \dots, y_{k-1})$ ;  $(d_0, d_1, d_2, \dots, d_{k-1})$  represents the expected output of the training sample. The weight from the input layer unit  $i$  to the hidden layer unit  $j$  is  $V_{ij}$ , and the weight from the hidden layer unit  $j$  to the output layer unit  $k$  is  $W_{jk}$  and  $\theta_j$  and  $\theta_k$ ; the hidden layer unit and the output layer unit are both represented by these symbols. Therefore, the network's hidden layer unit output is

$$h_j = f\left(\sum_{i=0}^{I-1} v_{ij}x_i - \theta_j\right). \quad (6)$$

Each unit in the output layer has the following value as its output:

$$y_k = f\left(\sum_{j=0}^{J-1} w_{jk}h_j - \theta_k\right). \quad (7)$$

**3.2.2. Learning Algorithm of Standard BP Network.** Two stages are involved in the BP algorithm. First, the input sample is fed into an output layer, where it is processed by a layer-by-layer method and finally output. The weight coefficient of this process remains unchanged. Second, if the output does not match the desired output, backpropagation is entered. To reduce the deviation signal, the second stage (also known as the backpropagation process)

TABLE 2: Normalized training data.

Enter	1	2	3	4	5	6	7	8
$X_1$	0.53	0.64	0.58	0.66	0.96	0.82	0.72	0.59
$X_2$	0.61	0.53	0.68	0.88	0.73	0.99	0.93	0.59
$X_3$	0.73	0.61	0.58	0.97	0.85	0.75	0.63	0.67
$X_4$	0.62	0.85	0.94	0.73	0.59	0.82	0.71	0.66
$X_5$	0.55	0.97	0.49	0.53	0.84	0.45	0.64	0.77
$X_6$	0.58	0.99	0.86	0.56	0.78	0.75	0.67	0.54
$X_7$	0.53	0.64	0.58	0.66	0.96	0.82	0.72	0.59
$X_8$	0.61	0.53	0.68	0.88	0.73	0.99	0.93	0.59
$X_9$	0.58	0.99	0.86	0.56	0.78	0.75	0.67	0.54
$X_{10}$	0.62	0.85	0.94	0.73	0.59	0.82	0.71	0.66
$X_{11}$	0.53	0.64	0.58	0.66	0.96	0.82	0.72	0.59
$X_{12}$	0.63	0.71	0.98	0.87	0.75	0.65	0.63	0.65

utilizes the error calculated at each concealed layer to advance the weights of the preceding layer. The network weight adjustment adopts the Delta learning rule; that is, the gradient along the error surface descends the fastest according to the gradient method, so as to minimize the network error.

*Backpropagation stage:* the deviation signal is transferred backward according to the original forward propagation route, and each hidden layer's weight coefficient is changed to minimize the deviation signal. The ideal gradient descent technique is the most popular approach to determining the value with the lowest variance. The weight adjustment formula between the output layer and

TABLE 3: Validation data after normalization.

Enter	1	2	3	4	5
$X_1$	0.55	0.68	0.57	0.58	0.96
$X_2$	0.66	0.59	0.72	0.88	0.96
$X_3$	0.78	0.64	0.59	0.96	0.85
$X_4$	0.58	0.75	0.93	0.65	0.68
$X_5$	0.59	0.99	0.55	0.67	0.79
$X_6$	0.57	0.91	0.79	0.82	0.74
$X_7$	0.65	0.58	0.77	0.98	0.66
$X_8$	0.76	0.69	0.52	0.98	0.86
$X_9$	0.68	0.74	0.99	0.56	0.85
$X_{10}$	0.78	0.95	0.63	0.75	0.58
$X_{11}$	0.89	0.59	0.95	0.77	0.69
$X_{12}$	0.67	0.81	0.99	0.72	0.84

the hidden layer is shown in the following equation. The correction value for each  $\omega_{jk}$  is

$$\Delta\omega_{jk} = -\eta \frac{\partial E}{\partial \omega_{jk}} = -\frac{\partial E}{\partial \text{net}_k} \cdot \frac{\partial \text{net}_k}{\partial \omega_{jk}} = \eta \delta_k o_j. \quad (8)$$

If the activation function of each layer of the BP neural network takes the unipolar sigmoid function, that is,

$$f(\text{net}) = \frac{1}{1 + e^{-\text{net}}}. \quad (9)$$

For the input layer,

$$\Delta\omega_{jk} = \eta o_j (d_k - o_k) o_k (1 - o_k). \quad (10)$$

For the hidden layer,

$$\Delta v_{jk} = \eta o_j \left( (1 - o_j) \sum_{k=0}^{K-1} \delta_k \omega_{jk} o_i \right). \quad (11)$$

**3.2.3. Limitations and Improvement Methods of BP Network.** The BP network is the most commonly utilized and has shown to be a worthwhile investment in the field. There are a slew of issues with the algorithm, though. Particularly problematic for BP's network are these five issues, some of which are quite significant. These five questions are briefly discussed below.

(1) The problem of convergence speed

The biggest weakness of the BP algorithm is that its training is difficult to master. Algorithm training takes a long time, particularly after the network training has progressed to a certain point; its convergence speed may drop to a point where it is difficult to grasp, unbearable point.

(2) The BP algorithm employs the steepest descent approach to solve the local minimum point issue

The slope of the error surface is used to estimate its training. In a high-dimensional space, the error surface of a complex network may be exceedingly complicated and uneven. Many local minimums are disseminated across the network during training. With the existing approach, it is very difficult to get out of a local minimum.

(3) The problem of network paralysis

The weight may become very large during training, causing the neuron's network input to become very large, causing the derivative function of its activation function to have a tiny value at this moment. At this time, the training step length will change is very small, which in turn causes the training speed to drop very low, eventually causing the network to stop converging.

In order to overcome the problems of slow results and local minima of the BP algorithm, many scholars have revised the BP algorithm from different aspects. The following are some commonly used improved algorithms:

(1) When the traditional BP method updates the weights, it does so exclusively based on the error's gradient descent direction at time  $t$ , which may cause the training process to oscillate and converge slowly based on the enhanced gradient descent technique. The improved technique is based on the standard gradient descent approach, which means that each time the network weights and thresholds are corrected, the previous learning's correction amount is added in a set proportion, accelerating network learning convergence

(2) The BP algorithm and simulated annealing method are combined to form a new algorithm. It can not only take into account the advantages that the adjustment amount of the connection weight of the BP algorithm is determined but also take into account the randomness and heuristics of the adjustment of the connection weight in the simulated annealing algorithm. As a result, by dividing the change of a connection weight into two parts, the BP method can give the direct calculation part, while the simulated annealing approach can supply the random component [19]. The connection weight  $\omega_{ij}$  between the neurons  $AN_i$  and  $AN_j$  in the network is adjusted by the following formula:

$$\Delta\omega_{ij} = \alpha \left( (1 - \beta) \delta_j o_i + \beta \Delta\omega'_{ij} \right) + (1 - \alpha) \Delta\omega''_{ij}, \quad (12)$$

where  $\omega'_{ij}$  is the adjustment amount of the connection weight  $\omega_{ij}$  obtained according to the simulated annealing algorithm and  $\omega''_{ij}$  is the last modification amount of  $\omega_{ij}$ ;  $\alpha \in (0, 1)$  is the learning rate. Here, it simultaneously also plays the role

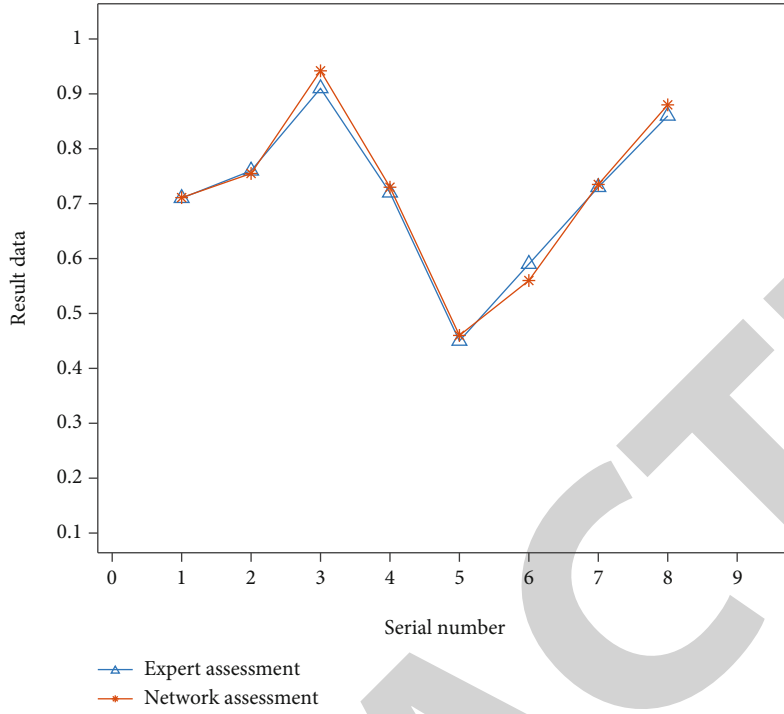


FIGURE 6: Comparison of neural network training results and actual evaluation results.

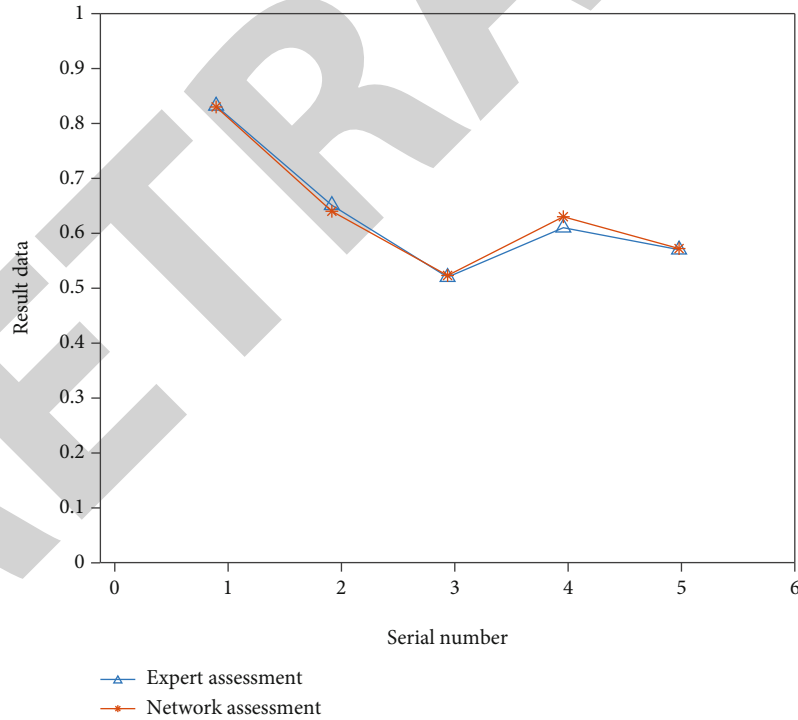


FIGURE 7: Test set test results compared to actual evaluation.

of weight distribution of “direct part” and “random part”;  $\beta \in (0, 1)$  is the impulse coefficient

$$\omega'_{ij} = T \tan(p(\Delta\omega)). \quad (13)$$

$p(\Delta\omega)$  is randomly selected in the uniform distribution interval  $[-0.5, 0.5]$ ;  $T$  is annealing temperature.

$$T = \frac{T_0}{1+t}, \quad (14)$$

where  $T$  is the initial temperature and  $t$  is the number of annealing.

### 3.3. Teaching Quality Evaluation Model Cased on Neural Network

**3.3.1. Vocational School Teaching Quality Evaluation Index System.** To reflect the scientificity, fairness, and rationality of teaching quality evaluation, the index system plays a key role. Different colleges and universities have different divisions of labor, positioning, and their own characteristics, and different indicators should be used for evaluation. Therefore, the establishment of a scientific and appropriate assessment index system for various colleges and institutions is necessary. The so-called scientific principle means that the established indicators and standards must reflect the development goals of education and the objective laws of teaching. Specifically, the evaluation index should be consistent with the overall goal of education and teaching; that is, whether the goal is correct or not should be measured by the correct direction. If the indicators violate the educational goals, it will lead to inaccurate goals and mistakes in decision-making and eventually lead to the wrong way of teaching. Teaching is guided by the evaluation index. A teacher's attention will be focused on what metrics are used in evaluations and assessments. Therefore, the selection and creation of indicators are critical. Reflecting the nature of education and selecting typical and objective indicators as well as paying attention to the leadership role are all necessary parts of the process. Otherwise, too simple and excessive indicators will make teaching evaluation useless.

According to the assessment index method for teaching work level in the normal colleges and universities, this paper strives to reflect the principles of scientificity, comprehensiveness, accuracy, and measurable operability and designs the index system into the following 12 indicators. Table 1 shows the index system that defines the network structure of the model for evaluating teaching quality.

**3.3.2. Normalization of Input Indicators.** Since the input of each indicator is obtained by students' scoring using the percentage system, the magnitude of each component's value is vastly different from the next. One possible consequence of using raw data directly is that the neuron's effective processing range may be exceeded due to the so-called "saturation phenomenon," which occurs when an amount of raw input is applied without any treatment. Even though the total value of the original data is not excessive, the network's influence may be larger than the impact of other components because of a component's excessive size, causing other components to lose control of the network. The neural network's input samples must, therefore, be normalized. For the neural network, the input should be normalized to  $[0, 1]$ . Because sigmoid function is a linear transformation of data processing, the maximum-minimum approach is adopted in this work for normalizing because it can better keep its original meaning

and will not cause information loss. In this work, the input normalization formula is as follows:

$$X = \frac{I - I_{\min}}{I_{\max} - I_{\min}}. \quad (15)$$

**3.3.3. Evaluation Model Based on Improved BP Neural Network.** The BP neural network has the following characteristics:

- (1) The advantage of the neural network is that it has the ability to simulate multiple variables without making complicated correlation assumptions about the input variables
- (2) One hidden layer is all that is needed to estimate any continuous function on an enclosed area with any degree of accuracy if the number of hidden nodes is enough
- (3) The generalization ability of BP neural network. After the neural network is trained, it does not respond to small changes in the input, which reflects the inaccuracy of its operation. An inaccuracy is a flaw, yet in certain instances, the system's performance may benefit from it. The purpose of this research is to develop a model for evaluating the quality of teaching by including the BP neural network [20, 21]

The challenge of determining the best model structure design is critical. The number of network trainings may be reduced, and the accuracy of network learning can be improved by making the right decision. This covers the kind of connection, the network level, and how many nodes are in each tier (that is, to determine the number of neurons in the input layer, hidden layer, and output layer). A nonlinear mapping between input (teaching quality evaluation index) and output (final assessment result of instructors' teaching quality) may be used to describe the challenge in teaching quality evaluation. If you want the most accurate approximation possible, a three-layer BP network topology is the best choice for this study. Figure 3 shows the BP neural network model for the teaching quality evaluation system, which may be summarized as follows. The realization process of the whole system is shown in Figure 4.

## 4. Experiment and Analysis

**4.1. Determination of the Number of Neurons in Each Layer.** Determination of the number of neurons in the input layer: The number of secondary indicators in the theoretical teaching quality evaluation system is 12, so the number of neurons in the input layer is set to 12. In the determination of the number of neurons in the hidden layer: calculated according to the empirical formula, when the initial number of nodes in the hidden layer is 5, multiple network structures are set up, and the number of nodes in the hidden layer of each network is increased by 1. The experimental results are shown in Figure 5; it can be seen that when the number

of hidden layer nodes is 5, the error is the smallest, so the number of hidden layer nodes of the BP neural network is set to 5. In the determination of the number of neurons in the output layer, the output target is the teaching quality evaluation result, so the output the layer node is 1.

**4.2. Preparation and Training of Sample Library.** It is critical to have samples accessible when training an artificial neural network. The quality of the sample selection has a direct impact on the neural network's training results. The selection of samples should be based on representative samples based on summing and analysis. Students in the classroom are given a questionnaire based on the teaching quality assessment indicators, which allows them to choose and rate different aspects of their instructors' performance. It is like having a lot of judges in each classroom since there are so many kids. The average value of the instructor's 12 input indications is calculated using the five highest and the five lowest scores, so that certain students' unreliable evaluations of the teacher may be discarded. Rather on relying on a predetermined set of output indicators, this study relies on data from actual classes to train a neural network using evaluations from the teacher oversight group. Although the students write out the teacher's indications, the ultimate assessment outcome reflects the evaluation thoughts of specialists in the supervisory team's group.

The obtained data is standardized using the index system's standardization process. The neural network will be able to handle these data more easily if they are converted to binary data. Tables 2 and 3 show the results of the data processing on the samples. Use the training data in Table 2 and the verification data in Table 3 to check the neural network model's prediction results.

**4.3. Simulation Experiments and Results.** MATLAB's neural network toolbox offers implementations of different neural network algorithm applications. The initialization of a BP neural network for Matlab typically consists of four steps: The establishment of the network is the next step. The third step is a network simulation. The network must be trained as a fourth step. An example of a simulation would be to read in the training data, create an appropriate neural network model using the above-mentioned model structure, and then begin training the model using these parameters. A neural network model is created, validation data is read in, and the predicted value is produced by the network computation when the training is complete.

After the network training, the simulation results were evaluated and the expert results of the five test sets were evaluated (see Figures 6 and 7). All of the training samples were found to be extremely near to expert assessment findings, as shown in Figures 6 and 7, and this was also true for the five simulated test sets. Experimental evidence shows that the BP neural network-based model for evaluating vocational education quality has training and prediction accuracy that is totally acceptable and that the model is a sensible and viable one.

## 5. Conclusion

Because of its great nonlinear learning ability and fault tolerance to noisy input, the BP neural network is the most extensively used artificial neural network method in data mining applications. This paper incorporates the theory of artificial neural networks into the quality evaluation of vocational education and teaching reform, based on extensive research on artificial neural network algorithms. The characteristics of this system are as follows: a comprehensive overview of several commonly used artificial neural network algorithms and a focus on the BP network model structure and learning algorithm; an upgraded version of the BP neural network is proposed in this research to address the issues of poor convergence speed and local minimum points and is used to combine the BP algorithm with the simulated annealing method to form a new algorithm. It can take into account not only the benefits of determining the connection weight adjustment amount in the BP algorithm but also the randomness and heuristics of determining the connection weight adjustment (amount) in the simulated annealing approach. Students of different majors have varied inclinations for different courses because to the randomization of students in the process of evaluating teaching, and due to the involvement of some human variables, students' scores cannot really reflect the actual teaching effect. This study incorporates artificial neural networks into the assessment of teaching quality by utilizing their nonlinear learning ability and fault tolerance. An assessment system for vocational education quality is presented in this research, which shows how the functions of data collecting and evaluation findings may be realized. The teaching quality assessment model built by utilizing neural network gives full play to the benefits of neural network. It is a new way to measure the quality of vocational education.

## Data Availability

The datasets used during the current study are available from the corresponding author on reasonable request.

## Conflicts of Interest

The authors declare that they have no conflict of interest.

## Acknowledgments

This work was supported by "Research on the Construction Strategy of Entrepreneurial Education Ecosystem in Higher Vocational Colleges," which is the 2021 Chinese Vocational Education Research Project of Zhejiang Province (project number: ZJCV2021C34).

## References

- [1] R. Hilal, "Vocational education and training for women and youth in Palestine: poverty reduction and gender equality under occupation," *International Journal of Educational Development*, vol. 32, no. 5, pp. 686–695, 2012.



## Research Article

# Effect Analysis of Positive Molecular Therapy in Surgical Nursing Based on Data Transformation Analysis

Yuan Liu , Sumei Wu, Guifen Wang, Xiaoxue Sun, Lei Liu, and Yaling Zhao

Department of Cardiothoracic Surgery, Tangshan People's Hospital of Hebei Province, Tangshan, Hebei 063000, China

Correspondence should be addressed to Yuan Liu; [ly15333251719@sina.com](mailto:ly15333251719@sina.com)

Received 16 May 2022; Revised 10 June 2022; Accepted 13 June 2022; Published 1 July 2022

Academic Editor: Naeem Jan

Copyright © 2022 Yuan Liu et al. This is an open access article distributed under the Creative Commons Attribution License, which permits unrestricted use, distribution, and reproduction in any medium, provided the original work is properly cited.

This paper briefly introduces the concept, classification, and mechanism of action of positive thinking therapy; reviews the application and research progress of positive thinking therapy in perioperative care of surgical patients at home and abroad; presents the shortcomings and defects in the development; and aims to provide intervention, reference, and basis for the development of positive thinking therapy in perioperative care of surgical patients. One hundred and eight patients are undergoing PCI surgery in our cardiology department; 50 patients undergoing percutaneous coronary intervention were selected as the control group, and 58 patients undergoing percutaneous coronary intervention were selected as the observation group. Traditional health education was employed in the control group, while empowerment education based on timing theory was used in the observation group. The two groups were observed and compared in terms of self-care competence, anxiety and depression, medication adherence score, and exercise adherence. *Conclusion.* Empowerment education based on timing theory can improve self-care ability of PCI patients, reduce patients' anxiety and depression, and improve patients' medication and exercise compliance.

## 1. Introduction

With the development of modern medical technology, surgical treatment has become a common method of treatment for various surgical diseases, and quality perioperative management provides an important guarantee for the success of surgery and the patient's future recovery. Most patients face surgery with anxiety, fear, and other adverse emotions due to concerns about the surgical outcome and recovery, causing adverse reactions of the body such as increased heart rate, elevated blood pressure, and flushing, thus affecting the surgical treatment and postoperative recovery [1]. As the scope of medical exploration continues to expand, "positive thinking intervention," which is an extension of psychology, has been gradually used in clinical research. In recent years, interventions based on positive thinking, such as meditation and stress reduction, have been used in the perioperative period to guide patients to face negative emotional disturbances objectively, relieve psychological stress, and reduce postoperative pain, which play an important role in the operation and postoperative recovery [2]. In this

paper, we review the relevant studies at home and abroad and aim to provide reference for the future application of positive thinking therapy in the perioperative period.

Since the introduction of positive thinking, psychologists and medical doctors have removed its religious components and applied it to clinical practice. Among them, MBSR and MBCT are the most commonly used, and MBSR and MBCT are currently the most mature and systematic positive thinking interventions [3]. Overseas traditional MBSR and MBCT are group training courses, mostly using the intervention method created by Kabat-Zinn that has a strict training cycle and training courses, the training cycle is generally 8 weeks, once a week, 2.5~3 h each time, and each week there are different types of training methods and coursework, and requires the course instructor to have professional knowledge and skills [4]. In recent years, China has introduced positive thinking into the medical field, in cardiovascular disease, diabetes, cancer, and other clinical diseases to explore, but its adopted treatment is slightly different from foreign countries; the whole course of treatment is 8 weeks, once a week, each time 2.5-3.5 h, requiring 45 min of formal

practice and about 10 min of informal practice every day, and in the 6th week a full day retreat (7.5h). With the continuous improvement of the concept of positive thinking, DBT and ACT have been gradually promoted in clinical practice in recent years and are now mainly used in the treatment of patients with psychiatric disorders such as borderline personality disorder. DBT and ACT can help them to improve their tolerance of negative feelings, reduce behavioral impulses, and enhance their ability to cope effectively with illness [5]. As an important method of psychological treatment for psychological disorders, positive thinking therapy has also played a key role in promoting patients' physical and mental health in clinical practice [6]. Domestic and international studies have shown that the interventions of positive thinking therapy in hypertension, diabetes, chronic pain, cancer, chronic inflammation, and perioperative patients can effectively relieve patients' physical pain, improve patients' emotional disorders, reduce psychological stress, and improve the quality of daily life, which have shown good results in clinical application [7].

Surgery is an invasive treatment, and as a serious source of psychological stress, it can adversely affect the patient's nervous system, endocrine system, and circulatory system, etc. The preoperative stress and anxiety and postoperative physiological trauma can also directly affect the patient's normal physiological activities [8, 9]. In order to solve the psychophysiological problems of patients, clinical workers need to adopt various ways to alleviate the various adverse reactions of patients in the perioperative period [10]. Currently, positive thinking therapies are implemented in the perioperative period in the form of body scans, positive breathing, positive meditation, walking meditation, and positive yoga. Most patients experience anxiety and depression as a result of the invasive nature of surgery and their own stress reactions. Some studies have found that anxiety and depression can increase sympathetic nerve tone and catecholamine secretion, which can cause palpitations, chest tightness, and even a sense of dying, which can seriously affect the operation and postoperative recovery [11]. In recent years, positive thinking therapy has been gradually applied to the guidance of perioperative management of surgical patients. In [12], an 8-week course of standard positive mindfulness stress reduction (tmbsr) was applied to patients awaiting renal transplantation via teleconferencing, and the results showed that TMBSR was effective in helping patients to reduce their preoperative anxiety and discomfort. In a controlled trial of perioperative orthostatic stress reduction therapy in 200 patients undergoing elective surgery, [13] showed that the preoperative systolic blood pressure and heart rate were more stable in the observation group (102 patients) than in the control group (98 patients), and the preoperative anxiety and depression scores in the observation group were significantly lower than those in the control group, which is consistent with the study by [14] and others.

The team of [15] used positive meditation training combined with guided psychology on perioperative patients in general surgery and found that the positive meditation training improved the positive thinking ability and positive thinking state of perioperative patients in general surgery,

allowing them to better control their negative emotions and psychological reactions. Positive meditation therapy can improve negative psychology and regulate body state for preoperative patients, according to the findings of the above study [16]. At present, China is facing the problems of large medical population, shortage of medical resources, shortage of medical and nursing staff, lack of comprehensive attention to patients' psychological problems, etc. Positive thinking therapy is simple, green, and can compensate for the shortage of medical and nursing staff to a certain extent and can improve the psychological intervention of medical and nursing staff to patients, which has good clinical feasibility [17]. However, the sample size of current studies is generally small, and there is a lack of high quality and standard randomized controlled trials, and the effectiveness of orthomolecular therapy for different surgical diseases remains to be investigated.

The research is organized as follows: the optimization algorithms are presented in Section 2. Section 3 analyzes some of the linear optimization problem. Section 4 discusses the study subjects. In Section 5, results and discussion were explored in depth. Section 6 proposed the discussion. Finally, in Section 7, the research work is concluded.

## 2. Optimization Algorithms

**2.1. Standard Particle Swarm Algorithm.** Let the current position and velocity of the  $i$ th particle of population size  $N$  be  $X_i = (x_{i1}, x_{i2}, \dots, x_{iD})$  and  $a_j \leq b_j$ ,  $V_i = (v_{i1}, v_{i2}, \dots, v_{iD})$ , respectively, and the best position of its current search is  $p_{best}$ , and the best position of all subcurrent searches is  $g_{best}$ . The  $j$ th dimensional state ( $1 \leq j \leq n$ ) of the  $k+1$ th iteration of particles is updated according to the following formula:

$$v_{ij}^{k+1} = \omega v_{ij}^k + C_1 R_1 (p_{best} - x_{ij}^k) + C_2 R_2 (g_{best} - x_{ij}^k), \quad (1)$$

$$x_{ij}^{k+1} = x_{ij}^k + v_{ij}^k, \quad (2)$$

$$\begin{cases} v_{ij}^{k+1} = v_{max}, & \text{if } v_{ij}^{k+1} > v_{max}, \\ v_{ij}^{k+1} = -v_{max}, & \text{if } v_{ij}^{k+1} < -v_{max}, \end{cases} \quad (3)$$

$$\begin{cases} x_{ij}^{k+1} = a_j, & \text{if } x_{ij}^{k+1} < a_j, \\ x_{ij}^{k+1} = b_j, & \text{if } x_{ij}^{k+1} > b_j, \end{cases} \quad (4)$$

where  $i = 1, 2, \dots, N, j = 1, 2, \dots, D$ .

Parameter description  $\omega$  is called the inertia weight, which determines the influence of the particle historical velocity information current velocity information.  $C_1, C_2$  is called the learning factor, which indicates the degree to which the particle is influenced by individual cognition and social cognition, and is usually set to  $C_1 = C_2 = 2$ .  $R_1, R_2$  indicates a random number uniformly distributed between [0.1]. In addition, the particle  $i$  is constantly adjusting its position according to the velocity and is limited by the maximum velocity  $v_{max}$  which is usually set to 10%-100% of the variation range per dimension.

**2.2. Monte Carlo Algorithm.** The Monte Carlo approach, also known as random simulation (Randulation), is a series of numerical methods for solving nonlinear problems. It is derived from the random process of roulette and coin tossing. The principle of Monte Carlo algorithm is as follows: statistical experiments and random simulation as a means, from the probability distribution of random variables through the method of randomly selected numbers, to produce a random sequence of numbers consistent with the characteristics of the probability distribution of the random variables, as the infant sequence for simulation.

### 3. Linear Optimization Problem

The first and second steps of the calibration of the nonlinear visual model are performed separately for the linear initial value solution and the initial nonlinear optimization of the NIE model, respectively. The parameters of the calibration are optimized in the process. According to the camera model, from the known object feature points projected onto the image plane, the model image coordinates of the feature points  $(U_i, V_i)$ , the model image coordinates  $(U_i, V_i)$  and the actual camera detected image coordinates, and there are residuals; the purpose of nonlinear optimization is to minimize this residual, so that the parameters minimize the residuals for the camera parameter values. The analytical expression of the objective function of the optimization is

$$F = \min \sum_{i=1}^n \sum_{j=1}^n d(Q(a_j, b_j), x_{ij})^2, \quad (5)$$

where  $x_{ij}$  denotes the 2D image point coordinates of the  $i$ th spatial point on the first picture, which is extracted directly from the image.  $Q(a_j, b_j)$  is the projected coordinates obtained by taking the known 3D point scale and the external parameter values, according to the projection relation.  $a_j$  denotes the first picture, and  $b_j$  denotes the coordinates of the  $i$ th 3D point.  $d(x, y)$  denotes the Euclidean distance of these two  $x, y$  vectors. The goal of the optimization is to minimize the residuals of the 2D coordinates obtained by these two different paths.

**3.1. Algorithm Flow.** The MPSO algorithm steps are as follows: the algorithm uses linear decreasing weight particle swarm for rough search at the early stage of evolution and improves the solution accuracy by using Monte Carlo algorithm for random search at the later stage.

**Step 1.** The particle population (population size in  $N$ ) for each particle in the initialization range for the speed and position of random initialization to ensure population variety, all particle positions uniformly distributed in the search area particle positions are initialized according to the following formula:

$$x_{ij} = a_j + (i - 1) \times (b_j - a_j) / N + ((b_j - a_j) / N) \times R, \quad (6)$$

where  $R$  is the random number  $i = 1, 2, \dots, N, j = 1, 2, \dots, D$  evenly distributed between  $[0, 1]$ .

**Step 2.** Calculate the adaptation values of all particles.

**Step 3.** Update the best position  $p_{\text{best}}$  experienced by each particle and the best position  $g_{\text{best}}$  experienced by all particles according to the current state of the particle population.

**Step 4.** Calculate the inertia weights according to equation (7) to update the velocity and position of particles according to equations (8) and (2), and use equations (3) and (4) to cross the boundary.

$$\omega^k = \omega_{\text{max}} - ((\omega_{\text{max}} - \omega_{\text{min}}) / it_{\text{max}}) \times k, \quad (7)$$

$$v_{ij}^{k+1} = \omega^k v_{ij}^k + C_1 R_1 (p_{\text{best}ij} - x_{ij}^k) + C_2 R_2 (g_{\text{best}ij} - x_{ij}^k). \quad (8)$$

**Step 5.** When the number of iterations does not reach the maximum number of iterations  $it_{\text{max}}$ , then go to Step 2; if it reaches the maximum number of iterations, then go to Step 6.

**Step 6.** Make  $j = 1$  and  $j < 10^4, k = 1, m_1 = m_2 = \dots = m_D = 1, x^j = g_{\text{best}} = (x_1^j, x_2^j, \dots, x_D^j), B_i = (b(i) - a(i)), i = 1, 2, \dots, D, F_1 = f(x^j)$ .

**Step 7.**  $m_k = m_k + 1$ , if  $m_k > 10^5$ , and  $B_k > \varepsilon$ , so that  $B_k = B_k / 2, m_k = 0$ .

**Step 8.** Generate a random number  $x_k^j = x_k^{j-1} + r_k^j, F_2 \geq F_1 = F(x^j)$  according to uniform distribution on  $(-B_k, B_k)$ , make  $x_k^j = x_k^{j-1} + r_k^j$ , and calculate  $F_2 = F(x^j)$ ; if  $F_2 \geq F_1$ , make  $x_k^j = x_k^j - r_k^j$ , and return to Step 7; otherwise, make  $F_2 = F, k = k + 1$ ; if  $K > D$ , make  $k = 1, j = j + 1, x_k^j = x_k^{j-1}, k = 1, 2, \dots, D$ .

**Step 9.** Check whether the preset precision  $\varepsilon$  and the maximum number of iterations are reached, if not, and  $j < 10^4$ , then return to Step 7; otherwise,  $x^j = (x_1^j, x_2^j, \dots, x_D^j)$  will be the final value of  $F$  solution.

### 4. Study Subjects

Patients undergoing percutaneous coronary intervention in the cardiology department of our hospital were selected as the study subjects. Inclusion criteria are as follows: (1) confirmed diagnosis of coronary artery disease, (2) good understanding and communication skills, and (3) informed consent of the patients and their families and willingness to cooperate with this study. Exclusion criteria are as follows: (1) combined with other cardiac diseases other than coronary heart disease; (2) suffering from cognitive dysfunction or psychological or psychiatric diseases; (3) combined with other serious physical diseases such as tumor, liver, and

kidney insufficiency; and (4) patients with joint, muscle, neurological, and other diseases that cannot cooperate with exercise rehabilitation. Exclusion criteria are as follows: (1) only contrast surgery that was performed on patients who did not fit the criteria for PCI procedure; (2) postoperative complications such as bleeding, restenosis, and occlusion of the implanted stent after PCI; and (3) patients who withdrew voluntarily. The final 108 patients were included in the study, 50 patients with percutaneous coronary intervention in March-May 2019 as the control group and 58 patients with percutaneous coronary intervention in June-August 2019 as the observation group. There was no statistically significant difference between the general data of the 2 groups such as gender, age, education, smoking history, drinking history, and number of stents ( $P > 0.05$ ). The details are shown in Table 1.

**4.1. Methods.** A total of four face-to-face health education sessions were conducted during hospitalization, each for about 30 min. They were carried out by charge nurses with clinical experience and were identical to those in the observation group. Patients and family members received information regarding coronary heart disease and general health education materials on the day of admission; 1 day before surgery, the process and preoperative preparation were explained, and patients were taught psychological relaxation techniques; on the day after surgery, skin care at the puncture site, the importance of postoperative medication; the effects of aspirin, clopidogrel, and other drugs; and the observation and treatment of adverse reactions were introduced; 1 d before discharge, a manual on rehabilitation exercises was distributed. Patients were followed up by telephone once a month for 3 months. The follow-up included the implementation of rehabilitation exercises, diet, medication standardization, and self-monitoring of diseases such as blood pressure and blood glucose.

**4.2. Observation Group.** Empowerment education research group was established including the director of the cardiology department (professor and master's supervisor), the head nurse (supervising nurse with more than 20 years of clinical work experience), 3 charge nurses (with more than 10 years of cardiology nursing experience), 2 nurses of the cardiac rehabilitation center (with provincial specialist nurse certificate), 2 nursing master students, and 1 psychological counselor (with national level 2 psychological counselor certificate). All team members underwent standardized training and passed the examination and were proficient in the intervention process.

The timing theory illness stage division was used as a reference in this investigation. To establish the intervention strategy for this study, the team members conducted a local and international literature search, clinical investigation with the features of PCI patients, expert consultation, and preexperimentation. This includes (1) the division of disease stages: diagnostic period (from disease onset to definite diagnosis), PCI perioperative period (patient's decision to operate to postoperative stabilization), discharge preparation period (patient's treatment is about to end to discharge),

adjustment period (after discharge to 1 month), and adaptation period (1 month to 3 months after discharge). (2) Determining the content of empowerment education includes as follows: (a) For question identification, the interventionist uses in-depth conversation with the patient using empathy and emotional support, asks the patient targeted questions, and understands the patient's current needs based on the patient's responses. (b) For emotional expression, start with an open-ended topic, induce the patient to tell or vent his emotions, do not interrupt the patient easily, pay attention to listening and responding at the right time, and explore the patient's innermost emotions. (c) For goal setting, group members act as a supporting role, actively provide medical information to support the patient, and the patient proposes goals. Team members help analyze the feasibility of the goals according to the patient's actual situation and make adjustments if necessary. (d) Develop a plan, in which the researcher helps the patient to develop a health promotion plan based on the set goals, and the patient chooses the method that meets his or her wishes. The main purpose of the program is to teach the researcher the relevant knowledge, the patient's participation in the discussion, and the training of relevant coping skills. (e) Behavioral assessments were carried out on a regular basis to track the improvement of patients and their families. If the goals are not met, actively seek out the reasons and make changes as soon as possible to boost the patient's self-esteem and treatment compliance.

The intervention was carried out by the investigator herself and a uniformly trained specialist nurse from the study team, with team members supervising throughout. The intervention was divided into in-hospital interventions: the diagnostic period, the PCI perioperative period, and the discharge preparation period. The intervention time was mainly focused around 20:00. The interventions were conducted 1 to 2 times per phase, each time for 30 to 45 min. The interventions were conducted in a face-to-face one-to-one format, mainly in the departmental demonstration room. Out-of-hospital interventions include adjustment and adaptation periods. The intervention time was agreed with the patient in advance, with one telephone follow-up intervention and one home visit per phase. Each visit was 15-30 min.

**4.3. Observation Index.** The Exercise of Self-Care Agency (ESCA) scale was developed by the American scholars Kearney and Fleischer in 1979 and is now widely used to test the self-care ability of patients with coronary heart disease in China. Self-concept, self-care responsibility, self-care abilities, and health knowledge are among the 43 items and four dimensions. A 5-point Likert scale was utilized, with a score ranging from "extremely unlike me" to "quite like me." The higher the total score, the better the patient's ability to care for themselves. The Cronbach  $\alpha$  coefficient of the English version of the scale was 0.862, which was translated into Chinese by Hsin-Hung in Taiwan. Its Cronbach  $\alpha$  coefficient was 0.83-0.98. It was assessed before the intervention, at the time of discharge, at the end of 1 month after discharge, and at the end of 3 months after discharge.

TABLE 1: Comparison of general information of patients in 2 groups with percutaneous coronary intervention.

Group	Observation group ( $n = 58$ )	Control group ( $n = 50$ )	Statistic	$P$
Age ( $\bar{X} \pm S$ years)	61.33 $\pm$ 8.69	60.92 $\pm$ 8.05	$t = 0.101$	0.919
Gender	31	28	$\chi^2 = 0.015$	0.904
Male	27	22		
Female				
Educational level	46	41	$\chi^2 = 0.749$	0.402
High school or below	14	7		
College or above				
Course of disease (years)			$\chi^2 = 0.588$	0.445
$\leq 5$	38	38		
$> 5$	18	14		
Disease type			$\chi^2 = 0.521$	0.482
Angina pectoris	27	18		
Myocardial infarction	31	32		
Disease severity			$\chi^2 = 0.199$	0.651
Mild	35	28		
Moderate and severe	24	21		
Number of implanted stents			$\chi^2 = 0.259$	0.611
$\leq 3$	33	27		
$> 3$	23	25		
Body mass index			$\chi^2 = 0.071$	0.794
$< 24$	15	10		
$\geq 24$	45	38		
Smoking history			$\chi^2 = 0.028$	0.871
Yes	37	33		
No	19	19		
Drinking history			$\chi^2 = 0.471$	0.497
Yes	26	21		
No	32	29		

The Self-Rating Anxiety Scale (SAS) and the Self-Rating Depression Scale (SDS) developed by Zung et al. were used to assess the subjective feelings of individuals with anxiety/depression tendencies. The 4-point Likert scale was used for both the SAS and the SDS.

**4.3.1. Medication Adherence.** The Morisky Medication Adherence Questionnaire was developed by Prof. Morisky. This questionnaire was used to measure medication adherence in patients with chronic diseases. There are 8 items, including whether patients forget to take their medication, whether they stop taking their medication or reduce their dose, and whether they carry their medication with them when they go out for a long period of time. A dichotomous scale was used, with a "1/0" score for each "yes/no" answer and a total score of 0 to 8. The higher the score, the better the patient's medication adherence, and the Cronbach  $\alpha$  coefficient of the scale was 0.72. At discharge, at the end of the first month after discharge, and at the end of the second month after discharge. The assessment was performed at the time of discharge, at

the end of 1 month after discharge, and at the end of 3 months after discharge.

**4.3.2. Exercise Compliance.** According to the expert consensus on exercise rehabilitation after PCI, patients were emphasized to exercise at least 3 times per week for at least 30 min each time for 3 months. Patients were considered to be in good compliance if they completed 80 percent or more of the total weekly recommended exercise time, good compliance if they completed 60 percent or more of the total weekly recommended exercise time, and poor compliance if they completed less than 60 percent of the total weekly recommended exercise time. The assessment was recorded at the completion of the intervention.

**4.3.3. Data Collection Method.** The data were collected by the investigator himself, and the baseline data were collected face-to-face on the day of admission for both groups of patients. The patients' self-care scores, anxiety-depression scores, and medication adherence scores were collected again on the day of discharge, and the patients' self-care

TABLE 2: Comparison of self-care ability scores of patients with percutaneous coronary intervention in 2 groups ( $\bar{X} \pm S$ , points).

Group	<i>n</i>	Before intervention	At the end of discharge	One month after discharge	Three months after discharge	Total	<i>F</i>	<i>P</i>
Self-concept								
Observation group	58	14.91 ± 1.60	16.60 ± 1.99	18.23 ± 2.14	19.11 ± 2.08	18.01 ± 1.91	259.382	<0.001
Control group	50	15.63 ± 2.22	15.77 ± 3.14	15.78 ± 3.26	15.29 ± 1.88	15.05 ± 1.04	38.839	<0.001
Total		14.69 ± 2.01	16.07 ± 2.11	17.02 ± 2.63	17.33 ± 2.73	16.51 ± 2.14	242.119	<0.001 <sup>#</sup>
<i>F</i>		0.933	2.951	6.190	9.651	27.337	109.131	<0.001*
<i>P</i>		0.361	0.004	<0.001	<0.001	0.001 <sup>#</sup>		
Sense of self-care responsibility								
Observation group	58	11.52 ± 1.22	13.12 ± 1.02	14.03 ± 1.13	12.09 ± 1.16	10.97 ± 1.36	286.991	<0.001
Control group	50	9.69 ± 1.96	10.13 ± 1.52	10.91 ± 1.41	11.65 ± 1.55	10.69 ± 1.55	48.851	<0.001
Total		9.55 ± 2.12	11.01 ± 1.51	12.09 ± 1.63	12.93 ± 1.86	11.53 ± 1.23	288.911	<0.001 <sup>#</sup>
<i>F</i>		1.179	5.251	9.335	9.324	28.998	55.055	<0.001*
<i>P</i>		0.240	<0.001	<0.001	<0.001	0.001 <sup>#</sup>		
Self-care skills								
Observation group	58	21.61 ± 3.40	23.78 ± 3.01	25.39 ± 4.11	26.51 ± 3.39	24.88 ± 2.57	2829.799	<0.001
Control group	50	21.03 ± 2.38	22.11 ± 2.91	23.19 ± 2.85	23.09 ± 2.85	22.11 ± 2.85	151.737	<0.001
Total		21.41 ± 2.78	22.97 ± 3.11	24.48 ± 3.09	24.93 ± 3.26	23.57 ± 3.02	1288.541	<0.001 <sup>#</sup>
<i>F</i>		1.132	2.855	4.384	6.381	14.424	183.819	<0.001*
<i>P</i>		0.261	0.049	<0.001	<0.001	0.001 <sup>#</sup>		
Health knowledge level								
Observation group	58	25.71 ± 2.21	27.53 ± 2.36	29.37 ± 2.59	30.69 ± 2.81	28.35 ± 2.31	464.733	<0.001
Control group	50	25.37 ± 2.13	25.81 ± 2.13	27.21 ± 2.69	26.45 ± 2.56	26.31 ± 2.51	52.451	<0.001
Total		25.57 ± 3.01	26.39 ± 2.39	28.39 ± 2.89	28.39 ± 3.26	12.36 ± 2.63	355.205	<0.001 <sup>#</sup>
<i>F</i>		0.743	4.143	4.186	7.222	18.651	101.567	<0.001*
<i>P</i>		0.459	<0.001	<0.001	<0.001	0.001 <sup>#</sup>		
Total score								
Observation group	58	71.89 ± 3.86	79.81 ± 6.23	86.53 ± 4.28	89.79 ± 4.25	82.19 ± 4.21	353.555	<0.001
Control group	50	71.23 ± 3.49	74.19 ± 6.11	77.39 ± 5.19	76.87 ± 5.22	77.81 ± 4.96	37.062	<0.001
Total		71.69 ± 3.69	77.14 ± 6.35	82.22 ± 6.59	83.71 ± 7.78	78.39 ± 6.31	293.233	<0.001 <sup>#</sup>
<i>F</i>		0.888	4.985	10.312	14.711	88.001	170.606	<0.001*
<i>P</i>		0.441	<0.001	<0.001	<0.001	0.001 <sup>#</sup>		

Note: # indicates the main effect; \* indicates the interaction effect.

scores, anxiety-depression scores, and medication adherence scores were collected by micromail or home visits at 1 month and 3 months of discharge, respectively; and the patients' exercise adherence was evaluated by the exercise diary filled by the patients at 3 months of discharge.

## 5. Results

**5.1. Comparison of Self-Care Competency Scores.** Using repeated measures ANOVA, spherical tests were performed for self-concept, self-care responsibility, self-care skills and health knowledge, and total scores of PCI patients ( $W = 0.232, 0.193, 0.155, 0.205, \text{ and } 0.039, P < 0.001$ ), respectively. Geisser corrected the results, and the patients in the observation group had higher scores on all dimen-

sions and total scores than the control group ( $F = 27.337, 28.998, 14.424, 18.651, \text{ and } 88.001, P < 0.001$ ). The differences in the scores and total scores of the dimensions of self-care competency at different time points were statistically significant ( $F = 242.119, 288.911, 1288.541, 355.205, \text{ and } 293.233, P < 0.001$ ); there was a more reciprocal effect between groups and time ( $F = 109.131, 55.055, 183.819, 101.567, \text{ and } 70.606, P < 0.001$ ). There was no statistically significant difference between the scores and total scores of self-care ability of the two groups before the intervention ( $P > 0.05$ ); there was a statistically significant difference between the scores and total scores of self-care ability of the two groups at discharge, at the end of 1 month after discharge, and at the end of 3 months after discharge ( $P < 0.05$ ). The details are shown in Table 2.

TABLE 3: Comparison of the anxiety-depression scores of patients with percutaneous coronary intervention in 2 groups with the Chinese adult normative score ( $\bar{X} \pm S$ , points).

Group	$n$	Before intervention	At the end of discharge	One month after discharge	Three months after discharge
Anxiety score					
Observation group	58	57.44 $\pm$ 4.33	55.25 $\pm$ 5.29	50.33 $\pm$ 5.17	46.61 $\pm$ 5.83
Control group	50	57.67 $\pm$ 4.32	56.89 $\pm$ 3.31	55.69 $\pm$ 3.31	53.19 $\pm$ 4.38
Norm	1168	28.88 $\pm$ 10.19	28.88 $\pm$ 10.19	28.88 $\pm$ 10.19	28.88 $\pm$ 10.19
$t_1$		30.901	24.798	20.612	16.011
$P_1$		<0.001	<0.001	<0.001	<0.001
$t_2$		32.001	32.659	30.712	27.123
$P_2$		<0.001	<0.001	<0.001	<0.001
Depression score					
Observation group	58	56.39 $\pm$ 4.19	54.44 $\pm$ 4.32	50.31 $\pm$ 4.50	47.98 $\pm$ 4.69
Control group	50	56.386 $\pm$ 4.23	58.03 $\pm$ 3.37	56.07 $\pm$ 3.34	55.51 $\pm$ 3.27
Norm	1355	33.51 $\pm$ 8.62	33.51 $\pm$ 8.62	33.51 $\pm$ 8.62	33.51 $\pm$ 8.62
$t_3$		22.601	19.333	15.991	13.159
$P_3$		<0.001	<0.001	<0.001	<0.001
$t_4$		22.687	25.123	23.512	21.457
$P_4$		<0.001	<0.001	<0.001	<0.001

Note:  $t_1, t_2$  indicates the comparison of SAS observation group and control group with the Chinese adult norm;  $t_3, t_4$  indicates the comparison of SDS observation group and control group with the Chinese adult norm.

TABLE 4: Comparison of anxiety and depression scores between the 2 groups of patients undergoing percutaneous coronary intervention ( $\bar{X} \pm S$ , points).

Group	$n$	Before intervention	At the end of discharge	One month after discharge	Three months after discharge	Total	$F$	$P$
Anxiety score								
Observation group	58	57.41 $\pm$ 4.21	55.12 $\pm$ 5.22	50.32 $\pm$ 5.33	47.11 $\pm$ 5.69	53.09 $\pm$ 5.41	209.123	<0.001
Control group	50	57.99 $\pm$ 3.98	57.01 $\pm$ 3.19	55.63 $\pm$ 3.49	54.11 $\pm$ 4.31	55.99 $\pm$ 5.39	35.889	<0.001
Total		57.59 $\pm$ 4.31	55.50 $\pm$ 4.61	52.88 $\pm$ 5.31	49.68 $\pm$ 6.19	54.01 $\pm$ 1.13	206.228 <sup>#</sup>	<0.001 <sup>#</sup>
$F$		0.599	2.858	6.085	6.940	22.751 <sup>#</sup>	36.111*	<0.001*
$P$		0.539	0.049	<0.001	<0.001	0.001 <sup>#</sup>		
Depression score								
Observation group	58	56.29 $\pm$ 4.11	54.44 $\pm$ 4.29	50.39 $\pm$ 4.50	48.11 $\pm$ 4.63	52.33 $\pm$ 3.39	1104.007	<0.001
Control group	50	57.09 $\pm$ 4.26	58.13 $\pm$ 3.41	56.08 $\pm$ 3.21	54.26 $\pm$ 3.30	57.01 $\pm$ 3.54	84.001	<0.001
Total		56.66 $\pm$ 4.13	55.51 $\pm$ 3.39	52.21 $\pm$ 5.51	50.82 $\pm$ 5.21	54.00 $\pm$ 4.13	829.213 <sup>#</sup>	<0.001 <sup>#</sup>
$F$		0.719	6.342	7.349	8.999	34.351 <sup>#</sup>	223.733*	<0.001*
$P$		<0.001	<0.001	<0.001	<0.001	0.001 <sup>#</sup>		

Note: # indicates the main effect; \* indicates the interaction effect.

5.2. *Anxiety and Depression Scores.* Anxiety and depression scores of patients are undergoing percutaneous coronary intervention in 2 groups.

The Chinese adult anxiety normative score was  $28.88 \pm 10.19$ , and the Chinese adult depression normative score was  $33.51 \pm 8.62$ , which were lower than the anxiety and depression scores of patients in the 2 groups in this study at each time point, and the differences were statistically significant ( $P < 0.001$ ). See Table 3.

5.3. *Comparison of Anxiety and Depression.* The comparison of anxiety and depression scores between 2 groups of patients is undergoing percutaneous coronary intervention.

First by spherical test ( $W = 0.026$  and  $0.030$ ,  $P < 0.001$ ), the spherical test was not satisfied ( $P < 0.10$ ). After using the Greenhouse-Geisser correction, the SAS and SDS scores were higher in the observation group than in the control group ( $F = 22.751$  and  $34.351$ ,  $P < 0.001$ ). The differences in SAS and SDS scores at different time points were

TABLE 5: Comparison of medication adherence scores between the 2 groups of patients undergoing percutaneous coronary intervention ( $\bar{X} \pm S$ , points).

Group	<i>n</i>	At the end of discharge	One month after discharge	Three months after discharge	Total	<i>F</i>	<i>P</i>
Observation group	58	6.44 ± 0.79	6.69 ± 0.83	6.37 ± 0.88	6.56 ± 0.81	18.537	<0.001
Control group	50	6.51 ± 0.87	6.17 ± 0.99	5.35 ± 0.73	6.04 ± 0.87	51.001	<0.001
Total		6.47 ± 0.86	6.55 ± 0.94	5.91 ± 0.93	6.18 ± 0.99	58.232*	<0.001 <sup>#</sup>
<i>F</i>		0.423	3.129	7.311	12.235 <sup>#</sup>	38.713*	<0.001*
<i>P</i>		<0.001	<0.001	<0.001	0.001 <sup>#</sup>		

Note: # indicates the main effect; \* indicates the interaction effect.

statistically significant ( $F = 206.228$  and  $829.213$ ,  $P < 0.001$ ); there was an interaction between group and time ( $F = 36.111$  and  $223.733$ ,  $P < 0.001$ ). There was no statistically significant difference between the SAS scores and SDS scores of the 2 groups before the intervention ( $P > 0.05$ ). There was a statistically significant difference between the self-SAS and SDS scores of the two groups at discharge, one month after discharge, and three months after discharge ( $P < 0.05$ ). Details are shown in Table 4.

The sphericity test was first tested ( $W = 0.746$ ,  $P < 0.001$ ), and the sphericity test was not satisfied ( $P < 0.10$ ). The results were corrected using the Greenhouse-Geisser correction, and the patients in the observation group had higher medication adherence than the control group ( $F = 12.235$ ,  $P < 0.001$ ). The difference in scores at different time points was statistically significant ( $F = 58.232$ ,  $P < 0.001$ ); group and time had a more reciprocal effect ( $F = 38.713$ ,  $P < 0.001$ ). There was no statistically significant difference between the scores of the 2 groups at the time of discharge ( $P > 0.05$ ); at the end of 1 month after discharge and at the end of 3 months after discharge, there was a statistically significant difference between the scores of the 2 groups ( $P < 0.05$ ). Details are shown in Table 5.

The comparison of exercise compliance between the 2 groups of patients is undergoing percutaneous coronary intervention. The differences in exercise compliance between the 2 groups of patients were statistically significant ( $P < 0.05$ ), as shown in Table 6.

## 6. Discussion

In postoperative patients, wound pain, tubing restrictions, and concerns about recovery can affect the psychological, physical, and social recovery of patients. The application of positive thinking therapy and progressive muscle relaxation training to postoperative rehabilitation of patients undergoing cardiothoracic surgery was found to be effective in reducing postoperative physical and psychological problems, as well as improving the quality of sleep and psychological mood of patients, according to a study by [18]. In a study by [19], it was concluded that positive stress reduction therapy was effective in reducing perceived stress levels in postoperative breast cancer patients, and [20] confirmed the long-term effects of positive stress therapy in improving postoperative anxiety and depression in breast cancer

TABLE 6: Comparison of exercise compliance levels between the 2 groups of patients undergoing percutaneous coronary intervention (cases).

Group	<i>n</i>	Good	Excellent	Bad
Observation group	58	29	20	9
Control group	50	21	12	17
<i>Z</i>			2.089	
<i>P</i>			0.037	

patients up to 1 year after the intervention. Furthermore, a number of studies have found that incorporating orthomolecular therapy into the postoperative care of patients undergoing surgical procedures such as hip replacement, cranial surgery, and radical esophageal cancer improves patients' perception and orthomolecular level, improves their pain experience, and promotes wound healing, all of which have a positive effect on their recovery. This may be related to the neuromodulation mechanism of orthomolecular therapy, but the details need to be further investigated. The above results suggest that positive thinking therapy has positive significance in promoting postoperative recovery, not only reducing body pain and relieving postoperative psychological stress, but also improving patients' quality of life. However, in most of the studies, the implementers did not receive systematic training in orthomolecular therapy and did not obtain the corresponding qualification, and there is a lack of unified protocols and consistent evaluation indexes in each region and hospital, so it is impossible to accurately understand the patient's compliance and intervention effect [21–24].

## 7. Conclusion

Positive thinking therapy, as a new psychological intervention, has played a positive role in promoting perioperative surgery and postoperative recovery. However, due to the small sample size, most of the studies in China are cross-sectional studies with small samples, and there is a lack of postintervention evaluation tools and long-term postoperative follow-up of the patients, which makes it impossible to comprehensively evaluate the intervention effects. Furthermore, the current study's participants were mostly adults, and more research is needed to see if the



positive thinking intervention strategy can be used with youngsters. Future studies should increase the sample size and strengthen the follow-up, and we should combine it with the “clown boil method” to conduct trials in children. We should also cultivate a specialized positive thinking intervention team, establish specific local measurement criteria based on the domestic environment, follow up the patients, and evaluate the intervention effect. It should also be fully integrated with the characteristics of hospital departments and patient care in China and be used as a powerful intervention tool to promote the development of positive thinking intervention in clinical practice.

### Data Availability

The dataset used in this paper are available from the corresponding author upon request.

### Conflicts of Interest

The authors declared that they have no conflicts of interest regarding this work.

### Acknowledgments

This work was supported by the Scientific Research Project of Hebei Provincial Health Commission in 2019. The topic is “Application of mindfulness decompression training in perioperative period of cardiac surgery” (No. 20191602).

### References

- [1] Y. Voigt and D. Jahn-Falk, “Analysis of the effect of the intensity of treatment on the success of treatment - an economic evaluation of the therapy of the left displacement of the abomasum,” *Tierärztliche Umschau*, vol. 62, no. 7, pp. 347–353, 2007.
- [2] X. Lyu, C. Sun, Z. Dong, and Y. Wu, “Analysis of the effect of a root cause analysis in elderly patients with acute pancreatitis: a randomized trial,” *Annals of Palliative Medicine*, vol. 10, no. 5, pp. 5738–5745, 2021.
- [3] F. J. Carabantes, M. D. Matas, F. Rius et al., “Analysis of the effect of chemotherapy (ct) on erythropoietin (epo) synthesis in cancer patients (pts),” *European Journal of Cancer*, vol. 35, pp. S364–S365, 1999.
- [4] P. Leher, “An individual patient data meta-analysis on the effect of racecadotril in acute watery diarrhea of children, based on 1612 patients on 12 randomized studies,” *Pediatric Research*, vol. 79, no. 3, pp. 510–510, 2016.
- [5] N. A. Gerasimova, M. I. Korenevskaja, S. M. Dul’Tsina, L. G. Kovaleva, and E. I. Terent’Eva, “Analysis of the effect of rubomycin in cell cultures from patients with acute leukemia,” *Laboratornoe Delo*, vol. 10, pp. 605–608, 1971.
- [6] J. Tabernero, A. F. Sobrero, C. Borg, A. Ohtsu, and E. V. Cutsem, “Exploratory analysis of the effect of ftd/tpi in patients treated in recourse by prognostic factors,” *Journal of Clinical Oncology*, vol. 37, 4\_suppl, p. 677, 2019.
- [7] A. K. Bekhet and J. A. Zauszniewski, “Measuring use of positive thinking skills: psychometric testing of a new scale,” *Western Journal of Nursing Research*, vol. 35, no. 8, pp. 1074–1093, 2013.
- [8] F. Karimi Azar, P. Abdoltajedini, and M. Azmoudeh, “Comparison of the effectiveness of positive thinking skills training and acceptance/commitment therapy on self-disability of shy female students,” *Community Health Journal*, vol. 15, no. 1, pp. 61–71.
- [9] J. L. Clore and S. T. Gaynor, “Cognitive modification versus therapeutic support for internalizing distress and positive thinking: a randomized technique evaluation trial,” *Cognitive Therapy and Research*, vol. 36, no. 1, pp. 58–71, 2012.
- [10] P. T. Meskaran, R. Hassanzadeh, and Y. Dousti, “Study of music therapy on female students extent of positive thinking,” *International Journal of Basic Sciences and Applied Research*, vol. 3, no. 6, pp. 344–348, 2014.
- [11] E. Golpasha and M. H. Asayesh, “The efficacy of religion based cognitive behavioral therapy with focus on forgiveness and positive thinking techniques on depression and anxiety signs: a case study,” *Journal of Islamic Psychology*, vol. 2, no. 3, pp. 138–165, 2016.
- [12] S. Makaremnia, M. Dehghan Manshadi, and Z. Khademian, “Effects of a positive thinking program on hope and sleep quality in Iranian patients with thalassemia: a randomized clinical trial,” *BMC psychology*, vol. 9, no. 1, pp. 1–10, 2021.
- [13] F. Hamidi, M. Otaghi, and F. M. Paz, “Effectiveness of positive thinking training on self-assertiveness of teenage girls,” *Women’s Health Bulletin*, vol. 7, no. 1, pp. 11–17, 2020.
- [14] I. Butmanowicz-Dębicka, “Positive thinking – an universal cure for modern-day diseases?,” *Studia Humanistyczne AGH (od 2012)*, vol. 17, no. 1, pp. 37–48, 2018.
- [15] A. Ashrafi Hafez, P. Asmand, S. R. Mousavi Moghadam, and K. Sayemiri, “Positive thinking effect in reducing marital disputes in married students,” *Medical Science Journal of Islamic Azad University-Tehran Medical Branch*, vol. 23, no. 4, pp. 49–53, 2014.
- [16] S. Safari and B. Akbari, “The effectiveness of positive thinking training on psychological well-being and quality of life in the elderly,” *Avicenna Journal of Neuro Psycho Physiology*, vol. 5, no. 3, pp. 113–122, 2018.
- [17] J. Li, Z. Zhou, J. Wu et al., “Decentralized on-demand energy supply for blockchain in internet of things: a microgrids approach,” *IEEE transactions on computational social systems*, vol. 6, no. 6, pp. 1395–1406, 2019.
- [18] W. Duan, J. Gu, M. Wen, G. Zhang, Y. Ji, and S. Mumtaz, “Emerging technologies for 5G-IoV networks: applications, trends and opportunities,” *IEEE Network*, vol. 34, no. 5, pp. 283–289, 2020.
- [19] F. M. A. Abd Algalil and S. P. Zambare, “New species of flesh fly (Diptera: Sarcophagidae) Sarcophaga (Liosarcophaga) geetai in India,” *J Entomol Zool Stud*, vol. 4, no. 3, pp. 314–318, 2016.
- [20] P. An, Z. Wang, and C. Zhang, “Ensemble unsupervised autoencoders and Gaussian mixture model for cyberattack detection,” *Information Processing & Management*, vol. 59, no. 2, p. 102844, 2022.
- [21] M. Radlett, “Smile or die: how positive thinking fooled America and the world,” *Existential Analysis*, vol. 22, no. 1, pp. 186–191, 2011.
- [22] M. Muñoz, S. Gómez-Ramírez, S. Kozek-Langenecker et al., “‘Fit to fly’: overcoming barriers to preoperative haemoglobin optimization in surgical patients<sup>†</sup>,” *British Journal of Anaesthesia*, vol. 115, no. 1, pp. 15–24, 2015.

- [23] N. A. Khan, O. Ibrahim Khalaf, C. Andrés Tavera Romero, M. Sulaiman, and M. A. Bakar, "Application of intelligent paradigm through neural networks for numerical solution of multi-order fractional differential equations," *Computational Intelligence and Neuroscience*, vol. 2022, 16 pages, 2022.
- [24] H. S. Gill, O. I. Khalaf, Y. Alotaibi, S. Alghamdi, and F. Alassery, "Fruit image classification using deep learning," *CMC-Computers, Materials & Continua*, vol. 71, no. 3, pp. 5135–5150, 2022.

## Research Article

# Q-Switched Laser Combined with Intense Pulsed Laser in the Treatment of Melasma Based on Reflection Confocal Microscope

Jiali Xu and Yijing Pu 

Tonglu County First People's Hospital, Zhejiang Hangzhou, Tonglu 311500, China

Correspondence should be addressed to Yijing Pu; 1931031204@siit.edu.cn

Received 12 April 2022; Revised 3 May 2022; Accepted 7 May 2022; Published 1 July 2022

Academic Editor: Naeem Jan

Copyright © 2022 Jiali Xu and Yijing Pu. This is an open access article distributed under the Creative Commons Attribution License, which permits unrestricted use, distribution, and reproduction in any medium, provided the original work is properly cited.

Chloasma is a prevalent clinical hyperpigmentation skin disorder that causes symmetrical brown to tan patches on the cheeks, as well as the neck and forearms on rare occasions. The pathophysiology of this condition is complicated, and there is now no cure. Under the light microscope, the full-thickness melanin of the epidermis in the skin lesions was increased, and the dermal chromophages increased. At present, the treatment of melasma mainly includes topical drugs, chemical peels, systemic drugs, laser therapy, and traditional Chinese medicine. With the development of medical technology, intense pulsed light and Q-switched laser have been widely used in the treatment of melasma, which can emit laser beams to penetrate the dermis uniformly to treat deep pigmented lesions in the dermis. After a stable treatment outcome for melasma is achieved, it is important to minimize side effects such as postinflammatory hyperpigmentation and skin irritation. Therefore, this paper uses a reflection confocal microscope to establish an evaluation index system and then uses a neural network to evaluate the treatment effect. The work of this paper is as follows: (1) this paper introduces various methods of treating melasma at home and abroad and focuses on the application of intense pulsed light therapy and low-energy Q-switched Nd: YAG laser in the treatment of melasma. (2) In this paper, the case data samples are trained with the designed BP network to obtain a reliable evaluation network model. (3) The results and mistakes of the evaluation are produced by training the genetic algorithm optimized backpropagation (GA-BP) network structure model to evaluate the treatment effect of chloasma. Finally, it has been demonstrated that the GA-BP network has great accuracy and stability.

## 1. Introduction

Chloasma is a pigmented skin disease. The pigmented spots are usually light brown or dark brown and distributed symmetrically on the cheekbones, forehead, and eyebrows and around the eyes and can also involve the dorsum of the nose, the alars of the nose, and the upper lip and lower whiskers. The border of the stain is clear or diffuse, the surface is free of inflammatory dandruff and flat to the skin surface, and most patients do not have any symptoms. Chloasma is more common in young and middle-aged women with darker skin and less common in men. Modern medicine believes that the pathogenesis of chloasma is extremely complex, and the latest research shows that the formation of chloasma may be related to local inflammation. Chloasma is characterized by an increase in melanin in the basal layer and acanthus layer

of the epidermis, the number of melanocytes is normal or increased, the cell body is enlarged, the dendrites are obvious, and pigmented disease is characterized by histological features of free melanin granules in the upper dermis or phagocytosis by melanophagocytes. UV rays, hereditary factors, endocrine factors, cosmetics, uterine and ovarian illnesses, hepatitis A and B, oral contraceptives, and phototoxic medicines are the most common causes of chloasma. UV radiation, hereditary factors, endocrine factors, and cosmetics are the most important among these factors [1]. At present, the methods of treating melasma mainly include topical depigmentation agents, oral drugs, chemical peeling, and traditional Chinese medicine treatment. In recent years, technologies such as laser, intense pulsed light, microneedle introduction, and radio frequency technology have been increasingly applied to the treatment of melasma,

and good results have been achieved [2]. Intense pulsed light is a broad-spectrum light in the 500-1200 nm band. According to selective photothermolysis theory, the pigment agglomeration preferentially absorbs laser energy after being irradiated with a specific wavelength of laser light, which can cause a blasting effect quickly, and then changes. The superficial ones are excreted with the skin flakes, and the deep ones are transported away with the lymphatic/blood circulation, so that they can be used to treat pigmented diseases [3]. However, the absorption of light by melanin is not limited to a single wavelength: in the wavelength range of 500-1200 nm, structures containing melanin can absorb the energy of light and cause photothermal decomposition [4]. However, since melasma melanocytes are unstable, it is an unstable disease, and any stimulation may aggravate the melasma, so the treatment of melasma needs to be gentle. The pulse width of the Q-switched laser is as short as nanoseconds, which is smaller than the thermal relaxation time of the melanin particles. The extremely high peak power can cause the melanin particles to be heated and exploded instantaneously. The treatment of sexually enhanced skin disease provides a new idea [5]. It avoids uneven distribution of energy, the treatment is relatively gentle, and the postoperative inflammatory response is mild. Therefore, the Q-switched ruby laser in the fractional mode is relatively safe for the treatment of melasma, and the incidence of side effects such as erythema, hyperpigmentation, and hypopigmentation is low [6]. In order to confirm the efficacy and safety of intense pulsed light and Q-switched laser in the treatment of melasma and to further explore its effects on melanocytes and melanin granules. In this paper, the RCM is used for postoperative observation. It has the characteristics of instant, noninvasive, and dynamic, and the detection depth can reach 300-500  $\mu\text{m}$ . The imaging resolution is high, and the epidermis and superficial dermis can be clearly observed. Then, use the neural network to analyze the obtained data, and finally, output the predicted value of the treatment effect of the Q-switched laser combined with the intense pulsed laser on melasma.

The application of intense pulsed light therapy and low-energy Q-switched Nd: YAG laser in the treatment of melasma is the emphasis of this paper, which introduces several methods of treating melasma at home and abroad. To obtain a reliable diagnosis and evaluation network model, the reliable diagnostic and evaluation case data samples are trained with the designed backpropagation neural network (BPNN) in this paper.

The paper arrangements are as follows: Section 2 describes the related work. Section 3 defines the various methods. Section 4 analyzes the experimental analysis. Section 5 concludes the article.

## 2. Related Work

The pulse width of the Q-switched laser is nanoseconds. Since its wavelength is within the wavelength range absorbed by melanosomes and the pulse width is smaller than the thermal relaxation time of melanosomes, melanosomes selectively absorb light instantaneously. It can be raised to a very high temperature, and then, the melanin particles

are smashed and disintegrated under the action of strong mechanical waves and are swallowed by macrophages, and the surrounding healthy tissues are not damaged. Q-switched laser is a classic laser for the treatment of pigmented diseases. There are many studies at home and abroad, but it also has a series of shortcomings, such as easy to cause pigmentation and hypopigmentation. Large-spot, low-energy, long-wavelength O-switched lasers have been utilized to treat pigmented illnesses in recent years to avoid the emergence of negative effects. The researchers applied a Q-switched fractional ruby laser with an energy of 2-3 J/cm<sup>2</sup> to Asian female patients for 6 treatments at two-week intervals and concluded that a large-spot, low-energy Q-switched fractional ruby laser can effectively treat yellow for chloasma; from the histopathological point of view, the epidermal pigmentation was reduced after treatment, and the pigment content in the basal layer of the epidermis was reduced [7].

Reference [8] used the same kind of laser treatment, the energy was 4-8 J/cm<sup>2</sup>, and the subjects were all Caucasians, and the study showed that the treatment consequence was remarkable. However, its exact mechanism of action remains to be further explored. In addition, the high recurrence rate after laser treatment is an urgent problem to be solved. The curative effect of Q-switched 1064 nm laser and fractional 1064 nm laser was compared and it was concluded that there was no significant difference in the total effective rate of the two groups in the treatment of melasma, and the recurrence rate was low during the 1-year follow-up. Among them, the skin reaction after fractional 1064 nm laser treatment is mild, has less complication, has high comfort, and has a good application prospect. Reference [9] divided the subjects into 3 groups. The first group applied low-energy Nd: YAG laser once a week. The second group was treated with fruit acid once every 2 weeks, and the third group was treated with high-energy Nd: YAG laser once every 2 weeks. The results showed that the treatment effect of the first group was the best, followed by the second group, and finally the third group. Low-energy Nd: YAG laser is safe and effective in the treatment of melasma. Reference [10] treated melasma with a high-energy Nd: YAG laser, which resulted in increased pigmentation and new pigmentation. In reference [11], in order to explore the freckle removal mechanism of Nd: YAG laser, before treatment, after 5 times of treatment, and after 9 times of treatment, the pigmented skin was observed by an in vivo confocal microscope, which clearly and intuitively showed the mechanism of action. Strong light therapy for chloasma has been widely used in clinical practice. It is a broad-spectrum visible light with relatively concentrated wavelength and adjustable pulse width. The continuous wavelength is 500-1200 nm. Melanocytes in skin lesions selectively absorb some wavelengths of strong light. The photothermal effect is generated after the light is exposed, and it is broken and necrotic. The superficial pigment tissue is damaged and necrotic, and phagocytes phagocytose and expel the deep pigment. After severe light exposure to pigmentation, immediate deepening of the pigmentation and localized skin erythema appear. Strong light and Q-switched lasers were examined for their effectiveness in the treatment of melasma. Patients with melasma were

treated using a combination of a bright light and a Q-switched laser. There was a statistically significant difference in the overall effectiveness of therapy between the bright light and Q-switch groups, but there was no significant difference in postoperative recurrence rates between the two groups, according to the data. Epidermal pigmentation and vascular disease can be effectively treated with bright light, although the impact on dermal pigmentation is minimal [12]

Treatment with the Q-switched Nd: YAG laser is the gold standard for chloasma; however, it is time unbearable and taxing on patients. Combining these two lasers to remove melasma can enhance the consequence. The experiment of reference [13] confirmed this point. The researchers first performed a bright light treatment on the subjects and then started the Q-switched Nd: YAG laser treatment two weeks later, a total of 4 times, with an interval of one week. The results showed that the curative effect was significant and the recurrence was effectively suppressed. It was concluded that the combination of the two and a single treatment was safe and effective with minimal adverse effects and that the Q-switched Nd: YAG laser paired with powerful pulsed light is worthy of promotion. Q-switched Nd: YAG laser and nonablative fractional 1550 nm laser were used for the treatment of freckles. Nonablative fractional laser was not found to have an auxiliary effect when Nd: YAG laser was used to treat melasma, and the effect of combined treatment was not significantly different from that of Nd: YAG laser treatment alone, according to the subjects [14]. Although laser treatment of melasma is effective, it also has different degrees of side effects. The recurrence rate of strong light therapy is relatively low, the recurrence rate of Q-switched laser is high, and it is easy to produce pigmentation. Fractional laser therapy has a high probability of postinflammatory pigmentation, and the pain is severe during treatment. In general, laser therapy is safer and more effective for light-skinned patients, but it should be used with caution in dark-skinned patients. With the introduction of new treatment theories and the emergence of new treatment instruments, laser treatment of melasma will become more and more important [15–18]. The organic and reasonable combination of various instruments will further improve the efficacy of the laser and reduce the side effects of laser treatment. Different pathological types and different skin types have different optimal responses to the instrument, and the optimal therapeutic parameters of various instruments for treating melasma in different periods are also different.

### 3. Method

This section discusses the BP neural network and defines the improvement of BP algorithm. They examine the treatment effect evaluation index system.

**3.1. BP Neural Network.** They discuss the establishment of the BP network model.

**3.1.1. BP Neural Network Model.** The learning of the BP network in the ANN uses the error backpropagation algorithm, which is one of the most mature and perfect artificial neural networks at present. It is categorized by a simple structure

and self-learning and parallel processing abilities; because it belongs to the classifier, it can form any decision-making area. The commonly used BP network is a three-layer structure. Forward propagation and backpropagation constitute the learning process of the BP network, each layer of the network has one or more neuron nodes, and the information is composed of the input layer which is passed to the output layer through each hidden layer, and the connection weight is used to represent the strength of the connection between the layers. The back-propagation learning method, or BP algorithm, may be used to alter the network's link weight such that the mapping relationship between the provided input and output of the network can be determined. There is no longer any room for mistake. The following relationship applies to the output layer:

$$O_k = f(neL_k), \quad k = 1, 2, \dots, l, \quad (1)$$

$$neL_k = \sum_{j=1}^m w_{jk} y_j, \quad k = 1, 2, \dots, l. \quad (2)$$

For the hidden layer, there are the following relationships:

$$y_j = f(neL_j), \quad j = 1, 2, \dots, m, \quad (3)$$

$$neL_j = \sum_{i=1}^n v_{ij} x_i, \quad j = 1, 2, \dots, m.$$

In the above two formulas, let the transition number  $f(x)$  be a unipolar sigmoid function:

$$f(x) = \frac{1}{1 + e^{-x}}. \quad (4)$$

Formulas (1)–(4) together constitute the mathematical model of the three-layer perceptron.

**3.1.2. The Learning Process of the BP Network.** The primary goal of the BP training procedure is to provide a certain input sample and get a specific output. Until a predefined error value is reached, the weights are modified based on the difference between the actual and predicted output values. The method is based on continuously modifying the threshold's weights and network parameters by propagating the error on one side and correcting the error on the other. For each training, it executes two propagation computations. The specific process is shown in Figure 1.

If the network output is not equal to the expected output, there will be an output error  $E$ , which is defined as follows:

$$E = \frac{1}{2} (b - O)^2 = \frac{1}{2} \sum_{k=1}^l (b_k - O_k)^2. \quad (5)$$

Expand the above error definition to the hidden layer; then,

$$E = \frac{1}{2} \sum_{k=1}^l \left[ b_k - f \left( \sum_{j=0}^m w_{jk} y_j \right) \right]^2. \quad (6)$$

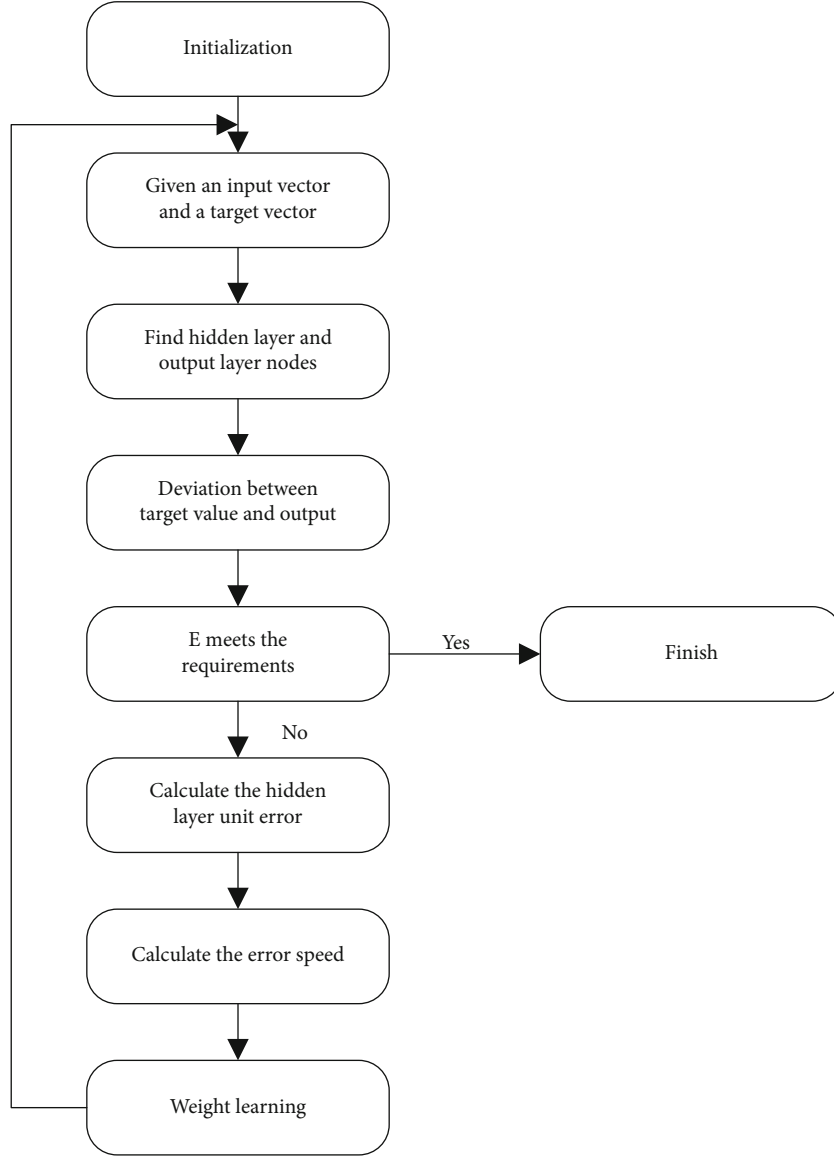


FIGURE 1: Network error definition and weight adjustment ideas.

Expanding further to the input layer, then

$$E = \frac{1}{2} \sum_{k=1}^l \left\{ b_k - f \left[ \left( \sum_{j=0}^m w_{jk} f \left( \sum_{i=0}^m v_{ij} x_i \right) \right) \right] \right\}^2. \quad (7)$$

This shows that the network error depends on the weights of each layer; hence, modifying the weights may affect error. Adjusting the weights is a continuous process of reducing the error; hence, the weight adjustment should be proportionate to the error gradient:

$$\begin{aligned} \Delta w_{jk} &= \frac{-\mu \partial E}{\partial w_{jk}}, \quad j = 0, 1, 2, \dots, m, k = 1, 2, \dots, l, \\ \Delta v_{ij} &= \frac{-\mu \partial E}{\partial v_{ij}}, \quad i = 0, 1, 2, \dots, n, j = 1, 2, \dots, m, \end{aligned} \quad (8)$$

where  $-$  represents the gradient descent and the constant  $\mu$  belongs to the number between (0, 1).

**3.1.3. The Establishment of the BP Network Model.** It is possible to choose the number of hidden layers and neurons at random in principle, but in practice, it is best to base this decision on the specifics of the problem at hand. For networks with a large number of hidden layers, training time is required since they are more likely to fall into a local minimum during training. After multiple testing, however, it was discovered that using a three-layer neural network was more accurate. Second, estimate the number of neurons in the output layer and input layer based on the data to be collected and the important elements influencing this layer as well as the feasibility of acquiring these influencing factor data. The hidden layer nodes may be identified without rules by counting the input and output nodes. Input nodes are the patient's important data, output nodes are the evaluation

result, and hidden layer nodes can be identified without rules by counting the input and output nodes. The following formula may be used to determine the implicitly three-layer network according to the Kolmogorov theorem:

$$H = \sqrt{m + n} + a, \quad (9)$$

where  $H$  represents the number of neurons in the hidden layer,  $m$  represents the number of neurons in the input layer,  $n$  is the number of neurons in the output layer, and  $a$  is a constant ranging from 1 to 10.

*3.1.4. Processing the Input Data of the BP Network.* Due to the characteristics of the BP network itself, the selection of sample data has a great influence on the convergence speed and prediction accuracy. The saturation of the output function curve is caused by too large or too small input, so, in order to avoid the saturation area at both ends of the function and make the input play a strong role, it is necessary to normalize the input of the network. The formula for processing is as follows:

$$X = \frac{I - I_{\min}}{I_{\max} - I_{\min}}, \quad (10)$$

where  $I$  represents the unprocessed neural network input value;  $X$  represents the smoothed neural network input value; and  $I_{\max}$  and  $I_{\min}$  are the maximum and minimum input values of the network input, respectively.

*3.1.5. Select the Learning Rate.* Training weight changes are dictated by the learning rate: a low learning rate may lead to a lengthy training period and an inefficient convergence rate, while a high learning rate may cause the system to malfunction. As a result, a low learning rate is often used in order to maintain system stability. There is a choice of a learning rate ranging from 0.01 to 0.7. The learning rate of 0.2 is chosen in this study based on the actual training circumstances

*3.2. Improvement of the BP Algorithm.* Although the BP neural network has many remarkable features, it also has certain limitations: the hypersurface of multiple local minimum points constitutes the connection weight space formed by the global error  $E$  of the BP network, but the essence of the training method currently used by the BPNN is as follows: the method to search for the optimal connection weight in the connection weight space formed by the global error  $E$  is a point-to-point search. Because the network structure parameters at the start of the BPNN training are randomly assigned values, the BPNN cannot avoid slipping into a local minimum. Therefore, in the search process, it is very important to determine the position of the starting point. To eliminate the shortcoming that BPNN is easy to fall into local minima, it is necessary to improve the training method of BPNN, overcome the blindness and randomness of network structure parameters given at the beginning of network training, and let BPNN training start at the beginning. The weight falls on the global optimal peak area in the connection weight space formed by the global error  $E$ . When the

BPNN is used for diagnosis and evaluation, the parameters of the obtained problem network model are easy to fall into local minima, and the network diagnosis and evaluation model cannot achieve satisfactory diagnosis and evaluation results every time, so it is necessary to improve the shortcomings of the BPNN that is easy to fall into local minima.

*3.2.1. Genetic Algorithms.* Genetic algorithm (GA) is a global optimization algorithm. Its objective function does not need to be continuous or differentiable. It is different from the single-point search method in that it uses a method of parallel processing of multiple individuals in the search space. It has good global search performance and can effectively reduce the possibility of falling into local minima. It is mainly used in three aspects of neural network: optimization of connection weights, optimization of learning rules, and optimization of network structure, and the most important one is the weight of training neural network. In essence, genetic algorithms are used to replace some classic learning algorithms. The neural network's connection weights are where all of the system's knowledge is spread. Using a certain weight change rule is the traditional method to obtain the weights. The training process of the BPNN is as follows: continuously adjust the weights during training, and finally, get a good weight distribution, but if the training time is too long, it may fall into a local minimum value, so that a suitable weight distribution cannot be obtained. To solve this problem, GA can be used to optimize the connection weight. The process of combining GA and BP algorithm for neural network training is as follows: the algorithm parameters used in the training process are very sensitive to the results of BP algorithm and GA, and the result of BP algorithm is the same as the initial state of the network. At the beginning of the genetic algorithm, the optimal weight distribution range of the network is obtained by searching the weight space formed by the global error  $E$  of the BPNN, and then, the BP algorithm is used to find the optimal solution in the optimal weight distribution range. Finally, it is concluded that the combination of BP algorithm and GA is a feasible way for the hybrid training of neural network, and the combined algorithm is called GA-BP algorithm.

*3.2.2. Design of the GA-BP Algorithm.* The main idea of using genetic algorithm to optimize the diagnosis and evaluation model of BPNN is as follows; based on BNN, the input and expected output of BPNN are normalized data. In this process, the BP algorithm is combined with the GA, and the gradient information of the BP algorithm, the advantages of strong local search ability, and the characteristics of the GA with high search efficiency and global search ability are used to train the neural network, so as to eliminate the BNN. In lattice training, the drawback is that it is simple to slip into the minimal value. Figure 2 depicts the GA-functional BP's modules. It is made up of four essential components: input parameter preprocessing, output data restoration, neural network subfunction module, and GA-BPNN learning algorithm. The parameters of the grid model are continuously changed by training with known samples,

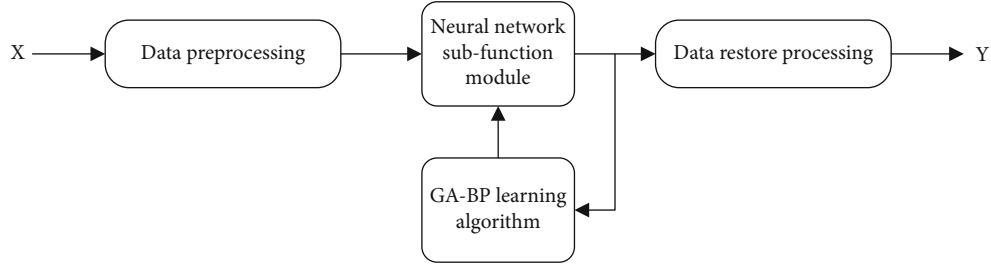


FIGURE 2: GA-BP neural network model structure diagram.

and the model can be used to diagnose and evaluate the therapy effect of unknown disorders.

The stages of genetic algorithm optimization of neural network connection weight are as follows: (1) for a set of randomly generated distribution weights, for each weight (or threshold) in this group, use the coding scheme to encode, so as to build each code chain; for the case where the training rules and network structure have been determined, this code chain corresponds to a neural network whose weights and thresholds take specific values. (2) Calculate the neural network's error function and its fitness function value. The less fit you are, the greater the mistake you make. (3) Next generation inherits a fitness function value from the greatest person. (4) In order to create the next generation of organisms, genetic operators such as crossover and mutation are utilized. (5) Repeat the above process to continuously evolve the initially determined set of weight distributions until the training target meets the requirements.

### 3.2.3. Implementation of GA-BP Algorithm Neural Network

- (1) Coding of network structure parameters: the GA is used to improve the BP algorithm, but the network structure parameters are dry. Genetic operations cannot directly deal with it, so it is necessary to encode the network structure parameters before training to convert it into the genes of chromosomes composed of a certain structure. The real number encoding scheme and the binary encoding scheme are mostly these two procedures to encode the weights and thresholds in the network. Although the binary encoding is simple and common, its disadvantages are as follows: low precision, encoding strings is very long, and the real encoding scheme does not have this disadvantage; it is intuitive. There will be no situation of insufficient precision, and it needs a special genetic operation design for one-dimensional real numbers. This design chooses the real number coding scheme, which can speed up the evolution
- (2) Select the fitness function: most of the genetic algorithm searches do not need external information, as long as the fitness function is used as the basis; the fitness value of each individual in the population is used to search. The fitness function used in this study is

$$f = \frac{1}{E}, \quad (11)$$

TABLE 1: Range of MASI reduction rate and treatment effect.

Treatment effect	MASI decline rate range
Basically healed	MASI decline rate $\geq 90\%$
Effective	MASI decline rate 50%~89%
Get better	MASI decline rate 10%~49%
Invalid	MASI decline rate $< 10\%$

where  $E$  is the global error. From formula (11), it can be known that the smaller the global error  $E$  is, the stronger the adaptability is

- (3) Selection operator: evaluate each weight and threshold, and select the probability  $P_i$  as follows:

$$P_i = \frac{f_i}{\sum_{i=1}^m f_i}, \quad (12)$$

where  $f_i$  represents the fitness value of the individual

- (4) Crossover and mutation operation: these two factors have a great influence on the running performance of heredity, and a relatively small crossover rate is selected. And the mutation rate can increase the chance of individuals to transfer to the next generation. This choice is used for solutions with high ability, conversely, to eliminate solutions of individuals with low fitness ability. It is necessary to choose a relatively high crossover rate and mutation rate. The operation methods of the adaptive crossover rate  $P_c$  and mutation rate  $P_m$  used in this design are as follows:

$$P_c = \frac{C}{f_{\max} - f_a},$$

$$P_m = \frac{d}{f_{\max} - f_a}, \quad (13)$$

where  $c$  and  $d$  are constants less than 1,  $f_{\max}$  is the maximum fitness value, and  $f_a$  is the average fitness value

- (5) Determine genetic manipulation control parameters: mutation probability, crossover probability, and population size are three parameters to be controlled by the genetic algorithm. The setting of the values of these three parameters has a direct effect on the



TABLE 2: Scoring criteria of each parameter of RCM.

Parameters	1	2	3	4
Epidermal pigmentation	<25.0%	26.0%-50.0%	51.0%-75.0%	76.0%-100%
Dendritic cells	None	≤5	≤15	>15
Melanophages	None	≤5	≤10	>10
Solar elastosis	Normal	Mild	Moderate	Serious
Vascularity	Normal	Mild	Moderate	Serious

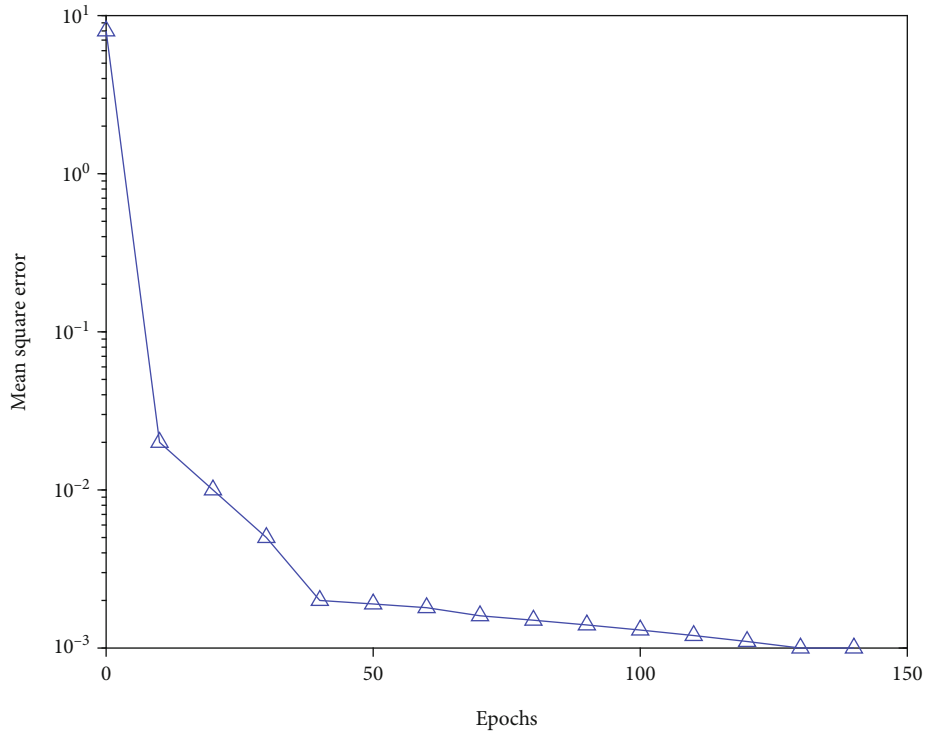


FIGURE 3: When the training curve is 138 steps, the convergence reaches the set accuracy.

execution result of the genetic algorithm. For the size of the group; if the size is larger, the diversity of individuals in the group will be more, so although it is easy to find the global optimum, if it is too large, it will increase the calculation and cause the speed of finding the global optimum to be very slow. If the population size is too small, the search space range of the GA will be limited, which will lead to premature convergence. The population is estimated to be in the range of 20 to 100 people. The chosen group size is 20 since it meets the requirements of this design. If the crossover probability is very high, the individual structure of high fitness will be destroyed; if the crossover probability is too low, global search will be difficult. The crossover probability should, in general, be between 0.4 and 0.99; in this example, it is set to 0.5. For mutation operators, if the mutation probability is too high, the grid's evolutionary algorithm will fail, and the network will devolve into a pure random search; if the mutation probability is too low, new mutations will be difficult to generate

### 3.3. Treatment Effect Evaluation Index System

- (1) MASI scoring method. According to the MASI international evaluation standard, the facial skin is divided into four areas, namely, the forehead, right cheek, left cheek, and mandible; the three indicators for evaluating the severity of skin lesions are skin lesion area percentage, color, and consistency of color distribution

$$M = 0.3[(DF + HF)AF + (DMR + MR)AMR + (DML + HML)AML] + 0.1(DC + HC)AC, \quad (14)$$

where  $M$  is MASI,  $D$  is color,  $H$  is consistency,  $A$  is area,  $F$  is forehead,  $MR$  is right cheek,  $ML$  is left cheek, and  $C$  is jaw.

$$\text{MASI reduction rate} = \frac{V_b - V_a}{V_a}, \quad (15)$$

TABLE 3: Validation results of the BP network model.

Sample	Expected output	BP model output	Error
1	0.151	0.125	0.024
2	0.243	0.273	0.033
3	0.060	0.092	0.032
4	0.192	0.214	0.024
5	0.533	0.483	0.046
6	0.582	0.561	0.018
7	0.422	0.442	0.022
8	0.3704	0.451	0.081
9	0.450	0.472	0.022
10	1.161	0.127	1.032

where  $V_b$  is value before treatment and  $V_a$  is value after treatment. See Table 1 for details.

- (2) RCM scoring method. The laser beam scans from the spinous layer to the basal layer, mainly to observe the pigment density, cell brightness, and cell morphology; scans to the epidermis junction to observe the brightness of the pigment ring; and scans to the superficial dermis to observe inflammatory cells and melanocytes, elastic fibers, and blood vessels. Before treatment, the values were calculated after 2, 5, and 10 treatments. This experiment mainly observed 5 items of epidermal pigmentation density, number of dendritic cells and melanophages, elastic fibrosis, and vascular proliferation. The specific scoring standards are shown in Table 2

In this paper, the five indicators of RCM score are selected as input, and the treatment effect of four grades is used as output.

#### 4. Experiment and Analysis

Here, the experimental results of BP algorithm are discussed, and the GA-BP algorithm experimental results are defined.

*4.1. Experimental Results of the BP Algorithm.* Valuable samples were formed through case records of dermatological patients in a tertiary hospital. From the 240 samples of reliably diagnosed cases, 200 were randomly selected as training samples and the remaining 40 as test samples. After 1000 iterations of BP neural network learning, the network performance target is set to 0.001, and the learning rate is set to 0.2. After training the BP network with the training samples, the test sample results are shown in Figure 3.

From the comparison error output in Table 3, it can be seen that most of the errors between the actual value of the patient's condition and the diagnostic value are not large, and one of the errors is large because a minimum value appears during network training. A small amount of error may be largely affected by the number of selected learning samples. In general, the construction and training of this BP network are feasible.

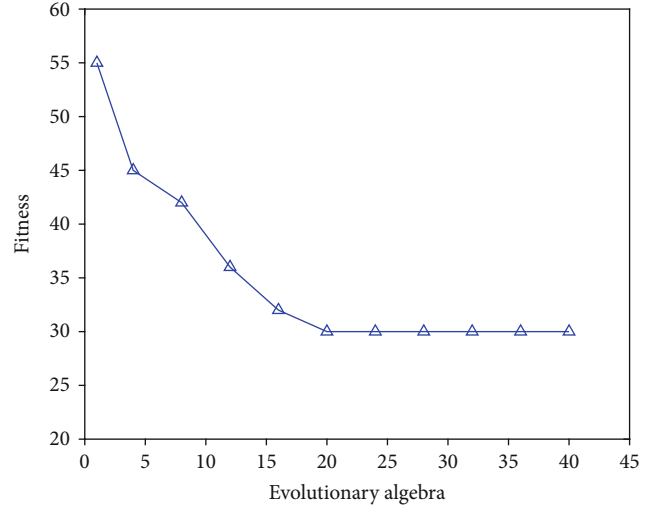


FIGURE 4: Variation of fitness curve when the genetic algorithm optimizes neural network.

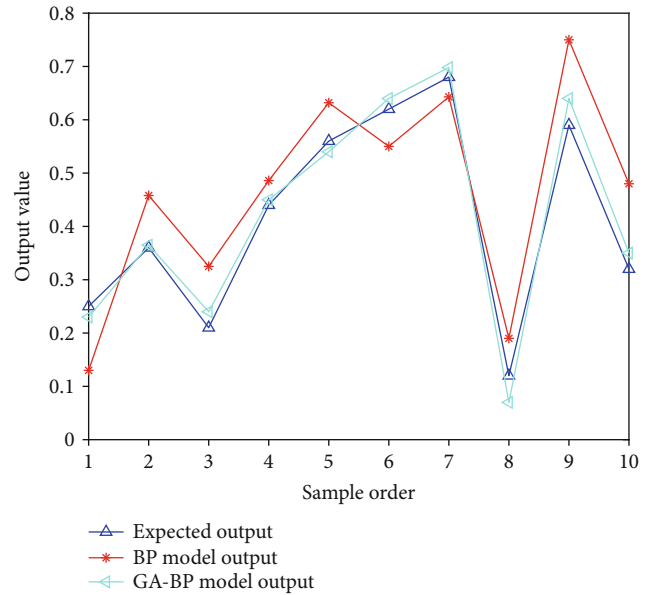


FIGURE 5: Comparison between the output of different models and the expected output.

*4.2. GA-BP Algorithm Experimental Results.* The parameters of the genetic algorithm are selected as follows: the number of iterations is 40, the population size is 20, the crossover probability is 0.3, and the mutation probability is 0.01. First, randomly produce an initial population with an individual code length of 100; then, use the genetic algorithm to iterate 40 times to attain excellent individuals according to the modifications in the fitness function; decode the best individual found and assign it to the BP network; use the train function to train the network; and then, input the normalized test data into the trained network. Using the sim function for prediction, the normalized diagnostic values of 10 test samples will be obtained, which can be denormalized

by mapminmax. Figure 4 shows the fitness change curve when the genetic algorithm optimizes the neural network. It can be found from the figure that the 6th generation is a turning point of the fitness curve, from the initial fitness value of 55 to 30, indicating that after 6 generations of evolution, the GA-BP network has acquired better individuals.

It can be seen from Figure 5 that the optimized GA-BP network is superior to the traditional BPNN under the same training conditions. The output of the BPNN is always changing, and the output of the GA-BP network, on the other hand, is rather steady despite the outcomes of repeated tests. GA-BP network output is less volatile and stable compared to the classic BP. The BP network has an average error of 0.325, whereas the GA-BP network has an average error of 0.156. The GA-BP network is shown to be more accurate than the BP network. It can be seen from the above analysis that compared with the traditional BPNN, the use of the GA-BP network to establish a diagnostic model overcomes the inherent defects of the traditional BPNN and has the advantages of higher accuracy and better stability. Therefore, the GA-BP network can be used to evaluate the effect of laser treatment of melasma.

## 5. Conclusion

There are different forms of face pigment spots induced by various lasers, including chloasma, freckles, black spots, and sequelae, with chloasma being the most prevalent. Chloasma is a light brown to dark brown hyperpigmented skin illness with well-defined patches that are symmetrically distributed over the forehead, neck, around the eyes, around the lips, and other areas and vary in size and shape. It has no inflammatory manifestations, no dandruff, and no symptoms. Chloasma is more common in middle-aged persons, particularly women, and it lasts an average of 96.3 months. There are many ways to treat melasma: such as drug treatment, laser treatment, and Chinese medicine treatment. Among them, intense pulsed light therapy and low-energy Q-switched Nd: YAG laser have been widely used in the treatment of melasma, which can emit laser beams to penetrate the dermis uniformly to treat deep pigmented lesions in the dermis. After a stable treatment outcome for melasma is achieved, it is important to minimize side effects such as postinflammatory hyperpigmentation and skin irritation. Therefore, this paper uses RCM to establish an evaluation index system and then uses a neural network to evaluate the treatment effect. The work of this paper is as follows: (1) this paper introduces various methods of treating melasma at home and abroad and focuses on the application of intense pulsed light therapy and low-energy Q-switched Nd: YAG laser in the treatment of melasma. (2) In this paper, the reliable diagnosis and evaluation case data samples are trained with the designed BPNN to obtain a reliable diagnosis and evaluation network model. (3) By training the GA-BP network structure model to evaluate the treatment effect of chloasma, the results and errors of the evaluation are obtained. Finally, it is proved that the GA-BP network has the advantages of high precision and good stability, so

it can be used to evaluate the effect of laser treatment of melasma.

## Data Availability

The datasets used during the current study are available from the corresponding author on reasonable request.

## Conflicts of Interest

The authors declare that they have no conflict of interest.

## References

- [1] Y. E. Shilong, "Discussion on the etiological factors and pathogenesis of chloasma," *China Journal of Traditional Chinese Medicine and Pharmacy*, vol. 9, 2006.
- [2] S. Rivas and G. Pandya, "Treatment of melasma with topical agents, peels and lasers: an evidence-based review," *American Journal of Clinical Dermatology*, vol. 14, no. 5, pp. 359–376, 2013.
- [3] R. Anderson and A. Parrish, "Selective photothermolysis: precise microsurgery by selective absorption of pulsed radiation," *Science*, vol. 220, no. 4596, pp. 524–527, 1983.
- [4] B. Altshuler, R. Anderson, D. Manstein, H. H. Zenzie, and M. Z. Smirnov, "Extended theory of selective photothermolysis," *Lasers in Surgery and Medicine*, vol. 29, no. 5, pp. 416–432, 2001.
- [5] S. Hilton, H. Heise, A. Bühren, H. Schrumpf, E. Bölke, and P. A. Gerber, "Treatment of melasma in Caucasian patients using a novel 694-nm Q-switched ruby fractional laser," *European Journal of Medical Research*, vol. 18, no. 1, pp. 1–5, 2013.
- [6] K. Naito, "Fractional photothermolysis treatment for resistant melasma in Chinese females," *Journal of Cosmetic and Laser Therapy*, vol. 9, no. 3, pp. 161–163, 2007.
- [7] R. Manaloto and T. Alster, "Erbium: YAG laser resurfacing for refractory melasma," *Dermatologic Surgery*, vol. 25, no. 2, pp. 121–123, 1999.
- [8] W. S. Jang, C. K. Lee, B. J. Kim, and M. N. Kim, "Efficacy of 694-nm Q-switched ruby fractional laser treatment of melasma in female Korean patients," *Dermatologic Surgery*, vol. 37, no. 8, pp. 1133–1140, 2011.
- [9] K. Kar, A. Chauhan, and L. Gupta, "A comparative study on efficacy of high and low fluence Q-switched Nd: YAG laser and glycolic acid peel in melasma," *Indian Journal of Dermatology, Venereology and Leprology*, vol. 78, no. 2, pp. 165–171, 2012.
- [10] J. Lee, J. Kim, K. Noh, and S. E. Chang, "Formation of new melasma lesions in the periorbital area following high-fluence, 1064-nm, Q-switched Nd:YAG laser," *Journal of Cosmetic and Laser Therapy*, vol. 15, no. 3, pp. 165–166, 2013.
- [11] C. Longo, G. Pellacani, A. Tourlaki, M. Galimberti, and P. L. Bencini, "Melasma and low-energy Q-switched laser: treatment assessment by means of in vivo confocal microscopy," *Lasers in Medical Science*, vol. 29, no. 3, pp. 1159–1163, 2014.
- [12] R. Wanitphakdeedecha, W. Manuskiatti, S. Siriphukpong, and M. T. Chen, "Treatment of melasma using variable square pulse Er: YAG laser resurfacing," *Dermatologic Surgery*, vol. 35, no. 3, pp. 475–482, 2009.

- [13] J. Pei, K. Zhong, M. A. Jan, and J. Li, "Personalized federated learning framework for network traffic anomaly detection," *Computer Networks*, vol. 209, p. 108906, 2022.
- [14] H. S. Kim, E. K. Kim, K. E. Jung, Y. M. Park, H. O. Kim, and J. Y. Lee, "A split-face comparison of low-fluence Q-switched Nd: YAG laser plus 1550 nm fractional photothermolysis vs. Q-switched Nd: YAG monotherapy for facial melasma in Asian skin," *Journal of Cosmetic and Laser Therapy*, vol. 15, no. 3, pp. 143–149, 2013.
- [15] K. Chandra, S. Marcano, S. Mumtaz, R. V. Prasad, and H. L. Christiansen, "Unveiling capacity gains in ultradense networks: using mm-wave NOMA," *IEEE Vehicular Technology Magazine*, vol. 13, no. 2, pp. 75–83, 2018.
- [16] J. Du, C. Jiang, Z. Han, H. Zhang, S. Mumtaz, and Y. Ren, "Contract mechanism and performance analysis for data transaction in mobile social networks," *IEEE Transactions on Network Science and Engineering*, vol. 6, no. 2, pp. 103–115, 2017.
- [17] K. Shankar, K. Godse, S. Aurangabadkar et al., "Evidence-based treatment for melasma: expert opinion and a review," *Dermatology and Therapy*, vol. 4, no. 2, pp. 165–186, 2014.
- [18] P. Arora, R. Sarkar, K. Garg, and L. Arya, "Lasers for treatment of melasma and post-inflammatory hyperpigmentation," *Journal of Cutaneous and Aesthetic Surgery*, vol. 5, no. 2, pp. 93–103, 2012.

## Research Article

# Effects of Knee Debridement with Flurbiprofen on Knee Function, Inflammatory Levels, and Bone Metabolism Activity in Patients with Knee Osteoarthritis

Tao Lin, Zemiao Liu , Wei Ji, and Peng Zhang

Department of Joint Surgery, Qilu Hospital (Qingdao), Cheeloo College of Medicine, Shandong University, 266035 Qingdao, Shandong Province, China

Correspondence should be addressed to Zemiao Liu; [liuzemiao@sdqiluhospital.cn](mailto:liuzemiao@sdqiluhospital.cn)

Received 16 May 2022; Revised 10 June 2022; Accepted 13 June 2022; Published 1 July 2022

Academic Editor: Naeem Jan

Copyright © 2022 Tao Lin et al. This is an open access article distributed under the Creative Commons Attribution License, which permits unrestricted use, distribution, and reproduction in any medium, provided the original work is properly cited.

**Objective.** The objective of this study is to explore the effects of knee debridement with flurbiprofen on the knee function, inflammatory levels, and bone metabolism activity in patients with knee osteoarthritis. **Methods.** 110 patients with knee osteoarthritis who underwent arthroscopic debridement in our hospital from 2020.01 to 2022.01 were selected for retrospective analysis. Based on whether or not flurbiprofen was used in combination during the perioperative phase, the patients were divided into the control group (only arthroscopic debridement of the knee) and the research group (flurbiprofen with arthroscopic debridement of the knee), with 55 cases in each group. The indexes such as knee function, inflammatory levels, and bone metabolism activity of the two groups were analyzed. **Results.** According to hospital for special surgery (HSS) evaluation for knee function, most patients in the control group were assessed as “moderate,” while patients in the research group were mainly focused on “excellent” and “good,” and their excellent and good rates were remarkably higher than those in the control group ( $P < 0.05$ ). There were no significant variations in bone metabolism indices such as osteoprotegerin levels (OPG), insulin-like growth factor-1 (IGF-1),  $\beta$ -isomerized C-terminal telopeptide ( $\beta$ -CTX), and receptor activator of nuclear factor- $\kappa$ B ligand (RANKL) before treatment between both groups ( $P > 0.05$ ), with higher OPG, IGF-1 levels, and remarkably lower  $\beta$ -CTX, RANKL levels in the research group than those in the control group after treatment ( $P < 0.05$ ). There were no remarkable differences in pain between both groups before treatment ( $P > 0.05$ ), while at 24 h and 48 h after surgery, the VAS scores in the research group were remarkably lower than those in the control group ( $P < 0.05$ ). In terms of inflammatory factors, the levels of interleukin- $1\beta$  (IL- $1\beta$ ), tumor necrosis factor- $\alpha$  (TNF- $\alpha$ ), and cyclooxygenase-2 (COX-2) in the research group were remarkably lower than those in the control group after treatment ( $P < 0.05$ ). **Conclusion.** Arthroscopy coupled with flurbiprofen provides a good analgesic effect in the therapeutic treatment of patients with knee osteoarthritis, which contributes to the recovery of knee function with definite results. Its mechanism may be associated with the control of inflammatory response and the regulation of bone metabolism disorder.

## 1. Introduction

Knee osteoarthritis is a chronic joint disease of the knee where the inflammation progresses slowly, and symptoms such as knee pain, swelling, stiffness, and deformity gradually develop, which affect the daily activities of patients and may render them completely immobile in the worst-case scenario [1–3]. Currently, the treatment of knee osteoarthritis is aimed at relieving pain, delaying disease progression, correcting deformities, improving or restoring joint func-

tion, and improving patients' quality of life. In clinical practice, laddering, personalized, and comprehensive treatments are taken as the leading treatment protocols, including four levels of basic, pharmacological, restorative, and reconstructive treatment [4–6]. Basic treatment, which is suitable for all patients with knee osteoarthritis, is only required by very few patients in the early stages with mild symptoms in the form of health education, exercise, and physical therapy. Most patients with clinical diagnosis need to receive pharmacological, restorative, or even reconstructive treatment.

Pharmacological treatment includes many types such as external use, oral administration, intravenous infusion, and intraarticular injection, for the main purpose of analgesia and symptom relief. Restorative treatment like arthroscopic debridement can remove many pain-causing factors, control the disease, prolong the use of joints, and avoid premature joint replacement surgery [7–9]. However, knee debridement cannot cure the disease, and many patients still have obvious joint swelling and pain after surgery. Since knee debridement is performed under local anesthesia, the perioperative analgesic management of such patients is particularly important for the prognosis and has always been a major clinical research challenge. Flurbiprofen is a nonsteroidal anti-inflammatory analgesic drug with certain targeting effects, and several studies have shown its good efficacy on the pain after orthopedic surgery [10, 11]. It can be used for preemptive analgesia or postoperative analgesia, but there are few studies on flurbiprofen-assisted arthroscopic debridement for knee osteoarthritis. This study intends to observe the effects of flurbiprofen on knee function and bone metabolism indexes in patients with knee osteoarthritis during the perioperative period of arthroscopic debridement.

The paper's organization paragraph is as follows: The materials and methods are presented in Section 1. Section 2, discusses the experiments and results. Finally, in Section 3, the research work is concluded with discussion.

## 2. Materials and Methods

**2.1. Inclusion and Exclusion Criteria.** Inclusion criteria are as follows: ① The patients met the therapeutic indications of knee arthroscopic debridement; ② the patients were aged  $\geq 50$ ; ③ the patients had no contraindications to flurbiprofen; ④ the patients were ranked in class I-II by ASA; ⑤ the patients had no peripheral neuropathy; ⑥ the patients had no history of peptic ulcer; and ⑦ the patients and their family members knew the study protocol and signed the consent form.

Exclusion criteria are as follows: ① patients with abnormal coagulation function; ② patients with cardiac or renal insufficiency; ③ patients with immune or infectious diseases; ④ patients with cognitive impairment or psychiatric diseases; ⑤ patients who dropped out after surgery; ⑥ patients with a history of allergy to nonsteroidal anti-inflammatory drugs; and ⑦ patients with long-term preoperative use of other analgesic drugs.

**2.2. Selection and Grouping of Patients.** The research objects were selected from the patients with knee osteoarthritis who underwent arthroscopic debridement in our hospital from 2020.01 to 2022.01, with the total sample size of 110 cases. The patients were grouped according to whether flurbiprofen was used in combination during the perioperative period. In other words, the patients who underwent arthroscopic debridement of the knee only were placed in the control group, and those who also received flurbiprofen treatment were placed in the research group, with 55 cases in each group. The study conformed to the ethical and moral

standards of our hospital and was approved by the Ethics Committee.

### 2.3. Method

**2.3.1. Arthroscopic Debridement.** Continuous epidural anesthesia or subarachnoid block anesthesia was administered, and balloon tourniquets (37.2-43.9 kPa) were used. The approaches for knee followed Jackson's standard. Arthroscope and surgical instruments were placed medially and laterally under the patella, and 1 L of 0.1% epinephrine injection and 3000 ml of normal saline were perfused through the suprapatellar lateral incision. The intraarticular conditions were explored under an arthroscope, with several treatments as follows: ① Treatment of cartilage injury. Cartilage injury was graded by Outerbridge scale. Injury of grade 1 was not treated specially; injury of grades 2-3 was trimmed with a cartilage shaver and treated with radiofrequency and gasification; grade 4 injuries were treated with a curette or nucleus pulposus clamp to remove the unstable cartilage edge, followed by radiofrequency, gasification, and solidification. ② Treatment of lateral patellar retinaculum. The patients who had obvious patellar subluxation or lateral tilt, and reduced mobility with obvious tenderness over lateral retinaculum by preoperative axial X-ray, and had degeneration of the lateral cartilage with intact medial cartilage according to arthroscopy, were treated with lateral retinacular release. ③ Treatment of osteophytes. Osteophytes that blocked flexion and extension of joints and caused frictional damage on articular cartilage surface were removed by grinding. ④ Treatment of hyperplastic synovium. Severely congested and edematous synovium, significantly thickened infrapatellar fat pad, and fat pad or synovium that affected joint flexion and extension and had obvious tenderness before surgery were moderately shaved and resected. ⑤ Treatment of meniscus injury. Partial or subtotal resection was conducted in the patients who had degenerative meniscus tears, trying to retain the anterior horn and removing the free body and debris. After cleaning, the joint cavity was repeatedly flushed with plenty of normal saline, and the knee joint was bandaged. All patients received arthroscopic debridement of the knee by the same group of physicians.

**2.3.2. Flurbiprofen.** 50 mg of flurbiprofen was intravenously injected before surgery (specification. 5 ml: 50 mg, Beijing Tide Pharmaceutical Co., Ltd., NMPA Approval No. H20041508) for analgesia. For 24-h postoperative continuous analgesia, the analgesic pumps were given 100 mL of 0.2% ropivacaine, and flurbiprofen was injected intravenously once every 12 h, with 50 mg each time.

### 2.4. Observation Indexes

**2.4.1. General Data.** Age, BMI, gender, affected side, underlying diseases (diabetes, hypertension, and hyperlipidemia), ASA classification, and K-L classification were the main statistical data.

**2.4.2. Knee Function.** After treatment, the patients' knee function was evaluated according to the hospital for special

surgery (HSS) scoring system, where the six evaluation dimensions included pain (30 points), function (22 points), range of motion (18 points), muscle strength (10 points), knee flexion deformity (10 points), and knee instability (10 points). Knee function was graded and scored by the clinical efficacy, with 85 points or more as excellent; 70-84 as good; 60-69 as moderate; and below 59 as poor.

3 ml fasting venous blood of the patients was taken in the early morning. The levels of interleukin-1 $\beta$  (IL-1 $\beta$ ), tumor necrosis factor- $\alpha$  (TNF- $\alpha$ ), cyclooxygenase-2 (COX-2), insulin-like growth factor-1 (IGF-1), osteoprotegerin (OPG), and receptor activator of nuclear factor- $\kappa$ B ligand (RANKL) were detected based on enzyme-linked immunosorbent assay. The level of  $\beta$ -isomerized C-terminal telopeptide ( $\beta$ -CTX) was detected by electrochemiluminescence immunoassay.

**2.4.3. Pain.** The patients' degree of pain was evaluated by visual analog scale (VAS) which uses a 10-cm-long straight line or ruler with 0 reflecting "no pain" and 10 reflecting the "worst pain" at either end. The patients marked the numbers on the straight line according to the pain they felt to indicate the intensity of pain and the degree of psychological displeasure, with 0 as no pain, 1-3 as mild pain, 4-6 as moderate pain, 7-9 as severe pain, and 10 as intolerable pain, i.e., severe pain.

**2.5. Statistical Disposal.** In this study, the differences between both groups were calculated by SPSS20.0, with the images edited based on GraphPad Prism 7 (GraphPad Software, San Diego, USA). The research data consisted of count data and measurement data, which were expressed as [ $n$  (%)] and ( $\bar{x} \pm s$ ) and tested by  $X^2$  and  $t$  tests. The differences were statistically remarkable when  $P < 0.05$ .

### 3. Results

**3.1. General Data.** There is no remarkable difference in the data such as mean age, BMI, gender, affected side, underlying diseases (diabetes, hypertension, hyperlipidemia), ASA classification, and K-L classification between both groups ( $P > 0.05$ ), which was detailed in Table 1.

**3.2. Knee Function.** According to the HSS evaluation for knee function, most patients in the control group are assessed as "moderate," while patients in the research group are mainly focused on "excellent" and "good," and their excellent and good rates are remarkably higher than those in the control group ( $P < 0.05$ ), which is detailed in Table 2.

**3.3. Bone Metabolism.** There is no remarkable difference in the levels of bone metabolism indexes such as OPG, IGF-1,  $\beta$ -CTX, and RANKL between both groups before treatment ( $P > 0.05$ ), with higher OPG, IGF-1 levels, and remarkably lower  $\beta$ -CTX, RANKL levels in the research group than those in the control group after treatment ( $P < 0.05$ ), which is detailed in Table 3.

**3.4. Pain.** There are no remarkable differences in pain between both groups before treatment ( $P > 0.05$ ), while at

TABLE 1: Comparison of general data ( $n = 55$ ).

Observation indexes	Control group	Research group	$X^2/t$	$P$
Age (years)	62.20 $\pm$ 4.70	61.95 $\pm$ 4.57	0.283	0.778
BMI (kg/m <sup>2</sup> )	23.15 $\pm$ 3.01	23.26 $\pm$ 3.04	0.191	0.849
Gender			0.334	0.563
Male	25 (45.54)	22 (40.00)		
Female	30 (54.55)	33 (60.00)		
Affected side				
Left side	21 (38.18)	17 (30.91)	0.643	0.423
Right side	27 (49.09)	30 (54.55)	0.328	0.567
Both sides	7 (12.73)	8 (14.55)	0.077	0.781
Underlying diseases				
Diabetes	27 (49.09)	25 (45.45)	0.146	0.702
Hypertension	29 (52.73)	30 (54.55)	0.037	0.848
Hyperlipidemia	24 (43.64)	23 (41.82)	0.037	0.847
ASA classification			0.334	0.563
Class I	22 (40.00)	25 (45.45)		
Class II	33 (60.00)	30 (54.55)		
K-L classification				
Class II	24 (43.64)	26 (47.27)	0.147	0.702
Class III	25 (45.45)	24 (43.64)	0.037	0.848
Class IV	6 (10.91)	5 (9.09)	0.101	0.751

24 h and 48 h after surgery, the VAS scores in the research group are remarkably lower than those in the control group ( $P < 0.05$ ), which is detailed in Figure 1.

**3.5. Inflammatory Factor Levels.** In terms of inflammatory factors, the levels of IL-1 $\beta$ , TNF- $\alpha$ , and COX-2 in the research group are remarkably lower than those in the control group after treatment ( $P < 0.05$ ), with statistically remarkable differences, which is shown in Table 4.

### 4. Discussion

Arthroscopic debridement has the advantages of minimal invasion, rapid postoperative recovery, and low cost, making it one of the common treatments for knee osteoarthritis. But the invasive nature of arthroscopic debridement inevitably leads to the intraoperative damage of intraarticular tissues which induces local swelling, adhesions, and inflammatory reactions. Furthermore, arthroscopic debridement, which is frequently accompanied with medicines for total treatment in clinic, is often challenging for patients with severe knee osteoarthritis to achieve excellent results [12–14]. In addition, perioperative analgesia for such patients is also an important way to alleviate postoperative pain and guarantee that the early postoperative functional exercise goes through smoothly. According to relevant reports, most patients with knee osteoarthritis show obvious local inflammatory injury and severe postoperative pain after arthroscopic debridement, which is attributed to intraoperative tissue damage

TABLE 2: Results of HSS evaluation.

Groups	Excellent	Good	Moderate	Poor	Excellent and good rate
Control group	8 (14.55)	11 (20.00)	25 (45.45)	11 (20.00)	19 (34.55)
Research group	19 (34.55)	22 (40.00)	10 (18.18)	4 (7.27)	41 (74.55)
$\chi^2$					17.747
$P$					<0.001

TABLE 3: Results of bone metabolism indexes.

Indexes	Control group	Research group	$t$	$P$
OPG (pg/ml)				
Before treatment	3.12 ± 0.71	3.16 ± 0.82	0.273	0.785
After treatment	4.63 ± 0.72	5.41 ± 0.66	5.922	<0.001
IGF-1 ( $\mu\text{g/L}$ )				
Before treatment	75.56 ± 6.32	75.82 ± 6.50	0.213	0.832
After treatment	86.25 ± 7.91	92.03 ± 8.01	3.808	<0.001
$\beta$ -CTX (pg/ml)				
Before treatment	0.92 ± 0.25	0.93 ± 0.24	0.214	0.831
After treatment	0.75 ± 0.21	0.45 ± 0.12	9.199	<0.001
RANKL (pg/ml)				
Before treatment	48.75 ± 4.15	48.62 ± 4.08	0.166	0.869
After treatment	38.56 ± 3.15	30.01 ± 2.43	15.938	<0.001

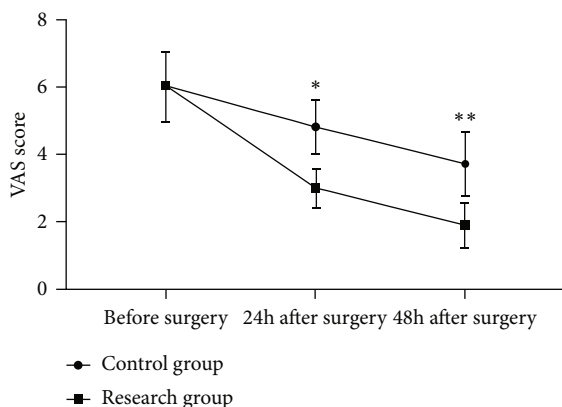


FIGURE 1: Results of VAS scores. Notes: The transverse axis was time points, and the longitudinal axis was the VAS score (points). The VAS scores in the control group before surgery, 24 h after surgery, and 48 h after surgery were (6.07 ± 1.09) points, (4.82 ± 0.81) points, and (3.73 ± 1.02) points, respectively. The VAS scores in the research group before surgery, 24 h after surgery, and 48 h after surgery were (6.07 ± 1.04) points, (2.95 ± 0.62) points, and (1.87 ± 0.74) points, respectively. \* suggested remarkable differences in the VAS scores at 24 h after surgery between both groups ( $t = 13.596$ ,  $P < 0.001$ ). \*\* suggested remarkable differences in the VAS scores at 48 h after surgery between both groups ( $t = 10.946$ ,  $P < 0.001$ ).

and inflammatory response. Flurbiprofen is a nonselective, nonsteroidal anti-inflammatory drug that targets injury sites of tissues and vessels, selectively reduces the level of inflammatory factors in the blood circulation, and has certain targeted anti-inflammatory and analgesia effects which have

been demonstrated in several postoperative analgesia studies [15–17]. In this study, patients with knee osteoarthritis in our hospital were chosen as the subjects for research, in order to further explore the effects of arthroscopic debridement with flurbiprofen on knee function and bone metabolism indexes and its mechanism.

During the perioperative period of arthroscopic debridement, the patients in the research group were given flurbiprofen. There were no remarkable differences in pain between both groups before treatment ( $P > 0.05$ ), while at 24 h and 48 h after surgery, the VAS scores in the research group were remarkably lower than those in the control group ( $P < 0.05$ ), which was consistent with the report of Nichilas Bene et al. [18]. As a nonsteroidal anti-inflammatory analgesic, flurbiprofen can reduce prostaglandin production by inhibiting central and peripheral cyclooxygenase, achieving analgesic effects, and reducing nociceptive sensitivity caused by surgical stimulation, as well as suppressing the release of inflammatory factors. Subsequently, this study found that the levels of inflammatory factors such as IL-1 $\beta$ , TNF- $\alpha$ , and COX-2 were remarkably lower in the research group than in the control group after treatment ( $P < 0.05$ ). The occurrence of knee osteoarthritis is mainly related to degenerative joint lesions or metabolic disorders, while inflammatory factors also play an important role in it. TNF- $\alpha$  is a pro-inflammatory cytokine that can increase osteoclast activity and inhibit osteoblast activity, inhibit the synthesis of proteoglycans and cartilage collagen, and is involved in the occurrence and development of knee osteoarthritis. IL-1 $\beta$  is a hormone-like peptide inflammatory factor, which also participates in the process of cartilage apoptosis. COX-2 is a



TABLE 4: Results of inflammatory factor levels.

Groups	Cases	IL-1 $\beta$ (ng/L)	TNF- $\alpha$ (pg/ml)	COX-2 (pg/ml)
Control group	55	4.79 $\pm$ 1.07	7.02 $\pm$ 1.28	16.65 $\pm$ 2.34
Research group	55	3.72 $\pm$ 1.05	5.47 $\pm$ 1.19	12.43 $\pm$ 2.10
<i>t</i>		5.293	6.577	9.954
<i>P</i>		<0.001	<0.001	<0.001

rate-limiting enzyme synthesized by prostaglandins, which is highly expressed under the induction of IL-1, TNF- $\alpha$ , or other cytokines. Some studies have found that the high expression of COX-2 in local joint is an important factor leading to knee osteoarthritis, whose progression is also accompanied by the further increased expression level of COX-2 [19–21]. As a result, the findings suggest that combining flurbiprofen perioperatively with arthroscopic debridement in individuals with knee osteoarthritis is helpful, especially for reducing the expression of IL-1 $\beta$ , TNF- $\alpha$ , COX-2, and other inflammatory factors. In addition, the imbalance of bone metabolism is also an important aspect reflecting local bone destruction and systemic bone loss in patients with osteoarthritis. Osteogenesis-osteolysis imbalance is mainly manifested as bone reconstruction, abnormal activation of osteoclasts, and imbalance of bone resorption and bone formation, and thus, the levels of OPG, IGF-1,  $\beta$ -CTX, RANKL, and other bone metabolism indexes in peripheral serum will change abnormally. This study found that the levels of OPG and IGF-1 were higher ( $P < 0.05$ ), and the levels of  $\beta$ -CTX and RANKL were remarkably lower ( $P < 0.05$ ) in the research group than in the control group after treatment.  $\beta$ -CTX is a bone resorption marker and shows a remarkable positive correlation with the degree of joint pain and swelling in patients. IGF-1 can reflect the activity of osteoblasts and has a significant role in the repair of damaged cartilage. OPG can block the binding of RANKL to RANK, inhibit osteoclast differentiation and maturation, and thus inhibit bone resorption [22–25]. The findings show that flurbiprofen combined with arthroscopic debridement is more effective in managing bone metabolism abnormalities and enhancing knee function recovery in patients with knee osteoarthritis. Then, according to the HSS evaluation for knee function, it was found that most patients in the control group were assessed as “moderate,” while patients in the research group were mainly focused on “excellent” and “good,” and their excellent and good rates were remarkably higher than those in the control group ( $P < 0.05$ ). It suggested that flurbiprofen combined with arthroscopic debridement is effective in patients with knee osteoarthritis and has a greater potential application for their prognostic recovery.

To sum up, for patients with knee osteoarthritis, flurbiprofen combined with arthroscopic debridement is effective and has good analgesic effect, which contributes to the recovery of knee function. Its mechanism may be associated with the control of inflammatory reaction and the regulation of bone metabolism disorder.

## Data Availability

Data to support the findings of this study is available on reasonable request from the corresponding author.

## Conflicts of Interest

The authors have no conflicts of interest to declare.

## References

- [1] C. Yiallourides and P. A. Naylor, “Time-frequency analysis and parameterisation of knee sounds for non-invasive detection of osteoarthritis,” *IEEE Transactions on Biomedical Engineering*, vol. 68, no. 4, pp. 1250–1261, 2021.
- [2] C. Nguyen and F. Rannou, “The safety of intra-articular injections for the treatment of knee osteoarthritis: a critical narrative review,” *Expert Opinion on Drug Safety*, vol. 16, no. 8, pp. 897–902, 2017.
- [3] J. Boonhong, P. Suntornpiyapan, and A. Piriyaajakul, “Ultrasound combined transcutaneous electrical nerve stimulation (UltraTENS) versus phonophoresis of piroxicam (PhP) in symptomatic knee osteoarthritis: a randomized double-blind, controlled trial,” *Journal of Back and Musculoskeletal Rehabilitation*, vol. 31, no. 3, pp. 507–513, 2018.
- [4] K. Mukhopadhyay, P. Ghosh, P. Ghorai, A. Hazra, and A. K. Das, “Oxaceprol versus tramadol for knee osteoarthritis: a randomized controlled trial,” *Indian Journal of Pharmacology*, vol. 50, no. 5, pp. 266–272, 2018.
- [5] S. Singh, M. Pattnaik, P. Mohanty, and G. S. Ganesh, “Effectiveness of hip abductor strengthening on health status, strength, endurance and six minute walk test in participants with medial compartment symptomatic knee osteoarthritis,” *Journal of Back and Musculoskeletal Rehabilitation*, vol. 29, no. 1, pp. 65–75, 2016.
- [6] S. H. Kim, W.-S. Cho, H.-Y. Joungh, Y. E. Choi, and M. Jung, “Perfusion of the rotator cuff tendon according to the repair configuration using an indocyanine green fluorescence arthroscope: a preliminary report,” *American Journal of Sports Medicine*, vol. 45, no. 3, pp. 659–665, 2017.
- [7] N. Kim and S. B. Jung, “Percutaneous unilateral biportal endoscopic spine surgery using a 30-degree arthroscope in patients with severe lumbar spinal stenosis—a technical note,” *Clinical Spine Surgery*, vol. 32, no. 8, pp. 324–329, 2019.
- [8] B. C. Kwon, J.-K. Lee, S. Y. Lee, and J. Y. Hwang, “Does use of the 70° arthroscope improve the outcomes of arthroscopic debridement for chronic recalcitrant tennis elbow?,” *Journal of Shoulder and Elbow Surgery*, vol. 28, no. 9, pp. 1750–1757, 2019.
- [9] E. P. Wahl, R. P. Coughlin, D. T. Mickelson, C. L. Green, and G. E. Garrigues, “How arthroscope orientation affects

- performance,” *The Journal of Bone and Joint Surgery. American Volume*, vol. 101, no. 4, p. e14, 2019.
- [10] P. P. Mariani, “The 45 degrees arthroscope: a forgotten scope in knee surgery,” *Revue de Chirurgie Orthopédique et Traumatologique*, vol. 105, no. 4, p. 461, 2019.
- [11] N. Maffulli, “Editorial commentary: hip trochanteric bursitis and femoroacetabular impingement: the arthroscope is only the tool,” *Arthroscopy*, vol. 34, no. 5, pp. 1461–1462, 2018.
- [12] J. Dahmen, G. M. M. J. Kerkhoffs, and C. J. A. van Bergen, “Editorial commentary: how far can the arthroscope reach in the ankle joint?,” *Arthroscopy: The Journal of Arthroscopic and Related Surgery*, vol. 37, no. 4, pp. 1258–1260, 2021.
- [13] B. Koc, N. Somorjai, E. P. Kiesouw et al., “Endoscopic debridement and fibrin glue injection of a chronic Morel-Lavallee lesion of the knee in a professional soccer player: a case report and literature review,” *The Knee*, vol. 24, no. 1, pp. 144–148, 2017.
- [14] C. S. Ottesen, A. Troelsen, H. Sandholdt, S. Jacobsen, H. Husted, and K. Gromov, “Acceptable success rate in patients with periprosthetic knee joint infection treated with debridement, antibiotics, and implant retention,” *The Journal of Arthroplasty*, vol. 34, no. 2, pp. 365–368, 2019.
- [15] H. Vahedi, A. Aali-Rezaie, A. Shahi, and J. D. Conway, “Irrigation, debridement, and implant retention for recurrence of periprosthetic joint infection following two-stage revision total knee arthroplasty: a matched cohort study,” *The Journal of Arthroplasty*, vol. 34, no. 8, pp. 1772–1775, 2019.
- [16] A. F. Duque, Z. D. Post, R. W. Lutz, F. R. Orozco, S. H. Pulido, and A. C. Ong, “Is there still a role for irrigation and debridement with liner exchange in acute periprosthetic total knee infection?,” *The Journal of Arthroplasty*, vol. 32, no. 4, pp. 1280–1284, 2017.
- [17] M. Jourdan, “Risk factors for repeat debridement, spacer retention, amputation, arthrodesis, and mortality after removal of an infected total knee arthroplasty with spacer placement,” *The Journal of Arthroplasty*, vol. 33, no. 2, pp. 515–520, 2018.
- [18] N. Bene, X. Li, and S. Nandi, “Factors affecting failure of irrigation and debridement with liner exchange in total knee arthroplasty infection,” *The Knee*, vol. 25, no. 5, pp. 932–938, 2018.
- [19] K. L. Urish, A. G. Bullock, A. M. Kreger et al., “A multicenter study of irrigation and debridement in total knee arthroplasty periprosthetic joint infection: treatment failure is high,” *The Journal of Arthroplasty*, vol. 33, no. 4, pp. 1154–1159, 2018.
- [20] J. Manrique, G. A. Komnos, T. L. Tan, S. Sedgh, N. Shohat, and J. Parvizi, “Outcomes of superficial and deep irrigation and debridement in total hip and knee arthroplasty,” *The Journal of Arthroplasty*, vol. 34, no. 7, pp. 1452–1457, 2019.
- [21] S. Paliwal, A. Tilak, J. Sharma et al., “Flurbiprofen-loaded ethanolic liposome particles for biomedical applications,” *Journal of Microbiological Methods*, vol. 161, pp. 18–27, 2019.
- [22] N. Isiklan and U. H. Erol, “Design and evaluation of temperature-responsive chitosan/hydroxypropyl cellulose blend nanospheres for sustainable flurbiprofen release,” *International Journal of Biological Macromolecules: Structure, Function and Interactions*, vol. 159, pp. 751–762, 2020.
- [23] S. Pande, J. Vashi, and A. Solanki, “Formulation and characterization of ileo-colonic targeted mucoadhesive microspheres containing flurbiprofen for treatment of ulcerative colitis,” *Research Journal of Pharmacy and Technology*, vol. 13, no. 7, pp. 3377–3382, 2020.
- [24] M. Alokour and E. Yilmaz, “A polymer hybrid film based on poly(vinyl cinnamate) and poly(2-hydroxy ethyl methacrylate) for controlled flurbiprofen release,” *Journal of Polymer Research*, vol. 28, no. 4, 2021.
- [25] A. N. Oktay, A. Karakucuk, S. Ilbasmis-Tamer, and N. Celebi, “Dermal flurbiprofen nanosuspensions: optimization with design of experiment approach and *in vitro* evaluation,” *European Journal of Pharmaceutical Sciences*, vol. 122, pp. 254–263, 2018.

## Research Article

# Enteral Nutrition: Based on the Combination of Nutrison Fibre and TPF-DM with A Marine Biological-Based Active Polysaccharide Preparation

Qiuyue Tang and Yaqin Cheng 

Department of Neurology, Affiliated Hospital of Nantong University, Nantong, Jiangsu 226000, China

Correspondence should be addressed to Yaqin Cheng; [c15862717955@sina.com](mailto:c15862717955@sina.com)

Received 10 May 2022; Revised 1 June 2022; Accepted 8 June 2022; Published 30 June 2022

Academic Editor: Naeem Jan

Copyright © 2022 Qiuyue Tang and Yaqin Cheng. This is an open access article distributed under the Creative Commons Attribution License, which permits unrestricted use, distribution, and reproduction in any medium, provided the original work is properly cited.

Good nutrition is essential for human growth, wound healing, and spiritual vitality. However, some individuals are unable to eat or experience gastrointestinal problems such as severe diarrhea, vomiting, gastric retention, and even gastrointestinal bleeding for a variety of causes. Therefore, it has important clinical significance to provide patients with required nutrients and maintain the integrity of the body's tissues and organs through enteral nutrition. Based on this, this work uses a dual carrier of polylactic acid (PLA) and polyvinyl alcohol (PVA) to carry marine biopolysaccharides combined with sodium alginate (PSS) and successfully obtains the intestinal tract based on marine bioactive polysaccharides. Nutritional oral biological preparations (PSS-PLA/PVA) also cooperate with enteral nutritional suspension (diabetes) (TPF-DM) and Nutrison fibre to provide enteral nutritional support for critically ill patients. PSS-PLA/PVA has been shown in clinical studies to increase the effect of enteral nutrition support, the function of intestinal T lymphatic tissue, and the ability to control immunological function, indicating that it is worthy of further clinical development.

## 1. Introduction

As a disease with high mortality and disability rate among middle-aged and elderly people, the incidence rate of neurocritical disease, with the development of population aging, is gradually increasing. The main clinical features are impaired cognitive function, central fever, dysphagia, and limb dysfunction. In addition, neurocritical illness is prone to induce severe stress reactions, accelerates the body's metabolic decomposition, and causes complications such as malnutrition and hypoproteinemia in patients, which are the primary factors restricting the prognosis and survival rate of patients. Compared with other diseases, critically ill patients are susceptible to the effects of drugs and stress reactions, leading to impaired gastrointestinal function, leading to diarrhea, vomiting, gastric retention, and even gastrointestinal bleeding [1, 2]. Therefore,

nutritional support is necessary to regulate the immune function of the patient's body and maintain the functional integrity of the body's tissues and organs [3–6].

Nutritional support can be divided into two types, enteral and parenteral [7]. Vitamins, calories, electrolytes, amino acids, and trace elements are delivered to patients via intravenous channels through parenteral nutrition [8–11]. However, using parenteral nutrition exclusively will make it more difficult to maintain patients' nutritional status and raise the risk of problems [12–15]. Enteral nutrition (EN) is a way to provide patients with required nutrients through the gastrointestinal route [16, 17]. In the early stages of neurocritical patients, enteral nutrition can better maintain the integrity of the body's tissues and organs than parenteral nutrition and has a nonnegligible impact on the prognosis of patients [18]. In addition, enteral nutrition in the early stage of the patient can effectively increase the

blood flow of the gastric mucosa and maintain the barrier function of the gastrointestinal mucosa. At the same time, food entering the gastrointestinal tract can also stimulate the body's advocacy-neuro-endocrine immune axis, effectively preventing the liver cholestasis situation. In addition, enteral nutrition can slow down the body's stress response, maintain the function of the intestinal mucosa, and reduce the occurrence of side effects such as gastrointestinal bleeding [19]. Enteral nutritional suspension (diabetes) (TPF-DM) and Nutrison fibre are commonly used clinical enteral nutrition drugs. In addition to supplying energy to the body, they can also control the patient's blood sugar and blood lipids and have a better therapeutic effect on critically ill patients. However, the use of TPF-DM and Nutrison fibre alone can easily produce side effects such as abdominal distension, diarrhea, and malabsorption. Therefore, how to improve this phenomenon is a hot issue of current research.

According to various sources, marine biological polysaccharides can be classified as marine plant polysaccharides, marine animal polysaccharides, and marine microbial polysaccharides [20–22]. The most researched marine polysaccharides include algae polysaccharides, scallop glycosaminoglycans, mussel polysaccharides, abalone polysaccharides, and YCP polysaccharides extracted from the mycelium of marine fungus Ys4108. Because of its unique chemical composition and structure, marine biopolysaccharides usually have antioxidant, antithrombotic, immune regulation, cholesterol-lowering, and antitumor effects [23–25]. It possesses dietary fibre qualities, and as an EN preparation, it can aid in the absorption of carbs, lipids, vitamins, and minerals by the body. At the same time, by increasing the activity of immune cells, marine polysaccharides can increase the secretion of cytokines, causing the body to manufacture antibodies to improve immunological function. In addition, the dietary fibre components contained in marine biopolysaccharides can effectively control the increase in blood sugar and improve glucose tolerance and cholesterol content. Therefore, in this work, sodium alginate (PSS) was selected as the main component of marine biobased active polysaccharide enteral nutrition preparation, and polylactic acid (PLA) and polyvinyl alcohol (PVA) were used as drug carriers to prepare a new type of marine organism. Active polysaccharide oral preparation was used in combination with TPF-DM and Nutrison fibre, in order to improve the side effects of TPF-DM and Nutrison fibre as enteral nutrition preparations and to investigate its application effect in neurocritical patients.

The paper is organized as follows: the materials and methods are presented in Section 2. Section 3 discusses the experimental analysis and results of the proposed concepts. Finally, in Section 4, the research work is concluded.

## 2. Materials and Methods

In this section, we define the reagents, instruments, preparation of PSS-PLA/PVA, analysis of PSS-PLA/PVA drug release ability *in vitro*, clinical research, and statistical analysis in detail.

**2.1. Reagents.** PSS was purchased from Shanghai Fusheng Industrial Co., Ltd. (Shanghai, China). PLA and PVA are provided by Wuhan Haishan Technology Co., Ltd. (Hubei, China). Dichloromethane, hydrochloric acid, potassium dihydrogen phosphate, and sodium hydroxide were purchased from Jinan Chuangshi Chemical Co., Ltd. (Shandong, China). Trypsin and pepsin were produced by Wuhan Zeshancheng Biomedical Technology Co., Ltd. (Hubei, China). TPF-DM and Nutrison fibre were provided by Nutricia Pharmaceutical (Wuxi) Co., Ltd. (Jiangsu, China).

**2.2. Instrument.** The KQ-500E ultrasonic cleaner was purchased from Kunshan Ultrasonic Instrument Co., Ltd. (Jiangsu, China). The micro high-speed refrigerated centrifuge C1650R-230V was provided by Lepto Scientific Instruments (Beijing) Co., Ltd. (Beijing, China). Carl Zeiss provided the SIGMA 500 field emission scanning electron microscope (Oberkochen, Germany). Particle Sizing Systems sold the AccuSizer780 AD multipurpose automatic counting particle size detector (Florida, USA). An Oulaibo constant temperature oscillator OLB-100B was purchased from Jinan Oulaibo Scientific Instrument Co., Ltd. (Shandong, Jinan).

**2.3. Preparation of PSS-PLA/PVA.** PSS-PLA is prepared by a double emulsification solvent evaporation method. 50 mg of PSS was dissolved in 1.0 mL of double-distilled water to prepare the PSS solution. Prepare a PLA solution with a concentration of 40 mg/mL using dichloromethane as the solvent. And use double-distilled water to prepare 4.0 mg/mL and 1.0 mg/mL PVA solutions. The PSS solution was progressively dripped into the PLA solution under ultrasonography in an ice bath to obtain a uniformly dispersed emulsion. Under the same conditions, it was slowly added to the 4.0 mg/mL PVA solution and added to 1.0 mg/mL PVA solution under the condition of stirring in the ice bath. Stir overnight, then freeze centrifugation at 12,000 rpm for 20 min, discard the supernatant, wash the precipitate with double-distilled water, and freeze-dry to obtain the PSS-PLA/PVA oral preparation. And use the field emission scanning electron microscope SIGMA 500 to characterize it.

**2.4. Analysis of PSS-PLA/PVA Drug Release Ability *In Vitro*.** The artificial gastric juice is prepared by adding 8.2 mL of dilute hydrochloric acid and 5.0 g of pepsin to 400 mL of double-distilled water. After stirring, add double-distilled water and dilute to 500 mL. The artificial intestinal juice is prepared by dissolving 3.9 g of potassium dihydrogen phosphate in 250 mL of double-distilled water, using 0.1 mol/L sodium hydroxide to adjust the pH = 6.8, and dissolving another 5.0 g of trypsin in double-distilled water. After mixing the two solutions, dilute to 500 mL with double-distilled water to obtain artificial intestinal juice. Place the PSS-PLA/PVA preparation in 10 mL of artificial gastric juice or artificial intestinal juice, and oscillate at a speed of 150 rpm in a constant temperature shaker at 37°C. Take out 1.0 mL of artificial intestinal juice or gastric juice at 120, 240, 480, and 720 min, and centrifuge at 12,000 rpm. Take the

TABLE 1: General data analysis.

	Group			
	Low risk 1 ( $n = 94$ )	Low risk 2 ( $n = 85$ )	High risk 1 ( $n = 77$ )	High risk 2 ( $n = 77$ )
Sex				
Male	58	61	52	48
Female	26	24	25	29
Age (years)	$55.44 \pm 11.52$	$57.63 \pm 10.69$	$72.17 \pm 11.68$	$71.56 \pm 11.68$
NRS2002 score	2	2	$3.25 \pm 0.62$	$3.56 \pm 0.73$
NIHSS score	$8.89 \pm 5.30$	$8.67 \pm 4.28$	$13.56 \pm 10.74$	$13.68 \pm 9.84$
GCS score	$11.64 \pm 3.44$	$12.65 \pm 3.39$	$10.36 \pm 4.37$	$10.68 \pm 4.59$

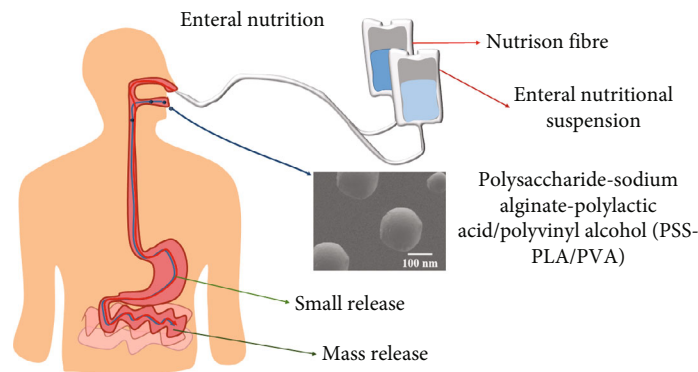


FIGURE 1: Enteral nutrition administration and absorption route.

supernatant to detect its absorbance at 490 nm, and calculate the PSS-PLA/PVA preparation in the artificial gastric juice and cumulative release rate in intestinal juice.

**2.5. Clinical Research.** In this section, we define the general data analysis, treatment method, and observation index in detail.

**2.5.1. General Data Analysis.** A total of 323 neurocritical patients who were treated in our hospital from December 2019 to February 2021 were selected, including 219 male patients and 104 female patients, with an average age of  $63.4 \pm 14.6$  years. The specific patient information is recorded in Table 1.

Before the patients receive enteral nutrition support, use the Acute Physiology and Chronic Health Score II (APACHE II) to make a comprehensive assessment of their vital signs, oxygenation, whether there is chronic organ dysfunction, whether they are in a state of immunosuppression, etc., where APACHE II score  $\geq 16$  points can be included in the observation. In addition, patients with severe heart disease, digestive system disease, endocrine disease, liver and kidney dysfunction, and unstable vascular dynamics besides neurocritical disease were not included in the observation. Relevant clinical treatments in this study have been approved by the hospital ethics committee, and all patients and their families have signed an informed consent form.

**2.5.2. Treatment Method.** All patients were divided into four groups according to the nutritional risk screening score

before enteral nutrition support (NRS2002) and different nutritional support methods, and the total calories of enteral nutrition was 25 kcal/(kg·d), with continuous treatment for 7 days. Among them, the group with the NRS2002 score  $< 3$  points and two enteral nutrition suspensions (TPF-DM and Nutrison fibre) is low-risk group 1, and two enteral nutrition suspensions plus PSS-PLA/PVA oral preparations are used. The second group is the low-risk group; the group with NRS2002 score  $\geq 3$  and two enteral nutrition suspensions is high-risk group 1, and the group is treated with two enteral nutrition suspensions plus PSS-PLA/PVA oral preparations. Its treatment mechanism for patients is shown in Figure 1.

**2.5.3. Observation Index.** Before and after the nutritional support was given, the patient's albumin (ALB), prealbumin (pre-ALB), and hemoglobin (HB) were tested for biochemical indicators used to evaluate the patient's nutritional support. Also, the total number of T lymphocytes (TLC) levels is used to evaluate the effect of enteral nutrition on lymphocyte function, and the levels of IgA, IgG, and IgM are used to evaluate the effect of enteral nutrition on the immune function of critically ill patients. Furthermore, gastrointestinal symptoms such as gastrointestinal haemorrhage, diarrhea, constipation, lung infection, vomiting, and stomach retention were recorded.

**2.6. Statistical Analysis.** Use SPSS 22.0 to process and analyze the data involved in this research. Quantitative variables are expressed as mean  $\pm$  standard deviation, and qualitative

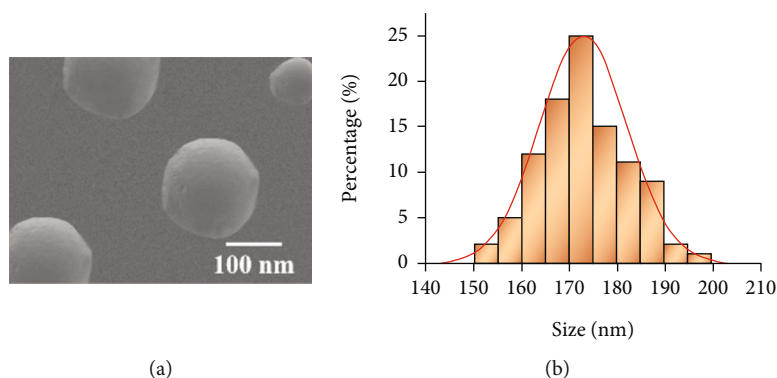


FIGURE 2: Characterization of a novel oral preparation of marine biologically active polysaccharide-sodium alginate-poly(lactic acid)/poly(vinyl alcohol) (PSS-PLA/PVA): (a) electron microscopy characterization diagram; (b) graph of particle size distribution.

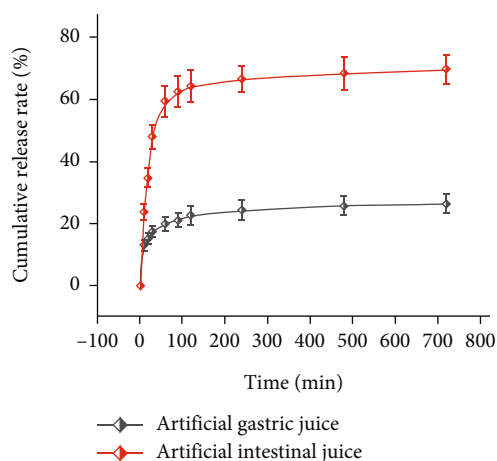


FIGURE 3: Analysis of the cumulative release rate of polysaccharide-sodium alginate-poly(lactic acid)/poly(vinyl alcohol) (PSS-PLA/PVA) in artificial gastric juice and artificial intestinal juice.

variables are described by frequency distribution and percentage (%). The  $t$ -test is used for the analysis of quantitative variables, and the analysis of qualitative variables uses the  $\chi^2$  test.  $P < 0.05$  indicates statistical significance.

### 3. Results and Discussion

**3.1. PSS-PLA/PVA Morphology Characteristics.** The morphology of the marine biobased active polysaccharide preparation—PSS-PLA/PVA preparation—was characterized by scanning electron microscopy. Figure 2 shows that the whole of PSS-PLA/PVA is spherical and evenly dispersed. The particle size distribution results show that the average particle size of PSS-PLA/PVA is  $173.52 \pm 23.69$  nm, and the average potential is  $-19.63 \pm 3.62$  mV. Its small particle size can be effectively absorbed by the body and improve the effect of enteral nutrition.

**3.2. In Vitro Release Effect of PSS-PLA/PVA.** In order to simulate the release of PSS-PLA/PVA in the body, the cumulative release rate of PSS-PLA/PVA in artificial gastric juice

and artificial intestinal juice was investigated, respectively (Figure 3). The results show that the drug release rate of PSS-PLA/PVA is faster at 0–60 min and then tends to be flat, and the cumulative release of PSS-PLA/PVA in artificial gastric juice at 720 min is only 26.31%, while at 720 min, the cumulative release amount in artificial intestinal fluid was 69.62%. This result proves that compared with gastric juice, PSS-PLA/PVA is easier to release in the intestine and can meet its enteral nutrition standard.

**3.3. Evaluation of the Effect of Enteral Nutrition.** In order to evaluate the effects of PSS-PLA/PVA oral preparations on enteral nutrition, ALB, HB, and pre-ALB were used as nutritional evaluation indicators to investigate their therapeutic effects on patients with different risk levels (Figure 4). The treatment results showed that each group of drugs had a significant therapeutic effect on neurocritical patients ( $P < 0.05$ ). In addition, the same drug has different effects on the low-risk group and the high-risk group, and it has a better therapeutic effect on patients in the high-risk group. In addition, compared with only using TPF-DM and Nutrison fibre, the addition of PSS-PLA/PVA oral preparations can improve the patient's enteral nutrition absorption.

**3.4. T Lymphocyte Function Evaluation.** TLC is employed as an evaluation index to evaluate the impact of different medicines on the T lymphatic function of neurocritical patients with varied risks, because enteral nutrition can sustain the function of the intestinal lymphatic tissue of patients (Figure 5). The results showed that compared with before treatment, the number of TLC in neurocritical patients with different risk levels increased after different drug treatments ( $P < 0.05$ ). And compared with only using TPF-DM and Nutrison fibre, the combination of TPF-DM and Nutrison fibre with PSS-PLA/PVA oral preparation has better therapeutic effect.

**3.5. Patient's Immune Function Regulation.** IgA, IgG, and IgM are all types of immunoglobulins. Therefore, this study used the levels of IgA, IgG, and IgM in neurocritically ill patients as indicators to investigate the effect of enteral nutrition on the immune function of patients (Figure 6). The findings revealed that after therapy, the

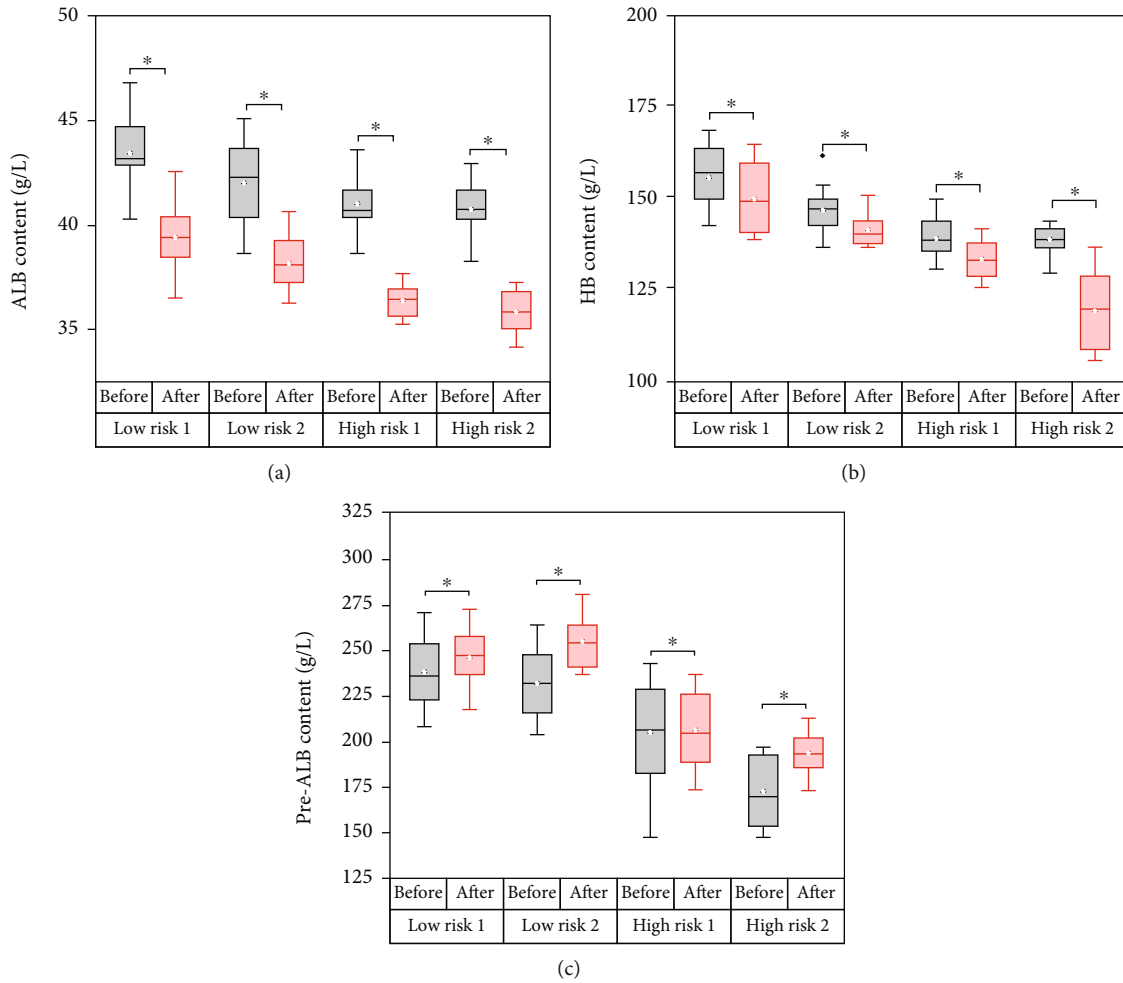


FIGURE 4: The effect of enteral nutrition on nutritional evaluation indexes of patients with different degrees of risk: (a) the effect on albumin (ALB) content; (b) the effect on hemoglobin (HB) content; (c) the effect on prealbumin (pre-ALB) content. \*  $P < 0.05$ .

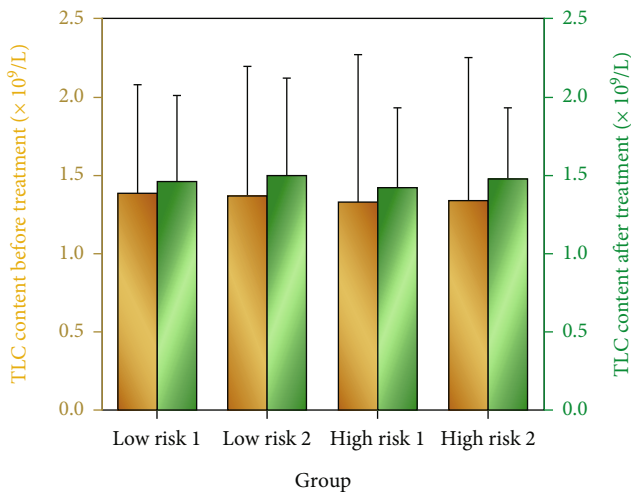


FIGURE 5: The effect of enteral nutrition on the total number of T cells (TLC) in patients with different degrees of risk.

immunoglobulin levels of patients in each group increased ( $P < 0.05$ ), with the increase being more pronounced in the high-risk group. In addition, the addition of PSS-PLA/PVA oral preparations can improve the regulatory effect of TPF-DM and Nutrison fibre on immune function.

**3.6. Incidence of Gastrointestinal Reactions in Patients.** As neurocritical patients are prone to adverse reactions such as diarrhea, constipation, vomiting, lung infection, gastrointestinal bleeding, gastric retention, and even death after treatment, the influence of enteral nutrition on the incidence of adverse reactions was investigated (Figure 7). The results show that the addition of PSS-PLA/PVA oral preparations can reduce the occurrence of adverse reactions.

**3.7. Discussion.** In the care of critically ill patients, malnutrition usually leads to reduced efficacy of drug treatment and some side effects. Therefore, strengthening the nutritional support for critically ill patients is essential. Studies have found that enteral nutrition can effectively improve the metabolic abnormalities of critically ill patients and reduce the risk of complications during treatment [26], especially in patients with neurological diseases such as stroke and

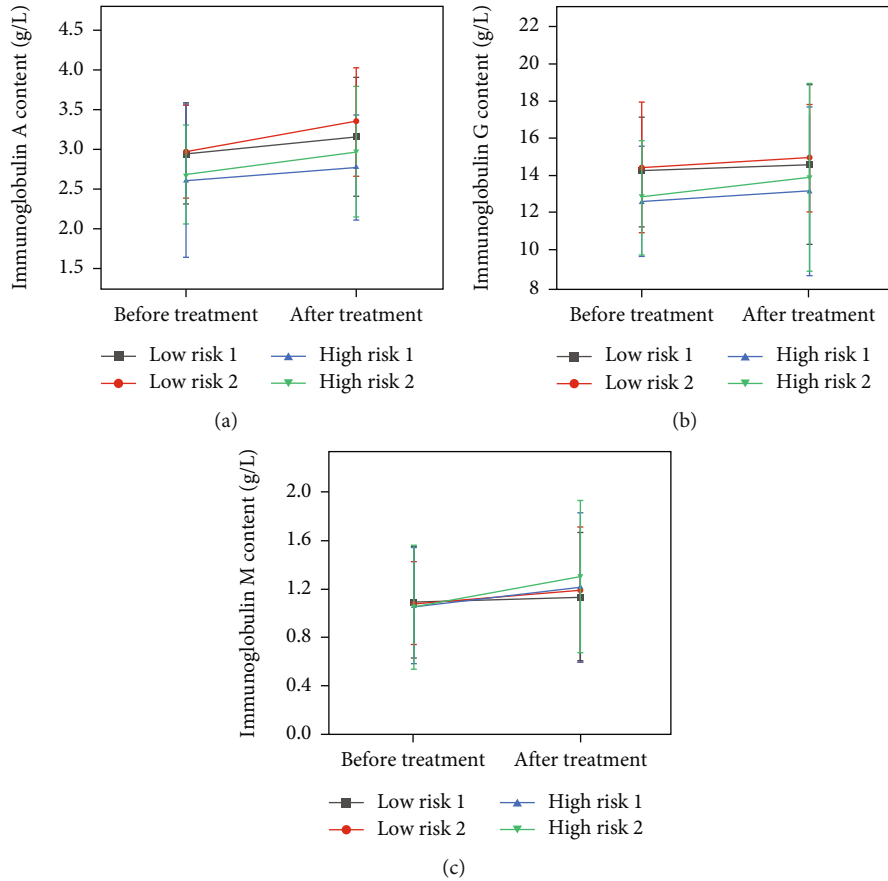


FIGURE 6: The effect of enteral nutrition on the immune function of patients with different degrees of risk: (a) the effect on immunoglobulin A content; (b) the effect on immunoglobulin G content; (c) the effect on immunoglobulin M content.

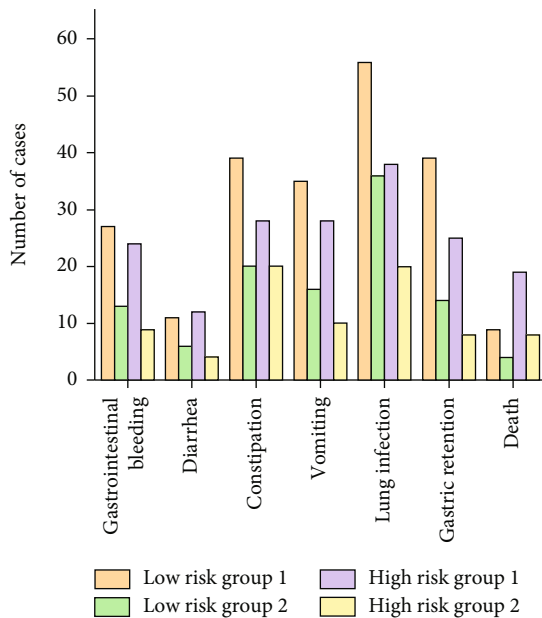


FIGURE 7: The effect of enteral nutrition on the incidence of gastrointestinal reactions in patients.

dementia and patients who require mechanical ventilation [27–29]. Enteral nutrition can be divided into two types: oral and via catheter. Oral administration is typically utilised for patients who are able to swallow on their own, whereas transcatheter infusion is separated into a nasogastric tube and oral feeding tube. Patients who require short-term enteral nutrition support should use a nasogastric tube, whereas patients who require long-term enteral nutrition support should use an oral feeding tube. It is suitable for patients who have undergone partial or complete gastrectomy and who are at risk of aspiration.

In this work, two types of enteral nutrition were used to provide nutritional support to patients undergoing neurocritical treatment. One of the enteral nutrition support methods is the combined use of TPF-DM and Nutrison fibre, and the other enteral nutrition support method is the use of Nutrison fibre and TPF-DM in combination with a marine biobased active polysaccharide preparation-PSS-PLA/PVA oral preparation. According to the NRS2002 score, patients were divided into low-risk and high-risk groups. Nutrition evaluation indicators such as ALB, pre-ALB, HB, TLC levels, and IgA, IgA, and IgA used to evaluate the regulatory effects of enteral nutrition on the immune function of critically ill patients were used. The detection results of IgG and IgM levels can find that each group of drugs has a significant therapeutic effect



on neurocritical patients ( $P < 0.05$ ). And the same drugs are more effective in treating patients in the high-risk group. Furthermore, when compared to only using TPF-DM and Nutrison fibre, adding PSS-PLA/PVA oral preparations can improve the patient's enteral nutrition support effect, maintain the function of intestinal T lymphatic tissue, and regulate the immune function of critically ill patients. In addition, the addition of PSS-PLA/PVA oral preparations can also effectively reduce the incidence of gastrointestinal reactions such as gastrointestinal bleeding, diarrhea, constipation, lung infection, vomiting, and gastric retention. This discovery provides a new way of enteral nutrition support for clinically critically ill patients.

#### 4. Conclusion

PSS was used as the principal component of a marine bioactive polysaccharide enteral nutrition preparation in this work, with PLA and PVA serving as drug transporters to create a new form of marine bioactive polysaccharide oral preparation. The results show that compared with the combined effect of TPF-DM and Nutrison fibre, the addition of PSS-PLA/PVA has better enteral nutrition support effect for patients with different risk levels of neurocritical patients, maintaining the function of intestinal T lymphatic tissue and regulating the immune function of neurocritical patients. It is worthy of further clinical promotion and use.

#### Data Availability

The dataset used in this paper are available from the corresponding author upon request.

#### Conflicts of Interest

The authors declared that they have no conflicts of interest regarding this work.

#### Acknowledgments

This work was supported by Standardized diagnosis and treatment of standardized nutritional management in critically ill neurological patients (MS22020012).



#### References

- [1] S. Livesay, H. Fried, D. Gagnon et al., "Clinical performance measures for neurocritical care: a statement for healthcare professionals from the neurocritical care society," *Neurocritical Care*, vol. 32, no. 1, pp. 5–79, 2020.
- [2] C. M. Schirmer, J. Kornbluth, C. B. Heilman, and A. Bhardwaj, "Gastrointestinal prophylaxis in neurocritical care," *Neurocritical Care*, vol. 16, no. 1, pp. 184–193, 2012.
- [3] R. T. Xu, C. H. Tan, J. J. Zhu et al., "Dysbiosis of the intestinal microbiota in neurocritically ill patients and the risk for death," *Critical Care*, vol. 23, no. 1, p. 195, 2019.
- [4] T. J. Puzio and R. A. Kozar, "Nutrition in the critically ill surgical patient," *Current Opinion in Critical Care*, vol. 26, no. 6, pp. 622–627, 2020.
- [5] P. A. Abdelmalik, S. Dempsey, and W. Ziai, "Nutritional and bioenergetic considerations in critically ill patients with acute neurological injury," *Neurocritical Care*, vol. 27, no. 2, pp. 276–286, 2017.
- [6] D. E. Bear, L. Wandrag, J. L. Merriweather et al., "The role of nutritional support in the physical and functional recovery of critically ill patients: a narrative review," *Critical Care*, vol. 21, no. 1, 2017.
- [7] M. V. Viana, O. Pantet, G. Bagnoud et al., "Metabolic and nutritional characteristics of long-stay critically ill patients," *Clinical Medicine*, vol. 8, no. 7, 2019.
- [8] M. D. Tadlock, M. Hannon, K. Davis et al., "Nutritional support using enteral and parenteral methods," *Military Medicine*, vol. 183, supplement\_2, pp. 153–160, 2018.
- [9] I. Baiu and D. A. Spain, "Parenteral nutrition," *The Journal of the American Medical Association*, vol. 321, no. 21, 2019.
- [10] M. Hellerman Itzhaki and P. Singer, "Advances in medical nutrition therapy: parenteral nutrition," *Nutrients*, vol. 12, no. 3, p. 717, 2020.
- [11] J. Gunst and G. Van Den Berghe, "Parenteral nutrition in the critically ill," *Current Opinion in Critical Care*, vol. 23, no. 2, pp. 149–158, 2017.
- [12] K. H. Mcgrath, "Parenteral nutrition use in children with cancer," *Pediatric Blood & Cancer*, vol. 66, no. 12, 2019.
- [13] N. J. Van, M. Voigt, E. Song et al., "Parenteral nutrition and cardiotoxicity," *Cardiovascular Toxicology*, vol. 21, no. 4, pp. 265–271, 2021.
- [14] J. Davila and D. Konrad, "Metabolic complications of home parenteral nutrition," *Nutrition in Clinical Practice*, vol. 32, no. 6, pp. 753–768, 2017.
- [15] M. Dibb and S. Lal, "Home parenteral nutrition: vascular access and related complications," *Nutrition in Clinical Practice*, vol. 32, no. 6, pp. 769–776, 2017.
- [16] D. M. Solomon, J. M. Hollands, L. Pontiggia, J. J. Delic, and A. L. Bingham, "Metabolic complications occur more frequently in older patients receiving parenteral nutrition," *Nutrition in Clinical Practice*, vol. 35, no. 4, pp. 627–633, 2020.
- [17] I. Baiu and D. A. Spain, "Enteral nutrition," *The Journal of the American Medical Association*, vol. 321, no. 20, 2019.
- [18] A. Vanblarcom and M. A. Mccoy, "New nutrition guidelines: promoting enteral nutrition via a nutrition bundle," *Critical Care Nurse*, vol. 38, no. 3, pp. 46–52, 2018.
- [19] O. Ojo and J. Brooke, "Recent advances in enteral nutrition," *Nutrients*, vol. 8, no. 11, p. 709, 2016.
- [20] E. Pash, "Enteral nutrition: options for short-term access," *Nutrition in Clinical Practice*, vol. 33, no. 2, pp. 170–176, 2018.
- [21] P. Laurienzo, "Marine polysaccharides in pharmaceutical applications: an overview," *Marine Drugs*, vol. 8, no. 9, pp. 2435–2465, 2010.
- [22] Y. E. Lee, H. Kim, C. Seo et al., "Marine polysaccharides: therapeutic efficacy and biomedical applications," *Archives of Pharmacological Research*, vol. 40, no. 9, pp. 1006–1020, 2017.
- [23] Q. M. Shi, A. J. Wang, Z. H. Lu, C. J. Qin, J. Hu, and J. Yin, "Overview on the antiviral activities and mechanisms of marine polysaccharides from seaweeds," *Carbohydrate Research*, vol. 453, pp. 1–9, 2017.
- [24] L. X. Zheng, X. Q. Chen, and K. L. Cheong, "Current trends in marine algae polysaccharides: the digestive tract, microbial catabolism, and prebiotic potential," *International Journal of Biological Macromolecules*, vol. 151, pp. 344–354, 2020.

- [25] C. Arnosti, M. Wietz, T. Brinkhoff et al., “The biogeochemistry of marine polysaccharides: sources, inventories, and bacterial drivers of the carbohydrate cycle,” *Annual Review of Marine Science*, vol. 13, no. 1, pp. 81–108, 2021.
- [26] N. Bibi and W. Bin, “Structure, biological properties and applications of marine-derived polysaccharides,” *Current Organic Chemistry*, vol. 20, no. 19, pp. 2002–2012, 2016.
- [27] C. O’leary-Kelley and K. Bawel-Brinkley, “Nutrition support protocols: enhancing delivery of enteral nutrition,” *Critical Care Nurse*, vol. 37, no. 2, pp. e15–e23, 2017.
- [28] D. B. Schwartz, “Enteral nutrition and dementia integrating ethics,” *Nutrition in Clinical Practice*, vol. 33, no. 3, pp. 377–387, 2018.
- [29] K. Allen and L. Hoffman, “Enteral nutrition in the mechanically ventilated patient,” *Nutrition in Clinical Practice*, vol. 34, no. 4, pp. 540–557, 2019.

## Research Article

# Application Effect of Dexmedetomidine and Dezocine in Patients Undergoing Lung Cancer Surgery under General Anesthesia and Analysis of Their Roles in Recovery Time and Cognitive Function

Jie Ding,<sup>1,2</sup> Mengqi Zhu,<sup>1,2</sup> Hu Lv,<sup>1,2</sup> Jun Zhang <sup>1,2</sup> and Wei Chen <sup>1,2</sup>

<sup>1</sup>Department of Anesthesiology, Fudan University Shanghai Cancer Center, Shanghai 200032, China

<sup>2</sup>Department of Oncology, Shanghai Medical College, Fudan University, Shanghai 200032, China

Correspondence should be addressed to Jun Zhang; zhangjun@shca.net.cn and Wei Chen; chenwei\_fdu@fudan.edu.cn

Received 18 May 2022; Revised 13 June 2022; Accepted 16 June 2022; Published 30 June 2022

Academic Editor: Naeem Jan

Copyright © 2022 Jie Ding et al. This is an open access article distributed under the Creative Commons Attribution License, which permits unrestricted use, distribution, and reproduction in any medium, provided the original work is properly cited.

**Objective.** To explore the application influence of dexmedetomidine (DEX) and dezocine in patients undergoing lung cancer surgery under general anesthesia and analysis of their roles in recovery time and cognitive function. **Methods.** A total of 120 patients who accepted thoracoscopic pulmonary wedge resection in our hospital from November 2021 to April 2022 were selected and randomly divided into group A ( $n=60$ ) and group B ( $n=60$ ). DEX combined with dezocine-assisted anesthesia was performed to group A, and the equal dose of normal saline was administered to group B, so as to compare their inflammatory influence level, brain function, arterial blood gas index, and cognitive function. **Results.** Compared with group B, group A obtained significantly lower intraoperative and postoperative inflammatory factor levels ( $P < 0.001$ ), better postoperative brain function and arterial blood gas index ( $P < 0.001$ ), and lower Loewenstein Occupational Therapy Cognitive Assessment (LOTCA) scores after surgery ( $P < 0.001$ ). Combining DEX with dezocine-assisted general anesthesia can improve the inflammatory factors level of patients undergoing lung cancer surgery and maintain their brain function and oxygen saturation, so that they have better postoperative cognitive function. Therefore, such anesthesia modality should be promoted in practice.

## 1. Introduction

Lung cancer is one of the most lethal malignancies, and in current practice, the prognosis of early-stage patients is improved mostly by thoracoscopic pulmonary wedge resection. However, surgical treatment involves general anesthesia, which can easily lead to immune response, stress reaction, and significant modification in hemodynamics during surgery, and in severe cases, hypoxaemia may even occur, causing injury in multiple organs such as the lung and brain and threatening patients' prognosis [1–3]. Administering safe and effective adjuvant anesthetic drugs is an important measure to reduce intraoperative stress in patients, but studies have shown that drugs such as fentanyl can cause neuronal apoptosis in encephalic region [4], while isoflurane, etc. may affect the cognitive function [5], resulting in perioperative delirium; hence, with such limited function of the said drugs, the cardiocerebral vascular system of patients

cannot be adequately protected. Dexmedetomidine (DEX) is a recent research hotspot in anesthesia, because it can not only alleviate vasoconstriction and blood pressure fluctuation induced by  $\alpha_1$  epinephrine and improve the oxygen saturation for patients undergoing one-lung ventilation [6, 7], but also suppress the secretion frequency of noradrenaline by virtue of its high  $\alpha_2$  epinephrine affinity, impair the stress response, and then protect the cardiocerebral vascular system in patients [8, 9]. On the basis of DEX, additionally administrating dezocine, a mixed opiate receptor agonist-antagonist, can have the effect of postoperative analgesia and lower the possibility of cognitive dysfunction.

There have been previous studies combining DEX with dezocine, but most attentive on their analgesic and sedative functions [10, 11], and none has explored their protective effects in assisting anesthesia on organ function in lung cancer patients who accepted surgery. Based on this, the actual application

consequence was investigated in this study, with the results reported below.

The occurrence of cognitive dysfunction is related to many influences, and analysis of the mechanism of DEX combined with dezocine on cognitive dysfunction revealed that such combination can decrease the inflammatory response, protect multiple organs and systems, and greatly improve the brain function, lung function, cardiovascular system, and CNS.

## 2. Materials and Methods

**2.1. General Information.** 120 patients who recognized thoracoscopic pulmonary wedge resection in our hospital from November 2021 to April 2022 were nominated and equally divided into group A and group B by random number way. No statistical differences were presented in the comparison of their general information ( $P > 0.05$ ), see Table 1. The study was approved by the ethics committee of Fudan University Shanghai Cancer Center (approval No. 2111246-14; clinical trial registration No. ChiCTR2200056217).

**2.2. Inclusion Criteria.** The inclusion criteria of the study were as follows.

- (1) The patients, who had lung cancer and underwent endoscopy, signed the informed consent
- (2) The patients were at least 50 years old
- (3) The patients' physical status was class I-II according to the American Society of Anaesthesiologists (ASA) classification [12]
- (4) The patients' heart function was class I-II according to the New York Heart Association (NYHA) Functional Classification [10] and
- (5) The patients' Child-Pugh scores were class A and B [13]

**2.3. Exclusion Criteria.** The exclusion criteria for the patients of the study were as follows.

- (1) Age < 50 years
- (2) BMI < 18.5 or > 40 kg/m<sup>2</sup> [14]
- (3) Preoperative disturbance of consciousness and cognitive dysfunction
- (4) Coronary heart disease, severe arrhythmia, cardiopulmonary dysfunction, and cerebrovascular accidents
- (5) Anemia
- (6) Hyperglycemia
- (7) Liver and kidney dysfunction
- (8) Asthma, COPD, or presence of above moderate ventilatory dysfunction according to the lung function test results and
- (9) Speech disorder, seeing-hearing dysfunction

**2.4. Methods.** After entering the operating room, all patients were noticed for mean arterial pressure (MAP), heart rate (HR), electrocardiogram (ECG), and oxygen saturation, their vein passages were established, and a face mask was put on for oxygen inhalation. For patients in group A before surgery, 0.1 mg/kg of dezocine (manufacturer: Yangtze River Pharmaceutical (Group) Co., Ltd.; NMPA Approval No. H20080329) was diluted to 6 ml with normal saline and infused within 3 minutes, then the loading dose of 0.7  $\mu$ g/kg of DEX (manufacturer: Cisen Pharmaceutical Co., Ltd.; NMPA Approval No. H20130027) was diluted to 20 ml with normal saline and infused intravenously for 10 minutes. After the beginning of surgery, 0.3  $\mu$ g/(kg•h) of DEX was pump-injected at a constant rate to patients in group A, and at the same time, equal volume of normal saline was administered to patients in group B. For anesthesia induction of patients in the two groups, 0.03 mg/kg of midazolam (manufacturer: Jiangsu Nhwa Pharmaceutical Co., Ltd.; NMPA Approval No. H10980026), 0.3  $\mu$ g/kg of sufentanil (manufacturer: Yichang Humanwell Pharmaceutical Co., Ltd.; NMPA Approval No. H20054171), TCI 3~4  $\mu$ g/ml of propofol (manufacturer: Jiangsu Nhwa Pharmaceutical Co., Ltd.; NMPA Approval No. H20123138), and 0.6 mg/kg of rocuronium (manufacturer: Zhejiang Xianju Pharmaceutical Co., Ltd.; NMPA Approval No. H20123188) were administered. And for intraoperative anesthesia maintenance, 2.5-4  $\mu$ g/ml of propofol and TCI 2-4 ng/ml of remifentanil were administered, and additional 0.2 mg/kg of rocuronium could be given as needed.

Intraoperative parameters: tidal volume was 6 ml/kg, PEEP was 3-5 mmHg, air/oxygen mixture was given, oxygen flow rate was 2 L/min, EtCO<sub>2</sub> was maintained at 35~45 mmHg, and Narcotrend was 40~60.

**2.5. Observation Criteria.**

- (1) **Inflammatory factor level.** Before surgery ( $T_1$ ), during surgery ( $T_2$ ), at the end of surgery ( $T_3$ ), and 1 d after surgery ( $T_4$ ), 20 ml of vein blood was strained from the patients to extent the levels of interleukin-1 $\beta$  (IL-1 $\beta$ ), interleukin-6 (IL-6), interleukin-10 (IL-10), and tumor necrosis factor- $\alpha$  (TNF- $\alpha$ ) with the ELISA method (kits manufactured: Beijing Kewei Clinical Diagnostic Reagent Inc.; NMPA Approval No. S20060028)
- (2) **Brain function.** At  $T_1$ ,  $T_3$ , and  $T_4$ , 15 ml of vein blood was drawn from the patients to measure the levels of serum S100 $\beta$  protein and neuron-specific enolase (NSE) with the ELISA method, and their cerebral extraction of oxygen (CEO<sub>2</sub>) at the same moments was detected with the blood gas analyzer (GEM3000, Beckman Coulter Life Science, IN, USA; NMPA (I) 20082401894)
- (3) **Arterial blood gas indexes.** At  $T_1$ ,  $T_3$ , and  $T_4$ , the oxygen partial pressure (PaO<sub>2</sub>), carbon dioxide partial pressure (PaCO<sub>2</sub>), and lactate level (LAC) in patients were measured

TABLE 1: Comparison of patients' general information.

Group	Group A ( $n=60$ )	Group B ( $n=60$ )	$X^2/t$	$P$
Gender			0.03	0.85
Male	35	36		
Female	25	24		
Age (years old)				
Range	60-76	60-74		
Mean age	$68.26 \pm 5.54$	$68.52 \pm 5.21$	0.26	0.79
Mean body weight (kg)	$54.98 \pm 2.65$	$54.54 \pm 2.57$	0.92	0.36
Complications				
Chronic bronchitis	8	9	0.07	0.79
Chronic obstructive pulmonary disease	10	9	0.06	0.80
Mean duration of disease (years)	$4.21 \pm 0.68$	$4.10 \pm 0.56$	0.97	0.33
Anesthesia grade			0.04	0.85
I	38	39		
II	22	21		
Tumor stage				
II	21	22	0.04	0.85
III	25	24	0.03	0.85
IV	14	14	0.00	1.00
Mean BMI ( $\text{kg}/\text{m}^2$ )	$22.65 \pm 2.51$	$22.68 \pm 2.50$	0.07	0.95
Place of residence			0.04	0.85
Urban area	40	41		
Rural area	20	19		
Monthly income (yuan)			0.04	0.85
$\geq 4,000$	38	37		
$< 4,000$	22	23		
Living habit				
Smoking history	42	40	0.15	0.69
Drinking history	35	34	0.03	0.85
Educational degree			0.14	0.71
Senior high school and below	23	25		
College and above	37	35		

- (4) **Cognitive function.** The cognitive function in patients at  $T_1$  and  $T_4$  was evaluated and compared with the Loewenstein Occupational Therapy Cognitive Assessment (LOTCA) [15, 16], which covered orientation (1-8 points), awareness (1-4 points), visuomotor construction (1-4 points), and thinking operations (1-4 points) and contained 20 items. The lower scores denoted that the patients' cognitive function was better

2.6. *Statistical Processing.* In this study, the data processing software was SPSS20.0, the picture drawing software was GraphPad Prism 7 (GraphPad Software, San Diego, USA), items included were enumeration data and measurement data, methods used were  $X^2$  test and  $t$ -test, and differences were considered statistically significant at  $P < 0.05$ .

### 3. Results

3.1. *Comparison of Inflammatory Factor Levels.* Group A obtained expressively lower intraoperative and postoperative inflammatory factor levels than group B ( $P < 0.001$ ), see Figure 1.

Figure 1(a) shows the serum IL- $1\beta$  level. At  $T_1$ , the IL- $1\beta$  levels of both groups were not significantly different ( $6.01 \pm 0.98$  vs  $6.00 \pm 0.89$ ,  $P > 0.05$ ); at  $T_2$ ,  $T_3$ , and  $T_4$ , the IL- $1\beta$  levels of group A were remarkably lower than those of group B ( $9.54 \pm 1.10$  vs  $14.65 \pm 1.26$ ,  $6.98 \pm 0.87$  vs  $9.10 \pm 0.95$ ,  $6.75 \pm 0.68$  vs  $8.65 \pm 0.99$ ,  $P < 0.001$ ).

Figure 1(b) shows the serum IL-6 level. At  $T_1$ , the IL-6 levels of both groups were not significantly different ( $59.65 \pm 6.87$  vs  $59.21 \pm 5.88$ ,  $P > 0.05$ ); at  $T_2$ ,  $T_3$ , and  $T_4$ , the IL-6 levels of group A were remarkably lower than those of group B ( $120.65 \pm 12.98$  vs  $160.98 \pm 15.98$ ,  $105.69 \pm 8.65$  vs  $145.68 \pm 12.68$ ,  $89.98 \pm 5.87$  vs  $139.98 \pm 10.65$ ,  $P < 0.001$ ).

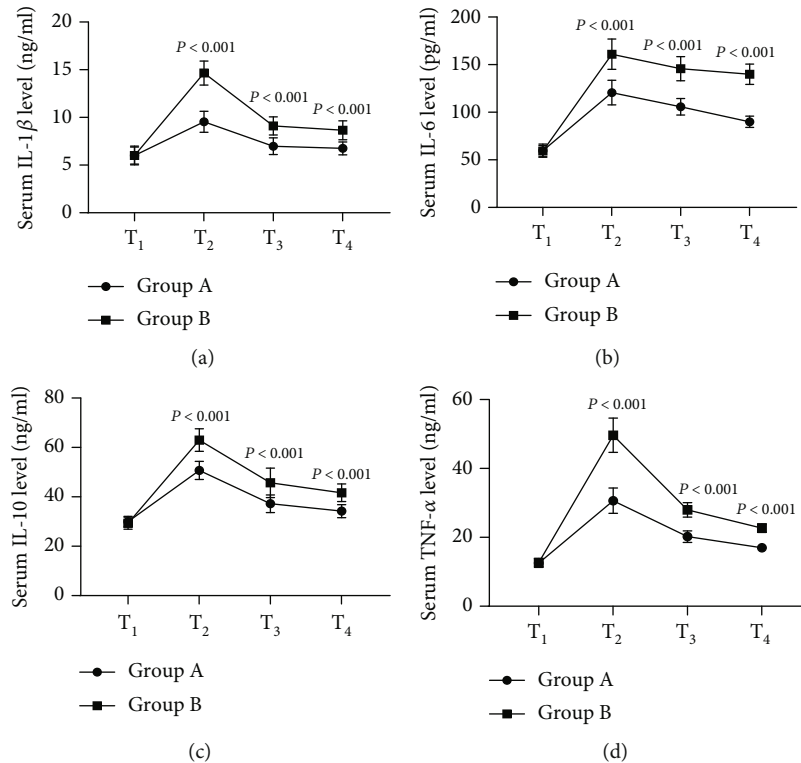


FIGURE 1: Comparison of inflammatory factor levels ( $\bar{x} \pm s$ ). Note: In Figure 1, the horizontal axis from left to right showed T<sub>1</sub>, T<sub>2</sub>, T<sub>3</sub>, and T<sub>4</sub>, the lines with dots denoted group A, and the lines with blocks denoted group B.

Figure 1(c) shows the serum IL-10 level. At T<sub>1</sub>, the IL-10 levels of both groups were not significantly different ( $29.98 \pm 2.15$  vs  $29.32 \pm 2.44$ ,  $P > 0.05$ ); at T<sub>2</sub>, T<sub>3</sub>, and T<sub>4</sub>, the IL-10 levels of group A were remarkably lower than those of group B ( $50.68 \pm 3.68$  vs  $62.98 \pm 4.56$ ,  $37.21 \pm 3.58$  vs  $45.68 \pm 5.98$ ,  $34.21 \pm 2.65$  vs  $41.65 \pm 3.58$ ,  $P < 0.001$ ).

Figure 1(d) shows the serum TNF- $\alpha$  level. At T<sub>1</sub>, the TNF- $\alpha$  levels of both groups were not significantly different ( $12.54 \pm 1.26$  vs  $12.65 \pm 1.22$ ,  $P > 0.05$ ); at T<sub>2</sub>, T<sub>3</sub>, and T<sub>4</sub>, the TNF- $\alpha$  levels of group A were remarkably lower than those of group B ( $30.65 \pm 3.68$  vs  $49.65 \pm 4.98$ ,  $20.21 \pm 1.68$  vs  $27.98 \pm 2.10$ ,  $16.98 \pm 1.11$  vs  $22.68 \pm 1.24$ ,  $P < 0.001$ ).

**3.2. Comparison of Brain Function.** After surgery, the brain function of group A was clearly better than that of group B ( $P < 0.001$ ), see Figure 2.

Figure 2(a) shows the serum S100 $\beta$  level. At T<sub>1</sub>, the S100 $\beta$  levels of both groups were not significantly different ( $0.49 \pm 0.10$  vs  $0.48 \pm 0.09$ ,  $P > 0.05$ ); at T<sub>3</sub> and T<sub>4</sub>, the S100 $\beta$  levels of group A were remarkably lower than those of group B ( $1.10 \pm 0.11$  vs  $1.89 \pm 0.21$ ,  $0.76 \pm 0.05$  vs  $1.54 \pm 0.20$ ,  $P < 0.001$ ).

Figure 2(b) shows the serum NSE level. At T<sub>1</sub>, the NSE levels of both groups were not significantly different ( $5.12 \pm 0.32$  vs  $5.11 \pm 0.28$ ,  $P > 0.05$ ); at T<sub>3</sub> and T<sub>4</sub>, the NSE levels of group A were remarkably lower than those of group B ( $12.98 \pm 2.54$  vs  $19.65 \pm 2.58$ ,  $15.11 \pm 3.58$  vs  $18.26 \pm 4.21$ ,  $P < 0.001$ ).

Figure 2(c) shows the CEO<sub>2</sub> level. At T<sub>1</sub>, the CEO<sub>2</sub> levels of both groups were not significantly different ( $36.54 \pm 5.65$

vs  $36.98 \pm 5.26$ ,  $P > 0.05$ ); at T<sub>3</sub> and T<sub>4</sub>, the CEO<sub>2</sub> levels of group A were remarkably lower than those of group B ( $38.21 \pm 5.14$  vs  $49.65 \pm 5.32$ ,  $41.98 \pm 4.68$  vs  $48.99 \pm 4.41$ ,  $P < 0.001$ ).

**3.3. Comparison of Arterial Blood Gas Indexes.** The postoperative arterial blood gas indexes of group A were significantly better than those of group B ( $P < 0.001$ ), see Figure 3.

Figure 3(a) shows the PaO<sub>2</sub> level. At T<sub>1</sub>, the PaO<sub>2</sub> levels of both groups were not significantly different ( $100.56 \pm 10.65$  vs  $101.98 \pm 11.26$ ,  $P > 0.05$ ); at T<sub>3</sub> and T<sub>4</sub>, the PaO<sub>2</sub> levels of group A were remarkably higher than those of group B ( $380.65 \pm 20.68$  vs  $328.98 \pm 26.68$ ,  $100.23 \pm 11.24$  vs  $82.65 \pm 10.68$ ,  $P < 0.001$ ).

Figure 3(b) shows the PaCO<sub>2</sub> level. At T<sub>1</sub>, the PaCO<sub>2</sub> levels of both groups were not significantly different ( $43.65 \pm 3.68$  vs  $43.96 \pm 3.55$ ,  $P > 0.05$ ); at T<sub>3</sub> and T<sub>4</sub>, the PaCO<sub>2</sub> levels of group A were remarkably higher than those of group B ( $39.24 \pm 3.21$  vs  $30.68 \pm 2.88$ ,  $42.10 \pm 2.65$  vs  $36.98 \pm 3.54$ ,  $P < 0.001$ ).

Figure 3(c) shows the LAC level. At T<sub>1</sub>, the LAC levels of both groups were not significantly different ( $0.87 \pm 0.10$  vs  $0.89 \pm 0.09$ ,  $P > 0.05$ ); at T<sub>3</sub> and T<sub>4</sub>, the LAC levels of group A were remarkably lower than those of group B ( $1.32 \pm 0.11$  vs  $1.42 \pm 0.10$ ,  $0.99 \pm 0.10$  vs  $1.20 \pm 0.15$ ,  $P < 0.001$ ).

**3.4. Comparison of Cognitive Function.** After surgery, group A obtained significantly lower LOTCA score than group B ( $P < 0.001$ ), see Table 2.

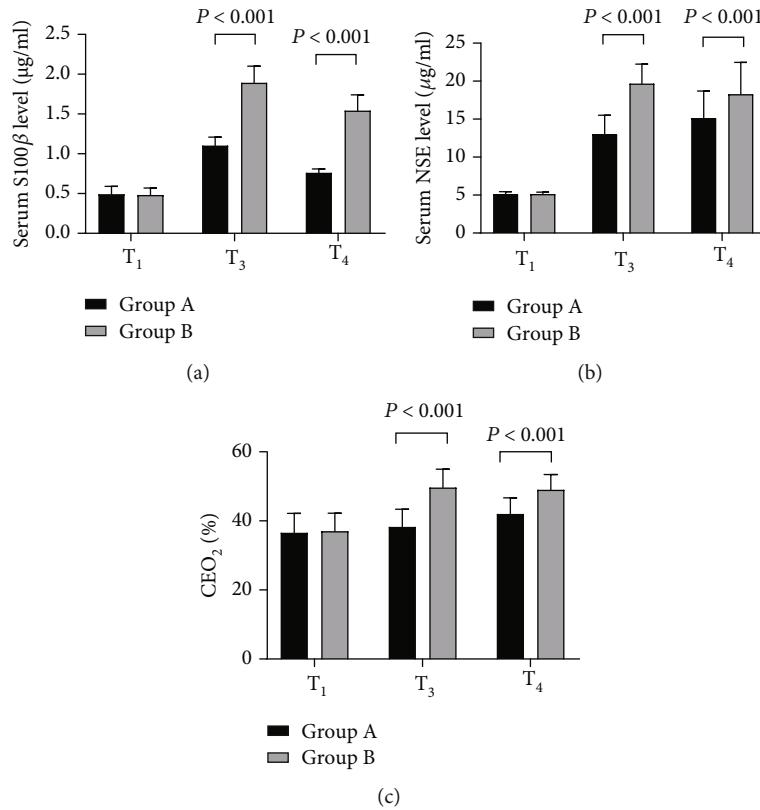


FIGURE 2: Comparison of brain function ( $\bar{x} \pm s$ ). Note: In Figure 2, the horizontal axis showed T<sub>1</sub>, T<sub>3</sub>, and T<sub>4</sub>, the black areas denoted group A, and the gray areas denoted group B.

#### 4. Discussion

Surgery can efficiently resect tumor tissue and dissect metastatic lymph nodes in lung cancer patients, but it is moderately traumatic and can trigger nonspecific reactions in the body, resulting in hemodynamics changes and fluctuating vital signs in patients, and even convincing ischemic damage in severe cases, which in turn elevates the inflammatory level and makes patients experience multiple complications such as organ dysfunction. Cognitive dysfunction is one of the most common postoperative complications of lung cancer [17], which increases the late mortality of patients. Factors such as stress reaction, surgical trauma, deterioration of cerebrovascular microcirculation, and hypoxemia can raise the possibility of cognitive dysfunction [18]. Anesthetic drugs can directly affect this complication by acting on the central nervous system (CNS) [19], so selecting suitable anesthetic adjuncts is beneficial to reduce the odds of cognitive dysfunction and improve patient outcomes.

The anesthetic drugs selected in this study were DEX, a widely used sedative agent in the clinic with significant efficacy in sedation, analgesia, and reducing stress reactions, and dezocine, a strong analgesic [20]. The study results showed that after surgery, group A obtained lower scores on LOTCA (with additional items such as spatial perception and thinking operations) compared with the mini-mental state examination (MMSE) than group B ( $P < 0.001$ ), fully

demonstrating that the cognitive function of group A was more ideal. Based on the results, it could be estimated that the mechanisms of lowering the odds of cognitive function by combining DEX with dezocine were as follows.

- (1) DEX, an  $\alpha_2$ -adrenoceptor agonist, could suppress the sympathetic nerve impulse in CNS and lift the activity of vagus nerve, thereby lowering the odds of hypotension while maintaining the cerebral oxygen metabolism, alleviating cerebral perfusion damage, and then protecting the brain function. The S100 $\beta$  (a nerve cell injury marker) and NSE (a soluble plasmin) selected in this study could enter the peripheral blood when the nerve cells were injured. The results presented that the postoperative brain function indexes of group A were significantly better than those of group B ( $P < 0.001$ ), denoting that DEX well-protected the brain function
- (2) When activating the  $\alpha_2$  adrenergic receptor agonist, DEX could lower the secretion frequency of noradrenaline and control the autonomic nervous reflex, while dezocine, the opiate receptor agonist-antagonist, could maintain stable hemodynamics, so combining the two could sufficiently alleviate the perioperative stress response of lung cancer patients and lower their angiotensin II level [21]

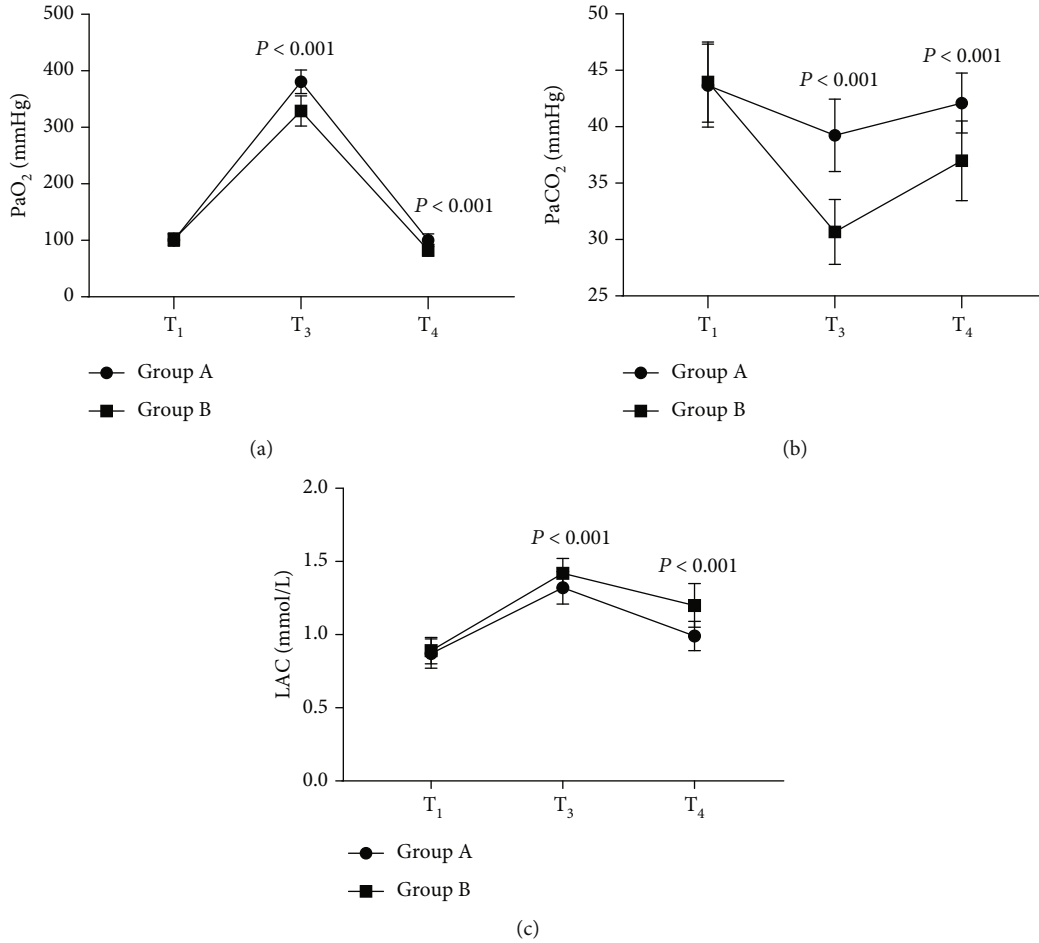


FIGURE 3: Comparison of arterial blood gas indexes ( $\bar{x} \pm s$ ). Note: In Figure 3, the horizontal axis from left to right indicated T<sub>1</sub>, T<sub>3</sub>, and T<sub>4</sub>, the lines with dots denoted group A, and the lines with blocks denoted group B.

TABLE 2: Comparison of LOTCA scores ( $\bar{x} \pm s$ , points).

Category	Group A		Group B		<i>t</i>	<i>P</i>
LOTCA	T <sub>1</sub>	79.65 ± 5.98	T <sub>1</sub>	79.54 ± 5.24	0.11	0.92
	T <sub>4</sub>	48.65 ± 5.62	T <sub>4</sub>	60.11 ± 5.36	11.43	< 0.001
	<i>t</i>	29.261	<i>t</i>	20.078		
	<i>P</i>	< 0.001	<i>P</i>	< 0.001		

(3) Surgical stress caused the release of TNF- $\alpha$  and other inflammatory factors and inflammatory reactions could damage the cardiocerebral vascular system in patients and trigger astrocyte activation in the CNS. Moon T and other scholars found that TNF- $\alpha$  could worsen cognitive function in patients [22], while the study by scholars Gao S et al. showed that DEX reduced the release of inflammatory mediators in toxin-induced shock rats [23], decreased the level of TNF- $\alpha$  and other inflammatory factors, and avoided mediating the memory loss reactions in CNS. This study also presented that group A obtained significantly lower intraoperative and post-operative inflammatory factor levels than group B

( $P < 0.001$ ), which was consistent with the general findings in academia

(4) Lung cancer surgery required one-lung ventilation with endotracheal intubation, which impaired the patients' intra-pulmonary gas diffusion function and reduced the gas exchange capacity between pulmonary alveolar and pulmonary capillary, so the patients were prone to hypoxaemia triggered by oxygenation decline. Scholar S. L. Zong research found that DEX, which had a slight effect on the respiratory center, was able to improve the arterial blood gas indicators and alleviate pulmonary infection in patients [24], and the respiration would not be inhibited by low-



dose dezocine, so the combination of the two drugs could effectively maintain respiratory movement, alleviate lung injury, and improve lung and brain micro-circulation with better  $\text{CeO}_2$ ; accordingly, the rate of cognitive impairment was reduced

The occurrence of cognitive dysfunction is related to many factors, and analysis of the mechanism of DEX combined with dezocine on cognitive dysfunction revealed that such combination can reduce the inflammatory response, protect multiple organs and systems, and greatly improve the brain function, lung function, cardiovascular system, and CNS. At present, most Chinese lung cancer patients are elderly who have poor body organs combined with multiple complications and are extremely prone to postoperative cognitive dysfunction and organ dysfunction. With DEX and dezocine-assisted anesthesia, the odds of postoperative complications can be efficiently reduced and the long-term prognosis of patients can be guaranteed. It should be noted that no adverse consequence-related research was done in this study, and general findings in academia showed that the combination did not increase the chance of adverse effects, but whether the applied dose of DEX and dezocine could affect the safety needs to be further explored.

## 5. Conclusion

Combining DEX with dezocine-assisted anesthesia can lower the perioperative inflammatory factor level, guarantee the brain function and oxygen saturation, and ensure better postoperative cognitive function in lung cancer patients undergoing surgery, which should be promoted in practice.

## Data Availability

Data to support the findings of this study is available on reasonable request from the corresponding author.

## Conflicts of Interest

The authors have no conflicts of interest to declare.

## Authors' Contributions

Jie Ding and Mengqi Zhu contributed equally to this article as first author.

## Acknowledgments

This research was funded by the Natural Science Foundation of Shanghai, grant number 21ZR1414000.

## References

- [1] H. X. Shi, W. F. Du XJ, Y. J. Hu, and W. D. Mi, "Dexmedetomidine for early postoperative cognitive dysfunction after video-assisted thoracoscopic lobectomy in elderly male patients with lung cancer," *Medicine*, vol. 99, no. 36, p. e21691, 2020.
- [2] F. Hetta, M. Fares, M. Abedalmohsen, A. H. Abdel-Wahab, G. M. Abo Elfadl, and W. N. Ali, "Epidural dexmedetomidine infusion for perioperative analgesia in patients undergoing abdominal cancer surgery: randomized trial," *Journal of Pain Research*, vol. Volume 11, pp. 2675–2685, 2018.
- [3] J. Freeman and J. Buggy, "Modelling the effects of perioperative interventions on cancer outcome: lessons from dexmedetomidine," *British Journal of Anaesthesia*, vol. 120, no. 1, pp. 15–17, 2018.
- [4] T. Gondo, T. Sonoo, H. Hashimoto, and K. Nakamura, "Chemoradiation therapy for oesophageal cancer with airway stenosis under mechanical ventilation with light sedation using dexmedetomidine alone," *BMJ case reports*, vol. 13, no. 8, p. e234507, 2020.
- [5] A. A. Saleh, A. Sultan, M. A. Hammouda, A. Shawki, and M. A. El Ghaffar, "Value of adding dexmedetomidine in endoscopic ultrasound-guided celiac plexus neurolysis for treatment of pancreatic cancer-associated pain," *Journal of Gastrointestinal Cancer*, vol. 52, no. 2, pp. 682–689, 2021.
- [6] Z. Liu, Q. Jia, and X. Yang, "Awake intubation and extraluminal use of Uniblocker for one-lung ventilation in a patient with a large mediastinal mass a case report," *BMC Anesthesiology*, vol. 20, no. 1, p. 125, 2020.
- [7] K. M. Fares, S. A. Mohamed, A. M. Abd El-Rahman, R. M. AbdeLemam, and A. M. Osman, "Analgesic effect of intrathecal fentanyl vs dexmedetomidine as adjuvants to bupivacaine following abdominal surgery for cancer in children, a randomized trial," *Pain Medicine*, vol. 11, p. 11, 2020.
- [8] Y. Chen, H. Li, C. Tan et al., "Dexmedetomidine enhances hypoxia-induced cancer cell progression," *Experimental and Therapeutic Medicine*, vol. 18, no. 6, 2019.
- [9] X. Su, Y. Fan, L. Yang et al., "Dexmedetomidine expands monocytic myeloid-derived suppressor cells and promotes tumour metastasis after lung cancer surgery," *Journal of Translational Medicine*, vol. 16, no. 1, p. 347, 2018.
- [10] H. Lavon, P. Matzner, A. Benbenishty et al., "Dexmedetomidine promotes metastasis in rodent models of breast, lung, and colon cancers," *BJA British Journal of Anaesthesia*, vol. 120, no. 1, pp. 188–196, 2018.
- [11] C. Wang, T. Dato, H. Zhao et al., "Midazolam and dexmedetomidine affect neuroglioma and lung carcinoma cell biology in vitro and in vivo," *Anesthesiology*, vol. 129, no. 5, pp. 1000–1014, 2018.
- [12] P. Forget, M. Berlière, A. Poncelet, and M. de Kock, "Effect of clonidine on oncological outcomes after breast and lung cancer surgery," *British Journal of Anaesthesia*, vol. 121, no. 1, pp. 103–104, 2018.
- [13] G. Connolly, S. Tan, B. Mastrogiacomo et al., "Intraoperative opioid exposure, tumour genomic alterations, and survival differences in people with lung adenocarcinoma," *BJA British Journal of Anaesthesia*, vol. 127, no. 1, pp. 75–84, 2021.
- [14] J. Arends and D. Tobias, "Hypothermia following spinal anesthesia in an infant: potential impact of intravenous dexmedetomidine and intrathecal clonidine," *Journal of Medical Cases*, vol. 10, no. 11, pp. 319–322, 2019.
- [15] K. Ankita, S. Tandon, and T. Kandy, "Extradural anesthesia in a case of mild head injury," *Cureus*, vol. 13, no. 7, 2021.
- [16] X. Wang, K. Wang, B. Wang et al., "Effect of oxycodone combined with dexmedetomidine for intravenous patient-controlled analgesia after video-assisted thoracoscopic lobectomy," *Journal of Cardiothoracic & Vascular Anesthesia*, vol. 30, no. 4, pp. 1015–1021, 2016.

- [17] X. Zhao, Y. Li, Y. Kong, L. Zhang, and X. H. Wen, "Anesthetic management of off-pump simultaneous coronary artery bypass grafting and lobectomy: case report and literature review," *Medicine*, vol. 96, no. 50, article e8780, 2017.
- [18] H. Lee, N. Kim, Y. Lee, M. G. Ban, and Y. J. Oh, "Effects of dexmedetomidine on oxygenation and lung mechanics in patients with moderate chronic obstructive pulmonary disease undergoing lung cancer surgery: a randomised double-blinded trial," *European Journal of Anaesthesiology*, vol. 33, no. 4, pp. 275–282, 2016.
- [19] J. Cui, H. Zhao, B. Yi, J. Zeng, K. Lu, and D. Ma, "Dexmedetomidine attenuates bilirubin-induced lung alveolar epithelial cell death in vitro and in vivo," *Critical Care Medicine*, vol. 43, no. 9, pp. e356–e368, 2015.
- [20] R. S. Herbst, R. Ansari, F. Bustin et al., "Efficacy of bevacizumab plus erlotinib versus erlotinib alone in advanced non-small-cell lung cancer after failure of standard first-line chemotherapy (BeTa): a double-blind, placebo-controlled, phase 3 trial," *The Lancet*, vol. 377, no. 9780, pp. 1846–1854, 2011.
- [21] J. Sarvesvaran, J. J. Goings, R. Milroy, S. B. Kaye, and W. N. Keith, "Is small cell lung cancer the perfect target for anti-telomerase treatment?," *Carcinogenesis*, vol. 20, no. 8, pp. 1649–1652, 1999.
- [22] T. Moon, J. Y. Tsai, S. Vachhani et al., "The use of intraoperative dexmedetomidine is not associated with a reduction in acute kidney injury after lung cancer surgery," *Journal of Cardiothoracic & Vascular Anesthesia*, vol. 30, no. 1, pp. 51–55, 2016.
- [23] S. Gao, Y. Wang, J. Zhao, and A. Su, "Effects of dexmedetomidine pretreatment on heme oxygenase-1 expression and oxidative stress during one-lung ventilation," *International Journal of Clinical & Experimental Pathology*, vol. 8, no. 3, pp. 3144–3149, 2015.
- [24] S. L. Zong, J. Du, Y. Chen, and H. Tao, "Application effect of dexmedetomidine combined with flurbiprofen axetil and flurbiprofen axetil monotherapy in radical operation of lung cancer and evaluation of the immune function," *J BUON*, vol. 26, pp. 1432–1439, 2021.

## Research Article

# Clinical Features of Acute Coronary Syndrome in Patients with Coronary Heart Disease and Its Correlation with Tumour Necrosis Factor in Cardiology

Run Guo, Tingting Wu, Nan Zheng, Yanfang Wan, and Jun Wang 

Department of Cardiovascular Medicine, Cangzhou Central Hospital, Cangzhou, 061000 Hebei, China

Correspondence should be addressed to Jun Wang; 17085208210010@hainanu.edu.cn

Received 24 April 2022; Revised 16 May 2022; Accepted 19 May 2022; Published 30 June 2022

Academic Editor: Naeem Jan

Copyright © 2022 Run Guo et al. This is an open access article distributed under the Creative Commons Attribution License, which permits unrestricted use, distribution, and reproduction in any medium, provided the original work is properly cited.

Tumour necrosis factor (TNF) levels are higher in patients who have experienced an acute ischemic stroke. Greater levels of TNF may not be linked to an increased risk of recurrent coronary events in the stable phase after myocardial ischemia (MI). Coronary atheroma is connected to endothelial and smooth muscle cells, as well as macrophages that emit the multifunctional cytokine tumour necrosis factor (TNF). Transplanted tumours become more vulnerable when TNF- $\alpha$  was first recognized to have a function in hemorrhagic necrosis. TNF- $\alpha$  has been demonstrated to induce heart failure, pulmonary edoema, and cardiomyopathy in people with advanced heart failure when it is elevated in the bloodstream. It has been postulated that prolonged overexpression of TNF- $\alpha$  after ischemia may contribute to poor cardiac outcomes by increasing TNF- $\alpha$  when the myocardium undergoes both temporary ischemia and reperfusion. A rise in TNF levels has been seen after a myocardial infarction, but it is unclear if these higher levels, found months after the initial event, are associated with an increased risk of subsequent heart attacks. We looked at TNF levels in the blood of 270 patients with coronary heart disease in the Chinese Hypertension League's Cholesterol and Recurrent Events (CARE) experiment to see if this notion held true. Recurrent coronary syndrome and coronary mortality were monitored prospectively in the participants. The min max imbalance normalization can be used to assess a patient's baseline characteristics, including hormone and cholesterol test results. Type 2 stimulant connection to aggregate the TNF-signaling qualities and fuzzy techniques was applied. There may now be enough preliminary evidence from the crucial bundle neural network analysis to identify the risk of coronary heart disease associated with TNF pregeneration studies. The tests were assessed using a variety of methods and performance metrics in a Matlab environment.

## 1. Introduction

In addition to hypertension, dyslipidemia, diabetes, ischemic heart disease, postpartum cardiomyopathy, and congenital defects, a number of variables contribute to the onset of acute coronary syndrome. Heart tissue injury may be refurbished by activating the heart's innate immune system. Innate immunity is activated following heart damage, as shown by an increase in the repertory of proinflammatory cytokines. Heart stress is associated with the production of proinflammatory cytokines, such as TNF- $\alpha$ , TGF- $\beta$ , and the interleukin (IL) family, which includes IL-1, 12, 8, and 18. Proinflammatory cytokines, which have been demon-

strated to have beneficial effects on tissue repair, play a role in cardiac remodeling. An injury's anti-inflammatory response occurs after the initial proinflammatory stage, which is becoming more obvious. Localized smooth muscle injury and increased leukocyte extravasation prolong the proinflammatory cycle because of the diverse and unique nature of cardiac stress, which increases the proinflammatory response. Chronic inflammation, which is aggravated by diseases like hypertension, diabetes, and other comorbidities, may result if the proinflammatory process is allowed to continue unchecked. A supply of proinflammatory cytokines must be established in heart tissue by macrophages in order to sustain chronic inflammation. Excessive production and

discharge into the circulation of cytokines put other organs at danger. TNF- $\alpha$  and IL-6 have been suggested as potential markers of heart failure in a number of studies. Furthermore, endothelial and smooth muscle cells, as well as macrophages, generate tumour necrosis factor- (TNF- $\alpha$ ), a multifunctional circulating cytokine, which is associated with coronary atherosclerosis. When TNF- $\alpha$  was originally recognized to have a role in hemorrhagic necrosis, transplanted tumours were shown to be more vulnerable. TNF- $\alpha$ , for instance, is elevated in severe heart failure and may induce pulmonary edoema, left ventricular dysfunction, and cardiomyopathy in experimental settings. TNF- $\alpha$  over-expression during ischemia has been hypothesized to contribute to poor cardiac outcomes. Both transient cardiac ischemia and reperfusion cause an increase in TNF- $\alpha$  level in the myocardium. However, it is not known whether higher TNF- $\alpha$  levels discovered months after a MI are connected to an increased risk of recurrent coronary events. This has been seen in several studies. This hypothesis was tested by including patients with increased levels of TNF- $\alpha$  in the Cholesterol and Recurrent Events (CARE) experiment. The goal of this study was to identify recurrences of MI and cardiac death in patients with acute coronary syndromes. To identify patients who had recurrent coronary episodes and those who did not, we examined post-MI TNF- $\alpha$  level in nested case-control analysis using the paramount bundle neural network (PBNN).

The paper's arrangement is as follows: Related work is summarized briefly in Section 2. Problem statement is described in Section 3. The implemented methods for performance analysis are presented in Section 4. Section 5 concludes the paper.

## 2. Related Works

More research on TNF production and its link to cardiovascular disease has been published by other authors. The author of [1] looked into these abnormalities in metabolism and fibrinolysis to see if TNF was involved. TNF levels were measured in 45-year-old male postinfarction patients and matched population-based controls. Patients had greater TNF plasma levels (4.1-4.6) than healthy controls (2.5-0.4 pg/mL). People with hyperlipidemia were shown to have higher levels of TNF- $\alpha$ , which was associated to higher levels of VLDL triglyceride and HDL cholesterol. This medication lowered VLDL triglyceride levels and elevated HDL cholesterol, but it had no impact on TNF- $\alpha$  concentrations. TNF concentrations were connected to glucose and proinsulin levels before and after glucose ingestion, as well as glucose and proinsulin levels after glucose consumption. In [2], this study employed CTRP 9 as well as pentraxin 3 (PTX3) to examine the diagnostic and prognostic value of C1q/tumour necrosis factor-related protein 9 in patients with acute coronary syndromes (ACS). A total of 137 people were found to have heart disease or chest pain. We divided those with ACS into one group and those with noncardiac chest pain (NCCP) into another group as "controls." An ELISA test was performed to check the blood levels of CTRP9 and PTX3 to see how they compare to other ACS-related indices

and whether or not they may be utilized to diagnose ACS and predict a poor prognosis. In [3], lncRNA MALAT1 and miR-125b were examined in connection to coronary heart disease risk, severity, and prognosis in order to assess the association between these two genes (CHD). In [4], among individuals from the Saudi population, the author found a link between serum tumour necrosis factor- (TNF- $\alpha$ ) and metabolic syndrome (MetS) components. In [5], the author examined the expression of lncRNA-FA2H-2 and its association with inflammatory markers in individuals with coronary heart disease (CHD). In [6], TNF- $\alpha$  expression in SCAD was investigated using metabolic, inflammatory, and microRNA (miRNA) markers. Researchers enlisted patients with SCAD, who were then tested for their metabolic and inflammatory profiles. To determine the presence of TNF, an enzyme-linked immunosorbent assay was performed. The relative levels of expression of MiRNAs associated with inflammation and/or atherosclerosis were assessed. In [7], a biomarker for distinguishing ACS-related chest pain from non-ACS-related chest pain may be plasma sTREM-1, according to the author. To see whether plasma sTREM-1 levels might be used to predict 30-day and six-month cardiovascular outcomes in patients with early-stage ACS, the researchers set out to do this study. In [8], swine farm workers who smoke may be affected by TNF gene polymorphisms, the study's author claims. Researchers in Saskatchewan polled more than 400 full-time swine farm workers and 411 nonfarming rural inhabitants. As part of the trial, researchers collected information about participants' demographics and lifestyle, as well as lung function and blood samples. Several linear regressions were used in the statistical analysis. Polymorphisms in the promoter of the TNF gene were investigated for three different variations. In [9], patients with acute myocardial infarction (AMI) who has periodontitis and systemic inflammation are examined by the author for their relationship to a variety of indications of heart disease. In [10], molecular targets for heart disease and the molecular mechanisms that underpin it are the focus of this research. The GSE66360, GSE19339, and GSE97320 array datasets were obtained from individuals with CAD. Gene expression profiles were generated and important modules associated with coronary heart disease were revealed by weighted gene coexpression network analysis using normalizing and decreasing inconsistencies between the three datasets (WGCNA). DAVID's database for annotating, visualizing, and integrating discovery (GO) functional and KEGG pathway enrichment studies was used to identify statistically significant genetic clusters. In [11], the author's purpose was to employ intravascular ultrasound (IVUS) images and deep learning convolutional neural networks to analyze the risk factors for adverse cardiovascular events (ACVEs) in elderly patients with coronary heart disease (CHD) following percutaneous coronary intervention (PCI) (CNNs). In [12], psoriasis patients on TNFi therapy may be at decreased risk of suffering a significant adverse cardiovascular event, according to the author's research (MACE). In their retrospective cohort study using the KPSC health plan, they found at least three ICD-9 psoriasis diagnoses but no preceding MACE

codes. In the study population, multivariable Cox regression was utilized to investigate the hazard ratios (HR) of MACE associated with TNFi use. In [13], meta-analysis was undertaken by the author to examine the risk of MACEs in adult plaque psoriasis patients who are exposed to biologic therapies. In [14], the author assessed the prognostic importance of EAT volume and attenuation values derived from non-contrast cardiac computed tomography. In [15], in this study, the CT plaque characteristics of ACS patients were analyzed to identify possible culprit lesions (CLs) [16]. The level of platelet activation and inflammatory reaction in coronary artery lesions in acute coronary syndrome could be predicted by serum PDGF contents in peripheral blood as well as coronary arteries, according to research findings. In patients with acute myocardial infarction, coronary sinus Ang-1 amounts may represent the seriousness of lesions. PDGF as well as Ang-1 could be designed to estimate the degree and prognosis of acute coronary syndrome patients [17]. Via many points of system interaction for miRNA control, circRNAs were implicated in the formation and progression of ACS. They believe that circRNAs could be used as a therapeutic avenue for a pathophysiological process of ACS, and that they could possibly be used as diagnosis and therapy biomarkers. They shall conduct *in vitro* and *in vivo* experiments in the long term to confirm the role of circRNAs throughout the atherosclerotic process of ACS [18]. In China, the most common way for treating CHD would be to accurately diagnose the condition utilizing contemporary medicine to assess syndrome distinction and then combining that with TCM. circRNAs as well as miRNAs were involved in the control of AS genesis and growth in various studies. CircRNA and miRNA are essential regulators of vascular function and structure, including in the development of CHD and AS [19]. Recurrent CV incidents, DR, and DN have all been highly linked with the duration of T2DM in a group with current ACS and T2DM. The existence from either DR or DN has been implicated as the cause of recurring CV incidents. Because the length of T2DM, although maintained a strong independent indicator of recurrent CV incidents, was adjusted out of the equation, the link with DR and/or DN and all these incidents were unlikely to be causal [20]. In ACS, there may be a great desire for a consistent, available, noninvasive, and hematological prognostic marker that may detect individuals with high cardiovascular disease risk and adapt treatment to particular requirements in prevention [21]. The chances of having UGIB paired with ACS were higher throughout the corresponding time while hospitalized, according to this report. Raised fibrinogen and RDW, in association with fundamental heart attacks, syncope, a large reduction in haemoglobin, and high total bilirubin levels, may alert individuals to the possibility of ACS. Individuals with UGIB can then use the Rockall rating and the Glasgow Blatchford rating to forecast the danger of UGIB paired with ACS in a timely way.

### 3. Problem Statement

Congestive heart failure is associated with an increased production of proinflammatory cytokines. TNF is an important proinflammatory cytokine that causes heart failure by sup-

pressing the body's natural anti-inflammatory responses and disrupting the homeostatic system. In this review, we lay forth the current understanding of how TNF causes heart failure. TNF and IL-6 biomarkers have been connected to the severity of heart failure, suggesting that they could be employed as biomarkers in the future. The mechanisms by which TNF leads to cardiac dysfunction and failure have been the subject of recent research. However, the algorithm's participation in the current technique was little, and it will take longer to complete the procedure. Thus, an effective technique is needed to address all of the current research gaps.

*3.1. Proposed Methodology.* To better understand the relationship between TNF and heart failure, researchers have examined the cytokine's potential therapeutic uses and as a biomarker for the disease. TNF- $\alpha$  signalling in cells is mediated in part by NF- $\kappa$ B, highlighting the dual function of TNF- $\alpha$  in cardiac physiology and disease once again. Two cognate receptors, TNF receptor 1 or 2, mediate TNF's biological actions farther down the line (TNFR1 or 2). TNF-induced TNFR1 activation is supposed to be harmful, whereas TNFR2-induced activation is thought to be beneficial, and the relative ratio of their expression in a given tissue system may alter phenotypes.

The TNF production process is depicted in Figure 1. It is also known that various cells can shed soluble TNFR1 or TNFR2 to produce TNFR1 or TNFR2 signalling molecules (sTNFRs). As a result, the pool of TNF accessible for binding and activating cell membrane TNFRs may be depleted. The importance of these sTNFRs in overall cardiac pathophysiology, however, has yet to be determined. TNF- $\alpha$  is an inflammatory ligand that comes in two forms: membrane-bound and secreted. This further complicates pathophysiology development. Even while TNF signalling is complicated, several studies have demonstrated that cardiomyocyte-specific production of TNF causes in reduced cardiac function that is dose dependent on the genetic. It will be mentioned later in the review how studies have consistently established that TNF- $\alpha$  exerts unfavourable inotrope effects *in vitro* and *in vivo*. Evidence like this suggests that TNF's proinflammatory effects on the beta-adrenergic receptor (AR) system may be the cause of the adverse inotropic phenotype associated with acute coronary syndrome. The overall representation of the suggested framework is illustrated in Figure 2.

*3.1.1. Dataset.* The CARE trial, which assessed the efficiency of 40 mg of pravastatin daily in the secondary prevention of cardiovascular disease, was utilized by the researchers for this investigation, which included 4159 persons who previously had a MI. Double-blind placebo control was used in the experiment's design. Ejection fraction of at least 25% and absence of clinical signs of congestive heart failure made post-MI patients between the ages of 21 and 75 years eligible for CARE if the qualifying index event occurred between 3 and 20 months before randomization. In this investigation, death from cardiovascular disease was the primary metric of interest. It was required that participants in the CARE study have an LDL cholesterol level between 115 and

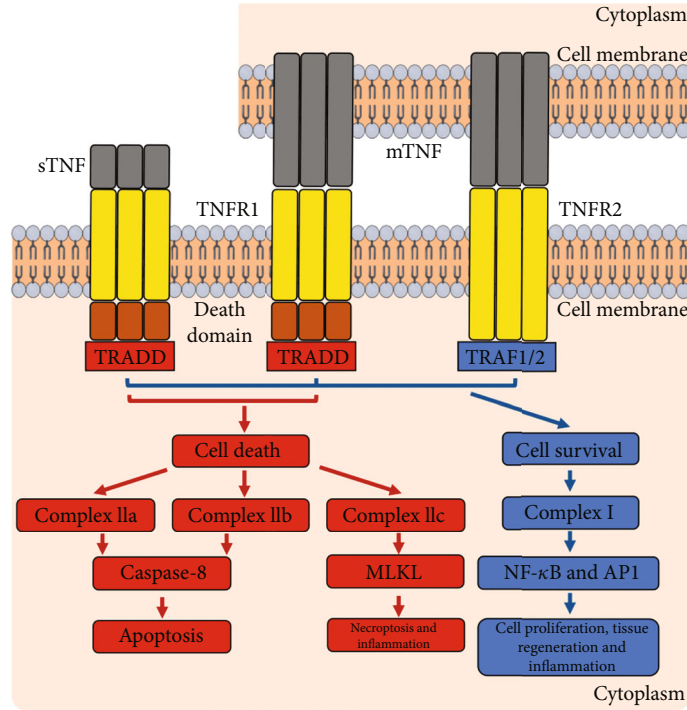


FIGURE 1: TNF-α production.

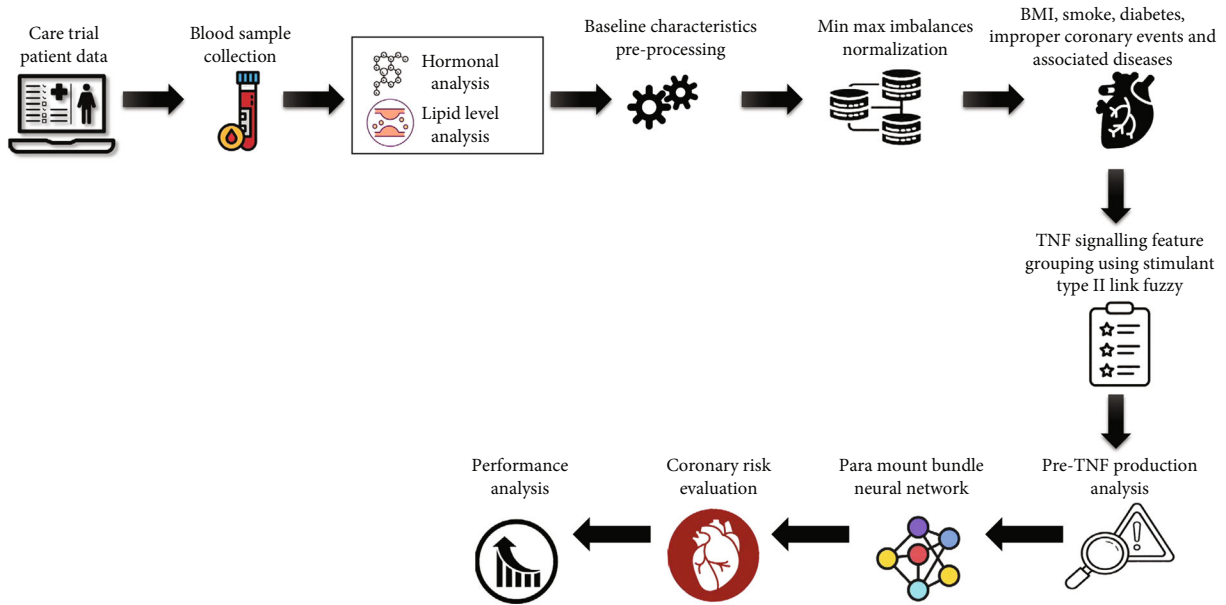


FIGURE 2: Schematic representation of the suggested methodology.

175 mg/dL to be eligible for randomization. Prerandomization visits were used to collect blood samples. For the duration of the testing process, samples were stored at 80°C. Prior to randomization, the cytokine TNF-α was examined in CARE study participants with recurrent MI or death from coronary heart disease during a 5-year follow-up period (cases) and 272 age- and sex-matched study participants who had no recurrent coronary events throughout the pre-randomization period (controls). Each case and control per-

son’s frozen plasma was tested for TNF using commercially available quantitative enzyme immunoassays. TNF concentrations as low as 0.1 pg/mL have been detected, with a coefficient of variance ranging from 5% to 8%. Blood samples were evaluated in pairs in order to reduce inter-assay variability and eliminate systematic bias. The lab staff had no idea whether the samples were from a case or a control group. TNF-α, total lipid, blood pressure, and future TNF-α production variations between case and control

individuals were assessed using the critical bundle neural network. Based on their medical histories, the patients were divided into two groups: A (136) and B (64). A greater number of abnormal coronary events or symptoms were seen in group A, whereas a greater number of abnormal coronary events or symptoms were observed in group B. The patient characteristics are represented in Table 1.

**3.1.2. Preprocessing.** Sizing distance and error analysis are two primary preprocessing theories that are used to establish relationships that allow accurate predictions to be made from data collected on processes or models, as well as to determine the type of relationship between each piece of information in order to collect the most relevant data for analysis. The data dimensions in which each relevant quantity involved in phenomena is represented provide the basis for error analysis. Because of this, one of the primary purposes of employing min max imbalance normalization is to produce an ordered errorless result from dimensionless words that can be analyzed. It was necessary to first set up the dimensionless variables in this example by,

$$\text{Ord} := O(A(Q) = +|Q(T) = w) - O(A(Q) = +|Q(T) = b), \quad (1)$$

where  $A$  = order function,  $q$  is the iterative error,  $w$  is the data variation,  $T$  is the dimensionless terms, and  $b$  is the backorder error.

Equation (1) can be re-arranged as follows,

$$\text{ord}(D) := \frac{|\{Q \in D|Q(T) = w, Q(\text{Class}) = +\}|}{|Q \in D|Q(T) = w|} - \frac{|\{Q \in D|Q(T) = b, Q(\text{Class}) = +\}|}{|Q \in D|Q(T) = b|}. \quad (2)$$

Once the similitude distance between the two sets of data has been determined, the similarity between them may be calculated,

$$\text{dis}(a_{T=b})(A, D) := \frac{|Q \in D|Q(T) = w, A(Q) = +|}{|Q \in D|Q(T) = w|} - \frac{|Q \in D|Q(T) = b, A(Q) = +|}{|Q \in D|Q(T) = b|}. \quad (3)$$

To arrange the equation in a proper format, there is a need to calculate the hat matrix,

$$\frac{\bar{q}_1 - \bar{q}_2}{\sqrt{(t_1^2/n_1) + (t_2^2/n_2)}} = \frac{\text{dis}_{\text{hat}=g}}{\sqrt{(t_1^2/n_1) + (t_2^2/n_2)}} * \frac{\bar{q}_1 - \bar{q}_2 - d_0}{\sqrt{(t_1^2/n_1) + (t_2^2/n_2)}}, \quad (4)$$

where

$$\begin{aligned} \bar{q}_1 &:= \{Q \in D|Q(T) = b\}, \\ \bar{q}_2 &:= \{Q \in D|Q(T) = w\}. \end{aligned} \quad (5)$$

Finally, the ordered equation was in the form of,

$$\text{acc}(A^{\text{Perf}}) - \text{acc}(A) = \frac{\min(d_b, d_w)}{d} 2 \frac{d_b d_w}{d} (\text{disc}(A^{\text{Perf}}) - \text{disc}(A)), \quad (6)$$

where

$$\begin{aligned} \text{acc}(A) &= \frac{t_o + t_n}{d} = \frac{to_b + tn_b + to_w + tn_w}{d}, \\ \text{dist}(A) &= \frac{to_w + go_w}{d_w} - \frac{to_b + go_b}{d_o}. \end{aligned} \quad (7)$$

**3.2. Feature Grouping.** Let us assume that  $A$  is a discrete random variable that can take one of  $b_1 \dots b_n$  values from the set of classes. In this example, assume that  $W$  is a random variable that spans throughout the set of words  $W = W_1 \dots W_n$ . It is possible to estimate the joint distribution  $p(j, W)$  using the training dataset. There are  $k$  clusters  $W_1, \dots, W_n$  of TNF signalling characteristics data. We employed stimulation type 2 links fuzzy to reduce the number of signals and the size of the model.  $W$  should be given a random range of values.

$$\begin{aligned} \vec{A} &= \vec{c} \cdot \vec{P}^*(j) - \vec{P}(j), \\ \vec{P}(j+1) &= \vec{P}^*(j) - \vec{a} \cdot \vec{E}. \end{aligned} \quad (8)$$

We employ a fuzzy measure approach to match the characteristics of clusters. Although it is ideal to conserve all mutual information when building clusters of signalling features, this is impossible since a clustering inevitably reduces mutual information. If the amount of data clusters is known, then we should try to identify a grouping that reduces signalling information as little as possible.

$$\begin{aligned} \vec{P} &= 2 \cdot \vec{r}_1, \\ \vec{A} &= 2 \vec{d} \cdot \vec{r}_2 - \vec{d}. \end{aligned} \quad (9)$$

Our algorithm explicitly minimizes the objective function,

$$\left\{ \begin{array}{l} \frac{to_b + (n_b - go_b) + to_w + (n_w - go_w)}{d} = \text{dist}(A) \\ 0 \leq to_b \leq o_b \\ 0 \leq to_b \leq n_b \\ 0 \leq to_w \leq o_w \\ 0 \leq to_w \leq n_w \end{array} \right. \quad (10)$$

There are two kinds of distances that must be calculated for each candidate: minimum and maximum. For any pair of clusters, the inter-cluster distance between them may be

TABLE 1: Patient characteristics.

	Total number of cases ( $n=272$ )	Control patients ( $n=272$ )	Value of $P$
Age in years	50.11 ± 10.80	60.00 ± 9.44	...
Sex	82.90	79.82	...
Smoking status,%	–	–	–
Never	20.44	20.72	0.09
Past	54.62	65.91	–
Current	18.61	14.22	–
Level of diabetes	30.11	20.44	0.004
Body metabolic index, kg/m <sup>2</sup>	26.72 ± 5.93	28.55 ± 7.22	0.01
Amount of the blood pressure, mm, hg	–	–	–
Systolic pressure	126.61 ± 18.52	127.90 ± 17.63	0.80
Diastolic pressure	89.11 ± 11.00	79.44 ± 18.62	0.92
Lipid fractions level, mg/dL	–	–	–
Total cholesterol level	209.82 ± 17.81	207.44 ± 18.44	0.44
LDL cholesterol	140.33 ± 14.92	139.33 ± 12.92	0.43
HDL cholesterol	38.22 ± 8.71	39.22 ± 8.55	0.44
Triglycerides	146.55 ± 18.44	149.62 ± 69.55	0.40

determined.

$$\text{Cluster} = kA = 2 \left\lfloor \log_2 \left( \frac{\text{dist}(A)}{a^m} \right)^{1/c} \right\rfloor. \quad (11)$$

Features that may be included include pruning with a minimum distance larger than feature distance,

$$c = \min_k \left[ \sigma \left( \frac{\text{dis}}{m \times k^c} \right) \right]. \quad (12)$$

If any data prototype may possibly be closer to a given subspace than any other data prototype, the above technique ensures that no feature is trimmed.

$$c_{Us} = C.RT \wedge 2 \frac{1}{uck}. \quad (13)$$

The algorithm iterates until a termination condition is reached, at which point it ceases to operate. The number of points, the linear sum of the points, and the square sum of the points are maintained for each cluster. It is now in the form of a grouping equation,

$$\text{Cluster features} = c \times m \times k^c + \zeta. \quad (14)$$

Finally, the features can be clustered together and form new signaling feature centroid.

**3.3. Risk Evaluation.** This is the last stage of the process in which the TNF- $\alpha$ . After extraction of the features, depending upon the presignaling factor, the level of the production probability of the TNF- $\alpha$  can be calculated. It determines

the optimal value for each cluster unit,

$$g_1(s) = \frac{\sum_{i \in C_s} \left[ \overrightarrow{\text{PBNN}} \left\{ GC_{\theta_q}(q_i) \right\} \oplus \overleftarrow{\text{PBNN}} \left\{ GC_{\theta_q}(q_i) \right\} \right]}{|C_s|}. \quad (15)$$

All points in the hyperplane fulfil the equation  $g_1(s)=0$  that forms the decision boundary between the two classes,

$$Z_i g_i = \sigma \left( \overline{U}_z GC_{\theta_q}(q_i) + W_z t_{i-1} + b_g b_z \right). \quad (16)$$

Let  $Z_i g_i$  be the hyper planes which will form a planar area over angle separation, where

$$z_i = \sigma \left( \overline{U}_o GC_{\theta_q}(q_i) + W_o t_{i-1} + b_o \right), \quad (17)$$

$$\widehat{Z}_i = \tan \left( \overline{U}_c GC_{\theta_q}(q_i) + W_c t_{i-1} + b_c \right).$$

The output  $c_i$  may be determined by using the sigmoid function, which computes the output of a neuron.

$$c_i = g_i \circ c_{i-1} + z_i \circ \widehat{c}_i. \quad (18)$$

After the feed-forward process is completed, the back-propagation process starts. Let  $\overrightarrow{Y}$  represent the error-sensitivity and to represent the desired output of a neuron in the output layer. Thus,

$$\overrightarrow{Y}(t+1) t_i = \tan(c_i) \circ o_i. \quad (19)$$



```

Input: Testing set  $g_1(s)$ 
Output: Feature subset  $\vec{Y}(t+1)t_i$ 
Initialize the parameter
    Calculate the optimal val()
    If
    So  $g_1(s)$ 
        
$$g_1(s) = \sum_{i \in C_s} [\overline{\text{PBNN}}\{GC_{\theta_q}(q_i)\} \oplus \overline{\text{PBNN}}\{GC_{\theta_q}(q_i)\}] / |C_s|$$

And
    Hyper planes (**) cross flg\
        
$$Z_i g_i = \sigma(U_z GC_{\theta_q}(q_i) + W_z t_{i-1} + b_g b_z)$$

Else
    Propagation process
        update
            
$$\vec{Y}(t+1)t_i = \text{tant}(c_i)^\circ o_i$$

Else if
    return
        <planes> variable factor
        Value <exceed>
        Probability score cal(&*)
        Weight score evaluation
            maximize  $\{\sum_j \sum_{i,i'} s_{i,i',j} U_{i,i'}\}$  subject to  $\sum_{i,i'} U_{i,i'}^2 \leq 1$ .
            maximize  $\{\sum_j w_j \sum_{i,i'} s_{i,i',j} U_{i,i'}\}$  subject to  $\sum_{i,i'} U_{i,i'}^2 \leq 1, \|t\|^2 \leq 1, \|W\|_1$ 
                
$$\leq m, w_j \geq 0 \forall j.$$

End
end

```

ALGORITHM 1: Paramount bundle neural network.

After  $\vec{Y}$  is computed, the weights and biases of each neuron are tuned into backpropagation process by using

$$\begin{aligned}
 & \text{maximize} \left\{ \sum_j \sum_{i,i'} s_{i,i',j} U_{i,i'} \right\} \text{subject to } \sum_{i,i'} U_{i,i'}^2 \leq 1, \\
 & \text{maximize} \left\{ \sum_j w_j \sum_{i,i'} s_{i,i',j} U_{i,i'} \right\} \text{subject to } \sum_{i,i'} U_{i,i'}^2 \leq 1, \|t\|^2 \leq 1, \|W\|_1 \\
 & \leq m, w_j \geq 0 \forall j.
 \end{aligned} \tag{20}$$

As soon as the first input vector has finished fine-tuning the network, the next round of input vectors is ready to be run. Until the network is satisfied with a single output or numerous outputs, the input continues training the networks. Finally depending upon the feature extracted, the TNF $_{\alpha}$  production can be predicted and its severity level can be determined. Depending upon the risk evaluated, it was revealed that the person having the elevated level of the TNF $_{\alpha}$  has the increase risk of coronary syndrome and also those persons have higher risk of getting abnormal hear events in the future due to the elevated upregulated TNF $_{\alpha}$  which was evaluated using the paramount bundle neural network.

#### 4. Performance Analysis

In this section, the overall TNF- $\alpha$  and lipid levels among study participants were normally evaluated to illustrate their future risk over abnormal coronary events.

Acute coronary syndrome patients were separated into two groups, and their data was collated. Two groups of patients may be shown in Figure 3 with a significant difference in average age and blood pressure. Patients in groups A and B had similar systolic blood pressure readings (58.2 mmHg and 52 mmHg, respectively), as shown by their similar ages.

Figure 4 shows cardiac activity. According to the findings of the research, some people developed heart failure, a myocardial infarction, typical angina, and sudden cardiac death. Heart failure and myocardial infarction were the second and third most prevalent conditions, respectively.

According to the findings, HDL C content was low in both groups A and B before the formation of the coronary syndrome, but it increased considerably following these cardiac events (as shown in Figure 5).

TNF levels were low in both groups before the onset of the cardiac syndrome; however, following the occurrence of the cardiac events, TNF levels increased (Figure 6).

Detection rates for eccentric plaques were compared, as seen in Figure 7. The comparison data indicated that 55.9% and 40.1 percent of the patients in groups A and EB had eccentric plaques.

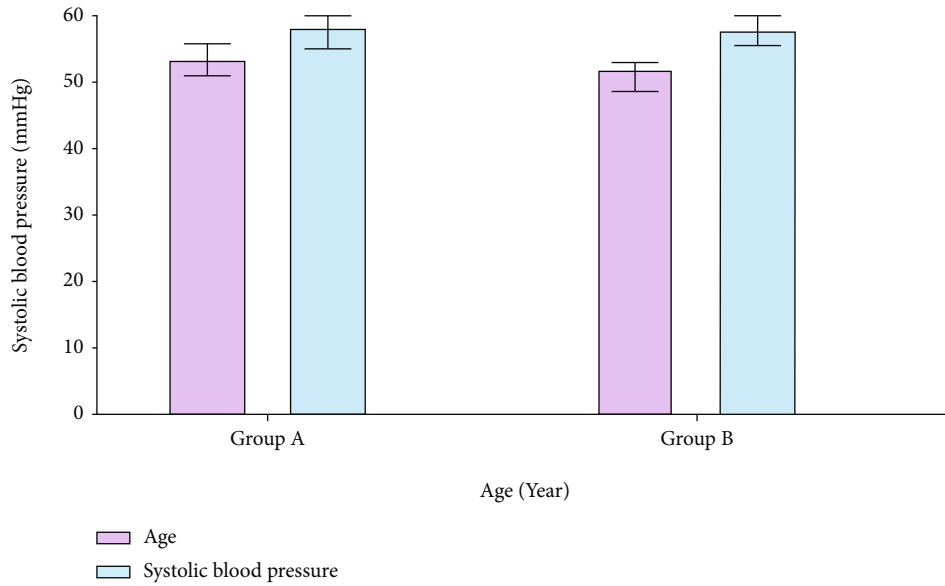


FIGURE 3: Age vs. systolic blood pressure.

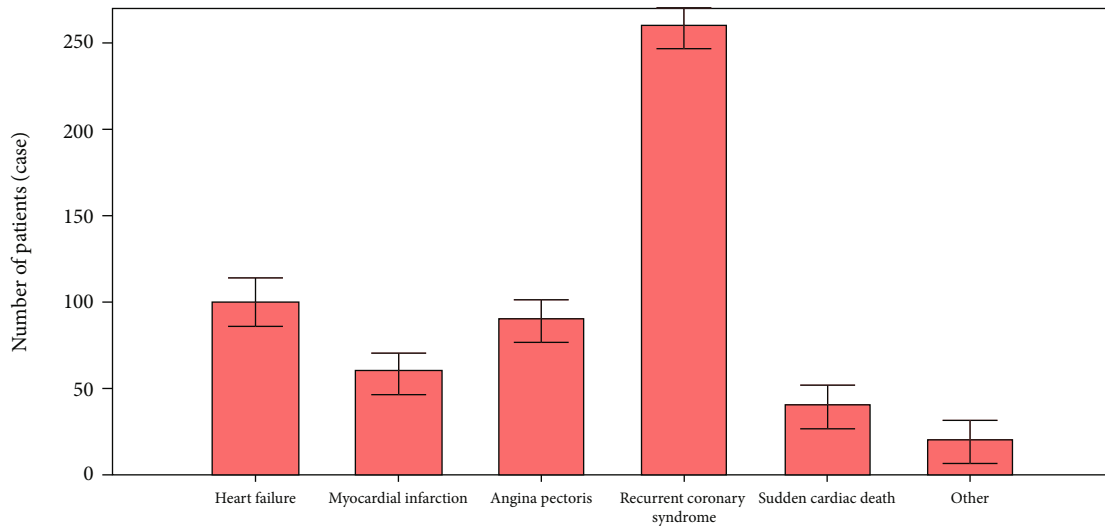


FIGURE 4: Cardiac abnormal events.

We can see how different techniques have found different parts of a tumour in Figure 8 (the diameter of the narrowest section). A and B lesions with 2.4 and 2.5 millimetre diameters were revealed to be the two narrowest.

Diastolic blood pressure and thyroglobulin (TG) levels were measured and compared between the two groups (see Figure 9). There were diastolic blood pressure values of 80.38 8.2 mmHg and 84.1 7.8 mmHg, respectively, in groups A and D with TG concentrations of 1.48 and 0.38 mmol/L, respectively. Diastolic blood pressure and serum TG levels were substantially different between the two groups as a consequence (Figure 10).

Prior to the coronary syndrome, group A and group B had CRP levels of 58.5 mmol/L and 59.3 mmol/L, respectively; group B had levels of 70.9 and 78.2. This study found

that CRP levels were significantly higher in both groups of patients prior to the onset of coronary syndrome.

Figure 11 shows the comparison results of the detection rate of centripetal plaque. It indicated that the detection rates in group A (48.2%) were obviously lower than those in group B (79.1%).

In Figure 12, you can observe a comparison of LDL-C values in two groups of individuals before and during a coronary syndrome. Before and after the syndrome, LDL-C levels in groups A and B were 2.76 mmol/L and 2.87 mmol/L, respectively; after assessing hormone levels, the probability of cytokine synthesis was predicted using the paramount bundle neural network.

As of from the result obtained from Figure 13, the group B people have the higher risk over abnormal coronary events. From the result obtained, the proposed algorithm

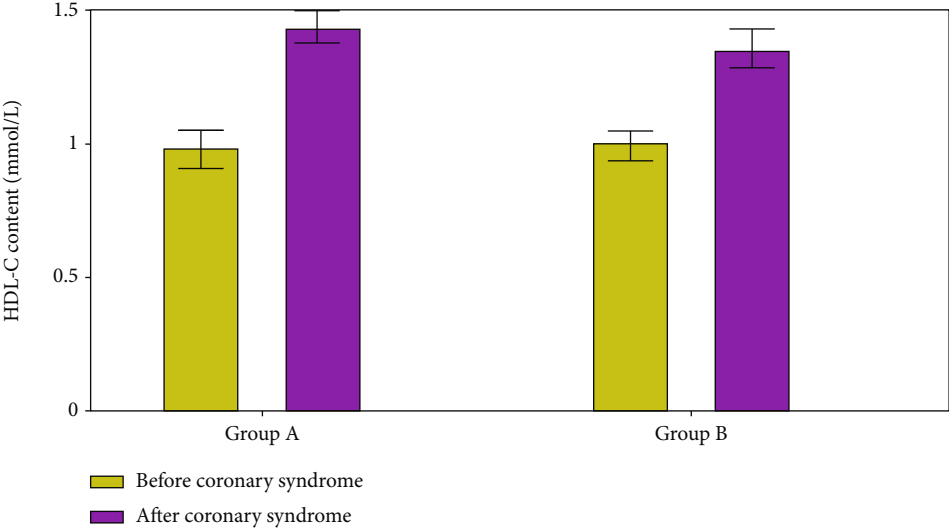


FIGURE 5: HDL C content evaluation.

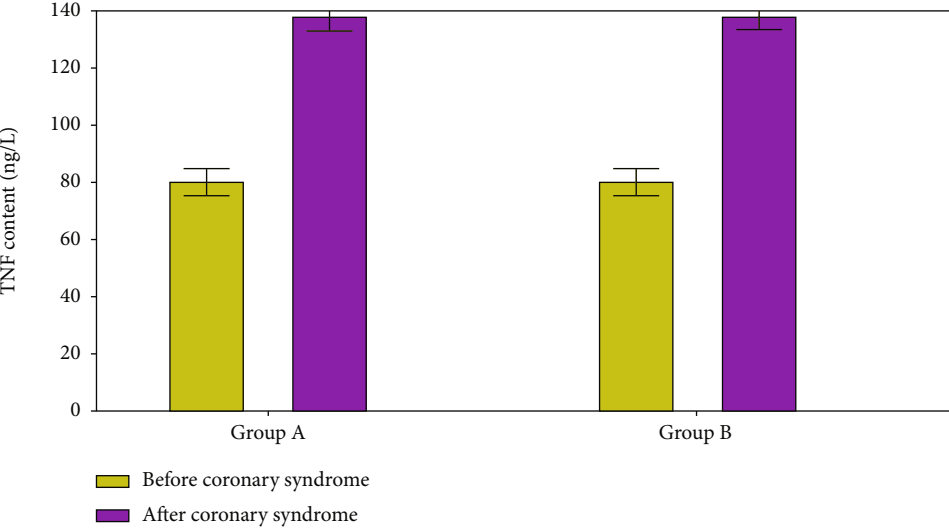


FIGURE 6: TNF level evaluation.

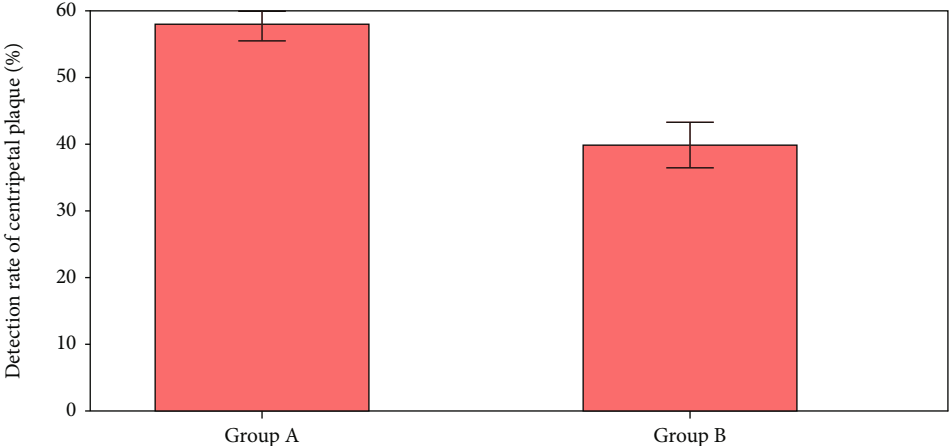


FIGURE 7: Detection rate of centripetal plaque.

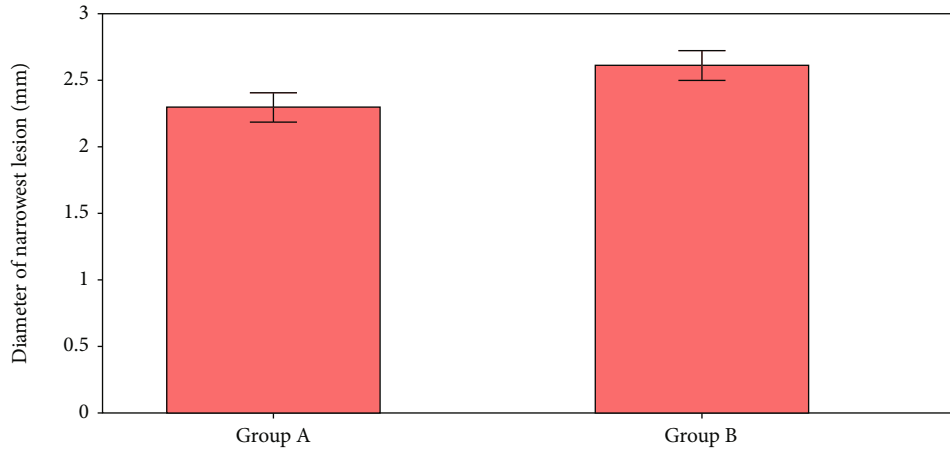


FIGURE 8: Diameter of narrowest lesion calculation.

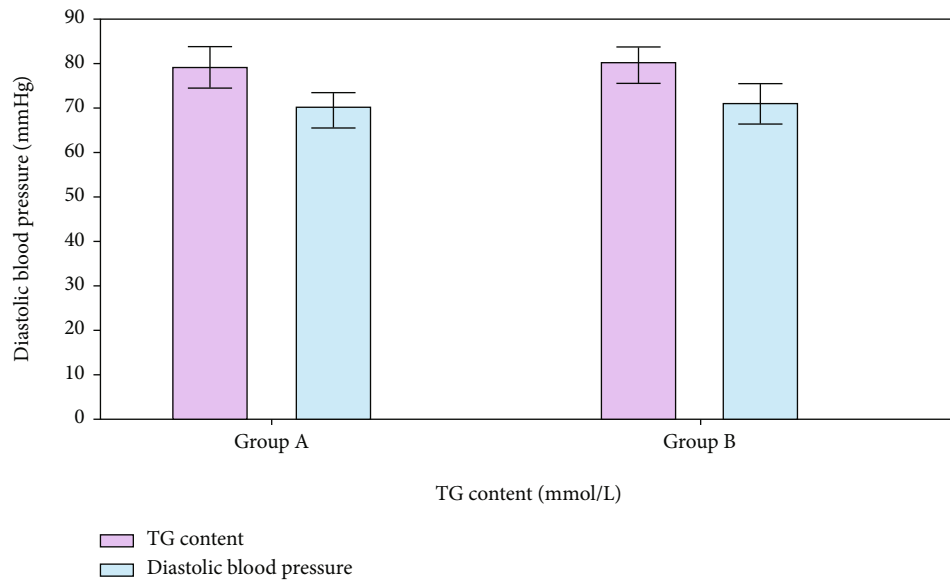


FIGURE 9: TG content vs. diastolic blood pressure.

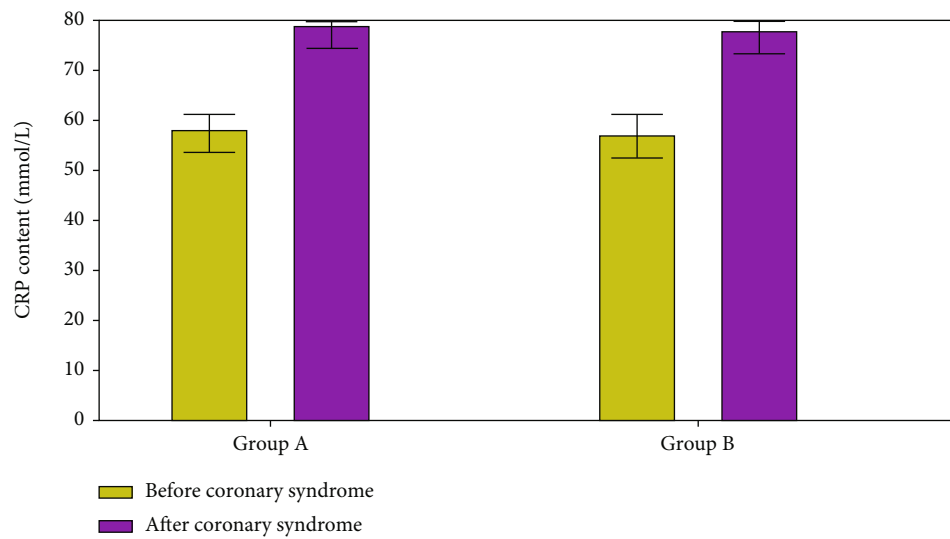


FIGURE 10: CRP content evaluations.

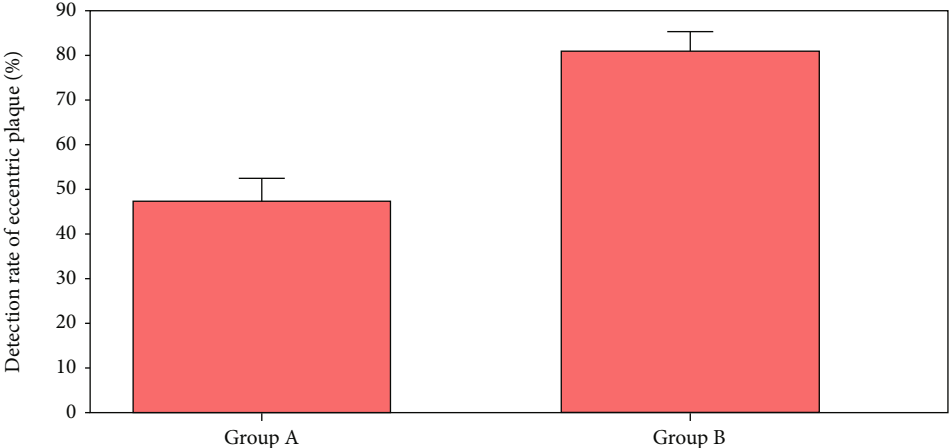


FIGURE 11: Detection rate of eccentric plaque.

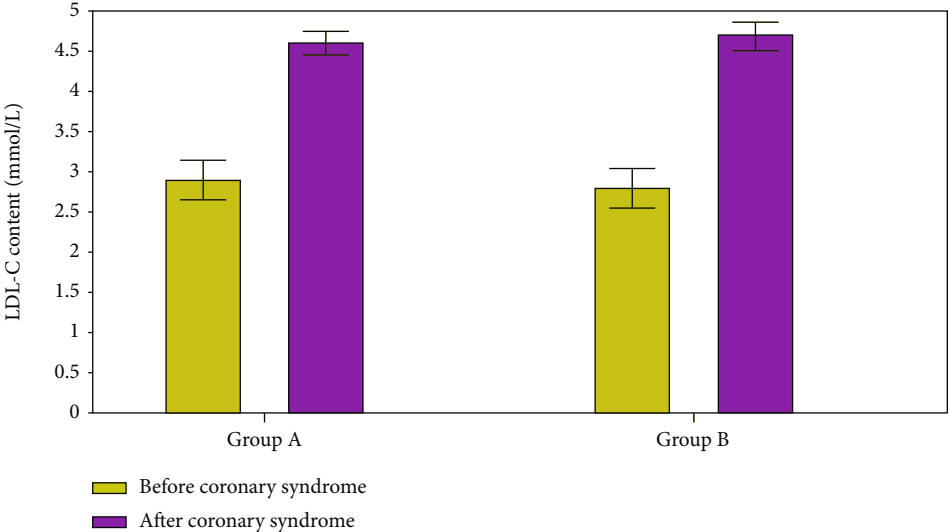


FIGURE 12: LDL-C content evaluation.

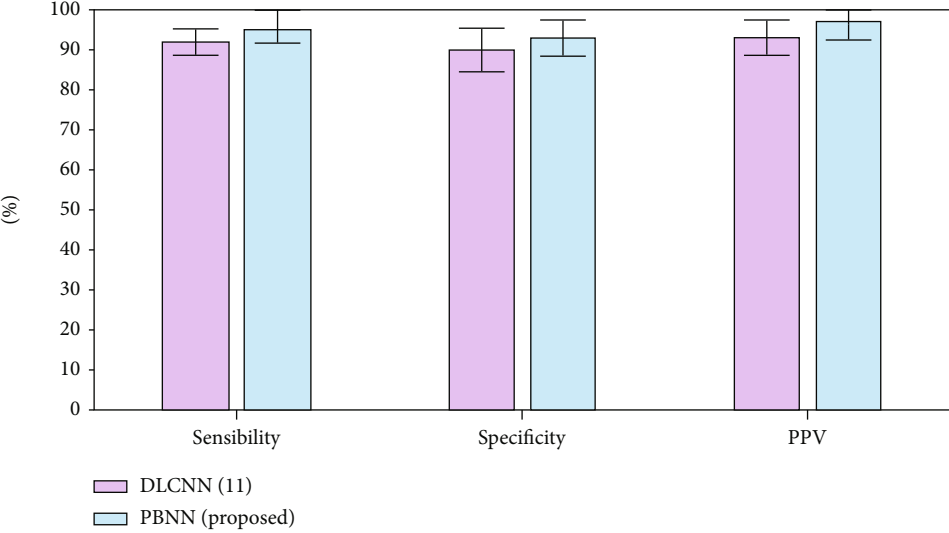


FIGURE 13: Performance metrics evaluation.

can predict the risk level of the patient and their future TNF production rate precisely when compared to other existing mechanisms.

## 5. Conclusions

Patients with an acute coronary syndrome were the focus of this investigation. A control group (group A) and an experimental group (group B) were formed by drawing lots from a hat (group B). These individuals' diagnoses were aided by laboratory testing and a thorough learning evaluation. The accuracy of TNF was compared to traditional methods. For the detection of TNF, a learning algorithm-based prediction technique showed high specificity, accuracy, and sensitivity. Acute coronary syndrome (ACS) may now be clinically identified and treated as a result of the results of this study.

## Data Availability

The labeled datasets used to support the findings of this study are available from the corresponding author upon request.

## Conflicts of Interest

The authors declare no conflicts of interest.

## Acknowledgments

This work was supported by the Cangzhou Science and Technology Support Project, Influence of anxiety and depression on Lp-PLA 2 and endothelial function in patients with acute coronary syndrome impact research (Project No. 162302172).

## References

- [1] S. Jovinge, A. Hamsten, P. Tornvall et al., "Evidence for a role of tumor necrosis factor  $\alpha$  in disturbances of triglyceride and glucose metabolism predisposing to coronary heart disease," *Metabolism*, vol. 47, no. 1, pp. 113–118, 1998.
- [2] N. Jiang, S. Zhou, G. Wang, N. Jiang, H. Wang, and F. Zhao, "Diagnostic value and prognostic significance of CTRP9 combined with pentraxin-3 in acute coronary syndrome," *Experimental and Therapeutic Medicine*, vol. 21, no. 3, pp. 1–1, 2021.
- [3] F. Lv, L. Liu, Q. Feng, and X. Yang, "Long non-coding RNA MALAT1 and its target microRNA-125b associate with disease risk, severity, and major adverse cardiovascular event of coronary heart disease," *Journal of Clinical Laboratory Analysis*, vol. 35, no. 4, article e23593, 2021.
- [4] M. Ullah, B. Alzahrani, A. Alsrhani, M. Atif, A. Alameen, and H. Ejaz, "Determination of serum tumor necrosis factor- $\alpha$  (TNF- $\alpha$ ) levels in metabolic syndrome patients from Saudi population," *Pakistan Journal of Medical Sciences*, vol. 37, no. 3, p. 700, 2021.
- [5] F. Guo, Y. Sha, B. Hu, and G. Li, "Correlation of long non-coding RNA LncRNA-FA2H-2 with inflammatory markers in the peripheral blood of patients with coronary heart disease," *Frontiers in Cardiovascular Medicine*, vol. 8, p. 611, 2021.
- [6] T. Pereira, P. Napoleão, M. Costa et al., "Association between miR-146a and tumor necrosis factor alpha (TNF- $\alpha$ ) in stable coronary artery disease," *Medicina*, vol. 57, no. 6, p. 575, 2021.
- [7] S. Shiber, V. Kliminski, K. Orvin et al., "Elevated plasma soluble triggering receptor expressed on myeloid cells-1 level in patients with acute coronary syndrome (ACS): a biomarker of disease severity and outcome," *Mediators of Inflammation*, vol. 2021, Article ID 8872686, 9 pages, 2021.
- [8] Z. Gao, J. Dosman, C. Rennie et al., "Effects of tumor necrosis factor (TNF) gene polymorphisms on the association between smoking and lung function among workers in swine operations," *Journal of Toxicology and Environmental Health, Part A*, vol. 84, no. 13, pp. 536–552, 2021.
- [9] A. Wojtkowska, T. Zapolski, J. Wysokińska-Miszczuk, and A. Wysokiński, "The inflammation link between periodontal disease and coronary atherosclerosis in patients with acute coronary syndromes: case-control study," *BMC Oral Health*, vol. 21, no. 1, pp. 1–17, 2021.
- [10] P. Zheng, L. Chen, Y. Guan, and P. Liu, "Weighted gene co-expression network analysis identifies specific modules and hub genes related to coronary artery disease," *Scientific Reports*, vol. 11, no. 1, pp. 1–13, 2021.
- [11] S. Wang, "Deep learning-based assessment of adverse cardiovascular events in elderly patients with coronary heart disease after percutaneous coronary intervention using intravascular ultrasound images," *Scientific Programming*, vol. 2021, Article ID 3314457, 8 pages, 2021.
- [12] J. Wu, A. Joshi, S. Reddy et al., "Anti-inflammatory therapy with tumour necrosis factor inhibitors is associated with reduced risk of major adverse cardiovascular events in psoriasis," *Journal of the European Academy of Dermatology and Venereology*, vol. 32, no. 8, pp. 1320–1326, 2018.
- [13] W. Rungapiromnan, Z. Yiu, R. Warren, C. Griffiths, and D. Ashcroft, "Impact of biologic therapies on risk of major adverse cardiovascular events in patients with psoriasis: systematic review and meta-analysis of randomized controlled trials," *British Journal of Dermatology*, vol. 176, no. 4, pp. 890–901, 2017.
- [14] E. Eisenberg, P. A. McElhinney, F. Commandeur et al., "Deep learning-based quantification of epicardial adipose tissue volume and attenuation predicts major adverse cardiovascular events in asymptomatic subjects," *Cardiovascular Imaging*, vol. 13, no. 2, article e009829, 2020.
- [15] S. Al'Aref, G. Singh, W. Choi et al., "A boosted ensemble algorithm for determination of plaque stability in high-risk patients on coronary CTA," *Cardiovascular Imaging*, vol. 13, no. 10, pp. 2162–2173, 2020.
- [16] S. Pang, Z. Tao, X. Min et al., "Correlation between the serum platelet-derived growth factor, angiotensin-1, and severity of coronary heart disease," *Cardiology Research and Practice*, vol. 2020, Article ID 3602608, 9 pages, 2020.
- [17] F. Lin, Y. Yang, Q. Guo et al., "Analysis of the molecular mechanism of acute coronary syndrome based on circRNA-miRNA network regulation," *Evidence-based Complementary and Alternative Medicine*, vol. 2020, Article ID 1584052, 17 pages, 2020.
- [18] F. Lin, W. Chen, A. Zhao et al., "Advances in research on the circRNA-miRNA-mRNA network in coronary heart disease treated with traditional Chinese medicine," *Evidence-based Complementary and Alternative Medicine*, vol. 2020, Article ID 8048691, 10 pages, 2020.

- [19] P. Seferovic, R. Bentley-Lewis, B. Claggett et al., “Retinopathy, neuropathy, and subsequent cardiovascular events in patients with type 2 diabetes and acute coronary syndrome in the ELIXA: the importance of disease duration,” *Journal of Diabetes Research*, vol. 2018, Article ID 1631263, 9 pages, 2018.
- [20] J. Budzianowski, K. Pieszko, P. Burchardt, J. Rzeźniczak, and J. Hiczkiewicz, “The role of hematological indices in patients with acute coronary syndrome,” *Disease Markers*, vol. 2017, 9 pages, 2017.
- [21] T. Chi, Q. Zhao, and P. Wang, “Risk factors for acute coronary syndrome in upper gastrointestinal bleeding patients,” *Gastroenterology Research and Practice*, vol. 2021, Article ID 8816805, 12 pages, 2021.

## Research Article

# Correlation of Inpatients Suffering from Acute Acalculous Cholecystitis during ICU Treatment with Acute Physiology and Chronic Health Evaluation II Score, Duration of Ventilator Use, and Time on Total Parenteral Nutrition

Yunfeng Zhang, Kaixian Wang, Yuhui Wang, and Yang Liu 

Department of Critical Care Medicine, Tangshan Workers Hospital, Tangshan, 063000 Hebei, China

Correspondence should be addressed to Yang Liu; liuyang@120org.com.cn

Received 25 May 2022; Revised 16 June 2022; Accepted 21 June 2022; Published 30 June 2022

Academic Editor: Naeem Jan

Copyright © 2022 Yunfeng Zhang et al. This is an open access article distributed under the Creative Commons Attribution License, which permits unrestricted use, distribution, and reproduction in any medium, provided the original work is properly cited.

**Objective.** To explore the correlation of inpatients suffering from acute acalculous cholecystitis (AAC) during ICU treatment with Acute Physiology and Chronic Health Evaluation II (APACHE-II) score, duration of ventilator use, and time on total parenteral nutrition (TPN). **Methods.** From March 2016 to March 2022, the clinical data of 47 patients with AAC who received ICU treatment in our hospital were retrospectively reviewed, and these patients were included in the AAC group. Another 36 patients treated in the ICU in the same period with age and gender matching with those in the AAC group were selected as the non-AAC group. Patients' various clinical data were recorded to analyze the correlation of AAC with APACHE-II score, duration of ventilator use, and time on TPN. **Results.** The shock time, duration of ventilator usage, and duration of sedative medicine use were all substantially longer in the AAC group than in the non-AAC group, according to the univariate analysis ( $P < 0.05$ ); the amount of norepinephrine used, white blood cell count, C-reactive protein (CRP) amount, and APACHE-II score were significantly higher in the AAC group than in the non-AAC group ( $P < 0.05$ ); between the two groups, the time on TPN and fasting time were different, but with no statistical significance ( $P > 0.05$ ); after performing Spearman's correlation with the significantly between-group different indicators, the result showed that the amount of norepinephrine used, duration of ventilator use, white blood cell count, and CRP amount were significantly correlated with the occurrence of AAC, and the correlation was positive ( $P$  all  $< 0.001$ ). **Conclusion.** The APACHE-II score and time on TPN are not significantly correlated with the occurrence of AAC; and the amount of norepinephrine used, duration of ventilator use, white blood cell count, and serum CRP are positively correlated with the occurrence of AAC. Measuring the variations in the levels of various markers can signal the onset of AAC or reflect the state and prognosis, suggesting a possible application in clinic-based targeted prevention and treatment of AAC.

## 1. Introduction

Acute acalculous cholecystitis (AAC) is a clinical emergency with lower morbidity, which tends to occur in critically ill patients with severe trauma, burns, shock, hypotension, or after major surgery, is featured with insidious onset, atypical clinical presentation, and rapid progression of the condition, and easily causes perforated gangrene and other complica-

tions, leading to a high clinical mortality [1–4]. Most patients treated in ICU inpatient areas are critically ill with complex condition and often accompanied by multivisceral dysfunction, so they are at high risk for AAC; in addition, patients who undergo the therapeutic means such as sedation and mechanical ventilation often have disorders of consciousness, and thus, the condition of AAC is not easily perceived, resulting in a prolonged disease course and a high clinical mortality



rate of 45-50% [5–8]. To enable clinicians to better monitor patients' gallbladder changes, control patients' conditions, and realize early detection, diagnosis, and treatment of AAC, a detailed analysis of each risk factor that can easily trigger AAC is required.

Many reports on AAC in recent years have shown that the incidence of AAC is clearly increasing, not only in critically ill patients like trauma and burns but also in patients with basic diseases like diabetes, hypertension, chronic bronchitis, and systemic lupus erythematosus, and that the disease group is becoming younger and younger [9–11]. However, the current published works on AAC in China are focused on disease diagnosis and treatment and technology update, promoting the development of curation, but there are few reports on analyzing the risk factors triggering AAC. To explore the factors that contribute to the development of AAC in critically ill patients, the study retrospectively analyzed the patients treated in our ICU to reduce their length of stay in the ICU and lower the case fatality rate of AAC in ICU patients.

## 2. Materials and Methods

### 2.1. Selection of Study Subjects in the AAC Group

- (1) The patients were ICU inpatients and treated in ICU for more than 24 h
- (2) The patients met the diagnosis criteria for AAC [12]
- (3) The patients were clearly diagnosed with normal gallbladder on admission and then were diagnosed with AAC during ICU treatment
- (4) The patients were at least 18 years old
- (5) The patients did not have severe cirrhosis, liver failure, acute leukemia, and other diseases
- (6) The patients were confirmed to have no cholelithiasis and choledocholith after imaging examination
- (7) The patients did not have the history of cholecystectomy
- (8) The patients had complete clinical data
- (9) The patients and their family members understood the study and signed the informed consent

Finally, 47 AAC patients who were treated in our hospital from March 2016 to March 2022 and met the study criteria were selected as the AAC group.

### 2.2. Selection of Study Subjects of the Non-AAC Group

- (1) The patients were treated in the ICU in the same period with age and gender matching with those in the AAC group
- (2) The patients did not have AAC during ICU treatment

The clinical data of 36 non-AAC patients were selected for the retrospective analysis study and set as the non-AAC group.

**2.3. Ethical and Moral Standards.** The study plan was reviewed, approved, and monitored by the Hospital Ethics Committee; and the ethical and moral standards met the World Medical Association Declaration of Helsinki (2013) [13].

### 2.4. Study Contents

**2.4.1. General Data.** The age, body mass index (BMI), gender, length of hospital stay, smoking, drinking, nationality, place of residence, and other general data of patients in the two groups were recorded to clarify the balance and comparability of the two groups by statistical analysis.

**2.4.2. Clinical Data.** Based on the early data analysis and summary of previous studies, the risk factors that might cause AAC were used for further between-group comparison and analysis, including the shock time, amount of noradrenaline used, duration of ventilation use, white blood cell count, C-reactive protein (CRP), the Acute Physiology and Chronic Health Evaluation II (APACHE-II) score, time on total parenteral nutrition (TPN), length of sedative medication use, and fasting time.

**2.4.3. Correlation Analysis.** To clarify the association between each metric and AAC, the above indicators that showed significant differences were subjected to correlation analysis using the statistical tool Spearman. Spearman's rank correlation coefficient is a nonparametric measure of the dependency of two variables, and the correlation of two statistical variables was evaluated using a monotonic equation.

**2.5. Statistical Processing.** In this study, the data processing software was SPSS 22.0, which was mainly used to calculate the between-group differences of data, the picture drawing software was GraphPad Prism 7 (GraphPad Software, San Diego, USA), the items included were enumeration data and measurement data, which were expressed by  $n$  (%) and  $(\bar{x} \pm s)$  and examined by  $X^2$  test and  $t$ -test, respectively, and met normal distribution, and between-group differences were considered statistically significant at  $P < 0.05$ .

## 3. Results

**3.1. General Data.** The patients' age, BMI, gender, length of hospital stay, smoking, drinking, nationality, place of residence, and other general data were not statistically different between the two groups ( $P < 0.05$ ), presenting comparability. See Table 1 for the specific data.

**3.2. Clinical Data.** The shock time, duration of ventilator use, and duration of sedative medication use were significantly longer in the AAC group than in the non-AAC group ( $P < 0.05$ ); the amount of norepinephrine used, white blood cell count, CRP amount, and APACHE-II score were significantly higher in the AAC group than in the non-AAC group ( $P < 0.05$ ); between the two groups, the time on TPN and fasting time were different, but with no statistical significance ( $P > 0.05$ ). See Table 2.

TABLE 1: Between-group comparison of patients' general data.

Observation indicators	AAC group ( $n = 47$ )	Non-AAC group ( $n = 36$ )	$X^2/t$	$P$
Age (years)	63.15 ± 13.860	66.56 ± 15.230	1.064	0.290
BMI (kg/m <sup>2</sup> )	23.97 ± 3.120	24.06 ± 3.150	0.130	0.897
Length of hospital stay (d)	36.91 ± 46.300	22.97 ± 15.560	1.731	0.087
Gender			1.030	0.310
Male	30 (63.83)	19 (52.78)		
Female	17 (36.17)	17 (47.22)		
Smoking			0.001	0.973
Yes	9 (19.15)	7 (19.44)		
No	38 (80.85)	29 (80.56)		
Drinking			0.124	0.724
Yes	5 (10.64)	3 (8.33)		
No	42 (89.36)	33 (91.67)		
Nationality			0.578	0.447
Minorities	3 (6.38)	1 (2.78)		
Han	44 (93.62)	35 (97.22)		
Place of residence			0.218	0.640
Urban area	25 (53.19)	21 (58.33)		
Rural area	22 (46.81)	15 (41.67)		

TABLE 2: Between-group comparison of clinical data.

Observation indicator	AAC group	Non-AAC group	$X^2/t$	$P$
Shock time (d)	2.45 ± 1.07	1.11 ± 0.70	6.517	<0.001
Amount of norepinephrine used ( $\mu\text{g}/\text{kg}$ )	32.53 ± 9.16	11.25 ± 4.10	12.966	<0.001
Duration of ventilator use (d)	8.81 ± 1.45	2.08 ± 0.64	25.951	<0.001
White blood cell count ( $\times 10^9/\text{L}$ )	13.83 ± 4.34	7.55 ± 2.49	7.753	<0.001
CRP amount (mg/L)	105.40 ± 10.51	30.10 ± 6.81	37.370	<0.001
APACHE-II score	23.55 ± 5.03	18.69 ± 5.66	4.131	<0.001
Duration of sedative medication use (d)	6.83 ± 2.13	3.11 ± 0.97	9.725	<0.001
Time on TPN (d)	3.13 ± 1.23	2.64 ± 1.08	1.895	0.062
Fasting time (d)	4.15 ± 1.60	3.53 ± 1.26	1.914	0.059

3.3. *Correlation Analysis.* After performing Spearman's correlation with the significantly between-group different indicators, including the amount of norepinephrine used, duration of ventilator use, white blood cell count, CRP amount, APACHE-II score, and duration of sedative medication use, it was found that the amount of norepinephrine used, duration of ventilator use, white blood cell count, and CRP amount were significantly correlated with the occurrence of AAC, and the correlation was positive ( $P$  all <0.001). See Table 3 for details.

#### 4. Discussion

In contrast to calculous cholecystitis, AAC has an urgent onset, atypical symptoms, and rapid disease progression and is often accompanied by severe complications such as gangrene of gallbladder, perforation of gallbladder, and peritonitis, making it

one of the important causes of death in patients [14–16]. Most ICU patients are acutely and critically ill with multiple organ dysfunction, making them vulnerable to AAC. These patients are unable to express their symptoms on their own, which, when combined with pharmaceutical interventions, examination limitations, and other factors, leads to delayed diagnosis and treatment, resulting in a high clinical mortality rate for AAC patients [17–20]. In recent years, increasing attention has been paid to AAC in clinic to clarify the potential pathogenic factors of AAC, and the development of targeted preventive measures for patients at high risk of AAC is urgent. However, current published works on AAC mostly focus on disease diagnosis and treatment, and there are still few studies on risk factors and correlation of AAC incidence. Based on this, a study of 83 patients admitted to our ICU ward was conducted with the aim of investigating common risk factors predisposing

TABLE 3: Spearman's correlation.

Test variable	<i>N</i>	Correlation coefficient	Sig. (two-sided)
Amount of norepinephrine used ( $\mu\text{g}/\text{kg}$ )	83	0.827*	0.000
Duration of ventilator use (d)	83	0.870*	0.000
White blood cell count ( $\times 10^9/\text{L}$ )	83	0.661*	0.000
CRP amount (mg/L)	83	0.858*	0.000

Note: \* denoted significant correlation at a confidence level (two-sided) of 0.001.

to AAC and the correlation between the occurrence of AAC and APACHE-II score, duration of ventilator use, and time on TPN. Clinical data from 44 patients were collected early in the investigation for a small retrospective analysis, and the link of parameters including shock duration, norepinephrine dose, and ventilator use with the development of AAC in ICU patients was studied for the first time herein.

After further expanding the sample size, it was concluded that according to the univariate analysis, the shock time, duration of ventilator use, and duration of sedative medication use were significantly longer in the AAC group than in the non-AAC group ( $P < 0.05$ ); the amount of norepinephrine used, white blood cell count, CRP amount, and APACHE-II score were significantly higher in the AAC group than in the non-AAC group ( $P < 0.05$ ); and between the two groups, the time on TPN and fasting time were different, but with no statistical significance ( $P > 0.05$ ), which was consistent with the previous studies [21]. With further analysis, the following can be concluded. (1) Patients with shock are more prone to develop AAC, according to some published studies, because vasodilation and improved blood flow result in the reperfusion of blood with many inflammatory mediators, causing gallbladder injury and increasing gallbladder inflammation. In the univariate analysis of the study, the shock time was significantly different between the two groups, but it was not observed by Spearman's correlation, and it may be that the evaluation of shock time in patients was biased by drug treatment, and in such cases, gallbladder monitoring in shock patients should be enhanced in the clinic, and follow-up studies with larger sample size are required for verification.

(2) Norepinephrine is one of the common drugs to correct shock and a necessary drug for patients in ICU to maintain blood pressure and ensure blood supply to important organs. High dosages of norepinephrine will increase peripheral vascular resistance, constrict the flow of blood vessels to the gallbladder, create gallbladder blood supply problems and mucosal ischemia, and worsen gallbladder inflammation. Spearman's correlation analysis showed that norepinephrine dosage was positively associated with AAC, indicating that norepinephrine dosage is an important risk factor contributing to the development of AAC, and therefore, for ICU patients who need elevation of blood pressure by drugs such as norepinephrine, dynamic monitoring of their gallbladder should be enhanced to facilitate early detection of AAC and to apply targeted control measures.

(3) Although sedation and analgesia are important therapeutic linkages for ICU patients and are advantageous to their early recovery, sedative medicines have unavoidable

side effects, such as gastrointestinal depression. Decreased gastrin can directly lead to insufficient secretion of cholecystokinin, failure of normal contraction of the gallbladder, bile retention in the gallbladder, absorption of bile water by gallbladder epithelial cells, and viscous bile that is difficult to excrete, causing cholestasis and aggravating damage to the gallbladder mucosa and proinflammatory reactions. Spearman analysis indicated that there was no significant correlation between the sedative drug dosage and AAC, which may be related to some factors such as patients' dosage difference and sample size.

(4) Assisted breathing by mechanical ventilation can cause increased intra-abdominal pressure, while continuous intra-abdominal hypertension can affect the blood supply to the intestine, causing ischemia and hypoxia of the intestinal mucosa and mucosal necrosis and sloughing and disrupting the intestinal mucosal barrier; in addition, continuous increased pressure in the abdominal cavity can also promote the passage of bacteria through the lymphatic system or blood into the biliary tract, causing bacterial infection in the gallbladder. Spearman's correlation analysis showed that the duration of ventilator use was positively correlated with AAC and was a significant risk factor for inducing AAC, so close attention should be paid to ICU patients receiving continuous mechanical ventilation in clinical treatment, so as to monitor gallbladder changes and prevent AAC occurrence.

(5) White blood cell count is an important observation indicator in cholecystitis patients, and this study confirmed that white blood cell count was positively associated with the occurrence of AAC. It is because individuals with AAC frequently have necrosis and perforation of the gallbladder wall, and gallbladder inflammation can quickly disseminate to the abdominal cavity, causing localised or diffuse peritonitis. Therefore, white blood cell count can be used as an important indicator to monitor changes in the gallbladder in ICU patients to suggest the lesion.

(6) CRP is one of the systemic inflammatory indicators for monitoring cholecystitis and a highly sensitive protein produced by the human liver, which is significantly higher in the acute phase of the inflammatory response, making it a marker of the systemic inflammatory response. When the body is stimulated by bacterial infection or bacteria or aseptic inflammatory stimuli such as atherosclerosis and cerebral infarction, CRP binds to lipoproteins, the complement system is activated, many inflammatory mediators are produced, and oxygen free radicals are released, causing damage to the vascular intima and increased vascular permeability and aggravating the systemic inflammatory response. Spearman analysis showed that CRP was positively correlated with AAC and an important indicator to alert the occurrence of AAC, so targeted prevention

initiatives should be taken and close attention to gallbladder changes should be paid for patients with progressive elevation of CRP in the ICU.

(7) The APACHE-II score consists of the acute physiology score (APS), age, and chronic physiology score (CPS). It is thought that the severity of an acute disease can be determined by measuring the degree of irregularity in a number of physiological indicators, which is a commonly used index in the ICU to assess the severity of illness in ICU patients, with higher scores indicating greater severity of illness and needing more intense monitoring and treatment. In this study, the APACHE-II scores of both groups were high and generally above 15 points, and the overall baseline value was high; hence, the correlation was not significant.

(8) TPN and fasting will irritate patients' gastrointestinal tract, affect the peristalsis of the gastrointestinal tract, and then change the normal gallbladder movement rhythm, affecting bile discharge and causing congestion and edema of the gallbladder mucosa and a series of acute inflammatory reactions, which, combined with the use of sedative medications, can easily trigger obstruction at the common bile duct opening and increase the risk of AAC. Relevant animal experimental studies also confirmed that TPN and fasting easily induced cholestasis [22–25]. However, because of the diverse disease kinds of patients in each group and because patients with gastrointestinal disease usually had a longer period of TPN and fasting, significance was not presented in this study.

In conclusion, the APACHE-II score and time on TPN are not significantly correlated with the occurrence of AAC; and the amount of norepinephrine used, duration of ventilator used, white blood cell count, and serum CRP are positively correlated with AAC. Measuring the variations in the levels of various markers can signal the onset of AAC or reflect the state and prognosis, suggesting a possible application in clinic-based targeted prevention and treatment of AAC.

## Data Availability

Data to support the findings of this study is available on reasonable request from the corresponding author.

## Conflicts of Interest

The authors do not have conflicts of interest to declare.

## References

- [1] P. Paci, N. E. Mayo, P. A. Kaneva, J. F. Fiore, G. M. Fried, and L. S. Feldman, "Determinants of variability in management of acute calculous cholecystitis," *Surgical Endoscopy*, vol. 32, no. 4, pp. 1858–1866, 2018.
- [2] A. S. O. Tang, T. S. Leong, L. P. Chew, and H. H. Chua, "Successful non-surgical treatment of an acute calculous cholecystitis in a myeloma patient with Covid-19: case report," *Clinical Medicine*, vol. 3, no. 2, pp. 666–669, 2021.
- [3] S. Y. Turiño, D. M. Shabanzadeh, N. M. Eichen, S. L. Jørgensen, L. T. Sørensen, and L. N. Jørgensen, "Percutaneous cholecystostomy versus conservative treatment for acute cholecystitis: a cohort study," *Journal of Gastrointestinal Surgery: Official Journal of the Society for Surgery of the Alimentary Tract*, vol. 23, no. 2, pp. 297–303, 2019.
- [4] Z. Zhang, Y. He, X. L. Zhu et al., "Acute cholecystitis following allogeneic hematopoietic stem cell transplantation: clinical features, outcomes, risk factors, and prediction model," *Journal of the American Society for Blood and Marrow Transplantation*, vol. 27, no. 3, pp. 253–254, 2021.
- [5] K. Gandhi, R. Du Plessis, J. Klopper, and C. Kloppers, "Percutaneous cholecystostomy placement in cases of non-operative cholecystitis: a retrospective cohort analysis," *World Journal of Surgery*, vol. 44, no. 12, pp. 4077–4085, 2020.
- [6] A. M. González-Castillo, J. Sancho-Insenser, D. Miguel-Palacio et al., "Mortality risk estimation in acute calculous cholecystitis: beyond the Tokyo Guidelines," *World Journal of Emergency Surgery*, vol. 16, no. 1, 2021.
- [7] C. S. Loozen, J. E. Oor, B. van Ramshorst, H. C. van Santvoort, and D. Boerma, "Conservative treatment of acute cholecystitis: a systematic review and pooled analysis," *Surgical Endoscopy*, vol. 31, no. 2, pp. 504–515, 2017.
- [8] S. Bourikian, R. J. Anand, M. Aboutanos, L. G. Wolfe, and P. Ferrada, "Risk factors for acute gangrenous cholecystitis in emergency general surgery patients," *The American Journal of Surgery*, vol. 210, no. 4, pp. 730–733, 2015.
- [9] A. Tufo, M. Pisano, L. Ansaloni et al., "Risk prediction in acute calculous cholecystitis: a systematic review and meta-analysis of prognostic factors and predictive models," *Journal of Laparoendoscopic & Advanced Surgical Techniques*, vol. 31, no. 1, pp. 41–53, 2021.
- [10] M. Takinami, G. Murohisa, Y. Yoshizawa, E. Shimizu, and M. Nagasawa, "Risk factors for cholecystitis after stent placement in patients with distal malignant biliary obstruction," *Journal of Hepato-Biliary-Pancreatic Sciences*, vol. 27, no. 8, pp. 470–476, 2020.
- [11] J. W. Han, Y. H. Choi, I. S. Lee et al., "Early laparoscopic cholecystectomy following percutaneous transhepatic gallbladder drainage is feasible in low-risk patients with acute cholecystitis," *Journal of Hepato-Biliary-Pancreatic Sciences*, vol. 28, no. 6, pp. 515–523, 2021.
- [12] J. K. Park, J. I. Yang, J. W. Wi et al., "Long-term outcome and recurrence factors after percutaneous cholecystostomy as a definitive treatment for acute cholecystitis," *Journal of Gastroenterology and Hepatology*, vol. 34, no. 4, pp. 784–790, 2019.
- [13] World Medical Association, "World Medical Association Declaration of Helsinki: ethical principles for medical research involving human subjects," *Journal of the American Medical Association*, vol. 310, no. 20, pp. 2191–2194, 2013.
- [14] R. Hirohata, T. Abe, H. Amano et al., "Identification of risk factors for open conversion from laparoscopic cholecystectomy for acute cholecystitis based on computed tomography findings," *Surgery Today*, vol. 50, no. 12, pp. 1657–1663, 2020.
- [15] K. Inoue, T. Ueno, D. Douchi et al., "Risk factors for difficulty of laparoscopic cholecystectomy in grade II acute cholecystitis according to the Tokyo guidelines 2013," *BMC Surgery*, vol. 17, no. 1, pp. 1–8, 2017.
- [16] A. Escartín, M. González, E. Cuello et al., "Acute cholecystitis in very elderly patients: disease management, outcomes, and risk factors for complications," *Surgery Research and Practice*, vol. 2019, Article ID 9709242, 2019.
- [17] A. D. Szvalb and D. P. Kontoyiannis, "Acute acalculous cholecystitis due to *Fusarium* species and review of the literature on fungal cholecystitis," *Mycoses: Diagnosis, Therapy*

- And Prophylaxis Of Fungal Diseases*, vol. 62, no. 9, pp. 847–853, 2019.
- [18] R. Z. Panni and S. M. Strasberg, “Preoperative predictors of conversion as indicators of local inflammation in acute cholecystitis: strategies for future studies to develop quantitative predictors,” *Journal of Hepato-Biliary-Pancreatic Sciences*, vol. 25, no. 1, pp. 101–108, 2018.
- [19] N. Sakata, Y. Okumura, K. Fushimi, M. Nakanishi, and A. Ogawa, “Dementia and risk of 30-day readmission in older adults after discharge from acute care hospitals,” *Journal of the American Geriatrics Society*, vol. 66, no. 5, pp. 871–878, 2018.
- [20] M. Portinari, M. Scagliarini, G. Valpiani et al., “Do I need to operate on that in the middle of the night? Development of a nomogram for the diagnosis of severe acute cholecystitis,” *Journal of Gastrointestinal Surgery*, vol. 22, no. 6, pp. 1016–1025, 2018.
- [21] W. Lei, M. Jianbao, and S. Kangjie, “Diagnosis and treatment of 29 cases of acute non calculous cholecystitis,” *Journal of Hepatobiliary Surgery*, vol. 22, no. 5, pp. 363–365, 2014.
- [22] Y. Kawamoto, T. Fujikawa, Y. Sakamoto et al., “Effect of antithrombic therapy on bleeding complications in patients receiving emergency cholecystectomy for acute cholecystitis,” *Journal of Hepato-Biliary-Pancreatic Sciences*, vol. 25, no. 11, pp. 518–526, 2018.
- [23] A. Bonaventura, I. Leale, F. Carbone et al., “Pre-surgery age-adjusted Charlson comorbidity index is associated with worse outcomes in acute cholecystitis,” *Digestive And Liver Disease*, vol. 51, no. 6, pp. 858–863, 2019.
- [24] B. Joseph, F. Jehan, M. Dacey et al., “Evaluating the relevance of the 2013 Tokyo Guidelines for the diagnosis and management of cholecystitis,” *Journal of the American College of Surgeons*, vol. 227, no. 1, pp. 38–43e1, 2018.
- [25] M. Barabino, G. Piccolo, A. Trizzino et al., “COVID-19 outbreak and acute cholecystitis in a Hub Hospital in Milan: wider indications for percutaneous cholecystostomy,” *BMC Surgery*, vol. 21, no. 1, 2021.

## Research Article

# Effect of Predictive Nursing Combined with Early Drinking Water Therapy on Patients with Urinary Retention after Vaginal Delivery

Gaiying Cui , Yong Zhang, Zhaoxia Liu, Xia Li, and Manting Sha 

Shijiazhuang Fourth Hospital, China

Correspondence should be addressed to Manting Sha; [mantohptd901802@163.com](mailto:mantohptd901802@163.com)

Received 6 April 2022; Revised 10 May 2022; Accepted 13 May 2022; Published 30 June 2022

Academic Editor: Naeem Jan

Copyright © 2022 Gaiying Cui et al. This is an open access article distributed under the Creative Commons Attribution License, which permits unrestricted use, distribution, and reproduction in any medium, provided the original work is properly cited.

The aim of this study is to analyze the effect of predictive nursing combined with early drinking water therapy on patients with urinary retention after vaginal delivery. A total of 600 women who gave birth in our hospital from July 2019 to July 2020 were selected as the research objects. A double-blind method was adopted to divide them into a control group and observation group, 300 cases in each group. In the control group, routine nursing was given. In the observation group, (1) predictive nursing measures were used before surgery. (2) The postoperative observation group used early drinking water therapy; the incidence of urinary retention, the effective rate of urination, postpartum haemorrhage, and the treatment of urinary retention were compared between the two groups. In the observation group, the number of urinary retention was 17, and the incidence of urinary retention was 5.67%. The urination efficiency of the observation group was 98.33%; the urination efficiency of the control group was 86.33%; comparison results showed that  $P < 0.05$ . The 24 h postpartum haemorrhage of the observation group was 1.33%; the 24 h postpartum haemorrhage of the control group was 2.66%. Uroschisis therapy was performed in 17 patients in the observation group and 44 patients in the control group. The observation group had an 88.24 percent treatment rate, while the control group had a 72.73 percent treatment rate.  $P < 0.05$  indicated that the difference was statistically significant.

## 1. Introduction

Postpartum retention refers to inability to urinate by oneself or inability to urinate properly for 6-8 hours after delivery, which is one of the common complications of postpartum [1]. It is a disease caused by bladder muscle paralysis caused by uterine pressure on bladder and pelvic nerve plexus during childbirth. Common reasons are being not used to urination in bed, sudden abdominal pressure, pain, psychological factor, and so on, which affect the recovery of patients after childbirth [2]. It has been reported in the literature that the incidence of postpartum urinary retention in vaginal delivery women is about 12~18% [3]. At present, there is no specific treatment to prevent and treat postpartum urinary retention. The traditional noninvasive method is induced urination, but its success rate is low [4, 5]. However, retention of urinary catheters can easily cause urinary tract infections. Studies have shown that urinary tract infections

caused by urinary catheters account for 60% to 80% of patients with urinary tract infections. Effective clinical measures should be taken to prevent urinary retention [6, 7].

Predictive nursing also known as advanced nursing takes preventive measures to reduce or avoid the occurrence of complications to a certain extent [8].

Studying on the effect of predictive nursing combined with early drinking water therapy on patients with urinary retention after vaginal delivery obtained good results. Predictive nursing combined with early drinking water therapy for the prevention and treatment of urine retention after vaginal delivery could effectively avoid urinary retention and improve the effective rate of urination. Expectant mothers should be encouraged to communicate with more experienced pregnant ladies.

The paper is arranged as follows: Section 2 discusses the materials and methods in detail. Section 3 analyzes the experiments and result. Section 4 concludes the article.

## 2. Materials and Methods

**2.1. General Information.** A total of 600 women who gave birth in our hospital from July 2019 to July 2020 were selected as the research objects. A double-blind method was adopted to divide them into a control group and observation group, 300 cases in each group. The control group was aged from 23 to 35, with an average age of 27.4. There were 180 parturient women, and the remaining 120 were parturient women; the observation group was 24 to 34 years old, with an average age of 27.2 years. There were 168 women who had already undergone parturition, and the remaining 132 were primiparous women. There was no statistically significant difference in general information between the two groups of patients ( $P > 0.05$ ).

- (1) Diagnostic criteria: this refers to the diagnostic criteria for postpartum urinary retention in obstetrics and gynaecology in integrated traditional Chinese and Western medicine [9]. (1) 6 hours after delivery, urine dropped or became obstructed, and abdominal distension was acute and painful. (2) The lower abdomen was bulging, and the bladder was full and tender
- (2) Inclusion criteria: (1) primiparous women who gave birth vaginally <35 years old; (2) people with clear consciousness, able to cooperate with treatment, and without other diseases such as urinary tract infection; and (3) women who volunteered to participate in this trial and signed informed consent
- (3) Exclusion criteria: (1) having mental illness and unable to cooperate with the treatment, (2) combined with urinary system diseases, (3) severe postpartum complications, (4) persons with serious cardiopulmonary diseases, and (5) people with severe blood clotting disorder

### 2.2. Methods

**2.2.1. Control Group.** Routine care was given. Patients and their families are informed about the common clinical signs of postpartum urine retention. The difficulties to be handled prior to childbirth as well the importance of breastfeeding were explained. After childbirth, the nursing staff should understand the vaginal bleeding of the mother and understand whether she had urinated 6 hours after delivery.

**2.2.2. Observation Group.** (1) Predictive nursing measures were used before surgery. In this group, predictive nursing measures were added, and the nursing content was as follows: (a) Physical status assessment: after admission, the patient's physical condition should be evaluated to understand the postpartum recovery of the patient. Under good condition, the patient could be assisted to get out of bed to urinate or raise the head of the bed to urinate on the bed. (b) Cognitive intervention: before giving birth, pregnant women should be informed of the causes of urinary retention and the importance of successful urination after surgery. Expectant mothers should be encouraged to commu-

nicate with more experienced pregnant ladies. Parturient women cooperated with medical staff to train and prevent postpartum urinary retention [10]. (c) Psychological intervention: medical staff should understand the psychological conditions of patients. Some maternal medical staff with fear and anxiety due to excessive worry should take appropriate measures to help the pregnant women stabilize their emotions, allowing women to have the best condition for surgery and gradually building up women's self-confidence in autonomous urination [11]. (4) In-bed urination training: medical staff needed to train the mother to urinate in bed and use toilets. This training was required three days before the operation. Training should be at least 2 to 3 times a day until the woman was ready to go to bed and defecate [12].

(2) The postoperative observation group was treated with early drinking water therapy. (a) Drinking water during labor: the puerpera is encouraged to drink water regularly and relieve urine once every 2~4 h. (b) Drinking water after delivery: during observation in the delivery room 2 h after delivery, the midwife guided the puerpera to water therapy in order to make the puerpera urinate as soon as possible. The specific methods are as follows: drinking 300~500 ml of warm water within 30 min after delivery, drinking 200~300 ml of warm water again 1 h after delivery, assisting the puerpera on their first pee by specially assigned personnel when the bladder is semifull or 1.5 h postpartum, and timely evaluation of bladder filling status during drinking water. (c) Urination training: while the patient was urinating, the medical staff could make the patient listen to the water to induce urination, and warm water could also be used to flush the perineum to stimulate urination. (d) Massage: the bladder area and uterus floor of the puerpera were massaged for 10 min/time, once every 0.5 h. The intensity was within the range of maternal tolerance. Massage action should not be too rough, and pay attention to the bladder area in the process of massage without swelling.

**2.3. Observational Index.** The first urination and urine volume were recorded, and the volume of vaginal bleeding 24 hours after delivery was measured.

- (1) Incidence of urinary retention = number of cases of urinary retention/total cases  $\times$  100%
- (2) Effective rate of urination = (number of significant cases + number of effective cases)/total cases  $\times$  100%. The first urination volume > 500 ml was significant. The first urination volume of 100~500 ml was effective; the first urination volume < 100 ml was invalid
- (3) Postpartum haemorrhage: blood loss within 24 h after delivery is  $\geq$ 500 ml
- (4) Uroschisis therapy: based on the bladder residual urine measured during the first and second urination after delivery and b-ultrasound after urination, the therapeutic effect of prevention of postpartum pigmentation was classified as special effect, obvious effect, effective, and invalid: special effects—urinary bladder residual urine volume  $\leq$  50 ml after urination

TABLE 1: Results of the incidence of urinary retention.

Groups	<i>n</i>	First urination time	Urination			
			0-4 h	4-6 h	Urinary retention	Incidence of urinary retention
Observation group	300	2.08 ± 1.02	274	9	17	5.67%
Control group	300	2.07 ± 1.41	231	25	44	14.67%

TABLE 2: Results of the urination efficiency.

Groups	<i>n</i>	Special effect	Obvious effect	Effective	Invalid
Observation group	300	90.0	205	5	98.333
Control group	300	73.1	186	41	86.333

TABLE 3: Results of postpartum haemorrhage.

Groups	<i>n</i>	2 h postpartum haemorrhage	24 h postpartum haemorrhage
Observation group	300	179.540 ± 12.161	4 (1.333)
Control group	300	18.533 ± 12.033	8 (2.662)

TABLE 4: Results of uroschesis therapy.

Groups	<i>n</i>	Special effect	Obvious effect	Effective	Invalid	Rate
Observation group	17	4	6	5	2	88.24%
Control group	44	8	13	11	12	72.73%

within 2 h after delivery; obvious effect—the residual urine volume ( $\leq 50$  ml) of the bladder after urination within 2-4 h after postpartum; effective—bladder residual urine volume  $\leq 50$  ml after urination within 4-6 h after postpartum; and invalid—those that did not meet the above criteria. For the first urination time  $> 6$  hours, it was recorded as urinary retention and its incidence is counted

**2.4. Statistical Methods.** Using SPSS 22 statistical software, data were processed. Statistical data were compared by the  $\chi^2$  test. Measurement data were represented by  $x \pm s$ , using the *t*-test.  $P < 0.05$  meant that the difference was statistically significant.

### 3. Results

**3.1. Results of the Incidence of Urinary Retention.** In the observation group, the number of urinary retention was 17, and the incidence of urinary retention was 5.67%; in the control group, the number of urinary retention was 44, and the incidence of urinary retention was 14.67%. Results of the incidence of urinary retention are shown in Table 1.

**3.2. Results of the Urination Efficiency.** The urination efficiency of the observation group was 98.33%, and the urination efficiency of the control group was 86.33%; comparison results showed that  $P < 0.05$ . Results of the urination efficiency are shown in Table 2.

**3.3. Results of Postpartum Haemorrhage.** The 24 h postpartum haemorrhage of the observation group was 1.33%; the 24 h postpartum haemorrhage of the control group was 2.66%. Results of postpartum haemorrhage are shown in Table 3.

**3.4. Results of Uroschesis Therapy.** Uroschesis therapy was performed in 17 patients in the observation group and 44 patients in the control group. The treatment rate in the observation group was 88.24%; the treatment rate of the control group was 72.73. The difference was statistically significant ( $P < 0.05$ ). Results of urinary retention therapy are shown in Table 4.

Postpartum nervous tension and bladder compression during delivery can lead to bladder mucosa edema and congestion, decreased bladder muscle tension, or decreased pelvic pressure, resulting in urinary retention [13, 14]. Among the causes of patients with urinary retention, the main reasons are being unaccustomed to urinating in bed, sudden drop in abdominal pressure, pain, and psychological reasons [15]. At the same time, due to the lack of knowledge of postpartum health care, women and their families do not understand the importance of urinating as soon as possible after delivery. Inadequate or excessive drinking of water, failure to urinate regularly, and an over-filled bladder lead to urinary tract infections and increased rates of postpartum bleeding; thus, the recovery time of the patient's follow-up palmitis can be increased [16, 17]. Predictive nursing primarily uses health disease knowledge



education and psychological intervention so that pregnant women can make appropriate preparations ahead of time, which can relieve the stress of patients entering the ward for the first time, establish harmonious medical care, and improve the pregnant women's trust and cooperation [18]. At the same time, the puerpera should be treated with drinking water therapy to make the puerpera feel like urinating as soon as possible. When the bladder is in a semifilled state or 1.5 to 2 hours after delivery, a person will help the puerpera to urinate, reducing the time it takes to urinate for the first time and recovering urinary function as soon as feasible [19, 20].

According to the findings, there were 17 cases of urine retention in the observation group, and the incidence of urinary retention was 5.67 percent; in the control group, the number of urinary retention was 44, and the incidence of urinary retention was 14.67%. The urination efficiency of the observation group was 98.33%, and the urination efficiency of the control group was 86.33%; comparison results showed that  $P < 0.05$ . The 24h postpartum haemorrhage of the observation group was 1.33%; the 24h postpartum haemorrhage of the control group was 2.66%. Uroschisis therapy was performed in 17 patients in the observation group and 44 patients in the control group. The treatment rate in the observation group was 88.24%; the treatment rate of the control group was 72.73. The difference was statistically significant ( $P < 0.05$ ).

#### 4. Conclusion

To sum up, the application of predictive nursing combined with early drinking water therapy for the prevention and treatment of urinary retention after vaginal delivery could effectively prevent the occurrence of urinary retention after vaginal delivery and improve the effective rate of urination. It not only did not increase the incidence of postpartum haemorrhage at 2h or 24h but also improved the therapeutic effect of urination, and it was worth promoting.

#### Data Availability

The datasets used during the present study are available from the corresponding author upon reasonable request.

#### Conflicts of Interest

The authors declare that they have no conflicts of interest.

#### Authors' Contributions

Yong Zhang contributed equally to this work.

#### Funding

This study was supported by the High risk factors and intervention effects of postpartum urinary retention during vaginal delivery (181461413).

#### References

- [1] F. E. Mulder, R. A. Hakvoort, J. P. De Bruin, E. W. Janszen, J. A. Van Der Post, and J. P. Roovers, "Long-term micturition problems of asymptomatic postpartum urinary retention: a prospective case-control study," *International Urogynecology Journal*, vol. 29, no. 4, pp. 481–488, 2017.
- [2] M. Polat, M. B. Şentürk, Ç. Pulatoğlu, O. Doğan, Ç. Kılıççı, and M. Ş. Budak, "Postpartum urinary retention: evaluation of risk factors," *Turkish Journal of Obstetrics & Gynecology*, vol. 15, no. 2, pp. 70–74, 2018.
- [3] A. Tan, L. Zhou, P. Hu, and Y. Liu, "Application of "Chang Chang circle" in prevention of postpartum urinary retention," *Chinese Medical Science*, vol. 8, no. 14, pp. 156–158, 2018.
- [4] P. Milart, B. Wozniakowska, P. Czuczwar, W. Wrona, and T. Paszkowski, "Extensive postpartum urinary retention successfully treated with clean intermittent catheterization," *Ginekologia Polska*, vol. 89, no. 3, pp. 174–174, 2018.
- [5] A. Pannullo and A. Hill, "Physical therapy interventions for prolonged postpartum urinary retention," *Journal of Women's Health Physical Therapy*, vol. 42, no. 1, pp. 23–31, 2018.
- [6] T. Beaumont, "Prevalence and outcome of postpartum urinary retention at an Australian hospital," *Midwifery*, vol. 70, pp. 92–99, 2019.
- [7] F. Shanti, F. Meghan, and M. Hupe, "Clinical pharmacology online databases pharmaceutical drugs point-of-care systems predictive auto-suggest product evaluation," *Medical Reference Services Quarterly*, vol. 37, no. 4, pp. 386–396, 2018.
- [8] G. Diego, B. Marta, G. Sara et al., "Predictive tools in the care of blood donors: prevention of vasovagal syndrome," *Studies in Health Technology and Informatics*, vol. 250, pp. 174–177, 2018.
- [9] D. Huang, "Observation on the curative effect of combined traditional Chinese and western medicine on postpartum urinary retention," *TCM Clinical Research*, vol. 10, no. 26, pp. 63–66, 2018.
- [10] B. Teimoori and A. Esmailzadeh, "A large uterine leiomyoma leading to non-puerperal uterine inversion: a case report," *International Journal of Reproductive Biomedicine*, vol. 15, no. 1, pp. 55–56, 2017.
- [11] H. D. Kwon and O. S. Yoo, "Retention of capable new employees under uncertainty: impact of strategic interactions," *IJSE Transactions*, vol. 49, no. 10, pp. 927–941, 2017.
- [12] G. Fabio, B. Ivano, T. Antonello, Q. Lai, and J. Andreuccetti, "Early and late effects of the sequential transfixated stich technique for the treatment of the symptomatic rectocele without rectal mucosa prolapse," *Minerva Chirurgica*, vol. 75, no. 2, pp. 83–91, 2020.
- [13] G. Lamblin, G. Chene, C. Aeberli et al., "Identification of risk factors for postpartum urinary retention following vaginal deliveries: a retrospective case-control study," *European Journal of Obstetrics, Gynecology, and Reproductive Biology*, vol. 243, pp. 7–11, 2019.
- [14] A. G. Kenny, O. Pellerin, G. Amouyal et al., "Prostate artery embolization in patients with acute urinary retention," *The American Journal of Medicine*, vol. 132, no. 11, pp. e786–e790, 2019.
- [15] K. Agrawal, S. Majhi, and R. Garg, "Post-operative urinary retention: review of literature," *World Journal of Anesthesiology*, vol. 8, no. 1, pp. 1–12, 2019.

- [16] G. Wang, "Predictive nursing to prevent postpartum urinary retention nursing experience," *Journal of Rare and Uncommon Diseases*, vol. 25, no. 5, pp. 88-89, 2018.
- [17] N. Crain and T. Tejirian, "Impact of intraoperative Foley catheters on postoperative urinary retention after inguinal hernia surgery," *The American Surgeon*, vol. 85, no. 10, pp. 1099-1103, 2019.
- [18] M. Kristina, V. Van, A. Grob, K. Schweitzer, C. H. van der Vaart, and M. Withagen, "Changes in the mean echogenicity and area of the urethra during pregnancy and after delivery," *European Journal of Obstetrics & Gynecology & Reproductive Biology*, vol. 211, pp. 208-209, 2017.
- [19] Q. Sun, "The preventive effect of predictive nursing intervention on postpartum urinary retention in women with natural childbirth," *Journal of Practical Clinical Nursing*, vol. 24, pp. 111-112, 2018.
- [20] H. Hilton, L. Boesby, and E. Nelveg, "Severe hyponatremia precipitated by acute urinary retention in a patient with psychogenic polydipsia," *Case Reports in Nephrology*, vol. 2020, Article ID 8792897, 4 pages, 2020.

## Retraction

# Retracted: Online Education Satisfaction Assessment Based on Machine Learning Model in Wireless Network Environment

### Computational and Mathematical Methods in Medicine

Received 17 October 2023; Accepted 17 October 2023; Published 18 October 2023

Copyright © 2023 Computational and Mathematical Methods in Medicine. This is an open access article distributed under the Creative Commons Attribution License, which permits unrestricted use, distribution, and reproduction in any medium, provided the original work is properly cited.

This article has been retracted by Hindawi following an investigation undertaken by the publisher [1]. This investigation has uncovered evidence of one or more of the following indicators of systematic manipulation of the publication process:

- (1) Discrepancies in scope
- (2) Discrepancies in the description of the research reported
- (3) Discrepancies between the availability of data and the research described
- (4) Inappropriate citations
- (5) Incoherent, meaningless and/or irrelevant content included in the article
- (6) Peer-review manipulation

The presence of these indicators undermines our confidence in the integrity of the article's content and we cannot, therefore, vouch for its reliability. Please note that this notice is intended solely to alert readers that the content of this article is unreliable. We have not investigated whether authors were aware of or involved in the systematic manipulation of the publication process.

Wiley and Hindawi regrets that the usual quality checks did not identify these issues before publication and have since put additional measures in place to safeguard research integrity.

We wish to credit our own Research Integrity and Research Publishing teams and anonymous and named external researchers and research integrity experts for contributing to this investigation.

The corresponding author, as the representative of all authors, has been given the opportunity to register their agreement or disagreement to this retraction. We have kept a record of any response received.

### References

- [1] J. Qin, "Online Education Satisfaction Assessment Based on Machine Learning Model in Wireless Network Environment," *Computational and Mathematical Methods in Medicine*, vol. 2022, Article ID 7958932, 11 pages, 2022.

## Research Article

# Online Education Satisfaction Assessment Based on Machine Learning Model in Wireless Network Environment

Jing Qin 

*Criminal Investigation Police University of China, Shenyang, 110854 Liaoning, China*

Correspondence should be addressed to Jing Qin; [qinjing@cipuc.edu.cn](mailto:qinjing@cipuc.edu.cn)

Received 19 April 2022; Revised 12 May 2022; Accepted 19 May 2022; Published 29 June 2022

Academic Editor: Naeem Jan

Copyright © 2022 Jing Qin. This is an open access article distributed under the Creative Commons Attribution License, which permits unrestricted use, distribution, and reproduction in any medium, provided the original work is properly cited.

With the development of wireless network technology, the transformation of educational concepts, the upgrading of users' educational needs, and the transformation of lifestyles, online education has made great strides forward. However, due to the rapid growth of online education in my country, many regulatory systems have not kept pace with the development of online education, resulting in low user experience and satisfaction with online education. The establishment of a user satisfaction model is beneficial for attracting attention and thinking about research in the field of online education service quality, assisting enterprises in recognizing the specific impact of various factors in services, accelerating service quality improvement, and assisting in the formulation of industry norms and improving enterprise competitiveness, all of which help students acquire knowledge more easily. In the era of big data, traditional satisfaction evaluation methods have many drawbacks, so more and more machine learning methods are applied to satisfaction evaluation models. This paper takes the research of machine learning algorithm as the core to carry out the research work, uses the cost-sensitive idea to improve the decision tree, considers the cost of different types of classification errors, and uses the random forest principle to integrate the generated decision tree, thereby improving the accuracy of the model. The model has better stability, and the validity of the model is verified by experiments. For a follow-up in-depth investigation of online education satisfaction rating technology, the linked work of this paper has certain reference and reference value.

## 1. Introduction

The use of smartphones and tablet computers has grown in popularity as the mobile Internet has become more popular and network costs for 4G and 5G networks have decreased, and more people are turning to the convenient and fast mobile Internet to access information. "Internet + education" has also emerged, and online education is setting off a profound revolution in learning methods. Online education gives full play to the advantages of wide network dissemination and rapid information update, realizes the sharing of learning resources, and meets the learning needs of learners anytime, anywhere. In recent years, the impact of the pandemic has further promoted the development of online education, and various online education platforms have emerged. However, online education platforms are heating up, and platform competition is escalating, but what follows is that the quality of online education platforms is

mixed. Therefore, the analysis of the service quality and user satisfaction of education platforms must be carried out on a daily basis.

How to make online education develop better and faster, benefit more people, and explore issues related to online education satisfaction are of great significance to theoretical basic research, enterprises, and users. The influencing variables of service quality, evaluation methodologies, and evaluation indicators are employed in the online education business on a theoretical foundation. Establishing a sound evaluation index system that adapts to the influencing factors of online education and measures it quantitatively can not only pique everyone's interest and stimulate thought in the field of online education service quality research, but also deepen the subdivision of this subdivision as technical conditions improve. For enterprises, if they recognize the specific influence of various factors in service quality, they can tilt their investment, accelerate the improvement of service

quality, improve user satisfaction, enhance the stickiness between users and enterprises, and increase the influence of word-of-mouth communication, which is conducive to formulating the service quality standards of the enterprise or the industry, strengthening the core competitiveness of the enterprise, and improving the industry status of the enterprise. For users, it is possible to gain more knowledge from online learning, and it is more convenient to use. Their explicit and implicit needs can be accurately met. Give full play to the high efficiency and low price of online education, and bring practical convenience to the majority of students. It saves the family's expenses on educational tuition and provides an important supplement to school education. Therefore, online education satisfaction research is a realistic topic.

With the continuous development of scientific computing methods, relevant statistical prediction researchers have turned their attention to the study of machine learning models. In the current era of Internet communication with many data dimensions and huge amounts of data, traditional mathematical statistical models are no longer sufficient to analyze and mine potential mathematical relationships and correlations between independent variables in data. Compared with other traditional statistical models, machine learning models have the following significant advantages: high accuracy, automated calculation, fast calculation speed, and custom features. Common algorithms include decision tree, Bayesian classification algorithm [1], artificial neural network [2], K nearest neighbors [3], and support vector machine [4]. Based on this, this paper establishes a user satisfaction evaluation model based on the decision tree algorithm in machine learning theory and improves the decision tree algorithm.

This research develops a machine learning-based online education satisfaction rating model, presents a decision tree-based mobile Internet satisfaction evaluation model, and enhances the decision tree algorithm. The improved method outperforms the BP neural network algorithm, Bayesian algorithm, and XGBoost algorithm in the experiments.

The paper arrangements are as follows: Section 2 describes the related work. Section 3 discusses the basic algorithms and principles. Section 4 examines the satisfaction evaluation algorithm based on decision tree. Section 5 analyzes the experiments and results. Section 6 concludes the article.

## 2. Related Work

This section discusses the research on machine learning in the field of customer satisfaction. They analyze the research on user satisfaction of online education.

*2.1. Research on Machine Learning in the Field of Customer Satisfaction.* Liu Yang conducts research on user satisfaction of telecom operators, forms experimental data sets through satisfaction attribute selection and questionnaires, uses random forest algorithm to build prediction models, and uses multi-label classification algorithm to optimize the model [5]. Liu Fan conducts research on user satisfaction in the telecommunications industry and integrates various business processes based on the prediction results of logistic

regression to obtain a prediction model of telecommunications user satisfaction [6].

Taking Jingdong Mall as the research object, Fan Miaomiao uses crawler technology to capture a large number of online customer reviews. Through word frequency analysis and topic semantic mining on the content of the reviews, combined with the logistics service satisfaction theory and LDA topic model, the logistics service satisfaction is established.

QIY and LIH have captured the stockholders' evaluations of a company's stock online, quantified the evaluation information using sentiment analysis, and used complex networks to study the conduction characteristics of stockholders' emotions [7]. Schumaker and Chen studied financial news articles through text table features and statistical machine learning and constructed a stock quantitative forecast system based on financial news [8].

Most studies collect data such as consumer behavior records, surveys, and online evaluations and use logistic regression, time series, neural network, and text mining methods to conduct factor analysis and forecast research on customer satisfaction. There is a scarcity of research on consumer satisfaction in online education compared to businesses like telecoms and e-commerce. Figure 1 show the workflow of machine learning:

*2.2. Research on User Satisfaction of Online Education.* Mei Lick Cheok and Su Luan Wong based on the review of past research on the satisfaction of using information technology system and established a theoretical model of the influencing factors of the satisfaction of online learning in middle school teachers and teaching. Three groups of potential factors affecting secondary school teacher satisfaction were identified. This study proposes a theoretical framework outlining the predictive potential of three key sets of factors for secondary school teachers' online learning satisfaction. It is believed that these factors can be considered when formulating future CPD curriculum and intervention plans and when proposing new curriculum innovations [9, 10].

Eshun and Amofa [11] used an online learning management system to determine the perceived value of multigenerational student groups' educational experiences. They discovered that the curriculum content design of students' online courses, as well as their preference for the classroom environment, resulted in varying levels of student satisfaction and concluded that based on multiple studies. The development of student groups in a contextualized online teaching model can be utilized as a tactic to increase students' learning experience and satisfaction. Kuo et al. [12] tested the student satisfaction model and tested the regression model with a hierarchical linear model, and the results showed that in terms of improving student satisfaction, the improvement of learner interaction with course content was the most promising, while in the course setting, the interaction between learners is negligible. Hsu et al. [13] applied basic psychological needs to online education courses, compared the motivational models of online learning and face-to-face learning, and concluded that whether students' needs are met has an impact on students' learning motivation and learning outcomes. Eom et al. [14] and

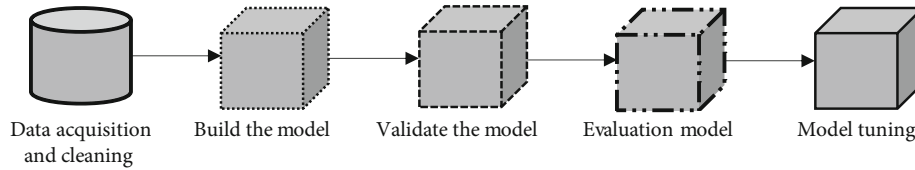


FIGURE 1: Machine learning workflow.

Harvey et al. [15] used factor analysis and structural equation modeling, respectively, to study the reasons that affect satisfaction and the effect of learning. Eom found that the most important factors affecting the satisfaction of online education platforms and students' learning effects are course design, teacher level and personality, and teacher-student interaction in the classroom; Harvey found that students' satisfaction with online education platforms is not related to the gender of users relationship and found three significant antecedents affecting male and female student satisfaction: word of mouth, facilities, and teachers. Ozyurt [16] collected data using the online education student satisfaction scale and clustered it using the Ward method in the hierarchical clustering method. Graber [17] adopted a quasi-experimental, post hoc comparison research design, using two groups of post hoc tests to compare the effectiveness of brick-and-mortar classrooms and online education in delivering knowledge to students through comprehensive grade point averages, class scores, and student satisfaction survey results. Effectiveness and student satisfaction validate the feasibility of conducting online education, as shown in Figure 2.

Xu Zheng analyzed the characteristics and essence of "Internet +" and regarded "Internet + education" as a kind of integration, which is the deployment and optimization of educational resources once again, which can reduce the entry threshold for users to learn and improve the learning effect. "Internet + education" is O2O under different conditions, with both online supplements and offline foundations. Users of online educational institutions are a special type of users, and their learning and consumption are more passive. Therefore, the teacher's responsibility is not only to simply teach and solve puzzles, but also to supervise and bring about the purpose of students' learning [18].

In the research on user satisfaction evaluation of multimedia courseware resources, Lenny conducted a questionnaire survey on users according to the four influencing factors of multimedia user satisfaction. Its influencing factors are content, interactivity, vividness, and graphic quality [19].

Fernando et al. believed that by surveying learners with distance education experience, they analyzed the influencing factors of distance education user satisfaction: the quality of resource content, the value of content, the availability of resources, and the innovation of resources [20].

The terms "digital natives" and "digital immigrants" were coined by the well-known learning software creator MP Translated (2009) and others to reflect the vast differences in digital technologies between today's individuals and their forefathers. People nowadays want to be a part of new experiences with interactivity, immediacy, virtuality,

control, and participation. These all fit perfectly with the characteristics of online education courses [21].

Jon Bergmann and Aaron Sams, according to the educational goal theory of the famous American educational psychologist Benjamin Samuel Bloom, found that although online education methods have adjusted and screened advantageous educational resources, online education can only achieve knowledge and comprehension; there is no guarantee of real outcomes of learning. Jon Bergmann and Aaron Sams then put forward a new educational model theory—Flipped Class. Its core concept is to allow learners to learn actively, participate actively, blended curriculum design and Podcasting classroom [22].

### 3. Basic Algorithms and Principles

Here, it discusses the evaluation method of satisfaction evaluation accuracy. They define the introduction to decision trees.

*3.1. Evaluation Method of Satisfaction Evaluation Accuracy.* The index characteristics of the accuracy, recall, precision, and error rate of the prediction results can usually reflect the good replacement of the model. And these indicator features can be reflected by confusion matrix [23].

Confusion matrix is to analyze the actual value of the sample and the predicted value of the model. If the actual sample is 0, it is a negative example, and if it is 1, it is a positive example. If the predicted class is wrong, it is false, and the prediction is correct, it is real. The final confusion matrix is shown in Table 1.

*3.1.1. Accuracy and Error Rate.* Accuracy refers to the probability that the model predicts correctly, and its formula is as follows:

$$Accuracy = \frac{TP + TN}{C}, \quad (1)$$

where  $C$  is the total number of samples.

Similarly, the error rate refers to the probability that the model predicts incorrectly, and its formula is as follows:

$$Error = \frac{FP + FN}{C}. \quad (2)$$

*3.1.2. Precision and Recall.* In practical applications, the accuracy and error rate alone cannot reflect the speed of the model, and customers pay different attention to the positive and negative examples of the target variable. Therefore, we must also consider precision rate.

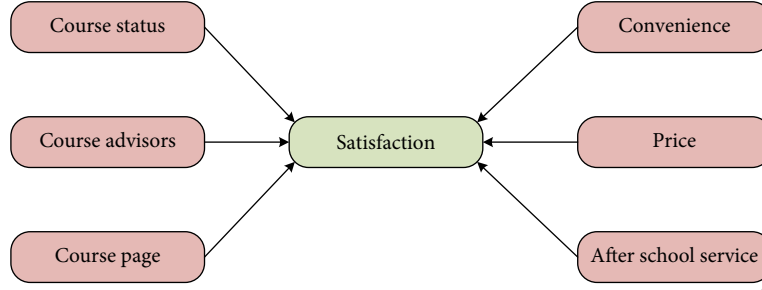


FIGURE 2: Online education user satisfaction evaluation index model.

TABLE 1: Con fusion matrix.

		True class	
		0	1
Predicted class	0	TN	FN
	1	FP	TP

Precision describes the ratio of the number of samples predicted to be positive and actually positive (TP) to the total number of samples predicted to be positive ( $TP + FP$ ) by the model, which is as follows:

$$Precision = \frac{TP}{TP + FP}. \quad (3)$$

This indicator represents the proportion of samples predicted as positive by the classifier that are actually positive.

Recall describes the ratio of the number of samples that the model predicts to be positive and are actually positive to the total number of samples that are actually positive in the test dataset, which is as follows:

$$Recall = \frac{TP}{TP + FN}. \quad (4)$$

This indicator represents the proportion of positive samples that the classifier predicts correctly, accounting for the actual positive samples. Since the positive and negative samples of the data set used in this paper are unbalanced, and the education satisfaction research will pay more attention to those “dissatisfied” user evaluation data, the evaluation criteria of the satisfaction model in this paper are mainly based on recall rate and accuracy rate, as a supplement.

**3.2. Introduction to Decision Trees.** Decision trees use tree structures to model the relationship between sample features and potential outcomes. Among them, each internal node (non-leaf node) represents a test on a feature, each branch represents an output of the test, each leaf node stores a class label, and the vertex of the tree is the root node. As shown in Figure 3, this is a sales decision tree model of a certain product, which predicts whether customers will buy a certain product according to customer characteristics. The rectangles represent the non-leaf nodes of the tree, and the ellipses represent its leaf nodes.

The decision tree processing problem is generally divided into the following two steps:

- (i) First, learn the training set to establish a decision tree classification model
- (ii) Use the established decision tree classification model to classify samples of unknown types

**3.2.1. Decision Tree Generation.** The establishment of a decision tree model is a recursive process that needs to repeatedly decompose the data into smaller subsets, and the process does not stop until the resulting subsets meet a stopping criterion. The root node represents the entire data set. At this time, there is no data decomposition. The decision tree selects a feature to decompose the data set. The first group of decisions is formed by dividing all of the data into separate subsets based on the value of the feature. Continue to decompose the data according to different feature values along each branch until the stopping condition is satisfied. If the node reaches the stop condition and no longer decomposes, the node becomes a leaf node. Each leaf node is a label, and the label is determined according to the category of the instance that is assigned to the node. The result of the decision tree model establishment is to establish a decision tree that can predict and classify unclassified samples, and its establishment process follows the idea of “divide and conquer.” The construction of a decision tree is a recursive process, and the decision tree algorithm returns recursion in three situations:

- (1) The samples contained in the nodes belong to the same category
- (2) The current attribute set is an empty set, or all samples in the node have the same value on this attribute
- (3) The current node does not contain any samples, that is, the sample set is empty

Through the learning of the data set, a tree can be established to classify unknown types of samples. When classifying a sample, first start from the top level of the decision tree, test the attributes of the sample, and judge that the sample should walk down the branch of the decision tree according to the attribute value. Each non-leaf node of the decision tree will test the data attributes until the sample reaches a leaf node of the decision tree and the classification is completed.

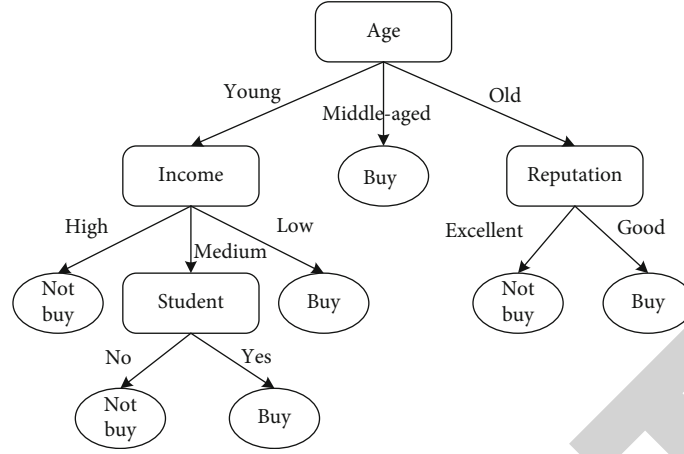


FIGURE 3: Decision tree model.

Then, the type of the sample is the type marked by the leaf node.

**3.2.2. Decision-Making Optimal Attributes Selection.** The key to the establishment of the decision tree model lies in the selection of the optimal attribute. There are many ways to choose the optimal attribute of the decision tree. The most classic ones are information entropy, information increase, and information gain rate. At the same time, these three concepts are also the cornerstone of ID3 algorithm and C4.5 algorithm. The information gain rate is the splitting index of C4.5. The main function of information entropy is to judge the purity of the sample type in the sample set, assuming the current sample set the proportion of the  $k$ th class samples in  $D$  is  $p_k (k = 1, 2, 3, \dots, |y|)$ , then the information entropy of  $D$  is expressed as

$$Ent(D) = - \sum_{k=1}^y p_k \log_2 p_k. \quad (5)$$

From Formula (5) that when the purity of sample  $D$  is higher, the value of  $Ent(D)$  is smaller, and the minimum value is 0. When the purity of  $D$  is lower, the value of  $Ent(D)$  is larger, and the maximum value is 1.

When using a decision tree algorithm to select optimal attributes, the higher the purity of the target variable, the better. Therefore, the concept of information gain is introduced to measure the effect of splitting according to attributes.

Assuming that the discrete attribute  $A$  has  $v$  possible values  $\{A_1, A_2, A_3, \dots, A_v\}$ , if the sample set  $D$  is divided by the attribute  $A$ ,  $v$  branch nodes will be generated, of which the  $v$  branch node contains all the values in the attribute  $A$  in  $D$ . The value of the sample  $A_v$  is denoted as  $D_v$ . We can calculate the information entropy of  $D_v$  according to Equation (5). Considering that the number of samples contained in different branch nodes is different, assign weights to the branch nodes  $|D_v|/|D|$ .  $D$  indicates the number of samples in the set  $D_v$ . That is, the branch node with more samples has a greater influence, so the calculation is based on the

attribute the information gain obtained by dividing the sample set  $D$  by  $A$ :

$$Gain(D, a) = Ent(D) - \sum_{v=1}^v \frac{|D_v|}{|D|} Ent(D_v). \quad (6)$$

To a certain extent, the information gain represents the purity improvement brought by classifying the sample set by attributes. That is to say, dividing the samples according to the information gain can increase the proportion of samples of the same type in the samples. As a result, the widely used ID3 method chooses partition attributes based on information gain. Of course, selecting the best attributes for a decision tree is an NP problem, and there are disadvantages to using information gain as the best attribute selection approach for samples: This method tends to choose attributes with more values as split points. To reduce this preference, the C4.5 algorithm refers to the information gain rate as a splitting index to select the optimal splitting attribute. The information gain rate is defined as

$$Gain\_ration(D, a) = \frac{Gain(D, a)}{IV(a)}, \quad (7)$$

$$IV(a) = - \sum_{v=1}^v \frac{|D_v|}{|D|} \log_2 \frac{|D_v|}{|D|}.$$

According to the different optimal attribute selection criteria, the decision tree algorithm can be divided into three types: ID3, C4.5, and CART [24]. These three decision tree algorithms have become the most classic decision tree algorithms.

#### 4. Satisfaction Evaluation Algorithm Based on Decision Tree

This paper mainly uses the decision tree algorithm to establish a satisfaction evaluation model and optimizes it according to the characteristics of the data set so that it has a good classification performance.



4.1. C 4.5 *Introduction to Algorithms*. The C4.5 decision tree algorithm has a good classification effect and visualization effect, so it is widely used. However, due to the imbalance in the number of positive and negative samples in the data set in this paper, it is not possible to directly use the traditional C4.5 decision tree algorithm for modeling. A good classification effect is achieved. The reasons are as follows:

- (1) The positive and negative samples of the data set used in this paper are extremely unbalanced. The classic C4.5 approach classifies the leaf nodes and prunes the decision tree based on the lowest error rate, biasing the decision tree's prediction result towards the data. There are numerous types. For example, the number of positive samples in a test set is 90, and the number of negative samples is 10. If the model predicts all the samples in the test set as positive samples, the accuracy of the model can also reach 90%. But this obviously does not make any sense. In real life, the cost of misjudging a sample type as another type is different. For example, predicting a cancer patient as a normal person and predicting a normal person as a cancer patient, obviously the former will cause more serious consequences. The cost of misclassification is different, and it is obviously not advisable to use the lowest error rate as the original criterion
- (2) A vast number of studies reveal that a single machine learning model's classification effect is not perfect, that it is prone to overfitting, and that its classification accuracy is limited regardless of which aspect is improved for a single learner. The model's evaluation accuracy can be improved by combining multiple models. Based on the above points, this paper mainly improves the C4.5 algorithm as follows: (1) Introduce a cost-sensitive mechanism to optimize the algorithm, and (2) use the idea of random forest integrate decision trees

#### 4.2. C 4.5 *Algorithm Optimization*

4.2.1. *Cost-Sensitive Decision Tree*. The positive and negative samples of the data set used in this paper are unbalanced. The traditional C4.5 decision tree algorithm performs leaf node labeling and model pruning optimization according to the minimum error rate, which cannot meet the requirements of satisfaction evaluation. All this paper introduces a cost-sensitive mechanism. Misclassification of different sorts of samples generates varying costs; hence, it is cost-sensitive. Cost-sensitive decision tree is an extension of decision tree learning, which optimizes the labeling and pruning of leaf nodes based on the minimum misclassification cost, rather than the traditional minimum error rate. In recent years, cost sensitivity has attracted extensive research since it was proposed in 2001 and achieved fruitful research results. Cost sensitivity has become a very effective way to solve the imbalance of sample distribution. This paper uses the cost-sensitive idea to improve the C4.5 decision tree algorithm to achieve a more accurate evaluation of mobile Internet satisfaction. The main ideas are as follows:

- (1) First, a cost-sensitive mechanism is introduced, and the minimum cost is used as the criterion when marking leaf nodes, rather than the original error rate
- (2) The construction of the decision tree is ended in advance by setting the minimum number of leaf node samples, avoiding over-fitting caused by over-refinement of the decision tree production process
- (3) This paper mainly adopts the post-pruning method to prune the decision tree, traverses each node of the decision tree in a bottom-up manner, calculates the misclassification cost of the current node, and then calculates and subtracts a certain branch. The misclassification cost before and after changes. If the pruned decision tree has a lower misclassification cost, it will be pruned, resulting in a smaller decision tree with a lower misclassification cost. Several related concepts are now introduced as follows:

*Definition 1.* Error cost matrix: Suppose that there are  $n$  kinds of classification marks in the training set  $T$ , the  $p_1, p_2, p_3, \dots, p_n$  current node is  $k$ , then define the cost loss matrix  $CM$  as

$$CM = \begin{bmatrix} 0 & \cdots & P_{1n} \\ \vdots & \ddots & \vdots \\ P_{n1} & \cdots & 0 \end{bmatrix}. \quad (8)$$

Among them, when  $i$  is not equal to  $j$ , it indicates the classification cost generated when  $p_{ij}$  the sample with the  $p_j$  actual category is judged to be a category  $p_i$ . When  $i = j$ , it indicates that the current node is correctly classified, and there is no misclassification cost, so it is 0. In leaf node labeling algorithm, the decision tree algorithm will return recursion in three cases:

- (1) The samples contained in the nodes belong to the same category
- (2) The current attribute set is an empty set, or all samples in the node have the same value on this attribute
- (3) The current node does not contain any samples, that is, the sample set is empty

*Definition 2.* Node misclassification cost: Assuming that the training set is  $T$ , there are  $m$  types in a node of the generated decision tree, and their category flags are, respectively,  $p_1, p_2, p_3, p_4, \dots, p_m$ , and the number of samples in each category is  $n_1, n_2, n_3, \dots, n_m$ . Assuming that the type of decision tree marked for the current node is  $p_i$ , the misclassification cost (CL) of its node is defined as

$$CL = \sum_{k=1}^m n_k * p_{ki}. \quad (9)$$

In order to prevent overfitting caused by too many branches of the decision tree, this paper adds a recursive

return condition, that is, to set the minimum number of leaf node samples  $\text{min\_Num}$ , when the sample contained in the current node is less than  $\text{min\_Num}$ , the recursion ends, and the node is marked as a leaf node. The labeled class is the class with the least classification cost.

In decision tree pruning, the traditional post-pruning method is to first generate a complete tree from the training set and then judge whether to prune according to the lowest classification error rate. If the error rate after pruning is lower than the error rate before pruning, this subtree is replaced with a leaf node, and the type of the node is marked as the type with the most samples. Pruning is not done if the mistake rate after pruning is higher than the error rate before pruning. The typical pruning method ignores the various costs associated with various types of misclassification. This paper improves the traditional pruning algorithm by considering the cost of various types of misclassification.

The specific pruning process is as follows: starting from the leaf node of the decision tree, each inner node of each layer is judged from bottom to top.

Step 1: Calculate the misclassification cost of each subtree node that may be pruned according to Formula (1)

Step 2: Calculate the misclassification cost of the subtree if it is not pruned according to Formula (2)

Step 3: Compare the misclassification cost of the subtree with the misclassification cost after the subtree is pruned and marked as a leaf node. If the former is greater than the latter, the subtree is turned into a leaf node, and the node is marked according to the minimum misclassification cost

Step 4: Repeat the above process until continuing pruning will increase the misclassification cost

The decision tree pruning can not only generate a decision tree with smaller scale and better generalization performance, but also can increase the number of classification of minority class samples by introducing the idea of cost sensitivity.

**4.2.2. Ensemble Method Based on Random Forest.** Many studies have proven that a single learner can no longer match people's categorization criteria, necessitating the use of numerous classifiers to create a high-performance combination model, or ensemble learning approach. Figure 4 depicts the overall architecture of ensemble learning. The integration method in this paper adopts the idea of random forest to integrate the optimized decision tree generated by training.

Random forest is a variant [25], which mainly introduces random attribute selection on the basis of bagging ensemble. The basic idea of random forest is as follows: First, use the bootstrap sampling method to extract  $k$  sample sets from the original data set, and then establish  $k$  decision tree models for these  $k$  sample sets, respectively. Because random forests introduce random attribute selection, for each node of each decision tree, first randomly select a subset of the attributes from the node's attribute set as an attribute subset, and then partition the subset into optimal attributes. In the

final prediction, the prediction results of the  $k$  decision trees are integrated by voting. The main idea of random forest is shown in Figure 5.

The data set used in this paper has the problem of imbalance of positive and negative samples. Although a cost-sensitive mechanism is introduced in Section 4.2.2, due to the large gap between positive and negative sample data, the corresponding value in the corresponding cost matrix is misclassified. It will also be very vast, resulting in a high error rate and a lot of unpredictability, even though the cost-sensitive decision tree can classify rare class samples well. Furthermore, the data set in this paper is very large. If the model is trained on the original data set, the time efficiency will be very low. Therefore, before generating the cost-sensitive decision tree, this paper uses the sampling method to reduce the positive and negative ratio of the training samples. The specific implementation is as follows: random forest for random sampling of datasets, the data which are first divided into large class datasets and rare class datasets by type. Then, random sampling is performed on the large class dataset and rare class dataset respectively. Then, the randomly sampled sets are combined into a decision tree training set, as shown in Figure 6. The steps of the random forest ensemble method in this paper are as follows:

Step 1: Input the sample set  $D$ , and divide the sample set  $D$  into large class sample sets  $D_1$  and rare class sample sets  $D_2$

Step 2: Perform random sampling with replacement in  $D_1'$  proportion to the large sample set to generate a new sample set. Perform random sampling with replacement  $P_1$  in proportion to the rare sample set to  $P_2$  generate a new sample set  $D_2'$

Step 3: Combine the sample set  $D_1'$  and  $D_2'$ , and combine the decision tree training set

Step 4: If the sample data contains  $n$  attribute values, then the decision tree randomly selects  $m$  attributes ( $m < n$ ) during node splitting and selects the optimal attribute for division on this  $m$  attributes

Step 5: Repeat Steps 2–4 to generate  $k$  decision trees

Step 6: Summarize the classification results of the  $k$  decision trees. The way of summarizing is to use the method of "majority voting" to determine the final classification result

## 5. Experiments and Results

This section examines the integrated learning. They analyze the comparison of other algorithms.

**5.1. Integrated Learning.** In this paper, the ensemble learning adopts the idea of random forest to integrate the decision tree model. The steps are when randomly sampling the data

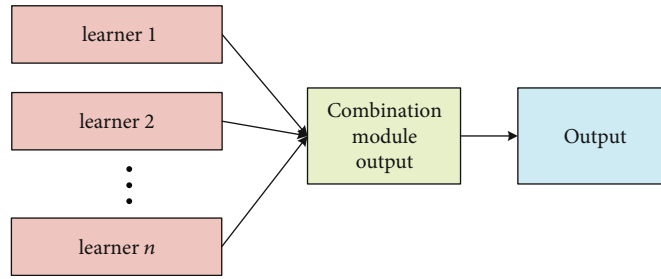


FIGURE 4: Ensemble learning model.

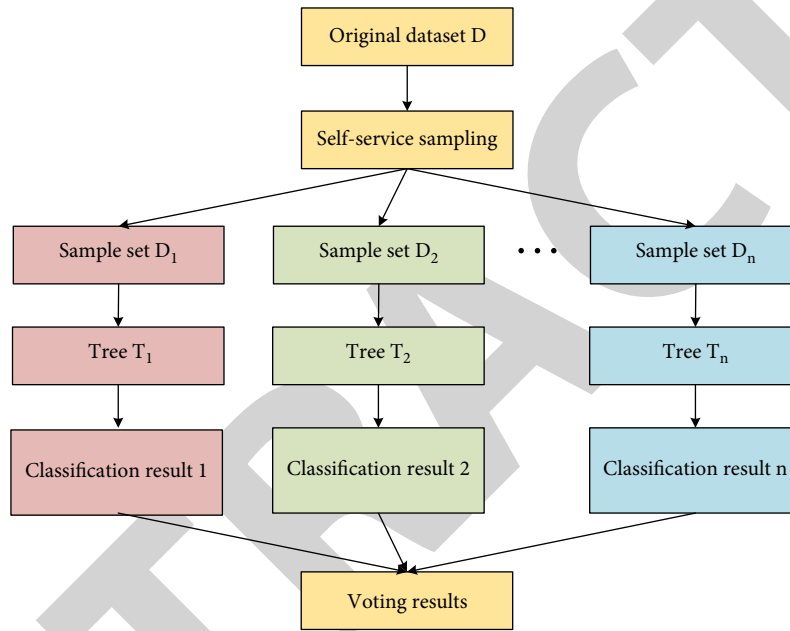


FIGURE 5: Random forest algorithm model.

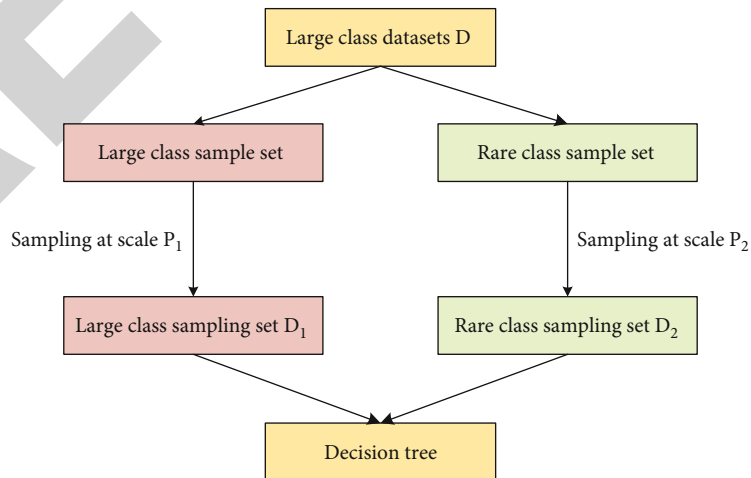


FIGURE 6: Sampling.

TABLE 2: Algorithm performance comparison.

	C4.5		Cost-sensitive decision tree		Random forest	
	Accuracy	Recall	Accuracy	Recall	Accuracy	Recall
1	0.9637	0.3118	0.8110	0.6058	0.9011	0.7158
2	0.9642	0.3574	0.7522	0.7623	0.8322	0.7521
3	0.9634	0.3234	0.7942	0.7221	0.8042	0.7408
4	0.9637	0.3834	0.7866	0.7208	0.7966	0.7565
5	0.9642	0.3534	0.8366	0.6765	0.8409	0.7508
6	0.9634	0.3334	0.8166	0.7008	0.8242	0.7367
7	0.9637	0.3634	0.7966	0.6901	0.8342	0.7408
8	0.9642	0.3834	0.7966	0.7208	0.8366	0.7208
9	0.9634	0.3334	0.8266	0.6208	0.8766	0.7308
10	0.9615	0.3234	0.8166	0.7108	0.8205	0.7367
Average value	0.9635	0.3466	0.8225	0.6931	0.8205	0.7367
Standard deviation	0.000789	0.02406	0.04314	0.04547	0.01653	0.0134

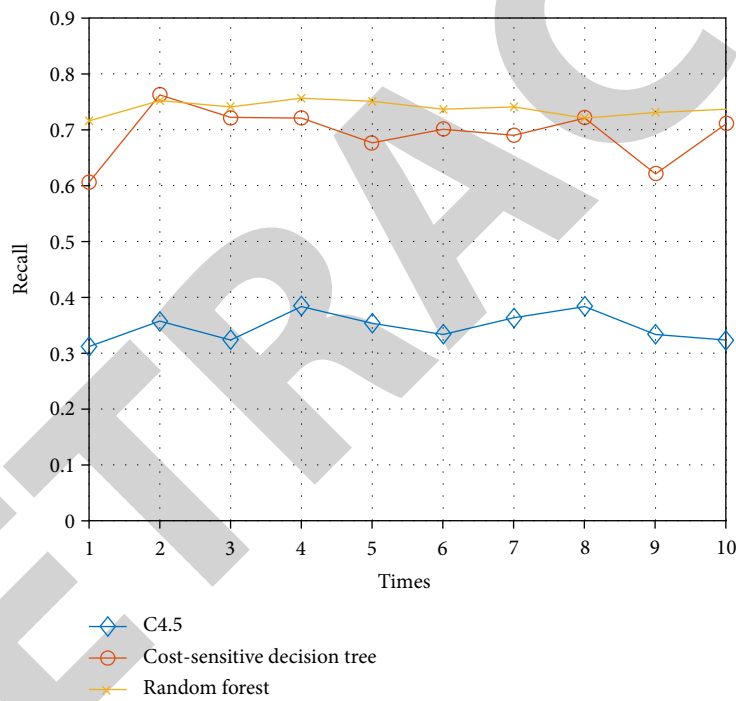


FIGURE 7: Recall comparison.

set, first divide the data into large-class data sets and rare-class data sets by type, and then separate the large-class samples. Sets and rare class samples are sampled, and finally the sampled data sets are combined for decision tree training.

In the experiment, the ratio of positive and negative samples in the training set of a decision tree is 20:1, and the number of experiments is 10 times. The performance comparison of each algorithm is shown in Table 2. Figure 7 shows the recall comparison between algorithms, and Figure 8 shows the accuracy comparison between algorithms.

From Table 2 that the cost-sensitive decision tree can greatly improve the recall rate of the model, but the range of its accuracy and recall rate fluctuates greatly. After the

decision tree model integrates the classification results based on the random forest method, although the recall rate cannot be significantly improved, the accuracy and recall rate fluctuate less. Therefore, using the random forest method to integrate the decision tree model can not only improve the accuracy of the model, but also increase the stability of the model.

*5.2. Comparison of Other Algorithms.* Finally, in order to verify the performance of the algorithm in this paper, compared with other mainstream classification learners, other algorithms are used: BP neural network algorithm, Elman neural network algorithm, mlp multilayer perceptron, naive Bayes, XGBoost algorithm.

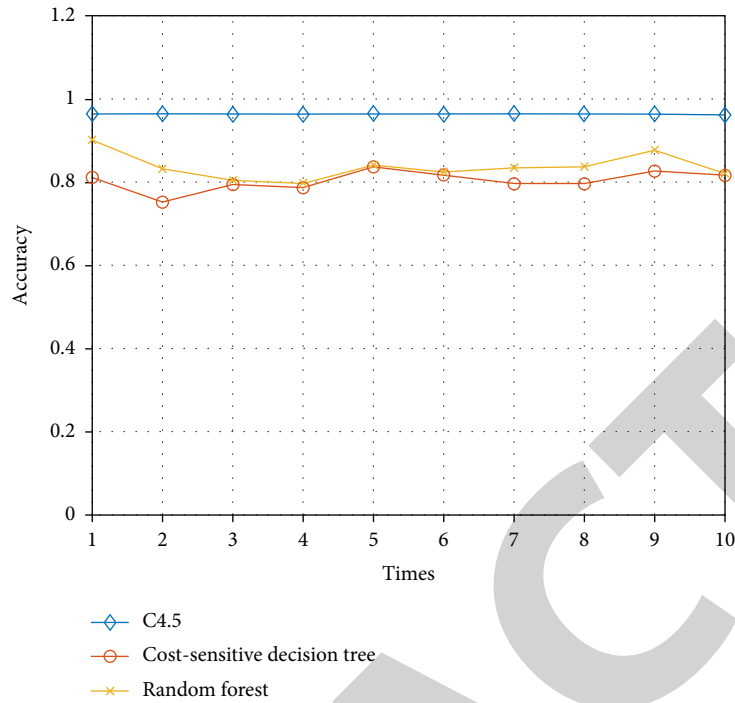


FIGURE 8: Accuracy comparison.

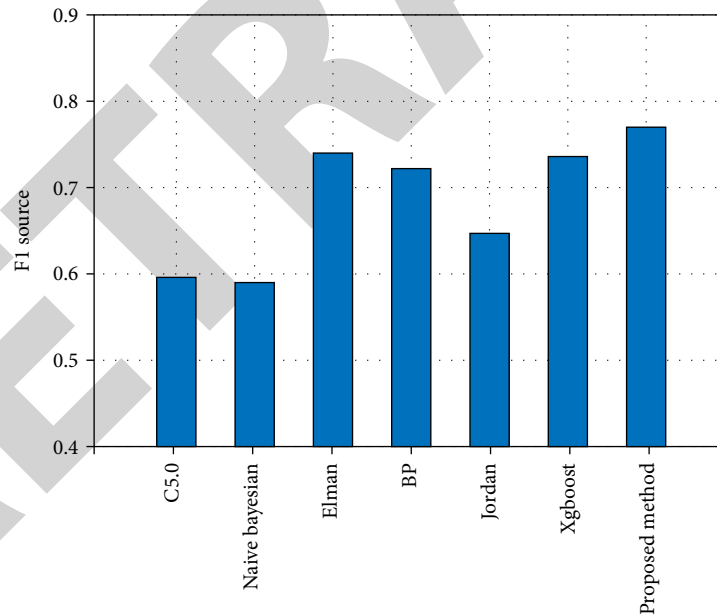


FIGURE 9: Compare with other algorithms.

The algorithm optimized in this study does not have the best accuracy or recall when compared to other algorithms, but it does have the highest F1 source, as seen in Figure 9. That is to say, this paper introduces cost-sensitive ideas to improve the algorithm, which can more accurately find customers who evaluate the mobile Internet as “dissatisfied”. The model has better classification performance.

## 6. Conclusion

The traditional education sector has been greatly influenced by the online education industry. With the rapid advancement of Internet and mobile terminal technologies, the online education market has seen the introduction of more and better course items. The cost of instruction is lower,

## Retraction

# Retracted: Application of Sandplay Therapy in the Mental Health Education of Vocational College Students

### Computational and Mathematical Methods in Medicine

Received 25 July 2023; Accepted 25 July 2023; Published 26 July 2023

Copyright © 2023 Computational and Mathematical Methods in Medicine. This is an open access article distributed under the Creative Commons Attribution License, which permits unrestricted use, distribution, and reproduction in any medium, provided the original work is properly cited.

This article has been retracted by Hindawi following an investigation undertaken by the publisher [1]. This investigation has uncovered evidence of one or more of the following indicators of systematic manipulation of the publication process:

- (1) Discrepancies in scope
- (2) Discrepancies in the description of the research reported
- (3) Discrepancies between the availability of data and the research described
- (4) Inappropriate citations
- (5) Incoherent, meaningless and/or irrelevant content included in the article
- (6) Peer-review manipulation

The presence of these indicators undermines our confidence in the integrity of the article's content and we cannot, therefore, vouch for its reliability. Please note that this notice is intended solely to alert readers that the content of this article is unreliable. We have not investigated whether authors were aware of or involved in the systematic manipulation of the publication process.

In addition, our investigation has also shown that one or more of the following human-subject reporting requirements has not been met in this article: ethical approval by an Institutional Review Board (IRB) committee or equivalent, patient/participant consent to participate, and/or agreement to publish patient/participant details (where relevant).

Wiley and Hindawi regrets that the usual quality checks did not identify these issues before publication and have since put additional measures in place to safeguard research integrity.

We wish to credit our own Research Integrity and Research Publishing teams and anonymous and named external researchers and research integrity experts for contributing to this investigation.

The corresponding author, as the representative of all authors, has been given the opportunity to register their agreement or disagreement to this retraction. We have kept a record of any response received.

### References

- [1] X. Xu, Y. Zhang, and L. Liu, "Application of Sandplay Therapy in the Mental Health Education of Vocational College Students," *Computational and Mathematical Methods in Medicine*, vol. 2022, Article ID 6141326, 5 pages, 2022.

## Research Article

# Application of Sandplay Therapy in the Mental Health Education of Vocational College Students

Xiaojing Xu , Yanhua Zhang, and Libin Liu

Shaanxi Business College, China

Correspondence should be addressed to Xiaojing Xu; [xuxiaojing202012@163.com](mailto:xuxiaojing202012@163.com)

Received 7 April 2022; Revised 28 May 2022; Accepted 16 June 2022; Published 29 June 2022

Academic Editor: Naeem Jan

Copyright © 2022 Xiaojing Xu et al. This is an open access article distributed under the Creative Commons Attribution License, which permits unrestricted use, distribution, and reproduction in any medium, provided the original work is properly cited.

**Objective.** To analyze the application and effect of sandplay therapy in higher vocational students' mental health. **Method.** 350 sophomores of 2019 in a higher vocational college were randomly selected, and 72 subjects of depressed students ( $SAS \geq 50$ ) were selected from 350 sophomores and randomly divided into the intervention group and the control group, each group 9, preparing one set of chamber equipment, adopting the same group before and after test experiment design. The intervention group was, respectively, given 8 individual box court game tutoring, once a week for each person. The control group did not intervene. By comparing the intervention group with the control group, the intervention effect of sandplay therapy on anxiety of experimental group members was investigated. **Results.** Among 350 respondents, 72 had SAS scores  $\geq 50$ , and the incidence of anxiety symptoms was 20.57%. Since there was only 1 case with SAS score  $\geq 70$ , it was incorporated into the group with SAS score ranging from 60 to 59. After treatment, SAS scores of students with mild to moderate anxiety in the intervention group decreased, and the difference was statistically significant. The difference before and after control group was not statistically significant. After sandplay therapy, the differences in SAS scores between the intervention group and the control group were found to be statistically significant for both mild and moderate anxiety. **Conclusion.** Sandplay therapy in the higher vocational college students' mental health education could promote the mental health of students, and it effectively improves students' psychological quality.

## 1. Introduction

With the changes of learning pressure and social environment in colleges and universities, the psychological diseases of college students show an increasing trend (depression, anxiety disorder, bipolar disorder, etc.) [1, 2]. Sandplay therapy is a kind of psychotherapy in which an individual, accompanied by the therapist, selects toys from the toy shelf freely and performs self-expression in a special box filled with fine sand [3]. In 1954, combining Jung's analytical psychology and projection techniques, Dore M. Kalf developed Lowenfeld's "The World Technique," it was introduced to Japan by a Japanese clinical psychologist, and Zhang Risheng introduced it to China in 1998 [4]. Sandplay therapy creates "free and protected spaces" through sand, water, and toys, providing visitors with the possibility of expressing unintentional processes [5]. The visitors solve their personality problem on this basis, and the symptoms

are also eliminated [6], thereby improving or eliminating psychological disorders such as anxiety and depression [7]. The sandplay therapy itself is nonverbal and nondirective. The client expresses his emotions in the chamber consciously or unconsciously. In the face of the sandplay works created by himself, through sharing and analysis with the therapist, the visitor will have awareness of his own cognition and emotions, so as to improve or eliminate his anxiety, depression, and other psychological disorders [8, 9]. At the initial stage of group sandplay therapy intervention, trauma themes such as division and hostility often appear. After the implementation of group sandplay therapy intervention, the sensitivity level of students' interpersonal relationship has decreased significantly, and their personal sense of discomfort and inferiority have improved. Group sandplay therapy shows a certain curative effect. Sandplay therapy is one of the important methods of emotional management education [10, 11]. Sandplay therapy can help

college students find their own problems, rebuild their cognition, and vent their emotions [12]. The mental health education of higher vocational students is of particularity. Its treatment targets are mainly growing and developing college students. Most of their psychological problems are developmental problems. Therefore, sandplay therapy can be used in college mental health education. This study selected 350 sophomore depressed students from our school to conduct a sandplay analysis.

## 2. Materials and Methods

*2.1. Research Object.* 350 sophomores of 2019 in a higher vocational college were randomly selected, and 72 subjects of depressed students ( $SAS \geq 50$ ) were selected from 350. Among them, there were 40 girls and 32 boys, aged from 20 to 22 years. The average age of the subjects was 21.24 years. The subjects were randomly divided into the intervention group and control group, each group 9. Basic information of research object is shown in Table 1:

### 2.2. Methods

*2.2.1. Equipment Preparation.* One set of box court equipment includes (1) 1 sandplay sandbox, (2) 2 toy racks, (3) about 1,000 toys, (4) one digital camera used for taking pictures in the gallery, and (5) forms recording relevant data and psychological support teachers for record the characteristics of the works and the process of the works.

*2.2.2. Testing Process.* All students completed the SAS scale before and after sandplay therapy, once a week per person. The control group did not intervene. By comparing the intervention group with the control group, the intervention effect of sandplay therapy on anxiety of the experimental group members was investigated. The specific experimental process is shown in Figure 1:

- (1) Preimplementation test: SAS (self-rating anxiety scale) [13] was used to screen the subjects (according to the diagnostic criteria of the self-rating anxiety scale in the behavioral medicine scale manual, the standard score of the self-rating anxiety scale  $\geq 50$  was taken as the standard for the diagnosis of anxiety disorders)
- (2) Sandplay intervention: choose a suitable venue, equipped with professional psychological instructors, test the students according to the norms of sand table play therapy, and record the relevant data of the test. The specific implementation process of sandplay therapy is shown in Figure 2:

- (i) Choosing dry or wet sand: guiding: "Please choose dry sand or wet sand. The wet sand ratio is easier to accumulate, but it is harder and cooler. And the dry sand is softer, but less likely to build up. You can choose any kind of sand"

- (ii) Feeling sand guiding: "Close eyes and adjust breathing, feel the texture and the temperature of the sand with your hands, Feel what the sand says and let your imagination fly"
- (iii) Sandplay works: guiding: "Please put these toys in the sandbox and do whatever you want." The subjects created freely. In this process, the subjects were not allowed to communicate with each other to avoid understanding each other's intentions, but the subjects could simply interact with the psychological teacher. Psychological teachers make simple records. If subjects do not take the initiative to communicate with psychological teachers, psychological teachers do not take the initiative to communicate with subjects
- (iv) Appreciating and experiencing works: guiding: "This is your own world, please experience the feelings this world brings to you."
- (v) Understanding and dialogue: having a dialogue about sandplay works, understanding the theme, content, and information about the mental state of the visitor. The last producer in the last round could have a modification opportunity, and after the production is finished. He could make some adjustments to the whole work, but he could not put toys. After the above operations, the team members and the team leader sat around the sandplay, told each other's intentions and feelings in combination with the order in which the toys were placed, and conducted an in-depth discussions. The discussion extended to the individual level. Finally, the group members jointly propositioned the sandplay works
- (vi) Photo record: the healer would take photos and record the box court works from different angles from directly below, left and right. And ask any subject in the group to choose any angle to take partial or overall photos of the work. It was up to the visitor to decide whether to demolish the work by himself or with the consultant
- (3) Implement posttesting: immediately after completion, the intervention group and the control group were given SAS, and the intervention group members were asked to fill in the self-reflection questionnaire
- (4) Follow-up visit: one month after the end, contact the two groups of testers and perform the SAS test again

*2.3. Observation Index.* SAS included 20 entries, each item was equivalent to a related symptom and was scored on a scale of 1 to 4. Among them, forward scoring questions were counted as 1, 2, 3, and 4 points. Reverse scoring questions were scored according to 4, 3, 2, and 1. Among them 5, 9, 13, 17, and 19 were entitled reverse in foreword score. The scoring standard was  $<50$ , indicating no anxiety. A standard



TABLE 1: Basic information of research object.

Groups	Gender		$\chi^2$	$P$	Age ( $x \pm s$ )	$\chi^2$	$P$
	Male	Female					
Intervention group	12	24	2.145	>0.05	19.02 $\pm$ 0.39	1.251	>0.05
Control group	20	16			19.12 $\pm$ 0.28		

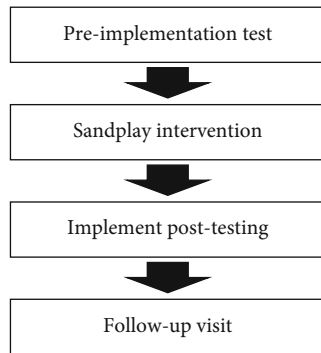


FIGURE 1: Experimental process.

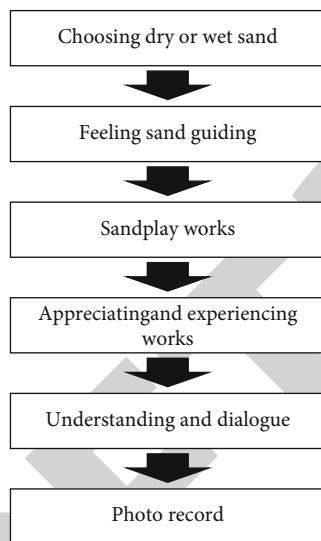


FIGURE 2: The implementation process of sandplay therapy.

score  $\geq 50$  and  $<59$  was classified as mild anxiety. Standard score  $\geq 60$  and  $<69$  was classified as moderate anxiety. A standard score greater than or equal to 70 indicates severe anxiety.

2.4. *Statistical Method.* SPSS 13.0 software was used for descriptive analysis and  $t$  test of the survey data.

### 3. Results

3.1. *Anxiety Detection Rate.* Among 350 vocational college students, 350 questionnaires had been recovered, and 336 were valid. The qualified rate of questionnaires was 96.00%. Among the 336 valid questionnaire respondents, 72 had SAS scores  $\geq 50$ , and the incidence of anxiety symptoms was

TABLE 2: Anxiety detection rate.

Groups	Intervention group	Control group
Gender		
Male	12	20
Female	24	16
SAS (50~59)		
Students ( $n$ )		48
Rate (%)		66.67
SAS (60~69)		
Students ( $n$ )		20
Rate (%)		27.78
SAS (>70)		
Students ( $n$ )		4
Rate (%)		5.55

25.00%. The incidence was 20.00% (34/170) for male students and 22.89% (38/166) for female students, with no statistically significant difference between the sexes ( $P > 0.05$ ). Anxiety detection rate is shown in Table 2:

3.2. *Effects of Sandplay Therapy.* Since there was only 1 case with SAS score  $\geq 70$ . It has been incorporated into the group with SAS score ranging from 60 to 59. After treatment, SAS scores of mild to moderate anxiety students in the intervention group decreased, and the difference was statistically significant. The difference before and after control group was not statistically significant. After sandplay therapy, the differences in SAS scores between the intervention group and the control group were found to be statistically significant for both mild and moderate anxiety. Comparison of SAS scores of the two groups before and after treatment is shown in Table 3:

### 4. Discussion

Mental health affects the life and study of higher vocational students. However, mental diseases have no obvious signs, so they are hidden and difficult to find. In addition, most vocational college students with mental diseases are unwilling to tell their parents and teachers, so colleges and families should pay attention to the mental health of vocational college students [14]. Sandplay therapy is an effective method to improve college students' unhealthy mental states, such as interpersonal maladjustment, anxiety, and attention deficits. Group sandplay therapy takes the group as the activity unit, and sandplay therapy in the group situation can promote interpersonal interaction, which has been proved to be effective [15]. Students in vocational colleges are in adolescence, and their physiological development has been basically mature, but their psychology is still immature, their ideas are also in the social survival of the fittest, and fair competition is constantly being tempered and tempered

TABLE 3: Comparison of SAS scores of the two groups before and after treatment.

SAS	Phase	Intervention group	Control group	<i>t</i>	<i>P</i>
50-59	Before treatment	55.35 ± 4.36	55.14 ± 4.28	1.80	>0.05
	After treatment	50.23 ± 5.47	54.87 ± 4.45	3.75	<0.05
60~69 and ≥70	Before treatment	64.86 ± 5.15	66.18 ± 5.06	1.68	>0.05
	After treatment	62.08 ± 6.32	65.75 ± 5.62	4.01	<0.05

[16]. Due to the lack of a complete and rational understanding of the society in the process of ideological growth of vocational college students, it is inevitable for vocational college students to have anxiety in the positive, confused, wait-and-see, and even negative and dispirited psychology. The faster the social change, the stronger the anxiety [17]. The quantitative and qualitative results of group integrated sand table play therapy are analyzed by using the dynamic Jiugongge analysis technology of sand table works, which proves that group integrated sand table play therapy has certain applicability and effectiveness in improving the self-identity of higher vocational students [18]. Group sandplay games refer to group members building sand tables in a common sandbox. The creation process needs to be based on certain principles and during the entire placement process. Team members are not allowed to communicate and interact in any form and play alone [19]. Group sandplay games can provide higher vocational students with a creative and free psychological space full of support from group members and help them relieve pressure [20, 21]. The context and form of the game itself can help vocational students to vent their internal psychological conflicts and psychological pressures. The projection of the sandplay table can help vocational students to understand themselves more comprehensively [22, 23]. After the tester completes the sandplay work creation, the psychological teachers should communicate with the tester. Psychological teachers should understand and record the inner world of the test taker, so as to prepare for the analysis of the psychological status of the test taker and the follow-up after the test [24, 25]. For example, when the tester places sand tools in the courtyard, the psychological teachers analyze the image on the right side and may reflect that the external world who pursues is practical and shared [26]. It is also very important for higher vocational students to follow up after receiving sandplay therapy. Schools can organize full-time teachers to carry out work to maintain the sustainability of the effect of sandplay therapy [27, 28]. Related theoretical and practical research explored the effectiveness of sandplay therapy as a psychological counseling model in colleges and universities and also verified the role of sandplay therapy in college mental health education [29, 30].

## 5. Conclusion

Research in this paper showed that among 350 subjects, 72 had SAS scores  $\geq 50$ , and the subjects with anxiety symptoms accounted for 20.57% of the total sample. Since there was only 1 case with SAS score  $\geq 70$ , it was incorporated into

the group with SAS score ranging from 60 to 59. After treatment, SAS scores of students with mild to moderate anxiety in the intervention group decreased, and the difference was statistically significant. The difference before and after control group was not statistically significant. After sandplay therapy, the differences in SAS scores between the intervention group and the control group were found to be statistically significant for both mild and moderate anxiety.

According to the summary, the sandplay therapy is effective in promoting the mental health of college students and optimizing the mental health of college students. However, college students' mental health support should be a multi-channel positive behavior, including family and school. The methods of mental health support should also be diversified. Colleges and mental health teachers should pay attention to adopting personalized methods of mental health support according to the special circumstances of college students.

## Data Availability

The data used to support the findings of this study are included within the article.

## Conflicts of Interest

The authors declare that there are no conflicts of interest regarding the publication of this paper.

## References

- [1] H. Qiuyue, M. Yidan, and W. Li, "A review of the research on the public stigma of college students' mental diseases in China," *Psychological Monthly*, vol. 17, no. 3, pp. 234–237, 2022.
- [2] L. Xuanying and X. Dan, "On the countermeasures of common psychological problems and the treatment of psychological diseases of college students," *Agricultural network information*, vol. 4, pp. 124–127, 2017.
- [3] S. Yuan, L. Yuxia, and Y. Jun, "Chinese name, definition and interpretation of sandplay therapy," *Psychological Monthly*, vol. 17, no. 1, pp. 230–233, 2022.
- [4] K. R. Choi, "A case study of bibliodrama in individual counseling with a sand play therapy," *Korean Journal of Christian Counseling*, vol. 29, no. 4, pp. 147–174, 2018.
- [5] K. Doyle and L. E. Magor-Blatch, "'Even adults need to play': sandplay therapy with an adult survivor of childhood abuse," *International Journal of Play Therapy*, vol. 26, no. 1, pp. 12–22, 2017.

## Retraction

# Retracted: UAV Communication Network Modeling and Energy Consumption Optimization Based on Routing Algorithm

### Computational and Mathematical Methods in Medicine

Received 1 August 2023; Accepted 1 August 2023; Published 2 August 2023

Copyright © 2023 Computational and Mathematical Methods in Medicine. This is an open access article distributed under the Creative Commons Attribution License, which permits unrestricted use, distribution, and reproduction in any medium, provided the original work is properly cited.

This article has been retracted by Hindawi following an investigation undertaken by the publisher [1]. This investigation has uncovered evidence of one or more of the following indicators of systematic manipulation of the publication process:

- (1) Discrepancies in scope
- (2) Discrepancies in the description of the research reported
- (3) Discrepancies between the availability of data and the research described
- (4) Inappropriate citations
- (5) Incoherent, meaningless and/or irrelevant content included in the article
- (6) Peer-review manipulation

The presence of these indicators undermines our confidence in the integrity of the article's content and we cannot, therefore, vouch for its reliability. Please note that this notice is intended solely to alert readers that the content of this article is unreliable. We have not investigated whether authors were aware of or involved in the systematic manipulation of the publication process.

Wiley and Hindawi regrets that the usual quality checks did not identify these issues before publication and have since put additional measures in place to safeguard research integrity.

We wish to credit our own Research Integrity and Research Publishing teams and anonymous and named external researchers and research integrity experts for contributing to this investigation.

The corresponding author, as the representative of all authors, has been given the opportunity to register their agreement or disagreement to this retraction. We have kept a record of any response received.

### References

- [1] R. Zhuo, S. Song, and Y. Xu, "UAV Communication Network Modeling and Energy Consumption Optimization Based on Routing Algorithm," *Computational and Mathematical Methods in Medicine*, vol. 2022, Article ID 4782850, 10 pages, 2022.

## Research Article

# UAV Communication Network Modeling and Energy Consumption Optimization Based on Routing Algorithm

Ran Zhuo<sup>1</sup>, Shiqian Song<sup>2</sup>, and Yejun Xu<sup>2</sup>

<sup>1</sup>Fundamental Experimental Teaching Department, Nanjing University of Aeronautics and Astronautics, Nanjing, 211100 Jiangsu, China

<sup>2</sup>Yangzhou Marine Electronic Instruments Institute, Yangzhou, 225101 Jiangsu, China

Correspondence should be addressed to Ran Zhuo; [zhuoran@nuaa.edu.cn](mailto:zhuoran@nuaa.edu.cn)

Received 27 April 2022; Revised 24 May 2022; Accepted 27 May 2022; Published 28 June 2022

Academic Editor: Naeem Jan

Copyright © 2022 Ran Zhuo et al. This is an open access article distributed under the Creative Commons Attribution License, which permits unrestricted use, distribution, and reproduction in any medium, provided the original work is properly cited.

Topological information is provided, and research on the design of routing protocols for UAV self-assembling networks is conducted, in order to enable fleet communication transfer between UAVs and UAVs and enhance their communication transmission rate in the self-assembling network. A new routing protocol is proposed through greedy forwarding and peripheral forwarding of UAV self-assembling network communication data, UAV self-assembling network planarization processing, dynamic adjustment of routing mode based on topological information, and routing protocol decision content generation. The proposed network is described using stochastic geometry theory, with the UAV and building locations modeled as two independently distributed Poisson point processes and the building shape modeled as a rectangular body with height obeying the Rayleigh distribution. An estimated equation for typical user coverage is produced using this model. The simulation results show that the approximate expression matches with the simulation results with reduced computational complexity, which verifies the validity of the approximate analysis. By comparing it with the clustering-based routing protocol, it is concluded that the new routing protocol conditions for UAV self-assembly network can realize the communication transmission between UAVs and drones and further promote their communication transmission rate.

## 1. Introduction

The existing unmanned aerial vehicle (UAV) autonomous network is generated on the basis of Ad network, which can realize the centerless and self-organized communication transmission method without relying on ground communication equipment in practical applications. However, this network structure has no central node in the process of communication transmission, so each communication node is able to join and leave the network freely, which makes the communication capability of the UAV itself reduce and has the problem of drastic changes in network topology. Both for the security of communication data information and for the operation of the UAV itself, there is a certain negative impact. Therefore, to address this problem, this paper carries out research on the design of UAV self-assembling network routing protocols based on the introduction of topology information technology [1–3].

Based on the topological information of UAV self-assembling network routing protocol design, UAV self-assembling network communication data greedy forwarding, and peripheral forwarding according to the communication transmission between UAV and UAV swarm, the communication data forwarding mode should be designed according to the actual situation, combined with the spatial characteristics of UAV in the process of operation; two forwarding modes are designed from two aspects, namely, greedy forwarding and peripheral forwarding [4–6]. The first one is greedy forwarding: in the UAV self-organizing network structure, the neighboring transmission node with the smallest spatial linear distance between the local neighbor table and the transmission target node is selected from the transmission node as the next data delivery node, and the node is also taken as the core node in the routing protocol. The overall flow diagram of greedy forwarding is shown in Figure 1.

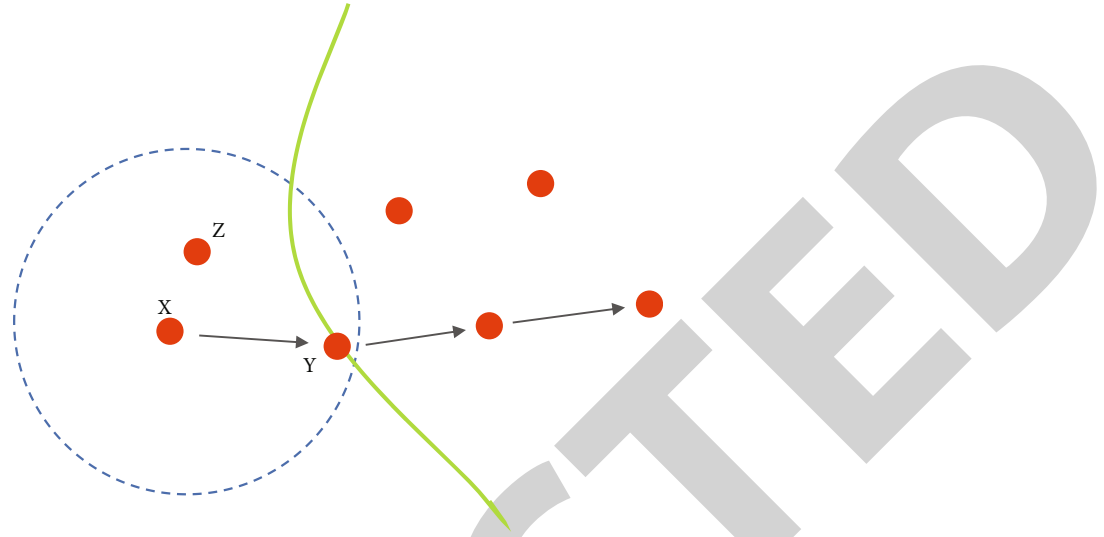


FIGURE 1: UAV self-organizing network communication data forwarding process diagram.

Combined with the content shown in Figure 1,  $X$  is taken as the data packet that needs to be transmitted for communication, the dashed circle in Figure 1 indicates the communication coverage of UAV A, and the solid arc indicates the arc with a point  $D$  of the communication coverage of another UAV B as the center of the circle and the line segment  $d(D, Y)$  as the diameter [7]. When packet  $X$  receives the data that needs to be transmitted, then the lowest distance can be selected by means of a straight-line distance calculation between  $Y$  and  $D$ , and the node corresponding to the shortest distance can be used as the next greedy forwarding node. Combined with the forwarding process discussed above, the delivery of packets is completed. In practical applications, greedy forwarding only needs to obtain the spatial geographic information of neighboring UAVs to achieve the selection of communication transmission paths. The second type is peripheral forwarding: this forwarding method is applicable to the forwarding needs that are smaller than the straight-line distance between each node in the above greedy forwarding, so it can be regarded as a way of in-place forwarding. When the distance of communication data transmission is insufficient, the packets will encounter routing hole problem during transmission and thus cannot be carried out according to the above greedy forwarding method [8–10]. A right-hand rule for perimeter forwarding is established to prevent routing holes when UAVs are sent in a self-organizing network, and a sequence of traversal operations is completed in a clockwise direction, forming a polygon region in the process. In the process of transmission, the source node gives a decision based on the routing information in the neighbor table and completes the next communication packet forwarding. When the next node receives the packet, the above operation is repeated to find the best next transmission node and so on until the packet is transmitted to the UAV destination node to realize the forwarding of UAV packets in the self-organizing network [10].

UAV self-organizing network is one of the typical applications of mobile self-organizing network in UAV field. With the characteristics of self-organization, mobility, topological dynamics, and high destructive resistance, UAV self-organizing network has a wide range of applications in both military and civilian fields, such as geological survey, rescue and disaster relief, regional reconnaissance, and unmanned cluster cooperative operations. The topology of UAV self-organizing networks is mainly divided into flat network structure and hierarchical network structure, and the hierarchical network structure is more suitable for UAV self-organizing networks of medium scale and above. In the hierarchical network structure, the network nodes are divided into several clusters, and each cluster has a cluster head node and several cluster member nodes, where the cluster head node is responsible for managing the other nodes in the cluster and communicating with the cluster head nodes of other clusters, and when the cluster member nodes need to communicate with other nodes, they first send messages to their cluster heads, and then, the cluster heads forward the messages to the destination nodes. Because of the open wireless communication environment and the flexible and changeable collaboration mode, the UAV self-assembled network is vulnerable to internal and external attacks in the process of constructing topology and establishing routes. In the process of network topology construction, the main security threats faced by UAV self-assembled networks include tampering attacks and impersonation attacks. If the integrity of topology construction messages is compromised, it will lead to wrong data being used for network topology construction, forming an invalid or inefficient topology structure [11–13]. The existing work on security protection of UAV self-assembling network mainly focuses on identity legitimacy verification, message confidentiality protection, message integrity protection, malicious node detection, and other areas when messages are transmitted between nodes after the network topology is established and lacks message

security protection mechanisms for the process of network topology establishment, and the existing few security protection schemes for topology messages are applicable to the UAV self-assembling network with flat network structure and cannot be directly applied to the hierarchical network. The few existing security protection schemes for topology messages are all applicable to the UAV self-assembled network of flat network structure and cannot be directly applied to hierarchical network structure.

This paper is organized such that Section 2 defines some related work. Section 3 proposes the main methods of the study. Section 3 also explains the methods of the proposed work. Section 3.5 defines the experiment and analysis of the proposed work. Finally, the paper ends with a conclusion in Section 4.

## 2. Related Work

In this section, we define the UAV communication network modeling and UAV communication routing.

*2.1. UAV Communication Network Modeling.* The rise of diversified application services is accompanied by the proliferation of end-users, and the massive number of connections and differentiated network demands places greater demands on wireless communication network systems. With the advantages of high mobility, easy deployment, and low cost [14, 15], UAV-based network communication solutions have emerged and gradually attracted the attention of researchers, and more and more research has been conducted. Although UAV-based communication makes up for the shortcomings of current wireless network systems and can provide flexible, reliable, and on-demand communication network services for end devices, the energy consumption and endurance problems of UAVs and the differentiated ground service requirements make it possible to improve transmission efficiency, access efficiency, and computational efficiency from three aspects: UAV network location deployment, network connection establishment, and network service provision. The research on UAV-based energy-efficient communication strategies has become a major hot area of current research. This section first summarizes the existing research on UAV-based communication to improve transmission efficiency and achieve energy-efficient network dynamic location deployment; then, it introduces the existing research on how to improve access efficiency and achieve energy-efficient access of ground devices for the scenario of massive ground devices accessing the network. Finally, it focuses on data computation offloading services for the provision of UAV-based communication network services. A synopsis of existing research on how to ensure computational efficiency and implement energy-efficient computational offloading using UAVs is presented. We examine the inadequacies of existing solutions and conduct out follow-up work to address the existing issues [16, 17].

After completing the deployment of UAV-based energy-efficient optimization, how to establish the network connection between ground terminal devices and UAV-based com-

munication platform becomes the next issue to be considered, especially for the mass-connected IoT terminal devices, which are often in remote areas and have extremely high requirements for energy consumption. However, because of the disparity between the large number of ground terminal users and limited wireless network access resources, as well as UAV range time, reducing access network congestion and overload, improving access resource utilization and terminal device access success rate, increasing access efficiency, and realizing energy-efficient network connection establishment based on UAVs are a critical problem that requires immediate attention. It has attracted a lot of discussion and attention in academia and industry. According to the difference in the location of the triggering network connection establishment service, the research of energy-efficient network connection establishment can be divided into push-type and pull-up-type energy-efficient network connection establishment schemes to alleviate access congestion and improve access efficiency at the same time.

After completing the deployment of UAV-based energy-efficient optimization, the next issue to consider is how to establish network connections between ground terminal devices and UAV-based communication platforms. This is especially important for mass-connected IoT terminal devices, which are often in remote areas and have extremely high energy consumption requirements, so UAVs' flexible mobility makes them an important means of assisting in IoT network access. A crucial means of increasing capacity [18, 19]. However, the contradiction between the huge number of ground terminal users and limited wireless network access resources and UAV range time makes how to reduce access network congestion and overload, improve access resource utilization and terminal device access success rate, increase access efficiency, and realize energy-efficient network connection establishment based on UAVs an important problem that needs to be solved urgently and has attracted much discussion and attention in academia and industry. It has attracted a lot of discussion and attention in academia and industry. According to the difference in the location of the triggering network connection establishment service, the research of energy-efficient network connection establishment can be divided into push-type and pull-up-type energy-efficient network connection establishment schemes to alleviate access congestion and improve access efficiency at the same time. The UAV communication schematic is shown in Figure 2.

*2.2. UAV Communication Routing.* With the increasingly widespread application of UAV self-assembly networks, domestic and foreign scholars have proposed a large number of UAV self-assembly network routing protocols; however, there is less research on the security protection mechanism of routing protocols, and if the integrity of information in the routing establishment process cannot be guaranteed, malicious information may be used to establish the network topology and routing path process, which leads to unstable network topology, inefficient routing, and other problems. This can have a significant negative impact on network performance [20].

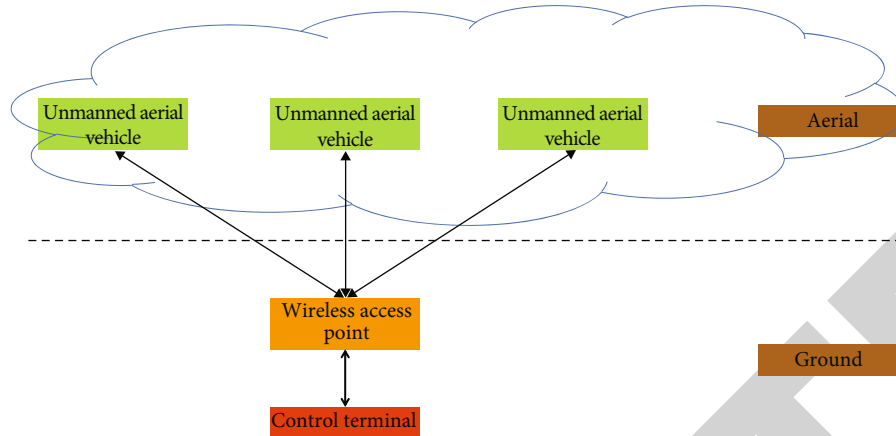


FIGURE 2: UAV communication schematic.

The routing protocols of UAV self-assembled networks can be split into two categories based on network topology: nonhierarchical routing protocols and hierarchical routing protocols. Among them, the nonhierarchical routing protocols are applicable to the planar network structure, in which all nodes in the network have equal status and have the function of forwarding and routing, and the existing classical protocols include on-demand distance vector routing, optimal link state routing protocol, dynamic source routing protocol, geolocation routing protocol GPSR, and secure routing algorithm of aerial self-assembling network based on geolocation integrated selection of the next hop. However, in complex mission scenarios, with the increase of the number of UAV nodes in UAV self-assembling networks, hierarchical routing protocols have become a hot spot for research in order to balance the UAV node load and improve the stability of the network. The existing classical hierarchical routing protocols mainly include lowest ID clustering algorithm with the unique identifier ID number of network nodes as a factor and mobility prediction-based clustering algorithm that considers node movement factors. Weight-based clustering algorithm uses node energy, node degree, distance between nodes, and node movement speed as measurement criterion for nodes to run for cluster head. The reliability-based clustering algorithm divides the clustered network with node energy, link retention rate, node degree, and communication volume as factors and adjusts the weight of each factor in the clustering process with the objectives of enhancing topology stability, saving energy, and improving service quality, respectively, to achieve network topology stability, reducing energy consumption or improving network service quality to the maximum extent. In the above hierarchical routing protocols, the formation of routes is built on the basis of building a hierarchical topology of the network, i.e., completing the clustering of network nodes [18].

In UAV self-assembled network routing security protection mechanism, attackers may launch a sequence of malicious actions to disrupt the routing system by eavesdropping on the control information at the network layer, making UAV networks communicating through wire-

less media more vulnerable to attacks than cable networks. Exposed to the vulnerable wireless environment, the network information security transmission of wireless self-assembled networks must satisfy both the security of data communication and the security of routing protocols. Currently, several schemes have been proposed to protect the routing protocols of UAV self-assembled networks. Manel proposes security enhancement methods for AODV protocols to protect the security of route discovery phase information and routing error information. We found that there is less research on the security protection mechanism for hierarchical routing protocols, and there is an urgent need to design an efficient and lightweight security protection mechanism for hierarchical routing protocols to ensure the integrity of the topology construction information transmitted between nodes during the construction of the network topology and to avoid the formation of inefficient or invalid topologies due to malicious attacks or failures that cause erroneous information to be used in the topology construction process and have negative impact on the upper layer services. In terms of data integrity protection, blockchain is increasingly being utilized to preserve the integrity of information due to its traceability and tamper-evident qualities, in addition to the use of hash functions and digital signature technology. In response to the current problem of the lack of security protection mechanism of the hierarchical UAV self-organizing network routing protocol, this paper proposes a security protection scheme for routing messages in the hierarchical routing protocol of the UAV self-organizing network. The scheme can guarantee the integrity of the interaction messages between nodes in the topology establishment process of the hierarchical network structured UAV self-organized network. In the scheme, blockchain technology is used to store static topology messages and verify and ensure their integrity, while reducing the resource overhead of the proposed scheme.

### 3. Methods

In the method section, we discuss the model structure, antenna model, channel model, and channel model in detail.

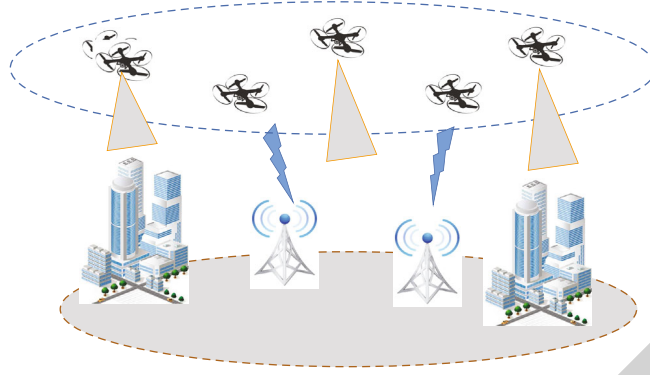


FIGURE 3: Model architecture.

**3.1. Model Structure.** A UAV wireless communication network in the 3D environment of a building is selected as the research object, and its system framework is shown in Figure 3. Firstly, consider buildings in cities, which are generally assumed to be rectangular in shape; their horizontal dimensions, heights, and orientations are random and mutually independent; and the central points constitute a uniform Poisson point process in the 2D plane with intensity  $\lambda B$ . Assume that the distribution of the length  $L$  and width  $W$  of each building obeys specific probability density functions  $f_L(y)$  and  $f_W(y)$  with expectations which are  $E[L]$  and  $E[W]$ . The orientation angle of the building is denoted by  $\varphi$ , which is uniformly distributed on  $(0, 2\pi]$ . The height  $h_B$  of the building obeys the Rayleigh distribution, and its probability density function is

$$f_{H_B}(h_B) = \frac{h_B}{\sigma^2} e^{-(h_B^2/2\sigma^2)}. \quad (1)$$

**3.2. Antenna Model.** In order to compensate for the high road loss characteristics of millimeter wave, it is assumed that both UAV and user are assembled with uniform planar square array (UPA) to achieve directional beam assignment, and the antenna gain is a complex function defined by the antenna azimuth and elevation angles. Using beam alignment and tracking techniques, it is assumed that the antenna main flaps at the transmitter and receiver ends can be perfectly aligned to achieve the maximum power gain. In the azimuth plane, the half-power beamwidths of the UAV antenna and the user antenna can be denoted as  $\theta_A^a$  and  $\theta_U^a$ , respectively, and the corresponding half-power beamwidths in the elevation plane are  $\theta_A^e$  and  $\theta_U^e$ , respectively, and the main flap gains of the UAV and user antennas are  $G_A$  and  $G_U$ , and the side flap gains are  $G_A$  and  $G_U$ , respectively, and the probability distribution function of the total antenna gain  $G$  received at the receiving end is

$$G = \begin{cases} G_A G_U, \zeta_1 = p_1 p_2, \\ g_A G_U, \zeta_2 = (1 - p_1) p_2, \\ G_A g_U, \zeta_3 = p_1 (1 - p_2), \\ g_A g_U, \zeta_4 = (1 - p_1) (1 - p_2). \end{cases} \quad (2)$$

$\zeta_i$  ( $i = 1, 2, 3, 4$ ) is the distribution probability of  $G$ ;  $p_1$  and  $p_2$  are the probabilities of antenna main flap alignment at the UAV side and the user side, respectively. The subscript  $c \in \{A, U\}$  is used to denote the UAV side and user side.

$$p_1 \& = \frac{\theta_A^a \theta_A^e}{2\pi \pi},$$

$$p_2 \& = \frac{\theta_U^a \theta_U^e}{2\pi \pi},$$

$$G_c \& = N_c, \quad c \in \{A, U\},$$

$$g_c \& = \frac{\sqrt{N_c} - (\sqrt{3}/2\pi) N_c \sin(\sqrt{3}/2 \sqrt{N_c})}{\sqrt{N_c} - (\sqrt{3}/2\pi) \sin(\sqrt{3}/2 \sqrt{N_c})}, \quad c \in \{A, U\}. \quad (3)$$

**3.3. Channel Model.** The large-scale fading term and the small-scale fading term of the millimeter-wave channel are considered comprehensively. The large-scale fading caused by path loss can be expressed as  $(d) = d - \alpha$ , where  $d$  is the distance from the UAV to the user and  $\alpha$  is the path loss index of the channel. Assumption 1 implies that the structures along the millimeter-wave communication link entirely block the millimeter-wave signal; i.e., the millimeter wave cannot pass through. For Assumption 2, the small-scale fading channel is a *Nakagami* channel, and the channel power gain is a gamma random variable  $z$  with probability density function

$$f_Z(z) = \frac{m^m z^{m-1}}{\Gamma(m)} \exp(-mz), \quad (4)$$

where  $m$  is the shape factor of Nakagami channel and  $\Gamma(m)$  is the gamma function of  $m$ .

**3.4. Performance Optimization.** Since both the UAV and the user are equipped with directional antennas in the system, the ambient noise in the system is negligible compared to the power of the interference. Therefore, only the signal-to-interference ratio (SIR) received at the user side is considered as a parameter for performance evaluation. Under the



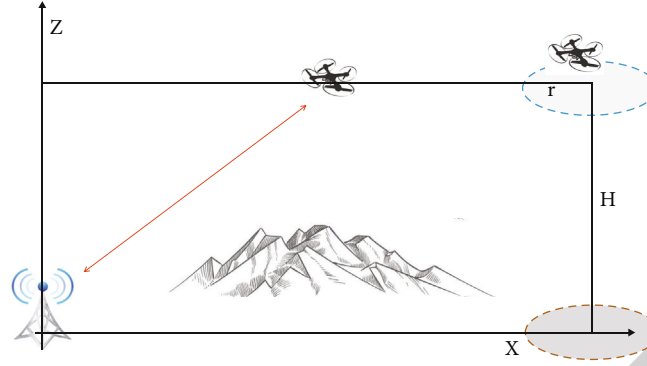


FIGURE 4: The basic model of the UAV network.

3D network model and the corresponding assumptions, the SIR received by a typical user in the downlink can be expressed as

$$\text{SIR} = \frac{G_1 z_0 [(h_A - h_U)^2 + R_0^2]^{-(\alpha/2)}}{\sum_{i \in \Psi \setminus 0} G_i z_i [(h_A - h_U)^2 + R_i^2]^{-(\alpha/2)} S_i}, \quad (5)$$

where  $R_0$  and  $R_i$  are the horizontal distances from the typical user to the serving drone and the interfering drone  $i$ , respectively;  $S_i$  is the total penetration power loss caused by the buildings on the  $OX_i$  link; and  $z_0$  and  $z_i$  are the small-scale fading terms of the serving link and the interfering link, respectively. Interference can be expressed as

$$I = \sum_{i \in \Psi \setminus 0} G_i z_i [(h_A - h_U)^2 + R_i^2]^{-(\alpha/2)} S_i. \quad (6)$$

Then, the coverage can be further expressed as

$$\begin{aligned} \mathbb{P}_{\text{COV}}(T) &= \mathbb{P}(\text{SIR} > T) = \mathbb{E}_x [P(\text{SIR} > T)] \\ &= \int_0^\infty \mathbb{P}(\text{SIR} > T | R_0 = x) f_R(x) dx \\ &= \int_0^\infty \mathbb{P}\left\{z_0 > T G_1^{-1} [(h_A - h_U)^2 + x^2]^{\alpha/2} I\right\} f_R(x) dx, \end{aligned} \quad (7)$$

where  $f_R(x)$  is the probability density function of the distance from a typical user to the unobstructed and closest UAV and  $T$  is the signal-to-media ratio threshold at the receiver side that can correctly demodulate the signal. Since the small-scale fading channel from the UAV to the user is a *Nakagami* channel, i.e., the power gain  $z_0$  is a random variable obeying a gamma distribution.

**3.5. Air-to-Ground Channel Modeling.** Figure 4 depicts the basic model of the UAV network. This UAV network consists of an observation UAV A, a relay UAV R based on the decode-and-forward collaboration approach, and a base station B. The UAV A flies over the observation area and collects observation information, and since the direct connection between UAV A and base station B is blocked by obstacles such as mountains or buildings, the collected infor-

mation needs to be delivered to base station B through the relay UAV R. The UAVs are set to be configured with an unlimited size data buffer, and the data that UAV A or R cannot deliver to the target in time due to the channel capacity limitation that can be cached in the buffer. To facilitate the analysis, a 3D Cartesian coordinate system scenario is considered in this chapter. UAV A makes a circular motion of radius  $r$  over the observation area; it flies at a fixed altitude  $H$  and has a fixed velocity  $V$ . Therefore, the period of UAV A flying for one week can be derived.

$$T_0 = \frac{2\pi r}{V_0}. \quad (8)$$

Since the UAV often flies at high altitude, the flight height  $H$  of the UAV is much greater than the height of the base station B. Therefore, the height of the base station B can be ignored in the analysis. It can be obtained that the coordinates of B can be expressed as  $O(0, 0, 0)$ , and the horizontal distance from base station B to the center of UAV A's flight trajectory circle  $O'$  is  $D$ . Therefore, the coordinates of the center of A's flight trajectory circle can be expressed as  $O'(D, 0, H)$ . The relay UAV R is free to fly in the space between A and B, but the flight altitude of R is always kept the same as that of A, which is  $H$ . Meanwhile, the maximum flight speed of the UAV R is limited to dagger. The overall operation time of the relay UAV is assumed to be  $T$ , while the takeoff and landing phases of the UAV are not considered. Therefore, at time  $t$ , the time-varying coordinates of UAV A can be expressed as  $X_A(t), Y_A(t), H$ , while the time-varying coordinates of UAV R can be expressed as, where  $t$  takes values in the range  $[0, T]$ . To facilitate the calculation, the operation time  $T$  of the relay UAV is evenly divided into  $N$  equal parts, and each time slot can be denoted as  $t_0 = T/N$ . When  $N$  is taken large enough, the positions of the UAV A and the relay R can be regarded as fixed in each time slot  $t_0$ . Due to the good mobility of UAVs, the communication links of UAV networks can avoid obstacles in most cases, so it is assumed that the communication channels from A to R and R to B are mainly composed of line-of-sight channels. In addition, the Doppler effect is assumed to be perfectly compensated at both the receiving end R and B and does not need to be considered.

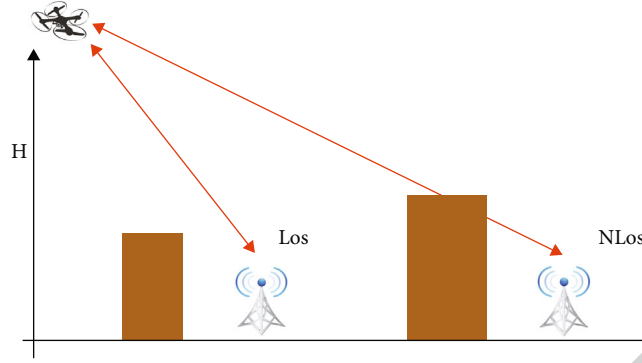


FIGURE 5: UAV-based wireless signal propagation for communication platforms in urban environments.

TABLE 1: UAV self-assembling network structure and TCP/IP correspondence in the experimental environment.

Self-organizing network architecture	TCP architecture	IP architecture
Application layer	Application layer	Application layer
Representation layer	Application layer	Application layer
Session layer	Application layer	Application layer
Transport layer	Proxy layer	Transport layer
Network layer	Proxy layer	Network layer
Link layer	Nodes and connections	Physical layer
Physical layer	Nodes and connections	Physical layer

TABLE 2: Experimental hardware environment.

Operating system	Windows 10
CPU	Intel(R) Core(TM) i5-9400F CPU @ 2.90 GHz
Memory	8.00GB (RAM)

The relay UAV  $R$  operates in full duplex mode and uses frequency division duplex technology, where the bandwidth of the transmit channel is equal to the bandwidth of the receive channel. In this chapter, it is assumed that the transmit power of all UAVs is certain, as

$$P_A = P_R = P_0, \quad (9)$$

where  $P_A$  denotes the transmit power of the observation UAV  $A$ ,  $P_R$  denotes the transmit power of the relay UAV  $R$ , and  $P_0$  denotes the fixed transmit power, which is a constant. In addition, the noise power is also assumed to be con-

TABLE 3: Communication transmission rate of each hierarchy of UAV network.

Hierarchy	This article routing protocol V value	Cluster-based routing protocol
Application layer	12.26 Mbit/s	1.23 Mbit/s
Representation layer	15.26 Mbit/s	1.20 Mbit/s
Session layer	18.26 Mbit/s	1.02 Mbit/s
Transport layer	11.23 Mbit/s	1.23 Mbit/s
Network layer	15.26 Mbit/s	2.25 Mbit/s
Link layer	13.14 Mbit/s	1.85 Mbit/s
Physical layer	15.36 Mbit/s	1.67 Mbit/s

stant, as

$$P_{N,A} = P_{N,R} = P_{N,B} = P_N, \quad (10)$$

where  $P_{N,A}$  denotes the noise power at UAV  $A$ ,  $P_{N,R}$  denotes the noise power at relay UAV  $R$ ,  $P_{N,B}$  denotes the noise power at the base station, and  $P_N$  denotes the fixed noise power, which is a constant. Since the bandwidth of the communication channel is fixed in this UAV network, it is known that the performance of the communication link is related to the signal-to-noise ratio at the receiving end according to the Shannon formula, according to the free-space path loss model.

The air-to-ground channel for UAV-based communication can be divided into two parts: LoS and non-line of sight. LoS communication is the wireless signal propagating in a straight line between the transmitter and the receiver with no obstacle occlusion  $W$ . NLoS communication is the wireless signal propagating between the transmitter and the receiving end which propagates with obstacle occlusion  $W$ . Take the Makoto city environment as an example, the air-to-ground channel of the UAV-based communication platform. Suppose the coordinates of a certain UAV are  $(x_u, y_u, h)$  and the coordinates where the user communicating with this UAV is located are  $(x_g, y_g, 0)$ . When the wireless signal propagates in free space, the signal does not undergo the

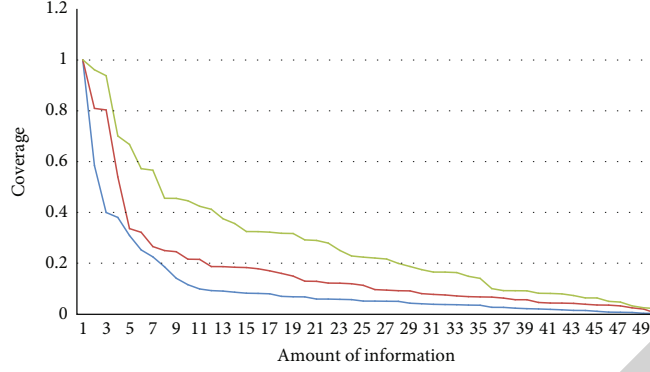


FIGURE 6: Coverage with different numbers of antenna arrays.

process of scattering, refraction, and diffraction, nor is it absorbed, and the path loss of the channel obeys the Gaussian distribution  $N$ .  $\mathcal{E}$  represents one of two channel types LoS and NLoS, i.e.,  $\mathcal{E} \in \{\text{LoS}, \text{NLoS}\}$  air-to-ground channel of a UAV-based communication platform. The path loss (in dB) in the LoS link and NLoS link cases is

$$\begin{aligned} L_{\text{LoS}} &= L_{\text{FS}} + \eta_{\text{LoS}}, \\ L_{\text{NLoS}} &= L_{\text{FS}} + \eta_{\text{NLoS}}. \end{aligned} \quad (11)$$

The wireless signal propagation of the UAV-based communication platform in the urban environment is shown in Figure 5. The flight energy consumption of UAVs has a significant impact on the UAV endurance and greatly affects the efficiency of UAV-based communication. In simple terms, the flight energy consumption of UAV is related to its load as well as flight speed, and some related studies have modeled the energy consumption of UAVs simply as a model related to the mass and flight speed of UAVs [8-11]. Assume that the flight time of the UAV is  $t$  and the flight speed at moment  $f$  is  $v(f)$ . The simple flight energy consumption model of the drone is

$$L_{\text{FS}} = \left( \frac{4\pi d f}{c} \right)^2, \quad (12)$$

where  $M$  is the mass of the UAV. Although the simple energy consumption model is generally applied to the energy consumption model of UAVs, however, different types of UAVs are constructed differently and have different power systems, so the energy consumption models of different types of UAVs need to be considered. In this paper, the energy consumption models of fixed-wing UAVs and rotary-wing UAVs are introduced, respectively.

## 4. Experiments and Results

**4.1. Experimental Setup.** After completing the theoretical design of the topology-based routing protocol, the following comparison experiments are conducted to investigate the performance of the routing protocol in practical applications: the topology-based routing protocol and the cluster-based routing protocol proposed in this paper are intro-

duced into two UAV devices of identical models and performance. In order to evaluate the performance of the two routing protocols in the UAV self-assembly network, an NS2 simulation device is installed in the Cygwin environment. The device is written in C++ using Otdl, and it is applied to the experimental environment of this paper to realize the simulation of UAV self-assembly network. The experimental environment built on the basis of this device contains a total of seven layers of network structure, whose corresponding TCP/IP relations are shown in Table 1. The hardware environment is shown in Table 2.

According to the contents in Table 1, after clarifying the correspondence between the UAV self-assembled network structure and TCP/IP, the communication transmission rate of each hierarchical structure of the self-assembled network is calculated under the transmission conditions of the two routing protocols, and its calculation formula is as follows:

$$V = \frac{M \cdot \chi}{s} \log_2 K. \quad (13)$$

$V$  denotes the communication transmission rate of each hierarchical structure of the UAV self-assembled network;  $M$  denotes the total amount of communication data generated in the communication process between UAVs;  $\chi$  denotes the baud rate of data in the transmission process;  $s$  denotes the transmission time of data in each hierarchical structure; and  $K$  denotes the effective discrete value of communication data. The communication transmission rate of each level of the UAV self-assembly network under the two routing protocols is calculated.

**4.2. Experimental Results and Analysis.** To facilitate the comparison of the application performance of the two routing protocols, the calculated experimental results are recorded as shown in Table 3.  $K$  is denoted as the effective discrete value of the communication data. The communication transmission rate of the UAV self-assembly network at the starting level of the two routing protocols is calculated.

Therefore, the results obtained from the above experiments prove that the communication transmission rate of the seven levels of the UAV self-assembly network exceeds 12.00 Mbit/s under the conditions of the routing protocol in this paper; the highest communication transmission rate

of the seven levels of the UAV self-assembly network is only 2.25 Mbit/s under the conditions of the routing protocol based on clustering. Therefore, the above experimental results prove that the routing protocol designed in this paper can achieve the communication transmission between UAVs and UAVs and achieve the application effect of efficient information transmission after the introduction of topology information technology.

Figure 6 shows the theoretical results and simulation results with good approximation. As the number of antenna array subunits equipped with UAV increases, the coverage of users corresponding to the same SIR threshold  $T$  also increases. This is due to the increase in the number of antenna arrays at the UAV end, which makes the antenna gain at the transmitting end larger, and the total gain of the useful signal received at the receiving end also increases, although the signal gain of the interfering UAV also increases, but because the main flap width of the directional antenna is narrow and randomly pointing, when the number of antenna arrays increases from 4 to 32, the probability of the main flap beam alignment between the transmitting end of the interfering UAV and the receiving end of the downlink user. Because the probability of the interference drone transmitter's primary flap beam alignment with the downlink user receiver drops from  $5.8 \times 10^{-3}$  to  $7.2 \times 10^{-4}$ , the impact of interference gain on user coverage performance is substantially smaller than that of usable signal gain. In addition, it can be seen from Figure 6 that when the threshold  $T$  of SIR is taken as 0 dB, the coverage rates at different numbers of antenna arrays are close to 1. This indicates that the number of antenna arrays of UAVs deployed in the area with lower quality of service requirements (i.e., lower SIR threshold) can be reduced, which can reduce the operator cost without affecting the system performance. And when the threshold of SIR is equal to 10 dB, the coverage rates corresponding to different antenna array numbers show significant differences, and the systems with antenna array numbers of 4 and 8 only correspond to coverage rates of 0.6 and 0.8. Therefore, in order to meet the areas with higher quality of service requirements, the number of antenna arrays of UAV-carrying antennas should be no less than 16.

## 5. Conclusion

We conduct research on the design of their routing protocols in this paper, based on clarifying the operation mechanism of UAV self-assembling networks. We also incorporate topological information into the research process to achieve dynamic routing technique adjustment. When the routing protocol proposed in this paper is applied to the actual UAV self-assembling network, the routing mode can be dynamically adjusted based on the specific needs of communication transmission, allowing the routing mode to be dynamically adjusted to provide the required conditions for different transmissions and achieving an overall improvement in communication transmission rate. However, there are still many problems that need to be explored in the research process, such as the uncertainty of

the motion law of the transmission nodes in the UAV self-assembling network; the transmission process should also be combined with a variety of motion models for improvement. As a result, in-depth research will be undertaken in the future to address the aforementioned issues, with the goal of boosting the routing protocol's perfection.

## Data Availability

The datasets used during the current study are available from the corresponding author on reasonable request.

## Conflicts of Interest

The authors declare that they have no conflict of interest.

## References

- [1] F. Aadil, A. Raza, M. F. Khan, M. Maqsood, I. Mehmood, and S. Rho, "Energy aware cluster-based routing in flying ad-hoc networks," *Sensors*, vol. 18, no. 5, p. 1413, 2018.
- [2] H. Nawaz, H. M. Ali, and A. A. Laghari, "UAV communication networks issues: a review," *Archives of Computational Methods in Engineering*, vol. 28, no. 3, pp. 1349–1369, 2021.
- [3] A. Rovira-Sugranes, A. Razi, F. Afghah, and J. Chakareski, "A review of AI-enabled routing protocols for UAV networks: trends, challenges, and future outlook," *Ad Hoc Networks*, vol. 130, p. 102790, 2022.
- [4] Z. Yang, H. Liu, Y. Chen, X. Zhu, Y. Ning, and W. Zhu, "UEE-RPL: a UAV-based energy efficient routing for Internet of Things," *IEEE Transactions on Green Communications and Networking*, vol. 5, no. 3, pp. 1333–1344, 2021.
- [5] H. I. Minhas, R. Ahmad, W. Ahmed, M. Waheed, M. M. Alam, and S. T. Gul, "A reinforcement learning routing protocol for UAV aided public safety networks," *Sensors*, vol. 21, no. 12, p. 4121, 2021.
- [6] Z. Zhu, L. P. Qian, J. Shen, L. Huang, and Y. Wu, "Joint optimisation of UAV grouping and energy consumption in MEC-enabled UAV communication networks," *IET Communications*, vol. 14, no. 16, pp. 2723–2730, 2020.
- [7] A. Rovira-Sugranes, F. Afghah, J. Qu, and A. Razi, "Fully-echoed Q-routing with simulated annealing inference for flying adhoc networks," *IEEE Transactions on Network Science and Engineering*, vol. 8, no. 3, pp. 2223–2234, 2021.
- [8] M. Y. Arafat and S. Moh, "A survey on cluster-based routing protocols for unmanned aerial vehicle networks," *IEEE Access*, vol. 7, pp. 498–516, 2019.
- [9] H. Nawaz and H. M. Ali, "Implementation of cross layer design for efficient power and routing in UAV communication networks," *Studies Information Control*, vol. 29, no. 1, pp. 111–120, 2020.
- [10] J. Liu, Q. Wang, C. T. He et al., "QMR:Q-learning based multi-objective optimization routing protocol for flying ad hoc networks," *Computer Communications*, vol. 150, pp. 304–316, 2020.
- [11] A. H. Wheeb, R. Nordin, A. A. Samah, M. H. Alsharif, and M. A. Khan, "Topology-based routing protocols and mobility models for flying ad hoc networks: a contemporary review and future research directions," *Drones*, vol. 6, no. 1, p. 9, 2022.

## Retraction

# Retracted: Evaluation of Football Teaching Quality Based on Big Data

### Computational and Mathematical Methods in Medicine

Received 17 October 2023; Accepted 17 October 2023; Published 18 October 2023

Copyright © 2023 Computational and Mathematical Methods in Medicine. This is an open access article distributed under the Creative Commons Attribution License, which permits unrestricted use, distribution, and reproduction in any medium, provided the original work is properly cited.

This article has been retracted by Hindawi following an investigation undertaken by the publisher [1]. This investigation has uncovered evidence of one or more of the following indicators of systematic manipulation of the publication process:

- (1) Discrepancies in scope
- (2) Discrepancies in the description of the research reported
- (3) Discrepancies between the availability of data and the research described
- (4) Inappropriate citations
- (5) Incoherent, meaningless and/or irrelevant content included in the article
- (6) Peer-review manipulation

The presence of these indicators undermines our confidence in the integrity of the article's content and we cannot, therefore, vouch for its reliability. Please note that this notice is intended solely to alert readers that the content of this article is unreliable. We have not investigated whether authors were aware of or involved in the systematic manipulation of the publication process.

In addition, our investigation has also shown that one or more of the following human-subject reporting requirements has not been met in this article: ethical approval by an Institutional Review Board (IRB) committee or equivalent, patient/participant consent to participate, and/or agreement to publish patient/participant details (where relevant).

Wiley and Hindawi regrets that the usual quality checks did not identify these issues before publication and have since put additional measures in place to safeguard research integrity.

We wish to credit our own Research Integrity and Research Publishing teams and anonymous and named external researchers and research integrity experts for contributing to this investigation.

The corresponding author, as the representative of all authors, has been given the opportunity to register their agreement or disagreement to this retraction. We have kept a record of any response received.

### References

- [1] Y. Long and W. Zhai, "Evaluation of Football Teaching Quality Based on Big Data," *Computational and Mathematical Methods in Medicine*, vol. 2022, Article ID 7174246, 10 pages, 2022.

## Research Article

# Evaluation of Football Teaching Quality Based on Big Data

Yue Long and Wei Zhai 

Football College, Wuhan Sports University, Wuhan Hubei 430077, China

Correspondence should be addressed to Wei Zhai; 2008053@whsu.edu.cn

Received 27 April 2022; Revised 21 May 2022; Accepted 24 May 2022; Published 28 June 2022

Academic Editor: Naeem Jan

Copyright © 2022 Yue Long and Wei Zhai. This is an open access article distributed under the Creative Commons Attribution License, which permits unrestricted use, distribution, and reproduction in any medium, provided the original work is properly cited.

The arrival of the big data era has opened up new avenues for assessing the quality of physical education instruction. Using big data to explore these systems may help improve the quality of physical education itself, in addition to assisting schools in developing quality assessment systems for physical education. More and more schools are making football a compulsory part of their physical education and wellness curriculum. Therefore, this study used the methods of literature materials, expert interviews, questionnaires, and Delphi method to determine the evaluation indicators and index weight coefficients of football teaching and borrowed the application background of big data to initially explore the construction of a football teaching quality evaluation system. To this end, this paper completes the following tasks: (1) The current state of football teaching quality evaluation studies in the United States and internationally is summarized. (2) A football teaching quality evaluation system based on the background of big data is constructed. (3) Our experiments show that the assessment approach described in this study is scientifically and rationally distributed and can accurately represent all components of physical education. As a result, evaluating football instruction using big data is a possibility.

## 1. Introduction

Assessment of football instruction is a crucial step in football teaching. How and what evaluations are conducted have a direct bearing on the quality of high school football instruction, as well as the growth and development of PE instructors and their pupils. School football teachers are now evaluated mostly on their students' online feedback at the conclusion of each semester. A student's grade in physical education is based on their performance in class and on assessments given by the school itself. It is now time to get the physical education teacher's teaching score for this semester. As a result, the reform and growth of football instruction in schools in my nation is being held back by this paradigm [1]. Because of this, colleges and universities are increasingly focused on developing an assessment system for physical education instructors and students that allows for more active participation in the process of teaching feedback. There has been a dramatic rise of science and technology in our planet, the means of information circulation are becoming more and more diverse, and the amount of infor-

mation exchange between people is growing rapidly. People in China and others can get real-time news, they can do online shopping through APPs such as Taobao and <https://jd.com/>, and they can inquire about all kinds of information they want through APPs such as Baidu and Zhihu. Therefore, under the background of the rapid popularization of mobile intelligent terminals, the vigorous development of mobile Internet, and the rise of the Internet of Things, big data is generated and developed. My country values big data innovation and incorporates it into its long-term growth objectives as a result of this strategy [2]. The introduction of big data applications has made it possible to automate the evaluation of physical education programs in schools. Physical education assessment may benefit from big data by providing a significant quantity of data support and, as a consequence, become more scientific and fair. Thanks to big data, physical education assessment can provide even more insight into the effectiveness of its methods. It is all about the technology here; it is all about the systems. The present physical education assessment system has been challenged by big data. A university that fulfills the needs of the

big data age is reliable and operable and really supports the growth of students and physical education instructors and thus is required to be investigated. The assessment mechanism for physical education is essential. The purpose of this study is as follows:

- (1) To investigate and analyze the current situation of football teaching evaluation in some schools; the purpose is to solve the existing problems of the school football teaching evaluation system in our country and provide a small reference for the reform of the system
- (2) This research uses the Delphi method and AHP to determine the index and index weight coefficient of the football teaching evaluation system; its purpose is to provide a more reliable, scientific, and reasonable method for the determination of football teaching evaluation index and index weight coefficient
- (3) This study investigates the construction of a football teaching evaluation system using relevant big data knowledge in order to provide a new idea for the construction of a football teaching evaluation system, thereby promoting the implementation of sports teaching evaluation and providing relevant research. Through interdisciplinary research, this study applies the relevant knowledge of big data to football teaching evaluation, enriches the content of football teaching evaluation, and provides a certain reference for the study of football teaching evaluation

In addition, the study looks into using big data to create an assessment system for football instructors, as well as providing ideas and techniques for reforming the football teaching evaluation system in the age of big data. The value of this study lies in the timely feedback of the evaluation results of football teaching, so that physical education instructors are able to recognize the benefits and drawbacks of the teaching process and remedy them in time, thus enhancing the quality of education and instruction. The relevance and efficacy of football education are improved by helping schools adapt their objectives in a timely way. Students and instructors of physical education are enthused about sports evaluation, and schools are encouraged to use football evaluation, thereby promoting the process of reforming the physical education evaluation system [3]. This level is marked by equal attention to theory and practice, as well as the gradual adoption of behavioral features of physical education teachers' instruction as assessment indicators [4]. Third, in 1998, South Korea implemented the implementation evaluation method for primary school students, which comprehensively evaluated the changes and development of students' individual physical, mental, and athletic abilities [5–7].

The paragraph organization is as follows: Section 2 gives an overview of the related work. Section 3 discusses the methods of the proposed concepts. Section 4 discusses the experiments and results. Section 5 concludes the article.

## 2. Related Work

There are many studies on physical education evaluation in China. As of February 2022, CNKI used “physical education evaluation” as the key word to retrieve more than 4,000 related literatures, including doctoral and master's theses, and journal literatures. It can be seen that the research on “physical education evaluation” has become a hot field of research today. This research has organized and analyzed the relevant materials collected. The assessment of domestic physical education instruction following my country's reform and opening up may be split into three stages: the first, the evaluation of instructors in this time; the second, the evaluation of students; and the third, the evaluation of programs. The school splits its assessment indicators into first- and second-level categories based on their degree of empirical support. Second, in the stage of regularization, the physical education evaluation in this period is more systematic, standardized, and open. Established in 1994, the Higher Education Research and Evaluation Association of the China Higher Education Society provides an organizational guarantee for teaching evaluation. This stage has the characteristics of paying equal attention to both theory and practice and gradually began to use the behavioral characteristics of physical education teachers' teaching as indicators for evaluation [4].

Now in 2001, a large number of academics have conducted a study on the assessment of physical education, and this evaluation has since spread throughout the nation. Teaching quality is an essential factor in the assessment of physical education teachers by colleges and universities [5]. As a result, several academics have turned their focus to the assessment of physical education (PE) teacher effectiveness. According to a review of the available literature, the majority of the international research on the assessment of physical education instruction has come from the United States, Japan, South Korea, Germany, and the United Kingdom. First, the physical education evaluation in the United States is mainly aimed at primary and secondary schools. Individual assessment should be used instead of a uniform evaluation standard in the evaluation of physical education. When it comes to evaluating students' performance and abilities in physical education in Japanese schools, pleasant sports are the norm, and this is reflected in the assessment of physical education, with thinking, judgment, knowledge, and understanding as the main content [6]. Third, in 1998, South Korea implemented the implementation evaluation method for primary school students, which comprehensively evaluated the changes and development of students' individual physical, mental, and athletic abilities [7]. Fourth, school sports in Germany attaches great importance to cultivating students' habit of self-exercise and strives to strengthen the communication and connection between school sports and social sports. Finally, the assessment of physical education in the United Kingdom emphasizes the need of developing students' initiative, awareness, and creativity [8]. Regarding the research status of big data in the field of sports, up to now, in the domestic research on big data, CNKI uses “big data” as the key word for retrieval, and the literature

classification is set to “sports” to obtain more than 500 related documents. In 2012, my nation started to use big data-related expertise in sports research. Many sports researchers and academics in my nation have turned to big data applications since 2012, notably in the last three years. Many in the sports sector feel that by focusing on “big data,” the current age of big data will provide significant potential for the industry. The themes include “Big Data Era,” “Sports,” “Sports Industry,” “World Cup,” “Ball Games,” “Competitive Sports,” and “Sports Events.” In the fields of industry, competitive sports, and sports events, there are only 9 literatures on “physical education”; even fewer publications exist on the assessment of physical education.

According to some domestic researchers, contemporary civilization has made it easier to communicate knowledge. In a world of big data, it is possible to conduct a more scientific and unbiased assessment of college and university physical education programs since the quantity of data available has grown exponentially [9]. As a result, big data should be used to evaluate physical education in colleges and universities. To summarize, most research into the use of big data in sports in my country is theoretical, and there are few practical studies on the subject. Big data may be both an advantage and a hindrance when it comes to physical education assessment in my nation, where there is little research on football teacher evaluation. International research on the use of big data in sports is few and far between, but big data has been utilized in a variety of ways, and sporting events and sports are the most common. It has been shown that theoretical models of tactical decision-making in team sports benefit from contemporary machine learning and big data approaches. Reference [10] proposes a project aimed at introducing big data techniques into elite football research technical analysis. Volleyball teams may enhance their overall performance by using a computer-aided analysis tool (CAAT) to evaluate the underlying patterns that contribute to victories and defeats. Therefore, due to the scarcity of research in other countries on the use of big data for assessment in physical education, it is necessary for us to learn from other nations’ experience with big data applications for other sports [11].

### 3. Method

In this section, we discuss the experimental method, construction of teaching quality evaluation system, weight distribution of teaching evaluation index system, and framework of evaluation system in the context of big data in depth.

#### 3.1. Experimental Method

**3.1.1. Documentation Method.** With the help of university libraries and Internet tools such as CNKI and Web of Science database, a large number of books, journals, and literature materials are consulted, and the consulted materials are organized to analyze physical education teaching evaluation, big data, and big data at home and abroad. According to the needs of the paper, we use “Physical Education Evaluation”

and “Big Data” as the search keywords in CNKI (China National Knowledge Infrastructure) and “Big Data” in Web of Science. This paper focuses on 12 master’s theses, 15 other documents, 3 foreign language documents, and 2 documents in the Web of Science database. *Architecting Big Data: Big Data Technology and Algorithm Analysis* and other books have provided a lot of precious inspiration and reference opinions, which provide reference and theoretical support for the research of this paper.

**3.1.2. Questionnaire Survey Method.** Aiming at the current situation of teaching evaluation in a province, this paper selects physical education teachers and students from 5 schools to conduct a questionnaire survey on the relevant content of the implementation of sports evaluation. Six physical education teachers were selected from each school, and a total of 30 teachers were sent out for teacher questionnaires; each school selected 100 students, divided according to the ratio of boys and girls and grades, including 50 boys and 50 girls. By referring to the relevant literature, the first drafts of the questionnaires for physical education teachers and students were compiled. After listening to the suggestions of 100 experts and tutors, the contents of the questionnaires were revised, and the questionnaires were finally determined. Questionnaires were distributed to 30 physical education teachers and 500 students by way of face-to-face distribution. Its efficiency and recovery rate have reached 100%.

During this research, a questionnaire validity survey was done on 10 experts in the area of physical education in order to confirm its validity. Experts who thought the questionnaire design was reasonable accounted for 70% and 30% were basically reasonable. Therefore, the designed status questionnaire was basically recognized by experts, and its validity was high. In order to test the overall reliability of the questionnaire, the method of retest reliability was used. At an interval of 15 days, 5 copies of the teacher questionnaire and 10 copies of the student questionnaire were distributed again. The one-time coefficient of the current situation questionnaire for sports is 0.864, and the one-time coefficient of the current situation questionnaire for students is 0.811, both of which are  $>0.75$ , so the reliability of this questionnaire is high. In order to determine the indicators and weight coefficients of the school physical education teaching evaluation system, this paper conducted an indicator questionnaire survey and indicator weight consultation among 22 experts in the field of physical education. As a result of a thorough review of relevant literature and resources, as well as interviews with experts, accordingly, evaluation index and weight survey tables for the physical education teacher’s teaching evaluation and the student’s assessment of physical education were created. In both the teacher and student teaching evaluation index tables, there are three first-level indicators and fourteen second-level indicators for physical education introduction.

**3.1.3. Delphi and AHP.** The Delphi method involves conducting two rounds of expert surveys among 22 experts in the field of physical education: the first round involves



carefully analyzing and comparing the initially formulated indicators, assigning values based on the importance of each indicator by experts, performing the relevant consistency test, and finally making certain modifications to the indicators based on expert opinions. In the second round of expert survey, according to the assignment of the importance of each index by experts, the relevant consistency test was carried out. Using big data, the index method for evaluating college physical education teachers was eventually established [12].

To begin, a hierarchical structure model of college sports assessment indicators is created using big data, and then, the judgment matrix for each level is created. Check each level once more and then calculate the weight value of each indicator for each level. The weight value of the index is used to determine the degree of its influence on physical education assessment [13, 14].

### 3.2. Construction of Teaching Quality Evaluation System

#### 3.2.1. Characteristics and Principles of System Construction.

With the rise of big data, the football teaching evaluation system may be reconstructed utilizing big data technology. Football teaching evaluation system qualities are outlined within the context of big data research and analysis: To begin, the appraisal is based on both personal experience and factual evidence. Second, the evaluation method changes from summative evaluation to accompanying evaluation. Third, the evaluation content is from singleness to diversity evaluation. Fourth, the evaluation methods have changed from manual evaluation to intelligent evaluation. The design of the football teaching assessment system should be founded on the theoretical foundation, beginning with all parts of the physical education process, and primarily satisfy the following guidelines:

- (1) The scientific and objective principles
- (2) The idea that everything should be included
- (3) The idea of bringing together commonalities and uniqueness in a harmonious way
- (4) The openness and timeliness of communication [15]

#### 3.2.2. Design of the System of Football Teaching Evaluation Indicators.

Based on a study of physical education teaching evaluations in colleges and universities, a physical education teacher teaching evaluation index and a student physical education teaching evaluation index system might be constructed, as well as experts' recommendations and design principles for a big data-era evaluation system. This system is broken into three parts: the first- and second-level indices and descriptions of the indices in question. Physical education teachers' teaching evaluation index system contains 3 first-level indices, and students' teaching evaluation index system includes 3 first-level indices and 10 secondary indices. Using SPSS statistical software, we do parameter analysis on the computer to determine the relevance of each indicator in the assessment system, as assigned by 22 experts.

The response rate to the expert consultation form is measured by the expert excitement coefficient. The greater the response rate, the more excited the experts are about answering questions. The formula is as follows:  $J = n/N$ , where  $N$  is the total number of experts and  $n$  is the number of experts that participated. In this study, the recovery and effectiveness rates of the two rounds were 100% and 100% and 90.91% and 100%, respectively, which fulfilled the requirements of this research. The lower the coefficient of variation, the better the coordination of specialists [16]. If the standard deviation is greater than 0.25, it is considered that the degree of coordination is not high. The calculation formula is

$$V_j = \frac{S_j}{M_j}, \quad (1)$$

$$M_j = \frac{1}{n} \sum_{j=1}^n X_j, \quad (2)$$

$$S_j = \sqrt{\frac{1}{n-1} \sum_{i=1}^n (X_i - M_j)^2}, \quad (3)$$

where  $V_j$  represents the coefficient of variation,  $S_j$  represents the standard deviation, and  $M_j$  represents the arithmetic mean, the smaller the coefficient of variation.

The Kendall harmony coefficient (KHC)  $W$  value can test whether the evaluation results of experts on the indicators are consistent. It is between 0 and 1, with higher values indicating more stability. When the  $P$  value is more than or equal to 0.05, the results are not consistent with Kendall's harmony coefficient; however, a  $P$  value of 0.05 indicates that the results are. The following is the formula for calculating the value:

$$W = \frac{S}{(1/12) \left[ K^2 (N^3 - N) - K \sum_{i=1}^K T_i \right]}, \quad (4)$$

$$S = \sum_{i=1}^n (R_i - \bar{R}_i)^2, \quad (5)$$

$$T_i = \sum_{j=1}^{M_i} (N_{ij}^3 - N_{ij}), \quad (6)$$

$$X^2 = K(N-1)W, \quad (7)$$

where  $N$  represents the number of indicators evaluated,  $K$  represents the number of experts participating in the evaluation,  $S$  represents the sum of the grades of each evaluated indicator  $R_i$  and the average of all these sums  $\bar{R}_i$  is the sum of squared deviations, and  $T_i$  represents the correction coefficient.

3.2.3. Determination of the Evaluation Index System of Football Teaching. After two rounds of expert index questionnaire investigation and demonstration, data statistics, and analysis, we have finally figured out how to evaluate

TABLE 1: Physical education teacher teaching evaluation index system.

First-level indicator	Secondary indicators
Teaching preparation A1	Preparation before class B1
	Lesson plan writing B2
	Teaching etiquette B3
	Classroom routine B4
	Teaching attitude B5
Teaching process A2	Teaching organization B6
	Teaching methods B7
	Teaching content B8
	Exercise load B9
	Classroom atmosphere B10
Teaching effect A3	Exercise awareness to develop B11
	Soccer skills B12
	Physical fitness B13
	Basic knowledge of sports theory B14

TABLE 2: Student football teaching evaluation index system.

First-level indicator	Secondary indicators
Learn to prepare C1	Preparation before class D1
	Teaching etiquette D2
	Classroom routine D3
Learning process C2	Learning attitude D4
	Cooperative spirit D5
	Classroom atmosphere D6
	Exercise awareness to develop D7
Learning effect C3	Soccer skills D8
	Physical fitness D9
	Basic knowledge of sports theory D10

TABLE 3: RI value table.

Order	1	2	3	4	5	6	7	8	9	10
RI	0.00	0.00	0.59	0.91	1.13	1.22	1.33	1.53	1.46	1.50

the physical education instructor (Table 1) and how to evaluate the student physical education teaching assessment system (Table 2).

3.3. *Weight Distribution of Teaching Evaluation Index System.* Using the Analytic Hierarchy Process (AHP), the weight coefficient of the evaluation index is calculated and determined. Using the analytic hierarchy approach, one may examine correlations between evaluation indicators, quantify the final findings, and then calculate each indicator’s weight coefficient. The AHP technique is employed in order to establish the indicator weight, which assures that the indicator weight is reasonable and scientifically determined [17].

3.3.1. *Steps of the AHP Method*

(1) *Build an Evaluation System.* Through two rounds of expert index questionnaire research, the obtained indices are analyzed.

(2) *Build a Hierarchy Model.* From the very top to the very bottom, the important indicators are categorized according to their many features and relative relevance.

(3) *Create a Judgment Matrix for the Results.* In order to create a judgment matrix, all evaluation indications are compared at the same level generally; the 1-9 scale method proposed by Saaty is used, such as the comparison of two indicators A and B.

(4) *Calculate the Weight Vector and Consistency Check.* The matrix’s largest eigenvalue is max, and its formula is as follows: consistency ratio (CR) and consistency indicator (CI) are used in the calculation  $CR = CI/RI$ .

$$\lambda_{\max} = \frac{1}{n} \sum_i \frac{(Aw)_i}{wi}, CI = \lambda_{\max} - \frac{n}{n-1}, \quad (8)$$

where Aw is the product of the judgment matrix and the eigenvector and RI is the average random consistency index, which can be obtained through the difference table (see Table 3).

3.3.2. *An Evaluation Index’s Weighted Coefficient May Be Calculated.* The weight coefficient of the physical education teacher’s teaching evaluation index is as follows: First, according to the Saaty 1-9 level judgment matrix standard degree table, the second round of the index weight consultation table, and 20 experts’ scores, we establish the physical education teacher’s teaching evaluation index system at all levels of judgment moments. Next, we enter the data of the judgment matrix of the first-level indicators in the Excel sheet and calculate the values of the in-row multiplication, the n-th power, the weight value W,  $\lambda_{\max}$ , CI, CR, etc. The weights of the first-level indicators of the PE teacher’s teaching evaluation index system are  $W1 = 0.12$ ,  $W2 = 0.65$ , and  $W3 = 0.23$ .  $CR = 0.0036 < 0.1$ , so it indicates that the first-level index judgment matrix passes the one-time test. Finally, the weight coefficients of the remaining three rectangular matrices and the corresponding weight coefficients of the matrices established by the secondary indicators B1 to B14 are calculated in the Excel sheet according to the above method, and the weight table of the teaching evaluation index system for physical education teachers is obtained.

The weight coefficient of the student physical education evaluation index is as follows: using the above method, we calculate the weight table of the student physical education evaluation index system.

3.4. *Framework of Evaluation System in the Context of Big Data.* According to the subject, evaluation can be divided into two categories: one is self-evaluation and the other is evaluation of others [18]. Teaching and learning are two of

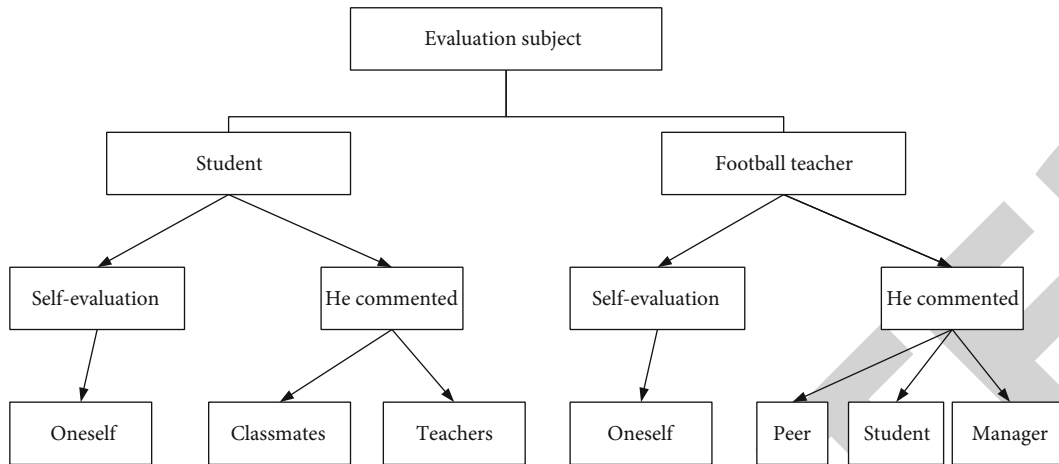


FIGURE 1: Framework of football teaching evaluation system.

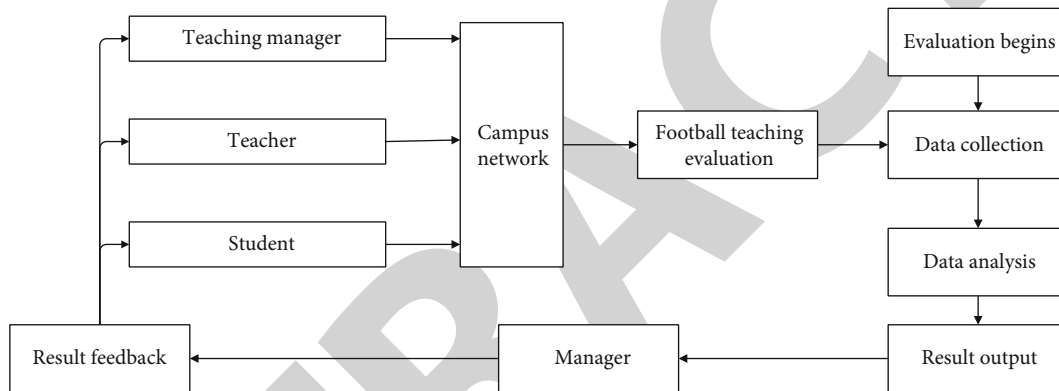


FIGURE 2: Football teaching evaluation process.

the most important criteria in evaluating a teacher's ability to educate. Therefore, we should realize that different evaluation subjects have different roles at the process of developing an assessment system for physical education in colleges and universities and clarify the commonality and individuality among the subjects through evaluation indicators and indicator weights. In this study, we selected four evaluation subjects including physical education instructors, students, and other members of the school's physical education department. The specific framework is shown in Figure 1.

### 3.4.1. Physical Education Evaluation Activities for Students

- (1) In this context, students' self-evaluation refers to students' self-awareness of their own learning process. Students who regularly do self-assessments have a better understanding of their own shortcomings and how to overcome them. As shown by the evaluation indicators, students perform an in-depth investigation of themselves as well as an overall assessment. The goal of this exercise is to help students better understand their learning preferences and methods, as well as their own strengths and shortcomings, to make the most of their own self-directed learning potential. Using your own teaching

account, students may access a whiteboard for self-evaluation of their classroom experiences

- (2) Students are divided into equal groups for the purposes of group teaching assessment, and the group members use a one-to-one evaluation approach to assess each other's performance on the indicators. Additionally, kids will be more enthusiastic in sports learning as a result, as well as be able to share their own learning techniques with other students. It is thus possible to get additional information about how physical education is affecting the school's livestock by doing a group review. Students use the teaching evaluation account to rate their classmates in physical education classes. Teachers submit the information about the class ahead of time
- (3) Physical education teachers' evaluation activities: in the activities of physical education evaluation for students, physical education teachers are the subject of evaluation, whereas the focus is on the pupils themselves. Teachers' evaluations of pupils in physical education are the most authentic, clear, and convincing. PE instructors have the largest impact on students' physical education instruction. As a result, the assessment of physical education instructors is a

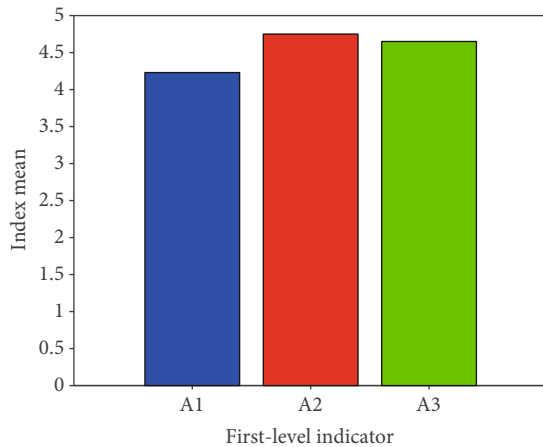


FIGURE 3: Comparison of the first-level index parameters of teacher evaluation (N = 20).

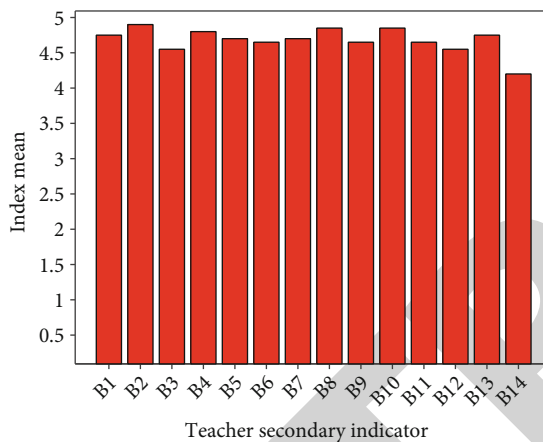


FIGURE 4: Second-level index parameters of teacher teaching evaluation (N = 20).

TABLE 4: Consistency test of primary and secondary indicators.

Index	KHC	Chi-square value	P value
First-level indicator	0.43	17.84	0.0002 < 0.05
Secondary indicators	0.37	92.19	<0.05

critical component in assessing students’ progress in physical education. In this study, physical education teachers can log in to the teacher system to evaluate physical education teaching for the students in their substitute classes

### 3.4.2. Teaching Evaluation Activities for Physical Education Teachers

(1) *Physical Education Teachers’ Self-Evaluation Activities.* The main approach of teaching quality evaluation is physical education instructors’ self-evaluation, which refers to a physical education teacher’s understanding of the quality of self-teaching. When PE teachers conduct self-evaluation,

they can clearly recognize their own deficiencies in the process of physical education and improve themselves. Physical education teachers log in to the teacher system to conduct self-evaluation on their class situations.

(2) *Activity-Based Evaluations of Physical Education Instruction by Students.* Students and physical education teachers are in close touch, and student evaluations of physical education instructors are the most compelling. As a result, it is impossible to disregard the assessment actions of pupils. When evaluating student-taught sessions, it is critical to distinguish between physical education instructors and students. Students are the subject, and they take action against the teachers. Students can rate the physical education teacher’s class using their teaching evaluation account.

(3) *Peer Evaluation of Teaching Activities.* Peer physical education instructors are the topic of the assessment process, while the assessed physical education teachers are the object of the evaluation procedure. There are no subjective evaluations in peer evaluations; thus, the individual physical education classroom survey is not taken into account by the peer instructors. Peer physical education teachers can conduct physical education teaching evaluation on physical education teachers by way of audition.

(4) *Teaching Evaluation Activities by the Personnel of the Competent Department of Physical Education.* First, the personnel of the competent department of physical education are familiar with the content and goals of physical education, and secondly, the personnel of the competent department of physical education can directly grasp the first-hand information of physical education teachers, so their evaluation is authoritative. Physical education department staff can evaluate physical education teachers’ classes through random checks and auditions.

3.4.3. *Explore the Construction of Football Teaching Evaluation Process.* Analysis of the present state of school teaching evaluation implementation shows that the assessment procedure for football is built on the use of big data. Teachers, administrators, and students are the primary beneficiaries of this tool. Collection, analysis, and interpretation of data make up the assessment process. In Figure 2, you can see the specifics of the output and result feedback in action.

## 4. Experiment and Analysis

In this chapter, we define the survey results and analysis of teacher evaluation indicators, survey results and analysis of student evaluation indicators, and indicator weight coefficient results in detail.

4.1. *Survey Results and Analysis of Teacher Evaluation Indicators.* Taking the evaluation results of the first- and second-level indicators of teachers by experts into the previous method for calculation, the following results were obtained: after two rounds of investigation, it was

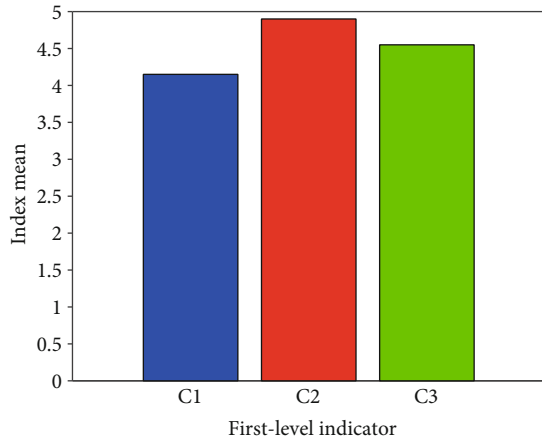


FIGURE 5: Comparison of primary indicators of student evaluation.

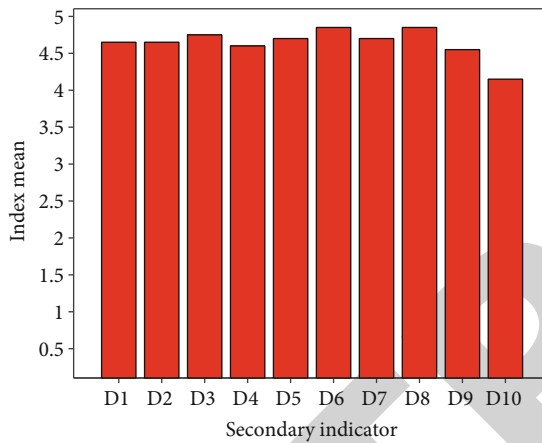


FIGURE 6: Comparison of secondary indicators of student evaluation.

TABLE 5: Consistency test of primary and secondary indicators.

Index	KHC	Chi-square value	<i>P</i> value
First-level indicator	0.45	18.14	0.0002 < 0.05
Secondary indicators	0.44	81.63	<0.05

determined that the first-level indicators of football teachers’ teaching evaluation included three items—the process of preparing to teach, the actual act of instructing, and the impact of that instruction. Preclass preparation, lesson plan composition, teaching etiquette, classroom routine, teaching attitude, teaching organization, teaching style, teaching material, and exercise load are secondary indicators used to evaluate football instructors, classroom atmosphere, sports skills, exercise awareness, and physical fitness; these are the 14 items of quality and theoretical basic knowledge. The parameter values of its primary and secondary indicators are shown in Figures 3 and 4.

Figure 3 shows that the parameters of the first-level indicators of teachers’ teaching evaluation all exceed 4. Among

them, the parameters of the teaching process and teaching effect even exceed 4.5, which show that experts have a high degree of recognition of these two items. Secondly, the Kendall harmony coefficient was 0.42, with a *P* value of 0.05 suggesting a substantial and well-coordinated set of expert evaluations. Teaching preparation, teaching method, and teaching impact are the three primary measures used to evaluate the effectiveness of football instructors in the classroom. Figure 4 shows that the parameters of the secondary indicators of teacher teaching evaluation also exceed 4, indicating that 14 secondary indicators have been recognized by experts. Secondly, the Kendall harmony coefficient rose to 0.35, which was greatly improved compared with the first round, indicating that the expert opinions were more coordinated. The chi-square value was 92.19, and the significance test *P* was much less than 0.05, indicating that the expert evaluation results were consistent. Finally, the secondary indicators of teacher teaching evaluation are these 14 items, and the consistency test statistical table of the primary and secondary indicators is shown in Table 4.

4.2. Survey Results and Analysis of Student Evaluation Indicators. After two rounds of investigation, it was determined that the first-level indicators of students’ football teaching evaluation were learning preparation, learning process, and learning effect. Preclass preparation, learning etiquette, classroom routine, learning attitude, emotional cooperation spirit, classroom atmosphere, sports skills, training awareness, physical quality, and basic knowledge of sports theory are the secondary indicators used to determine students’ physical education teaching evaluation. The comparison of its primary and secondary index parameters is shown in Figures 5 and 6.

Figure 5 shows that after two rounds of investigation, the parameters have obvious changes. The average of the three indicators of learning preparation, learning process, and learning effect increased, and the coefficient of variation decreased. Among them, the index of learning preparation increased “learning etiquette,” the mean increased to 4.05, and the coefficient of variation decreased to 0.19. The mean of the effect index increased to 4.55, and the coefficient of variation decreased to 0.11. Secondly, according to the Kendall harmony coefficient, the assessment findings of experts were coordinated and consistent. The Kendall harmony coefficient achieved 0.45, *P*0.05. Finally, we determine the first-level indicators of students’ PE teaching evaluation as learning preparation, learning process, and learning effect. This is shown by Figure 6. The averages of all indicators evaluated by students are all over 4, and the coefficients of variation are all less than 0.25, indicating that after these two rounds of expert indicator questionnaire surveys, experts have detected all ten secondary indications. First of all, the Kendall harmony coefficient shows that the expert survey findings are well coordinated, with a value of 0.44; the chi-square value is 81.63; and the significance test *P* is less than 0.05, indicating that the expert survey results are significant. Finally, we determine the secondary indicators of students’ PE teaching evaluation as these 10 items. The consistency test of the primary and secondary indicators of

TABLE 6: The weight of teachers' primary and secondary indicators.

First-level indicator	Index weight	Secondary indicators	Index weight
A1	0.13	B1	0.16
		B2	0.74
		B3	0.11
		B4	0.01
		B5	0.12
A2	0.67	B6	0.25
		B7	0.23
		B8	0.24
		B9	0.07
		B10	0.04
A3	0.20	B11	0.06
		B12	0.32
		B13	0.57
		B14	0.05

TABLE 7: Weights of primary and secondary indicators of students.

First-level indicator	Index weight	Secondary indicators	Index weight
C1	0.07	D1	0.76
		D2	0.24
		D3	0.12
C2	0.65	D4	0.20
		D5	0.60
		D6	0.08
		D7	0.13
C3	0.28	D8	0.30
		D9	0.46
		D10	0.11

student physical education teaching evaluation is shown in Table 5.

**4.3. Indicator Weight Coefficient Results.** The weights of various indicators of teachers and students in football teaching are calculated by the AHP method mentioned above, as shown in Tables 6 and 7.

## 5. Conclusion

In the current state of school physical education evaluation, there are numerous challenges that divert from the original intent of the discipline, including a single subject and model, unscientific techniques, a lack of originality in standards, an inadequate assurance system, and an unsatisfactory feedback mechanism; all contribute to the lack of individuality in standards. As a result, it is inextricably related to my country's long-established, centralized, and consistent educational administration structure. The study's index weight coefficient distribution is more scientific and sensible

because big data was used to construct evaluation indicators that could reflect practically every aspect of football instruction. As a result, big data can be utilized to assess physical education. The bulk of persons being evaluated for their work in the field of physical education in the context of big data applications is physical education instructors, students, peers, and employees in physical education departments. Data collection, data analysis, result output, and feedback are all components of a school physical education teaching evaluation system. In order to get reliable findings, data collection must be thorough, data analysis must be scientific, and feedback must be prompt and accurate. The assessment of physical education is incomplete without each connection.

## Data Availability

The datasets used during the current study are available from the corresponding author on reasonable request.

## Conflicts of Interest

The authors declare that they have no conflict of interest.

## References

- [1] E. Scase, J. Cook, M. Makdissi, B. Gabbe, L. Shuck, and W. Payne, "Teaching landing skills in elite junior Australian football: evaluation of an injury prevention strategy COMMENTARY," *British Journal of Sports Medicine*, vol. 40, no. 10, pp. 834–838, 2006.
- [2] L. Wu, D. Sun, P. Ren, D. Sun, and H. Xiong, "Mobile intelligent terminal based remote monitoring and management system," *Experimental Technology & Management*, vol. 43, no. 4, pp. 56–59, 2013.
- [3] J. Pei, K. Zhong, M. A. Jan, and J. Li, "Personalized federated learning framework for network traffic anomaly detection," *Computer Networks*, vol. 209, p. 108906, 2022.
- [4] G. L. Huang, "Discussion on teaching evaluation of teachers in private colleges and universities in my country," *Henan Education Mid*, vol. 9, pp. 8–9, 2012.
- [5] M. E. Lockheed and A. Komenan, "Teaching quality and student achievement in Africa: the case of Nigeria and Swaziland," *Teaching & Teacher Education*, vol. 5, no. 2, pp. 93–113, 1989.
- [6] S. M. Lee, C. R. Burgeson, J. E. Fulton, and C. G. Spain, "Physical education and activity: results from the school health policies and programs study 2000," *Journal of Physical Education Recreation & Dance*, vol. 74, no. 1, pp. 20–36, 2003.
- [7] S. Biddle, C. Wang, N. Chatzisarantis, and C. M. Spray, "Motivation for physical activity in young people: entity and incremental beliefs about athletic ability," *Journal of Sports Sciences*, vol. 21, no. 12, pp. 973–989, 2003.
- [8] W. Duan, J. Gu, M. Wen, G. Zhang, Y. Ji, and S. Mumtaz, "Emerging technologies for 5G-IoV networks: applications, trends and opportunities," *IEEE Network*, vol. 34, no. 5, pp. 283–289, 2020.
- [9] Y. Wu, W. Zhang, J. Shen, Z. Mo, and Y. Peng, "Smart city with Chinese characteristics against the background of big data: idea, action and risk," *Journal of Cleaner Production*, vol. 173, pp. 60–66, 2018.

## Retraction

# Retracted: Exploration of the Cultivation Path of Medical Students' Politico-Ideological and Humanistic Quality Based on Deep Learning

### Computational and Mathematical Methods in Medicine

Received 1 August 2023; Accepted 1 August 2023; Published 2 August 2023

Copyright © 2023 Computational and Mathematical Methods in Medicine. This is an open access article distributed under the Creative Commons Attribution License, which permits unrestricted use, distribution, and reproduction in any medium, provided the original work is properly cited.

This article has been retracted by Hindawi following an investigation undertaken by the publisher [1]. This investigation has uncovered evidence of one or more of the following indicators of systematic manipulation of the publication process:

- (1) Discrepancies in scope
- (2) Discrepancies in the description of the research reported
- (3) Discrepancies between the availability of data and the research described
- (4) Inappropriate citations
- (5) Incoherent, meaningless and/or irrelevant content included in the article
- (6) Peer-review manipulation

The presence of these indicators undermines our confidence in the integrity of the article's content and we cannot, therefore, vouch for its reliability. Please note that this notice is intended solely to alert readers that the content of this article is unreliable. We have not investigated whether authors were aware of or involved in the systematic manipulation of the publication process.

In addition, our investigation has also shown that one or more of the following human-subject reporting requirements has not been met in this article: ethical approval by an Institutional Review Board (IRB) committee or equivalent, patient/participant consent to participate, and/or agreement to publish patient/participant details (where relevant).

Wiley and Hindawi regrets that the usual quality checks did not identify these issues before publication and have since put additional measures in place to safeguard research integrity.

We wish to credit our own Research Integrity and Research Publishing teams and anonymous and named external researchers and research integrity experts for contributing to this investigation.

The corresponding author, as the representative of all authors, has been given the opportunity to register their agreement or disagreement to this retraction. We have kept a record of any response received.

### References

- [1] S. Xue and S. Li, "Exploration of the Cultivation Path of Medical Students' Politico-Ideological and Humanistic Quality Based on Deep Learning," *Computational and Mathematical Methods in Medicine*, vol. 2022, Article ID 5766675, 9 pages, 2022.

## Research Article

# Exploration of the Cultivation Path of Medical Students' Politico-Ideological and Humanistic Quality Based on Deep Learning

Sainan Xue and Shuang Li 

College of Nursing, Inner Mongolia Medical University, Hohhot, Inner Mongolia Autonomous Region 010059, China

Correspondence should be addressed to Shuang Li; 20120162@immu.edu.cn

Received 21 April 2022; Revised 18 May 2022; Accepted 23 May 2022; Published 28 June 2022

Academic Editor: Naeem Jan

Copyright © 2022 Sainan Xue and Shuang Li. This is an open access article distributed under the Creative Commons Attribution License, which permits unrestricted use, distribution, and reproduction in any medium, provided the original work is properly cited.

Medical talent development has its own characteristics, which means that political-ideological education in medical colleges must establish a development model that reflects these characteristics. In a methodological sense, research on the development of politico-ideological education in medical colleges should adhere to the coordinated development of politico-ideological education in medical colleges, which follows the requirements of the current situation and the three laws of politico-ideological education in medical colleges, namely, the requirements of the law of politico-ideological education, the law of teaching and educating people, and the law of study. In practice, in view of the practical contradictions in the politico-ideological work of medical colleges and universities at the present stage, explore the collaborative education mechanism of medical colleges and universities, constantly enrich the ways and methods of politico-ideological work in medical colleges and universities, improve the affinity, pertinence, and effectiveness of politico-ideological education, and constantly open up a new situation of politico-ideological education in colleges and universities. This work offers a path exploration approach based on deep learning for cultivating the political-ideological, and humanistic qualities of medical students' curriculum, and the model's performance is proven by simulation trials.

## 1. Introduction

The Communist Party of China has always attached great importance to politico-ideological work. The discipline of politico-ideological education was established in the early 1980s, and the politico-ideological work in colleges and universities began to be highly valued in the late 1980s [1]. The discipline of politico-ideological education has developed rapidly at this stage, and the discipline system, content, media, and means of politico-ideological education are also constantly improving. At the same time, under the background of the rapid development of economy and society, the rapid change of science and technology, and the continuous improvement of the level of opening to the outside world in the period of social transformation, there are many challenges and problems in the continuous development and self-improvement of politico-ideological education in colleges and universities [2], including the challenge of the

development concept of western universities, the challenge of hostile forces at home and abroad, the challenge of multiple ideologies and values, and the challenge of new media. The unique history, culture, and national conditions determine that we must take our own path of higher education development [3]. Do a good job of running socialist colleges and universities with Chinese characteristics and putting them in a strong position to follow the party's leadership. Fully implementing the party's education policy, policy, and line, continuously strengthening and improving politico-ideological education, always adhering to the correct direction of educating people, and comprehensively improving the politico-ideological work of colleges and universities are all critical [4]. The significance and ways of humanistic quality and politico-ideological education in colleges and universities are shown in Figure 1.

It is of great significance to fully implement the party's education policy, policy, and line, continuously strengthen



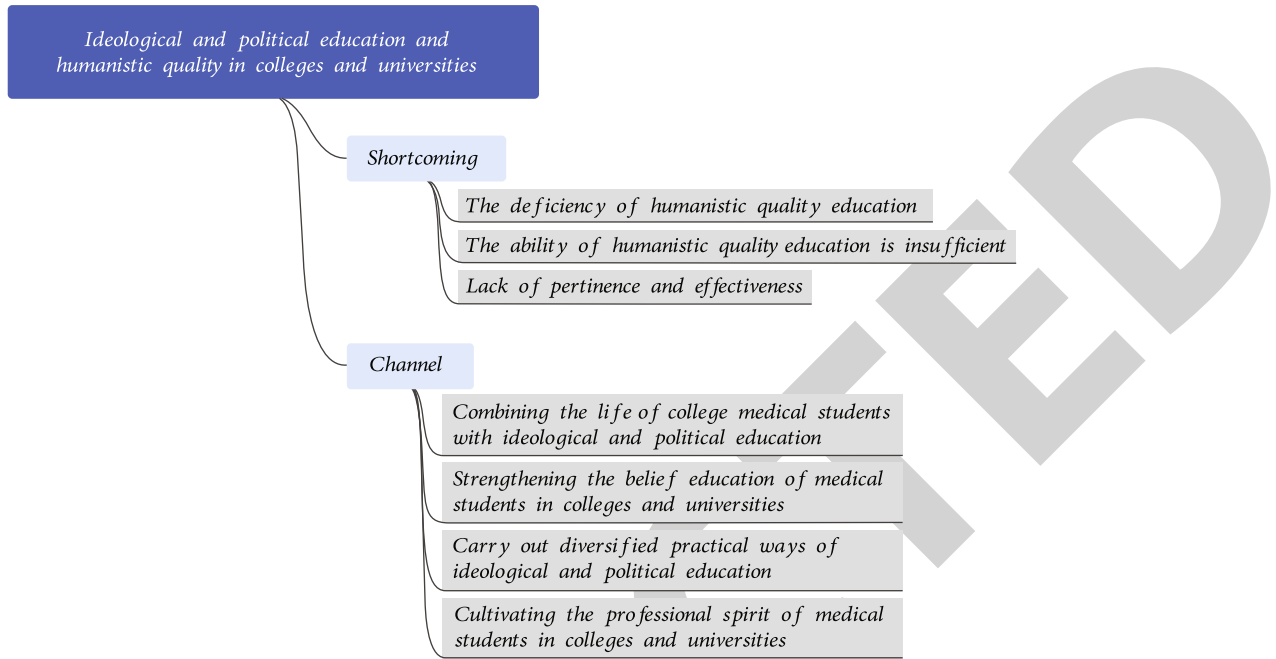


FIGURE 1: The significance and ways of humanistic quality and politico-ideological education in colleges and universities.

and improve politico-ideological education, always adhere to the correct direction of educating people, and comprehensively improve the politico-ideological work of colleges and universities [5]. It is conducive to solving the current politico-ideological education dilemma and enhancing the effectiveness of politico-ideological education in medical schools. It is conducive to the issue of improving the ideological and moral quality of medical students and implementing the concept of synergy in the politico-ideological education of medical schools [6]. Through the organic integration of curriculum thinking and political science courses, which can better penetrate the notion of educational thought, the organic integration of medical professional teaching and political-ideological education teaching can be realized. Teaching through practice bases, such as university hospital internships and community clinics, cultivates the spirit of medicine, enhances the apprehension of the meaning of life, helps motivate the learning of professional skills, and facilitates the cultivation of new medical talents with both virtues and talents [7]. The research on the collaborative development of politico-ideological education in medical schools under the pattern of “Big Thinking and Politics” is conducive to building a smooth communication channel in education and teaching, bringing into play the affinity of politico-ideological work, enhancing the effectiveness of education, and facilitating the integration of the links and communication among the constituent elements and departments in the current education system, so as to bring into play the proper functions of each subsystem.

Compared with the traditional politico-ideological education mode, the “great politico-ideological” education mode has its own characteristics [8]. First of all, the education mode under the “great politico-ideological” pattern has the universality of personnel participation. In terms of partici-

pants, the education mode under the “great politico-ideological” pattern is not limited to full-time teachers of politico-ideological theory courses but requires the teaching staff of the whole school to participate in the politico-ideological work of college students. Secondly, the educational mode under the pattern of “great thought and politics” has the extensive use of time and space. Colleges and universities should shoulder the task of educating people all the time from entering the school to graduation and in all educational links. In talent training, education, and teaching, we should adhere to the principle of education first and moral education first and pay attention to and implement the infiltration method of politico-ideological education [9]. Thirdly, due to the pertinence and openness of the content system, the politico-ideological education in colleges and universities has vitality. It must keep up with the pace of the times and always adhere to being close to reality and life [10]. The politico-ideological education should be targeted and the content selection of politico-ideological education should be open. Politico-ideological education should face the world and the future, absorb the advanced achievements of human civilization to the greatest extent, release the attraction and appeal of politico-ideological education to the greatest extent, and improve the affinity of politico-ideological education. Finally, the platform makes use of the complementarity of virtual reality [11]. In terms of educational methods and means, based on the characteristics of the network era, integrate the real platform and virtual platform, and strive to truly promote the cultivation of morality in the complementary advantages of multiple platforms.

The arrangements of the paper are as follows: Section 2 discusses the related work. Section 3 describes the design of application model. Section 4 examines the experiments and results; section 5 concludes the article.

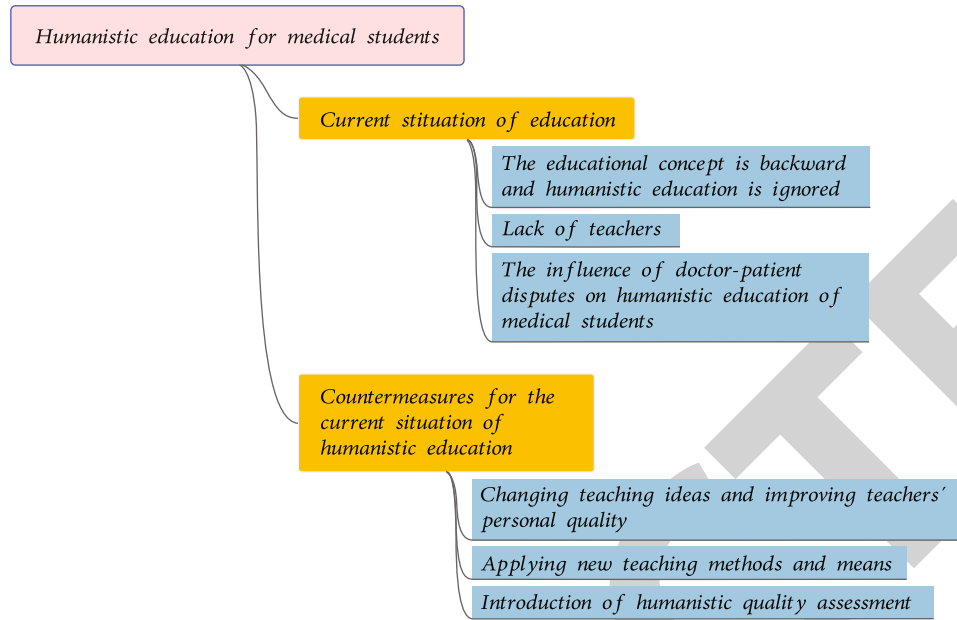


FIGURE 2: The current situation of humanistic education for medical students.

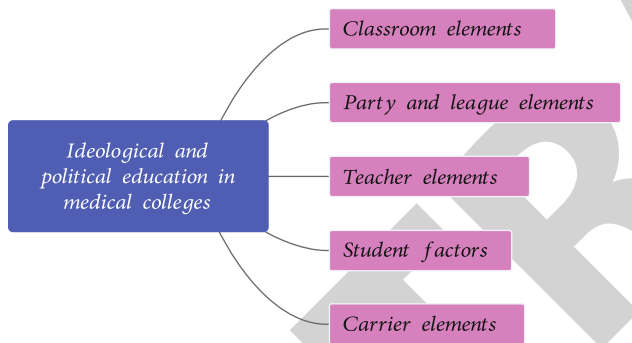


FIGURE 3: The structure of politico-ideological education in medical colleges.

## 2. Related Work

**2.1. Research Status of Humanistic Quality Education for Medical Students.** Medical students' humanistic education needs to go through two stages: the classroom learning stage and the clinical practice stage. Similar to the current situation the biomedical model is still dominant in clinics, China's medical education has not gotten rid of the traditional biomedical education model. In the classroom learning stage, whether it is basic medical courses or clinical courses, teachers only pay attention to the explanation of medical knowledge [12]. Ignoring the explanation of humanistic knowledge combined with clinical practice leads medical students to know little about doctor-patient communication skills and the complex doctor-patient relationships. Clinical practice is an important period for medical students to learn. It is a key stage to combine the theoretical knowledge of classroom learning with clinical practice. However, at present, the humanistic education of medical students in clinical practice has not been paid attention to

[13]. The current situation of humanistic education for medical students is shown in Figure 2.

Most of the teachers in clinical teaching units have been used to the disease-centered biomedical model. They believe that medical knowledge and technology are the most important. Students with solid clinical knowledge and skills can be competent for clinical work. Most of the clinical teaching teachers are frontline clinical doctors. They are nervous and do not have enough time to lead students to communicate with patients on the spot [14]. However, students' work stays on the writing of medical documents. Some teaching teachers have insufficient humanistic knowledge reserves and cannot play an exemplary role for students. Some teachers are afraid of medical disputes and dare not let medical students contact patients, which deprives medical students of the opportunity to combine the learned humanistic knowledge with clinical practice and cannot effectively transform it into clinical ability. All of these hinder the improvement of medical students' humanistic quality and make students have the idea of emphasizing technology over humanities [15]. Teachers are the key factor in the cultivation of the humanistic quality of medical students. At present, the number of teachers in medical colleges in China is insufficient and the structure of teachers is unreasonable. Teachers of general medical courses graduated from medical colleges and universities, with good medical professional knowledge, but lack humanistic knowledge [16]. Humanities teachers graduated from nonmedical colleges and lack a comprehensive and systematic understanding of medical knowledge. Teachers act in their own way and lack communication and exchange, so they cannot organically combine the medical knowledge and humanistic knowledge learned by students. The frequent occurrence of doctor-patient disputes, especially violent medical injuries, has a certain negative impact on the humanistic education

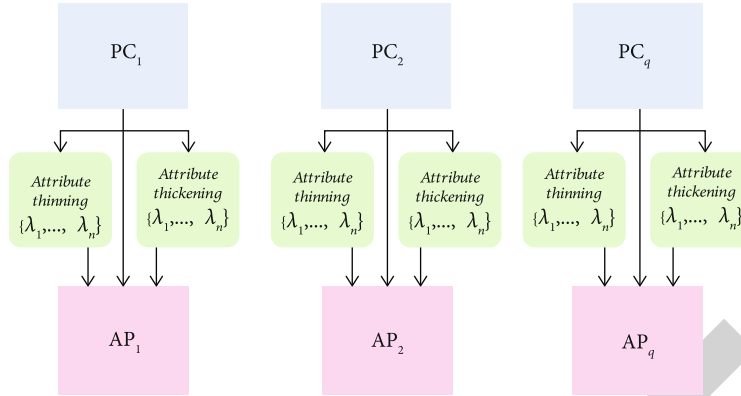


FIGURE 4: Diagram of the composite kernel function of the depth method.

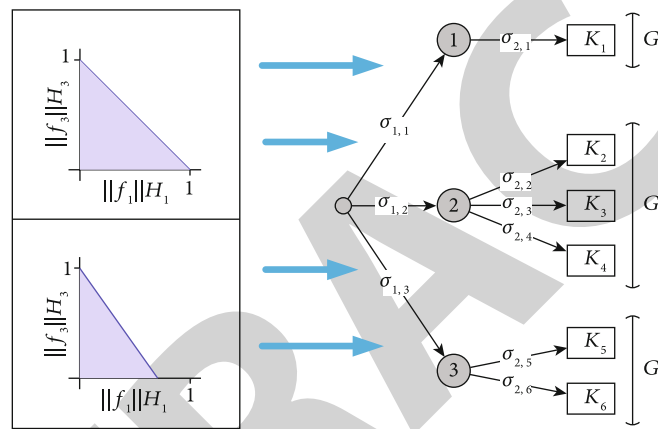


FIGURE 5: The cross-layer connection structure of the residual network.

of medical students [17]. On the one hand, it makes them lack confidence and even fear about the career they want to engage in the future, which leads some medical students to switch to other careers after leaving school [18]. On the other hand, in order to avoid the occurrence of medical disputes, some clinical practice units dare not let interns operate or communicate with patients, which deprives them of a great opportunity to integrate theory with practice.

**2.2. Research Status of Politico-Ideological Education for Medical Students.** In fact, in clinical work, we often find that some patients are resistant to interns and unwilling to cooperate with their diagnosis and treatment activities, so they cannot master doctor-patient communication skills well [19]. The lack of doctor-patient communication skills of medical students is easy to cause contradictions with patients in their contact with patients and leads to doctor-patient disputes. This will create a vicious cycle that is not helpful to the development of a positive doctor-patient relationship. Medical colleges and universities, like the majority of colleges and universities, struggle with issues such as ideological imbalance between teachers and students, a single teaching paradigm, and a lack of an overarching idea of politico-ideological education [20]. At the same time, the problems of politico-ideological education in medical colleges still have their particularity, the lack of personality in

politico-ideological education, and so on. The above problems pose a great challenge to the effectiveness of politico-ideological education in medical colleges. It is urgent to change the development mode of politico-ideological education in medical colleges and take coordinated development as the methodological guidance [21]. The coordinated development of politico-ideological education in medical colleges and universities refers to taking the concept of coordinated development as the methodological guidance of the action of politico-ideological education in medical colleges and universities in order to achieve the goal of politico-ideological education [22]. The structure of politico-ideological education in medical colleges is shown in Figure 3.

The coordinated development of politico-ideological education in medical colleges can learn from various educational media, educational subjects, and other favorable factors and operate in a coordinated and orderly manner [23]. Thus, the functions of each part can be brought into full play, and the goal of politico-ideological education in medical colleges can be optimally and effectively realized. Professional course teachers and politico-ideological theory teachers should cooperate to educate people and do well the politico-ideological work in medical colleges and universities [9]. We should follow the law of politico-ideological work, the law of teaching and educating people, and the law of students' growth and constantly improve the ability

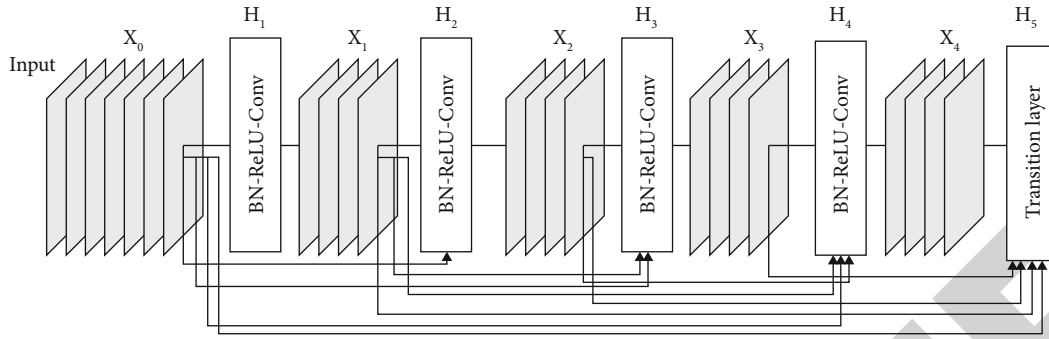


FIGURE 6: The convolutional neural network containing one or more dense modules.

TABLE 1: The current situation of politico-ideological integration of the curriculum.

	Freshman	Sophomore	Junior
Integration into curriculum thought and politics	11	14	9
Not integrated into the curriculum of politico-ideological education	21	18	23

and level of politico-ideological work. To make good use of the classroom as the main channel, the theory course of politico-ideological education should be strengthened in improvement, enhance the affinity and pertinence of politico-ideological education, and meet the needs and expectations of student’s growth and development [24]. Educators are the first to receive an education. Only under the guidance of educators with noble moral quality and keeping pace with the times, can they smoothly interact with the educated in the process of education, so as to improve students’ ideological and moral quality. The success of this interaction ultimately depends on the teacher as the leader of education [25].

*2.3. Research Status of Deep Learning.* How to transfer the input data from the original space to the high-dimensional space, which can distinguish two types of complicated sample data without requiring any implicit mapping kernel function [26], is a problem worth considering. A good way to overcome this problem is to utilize a deep neural network to map the samples from input space to feature space, which will improve the classification effect. Generally speaking, for a given number of training samples, if they lack other prior knowledge, people prefer to use a small number of calculation units to establish the compact expression of the objective function in order to obtain better generalization ability. Deep learning takes the original form of data as the input of the algorithm [27]. The original data is abstracted layer by layer as the final feature representation required by its own task and finally ends with the mapping from the feature to the task target. In particular, experience has proved that the two-stage strategy composed of unsupervised pretraining and supervised tuning is not only effective for overcoming the training difficulties of deep networks but also endows deep networks with superior feature learning ability. Then, many new depth structures were established. Meanwhile, at last year’s international top conference on

computer vision and pattern recognition, researchers announced the end of the ImageNet challenge [28]. Even though it has only been around for eight years, it has accomplished incredible things. Machine learning has advanced in the disciplines of computer vision, speech recognition, and natural language processing, while the outcomes of picture categorization and target identification have made significant advances.

Among them, the key is that the neural network has ushered in its spring again after a long cold winter. Although deep learning can automatically obtain features of different scales from simple to abstract when using the extracted features for classification or recognition, a deep neural network uses the feature of the last hidden layer for classification, that is, using the feature of a single scale for classification [29]. This is because, in the deep neural network, a layer is connected with its front and rear adjacent layers, that is, it can only receive input from the adjacent previous layer.

### 3. Design of Application Model

Based on deep learning, this paper focuses on the kernel mapping structure and spanning structure model of the deep neural network, in order to effectively solve the shortcomings of the original method, improve the performance and generalization ability of the deep neural network, and finally promote the improvement and development of deep neural network model. This research plays a positive role in promoting the development of deep neural networks, especially multilayer perceptron and convolutional neural network models. Combined with the research focus of this paper, some representative works in multicore learning and cross-connected convolution neural networks are introduced in detail. Among them, the research of multicore learning is mainly divided into the research of learning methods of multicore learning and the research of training methods of

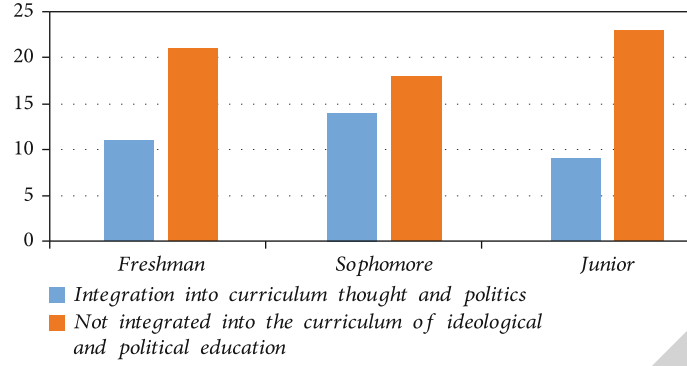


FIGURE 7: The current situation of politico-ideological integration of the curriculum.

TABLE 2: The statistics of politico-ideological elements in the end part.

Category	Relaxation activities	Mutual evaluation	Class summary	Job arrangement	Interaction
Numbers	22	34	342	21	35
Percentage	28.21%	43.59%	41.05%	26.92%	44.87%

multicore learning. The three representative models of cross-connected convolutional neural networks are fast track network, residual network, and densely connected network. When the compound nucleus is applied to the task of gene function classification, the classification accuracy is higher than that of a single nucleus. The mathematical expression is as follows:

$$\begin{aligned} K_{\text{comb}} &= K_1(\mathbf{x}_1 + \mathbf{x}_2) + K_2(\mathbf{x}_1 + \mathbf{x}_2), \\ K_{\text{comb}} &= K_1(\mathbf{x}_1 + \mathbf{x}_2) \cdot K_2(\mathbf{x}_1 + \mathbf{x}_2). \end{aligned} \quad (1)$$

Then, the combination coefficient is directly calculated through a heuristic process, and its mathematical expression is as follows:

$$A(\mathbf{K}, \mathbf{K}_t) = \frac{\langle \mathbf{K}, \mathbf{K}_t \rangle_F}{\sqrt{\langle \mathbf{K}, \mathbf{K} \rangle_F \langle \mathbf{K}_t, \mathbf{K}_t \rangle_F}}. \quad (2)$$

The weight in the classification function leads to the combination kernel function with worse performance. Therefore, the kernel matrix is obtained first.

$$\mathbf{K}^c = \mathbf{K} - \frac{1}{n} \mathbf{1} \cdot \mathbf{1}^T \cdot \mathbf{K} - \frac{1}{n} \mathbf{K} \cdot \mathbf{1} \cdot \mathbf{1}^T + \frac{1}{n^2} (\mathbf{1}^T \cdot \mathbf{K} \cdot \mathbf{1}) \cdot \mathbf{1} \cdot \mathbf{1}^T. \quad (3)$$

Then, calculate the combination coefficient as shown below, and a more reasonable combination kernel function can be obtained.

$$\theta_m = \frac{A(\mathbf{K}_m^c, \mathbf{K}_t^c)}{\sum_{i=1}^M A(\mathbf{K}_i^c, \mathbf{K}_t^c)}. \quad (4)$$

The optimization method also expresses the composite kernel function as a nonnegative linear combination of a

set of basis kernels. The difference is that it calculates the combination coefficient through some optimization criterion.

$$\begin{aligned} \max \quad & \sum_{m=1}^M \theta_m \mathbf{y}^T \mathbf{K}_m \mathbf{y} \\ \text{s.t.} \quad & \sum_{m=1}^M \sum_{i=1}^M \theta_m \theta_i \langle \mathbf{K}_m, \mathbf{K}_i \rangle_F = c \\ & \theta \in \mathbf{R}_+^M \end{aligned} \quad (5)$$

By solving the programming problem represented by the above formula, the combination coefficient can be obtained. Moreover, the optimization method can also express the composite kernel function as the nonlinear combination of the base kernel. The mathematical expression of its objective function is as follows:

$$\begin{aligned} \min_{\mathbf{w}, b, \theta} \quad & \frac{1}{2} \mathbf{W}^T \mathbf{W} + \sum_l L(y^l, f(\mathbf{x}^l)) + r(\theta) \\ \text{s.t.} \quad & \theta \in \mathbf{R}_+^M \end{aligned} \quad (6)$$

Kernel functions can have a variety of forms, commonly used for the following mathematical expressions:

$$K_{\text{comb}}(\mathbf{x}_i, \mathbf{x}_j) = \left( d_0 + \sum_{m=1}^M \theta_m \mathbf{x}_i^T \mathbf{x}_j \right)^q. \quad (7)$$

The depth method is to stack multiple basis kernels in depth to obtain the composite kernel function and then use some criteria to solve the parameters. The structural block diagram of the composite kernel function of the depth method is shown in Figure 4.

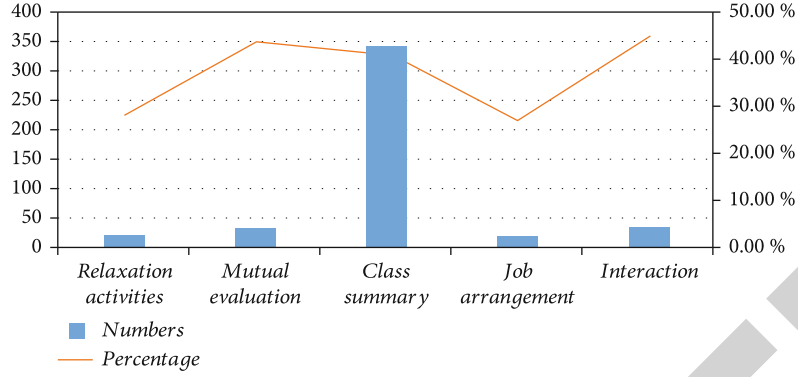


FIGURE 8: The statistics of politico-ideological elements in the end part.

The optimization problem of multilayer and multicore learning of  $j$ -layer can be expressed as

$$\min_{K \in \mathcal{K}^{(1)}} \min_{f \in \mathcal{H}_K} \lambda \|f\|_{\mathcal{H}_K} + \sum_{l=1}^N L(y^l f(\mathbf{x}^l)). \quad (8)$$

Specifically, the mathematical of the decision function can be expressed as

$$\mathcal{H}^{(2)} = \left\{ K^{(2)}(\mathbf{x}_i, \mathbf{x}_j; \boldsymbol{\theta}) = \exp \left( \sum_{m=1}^M \theta_m K_m^{(1)}(\mathbf{x}_i, \mathbf{x}_j) \right) \right\}. \quad (9)$$

At this time, the mathematical expression of the objective function is

$$\min_{K \in \mathcal{H}^{(2)}} \min_{f \in \mathcal{H}_K} \frac{1}{2} \|f\|_{\mathcal{H}_K}^2 + C \sum_{l=1}^N \max(0, 1 - y^l f(\mathbf{x}^l)) + \sum_{m=1}^M \theta_m. \quad (10)$$

Firstly, the base core is selected, and then, the selected base core is combined in a linear or nonlinear way to obtain the composite core. However, research shows that the composite kernel generated by multicore learning is not always better than the base kernel, one possible reason is that the network structure of multicore learning is shallow and has certain limitations, which is not enough to express relatively complex composite kernel functions through the linear or nonlinear combination of base kernels. Most of the current multicore learning methods convert the problem to dual space and use a two-step method to solve the parameters. This will cause misunderstanding among readers to a certain extent. For solving the kernel learning method, we must convert it to dual space for the solution. The cross-layer connection structure of the residual network is shown in Figure 5.

The traditional deep neural network only allows the structure connected by adjacent layers, which limits its integration of multiscale features for classification or recognition. In the fast-track network, information can flow across layers directly behind layers without obstacles, and its math-

ematical expression is as follows:

$$\mathbf{y} = H(\mathbf{x}, \mathbf{W}_H) \circ T(\mathbf{x}, \mathbf{W}_T) + \mathbf{x} \circ C(\mathbf{x}, \mathbf{W}_C). \quad (11)$$

By multiplying element by element, the fast tracklayer can be simplified to

$$\mathbf{y} = H(\mathbf{x}, \mathbf{W}_H) \circ T(\mathbf{x}, \mathbf{W}_T) + \mathbf{x} \circ (1 - T(\mathbf{x}, \mathbf{W}_H)). \quad (12)$$

Another treatment is to change the dimension of the ordinary layer first and then stack the fast track layer. Based on these two processes, a similar fast tracklayer can be constructed by using the idea of shared weight and receptive field in a convolutional neural network. Once convergence begins, degradation problems may also occur. The degradation problem is that as the depth increases, the accuracy quickly reaches saturation and then degenerates rapidly. Unexpectedly, this degradation is not caused by overfitting, because increasing the number of layers will lead to a higher error rate. The introduction of identity transformation can make the adjustment of network. Parameters more effective, i.e., the mapping is more sensitive to output change after the introduction of residual. In terms of back-propagation, identity mapping allows for direct propagation and the addition of the error term to the front layer, removing gradient reduction and explosion issues. In short, residuals allow you to remove the same main part while highlighting minor differences. According to research on residual networks, even networks with hundreds of layers can be trained reliably and successfully provided cross-layer connections are added between levels. Broadly speaking, a dense network refers to a convolutional neural network containing one or more dense modules, as shown in Figure 6.

This control of growth rate cannot only reduce the parameters of the dense network but also ensure the performance of the dense network. However, dense networks simply splice features of different scales, which may lead to feature redundancy. In addition, the dense network consumes a lot of memory during training. The usual approach is to design a cross-connect structure carefully for a given task. This approach usually achieves good results but does not provide people with the difference between the results of different cross-connect methods.

To sum up, this paper proposes a deep neural mapping support vector machine model. The model uses a deep neural network to explicitly represent the kernel mapping and maps the input from the original space to the feature space. In fact, kernel mapping is an explicit function represented by a deep neural network.

#### 4. Experiments and Results

In order to accurately understand the current situation of the implementation of curriculum politico-ideological education, a questionnaire survey was conducted on the teaching front-line teachers of the teaching part of 8 medical colleges in Shandong and some students in freshman, sophomore, and junior grades, and field visits were conducted to investigate the politico-ideological classroom of relevant schools. The teaching records of politico-ideological education were included in the scope of this study, so as to master the specific implementation of curriculum politico-ideological education such as students' cognitive status and teachers' cognitive status. Starting with the current situation of curriculum politico-ideological education, this paper deeply explores and analyzes the bottlenecks and reasons encountered in the implementation process, puts forward reasonable solutions for the implementation of curriculum politico-ideological education in the classroom, and puts forward measures to improve the quality of curriculum politico-ideological education, so as to integrate teaching with politico-ideological education and improve the ideological and moral level of medical students. The current situation of politico-ideological integration is shown in Table 1 and Figure 7.

The results show that in the implementation of curriculum thought and politics, the integration of physical education in sophomore is the best, followed by the freshman, and the integration of junior is slightly worse. On the one hand, it may be related to the learning pressure of students. Compared with freshmen and sophomores, junior students are facing great pressure of graduation. The focus of learning is on the subjects of cultural courses, which requires a lot of time to study and review cultural courses. On the other hand, some politico-ideological courses may be replaced by other teachers, resulting in the reduction of students' politico-ideological courses. At the same time, in order to serve other courses, teachers only complete teaching tasks in class, only pay attention to the teaching of skills and ignore the guidance of values, which makes it difficult to implement curriculum politico-ideological education in the third grade. In contrast, freshmen and sophomores face less pressure. Sophomores have adapted to the school environment, have a certain sports foundation, and have stronger autonomy in choosing learning content, so it is easier to implement curriculum thought and politics. Through the investigation, it is found that in terms of the ways to receive politico-ideological education, students believe that politico-ideological course is the main way to carry out politico-ideological education, followed by the infiltration in various disciplines, indicating two problems: one is that high school students lack ideological education at present, and the other

is that the school does not pay attention to carrying out ideological education. The statistics of politico-ideological elements in the end part are shown in Table 2 and Figure 8.

From the results of teachers' questionnaire statistics, first, in terms of teachers' cognition, teachers believe that the current way for students to receive ideological education is through the penetration of various disciplines. Secondly, most teachers affirmed the suitability and necessity of curriculum politico-ideological infiltration into the classroom and said that they would implement it in the follow-up classroom, but on the whole, teachers' understanding of curriculum politico-ideological is not enough.

#### 5. Conclusion

People benefit from political-ideological education. The work of being a man is difficult, and the ideological work of being a man is even more difficult. In general, political-ideological education integrates individual differences with society's mainstream values. Individuals have subjective initiative, and there are still some distinctions among them. Medical colleges and universities should be transformed into model places of stability and unity in order to cultivate a pleasant and welcoming environment. The politico-ideological education in medical colleges and universities should proceed from reality and integrate theory with practice. Based on this, this paper proposes a path exploration method for the cultivation of politico-ideological, and humanistic quality of medical students' curriculum based on deep learning, and the effectiveness of the model is verified by simulation experiments.

The research on the coordinated development of politico-ideological education in medical colleges is a research focusing on practice and application. In the future, we should continue to think about how to do a good job in the politico-ideological education in medical colleges and improve the affinity and pertinence of the politico-ideological education in medical colleges. Politico-ideological educators should have strong theoretical literacy and actively make use of the collaborative resources of Politico-ideological education with the characteristics and advantages of medical colleges. Finally, we should constantly improve our comprehensive ability to obtain and process information and be good at using new media. Other fields' mature theoretical and practical experience have been incorporated by the subject of political-ideological education. At home and abroad, dialectically treat and absorb ideological culture, science, and technology, and the discipline of politico-ideological education is expected to grow by leaps and bounds only via continual learning.

#### Data Availability

The datasets used during the current study are available from the corresponding author on reasonable request.

#### Conflicts of Interest

The authors declare that they have no conflict of interest.

## Research Article

# Identification of Key Genes in Severe Burns by Using Weighted Gene Coexpression Network Analysis

ZhiHui Guo , YuJiao Zhang, ZhiGuo Ming, ZhenMing Hao, and Peng Duan

Burns Department, General Hospital of TISCO, Taiyuan, 030003 Shanxi, China

Correspondence should be addressed to ZhiHui Guo; 201701370106@lzpcc.edu.cn

Received 22 April 2022; Revised 12 May 2022; Accepted 19 May 2022; Published 28 June 2022

Academic Editor: Naeem Jan

Copyright © 2022 ZhiHui Guo et al. This is an open access article distributed under the Creative Commons Attribution License, which permits unrestricted use, distribution, and reproduction in any medium, provided the original work is properly cited.

The aims of this work were to explore the use of weighted gene coexpression network analysis (WGCNA) for identifying the key genes in severe burns and to provide a reference for finding therapeutic targets for burn wounds. The GSE8056 dataset was selected from the gene expression database of the US National Center for Biotechnology Information for analysis, and a WGCNA network was constructed to screen differentially expressed genes (DEGs). Gene Ontology and pathway enrichment of DEGs were analyzed, and protein interaction network was constructed. A burn mouse model was constructed, and the burn tissue was taken to identify the expression levels of differentially expressed genes. The results showed that the optimal soft threshold for constructing the WGCNA network was 9. 10 coexpressed gene modules were identified, among which the green, brown, and gray modules had the largest number of burn-related genes. The DEGs were mainly related to immune cell activation, inflammatory response, and immune response, and they were enriched in PD-1/PD-L1, Toll-like receptor, p53, and nuclear factor-kappa B (NF- $\kappa$ B) signaling pathways. 5 DEGs were screened and identified, namely, Jun protooncogene (JUN), signal transducer and activator of transcription 1 (STAT1), BCL2 apoptosis regulator (Bcl2), matrix metalloproteinase 9 (MMP9), and Toll-like receptor 2 (TLR2). Compared with skin tissue of normal mouse, the messenger ribose nucleic acid (mRNA) and protein expression levels (PEL) of STAT1 and Bcl2 in burn tissue were greatly decreased, while those of JUN, MMP9, and TLR2 were increased obviously ( $p < 0.05$ ). In conclusion, STAT1, Bcl2, JUN, MMP9, and TLR2 can be potential biological targets for the treatment of severe burn wounds.

## 1. Introduction

Burn is a very special trauma, and its incidence is closely related to emergencies, traffic accidents, and daily life [1]. Severe burns can result in the loss of limb function and even death [2]. Burn patients will suffer physical and psychological harm if they receive a significant number of skin grafts, harsh physical therapy, or long-term rehabilitation treatment [3, 4]. Large-scale burns will cause a series of immunological and pathophysiological changes in the body, which will eventually lead to the disorder of the immune system [5]. Therefore, some scholars believe that the disturbance of immune system function after burn is an important factor leading to severe infection, multiorgan/system dysfunction, or death after burn [6]. Factors such as large-area tissue necrosis, stress response, shock, infection, or nutritional deficiency after burns, together with subsequent treatment,

will change the microenvironment of immune cells in the body [7, 8]. Therefore, although burn treatment techniques can improve the clinical symptoms and prognosis of patients to a certain extent, they cannot reduce the mortality of patients [9]. Therefore, it is urgent to understand the specific mechanism of maintaining and regulating immune dysfunction in burn patients and to find corresponding treatment methods.

Because gene chip and sequencing technologies can directly examine transcriptome data, it has become the primary tool for investigating the molecular mechanisms underlying life activities [10]. It is difficult to dig out the underlying molecular mechanisms by simply analyzing the transcriptome of a single tissue or sample. However, analyzing biological networks can reflect the interaction between different biomolecules at the system level, but cannot provide possibilities for exploring complex biological



phenomena [11]. Weighted gene coexpression network analysis (WGCNA) can identify coexpression modules in multiple biological samples based on the correlation between different gene expression profiles and find coexpression modules that are highly related to them after phenotypic correlation [12]. Compared with other coexpression analysis methods, the WGCNA network uses a soft threshold method to provide the sensitivity of the network to module identification, so the network has been widely used in the analysis of coexpression patterns in various organisms [13, 14]. The approach uses an approximate scale-free topology to generate the soft threshold and then replaces the previous traditional algorithm's hard threshold [15–18].

Therefore, the WGCNA method is adopted systematically to explore the expression patterns of severe burn tissue and normal tissue in this work, aiming to find the key genes of severe burn wound healing and provide a molecular-level theoretical basis for the search for clinical therapeutic targets of burn wounds.

This paper is organized as follows: Section 2 presents the materials and methods of the proposed concepts. Section 3 describes the statistical analysis and results. Section 4 presents the discussion of the whole paper. Section 5 summarizes this paper and offers directions for future work.

## 2. Materials and Methods

**2.1. Basis of the WGCNA Algorithm.** WGCNA belongs to a class of gene coexpression networks. The algorithm introduces an approximate scale-free topology to accurately calculate the soft threshold and then replaces the hard threshold of the previous traditional algorithm [15]. Compared with random networks, scale-free topology is more realistic. After standardization of the experimental data, WGCNA analysis can be performed. The specific analysis process is shown in Figure 1.

The coexpression network was adopted to construct a matrix  $A$  of the expression levels of samples and related genes. It was assumed that the gene was represented by  $i$ , and the sample size detection value was  $j$ ; the mathematical expression of the matrix could be given as follows:

$$A = \{a_{ij}\} = \{a_1, a_2, \dots, a_n\}. \quad (1)$$

After transformation of expression profile data matrix and calculation of the correlation between genes using matrix operations, the coexpression similarity can be defined using the absoluteness of the correlation coefficient:

$$\text{Similarity}_{ij} = |\text{cor}(a_i, a_j)|. \quad (2)$$

In Equation (2) above,  $\text{Similarity}_{ij}$  represented the similarity of the expression profiles of genes  $i$  and  $j$ , and the value ranged from 0 to 1.

The similarity matrix was converted to an adjacency matrix, and then, the WGCNA weighting coefficient  $\beta$  could

be determined based on the Pareto distribution law:

$$N_{ij} = \text{Similarity}_{ij}^\beta. \quad (3)$$

In the above Equation (3),  $N_{ij}$  was an adjacency matrix, and  $\beta$  was a weighting coefficient or a soft threshold.

To determine the dissimilarity of the highly connected gene forming modules in the constructed network, the adjacency matrix can be converted into a topological matrix, and then, topological reconstruction can be selected to calculate the degree of intergene association. The equation for calculating topological overlap was defined as follows:

$$\omega_{ij} = \frac{L_{ij} + N_{ij}}{\min\{k_i, k_j\} + 1 - N_{ij}}, \quad (4)$$

$$L_{ij} = \sum_u n_{iu}n_{ju}. \quad (5)$$

In Equation (4) above,  $L_{ij}$  was the sum of the products of adjacency coefficients of gene  $i$  and  $j$  connecting nodes, and  $k$  referred to the sum of adjacency coefficients of gene connecting nodes. When  $\omega_{ij} = 1$ , it meant that genes  $i$  and  $j$  were connected to all genes; when  $\omega_{ij} = 0$ , it meant that genes  $i$  and  $j$  were not connected to all genes.

The WGCNA required to use the dissimilarity calculated by the topological overlap method for hierarchical clustering and then obtain different gene modules of different branches [16]. The dynamic pruning was applied for the construction of cluster numbers to mine more modules. Gene coexpression network was to use systems biology methods to search for highly correlated modules. WGCNA can continuously approximate genes into a scale-free topology network through a weighted method and then construct a coexpression network and find hub genes in modules of interest [17]. Hub genes can be searched by threshold setting or by using function network screening.

**2.2. Selection of Materials for WGCNA.** The microarray data related to burns were screened from the gene expression database of the National Center for Biotechnology Information (NCBI) (<http://www.ncbi.nlm.nih.gov/geo/>), and GSE8056 was finally selected as the research object according to the research subjects and sample size. The samples in this dataset were derived from the skin samples of burn patients quickly obtained in the operating room and then detected and analyzed by high-throughput chips. The dataset contained a total of 12 samples, which were the normal group (accession numbers: GSM198875, GSM198876, and GSM198877) and the burn group (accession numbers: GSM198866, GSM198867, GSM198868, GSM198869, GSM198870, GSM198871, GSM198872, GSM198873, and GSM198874). Relevant gene records with  $p$  values less than 0.05 were selected and included in the WGCNA.

**2.3. Construction of WGCNA.** The “Flash Clust” software in the R language package was used for cluster analysis of the included samples, and the “Pick Soft Threshold” function

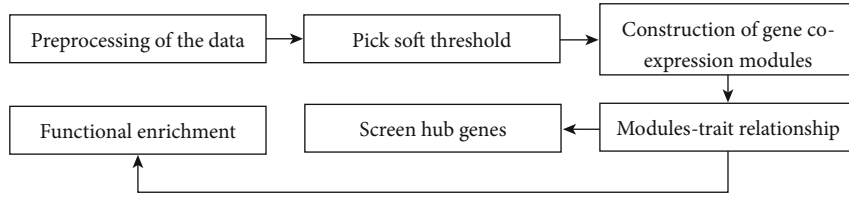


FIGURE 1: The specific analysis process of WGCNA.

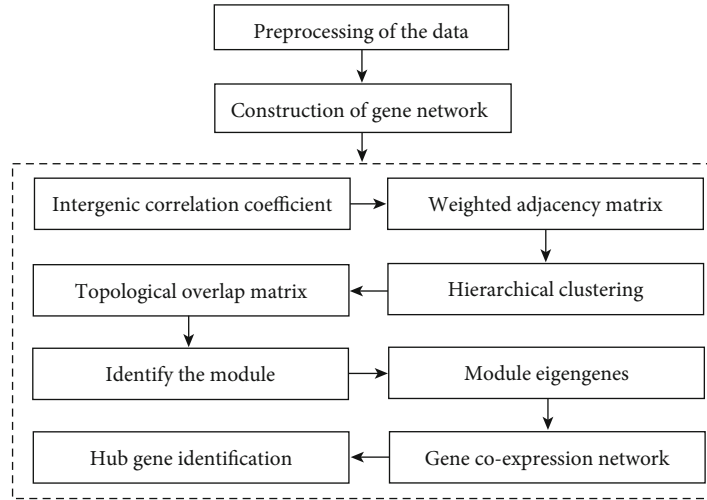


FIGURE 2: The specific flow of burn-related gene analysis using WGCNA.

TABLE 1: The quantitative primers of DEGs.

Gene name	Primer sequence (5'→3')	Size of product (bp)
STAT1 decreased	F: TACGGAAGCAAGCGTAATCT	219
	R: TGCACATGACTTGATCCTTCAC	
JUN increased	F: GTGTGGGACGACGATCAAAAG	151
	R: TGACCACTAACAGGGAAGGAC	
Bcl2 decreased	F: ACGTGGACCTCATGGAGTG	129
	R: TGTGTATAGCAATCCCAGGCA	
MMP9 increased	F: GCAGAGGCATACTTGTACCG	229
	R: TGATGTTATGATGGTCCCCTTG	
TLR2 increased	F: CTCTCAGCAAACGCTGTTCT	237
	R: GCGTCTCCCTCTATTGTATTG	
GAPDH	F: TGGCCTCCGTGTTCTAC	178
	R: GAGTTGCTGTTGAAGTCGCA	

was to adjust the weight of the weighting coefficient  $\beta$ . The matrix with correlation and adjacent relationship was calculated as a topological overlap matrix (TOM) using WGCNA, and the dissimilarity was calculated. The dissimilarity was undertaken as a distance metric to perform hierarchical clustering of genes and obtain identification modules, cluster markers, and merge highly similar modules. The “Plot Dendro and Color” function was selected to visualize the gene module and select the target genes within the module to draw a heat map. Finally, the genes in the modules closely related to severe burn were found, and the cluster analysis

of the relationship heat map was performed on the clinical characteristics. The specific flow of burn-related gene analysis using WGCNA is shown in Figure 2.

2.4. Screening of DEGs. Background correction of raw data was performed using robust multiarray average software, and DEGs were obtained using independent samples *t*-test and fold method. Comparative analysis of DEGs in burn tissue and normal tissue was performed using the analysis tool that came with the gene expression database in the NCBI dataset. The screening conditions were set as:

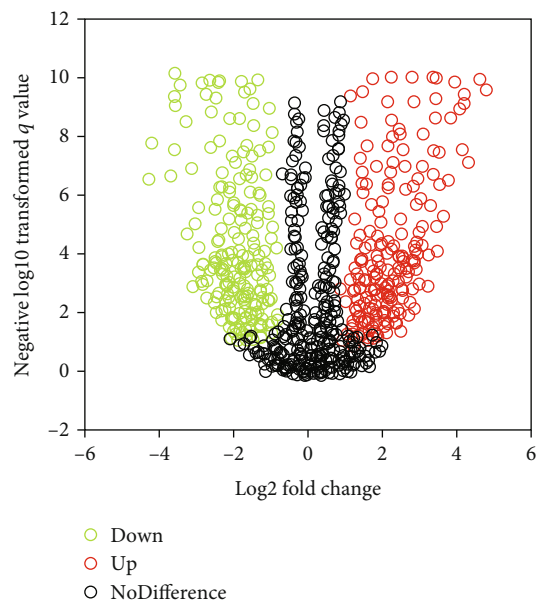


FIGURE 3: Volcano plot analysis of DEGs. Genes with no statistically great difference were marked in black, genes with low expression and statistically obvious difference were marked in green, and genes with high expression and statistically remarkable difference were marked in red.

- (1) The corrected  $p$  value (the adj  $p$  value) was less than 0.05
- (2) The absolute value of the log gene expression fold difference ( $|\log FC|$ ) was  $\geq 1.5$

**2.5. Analysis on Gene Ontology and Pathway Enrichment of DEGs.** Gene Ontology can be used for functional annotation of genes. The functional enrichment analysis of Gene Ontology included molecular function (MF), biological process (BP), and cellular component (CC). The gene set enrichment analysis software and profiler online tool were adopted in this work for enrichment analysis and annotations of the module and Kyoto Encyclopedia of Genes and Genomes (KEGG).

**2.6. Construction and Analysis on Protein Interaction Network of DEGs.** The STRING database can be selected to predict the functional correlation between proteins, and its prediction accuracy for genes was as high as 80% or more. The protein-protein interaction network of DEGs obtained by screening was constructed using the STRING 11.0 online tool (<https://cn.string-db.org/>). Protein interactions with confidence greater than 0.5 were selected from the protein-protein interaction network. The DEGs protein interaction network was constructed using Cytoscape software.

## 2.7. Identification of DEGs

**2.7.1. Construction of Burn Animal Model.** 20 healthy adult BALB/c mice, male or female, were selected as research subjects. Mice were randomly rolled into a control group and a burn group. The control mice were not given any medication and were fed normally. Mice in the burn model were

anesthetized by intraperitoneal injection of 50 mg/kg 1% sodium pentobarbital. The back skin was prepared, and the hair was removed; the mice were fixed on the operating table, and the depilated area was scalded continuously for 15 s with 97°C hot water to obtain a third-degree burn model. Immediately after modeling, 1 mL of 0.9% sterile normal saline was intraperitoneally injected for antishock treatment, and the wounds were disinfected with iodophor disinfectant.

**2.7.2. Real-Time Fluorescence Quantitative Polymerase Chain Reaction (rt-qPCR).** After 15 days of modeling, the back skin tissue of the same part of the two groups of mice was taken. After the blood was flushed with phosphate buffer, it was snap frozen in liquid nitrogen. After fully grinding the tissue, the Trizol method was used to extract total RNA from the tissue, and the concentration, purity, and integrity of the extracted RNA were detected. Using the extracted RNA as a template, reverse transcription of cDNA was performed according to the instructions of the PrimeScript™ RT reagent Kit with gDNA Eraser (perfect real-time) kit (Takara, Japan). Then, quantitative detection of the target gene was performed according to the instructions of the TB Green® Premix Ex Taq™ II (Tli RNaseH Plus) kit (Takara, Japan). The reaction system was set as follows: 10  $\mu$ L TB green Premix Ex Taq™ II reagent, 0.8  $\mu$ L upstream primer, 0.8  $\mu$ L downstream primer, 0.4  $\mu$ L ROX Reference Dye, 2  $\mu$ L cDNA template, and 6  $\mu$ L ddH<sub>2</sub>O. Quantitative primers were designed and synthesized by Shanghai Sangon Bioengineering Co., Ltd. The primer information was shown in Table 1.

**2.7.3. Western Blot.** The tissue was crushed thoroughly, and RIPA reagent was applied for protein extraction in the frozen skin tissue from the back of the mouse. The protein concentration of the extracted sample was determined according to the instructions of the BCA kit, the corresponding stacking gel and separating gel were prepared, and the sample protein was loaded and electrophoresed. After the target protein band was transferred to the membrane, a blocking solution containing 5% nonfat milk powder was used for blocking treatment at room temperature for 1 hour. After washed, add diluted primary antibodies; rabbit monoclonal STAT1 (1:2000), rabbit monoclonal JUN (1:5000), rabbit monoclonal Bcl2 (1:2000), rabbit monoclonal MMP9 (1:2000), rabbit monoclonal TLR2 (1:1000), and mouse monoclonal  $\beta$ -actin (1:5000) were incubated at 4°C for 12 hours. After recovery of the antibody, it can add the diluted secondary antibody, horseradish peroxidase-labeled goat anti-mouse IgG (1:10000), and incubate at room temperature for 1 hour in the dark. In addition, the target protein band was developed according to the instructions of the ECL chemiluminescence kit. The ImageJ software in the gel imager was adopted to measure the gray value of the target protein band, and  $\beta$ -actin was undertaken as the internal reference gene to detect the relative expression level of the target protein.

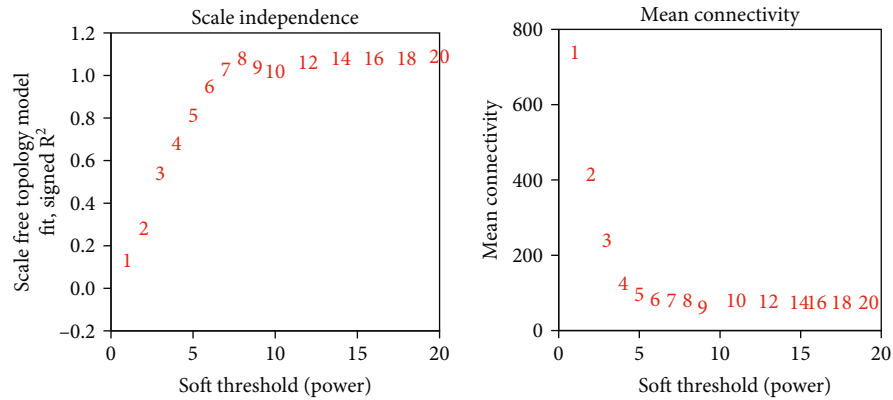


FIGURE 4: Soft threshold determination of WGCNA networks.

### 3. Statistical Analysis

SPSS 22.0 was used for data processing and statistical analysis. In the rt-qPCR detection results, the  $2^{-\Delta\Delta CT}$  method was applied to calculate the relative mRNA expression level of target gene, where  $\Delta CT \text{ value} = CT_{\text{target gene}} - C T_{\text{internal reference gene}}$ ,  $2^{-\Delta\Delta CT} = \Delta CT_{\text{burn group}} - \Delta C T_{\text{control group}}$ . The relative expression levels of mRNA and protein were compared between groups using independent samples  $t$  test, and expressed as mean  $\pm$  standard deviation.  $p < 0.05$  was considered to be statistically significant.

### 4. Results

**4.1. Construction of WGCNA Network.** Screening from the dataset, 563 DEGs were obtained, and the volcano plot of DEGs was shown in Figure 3. As it was given, the clustering results of the genes screened from the dataset had no obvious outlier samples, so they can be included in the subsequent WGCNA.

To improve the analysis effect of constructing the WGCNA model, the relationship between the soft threshold and the correlation coefficient (the left of Figure 4) and the relationship between the soft threshold and the mean value of the gene connection coefficient (the right of Figure 4) were plotted. It can be found that when the weighting coefficient  $\beta$  (i.e., soft threshold) in the WGCNA model was 9, the correlation coefficient and gene average connection coefficient of the constructed model were optimal. Therefore,  $\beta = 9$  was subsequently set for analysis.

**4.2. Clinical Correlation Analysis Based on WGCNA Network.** The correlation between external information and network modules was found from the gene coexpression network, and then, the network modules with high similarity were found. When  $\beta = 9$  in the WGCNA network, the squared value of the correlation coefficient between  $\log(k)$  and  $\log[p(k)]$  was greater than 0.9, and then, the constructed WGCNA network is shown in Figure 5.

Subsequently, the correlation heat map and cluster analysis of the WGCNA network module were constructed, and the results were given in Figure 6. As the figure revealed, 10 corresponding modules were screened in this work, and the

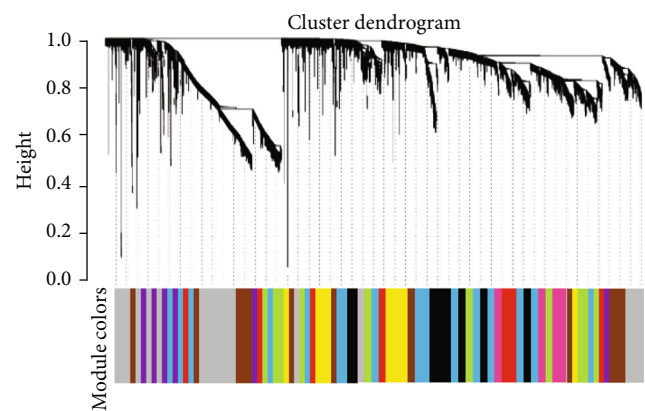


FIGURE 5: WGCNA network module of DEGs in burn tissue and normal tissue.

clinical characteristics were highly correlated with the green, brown, and gray modules in the WGCNA network.

**4.3. Analysis on Burn DEGs Based on WGCNA Network.** The WGCNA network was utilized to determine the key and differentially expressed genes, and Gene Ontology and KEGG tools were employed to undertake functional annotation of DEGs and enrichment analysis of signaling pathways. Figure 7 depicts the outcomes. As can be known from Figure 7(a), DEGs were mainly enriched for molecular functions such as replicative senescence, bacterial response to acyl bacterial lip peptides, and Toll-like receptor signaling pathways. They were mainly enriched for biological processes such as CCR5 chemokine receptor binding, histone kinase activity, and lipopeptide binding, and they were enriched for cell components such as cyclin B1-cdk1 complex and dependent protein kinase holoenzyme complex. As demonstrated in Figure 7(b), DEGs were mainly located in the PD-1/PD-L1 pathway, the AGE-RAGE pathway, the Toll-like receptor signaling pathway, the p53 signaling pathway, or the NF- $\kappa$ B signaling pathway.

The genes highly related to burns were found through the identification module, and the top 10 DEGs were selected using functional clustering analysis. The results were illustrated in Table 2. The top 10 DEGs were mainly

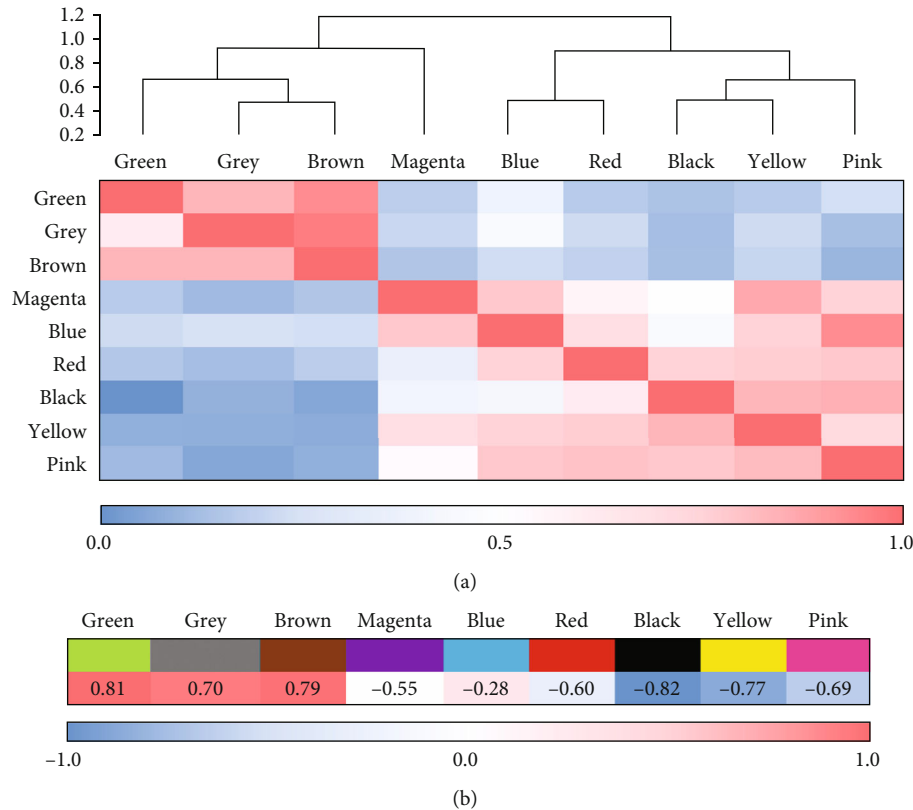


FIGURE 6: Modules of WGCNA network and its interaction analysis with clinical characteristics. (a) The interaction among different network modules and (b) the association between network modules and clinical features.

located in the green, brown, and gray modules of the WGCNA network.

**4.4. Analysis on Protein Interaction Network of DEGs in Burn Tissue.** The protein-protein interaction network of DEGs was constructed using STRING online software, and the results are illustrated in Figure 8. Figure 8(a) revealed the overall analysis results of DEGs protein-protein interaction network. Except for STEAP4, LMO7, BTBD17, and AMPD3 genes that were not related to other genes, there was an interaction among the proteins of other genes.

JUN, STAT1, Bcl2, MMP9, and TLR gene subprotein were selected for the construction of protein interaction network. Figure 8(b) suggested that the JUN gene was closely related to CTNBN1, EP300, SMAD3, ATF2, FOS, FOSL1, BATF3, ATF3, and FOSL2. STAT1 gene was closely related to IFNGR1, JAK2, IRF9, IFNAR1, IRF1, JAK1, CREBBP, EP300, PIAS1, and KPNA1. The Bcl2 gene was closely correlated to BBC3, TP53, Bcl2L11, BAX, BAD, BIK, BID, Bcl2L1, FKBP8, and BECN1. MMP9 gene was closely correlated with CD44, TIMP1, SDC1, CDH1, VEGFA, PLG, TIMP3, TGFBI, LCN2, and IL6. TLR2 gene was closely related to IRAK1, HMGB1, LY96, CLEC7A, HSP90B1, HSPD1, VCAN, CD14, TollIP, and TIRAP.

**4.5. Identification of Burn DEGs.** First, rt-qPCR was used to detect the differences in the mRNA expression levels of STAT1, JUN, Bcl2, MMP9, and TLR2 in the burn tissue of mice in the control group and the burn group. The results

demonstrated in Figure 9 revealed that compared with the control group, the mRNA expression levels of STAT1 and Bcl2 in the burn group were decreased, while those of JUN, MMP9, and TLR2 were increased ( $p < 0.05$ ).

Western blot detected the differences in PELs of STAT1, JUN, Bcl2, MMP9, and TLR2 in the tissues of mice, and the results were shown in Figure 10. Compared with the control group, the PELs of STAT1 and Bcl2 in the burn group were decreased, while the PELs of JUN, MMP9, and TLR2 were greatly increased ( $p < 0.05$ ).

## 5. Discussion

Burn is a very common disease, and most patients have burns of grade 2 and above [18]. Scar is one of the most common complications of burn patients during rehabilitation, which seriously affects the rehabilitation effect and quality of life of patients [19]. Therefore, this work is of great significance to explore the potential therapeutic targets in the process of wound healing after burn injury and to improve the prognosis of burn patients. In this work, based on WGCNA analysis, the related gene modules of wound healing after burn were searched, and the expression status of DEGs was explored by bioinformatics analysis method, aiming to provide reference materials for the improvement of wound healing effect.

Based on WGCNA, multiple DEGs were obtained, and Gene Ontology functional annotation of these genes [20] and enrichment analysis of KEGG signaling pathway [21]

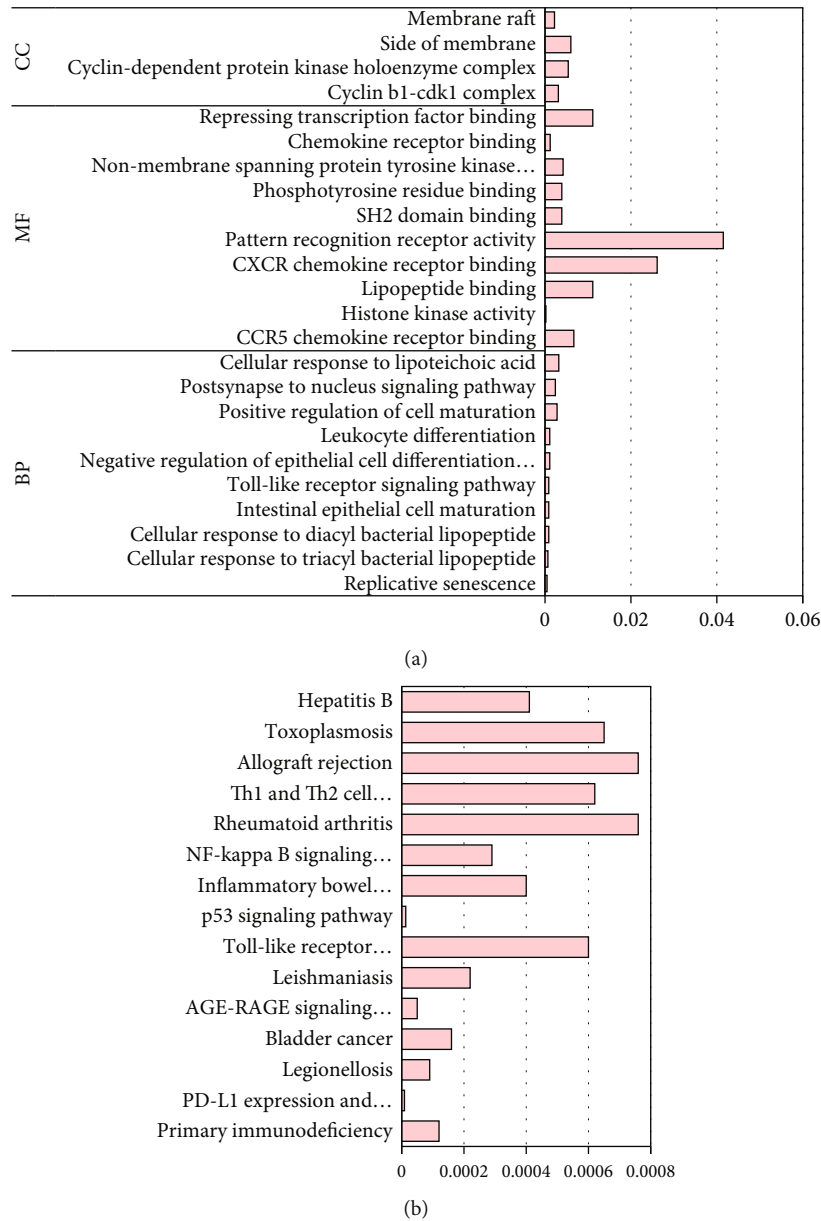


FIGURE 7: Gene Ontology and KEGG analysis of DEGs. (a) The Gene Ontology analysis result of DEGs and (b) the KEGG analysis result of DEGs.

TABLE 2: Information of the top 10 DEGs.

Gene ID	Gene	Full name of the gene	Module	Regulation
ENSG00000177606	JUN	Jun protooncogene	Green	Up
ENSG00000115415	STAT1	Signal transducer and activator of transcription 1	Grey	Down
ENSG00000171791	Bcl2	BCL2 apoptosis regulator	Green	Down
ENSG00000100985	MMP9	Matrix metalloproteinase 9	Green	UP
ENSG00000137462	TLR2	Toll-like receptor 2	Brown	UP
ENSG00000096968	JAK2	Janus kinase 2	Brown	UP
ENSG00000170458	CD14	CD14 molecule	Green	UP
ENSG00000170312	CDK1	Cyclin-dependent kinase 1	Brown	Up
ENSG00000168610	STAT3	Signal transducer and activator of transcription 3	Brown	Up
ENSG00000177455	CD19	CD19 molecule	Green	Down

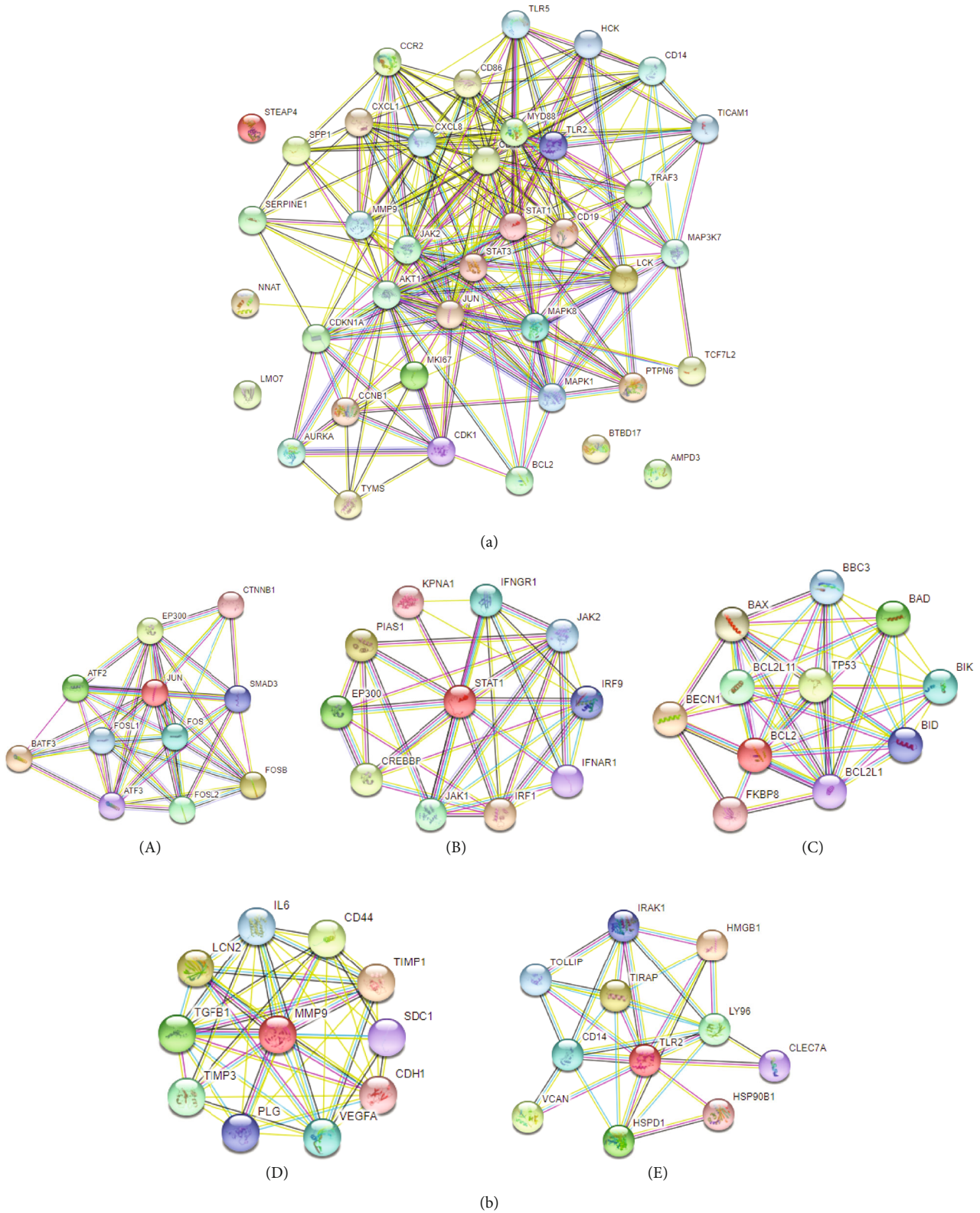


FIGURE 8: DEGs have a complex protein interaction network. The total protein-protein interaction network was depicted in (a); (b) diagram of the subprotein-protein interaction network, where A was the JUN gene, B was the STAT1 gene, C referred to the Bcl2 gene, D represented the MMP9 gene, and E stood for the TLR2 gene.

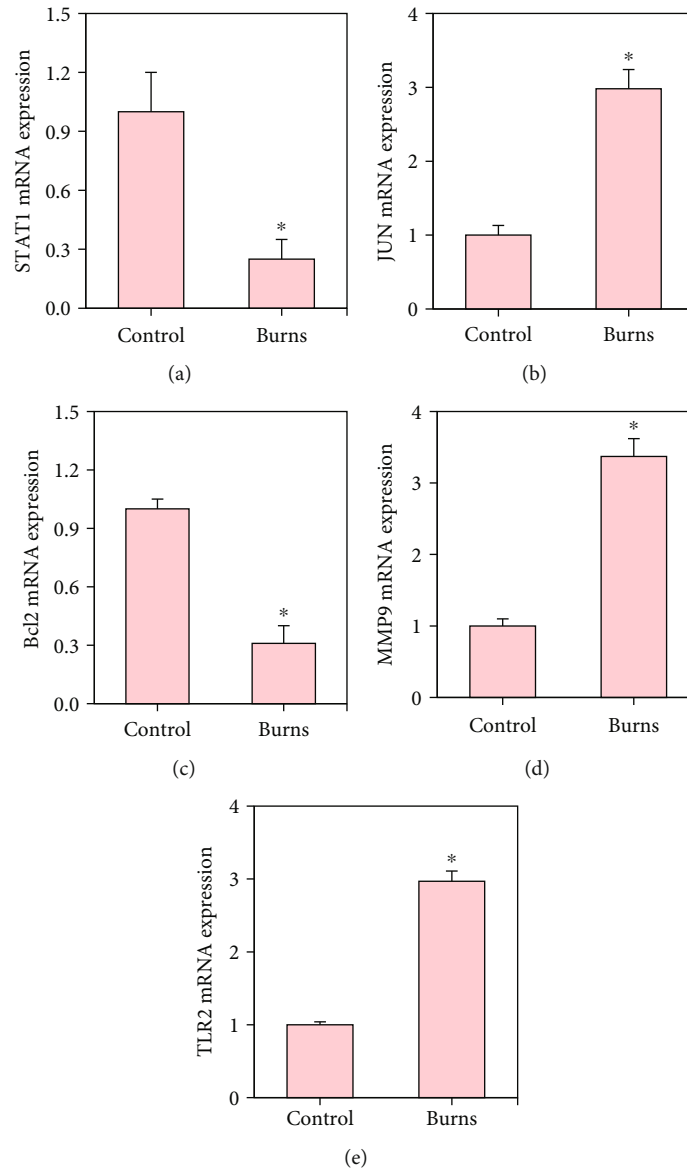


FIGURE 9: Detection results of mRNA expression levels of DEGs. (a–e) The detected values of STAT1, JUN, Bcl2, MMP9, and TLR2, respectively, and \* indicated a statistically obvious difference between groups ( $p < 0.05$ ).

were performed. The results of Gene Ontology analysis showed that DEGs after burn were related to immune system function, metabolic process, and cellular biological regulation. The results of KEGG pathway enrichment analysis showed that DEGs after burn were mainly located in the Toll-like receptor [22], p53 [23], PD-1/PD-L1 [24], and NF- $\kappa$ B [25]. Toll-like receptor signaling pathway can activate bacterial membrane components and promote the activation of MAPK signaling pathway, which in turn triggers the body's inherent immune response and increases the production of proinflammatory factors [26].

Subsequently, five DEGs were screened for expression level verification. The STAT protein family can participate in the binding of different cytokines or growth factors, which can be activated by a variety of cytokines and mediate the expression of multiple genes in response to pathogen invasion [27]. STAT1 plays an important role in antigen presen-

tation and B cell development [28]. Studies have shown that the decrease in the expression level of STAT1 can lead to a decrease in the expression level of IgG, which in turn increases the susceptibility of the body to the virus [29]. JUN is a stress-activated protein kinase, which plays an important role in the process of apoptosis [30]. Studies have confirmed that after inhibiting the expression of JUN, the content of proinflammatory factors such as IL-6 will also decrease, while the content of anti-inflammatory factors such as IL-10 will increase [31]. Bcl2 is also one of the serious hot spots in the process of apoptosis, and it mainly plays the role of inhibiting apoptosis and promoting apoptosis [32]. MMP9 can activate the functions of cytokines and chemokines, so it is involved in the processes of skin wound inflammatory response, matrix remodeling, and epithelialization [33]. Toll-like receptors can selectively recognize microorganisms and their tissue components, and TLR2



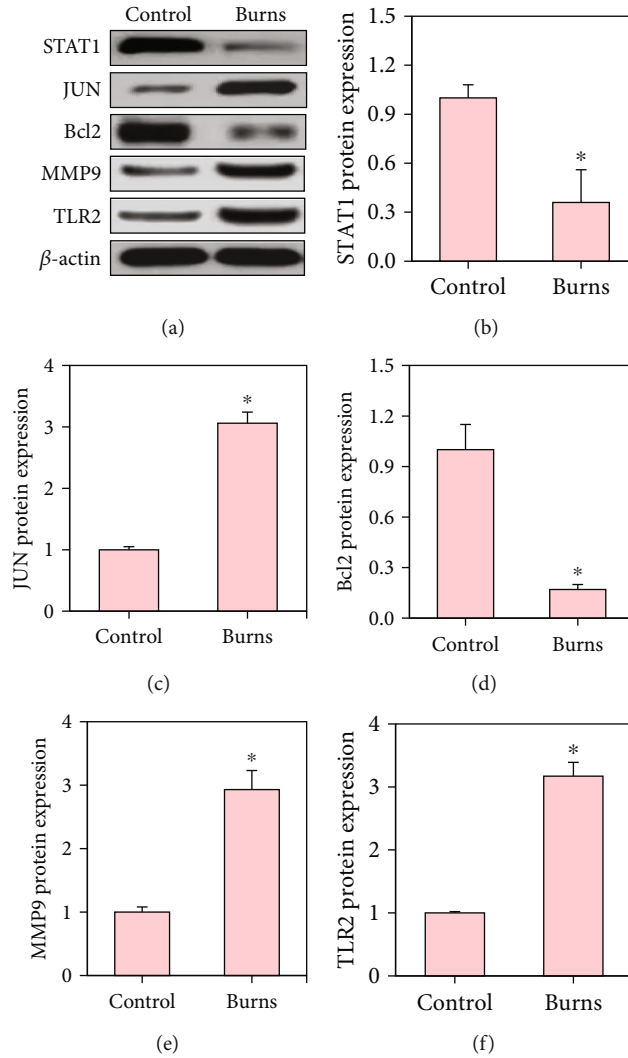


FIGURE 10: Detection results of PELs of DEGs. (a-f) The detected values of STAT1, JUN, Bcl2, MMP9, and TLR2, respectively, and \* indicated a statistically obvious difference between groups ( $p < 0.05$ ).

plays an important role in the activation of cells by Gram-positive bacteria [34]. The results of this work suggested that the expression levels of STAT1 and Bcl2 in burn tissue were much lower than compared to the normal tissue, while the levels of JUN, MMP9, and TLR2 were remarkably higher. The above results suggest that the body after burn may inhibit the proliferation of immune cells, promote cell apoptosis, reduce the body's immunity, and then, reduce the resistance to external pathogens. The increased expression of JUN in burn tissue triggers the excessive release of pro-inflammatory factors in the body, which in turn leads to a severe inflammatory response in the body. Therefore, the continuous high expression of inflammatory factors such as JUN, MMP9, and TLR2 in burn wounds tissue may slow down the speed of wound healing.

## 6. Conclusions

WGCNA and other bioinformatics analysis approaches were used to investigate the features of DEGs in burn tissue in this study. According to the WGCNA mining results, ten network

modules were discovered to be strongly associated to postburn wound healing, with the green, brown, and grey modules having the most DEGs. The Gene Ontology and KEGG analysis of DEGs found that these genes were mainly functionally annotated as immune cell activation, inflammatory response, and immune response, etc., and were mainly enriched in PD-1/PD-L1, Toll-like receptor signaling, p53, and NF- $\kappa$ B. Later, it was found that the wound healing effect after burn was closely related to genes such as STAT1, JUN, Bcl2, MMP9, and TLR2. However, it only used published data to analyze gene co-expression networks in this work. Clinical tissue samples would be acquired for transcriptase analysis in the follow-up study, and WGCNA would be built and examined again. The results of this work were aimed at finding potential targets for wound healing after burns and providing reference data for improving the prognosis of burn patients.

## Data Availability

The data used to support the findings of this study are available from the corresponding author upon request.

## Conflicts of Interest

The authors declare that they have no conflicts of interest.

## Authors' Contributions

ZhiHui Guo and YuJiao Zhang are both 1st authors of this paper.

## References

- [1] R. P. Clayton, P. Wurzer, C. R. Andersen, R. P. Mlcak, D. N. Herndon, and O. E. Suman, "Effects of different duration exercise programs in children with severe burns," *Burns: Journal of the International Society for Burn Injuries*, vol. 43, no. 4, pp. 796–803, 2017.
- [2] M. K. Arbuthnot and A. V. Garcia, "Early resuscitation and management of severe pediatric burns," *Seminars in Pediatric Surgery*, vol. 28, no. 1, pp. 73–78, 2019.
- [3] X. X. Wang, M. J. Zhang, and X. B. Li, "Advances in the research of zinc deficiency and zinc supplementation treatment in patients with severe burns," *Chinese Journal of Burns*, vol. 34, no. 1, pp. 57–59, 2018.
- [4] L. Roshangar, J. Soleimani Rad, R. Kheirjou, M. Reza Ranjesh, and A. Ferdowsi Khosroshahi, "Skin burns: review of molecular mechanisms and therapeutic approaches," *Wounds: a compendium of clinical research and practice*, vol. 31, no. 12, pp. 308–315, 2019.
- [5] S. Tejiram, K. S. Romanowski, and T. L. Palmieri, "Initial management of severe burn injury," *Current Opinion in Critical Care*, vol. 25, no. 6, pp. 647–652, 2019.
- [6] F. E. Rodger and I. Taggart, "Seasonal flu-vaccination in the immunocompromised burns patient," *Burns: Journal of the International Society for Burn Injuries*, vol. 46, no. 1, pp. 178–181, 2020.
- [7] Y. M. Yao and Y. Y. Luan, "New understanding on the immunity for severe infections and complications in burns and trauma," *Chinese Journal of Burns*, vol. 37, no. 6, pp. 519–523, 2021.
- [8] D. G. Greenhalgh, "Management of burns," *The New England Journal of Medicine*, vol. 380, no. 24, pp. 2349–2359, 2019.
- [9] A. M. Strobel and R. Fey, "Emergency care of pediatric burns," *Emergency Medicine Clinics of North America*, vol. 36, no. 2, pp. 441–458, 2018.
- [10] J. A. Barrera, A. A. Trotsyuk, Z. N. Maan et al., "Adipose-derived stromal cells seeded in pullulan-collagen hydrogels improve healing in murine burns," *Tissue Engineering. Part A*, vol. 27, no. 11–12, pp. 844–856, 2021.
- [11] G. Tang, T. Zhang, X. Wang et al., "Sub-pathway analysis for severe burns injury patients: identification of potential key lncRNAs by analyzing lncRNA-mRNA profile," *Experimental and Therapeutic Medicine*, vol. 15, no. 6, pp. 5281–5287, 2018.
- [12] Z. Tian, W. He, J. Tang et al., "Identification of important modules and biomarkers in breast cancer based on WGCNA," *Oncotargets and Therapy*, vol. 13, pp. 6805–6817, 2020.
- [13] A. S. Nangraj, G. Selvaraj, S. Kaliyamurthi, A. C. Kaushik, W. C. Cho, and D. Q. Wei, "Integrated PPI- and WGCNA-retrieval of hub gene signatures shared between Barrett's esophagus and esophageal adenocarcinoma," *Frontiers in Pharmacology*, vol. 11, p. 881, 2020.
- [14] G. Pei, L. Chen, and W. Zhang, "WGCNA application to proteomic and metabolomic data analysis," *Methods in Enzymology*, vol. 585, pp. 135–158, 2017.
- [15] M. Wang, L. Wang, L. Pu et al., "LncRNAs related key pathways and genes in ischemic stroke by weighted gene co-expression network analysis (WGCNA)," *Genomics*, vol. 112, no. 3, pp. 2302–2308, 2020.
- [16] F. Haase, B. S. Gloss, P. Tam, and W. A. Gold, "WGCNA identifies translational and proteasome-ubiquitin dysfunction in rett syndrome," *International Journal of Molecular Sciences*, vol. 22, no. 18, p. 9954, 2021.
- [17] Z. Rezaei, J. Ranjbaran, H. Safarpour et al., "Identification of early diagnostic biomarkers via WGCNA in gastric cancer," *Biomedicine & Pharmacotherapy*, vol. 145, article 112477, 2022.
- [18] E. E. Tredget, J. W. Shupp, and J. C. Schneider, "Scar management following burn injury," *Journal of burn care & research: official publication of the American Burn Association*, vol. 38, no. 3, pp. 146–147, 2017.
- [19] Y. S. Cho, J. H. Jeon, A. Hong et al., "The effect of burn rehabilitation massage therapy on hypertrophic scar after burn: a randomized controlled trial," *Burns: Journal of the International Society for Burn Injuries*, vol. 40, no. 8, pp. 1513–1520, 2014.
- [20] G. Tang, T. Zhang, X. Wang et al., "Analysis of differentially expressed genes in white blood cells isolated from patients with major burn injuries," *Experimental and Therapeutic Medicine*, vol. 14, no. 4, pp. 2931–2936, 2017.
- [21] H. Jin, Y. Gao, Z. Lu, Q. Zhou, P. Shi, and L. Yang, "Screening genes related with leukocyte responses early after burn injury: analysis of differentially gene expression profiling data in mice," *Journal of Southern Medical University*, vol. 35, no. 12, pp. 1775–1781, 2015.
- [22] P. D'Arpa and K. P. Leung, "Toll-like receptor signaling in burn wound healing and scarring," *Advances in Wound Care*, vol. 6, no. 10, pp. 330–343, 2017.
- [23] H. Nakazawa, K. Chang, S. Shinozaki et al., "iNOS as a driver of inflammation and apoptosis in mouse skeletal muscle after burn injury: possible involvement of Sirt1 S-nitrosylation-mediated acetylation of p65 NF- $\kappa$ B and p53," *PLoS One*, vol. 12, no. 1, article e0170391, 2017.
- [24] N. K. Patil, L. Luan, J. K. Bohannon, A. Hernandez, Y. Guo, and E. R. Sherwood, "Frontline science: anti-PD-L1 protects against infection with common bacterial pathogens after burn injury," *Journal of Leukocyte Biology*, vol. 103, no. 1, pp. 23–33, 2018.
- [25] B. George, T. VSuchithra, and N. Bhatia, "Burn injury induces elevated inflammatory traffic: the role of NF- $\kappa$ B," *Inflammation Research: Official Journal of the European Histamine Research Society*, vol. 70, no. 1, pp. 51–65, 2021.
- [26] P. Guo, "Weighted gene co-expression network analysis of methylated genes in burn scar tissue," *Chinese Journal of Burns*, vol. 37, no. 12, pp. 1185–1190, 2021.
- [27] Q. Zou, Y. B. Gao, H. Jin, Z. Y. Lu, P. W. Shi, and L. Yang, "Screening of biomarkers related with leukocyte responses early after burn injury in mice by differential gene expression profiling," *Journal of Southern Medical University*, vol. 37, no. 6, pp. 767–773, 2017.
- [28] A. N. Guillory, R. P. Clayton, D. N. Herndon, and C. Finnerty, "Cardiovascular dysfunction following burn injury: what we have learned from rat and mouse models," *International Journal of Molecular Sciences*, vol. 17, no. 1, p. 53, 2016.

- [29] Y. Gao, W. Nai, L. Yang et al., “Construction of an immunorelated protein-protein interaction network for clarifying the mechanism of burn,” *Burns: Journal of the International Society for Burn Injuries*, vol. 42, no. 2, pp. 405–413, 2016.
- [30] H. Ye, U. K. Rahul, U. Kruger et al., “Raman spectroscopy accurately classifies burn severity in an ex vivo model,” *Burns: Journal of the International Society for Burn Injuries*, vol. 47, no. 4, pp. 812–820, 2021.
- [31] S. Aslam, I. Khan, F. Jameel, M. B. Zaidi, and A. Salim, “Umbilical cord-derived mesenchymal stem cells preconditioned with isorhamnetin: potential therapy for burn wounds,” *World Journal of Stem Cells*, vol. 12, no. 12, pp. 1652–1666, 2020.
- [32] C. Sharma, G. P. Dobson, L. M. Davenport, J. L. Morris, and H. L. Letson, “The role of matrix metalloproteinase-9 and its inhibitor TIMP-1 in burn injury: a systematic review,” *International Journal of Burns and Trauma*, vol. 11, no. 4, pp. 275–288, 2021.
- [33] R. F. Oppeltz, M. Rani, Q. Zhang, and M. G. Schwacha, “Burn-induced alterations in toll-like receptor-mediated responses by bronchoalveolar lavage cells,” *Cytokine*, vol. 55, no. 3, pp. 396–401, 2011.
- [34] A. Agrawal, J. Ding, B. Agrawal, P. O. Kwan, and E. E. Tredget, “Stimulation of toll-like receptor pathways by burn eschar tissue as a possible mechanism for hypertrophic scarring,” *Wound Repair and Regeneration*, vol. 29, no. 5, pp. 810–819, 2021.

## Research Article

# Imaging Diagnosis of Primary Liver Cancer Using Magnetic Resonance Dilated Weighted Imaging and the Treatment Effect of Sorafenib

Bin Fan,<sup>1</sup> Yunyi Zhang,<sup>2</sup> and Shuai Guo <sup>3</sup>

<sup>1</sup>General Surgery, The First Affiliated Hospital of Northwest University (Xi'an No. 1 Hospital), Xi'an, 710000 Shaanxi, China

<sup>2</sup>Public Health and Management Department, Ningxia Medical University, Yinchuan, 750001 Ningxia, China

<sup>3</sup>Oncology Department, Huyi District People's Hospital, Xi'an, 710000 Shaanxi, China

Correspondence should be addressed to Shuai Guo; 201701330128@lzpcc.edu.cn

Received 5 May 2022; Revised 25 May 2022; Accepted 28 May 2022; Published 28 June 2022

Academic Editor: Naeem Jan

Copyright © 2022 Bin Fan et al. This is an open access article distributed under the Creative Commons Attribution License, which permits unrestricted use, distribution, and reproduction in any medium, provided the original work is properly cited.

**Objective.** This work explores the application value of dilated weighted imaging (DWI) in the diagnosis of primary liver cancer (PLC) and the effect of sorafenib in the treatment of PLC. **Methods.** 88 patients with PLC who were treated in The First Affiliated Hospital of Northwest University from March 2019 to March 2021 were selected and randomly rolled into an experimental group and a control group, with 44 cases in each group. Patients in both groups were treated with transcatheter arterial chemoembolization (TACE), and the patients in the experimental group were treated with oral sorafenib on the basis of TACE. The indicators of complications, short-term efficacy (STE), and long-term efficacy (LTE) of the two groups were observed. All patients received DWI and magnetic resonance (MR) plain scan. The diagnostic accuracy and misdiagnosis rate of the two methods in diagnosing the PLC were compared. **Results.** The accuracy, specificity, and sensitivity of MR plain scan were 68%, 88%, and 89%, respectively, while those of DWI were 96%, 95%, and 94.2%, respectively. It indicated that the accuracy, specificity, and sensitivity of DWI in diagnosing lesions were better than those of MR plain scan, especially the diagnostic accuracy ( $P < 0.05$ ). The objective response rate (ORR) and disease control rate (DCR) of the STE in the experimental group were 30% and 97%, respectively, and those in the control group were 6% and 54.5%, respectively. The experimental group's mean progression-free survival (mPFS) and mean overall survival (mOS) were 12 and 25 months, respectively, while the control group's were 8 and 19 months, respectively. It was concluded that the mPFS and mOS of patients receiving TACE combined with oral sorafenib were much higher than those receiving TACE only ( $P < 0.05$ ). **Conclusion.** DWI and TACE combined with sorafenib had high application value in the diagnosis and treatment of PLC.

## 1. Introduction

Primary liver cancer (PLC) is one of the malignant tumors with the highest incidence in the world. Clinical statistics show that 4.7% of new cancer patients are liver cancer patients each year, and liver cancer patients account for 8.2% of the number of cancer deaths each year. According to statistics from the World Health Organization (WHO), liver cancer has become one of the six major cancers in the world and the fourth leading cause of cancer-related death in 2018 [1–3]. The WHO also said that in the next few years, the incidence and death of liver cancer will continue to increase

and rise. The incidence of liver cancer is affected by factors such as geographical location, ethnicity, economy, and food culture. Therefore, PLC has different incidence rates in different countries. Epidemiological survey results show that the incidence of PLC in Asia is relatively high, and the reason may be closely related to the relatively large population base in Asia [4]. The common cause of PLC is chronic liver disease caused by hepatitis virus. However, factors such as alcoholic liver disease, obesity, type 2 diabetes, and nonalcoholic fatty liver disease are also closely related to the occurrence of liver cancer. The main causes of liver cancer vary in different regions. In China, the biggest risk factors are hepatitis B infection and aflatoxin

poisoning. Hepatitis C infection is the leading cause of death in Japan and Egypt. Obesity is the main reason for the increase in the incidence of liver cancer in areas with low incidence of liver cancer [5–7]. Epidemiological survey statistics show that the incidence of liver cancer in my country accounts for more than 50% of the world's, and liver cancer-related mortality ranks third in the world. At present, liver resection or liver transplantation is still the main method to ensure the long-term survival of PLC patients. However, clinical studies have shown that the early onset of PLC is relatively insidious, with no obvious clinical symptoms or even asymptomatic. This has led to the fact that most patients have already developed their disease in the middle and late stages when they come to see a doctor and have already lost the opportunity for surgical treatment. Clinical studies have shown that only less than 1/5 of patients can obtain the opportunity for surgery [8–10]. Despite the further development of medical technology in recent years, the treatment methods of PLC have gradually diversified. However, there is still no reliable and practical way for increasing patient survival rates. Liver cancer is characterised by a high blood supply, recurrence, and angiogenesis, according to clinical trials. Even in patients who have undergone surgical treatment, nearly 40% of patients relapse one year after surgery. 10% to 20% of patients have recurrence even after liver transplantation. China is a large hepatitis B country with a large population and a serious aging population. Generally speaking, the form of PLC is very serious [11].

Because PLC is usually found in the middle and late stages, many patients cannot be treated with surgery. Therefore, non-surgical treatment is often used in the clinical treatment of PLC. Transcatheter arterial chemoembolization (TACE) is the most common treatment for hepatocellular carcinoma besides surgery. This method is to inject chemotherapy drugs such as doxorubicin, epirubicin, and cisplatin into tumor blood vessels and then embolize them with materials such as gelatin sponge [12]. The method has the advantages of less trauma, clear effect, wide application range, and high repeatability. However, this method also has some disadvantages, such as poor deposition of lipiodol and inability to completely embolize blood vessels. Based on the above shortcomings and the influence of the rich blood supply and angiogenesis of the PLC tumor itself, a single TACE treatment often fails to achieve the desired therapeutic effect. Therefore, TACE is often combined with other therapeutic methods to treat the PLC in clinical practice. Clinical studies have shown that TACE combined with systemic therapy can significantly prolong the survival of patients with advanced disease [13]. Sorafenib and apatinib are common oral targeted drugs in clinical practice. Among them, sorafenib is the first drug used in the systemic treatment of patients with advanced PLC and has shown good efficacy. It has been approved for first-line treatment of PLC. As an oral multienzyme inhibitor, sorafenib can act on tumor tissue and tissue blood vessels. It can block the formation of tumor angiogenesis, thereby inhibiting the growth of tumor tissue. Theoretically, the combination of TACE therapy and sorafenib can improve the prognosis of patients with advanced PLC. However, there is still a lack of effective large-scale clinical studies on this method, so further research is needed [14].

Computed tomography (CT) scan and enhancement, which can properly depict the number, size, shape, and deposition status of lipiodol, are currently the most effective and widely used procedures for the diagnosis and evaluation of the curative effect of PLC. However, due to the interference of high-density lipiodol, the density of the active tumor tissue lock may be misdiagnosed and missed. Ultrasound can observe the blood supply of tumors, but due to the influence of lipiodol, it is prone to chaotic strong echo reflections and limited spatial resolution of ultrasound [15]. Conventional magnetic resonance imaging (MRI) can detect tumor tissue but cannot differentiate between necrotic and viable parts. In recent years, magnetic resonance (MR) technology has developed rapidly. Some new technologies have been applied and developed, and people are gradually entering the era of diagnosing the PLC and evaluating the curative effect at the molecular level of functional status. Diffusion-weighted imaging (DWI) is one of them. DWI has a high sensitivity to Brownian motion of water molecules, and it is currently the only noninvasive method that can evaluate and identify the diffusion motion of water molecules in live tissue [16]. DWI can distinguish necrotic and residual viable tumor cells. The apparent diffusion coefficient (ADC) map can prove the signal difference between the two through quantitative analysis. The application of DWI technology may be able to solve the problem that conventional CT and MRI scans cannot quantitatively analyze tumor necrosis [17].

PLC patients were enrolled in this study and assigned to one of two groups: experimental or control. Patients in the experimental group received TACE in combination with sorafenib, while those in the control group received simply TACE. At the same time, all patients were diagnosed and evaluated by DWI technology, and the results were analyzed. This work is aimed at offering a reference and basis for clinical treatment and diagnosis of PLC.

The paper's organization paragraph is as follows: The materials and methods are presented in Section 2. Section 3 presents the experimental results of the proposed work. Section 4 consists of the discussion section. Finally, in Section 5, the research work is concluded.

## 2. Materials and Methods

*2.1. Research Objects.* 88 PLC patients treated in The First Affiliated Hospital of Northwest University from March 2019 to March 2021 were selected, and they were rolled randomly into an experimental group and a control group, with 44 cases in each group. Patients included had to meet the following conditions: patients who were pathologically or clinically diagnosed as PLC, which could not be treated by surgery; patients with Barcelona liver cancer clinical stage (BCLC) of stage C; patients with estimated survival time of greater than 3 months; patients with no abnormality in blood routine, renal function, electrocardiogram, and other examinations before receiving treatment; and patients with no contraindications related to TACE and oral targeted drugs. Patients satisfying the below items had to be excluded: patients with or ever suffering from other malignant tumors;

TABLE 1: Evaluation criteria of RECIST1.1.

Efficacy classification	Symptom descriptions
Progressive disease (PD)	The largest diameter and the lowest increase of the target lesion was $\geq 20\%$ or the new lesion was found
Stable disease (SD)	The largest diameter and decrease in diameter of the target lesion did not reach PR or the enlargement diameter did not reach PD
Partial response (PR)	The largest diameter and decrease in diameter of the target lesion reached $\geq 30\%$ and maintained for more than 4 weeks
Complete response (CR)	All target lesions disappeared, no new lesions appeared, and the tumor markers were normal and maintained for more than 4 weeks

Note: PR+CR was ORR; total DCR was the value of SD+PR+CR.

TABLE 2: General data of patients.

Indicator		Experimental group ( $n = 44$ )	Control group ( $n = 44$ )	$\chi^2/t$	$P$
Age (years)		$55.3 \pm 11.4$	$55.2 \pm 12.2$	0.712	0.623
Gender	Males	15	18	—	—
	Females	19	14	—	—
				0.08	0.99
Hepatitis B carriers	Yes	25	26		
	No	19	18		
				3.32	0.28
HBV replication	Yes	20	23		
	No	24	21		
				0.66	0.82
Vascular invasion	Yes	21	17		
	No	23	27		
				0.33	0.73
Distant metastasis	Yes	25	23		
	No	19	21		
				0.068	1.03
TACE times	$5.52 \pm 3.88$	$4.33 \pm 4.13$			

patients with severe liver damage; patients with severe heart, lung, kidney, or other systemic diseases; patients who received chemotherapy, radiotherapy, or other antitumor treatments; pregnant and breastfeeding females; and patients with a personal or family history of mental illness. All experiments in this work obtained patient informed consent and met the requirements of medical ethics.

**2.2. Treatment Methods.** All patients were treated with TACE. The patients in the experimental group were treated with oral sorafenib on the basis of TACE treatment. The detailed treatment process was as follows:

*TACE treatment:* angiography was performed through the celiac or common hepatic arteries using the Seldinger cannulation procedure. It could implant the catheter tip in the blood supply vessel, inject lipiodol and chemotherapeutic medications, and then employ gelatin sponge particles to embolize blood vessels once the tumor location, size, blood supply source, and other information were clearly understood. In addition, postoperative symptomatic and supportive treat-

ment was performed. The specific dosage and treatment cycle of chemotherapeutic drugs were determined by the attending physician on the basis of the patient's review indicators.

*Sorafenib treatment:* the sorafenib tosylate tablets (Nexavar, Bayer Schering Pharmaceuticals, Imported Drug Registration Certificate No. H20160201, specification  $0.2 \text{ g} \times 60$  tablets/box, 5700 yuan/box) were adopted. The patient was required to take sorafenib tosylate tablets orally within 1 week after receiving TACE treatment, taking  $0.4 \text{ g}$  each time, twice a day. If any grade 3-4 adverse reactions related to medication occurred, the drug can be adjusted according to the specific situation of the patient. The dose was adjusted to  $0.4 \text{ g/time}$ , once a day.

**2.3. MRI Examination.** The instruments included GE Signa Excite 1.5T superconducting MR scanner and 8-channel phased array soft body coil, TOSHIBA-SDF digital subtraction angiography system, and Marconi CT-Twin flash CT scanner.

The patient should fast for 6 hours prior to the assessment. The patient should practise holding their breath before

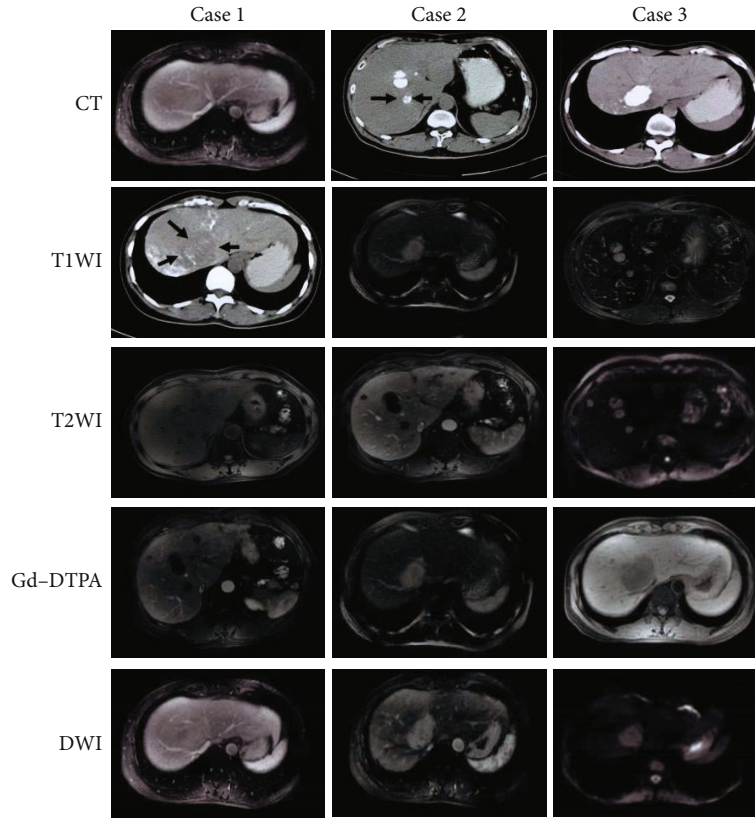


FIGURE 1: Imaging images of typical cases.

the scan. All of the patients had standard MRI scans first, followed by T1WI cross-sectional suppression sequences, diffusion-weighted imaging, and finally cross-sectional dynamic contrast-enhanced images. The layer thickness of each sequence was 8 mm, layer spacing was 2 mm, field of view (FOV) was 34~40 cm, and all were replicated to keep consistency. The specific imaging sequence and scanning parameters were as follows: FSPGR sequence T1WI: the time of repetition (TR) was 150 ms, time of echo (TE) was 4.2 ms, width of band (WB) was 41.7 kHz, flip angle was 85°, and matrix was 288 × 192. FRFSE (RT) sequence T2WI: TR was 6000 ms, TE was 87.1 ms, WB was 62.5 kHz, FOV was 34~40 cm, and matrix was 320 × 192. SE-EPI sequence diffusion-weighted imaging: TR was 1200 ms, TE was 59.0 ms, FOV was 35~38 cm, matrix was 128 × 128, number of excitations (NEX) was 4, and 3 different diffusion sensitivity factor  $b$  values were selected: 1000, 500, and 300 s/mm<sup>2</sup> scan once each. At the same time, the diffusion gradient took three X, Y, and Z orientations. FSPGR sequence dynamic enhanced scan: TR was 125 ms, TE was 2.9 ms, WB was 83.33 kHz, FOV was 30~38 cm, flip angle was 80°, and matrix was 288 × 192. The contrast agent was Gd-DTPA, the dose was calculated according to 0.2 mL/kg body weight, and the injection rate was 3 mL/s. After bolus injection through the antecubital vein, three rounds of sampling were performed at 15~18 s, 50~65 s, and 90~120 s, respectively.

**2.4. Image Analysis and Judgment Criteria.** Two experienced radiologists, combined with CT images, MRI plain scans, DWI images, and DSA angiography images, comprehensively

analyzed the T1WI, T2WI, dynamic enhancement performance, and tumor blood supply staining to the necrosis, residual, and recurrence of the tumor. The results were compared with those of DWI images. The judging criteria were as follows. Residual tumor: after 1 month of treatment, MRI showed enhancement of the lesion, and DSA showed tumor staining. Tumor coagulation necrosis: after 1-3 months of treatment, MRI showed no enhancement of the lesion and no tumor staining on DSA. Tumor recurrence: new lesions appeared after complete necrosis of the tumor, MRI showed enhancement, and DSA showed tumor staining.

**2.5. Evaluation of Treatment Effect.** The patients were followed up by telephone, and the main items of follow-up were adverse reactions, liver-enhanced CT, DWI, and DSA angiography. The primary endpoint was OS. The measurement method of the maximum diameter of the target lesion in the same patient should be the same, and then, the RECIST1.1 standard was used to evaluate the efficacy of the patient. The specific efficacy evaluation methods are shown in Table 1.

**2.6. Statistical Methods.** All data analysis was completed by SPSS19.0. The measurement data were expressed in the form of mean ± standard deviation, and the test method was an independent sample  $t$ -test. The count data was expressed as frequency, and the comparison between groups was done

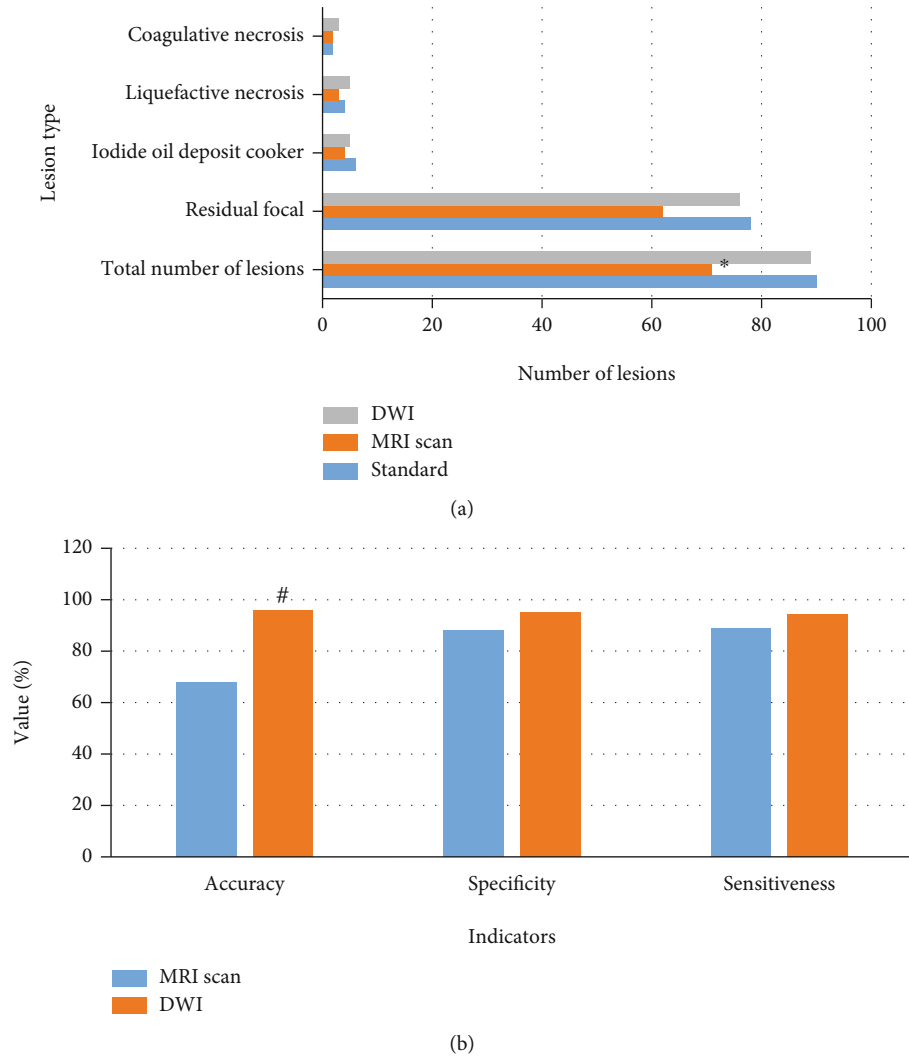


FIGURE 2: Display of correct diagnosis results of lesions. Note: \* and # suggested  $P < 0.05$  compared with the standard value and the MR plain scan, respectively.

by the chi-squared test.  $P < 0.05$  meant the difference was statistically significant.

### 3. Results

3.1. *General Data of Patients.* Table 2 shows the general information for the two patient groups. It revealed that the experimental group consisted of 15 male and 19 female patients, with an average age of 48 years which was  $55.3 \pm 11.4$ , and the number of TACE times was  $5.52 \pm 3.88$ . The control group included 18 male patients and 14 female patients, the average age of the patients was  $55.2 \pm 12.2$ , and the number of TACE was  $4.33 \pm 4.13$ . The two groups of patients had no discernible differences in general data, and they were comparable.

3.2. *Imaging Image Display of Typical Cases.* The imaging images of typical cases are shown in Figure 1. It illustrated that the CT images of the patients generally showed round-shaped low-density lesions with a small amount of lipiodol deposition inside. MRI T1WI and T2WI lesions showed low T1WI and high T2WI signals. On dynamic contrast-enhanced magnetic

resonance imaging, the lesions showed a marked enhancement in the arterial phase, and the enhancement in the portal venous phase and the delayed phase rapidly decreased and showed isointensity. DWI showed marked hyperintensity.

3.3. *Correct Results of DWI in the Diagnosis of Various Lesions.* The results of the correct diagnosis of the lesions are shown in Figure 2. It demonstrated that 90 lesions were found in this work, including 78 residual lesions, 6 lipiodol deposition lesions, 4 liquefaction lesions, and 2 coagulation necrosis lesions. 71 lesions were diagnosed by MR plain scan, including 62 residual lesions, 4 lipiodol deposition lesions, 3 liquefaction lesions, and 2 coagulation necrosis lesions. 89 lesions were diagnosed with DWI, including 76 residual lesions, 5 lipiodol deposition lesions, 5 liquefied lesions, and 3 coagulation necrosis lesions. The diagnostic results of the two methods were compared with the real data, the difference between the MR plain scan and the real data was large ( $P < 0.05$ ), and the DWI diagnostic results were closer to the real data. Figure 2(b) shows that the MR plain scan's accuracy, specificity, and sensitivity for diagnosing



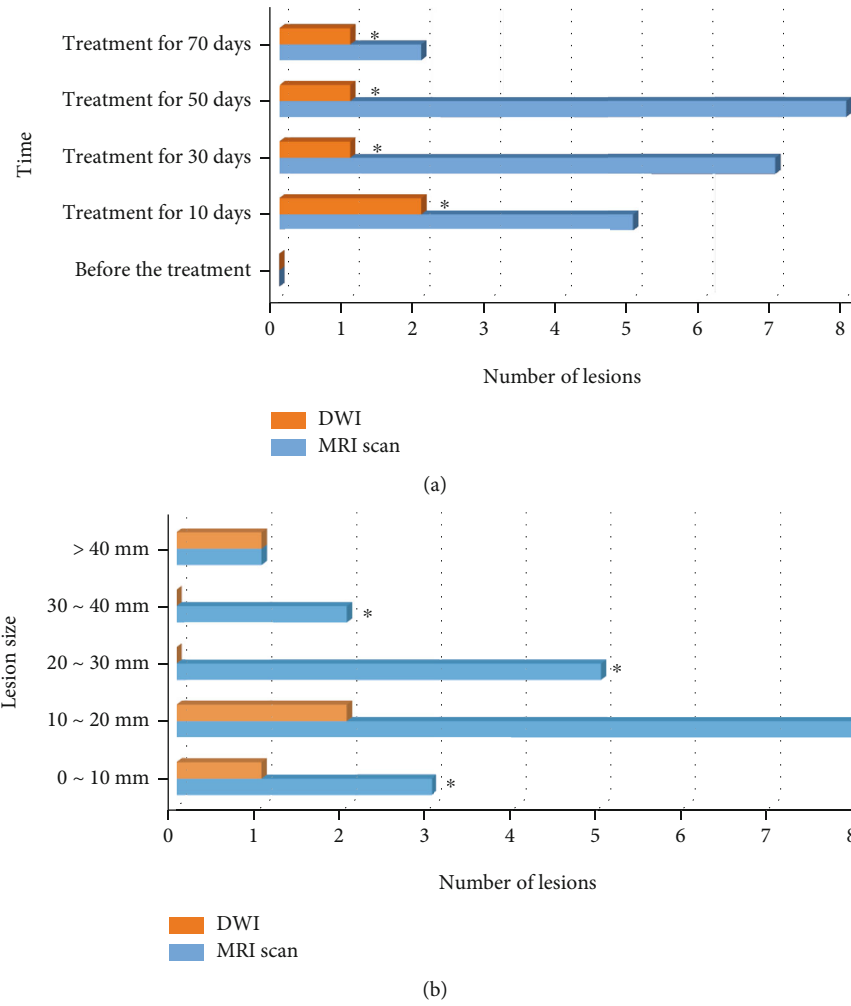


FIGURE 3: The misdiagnosis of lesions of two methods. Note: \* meant  $P < 0.05$  in contrast to DWI.

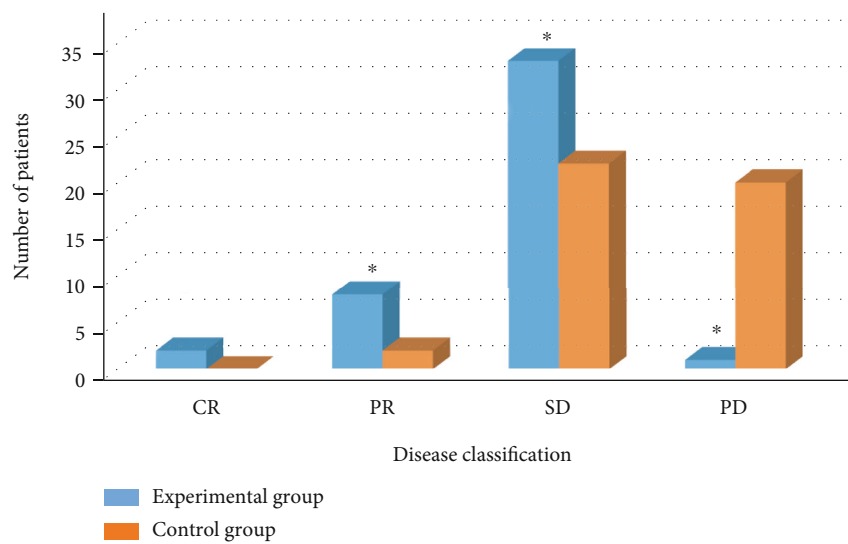


FIGURE 4: The number of patients in each stage of the two groups of patients. Note: \* meant  $P < 0.05$  compared with the control group.

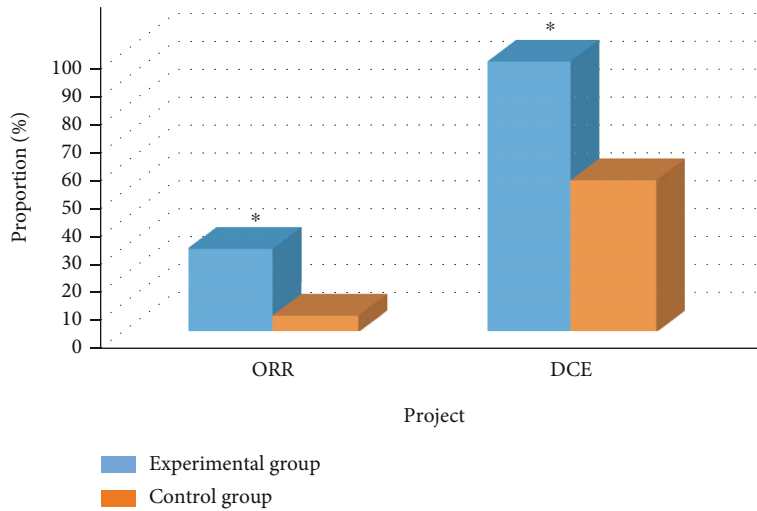


FIGURE 5: Comparison of ORR and DCR of patients. Note: \* meant  $P < 0.05$  compared with the control group.

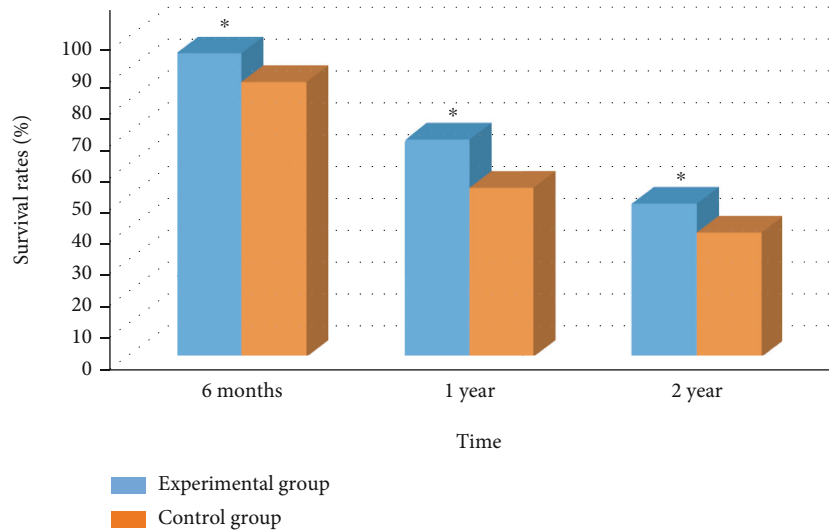


FIGURE 6: Survival rates of patients in the two groups at different time periods. Note: \* meant  $P < 0.05$  compared with the control group.

lesions were 68%, 88%, and 89%, respectively, whereas the DWI's accuracy, specificity, and sensitivity for diagnosing lesions were 96%, 95%, and 94.2%, respectively. It suggested that the accuracy, specificity, and sensitivity of DWI in diagnosing lesions were better than those of MR plain scan, especially that the accuracy was much better than that of MR plain scan ( $P < 0.05$ ).

**3.4. The Misdiagnosis of Lesions in Two Methods.** The misdiagnosis of lesions by the two methods is shown in Figure 3. It revealed that the number of MR misdiagnosed lesions before treatment, 10 days, 30 days, 50 days, and 70 days of treatment was 0, 5, 7, 8, and 2, respectively. The number of DWI misdiagnosed lesions was 0, 2, 1, and 1, respectively. The number of DWI misdiagnosed lesions in each time period was less than that of MR plain scan ( $P < 0.05$ ). The number of MR misdiagnosed lesions with diameters of 0-10 mm, 10-20 mm, 20-30 mm, 30-40 mm, and more than 40 mm was 3, 8, 5, 2, and 1, respectively. The number of misdiagnosed lesions on DWI

was 1, 2, 0, 0, and 1, respectively. It meant that the number of lesions misdiagnosed on DWI was less than that on MR plain scan for lesions with different diameters ( $P < 0.05$ ).

**3.5. Comparison of STE between Two Groups of Patients.** The comparison results of STE in the two groups of patients are shown in Figures 4 and 5. The numbers of CR, PR, SD, and PD patients in the experimental group were 2, 8, 33, and 1, respectively, and the ORR and DCR were 30% and 97%, respectively [18]. The numbers of CR, PR, SD, and PD patients in the control group were 0, 2, 22, and 20, respectively, and the ORR and DCR were 6% and 54.5%, respectively.

**3.6. Comparison of LTE between Two Groups of Patients.** Figures 6 and 7 show the LTE comparison results of the two groups of patients. The 6-month, 1-year, and 2-year survival rates of the experimental group were 95%, 68%, and 48%, respectively, while those in the control group were 86%, 53%, and 39%, respectively. Comparison showed that the survival

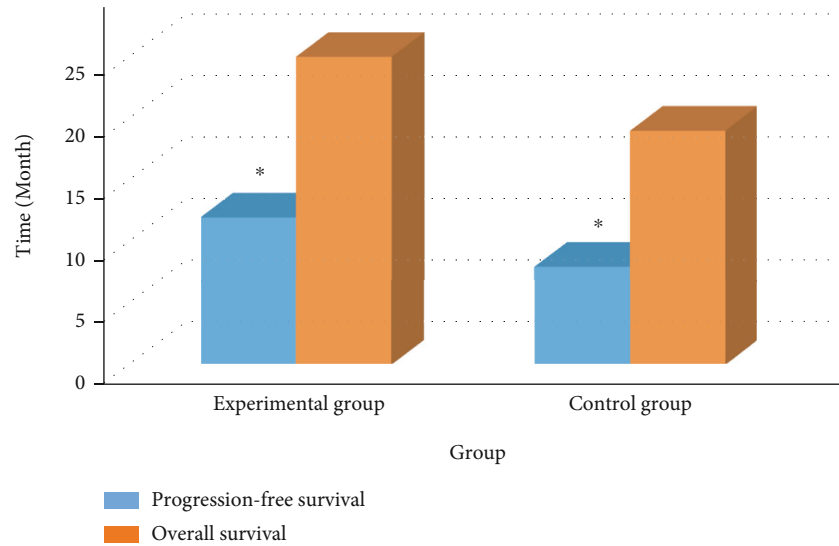


FIGURE 7: Comparison of mPFS and mOS of patients. Note: \* meant  $P < 0.05$  compared with the control group.

rate of the experimental group in each time period was higher obviously than that of the control group ( $P < 0.05$ ). The mPFS and mOS of the experimental group were 12 months and 25 months, respectively, while those were 8 months and 19 months, respectively, in the controls. The mPFS and mOS of the experimental group were greatly higher ( $P < 0.05$ ).

**3.7. Comparison on AFP.** The AFP comparison results of the two groups of patients before and after treatment are shown in Figure 8. The figure illustrated that the pretreatment AFP of the experimental group and the control group was 715 and 697, respectively, and the posttreatment AFPs were 201 and 251, respectively. The intragroup comparison showed that the two groups of AFP were removed from the shelves after treatment, and the decrease in the experimental group was greater. No great difference in AFP was found between the two groups before treatment. After treatment, the AFP of the experimental group was remarkably higher.

**3.8. Comparison of Complications between the Two Groups of Patients.** The comparison results of complications between the two groups are shown in Figure 9. The number of patients in the experimental group with complications such as hand-foot syndrome, fatigue, hypertension, diarrhea, proteinuria, bone marrow suppression, and elevated transaminase was 1, 3, 0, 1, 0, and 1, respectively. The incidence of the disease was 13.6%. The number of patients in the control group with complications such as hand-foot syndrome, fatigue, hypertension, diarrhea, proteinuria, bone marrow suppression, and elevated transaminase was 2, 2, 1, 0, 0, and 2, respectively. The incidence of the disease was 15.9%. The difference in the incidence of complications was not obvious between the two groups.

#### 4. Discussion

PLC is one of the common cancers that threaten human life and health. Clinical statistics show that the annual new cases of PLC in the world are 841,000, ranking 6th in the global

incidence of malignant tumors, and the annual death cases are 781,000, ranking 4th in malignant tumors. In China, the proportion of new cases every year is 46.6%, and the proportion of deaths is 54.6%. In general, PLC has the characteristics of high malignancy, rapid progression, and insidious onset. It has caused a huge threat to the life safety of our people and also caused a huge economic burden [19].

At present, the common treatment methods for PLC include surgical treatment, local treatment, and systemic treatment. Surgery is still the main method for the treatment of PLC at present, and it is also the preferred treatment method for patients with PLC. Generally, liver resection and liver transplantation are commonly used. However, PLC has the characteristics of multicenter, which leads to the recurrence of nearly 40% of patients one year after surgery and more than 50% to 70% of patients after 5 years of surgery [20]. Even after liver transplantation, 10% to 20% of patients relapse. In addition, PLC also has the characteristics of insidious onset. Many patients have developed to the middle and late stages of PLC when they are diagnosed with PLC and have missed the opportunity for surgery and cannot be treated with surgery. For these patients, interventional therapy represented by TACE has become the preferred treatment method [18]. These methods have the advantages of minimally invasive, clear curative effect, and strong practicability, so they have been widely used in clinical practice. Numerous clinical studies have shown that TACE can significantly prolong the survival of patients, and the cumulative 1-, 3-, and 5-year survival rates are 57%-100%, 31%-52%, and 26%-34%, respectively. However, TACE embolization of blood vessels is not complete, so TACE is often combined with other treatment methods to treat liver cancer. Systemic therapy is the most prominent and most concerned area in clinical trials in recent years [21]. The efficacy of multikinase receptor inhibitors and monoclonal antibodies on advanced liver cancer has been confirmed. Sorafenib is the first targeted drug approved for the treatment of advanced liver cancer. Randomized double-blind trials in Europe, America, and Asia Pacific have

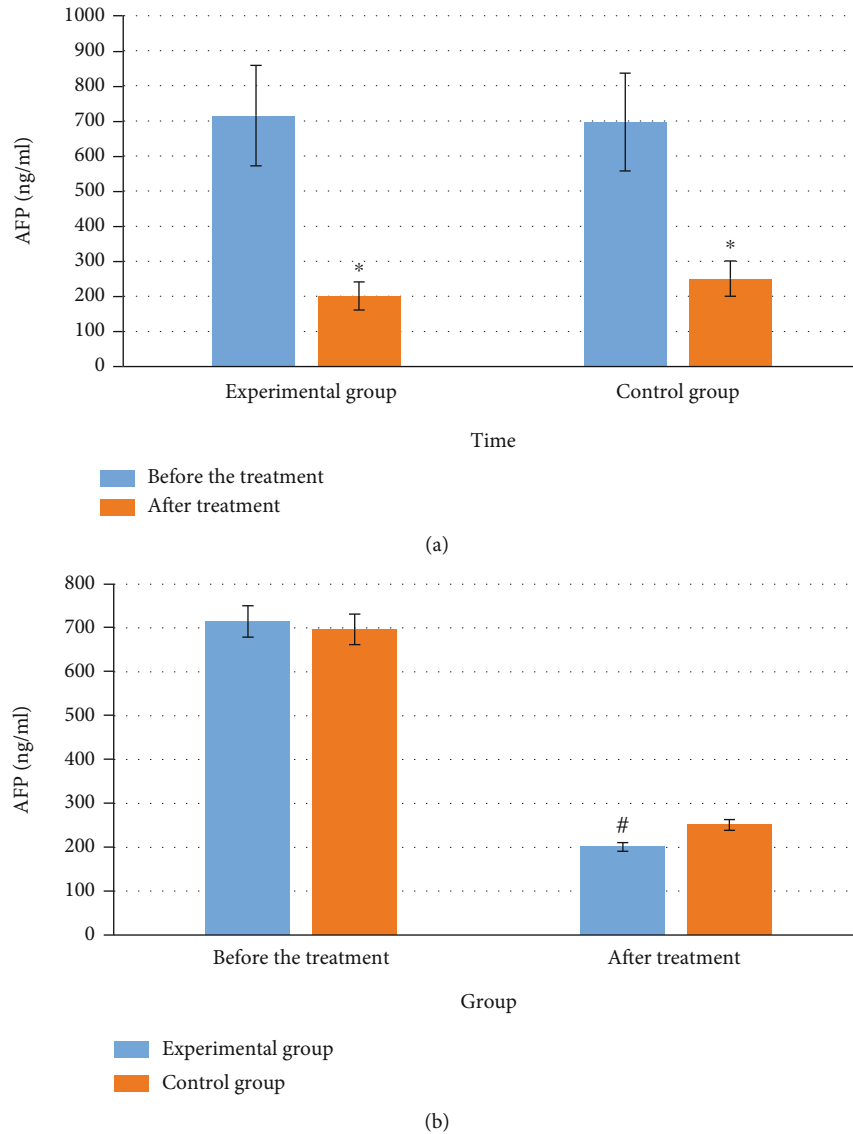


FIGURE 8: Comparison of AFP of patients. Note: # and \* meant  $P < 0.05$  in contrast to the control group and the value before treatment, respectively.

confirmed that sorafenib can significantly prolong the effective survival of advanced liver cancer [22]. Scholars in North America, Europe, and Australia compared sorafenib with placebo, and the results showed that patients using sorafenib had a median overall survival improvement of 10.7 months compared with placebo, compared with 7.9 months for placebo; sorafenib also successfully extended patients' median progression-free time from 2.8 months to 5.5 months. Similar experiments were conducted in China and South Korea, again demonstrating the effectiveness of sorafenib. Theoretically, combining TACE with sorafenib could improve the survival rate of PLC patients. However, large-scale clinical studies are needed to confirm its efficacy [23, 24]. In this work, patients with PLC who missed the opportunity for surgery were selected as the research objects, and the patients were randomly rolled into an experimental group and a control group. The patients in the experimental group were treated with TACE+sorafenib, and the patients in the control group were

treated with TACE alone. No obvious difference was found in the incidence of complications between the two groups, but both STE and LTE in the experimental group were significantly better. AFP decreased significantly more in the experimental group. This shows that the TACE+sorafenib treatment regimen can improve the survival rate and quality of life in patients with PLC effectively and greatly.

The most commonly used examination methods for the diagnosis and efficacy evaluation of PLC are CT scan and MRI. It can better detect and evaluate the number, size, shape, and lipiodol deposition of lesions. However, it also has certain defects. For example, under the influence of high-density lipiodol, the dominant density of some active tumor tissues is masked [25, 26]. Ultrasound and DSA have the disadvantage of not being able to assess the degree of tumor necrosis, and DSA is an invasive test. PET/CT has limited sensitivity and specificity. Compared with the above recurrence, MRI has the advantages of good tissue resolution, no radiation, and

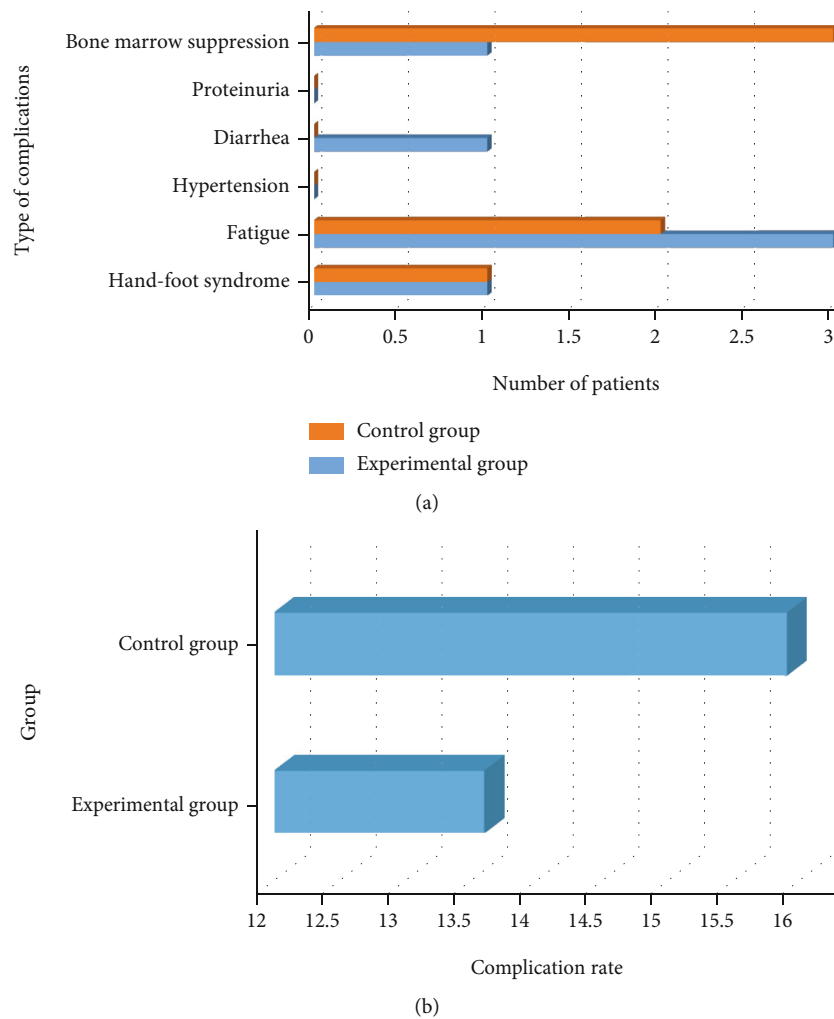


FIGURE 9: Complications of the two groups of patients: (a) number of people; (b) proportion.

MRI signal not affected by lipiodol. It has gradually received extensive attention and application in the diagnosis and efficacy evaluation of liver cancer [27–29]. DWI can detect the motion state of water molecules in biological tissues, and the motion state of water molecules is closely related to tissue structure, biochemical properties, intracellular and extracellular volume changes, and extracellular space morphological changes. It can be said that this sequence can not only observe the morphological changes but also quantitatively analyze the tissue to achieve dual imaging of morphology and function [30]. Therefore, the introduction of DWI technology into the diagnosis of PLC may be able to achieve accurate qualitative analysis of PLC. In this work, DWI technology was introduced into the diagnosis of liver cancer patients, and its diagnostic effect was compared with the results of MR plain scan. The results suggested that the DWI diagnosis results were closer to the real data, and the misdiagnosis rate was lower. This shows that DWI diagnosis shows better performance in the diagnosis of PLC.

## 5. Conclusions

Patients with PLC who missed out on surgery were used as research subjects in this study, and they were assigned to the

experimental and control groups at random. The patients in the experimental group were treated with TACE+sorafenib, and the patients in the control group were treated with TACE alone. Simultaneously, DWI technology was brought into the diagnosis of PLC patients, and its diagnostic effect was compared to that of an MR plain scan. According to the findings, there was no significant difference in the incidence of problems between the two groups, but the experimental group's STE and LTE were much better. In addition, AFP decreased significantly more in the experimental group. This shows that the TACE +sorafenib treatment regimen can improve the survival rate and quality of life in patients with PLC effectively. The DWI diagnosis results were closer to the real data, and the misdiagnosis rate was lower. To sum up, DWI had a good diagnostic efficiency for PLC, and TACE combined with sorafenib had a good therapeutic effect on PLC. There were still some limitations and shortcomings in this work. For example, it only compared the therapeutic effect of TACE alone and TACE combined with sorafenib. There was no comparison of the therapeutic effects of other medicines, such as apatinib coupled with TACE. As a result, the treatment technique suggested may not be the best option. Furthermore, only the findings of DWI and MR plain scan were compared and studied in the research on PLC

diagnosis methods, in order to introduce more inspection methods. Failure to introduce more inspection methods may lead to insufficient objective and comprehensive research results. Future study and work would improve the above problems and conduct further in-depth research.

## Data Availability

The data used to support the findings of this study are available from the corresponding author upon request.

## Conflicts of Interest

The authors declare that they have no conflicts of interest.

## References

- [1] J. Zhang, X. Wang, L. Zhang et al., “Radiomics predict postoperative survival of patients with primary liver cancer with different pathological types,” *Annals of Translational Medicine*, vol. 8, no. 13, p. 820, 2020.
- [2] S. Li, S. Shi, A. Li, H. Liu, and L. Cai, “Diffusion-weighted magnetic resonance imaging in assessment of primary liver cancer after HIFU treatment,” *Journal of the College of Physicians and Surgeons–Pakistan*, vol. 29, no. 4, pp. 305–308, 2019.
- [3] Y. Liu, S. Wang, X. Zhao et al., “Predicting clinical efficacy of vascular disrupting agents in rodent models of primary and secondary liver cancers: an overview with imaging-histopathology correlation,” *Diagnostics*, vol. 10, no. 2, p. 78, 2020.
- [4] D. M. Riviere, E. J. M. van Geenen, B. M. van der Kolk et al., “Improving preoperative detection of synchronous liver metastases in pancreatic cancer with combined contrast-enhanced and diffusion-weighted MRI,” *Abdominal Radiology*, vol. 44, no. 5, pp. 1756–1765, 2019.
- [5] H. H. Chong, L. Yang, R. F. Sheng et al., “Multi-scale and multi-parametric radiomics of gadoxetate disodium-enhanced MRI predicts microvascular invasion and outcome in patients with solitary hepatocellular carcinoma  $\leq 5$  cm,” *European Radiology*, vol. 31, no. 7, pp. 4824–4838, 2021.
- [6] Q. Song, Y. Guo, X. Yao et al., “Comparative study of evaluating the microcirculatory function status of primary small HCC between the CE (DCE-MRI) and non-CE (IVIM-DWI) MR perfusion imaging,” *Abdominal Radiology*, vol. 46, no. 6, pp. 2575–2583, 2021.
- [7] S. B. Hong, S. H. Choi, K. W. Kim et al., “Diagnostic performance of [ $^{18}$ F]FDG-PET/MRI for liver metastasis in patients with primary malignancy: a systematic review and meta-analysis,” *European Radiology*, vol. 29, no. 7, pp. 3553–3563, 2019.
- [8] S. Keller, J. Chapiro, J. Brangsch et al., “Quantitative MRI for assessment of treatment outcomes in a rabbit VX2 hepatic tumor model,” *Journal of Magnetic Resonance Imaging*, vol. 52, no. 3, pp. 668–685, 2020.
- [9] S. Colagrande, L. Calistri, G. Grazzini et al., “MRI features of primary hepatic lymphoma,” *Abdominal Radiology*, vol. 43, no. 9, pp. 2277–2287, 2018.
- [10] S. Lewis, S. Peti, S. J. Hectors et al., “Volumetric quantitative histogram analysis using diffusion-weighted magnetic resonance imaging to differentiate HCC from other primary liver cancers,” *Abdominal Radiology*, vol. 44, no. 3, pp. 912–922, 2019.
- [11] S. V. Kushchayev, Y. S. Kushchayeva, S. H. Tella, T. Glushko, K. Pacak, and O. M. Teytelboym, “Medullary thyroid carcinoma: an update on imaging,” *Journal of Thyroid Research*, vol. 2019, Article ID 1893047, 2019.
- [12] J. Podgórska, K. Pasicz, W. Skrzyński et al., “Perfusion-diffusion ratio: a new IVIM approach in differentiating solid benign and malignant primary lesions of the liver,” *BioMed Research International*, vol. 2022, Article ID 2957759, 2022.
- [13] S. X. Hu, K. Yang, X. R. Wang et al., “Application of MRI-based radiomics models in the assessment of hepatic metastasis of rectal cancer,” *Sichuan Da Xue Xue Bao. Yi Xue Ban*, vol. 52, no. 2, pp. 311–318, 2021.
- [14] B. Hazhirkarzar, P. Khoshpouri, M. Shaghghi, M. A. Ghasabeh, T. M. Pawlik, and I. R. Kamel, “Current state of the art imaging approaches for colorectal liver metastasis,” *Hepatobiliary Surgery and Nutrition*, vol. 9, no. 1, pp. 35–48, 2020.
- [15] H. X. Hu and T. Yu, “Primary hepatic neuroendocrine tumors,” *Medicine*, vol. 98, no. 50, article e18278, 2019.
- [16] M. Zarghampour, D. F. Fouladi, A. Pandey et al., “Utility of volumetric contrast-enhanced and diffusion-weighted MRI in differentiating between common primary hypervascular liver tumors,” *Journal of Magnetic Resonance Imaging*, vol. 48, no. 4, pp. 1080–1090, 2018.
- [17] N. Zhou, A. Hu, Z. Shi et al., “Inter-observer agreement of computed tomography and magnetic resonance imaging on gross tumor volume delineation of intrahepatic cholangiocarcinoma: an initial study,” *Quantitative Imaging in Medicine and Surgery*, vol. 11, no. 2, pp. 579–585, 2021.
- [18] N. Spahr, S. Thoduka, N. Abolmaali, R. Kikinis, and A. Schenk, “Multimodal image registration for liver radioembolization planning and patient assessment,” *International Journal of Computer Assisted Radiology and Surgery*, vol. 14, no. 2, pp. 215–225, 2019.
- [19] N. Vietti Violi, S. Lewis, J. Liao et al., “Gadoxetate-enhanced abbreviated MRI is highly accurate for hepatocellular carcinoma screening,” *European Radiology*, vol. 30, no. 11, pp. 6003–6013, 2020.
- [20] J. Ricke, I. G. Steffen, I. Bargellini et al., “Gadoxetic acid-based hepatobiliary MRI in hepatocellular carcinoma,” *JHEP Reports*, vol. 2, no. 6, article 100173, 2020.
- [21] S. Connor, C. Sit, M. Anjari et al., “Correlations between DW-MRI and  $^{18}$ F-FDG PET/CT parameters in head and neck squamous cell carcinoma following definitive chemo-radiotherapy,” *Cancer Reports*, vol. 4, no. 4, article e1360, 2021.
- [22] K. Yugawa, T. Yoshizumi, N. Harada et al., “Multiple hepatic sclerosing hemangiomas: a case report and review of the literature,” *Surgical Case Reports*, vol. 4, no. 1, p. 60, 2018.
- [23] J. P. Pennings, R. J. de Haas, K. J. A. Murshid, K. P. de Jong, R. A. J. O. Dierckx, and T. C. Kwee, “FDG-avid presacral soft tissue mass in previously treated rectal cancer: diagnostic outcome and additional value of MRI, including diffusion-weighted imaging,” *European Journal of Surgical Oncology*, vol. 45, no. 4, pp. 606–612, 2019.
- [24] S. H. Park, B. Kim, S. Y. Kim et al., “Characterizing computed tomography-detected arterial hyperenhancing-only lesions in patients at risk of hepatocellular carcinoma: can non-contrast magnetic resonance imaging be used for sequential imaging?,” *Korean Journal of Radiology*, vol. 21, no. 3, pp. 280–289, 2020.
- [25] C. C. Pieper, A. M. Sprinkart, G. M. Kukuk, and P. Mürtz, “Short-term measurement repeatability of a simplified intra-voxel incoherent motion (IVIM) analysis for routine clinical

- diffusion-weighted imaging in malignant liver lesions and liver parenchyma at 1.5 T,” *RöFo - Fortschritte auf dem Gebiet der Röntgenstrahlen und der bildgebenden Verfahren*, vol. 191, no. 3, pp. 199–208, 2019.
- [26] N. Yang, J. Gong, L. Yao et al., “Magnetic resonance imaging-guided microwave ablation of hepatic malignancies: feasibility, efficacy, safety, and follow-up,” *Journal of Cancer Research and Therapeutics*, vol. 16, no. 5, pp. 1151–1156, 2020.
- [27] J. Fu, M. J. Fang, D. Dong et al., “Heterogeneity of metastatic gastrointestinal stromal tumor on texture analysis: DWI texture as potential biomarker of overall survival,” *European Journal of Radiology*, vol. 125, article 108825, 2020.
- [28] G. Usui, H. Hashimoto, M. Kusakabe et al., “Intrahepatic carcinosarcoma with cholangiocarcinoma elements and prominent bile duct spread,” *International Journal of Surgical Pathology*, vol. 27, no. 8, pp. 900–906, 2019.
- [29] M. V. Chan, Y. R. Huo, N. Trieu et al., “Noncontrast MRI for hepatocellular carcinoma detection: a systematic review and meta-analysis - a potential surveillance tool?,” *Clinical Gastroenterology and Hepatology*, vol. 20, no. 1, pp. 44–56.e2, 2022.
- [30] Y. Liu, F. De Keyser, Y. Wang et al., “The first study on therapeutic efficacies of a vascular disrupting agent CA4P among primary hepatocellular carcinomas with a full spectrum of differentiation and vascularity: correlation of MRI-microangiography- histopathology in rats,” *International Journal of Cancer*, vol. 143, no. 7, pp. 1817–1828, 2018.

## Retraction

# Retracted: Monitoring Mycoplasma pneumoniae-Specific Antibody, C-Reactive Protein, and Procalcitonin Levels in Children with Mycoplasma Pneumonia Is Important

### Computational and Mathematical Methods in Medicine

Received 25 July 2023; Accepted 25 July 2023; Published 26 July 2023

Copyright © 2023 Computational and Mathematical Methods in Medicine. This is an open access article distributed under the Creative Commons Attribution License, which permits unrestricted use, distribution, and reproduction in any medium, provided the original work is properly cited.

This article has been retracted by Hindawi following an investigation undertaken by the publisher [1]. This investigation has uncovered evidence of one or more of the following indicators of systematic manipulation of the publication process:

- (1) Discrepancies in scope
- (2) Discrepancies in the description of the research reported
- (3) Discrepancies between the availability of data and the research described
- (4) Inappropriate citations
- (5) Incoherent, meaningless and/or irrelevant content included in the article
- (6) Peer-review manipulation

The presence of these indicators undermines our confidence in the integrity of the article's content and we cannot, therefore, vouch for its reliability. Please note that this notice is intended solely to alert readers that the content of this article is unreliable. We have not investigated whether authors were aware of or involved in the systematic manipulation of the publication process.

In addition, our investigation has also shown that one or more of the following human-subject reporting requirements has not been met in this article: ethical approval by an Institutional Review Board (IRB) committee or equivalent, patient/participant consent to participate, and/or agreement to publish patient/participant details (where relevant).

Wiley and Hindawi regrets that the usual quality checks did not identify these issues before publication and have since put additional measures in place to safeguard research integrity.

We wish to credit our own Research Integrity and Research Publishing teams and anonymous and named external researchers and research integrity experts for contributing to this investigation.

The corresponding author, as the representative of all authors, has been given the opportunity to register their agreement or disagreement to this retraction. We have kept a record of any response received.

### References

- [1] X. Cao, "Monitoring Mycoplasma pneumoniae-Specific Antibody, C-Reactive Protein, and Procalcitonin Levels in Children with Mycoplasma Pneumonia Is Important," *Computational and Mathematical Methods in Medicine*, vol. 2022, Article ID 7976858, 7 pages, 2022.



## Research Article

# Monitoring Mycoplasma pneumoniae-Specific Antibody, C-Reactive Protein, and Procalcitonin Levels in Children with Mycoplasma Pneumonia Is Important

Xinying Cao 

School of Harbin Medical University, China

Correspondence should be addressed to Xinying Cao; [fj-yjs2020022080@hmdq.edu.cn](mailto:fj-yjs2020022080@hmdq.edu.cn)

Received 19 April 2022; Revised 10 May 2022; Accepted 2 June 2022; Published 28 June 2022

Academic Editor: Naeem Jan

Copyright © 2022 Xinying Cao. This is an open access article distributed under the Creative Commons Attribution License, which permits unrestricted use, distribution, and reproduction in any medium, provided the original work is properly cited.

The goal of this study was to see how important it is to monitor Mycoplasma pneumoniae-specific antibody IgM, C-reactive protein, and procalcitonin levels in the blood of kids with Mycoplasma pneumoniae pneumonia as a reference for clinical diagnosis and treatment. The study group consisted of 96 children who had mycoplasma pneumonia in our hospital between May 2020 and May 2021, and the control group consisted of 96 healthy children who had a routine physical examination in our hospital at the same time. C-reactive protein and procalcitonin were measured and compared. The application value of single detection and combined detection of Mycoplasma pneumoniae-specific antibody IgM, C-reactive protein, and procalcitonin in the diagnosis of Mycoplasma pneumoniae pneumonia was evaluated based on clinical diagnosis results. The detection values of C-reactive protein and procalcitonin in the study group were higher than those in the recovery period and the control group,  $P < 0.05$ ; the detection values of C-reactive protein and procalcitonin in the study group were higher than those in the control group,  $P < 0.05$ . The combination detection of Mycoplasma pneumoniae-specific antibody IgM, C-reactive protein, and procalcitonin had a greater diagnostic accuracy than single detection ( $P < 0.05$ ). The sensitivity was higher than C-reactive protein and procalcitonin ( $P < 0.05$ ); the specificity and positive predictive value were higher than Mycoplasma pneumoniae-specific antibody IgM ( $P < 0.05$ ); and the negative predictive value was higher than procalcitonin ( $P < 0.05$ ). The clinical value of combining the detection of Mycoplasma pneumoniae-specific antibody IgM, C-reactive protein, and procalcitonin in the diagnosis of Mycoplasma pneumoniae pneumonia in children is higher than that of single item detection, and it can provide a reliable clinical reference, as well as aid in evaluating the recovery effect of children, and it is worthy of application.

## 1. Introduction

In pediatrics, mycoplasma pneumonia is a frequent respiratory disease that affects school-aged and preschool children. Mycoplasma pneumonia is greatly affected by seasonal changes, children's physical resistance, and other factors. Mycoplasma pneumonia is characterized by rapid onset, long treatment cycle, and the need for continuous medication. In addition, the emotional instability caused by cough and fever in sick children also increases the difficulty of treatment [1]. Infection with Mycoplasma pneumoniae is

the main cause of the disease. Because of their young respiratory systems, poor respiratory function, and inadequate immunity, children are more likely to contract the disease [2]. The disease's symptoms appear gradually. Weariness, faintness, and sluggishness are common in mild patients. An MP infection might be hazardous in some situations. If you have asthma, MP could make your symptoms worse. MP can possibly develop into a more serious pneumonia. MP complications include respiratory failure, lung abscess, acute respiratory distress syndrome, lung consolidation, and bronchiolitis obliterans. Symptoms such as dyspnea,

headache, fever, and cough are common among severe patients. During auscultating lung sounds, tubular breath sounds and wet rales are common clinical symptoms.

Untimely or ineffective treatment can worsen the condition, harm small airway and respiratory function, and even cause encephalitis, myocarditis, and other complications [3]. *Mycoplasma pneumoniae* has obvious symptoms such as persistent high fever and aggravated cough. If it is not treated in time, it may form lobar pneumonia. At the same time, *Mycoplasma pneumoniae* infection can also cause myocardial damage and liver function damage and seriously reduce the diet and mental state of children. Some children will cause central nervous system infection, and the infection of *Mycoplasma pneumoniae* encephalitis will affect life safety [4]. As a result, in clinical treatment, it is critical to diagnose and treat *Mycoplasma pneumoniae* as soon as feasible. The clinical value of combining the detection of *Mycoplasma pneumoniae*-specific antibody IgM, C-reactive protein, and procalcitonin in the diagnosis of *Mycoplasma pneumoniae* pneumonia in children is higher than single item detection, and it can provide a reliable clinical reference, as well as aid in evaluating the recovery effect of children, and it is worthy of application.

In recent years, projects based on serum targets such as *Mycoplasma pneumoniae*-specific antibody, C-reactive protein, and procalcitonin, among others, have been developed to provide a reliable diagnostic basis for clinics, which is critical for improving *Mycoplasma pneumoniae* clinical diagnostic efficiency [5–7]. The variance of *Mycoplasma pneumoniae* specific antibody, C-reactive protein, and procalcitonin in the blood of 96 children with *Mycoplasma pneumoniae* and 96 healthy children was compared by pediatricians at our hospital. Monitoring the levels of *Mycoplasma pneumoniae*-specific antibody, C-reactive protein, and procalcitonin in children with *Mycoplasma pneumoniae* pneumonia is helpful for the diagnosis of *Mycoplasma pneumoniae* pneumonia and the evaluation of children's condition. The main structure and ideas of this study are shown in Figure 1.

## 2. Materials and Methods

**2.1. General Information.** From May 2020 to May 2021, we evaluated the medical records of all children with *Mycoplasma pneumoniae* admitted to our department, and 96 patients with *Mycoplasma pneumoniae* diagnosed and treated in our hospital's pediatrics were placed into the study group. There were 51 girls and 45 boys; the age ranged from 1 to 14 ( $6.13 \pm 1.02$ ) years. The conditions of the group are as follows:

### 2.1.1. Inclusion Criteria

- (1) Integral medical records
- (2) Confirmed by laboratory and imaging examinations, meeting the requirements of diagnosis regulations in *Zhu Futang Practice of Pediatrics* (8th Edition) [8];

- (3) Family members know about the study and voluntarily participate it

### 2.1.2. Exclusion Criteria

- (1) Congenital diseases
- (2) Serious organ dysfunction
- (3) Serious diseases synthesizing other organs
- (4) Systemic immune diseases
- (5) Blood system diseases
- (6) Cancer
- (7) Mental diseases
- (8) Allergy to therapeutic drugs

In addition, 96 healthy children who underwent routine physical examination in pediatrics of our hospital meanwhile were classified into the control group. There were 50 girls and 46 boys; the age ranged from 1 to 14 ( $6.16 \pm 1.00$ ) years. The conditions of the control group are as follows:

### 2.1.3. Inclusion Criteria

- (1) Integral physical examination data
- (2) Good physical condition
- (3) Family members knew about the study and participated voluntarily

### 2.1.4. Exclusion Criteria

- (1) *Mycoplasma pneumoniae*
- (2) Congenital diseases
- (3) Severe organ dysfunction
- (4) Severe diseases synthesizing other organs
- (5) Systemic immune diseases
- (6) Blood system diseases
- (7) Cancer
- (8) Mental diseases

*P* values are the same in the comparison of gender and age between the two groups that is  $>0.05$ .

**2.2. Methods.** The children in the study group collected 2~3ml of upper limb venous blood on an empty stomach at the beginning of admission (acute stage) and recovery stage, and the children in the control group collected 2~3 ml of upper limb venous blood on an empty stomach at one time. The blood samples were centrifuged, placed in a vacuum tube, posited for 30 min, centrifuged at 3500 r/min for 10 min, and the supernatant was extracted for later testing. In the detection of *Mycoplasma pneumoniae*-

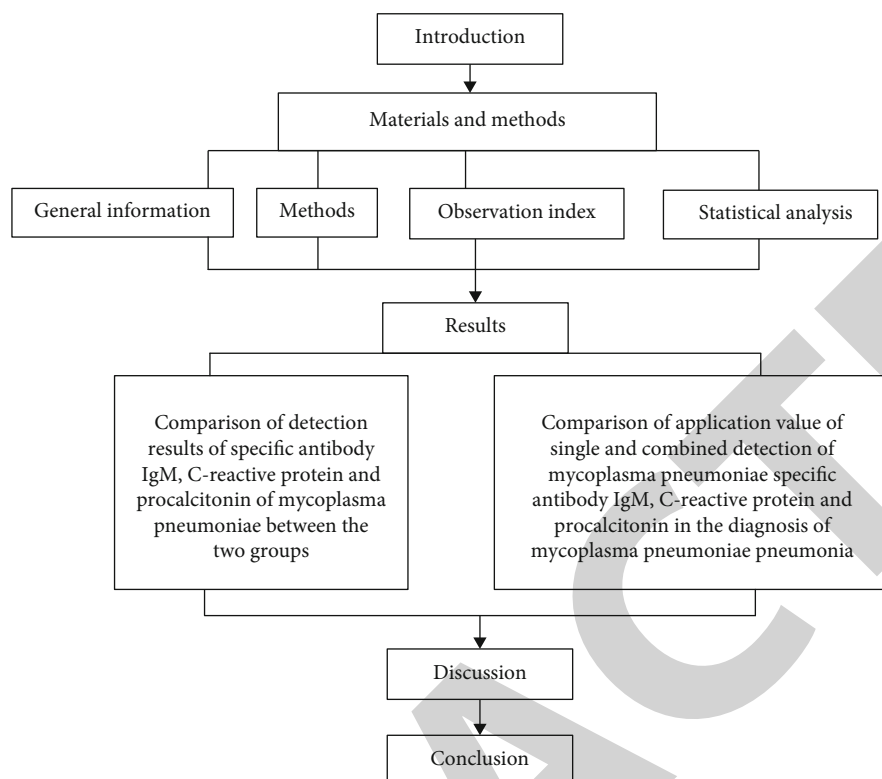


FIGURE 1: Structure of this study.

specific antibody IgM, indirect enzyme-linked immunosorbent assay is used for detection. The kit is provided by the Shanghai Hushang Biotechnology Co., Ltd. It is regarded positive if the detection well's color rendering is better than the control well's. Immune scattering turbidimetry is used to identify C-reactive protein, which is detected with the Nephstar Plus device. The kit is provided by Siemens Medical Diagnostic Products (Shanghai) Co., Ltd. The result of detection is considered positive if the detection value is  $>8$  mg/l [9]. In procalcitonin detection, chemiluminescence method is used for detection with Roche Cobas e601 electrochemiluminescence immunoanalyzer, and the kit is provided by Merier Diagnostic Products (Shanghai) Co., Ltd; the test value  $>0.5$  ng/ml is considered positive [10].

### 2.3. Observation Index

- (1) Compare the detection results of specific antibody IgM, C-reactive protein, and procalcitonin of Mycoplasma pneumoniae between the two groups
- (2) Based on the clinical diagnosis results, the application value of single and joint detection of Mycoplasma pneumoniae-specific antibody IgM, C-reactive protein, and procalcitonin in the diagnosis of Mycoplasma pneumoniae pneumonia were evaluated, and the accuracy, sensitivity, specificity, positive predictive value, and negative predictive value were calculated

**2.4. Statistical Analysis.** Statistical data analysis was performed with SPSS 22.0; normally enumeration data are expressed as % and inspected by chi-square test, and the data are expressed in  $(\pm s)$  and performed by *t*-test. A *P* value of  $<0.05$  was considered statistically significant.

## 3. Results

**3.1. Comparison of Detection Results of Specific Antibody IgM, C-Reactive Protein, and Procalcitonin of Mycoplasma pneumoniae between the Two Groups.** At the time of admission, the study group had higher rates of positive Mycoplasma pneumoniae-specific antibodies IgM, C-reactive protein, and procalcitonin, as well as higher detection values of C-reactive protein and procalcitonin, than the recovery group and the control group ( $P < 0.05$ ). The detection values of C-reactive protein and procalcitonin in the study group were higher than those in the control group ( $P < 0.05$ ). They are presented in Table 1.

**3.2. Comparison of Application Value of Single and Combined Detection of Mycoplasma pneumoniae-Specific Antibody IgM, C-Reactive Protein, and Procalcitonin in the Diagnosis of Mycoplasma pneumoniae Pneumonia.** The diagnostic accuracy of combined detection of Mycoplasma pneumoniae-specific antibody IgM, C-reactive protein, and procalcitonin was higher than that of single detection ( $P < 0.05$ ); the sensitivity was higher than that of C-reactive protein and procalcitonin ( $P < 0.05$ ); the specificity

TABLE 1: Comparison of detection results of specific antibody IgM, C-reactive protein and procalcitonin of Mycoplasma pneumoniae between the two groups.

Group	Time	Case number	Positive detection rate of Mycoplasma pneumoniae-specific antibody IgM [n (%)]		C-reactive protein		Procalcitonin	
			Detection value ( $\bar{x} \pm s$ , mg/l)	Detection value ( $\bar{x} \pm s$ , ng/ml)	Positive detection rate [n (%)]	Detection value ( $\bar{x} \pm s$ , ng/ml)	Positive detection rate [n (%)]	
Study group	Initial hospitalization	96	68 (70.83)	17.72 $\pm$ 5.15	60 (62.50)	0.58 $\pm$ 0.17	33 (34.38)	
	Convalescence	96	13 (13.54)	7.86 $\pm$ 2.94	8 (8.33)	0.17 $\pm$ 0.03	4 (4.17)	
Control group	—	96	6 (6.25)	3.14 $\pm$ 0.78	2 (2.08)	0.12 $\pm$ 0.02	1 (1.04)	
	Initial hospitalization and convalescence of the study group	—	64.598	16.291	64.733	23.271	28.156	
$\chi^2/t$ value (initial hospitalization and convalescence of the study group)		—	$\leq 0.001$	$\leq 0.001$	$\leq 0.001$	$\leq 0.001$	$\leq 0.001$	
$P$ value (initial hospitalization and convalescence of the study group)		—	84.522	27.426	80.135	26.331	36.599	
$\chi^2/t$ value (initial hospitalization of hospitalization of study group and control group)		—	$\leq 0.001$	$\leq 0.001$	$\leq 0.001$	$\leq 0.001$	$\leq 0.001$	
$P$ value (initial hospitalization of study group and control group)		—	2.862	15.204	3.798	13.587	1.848	
$\chi^2/t$ value (convalescence of study group and control group)		—	0.091	$\leq 0.001$	0.051	$\leq 0.001$	0.174	
$P$ value (convalescence of study group and control group)		—						

TABLE 2: Comparison of diagnosis results of *Mycoplasma pneumoniae*-specific antibody IgM, C-reactive protein, and procalcitonin by single detection and combined detection ( $n$ ).

Diagnostic results	Mycoplasma pneumoniae-specific antibody IgM		C-reactive protein		Procalcitonin		Joint detection		Total
	Positive	Negative	Positive	Negative	Positive	Negative	Positive	Negative	
Positive	68	28	60	36	33	63	76	20	96
Negative	6	90	2	94	1	95	0	96	96
Total	74	118	62	130	34	158	76	116	192

TABLE 3: Comparison of application value of single and combined detection of *Mycoplasma pneumoniae*-specific antibody IgM, C-reactive protein, and procalcitonin in the diagnosis of *Mycoplasma pneumoniae* pneumonia [% ( $n/N$ )].

Test method	Accuracy rate	Sensitivity	Specificity	Positive predictive value	Negative predictive value
Mycoplasma pneumoniae-specific antibody IgM	82.29 (158/192)	70.83 (68/96)	93.75 (90/96)	91.89 (68/74)	76.27 (90/118)
C-reactive protein	80.21 (154/192)	62.50 (60/96)	97.92 (94/96)	96.77 (60/62)	72.31 (94/130)
Procalcitonin	66.67 (128/192)	34.38 (33/96)	98.96 (95/96)	97.06 (33/34)	60.13 (95/158)
Joint detection	89.58 (172/192)	79.17 (76/96)	100.00 (96/96)	100.00 (76/76)	82.76 (96/116)
$\chi^2$ value (Mycoplasma pneumoniae-specific antibody IgM and joint detection)	4.224	1.778	5.813	6.419	1.510
$P$ value (Mycoplasma pneumoniae-specific antibody IgM and joint detection)	0.040	0.182	0.016	0.011	0.219
$\chi^2$ value (C-reactive protein and joint detection)	6.580	6.454	1.895	2.488	3.808
$P$ value (C-reactive protein and joint detection)	0.010	0.011	0.169	0.115	0.051
$\chi^2$ value (procalcitonin and joint detection)	29.501	39.240	0.943	2.256	16.226
$P$ value (procalcitonin and joint detection)	$\leq 0.001$	$\leq 0.001$	0.332	0.133	$\leq 0.001$

and positive predictive value were higher than those of *Mycoplasma pneumoniae*-specific antibody IgM ( $P < 0.05$ ); the negative predictive value was higher than that of procalcitonin ( $P < 0.05$ ). They are presented in Tables 2 and 3.

#### 4. Discussion

The gold standard for clinical diagnosis of *Mycoplasma pneumoniae* is isolating culture. However, because *Mycoplasma pneumoniae* grows slowly and takes a long time to isolate, it cannot produce results rapidly, which is inconvenient for early disease therapy, resulting in its limited clinical application [11]. With the deepening of relevant researches, it is considered that *Mycoplasma pneumoniae*-specific antibody, C-reactive protein, and procalcitonin can play an important role in the diagnosis and efficacy evaluation of *Mycoplasma pneumoniae* pneumonia in children and are important supplementary indicators for the isolation and culture of *Mycoplasma pneumoniae* [12–14]. After infection with *Mycoplasma pneumoniae* in humans, specific IgM, IgG, and IgA antibodies will be produced in them, of which IgM antibodies appear first. Under normal

circumstances, they only exist in serum 60–90 days after infection, so they have become an effective marker of recent infection [15, 16]. Relevant studies have also found that the incubation period of *Mycoplasma pneumoniae* infection is 14–21 days, and the IgM antibody in children's serum has reached a very high level when they have symptoms [17]. C-reactive protein (CRP) is a liver-produced acute phase reactive protein that can bind with choline phosphate in bacterial cell walls to activate complement activity and regulate cell phagocytosis [18]. When the body is stressed by an inflammatory reaction, the liver produces a huge amount of C-reactive protein, resulting in a considerable increase in its expression level [19]. The sensitivity of C-reactive protein is high, and its detection value is not affected by the patient's age, gender, body temperature, and other factors. Procalcitonin, a precursor of calcitonin, is a protein secreted by thyroid C cells. The body generally cannot detect PCT under healthy conditions. When the body has inflammation or infection, it will release a large number of inflammatory cytokines. The combination of inflammatory cytokines and bacterial toxins will produce a large number of procalcitonin, resulting in a significant

increase in its detection value. Studies have found that the higher the detection value of procalcitonin, the more serious the infection [20]. At present, it is generally believed that when antibiotics are used in clinical treatment of mycoplasma pneumonia in children, procalcitonin level can be used as a reference index to provide medication guidance. Once the serum procalcitonin of children reaches 0.5 ng/ml, it should be used in time, so as to shorten the antibacterial course and improve the overall curative effect [21]. Through the use of appropriate dose of budesonide atomization therapy combined with azithromycin administration, it has obvious effect on children with mycoplasma pneumonia, which can quickly alleviate children's cough and improve the clinical efficacy [22]. The use of montelukast sodium chewing combined with azithromycin administration has a significant effect on children with mycoplasma pneumonia, which can effectively improve patients' lung function and alleviate the symptoms of mycoplasma pneumonia [23].

The findings of this study revealed that the positive rates of *Mycoplasma pneumoniae*-specific antibody IgM, C-reactive protein, and procalcitonin, as well as the detection values of C-reactive protein and procalcitonin, were higher in the study group at the start of hospitalization than in the recovery period and control group, implying the high expression of *Mycoplasma pneumoniae*-specific antibody IgM, C-reactive protein, and procalcitonin in children with myco, while the detection values of the three indexes of children have decreased significantly after treatments, and the positive detection rate has no significant difference compared with the control group. In case of that, it is considered that the specific antibodies IgM, C-reactive protein, and procalcitonin of *Mycoplasma pneumoniae* can be used as reference indexes for clinical diagnosis and curative effect evaluation of children with *Mycoplasma pneumoniae* pneumonia. The results of diagnostic analysis showed that compared with the detection of each single index, the accuracy of the three indexes after the joint detection in the diagnosis of mycoplasma pneumonia was significantly higher, and the sensitivity, specificity, positive predictive value, and negative predictive value were improved in varying degrees, indicating that the joint detection can further improve the accuracy of diagnostic results and provide more accurate reference basis for clinical practice.

## 5. Conclusion

As a consequence, combining the detection of *Mycoplasma pneumoniae*-specific antibody, C-reactive protein, and procalcitonin in the diagnosis of children with *Mycoplasma pneumoniae* pneumonia has a higher clinical application value than single item detection, which can provide a reliable reference basis for clinical practice and aid in evaluating the recovery effect of children, and is worthy of application. The emotional instability of children with mycoplasma infection, persistent fever, and cough affect the treatment and diet of children. We can consider increasing nutritional supplement and related psychological support to speed up the recovery of children.

## Data Availability

The data used to support the findings of this study are included within the article.

## Conflicts of Interest

The author declares that they have no conflicts of interest.

## References

- [1] T. Changming and T. Yuan, "Expression of Th17 and Treg cell subsets and cytokines in peripheral blood of children with *Mycoplasma pneumoniae* and study on CRP and PCT levels," *Journal of Modern Laboratory Medicine*, vol. 34, no. 4, pp. 108–111, 2019.
- [2] X. Ji and L. Siyu, "The value of combined detection of procalcitonin, C-reactive protein and serum amyloid protein A in early diagnosis of infantile bacterial infectious diseases," *Chinese Journal of Health Laboratory Technology*, vol. 28, no. 8, pp. 967–969, 2018.
- [3] H. Ting, H. Haiyan, W. Jing, R. Qiangquan, and Q. Yao, "Clinical significance of serum procalcitonin and C-reactive protein levels in children with mycoplasma pneumonia," *Journal of Clinical Research*, vol. 2, no. 14, pp. 99–100, 2017.
- [4] X. Aili, X. Qun, Z. Zhen, Y. Mei, and Z. Rui, "The clinical significance of the serum level changes of procalcitonin and C-reactive protein in children with *Mycoplasma pneumoniae* pneumonia," *Journal of Bengbu Medical College*, vol. 43, no. 4, pp. 488–490, 2018.
- [5] F. Cheng and S. Jun, "Detection value of *Mycoplasma pneumoniae* IgM, IgG, serum CRP and PCT levels in diagnosis and treatment of *Mycoplasma pneumoniae* pneumonia in children," *Journal of North Sichuan Medical College*, vol. 35, no. 2, pp. 321–323, 2020.
- [6] L. Qi and G. Hongli, "Changes and significance procalcitonin, C-reactive protein, T-lymphocyte subsets, and immunoglobulin in children with mycoplasma pneumonia," *Hainan Medical Journal*, vol. 31, no. 11, pp. 1408–1411, 2020.
- [7] H. Xiao, W. Shaofen, and Z. Junying, "Clinical value of early differential diagnosis of children's pneumonia by cellular immune index, serum hs CRP and PCT," *Experimental and Laboratory Medicine*, vol. 38, no. 3, pp. 530–532, 2020.
- [8] J. Zaifang, S. Kunling, and S. Ying, *Zhu Futang Practice of Pediatrics*, People's Publishing House, 8th edition, 2015.
- [9] Z. Weidong, L. Yujuan, Z. Yunmei, L. Su, and T. Wei, "Changes and clinical significance of procalcitonin C-reactive protein in children with *Mycoplasma pneumoniae* pneumonia," *Journal of Yichun University*, vol. 40, no. 12, pp. 73–75, 2018.
- [10] Z. Jinbao, L. Tianming, L. Caihong, M. Shuhong, and W. Jianguan, "Clinical significance of changes of procalcitonin, high-sensitivity C-reactive protein and T cell subsets in children with different pneumonia," *Chinese Journal of Laboratory Diagnosis*, vol. 22, no. 11, pp. 1960–1962, 2018.
- [11] S. Jingwei, P. Wansheng, H. Yuzhu, L. Na, and L. Jiachen, "Changes and clinical significance of hypersensitive CRP, PCT and WBC in children with *Mycoplasma pneumoniae* pneumonia complicated with systemic inflammatory response syndrome," *Chinese Journal of General Practice*, vol. 17, no. 2, pp. 245–247, 2019.

## Research Article

# Fetal and Neonatal Middle Cerebral Artery Hemodynamic Changes and Significance under Ultrasound Detection in Hypertensive Disorder Complicating Pregnancy Patients with Different Severities

Pei Zhou, Yi Sun, Yongpan Tan, Yanru An, Xingxing Wang, and Lufang Wang 

Department of Ultrasound, The Fourth Hospital of Shijiazhuang, Shijiazhuang, 050000 Hebei, China

Correspondence should be addressed to Lufang Wang; 1931011128@siit.edu.cn

Received 22 April 2022; Revised 16 May 2022; Accepted 20 May 2022; Published 27 June 2022

Academic Editor: Naeem Jan

Copyright © 2022 Pei Zhou et al. This is an open access article distributed under the Creative Commons Attribution License, which permits unrestricted use, distribution, and reproduction in any medium, provided the original work is properly cited.

Colour Doppler ultrasound was applied for monitoring the hemodynamic parameters of fetal uterine artery (UtA), umbilical artery (UA), and middle cerebral artery (MCA) during pregnancy. In hypertension disease complicating pregnancy, these hemodynamic measures and their therapeutic applicability value were reviewed (HDCP). 120 singleton pregnant women were chosen, with 40 cases of mild preeclampsia (mild group), 40 cases of severe preeclampsia (severe group), and 40 normal control pregnant women (control group). The hemodynamic parameters of UtA, MCA, and UA were monitored in the three groups, including pulsatility index (PI), resistance index (RI), and the systolic/diastolic velocity (S/D). The parameters PI, RI, S/D, and venous catheter shunt rate ( $Q_{dv}/Q_{uv}$ ) of UtA and UA in the severe group were higher than those in the normal group and the mild group, showing the differences statistically significant ( $P < 0.05$ ). The PI, RI, and S/D of MCA in the severe group were lower than those in the normal group and the mild group ( $P < 0.05$ ). The changing trends of PI, RI, and S/D in the severe group were all first increased and then decreased in the early, middle, and later pregnancy ( $P < 0.05$ ). The area under the curve (AUC) was 0.98 in the receiver operating characteristic (ROC) curve created using a combination of hemodynamic measures and pregnancy outcomes, and the sensitivity and specificity for predicting bad outcomes were 94.7 percent and 96.4 percent, respectively. Colour Doppler ultrasound may accurately detect changes in the PI, RI, and S/D of UtA, MCA, and UA in pregnant women and serve as a reference for determining the intrauterine state of the fetuses and predicting bad pregnancy outcomes. In particular, the parameters in later pregnancy were higher worthy of diagnostic value for adverse pregnancy outcomes. The combination of various parameters could make an improvement of the diagnostic accuracy and provide a basis for guiding treatment as well as determining the optimal timing of delivery.

## 1. Introduction

Hypertensive disorder complicating pregnancy (HDCP) is a group of diseases that coexist with pregnancy and elevated blood pressure, with an incidence of about 5% to 12%. It seriously affects the health of mothers and fetuses and is one of the important causes of maternal and fetal death [1–3]. The common methods for monitoring fetal intrauterine status include fetal movement counting, electronic fetal heart rate monitoring, fetal scalp blood gas analysis, fetal electrocardiogram, ultrasound, and amniocentesis. With ultrasound, not only the intrauterine growth of the fetus but also the fetal position,

placental position, amniotic fluid volume, and placental maturity can be determined; it is the most common imaging method in obstetrics [4, 5]. As colour Doppler flow imaging (CDFI) is combined with conventional two-dimensional ultrasound, the distribution of blood flow can be displayed, and the velocity of blood flow can be quantitatively measured. Thus, the distribution and passages of blood flow in blood vessels are shown more comprehensively [6].

Blood flow of umbilical artery (UA) has a wide range of applications clinically. By monitoring fetal UA blood flow parameters, placental blood perfusion and placental peripheral microcirculation resistance are evaluated, which is to judge

TABLE 1: Comparison of the mean age and mean gestational age ( $\bar{x} \pm s$ ).

Groups	Cases ( $n$ )	Mean age (years old)	Mean gestational age (weeks)
Control group	30	$28.89 \pm 2.360$	$32.67 \pm 0.782$
Mild group	30	$27.68 \pm 2.644$	$32.36 \pm 0.563$
Severe group	30	$28.79 \pm 2.571$	$32.61 \pm 0.451$

fetal intrauterine status and predict pregnancy outcome [7–9]. The uterine artery (UtA) is the main blood vessel for blood circulation between the uterus and the placenta and is a crucial bridge between the fete and the mother. Both the diameter of the UtA and the blood flow velocity increase to meet the blood supply for the growth and development of the fetuses [10]. The fetal MCA expands to the internal carotid artery, and its oxygen supply occupies about 80% of the entire brain. Since the fetal brain is the most sensitive to intrauterine hypoxia, monitoring the blood flow parameters of the MCA can reflect the developmental status of fetal cerebral circulation directly, having a certain clinical value in assessing fetal intrauterine conditions and predicting pregnancy outcomes [11–13]. By detecting the blood flow parameters pulsatility index (PI), resistance index (RI), and the ratio of systolic peak velocity to diastolic end velocity (S/D) of fetal-related blood vessels like UtA, MCA, and UA, an objective basis can be obtained for determining the intrauterine status of the fetuses, guiding clinical treatment, and predicting pregnancy outcomes [14–17].

The blood flow parameters UtA, MCA, and UA in 120 pregnant women with singleton pregnancy were monitored and analysed in this research. It was aimed at the changes in blood flow parameters of UtA, MCA, and UA in HDCP patients and their correlation with pregnancy outcomes. It was expected to give a diagnostic basis for clinical application. The later-stage markers demonstrated a higher diagnostic value for negative pregnancy outcomes. All of the parameters together could increase diagnostic accuracy and offer a foundation for guiding treatment and identifying the ideal delivery time. The disadvantages of this study were that the measurements of several parameters might be affected by frequent fetal movement. The angle of sampling between the sound beam and the blood flow should be exact, and there may be minor mistakes.

The arrangements of the paper are as follows: Section 2 discusses the materials and methods. Section 3 describes the results and discussion. Section 4 examines the sensitivity and specificity of the combination of all parameters in diagnosing adverse pregnancy outcomes. Section 5 concludes the article.

## 2. Materials and Methods

*2.1. Research Objects.* 120 pregnant women were chosen as they went to the Fourth Hospital of Shijiazhuang for prenatal examination from November 2019 to December 2021. They had the singleton pregnancy at 32–34 weeks, including

40 cases with mild preeclampsia (mild group), 40 with severe eclampsia (severe group), and 40 normal pregnant women (control group). All cases were followed up to the end of their pregnancy. Their age ranged from 22 to 35 years old, with a mean value of  $28.45 \pm 2.36$  years old. The gestational age was varied from 28 to 40 weeks, with  $35.42 \pm 4.3$  weeks on average. Mild and severe preeclampsia in these cases conformed to the classification of HDCP in the 8th edition of Obstetrics and Gynecology [18]. This research had been approved by the Medical Ethics Committee of the Fourth Hospital of Shijiazhuang, and the patients and their families were informed about the research situation and signed the informed consents.

Inclusion criteria were listed as below.

- (1) Pregnant women went with the complete medical records, went for obstetric examination regularly, and received institutional delivery
- (2) They were health previously, with no smoking, alcohol abuse, and other bad habits
- (3) Their menstruation was regular, and the last menstrual period was clear; under early pregnancy ultrasound examination, the fetal size and menopause cycle were matched
- (4) They had no special medication history during pregnancy, and the fetuses got no congenital developmental malformation

The following were the exclusion criteria.

- (1) Ultrasound examination revealed fetal congenital abnormality or abnormal placenta
- (2) Ultrasound examination showed there were twins or multiples
- (3) The patients were accompanied with genital malformations or genital diseases
- (4) The patients had an acute infectious disease
- (5) They had a history of lower abdominal and pelvic surgery in the past
- (6) Patients went with obesity

*2.2. Examination Methods.* The probe frequency was 3.5 MHz, the sample volume was 2 mm, and the angle between the sound beam and blood flow was  $30^\circ$  using the Philips-IU22 full digital colour Doppler ultrasound diagnostic apparatus made in the Netherlands. Before the examination, all pregnant women emptied their urine and underwent routine obstetric ultrasound examination in the supine position. The fetal biparietal diameter (BPD), head circumference (HC), abdominal circumference (AC), femoral length (FL), and more growth indexes were examined. The fetal position and placental position were observed, and fetal heart rate, amniotic fluid volume, and more were monitored. After routine obstetric ultrasound examination, CDFI was performed for the measurement of the blood flow



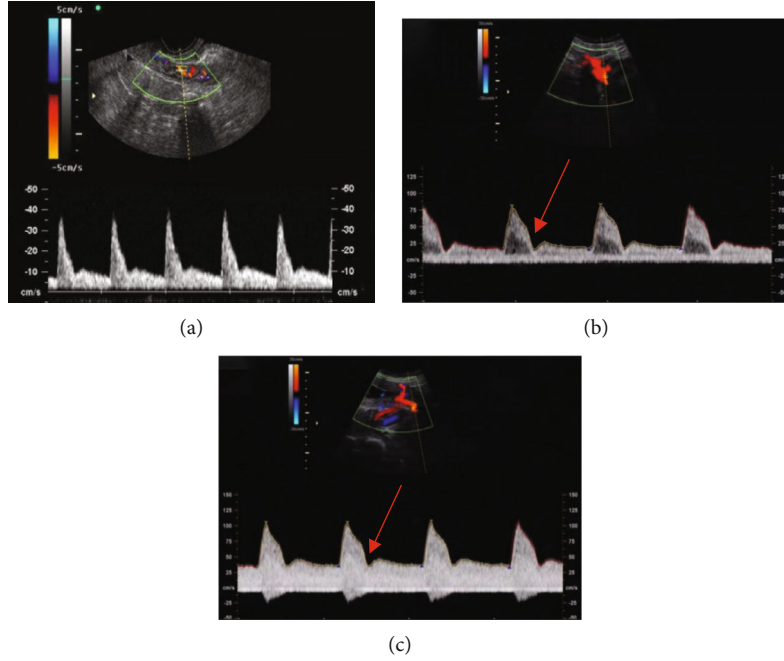


FIGURE 1: The blood flow spectra of fetal UtA. (a) Doppler waveform of UtA blood flow of pregnant women measured by transabdominal ultrasound in the control group. (b) Doppler waveform of abnormal UtA blood flow in the mild group. (c) Doppler waveform of abnormal UtA blood flow in the severe group. The red arrow indicated the diastolic notch.

parameters PI, RI, and S/D of UtA, MCA, and UA and the maximum flow rate (V1) and inner diameter (D1) of umbilical vein (UV), as well as the maximum flow rate (V2) and inner diameter (D2) of ductus venosus (DV). All these were measured independently by the same experienced sonographer.

The blood flow volume of UV ( $Q_{uv}$ ), the ductus-venous blood flow volume ( $Q_{dv}$ ), and the venous catheter shunt rate ( $Q_{dv}/Q_{uv}$ ) were calculated, respectively, as follows.

$$Q_{uv} = 0.5 \times V1 \times \pi \times \left(\frac{D1}{2}\right)^2, \quad (1)$$

$$Q_{dv} = 0.5 \times V2 \times \pi \times \left(\frac{D2}{2}\right)^2, \quad (2)$$

$$\text{Venous catheter shunt rate} = \frac{Q_{dv}}{Q_{uv}}. \quad (3)$$

**2.3. Detection of Blood Flow Parameters of UtA, MCA, and UA.** First, two-dimensional ultrasound was applied to display UtA on both sides of the junction of the uterus and cervix through the abdomen. Then, CDFI was performed for the blood flow signal of UtA. 1-2 cm away from the internal iliac artery, the site in UtA was taken as the sampling point. The sample volume was set at 2 mm, and the angle between the sound beam and the blood flow was set at 30 degrees. Five or more distinct and stable characteristic spectra were collected before the image was locked.

The standard section for BPD measurement was chosen, and the probe moved along the BPD section toward the skull base. The large sphenoid bone was found between the ante-

rior and middle cranial fossa, and CDFI was used for displaying the blood flow in the circle of Willis. Additionally, MCA originating from the left and right sides of the circle of Willis was also displayed. The midsection of the MCA was taken as the sampling point, the sampling volume was set to 2 mm, and the angle between the blood flow direction the sound beam was  $<60^\circ$ . The images were frozen after the obtainment of 5 or more clear and stable characteristic spectra.

The free umbilical cord close to the placenta and not tortuous and knotted was selected, and the inside of the UA was the sampling point. With the sampling volume of 2 mm and the angle between the sound beam direction and the blood flow direction  $<30^\circ$ , the images turned to be frozen after at least 5 clear and stable characteristic spectra were worked out.

The instrument measured RI, PI, and S/D of UtA, MCA, as well as UA automatically, each parameter was measured 3 times, and the mean value was taken and recorded.

**2.4. Evaluation Criteria for Adverse Pregnancy Outcomes.** Premature birth was defined as a delivery with the gestation over 28 weeks but less than 37 weeks. The Apgar score was a scoring system of 5 signs after birth, including heart rate, breathing, muscular tension, laryngeal reflex, and skin colour. Fetal growth restriction (FGR) was the impaired fetal growth potential, and the fetal weight estimated was less than the 10% of that with the same gestational age.

Diagnostic criteria for fetal intrauterine distress (FIUD) were explained as follows.

- (1) Fetal movement decreased or disappeared: the fetal movement counting  $< 10$  times/2 h or got a decrease

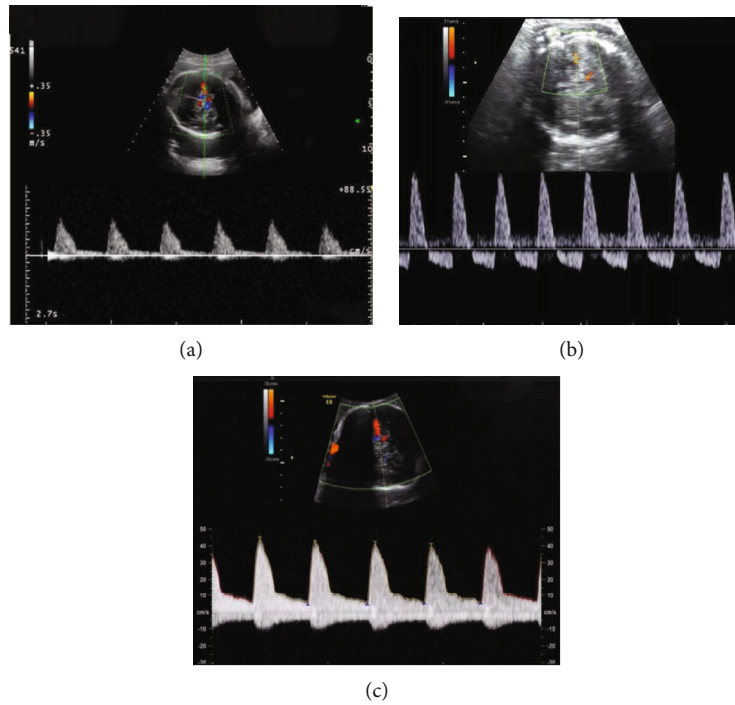


FIGURE 2: Blood flow spectra of fetal MCA. (a) Doppler waveform of MCA blood flow in pregnant women under transabdominal ultrasound in the normal group. (b) Doppler waveform of abnormal MCA blood flow in the mild group. (c) Doppler waveform of MCA blood flow abnormality in the severe group.

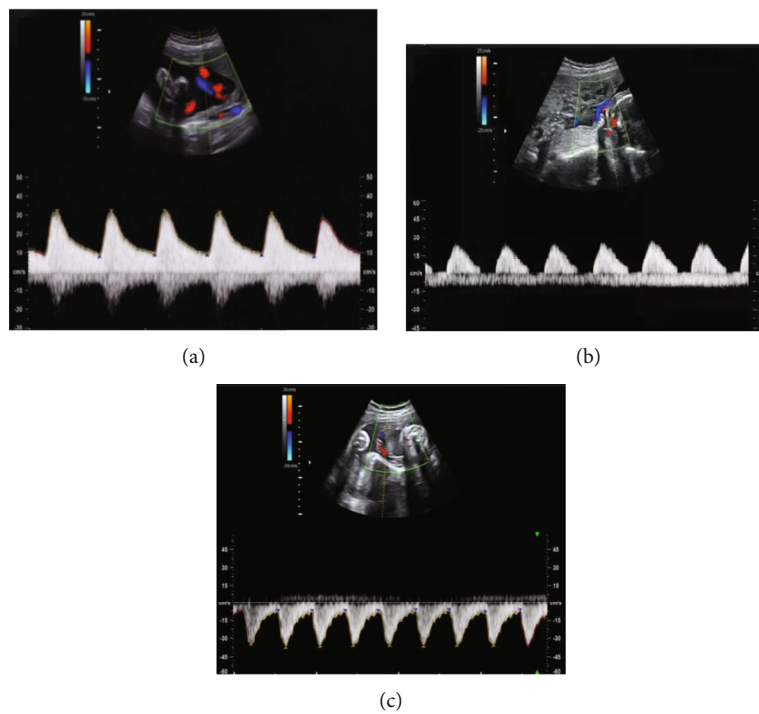


FIGURE 3: Blood flow spectra of fetal UA measured by transabdominal ultrasound. (a) Doppler waveform of UA blood flow in the normal group. (b) Doppler waveform of abnormal UA blood flow in the mild group. Diastolic blood flow signal of UA disappeared. (c) Doppler waveform of abnormal UA blood flow in the severe group. The UA diastolic blood flow signal was reversed.

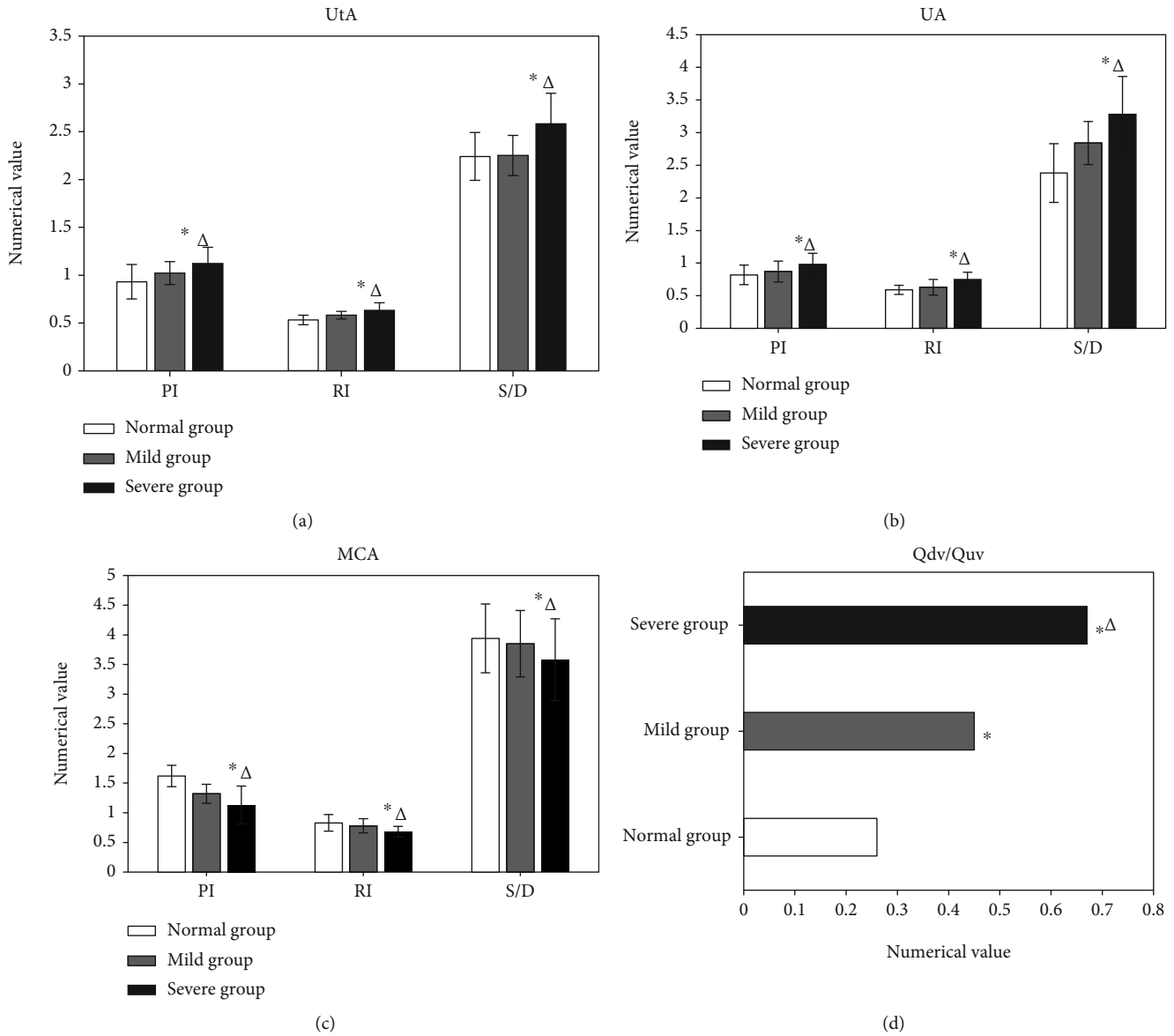


FIGURE 4: Comparison of fetal blood flow parameters. (a) Comparison of fetal blood flow parameters of UtA. (b) Comparison of those of UA. (c) Comparison of those of MCA. (d) Comparison of the fetal Qdv/Quv. Note: \* and Δ marked the statistical differences in comparison with the normal and mild groups, respectively ( $P < 0.05$ ).

of 50%, which indicated the possibility of fetal hypoxia

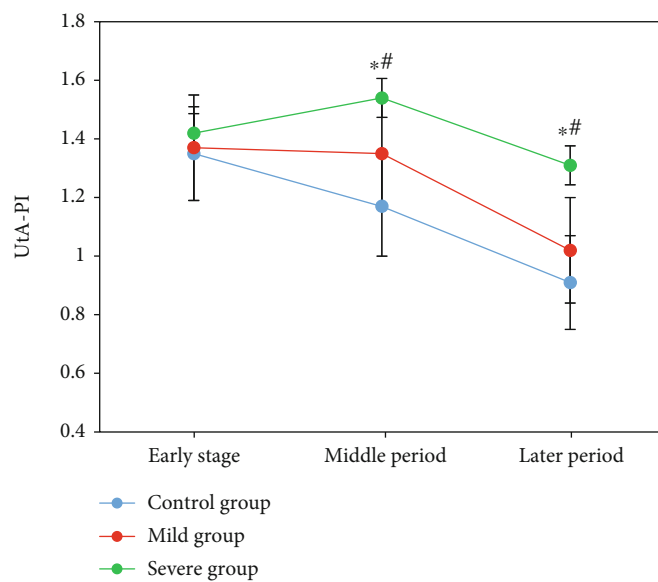
- (2) Abnormal nonstress test results also indicated the possibility of fetal hypoxia, but the false positive rate was high; thus, it is needed to be reviewed
- (3) For the fetal biophysical score, 5-6 points indicated a suspected fetal hypoxia
- (4) Abnormal blood flow was presented in fetal CDFI: the ratio value of S/D increased, indicating insufficient placental blood perfusion and fetal hypoxia

**2.5. Pregnancy Outcomes in Follow-Ups.** When premature birth, FIUD, FGR, or neonatal asphyxia occurred, a poor pregnancy outcome was identified. In the follow-ups of perinatal

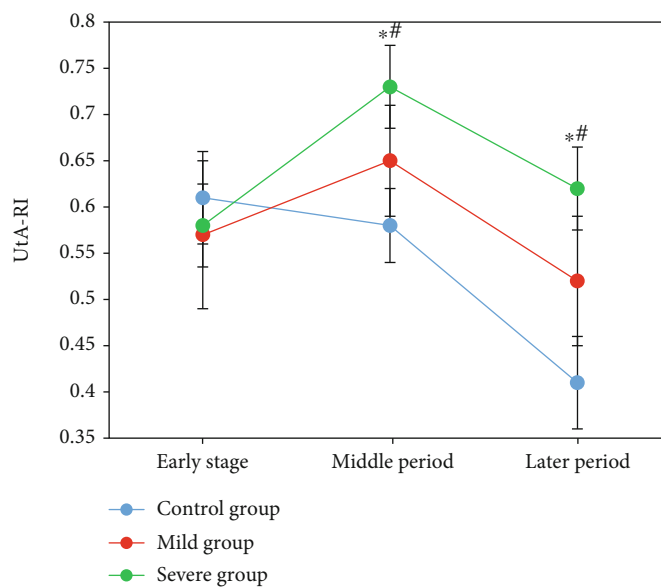
prognosis, it was known whether there was a FIUD, neonatal asphyxia, FGR, and delivery gestational age. The perinatal outcomes of pregnant women were followed up; related indexes, maternal weeks at delivery, neonatal weight, pH value of UA, 5 min Apgar score, and placental weight, were recorded.

Adverse perinatal outcomes were divided into mild ones and the severe ones. Mild adverse outcomes included premature birth, pH of UA < 7.20, and birth weight < 2.5 kg. Severe adverse outcomes included intrauterine stillbirth, fetal death after birth, birth weight < 1.5 kg, and Apgar score  $\leq 7.5$  minutes after the birth.

**2.6. Statistical Processing.** All the data in this work were expressed as mean  $\pm$  standard deviation ( $\bar{x} \pm s$ ), and SPSS 19.0 was used for data analysis. Pairwise comparisons were performed using  $t$  test, and comparisons between or among



(a)



(b)

FIGURE 5: Continued.

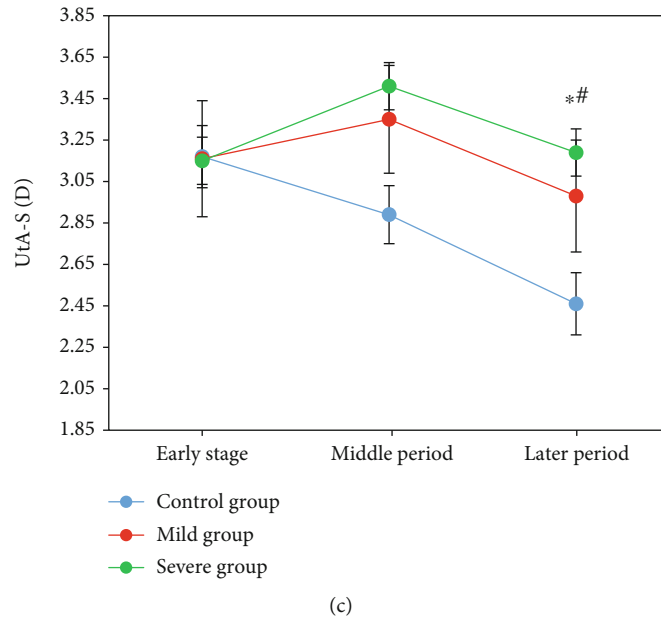


FIGURE 5: Comparison of blood flow parameters PI, RI, and S/D of UtA in different stages. (a) PI comparison. (b) RI comparison. (c) S/D comparison. Note: \* and # indicated the significant difference statistically compared with the early and middle stages, respectively,  $P < 0.05$ .

groups were made using one-way analysis of variance. Logistic binary regression was used for the analysis of the related factors of poor perinatal prognosis. If  $P < 0.05$ , the difference was thought to be statistically significant.

### 3. Results and Discussion

**3.1. Comparison of Mean Age and Gestational Age among Three Groups.** There was not a significant difference in the mean age and mean gestational age among the three groups ( $P > 0.05$ ), as listed in Table 1.

**3.2. Blood Flow Spectra of Fetal UtA, MCA, and UA.** The Doppler ultrasound spectral waveform of UtA was characterized by high resistance and low diastolic components in early pregnant women, and it was hump-shaped in the diastolic phase (two-peak continuous spectrum). In HDCP patients, intrauterine hypoxia was observed; diastolic notch was in UtA, which is presented in Figure 1.

For the measurement of fetal MCA, the Doppler sampling volume was in the middle of the artery. In the standard BPD section, the probe was moved parallel to the fetal skull base until the paired greater wings of sphenoid bone appeared between the anterior and the middle cranial fossae. CDFI showed the arterial ring of Willis; MCA originated from the left and right sides of the middle of the arterial ring and runs to the brain bilaterally, deviating to the frontal direction slightly. As shown in Figure 2, the blood flow resistance of fetal MCA in HDCP patients was lowered. The placental resistance was reflected in the blood flow of UA, and the partial diastolic blood flow spectrum of the fetal UA was absent or inverted in HDCP patients, as shown in Figure 3.

With the widespread use of colour Doppler ultrasound in prenatal diagnosis in recent years, clinical research in

obstetrics and gynecology has gradually focused on the relationship between maternal and fetal ultrasound blood flow parameters, as well as the occurrence and progression of adverse pregnancy outcomes. Ultrasound detection indices can now be used as supplemental indices for HDCP diagnosis and treatment [19–21]. Abnormal UA spectrum is associated with placental 3rd-grade villous stem occlusion. With the development of the disease, the structure of the placental villi vessels changes, and the number of placental 3rd-grade villous stem arterioles decreases notably. The interstitial fibrosis worsens, and fibrous material is deposited, reducing the volume of fetal placental blood circulation and impeding fetal growth and development. Rubin et al. [22] pointed out that venous blood flow was reduced in fetuses with abnormal Doppler spectra of UA significantly. In the waveform of DV, the degree of downward deflection is proportional to the risk of fetal death or multisystem organ failure. Studies have shown that abnormal DV waveforms are strongly associated with fetal death.

**3.3. Comparison of Blood Flow Parameters PI, RI, and S/D in Three Groups of UtA, UA, and MCA.** The blood flow parameters PI, RI, S/D, and Qdv/Quv of UtA and UA were higher in the severe group than those in the control group and the mild group; the differences were all of statistical significance ( $P < 0.05$ ) in Figures 4(a), 4(b), and 4(d). PI, RI, and S/D of MCA were lower in the severe group than those in the control group and mild group, suggesting the difference significant statistically ( $P < 0.05$ ), shown in Figure 4(c).

In clinical practise, fetal UA blood flow measurements are crucial indicators of placental function alterations. Ciobanu et al. [23] found that for patients with abnormal UA blood flow resistance during pregnancy, the mean gestational age of delivery was significantly shortened after treatment, and the incidences of FIUD and neonatal asphyxia

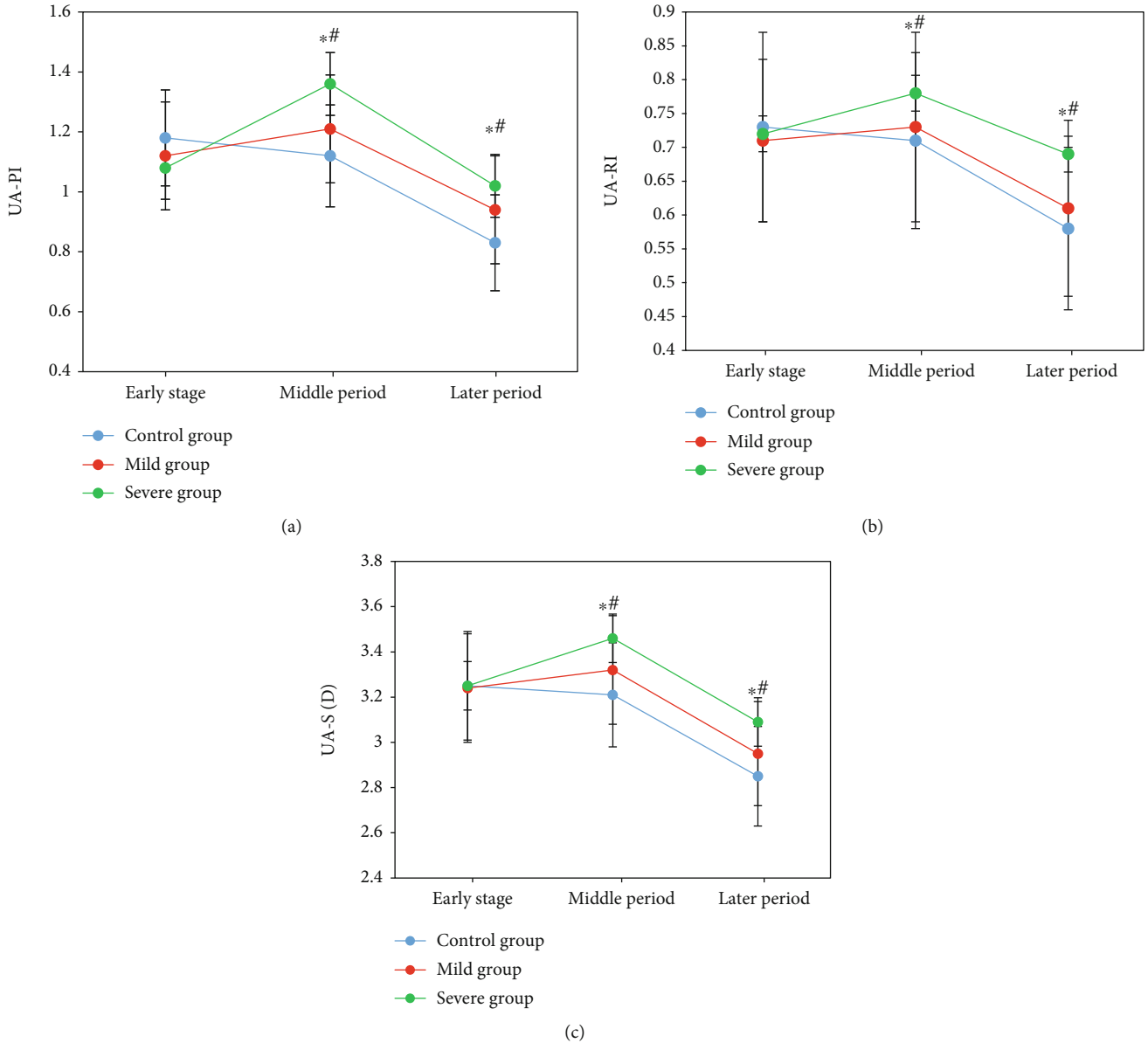


FIGURE 6: Comparison of blood flow parameters PI, RI, and S/D of UA in different periods. (a) PI comparison. (b) RI comparison. (c) S/D comparison. Note: \* indicated there was a significant difference statistically compared with the early stage, while # indicated the same compared with those in the middle stage,  $P < 0.05$ .

were significantly increased, even if the patients' UA resistance recovered to normal. The major blood artery supplying the cerebral hemisphere is the fetal MCA. Kim J et al. [24] come up with that RI of MCA had bidirectional changes; that is, the resistance decreased with hypoxia compensation and increased with decompensation. Among the cases here, blood flow parameters of MCA became decreased in the severe group, indicating that the MCA could reflect the severity of HDCP.

Changes in blood flow of UA are the earliest identifiable Doppler signals of early placental insufficiency. During normal fetal growth and development, the Qdv/Quv plays a vital role in regulating [22, 25, 26]. When the fetus is hypoxic, the DV dilates, the proportion of blood flow from UV into DV increases, and the Qdv/Quv increases sharply. Pinter et al.

[27] suggested that fetal venous blood flow change was superior to arterial blood flow change in predicting adverse pregnancy outcomes. For cases in both the mild and the severe groups, the Qdv/Quv was increased compared with that of the normal control pregnant women, which was consistent with the description of the above research. Measurement of DV hemodynamics contributes to the understanding of the pathological state of the fetal circulation, deepening the understanding of hemodynamics in many fetal diseases.

**3.4. Comparison of PI, RI, and S/D of UtA, UA, and MCA in Different Pregnancy Periods.** In early pregnancy, no significant difference was observed in PI, RI, and S/D of UtA among the three groups ( $P > 0.05$ ). All of PI, RI, and S/D increased first and then decreased in the early, middle, and later pregnancy

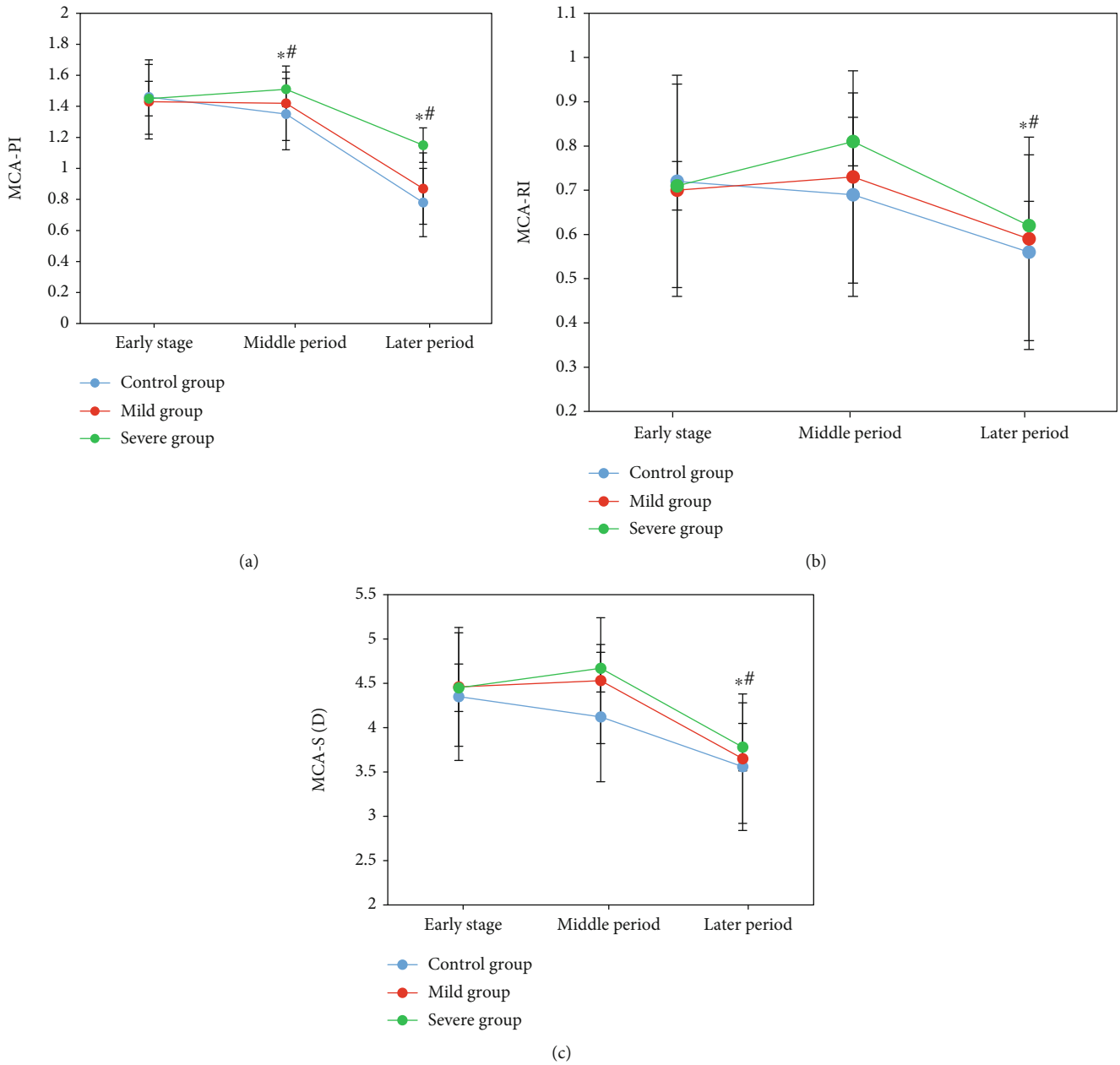


FIGURE 7: Comparison of PI, RI, and S/D of MCA in different stages. (a) Comparison of PI. (b) Comparison of RI. (c) Comparison of S/D. Note: \* and # pointed out the differences significant statistically in comparison with those in the early and middle stages, respectively,  $P < 0.05$ .

TABLE 2: Comparison of pregnancy outcomes of fetuses ( $n$ , %).

	Control group ( $n = 40$ )	Mild group ( $n = 40$ )	Severe group ( $n = 40$ )	$F$	$P$
Premature birth	2 (5)	11 (27.5)	17 (42.5)	8.37	0.002
FIUD	0	8 (20.0)	18 (45.0)	10.29	0.000
FGR	1 (2.5)	4 (10.1)	13 (32.5)	9.36	0.001
Neonatal asphyxia	0	6 (15.2)	16 (40.2)	11.37	0.000

in the severe group, with the difference significant statistically ( $P < 0.05$ ). In the middle and later stages, those were higher than those in the mild and the control groups, as the differences were of statistical significance ( $P < 0.05$ ). PI, RI, and S/D were gradually decreasing in the three stages of pregnancy in the control group, showing the significant differences statistically ( $P < 0.05$ ) as presented in Figure 5.

The PI, RI, and S/D of UA in the middle and later stages of pregnancy declined steadily in both the mild and severe groups, with statistically significant differences ( $P < 0.05$ ). In the later stage, the severe group's PI, RI, and S/D were higher than the control group's, statistically and substantially ( $P < 0.05$ ) in Figure 6.

TABLE 3: Comparison of perinatal prognosis ( $n$ , %).

	Control group ( $n = 40$ )	Mild group ( $n = 40$ )	Severe group ( $n = 40$ )	$F$	$P$
Weeks of delivery (weeks)	$36.7 \pm 3.2$	$33.2 \pm 2.6$	$32.1 \pm 2.5^{*\Delta}$	8.352	0.000
Birth weight (g)	$2926.1 \pm 634.3$	$2743.8 \pm 73.2$	$2171.1 \pm 745.3^{*\Delta}$	11.293	0.001
pH of UA	$7.3 \pm 0.1$	$7.1 \pm 0.2$	$6.8 \pm 0.1^{*\Delta}$	9.362	0.001
Apgar score (points)	$10.0 \pm 0.0$	$10.0 \pm 0.0$	$8.3 \pm 2.7^{*\Delta}$	10.281	0.002
Placental weight (g)	$578.91 \pm 132.6$	$553.2 \pm 121.7$	$468.9 \pm 102.4^{*\Delta}$	11.381	0.000

Note:  $^{*\Delta}$  indicated that a difference significant statistically was shown compared with the control group and mild group, respectively,  $P < 0.05$ .

TABLE 4: AUC, optimal cut-off value, sensitivity, and specificity with blood flow parameters and pregnancy outcomes of UtA, MCA, and UA.

Test variables	AUC	Optimal cut-off value	Sensitivity (%)	Specificity (%)
UtA-PI	0.78	1.17	80.2	72.1
UtA-RI	0.72	0.67	53.8	86.7
UtA-S/D	0.71	2.68	78.3	54.6
UA-PI	0.82	0.95	73.2	77.2
UA-RI	0.76	0.64	63.2	75.8
UA-S/D	0.68	2.83	72.4	68.3
MCA-PI	0.81	1.67	68.7	83.2
MCA-RI	0.73	0.68	89.4	58.7
MCA-S/D	0.86	3.63	87.5	78.6
Combination of all parameters	0.98	/	94.7	96.4

PI, RI, and S/D of MCA were all decreased gradually in the three groups in the middle and later pregnancy; the differences were also proved significant statistically ( $P < 0.05$ ). Higher than those in the control group, PI, RI, and S/D were much different in the severe group in the middle and later stages statistically and significantly ( $P < 0.05$ ), which are presented in Figure 7.

Under normal circumstances, blood flow parameters of UtA should go down gradually with gestational time. In this work, blood flow parameters PI, RI, and S/D of UtA gradually decreased with the increase of gestational age in the normal control group. But those increased first and decreased then from the early stage to the middle stage in the severe group, higher than those of the control group notably except in the early pregnancy ( $P < 0.05$ ). With the development of embryos during normal pregnancy, placental trophoblast cells infiltrate continuously, UtA vascular remodelling is strengthened, the lumen is continuously enlarged, and the elasticity of the vascular wall is reduced. Uterine blood flow changes to low resistance and high flow rate from the high resistance and low flow rate before pregnancy [28–30]. The placental trophoblasts of pregnant women with HDCP have insufficient ability to infiltrate the arteries, the strength and quantity of vascular remodelling are also insufficient, the muscle layer of the vascular wall still maintains a large elasticity, and the vascular resistance goes up. PI, RI, and S/D values increase under the Doppler ultrasound quantitative analysis. The measurement of UA hemodynamic parameters can reflect the circulatory status between the fetus and the placenta. The results of this work demonstrated that the PI, RI, and S/D of UA increased abnormally in the control group in the middle and later stages of pregnancy. This

indicated that the blood flow resistance of UA in HDCP patients was greater with less blood flow volume, because of the circulatory disorders in the fetus caused by the increased placental resistance.

**3.5. Comparison of Fetal Pregnancy Outcomes.** Among the 40 cases in the control group, there were 3 cases got abnormal pregnancy outcomes (including 2 cases with premature birth and 1 case with FGR); the incidence was 7.5%. In the mild group, 13 cases had abnormal pregnancy outcomes (11 cases of premature birth, 8 cases of FGR, 4 cases of FIUD, and 6 cases of neonatal asphyxia), with the incidence of 32.5%. In the severe group, 19 cases suffered from abnormal pregnancy outcomes (premature birth in 17 cases, FGR in 18 cases, FIUD in 13 cases, and neonatal asphyxia in 16 cases), working out an incidence of 47.50%. The incidence of abnormal pregnancy outcomes was higher markedly in the severe group than that in the mild and the control groups, suggesting the significant differences statistically ( $P < 0.05$ ). Detailed data are shown in Table 2.

**3.6. Comparison of Perinatal Prognosis.** There were big statistical differences in the weeks of delivery, birth weight, pH value of UA, Apgar score, and placental weight of neonates among three groups ( $P < 0.05$ ). Between the mild group and the control group, no statistical difference was found ( $P > 0.05$ ) as displayed in Table 3.

The placenta's size is critical for supporting appropriate fetal growth. The weight of the placenta in the normal pregnancy group was substantially higher than that in the HDCP



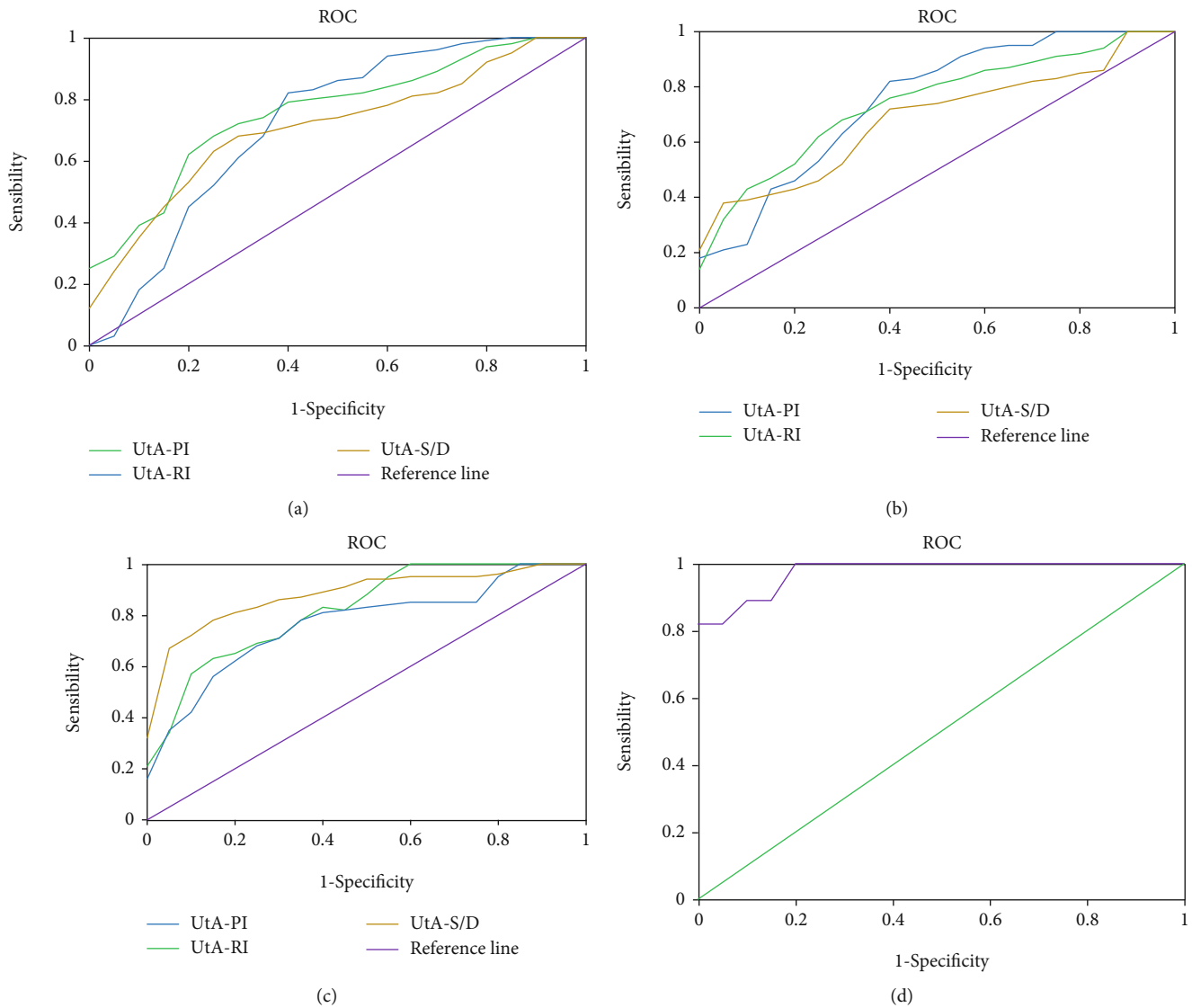


FIGURE 8: ROC curves of UtA, MCA, and UA blood flow parameters as well as pregnancy outcomes. (a) ROC curves of UtA drawn under blood flow parameters and pregnancy outcomes. (b) ROC curves of UA. (c) ROC curves of MCA. (d) Blood flow parameter combined with pregnancy outcomes.

group, according to Esposito et al. [31]. The severe group had significantly lower weeks of delivery, placental weight, and neonatal birth weight than the normal and mild groups, which was consistent with the previous study. The reason may be that the total number of villi in the placenta increases with the weight of the placenta.

**3.7. Blood Flow Parameters of UtA, UA, and MCA in the Diagnosis of Adverse Pregnancy Outcomes.** Table 4 displays the AUC, appropriate cut-off value, sensitivity, and specificity of pregnancy outcomes, as well as UtA, MCA, and UA blood flow parameters. For the ROC curve, the optimal cut-off value of PI was 1.17, and the AUC was 0.78; the sensitivity and specificity were 80.2% and 72.1% for predicting adverse pregnancy outcomes, respectively. Of RI, the optimal cut-off value and AUC were 0.67 and 0.72, respectively; the sensitivity and specificity were 53.8% and 86.7%, respectively. Of S/D, the optimal cut-off value, AUC, sensitivity, and specificity were 2.68, 0.71,

78.3%, and 54.6%, respectively. PI had the most diagnostic value, as shown in Figure 8(a).

The appropriate cut-off value and AUC of PI were 0.95 and 0.82, respectively, with the ROC curve drawn by PI, RI, and S/D of UA as well as pregnancy outcomes; the sensitivity and specificity of PI for predicting bad pregnancy outcomes were 73.2 percent and 77.2 percent, respectively. The optimal cut-off value, AUC, sensitivity, and specificity of RI were 0.64, 0.76, 63.2%, and 75.8%, respectively. Those of S/D were 2.83, 0.68, 72.4%, and 68.3%, respectively. PI had the most diagnostic value of UA, which are shown in Figure 8(b).

With the ROC curve of MCA, the four indexes of PI were 1.67, 0.81, 68.7%, and 83.2%, respectively. Of RI, those were 0.68, 0.73, 89.4%, and 58.7%, respectively. Of S/D, those were 3.63, 0.86, 87.5%, and 78.6%, respectively. S/D showed the most diagnostic value of MCA, as it could be found in Figure 8(c).

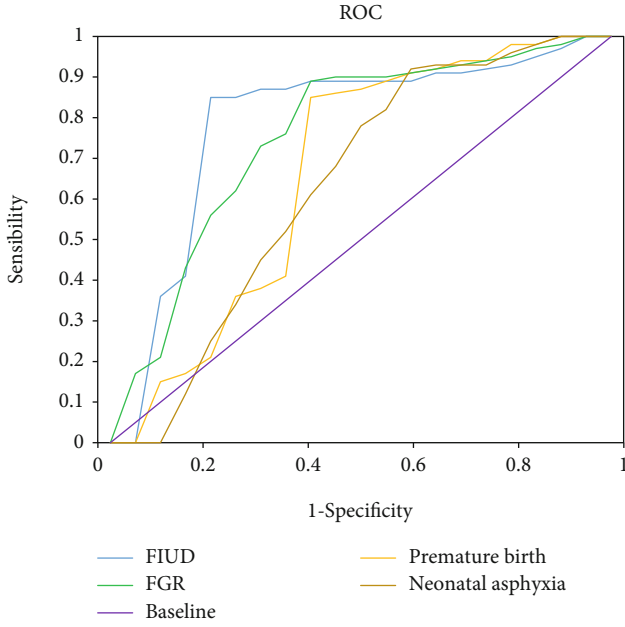


FIGURE 9: ROC curves drawn under the combined diagnosis with all parameters of adverse pregnancy outcomes.

TABLE 5: AUC, sensitivity, and specificity of the combined diagnosis for adverse pregnancy outcomes with UtA, UA, and MCA parameters.

Test variables	AUC	Sensitivity (%)	Specificity (%)
FIUD	0.89	86.3	88.4
Premature birth	0.72	89.2	51.2
FGR	0.63	94.6	39.2
Neonatal asphyxia	0.73	87.4	54.4

TABLE 6: Correlation between fetal hemodynamic parameters and poor perinatal prognosis.

Independent variables	$\beta$	Wald value	df	OR	$P$
Qdv/Quv	4.372	3.281	1	2.837	0.021
UtA-PI	2.271	4.872	1	3.782	0.001
UtA-RI	2.361	5.383	1	2.873	0.000
UtA-S/D	2.783	6.787	1	1.987	0.001
UA-PI	3.827	7.832	1	3.822	0.001
UA-RI	3.892	6.785	1	2.861	0.011
UA-S/D	2.371	7.684	1	0.563	0.002
MCA-PI	-1.982	7.982	1	0.462	0.004
MCA-RI	-4.381	6.483	1	0.632	0.006
MCA-S/D	-2.986	7.842	1	0.271	0.000

The AUC was 0.98 in the ROC curve created by combining blood flow characteristics and pregnancy outcomes, and the sensitivity and specificity for predicting bad outcomes were 94.7 percent and 96.4 percent, respectively. When compared to a single blood flow parameter, the diagnostic value was higher, as illustrated in Figure 8(d).

Prasad et al. [32] reported that the continuous increase of UtA-PI predicted abnormal changes in vascular resistance, and dynamic monitoring of S/D could understand the uterine-placental circulation status. Elevated UtA-RI was the best predictor of severe FGR in high-risk groups, which illustrated that the blood flow parameters were complementary to each other and could evaluate and predict adverse pregnancy outcomes objectively.

#### 4. Sensitivity and Specificity of the Combination of All Parameters in Diagnosing Adverse Pregnancy Outcomes

The combination of all the parameters showed the highest diagnostic value for FIUD, with an AUC of 0.89; its sensitivity and specificity were 86.3% and 88.4%, respectively. In this case, the AUC for FGR was 0.63, with the highest diagnostic sensitivity of 94.6%; but its specificity was a little lower, which reached 39.2% merely. These results are represented in Figure 9 and Table 5 in details.

4.1. *Correlation between Fetal Hemodynamic Parameters and Poor Perinatal Prognosis.* Logistic binary regression analysis was performed with the Qdv/Quv as well as hemodynamic parameters of UtA, UA, and MCA as independent variables, and whether an adverse perinatal outcome occurred was taken as the dependent variable. It was illustrated that poor perinatal prognosis was correlated with fetal Qdv/Quv as well as blood flow parameters PI, RI, and S/D of UtA, UA, and MCA ( $P < 0.05$ ), as suggested in Table 6.

In correlation analysis, the poor perinatal prognosis was demonstrated to be correlated with fetal hemodynamic parameters of UtA, UA, and MCA and Qdv/Quv. These indexes could be auxiliary indexes for the evaluation of patients' condition and the prediction of perinatal prognosis, consistent with what was found by Maged et al. [33].

#### 5. Conclusions

As the blood flow parameters of UtA, MCA, and UA in 120 pregnant women with singleton pregnancy were monitored and analysed, this work was aimed at exploring these blood flow parameters in HDCP patients and their correlations with pregnancy outcomes. Colour Doppler ultrasound could be utilised to detect PI, RI, and S/D of UtA, MCA, and UA in pregnant women, providing a baseline for measuring the fetus' intrauterine state and predicting negative pregnancy outcomes. The parameters in the later stage had the higher diagnostic value of adverse pregnancy outcomes. The combination of all the parameters could improve the diagnostic accuracy and provide a basis for guiding treatment and determining the best timing of delivery. The disadvantages of this research lay in that frequent fetal movement would affect the measurement of various parameters. The angle of the sampling between the sound beam and blood flow should be strictly required, and there might be slight errors. Furthermore, the sample size was small, resulting in some discrepancies in the results. In the future, larger sample sizes

will be required for more complete studies and more valuable research outcomes. In conclusion, this work could provide reference for early prevention, early detection, and early treatment of HDGP, so as to improve adverse pregnancy outcomes.

## Data Availability

The data used to support the findings of the study are included within the article.

## Conflicts of Interest

The authors declare no conflicts of interest.

## Authors' Contributions

Pei Zhou and Yi Sun are both co-first authors of this paper.

## References

- [1] A. Sinkey, N. Battarbee, A. Bello, C. W. Ives, S. Oparil, and A. T. N. Tita, "Prevention, diagnosis, and management of hypertensive disorders of pregnancy: a comparison of international guidelines," *Current Hypertension Reports*, vol. 22, no. 9, p. 66, 2020.
- [2] M. Hauspurg, J. Countouris, and M. Catov, "Hypertensive disorders of pregnancy and future maternal health: how can the evidence guide postpartum management?," *Current Hypertension Reports*, vol. 21, no. 12, p. 96, 2019.
- [3] I. Behrens, S. Basit, M. Melbye et al., "Risk of post-pregnancy hypertension in women with a history of hypertensive disorders of pregnancy: nationwide cohort study," *BMJ*, vol. no. 358, article j3078, 2017.
- [4] U. Ukah, D. A. de Silva, B. Payne et al., "Prediction of adverse maternal outcomes from pre-eclampsia and other hypertensive disorders of pregnancy: a systematic review," *Pregnancy Hypertens*, vol. 11, pp. 115–123, 2018.
- [5] E. Jones, T. Hernandez, J. Edmonds, and E. P. Ferranti, "Continued disparities in postpartum follow-up and screening among women with gestational diabetes and hypertensive disorders of pregnancy: a systematic review," *The Journal of Perinatal & Neonatal Nursing*, vol. 33, no. 2, pp. 136–148, 2019.
- [6] A. Gebremedhin, K. Regan, S. Ball et al., "Interpregnancy interval and hypertensive disorders of pregnancy: a population-based cohort study," *Paediatric and Perinatal Epidemiology*, vol. 35, no. 4, pp. 404–414, 2021.
- [7] J. Semmler, S. Abdel-Aziz, S. Anzoategui, H. Zhang, K. H. Nicolaides, and M. Charakida, "Influence of birth weight on fetal cardiac indices at 35–37 weeks' gestation," *Ultrasound in Obstetrics & Gynecology*, vol. 57, no. 2, pp. 266–272, 2021.
- [8] S. Ali, S. Heuving, M. Kawooya et al., "Prognostic accuracy of antenatal Doppler ultrasound for adverse perinatal outcomes in low-income and middle-income countries: a systematic review," *BMJ Open*, vol. 11, no. 12, article e049799, 2021.
- [9] R. Ayaz, T. Günay, D. Yardımcı, A. Turgut, and H. Ankaralı, "The effect of 75-g oral glucose tolerance test on maternal and foetal Doppler parameters in healthy pregnancies: a cross-sectional observational study," *Journal of Obstetrics and Gynaecology*, vol. 41, no. 1, pp. 83–88, 2021.
- [10] M. Gómez-Roig, E. Mazarico, D. Cuadras et al., "Placental chemical elements concentration in small fetuses and its relationship with Doppler markers of placental function," *Placenta*, vol. 110, pp. 1–8, 2021.
- [11] C. Monaghan, J. Binder, B. Thilaganathan, J. Morales-Roselló, and A. Khalil, "Perinatal loss at term: role of uteroplacental and fetal Doppler assessment," *Ultrasound in Obstetrics & Gynecology*, vol. 52, no. 1, pp. 72–77, 2018.
- [12] C. Paules, L. Youssef, C. Rovira et al., "Distinctive patterns of placental lesions in pre-eclampsia vs small-for-gestational age and their association with fetoplacental Doppler," *Ultrasound in Obstetrics & Gynecology*, vol. 54, no. 5, pp. 609–616, 2019.
- [13] Z. Wei, M. Mu, M. Li, J. Li, and Y. Cui, "Color Doppler ultrasound detection of hemodynamic changes in pregnant women with GDM and analysis of their influence on pregnancy outcomes," *American Journal of Translational Research*, vol. 13, no. 4, pp. 3330–3336, 2021.
- [14] H. Lee, S. Lee, J. Ko, S. J. Kim, and J. E. Shin, "Association between fetoplacental Doppler results, placental pathology, and angiogenic factors among pregnant women with anxiety," *Taiwanese Journal of Obstetrics & Gynecology*, vol. 59, no. 6, pp. 842–847, 2020.
- [15] L. Roberts, H. Ling, L. Poon, K. H. Nicolaides, and N. A. Kametas, "Maternal hemodynamics, fetal biometry and Doppler indices in pregnancies followed up for suspected fetal growth restriction," *Ultrasound in Obstetrics & Gynecology*, vol. 52, no. 4, pp. 507–514, 2018.
- [16] A. Ciobanu, A. Rouvali, A. Syngelaki, R. Akolekar, and K. H. Nicolaides, "Prediction of small for gestational age neonates: screening by maternal factors, fetal biometry, and biomarkers at 35–37 weeks' gestation," *American Journal of Obstetrics and Gynecology*, vol. 220, no. 5, pp. 486.e1–486.e11, 2019.
- [17] L. Nader, P. Zielinsky, A. Naujorks et al., "Behaviour of the foramen ovale flow in fetuses with intrauterine growth restriction," *Obstetrics and Gynecology International*, vol. 2018, Article ID 1496903, 6 pages, 2018.
- [18] T. Ton, M. Bennett, D. Incerti et al., "Maternal and infant adverse outcomes associated with mild and severe preeclampsia during the first year after delivery in the United States," *American Journal of Perinatology*, vol. 37, no. 4, pp. 398–408, 2020.
- [19] D. Martino, E. Ferrazzi, M. Garbin et al., "Multivariable evaluation of maternal hemodynamic profile in pregnancy complicated by fetal growth restriction: prospective study," *Ultrasound in Obstetrics & Gynecology*, vol. 54, no. 6, pp. 732–739, 2019.
- [20] M. Zijl, B. Koullali, J. Mol, R. J. Snijders, B. M. Kazemier, and E. Pajkrt, "The predictive capacity of uterine artery Doppler for preterm birth—a cohort study," *Acta Obstetrica et Gynecologica Scandinavica*, vol. 99, no. 4, pp. 494–502, 2020.
- [21] H. Liu and J. Liu, "Improved support vector machine algorithm based on the influence of gestational diabetes mellitus on the outcome of perinatal outcome by ultrasound imaging," *Pakistan Journal of Medical Sciences*, vol. 37, no. 6, pp. 1625–1629, 2021.
- [22] J. Rubin, S. Li, J. Fowlkes et al., "Comparison of variations between spectral Doppler and Gaussian surface integration methods for umbilical vein blood volume flow," *Journal of Ultrasound in Medicine*, vol. 40, no. 2, pp. 369–376, 2021.
- [23] A. Ciobanu, A. Wright, A. Syngelaki, D. Wright, R. Akolekar, and K. H. Nicolaides, "Fetal Medicine Foundation reference ranges for umbilical artery and middle cerebral artery

- pulsatility index and cerebroplacental ratio,” *Ultrasound in Obstetrics & Gynecology*, vol. 53, no. 4, pp. 465–472, 2019.
- [24] J. Kim, S. Ha, W. Jin et al., “Color Doppler ultrasonography for predicting the patency of anastomosis after superficial temporal to middle cerebral artery bypass surgery,” *Acta Neurochirurgica*, vol. 163, no. 5, pp. 1503–1513, 2021.
- [25] M. Wu, Y. Lin, F. Lei, Y. Yang, L. Yu, and X. Liu, “Diagnostic value of prenatal ultrasound for detecting abnormal fetal blood flow,” *American Journal of Translational Research*, vol. 13, no. 5, pp. 5094–5100, 2021.
- [26] Q. Yin, Y. Zhang, Q. Ma, L. Gao, P. Li, and X. Chen, “The clinical value of blood flow parameters of the umbilical artery and middle cerebral artery for assessing fetal distress,” *American Journal of Translational Research*, vol. 13, no. 5, pp. 5280–5286, 2021.
- [27] S. Pinter, O. Kripfgans, C. Treadwell, A. W. Kneitel, J. B. Fowlkes, and J. M. Rubin, “Evaluation of umbilical vein blood volume flow in preeclampsia by angle-independent 3D sonography,” *Journal of Ultrasound in Medicine*, vol. 37, no. 7, pp. 1633–1640, 2018.
- [28] T. Avitan, A. Sanders, U. Brain, D. Rurak, T. F. Oberlander, and K. Lim, “Variations from morning to afternoon of middle cerebral and umbilical artery blood flow, and fetal heart rate variability, and fetal characteristics in the normally developing fetus,” *Journal of Clinical Ultrasound*, vol. 46, no. 4, pp. 235–240, 2018.
- [29] H. G. Herman, E. Barber, R. Gasnier et al., “Placental pathology and neonatal outcome in small for gestational age pregnancies with and without abnormal umbilical artery Doppler flow,” *European Journal of Obstetrics, Gynecology, and Reproductive Biology*, vol. 222, pp. 52–56, 2018.
- [30] A. Abdallah, A. Eldorf, S. Sallam et al., “Nuchal cord: impact of umbilical artery Doppler indices on intrapartum and neonatal outcomes: a prospective cohort study,” *The Journal of Maternal-Fetal & Neonatal Medicine*, vol. 32, no. 20, pp. 3367–3378, 2019.
- [31] L. Esposito, A. Salzano, M. Russo et al., “Corpus luteum color Doppler ultrasound and pregnancy outcome in buffalo during the transitional period,” *Animals (Basel)*, vol. 10, no. 7, p. 1181, 2020.
- [32] S. Prasad, R. Goyal, Y. Kumar et al., “The relationship between uterine artery two-dimensional color Doppler measurement and pregnancy outcome: a prospective observational study,” *Journal of Reproduction & Infertility*, vol. 18, no. 2, pp. 251–256, 2017.
- [33] A. Maged, H. Abdelaal, E. Salah et al., “Prevalence and diagnostic accuracy of Doppler ultrasound of placenta accreta in Egypt,” *The Journal of Maternal-Fetal & Neonatal Medicine*, vol. 31, no. 7, pp. 933–939, 2018.

## Research Article

# MicroRNA-17-5p Protects against Propofol Anesthesia-Induced Neurotoxicity and Autophagy Impairment via Targeting BCL2L11

Mingyu Xiu, Hengfei Luan, Xiaojiao Gu, Chuang Liu, and Deming Xu 

Department of Anesthesiology, The First People's Hospital of Lianyungang, Lianyungang 222000, China

Correspondence should be addressed to Deming Xu; 1527840997@qq.com

Received 14 May 2022; Revised 6 June 2022; Accepted 9 June 2022; Published 28 June 2022

Academic Editor: Naeem Jan

Copyright © 2022 Mingyu Xiu et al. This is an open access article distributed under the Creative Commons Attribution License, which permits unrestricted use, distribution, and reproduction in any medium, provided the original work is properly cited.

**Background.** Propofol (PPF) has been shown in studies to cause cognitive impairment and neuronal cell death in developing animals. PPF has been demonstrated to decrease the expression of microRNA-17-5p (miR-17-5p) in a recent study. Nonetheless, the function of miR-17-5p in PPF-induced neurotoxicity and related mechanisms is uncharacterized. **Methods.** After the induction of neurotoxicity by treating the SH-SY5Y cells with PPF, qRT-PCR was conducted to evaluate the level of miR-17-5p. Using MTT and flow cytometry, cell viability and apoptosis rate were assessed, respectively. Interaction between miR-17-5p and BCL2 like 11 was (BCL2L11) studied using a Luciferase reporter assay. With the help of western blot analysis, we determined the level of proteins of apoptosis-related genes and autophagy-related markers. **Results.** In SH-SY5Y cells, PPF treatment induced neurotoxicity and downregulated miR-17-5p expression. In SH-SY5Y cells post-PPF exposure, overexpression of miR-17-5p increased cell viability and decreased apoptosis. Consistently, miR-17-5p mimics mitigated PPF-generated autophagy via inhibition of Atg5, Beclin1, and LC3II/I level and elevation of p62 protein expression. In addition, BCL2L11, which was highly expressed in PPF-treated SH-SY5Y cells, was directly targeted by miR-17-5p. Further, in PPF-treated SH-SY5Y cells, overexpressed BCL2L11 counteracted the suppressing behavior of miR-17-5p elevation on PPF-induced apoptosis. **Conclusion.** Overexpressed miR-17-5p alleviates PPF exposure-induced neurotoxicity and autophagy in SH-SY5Y cells via binding to BCL2L11, suggesting the possibility that miR-17-5p can serve as a candidate in the treatment of neurotoxicity (caused by PPF).

## 1. Introduction

Ever-increasing evidence reveals that different kinds of anesthetics can lead to long-term cognitive dysfunction and adverse effects on the development of neurons [1]. In addition, anesthesia often causes developmental neurotoxicity such as neurodegeneration, neurogenetic change, synaptogenesis, and brain circuit damage [2]. Based on the rapid onset and minimal negative postoperative effects, PPF is widely used to induce and maintain sedation as well as anesthesia [3]. PPF is still an anesthetic that should be used with caution in most clinical paediatric settings since it always causes bradycardia, heart failure, metabolic acidosis, and other complications [4, 5]. In developing mice, even subanesthetic doses of PPF can cause cell death, aberrant dendrite formation, and cognitive impairment, according to documents [6, 7]. All these effects raise concerns about the safety of PPF in paediatric anesthesia.

Clinical studies have attributed neurotoxicity and neurogenic injury to PPF [8, 9]. The complex mechanisms of neurotoxicity induced by PPF include intracellular calcium dysregulation, mitochondrial division, neuroinflammation, and abnormal neurotrophic protein expression [10–12]. Recent research has revealed that the mechanisms underlying PPF may exert a role in the establishment of novel effective therapeutic methods to avoid neurotoxicity in the underdevelopment brain [13]. Therefore, biological biomarkers must be investigated in order to prevent and treat neurotoxicity caused by PPF exposure.

miRNAs, which are endogenous noncoding RNA molecules with lengths ranging from 18 to 25 nucleotides, can regulate various biological processes via targeting and regulating the downstream messenger RNAs (mRNAs) expression at the posttranscriptional level [14–16]. Plenty of studies have identified the influence of miRNAs in the

modulation of neurotoxicity mediated by PPF. For example, miR-582-5p mitigates PPF-generated neuron apoptosis by inhibition of ROCK1 in newborn rats [17]. PPF anesthesia reduces the expression of miR-132 and decreases the number of dendritic spines in the hippocampus [18]. miR-141-3p knockdown alleviates PPF-mediated inhibition on neural stem cell neurogenesis by targeting IGF2BP2 [19]. As previously reported, miRNAs also participate in the process of PPF-mediated autophagy. Downregulated endogenous expression of miR-20b weakens the protective role of PPF and causes accentuation on autophagy [20]. Interestingly, miR-17-5p has been validated to bind with STAT3 and thus regulating the growth of cortical neuron neurite [21]. In addition, miR-17-5p, which displays low level after PPF treatment, is involved in cardiomyocyte apoptosis induced by ischemia/reperfusion (I/R) [22]. Though, the biological functionality, as well as molecular mechanisms of miR-17-5p in PPF-induced neurotoxicity, has not been evaluated.

BCL2-like 11 (BCL2L11), a member of the Bcl-2 family, is found on chromosome 2q12-q13. BCL2L11 is anticipated to share a binding site with miR-17-5p, according to bioinformatics analysis. The human BCL2L11 gene comprises important death-decision makers in the process of apoptosis [23]. BCL2L11 abrogates miR-92a-induced suppression on cell apoptosis and caspase-3/7 activity [24]. Nonetheless, the BCL2L11 role in PPF-induced neurotoxicity remains unclear.

In our current investigation, what we intended to decipher is the functionality of miR-17-5p in regulating PPF-treated SH-SY5Y cell apoptosis and autophagy and the underlying mechanisms associated with miR-17-5p. The current study may explore a new candidate target for treating neurotoxicity (caused by PPF exposure).

The paper's organization paragraph is as follows: the materials and methods are presented in Section 2. Section 3 discusses the experiments and results. Finally, in Section 4, the research work is concluded with discussion.

## 2. Materials and Methods

**2.1. Cell Culture.** We purchased the human neuroblastoma SH-SY5Y cell line from China Center for Type Culture Collection (CCTCC) and plated in 96-well plates (BD Biosciences, USA) and incubated in DMEM (Invitrogen, USA) containing FBS (10%) (Invitrogen) and penicillin (100 U/mL) (LianShuo, Shanghai, China) under humid conditions with 5% CO<sub>2</sub> at 37°C. 1, 5, 10, and 20 µg/ml PPF (2,6-diisopropylphenol, Merck & Co., USA) were utilized for the overnight treatment of SH-SY5Y cells, and phosphate buffer was used as a blank control.

**2.2. Cell Transfection.** RiboBio (Guangzhou, China) provided the miR-17-5p mimics and negative control (NC) used for the overexpression of miR-17-5p and as the control, respectively. pcDNA3.1/BCL2L11 was used to increase BCL2L11 expression, with an empty vector pcDNA3.1 (GenePharma). We transfected the miR-17-5p and NC mimics (50 nM each) pcDNA3.1/BCL2L11 (10 nM) or empty pcDNA3.1 (10 nM) in SH-SY5Y cells with Lipofectamine 2000 for 48 h. The cells

transfected by Lipofectamine 2000 with scrambled sequences served as NC.

**2.3. 3-(4,5-Dimethylthiazol-2-yl)-2,5-Diphenyltetrazolium Bromide (MTT) Assay.** With the help of the MTT assay, we performed the identification of SH-SY5Y cell viability as instructed by the supplier. In 96-well plates, the SH-SY5Y (5 × 10<sup>4</sup> cells/well) cells were seeded. After cell transfection, the cell viability with or without PPF treatment was detected using a MTT kit (Promega, USA), followed by adding the solution of MTT (20 µl, 0.5 mg/ml) into each well for continuous cell culturation for 4 h. Formazan crystals were dissolved by carefully removing the medium, adding 100 µL dimethyl sulfoxide and incubating the cells at 37°C for 10 min. Through a microplate reader (Thermo Fisher Scientific), the O.D. was achieved at 570 nm.

**2.4. Isolation of RNA and qRT-PCR Evaluations.** The Ultra HiFidelity PCR Kit (Tiangen) was utilized for total RNA extraction. RNA concentrations were quantified by Nanodrop (Thermo Fisher Scientific, USA). We adopted the TaqMan miRNA reverse transcription kit (Beyotime) to reverse transcribe RNA (total of 1 µg) to cDNA. The qRT-PCR was then conducted via SYBR Green (Takara, Dalian, China) on Applied Biosystems (Thermo Fisher Scientific). Detailed conditions were that 10 min at 95°C, and 40 cycles at 95°C for 10 sec and at 60°C for 30 sec (for MIDN, MYLIP, BCL2L11 and glyceraldehyde-3-phosphate dehydrogenase (GAPDH)), 10 min at 95°C, and 40 cycles at 95°C for 10 sec and 2 at 60°C and 1 min at 95°C, 30 sec at 55°C, and 30 sec at 95°C (for miR-17-5p). Calculation for the relative gene expression was achieved via 2<sup>-ΔΔCt</sup> method [25]. U6 and GAPDH were, respectively, utilized as the internal references for miR-17-5p and BCL2L11. The study includes the underlined primer sequences: miR-17-5p forward: 5'-CCGGGTCAGAATAATGTCAAAGTGCTTACAGTGCAGGTAGTGATATGTGCATCTACTGCAGTGAAGGCACTTGTAGCATTATGGTGACTTTTTG-3', reverse: 5'-AATTCAAAAAGTCACCATAATGCTACAAGTGCCTTCACTGCAGTAGATGCACATATCACTACCTGCAGTGAAGCACTTTGACATTATTCTGAC-3'; BCL2L11 forward: 5'-CAAGGAGGATGCCTCTTCC-3', reverse: 5'-CTTCCTGAGACCTGCTGTC-3'; GAPDH forward, 5'-CCTCCTGTTTCGACAGTCAG-3', reverse: 5'-CATACGACTGCAAAGACCC-3'; U6 forward: 5'-CTTTGGCAGCACATATACCA-3', reverse: 5'-CTCATTGAGAGGCCATGCT-3'.

**2.5. Flow Cytometry (FC) Analysis.** With the help of the Annexin V-FITC Apoptosis Detection Kit (Vazyme, Nanjing, China), we analyzed the SH-SY5Y cell apoptosis. The cells were centrifuged and resuspended in binding buffer after being treated with PPF (100 µl) (MultiSciences, Hangzhou, China). Then, we added the Annexin V-FITC and PI (5 µl each) reagents into the cells for culturation for 15 min with light. Analyzation of cell apoptosis was achieved using FACS flow cytometer (Attune, Life Technologies, Germany).

**2.6. Western Blot (WB) Analysis.** After PBS washing, the centrifugation (at  $10,000\times g$ ) of lysed cells was carried out for 10 min at  $4^{\circ}\text{C}$ . A Bradford Protein Assay kit (Invitrogen, USA) was adopted for the determination of total protein concentrations. We separated the protein samples ( $25\ \mu\text{g}$ ) by SDS-PAGE (10%), followed by transferring them onto PVDF membranes (Standards, Shanghai, China) that were subsequently sealed with skimmed milk (5%) at  $37^{\circ}\text{C}$  for 1.5 h. Incubation of the membranes was performed with primary antibodies against Bcl-2 (1:1000 dilution, ab32124, Abcam), Bax (1:5000 dilution, ab32503, Abcam), Cleaved-caspase-3 (1:500 dilution, ab32042, Abcam), Atg5 (1:5000 dilution, ab108327, Abcam), Beclin 1 (1:2000 dilution, ab207612, Abcam), LC3 (0.5– $2\ \mu\text{g}/\text{ml}$ , ab48394, Abcam), p62 (1:10000 dilution, ab109012, Abcam), BCL2L11 (1:1000 dilution, ab32158, Abcam), and GAPDH (1:2500 dilution, ab9485, Abcam) for 24 hrs at  $4^{\circ}\text{C}$ . After that, the membrane was incubated with the secondary antibody at  $37^{\circ}\text{C}$  for 2 h. An enhanced chemiluminescence kit (Takara, Dalian, China) and ImageJ software [26] were, respectively, utilized for signal visualization and blot analyzation.

**2.7. Dual-Luciferase Reporter (DLR) Assay.** DNA sequencing was used for confirming the wild type (WT) and mutant (Mut) 3'-UTR sequences of BCL2L11. The BCL2L11-WT and BCL2L11-Mut vectors were constructed by amplifying and inserting the WT and Mut 3'-UTR sequences of BCL2L11 into the luciferase reporter pmirGLO (Promega, USA). In 96 well-plates, SH-SY5Y cells were plated and grown for 24 h at  $37^{\circ}\text{C}$ . After removing the culture medium, Lipofectamine 2000 was adopted for cotransfection of BCL2L11-WT or BCL2L11-Mut vectors with mimics (miR-17-5p or NC) in SH-SY5Y cells. Post 48 h of transfection, we used a DLR Assay Kit (Promega, USA) to determine the relative luciferase activity (LA) of BCL2L11-WT and BCL2L11-Mut vectors with Renilla LA as normalization.

**2.8. Statistical Analysis.** Each analysis was done three times, and the results were expressed as mean standard deviation. In order to perform the statistical analysis, we used GraphPad Prism 6.0 (USA). The one-way ANOVA or Student's *t* test, followed by Tukey's post hoc test, was utilized to analyze variations between two or more groups. Less than a 0.05 *p* value indicates statistical significance.

### 3. Results

**3.1. PPF Treatment Induces Neurotoxicity in SH-SY5Y Cells and Downregulated miR-17-5p Expression.** For investigating the impact of neurotoxicity caused by anesthesia, SH-SY5Y cells were exposed to PPF or phosphate buffer treatment (1, 5, 10, or  $20\ \mu\text{g}/\text{ml}$ ), followed by in vitro evaluation of their cell viability. MTT assay illuminated that compared with the cells treated with phosphate buffer, and the viability of the SH-SY5Y cells was inhibited by 5, 10, and  $20\ \mu\text{g}/\text{ml}$  of PPF, suggesting that PPF treatment resulted in neurotoxicity in SH-SY5Y cells (Figure 1(a)). The miR-17-5p level was further tested by qRT-PCR. The results of qRT-PCR revealed a dose-dependent lower trend in miR-17-5p concentrations in

SH-SY5Y cells (exposed to PPF) relative to the control (Figure 1(b)). Because the SH-SY5Y cell's viability was approximately 50% at  $10\ \mu\text{g}/\text{ml}$  of PPF, PPF at a  $10\ \mu\text{g}/\text{ml}$  dose was selected for subsequent cellular experiments. The viability of SH-SY5Y cells was then tested at 0, 6, 12, 24, and 48 h. As a result, SH-SY5Y cell viability was reduced at 12, 24, and 48 h when compared to the NC group (Figure 1(c)). Consistently, the expression level of miR-17-5p was also downregulated with the increase of time after  $10\ \mu\text{g}/\text{ml}$  of PPF treatment (Figure 1(d)). There was a dose and time-dependent decrease in miR-17-5p expression following PPF treatment of SH-SY5Y cells, as demonstrated by the above results.

**3.2. miR-17-5p Alleviates PPF-Induced SH-SY5Y Cell Injury.** Subsequently, miR-17-5p mimic transfection was carried out with the aim of probing into the effect of the miR-17-5p upregulation on PPF-injured SH-SY5Y cells. Notably, significantly elevated expression of miR-17-5p was indicated in SH-SY5Y cells (exposed to PPF) after miR-17-5p mimic transfection than with the transfection of NC mimics (Figure 2(a)). For the assessment of the fact that whether miR-17-5p exerts the regulatory function in PPF-induced neurotoxicity, MTT assay was conducted. The observed results indicated the elevation of miR-17-5p significantly rescued PPF-injured cell viability (Figure 2(b)). In addition, the apoptosis of SH-SY5Y cells was investigated by FC and WB analysis, which demonstrated that PPF treatment significantly increased cell apoptosis rate as compared to the Con + NC mimic group. Overexpressed miR-17-5p was responsible for increased apoptosis in PPF-treated cells (Figures 2(c) and 2(d)). The protein levels of the markers associated with apoptosis (Bax and Cleaved-caspase-3) were downregulated after PPF treatment, but the reduced levels were reversed with the miR-17-5p mimic transfection. In contrast, overexpressed miR-17-5p partially abrogated the promoting impact of PPF-treatment on the protein levels of Bax, a marker associated with apoptosis (Figure 2(e)). Conclusively, overexpressed miR-17-5p mitigated PPF-injured SH-SY5Y cells and inhibited PPF-induced neuron apoptosis.

**3.3. miR-17-5p Inhibits PPF-Induced Autophagy in SH-SY5Y.** Previous research has identified that miR-17-5p possesses antiautophagy effect in human diseases [27, 28]. Therefore, we examined the protein levels of markers related to autophagy (Atg5, Beclin1, p62, and LC3) in SH-SY5Y cells. Specifically, Beclin1 serves as a marker for autophagy. LC3II/I and p62 are markers of early and late autophagy, accordingly. When compared to the Con + NC mimic group, aberrant autophagy was seen in the propofol + NC mimic group, including enhanced levels of autophagy of Atg5, Beclin1, and LC3II/I ratios and decreased level of p62 protein. Interestingly, comparing with the propofol + NC mimic group, transfecting miR-124 mimics significantly reduced the protein levels of Atg5, Beclin-1, and LC3II/I ratios and restored p62 protein levels (Figures 3(a)–3(e)). These findings elaborated the implication of miR-17-5p in the suppression of autophagy.

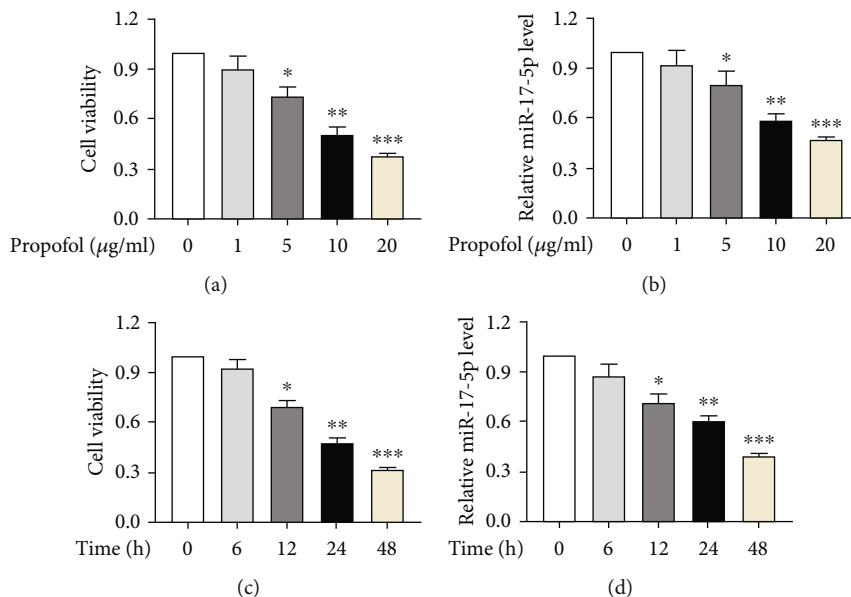


FIGURE 1: PPF treatment induces neurotoxicity in SH-SY5Y cells and downregulates miR-17-5p expression. (a) MTT assay was conducted to evaluate the survival of SH-SY5Y cells exposed to elevated concentrations (1, 5, 10, or 20  $\mu\text{g/ml}$ ) of PPF. (b) The level of miR-17-5p after treatment with elevated concentrations (1, 5, 10, or 20  $\mu\text{g/ml}$ ) of PPF by qRT-PCR. (c) The SH-SY5Y cells after treatment with 10  $\mu\text{g/ml}$  of PPF for 0, 6, 12, 24, and 48 h were used for an MTT assay to determine their viability. (d) The miR-17-5p level in SH-SY5Y cell postexposure with 10  $\mu\text{g/ml}$  of PPF at different time points was subjected for qRT-PCR evaluations. \*  $p$ , \*\*  $p$ , and \*\*\*  $p$  values less than 0.05, 0.01, and 0.001, accordingly.

**3.4. miR-17-5p Targets BCL2L11 in SH-SY5Y.** To probe into the underlying mechanism through which miR-17-5p alleviates PPF-induced neurotoxicity, prediction of downstream targets of miR-17-5p was carried out via starBase online website (<https://starbase.sysu.edu.cn/>) with the screening condition of AgoExpNum > 60. The predicted results manifested that miR-17-5p shares 3'-UTR binding sites with MIDN, MYLIP, and BCL2L11. By performing qRT-PCR, the levels of MIDN, MYLIP, and BCL2L11 mRNA expression in SH-SY5Y cells were assessed, and only BCL2L11 level was decreased in SH-SY5Y cells after miR-17-5p mimic transfection relative to the NC mimic-transfected cells (Figure 4(a)). WB analysis was used to examine the amounts of BCL2L11 protein in SH-SY5Y cells. Upregulation of miR-17-5p dramatically reduced BCL2L11 protein levels, according to the findings (Figures 4(b) and 4(c)). An LR assay was conducted in order to validate that the 3'-UTR sequence of BCL2L11 is specifically targeted by miR-17-5p. Predicted pairing target region of BCL2L11 and miR-17-5p was presented in Figure 4(d). It was found that compared to luciferase activity (LA) in cells cotransfected with NC mimics and BCL2L11-WT, the LA was inhibited significantly after being cotransfected with miR-17-5p mimics and WT BCL2L11 3'-UTR; however, luciferase activity was not significantly changed in cells cotransfected with Mut BCL2L11 3'-UTR and miR-17-5p mimics or NC mimics (Figure 4(e)). Subsequent qRT-PCR and WB analyses exhibited an elevated level of BCL2L11 at both transcriptional and translational levels after treatment with PPF (Figures 4(f) and 4(g)). All these experiments illumi-

nated that miR-17-5p bound with BCL2L11 in SH-SY5Y cells and PPF induced the elevation of BCL2L11 expression.

**3.5. miR-17-5p Targets BCL2L11 to Regulate SH-SY5Y Cell Viability and Apoptosis.** To further explore whether miR-17-5p modulates cell viability and apoptosis via targeting BCL2L11, we conducted several rescue experiments using SH-SY5Y cells. qRT-PCR illuminated that BCL2L11 expression was elevated by transfecting pcDNA3.1/BCL2L11 (Figure 5(a)). Similar results were observed in WB analysis that BCL2L11 protein level was increased after pcDNA3.1/BCL2L11 transfection (Figure 5(b)). MTT assay indicated the enhanced level of miR-17-5p exerts the promotive impact on the viability of the SH-SY5Y cells, but this effect was countered after transfection of pcDNA3.1/BCL2L11 (Figure 5(c)). BCL2L11 overexpression counteracted the inhibitory effect of overexpressed miR-17-5p on cell apoptosis, according to FC analysis (Figure 5(d)). Furthermore, WB analysis revealed that increased BCL2L11 partially reversed the miR-17-5p-mediated reduction of Bax and Cleaved-caspase-3 protein levels. In contrast, overexpressed BCL2L11 offsets miR-17-5p elevation-induced promotion on Bcl-2 protein level (Figure 5(e)). Thus, miR-17-5p exerted a protective role in SH-SY5Y cells by downregulating BCL2L11.

## 4. Discussion

Recently conducted preclinical and clinical studies revealed that neonatal prolonged or repeated exposure to anesthesia leads to the increased risk for acute neurotoxicity and long-term cognitive impairment [29]. There is currently no effective way to



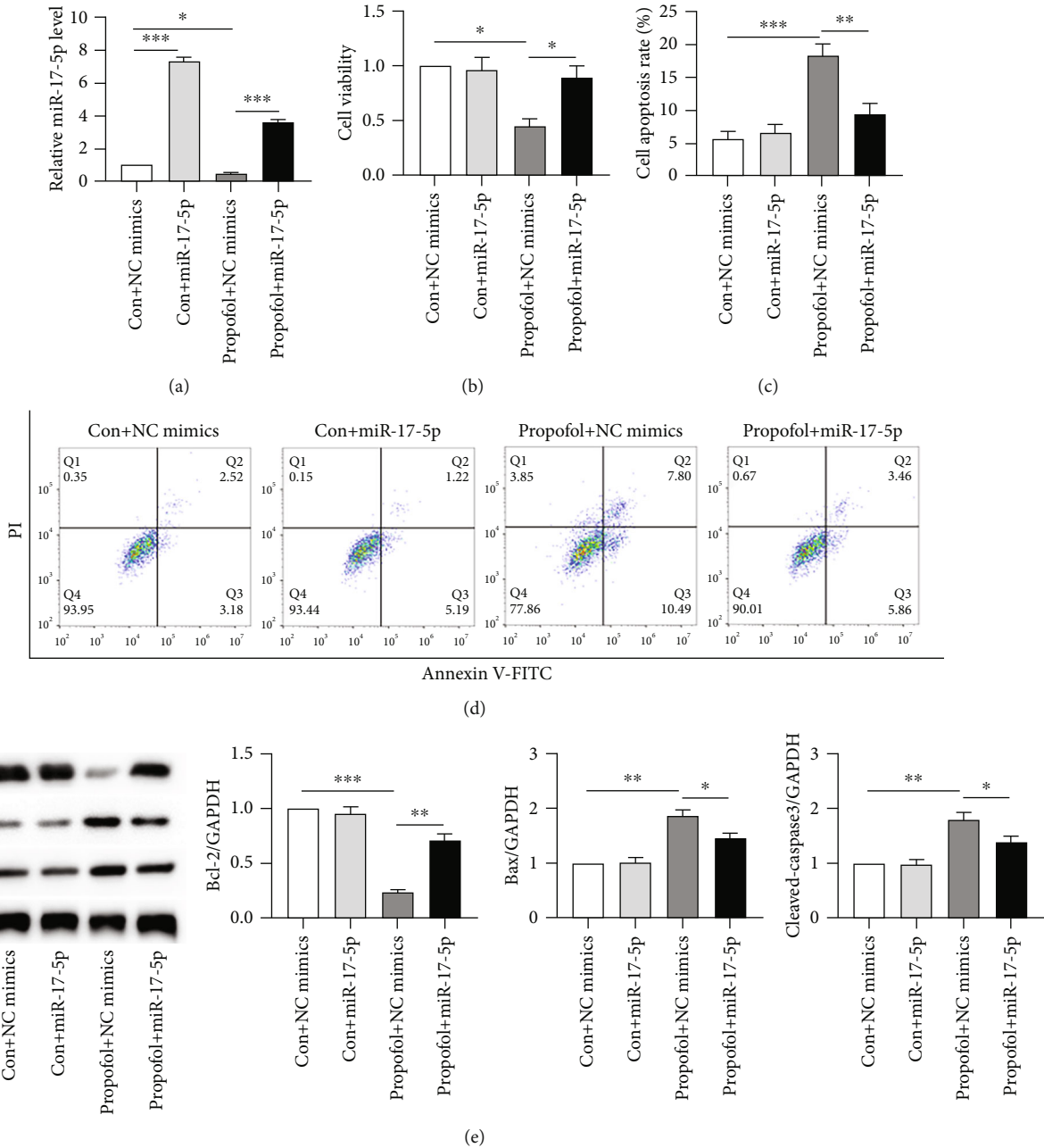


FIGURE 2: Functional experiments focusing on the impact of miR-17-5p on PPF-caused neurotoxicity. (a) By utilizing qRT-PCR, the miR-17-5p transcriptional level was examined in SH-SY5Y cells with or without 10  $\mu$ g/ml of PPF treatment posttransfection with miR-17-5p or NC mimics. (b) The survival of SH-SY5Y cells was measured via MTT in the groups of Con + NC mimics, Con + miR - 17 - 5p, propofol + NC mimics, and propofol + miR - 17 - 5p. (c, d) FC analysis was conducted to assess the apoptosis process in the abovementioned groups. (e) Representative results of WB showed the translational levels of Bcl-2, Cleaved-caspase-3, and Bax in various groups. \*  $p$ , \*\*  $p$ , and \*\*\*  $p$  values less than 0.05, 0.01, and 0.001, accordingly.

prevent anesthesia-induced neurotoxicity and cognitive impairments [29]. However, because the use of anesthetics is inevitable in many paediatric procedures, researching techniques to decrease neurotoxicity induced by anesthetics is critical. It has been revealed by previous research that SH-SY5Y human neuroblastoma cells are sensitive to anesthetic-induced neurotoxicity [30]. Hence, SH-SY5Y cells were selected to conduct *in vitro* experiments. PPF, as an effective inducer of nerve injury, can bring about neuron apoptosis and autophagy [31]. Clinical stud-

ies also revealed the neuroprotective effects of PPF that PPF treatment protects against I/R or hypoxic injury [32, 33]. In our exploration, the PPF effect on SH-SY5Y cells was first determined by MTT assay, FC, and WS analysis. Findings demonstrated that PPF dose- and time-dependently suppressed the viability of the SH-SY5Y cells. The results are consistent with a recent report showing the inhibition of SH-SY5Y cell viability with the increased PPF concentration [34]. Additionally, after PPF treatment, cell apoptosis rate and autophagy were

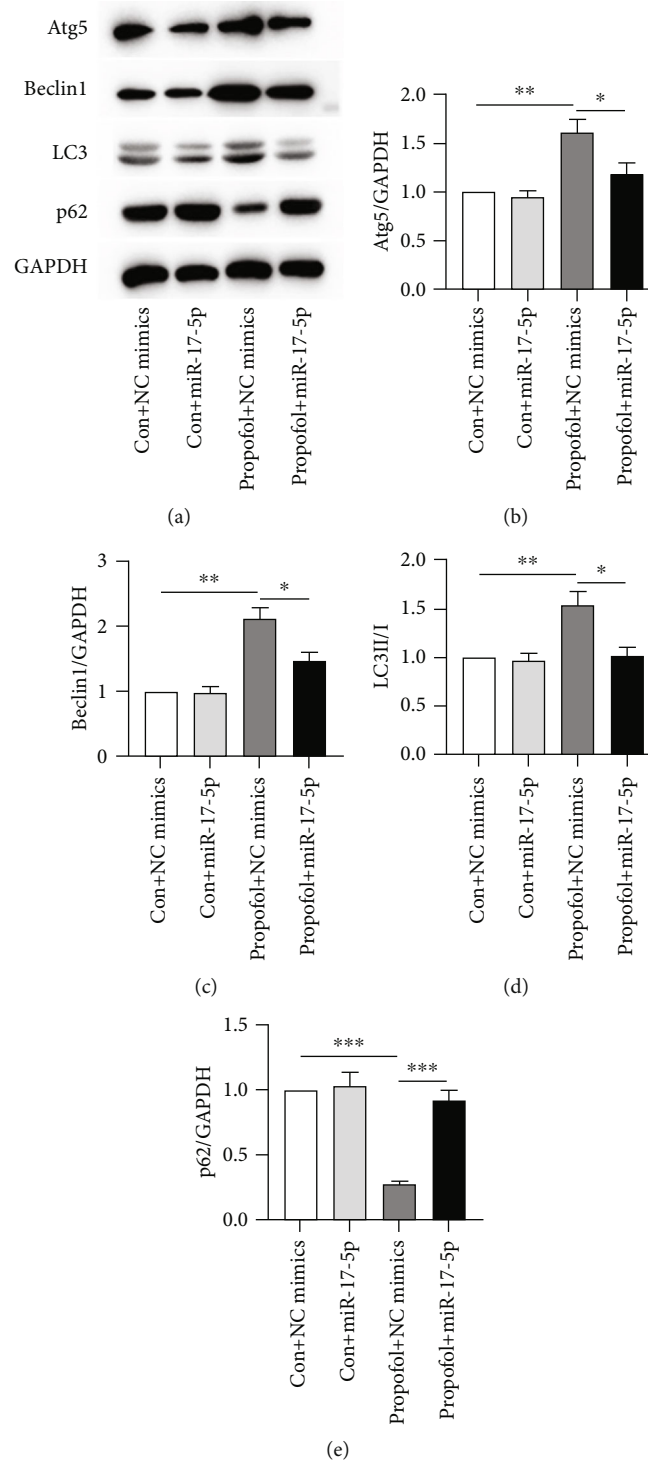


FIGURE 3: miR-17-5p inhibits PPF-induced autophagy in SH-SY5Y. (a)–(e) Protein levels of proteins related to autophagy (Atg5, Beclin1, LC3, and p62) in transfected SH-SY5Y cells with miR-17-5p or NC mimics with or without PPF (10  $\mu\text{g}/\text{ml}$ ) were measured by WB. \*  $p$ , \*\*  $p$ , and \*\*\*  $p$  values less than 0.05, 0.01, and 0.001, accordingly.

significantly elevated. Our results verified that PPF treatment induced obvious neurotoxicity in SH-SY5Y cells.

Previous documents have illuminated that miRNAs showed expression levels in the nervous system and implicated in the development of neurological diseases [35, 36]. miR-214-5p reduces contents of serum inflammatory factors

and alleviates the cognitive impairment by targeting SUZ12 in Alzheimer's disease mice [37]. miR-23b knockdown alleviates ischemic brain injury via elevating the level of nuclear factor erythroid 2-related factor 2 [38]. Upregulation of miR-29a mitigates aluminum-induced injury to primary hippocampal neurons [39]. miR-17-5p expression is

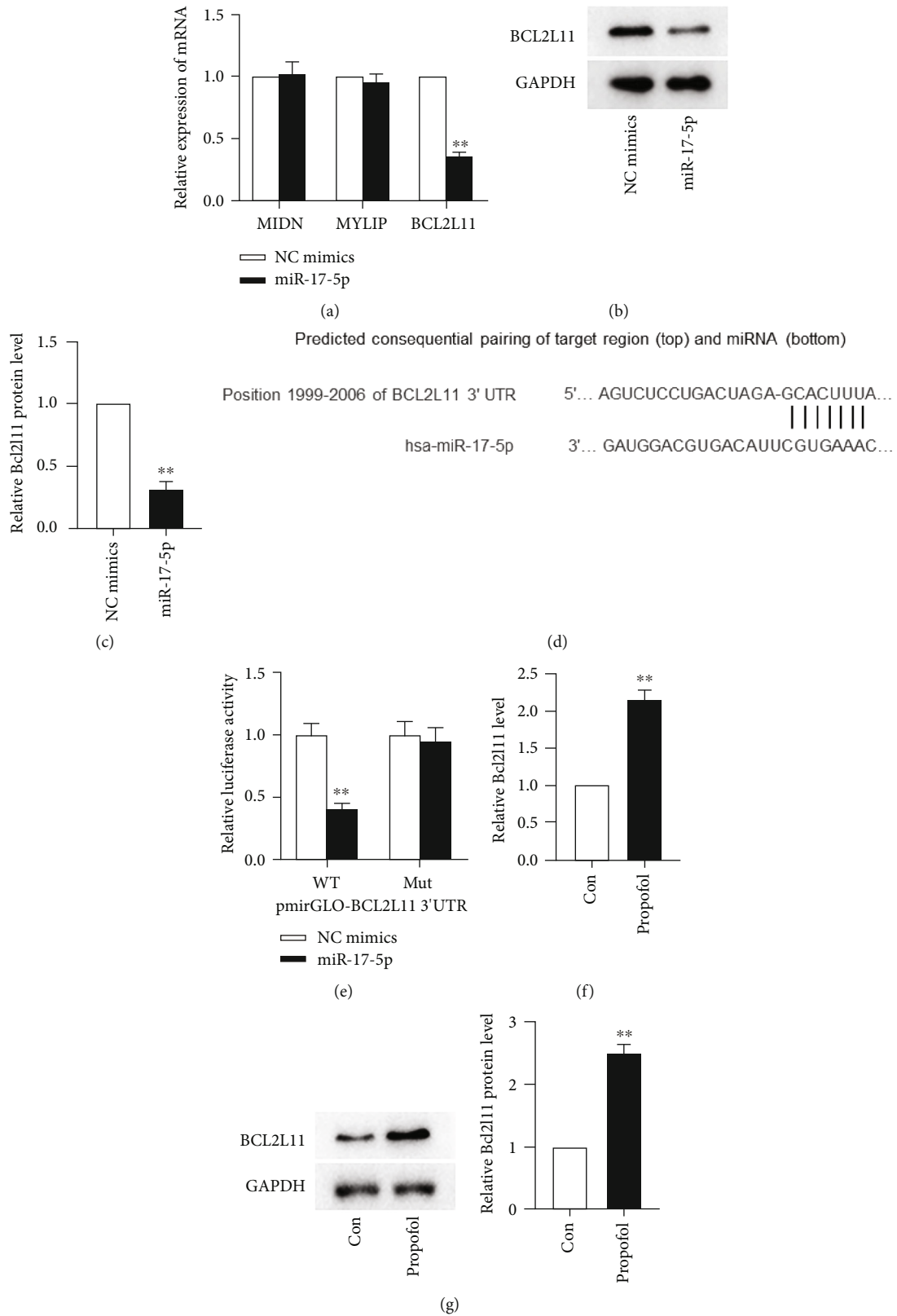


FIGURE 4: BCL2L11 is directly targeted by miR-17-5p in SH-SY5Y. (a) qRT-PCR examined the level of MIND, MYLIP, and BCL2L11 in SH-SY5Y cells with miR-17-5p or NC mimic transfection. (b, c) BCL2L11 protein levels were measured in SH-SY5Y cell posttransfection with miR-17-5p or NC mimics by WB. (d) Predicated binding region between miR-17-5p and BCL2L11 through Targetscan. (e) Validation of the combination between miR-17-5p and BCL2L11 via DLR assay. (f, g) BCL2L11 transcriptional and translational level was tested in SH-SY5Y cells treated with PPF or phosphate buffer by qRT-PCR and WB analysis, respectively. \*\* $p < 0.01$ .

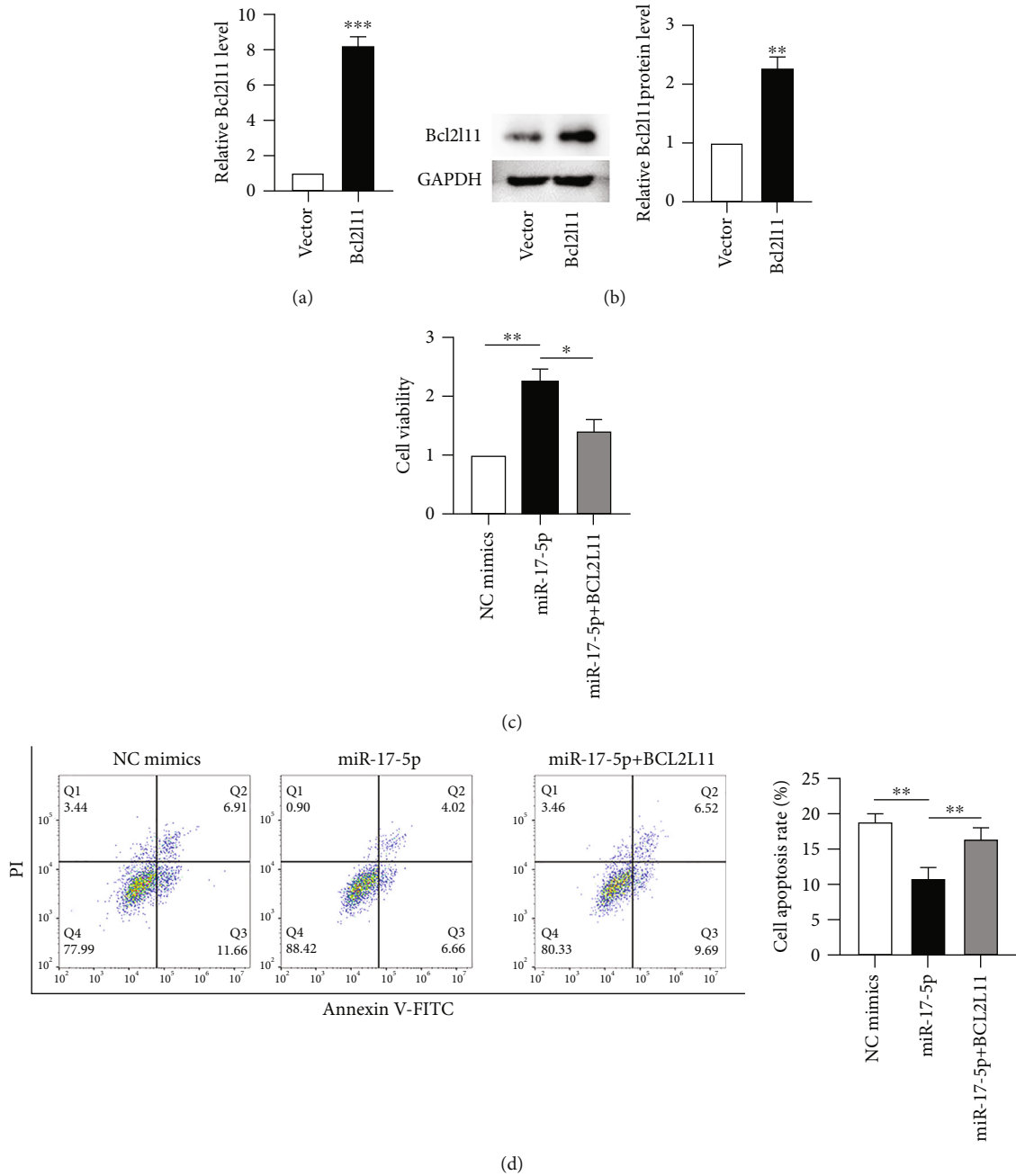


FIGURE 5: Continued.

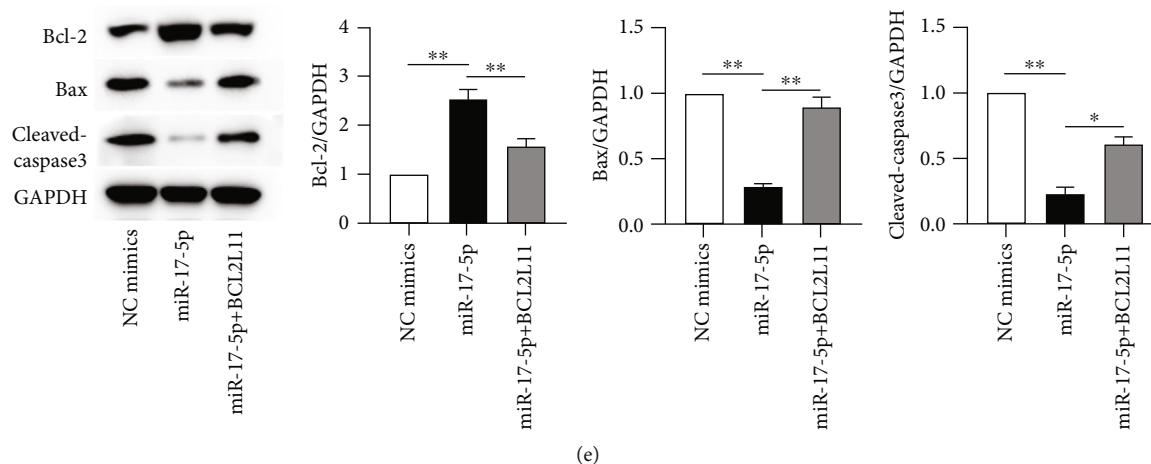


FIGURE 5: The influence of miR-17-5p on SH-SY5Y viability and apoptosis via modulating BCL2L11. Postexposure with PPF (10  $\mu\text{g/ml}$ ) for 24 h, rescue experiments were conducted. (a, b) Overexpression efficacy of BCL2L11 in SH-SY5Y cells was, respectively, evaluated by qRT-PCR and WB evaluations. (c, d) MTT assay and FC analysis were performed for evaluating SH-SY5Y cell viability and apoptosis after transfection of NC mimics, miR-17-5p mimics, and miR-17-5p mimics + pcDNA3.1/BCL2L11. (e) The translational levels of Bcl-2, Bax, and Cleaved-caspase-3 were estimated by WB in SH-SY5Y cells with plasmids transfection. \*  $p$ , \*\*  $p$ , and \*\*\*  $p$  values less than 0.05, 0.01, and 0.001, accordingly.

downregulated in paraquat-induced neuro-2a cells, and miR-17-5p depletion has a critical role in dopaminergic neurodegeneration induced by paraquat [40, 41]. The level of miR-17-5p in SH-SY5Y cells exposed to various PPF doses was detected, and the results presented the time- and dose-dependent decrease in its expression. The expression of miR175p increased the survival of PPF-treated cells and inhibited the apoptotic and autophagic processes in SH-SY5Y cells treated with PPF. These discoveries reveal that miR-17-5p is able to play a neuroprotective function in neurotoxicity (caused by PPF) by suppression of apoptotic process and autophagy in SH-SY5Y cells.

Plenty of documents have identified that miRNAs possess the ability to target various mRNAs and modulate the expression of genes to repair neuronal damage in neurodegenerative diseases [42]. By using bioinformatics analysis tools, BCL2L11 was predicted as the downstream target of miR-17-5p. Herein, BCL2L11, which presented elevated expression after PPF treatment, was validated to be directly targeted by miR-17-5p in SH-SY5Y cells. BCL2L11 is believed to play the role of apoptosis facilitator in many diseases [43]. For example, inhibition of BCL2L11 reduces neuron apoptosis in Alzheimer's diseases [44]. In addition, overexpression of BCL2L11 eliminates the miR-338-5p protective role against apoptosis of neurons [45]. Consistent with previous research, our results illuminated that in PPF-treated SH-SY5Y cells, overexpression of BCL2L11 reversed the rise in cell survival and the decrease in apoptotic process in context of miR-17-5p overexpression suggesting the potential of miR-17-5p to alleviate PPF exposure-caused the SH-SY5Y cells apoptosis by targeting BCL2L11.

Finally, our research looked at the role of miR-17-5p in PPF-induced apoptosis, autophagy, and the associated mechanism. The results showed that miR-17-5p, by inhibiting BCL2L11, reduced PPF-induced cell damage. Our study innovatively demonstrated that miR-17-5p may serve as a therapeutic target for the treatment of neurotoxicity caused

by PPF. Nonetheless, there were few limitations to this study. First, the protective role of miR-17-5p in SH-SY5Y cells (PPF-induced) was just validated by *in vitro* experiments, and *in vivo* studies are required to evaluate whether miR-17-5p exerts protective function in PPF-induced animal models. Second, due to the complexity of molecular mechanisms, the upstream molecules or downstream signaling pathways of the miR-17-5p/BCL2L11 axis still need further exploration.

## Data Availability

Data will be provided upon request to the authors.

## Conflicts of Interest

The authors declare that they have no conflicts of interest.

## Acknowledgments

The authors appreciate all the participants providing supports for this study.

## References

- [1] Y. Yan, S. Qiao, C. Kikuchi et al., "Propofol induces apoptosis of neurons but not astrocytes, oligodendrocytes, or neural stem cells in the neonatal mouse hippocampus," *Brain Sciences*, vol. 7, no. 12, p. 130, 2017.
- [2] S. Q. Zheng, L. X. An, X. Cheng, and Y. J. Wang, "Sevoflurane causes neuronal apoptosis and adaptability changes of neonatal rats," *Acta Anaesthesiologica Scandinavica*, vol. 57, no. 9, pp. 1167–1174, 2013.
- [3] V. Chidambaran, A. Costandi, and A. D'Mello, "Propofol: a review of its role in pediatric anesthesia and sedation," *CNS Drugs*, vol. 29, no. 7, pp. 543–563, 2015.

- [4] P. C. Kam and D. Cardone, "Propofol infusion syndrome," *Anaesthesia*, vol. 62, no. 7, pp. 690–701, 2007.
- [5] A. Krajčová, P. Waldauf, M. Anděl, and F. Duška, "Propofol infusion syndrome: a structured review of experimental studies and 153 published case reports," *Critical Care*, vol. 19, no. 1, p. 398, 2015.
- [6] C. Creeley, K. Dikranian, G. Dissen, L. Martin, J. Olney, and A. Brambrink, "Propofol-induced apoptosis of neurones and oligodendrocytes in fetal and neonatal rhesus macaque brain," *British Journal of Anaesthesia*, vol. 110, pp. i29–i38, 2013.
- [7] J. Wan, C. M. Shen, Y. Wang et al., "Repeated exposure to propofol in the neonatal period impairs hippocampal synaptic plasticity and the recognition function of rats in adulthood," *Brain Research Bulletin*, vol. 169, pp. 63–72, 2021.
- [8] M. Xiong, L. Zhang, J. Li, J. Eloy, J. Ye, and A. Bekker, "Propofol-induced neurotoxicity in the fetal animal brain and developments in modifying these effects—an updated review of propofol fetal exposure in laboratory animal studies," *Brain Sciences*, vol. 6, no. 2, p. 11, 2016.
- [9] A. L. Brotherton, E. P. Hamilton, H. G. Kloss, and D. A. Hammond, "Propofol for treatment of refractory alcohol withdrawal syndrome: a review of the literature," *Pharmacotherapy*, vol. 36, no. 4, pp. 433–442, 2016.
- [10] M. Yang, Y. Wang, G. Liang, Z. Xu, C. T. Chu, and H. Wei, "Alzheimer's disease presenilin-1 mutation sensitizes neurons to impaired autophagy flux and propofol neurotoxicity: role of calcium dysregulation," *Journal of Alzheimer's Disease*, vol. 67, no. 1, pp. 137–147, 2019.
- [11] H. S. Zhang, C. D. Liu, M. C. Zheng, H. T. Zhao, and X. J. Liu, "Propofol alleviates hypoxic neuronal injury by inhibiting high levels of mitochondrial fusion and fission," *European Review for Medical and Pharmacological Sciences*, vol. 24, no. 18, pp. 9650–9657, 2020.
- [12] M. Wang, L. Suo, S. Yang, and W. Zhang, "CircRNA 001372 reduces inflammation in propofol-induced neuroinflammation and neural apoptosis through PI3CA/Akt/NF- $\kappa$ B by miRNA-148b-3p," *Journal of Investigative Surgery*, vol. 34, no. 11, pp. 1167–1177, 2021.
- [13] Z. J. Bosnjak, S. Logan, Y. Liu, and X. Bai, "Recent insights into molecular mechanisms of propofol-induced developmental neurotoxicity: implications for the protective strategies," *Anesthesia and Analgesia*, vol. 123, no. 5, pp. 1286–1296, 2016.
- [14] M. R. Fabian, N. Sonenberg, and W. Filipowicz, "Regulation of mRNA translation and stability by microRNAs," *Annual Review of Biochemistry*, vol. 79, no. 1, pp. 351–379, 2010.
- [15] G. C. Shukla, J. Singh, and S. Barik, "MicroRNAs: processing, maturation, target recognition and regulatory functions," *Molecular and Cellular Pharmacology*, vol. 3, no. 3, pp. 83–92, 2011.
- [16] T. X. Lu and M. E. Rothenberg, "MicroRNA," *The Journal of Allergy and Clinical Immunology*, vol. 141, no. 4, pp. 1202–1207, 2018.
- [17] Z. Zhang, Y. Xu, S. Chi, and L. Cui, "MicroRNA-582-5p reduces propofol-induced apoptosis in developing neurons by targeting ROCK1," *Current Neurovascular Research*, vol. 17, no. 2, pp. 140–146, 2020.
- [18] S. Zhang, Z. Liang, W. Sun, and L. Pei, "Repeated propofol anesthesia induced downregulation of hippocampal miR-132 and learning and memory impairment of rats," *Brain Research*, vol. 1670, pp. 156–164, 2017.
- [19] Q. Jiang, Y. Wang, and X. Shi, "Propofol inhibits neurogenesis of rat neural stem cells by upregulating microRNA-141-3p," *Stem Cells and Development*, vol. 26, no. 3, pp. 189–196, 2017.
- [20] Y. Lu, S. Wang, S. Cai et al., "Propofol-induced miR-20b expression initiates endogenous cellular signal changes mitigating hypoxia/re-oxygenation-induced endothelial autophagy in vitro," *Cell Death & Disease*, vol. 11, no. 8, p. 681, 2020.
- [21] J. Ye, J. Zhu, H. Chen et al., "A novel lncRNA-LINC01116 regulates tumorigenesis of glioma by targeting VEGFA," *International Journal of Cancer*, vol. 146, no. 1, pp. 248–261, 2020.
- [22] J. Chen, X. Li, F. Zhao, and Y. Hu, "HOTAIR/miR-17-5p axis is involved in the propofol-mediated cardioprotection against ischemia/reperfusion injury," *Clinical Interventions in Aging*, vol. Volume 16, pp. 621–632, 2021.
- [23] A. C. Faber, H. Ebi, C. Costa, and J. A. Engelman, "Apoptosis in targeted therapy responses: the role of BIM," *Advances in Pharmacology*, vol. 65, pp. 519–542, 2012.
- [24] H. Niu, K. Wang, A. Zhang et al., "miR-92a is a critical regulator of the apoptosis pathway in glioblastoma with inverse expression of BCL2L1," *Oncology Reports*, vol. 28, no. 5, pp. 1771–1777, 2012.
- [25] J. C. Doré, T. Ojasoo, and M. Thireau, "Using the volumetric indices of telencephalic structures to distinguish *Salamandridae* and *Plethodontidae*: comparison of three statistical methods," *Journal of Theoretical Biology*, vol. 214, no. 3, pp. 427–439, 2002.
- [26] E. Y. Rha, J. M. Kim, and G. Yoo, "Volume measurement of various tissues using the image J software," *The Journal of Craniofacial Surgery*, vol. 26, no. 6, pp. e505–e516, 2015.
- [27] F. Pang, C. Liu, Y. Cui et al., "miR-17-5p promotes proliferation and migration of CAL-27 human tongue squamous cell carcinoma cells involved in autophagy inhibition under hypoxia," *International Journal of Clinical and Experimental Pathology*, vol. 12, no. 6, pp. 2084–2091, 2019.
- [28] X. Xu, Y. L. Su, J. Y. Shi, Q. Lu, and C. Chen, "MicroRNA-17-5p promotes cardiac hypertrophy by targeting Mfn2 to inhibit autophagy," *Cardiovascular Toxicology*, vol. 21, no. 9, pp. 759–771, 2021.
- [29] C. L. Dai, H. Li, X. Hu et al., "Neonatal exposure to anesthesia leads to cognitive deficits in old age: prevention with intranasal administration of insulin in mice," *Neurotoxicity Research*, vol. 38, no. 2, pp. 299–311, 2020.
- [30] Z. Li, Q. Pei, L. Cao, L. Xu, B. Zhang, and S. Liu, "Propofol increases  $\mu$ -opioid receptor expression in SH-SY5Y human neuroblastoma cells," *Molecular Medicine Reports*, vol. 6, no. 6, pp. 1333–1336, 2012.
- [31] J. Liang, S. Zhang, W. Wang et al., "Long non-coding RNA DSCAM-AS1 contributes to the tumorigenesis of cervical cancer by targeting miR-877-5p/ATXN7L3 axis," *Bioscience reports*, vol. 40, no. 1, 2020.
- [32] M. A. Hausburg, K. L. Banton, P. E. Roman et al., "Effects of propofol on ischemia-reperfusion and traumatic brain injury," *Journal of Critical Care*, vol. 56, pp. 281–287, 2020.
- [33] Z. Liu, J. H. Chen, W. Z. Yuan et al., "Nuclear factor I/B promotes colorectal cancer cell proliferation, epithelial-mesenchymal transition and 5-fluorouracil resistance," *Cancer Science*, vol. 110, no. 1, pp. 86–98, 2019.
- [34] Y. Yao and J. J. Zhang, "Propofol induces oxidative stress and apoptosis in vitro via regulating miR-363-3p/CREB signalling axis," *Cell Biochemistry and Function*, vol. 38, no. 8, pp. 1119–1128, 2020.

- [35] R. Johnson, C. Zuccato, N. D. Belyaev, D. J. Guest, E. Cattaneo, and N. J. Buckley, "A microRNA-based gene dysregulation pathway in Huntington's disease," *Neurobiology of Disease*, vol. 29, no. 3, pp. 438–445, 2008.
- [36] S. S. Hébert, K. Horré, L. Nicolai et al., "Loss of microRNA cluster miR-29a/b-1 in sporadic Alzheimer's disease correlates with increased BACE1/beta-secretase expression," *Proceedings of the National Academy of Sciences of the United States of America*, vol. 105, no. 17, pp. 6415–6420, 2008.
- [37] G. Hu, Z. Shi, W. Shao, and B. Xu, "MicroRNA-214-5p involves in the protection effect of dexmedetomidine against neurological injury in Alzheimer's disease via targeting the suppressor of zest 12," *Brain research bulletin*, vol. 178, pp. 164–172, 2022.
- [38] R. Xin, D. Qu, S. Su, B. Zhao, and D. Chen, "Downregulation of miR-23b by transcription factor c-Myc alleviates ischemic brain injury by upregulating Nrf2," *International Journal of Biological Sciences*, vol. 17, no. 13, pp. 3659–3671, 2021.
- [39] H. Zhang, X. Cai, C. Xiang, Y. Han, and Q. Niu, "miR-29a and the PTEN-GSK3 $\beta$  axis are involved in aluminum-induced damage to primary hippocampal neuronal networks," *Ecotoxicology and Environmental Safety*, vol. 224, article 112701, 2021.
- [40] Y. Zhan, Z. Guo, F. Zheng et al., "Reactive oxygen species regulate miR-17-5p expression via DNA methylation in paraquat-induced nerve cell damage," *Environmental Toxicology*, vol. 35, no. 12, pp. 1364–1373, 2020.
- [41] Q. Wang, Y. Zhan, N. Ren et al., "Paraquat and MPTP alter microRNA expression profiles, and downregulated expression of miR-17-5p contributes to PQ-induced dopaminergic neurodegeneration," *Journal of Applied Toxicology*, vol. 38, no. 5, pp. 665–677, 2018.
- [42] R. Su, P. Sun, D. Zhang, W. Xiao, C. Feng, and L. Zhong, "Neuroprotective effect of miR-410-3p against sevoflurane anesthesia-induced cognitive dysfunction in rats through PI3K/Akt signaling pathway via targeting C-X-C motif chemokine receptor 5," *Genes Genomics*, vol. 41, no. 10, pp. 1223–1231, 2019.
- [43] Y. Zhao, L. Zhu, S. Yu, J. Zhu, and C. Wang, "CaMKII inhibition promotes neuronal apoptosis by transcriptionally upregulating Bim expression," *Neuroreport*, vol. 27, no. 14, pp. 1018–1023, 2016.
- [44] R. Malishev, S. Nandi, D. Śmiłowicz et al., "Interactions between BIM protein and beta-amyloid may reveal a crucial missing link between Alzheimer's disease and neuronal cell death," *ACS Chemical Neuroscience*, vol. 10, no. 8, pp. 3555–3564, 2019.
- [45] J. Li, D. Li, H. Zhou et al., "MicroRNA-338-5p alleviates neuronal apoptosis via directly targeting BCL2L1 in APP/PS1 mice," *Aging (Albany NY)*, vol. 12, no. 20, pp. 20728–20742, 2020.

## Research Article

# Clinical Usage of Different Doses of Cis-Atracurium in Intracranial Aneurysm Surgery and Its Effect on Motor-Evoked Potentials

Zhongyuan Qiao and Rong Fan 

Anesthesiology Department, The First Affiliated Hospital of Northwest University (Xi'an No. 1 Hospital), Xi'an, 710000 Shaanxi, China

Correspondence should be addressed to Rong Fan; 0121063@yzpc.edu.cn

Received 5 May 2022; Revised 24 May 2022; Accepted 26 May 2022; Published 28 June 2022

Academic Editor: Naeem Jan

Copyright © 2022 Zhongyuan Qiao and Rong Fan. This is an open access article distributed under the Creative Commons Attribution License, which permits unrestricted use, distribution, and reproduction in any medium, provided the original work is properly cited.

The objective of this work was to investigate the effect of different doses of cis-atracurium on patients undergoing general anesthesia induction (GAI) during intracranial aneurysm surgery (ICAS). In this work, 90 patients who underwent ICAS under the elective motor-evoked potential (MEP) monitoring in the First Affiliated Hospital of Northwest University (Xi'an No. 1 Hospital) from January 2021 to May 2022 were enrolled as the research objects. Randomly, they were rolled into a S1 group (30 cases, 2 times 95% effective dose (ED95) cis-atracurium), a S2 group (30 cases, 3 times ED95 cis-atracurium), and a S3 group (30 cases, 4 times ED95 cis-atracurium). The endotracheal intubation conditions, the train-of-four (TOF) rate (TOFR), body movement, and spontaneous breathing were compared among the three groups of patients. The results showed that the MEP inhibition time of the patients in the S3 group was much longer than that of the S1 and S2 groups, but it showed no significant difference between the S1 group and S2 group ( $P > 0.05$ ). The good rates of endotracheal intubation conditions in the S2 group (100%) and S3 group (100%) were obviously higher than the rate in the S1 group (43.33%). The TOFRs of patients in S2 and S3 groups at time t2 and t3 were lower obviously to that at time t0, while the TOFRs of patients in S3 group at time t2 and t3 were still lower in contrast to the S2 group ( $P < 0.05$ ). The mean arterial pressure (MAP) and heart rate (HR) of patients in all groups were lower at t1, t2, and t3 than at t0 ( $P < 0.05$ ), while the differences among different groups were not remarkable ( $P > 0.05$ ). Finally, using 3 times ED95 cis-atracurium for GAI could reduce the risk of intraoperative body movement and spontaneous breathing, as well as the residual degree of muscle relaxation, in patients with ICAS, without affecting MEP monitoring, improving endotracheal intubation conditions, and increasing safety during open neurosurgery operations.

## 1. Introduction

Intracranial aneurysm generally refers to the abnormal bulge of the intracranial artery wall, which is the first cause of subarachnoid haemorrhage [1]. Due to the weak structure and poor elasticity of the blood vessel wall of a cerebral aneurysm, it is possible that the rupture of the cerebral aneurysm may occur when the mean arterial pressure (MAP) increases during emotional agitation, forced defecation, fatigue, etc., so the incidence rate is extremely high. Outside of the cerebral blood arteries, the incidence of cerebral haemorrhage

(subarachnoid haemorrhage) produced by cerebral aneurysm is currently second only to cerebral thrombosis and hypertensive cerebral haemorrhage, and the fatality rate is first [2–4]. Most intracranial aneurysms occur in middle-aged and elderly women between the ages of 40 and 60. At present, the etiology of intracranial aneurysms is still unclear. Most scholars believe that intracranial aneurysms are caused by local congenital defects in the intracranial arterial wall and increased intraluminal pressure. Hypertension, cerebral arteriosclerosis, and vasculitis are associated with the occurrence and development of aneurysms [5, 6].



Intracranial aneurysms are usually minor and cause no symptoms. Aneurysms are discovered in two ways: when they rupture and bleed, creating a severe headache or coma, and when they compress and create a sequence of symptoms [7]. Although the process of aneurysm rupture and bleeding lasts only a few seconds, it can bring a series of serious consequences, so once the intracranial aneurysm lesion is detected, it should be treated as soon as possible [8].

Clinical treatment of intracranial aneurysms mainly includes open surgical treatment (clamping, wrapping), endovascular interventional treatment (coils, blood flow guide devices, liquid embolic agents, stents, etc.), and conservative treatment to control the risk factors [9, 10]. Clipping is to select the appropriate aneurysm to clip the aneurysm according to the orientation of the aneurysm and the length of the aneurysm neck. It is a common method for the treatment of intracranial aneurysms. If it is closed, aneurysm wrapping will be used. Endovascular interventional therapy is a new alternative treatment for inoperable patients, mainly by implanting coils, stents, balloons, liquid glue, and other materials for aneurysm treatment [11–13]. Interventional therapy, on the other hand, has a dismal prognosis. Some people, for example, will have increased blood viscosity. When the blood arteries in the head narrow and spasm, the blood flow rate slows, increasing the risk of a head blood vessel infarction. In addition, patients may also experience hemiplegia, aphasia, intellectual disability, and movement disorders [14–16]. Unfortunately, these conventional treatments all have many difficulties for giant intracranial aneurysms, such as huge aneurysm, thin wall, easy rupture and bleeding, wide aneurysm neck, difficult or impossible to clip. It is not suitable for tamponade, or the pituitary gland is still compressed after tamponade, and it is difficult to improve the symptoms of patients [17, 18].

The motor-evoked potential (MEP), which can reflect the integrity of the descending pathway of anterior spinal cord motor conduction and is used clinically to assess the integrity of the patient's motor function in real time, is one of the key elements to be monitored in neurosurgery. As a result, improving the accuracy of MEP intraoperative monitoring is an area that requires focus [19, 20]. There are many factors that affect MEP, such as anesthesia drugs, pacemakers, and surgical operations, among which anesthesia drugs have the greatest impact. Cis-atracurium is a synthetic bisquaternary ammonium ester type benzyl isoquinoline compound, which is a medium-acting nondepolarizing muscle relaxant, can act through competitive binding with cholinergic receptors, has a rapid onset of action, and has a good muscle relaxation effect, and is widely used in clinical anesthesia [21–23]. As a result, 90 ICAS patients who underwent MEP monitoring in our hospital were chosen as research subjects and divided into three groups: S1 (2 times the 95 percent effective dose (ED95) cis-atracurium), S2 (3 times ED95 cis-atracurium), and S3 (4 times ED95 cis-atracurium), each having 30 cases [24, 25]. It compared the general data, endotracheal intubation conditions, hemodynamic indexes, respiratory function indexes, train-of-four (TOF) ratio (TOFR), body movement, and spontaneous breathing conditions of the three groups of patients, so as to deeply

analyze the effects of different doses of cis-atracurium on GAI of patients with ICAS.

## 2. Materials and Methods

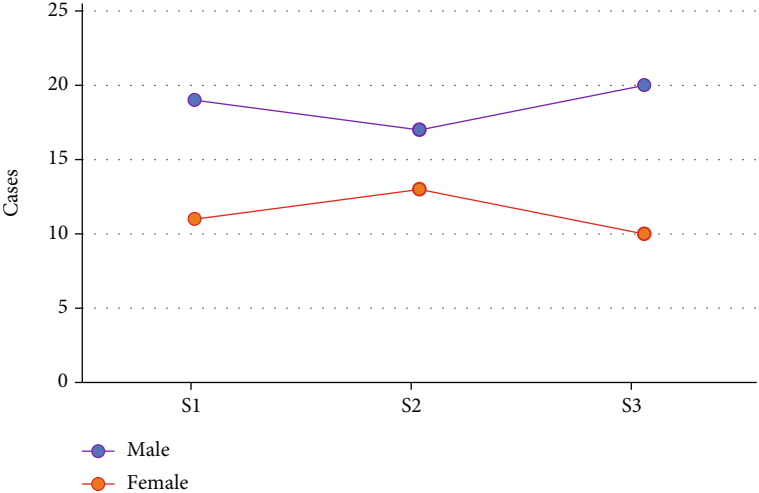
*2.1. Research Objects.* 90 ICAS patients who underwent MEP monitoring in the First Affiliated Hospital of Northwest University (Xi'an No. 1 Hospital) from January 2021 to May 2022 were selected as the research subjects. The experiment had been approved by the Ethics Committee of the First Affiliated Hospital of Northwest University (Xi'an No. 1 Hospital), and the informed consents had been obtained from all patients and their families

Patients enrolled had to meet the following criteria: patients who were older than 18 years old, patients who were determined as American Society of Anesthesiologists (ASA) grade I or II, persons with normal body temperature, patients with complete clinical data, and patients with normal communication.

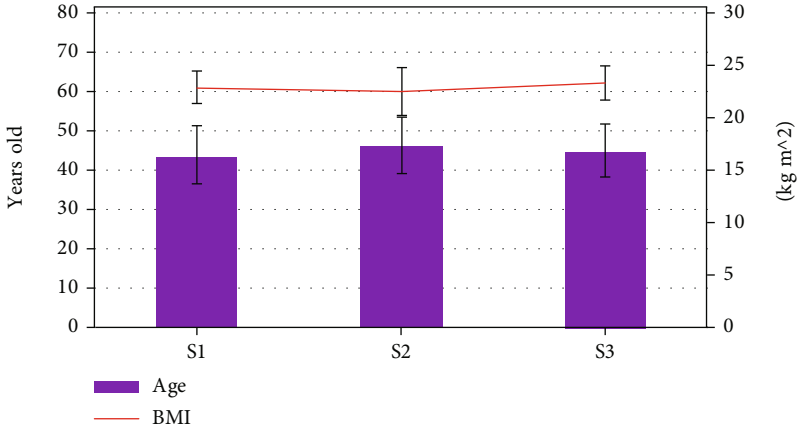
Patients satisfying below conditions had to be excluded from this work: patients with moderate to severe anemia; patients with difficult airway; patients with infection at the monitoring site; patients with severe heart, liver, and kidney disease; patients complicated with mental illness; patients who are allergic to anesthetics; and patients with malignant tumors or other malignant diseases.

*2.2. Grouping of Objects.* The patients were divided into 30 cases in the S1 group, 30 cases in the S2 group, and 30 cases in the S3 group by a random number table method. Patients in group S1 were treated with 2 times the 95% effective dose (ED95) cis-atracurium; patients in group S2 were treated with 3 times ED95 cis-atracurium; and patients in group S3 were treated with 4 times ED95 cis-atracurium.

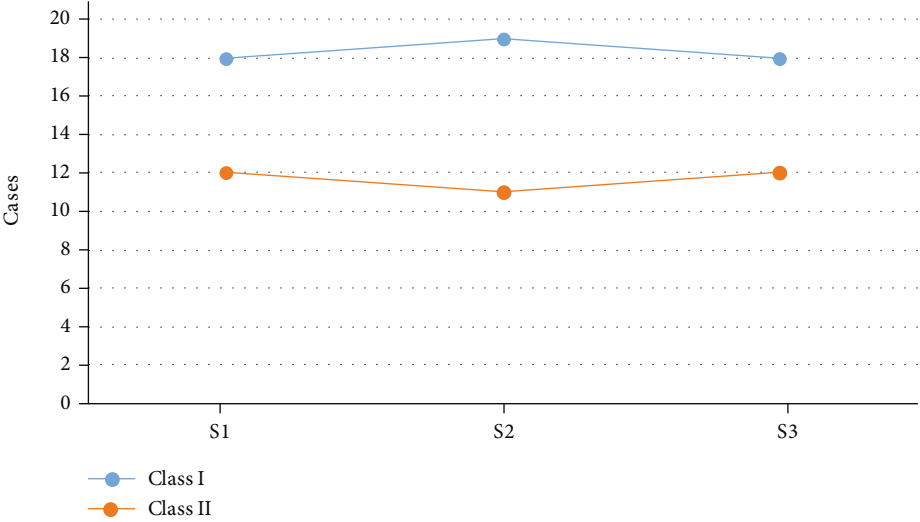
*2.3. Anesthesia Method.* Firstly, before the surgery, the patient was allowed to fast for 8 hours and water for 5 hours. The electrocardiogram, heart rate (HR), MAP, and other physical indicators of patients should be monitored after they entered the operation room. They all received intravenous anesthesia, intravenous infusion of 0.4 mg of scopolamine before anesthesia. Secondly, during the anesthesia, 0.04 mg/kg of midazolam and 1.5 mg/kg of propofol were intravenously injected in sequence. After the patient lost consciousness, 0.4  $\mu$ g/kg of sufentanil was intravenously injected, and electrophysiological monitor was performed. Thirdly, different doses of cis-atracurium were intravenously injected to the corresponding patients, and the tracheal intubation was performed through the mouth (dyclonine hydrochloride mucilage was applied to the surface of the tracheal tube) after the drug took effect. Fourthly, it could select the appropriate size catheter according to the individual situation of the patient, adjust the depth of tracheal intubation by auscultation, and perform mechanically controlled ventilation after fixation. Respiratory parameters were set as follows: the tidal volume was 8.5–10.5 mL/kg, the respiratory rate was 10–12 times/min, and the oxygen flow was 1.5 L/min. Fifthly, during the surgery, the end-tidal carbon dioxide should be maintained at a level of about 35 mmHg, and the



(a)

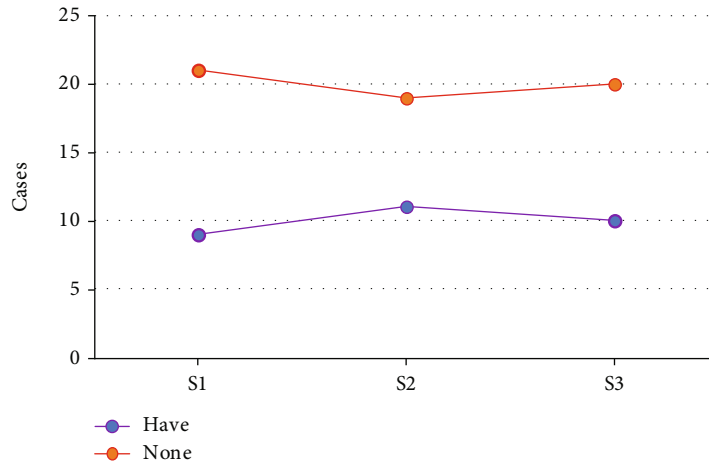


(b)

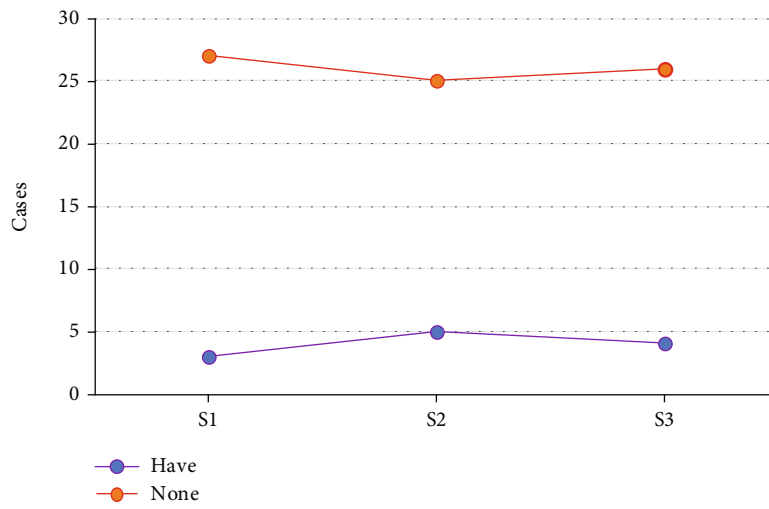


(c)

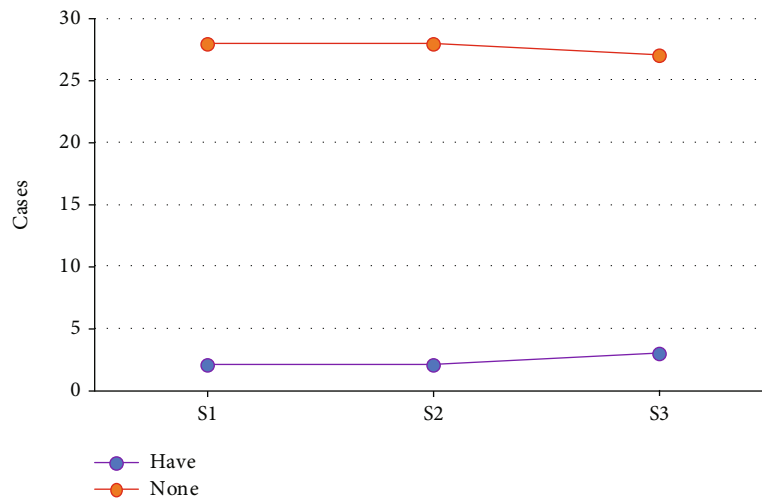
FIGURE 1: Continued.



(d)



(e)



(f)

FIGURE 1: Comparison on the general data of patients ((a) is the comparison on number of male and female cases; (b) shows the comparison of the average age and BMI; (c) illustrates the comparison of the ASA classification; (d–f) compare the number of hypertension, diabetes, and CHD, respectively).

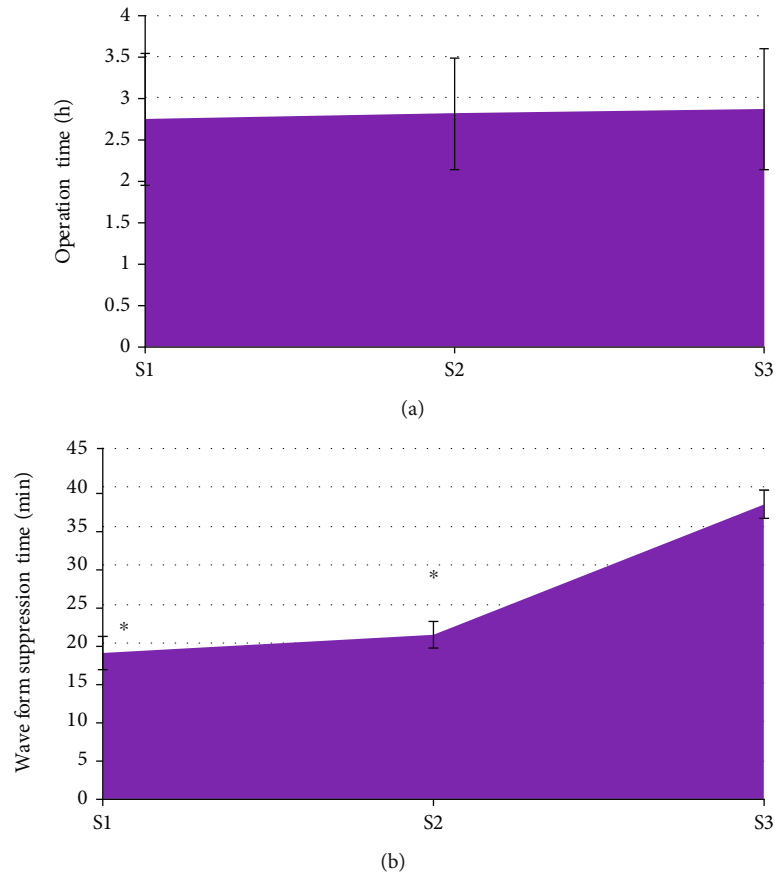


FIGURE 2: Comparison of operation time and MEP inhibition time ((a) compares the operation time; (b) compares the MEP inhibition time).

fluid infusion rate should be adjusted according to the patient's MAP and HR in real time to maintain hemodynamic balance. Half an hour before the end of surgery, the patient should be given 4 mg of dezocine and 0.02 mg/kg of tropisetron. Propofol and sufentanil injections were stopped 10 minutes before the end of surgery. After the patient regained spontaneous breathing, neostigmine and atropine were administered intravenously, and tracheal extubation was performed after the patient was completely awake.

**2.4. MEP Monitoring.** MEP monitoring was performed using a 32-channel bioelectrophysiological signal analysis system XLTEK32 (GE, USA). Firstly, the abductor pollicis brevis muscle, the abductor pollicis muscle of the upper extremity, and the abductor pollicis muscle of the lower extremity were selected as the monitoring sites, and the spiral electrode was used as the scalp stimulation electrode. The line was placed on the shoulders of the changer. The stimulation parameters were set as follows: the stimulation intensity was about 120 V, the stimulation frequency was 5-10 times, the stimulation interval was 2-3.5 ms, and the pulse was 45  $\mu$ s. It should record the compound muscle action potential at the corresponding muscle position at the speed of 8 ms/div, the filter of 50-2500 HZ, and the display gain of 45  $\mu$ V/div. The electrodes can be stimulated after the intravenous injection of cis-atracurium.

**2.5. Intraoperative Emergency Response Measures.** The following are the emergency response measures: (1) If the patient recovered spontaneous breathing during the operation, the ventilator can be adjusted to manual assisted ventilation mode, and about 30 mg of propofol can be intravenously infused. It can adjust to the mechanically controlled ventilation mode when the patient has no spontaneous breathing. (2) If the patient had body movement during the surgery, it could inject about 30 mg of propofol and temporarily stop the MEP monitoring. (3) When the patient's MAP decreased by more than 30% (compared to the baseline value), appropriate fluid replacement was required, and norepinephrine bitartrate (3  $\mu$ g single injection) was used as appropriate; if the patient's MAP increased by more than 30% (compared to the baseline value), which can deepen the degree of anesthesia and use vasoactive drugs as appropriate. (4) If the patient's HR decreased by more than 30% (compared to the basal value), it could give the patient 0.4 mg of atropine; if the patient's HR increased by more than 30% (compared to the basal value), appropriate fluids can be added to maintain a sufficient degree of anesthesia and as appropriately adopt the  $\beta$ -blockers.

**2.6. Observation Indexes.** The general information of the patients (age, gender, height, weight, hypertension, diabetes, and coronary heart disease (CHD)) was collected. MAP, HR,

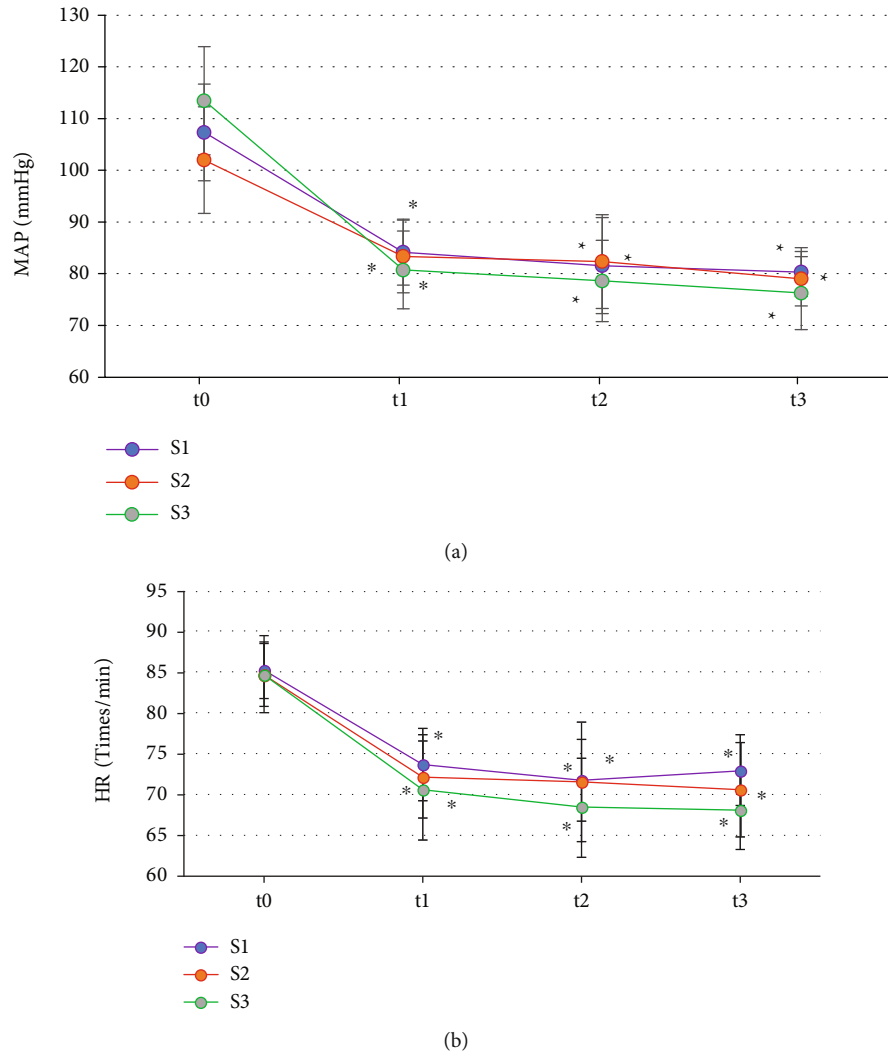


FIGURE 3: Comparison of MAP and HR at different times ((a) compares the MAP, and (b) compares the HR) Note: \* indicates  $P < 0.05$  compared with the values at time t0.

pulse oxygen saturation ( $SpO_2$ ), partial pressure of carbon dioxide in end-expiratory gas ( $PETCO_2$ ), and peak airway pressure (Peak) were recorded at different times (when entering the room (t0), immediately after endotracheal intubation (t1), 5 minutes after endotracheal intubation (t2), and release of MEP waveform (t3)). The TOF-Watch SX acceleration muscle relaxation monitor was used to evaluate the residual effect of the patient's muscle relaxation, and TOFR was calculated. Cooper's scoring method [22] was adopted to evaluate endotracheal intubation conditions, including the sum of three scores: laryngoscopy, glottis opening, and closing and intubation response. The suppression time and operation time of the patient's MEP waveform were recorded.

**2.7. Statistical Methods.** SPSS19.0 was used for data processing in this work. Measurement data were expressed in the form of mean  $\pm$  standard deviation ( $\bar{x} \pm s$ ), and enumeration data were expressed as percentage (%). Pairwise comparisons were made using one-way ANOVA. The difference was statistically significant at  $P < 0.05$ .

### 3. Results and Discussion

**3.1. Comparison on General Data of Patients in Different Groups.** As shown in Figure 1 below, there were no statistically obvious differences in the ratio of males and females, average age, body mass index (BMI), hypertension, diabetes, and CHD among three groups ( $P > 0.05$ ).

**3.2. Comparison of Perioperative Conditions of Patients.** As shown in Figure 2 below, the operation time showed no great difference among the S1, S2, and S3 groups ( $P > 0.05$ ). The MEP inhibition time of the S3 group was the longest among all groups ( $P < 0.05$ ), while it showed no obvious different between the S1 and S2 groups ( $P > 0.05$ ).

As illustrated in Figure 3, the pairwise comparison of MAP and HR at t0 in the three groups of patients showed the difference was not statistically notable ( $P > 0.05$ ); those at t1, t2, and t3 were lower than at t0 time ( $P < 0.05$ ); and no remarkable difference was found among the three groups at t1, t2, and t3 ( $P > 0.05$ ).

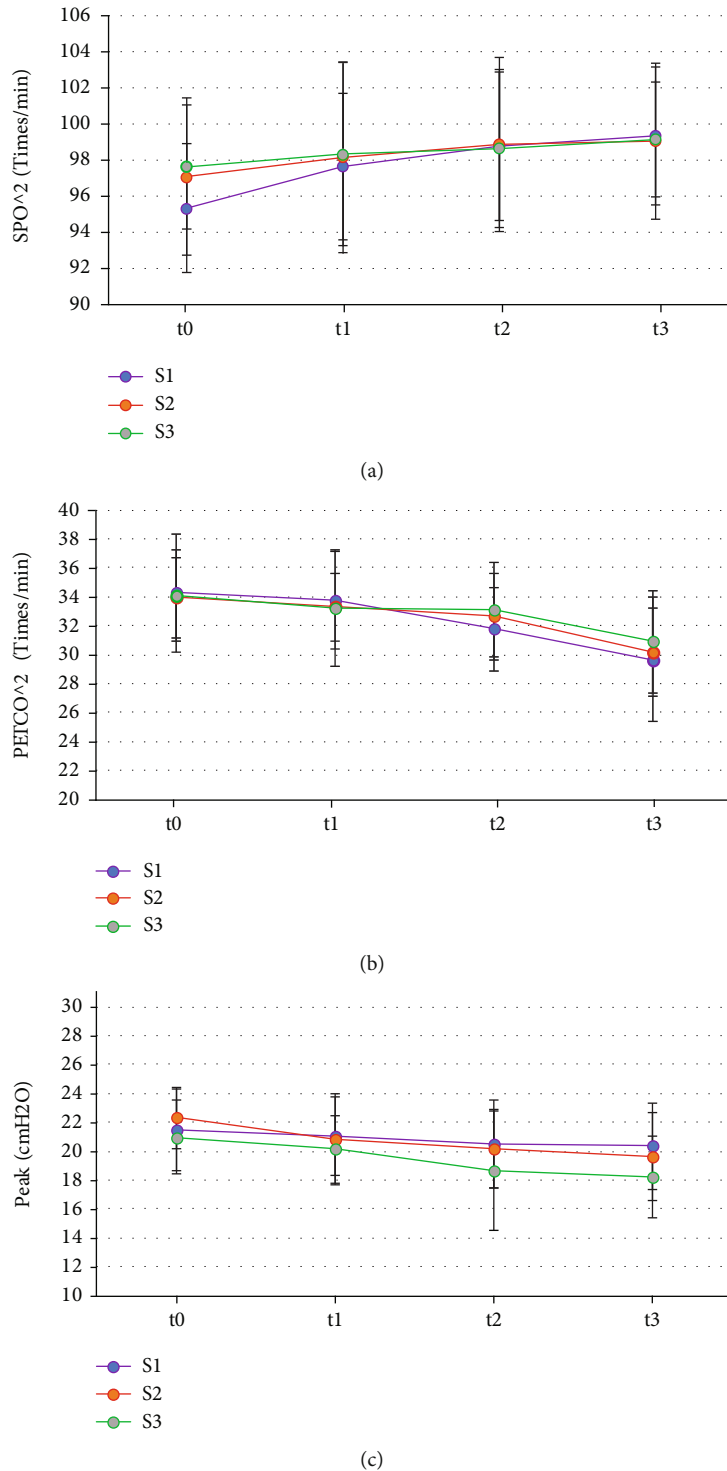


FIGURE 4: Comparison on SpO<sub>2</sub>, PETCO<sub>2</sub>, and peak ((a-c) compare the SpO<sub>2</sub>, PETCO<sub>2</sub>, and peak, respectively).

As demonstrated in Figure 4, the pairwise comparisons of SpO<sub>2</sub>, PETCO<sub>2</sub>, and peak among all groups showed no obvious difference at all time points ( $P > 0.05$ ).

As given in Figure 5, the TOFRs of the three groups of patients at time t0 were not different greatly ( $P > 0.05$ ); the TOFRs in the S2 groups and the S3 group at time t2 and

t3 decreased than those before surgery ( $P < 0.05$ ), while those in the S3 group were lower in contrast to those in the S2 group at both t2 and t3 ( $P < 0.05$ ).

As shown in Tables 1 and 2, patients in group S1 did not experience body movement or spontaneous breathing at time t0, t1, and t2, while at t3, 3 patients had body

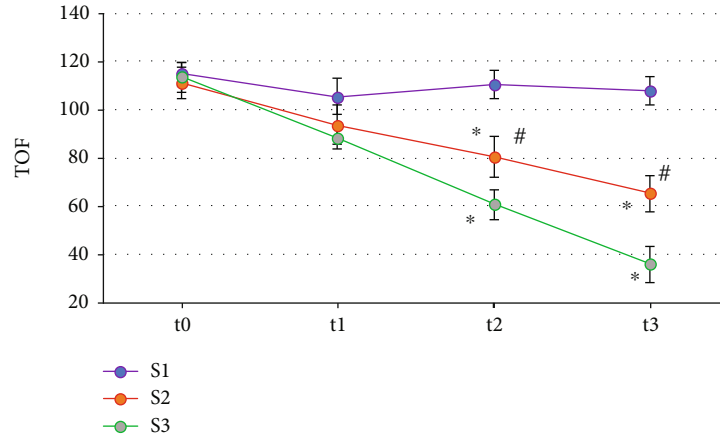


FIGURE 5: Comparison of TOF values of three groups of patients at different times. Note: \* and # mean  $P < 0.05$  in contrast to the values at t0 and S3 group, respectively.

TABLE 1: Statistics on body movement of patients.

Time	S1 group	S2 group	S3 group
t0	30	30	30
t1	0	0	0
t2	0	0	0
t3	3	0	0

TABLE 2: Statistics on spontaneous breathing of patients.

Time	S1 group	S2 group	S3 group
t0	30	30	30
t1	0	0	0
t2	0	0	0
t3	2	0	0

movement and 2 patients had spontaneous breathing. Patients in groups S2 and S3 did not experience body movement or spontaneous breathing at all time points.

Figure 6 shows the comparison of the dosage of propofol and sufentanil among the three groups of patients. The dosage of propofol in patients with S1 was  $734.65 \pm 102.34$  mg, and the dosage of sufentanil was  $2.04 \pm 0.25$  mg. The dosages of propofol and sufentanil in the S2 group were  $679.25 \pm 97.54$  mg and  $1.87 \pm 0.18$  mg, respectively; the dosages of propofol and sufentanil in S3 group were  $678.05 \pm 99.25$  mg and  $1.79 \pm 0.38$  mg, respectively. The analysis showed no visible difference in the doses of propofol and sufentanil among the three groups of patients ( $P > 0.05$ ).

**3.3. Comparison of Intraoperative Endotracheal Intubation Conditions.** Figure 7 shows the comparison of the endotracheal intubation conditions of the three groups of patients. It showed that the patients in the S1 group had excellent endotracheal intubation circumstances in six cases, good in seven, moderate in eleven, and poor in six. The endotracheal intubation conditions of the patients in the S2 group were

excellent in 23 cases, good in 7 cases, moderate in 0 cases, and poor in 0 cases. In the S3 group, the endotracheal intubation conditions were excellent in 24 cases, good in 6 cases, moderate in 0 cases, and poor in 0 cases. The analysis showed that the excellent and good rates of endotracheal intubation conditions of patients in S2 group (100%) and S3 group (100%) were absolutely higher in contrast to those in S1 group (43.33%), showing statistically visible differences ( $P < 0.05$ ).

## 4. Discussion

Intracranial aneurysm is a clinical disease with a very high morbidity and mortality rate. Although aneurysm is not a tumor, it is much more dangerous than a tumor [23, 24]. However, because the human brain is such a complicated organ, even minor injury might impair the patient's neurological function, so the procedure must be done with extraordinary precision. In ICAS, neurophysiological monitoring is the gold standard for detecting nerve injury induced by various variables in time for scientific intervention [25, 26]. Muscle relaxants are a major factor affecting the accuracy of MEP monitoring. Therefore, this work included 90 ICAS patients who underwent MEP monitoring in our hospital from January 2021 to May 2022 and divided the patients into a S1 group (2 times ED95 cis-atracurium), a S2 group (3 times ED95 cis-atracurium), and a S3 group (4 times ED95 cis-atracurium) for comparative analysis, with 30 cases in each group. Firstly, the basic data of the three groups of patients were compared, and it was found that the ratio of males and females, average age, BMI, hypertension, diabetes, and CHD in the S1, S2, and S3 groups were not greatly different ( $P > 0.05$ ). This provides a reliable basis for follow-up research.

Then, it analyzed the perioperative conditions of the three groups of patients. Firstly, difference in the operation time between the three groups of patients in the S1, S2, and S3 groups was not great ( $P > 0.05$ ). This is similar to the findings of Pressman et al. [27], indicating that the dose of cis-atracurium does not differ in terms of ICAS length.

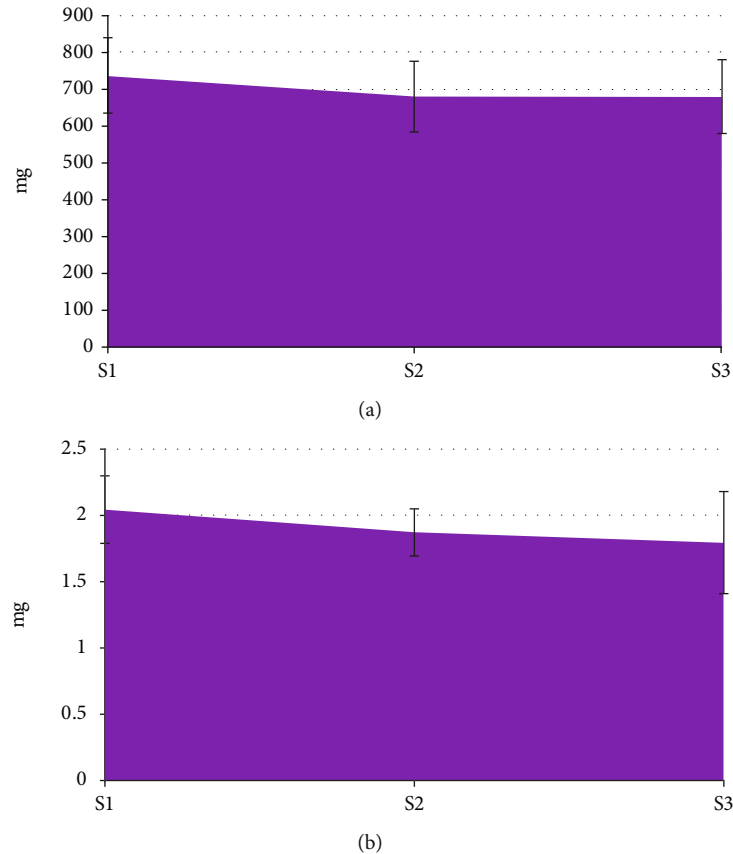


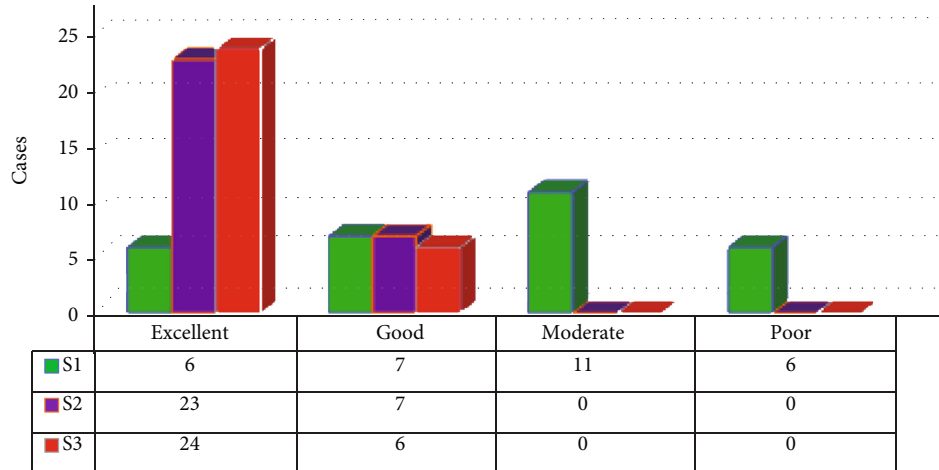
FIGURE 6: Comparison of the dosage of propofol and sufentanil ((a) shows the comparison of propofol; and (b) illustrates the comparison of sufentanil).

The MEP inhibition time of the S3 group was the longest to the S1 and S2 groups; it was not greatly different between the S1 and S2 groups ( $P > 0.05$ ). This suggests that when the induction dose is increased from 2 times ED95 cis-atracurium to 3 times ED95 cis-atracurium, the inhibition time of MEP waveform will not be significantly prolonged; and the 4 times ED95 cis-atracurium could result in a substantial prolongation of the suppression time of the MEP waveform. Such results suggest that the doses of 2 times ED95 cis-atracurium and 3 times ED95 cis-atracurium will not affect MEP and are suitable for use in neurosurgery ICAS. The comparison on endotracheal intubation conditions of the three groups of patients revealed that in the S1 group it was excellent in 6 cases, good in 7 cases, moderate in 11 cases, and poor in 6 cases; it was excellent in 23 cases, good in 7 cases, fair in 0 cases, and poor in 0 cases in S2 group; and it was excellent in 24 cases, good in 6 cases, moderate in 0 cases, and poor in 0 cases in S3 group. The analysis showed that the excellent and good rates of endotracheal intubation conditions in the S2 group and the S3 group (both were 100%) were absolutely higher compared with the S1 group (43.33%), and the differences were statistically notable ( $P < 0.05$ ). Such results suggest that 2 times ED95 cis-atracurium doses had poor endotracheal intubation conditions. Furthermore, at time t0, t1, and t2, patients in the S1 group did not have any body movement or spontaneous breathing. Three patients experienced body movement, and

two had spontaneous breathing at time t3. At t0, t1, t2, and t3, no body movement or spontaneous breathing occurred in groups S2 and S3. Such results further indicate that 3 times ED95 cis-atracurium and 4 times ED95 cis-atracurium are better than 2 times ED95 cis-atracurium for maintaining the patient's intraoperative condition [28]. Based on the above results, it can be known that the anesthetic dose of 3 times ED95 cis-atracurium is the most suitable for ICAS.

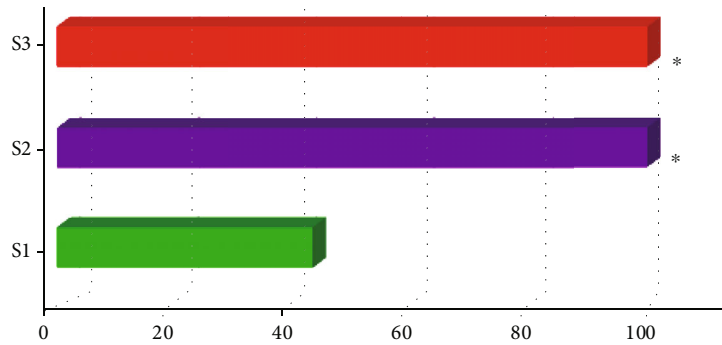
During the surgery, the reduction of MAP in patients often exceeds the clinical standard and affects the hemodynamics of patients, so intraoperative monitoring of hypotension is very important [29]. It was found in this work that the MAP and HR of the three groups of patients at t1, t2, and t3 were decreased compared with those at t0, while the differences between groups at t1, t2, and t3 were not statistically obvious ( $P > 0.05$ ). The use of intraoperative anesthetics can make the MAP of the patients drop to a certain extent, which is a normal clinical manifestation. The results indicate that the dose of cis-atracurium does not affect the hemodynamic changes of the patients. In addition, this work found that the  $SpO_2$ ,  $PETCO_2$ , and peak at t1, t2, and t3 of the three groups of patients were not observably different from those at t0 ( $P > 0.05$ ). No statistically remarkable difference among the three groups in  $SpO_2$ ,  $PETCO_2$ , and peak was found at time t1, t2, and t3 ( $P > 0.05$ ).  $SpO_2$ ,  $PETCO_2$ , and peak are all main indicators of respiratory function





■ S1  
■ S2  
■ S3

(a)



(b)

FIGURE 7: Comparison of intraoperative endotracheal intubation conditions among three groups of patients ((a) shows the number of excellent, moderate, and poor cases; (b) shows the excellent and good rate) Note: \* indicates that the difference was statistically great compared with the S1 group ( $P < 0.05$ ).

monitoring during surgery.  $PETCO_2$  refers to the carbon dioxide partial pressure or carbon dioxide concentration in the mixed alveolar air exhaled at the end of expiration. It is often used to evaluate patients' ventilatory function, circulatory function, pulmonary blood flow, alveolar ventilation, subtle repeated inhalation, and the patency of the entire airway and breathing circuit.  $SpO_2$  is the percentage of oxyhemoglobin in the blood to the total hemoglobin volume, which is used to assess the patient's breathing and circulation. Peak airway pressure is the highest pressure experienced during ventilator insufflation, and it is determined by lung compliance, airway resistance, tidal volume, and other factors [30]. As a result, the findings suggest that the incidence of intraoperative respiratory depression in patients is unrelated to the use of various cis-atracurium doses and that the analysis could be induced by intravenous injections of propofol and sufentanil. The TOFRs of patients in the S2 and S3 groups at time t2 and t3 were much lower than those at time t0, while the TOFRs of patients in group S3 at time t2 and t3 were not as high as those in group S2, and the differences were obvious ( $P < 0.05$ ). Such conclusions are similar

to the results of Ding et al. [31]. The TOFR represents the degree of blockade of the presynaptic receptors, indicating that 2 times ED95 cis-atracurium and 3 times ED95 cis-atracurium can reduce the residual degree of muscle relaxation and improve intracranial surgical openness without affecting MEP monitoring, improving the safety during the ICAS.

## 5. Conclusions

From January 2021 to May 2022, 90 ICAS patients underwent MEP monitoring at Northwest University's First Affiliated Hospital (Xi'an No. 1 Hospital). The patients were randomly assigned to one of three groups: S1 (2 times ED95 cis-atracurium), S2 (3 times ED95 cis-atracurium), and S3 (4 times ED95 cis-atracurium). The general data, endotracheal intubation conditions, TOFR, body movement, spontaneous breathing, and hemodynamic indicators were compared among the three groups of patients. Finally, it was found that GAI using 3 times ED95 cis-atracurium can reduce the risk of intraoperative body movement and

spontaneous breathing and the residual degree of muscle relaxation in patients with intracranial aneurysm and improve endotracheal intubation conditions without affecting MEP monitoring and hemodynamics, enhancing the safety during open neurosurgery procedures. However, the sample size of patients included was small, and the source was single, which may have some influence on the results. Moreover, no follow-up observation of patients' postoperative conditions was conducted, and there was a lack of patient prognosis data using different doses of cis-atracurium. As a result, in future studies, it will consider using more case data in the analysis to further investigate the best cis-atracurium dose. In conclusion, the results of this work could provide a reference for the dose selection of GAI muscle relaxants in ICAS.

## Data Availability

The data used to support the findings of this study are available from the corresponding author upon request.

## Conflicts of Interest

The authors declare that they have no known competing financial interests.


## References

- [1] O. K. Kwon, "Headache and aneurysm," *Neuroimaging Clinics of North America*, vol. 29, no. 2, pp. 255–260, 2019.
- [2] F. Shikata, K. Shimada, H. Sato et al., "Potential influences of gut microbiota on the formation of intracranial aneurysm," *Hypertension*, vol. 73, no. 2, pp. 491–496, 2019.
- [3] H. J. Liu, H. Zhou, D. L. Lu et al., "Intracranial mirror aneurysm: epidemiology, rupture risk, new imaging, controversies, and treatment strategies," *World Neurosurgery*, vol. 127, pp. 165–175, 2019.
- [4] A. Shrivastava, R. Mishra, L. R. M. Salazar, P. Chouksey, S. Raj, and A. Agrawal, "Enigma of what is known about intracranial aneurysm occlusion with endovascular devices," *Journal of Stroke and Cerebrovascular Diseases*, vol. 30, no. 6, article 105737, 2021.
- [5] T. Sharma, K. K. Datta, M. Kumar et al., "Intracranial aneurysm biomarker candidates identified by a proteome-wide study," *OMICS*, vol. 24, no. 8, pp. 483–492, 2020.
- [6] C. S. Lozano, A. M. Lozano, and J. Spears, "The changing landscape of treatment for intracranial aneurysm," *The Canadian Journal of Neurological Sciences*, vol. 46, no. 2, pp. 159–165, 2019.
- [7] S. Boissonneau, T. Graillon, M. Meyer, H. Brunel, S. Fuentes, and H. Dufour, "Intracranial giant mycotic aneurysm without endocarditis and vasculitis: report of rare entity and review of literature," *World Neurosurgery*, vol. 119, pp. 353–357, 2018.
- [8] K. Shimizu, M. Kushamae, T. Mizutani, and T. Aoki, "Intracranial aneurysm as a macrophage-mediated inflammatory disease," *Neurologia Medico-Chirurgica (Tokyo)*, vol. 59, no. 4, pp. 126–132, 2019.
- [9] N. Juchler, S. Schilling, P. Bijlenga et al., "Shape irregularity of the intracranial aneurysm lumen exhibits diagnostic value," *Acta Neurochirurgica*, vol. 162, no. 9, pp. 2261–2270, 2020.
- [10] V. Rantasalo, J. Gunn, T. Kiviniemi et al., "Intracranial aneurysm is predicted by abdominal aortic calcification index: a retrospective case-control study," *Atherosclerosis*, vol. 334, pp. 30–38, 2021.
- [11] H. Miyata, K. Shimizu, H. Koseki et al., "Real-time imaging of an experimental intracranial aneurysm in rats," *Neurologia Medico-Chirurgica (Tokyo)*, vol. 59, no. 1, pp. 19–26, 2019.
- [12] Z. Li, G. Huo, Y. Feng, and Z. Ma, "Application of virtual reality based on 3D-CTA in intracranial aneurysm surgery," *Journal of Healthcare Engineering*, vol. 2021, Article ID 9913949, 11 pages, 2021.
- [13] H. Tang, Y. Luo, Q. Zuo et al., "Current understanding of the molecular mechanism between hemodynamic-induced intracranial aneurysm and inflammation," *Current Protein & Peptide Science*, vol. 20, no. 8, pp. 789–798, 2019.
- [14] Y. Liu, Y. Song, P. Liu et al., "Comparative bioinformatics analysis between proteomes of rabbit aneurysm model and human intracranial aneurysm with label-free quantitative proteomics," *CNS Neuroscience & Therapeutics*, vol. 27, no. 1, pp. 101–112, 2021.
- [15] Y. Wang, C. Yuan, S. Shen, L. Xu, and H. Duan, "Whether intracranial aneurysm could be well treated by flow diversion: a comprehensive meta-analysis of large-sample studies including anterior and posterior circulation," *BioMed Research International*, vol. 2021, Article ID 6637780, 8 pages, 2021.
- [16] H. Hayashi, J. F. Bebawy, A. Koht, and L. B. Hemmer, "Cautionary findings for motor evoked potential monitoring in intracranial aneurysm surgery after a single administration of rocuronium to facilitate tracheal intubation," *Journal of Clinical Monitoring and Computing*, vol. 35, no. 4, pp. 903–911, 2021.
- [17] D. Park, B. H. Kim, S. E. Lee et al., "Usefulness of intraoperative neurophysiological monitoring during the clipping of unruptured intracranial aneurysm: diagnostic efficacy and detailed protocol," *Frontiers in Surgery*, vol. 8, no. 631053, 2021.
- [18] D. Guo, X. Fan, H. You et al., "Prediction of postoperative motor deficits using intraoperative motor-evoked potentials in middle cerebral artery aneurysm," *Neurosurgical Review*, vol. 44, no. 1, pp. 495–501, 2021.
- [19] H. S. Byoun, C. W. Oh, O. K. Kwon et al., "Intraoperative neuromonitoring during microsurgical clipping for unruptured anterior choroidal artery aneurysm," *Clinical Neurology and Neurosurgery*, vol. 186, article 105503, 2019.
- [20] N. Aygun, M. Kostek, A. Isgor, and M. Uludag, "Recent developments of intraoperative neuromonitoring in thyroidectomy," *The Medical Bulletin of Sisli Etfal Hospital*, vol. 55, no. 3, pp. 273–285, 2021.
- [21] P. Gurung, Y. Motoyama, T. Takatani et al., "Transient augmentation of intraoperative motor evoked potentials during middle cerebral artery aneurysm surgery," *World Neurosurgery*, vol. 130, pp. e127–e132, 2019.
- [22] T. Greve, V. M. Stoecklein, F. Dorn et al., "Introduction of intraoperative neuromonitoring does not necessarily improve overall long-term outcome in elective aneurysm clipping," *Journal of Neurosurgery*, vol. 132, no. 4, pp. 1188–1196, 2019.
- [23] J. Chung, W. Park, S. H. Hong et al., "Intraoperative use of transcranial motor/sensory evoked potential monitoring in the clipping of intracranial aneurysms: evaluation of false-positive and false-negative cases," *Journal of Neurosurgery*, vol. 130, no. 3, pp. 936–948, 2019.

- [24] I. Oran, C. Cinar, M. Gok, and F. Duzgun, “Aggregometry response to half-dose prasugrel in flow-diverting stent implantation,” *Clinical Neuroradiology*, vol. 30, no. 3, pp. 463–469, 2020.
- [25] R. Post, I. A. J. Zijlstra, R. V. D. Berg, B. A. Coert, D. Verbaan, and W. P. Vandertop, “High-dose nadroparin following endovascular aneurysm treatment benefits outcome after aneurysmal subarachnoid hemorrhage,” *Neurosurgery*, vol. 83, no. 2, pp. 281–287, 2018.
- [26] A. Can, V. M. Castro, Y. H. Ozdemir et al., “Association of intracranial aneurysm rupture with smoking duration, intensity, and cessation,” *Neurology*, vol. 89, no. 13, pp. 1408–1415, 2017.
- [27] E. Pressman, C. A. De la Garza, F. Chin et al., “Nuisance bleeding complications in patients with cerebral aneurysm treated with pipeline embolization device,” *Journal of Neurointerventional Surgery*, vol. 13, no. 3, pp. 247–250, 2021.
- [28] X. Feng, Z. Qian, B. Zhang et al., “Number of cigarettes smoked per day, smoking index, and intracranial aneurysm rupture: a case-control study,” *Frontiers in Neurology*, vol. 9, p. 380, 2018.
- [29] F. Cagnazzo, P. Perrini, P. H. Lefevre et al., “Comparison of prasugrel and clopidogrel used as antiplatelet medication for endovascular treatment of unruptured intracranial aneurysms: a meta-analysis,” *AJNR. American Journal of Neuroradiology*, vol. 40, no. 4, pp. 681–686, 2019.
- [30] J. Song, Y. Q. Xue, Y. J. Wang, P. Xu, D. K. Sun, and W. Chen, “An update on the efficacy and safety profile of clazosentan in cerebral vasospasm after aneurysmal subarachnoid hemorrhage: a meta-analysis,” *World Neurosurgery*, vol. 123, pp. e235–e244, 2019.
- [31] D. Ding, C. J. Chen, R. M. Starke et al., “Risk of brain arteriovenous malformation hemorrhage before and after stereotactic radiosurgery,” *Stroke*, vol. 50, no. 6, pp. 1384–1391, 2019.

## Research Article

# Pharmacokinetics of Veratramine and Jervine from Alcohol Extracts of Radix Veratri

Song Wang,<sup>1,2</sup> Jiali Cui,<sup>1,3</sup> Gaoqiong Zhao,<sup>1,3</sup> Hongbin Liu,<sup>1,3</sup> and Jingkun Wang<sup>1,3</sup> 

<sup>1</sup>Yunnan Institute of Materia Medica, Kunming, 650111 Yunnan, China

<sup>2</sup>Yunnan Technology and Business University, 651701, China

<sup>3</sup>Yunnan Province Company Key Laboratory for TCM and Ethnic Drug of New Drug Creation, 650111, China

Correspondence should be addressed to Jingkun Wang; 854745@stu.ahu.edu.cn

Received 9 May 2022; Revised 29 May 2022; Accepted 31 May 2022; Published 23 June 2022

Academic Editor: Naeem Jan

Copyright © 2022 Song Wang et al. This is an open access article distributed under the Creative Commons Attribution License, which permits unrestricted use, distribution, and reproduction in any medium, provided the original work is properly cited.

**Background.** Chinese *Materia Medica* and Jiangsu New Medical College record that Radix Veratri root is *Liliaceae Veratrum taliense* Loses. f. and the root of *Veratrum stenophyllum* Diels. According to traditional Chinese medicine (TCM) example, Radix Veratri is a *Liliaceae* plant *Veratrum taliense*. Another literature pointed out that the aliases of *Veratrum taliense* and *Veratrum angustifolia* are both Radix Veratri, and their effects are basically the same. The main active ingredient of *Veratrum* is veratramine, of which veratramine and Jervine are higher in content, reaching 24.60% and 21.28% of the total alkaloids, respectively. *Veratrum* alkaloids are both toxic and effective ingredients. In addition to its good clinical efficacy, attention should also be paid to its pharmacokinetic characteristics in vivo. It is particularly important to study the pharmacokinetic characteristics of veratramine and Jervine in vivo. **Objective.** The goal of this study was to develop a simple and effective method for measuring veratramine and Jervine in rat plasma at the same time. This method was used to study the pharmacokinetic characteristics of veratramine and Jervine in the alcohol extract of Radix Veratri in rats, to provide a reasonable basis for the clinical use of Radix Veratri. **Methods.** Eighteen SD rats were randomly assigned into three groups, half male and half female, and were given 0.04 g/kg, 0.08 g/kg, and 0.16 g/kg Radix Veratri alcohol extract, respectively. Blood samples were collected at different time points and were analyzed by LC-MS/MS after protein precipitation. Bullatine was set as the internal standard; the plasma samples were extracted with ethyl acetate. After the sample was processed, acetonitrile-10 mM ammonium acetate, whose pH was adjusted to 8.8 with ammonia water, was taken as the mobile phase. Veratramine quantitative ion pair was 410.1 → 295.1 m/z, Jervine quantitative ion pair was 426.2 → 114.1 m/z, and Bullatine B (IS) quantitative ion pair was 438.2 → 420.1 m/z. In the positive ion mode, the multireaction monitoring (MRM) mode was used to determine the blood concentration of veratramine and Jervine. DAS 3.3.0 was used to calculate the relevant pharmacokinetic parameters. **Results.** Veratramine had a good linear relationship in the concentration range of 0.0745~18.2 ng/mL, and that of Jervine was 1.11~108 ng/mL. The correlation coefficient  $r$  of three consecutive batches of the standard curve was greater than 0.995. Veratramine's lower quantification limit was 0.745 ng/mL, Jervine's was 1.11 ng/mL, and precision and accuracy were both less than 15%. The accuracy of veratramine was between 88.96% and 101.85%, and the accuracy of Jervine was between 92.96% and 104.50%. This method was adopted for the pharmacokinetic study of alcohol extracts of Radix Veratri. The results showed that only  $C_{\max}$  of veratramine female rats did not show linear kinetic characteristics in the dose range of Radix Veratri alcohol extract from 0.04 g/kg to 0.16 g/kg. For  $AUC_{0-t}$  and  $C_{\max}$  of veratramine and Jervine, it could not determine whether the Radix Veratri alcohol extract showed linear kinetic characteristics within the dosage range of 0.04 g/kg~0.16 g/kg. Veratramine and Jervine showed obvious gender differences in the absorption and elimination stages. The absorption rate of veratramine and Jervine by male mice was about 10 times higher than that of female mice, and the elimination rate of male mice is about 20 times lower than that of female mice. It was suggested that the clinical application of the steroidal alkaloids veratramine and Jervine in Radix Veratri required rational use of drugs based on gender. **Conclusion.** An LC-MS/MS analysis method suitable for the pharmacokinetic study of veratramine and Jervine in Radix Veratri in SD rats was established to provide a basis for in vivo pharmacokinetic studies. The pharmacokinetic characteristics of veratramine and Jervine in the alcohol extract of Radix Veratri were significantly different in female and male rats. During the clinical use of Radix Veratri, it should pay close attention to the obvious gender differences that may occur after the medication.

## 1. Introduction

Radix Veratri is also known as small Veratri, Veratrum, small brown bag, human hair, etc. The taste is bitter, cool in nature, and highly toxic. It has the effects of dispelling blood stasis and swelling, analgesic and hemostasis, lowering blood pressure [1–3], expectorant, and resuscitation. Indications are traumatic injuries, fractures, paraplegia, epilepsy, rheumatic pain, traumatic bleeding, etc., and it is also used to treat cancer in the folk [4–8]. The main active ingredients of Veratrum are steroidal alkaloids, among which the content of veratramine and Jervine is relatively high, reaching 24.60% and 21.28% of total alkaloids, which has antitumor and antibacterial effects [9, 10]. Veratramine and Jervine can specifically bind to the upstream activator of the Hh pathway, Smo, to inhibit the transmission of pathway signals, thereby inhibiting the proliferation effect of tumor cells [11, 12]. Moreover, veratramine and Jervine are also toxic components, and the toxicity is strong, mainly manifested as teratogenicity, reproductive toxicity, etc. [9, 13, 14]. Radix Veratri is used as a special Yi medicine for the treatment of bruises. In addition to its good clinical efficacy, attention should also be paid to its pharmacokinetic characteristics in the body. In particular, the research on the in vivo pharmacokinetic characteristics of compounds that contain both effective and toxic ingredients is particularly important. This work was developed to establish an HPLC-MS/MS method for the determination of veratramine and Jervine in rat plasma, and a systematic methodological verification was conducted. The pharmacokinetic characteristics of veratramine and Jervine in the alcohol extract of Radix Veratri in rats at different dosage levels were systematically studied. The confidence interval method was used for statistical analysis of the obtained pharmacokinetic parameters [15–19]. The dose range in which veratramine and Jervine exhibited linear dynamic characteristics of the dose-exposure level was explored. In addition, the pharmacokinetic parameters of Radix Veratri alcohol extract at different doses were analyzed and compared [5, 20, 21]. The above studies can provide references for the follow-up safety evaluation and clinical medication of veratramine and Jervine.

The paper's organization paragraph is as follows: The materials and methods are presented first. Second are experimental results of the proposed work. Thirdly, it consists of the results and discussion sections. Finally, the research work is concluded.

## 2. Materials and Methods

**2.1. Chemicals and Reagents.** Veratramine and Jervine reference substances' purity was no less than 98%, which were purchased from Nanjing SenBeiJia Biological Technology Co., Ltd. (batch number: SBJ150701, SBJ150625). Bullatine B (internal standard, purity no less than 98%) was purchased from the Beijing Shengshikangpu Chemical Technology Research Institute (batch number: N-019-150906). Heparin sodium (chromatographically pure) was purchased from Aladdin (batch number: C162031). Ammonium acetate

(chromatographically pure) was purchased from Aladdin (batch number: k1616041). Methanol (chromatographically pure) was purchased from MERCK (batch number: I0887507 717). Sinopharm Chemical Reagent Co., Ltd. provided analytical pure ethyl acetate (batch number: 20170824). Sichuan Xilong Chemical Co., Ltd. provided the ammonia (analytical pure) (batch number: 150324). The water was ultrapure water made by the Drug Safety Evaluation Center of Yunnan Institute of Materia Medica.

**2.2. Liquid Mass Spectrometry Instruments and Conditions.** The researchers used an API-3200 triple quadrupole tandem mass spectrometer and an electrospray ionisation ion source (ESI). Multiple reaction monitoring (MRM) was used to quantify the sample, which was separated on an Agilent ZORBAX Extend C18 column. The mobile phase was A (10 mmol/L ammonium acetate) and B (acetonitrile), 0–0.2 min, 10% B; 0.2–2 min, 10%–90% B; 2–5 min, 90% B; 5–5.1 min, 90%–10%B; and 5.1–7.5 min, 10%B. The flow rate was 0.4 mL/min, the column temperature was set to 20°C, and the measurement solution was 10  $\mu$ L. The mass spectrum parameters were as follows: veratramine  $m/z$ : 410.1  $\rightarrow$  295.1, Jervine  $m/z$ : 426.2  $\rightarrow$  114.1, and Bullatine B  $m/z$ : 438.2  $\rightarrow$  420.1. Ion source parameters were as follows: CUR: 20.00 psi, IS: 5,500.00 V, TEM: 500.0°C, GS1: 50.0 psi, GS2: 50.0 psi, CAD: medium, and interface heater(ihe): on.

**2.3. Preparation of Standard Solutions and Quality Control Samples.** 5.45 mg and 5.53 mg of veratramine reference substance and 4.96 mg and 5.13 mg Jervine reference substance were taken, two copies each. Methanol was diluted to stock solutions with concentrations of 545  $\mu$ g/mL, 553  $\mu$ g/mL, 496  $\mu$ g/mL, and 513  $\mu$ g/mL. Diluted with methanol, the concentrations of veratramine were 0.745, 2.24, 6.70, 20.2, 60.5, and 182 ng/mL; those of Jervine standard working fluid were 11.1, 27.8, 69.5, 174, 434, and 1,080 ng/mL; those of veratramine were 0.745, 2.70, 25.6, and 143 ng/mL; and those of Jervine quality control working solution were 1.11, 31.6, 194, and 724 ng/mL. Quality control samples were used for precision, accuracy, matrix effect, recovery, and stability investigations. The same method was used to prepare Bullatine B (IS) internal standard working solution with a concentration of 128 ng/mL, and all working solutions were stored in a refrigerator at 2–8°C.

**2.4. Preparation of Plasma Samples.** 10  $\mu$ L internal standard working solution was added into a 2 mL EP tube, blown and dried with nitrogen at room temperature, and added with 100  $\mu$ L of plasma sample mixed in vortex for 2 min. Then, 40  $\mu$ L 25% ammonia water was added and mixed in vortex for 1 min, and 1 mL ethyl acetate was added and mixed in vortex for 3 min and centrifuged at 6,000 r/min at room temperature for 10 min. 600  $\mu$ L of the supernatant was taken and blown and dried with nitrogen at room temperature. It was reconstituted with 150  $\mu$ L methanol and mixed in vortex for 2 minutes and centrifuged at 15,000 r/min at room temperature for 10 minutes, and the supernatant was taken for analysis.

## 2.5. Mass Spectrometry Method Validation

**2.5.1. Specificity.** It was fully verified according to the US Food and Drug Administration's bioanalytical method verification guidelines, as illustrated in Figures 1 and 2. Under the selected chromatographic conditions, the peak times of veratramine, Jervine, and Bullatine B were 3.84 min, 3.81 min, and 3.21 min, respectively. Endogenous substances in plasma did not affect the detection of veratramine, Jervine, and internal standard Bullatine.

**2.5.2. Standard Curve and Lower Limit of Quantification.** The standard curve was obtained by measuring no less than six points for each compound. The veratramine concentrations were 0.0745, 0.224, 0.670, 2.02, 6.05, and 18.2 ng/mL, respectively. The Jervine concentrations were 1.11, 2.78, 6.95, 17.4, 43.4, and 108 ng/mL, respectively. The lowest detectable concentration was used to define the lower limit of quantification. It was also repeated six times to ensure precision and accuracy. The veratramine standard curve was  $y = 0.291x + 17.1 \times 10^{-4}$  ( $r = 0.9965$ ). The Jervine standard curve was  $y = 0.0462x - 5.51 \times 10^{-3}$  ( $r = 0.9981$ ). The lower limits of quantification of veratramine and Jervine were 0.0745 and 1.11 ng/mL, respectively, and those of RSD% were 5.49% and 0.12%, respectively.

**2.5.3. Precision and Accuracy.** The accuracy and precision of intraday ( $n = 6$ ) and intraday ( $n = 6$ ) were determined after four concentrations of quality control samples were measured, those of veratramine were 0.745, 2.70, 25.6, and 143 ng/mL, respectively, and those of Jervine were 1.11, 31.6, 194, and 724 ng/mL, respectively (Table 1). The absolute value of the relative deviation was not higher than 15%, the accuracy of veratramine was 88.96%~101.85%, and that of Jervine was 92.96%~104.50%. The results showed that the accuracy and precision of this method met the requirements of biological sample analysis.

**2.6. Extraction Recovery Rate and Matrix Effect.** The extraction recovery rate of veratramine and Jervine at three concentrations ( $n = 6$ ) was veratramine of 2.70, 25.6, and 143 ng/mL, respectively, and Jervine of 31.6, 194, and 724 ng/mL, respectively. The extraction recoveries of the two compounds were veratramine of 81.22%~94.42% and Jervine of 81.65%~87.98% (Table 2). The matrix had no influence on veratramine, Jervine, or the internal standard Bullatine B, and it had the same effect on each concentration, meeting the pharmacokinetic analysis and detection requirements.

**2.7. Stability.** The stability of plasma samples stored at room temperature and 2-8°C for 48 hours and 5 days at room temperature is illustrated in Table 3. The untreated plasma samples were kept at room temperature for 20 hours and -20°C for 20 hours, 34 days, and 34 days, respectively. Three freeze-thaw cycles were performed to verify the stability (Table 4). Under the above settings, the relative standard deviations were all less than 15%, and the samples were stable enough to meet the requirements of pharmacokinetic analysis and testing.

## 2.8. Pharmacokinetic Studies

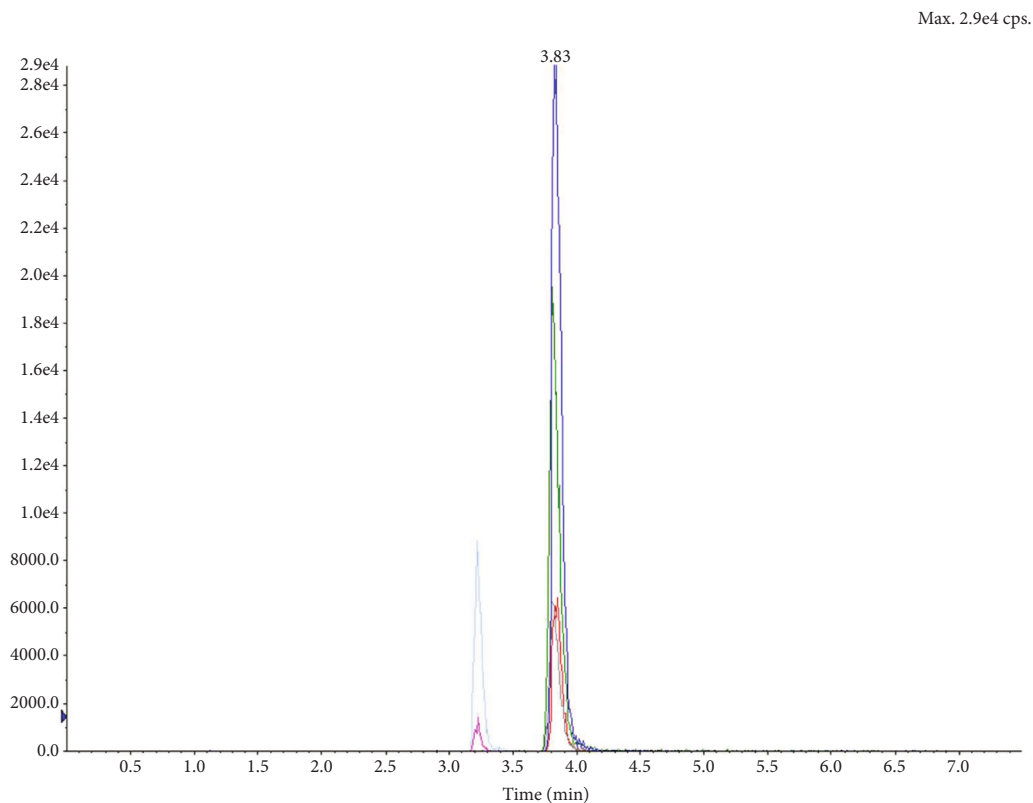
**2.8.1. Extraction Preparation.** Radix Veratri coarse powder was taken, added with six times 65% ethanol and heated under reflux for extraction three times, 1 h each time, and filtered, and then, the filtrates were combined. The ethanol was recovered under reduced pressure, concentrated into a thick paste, dried under reduced pressure at 70°C, and crushed into final products. The contents of veratramine and Jervine in the extract measured by the HPLC-UV method were 2.69% and 1.79%, respectively.

**2.8.2. Drug Administration.** 0.0805 g, 0.1601 g, and 0.3214 g of alcohol extracts were put into a mortar and ground thoroughly. During the grinding, 20 mL of 0.05% sodium carboxymethyl cellulose was added, which was ground to a uniform suspension and placed in a refrigerator at 2~8°C. Each SD rat was given a single dose, and the administration volume was 10 mL/kg. According to this method, the dosage of Radix Veratri alcohol extract was 0.04 g/kg, 0.08 g/kg, and 0.16 g/kg, respectively. The corresponding veratramine doses were 0.108, 0.215, and 0.430 mg/mL, and the Jervine doses were 0.072, 0.143, and 0.286 mg/mL, respectively.

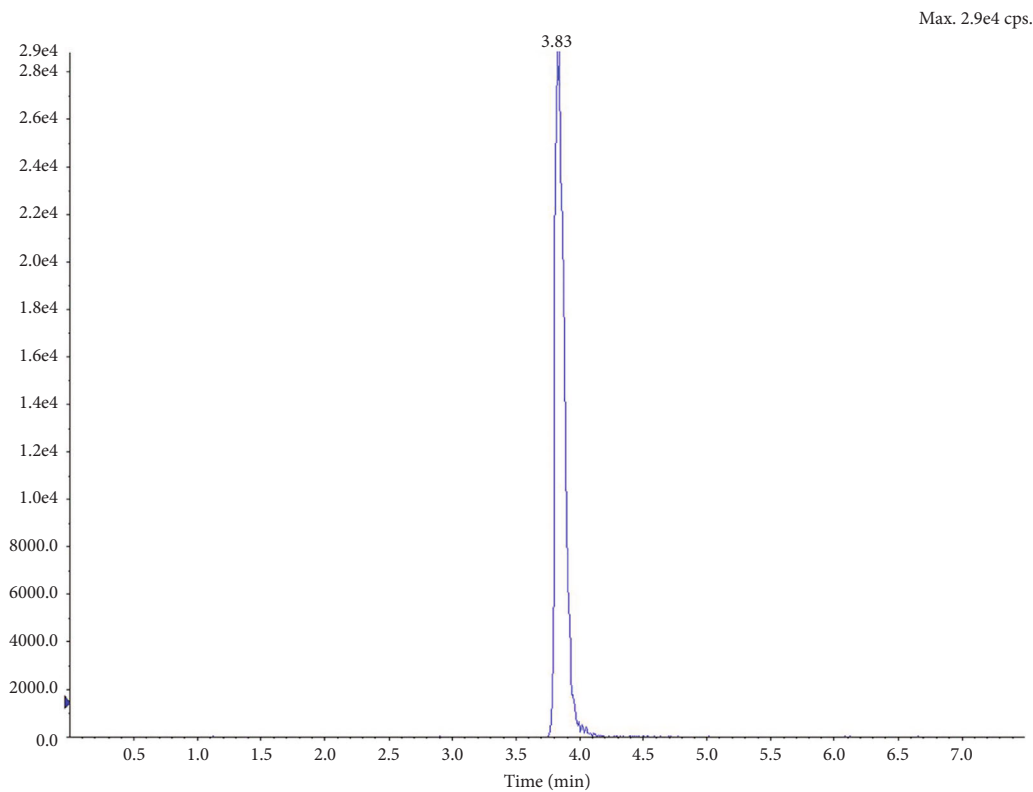
**2.9. Animal Experiments and Sample Collection.** After the ethical approval, a total of 18 healthy SPF SD rats were taken, the license number was SCXK (Sichuan) 2015-030, and the laboratory animal quality certificate number was No. 51203500004128. There are 9 females and 9 males each, 7-8 weeks, the weight range of female rats was 200-230 g, and the weight range of male rats was 200-230 g. The weight difference of the grouped animals was not more than 20% of the average weight of all animals, and they were rolled into low, medium, and high dose groups, with half males and half females. Samples were collected at 0.15, 0.5, 1, 3, 6, 9, 18, 30, 48, 72, and 96 h before intragastric administration (0 h) and after administration. 0.3 mL of blood was collected from the rat's retroorbital venous plexus, placed in a centrifuge tube soaked in 2 mL of heparin sodium, and centrifuged (3,000 rpm/min) for 15 min, and the plasma was frozen and stored at -20°C for testing.

**2.10. Data Analysis.** The pharmacokinetic parameters were calculated using the DAS 3.3.0 pharmacokinetic program to calculate the main pharmacokinetic parameters  $AUC_{0-t}$ ,  $AUC_{0-\infty}$ , and  $T_{1/2}$ .  $C_{max}$  and  $T_{max}$  adopted actual measured values, and other pharmacokinetic parameters adopted statistical moment parameters.

Power function model  $PK = \alpha \cdot D^\beta$  ( $D$  was the dose, while  $\alpha$  and  $\beta$  were constants) was used for multidose linear relationship analysis.  $\alpha$ ,  $\beta$ , and the 90% confidence interval (90% CI) of the  $\beta$  value in the power function model were calculated using the DAS 3.3.0 pharmacokinetic program. The linear judgment interval after the criterion was changed using the DAS 3.3.0 pharmacokinetic program was 0.839-1.161, based on the bioequivalence criterion of 0.8 to 1.25. When the 90% CI of the  $\beta$  value fell within the linear judgment interval, the linear relationship was considered to be established; otherwise, the linear relationship did not hold.

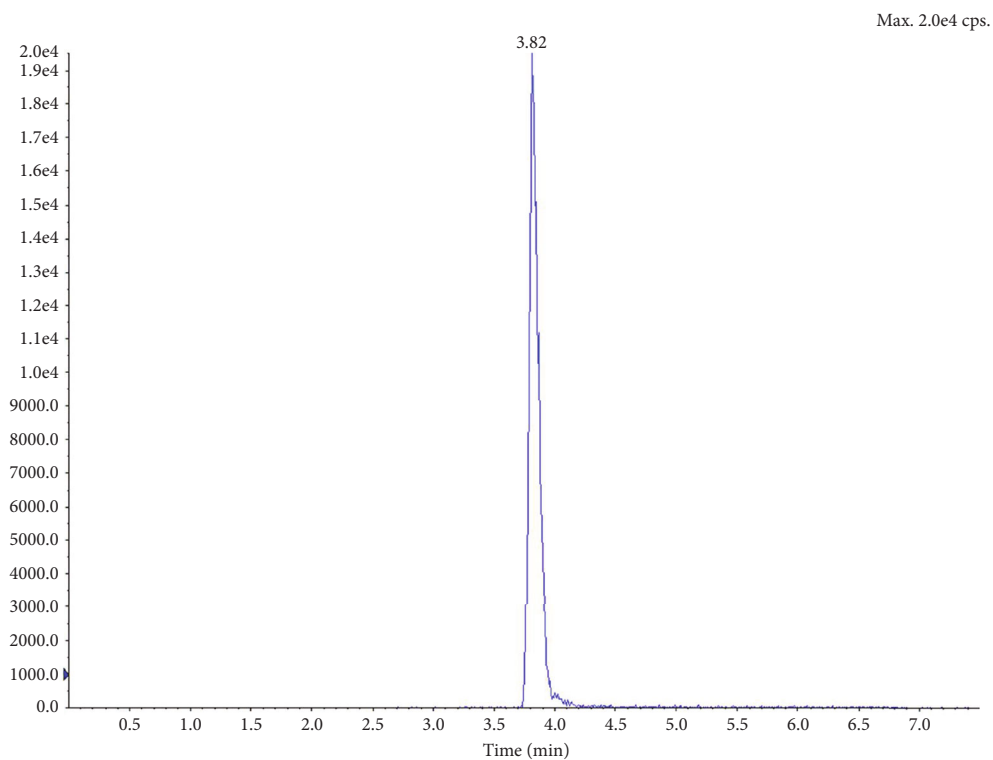


(a)

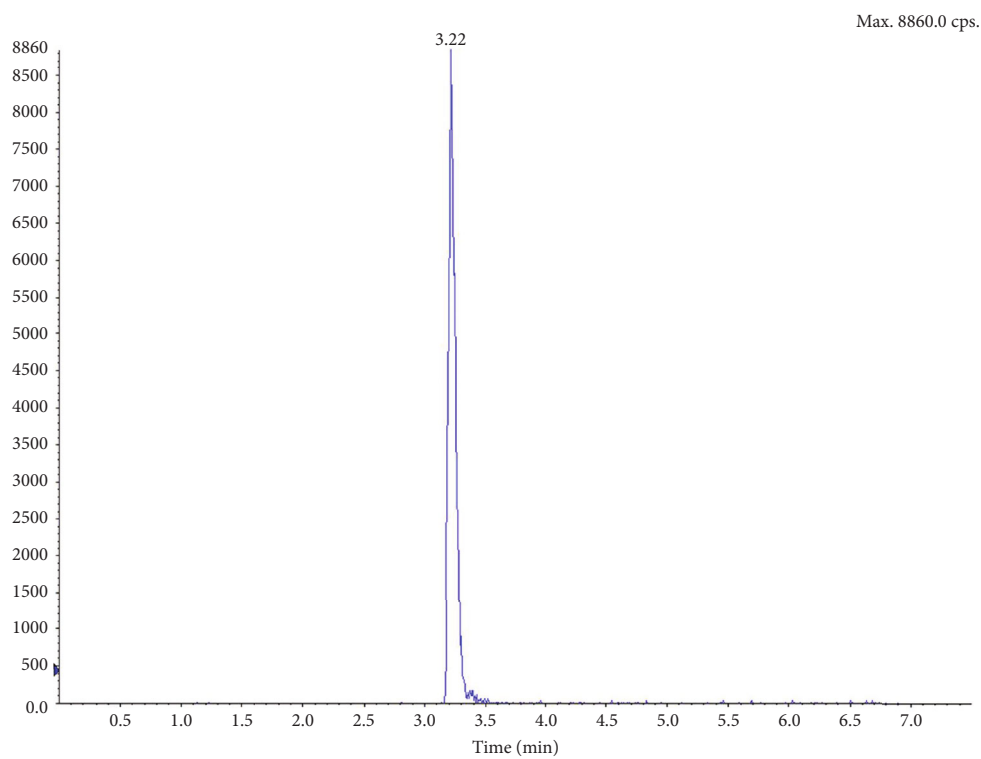


(b)

FIGURE 1: Continued.



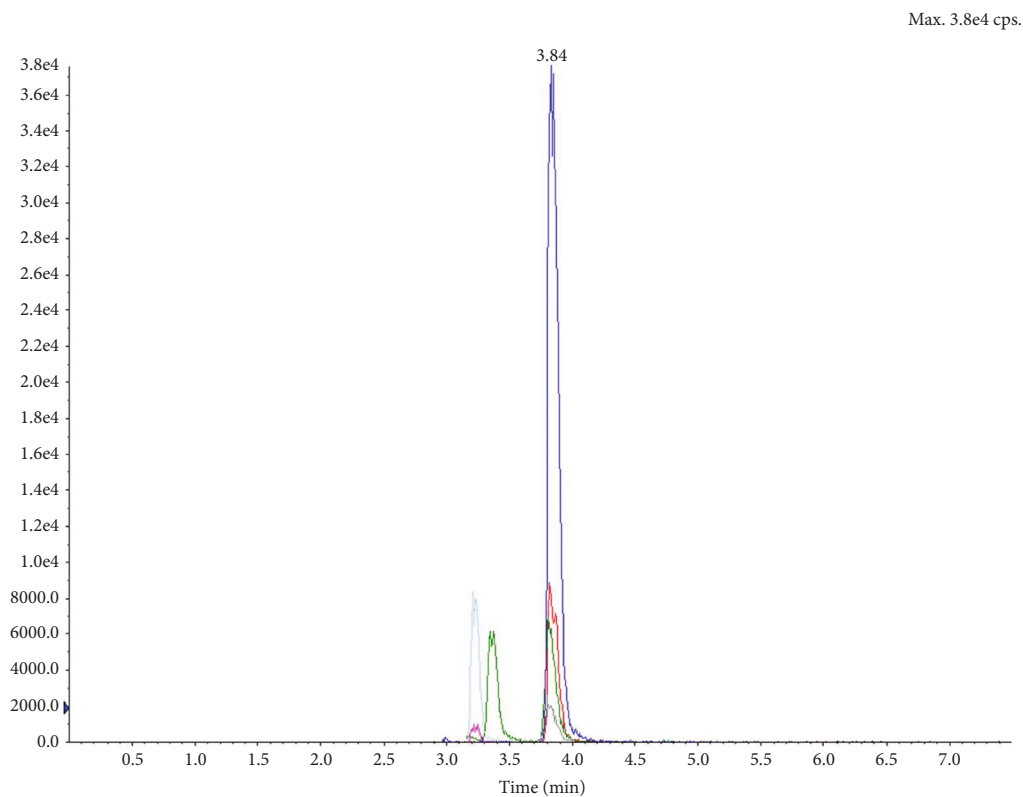
(c)



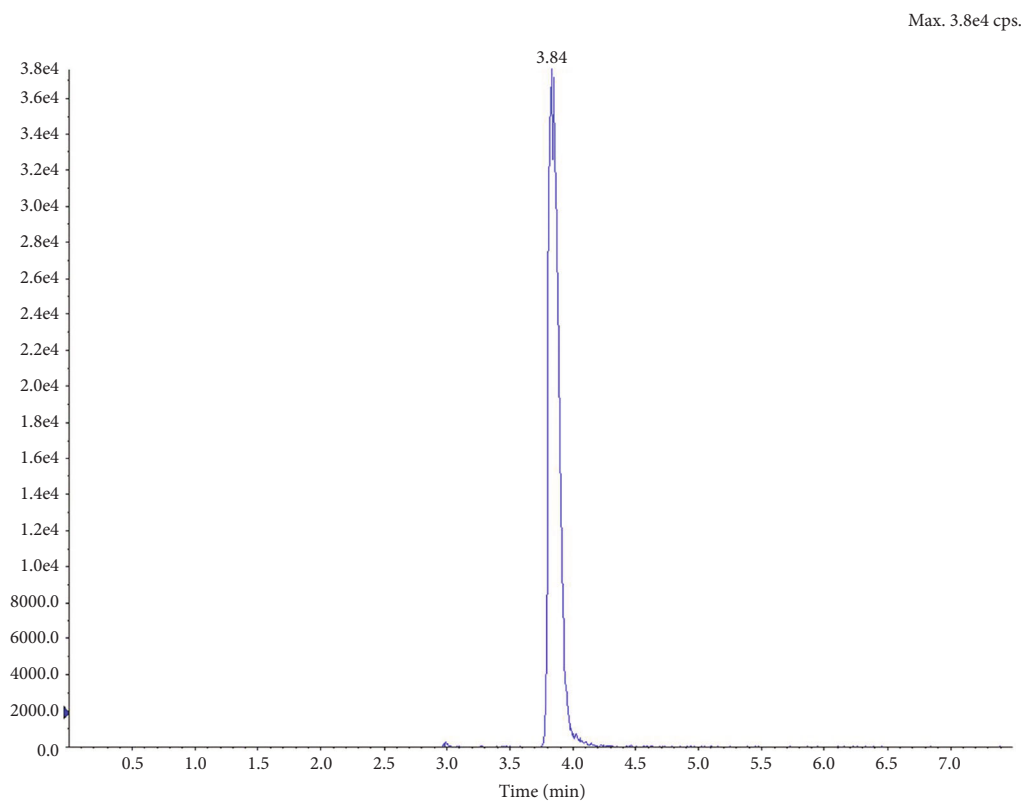
(d)

FIGURE 1: (a) Total ion current diagram of blank plasma plus veratramine  $m/z$ : 426.2/114.1, Jervine  $m/z$ : 426.2/114.1, and Bullatine B  $m/z$ : 438.2/420.1; (b) the ion current diagram of extracted veratramine  $m/z$ : 410.1/295.1; (c) the ion current diagram of extracted Jervine  $m/z$ : 426.2/114.1; (d) the ion current diagram of extracted Bullatine B  $m/z$ : 438.2/420.1.



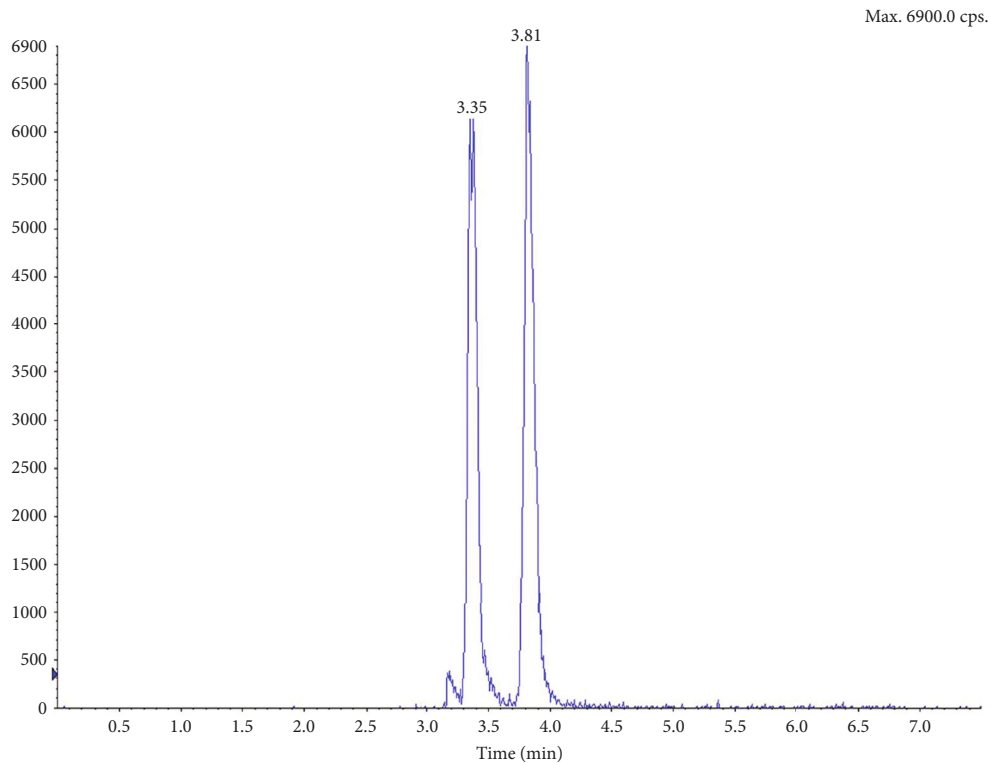


(a)

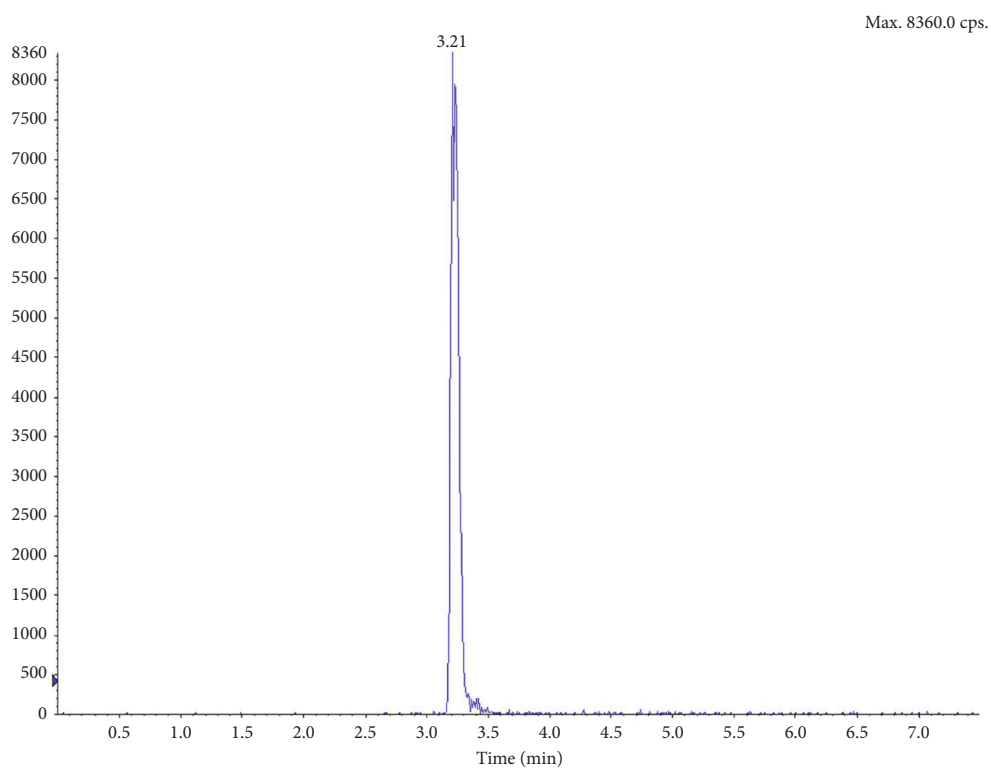


(b)

FIGURE 2: Continued.



(c)



(d)

FIGURE 2: (a) Total ion current diagram of 1 h unknown concentration of plasma sample of formal experiment No. 22 rat; (b) the ion current diagram of extracted veratramine  $m/z$ : 410.1/295.1; (c) the ion current diagram of extracted Jervine  $m/z$ : 426.2/114.1; (d) the ion current diagram of extracted Bullatine B  $m/z$ : 438.2/420.1.

TABLE 1: Precision and accuracy.

Compound	Concentration (ng/mL)	Accuracy (RE%)	Intraday precision (RSD%)	Daytime precision (RSD%)
VER	0.745	96.51	06.54	09.21
	02.70	98.52	06.02	97.78
	25.6	95.70	05.31	99.22
	143	96.71	11.93	94.62
JER	01.11	102.70	07.11	100.18
	31.6	100.32	08.52	99.05
	194	101.10	04.08	102.20
	724	92.96	13.19	94.61

TABLE 2: Extraction recovery rate and matrix effect.

Compound	Concentration (ng/mL)	Recovery rate (%) ( $\pm$ SD)	Matrix effect (%) ( $\pm$ SD)
VER	2.70	94.42 $\pm$ 0.01	116.22 $\pm$ 13.10
	25.60	81.22 $\pm$ 0.06	117.08 $\pm$ 8.26
	143	93.29 $\pm$ 0.26	110.44 $\pm$ 8.02
JER	31.60	87.98 $\pm$ 0.01	137.15 $\pm$ 15.86
	194	81.65 $\pm$ 0.07	143.50 $\pm$ 5.02
	724	84.90 $\pm$ 0.22	130.63 $\pm$ 7.46

TABLE 3: Stability of plasma samples after treatment.

Compound	Room temperature 48 h		Conditions 2~8°C 48 h		Room temperature 5 d	
	Accuracy	RSD%	Accuracy	RSD%	Accuracy	RSD%
VER	-2.22%	6.44%	6.30%	5.92%	5.19%	4.93%
	-4.69%	5.47%	-0.39%	5.10%	3.12%	7.20%
	-4.90%	13.01%	-1.40%	7.16%	0.70%	9.44%
JER	0.95%	9.31%	7.91%	8.27%	-1.27%	8.91%
	-5.46%	4.53%	4.12%	7.26%	-9.79%	3.20%
	-0.81%	14.70%	-3.18%	9.67%	-11.60%	2.09%

TABLE 4: Stability of plasma samples before treatment.

Compound	Conditions							
	Room temperature 20 h		-20°C 20 h		-20°C 34 d		-20°C 34 d freeze-thaw three times	
	Accuracy	RSD%	Accuracy	RSD%	Accuracy	RSD%	Accuracy	RSD%
VER	7.41%	8.62%	8.15%	12.67%	2.59%	10.47%	-5.92%	7.48%
	3.52%	5.66%	3.52%	10.19%	-3.52%	10.12%	-1.17%	6.72%
	2.80%	10.48%	10.49%	12.53%	10.49%	11.93%	-1.40%	5.53%
JER	7.91%	4.16%	14.87%	10.22%	-4.11%	10.59%	0.63%	8.43%
	-0.21%	4.80%	-0.52%	11.66%	-2.06%	5.78%	-3.61%	7.70%
	-1.10%	14.28%	2.35%	11.40%	-7.46%	4.10%	-5.39%	5.08%

### 3. Results

The absorption rate of male mice was higher than that of female mice, and the elimination rate of male mice was

lower than that of female mice, showing obvious gender differences in veratramine (Figure 3) and Jervine (Figure 4). At the different doses designed in this experiment, there were obvious gender differences. The drug exposure of

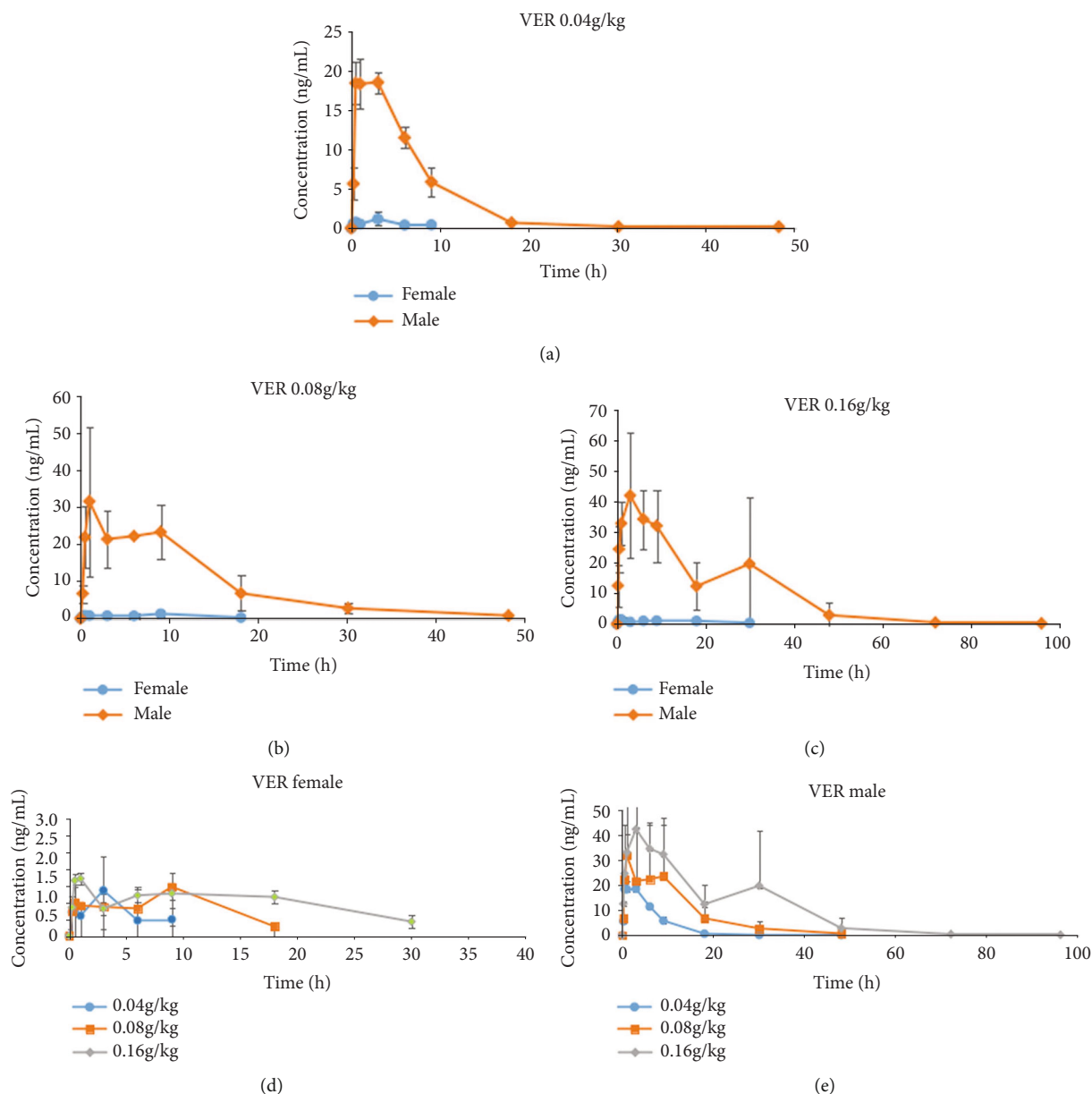


FIGURE 3: (a) Female and male average drug-time curve of 0.04 g/kg VER; (b) female and male average drug-time curve of 0.08 g/kg VER; (c) female and male average drug-time curve of 0.16 g/kg VER; (d) VER female average drug-time curve; (e) VER male average drug-time curve.

veratramine in male rats was much higher than that in female rats. With the increase of the administered dose, the exposure dose of veratramine to both male and female rats also increased. The absorption, distribution, and elimination of veratramine in rats can be affected by some molecules that were inadvertently removed during the extraction process. Furthermore, this effect was more noticeable throughout the stage of drug distribution. Jervine drug exposure was substantially higher in male rats than in female rats. The exposure dose of female and male rats to the Jervine medication increased as the provided dose was increased. Certain compounds that were inevitably extracted during the extraction process can affect the

absorption, distribution, and elimination of Jervine in rats. Unlike veratramine, however, this effect was more obvious in the drug elimination phase. The main pharmacokinetic parameters of Radix Veratri alcohol extract low, medium, and high dose groups were analyzed to compare the results (Table 5).

3.1. Linear Dynamic Judgment. DAS 3.3.0 was employed, the Power Model in the hypothesis test method was used according to the standard of 0.8~1.25, and the linear interval calculated by  $1 \pm \ln(\theta L)/\ln(DH/DL) < \beta < 1 \pm \ln(\theta H)/\ln(DH/DL)$  should be between 0.839 and 1.161. The results of determinations of whether veratramine and Jervine in

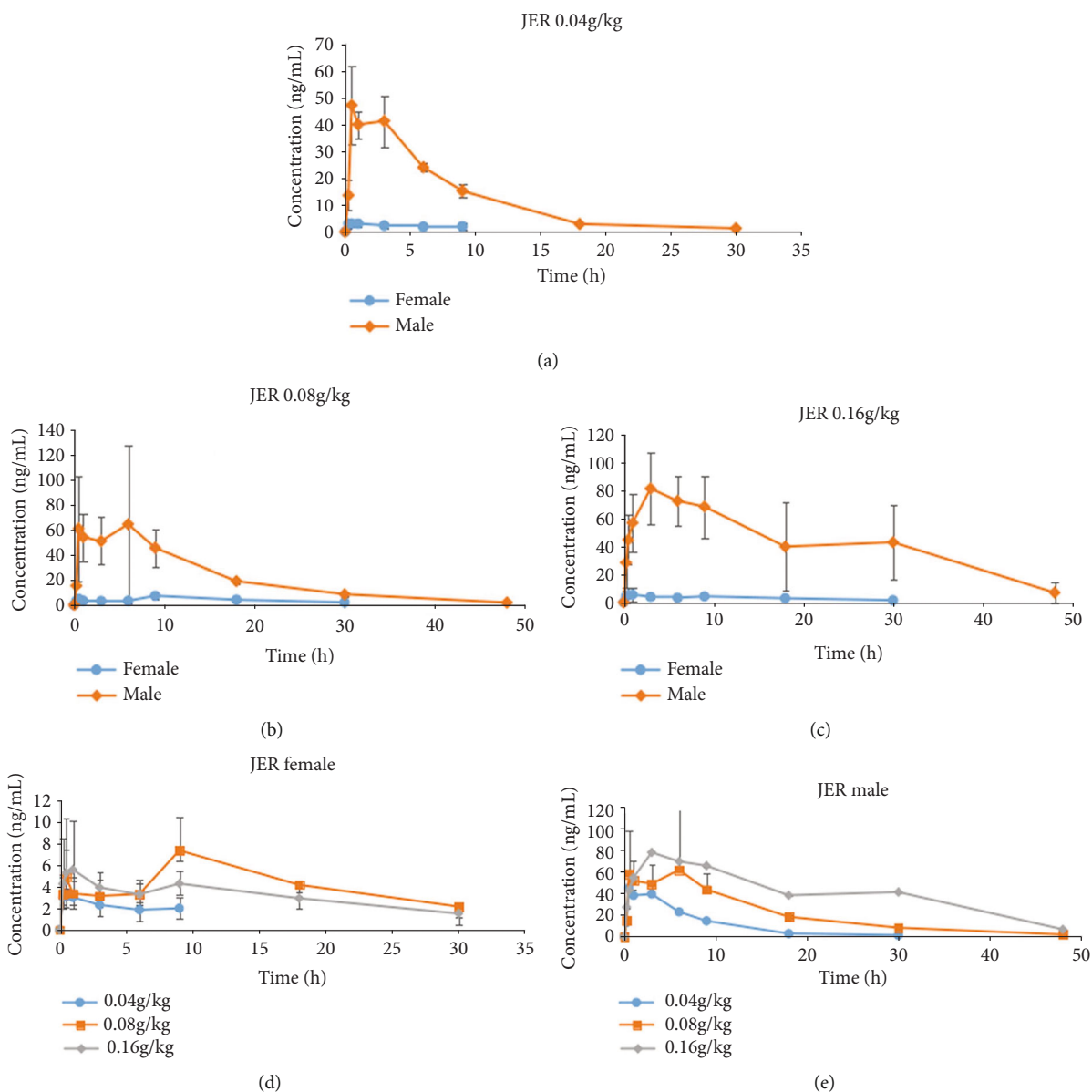


FIGURE 4: (a) Female and male average drug-time curve of 0.04 g/kg JER; (b) female and male average drug-time curve of 0.08 g/kg JER; (c) female and male average drug-time curve of 0.16 g/kg JER; (d) JER female average drug-time curve; (e) JER male average drug-time curve.

the alcohol extract of Radix Veratri showed linear kinetic characteristics within the dose range of 0.04 g/kg to 0.16 g/kg are presented in Table 6.

#### 4. Discussion

In the initial selection of internal standards, the first selected compounds were aconitine, hyaconitine, Bullatine A, Wilforgine, and Bullatine B. The response of aconitine and hyaconitine could not reach the linear medium concentration, and the response was extremely unstable. Although Bullatine A and Wilforgine could achieve the required response, their chromatographic peaks were far from the target peak, and the analysis time was long, which increased the

experimental cost. The peak shape of Bullatine B was good, it can be completely separated from the target peak, and it can be better dissolved in the sample. After testing, there was no Bullatine B in Radix Veratri, so Bullatine B was selected as the internal standard.

$C_{max}$  of veratramine female rats did not show linear kinetic characteristics within the dosage range of 0.04 g/kg~0.16 g/kg of Radix Veratri alcohol extract. For others, it cannot be judged whether  $AUC_{0-t}$  and  $C_{max}$  were linear kinetic characteristics within the dosage range of 0.04 g/kg~0.16 g/kg of Radix Veratri alcohol extract.

In the low-dose group, middle-dose group, and high-dose group, the average  $AUC_{0-t}$  and average  $C_{max}$  of males were much higher than those of females. Female rats have

TABLE 5: Comparison of main pharmacokinetic parameters of Radix Veratri alcohol extract.

Compound	Group	Gender	$C_{max}$	$T_{max}$	$T_{1/2}$	$AUC_{0-t}$ ( $\mu\text{g/L}\cdot\text{h}$ )	$AUC_{0-\infty}$ ( $\mu\text{g/L}\cdot\text{h}$ )	$MRT_{0-t}$ (h)	$MRT_{0-\infty}$ (h)	$V_z/F$ (L/kg)	$CL_z/F$ (L/h/kg)	
VER	—	♀♂	$10.8 \pm 10.3$	$1.83 \pm 1.29$	$3.71 \pm 0.917$	$81 \pm 83$	$82 \pm 83$	$4.88 \pm 1.88$	$5.63 \pm 0.583$	$14779 \pm 15974$	$3234 \pm 3421$	
			$18.7 \pm 21.8$	$5.25 \pm 3.74$	$7.25 \pm 3.08$	$220 \pm 543$	$225 \pm 246$	$8.70 \pm 2.49$	$10.63 \pm 3$	$29509 \pm 34086$	$3948 \pm 5244$	
			$24.5 \pm 26.8$	$7.42 \pm 11.51$	$14.26 \pm 11.94$	$488 \pm 594$	$492 \pm 591$	$15.68 \pm 5.4$	$22.19 \pm 15.25$	$54120 \pm 72536$	$2365 \pm 2541$	
	$0.04 \text{ g/kg}$		♀	$1.40 \pm 0.735$	$2.17 \pm 1.44$	$3.06 \pm 0.80$	$6 \pm 2$	$7 \pm 2$	$3.84 \pm 0.19$	$5.26 \pm 0.55$	$27931 \pm 10901$	$6211 \pm 637$
	$0.08 \text{ g/kg}$		♀	$1.38 \pm 0.208$	$5.17 \pm 4.31$	$6.04 \pm 4.08$	$11 \pm 5$	$13 \pm 6$	$6.75 \pm 0.81$	$9.77 \pm 4.16$	$56524 \pm 26712$	$7699 \pm 5153$
	$0.16 \text{ g/kg}$		♀	$1.93 \pm 0.717$	$3.50 \pm 4.77$	$18.23 \pm 16.93$	$30 \pm 9$	$38 \pm 12$	$15.32 \pm 3.98$	$28.24 \pm 20.38$	$105156 \pm 73053$	$4509 \pm 1528$
	$0.04 \text{ g/kg}$		♂	$20.2 \pm 0.939$	$1.50 \pm 1.32$	$4.35 \pm 0.46$	$157 \pm 17$	$157 \pm 17$	$5.92 \pm 0.44$	$6.01 \pm 0.35$	$1628 \pm 367$	$257 \pm 30$
	$0.08 \text{ g/kg}$		♂	$36.1 \pm 16.8$	$5.33 \pm 4.04$	$8.46 \pm 1.62$	$429 \pm 127$	$436 \pm 130$	$10.65 \pm 1.85$	$11.49 \pm 1.73$	$2495 \pm 1303$	$197 \pm 71$
	$0.16 \text{ g/kg}$		♂	$47.1 \pm 16.5$	$11.33 \pm 16.20$	$10.28 \pm 4.72$	$946 \pm 502$	$947 \pm 503$	$16.05 \pm 7.52$	$16.14 \pm 7.50$	$3084 \pm 1742$	$221 \pm 152$
	JER	—	♀♂	$26.6 \pm 26.2$	$0.71 \pm 0.33$	$11.10 \pm 16.86$	$196 \pm 193$	$218 \pm 179$	$5.28 \pm 1.24$	$16.30 \pm 24.25$	$6571 \pm 8482$	$606 \pm 711$
$45.2 \pm 51.2$				$4.33 \pm 4.17$	$20.08 \pm 24.28$	$572 \pm 550$	$660 \pm 500$	$11.96 \pm 4.65$	$30.35 \pm 34.43$	$6270 \pm 6922$	$240 \pm 232$	
$44.9 \pm 45.1$				$8.25 \pm 11.13$	$29.47 \pm 41.47$	$1100 \pm 1225$	$1361 \pm 1462$	$14.03 \pm 5.07$	$45.08 \pm 58.76$	$16572 \pm 19840$	$501 \pm 579$	
$0.04 \text{ g/kg}$			♀	$3.64 \pm 1.59$	$0.58 \pm 0.38$	$17.49 \pm 24.18$	$20 \pm 5$	$57 \pm 51$	$4.18 \pm 0.38$	$25.77 \pm 34.65$	$12439 \pm 8746$	$1106 \pm 717$
$0.08 \text{ g/kg}$			♀	$7.72 \pm 2.79$	$3.33 \pm 4.91$	$30.91 \pm 33.43$	$113 \pm 78$	$258 \pm 156$	$11.61 \pm 7.15$	$46.79 \pm 46.33$	$11453 \pm 6244$	$401 \pm 239$
$0.16 \text{ g/kg}$			♀	$6.16 \pm 4.15$	$5.17 \pm 4.31$	$46.30 \pm 58.01$	$86 \pm 36$	$264 \pm 230$	$10.94 \pm 1.62$	$68.22 \pm 83.70$	$31977 \pm 16494$	$922 \pm 553$
$0.04 \text{ g/kg}$			♂	$49.5 \pm 11.9$	$0.83 \pm 0.29$	$4.61 \pm 1.22$	$372 \pm 17$	$378 \pm 17$	$6.38 \pm 0.25$	$6.83 \pm 0.75$	$703 \pm 108$	$106 \pm 5$
$0.08 \text{ g/kg}$			♂	$82.8 \pm 48.3$	$5.33 \pm 4.04$	$9.26 \pm 2.17$	$1032 \pm 344$	$1063 \pm 337$	$12.32 \pm 1.61$	$13.92 \pm 2.54$	$1087 \pm 458$	$80 \pm 21$
$0.16 \text{ g/kg}$			♂	$83.6 \pm 23.6$	$11.33 \pm 16.20$	$12.64 \pm 9.24$	$2114 \pm 816$	$2459 \pm 1296$	$17.13 \pm 5.73$	$23.37 \pm 10.91$	$1168 \pm 381$	$80 \pm 46$

TABLE 6: Judgment and statistics of the linear kinetic relationship between veratramine and Jervine in the alcohol extract of Radix Veratri.

Compound	Gender	Pharmacokinetic parameters	$\alpha$	$\beta$	$r$ (correlation coefficient)	Judgment interval	Beta value 95% confidence interval	Judgment result
VER	Female	$AUC_{0-t}$	5.465	1.186	0.88	0.839-1.161	0.613-1.759	Fail to judge
		$C_{max}$	1.083	0.274	0.428	0.839-1.161	-0.243-0.792	No
	Male	$AUC_{0-t}$	8.996	1.212	0.889	0.839-1.161	0.654-1.770	Fail to judge
		$C_{max}$	4.912	0.581	0.768	0.839-1.161	0.148-1.014	Fail to judge
JER	Female	$AUC_{0-t}$	6.558	1.026	0.692	0.839-1.161	0.069-1.984	Fail to judge
		$C_{max}$	2.472	0.333	0.357	0.839-1.161	-0.446-1.112	Fail to judge
	Male	$AUC_{0-t}$	9.863	1.210	0.933	0.839-1.161	0.793-1.627	Fail to judge
		$C_{max}$	5.14	0.374	0.544	0.839-1.161	-0.141-0.888	Fail to judge

considerably greater  $CL_z/F$  clearance rates of veratramine and Jervine than male rats. However, there was no discernible variation in the half-life of veratramine in male and female rats, while the half-life of Jervine was considerably different in female and male rats. This was due to the fact that female rats had a considerably higher volume of veratramine dispersion than male rats, and Jervine was removed faster in female rats than in male rats. The above situation showed that after administration of the alcohol extract of Radix Veratri, veratramine and Jervine were more widely distributed in female rats than in male rats, but the clearance rate was much lower than that in female rats. In addition, at the dosage designed in this experiment, the average  $AUC_{0-t}$  and average  $C_{max}$  of males were much higher than that of females. The drug exposure in male rats was much higher than that of female rats, but the clearance rate was much lower than that of female rats. Male rats were more prone to accumulate toxicity in the course of long-term administration, and the symptoms of toxicity were greater than that of females.

## 5. Conclusion

The blood drug concentration and main pharmacokinetic parameters of the Radix Veratri alcohol extract group were analyzed. The absorption rate of veratramine and Jervine by males was higher than that of female rats. Although Bullatine A and Wilforgine were able to provide the desired response, their chromatographic peaks were distant from the intended peak, and the analysis time was considerable, increasing the expense of the experiment. Male mice had a lower elimination rate than female mice, indicating clear gender differences. Finally, the clinical usage of the steroidal alkaloids veratramine and Jervine in Radix Veratri necessitates gender-based medication selection.

## Data Availability

The datasets used during the current study are available from the corresponding author on reasonable request.

## Conflicts of Interest

The authors declare that they have no conflict of interest.

## Acknowledgments

This work was supported by the Capacity Building project of the Third-party Public Technology Service Platform of Yunnan Institute of Materia Medica, Plan of Innovation Orientation and Cultivating Technology-based Enterprises of Yunnan Science and Technology Plan (Project Number: 202104AR040002).

## References

- [1] L. Gao, L. Peng, C. Zhao, D. Fu, J. Wang, and Z. Zhu, "Medicinal experience, toxicity and efficacy of five types of Yunnan ethnic medicine," *Chinese Journal of Pharmacology and Toxicology*, vol. 6, pp. 503–507, 2017.
- [2] X. He, J. Fang, L. Huang, J. Wang, and X. Huang, "Sophora flavescens Ait.: traditional usage, phytochemistry and pharmacology of an important traditional Chinese medicine," *Journal of Ethnopharmacology*, vol. 172, pp. 10–29, 2015.
- [3] X. Li, D. Wu, J. Niu et al., "Intestinal flora: a pivotal role in investigation of traditional Chinese medicine," *The American Journal of Chinese Medicine*, vol. 49, no. 2, pp. 237–268, 2021.
- [4] Y. Cong, Y. Wu, S. Shen, X. Liu, and J. Guo, "A structure-activity relationship between the Veratrum alkaloids on the antihypertension and DNA damage activity in mice," *Chemistry & Biodiversity*, vol. 17, no. 2, article e1900473, 2020.
- [5] P. Huang, J. W. Gao, Z. Shi et al., "A novel UPLC-MS/MS method for simultaneous quantification of rhein, emodin, berberine and baicalin in rat plasma and its application in a pharmacokinetic study," *Bioanalysis*, vol. 4, no. 10, pp. 1205–1213, 2012.
- [6] Q. Li, Y. L. Zhao, C. B. Long, P. F. Zhu, Y. P. Liu, and X. D. Luo, "Seven new veratramine-type alkaloids with potent analgesic effect from *Veratrum taliense*," *Journal of Ethnopharmacology*, vol. 244, article 112137, 2019.
- [7] P. Jiaming, Z. Kaiyang, A. J. Mian, and L. Jinhai, "Personalized federated learning framework for network traffic anomaly detection," *Computer Networks*, vol. 209, article 108906, 2022.

- [8] Q. Wang, W. Li, M. Yang, Y. Chen, D. Zhang, and M. Li, "Study on the antihypertensive effect of Veratramine," *Chinese Journal of Gerontology*, vol. 31, pp. 3112–3114, 2011.
- [9] L. Wang, L. Y. Li, and Y. Liu, "Hypotensive effect and toxicology of total alkaloids and veratramine from roots and rhizomes of *Veratrum nigrum* L. in spontaneously hypertensive rats," *Pharmazie*, vol. 63, no. 8, pp. 606–610, 2008.
- [10] G. Zhao, R. Peng, Z. Ji, and C. Hu, "Antihypertensive effect and mechanism of three kinds of domestic veratrine (*Veratrum schindler* Loes. f., *V. puberulum* Loes. f., *V. maackii* Regel)," *Acta Pharmaceutica Sinica*, vol. IX, pp. 591–597, 1962.
- [11] E. Meilman, "The management of hypertensive cardiovascular disease," *Circulation*, vol. 13, no. 4, pp. 596–607, 1956.
- [12] E. D. Freis and J. R. Stanton, "A clinical evaluation of *Veratrum viride* in the treatment of essential hypertension," *American Heart Journal*, vol. 36, no. 5, pp. 723–738, 1948.
- [13] W. S. Coe, M. M. Best, and J. M. Kinsman, "Veratrum viride in the treatment of hypertensive vascular disease," *Journal of the American Medical Association*, vol. 143, no. 1, pp. 5–7, 1950.
- [14] P. Xue, L. Zhao, Y. Wang, Z. Hou, F. Zhang, and X. Yang, "Reducing the damage of quinoa saponins on human gastric mucosal cells by a heating process," *Food Science & Nutrition*, vol. 8, no. 1, pp. 500–510, 2020.
- [15] H. J. Jung, H. J. Jang, and T. H. Kwon, "Aquaporins implicated in the cell proliferation and the signaling pathways of cell stemness," *Biochimie*, vol. 188, pp. 52–60, 2021.
- [16] J. Tang, H. L. Li, Y. H. Shen et al., "Antitumor activity of extracts and compounds from the rhizomes of *Veratrum dahuricum*," *Phytotherapy Research*, vol. 22, no. 8, pp. 1093–1096, 2008.
- [17] H. Kayed, P. Meyer, Y. He et al., "Evaluation of the metabolic response to cyclophamide therapy in pancreatic cancer xenografts using a clinical PET-CT system," *Translational Oncology*, vol. 5, no. 5, pp. 335–343, 2012.
- [18] D. G. Barceloux, *Medical toxicology of natural substances: foods, fungi, medicinal herbs, plants, and venomous animals*, John Wiley & Sons, 2008.
- [19] A. R. Toogood, *Gardener's Encyclopedia of Perennials*, Gallery Books, 1989.
- [20] K. R. Patel, V. A. Brown, D. J. L. Jones et al., "Clinical pharmacology of resveratrol and its metabolites in colorectal cancer patients," *Cancer Research*, vol. 70, no. 19, pp. 7392–7399, 2010.
- [21] Y. Xu, X. Li, T. Chen et al., "Incompatibility mechanism between *Radix Paeoniae Alba* and *Veratrum nigrum* focusing on estrogen-estrogen receptor pathway in immature/ovariectomized mice," *Rejuvenation Research*, vol. 22, no. 6, pp. 465–477, 2019.



## Research Article

# The Effect of Acceptance and Commitment Therapy on Psychological Nursing of Acute Cerebral Infarction with Insomnia, Anxiety, and Depression

Xinyu Wang,<sup>1</sup> Jie Chen,<sup>1</sup> Yun-e Liu,<sup>2</sup> and Yan Wu<sup>3</sup> 

<sup>1</sup>Department of Outpatient, PLA Rocket Force Characteristic Medical Center, Beijing 100088, China

<sup>2</sup>Department of Vascular Neurosurgery, PLA Rocket Force Characteristic Medical Center, Beijing 100088, China

<sup>3</sup>Department of Neurology, PLA Rocket Force Characteristic Medical Center, Beijing 100088, China

Correspondence should be addressed to Yan Wu; 11131337@stu.wxlc.edu.cn

Received 5 May 2022; Revised 26 May 2022; Accepted 30 May 2022; Published 22 June 2022

Academic Editor: Naeem Jan

Copyright © 2022 Xinyu Wang et al. This is an open access article distributed under the Creative Commons Attribution License, which permits unrestricted use, distribution, and reproduction in any medium, provided the original work is properly cited.

Acute cerebral infarction (ACI) is a kind of stroke, mostly suffering from insomnia, anxiety, and depression; therefore, the importance of psychological nursing in such patients is a necessary mean. Acceptance and commitment therapy (ACT) is a psychological theory which advocates embracing pain, improving the ability to face pain, with the goal of improving psychological flexibility, so as to reduce the negative impact of pain on personal life. To explore the effect of psychological nursing intervention on ACI patients with anxiety, depression and insomnia are based on acceptance and commitment therapy. A randomized clinical trial study was conducted on 140 eligible ACI patients suffering from insomnia, anxiety, and depression who were selected using easy sampling methods and allocated randomly into two groups of observation and control. The data were collect through demographic questionnaires, the summary of Pittsburgh sleep quality index (PSQI), Athens Insomnia Scale (AIS), Acceptance and Action Questionnaire-II (AAQ-II), Cognitive Fusion Questionnaires (CFQ), Self-Rating Depression Scale (SDS), and Self-Rating Anxiety Scale (SAS). The observation group received ACT treatment, while the control group received standard care. The scores of AAQ-II and CFQ were significantly decreased in the observation group, indicating that psychological flexibility was improved ( $P < 0.05$ ); the scores of SAS and SDS were significantly decreased in the observation group; and the scores of PSQI and AIS were significantly decreased in the observation group. The difference between the two groups was verified by *t*-test.

## 1. Introduction

Acute cerebral infarction (ACI) is a cerebrovascular disease with complex pathogenesis [1]. ACI patients are prone to insomnia under the action of multiple factors, leading to poor sleep quality and even secondary ACI [2]. Studies have shown that up to 56% of ACI patients suffer from insomnia [3]. ACI patients with anxiety, depression, emotional imbalance, anger tendency, etc., unable to contact with the status quo or achieve the target and value, namely, psychological flexibility was decreased. They lack the ability to adjust their negative emotions, cannot accept the status quo, correctly understand the significance of rehabilitation training, and resistance to the status quo or unable to do anything about

the ambivalence; this psychological state is inflexibility. Thus, it causes a series of psychological problems such as ineffective denial, adjustment disorder, self-image disorder, anxiety, and mental distress. These psychological problems will lead to insomnia, reduced sleep quality, and affect the prognosis of patients. However, the severity of these psychological problems is far from anxiety, depression, and other aspects of psychiatric diagnosis, but requiring nursing staff to implement psychological nursing. Acceptance and Commitment Therapy (ACT) [4] advocates embracing pain and improving the ability to face pain, aiming at improving psychological flexibility, so as to reduce the negative impact of pain on personal life. The ACT theory includes 6 parts: flexible attention to the present moment, acceptance, cognitive

defusion, self-as-context, committed action, and valuing. Many studies [5–11] have applied it to the psychological care of patients and their families, such as relieving the fear of patients with recurrent oral cancer, improving the self-management ability of patients with chronic diseases, alleviating the mental health problems of the population such as maternal depression after painless delivery, or improving the self-management ability of patients with diabetes.

An 8-week ACT therapy course decreased stress and other psychological health indices in people with IBD in a randomized controlled experiment. They have all had a positive psychological nursing effect in a short amount of time, namely, during their hospital stay, and they have all focused on enhancing psychological flexibility, improving sleep and other health issues, and boosting patients' quality of life. ACT has been found in studies to enhance not only physical function but also a variety of mental health issues [12]. Many studies at home and abroad have shown that psychological flexibility reflects mental health level to some extent [13]. However, we found no studies that applied this model to ACI patients such as those with insomnia, anxiety, and depression. Therefore, the present study aims to examine the effects of interventions according to ACT on psychological nursing.

The following is a summary of the research: Section 2 contains the patients and methods. Section 3 discusses the results and experiments. Section 4 consists of the discussion section; finally, the conclusion brings the paper to a finish in Section 5.

## 2. Patients and Methods

**2.1. Trial Design and Participants.** This study was a randomized clinical trial. 100 patients were enrolled in the study including 50 patients for the observation group and 50 patients for the control one. Two groups of patients were selected and randomly assigned to observation and control groups. Patients in the observation group received psychological nursing which based on ACT and were carried out according to the nursing steps of assessment, diagnosis, planning, implementation, and evaluation; patients in control group received traditional psychological nursing which included assessment, comfort, communication, and music therapy. Observation group comprised 39 cases of male and 11 cases of female, with an average age of 62.04 years old. Control group consisted of 38 cases of male and 12 cases of female, with an average age of 60.86 years old, and the self-care model components in the two groups were compared using independent samples *t*-test or Chi-squared test. As revealed, no significant difference was evident prior to intervention in terms of gender ( $P = 0.812$ ) and age ( $P = 0.798$ ). Anxiety, depression, insomnia, and psychological flexibility were compared between the two groups before and after 1 month of psychological nursing.

**2.2. Selection Criteria.** The inclusion criteria were as follows: (1) over 18 under 75 years of age, (2) the vital signs were stable, (3) be able to communicate face to face normally, (4)  $PSQI \geq 11$  points and  $AIS \geq 6$  points, (5)  $SAS \geq 49$  points,

and  $SDS \geq 53$  points. Exclusion criteria consisted (1) previous history of mental illness (such as bipolar disorder) or dementia, history of use of psychiatric drugs or sedatives within 6 months, or use of antidepressants and other drugs; (2) transient cerebral ischemia patients; (3) severe anxiety and depression ( $SAS \geq 69$ ,  $SDS \geq 73$ ); (4) a history of substance abuse or dependence; (5) psychotherapy in the past 3 months.

### 2.3. Data Collection and Statistical Analysis

#### 2.3.1. Data Collection Tools

- (1) *PSQI*. The scale [14] can be used to assess sleep quality in patients with sleep disorders and mental disorders, as well as in typical persons; the total score ranges from 0 to 21, with higher scores indicating poorer sleep quality
- (2) *AIS*. There are 8 items in this scale [15], and each item can be divided into four grades from none to severe: 0, 1, 2, and 3. And the total score is less than 4: no sleep disorder; if the total score is 6: suspicious insomnia; if the total score is above 6: insomnia. The main content of this scale is the subjective feeling of sleep
- (3) *SAS*. The scale contains 20 items [16] to reflect the subjective feelings of anxiety and adopts 4-level scoring. Reverse scoring is required for the 5th, 9th, 13th, 17th, and 19th; and normal scoring is required for the rest. The total score of 20 items is rough, which is multiplied by 1.25 for standard score. The standard score is based on a cutoff of 50, a score below 49 is normal, a score between 50 and 59 is mild anxiety, a score between 60 and 69 is moderate anxiety, and a score above 69 is severe anxiety
- (4) *SDS*. This scale was compiled in 1965 and contains 20 items to reflect subjective feelings of depression [17]. It adopts a 4-level score, among which 10 items need reverse score and the rest are normal score. The total score of 20 items is rough score, which is multiplied by 1.25 for standard score. The cutoff score was 53, with a score below 53 considered normal, 53-62 considered mild depression, 63-72 considered moderate depression, and 73 or above considered major depression
- (5) *AAQ-II*. The questionnaire is designed to assess the degree of "empirical avoidance." There are seven items on the scale, ranging from 1 (never) to 7 (always). The higher the score, the more empirical avoidance is present. "Empirical avoidance" [18] is an act that people attempts to change the form, frequency, or sensitivity of their internal experiences (such as thoughts, emotions, and somatosensory sensations) in their minds, even if doing it can lead to actions that are inconsistent with their personal values or goals (such as giving up pursuing a long-term goal in order to avoiding anxiety)

- (6) *CFQ*. “Cognitive Fusion” is the tendency of people’s behavior to be excessively controlled by language rules and thought content, which will enable individuals to automatically extract the literal meaning of thought events, and thus unable to guide their behavior with the direct experience of the “here and now” [19]. There are 9 items in the scale [20], with points from 1 (never) to 7 (always), the score higher, the degree deeper of cognitive fusion

2.3.2. *Statistical Analysis*. Double entry for verification data, SPSS 22.0 was used for data analysis, and the data was checked by statistical experts. The measurement data is described by the mean  $\pm$  standard deviation (SD). And the enumeration data is described by frequency and composition ratio. *T*-test and nonparametric tests were used for measurement data, and chi-squared test was used for enumeration data.  $P < 0.05$  was considered as significant difference.

#### 2.4. Intervention Measures in Observation Group

2.4.1. *Psychological Nursing Assessment*. Psychological flexibility, anxiety, depression, and insomnia were evaluated with the scale before intervention. There was no significant difference in scores between the two groups, as shown in Table 1. Patients were closely observed and communicated frequently to find out their negative emotions, and some common negative statements and body language were recorded for psychological nursing evaluation to facilitate diagnosis.

2.4.2. *Psychological Nursing Diagnosis*. In combination with the psychological nursing evaluation content and clinical commonly used psychological nursing diagnosis, PES structure is used to carry out psychological nursing diagnosis, and generalized diagnosis of patients is summarized, as shown in Table 2. The psychological nursing diagnosis of PES structure corresponded to the contents of psychological nursing evaluation and the six problems of psychological flexibility, and the various symptoms or signs in the psychological nursing diagnosis of PES structure belonged to the symptoms of psychological inflexibility. The details are shown in Table 3.

The “symptoms” in Table 3 are compared with those in Table 2. For example, “P-① -S-c” is the “symptom- c(Willfully ignoring certain symptoms and dangers)” in “item S” corresponding to “① invalid denial” of “item P” in Table 2.

2.4.3. *Planning and Implementation*. According to the basic concept of the psychological nursing plan, this study’s psychological plan includes the following: ACT psychological nursing diagnosis, predicted goals, psychological nursing measures, and evaluation,

- (1) *Nursing Diagnosis*. The patient’s ACT psychological nursing diagnosis is summarized according to the results of the assessment and diagnosis. The reduced psychological flexibility leads to anxiety, depression, and insomnia

TABLE 1: Comparison of scales before psychological nursing.

Item	Scores (min-max)		Z	P value
	Observation group	Control group		
SAS	61.00 (60-66)	61.50 (60-66)	-0.240	0.811
SDS	67.50 (62-72)	67.00 (63-72)	-0.021	0.983
PSQI	15.00 (11-19)	14.00 (11-18)	-1.139	0.255
AIS	13.00 (8-17)	12.00 (8-17)	-1.439	0.150
AAQ-II	40.00 (34-47)	39.00 (34-47)	-1.087	0.277
CFQ	55.00 (45-64)	54.50 (45-64)	-0.674	0.500

- (2) *Expected Goals and Measures*. According to ACT, psychological nursing measures are formulated and divided into 7 units, as shown in Table 4

### 3. Results

The comparison of the results of the two groups 1 month after intervention is also the evaluation process of psychological nursing. Compared with before intervention, the scores of both groups are improved, but the observation group is significantly better than the control group, as shown in Table 5.

### 4. Discussion

There were 6 psychological nursing diagnoses in this study, and after removing the overlapping etiology, there were still 20 etiologies (E) and 21 symptoms (S). However, when ACT was diagnosed with psychological nursing for patients, there were only one problem of reduced psychological flexibility, and there were 6 manifestations of low psychological flexibility. Patients suffered from experience avoidance, cognitive fusion, and psychological inflexibility, according to the findings of this study. Acceptance and action refer to the patient’s desire to feel their feelings and move on from those undesirable psychological experiences. Acceptance and action in this study refer to patients’ acknowledgment of their sickness, as well as their negative emotions and symptoms following the illness. In this situation, they can still have a good living state and beliefs in a worse living environment than before the illness.

In this study, ACI patients often held a pessimistic attitude towards the prognosis of the disease, believing that the disease was worthless because of the inconvenience of movement after the disease. Because ACI is a chronic disease with a high disability rate, many middle-aged and elderly people will change their roles and reduce their adaptability, which causes its occurrence anxiety depression and causes insomnia. By contrast, ACT makes psycho-care diagnosis simpler, attributes all symptoms to a single problem of “reduced mental mobility,” and develops a more comprehensive program that starts with six signs of low mental mobility.

If a mental care program is developed based on the diagnosis of psychological care for 6 health problems (P), 21 symptoms (S) resulting from 20 causes (E) need to be

TABLE 2: Psychological nursing diagnosis for patients.

P (problem)	E (etiology)	S (signs and symptoms)
(1) Invalid denied	(a) Relating to the generation of denial of a particular scene (b) Associated with the observed overstimulation of the disease (c) Associated with ACI	(a) Delay or refuse rehabilitation training (b) Refusing to talk about the pain caused by the disease, and making gestures or remarks of dismissal when talking about painful things (c) Willfully ignoring certain symptoms and dangers
(2) Impaired adjustment	(a) Associated with impaired physical mobility after ACI that causes changes in lifestyle (b) Associated with damage to self-esteem (c) Related to insufficient support systems	(a) Self-reported inability to accept changes in health status (b) Too long denial of changes in health status, showing anger (c) Lack of practical action to solve the problem and future-oriented requirements
(3) Self-image disorder	(a) Associated with ACI (b) Related to mental stress from social environment (c) Conflicts with others' acceptance of human appearance (d) Related to patients' expectations of appearance and activity requirements	(a) Negative responses to existing changes in bodily function, feelings of shame, guilt, and disgust (b) Avoid talking about the function of altered parts of the body (c) Have pain, depression, sadness, and other negative emotions (d) Avoid social contact
(4) Presentimental sadness	(a) Relating to the loss of work capacity and social status (b) Relating to the prospect of loss of property (c) Relating to the lack of effective support (d) Associated with a lack of experience in dealing with ACI (e) Associated with ACI	(a) The patient has a premonition that important things will be lost and shows negative emotions about the expected loss (b) Withdrawal behavior, loss of interest in life, changes in daily activities, and ambivalence (c) Excessive emotional reaction, denial, self-blame, depression, anger, and anxiety (d) Changes in physiological function and sleep disorders
(5) Spiritual distress	(a) Associated with life-threatening (b) Related to the loss of some self-care ability and social status (c) The value of fuzzy	(a) Abnormal behavior and emotions, crying, withdrawal, anxiety, depression, anger, and denial (b) Significant changes in sleep and mental outlook (c) Express doubts about their own values and thus feel spiritually empty (d) Seek spiritual sustenance and spiritual help
(6) Anxiety	(a) Relating to a premonition that the patient's health is at risk (b) Associated with threats to self-concept (c) Associated with a premonition of misfortune	(a) Abnormal emotions and behaviors such as speaking too fast, helplessness, and self-accusation (b) Too much attention to oneself and self-reported worries and worries (c) Inability to concentrate, repeat aimless movements, and avoid behavior

TABLE 3: Psychological inflexibility problems for patients.

Psychological inflexibility	Symptoms	Emotional symptoms	Physical symptoms
Cognitive fusion	P-①-S-c,P-④-S-a		
Experiential avoidance	P-①-S-b,P-③-S-bd, P-⑤-S-a,P-⑥-S-a	Moderate anxiety	
Self-as-content	P-③-S-a,P-⑥-S-b	Moderate depression	Insomnia
Inflexible attention	P-②-S-ab,P-④-S-a	P-③-S-c	P-④-S-d
Lack of contact with chosen values	P-④-S-b,P-⑤-S-cd,P-⑥-S-c	P-④-S-c	P-⑤-S-b
Avoidant persistence	P-①-S-a,P-②-S-c	P-⑤-S-a	

addressed, involving more psychological techniques and psychological nursing techniques. Make the plan long and complicated, without a full set of scientific theory support. And ACT is only to counter the problem of psychological flexibility, improve psychological flexibility, not committed to solve the symptoms, but has the abilities such as acceptance of the status quo, let patients see negative thoughts

in the mind of the border, better aware of the current situation, in this kind of situation, has the ability to face the pain, solve the symptoms that are caused by negative emotions, to relieve negative emotions and improve clinical purpose of adverse symptoms. A great number of research have indicated that strengthening patients' psychological flexibility is critical to resolving the symptoms of psychological issues.

TABLE 4: ACT psychological nursing measures.

Times	Unit content
No. 1	Get of your mind, understand ACI
<p>Basis: ACT—cognitive defusion</p> <p>Location: ward; time: after the end of basic treatment in the morning; supplies: knowledge album, mobile phone.</p> <p>(1) Encourage patients to express their views on ACI and their understanding of its health knowledge.</p> <p>(2) Ask the usual way to understand ACI and help patients distinguish the true and false online information, so as to avoid network fraud.</p> <p>(3) Health education: use picture books of ACI knowledge with pictures and pictures to explain the knowledge of ACI symptoms to patients, including the inducing factors of ACI, the inevitability of disease recurrence and impaired limb function after ACI, and the methods of limb rehabilitation training.</p> <p>(4) Use stories or metaphors to help patients understand that ideas are ideas, the status quo is the status quo, and ideas cannot exist without the context of the status quo.</p> <p>Objective: after the first psychological nursing, patients can correctly understand the disease, to help patients pull open the distance between the ideas and status quo.</p>	
No. 2	Into your life, accept status quo
<p>Basis: ACT—acceptance</p> <p>Location: experimental ward (warm, safe and private environment); time: after the basic treatment in the afternoon, before dinner; equipment: wireless audio.</p> <p>(1) Encourage patients to express ideas: encourage patients to describe their own worries or fears after the occurrence of the disease thoughts, inner feelings, such as disease treatment, work, life, intimate relationship, and other aspects.</p> <p>(2) Negative thoughts normalization: tell patients in the face of the disease, negative emotions is a normal reaction, is the psychological defense instinct, and dos not resist, so as to reduce some unnecessary negative emotions and psychological burden and avoid thinking in the exhaustive.</p> <p>(3) Positive thoughts: encourage patients to share the measures taken to deal with the above thoughts or feelings and the effect and praise the positive behavior.</p> <p>(4) Accept the status quo: let the patient close his eyes, take a deep breath, and choose a comfortable and relaxed posture to lie or sit well and guide. Allow them to comprehend that inner suffering is common and that we all experience bad feelings when confronted with such issues. Only by embracing the existing quo can you improve yourself by feeling pleased and calm rather than suffering.</p> <p>(5) Let patients say to themselves: because I have to face the disease seriously, so I am anxious; I could not sleep because I was trying to figure out how to live my life. Because I realize how important health is, I cannot get depressed.</p> <p>Objective: after the second psychological care, patients learn to accept the status quo and remain open to the inner experience they previously avoided.</p>	
No. 3	Observe the self, understand the self
<p>Basis: ACT—self-as-context</p> <p>Location: experimental ward; time: after basic treatment in the morning; equipment: white paper, pencil, paper, and glue.</p> <p>(1) Self-portrait: let the patient draw a self-portrait of himself on the paper, a simple outline can be.</p> <p>(2) Write labels: write their own or others' views on their own, their eating habits, living habits, mentality, personality, occupation, etc., the more complete the better.</p> <p>(3) Labeling: ask the patient to stick these labels on their self-portrait.</p> <p>(4) Guide the patient to remove the label</p> <p>(5) Let the patient tear the label when retelling: this is not me, other people's view is only other people's view; this is not me, I just occasionally have anxiety, need to change; this is not me. Depression is not good for recovery and needs to change. This is not me, I believe I can change bad habits, I am changing. This is not me, the disease is just accidental, not inevitable, I will change.</p> <p>Objective: after the third psychological nursing, patients learn to observe themselves and understand themselves. Let patients realize that "I am who I am"</p>	
No. 4	Flexible attention to the now
<p>Basis: ACT—flexible attention to the now</p> <p>Location: experimental ward; time: after the basic treatment in the afternoon, before dinner; equipment: wireless audio</p> <p>(1) Guide patients to perceive the present: mobilize the five senses, namely, touch, hearing, smell, vision, and taste. First deep breath smooth mood, guide the patient gently close your eyes and experience the feeling of body contact with the bed/floor/seat, experience the temperature of the room, listen to the voices around, trying to explore in the environment, slowly open your eyes, can be seen inside view of the color, and touch the objects around, hand experience and items, the sense of touch.</p> <p>(2) Encourage the patient to describe the current feelings: guide the patient to describe in as much detail as possible.</p>	

TABLE 4: Continued.

Times	Unit content
(3) Be aware of other guides of the present moment: every morning, tell yourself, "I see the light, the darkness will pass, and I will be better." Every time you eat, tell yourself, "I am replacing nutrition in order to recover quickly." Every day when receiving infusion therapy, tell yourself, "I will actively work with the medical staff, we will fight the sickness together, I have the courage, and I will be better." Every time I take a test, I tell myself not to worry; if it's good to find the problem, please assist me in finding the hidden trouble; tell yourself this every day before going to bed: I should rest, rest is to raise enough spirit, believe that tomorrow will be better. Objective: after the 4th psychological care, patients can be aware of the present and strengthen the positive belief.	
No. 5 Basis: ACT—valuing Location: experimental ward; time: after the basic treatment in the afternoon, before dinner; equipment: white paper, pencil, and paper basket. (1) Clarification value (2) Help patients to clarify their self-worth: help patients to clarify what is the most important value at present. If your life were a book or a TV show, what would you want the ending to be? According to the patient's answer, guide the patient's positive value direction. Objective: after the fifth psychological nursing, patients clear self-worth direction, and have a positive attitude to face the status quo.	Clarify values, clarify direction
No. 6 Basis: ACT—committed action Location: experimental ward; time: after the basic treatment in the afternoon, before dinner; equipment: white paper and pencil. (1) Goal setting: to help patients develop specific goals based on value orientation, so that patients are in the leading position in the development of specific plans. Help patients to select suitable and difficult goals for their current situation. (2) Commitment to action: in the training or in the realization of the goal, there may be setbacks, once again triggered negative emotions, and actively guide the patient. Objective: after the 6th psychological care, patients make goals in line with their current situation, and commit to action	Set goals, commit to action
No. 7 Basis: ACT—mindfulness and acceptance Location: experimental ward; time: after dinner; equipment: wireless audio. (1) To guide patients with abdominal breathing: use music with guidance language to focus patients' attention on breathing and every part of the body, relax the body, and avoid entering complex inner activities again. Guide words (speaking slowly): choose a comfortable lying position, preferably a supine position, close your eyes, take a deep breath, put your hands on your abdomen, feel the breath, breath and breath. (2) Let the patient be familiar with the music and guide language to relax the body: slowly speak each part of the patient's body, let the patient be familiar with the guide language, to avoid the patient cannot keep up with the guide language and anxious. Let patients relax their body and mind and sleep peacefully. (3) Recommend some hypnotic guidance to patients Objective: after the 7th psychological nursing, patients learn relaxation techniques.	Relax and sleep peacefully

The use of ACT in the development of a psychological nursing plan so that patients take the initiative to accept negative emotions and problems, and in this situation, to find their own value direction and put it into action in order to alleviate negative emotions, improve insomnia, and improve their quality of life. Higher psychological flexibility enables patients to face life more positively in painful situations and reduces the generation of negative emotions and the impact of negative emotions. Studies have shown that psychological flexibility reflects mental health.

ACT is a professional psychological technique with scientific theoretical basis and a complete practical process to support its use in psychological nursing. This study standardized the process of psychological nursing, diagnosed patients with common problems, and preliminarily con-

structed a more professional and detailed program, and the application effect is good, and patients' psychological flexibility can be improved, relieve anxiety and depression, and improve insomnia symptoms. However, in the specific implementation, there are still some personalized problems. More attention should be paid to patients' psychological flexibility, more care should be given to patients, social support should be strengthened, value direction should be found in the hardship, and action should be taken to lead a positive and optimistic life in order to train medical staff to learn ACT. However, this study was only initially applied in ACI patients, and the acceptance of ACT psychological nursing among patients of different ages should be further explored to develop a scale to measure the psychological flexibility of sACI patients for a

TABLE 5: Comparison of scales after 1 month of psychological nursing.

Item	Scores (min-max)		Z	P value
	Observation group	Control group		
SAS	51.00 (45-58)	58.00 (52-61)	-8.041	0.001
SDS	53.00 (45-60)	59.00 (54-63)	-8.042	0.001
PSQI	7.00 (4-11)	9 (4-13)	-4.331	0.001
AIS	3.00 (1-6)	6.50 (4-11)	-8.221	0.001
AAQ-II	20.00 (17-24)	31.00 (19-39)	-8.403	0.001
CFQ	22.00 (17-29)	40.00 (20-51)	-8.367	0.001

more detailed and accurate measurement. And explore the psychological nursing effect of the best nursing frequency, in order to clinical work for reference.

## 5. Conclusion

In general, using ACT in psychological nursing can help ACI patients improve their mental flexibility, decrease negative emotions like anxiety and depression, and improve insomnia symptoms, sleep quality, and overall quality of life. At the same time, the process and scientific basis of psychological nursing plan formulation are explained. This study is innovative and reproducible and has certain clinical significance. And “ACT → psychological nursing → psychological flexibility → relief of negative emotions → improvement of adverse symptoms” can be used as a new way to explore psychological nursing.

## Data Availability

All data included in this study are available upon request by contacting with the corresponding authors.

## Conflicts of Interest

The authors declare that they have no conflicts of interest.

## Acknowledgments

The authors are thankful for the participants who participated in the study. Their sincere appreciation also goes to the management of the hospitals for giving administrative approval for the research.

## References

- [1] Z. Sun, Q. Xu, G. Gao, M. Zhao, and C. Sun, “Clinical observation in edaravone treatment for acute cerebral infarction,” *Nigerian Journal of Clinical Practice*, vol. 22, no. 10, pp. 1324–1327, 2019.
- [2] D. M. Hermann and C. L. Bassetti, “Sleep-related breathing and sleep-wake disturbances in ischemic stroke,” *Neurology*, vol. 73, no. 16, pp. 1313–1322, 2009.
- [3] C. C. Guo and Y. L. Wang, “Research progress and treatment status of insomnia after stroke,” *World Latest Medicine Information*, vol. 18, no. 88, pp. 114–115, 2018.
- [4] H. Sc, K. Strosahl, and K. G. Wilson, *Acceptance and Commitment Therapy: An Experiential Approach to Behavior Change*, vol. 9, no. 2, 1999, Guilford Press, New York, 1999.
- [5] M. P. Twohig and M. E. Levin, “Acceptance and commitment therapy as a treatment for anxiety and depression: a review,” *The Psychiatric Clinics of North America*, vol. 40, no. 4, pp. 751–770, 2017.
- [6] L. S. Hughes, J. Clark, J. A. Colclough, E. Dale, and D. McMillan, “Acceptance and commitment therapy (ACT) for chronic pain,” *The Clinical Journal of Pain*, vol. 33, no. 6, pp. 552–568, 2017.
- [7] B. Wynne, L. McHugh, W. Gao et al., “Acceptance and commitment therapy reduces psychological stress in patients with inflammatory bowel diseases,” *Gastroenterology*, vol. 156, no. 4, pp. 935–945.e1, 2019.
- [8] S. A. Johns, P. V. Stutz, T. L. Talib et al., “Acceptance and commitment therapy for breast cancer survivors with fear of cancer recurrence: a 3-arm pilot randomized controlled trial,” *Cancer*, vol. 126, no. 1, pp. 211–218, 2020.
- [9] A. A. Taheri, A. A. Foroughi, Y. Mohammadian et al., “The effectiveness of acceptance and commitment therapy on pain acceptance and pain perception in patients with painful diabetic neuropathy: a randomized controlled trial,” *Diabetes Therapy*, vol. 11, no. 8, pp. 1695–1708, 2020.
- [10] R. Wang, Y. J. Liu, and E. H. Yong, “Effects of acceptance and commitment therapy on anxiety and depression in infertile patients and their quality of life,” *Hebei Medical Journal*, vol. 39, no. 22, pp. 3430–3432, 2017.
- [11] Y. Wang, “Application of admission and commitment therapy in self-management of patients with chronic obstructive pulmonary disease (COPD),” *Guide of China Medicine*, vol. 14, no. 32, pp. 198–199, 2016.
- [12] A. Spidel, T. Lecomte, D. Kealy, and I. Daigneault, “Acceptance and commitment therapy for psychosis and trauma: improvement in psychiatric symptoms, emotion regulation, and treatment compliance following a brief group intervention,” *Psychology and Psychotherapy: Theory, Research and Practice*, vol. 91, no. 2, pp. 248–261, 2018.
- [13] T. B. Kashdan and J. Rottenberg, “Psychological flexibility as a fundamental aspect of health,” *Clinical Psychology Review*, vol. 30, no. 7, pp. 865–878, 2010.
- [14] L. U. Taoying, L. I. Yan, P. Xia, G. Zhang, and W. U. Darong, “Reliability and validity analysis of Pittsburgh sleep quality index,” *Chongqing medical*, vol. 43, no. 3, pp. 260–263, 2014.
- [15] C. R. Soldatos, D. G. Dikeos, and T. J. Paparrigopoulos, “Athens insomnia scale: validation of an instrument based on ICD-10 criteria,” *Journal of Psychosomatic Research*, vol. 48, no. 6, pp. 555–560, 2000.

- [16] D. A. Dunstan and N. Scott, "Norms for Zung's self-rating anxiety scale," *BMC Psychiatry*, vol. 20, no. 1, p. 90, 2020.
- [17] W. W. Zung, "A self-rating depression scale," *Archives of General Psychiatry*, vol. 12, no. 1, pp. 63–70, 1965.
- [18] J. Cao, Y. Ji, and Z. H. Zhu, "The second Chinese version of the acceptance and action questionnaire assessed the reliability and validity of college students," *Chinese Mental Health Journal*, vol. 27, no. 11, pp. 873–877, 2013.
- [19] S. C. Hayes, K. G. Wilson, E. V. Gifford, V. M. Follette, and K. Strosahl, "Experimental avoidance and behavioral disorders: a functional dimensional approach to diagnosis and treatment," *Journal of Consulting and Clinical Psychology*, vol. 64, no. 6, pp. 1152–1168, 1996.
- [20] W. C. Zhang, Y. Ji, and X. Li, "Reliability and validity analysis of the Chinese version of cognitive fusion questionnaire," *Chinese Mental Health Journal*, vol. 28, no. 1, pp. 40–44, 2014.



## Research Article

# Prediction Model Construction for Ischemic Stroke Recurrence with BP Network and Multivariate Logistic Regression and Effect of Individualized Health Education

Ting Lu  and Yun Wang 

*Department of Neurology Nursing, Sichuan Provincial People's Hospital, University of Electronic Science and Technology of China, Chinese Academy of Sciences Sichuan Translational Medicine Research Hospital, Chengdu, Sichuan 610072, China*

Correspondence should be addressed to Yun Wang; wangyun@med.uestc.edu.cn

Received 11 May 2022; Revised 1 June 2022; Accepted 4 June 2022; Published 22 June 2022

Academic Editor: Naeem Jan

Copyright © 2022 Ting Lu and Yun Wang. This is an open access article distributed under the Creative Commons Attribution License, which permits unrestricted use, distribution, and reproduction in any medium, provided the original work is properly cited.

Stroke is an acute cerebrovascular disease caused by the rapid rupture or blockage of intracranial blood vessels for a variety of reasons, preventing blood from flowing into the brain and causing damage to brain tissue. The global burden of stroke disease is quickly increasing, and ischemic stroke (IS) accounts for 60 percent to 70 percent of all strokes, owing to the prevalence of people's bad lifestyles and the intensity of global ageing. Although most IS patients have received effective treatment, many patients still have certain dysfunction or death after treatment, and the recurrence rate is about 18%, which brings a heavy economic burden to society and families. Therefore, it is urgent to build a postoperative prediction model for IS, so as to take targeted clinical intervention measures, which has extremely important practical significance for improving the prognosis of IS. The following work has been done in this paper: (1) the theoretical background for the BP prediction model and logistic regression prediction model suggested in this work is offered, as well as the research progress and related technologies of IS recurrence prediction by domestic and foreign academics. (2) The basic principles of BPNN and logistic regression are introduced, and the logistic multifactor predictor is constructed. (3) The experimental results show that the consistency rate, sensitivity, and specificity of the prediction results of BPNN are higher than those of logistic regression, indicating that for diseases such as IS, which have many pathogenic factors and complex relationships between factors, the fitting effect of BPNN model is better than that of the logistic regression model.

## 1. Introduction

Stroke follows cardiovascular disease as the major cause of mortality globally. There are about 2.4 million new stroke patients in my country every year, about 1.1 million deaths, and about 11 million poststroke survivors, of which about 70% are IS. IS refers to the ischemic necrosis or softening of the brain tissue caused by ischemia and hypoxia caused by various reasons. About 75% of IS patients have different degrees of dysfunction after the onset of the disease, which brings a heavy burden to the family and society, and IS is prone to relapse within 1 year after the onset of IS. The recurrence rates were 10.9%, 13.4%, and 14.7%, respectively [1]. In the first year after the onset of acute ischemic stroke, 1

in 18 people has a recurrent stroke. The harm caused by the recurrence of IS is far greater than that of the first stroke. The neurological damage caused by the recurrent stroke is more serious and more refractory and has a higher mortality rate than the first stroke. It is one of the main causes of death, rehospitalization, and long-term disability. Cumulative mortality after relapse more than doubled compared with first-episode stroke, and the risk of death increased approximately 17-fold. Reducing the recurrence rate of IS is the key to improving the prognosis of stroke, and secondary prevention of stroke can reduce the risk of IS recurrence by about 13% to 67%. Risk prediction of IS recurrence is the key to effective clinical secondary prevention and the most effective means to reduce the fatality and disability rate of

patients [2, 3]. There are two main issues to consider in IS recurrence risk prediction: the first is the selection of IS recurrence risk predictors. The screening of predictive factors is an important step in the construction of predictive models, and the effect of predictive models depends on the accuracy and sensitivity of the predictive factors. There are many studies on the risk factors of IS recurrence, but the research results are affected by regions, medical policies, social economy, etc., and the research results are different.

It is difficult to predict the screening of IS recurrence risk factors. The risk prediction of IS recurrence is mainly based on clinical factors. The results of risk verification showed that the AUC values of the area under the ROC curve were all 0.59. The model did not cover all risk factors and had a limited predictive impact, making it difficult to meet clinical needs [4]. Scholars have increasingly employed biomarkers, imaging markers, and TCM syndrome distinguishing signals to the risk prediction of IS recurrence, improving the prediction effect in recent years. The method for building the IS recurrence risk prediction model is the second. Traditional statistical methods for developing prediction models, such as Cox proportional hazards regression analysis and logistic regression analysis, are currently the most popular. Traditional statistical methods, on the other hand, have stringent data-type restrictions and have little impact on data mining when dealing with clinical recurrence data. Machine learning has started to be used to illness risk prediction with the progress of computer technology and smart medical care. Multidisciplinary in nature, machine learning draws on a variety of fields, including probability and statistics, approximation theory, convex analysis, and theory of algorithm complexity. The artificial intelligence of a computer may be realized via the machine's ability to learn from the data's inherent regularity information and gain new experience and knowledge [5, 6]. Machine learning algorithms have the characteristics of high efficiency and accuracy in processing big data, and the prediction effect is better than traditional statistical methods [7]. The disease risk prediction model built with BPNN, SVM algorithm, XGBoost algorithm, and other machine learning algorithms outperforms established statistical methods such as the logistic regression model and the Cox proportional hazards regression model [8]. As a result, this work used prospectively gathered medical-related data from IS patients, applied multivariate analysis to screen out risk factors affecting IS prognosis, and built a machine learning algorithm-based risk prediction for ischemic stroke with a bad prognosis. The model can quickly predict and identify the risk of poor functional recovery of IS patients in the early stage of disease diagnosis and treatment, scientifically assist the selection of clinical treatment plans, improve the prognosis of stroke patients, reduce the disability rate of stroke, and improve the quality of medical care, and it provides a new idea for predicting the prognosis of IS.

The following is the paper's organisation paragraph: in Section 2, the related work is provided. The suggested work's approaches are examined in Section 3. The experiments and results are discussed in Section 4. Finally, the research is completed in Section 5.

## 2. Related Work

A large number of studies have shown that the prognosis of ischemic stroke is affected by factors such as age, family history, smoking, drinking, hypertension, abnormal lipid metabolism, abnormal glucose metabolism, and hyperhomocysteinemia. This provides a good basis for the risk prediction study of poor prognosis of ischemic stroke [9, 10]. At present, traditional evaluation tools, such as Essen scale, ABCD2 scale, and SPI-II scale, are mainly used in clinical practice for ischemic stroke to predict the recurrence risk of patients. ESRS is based on the stroke prediction model developed by the CAPRIE Institute. The higher the score, the greater the risk of stroke recurrence. The Essen score is currently the most commonly used scale in the world to predict the long-term recurrence risk of stroke [11]. Reference [12] developed the ABCD2 scoring method based on the ABCD scoring system proposed by the "Oxfordshire Community Stroke Project" study to assess the risk of stroke in patients with transient ischemic attack. Reference [13] proposed the SPI-III scale in 2000 to assess the long-term recurrence risk of stroke patients. Age over 70, diabetes, coronary heart disease, and a history of stroke are all listed as risk factors for stroke recurrence in the evaluation tool. Using manual or traditional statistical analysis methods, the above-mentioned scoring scales combine several risk factors that affect stroke prognosis and assign varying weights to each risk factor. Diverse groups of people have different lifestyles; thus, it is still unclear whether the weights allocated to these aspects are appropriate for Chinese people. At present, for the prediction of IS prognosis, domestic and foreign scholars still mostly use retrospective cohort studies to construct a risk prediction model for poor stroke prognosis based on traditional statistical analysis of logistic regression and Cox regression [14, 15]. The medical and health sector has entered the age of big data as a result of the fast growth of medical and health informatization building. Machine learning algorithms have been extensively employed in the medical industry, such as illness prediction, disease prognosis evaluation, disease auxiliary diagnosis, and health management, in the face of these large data with huge volume, varied kinds, and high hidden value [16]. This is because machine learning algorithms can take into account more variables and effectively reflect the unpredictable and complex nature of the human body than traditional prediction models that only consider one or two variables. A multilayer feedforward neural network known as the BPNN was initially suggested by researchers in 1986, and it has since become the most widely used neural system model in neuroscience [17]. BPNN does not have high requirements for data types and has strong nonlinear mapping ability and adaptive ability, which can effectively dig out the influencing factors related to the occurrence of diseases from the complicated medical big data and scientifically evaluate the occurrence of disease risk [18]. Reference [19] used BPNN and logistic regression model to construct a risk prediction model for spontaneous hemorrhagic transformation in ischemic stroke patients, respectively. The results showed that the predictive performance of BPNN was better than

that of the logistic regression model. Random forest is a supervised learning ensemble algorithm proposed by reference [19] in 1995. Because of its great antinoise capabilities and difficult overfitting, the algorithm is commonly employed in illness risk prediction. The random forest model outperforms the BPNN model and the logistic regression model in predicting the risk of coronary stenosis, according to academic research, and its AUC values are 0.752, 0.723, and 0.739, respectively. Based on the current research status at home and abroad, various traditional risk scale scores have achieved certain results in the prognosis prediction of ischemic stroke, but various scales only include simple indicators such as age and past medical history, and the prediction accuracy is often low and cannot fully explain whether there is an interaction between the indicators. In addition, the existing studies also have problems such as small sample size, single center, retrospective studies, and low data quality and sample representativeness [20]. Because of the fast growth of data mining technology and the increasing amount of data in electronic medical records, the use of machine learning in the area of illness prognostic prediction has made significant strides [21–24]. There are still few studies on prognosis prediction of hemorrhagic stroke patients, and further research is needed.

### 3. Method

*3.1. The Basic Principle of Artificial Neural Network.* Analogous neural networks (ANNs) are mathematical models of the brain’s synaptic connections. Modern neuroscience research has resulted in the reduction, abstraction, and modeling of the structure and function of the biological nerve system of the human brain, which reflects the human brain’s essential properties. This nonlinear network system is made up of a large number of small basic units called neurons that are connected in a way that resembles how the human brain processes information and distributes processing. ANN does not use mathematical methods for precise calculation, nor does it need to predetermine basic functions like regression equations, but directly train the neural network with data or signal samples, and obtain a response after a limited number of iterative calculations. Another advantage of the neural network method is that it requires no prior information and offers self-learning, self-adaptation, and fault tolerance, making it ideal for multivariate pattern identification. It provides a new way to solve the uncertainty, ambiguity, and dynamic complexity in hygiene evaluation. At present, it has been widely used in the prediction, diagnosis, image processing, and other aspects of diseases in the medical field, especially the error backpropagation algorithm which is more widely used.

*3.1.1. Backpropagation BP Network Algorithm.* The error backpropagation technique was first published by Paul Werbos in 1974, although it was not extensively used at the time. BPNN is a multilayer forward neural network based on this approach. It was not until the mid-1980s that some scholars conducted further research on the BP algorithm and wrote the BP algorithm into the book “Parallel Distributed Pro-

cessing,” and the BP algorithm was not widely known. BPNN is a typical multilayer feedforward neural network using a teacher-supervised learning algorithm. It has powerful computing power and can master the input-output mapping relationship implied by the learning sample through training and has a wide range of applications in classification and prediction. Parallel networks are used in the BPNN. Hidden node output signals are passed to the output node, and eventually, the output result is supplied. Forward propagation and backward propagation of errors are both used in the algorithm’s learning phase. A forward propagation method is used to process input information from the input layer to the hidden layer and transmit it to the output layer. A neuron’s current state solely influences the following neuron’s current state. In the event that the desired output result cannot be attained in the output layer, the error signal is returned over the original connection channel and is then processed via backpropagation. The mean square of the error is reduced by adjusting the weights of neurons in each layer. BPNN’s excellent nonlinear mapping ability and generalization function have been shown by neural network theory. A three-layer network may realize any continuous function or mapping.

*3.1.2. BP Network Structure.* BPNN is by far the most famous and widely used neural network. Theoretically, the complex nonlinear relationship can be fully described by a three-layer feedforward network. An input layer, a hidden layer, and an output layer are the three layers that make up a network. The topology of a typical BPNN is shown in Figure 1.

Because of this, the BP algorithm alters its weights and biases in the opposite direction of gradient, which is similar to how a linear network’s learning algorithm works. A mathematical formula for the BP algorithm’s iterative computation is as follows:

$$x_{k+1} = x_k - \nu g_r, \quad (1)$$

where  $x_k$  represents the current weight and bias,  $x_{k+1}$  represents the next weight and bias generated by iteration,  $g_r$  is the gradient of the current error function, and  $\nu$  represents the learning rate.

Using an example of a BPNN with two hidden layers and four total layers of neurons, we can figure out how the learning process works in this section.  $M$  is the number of inputs, and  $m$  is the identifier for any one of them. An  $I$  represents one of the  $I$  neurons in the first hidden layer, which has  $I$  neurons in total. There are a total of  $j$  neurons in the second hidden layer, each of which has been labeled with  $j$ . There are  $P$  neurons in the output layer, each of which is symbolized by the letter  $p$ .  $w_{mi}$  is the weight between the  $m$ th neuron in the input layer and the first hidden layer, which is indicated as the weight output from the  $m$ th neuron to the first hidden layer.  $w_{ij}$  Denotes the weight between the first and second hidden layers. Input and output weights are indicated by  $w_{ip}$  and  $w_{jp}$ , respectively.

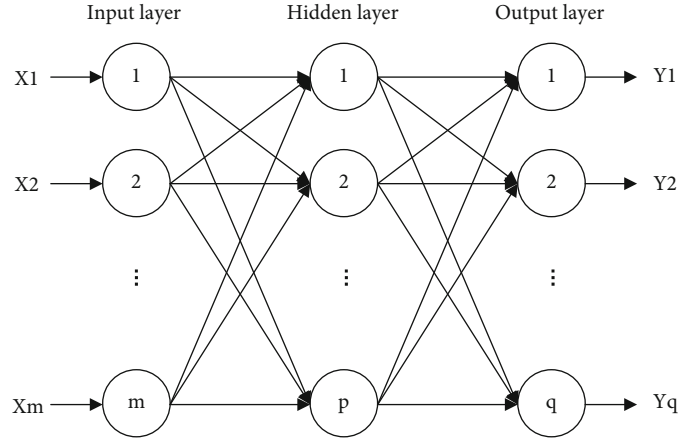


FIGURE 1: BP algorithm network structure.

TABLE 1: 16-item univariate logistic regression results.

Factors	<i>B</i>	S.E.	Wald	<i>P</i>	OR	OR (95% CI)
Age	0.045	0.006	23.12	<0.001	1.036	1.018-1.055
Systolic pressure	0.025	0.003	20.65	<0.001	1.015	1.005-1.028
Diastolic pressure	0.047	0.005	35.78	<0.001	1.040	1.022-1.055
Language disability	0.762	0.180	12.54	<0.001	2.169	1.460-2.221
CA	0.518	0.170	6.57	0.006	1.698	1.142-2.515
Hypertension	0.529	0.165	7.02	0.005	1.712	1.162-2.522
Hyperlipidemia	0.785	0.327	4.28	0.010	2.216	1.120-4.375
Smoking	0.219	0.096	4.18	0.011	1.289	1.028-1.627
Drinking	0.488	0.205	4.30	0.010	1.661	1.073-2.572
ADL	0.327	0.104	8.53	0.002	1.428	1.131-1.815
Triglycerides	0.216	0.085	4.12	0.012	1.274	1.025-1.582
LDL	0.184	0.082	3.21	0.026	1.243	1.002-1.538
Total cholesterol	0.152	0.068	3.79	0.017	1.204	1.010-1.436
Take aspirin regularly	-0.181	0.085	3.22	0.026	0.685	0.530-0.975
Sleeping	-0.344	0.117	6.85	0.006	0.578	0.514-0.887
Confidence	-0.415	0.178	4.48	0.010	0.522	0.427-0.918

The neuron input is denoted as  $Z$ , the output is denoted as  $O$ , and  $Z_i^l$  represents the input of the  $i^{\text{th}}$  neuron in the first hidden layer. Let the transfer function of all neurons be the sigmoid function. The training sample set is  $X = (X_1, X_2, \dots, X_N)$ , and any training sample  $X_k$  is an  $M$ -dimensional vector, that is,  $X = (X_{k1}, X_{k2}, \dots, X_{km})$  ( $k = 1, 2, \dots, N$ ); the expected response is  $d_k$ , and the actual output is  $Y_k$ . Let  $n$  be the number of iterations, and both the weights and the actual output are functions of  $n$ . When the network input training sample is  $X = (X_{k1}, X_{k2}, \dots, X_{km})$ , the network signal is transmitted in a forward manner. For the intermediate value of each layer, the expression can be written as follows.

The input of the  $i^{\text{th}}$  neuron in the first hidden layer is

$$Z_i^l = \sum_{m=1}^M w_{mi} x_{km}. \quad (2)$$

The output of the  $i^{\text{th}}$  neuron in the first hidden layer is

$$O_i^l = f \left( \sum_{m=1}^M w_{mi} x_{km} \right). \quad (3)$$

The output of the  $j^{\text{th}}$  neuron in the second hidden layer is

$$O_j^l = f \left( \sum_{i=1}^I w_{ij} O_i^l \right). \quad (4)$$

The input of the  $p^{\text{th}}$  neuron in the output layer is

$$Z_p^p = \sum_{j=1}^J w_{jp} O_j^l. \quad (5)$$

TABLE 2: Multivariate logistic regression results of recurrence in patients with IS.

Factors	$B$	S.E.	Wald	$P$	OR	OR (95% CI)
Age	0.045	0.006	23.12	<0.001	1.036	1.018-1.055
Diastolic pressure	0.047	0.005	35.78	<0.001	1.040	1.022-1.055
Language disability	0.762	0.180	12.54	<0.001	2.169	1.460-2.221
Drinking	0.488	0.205	4.30	0.010	1.661	1.073-2.572
Triglycerides	0.216	0.085	4.12	0.012	1.274	1.025-1.582
Take aspirin regularly	-0.181	0.085	3.22	0.026	0.685	0.530-0.975
Sleeping	-0.344	0.117	6.85	0.006	0.578	0.514-0.887

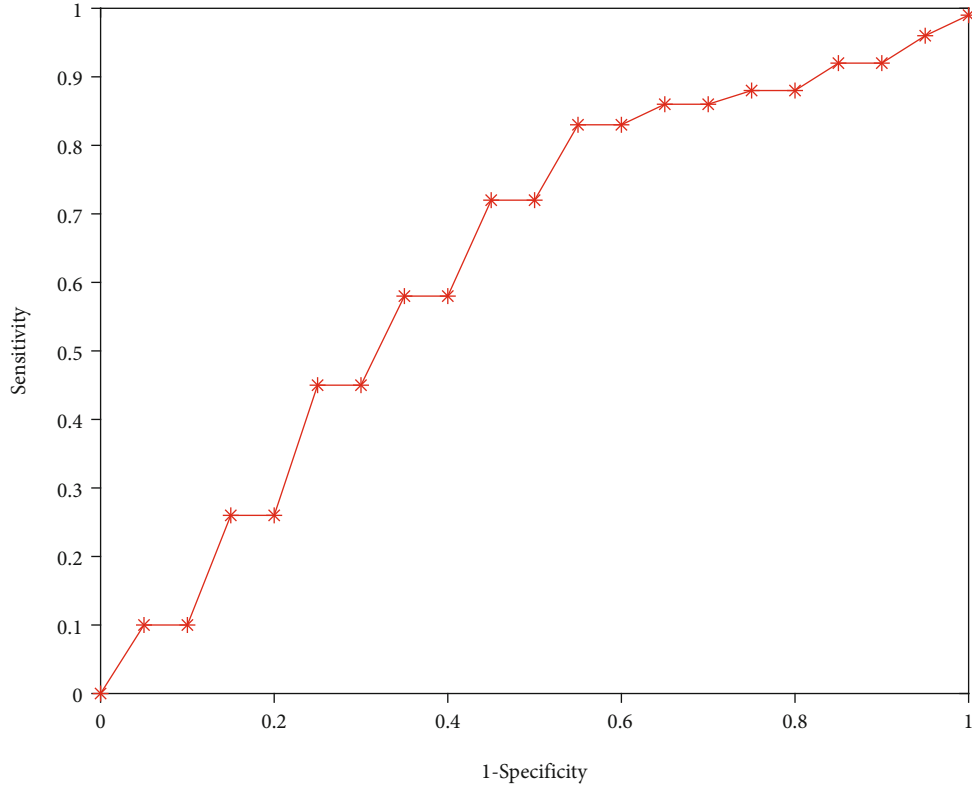


FIGURE 2: ROC curve of test set multivariate logistic regression.

The output of the  $p^{\text{th}}$  neuron in the output layer, that is, the network output, is

$$y_{kp} = O_p^p = f\left(\sum_{j=1}^J w_{jp} O_j^I\right). \quad (6)$$

The output error of the  $p^{\text{th}}$  neuron in the output layer is

$$e(n) = d_{kp}(n) - y_{kp}(n). \quad (7)$$

Define the error energy as  $e$ , and the sum of the error energy of all neurons in the output layer is

$$E(n) = \frac{1}{2} \sum_{p=1}^P e^2(n). \quad (8)$$

TABLE 3: Area under ROC curve of the logistic regression model and related results.

AUC	95% CI	Accuracy	Sensitivity	Specificity	Youden's index
0.735	0.496-0.825	82.5%	63.2%	75.6%	38.2%

The error is opposite to the signal and propagates from back to front, and in the process of backpropagation, the weights and biases are modified layer by layer. The adjustment process of backpropagation and error is calculated below.

**3.1.3. Weight Adjustment.** A partial differential of output error energy compared to the predicted response to weight is used in the BP algorithm, and the sign of this difference

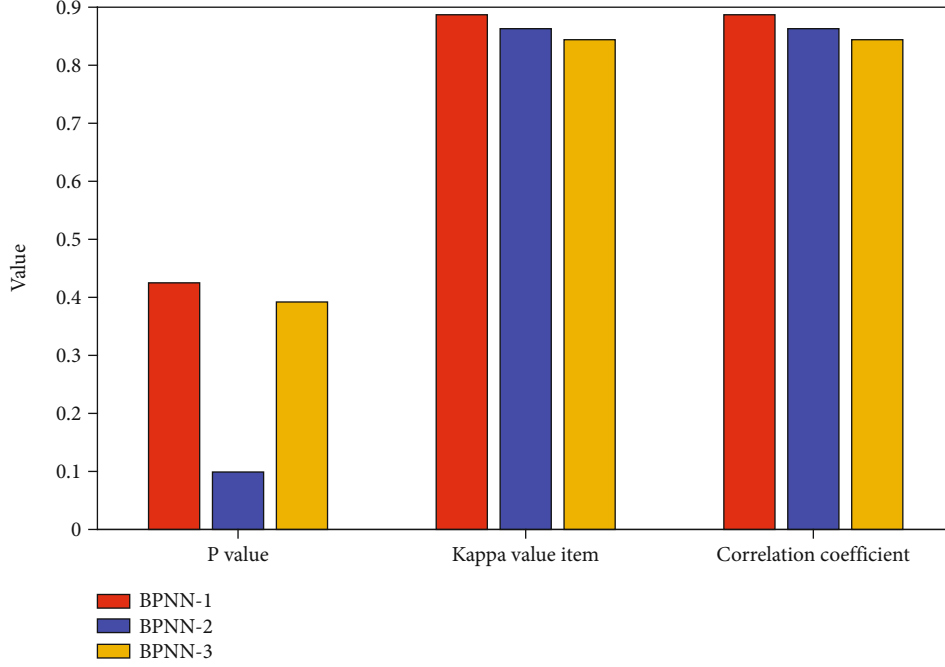


FIGURE 3: Result comparison of BP models with different numbers of hidden layers.

is used to alter weight. Following is the calculation of this partial differential's value. According to the learning rule of gradient descent, the correction amount of  $w_{jp}$  is

$$\Delta w_{jp}(n) = -\lambda \frac{\partial E(n)}{\partial w_{jp}(n)} = \theta_p^P(n) \cdot O_j^I(n), \quad (9)$$

where  $\lambda$  is the learning step size,  $p$  is the local gradient, and  $\theta_p^P(n)$  can be obtained according to the forward propagation process of the signal. Thus, the next iteration value of  $w_{jp}$  is calculated.

Get the next iteration value of the weight  $w_{jp}(n+1)$  before the hidden layer  $J$  and the output layer  $P$ :

$$w_{jp}(n+1) = w_{jp}(n) + \Delta w_{jp}(n). \quad (10)$$

In the same way, the next iteration value of the weight  $w_{ij}(n)$  before the hidden layer  $I$  and the hidden layer  $J$  can be obtained:

$$w_{ij}(n+1) = w_{ij}(n) + \Delta w_{ij}(n). \quad (11)$$

Through the following iterative formula, the weight between the input layer  $M$  and the hidden layer  $I$  of the next iteration can be obtained.

$$w_{mi}(n+1) = w_{mi}(n) + \Delta w_{mi}(n). \quad (12)$$

The above is the weight iteration formula of the learning rule of the full sigmoid transfer function BPNN including two hidden layers.

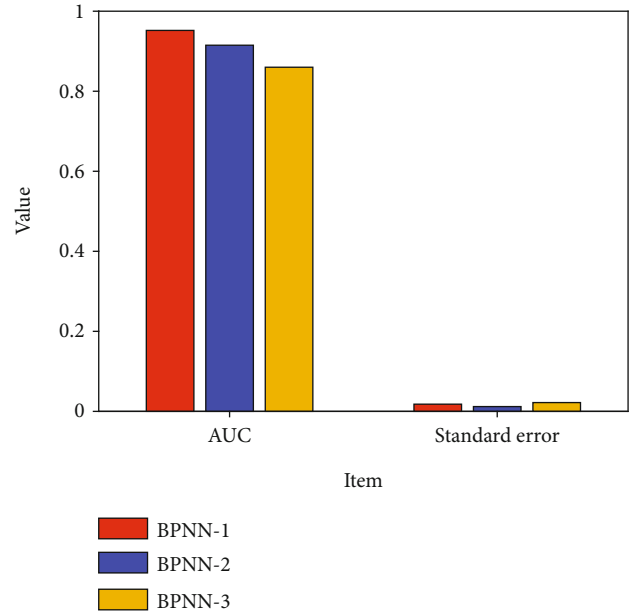


FIGURE 4: AUC and standard errors of BP models with different hidden layers.

### 3.2. Basic Principles of Logistic Regression

**3.2.1. Logistic Regression Model.** One way to look at the connection between binary data and some of their influencing elements is through a probabilistic nonlinear regression approach known as logistic regression (LR). It is often used in epidemiological research to examine the quantitative association between illnesses and other risk variables. Let

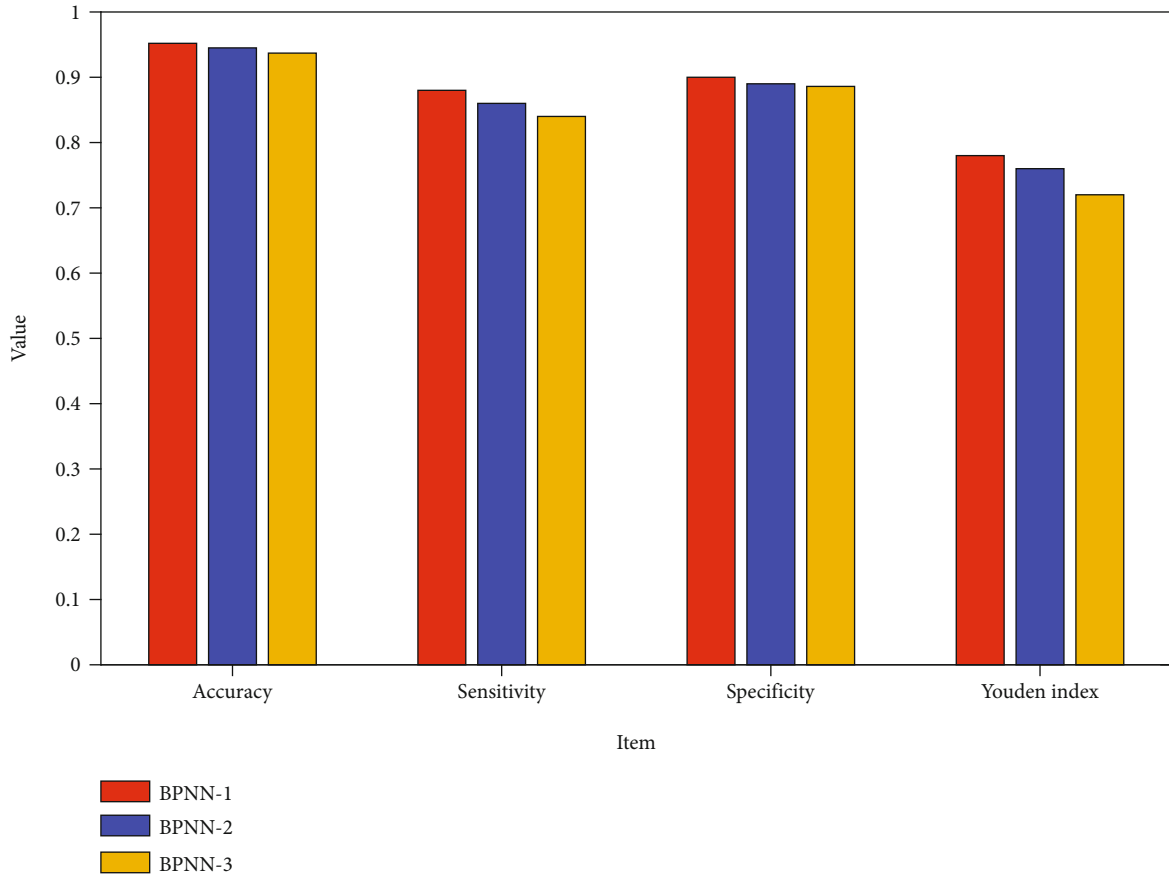


FIGURE 5: Prediction accuracy indicator of BP models with different hidden layers.

the dependent variable  $Y$  be a binary variable whose value is

$$Y = \begin{cases} 1, & \text{negative result,} \\ 0, & \text{positive result.} \end{cases} \quad (13)$$

There are also  $m$  independent variables ( $X_1, X_2 \dots X_m$ ) that affect the value of  $Y$ . Note that  $P = P(Y = 1 | X_1, X_2 \dots X_m)$  represents the probability of a positive result under the action of  $m$  independent variables, and the logistic regression model can be expressed as

$$P = \frac{1}{1 + \exp(\alpha_0 + \alpha_1 X_1 + \alpha_2 X_2 + \dots + \alpha_m X_m)}, \quad (14)$$

where  $\alpha_0$  is the constant term and  $\alpha_1, \alpha_2, \dots, \alpha_m$  is the regression coefficient. If  $L$  is used to represent the linear combination of  $m$  independent variables,

$$L = \alpha_0 + \alpha_1 X_1 + \alpha_2 X_2 + \dots + \alpha_m X_m. \quad (15)$$

Transforming formula (14), the logistic regression model can be expressed as the following linear form:

$$\ln\left(\frac{P}{1-P}\right) = \alpha_0 + \alpha_1 X_1 + \alpha_2 X_2 + \dots + \alpha_m X_m. \quad (16)$$

TABLE 4: Area under ROC curve of BP neural network and related results.

AUC	95% CI	Accuracy	Sensitivity	Specificity	Youden's index
0.796	0.658-0.912	86.8%	82.1%	80.5%	64.7%

The left end of formula (16) is the natural logarithm of the ratio of the probability of positive and negative results, which is called the logit transformation of  $P$ , and is recorded as  $\text{logit}P$ . It can be seen that although the value range of probability  $P$  is between 0 and 1,  $\text{logit}P$  has no numerical limit.

**3.2.2. Logistic Regression Modeling.** A logistic regression model was developed using 500 patients acquired from a retrospective investigation as training samples. To examine the prediction performance, 200 patients from a prospective inquiry were employed as prediction samples, which were substituted into the developed model. Using the selected training samples, univariate logistic regression analysis was performed on the patients' basic information, clinical information, clinical biochemical indicators, postdischarge rehabilitation, and living conditions. For factor logistic regression model, see Table 1. Multifactor screening was

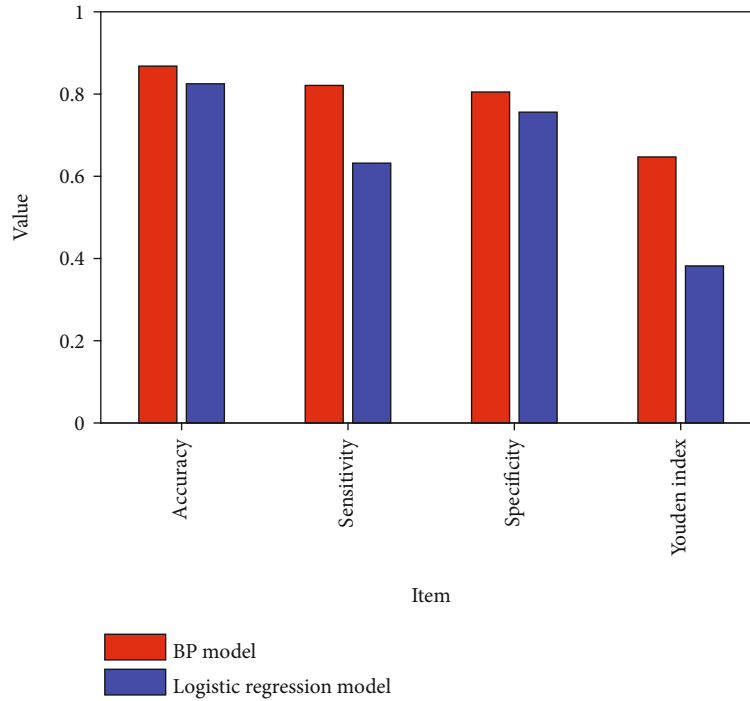


FIGURE 6: Comparison of various indicators between the BP model and logistic regression.

carried out, and the forward method based on partial maximum likelihood estimation was used. With  $\alpha = 0.05$  as the inclusion criterion and  $\alpha = 0.10$  as the exclusion criterion, a logistic regression model for predicting the recurrence of ischemic stroke patients was established. There are 7 factors that finally entered the model (see Table 2).

## 4. Experiment and Analysis

**4.1. Multivariate Logistic Regression Results.** From the 7 influencing factors screened above, a logistic regression model is established, and its expression is  $\text{logit}(P) = -6.765 + 0.045x_1 + 0.047x_2 + 0.762x_3 + 0.488x_4 - 0.216x_5 - 0.181x_6 - 0.344x_7$ ; in the formula,  $x_1, x_2, x_3, x_4, x_5, x_6$ , and  $x_7$  represent 7 factors of age, diastolic blood pressure, language barrier, alcohol consumption, triglyceride, aspirin, and sleep, respectively. Substitute 200 test samples into the logistic model established above, draw the ROC curve as shown in Figure 2, and calculate the area under the curve (AUC): AUC is 0.735, the prediction accuracy rate is 82.5%, and the sensitivity and specificity are 63.2% and 75.6%, respectively. Youden index is 38.2% (see Table 3).

### 4.2. BP Neural Network Modeling Results

**4.2.1. Establishment and Training of the Network Model.** 500 retrospectively investigated cases were used as the training set, and 200 prospectively investigated patients were used as the testing set. In order to simplify the calculation and prevent unnecessary overfitting, logistic regression was used to screen all factors by single factor in this study, and all 16 factors screened out by a single factor were used as input variables, that is, the input layer neurons  $n = 16$ . Modeling

is done using three distinct types of simple BPNN models with varied amounts of hidden layers. The number of hidden layer nodes is calculated using the trial and error method in this study, with the first hidden layer node being defined as 8 and the second and third layers being reduced layer by layer to 6 and 3, respectively. At the same time, the maximum training error is to be selected as 0.001, the initial learning rate is 0.15, the minimum learning rate is 0.001, the maximum learning rate is 0.2, and the kinetic energy term  $\alpha = 0.95$ .

**4.2.2. BP Neural Network Modeling Results.** There is no statistically significant difference between the prediction results of the training set and the actual results of each model ( $P > 0.05$ ), and the kappa values are all greater than 0.7, indicating that the prediction results are more consistent with the actual results. See Figure 3, so it can also be considered that the number of different hidden layers has little effect on the prediction results of the test set samples.

**4.2.3. Comparison of the Area under the ROC Curve of the Three BPNN Models.** The predicted probability and actual results of the three BPNN models are used to make the ROC curve. The experimental results are shown in Figure 4. It can be seen that the prediction accuracy of BPNN-1 is higher than that of the other two models.

**4.2.4. Comparison of Prediction Accuracy and Validity of Models with Different Numbers of Hidden Layers.** The prediction accuracy rates of each model are 95.2%, 94.5%, and 93.7%, respectively, and there is no statistical significance between the three accuracy rates. It can be seen that there



is no difference in the prediction accuracy of the BPNN with different hidden layers. The results are shown in Figure 5.

**4.2.5. Analysis of Influencing Factors of BPNN.** Increasing the number of hidden layers cannot improve the prediction effect of BPNN and may even affect the accuracy of model prediction. At the same time, the modeling time of a single hidden layer is short, and overfitting is not easy to occur. Choose a BPNN with one hidden layer. According to the influence degree of the imported influencing factors on the network, the top three influencing factors with the highest degree of influence are ADL, diastolic blood pressure, and aspirin consumption.

**4.2.6. Predictive Validity and Area under the ROC Curve of the Test Set of the BPNN Model.** Substitute the data of the test set into the trained neural network model, and draw the ROC curve. The area under the ROC curve was calculated to be 0.796, and the calculated agreement of the model prediction was 86.8%, the sensitivity was 82.1%, the specificity was 80.5%, and the Youden index was 64.7%. The specific results are shown in Table 4.

**4.3. Comparison Results between BP Neural Network and Logistic Regression.** Compared with the logistic regression prediction model, the product under the ROC curve of the BPNN prediction result was 0.796, which was greater than the 0.735 obtained by the logistic regression prediction model, and the difference was statistically significant when comparing the area under the curve of the two models. The accuracy rate, sensitivity, specificity, and Youden index of the BPNN are also higher than those of the logistic regression model, so the prediction effect of the BPNN is better than that of the logistic regression, as shown in Figure 6.

## 5. Conclusion

The continuous development of my country's social economy has improved the living standards of residents. Because of the prevalence of unhealthy lifestyles in my country, the incidence of stroke has continued to climb, and the age of onset has gradually decreased. Stroke has had a significant impact on our people's health. In my country, it has become one of the most serious public health issues. The latest data from the Global Burden of Disease Study show that from 2005 to 2017, the incidence of ischemic stroke in my country was on the rise. In 2017, there were 156 new ischemic strokes per 100,000 people in my country. Research shows that the disability-adjusted life years lost due to stroke in my country ranks first among all diseases, with a recurrence rate of 9.7% within three months of onset and a disability rate of 37.1%. Because BPNN has been paid more and more attention by medical workers in disease prediction, people often use it to compare with the logistic regression model. The advantages of the logistic regression model are that it is simple and easy to use, the quantitative interpretation of the individual effects of factors is clear, the approximate estimation of the relative risk can be directly obtained, and the methodology of the quantitative dependence of variables can be established. The neural network model uses the infor-

mation theory method, along with a human-like thinking mode, to develop the network by learning existing examples. It has a strong ability to solve the collinear effect and interaction between variables, and it has no restrictions on the distribution of data and can make full use of data information, with strong fault tolerance. As a nonlinear mathematical model, neural networks aid in the discovery of undiscovered correlations among various variables. Therefore, the following work is done in this paper: (1) the research progress and related technologies of IS recurrence prediction by domestic and foreign scholars are introduced, and the theoretical basis for the BP prediction model and logistic regression prediction model proposed in this paper is provided. (2) The basic principles of BPNN and logistic regression are introduced, and the logistic multifactor predictor is constructed. (3) The experimental results are that the area under the ROC curve of the logistic regression prediction model is 0.735, and the area under the ROC curve of the BPNN prediction results is 0.796. The Youden indices of BPNN and logistic regression are 64.7% and 38.2%, respectively, indicating that the prediction effect of BPNN is better than that of logistic regression. The consistency rate, sensitivity, and specificity of BPNN prediction results are greater than those of logistic regression, showing that the BPNN model has a superior fitting effect for disorders like ischemic stroke, which have many pathogenic components and complex connections between them.

## Data Availability

The datasets used during the current study are available from the corresponding author on reasonable request.

## Conflicts of Interest

The authors declare that they have no conflict of interest.

## References

- [1] W. Wang, B. Jiang, H. Sun et al., "Prevalence, incidence, and mortality of stroke in China," *Circulation*, vol. 135, no. 8, pp. 759–771, 2017.
- [2] K. Kang, T. H. Park, N. Kim et al., "Recurrent stroke, myocardial infarction, and major vascular events during the first year after acute ischemic stroke: the multicenter prospective observational study about recurrence and its determinants after acute ischemic stroke I," *Journal of Stroke and Cerebrovascular Diseases*, vol. 25, no. 3, pp. 656–664, 2016.
- [3] W. N. Kernan, R. I. Horwitz, L. M. Brass, C. M. Viscoli, and K. J. Taylor, "A prognostic system for transient ischemia or minor stroke," *Annals of Internal Medicine*, vol. 114, no. 7, pp. 552–557, 1991.
- [4] Y. Liu and X. G. Gao, "Role of ESSEN and SPI-II scores in predicting the long-term recurrent rate of ischemic stroke," *Chinese Journal of Geriatric Heart Brain and Vessel Diseases*, vol. 16, no. 12, article 3, 2014.
- [5] S. Sumi, H. Origasa, K. Houkin et al., "A modified Essen stroke risk score for predicting recurrent cardiovascular events: development and validation," *International Journal of Stroke*, vol. 8, no. 4, pp. 251–257, 2013.

- [6] X. Ling, S. M. Yan, B. Shen, and X. Yang, "A modified Essen Stroke Risk Score for predicting recurrent ischemic stroke at one year," *Neurological Research*, vol. 40, no. 3, pp. 204–210, 2018.
- [7] I. Fernández-Cadenas, M. Mendióroz, D. Giralt et al., "GRE-COS project (genotyping recurrence risk of stroke)," *Stroke*, vol. 48, no. 5, pp. 1147–1153, 2017.
- [8] Z. Zhang, G. Xu, B. Cai, H. Zhang, W. Zhu, and X. Liu, "Genetic variants in microRNAs predict recurrence of ischemic stroke," *Molecular Neurobiology*, vol. 54, no. 4, pp. 2776–2780, 2017.
- [9] R. R. Bretón and J. C. G. Rodríguez, "Excitotoxicity and oxidative stress in acute ischemic stroke," *Acute Ischemic Stroke*, vol. 200, 2012.
- [10] Y. Fu, Q. Liu, J. Anrather, and F. D. Shi, "Immune interventions in stroke," *Nature Reviews Neurology*, vol. 11, no. 9, pp. 524–535, 2015.
- [11] L. Belayev, S. H. Hong, H. Menghani et al., "Docosanoids promote neurogenesis and angiogenesis, blood-brain barrier integrity, penumbra protection, and neurobehavioral recovery after experimental ischemic stroke," *Molecular Neurobiology*, vol. 55, no. 8, pp. 7090–7106, 2018.
- [12] K. X. Jin, J. Y. Ding, and R. Meng, "Application of magnetic resonance perfusion imaging in early warning and prognosis of ischemic stroke," *Chinese Journal of Geriatric Heart Brain and Vessel Diseases*, vol. 22, no. 2, pp. 216–218, 2020.
- [13] W. N. Kernan, B. Ovbiagele, H. R. Black et al., "Guidelines for the prevention of stroke in patients with stroke and transient ischemic attack," *Stroke*, vol. 45, no. 7, pp. 2160–2236, 2014.
- [14] Group I S T C, "The International Stroke Trial (IST): a randomised trial of aspirin, subcutaneous heparin, both, or neither among 19 435 patients with acute ischaemic stroke," *The Lancet*, vol. 349, no. 9065, pp. 1569–1581, 1997.
- [15] A. Wutzler, C. Krogias, A. Grau, R. Veltkamp, P. U. Heuschmann, and K. G. Haeusler, "Stroke prevention in patients with acute ischemic stroke and atrial fibrillation in Germany - a cross sectional survey," *BMC Neurology*, vol. 19, no. 1, pp. 1–4, 2019.
- [16] W. Hacke, M. Kaste, E. Bluhmki et al., "Thrombolysis with alteplase 3 to 4.5 hours after acute ischemic stroke," *New England Journal of Medicine*, vol. 359, no. 13, pp. 1317–1329, 2008.
- [17] I. Deguchi and M. Takao, "Reduced doses of direct oral anticoagulants in ischemic stroke patients with nonvalvular atrial fibrillation," *Journal of Stroke and Cerebrovascular Diseases*, vol. 28, no. 2, pp. 354–359, 2019.
- [18] M. S. Dharmoon, W. Tai, B. Boden-Albala et al., "Risk of myocardial infarction or vascular death after first ischemic stroke," *Stroke*, vol. 38, no. 6, pp. 1752–1758, 2007.
- [19] L. Liu, Z. Wang, L. Gong et al., "Blood pressure reduction for the secondary prevention of stroke: a Chinese trial and a systematic review of the literature," *Hypertension Research*, vol. 32, no. 11, pp. 1032–1040, 2009.
- [20] Q. Jia, X. Zhao, C. Wang et al., "Diabetes and poor outcomes within 6 months after acute ischemic stroke," *Stroke*, vol. 42, no. 10, pp. 2758–2762, 2011.
- [21] J. Pei, K. Zhong, M. A. Jan, and J. Li, "Personalized federated learning framework for network traffic anomaly detection," *Computer Networks*, vol. 209, p. 108906, 2022.
- [22] D. Jiang, F. Wang, Z. Lv et al., "QoE-aware efficient content distribution scheme for satellite-terrestrial networks," *IEEE Transactions on Mobile Computing*, 2021.
- [23] G. Cai, Y. Fang, J. Wen, S. Mumtaz, Y. Song, and V. Frascolla, "Multi-carrier M-ary DCSK system with code index modulation: an efficient solution for chaotic communications," *IEEE Journal of Selected Topics in Signal Processing*, vol. 13, no. 6, pp. 1375–1386, 2019.
- [24] J. Pang, N. Zhang, Q. Xiao, F. Qi, and X. Xue, "A new intelligent and data-driven product quality control system of industrial valve manufacturing process in CPS," *Computer Communications*, vol. 175, pp. 25–34, 2021.

## Research Article

# Effect of Physical Exercise Intervention Based on Improved Neural Network on College Students' Mental Health

**Linlin Cai** 

*Nanjing Medical University, Nanjing, 210000 Jiangsu, China*

Correspondence should be addressed to Linlin Cai; [linlincai1377@njmu.edu.cn](mailto:linlincai1377@njmu.edu.cn)

Received 20 April 2022; Revised 16 May 2022; Accepted 20 May 2022; Published 21 June 2022

Academic Editor: Naeem Jan

Copyright © 2022 Linlin Cai. This is an open access article distributed under the Creative Commons Attribution License, which permits unrestricted use, distribution, and reproduction in any medium, provided the original work is properly cited.

Physical exercise refers to various physical exercises carried out through certain means and methods. Physical exercise can not only achieve the purpose of strengthening the body and health but also make people face challenges in physical and mental sports, and the resulting psychological satisfaction and excitement make exercisers happy physically and mentally. Physical activity has a certain appeal that makes it one of the most effective ways for modern people to alleviate mental illnesses. The human brain's reaction time is linked to its thinking speed and intelligence. Regular physical activity can increase human brain cell reaction time and completely utilize human brain capacity, which is beneficial to the healthy development of human attention, memory, imagination, and thinking ability. Scientific and reasonable physical exercise is also an important means to improve people's intelligence levels. Everyone's physical health level is closely related to their mental health. A healthy mind comes from a healthy body. A large number of scientific studies have confirmed that reasonably arranging the contents and methods of physical exercise according to their own health level and psychological state cannot only enhance the physique of college students but also cultivate their excellent personality. Firstly, this paper summarizes the influence of physical exercise on mental health. The ways of employing physical exercise to improve and improve the mental health of college students are presented in this study. Then, this paper proposes a physical exercise intervention based on an improved neural network (NN), which has an impact on the mental health level of college students, and the effectiveness of this model is verified by simulation experiments.

## 1. Introduction

Nowadays, with the rapid development of the social economy, the stress events faced by college students will also increase in a complex environment. When people encounter stressful events in life, they will have a sense of stress [1]. When people do not know how to face this sense of pressure, they will have all kinds of negative emotions. The National Health Commission released the content on the development of teenagers' mental health, pointing out that with the rapid development of the economy and society, various complex relationships between adults will involve teenagers, and they will also face environmental changes and complex

interpersonal communication, which will put pressure on them [2]. The psychological and physiological development of college students in this period is not fully mature. They are more likely to feel pressure and develop psychological and behavioral difficulties, such as irritation and anxiety, when their living environment changes [3]. In recent years, negative emotions have also received extensive attention in the field of psychology. Previous studies have shown that college students' stress events lead to the rise of psychological pressure, and the impact of the increase of psychological pressure on negative emotions is also gradually increasing [4]. The relationship between physical exercise and students' mental health is shown in Figure 1.

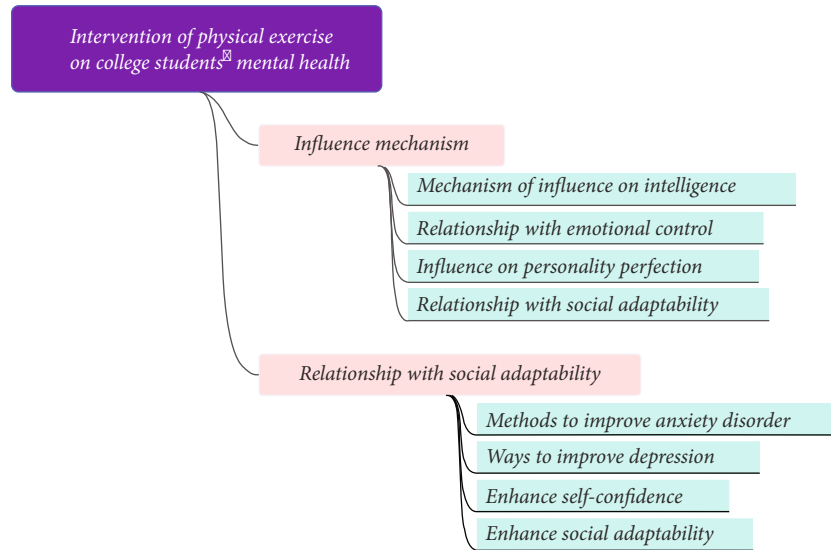


FIGURE 1: The relationship between physical exercise and students' mental health.

The proportion of negative emotions caused by psychological pressure is as high as more than 20%, mainly because college students are prone to negative emotions such as anger, anxiety, and depression in the face of various stress events [5]. Foreign researchers have found that stress can predict negative emotions; at the same time, some studies have found that the pressure perceived by individuals in daily life can positively predict a series of negative emotions such as worry and anger. Therefore, it is necessary to adopt effective regulation methods to regulate and guide college students' psychological pressure and negative emotions, so as to enhance the development of physical and mental health [6]. Physical exercise, as a means of control, has been demonstrated in some studies to be more sensitive to the impact of individual mood in the field of mental health; both short-term exercise and long-term exercise can alleviate the negative emotional state caused by psychological pressure [7]. In an experimental study, the meta-analysis of the impact of stressors on emotion pointed out that when subjects respond to stressors, their negative emotions will also increase. In daily life, college students' psychological stress, negative emotion, and physical exercise are different [8]. By tracking and measuring them, this paper explores the relationship between college students' psychological stress and negative emotion, and the impact of psychological stress on a negative emotion further enriches the relevant research on the relationship between college students' psychological stress and negative emotion and explores the regulatory effect of physical exercise between psychological stress and negative emotion. It serves as a vital foundation for future daily follow-up study in this sector [9].

This paper proposes a physical exercise intervention based on an improved NN, which has an impact on the mental health level of college students. Track and measure the daily psychological pressure, negative emotion, and physical exercise of college students, understand the overall situation of college students in these three aspects, deeply analyze the relationship between psychological pressure

and negative emotion and the impact of psychological pressure on a negative emotion, and explore the regulatory effect of physical exercise on their relationship. At the same time, it puts forward reasonable suggestions for improving college students' psychological pressure and negative emotional state and promoting their physical and mental health.

The arrangements of the paper are as follows: Section 2 discusses the related work. Section 3 defines the design of application model. Section 4 examines the experiments and results. Section 5 concludes the article.

## 2. Related Work

*2.1. Effect of Sports Intervention on Psychological Stress of College Students.* Compared with teenagers, college students enjoy higher freedom of activities. They choose their own way of life according to their own principles, schedules, and likes and dislikes. They can control their leisure time and choose their favorite exercise environment and exercise methods [10]. They can arrange the time according to their own schedule, regularly participate in physical exercise, master the skills needed for lifelong physical exercise, and may eventually become a lifelong sports population. Therefore, it is particularly important to increase the frequency of physical exercise during college. However, research shows that the frequency of physical exercise decreases with age [11]. Generally speaking, from children to teenagers, from teenagers to college students, and from college students to adults, the frequency of physical exercise is getting lower and lower. Researchers conducted a survey on the reasons for the formation of exercise habits among college students. The results found that students who participated in a course on jogging and health knowledge may have a more positive attitude towards physical exercise and are more likely to become a person who adheres to jogging as a way of fitness [12]. The mechanism of physical exercise affecting psychological stress is shown in Figure 2.

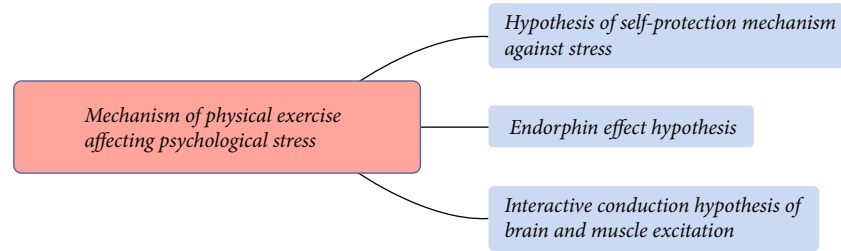


FIGURE 2: The mechanism of physical exercise affecting psychological stress.

Regular physical exercise increases the nerve excitation conduction frequency between brain and muscle, promotes the increase of brain nerve excitation, and then inhibits the level of individual psychological pressure [13]. There is an obvious item effect of sports on psychological stress: it may be related to the item group characteristics of sports. According to the event group theory, football and basketball belong to skill-dominated the same field antagonistic projects. The characteristics of this event group are high exercise intensity, which can make the exerciser focus on the limited stimulus sources during the exercise, and then lose the feeling of time. Integrate oneself organically with the environment so that the body and soul are in a balanced state with a strong sense of control and ability [14].

Volleyball, table tennis, and badminton belong to skill-oriented net separated antagonistic events, which are characterized by strong confrontation and sports load. In the process of exercise, exercisers communicate through body language. The sense of joy after victory or the negative mood after failure makes physical activities stimulate the nervous system, which is conducive to the individual getting rid of the paranoid symptoms of depressed thoughts and delusions [15]. Roller skating belongs to endurance events dominated by physical fitness. This group belongs to aerobic exercise. Aerobic exercise has a good therapeutic effect on mild to moderate anxiety and depression. Wushu belongs to the skill-oriented project, which is difficult to express beauty. The characteristics of the project can improve the flexibility and balance of the exerciser's nervous system, effectively enhance the individual's self-control ability, and significantly promote the adjustment of individual psychological states [16]. Individuals can improve their self-awareness and self-awareness in their interpersonal communication and then adjust their adaptive adjustments in the objective environment, which is crucial in improving individual psychological difficulties and development.

**2.2. Effect of the Exercise Intervention on College Students' Health Belief.** Health belief can not only affect the behavior of individuals participating in physical exercise but also effectively improve the level of individual health belief through sports intervention [17]. There is no systematic research and explanation on the mechanism of sports affecting health belief, but it can be explained according to three theories. First, there is social cognitive theory, which maintains that human activities are the outcome of interactions between people, their behavior, and their surroundings. Individuals increasingly realise the function and importance

of physical activity in sports and believe that physical activity can successfully avoid their personal risks and diseases, resulting in an increase in individual health belief [18]. Second, the theory of planned behavior holds that attitude has the function of behavior belief, which enables individuals to perceive the advantages and disadvantages of physical exercise behavior when participating in sports, so as to recognize physical exercise behavior and improve the level of individual health belief [19]. Third, the theory of protective motivation holds that the comprehensive perception of efficacy and response cost produces stress evaluation. When the internal reward and external reward system of individual health behavior perceive that physical exercise can reduce the severity and susceptibility of individual diseases, the comprehensive perception of reward and fear will produce benign evaluation, so as to improve the level of individual health belief [20].

College students' perceptions of physical activity are not limited to certain sports, such as aerobics. This study is significant because it demonstrates that previously acquired knowledge about physical activity and health can be carried over from college to adulthood. In other words, if a person takes physical exercise as an important part of his life in college, this lifestyle is more likely to last for the rest of his life [21]. Then, scholars compared the physical exercise of students from four different universities, which have different requirements for physical education. The results show that the subjects from schools with high requirements for physical education have a higher level of physical exercise than other subjects and are better than other subjects in mastering physical exercise knowledge, attitude towards physical education, and exercise habits. At the same time, the research also shows that subjects from schools with high requirements for physical education are relatively more active in physical exercise and tend to show a high desire for exercise [22]. The impact of an exercise intervention on college students' health beliefs is shown in Figure 3.

**2.3. Research Status of Improved Neural Network.** The NN is a system that simulates the results and functions of the human brain NN. Good self-learning, self-organization, fault tolerance, and the ability to simulate nonlinear relations make NNs widely used in the field of science and technology [23]. It has been proved that a simple three-layer feedforward NN using a sigmoid response function can approximate any nonlinear function. The superior performance of NNs largely depends on the learning of weights [24]. The most widely used weight learning method is the

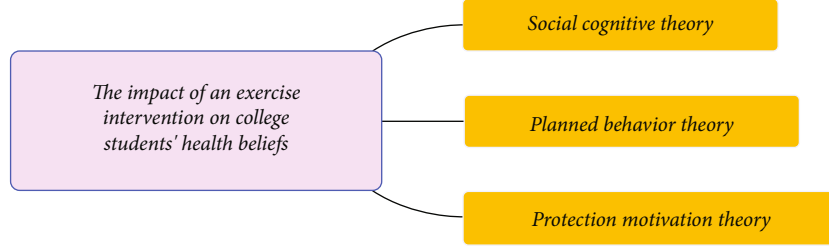


FIGURE 3: The impact of an exercise intervention on college students' health beliefs.

BP algorithm, which uses the response propagation of error to adjust the weight. However, the BP algorithm is powerless for systems that cannot determine gradient information [25].

Many academics have begun to examine utilizing the particle swarm optimization algorithm to alter the weight of NN, and the particle swarm optimization method can also optimize the structure of the NN [26], due to its development as a good global convergence approach that is simple to implement. So far, there are two main methods to train NNs with particle swarm optimization algorithms: to train the weights of NNs with particle swarm optimization algorithms [27]. One is to combine the particle swarm optimization algorithm with the BP algorithm, using the powerful global search ability of the particle swarm optimization algorithm and the good local search characteristics of the BP algorithm [28]. When the particle swarm optimization algorithm converges to a certain degree, the BP algorithm is used to continue to search for the global best of particle swarm optimization and finally get the global optimal solution [29].

### 3. Design of Application Model

**3.1. Basic Particle Swarm Optimization Algorithm.** The particle swarm optimization algorithm updates iteratively from the initial random position until it finds the global optimal position, that is, the global optimal solution of the problem. The particle swarm optimization algorithm is a random search optimization algorithm, which has good global convergence for multimodal problems. The updated formula is as follows:

$$\begin{aligned} v_{i,d}^{k+1} &= v_{i,d}^k + c_1 \times r_1 \times (p_{i,d}^k - x_{i,d}^k) + c_2 \times r_2 \times (p_{g,d}^k - x_{i,d}^k), \\ x_{i,d}^{k+1} &= x_{i,d}^k + v_{i,d}^{k+1}. \end{aligned} \quad (1)$$

The speed update of particle swarm optimization is divided into three parts: the first portion is the particle's speed before iteration; the second part is the cognitive part, which is the particle's best location; and the third part is the social part, which is the particle's best position in the particle group. Figure 4 depicts the basic flow of the particle swarm optimization technique.

Unless the optimal solution of the problem is on the trajectory of particle swarm optimization, the particle swarm will fly down at the current speed and in the same direction

until it hits the edge of the search; particle swarm optimization algorithm cannot find the optimal solution, and the optimal solution must be almost impossible on the trajectory of particle swarm optimization. In order to achieve a better balance between local search and global search, inertia weight factor is introduced into the basic particle swarm optimization algorithm. The mathematical expression is as follows:

$$v_{i,d}^{k+1} = w^* v_{i,d}^k + c_1 \times r_1 \times (p_{i,d}^k - x_{i,d}^k) + c_2 \times r_2 \times (p_{g,d}^k - x_{i,d}^k). \quad (2)$$

The inertia weight factor decreases linearly, as shown below.

$$w(k) = -0.5 \left( \frac{k}{\text{max number}} \right) + 0.9. \quad (3)$$

The decreasing inertia weight factor makes the algorithm has better global search ability in the early stage and better convergence in the later stage, but the convergence speed is relatively slow. The increasing inertia weight factor makes the algorithm to converge quickly in the early stage. The inertia weight factor that increases first and then decreases is shown in the figure below.

$$w(k) = \begin{cases} 1 \times \frac{k}{\text{max number}} + 0.4, & 0 \leq \frac{k}{\text{max number}} \leq 0.5, \\ -1 \times \frac{k}{\text{max number}} + 1.4, & 0.5 \leq \frac{k}{\text{max number}} \leq 1. \end{cases} \quad (4)$$

In the whole iterative process, the initial  $W$  is large, and the particles fly rapidly all over the whole search space. After reaching the iterative threshold, the inertia weight will be limited to  $FW$ , and the particles maintain a certain speed to find the global optimal value in the neighborhood of the optimal value. The values of uniformly distributed random inertia weight factors vary according to whether the global optimal particle position changes, as shown in the following:

$$\text{If } \Delta g \text{ best} = 0, w = \text{rand}(r_1, r_2); \text{ else } w = \text{rand}(r_3, r_4). \quad (5)$$

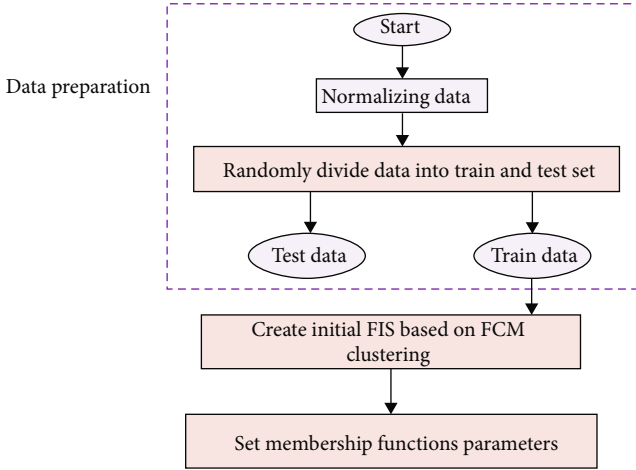


FIGURE 4: The basic flow of particle swarm optimization algorithm.

The change rate of the optimal fitness value is shown in the following formula.

$$k = \frac{f(t) - f(t-10)}{f(t-10)}. \quad (6)$$

The convergence of particles can be seen from its change. If the parameter setting is unreasonable, the speed of particles will increase or decrease rapidly. The ideal velocity of a particle swarm is to start relatively large, get smaller and smaller, and finally become 0. The inertia weight formula is as follows.

$$\begin{cases} w(t+1) = \max \{w(t) - \sigma \times \text{rand}, w_{\min}\}, & v_{\text{ave}}(t+1) > v_{\text{ideal}}(t+1), \\ w(t+1) = \min \{w(t+1) + \sigma \times \text{rand}, w_{\max}\}, & v_{\text{ave}}(t+1) \leq v_{\text{ideal}}(t+1). \end{cases} \quad (7)$$

When the position of the particle swarm does not change in a continuous number of iterations, the  $k$ -dimension of the optimal particle position is randomly taken and replaced with a random number with a certain probability. The average particle spacing formula is as follows.

$$D(t) = \left( \frac{1}{M \cdot L} \right) \sum_{i=1}^M \sqrt{\sum_{d=1}^D (x_{id}^t - \bar{p}_d)^2}. \quad (8)$$

No matter which mutation operation is adopted, the adaptive mutation operator actually uses an evaluation mechanism to randomly change the position of the optimal particle when the algorithm falls premature. In this case, similar to the multiobjective constraint processing method, all constraint functions are treated as an objective function. When there is a dominant relationship, the multiobjective constraint processing method is used for individual comparison.

**3.2. Particle Swarm Optimization Improved Neural Network.** The NN was trained using the particle swarm optimization approach, which included weight training and structural

correction. The optimization problem of finding the ideal continuous weight for NNs is essentially a continuous and difficult optimization problem. However, the possibility of a single restricted infeasible solution in the individual optimal solution may not be the most effective method, because, under this idea, the information of some important infeasible solutions cannot be used, such as the infeasible solutions with small objective function values, which may be closer to the global optimal solution than some feasible solutions. Therefore, it is very necessary to allow the infeasible solution as the guiding position with a certain probability under certain conditions. When using the particle swarm optimization algorithm to train the weights of the NN, the first is the coding of particle swarm optimization, as shown in Figure 5.

The position of each particle represents the value of all weights of a group of NNs. The specific coding method is as follows.

$$\text{particle}(i) = (w_{31} w_{32} w_{41} w_{42} w_{51} w_{52} w_{61} w_{62} w_{63}). \quad (9)$$

After particle swarm optimization coding, the error criterion function in the BP algorithm is taken as the particle fitness function, and then, the optimization is carried out according to the basic particle swarm optimization process. Finally, the location of the globally optimal particle is the ownership value of the NN. The speed update formula for connecting variables is as follows.

$$v_{ih} \leftarrow w * v_{ih} + c_1 * \text{rand} * (p_i - \delta_{ih}) + c_2 * \text{rand} * (g - \delta_{ih}). \quad (10)$$

The output of each node is calculated according to the following equation:

$$Q_i^1 = \mu_{A_i}(x) = \frac{1}{1 + [(x - v_i)/\sigma_i]^b}. \quad (11)$$

The two successive changes of weight can be regarded as the change of particle velocity, as shown as follows:

$$Q_i^2 = w_i = \mu_{A_i}(x) \mu_{B_i}(y), i = 1, 2. \quad (12)$$

The outputs are normalized firing strengths, as shown as follows:

$$Q_i^4 = \bar{w}_i f_i = \bar{w}_i (p_i x + q_i y + r_i), i = 1, 2. \quad (13)$$

The summation of all input signals as the overall output is shown as follows:

$$Q_i^5 = \text{overall output} = \sum_i \bar{w}_i f_i = \frac{\sum_i w_i f_i}{\sum_i w_i}. \quad (14)$$

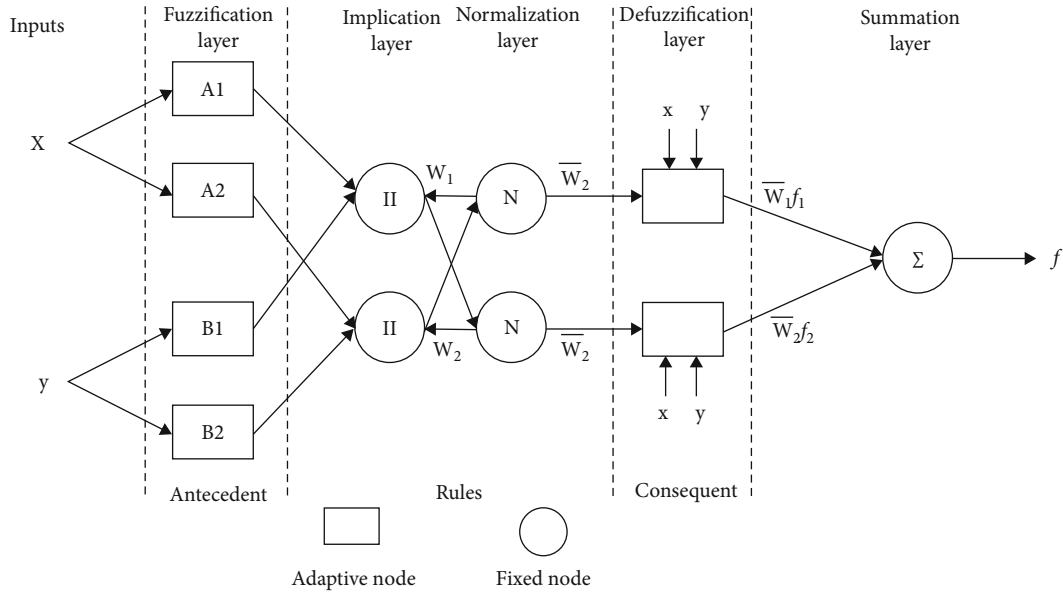


FIGURE 5: Particle swarm optimization NN structure diagram.

The inertia weights can be presented as follows:

$$\Delta\omega_2 = \lambda_1 e(k)x'_j + \lambda_2 [c_1 r_1 (\omega_2(b) - \omega_2) + c_2 r_2 (\omega_2(g) - \omega_2)]. \quad (15)$$

However, the current particle swarm optimization algorithm needs a lot of calculation when optimizing the structure of the NN, and it is difficult to meet the requirements for some problems that need online learning. One location is a feasible solution, and the other location is an infeasible solution. When this happens, in order to avoid the problem that the algorithm cannot jump out of the local extreme point due to the loss of important infeasible solution information, in the early stage of evolution, it is allowed to accept the infeasible solution with a certain probability when the function value of the infeasible solution is less than the function value of the feasible solution. However, in the later stage of the algorithm, in order to better carry out local mining, the emergence of the infeasible solution is unbearable; therefore, the probability of accepting an infeasible solution decreases to 0. At this time, it is obviously unreasonable to only consider the size of constraint violation degree and ignore the optimization function of function. Therefore, in this case, how to reasonably balance the relationship between function value and constraint violation degree and select a more reasonable position as the individual optimal guidance position is very important. In order to better evolve continuous variables and discrete variables, this algorithm uses the PSO algorithm with outstanding performance to solve continuous optimization to deal with the optimization of continuous variables, uses the GA algorithm which is mature to solve discrete optimization to deal with the evolution of discrete variables, and organically combines the two by means of collaborative crossover.

#### 4. Experiments and Results

Physical exercise refers to the process in which people produce a series of stimuli to various organ systems through scientific activities, promote a series of adaptive changes and reactions to the human body's morphological structure and physiological function, and improve health and physique. Exercise time is usually related to people's exercise load, which is mainly manifested in that if the exercise load is large, the exercise time is short. The analysis of each physical exercise time of college students is shown in Table 1 and Figure 6.

The study found that college students have sufficient physical exercise time. Those who exercise more than 30 minutes each time account for 55% of the total survey, of which 36% are in 30-60 minutes. Boys have more exercise time than girls in general. There are significant differences in physical exercise time between the sexes. Exercise intensity plays a very important role in improving and improving college students' mental health. Different physical exercise intensities will have different effects on the mental health level of college students; that is, the psychological status of students varies with the intensity of physical exercise. The intensity of each physical exercise of college students is shown in Table 2 Figure 7 and Figure 8.

The study found that nearly 80% of students said that the intensity of each exercise can reach more than medium intensity, that is, slight sweating all over the body. 36% of the students said they could reach the level of exhaustion every time they exercised. However, studies have shown that the effect of moderate-intensity physical exercise on educating the mental health of college boys is significantly higher than that of low-intensity and high-intensity physical exercise. It is suitable for college girls to use a lower moderate amount of exercise, and the suitability of exercise intensity is the guarantees of good mental health effect. The research



TABLE 1: Analysis of physical exercise time of college students.

Exercise time	Man	Woman	Total
10 min~ 30 min	17%	28%	45%
30 min~ 60 min	21%	15%	36%
More than 60 minutes	13%	6%	19%
Total	51%	49%	100%

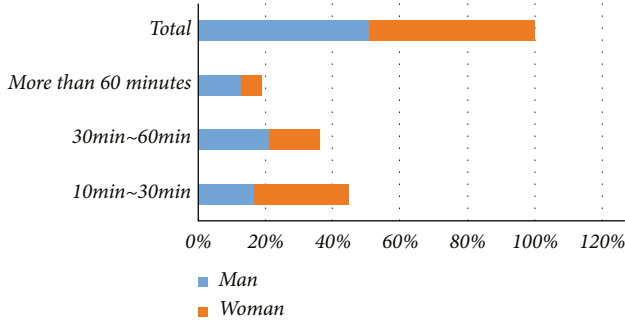


FIGURE 6: Analysis of physical exercise time of college students.

TABLE 2: The intensity of each physical exercise of college students.

Exercise time	Man	Woman	Total
High strength	21%	15%	36%
Medium strength	23%	20%	43%
Small strength	6%	9%	15%
Other	1%	5%	6%
Total	51%	49%	100%

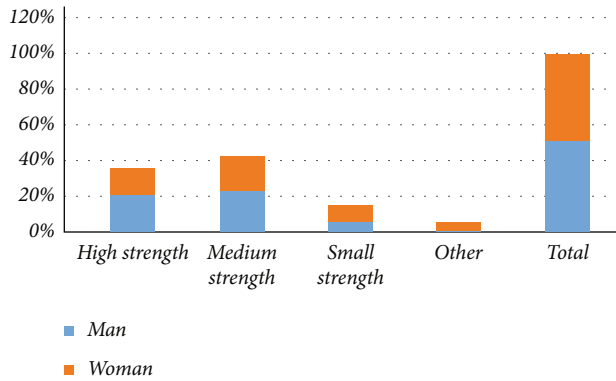


FIGURE 7: The intensity of each physical exercise of college students.

shows that the exercise intensity of college boys is generally higher than that of girls, and girls are mainly in the exercise mode below medium intensity. There is a significant difference between exercise intensity and students' gender. Self-stress assessment is to use the self-stress assessment test form to let students fill in the form and answer according to the actual situation, calculate the total score according to the corresponding bisection standard, and then evaluate the degree of stress they feel according to the corresponding score segment. The study found that the mental health level of college students is low, in which only 5% and 25% of the

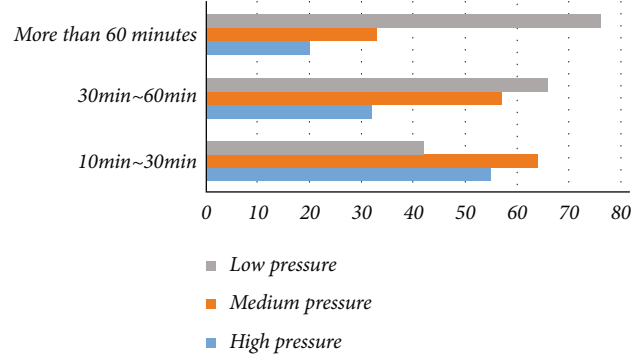


FIGURE 8: The relationship between college students' self-stress test and exercise time.

TABLE 3: The relationship between college students' self-stress test and exercise time.

Exercise time	High pressure	Medium pressure	Low pressure
10 min~ 30 min	55	64	42
30 min~ 60 min	32	57	66
More than 60 minutes	20	33	76

students feel no pressure or feel less pressure, while the number of students with moderate self-pressure accounts for 46% of the total survey, and 18% of the students feel greater self-pressure. The relationship between college students' self-stress test and exercise time is shown in Table 3.

Physical activity is not only beneficial to college students' intellectual growth, but it also has a clear influence on reducing anxiety, building a positive self-concept, and removing psychological barriers, as evidenced by the findings. In the process of exercise, it improves the level of college students' health belief, makes individuals subjectively evaluate psychological stress, and has a great negative impact on health caused by illness so that the health belief that avoiding psychological stress is good for personal health regulates the process of exercise to improve psychological stress. Taking the students in five colleges and universities in Jiangsu Province as the survey object, this paper studies the intervention of physical exercise on college students' mental health by using the methods of literature, investigation, mathematical statistics, and logical analysis.

### 5. Conclusion

College students are a special group, and their physical and mental health is the basis for success. Their physical appearance and health are directly tied to the future health, scientific, and technical benefits of high-tech teams. We require physical exercise to strengthen our bodies because our daily studies and lives prevent us from moving for long periods of time. This research suggests a physical exercise intervention based on enhanced NN that has an effect on college students' mental health. To sum up, the appropriate sports plan can help college students carry out scientific and reasonable

exercises. This kind of physical exercise mode has stronger pertinence and is effective in improving and improving the mental health level of college students.

At present, medical psychology has achieved certain results in the diagnosis and treatment of mental diseases, but the particularity of physical exercise cannot be compared with other ways to improve and treat mental diseases. For college students, it is more effective and useful. College students are frequently impacted by emotional oscillations and excessive mental tension due to the quick speed of work and living in today's culture, as well as severe rivalry. College students can formulate appropriate physical exercise methods to improve their mental health level according to their own physical conditions, health status, interests, and hobbies and make timely adjustments and interventions for their psychological and emotional adverse reactions, so as to make their physical and mental relaxation moderate and always maintain a relatively stable state. Because physical exercise has high application value and theoretical research value to promote the level of mental health, we should constantly explore this field and study more effective means and methods to improve the level of mental health.

### Data Availability

The datasets used during the current study are available from the corresponding author on reasonable request.

### Conflicts of Interest

The author declares that he has no conflict of interest.

### References

- [1] P. Veliz, Q. Epstein-Ngo, E. Austic, C. Boyd, and S. E. McCabe, "Opioid use among interscholastic sports participants: an exploratory study from a sample of college students," *Research Quarterly for Exercise and Sport*, vol. 86, no. 2, pp. 205–211, 2015.
- [2] P. Liu, "Research on college students' conformity in sports," *Creative Education*, vol. 7, no. 3, pp. 449–452, 2016.
- [3] J. Han and H. Lee, "A study on structural relations among the social support, self-esteem, and college life adjustment of college students participating in convergence leisure sports activities," *Journal of Digital Convergence*, vol. 13, no. 8, pp. 515–523, 2015.
- [4] R. J. Martin, S. E. Nelson, A. R. Gallucci, and J. G. L. Lee, "Daily and season-long fantasy sports participation and gambling-related problems among a sample of college students at three universities," *International Gambling Studies*, vol. 18, no. 3, pp. 395–407, 2018.
- [5] J. Odat, "The reasons for the reluctance of Princess Alia University college students' from practicing sports activities," *International Education Studies*, vol. 8, no. 4, pp. 40–51, 2015.
- [6] M. Ulukan, Y. Şahinler, and R. Eynur, "Investigation of happiness levels of physical education and sports college students," *International Journal of Psychology and Educational Studies*, vol. 7, no. 4, pp. 73–83, 2020.
- [7] A. Garcia, H. Huerta, J. Ramirez, and O. E. Patrón, "Contexts that matter to the leadership development of Latino male college students: a mixed methods perspective," *Journal of College Student Development*, vol. 58, no. 1, pp. 1–18, 2017.
- [8] J. Boehmer, "Does the game really change? How students consume mediated sports in the age of social media," *Communication & Sport*, vol. 4, no. 4, pp. 460–483, 2016.
- [9] C. Yake, "Influence of tobacco on physical fitness recovery of college students after sports," *Tobacco Regulatory Science*, vol. 7, no. 5, pp. 3445–3451, 2021.
- [10] T. Li and J. Song, "Research on promotion methods of positive mental health of college students under the model of ecological sports teaching," *Ekoloji*, vol. 28, no. 107, pp. 1861–1868, 2019.
- [11] Y. Liang, J. Zhang, Y. Cui, and R. Yuan, "Experimental study for cultivating college students' sports motivation in sport education model," *Advances in Physical Education*, vol. 6, no. 3, pp. 169–177, 2016.
- [12] Z. Liu and B. Hu, "A novel evaluation technology to the sports teaching effect of college students based on improved ELEC-TRE method," *Journal of Computational and Theoretical Nanoscience*, vol. 13, no. 5, pp. 3451–3457, 2016.
- [13] S. Gu and X. Shi, "Investigation and research on present situation of college students group participating in sports tourism in Shanxi Province," *Journal of Human Movement Science*, vol. 2, no. 3, pp. 20–27, 2021.
- [14] L. Marchica and J. Derevensky, "Fantasy sports: a growing concern among college student-athletes," *International Journal of Mental Health and Addiction*, vol. 14, no. 5, pp. 635–645, 2016.
- [15] M. Yasar and M. Turgut, "Unemployment anxiety of last year college students," *Cypriot Journal of Educational Sciences*, vol. 15, no. 1, pp. 56–64, 2020.
- [16] J. Xu, "A study of extension strategies of multimedia online teaching platform in sports teaching of universities," *Journal of Computational and Theoretical Nanoscience*, vol. 14, no. 1, pp. 94–98, 2017.
- [17] C. Hsu, Y. Huang, and Y. Lee, "Research on the motivation and attitude of college students' physical education in Taiwan," *International Journal of Physical Education, Fitness and Sports*, vol. 8, no. 1, pp. 95–109, 2019.
- [18] A. Bryant and D. Clement, "Coping strategies of female peer leaders participating in college club sports," *Recreational Sports Journal*, vol. 39, no. 1, pp. 16–26, 2015.
- [19] Y. Ren, R. Tang, and X. Jiang, "Three track teaching mode of sports anatomy based on innovative theory," *International Journal of Emerging Technologies in Learning (iJET)*, vol. 15, no. 24, pp. 75–88, 2020.
- [20] A. Wilson, K. Kamara, Z. Papalia, M. Bopp, and C. M. Bopp, "Changes in hypertension diagnostic criteria enhance early identification of at risk college students," *Translational Journal of the American College of Sports Medicine*, vol. 5, no. 1, pp. 1–5, 2020.
- [21] D. Engquist, A. Smith, J. Chimera, and M. Warren, "Performance comparison of student-athletes and general college students on the functional movement screen and the Y balance test," *The Journal of Strength & Conditioning Research*, vol. 29, no. 8, pp. 2296–2303, 2015.
- [22] M. McElveen and K. Ibele, "Retention and academic success of first-year student-athletes and intramural sports participants," *Recreational Sports Journal*, vol. 43, no. 1, pp. 5–11, 2019.
- [23] N. Yu, Y. Zhai, Y. Yuan, and Z. Wang, "A bionic robot navigation algorithm based on cognitive mechanism of

- hippocampus,” *IEEE Transactions on Automation Science and Engineering*, vol. 16, no. 4, pp. 1640–1652, 2019.
- [24] B. Gordan, D. J. Armaghani, M. Hajihassani, and M. Monjezi, “Prediction of seismic slope stability through combination of particle swarm optimization and neural network,” *Engineering with Computers*, vol. 32, no. 1, pp. 85–97, 2016.
- [25] R. Taormina and K. Chau, “Neural network river forecasting with multi-objective fully informed particle swarm optimization,” *Journal of Hydroinformatics*, vol. 17, no. 1, pp. 99–113, 2015.
- [26] T. Liu and S. Yin, “An improved particle swarm optimization algorithm used for BP neural network and multimedia course-ware evaluation,” *Multimedia Tools and Applications*, vol. 76, no. 9, pp. 11961–11974, 2017.
- [27] S. Chatterjee, S. Sarkar, S. Hore, N. Dey, A. S. Ashour, and V. E. Balas, “Particle swarm optimization trained neural network for structural failure prediction of multistoried RC buildings,” *Neural Computing and Applications*, vol. 28, no. 8, pp. 2005–2016, 2017.
- [28] L. Yang and H. Chen, “Fault diagnosis of gearbox based on RBF-PF and particle swarm optimization wavelet neural network,” *Neural Computing and Applications*, vol. 31, no. 9, pp. 4463–4478, 2019.
- [29] A. Ahmadi, R. Soleimani, M. Lee, T. Kashiwao, and A. Bahadori, “Determination of oil well production performance using artificial neural network (ANN) linked to the particle swarm optimization (PSO) tool,” *Petroleum*, vol. 1, no. 2, pp. 118–132, 2015.

## Research Article

# Prediction of Ischemic Stroke Recurrence Based on COX Proportional Risk Regression Model and Evaluation of the Effectiveness of Patient Intensive Care Interventions

Yun Wang  and Ting Lu 

*Department of Neurology Nursing, Sichuan Provincial People's Hospital, University of Electronic Science and Technology of China, Chinese Academy of Sciences Sichuan Translational Medicine Research Hospital, Chengdu, Sichuan 610072, China*

Correspondence should be addressed to Ting Lu; [luting@med.uestc.edu.cn](mailto:luting@med.uestc.edu.cn)

Received 11 May 2022; Revised 1 June 2022; Accepted 4 June 2022; Published 20 June 2022

Academic Editor: Naeem Jan

Copyright © 2022 Yun Wang and Ting Lu. This is an open access article distributed under the Creative Commons Attribution License, which permits unrestricted use, distribution, and reproduction in any medium, provided the original work is properly cited.

With the continuous improvement of medical technology and the aging of the population, the death rate of stroke is gradually decreasing, but the recurrence rate is still high, and the number of recurrences is increasing, resulting in disability and other symptoms, which brings great burden and distress to patients and their families. As the number of strokes increases, neurological impairment becomes more and more severe, affecting patients' ability to live, socialize, and work, and seriously reducing their quality of life. Clustered care is a combination of evidence-based linked interventions and a multidisciplinary team providing the best possible care through evidence-based research and highly operational practice, and it can improve outcomes for ischemic stroke patients more than implementation alone. This paper presents a Cox proportional risk regression-based model, using it to build the most used semi-parametric model for multifactorial survival analysis, due to its advantages of both parametric and nonparametric models, and to analyze the factors influencing survival time in study subjects with incomplete data. The proposed strategy has been found to be useful in predicting ischemic stroke recurrence and cluster care interventions for patients.

## 1. Introduction

Currently, the treatment strategy of ischemic stroke is to improve cerebral blood circulation, restore blood flow in obstructed blood vessels as early as possible, ensure the stability of cerebral blood flow, and reduce neurological damage through pharmacological thrombolysis or mechanical embolization. The advantages, disadvantages, and research progress of cerebral blood circulation improvement therapy, neuroprotective therapy, and preventive therapy for IS are reviewed in order to provide new ideas for the development of IS prevention strategies and therapeutic drugs [1–3].

Irreversible necrosis will develop in the ischemic core area of brain tissue after the development of IS. It is possible to successfully reduce cerebral ischemia damage and recover the structure and function of brain tissue if cerebral blood circulation can be improved promptly within the therapy

time window. Measures like thrombus clearance and vasodilation are frequently employed in clinical practice to improve cerebral blood circulation. Within the therapeutic time window, thrombus removal is the most effective way to restore blood flow to the ischemic area. In clinical practice, thrombus removal therapy includes intravenous thrombolysis and endovascular intervention [4–6]. The major thrombolytic method is intravenous thrombolysis using tissue-type fibrinogen activator, which is straightforward, quick, and relatively safe within the therapeutic time window. In addition, neuroprotective agents are a promising IS treatment strategy, which can reduce the extent and degree of neuronal cell death after IS to play an anti-IS role. The main symptoms of ischemic stroke are shown in Figure 1.

Therefore, the clinical translation of neuroprotective agents has become a hot topic of research. The use of tPA

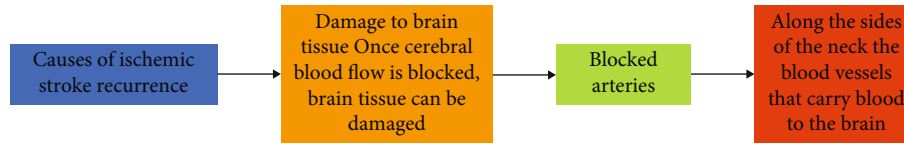


FIGURE 1: Main symptoms of ischemic stroke.

beyond the time window (6 h) will lead to an increased risk of hemorrhagic transformation and mortality by four; therefore, only 1% of patients benefit from clinical treatment with t-PA intravenous thrombolysis. There is no significant thrombolytic effect with intravenous thrombolysis for vascular occlusion caused by platelet-rich emboli, old emboli, calcified emboli, or fat emboli. With the maturity of medical imaging technology, scholars found that there exists part of the ischemic semi dark zone with mainly apoptotic neurons in the marginal zone between the normal zone around the central area of ischemia and the ischemic zone, and restoring the blood flow state of the ischemic semi dark zone can stop its transformation into necrotic tissue. Therefore, the brain tissue density and gray-white matter interface of the insular zone after 4.5 h of IS attack were observed with the cooperation of imaging, and patients with small infarct core volume and disproportionate cerebral infarct area were selected for intravenous thrombolytic therapy by assessing the size of salvageable brain tissue. The thrombolytic effect and prognosis were good [7]. One study used CT/magnetic resonance perfusion imaging and RAPID automated software to assess the degree and extent of cerebral ischemia, identify salvageable brain tissue, and screen patients with a perfusion defect-core ischemic area mismatch for t-PA intravenous thrombolysis and showed that good outcomes and prognosis were still achieved by extending the thrombolysis time window to 9 h in the screened patients.

In China, where the nurse-patient ratio is severely imbalanced, targeted evidence-based practice is more conducive to rational deployment of medical resources to improve the quality-of-care delivery in terms of quantity and quality. The development of a clustered nursing intervention program as a link in the distribution of evidence for JBI evidence-based nursing practice integrates evidence into clinical practice in a way that supports nursing interventions' scientific basis in clinical implementation [8, 9]. Clustered care is the construction of specific task lists and standardized care processes. Each care intervention in a structured program is based on high-level clinical evidence, and its effects are greater than the effects of individual interventions through integration, which can be targeted to provide patients with safer and more reliable care and to achieve the best possible outcomes. The single-patient cluster care interventions are not static but are implemented in a way that considers clinical realities and patient wishes. Both patients and caregivers are involved in the health management process, and each intervention is evaluable, providing feedback to clinical staff, improving the quality of clinical care, enhancing the patient-nurse relationship, and increasing patient compliance and satisfaction [10]. Currently, traditional empirical nursing approaches are used to avoid

lower extremity DVT in acute ischemic stroke patients, and a scientific preventative system has yet to be developed. The use of mechanical prophylaxis, pharmacological prophylaxis, and early activity alone can improve one aspect of the cause of lower extremity DVT and thus prevent thrombosis, which has been verified in clinical studies. For example, early functional exercise and intermittent pneumatic compression devices can improve the flow rate of blood in patients' lower extremities, accelerate blood flow, avoid blood stagnation in the lower extremities, and prevent the aggregation of clotting factors while through drugs can not only improve the hypercoagulable state of blood, but also increase the risk of bleeding in patients, and how to make the benefits of drug prophylaxis outweigh the risks in patients is still controversial. The occurrence of LDVT is based on high blood viscosity, slow blood flow, and vascular wall. The interconnection and interaction between the three main etiologies of LDVT lead to abnormal clotting of blood to form emboli and impede blood flow. The risk of lower extremity DVT in patients with acute ischemic stroke can be more effectively prevented through the development and implementation of a cluster care intervention program and enhanced health education for patients and caregivers [11].

The Cox proportional risk regression model, also known as Cox regression, was proposed in 1972 and is now the most widely used and classic modelling method in survival analysis. It is primarily used in the medical field for the analysis of prognostic factors in oncology and other chronic diseases, as well as the evaluation of clinical outcomes and etiologic exploration. The application of the Cox proportional risk regression model is limited to some extent by the presence of nonlinear effects between the independent and dependent variables. However, compared with the Kaplan-Meier method, it can satisfy the simultaneous analysis of multiple variables and also analyze the effects of continuous variables on survival outcomes. In this paper, we propose a COX-based proportional risk regression model for ischemic stroke recurrence prediction and patient clustering care intervention.

The paper's organization paragraph is as follows: The related work is presented in Section 2 as well as ischemic stroke disease and bundled patient care. Section 3 analyzes the methods of the proposed work. Section 4, discusses the experiments and results. Finally, in Section 5, the research work is concluded.

## 2. Related Work

In this section, we define the ischemic stroke disease, and bundled patient care in depth.

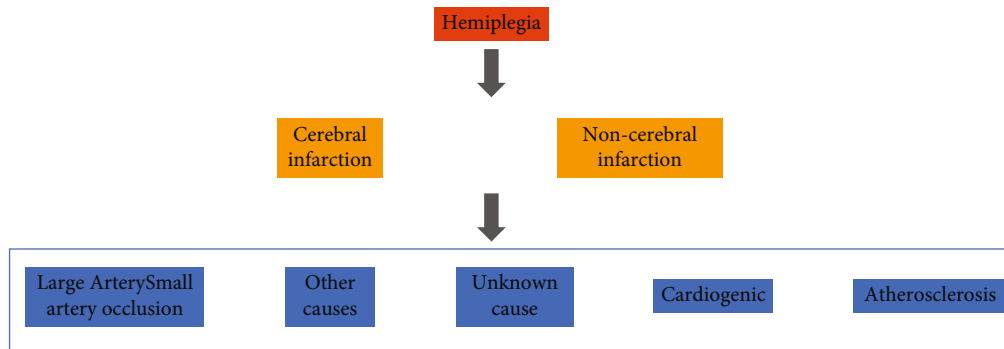


FIGURE 2: Ischemic stroke diagnostic process.

**2.1. Ischemic Stroke Disease.** Stroke is currently the number one disease causing death among Chinese residents. Ischemic strokes account for about 80% of all stroke cases and are characterized by high mortality, disability and recurrence rates, posing a huge burden to the world. Currently, the incidence of ischemic stroke is decreasing year by year in developed countries worldwide, but it is still on the rise in China, making the task of prevention and treatment very difficult. Nerve cells in the brain are highly intolerant to ischemia and hypoxia, and rapid and effective intervention in the acute phase is a key aspect to improve the prognosis of patients with ischemic stroke [12, 13].

The half-life of rt-PA is only 3-5 min, which requires continuous intravenous drip administration, and for strokes caused by acute occlusion of large vessels, the rate of revascularization after rt-PA intravenous thrombolysis does not exceed 25%. Therefore, the search for a drug with a wider therapeutic window, a simpler method of administration (e.g., intravenous push), and a higher revascularization rate has become the goal. The new thrombolytic drugs tenecteplase, a recombinant product, and desmopressin, derived from the saliva of vampire bats, both have higher fibrin specificity and longer half-life than rt-PA; however, whether these drugs are more effective than rt-PA remains to be confirmed in more clinical studies. Endovascular therapy, as opposed to intravenous thrombolytic therapy, provides direct local intervention in thrombosis and theoretically allows for more rapid and effective opening of occluded vessels. Prior to the advent of thrombolytic devices, intra-arterial thrombolysis was used with a view to intervene locally on the thrombus. The ischemic stroke diagnosis process is shown in Figure 2.

The Study of the Use of Recombinant Urokinase Pro in Acute Cerebral Thromboembolism (PROACT)-II has demonstrated that intra-arterial local instillation of urokinase pro has a high rate of revascularization, but with a concomitant increased risk of intracranial hemorrhage. Mechanical thrombolysis relies on local mechanical force to remove the thrombus, theoretically avoiding the effect of drugs on coagulation and thus reducing the risk of bleeding. Mechanical thrombolysis based on intravenous thrombolysis improves the revascularization rate significantly when compared to intravenous thrombolysis alone, while the proportion of patients with 90-day modified Rankin Scale (mRS)

scores 0-2 increases significantly, and the risk of bleeding even tends to decrease, demonstrating that thrombolysis [14–16]. Therefore, endovascular therapy is the second breakthrough in the field of ischemic stroke treatment after rt-PA intravenous thrombolysis. Endovascular techniques include intra-arterial thrombolysis and stent retrieval, the latter of which has evolved into thrombus aspiration and Solombra techniques to further improve recanalization rates, reduce the risk of distal embolism, and mitigate mechanical damage to the cerebral vasculature. Compared with intravenous thrombolysis, thrombectomy has significantly improved the recanalization rate, even up to 90% or more. Further meta-analysis showed that thrombolysis is a highly effective treatment for achieving good clinical outcome, and the treatment time window can be further extended to 7.3 h. For patients with acute occlusion of large cerebral vessels within the thrombolysis time window, bridging therapy remains the gold standard, but it is still controversial whether endovascular treatment should be performed directly instead of intravenous thrombolysis. Some studies suggest that bridging within the time window of thrombolysis is not superior to direct endovascular therapy for ischemic stroke with large vessel occlusion in the anterior circulation, but there are no additional clinical studies to confirm this conclusion [17, 18].

The limited time window for stroke treatment requires that stroke patients be identified and recognized as soon as possible and that emergency systems transport stroke patients to the nearest stroke center as soon as possible. Therefore, it is important to establish a regionalized stroke care network. Primary stroke centers within the network should provide plain-scan computed tomography (CT) and intravenous thrombolysis, while advanced stroke centers should provide more comprehensive neuroimaging, including magnetic resonance imaging, CT angiography, and digital subtraction angiography, with formally trained neurovascular interventionalists, stroke physicians, neurosurgeons, neurologists, and neurocritical care physicians. The mobile CT system allows patients to be seen at the same time. The use of mobile CT allows patients to receive an initial imaging evaluation in the ambulance, while the telemedicine consultation system allows specialists to direct emergency physicians to initiate rt-PA IV thrombolysis prior to transport at any time.

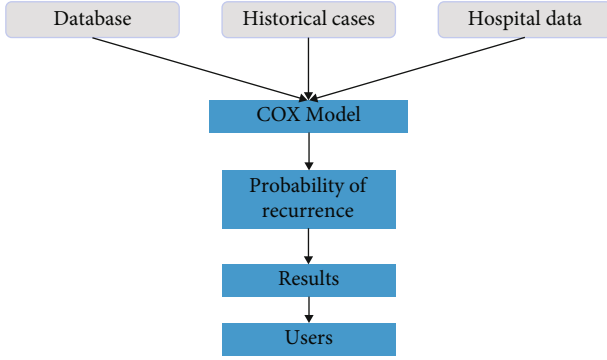


FIGURE 3: Patient intensive care intervention process.

2.2. *Bundled Patient Care.* Bundle of care is a collection of evidence-based interventions offered by a multidisciplinary team using evidence-based research and practice to provide the best possible care, is highly actionable, and can enhance patient outcomes more effectively than if executed separately. The patient cluster care intervention process is shown in Figure 3.

The following factors were generally considered: whether the patient directly benefited, whether the number of days in the hospital was shortened, whether the cost was reduced, and whether the utilization of health care resources was improved. Timely feedback on the results of the implementation of cluster-based care and continuous promotion of its application in clinical practice [19]. Evidence-based care is a nursing concept that has played a huge role in the development of nursing specialization worldwide and has increased as the impact of evidence-based medicine has grown on the medical community. The core idea of evidence-based nursing is the judicious, explicit, and judicious application of the best research evidence to provide the best care for patients with the goal of achieving the best possible recovery outcomes. Evidence-based nursing is primarily a clinical practice based on scientific evidence, combining subjective and objective patient data, clinical experience, and the application of best practice evidence to clinical care and as a basis for clinical care decisions. Cluster-based care is the introduction of evidence-based concepts into clinical practice and the creation of best practice guidelines for the care of patients with prevalent nursing problems or a certain disease, which are highly operational, reliable, and scientific, and their joint interventions are more effective in improving the quality of patient care than individual interventions. The most important feature of clustered care is its ability to integrate with clinical practice, i.e., to apply high-quality evidence that is consistent with clinical scenarios and patient preferences and wishes, thereby promoting the standardization and effectiveness of clinical care practices and improving patient outcomes. In summary, the most important advantage of cluster-based care is that it is based on a combination of patient preferences and clinical scenarios that address the many influencing factors and difficult care issues. Clustered care is supported by evidence-based theory and aims to provide the best and most complete care possible for the patient. It

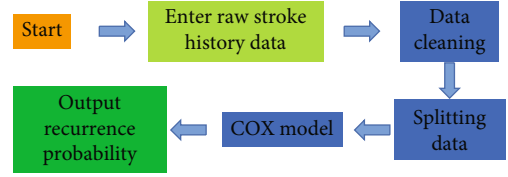


FIGURE 4: COX model recurrence prediction process.

is applied in patients with AIS dysphagia, combining effective interventions and maximizing the impact of each intervention to reduce the incidence of adverse events and improve the patient's recovery outcome. Cluster-based care requires nursing staff to continuously summarize lessons learned and grasp the evidence-based basis when implementing interventions and to give the best care plan based on the original nursing evidence [20, 21].

The concept of clustered care originated from the 1996 to 1998 policy on medical care, stating that evidence-based principles should be followed before all measures are carried out to promote the quality of care. Currently, the international application of clustered care is focused on critical care, emergency care, catheter-associated bloodstream infections, and sepsis, where the rate of catheter-associated bloodstream infections is increasing year by year, accompanied by increased mortality, disability, and length of stay, so clustered care interventions, such as skin preparation with chlorhexidine gluconate, maximizing sterile barriers during placement, selection of subclavian vein placement, hand hygiene, and daily catheterization, which have been categorized by the IHI as central venous catheterization care interventions, have been effective in reducing the incidence of catheter-associated bloodstream infections and improving the quality of life of patients.

### 3. Methods

In the method section, we define the model assumptions and their tests, parameter interpretation, parameter estimation and hypothesis testing, and implementation of a centralized nursing intervention program in detail.

3.1. *Model Assumptions and their Tests.* The COX model recurrence prediction process is shown in Figure 4. The Cox proportional risk regression model is as follows:

$$h(t) = h_0(t) \exp(\beta_1 X_1 + \beta_2 X_2 + \dots + \beta_p X_p). \quad (1)$$

From the Cox proportional risk regression model, the ratio of any two individual risk functions, i.e., the risk ratio, is

$$\begin{aligned} \text{HR} &= \frac{h_i(t)}{h_j(t)} = \frac{h_0(t) \exp(\beta_1 X_{i1} + \beta_2 X_{i2} + \dots + \beta_p X_{ip})}{h_0(t) \exp(\beta_1 X_{j1} + \beta_2 X_{j2} + \dots + \beta_p X_{jp})} \\ &= \exp \left[ \beta_1 (X_{i1} - X_{j1}) + \beta_2 (X_{i2} - X_{j2}) + \dots \right. \\ &\quad \left. + \beta_p (X_{ip} - X_{jp}) \right], i, j = 1, 2, \dots, n. \end{aligned} \quad (2)$$

The ratio is independent of  $h_0(t)$  and independent of time  $t$ . That is, the effects of the independent variables in the model do not change with time, and the risk of recurrence for a patient with a particular prognostic factor vector remains in a constant ratio at all-time points to the risk of recurrence for a patient with another particular prognostic factor vector, a situation known as proportional risk. The test for the PH assumption consists of a graphical method and a test method. The graphical method involves observing the distribution or trend of the scattered points in the scatter plot, primarily the COX-KM survival curve, and the graphical method based on the cumulative risk function, the Schoenfeld residual plot, and the Score residual plot to determine whether the survival time satisfies or approximates the PH assumption. The test method is to determine whether the PH assumption is satisfied or approximately satisfied based on the magnitude of the test statistic and the corresponding  $p$  value, mainly the time covariance method, linear correlation test, weighted residual score test, and the third spline function method. Due to the limitation of space, only the COX-KM survival curve and the graphical method based on the cumulative risk function are introduced here, and readers interested in other methods can refer to the literature.

The COX-KM survival curve method is to observe the Kaplan-Meier survival curves grouped by that variable (meaning the independent variable to be examined), and if the survival curves are significantly crossed, the PH assumption is not satisfied. The graphical method based on the cumulative risk function is to plot the survival curves for each group of the categorical covariate with the survival time  $t$  as the horizontal axis and the log survival  $\ln[-\ln \hat{S}(t)]$  as the vertical axis, and the PH assumption is satisfied if the curves corresponding to each group of the covariate are approximately parallel or equidistant. For continuous variables, the variable can be discrete, and the COX-KM survival curves or  $\ln[-\ln \hat{S}(t)]$  plotted against survival time  $t$  for each group can be compared, or the interaction term of continuous variables with log survival time can be put into the regression model, and if the interaction term is not statistically significant, the PH assumption is satisfied. If all covariates (meaning independent variables or influences other than time  $t$ ) satisfy or approximately satisfy the PH assumption, the Cox proportional risk regression model can be applied directly.

**3.2. Parameter Interpretation.** Let  $\beta$  represent the absolute value of the difference in the value of the  $i^{th}$  independent variable taken on two different individuals, under the condition that the other independent variables take the same value, the variable  $\beta$ , the natural logarithm of the risk ratio caused by each unit increase  $\beta$  in the Cox proportional risk regression model, that is,  $\ln HR_i = \beta_i$ . When  $\beta > 0$ ,  $HR > 1$ , indicating that when  $X$  increases, the risk function increases, and  $X$  is risk factor (its real meaning is: such factors take high level relative to take low level risk increase); when  $\beta < 0$ ,  $HR < 1$ , it means that when  $X$  increases, the risk func-

tion decreases, and  $X$  is a protective factor (its real meaning is: such factors take high level relative to take low level risk decrease); when  $\beta = 0$ ,  $HR = 1$ , it means that when  $X$  increases, the risk function remains unchanged, and  $X$  is a factor with no effect on survival time factors that have no effect on survival time.

**3.3. Parameter Estimation and Hypothesis Testing.** The estimation of the partial regression coefficients  $\beta_1, \beta_2, \dots, \beta_p$  needs to be obtained with the maximum likelihood estimation method with the help of the partial likelihood function. The partial likelihood function is calculated as follows:

$$L = q_1 q_2 \cdots q_i \cdots q_k = \prod_{i=1}^k q_i \tag{3}$$

$$= \prod_{i=1}^k \frac{\exp(\beta_1 X_{i1} + \beta_2 X_{i2} + \cdots + \beta_p X_{ip})}{\sum_{S \in R(t_i)} \exp(\beta_1 X_{s1} + \beta_2 X_{s2} + \cdots + \beta_p X_{sp})}$$

The baseline risk function  $h_j(t)$  in the denominator resists  $j = i$  elimination. Taking the logarithm of the partial likelihood function, the logarithmic partial likelihood function  $\ln L$  is obtained, and the solution of  $\ln L$  with the first-order partial derivative of 0 with respect to  $\beta_p$  is obtained (usually a nonlinear iterative algorithm is required, which is omitted here).

The maximum likelihood estimate  $b$  of  $\beta$  is then obtained. The hypothesis testing approach is comparable to logistic regression analysis, with likelihood ratio test, Wald test, and score test, and the detailed theory is ignored here; both parameter estimation and hypothesis testing may be done quickly with statistical software.

For 0-1 variables (i.e., two-sample survival information), the following expressions hold when the PH assumptions are satisfied:

$$h(t) = h_0(t) \exp(\beta x),$$

$$H(t) = H_0(t) \exp(\beta x), \tag{4}$$

$$\log H(t) = \log H_0(t) + \beta x$$

$$\log[-\log S(t)] = \log[-\log S_0(t)].$$

For a numerical variable Cox model, the data can be divided into layers based on a numerical variable within the model, and the Cox model is fitted to each layer separately. If the values of each layer are similar to the original model and the plot of  $\log H(t)$  or  $\log[-\log S(t)]$  against  $t$  for each layer is approximately parallel, then the risk rate is proportional, and it is appropriate to introduce this variable in the model. This method can also be used for the PH assumption when graphing  $k$  covariates. Assuming that there are  $M$  subgroups based on combinations of values of the  $k$  variables, the  $m$ -th subgroup will contain individuals with covariate characteristic  $X$ . The survival curve is estimated within each subgroup by a nonparametric method, i.e., the Kaplan-Meier method, and the  $M$  groups, can be considered proportional if the plot of the  $M$  log



cumulative risk functions  $\log [-\log S(t)]$  against  $t$  is approximately parallel:

$$\begin{aligned}\hat{w}(t) &= \frac{\hat{H}_1(t)}{\hat{H}_0(t)} = \exp(\hat{\beta}), \\ \hat{r}(t) &= \log [-\log \hat{S}_1(t)] - \log [-\log \hat{S}_0(t)].\end{aligned}\quad (5)$$

Then, the graph of  $\hat{w}(t)$  or  $\hat{r}(t)$  versus  $t$  can be used to evaluate whether the PH assumption is satisfied. It is characterized by the evaluation of the constancy of one curve instead of comparing the parallelism of two curves. The scatter plot fluctuates randomly around the center  $\exp(\hat{\beta})$  or  $\hat{\beta}$  under the PH assumption. Note that if  $\beta(t) = \log [h_1(t)/h_0(t)]$ ,  $\log [H_1(t)/H_0(t)] = \log [h_1(t)/h_0(t)]$  when the PH assumption is satisfied, and not when the PH assumption is satisfied, because  $\log [H_1(t)/H_0(t)] \neq \log [h_1(t)/h_0(t)]$ , so  $f(t) \neq B(t)$ , we cannot infer from (t) from the shape of (1), i.e., such graphs can only give disproportionate baseline risk for each stratum, but not detailed information about the type of deviated risk, which is exactly what we need.

**3.4. Implementation of a Centralized Nursing Intervention Program.** Although DVT prophylaxis has been carried out for many years, it is now commonly believed that DVT occurs mostly in surgical patients, ignoring internal medicine, which lacks awareness of DVT prophylaxis, and even lacks the organizational awareness of multidisciplinary joint DVT prophylaxis. The clinical nursing staff has the most contact time with patients, and the nursing staff has perfect knowledge of thrombosis prevention, which is helpful for early clinical detection of thrombosis risk and prevention. By forming an evidence-based care practice group for prevention of lower extremity DVT in patients with acute ischemic stroke, including evidence-based medical experts, clinical specialists, nursing managers, and nurse specialists, the multidisciplinary team provided a more scientific approach to the construction of the program, increased clinical caregivers' awareness of thrombosis prevention, and ensured the feasibility of the program for clinical research so that patients could receive continuous professional care. The program has improved the awareness of clinical staff on thrombosis prevention, ensured the feasibility of clinical research, and provided patients with continuous professional care.

## 4. Experiments and Results

In this part, we describe the dataset, experimental setup, basic data characteristics, and experimental results in detail.

**4.1. Dataset.** The chronic disease morbidity and mortality surveillance system of a city in China was relied on to construct a cohort of ischemic stroke cases in the city from 2014 to 2018. A total of 16,383 ischemic stroke cases were included according to the International Classification of Diseases criteria for all household residents with stroke estab-

lished from January 1, 2014, to December 31, 2018, excluding missing or abnormal data.

**4.2. Experimental Setup.** The assessment indexes were measures of vegetation cover, using normalized difference vegetation index (ND-VI), enhanced vegetation index (EVI), and soil adjusted vegetation index (Soi NDVI is the ratio of near-infrared to visible red irradiation, and SAVI is like NDVI with the addition of a soil brightness correction factor). EVI corrects for atmospheric aerosol scattering and soil background based on NDVI and is commonly used in areas with dense vegetation. The values of NDVI, EVI, and SAVI were extracted using ENVI5.3 and ArcGIS10.2 software.

The graph was created using research literature to identify the exposure and result between the intervening factors and to select a minimal set of more appropriate covariates to correct for confounding. According to the DAG plot, age, sex, population density, spatial GDP, walking index, and road density were ultimately selected as the minimum adjusted set on the causal pathway between vegetation cover and stroke death.

Statistical treatment for basic characteristics of the study population, quantitative information was described using (mean  $\pm$  standard deviation), and qualitative information was described using number of cases and percentages. The Cox proportional risk model was used to quantify the risk ratio of changes in vegetation index to mortality and then adjusted for age, sex, population density, spatial GDP, road density, and walking index. The first quartile (Q1) of NDVI, EVI, and SAVI were used as reference values, respectively, and the 95% confidence interval (CI) of the risk ratio (HR) between quartile (Q2, Q3, Q4) of NDVI, EVI, and SAVI and death from ischemic stroke were reported separately.

**4.3. Basic Data Characteristics.** 16383 patients with ischemic stroke and 3697 deaths due to ischemic stroke were included, after quadrating the cumulative mean NDVI, EVI, and SAVI from 2014 to 2018. Among them, 8471 new cases of ischemic stroke in men and 12797 new cases of ischemic stroke  $\geq 60$  years old were included.

**4.4. Experimental Results.** The error drop of the model training process is shown in Figure 5. Cox proportional risk regression model analysis of NDVI and risk of recurrence in patients with ischemic stroke quadrupled NDVI and calculated ORs and 95% CIs for Q2 and Q3, using the Q1 group as reference. 1237 deaths from ischemic stroke were recorded in the Q1 group, 843 deaths from ischemic stroke in the Q2 group, 923 deaths from ischemic stroke in the Q3 group, and 694 deaths from ischemic stroke in the Q4 group. Ischemic stroke claimed the lives of 694 people in the Q4 group. The NDVI-Q4 level was the most protective against death in individuals with ischemic stroke in both the adjusted and unadjusted models for different NDVI levels. In unadjusted model 1, patients with ischemic stroke residing at NDVI-Q4 levels had the lowest risk of recurrence (HR = 0.67, 95% CI: 0.61-0.74), and in model 2, patients with ischemic stroke residing at ND-VI-Q4 levels had the

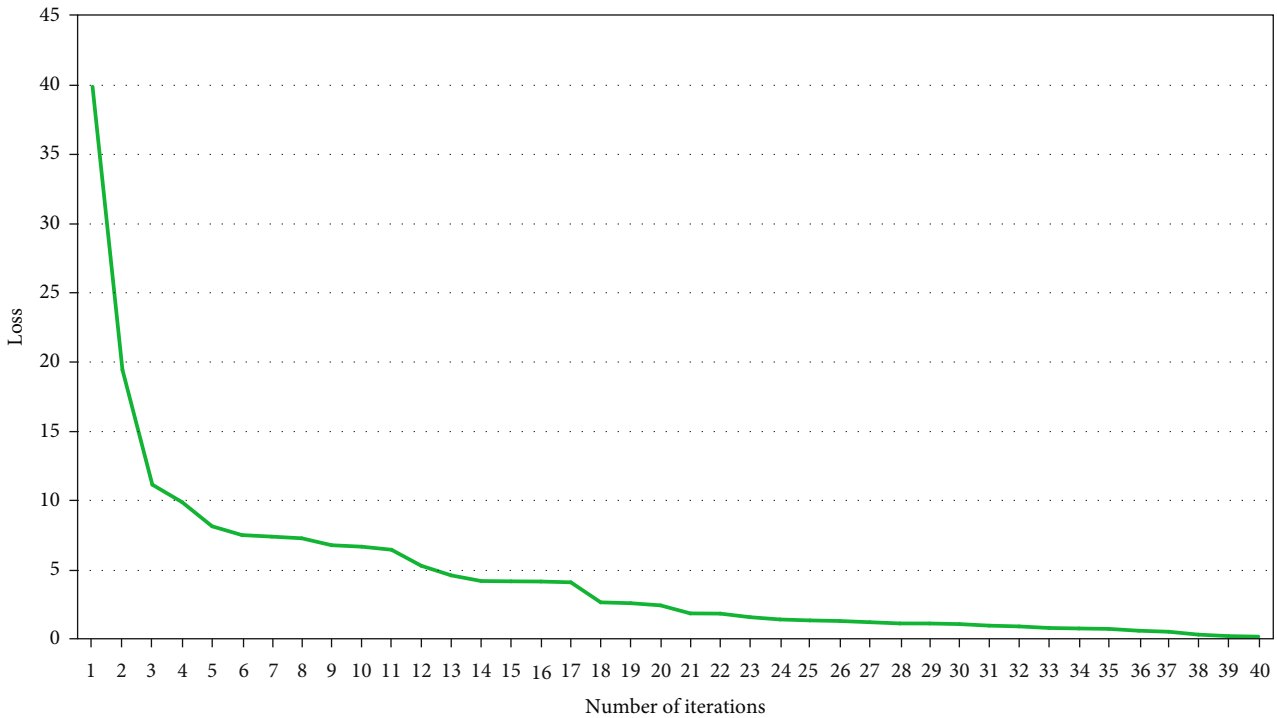


FIGURE 5: Error drop diagram of model training process.

TABLE 1: Cox proportional risk model analysis of NDVI and risk of recurrence in patients with ischemic stroke.

Models	Q1	Quadratic quartiles of NDVI (HR, 95% CI)		
		95% CI of Q2HR	95% CI of Q3 HR	95% CI of Q4 HR
Model 1	1	0.68 (0.63~0.75)	0.79 (0.72~0.86)	0.67 (0.61~0.74)
Model 2	1	0.68 (0.62~0.74)	0.77 (0.71~0.84)	0.67 (0.61~0.73)
Model 3	1	0.71 (0.65~0.78)	0.74 (0.68~0.81)	0.63 (0.57~0.69)

risk of recurrence was lowest in model 2 (HR = 0.67, 95% CI: 0.61-0.73). In model 3, patients with ischemic stroke at the NDVI-Q4 level had the lowest risk of recurrence (HR = 0.63, 95% CI: 0.57 to 0.69) (see Table 1). The performance improvement of the model training process is shown in Figure 6.

Cox proportional risk regression model analysis of EVI and risk of recurrence in patients with ischemic stroke quadrupled the EVI and calculated the OR and 95% CI for Q2 and Q3 using the Q1 group as reference. 1324 deaths from ischemic stroke were recorded in the Q1 group, 818 deaths from ischemic stroke in the Q2 group, 851 deaths from ischemic stroke in the Q3 group, and 851 deaths from ischemic stroke in the Q4 group. The number of deaths from ischemic stroke was 704. In both adjusted and unadjusted models, for different EVI levels, the EVI-Q4 level was the most protective against death in patients with ischemic stroke. In unadjusted model 1, patients with ischemic stroke residing at EVI-Q4 levels had the lowest risk of recurrence (HR = 0.61, 95% CI: 0.55 to 0.66), and in model 2, patients with ischemic stroke residing at EVI-Q4 levels had the lowest risk of recurrence (HR = 0.60, 95% CI: 0.55 to 0.66). The

risk of recurrence was lowest in patients with ischemic stroke at the EVI-Q4 level in model 3 (HR = 0.58, 95% CI: 0.53 to 0.63) (see Table 2).

Cox proportional risk regression model analysis of SAVI and the risk of recurrence in patients with ischemic stroke quadrupled SAVI, and the ORs and 95% CIs were calculated for Q2 and Q3 using the Q1 group as a reference. 1108 deaths from ischemic stroke were recorded in the Q1 group, 830 deaths from ischemic stroke in the Q2 group, 915 deaths from ischemic stroke in the Q3 group, and 915 deaths from ischemic stroke in the Q4. The number of deaths from ischemic stroke in the Q4 group was 844. In both adjusted and unadjusted models, for different SAVI levels, SAVI-Q2 levels were the most protective against death in patients with ischemic stroke. In unadjusted model 1, patients with ischemic stroke residing at SAVI-Q2 levels had the lowest risk of recurrence (HR = 0.75, 95% CI: 0.69 to 0.83), and in model 2, patients with ischemic stroke residing at SAVI-Q2 levels had the lowest risk of recurrence (HR = 0.75, 95% CI: 0.68 to 0.83). The risk of recurrence was lowest in patients with ischemic stroke at the SAVI-Q2 level in model 3 (HR = 0.79, 95% CI: 0.72 to 0.86) (see Table 3).

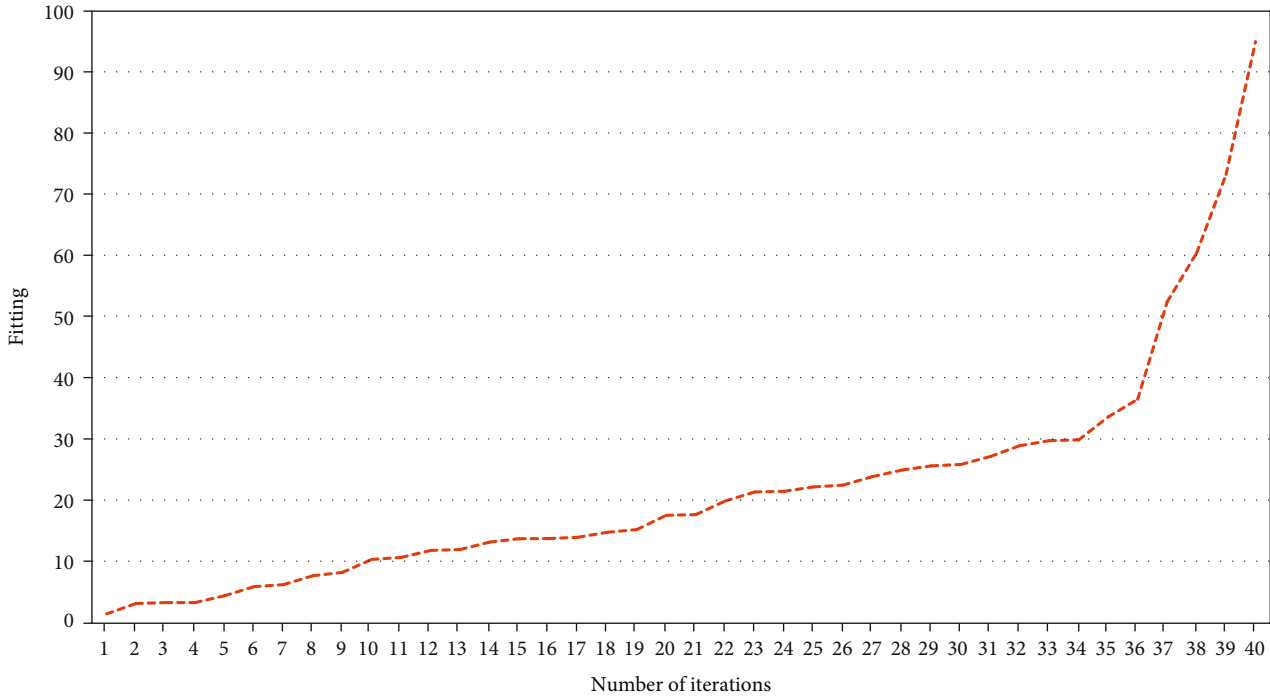


FIGURE 6: Model training process performance improvement chart.

TABLE 2: Results of a Cox proportional risk model analysis of EVI and risk of recurrence in patients with ischemic stroke.

Models	Q1	Quadratic quartiles of EVI (HR, 95% CI)		
		95% CI of Q2HR	95% CI for Q3 HR	95% CI of Q4 HR
Model 1	1	0.64(0.58 to 0.69)	0.69 (0.64~0.76)	0.61 (0.55~0.66)
Model 2	1	0.63(0.58~0.69)	0.69 (0.63~0.75)	0.60 (0.55~0.66)
Model 3	1	0.67(0.62~0.74)	0.67 (0.62~0.73)	0.58 (0.53~0.63)

TABLE 3: Results of a Cox proportional risk model analysis of SAVI and risk of recurrence in patients with ischemic stroke.

Models	Q1	Quadratic quartiles of SAVI (HR, 95% CI)		
		95% CI of Q2HR	95% CI for Q3 HR	95% CI of Q4 HR
Model 1	1	0.75 (0.69~0.83)	0.88 (0.80~0.96)	0.89 (0.81~0.97)
Model 2	1	0.75 (0.68~0.82)	0.86 (0.79~0.94)	0.88 (0.80~0.96)
Model 3	1	0.79 (0.72~0.86)	0.84 (0.77~0.91)	0.83 (0.76~0.91)

### 5. Conclusion

Clinical utility and extrinsic realism must be considered while evaluating ischemic stroke recurrence prediction models. Clinical usefulness is required for physician approval and use. Firstly, the prediction model should have clinical significance and application value, and secondly, the variables of the model should be easy to collect in the clinical setting, i.e., clinical applicability. Especially for emergency patients or newly admitted patients, good prediction results of the prediction model can guide physicians to make decisions, direct clinical treatment, and secondary prevention and prevent recurrence.

In this study, a hospital-based prospective cohort study was conducted with a 4-year follow-up, and the Cox propor-

tional risk regression model was applied to establish individual equations for ischemic stroke recurrence, and the final variables entered into the main effect equation were as follows: age, heart disease, hypertension, diabetes mellitus, and TC. We also verified the model’s external truthfulness, which is one of the most critical requirements for doctors to accept and use it. The established prediction model was initially utilized to forecast the 4-year recurrence rate of ischemic stroke patients, and it has good extrinsic realism and is simple to use with high accuracy, making it ideal for further validation and application promotion.

The construction of a clustered care intervention protocol for lower extremity deep vein thrombosis in patients with ischemic stroke has some clinical applicability and validity. The protocol is based on high-quality evidence,

which has changed the status quo of traditional empirical nursing care, promoted the scientific of clinical nursing decisions, ensured the safety of nursing practice, and improved the quality of clinical nursing services. This intensive care intervention program reduces the risk of lower limb deep vein thrombosis in patients with ischemic stroke, improves patients' coagulation function, and facilitates the functional recovery of patients' lower limbs by improving muscle strength, neurological deficits, and functional disability levels, making it clinically valuable.

## Data Availability

The datasets used during the current study are available from the corresponding author on reasonable request.

## Conflicts of Interest

The authors declare that they have no conflict of interest.

## References

- [1] B. Ji, Y. Li, D. Cao, C. Li, S. Mumtaz, and D. Wang, "Secrecy performance analysis of UAV assisted relay transmission for cognitive network with energy harvesting," *IEEE Transactions on Vehicular Technology*, vol. 69, no. 7, pp. 7404–7415, 2020.
- [2] X. Lin, J. Wu, S. Mumtaz, S. Garg, J. Li, and M. Guizani, "Blockchain-based on-demand computing resource trading in IoV-assisted smart city," *IEEE Transactions on Emerging Topics in Computing*, vol. 9, no. 3, pp. 1373–1385, 2021.
- [3] J. Li, Z. Zhou, J. Wu et al., "Decentralized on-demand energy supply for blockchain in internet of things: a microgrids approach," *IEEE Transactions on Computational Social Systems*, vol. 6, no. 6, pp. 1395–1406, 2019.
- [4] K. Yuan, J. Chen, P. Xu et al., "A nomogram for predicting stroke recurrence among young adults," *Stroke*, vol. 51, no. 6, pp. 1865–1867, 2020.
- [5] J. Liu, Y. Yang, K. Yan, C. Zhu, and M. Jiang, "Development and validation of nomograms for predicting stroke recurrence after first episode ischemic stroke," *Journal of Southern Medical University*, vol. 42, no. 1, pp. 130–136, 2022.
- [6] X. Song, X. Zhao, D. S. Liebeskind et al., "Incremental value of plaque enhancement in predicting stroke recurrence in symptomatic intracranial atherosclerosis," *Neuroradiology*, vol. 62, no. 9, pp. 1123–1131, 2020.
- [7] M. Wu, X. Zhang, J. Chen et al., "A score of low-grade inflammation for predicting stroke recurrence in patients with ischemic stroke," *Journal of Inflammation Research*, vol. 14, pp. 4605–4614, 2021.
- [8] Y. Y. Chen, Z. S. Ye, N. G. Xia, and Y. Xu, "TMAO as a novel predictor of major adverse vascular events and recurrence in patients with large artery atherosclerotic ischemic stroke," *Clinical and Applied Thrombosis/Hemostasis*, vol. 28, 2022.
- [9] Z. X. Huang, S. Yuan, D. Li, H. Hao, Z. Liu, and J. Lin, "A nomogram to predict lifestyle factors for recurrence of large-vessel ischemic stroke," *Risk Management and Healthcare Policy*, vol. 14, pp. 365–377, 2021.
- [10] X. M. Li, X. Wang, X. W. Feng et al., "Serum interleukin-33 as a novel marker for long-term prognosis and recurrence in acute ischemic stroke patients," *Brain and Behavior*, vol. 9, no. 9, article e01369, 2019.
- [11] N. Hashimoto, T. Watanabe, H. Tamura et al., "Left atrial remodeling index is a feasible predictor of poor prognosis in patients with acute ischemic stroke," *Heart and Vessels*, vol. 34, no. 12, pp. 1936–1943, 2019.
- [12] X. Han, J. Cai, Y. Li et al., "Baseline objective malnutritional indices as immune-nutritional predictors of long-term recurrence in patients with acute ischemic stroke," *Nutrients*, vol. 14, no. 7, p. 1337, 2022.
- [13] X. Yang, G. Wang, J. Jing et al., "Association of triglyceride-glucose index and stroke recurrence among nondiabetic patients with acute ischemic stroke," *BMC Neurology*, vol. 22, no. 1, pp. 1–9, 2022.
- [14] Y. Shojima, Y. Ueno, R. Tanaka et al., "Eicosapentaenoic-to-arachidonic acid ratio predicts mortality and recurrent vascular events in ischemic stroke patients," *Journal of Atherosclerosis and Thrombosis*, vol. 27, no. 9, pp. 969–977, 2020.
- [15] Y. H. Chan, C. M. Schooling, J. Zhao et al., "Mendelian randomization focused analysis of vitamin D on the secondary prevention of ischemic stroke," *Stroke*, vol. 52, no. 12, pp. 3926–3937, 2021.
- [16] X. Liu, Q. Wang, J. Zhao, H. Chang, and R. Zhu, "Inflammation-related circRNA polymorphism and ischemic stroke prognosis," *Journal of Molecular Neuroscience*, vol. 71, no. 10, pp. 2126–2133, 2021.
- [17] L. M'barek, S. Sakka, F. Megdiche et al., "Traditional risk factors and combined genetic markers of recurrent ischemic stroke in adults," *Journal of Thrombosis and Haemostasis*, vol. 19, no. 10, pp. 2596–2604, 2021.
- [18] R. Zhu, T. Xiao, Q. Wang, Y. Zhao, and X. Liu, "Genetic polymorphisms in lncRNAs predict recurrence of ischemic stroke," *Metabolic Brain Disease*, vol. 36, no. 6, pp. 1353–1359, 2021.
- [19] A. C. Kirkpatrick, A. S. Vincent, G. L. Dale, and C. I. Prodan, "Increased platelet procoagulant potential predicts recurrent stroke and TIA after lacunar infarction," *Journal of Thrombosis and Haemostasis*, vol. 18, no. 3, pp. 660–668, 2020.
- [20] G. Georgiopoulos, G. Ntaios, K. Stamatelopoulou et al., "Comparison of risk scores for the prediction of the overall cardiovascular risk in patients with ischemic stroke: the Athens stroke registry," *Journal of Stroke and Cerebrovascular Diseases*, vol. 28, no. 12, article 104415, 2019.
- [21] J. Jing, Y. Suo, A. Wang et al., "Imaging parameters predict recurrence after transient ischemic attack or minor stroke stratified by ABCD2 Score," *Stroke*, vol. 52, no. 6, pp. 2007–2015, 2021.

## Research Article

# Stability Analysis of Geotechnical Landslide Based on GA-BP Neural Network Model

Jin Xu <sup>1</sup> and Yanna Zhao<sup>2</sup>

<sup>1</sup>School of Civil Engineering, Xuchang University, Xuchang, Henan, China

<sup>2</sup>Xuchang Jinke Resource Recycling Co., Ltd., Xuchang, Henan, China

Correspondence should be addressed to Jin Xu; xuj@xcu.edu.cn

Received 19 April 2022; Revised 14 May 2022; Accepted 19 May 2022; Published 20 June 2022

Academic Editor: Naeem Jan

Copyright © 2022 Jin Xu and Yanna Zhao. This is an open access article distributed under the Creative Commons Attribution License, which permits unrestricted use, distribution, and reproduction in any medium, provided the original work is properly cited.

Rock and soil landslides, a regular geological disaster in engineering construction, endanger national property and, in severe circumstances, result in a huge number of casualties. A set of methods for landslide stability analysis and prediction has been established, with the academic idea of “geological process mechanism analysis-quantitative evaluation” at its core, combined with detailed field investigation of geological hazards, forming a relatively complete technical route for research on landslide stability analysis. The work of this paper can be summarized as follows: (1) Introduce the research status of geotechnical landslide stability at home and abroad and the current development trend of neural network. (2) Through the collected sample database, take the training function and the number of hidden layer neurons as variables to optimize the BP neural network, and combine the optimized BP neural network with the genetic algorithm to construct the GA-BP neural network. (3) The stability coefficients of the BP neural network, the genetic algorithm based back propagation neural network (GA-BPNN), and the limit equilibrium technique are analyzed and compared. The findings imply that landslide stability can be assessed using neural networks. GA-BPNN is a viable alternative to back propagation neural network (BPNN). The algorithm is more accurate, has a faster convergence rate, and is more stable.

## 1. Introduction

Geotechnical landslide is a geological phenomenon of sliding of the slope rock and soil along the through shear plane caused by natural geological action and human engineering activities. Landslide instability and damage cause heavy losses and disasters. The EM-DAT catastrophe database estimates that 8,658 persons perished as a direct result of landslide activity throughout the globe during 1990 and 1991 [1]. “The Durham Fatal Landslide Database” (DFLD) database indicates that the death toll from landslide events between 1980 and 2000 was about 72,000 worldwide, or about 3,400 per year, a figure that is considered a significant underestimation of landslide hazard outcomes because the underreporting of small events (events with very low mortality rates) and events that occur in very remote areas keeps the count far below the actual number [2]. Landslide geological disasters are widely distributed in my country. According

to statistics from the Ministry of Land and Resources, mountains in my country account for about 33% of the country's land area, plateaus account for 26%, and hills account for 10%. Usually people refer to mountains, hills, and relatively rugged plateaus as mountainous areas. Mountainous areas in my country account for more than two-thirds of the country's land area. One of the important reasons for the underdeveloped economy in the vast mountainous areas of our country is the poor topographic and geological conditions and the backward infrastructure, especially the transportation facilities. In order to fundamentally enhance the economic growth of these places, the state has been concentrating larger efforts in recent years and for a long time in the future to establish various infrastructures in these areas. There are many geological threats in large areas of mountainous areas. Various engineering constructions in the mountainous areas have more and more disturbances to the natural geology, coupled with natural factors such as

climate change and seismic activity, resulting in frequent occurrence of geological disasters such as rock and soil landslides, hindering and limiting the occurrence of geological disasters. The development and construction of mountainous areas, especially in recent years, the rural highway network and the “eight vertical and eight horizontal” high-speed railway network, as the main artery of the national economy and the construction of major livelihood projects, are in full swing. Geotechnical landslides have been listed as one of the major geological disasters in my country, and key research has been carried out. The prediction and control of landslides has always been an important research direction in the field of geotechnical engineering. In order to better provide a basis for landslide prevention and control, it is necessary to deeply understand the mechanical mechanism and failure process of landslide instability and establish accurate stability evaluation standards to achieve scientific prevention and control and reduce and eliminate landslide disasters in engineering construction. Slope stability is a means of determining prevention measures and engineering quantities. The calculation of landslide safety factor is the basis for control design. Stability calculation is the core of slope stability analysis. Slope stability is a state that indicates whether the slope is safe or not and the degree of safety. The result of treatment should be to make the slope reach the safety standard state. Since slope rock and soil is a complex geological medium, it is difficult to obtain quantitative values accurately, so qualitative analysis based on geological statistics and experience should be combined with quantitative calculation. In the semiquantitative evaluation method, there is also the problem of artificially quantifying each factor index and determining the weight of the factor based on experience, which is difficult to truly reflect the actual situation. With the deepening of research, the phenomenon of interdisciplinary is becoming more and more common, so it has become a trend to study the stability of rock and soil landslides with new analytical methods. This paper mainly improves the traditional BP neural network based on the genetic algorithm, and applies the GA-BP neural network to the stability analysis of the landslide, aiming to seek a way to improve the prediction accuracy.

The paper organizations are as follows: Section 2 defines the related work. Section 3 discusses the methods of the proposed concepts. Section 4 discusses the analysis of experimental and discussions. Section 5 concludes the article.

## 2. Related Work

The landslide mechanism is the physical and mechanical nature and laws of the whole process of the slope under certain geological structure conditions, from stable to unstable state under the action of various factors, and then to a new stable state or permanent instability. The concept of progressive failure of soil was first proposed by reference [3, 4]. The theory of stress differentiation and shear strength redistribution was used to explain the progressive failure, and it was pointed out that its essence was that the soil flowed from the initial strength state to the plastic flow, but only limited to the brittle clay range at that time. It is reference [5] that

really applies the concept of progressive failure to slope analysis. By analyzing and studying the long-term stability of soil slopes, and analyzing the results of a large number of field direct shear tests, it is pointed out that the slope deformation changes from local to overall through failure. In the process, the research on the gradual development of the slope is developed on the basis of the traditional static research. After that, the gradual failure of the slope has made more development, and reference [6] studied the gradual failure mechanism of the slope from the perspective of failure criteria and stress-strain relationship according to the experimental study of soil strength. Reference [7] established a mechanical model of progressive failure of excavation slopes according to the strain softening characteristics of soil under fatigue load and considered that the discontinuity of the slope soil resulted in progressive failure. Reference [8] analyzes the development of cracks in the slope, applying various parameter combinations to represent the peak and residual shear strength conditions along the cracked and uncracked parts of the critical surface, and analyzes the progressive failure process. Reference [9, 10] established a calculation model for the gradual development of the slope from the toe to the top and explained the progressive failure mechanism from the perspective of probability analysis.

The stability analysis of rock and soil landslides has a research history of more than a century, and many scholars have achieved a series of achievements, forming the theoretical basis of slope analysis. There are currently a variety of methods for assessing the stability of geotechnical landslides, the most common of which are the geological analysis method, empirical analogy method, structural analysis method, limit equilibrium analysis method, numerical analysis method, and probability analysis method, the first three of which are qualitative analysis methods. However, the latter three are used more in the stability evaluation of rock and soil landslides. The limit equilibrium method regards the sliding body as a rigid body and analyzes its equilibrium state along the sliding surface. The commonly used methods include the Janbu method, the simplified Bishop method, the wedge body method, the transfer coefficient method, the Fellenius method, and the Sama method. These methods are all based on the limit equilibrium state, treat the rock and soil mass as a rigid body, and assume that the sliding zone as a whole reaches a critical state, which is far from reality in many cases and cannot reflect the real stress-strain relationship inside the rock and soil mass. A large number of studies have shown that the deformation and failure of slopes are a gradual process. Some scholars have extended the limit equilibrium method combined with the change of strength parameters and developed a system of gradual development research on the basis of traditional static research. Skempton put forward the concept of gradual failure of slope through the analysis and research of soil slope and developed the research of gradual development on the basis of traditional static research. Reference [11–13] considered the softening characteristics of soil strength parameters, and considered the mechanical mechanism and failure evolution process of the gradual development of the slope, and extended the limit equilibrium

analysis method. The numerical analysis strength reduction method can calculate the stability of the slope in combination with the constitutive relationship of the rock and soil mass and can reflect the gradual failure process of the slope to a certain extent. The area where the shear strength is exceeded is the failure area. Reference [14] proposed the strength reduction method, which has been widely used in the numerical calculation of slope stability and is also developing continuously; the strength reduction method provides convenience for the calculation of various complex slopes; and the calculation amount and accuracy are guaranteed to a certain extent. The determination of the final result of the strength reduction method depends on the selection of the calculation termination conditions, that is, the choice of the instability criterion. Reference [15] takes the nonconvergence of a certain number of nonlinear iterative calculations as the instability criterion, and uses a large number of strength reduction methods and numerical calculations to demonstrate its feasibility [16]. Geological issues such as earthquakes, geophysical research, and geological hazard prevention and prediction have recently used neural network theory. In terms of geological disaster prevention and prediction, the application of domestic BP neural network can be roughly divided into three stages: understanding, development, and extension. The cognitive stage is the enlightenment period for the application of BP neural network to geological disasters. This period mainly provides a theoretical basis and is not used in practical engineering applications; in the development stage, geologists use BP neural network to solve landslides, land subsidence, and sand liquefaction. Extension of the BP neural network to a new study stage was made possible by geologists combining ideas and technology from other disciplines to create new research approaches [17]. Neural networks are projected to have a wide range of applications in multivariate analysis, parameter prediction, inversion, and factor sensitivity analysis in engineering geological issues. The danger elements impacting landslide stability were discovered after a thorough review of landslide stability assessment methodologies. Researchers have developed a novel approach for analyzing slope stress by combining discrete element computation with neural network prediction; an assessment model for town landslides' stability was developed by researchers using BP neural networks; and the forecast findings were in line with the actual circumstances. Abroad, a research group of scientists had insight into the importance of neural network information processing, and established a parallel and distributed processing (PDP) group in 1982 to explore parallel distributed processing technology, and three years later, the BP network learning algorithm was researched, and Minsky's multilayer network vision was realized [18]. Subsequently, reference [19] published three academic papers on the application of neural networks in distinguishing earthquakes from blasting. Reference [20] used a new method of GIS combined with artificial neural network model earlier to evaluate the landslide risk in the Boeun area of Korea. It can be seen from the above that in recent years, scholars at home and abroad have achieved many research results in engineering applications using BP neural network, espe-

cially the improvement of BP neural network combined with other disciplines. There are few studies related to prediction [21, 22].

### 3. Method

#### 3.1. Construction of BP Neural Network Model

*3.1.1. Principle of BP Neural Network Algorithm.* The following nodes make up the BP neural network: In other words, a BP neural network is used to teach the error back propagation method. The training process is divided into two stages. To determine your mistake, start by comparing your output value to a real-world value. The BP neural network has three layers: an input layer, a hidden layer, and an output layer. The training data enters the model through the input layer, which acts as a buffer for the data. It is up to the user to decide how many layers of the hidden layer they want, and the number of neurons in each layer is determined empirically by training and testing the model many times with different combinations of input data parameters. The input layer sends data to the hidden layer, which transforms it before passing it on to the output layer, which generates the forward-propagated data. The activation function of the output layer transforms data that has been passed from the hidden layer. The network performs the error back propagation process when the difference between the output result and the measured value is too large. The BP neural network gradient descent algorithm is used to correct each layer's weights and thresholds, and then, forward prediction is performed once more. End the training session now. The structure of the BPNN model is shown in Figure 1.

*3.1.2. BP Neural Network Parameter Selection.* Many variables must be taken into account while creating a BP neural network model. The number of hidden layers, the number of neurons in the hidden layer, the starting weights, the activation function, the anticipated error, the learning rate, and the number of repetitions of learning, among other factors, are not precisely described.

Since there is just one hidden layer in the BP neural network, it is unknown how many layers it may have. However, this is plausible. If you have a three-layer BP neural network with only a single hidden layer, you can complete any nonlinear mapping, even if the nonlinear map goes from  $n$  to  $m$  dimensions. Despite the fact that the BP neural network's three layers can approximate any nonlinear mapping, there is a large difference between the output result and the actual value and a poor degree of accuracy in identification. Allowing for a greater number of hidden layers helps alleviate this drawback. A more complicated BPNN structure results from adding more hidden layers, since the weight training time for neuron connections across layers increases as more layers are added. Although adding more hidden layers improves the BP network's output accuracy, it is simpler to see and change the network training effect when there are more neurons in each layer. Therefore, increasing the number of hidden layers is the best method for reducing network training error.

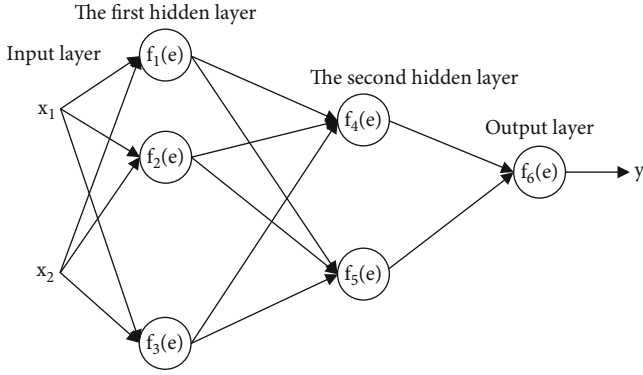


FIGURE 1: The structure of the BP neural network model.

The buried layer's neuron count is as follows: It is necessary to start with a small hidden layer to train and debug the neural network and then increase the number of neurons in the hidden layer until it performs to specifications. Increase the number of hidden layers if it does not work. It has been found that the process of adding hidden layer nodes is significantly easier than the process of adding hidden layers. If you have just one hidden layer in your neural network, you may use this method to figure out the number of nodes in the hidden layer's first layer.

$$z = \sqrt{q + p} + a, \quad (1)$$

where  $p$  and  $q$  represent the number of nodes in the input layer and output layer, respectively, and  $a$  is a constant with a value range of  $(1, 0)$ .

Activation function, learning rate, and expected error: The activation function is introduced into the BP neural network because the BP neural network model studies nonlinear problems, and the nonlinear function is introduced to increase nonlinear factors. When the activation function is introduced into the BP neural network, the network becomes more complex than before, thus improving the expressive ability of the network. However, there are certain restrictions when choosing the activation function; that is, the function must be derivable and continuous. There is an activation function for this paper's hidden layer that is called tansig, and its value range is between 1 and 1. Due to the fact that the normalized data in this study fall between -1 and 1, the output layer picks the purelin function, which is linear, in the MATLAB toolbox in order to expand the range of values for the output. For the tansig function, the following expression is appropriate:

$$f(x) = \frac{e^x - e^{-x}}{e^x + e^{-x}}, \quad (2)$$

It can be obtained by simple operation.  $f(x) \in (-1, 1)$ .

The mathematical equation for the first derivative of tansig is

$$f'(x) = \frac{4}{(e^x + e^{-x})^2} \tanh(x) = \text{sech}(x)^2. \quad (3)$$

A significant aspect in the BP neural network's success is its ability to adapt to changes in the model's weights throughout the training phase. If the learning rate is too high, the weights will change more often, resulting in a bigger change each time they are updated, and it is very likely that the optimal weights cannot be found or not easily found, and even the BP neural network will collapse. If the learning rate is too small, the time for each training weight update will be longer, reducing the convergence speed of the network. In practical applications, even if the learning rate is too small, it will affect the convergence speed of the network, but this method avoids the local optimal solution of the trained network, so a relatively small learning rate is often selected. The value range of the learning rate in the BPNN model is commonly found to be between 0.01 and 0.08. This article regularly trains the existing BP neural network-based geotechnical landslide prediction model with a learning rate of 0.01, and its performance is superior.

The expected error is very important for the BP neural network. It is an evaluation criterion for the excellent performance of the network model. In order to make the error of the BP neural network relatively small, the network structure and performance must be paid to a certain extent, increasing the number of hidden layers of the network or increasing the number of neurons in the hidden layer and consuming more training and learning time. In order to reduce the cost of the network, it is necessary to work on the expected error function. There are three kinds of error functions commonly used in BP neural network, and the following is the comparison of these three error functions. The error function commonly used in the BP network model is the formula  $E_{p1}$ :

$$E_{p1} = \frac{1}{2} \sum_{j=1}^m (t_j^p - y_j^p)^2, \quad (4)$$

where  $m$  is the number of neurons in the output layer;  $p$  is the number of training samples;  $E_p$  is the error of the  $p$  data of the training sample;  $t_j^p$  is the true value; and  $y_j^p$  is the output value.

Each time the BP neural network updates the weights, it will be affected by each sample. However, there are certain disadvantages in using this error function. It only considers the influence of the current sample on the weights, and does not consider the influences of other samples on the modified weights. Therefore, this error function will increase the training times of the BP neural network. The cumulative error  $E_{p2}$  is a global error function, which is defined as follows:

$$E_{p2} = \frac{1}{2} \sum_{p=1}^p \sum_{j=1}^m (t_j^p - y_j^p)^2 = \sum_{p=1}^p E_{p1}, \quad (5)$$

where  $p$  represents the data of  $p$  training samples;  $E_{p2}$  represents the expected error of the  $p$ -th training sample;  $\text{MSE} = 1$



$1/mp \sum_{p=1}^p \sum_{j=1}^m (y'_{pj} - y_{pj})^2$  represents the real value;  $y'_j$  represents the output value of each loop; and  $m$  represents the number of neurons in the output layer.

The role of the global error function is to reduce the global error of the system. If it is only used in a sample, it can only improve the global error accuracy of the sample, and cannot affect the error of each sample. In addition, it cannot be compared with the performance of other networks, because the error values are different for  $m$  and  $p$  in the formula on different networks; when  $m$  is constant, the larger  $p$  is, the larger the global error  $E_{p2}$  is; when  $p$  is changed, the larger  $m$  is, the larger the global error  $E_{p2}$  is. The mean square error function of the BP network is

$$\text{MSE} = \frac{1}{mp} \sum_{p=1}^p \sum_{j=1}^m (y'_{pj} - y_{pj})^2, \quad (6)$$

where  $m$  represents the number of neuron nodes in the output layer;  $p$  represents the number of samples;  $y'_{pj}$  represents the true value; and  $y_{pj}$  represents each training value.

**3.1.3. Limitations of BP Neural Networks.** Although the BP neural network has many advantages and has been widely used and promoted, there are still some limitations in terms of its structure and performance. The problems mainly include the following aspects.

- (1) Since the learning rate of the network cannot be selected too large, the BP neural network training takes a long time
- (2) The BP neural network algorithm may generate a local minimum solution, because the gradient descent method may be used to obtain a local minimum solution when updating the weights. As an optimal solution, the BP neural network will make the weights converge to a certain value, but not necessarily the global optimal value
- (3) The hidden layer of the BP neural network finally uses several layers and the number of neurons in each layer. Only a few can make the network performance optimal, so far there is no clear formula or theory, and their numbers are determined by users using empirical formulas and repeated training. Therefore, the network performance is uncertain. If there are too many hidden layers and nodes in each layer, the system will be too complicated, and the training speed will be slow; otherwise, the target curve cannot be better fitted
- (4) The predicted value of BP neural network is unstable. For the same training samples and prediction samples, the results of each prediction are different

**3.2. Establish a Neural Network Based on GA-BP.** The BP neural network must be tuned because of its high volatility and proclivity for local optimal solutions. The genetic algorithm has global search ability and can improve the defects

of the BP model, so this paper uses the genetic algorithm to optimize the BP neural network.

**3.2.1. Principle of Genetic Algorithm.** The calculation process of genetic algorithm is mainly composed of coding, population initialization, fitness function evaluation, selection, crossover, mutation, and other modules. The following is a detailed discussion of each module of the genetic algorithm. For coding, before carrying out the genetic algorithm, an important work must be done to the solution of the problem, which is to encode it into a symbol that the genetic algorithm can operate, that is, the chromosome string. Binary, floating-point, mixed encoding, and other methods can be used to encode the issue solution, with floating-point encoding having the maximum accuracy. For the initial population, the convergence speed of the genetic algorithm and the accuracy of the feasible solution must be guaranteed, and the precondition is that the size of the population should be appropriate. If the size selection of the population is too large, individuals with low fitness will be eliminated early in the process of genetic algorithm optimization, the diversity of the population will be reduced prematurely, and the distribution of feasible solutions will become sparse. The number of local solutions is reduced, and the operation process will also converge prematurely, and the global optimal solution of the problem will be difficult to search. Similar to the requirements of BP neural network training samples, as the input of genetic algorithm, the distribution of individuals in the population and the characteristics of the population should be rich, and these two aspects must be considered when selecting input data. When the starting population's features are basic, the genetic algorithm is prone to premature and local convergence, which affects the accuracy of the algorithm optimization; thus, attempt to make the initial population's individual characters as rich as possible. However, a diverse distribution of population individuals can overcome the lack of a single individual trait, even if the population is scattered in the entire search space. Usually, the initial population size is selected in the range of 20 to 100. In the design of the fitness function, the fitness is an evaluation of the ability of the individual population to adapt to the natural environment. Similarly, the fitness function is also an evaluation of the adaptive ability of the individual in the evolutionary process of the genetic algorithm. History has proved that organisms follow a law in the process of evolution; that is, the driving force and purpose of evolution are to evolve in the direction of adapting to the current living conditions. Genetic algorithm is a simulation of biological evolution, and the convergence of objective function can be regarded as the goal and motivation of evolution. The genetic algorithm population solely executes optimization calculations using its own fitness function during evolution, and does not seek input from the outside environment. As a result, the fitness function used in the genetic algorithm has a significant impact on the algorithm's performance. Usually, the reciprocal of the objective function is used as the objective function of the genetic algorithm, as follows:

$$F(f(x)) = \frac{1}{1 + c + f(x)} \quad c \geq 0, c + f(x) \geq 0. \quad (7)$$

For selection, selection is also called regeneration or replication. The step is that the individual string randomly selects a certain individual from the parent population as the genetic information of the offspring according to the size of the fitness to replicate. The selection operation has a decisive influence on the size of the crossover individual and its offspring. In crossover, the genetic information of the individual will be passed on to the next generation in the process of evolution, and at the same time, each generation of individuals will change themselves in order to adapt to the surrounding environment. Therefore, the crossover operator can be understood through this concept. The function of the crossover operator is to make the next generation appear new individuals that are different from the previous generation. After generations of evolution, the crossover operator continuously adds new individuals to the population to participate in the calculation and eliminates the old individuals. According to the rules of biological inheritance, the exchange of genetic information between two combined individuals will generate two completely new individuals, and this operation will be repeated between the new individuals until it converges to the optimal solution. In mutation, for biological evolution, the probability of mutation is very small. Similarly, in genetic algorithm, mutation operation will randomly replace the value of chromosome string, but the probability of this operation is very small. For example, a mutation operation replaces 0s with 1s on a string of binary chromosomes with a probability of 0.1. The influence of mutation operation on the optimization of genetic algorithm should not be underestimated. First, it can make the local search of the algorithm more thorough and increase the search accuracy and the speed of the local optimal solution, preventing premature convergence of the algorithm.

3.3.2. *Genetic Algorithm Framework Process.* The genetic algorithm framework process is shown in Figure 2.

### 3.3. BP Neural Network Based on Genetic Algorithm

3.3.1. *The Basic Principle of GA-BP Algorithm.* Due to the fact that its method can map the nonlinear connection between input and output of any issue, BP neural network is extensively employed in a broad range of industries. It is simple to slip into the local minimum value using the typical BP neural network, and it takes an extremely lengthy time to train. Consequently, it is vital to strengthen and optimize the BP network in order to overcome its weaknesses. Genetic algorithms are employed to optimize the BP network in this article, creating the GA-BP network model. To begin, the BP network uses the genetic algorithm to optimize its initial weights, and then, the BP network uses its own method to train weights and thresholds that match the error criteria based on those optimized starting weights. The research reveals that the GA-BP algorithm can improve the classic BP network model's existing flaws, and it is currently the most often used BP network optimization approach. The operation flow of the GA-BP algorithm is shown in Figure 3.

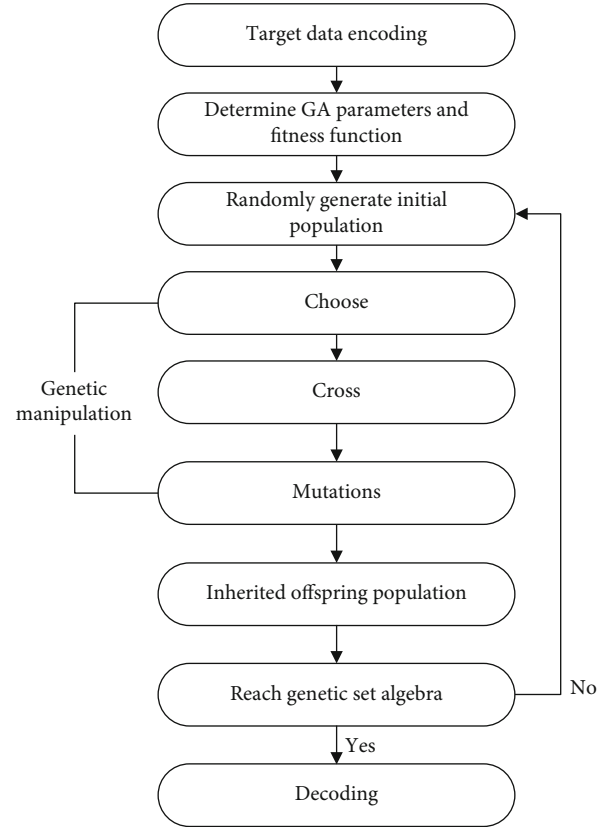


FIGURE 2: Genetic algorithm framework process.

3.3.2. *Optimizing the GA-BP Algorithm.* Whether the appropriate crossover operator  $P_c$  and mutation operator  $P_m$  can be selected has a great impact on the performance of the genetic algorithm. The reason why the genetic algorithm can generate new individuals, the crossover algorithm plays a decisive role. Through crossover operation, excellent traits can be combined advantageously and be inherited to the next generation with higher fitness value. Therefore, in order to obtain as many optimal individuals as possible, the value of  $P_c$  is usually relatively large. However, if the value of  $P_c$  is too large, excellent parent individuals will be included in the crossover category, which will destroy the preservation mechanism of excellent individuals and slow down the evolution rate. If the value of  $P_c$  is selected too small, the growth rate of new individuals in the population will become very slow, and the process of GA optimization will take too long. The usual range for the probability of  $P_c$  is (0.40, 0.99). Mutation  $P_m$  is one of the methods to avoid prematurity in the genetic algorithm, and it is also an important method for the population to generate new individuals. However, the probability of mutation in nature is very small. In order to improve the effect of mutation in the genetic algorithm, its value will be appropriately increased. However, if the value of  $P_m$  is too large, it loses its original significance in genetics; on the contrary, if the value of  $P_m$  is small, the precocious effect of mutation suppression genetic algorithm will no longer exist.  $P_m$  usually takes the value (0.0001, 0.1).

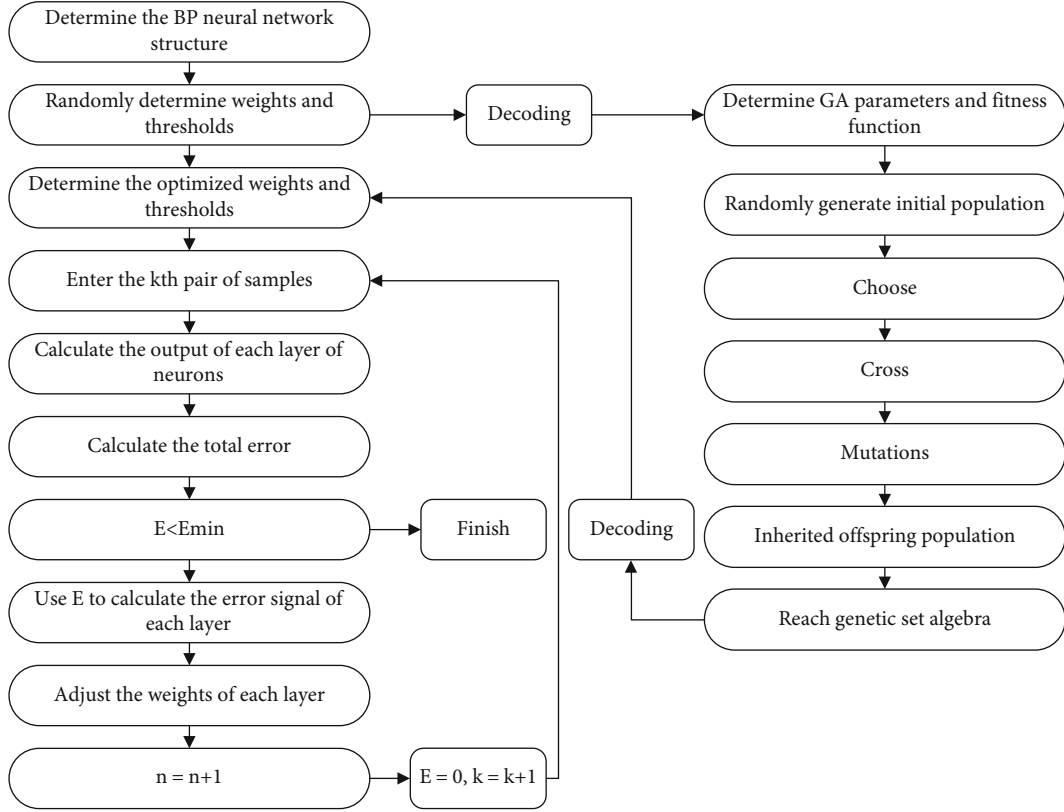


FIGURE 3: Operation flow of the GA-BP algorithm.

When the probability of crossover and mutation is determined, individuals with particularly high fitness may occupy all the positions of the population after several generations of inheritance, which makes the genetic algorithm converge prematurely, resulting in a high probability of obtaining a local minimum value. By analyzing this phenomenon, it is concluded that once the algorithm appears precocious, the fitness of many individuals in the population is very close. At this time, the fitness variance value of the population is very small, so the variance characteristics at this time can be used as a precocious evaluation index. For ease of calculation, let

$$E_2 = \frac{1}{M} \sum_{i=1}^M |f_i - f_{\text{avg}}|, \quad (8)$$

where  $E_2$  is less than a certain value, the genetic algorithm is judged to be premature, and then, the processing measures are taken. In this paper, the adaptive crossover and mutation algorithm are used to realize the connection between the probability change of the genetic operator and the individual fitness. The optimized algorithm is shown in the formula.

$$P_{ci} = P_c \times \left(1 - \frac{f(x_i)}{\sum_{i=1}^M f(x_i)}\right), \quad (9)$$

$$P_{mi} = P_m \times \left(1 - \frac{f(x_i)}{\sum_{i=1}^M f(x_i)}\right), \quad (10)$$

where  $P_{ci}$  and  $P_{mi}$  are the crossover and mutation probabilities of the  $i$ -th individual after optimization and  $P_c$  and  $P_m$  are the crossover and mutation probabilities of the original entire population, respectively. It can be calculated from the formula that when the population is precocious, the probability of individuals in the population being genetically manipulated will decrease as the fitness increases. Individuals with very small fitness will not be eliminated completely because their value is too small, which enriches the diversity of the population. The biggest difference from the traditional algorithm is that the probability of the improved crossover and mutation operator will change with the change of the individual itself. Therefore, the genetic algorithm optimized by using the genetic operator is more in line with the evolutionary rules of biology and has obvious inhibitory effect on the precocious phenomenon.

#### 4. Experiments and Discussions

In the experimental and discussions section, we define the example analysis of geotechnical landslide, stability analysis of geotechnical landslides by BP neural network, stability analysis of GA-BP neural network, and comparison of two stability evaluation methods.

**4.1. Example Analysis of Geotechnical Landslide.** This paper takes a soil slope as an example. The slope aspect is about  $12^\circ$ , the rear elevation is more than 450 m, the slope is 26-29°, the elevation is between 423 and 456 m, and the terrain slope is about  $23.5^\circ$ . The landslide is the Quaternary loose

TABLE 1: Prediction stability coefficient of BP neural network.

Serial number	Predictive value	Actual value	Absolute difference	Relatively poor
1	0.999	0.995	0.003	0.36%
2	0.998	0.995	0.003	0.33%
3	1.042	0.995	0.046	4.48%
4	1.098	0.995	0.102	9.36%
5	0.999	0.995	0.003	0.37%
6	0.999	0.995	0.004	0.40%
7	1.003	0.995	0.007	0.77%
8	1.006	0.995	0.011	1.12%
9	1.092	0.995	0.096	8.86%
10	1.003	0.995	0.007	0.75%

gravel soil sliding and deforming along the top surface of the bedrock. The plane is approximately rectangular. The elevation of the Yellow Sea at the front edge is 425 m, and the elevation of the Yellow Sea at the trailing edge is 455 m. The width of the front and rear edges is about 80 m, and the middle is slightly wider. Calculated by the limit equilibrium algorithm, the stability coefficient of the landslide is 0.9956, and there is the possibility of overall slippage.

**4.2. Stability Analysis of Geotechnical Landslides by BP Neural Network.** Since the weights and thresholds of the neural network are randomly generated at the beginning of training, the results of each network training cannot be guaranteed to be consistent, and sometimes even large errors may occur; the trainlm function trains the neural network with high prediction accuracy for training samples, but not consistently high for detection samples. Therefore, in order to ensure the accuracy of the results, this paper makes 10 correlation predictions and then takes the average value. The results of the 10 operations are shown in Table 1.

The mean of the 10 sets of predicted values is 1.0243, the absolute error is 0.0287, and the relative error is 2.68%. As can be seen from the table, compared with the limit equilibrium method, the single maximum error of the BP neural network reaches 9.36%, but the average relative error is only 2.68%, and the prediction accuracy is relatively high.

**4.3. Stability Analysis of GA-BP Neural Network.** In order to reduce the random error of a single prediction, the GA-BP neural network also made 10 correlation predictions for the landslide and then took the average value. The operation results of its 10 predictions are shown in Table 2.

It can be seen from the table that the relative error of the predicted value of GA-BP neural network is between 0.10% and 3.86%, the error is small, and the stability is better. Its mean is 1.0078, the mean absolute error is 0.0122, and the mean relative error is 1.19%.

**4.4. Comparison of Two Stability Evaluation Methods.** The comparison between the absolute error and the relative error of the BP neural network and the GA-BP neural network stability evaluation method are shown in Figures 4 and 5.

TABLE 2: Predicted stability coefficient of GA-BP neural network.

Serial number	Predictive value	Actual value	Absolute difference	Relatively poor
1	0.998	0.995	0.003	0.31%
2	1.023	0.995	0.027	2.69%
3	0.996	0.995	0.001	0.10%
4	1.001	0.995	0.005	0.55%
5	0.997	0.995	0.001	0.14%
6	1.026	0.995	0.030	2.99%
7	0.999	0.995	0.004	0.42%
8	1.001	0.995	0.005	0.56%
9	0.998	0.995	0.003	0.32%
10	1.035	0.995	0.040	3.86%

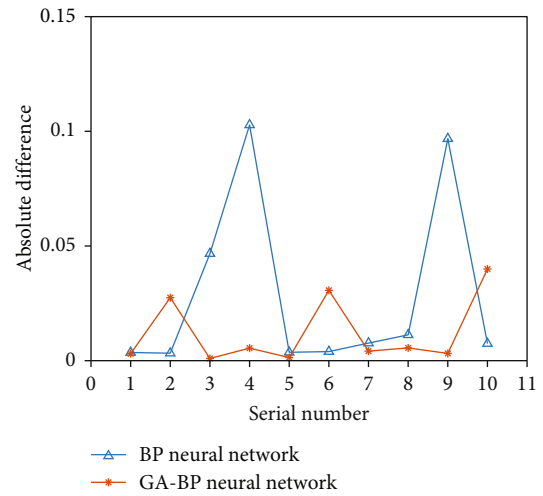


FIGURE 4: Comparison of absolute differences between the two methods.

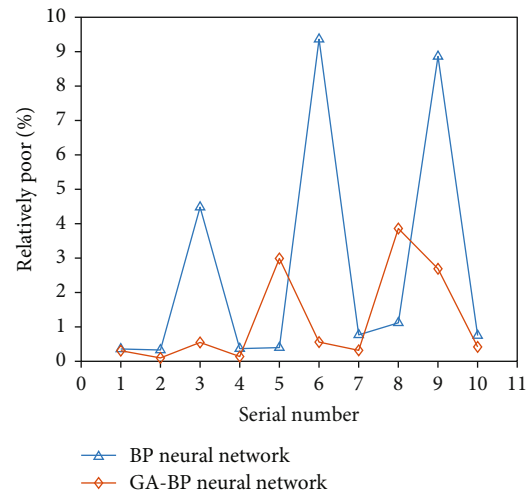


FIGURE 5: Changes in relative difference between the two methods.

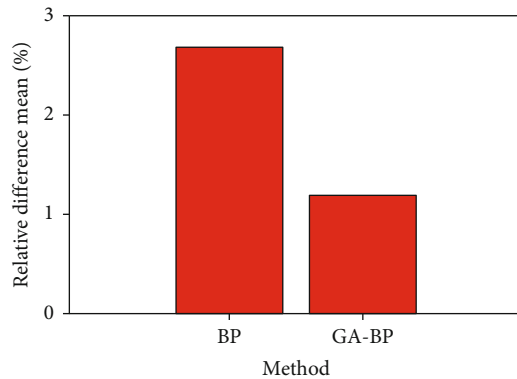


FIGURE 6: Average comparison of relative errors between the two.

It can be seen from the figure that the GA-BP neural network algorithm has faster convergence speed, higher accuracy, and better stability than the BP neural network algorithm. The average comparison of the relative errors between the two is shown in Figure 6.

## 5. Conclusion

This paper firstly introduces the basic knowledge of BPNN from the research history, application research, and other aspects; clarifies the origin, definition, characteristics, application, and existing defects of BPNN; and determines the BPNN in this research. Because of the neural network model structure, using neural networks in the analysis and prediction of rock and soil landslides has a strong theoretical basis. The genetic algorithm's premise is also examined, and a neural network based on GA-BP is built and optimized. The two stability evaluation methods and the traditional limit equilibrium method are used in the actual geotechnical measurement, and the results are as follows:

- (1) The GA-based BP neural network can effectively improve the convergence speed of the network, improve the solution space of the network, and overcome the problem that it is easy to fall into local minima, thereby improving the prediction accuracy of the network
- (2) The training process of the BP neural network is greatly affected by the initial weights and thresholds. In addition to the insufficient number of samples and incomplete input parameters, in practical applications, there is a large error in the single training result of the neural network, and the method of averaging multiple training results can effectively reduce this error, thereby improving the prediction accuracy
- (3) The results show that utilizing methods like the BPNN algorithm and the GA-BPNN algorithm, neural networks can be utilized to analyze the stability of the Baitupo landslide using the limit equilibrium approach. The GA-BPNN algorithm provides a quicker convergence time, more accuracy, better sta-

bility, and more dependable outputs compared to the BP neural network method

- (4) The landslide stability calculation shows that the landslide is in an understable state as a whole under natural working conditions, and there is a possibility of overall slippage
- (5) The sample database in this work selects 9 characteristics that affect landslide stability; however, the rock mass structure, geological structure, and other issues that are difficult to measure have not been taken into account, which will invariably have an impact on the results. Therefore, the scientific selection of influencing factors will be a reasonable quantification of non-quantitative factors and is a problem worthy of further study

## Data Availability

The datasets used during the current study are available from the corresponding author on reasonable request.

## Conflicts of Interest

Declares that he has no conflict of interest.

## References

- [1] R. Andrewwinner and S. S. Chandrasekaran, "Investigation on the failure mechanism of rainfall-induced long-runout landslide at Upputhode, Kerala State of India," *Land*, vol. 10, no. 11, p. 1212, 2021.
- [2] P. O. Falae, R. K. Dash, M. Samanta, and D. P. Kanungo, "Geo-integrated assessment of the landslide zone around Gadora along NH 58 of the Garhwal Himalayas, India," *Near Surface Geophysics*, vol. 19, no. 2, pp. 183–198, 2021.
- [3] D. R. Pathak, H. N. Gharti, and A. Hiratsuka, "Stochastic modeling of progressive failure in heterogeneous soil slope," *Geotechnical & Geological Engineering*, vol. 26, no. 2, pp. 113–120, 2008.
- [4] F. Zhang, A. Yashima, H. Osaki, T. Adachi, and F. Oka, "Numerical Simulation of Progressive Failure in Cut Slope of Soft Rock Using a Soil-Water Coupled Finite Element Analysis," *Journal of the Japanese Geotechnical Society*, vol. 43, no. 5, pp. 119–131, 2003.
- [5] J. M. Vierling and R. H. Fennell, "Histopathology of early and late human hepatic allograft rejection: evidence of progressive destruction of interlobular bile ducts," *Hepatology*, vol. 5, no. 6, pp. 1076–1082, 1985.
- [6] J. M. Duncan and S. G. Wright, *Soil Strength and Slope Stability*, John Wiley & Sons, United States, 2014.
- [7] D. M. Hume and R. H. Egdahl, "Progressive destruction of renal homografts isolated from the regional lymphatics of the host. [J]," *Surgery*, vol. 38, no. 1, pp. 194–214, 1955.
- [8] H. Lu, Y. Gao, and D. Gan, "Occurrence and control mechanisms of slope crack at tunnel entrance," *Journal of Highway and Transportation Research and Development*, vol. 30, no. 2, pp. 69–76, 2013.
- [9] M. T. Harris, "The foreslope and toe-of-slope facies of the middle triassic Latemar buildup (Dolomites, northern Italy)," *Journal of Sedimentary Research*, vol. 64, pp. 132–145, 1994.

- [10] G. L. Bracco Gartner, M. Morsilli, W. Schlager, and A. Bosellini, "Toe-of-slope of a Cretaceous carbonate platform in outcrop, seismic model and offshore seismic data (Apulia, Italy) [J]," *International Journal of Earth Sciences*, vol. 91, no. 2, pp. 315–330, 2002.
- [11] Q. Zhang, "Block-dividing limit equilibrium analysis method with multiple sliding-planes," *Chinese Journal of Rock Mechanics and Engineering*, vol. 26, no. 8, pp. 1625–1632, 2007.
- [12] S. N. Wang, C. Shi, Y. L. Zhang, and K. H. Chen, "Numerical limit equilibrium analysis method of slope stability based on particle swarm optimization," *Applied Mechanics and Materials*, vol. 353-356, pp. 247–251, 2013.
- [13] H. B. Xue, C. M. Zhang, and F. N. Dang, "Limit equilibrium analysis method for loess slopes considering spatial-temporal evolution laws of parameters," *Chinese Journal of Geotechnical Engineering*, vol. 40, pp. 162–166, 2018.
- [14] L. Y. Zhang, Y. R. Zheng, S. Zhao, and W. Shi, "The feasibility study of strength-reduction method with FEM for calculating safety factors of soil slope stability," *Journal of Hydraulic Engineering*, vol. 1, no. 1, pp. 21–26, 2003.
- [15] K. Yamazaki and T. Saeki, "Adaptive mesh generation within nonlinear iterative calculations for analyses of electric machines [J]," *IEEE Transactions on Magnetics*, vol. 39, no. 3, pp. 1654–1657, 2003.
- [16] K. Ying, P. Chen, and H. Yu, "Analysis of rock high-slope stability based on a particle flow code strength reduction method," *Electronic Journal of Geotechnical Engineering*, vol. 20, no. 28, pp. 13421–13430, 2015.
- [17] X. Zhi, "BP neural network with rough set for short term load forecasting," *Expert Systems with Applications an International Journal*, vol. 36, no. 1, pp. 273–279, 2009.
- [18] D. E. Rumelhart, J. L. McClelland, and PDP Research Group, *Parallel Distributed Processing: Explorations in the Microstructure of Cognition*, MIT Press, Cambridge, 1987.
- [19] F. Dowla, F. Taylor, and R. Anderaon, "Selamic discrimination with artificia neural: preliminary results with regional spectral date bull seiam," *Soc.AM*, vol. 8, no. 4, pp. 1346–1373, 1990.
- [20] S. Wang, N. Zhang, L. Wu, and Y. Wang, "Wind speed forecasting based on the hybrid ensemble empirical mode decomposition and GA-BP neural network method," *Renewable Energy*, vol. 94, pp. 629–636, 2016.
- [21] K. Chandra, A. S. Marcano, S. Mumtaz, R. V. Prasad, and H. L. Christiansen, "Unveiling capacity gains in ultradense networks: using mm-wave NOMA[J]," *IEEE Vehicular Technology Magazine*, vol. 13, no. 2, pp. 75–83, 2018.
- [22] J. Du, C. Jiang, Z. Han, H. Zhang, S. Mumtaz, and Y. Ren, "Contract mechanism and performance analysis for data transaction in mobile social networks," *IEEE Transactions on Network Science and Engineering*, vol. 6, no. 2, pp. 103–115, 2019.

## Research Article

# Research on Forest Conversation Analysis Using Autoregressive Neural Network-Based Model

Tianhao Ma,<sup>1</sup> Yuchen She,<sup>2</sup> and Junang Liu <sup>1</sup>

<sup>1</sup>College of Forestry, Central South University of Forestry and Technology, Changsha, 410004 Hunan, China

<sup>2</sup>Central South Inventory and Planning Institute of National Forestry and Grassland Administration, Changsha, 410014 Hunan, China

Correspondence should be addressed to Junang Liu; [junangliu@stu.cpu.edu.cn](mailto:junangliu@stu.cpu.edu.cn)

Received 6 April 2022; Revised 11 May 2022; Accepted 16 May 2022; Published 20 June 2022

Academic Editor: Naeem Jan

Copyright © 2022 Tianhao Ma et al. This is an open access article distributed under the Creative Commons Attribution License, which permits unrestricted use, distribution, and reproduction in any medium, provided the original work is properly cited.

Forest biodiversity is an important component of biological diversity that should not be disregarded. The question of how to evaluate it has sparked scholarly inquiry and discussion. The purpose of this paper is to describe the principles of general linear regression, the selection of model variables in OLS autoregressive modelling, model coefficient testing, analysis of variance of autoregressive models, and model evaluation indicators in order to clarify the suitability of GWR models for solving biomass-related data problems. The GWR 4.0 program was used to create a spatially weighted autoregressive model. Model testing and an accuracy analysis were performed on the model. Following a comparison and study with the general linear regression model, it was discovered that the geographically weighted autoregressive model is better suited to defining spatially correlated data than the general linear regression model.

## 1. Introduction

Since the industrial revolution, the impact of human activities on the biosphere has spread from local to global, especially the concentration of  $CO_2$ ,  $CH_4$  and other greenhouse gases in the atmosphere is increasing year by year, resulting in a continuous increase in global temperature [1]. The rise in global temperature will lead to a rise in sea level, an uneven distribution of precipitation, increased desertification and natural disasters, which will seriously affect the development of national economies [2].

Forest biomass is the carrier of the carbon cycle in forest ecosystems and an important parameter for assessing the forest carbon cycle [3]. There are basically three traditional ways to study forest biomass: firstly, the micrometeorological field method, which combines the rules of micrometeorological field with wind direction, wind speed and temperature; secondly, the carbon dioxide balance method, which measures the change of carbon dioxide in the ecosystem; and thirdly, the direct harvesting method, which investigates the existing biomass of the forest, although this

method is more accurate, it is difficult to use because of the large workload, complicated process and long period; Accurate determination of forest biomass is important for both production and theoretical research, and has been valued by ecologists and foresters worldwide [4]. The use of forest biomass models to estimate biomass has become a popular method.

There are three basic types of forest biomass models: linear models, non-linear models and polynomial models. These models are based on the basic assumption that the biomass distribution is random and do not take into account the spatial non-stationarity of the study variables [5]. It has been found that the spatial correlation between many sample data is due to the proximity of geographical locations; in order to take into account the spatial correlation of data when studying biomass distribution, In recent years, the evaluation of forest biodiversity has been studied more from a systemic perspective, and the factors affecting the evaluation include not only natural factors, but also various factors such as human, social and economic development [6]. The methods proposed to prevent the decline of biodiversity

include not only natural measures, but also socio-economic and cultural measures. For example, concluded that the decline of species and biological assets is mainly caused by the neglect of ecological values other than private interests, and proposed that ecosystems and biodiversity the scientific assessment process for ecosystems and biodiversity is policy change [7]. Studies by [8, 9] also show that habitat loss and habitat fragmentation are major contributors to environmental degradation and biodiversity loss. In addition, it is difficult to know the exact number of species, ecosystems and genes in forest biodiversity, no matter how it is evaluated, and its evaluation is a typical ‘black box’ system [10]. The evaluation of forest biodiversity is a typical “black box” system, and the “black box” theory should be applied to evaluate changes in forest biodiversity through the pressure-state and response caused by human socio-economic activities [11]. The author takes the biodiversity of forest nature reserves as the research object, collects relevant information based on the data of the seven national forest resources inventories, and establishes a differential equation between biodiversity changes and economic development in forest nature reserves at the national level to find out the optimal price for forest biodiversity value evaluation, with a view to providing a basis for biodiversity value compensation and management [12].

The paper’s organization paragraph is as follows: The related work is presented in Section 2. Section 3 analyzes the geographically weighted regression of the proposed work. Section 4, discusses the comparative analysis of results. Finally, in Section 5, the research work is concluded.

## 2. Related Work

In a study of the application of geographically weighted autoregressive models, [13] for the first time used a geographically weighted regression model to study the distribution of disease and compared it with the traditional least squares method, showing that the residuals of the method were much smaller than those of the ordinary linear regression model. [14] Established a spatial relationship between China’s GDP and the variation of each province. The usual regression analysis assumes that the regression coefficients are consistent across regions, but in actual geographical space, the impact of a certain factor on the level of industrialization development is not entirely consistent across regions. This method is a good way to analyses the relationship between the local economy and the overall economy and the process of change. [In Sendai, Japan, he studied the spatial variation of the heat island effect in the city and showed that the same spatial variation in urban temperature trends could be addressed by a geographically weighted autoregressive model. [15] Used the geographically weighted autoregressive principle to model the relationship between climate and elevation in the UK, and showed that the model fit was very well matched to reality. [16] used a GWR model to successfully solve the spatial distribution pattern of vegetation. In the same year, [17, 18] applied this method to the analysis of regional industrialisation and his results showed that the level of industrialisation varied significantly spatially

due to environmental influences. [8] applied this method to traffic, studying the relationship between average visual traffic and environmental factors, and thus predicting future traffic congestion levels in different regions [19].

In general, a lot of research has been done in geographically weighted regression at home and abroad, and a lot of results have been achieved. However, forest biomass distribution research is limited to classic geostatistical approaches and remote sensing spectral analysis, which leaves a lot to be desired. Geographically weighted regression models have great advantages in solving the spatial distribution of geographic things, especially the new geographically weighted regression models, whose powerful function type is getting more and more attention and application [19]. Therefore, the geographically weighted regression models used in this paper simulate the spatial distribution of forest biomass, and it is important to analyze the advantages and disadvantages of geographically weighted regression models in the spatial distribution of forest biomass [20–22].

## 3. Geographically Weighted Regression

In forest manager surveys, the distribution characteristics of all the data we collect often vary depending on location. Traditional regression analysis methods ignore the relationship between parameter estimates and the geographical location of data collection and fail to represent the spatial sub-characteristics of the data. To address this problem.

*3.1. Geographically Weighted Regression Model Basis.* It has the following basic form:

$$y_i = \beta_0(u_i, v_i) + \sum_{k=1}^p \beta_k(u_i, v_i)x_{ik} + \varepsilon_i \quad i = 1, 2 \dots, n \quad (1)$$

Where  $(u_i, v_i)$  is the geographical coordinate of the  $i$ th sampling point,  $\beta_k(u_i, v_i)$  is the  $k$ th regression coefficient on the  $i$ th sampling point,  $\varepsilon_i$  is the random error term, and the underlying assumption is that it follows a normal distribution, i.e.

$$\varepsilon_i \sim N(0, \sigma^2) \text{Cov}(\varepsilon_i, \varepsilon_j) = 0 (i \neq j) \quad (2)$$

Equation (2) can also be written as:

$$y_i = \beta_{i0} + \sum_{k=1}^p \beta_{ik}x_{ik} + \varepsilon_i \quad i = 1, 2 \dots, n \quad (3)$$

If  $\beta_{1k} = \beta_{2k} = \dots = \beta_{nk}$ , then the GWmin model is the same as the general linear regression model, i.e, which will W better reflect the spatial variation patterns of the study variables. To simplify the calculation process, Brunson et al. introduced a spatial weight  $w_{ij}$  into the model so that the regression parameters at point  $i$  would have to make

$$\sum_{j=1}^n w_{ij} \left( y_j - \beta_{i0} - \sum_{k=1}^p \beta_{ik}x_{ik} \right)^2 \quad (4)$$



The estimated value of the regression parameter is calculated when the minimum value is taken as  $\hat{\beta}(u_i, v_i)$ , where  $w_{ij}$  is the geographical weight, the size of which increases as the geographical distance between point i and point j decreases.

The estimated value of the regression parameter  $\hat{\beta}(u_i, v_i)$  at observation point i is:

$$\hat{\beta}(u_i, v_i) = \left( X' W(u_i, v_i) X \right)^{-1} X' W(u_i, v_i) Y \quad (5)$$

Of which:

$$X = \begin{bmatrix} 1 & x_{11} & \cdots & x_{1k} \\ 1 & x_{21} & \cdots & x_{2k} \\ \cdots & \cdots & \cdots & \cdots \\ 1 & x_{n1} & \cdots & x_{nk} \end{bmatrix}, W(u_i, v_i) = W_i \quad (6)$$

$$= \begin{bmatrix} w_{i1} & 0 & \cdots & 0 \\ \cdots & w_{i2} & \cdots & 0 \\ \cdots & \cdots & \cdots & \cdots \\ 0 & 0 & \cdots & w_{in} \end{bmatrix}$$

$$\beta = \begin{bmatrix} \beta_0(u_1, v_1) & \beta_1(u_1, v_1) & \cdots & \beta_k(u_1, v_1) \\ \beta_0(u_2, v_2) & \beta_1(u_2, v_2) & \cdots & \beta_k(u_2, v_2) \\ \cdots & \cdots & \cdots & \cdots \\ \beta_0(u_n, v_n) & \beta_1(u_n, v_n) & \cdots & \beta_k(u_n, v_n) \end{bmatrix}, Y = \begin{bmatrix} y_1 \\ y_2 \\ \cdots \\ y_n \end{bmatrix} \quad (7)$$

n is the number of sample sites,  $\hat{\beta}$  is the estimated value of the regression coefficient slice, and k is the number of independent variables.  $w_{ij}$  ( $j = 1, 2, \dots, n$ ) is the weight given to sample point j when fitting the model at observation i.

$X_i$  is the vector consisting of the ith observed independent variable factor, and according to Equation (7), the fitted value  $\hat{y}_i$  is obtained as

$$\hat{y}_i = X_i \hat{\beta}(u_i, v_i) = X_i \left( X' W(u_i, v_i) X \right)^{-1} X' W(u_i, v_i) Y \quad (8)$$

The matrix shape of the fitted values can be expressed as follows:

$$\hat{Y} = \begin{bmatrix} X_1 \left( X' W(u_1, v_1) X \right)^{-1} X' W(u_1, v_1) \\ X_2 \left( X' W(u_2, v_2) X \right)^{-1} X' W(u_2, v_2) \\ \cdots \\ X_n \left( X' W(u_n, v_n) X \right)^{-1} X' W(u_n, v_n) \end{bmatrix} Y = SY \quad (9)$$

Where

$$S = \begin{bmatrix} X_1 \left( X' W(u_1, v_1) X \right)^{-1} X' W(u_1, v_1) \\ X_2 \left( X' W(u_2, v_2) X \right)^{-1} X' W(u_2, v_2) \\ \cdots \\ X_n \left( X' W(u_n, v_n) X \right)^{-1} X' W(u_n, v_n) \end{bmatrix} \quad (10)$$

is the spatial hat matrix of the geographically weighted back coincidence fit.

**3.2. Selection of Spatial Enumeration Functions.** The spatial weights are used to represent the degree of relationship prior to the regression point's neighboring point j. Equation Equation (9) provides the definition of spatial weights, which is used to calculate the GWR model's regression parameters. The following four spatial weight functions are commonly used, respectively.

**3.2.1. Distance Threshold Method.** Distance threshold method is actually given a distance D, such as is less than the distance D is considered to be the weight of 1, otherwise the weight is considered to be 0, that is, the points beyond the distance is considered irrelevant to the current point, the distance outside the point does not participate in the model fitting calculation. The formula is expressed as follows:

$$w_{ij} = \begin{cases} 1 & d_{ij} \leq D \\ 0 & d_{ij} > D \end{cases} \quad (11)$$

**3.2.2. The Inverse Distance Method.** The inverse distance method was proposed by the scholar Tobler and the formula is expressed as follows:

$$w_{ij} = 1/d_{ij}^\alpha \quad (12)$$

Where  $\alpha$  is a constant that is determined by the situation. The formula above shows that the closer the point is to the center, the more weight it receives. Tobler proposed it mostly based on the first law of geography. The inverse distance method is much better than the distance threshold, but the only drawback is that if the regression points overlap with the sample data points  $d_{ij}^\alpha = 0$ , then the weights appear to be infinite at this point. If this point is removed, the accuracy of the parameter estimation is reduced, so this method is also not applicable to GWR models.

$$w_{ij} = \exp \left( -(d_{ij}/b)^2 \right) \quad (13)$$

Where b is the bandwidth. From the formula, the larger the bandwidth, the slower the decay of the weights, and vice versa. If  $b=0$ , then  $w_{ij} = 1$ , which means that the weight at regression point i is 1 and the weights at other observation points tend to be 0, the fit becomes a local fit. If b is infinite, then the weights at all observation points converge to 1, and

the fit is in fact a global fit. If the bandwidth is fixed, the  $w_{ij} = 1$  weights reach a maximum when  $d_{ij} = 0$ ;  $w_{ij}$  decreases as the distance between the sample point and the regression point increases.

3.2.3. *Truncated Function Method (Bi-Square)*. Gaussian function will be the sample data involved in the calculation, while the truncated function only calculates the distance less than the bandwidth of the sample data, truncated function is to improve the efficiency of the calculation of Gaussian function of the improved type, the form of the following:

$$w_{ij} = \begin{cases} \left[1 - (d_{ij}/b)^2\right]^2 & d_{ij} \leq b \\ 0 & d_{ij} > b \end{cases} \quad (14)$$

3.3. *Geographically Weighted Regression Model Implementation Method*. In this paper, the geo-weighted regression model was calculated using GWR4.0, a Gaussian kernel function was used for the fitting process, and C V was used as the evaluation index to select the best bandwidth. The dependent variable of the model was the forest biomass of each sample plot, the environmental factor Elevation and the average diameter at breast height (AVER DBH) of the stand were used as independent variables. The GWR model was expressed as follows: the biomass  $y_i$  per hectare of sample plot number  $i$  was expressed as the sum of the product of the  $j$ th independent variable  $x_{ij}$  ( $j = 0, 1, 2$ ) and the corresponding coefficient ( $\beta_{ij}$ ,  $j = 0, 1, 2$ ), and  $\varepsilon$  was the model residual.

$$y_i = \beta_{i0} + \beta_{i1}x_{i1} + \beta_{i2}x_{i2} \quad (15)$$

Where  $y_i$  is the biomass per hectare in plot  $i$ ,  $x_{i1}$  is the elevation of plot  $i$ ,  $x_{i2}$  is the mean diameter at breast height in plot  $i$  and  $\varepsilon$  is the model residual.

A weighting function is used in the GWR model to quantify the effect of each site biomass on the forest biomass of the sample site. The weight function chosen in this paper is a Gaussian function with a bandwidth of 1083 m and the weight function is shown below:

$$w_{ij} = e^{-\left(\frac{d_{ij}}{1083}\right)^2} \quad (16)$$

#### 4. Comparative Analysis of Results

The five evaluation indicators for the two models are given in Table 1. From the table, it can be seen that the AIC value of the GWR model is 18.325 smaller than the ALC value of the OLS model. In addition, the AICc and CV of the local model are much smaller than those of the traditional linear regression model, which further indicates that the local model has improved the accuracy of biomass estimation, and that the R2 and R2-squared values have increased further compared to those of the OLS model. Because the geographically weighted regression model handles spatial unsteadiness in its modelling, these measures suggest that

TABLE 1: Two model fit statistics.

Model	AIC	AICc	R <sup>2</sup>	R <sup>2</sup> <sub>adj</sub>	CV
OLS	1324.741	1223.147	0.554	0.521	2164.010
GWR	1305.421	1254.291	0.745	0.654	1954.623

the GwR model's model accuracy, predictive power, and precision are substantially higher than those of the OLS model.

The estimated values, standard errors, p-values,  $\beta - 1 \times SD$  and  $\beta + 1 \times SD$  of the least squares model coefficients are shown in Table 2. For the general linear regression model, the model coefficients showed significant correlation at the  $\alpha = 0.05$  level of significance.

In terms of model coefficients, mean diameter at breast height was the most important factor. Another important factor is elevation. The data show that forest biomass is higher at higher elevations and lower at lower elevations. Lower elevations are flatter and more heavily damaged by humans, but higher elevations have steeper slopes and are less prone to tree removal, resulting in larger forest biomass. The GWwR model is a local regression model in which a set of local regression parameters is calculated for each regression point, and the variation between the regression parameters can explain the spatial non-stationarity of the predictors very well. The spatial non-stationarity of the study factors can be well explained by the variation between regression parameters. The results of the geographically weighted regressions for the Liangshui National Nature Reserve include: maximum, minimum, median, 25% quantile (Q1) and 75% quantile (Q3). As shown in Table 3.

National studies have found that the median GWR model coefficient is similar to the OLS model coefficient; between Q1 (25% quantile) and Q3 (75% quantile) 50% of the GwR model coefficients are included. If the data meet the basic assumption of a normal distribution, with 68% of the OS model coefficients included within  $\pm 1$  standard deviation of the model coefficients, it is generally accepted that if there is no non-stationarity in the spatial distribution of the data, then the geo-weighted regression model coefficients Q1 and Q3 should be included within  $\pm 1$  standard deviation of the least squares model coefficients. If Q1 or Q3 do not fall within the range  $[\beta - 1 \times SDB + 1 \times SD]$ , then there is non-stationarity in the spatial distribution of the study variables. 1 For example, the range of Q1 to Q3 for the coefficients of the AVER DBH values in the geo-weighted regression is 5.04 to 7.7 [22–25].

This demonstrates the spatial non-stationarity of the relationship between the mean diameter at breast height and the elevation coefficients. With the development of GIS technology, the spatial variation of the coefficients of the geo-weighted regression model can be visualised using GIS technology to produce maps. Figures 1 and 2 use maps to depict the spatial distribution patterns of these regression coefficients. The mean diameter at breast height of the sample plots is generally positive throughout the study area, whereas elevation varies from negative to positive in different areas.

The scatter plots of the residuals of the GWR model and the OLS model are shown in Figures 3 and 4, respectively.

TABLE 2: Linear back old model coefficients, standard errors and  $p$ -values.

Variable	Estimate	StandardError	T value	Pr > t	$\beta-1 \times SD$	$\beta+1 \times SD$
Intercept	-54.021	23.412	-2.010	0.0214	-75.241	-31.247
Elevation	0.157	0.0640	2.630	0.008	0.099	0.214
AVER_DBH	6.321	0.5620	11.24	<0.001	5.741	6.852

TABLE 3: Estimated values of the 3GTO model parameters.

Variable	Mean	Standard	Min	Lwr quartile	Median	Upr quartile	Max
Intercept	-32.14	76.54	-214.75	-74.40	-74.23	1.15	189.61
Elevation	0.09	0.23	-0.35	-0.480	0.07	0.25	0.60
AVER_DBH	6.50	1.47	0.23	5.240	7.01	7.80	10.54

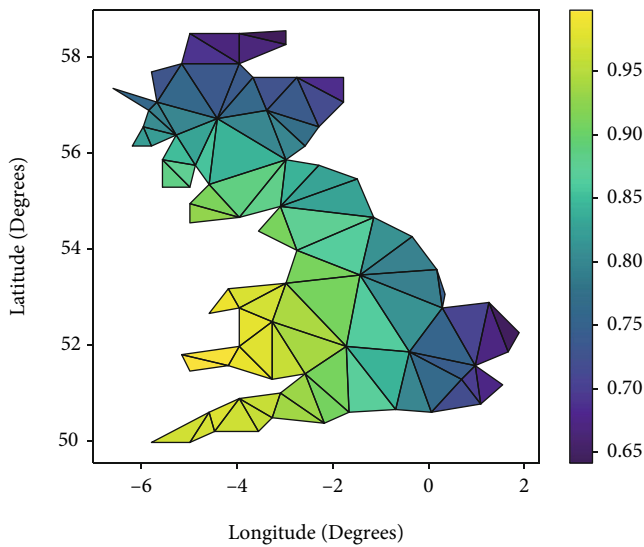


FIGURE 1: Spatial distribution of regression coefficients.

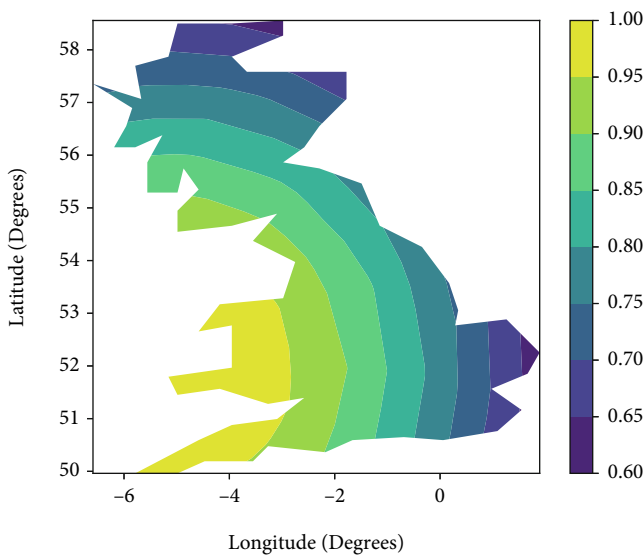


FIGURE 2: Spatial distribution of elevation regression coefficients.

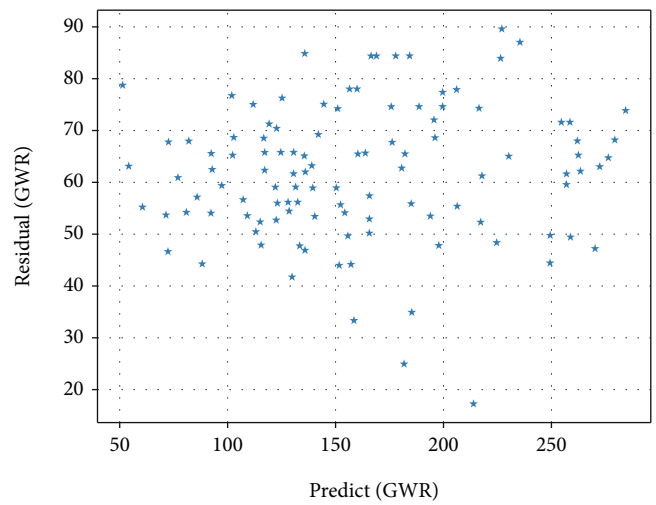


FIGURE 3: GWR residual distribution.

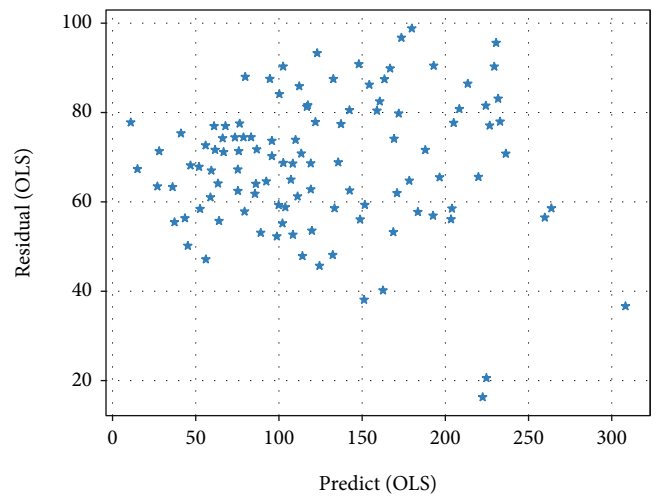


FIGURE 4: OLS Residuals Distribution Chart.

This indicates that the GWR model is more accurate and solves the heteroskedasticity problem to a certain extent.

Local residuals spatial correlation analysis Global Moran's I can only reflect the spatial correlation of the study variables as a whole. The local Moran's I statistic was introduced

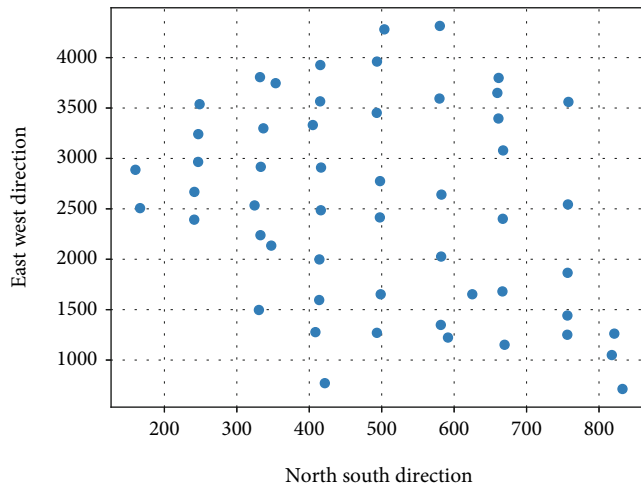


FIGURE 5: OLS residual local spatial correlation.

in this research to further investigate the spatial correlation of model residuals in different regions. In order to make comparative analysis easier, a bandwidth of 1083 m was selected and the local Moran's I statistic of the residuals was calculated using the EXCEL plug-in ROOTCASE, and finally the Moran's I was plotted using the bubble chart tool in EXCEL. The results are shown in Figure 5.

## 5. Conclusions

The fundamentals of general linear auto regression, model variable selection in OLS regression modelling, model coefficient tests, regression model analysis of variance, and model evaluation indicators are all covered in this work. The weighting function selection procedure in the geographically weighted regression model is presented, as well as the pros and disadvantages of each weighting function, and the Gaussian function is finally chosen as the weighting function in this study. The selection methods and criteria of different bandwidths are presented, and after comparison, the model finally decides to choose 1083 m as the bandwidth to achieve forest value protection.

## Data Availability

The datasets used during the current study are available from the corresponding author on reasonable request.

## Conflicts of Interest

Declares that he has no conflict of interest.

## References

- [1] J. Zhang, H. Qiu, X. Li et al., "Real-time nowcasting of microbiological water quality at recreational beaches: a wavelet and artificial neural network-based hybrid modeling approach," *Environmental Science & Technology*, vol. 52, no. 15, pp. 8446–8455, 2018.
- [2] L. Wen and X. Yuan, "Forecasting CO<sub>2</sub> emissions in Chinas commercial department, through BP neural network based on random forest and PSO," *Science of the Total Environment*, vol. 718, p. 137194, 2020.
- [3] V. Nourani, A. H. Baghanam, J. Adamowski, and M. Gebremichael, "Using self-organizing maps and wavelet transforms for space-time pre- processing of satellite precipitation and runoff data in neural network based rainfall-runoff modeling," *Journal of Hydrology*, vol. 476, pp. 228–243, 2013.
- [4] Y. C. Hu, "Electricity consumption prediction using a neural-network-based grey forecasting approach," *Journal of the Operational Research Society*, vol. 68, no. 10, pp. 1259–1264, 2017.
- [5] J. Yang, Y. Guo, and W. Zhao, "Long short-term memory neural network based fault detection and isolation for electro-mechanical actuators," *Neurocomputing*, vol. 360, pp. 85–96, 2019.
- [6] E. Ramos-Pérez, P. J. Alonso-González, and J. J. Núñez-Velázquez, "Multi-transformer: a new neural network-based architecture for forecasting S&P Volatility," *Mathematics*, vol. 9, no. 15, p. 1794, 2021.
- [7] G. Huang, X. Li, B. Zhang, and J. Ren, "PM2. 5 concentration forecasting at surface monitoring sites using GRU neural network based on empirical mode decomposition," *Science of the Total Environment*, vol. 768, article 144516, 2021.
- [8] Z. Khan, S. M. Khan, K. Dey, and M. Chowdhury, "Development and evaluation of recurrent neural network-based models for hourly traffic volume and annual average daily traffic prediction," *Transportation Research Record*, vol. 2673, no. 7, pp. 489–503, 2019.
- [9] B. Mishra, N. K. Tripathi, and M. S. Babel, "An artificial neural network-based snow cover predictive modeling in the higher Himalayas," *Journal of Mountain Science*, vol. 11, no. 4, pp. 825–837, 2014.
- [10] D. Wu, C. Zhang, L. Ji, R. Ran, H. Wu, and Y. Xu, "Forest fire recognition based on feature extraction from multi-view images," *Traitement du Signal*, vol. 38, no. 3, pp. 775–783, 2021.
- [11] L. Wang, C. Zhang, Q. Chen et al., "A Communication Strategy of Proactive Nodes Based on Loop Theorem in Wireless Sensor Networks," in *2018 Ninth international conference on intelligent control and information processing (ICICIP)*, pp. 160–167, Wanzhou, China, 2018.
- [12] S. M. Pappada, B. D. Cameron, P. M. Rosman et al., "Neural network-based real-time prediction of glucose in patients with insulin-dependent diabetes," *Diabetes Technology & Therapeutics*, vol. 13, no. 2, pp. 135–141, 2011.
- [13] Y. C. Hu and P. Jiang, "Forecasting energy demand using neural-network-based grey residual modification models," *Journal of the Operational Research Society*, vol. 68, no. 5, pp. 556–565, 2017.
- [14] S. Xie, W. Wu, S. Mooser, Q. J. Wang, R. Nathan, and Y. Huang, "Artificial neural network based hybrid modeling approach for flood inundation modeling," *Journal of Hydrology*, vol. 592, article 125605, 2021.
- [15] Z. Boussaada, O. Curea, A. Remaci, H. Camblong, and N. Mrabet Bellaaj, "A nonlinear autoregressive exogenous (NARX) neural network model for the prediction of the daily direct solar radiation," *Energies*, vol. 11, no. 3, p. 620, 2018.
- [16] F. Nunno, F. Granata, R. Gargano, and G. de Marinis, "Prediction of spring flows using nonlinear autoregressive exogenous (NARX) neural network models," *Environmental Monitoring and Assessment*, vol. 193, no. 6, pp. 1–17, 2021.

- [17] F. Ullah, S. Jabbar, and L. Mostarda, "An intelligent decision support system for software plagiarism detection in academia," *International Journal of Intelligent Systems*, vol. 36, no. 6, pp. 2730–2752, 2021.
- [18] Ö. Ö. Bozkurt, G. Biricik, and Z. C. Tayşi, "Artificial neural network and SARIMA based models for power load forecasting in Turkish electricity market," *PLoS One*, vol. 12, no. 4, article e0175915, 2017.
- [19] J. G. Jetcheva, M. Majidpour, and W. P. Chen, "Neural network model ensembles for building-level electricity load forecasts," *Energy and Buildings*, vol. 84, pp. 214–223, 2014.
- [20] I. Oksuz and U. Ugurlu, "Neural network based model comparison for intraday electricity price forecasting," *Energies*, vol. 12, no. 23, p. 4557, 2019.
- [21] S. Poornima and M. Pushpalatha, "Prediction of rainfall using intensified LSTM based recurrent neural network with weighted linear units," *Atmosphere*, vol. 10, no. 11, p. 668, 2019.
- [22] C. M. Song, "Data construction methodology for convolution neural network based daily runoff prediction and assessment of its applicability," *Journal of Hydrology*, vol. 605, p. 127324, 2022.
- [23] F. Ullah, F. Al-Turjman, and A. Nayyar, "IoT-based green city architecture using secured and sustainable android services," *Environmental Technology and Innovation*, vol. 20, p. 101091, 2020.
- [24] R. Ali, A. Ali, F. Iqbal, A. M. Khattak, and S. Aleem, "A systematic review of artificial intelligence and machine learning techniques for cyber security," in *Communications in Computer and Information Science*, pp. 584–593, Springer, Singapore, 2019.
- [25] R. Ali, A. M. Khatak, F. Chow, and S. Lee, "A case-based meta-learning and reasoning framework for classifiers selection," in *Proceedings of the 12th International Conference on Ubiquitous Information Management and Communication*, pp. 1–6, Langkawi, Malaysia, January 2018.

## Research Article

# The Modeling Analysis and Effect of CHI3L1 and CD31-Marked Microvessel Density in the Occurrence and Development of Cervical Squamous Cell Carcinoma

Yanzi Qin <sup>1</sup> and Wenjun Zhao<sup>2</sup>

<sup>1</sup>Department of Pathology, The First Affiliated Hospital of Bengbu Medical College, Bengbu, 233000 Anhui, China

<sup>2</sup>Department of Emergency Internal Medicine, The Third the People's Hospital of Bengbu, Bengbu, 233000 Anhui, China

Correspondence should be addressed to Yanzi Qin; 0100203@bbmc.edu.cn

Received 13 May 2022; Revised 31 May 2022; Accepted 3 June 2022; Published 18 June 2022

Academic Editor: Naeem Jan

Copyright © 2022 Yanzi Qin and Wenjun Zhao. This is an open access article distributed under the Creative Commons Attribution License, which permits unrestricted use, distribution, and reproduction in any medium, provided the original work is properly cited.

**Background.** Chitinase-3-like protein 1 (CHI3L1) has been identified as a novel tumor marker in several cancers. The objective of this study was to detect the expression of Chitinase-3-like protein 1 (CHI3L1) and CD31-labeled microvessel density (MVD) in cervical squamous cell carcinoma (CSCC) and to assess its prognostic impact. **Methods.** Elivision™ plus immunohistochemical method was used to detect CHI3L1 expression and MVD in different cervical tissues. We analyzed the relationship between CHI3L1 and MVD in CSCC tissues and investigated the relationship between CHI3L1, MVD, and clinicopathological parameters. Univariate and multivariate survival analyses were performed to assess the impact on progression-free survival (PFS) and overall survival (OS). **Results.** The positive expression rate of CHI3L1 protein in CSCC tissues (69.9%, 72/103) was significantly higher than that in high-grade cervical intraepithelial lesions (53.3%, 32/60), low-grade cervical intraepithelial lesions (25%, 15/60), and normal cervical tissues (16.7%, 10/60). MVD values ranged from 6 to 64 in CSCC, and no microvascular formation was observed in normal cervical tissues, high-grade intraepithelial lesions, or low-grade intraepithelial lesions. The high expression of CHI3L1 and MVD was significantly correlated with the invasion depth, differentiation degree, vascular invasion, and lymph node metastasis of CSCC (all  $P < 0.05$ ). In CSCC, the expression of MVD in the CHI3L1 high-expression group ( $41.35 \pm 9.056$ ) was significantly higher than that in the CHI3L1 low-expression group ( $23.26 \pm 11.000$ ,  $P < 0.05$ ). On univariate Kaplan-Meier analysis, FIGO stage, tumor diameter, lymph node metastasis, vascular invasion, CHI3L1, and MVD of CSCC were related to the prognosis of PFS and OS (all  $P < 0.05$ ); however, CHI3L1 and MVD were not independent prognostic factors. **Conclusion.** CHI3L1 may be involved in the progression of cervical cancer. Its high expression can promote neovascularization in the tumor microenvironment. CHI3L1 is a potential therapeutic target in the context of cervical cancer.

## 1. Introduction

Globally, cervical cancer is one of the most common cancers and among the most common causes of cancer-associated mortality in women. The incidence of cervical cancer is particularly high in underdeveloped settings [1]. An estimated 600000 women worldwide are diagnosed with cervical cancer every year, and more than half of these die of this disease [2]. The main reasons for the deterioration of cervical cancer are infiltration and metastasis, resulting in a poor prognosis. Finding possible molecular targets that lead to the incidence

and progression of cervical cancer is therefore crucial for the treatment and evaluation of cervical cancer patients in the future. Cervical cancer includes squamous cell carcinoma and adenocarcinoma, among which cervical squamous cell carcinoma (CSCC) is the most important histological type.

Chitinase-3-like protein 1 (CHI3L1, also known as YKL-40), is located on human chromosome 1q32 [3]. As an important growth factor for connective tissue cells, CHI3L1 has been shown to regulate vascular endothelial growth factor and angiogenesis [4], differentiation, and proliferation of cells [5], reregulate the extracellular matrix [5], and activate Akt to par-

ticipate in the migration of vascular endothelial cells [5]. It has important roles in signaling [6], preventing apoptosis [7], promoting metastasis [8], and tumor progression [5, 9–12]. Studies have demonstrated the involvement of CHI3L1 in tumor angiogenesis [13] and the formation of angiogenic mimicry in cervical cancer [14].

In a hypoxic environment, malignant tumor cells secrete proangiogenic factors, which promote the migration of vascular endothelial cells and formation of new blood vessels. Microvessel development has the potential to create tumor vascular networks, deliver nutrients to tumors, and further infiltrate the surrounding matrix. Tumor occurrence and metastasis are both influenced by microvessel density (MVD) [15, 16]. Many studies have found that tumor microvessels are closely linked to clinical progression and prognosis in a variety of solid tumors and that the expression of endothelial cell markers can be utilized to quantify the formation of MVD in tumor tissue [17]. CD31, also known as platelet endothelial cell adhesion molecule-1 (PPECAM-1), as one of the specific markers of endothelial cells, is often used to count tumor microvessels in immunohistochemical experiments to evaluate tumor angiogenesis [18].

This study is aimed at detecting the expression of CHI3L1 and MVD in CSCC and at the same time clarifying the relationship between CHI3L1 and MVD and its impact on the progression and evolution of disease. Our findings may provide a combination of targeted molecular therapy for cervical cancer.

## 2. Materials and Methods

**2.1. Patients and Specimens.** Paraffin archived specimens of 103 cases of CSCC tissues, 120 cases of cervical intraepithelial lesions (60 cases of high-grade intraepithelial lesions and 60 cases of low-grade intraepithelial lesions), and 60 cases of normal cervical epithelial tissues were retrospectively selected from the First Affiliated Hospital of Bengbu Medical College from January to December 2014. The pathological results of all cases were jointly diagnosed by two experienced senior pathologists, and all cases had complete clinical and follow-up data. Patients with CSCC were followed up until December 2021 or had died. In CSCC patients, the age ranged from 31 to 72 years, and the median age was 49 years old, mean  $\pm$  standard deviation (49.0  $\pm$  8.906) years old; tumor diameter is as follows: <2 cm in 10 cases,  $\geq$ 2 cm and <4 cm in 50 cases, and  $\geq$ 4 cm in 43 cases. The general types were endogenous infiltration in 24 cases, external lettuce flower in 30 cases, ulcer in 21 cases, and superficial erosion in 28 cases. Depth of infiltration is as follows: <1/2 full layer 42 cases,  $\geq$ 1/2 and <2/3 full layer 40 cases, and  $\geq$ 2/3 full layer 21 cases; degree of differentiation is as follows: high differentiation in 9 cases, medium differentiation in 63 cases, and low differentiation in 31 cases; 27 cases had lymph node metastasis, and 76 cases had no lymph node metastasis. Vascular invasion is as follows: 68 cases were found to have tumor thrombus, and 35 cases were found to have no tumor thrombus. According to the 2018 International Federation of Gynecology and Obstetrics (FIGO) staging criteria [19], there are 3 cases of IA1, 3 cases of IA2, 23 cases of IB1, 11

cases of IB2, 10 cases of IB3, 16 cases of IIA1, 10 cases of IIA2, 1 case of IIIA, 16 cases of IIIC1, 7 cases of IIIC2, and 3 cases of IVA. For the convenience of data statistics, the cases in this study are divided into IA (IA1+IA2), IB (IB1+IB2+IB3), II (IIA1+IIA2), and III+IV (IIIA+IIIC1+IIIC2+IVA). All patients did not receive any radiotherapy or chemotherapy before surgery. The ethics committee of Bengbu Medical College has approved the implementation of this experiment.

**2.2. Immunohistochemistry.** The collected cervical tissues were fixed with 10% neutral formalin, paraffin-embedded, and sequentially sectioned (3–5  $\mu$ m thick sections). Tissue antigens were restored after deparaffinization and hydration of paraffin slices. Phosphate-buffered solution (PBS) was diluted three times to eliminate the PBS solution. Diluted with 50  $\mu$ l of primary antibody per section (CHI3L1, rabbit polyclonal, diluted 1:1000, Abcam, USA and CD31, rabbit polyclonal, diluted 1:200, Abcam, USA), overnight at 4°C. Wash with PBS 3 times, remove PBS solution, add 50  $\mu$ l polymer reinforcement to each section, incubate at room temperature for 20 min, and rinse with PBS 3 times. Remove PBS solution, add 50  $\mu$ l enzyme-labeled anti-mouse/rabbit polymer (secondary antibody) to each section, and incubate at room temperature for 30 min. Rinse with PBS 3 times. The slices were stained with DAB (3,3'-diaminobenzidine) and observed under a microlens for 3–5 minutes. Hematoxylin was restained and turned blue with PBS. PBS replaced primary antibodies as negative control and known positive tablets as a positive control. The above experiments were performed according to the Elivision™ Plus detection kit instructions (Fuzhou Maixin Co., Ltd., China).

**2.3. Positive Criteria for CHI3L1.** CHI3L1 positive particles are light yellow to brownish yellow, mainly located in the cytoplasm. Immunohistochemical labeling results were evaluated by the semiquantitative scoring method from staining intensity and staining range. We randomly selected five high-power fields (400x) in the tumor cell region, and 200 tumor cells were counted. According to the proportion of positive cells, the cells were divided into <5% as 0, 5%–25% as 1, 26%–50% as 2, 51%–75% as 3, and >75% as 4. Staining intensity of positive cells is as follows: no staining as 0, light yellow as 1, brown-yellow as 2, and tan as 3. When the two of the same case are multiplied, the standard of low expression or no expression is <3 points and the standard of high expression is  $\geq$ 3. All results were judged by the double-blind method and repeated three times.

**2.4. MVD Positive Evaluation Criteria.** MVD was counted by Weinner counting method [20]. At low magnification (100x), the area with the highest microvascular density was selected. At medium magnification (200x), the number of microvessels in 5 different fields was manually counted and the average value was MVD. CD31 was located in vascular endothelial cells, and a positive microvessel was counted as a single endothelial cell or endothelial cell cluster with positive staining. Inclusion criteria are as follows: endothelial cells with complete structural outline were stained, isolated

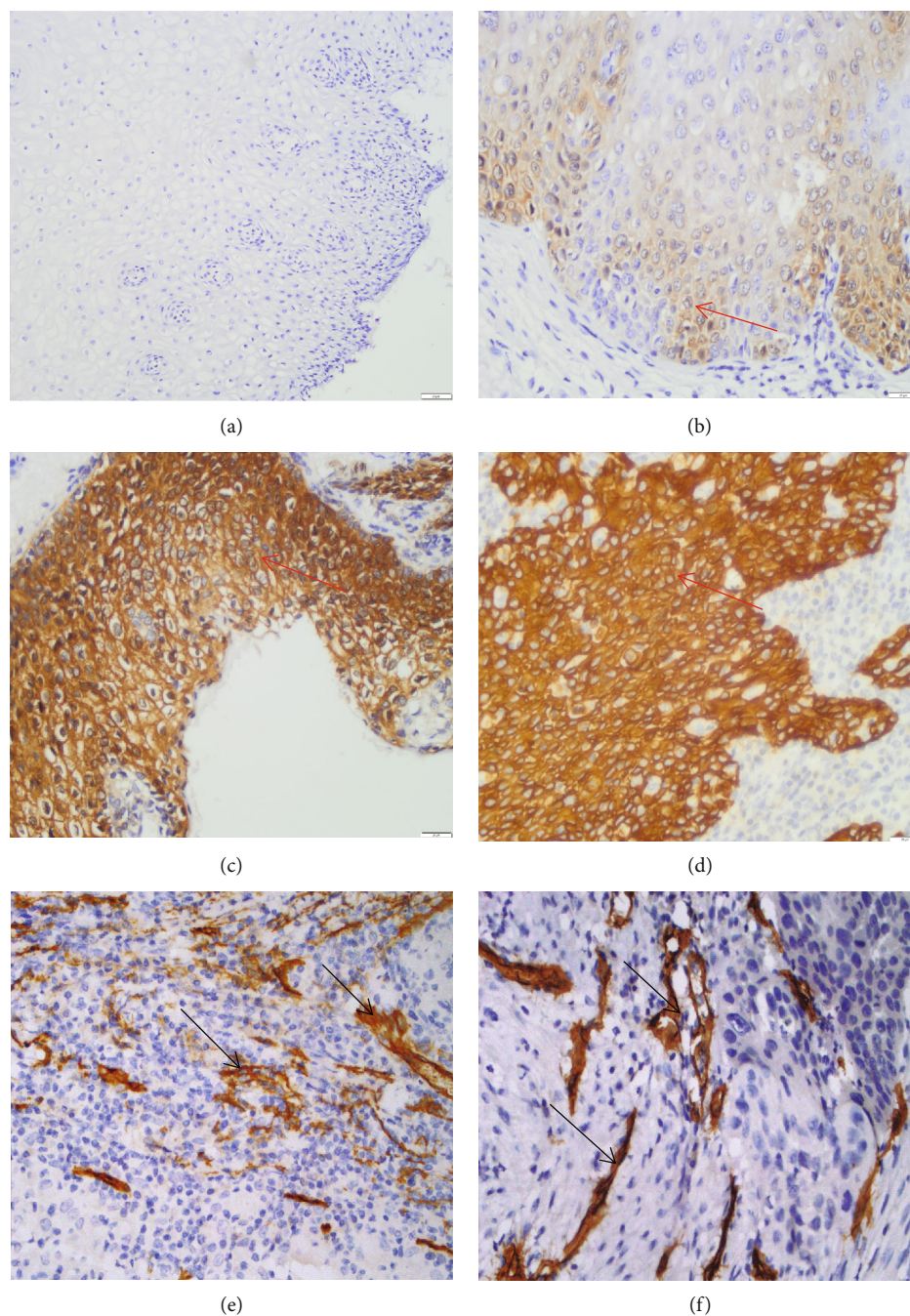


FIGURE 1: Immunohistochemical analysis of CHI3L1 and MVD expression in cervical squamous cell carcinoma (CSCC) and control groups ( $\times 400$  magnification). CHI3L1 was negatively expressed in (a) normal cervical tissue. CHI3L1 (red arrow) is brown or tan granules in the cytoplasm in (b) low-grade intraepithelial lesions, (c) high-grade intraepithelial lesions, and (d) ESCC, respectively. CD31-marked microvessels are expressed between nests of (e, f, black arrows) ESCC.

from adjacent microvessels showed single vascular endothelial cells or clusters of vascular endothelial cells and branching vascular structures with unconnected structures. Exclusion criteria are as follows: vessels with diameter  $\geq 8$  red blood cells, thick-walled smooth muscle vessels, and vessels in the sclerotic necrotic zone. All of the results were judged three times using the double-blind approach.

**2.5. Statistical Analysis.** All data were collected by SPSS26.0 (IBM Corp., Armonk, NY, USA) statistical software analysis. Statistically, the cut-off value is 0.05. When  $P < 0.05$ , it was statistically significant. *t*-test or Fisher's exact test was used for measurement data of both groups, one-way ANOVA was used for measurement data of multiple groups, and  $\chi^2$  test was used for counting data. The follow-up data were



TABLE 1: The relationship between CHI3L1, MVD, and clinicopathological parameters of cervical squamous cell carcinoma (CSCC).

Variable	CHI3L1		$\chi^2$	$P$	MVD	$t$ -test/ANOVA	$P$
	High expression	Low expression					
Age (years)			2.356	0.125		7.985	0.357
<50	37	21			34.88 ± 12.802		
≥50	35	10			37.22 ± 12.669		
Diameter (cm)			1.785	0.410		10.123	0.001
<2	6	4			20.60 ± 10.255		
≥2, <4	33	17			35.98 ± 11.531		
≥4	33	10			39.12 ± 12.204		
General type			2.522	0.471		2.068	0.109
Endogenous infiltration	15	9			34.38 ± 14.080		
External lettuce flower	24	6			38.57 ± 11.726		
Ulcer	15	6			39.29 ± 10.494		
Superficial erosion	18	10			31.82 ± 13.358		
Depth of infiltration			13.420	0.001		4.975	0.009
<1/2	21	21			31.31 ± 13.616		
≥1/2, 2/3	33	7			39.15 ± 11.116		
≥2/3	18	3			38.90 ± 11.458		
Differentiation			26.122	0.001		12.151	0.001
Well	1	8			21.44 ± 13.602		
Moderately	41	22			34.81 ± 12.076		
Poorly	30	1			42.32 ± 9.639		
Lymph node metastasis			4.062	0.044		4.570	0.001
Yes	23	4			44.70 ± 9.376		
No	49	27			32.78 ± 12.341		
Vascular invasion			31.967	0.001		7.985	0.001
Yes	60	8			41.56 ± 9.670		
No	12	23			24.91 ± 10.678		
FIGO stage			2.296	0.513		1.591	0.196
IA	3	3			26.17 ± 15.690		
IB	29	15			35.36 ± 11.654		
II	20	6			38.46 ± 11.863		
III+IV	20	7			36.48 ± 14.132		

TABLE 2: The relationship between CHI3L1 and MVD in CSCC.

Variable	MVD	$t$	$P$
CHI3L1		8.473	0.001
High expression	41.83 ± 10.024		
Low expression	23.03 ± 11.020		

analyzed by the Kaplan–Meier method for univariate survival and Cox regression analysis for multivariate survival.

### 3. Result

In this section, we explain the expression of CHI3L1 in different cervical tissues, the relationship between the expres-

sion of CHI3L1 in CSCC tissues and its clinical parameters in patients, and the expression of CD31-marked MVD in different cervical tissues in detail.

*3.1. Expression of CHI3L1 in Different Cervical Tissues.* The positive expression rate of CHI3L1 was 16.7% (10/60), 25% (15/60), 53.3% (32/60), and 69.9% (72/103) in normal cervical tissues, low-grade intraepithelial lesions, high-grade intraepithelial lesions, and CSCC, respectively. The positive expression of CHI3L1 in cervical tissues increased during the progression of malignant transformation ( $\chi^2 = 56.486$ ,  $P < 0.001$ ), which was statistically significant. Meanwhile, the positive expression rate of CHI3L1 in CSCC tissues was significantly higher than that in normal cervical tissues, low-grade intraepithelial lesions, and high-grade

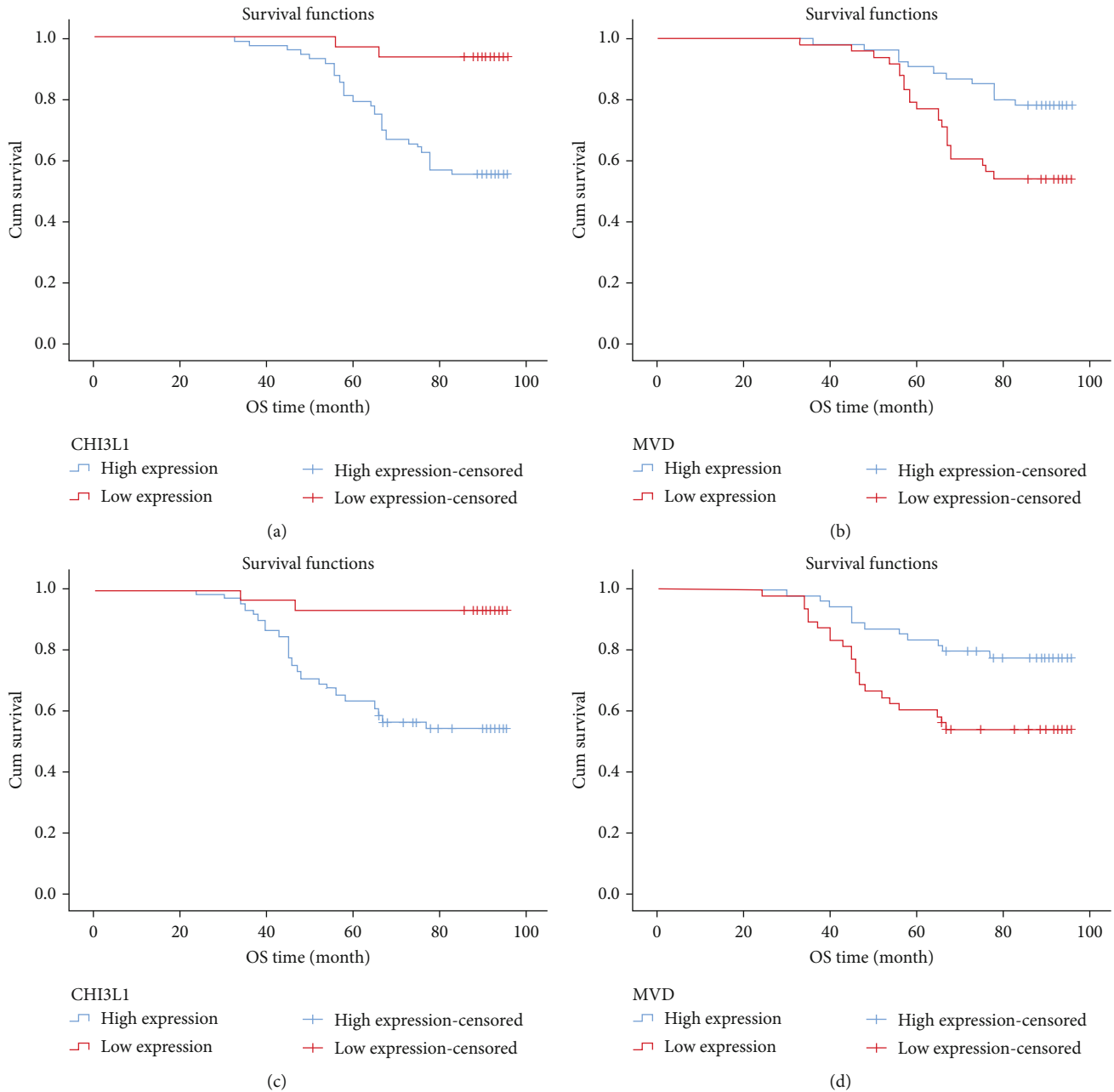


FIGURE 2: Kaplan–Meier analysis of the survival rates of patients with CSCC: (a) lower overall survival (OS) of patients with positive CHI3L1 expression (log – rank = 12.655,  $P < 0.001$ ), (b) lower OS of patients with positive MVD expression (log – rank = 7.248,  $P = 0.007$ ), (c) progression-free survival (PFS) of patients in relation to CHI3L1 (log – rank = 24.431,  $P < 0.001$ ), and (d) lower PFS of patients with positive MVD expression (log – rank = 8.522,  $P = 0.004$ ).

intraepithelial lesions ( $\chi^2 = 42.983$ ,  $\chi^2 = 30.718$ , and  $\chi^2 = 4.507$ , all  $P < 0.05$ ). The positive expression of CHI3L1 in high-grade intraepithelial lesions was significantly higher than that in normal cervical tissues and low-grade intraepithelial lesions ( $\chi^2 = 17.729$  and  $\chi^2 = 10.108$ , both  $P < 0.05$ ). However, there was no significant difference in the positive expression of CHI3L1 between low-grade intraepithelial lesions and normal cervical tissue, as shown in Figure 1.

3.2. The Relationship between the Expression of CHI3L1 in CSCC Tissues and Its Clinical Parameters of Patients. The

results showed that in CSCC tissues, the positive expression rate of CHI3L1 was significantly correlated with the depth of tumor invasion, degree of differentiation, vascular invasion, and lymph node metastasis (all  $P < 0.05$ ), but not with the patient’s age, tumor diameter, gross type, and FIGO stage (all  $P > 0.05$ ). With the deepening of tumor infiltration, especially the infiltration depth of more than 2/3 of the full thickness, the positive rate of CHI3L1 (85.7%, 18/21) was significantly higher than that of the infiltration depth of less than 1/2 of the full thickness (50%, 21/42) and the positive rate of more than 1/2 but less than 2/3 full-thickness

TABLE 3: Results of multivariate Cox regression analysis of overall survival (OS).

	B	SE	Wald	df	P	Exp (B)	95.0% CI for Exp (B)	
							Lower	Upper
Age (years)	0.505	0.384	1.732	1	0.188	1.657	0.781	3.514
FIGO stage	-0.817	0.545	2.250	1	0.134	0.442	0.152	1.285
Diameter (cm)	0.551	0.392	1.972	1	0.160	1.735	0.804	3.745
Depth of infiltration	-0.282	0.286	.973	1	0.324	0.754	0.431	1.321
Differentiated	0.433	0.396	1.197	1	0.274	1.542	0.710	3.352
Lymph node metastasis	-2.618	1.075	5.927	1	0.015	0.073	0.009	0.600
General type	-0.456	0.325	1.970	1	0.160	0.634	0.335	1.198
Vascular invasion	-0.946	0.886	1.140	1	0.286	0.388	0.068	2.204
CHI3L1	-1.219	0.816	2.232	1	0.135	0.296	0.060	1.463
MVD	0.587	0.446	1.731	1	0.188	1.798	0.750	4.312

(82.5%, 33/40). The positive rate of CHI3L1 in poorly differentiated tissues (96.7%, 30/31) was significantly higher than that in well-differentiated tissues (11.1%, 1/9) and moderately differentiated tissues (65.1%, 41/63). The CHI3L1 protein-positive rate in patients with lymph node metastasis (85.2%, 23/27) was significantly higher than that in patients without lymph node metastasis (64.5%, 49/76). The positive rate (88.2%, 60/68) was higher than the positive rate of patients without intravascular tumor thrombus (34.3%, 12/35). The above data are shown in Table 1.

**3.3. Expression of CD31-Marked MVD in Different Cervical Tissues.** In 103 cases of CSCC tissues, MVD was mainly characterized by irregular morphology, increased number, and disorganized branching and was concentrated at the edge of tumor invasion. MVD values ranged from 6 to 64, with the median value of 36 as the truncated value. MVD in the high-expression group was  $\geq 36$ , and MVD in the low-expression group was  $< 36$ , as shown in Figures 1(e) and 1(f). No microvascular formation was detected in normal cervical tissues, low-grade intraepithelial lesions, and high-grade intraepithelial lesions, and only CD31-marked MVD was detected in CSCC tissues, suggesting that the production of MVD generation increased significantly after cervical tissue carcinogenesis.

**3.4. The Relationship between the Expression of MVD in CSCC Tissues and Its Clinicopathological Parameters.** Further analysis showed that MVD expression in CSCC tissues was correlated with tumor size, invasion depth, differentiation type, vascular invasion, and lymph node metastasis ( $P < 0.05$ ), but not with age, tumor gross type, and FIGO stage ( $P > 0.05$ ). With the increase in tumor diameter, the MVD value increased gradually ( $F = 10.123$ ,  $P < 0.05$ ). The MVD value of cases with invasion depth of tumor invasion was 1/2 of the full layer ( $\geq 2/3$  full layer,  $38.90 \pm 11.458$  and  $\geq 1/2$  and  $< 2/3$  full layer,  $39.15 \pm 11.116$ ) was significantly higher than that of cases with invasion depth of  $< 1/2$  full layer ( $31.31 \pm 13.616$ ). The more poorly differentiated the tumor was, the higher the MVD value was ( $F = 12.151$ ,  $P < 0.05$ ). The MVD value of the CSCC patients with lymph node metastasis ( $44.70 \pm 9.376$ ) was significantly higher

than that of patients without lymph node metastasis ( $32.78 \pm 12.341$ ). The MVD value of CSCC with vascular invasion ( $41.56 \pm 9.670$ ) was significantly higher than that of CSCC without vascular invasion ( $24.91 \pm 10.678$ ). The above data are shown in Table 1.

**3.5. The Relationship between CHI3L1 and MVD in CSCC Tissue.** CSCC tissues were divided into two groups: the high CHI3L1 expression group and the low CHI3L1 expression group. MVD value of the high-expression group of CHI3L1 was  $41.83 \pm 10.024$ , while that of the low-expression group of CHI3L1 was  $23.03 \pm 11.020$ , and the difference was statistically significant ( $t = 8.473$ ,  $P < 0.05$ ). The positive rate of MVD in the group with high CHI3L1 expression was higher than that in the group with low CHI3L1 expression, as shown in Table 2.

**3.6. Prognosis.** The overall survival (OS) and progression-free survival (PFS) after operation in 103 patients were evaluated to see if there was a link between the expression of CHI3L1 and MVD in CSCC and patient survival. Kaplan-Meier (log-rank) survival analysis was performed on the relevant data. The results showed that the OS survival time of CSCC patients over five years after operation was  $82.42 \pm 15.789$  months, and the OS survival rate over five years was 66.9% (69/103). The survival time of PFS was  $74.63 \pm 21.630$  months, and the survival rate of PFS over five years was 50.4% (52/103). FIGO stage (log-rank = 26.469,  $P < 0.001$ ), tumor diameter (log-rank = 8.779,  $P = 0.012$ ), depth of invasion (log-rank = 6.108,  $P = 0.047$ ), degree of differentiation (log-rank = 7.689,  $P = 0.021$ ), lymph node metastasis (log-rank = 33.316,  $P < 0.001$ ), vascular invasion (log-rank = 17.062,  $P < 0.001$ ), CHI3L1 expression (log-rank = 12.655,  $P < 0.001$ , Figure 2(a)), and MVD expression (log-rank = 7.248,  $P = 0.007$ , Figure 2(b)) correlated with OS prognosis ( $P < 0.05$ ). FIGO stage (log-rank = 13.084,  $P < 0.001$ ), tumor diameter (log-rank = 14.211,  $P = 0.001$ ), depth of invasion (log-rank = 6.108,  $P = 0.047$ ), degree of differentiation (log-rank = 13.084,  $P = 0.001$ ), lymph node metastasis (log-rank = 39.522,  $P < 0.001$ ), vascular invasion (log-rank = 25.180,  $P < 0.001$ ), CHI3L1 expression

TABLE 4: Results of multivariate Cox regression analysis of progression-free survival (PFS).

	<i>B</i>	SE	Wald	df	<i>P</i>	Exp ( <i>B</i> )	95.0% CI for Exp ( <i>B</i> )	
							Lower	Upper
Age (years)	0.130	0.313	0.171	1	0.679	1.138	0.616	2.103
FIGO stage	-0.387	0.415	0.867	1	0.352	0.679	0.301	1.533
Diameter (cm)	0.592	0.308	3.691	1	0.055	1.808	0.988	3.307
Depth of infiltration	-0.365	0.233	2.454	1	0.117	0.694	0.440	1.096
Differentiated	0.401	0.337	1.414	1	0.234	1.494	0.771	2.893
Lymph node metastasis	-1.792	0.807	4.931	1	0.026	0.167	0.034	0.810
General type	-0.618	0.273	5.123	1	0.024	0.539	0.316	0.921
Vascular invasion	-0.564	0.608	0.859	1	0.354	0.569	0.173	1.875
CHI3L1	-1.867	0.676	7.617	1	0.006	0.155	0.041	0.582
MVD	0.502	0.357	1.972	1	0.160	1.652	0.820	3.328

(log – rank = 24.431,  $P < 0.001$ , as shown in Figure 2(c)), and MVD expression (log – rank = 8.522,  $P = 0.004$ , as shown in Figure 2(d)) were correlated with PFS prognosis ( $P < 0.05$ ). Cox multivariate analysis is shown in Tables 3 and 4.

#### 4. Discussion and Conclusion

CHI3L1 can be expressed and secreted by a variety of cells, including macrophages, neutrophils, epithelial cells, smooth muscle cells, chondrocytes, and tumor cells [21]. In recent years, more and more investigations on CHI3L1 in malignant tumors have been conducted. Serum CHI3L1 levels are significantly increased in endometrial cancer, melanoma, colorectal cancer, lung cancer, and breast cancer [22–24]. Increased serum CHI3L1 protein level in patients with CSCC and cervical adenocarcinoma was shown to lead to aggravation of cervical cancer, resulting in poorer prognosis and shorter survival [25, 26]. The expression level of CHI3L1 protein in cervical cancer tissues was also shown to be significantly higher than that in normal cervical tissues [13]. Although several studies have demonstrated the involvement of high expression of serum CHI3L1 protein in the growth, proliferation, infiltration, and metastasis of cervical cancer [21, 25, 26], the relationship between the expression level of CHI3L1 protein and the specific clinicopathological parameters of cervical cancer patients from the perspective of histology is not well characterized. Only Ngernyung et al. [13] reported a much higher positivity rate of CHI3L1 in cervical cancer patients with regional lymph node and organ metastasis compared to that in patients with nonmetastatic disease, which is consistent with the results of the present study. In the present study, we detected the expression level of CHI3L1 in different cervical tissue samples and confirmed that the positive expression rate of CHI3L1 in CSCC tissues was significantly higher than that in cervical intraepithelial lesions and normal cervical tissues, which was consistent with the results reported above [13]. The presence of lymph node metastases in CSCC patients enhanced the expression level of the CHI3L1 protein, according to this study ( $P < 0.05$ ). Meanwhile, it was confirmed for the first time in this study that the protein

level of CHI3L1 was significantly increased with the lower differentiation degree of CSCC, the deepening of tumor invasion depth or vascular invasion (all  $P < 0.05$ ). These findings suggest that dynamic monitoring of the positive expression level of CHI3L1 in cervical tissue may predict whether the cervix will undergo malignant changes, so CHI3L1 may become a candidate gene for predicting cervical cancer. The high expression of CHI3L1 protein is closely related to lymph node metastasis and tumor invasion of cervical cancer, which may aggravate the progression of cervical cancer.

How does CHI3L1 participate in the occurrence and progression of cervical cancer, and what is the specific mechanism? One of the leading causes of death in cancer patients is tumor metastasis and dissemination. Microangiogenesis and dietary factors are primarily used by lymph node metastases and hematogenous dissemination to offer ample blood supply. Tumor metastasis and spread are one of the causes of death in cancer patients. Lymph node metastasis and hematogenous dissemination mainly rely on microangiogenesis to provide abundant blood supply and nutritional factors. Growth and migration cannot leave the blood vessels that provide nutrients and energy. In order to ensure the survival and growth of malignant tumor cells, a continuous blood supply is required, and a good blood supply can further maintain and promote the growth of malignant tumor cells. Genogenesis plays an extremely important role in the occurrence and development of tumor tissues [27]. It has been reported that CHI3L1 plays a key role in tumor development by promoting tumor angiogenesis [6, 28]. Based on this, the relationship between MVD and clinicopathological parameters of CSCC and CHI3L1 was also detected in this study. No microvascular formation was observed in the control tissues (cervical intraepithelial lesions and normal cervical tissues), while a higher number of MVD was observed in cervical tissues, which is consistent with previous reports [13]. This experiment showed that the number of MVD would increase with the increase of tumor, the deepening of invasion depth, the lower degree of differentiation, lymph node metastasis, and vascular invasion, suggesting that the occurrence and deterioration of CSCC are closely related to the formation of neovascularization.

This study was the first to explore the effects of CHI3L1 and MVD on the prognosis and survival of CSCC from the histological perspective. The study showed that the survival status of OS and PFS was related to the expression of CHI3L1 protein and MVD ( $P < 0.05$ ). However, CHI3L1 expression cannot be used as an independent prognostic factor for OS and DFS in CSCC patients, nor can MVD expression be used as an independent prognostic factor for OS in CSCC patients, while MVD expression level can be used as an independent factor to evaluate the survival of PFS. It is suggested that high expression of CHI3L1 protein and MVD may indicate poor prognosis of CSCC patients, but neither of them can be used as independent prognostic criteria for CSCC. A similar conclusion was obtained in detecting the influence of serum CHI3L1 expression level on the prognosis of cervical cancer [25]. Mitsuhashi et al. [25] showed in a retrospective study that high serum CHI3L1 protein level is a potential independent prognostic biomarker for assessing short-term OS before treatment in patients with CSCC and cervical adenocarcinoma. This study also confirmed that FIGO stage, tumor size, lymph node metastasis, and vascular invasion were correlated with the prognosis of OS and PFS in patients with ESCC ( $P < 0.05$ ), and these factors were key factors affecting the prognosis of patients.

In this study, the number of MVD in the high-expression group of CHI3L1 was significantly higher than that in the low-expression group of CHI3L1, suggesting that CHI3L1 may be involved in the occurrence and development of cervical cancer and promote tumor angiogenesis as an angiogenic factor. Ngernyuang et al. [13] also reached the same conclusion in previous studies. Studies have shown that CHI3L1 is involved in the adhesion and migration of vascular endothelial cells [4, 29]. Studies have shown that the addition of CHI3L1 recombinant protein in vitro promotes vascular endothelial cell migration and tubule formation, which are important steps in angiogenesis. Moreover, CHI3L1 can promote the secretion of vascular endothelial growth factor (VEGF) by U87 cells and accelerate tumor angiogenesis by cooperating with other proangiogenic factors [4]. CHI3L1 activates the activities of focal adhesion kinase (FAK) and extracellular regulated protein kinase (ex-tracellular signal regulated kinases-1, ERK-1)/(ex-tracellular signal regulated kinases-2, ERK-2). Increased VEGF and angiogenesis [30], in particular the membrane receptor syndeca-1 and integrin  $\alpha v \beta 5$ , act as triggering molecules to trigger the CHI3L1 signaling cascade. CHI3L1 binds to the receptor of advanced glycation endproducts (RAGE) and induces the proliferation of cancer cells. ERK1/2-MAPK (mitogen activated protein kinase) pathway plays a role in the downstream signal cascade of RAGE-CHI3L1 [30]. Therefore, the next step of this research group is to detect the relationship between CHI3L1 and MVD through in vitro experiments, to further analyze the role of CHI3L1 in the formation of new blood vessels in CSCC and to explore the mechanism of CHI3L1 involved in CSCC.

In general, the tumor size, FIGO stage, invasion depth, vascular invasion, lymph node metastasis, and differentiation degree of CSCC are all linked to high CHI3L1 and

MVD expression. The high expression of CHI3L1 and MVD may indicate a poor prognosis for patients, but it cannot be used as an independent prognostic factor to evaluate the prognosis of patients with cervical cancer. Studies have pointed out that the growth and progression of tumors can be effectively controlled by controlling tumor angiogenesis [31]. It seems plausible that targeted inhibition of CHI3L1 expression level may potentially control tumor neovascularization and inhibit generation of lymphatic vessels, so as to effectively control tumor growth and progression.

## Data Availability

All data generated or analyzed during this study are included in this published article.

## Ethical Approval

The authors are accountable for all aspects of the work in ensuring that questions related to the accuracy or integrity of any part of the work are appropriately investigated and resolved. This study was conducted with approval from the Ethics Committee of Bengbu Medical College (No. 055).

## Conflicts of Interest

The authors declare that they have no competing interests.

## Authors' Contributions

QYZ and ZWJ participated in the research design. QYZ and ZWJ performed the research and wrote the manuscript. QYZ contributed towards critically revising the manuscript.

## Acknowledgments

This work was funded by the Natural Science Key Project of Anhui Provincial Department of Education (KJ2019A0344) and the 512 Talent Cultivation Plan of Bengbu Medical College (by51201305).

## References

- [1] P. E. Castle, M. H. Einstein, and V. V. Sahasrabudde, "Cervical cancer prevention and control in women living with human immunodeficiency virus," *Ca: A Cancer Journal For Clinicians*, vol. 71, no. 6, pp. 505–526, 2021.
- [2] H. Sung, J. Ferlay, R. L. Siegel et al., "Global cancer statistics 2020: GLOBOCAN estimates of incidence and mortality worldwide for 36 cancers in 185 countries," *CA: a Cancer Journal for Clinicians*, vol. 71, no. 3, pp. 209–249, 2021.
- [3] C. G. Lee, S. C. A. Da, C. S. Dela Cruz et al., "Role of chitin and chitinase/chitinase-like proteins in inflammation, tissue remodeling, and injury," *Annual Review of Physiology*, vol. 73, no. 1, pp. 479–501, 2011.
- [4] M. Faibish, R. Francescone, B. Bentley, W. Yan, and R. Shao, "A YKL-40-neutralizing antibody blocks tumor angiogenesis and progression: a potential therapeutic agent in cancers," *Molecular Cancer Therapeutics*, vol. 10, no. 5, pp. 742–751, 2011.

- [5] D. Low, R. Subramaniam, L. Lin et al., "Chitinase 3-like 1 induces survival and proliferation of intestinal epithelial cells during chronic inflammation and colitis-associated cancer by regulating S100A9," *Oncotarget*, vol. 6, no. 34, pp. 36535–36550, 2015.
- [6] R. Shao, K. Hamel, L. Petersen et al., "YKL-40, a secreted glycoprotein, promotes tumor angiogenesis," *Oncogene*, vol. 28, no. 50, pp. 4456–4468, 2009.
- [7] C. G. Lee, D. Hartl, G. R. Lee et al., "Role of breast regression protein 39 (BRP-39)/chitinase 3-like-1 in Th2 and IL-13-induced tissue responses and apoptosis," *Journal of Experimental Medicine*, vol. 206, no. 5, pp. 1149–1166, 2009.
- [8] Y. Chen, S. Zhang, Q. Wang, and X. Zhang, "Tumor-recruited M2 macrophages promote gastric and breast cancer metastasis via M2 macrophage-secreted CHI3L1 protein," *Journal of Hematology & Oncology*, vol. 10, no. 1, p. 36, 2017.
- [9] S. Libreros and V. Iragavarapu-Charyulu, "YKL-40/CHI3L1 drives inflammation on the road of tumor progression," *Journal of Leukocyte Biology*, vol. 98, no. 6, pp. 931–936, 2015.
- [10] S. Libreros, R. Garcia-Areas, Y. Shibata, R. Carrio, M. Torroella-Kouri, and V. Iragavarapu-Charyulu, "Induction of proinflammatory mediators by CHI3L1 is reduced by chitin treatment: decreased tumor metastasis in a breast cancer model," *International Journal of Cancer*, vol. 131, no. 2, pp. 377–386, 2012.
- [11] G. Hamilton and B. Rath, "Circulating tumor cell interactions with macrophages: implications for biology and treatment," *Translational Lung Cancer Research*, vol. 6, no. 4, pp. 418–430, 2017.
- [12] D. H. Kim, H. J. Park, S. Lim et al., "Regulation of chitinase-3-like-1 in T cell elicits Th1 and cytotoxic responses to inhibit lung metastasis," *Nature Communications*, vol. 9, no. 1, p. 503, 2018.
- [13] N. Ngernyuang, R. A. Francescone, P. Jearanaikoon et al., "Chitinase 3 like 1 is associated with tumor angiogenesis in cervical cancer," *The International Journal of Biochemistry & Cell Biology*, vol. 51, pp. 45–52, 2014.
- [14] N. Ngernyuang, R. Shao, K. Suwannarurk, and T. Limpaboon, "Chitinase 3 like 1 (CHI3L1) promotes vasculogenic mimicry formation in cervical cancer," *Pathology*, vol. 50, no. 3, pp. 293–297, 2018.
- [15] A. L. Jackson, E. L. Eisenhauer, and T. J. Herzog, "Emerging therapies: angiogenesis inhibitors for ovarian cancer," *Expert Opinion on Emerging Drugs*, vol. 20, no. 2, pp. 331–346, 2015.
- [16] J. Hasan, R. Byers, and G. C. Jayson, "Intra-tumoural microvessel density in human solid tumours," *British Journal of Cancer*, vol. 86, no. 10, pp. 1566–1577, 2002.
- [17] C. N. Rathcke, J. Holmkvist, L. L. Husmoen et al., "Association of polymorphisms of the CHI3L1 gene with asthma and atopy: a populations-based study of 6514 Danish adults," *PLoS One*, vol. 4, no. 7, p. e6106, 2009.
- [18] J. Y. Wang, X. Y. Xu, J. H. Jia, C. H. Wu, and R. W. Ge, "Expressions of SE-1, CD31 and CD105 in the vascular endothelial cells and serum of rat with hepatocellular carcinoma," *Chinese Medical Journal*, vol. 123, no. 6, pp. 730–733, 2010.
- [19] N. Bhatla and L. Denny, "FIGO cancer report 2018," *International Journal of Gynaecology and Obstetrics*, vol. 143, Supplement 2, pp. 2–3, 2018.
- [20] N. Weidner, J. Folkman, F. Pozza et al., "Tumor angiogenesis: a new significant and independent prognostic indicator in early-stage breast carcinoma," *Journal of the National Cancer Institute*, vol. 84, no. 24, pp. 1875–1887, 1992.
- [21] J. S. Johansen, B. V. Jensen, A. Roslind, D. Nielsen, and P. A. Price, "Serum YKL-40, a new prognostic biomarker in cancer patients?," *Cancer Epidemiology, Biomarkers & Prevention*, vol. 15, no. 2, pp. 194–202, 2006.
- [22] M. K. Boisen, C. V. Madsen, C. Dehlendorff, A. Jakobsen, J. S. Johansen, and K. D. Steffensen, "The prognostic value of plasma YKL-40 in patients with chemotherapy-resistant ovarian cancer treated with bevacizumab," *International Journal of Gynecological Cancer*, vol. 26, no. 8, pp. 1390–1398, 2016.
- [23] B. Kotowicz, M. Fuksiewicz, J. Jonska-Gmyrek, M. Wagrodzki, and M. Kowalska, "Preoperative serum levels of YKL 40 and CA125 as a prognostic indicators in patients with endometrial cancer," *European Journal of Obstetrics, Gynecology, and Reproductive Biology*, vol. 215, pp. 141–147, 2017.
- [24] I. Lugowska, M. Kowalska, M. Fuksiewicz et al., "Serum markers in early-stage and locally advanced melanoma," *Tumor Biology*, vol. 36, no. 11, pp. 8277–8285, 2015.
- [25] A. Mitsuhashi, H. Matsui, H. Usui et al., "Serum YKL-40 as a marker for cervical adenocarcinoma," *Annals of Oncology*, vol. 20, no. 1, pp. 71–77, 2009.
- [26] A. Roslind, C. Palle, J. S. Johansen, I. J. Christensen, H. J. Nielsen, and B. J. Mosgaard, "Prognostic utility of serum YKL-40 in patients with cervical cancer," *Scandinavian Journal of Clinical and Laboratory Investigation*, vol. 80, no. 8, pp. 687–693, 2020.
- [27] T. C. Liu, X. Jin, Y. Wang, and K. Wang, "Role of epidermal growth factor receptor in lung cancer and targeted therapies," *American Journal Of Cancer Research*, vol. 7, no. 2, pp. 187–202, 2017.
- [28] M. Faibish, R. Francescone, B. Bentley, W. Yan, and R. Shao, "A YKL-40-neutralizing antibody blocks tumor angiogenesis and progression: a potential therapeutic agent in cancers," *Mol Cancer Ther*, vol. 10, no. 5, pp. 742–751, 2011.
- [29] K. M. Malinda, L. Ponce, H. K. Kleinman, L. M. Shackelton, and A. J. Millis, "Gp38k, a protein synthesized by vascular smooth muscle cells, stimulates directional migration of human umbilical vein endothelial cells," *Experimental Cell Research*, vol. 250, no. 1, pp. 168–173, 1999.
- [30] R. A. Francescone, S. Scully, M. Faibish et al., "Role of YKL-40 in the angiogenesis, radioresistance, and progression of glioblastoma," *Journal of Biological Chemistry*, vol. 286, no. 17, pp. 15332–15343, 2011.
- [31] N. Khromova, P. Kopnin, V. Rybko, and B. P. Kopnin, "Down-regulation of VEGF-C expression in lung and colon cancer cells decelerates tumor growth and inhibits metastasis via multiple mechanisms," *Oncogene*, vol. 31, no. 11, pp. 1389–1397, 2012.

## Research Article

# Efficacy of Digestive Endoscope Based on Artificial Intelligence System in Diagnosing Early Esophageal Carcinoma

Zhentao Zhao,<sup>1</sup> Meng Li,<sup>2</sup> Ping Liu,<sup>3</sup> Jingfang Yu,<sup>4</sup> and Hua Zhao <sup>1</sup>

<sup>1</sup>Endoscopic Diagnosis and Treatment Department, The Second Affiliated Hospital of Shandong University of Traditional Chinese Medicine, 250001 Jinan City, Shandong Province, China

<sup>2</sup>Office of Invitation to Bid, The Second Affiliated Hospital of Shandong University of Traditional Chinese Medicine, 250001 Jinan City, Shandong Province, China

<sup>3</sup>Radiology Department, The Second Affiliated Hospital of Shandong University of Traditional Chinese Medicine, 250001 Jinan City, Shandong Province, China

<sup>4</sup>Department of Spleen, Stomach and Liver Diseases, The Second Affiliated Hospital of Shandong University of Traditional Chinese Medicine, 250001 Jinan City, Shandong Province, China

Correspondence should be addressed to Hua Zhao; zhaohua@zydey.org.cn

Received 12 May 2022; Revised 30 May 2022; Accepted 2 June 2022; Published 18 June 2022

Academic Editor: Naeem Jan

Copyright © 2022 Zhentao Zhao et al. This is an open access article distributed under the Creative Commons Attribution License, which permits unrestricted use, distribution, and reproduction in any medium, provided the original work is properly cited.

**Objective.** To explore the efficacy of digestive endoscopy (DEN) based on artificial intelligence (AI) system in diagnosing early esophageal carcinoma. **Methods.** The clinical data of 300 patients with suspected esophageal carcinoma treated in our hospital from January 2018 to January 2020 were retrospectively analyzed; among them, 198 were diagnosed with esophageal carcinoma after pathological examination, and 102 had benign esophageal lesion. An AI system based on convolutional neural network (CNN) was adopted to assess the DEN images of patients with early esophageal carcinoma. A total of 200 patients (148 with early esophageal carcinoma and 52 with benign esophageal lesion) were selected as the learning group for the Inception V3 image classification system to learn; and the rest 100 patients (50 with early esophageal carcinoma and 50 with benign esophageal lesion) were included in the diagnosis group for the Inception V3 system to assist the narrow-band imaging (NBI) with diagnosis. The diagnosis results from Inception V3-assisted NBI were compared with those from imaging physicians, and the diagnostic efficacy diagram was drawn. **Results.** The diagnosis rate of AI-NBI was significantly faster than that of physician diagnosis ( $0.02 \pm 0.01$  vs.  $5.65 \pm 0.32$  s (mean rate of two physicians),  $P < 0.001$ ); between AI-NBI diagnosis and physician diagnosis, no statistical differences in sensitivity (90.0% vs. 92.0%), specificity (92.0% vs. 94.0%), and accuracy (91.0% vs. 93.0%) were observed ( $P > 0.05$ ); and according to the ROC curves, AUC (95% CI) of AI-NBI diagnosis = 0.910 (0.845-0.975), and AUC (95% CI) of physician diagnosis = 0.930 (0.872-0.988). **Conclusion.** CNN-based AI system can assist NBI in screening early esophageal carcinoma, which has a good application prospect in the clinical diagnosis of early esophageal carcinoma.

## 1. Introduction

Esophageal carcinoma is a malignant tumor originating at the mucosal or glandular epithelium of the esophagus [1, 2]. According to epidemiological survey data, the incidence of esophageal carcinoma ranks eighth among all malignant tumors worldwide [3], the incidence in East Asia has been consistently higher than the world average due to the special

dietary habits, and in China in 2018, new cases and deaths of esophageal carcinoma accounted for 53.7% and 55.7% of the global total, respectively, with esophageal carcinoma burden about two times the world level [4, 5]. Early diagnosis and treatment is key to reducing such burden in China [6, 7]. Currently, endoscopy, a set of devices for the diagnosis and treatment of digestive diseases by direct acquisition of images of the alimentary tract and digestive organs through the

alimentary tract, has become a main method for diagnosis of early esophageal carcinoma in practice. Chromoendoscopy, high-frequency micro probe ultrasonic endoscopy, and electronic staining are common clinical examination modalities. Among them, narrow-band imaging (NBI) is one of the most widely used endoscopic optical staining techniques at present, which, by combining with magnifying endoscopy, can clearly present subtle changes of the capillaries and mucosa within the epithelial papilla with the help of a spectral combination and then effectively improve the detection rate of superficial neoplastic lesions under endoscopy [8], and therefore, it is often used in the clinical diagnosis of early esophageal carcinoma.

In recent years, the development of artificial intelligence (AI) has allowed NBI examinations to be further optimized, and AI model relying on convolutional neural network (CNN) can precisely identify NBI endoscopic images of cancer patients and improve the diagnostic efficiency of NBI [9]. The diagnostic value of the current AI model in gastrointestinal malignancies, such as colorectal cancer and gastric cancer, has been confirmed by literature at home and abroad [10], and Tan et al. reported that the CNN-based AI model had a sensitivity of 90.12% and a specificity of 91.53% for the interpretation of NBI endoscopy in patients with laryngeal cancer [11], with exact application value. Based on this, the study combined AI system with NBI and selected 200 patients (148 with early esophageal carcinoma and 52 with benign esophageal lesion) as the learning group for the Inception V3 image classification system to learn and included another 100 patients (50 with early esophageal carcinoma and 50 with benign esophageal lesion) in the diagnosis group for the Inception V3 system to assist the narrow-band imaging (NBI) with diagnosis, aiming to improve the efficacy of diagnosing early esophageal carcinoma and provide theoretical support for practice and application. The flow diagram of the study is detailed in Figure 1.

## 2. Materials and Methods

**2.1. Study Design.** It was a retrospective study conducted in our hospital from January 2018 to January 2020 to explore the clinical application value of AI system combined with DEN in diagnosing early esophageal carcinoma.

**2.2. Inclusion and Exclusion Criteria.** Inclusion criteria of the study were as follows. (1) The patients were found to have suspected mucosal lesion in the esophagus such as rough, erosive, and mildly protruded mucosa after general white light gastroscopy; (2) the patients were at least 18 years old and voluntarily joined the study; and (3) the patients were treated in our hospital in the whole course and had complete clinical data.

Exclusion criteria of the study were as follows. (1) The patients had clearly diagnosed diseases such as polyp and diverticulum of the esophagus; (2) the patients were in the progressive period of esophageal carcinoma or had accepted treatments such as esophageal carcinoma surgery or chemotherapy before; (3) the patients had obviously extended coagulogram; (4) the patients had severe organic diseases that might affect the accuracy of study results; (5) the patients

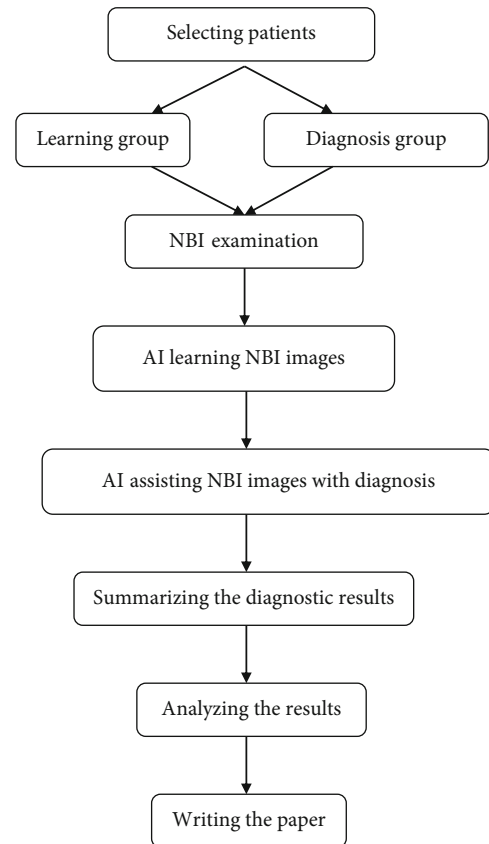


FIGURE 1: Flow diagram of the study.

were pregnant or lactating women; (6) the patients could not tolerate with the NBI examination; and (7) the patients could not communicate with others due to factors such as mental diseases.

**2.3. General Data.** A total of 300 patients with suspected esophageal carcinoma were included in the study; among them, 198 were diagnosed with esophageal carcinoma after pathological examination, and 102 had benign esophageal lesion. A total of 200 patients (148 with early esophageal carcinoma and 52 with benign esophageal lesion) were selected as the learning group for the Inception V3 image classification system to learn; and the rest 100 patients (50 with early esophageal carcinoma and 50 with benign esophageal lesion) were included in the diagnosis group for the Inception V3 system to assist NBI with diagnosis. By collecting the socio-demographic data and clinical manifestation data, it could be concluded that patients with early esophageal carcinoma included in the study (128 males and 70 females) had a mean age of  $68.14 \pm 9.20$  years, and among them, 28 patients had lesion at the median esophagus, 90 patients at the upper esophagus, and 80 patients at the lower esophagus; according to Vienna Classification, 198 patients had high-grade intraepithelial neoplasia (108 with severe atypical hyperplasia and 90 with carcinoma in situ); and the length of patients' lesion was  $13.11 \pm 2.65$  mm. Patients with benign esophageal lesion (72 males and 30 females) had a mean age of  $69.17 \pm 9.48$  years, and according to Vienna Classification, 70 patients had low-



TABLE 1: Analysis of diagnosis results from AI-NBI and physicians.

Group	AI-NBI	Physicians
Sensitivity	90.0 (45/50)	92.0 (46/50)
Specificity	92.0 (46/50)	94.0 (47/50)
Positive predictive value	91.8 (45/49)	93.9 (46/49)
Negative predictive value	90.2 (46/51)	92.2 (47/51)
Accuracy rate	91.0 (91/100)	93.0 (93/100)

grade intraepithelial neoplasia (40 with mild atypical hyperplasia and 30 with moderate atypical hyperplasia), and 32 patients had inflammatory lesions.

**2.4. Moral Consideration.** The study met the principles in *World Medical Association Declaration of Helsinki (2013)* [12] and followed the generally recognized scientific principles and codes of ethics. The patients included understood the study purpose, meaning, contents, and confidentiality and signed the informed consent.

## 2.5. Methods

**2.5.1. NBI.** The Olympus GIF-H290 endoscopy (Olympus Corporation; NMPA Registration (I) no. 20153223719) and Olympus CV-290SL NBI endoscopy examination system (Olympus Corporation; NMPA Registration (I) no. 20153223192) were adopted. Routine fasting and water deprivation were performed to patients, and 15 min before examination, patients took lidocaine mucilage (Zhejiang Kangde Pharmaceutical Co., Ltd.; NMPA approval no. H20066381), and then, endoscopy examination was performed by endoscopists from the department of digestive medicine with the following steps. Patients were in the left lateral position. First, the scope was entered to the descendant duodenum and then slowly retracted, during which pumping was constantly conducted to expose the gastric cavity and esophageal cavity, and after the scope reached the esophagus, the esophageal mucosa was first observed with white light; when the lesion position was found, it was flushed with dimethyl silicone oil and normal saline, and observation was performed again after removing esophageal mucus. Two physicians used magnifying endoscopy to observe the capillary loops and mucosal microstructure within the papilla of esophageal epithelium to observe the lesion area and then draw corresponding conclusions, which were determined by discussion in case of inconsistency.

**2.5.2. Algorithm Construction.** The Inception V3 image classification system (Google, California, USA) based on Google Net model was adopted, ImageNet 2012 Challenge training dataset was used, Net was adjusted in NBI image data, algorithm was trained by RMSprop, and the diagnosis model was TensorFlow 1.6. The NBI image data were complete images and marked as pathological benign or malignant for the system to learn, so that the predictive value was infinitely close to the target value, and then, the NBI images of the diagnosis group were interpreted.

## 2.6. Observation Criteria

**2.6.1. Diagnosis Results.** The diagnosis results from AI-NBI and physicians were recorded, i.e., the number of positive and negative patients obtained by different diagnostic methods.

**2.6.2. Diagnostic Efficacy.** The diagnostic efficacy of different diagnosis modalities was calculated. (1) Sensitivity: number of true positive cases/(number of true positive cases + number of false negative cases) \* 100%; (2) specificity: number of true negative cases/(number of true negative cases + number of false positive cases) \* 100%; (3) positive predictive value (PPV): number of true positive cases/(number of true positive cases + number of false positive cases); and (4) negative predictive value (NPV): number of true negative cases/(number of false negative cases + number of true positive cases).

**2.6.3. ROC Curve.** The ROC curves of the two diagnosis modalities were plotted by recording the positive and negative results from imaging examination into SPSS20.0 and using the ROC analysis method.

**2.7. Statistical Processing.** In this study, the data processing software was SPSS20.0, the picture drawing software was GraphPad Prism 7 (GraphPad Software, San Diego, USA), the item included was enumeration data, the method used was  $X^2$  test, and differences were considered statistically significant at  $P < 0.05$ .

## 3. Results

**3.1. Diagnostic Results.** The diagnosis rate of AI-NBI was significantly faster than that of physicians ( $0.02 \pm 0.01$  vs.  $5.65 \pm 0.32$  s (mean rate of two physicians),  $P < 0.001$ ). See Table 1 for the diagnosis results from AI-NBI and physicians.

**3.2. Diagnostic Efficacy.** Between AI-NBI diagnosis and physician diagnosis, no statistical differences in the sensitivity (90.0% vs. 92.0%), specificity (92.0% vs. 94.0%), and accuracy (91.0% vs. 93.0%) were observed ( $P > 0.05$ ). See Table 2.

**3.3. ROC Curve.** According to the ROC curves, AUC (95% CI) of AI-NBI diagnosis = 0.910 (0.845-0.975), and AUC (95% CI) of physician diagnosis = 0.930 (0.872-0.988), as detailed in Figure 2.

## 4. Discussion

Early esophageal cancer refers to esophageal carcinoma with severe dysplasia, lesions confined within the mucosal layer, and no lymph node metastasis, which can be cured by endoscopic minimally invasive treatment with little trauma, rapid recovery, and a 5-year survival rate more than 90.0% [13], so improving the early detection rate of esophageal carcinoma is key to safeguarding patient outcome. As esophageal carcinoma is mainly squamous cell carcinoma [14], Lugo's solution iodine staining is currently the most common clinical diagnostic method at this stage, which, although has high

TABLE 2: Analysis of diagnostic efficacy of AI-NBI and physicians.

Group	Sensitivity (%)	Specificity (%)	PPV (%)	NPV (%)	Accuracy (%)
AI-NBI	90.0 (45/50)	92.0 (46/50)	91.8 (45/49)	90.2 (46/51)	91.0 (91/100)
Physician diagnosis	92.0 (46/50)	94.0 (47/50)	93.9 (46/49)	92.2 (47/51)	93.0 (93/100)

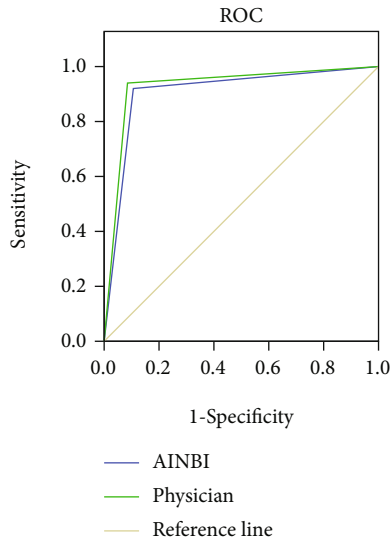


FIGURE 2: ROC curves of AI-NBI diagnosis and physician diagnosis.

sensitivity, is limited in clinical application due to its susceptibility to trigger burning sensation and allergic reactions in the stomach [15]. With the continuous advancement of DEN, NBI is developing rapidly, which can apply filters to filter the broad-band spectrum of endoscopic light sources and leave a narrow-band spectrum of green light and blue light and then fully exhibit the subtle changes of the mucosa and the capillaries within the epithelial papilla [16]. When combined with magnifying endoscopy, the contrast of the superficial and underlying blood vessels in the esophageal mucosa can be greatly enhanced, which will facilitate the initial histological diagnosis of early esophageal lesions by clinicians, thereby guiding lesion targeted biopsy and reducing the number of biopsies [17, 18]. Not only that, NBI also has advantages such as easy operation and no adverse reactions induced by chemical stains, so currently, it has been widely used in the clinical diagnosis of Barrett's esophagus early carcinogenesis, early esophageal squamous cell carcinoma, and early esophageal adenocarcinoma.

The report by Liu concluded that the sensitivity and specificity of NBI diagnosing Barrett's esophagus early carcinogenesis were, respectively, 97.0% and 94.0% [19], indicating desirable sensitivity but a certain false positive rate, which was close to the results of Lugo's solution iodine staining. Zhang S.M. et al. showed that the sensitivity of NBI for the diagnosis of esophageal squamous high-grade intraepithelial neoplasia varied greatly, reaching up to 100.0% by experienced endoscopists and only 69.0% by inexperienced physicians [20], indicating that the examination results of

NBI are still influenced by the subjective factors of endoscopists. Because clinical upper DEN needs to be done by endoscopists, and diagnosis relies entirely on the endoscopist's visual interpretation and pathological biopsy, the essence is continuously accumulating experience to enhance accuracy. Although endoscopists can fully master the technique of DEN after years of training, the possibility of misdiagnosis and erroneous diagnosis still cannot be excluded. To improve the objectivity and efficiency of diagnosis, AI-assisted DEN has become a hot spot in recent clinical research. AI can enhance its own performance in a way that it learns data without explicit instruction, and feature learning enables AI to actively learn and recognize features in image data, thereby automatically inferring input and output values [21]. On a technical level, such deep learning modality can adopt CNN to analyze complex information, making AI an intelligent system to assist diagnosis, which is beneficial to reduce the study cost of endoscopists, and facilitate the faster application of new technologies such as NBI into practice.

At present, the effectiveness of AI-NBI in the diagnosis of gastrointestinal tumors such as gastric cancer and colorectal cancer has been demonstrated [22]; scholars Barragán-Montero et al. showed that the accuracy of IMRI deep learning-based AI system in diagnosing esophageal cancer was superior to that of 4 endoscopists [23] and that this technique could further determine the depth of invasion of early esophageal carcinoma, proving that AI system can compensate for the shortcomings of incomplete visual capture in humans and assist endoscopists in DEN for precise diagnosis. Scholars Pham et al. constructed an AI model based on CNN and found that its sensitivity for detecting melanoma was 98.0% and the detection rate was significantly higher than endoscopists [24], and this study also found that the diagnosis rate of AI-NBI was  $0.02 \pm 0.01$  s, significantly faster than that of physicians ( $P < 0.001$ ). Zhang S.M. et al. adopted a great number of samples to construct an AI model to learn 8,428 endoscopic images of patients with esophageal carcinoma, and the results showed that the sensitivity of AI diagnosis was 98.0% and the PPV was 40.0% [20]. Based on the features of AI learning, the PPV will continuously increase with the number of samples, and with the building of IOT data platform, the accuracy of AI also elevates. The study showed that the sensitivity, specificity, and accuracy of AI-NBI diagnosis were, respectively, 90.0%, 92.0%, and 91.0%, and  $AUC (95\%CI) = 0.910 (0.845-0.975)$ , while the  $AUC (95\% CI)$  of physician diagnosis = 0.930 (0.872-0.988), demonstrating that AI system under deep learning could better improve the positive rate of NBI. The future direction should be to achieve real-time diagnosis and make the best use of the advantages of AI technology to reduce the esophageal carcinoma burden in China.

## 5. Conclusion

CNN-based AI system can assist NBI with screening early esophageal carcinoma, presenting a desirable diagnosis rate and a good application prospect in clinical diagnosis of early esophageal carcinoma.

## Data Availability

Data to support the findings of this study is available on reasonable request from the corresponding author.

## Conflicts of Interest

The authors have no conflicts of interest to declare.

## References

- [1] J. Li, J. Xu, Y. Zheng et al., “Esophageal cancer: epidemiology, risk factors and screening,” *Chinese Journal of Cancer Research*, vol. 33, no. 5, pp. 535–547, 2021.
- [2] Z. Jiang, J. Wang, Z. Shen, Z. Zhang, and S. Wang, “Characterization of esophageal microbiota in patients with esophagitis and esophageal squamous cell carcinoma,” *Frontiers in Cellular and Infection Microbiology*, vol. 11, article 774330, 2021.
- [3] S. Dhingra, F. Bahdi, S. B. May, and M. O. Othman, “Clinicopathologic correlations of superficial esophageal adenocarcinoma in endoscopic submucosal dissection specimens,” *Diagnostic Pathology*, vol. 16, no. 1, p. 111, 2021.
- [4] G. Mavrogenis, D. Ntourakis, Z. Wang et al., “The learning experience for endoscopic submucosal dissection in a non-academic western hospital: a single operator’s untutored, prevalence-based approach,” *Annals of Gastroenterology*, vol. 34, no. 6, pp. 836–844, 2021.
- [5] Y. Tanaka, T. Shimokawa, K. Harada, and K. Yoshida, “Effectiveness of elemental diets to prevent oral mucositis associated with cancer therapy: a meta-analysis,” *Clinical Nutrition ESPEN*, vol. 49, pp. 172–180, 2022.
- [6] L. Yong, “Artificial intelligence-assisted endoscopic detection of esophageal neoplasia in early stage: the next step,” *World Journal of Gastroenterology*, vol. 27, no. 14, pp. 1392–1405, 2021.
- [7] K. Ohnita, S. Higashi, S. Hirai et al., “Esophageal metastasis of renal cell carcinoma resected by endoscopic submucosal dissection: a case report,” *BMC Gastroenterology*, vol. 21, no. 1, p. 348, 2021.
- [8] D. Tang, L. Wang, J. Jiang et al., “A novel deep learning system for diagnosing early esophageal squamous cell carcinoma: a multicenter diagnostic study,” *Clinical and Translational Gastroenterology*, vol. 12, no. 8, p. e00393, 2021.
- [9] C. Niu, Y. Liu, J. Wang et al., “Risk factors for esophageal squamous cell carcinoma and its histological precursor lesions in China: a multicenter cross-sectional study,” *BMC Cancer*, vol. 21, no. 1, p. 1034, 2021.
- [10] R. Ishihara, J. Mizusawa, R. Kushima et al., “Assessment of the diagnostic performance of endoscopic ultrasonography after conventional endoscopy for the evaluation of esophageal squamous cell carcinoma invasion depth,” *JAMA Network Open*, vol. 4, no. 9, p. e2125317, 2021.
- [11] J. Q. Tan, Z. Li, G. Chen et al., “The natural compound from *Garcinia bracteata* mainly induces GSDME-mediated pyroptosis in esophageal cancer cells,” *Phytomedicine*, vol. 102, p. 154142, 2022.
- [12] World Medical Association, “World Medical Association Declaration of Helsinki: ethical principles for medical research involving human subjects,” *Journal of the American Medical Association*, vol. 310, no. 20, pp. 2191–2194, 2013.
- [13] S. Kuntz, E. Kriehoff-Henning, J. N. Kather et al., “Gastrointestinal cancer classification and prognostication from histology using deep learning: systematic review,” *European Journal of Cancer*, vol. 155, pp. 200–215, 2021.
- [14] M. X. Li, X. M. Sun, W. G. Cheng et al., “Using a machine learning approach to identify key prognostic molecules for esophageal squamous cell carcinoma,” *BMC Cancer*, vol. 21, no. 1, pp. 1–11, 2021.
- [15] K. E. Shin, “Epidural abscess formation after chemoradiation therapy for esophageal cancer: a case report and literature review,” *Medicine (Baltimore)*, vol. 101, no. 21, p. e29426, 2022.
- [16] V. J. Grille, S. Campbell, J. F. Gibbs, and T. L. Bauer, “Esophageal cancer: the rise of adenocarcinoma over squamous cell carcinoma in the Asian belt,” *Journal of Gastrointestinal Oncology*, vol. 12, no. S2, pp. S339–S349, 2021.
- [17] K. M. Bhatti, Z. S. Khanzada, M. Kuzman, S. M. Ali, S. Y. Iftikhar, and P. Small, “Diagnostic performance of artificial intelligence-based models for the detection of early esophageal cancers in Barret’s esophagus: a meta-analysis of patient-based studies,” *Cureus*, vol. 13, p. e15447, 2021.
- [18] C. R. A. Lesmana, M. S. Paramitha, and R. A. Gani, “The role of interventional endoscopic ultrasound in liver diseases: what have we learnt,” *Canadian Journal of Gastroenterology and Hepatology*, vol. 2021, Article ID 9948979, 8 pages, 2021.
- [19] Y. Liu, “Artificial intelligence-assisted endoscopic detection of esophageal neoplasia in early stage: the next step,” *World Journal of Gastroenterology*, vol. 27, no. 14, pp. 1392–1405, 2021.
- [20] S. M. Zhang, Y. J. Wang, and S. T. Zhang, “Accuracy of artificial intelligence-assisted detection of esophageal cancer and neoplasms on endoscopic images: a systematic review and meta-analysis,” *Journal of Digestive Diseases*, vol. 22, no. 6, pp. 318–328, 2021.
- [21] C. N. Ekeke, E. G. Chan, T. Fabian, M. Villa-Sanchez, and J. D. Luketich, “Recommendations for surveillance and management of recurrent esophageal cancer following endoscopic therapies,” *The Surgical Clinics of North America*, vol. 101, no. 3, pp. 415–426, 2021.
- [22] A. L. Klamt, J. L. Neyeloff, L. M. Santos, G. da Silva Mazzini, V. J. Campos, and R. R. Gurski, “Echoendoscopy in preoperative evaluation of esophageal adenocarcinoma and gastroesophageal junction: systematic review and meta-analysis,” *Ultrasound in Medicine & Biology*, vol. 47, no. 7, pp. 1657–1669, 2021.
- [23] A. M. Barragán-Montero, M. Thomas, G. Defraene et al., “Deep learning dose prediction for IMRT of esophageal cancer: the effect of data quality and quantity on model performance,” *Physica Medica*, vol. 83, pp. 52–63, 2021.
- [24] T. C. Pham, C. M. Luong, V. D. Hoang, and A. Doucet, “AI outperformed every dermatologist in dermoscopic melanoma diagnosis, using an optimized deep-CNN architecture with custom mini-batch logic and loss function,” *Scientific Reports*, vol. 11, no. 1, pp. 1–13, 2021.

## Research Article

# Influences of Magnetic Resonance Imaging Superresolution Algorithm-Based Transition Care on Prognosis of Children with Severe Viral Encephalitis

Yan Wang, Yan Zhang, and Ling Su 

Department of Infusion Room of Emergency, Children's Hospital of Nanjing Medical University, Nanjing, 210000 Jiangsu Province, China

Correspondence should be addressed to Ling Su; [weiyang990947111384@163.com](mailto:weiyang990947111384@163.com)

Received 24 April 2022; Revised 20 May 2022; Accepted 23 May 2022; Published 17 June 2022

Academic Editor: Naeem Jan

Copyright © 2022 Yan Wang et al. This is an open access article distributed under the Creative Commons Attribution License, which permits unrestricted use, distribution, and reproduction in any medium, provided the original work is properly cited.

**Objective.** Its goal was to see how convolutional neural network- (CNN-) based superresolution (SR) technology magnetic resonance imaging- (MRI-) assisted transition care (TC) affected the prognosis of children with severe viral encephalitis (SVE) and how effective it was. **Methods.** 90 SVE children were selected as the research objects and divided into control group (39 cases receiving conventional nursing intervention) and observation group (51 cases performed with conventional nursing intervention and TC intervention) according to their nursing purpose. Based on SR-CNN-optimized MRI images, diagnosis was implemented. Life treatment and sequelae in two groups were compared. **Results.** After the processing by CNN algorithm-based SR, peak signal to noise ratio (PSNR) (40.08 dB) and structural similarity (SSIM) (0.98) of MRI images were both higher than those of fully connected neural network (FNN) (38.01 dB, 0.93) and recurrent neural network (RNN) (37.21 dB, 0.93) algorithms. Diagnostic sensitivity (95.34%), specificity (75%), and accuracy (94.44%) of MRI images were obviously superior to those of conventional MRI (81.40%, 50%, and 80%). PedsQLTM 4.0 scores of the observation group 1 to 3 months after discharge were all higher than those of the control group ( $54.55 \pm 5.76$  vs.  $52.32 \pm 5.12$  and  $66.32 \pm 8.89$  vs.  $55.02 \pm 5.87$ ). Sequela incidence in the observation group (13.73%) was apparently lower than that in the control group (43.59%) ( $P < 0.05$ ). **Conclusion.** (1) SR-CNN algorithm could increase the definition and diagnostic ability of MRI images. (2) TC could reduce sequelae incidence among SVE children and improve their quality of life (QOL).

## 1. Introduction

Viral encephalitis is an inflammatory lesion of the brain parenchyma mainly caused by viral infection, including herpes simplex virus, arbovirus, and other common viruses. It is the commonest disease among children [1, 2]. Viral encephalitis is featured with sudden onset, rapid development, and high mortality, especially severe viral encephalitis (SVE) [3]. Children with SVE usually suffer from epilepsy, mental retardation, paralysis, dyskinesia, and other sequelae, which cause huge burden to families. Therefore, definite diagnosis and out-of-hospital care are very important for SVE children [4].

According to several research, a thorough systematic nursing intervention (mental nursing and rehabilitation

guidance) for children with SVE sequela after discharge could enhance their prognosis and quality of life (QOL) [5]. Based on the preceding findings, American specialists propose transition care (TC). TC was aimed at enabling patients to receive collaborative and transition care on different sites [6]. TC focuses on long-term nursing and enhances the self-care abilities of patients and their family members under the guidance of evidence-based basis. Besides, it was shown that TC mode can evidently enhance functional activities, compliance, and QOL of patients [7]. TC mode is gradually developed towards China. At present, the study on the application of TC focuses mainly on postpartum [8] and chronic diseases [9]. The studies on its application in SVE sequela among children.

In terms of the diagnosis of viral encephalitis, imaging technologies currently show good application values. Magnetic resonance imaging (MRI) is one of them [10]. It is proposed in a large number of studies that MRI examination demonstrates significant clinical application values in the diagnosis and differential diagnosis of viral encephalitis in children [11, 12]. In addition, MRI images possess high resolution. However, an MRI image with higher resolution indicates longer acquisition time and higher requirement for devices due to hardware, physical, and physiological limitations. With the studies in recent years, superresolution (SR) technology is put forward. SR technology assesses low resolution (LR) images and then transmits the result to high resolution (HR) images to minimize the error between HR images and original images [13]. With the emergence of deep learning (DL), SR technology is further optimized [14]. Convolutional neural network (CNN) algorithm is a widely applied SR technology. Relevant studies reveal that CNN algorithm shows excellent performance in image processing [15].

CNN-based SR technology (SR-CNN) was adopted to optimize MRI images, assist TC in carrying out the prognosis and nursing of SVE children, and assess the application effects on the improvement of SVE sequela among children, which are aimed to provide more effective therapeutic and nursing methods for the children with viral encephalitis, reduce the incidence of SVE sequela, and improve the daily QOL of SVE children.

The following is the paper's organization paragraph: In Section 2, the research method is provided. The experimental results are examined in Section 3. Section 4 consists of the discussion section. Finally, the research job is completed in Section 5.

## 2. Research Methods

**2.1. Research Objects.** A total of 90 SVE youngsters were chosen as research subjects, with 49 boys and 41 females hospitalized to our hospital between March 2020 and March 2021. Their average age was between 5 and 14 with the average of  $8.98 \pm 1.08$ . There were 78 children with clinical fever, 26 with vomiting, 58 with convulsion, 31 with coma, 12 with limb disorder, 23 infected by herpes simplex virus, 31 with infected by adenovirus, 19 infected by cytomegalovirus, and 11 for other reasons. The children were divided into two groups depending on the intentions of the children and their families: control group (39 cases with typical nursing intervention after discharge) and observation group (51 cases receiving TC intervention based on conventional nursing). SR-CNN-based MRI images were utilized to diagnose the patients in two groups. Besides, the prognosis of the two groups was compared. The implementation of the research had been approved by relevant Medical Ethics Committee.

The patients were included based on the following standards.

- (A) All children could engage in the research and communication with certain understanding ability

- (B) Children's parents did not suffer from cognitive or speech dysfunction
- (C) Children volunteered to participate in the research and had signed informed consent
- (D) All children conformed to the standard of viral encephalitis in *neurology* [16]

The patients were excluded based on the following standards.

- (A) Children themselves sufferer from other central nervous diseases or chronic diseases
- (B) Children suffered from severe epidemic encephalitis type B
- (C) Children did not participate in a complete study

**2.2. CNN Algorithm-Based SR Technology.** CNN algorithm currently shows good application effects in various fields. As a feedforward neural network (FNN), CNN mainly consists of three components, including convolutional layer, pooling layer, and fully connected layer, as shown in Figure 1.

Convolutional layer is made up of convolution kernel and activation function. Its main function is the extraction of the features of target images. Convolutional kernel recognizes the features of images, and activation function obtains multidimensional images. The specific calculation method is shown as follows:

$$S = \int_L^{L-1} \int_W^{W-1} P \bullet \omega + b. \quad (1)$$

In equation (1),  $P$  represents the input target image.  $S$  refers to the output image.  $L$  and  $W$  denote the length and width of the image, respectively.  $\omega$  stands for convolutional kernel.  $b$  represents bias.  $\bullet$  is the convolution operation. In convolutional layer, the convolution operation is performed on  $P$  and  $\omega$  according to bitwise multiplication. The calculation method is expressed as follows:

$$S' = Q_1 \times \omega + Q_2 \times \omega + \dots + Q_n \times \omega. \quad (2)$$

In equation (2),  $Q$  represents the image region,  $n$  refers to the number of regions, and  $S'$  denotes the output convolution feature diagram.

The main function of the pooling layer is the sampling of feature images to reduce training parameters as well as computation and avoid overfitting. The pooling layer is mainly divided into maximum pooling layer and average pooling layer. Figure 2 demonstrates the specific calculation process.

The white region in Figure 2 is set as the example. The pooling process of the average is expressed as follows:

$$P' = \frac{p4 + p5 + p5 + p6}{4}. \quad (3)$$

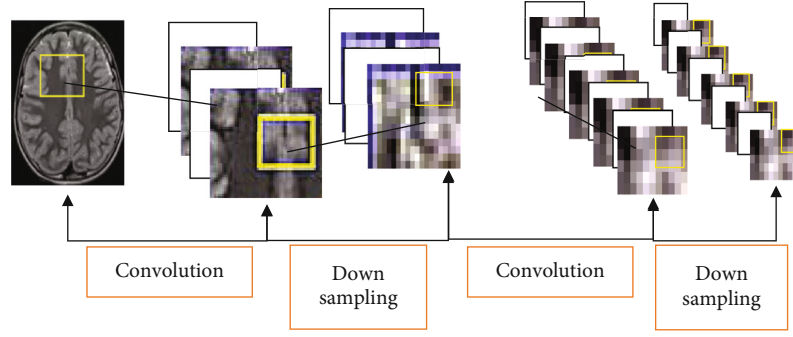


FIGURE 1: CNN action process (inside the yellow boxes are the captured feature images).

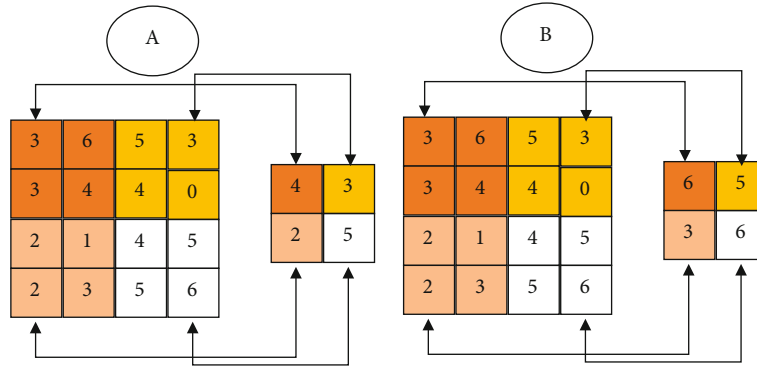


FIGURE 2: Pooling layer action process: (a) average pooling; (b) maximum pooling.

The above equation is simplified as follows:

$$\frac{4 + 5 + 5 + 6}{4} = 5. \quad (4)$$

The pooling process of the maximum is expressed as follows:

$$P' = \{p4 < p5 = p5 < p6\} P' = p_{\max}. \quad (5)$$

The above equation is simplified as follows:

$$P' = 6(4 < 5 = 5 < 6). \quad (6)$$

In equation (6),  $P'$  represents the pooling value of output image features,  $p$  denotes the pooling value in the picture of an image region, and  $P_{\max}$  refers to the maximum.

The main function of fully connected layer is the connection of all feature images and the classification of these images to obtain the results by classifier.

In image reconstruction, SR technology reversely obtains HR images from LR images. The key step is upsampling, which is also the main action step of CNN algorithm. The upper sampling layer is divided into preupsampling (the images of the same size as target images are obtained from LR images, and their features are extracted, and their display effects are enhanced), postupsampling (the size of input images is kept the same), progressive upsampling (the reconstructed images are gradually enlarged to 2 times to obtain the images with different resolutions), and iterative up-

down sampling (the features of HR images at different stages are obtained). According to the operation methods of upper sampling layer, it can also be divided into deconvolution layer and subpixel layer.

The main operation of deconvolution layer is enlargement-zero-padding-convolution. It is assumed that the original image  $T$  is  $m \times n$ , enlarged image  $T'$  is specifically expressed as follows:

$$T' = (m + m \times 1) \times (n + n \times 1). \quad (7)$$

The image  $T''$  obtained by zero-padding is expressed as follows:

$$T'' = (m + m \times 1 + 1) \times (n + n \times 1 + 1). \quad (8)$$

Convolution refers to the convolutional image obtained by calculation according to CNN algorithm.

The main function of subpixel layer is the rearrangement of the image features obtained by convolution to acquire high-resolution images.

CNN algorithm-based SR image is assessed by peak signal to noise ratio (PSNR), structural similarity (SSIM), and its diagnostic efficacy.

$$\text{PSNR} = 10 * \log_{10} \left( \frac{(2^B - 1)^2}{(1/mn) \sum_{i=0}^{m-1} \sum_{l=0}^{n-1} (C - U)} \right), \quad (9)$$

where  $2^B - 1$  denotes the maximum pixel value of the

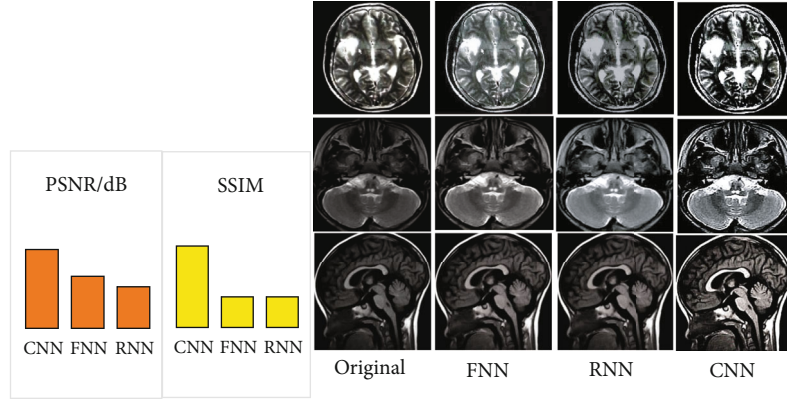


FIGURE 3: PSNR and SSIM results as well as the comparison of processing effects (the images in line 1 were taken from diagonal plane, those in line 2 were taken from transverse slope, and those in line 3 were taken from sagittal view).

image,  $n$  refers to the binary number of pixel value,  $m$  represents the number of image samples,  $i$  and  $l$  stand for certain pixel point in the image,  $C$  refers to clear image, and  $U$  means noisy image.

$$\text{SSIM}(C, U) = \frac{2\alpha_C\alpha_U + B}{\alpha_C^2 + \alpha_U^2 + B}, \quad (10)$$

$$\alpha_C = \frac{1}{H \times W} \sum_{i=1}^H \sum_{l=1}^W C, \quad (11)$$

$$\alpha_U = \frac{1}{H \times W} \sum_{i=1}^H \sum_{l=1}^W U, \quad (12)$$

where  $H \times W$  denotes the images size,  $\alpha$  represents the average value, and  $B$  refers to the constant.

Greater PSNR and SSIM values indicate better processing effect on images.

**2.3. MRI Examination.** The examination of all children was performed by one magnetic resonance scanner and review by one surgeon. The films were reviewed by two experienced (20 years or more) clinicians. Siemens superconducting magnetic resonance scanner (model number was Magnetom Impct 1.0 T, spin echo, Germany) was adopted. The scanning parameters were set as follows. The thickness was 2.5 mm, layer-to-layer spacing was 3 mm, and time of repetition (TR) was 0.6 s and 3.4 s. Time of echo (TE) was 15 sm and 89 sm. Scanning planes included cross plane, sagittal plane, and coronal plane. Scanning sequences included T1WI and T2WI. The process of enhanced scanning was as follows. The contrast agent (Gd-DTPA, 0.2 mL/kg) was injected intravenously. The obtained images were processed by MRI and then optimized by CNN algorithm-based SR technology.

**2.4. Nursing Methods.** The children in the control group were performed with conventional nursing. The information about the patients' disease was obtained by phone 3 days after discharge, including diet, physical condition, and activity level. According to the obtained information, the corresponding nursing guidance was offered. The patients were told to visit outpatient department for review after 1 month and 3 months.

The children in the observation group received TC based on the nursing method for the control group. Firstly, a special TC team was composed of chief physicians, supervisor nurses, nursing graduates, therapists, and psychologists at pediatric department. Secondly, scales of pediatric quality of life inventory version 4.0 (PedsQL™ 4.0) [17] assessment was conducted on the patients before discharge and then set up health files, formulated discharge plans, and handed out record books to the patients' parents to prompt them to record their children's daily health status. Finally, to promote contact between patients' parents and medical nursing workers, a network video technique was used to provide SVE advice and training 2 to 3 weeks following discharge. Finally, the patients were informed that a follow-up visit would be scheduled one month after discharge. Besides, a target nursing scheme was formulated according to the result of the follow-up visit. Fifthly, home nursing guidance was carried out 2 months after discharge. Besides, psychological nursing intervention was performed according to the specific situations. Finally, the patients were informed of review 3 months after discharge, and nerve physique examination was also needed.

PedsQL™ 4.0 scores of the children in two groups at discharge, 1 month after discharge, and 3 months after discharge were compared. In addition, the incidence probability of patients' sequela (aphasia, acroparalysis, consciousness disorder, psychiatric disorders, dementia, epilepsy, deafness, impaired vision, and facial nerve numbness) 3 months after discharge was also compared.

**2.5. Statistical Methods.** The original data were input into the SPSS 22.0 statistical software for data analysis. Measurement data were expressed by mean  $\pm$  standard deviation ( $\bar{x} \pm s$ ). Independent sample  $t$ -test was used for pairwise comparison. Enumeration data were denoted by frequency and percentage (%).  $\chi^2$  test was utilized for pairwise comparison.  $P < 0.05$  indicated that the differences were statistically significant.

### 3. Results

**3.1. Comparison of Algorithm Performance.** MRI images of 3 children with viral encephalitis were used as the sample, and the optimization performance of CNN algorithm, fully

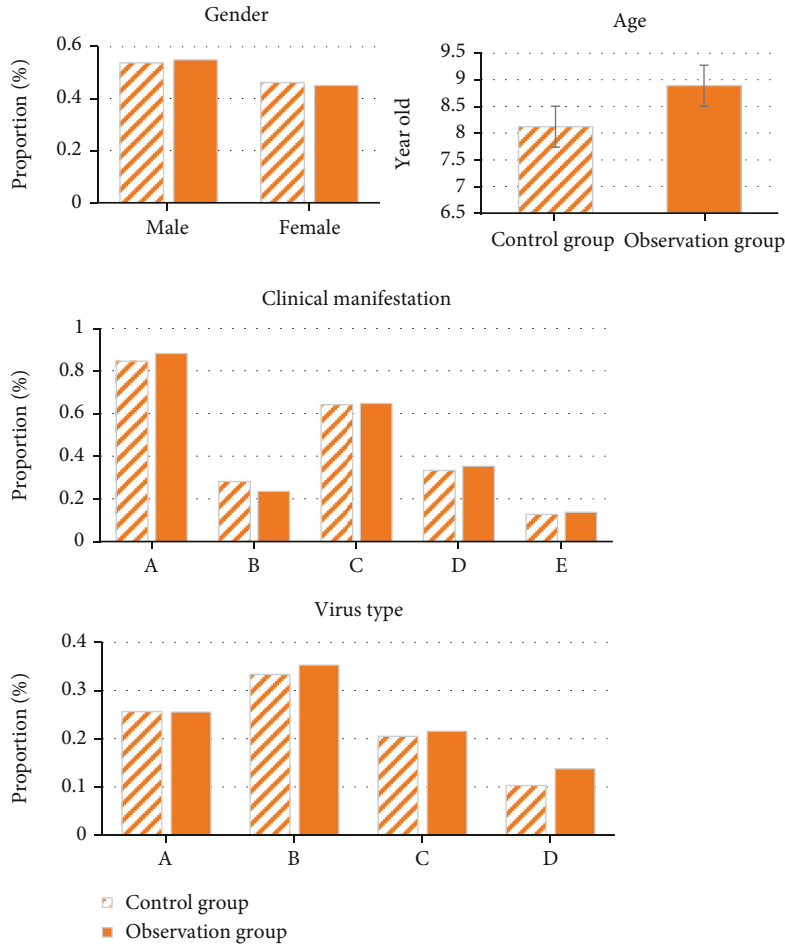


FIGURE 4: Comparison of general data (A represents fever, B denotes vomiting, C refers to convulsion, D means coma, and E indicates limb disorders) (A represents herpes simplex virus, B denotes adenovirus, C refers to cytomegalovirus, and D stands for other viruses).

TABLE 1: Diagnostic results of SR-CNN-based MRI images.

		Cerebral effusion examination ( <i>n</i> = 90 cases)		Total
		Positive	Negative	
SR-CNN-based MRI ( <i>n</i> = 90 cases)	Positive	82	01	83
	Negative	04	03	07
Total		86	04	90

TABLE 2: Diagnostic results of conventional MRI images.

		Cerebral effusion examination ( <i>n</i> = 90 cases)		Total
		Positive	Negative	
Conventional MRI ( <i>n</i> = 90 cases)	Positive	70	02	72
	Negative	16	02	18
Total		86	04	90

connected neural network (FNN) [18], and recurrent neural network (RNN) [19] for SR technology was compared. The result showed that the average PSNR and SSIM values of

MRI images processed by CNN algorithm-based SR technology were 40.08 dB and 0.98, respectively. Those processed by FNN algorithm-based SR technology were 38.01 dB and



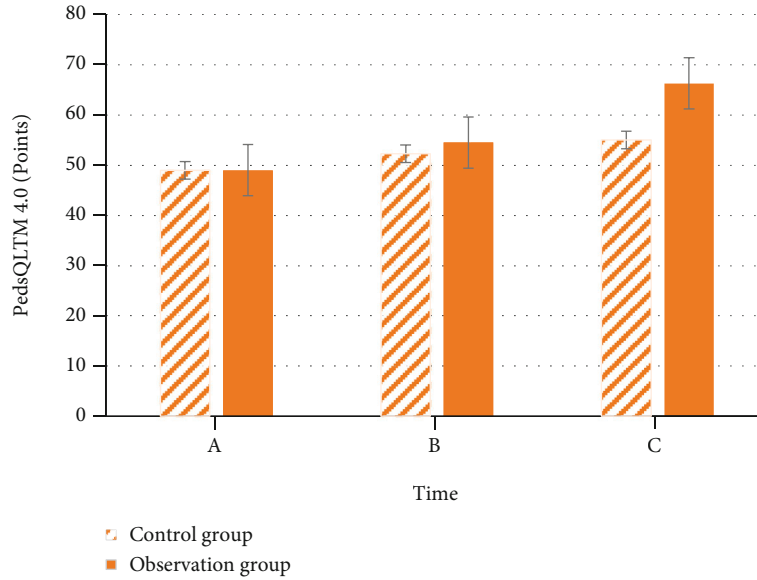


FIGURE 5: Comparison of PedsQLTM 4.0 scores (A represents PedsQLTM 4.0 scores at discharge, B denotes those 1 month after discharge, and C refers to those 3 months after discharge).

TABLE 3: Incidence of sequelae.

	Control group ( $n = 39$ cases)	Observation group ( $n = 51$ cases)	Total
Aphasia	04	01	05
Acroparalysis	02	01	03
Consciousness disorder	00	0	0
Psychiatric disorders	0	0	0
Dementia	01	0	01
Epilepsy	01	0	01
Deafness	02	02	04
Impaired vision	03	01	04
Facial nerve numbness	04	02	06
Total	17	07	24

0.93, respectively. Those processed by RNN algorithm-based SR technology were 37.21 dB and 0.93, respectively. According to the comparison, PSNR and SSIM of the images processed by CNN algorithm-based SR were both higher than those processed by FNN algorithm- and RNN algorithm-based SR, as Figure 3 illustrates. Figure 4 displays the processing effects of three algorithms on images. It was demonstrated that MRI images processed by CNN algorithm-based SR technology showed higher definition.

**3.2. Diagnostic Efficacy of SR Algorithm-Based MRI Images.** According to the results of cerebral effusion examination, the diagnostic effect of MRI images on 90 included children with viral encephalitis was assessed and compared with that of conventional MRI images (the children diagnosed with viral encephalitis were positive, otherwise negative), as

Tables 1 and 2. According to the calculation results, the diagnostic sensitivity, specificity, and accuracy of SR-CNN algorithm-based MRI images reached 95.34%, 75%, and 94.44%, respectively. Those of conventional MRI images amounted to 81.40%, 50%, and 80%, respectively. Apparently, the diagnostic efficacy of SR-CNN algorithm-based MRI images was superior to that of conventional MRI, indicating certain accuracy of the research.

**3.3. Comparison of General Data.** Figure 4 shows the statistical comparison of general clinical data on the patients in two groups. In terms of gender distribution, the proportions of male and female children in the control group were 53.85% and 46.15%, respectively. In the observation group, the proportions of male and female children reached 54.90% and 45.10%, respectively. The gender distribution in the two groups showed no remarkable statistical significance ( $P < 0.05$ ). As for average age, the average age of the children in the control group was  $8.12 \pm 1.68$ , and that in the observation group amounted to  $8.89 \pm 0.99$ . The comparison of the average age between two groups revealed no notable statistical difference ( $P < 0.05$ ). With respect to the distribution of clinical manifestations, the proportions of clinical manifestations of fever, vomiting, convulsion, coma, and limb disorders in the control group were 84.62%, 28.21%, 64.10%, 33.33%, and 12.82%, respectively. Those in the observation group were 88.24%, 23.53%, 64.71%, 35.29%, and 13.73%, respectively. The comparison indicated no evident statistical difference ( $P < 0.05$ ). As to virus type distribution, the proportions of herpes simplex virus, adenovirus, cytomegalovirus, and other viruses in the control group reached 25.64%, 33.33%, 20.51%, and 10.26%, respectively. Those in the observation group amounted to 25.49%, 35.29%, 21.57%, and 13.73%, respectively. The comparison showed no statistical difference ( $P < 0.05$ ). The above results suggested that the research was feasible to some extent.

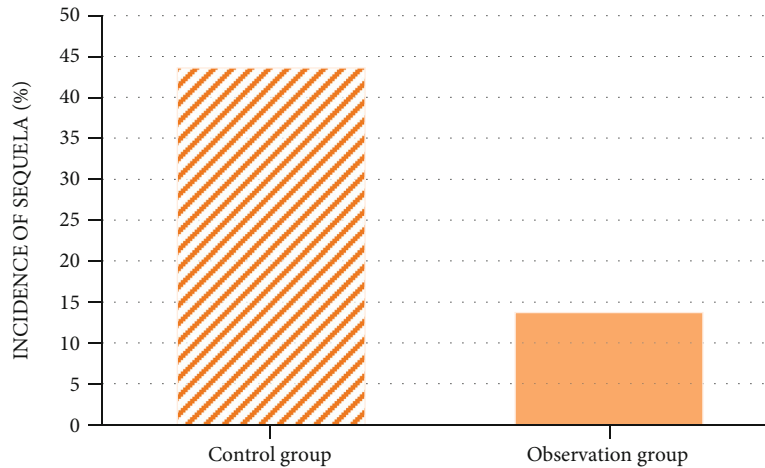


FIGURE 6: Comparison of incidence of sequelae.

**3.4. PedsQLTM 4.0 Scores.** Figure 5 displays the comparison of PedsQLTM 4.0 scoring results of the children in two groups at discharge, 1 month after discharge, and 3 months after discharge. There was no discernible difference in PedsQLTM 4.0 scores between control group ( $48.99 \pm 4.91$ ) and observation group ( $49.03 \pm 4.32$ ) at discharge ( $P < 0.05$ ). PedsQLTM 4.0 scores of the children in the control group 1 month and 3 months after discharge were  $52.32 \pm 5.12$  and  $55.02 \pm 5.87$ , respectively. Those in the observation group reached  $54.55 \pm 5.76$  and  $66.32 \pm 8.89$ , respectively. PedsQLTM 4.0 scores in the two groups were both improved compared with those before discharge. Besides, PedsQLTM 4.0 scores of the observation group 1 month and 3 months after discharge were both superior to those of the control group ( $P < 0.05$ ).

**3.5. Incidence of Sequelae.** Table 3 displays the incidence of various sequelae among the children in two groups. According to the calculations, the incidence of sequelae in the control group was 43.59% percent, while it was 13.73% in the observation group. The incidence of sequelae in latter group was apparently lower than that in former one ( $P < 0.05$ ), as Figure 6 presents.

## 4. Discussion

With the development of current medical industry, the need for high-resolution images by the diagnosis and treatment of clinical diseases is becoming more and more urgent. Deep learning method is of great significance to the reconstruction of SR images. Multiple research have suggested that deep learning-based neural network algorithms, particularly the CNN method, have considerable optimization impacts in the medical imaging SR field [20–22]. The processing effect of SR technology based on the CNN algorithm was compared to that of SR technology based on the FNN and RNN algorithms. The results demonstrated that PSNR (40.08 dB) and SSIM (0.98) of MRI images processed by CNN algorithm-based SR were both higher than those processed by FNN algorithm- ( $38.01$  dB and  $0.93$ ) and CNN

algorithm-based SR ( $37.21$  dB and  $0.93$ ). MRI images processed by CNN algorithm-based SR showed the highest definition, which indicated that CNN algorithm improved the image reconstruction effects of SR technology very well. The result was consistent with the conclusions of most relevant studies [23, 24]. In addition, it was concluded that the diagnostic sensitivity (95.34%), specificity (75%), and accuracy (94.44%) of SR-CNN algorithm-based MRI images were obviously superior to those of conventional MRI (81.40%, 50%, and 80%). The conclusion revealed that SR-CNN algorithm-based MRI images could improve the diagnostic effect of MRI images, which was consistent with the outcomes of the studies conducted by Yan et al. [25] and Park et al. [26] and provided the basis for the accuracy of subsequent studies.

Based on the above research results, the effect of TC on children with SVE was investigated and compared with conventional nursing effect. It was pointed out in some studies that TC technology was not only very practical but also could reduce health care costs [27]. The systematic analysis of the consumption of health care costs was not involved in the research. However, the nursing effects of TC on QOL of SVE children after discharge and sequelae were compared. The results suggested that PedsQLTM 4.0 scores of the children in the observation group 1 month and 3 months after discharge were both superior to those in the control group ( $54.55 \pm 5.76$  vs.  $52.32 \pm 5.12$  and  $66.32 \pm 8.89$  vs.  $55.02 \pm 5.87$ ). The incidence of sequelae in the observation group (13.73%) was obviously lower than that in control group (43.59%) ( $P < 0.05$ ), which implied that reasonable and normative physiological and psychological nursing based on detailed record and understanding of children's disease was more conducive to the recovery of the children and reduced the incidence probability of sequelae among them. According to the study conducted by Chen et al. [28], TC exerted a profound influence on the nursing of stroke patients. Besides, it was put forward in multiple studies that TC was needed in the late care for many diseases [29]. Van et al. [30] also pointed out in their study that TC could not only effectively reduce medical system cost but also enhanced the effective rate of the treatment for patients

and reduce patient readmission rate. The results of the above studies were all consistent with the research outcome and gave good support to the research.

## 5. Conclusion

After the examination on SVE patients with SR-CNN algorithm-based MRI images, TC was adopted to carry out prognostic care for SVE children. The results were as follows.

- (A) SR-CNN algorithm could enhance the definition and diagnostic efficacy of MRI images
- (B) TC could reduce the incidence of sequelae among SVE children and improved their QOL

Nonetheless, the impact of diagnostic accuracy on nursing effects was left out of the study, making it incomplete. As a result, more research was required. It could not be underestimated that the application of TC in sequela nursing for SVE children after discharge was advanced, and the application prospect was worth expectation.

## Data Availability

The datasets used and analyzed during the current study are available from the corresponding author on reasonable request.

## Conflicts of Interest

The authors declare that they have no conflicts of interest.

## Authors' Contributions

Yan Wang and Yan Zhang contributed equally to this work.

## References

- [1] A. J. Aksamit, "Treatment of viral encephalitis," *Neurologic Clinics*, vol. 39, no. 1, pp. 197–207, 2021.
- [2] B. K. Costa and D. K. Sato, "Encefalite viral: uma revisao pratica sobre abordagem diagnostica e tratamento," *Jornal de Pediatria*, vol. 96, Suppl 1, pp. 12–19, 2020.
- [3] O. L. Gern, F. Mulenge, A. Pavlou et al., "Toll-like receptors in viral encephalitis," *Viruses*, vol. 13, no. 10, article ???, 2021.
- [4] T. Khushafa, L. Jing, Z. Zhaojun, S. Jiameng, and Z. Haixia, "Insights into the biomarkers of viral encephalitis from clinical patients," *Pathogens and Disease*, vol. 79, no. 1, article ftaa073, 2021.
- [5] K. Haraldstad, A. Wahl, R. Andenaes et al., "A systematic review of quality of life research in medicine and health sciences," *Quality of life Research*, vol. 28, no. 10, pp. 2641–2650, 2019.
- [6] F. Wells and J. Manning, "Transition of care from children's to adult services," *Nursing Children and Young People*, vol. 29, no. 8, pp. 30–34, 2017.
- [7] A. Coffey, H. Mulcahy, E. Savage et al., "Transitional care interventions: relevance for nursing in the community," *Public Health Nursing*, vol. 34, no. 5, pp. 454–460, 2017.
- [8] M. Shankar, C. S. Chan, S. M. Frayne, D. M. Panelli, C. S. Phibbs, and J. G. Shaw, "Postpartum transition of care: racial/ethnic gaps in veterans' re-engagement in VA primary care after pregnancy," *Women's Health Issues*, vol. 31, no. 6, pp. 603–609, 2021.
- [9] H. Aboumatar, M. Naqibuddin, S. Chung et al., "Effect of a hospital-initiated program combining transitional care and long-term self-management support on outcomes of patients hospitalized with chronic obstructive pulmonary disease: a randomized clinical trial," *JAMA*, vol. 322, no. 14, pp. 1371–1380, 2019.
- [10] J. P. Stahl and A. Mailles, "Herpes simplex virus encephalitis update," *Current Opinion in Infectious Diseases*, vol. 32, no. 3, pp. 239–243, 2019.
- [11] A. A. Rabinstein, "Herpes virus encephalitis in adults: current knowledge and old myths," *Neurologic Clinics*, vol. 35, no. 4, pp. 695–705, 2017.
- [12] Q. Ren, L. Guo, X. Liu et al., "Analysis of the effect of incentive nursing intervention in children with severe viral encephalitis and myocarditis during rehabilitation based on diffusion weighted MRI," *Journal of Healthcare Engineering*, vol. 2021, Article ID 9993264, 8 pages, 2021.
- [13] S. Park, H. M. Gach, S. Kim, S. J. Lee, and Y. Motai, "Autoencoder-inspired convolutional network-based super-resolution method in MRI," *IEEE Journal of Translational Engineering in Health and Medicine*, vol. 9, article 1800113, pp. 1–13, 2021.
- [14] M. Hu, Y. Zhong, S. Xie, H. Lv, and Z. Lv, "Fuzzy system based medical image processing for brain disease prediction," *Frontiers in Neuroscience*, vol. 15, article 714318, 2021.
- [15] C. Zhao, B. E. Dewey, D. L. Pham, P. A. Calabresi, D. S. Reich, and J. L. Prince, "SMORE: a self-supervised anti-aliasing and super-resolution algorithm for MRI using deep learning," *IEEE transactions on medical imaging*, vol. 40, no. 3, pp. 805–817, 2021.
- [16] A. Venkatesan and O. C. Murphy, "Viral encephalitis," *Neurologic Clinics*, vol. 36, no. 4, pp. 705–724, 2018.
- [17] I. Sato, T. Soejima, M. Ikeda, K. Kobayashi, A. Setoyama, and K. Kamibeppu, "Reliability and validity of the Japanese version of the Pediatric Quality of Life Inventory Infant Scales," *Journal of patient-reported outcomes*, vol. 6, no. 1, p. 10, 2022.
- [18] E. Ozanich, P. Gerstoft, and H. Niu, "A feedforward neural network for direction-of-arrival estimation," *The Journal of the Acoustical Society of America*, vol. 147, no. 3, pp. 2035–2048, 2020.
- [19] E. Z. Chen, P. Wang, X. Chen, T. Chen, and S. Sun, "Pyramid convolutional RNN for MRI image reconstruction," *IEEE Transactions on Medical Imaging*, vol. PP, p. 1, 2022.
- [20] J. M. Goo, "Deep learning-based super-resolution algorithm: potential in the management of subsolid nodules," *Radiology*, vol. 299, no. 1, pp. 220–221, 2021.
- [21] L. Fang, F. Monroe, S. W. Novak et al., "Deep learning-based point-scanning super-resolution imaging," *Nature methods*, vol. 18, no. 4, pp. 406–416, 2021.
- [22] R. J. G. Sloun, O. Solomon, M. Bruce et al., "Super-resolution ultrasound localization microscopy through deep learning," *IEEE Transactions on Medical Imaging*, vol. 40, no. 3, pp. 829–839, 2021.
- [23] N. Rybnikova, E. M. Mirkes, and A. N. Gorban, "CNN-based spectral super-resolution of panchromatic night-time light imagery: city-size-associated neighborhood effects," *Sensors*, vol. 21, no. 22, article 7662, 2021.

- [24] X. Guo, X. Sang, D. Chen et al., “Real-time optical reconstruction for a three-dimensional light-field display based on path-tracing and CNN super-resolution,” *Optics Express*, vol. 29, no. 23, pp. 37862–37876, 2021.
- [25] Y. Yan, W. Ren, X. Hu, K. Li, H. Shen, and X. Cao, “SRGAT: single image super-resolution with graph attention network,” *IEEE Transactions on Image Processing*, vol. 30, pp. 4905–4918, 2021.
- [26] J. Park, D. Hwang, K. Y. Kim, S. K. Kang, Y. K. Kim, and J. S. Lee, “Computed tomography super-resolution using deep convolutional neural network,” *Physics in Medicine and Biology*, vol. 63, no. 14, p. 145011, 2018.
- [27] T. M. O. Menezes, A. L. B. Oliveira, L. B. Santos, R. A. Freitas, L. C. Pedreira, and S. M. Veras, “Hospital transition care for the elderly: an integrative review,” *Revista Brasileira de Enfermagem*, vol. 72, suppl 2, pp. 294–301, 2019.
- [28] L. Chen, L. D. Xiao, and D. Chamberlain, “An integrative review: challenges and opportunities for stroke survivors and caregivers in hospital to home transition care,” *Journal of Advanced Nursing*, vol. 76, no. 9, pp. 2253–2265, 2020.
- [29] C. Barnabe, K. Chomistek, N. Luca et al., “National priorities for high-quality rheumatology transition care for youth in Canada,” *The Journal of Rheumatology*, vol. 48, no. 3, pp. 426–433, 2021.
- [30] S. Van, T. Rahman, O. Mytton et al., “Comparative effectiveness of transitional care services in patients discharged from the hospital with heart failure: a systematic review and network meta-analysis,” *European Journal of Heart Failure*, vol. 19, no. 11, pp. 1427–1443, 2017.

## Retraction

# Retracted: Analysis of Legal Attributes and Rights Attributes of Personal Information from the Perspective of Big Data

### Computational and Mathematical Methods in Medicine

Received 25 July 2023; Accepted 25 July 2023; Published 26 July 2023

Copyright © 2023 Computational and Mathematical Methods in Medicine. This is an open access article distributed under the Creative Commons Attribution License, which permits unrestricted use, distribution, and reproduction in any medium, provided the original work is properly cited.

This article has been retracted by Hindawi following an investigation undertaken by the publisher [1]. This investigation has uncovered evidence of one or more of the following indicators of systematic manipulation of the publication process:

- (1) Discrepancies in scope
- (2) Discrepancies in the description of the research reported
- (3) Discrepancies between the availability of data and the research described
- (4) Inappropriate citations
- (5) Incoherent, meaningless and/or irrelevant content included in the article
- (6) Peer-review manipulation

The presence of these indicators undermines our confidence in the integrity of the article's content and we cannot, therefore, vouch for its reliability. Please note that this notice is intended solely to alert readers that the content of this article is unreliable. We have not investigated whether authors were aware of or involved in the systematic manipulation of the publication process.

In addition, our investigation has also shown that one or more of the following human-subject reporting requirements has not been met in this article: ethical approval by an Institutional Review Board (IRB) committee or equivalent, patient/participant consent to participate, and/or agreement to publish patient/participant details (where relevant).

Wiley and Hindawi regrets that the usual quality checks did not identify these issues before publication and have since put additional measures in place to safeguard research integrity.

We wish to credit our own Research Integrity and Research Publishing teams and anonymous and named external researchers and research integrity experts for contributing to this investigation.

The corresponding author, as the representative of all authors, has been given the opportunity to register their agreement or disagreement to this retraction. We have kept a record of any response received.

### References

- [1] J. Yan, "Analysis of Legal Attributes and Rights Attributes of Personal Information from the Perspective of Big Data," *Computational and Mathematical Methods in Medicine*, vol. 2022, Article ID 9731414, 10 pages, 2022.

## Research Article

# Analysis of Legal Attributes and Rights Attributes of Personal Information from the Perspective of Big Data

Jingzhong Yan <sup>1,2</sup>

<sup>1</sup>*Kenneth Wang School of Law, Soochow University, Suzhou, Jiangsu 215007, China*

<sup>2</sup>*Business School, Suqian University, Suqian, Jiangsu 223800, China*

Correspondence should be addressed to Jingzhong Yan; 21068@squ.edu.cn

Received 24 April 2022; Revised 20 May 2022; Accepted 24 May 2022; Published 17 June 2022

Academic Editor: Naeem Jan

Copyright © 2022 Jingzhong Yan. This is an open access article distributed under the Creative Commons Attribution License, which permits unrestricted use, distribution, and reproduction in any medium, provided the original work is properly cited.

With the popularization and rapid development of Internet technology (IT), social activities based on the exchange of personal information are rapidly popularizing. Although the free flow of a huge volume of personal data meets the needs of information exchange, its illicit use poses legal risks to rights holders and infringes on the applicable rights and interests of the information subject. The ambiguity of the right attribute and legal attribute of personal information leads to the scattered protection of personal information in the legislative system in different legal norms. Based on this background, this paper constructs an evaluation index based on the legal attributes and rights attributes of personal information rights and proposes a rationality evaluation method for the attributes of personal information rights based on neural networks. The completed work is as follows: (1) focusing on the legal attributes and the right attribute is discussed in detail, and the dissimilar views of scholars at home and abroad are presented. (2) The back propagation neural network (BPNN) model structure required in this study is defined, and the evaluation index based on the legal attribute and right attribute of personal information right is produced. (3) Use big data technology to collect relevant data and compare the results obtained by the BPNN model with the results obtained by the improved BPNN model. The results show that the improved BPNN evaluate model has smaller error and higher accuracy.

## 1. Introduction

With the development of the Internet, more and more attention has been paid to the protection of personal information, which is closely related to the characteristics of the relevant subjects, and can accurately identify the identity of the information subject, thus reflecting the particularity of the subject in society, including the identity of the individual, family, property status, and medical health. Article 111 of the “General Principles of Civil Law” has formulated a special law for the protection of personal information. This article clarifies the relevant guidelines that others should follow when using citizens’ information [1]. In the information age, this is the era’s necessity for the security of personal information, and it expresses society’s intent. The legislative spirit of this article is to affirm that personal information is a private interest enjoyed by natural persons in accordance with the law, and such private interests are protected by legal coercive force, which also ensures the freedom of natural persons to exer-

cise personal rights within a certain range. At the same time, the right to personal information has the attribute of will-power. In this regard, the right to personal information should belong to a civil right, not a general legal interest. First of all, the right to personal information protects the specific interests of natural persons and is a collection of natural persons’ spiritual interests and property interests. The “General Principles of Civil Law” provides legal protection for such specific interests [2]. Personal information encapsulates the private interests of natural persons; therefore, the subject of personal information should be safeguarded under the right to personal information. This kind of private interest is mainly reflected in two aspects: on the one hand, when personal information is infringed by others, the natural person can request the relevant authorities to protect it, and at the same time, it can also require the relevant infringer to act or refrain from taking certain actions, so that the right holder can independently decide how your personal information will be used. This not only reflects the freedom of

civil subjects to exercise relief methods when they are violated but also demonstrates the personal dignity and personal interests of civil subjects but also shows the protection of civil subjects by laws and regulations, and it is guaranteed that civil subjects can realize their relevant legal interests of personality in civil activities. On the other hand, the law allows the right holder to freely dominate and control personal information within a certain range, which is mainly manifested in the commercial use of the personal information by the right holder, and in the process realizes a certain property value of the personal information, which reflects the freedom of civil subjects to exercise civil rights [3]. Secondly, the right to personal information has the attribute of willpower, and the essential attribute of civil rights is the willpower, which is the right granted by the law to civil subjects to make independent decisions within a specific range. This attribute of willpower is the fundamental characteristic of civil rights, and it is also the fundamental characteristic that distinguishes civil rights from general legal interests [4]. For example, in the theory of ownership, the right holder can independently control and dominate the property and exclude the interference of others, thus realizing the fundamental value of the property [5]. Whether the right to personal information can be recognized as a civil right, we must first analyze whether it conforms to the essential attributes of civil rights. Personal information is owned by natural persons, and natural persons can autonomously control and dominate within a specific range and can disclose their information or use it commercially. In order to realize its interests, it reflects the right of natural persons to independently decide how to use personal information, and it is a manifestation of the free development of the personal freedom of the subject of personal information within a certain range [6]. Furthermore, when personal information is disturbed, the right holder can request the counterparty to variation and delete it or request the state agency for compulsory protection, which demonstrates the personal dignity of the natural person. The control and domination of personal information by natural persons also reflect the free exercise of personality power within a certain range [7]. In other words, the right to personal information has already demonstrated a positive willpower, that is, the willpower of self-determination; so, it is a civil right. The theoretical significance of this thesis is to clarify the legal and power attributes of personal information right from the perspective of private law through the specific sorting and analysis of domestic and foreign theories. The location and choice of personal information legislation are determined by the legal attribute of personal information right and the attribution of power attribute. This paper will conduct in-depth research on this theoretical issue and use neural network technology to analyze the rationality of the attribute of personal information right. Therefore, accurately judging its legal attributes is the actual problem of this paper. Article 111 of the General Principles of Civil Law has made relevant rules for the protection of personal information. Therefore, before formulating systematic and comprehensive relevant laws and regulations, defining its attributes is the first step. For the issues to be discussed, more reasonable laws and regula-

tions can be formulated only by clarifying the nature of their rights. Reference [8] believes that personal data refers to any information that has a relationship with a natural person that can be identified or can be identified. A natural person who can be identified refers to one of a series of factors that can directly participate or indirectly refer to its own identification number and its own unique physical, cultural, spiritual, physiological, economic, and social identification and other factors, one or several people who can confirm its identity.

## 2. Related Work

Due to the development of network technology and the speed of changes in the times, personal information itself has great economic value, and there are continuous cases of personal information infringement. People have begun to pay attention to issues with personal information, and the protection of personal information has been a hot topic in academia in recent years, with experts holding a variety of viewpoints and beliefs. At the same time, reference [9] also has a similar definition of the concept of personal information. It believes that the scope of personal information generally includes a natural person's address, name, ID number, personnel records, and birth date medical records and photos and a series of individual or specific personal information that can be identified individually or compared with other information. It is commonly used in the academic community to refer to whether there is a direct relationship between individuals and personal information and to divide personal information into two categories: sensitive information and nonsensitive information [10]. Furthermore, our country's current national standards, "Guidelines for Personal Information Protection" and "Personal Information Security Specifications," use approaches such identifying connotations and examples for personal sensitive information. Among them, sensitive personal information, if leaked or modified, will have a negative impact on the subject of personal information related to identity. Compared with domestic research, foreign research on personal information started earlier and has a long time, and the personal information legislative protection system is more comprehensive. Looking at the experiences of various countries, in terms of the current international environment, almost all countries in the world protect personal information. Reference [11] officially published "On the Right to Privacy" in 1890, which triggered discussions on the right to privacy in domestic theoretical circles. Since then, the United States has promulgated a special law on the right to privacy, and personal information has been included in the scope of this law in terms of privacy. Reference [12] believes that with the expansion of personal social interpersonal relationships, personal information plays an increasingly important role in social interaction, the relationship between privacy and social interaction is becoming increasingly close, individuals have the right to privacy so that individuals can control the dissemination of their personal information, and the use of third parties is restricted. In actuality, American law has enlarged the area of protection of the right to privacy, and

the information subject can freely use and control the information, according to reference [13], which also defaults to the view that privacy is a property of personal information. Individuals can restrict the scope of information activities within the legal limits, according to reference [4], which is an expression of the right to privacy. In terms of personal information protection, as the economization of personality rights progresses, personal information increasingly represents property interests, and a brand-new right, the right of publicity, has evolved in the theoretical circle. The United States uses the right of privacy and the right of publicity to protect the personal interests and property interests embodied in personal information, respectively. In terms of data protection legislation, the United States adopts a segmented legislative approach. Reference [14] believes that the protection of personal information in the United States mainly relies on industry self-discipline, the protection of personal information is scattered in the laws of various states, and the fragmented and fragmented model cannot effectively protect the personal information of its citizens. Reference [15] believes that a right to be forgotten system should be established in line with national conditions. Reference [16] analyzes from the perspective of protecting personal dignity and personal freedom and believes that the essence of protection of personal information rights in European and American countries is to take it as an independent personality interest and incorporate it into the protection of privacy rights. In Germany, personal information is positioned and protected by law in the protection mode of personality rights. The legal interests protected are general personality interests, and Germany is a typical representative. Reference [17] believes that the “other rights” stipulated in article 823 of the “German Civil Code” do not include the right to personal information, and that personal information that reflects the interests of general personality is essentially a system of general personality rights. Reference [18] in his book “The Munich Commentary on the German Civil Code” believes that the right to personal information belongs to the category of “other rights” stipulated in article 823 of the “German Civil Code” and belongs to a separate right. Reference [19] believes that under the framework of German law, whether the right to personal information belongs to the “other rights” in article 823 of the “German Civil Code” or the general system of personality rights, different views on the attributes of the right to personal information will lead to the same conclusion which is that the right to personal information is an absolute right. In terms of German judicial practice, the 1983 “census case” gave birth to a new concept of rights, namely, “information self-determination,” and the right to personal information began to develop in the direction of constitutional rights. At the same time, the Federal Court, based on the “German Basic Law,” affirmed the important value of the right to personal information in protecting personal dignity and personal freedom. From the perspective of doctrine and precedent, Germany recognizes the right attribute of personal information right as a general personality right and realizes the protection of personal information with the use of “information self-determination right.” By analyzing the status quo of per-

sonal information rights at home and abroad, it is determined that its legal attributes are mainly the theory of privacy rights, the theory of general personality rights, the theory of specific personality rights, the theory of property rights, and the theory of dual rights. Extraterritorial law mainly identifies the legal attributes of personal information rights as privacy rights and publicity rights, general personality rights, and basic human rights [20–23]. There is a certain gap between the domestic legal tradition and the foreign legislative environment; so, these theories cannot be used for reference. Considering the development trend of personality rights in the new era, it should be considered that certain personality elements reflect certain property interests.

### 3. Method

Here, it discusses the BP neural network. They evaluate the legal attributes and rights attributes of personal information.

*3.1. Back Propagation (BP) Neural Network.* In this subsection, analyze the definition and characteristics of BP network. They define the structure of BP neural network and also discussing the BPNN algorithm. They examine the deficiencies and applications of BPNN.

*3.1.1. Definition and Characteristics of BP Network.* In the mid-1980s, different scholars independently discovered and proposed the BP algorithm. In 1986, Rumelhart and McClelland published a book titled “Parallel Distributed Processing: Exploration in the Microstructures of Cognition” that had a significant effect on the BP algorithm’s implementation. Later, the development of the BP algorithm benefited in the advancement of neural networks by addressing the multilayer perceptron learning problem. The BPNN, a multilayer feed-forward network for algorithm training based on error back propagation, was established in 1986 by a group of academics led by Rumelhart and McClelland. It is one of the most popular neural network models out there. The forward and backward propagations of error are the two main components of BPNN. A neuron in the input layer receives input signals from the external environment and passes them on to a neighboring one or more hidden layers of neurons in the middle layer, which process the transformed data. The middle layer can be a single hidden layer or a multihidden layer structure, depending on the needs of the input signal changes. Direct transmission of learning to the output neurons takes place in a single-layer neural network. A multihidden layer neural network uses a forward propagation method to learn from the previous hidden layer, and then the output layer sends the processing results to the external world. Back propagation of the mistake occurs if the actual output value does not match the predicted output value. Output errors are used to adjust the weights of each layer in the form of error gradient descent, while the error is reversely communicated to the hidden and the input layers. Network learning is an ongoing process in which weights are continually adjusted in order to propagate information and correct faults in a neural network’s hidden and output layers. In order for this process to continue, the operator must



either be satisfied with the output error or a certain number of learning cycles have been completed.

The information processing technique of BPNN has the following characteristics:

- (1) Information distributed storage: the BPNN simulates the characteristics of the human brain to store information on the connection strength between neurons and stores the information on the connection weight and distributes it in the network
- (2) Parallel processing of information: although the speed of human brain neurons transmitting signals is not as fast as that of computers, the human brain can quickly judge and deal with many problems because of its unique properties, which is unmatched by computers. BPNN simulates the human brain to run parallel processing to improve processing power
- (3) It is fault-tolerant: the BPNN simulates the automatic repair characteristics of the biological nervous system, and the damage of some neurons does not affect the overall error
- (4) It has the ability of self-learning, self-organization, and self-adaptation. The BPNN can continuously adjust the weights of each layer to adapt to different external environments during learning or training. Under different learning methods, the BPNN can play different network functions. In addition, after training and learning, the BPNN can remember inventory characteristics like as weight matrices and neuron conversion function coefficients and adjust this memory to the inventory, and it may store the system's information distribution in the weight matrix and these coefficients. Changes in the environment are constantly reflected in inventory characteristics, which aid our inventory analysis. BPNN is the core part of the forward neural network. In fact, in the practical application of artificial neural network (ANN), the application of BPNN accounts for a large part of the ANN model. It fully reflects the best part of ANN

**3.1.2. Structure of BP Neural Network.** Neural networks with several layers are called BPNNs because of their structure. It has three parts: input layer, hidden layer, and output layer. The concealed layer is separated into a single layer and a multilayer structure. For each layer, weights link each node to the next, and each node has a threshold and transfer function for the output layer. The transfer function of BPNN should be differentiable everywhere.

*Input layer:* the input variable of the BPNN is a variable that has a great influence on the output variable and can be extracted with specific values. In addition, as the input variables of the BPNN, the two must be uncorrelated or the correlation is very small.

*Hidden layer:* extracting and storing internal rules from the sample is what this node is all about. For each hidden layer node, there are numerous weights, and each weight promotes

network mapping. Generally speaking, complex nonlinear functions with many fluctuations and large amplitude changes require the network to have more hidden layer nodes to enhance its mapping ability. Whether the number of hidden layer nodes is optimal depends on the following factors:

- (1) The number of input and output layer nodes
- (2) The number of training samples
- (3) The noise in the target output
- (4) The function to be learned by the neural network or the complexity of the classification problem
- (5) The structure of the network
- (6) The activation function adopted by the hidden layer nodes
- (7) The training algorithm
- (8) The regularization

*Output layer:* generally speaking, the output volume represents the functional goal of the system to be expressed. Under normal circumstances, the output variable is a numerical value, and the system needs to analyze, compare, and study this numerical value. The selection of output variables is relatively simple, and there can be multiple output variables.

### 3.1.3. BPNN Algorithm

- (1) Introduction of the neural network algorithm: in 1974, Werbos first proposed the idea of the BP algorithm. Moreover, some other scholars also proposed the BP algorithm in the same period. However, this algorithm has not received the attention of the theoretical community until Rumelhart et al. began to study again. The BP algorithm mainly uses the LMS learning algorithm, which makes the actual result value infinitely close to the expected result value through the gradient search technology. The learning process of BPNN is a process in which the error is propagated backward, and the weights are constantly revised. Figure 1 shows the algorithm flow of BPNN

In a multilayer ANN, there are two types of signals that are exchanged. When a first-order digital signal is applied to a second-order digital signal and then to a third-order digital signal, the working signal is formed. Input variables and weights of connections determine this. The error signal is the signal from the output layer to the input layer that reflects the difference between the predicted output and the actual output of the neural network. The forward propagation of the input signal and the reverse propagation of the error signal comprise the BP learning algorithm, an iterative process. Its learning method is as follows. The input signal is sent via the transmission process of the input layer-hidden layer-output layer, and the output signal is created at the output layer port. As long as the signal is being sent forward, the network's weights remain constant; therefore, the

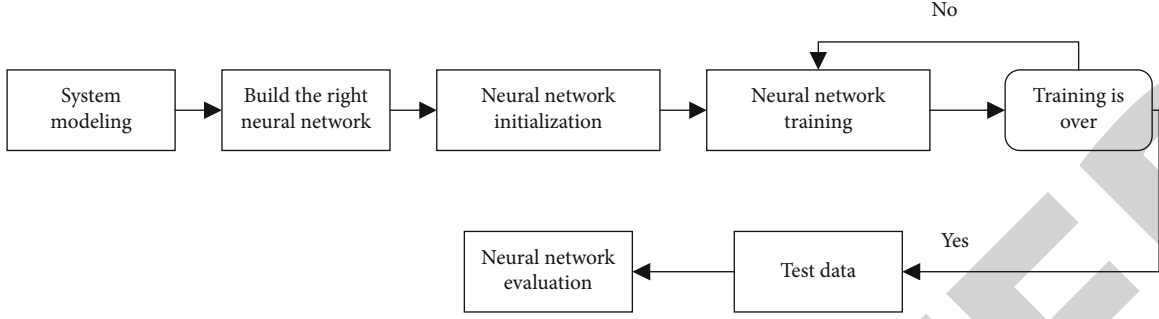


FIGURE 1: BP neural network algorithm flow.

activity in any given layer of neurons has no effect on the activity in the layer above it. The error signal is transmitted to back propagation if the intended output is not achieved at the output layer. The error signal is the difference between the network's actual output and its predicted output. The back propagation of the error signal occurs when the signal travels from the output layer to the hidden layer to the input layer. Weights in the network are recalculated during the back propagation of error signals. Weights are constantly adjusted to bring the network's output closer to the desired output.

- (2) Although the improved BP algorithm of the neural network algorithm has been widely used, it also has its own limitations and shortcomings, such as slow training speed, easy to fall into the minimum point, and low generalization ability. With the continuous in-depth study of the BP algorithm by experts and scholars, many improvement methods have emerged: adaptive learning rate modification and additional momentum methods, for example. First, the adaptive learning rate adjustment method is introduced. There is an optimal learning rate for each specific link of the neural network; so, there are several different learning rates in different stages of a neural network. In order to change this situation and speed up the convergence process, the method of adaptively changing the learning rate came into being. The network automatically adjusts to different learning rates at different stages of neural network training. The adjustment formula is as follows:

$$\theta(t+1) = \begin{cases} 1.15\theta(t) & E(t+1) < E(t), \\ 0.75\theta(t) & E(t+1) > 1.14E(t), \\ \theta(t) & \text{others} \end{cases} \quad (1)$$

where  $\theta$  is the learning rate, which can be automatically adjusted according to the size of the error  $E$ .

The second is the additional momentum method. When the neural network uses the additional momentum method to modify the weights of the network, the effect of the error on the gradient and the influence of the change trend on the error surface must be considered. If additional momentum is applied, the network is able to avoid getting stuck in local

minima and possibly slip through it. The weight adjustment formula with additional momentum factor is

$$\begin{cases} \Delta w_{ij}(t+1) = (1 - m_a)\theta S_i O_j + m_a \Delta w_{ij}(t), \\ \Delta v_{ij}(t+1) = (1 - m_a)\theta S_i + m_a \Delta v_{ij}(t), \end{cases} \quad (2)$$

where  $O_j$  is the input of the  $j$ -th neuron in the input layer,  $S_i$  is the error signal output by the  $i$ th neuron, and  $m_a$  is the momentum factor, generally around 0.95.

**3.1.4. Deficiencies and Applications of BPNN.** Although BPNN has been widely used in the field of prediction, it still cannot cover up the defects of neural network more or less.

- (1) The learning rate of ordinary BP neural network is fixed, which leads to slow network convergence and long training time. The learning rate is too small so that the training time of BPNN can be too long. We can use varying learning rates or adaptive learning rates to improve BPNN
- (2) The BP algorithm can converge the weights to a value that is likely to be a local minimum rather than a global minimum. We can solve this problem with the additional momentum method
- (3) The number of layers and nodes of the hidden layer of the neural network can only be determined through experience or through experiments one by one, which will make the BPNN, have great redundancy, and increase the pressure of network learning to a certain extent
- (4) The learning and memory of the network are unstable. The neural network cannot memorize the previous weights and thresholds. If the sample data changes, the neural network has to start training again. But better weights for prediction, classification, or vergence can be saved. The main application of BPNN is as follows:
  - (i) Function approximation: train a grid to approximate a function with training samples consisting of input variables and output variables
  - (ii) Pattern recognition: using a pending output variable to associate it with an input variable

- (iii) Categorize: categorize the appropriate way of defining the input variables
- (iv) Data compression: to facilitate transmission or storage, the dimension of output variables can be reduced

3.2. *Legal Attributes and Rights Attributes of Personal Information.* Here, defining the concept of the human right to information, they analyze the dispute over personality rights.

3.2.1. *The Concept of the Human Right to Information.* The connotation of right is the premise of researching the attribute of a right, and the research on the attribute of personal information right needs to start from its concept. “The General Provisions of the Civil Law” promulgated in 2017 used the expression of personal information in civil legislation for the first time and made it the basis and core concept of article 111, but “The General Provisions of the Civil Law” did not further explain this concept. The concept of personal information first appeared in the data protection proposed in the “International Human Rights Conference” convened by the United Nations in 1968. The expressions of each country vary slightly when compared to the regulations of other countries. Personal information is used in Japan, while personal data is used in Germany and the European Union; personal privacy is used in the United States, replacing personal information with privacy. Different cultural and legal tradition backgrounds in different countries lead to different expressions of data protection, and different expressions are only the relationship between essence and appearance; they are the specific manifestations of information. Based on the above considerations, personal information can better reflect the fundamental rights and interests protected by law. The huge rights system of civil law endows citizens with various rights, and each right is generated based on a specific legal relationship generated by a specific behavior. It takes a long period of development to form a specific right and then join the civil law in the rights system. The most important thing to study a right is to explore its inherent legal attributes. Only by grasping the attributes of a right can the right solve the problems encountered in the real society.

### 3.2.2. *Dispute over Personality Rights*

(1) *The General Theory of Personality Rights.* Some scholars believe that personal dignity, equality, and freedom can well protect personal information rights under the theory of general personality rights. The specific reasons are as follows: first, with the development of today’s social economy, the nature of the identifiability of personal information rights determines as its scope becomes wider and wider, and it is difficult for a specific personality right to effectively protect the increasingly complex and changing personal information rights, while the openness and inclusiveness of general personality rights in the content of rights can be protected in specific personality rights. Secondly, general

personality rights can effectively protect the personal dignity and freedom of natural persons. If the right to personal information falls under the category of general personality rights, it can be adequately safeguarded under the current legal system without the need to create new special rights, which would jeopardize the current system’s stability. Finally, there are pertinent practice cases to refer to. For example, in “Ren v. Beijing Baidu Netcom Technology Co., Ltd. Dispute on General Personality Rights,” the plaintiff tried to use the general personality right to claim the “right to be forgotten,” but the law of our country did not provide for this right, and the court finally decided that it was not necessary for protection and did not support it.

(2) *The Theory of Specific Personality Rights.* Some scholars hold the view of specific personality rights for the following reasons: first of all, there are many differences between personal information rights and privacy rights in terms of attributes, objects, and protection methods, and traditional methods of protecting privacy rights and traditional legal protection methods cannot continue to be used. It is easy to cause judicial loopholes, resulting in the inability to effectively protect the right to personal information. It is necessary to defend the personal information of natural persons with a new definite personality right that is different from the right to privacy. Secondly, the development of the market makes personal information generate commercial value. Personal information right not only reflects the interests of personality rights but also reflects certain property interests. The right holder can obtain certain economic remuneration by selling, using, and other means, but it should not be considered that personal information right belongs to the scope of property rights, and its essence still belongs to specific personality rights, while economic value is one of the manifestations in the process of social development. Finally, specific personality rights can coexist with property interests. Personality interests and property interests are not an either-or relationship. With the development of society, there will be more civil rights to reflect the emerging new interests, but this does not affect the original positioning of the rights. The nature of specific personality rights can better safeguard personal information rights.

(3) *Privacy Right Theory.* Scholars who hold a privacy point of view are inevitably influenced by the protection of personal information in the United States and believe that first, in the age of information networks, individuals’ attitudes towards personal information related to themselves have undergone a significant change. Second, article 2 of the “Tort Liability Law” specifies the legal attitude toward the protection of the right to privacy. As a result, if the right to personal information is linked to the right to privacy, the right to privacy can be utilized to safeguard it directly without the need to invoke the right to privacy in principle or practice. New rights and solutions, without having to seek new legislation, can leverage mature privacy protection models to maintain legal stability. Finally, in my country’s judicial practice, for personal information infringement cases, there are cases based on the right of

TABLE 1: Personal information right attribute assessment system.

First-level indicator	Secondary indicators	Label
General personality rights	Protect human dignity and freedom	X1
	Equal rights of individuals	X2
	Support the right to be forgotten	X3
Specific personality rights	Enjoy personal interests such as privacy and name	X4
	Enjoy personal interests such as life and health	X5
	Enjoy personal benefits such as reputation and honor	X6
	Include an individual's private life	X7
Privacy rights	Use of personal information, such as sale and transfer	X8
	Insulting information reduces social evaluation	X9
Property rights	Personal information has commercial value	X10
	Collect personal information to meet interests	X11

reputation and the right of portrait, but most cases still use the right of privacy as the cause of the case to define the nature of the case, and the right to privacy is more accustomed to use in practice.

(4) *Property Rights Theory*. Scholars arguing for this theory advocate the right attribute of property rights and believe that in the face of the property interests that constantly reflected by personal information, the traditional personality rights model cannot provide a reasonable explanation for this nor can it be fully protected by the use of personality rights. Therefore, the right attribute of the property right provides effective protection for personal information, and the main reasons are as follows: first, property interests are constantly highlighted. With the development of the market and the wide application of big data, the commercial value of personal information exists as a resource. To some extent, mastering personal knowledge entails mastering future market wealth. The property attribute of personal information rights is becoming increasingly important as data analysis may help corporations change product structure and build individualized marketing campaigns for different consumers, among other things. Secondly, the attribute of property right is a supplement to the theory of personality right. Under the personality rights model, personal information is closely integrated with the subject of rights, has a strong dependence, and cannot exist independently of the subject. However, since entering the era of big data, commercial exchanges have made the commercial value reflected in the information continue to highlight, resulting in many criminals illegally using a large amount of personal information. Therefore, for the separation status of personal information, the use of property rights attributes is an extension and supplement to the traditional theory of personality rights. Finally, attributing personal information rights to property rights is more conducive to the protection of rights subjects. Personal information is vulnerable to illegal infringement in the process of collection and use. Protecting personal information rights in a property rights model can effectively provide adequate protection at all stages of personal information circulation.

According to the various theories of different scholars above, and combined with the specific conditions of the country, this paper constructs a personal information right attribute evaluation system suitable for neural network evaluation, as shown in Table 1. By analyzing the right-related characteristics in the attribute of personal information rights, the rationality of the attribute is judged.

#### 4. Experiment and Analysis

Here, it analyzes the dataset sources and defines the BP neural network evaluation model construction. They evaluate the contrastive experiment of BP neural network and the improved model.

4.1. *Dataset Sources*. According to the analysis of the legal attributes and rights attributes of personal information rights in Chapter 3, this paper designs relevant questionnaires and collects and extracts the required data through big data technology. There are 180 groups of data collected, of which 150 groups use as the training set, and 30 groups were used as the test set.

##### 4.2. BP Neural Network Evaluation Model Construction

4.2.1. *Input and Output Layers*. The input layer neurons of the BPNN are the attribute indicators of the personal information analyzed in this paper. In the third chapter, 11 attribute indicators of personal information are analyzed. Therefore, we can set the number of neurons in the input layer of the BPNN to 11 and the number of neurons in the output layer to be 1.

4.2.2. *Hidden Layer*. This paper designs a 3-layer BPNN model consisting of an input layer, a hidden layer, and an output layer. The number of hidden layer nodes can be selected by the following formula:

$$H = \sqrt{m + n} + a, \quad (3)$$

where  $H$  represents the number of hidden layer nodes,  $m$  represents the number of neurons in the output layer of

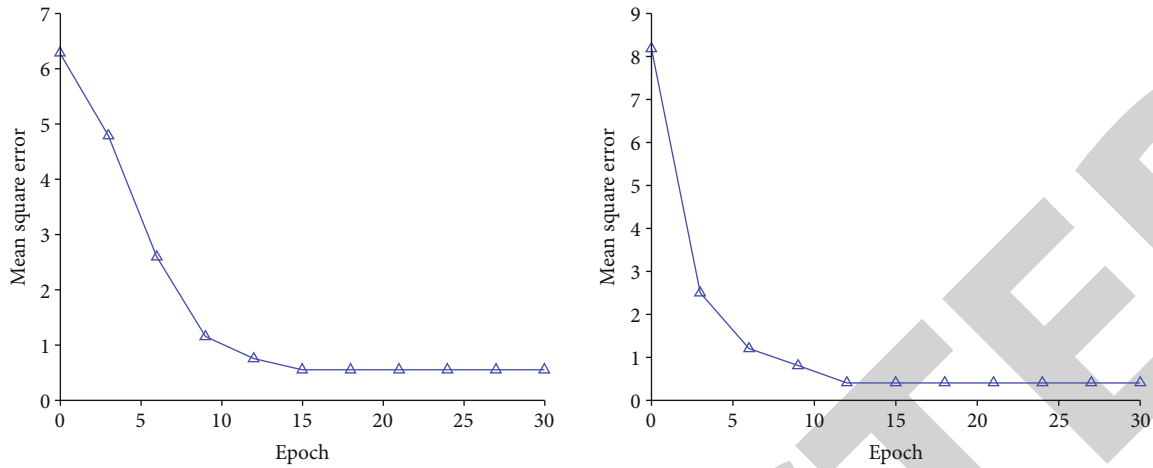


FIGURE 2: Training effect when  $N = 4$  and  $N = 6$ .

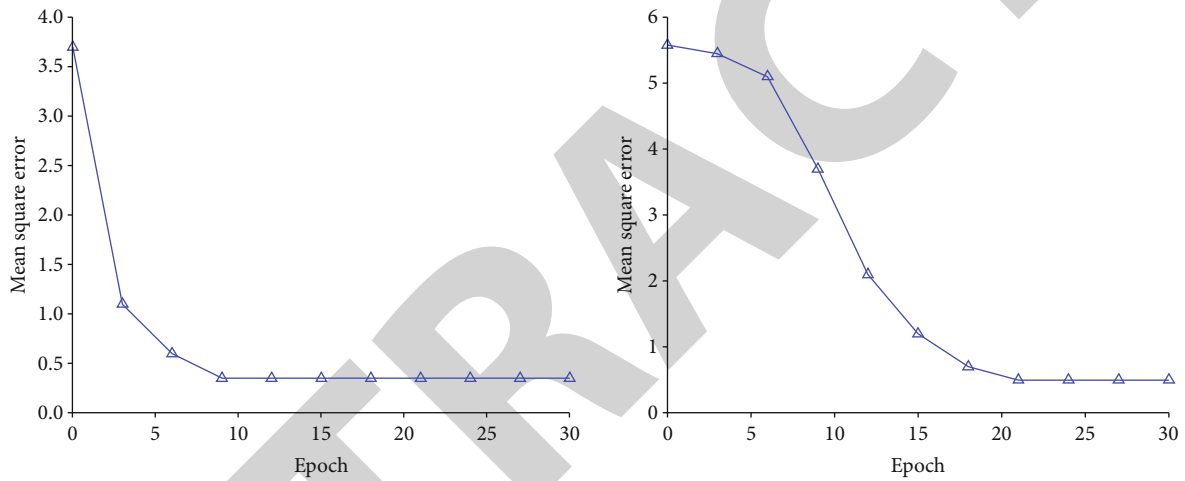


FIGURE 3: Training effect when  $N = 8$  and  $N = 10$ .

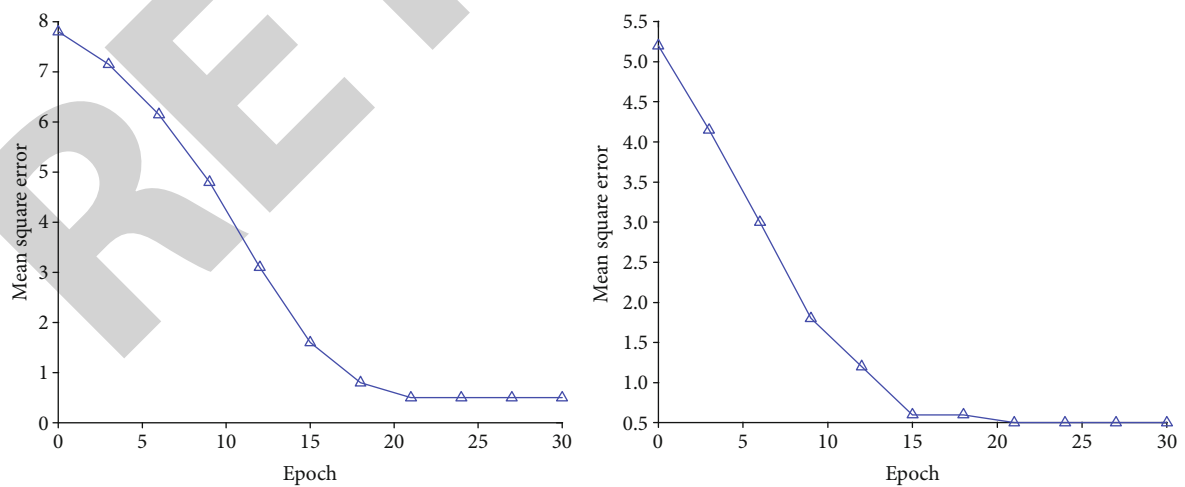


FIGURE 4: Training effect when  $N = 12$  and  $N = 14$ .

the neural network,  $n$  represents the number of neurons in the input layer of the neural network, and  $a$  represents a constant in the range [1–9, 24].

Then, the number of hidden layer nodes of the BPNN in this paper is in the range of [3–13]; so, the trial and error method is used to determine the specific value. Select the

TABLE 2: Comparison of the evaluation results of the two models with the actual results.

Number	1	2	3	4	5	6	7	8
Actual result	0.812	0.658	0.735	0.859	0.882	0.912	0.622	0.698
BP model	0.785	0.672	0.721	0.828	0.852	0.933	0.665	0.660
Improved BP model	0.821	0.659	0.740	0.849	0.895	0.908	0.638	0.705

number of nodes to be 4, 6, 8, 10, 12, and 14 to conduct experiments. The experimental results are shown in Figures 2–4. Finally, the number of nodes selected is 8.

**4.3. Contrastive Experiment of BP Neural Network and the Improved Model.** After the structural analysis of the BPNN, through the training of the training samples, the BPNN fully absorbed the fuzzy and complex laws contained in the training samples. Therefore, using the trained BPNN model to simulate the test samples has a relatively high accuracy. The accuracy of the trained BPNN is uncertain. Here, we must pass the test of the test sample to be sure. The main content of this section is to use 30 sets of test samples to test the trained network and observe its prediction results. Some results are shown in Table 2.

From the results in Table 2, it can be found that the improved BPNN model has smaller error, higher accuracy, and better evaluation effect.

## 5. Conclusion

The fundamental difficulties that must be resolved in the creation of personal information protection legislation are the legal qualities and rights attributes of personal information rights, which are also contentious questions among scholars. There are “basic rights theory” and “private law rights theory,” which comprises “property rights theory,” “personality rights theory,” and “privacy rights theory,” among other things. The “basic rights theory” and the “private law rights theory” genuinely entail the problem of where to place personal information rights for protection when deciding between public and private rights. There is no essential contradiction and can coexist at the same time. The right to personal information can and should be a fundamental right of citizens. However, due to the lack of clear provisions on personal information rights in my country’s constitution, coupled with the delay of my country’s constitutional interpretation system and the imperfect constitutional litigation mechanism, the right to personal information cannot actually become a basic right in my country. The emergence of commercial entities among the infringing entities and the balance of interests between protecting individual rights and the effective flow of information make it possible for them to be protected in a timely and effective manner only if they are regarded as a private law right in legal policies. Even so, the protection of personal information from administrative, criminal, and other fields is still necessary. This paper builds an assessment index based on the legal qualities and rights attributes of personal information rights and presents a neural network-based rationality evaluation approach

for the attributes of personal information rights. The completed work is as follows:

- (1) Focusing on the legal attributes and the rights attributes is discussed in detail. First of all, the different viewpoints of scholars at home and abroad are introduced one by one, and they are analyzed one by one. Then, summarize and analyze many academic viewpoints and put forward the viewpoints of this paper and demonstrate
- (2) The evaluation index based on the legal attribute and right attribute of personal information right is constructed, and the BPN model structure required in this paper is determined
- (3) Compare the results obtained by the BPNN model with the results obtained by the improved BPNN model. The results show that the improved BPNN model has smaller error, higher accuracy, and better evaluation effect

## Data Availability

The datasets used during the current study are available from the corresponding author on reasonable request.

## Conflicts of Interest

The author declares that he has no conflict of interest.

## Acknowledgments

This work was supported by the Project of Philosophy and Social Science Foundation of Jiangsu Province, China, “Research on the legal mechanism of social credit system in Jiangsu province—analysis of the legal problems in the construction of social credit system in Jiangsu Province” (2019SJA2007).

## References

- [1] X. Liang, ““General provisions of the civil law of the People’s Republic of China (draft)”: interpretation, comments and suggestions for amendment,” *ECUPL Journal*, vol. 19, no. 5, p. 20, 2016.
- [2] J. Fenrich, “Common law protection of Individuals’ rights in personal information,” *Fordham Law Review*, vol. 65, p. 951, 1996.
- [3] A. Miller, “What do we worry about when we worry about price discrimination—the law and ethics of using personal information for pricing,” *Journal of Technology Law & Policy*, vol. 19, p. 41, 2014.

## *Retraction*

# **Retracted: Integrated Design and Development of Intelligent Scenic Area Rural Tourism Information Service Based on Hybrid Cloud**

### **Computational and Mathematical Methods in Medicine**

Received 1 August 2023; Accepted 1 August 2023; Published 2 August 2023

Copyright © 2023 Computational and Mathematical Methods in Medicine. This is an open access article distributed under the Creative Commons Attribution License, which permits unrestricted use, distribution, and reproduction in any medium, provided the original work is properly cited.

This article has been retracted by Hindawi following an investigation undertaken by the publisher [1]. This investigation has uncovered evidence of one or more of the following indicators of systematic manipulation of the publication process:

- (1) Discrepancies in scope
- (2) Discrepancies in the description of the research reported
- (3) Discrepancies between the availability of data and the research described
- (4) Inappropriate citations
- (5) Incoherent, meaningless and/or irrelevant content included in the article
- (6) Peer-review manipulation

The presence of these indicators undermines our confidence in the integrity of the article's content and we cannot, therefore, vouch for its reliability. Please note that this notice is intended solely to alert readers that the content of this article is unreliable. We have not investigated whether authors were aware of or involved in the systematic manipulation of the publication process.

Wiley and Hindawi regrets that the usual quality checks did not identify these issues before publication and have since put additional measures in place to safeguard research integrity.

We wish to credit our own Research Integrity and Research Publishing teams and anonymous and named external researchers and research integrity experts for contributing to this investigation.

The corresponding author, as the representative of all authors, has been given the opportunity to register their agreement or disagreement to this retraction. We have kept a record of any response received.

### **References**

- [1] H. Zhang and M. Li, "Integrated Design and Development of Intelligent Scenic Area Rural Tourism Information Service Based on Hybrid Cloud," *Computational and Mathematical Methods in Medicine*, vol. 2022, Article ID 5316304, 9 pages, 2022.

## Research Article

# Integrated Design and Development of Intelligent Scenic Area Rural Tourism Information Service Based on Hybrid Cloud

Hong Zhang  and Mingyang Li

Business School, Dalian University of Foreign Languages, Dalian 116044, China

Correspondence should be addressed to Hong Zhang; zhanghong@dlufl.edu.cn

Received 9 May 2022; Revised 27 May 2022; Accepted 30 May 2022; Published 16 June 2022

Academic Editor: Naeem Jan

Copyright © 2022 Hong Zhang and Mingyang Li. This is an open access article distributed under the Creative Commons Attribution License, which permits unrestricted use, distribution, and reproduction in any medium, provided the original work is properly cited.

Although the “Internet+” technologies (big data and cloud computing) have been implemented in many industries, each industry involved in rural tourism economic information services has its own database, and there are still vast economic information resources that have not been exploited. Z travel agency through rural tourism enterprise third-party information services and mobile context-awareness-based Z travel has achieved good economic and social benefits by deep value mining and innovative application of the existing data of the enterprise through the third-party information service of rural tourism enterprises and mobile context-aware travel recommendation service. It clearly demonstrates that, in order to maximise the benefits of economic data, rural tourist businesses should focus not only on the application of new technologies and methodologies but also on the core of demand and data-driven and thoroughly investigate the potential value of current data. This paper mainly analyzes the problems related to how rural tourism can be upgraded under the smart tourism platform, with the aim of improving the development of China’s rural tourism industry with the help of an integrated smart tourism platform, and proposes a hybrid cloud-based integrated system of smart scenic rural tourism information services, which can meet the actual use needs of rural tourism, with good shared service effect and platform application performance, and promote the development of rural tourism and resource utilization rate.

## 1. Introduction

The rise of the smart tourism model provides a new opportunity for rural tourism information construction, and the full integration of rural tourism information technology and smart tourism development is beneficial to the realization of rural tourism industry development systemic linkage, but also the future of rural tourism economic construction indispensable main content, to enhance the impact of rural tourism, has important significance [1–3].

International rural tourism information technology started earlier, and in the late 1990s, some developed countries have formed the prototype of intelligent tourism. With the improvement of the level of information development and the popularization of intelligent technology, intelligent tourism development has become the main form of rural tourism development in some international developed countries.

Among them, the customised service model [4, 5], which analyses the market demand of tourism consumers to develop tourism programs and carry out the entire process of tourism management services from the perspective of consumers, effectively improving the accuracy of the positioning of the rural tourism industry and providing a strong guarantee for the expansion of potential consumer groups, is widely used in the development of intelligent tourism in Western Europe. In contrast to developed countries in Western Europe, the use of intelligent tourism technology in the development of rural tourism information technology in some North American countries is primarily reflected in the fields of marketing advertising and advertising information propaganda, with the use of information technology and intelligent technology in rural tourism services being relatively limited. This difference is mainly due to the different economic development patterns and economic development systems in different regions, so that each region must



choose the appropriate way to carry out rural tourism informatization construction based on its own conditions, thus promoting the formation of a diversified rural tourism informatization development pattern worldwide. China's domestic rural tourism information construction started nearly 20 years later than the international developed countries, the early stage of development level is particularly lagging behind, and development resources are limited to economic development areas. Rural tourism informatization development has become the basis of modern rural tourism economic construction in China, influenced by the level of information technology development and the soft power of information management, especially in Central China, South China, and Southwest China, where rural tourism informatization development is relatively high. It is due to the development of information technology and the wide application of Internet technology that China's information-based rural tourism construction was formed with local characteristics and cultural style. With the launch of many domestic tourism apps in recent years, the development of rural smart tourism has gradually been emphasized by all regions and has become a major thrust for regional economic development. Although China's current rural intelligent tourism development is relatively good, there are still some basic problems to be solved, which is also an important factor hindering the development of China's rural tourism information construction [6, 7]. The basic features of cloud computing are shown in Figure 1.

China and governments at all levels have deployed the rural revitalization strategy, and rural revitalization has become an important grasp of China's three agricultural works during the period of China's rural transformation and development. Economic revitalization is the foundation of rural revitalization, and rural tourism industry has become an important way to promote rural economic revitalization and industrial prosperity because of its diversified resource elements input requirements to integrate rural natural ecology and traditional culture and plays a pivotal role in the transformation of modern rural production mode and industrial structure. And with the development of modern technologies such as big data and Internet of Things, rural tourism development has advanced with the times, through the deep integration of technology and tourism, not only to achieve the systematic integration of tourism resources but also through the application of big data, cloud computing, artificial intelligence technology, etc. [8, 9], to improve tourism infrastructure, enhance tourism experience, and promote services with technology, forming a new tourism industry of wisdom, information, and personalization and creating a wisdom tourism. With the help of wisdom tourism-related technology and production and management system, we improve the rural tourism service system, consolidate the technical foundation of rural tourism development, promote the construction of tourism-oriented villages with wisdom tourism, realize rural affluence, rural income, and ecological improvement with the new mode of tourism industry development, and provide the industrial foundation for comprehensive rural revitalization. This paper focuses on the overall architecture of the

wisdom tourism hybrid platform and proposes a hybrid cloud-based integrated architecture of wisdom scenic rural tourism information service, which realizes the virtualization management of rural tourism resources through cloud computing to achieve unified sales, service, and management of rural tourism resources. As an important service industry, exploring a cloud computing application scheme suitable for rural tourism scenic areas is an important element of future smart tourism construction. The deployment strategy of hybrid cloud is analyzed, and the effectiveness of the method in this paper is verified through experiments.

The following is the paper's organization paragraph: Section 2 discusses the related work. The suggested work's approaches are examined in Section 3. The trials and results are discussed in Section 4. Finally, the research job is completed in Section 5.

## 2. Related Work

*2.1. Rural Intelligent Tourism Construction.* There will very certainly be a lot of infrastructure rehabilitation and industrial development as part of the process of rejuvenating the countryside and boosting rural tourism. To avoid destroying the original rural landscape and cultural traditions during construction and development, intelligent tourism technology can be used to achieve sustainable utilization, such as using mapping and positioning technology in intelligent tourism, applying satellite remote sensing mapping, drone mapping, tilt photography technology, and Baidoo precise positioning technology in large regional project implementation monitors. In terms of monitoring regional project implementation, land resource protection, and use, as well as environmental protection of rural villages and restoration of ancient buildings, tourism development and utilization can be realized without changing the original rural landscape, and the authenticity of tourism resources can be protected as much as possible. For the intangible cultural heritage, mainly intangible cultural heritage, which is widely inherited in the countryside, big data technologies such as database, knowledge mapping, block chain, and other technologies in smart tourism can be used to achieve sustainable utilization of traditional rural culture. The purpose of wisdom tourism development for rural tourism system construction is to carry out scientific wisdom tourism development management layout according to the characteristics of rural tourism information development, promote the diversified design of wisdom tourism content [10–13], and develop wisdom tourism strategies centered on rural tourism development. For example, vigorously promote rural tourism with some companies to enhance tourism market resources to rural tourism construction, using joint development with relevant enterprises to achieve the synchronization of rural tourism and wisdom tourism development content, so that rural tourism information construction can benefit from mobile Internet for effective information promotion. On the one hand, to meet the basic needs of rural tourism informatization construction; on the other hand, to improve the perfection of industrial content of wisdom tourism development, so that rural tourism

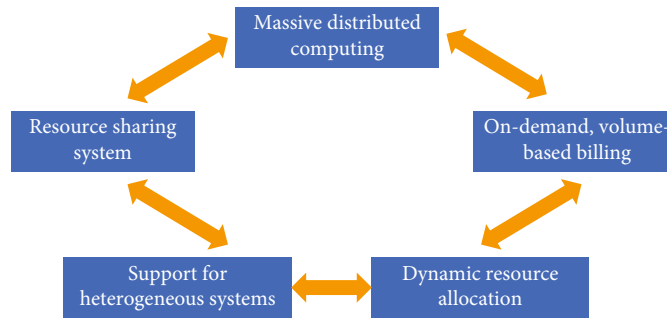


FIGURE 1: Map of the basic features of cloud computing.

informatization development and wisdom tourism industry layout can effectively achieve mutual benefit and win-win situation. To strengthen rural tourism informatization of wisdom tourism synergistic development mainly tourism development marketing, service management and tourism project design, and other levels to achieve synergistic development and wisdom tourism as a carrier to rural tourism service information conduction, the process of rural tourism informatization construction mainly plays a terminal service management role, that is, to achieve offline tourism services and management planning [14–17]. Rural tourism information development background and intelligent tourism industry integration should give rural tourism certain help in tourism development innovation. For example, in travel mode, travel items and travel content can be adjusted according to the needs of travel consumer groups. Through the smart tourism data platform and information management, it is possible to ensure that the content of tourism projects and publicity content remain unified, so that the construction of rural tourism information and the integration of smart tourism can ensure a consistent pace, keep pace with the times [18], and promote industrial construction and development.

**2.2. Hybrid Cloud.** The industry has progressed from simple computing virtualization to the cloud of the entire data center, employing a software-defined approach to automate and scale the administration of computing, network, and storage resources in the data center. A multi-AZ interoperable resource sharing paradigm has been adopted across various cloud data centers by large companies with numerous data centers. Today, an increasing number of businesses are combining clouds from various providers to solve specific business concerns. The evolution from traditional IT to the cloud has given birth to a large number of different cloud technologies (see Figure 2) [19–21]. The most basic categories include traditional IT environments, private clouds built by enterprises, hosted clouds built by service providers for specific enterprises, and public clouds built by service providers for the general public. Each production environment in turn has different technology choices and feature options, both large and small, framing an exceptionally complex application deployment relationship. In the short and medium term, different enterprises and different applications have their own intrinsic reasons for choosing different

execution environments and cannot simply choose one and discard the others.

At this stage, enterprises usually use three types of computing resources, namely, dedicated server resources running in enterprise data, virtual resource pools established on the basis of private clouds in enterprise data centers, and computing resources provided by public cloud providers [22]. For these three different types of enterprise computing resources, it is less cost-effective to use a private cloud that consumes a lot of resources to run enterprise applications that would be more efficiently run on a public cloud platform, but some enterprise-critical applications must be run in a private cloud environment. The advantage of hybrid cloud is that it can adapt to the needs of enterprises for different platforms, providing both the security and convenience and management and operation and maintenance levels of a private cloud and the openness and convenience of a public cloud, and is now considered to be the mainstream business cloud solution that enterprises will increasingly adopt in the future. These platforms operate independently of each other and are interconnected, allowing data to be shared as required to meet service agreements [23]. Deploying a successful hybrid cloud starts with a good understanding of which datasets and applications are best suited to run in a private cloud environment and which can be delivered to a trusted cloud service provider to ensure that a fully integrated platform can be provided to the enterprise. A trusted partner can help identify and articulate the reasons for a well-performing business, in addition to helping oversee a catalog of service portfolios, including creating metrics and portfolio management. Finally, the partner can help select a portfolio of services for delivery models such as financial, compliance, security, and workload. The specific hybrid cloud deployment strategy is shown in Figure 3.

### 3. Methodology

**3.1. Hybrid Cloud Platform Architecture Design.** Both public and private clouds offer infrastructure resources including processing, storage, and networking, as well as open APIs for consumers to employ. However, each cloud provider's APIs are distinct, and there is no consistent standard, which makes adapting heterogeneous clouds a difficult task for customers. Therefore, in this paper, we build independent Kubernetes container clusters in each cloud provider, such

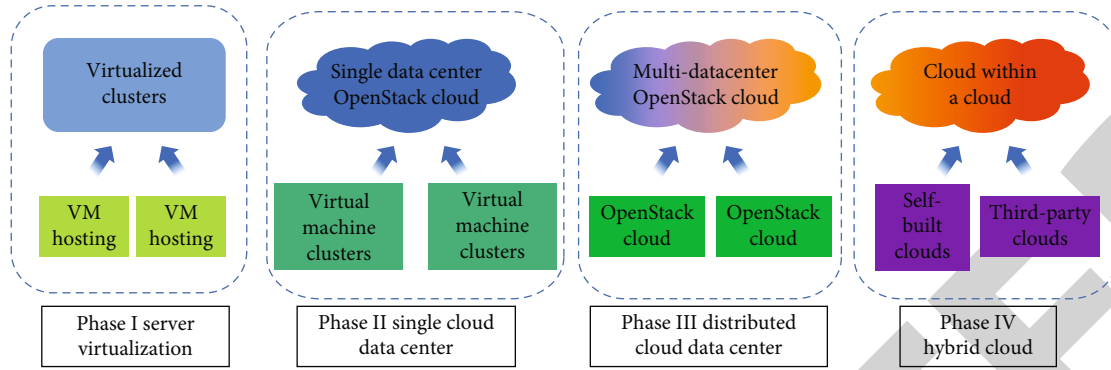


FIGURE 2: Cloud computing trends.



FIGURE 3: Hybrid cloud deployment strategy flowchart.

as public and private clouds, and then design and implement a unified global controller to manage and schedule the Kubernetes container clusters on each heterogeneous cloud at the upper layer. This ensures API homogeneity across the underlying heterogeneous clouds, as well as the simplicity of cross-cloud deployment, migration, and business elastic scalability. Figure 4 depicts the full hybrid cloud platform architecture.

The hybrid cloud management platform mainly manages application publishing and resource scheduling of container clusters on the underlying heterogeneous cloud and contains four modules: API, scheduler, controller, and database. The API is mainly used to receive commands from the front-end, the scheduler is used to schedule Kubernetes clusters in the heterogeneous cloud, the controller is used to handle business logic, and the database is used to persistently store resource data managed by the platform. The underlying public or private cloud Kubernetes cluster mainly manages the scheduling and dispatching of resources of a single container cluster, including master and node nodes. Master mainly controls the resource scheduling of a single cluster, and node runs the actual business container as a working node.

**3.2. Heterogeneous Kubernetes Access Design.** To deploy Kubernetes on each heterogeneous cloud infrastructure of the user, the upper global controller needs to add the platform address, port and Barberton of each Kubernetes cluster, etc. The upper controller makes calls through the standard API and the underlying Kubernetes. Namespaces of Kubernetes represent namespaces, which are mainly used to achieve resource isolation of tenants. Nodes represent host nodes in the cluster, which are the bearers of resource scheduling. Deployments are primarily used to manage the number of copies of applications. Pods are the smallest units for application operation and scheduling. Services are services that can expose access portals for back-end applica-

tions. Figure 5 depicts a schematic diagram of cloud data transfer and exchange.

**3.3. Hybrid Cloud Framework Application Performance Analysis.** Considering the economic cost and time cost, often different cloud service models are used to accomplish big data analysis. Therefore, the hybrid cloud platform should give the estimated computational resources and computation time to the user before the user submits the data with the target problem to determine the required virtual machine configuration. Initially, the MapReduce application is deployed on  $N$  internal private cloud VMs, and all the initial invariant data is stored in a distributed manner. When there are  $M$  external public cloud VMs scaled to support  $N$  internal VMs for big data analytics tasks, the perception policy rescales the deployment of MapReduce applications and iterates the MapReduce-based big data analytics application on the generated hybrid cloud platform. For analysis, let the internal VMs have the same configuration capability as external VMs, and users can trace the historical state of the application or have access to the following MapReduce performance metrics: the total number of map/reduce tasks, denoted as PM and PR; the number of physical slots for performing map/reduce tasks, denoted as  $k_M$  and  $k_R$ ; the average time to execute map, reduce, and scheduling tasks, denoted as AM, AR, and AS; and the average amount of scheduling data per execution of map, reduce, and scheduling tasks, denoted as DM, DR, and DS. In addition, let the dynamic behavior of the big data analysis application at runtime be measurable; i.e., the first iteration process is known a priori, while the input data volume, newly generated data volume, and computational complexity during each subsequent MapReduce operation are independent of each other. The internal virtual machine performance evaluation metrics are used in the  $i^{\text{th}}$  map operation, and the set of tasks with the number  $\text{Num}_{M,i}$  is assigned to  $k_{M,i}$  physical machines using a greedy allocation strategy. In this process,

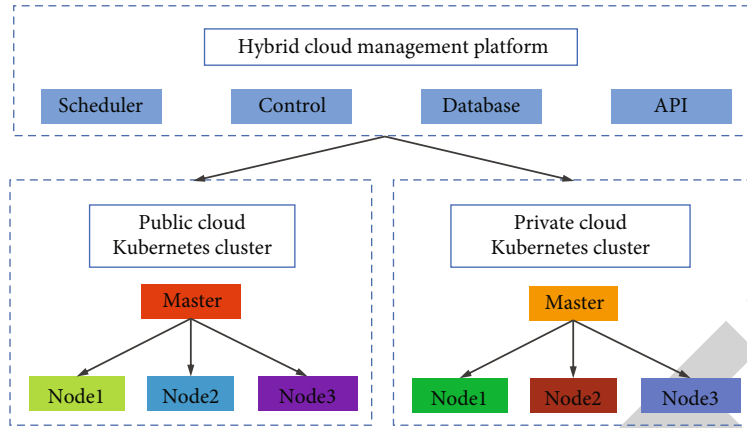


FIGURE 4: Overall hybrid cloud platform architecture.

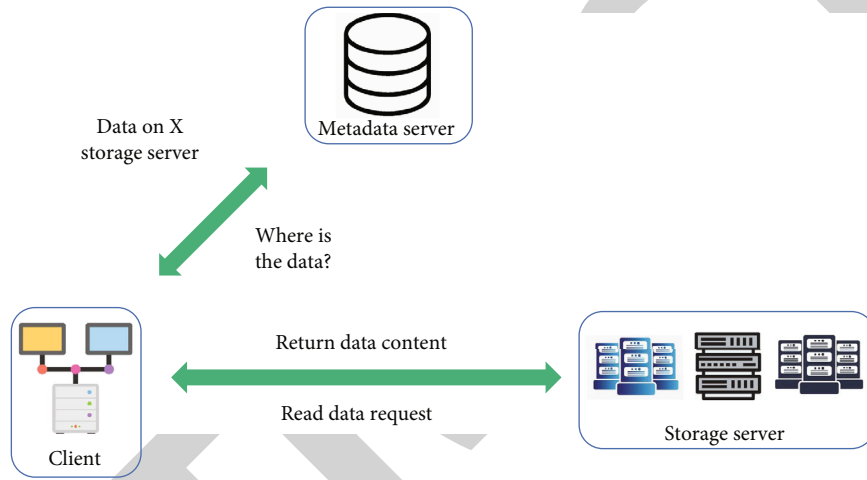


FIGURE 5: Sharing of data.

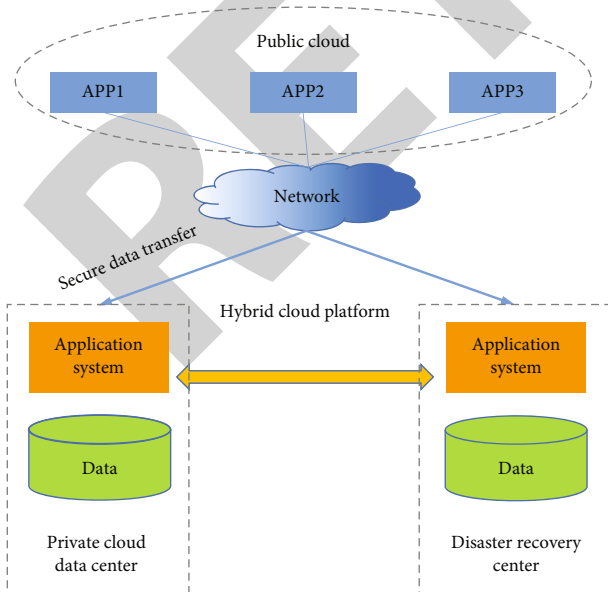


FIGURE 6: Hybrid cloud disaster recovery solution.

the task scheduling operation needs to be started first, so extra time is introduced and its time overhead needs to be considered separately, and its execution time is noted as  $T_l$ , whose value is related to the physical device performance and software system working mechanism, and can be considered as a constant. The theoretical lower bound on the execution time of subsequent task execution occurs in the case that the slowest task is scheduled to be executed last, while the previous  $\text{Num}_{R,i}$  tasks have already been executed. Therefore, the theoretical maximum execution time of the  $i^{\text{th}}$  map operation is

$$T_{M,i}^{\max} = \frac{(\text{Num}_{M,i} - 2)\bar{\tau}}{k_{M,i}} + \tau_{\max}, \quad (1)$$

where  $\tau$  is now the average execution time of the task and  $\tau_{\max}$  is the slowest execution time of the task. Further, its minimum execution delay occurs when the workload is fully balanced, and all tasks are executed with normal efficiency. Therefore, the theoretical minimum execution time of the

TABLE 1: Experimental dataset.

Statistics	Number of species	Query the records	Average record	Related documentation	Average kind	Different words
User 1	11	49	4.50	335	1.10	7965
User 2	09	52	6.10	168	01	6248
User 3	07	62	7.20	276	10	6689
User 4	08	49	5.20	103	1.20	4893
User 5	12	69	6.90	158	1.10	4903
User 6	09	39	4.50	164	01	4405
User 7	10	32	3.80	213	01	4498

TABLE 2: Accuracy comparison results.

Accuracy	User 1	User 2	User 3	User 4	User 5	User 6	User 7
Rocchio	0.65	0.71	0.89	0.72	0.81	0.70	0.69
Proposed algorithm	0.85	0.89	0.92	0.80	0.83	0.95	0.78

TABLE 3: Comparison of average accuracy of different algorithms.

Method	Personal characteristics match	Universal feature matching	Mixed feature matching 1	Mixed feature matching 2	Mixed feature matching 3
Accuracy	0.7658	0.9046	0.7051	0.9158	0.8957

TABLE 4: Average completion time per iteration of TestDFSIO.

Configuration serial number	Configure	Time per iteration/min	$\beta$
Configuration 1	3-on-0-off	6.90	3.40
Configuration 2	3-on-3-off	11.80	3.41
Configuration 3	3-on-6-off	11.90	3.38
Configuration 4	3on-9-off	11.60	3.45
Configuration 5	3-on-12-off	12.05	3.42

$i^{\text{th}}$  map operation as

$$T_{M_-}^{\min} = \frac{(\text{Num}_{M_-} - 1)\bar{\tau}}{k_{M_i}}. \quad (2)$$

Since the reduce and map operations in MapReduce are independent of each other but do not require task scheduling operations again, the minimum and maximum execution times for the  $i^{\text{th}}$  reduce operation are

$$\begin{cases} T_{R_-}^{\max} = \frac{(\text{Num}_{R_i} - 1)\bar{\tau}}{k_{R_-}} + \tau_{\max}, \\ T_{R_-}^{\min} = \frac{\text{Num}_{R_-}\bar{\tau}}{k_{R_i}}, \end{cases} \quad (3)$$

where  $T_{R_-}^{\max}$  and  $T_{R_-}^{\min}$  are the theoretical upper and lower bounds of the execution time of the  $i^{\text{th}}$  reduce operation,

$\text{Num}_{M_i}$  is the number of tasks in the  $i^{\text{th}}$  reduce operation, and  $k_{R_i}$  is the number of physical machines in the  $i^{\text{th}}$  reduce operation. In summary, for the  $i^{\text{th}}$  iteration process, the lower bound on the time delay required to complete its execution can be estimated by the following equation

$$T_i^{\max} = T_{M_-}^{\max} + T_{R_-}^{\max} + T_1. \quad (4)$$

For a big data analysis application with iteration  $I$ , the total completion time can be estimated by the following equation.

$$T^{\max} = \sum_{i=1}^I (T_{M_-}^{\max} + T_{R_-}^{\max}) + IT_1. \quad (5)$$

**3.4. Rural Tourism Information Ranking.** Let the length of all retrieval result lists be  $N$ . The rating of the  $i^{\text{th}}$  data in the list is  $(N - i + 1)$ , so the first data in the retrieval result list with the highest rating can be obtained as  $N$  and the last data with the lowest rating. Assuming that a data appears more times in different retrieval result lists, the rating of the data can be expressed as the sum of the rating values of each retrieval queue. Then, the data that appears in all of the multiple retrieval result lists has a higher rating than the one that appears individually. The total score is obtained by first scoring each retrieval result data, and then, the data appearing in different retrieval result queues are summed into a list and sorted according to the weight value from largest to smallest. Let  $MM$  be the amount of data in the longest retrieval return list. In this paper, the longest retrieval chain is  $NC$ , i.e.,  $M = MO$ . For the  $j$ -th retrieval result list, let the rating base

be  $W_j$ , and let the rating of the  $i^{\text{th}}$  data in the  $j$ -th column be  $W_j \cdot (MM - i + 1)$ . The relevance of the search term to its corresponding search category  $C$  and the amount of data in the retrieval queue will have an impact on the scoring base  $W_j$ . The retrieval queue scoring base  $W_j$  is shown as follows:

$$W_j = \text{rank}_C \cdot \sqrt{\text{sim}_C} \cdot \text{num}_C, \quad (6)$$

where assuming the best similarity between retrieval category  $C$  and retrieval keywords,  $\text{rank}_C$  is 1. In the second rank,  $\text{rank}_C$  is 0.5, and in the third rank,  $\text{rank}_C$  is 0.25.  $\text{sim}_C$  is  $\text{Sim}(q, c)$ , and  $\text{num}_C$  indicates the number of data in the retrieval list. If a retrieval result list is not summed by retrieval category,  $\text{rank}_C$  is 0.5 and  $\text{sim}_C$  is 0.1.

**3.5. Realize Off-site Disaster Recovery.** A new private cloud data center is built off-site, and public cloud services are rented to form a “hybrid cloud” architecture. At the same time, the local data center of the health Bureau is used as the disaster recovery center, which eventually forms a “hybrid cloud” based two-location, three-center architecture. The existing hardware and network resources are fully protected, and under the cloud environment of the new data center, the appropriate level of protection is provided for each level of business, and the colocation and off-site disaster recovery of business and data backup are completed. The core key services of the new private cloud data center are built in 1:1 mode, which can realize business-level disaster recovery, and when the main system fails, the backup system takes over the business without losing business data. In addition, in order to avoid the hidden danger of data loss caused by natural disasters, the local server room of the health Bureau is used as the disaster recovery center, and a flexible deployment backup strategy is adopted, so that when the private cloud data center fails, no data can be lost, storage level disaster recovery can be realized, and the local data center has the ability to quickly resume business. The hybrid cloud disaster recovery solution is shown in Figure 6.

## 4. Experiments and Results

**4.1. Dataset.** In order to verify the effectiveness of the algorithm proposed in this paper, cross-simulation tests are conducted. The user’s rural tourism retrieval records were all divided into 10 subsets, each with the same number of tourism retrieval records. The retrieval algorithm was repeated 10 times for each different subset of data, and 9 of them were used as the training set. For the training set, the matrix  $DT_{\text{train}}$  and matrix  $DC_{\text{train}}$  are built using the method proposed in this paper, and the matrix  $DT_{\text{test}}$  and matrix  $DC_{\text{test}}$  are built according to the test set. Once the individual retrieval feature matrix  $M$  is constructed, the relevance of the retrieval categories in the  $DT_{\text{test}}$  matrix and  $DC_{\text{test}}$  matrix to the retrieval keywords is obtained, and the relevance score is performed. The experiments are from a travel information website, and the statistical results are shown in Table 1.

**4.2. Experimental Results.** For each user’s retrieval, the algorithm feeds the user 3 categories with high relevance to the

retrieved term, and the following equation is used to score the relevance of the retrieved category to the retrieved keyword.

$$\text{Accuracy} = \frac{\sum_{C \in \text{top3}} \text{score}_{ci}}{n}, \quad (7)$$

$$\text{score}_{ci} = \frac{1}{1 + \text{rank}_{ci} - \text{ideal\_rank}_{ci}},$$

where  $n$  denotes the number of all retrieval categories related to the retrieved keywords,  $\text{score}_{ci}$  denotes the rating of the top three retrieval categories  $ci$  in terms of relevance,  $\text{rank}_{ci}$  denotes the ranking of retrieval categories  $ci$ , and  $\text{ideal\_rank}_{ci}$  denotes the highest ranking that retrieval categories  $ci$  may receive. The feature matrix simulation experiments use the Rocchio algorithm and the Im-Rocchio algorithm proposed in this paper to calculate the user retrieval feature matrix  $M$ , respectively, and then, use the user retrieval feature matching algorithm to perform category matching and calculate the matching accuracy. From the results in Table 2, we can see that the average retrieval accuracy of the Im-Rocchio algorithm proposed in this paper is higher than that of the standard Rocchio algorithm.

Feature matching simulation experiments are first conducted using the experimental dataset to compare user retrieval feature matching, generic retrieval feature matching, and 3 kinds of mixed feature threshold extraction matching, and the average accuracy of retrieval results is counted, as shown in Table 3. From the results in Table 3, we can see that the precision of the three-hybrid feature threshold extraction matching algorithms is not much different, but all of them are more precise than the user retrieval feature matching and universal retrieval feature matching, so the hybrid feature threshold extraction matching algorithm is better than the other algorithms. In addition, user retrieval feature matching is better than generic retrieval feature matching. To further validate the performance of the algorithm, the hybrid feature threshold extraction matching algorithm is considered and the training set is gradually increased. The above experiments show that when the data training set is small, the user retrieval feature matching algorithm is less accurate than the general-purpose retrieval matching algorithm. Even when the training set is small, the hybrid feature threshold extraction matching algorithm still achieves better results. When the training set is gradually increased, the accuracy of both the user retrieval feature matching strategy and the hybrid feature threshold extraction matching strategy increases.

**4.3. Hybrid Cloud Performance Testing.** In this experiment, the size of the input data volume used is 20 GB, and the size of the data volume processed by each mapping processor varies randomly, which equates to the number of mapping processors varying randomly. As a result, the following is the data sample creation process utilized to construct the random forest algorithm: First, HDFS is installed on three virtual machines in the internal virtual cloud and configured to generate data blocks using TestDFSIO. After the initial

data is written, the HDFS deployed on the internal private cloud VMs can be further extended and deployed to the external public cloud VMs; second, during the load balancing phase, another TestDFSIO program is made to start at the same time. At the same time, at least one copy of each data block stored internally during the load balancing phase is moved to the externally deployed VMs. During the experimental run, the amount of data migrated to the external public cloud in the load balancing phase is recorded, thus forming a data sample containing different VM configuration scenarios and the performance of the corresponding algorithms. The proposed steps are then applied to construct a random forest. Denote the configuration scheme with  $N$  virtual machines deployed on the internal private cloud and  $M$  virtual machines deployed on the external public cloud as  $N$ -on- $M$ -off. Let  $M = 0$  denote the traditional single cloud storage scheme in the benchmark case, existing methods as a comparison, and  $M > 0$  denote the proposed hybrid cloud storage scenario. The TestDFSIO experiments in the baseline and hybrid configuration scenarios are repeatedly executed 10 times, and these results are computed for the parameter  $\beta$ . Table 4 gives the correspondence between the data transfer time and the load balancing time under the indicated partial configuration scenarios. Among them are configuration 1: 3-on-0-off; configuration 2: 3-on-3-off; configuration 3: 3-on-6-off; and configuration 4: 3-on-9-off. It can be seen that the hybrid cloud model, where the rack-aware policy-based data migration storage and load balancing significantly take up physical overhead, reduces concurrent read throughput, and the load balancing overhead time rises by more than 40.5 percent compared to the single cloud model.

## 5. Conclusion

The importance of rural tourism to rural revitalization is largely due to its high industrial correlation feature, which relates to transportation, accommodation, medical care, entertainment, catering, and a series of other supporting industries. Hybrid cloud platform has obvious technical and economic advantages because it combines the advantages of private cloud security and reliability and public cloud computing power. However, running intensive data businesses such as big data analytics under the hybrid cloud framework is still in its infancy, and there are difficulties in mismatching the underlying data storage with advanced applications and inaccurate application execution time prediction. The cloud platform is a new type of sharing infrastructure that employs cloud computing technology to gather a huge number of online resources and manages them automatically with software. The hybrid cloud-based integrated system of information services for rural tourism in smart scenic areas designed in this paper can use the hybrid cloud platform to get a large number of available resources in rural tourism and use software to manage them automatically. The test of this paper shows that the platform shares a relatively large number of resources and has comprehensive contents to meet the needs of users, and the rural tourism

resources have good sharing application effects, which can improve the economic benefits of rural tourism.

## Data Availability

The datasets used during the current study are available from the corresponding author on reasonable request.

## Conflicts of Interest

The authors declare that they have no conflict of interest.

## Acknowledgments

This work was sponsored in part by the Research on the Spatial Layout and Coordinated Development of Urban Tourism Industry in Liaoning Province (L21BGL015).

## References

- [1] J. Li, Z. Zhou, J. Wu et al., "Decentralized on-demand energy supply for blockchain in Internet of Things: a microgrids approach," *IEEE transactions on computational social systems*, vol. 6, no. 6, pp. 1395–1406, 2019.
- [2] D. Jiang, F. Wang, Z. Lv et al., "QoE-aware efficient content distribution scheme for satellite-terrestrial networks," *IEEE Transactions on Mobile Computing*, p. 1, 2021.
- [3] R. H. Tsaih and C. C. Hsu, "Artificial intelligence in smart tourism: a conceptual framework," *Artificial Intelligence*, vol. 2, 2018.
- [4] Y. Zhao, Y. Han, and Y. Wang, "How to establish the wisdom of rural tourism based on "Internet+": taking coastal areas in Shandong province for example," *Journal of Coastal Research*, vol. 103, no. sp1, pp. 1047–1050, 2020.
- [5] U. Gretzel and C. Koo, "Smart tourism cities: a duality of place where technology supports the convergence of touristic and residential experiences," *Asia Pacific Journal of Tourism Research*, vol. 26, no. 4, pp. 352–364, 2021.
- [6] A. E. Arenas, J. M. Goh, and A. Urueña, "How does IT affect design centrality approaches: evidence from Spain's smart tourism ecosystem," *International Journal of Information Management*, vol. 45, pp. 149–162, 2019.
- [7] R. Hassannia, A. Vatankeh Barenji, Z. Li, and H. Alipour, "Web-based recommendation system for smart tourism: multi-agent technology," *Sustainability*, vol. 11, no. 2, p. 323, 2019.
- [8] L. P. M. da Costa, E. Alén-González, and L. D. F. V. de Azevedo, "Digital technology in a smart tourist destination: the case of Porto," *Journal of Urban Technology*, vol. 25, no. 1, pp. 75–97, 2018.
- [9] A. Mandić and D. G. Praničević, "Progress on the role of ICTs in establishing destination appeal: implications for smart tourism destination development," *Journal of Hospitality and Tourism Technology*, vol. 10, no. 4, pp. 791–813, 2019.
- [10] I. S. Tukhliev and A. N. Muhamadiyev, "Smart-tourism experience in geo information systems," *Theoretical & Applied Science*, vol. 72, no. 4, pp. 501–504, 2019.
- [11] G. Baralla, A. Pinna, R. Tonelli, M. Marchesi, and S. Ibaa, "Ensuring transparency and traceability of food local products: a blockchain application to a smart tourism region," *Concurrency and Computation: Practice and Experience*, vol. 33, no. 1, article e5857, 2021.

## Retraction

# Retracted: Application Effect Analysis of Clinical Nursing Pathway in the Care of Neonatal Hypoxic-Ischemic Encephalopathy

### Computational and Mathematical Methods in Medicine

Received 25 July 2023; Accepted 25 July 2023; Published 26 July 2023

Copyright © 2023 Computational and Mathematical Methods in Medicine. This is an open access article distributed under the Creative Commons Attribution License, which permits unrestricted use, distribution, and reproduction in any medium, provided the original work is properly cited.

This article has been retracted by Hindawi following an investigation undertaken by the publisher [1]. This investigation has uncovered evidence of one or more of the following indicators of systematic manipulation of the publication process:

- (1) Discrepancies in scope
- (2) Discrepancies in the description of the research reported
- (3) Discrepancies between the availability of data and the research described
- (4) Inappropriate citations
- (5) Incoherent, meaningless and/or irrelevant content included in the article
- (6) Peer-review manipulation

The presence of these indicators undermines our confidence in the integrity of the article's content and we cannot, therefore, vouch for its reliability. Please note that this notice is intended solely to alert readers that the content of this article is unreliable. We have not investigated whether authors were aware of or involved in the systematic manipulation of the publication process.

Wiley and Hindawi regrets that the usual quality checks did not identify these issues before publication and have since put additional measures in place to safeguard research integrity.

We wish to credit our own Research Integrity and Research Publishing teams and anonymous and named external researchers and research integrity experts for contributing to this investigation.

The corresponding author, as the representative of all authors, has been given the opportunity to register their agreement or disagreement to this retraction. We have kept a record of any response received.

### References

- [1] X. Zhang and H. Wang, "Application Effect Analysis of Clinical Nursing Pathway in the Care of Neonatal Hypoxic-Ischemic Encephalopathy," *Computational and Mathematical Methods in Medicine*, vol. 2022, Article ID 9379361, 6 pages, 2022.



## Research Article

# Application Effect Analysis of Clinical Nursing Pathway in the Care of Neonatal Hypoxic-Ischemic Encephalopathy

Xiaoyu Zhang and Hai Wang 

Department of Obstetrics, The First Affiliated Hospital of Heilongjiang University of Chinese Medicine, Harbin, 150040 Heilongjiang, China

Correspondence should be addressed to Hai Wang; wanghai576@163.com

Received 6 April 2022; Revised 12 May 2022; Accepted 16 May 2022; Published 16 June 2022

Academic Editor: Naeem Jan

Copyright © 2022 Xiaoyu Zhang and Hai Wang. This is an open access article distributed under the Creative Commons Attribution License, which permits unrestricted use, distribution, and reproduction in any medium, provided the original work is properly cited.

This research focuses on the effectiveness of the clinical nursing pathway (CNP) in the treatment of infant hypoxic-ischemic encephalopathy (NHIE). This research enrolled 120 cases of NHIE admitted to the First Affiliated Hospital of Heilongjiang University of Chinese Medicine, including 70 cases (research group, the Res) who received CNP intervention and 50 cases (control group, the Con) treated by routine nursing pathway intervention. The psychomotor development index (PDI), mental development index (MDI), neurodevelopment (ND), physique growth, and incidence of adverse events (AEs) were recorded and analyzed. The results identified that in comparison with the Con (1) the PDI and MDI were obviously better in the Res 6 months postintervention; (2) the Res had significantly superior ND of behavioral capacity, passive tone, active tone, primitive reflex, and general assessment 1 month after intervention, as well as physical development of body weight, height, and head circumference after 40 days of birth, (3) the incidence of total AEs within 40 days was statistically lower in the Res. As a result, CNP is considerably superior to the traditional nursing pathway in the treatment of NHIE, and it merits clinical promotion.

## 1. Introduction

Birth asphyxia is the most common risk factor for early neonatal death, followed by premature delivery, low birth weight, and infection [1]. The exploration of the pathological mechanism of neonatal asphyxia found that hypoxia and ischemia can make the nutrition and energy supply of the neonatal brain abnormal, which in turn leads to neuronal cell death, cell dysfunction, and neurodevelopmental defects [2]. Neonatal hypoxic-ischemic encephalopathy (NHIE) is one of the serious complications of perinatal asphyxia, and its etiology is related to impair ND [3]. According to statistics, about a quarter of NHIE cases will die during the neonatal period, and another quarter may develop long-term sequelae such as cerebral palsy, epilepsy, and sensory disturbance, which seriously compromise the healthy growth of children's body and mind [4]. Choosing appropriate and effective treatment methods is crucial to improve the prognosis of NHIE children, and the postnatal care of neonates with hypoxic-ischemic encephalopathy (HIE) is also critical

[5, 6]. Accordingly, we herein discuss the application effect of nursing intervention for NHIE, aiming at providing clinical reference for improving the neurological and physical development of HIE children, which is of positive significance for improving the prognosis of such neonates.

As far as the healthy development of families and even the country is concerned, improving the survival rate and long-term neurodevelopmental outcome of children with HIE has huge implications [7]. At present, routine nursing mainly focuses on targeted treatment or nutritional support, which has no significant effect on improving neither the ND nor the long-term ND outcome of HIE children [8]. The clinical nursing pathway (CNP) is mainly aimed at helping children with HIE improve their ND by providing the children's family members with disease introduction, oxygen guidance, and rehabilitation direction and giving sensory stimulation training to children during their hospitalization [9]. CNP is currently widely utilized in a variety of conditions, including advanced schistosomiasis ascites, acute bronchial asthma, and acute cerebral hemorrhage, with the

benefits of lower mortality, less adverse reactions, and faster resolution of clinical symptoms and indications [10–12]. In addition, CNP has been proved to facilitate neurological recovery and improve the curative effect and prognosis of childhood diseases (e.g., nephropathy) [13, 14]. We believe that CNP is effective and has positive significance for the ND and physique growth of HIE children. We hereby compare the application effect of CNP with routine nursing in the care of NHIE and report it.

This study is unique in that it examines the effectiveness and dependability of CNP in the care of NHIE from a variety of viewpoints, including PDI, MDI, ND, physical growth, and safety, providing fresh insights into nursing techniques for NHIE. There are various limitations to this study that will need to be addressed in future research.

## 2. Data and Methods

**2.1. General Data.** This research enrolled 120 cases of NHIE treated in the First Affiliated Hospital of Heilongjiang University of Chinese Medicine between December 2017 and December 2020 and assigned them into a research group (the Res,  $n = 70$ ) receiving CNP intervention and a control group (the Con,  $n = 50$ ) treated by routine nursing pathway intervention. The male-to-female ratio and the mean gestational age in the Res were 32:38 and  $39.17 \pm 2.89$  years, respectively, while in the Con they were 22:28 and  $39.43 \pm 2.73$  years, respectively. Inclusion criteria: diagnosis of HIE; no placenta residue during delivery; neonatal birth weight: 3-5 kg; voluntary participation of the neonate's family members, with the consent form provided; no maternal genetic diseases that can pass on to the baby. Exclusion criteria: severe multiple organ dysfunction, hematopathy or infectious diseases, neurologic disorders, other congenital diseases, and incomplete clinical data. This research was ethically ratified by the First Affiliated Hospital of Heilongjiang University of Chinese Medicine.

**2.2. Nursing Methods.** A standard nursing pathway intervention was given to the Con. Nurses treated hypoglycemia, hypotension, and acidosis; administered oxygen; and cleansed the respiratory secretions of infants on a regular basis to maintain the respiratory tract clear. Anti-infection treatment or nutritional support was given according to the presence of infection and malnutrition. Nursing staff also attached special importance to the mental state, vital signs, and skin color of neonates.

**2.2.1. CNP Was Implemented in the Res in addition to Routine Nursing.** (1) On the first day of admission, the neonates' families were introduced to the environmental function of the ward, the relevant matters that doctors and nurses were responsible for, and the work schedule and safety system. Besides, health education, etiology, and clinical symptoms of HIE as well as matters needing attention during hospitalization were disseminated to the neonates' families. (2) On the second day of admission, related knowledge of oxygen use was introduced to the neonates' families, and guidance was given to them so that they could under-

stand the knowledge of oxygen inhalation and the appropriate way of oxygen supply. Family members were also told to remove respiratory secretions as soon as possible to keep the respiratory tract clear and avoid suffocation while sleeping. (3) On day 3 after admission, some children with high fever were treated with mild hypothermia, and health education and publicity were given to the families of such children so that the families could have a certain understanding of the precautions when the children were cooled down and maintained. (4) On the fourth day of admission, children's sensory stimulation was strengthened for passive gymnastics training. (5) On day 5 after admission, family members were instructed in rehabilitation training, as early motor and perception training is helpful to promote the recovery of brain function. By patiently answering the illness of the newborns to the families, the nursing staff gained the trust and understanding of family members. In addition, parents were instructed to master the rehabilitation training measures during the convalescence period, so as to obtain parental cooperation and enhance their compliance with the regular follow-up.

### 2.3. Endpoints

**2.3.1. Mental Development Index (PDI) and Mental Development Index (MDI) [15].** The scores of these two indicators are above 120 points for excellent, 110-119 points for upper-middle intelligence, 90-109 points for moderate intelligence, 80-89 points for middle-lower points, 70-79 points for critical state, and below 69 points for mental retardation.

**2.3.2. ND.** The neonates were scored for their neurodevelopmental status using the Neonatal Behavioral Neurological Assessment (NBNA) [16] from the aspects of behavior, passive tone, active tone, primitive reflex, and general assessment. The score was proportional to the ND of children.

**2.3.3. Physique Growth.** It was evaluated by measuring the weight gain, height gain, and head circumference growth of children.

**2.3.4. Incidence of Adverse Events (AEs).** The cases of anemia, emaciation, malnutrition, growth retardation, cough and vomiting, hypotension, intracranial hypertension, and other AEs were observed and recorded.

**2.4. Statistical Processing.** The software used for data analysis and image description was SPSS v23.0 and GraphPad Prism v8.0, respectively. For counting data described in the form of number of cases/percentages ( $n(\%)$ ), either the chi-square test or the chi-square test with continuity correction (applied when the theoretical frequency in the chi-square test was less than 5) was used for intragroup comparisons. Mean  $\pm$  standard deviation (SD) was used to represent the measurement data, and the statistical methods for intergroup and intragroup (before and after treatment) comparisons were independent samples  $t$ -test and paired  $t$ -test, respectively.  $P < 0.05$  is regarded as the difference with statistical significance.

TABLE 1: Baseline data of patients in the two groups ( $n(\%)$ , mean  $\pm$  SD).

Variables	$n$	Control group ( $n = 50$ )	Research group ( $n = 70$ )	$\chi^2/t$	$P$
Gender				0.035	0.85
Male	54	22 (44.00)	32 (45.71)		
Female	66	28 (56.00)	38 (54.29)		
Gestational age (weeks)	120	39.43 $\pm$ 2.73	39.17 $\pm$ 2.89	0.504	0.62
Head circumference (cm)	120	33.90 $\pm$ 3.16	33.54 $\pm$ 3.21	0.610	0.54
Weight (kg)	120	3.41 $\pm$ 0.45	3.36 $\pm$ 0.42	0.624	0.53
Natural delivery				0.403	0.52
Yes	37	17 (34.00)	20 (28.57)		
No	83	33 (66.00)	50 (71.43)		
Symptoms				0.040	0.98
Seizures or hyperexcitability	35	15 (30.00)	20 (28.57)		
Lethargy	54	22 (44.00)	32 (45.71)		
Indifference or coma	31	13 (26.00)	18 (25.72)		

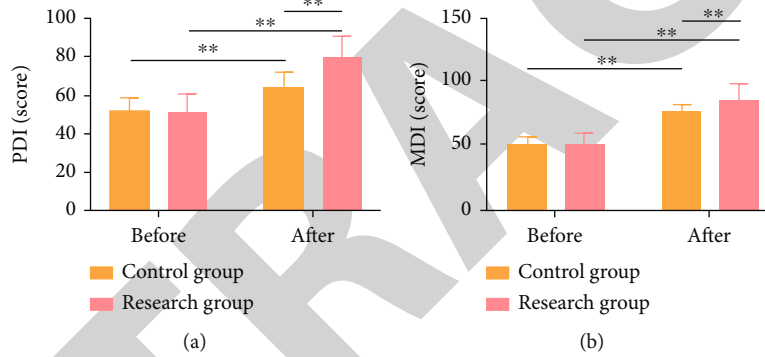


FIGURE 1: PDI and MDI of two groups of patients. (a) Comparative analysis of PDI between two groups of patients. (b) Comparative analysis of MDI between two groups of patients. Note:  $**P < 0.01$ .

### 3. Results

3.1. *General Data.* The two cohorts of patients were comparable in age, gestational age, head circumference, weight, natural delivery, and symptoms ( $P > 0.05$ ) (Table 1).

3.2. *Comparative Analysis of PDI and MDI between Two Groups of Patients.* We evaluated the psychomotor development (PMD) and intelligence development of the two groups of patients by PDI and MDI, respectively. The data showed no evident difference in PDI and MDI between groups before nursing ( $P > 0.05$ ) and notably elevated parameters after nursing, especially in the Res, with statistical significance ( $P < 0.05$ ) (Figure 1).

3.3. *ND of Two Groups of Patients.* We analyzed neonates' ND with the NBNA scale. The data identified significantly enhanced behavioral capacity, passive tone, active tone, primitive reflex, and general assessment in both groups after nursing; moreover, in comparison with the Con, the five indexes were higher in the Res at 2 weeks and 1 month of birth, with statistical significance ( $P < 0.05$ ) (Figure 2).

3.4. *Physique Growth of Two Groups of Patients.* We evaluate the physique growth of newborns through three indicators: weight gain, height gain, and head circumference growth. The Res had much higher weight gain, height rise, and head circumference growth than the Con, with statistical significance ( $P < 0.05$ ) (Figure 3).

3.5. *Incidence of AEs in Two Groups.* We observed and compared the incidence of AEs to evaluate the influence of different nursing intervention methods on AEs. The results identified a markedly lower incidence of AEs in the Res versus the Con (8.58% vs. 32.00%,  $P < 0.05$ ) (Table 2).

### 4. Discussion

HIE is a brain dysfunction related to oxygenation and blood flow insufficiency [17]. Our research has confirmed that CNP has a good application effect in the care of NHIE, which can significantly promote the PMD, intelligence development, ND, and physique growth of HIE children with a favorable safety profile.

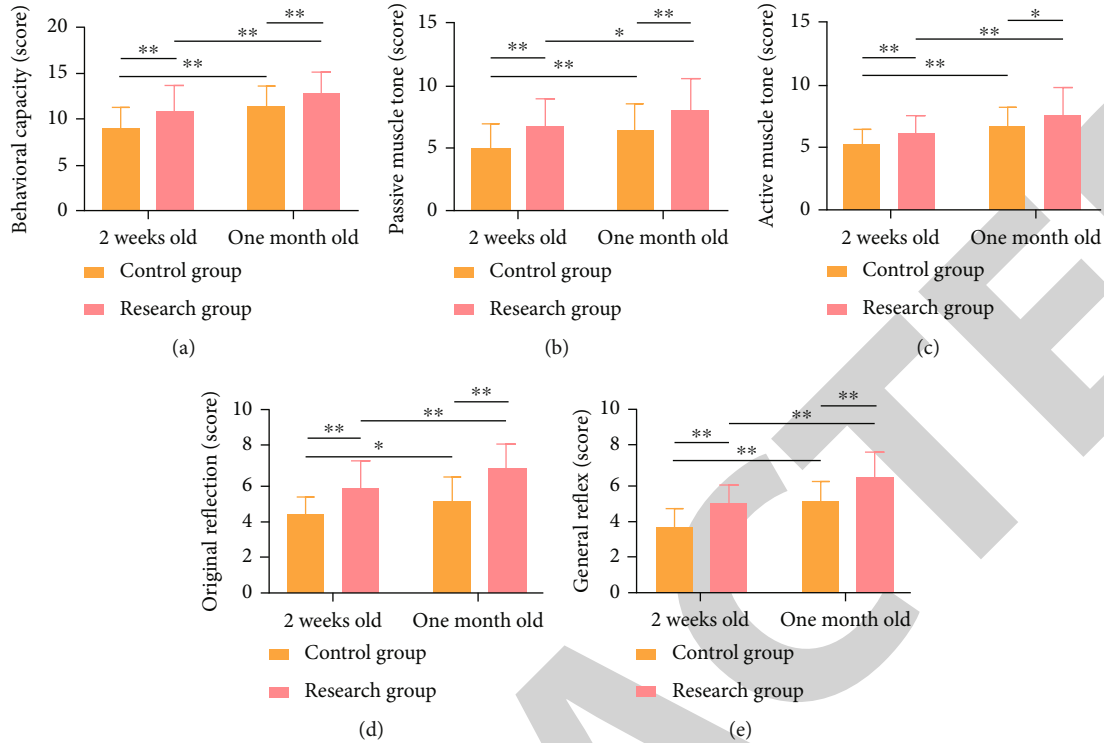


FIGURE 2: Neurodevelopment of two groups of patients. (a) Behavioral capacity of two groups of patients at 2 weeks and 1 month of birth. (b) Passive muscle tone of two groups of patients at 2 weeks of birth and 1 month of birth. (c) Active muscle tone of two groups of patients at 2 weeks and 1 month of birth. (d) The primitive reflex of two groups of patients at 2 weeks and 1 month of birth. (e) The general reflex of two groups of patients at 2 weeks and 1 month of birth. Note: \* $P < 0.05$ ; \*\* $P < 0.01$ .

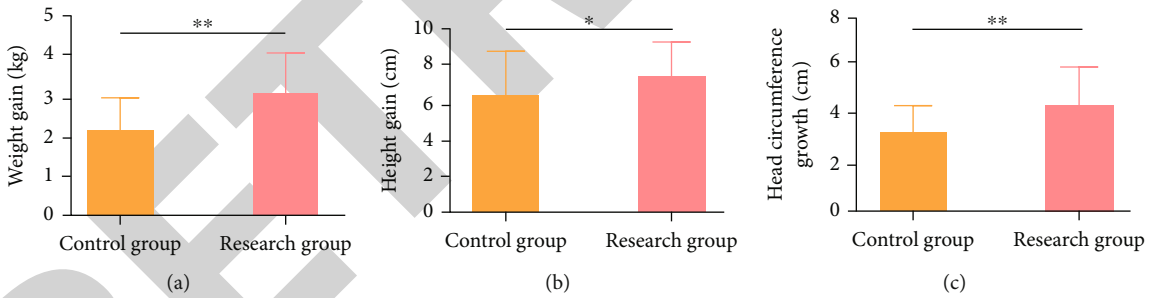


FIGURE 3: Physique growth of patients in two groups. (a) Weight gain of neonates in the two groups after 40 days of birth. (b) Height gain of neonates in the two groups after 40 days of birth. (c) Head circumference growth of neonates in the two groups after 40 days of birth. Note: \*\* $P < 0.01$ .

TABLE 2: Incidence of adverse events in two groups of patients ( $n(\%)$ ).

Categories	Control group ( $n = 50$ )	Research group ( $n = 70$ )	$\chi^2$ value	$P$ value
Anemia	2 (4.00)	1 (1.43)	—	—
Emaciation	3 (6.00)	1 (1.43)	—	—
Malnutrition	4 (8.00)	1 (1.43)	—	—
Growth retardation	3 (6.00)	2 (2.86)	—	—
Cough and vomiting	1 (2.00)	0 (0.00)	—	—
Hypotension	2 (4.00)	0 (0.00)	—	—
Intracranial hypertension	1 (2.00)	1 (1.43)	—	—
Total	16 (32.00)	6 (8.58)	10.693	0.001

Traditional nursing intervention has been shown to have several limitations, as the nursing procedure's basic thought cannot fully adjust to illness development or address patients' main clinical demands [18]. CNP, on the other hand, is a modern nursing model that emphasizes postadmission cognition, treatment, and rehabilitation guidance for hospitalized patients; it requires nurses to have professional knowledge reserves, and it meets the needs of patients by formulating reasonable and predictable nursing programmes [19]. In our study, the children who received routine nursing pathway were set as the Con, and those who received CNP were taken as the Res. The research data showed significantly elevated PDI and MDI scores in the Res after nursing, which was statistically higher than the Con, indicating that the CNP can significantly improve the PMD and intellectual development of patients. In terms of ND, the behavioral capacity, passive tone, active tone, primitive reflex, and general assessment in the Res were statistically better than those before treatment and the Con after nursing, suggesting that the CNP has significant positive significance for the ND of HIE children. Physically, more evident weight gain, height gain, and head circumference growth were observed in the Res, demonstrating that CNP is helpful to promote the physique growth of children with HIE. CNP's intervention in children's movement and perception training, as well as the guidance of rehabilitation training for children's family members, is credited with increasing children's nerve, intelligence, and motor development [20]. Finally, we assessed the safety of neonates in both groups and discovered that they were mostly malnourished, growth retarded, and emaciated. In addition, the Res had a significantly decreased overall incidence of AEs, implying that the CNP provides some assurance of postpartum child safety.

## 5. Conclusion

The novelty of this study lies in the analysis of the effectiveness and reliability of CNP in the care of NHIE from multiple perspectives of PDI, MDI, ND, physique growth, safety, etc., which provides new insights for the choice of nursing strategies for NHIE. This study also has several limitations, which need to be gradually addressed in future research. First, given the limited cases included, it is necessary to increase the sample size to improve the accuracy and universality of the research results. Second, there is no long-term follow-up. Supplementary examination of this feature can be used to assess children's long-term neurodevelopmental outcomes, which can help to enhance their long-term prognosis. Third, if the analysis of risk factors affecting neurological development of HIE children can be increased; the nursing strategy can be further optimized.

Evidence from this study shows that while reducing the incidence of AEs, CNP is beneficial to improve the PMD, intellectual development, ND, and physique growth of children with HIE, which provides new cognition for the management of NHIE and helps to improve the prognosis of children.

## Data Availability

The simulation experiment data used to support the findings of this study are available from the corresponding author upon request.

## Conflicts of Interest

The authors declare no competing interests.

## Authors' Contributions

Xiaoyu Zhang was responsible for methodology, investigation, data curation, original draft, writing, review, and editing. Hai Wang was responsible for review and editing, idea, supervision, review, and editing.

## Acknowledgments

I would like to express my gratitude to all those helped me during the writing of this thesis. I acknowledge the help of my colleagues, Wang Hai. They have offered me suggestion in academic studies.

## References

- [1] B. Olack, N. Santos, M. Inziani et al., "Causes of preterm and low birth weight neonatal mortality in a rural community in Kenya: evidence from verbal and social autopsy," *BMC Pregnancy Childbirth*, vol. 21, no. 1, p. 536, 2021.
- [2] M. Koehn, X. Chen, F. Logsdon, P. Lim, and S. Stonestreet, "Novel neuroprotective agents to treat neonatal hypoxic-ischemic encephalopathy: inter-alpha inhibitor proteins," *International Journal of Molecular Sciences*, vol. 21, no. 23, p. 9193, 2020.
- [3] I. Bersani, F. Piersigilli, D. Gazzolo et al., "Heart rate variability as possible marker of brain damage in neonates with hypoxic ischemic encephalopathy: a systematic review," *European Journal of Pediatrics*, vol. 180, no. 5, pp. 1335–1345, 2021.
- [4] S. Dumbuya, L. Chen, Y. Wu, and B. Wang, "The role of G-CSF neuroprotective effects in neonatal hypoxic-ischemic encephalopathy (HIE): current status," *Journal of Neuroinflammation*, vol. 18, no. 1, p. 55, 2021.
- [5] A. Kane, G. Vezina, T. Chang et al., "Early versus late brain magnetic resonance imaging after neonatal hypoxic ischemic encephalopathy treated with therapeutic hypothermia," *J Pediatr.*, vol. 232, pp. 73–79.e2, 2021.
- [6] J. Cooper, "Induced hypothermia for neonatal hypoxic-ischemic encephalopathy: pathophysiology, current treatment, and nursing considerations," *Neonatal Network*, vol. 30, no. 1, pp. 29–35, 2011.
- [7] Z. Wang, P. Zhang, W. Zhou et al., "Neonatal hypoxic-ischemic encephalopathy diagnosis and treatment: a national survey in China," *BMC Pediatrics*, vol. 21, no. 1, p. 261, 2021.
- [8] R. Synnes, J. Petrie, E. Grunau et al., "Canadian Neonatal Follow-Up Network Investigators. Family integrated care: very preterm neurodevelopmental outcomes at 18 months," *Archives of Disease in Childhood - Fetal and Neonatal Edition*, vol. 107, no. 1, pp. 76–81, 2022.
- [9] W. Li, J. Gao, S. Wei, and D. Wang, "Application values of clinical nursing pathway in patients with acute cerebral

## Retraction

# Retracted: Contemporary Value Assessment of Marxist Ideology under the Context of Deep Learning

### Computational and Mathematical Methods in Medicine

Received 1 August 2023; Accepted 1 August 2023; Published 2 August 2023

Copyright © 2023 Computational and Mathematical Methods in Medicine. This is an open access article distributed under the Creative Commons Attribution License, which permits unrestricted use, distribution, and reproduction in any medium, provided the original work is properly cited.

This article has been retracted by Hindawi following an investigation undertaken by the publisher [1]. This investigation has uncovered evidence of one or more of the following indicators of systematic manipulation of the publication process:

- (1) Discrepancies in scope
- (2) Discrepancies in the description of the research reported
- (3) Discrepancies between the availability of data and the research described
- (4) Inappropriate citations
- (5) Incoherent, meaningless and/or irrelevant content included in the article
- (6) Peer-review manipulation

The presence of these indicators undermines our confidence in the integrity of the article's content and we cannot, therefore, vouch for its reliability. Please note that this notice is intended solely to alert readers that the content of this article is unreliable. We have not investigated whether authors were aware of or involved in the systematic manipulation of the publication process.

Wiley and Hindawi regrets that the usual quality checks did not identify these issues before publication and have since put additional measures in place to safeguard research integrity.

We wish to credit our own Research Integrity and Research Publishing teams and anonymous and named external researchers and research integrity experts for contributing to this investigation.

The corresponding author, as the representative of all authors, has been given the opportunity to register their agreement or disagreement to this retraction. We have kept a record of any response received.

### References

- [1] J. Sun, "Contemporary Value Assessment of Marxist Ideology under the Context of Deep Learning," *Computational and Mathematical Methods in Medicine*, vol. 2022, Article ID 4654153, 10 pages, 2022.

## Research Article

# Contemporary Value Assessment of Marxist Ideology under the Context of Deep Learning

Jian Sun <sup>1,2</sup>

<sup>1</sup>School of Marxism, Nanjing University of Aeronautics and Astronautics, Nanjing Jiangsu 211170, China

<sup>2</sup>School of Marxism, Jiangsu Maritime Institute, Nanjing Jiangsu 211170, China

Correspondence should be addressed to Jian Sun; 20060034@jmi.edu.cn

Received 19 April 2022; Revised 12 May 2022; Accepted 18 May 2022; Published 15 June 2022

Academic Editor: Naeem Jan

Copyright © 2022 Jian Sun. This is an open access article distributed under the Creative Commons Attribution License, which permits unrestricted use, distribution, and reproduction in any medium, provided the original work is properly cited.

As a conceptual superstructure, ideology plays a very important role in national security, social stability, and healthy economic development. As a result, ideological work is critical to the Party's success, and the current focus of ideological work is to increase ideological risk prevention. The focus of ideological risk avoidance is gradually shifting to cyberspace as the Internet becomes the primary arena and forum for information interchange, value dissemination, and ideological exchanges. Deep learning, as a data processing technology, is characterized by deep data analysis and full generalization and can have an impact on ideological security work: on the one hand, it helps work subjects evaluate and count the process and effect of work in order to grasp the trend of public opinion; on the other hand, it helps work subjects understand and reflect on the inner logic and contemporary value of Marxist theory through diversified work platforms and diverse work methods and promotes work subjects' understanding of Marxist theory. On the other hand, through diversified working platforms and various working methods, we help the working targets to understand and reflect on the inner logic and contemporary values of Marxist theory and promote their true identification with socialist core values. Based on the impact of deep learning on work subjects and work objects, this paper proposes that Marxian ideological security workers can use it to effectively achieve good communication and contemporary value assessment among different work subjects, set specific indicators according to the division of labour, adopt different working methods according to the groups to which the learning objects belong, and establish a long-term evaluation mechanism in the process.

## 1. Introduction

Along with the accelerated pace of reform and opening, China's economic construction has grown rapidly, and the rapidly changing science and technology has continued to promote economic globalization, and various products from the west have flocked to China [1–3]. In the process of cultural globalization, different national cultures, which are the crystallization of the wisdom of the working people, intermingle and collide with each other. On the one hand, through the continuous exchange and integration of international and local Chinese cultures, we have been able to learn from and appreciate the excellent cultures of different nationalities. On the other hand, the continuous integration of foreign cultures challenges the traditional Chinese culture and has a great impact on the mainstream ideology of China, and various

western cultural ideologies impact the ideological consciousness of contemporary college students and affect their ideals and beliefs [2]. Vices such as greed for pleasure and obsession with online games seriously affect the normal study of college students and their desire to pursue ideals and benefit mankind. In today's era, in the face of the great adjustment and change of the world pattern, the frequent intermingling of various ideologies and cultures, and the rise of China, many developed countries are anxious in the international arena, and in the international arena, the western hostile forces are using all available forms to constantly infiltrate and invade China culturally and develop various cultural communication channels to spread their "free thinking" and "hedonism." They are trying to assimilate China ideologically and culturally by developing various cultural channels of communication and spreading their "free thinking" and "hedonism," and by

propagating their ideology. In China, with the rise of the market economy and the infiltration of western culture, the development of the Chinese cultural market has lagged and is relatively imperfect [4, 5].

Many young people have become confused about Chinese culture and lack self-confidence in their own outstanding culture, and at the same time, they have become skeptical of the core values of socialism with Chinese characteristics. Some college students are eager to learn about western culture and western festivals and worship everything in the west blindly. Culture carries the future destiny of the nation, and a country and a nation need strong cultural confidence if they want to be invincible in the forest of the world's nations. Cultural confidence is the correct examination and application of the history of the Chinese nation and is the cornerstone of national self-confidence, which must be nurtured in the practice of socialism with Chinese characteristics in the new era. By practicing cultural self-confidence, we can realize the grand blueprint of building a strong cultural nation [6, 7]. The logic of contemporary changes calls for great theories, and great theories keep advancing the emergence of practice. Under the increasingly fierce international competitive environment, studying the cultural self-confidence of college students is an inevitable requirement for realizing a strong cultural nation with Chinese characteristics. Only in this way can the nation have faith, the people have hope, and the country have strength.

The media industry, communication ecology, and public opinion environment are changing as a result of the iterative development of visual media and the rapid emergence of visual communication, and Internet users' "visual survival" is quietly affecting their cognitive habits and cognitive choices and, even to a degree, their intrinsic value judgment of information [8–10]. The Marxist materialistic dialectic emphasizes that things always have two sides, and it is necessary to grasp them comprehensively from both positive and negative aspects. Therefore, while we are happy to see a wide range of visual landscapes to enrich the online life of Internet users, we must also be aware that many visual information, although superficially no different from other information, contains elements of wrong social trends and antimainstream ideology and implies the realistic purpose of anti-Marxism, and the explosive and fissionable spread of such information is bound to cause ideological erosion to Internet users, leading to a continuous decline in the value of the majority of Internet users. The explosion and fission of this kind of information are destined to produce ideological erosion among netizens, resulting in a steady reduction in the value of most netizens and even a misguided ideological shift. In such circumstances, Internet ideology, as a conceptual superstructure built on an economic foundation, is today facing the hazards of metaphorization [10], fragmentation, and panentertainment, all of which are affecting and contesting mainstream ideology's dominance. Figure 1 shows the meaning of Marxist philosophy.

Internet users are no longer limited to getting information through old monotonous text media but are increasingly using innovative and dynamic visual media such as photographs and videos, thanks to the iterative updating of

mobile information technology. Visual media has arguably become the primary source of information for Internet users [11]. The rise of visual media in cyberspace has not only brought richer and more shocking online life experience for Internet users but also brought new impact and risk to network ideology, which to a certain extent affects the Party's dominance, initiative, and right to speak in network ideology work. The transmutation of the network communication pattern and netizens' access to information requires us to actively explore the use of new technological means to empower ideological work and further enhance the relevance, scientific, and longevity of network ideological risk prevention. As a cutting-edge application of artificial intelligence in the field of vision, visual recognition has the unique ability to intelligently acquire, identify, analyze, and interpret images and video images and is expected to become an important focus point for the innovation of network ideological risk prevention means under the new situation and environment. Therefore, based on the perspective of Marxist theory discipline, this study is dedicated to exploring the important role and realization mechanism of introducing visual recognition in network ideological risk prevention, so as to provide innovative ideas, useful suggestions, and reference paths for the practice of risk prevention in the ideological field as far as possible.

The organizational paragraph is given below: Section 2 contains the related work. Section 3 reviews the methods of the proposed work. Section 4 described the experimental design and results. Finally, the paper ends with the conclusion in Section 5.

## 2. Related Work

*2.1. Marxist Ideology.* Numerous practices have proven that Marxism is a universally applicable reality since the May Fourth Movement and the dissemination of Marx to China. No matter in the war years or in the socialist construction in peacetime [12–14], Marxism has always been a guiding light for the Chinese revolution, and only under the guidance of Marxism can the Chinese revolution be invincible. In the cultivation of cultural self-confidence of college students, adhering to the Marxist view of culture has a double significance. Ideological assessment indicators are shown in Figure 2.

It enriches the theory of cultural self-confidence of college students. Adhering to the Marxist cultural outlook and exploring the cultivation path of cultural confidence of college students not only enrich the connotation of cultural confidence of college students but also expand the theoretical scope of the Marxist cultural outlook. Cultural self-confidence has been mentioned by national leaders many times. Extensive and in-depth discussion on the cultural self-confidence of college students and new initiatives to adapt to the growth of college students under the threshold of Marxist cultural outlook are of great significance to the expansion of the breadth and depth of cultural self-confidence of college students and to the process of advancing Marxist cultural theory, which is not only beneficial to the cultivation of cultural self-confidence of college students but enables also college students to clearly understand the



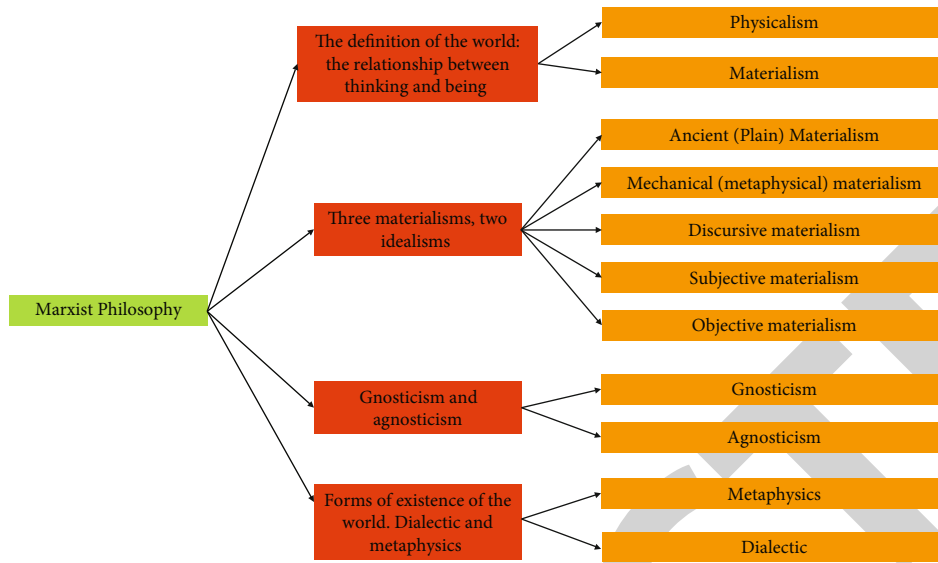


FIGURE 1: Marxist theory connotation.

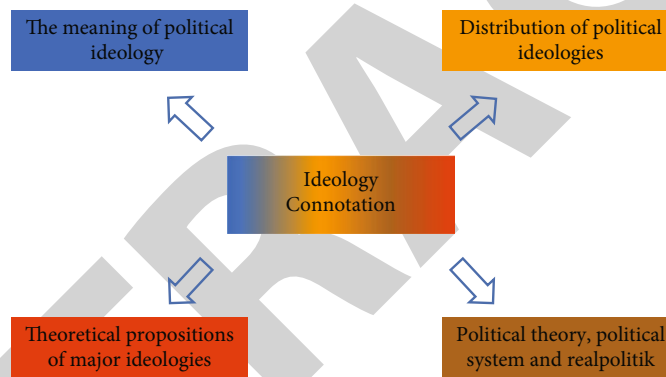


FIGURE 2: Ideological assessment indicators.

mainstream ideology of Chinese characteristics, which can stimulate the whole nation creativity and innovation of culture [14–16]. Second, it favors the advancement of ideological and political education disciplines in colleges and universities. Adhering to a Marxist view of culture and proposing countermeasures aimed at increasing college students’ cultural self-confidence can help to advance and improve college ideological education theory, provide a theoretical foundation for reforming college ideological education, and provide strategies for increasing college students’ cultural self-confidence. Adhering to the Marxist cultural view, the discussion on the cultivation of college students’ cultural self-confidence is conducive to improving the working methods and approaches of college political education, improving the level of college political education, consolidating the scientific research ability of college political education, and providing strong guarantee for the reform of college political education and the cultivation of talents, which can enhance the timeliness of college students’ political education in the new era and strengthen its teaching and education. It can enhance the timeliness of political education for college students in the new era and strengthen the

effectiveness of teaching and educating people [17–19]. Third, it demonstrates the profound effect of Marxist cultural perspectives. The discussion on topics connected to the road of nurturing cultural self-confidence among college students can strengthen the theory of Marxist cultural outlook and encourage the greater growth of advanced socialist culture, according to the Marxist cultural outlook. To cultivate the cultural self-confidence of college students, we have a deep cultural heritage and a strong base. The October Socialist Revolution in Russia promoted the progressive intellectuals in China to study and propagate Marxism, and the wide spread of Marxism in China laid the ideological foundation for the establishment of the Communist Party of China, and the Chinese Revolution has had a brand-new guiding ideology and direction since then. Marxist cultural theory is a classic reproduction of human cultural concepts. Starting from a materialistic historical view, it stands at the high point of human culture and reflects the characteristics of the times comprehensively and accurately, “caging heaven and earth within the form and thwarting all things in the brush,” gaining insight into the times, and meeting the light. Nowadays, under the new situation of promoting socialist

culture to a higher and deeper goal, adhering to the Marxist view of culture, further analyzing the confusion arising from the cultural self-confidence of college students, finding out where the problems lie, and proposing targeted cultivation programs not only manifest the profound practical logic and theoretical logic of Marxist cultural theory but also make rational thinking and theoretical responses to the cultivation of cultural self-confidence of college students, so that college students can continuously improve their cultural cultivation. It makes college students continuously improve their cultural cultivation [20].

It is conducive to the transmission of excellent Chinese culture. Guided by the Marxist view of culture, the study of cultural confidence of college students not only helps to inherit and carry forward the excellent Chinese traditional culture but also helps to forge a new splendor of Chinese culture and gives new vitality to the cultivation of enhancing cultural confidence of college students. As the times are changing and the society is changing, college students in the new era should adapt to the development of the times, bear in mind the origin and historical lineage of Chinese national culture, and make efforts to spread it. Only in this way can it be conducive to solving the problems of college students themselves and enhancing the timeliness of Civic Education, and only then can it be conducive to the enhancement of national cultural soft power and influence, strengthening the discourse of the Chinese nation in the international arena, enhancing the international status of the Chinese nation, and showing the style of a great nation for global peace. Second, it is conducive to the formation of a correct life orientation. Educators should appropriately guide college students to determine Marxism's ideology and the wonderful Chinese culture as their knowledge and absorb their comprehensive quality during the university time, which is the formation period of life outlook, world outlook, and values. They should supervise college students to perfect their overall value orientation, improve their cultural literacy, comprehensively strengthen the cultivation of their comprehensive quality, and promote their rational treatment of Chinese and western cultures. We should guide college students to correctly grasp the connotation of mainstream culture, to "look far ahead, be vigilant in peace, be brave in change, be brave in innovation, never be rigid, never be stagnant," so that under the guidance of Marxist cultural outlook [23], college students can strengthen their cultivation, correct their thinking, not be influenced by western nihilism and retrogressive, and, under the guidance of Marxist cultural outlook, be guided by a loud and clear voice. Under the guidance of the Marxist cultural concept, they will manifest the spiritual power of cultural confidence with a loud main theme and strong positive energy, so that Chinese culture will be more vigorous and vital.

*2.2. Deep Learning and Ideology.* Metaphor itself is simply a neutral linguistic method that can have both positive and negative effects. However, when metaphors are used in political topics, i.e., when political metaphors are created, they can pose ideological risks and threats. Before the era of visual communication, political metaphors mainly appeared in the

form of textual metaphors [16]. However, with the advent of the era of visual communication, a new type of political metaphor, visual metaphor, has emerged quietly, posing a new threat to online ideological security. Visual metaphors refer to the cultural behavior of using visual images such as pictures and videos to suggest people to perceive, imagine, and experience a viewpoint or value. Visual images may seem straightforward and simple, bringing a visual impact without conveying too much of a point of view or value, but they are not. Like words, visual images also can convey ideas and opinions and do so in a more subtle and flexible way. We should not underestimate the power of image cultures, especially dynamic ones, to influence emotions through images and thus to have a significant impact on systems of representation and value. Similarly, visual images are often used as a metaphor, and visual images have an ideology behind them. Therefore, it can be said that the content of visual images is to a large extent ideology and various social trends, which spread and spread in cyberspace by means of visual image shells, so that most Internet users "hear the thunder in silence." At present, visual metaphors have three main characteristics: first, they spread faster. Visual images have the advantage of being intuitive and dynamic, and their audiences are not restricted by age, region, culture, and occupation, so visual metaphors tend to spread faster and more widely. Second, they are more concealed. In the process of visual metaphors, negative factors are embedded in the visual information structure, which makes them appear calm and untouched on the surface, but in fact, they are treacherous and harmful. Third, it is more attractive. Visual metaphors are often set in the subject matter of interest to Internet users, which can be close to social hotspots and close the distance between the mind and the heart of Internet users, thus attracting them to browse and watch [22-23].

Hostile forces use metaphorical images to attack the mainstream ideology. The characteristics of visual metaphors largely give hostile forces an opportunity to take advantage of them. Hostile Chinese and international forces often target and choose the painful points, hot spots, and focal points of Internet users, especially the youth, and very cleverly express their so-called western "universal values," neoliberalism and other capitalist ideologies, and wrong social trends with false qualities through visual metaphors. They question the scientific, value, and legitimacy of the mainstream ideology; attack the Party's leadership and the existing institutional arrangement; and vilify the core socialist value system, with the intention of competing with the mainstream ideology for people's hearts and minds. In the communication of visual metaphors, very often, the content expressed by the content distributor does not stop after one simple transmission but is repeatedly transferred and even spread geometrically, so that the undesirable information content is constantly embedded in people's visual neurons, reaches people's minds, and influences their thoughts. Hostile forces are good at infiltrating through uninterrupted and elaborate visual content, like "boiling a frog in warm water" to poison the minds of Internet users, especially the youth, little by little for a long time, in an attempt to achieve the sinister purpose of identifying with their wrong ideas

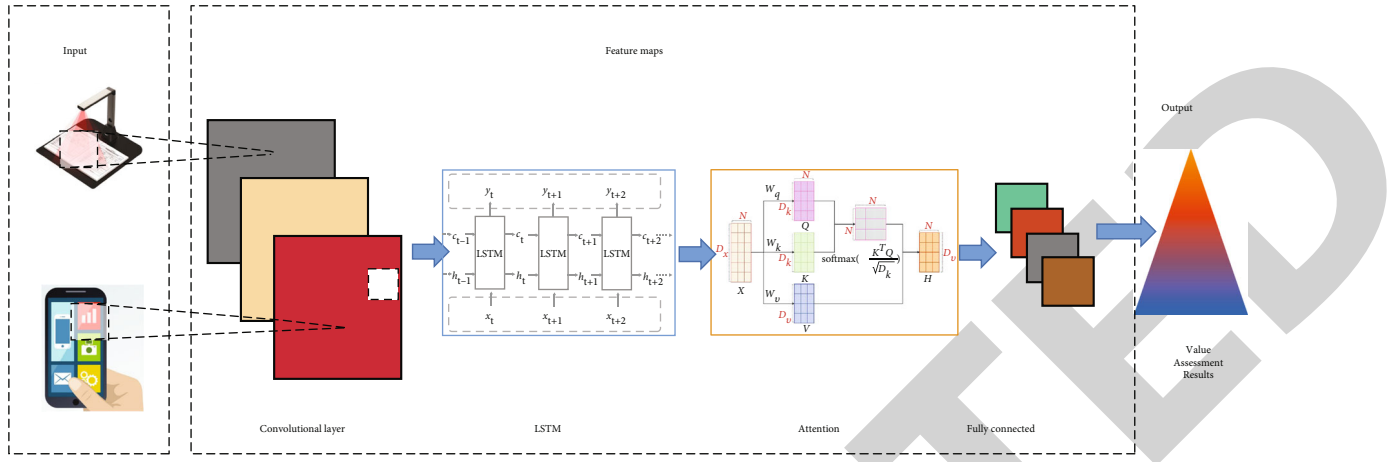


FIGURE 3: Model architecture.

and wrong values. Young Internet users, who are often weak in media literacy, are unwittingly incited and compelled by them, unable to discern between good and evil, resulting in ideological distortion and polarisation. At present, it is very difficult to control such visual metaphors. This is because, for textual metaphors, we can get better control by setting up sensitive words and keywords to retrieve and filter undesirable contents, but not for visual metaphors. The metaphorical connection is not natural but gradually built up during the communication process within the network circle, so it is extremely concealed and creates a more difficult governance problem. This makes it difficult to reach the crux of the problem by using traditional regulation and governance methods, and there is the disadvantage of treating the symptoms but not the root cause, with little effect. At present, almost all mobile social platforms take short videos as the first choice of information dissemination, forming a new pattern of short videos leading and influencing the communication style and content of cyberspace. The biggest feature of short video is to create a “light communication” mode with short duration and small length. This “short” and “light” determine that the content presentation of short videos must be fragmented, fragmentary, and incomplete. Video producers tend to large volume and long content through splicing, editing, compression, and other techniques to process and then produce a short video; a few minutes of content is often cut from several minutes or even hours of content. This content fragmentation problem is characterized by the commonality of short videos and the performance of many objects, and the effect is not the same. For the expression of life and leisure content, short video is the most suitable media tool. This is because the content of life and leisure does not seek to express the complete, logical, rational thinking, but the most important thing is to express the emotion; the most important thing is to be concise; the most important thing is to go straight to the subject; short video is suitable for this demand. For example, using short videos to watch TV series, movies, and variety shows can help Internet users with limited free time to focus on the main plot of the TV series, movies, and variety shows; using short videos to watch sports highlights can help Internet

users who miss the opportunity to experience live games to quickly view the highlights afterwards. However, for serious content and theoretical content, short videos add to the difficulty of expression, making it difficult to present the original content in a panoramic view and accurately express the true and perfect meaning of mainstream ideology.

### 3. Methods

In this section, we defined the model structure, data preprocessing, text features, word embedding, LSTM layer, and output layer in detail.

**3.1. Model Structure.** Traditional machine learning, according to previous research, always suffers from the problem that the influence of Marxian ideology recognition is restricted by the corpus size and feature selection, resulting in a lack of generalization ability in complicated recognition tasks. To address the above problems, a hybrid deep neural network-based sentiment recognition model for Chinese Marxian ideology text is proposed through the study of deep learning, as shown in Figures 3. The model integrates bi-LSTM, CNN, and with attention mechanism, which first obtains the contextual semantic features of the corpus and then extracts local semantic features, while giving r different schemes of attention to the feature information at each moment in order to get a better representation of text features and then further improve the accuracy of text sentiment recognition.

The model mainly consists of seven parts:

- (1) Input layer: acquisition of corpus data
- (2) Preprocessing layer: splitting words and removing irrelevant data
- (3) Bi-LSTM layer: extracting contextual semantic features of the corpus
- (4) Attention mechanism layer: obtaining weighted contextual semantic features with different focus representations of the sentence

- (5) kCNN layer: obtaining the final vector representation containing both contextual and local semantic features
- (6) Output layer: realize text recognition prediction

The steps are briefly described as follows:

- (1) Obtain real text corpus data through crawlers and other means
- (2) Preprocessing of the corpus such as word separation
- (3) Vectorized representation of the corpus text:
- (4) Build a Chinese text sentiment recognition model based on hybrid deep neural network
- (5) Designing the cost function and training the network with relevant algorithms
- (6) Validation of the model using the validation set corpus
- (7) Practical application of the model

### 3.2. Data Preprocessing

**3.2.1. Text Corpus Cleaning Preprocessing.** The main purpose is to carry out traditional and simplified conversion and remove duplicate data and irrelevant data in the Marxian ideological corpus, involving special symbols, text, HTML web tags, and other processing objects. The duplicate data may be the result of wrong crawling in the process of crawling data or due to the malicious brush reviews of the network water army; whatever the reason is, the same data need to be filtered. The original corpus sometimes also contains some meaningless text data, such as text content is full of numbers, letters, symbols, etc. This kind of corpus usually does not have much emotional information. If we do not filter out the repetitious and irrelevant data, it will inevitably impair the recognition effect, and these two types of data can be processed using Excel and other ways. The corpus is labeled with categories, such as good, medium, and bad reviews. The corpus is divided into words and deactivated using jieba. It is the process of cutting the text in the corpus into a series of sentences based on punctuation and then cutting the sentences into individual words, and it is found that the effect of precise mode of word separation is relatively good. Since some new Internet terms usually appear in the web text and the content is often colloquial, it is often necessary to load the user dictionary in order to make the word separation more accurate. User dictionaries are composed of unregistered words, user-built dictionaries, etc. In the user-built dictionaries, some domain-specific terms can be organized. The identification of unregistered words can be achieved by using fastText new word discovery algorithm, adding them to the user dictionary, then using sentiment polarity calculation algorithm to determine their sentiment polarity, and then adding them to the semantic sentiment dictionary if they are sentiment words. In addition, some common deactivated words should be removed in this process;

most of them are some auxiliary words, tone words, and some symbols, which not only do not provide help but also take up resources making the processing time grow. The removal of deactivated words can be done through the constructed deactivated word lexicon. To make the model work well for long text data, the corpus is further filtered with the TextRank algorithm to avoid the problem of “dimensional disaster” in the subsequent processing, the preprocessed corpus is divided into three parts: validation set, test set, and training set.

**3.3. Text Features.** In this paper, a new algorithm TextRank is used to achieve text feature extraction. The algorithm comes from the PageRank algorithm, which is a graph-based algorithm for calculating the importance ranking of web pages; it treats the whole network as a graph; the nodes are web pages; if there is a link relationship between two nodes, then there will be an edge between these two nodes. The importance of the pages  $S(V)$  is

$$S(V_i) = (1 - d) + d * \sum_{j \in \text{In}(v_i)} \frac{S(V_j)}{|\text{Out}(V_j)|}, \quad (1)$$

where  $d$  is the damping factor used for smoothing,  $S(V_j)$  indicates the existence of a collection of web pages pointing to the web page; links,  $\text{Out}(V_j)$  indicates the collection of web pages to which the web page  $V_j$  can jump, and  $|\text{Out}(V_j)|$  is the number of elements in the collection. The inspiration from the study of the PageRank algorithm is that for text, as long as the graph can be constructed from words/sentences, and then, the relationships between nodes in this graph can be determined by some method, such as word order relationships, semantic relationships, and content similarity; then, we can use the PageRank algorithm to get the core information such as keywords and key sentences in the corpus. Using sentences as nodes, we construct edges with the similarity relationship  $S(S_i, S_j)$  between sentences.

$$S(S_i, S_j) = \frac{|\{w_k | w_k \in S_i \& w_k \in S_j\}|}{\log(|S_i|) + \log(|S_j|)}. \quad (2)$$

Iterate the node weights until convergence; sort the node set weights in reverse order, and output the most important  $N$  results.

**3.4. Word Embedding.** In order to enable the computer to recognize and process Marxian ideological text content, the corpus first needs to be converted into digital form. The text data  $T$  with labels are loaded by batch, and then, the word embedding matrix  $E$  obtained by Word2Vec is mapped to map the text  $T$  containing the comment content  $D$  and the label content  $L$  into a three-dimensional vector matrix  $E$ . At this point, a vectorized text  $T_j = \{x_1, x_2, \dots, x_i, \dots, x_n\}$  containing  $n$  words denote  $E$  is described as follows:

$$E = (e_1, e_2, \dots, e_i, \dots, e_n), \quad (3)$$

$$e_i = w_{x_i} E_w,$$

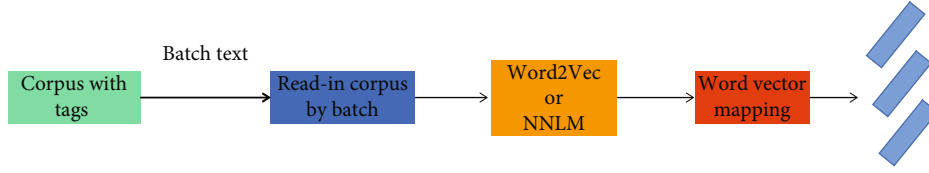


FIGURE 4: Text vectorization.

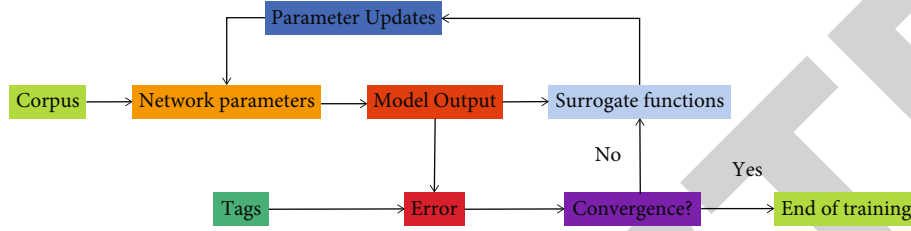


FIGURE 5: Training process.

TABLE 1: Corpus information.

Category	Good reviews (5 stars)/article	Moderate rating (3 stars)/article	Poor reviews (1 star)/article
Training set	600	600	600
Test set	150	150	150
Validation set	100	100	100

where  $E \in R^{\text{batch} \times S \times d}$ ,  $E_v \in R^{V_n \times d}$ , batch is the size of the batch data,  $S$  is the set text sequence threshold,  $d$  is the word vector dimension,  $V_w$  denotes the word embedding matrix size, and  $w$  is the index of the one-to-one correspondence between word  $x$  and  $E$ . The flow chart of text vectorization is shown in Figure 4.

**3.5. LSTM Layer.** When LSTM extracts the contextual semantic features of the text, the cell information at moment  $t$  is updated as follows:

$$\begin{aligned}
 i_t &= \sigma(W_{ei}e_t + W_{hi}h_{t-1} + b_i), \\
 f_t &= \sigma(W_{ef}e_t + W_{hf}h_{t-1} + b_f), \\
 g_t &= \tanh(W_{ec}e_t + W_{hc}h_{t-1} + b_c), \\
 c_t &= i_t g_t + f_t c_{t-1}, \\
 o_t &= \sigma(W_{eo}e_t + W_{ho}h_{t-1} + b_o), \\
 h_t &= o_t \tanh(c_t),
 \end{aligned} \tag{4}$$

where  $i_t$ ,  $f_t$ ,  $o_t$ , and  $g_t$  denote input gate, forget gate, output gate, and candidate gate, respectively;  $W_{ei}$ ,  $W_{hi}$ ,  $W_{ef}$ ,  $W_{hf}$ ,  $W_{ec}$ ,  $W_{eo}$ ,  $W_{ho}$ , and  $W_{hc}$  denote weights; and  $\sigma$  and  $\tanh$  are activation functions. However, LSTM only focuses on the temporal information and ignores the most important contextual information in the text. Bi-LSTM extends the one-way LSTM into a bidirectional structure, which retains the good performance of LSTM and can obtain the pre- and postcontextual information well. Input  $E$  into the forward

and backward structures of bi-LSTM, respectively, to get the forward and reverse hidden features, and the cascade is the output  $h$  at the  $i$ th moment, and finally, the output of each moment is spliced to get the contextual semantic features.

$$\begin{aligned}
 H &= (h_1, h_2, \dots, h_i \dots, h_n), \\
 h_i &= \left[ \vec{h}_i \oplus \bar{h}_i \right],
 \end{aligned} \tag{5}$$

where  $H \in R^{\text{batch} \times n \times 2d}$ ,  $\oplus$  is the splicing process, and  $n$  is the required time size and equal to the text sequence threshold.

**3.6. Output Layer.** Inputting  $C$  to the output layer, the output vector  $p(y)$  is obtained by determining the class to which the Marxian ideological text belongs through SoftMax. To prevent overfitting, the dropout technique, a common measure in neural network models, is used in this layer.

$$p(y) = \text{soft max}(W_c C_d + b_c), \tag{6}$$

where  $p(y) \in R^{\text{batch} \times \text{classes}}$ ,  $W_c \in R^{2n \times \text{classes}}$  and  $b_c$  are the weight matrix and bias matrix of the output layer, respectively; and classes are the number of recognition categories required by the task. Softmax is used to estimate the probability  $p(y)$  that the corpus text belongs to each target recognition category, and the label corresponding to the maximum probability  $y$  is selected from it as the final

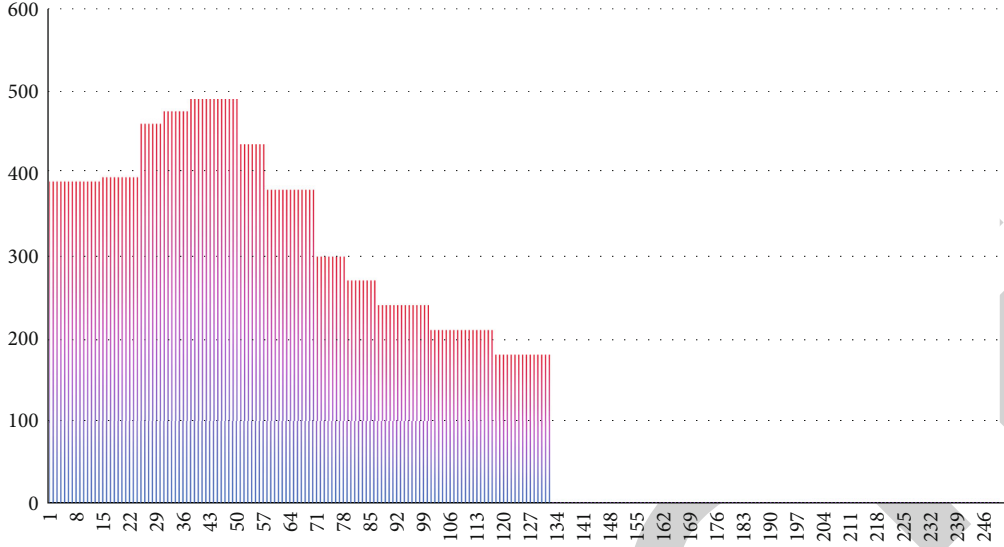


FIGURE 6: Sentence length distribution of the corpus.

TABLE 2: Performance comparison.

Models	Number of cycles	Training time (s)	Test time (s)	Accuracy rate	Recall rate	F1 value
CNN	3800	3594	36	0.89	0.89	0.89
LSTM	2300	33456	139	0.77	0.77	0.76
Bi-LSTM	4000	219008	1412	0.88	0.87	0.87
Bi-LSTM-attention	4000	206272	776	0.90	0.90	0.90
RCNN	1900	185709	2051	0.92	0.91	0.91
Proposed method	5000	162950	720	0.94	0.94	0.94

TABLE 3: Results of ablation experiments.

Models	P	R	F1
SVM + Word2vec + wordiness + adverb of degree + emotion + negation	0.88	0.78	0.81
SVM + Word2vec + transitive + wordiness + degree adverb + emotional word + negative word	0.89	0.86	0.88
SVM + Word2vec + conditionals + transitions + wordiness + degree adverbs + emotional words + negation	0.90	0.91	0.90
SVM + Word2vec + punctuation + conditional word + transitive + degree adverb + negative word + emotional word + negative word	0.86	0.88	0.85
NB + Word2vec + word vector averaging	0.76	0.74	0.75
NB + Word2vec + word vector "voting" method	0.77	0.82	0.80
NB + Word2vec + emotional words	0.98	0.96	0.99

recognition. The result is selected as the final recognition result.

$$y = \arg \max (p(y)). \quad (7)$$

In this paper, when training the model, the cost function  $J(\theta)$  is used as the crossentropy between the output of the model and the corpus labels, and the model parameter  $e$  is updated using the Adam optimizer with good performance

in deep learning, and the training process is shown in Figure 5.

$$J(\theta) = \frac{1}{N} E(D, L; \theta) + \frac{\lambda}{2} \|\theta\|^2, \quad (8)$$

$$E(D, L; \theta) = - \sum_{i=0}^N \{p(L_i) \log (y; \theta) + [1 - p(L_i)] \log [1 - (y; \theta)]\}.$$

## 4. Experiments and Results

In order to ensure the objectivity and authenticity of the experiment, the corpus used in this experiment was crawled using crawler technology to crawl the comment data about Marx's ideology-related content on a large Chinese social platform, and the basic information of the corpus is shown in Table 1, and Figure 6 shows the sentence length distribution of the corpus.

The experiment is implemented in TensorFlow deep learning framework using Python language and the specific experimental environment configuration. Table 2 shows that the experimental findings indicate good performance in both general and particular recognition outcomes for each category. The model also has higher recognition accuracy in real estate, lottery, finance, sports, and gaming, but lower recognition accuracy in society, science and technology, and other fields. The latter may be related to the constant emergence of new words and the rapid changes of current affairs and social hotspots, while new topics and new terms may not be recognized in time for the model that has been trained, so the performance in these fields will be slightly worse.

The results of the ablation experiments are shown in Table 3. As can be seen from Experiments 20 and 21, the  $F$ -value of bi-LSTM is improved by about 3% compared with LSTM, which indicates that bi-LSTM with two-layer network structure of forward and reverse can better obtain the contextual information of the text, so the accuracy will be improved, but the complexity is greater than that of LSTM network, resulting in a slightly longer computing time compared with LSTM. As can be seen from Experiments 21 and 22, using the attention mechanism after the bi-LSTM model leads to an improvement in the  $F$ -value of about 4%, which indicates that attention does have the ability to identify key information that can be helpful for the results. Due to the unique model parameter-sharing feature of CNN, it makes the recognition effect not the best, but it can greatly save the computing time. Experiments 19-23 show that the RCNN network, which combines the advantages of RNN (and its variants) and CNN, outperforms each network individually. From the whole Table 3, the network model proposed in this section has the highest accuracy, which indicates that the deep neural network obtained by integrating bi-LSTM and CNN and introducing the attention mechanism, using TextRank algorithm in the preprocessing process, and using dropout technique in order to avoid overfitting, L2 regularization, and early stopping three strategies is a very effective method for Chinese text sentiment recognition.

## 5. Conclusion

Marxism believes that society is constantly changing, developing, and moving forward. Ideological work must always adhere to the materialistic view of history, problem-oriented, advancing with the times, deepening understanding with the development of the times, constantly innovating ideas, and constantly updating the means. In this sense, the network ideological risk prevention is only a work in progress; there is no time to complete; we cannot let down our guard; we

must rely closely on new technological means to manage the network, especially the application of artificial intelligence to help network ideological work, to ensure that cyberspace adhere to the correct, mainstream orientation of public opinion and value orientation. Looking ahead, the new wave of technology, which has artificial intelligence at its core, will continue to make significant progress. Visual recognition technology will also usher in new iterations of upgrading opportunities, and we have reason to believe that the strong leadership of the Party, as well as the joint participation of multiple subjects, will help to accelerate this process. Artificial intelligence-supported network is a good technique to ensure that the network ideological risk prevention work to introduce the role of visual recognition will continue to improve. Work on preventing ideological risk will be more steady and widespread, and the Internet will be brighter, cleaner, and clearer.

## Data Availability

The datasets used during the current study are available from the corresponding author on reasonable request.

## Conflicts of Interest

The author declares that he has no conflict of interest.

## References

- [1] M. A. Peters, D. Neilson, and L. Jackson, "Post-marxism, humanism and (post)structuralism: educational philosophy and theory," *Educational Philosophy and Theory*, pp. 1-10, 2020.
- [2] M. A. Peters, "Affective capitalism, higher education and the constitution of the social body Althusser, Deleuze, and Negri on Spinoza and Marxism," *Educational Philosophy and Theory*, vol. 51, no. 5, pp. 465-473, 2019.
- [3] H. Dong, "Teaching design of "three-dimensional" blended ideological and political courses from the perspective of deep learning," *Security and Communication Networks*, vol. 2022, 9 pages, 2022.
- [4] J. Wei, "Video face recognition of virtual currency trading system based on deep learning algorithms," *IEEE Access*, vol. 9, pp. 32760-32773, 2021.
- [5] Q. Hou, "Research on the diagnosis of students' cognitive level based on deep learning," *Security and Communication Networks*, vol. 2021, 6 pages, 2021.
- [6] A. Ardill, "Deep critique: critical pedagogy, Marxism, and feminist standpoint theory in the corporate classroom," in *Teaching Marx & Critical Theory in the 21st century*, pp. 143-163, Brill, 2019.
- [7] Y. Wang and C. Ma, "Evaluation and analysis of college students' mental health from the perspective of deep learning," *Wireless Communications and Mobile Computing*, vol. 2022, 11 pages, 2022.
- [8] W. Feng and Y. Dai, "On the improvement of discourse affinity of ideological and political course in colleges and universities," *Journal of Frontiers in Educational Research*, vol. 1, no. 8, pp. 40-44, 2021.
- [9] J. Yin, "On the necessity of integrating excellent traditional culture guided by Marxism with ideological and political

## Retraction

# Retracted: Corpus-Driven Resource Recommendation Algorithm for English Online Autonomous Learning

### Computational and Mathematical Methods in Medicine

Received 25 July 2023; Accepted 25 July 2023; Published 26 July 2023

Copyright © 2023 Computational and Mathematical Methods in Medicine. This is an open access article distributed under the Creative Commons Attribution License, which permits unrestricted use, distribution, and reproduction in any medium, provided the original work is properly cited.

This article has been retracted by Hindawi following an investigation undertaken by the publisher [1]. This investigation has uncovered evidence of one or more of the following indicators of systematic manipulation of the publication process:

- (1) Discrepancies in scope
- (2) Discrepancies in the description of the research reported
- (3) Discrepancies between the availability of data and the research described
- (4) Inappropriate citations
- (5) Incoherent, meaningless and/or irrelevant content included in the article
- (6) Peer-review manipulation

The presence of these indicators undermines our confidence in the integrity of the article's content and we cannot, therefore, vouch for its reliability. Please note that this notice is intended solely to alert readers that the content of this article is unreliable. We have not investigated whether authors were aware of or involved in the systematic manipulation of the publication process.

Wiley and Hindawi regrets that the usual quality checks did not identify these issues before publication and have since put additional measures in place to safeguard research integrity.

We wish to credit our own Research Integrity and Research Publishing teams and anonymous and named external researchers and research integrity experts for contributing to this investigation.

The corresponding author, as the representative of all authors, has been given the opportunity to register their agreement or disagreement to this retraction. We have kept a record of any response received.

### References

- [1] L. Gu, "Corpus-Driven Resource Recommendation Algorithm for English Online Autonomous Learning," *Computational and Mathematical Methods in Medicine*, vol. 2022, Article ID 9369258, 10 pages, 2022.



## Research Article

# Corpus-Driven Resource Recommendation Algorithm for English Online Autonomous Learning

Ling Gu 

*School of Humanities and Law, Gannan University of Science and Technology, Ganzhou, Jiangxi 341000, China*

Correspondence should be addressed to Ling Gu; 9320030112@jxust.edu.cn

Received 26 April 2022; Revised 18 May 2022; Accepted 24 May 2022; Published 14 June 2022

Academic Editor: Naeem Jan

Copyright © 2022 Ling Gu. This is an open access article distributed under the Creative Commons Attribution License, which permits unrestricted use, distribution, and reproduction in any medium, provided the original work is properly cited.

One of the most significant aspects of English teaching, as well as the embodiment of students' comprehensive English skill, is the cultivation of English learning ability. Teachers of English should help students understand the topic's material and be able to convey, describe, and analyze the topic's substance, such as summarizing, subjective judgments analysis, and tale continuation. Students' English learning is restricted by the learning environment, teachers' quality, students' own ability, and other aspects. Furthermore, schools and families do not prioritize English learning, resulting in low teacher expectations for English instruction, as well as a lack of English practice and strategy training among students. In order to improve the inefficiency of English teaching, this paper combines corpus technology with English teaching and proposes an online autonomous learning resource recommendation algorithm. The model is optimized in the aspects of high efficiency, diversity, and timeliness of learning resource recommendation supported by deep learning technology. The model is pretrained through the processed dataset, and the algorithm designed in this study is compared with the classical algorithm to verify the rationality and effectiveness of the algorithm designed in this study. Based on the previous studies, this study attempts to apply the teaching model combining corpus and recommendation algorithm to online teaching, so as to optimize English teaching model and teaching methods.

## 1. Introduction

Corpus is a research resource for scientists to study language use and an important part of language teaching. In fact, European linguists represented by Geoffrey Leech began to propose that the application of corpus in language teaching would become an important part of corpus linguistics when corpus linguistics just came into the field of scientists. They propose that corpus can be applied in teaching from the following two perspectives: one is the indirect application of corpus, such as corpus dictionary, textbook compilation, and language software package and test and evaluation tool compilation. The other is direct corpus development, such as corpus teaching knowledge, corpus exploration methods, and the use of corpus resources.

With the deepening of linguists' research on corpus linguistics, corpus linguistics has been widely used in the research of second language teaching [1]. In English teach-

ing and research, corpus method is used to make the characteristics and development rules of students' language output be scientifically quantified, from subjective qualitative research to scientific quantified embodiment. This research paradigm fundamentally expands the approach to second language research, covering two main aspects, including language output and language error analysis. The application of this research method in English teaching is mainly embodied in "language error analysis," which is the corpus-based teaching model discussed in this paper.

The education industry has also jumped on the Internet bandwagon, launching a number of online learning platforms that allow users to take their courses without leaving home. The outbreak of COVID-19 in 2020 has also promoted the development of online courses. For students who cannot go back to school, the school has launched online classes for online teaching and online exams. Students' safety is maintained by this new online learning

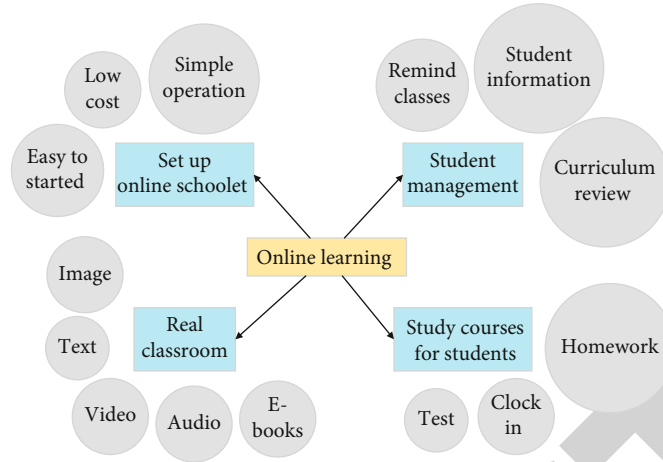


FIGURE 1: Characteristics of online learning.

approach, as is the efficiency and quality of studying at home [2]. Figure 1 depicts the characteristics of online learning in general. For starters, it has a larger learning resource base thanks to the Internet. Learners can make decisions based on their interests and present needs, allowing them to suit the various learning needs of users at various stages. Second, online learning can save time and resources. Through the tool of online courses on the Internet, users can choose a convenient place and study at an appropriate time. Compared with offline teaching in fixed time, fixed site, and huge number of personnel management, online learning makes it possible to study anytime and anywhere.

The proliferation of learning platforms has resulted in an increase in course resources. While they aid people in their learning, they also cause issues such as information overload. How people find the materials they are interested in and suitable for themselves from a large number of learning resources as well as how to find the courses to learn at the present stage is a major difficulty for online courses to improve users' learning efficiency. Among the common solutions to the problem of information overload, it is straightforward to use the methods of catalogs or search engines, which are important tools for obtaining information. Classified catalog in the format of a catalog, to classify the content according to the category of display. Users search resources according to the classification, which can further save the time of searching resources [3]. However, when the content is very large and the amount of data is very large, it becomes very difficult for users to find useful information, which consumes both time and energy. In the face of the challenge of massive data, search engines can better solve the problem of information search than classified directory. But users often do not have a good overview of what they are looking for, and if they do not enter accurate keywords in the search box, users may not be able to find what they need. In order to better deal with the problems brought by various information, the recommendation system appeared. It can not only solve the problem of massive data which is difficult to deal with in classified catalogue, but also solve the problem that users need accurate keywords

to search in search engine. It connects users to information to find value in it. This data make recommendations to users [4]. The application of recommendation system in online learning can better save the time for users to search for information and make it more convenient for users to find courses that meet their learning needs. For the course itself, it can also promote the further development and circulation of high-quality course resources, get rid of useless inferior courses, and promote the healthy development of the whole online learning environment.

Currently, the collaborative filtering algorithm has a positive impact on course recommendation, but it is not without flaws, such as recommendation accuracy and data scarcity. Collaborative filtering makes recommendations for users through a large number of rating data. However, in our real life, users do not score everything they touch, so the rating data of users on projects are not very complete, resulting in the problem of low accuracy of recommendations. In 2006, the concept of deep learning was proposed, and deep learning has brought vigorous vitality to the information technology industry [5]. In the image field, images and user preferences are put together through two subnetworks, and the distance between images and users is calculated to judge the similarity. The accuracy of image classification is improved by learning residual network. In the aspect of speech recognition, DNNs are successfully applied in the theory of acoustics.

Deep learning has strong learning ability. It can find deeper characteristics through a small number of individuals, so as to discover the nonlinear relationship between users and items and obtain more potential information between users and items. Using deep learning in recommendation algorithms can fully mine the features of various types of data, alleviate the problem of missing values in datasets, and improve the recommendation effect. In this paper, the recommendation algorithm and deep learning are combined to ensure better recommendation effect of course resources.

The use of recommendation algorithm in course resource suggestion is an important application of recommendation system in life, and this work has a good

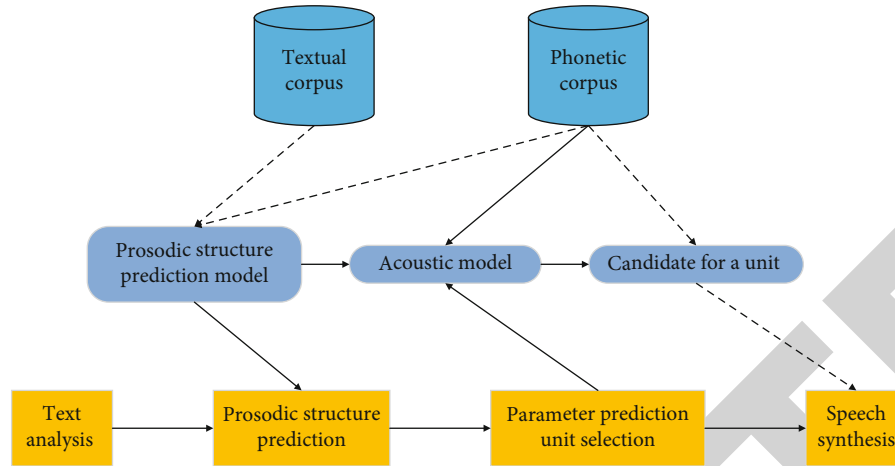


FIGURE 2: Processing flow of corpus data.

recommended effect. Curriculum resource recommendation for learners can suggest corresponding courses based on distinct learning demands, hence improving learning efficiency; for curriculum resources, it can speed up the removal of ineffective resources, which has great research relevance.

The paper arrangements are as follows: Section 2 discusses the related works. Section 3 examines the algorithm design. Section 4 evaluates the experiment and analysis. Section 5 concluded the article.

## 2. Related Works

**2.1. Research Status of Corpus.** John Sinclair, the pioneer of corpus linguistics, believes that “corpus is a collection of actual languages used in real life, which can reflect the characteristics of language in the process of use.” Yang pointed out that many linguists in China have also defined corpus, which is a large electronic text database of language that linguists randomly collect natural language according to the expression rules of language and store them together. GUI believes that corpus is a kind of language database, which is established by linguists to collect language materials by random sampling for language research.

Due to the limitations of science and technology, manual recovery was adopted for retrieval, which was the earliest corpus research adopted by linguists. After entering the twentieth century, corpus research had a preliminary development in the 1950s to 1970s. Quirk, a British grammar, compiled a Survey of English Usage while studying English grammar and produced an electronic version in the 1980s [6]. Since 1980s and 1990s, corpus-related research has developed vigorously, and countries, regions, and fields around the world have begun to build their own corpus, and the trend of internationalization has initially formed.

The application of corpus in the field of teaching is an important research direction of corpus research, and significant research results have been obtained in the application of corpus in language teaching. The data processing process of corpus is shown in Figure 2. Wu expounds the positive role of corpus in second language acquisition from the

aspects of grammar, vocabulary, error analysis, and independent learning. Xu from the angle of the corpus in the teaching of second language acquisition application points out the advantages of corpus.

In recent years, in the researches of scholars, corpus linguistics is increasingly combined with language teaching and presents a trend of diversification and automation, trying to explore the characteristics and development rules of inter-language students. The formal birth of corpus linguistics was in the 1980s, when the study of natural language texts was the main research direction. Its purpose is to provide objective evidence for linguistic research and guide the development of natural language.

In the early twenty-first century, some foreign scholars began to learn the teaching methods of corpus-assisted instruction. Tim Johns was a pioneer in this sector, and they were the first to use corpus-assisted instruction in classrooms. They advocate for “data-driven learning” and “classroom priming exercises.” Since then, researchers have shown that learners can use data from the database to improve learning. Some linguists point out that data-driven learning is consistent with current language learning theories, in which students learn to observe and summarize under their own guidance [7]. This indicates that language teaching assisted by corpus technology can strengthen students’ attention to a certain knowledge structure in the process of learning, thus promoting the improvement of students’ language learning ability. Criterion-E-Rater is a corpus-based automatic evaluation system that provides real-time communication about the grammatical structure, style, thinking structure, and content of essays, as well as overall grading of essays. Some studies have shown a high degree of consistency between this system and manual scoring, while other studies have found significant differences between the system and manual scoring, and their reliability is affected by the range of scoring. According to Liang, it is very important to analyze the advantages and disadvantages of the existing foreign automatic composition scoring system for the development of our own automatic scoring system [8]. However, due to the different technologies used, existing automated

evaluation systems abroad differs greatly in their ability to analyze the performance quality of words.

The experimental results show that students have an important influence on reducing grammatical errors, spelling errors, punctuation marks, and word arrangement, and corpus retrieval plays an important role in the interaction. Yoon examined the use of corpus by EFL learners in academic studies and found that the corpus method to cultivate second language ability is helpful and can enhance confidence. The case study shows that the use of corpus is not only supportive to solve academic problems, but also to improve students' comprehensive English language ability [9]. Foreign scholars conducted research on students learning English and a second language as their mother tongue, combined with corpus-related software, corpus-related retrieval, and education. Many studies have shown that by using corpus skills, students can improve their understanding of grammar and vocabulary, reduce writing errors, and increase their confidence by improving their skills. Scholars' flexible use of corpus technology and its integration with practical education provide inspiration for this research.

Recent trends in the number of papers published in major Chinese journals indicate that corpus linguistics has become an important tool for linguistic research. The study of corpus linguistics is still an important field in Chinese linguistics and has been developing rapidly [10]. Many Chinese scholars have made great efforts in using corpus as an auxiliary tool and method for language teaching and research. He investigated the application of corpus-assisted instruction in practical teaching and listed relevant examples in *Introduction to Corpus-Assisted English Teaching*. Attempts to introduce corpora into teaching continue. Theoretically, some researchers have discussed the current situation, characteristics, and advantages of corpus when writing scientific articles in English, as well as the methods of using corpus in teaching, encouraging more integration of corpus technology with second language teaching. Using corpus technology, remarkable achievements have been made in error analysis and feedback [11]. In the collection from the basic education phase to the stage of higher education of Chinese students to learn English composition of the material, there are millions of words and marked with the Chinese students in this corpus in English that often appear in the process of sixty-one types of errors, for Chinese corpus made outstanding contributions to the construction and teaching research.

*2.2. Research Status of Recommendation Algorithms.* In theory and method, Debnath studied the selection method of feature weight and its influence on the recommendation effect. Blanco combines the Semantic Web with content-based recommendation to provide users with recommendations based on the precise feature relationships contained in the Semantic Web. Noia further applies the latest Semantic Web of open Connected Data items to recommendations; Zenebe applies fuzzy set theory to the matching process of user and item feature sets to provide users with content-based recommendations [12]. Cramer looked at the impact of system transparency on user trust and acceptance in the context of content-based recommendations. In practical

application, Mooney studied and launched a content-based book recommendation system; Cano has introduced a content-based music recommendation system; Basu studied the application of social relationship information in the recommendation system, and Cantador further applied content-based recommendation to the social tag system, so as to recommend the most likely objects of interest to users for labeling. Chen studied the content-based e-commerce system; Phelan has studied content-based news recommendation systems.

Lemire proposed the famous Slope One series algorithms to simplify the regression function of collaborative filtering in order to further solve the problem of large amounts of similarity calculation, which achieved the same or even better effect than the original nearest neighbor based algorithm while greatly reducing calculation time and storage requirements. Item clustering was developed by Connor to simplify the complexity of similarity calculation [13]. Gong tried and compared the effects of clustering users and items separately. George uses the method of cross-clustering to cluster users and items at the same time and searches for neighbors on this basis. Ma proposed an accelerated algorithm to find the nearest neighbor and calculate the prediction score based on similarity threshold filtering. Zhou used Hadoop to research and constructs a parallel similarity calculation and collaborative filtering approach.

One of the most significant issues in collaborative filtering recommendation systems is cold start. Because new users have little or no past behavior records, collaborative filtering algorithms struggle to model their preferences when they first join the system. For example, in user-based collaborative filtering, similar neighbor users cannot be calculated for cold-start users because they have no historical scoring records. The same problem also exists in the collaborative filtering algorithm based on items. As there is almost no user rating for newly added items, it is difficult to be recommended by the algorithm. Gantner solved the cold start problem by learning attribute feature mapping. Zhang uses social tagging to alleviate the cold start problem; Bobadilla studied the application of neural network learning algorithm in cold start problem [14]. Leroy et al. studied the correlation prediction of cold start. Ahn proposed a heuristic similarity calculation method to solve the problem of cold startup for new users. Zhou proposed the functional matrix decomposition model, which uses the combination of decision tree and matrix decomposition to select appropriate items for users to score during the cold start process, so as to understand users' preferences as accurately as possible. Closely related to the cold start problem is the data sparsity of collaborative filtering [15]. Compared with the huge total number of items in the system, only a small part of items that each user has interacted with are evaluated. Data sparsity brings challenges to user preference modeling.

The benefit of content-based recommendation is that there is no problem with cold startup, but the construction of user and item portraits requires a lot of time and manpower; however, the recommendation based on collaborative filtering makes use of the wisdom of the group to carry out portrait and modeling of users and items, but it also has

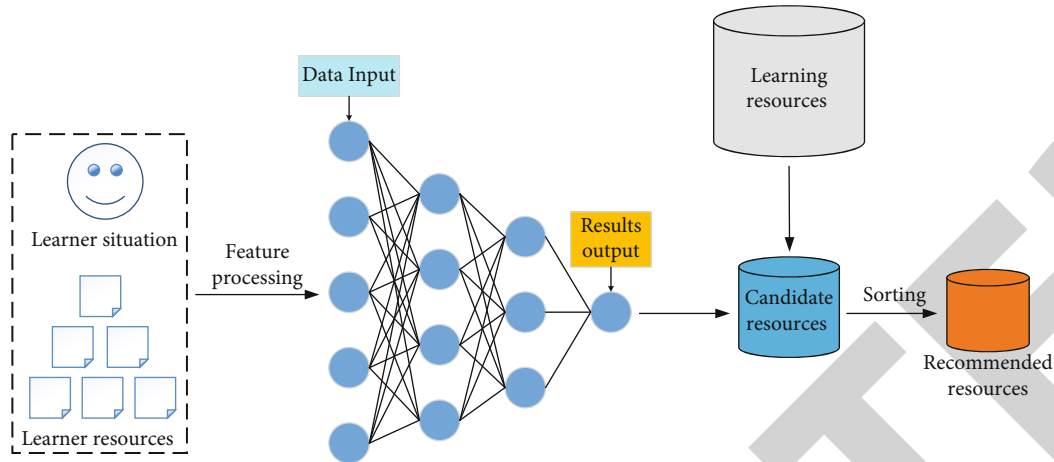


FIGURE 3: Block diagram of combination of deep learning and recommendation algorithm.

shortcomings such as cold start and data sparsity. Claypool then combines content-based and collaborative filtering recommendations for the task of news recommendation; Wang combined traditional user collaborative filtering and item collaborative filtering based on similarity fusion method. Good proposes a collaborative filtering framework combined with personal assistants. Pennock combines the nearest neighbor-based coco-co-filtering with the mode-based square method [16]. Melville proposed a collaborative filtering method based on content enhancement. Kim studied the mixed recommendation model based on decision tree. Popescul studied a probabilistic approach to hybrid recommendations.

The basic framework of the research on the combination of deep learning and recommendation algorithm is shown in Figure 3. Kim proposed a new context-aware recommendation model, convolution matrix decomposition model, which combined convolution neural network and probability matrix decomposition to solve the problem of sparse score. In other words, the features of learning resources were extracted by convolutional neural network, and then the learning resources were recommended based on the preferences of learners. Shu introduces convolutional neural network to extract text information from learning resources, realizes content-based recommendation algorithm, and improves the recommendation quality of learning resources. Mao designed a time model and constructed a dynamic convolutional recommendation model [17]. Zhang proposed a recommendation algorithm based on feedback information, which uses convolutional neural network to extract features from feedback information of learners' comments. Zhao uses information about users' use of resources between different domains to construct collaborative filtering recommenders by mining users' shared preferences between domains and unique preferences within domains through a novel multibranch neural network. In this recommendation method, input is processed by feature selection model, and output is processed by learner-learning resource association model to determine whether learning resources are recommended [18]. Combining natural language processing and

deep learning technology, he classifies new users, calculates the similarity of learning level between target users and other users in the classification, finds the similar user set through learning level similarity, and then determines the final similar user set through fusion calculation, so as to recommend learning resources.

### 3. Algorithm Design

Here, they discuss the algorithm requirements. They analyze the algorithm flow. They also examine the algorithm model.

**3.1. Algorithm Requirements.** There are many factors that affect accuracy, and the most important factors are learner characteristics, learning resource characteristics, situation characteristics, and recommendation method design. Incomplete feature mining, right feature selection, inappropriate feature processing, and unreasonable method design will all affect the accuracy of learning resource suggestion. The accuracy of learning resource suggestion can only be increased if features are correctly handled and recommendation techniques are properly built. If the feature engineering is done very well and the recommendation method is not designed properly, the result will be short board effect, or if the recommendation method is perfect but the feature engineering is not good, the short board effect will also be caused, affecting the accuracy of the recommendation of learning resources [19]. When designing the learning resource recommendation model, we should reduce the error between the predicted value of learner-learning resource score and the real value and improve the accuracy of the recommendation.

- (1) Accuracy is mainly used to evaluate the degree of matching between recommended learning resources and learners' learning interests. Accuracy is not only the primary goal of learning resource recommendation, but also the most important evaluation index of learning resource recommendation effect. It is also the basic requirement of learning resource

recommendation. The correctness of learning resource recommendations should be prioritized. As long as the recommended learning resources do not match learners or their matching degree is not high or suitable for learners, that is, the accuracy is not high, no matter how rich the other functions are, they are meaningless

- (2) Individuation is to recommend different learning resources according to different learners, that is, to recommend customized learning resources with each learner as the center. The personalized recommendation of learning resources is a significant goal, but the personalized recommendation of learning resources not only contains the personalized recommendation of recommended resources, but also contains the personalized recommendation of personalized learning resources, which should be personalized from numerous perspectives. Personalized recommendation of learning resources includes that the recommended learning resources are personalized and the recommendation process is personalized
- (3) High efficiency refers to the high efficiency of learning resource recommendation, that is, the relevant processing in the recommendation process is simple, the recommendation response time is short, and the resource recommendation page responds quickly. The growth rate of learning resources in the Internet era and the era of sharing is beyond our imagination [20]. Exponential growth is not an exaggeration. We should not only study the recommendation of learning resources at the level of ten thousand, but also study the learning resources at the level of one hundred thousand, one million, or even ten million. In the face of such a large number of learning resources, how to reduce the program processing time, reduce the response time, and improve the efficiency of recommendation is also what we need to consider
- (4) Diversity means that the learning resources recommended by learners are not immutable but will be appropriately expanded according to learners' learning interests, which not only matches the static and fixed learning interests of learners, but also matches the dynamic and changing learning interests of learners, so as to avoid excessive homogeneity of the recommended learning resources
- (5) Initiative is a recommended system at the right time to recommend suitable learning resources for learners to learn actively; the initiative also reflects timeliness, and related research suggests that actively recommending learning resources for learners at the proper time and place in a timely manner can have the effect of reminding learners to study and can increase mobile learning effect [21]. Relevant studies also show that actively pushing learning resources to appropriate learners can effectively improve the utilization rate of learning resources and improve the quality of learning resources

**3.2. Algorithm Flow.** The learning resource recommendation model based on deep neural network contains three core modules: resource filtering, resource recommendation, and resource display. The core of resource display is real-time push. The relevant algorithms involved in these three core modules will be explained below.

If massive learning resources are recommended directly through the deep neural network model or other neural network models, the model complexity will be increased, response time will be increased, and the recommendation efficiency of learning resources will be reduced. Therefore, this study proposes a resource filtering technique based on similarity ranking, which filters out most irrelevant learning resources or learning resources with low similarity with learners' learning interests before entering the deep neural network model for recommendation, thus reducing the input and output of the neural network model and decreasing the complexity. The similarity ranking method is that, with the help of natural language processing technology, existing text generation vectors such as learners' learning interest, names of learning resources, and themes of learning resources are calculated, and then the average value of existing text feature vectors such as names of learning resources and themes of learning resources is calculated to obtain a vector about learning resources. Then the cosine similarity of the learning interest vector and the learning resource vector is calculated, and the similarity of the learning resource name and the learning resource theme is compared with the learning interest of the learner [22]. Most of the irrelevant resources are filtered out, which is easy to process and fast to calculate. Meanwhile, in order to preferentially select the latest resources, a method of similarity reduction based on time factor is designed. The calculation method of similarity between learning resources and learners' learning interest is as follows:

$$S = \frac{A \cdot B}{\|A\| \times \|B\|}. \quad (1)$$

The filtering algorithm based on similarity ranking is equivalent to a simple content-based learning resource recommendation method.

Traditional learning resource recommendation approaches have low feature acquisition accuracy and require complex model building. A deep neural network model is a nonlinear model that can produce high-quality nonlinear relationships and data characteristics.

Studies on the recommendation of existing learning resources seldom consider the initiative and timeliness of resource recommendation. First, new resources suitable for learners are actively pushed to learners in time, and second, resources are timely pushed to learners at specific time of learning to improve learners' learning experience. The other is the timely push method based on deep neural network, which pushes specific learning resources at the time when learners are likely to learn.

Learning resources in order to timely push actively, this paper uses a timely push method based on the depth of the

neural network resources, through the existing situation, learning resources situation, and the learning environment data such as depth of training the neural network model, which make its study can effectively predict the interval of learning and then calculate the time of the next learning. The present learning time and the next learning time interval are the outputs, and the data processing and selection procedure are the same as the previous deep neural network. After predicting the learning interval of learners and calculating the next learning date, this study designed the following methods to calculate the learning time of learners on the day:

$$T = \max (n_i) \longrightarrow t_i (1 \leq i \leq 5). \quad (2)$$

**3.3. Algorithm Model.** The performance of recommendation algorithm is improved by introducing knowledge graph. After the model is given the item that has interacted with the user, the user's embedded table is finally obtained through the interaction calculation between the item vector and the items around the user. The network model can better capture the neighborhood information of the project, give the weight of the neighbor node and the aggregation of the neighbor node according to the specific relationship between the specific user and the map, and use the weighted result to represent the neighbor node to complete the calculation of the project vector. Both methods provide end-to-end recommendations that enable users and embedded representations of knowledge graph entities and relationships to become learnable vectors [23]. When aggregating the first-order or higher-order neighbor nodes of learning resources, the learner's embedded representation of the user is used to assign aggregation weight to it to expand its embedded representation. Finally, the interaction probability of learners and learning resources is calculated by embedding them.

From the perspective of learners, the KNDP model uses the relationship between entities in knowledge graph  $G$  to find the entity set  $K$  between  $m_{sl}=1$  and  $m_{sl}=0$  nodes, aggregates the information of entities and their neighbors in the set, and transmits its features to the target node through the knowledge graph, allowing learners' representation to be obtained. Fixed-size sampling is considered as the acceptance domain of this node in the neighbor entity set  $N(L)$  from the standpoint of learning resources, and the embedded representation of learning resources is obtained by aggregation with a given weight and  $L$ . Finally, the interaction probability of the two is obtained through the full connection layer. The overall algorithm model of this paper is shown in Figure 4.

## 4. Experiment and Analysis

**4.1. Experimental Environment and Dataset.** The experiment in this paper was carried out in PyCharm on 64-bit Windows 10 system, based on TensorFlow framework and Python 3.6 implementations, and the experimental environment is shown in Table 1.

The experiment uses MOOPer dataset. The dataset is divided into two parts: interactive data and knowledge

graph. There are three types of interactive data, namely, learner behavior, learner feedback, and system feedback. Learner behavior shows the interaction process with learning resources, learner feedback reflects their learning status and satisfaction, and systematic feedback data describes the result feedback of learners in the process of practice. The knowledge graph is formed by modeling the attribute information of curriculum, practice, level and knowledge point, and their relationship among them. The statistical information of the dataset after preprocessing is shown in Table 2.

**4.2. Comparison Model.** To verify the effectiveness of the algorithm, the proposed KNDP is compared with the following recent recommendation model. The parameter Settings of the comparison model are the same as those in the original text.

- (1) The improved deep neural network learning resource recommendation algorithm (UDN-CBR) takes learner information and learning resource information as input and obtains its feature vector through the full connection layer; at the same time, word2vec is introduced to get the text features of learning resources and fuse them with the feature vectors of learning resources. Finally, the scores are predicted by multi-layer perceptron network
- (2) KGCN: using the neighborhood information of the entity in the knowledge graph, the information of its neighbor nodes is aggregated into the node through graph convolution to enrich the representation of the project
- (3) Dual-end recommendation algorithm based on knowledge graph convolution network (DEKGCN): at the client end and the project end, the neighbor information is aggregated into the node by graph convolution, so as to obtain the embedded representation of the user and the project, and finally calculate the interaction probability of the two

**4.3. Experimental Results and Analysis.** The experiment in this paper divided interactive data into training sets, validation sets, and test sets in a ratio of 7:2:1 to train the model. When the number of fully connected layers is set to 4, the activation function of the nonlast layer is ReLU, and that of the last layer is tanh, and the learning rate is 0.001.

In the interaction rate prediction, the trained model is used to predict each interaction in the test set, and the AUC and ACC indicators are used to evaluate the model performance. For the Top-K recommendation task, the Top-K learning resources were recommended for learners in the test set, and the performance of the model was evaluated by using Precision@K and Recall@K indicators. The comparison results of AUC and ACC in interaction probability prediction are shown in Table 3. It can be seen from Table 3 that KNDP model achieves good performance in both ACC and AUC evaluation indicators and increases the AUC indicators by 2 to 7 percentage points compared

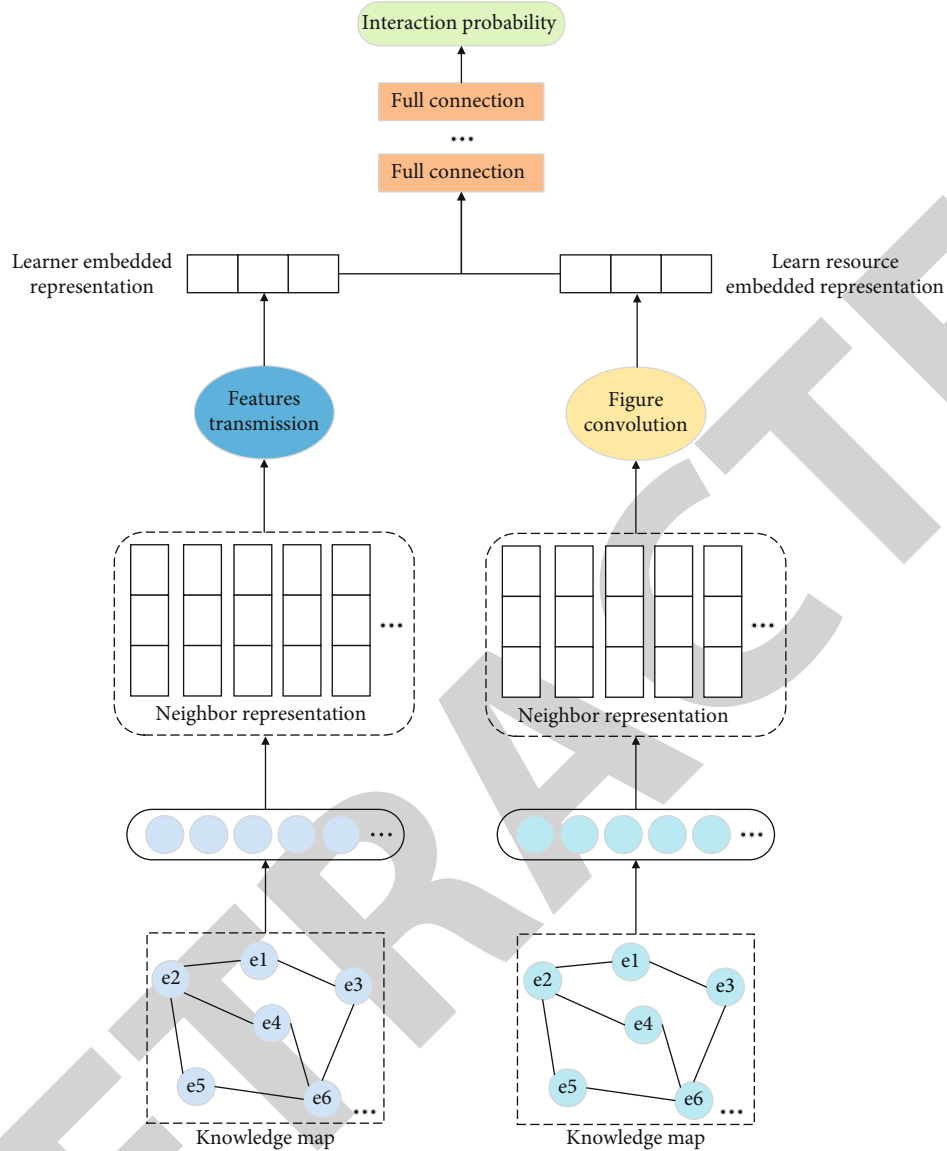


FIGURE 4: Overall algorithm model.

TABLE 1: Experimental environment.

System environment	Windows 10
GPU version	GTX1080Ti
Programming language	Python 3.6
TensorFlow version	TensorFlow 1.8
Anaconda version	Anaconda 4.9.2

with other benchmark models and increases by 1 percentage point to 4 percentage points in ACC indicators.

The comparison results of Precision@K in the Top-K task are shown in Figure 5. As can be seen from Figure 5, when  $K = 5$ , Precision@K of base-line DEKGCN is the best, and KDNP increases by 6% compared with Precision@K. When comparing experimental data, it can

be found that the baseline models KGCN and DEKGCN outperform the UDN-CBR model, implying that entity and relationship information in the knowledge graph helps to improve recommendation performance following knowledge graph introduction. Among them, DEKGCN starts from the client side and uses entities around learning resources to spread learners' preference information to calculate learners' vector representation. Its deficiency lies in that it does not use knowledge graph to improve the information quality of the project side.

The result of Recall@K in the Top-K task is shown in Figure 6. Base-line DEKGCN performed best at Recall@K, with KDNP up 11% each on Recall@K. The advantage of DEKGCN is that it considers both the client and the project. However, when aggregating the information of the client, it chooses to aggregate the demographic information of the user by constructing the user attribute



TABLE 2: Dataset statistics.

Interactive data		Knowledge map	
Learners number	45637	Types of entities	13
Learning resources number	5063	Entities number	60875
Interactions number	2651618	Relationship types	16
—	—	Relationship number	82174

TABLE 3: Performance comparison of AUC and ACC.

Model	AUC	ACC
UDN-CBR	0.852	0.811
KGCN	0.871	0.822
DEKGCN	0.911	0.833
KNDP	0.933	0.854

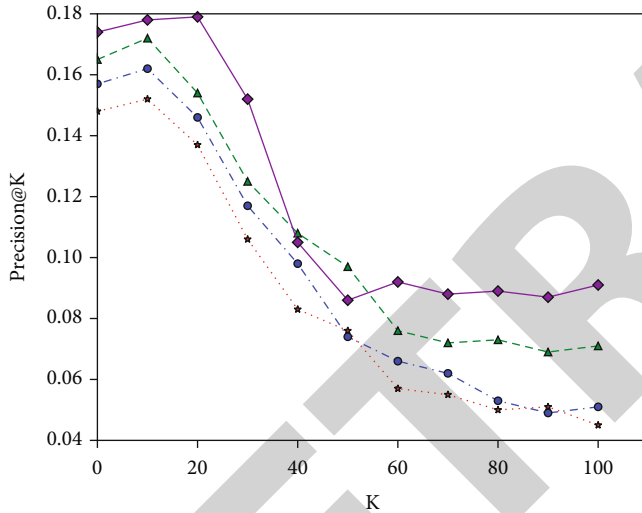


FIGURE 5: Precision of Top@K.

graph. This results in the lack of knowledge characteristic information on the user end, which leads to the lack of semantic richness of learners' embedded representation. The KNDP model proposed in this paper makes full use of the heterogeneous information of the knowledge graph on both the client and project sides and fuses the entity and neighbor information between the project and the learning target that the learner has interchanged with into the vector embedded representation of the learner, thus resulting in a significant improvement in performance.

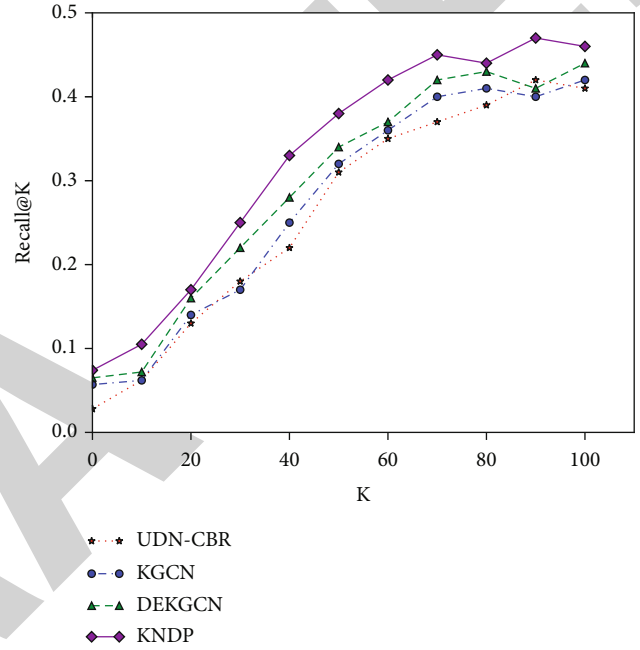


FIGURE 6: Recall of Top@K.

## 5. Conclusions

This research effectively improves the problem by applying corpus and deep learning technology to the suggestion of learning resources, in light of Chinese English teachers' weaknesses in teaching technology. The characteristics of learning resource suggestion are presented based on a thorough examination of the needs for learning resource recommendation, the principles of deep learning technology, and the deficiencies of previous research. At the same time, guided by relevant theories, a learning resource recommendation model based on deep neural network is constructed. Compared with existing studies, the model is optimized mainly from the aspects of high efficiency, diversity, and timeliness of learning resource recommendation supported by deep learning technology. For the three modules of resource filtering, resource recommendation, and resource display in the proposed model, a resource filtering algorithm based on similarity ranking and a resource recommendation and resource display algorithm based on deep neural network are designed. The experiment proves that the method in this paper has good recommendation effect, and the

## *Retraction*

# **Retracted: A Secure Private Cloud Storage Platform for English Education Resources Based on IoT Technology**

### **Computational and Mathematical Methods in Medicine**

Received 25 July 2023; Accepted 25 July 2023; Published 26 July 2023

Copyright © 2023 Computational and Mathematical Methods in Medicine. This is an open access article distributed under the Creative Commons Attribution License, which permits unrestricted use, distribution, and reproduction in any medium, provided the original work is properly cited.

This article has been retracted by Hindawi following an investigation undertaken by the publisher [1]. This investigation has uncovered evidence of one or more of the following indicators of systematic manipulation of the publication process:

- (1) Discrepancies in scope
- (2) Discrepancies in the description of the research reported
- (3) Discrepancies between the availability of data and the research described
- (4) Inappropriate citations
- (5) Incoherent, meaningless and/or irrelevant content included in the article
- (6) Peer-review manipulation

The presence of these indicators undermines our confidence in the integrity of the article's content and we cannot, therefore, vouch for its reliability. Please note that this notice is intended solely to alert readers that the content of this article is unreliable. We have not investigated whether authors were aware of or involved in the systematic manipulation of the publication process.

Wiley and Hindawi regrets that the usual quality checks did not identify these issues before publication and have since put additional measures in place to safeguard research integrity.

We wish to credit our own Research Integrity and Research Publishing teams and anonymous and named external researchers and research integrity experts for contributing to this investigation.

The corresponding author, as the representative of all authors, has been given the opportunity to register their agreement or disagreement to this retraction. We have kept a record of any response received.

### **References**

- [1] W. Li and Y. Guo, "A Secure Private Cloud Storage Platform for English Education Resources Based on IoT Technology," *Computational and Mathematical Methods in Medicine*, vol. 2022, Article ID 8453470, 12 pages, 2022.

## Research Article

# A Secure Private Cloud Storage Platform for English Education Resources Based on IoT Technology

Wei Li  and Ying Guo

*School of Foreign Studies, Tangshan Normal University, Tangshan Hebei 063000, China*

Correspondence should be addressed to Wei Li; [liwei@tstc.edu.cn](mailto:liwei@tstc.edu.cn)

Received 26 April 2022; Revised 18 May 2022; Accepted 21 May 2022; Published 14 June 2022

Academic Editor: Naeem Jan

Copyright © 2022 Wei Li and Ying Guo. This is an open access article distributed under the Creative Commons Attribution License, which permits unrestricted use, distribution, and reproduction in any medium, provided the original work is properly cited.

The contemporary ubiquitous “cloud” network knowledge and information resources, as well as ecological pedagogy theory, have enlarged teaching research’s perspective, widened teaching research’s innovation area, and created practical options for English classroom reform. Cloud education relies on the Internet of Things, cloud computing, and big data to have a huge impact on the English learning process. The key to the integration of English education resources is the storage of huge amount of English teaching data. Applying the technology and methods of cloud storage to the construction of English education resource integration can effectively save the educational resources of schools, improve the utilization rate of English education resources, and thus enhance the teaching level of English subjects. In this work, we examine the existing state of English education resource building and teaching administration and offer a way for creating a “private cloud” of English education materials. We not only examined the architecture and three-layer modules of cloud computing in depth, but we also analyzed the “private cloud” technology and built the cloud structure of English teaching materials on this foundation. We hope that this paper can help and inspire us to solve the problems of uneven distribution, irregular management, and difficult sharing in the construction of English education resources.

## 1. Introduction

With the continuous development of Internet of Things (IoT) technology and its educational application research, the promotion of IoT technology for educational management and educational teaching is becoming more and more obvious, and the popularization of IoT educational applications seems to be an inevitable trend [1]. The new IoT education application mode with education resource library as the core can greatly reduce the cost and technical threshold of IoT education application and make the popularization of IoT education application possible [2]. At present, various network educational resources, mainly network storage resources and educational resources that can be accessed through the net network, including various materials, multi-

media courseware, integrity training videos, and e-books, are intended to provide support for teachers and students’ use [3].

Traditional online English education resource platforms have many problems such as uneven distribution, irregular management, duplicate construction, difficulty in sharing, limited by storage capacity, and low security [4]. This makes it difficult for users to tap a large number of high-quality digital English education resources in the process of using them, and they are prone to low accuracy in information retrieval and low utilization of personalized resources [5]. However, the construction of English education resources is not a one-time performance completion, but a long-term process that must have long-term planning for sustainable development [6]. To eliminate the conventional closed model, data

silos, and open up the environment for exchanging educational resources, it is required to regularly update and adapt construction methodologies [7]. In addition, the construction of educational resources must take service teaching as the main goal, and the basic principles of integrated planning, clear division of labor, broadening mode, strengthening application, and continuous innovation should be done in the construction process [8]. The existing resources need to be organized in a reasonable order and sorted out, while continuously introducing the latest and foreign excellent achievements [9].

The purpose of using cloud computing to build an English education resource store is to serve many users at the same time [10]. The cloud computing system uses many technologies, among which virtualization, data storage, and cloud computing platform management are the most critical [11]. The cloud computing system uses redundant storage to ensure the reliability of data, and the distributed storage method can effectively store data [12]. The construction of an open English education resource platform based on cloud computing provides an important opportunity for the sharing of English education resources [13], and the basic architecture of cloud computing is shown in Figure 1. The feasibility analysis is as follows:

- (1) Expand the sharing of English education resources, avoid duplication of resources, and effectively improve the utilization of infrastructure. Since cloud computing supports crossplatform IoT terminal devices, the network can be used to share resources anytime and anywhere
- (2) Improving educational resource management. Through distributed and parallel computing, cloud computing analyzes and manages English education resources and stores and calculates them, and the high reliability can ensure the efficient operation of the open education resource platform

The goal of this study is to construct a “private cloud” environment and use cloud computing, a new Internet of Things technology, to overcome the shortcomings of the traditional English education resource platform. By establishing a large digital education platform for resource management and sharing, educational resources can be widely used. It can also serve as a reference for the development of cloud computing model education reform and information technology for English education.

The paper’s organization paragraph is as follows: the related work is presented in Section 2. Section 3 analyzes the architecture of the cloud platform. Section 4, discusses the design of English education resource storage system based on Eucalyptus private cloud platform. Finally, in Section 5, the research work is concluded.

## 2. Related Work

In this section, we define the analysis of the current situation of English online education resources, obstacles encountered in

the construction of English online educational resources, and advantages of private cloud-based English education resource construction in detail.

### 2.1. Analysis of the Current Situation of English Online Education Resources

*2.1.1. Analysis of Resource Management Model of Network Education on Various Platforms.* In terms of the current management modes of various English education resource repositories [14], they can be basically summarized into three types: centralized management, open management, and centralized plus open management. Centralized management emphasizes privacy and copyright protection [15], orderliness, and standardized use of educational resources to ensure security and effective use. With this approach, a single department is usually solely responsible for unified management. The model emphasizes that the characteristics of educational resources should fully reflect the professional advantages of each educational platform with distinctive cultural advantages. The disadvantage of this model, on the other hand, is the closed lack of openness. Because educational resources are often restricted to use within a single specific group, this greatly limits the space for utilization, is not conducive to fully reflecting their value, and is poorly shared. In the open management model, the idea is to open up. This management paradigm assigns different permissions to distinct groups of resource users and creates a security hierarchy for educational resources, allowing some users to have administrator privileges and upload resources. The advantage of open and interactive management is that users and managers can interact and by doing so, information resources can be continuously improved to a higher and higher level. It can truly reflect the needs of the users, and the resource effectiveness is fully reflected. The centralized management mode, together with completely open management, effectively avoids the disadvantages of both. Realizing openness in centralization and centralization in openness is the future development direction of education resource management model.

*2.1.2. Current Situation of the Development of English Online Education Resources on Various Platforms.* At present, the main form of network education resource construction is resource library [16]. From the construction of English education resource library of each platform, all of them have purchased online education resource library and online teaching platform [17]. Teachers, professionals, and software companies work together to integrate educational resources; conduct online courses, online teaching, and online course development; and build “high-quality courses.” From the perspective of the construction mode, there are mainly the following modes: (1) there are many companies engaged in research work in this area, they have made a large number of highly targeted teaching materials, direct purchase can save a lot of development costs in terms of manpower and financial resources, and these materials can be widely adapted to the majority of teachers’ requirements; (2) resource sharing with various professional open websites;

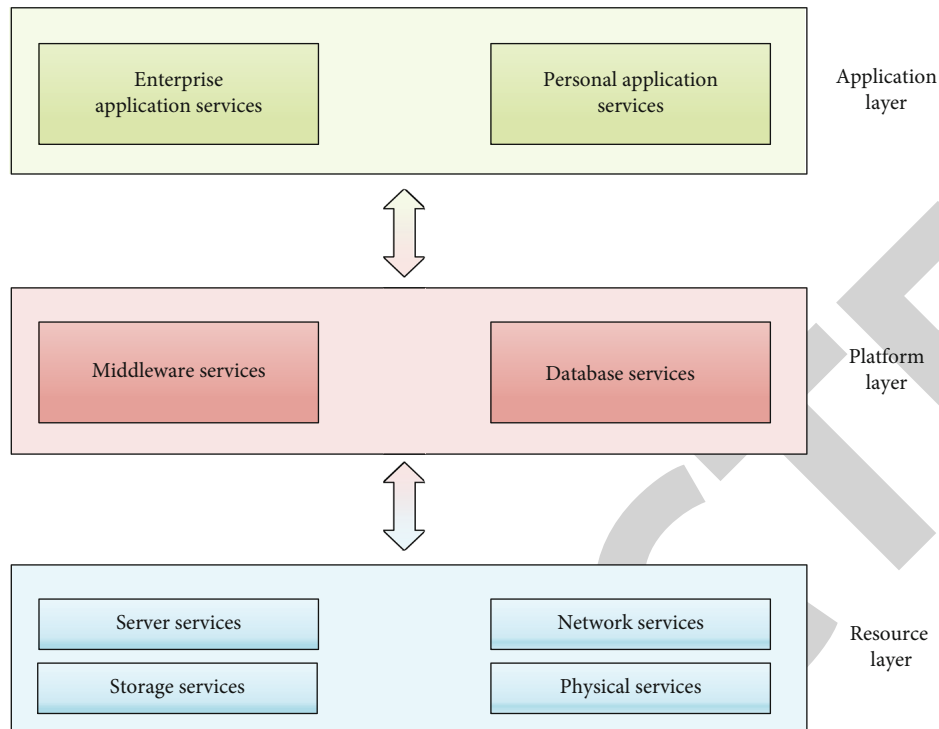


FIGURE 1: Cloud computing architecture.

and (3) mainly for each platform's own teaching philosophy and the needs of teaching teachers.

**2.2. Obstacles Encountered in the Construction of English Online Educational Resources.** According to the survey of educational resource libraries on various platforms, it is found that many inventories have problems in the following aspects.

- (1) Resource construction emphasizes quantity but neglects quality

Today's educational resource repositories range from tens of GB to several TB. The platforms often store large amounts of data with large storage capacity. Platforms often take the large data of storage capacity as a selling point and spend a lot of effort to collect more resources without paying attention to the quality of resources, resulting in impractical resource contents that do not meet the needs of teaching and learning, reducing the availability of resources and leading to the waste of resources.

- (2) Poor communication and interactive performance among users

The lack of communication between users and resource builders results in poor initiative of users, which prevents resource builders from getting timely feedback information. Because of the lack of systematic research and study to fully understand the needs of teachers and students in terms of usage, the dimension and depth of cooperation between resource builders and subject teachers are insufficient. The

bearers of resource construction are often prone to work behind closed doors, measuring the effectiveness of resources by their own standards of take and take, thus causing the repository to frequently fail to find the needed resources and frustrating the motivation of teachers and students to continue using them.

- (3) The efficiency and accuracy of educational resource retrieval is poor

The reason for this is mainly that the attribute labeling of resources is not rich and standard enough when data are stored. With the existing resources, it is too simple to provide query functions; it should provide a variety of query methods, such as keyword search, categorized information, combined query, tree view, search, and personalized full-text search.

**2.3. Advantages of Private Cloud-Based English Education Resource Construction.** Cloud computing services were applied to all areas of English platform education resource construction by building a private cloud environment inside the platform to facilitate the completion of daily teaching activities and provide an efficient and stable education resource application environment for teachers and students [18]. Building cloud-assisted teaching is a new concept that involves several disciplines, and its main research includes theories of cloud computing on traditional educational resources and various factors that affect the application of educational exploration teaching methods, cloud computing, etc. [19]. It also includes the use of information technology to create and manage current educational resources, as well

as the creation of new resource sharing models to ensure that educational resources are used to their full potential [20].

Private cloud education resource platform has the following advantages.

#### (1) Cost reduction

The English education resource platform built by applying cloud computing network can effectively control the demand for hardware and the resulting costs. In traditional servers providing network services, we often encounter various hardware failures caused by hard disk damage brought about by long-term use of the server, which may lead to data loss and bring us irreparable damage. With a server using cloud storage, such problems can be avoided. We store data in a unified cloud file, and file reads are done in the cloud. Since in cloud computing clusters, the hardware requirements for server equipment are not high, old equipment can be reused without the need to buy high-grade new equipment. Even various old inexpensive PCs can be incorporated into the cloud storage system. In this way, the procurement cost of each platform is reduced, while the service life of the hardware is greatly improved. In addition, virtualization technology can be used to consolidate the school's original group of server machines into a powerful cloud cluster through the configuration of virtualization software, which allows the school to save a lot of money in terms of hardware expenses and maintenance, etc.

#### (2) Easy sharing of resources

Working together and sharing resources, solving problems, and using resources in a virtual organization to fulfil the new needs of users are another significant element of cloud computing. Cloud computing is an integrated computing system in which users in a private cloud can share the same environment and access their desired resources at any time and from any location. At the same time, information and resources can be shared by writing a number of different computer applications that are based on the characteristics of cloud computing and allow users to access them independently for extensive collaborative learning through cooperation.

#### (3) Security

While cloud computing can improve business agility and efficiency, it can also introduce new risks and threats. Cloud users will face unprecedented challenges, not only in terms of technology, but also in terms of making significant changes in the process. Yet, a cloud-based English education resource platform eliminates the need to consider the current common security concerns regarding cloud computing in addition to the security issues common in traditional online education. On the one hand, because the cloud computing education platform is used by a single group, it is easy to implement regulatory control for users in the cloud platform. On the other hand, the architecture and design of the

cloud platform also fully consider the security policy and other related issues. In addition, the cloud platform uses user authentication and access control to control the security risks of each layer.

### 3. Architecture of the Cloud Platform

In this chapter, we define the private clouds, private cloud platform based on Eucalyptus infrastructure, Hadoop-based massive data storage platform, and HBase in depth.

*3.1. Private Clouds.* Private clouds are clouds for your own internal use and are deployed within the firewall of the English education platform's data center. Since it is built for the platform's separate use, it can effectively control data security and data quality in the private cloud. Based on the existing facilities, the platform can adopt the private cloud construction mode and deployment method that meet its own needs and combine the characteristics of cloud computing, as shown in Figure 2 for the private cloud deployment schematic.

The private cloud is deployed behind the user's firewall and is connected to the outside Internet via routing and firewall. Inside the firewall, the private cloud provides various cloud services to the IoT endpoints below. Private clouds have similar functionality to public cloud platforms, with common private cloud platforms such as IBM Cloud-Burst and Microsoft Windows Azure. A common private cloud architecture is shown in Figure 3.

From Figure 3, we see that the private cloud contains the following management platforms:

- (1) Resource management: computing, storage, network resources, applications, and operation (use) interface calls to achieve the management and monitoring of resources
- (2) Network management system: through the network management interface, used to receive a variety of information network management, including network configuration, network performance, and alarm information
- (3) Operation management: the private cloud operation management platform sends messages to users or operation managers
- (4) System management: the unified identity authentication method of single sign-on is used to enter the system management

Users can apply for and use resources through the private cloud platform, and operation managers can complete operation management operations for users and resources through the operation management portal of the private cloud operation management platform.

*3.2. Private Cloud Platform Based on Eucalyptus Infrastructure.* Eucalyptus is divided into five main parts, which collaborate with each other to provide services. They are Cloud Controller (CLC), Cluster Controller (CC), Node

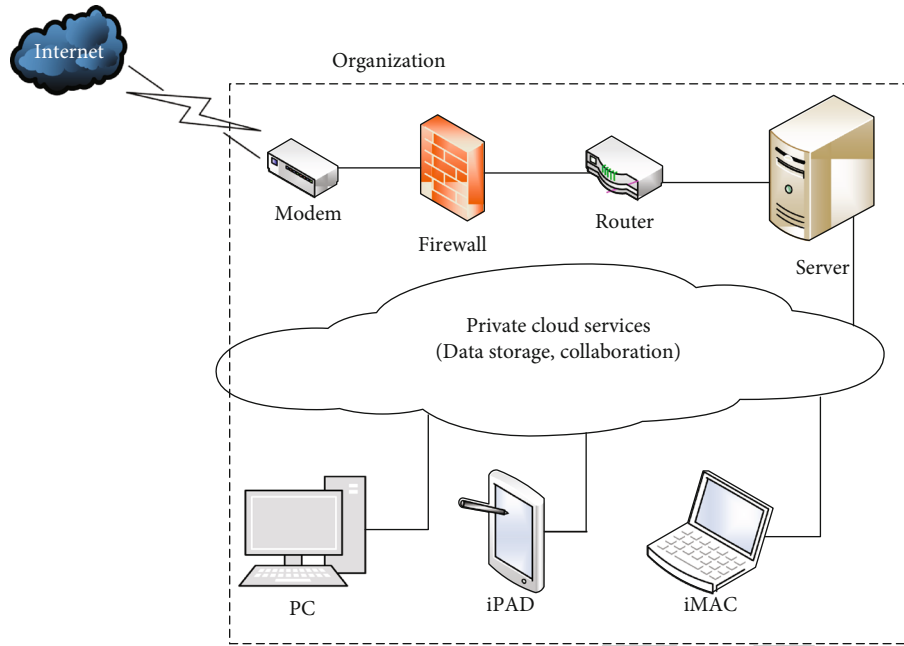


FIGURE 2: Private cloud deployment schematic.

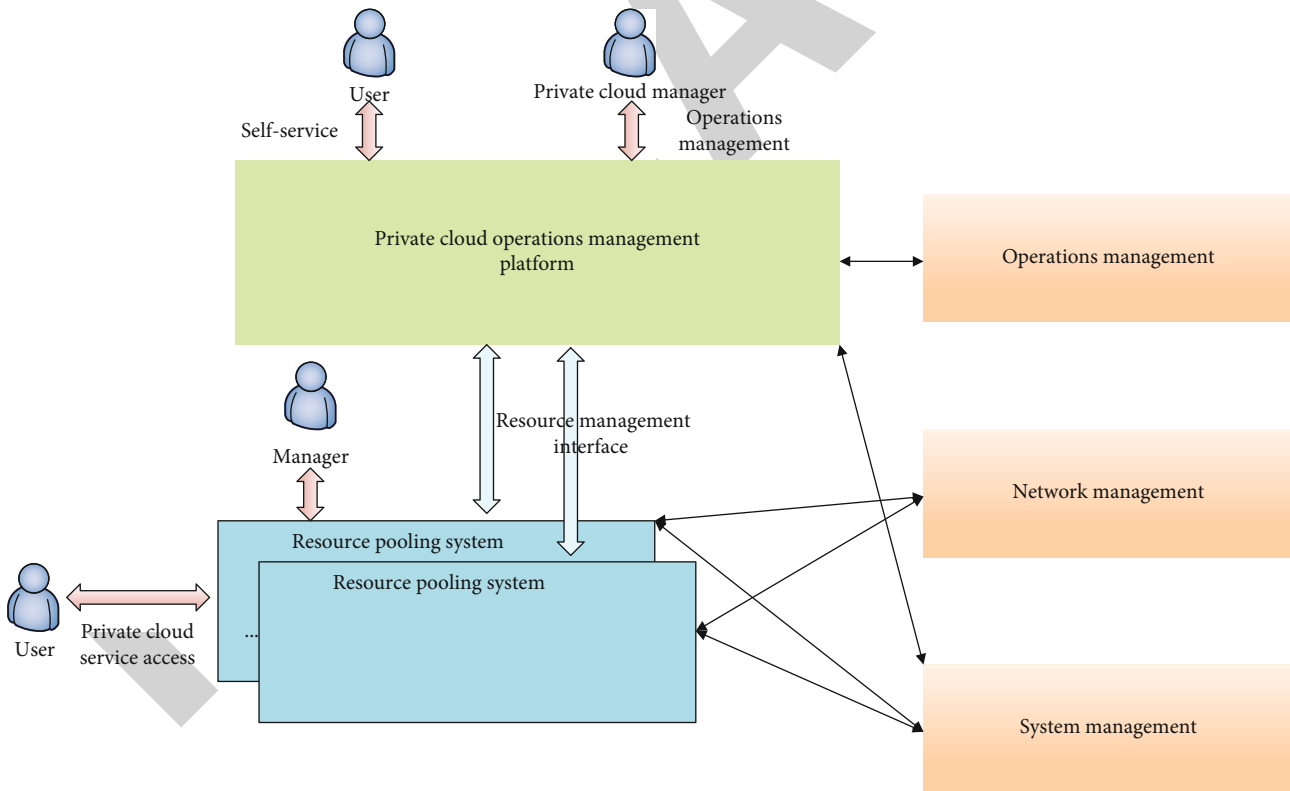


FIGURE 3: Private cloud architecture.

Controller (NC), Walrus Storage Controller, and Storage Controller (SC). Various components of Eucalyptus for flexible configuration of various topology administrators adjust the cloud platform configuration. Different levels of security are considered to meet security and management

needs. Eucalyptus can topologize one and multiple clusters. A single cluster requires at least two servers: a CC, SC, and CLC, and other small NCs; this configuration is mainly used for testing. In a multicluster deployment, different components (CC, SC, and NC) can be set to different machines.

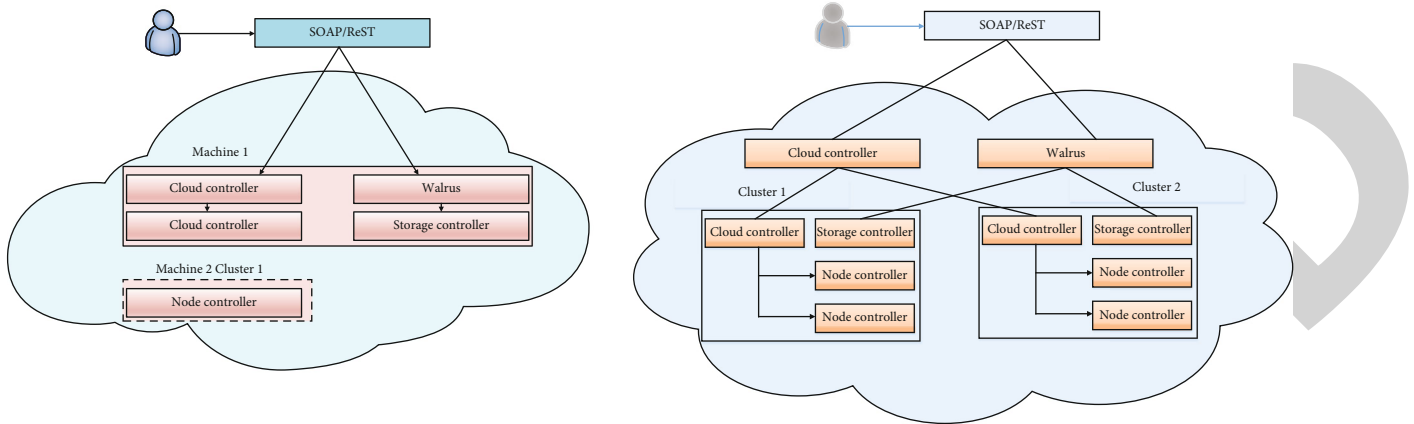


FIGURE 4: Eucalyptus single and multiclustertopologies.

If it is used for a large number of calculations, a multiclustertopology is most suitable. As demonstrated in Figure 4, resource allocation may be done across zones and nodes, and a node failure does not affect the entire cluster, leading to high availability, load balancing, and resource distribution among clusters to handle enormous data processing tasks.

**3.3. Hadoop-Based Massive Data Storage Platform.** Hadoop is a distributed system infrastructure in which users develop applications without the need to understand the detailed information system mastery. In Hadoop distributed applications, users can take full advantage of high-speed computing clusters and storage capabilities without having to understand the detailed information system mastery. HDFS is short for Hadoop's file system. HDFS is highly fault-tolerant, can be used on low-cost hardware, and has high access rates to applications. It can be used on low-cost hardware and has a high access rate to applications, making it suitable for applications with large amounts of data to compute.

HDFS, a distributed file system for use on general purpose hardware devices, is part of the composition and design of Nutch's search engine project under Hadoop. HDFS uses a master-slave architecture and is more like a hierarchical file system from the user's perspective. File commands to create, delete, move, or rename can be performed. Due to its own characteristics, HDFS is architected as a series of specific nodes. These nodes include a NameNode that provides metadata services and a series of DataNodes that provide storage blocks to accommodate applications with large data sets, as shown in Figure 5.

The files stored in HDFS are divided into 64M-sized chunks, which are then copied to multiple data nodes. The NameNode controls all file operations in HDFS, and all communication within HDFS uses the standard TCP/IP protocol.

**3.3.1. NameNode.** In Hadoop, the NameNode is the software that runs on the computer. The NameNode is the master server, responsible for managing files and namespaces, accessing clients, and the administrator of the entire system.

The NameNode determines whether data files are replicated to the DataNode.

The HDFS cluster has only one NameNode, thus simplifying the overall architecture of the system Hadoop, which manages all the metadata of the file system. The functions are composed of the following points:

- (1) The data NameNode in HDFS is used to maintain file system metadata, such as names, spaces, and data exchange information for data block mapping. It is also responsible for managing client access to files, such as opening files or directories, closing, and renaming
- (2) Detecting NameNode periodically collects the load on this DataNode node, during which the DataNode may lose contact with NameNode due to failure. If a heartbeat packet is lost, the lost DataNode is marked as failed and no new I/O requests are sent to them, while all data within this node will be cleared
- (3) Namespace management NameNode manages the system namespace. Any changes to the generated data are logged by the NameNode using EditLog. Also, the entire system uses FsImage for storage. NameNode stores the file system in the FsImage and logs it inside EditLog
- (4) Listening and processing requests to the client DataNode give NameNode the responsibility to monitor and process the requests. Based on the request, it reads and writes files, deletes them, and performs other file operations

**3.3.2. DataNode.** Each node of a DataNode deployment Hadoop cluster is a Hadoop instance, usually a piece of software running on a machine. A file is usually divided into several chunks of data, and one of the DataNode nodes is responsible for managing its own data storage and reading client requests. The DataNode receives read and write client requests and, together with the NameNode, creates, deletes,



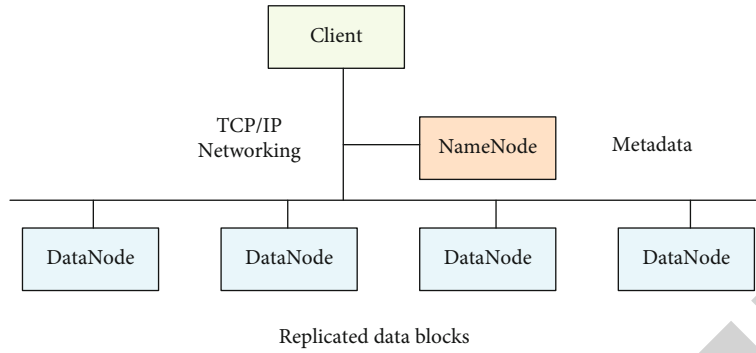


FIGURE 5: Simplified view of an HDFS cluster.

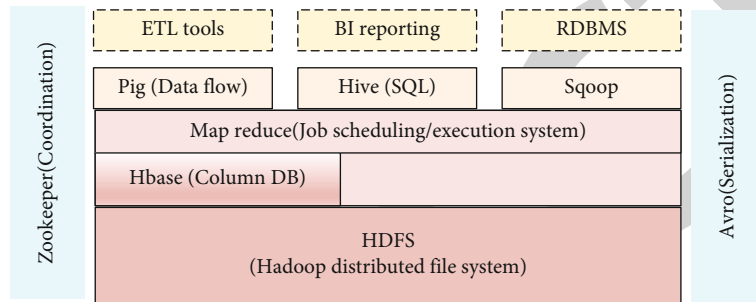


FIGURE 6: Hadoop system architecture.

and copies blocks of data. The functions of the data nodes are summarized as follows:

(1) Copy data

First, the file system server process on the client side gets a list of the blocks of data being copied from the NameNode, then copies the file blocks cached by the client to the first DataNode node, and simultaneously transfers that part to the second DataNode node. This is repeated until the copy of the file block and its data block is completed.

(2) Read and write data blocks

By contacting the client file system in the service process, when it receives a request for work from the client file system, the DataNode starts interacting with the NameNode to determine the need to create file blocks, delete, and copy, and after receiving permission from the NameNode, the DataNode client on the DataNode specified by the file system performs the specified operation.

(3) Send a heartbeat message and a block report to the NameNode

Each DataNode sends a message and file status report block to the NameNode periodically to determine the status of those DataNodes based on that report. In addition, the DataNode starts, begins scanning the local file system, and creates a list of all HDFS blocks, then sends a report to the NameNode.

3.4. *HBase*. HBase is an open-source distributed database storage schema, which also belongs to the Apache Hadoop project subproject. It is a highly reliable, high-performance, scalable, and powerful database system that can be built on servers that use it for the overall structure of a large data storage cluster. As shown in Figure 6, the HBase file storage system is Hadoop HDFS. Hadoop MapReduce is used to handle the massive data computation in HBase. Zookeeper is a unified scheduling collaboration service.

**4. Design of English Education Resource Storage System Based on Eucalyptus Private Cloud Platform**

In this section, we define the infrastructure layer design, platform service layer design, software service layer design, and database design in detail.

We share resources and enhance interaction for collaborative learning, and under the concept of computer-assisted teaching, this led to the design of a private cloud-based English education resource storage platform. The design idea not only integrates the theoretical research but also reflects the idea of preparation stage, and its overall architecture is shown in Figure 7.

*4.1. Design of Functional Submodules of Private Cloud-Based English Education Resource Storage Platform*

4.1.1. *Infrastructure Layer Design*. The core technologies of the private cloud-based English education resource storage

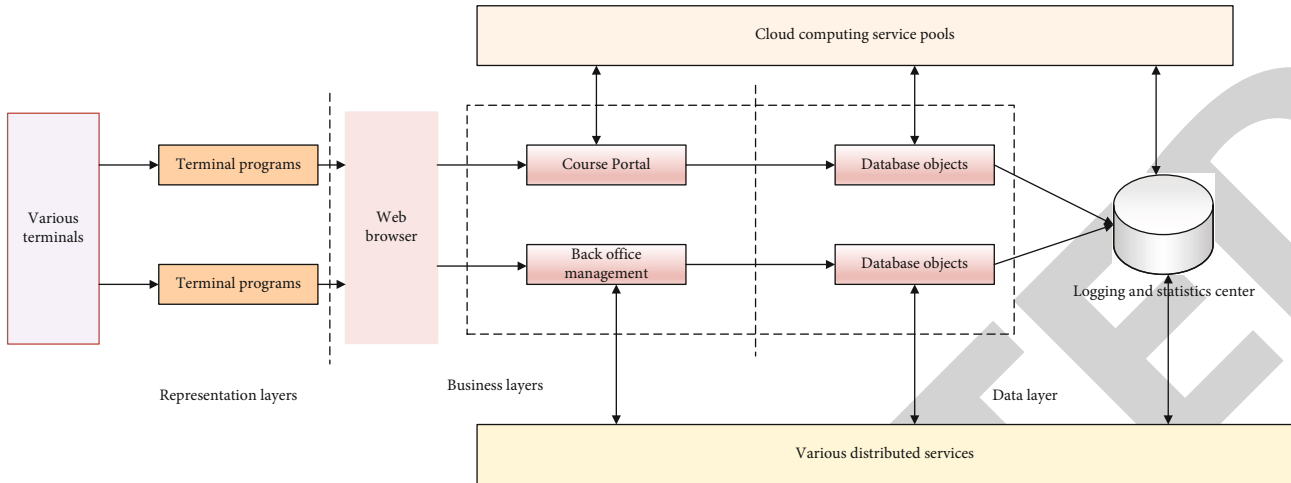


FIGURE 7: The architecture of English education resource storage platform in private cloud.

platform involve virtualization technology, data storage and management, device maintenance, redevelopment technology, and load balancing. Virtualization technology not only refers to the virtualization of applications but also can refer to the virtualization of hardware devices. In the infrastructure service layer, virtualization technology can set various resources into a virtual resource pool and complete the unified management maintenance and scheduling of resources. Users do not need to know and manage the devices in the infrastructure service layer, and they can just arrange the storage devices and install the operating system and client software according to their needs. The education resource sharing platform can scale and adjust the resources well by using the technology of virtualization, which provides a strong technical support for the dynamic management of cloud computing resources. The infrastructure service layer is shown in Figure 8.

**4.2. Platform Service Layer Design.** In the field of education and teaching, the service layer of the PaaS platform built is based on the cloud storage feature of educational resources. On this platform, cloud services integrating development, testing, and operation are provided for education practitioners, educational institutions, or enterprises. The PaaS platform service layer also includes the environment needed for developing the teaching resource cloud platform, such as development, testing, operation, and maintenance. The PaaS platform service layer also formulates standard Web protocols, data formats, SDKs, and APIs and encapsulates common functions into header files for developers to call, which greatly reduces the development cycle and difficulty of enterprises, facilitates future maintenance, and improves the utilization of educational resources. It also improves the utilization of educational resources. In the private cloud-based English education resource storage solution introduced in this paper, the architecture diagram of PaaS is given in Figure 9.

According to the given PaaS architecture diagram, PaaS is mainly composed of two parts, which are the base platform

and the service platform. The base platform generally provides environmental support for the development of application service software, such as performance management, storage management and computing, system billing, and forensic management and grid computing services, which are not visible to users. The service platform is mainly for user use and provides the environment required for application development, including development, testing, and running environments. During application development, both offline and online situations are supported. When the application is running, PaaS is in a hosted state and also features online automatic loading of the latest version of the application, real-time tracking, and traffic calculation.

**4.3. Software Service Layer Design.** The software service layer is a direct user-oriented platform on the configured education resource sharing platform. Users directly access resources, share resources, store resources, etc. after logging in through the login interface. The software service layer is user-oriented, and the user's perception and experience of using it are directly reflected in the application service, which is called the value source of the cloud platform client, where all the data and information of educational resources are stored, directly facing the user.

**4.3.1. Educational Resource Production System Design.** Aiming at the current problems of unreasonable information deployment, poor system operation, and poor human resource interactivity in the educational resource production system, the private cloud-based educational resource storage solution proposed in this paper can solve these problems well. By building a private cloud-based educational resource storage sharing platform, teachers and students can access a huge amount of teaching resources, which is convenient not only for teachers to teach production classes and assign after-class homework but also for students to finish their homework on time and submit it to teachers for review. In this cloud platform, students can also study according to their own needs and can leave

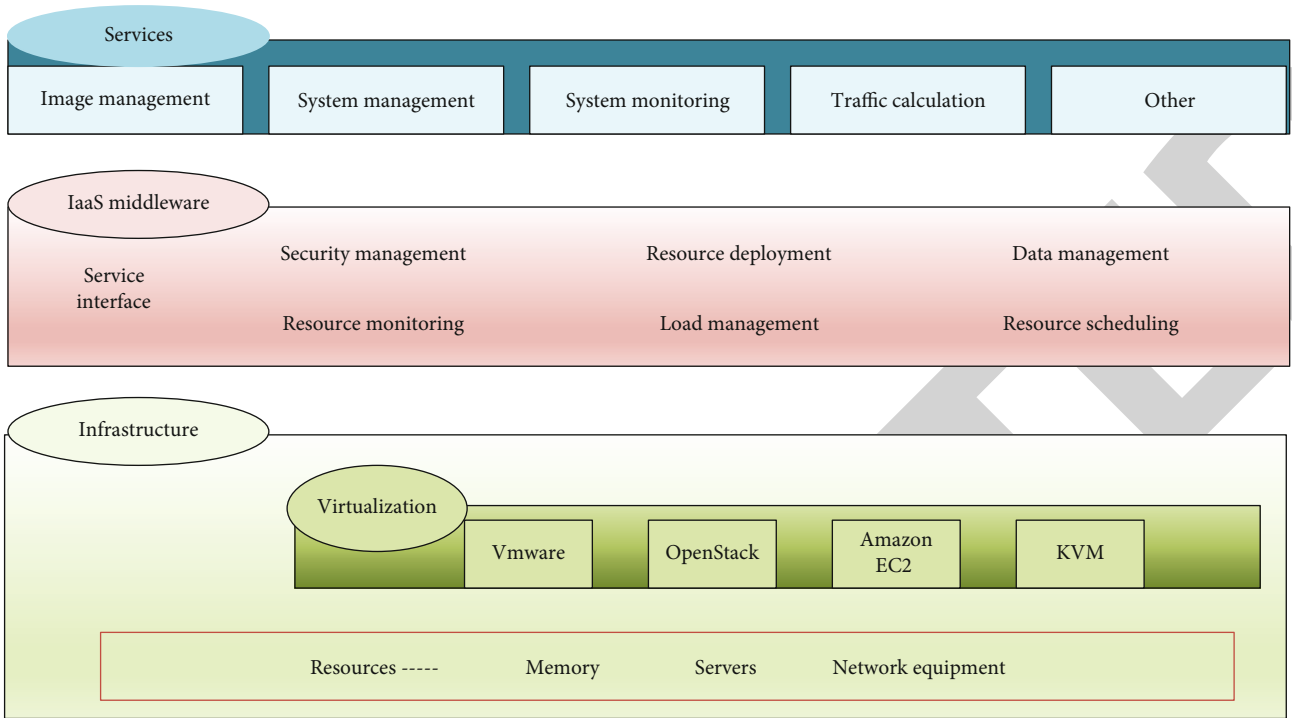


FIGURE 8: English education resource storage infrastructure service layer.

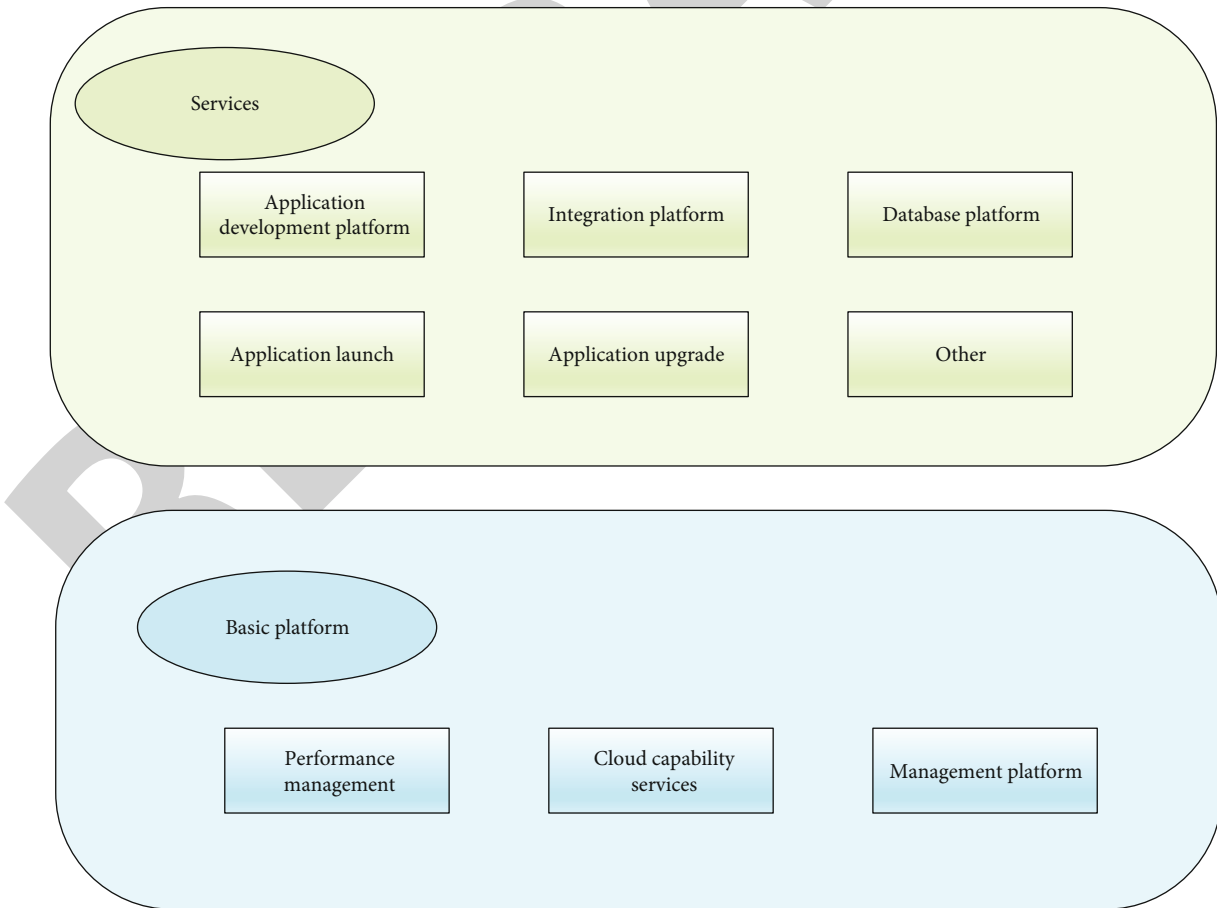


FIGURE 9: Education resource storage platform PaaS layer architecture diagram.

TABLE 1: User table.

Field	Type	Null	Default	Comments	MIME
id	Int (128)	No		Primary key	
User_name	Varchar (128)	No		User name	
Password	Varchar (128)	No		User password	
Priority	Tinyint (10)	Yes	NULL	User rights	

TABLE 2: User information form.

Field	Type	Null	Default	MIME
id	Int (8)	No		
User_id	Int (8)	No		
User_email	Varchar (40)	No		
User_name	Varchar (40)	Yes	Null	
User_address	Varchar (120)	Yes	Null	
User_sex	Varchar (4)	Yes	Null	
User_birthday	Varchar (20)	Yes	Null	
User_intro	Varchar (400)	Yes	Null	
User_time	Timestamp	No	Current_timestamp	
User_profession	Varchar (200)	Yes	Null	
User_label	Varchar (200)	Yes	Null	

TABLE 3: User resource table.

Field	Type	Null	Default	MIME
id	Int (11)	No		
User_id	Int (11)	No		
Resource_name	Varchar (128)	Yes	Null	
Resource_info	Text	Yes	Null	
Resource_type	Varchar (11)	Yes	Null	
Resource_grade	Varchar (11)	Yes	Null	
Resource_address	Varchar (128)	Yes	Null	
Resource_version	Varchar (64)	Yes	Null	
Resource_pub_sel	Varchar (11)	No	Null	
Resource_suit	Varchar (20)	Yes	Null	
Resource_discipline	Varchar (20)	Yes	Null	
Resource_edition	Varchar (20)	Yes	Null	
Resource_special	Varchar (20)	Yes	Null	
Resource_allow_download	Tinyint (1)	Yes	Null	
Resource_regi	Timestamp	No	Current_timestamp	
Resource_update	Timestamp	No	0000-00-00 00:00:00	

messages with their teachers about their confusion after studying, which strengthens the interaction between teachers and students and also helps teachers to better understand students and help them learn. At the same time, in order to build the educational resource system, three subsystems are given according to the classification of students' needs, which are courseware production, assessment, and management.

#### (1) Courseware production subsystem

The courseware production subsystem is mainly to provide convenient services for teaching staff, and it is a key part of the education resource cloud platform. There are various resources such as text, photos, audio files, and video files distributed on the network. Teachers can integrate these resources through the education resource sharing platform

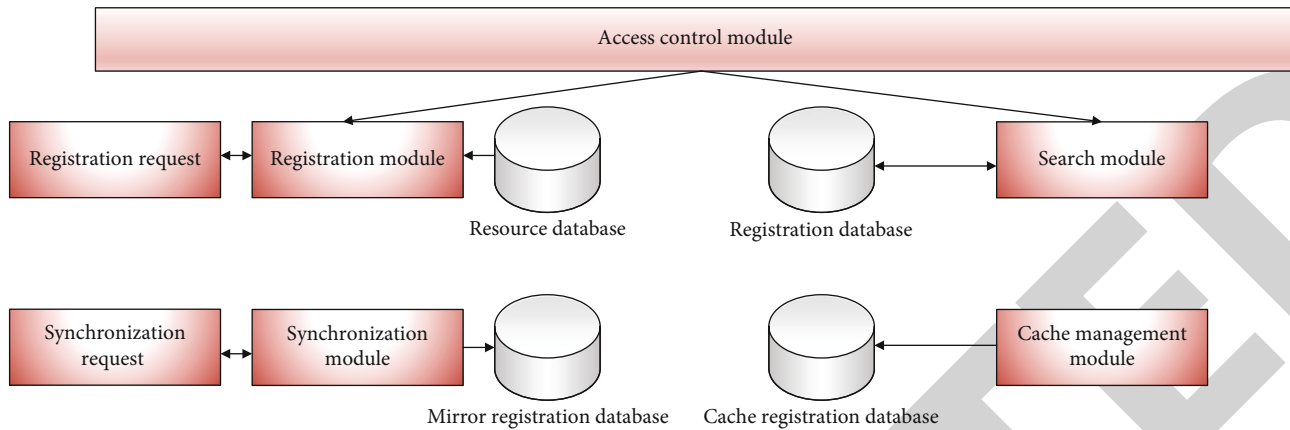


FIGURE 10: Educational resource management subsystem structure diagram.

and make an editable teaching file and then share this file on the education cloud platform for everyone's reference and learning.

### (2) Assessment subsystem

Because it is mainly for the pedagogue, the assessment subsystem is mainly to help teachers better assign homework and help students better complete their homework, and most importantly, teachers can see the homework in time after students finish it and also can review and interact online.

### (3) Educational resource management subsystem

The management subsystem is mainly responsible for the management and maintenance of the system. The system management includes the registration of new users and the permissions of student users and teacher users. In this system, users are allowed to share their own resources on the platform, and other users can access and study them. Figure 10 shows the infrastructure diagram of the educational resource management subsystem.

As can be seen from Figure 10, the management subsystem contains four modules, each of which implements a different function. Four databases with varied functionalities are also set up, with the main purpose of storing various types of data. The management subsystem's registration module performs resource verification, checks that there are no issues, and then determines it to be lawful before saving it in the database. At the same time, some annotated information about the resources will be stored in the registration database, which is convenient for the search module. The access control module is mainly to complete user verification, and those who pass the verification are normal users before they can manage the data resources. In the face of massive data, the cache module can exponentially improve the rate and accuracy of resource screening. The function of the synchronization module is to complete the mirror registration database and the cloud platform data information comparison.

**4.4. Database Design.** The information stored on the server of the English education resource cloud platform is mainly the information of network nodes, the information of materials uploaded by users, and some basic information filled in by users when they register. The following describes the design of database keywords involved in the education cloud platform. Table 1 is the user information table for the initially registered users; when there is a newly registered user, it is to be filled out according to the table information, mainly concerning the user name, password, and user rights. Table 2 is the user information table; this table is mainly used to store the user's private information, including birthday, home address, and hobbies. Table 3 is the resource table; this table stores the user's resource information, which involves whether the information is public or not, the type of information, etc.

## 5. Conclusion

Cloud storage technology and methodologies are being utilized to integrate English education resources as an emerging concept, which can significantly improve the usage rate of online platform English education resources and teaching efficiency. We provide a private cloud storage platform for English educational resources, combining cloud computing technologies, analyzing its architecture and execution, and implementing data transmission and storage using the Hadoop platform. The implementation of this platform is based on the existing mature cloud platform application examples and requires the synergy between various technologies such as multitenancy, distributed computing, and virtualization to build a cloud service platform for English education resource storage. This solution may open up new possibilities for the creation and distribution of English educational content.

### Data Availability

The datasets used during the current study are available from the corresponding author on reasonable request.

## Retraction

# Retracted: Evaluation and Analysis of Traditional Customary Law Based on the Perspective of Big Data

### Computational and Mathematical Methods in Medicine

Received 1 August 2023; Accepted 1 August 2023; Published 2 August 2023

Copyright © 2023 Computational and Mathematical Methods in Medicine. This is an open access article distributed under the Creative Commons Attribution License, which permits unrestricted use, distribution, and reproduction in any medium, provided the original work is properly cited.

This article has been retracted by Hindawi following an investigation undertaken by the publisher [1]. This investigation has uncovered evidence of one or more of the following indicators of systematic manipulation of the publication process:

- (1) Discrepancies in scope
- (2) Discrepancies in the description of the research reported
- (3) Discrepancies between the availability of data and the research described
- (4) Inappropriate citations
- (5) Incoherent, meaningless and/or irrelevant content included in the article
- (6) Peer-review manipulation

The presence of these indicators undermines our confidence in the integrity of the article's content and we cannot, therefore, vouch for its reliability. Please note that this notice is intended solely to alert readers that the content of this article is unreliable. We have not investigated whether authors were aware of or involved in the systematic manipulation of the publication process.

Wiley and Hindawi regrets that the usual quality checks did not identify these issues before publication and have since put additional measures in place to safeguard research integrity.

We wish to credit our own Research Integrity and Research Publishing teams and anonymous and named external researchers and research integrity experts for contributing to this investigation.

The corresponding author, as the representative of all authors, has been given the opportunity to register their agreement or disagreement to this retraction. We have kept a record of any response received.

### References

- [1] J. Yang and T. B. Chuan, "Evaluation and Analysis of Traditional Customary Law Based on the Perspective of Big Data," *Computational and Mathematical Methods in Medicine*, vol. 2022, Article ID 5088630, 10 pages, 2022.

## Research Article

# Evaluation and Analysis of Traditional Customary Law Based on the Perspective of Big Data

Juanjuan Yang <sup>1,2</sup> and Tee Boon Chuan<sup>1</sup>

<sup>1</sup>*Institute of Chinese Studies, Universiti Tunku Abdul Rahman, 43000 Kajang, Malaysia*

<sup>2</sup>*School of Marxism, HaiKou University of Economics, Haikou, 571000 Hainan, China*

Correspondence should be addressed to Juanjuan Yang; 201772513@yangtzeu.edu.cn

Received 25 April 2022; Revised 20 May 2022; Accepted 23 May 2022; Published 14 June 2022

Academic Editor: Naeem Jan

Copyright © 2022 Juanjuan Yang and Tee Boon Chuan. This is an open access article distributed under the Creative Commons Attribution License, which permits unrestricted use, distribution, and reproduction in any medium, provided the original work is properly cited.

Today's rule of law construction in China is walking between the conflict and coordination of factors such as reality and ideals, tradition and modernity, local and foreign, and local knowledge and universal principles, all while continuing to strengthen the unification of the legal system and advance the modernization of the rule of law. Traditional customary law, which is the most representative local resource culture, is unquestionably one of the most important themes in the formation of the rule of law. It has far-reaching significance for the development of ethnic jurisprudence, the reunderstanding of traditional culture, and the construction of ethnic unity and harmonious society. Based on this background, this paper uses big data technology to collect relevant experimental data and proposes a traditional customary law value assessment based on BPNN. The completed work is as follows: (1) this paper clarifies the concept of customary law and the difference between it and related concepts and introduces the domestic relevant research on traditional customary law and the interactive relationship between customary law and national law in dynamic legal practice and puts forward the status and influence of customary law in contemporary legal practice. (2) The related technologies of neural network are introduced, and a traditional customary value evaluation system that can be used for experiments is constructed. (3) Experiment with the designed data set to see if the BP model is feasible. The experimental results suggest that the model proposed in this study has a low error rate and performs well while evaluating traditional common law values.

## 1. Introduction

My country's legal circles have paid attention to customary law mainly since the 1990s. The study of Chinese customary law is mainly influenced by the western postmodern thought, which has formed the postmodern legal theory in the field of law. The core idea of postmodern legal theory holds that rational individuals as autonomous legal subjects do not exist, and modern society is illusory. People in the present social system are not "actual people," but appendages of the social structure, and the manner of their existence is rights [1, 2]. The universality of the law is a virtual "macrodiscourse," and the principles in the law are only an assumption. The process of modernizing the rule of law is also a process of training people to abandon specific and individual experiences, accept general rules, abandon the

rich and colorful human life, and accept standardized behavior patterns. Modern law has been influenced by postmodern jurisprudence. Individuals are independent, conscious, rational subjects, according to modern law [3]. Law progresses from lower to higher levels, and truth can be discovered by trial and error. Postmodern legal theory has brought methodological innovation to the legal circle in our nation which was previously dominated by modern legal theory and has extended the boundaries of legal research. The study of traditional customary law has caused a lot of disputes in the academic circles. Scholars hold different views on issues ranging from whether customary law is law to what is the significance of customary law to the construction of the rule of law. Domestic legal history and legal sociology scholars are the main force in the study of traditional customary law, and their research methods are mainly to find answers

from historical materials or start with the grass-roots judicial system, analyze the influence of customary law on grass-roots judicial adjudication, and study the interaction between traditional customary law and statutory law [4]. There are also scholars who doubt the practical significance of customary law research and even believe that customary law research is not only meaningless to the construction of the rule of law, but will even hinder the process of the construction of the rule of law. In view of the fact that a truly independent space for academic research has not yet been formed, it is generally believed that academic research should have practical significance, so this criticism also has considerable deterrence. Therefore, this article intends to give a little answer to this criticism. Although I do not agree that academic research must have so-called practical significance, I must insist on showing the truth of the facts. The issue of traditional customary law has such great significance to contemporary legal practice, and even the neglect of this issue is the crux of the repeated obstruction of the rule of law process [5]. Criticisms about traditional customary law research are inseparably linked to the current state of traditional customary law research. The current research is mainly carried out from a historical perspective, and some scholars describe the situation of customary law in rural justice from an empirical perspective, but they all give people a negative impression [6]. Traditional customary law is a phenomenon that has existed in history or still exists in areas where the rule of law is underdeveloped. Such research results inevitably lead to the view that traditional customary law is backward and contradicts the modernization of the rule of law, which is actually a misunderstanding of traditional customary law [7, 8]. Based on the shortcomings and misunderstandings of the current traditional customary law research, the main content of this paper is to discuss the important role of traditional customary law in legal practice, especially to reveal the operation of customary law in a modern rule of law society or developed areas under the rule of law. The reason forces us to reconsider the meaning and direction of the rule of law's modernization. Because theoretical circles have yet to form a unified authoritative view on the basic theory of customary law, this paper begins with the fundamental concept of traditional customary law, defines the concept and main characteristics of customary law, and distinguishes customary law from related concepts. In modern legal practice, the interaction between customary and national law is primarily expressed in the relationship between the two. Traditional customary law and national law are transformed into each other in legal practice. This interactive relationship may have a certain impact on the construction of the rule of law. In this context, based on big data technology, this paper uses neural network technology to evaluate and analyze the value of traditional customary law, so as to reveal the significance of traditional customary law to the construction of the rule of law in my country.

The following is the paper's organization paragraph: Section 2 discusses the associated work. The techniques of the proposed notions are examined in Section 3. The trials and results are discussed in Section 4. Finally, the research job is completed in Section 5.

## 2. Related Work

In a sense, the history and achievements of foreign legal circles studying customary law are mainly reflected in the field of legal anthropology. Therefore, it is necessary to review and sort out the history and development of legal anthropology in detail. Legal anthropology is a discipline at the edge of the two major disciplines of law and anthropology. It is a new discipline that jurists and anthropologists "interpenetrate" and cultivate on the edge of their respective disciplines [9]. For a jurist, the main sources of many legal formulations, revisions, and procedures, and their universal application, are found in the concepts and relationships embodied in everyday social life. It is this kinship between law and anthropology that drives anthropologists' attention to law. It also promotes jurists to attach importance to anthropological materials and methods and gradually forms an "emerging" interdisciplinary subject [10]. Reference [11] presents what he calls "relative, contingent relationships" that affect the legal basis, including climatic conditions, geographic environment, religious beliefs, and the political structure of a particular country. If the laws of one country can be adapted to another country, it is only very coincidental. Reference [12] believes that law is deeply rooted in the history of a particular nation, depends on the national spirit and national consciousness, and regards law as a part of the whole of social existence. From the perspective of discussing the status and role of the early human legal system in individuals of different civilizations, the dynamic research provides theoretical support. Reference [13] conducted field research and published "Crime and Customs in Primitive Society" in 1926, which is of epoch-making significance for the development of legal anthropology and the study of traditional customary law. Reference [14] believes that there is customary law, and divides the law into three types: customary law, bureaucratic law, and legal order. Reference [15] presents a very different view. In a broad sense, customary law secretly makes new laws, like the latent life of plants and animals before they are born, it is the life force of legal rules, its scope of application is infinite, and it is no exaggeration to say that it is the only source of law. Reference [16] identifies customary law as one of the two basic types of law alongside statute law and argues that customary law arises from an act generally observed where the actor does not consciously aim to create the law, but they must see their actions as conforming to binding norms rather than arbitrary choices, and customary law is equally valid. Reference [17] analyzes the meaning of custom for the formation of law, and the transitional boundaries between custom and law. Reference [18] conducted a comparative analysis of the external order and the internal order and conducted a comprehensive study of customary law including customs and conventions when discussing the internal order. For a long time, due to the constraints of the class view and the influence of the monistic theory of law, when discussing the creation of law and the origin of law, the legal circle in my country always believed that customary law was associated with the state, unique to class society, and recognized by the state. And the habit of implementation is



guaranteed by the coercive force of the state, while ignoring the objective existence of customary law and denying the category of customary law as law [19]. In the middle and late twentieth century, with the accelerated pace of reform and opening up, my country's humanities, social sciences, and other exchanges with the international community have increased, and the academic atmosphere has been unprecedentedly active. Domestic scholars began to reexamine the legal theory and research methods in our country, and more and more jurists advocated that the study of law should be related to a specific society, culture, system, etc. The de facto existence of customary law and legal pluralism has become an indisputable issue. Scholars have begun to focus on the analysis of the cultural background, functional mode, generation, and operation mechanism of customary law, especially the fate of customary law in the trend of legal unification, which is a hot spot that people are highly concerned about. Reference [20] expands the research horizon to the customary law of ethnic clans and villages, the customary law of industry, the customary law of religious monasteries, and the customary law of secret societies. It points out that minority customary law still largely dominates the minds of local people and is an effective mode of social control in minority areas. Reference [21–23] upholds the concept of legal pluralism and uses the concept of “folk law” from the perspectives of social, historical, and legal anthropology and combines a large number of rich historical facts and community cases. It makes an in-depth analysis of the status and function, operation and practice, and development and trend of national law and traditional customary law in rural society. Obviously, the views of the above parties cannot be reached, and the research methods used are also different, but most scholars recognize the existence of customary law and accept the fact of “law pluralism.” The research at this stage simply points out the relationship between traditional customary laws as a supplement to national law, but has never found a satisfactory solution to the problem of where customary law goes, thus revealing the significance of traditional customary law to the construction of the rule of law in our country.

### 3. Method

In this chapter, we discuss the introduction to artificial neural networks, network structure of BP neural network, the algorithm principle of BP neural network, deficiencies and improvements of BP neural network algorithm, and traditional and customary law value assessment system in depth.

**3.1. Introduction to Artificial Neural Networks.** The field of brain research developed the ANN data processing paradigm after studying biological neural networks in the brain. The human brain is a biological network structure made up of billions of neurons connected by complicated interconnections, as we all know. It is the source of tools for humans to carry out a series of daily activities such as memory, analysis, reasoning, and recognition. The processing speed of data information is also much higher than the processing speed of today's fastest computers. The basic unit of work of neural network in biology is biological neuron composed

of cell body and synapse. The intensity also changes continuously with the change of external stimuli, thereby realizing information storage and memory. When we see a familiar face or hear a familiar voice, it only takes a few hundred milliseconds for the biological neural network system to recognize it, which is a series of events. This ability of biological nerves, however, is not innate. Our brains have been constantly receiving information from the external environment since birth, and the connections between neurons in the brain are constantly altering, allowing us to store a great quantity of data. It is a learning process, and ultimately realize various mental activities such as thinking and emotions through these. Analogous to the behavior of information storage and processing of neurons in the human brain, an ANN model composed of a large number of artificial neurons through a certain connection method can theoretically achieve functions similar to biological neural networks. Neurons change their own structure by continuously receiving the “stimulation” of external data information, that is, the connection mode and connection strength between neurons. This change is reflected in the ANN as a change in the connection weight between neurons, through this change to process the input data information to achieve “learning” behavior. The ANN is realized by linear weighting and function mapping of the input signal, and the weight adjustment process is realized by a suitable learning algorithm to replicate the process of biological nerve cells receiving stimulation from other cells and creating output nerve signals. The data processing model established in this way is the ANN model. Although this bionic mathematical model is far from the true biological neural network, the current research results have been successfully applied to many solutions to practical problems.

**3.2. Introduction to BP Neural Network.** The neural network model can be divided into two types of network structure: feed-forward and feedback. In the feed-forward network structure, the neuron nodes of each layer will receive the input data of the previous layer and then use the linear weighting method to output the output as the input of the next layer through the function mapping. The whole process data flows in only one direction. Without the step of data feedback, the BPNN belongs to the feed-forward neural network. According to the learning method, the neural network model can be divided into supervised learning and unsupervised learning. Supervised learning means that the training and learning of the model need to be guided by the determined output data, so that the model can learn the relationship between the input and output values. The unsupervised model does not need it, and the algorithm of the BPNN belongs to the former. The BPNN is the core and essence of the entire ANN and has shown good performance in various fields such as identification, regression, and classification. Therefore, about 80% of the neural network models in practical applications take the form of BPNN or its related.

**3.2.1. Network Structure of BP Neural Network.** As a feed-forward neural network model, BPNN model consists of

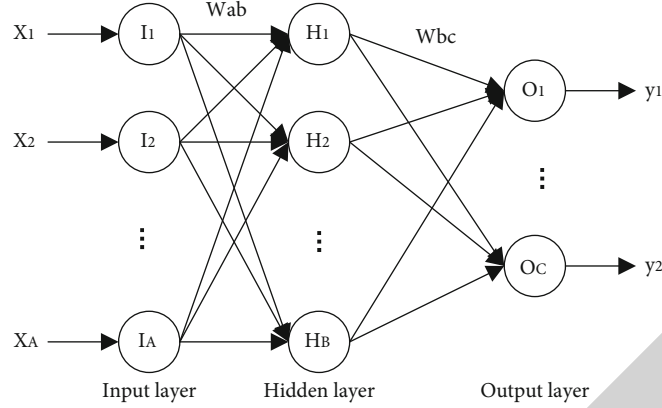


FIGURE 1: Schematic diagram of BP neural network structure.

three parts: input layer, hidden layer, and output layer. The hidden layer can have one or more layers, unlike the input and output layers, which both have just one layer. This article uses a single hidden layer to demonstrate the basic structure of the BPNN model, as shown in Figure 1, where  $x_A$  is the network structure's input data.  $I$  is the input layer of the network structure,  $W_{ab}$  is the connection weight of the input layer parameters to the hidden layer node,  $H$  is the hidden layer of the network structure,  $W_{bc}$  is the connection weight of the hidden layer node to the output layer node,  $O$  is the output layer of the network structure, and  $y_c$  is the actual output of the network structure.

**3.2.2. Characteristics of BP Neural Network.** In order to analyze the relationship between the input and the output in the BPNN, the network output is obtained by inputting the input data into the network model through the forward algorithm, and the error function between the actual output and the expected output of the network is established, also called the loss function. The function approximation can be achieved by continuously optimizing the algorithm to obtain the minimum value of the loss function, thereby reflecting the relationship between the input and output parameters. The specific algorithm principle and weight adjustment process will be given in the next section. The characteristics of the BPNN model can be roughly summarized as the following three points:

- (1) The network structure is composed of multiple layers, and there is no connection between all the neuron nodes in the same layer, and each adjacent layer has the connection which is fully connected, that is, all neuron nodes in the previous layer are connected to all neuron nodes in the next layer. This multilevel structure design can mine a large amount of information from the input data to complete complex tasks
- (2) The BPNN adopts the error back propagation algorithm. The input data is input from the input layer and propagates forward layer by layer through the

hidden layer to the output layer. After reaching the output layer, an error function is established, and the error reaches the input layer through the hidden layer, and the backward propagation in the reverse direction layer by layer continuously corrects the connection weights of the network. By iterating this process many times, you can eventually make the error smaller and smaller

- (3) Since the BPNN model needs to use the gradient descent algorithm to optimize the model, it is necessary to solve the partial derivative of the loss function. When no activation function is set, the neural network model is actually a linear weighting of parameters. When a differentiable activation function is set, the gradient descent algorithm can be used to optimize the model

**3.3. The Algorithm Principle of BP Neural Network.** As shown in Figure 2, we assume that there are an input neural parameters  $x_1, x_2, x_3, \dots, x_A$ , which are represented as  $[x_1, x_A]$  in the form of a matrix, and the input information and output information of each layer are represented by  $M$  and  $N$ , respectively, then the input information of the input layer is also the input information of the entire network, which can be expressed as:

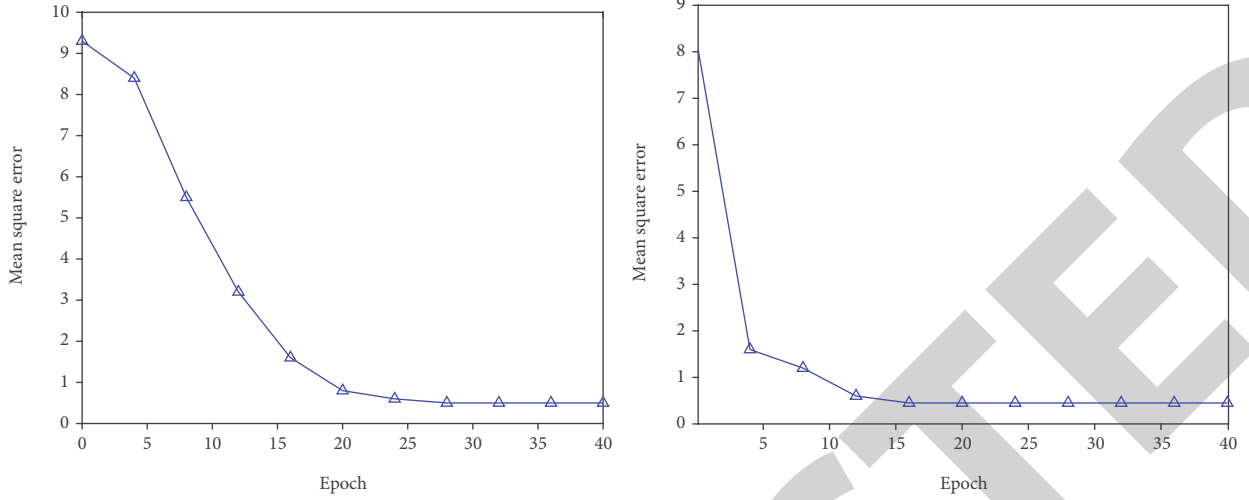
$$M_I = [x_1, x_A]. \quad (1)$$

The output information of the input layer is:

$$N_I = M_I = [x_1, x_A]. \quad (2)$$

Assuming that there are  $B$  neuron nodes in the hidden layer, the input of the  $b$ th neuron node of the hidden layer can be expressed as the weighted sum of the output  $N_I$  of the input layer and the sum of the bias term parameter  $p$ :

$$M_H^b = \sum_{a=1}^A W_{ab} \cdot N_I^a. \quad (3)$$


 FIGURE 2: Training effect when  $N = 4$  and  $N = 6$ .

Assuming that the activation function of the hidden layer is  $f$ , then the output of the  $b$ th neuron node of the hidden layer can be expressed as:

$$N_H^b = f(M_H^d). \quad (4)$$

Assuming that there are  $C$  neuron nodes in the output layer, the input of the  $c^{\text{th}}$  neuron node of the output layer can be expressed as the weighted sum of the output of the hidden layer and the sum of the bias term parameters:

$$P_O^c = \sum_{b=1}^B W_{bc} \cdot N_H^b + k. \quad (5)$$

Assuming that the activation function of the output layer is  $g$ , then the output of the  $c^{\text{th}}$  neuron node of the output layer, that is, the output of the network structure can be expressed as:

$$y_c = N_O^c = g(P_O^c). \quad (6)$$

In this way, we put input neural parameters  $x_1, x_2, x_3, \dots, x_A$  into the network structure, and the output of the network is  $y_1, y_2, y_3, \dots, y_c$ . Assuming that the expected output of the network structure is  $P_1, P_2, P_3, \dots, P_C$ , and the error of the  $c$ th neuron node of the output layer is  $E_c$ . It can be expressed as:

$$E_c = P_c - y_c. \quad (7)$$

The total error  $E$  of the network is the loss function, which can be expressed by the mean square error formula as:

$$E = \frac{1}{C} \sum_{c=1}^C E_c^2. \quad (8)$$

After the loss function of the network is obtained, the correction of the weights corresponding to the network parameters needs to be determined according to the loss function. The gradient of the loss function to the weight is calculated by the steepest descent method, and the weight is adjusted in the opposite direction of the gradient. The whole process is divided into two steps:

- (1) Adjust the connection weight  $W_{bc}$  from the hidden layer node to the output layer node
- (2) Adjust the connection weight  $W_{ab}$  from the input layer node to the hidden layer node. Make adjustments to  $W_{bc}$ . First, the formula for calculating the adjustment of the loss function to the weights is:

$$\Delta W_{bc} = -\mu \frac{\partial E}{\partial W_{bc}}, \quad (9)$$

where  $\mu$  is the step size of each adjustment of the weight, also called the learning rate.

Then, the expression of the relationship between the adjusted weight  $W_{bc}(n+1)$  and the adjusted weight  $W_{bc}(n)$  is:

$$W_{bc}(n+1) = W_{bc}(n) + \Delta W_{bc}. \quad (10)$$

In the process of adjusting the connection weight  $W_{bc}$  from the hidden layer node to the output layer node,  $N_H^b$  is the output value of the hidden layer node neuron, which can be regarded as an independent variable, and defines the concept of local gradient  $\lambda_O^c$ , which represents the required change in weights. The expression for the local gradient is:

$$\lambda_O^c = \frac{\partial E}{\partial M_O^c} = \frac{\partial E}{\partial E_c} \cdot \frac{\partial E_c}{\partial y_c} \cdot \frac{\partial y_c}{\partial M_O^c} = -2E_c g'(M_O^c). \quad (11)$$

Then, the amount of each adjustment of the weights can be expressed as:

$$\Delta W_{bc} = 2\mu\lambda_O^c N_H^b. \quad (12)$$

Adjust the connection weights  $W_{ab}$  of the connection weights from the input layer nodes to the hidden layer nodes. Similar situation with  $W_{bc}$

$$\Delta W_{ab} = 2\mu\lambda_H^b N_I^a. \quad (13)$$

In this way, the connection weights from the hidden layer nodes to the output layer nodes and the connection weights from the input layer nodes to the hidden layer nodes are adjusted in one round, and the error back propagation process of the first round is completed. The more complicated step in the whole process is that when adjusting the weight between the input layer and the hidden layer, since the hidden layer is invisible, the calculation of the local gradient needs to use the local gradient calculated in the previous step, that is, between the hidden layer and the output layer. The local gradient of BPNN can only be reversed in the process of weight adjustment. After adjusting and updating the weights of the network, a new error function is obtained through the forward propagation of the input information for the next round of weight adjustment. Through repeated iterations, the network error can be continuously reduced and the input is continuously approached. The functional relationship with the output, so as to realize the network function to achieve the purpose of classification or prediction.

### 3.4. Deficiencies and Improvements of BP Neural Network Algorithm

**3.4.1. Disadvantages of BP Algorithm.** Although the BP algorithm can approximate any complex functional relationship with arbitrary precision in theory, with more and more use, some shortcomings are gradually discovered, which are roughly summarized as more parameters, easy to fall into the local optimal solution and the three points of overfitting phenomenon:

- (1) The problem of more parameters. BPNN needs more parameters due to its structural characteristics, and the determination methods of many parameters are not very certain. Layer weights and learning rates, as well as the number of nodes in each nested layer, are all included in this list. When utilizing the BP method, the phenomena of “gradient diffusion” may arise if the number of network levels is too deep. Overlearning will occur if the number of nodes in the hidden layer is excessive. There is a risk of poor learning if the number of neurons is too low. As a result, if the learning rate is too high, the parameters may swing back and forth on either side of the optimum solution but fail to converge, or the learning

rate is too little. The optimal solution cannot be quickly converged within the number of iterations

- (2) The phenomenon of local optimal solution. Due to the setting of the initial weight, the BP algorithm may have a poor “initial position” of the loss function, and the learning process only converges to the local minimum value and does not reach the global minimum value; thus, the phenomenon of local optimal solution appears
- (3) Overfitting phenomenon. After the BP algorithm optimizes the set loss function on a certain training data set, the model may perform well on the training data, but perform poorly on the unknown data. The reason for this is that the model overly “remembers” each “random noise” part of the training data and neglects to “learn” general trends in the training data

**3.4.2. Improved Method of BP Algorithm.** Although the BP algorithm has flaws, scientists have continued to explore and improve it, and some enhanced approaches have demonstrated promising outcomes in practice.

- (1) Regarding the setting of the learning rate, the exponential decay method can be used to set the dynamic learning step size, and a larger learning rate can be set in the early stage of iterative learning to quickly obtain a relatively optimal solution and gradually decrease with the increase of the number of iterations. A small learning rate is used to ensure stable convergence in the end
- (2) In the case of local optimal solutions, the genetic algorithm can be used to “preprocess” the initial weights instead of using random weights to set the initial parameters, resulting in a loss function “initial position” that is a relatively ideal value, greatly improving the model’s stability and better predicting the function’s output
- (3) Regarding the overfitting problem, a regularization method can be used, and indicators can be added to describe the complexity of the model, through the idea of limiting the size of the weights to control that the model cannot arbitrarily learn “random noise” in the training data

**3.5. Traditional and Customary Law Value Assessment System.** In order to establish a reasonable traditional customary law value evaluation system, we must first discuss the value of traditional customary law.

**3.5.1. Control of Rural Society.** Rousseau has commented on the customary law, adding to these three a fourth, and the most important of all, which is neither inscribed in marble, it is not engraved on the bronze watch, in the folks’ hearts. If you want to discover what constitutes a nation’s genuine constitution and how the nation’s founding spirit may be preserved and replaced, you need to go no further than the power of habit. This is the power of habit. It can be said that

customs and customary laws formed based on customs and habits are an important part of ancient Chinese rituals. These customary laws arise from people's daily life and are the norm in people's daily life. Ancient China has a deep understanding of the role of rituals. It can be said that it is the first line of defense to prevent disputes and achieve a good social order, and it is the most important means of social control. From the point of view of the code of conduct alone, this is no different from the law, and the law is also a code of conduct. The difference between ritual and law is the power to maintain norms. The law is enforced by the power of the state. The state refers to political power. Tribes were also political power before the modern state was founded. This tangible authority is not required to keep the ritual going. It is tradition that maintains this norm. In fact, the content of traditional customary law is very rich, and its manifestations are also varied. The basis for its effectiveness may come from tradition and its social organization, or from the state. The source of law is customary law, which is a social norm, and there have been countries in history where a set of carefully formulated customary laws was more than enough to solve problems. Most of the countries in ancient times were rural societies with traditional customary law, so customary law played a central and leading role in their social control system.

*3.5.2. Demonstrate Psychological Conviction.* Like legal concepts, traditional customary law has many interpretations. In traditional Chinese jurisprudence, all laws are related to the state, and customary law is no exception. Therefore, customary law is a habit recognized by the state and guaranteed by the state's coercive force. It strictly distinguishes custom from customary law, and its scope is narrow. Whether this usage of customary law is appropriate or not is irrelevant. According to general terminology, as a norm of customary law, its effectiveness depends to a large extent on a similar mechanism of enforcement, albeit from consent rather than enactment. Habits are not characterized by any coercive mechanism. The Oxford Dictionary of Law is more open, when some custom and custom and prevailing practice has been established in a considerable part of the country, recognized and regarded as legally binding, as if it were based on written legislative rules, they can rightfully be called customary law. Here, its validity is based on people's "psychological conviction," as long as people are convinced of its legal effect, it is customary law. This conviction may come from coercive institutions, from natural laws, or from religion, etc.

*3.5.3. Improve the Binding Force of Custom.* In recent years, Chinese academics have steadily expanded the concept of customary law and collaborated in the research of customary law. In the opinion of some legal academics, national customary law is a code of behavior formed by people based on facts, experience, and a specific social authority that is apart from state statute law. He also summed up the characteristics of national customary law into six characteristics: rooted locality, content vitality, informality of procedure, regionality of jurisdiction, internal control of operation, and

TABLE 1: Traditional and customary law value assessment system.

Number	Index	Label
1	Maintain the creative spirit of a nation	X1
2	Prevent social disputes in rural areas	X2
3	Liveness of content	X3
4	Informality of procedure	X4
5	Territoriality of jurisdiction	X5
6	Operational internal control	X6
7	Maintained constancy	X7
8	Politically significant	X8
9	Contribute to the construction of sound laws	X9
10	Contribute to regional economic benefits	X10

constancy of maintenance. Some scholars define customary law as some custom practice and common practice recognized and regarded as legally binding. The sum of customary binding forces that preserve and regulate the relationship between a social organisation and its members is referred to as customary law. It is created by the members of the organisation or group to meet the organizations or group's production and survival demands. Certain regions are subject to mandated codes of behavior. The characteristics and manifestations of customary law are fully explored in "China Minority Customary Law Research," which has a stronger guiding role in understanding and interpreting customary law. Customary law is corresponding to the statutory law of the state. It comes from various social organizations and social authorities, regulates the behavior of all members of a certain social organization and social area, and is generally abided by them. Secondly, it must be clear that customary law is not created out of thin air; it comes from various habits that already exist in society. Lastly, customary law is both natural and customary, and it is also agreed upon by members of a specific social organization. It can be unwritten or written, and it must not be considered that customary law must be expressed in unwritten form. Customary law mainly relies on word of mouth and behavior to spread and inherit. In addition, some scholars believe that customary law is a code of conduct that is jointly confirmed by members of society and is applicable to a certain area in order to maintain social order, adjust, and deal with people's mutual relations within or between ethnic groups. This article still follows the habit of most Chinese and foreign scholars to call it "customary law" and believes that customary law is a habit of people and their communities in their mutual exchanges, with certain rights and obligations as the content and is established by people outside the country. A code of conduct that guarantees that it is generally followed in a certain area or group.

In this regard, our considerations are: first, the emergence of customary law is based on the premise of people's interaction with each other and is a code of conduct to clarify their mutual rights and obligations, rather than the premise of the formation of a state or other public authority, trying to expand the time limit of its existence as much as possible;

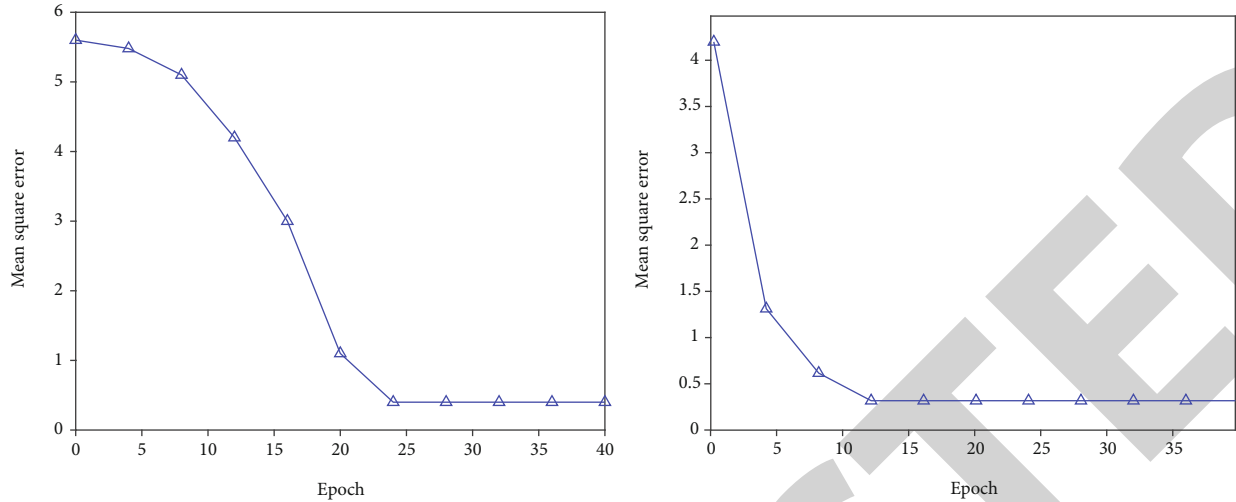


FIGURE 3: Training effect when  $N = 8$  and  $N = 10$ .

second, the inclusion of rights and obligations is to distinguish them from purely obligatory taboos, morals, and other norms, and their rights and obligations are not necessarily very clear and not necessarily equal, so the use of the word “must” is limited; thirdly, the way of enforcement outside the state is to distinguish between customary law and national law; the case law in the common law system and the custom recognized by the national legislative process are not in the scope of customary law, those who do not use “coercive force” but use coercive methods, including unorganized coercive methods such as pressure from religion, spirituality, and social public opinion; fourth, a specific region or community emphasizes that customary law is a type of local knowledge distinct from human beings’ universal natural law. For example, it is not a customary law for a group to wear clothes, and it may be a customary law not to wear it, to wear it less, or to wear it uniquely and nonnormative behavior towards specific people and things. To sum up, this paper constructs a traditional customary law value evaluation system, as shown in Table 1. According to the input indicator data, the output is finally set to three levels.

#### 4. Experiment and Analysis

In this section, we define the normalization of input and output variables, selection of data sources and network parameters, and determination of BP network verification model in depth.

**4.1. Normalization of Input and Output Variables.** When processing data with a neural network model, it is generally necessary to preprocess the data, and the most commonly used processing method is data normalization. The data normalization processing method refers to converting all input and output data to between 0 and 1 on the basis of ensuring that the characteristics of the data information remain unchanged. The reason for normalizing the data is that since the neural network often deals with nonlinear functions, it

can be seen in chapter 3, principles of network algorithms, that the nonlinear process is realized by the activation function of the network. The most commonly used activation function is the sigmoid function whose value range is  $[0, 1]$ . In the case of not normalizing the data, there may be a certain order of magnitude difference in the data, and the difference may be large. At this time, the data with a small value will produce small errors, while the data with a large number will produce a relatively large error. Also mentioned above, the training process of the neural network is based on the total error to adjust the weight of the neural network, which will cause the component with small error to account for a larger proportion of the total error than the component with large error in the total error. This is not conducive to the optimization of the network within a certain number of iterations. Normalizing the data can greatly reduce the impact of this problem on the model accuracy, which has been proved by the research of many scholars. Commonly used data normalization methods are mainly divided into maximum and minimum methods. Its normalization formula is as follows:

$$I = \frac{I - I_{\min}}{I_{\max} - I_{\min}}, \quad (14)$$

where  $I_{\max}$  and  $I_{\min}$  are the maximum and minimum values in the data sequence to be processed, respectively.

**4.2. Selection of Data Sources and Network Parameters.** According to the evaluation indicators constructed in chapter 3, this paper designs a related questionnaire and then uses the big data technology to obtain the data set required for the experiment, including 280 sets of data, of which 240 sets are used as training sets and 40 sets are used as test sets. The number of nodes in the hidden layer is another important parameter of the hidden layer, but the precise determination of the number of nodes is still a key problem to be solved so far. Similar to the number of hidden layers,

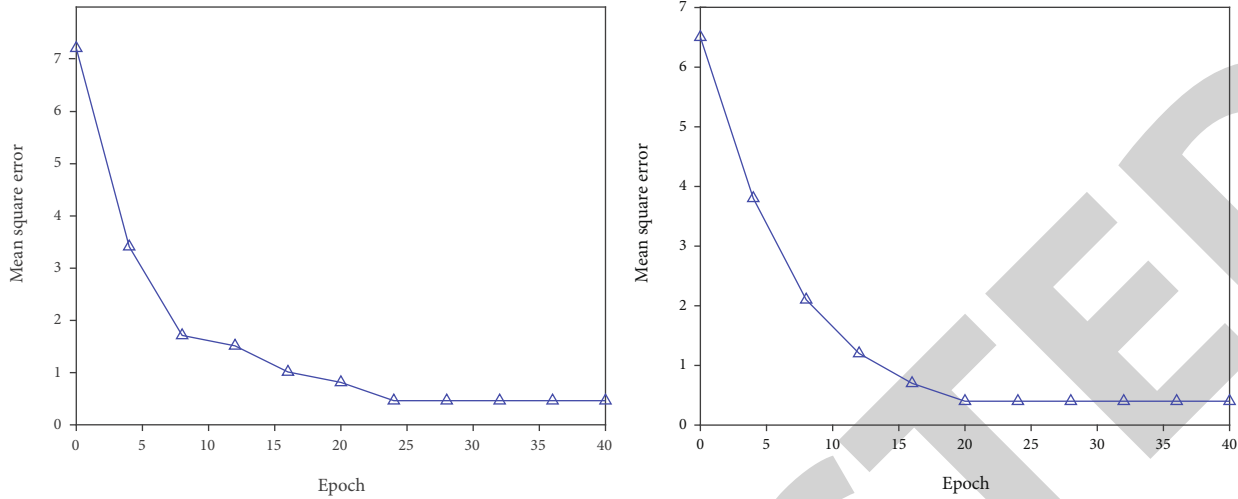


FIGURE 4: Training effect when  $N = 12$  and  $N = 14$ .

TABLE 2: The comparison between the expected output and the actual output.

Number	1	2	3	4	5	6	7	8
Actual output	0.815	0.728	0.691	0.885	0.762	0.785	0.693	0.919
Expected output	0.808	0.712	0.712	0.840	0.755	0.791	0.674	0.902
Error	0.007	0.016	0.021	0.045	0.007	0.006	0.019	0.017

the selection of points also has the same problem. Too few nodes will affect the learning ability of the network and cannot achieve the expected accuracy. Too many nodes will not only increase the training time but also may cause the network to fall into a local optimal solution. According to the successful cases studied by relevant scholars, the selection of the number of nodes is usually given by the following empirical formula:

$$H = \sqrt{m + n} + a, \tag{15}$$

where  $H$  is the number of nodes in the hidden layer,  $m$  is the number of neurons in the input layer,  $n$  is the number of neurons in the output layer, and  $a$  is a constant between 0 and 10.

The number of hidden layer nodes is estimated to be in the range of [4–14] using the algorithm above. As a result, the experiment is conducted using the trial and error approach, with the number of nodes chosen as 4, 6, 8, 10, 12, and 14 for the experiment. The results obtained are shown in Figures 2–4. Finally, according to the experimental results, the most suitable number of nodes is selected as 10.

**4.3. Determination of BP Network Verification Model.** The number of hidden layer nodes of the network model is 10, the number of input indicators is 10, and the test set is used for experiments. At this time, the actual output and expected output of the model are shown in Table 2. The network error is low, and the average prediction accuracy of the model is high. At this time, the network performance of the model

is better, and the functional relationship between input and output can be approximated with high precision.

### 5. Conclusion

As a legal phenomenon, traditional customary law plays a role similar to that of national law in the formation of order and the settlement of disputes. It is closely related to national law in various fields and has an important influence on contemporary legal practice. However, to some extent, the legal circle of our country only regards customary law as a historical phenomenon or a manifestation of backward legal system, which is a misunderstanding in the study of customary law. If customary law is a social order that emerges spontaneously, it is acknowledged by academics as having had a significant historical impact, as evidenced by a great number of historical and sociological research findings. The worth of conventional customary law is assessed using a neural network in this paper. The work done is as follows:

- (1) This paper clarifies the concept of customary law and the difference between it and related concepts, and introduces domestic and foreign research on traditional customary law and dynamic legal practice. The status and effect of customary law in current legal practice is proposed by the interaction link between customary law and national law
- (2) The related technologies of neural network are introduced and a traditional customary value

## Research Article

# Predictive Analysis of Hospital HIS System Usage Satisfaction Based on Machine Learning

Yuhang Hu<sup>1</sup> and Haotian Gan <sup>2</sup>

<sup>1</sup>Finance Section, The Second Affiliated Hospital of Qiqihar Medical University, Qiqihar, 161006 Heilongjiang, China

<sup>2</sup>Computer Centre, The Third Affiliated Hospital of Qiqihar Medical University, Qiqihar, 161006 Heilongjiang, China

Correspondence should be addressed to Haotian Gan; ganhao99@qmu.edu.cn

Received 19 April 2022; Revised 12 May 2022; Accepted 17 May 2022; Published 14 June 2022

Academic Editor: Naeem Jan

Copyright © 2022 Yuhang Hu and Haotian Gan. This is an open access article distributed under the Creative Commons Attribution License, which permits unrestricted use, distribution, and reproduction in any medium, provided the original work is properly cited.

Hospital information system (HIS) can provide a full range of information support for various hospital business activities and information collection, processing, and transmission, helping medical service providers. And HIS can reduce medical service costs and improve work efficiency, greatly reducing errors in diagnosis and treatment. Although the advantages of using the HIS are obvious, there are still some challenges in its use, the most prominent being how to make the medical staff use HIS effectively. Based on this background, this paper uses machine learning (ML) technology to predict and analyze the satisfaction of HIS use in hospitals and completes the following work: firstly, introduce the situation and development trend of HIS construction at home and abroad and provide theoretical basis for model design. The related development technologies are discussed and studied in detail. Second, the ML algorithm is used to provide a prediction strategy. The support vector machine (SVM) can handle small data sets well, and this study applies the AdaBoost technique to improve the model's generalization ability and accuracy. Lastly, a diversity metric is included to guarantee that the basic learner has good variety in order to increase the algorithm's performance. Accuracy rates may reach more than 95% in the case of tiny data sets, according to the self-built data set used for testing. This proves the superiority of the model proposed in this paper.

## 1. Introduction

The amount of scientific and technical objects that aid people's lives and work has steadily increased, and informatization has gradually supplanted the intrinsic conventional, with information systems being applied to all aspects of daily life, whether thoroughly or superficially. The deep integration of traditional medical care with information technology and the Internet has generated an entirely new revolution in the medical industry at hospitals, where our health and personal information are firmly linked. Hospitals at all levels have spent a great deal of money in the installation and development of HIS with the full backing of the government. Secondary and tertiary hospitals are now widely accepted, resulting in vastly improved medical care [1].

In 2018, the State Council issued several documents to emphasize the development and improvement of the "Internet+medical and health" service model and to improve the hospital informatization construction and convenience services [2]. HIS can provide comprehensive information support for various hospital operations and information collection, processing, and transmission, and help medical service providers such as doctors, nurses, and hospital management to obtain more timely, accurate, and complete medical information. The reduction of medical service costs and the improvement of work efficiency also greatly reduce the errors of diagnosis and treatment, and ultimately, the improvement of medical quality brings the improvement of patient satisfaction [3]. Despite the apparent benefits of employing the HIS, there are still certain difficulties



associated with its implementation. One of the most important is how to make HIS “effectively used” by its direct users, such as physicians, nurses, and hospital managers. Most hospitals these days gauge how well physicians are doing their jobs based on how long they spend treating patients and how accurate their diagnoses are. For the sake of the hospital’s efficiency and effectiveness, the HIS should be implemented in order to better support the hospital’s entire work flow. However, in their day-to-day duties as doctors, they must also deal with the unique challenges that come with working in a hospital and dealing with a variety of situations that arise due to the unique nature of patient care, including diagnosis, treatment, and follow-up. The standardization of most information systems means that they are not always able to assist medical professionals in dealing with a variety of unique scenarios. Instead, it increases their burden and, in certain cases, decreases their level of agency at work. Since many physicians and other system users, such as nurses, simply see the hospital information system as a tool they must use because of the hospital’s demands, they are unable to make full use of the system and fail to meet the goals of its deployment [4]. Because of this, it is critical to examine the way in which HIS is used and the impact it has on medical diagnosis and treatment, as well as hospital administration, and to perform an in-depth theoretical exploration of the elements and mechanisms that influence it. Scholars in both the United States and overseas tend to concentrate on how to get people to use information systems from the standpoint of frequency and length of usage, and they tend to focus on enterprise information systems rather than HIS. Studies on information systems’ postimplementation stages have become increasingly common in recent years, but there are few studies on the “effective use” of the system in terms of integrating the user’s personal characteristics, technical characteristics, and organizational environment in relation to medical scenarios. The research perspective of the “effective use” of the system to explore the influencing factors at different levels is even lacking [5, 6]. Therefore, starting from the special context of the application of information systems to hospitals, this paper explores how personal, technological, and environmental factors affect doctors, nurses, and hospital management based on the classic behavioral theory, technology acceptance model and its extended model. Medical service providers “effectively use” the hospital information system and then combine ML technology to predict and analyze the satisfaction with the use of the HIS, in order to promote the improvement of my country’s medical quality and the development of hospital informatization.

The paper organizations are as follows: Section 2 defines the related work. Section 3 discusses the methods of the proposed concepts. Section 4 discusses the analysis of experimental results. Section 5 concludes the article.

## 2. Related Work

The United States is the first country in the world to use the HIS [7]. The United States was the first to introduce computers into hospital management and financial work. After

computer engineers continued to improve the software, computers were expanded to all aspects of hospital work and used in various fields of hospitals, such as medical treatment, scientific research, and teaching. And management and other aspects have been comprehensively promoted and finally formed the so-called HIS system. The information system of American hospital is the originator of modern HIS. In the 1990s, the US Department of Defense developed and designed a new generation of HIS system for the US military in hundreds of hospitals and more than 500 clinics around the world [8]. The system can not only share the patient’s medical examination results, electronic medical records, and medical imaging data on the Internet, but its biggest feature is that it can realize telemedicine consultation among US military hospitals around the world [9]. HIS research and development in European countries started later but progressed quickly. Almost every European country has succeeded in implementing a standardized HIS, which requires connecting computer terminals across a LAN to build a regional network and then creating an HIS with systematic features. Denmark’s “Red System,” for example, and France’s “Integrated Hospital Information System” are two of the best examples [10]. A system called “SHINE” is currently being developed by the EU countries represented by Germany, France, the United Kingdom, and Italy, which not only maintains the functional characteristics of the hospital’s own information system but also shares information between hospitals in various countries via the Internet [11]. In general, the HIS research in developed countries in Europe and the United States is early and the development speed is fast. It was originally to meet the business needs of the rapid development of the hospital, but in turn, it has promoted the progress of the hospital’s work in the continuous practical application.

It is the informatization of hospitals in developed countries, an important part of modernization [12]. The development of hospital informatization can be roughly divided into three stages. The first stage is hospital administrative office management, the second stage is hospital information system, and the third stage is HIS that focuses on medical impact processing, unified medical language system, patient records. HIS is trending towards miniaturization, intelligence, and integration. In the early days of the founding of China, my country’s economic foundation and science and technology were relatively backward, and objective factors caused the research on HIS in my country to be nearly 20 years later than that of developed countries in Europe and America. In the 1990s, China began to develop its own HIS. The software enterprise units gradually develop my country’s independent HIS system. Although our country started late, the system function basically has the characteristics it should have. Compared with foreign medical standard systems, my country’s medical information does not have consistent standards for data information and business processes, which invisibly increases the difficulty and complexity of system development and hinders the sharing of medical information among hospitals [13–15]. Therefore, in the process of building hospital informatization, country should increase capital investment to improve hospital

information standardization. This can improve the information interface between the hospital and external institutions and truly realize the integration of hospital information [16, 17]. There are many HIS software development businesses on the market, and the standard specifications and module functionalities of the systems built by different companies are relatively different because there is no unified development standard and specification for the HIS at the moment. In recent years, the HIS has gotten increasingly difficult in order to fulfil modern hospital management, and it is no longer a solution for a single manufacturer. There is an integration problem in the application of products from different manufacturers in the same hospital. And because the functions of the HIS are gradually expanded, different modules use completely different hardware and software technologies, and may be developed by different manufacturers, the management of the entire information system is decentralized, and there is no natural relationship between modules. Moreover, most HIS use the method of parameter definition to solve the problem of software adaptability. Once the parameter definition cannot meet the needs of users, modifying the program may become a catastrophic task [18–21]. In order to meet the needs of parameter definition, the module is very complicated to write, and the modification is prone to new errors. The reason for this confusion is that each HIS development enterprise does not have a unified standard, which makes it difficult to transmit and share information in a “heterogeneous environment.” There is already a mature standard HL7 for text information exchange between HIS in the world. At the same time, there are relatively mature middleware technologies. These standards and technologies are used to build a middle-layer software, which can effectively integrate different information systems and realize the sharing of medical information quickly and easily.

### 3. Method

In this section, we defined the prediction problem analysis and algorithm selection, support vector machines, integrated learning, model creation and algorithm improvement, and hospital HIS use satisfaction index in detail.

#### 3.1. Prediction Problem Analysis and Algorithm Selection

**3.1.1. Prediction Problem Analysis.** The analysis of the satisfaction prediction problem of the HIS in the hospital in this paper is similar to the evaluation problem. The classification process is the prediction process in machine learning. A classification model with machine learning can predict satisfaction. Therefore, using the ML method to predict the satisfaction of hospital HIS use, it is necessary to select an appropriate algorithm and optimize the algorithm. Common ML methods and application scenarios are shown in Figure 1.

The problem of predicting the use satisfaction of hospital HIS is a multiclassification problem, and the classification algorithm in ML can be used. ML includes a variety of classification models and classification algorithms, such as SVM,

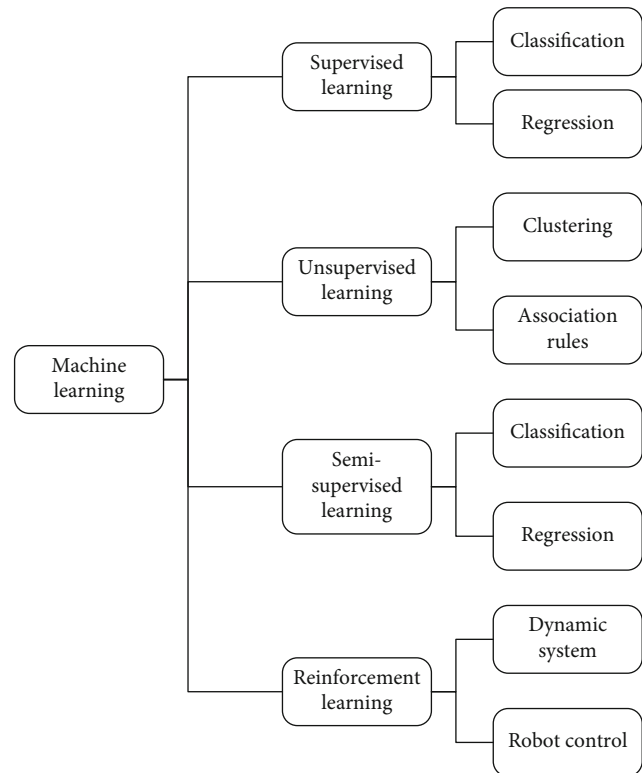


FIGURE 1: Application scenario of machine learning algorithms.

neural networks, clustering, naive Bayesian algorithms, logistic regression, and decision trees.

**3.1.2. Algorithm Selection.** By analyzing the commonly used ML classification algorithms and then selecting the appropriate algorithm, the classification algorithm used in this paper should first be a supervised learning algorithm. To evaluate the quality of college students’ training in this paper, it is first necessary to preprocess some sample data and analyze the sample data. Labeling is performed and then used for model training. Therefore, several commonly used supervised learning algorithms are compared here. The decision tree algorithm is prone to overfitting, and the accuracy is not high, and the recursive operation of the decision tree takes up a lot of memory. To improve the accuracy of the decision tree by means of ensemble learning, such as using the boosting algorithm, it is necessary to study the depth of the decision tree at this time, and the method is not simple and effective. For logistic regression, the samples need to be linearly separable or nearly linearly separable. When there are many data features, logistic regression is used for classification, and the classification task cannot be better completed due to the low accuracy. Bayesian classification mainly has the following shortcomings. First, because Bayesian classification is based on a probability model, using Bayesian classification requires probability assumptions. If the probability assumptions are not reasonable enough, the final result will be less accurate. At the same time, it is relatively difficult to assume that the probability is relatively difficult, and the data requirements are special. For the same

data, if its representation is different, the results will vary greatly. For neural networks, if the amount of data is large, its accuracy is high, but it requires huge data preprocessing work, and if the amount of data is not enough, it will lead to overfitting problems. At the same time, there is no standard for the selection of the number of neurons, and the selection of neurons will have a greater impact on the results. SVM has good generalization ability, is not sensitive to data, and has strong generalization ability on small data and is still applicable to linear inseparable cases, and the modeling is simple and efficient. Therefore, in this paper, support vector machine is selected as the hospital HIS use satisfaction prediction model. Since the accuracy of the SVM still has room for optimization, this paper uses the ensemble learning algorithm AdaBoost to optimize the SVM.

**3.2. Support Vector Machines.** SVMs mainly include support vector classification (SVC) and support vector regression (SVR). The SVC is used for classification problems, while the SVR is mainly used to solve nonlinear regression in regression problems. In this paper, the use satisfaction prediction problem of hospital HIS is essentially a classification problem from the perspective of ML. Therefore, for the ML model of hospital HIS use satisfaction prediction problem, the research should be carried out from the classification model. This paper mainly studies the SVC model.

**3.2.1. Algorithm Principle.** There are numerous strategies for solving classification problems among supervised learning algorithms. SVMs, for example, have a number of advantages when it comes to tackling classification problems, including high performance on small sample sets and strong generalization capabilities. SVM finds a plane in the sample space, called a hyperplane, so that as many samples belonging to different categories in the sample space can be correctly classified as possible. Finding the hyperplane requires training the model through the training data set and obtaining the hyperplane according to the characteristics of the training data set. After the hyperplane is obtained, it can be used to classify the sample data, and the category to which the test sample belongs is determined according to the position of the sample points in the sample data relative to the hyperplane in space. The sample data in the data set is composed of two parts: feature and category label. In this paper, the feature refers to the hospital HIS use satisfaction index, and the category label refers to the hospital HIS use satisfaction level. It is an ideal state for the hyperplane to perfectly classify the sample points, and many data in reality cannot be perfectly divided into different categories, that is, linear inseparability. In this case we have to allow a small number of points to be misclassified. According to the actual situation of the problem, "slack variables" are introduced to allow some sample points to be misclassified within an acceptable range. Searching for a hyperplane during training allows a small number of points that cannot be fully classified, so it is necessary to find the best possible hyperplane. In reality, data is a variety of data forms and dimensions and also has its own characteristics. Some data sets are inseparable in their original dimensions. For indivisible data,

it is usually to find a higher dimension so that the sample points can be mapped from the original dimension to higher dimensions so that the samples are separable. The algorithm grows more difficult as the number of dimensions increases, occasionally leading to insurmountable issues. At this point, we must apply the kernel function to map low-dimensional data to high-dimensional space in order to separate the data points in the high-dimensional space and avoid the problem of increasing the difficulty of calculation in the high-dimensional space. The selection of kernel function is very important for the performance of SVM. Inappropriate selection of kernel function will lead to poor final classification effect.

Let the hyperplane  $w^T x + b = 0$  in the space, where  $w$  the normal is vector and  $b$  is the displacement term. When the samples are linearly separable, there may be more than one hyperplane that can correctly classify the samples.

There are multiple hyperplanes that can correctly distinguish samples, and the hyperplane is the farthest from the points in the sample, which we call the optimal hyperplane. Let the distance from the sample to the optimal hyperplane be  $d$ , and the distance formula from the sample point to the optimal hyperplane can be obtained from the formula of the distance from the point to the plane as follows.

$$d = \frac{|w^T x + b|}{\|w\|}. \quad (1)$$

Let  $D$  be the training sample set,  $D = \{(x_i, y_i) | i = 1, 2, 3, \dots, n\}$ , where  $x_i \in R^{d_0}$ ,  $y_i \in \{-1, 1\}$ ,  $d_0$  is the input sample dimension, this paper refers to a scalar number, and  $n$  is the number of samples. If the hyperplane can correctly classify the samples,  $w^T x + b > 0$  can be obtained for the positive example, i.e.,  $y_i = +1$ , and  $w^T x + b < 0$  for the negative example. Therefore, for the positive and negative examples, the following formula can be obtained.

$$\begin{cases} w^T x_i + b \geq 1, & y_i = +1, \\ w^T x_i + b \leq -1, & y_i = -1. \end{cases} \quad (2)$$

In a schematic diagram of SVM with interval and hyperplane, there will be a point that is closest to the solid line in the hyperplane graph, and these sample points make the equal sign in formula (2) true. Such a sample point is called a support vector, and the distance and interval from the support vector to the hyperplane are represented by  $F$ , which can be calculated by

$$F = \frac{2}{\|w\|}, \quad (3)$$

when  $F$  achieves the maximum value, the support vector of the positive example and the support vector of the negative example are the farthest from the hyperplane, and the hyperplane can better classify the samples. Therefore, the search for the optimal hyperplane is converted into

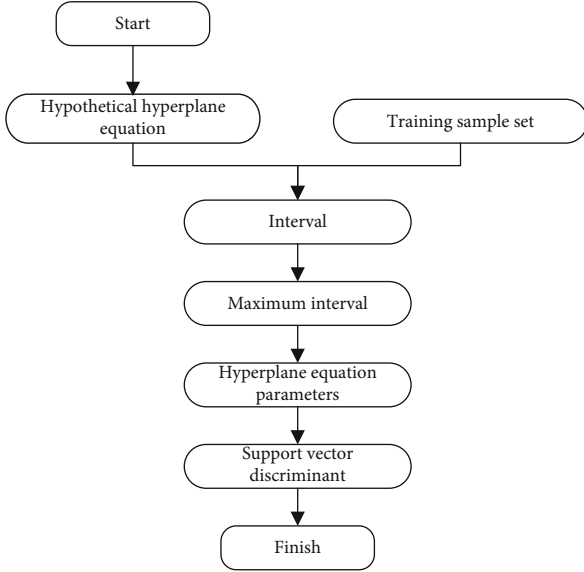


FIGURE 2: Support vector machine to solve the hyperplane flow chart.

the value of  $w$  and  $b$  when the value of  $F$  is maximized. In order to facilitate the calculation, it is converted into the following

$$\min_{w,b} \frac{1}{2} \|w\|^2, \text{ s.t. } y_i(w^T x_i + b) \geq 1, i = 1, 2, \dots, n. \quad (4)$$

The hyperplane can be obtained by solving the formula (4), and the classification of the samples can be realized according to the obtained hyperplane formula as a SVM model. Solving formula (4) usually uses the Lagrange multiplier method. Therefore, the first task of the SVM classification model is to use the training set data to determine the hyperplane and obtain the hyperplane formula. SVM can be simply understood as a mapping relationship from sample features to classification results. In this paper, it is a mapping relationship from the satisfaction prediction data used by the hospital HIS to the prediction results. SVM training refers to finding the connection between data features and classification outcomes by solving this mapping relationship using processed sample data. This paper uses Figure 2 to describe the process of SVM to solve hyperplane.

The solution of formula (4) is actually the solution of a quadratic programming problem, and its dual problem is obtained by using the Lagrange multiplier method, and the solution is solved by combining the KKT conditions. Using the Lagrange multiplier method to solve formula (4), the Lagrange function can be obtained as

$$L(w, b, \lambda) = \frac{1}{2} \|w\|^2 + \sum_{i=1}^n \lambda_i (1 - y_i (w^T x_i + b)). \quad (5)$$

Solving the partial derivatives of formula (5) yields

$$\frac{\partial L(w, b, \lambda)}{\partial w} = w - \sum_{i=1}^n \lambda_i y_i x_i, \quad (6)$$

$$\frac{\partial L(w, b, \lambda)}{\partial b} = \sum_{i=1}^n \lambda_i y_i. \quad (7)$$

By making formulas (6) and (7) zero, formulas (8) and (9) can be obtained as follows.

$$w = \sum_{i=1}^n \lambda_i y_i x_i, \quad (8)$$

$$0 = \sum_{i=1}^n \lambda_i y_i. \quad (9)$$

Simultaneous formulas (8) and (5), eliminating  $w$  and  $b$  in formula (5), the dual problem of formula (4) can be obtained

$$\max_{\lambda} \sum_{i=1}^n \lambda_i - \frac{1}{2} \sum_{i=1}^n \sum_{j=1}^n \lambda_i \lambda_j y_i y_j x_i^T x_j, \text{ s.t. } 0 = \sum_{i=1}^n \lambda_i y_i. \quad (10)$$

The solution of formula (10) satisfies the KKT condition, and the analysis shows that only the  $\lambda_i$  value corresponding to the support vector  $(x_i, y_i)$  is not 0, and the rest  $\lambda_i$  values are 0. After solving  $\lambda_i^*$ , the optimal  $w^*$  and  $b$  are obtained

$$w^* = \sum_{i=1}^n \lambda_i^* y_i x_i, \quad (11)$$

$$b = 1 - w^{*T} x. \quad (12)$$

The hyperplane formula can be obtained. For cases that are close to linearly separable or linearly inseparable in low dimensions, slack variables and kernel functions are introduced. There are many choices of kernel functions, and different kernel functions can be selected according to specific problems, or a new kernel function can be constructed. In the same way as the above solution method, after introducing the slack variable and the kernel function, the optimal classifier can be obtained by the Lagrange multiplier method, as shown in the following formula.

$$f(x) = \sum_{i=1}^n \lambda_i^* y_i K(x_i, x) + b^*. \quad (13)$$

**3.2.2. Support Vector Machine Multiclassification.** The SVM is a binary classifier, as shown by the analysis of the SVC principle, and the hospital HIS use satisfaction prediction problem in this paper is a multiclassification problem. In order to apply the SVM to the multiclassification problem, it is necessary to use SVMs to construct multiple classifiers. The usual methods include the direct method and the indirect method. Due to the high computational complexity of

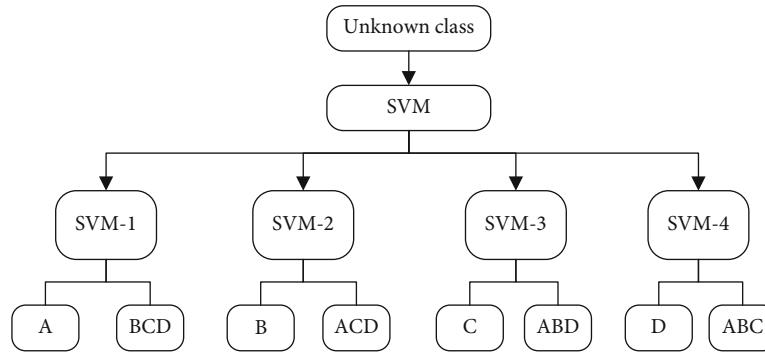


FIGURE 3: Schematic diagram of OVR strategy.

the direct method and the difficulty in implementation, the direct method is generally not used, and the indirect method is usually used to construct multiple classifiers. The indirect method has the following two strategies.

(1) *Indirect Multiclassification Strategy*. For other one-versus-rest (OVR) training samples, construct multiple SVMs to take a certain category as one class and train the other classes as one class, so that  $m$  categories are constructed by constructing  $m$  support vector machines. When classifying the samples, different SVMs on the sample classification decision function value classify the unknown samples into the class with the largest classification function value. The samples are separated into four groups in the hospital HIS use satisfaction prediction; therefore, the SVM is used for four categories of classification and a pair of additional classification algorithms are applied. Figure 3 is shown below. The four SVMs are SVM-1, SVM-2, SVM-3, and SVM-4, respectively, and the corresponding four categories are A, B, C, and D.

For a pair of other classification strategies, when classifying each class, there will be fewer positive samples than negative samples. When there are a lot of classes, the number of positive and negative samples in each binary classifier is asymmetric, which leads to classification and recognition. The difficulty increases, and the final output result is to make a decision by comparing the output results of several classifiers and selecting the maximum value. The output results of the same classifier are comparable, but the output results of different classifiers are not comparable, thus leading to wrong decisions.

(2) *Indirect Multiclassification Strategy*. For one-versus-one (OVO), the OVO classification method constructs an SVM classifier between any two categories, so that for multiclassification problems with  $m$  categories, in total,  $m(m-1)/2$  classifiers need to be constructed. When an unknown category is input,  $m(m-1)/2$  classifiers vote according to their respective classification results, and the final result is the category with the most votes. Taking the four classifications in this article as an example, the schematic diagram of the OVO classification method is shown in Figure 4.

This method is widely used and has high classification accuracy. However, due to the large number of classifiers constructed, the cost is also high. However, when the experimental conditions permit, this method can obtain higher accuracy. The categorization in this study will be done using the OVO approach, which has a high level of accuracy. And, compared to a pair of other approaches, there are only two extra classifiers because there are only four classification results. The computational cost is acceptable, and the classification accuracy should be improved as much as possible.

### 3.3. Integrated Learning

3.3.1. *Principle of Ensemble Learning*. Ensemble learning, in simple terms, is to combine multiple learners to improve the overall performance of multiple learning models. As a hotspot of ML, ensemble learning is listed by authoritative scholars as the first of the four research directions in the field of ML. Using the ensemble learning algorithm to integrate and combine simple learners, the learning effect and performance are improved. According to the different combination methods, ensemble learning can be divided into two categories: “homogeneous” and “heterogeneous.” The learners in the homogeneous ensemble method are of the same type, and the learners in the heterogeneous ensemble method are of different types, and the learners in the homogeneous ensemble method can also be called basic learners. The learners in heterogeneous ensembles are called “component learners” or individual learners.

3.3.2. *Ensemble Learning Category*. Homogeneous type of ensemble learning is usually used for different training sets or random sampling of the original data set, so that the training set on each individual learner is different. According to the techniques used by homogeneous types of individual learners to obtain different training samples, they can be divided into methods such as resampling the training set, manipulating input variables, and manipulating output targets. There are two generation methods for individual learners. If there is a strong dependency between individual learners, the generation method is serial. If there is no strong dependency, the individual learners can be generated in

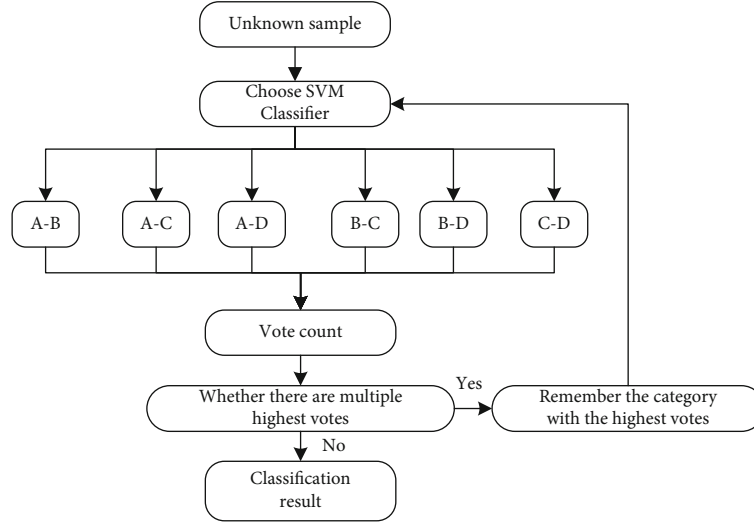


FIGURE 4: Schematic diagram of OVO classification method.

parallel. The former is represented by boosting, and the latter is represented by bagging and “random forest.”

**3.3.3. AdaBoost Algorithm.** With its solid theoretical foundation, high accuracy, and simplicity, AdaBoost, the most recognized algorithm in ensemble learning, has been widely applied in various domains and has achieved significant success. AdaBoost primarily uses numerous iterations to create an ensemble learning model. It can adjust the component learner in an adaptive way, and the AdaBoost algorithm updates the weight of the sample of each iteration.

**3.4. Model Creation and Algorithm Improvement.** There is currently no fixed method for the selection of the kernel function, which is usually selected based on experience and comparison. According to general experience, the selection of the kernel function usually first selects the linear kernel function, and if the effect is not ideal, the Gaussian kernel function can be used. The SVM kernel function that is not used for integration in this paper selects the linear kernel function for better classification. The linear kernel function is  $k$ , and the constant  $C$  and  $C \geq 0$  are introduced in the way of “soft interval,” and the slack variable  $r \geq 0$  is introduced. Through the method mentioned above, the final decision formula can be obtained as shown in formula (14), and the coefficients in the formula can be obtained by the data operation in the training set.

$$f(x) = \sum_{i=1}^n \lambda_i^* y_i K(x_i, x) + b^*, w^* = \sum_{i=1}^n \lambda_i^* y_i x_i, b^* = 1 - w^{*T} x \quad (14)$$

Part of the sample data is used as the test data, and the student’s index value is input into formula (14) to output the final discrimination result. In this paper, the OVO strategy is used to achieve multiclassification, and the accuracy of

the model is measured by comparing the output results with the actual category of the sample.

This section studies the integration of the AdaBoost algorithm and the SVM algorithm. By selecting the kernel function of the SVM and setting its parameters, the accuracy is reduced and the characteristics of the boosting algorithm are satisfied, thereby improving the performance of the integrated model. And the diversity measurement of the SVM algorithm makes it have better diversity and further improves the efficiency and performance of the integrated algorithm.

**3.4.1. Based on the Diversity of Learning Algorithms.** As the most famous algorithm in the boosting algorithm, AdaBoost has some characteristics of the boosting algorithm. The boosting algorithm requires the basic learners to have the characteristics of diversity. Only when the basic learners have good diversity can the ensemble learning model have better classification results. Therefore, its diversity is guaranteed, that is, the basic learners are not correlated, so that the performance of the final ensemble model can be optimized. Scholars have studied the diversity of base learners from different perspectives. The first is how to define the diversity of classifiers, what diversity is, how to measure it, and what conditions are met to be diverse. The second is how to introduce a diversity measure when creating an ensemble learning model to create a multiclassifier system. Finally, it is studied under which conditions the diversity of base classifiers achieves the optimal performance of the ensemble model. For the diversity of the ensemble learning AdaBoost-SVM base learner, we define it as follows. For the  $t$ th component classifier, the diversity  $d_t$  on the sample  $X_i$  is calculated by

$$d_t = \begin{cases} 0, & \text{if } h_t(X_i) = f(X_i), \\ 1, & \text{if } h_t(X_i) \neq f(X_i), \end{cases} \quad (15)$$

where  $h_t(X_i)$  is the output result of the  $t$ th classifier on sample  $X_i$ , and  $f(X_i)$  is the label of sample  $X_i$ . The diversity  $D_{iv}$

TABLE 1: Satisfaction index of hospital HIS system use.

First-level indicator	Secondary indicator	Label
System security	Use database super user login method	X1
	Program provides data backup function	X2
	Provide full monitoring of data modification	X3
System scalability	Provide various parameters to fully adjust system	X4
	Subsystems can operate individually or shared	X5
System maintainability	Provide various external interfaces	X6
	Easy and fast system installation	X7
	Provides tools for maintaining databases	X8
	Client and system automatic upgrade	X9
Software ease of use	Has a unified operation interface	X10
	With personalization function	X11
	Provide online help	X12
External interface	Statistics related system interface	X13
	With medical insurance interface	X14
	Disease control and health monitoring interface	X15

of the  $T$  component classifiers of AdaBoost-SVM on  $N$  samples can be calculated by

$$D_{iv} = \frac{1}{TN} \sum_{t=1}^T \sum_{i=1}^N d_t(X_i). \quad (16)$$

**3.4.2. Kernel Function and Parameters.** Boosting algorithm, as the learning algorithm of its basic learner, has poor classification performance, and the accuracy of classification is better than that of random guessing, that is to say, it requires a basic learner. The accuracy is just above 0.5. In general, SVM has a better classification effect. In this way, the integration of SVM algorithm with AdaBoost algorithm seems to be contrary to the principle of boosting. Therefore, if SVM is used as the base learner of the AdaBoost algorithm, then there must be a way to reduce the accuracy of SVM and be above 0.5. The research on the SVM algorithm shows that the accuracy of the SVM algorithm is affected by the selected kernel function and parameters. In the SVM that selects the Gaussian kernel function, the classification performance is affected by the regularization parameter  $C$  and the Gaussian bandwidth  $W$ . When the value of  $C$  is small, the performance of the algorithm is greatly affected by  $W$ . Therefore, when the value of  $C$  is roughly suitable, the performance of the algorithm can be more effectively changed by the value of parameter  $W$ . When the value of  $W$  is relatively large, the classification performance of SVM will be appropriately weakened. Therefore, at the beginning of the iteration of the AdaBoost algorithm, an appropriately large value of  $W$  should be given, and the value of  $W$  should be modified after each iteration.

**3.4.3. AdaBoost-SVM Algorithm.** We optimize AdaBoost-SVM through diversity and accuracy of base learners. For the diversity of each base learner, we will get a value  $D_{iv}$  that measures the diversity; it can be seen in the above algorithm

that a threshold DIV is set for diversity. If  $D_{iv}$  is greater than the threshold DIV set above, the current base learner can be added to the ensemble learning model as a new learner. Otherwise, the current base learner needs to be discarded. Compared with the original AdaBoost algorithm, the base learner has better diversity to build an ensemble learning model, and the generalization ability and efficiency of the final ensemble model will be improved.

**3.5. Hospital HIS Use Satisfaction Index.** For the prediction of hospital HIS usage satisfaction proposed by the subject of this paper, it is necessary to construct a quantifiable evaluation index. By referring to the relevant literature and combining with the development status of the hospital HIS, the constructed evaluation indicators are shown in Table 1.

## 4. Experiment and Analysis

In this section, we defined the data set and model training and experimental accuracy of different models in detailed.

**4.1. Data set and Model Training.** To verify the effectiveness of satisfaction prediction model proposed in this paper, this paper builds a dataset. This dataset contains 900 sets of data. This work uses Python and scikit-learn framework to construct a network. When the SVM selects the Gaussian kernel function,  $W = 35$ ,  $C = 1.4$ , and the number of basic learners is 8, the error rate of the model output reaches the lowest, and the final error rate output of the AdaBoost-SVM model is 0.05, that is, the accuracy rate is 0.95. The training results of the AdaBoost-SVM model are shown in Figure 5.

As can be observed from running data, the model's error rate on the test and training sets does not change whether there are 8 component learners in the model. In other words, after the 8 basic learners are built, the model's error rate approaches the ideal level under the specified parameters. The model's test set error rate is 0.05 when the curves are

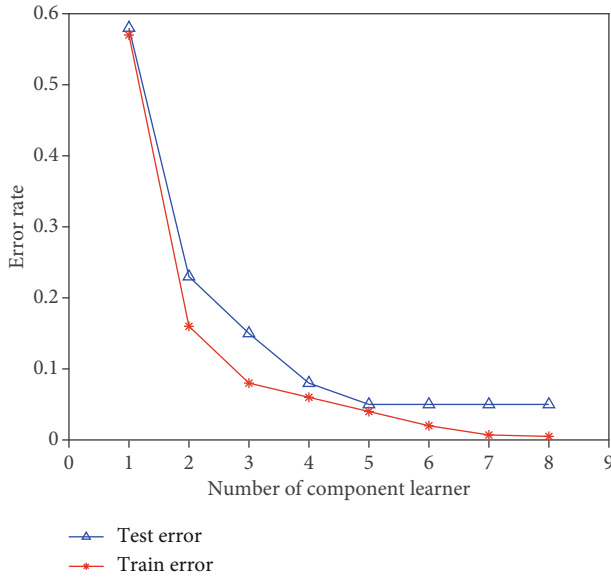


FIGURE 5: The training results of the AdaBoost-SVM model.

TABLE 2: Sample classification situation.

Satisfaction level	Number of samples	Evaluation results			
		A	B	C	D
A	30	26	01	02	01
B	30	0	29	01	01
C	30	0	01	28	01
D	30	02	0	0	28

balanced. The curve does not alter after increasing the number of base classifiers. As a result, there are eight primary classifiers. HIS-based AdaBoost-SVM assessment model is assessed using the data from the satisfaction data sample, except for training and test samples, with four sets of 30 samples each. Table 2 shows the test findings.

Table 2 shows the sample data for four categories, with 30 samples for each category to evaluate the model. After entering the model, for A-level satisfaction, the number of correct classifications is 26, and the number of wrong classifications is 4, of which 1 is wrongly classified into category B and 2 samples are wrongly classified into category C. In satisfaction level B, 29 samples were correctly classified and one sample was wrongly classified into class C. For C-level satisfaction, 28 samples were correctly classified, and the remaining two samples were wrongly classified into B and D categories, respectively. For D-level satisfaction, the number of correctly classified samples is 28 and the number of misclassified samples is 2 and misclassified into class A. It can be concluded that the AdaBoost-SVM evaluation model has good performance in both accuracy and recall. After training, the model can be easily used to predict the satisfaction of HIS usage.

4.2. *Experimental Accuracy of Different Models.* We use Python language to test the SVM, AdaBoost-SVM, and BP

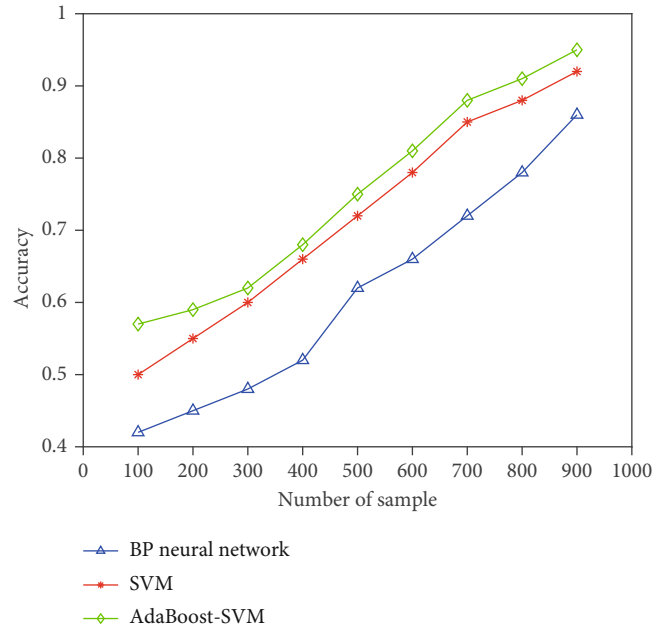


FIGURE 6: Experimental accuracy of different models.

neural network with the help of scikit-learn ML framework. The test data set still uses the data set built in this paper. There are 900 data samples in this data set, each sample has 4 features, and the samples have three categories in total. By testing the algorithm, the relationship between the accuracy of the algorithm and the number of samples can be obtained as shown in Figure 6. In the experiment, the parameter selection  $C$  of SVM is 10, the kernel function selects the Gaussian kernel function parameter  $W = 14$ , and the parameters in AdaBoost-SVM select  $C = 10$ ,  $W = 14$ , and  $DIV = 0.3$ . The activation function of the BP neural network uses the Relu activation function, and the threshold  $T = 0.005$ .

It can be seen from the test results that the accuracy rate of AdaBoost-SVM is the highest, and can reach more than 95%, and the accuracy rate of SVM is higher than that of BP neural network. Therefore, the AdaBoost-SVM algorithm is selected in this paper, which can reduce a lot of data preprocessing work and make the accuracy of the model to be optimal in the case of a small amount of data. It can effectively avoid heavy data processing work due to the need for a large number of data samples for model training in the prediction of hospital HIS use satisfaction.

## 5. Conclusion

The information era has arrived in the twenty-first century, and the HIS is a medical service-oriented information system that is part of this trend. Aside from some important manual procedures, most hospitals have essentially completed the transition from traditional management to computerized automatic management, which decreases medical staff workload and enhances labor efficiency and service quality. Accurate and standardized computerized management provides scientific data prediction and information



decision-making for the medical industry. HIS usage as a research context and the idea of user pleasure as a research object are examined in this study. Based on the technology acceptance model and rational and planned behavior theory, this research investigates the characteristics of the human, technical, and organizational environment that determine the successful use of HIS. In this paper, the current popular ML method is used to predict the current use satisfaction of HIS through the constructed HIS use satisfaction evaluation index. The work done in this thesis includes the following aspects: (1) introduce the current state of HIS construction at home and overseas, as well as the challenges that exist in our country's HIS, and make some recommendations. To prepare for the upcoming model design, the theoretical foundation and related development technologies required for model design are addressed and examined in depth; (2) analyze the prediction method and introduce the algorithm of machine learning as the prediction method. This work uses the AdaBoost method to select and integrate SVMs to increase accuracy and generalization even further since SVMs do well on small data sets and still have potential for improvement. This study picks the Gaussian kernel function and modifies the SVM parameters such that the SVM's accuracy may match the criteria of the AdaBoost method when it is employed as the base learner of the AdaBoost algorithm; and (3) a diversity metric is introduced to ensure that the basic learner has good diversity in order to increase the algorithm's performance. The accuracy rate of AdaBoost-SVM can reach more than 95% in the event of a little amount of data, according to the self-built data set used to test the algorithm. This demonstrates the model provided in this paper's superiority.

### Data Availability

The data sets used during the current study are available from the corresponding author on reasonable request.

### Conflicts of Interest

The authors declare that they have no conflict of interest.

### Acknowledgments

This work was supported by the Qiqihar Science and Technology Research project, Research on Investigation, Analysis, and Research on the Use Satisfaction of HIS System in a Third Class Hospital in Qiqihar (Project no. CSFGG-2021147).

### References

- [1] R. M. Gardner, T. A. Pryor, and H. R. Warner, "The HELP hospital information system: update 1998," *International Journal of Medical Informatics*, vol. 54, no. 3, pp. 169–182, 1999.
- [2] X. F. Wu and X. Ge, "Optimization of material management system based on integration of hospital information system," *China Medical Devices*, vol. 33, no. 5, pp. 183–185, 2018.
- [3] G. J. Kuperman, R. M. Gardner, and T. A. Pryor, *HELP: A dynamic hospital information system*, Springer Science & Business Media, 2013.
- [4] A. Ismail, A. T. Jamil, A. F. A. Rahman, J. M. A. Bakar, N. M. Saad, and H. Saadi, "The implementation of hospital information system (HIS) in tertiary hospitals in Malaysia: a qualitative study," *Malaysian Journal of Public Health Medicine*, vol. 10, no. 2, pp. 16–24, 2010.
- [5] P. W. Handayani, A. N. Hidayanto, A. A. Pinem, I. C. Hapsari, P. I. Sandhyaduhita, and I. Budi, "Acceptance model of a hospital information system," *International Journal of Medical Informatics*, vol. 99, pp. 11–28, 2017.
- [6] N. I. Ismail, N. H. Abdullah, A. Shamsudin, and N. A. N. Ariffin, "Implementation differences of Hospital Information System (HIS) in Malaysian public hospitals," *International Journal of Social Science and Humanity*, vol. 3, no. 2, pp. 115–120, 2013.
- [7] H. Ahmadi, M. Nilashi, and O. Ibrahim, "Organizational decision to adopt hospital information system: an empirical investigation in the case of Malaysian public hospitals," *International Journal of Medical Informatics*, vol. 84, no. 3, pp. 166–188, 2015.
- [8] J. F. Kurose and K. W. Ross, *Computer networking*, vol. 1, Higher Education Press, 2005.
- [9] R. D. Hertin and O. I. Al-Sanjary, "Performance of hospital information system in Malaysian public hospital: a review," *International Journal of Engineering & Technology*, vol. 7, no. 4.11, pp. 24–28, 2018.
- [10] H. W. Lee, T. Ramayah, and N. Zakaria, "External factors in hospital information system (HIS) adoption model: a case on Malaysia," *Journal of Medical Systems*, vol. 36, no. 4, pp. 2129–2140, 2012.
- [11] G. Yucel, S. Cebi, B. Hoegel, and A. F. Ozok, "A fuzzy risk assessment model for hospital information system implementation," *Expert Systems with Applications*, vol. 39, no. 1, pp. 1211–1218, 2012.
- [12] N. I. Ismail, N. H. Abdullah, and A. Shamsuddin, "adoption of hospital information system (HIS) in Malaysian public hospitals," *Procedia-Social and Behavioral Sciences*, vol. 172, pp. 336–343, 2015.
- [13] M. F. Collen, "A brief historical overview of hospital information system (HIS) evolution in the United States," *International Journal of Bio-Medical Computing*, vol. 29, no. 3-4, pp. 169–189, 1991.
- [14] C. S. Anthony, "Computer application in critical care medicine," *The journal of clinical information*, vol. 52, no. 1, pp. 100–102, 2001.
- [15] M. P. De, G. Quattrone, and D. Ursino, "Integration of the HL7 standard in a multiagent system to support personalized access to e-health services," *IEEE Transactions on Knowledge and Data Engineering*, vol. 23, no. 8, pp. 1244–1260, 2011.
- [16] S. Lanchaen, P. Suksawang, and T. Naenna, "Readiness assessment of information integration in a hospital using an analytic network process method for decision-making in a healthcare network," *International Journal of Engineering Business Management*, vol. 12, 2020.
- [17] Y. Chen, "A survey on industrial information integration 2016–2019," *Journal of Industrial Integration and Management*, vol. 5, no. 1, pp. 33–163, 2020.
- [18] B. Ji, Y. Li, D. Cao, C. Li, S. Mumtaz, and D. Wang, "Secrecy performance analysis of UAV assisted relay transmission for cognitive network with energy harvesting," *IEEE Transactions on Vehicular Technology*, vol. 69, no. 7, pp. 7404–7415, 2020.

- [19] X. Lin, J. Wu, S. Mumtaz, S. Garg, J. Li, and M. Guizani, "Blockchain-based on-demand computing resource trading in IoV-assisted smart city," *IEEE Transactions on Emerging Topics in Computing*, vol. 9, no. 3, pp. 1373–1385, 2021.
- [20] J. Pei, K. Zhong, M. A. Jan, and J. Li, "Personalized federated learning framework for network traffic anomaly detection," *Computer Networks*, vol. 209, article 108906, 2022.
- [21] R. Liu and L. Li, "Evaluation system for the talent training quality of higher education based on the combination of the subjective and objective evaluation method and AdaBoost-SVM," *Wireless Communications and Mobile Computing*, vol. 2022, Article ID 8022386, 13 pages, 2022.

## Retraction

# Retracted: Construction Method of Industrial College in Vocational Colleges Based on Cluster Analysis Algorithm

### Computational and Mathematical Methods in Medicine

Received 25 July 2023; Accepted 25 July 2023; Published 26 July 2023

Copyright © 2023 Computational and Mathematical Methods in Medicine. This is an open access article distributed under the Creative Commons Attribution License, which permits unrestricted use, distribution, and reproduction in any medium, provided the original work is properly cited.

This article has been retracted by Hindawi following an investigation undertaken by the publisher [1]. This investigation has uncovered evidence of one or more of the following indicators of systematic manipulation of the publication process:

- (1) Discrepancies in scope
- (2) Discrepancies in the description of the research reported
- (3) Discrepancies between the availability of data and the research described
- (4) Inappropriate citations
- (5) Incoherent, meaningless and/or irrelevant content included in the article
- (6) Peer-review manipulation

The presence of these indicators undermines our confidence in the integrity of the article's content and we cannot, therefore, vouch for its reliability. Please note that this notice is intended solely to alert readers that the content of this article is unreliable. We have not investigated whether authors were aware of or involved in the systematic manipulation of the publication process.

In addition, our investigation has also shown that one or more of the following human-subject reporting requirements has not been met in this article: ethical approval by an Institutional Review Board (IRB) committee or equivalent, patient/participant consent to participate, and/or agreement to publish patient/participant details (where relevant).

Wiley and Hindawi regrets that the usual quality checks did not identify these issues before publication and have

since put additional measures in place to safeguard research integrity.

We wish to credit our own Research Integrity and Research Publishing teams and anonymous and named external researchers and research integrity experts for contributing to this investigation.

The corresponding author, as the representative of all authors, has been given the opportunity to register their agreement or disagreement to this retraction. We have kept a record of any response received.

### References

- [1] X. Liu, "Construction Method of Industrial College in Vocational Colleges Based on Cluster Analysis Algorithm," *Computational and Mathematical Methods in Medicine*, vol. 2022, Article ID 3278395, 9 pages, 2022.

## Research Article

# Construction Method of Industrial College in Vocational Colleges Based on Cluster Analysis Algorithm

Xiaorong Liu 

Wuxi Vocational College of Science and Technology, Wuxi, 214028 Jiangsu, China

Correspondence should be addressed to Xiaorong Liu; 3101060@wxsc.edu.cn

Received 18 April 2022; Revised 14 May 2022; Accepted 18 May 2022; Published 13 June 2022

Academic Editor: Naeem Jan

Copyright © 2022 Xiaorong Liu. This is an open access article distributed under the Creative Commons Attribution License, which permits unrestricted use, distribution, and reproduction in any medium, provided the original work is properly cited.

In the context of the combination of industry and education, the construction of industrial colleges in vocational colleges can drive the scientific development of specialty settings in colleges and universities, and promote the way for colleges to expand students' practical teaching under the teaching of theoretical knowledge, and it is also an effective way for students to stimulate their learning enthusiasm and innovation enthusiasm. Colleges and universities can increase the direction and characteristics of specialist settings in colleges while enhancing instructors' professional level through school-business collaboration, and growing measures of talent training in colleges and universities plays a significant guiding role. The way to set up industrial colleges in vocational colleges reflects the development characteristics of talent training mode in the new era, and it is also an effective way to meet the practical training of students and the actual needs of society. It is a new school running mode of transforming productivity, cooperation, and mutual benefit, which is very worthy of promotion and development. This paper analyzes the problems existing in the construction of industrial colleges in vocational colleges in China and finds out the corresponding solutions. A path method of industrial college construction in vocational colleges based on the cluster analysis algorithm is proposed. The validity of this model is verified by experiments, which lays a foundation for the construction of industrial colleges in vocational colleges.

## 1. Introduction

For vocational colleges, the main purpose of training students is to shoulder the actual tasks in the actual work and be able to take the lead in the production, operation, and each job with professional knowledge, rich experience, and skilled technology [1]. The biggest difference between vocational education and ordinary higher education is that the talents trained belong to applied skilled talents, that is, they can combine professional knowledge with the practical operation. On the one hand, they complete the study of theoretical knowledge during school study; on the other hand, they complete the study, production, and service under the training mode of school-enterprise cooperation [2]. The college of the industry provides a practical and innovative platform for the majority of higher vocational students so that they can have a real simulated operation environment before they formally take up their jobs.

The way of talent training in vocational colleges is to face the market and serve the industry. Only when the talent training meets the actual needs of the current society and industry for talents can the effective development of individual talents be realized, and the teaching direction is suitable for post-application. Over the years, the development of vocational education in China has made continuous reform and innovation with the continuous transformation of the industrial structure, but it is still difficult to meet the actual needs of the market. The construction of industrial colleges in vocational colleges aims at the needs of enterprises and trains students. It is very necessary for students to adapt to industry standards in advance while cultivating professional knowledge [3]. This can not only improve the fit between the professional setting of vocational colleges and the industrial structure but also enable colleges to recognize the shortcomings of professional courses with the assistance of the industrial college, which plays a great role in promoting the

professional setting of colleges and market research [4]. At present, most of the industrial colleges of vocational colleges in China are carried out in the way of school-enterprise cooperation, in which enterprises provide venues, equipment, and technology, and colleges provide teaching venues and teaching teacher management content. This cooperation mode takes advantage of each other in terms of the management system, teacher team or training base construction has a strong educational purpose, and can develop strengths and avoid weaknesses at the same time [5]. The respective advantages of enterprises and colleges are reflected in the construction of industrial colleges, so as to realize the win-win strategy of education and production. For vocational colleges, it can not only have better practical significance in the overall professional setting and skill improvement but also play a great role in promoting the cultivation of double qualified education and enhancing the core competitiveness of the college [6]. The construction path of industrial colleges in vocational colleges is shown in Figure 1.

The industrial college of vocational colleges is neither a university nor a college of education in the traditional sense, but rather a learning organization that refers to the collaboration between schools and businesses to develop talent. It aims to provide college students with a high-quality and high-skilled learning system and strives to transform students' professional theoretical knowledge into practical operation ability. At present, China's higher vocational industrial colleges generally set up special venues in the college and build them in the form of joint secondary colleges with relevant enterprises in the industry, so as to provide students with practice places and create a practice platform [7]. Industry university cooperation is a new mode of contemporary vocational education. Under this mode, it provides a good development opportunity for the construction of industrial college of vocational colleges. However, it is undeniable that the institutional setting and management mode of enterprises and colleges are completely different [8]. The continuous development and prosperity of this educational mode also stimulate some contradictions in the system, institution, and management of the industrial college. If these contradictions are not solved, it is bound to restrict the daily management of the Institute of Technology to a great extent and seriously hinder the further deepening of school-enterprise cooperation.

The following is the paper's organization paragraph: Section 2 discusses the related work. The design of the application model is examined in Section 3. The experiments and results are discussed in Section 4. Finally, the research job is completed in Section 5.

## 2. Related Work

In this section, we explain the development status of industrial colleges in vocational colleges, research status of construction path of industrial college, and research status of clustering algorithm in detail.

*2.1. Development Status of Industrial Colleges in Vocational Colleges.* The school running mode of school-enterprise

cooperation is an effective carrier for the development of colleges and enterprises. It is not only a way for enterprises to cultivate talents but also a teaching measure for vocational colleges to actively set up professional industries [9]. The two sides can realize cooperation on the basis of mutual benefit and establish vocational colleges as a training base for professional and skilled talents. However, in terms of the current construction mode of industrial colleges in most vocational colleges, the school-enterprise cooperation is too unitary in form and content, taking the order type talent training and post-practice mode as the primary mode of cooperation, and the lack of deeper cooperation mode limits the way of industry education integration and talent transmission, which is not conducive to giving full play to the role of talent training base in vocational colleges [10]. The development status of the Institute of Technology is shown in Figure 2.

The main body of the construction of industrial college is implemented by the cooperation between enterprises and colleges. However, due to the great differences in the organization and management methods of both sides, the lack of a detailed management scheme and supervision system in the management of the industrial college is very disadvantageous from the perspective of enterprises or colleges. Enterprises cannot integrate into the management of industrial colleges, and colleges and universities cannot play a real educational role [11]. In the process of cooperation, there is a lack of detailed rules for the implementation of cooperation schemes, resulting in unclear rights and responsibilities and uneven distribution of interests, which is very likely to lead to the lack of implementation power of cooperation subjects, which fundamentally hinders the development of school-enterprise cooperation [12]. As the main mode of school-enterprise cooperation in vocational colleges at the present stage, the entrusted training order training mode will still have various teaching problems due to the immaturity of the educational mechanism, such as students' academic performance, behavior performance, implementation countermeasures, internship, and employment [13]. It is similar to the phenomenon of signing an employment agreement while ignoring academic performance and school behavior. Both students and parents believe that an employment agreement can ensure students' future employment, which has brought great trouble to vocational colleges in daily teaching management.

*2.2. Research Status of Construction Path of Industrial College.* The construction of mixed ownership industrial colleges in vocational colleges should be in line with the coordinated development of regional industrial clusters and the improvement of educational quality and the optimization of professional structure in vocational colleges [14]. It should not only accomplish scientific rationality of the best combination of industrial and educational elements but also achieve rapid resource structure and efficiency growth [15]. At the same time, we can achieve in-depth integration of talent training mode, curriculum system construction, teaching method reform, scientific research innovation, teacher team construction, and so on between industrial enterprises and

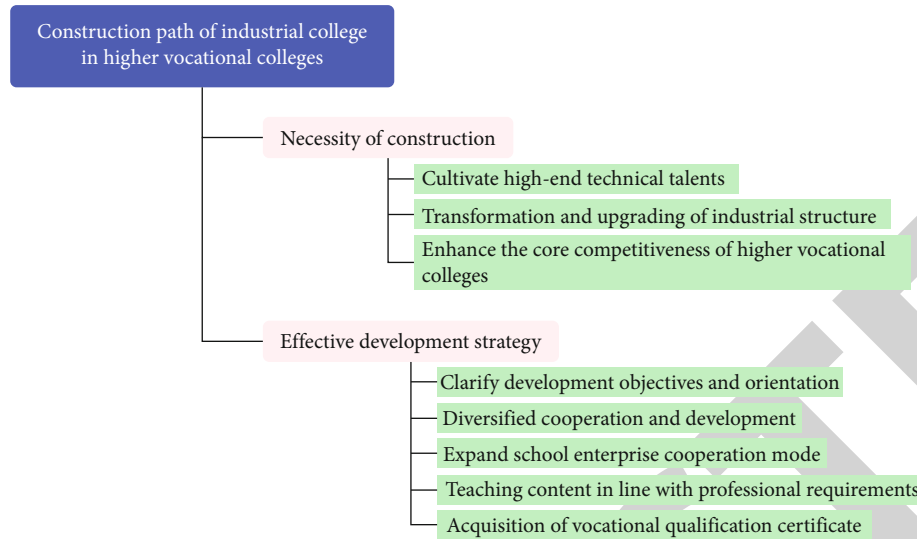


FIGURE 1: The construction path of industrial college in vocational colleges.

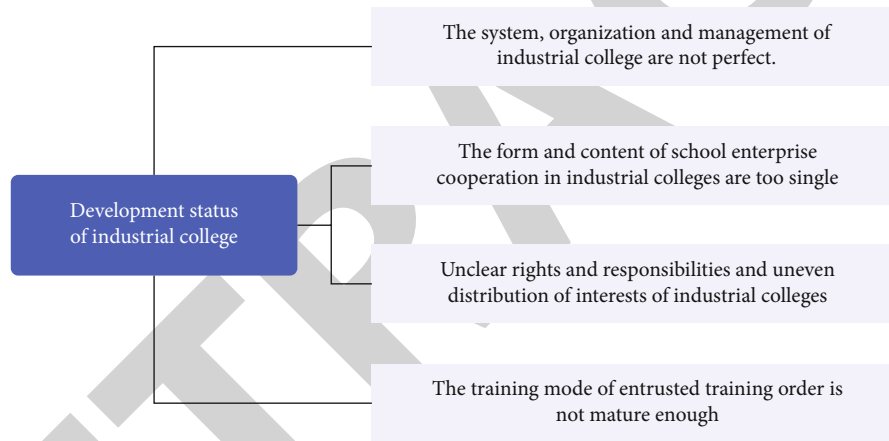


FIGURE 2: The development status of the Institute of Technology.

vocational colleges through mutual integration and derivation between industrial layout and related majors. To build a mixed ownership industrial college in vocational colleges, we must first clarify the essential attributes, main characteristics, and school running orientation of the mixed ownership industrial college, and scientifically understand the differences between the mixed ownership industrial college and the secondary college [16]. A secondary college is a secondary teaching unit attached to a higher vocational college. It is different from a mixed ownership industrial college in terms of property right structure, school running subject, founding purpose, and operating mechanism.

In addition, the establishment of a variety of industrial clusters and research institutes, as well as the close integration of various industrial clusters and industrial associations that hinder the sustainable development of the park, should break through the bottleneck of the main body of the park and the integration of multiple industries, institutions, and research institutes, as well as the close cooperation between the two sides [17], the development model of interoperabil-

ity and mutual progress. The establishment of corporate identity is fundamental for the mixed ownership industrial college to settle down. At present, under the legal system and framework of higher education in China, the legal person status of mixed ownership vocational colleges cannot be relied on, and the legal person status of mixed ownership industrial colleges is more difficult to determine. Vocational colleges are not-for-profit legal persons. Mixed ownership industrial colleges undertake the main function of public welfare vocational education [18]. It is obviously inappropriate to be positioned as for-profit legal persons; the participation of nonpublic capital such as industrial capital and private capital in running schools inevitably requires capital appreciation, which is not in line with the characteristics of nonprofit legal persons. Therefore, the mixed ownership industrial college can be positioned as a special legal person. As an independent educational and teaching institution, the college of mixed ownership industry is not for profit [19]. It is engaged in public welfare vocational education, technology development, social services, and other functions. It is

jointly funded and established with industrial enterprises, social organizations, and individuals, which is in line with the basic characteristics of special legal persons [20].

Therefore, the legal person status of mixed ownership industrial college must be clarified by special laws and regulations or clear provisions. Many existing education policy documents encourage the development of industrial colleges with mixed ownership characteristics. Only by issuing special policy documents on the legal personality of the college of mixed ownership industry can we clarify the legal personality of the college of mixed ownership industry from the legal level [21]. Due to the diversification of school running subjects, the mixed ownership industrial college should follow the dual development principles of market law and education law. Improving the management mechanism and building a modern governance structure is not only an important guarantee for the efficient operation of the industrial college but also a prerequisite for realizing the goal of talent training [22]. Second, we should effectively participate in the management of the mixed ownership industrial college as stakeholders. The construction path of the industrial college is shown in Figure 3.

*2.3. Research Status of Clustering Algorithm.* The standard NMF method's single nonnegative constraint beam cannot suit the needs of many fields; hence, there are still certain flaws and restrictions. Researchers develop a neighbor network and a weighted adjacency matrix based on the similarity between data points in order to mine the possible manifold structural information between high-dimensional data and suggest the graph's regular nonnegative matrix decomposition [23]. Considering that a single cluster center in NMF and GNMF is not enough to describe the complex structure of the original data, researchers use multiple center points to represent the category of samples, so as to propose the local center structure nonnegative matrix decomposition [24].

In order to adaptively learn the local manifold structure, the researchers propose the concept of adaptive neighborhood and adaptively assign neighbors to each data point, so as to propose a non-negative matrix decomposition with the adaptive domain. Generally speaking, the cluster center is surrounded by some points with low local density, and these points are far away from other high-density points [25]. Then, the researchers proposed the density peak algorithm, which calculates the distance of the nearest neighbor and arranges it according to the density to obtain multiple peak points of the data, so as to obtain the clustering center to realize the efficient clustering of the data [26]. However, the nearest neighbor graph constructed by GNMF is based on the traditional Euclidean distance, which sometimes cannot accurately describe the real distance between samples when dealing with complex data structures [27]. Furthermore, while the LCSNMF model stipulates the same number of centers for each cluster, the architecture of various clusters varies in practice. This description is obviously flawed [28].

Although the LCSNMF algorithm uses multiple center points to represent the sample points in a cluster, the struc-

ture of each cluster is different in practical application. It is obviously unreasonable to specify the same number of center points for different clusters, and the optimal clustering results cannot be obtained for the data with complex structures [29]. To solve this problem, this paper proposes PNMF. The density peak algorithm is used to locate numerous density peak points for the data set, and then the linear combination of density peak points is used to create cluster center points for clustering. The regular term is also integrated into the NMF framework [30], and the geodesic distance is used to generate the manifold nearest neighbor graph.

### 3. Design of Application Model

*3.1. Basic Principle of Clustering Algorithm.* The algorithm finds multiple density peak points of the data, constructs a bipartite graph with its peak points and sample points, constructs a data nearest neighbor graph based on geodesic distance, and integrates it into the nonnegative matrix decomposition model. Clustering is the process of grouping items into distinct classes or clusters based on their features and particular rules, with the goal of making data within each class as similar as feasible while data between classes is as dissimilar as possible. The general steps of clustering are shown in Figure 4.

Therefore, for the selection of density peak points, the local density of sample points and the distance from the density center are comprehensively considered. In practical application, the number of samples in different classes varies greatly, and the density is also different, which will lead to the uneven distribution of the selected peak points. Take all sample points as a candidate set of density peak points, then assess each sample point's local density and distance from the density center, and choose a sample point in order from large to small. The similarity measurement step is used to measure the similarity of different data in the same feature space.

Firstly, the local density of each sample point is calculated, and multiple density peaks are found from the data set by using the local density. It specifies multiple center points for each cluster and constructs a bipartite graph by using the density peak points and sample points. In addition, the geodesic distance under manifold structure is used to construct the nearest neighbor graph of data, so as to describe the local geometric relationship and make the distance between sample points more accurate. In order to prove the effectiveness of the algorithm, this paper compares the clustering effect of the algorithm on several facial data sets, and text and sound data sets. Experimental results show that PNMF has better clustering performance than other NMF algorithms. The clustering performance of GNMF and NMFAN based on the Euclidean distance nearest neighbor graph is not as good as that of PNMF based on the manifold distance nearest neighbor graph, which shows that the traditional Euclidean distance cannot well and accurately show the true distance between data in the face of more complex and high-dimensional data. Because of the limits of its cluster center selection, LCSNMF is less effective than

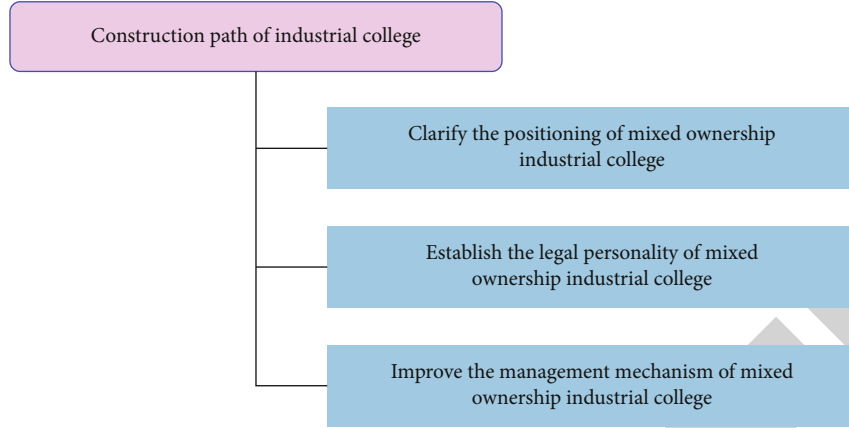


FIGURE 3: The construction path of the industrial college.

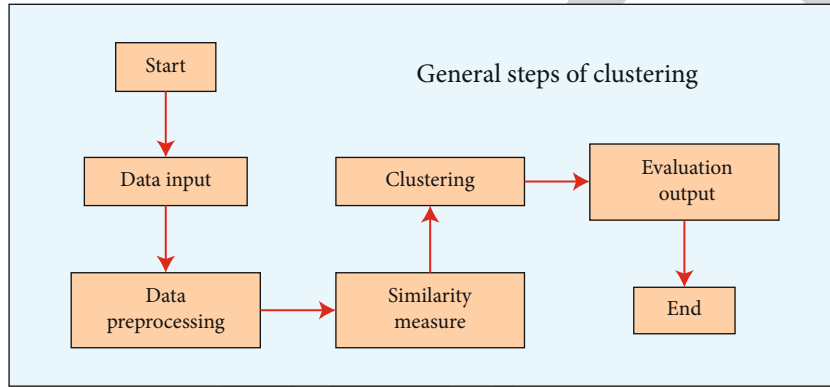


FIGURE 4: The general steps of clustering.

PNMF, while standard NMF clustering performs poorly due to a lack of constraints. The nonnegative matrix decomposition model is a common data dimensionality reduction method. In the research of existing nonnegative matrix decomposition algorithms for clustering, each category is generally represented by one or more designated central points.

The clustering algorithm based on the partition is to divide the data into  $k$  classes, and  $K$  should be less than the total number of data. The division method needs to know the number of clusters in advance, randomly select the initial cluster center, and the other objects will be divided into which class near the cluster center. Then, an objective function is optimized to iteratively find a new cluster center, and the remaining objects are classified until the cluster center is no longer changed or the number of iterations is reached. The partition-based clustering algorithm iterates continuously according to the optimization evaluation function, which is simple to calculate. It is suitable for large-scale data sets and spherical clusters. However, the number of clusters should be determined in advance and sensitive to the initial clustering center. The obtained solution is not necessarily the global optimal solution but maybe the local optimal solution. The probability that each data point is selected as the cluster center shall meet the following math-

ematical expression.

$$P_i = \frac{D(x_i)^2}{\sum_{i=1}^n D(x_i)^2}. \tag{1}$$

If the structure of the data set is unknown, we need to use internal measurement methods. To quantify clustering quality, we usually utilize the intracluster variance, which is the sum of squares of intracluster errors. Its mathematical expression is as follows.

$$V(C) = \sum_{C_k \in C} \sum_{i \in C_k} d(i, \mu_k)^2. \tag{2}$$

The effectiveness index is the linear combination of the average dispersion of clusters and the overall separation between clusters, which is defined as the following expression.

$$SD(C) = \alpha \text{Scat}(C) + \text{Dis}(C). \tag{3}$$

At present, most clustering algorithms need to customize some parameters, and the selection of these parameters directly affects the final clustering effect. Therefore, the



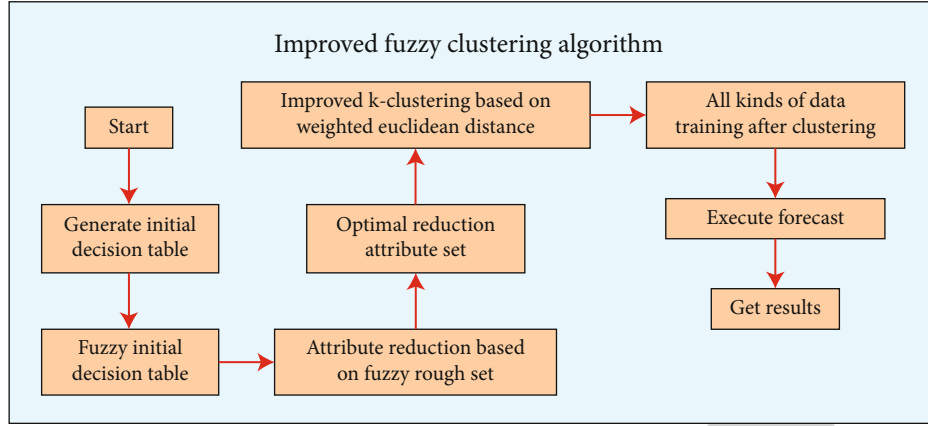


FIGURE 5: The flow of the improved fuzzy clustering algorithm.

TABLE 1: Analysis on output factors of high-level scientific research projects.

Project	NIVTC	WVTC	YITC	CEVTC
Innovation mechanism	12.30%	14.30%	13.50%	15.60%
Innovation platform	15.50%	12.30%	14.30%	15.30%
Teaching staff	29.80%	23.20%	22.50%	24.30%
Resource allocation	18.80%	19.20%	17.30%	16.30%
Cooperation ability	15.90%	16.20%	18.60%	18.20%
Transformation level	07.70%	14.80%	13.80%	10.30%

influence of these parameters should be considered when selecting the clustering quality measurement method. At the same time, these measurement standards can also help us set the parameter values. When choosing clustering quality evaluation methods, we should also consider the structure of the data itself. At present, there is no measurement method suitable for all application fields. We choose the appropriate measurement method according to the specific situation. When clustering data objects, we need to evaluate the difference between objects, that is, the commonly known distance. Among them, the Euclidean distance function is the most commonly used measurement method, and its expression is as follows.

$$d(i, j) = \left[ \sum_{k=1}^n (x_{ik} - x_{jk})^2 \right]^{1/2}. \quad (4)$$

In traditional clustering methods, each attribute of the object is treated equally, and their contribution to clustering is equal. However, in practical application, the internal properties of objects are different, and the importance of each attribute will be different.

**3.2. Improved Clustering Algorithm.** At present, the most popular fuzzy clustering algorithm is the fuzzy mean algorithm. Its goal is to minimize the criterion function and gradually obtain a more accurate membership matrix. It is easy to fall into the local optimal solution of the iterative center selection process. The goal of the FCM algorithm is

to find the optimal prototype matrix and the corresponding membership matrix to minimize the objective function given by the following formula.

$$J = \sum_{i=1}^C \sum_{j=1}^N (u_{ij})^m d_{ij}^2. \quad (5)$$

The parameter  $d_{ij}$  is obtained from the following formula:

$$d_{ij} = s_j - \beta_i. \quad (6)$$

After calculating the membership of all objects, you can calculate the new cluster prototype. When the prototype stabilizes, the process stops. In other words, the prototype generated in the previous iteration is very close to the prototype. In order to adjust the performance of particle swarm optimization and local search ability of particle swarm optimization in the search process, a simple and effective inertia weight adjustment strategy is introduced into the particle swarm optimization algorithm. The new function is as follows:

$$\omega_l(t) = (\ln(2.1 + t)) \wedge (-z). \quad (7)$$

New velocity formula and position formula using new inertia weight.

$$\begin{aligned} V_l(t+1) &= \omega(t)V_l(t) + c_1 R_{1l}(pbest_l(t) - X_l(t)) \\ &\quad + c_2 R_{2l}(gbest(t) - X_l(t))X_l(t+1) \\ &= X_l(t) \oplus V_l(t). \end{aligned} \quad (8)$$

The random value  $R$  is specified as a matrix to boost the randomness of particle swarm optimization. The random matrix of each particle is initialized with each iteration. Therefore, a group represents multiple candidate clustering centers of the data vector. Each data vector belongs to a cluster according to its membership function, so each data vector is given a fuzzy membership. In each iteration, each cluster has a cluster center, and a solution method of cluster

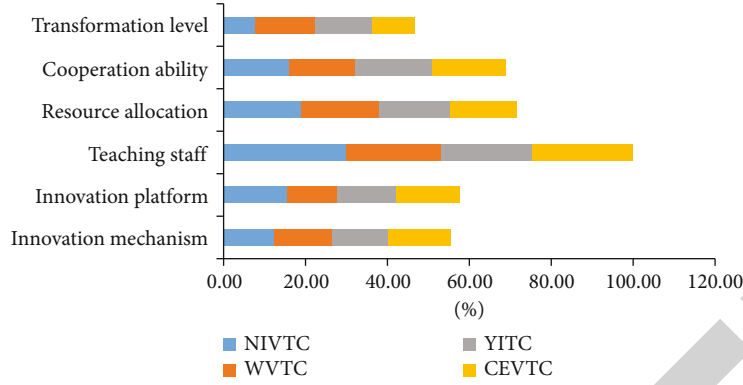


FIGURE 6: Analysis on output factors of high-level scientific research projects.

TABLE 2: Analysis on factors of high-end team construction.

Project	NIVTC	WVTC	YITC	CEVTC
Highly educated teachers	22.30%	20.30%	23.40%	21.60%
High-level talents	32.50%	32.10%	34.10%	35.50%
High-level team	26.80%	23.40%	22.70%	25.30%
Cultivation strength	18.40%	24.20%	19.80%	17.60%

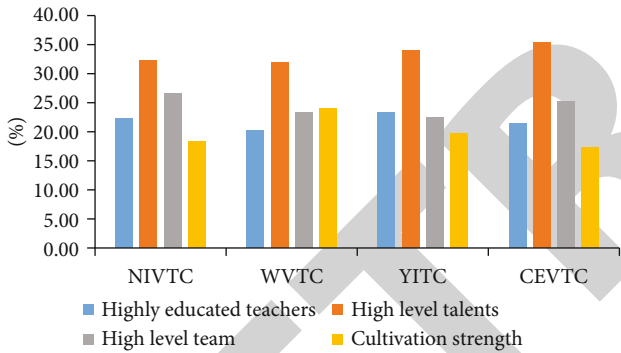


FIGURE 7: Analysis on factors of high-end team construction.

center vector is given. The fitness function for finding the generalized solution is expressed as:

$$f(X_i) = \frac{1}{J(X_i)}. \quad (9)$$

After the initial centroid is randomly selected in the traditional  $K$ -means clustering algorithm, the clustering results fluctuate greatly and the accuracy is low. The improved clustering proposed in this paper can optimize the initial centroid selection of the  $K$ -means clustering algorithm. The algorithm improves from the quantum revolving gate and changes the mutation strategy from the traditional nongate to the H gate. The improvement of the quantum revolving gate is to organically combine the three behaviors of foraging, clustering, and tail chasing in the fish school, and dynamically update the rotation angle with the increase of the number of iterations, so as to make the update of the next generation more reasonable. The algorithm, on the

other hand, will run out of memory as the amount of data grows. As a result, we must concentrate on how to solve such problems using the distributed computing architecture in order to increase the algorithm's performance. The flow of the improved fuzzy clustering algorithm is shown in Figure 5.

#### 4. Experiments and Results

This study adopts the methods of literature research, in-depth interview, investigation, and statistical analysis. The respondents of the questionnaire include 30 functional departments such as the academic affairs office, personnel office, science, and technology office, and student office of four vocational colleges: Nanjing Information Vocational and Technical College, Wuxi Vocational and Technical College, Yangzhou Industrial Vocational and Technical College and Changzhou Engineering Vocational and Technical College, with 300 student representatives. A total of 800 questionnaires were distributed to faculty and students of functional departments, and 750 questionnaires were recovered, of which 725 were valid, with an effective rate of 90%. However, the government's support for vocational colleges in terms of relevant policies and the coverage of special construction indicators needs to be improved, and the investment and support in the construction of high-level professional clusters and the integrated practice platform of industry education integration need to be strengthened. The analysis table of output factors of high-level scientific research projects and achievements is shown in Table 1 and Figure 6.

From the data analysis, the reason for the small number of high-level scientific research projects and achievements in some Jiangsu vocational colleges is that the mechanism and platform of collaborative innovation need to be improved, the innovation ability of scientific researchers and teams needs to be improved, and the effective allocation of scientific research resources needs to be strengthened. Therefore, the output of high-level scientific research papers and patents is still relatively rare. At the same time, it faces difficulties in the integration of industry and education and in-depth school-enterprise cooperation. It also needs to be strengthened in the service of scientific research

achievements to local economic and social development. The output of scientific research projects and achievements is an important quantitative index for the development of higher vocational education, and high-level projects and achievements are the key symbols of the scientific research level of the school. The factor analysis of high-end team construction is shown in Table 2 and Figure 7.

According to the data analysis, the reason why some high-level and high-end teachers in Jiangsu vocational colleges are weak is that the proportion of highly educated teachers and professors in the teaching team of vocational colleges is relatively weak, and the level of double qualified teachers with rich enterprise experience needs to be improved. Therefore, from the perspective of supply and demand, how strengthening the introduction of high-level talents and teams and cultivating high-level technical talents will become an important problem faced by high-level vocational colleges in Jiangsu Province. The factors affecting the education and teaching quality of some Jiangsu vocational colleges include the quality of students, professional construction, and talent training quality. The construction of professional and high-level teaching achievements is the key to promoting the high-level construction of Jiangsu. Nowadays, the professional construction of Jiangsu vocational colleges still does not break the technical barriers of majors. Only by integrating the advantages of existing majors and developing cross-new disciplines can we play the role of complementary advantages among majors and promote the development and construction of majors. At the same time, the high-level teaching achievements and awards need to be enhanced.

## 5. Conclusion

Industrial college is the most important carrier for vocational colleges to realize the integration of industry and education. It is also the base for cultivating high-quality skilled applied talents. To accelerate the construction of industrial colleges, we must establish a construction mechanism and action plan that will deepen the development path of vocational colleges' integration of industry and education, implement the innovative development concept, promote higher vocational industrial colleges to better serve the new mode of vocational colleges, enterprises, and industrial cooperation in running schools, and assist vocational colleges in achieving long-term success. This paper analyzes the problems existing in the construction of industrial colleges in vocational colleges in China and finds out the corresponding solutions. A path method of industrial college construction in vocational colleges based on the cluster analysis algorithm is proposed.

The construction of the higher vocational industrial college also needs the joint efforts of the government, administration, schools, and enterprises. Only by deepening the reform of vocational education and improving the joint school running mode of multiple subjects can we achieve the two-way balance between supply and demand of talent training. We must emphasize the role of vocational education in industrial development, as well as the complimen-

tary, balanced, and constraining link between the two. Throughout the entire process of running the Institute of Industry, the management idea of deep integration of industry and education, as well as collaborative innovation and development, will be applied. The Institute of Industry and Technology will exchange and integrate educational resources while also spearheading discipline and specialization construction reform. We also need to promote the goal of talent-oriented training, establish a stable professional teaching team, build a systematic standardized practical teaching site, and strengthen the function of school-enterprise coordinated development of industrial colleges.

## Data Availability

The data sets used during the current study are available from the corresponding author on reasonable request.

## Conflicts of Interest

The author declares that he has no conflict of interest.

## Acknowledgments



This work was supported by 2021 Jiangsu Province "14th five-year plan" Project: «Research and Practice on the construction path of Industrial College in Local Higher Vocational Colleges under the background of the Yangtze River Delta Integration» (No:D202103106).

## References

- [1] Y. Wang, "“Co-construction” to “symbiosis”: research on the integrated governance mechanism of industrial colleges in higher vocational colleges," *Journal of Contemporary Educational Research*, vol. 5, no. 9, pp. 142–146, 2021.
- [2] S. Shet and R. Narwade, "An empirical case study of material management in construction of industrial building by using various techniques," *International Journal of Civil Engineering and Technology*, vol. 7, no. 5, pp. 393–400, 2016.
- [3] W. Zhu and Y. Peng, "Research on the construction of industrial college in local undergraduate colleges and universities under the background of new engineering," *Journal of Higher Education Management*, vol. 12, no. 2, pp. 30–37, 2018.
- [4] M. Sarireh, "Optimum percentage of volcanic tuff in concrete production," *Yanbu Journal of Engineering and Science*, vol. 11, no. 1, pp. 43–50, 2015.
- [5] S. Zhang, C. Zhao, S. Wang, and F. Wang, "Pseudo time-slice construction using a variable moving window k nearest neighbor rule for sequential uneven phase division and batch process monitoring," *Industrial & Engineering Chemistry Research*, vol. 56, no. 3, pp. 728–740, 2017.
- [6] K. R. Kumar, G. Shyamala, P. O. Awoyera, K. Vedhasakthi, and O. B. Olalusi, "Cleaner production of self-compacting concrete with selected industrial rejects-an overview," *Silicon*, vol. 13, no. 8, pp. 2809–2820, 2021.
- [7] L. C. Jia, W. J. Sun, L. Xu et al., "Facile construction of a superhydrophobic surface on a textile with excellent electrical conductivity and stretchability," *Industrial & Engineering Chemistry Research*, vol. 59, no. 16, pp. 7546–7553, 2020.

## Research Article

# Inception-LSTM Human Motion Recognition with Channel Attention Mechanism

Yongtao Xu <sup>1,2</sup> and Liye Zhao <sup>1,2</sup>

<sup>1</sup>School of Instrument Science and Engineering, Southeast University, Nanjing 210096, China

<sup>2</sup>Key Laboratory of Micro-Inertial Instrument and Advanced Navigation Technology, Ministry of Education, Southeast University, Nanjing 210096, China

Correspondence should be addressed to Yongtao Xu; 220193315@seu.edu.cn and Liye Zhao; liyehao@seu.edu.cn

Received 15 April 2022; Revised 9 May 2022; Accepted 14 May 2022; Published 13 June 2022

Academic Editor: Naeem Jan

Copyright © 2022 Yongtao Xu and Liye Zhao. This is an open access article distributed under the Creative Commons Attribution License, which permits unrestricted use, distribution, and reproduction in any medium, provided the original work is properly cited.

An improved channel attention mechanism Inception-LSTM human motion recognition algorithm for inertial sensor signals is proposed to address the problems of high cost, many blind areas, and susceptibility to environmental effects in traditional video image-oriented human motion recognition algorithms. The proposed algorithm takes the inertial sensor signal as input, first extracts the spatial features of the sensor signal into the feature vector graph from multiple scales using the Inception parallel convolution structure, then uses the improved ECA (Efficient Channel Attention) channel attention module to extract the critical details of the feature vector graph of the sensor data, and finally uses the LSTM network to further extract the temporal features of the inertial sensor signals to achieve the classification and recognition of human motion posture. The experiment results demonstrate that 95.04% recognition accuracy on the public dataset PAMAP2 and 98.81% accuracy on the self-built dataset can be realized based on the algorithm model, indicating that the algorithm model has a superior recognition effect. In addition, the results of the visual analysis of channel attention weights show that the proposed model is interpretable for the recognition of human motions and is consistent with the living intuition.

## 1. Introduction

Lately, human motion recognition has turned into the most dynamic and famous area because of its wide application in true situations like medical care, smart home, and monitoring [1–3]. Traditional computer vision-based human motion recognition [4, 5] is limited in its effectiveness in the actual recognition process due to variations in illumination, complex background environments, and the influence of individual differences in objects. Compared with computer vision-based methods, inertial sensors have become increasingly important and started to be extensively applied in human motion recognition due to their low environmental coupling, high individual adaptability, and small size and low cost.

There are many existing studies on automatic human motion posture recognition based on inertial sensor data [6, 7], but accurate detection and recognition is still a chal-

lenge. The quality of the manually extracted signal features has a huge impact on the human motion recognition effect based on traditional machine learning algorithms (such as support vector machines [8] and random forests [9]), and thus, the professional knowledge in the field is required to transform sensor signal into corresponding feature expression for human motion recognition [10]. In addition, the elementary human postures can be represented effectually by the hand-made features, but they are unable to handle more complex motion patterns. In most cases, feature selection techniques are also needed to obtain significant features and reduce the dimension of feature space [11] to achieve optimal performance. To address these challenges, in-depth research on automatic feature extraction methods that do not require human intervention has become an active research area.

Convolutional neural networks (CNN) has emerged as a powerful tool in image processing and machine vision. When

used for human action recognition of inertial sensors, convolutional neural networks can automatically extract high-dimensional data features and thus can largely avoid the reliance on feature engineering. Also, due to its rich expressive power and spatial feature extraction capability, it can achieve better results than traditional machine learning algorithms when processing inertial sensor data [12]. However, in existing studies, researchers have mostly used serial convolutional structures to deepen the depth of convolution [13, 14], while there are fewer studies on parallel convolutional structures to widen the convolution width for processing inertial sensor data. An Inception neural network structure was proposed in the literature [15]. This structure is established on convolutional neural network and adopts multipath parallel convolution mode, which improves the utilization rate of computing resources in the network and fully extracts spatial features of data on multi-scale convolution kernel. It has excellent performance in the field of visual recognition and good scalability. LSTM is a special recurrent neural network (RNN) structure, which consists of a series of repeating neural networks combined in a chain. Its unique network structure makes it very sensitive to signals with temporal dependence. The attention mechanism is a widely studied network design approach in the fields of computer vision [16] and natural language processing [17]. Exhibiting a resemblance to human perception, the attention mechanism focuses upon the certain section of the objective region to magnify the key details of the object while abolishing other extraneous potentially baffling information, allowing neural network models to have a high level of interpretability. There are limited existing studies that apply attentional mechanisms to the field of inertial sensor action recognition. Literature [18] used a multi-head model based on the SENet (Squeeze Excitation Network) channel attention mechanism to extract features from inertial sensors signal and attained good recognition results on the UCI and WISDM datasets. Literature [19] used a dual attention approach combining channel attention and spatial attention to achieve good action classification results on all four publicly available datasets. In literature [20], based on SENet, an optimized channel attention mechanism model ECA is proposed, which significantly reduces the complexity of the model through cross-channel interaction of feature information and the performance of the model has been raised simultaneously.

In order to deal with the problem that the human motion recognition algorithm based on video images is vulnerable to uncertainties in the environment in applications, and to overcome the limitation that traditional machine learning algorithms require expert knowledge in related fields for manual feature extraction, this paper proposes an Inception-LSTM human motion recognition algorithm that introduces a channel attention mechanism based on inertial sensor signals. The proposed human motion recognition algorithm automatically extracts spatial features of inertial sensor data using Inception convolutional structure, extracts temporal features of data using LSTM, and introduces an improved ECA channel attention mechanism module between the two feature extraction networks to make the model focus more on the critical details of sensor data features, suppress non-key information, and improve motion recognition rate.

## 2. Model Construction of the Inception-LSTM Algorithm for Introducing Channel Attention

The proposed Inception-LSTM human motion recognition algorithm, which introduces the channel attention mechanism, extracts the features of sensor signals in three parts: the spatial features of inertial sensor signals are extracted using a spatial feature extraction network; the model converges its attention on the key details of each action using a modified ECA channel attention module; and the temporal dependencies hidden in sensor signals are extracted using a temporal feature extraction network.

*2.1. Spatial Feature Extraction Network.* The multiaxial data output of acceleration and gyroscope of inertial sensors allows them to collect rich spatial features in characterizing human activities. And CNN have significant advantages in extracting spatial features of signals. Each feature pixel in the current neuron of a CNN is mapped to the previous layer of neurons by a local receptive field and then obtained by a nonlinear activation function. The calculation is shown in Equation (1).

$$s(i, j) = \sigma \left( \sum_{m=1}^H \sum_{n=1}^K w_{m,n} x_{i+m, j+n} + b \right), \quad (1)$$

where  $s(i, j)$  is the feature pixel of the current neuron,  $\sigma$  is the nonlinear activation function,  $w$  is the weight matrix of the  $H \times K$  convolution kernel,  $b$  is the bias, and  $x$  is the local receptive field of the upper layer neuron. CNN represent the data by convolution in order to abstract the features of the signals. Generally, the performance of convolutional neural network can be enhanced through increasing the depth and node number of each layer in serial sequential manner, but this brings two drawbacks: first, the larger network size makes the model risk of overfitting. Second, the amount of nodes in the network is too large, which makes the computational resources exponentially increase.

The Inception convolutional structure changes the serial sequential connection between layers of the traditional convolutional model by distributing four different convolutional kernels—one  $1 \times 1$  convolution, one  $1 \times 1$  convolution in series with a  $3 \times 3$  convolution, one  $1 \times 1$  convolution in series with a  $5 \times 5$  convolution, and one  $3 \times 3$  maximum pooling layer in series with a  $1 \times 1$  convolution—on four different convolutional paths, and the input signals enter these 4 convolution paths in parallel in turn, and finally, the outputs of the 4 convolution results are stitched together and used as the input of the poststage network. This parallel convolution method can extract the spatial features of the input signal at different scales and give different weights to achieve a good recognition effect.

The proposed model in this paper adopts the Inception asymmetric convolution structure to construct a lightweight sensor signal space feature extraction module. As shown in Figure 1, from left to right, it is channel 1 to channel 4. Channel 1 performs two  $1 \times 1$  convolution operations, similar to the

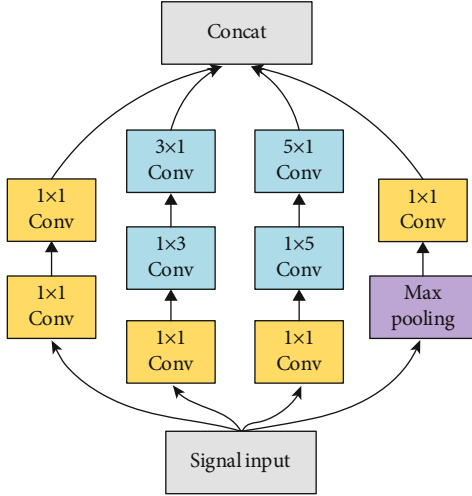


FIGURE 1: Inception asymmetric convolution structure.

fully connected operation in linear networks; channel 2 first performs a  $1 \times 1$  convolution operation, aiming to trim the number of parameters and quicken the training process. Then, one  $1 \times 3$  asymmetric convolution operation is performed to mine the feature information between acceleration and angular velocity of the inertial sensor and extract it into the feature vector graph through the convolution kernel of the lateral vector. Finally, a  $3 \times 1$  convolution operation is performed to get the signal features in the same inertial axes of adjacent time into the feature vector map through the convolution kernel of longitudinal vectors; channel 3 first performs a  $1 \times 1$  convolution operation with the same effect as in channel 2, then a  $1 \times 5$  lateral convolution operation to expand the interaxis data features in a larger range into the feature map, and finally a  $5 \times 1$  vertical convolution operation to fuse the temporal features of the data at a larger scale and add them to the feature map; channel 4 first introduces a maximum pooling layer to downsample the data samples composed of inertial sensor data to reduce the data dimensionality and compress the features and then performs a  $1 \times 1$  convolution operation. The four channels of the altered Inception structure are independent of each other and process the data in parallel, and finally, the data of the four channels are stitched together by channel dimension. This asymmetric convolution structure can obtain the spatial features of inertial sensor signals better.

**2.2. Channel Attention Mechanism.** In the purpose of improving the performance of the proposed algorithm for inertial sensor signal recognition, the ECA channel attention mechanism module is introduced in this paper. ECA is an optimized channel attention mechanism model. Based on SENet, ECA can realize a huge complexity reduction and performance improvement of the model by a local cross channel interaction strategy without no reduction of the dimension and self-adaptive selection of 1D convolution kernel size. For a feature graph input  $A \in R^{W \times H \times C}$  with channel number  $C$ , height  $H$ , and width  $W$ , ECA first performs a global average pooling to compress the information of each channel independently to obtain a feature strip with dimension  $1 \times 1 \times C$ . Then, the

1D convolution and nonlinear transformation are performed on the feature strip to obtain the attention weight  $\omega_i$  for each channel  $A_i$ . The weight  $\omega_i$  for channel  $A_i$  focuses only on the current channel  $A_i$  and its  $k$  neighboring channels and is calculated as shown in Equation (2).

$$\omega_i = \sigma \left( \sum_{j=1}^k \omega_i^j A_i^j \right), A_i^j \in \Omega_i^k, \quad (2)$$

where  $\Omega_i^k$  represents the set of  $k$  adjacent channels of  $A_i^j$ . The 1D convolution kernel size  $k$  is obtained by adaptive calculation of Equation (3), where  $\gamma = 2$ ,  $b = 1$ .

$$k = \psi(C) = \left\lfloor \frac{\log_2(C)}{\gamma} + \frac{b}{\gamma} \right\rfloor. \quad (3)$$

Based on the original ECA module, the proposed algorithm combines the inertial sensor signal to realize human motion recognition, and a channel feature extraction module is added in the later stage, as shown in Figure 2.

The algorithm put forward here is based on the original ECA module and combines the application context of human motion recognition with inertial sensor signals, adding a channel feature extraction module to its back-end, as shown in Figure 2.

The attention weights  $\omega_i$  obtained from the original ECA module after the 1D convolution and nonlinear transformation are first arranged in descending order according to their absolute value magnitudes to obtain the sequence  $\tilde{\omega}$  and its corresponding index. Then, the values of the first  $N$  sequences in sequence  $\tilde{\omega}$  and their index values are selected. At the end of the multiplication of the original feature map input  $A \in R^{W \times H \times C}$  with the attention weights  $\omega_i$ , the corresponding feature channels of the multiplication results are extracted according to the indexes of the obtained values of the first  $N$  sequences, and the output feature map  $A' \in R^{W \times H \times N}$  is finally obtained, where the parameter  $N$  is calculated by Equation (4).

$$N = k + \frac{\log_2(C)}{2} \Big|_{\text{even}}, \quad (4)$$

where even indicates that the result is taken as the closest even number. By this extraction of the main feature channels, the feature utilization efficiency of the deep neural network is improved, which in turn improves the recognition performance of the network.

**2.3. Temporal Feature Extraction Network.** The signals generated by inertial sensors have strong temporal dependence when the human body performs various action posture activities, and RNN has significant advantages in extracting temporal features of the signals. The temporal features extracting network in the algorithm proposed in this paper consist of LSTM. Unlike RNN, LSTM introduces the concepts of input gate, forgetting gate, and output gate for realizing the update

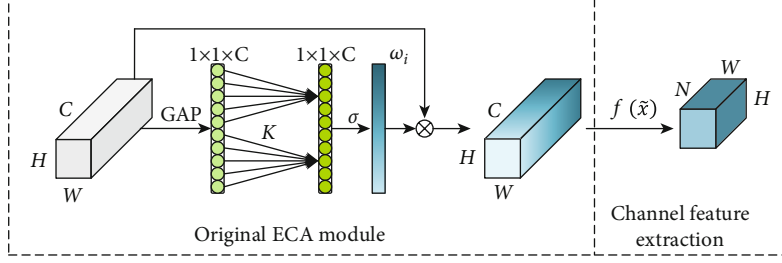


FIGURE 2: Improved ECA module structure.

and output of memory states. Its basic neural network unit structure is shown in Figure 3.

In Figure 3,  $c$  is the cell state, which is similar to an information pipeline that runs through the entire operation cycle of the LSTM. The three gate structures of the LSTM allow for the removal and addition of information in the cell, allowing for selective information flow.  $\sigma$  is a nonlinear activation function that maps the output value of the function between 0 and 1, with 0 indicating no information passes and 1 indicating all information passes.  $W$  is the weight matrix, and  $b$  is the bias vector.

First, the forgetting gate determines what kind of message will be discarded from the cell. The gate will read the hidden state  $h_{t-1}$  of the prior moment with input  $X_t$  and output a value between  $[0,1]$  and the cell state  $c_{t-1}$  of the prior moment by the  $\sigma$  function to do the element multiplication operation. The result of the output  $f_t$  of the forgetting gate is illustrated in Equation (5).

$$f_t = \sigma(W_f \times [h_{t-1}, X_t] + b_f). \quad (5)$$

Second, the input gate determines what new messages are to be stored in the cell state. The output of the  $\sigma$  function determines what values are to be updated and the tanh layer builds a new candidate cell state vector  $\tilde{c}_t$  to determine in which way to add the output to the cell state. The output  $i_t$  of the input gate, the candidate cell state vector  $\tilde{c}_t$ , is updated with the current cell state  $c_t$  as shown in Equation (6) to Equation (8).

$$i_t = \sigma(W_i \times [h_{t-1}, X_t] + b_i), \quad (6)$$

$$\tilde{c}_t = \tanh(W_c \times [h_{t-1}, X_t] + b_c), \quad (7)$$

$$c_t = f_t \times c_{t-1} + i_t \times \tilde{c}_t. \quad (8)$$

Finally, the output of the LSTM is obtained from the output gate  $o_t$ . The function  $\sigma$  determines which information will be output. The current cell state  $c_t$  is processed by tanh, and by the output of the  $\sigma$  function is multiplied by elements to obtain the final output  $h_t$  of the LSTM. The output  $o_t$  of the output gate and the final output  $h_t$  is illustrated according to Equation (9) to Equation (10).

$$o_t = \sigma(W_o \times [h_{t-1}, X_t] + b_o), \quad (9)$$

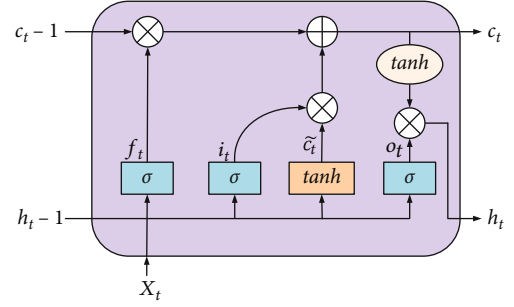


FIGURE 3: Internal structure of LSTM.

$$h_t = o_t \times \tanh(c_t). \quad (10)$$

The design of the three gates in the LSTM makes the structure highly sensitive when dealing with data with temporal dependencies. For the temporal feature extraction module, its input at each time step is derived from the feature vector map extracted by the predecessor improved ECA module. At each time step, the LSTM reads in the feature map input  $A' \in R^{W \times H \times N}$  line by line, and at time steps  $t_1$  to  $t_n$ , a total of  $n$  data frames of the feature maps are read in. The LSTM network is used to take into account the interaction between the timing dimensions of the upstream and downstream inertial sensor data frames and to better extract the timing features.

In summary, the architecture of the proposed algorithm in this paper is presented in Figure 4.

### 3. Experimental Design

**3.1. Experimental Data Acquisition.** In the purpose of verifying the effectiveness of the proposed human motion recognition algorithm model, the recognition performance of the algorithm model is tested on the public dataset PAMAP2 and the self-built motion posture dataset, respectively.

The PAMAP2 human activity monitoring dataset [21] includes 18 different physical activity postures (e.g. cycling, running, and walking). The dataset was obtained from nine persons wearing three inertial measurement units, one at the wrist of the subject's dominant arm, one at the chest, and one at the ankle of the subject's dominant side of the body. According to the experimental requirements, each person was required to conduct 12 different activities, including sitting, standing, walking up and down stairs, jumping rope,

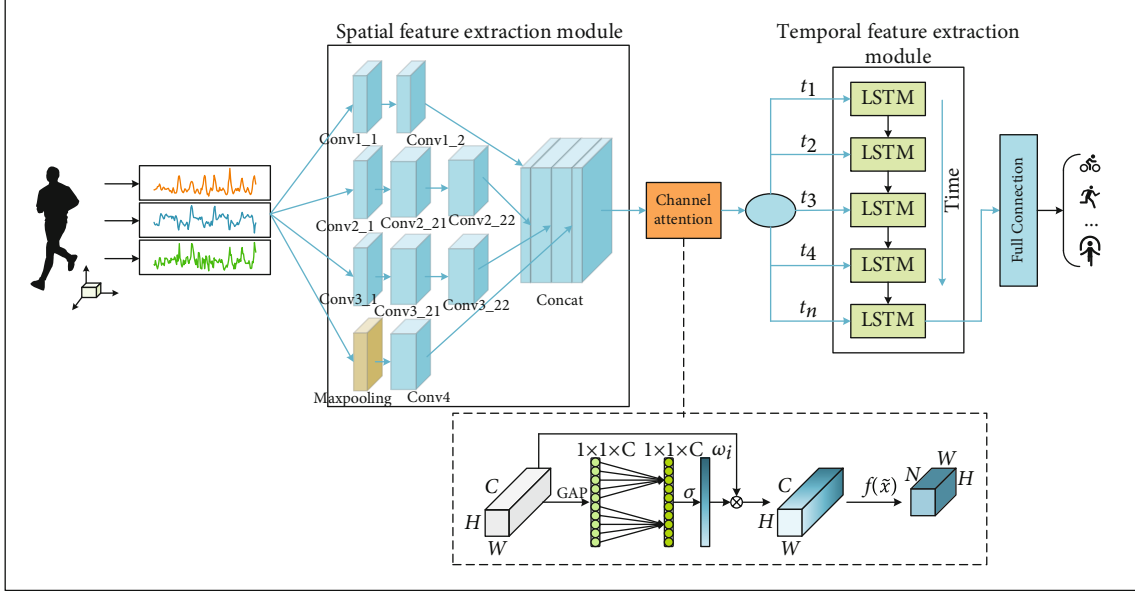


FIGURE 4: Inception-LSTM algorithm model with channel attention.

and running. In addition, a number of random activities were performed for each program, including cleaning the room, driving, and working in front of the computer. Each inertial measurement unit was used with a sampling frequency of 100 Hz, and at each moment, three inertial measurement units collected acceleration, gyroscope, magnetometer, and body temperature data from the different body parts of the subject's current activity. A total of 216,000 data from 9 subjects were selected for the training. In the experiment, the dataset was split into training dataset and test dataset based on 7:3.

In the purpose of further verifying recognition capability and data robustness of the proposed model, a self-built human activity dataset was constructed in this paper. Two inertial measurement units are installed on the abdomen and the upper side of the knee of the left leg of the experimental tester, as shown in Figure 5. Each inertial measurement unit can output 3-axis gyroscope and 3-axis acceleration signal of the current activity of the tester. According to the experimental requirements, the tester needs to complete seven prescribed movements including sitting, standing, going upstairs, going downstairs, walking, running, and cycling. The long-time movements (sitting, standing, walking, running, and riding) are recorded as a set of data every 3 min, and the short-time movements (going upstairs and downstairs) are recorded as a set every 5 s. The sampling frequency of the inertial measurement unit was set to 25 Hz, and finally, 52,500 action data were obtained. During the training process, the dataset is also split into training dataset and test dataset based on 7:3.

**3.2. Data Preprocessing.** The preprocessing of the data is mainly for the processing of the missing values of the data and the segmentation of the data. For the missing values of the data, this paper mainly uses the method of Equation (11) for linear interpolation, where  $y_i$  is the missing value of the inertial sensor to be interpolated at the moment  $x_i$ .

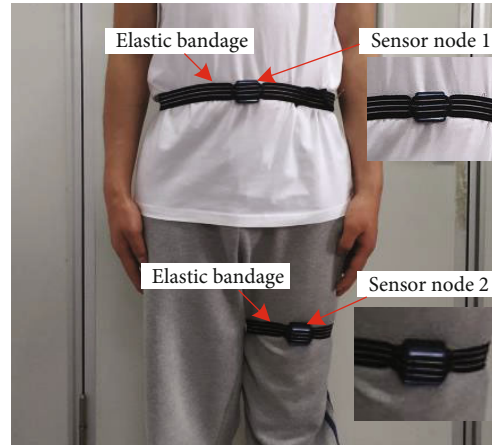


FIGURE 5: Schematic diagram of the sensor wearing.

$y_s$  and  $y_d$  are the normal output sensor values at both ends of the missing value.

$$y_i = y_s + \frac{y_d - y_s}{x_d - x_s} (x_i - x_s). \quad (11)$$

For data segmentation, an intelligent segmentation approach was used in literature [22] to adaptively adapt to human activity poses with different duration lengths, and good action recognition results were achieved under different conditions. However, the data segmentation method with fixed window size has obvious advantages in terms of computational efficiency, while it is easier to achieve end-to-end processing. Therefore, this paper uses the fixed-window-size strategy by referring to the approach in literature [23]. When the fixed window length is  $K$ , the data sequence for the same inertial measurement cell at the  $i$  window time is as follows:



$$\begin{cases} S_i^{a^x} = [a_t^x, a_{t+1}^x, \dots, a_{t+K-1}^x], \\ S_i^{a^y} = [a_t^y, a_{t+1}^y, \dots, a_{t+K-1}^y], \\ S_i^{a^z} = [a_t^z, a_{t+1}^z, \dots, a_{t+K-1}^z], \\ S_i^{g^x} = [g_t^x, g_{t+1}^x, \dots, g_{t+K-1}^x], \\ S_i^{g^y} = [g_t^y, g_{t+1}^y, \dots, g_{t+K-1}^y], \\ S_i^{g^z} = [g_t^z, g_{t+1}^z, \dots, g_{t+K-1}^z]. \end{cases} \quad (12)$$

Different window lengths  $K$  will have an impact on the accuracy, and the relationship between several groups of window lengths  $K$  and accuracy is obtained by comparing the experiments as shown in Figure 6.

As can be seen from Figure 6, on the PAMAP2 dataset, the accuracy can reach about 95% when  $K$  is 100. On the self-built dataset, the accuracy can reach about 98% when  $K$  is 50. Therefore, the model training process sets  $K$  to 100 and 50 on the PAMAP2 dataset and the self-built dataset, respectively.

**3.3. Model Training.** The specific design parameters of the proposed Inception-LSTM human motion recognition algorithm that introduces the channel attention mechanism are shown in Table 1. The model is based on the Windows platform, running in the Anaconda environment of Python 3.6 kernel, and is obtained by CPU-accelerated training. During the training process, the hyperparameters learning rate and the number of training iteration are set to 0.001 and 200 respectively.

## 4. Experimental Results and Analysis

**4.1. Evaluate Metrics.** In this paper, the performance of the algorithm model is measured by using the evaluation metrics of average accuracy, precision, recall, and F1 value. The calculation formulas are Equation (13) to Equation (16), respectively.

$$\text{Accuracy} = \frac{\text{TP} + \text{TN}}{\text{TP} + \text{TN} + \text{FP} + \text{FN}}, \quad (13)$$

$$\text{Precision} = \frac{\text{TP}}{\text{TP} + \text{FP}}, \quad (14)$$

$$\text{Recall} = \frac{\text{TP}}{\text{TP} + \text{FN}}, \quad (15)$$

$$\text{F1} = \frac{2 \times \text{Precision} \times \text{Recall}}{\text{Precision} + \text{Recall}}, \quad (16)$$

where TP means true positive, indicating a positive sample judged to be positive, TN means true negative, indicating a negative sample judged to be negative, FP means false positive, indicating a negative sample judged to be positive, and FN means false negative, indicating a positive sample judged to be negative.

**4.2. Performance on the PAMAP2.** In the purpose of observing the performance of the proposed algorithm on the public dataset PAMAP2, four algorithms, namely, the standard CNN net-

work, the LSTM network, the neural network without channel attention mechanism, and the neural network with the original ECA added in the proposed model, are also designed as the control experiment of the proposed algorithm model in this paper. Meanwhile, in the purpose of ensuring the fairness of the comparison experiment, the parameters of the convolutional layers of the standard CNN network are set to the serial sequential connection form of the parameters of the Inception convolutional structure in this model to ensure the consistent scale of the convolutional layers. The parameters of the rest of the neural network algorithms are set with the same values of the proposed model. All adjustable hyperparameters were kept consistent with the proposed model during the experiments. The results are displayed in Figure 7.

As is displayed in Figure 7, the neural network without ECA that combines the Inception parallel convolutional structure with LSTM has significantly higher recognition accuracy than the classical CNN with serial sequential connections and the LSTM neural network alone. Meanwhile, the model incorporating the channel attention mechanism performs significantly better than the ordinary neural network without the channel attention mechanism in terms of recognition accuracy. In addition, the improved ECA model with channel feature extraction proposed in this paper also has a certain improvement in action recognition accuracy compared with the unimproved original ECA.

The proposed algorithm in this paper is compared with other algorithms in existing studies using the same PAMAP2 dataset, and the comparison results are displayed in Table 2. As is seen in the table, the proposed Inception-LSTM human action recognition algorithm that introduces a channel attention mechanism improves 1.88% in recognition accuracy compared to the literature [19] that uses a dual attention mechanism and improves over the AttnSense model proposed in the literature [24] and the layered convolutional neural network model with local loss proposed in the literature [25] by 5.74% and 2.07%. Also, the increase in model size is almost negligible compared to the neural network without the use of ECA.

The confusion matrix of the algorithm proposed in this paper is displayed in Figure 8. From the figure, it can be observed that the recognition accuracy of the algorithm can reach more than 90% for most of the actions on the PAMAP2 dataset. Among them, the recognition accuracy of rope jumping and running actions can reach 100%. For some more confusing actions such as sitting, standing, and ironing, the recognition effect is poor. Sitting actions are easily misclassified as standing actions and standing actions are easily misclassified as ironing. The demarcation between such static actions is not obvious, so they are often misclassified by the model.

In order to visualize the model interpretability brought by the channel attention mechanism, this paper provides a visual analysis of channel attention weights to evaluate the influence of various body parts on motion recognition when the human body performs different motion postures, and the results are displayed in Figure 9.

In Figure 9, the shades of the sensor colors at different moments indicate how much attention the algorithm model

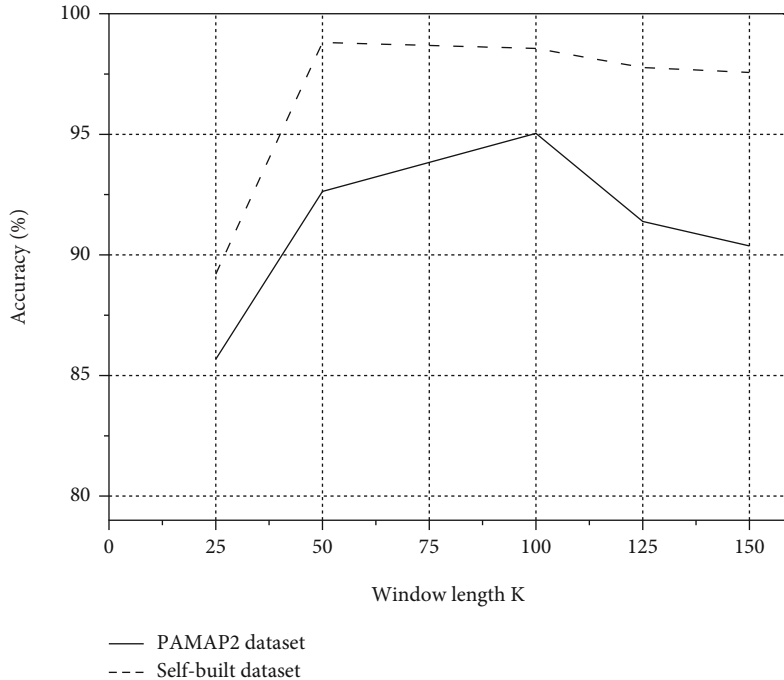


FIGURE 6: Influence of different window lengths on accuracy.

TABLE 1: The parameters of each layer of the proposed model.

Order number	Layer position	Size	Number of parameters
1	The convolutional layer, 1_1	[64, 1, 1, 1]	128
2	The convolutional layer, 1_2	[64, 64, 1, 1]	4160
3	The convolutional layer, 2_1	[64, 1, 1, 1]	128
4	Convolutional layer 2_21	[128, 64, 1, 3]	24704
5	Convolutional layer 2_22	[128, 128, 3, 1]	49280
6	The convolutional layer, 3_1	[64, 1, 1, 1]	128
7	Convolutional layer: 3_21	[128, 64, 1, 5]	41088
8	Convolutional layer 3_22	[128, 128, 5, 1]	82048
9	Maximum pooling layer	[64, 1, 3, 3]	0
10	Convolutional layer 4	[64, 1, 1, 1]	4160
11	Channel attention block	[1, 5]	385
12	Feature extraction layer	[9, 384, 1, 1]	3465
13	LSTM layer	[64, 18]	5312
14	Fully connected layer	[12, 64]	780

pays to the current activity on that component of the sensor. From the figure, it can be observed that the model proposed in this paper pays more attention to the  $x$ -axis component of the wrist sensor, the  $x$ -axis component of the chest sensor, and the  $z$ -axis component of the ankle sensor during the running activity. During the cycling activity, the model pays much attention to the  $x$ -axis and  $z$ -axis components of the ankle sensors. For the rope-jumping activity, the proposed model pays more attention to the  $y$ -axis and  $z$ -axis components of the wrist and the three axial components of the ankle. During the ironing activity, the model pays more

attention to the  $x$ -axis and  $y$ -axis components at the wrist. Thus, it can be observed that the algorithm incorporating the channel attention mechanism is interpretable in terms of action recognition results and is generally consistent with the life intuition.

*4.3. Performance on the Self-Built Dataset.* The same four neural network algorithms, standard CNN network, LSTM network, neural network without channel attention mechanism, and the proposed model with original ECA neural network, were designed as control experiments on the self-built

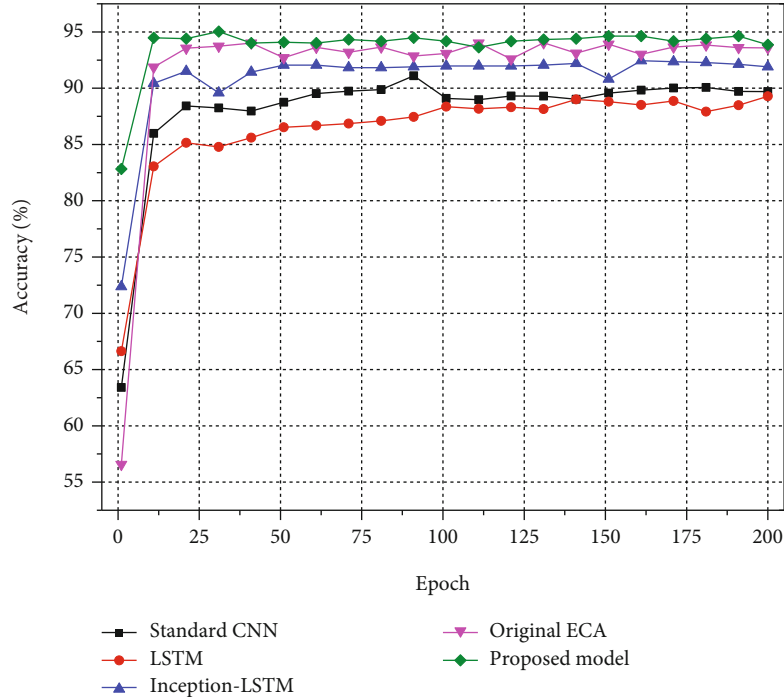


FIGURE 7: Accuracy of each model on PAMAP2 dataset.

TABLE 2: Experimental results of different models on PAMAP2.

Algorithm model	Accuracy	Precision	Recall	F1 value	Model size
Classics CNN	91.11%	91.41%	91.11%	91.26%	7.14 M
LSTM	89.28%	89.69%	89.28%	89.49%	0.37 M
Neural network without ECA	92.44%	92.93%	92.44%	92.68%	2.67 M
Original ECA	93.91%	94.04%	93.91%	93.97%	2.68 M
This article model	95.04%	95.06%	95.21%	95.13%	2.68 M
Literature: [24]	89.30%	—	—	—	—
Literature: [25]	92.97%	—	—	—	—
Literature: [19]	93.16%	—	—	—	3.51 M

dataset. The adjustable hyperparameters of the models and the scale of the models are kept consistent with the proposed model. The experimental results are displayed in Figure 10.

As it can be observed from Figure 10, the proposed model has some improvement in accuracy over the model using the original ECA. Meanwhile, the neural network incorporating the channel attention mechanism is overall more accurate and converges faster than the neural network without the channel attention mechanism. The experimental results and model sizes of the different models on the self-built dataset are presented in Table 3.

The confusion matrix for the proposed model to identify each action in the self-built dataset is displayed in Figure 11.

As can be observed from Figure 11, the proposed model can maintain high accuracy in recognizing all seven motions on the self-built dataset. Among them, the recognition accuracy of sitting still, running, and cycling reaches 100%. Among them, the

motion patterns of going upstairs, going downstairs, and walking are more similar, so the degree of confusion is higher.

The visualization results of the attention weights of the model are shown in Figure 12. As is shown in the figure, under the condition that the two inertial measurement units characterize the human activity posture, the channel attention model pays high attention to the signal component of the abdominal sensor  $x$ -axis when the human body is in the standing posture. During the upstairs activity, the channel attention model pays more attention to the signal components of the  $x$ -axis and  $z$ -axis of the leg sensors, which is consistent with the intuition of daily life.

## 5. Summary

In this paper, we propose the Inception-LSTM human motion recognition algorithm with the introduction of

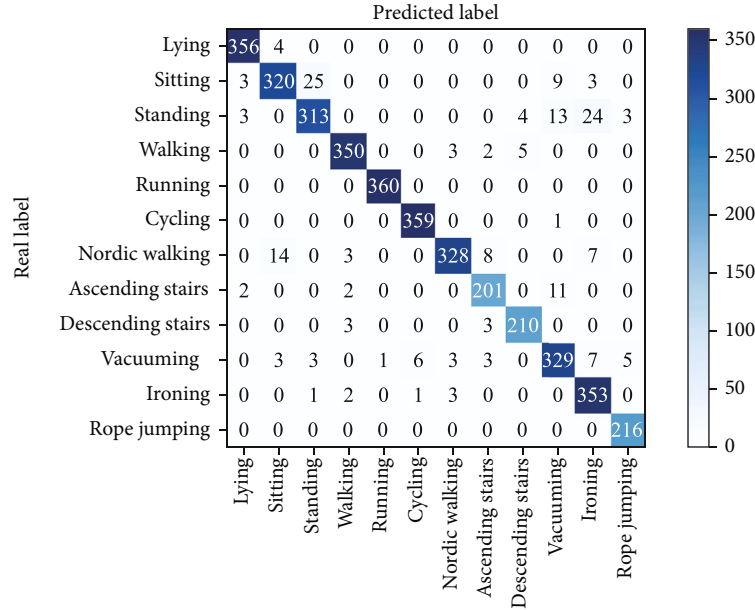


FIGURE 8: The confusion matrix of different motions of the proposed model on PAMAP2 dataset.

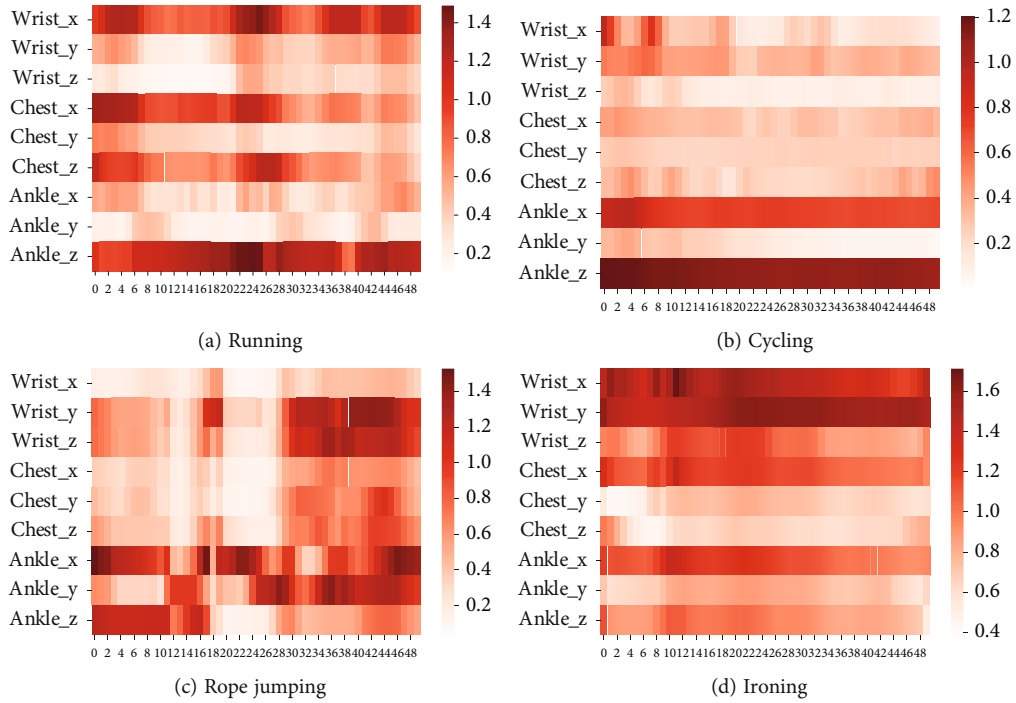


FIGURE 9: Visualization of channel attention weights of different motions on PAMAP2 dataset.

channel attention mechanism, which has two main features. One is to replace the traditional serial sequentially connected convolutional neural network with the Inception parallel convolutional structure to fully extract the spatial features of inertial sensors on multiple paths and scales and to join the LSTM network to extract the temporal features of the signals. Second, the channel attention mechanism ECA module is improved

and fused into the neural network model by combining the inertial sensor signal characteristics to improve the recognition efficiency and resource utilization of the model. The proposed algorithm is tested on the public dataset PAMAP2 and the self-built dataset, and good recognition results are achieved on both datasets. The accuracy of the proposed algorithm for human motion recognition is higher than that of standard

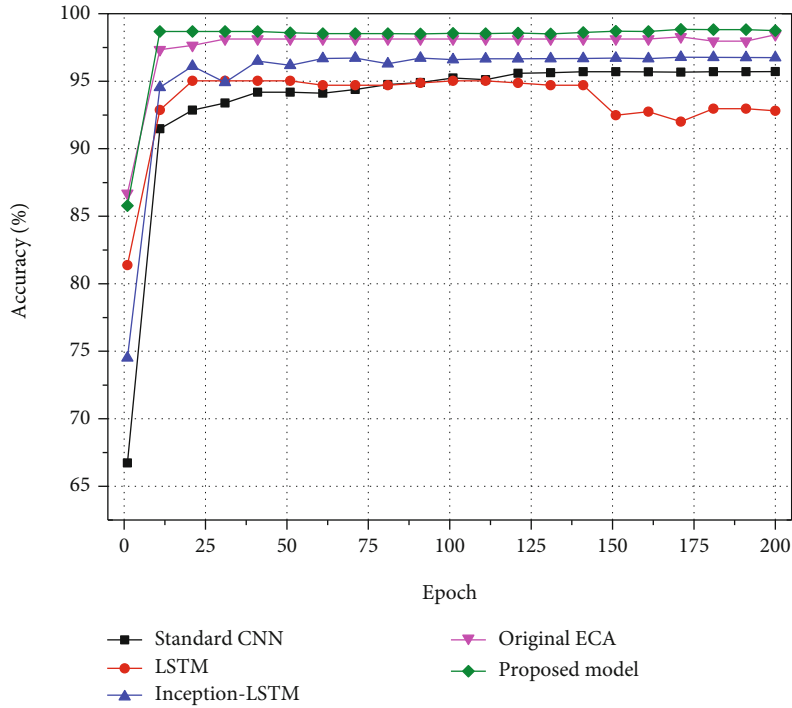


FIGURE 10: Accuracy of each model on self-built dataset.

TABLE 3: Experimental results of different models on self-built dataset.

Algorithm model	Accuracy	Precision	Recall	F1 value	Model size
Classics CNN	95.71%	96.12%	95.71%	95.91%	2.53 M
LSTM	95.02%	95.98%	95.02%	95.50%	0.34 M
Neural network without ECA	96.77%	96.85%	96.77%	96.81%	1.21 M
Original ECA	98.44%	98.54%	98.44%	98.49%	1.24 M
The proposed model	98.81%	98.81%	98.81%	98.81%	1.24 M

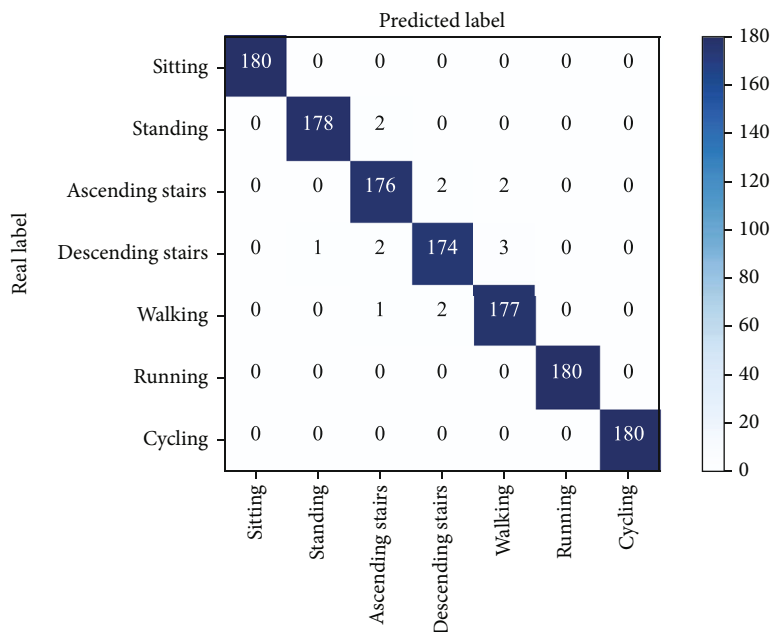


FIGURE 11: The confusion matrix of different motions of the proposed model on self-built dataset.

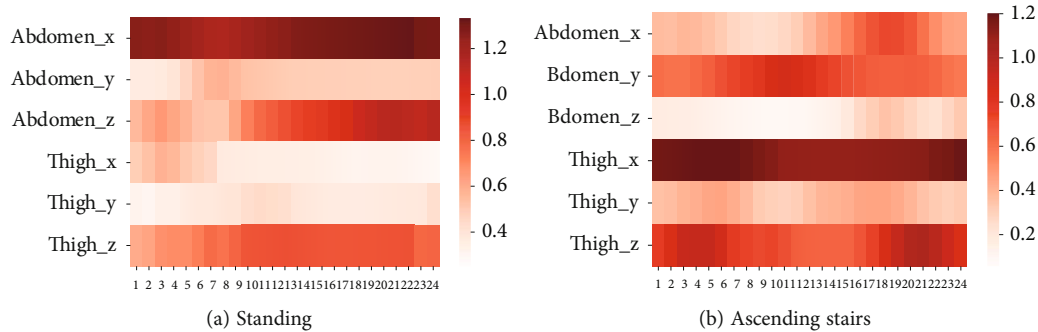


FIGURE 12: Visualization of channel attention weights of different motions on self-built dataset.

CNN, LSTM, and neural network models without using attention mechanism. Also, the improved ECA module has improved the recognition results compared with the original ECA module. In addition, the visual analysis of channel attention weights for several typical actions shows that the action recognition results of the proposed algorithm model are interpretable and consistent with the living intuition.

### Data Availability

The datasets used during the current study are available from the corresponding author on reasonable request.

### Conflicts of Interest

The authors declare that they have no conflicts of interest.

### References

- [1] L. Gao, G. Zhang, B. Yu, Z. Qiao, and J. Wang, "Wearable human motion posture capture and medical health monitoring based on wireless sensor networks," *Measurement*, vol. 166, no. 4, p. 108252, 2020.
- [2] G. Sprint, D. Cook, D. Weeks, J. Dahmen, and A. La Fleur, "Analyzing sensor-based time series data to track changes in physical activity during inpatient rehabilitation," *Sensors*, vol. 17, no. 10, p. 2219, 2017.
- [3] J. Li, X. Mao, L. Chen, and L. Wang, "Human interaction recognition fusing multiple features of depth sequences," *IET Computer Vision*, vol. 11, no. 7, pp. 560–566, 2017.
- [4] J. Liu, Y. Wang, Y. Liu, S. Xiang, and C. Pan, "3D PostureNet: a unified framework for skeleton-based posture recognition," *Pattern Recognition Letters*, vol. 140, no. 8, pp. 143–149, 2020.
- [5] L. Wang, L. Ge, R. Li, and Y. Fang, "Three-stream CNNs for action recognition," *Pattern Recognition Letters*, vol. 92, pp. 33–40, 2017.
- [6] H. Kale, P. Mandke, H. Mahajan, and V. Deshpande, "Human posture recognition using artificial neural networks," in *International Advance Computing Conference*, pp. 272–278, Greater Noida, India, 2018.
- [7] E. Fridrikzdottir and A. G. Bonomi, "Accelerometer-based human activity recognition for patient monitoring using a deep neural network," *Sensors*, vol. 20, no. 22, p. 6424, 2020.
- [8] L. Zhao and W. Chen, "Detection and recognition of human body posture in motion based on sensor technology," *IEEE Transactions on Electrical and Electronic Engineering*, vol. 15, no. 5, pp. 766–770, 2020.
- [9] G. M. Weiss, K. Yoneda, and T. Hayajneh, "Smartphone and smartwatch-based biometrics using activities of daily living," *IEEE Access*, vol. 7, pp. 133190–133202, 2019.
- [10] S. González, J. Sedano, J. R. Villar, E. Corchado, Á. Herrero, and B. Baruque, "Features and models for human activity recognition," *Neurocomputing*, vol. 167, no. 1, pp. 52–60, 2015.
- [11] I. Andrey, "Real-time human activity recognition from accelerometer data using convolutional neural networks," *Applied Soft Computing*, vol. 62, pp. 915–922, 2018.
- [12] W. Jiang and Z. Yin, "Human activity recognition using wearable sensors by deep convolutional neural networks," in *ACM international conference on multimedia*, pp. 1307–1310, Brisbane Australia, 2015.
- [13] M. Gil-Martín, R. San-Segundo, F. Fernández-Martínez, and J. Ferreiros-López, "Improving physical activity recognition using a new deep learning architecture and post-processing techniques," *Engineering Applications of Artificial Intelligence*, vol. 92, no. 92, pp. 103679–103689, 2020.
- [14] V. Bianchi, M. Bassoli, G. Lombardo, P. Fornacciarì, M. Mordonini, and I. de Munari, "IoT wearable sensor and deep learning: an integrated approach for personalized human activity recognition in a smart home environment," *IEEE Internet of Things Journal*, vol. 6, no. 5, pp. 8553–8562, 2019.
- [15] C. Szegedy, W. Liu, Y. Jia et al., "Going deeper with convolutions," in *Conference on computer vision and pattern recognition*, pp. 1–9, Boston, 2015.
- [16] W. Zhu, Z. Wang, R. Hu, and D. Li, "From semantic to spatial awareness: vehicle reidentification with multiple attention mechanisms," *IEEE Multimedia*, vol. 28, no. 3, pp. 32–41, 2021.
- [17] D. Jain, A. Kumar, and G. Garg, "Sarcasm detection in mash-up language using soft-attention based bi-directional LSTM and feature-rich CNN," *Applied Soft Computing*, vol. 91, pp. 106198–106208, 2020.
- [18] Z. N. Khan and J. Ahmad, "Attention induced multi-head convolutional neural network for human activity recognition," *Applied Soft Computing*, vol. 110, pp. 107671–107679, 2021.
- [19] W. Gao, L. Zhang, Q. Teng, J. He, and H. Wu, "DanHAR: dual attention network for multimodal human activity recognition using wearable sensors," *Applied Soft Computing*, vol. 111, pp. 107728–107739, 2021.
- [20] Q. Wang, B. Wu, P. Zhu, P. Li, W. Zuo, and Q. Hu, "ECA-Net: efficient channel attention for deep convolutional neural networks," in *Conference on computer vision and pattern recognition*, pp. 11531–11539, Seattle, 2020.

- [21] A. Reiss and D. Stricker, "Introducing a new benchmarked dataset for activity monitoring," in *International Symposium on Wearable Computers*, pp. 108-109, Newcastle, 2012.
- [22] C. Ma, W. Li, J. Cao, J. du, Q. Li, and R. Gravina, "Adaptive sliding window based activity recognition for assisted livings," *Information Fusion*, vol. 53, pp. 55-65, 2020.
- [23] H. Zhang, Z. Xiao, J. Wang, F. Li, and E. Szczerbicki, "A novel IoT-perceptive human activity recognition (HAR) approach using multihead convolutional attention," *IEEE Internet of Things Journal*, vol. 7, no. 2, pp. 1072-1080, 2020.
- [24] H. Ma, W. Li, X. Zhang, S. Gao, and S. Lu, "Attnsense: multi-level attention mechanism for multimodal human activity recognition," in *International joint conference on artificial intelligence*, pp. 3109-3115, Macao, 2019.
- [25] Q. Teng, K. Wang, L. Zhang, and J. He, "The layer-wise training convolutional neural networks using local loss for sensor-based human activity recognition," *IEEE Sensors Journal*, vol. 20, no. 13, pp. 7265-7274, 2020.

## Retraction

# Retracted: Text Feature Extraction for Public English Vocabulary Based on Wavelet Transform

### Computational and Mathematical Methods in Medicine

Received 19 September 2023; Accepted 19 September 2023; Published 20 September 2023

Copyright © 2023 Computational and Mathematical Methods in Medicine. This is an open access article distributed under the Creative Commons Attribution License, which permits unrestricted use, distribution, and reproduction in any medium, provided the original work is properly cited.

This article has been retracted by Hindawi following an investigation undertaken by the publisher [1]. This investigation has uncovered evidence of one or more of the following indicators of systematic manipulation of the publication process:

- (1) Discrepancies in scope
- (2) Discrepancies in the description of the research reported
- (3) Discrepancies between the availability of data and the research described
- (4) Inappropriate citations
- (5) Incoherent, meaningless and/or irrelevant content included in the article
- (6) Peer-review manipulation

The presence of these indicators undermines our confidence in the integrity of the article's content and we cannot, therefore, vouch for its reliability. Please note that this notice is intended solely to alert readers that the content of this article is unreliable. We have not investigated whether authors were aware of or involved in the systematic manipulation of the publication process.

Wiley and Hindawi regrets that the usual quality checks did not identify these issues before publication and have since put additional measures in place to safeguard research integrity.

We wish to credit our own Research Integrity and Research Publishing teams and anonymous and named external researchers and research integrity experts for contributing to this investigation.

The corresponding author, as the representative of all authors, has been given the opportunity to register their agreement or disagreement to this retraction. We have kept a record of any response received.

### References

- [1] D. Ye and X. Shi, "Text Feature Extraction for Public English Vocabulary Based on Wavelet Transform," *Computational and Mathematical Methods in Medicine*, vol. 2022, Article ID 7125242, 10 pages, 2022.



## Research Article

# Text Feature Extraction for Public English Vocabulary Based on Wavelet Transform

Di Ye  and Xiaojing Shi

School of Foreign Studies, Tangshan Normal University, Tangshan, Hebei 063000, China

Correspondence should be addressed to Di Ye; yedi@tstc.edu.cn

Received 26 April 2022; Revised 21 May 2022; Accepted 24 May 2022; Published 11 June 2022

Academic Editor: Naeem Jan

Copyright © 2022 Di Ye and Xiaojing Shi. This is an open access article distributed under the Creative Commons Attribution License, which permits unrestricted use, distribution, and reproduction in any medium, provided the original work is properly cited.

Text interpretation of public English vocabulary is a critical task in the subject of natural language processing, which uses technology to allow humans and computers to communicate effectively using natural language. Text feature extraction is one of the most fundamental and crucial elements in allowing computers to effectively grasp and read text. This paper proposes a text feature extraction method based on wavelet analysis that performs fast discrete wavelet transform and inverse discrete wavelet transform on the feature vectors under the traditional TF-IDF vector space model to address the problem of low feature differentiation of high-dimensional data in text feature extraction. In particular, due to the design of the Mallat algorithm, there is frequency aliasing in the signal decomposition process. This phenomenon is a problem that cannot be ignored when using wavelet analysis for feature extraction. Therefore, this paper proposes an improved inverse discrete wavelet transform method, in which the signal is decomposed by Mallat algorithm to obtain wavelet coefficients at each scale and then reconstructed to the required wavelet space coefficients according to the reconstruction method, and the reconstructed coefficients are used to analyze the signal at that scale instead of the wavelet coefficients obtained at the corresponding scale. Experiments on the public English vocabulary dataset reveal that the wavelet transform-based strategy suggested in this research outperforms existing feature extraction methods while maintaining greater classification accuracy while reducing the dimensionality of the TF-IDF vector space model.

## 1. Introduction

With the development of the Internet and the continuous updating of computers and information technology, the information stored on the network is becoming more and more abundant. The number of texts, as an effective expression of information, is also growing rapidly. In recent years, with the rise of cloud computing and big data, it has enabled the effective organization and management of huge amount of public English vocabulary texts. How to obtain effective information efficiently and accurately has become the main purpose of text mining, information retrieval, and network opinion analysis. The diversity, complexity, redundancy, and irregularity of public English lexical text data pose a great challenge for text understanding. The core of text understanding is to convert text data into signals that can be perceived and analyzed by computers through mathemat-

ical operations and to process them automatically to feed back the results depending on the task. In text understanding, one of the most fundamental and critical steps is text feature extraction. Therefore, feature reduction of complex feature space with high dimensionality of text becomes the main key point for text classification. The purpose of feature extraction is to effectively downscale the initial high-dimensional features and select an optimal subset of features from the high-dimensional feature space [1].

The vast amount of public English lexical texts on the Internet has brought about a rich corpus of resources but at the same time has made text perception, analysis, and processing a huge challenge. The first challenge is that any user can generate and disseminate data, the majority of which is text, resulting in the rapid growth of the text corpus; the second challenge is that behind the big data lies a large amount of repetitive and meaningless data, which is of mixed quality

and low value density. Finally, data exists in a variety of platforms, including structured data, semistructured data, and unstructured data, so “high feature dimensionality and complex structure” are the third challenge. The third challenge is “high feature dimensionality and complex structure.” Addressing these challenges is the main obstacle for text data analysis [2]. The feature vector space is usually formed by using a set of words of a text as attribute vectors. The original feature vector space of text contains all the attributes of words, which is high-dimensional and sparse, but not all attributes contribute to the classification decision. Therefore, it is necessary to effectively reduce the dimensionality of the high-dimensional text feature space and extract the best set of classification feature attributes without degrading the system performance.

In recent years, many scholars have proposed a large number of effective methods and techniques in text feature extraction to address these three challenges. Words in public English, as the most basic units in a text, are the smallest elements that constitute sentences and discourse. Feature extraction of words is usually called word-level representation, but the number of words in a text, no matter in English, is very large, and sequential coding of these words alone is not only labor-intensive but also difficult to reveal the semantic relationships between words, so a vectorized representation of word level with measurable semantic distance is very necessary. Specifically, given a semantic metric, each word or phrase is projected as a high-dimensional vector, and the space formed by these vectors is called the vector space at the word level, thus transforming the unstructured text into a manageable structured form. Public English lexical texts still have the common problems in text data analysis: high dimensionality and feature redundancy. Data compression has been one of the important application areas of wavelet analysis, and this has led to great social and economic benefits [3]. Compressed perception theory proves that a signal can be sampled at a lower frequency and reconstructed with high probability as long as the signal is sparse in some orthogonal space. Compressed perception theory can efficiently capture information from sparse signals and perceive measurements through noncorrelation, a property that makes compressed perception widely used in real-life applications. Compressed perception theory has brought a revolutionary breakthrough by solving the current bottleneck in information acquisition and processing technology and has received widespread attention from scholars in various countries, ranging from medical imaging and signal coding to astronomy and geophysics [4]. The Boolean model [5–7] is an early text representation paradigm that uses a collection of “1” and “0” variables to represent the feature items of the related text. However, regardless of semantic relevance, text features are now allocated equal weights by default, making the represented features unable to match the realistic meaning.

In this paper, to address the problems of high dimensionality and feature redundancy of public English lexical text, wavelet transform and inverse wavelet transform are performed on the feature vectors under the text vector space model, so that the text feature space dimensionality is

reduced. In particular, for the phenomenon of frequency aliasing in the signal decomposition process of Mallat algorithm, an improved algorithm model that can effectively eliminate frequency aliasing is proposed, expecting to achieve the purpose of accurate extraction of public English vocabulary text features, and the proposed method is verified based on the text classification task.

The paper’s divisional layout is as follows: the related work is presented in Section 2. Section 3 analyzes the algorithm design of the proposed work. Section 4, discusses the experimentation and results. Finally, in Section 5, the research work is concluded.

## 2. Related Works

*2.1. Text Feature Extraction.* After text preprocessing and representation, text information still belongs to a high-dimensional and highly sparse vector matrix, which makes the computer’s computation and learning training process more difficult, and the classification effect is poor. Text feature selection is required to achieve even more dimensionality reduction. Finding the ideal subset of features in the solution space comprising all feature subsets and selecting the most representative combination of features with the least amount of time are the key to feature selection. Since computer devices can only recognize mathematical symbols such as binary, the original text language should be converted into a computer-recognizable representation before using computers to study text information. Among the many text representation methods, the most effective and accurate method is to build a text representation model. A good text representation model not only affects the accuracy of text detection but also is related to the relevance of the semantic connection between text data. Thus, text representation models have an irreplaceable position in text analysis. Boolean model [5] is an early text representation model, which represents the feature items of the corresponding text by the set of “1” and “0” variables. However, at this time, the text features are assigned with equal weights by default regardless of semantic relevance, which makes the represented features unable to match the realistic meaning. The vector space model (VSM) was proposed by Huang et al. [6] and is one of the classical models in text representation. This model is also a statistical model based on bag of words [7], which compares the words in a text to a bag of balls and represents the text ignoring the order of word occurrence, which has the feature of simplicity and speed. However, the individual unordered individuals alone are also unable to solve the relationship between words, which in turn causes the problem of losing semantic information. The above two models generally suffer from two main problems of high dimensionality and vector sparsity in the process of representing text, which eventually leads to a large amount of computer resources being spent but instead results in poor text clustering accuracy. In recent years, research scholars have focused on how to reduce the complexity of the text representation model on the basis of ensuring that the clustering accuracy is not affected, and the main solutions can be broadly divided into two categories: feature

selection and feature extraction. Among them, feature selection is used to obtain a subset of features from the initial text feature data as the text representation according to certain rules. For example, the term frequency and inverse document frequency (TF-IDF) for text feature selection [8, 9] can be used to solve the problem of equal weights. It gives feature words weight coefficients based on the number of occurrences and relative relevance of a word in the text, with the goal of filtering out feature words that highlight the text topic. Scholars have suggested feature selection techniques such as the chi-square test [10], information gain [11], and mutual information [2] since then, all of which have achieved the goal of decreasing the complexity of the text representation model without affecting the semantics of the text. In contrast, in the feature extraction approach, the extracted features are not derived from a subset of the initial text features, but a new set of text features created based on the initial text features is used as the text representation. The current common feature extraction methods tend to utilize the core idea of stitching features, where individuals with little difference in nature in the features are fused into new feature items. The Dirichlet allocation topic model [12] and the random mapping model [13] have made significant contributions to the research development of feature extraction as representatives in feature extraction models. With the rapid development of deep learning in recent years, Mikolov et al. [14] proposed the Word2Vec model, which has made great progress in feature extraction techniques. The model represents text by converting words in text space to vector space and using low-dimensional numerical vectors. It overcomes the text vector dimensionality explosion and increases the accuracy of conveying the semantics of the original text by representing words as word vectors by exploiting semantic linkages between contexts. After that, Kim et al. [15] proposed the Doc2vec model for text semantic feature extraction. The above mathematical models based on deep learning reflect the current situation that deep learning knowledge is gradually integrated into text representation as well as feature extraction; however, the problem of large-scale data and computational hardware loss required by deep learning models is also more significant.

**2.2. Wavelet Transform.** The idea of wavelet transform comes from the method of stretching and translation, which is to compress and stretch the signal in the time axis; translation is to move the wavelet basis function in parallel with the waveform in the time auxiliary. In 1974, the French engineer Morlet first proposed wavelet transform, which was not available at that time. In 1974, the mathematician Meyer proved the existence of wavelet function and carried out an in-depth study in the theory. So far, wavelet transform theory has been widely used in signal analysis [16], image processing [17], fault diagnosis [18], and other engineering fields.

Since 1990, the wavelet transformation and its engineering applications have gradually received the attention of scientists from all over the world, and it is considered a major breakthrough to the Fourier transform. Wavelet transform is developed on the basis of Fourier transform, and they are

essentially different from each other in time and frequency domains. Wavelet transform provides an adaptive analysis method of simultaneous local changes in time and frequency domains, which can automatically adjust the time and frequency windows to meet the needs of practical engineering, no matter analyzing low-frequency or high-frequency local signals. Characterizing the singularity of the signal is another feature of wavelet transform, and the maximum value of wavelet transform modes of the fault signal at different decomposition scales can represent the sudden change of the signal. The application of wavelet transform theory to the field of signal processing has been developed rapidly in recent years, mainly including signal denoising, data compression, and fault diagnosis.

The wavelet is defined as follows: let  $\psi(t)$  be a square productable function,  $\psi(t) \in L^2(R)$ . Its Fourier transform  $\psi(\omega)$  is given by

$$C_\psi = \int_R \frac{|\widehat{\psi}(\omega)|^2}{|\omega|} d\omega < \infty, \quad (1)$$

calling  $\psi(t)$  as the base wavelet or mother wavelet; equation (1) is the tolerance condition of the wavelet function. Scaling and translating  $\psi(t)$ , the function  $\psi_{a,\tau}(t)$  is obtained as

$$\psi_{a,\tau}(t) = \frac{1}{\sqrt{|a|}} \psi\left(\frac{t-\tau}{a}\right), \quad a, \tau \in R; a \neq 0. \quad (2)$$

In formula (2),  $a$  and  $\tau$  are the scaling factor and translation factor, respectively. The wavelet transform is defined as follows: after translating the wavelet function  $\psi(t)$  by  $\tau$ , the inner product operation is done with the signal to be analyzed  $x(t)$  at different scales  $a$ , as shown in the following equation:

$$\text{WT}_x(a, \tau) = \frac{1}{\sqrt{a}} \int_{-\infty}^{+\infty} x(t) \psi^*\left(\frac{t-\tau}{a}\right) dt, \quad a > 0. \quad (3)$$

The equivalent frequency domain representation of equation (3) is shown in equation (4), where  $X(\omega)$ ,  $\psi(\omega)$  are the Fourier transforms of  $x(t)$  and  $\psi(t)$ , respectively.

$$\text{WT}_x(a, \tau) = \frac{\sqrt{a}}{2\pi} \int_{-\infty}^{+\infty} X(\omega) \psi^*(a\omega) e^{j\omega\tau} d\omega. \quad (4)$$

The wavelet transform can obtain a multiresolution description of the signal, and this description conforms to the general laws of human observation of the world. At the same time, wavelet transform has rich wavelet basis that can be adapted to signals with different characteristics. The features of wavelet and wavelet transform are (1) joint local analysis function in time domain and frequency domain; (2) multiresolution and multiscale analysis function; (3) a good local approximation basis for nonlinear system; and (4) fast algorithm based on conjugate mirror filter bank. At present, wavelet transform is widely used in industry, medical treatment, military, and other fields.

### 3. Algorithm Design

The vector space model simplifies text processing, and combinations between different words may achieve the effect of their alignment. However, its disadvantage is that the vector dimensions increase rapidly as the text set expands and the dictionary words increase. Because it is difficult for a single text vector to include all of the words in the dictionary, there are many dimensions with weight values of 0, resulting in high dimensionality and vector sparsity. Therefore, we need to reduce the dimensionality of the vectors in the traditional vector space model, which can be viewed as digital signals for text vectors. And wavelet analysis theory has strong advantages for digital signal processing. Existing theories and practices show that the transformed digital signal can be highly restored to the original signal, and wavelet analysis can uniquely capture the localization details, which makes it possible to operate in the wavelet transform space for this paper. In this paper, the DWT and IDWT methods used in this paper are performed on the vector space model to test the effectiveness of this text feature extraction method with the accuracy of text classification. The flow chart of the algorithm is shown in Figure 1. Firstly, the dataset is divided into words and a dictionary is constructed to obtain the TF-IDF feature space vectors; then, the obtained TF-IDF vectors are subjected to a one-dimensional discrete wavelet transform (DWT) to obtain the scale coefficients and wavelet coefficients; the scale coefficients and wavelet coefficients are summed up in the corresponding components to obtain the wavelet space vectors proposed in this paper. Finally, the scale coefficients and wavelet coefficients obtained in the previous step are summed up again by reducing the corresponding scale functions, and several of their middle dimensions are extracted from the obtained vectors to obtain the inverse discrete wavelet transform (IDWT) space vectors proposed in this paper.

**3.1. TF-IDF Feature Extraction.** Term frequency-inverse document frequency (TF-IDF) is one of the popular algorithms in the field of text mining, which is obtained by multiplying TF (word frequency) and IDF (inverse document rate) [19]. The actual meaning of TF is the probability of occurrence of a keyword in a document, as shown in equation (5). The more the keyword appears in a single text, the larger the TF value is, where  $n_{ij}$  denotes the number of occurrences of word  $t_i$  in text  $d_j$  and  $\sum_k n_{k,j}$  denotes the number of occurrences of all words in document  $d_j$ .

$$TF_{i,j} = \frac{n_{i,j}}{\sum_k n_{k,j}}. \quad (5)$$

The emergence of TF has led many scholars to use TF as a method for judging text similarity. Although this method can reflect the similarity of high-frequency words in each text, it can provide theoretical support for judging text similarity to a certain extent. However, there are many popular or basic words in all kinds of texts, so it is obvious that the TF frequency alone is not scientifically supported. Therefore, the IDF variable is introduced as the weight factor of TF,

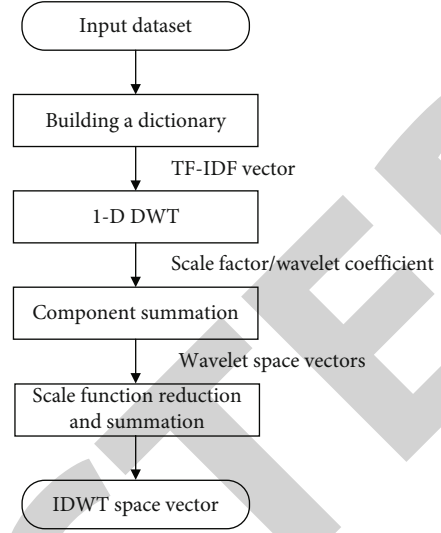


FIGURE 1: Flow chart of text feature extraction based on wavelet transform.

which is used to regulate the problem that the TF value is generally high among the texts of multiple categories. The IDF is calculated by taking the number of texts containing a certain keyword as the denominator and the number of texts in the corpus as the numerator, and the result of this fractional formula is taken as the logarithm to obtain the result of IDF, as shown in the following equation:

$$IDF = \log \frac{|D|}{1 + |\{j : t_i \in d_j\}|}. \quad (6)$$

In equation (6),  $D$  is the whole corpus and  $\{j : t_i \in d_j\}$  is the number of texts in which a word appears in the corpus. In order to avoid the situation that the denominator is 0 because the word does not exist in the corpus, the denominator is increased by 1. If a high-frequency word appears in a large number of texts in the corpus, it means that the word is less important for a single text and is not a keyword to be extracted. In this case, the IDF value of this word will be smaller, and the weight of this keyword will be reduced. For example, if all the texts in a corpus are about a person, the name of the person may appear in all the texts, and then, the IDF value will be very small. In summary, the formula of TF-IDF is shown in equation (7), which eliminates a large number of common words in the text while retaining high-frequency words and extracts words with a high degree of importance.

$$TF_{i,j} - IDF_i = TF_{i,j} \times IDF_{i,j}. \quad (7)$$

### 3.2. Improved Mallat Algorithm

**3.2.1. Traditional Mallat Algorithm.** The Mallat algorithm is a fast algorithm for wavelet analysis that introduces the idea of multiresolution analysis in the field of computer vision into wavelet analysis. However, the Mallat algorithm is implemented by using wavelet low-pass filters  $H$  and  $h$  and

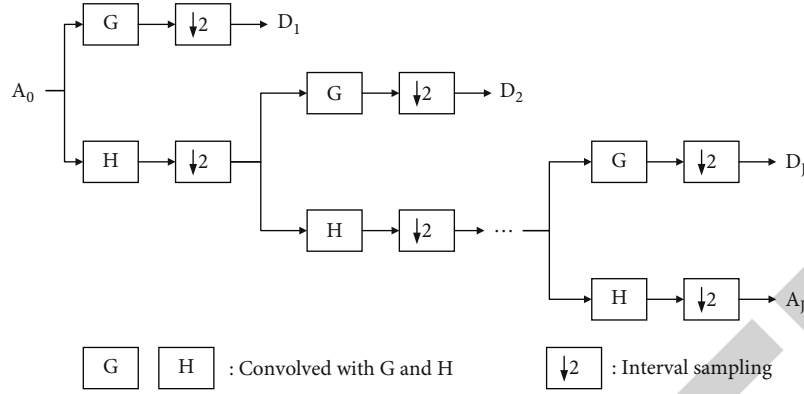


FIGURE 2: Decomposition process of Mallat two-dimensional tower wavelet transform.

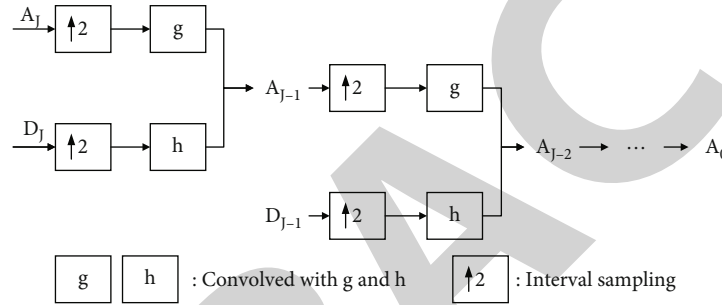


FIGURE 3: Reconstruction process of Mallat two-dimensional tower wavelet transform.

wavelet high-pass filters  $G$  and  $g$  corresponding to the scale function and wavelet function to filter the signal in low pass and high pass. For convenience, the scale function is referred to as the low-frequency subband and the wavelet function is referred to as the sub-high-frequency subband. The Mallat decomposition algorithm is as follows:

$$\begin{cases} A_0[f(t)] = f(t), \\ A_j[f(t)] = \sum_k H(2t-k)A_{j-1}[f(t)], \\ D_j[f(t)] = \sum_k G(2t-k)A_{j-1}[f(t)], \end{cases} \quad (8)$$

where  $t$  is the discrete time series number,  $t = 1, 2, \dots, N$ ;  $f(t)$  is the original signal;  $j$  is the number of layers,  $j = 1, 2, \dots, J$ ,  $J$  takes  $\lfloor \log_2 N \rfloor$ ;  $H$  and  $G$  are wavelet decomposition filters;  $A_j$  is the wavelet coefficient of the approximate part of the  $j$ th layer of the signal  $f(t)$ ; and  $D_j$  is the wavelet coefficient of the detailed part of the signal  $f(t)$  in layer  $j$ . The decomposition process of Mallat two-dimensional tower wavelet transform is shown in Figure 2.

Refactoring algorithm

$$A_j[f(t)] = 2 \left\{ \sum_k h(t-2k)A_{j+1}[f(t)] + \sum_k g(t-2k)D_{j+1}[f(t)] \right\}, \quad (9)$$

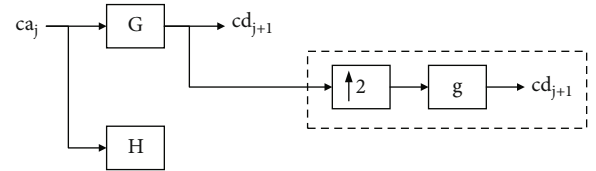
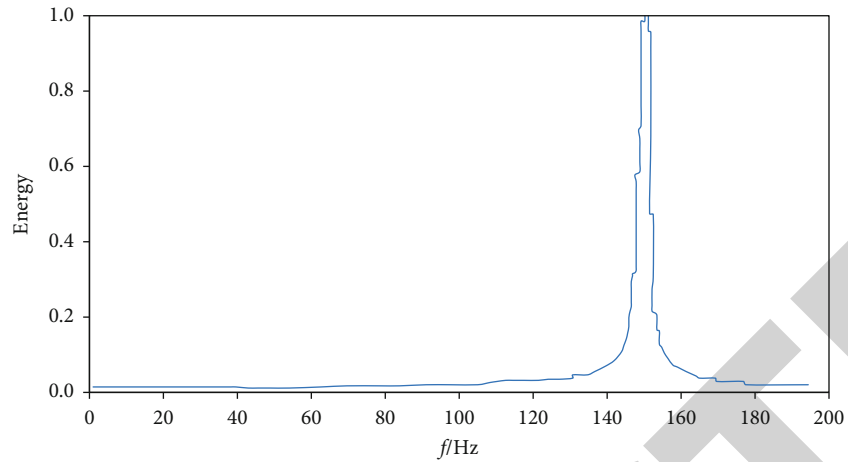


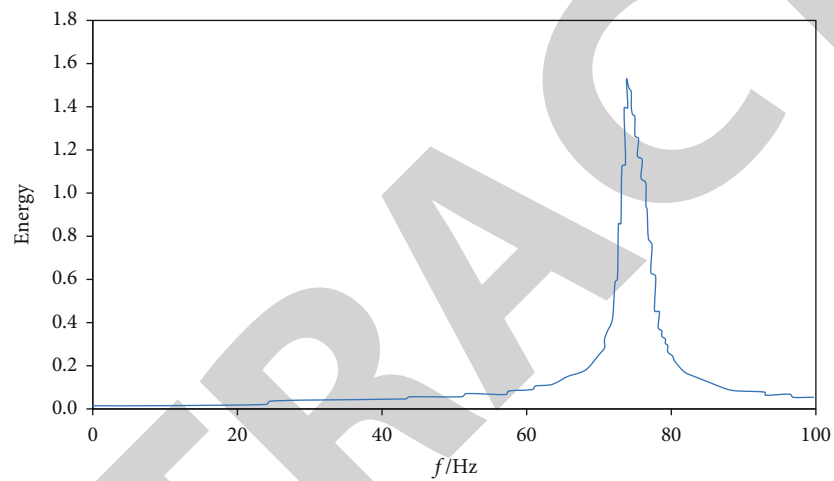
FIGURE 4: Improved Mallat decomposition algorithm model.

where  $j, J$  is the same as equation (8),  $j = J - 1, J - 2, \dots, 0$ ;  $h, g$  are wavelet reconstruction; and  $A_j$  and  $D_j$  have the same meaning as equation (2). The reconstruction process of Mallat two-dimensional tower wavelet transform is shown in Figure 3.

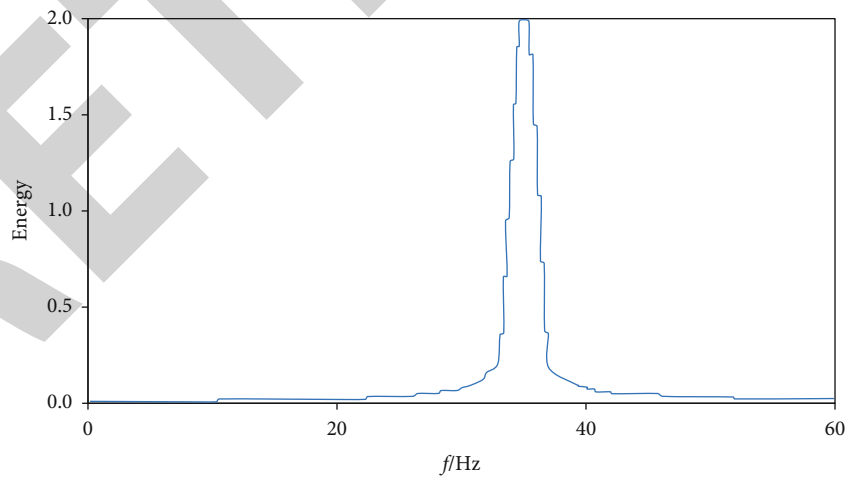
**3.2.2. Mallat Algorithm Analysis.** From Mallat's decomposition algorithm, it follows that the approximate part of the signal  $f(t)$  is at the  $2^j$ th scale ( $j$ th layer). The wavelet coefficients  $A_j$  of the low-frequency part are obtained by convolving the wavelet coefficients  $A_{j-1}$  of the approximate part of the  $2^{j-1}$  scale (the  $j-1$ th layer) with the decomposition filter  $H$ , and then, the convolution result is sampled at intervals. The wavelet coefficients  $D_j$  of the high-frequency part of the signal  $f(t)$  at the  $2^j$ th scale (the  $j$ th layer) are obtained by convolving the wavelet coefficients  $A_{j-1}$  of the



(a) cd1 spectrum



(b) cd2 spectrum



(c) cd3 spectrum

FIGURE 5: Simulation effect of the improved Mallat algorithm.

approximate part of the  $2^{j-1}$  scale (the  $j - 1$ th layer) with the decomposition filter  $G$  and then sampling the convolution result at intervals. It can be said that the Mallat algorithm is basically done in 3 steps:

- (1) Wavelet filtering (convolution)
- (2) Interval sampling
- (3) Interval zero interpolation

Therefore, the frequency overlap phenomenon is definitely generated during the above 3 steps. The interpolation of zeroes is a technique used in wavelet reconstruction, which does not affect the wavelet decomposition stage; i.e., it is not relevant to the problem discussed in this paper. In fact, the wavelet filter is not an ideal filter, and the nonideal frequency domain characteristics of the filter make it possible for the signal to be filtered with each bandlimited subband containing its neighboring subband components, thus generating the frequency aliasing phenomenon. However, considering the unevenness of frequency aliasing in each band-limited subband (approximate and detailed), there is almost no aliasing in the approximate band-limited subband. In fact, interval sampling is the root cause of frequency aliasing, because it violates Shannon’s sampling theorem. Therefore, if the original signal contains frequency components close to the sampling edge, the decomposition according to Mallat’s algorithm will definitely generate frequency aliasing imagination.

**3.2.3. Improved Mallat Algorithm.** After a thorough study of Mallat algorithm, it is clear that the implementation of Mallat algorithm inevitably generates frequency aliasing. We can see from the wavelet decomposition and reconstruction algorithms that the wavelet decomposition process is sampling at intervals and the reconstruction process is interpolating zeros at intervals; both processes cause frequency aliasing, but in different directions. That is to say, the decomposition process generated by the overlap in the reconstruction process has been corrected. However, this also provides an idea of how to solve the frequency aliasing phenomenon generated by Mallat decomposition algorithm: after decomposing the signal by Mallat algorithm to obtain wavelet coefficients at each scale and then reconstructing to the required wavelet space coefficients  $cd_j$  according to the reconstruction method and using the reconstructed coefficients  $cd_j$  to analyze the signal at that scale instead of the wavelet coefficients  $cd_j$  obtained at the corresponding scale. In this way, the effects of frequency aliasing can be better resolved to achieve the desired goal. In this paper, this algorithm is called subband signal reconstruction algorithm. The improved algorithm model is shown in Figure 4. Using this model, the TF-IDF features of the equation input are red decomposed and the simulation results show that the algorithm is practical and effective. Figure 5 shows the analysis of the TF-IDF feature vector using this algorithm and the spectral effect of the detailed signal  $d_j$ .

## 4. Experiments

**4.1. Experiment Preparation.** The text dataset of public English vocabulary used in this paper is a corpus retrieved from the web. It contains a total of 10,505 samples from eight categories: education, culture, finance and economics, science and technology, sports, military, agriculture, and politics. This data source is rich and suitable for the study of text classification. The number of samples in each cate-

TABLE 1: Text dataset of public English vocabulary.

Text category	Sample size
Education	1021
Culture	1568
Economic	1392
Science	1077
Sports	1408
Military	1390
Agricultural	1296
Political	1353
Total number	10505

TABLE 2: Average experimental results of internal category text classification.

Methodology	Precision	Recall	F1-score
SVD	0.875	0.859	0.867
ICA	0.826	0.847	0.836
PCA	0.883	0.862	0.872
Proposed	0.904	0.911	0.907

gory is shown in Table 1. Two major groups of experiments are conducted in this paper. The first set of experiments tests the classification performance of each training space when targeting internal samples (the test set and training set are from the same distribution), and 80% of the data in the experiments are used for the training set and the rest for testing; the second set of experiments verifies the superiority of the wavelet analysis method proposed in this paper for exotic samples. The text data with the categories of education, culture, finance and economics, science and technology, and sports are used as the training set, and the text data with the categories of military, agriculture, and politics are used as the test set (the training set and the test set are from different distributions). Singular value decomposition (SVD) [20], independent component analysis (ICA) [21], principal component analysis (PCA) [22] method, and the modified Mallat method in this paper were used to extract the feature vectors under the vector space (TF-IDF). The feature vectors (TF-IDF) of the vector space are extracted by dimensionality reduction. The accuracy of each space is measured using the KNN method (cosine distance as the similarity measure), and the dimensionality of SVD space, ICA space, and PCA space is consistent. In this paper, the precision, recall, and F1-score are used to evaluate the model performance. The accuracy rate indicates the percentage of correctly predicted results to the total samples; the precision rate indicates the number of correctly predicted samples among the samples predicted to be of that class; the recall rate is the probability of being predicted to be of that class among the samples that are actually of that class; both the precision rate and recall rate are considered simultaneously, so that both are simultaneously maximized and a balance is achieved.

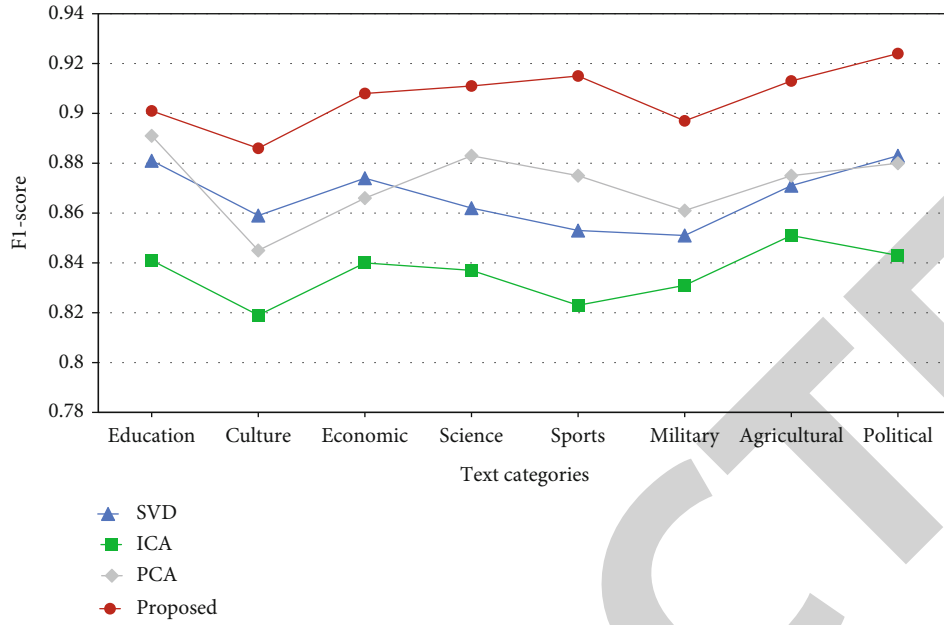


FIGURE 6: F1-score of various algorithms under different text categories.

TABLE 3: External category text classification effect.

Methodology	Criteria	Military	Agricultural	Political	Average
SVD	Precision	0.857	0.796	0.812	0.822
	Recall	0.802	0.812	0.824	0.813
	F1-score	0.829	0.804	0.818	0.817
ICA	Precision	0.849	0.786	0.805	0.813
	Recall	0.833	0.771	0.793	0.799
	F1-score	0.841	0.778	0.799	0.806
PCA	Precision	0.842	0.794	0.756	0.797
	Recall	0.829	0.772	0.743	0.781
	F1-score	0.835	0.783	0.749	0.789
Proposed	Precision	0.886	0.854	0.875	0.872
	Recall	0.875	0.889	0.832	0.865
	F1-score	0.88	0.871	0.853	0.868

**4.2. Internal Category Text Classification.** In this section, we conduct classification experiments on internal categories of public English lexical texts to verify the feature extraction effect. Since a total of 8 categories of training samples are used in this experiment, the average of precision rate, recall rate, and F1-score is taken as indicators to evaluate the effectiveness of each method. The classification results are shown in Table 2, and the F1-score of the method in this paper is improved by 04%, 7.10%, and 3.50% compared with that of SVD, ICA, and PCA, respectively. The results show that the wavelet transform-based feature extraction methods proposed in this paper can all obtain robust feature representations, which confirms the stability of the method.

In order to show more intuitively and clearly the effect of the improved feature extraction algorithm on the index

improvement of classifier classification, the F1-score of each algorithm under different categories is plotted in this paper based on the data in Table 2 as shown in Figure 6. It can be observed that the ICA and PCA methods have similar feature extraction ability for public English lexical texts, while the wavelet transform-based method proposed in this paper has the best feature extraction ability for each category. This is because the wavelet transform inherits and develops the localization idea of the short-time Fourier transform, overcomes the shortcomings such as the window size does not change with frequency, and can fully highlight the features of certain aspects of the problem through the transform. It can localize the analysis of time (space) frequency and gradually carry out multiscale refinement of the signal (function) through the telescopic translation



operation, finally achieving time subdivision at high frequencies and frequency subdivision at low frequencies, which can automatically adapt to the requirements of time-frequency signal analysis and thus can focus on any details of the signal.

**4.3. External Category Text Classification.** The second set of experiments is aimed at verifying the feature extraction ability of the algorithm for samples with different distributions from the training set. Table 3 shows the detailed classification accuracy of the three categories in the test set. From the table, it can be concluded that the proposed method based on the improved inverse discrete wavelet transform can have better feature extraction ability for unseen categories of text, while the SVD, ICA, and PCA algorithms depend on the characteristics of the training set.

## 5. Conclusions

In this paper, an improved inverse discrete wavelet transform text feature extraction method based on the Mallat algorithm is proposed for the problem that public English lexical text features have high dimensionality and the features contain redundant information. In this work, the wavelet transform is simply the sum of the respective components of the low-frequency and high-frequency vectors created by the one-dimensional discrete wavelet transform. After the one-dimensional discrete wavelet transform, the dimensionality of the low-frequency and high-frequency vectors is the same and around half of the original vectors, meeting the dimensionality reduction goal. We discover the primary reasons of frequency mixing in the Mallat algorithm in this work, based on an in-depth examination of the algorithm, and suggest a better model to solve the frequency mixing. Under certain circumstances, the proposed inverse wavelet space may have a higher accuracy for a specific classification category. Many low-dimensional feature extraction approaches lose crucial classification features; however, the highly sparse orthogonal wavelet space vector in this study, according to compressed perception theory, can reliably maintain the important properties of the most original feature vector. The next work is to check whether the feature extraction efficiency of wavelet analysis method has certain advantages in experiments and how to expand the specific conditions of this paper's inverse wavelet space to make its specific advantages greater.

## Data Availability

The datasets used during the current study are available from the corresponding author on reasonable request.

## Conflicts of Interest

The authors declare that they have no conflict of interest.

## References

- [1] K. Thirumoorthy and K. Muneeswaran, "Feature selection using hybrid poor and rich optimization algorithm for text classification," *Pattern Recognition Letters*, vol. 147, pp. 63–70, 2021.
- [2] X. Tang, Y. Dai, and Y. Xiang, "Feature selection based on feature interactions with application to text categorization," *Expert Systems with Applications*, vol. 120, pp. 207–216, 2019.
- [3] M. Andrecut, "Wavelet lossy compression of random data," *International Journal of Modern Physics C*, vol. 20, no. 1, pp. 109–116, 2009.
- [4] L. Li, Y. Fang, L. Liu, H. Peng, J. Kurths, and Y. Yang, "Overview of compressed sensing: sensing model, reconstruction algorithm, and its applications," *Applied Sciences*, vol. 10, no. 17, p. 5909, 2020.
- [5] B. Menaouer, S. Mohammed, and M. Nada, "Towards a model to improve Boolean knowledge mapping by using text mining and its applications," *International Journal of Information Retrieval Research (IJIRR)*, vol. 10, no. 3, pp. 35–56, 2020.
- [6] L. B. Huang, V. Balakrishnan, and R. G. Raj, "Improving the relevancy of document search using the multi-term adjacency keyword-order model," *Malaysian Journal of Computer Science*, vol. 25, no. 1, pp. 1–10, 2012.
- [7] D. Yan, K. Li, S. Gu, and L. Yang, "Network-based bag-of-words model for text classification," *IEEE Access*, vol. 8, pp. 82641–82652, 2020.
- [8] N. Azam and J. T. Yao, "Comparison of term frequency and document frequency based feature selection metrics in text categorization," *Expert Systems with Applications*, vol. 39, no. 5, pp. 4760–4768, 2012.
- [9] T. Peng, L. Liu, and W. Zuo, "PU text classification enhanced by term frequency-inverse document frequency- improved weighting," *Concurrency and Computation: Practice and Experience*, vol. 26, no. 3, pp. 728–741, 2014.
- [10] Y. Lu, M. Liang, Z. Ye, and L. Cao, "Improved particle swarm optimization algorithm and its application in text feature selection," *Applied Soft Computing*, vol. 35, pp. 629–636, 2015.
- [11] C. Shang, M. Li, S. Feng, Q. Jiang, and J. Fan, "Feature selection via maximizing global information gain for text classification," *Knowledge-Based Systems*, vol. 54, pp. 298–309, 2013.
- [12] N. Liu, X. J. Tang, Y. Lu, M. X. Li, H. W. Wang, and P. Xiao, "Topic-sensitive multi-document summarization algorithm," in *2014 sixth international symposium on parallel architectures, algorithms and programming*, pp. 69–74, Beijing China, 2014.
- [13] C. B. Do and A. Y. Ng, "Transfer learning for text classification," *Advances in Neural Information Processing Systems*, vol. 18, 2005.
- [14] S. Ji, N. Satish, S. Li, and P. K. Dubey, "Parallelizing word2vec in shared and distributed memory," *IEEE Transactions on Parallel and Distributed Systems*, vol. 30, no. 9, pp. 2090–2100, 2019.
- [15] D. Kim, D. Seo, S. Cho, and P. Kang, "Multi-co-training for document classification using various document representations: TF-IDF, LDA, and Doc2Vec," *Information Sciences*, vol. 477, pp. 15–29, 2019.
- [16] D. A. Slesarev and V. A. Barat, "Application of wavelet transform to the analysis of signals with pulsed components," *Measurement Techniques*, vol. 43, no. 8, pp. 696–699, 2000.

## Research Article

# Effect of Painless Rehabilitation Nursing for Hip Replacement Patients

Xiaona Zhao,<sup>1</sup> Ru Bai,<sup>2</sup> and Jing Yang<sup>3</sup> 

<sup>1</sup>Yuncheng Central Hospital, Yuncheng, China

<sup>2</sup>Yuncheng Vocational and Technical University, Yuncheng, China

<sup>3</sup>Nursing College of Shanxi Medical University, Shanxi, China

Correspondence should be addressed to Jing Yang; [jinggupaofei478@163.com](mailto:jinggupaofei478@163.com)

Received 7 April 2022; Revised 14 May 2022; Accepted 18 May 2022; Published 11 June 2022

Academic Editor: Naeem Jan

Copyright © 2022 Xiaona Zhao et al. This is an open access article distributed under the Creative Commons Attribution License, which permits unrestricted use, distribution, and reproduction in any medium, provided the original work is properly cited.

**Objective.** To analyze the effect of painless rehabilitation nursing for hip replacement patients. **Method.** 124 elderly patients who underwent total knee arthroplasty in our hospital from June 2019 to June 2020 were selected as study subjects. They were randomly divided into observation group and control group. The control group was given routine nursing care, and the observation group was given painless rehabilitation care on the basis of the control group. Knee circumference, knee pain, knee function, agitation and sleep duration were recorded and compared between the two groups. **Results.** The changes of knee circumference diametral in both groups were significantly decreased at 1, 3 and 7 days after operation; The changes of knee circumference diametral in the observation group were significantly smaller than those in the control group at 3,7 days after operation ( $P < 0.05$ ). VAS (Visual Analogue Scale) scores at 1, 3 and 7 d after operation were significantly decreased in both groups; The score of the observation group was significantly lower than that of the control group, and the difference was statistically significant ( $P < 0.05$ ). HSS (Hospital for special surgery) scores increased significantly in both groups at 1 week, 1 month, 3 months and 6 months after operation. All the comparisons were statistically significant ( $P < 0.05$ ); HSS scores of observation group were significantly higher than control group at 1 week, 1 month, 3 months and 6 months after surgery. The difference was statistically significant ( $P < 0.05$ ). The agitation rate of the observation group was lower than that of the control group ( $P < 0.05$ ). Compared with the control group, the sleep time of observation group increased significantly in each period, with statistically significant difference ( $P < 0.05$ ). **Conclusion.** Perioperative painless rehabilitation nursing interventions for patients with hip replacement could significantly relieve swelling and pain, it was helpful for the patients to recover the function of knee joint after operation and worthy of clinical application.

## 1. Introduction

In clinic, femoral neck fracture usually occurs in the elderly. Hip replacement is mainly used in the elderly patients with femoral neck fracture in clinical, mainly for the elderly patients over 50 years old. Due to the inability of the affected limb to walk with weight after fracture, it needs to stay in bed for a long time, but it is prone to serious bed complications such as bedsore, accumulated pneumonia, urinary tract infection and lower extremity deep venous thrombosis, which is difficult to care [1]. The treatment effect of acetabular degeneration, articular ankylosis, femoral head necrosis, femoral neck fracture and other symptoms is good, which

can effectively restore the patient's hip function [2]. The operation process of total hip arthroplasty is convenient and operable, and the incidence of postoperative adverse reactions is relatively low and the safety factor is high [3]. Hip arthroplasty is the most effective method for the treatment of hip disease and femoral neck fracture. This operation is to place a metal prosthesis similar to human bone and joint into the damaged joint surface. The ultimate purpose of hip arthroplasty is to restore joint function and eliminate pain, but the recovery of joint function after arthroplasty is closely related to patients' postoperative rehabilitation exercise [4]. Due to the poor physical quality of the elderly patients, the incidence of postoperative

complications is higher. Therefore, how to perform effective analgesia for patients with hip joint disease is of great significance [5, 6]. Early rehabilitation nursing intervention as soon as possible after the recovery of patients' consciousness can not only improve their psychological state, but also enhance the patients' attention to postoperative rehabilitation exercise, effectively alleviate their pain and create conditions for the smooth progress of follow-up rehabilitation exercise [7]. Studies have shown that painless rehabilitation care has a more prominent effect in preventing postoperative pain and can promote faster recovery of patients [8, 9].

To analyze the effect of painless rehabilitation nursing for hip replacement patients. 124 elderly patients who underwent total knee arthroplasty in our hospital from June 2019 to June 2020 were selected as study subjects. The indexes of knee circumference diameter and knee pain were observed 1, 3 and 7 days after operation; The indexes of knee function, agitation situation and sleep time were observed 1 week, 1 month and 3 months after operation. The application effect of painless rehabilitation nursing for hip replacement patients was discussed by analyzing the data of the above five observation indexes. The rest of our paper consists as section-2 illustrates materials and methods that we have used during our research work, section-3, makes a comparative analysis of the two groups of cases, section-4 is based on discussing and finally, we conclude our work in section-5.

The detailed research content is as follows:

## 2. Materials and Methods

**2.1. General Information.** According to the following exclusion criteria and inclusion criteria, 124 elderly patients who underwent total knee arthroplasty in our hospital from June 2019 to June 2020 were selected as study subjects.

### 2.1.1. Inclusion Criteria

- (1) No cognitive or mental disorders
- (2) Meeting the relevant indications for hip replacement [10];
- (3) American Association of Anesthesiologists (ASA) grade I~III [11].

### 2.1.2. Exclusion Criteria

- (1) Patients with malignant tumors, cognitive impairment, contraindications to anesthesia and incomplete clinical data
- (2) Preoperative analgesic drugs were used
- (3) Severe heart and lung dysfunction
- (4) Other persons who were not suitable to be enrolled

124 cases were divided into control group and observation group to be grouped by lot: In the control group, there were 62 cases, including 39 males and 23 females, the average age was  $(74.29 \pm 3.35)$  between 66 and 85 years old, the

body mass was 56~69 kg, with an average weight of  $(62.25 \pm 2.36)$  kg. In the observation group, there were 62 cases, including 33 males and 29 females, the average age was  $(73.24 \pm 3.32)$  between 64 and 85 years old, the body mass was 55~72 kg, with an average weight of  $(62.21 \pm 2.65)$  kg. Participants and their families were informed, and baseline information remained homogeneous between groups ( $P > 0.05$ ). The grouping details are shown in Table 1.

**2.2. Methods.** During the perioperative period, the observation group adopted conventional nursing, namely preoperative examination under the guidance of the responsible nurse, formulation of personalized diet plan, preoperative psychological counseling, and intraoperative cooperation with the attending physician to complete the operation. Paying close attention to the changes of vital signs, follow the doctor's advice for routine treatment and resume knee function exercise. In the control group, the following measures were added to the perioperative nursing of the observation group: Preoperative evaluation; Pain education; Pain management; Pain care; Rehabilitation; Nutritional support; Psychological support. Details of the above measures are as follows:

- (1) Preoperative evaluation. After admission, the patient's physical condition was comprehensively evaluated based on the patient's health status and examination results to ensure the patient's tolerance during the operation, and the patient's vital signs were monitored in detail and make detailed paper records. Ensure that patients receive adequate nutritional support, psychological preparation and adequate preoperative preparation
- (2) Pain education. For different fear levels of pain, publicity materials related to painless care are posted in the ward, pain education manuals are distributed to patients, and psychological communication is carried out with patients to help patients deepen their understanding of pain
- (3) Pain management. For preoperative analgesia, celecoxib (200 mg) was given to the patient 3 days before the operation, twice a day, for 1 week after the operation. During the operation, femoral nerve combined with sciatic nerve block anesthesia was performed on the basis of general anesthesia. Attention was paid to keep warm during the operation, and intraoperative infusion volume was controlled. After surgery, when the patient returned to the ward, multimodal postoperative pain control was performed, such as parecoxib intramuscular injection [12] (40 mg), 2 times/d, continuous 3 days; continuous ice application for 48 hours; The intravenous self-controlled analgesia pump was used continuously for 48 hours
- (4) Pain care. Instructing patients to keep warm and keep the surgical site clean to prevent infection, patients with severe pain could be treated with central analgesics or a combination of non-steroidal

TABLE 1: General Information of Cases.

Groups	Cases	Average age	Body mass(kg)
Observation group	33 males	73.24 ± 3.32	62.21 ± 2.65
	29 females		
Control group	39 males	74.29 ± 3.35	62.25 ± 2.36
	23 females		

anti-inflammatory analgesics [13] as prescribed by the doctor. For the pain caused by the postoperative incision and tight dressing, corresponding treatment could be given according to the specific situation, and the patient's pain symptoms should be evaluated in time. Letting patients relax their muscles by closing their eyes, meditation, deep breathing, sighing, and yawning to achieve the effect of pain relief. At the same time, various physical therapy methods such as cold compresses, ice compresses, hot compresses, appropriate relaxation of bandage and slight massage various physical treatment methods were used to relieve pain

- (5) Rehabilitation. Within 1 week after the operation, the patient was mainly manifested as local swelling and pain, and appropriate isometric exercises could be performed to help restore the original physiological function of the limb. Two weeks after the operation, the main symptoms were inflammation disappeared, callus formation and fracture end stability. There were moderate amount on the basis of muscle contraction exercise, gradually moving up and down joints. Prevent muscle atrophy
- (6) Nutritional support. If the patient had no symptoms of abdominal pain or abdominal distension 1 day after the operation, patient could eat an appropriate amount of fat-free or semi-liquid food. Under the guidance of the medical staff, patients were instructed to eat more light food which was easy to digest and rich in high quality protein, and eat more fresh vegetables and fruits
- (7) Psychological support. Guide patients to correctly face the pain caused by operation after operation; Face the difficulties encountered in recovery with a positive attitude; Provide psychological support for patients' family members in helping patients recover. Actively prevent patients from mental diseases such as depression and mania

Both groups were followed up for 5 months by telephone or outpatient follow-up, the follow-up period was from July 2020 to November 2020. And the recovery of knee joint function was recorded in detail.

2.3. *Observational Index.* Knee circumference, knee pain, knee function, agitation and sleep duration were compared between the two groups.

TABLE 2: Results of knee circumference diameter.

Groups	Cases	1d after operation	3d after operation	7d after operation
Observation group	62	29.71 ± 3.06	21.47 ± 2.29	14.26 ± 1.35
Control group	62	30.32 ± 3.34	25.34 ± 1.83	19.52 ± 1.91

TABLE 3: Results of knee pain.

Groups	Cases	1d after operation	3d after operation	7d after operation
Observation group	62	6.18 ± 1.33	3.32 ± 0.62	1.44 ± 0.36
Control group	62	6.14 ± 1.09	4.65 ± 0.85	2.69 ± 0.72

- (1) Knee circumference (1, 3, 7d postoperatively). Preoperative and postoperative circumference of affected knee joint 1,3,7 d were measured by scale method. To improve the measurement accuracy, gentian violet could be used to mark the upper edge of the skeleton and marked the upper edge of the skeleton at 2 cm. A soft tape measure was used to measure the circumference (mm) of the knee joint at 2 cm above the upper margin of the skeleton. The change of knee circumference diameter (mm) = the circumference diameter on the n day after surgery - the circumference diameter before surgery, in which n was 1, 3, 7d
- (2) Knee pain (1,3,7 d postoperatively). VAS Scale [14] (Visual Analogue Scale. This method is sensitive and comparable. Draw a 10 cm horizontal line on the paper. One end of the horizontal line is 0, indicating no pain; The other end is 10, indicating severe pain; The middle part indicates different degrees of pain.) was used to score the knee pain of the patients. 0~3 points: the patient had mild pain but can tolerate; 4~6 points: the patient's pain was more obvious, but could endure, if necessary, oral analgesic drugs; 7~10 points: The patient had more intense pain, pain severe unbearable
- (3) Knee function. HSS Scale [15] (Hospital for Special Surgery. The knee scoring system was proposed by the American Hospital for Special Surgery in 1976 to evaluate the preoperative and postoperative function of the knee. The main evaluation indexes include: pain, function, joint range of motion, muscle strength, knee flexion deformity and knee instability.) was used to score the knee joint function of the patients. There were 6 items including pain (30 points), function (22 points), activity (18 points), muscle strength (10 points), flexion deformity (10 points) and stability (10 points), and the scoring range was 0~100 points
- (4) Agitation condition. SAS (Sedative-Agitation Scale-A psychological scale used to measure the severity of anxiety and its changes during treatment. It is mainly used for efficacy evaluation, not for diagnosis.) [16] was used to evaluate, according to the level

TABLE 4: Results of knee function.

Groups	Cases	1week after operation	1month after operation	3months after operation	6months after operation
Observation group	62	61.82 ± 3.52	71.26 ± 3.91	84.52 ± 4.21	93.70 ± 5.35
Control group	62	48.63 ± 3.06	62.13 ± 3.29	70.25 ± 3.66	81.64 ± 5.04

TABLE 5: Result of agitation situation.

Groups	Cases	Normal	Mild agitation	Moderate agitation	Severe agitation	Agitation rate
Observation group	62	60	1	1	0	3.23%
Control group	62	52	6	2	2	16.13%
$\chi^2$	—	—	—	—	—	3.880
$P$	—	—	—	—	—	< 0.05

TABLE 6: Result of sleep time.

Groups	Cases	Pre-operation	Operation day	1d after operation
Observation group	62	4.23 ± 0.61	5.33 ± 0.62	6.01 ± 1.03
Control group	62	3.62 ± 0.75	3.97 ± 0.71	4.74 ± 0.91
$\chi^2$	—	5.364	9.602	7.623
$P$	—	< 0.05	< 0.05	< 0.05

of normal: in a quiet state, could easily wake up, and obeyed the command; Mild agitation: body agitation, emotional anxiety, after verbal reminder could keep quiet; Moderate agitation: repeated verbal reminders or protective restraint; Severe agitation: The patient was aggressive and struggles violently

$$\text{Agitation Rate} = (\text{Mild Agitation} + \text{Moderate Agitation} + \text{Severe Agitation}) / \text{total number} \times 100\% \quad (1)$$

(5) Sleep time. The sleep time of the patients before, after and 1d after the operation was recorded

2.4. *Statistical Method.* SPSS 19.0 statistical software was used for calculation and analysis. The measurement data were expressed as  $\bar{x} \pm s$ , t test was used for measurement data. Enumeration data was expressed in cases (%),  $\chi^2$  test was used for counting data.  $P < 0.05$  was considered statistically significant.

### 3. Results

3.1. *Results of Knee Circumference Diameter.* The changes of knee circumference diametral in both groups were significantly decreased at 1, 3 and 7 days after operation; The changes of knee circumference diametral in the observation group were significantly smaller than those in the control group at 3,7 days after operation ( $P < 0.05$ ). Results of knee circumference diameter was shown in Table 2:

3.2. *Results of Knee Pain.* VAS (Visual Analogue Scale) scores at 1, 3 and 7 d after operation were significantly decreased in both groups; The score of the observation

group was significantly lower than that of the control group, and the difference was statistically significant ( $P < 0.05$ ). Results of knee pain was shown in Table 3:

3.3. *Results of Knee Function.* HSS (Hospital for special surgery) scores increased significantly in both groups at 1 week, 1 month, 3 months and 6 months after operation. All the comparisons were statistically significant ( $P < 0.05$ ); HSS scores of observation group were significantly higher than control group at 1 week, 1 month, 3 months and 6 months after surgery. The difference was statistically significant ( $P < 0.05$ ). Results of knee function was shown in Table 4:

3.4. *Result of Agitation Situation.* The agitation rate of the observation group was lower than that of the control group ( $P < 0.05$ ). Result of agitation situation was shown in Table 5:

3.5. *Result of Sleep Time.* Compared with the control group, the sleep time of observation group increased significantly in each period, with statistically significant difference ( $P < 0.05$ ). Result of sleep time was shown in Table 6:

### 4. Discussion

For patients undergoing hip replacement operation, getting out of bed as soon as possible after surgery can effectively prevent deep vein thrombosis of the lower extremities [17]. Lower extremity deep venous thrombosis is the main complication of hip arthroplasty, but postoperative pain leads most patients to dread early functional exercise, which leads to a series of complications [18]. Pain affects the mood, confidence and expectation of future healthy life of patients undergoing hip arthroplasty. Therefore, pain is an important index that should be considered in postoperative nursing of patients undergoing hip arthroplasty [19]. Studies have

shown that good postoperative analgesia care can shorten the recovery time of patients and reduce the risk of postoperative complications [20]. The painless management system has been applied well in many departments. With the continuous improvement of medical standards in recent years, people's demand for quality of care has also been rising, and pain care has gradually attracted attention [21]. Traditional Chinese medicine physiotherapy, related gymnastics and targeted limb movements can have a certain effect on the postoperative rehabilitation of patients undergoing hip arthroplasty. Clinical studies have shown that effective psychological intervention and pain care can significantly reduce patients' negative emotions and pain response [22]. Continuous psychological counseling for patients after operation can alleviate the anxiety or depression of patients and contribute to the rehabilitation of patients [23]. Therefore, painless rehabilitation nursing of patients undergoing hip arthroplasty is one of the hotspots of orthopaedic nursing.

This study showed that the changes of knee circumference diametral in both groups were significantly decreased at 1, 3 and 7 days after operation; The changes of knee circumference diametral in the observation group were significantly smaller than those in the control group at 3,7 days after operation ( $P < 0.05$ ). VAS (Visual Analogue Scale) scores at 1, 3 and 7 d after operation were significantly decreased in both groups; The score of the observation group was significantly lower than that of the control group, and the difference was statistically significant ( $P < 0.05$ ). HSS scores increased significantly in both groups at 1 week, 1 month, 3 months and 6 months after operation. All the comparisons were statistically significant ( $P < 0.05$ ); HSS scores of observation group were significantly higher than control group at 1 week, 1 month, 3 months and 6 months after surgery. The difference was statistically significant ( $P < 0.05$ ). The agitation rate of the observation group was lower than that of the control group ( $P < 0.05$ ). Compared with the control group, the sleep time of observation group increased significantly in each period, with statistically significant difference ( $P < 0.05$ ).

## 5. Conclusion

To sum up, the perioperative painless rehabilitation nursing interventions for patients with hip joint replacement could significantly relieve swelling and pain. It is helpful to improve the prognosis of patients and accelerate the rehabilitation process of patients. It is of great significance to the establishment of a good and harmonious doctor-patient relationship. It was helpful for the patients to recover the function of knee joint after operation and it was worthy of clinical application.

However, due to the limitation of our time and experience, the sample size collected is small, and there is no in-depth use of SAS scale to study the postoperative mood of patients, which is the shortcomings of this study. We expect that future scholars can combine SAS scale to obtain postoperative emotion related indicators of patients, so as to improve the level of nursing service.

## Data Availability

The datasets used during the present study are available from the corresponding author upon reasonable request.

## Conflicts of Interest

The author declares that he has no conflict of interest.

## References

- [1] S. F. Harwin, M. Cadossi, A. Sambri et al., "Anterior approach in Total hip replacement," *Orthopedics*, vol. 40, no. 3, pp. 1–4, 2017.
- [2] D. C. McNabb, J. M. Jennings, D. L. Levy, T. M. Miner, C. C. Yang, and R. H. Kim, "Direct anterior hip replacement does not pose undue radiation exposure risk to the patient or surgeon," *The Journal of Bone and Joint Surgery*, vol. 99, no. 23, pp. 2020–2025, 2017.
- [3] H. Dongying, "Clinical intervention and effect of rapid rehabilitation nursing in patients with femoral neck fracture undergoing total hip arthroplasty Shanxi," *Journal of Medicine*, vol. 50, no. 6, pp. 1048–1049, 2021.
- [4] H. Lingli, Z. Yi, L. Mingshuang, and L. Huawei, "Effect of early rehabilitation nursing on rehabilitation effect and self-care ability of patients undergoing hip arthroplasty," *Nursing Practice and Research*, vol. 15, no. 8, pp. 78–79, 2018.
- [5] Y. N. T. V. D. Eeden, B. J. G. D. Turck, and F. M. C. V. D. Eeden, "24 hours stay after hip replacement," *Acta Orthopaedica*, vol. 88, no. 1, pp. 24–28, 2017.
- [6] P. A. Manner, "Editor's spotlight/take 5—2018 John Charnley award: analysis of US hip replacement bundled payments: physician-initiated episodes outperform hospital-initiated episodes," *Clinical Orthopaedics and Related Research*, vol. 477, no. 2, pp. 268–270, 2019.
- [7] C. Huiqing and Z. Chen, "Observation on the effect of early rehabilitation of elderly patients with total hip arthroplasty," *Dialysis and Artificial Organ*, vol. 32, no. 4, pp. 95–96 + 98, 2021.
- [8] L. Freeman Williamson and D. D. Kautz, "Trauma-informed care is the best clinical practice in rehabilitation nursing," *Rehabilitation Nursing*, vol. 43, no. 2, pp. 73–80, 2018.
- [9] Z. Xueqin, S. Yindi, X. Jie et al., "Application of painless rehabilitation nursing concept in the treatment of patients with lumbar intervertebral disc herniation," *U.S.-China International Trauma Journal*, vol. 17, no. 3, pp. 49–52, 2018.
- [10] M. E. Arakgi and R. M. Degen, "Approach to a failed hip arthroscopy," *Current Reviews in Musculoskeletal Medicine*, vol. 13, no. 3, pp. 233–239, 2020.
- [11] M. Mupparapu and S. R. Singer, "The American Society of Anesthesiologists (ASA) physical status classification system and its utilization for dental patient evaluation," *Quintessence International (Berlin, Germany: 1985)*, vol. 49, no. 4, pp. 255–256, 2018.
- [12] L. Yang, L. Jinfeng, L. Chunlian et al., "Optimization of perioperative analgesia management in elderly patients with total knee arthroplasty," *Chinese Journal of Anesthesiology*, vol. 39, no. 12, pp. 1456–1460, 2019.
- [13] J. Murrell, "Perioperative use of non-steroidal anti-inflammatory drugs in cats and dogs," *In Practice*, vol. 40, no. 8, pp. 314–325, 2018.

- [14] B. K. Wang, T. H. Liu, F. Xie, and Y. Q. Liu, "Pain vision system for evaluating chronic pain: a comparison with VAS scoring," *Pain Research & Management*, vol. 2020, no. 6, pp. 1–4, 2020.
- [15] V. J. Daniels, A. C. Strand, H. Lai, and T. Hillier, "Impact of tablet-scoring and immediate score sheet review on validity and educational impact in an internal medicine residency objective structured clinical exam (OSCE)," *Medical Teacher*, vol. 41, no. 9, pp. 1039–1044, 2019.
- [16] G. Lijuan and P. Lifei, "Analysis of the effect of adjusting sedative drug use according to human body normal rest and rest on mechanical ventilation patients in ICU," *Chinese General Practice*, vol. 17, no. 2, pp. 317–320, 2019.
- [17] C. Rivière, J. Y. Lazennec, C. Van Der Straeten, E. Auvinet, J. Cobb, and S. Muirhead-Allwood, "The influence of spine-hip relations on total hip replacement: a systematic review," *Orthopaedics & Traumatology: Surgery & Research*, vol. 103, no. 4, pp. 559–568, 2017.
- [18] C. L. McCarthy, Y. Uchihara, M. Vlychou, G. Grammatopoulos, and N. A. Athanasou, "Development of malignant lymphoma after metal-on-metal hip replacement: a case report and review of the literature," *Skeletal Radiology*, vol. 46, no. 6, pp. 831–836, 2017.
- [19] L. Ezquerro, M. P. Quilez, M. Á. Pérez, J. Albareda, and B. Seral, "Range of movement for impingement and dislocation avoidance in Total hip replacement predicted by finite element model," *Journal of Medical and Biological Engineering*, vol. 37, no. 1, pp. 26–34, 2017.
- [20] W. A. Yassin, A. R. Al-Mirah, A. A. Almoaish et al., "Cemented versus Cementless primary hip replacement: assessment of leg length inequality," *Journal of Young Pharmacists*, vol. 9, no. 3, pp. 327–331, 2017.
- [21] E. Sayit and Y. Terzi, "The effects of partial hip replacement surgery after hip fractures on complete blood count parameters in elderly," *International Journal of Clinical and Experimental Medicine*, vol. 10, no. 4, pp. 7157–7162, 2017.
- [22] S. Jie, Z. Jiangning, M. Tingting, and S. Xiaoli, "Discussion on the effectiveness of early analgesia and nursing psychological intervention to reduce pain and stress response in patients with severe multiple trauma," *Psychological Monthly*, vol. 14, no. 11, pp. 62–62, 2019.
- [23] Y. Zhenzhen, "Analysis of the effect of psychological nursing intervention on mental state, pain and nursing satisfaction after fracture operation," *Contemporary Nurse (Late Issue)*, vol. 26, no. 4, pp. 148–149, 2019.

## Retraction

# Retracted: Rural Planning Evaluation Based on Artificial Neural Network

### Computational and Mathematical Methods in Medicine

Received 25 July 2023; Accepted 25 July 2023; Published 26 July 2023

Copyright © 2023 Computational and Mathematical Methods in Medicine. This is an open access article distributed under the Creative Commons Attribution License, which permits unrestricted use, distribution, and reproduction in any medium, provided the original work is properly cited.

This article has been retracted by Hindawi following an investigation undertaken by the publisher [1]. This investigation has uncovered evidence of one or more of the following indicators of systematic manipulation of the publication process:

- (1) Discrepancies in scope
- (2) Discrepancies in the description of the research reported
- (3) Discrepancies between the availability of data and the research described
- (4) Inappropriate citations
- (5) Incoherent, meaningless and/or irrelevant content included in the article
- (6) Peer-review manipulation

The presence of these indicators undermines our confidence in the integrity of the article's content and we cannot, therefore, vouch for its reliability. Please note that this notice is intended solely to alert readers that the content of this article is unreliable. We have not investigated whether authors were aware of or involved in the systematic manipulation of the publication process.

Wiley and Hindawi regrets that the usual quality checks did not identify these issues before publication and have since put additional measures in place to safeguard research integrity.

We wish to credit our own Research Integrity and Research Publishing teams and anonymous and named external researchers and research integrity experts for contributing to this investigation.

The corresponding author, as the representative of all authors, has been given the opportunity to register their agreement or disagreement to this retraction. We have kept a record of any response received.

### References

- [1] Y. Liu and X. Huang, "Rural Planning Evaluation Based on Artificial Neural Network," *Computational and Mathematical Methods in Medicine*, vol. 2022, Article ID 9746362, 10 pages, 2022.



## Research Article

# Rural Planning Evaluation Based on Artificial Neural Network

Yumei Liu <sup>1,2</sup> and Xuezhou Huang<sup>1</sup>

<sup>1</sup>*School of Geography Science and Geomatics Engineering, Suzhou University of Science and Technology, Suzhou 215009, China*

<sup>2</sup>*Institute of Suzhou's Rural Revitalization Research, Suzhou 215009, China*

Correspondence should be addressed to Yumei Liu; plumyliu@usts.edu.cn

Received 24 April 2022; Revised 18 May 2022; Accepted 23 May 2022; Published 11 June 2022

Academic Editor: Naeem Jan

Copyright © 2022 Yumei Liu and Xuezhou Huang. This is an open access article distributed under the Creative Commons Attribution License, which permits unrestricted use, distribution, and reproduction in any medium, provided the original work is properly cited.

The continuation of human civilization is inseparable from the development and construction of rural areas, and infrastructure is the core of rural development. China has been building large-scale rural infrastructure in recent years. Rural infrastructure building, for example, is huge in both quantity and scope, but it is beset by challenges in its current construction and development, and it urgently requires suitable leadership. Planning assessment, as a technical method, can identify problems in regional development and is a powerful tool for evaluating the impact of planning and construction and promoting the development of complete new areas. This paper is aimed at the planning evaluation of rural construction and the evaluation of rural construction and guides the planning and implementation of the next step of rural construction, to assist China's supervision and inspection of rural construction effect and promote rural construction and development into a good track. In view of the low accuracy and efficiency of the current evaluation model of rural planning and the problem that a single neural network easily produces local extreme value, the neural network method is improved, and the application of LM-BP neural network in the evaluation model of rural planning is proposed. Input sample elements are five factors affecting rural construction, including industrial construction, population distribution, and utilization rate of large-scale facilities, construction of public facilities, and promotion effect of supporting policies. Output sample is the evaluation result. On this foundation, the LM-BP neural network was used to convert the training into a least square problem, and the LM method was used to redefine the number of hidden layer nodes, resulting in the construction of a rural planning evaluation model based on the LM-BP neural network. This approach is used to determine the outcomes of rural planning evaluations. The experimental results show that the designed evaluation model has a small evaluation error, has the advantage of high accuracy compared with similar models, and is a reliable evaluation model for rural planning.

## 1. Introduction

In the process of realization after reform and opening up, the Central Work Conference discussed the “new normal” at the end of 2014, pointing out the direction of China's future progress. The new normal emphasizes the innovation of GDP growth mode, believing that the fundamental significance lies in meeting the actual needs of human material and cultural life, rather than merely pursuing quantitative growth. Reflected in urban and rural planning, the new normal emphasizes the characteristics of conforming to social development and focusing on quality rather than quantity [1]. In the past ten years, for the development and the rural demand level, urban and rural planning and construction of

our country will focus on material space level; a large number of new area development, park construction, and large-scale and high strength facilities, beyond the living demand of residential development, emerge in endlessly; the focus of the urban and rural planning and construction shall be transferred accordingly; no need to pay attention to the growth of construction quantity. It requires control over the effectiveness and quality of construction. Instead of paying attention to the actual effect and profit of development and construction in the past, we should think about the rationality of planning and supervise and consider the implementation of planning.

Urban and rural planning evaluation started late in China, the theoretical basis is relatively weak, technology

and methods are not yet mature, and the research has focused on the overall plan level, with single evaluation type; the characteristic of the large arbitrariness, its theoretical research, and practice to a certain extent is disjointed, before the urban and rural planning act was issued, and there are no supervision and related legal requirements [2]. Under the new situation, China's planning evaluation needs to be developed urgently, and relevant theories and mechanism construction need to be improved to ensure that the effectiveness and quality of construction are controlled in the whole process of planning and implementation and play a good driving role in rural development.

As a new rural space, the development of rural new areas will inevitably encounter various problems and obstacles, especially the comprehensive new areas with complicated functions. Harbin New Area was planned in 1990 and started construction in 2000, but the development level is still not high due to the high threshold of crossing the river. New Area was founded in 2001, and the permanent population of New Area was only 300,000 in 2011, which was quite short of the planned target of 1.5 million. With the continuous increase of rural new areas, the problem of building without city and city without employment in rural new areas is becoming more and more serious, and the phenomenon of "ghost city" emerges in endlessly [3]. The reasons are worth pondering. Is it the original site selection, positioning, land use planning, and other planning problems, or is there insufficiency in the implementation process? Faced with several issues in the development bottleneck, China's comprehensive rural new areas must find appropriate countermeasures, supervise the compilation and execution of appropriate planning, revise and adapt the development direction and mode, and get through the current bottleneck phase.

"To evaluate" means to appraise and measure. Referring to the explanation in Ci Hai, "evaluation" includes two basic processes: "measuring and evaluating the value of things" and "making general inferences about the nature, quantity, and change of things based on the current situation." The Chinese "Evaluation" directly corresponds to English words such as Evaluation, Assessment, and Appraisal, which have different applications according to different contexts [4]. Among them, Evaluation is the most commonly used word to express the concept of Evaluation in western countries. Its etymology comes from "Value," which is an activity to judge the Value of people or things. The U.S. Department of State defines it as "a systematic information collection and analysis tool" that improves efficiency and provides decision makers with current and possible future information based on the characteristics and outcomes of programs, projects, and processes. Evaluation is often used as an English explanation in the studies of planning Evaluation by domestic scholars [5]. Reasonable evaluation of rural construction can provide powerful data support for rural construction. As shown in Figure 1, the evaluation model can play a role in all aspects of rural planning. Therefore, it is crucial to find high-quality evaluation methods for rural planning.

There are many existing evaluation methods in China. Wei et al. [6] adopts the evaluation model of rural planning

based on input-output analysis. From the input and output of buildings, the statistical data obtained from planning are relatively one-sided, leading to large errors in evaluation results. Liu et al. [7] proposed the loss assessment model based on maximum likelihood method, which easily falls into the state of local optimal solution, and the obtained assessment results have low credibility. Zhang et al. [8] uses the zoning classification method to evaluate the engineering planning and construction, starting from the factors that affect rural planning, in an attempt to fully grasp the situation of rural planning and accurately predict the evaluation results. However, because of overfitting in the training phase, this approach is prone to substantial errors in the evaluation outcomes. Hong-Juan conducted a preliminary study of the implementation evaluation of rural design [9] on the basis of emphasizing the importance of this evaluation. He drew important conclusions on the implementation level of rural design through an overall evaluation of the scope involved and an investigation of a typical case of a developed neighborhood. Planners can identify difficulties in the implementation process by conducting a rational review of rural design implementation. Taking the water supply special evaluation of new county as an example, Cheng et al. [10] evaluated the implementation results of the planning from three aspects of water source, water plant, and water distribution network and evaluated the main contents of the water supply special planning from the selection of water source, water consumption index, and daily variation coefficient. In the research method combining quantitative and qualitative methods, the evaluation results of each evaluation object are usually dimensionless in existing planning evaluation, and a group of results can be discussed under the same standard. Generally, three kinds of methods are used: grading evaluation, completion percentage calculation, and index deviation calculation. For example, in the comparative study method, the consistency between planning and construction implementation is usually compared, and the percentage of completion of each item is obtained according to land use classification, or the percentage of completion of major facility projects and the percentage of coverage of control regulations are obtained. For example, in the index system method, the effective degree of planning implementation is evaluated according to the grading evaluation method of "effective, general, and ineffective," and then, the comprehensive score is weighted by combining the evaluation of the percentage of completion. The questionnaire survey principle uses the survey statistical results to make equal-weight statistics of "excellent, general, and poor" and uses the method of graded evaluation to get the final results [11]. Other studies compare the deviation between the current rural construction, social development, and other indicators and the planning and score according to the percentage of deviation between the current value and the target value.

Aimed at the problems of rural planning evaluation model and method, in this paper, the neural network was improved, because the state of a single neural network easily trapped in local minima and convergence for a long time; to obtain the optimal evaluation results, the design is based on



FIGURE 1: Schematic diagram of the evaluation model applied to rural planning.

LM-BP neural network assessment model; this model has two characteristics, one of which is on the basis of neural network. Converting network training into least square problem can solve the protracted problem of rural planning evaluation. Second, the number of iterations of LM-BP neural network training is limited to avoid training falling into local extremum state. Therefore, the model in this paper can ensure the accuracy of evaluation and improve the efficiency of evaluation. Simulation experiments are carried out to verify the efficiency evaluation effect, providing a reliable analysis basis for rural planning and construction.

The arrangements of the paper are as follows: Section 2 discusses the related work. Section 3 discusses the algorithm design of the proposed work. Section 4 examines the experiments and results. Section 5 concludes the article.

## 2. Related Works

**2.1. Current Situation of Rural Planning Evaluation.** Western planning evaluation started in the 1950s, originated from the public policy evaluation of British and American countries, and experienced a process of transformation from rational planning to communicative planning in planning paradigm, from instrumental rationality to substantive rationality, and finally to communicative rationality. Based on these changes in the way of thinking, Guba and Lincoln [12] divides the evaluation into four stages from the value orientation in the fourth-generation evaluation: measurement, description, and judgment and value diversification [13]. In different stages, different viewpoints have emerged on the subject, object, and method of planning evaluation.

As for the subject of planning evaluation, Williams [14] distinguished each stage in the process of planning preparation and the relationship between evaluation executor and planner, as well as the time point of implementing evaluation and the specific content of evaluation. It is suggested that the evaluation criteria should be formulated by planners in the process of planning. As for the objects of planning evaluation, Kok et al. compared the development of planning evaluation and project evaluation at that time and believed that the evaluation before and during the implementation of planning evaluation had been marginalized [15]. De Oliveira et al. [16] takes a similar view, noting that

there has been more research on preimplementation evaluations than on the implementation and postimplementation phases. In terms of planning evaluation methods, according to Guba's [12] four-generation classification method, western planning evaluation ideas and methods can be divided into four categories of "measurement-description-judgment-value diversification" in chronological order. According to their own characteristics, these methods can be used in different stages of planning and implementation. The first generation of evaluation, represented by the cost-benefit method proposed by Hill and Wehman [17], was first applied to public policy evaluation, which was "measurement" oriented evaluation. Based on the thinking mode of instrumental rationality, the currency is taken as the unit of measurement to determine the most stable operation mode, which is generally applied to the development activities of public undertakings and infrastructure construction. A similar method is cost-effectiveness analysis. The second generation of assessments introduces "descriptions" of things that cannot be directly quantified, in order to judge the consistency between the current situation and the described goals [18]. It tries to go beyond simple positivism and combine rational measurement with evaluation of target effectiveness. The representative methods are target realization matrix method and multiple index evaluation method, which decompose the total goal into multiple indexes, measure the target realization degree of each index through cost and income and then determine the overall goal realization situation through the weight of each index. The third generation of evaluation goes beyond pure rational planning and begins to consider the "judgment" of object value. It believes that the value orientation of evaluation is different, and the value judgment results of planning results are also diverse. Planning balance sheet and environmental impact assessment are both third-generation methods [19]. PBS method is a CBA method incorporating social analysis, considering the externality of the project. The fourth-generation assessment is based on the concept of communicative planning and is characterized by "value diversification," emphasizing diverse participation, feasibility, and incremental development. Represented by the community impact analysis method proposed by Lichfield, it pursues a comprehensive, systematic, and composite analysis method.

The domestic research on planning evaluation started from the 1990s, and a series of related theoretical studies were carried out based on the western planning evaluation theory review. The focus is on the sorting and reference of relevant western theories and methods, the division of planning and evaluation stages, and the summary of research contents in each stage. Some scholars summarized relevant western theories in detail [20]. For example, Jenkins et al. [21] discussed the origin, theory, and content of modern planning evaluation in detail against the background of the mature planning evaluation system in the West. Song and Li [22] drew lessons from North American rural planning and evaluation experience and explored the development direction of planning and evaluation in China from the aspects of planning implementation subject, content of planning and evaluation, result expression, and public participation. Graymore et al. explored the planning evaluation methods in line with the development situation in China by sorting out the theoretical paradigms related to planning evaluation and the changing process of evaluation methods in western countries [23]. Represented by sun, domestic scholar's research content is more comprehensive; on the basis of summarizing the theories and methods of the western division of the type of planning evaluation, combined with its values and the paradigm shift, planning assessment and implementation effect evaluation put forward the corresponding ideas and methods and also stress the necessity and difficulty of planning evaluation research in China. Lu planning implementation evaluation can be divided into planning, planning, evaluation, planning, implementation, planning revision, and planning implementation after the completion of the five stages and put forward the measures for the rural planning and assessment of target oriented to promote rural planning form "compile-adjustment-evaluation" the virtuous circle, to cope with the problems in the planning and implementation stages. Through sorting out the planning time axis, McDonald et al. constructed a multiangle planning assessment model based on four factors, including technical means, planning objects, efficacy of the planning implementation stage, and postimplementation effect [24]. The special research of planning evaluation in "Overall Implementation and Technical Evaluation of Qingdao International Horticultural Expo Planning" suggests that the evaluation activities of rural planning should be discussed from three aspects: technical rationality, planning timeliness, and system coordination. In terms of technical rationality, it evaluates the scientific, feasibility, and rationality of the planning scheme from the aspects of environment, technology, and policy. In terms of planning effectiveness, the author examines the status quo of rural spatial development and the realization of rural spatial functions to judge whether planning can guide rural development. In terms of system coordination, short-term and long-term benefits, local and global benefits, and overall and group benefits of relevant planning should be considered to reflect their public policy attributes.

The western practice of planning evaluation is usually divided into three categories: planning preparation evaluation, planning implementation evaluation, and planning

effect evaluation. As its name implies, it is divided according to the different evaluation objects of different stages of planning. Planning preparation evaluation is generally used to express whether the planning scheme or text is reasonable, and its practice is mostly targeted at specific special planning schemes, such as the quality evaluation of planning text of disaster prevention planning in the United States, the planning preparation action plan evaluation of New York low-carbon planning, and the planning preparation action plan evaluation of Auburn city. The primary purpose of the plan implementation evaluation is to track and monitor whether the plan is being implemented as planned and, in practice, to evaluate the regulations governing rural growth in the United States [25]. In general, systematic index evaluation or quantitative method is used to evaluate the planning effect within a certain range, such as Talen's [26] evaluation of the implementation of public facilities layout in Pueblo, Colorado, USA. In terms of the domestic situation, the classification of planning evaluation practice is usually based on the planning level, which mainly involves four levels: macro regional planning level, overall planning level, detailed planning level, special planning level, and other levels. After the promulgation of the Urban and Rural Planning Law and the measures, the number of relevant practical studies in China has increased significantly. Scholars have paid more attention to the level of rural master planning, while the number of evaluation studies on the level of detailed planning is relatively small. The Review and Countermeasures of Shenzhen Rural Master Planning in 2002 is an earlier research document with the meaning of planning evaluation in China, appearing in the form of "planning review." At present, most of the research objects of planning evaluation practice in China are the villages at prefecture-level and above, and the evaluation methods are not systematic. Most of them are the evaluation after the implementation of planning, that is, the evaluation of planning implementation and the evaluation of planning effect.

## 2.2. Current Situation of Neural Network Evaluation Model.

It was Banerji and Fisher [27], a statistician, who first put forward the classification problem of assessment in 1936. At that time, the assessment business in the United States began to develop and the business of many financial structures also developed rapidly. Financial institutions began to assess users' information in the process of processing application information, and expert system was the earliest system used for assessment. The system is used to evaluate applicants. In 1941, statistician Durand [28] used the characteristic dimension to assess the default risk of applicants, which was then used by financial institutions to distinguish between good and bad applicants. In 1996, Henley and Hand [29] applied the improved  $K$ -nearest neighbor method to financial risk assessment, which improved the prediction accuracy of data compared with the previous method. In 2003, Li et al. [30] used the linear discriminant method to predict the data, and the experiment proved that the classification tree has better results than other traditional methods. In 2005, Shi et al. [31] first used logistic regression to remove the features with high correlation and applied the results to

artificial neural network to have better effect, so as to achieve the purpose of improving the effect of the model. In 2011, Buzius et al. [32] compared multiple classifiers through experimental research and carried out experiments on several commonly used classifiers. The results show that data modeling by machine learning has certain advantages, but it is still a complicated problem for classifier selection and model parameter tuning [33]. With the advent of the era of artificial intelligence, many scholars apply neural networks to evaluation models. In 2014, Oreski and Oreski [34] found that the data currently studied on financial institutions were all high-dimensional data, and too many irrelevant features might reduce the prediction accuracy of neural network. Oreski and Oreski [34] selects important features in data preprocessing through genetic algorithm and uses neural network modeling. In 2014, Fan et al. [35] used random forest as an evaluation model. Through experimental comparison, the model based on random forest has better generalization and prediction accuracy than the traditional single classifier model. Through the study of the literature, it was found that logistic regression and linear statistical method based on the current complex multidimensional nonlinear financial data have no good fitting effect; the traditional neural network to the dimensions of the data and data volumes have high requirements, such as random forests which also require a certain amount of data to get the ideal effect.

The standard particle swarm optimization algorithm is likely to have the same problem as gradient descent when solving space optimization; that is, particles trapped in local extremum cannot escape. Because each particle reduces the search space when exchanging information, it is possible that the particles still have a large space after convergent search. Many scholars' efforts in this area, such as adding iterative position changes in the late stage of the standard PSO algorithm, can enable particles with local convergence to jump out of the local optimal solution for global optimization. However, the effect of adding disturbed particles in the later stage is limited, because the earlier particles will quickly reduce the search range in the process of optimization. Some researchers increase the number of particles to cover a larger solution space and improve optimization outcomes. PSO, on the other hand, is still simple to fall into the local optimal solution as iteration times increase. The addition of genetic algorithm improves the possibility of searching global potential solutions, but its disadvantages are slow convergence rate and poor ability of searching local solutions.

Data is the basis of models. In planning evaluation, the security and privacy of data make it impossible to share data modeling, which is a limitation for the research in the field of evaluation models. In 2016, Google put forward the concept of federated learning, using the method of federated learning. In this application, the mobile phone, as the client participating in the modeling, trains the same model together under the coordination of the central server [36]. The author constructs a client-to-server architecture to protect data security, so that multiple clients can cooperate to train the model under the premise of ensuring data security.

In addition, in recent years, there are many studies that combine federated learning with specific systems and combine federated learning with system functions to ensure the security of data involved in training. Therefore, for the evaluation problem, it is necessary to start from the algorithm model and data at the present stage. The algorithm model requires to ensure the ability of fitting complex data and find potential laws from high-dimensional nonlinear data, so as to achieve accurate prediction [37]. On the other hand, in view of the security and privacy of the data of financial institutions, the data quantity of the training model is increased through federated learning, and the data quality is indirectly improved, so as to improve the effect of the model.

### 3. Algorithm Design

In this section, we define the traditional assessment model and LM-BP neural network evaluation model in detail.

*3.1. Traditional Assessment Model.* Design evaluation model using the error backpropagation algorithm with more multi-layer forward neural network (BP neural network), learning samples as input, and the corresponding expectations as output; the neural network weights and threshold depend on the realization and are expected to adjust the differential, the output value in line with expectations, and maximum output error sum of squares of the minimum [38]. Accordingly, the rural planning evaluation model based on neural network is constructed, as shown in Figure 2. In Figure 2, industrial construction, population distribution, utilization rate of large-scale facilities, construction of public facilities, and promotion effect of supporting policies are taken as input samples of the evaluation model.

Neural networks have strong adaptive capacity and higher level of generalization. Neural network was used to construct an evaluation model which can obtain more reliable evaluation result, but the state of single neural network is easily trapped in local minima and convergence when using long defects; to obtain the optimal evaluation results, the neural network is improved, and the evaluation model based on LM-BP neural network is obtained.

*3.2. LM-BP Neural Network Evaluation Model.* The LM algorithm is a nonlinear least squares method that uses a model function to evaluate parameter vectors using linear approximation. This step is finished in its field, and it changes network training into a least squares issue by ignoring derivative terms higher than bivalent. As a result, the LM-BP neural network can overcome the problem of classic neural networks' long convergence times. Based on the same sample capacity as a neural network, the LM-BP neural network is prone to falling into a local extremum state. This defect of LM-BP neural network can be avoided by setting the number of iterations. When the number of iterations of the LM-BP neural network reaches a certain limit, it is temporarily stopped. New weights and thresholds were assigned to the LM-BP neural network, and new iterative training was started until the desired results were obtained.

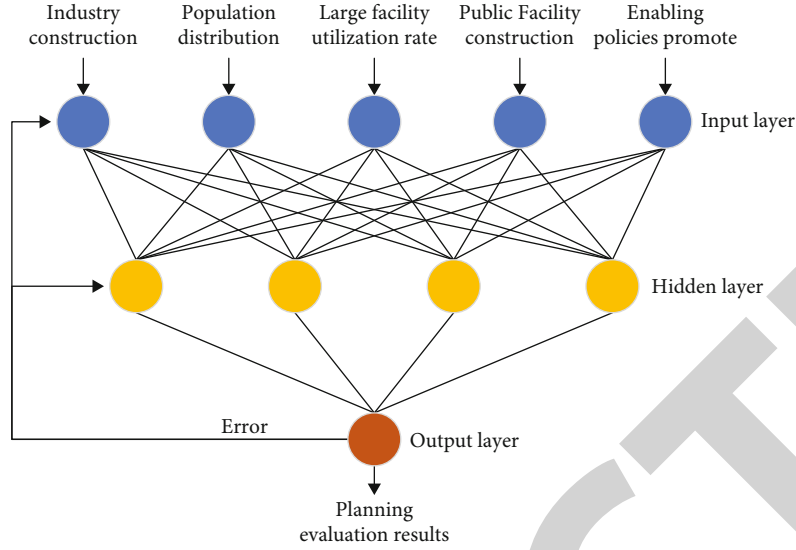


FIGURE 2: Neural network-based rural planning evaluation model.

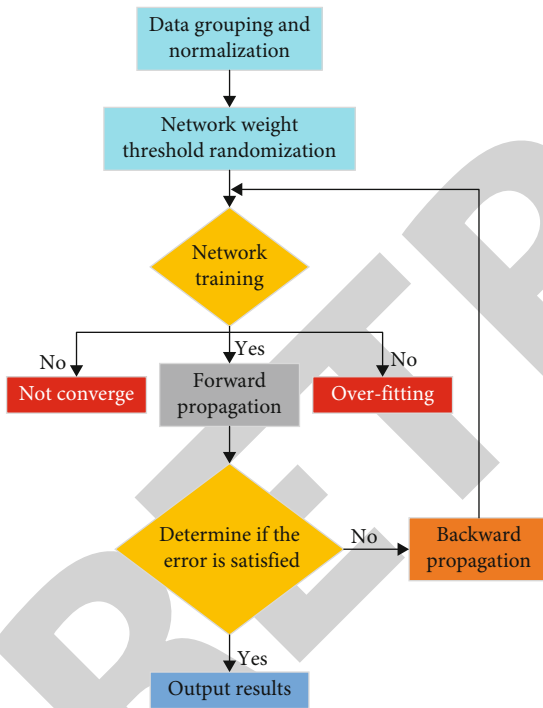


FIGURE 3: Training steps of LM-BP neural network.

The contradiction between high training accuracy and a large number of training samples results in overfitting of the network and the reduction of network generalization ability [39]. The problem of decreased generalization ability can be solved by setting verification samples. In the process of verification sample training, if the sample accuracy decreases with the improvement of network accuracy, the network training should be terminated immediately. The training steps of the LM-BP neural network are described in Figure 3. When the training error does not meet the expected standard, the network training is reconducted until

the sample training error meets the expected value, and the output model training results are obtained.

The LM-BP neural network evaluation model is designed. The number of input layer, hidden layer, and output layer is 1. The LM-BP evaluation model was trained using imitation software, and the number of hidden layer nodes was chosen to be 5 based on the findings of the optimal network training fitting [40]. The improved neural network evaluation model based on LM-BP is described in Figure 4.

In Figure 4, the five input nodes in the LM-BP neural network are industrial construction, population distribution, utilization rate of large-scale facilities, construction of public facilities, and promotion effect of supporting policies, and the last output node is the evaluation result. The weight matrix of LM-BP neural network from the input layer to hidden layer is described by  $IW \{1, 1\}$ , the threshold matrix is described by  $B \{1\}$ , the weight matrix from the hidden layer to output layer is described by  $LW \{2, 1\}$ , and the threshold matrix is described by  $B \{2\}$ .

Firstly, the correlation significance coefficient is obtained by using the following equation:

$$t_{nm} = \sum_{h=1}^p W_{nh} \frac{1 - e^{-W_{mh}}}{1 + e^{-W_{mh}}} \quad (1)$$

Secondly, equation (2) is used to obtain the correlation index:

$$T_{nm} = \left| \frac{1 - e^{-t_{mh}}}{1 + e^{-t_{mh}}} \right| \quad (2)$$

Finally, equation (3) is adopted to obtain the weight

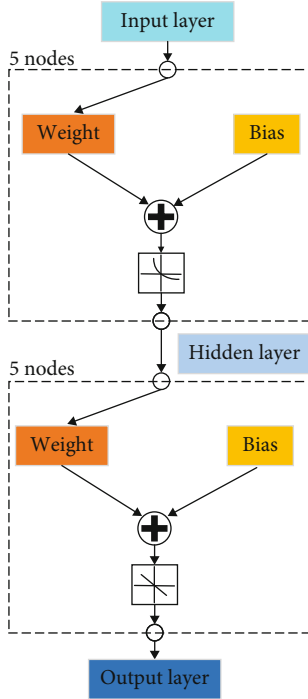


FIGURE 4: Improved neural network evaluation model based on LM-BP.

TABLE 1: Influence weights of input variables on output variables.

Input variables	Weights
Industry construction	0.134
Population distribution	0.175
Utilization rate of large facilities	0.096
Public facility construction	0.186
Effect of supporting policies to promote	0.169

index of the evaluation index:

$$G_{nm} = \frac{T_{nm}}{\sum_{n=1}^j T_{nm}}. \quad (3)$$

In the above formula, the input layer unit of LM-BP neural network is described by  $i$  and meets the conditions  $n = 1, 2, 3 \dots, i$ . The output layer unit of the LM-BP neural network is described by  $m$ , and  $m = 1$ . The weight value of the  $h$  th node of the hidden layer and the output layer of the improved LM-BP neural network is described by  $m_h$ ; the correlation significance coefficient and correlation index between the  $n_{th}$  input variable and the hidden layer are described by  $t_{nm}$  and  $T_{nm}$ , respectively; and the influence of the  $n_{th}$  input variable on the evaluation result of the output is described by  $g_{nm}$ . The neural network evaluation model based on LM-BP outputs the evaluation results. The LM-BP neural network rural planning evaluation model output evaluation results.

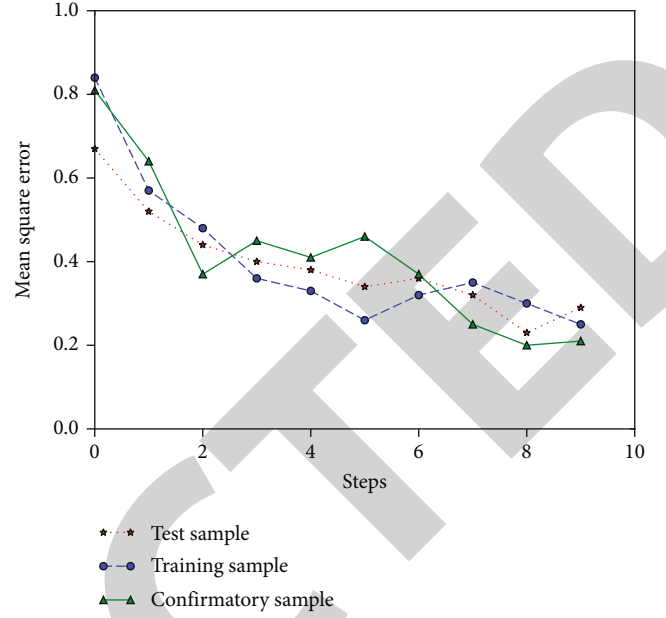


FIGURE 5: Comparison curves of training errors of three samples.

## 4. Experiments

In this chapter, we discuss the model prediction performance analysis and evaluating performance comparisons.

**4.1. Model Prediction Performance Analysis.** In order to verify the effectiveness of the proposed model in rural planning evaluation, a simulation experiment was carried out. The experimental sample is from the public data of rural planning evaluation in a certain region, and the sample records the data related to the construction and evaluation of the village from 2007 to 2016, with a total of 18 evaluations. 66% of the samples were used as training samples, 17% as testing samples, and the remaining 17% as verification samples. The scientific nature and reliability of the experiment can be assured after dimensionless processing of the experimental samples. If the sample error is set to increase for three consecutive times, the training will be stopped to prevent the faults produced by overfitting of the model in this paper. The model in this paper is used for sample training, and the weights of input variables on output variables are listed in Table 1.

The results are described in Figures 5 and 6, respectively. Figure 5 describes the training errors of the model in the training samples, test samples, and verification samples. It can be seen from Figure 5 that before the experimental step number is 6, with the increase of the experimental step number, the error of the three samples of the model training in this paper gradually decreases and reaches the optimal state of the current training error when the step number is 6, which verifies the optimal point of the strong generalizing energy of the model in this paper. Between steps 6 and 9, the error of the validation sample increases continuously, which is consistent with the phenomenon that the model in this paper is prone to overfitting in the sample training

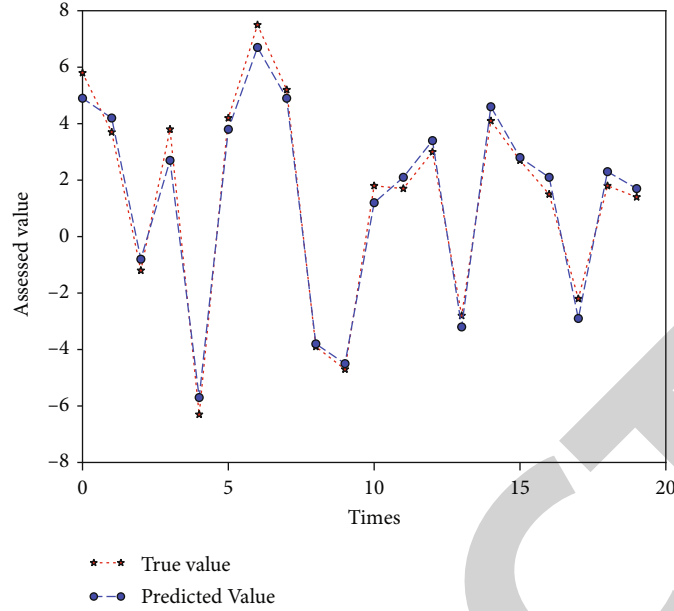


FIGURE 6: Comparison of predicted and actual values of the model in this paper.

TABLE 2: Relative error of the prediction sample.

Relative error	Test sample output	Test sample target
10.26%	86.50	79.40
6.81%	83.60	75.10
2.57%	88.70	86.80
1.39%	90.40	89.40
0.85%	89.20	88.50

TABLE 3: Relative errors of the model in this paper compared with the traditional model.

True value	Our model results	Relative error	Input-output model results	Relative error
78.20	83.70	7.90%	62.50	14.20%
85.60	81.50	8.50%	59.70	16.10%
67.50	62.80	5.20%	84.90	12.50%
76.40	78.60	8.60%	91.40	13.30%
83.70	88.40	4.70%	95.3	10.70%
87.90	82.30	6.30%	71.20	9.50%
84.30	87.10	1.40%	73.50	12.70%
77.80	76.10	3.80%	87.20	8.70%

process. During this process, the error of the training sample decreases gradually, while the error of the test sample increases gradually, which indicates that the model in this paper begins to overfit. Due to the relevant settings of the experiment to prevent overfitting, the experiment was stopped in time when the number of steps was 9, so as to avoid excessive error in sample training of the model in this paper, and the error of the training sample reached the target error value at this time.

Figure 6 shows the comparison between the predicted value and the actual value of the model in this paper. Figure 6 shows that the model prediction and the actual value are highly consistent; the abscissa describes the evaluation number of sample data and each assessment as a sample data, so the training samples for experiment 1~12 sample data confirm sample for 13~15 sample data, and prediction sample is 16~18 sample data. Figure 6 shows that the fitting degree of training and confirmation samples is good, and the actual value of data acquired from prediction samples is very consistent, based on this, which verifies the effectiveness and reliability of the model in this paper in rural planning evaluation.

In addition, the relative error of the evaluation results predicted by the model in this paper is described in Table 2. According to the data described in Table 2, with the progress of the test, the loss error of the model in this paper gradually decreases, and the error at the end of the experiment is only 0.85%, which can accurately achieve effective evaluation of rural planning.

**4.2. Evaluating Performance Comparisons.** To emphasize the model's benefits in this paper, a comparison experiment based on the input-output analysis and evaluation model was conducted, with data from a rural planning evaluation for 5 times or more from 2000 to 2018 chosen as the simulation experiment to increase the difficulty of sample training and planning evaluation and prediction. Industrial construction, population distribution, utilization rate of large-scale facilities, construction of public facilities, and promotion effect of supporting policies were taken as input variables of sample training, and planning evaluation was taken as output variables. Also, dimensionless operation was performed on experimental data to ensure the authenticity and reliability of experimental results.



The comparison between the evaluation results of the model in this paper and the evaluation model based on input-output analysis is listed in Table 3. As can be seen from Table 3, only in the third and seventh test, the evaluation error of the model in this paper is larger than 08%, which is 17.40% and 11.60%, respectively. The evaluation error of the model based on input-output analysis in these two tests is 13.40% and 18.70% higher than that of the model in this paper, respectively. In the other 5 tests, the evaluation error of the model in this paper is less than 06%, and in the sixth test, the error is the smallest, only 1.40%. At this time, the evaluation error of the model based on input-output analysis is 12.60%, much higher than that of the model in this paper. On the whole, the mean value of the evaluation error of the model in this paper is 5.60%, while that of the model based on input-output analysis is 8.90%, which is 6.70% higher than that of the model in this paper. Based on the above data, it can be seen that the model in this paper has high accuracy and small error in rural planning evaluation, so the evaluation performance of the model in this paper is better and has strong advantages compared with similar models.

The high evaluation accuracy of the model in this paper is because the model in this paper introduces LM algorithm on the basis of the single god meridian network and converts the network training into the least square problem. By setting the number of iterations, the LM-BP neural network is avoided to fall into the local extremum state, and the training accuracy of the model is improved.

## 5. Conclusions

This research presents an assessment model in light of the paucity of evaluation of rural planning in existing studies. A neural network evaluation model based on LM-BP is presented to increase the accuracy of rural planning evaluation. The model has three layers: input, hidden, and output. The five elements that influence rural planning are used as input samples, and estimation results are obtained via hidden layer learning. In this process, the model in this paper transforms the neural network training into the least square problem, which effectively shortens the network convergence time and improves the training efficiency, which is one of the characteristics of the model in this paper. At the same time, the model in this paper sets the iteration times of network training to avoid local extreme values of the LM-BP neural network. When the iteration times of LM-BP neural network training reach a fixed limit, the test is stopped, and new weights and thresholds are assigned to LM-BP neural network training to start new iterative training and stop when the desired results are obtained. This is another characteristic of the model in this paper. Through this step, the problem that the neural network easily falls into local extremum is solved. This methodology achieves efficient and accurate rural planning evaluation based on these two criteria. The findings demonstrate that this model's predicted value is nearly identical to the actual value, and it has a greater prediction accuracy than a similar model. This model meets the needs of planning evaluation in terms of

evaluation accuracy and efficiency and provides scientific analysis basis for rural planning.

## Data Availability

The datasets used during the current study are available from the corresponding author on reasonable request.

## Conflicts of Interest

The authors declare that they have no conflict of interest.

## References

- [1] Y. Liu, T. Luo, Z. Liu, X. Kong, J. Li, and R. Tan, "A comparative analysis of urban and rural construction land use change and driving forces: implications for urban-rural coordination development in Wuhan, Central China," *Habitat International*, vol. 47, pp. 113–125, 2015.
- [2] Q. He, S. Tan, C. Yin, and M. Zhou, "Collaborative optimization of rural residential land consolidation and urban construction land expansion: a case study of Huangpi in Wuhan, China," *Computers, Environment and Urban Systems*, vol. 74, pp. 218–228, 2019.
- [3] R. Pheasant, K. Horoshenkov, G. Watts, and B. Barrett, "The acoustic and visual factors influencing the construction of tranquil space in urban and rural environments tranquil spaces-quiet places?," *The Journal of the Acoustical Society of America*, vol. 123, no. 3, pp. 1446–1457, 2008.
- [4] Y. Tang, R. J. Mason, and P. Sun, "Interest distribution in the process of coordination of urban and rural construction land in China," *Habitat International*, vol. 36, no. 3, pp. 388–395, 2012.
- [5] W. S. Tang and H. Chung, "Rural–urban transition in China: illegal land use and construction," *Asia Pacific Viewpoint*, vol. 43, no. 1, pp. 43–62, 2002.
- [6] Y. Wei, C. Huang, J. Li, and L. Xie, "An evaluation model for urban carrying capacity: A case study of China's mega- cities," *Habitat International*, vol. 53, pp. 87–96, 2016.
- [7] J. Liu, Y. Liu, and X. Wang, "An environmental assessment model of construction and demolition waste based on system dynamics: a case study in Guangzhou," *Environmental Science and Pollution Research*, vol. 27, no. 30, pp. 37237–37259, 2020.
- [8] X. Zhang, S. Du, and Z. Zheng, "Heuristic sample learning for complex urban scenes: Application to urban functional-zone mapping with VHR images and POI data," *ISPRS Journal of Photogrammetry and Remote Sensing*, vol. 161, pp. 1–12, 2020.
- [9] X. Hong-Juan, "The study on rural transition and planning tactics in the Pearl Delta Area," *Modern Urban Research*, vol. 28, no. 6, pp. 41–45, 2013.
- [10] C. Y. Cheng and X. Qian, "Evaluation of emergency planning for water pollution incidents in reservoir based on fuzzy comprehensive assessment," *Procedia Environmental Sciences*, vol. 2, pp. 566–570, 2010.
- [11] Q. Yanbo, J. Guanghui, T. Yaya, Shang Ran, W. Shuwen, and L. Yuling, "Urban - rural construction land transition(URCLT) in Shandong Province of China: features measurement and mechanism exploration," *Habitat International*, vol. 86, pp. 101–115, 2019.
- [12] E. G. Guba and Y. S. Lincoln, *Fourth generation evaluation*, Sage, 1989.

## Retraction

# Retracted: Innovation of Ideological and Political Education Management of College Students Based on IOT Big Data Technology in a Wireless Network Environment

### Computational and Mathematical Methods in Medicine

Received 25 July 2023; Accepted 25 July 2023; Published 26 July 2023

Copyright © 2023 Computational and Mathematical Methods in Medicine. This is an open access article distributed under the Creative Commons Attribution License, which permits unrestricted use, distribution, and reproduction in any medium, provided the original work is properly cited.

This article has been retracted by Hindawi following an investigation undertaken by the publisher [1]. This investigation has uncovered evidence of one or more of the following indicators of systematic manipulation of the publication process:

- (1) Discrepancies in scope
- (2) Discrepancies in the description of the research reported
- (3) Discrepancies between the availability of data and the research described
- (4) Inappropriate citations
- (5) Incoherent, meaningless and/or irrelevant content included in the article
- (6) Peer-review manipulation

The presence of these indicators undermines our confidence in the integrity of the article's content and we cannot, therefore, vouch for its reliability. Please note that this notice is intended solely to alert readers that the content of this article is unreliable. We have not investigated whether authors were aware of or involved in the systematic manipulation of the publication process.

In addition, our investigation has also shown that one or more of the following human-subject reporting requirements has not been met in this article: ethical approval by an Institutional Review Board (IRB) committee or equivalent, patient/participant consent to participate, and/or agreement to publish patient/participant details (where relevant).

Wiley and Hindawi regrets that the usual quality checks did not identify these issues before publication and have since put additional measures in place to safeguard research integrity.

We wish to credit our own Research Integrity and Research Publishing teams and anonymous and named external researchers and research integrity experts for contributing to this investigation.

The corresponding author, as the representative of all authors, has been given the opportunity to register their agreement or disagreement to this retraction. We have kept a record of any response received.

### References

- [1] Z. Du, "Innovation of Ideological and Political Education Management of College Students Based on IOT Big Data Technology in a Wireless Network Environment," *Computational and Mathematical Methods in Medicine*, vol. 2022, Article ID 9585760, 8 pages, 2022.

## Research Article

# Innovation of Ideological and Political Education Management of College Students Based on IOT Big Data Technology in a Wireless Network Environment

Zheng Du 

Jinhua Education College, Jinhua, 321000 Zhejiang, China

Correspondence should be addressed to Zheng Du; 20050081@jhc.edu.cn

Received 1 April 2022; Revised 3 May 2022; Accepted 7 May 2022; Published 9 June 2022

Academic Editor: Naeem Jan

Copyright © 2022 Zheng Du. This is an open access article distributed under the Creative Commons Attribution License, which permits unrestricted use, distribution, and reproduction in any medium, provided the original work is properly cited.

Universities are not only the front line of national ideological and political works but also the gathering place of national talent training, which is of far-reaching significance to the national strategic development, and it is vital to do a good job of ideological and political education in universities for the construction and development of the country. “The university has become a place where wireless network technology can be used. The paper examines the current state of mobile learning in the United States and abroad, explains the principles for developing a mobile ideological and political learning system, designs and studies the system’s overall structure and functional modules, and shows how the system’s application can replace traditional ideological and political learning methods, allowing students to improve their ideological and political abilities using mobile devices.

## 1. Introduction

With the rapid development of information technology and the information industry, the demands on network communications are increasing and wireless networking technology is making up for the shortcomings of traditional network technology and a radio can be used to great effect both over long distances and in close proximity [1]. The uses are very similar to those of limited networks. The major difference lies in the transmission medium [2]. The use of radio technology instead of a network can be used as a backup to a wired network. Ideological and political education is to analyze the different kinds of human needs and then distinguish between reasonable and unreasonable needs and different levels of needs, so as to carry out ideological and political education and solve the problem of unmet needs or the problem of different needs being met one after another [3]. The leading role of the ideological and political education of university students is to play a positive role in promoting the comprehensive, coordinated, and sustainable development of students [4–7].

The Internet has gradually replaced the radio and television as the main channels for people, especially young people, to obtain information in their daily lives [8]. People have recognized the convenience of the Internet, and the ease of access to wireless networks implies that university students have more flexibility of choice [9]. Wireless network technology provides university students with access to information not only in terms of time and space but also in terms of content and form, providing them with a rich and complex range of sources from mobile phones, tablets, laptops, and desktop computers. While network technology is developing at a rapid pace, the network environment is not optimistic, especially as many unscrupulous elements are promoting extremist ideas on the network or taking advantage of students’ gullible personalities to commit network fraud [10].

It is more likely to be incited by socially undesirable ideas. Wireless network technology has not only brought the people the convenience of updating their thoughts [11]. Many unscrupulous elements precisely use college students’ ears to think simple and other characteristics, propagating their bad speech to achieve its profiteering to disturb the social order [12–15].

The teaching mode is more conservative compared to other disciplines. The content is more serious. There is a lot of theoretical content. Students find it difficult to understand. The efficiency of the classroom is low, and many of the ideological and political theory classes have become “disaster areas” where students are absent from the class. Students are active and have a strong sense of thinking. With the development of the times, students receive a huge amount of information, although they are young [16]. They are young, but their minds are mixed with a variety of ideas. To carry out ideological and political education work in colleges and universities means to do the work in the field of ideas and to guide students to receive advanced theoretical knowledge of the Communist Party of China. It is not a matter of forceful indoctrination, which would only cause resentment among students [17–20].

The paper arrangements are as follows:

Section 2 describes the ideological and political education in the environment of IoT. Section 3 defines the ideological and political education system design and implementation. Section 4 examines the intelligent recommendation algorithms for student development models based on learning trajectories. Section 5 analyzes the experimental results. Section 6 concludes the paper.

## 2. Ideological and Political Education in the Environment of IoT

This section discusses the analysis of the current situation and defines the research significance.

*2.1. Analysis of the Current Situation.* Since the 1970s, the emphasis on intelligent teaching systems has increased. In particular, Western countries such as the USA have attached particular importance to the development of intelligent education systems [21]. These countries have strong economic power, and science and technology have driven the development of intelligent market industries, as well as optimizing the design of intelligent education systems. With the advancement of the Internet of things technology, intelligent teaching systems are gradually being applied to school teaching in the United States, primarily for physics, chemistry, and other science services [22]. Intelligent science services can be simulated through the system to improve professional teaching services, and with the advancement of the Internet of things technology, intelligent teaching systems are gradually being applied to school teaching, with great success. Compared with this, China’s intelligent teaching system still needs a breakthrough to further strengthen and improve the service function of the intelligent teaching system to provide effective services for actual teaching. At present, China’s intelligent teaching system has made a breakthrough in technology, mainly in artificial intelligence technology to assist teachers in their daily work [23]. Combined with traditional education, intelligent education is a new type of education system based on computer technology, which emphasizes the organic combination of intelligent technology and education, teachers and teaching, etc. It can improve the education system, thus strengthening

the quality of teaching and improving students’ interest in learning and enabling systematic evaluation, allowing students to learn independently and understand and master students’ abilities, especially in ideological and political education, which must be pushed forward to strengthen students’ ideological and political competencies [24, 25].

*2.2. Research Significance.* It is true that our country already has numerous online ideological and political education websites. But there are still many problems that have been revealed, which seriously affect the use of the system by students. First of all, there are regional differences. The selectivity of the teaching textbooks in the intelligent system leads to different textbooks and learning contents, and different regions use different versions of teaching materials and training programs, leading to educational ideas and regions being in “opposition.”

## 3. Ideological and Political Education System Design and Implementation

*3.1. Overall System Design.* The ideological and political education system, according to the requirement analysis, is typically employed as a learning aid and must ensure that the user experience is effective while also ensuring that its objectives are performed to the greatest extent possible. In order to simplify the overall design requirements and to research on the existing system structure, the author starts from the role of the ideological and political education system crowd; it can be concluded that there are three types of users in the system, namely, system administrators, teacher users, and student users. Each of them has a different function. By integrating the functions that have overlapping needs, the following modules are finally obtained, which are described in detail in Figure 1.

### 3.2. Function Implementation

*3.2.1. Student Management.* Student management is more targeted and based mainly on the student learning content. Ideological and political education needs to take into account students’ ability to listen, read, and write. It should enable registration and login and the viewing and modification of personal information. Also, as the core content, students can view courseware, video tutorials, test questions, and complete online quizzes. They can also view website announcements and post online responses to messages, etc. These functions certify that students can access the learning end of the system to learn effectively and achieve the resolution of independent learning, as shown in Figure 2.

In the module ideological and political education system for students to learn the main module, students first have to register and select the appropriate class and subclass learning; students can be combined with the actual ideological and political levels of communication with the class teacher, at the same time, they can be based on the stage. The system may generate reports based on student grades, and students and teachers can efficiently analyze deficiencies and provide comments on study hours based on detailed data. In

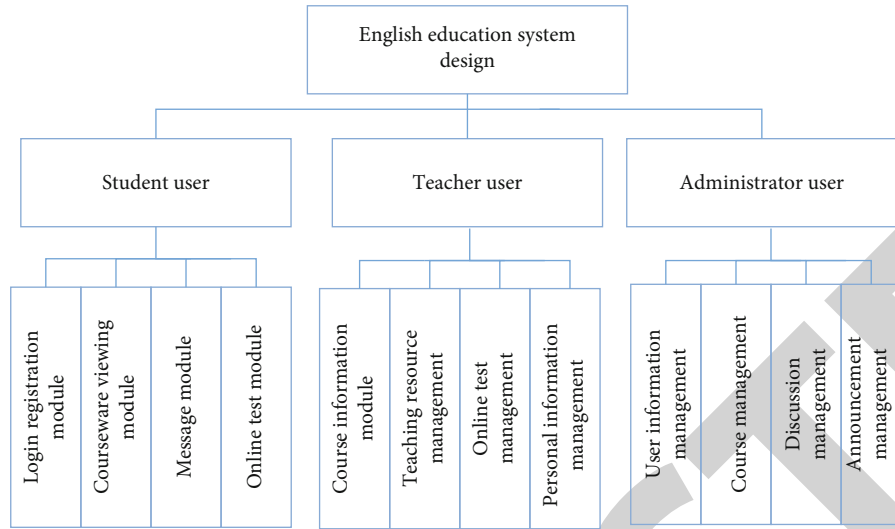


FIGURE 1: Overall design of the ideological and political education system.

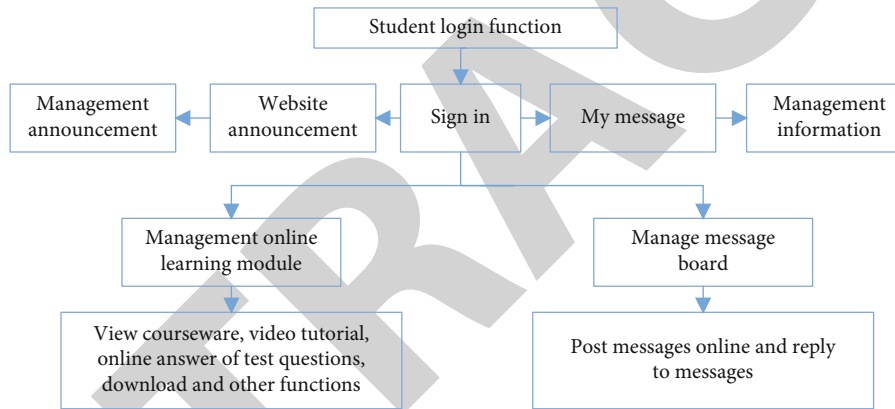


FIGURE 2: Diagram of student management.

In addition, students can upload teaching materials outside of the platform system to increase the extracurricular learning content, giving full play to the function of the ideological and political education system and thus improving students' ideological and political performance. The message board can post online, reply to messages, etc. Students can ask questions, communicate with teachers, and appear as a learning forum, while students can learn about grades, class assignments, news announcements, etc. on the message board, enabling them to keep abreast of their learning, consult with classmates and teachers, exchange learning experiences, and make full use of the system's functions [26, 27].

**3.2.2. Teacher Management/Administrator Management.** Teachers and administrators can act as the “decision makers” for the background functions. Both teachers and administrators have the ability to add, delete, and enter. The administrator can manage teacher information, student information, course information, data information, etc. in the system, as shown in Figure 3.

The administration centre is used by teachers to manage users, manage courseware, add assignments, and manage

online questions and other basic information management, and the administration message board has functions such as forum management and replying to messages. Therefore, the login functions of teachers and administrators have similarities and differences. Teachers mainly manage learning tests, teaching aids, and teaching resources, while administrators mainly add, modify, and delete information [28, 29].

#### 4. Intelligent Recommendation Algorithms for Student Development Models Based on Learning Trajectories

**4.1. Data Collection and Mining.** According to the results of the intelligent advice and the preferences of the students, the school completes the redesign of the student learning course system, provides for the appropriate professional learning, and realizes the innovation of the student training mode. The data source for this recommendation system is student information, book information, and borrowing information, and the differentiation and humanization of students' practical ties are enhanced through the use of intelligent analytic technology.

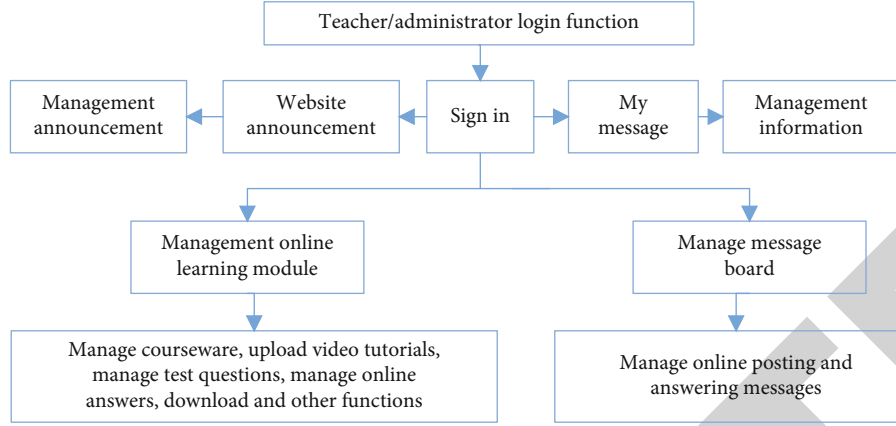


FIGURE 3: Diagram of teacher management/administrator management functions.

4.2. *Selection of Recommendation Algorithms.* The interest-based recommendation algorithm uses item-based collaborative filtering (item CF for short). The core of the algorithm is to use user behavior data to calculate the similarity between items and to make personalized recommendations based on the user's historical behavior and the item similarity matrix. When predicting user interests, it is important to consider weighing the user's recent behavior more heavily and adding temporal validity information to the user recommendation results. The core of the recommendation algorithm based on the learning trajectory is to mine the background data from students' history of book borrowing and Internet browsing on the campus for a more personalized and specialized course system, making student training more targeted and improving the quality of student training.

The item CF algorithm consists of two main steps.

(a) Calculate the similarity between items [30]

$$W(ij) = \frac{|N(i) \cap N(j)|}{\sqrt{|N(i)||N(j)|}}, \quad (1)$$

$$P(u, j) = \sum_{i \in S(j,k) \cap N(u)} W(j, i) * r(u, i).$$

#### 4.3. Improvements to Item CF

4.3.1. *Consider the Popularity of the Item [31].* In the calculation of item similarity, active users contribute more to the item similarity than inactive users and it can also be considered that the more popular the item is, the more it contributes to the calculation of item similarity. The formula for calculating item similarity is as follows:

$$w(i, j) = \frac{\sum_{u \in N(i) \cap N(j)} (1/\log(1 + |N(u)|))}{\sqrt{|N(i)||N(j)|}}, \quad (2)$$

where  $|N(u)|$  denotes the number of items of interest to user  $u$ .

4.3.2. *Time Context-Dependent Item CF Algorithm.* When calculating item similarity, it is also important to consider the effect of temporality. The closer to the current time, the more similar the item is to the user, and the formula for calculating similarity is as follows:

$$w(i, j) = \frac{\sum_{u \in N(i) \cap N(j)} \left( \frac{1/\log(1 + \alpha * |T_{u_i} - T_{u_j}|)}{\sqrt{|N(i)||N(j)|}} \right)}{\sqrt{|N(i)||N(j)|}}. \quad (3)$$

The recent behavior is more indicative of the user's current interest than the previous behavior, where the user's interest in the item  $P(u, i)$  is calculated using the following equation:

$$P(u, i) = \sum_{j \in S(i,k) \cap N(u)} W(i, j) * r(u, j) * \frac{1}{1 + \alpha(T_0 - T_{u_j})}. \quad (4)$$

## 5. Experimental Results

In the experiment, taking the software engineering course system as an example, the abovementioned recommendation algorithm is applied to improve and update the course system, which can obtain a course system more in line with individual characteristics.

As illustrated in Figure 4, the recommendation of online education is still hampered by transmission rate limitations, the use of teaching courseware, network speed issues, and other factors that impede learners' ability to learn online. As a result, in the Internet of things technology environment, an integrated examination of the ideological and political education system design is also required, so the paper uses based on B/S system framework structure construction and 3-layer logic structure, to further improve the security and applicability of the system, B/S system framework structure through the Java language programming run, can make it in the browser side, the server side of a large number of computing processing, easy to develop and maintain. Formation of the browser-side (B) - release instructions - server-side (S) - calculation results - The 3-layer structure

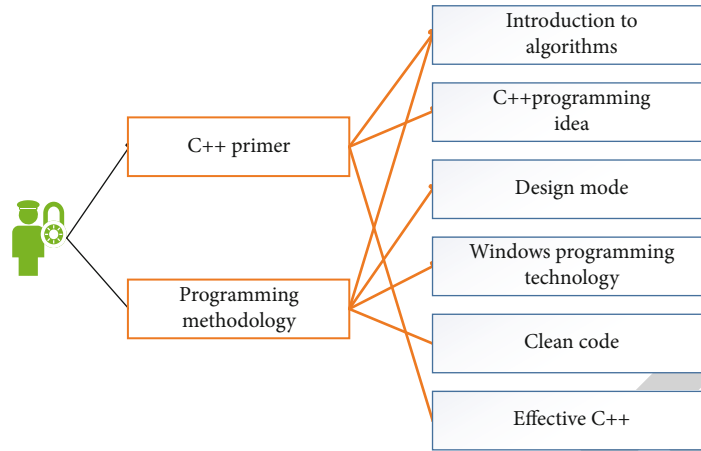


FIGURE 4: Diagram of the recommendation algorithm.

under the B/S system can form a highly cohesive and low-coupling state, further improving the performance of the ideological and political education system.

As seen in Figure 5, we believe that learning is tedious and ineffective. The “double-edged sword” of wireless network technology can be efficiently used by ideological and political education in higher education to construct an online learning platform, for example, by opening a WeChat account. Through the WeChat subscription number, we can publish weekly or monthly summaries of social and current affairs and the key arrangements of ideological and political work; we can also build a web space, upload the main contents of ideological and political education in the form of a journal, and require students to study online.

Figure 6 depicts the distribution of students’ learning interests as a useful tool for sorting out Internet information sources. Ideological and political educators in colleges and universities should pay greater attention to network information media and stay up to date on diverse topics in order to guide college students in determining what is right and incorrect. Many network information publishers are unconcerned about information’s accuracy and scientificity. As a college ideological and political educator, you should pay more attention to the information. In the classroom or during the evening roll call, they should analyze and explain inaccurate or radical comments to help students judge right and wrong. For example, during a certain period of time, students should not be misled by bad information on the Internet. For example, during a certain period of time, the international relations between China and Japan were tense. Many students on university campuses have been incited by “anti-Japanese” sentiments on the Internet. They were encouraged to take part in illegal demonstrations and even to vandalize Japanese cars and electrical shops. Ideological and political educators in universities should make use of evening roll calls and class meetings to analyze the situation. Guide students to be rational and patriotic. Avoid a situation that gets out of hand.

For example, they can check more classes, communicate more with college teachers, and strictly discipline the use of mobile phones in class, as shown in Figure 7, so as to reduce

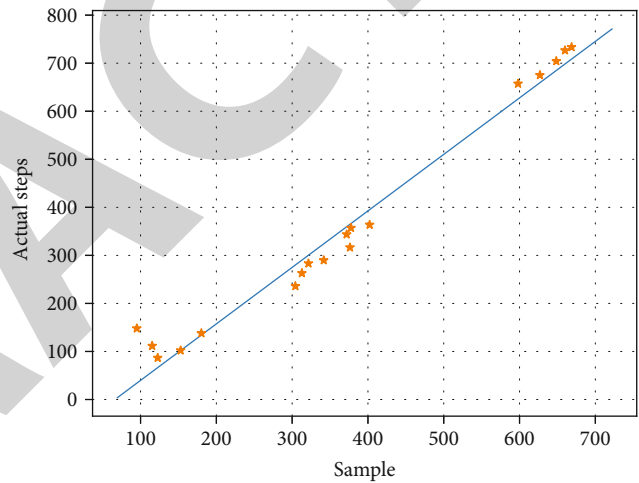


FIGURE 5: Student learning outcomes in Civics.

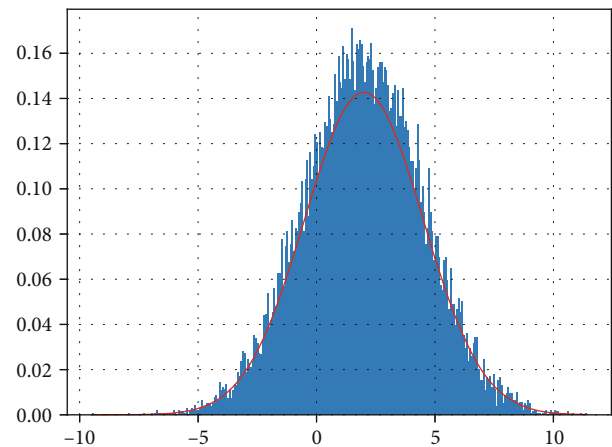


FIGURE 6: Distribution of learning interests.

the chances of students using their hand percussion in class and restore good classroom order. The majority of ideological and political educators in higher education are student

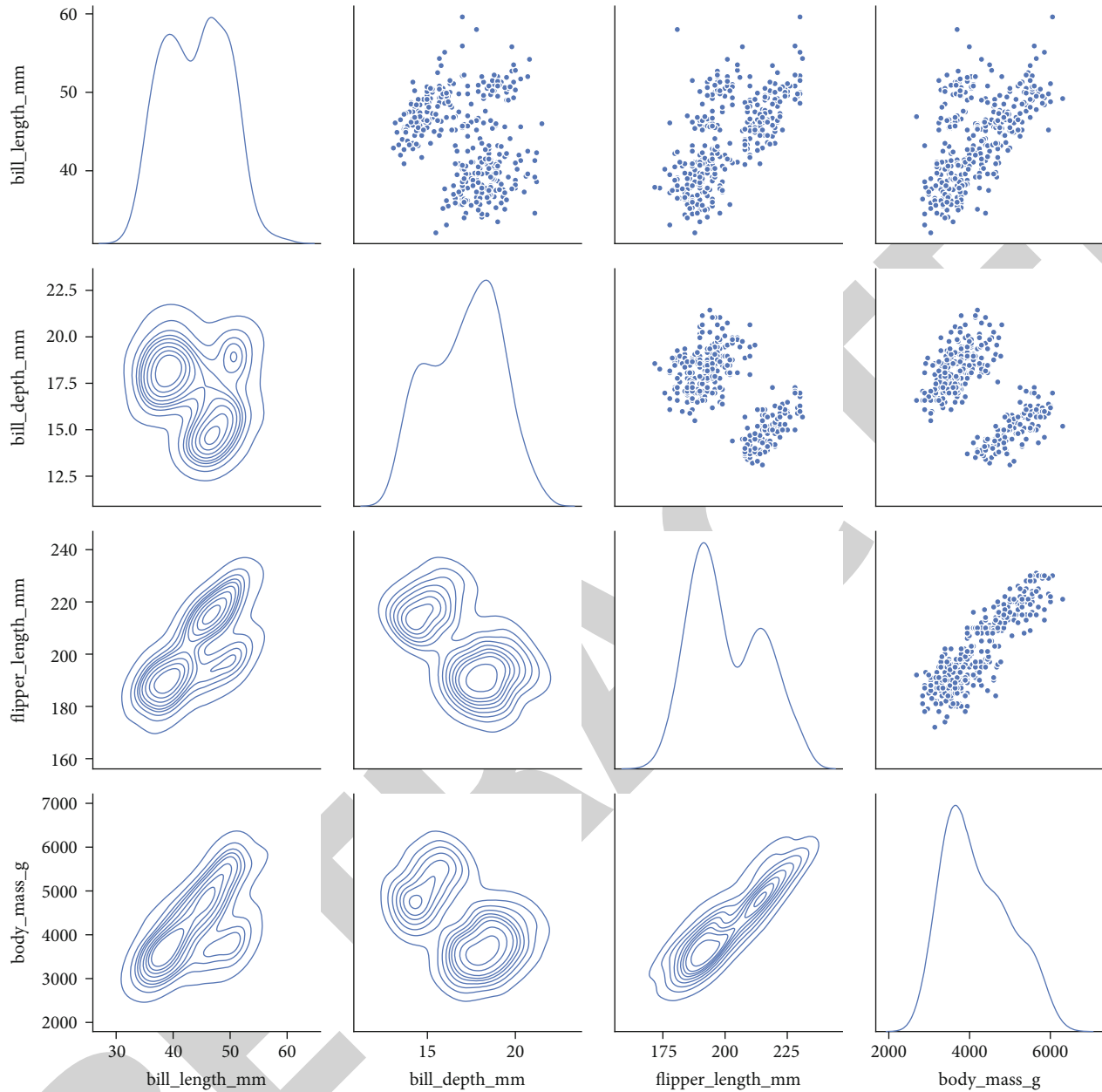


FIGURE 7: Student-teacher fit.

ideological and political counsellors, who have the most contact with students and can make use of opportunities such as evening roll calls or class meetings to strengthen education and propaganda for students to fully understand the autonomy and conscientiousness of learning.

## 6. Conclusions

With the development of Internet of things technology, education tends to be more technological and informational development, the application of the network education platform for ideological and political teaching has been achieved, and there is no doubt that the intelligent development of education is a change to the traditional ideological

and political teaching mode. The system not only provides students with individualized instruction, such as online learning, online testing, downloading, online question answering, and other services, but also serves as a showcase for wireless network technology as a gathering place for young talent. The work of ideological and political education in colleges and universities should make good use of this “double-edged sword,” so that it can play a positive role in promoting ideological and educational works.

## Data Availability

The datasets used during the current study are available from the corresponding author upon reasonable request.



## Conflicts of Interest

The author declares that there is no conflict of interest.

## References

- [1] F. Zeng and L. Liu, "Improving the quality of ideological and political education in colleges and universities in big data age," *Journal of Physics: Conference Series*, vol. 1852, no. 3, p. 032034, 2021.
- [2] C. Chen and W. Xu, "Innovation and application of college students' education and management based on big data," in *Proceedings of the 2020 The 3rd International Conference on Big Data and Education*, pp. 5–9, London, United Kingdom, 2020.
- [3] X. Pan, "Innovation of ideological and political education model in the context of big data," *International Conference on Machine Learning and Big Data Analytics for IoT Security and Privacy*, vol. 1282, pp. 326–331, 2020.
- [4] J. Wang and P. Wang, "Innovation research on big data-driven student management work in universities," in *2021 international wireless communications and mobile computing (IWCMC)*, Harbin City, China, 2021.
- [5] Y. Liu, "The innovation of college counsellor's work based on big data analysis," in *International Conference on Machine Learning and Big Data Analytics for IoT Security and Privacy*, pp. 235–241, Springer, Cham, 2020.
- [6] Q. Gao and L. Ai, "Problems of ideological and political education of college students in the era of big data," *Journal of Physics: Conference Series*, vol. 1852, no. 3, p. 032037, 2021.
- [7] D. Haoyun, "Exploration and innovation on ideological and political education from the perspective of big data," *Canadian Social Science*, vol. 11, no. 1, pp. 206–210, 2015.
- [8] S. Pu, "Political and ideological personnel management mode based on computer network," in *International Conference on Machine Learning and Big Data Analytics for IoT Security and Privacy*, vol. 1283, pp. 45–52, 2020.
- [9] Y. Cheng, "Research and design of aided instruction system of ideology course for college students based on big data analysis," in *2021 4th International Conference on Information Systems and Computer Aided Education*, pp. 341–344, Dalian, China, 2021.
- [10] L. Yalan, Z. Qingjie, and N. Lu, "Innovation of ideological and political education in big data age," *Canadian Social Science*, vol. 17, no. 1, pp. 38–43, 2021.
- [11] S. Che, M. Wang, and Y. Zhang, "Research on the strategies of college students' ideological and political education under the Internet background," in *2020 international conference on big data, artificial intelligence and internet of things engineering (ICBAIE)*, Fuzhou, China, 2020.
- [12] Z. Liu, "Research on informatization of educational management archives based on Internet+," in *2021 international conference on Internet, education and information technology (IEIT)*, Suzhou, China, 2021.
- [13] Y. Cui, "The influence of music appreciation courses on the formation of college students' ideological quality under the environment of big data," *Journal of Physics: Conference Series*, vol. 1533, no. 4, p. 042074, 2020.
- [14] J. Zhao, "Development and innovation of education management information in college with big data," in *International Conference on Machine Learning and Big Data Analytics for IoT Security and Privacy*, vol. 1282, pp. 308–313, 2020.
- [15] D. Lu and K. Wang, "Research on peer mutual aid psychological education of college students in the era of we media based on big data," in *2021 International Wireless Communications and Mobile Computing (IWCMC)*, pp. 1206–1209, Harbin City, China, 2021.
- [16] Y. Zhang, "Fusion development of ideological and political teaching with information technology in the big data era," *Journal of Physics: Conference Series*, no. 4, p. 042013, 2020.
- [17] G. Yun, V. Ravi, and K. Jumani, "Analysis of the teaching quality on deep learning-based innovative ideological political education platform," *Progress in Artificial Intelligence*, pp. 1–12, 2022.
- [18] B. Ji, Y. Li, C. Cao, S. Li, D. Mumtaz, and D. Wang, "Security performance analysis of UAV assisted relay transmission for cognitive network with energy harvesting," *IEEE Transactions on Vehicular Technology*, vol. 69, no. 7, pp. 7404–7415, 2020.
- [19] J. Lin, S. Wu, S. Mumtaz, J. Garg, and M. Li, "Blockchain-based on-demand computing resource trading in IoV-assisted smart city," *IEEE Transactions on Emerging Topics in Computing*, vol. 9, no. 3, pp. 1373–1385, 2021.
- [20] Z. W. Zhang, D. Wu, and C. J. Zhang, "Study of cellular traffic prediction based on multi-channel sparse LSTM," *Computer Science*, vol. 48, no. 6, pp. 296–300, 2021.
- [21] P. An, Z. Wang, and C. Zhang, "Ensemble unsupervised auto-encoders and Gaussian mixture model for cyberattack detection," *Information Processing & Management*, vol. 59, no. 2, article 102844, 2022.
- [22] J. Li, Z. Zhou, J. Wu et al., "Decentralized on-demand energy supply for blockchain in Internet of things: a microgrids approach," *IEEE Transactions on Computational Social Systems*, vol. 6, no. 6, pp. 1395–1406, 2019.
- [23] V. Thakuriah, Y. Tilahun, and M. Zellner, "Big data and urban informatics: innovations and challenges to urban planning and knowledge discovery," *Seeing Cities through Big Data*, pp. 11–45, 2017.
- [24] C. Zhang, "Application of big data technology in financial management teaching," in *2021 International Wireless Communications and Mobile Computing (IWCMC)*, pp. 1506–1509, Harbin City, China, 2021.
- [25] T. Qian and Q. Zhang, "Research on teaching management of applied university based on big data," in *the international conference on cyber security intelligence and analytics*, vol. 1343, 2021.
- [26] S. Liu, "Research on university ideological and political education based on big data information teaching mode," in *2020 international conference on computers, information processing and advanced education (CIPAE)*, pp. 280–285, Ottawa, ON, Canada, 2020.
- [27] F. Liu, "Design of innovation and entrepreneurship teaching system for ideological and political courses in universities based on online and offline integration," in *International Conference on E-Learning, E-Education, and Online Training*, vol. 389, pp. 344–354, 2021.
- [28] Z. Ma, J. Guan, and R. Li, "Research on innovative teaching mode of art education in the age of convergence of media," *International Journal of Emerging Technologies in Learning (iJET)*, vol. 16, no. 2, pp. 272–284, 2021.
- [29] D. Qianqiu, "Exploration on the cultivation of college students' leadership under the smart campus system," in *2020 International Conference on Modern Education and Information Management (ICMEIM)*, pp. 76–79, Dalian, China, 2020.

## Research Article

# Application of New Media in Student Management from the Perspective of Deep Learning and Evaluation and Analysis of Practical Effects

Danjun Ji, Xuejiao Wang, and Tianyu Zhang 

*School of Literature and Journalism, Sanjiang University, Nanjing, Jiangsu 210012, China*

Correspondence should be addressed to Tianyu Zhang; 2009040141@st.btbu.edu.cn

Received 27 April 2022; Revised 24 May 2022; Accepted 28 May 2022; Published 9 June 2022

Academic Editor: Naeem Jan

Copyright © 2022 Danjun Ji et al. This is an open access article distributed under the Creative Commons Attribution License, which permits unrestricted use, distribution, and reproduction in any medium, provided the original work is properly cited.

New media has become incorporated into people's lives as a result of its advent and great popularity. Students make substantial use of new media, and using it for student management necessitates social attention and assistance. It has to do with the management effect of colleges and universities, as well as the development of college students and societal harmony and advancement. Under the new media environment, student management workers should apply new media to daily student management work on the basis of traditional student management work methods, carry out new extensions and expansions, and use various forms of new media platforms as working methods and means. To carry out student work to improve the efficiency and effectiveness of student management work, in this context, this paper uses deep learning to carry out the application and practical effect evaluation of new media in student management and completes the following work: (1) This paper examines and discusses the development history, concept, connotation, and characteristics of new media using the literature analysis approach. The literature is used to synthesize the study findings of contemporary academic circles on the management of student issues in the new media environment. (2) The related technologies of BPNN are introduced, the evaluation index of the application effect of new media on student management work is constructed, and then, the appropriate BPNN structure is designed. (3) Experiments are carried out with the self-designed data set. The results of the experiments reveal that the model proposed in this research has a low error and good performance.

## 1. Introduction

In this rapidly developing society of digital technology and new media technology, all kinds of media information have enriched people's information resources. The majority of young college students are one of the groups that use new media widely and have been integrated into the new media era [1]. How to use new media to serve student management and open up a new situation of new media platform education has become a new topic for student management workers in colleges and universities. There are now over 750 million Chinese netizens, 720 million mobile netizens, and more than 50 percent Internet penetration in China, according to a CNNIC report issued in August 2017 entitled "Statistics on the Internet Development in China." In terms

of age structure, Chinese netizens are mainly 10-39 years old, accounting for about 70% of the total, among which the 20-29 age group accounts for the highest proportion of netizens, close to 30. In terms of occupational structure, netizens have the largest group of middle school students, accounting for about 25%. Among the student groups of Chinese netizens, college students are one of the subjects who use new media. The emergence of new media has changed the way of information production and dissemination and has formed a variety of publicity media including Weibo, WeChat public account, and website, which has brought an impact on the management of college students [2]. For example, many colleges and universities still use traditional management methods, mainly relying on manpower management. But it is more of an opportunity. College

students born in the Internet age have taken the Internet and new media as part of their lives and have completely accepted new media.

New media provides colleges and universities with a more efficient and convenient management method, which enables the dissemination of traditional media content information from chain-like dissemination to network dissemination, which speeds up the speed and breadth of information dissemination and expands the influence of information [3]. The management of students in colleges and universities should make full use of this information dissemination tool to realize the informatization of student management. It is practical and feasible to use new media for student management, and it has a certain material basis. At present, “post-90s” college students are the main body of contact and use of new media, and mobile phones and tablet computers are the main forms of new media, and these new media terminals are widely owned by college students and young teachers, especially college students’ mobile phone ownership rate is very high, which lays a solid material foundation for the application of new media to student management [4]. To break through the restrictions of time and distance, the new media can be easily carried and used, and the costs of new media information transmission are cheap, paving the way for the use of new media in student management. According to the “Higher Education Law” of my nation, the purpose of higher education is to educate highly skilled specialists with a creative spirit and practical aptitude, to foster a culture of science and technology, and to advance socialist modernization [5]. Numerous educational institutions use new media in their everyday operations to better manage college students, and this has resulted in an increase in student management efficiency as well as an increase in the effectiveness of the methods they use. The emergence of new media has also made it more difficult for colleges and universities to govern their operations, and many institutions lack the backing of solid ideas and management practices [6]. This paper takes the management of college students as the research object and analyzes the relatively backward management mode in the new media environment.

It argues that current management is complicated by the management environment, that managers lack knowledge of new media management, that managers’ authority has eroded, and that individual students are preoccupied with issues such as the network, and then proposes a path for innovative management, and then uses deep learning to evaluate the value of new media in student management work. Dissemination of information occurs quickly and over a broad spectrum in the new media environment. In order to effectively manage college students, a university student management system must incorporate new media, constantly innovate management concepts and methods, fully utilize new media, and correctly understand the characteristics, development laws, and trends of new media. Excellent student management is a must in the age of social media [7]. As a result, one of the most pressing concerns confronting today’s student employees is how to make the best use of digital media in overseeing college students.

The paper’s organization paragraph is as follows: The related work is presented in Section 2. Section 3 analyzes the methods of the proposed work. Section 4 discusses the experiments and results. Finally, in Section 5, the research work is concluded.

## 2. Related Work

Although the time from the emergence, development, and widespread application of new media is relatively short, it has already received widespread attention from the society. Domestic scholars engaged in new media research have already formed a lot of research results. Regarding the definition of the concept of new media, scholars differ in terms of understanding and interpretation. At present, the academic circle has not formed a relatively unified concept expression. Reference [8] explains the concept of new media from four aspects: first, new media should be digital and highly interactive; second, new media is changing with technological development; third, so-called new media should adopt international standards as the judgment criteria; fourth, terminals are used to access information and services provided by terminals in new media. Reference [9] believes that the concept of new media is constantly developing, and new media has different forms of expression in different time periods. There are two types of new media: broad and narrow. In the broad sense, “new media” refers to new forms of communication or media based on digital, network, and other technologies; in the restricted sense, “new media” refers to “developing media.” Compared with traditional media such as newspapers, TV, and radio, new media is a communication platform that provides users with information and services based on digital technology, using mobile communication channels such as the Internet, and using computers and mobile phones as terminals [10]. Regarding the research on the manifestations of new media, reference [11] believes that the manifestations of new media include teletext, optical fiber cable communication network, computer communication network, TV, mobile phone, large-scale computer database communication system, multimedia information interactive platform, satellite live TV system, Internet, and multimedia technology broadcasting. There has been much study done on the coupling of new media and higher education, with an emphasis on the influence of new media on college students’ ideological and political education, and how to lead college students ideologically in the new media environment. Most of the research is still at the level of theoretical research, and there are very few researches that really apply and test new media in practical work. There is a lot of attention on two components of college student affairs management research.

On one side, it highlights and examines problems with college and university administration’s student affairs policies. According to reference, traditional college student affairs management in our country has flaws with the system, concept, and team structure. College administrators should adopt the management philosophy of “people-oriented” so that students have greater possibilities to participate in school management. Provide students with a good

campus environment, cultivate students' self-awareness, encourage students to start their own businesses, and provide students with a platform for free development. On the other hand, it studies the management mode of college students. Reference [12] proposed that colleges and universities should change the simple management method, add services to the traditional "education-management" model, and take "student development" as the core of student management. Research on new media and student affairs management. The rise and wide application of new media in China has been relatively short. In recent years, my country's new media technology has made great progress, but the systematic research on new media applications is in its infancy. Reference [13] analyzed the impact of new media on the management of student affairs in colleges and universities and summed up three ways that current college student affairs management workers treat new media: one is to resist some new media with bad information; tired of dealing with the negative information on the new media; and thirdly, only hope to release information through some functions of the new media.

Reference [14] analyzed the characteristics of new media and the impact of new media on college students and analyzed the student service mechanism, news release mechanism, opinion hearing mechanism, leadership reception mechanism, democratic evaluation mechanism, emergency handling mechanism, and network literacy. The establishment of management mechanism makes suggestions to colleges and universities. According to reference [15], new media will present chances and problems for college students' work. New media qualities such as immediacy, variety, and equal communication, for example, provide a new platform for the creation of working methods and student affairs management methods in colleges and universities. In the United States, student management work is called student affairs management, which is similar to the student management work in Chinese universities in terms of work object, nature, content, and scope [16]. Reference [17] defines student affairs as follows. Student affairs are used to describe the organizational units and machines that are responsible for students' extraclassroom education and also include in-classroom education. In the management of student affairs in western developed countries, especially in the higher education in the United States, there is already a relatively complete theoretical and practical system, and the enterprising spirit and open tradition have achieved the first-class education status of the United States. The United States is a multiethnic and multicultural country, and politically, it is a country of decentralization. In this context, the management of student affairs in American colleges and universities presents the characteristics of diversity and individuality. The United States comprehensively promotes the concept of student development, educating students and serving students at the same time, and has made a new interpretation of the connotation of higher education [18–20]. By combing the above literature, it is found that scholars have paid attention to the impact of new media on colleges and universities and have carried out relevant research on how to apply new media. Studies into how students' political

and ideological perspectives are being shaped in the new media era have been quite methodical and thorough, resulting in a wealth of theoretically sound study findings

### 3. Method

In this section, we define the basic theory of BP neural network, evaluation of the application effect of new media in student management, and construction of the evaluation model in detail.

*3.1. The Basic Theory of BP Neural Network.* BPNN is one of many branches of neural network. As far as the current research situation at home and abroad, it is a relatively mature theory. The BPNN performs calculation and fitting on a large amount of data, and each calculation will modify the internal parameters to increase the overall fitting effect of the model, so that the output results continue to approach the real data. The general BPNN structure consists of three parts. The first part is the input layer, which is the input end of data import and is an  $N$ -dimensional vector; the second part is the hidden layer. The hidden layer can be a multilayer network, but the middle layer of the general one-layer structure is enough to fit any mapping relationship; the third part is the output layer, which is the mapping result of the input data, which is an  $N$ -dimensional vector. A simple neural network model with one layer in the middle is shown in Figure 1. In the network structure, the units of the same layer are not connected to each other, and the units of the adjacent layers have a transfer connection.

The mathematical model of the neuron unit is as follows:

$$y = f \left[ \sum_{i=1}^n w_i x_i - \lambda \right], \quad (1)$$

where  $y$  is the output value of the neuron in the backward direction,  $w_i$  is the connection weight coefficient between the neural unit in the front layer and the neural unit in the rear layer,  $\sum w_i$  is the weighted summation value,  $\lambda$  is the threshold set by the neural network, and  $f$  is the activation function of the neural unit. The backward output value  $\sum w_i x_i$  adjusted by the weight coefficient is compared with the set threshold  $\lambda$ .

After meeting certain conditions, the neural unit will work; otherwise, it will remain static. This working mode is essentially the input data. Perform category filtering to obtain different expected output values for input values in different categories. In a neural network, information is passed backward through the input layer through connection weight adjustment, and the neuron is activated when the weighted sum value satisfies the threshold condition.

The BPNN goes through the forward propagation process and the back propagation algorithm. The neural network first randomly assigns adjustment coefficients to the forward pass between each level and then fits the data samples. According to the comparison error between the output result and the given result, the weights of each layer are adjusted in a specific direction from the first layer along

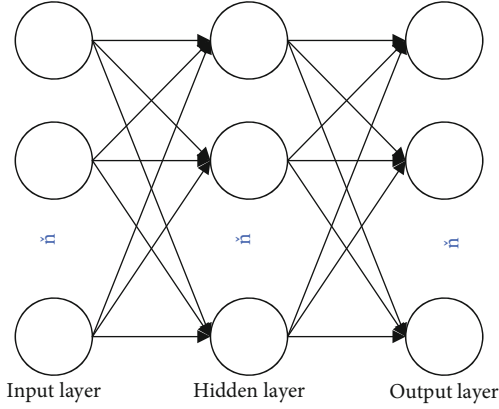


FIGURE 1: Neural network model diagram.

the middle layer to the last layer until the error reaches an ideal level. This algorithm is the error back propagation algorithm, namely, BP algorithm, and its related theory is as follows. Because the three-layer neural network is enough to simulate any mapping relationship, it is assumed that there is a three-layer network, the number of units in the first layer is  $m$ , the number of units in the second layer is  $z$ , and the number of units in the last layer is  $s$ .  $X_1, X_2, \dots, X_m$  are input data;  $H_1, H_2, \dots, H_z$  are the back-transmission data of the intermediate layer; and  $y_1, y_2, \dots, y_s$  are output data. The adjustment coefficient from the  $m$ -th first-layer unit to the  $z$ -th intermediate-layer unit is  $w_{mz}$ , the threshold of the  $z$ -th unit in the intermediate layer is  $\theta_z$ , the adjustment coefficient from the  $z$ -th intermediate-layer unit to the  $s$ -th last-layer unit is  $R_{zs}$ , and the last threshold of the  $s$ -th unit of the layer is  $\varphi_s$ ; the transfer function from the first layer to the middle layer is  $f_1$ , and the transfer function from the middle layer to the last layer is  $f_2$ . Here, tansig is selected as the transfer function for  $f_1$  and  $f_2$ . The input of the  $z$ -th unit of the second layer can be obtained:

$$\text{Net}_{\text{in}1z} = \sum_{i=1}^m x_i \cdot w_{iz}. \quad (2)$$

The output of the  $z$ -th unit of the second layer is as follows:

$$H_z = f_1[\text{Net}_{\text{in}1z} - \theta_z]. \quad (3)$$

The input to the  $s$ -th unit of the last layer is as follows:

$$\text{Net}_{\text{in}2s} = \sum_{i=1}^z H_i \cdot R_{is}. \quad (4)$$

The output of the  $s$ -th unit in the last layer is as follows:

$$Y_s = f_2[\text{Net}_{\text{in}2s} - \varphi_s]. \quad (5)$$

The output of the neural network is

$$O_s = (Y_1, Y_2, \dots, Y_s). \quad (6)$$

Calculate the error of the prediction result with the least square method:

$$E_k = \frac{1}{2} \sum_{i=1}^s (Y_i - y_i)^2. \quad (7)$$

Now adjust the parameter value according to the obtained error to reduce  $E_k$  and improve the explanatory power of the model. Obtain the partial derivative for the parameter Param that needs to be adjusted, so that the parameter changes in the opposite direction of the positive and negative signs of the partial derivative. At this time, the value of each unit change of the parameter operation is  $\partial E_k / \partial \text{Param}$ . At the same time, in order to prevent the change rate from being too fast to miss the optimal parameter setting or the solution speed that is too slow, a reasonable learning rate  $\alpha$  needs to be set. The parameter adjustment formula at this time is

$$\text{Param}' = \text{Param} - \alpha \frac{\partial E_k}{\partial \text{Param}}. \quad (8)$$

The weight adjustment from the second layer to the last layer can be obtained accordingly:

$$R'_{zs} = R_{zs} - \alpha \frac{\partial E_k}{\partial R_{zs}}. \quad (9)$$

The adjustment coefficient correction value  $\Delta R_{zs}$  from the  $z$ -th unit of the second layer to the  $s$ -th unit of the last layer is

$$\Delta R_{zs} = -\alpha \frac{\partial E_k}{\partial R_{zs}} = -\alpha \frac{\partial E_k}{\partial Y_s} \cdot \frac{\partial Y_s}{\partial \text{Net}_{\text{in}2s}} \cdot \frac{\partial \text{Net}_{\text{in}2s}}{\partial R_{zs}}. \quad (10)$$

Of which there are

$$\frac{\partial E_k}{\partial Y_s} = Y_s - y_s. \quad (11)$$

The above is the mathematical principle of the BP algorithm for parameter correction. Using the relevant network, generally only need to set the relevant index parameters, and then, the adjustment between the layers of the BPNN can be adjusted by fitting the abovementioned correction model with sufficient sample data. The coefficient is corrected and calculated, and the nonlinear mapping relationship between the input information and the output information is simulated and fitted.

### 3.2. Evaluation of the Application Effect of New Media in Student Management

**3.2.1. Diversified Types of New Media.** The "Regulations on the Administration of Students in Ordinary Institutions of Higher Education" pointed out that the management of students is to maintain the normal order of education, teaching, and life in ordinary institutions of higher learning; protect the legitimate rights and interests of students; and cultivate

socialist builders who develop in an all-round way in terms of morality, intelligence, physique, beauty, and successor. The supervision of college students is an important aspect of college administration. Because of the rapid increase of informatization and digitalization, students at colleges and universities are increasingly using mobile devices on campus, such as smartphones and tablet computers. New media is subtly changing the traditional management model of college students. Taking a university as an example, this paper investigates the current situation of using new media to carry out student management, the problems existing in the process of using new media for student management, and analyzes the reasons. The types of new media used are diversified. Currently, the more popular new media softwares include instant messaging software, video software, dating software, etc. The instant messaging software developed by Tencent is the most widely used, and QQ and WeChat are the most representative. Users can communicate instantly through mobile digital media by sending pictures, expressions, audio, video, etc. A whopping 889 million people use WeChat on a monthly basis as of December 2016. For chatting with pals, WeChat is a cutting-edge social networking app. Users can add friends and follow public platforms by searching WeChat, sharing WeChat, shaking, scanning QR code, etc., and can share with your friends by posting text, pictures, and videos in your moments. From the perspective of college student management, the WeChat platform, as a management tool, has been valued by many colleges and universities, and they have begun to use the WeChat platform to serve the management of students. We discovered through research and interviews that a certain school has begun to experiment with new media platforms to help with student management, and the sorts of use are becoming broader. The main forms of use include the establishment of theme education websites specially used for student management, such as the website of the Ministry of Student Affairs and the National Defense Education website. Different education systems also provide management services for college students through various forms such as QQ, WeChat, Weibo, and forums. Students' questionnaires can reflect this conclusion. In the interviews with teachers, the vast majority of teachers choose instant messaging tools and Weibo, post bar, forums, etc. These data show that colleges and universities have begun to use a variety of new media platforms to carry out student management work and have achieved certain results.

*3.2.2. Changes to Student Management by New Media.* Through interviews and questionnaires, we learned that the student management work of a certain school is making continuous progress relying on new media platforms. The specific manifestations are as follows:

- (1) New media promotes the digitalization and networking of student management work. We have entered the digital age, and new media makes student management work to be digitalized and networked. In the past, in order to understand the basic situation of students, the collection of student information

was in the form of a paper information registration form. The student information is now almost entirely computerized. Student information, namely, basic student information, rewards and punishments, mental health, employment, and so on, is all provided to the data platform of a digital campus of a particular school. When you need to access student information, you can utilize it to quickly search for digital data, making student management more efficient and eliminating the need for significant human labor. It simplifies a lot of repetitive work, saves manpower, reduces workload, avoids mistakes in some work, improves work efficiency, and expands the work extension space of student administrators

- (2) The new media provides a broader working platform for the management of college students. The traditional management platform for college students mainly include class meetings, school newspapers, publicity boards, symposiums, interviews, etc. These methods are limited by time and space and are relatively simple and often do not receive good educational effects. With the advent of new media, college students now have access to a platform for political and ideological education that was previously unattainable due to the constraints of time and geography. Relying on information technology, new media has the advantages of rich resources, strong interaction, and rapid dissemination compared with traditional media, creating a brand-new educational platform for college students and enabling student management workers to have a better understanding of students' needs channel. On this working platform, student management workers can carry out their work in a timely and comprehensive manner. Teachers and students can be friends on QQ and WeChat and engage on Weibo, allowing teachers to provide immediate and focused counsel to problems as they develop, influencing students' behavior, changing bad habits, and helping them progress. Student management staff use the new media platform to gather useful material to assist college students in growing up healthy and then broadcast it on the platform via text, video, audio, photos, and other means. According to statistics, there are 9 WeChat official accounts at various levels in a school, and each department also has its own WeChat official account. These official accounts have their own characteristics and push department news, student management, and student growth-related knowledge, which has a great impact on students
- (3) The new media has changed the working methods of the management of college students and promoted the communication between teachers and students. The new media has expanded the ideas of student management, integrated it into the management of students, and completely innovated the way of education. Before the new media era, an educational model centered on management educators, teaching

TABLE 1: Application of new media in student management and evaluation indicators.

Index	Label
Accelerate the collection of student information	I <sub>1</sub>
Pay attention to students' mental health in a timely manner	I <sub>2</sub>
It is convenient to record and publish reward and punishment information	I <sub>3</sub>
Follow up on student employment in a timely manner	I <sub>4</sub>
Expanded work extension space for student administrators	I <sub>5</sub>
Provide a broader working platform for college students' management work	I <sub>6</sub>
Expanded the space of ideological and political education work	I <sub>7</sub>
Timely push college-related news	I <sub>8</sub>
Flexible and diverse educational methods	I <sub>9</sub>
Students are more willing to accept new media methods	I <sub>10</sub>
Integrate various educational forces	I <sub>11</sub>
Facilitate the organization of various new media-related events	I <sub>12</sub>

materials, and classrooms was formed. To carry out managerial activities, managers primarily employed theoretical instillation and preaching. Students are in a submissive position and passively take information. Student administrators are frequently "arrogant" and require students to be managed. This concept has been dramatically transformed by the advent of new media. Workers in student management have modified their teaching techniques, included new media elements, and acted as guides in educational management activities. As a new working platform for college students' management job, new media tools like WeChat and Weibo have proved their merits. Students are ready to adopt a number of media formats in addition to conventional written language and text. For example, you can grasp the student's ideological dynamics by checking the students' QQ, Weibo, and WeChat. Send information through WeChat groups, forums, etc., and publish class dynamics, so that students can better participate in student management. The new media has provided more diverse and convenient working platforms for student management, changed the working methods of college students' management, and promoted the communication between teachers and students

- (4) The new media has formed a harmonious joint management environment. The so-called educational synergy is the comprehensive effect produced by the implementation of comprehensive education within a certain period of time and under certain conditions. This comprehensive effect is not the sum of the individual educational functions in comprehensive education, but a new educational force that is much larger than the individual educational functions. The student management work in colleges and universities can only form an educational synergy if they receive more support. New media can bind together the forces of education. First of all, parents do not need to go to school, but through

new media platforms such as WeChat and blogs, they can easily understand the situation of students in school and give feedback on problems that arise, thus forming a harmonious educational joint force between the school and parents. This new educational synergy breaks through the limitations of the traditional education model, effectively realizes the cooperation between the school and the family, and maximizes the effect of student education. Second, new media enhances cohesion. To increase their popularity and competitiveness, numerous colleges and universities now display their style through multimedia platforms such as campus networks, WeChat public platforms, and post bars. Students enthusiastically participated in many events such as college style and contestant voting, which improved the school's external image. The style is displayed inside the school via the new media platform. Activities such as the selection of "the most beautiful counselor" and "the most American military instructor" conducted by a school have enhanced cohesion within a certain range, spread positive energy, and also played a supervisory role, which is conducive to the formation of a harmonious management environment

- (5) Crisis public relation events in the age of traditional media have few communication channels, slow speed, narrow scope, and passive acceptance of information by the audience. The new media has changed the communication relationship between the media and the audience and changed the traditional discourse environment. As soon as the material is provided through new media, it is easy for other media outlets to cite and distribute it. Information is being disseminated more quickly and with a broader breadth. The audience can express their own opinions, and positive public opinion and negative public opinion are tit-for-tat, which increases the difficulty of management. As university administrators, when dealing with crisis events, they should

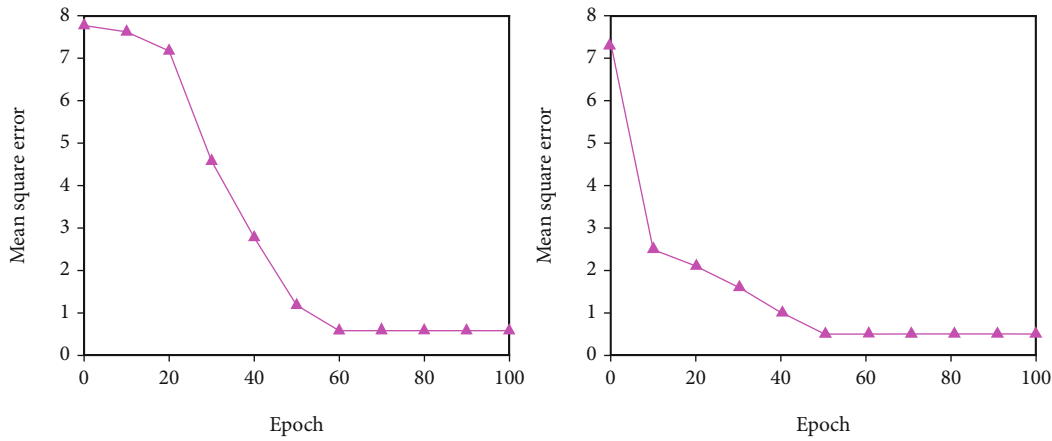


FIGURE 2: Training effect when  $N = 5$  and  $N = 7$ .

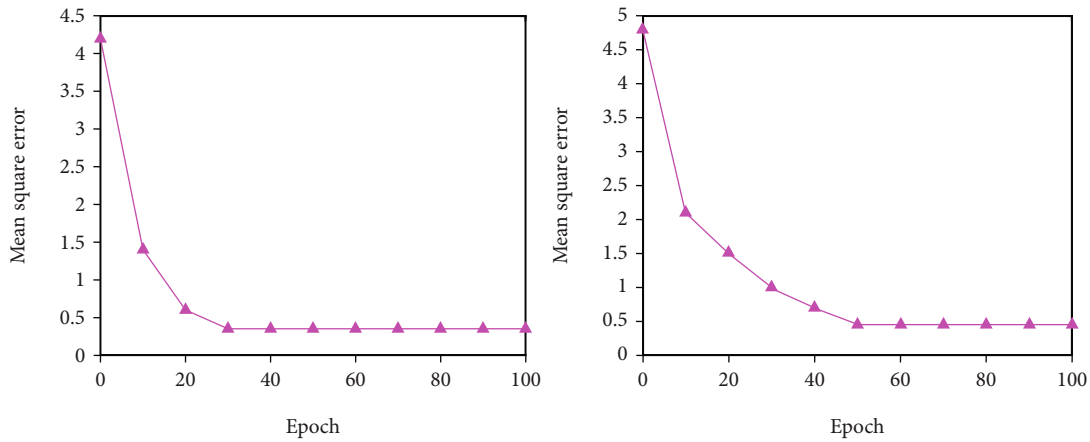


FIGURE 3: Training effect when  $N = 9$  and  $N = 11$ .

seize the right to speak as soon as possible, publish the real information of the event through new media, express their position, establish their authority in the online battlefield, guide students to correctly view emergencies, prevent students from obeying gossip and fake news, and avoid spreading the truth and triggering the escalation of the incident. Among the students of a certain school, there was a rumor that the dormitory would be adjusted on a large scale, which caused the discussion and anxiety of the majority of students. After learning about it, the student office swiftly posted official news via the WeChat public account, thereby stopping the spread of misinformation and restoring normal classroom management procedures

Through the above discussion, it can be seen that new media has been widely used in student management and has produced a very positive effect. Therefore, this paper constructs the application and effect evaluation indicators of new media in student management, as shown in Table 1. According to the corresponding input indicators, different levels of evaluation results can be obtained, which are divided into three levels.

### 3.3. Construction of the Evaluation Model

#### 3.3.1. Building the Model Framework

(1) *The Number of Layers of the BPNN Is Determined.* According to the basic theory above, this paper selects a three-layer network structure that can simulate any nonlinear mapping function, that is, a single hidden layer structure.

(2) *Determination of the Number of Input Layer Units.* According to the analysis of this paper, there are 12 indicators for the application and effect evaluation of new media in student management. Therefore, this paper sets the number of neurons in the input layer to 12.

(3) *Determination of the Number of Output Layer Units.* The purpose of constructing the BPNN model in this paper is to use relevant data to evaluate the effect of new media in student management. Therefore, the number of neurons in the output layer is 1, which is the effect level.

(4) *Calculation of the Total Number of Hidden Layer Units to Be Used.* Neural networks are better able to explain nonlinear mapping relationships when they include more hidden



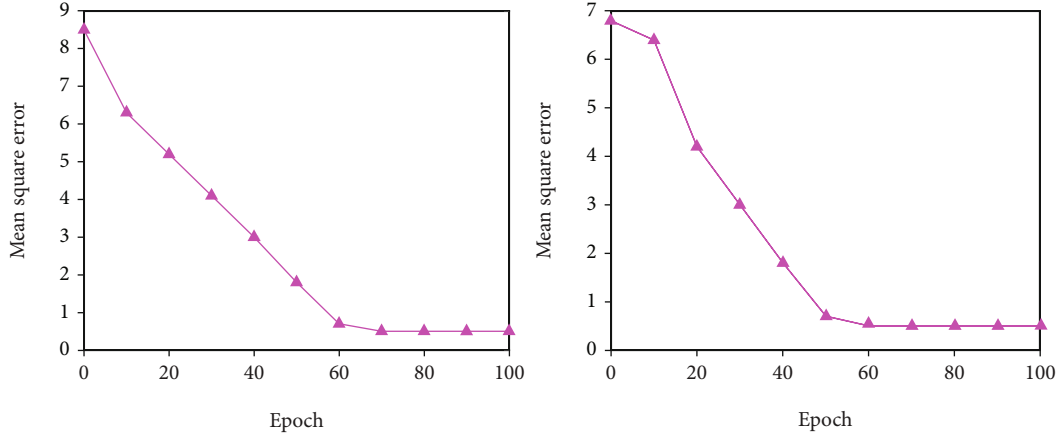


FIGURE 4: Training effect when  $N = 13$  and  $N = 15$ .

layer units. But excessive number of units will lower model training's efficiency. And the number of hidden layer units must be less than  $N - 1$ , where  $N$  is the number of training samples; otherwise, the built model cannot be generalized. This article is based on the following empirical formula:

$$h = \sqrt{m + n} + a, \quad (12)$$

where  $h$  is the number of hidden layer units,  $m$  is the number of input layer units,  $n$  is the number of output layer units, and  $a$  is an integer in the interval  $[1, 9]$ .

Start with 5 units and increase to 15 in turn to test the influence of different numbers of units on the model error, and select the number of optimal results as the number of middle-level units.

(5) *Determination of Activation Function.* In this paper, the tansig function is selected as the transfer function.

(6) *Determination of Other Parameters.* In this paper, the trainingdx algorithm is selected as the learning algorithm of the BPNN. The algorithm has a momentum project and can achieve self-adaptive adjustment. In this paper, the training accuracy is set to  $1e^{-5}$ ; that is, the error level is below 0.00001. The learning rate setting range is (0.1, 0.9), and the learning rate is the convergence distance of the model when the correction calculation is performed. A smaller learning rate will reduce the training efficiency, and a larger learning rate is not conducive to finding the optimal weight matrix. Different learning rates are tested, and the settings are selected to make the model training the most effective learning rate. Other parameters are set according to the default parameters of MATLAB and do not change.

(7) *The Input Layer of the Final Constructed Model.* The input layer of the final constructed model framework is set with 12 units, representing 12 evaluation indicators. The output layer sets 1 unit, which represents the level of the effect. The number of units in the middle layer needs to be further

confirmed in the empirical process. The transfer functions from the input layer unit to the middle layer unit and the middle layer unit to the output layer unit are all tansig functions, and the learning algorithm is the trainingdx algorithm.

### 3.3.2. Simulation of the Model

(1) *Preprocessing of Sample Data.* Because the meanings of the data in each dimension in the indicator system are different, the units used are also very different. At the same time, the internal transfer of the model and the range of the activation function have limits. To construct a real mapping relationship, it is necessary to standardize the input range. The processed input will render the built model meaningless, and the input data needs to be processed. The processing method selected in this paper is normalization processing, which converts data of different dimensions into similar data structures.

(2) *BPNN Training.* In this paper, a trainable feedforward neural network is established through the newf function, and then, the trained model is saved.

(3) *Simulation Output.* Input the data of the sample to be tested into the trained BPNN, use the neural network model to calculate the predicted target value through the sim function, and then denormalize the predicted value to obtain the evaluation value. It is the evaluation value of the application and effect of new media on student management work.

## 4. Experiment and Analysis

4.1. *Dataset and Simulation of BP Neural Network Model.* All of the experimental data in this study comes from a university questionnaire survey, and the necessary big data is then arranged into a data set of 200 training sets and 40 test sets. The analog input command sets the relevant basic parameters. Since the predicted target value is based on the effect evaluation level, the output dimension is 1. The transfer function between each level adopts the tansig function. The result update frequency display is set to update the

TABLE 2: Comparison of BP model output and expert evaluation results.

Number	1	2	3	4	5	6	7	8
Expert evaluation	0.75	0.77	0.85	0.88	0.92	0.63	0.71	0.66
Model output	0.73	0.76	0.85	0.90	0.92	0.61	0.73	0.65

training results every 400 iterations. Due to the complexity of the sample data, in order to obtain more accurate training results, the number of iterations of the initial training is set to 5000 times. The training error target of the neural network is set to  $1e^{-5}$ , which is 0.00001. This error level can better reflect the simulation degree of the model and increase the reliability of the model. The gradient index used to detect the generalization ability of the model is set to  $1e^{-6}$ . The generalization ability index is used to prevent the model from falling into a local minimum. The model stops running when the error reduction degree of the model training does not meet the defined generalization ability index. The trial-and-error method was used to conduct experiments with various numbers of middle-layer units, and the number of hidden layer units that made the model fit ideally was chosen as the number of middle-layer units in the BPNN model in this study. The relationship between the number of hidden layer units and the training error is shown in Figures 2–4. The number of nodes chosen for trials is 5, 7, 9, 11, 13, and 15. The training error reaches a minimum value when the number of hidden layer units is 9, as seen in the figure; hence, this study sets the number of hidden layer units to 9.

After trial-and-error experiments, it was found that too large a learning rate could easily make the neural network fall into a local minimum. When the learning rate is 0.4, the training error reaches the maximum value, and when the learning rate is 0.1, 0.2, 0.4, 0.5, and 0.7, the training error is very close, because the smaller the learning rate, the less likely the model will fall into the regional minimum value. Therefore, in order to obtain a better training effect, this paper sets the learning rate to 0.1.

The number of hidden layer units is set to 9 as described above, and the learning rate of the model is set to 0.1. After setting the relevant basic parameters, use the `newff` command to construct the BPNN, and set the neural network training function to the `trainingdx` function. After constructing the BPNN, use the `train` command to run the MATLABR2020b program to train the model. The model's interpretation degree when the training is completed is  $R = 0.9999$ , according to the program's running results. The model's training accuracy is very good, and it has a strong ability to sample data, as can be observed. The trained evaluation model can better reflect the nonlinear mapping relationship between the input index and the output index of the sample data. Store the trained BPNN model. At this time, the BPNN model has been completed. You can input new sample data through the model to predict the evaluation level of the application effect of the new sample.

4.2. *Experimental Results of the BP Model.* Input the sample data to be tested, use the `sim` simulation function to input

the data, output the evaluation result data through the BPNN model, and then denormalize the obtained predicted output value through the `postmnmx` inverse normalization function, and finally obtain the predicted output value to be tested. The BPNN model predicts the sample output value, which is the evaluation level of the application influence of new media in student management job. The results of this evaluation are shown in Table 2. The relevant data will be graded by school leaders and experts engaged in student management and compared with the experimental results obtained by the BPNN proposed in this paper. It can be seen from the experimental results that the error between the results obtained by the model proposed in this paper and the results evaluated by experts is very small, indicating that the BP model has superior performance.

## 5. Conclusion

New media has infiltrated every nook and cranny of people's lives, impacting every element of their existence. College students' thinking, study, living, and behavior habits have all been substantially influenced by the use of new media. The new media has opened up a plethora of possibilities for student affairs management, increased work efficiency, and reduced the gap between students and professors. Student affairs management is no longer limited by time and space, so that student affairs management workers can communicate with students, understand and mastering the situation of students, and also provide a convenient channel for students to communicate with student affairs management workers on an equal footing. The diversity of new media also provides a good platform for innovation in student affairs management. But at the same time, we cannot ignore the negative impact of new media on student affairs management. The intricate information provided by the new media dazzles the students who are not strong in screening ability and are easily confused and misled, which affects the growth and success of college students. As a result, it is critical to employ new media in student affairs administration. This study looks into and evaluates the current state of college students' use of new media, as well as the importance of incorporating new media into college student affairs management. The neural network is used to evaluate the effect of new media in student management, and the following work is finally completed: (1) This paper uses the literature analysis method to systematically study the development history, concept, connotation, and characteristics of new media and conduct a more in-depth study discussion. The research results of the current academic circles on the management of student affairs in the new media environment are summarized by referring to the literature. (2) The relevant BPNN technologies are introduced, followed by the construction of an assessment index for the application effect of new media on student management work and the design of an appropriate BP network structure. (3) Experiments are carried out with the self-designed data set. The experimental results show that the model designed in this paper has a small error and good performance.

## Data Availability

The datasets used during the current study are available from the corresponding author on reasonable request.

## Conflicts of Interest

The authors declare that they have no conflicts of interest.

## References

- [1] C. C. Self, "Hegel, Habermas, and community: the public in the new media era," *International Journal of Strategic Communication*, vol. 4, no. 2, pp. 78–92, 2010.
- [2] Q. Y. Guo, "Student management in the new media environment," *Journal of Chifeng University*, vol. 37, no. 8, pp. 241–242, 2016.
- [3] Y. Yu, "On the ideological and political education of college students in the new media era," *Open Journal of Social Sciences*, vol. 10, no. 1, pp. 1–14, 2022.
- [4] Z. Yin, "New media perspective of the process of university emergency management information and its optimization," *Agro Food Industry Hi-Tech*, vol. 28, no. 1, pp. 3190–3191, 2017.
- [5] Y. Richen, "Research on the innovative path of ideological and political work of college students of ethnic minorities from the perspective of national unity," *The Theory and Practice of Innovation and Entrepreneurship*, vol. 3, no. 12, p. 131, 2020.
- [6] M. Gong and L. Zuo, "Research on college students' ideological and political education in the new media era," *Creative Education*, vol. 11, no. 6, pp. 881–884, 2020.
- [7] L. Zhang, "Analysis on penetrative effects of new media on ideological and political education of universities and colleges," *Open Journal of Social Sciences*, vol. 3, no. 12, pp. 207–211, 2015.
- [8] Y. Zhang, "Research on the innovation of college students' ideological and political education in big data era," *DEStech Transactions on Computer Science and Engineering*, vol. 21, p. 143, 2017.
- [9] W. Hengbing, "The mechanism of ideological-political education exchange and sharing platform in colleges under the new media era based on Internet web technology," *Revista de Cercetare și Intervenție Socială*, vol. 63, pp. 85–104, 2018.
- [10] J. Song and J. Li, "Research on the coordinated development of multiple platforms of ideological and political courses in the new era," *Open Access Library Journal*, vol. 9, no. 3, pp. 1–7, 2022.
- [11] Z. Li, J. Zhang, and B. Duan, "Means of ideological and political education in colleges and universities under the new media environment," *Transactions on Computer Science and Technology*, vol. 7, no. 1, p. 5, 2019.
- [12] H. Ai, "The influence of new media on college students' ideological and political education and the countermeasures," *Journal of Contemporary Educational Research*, vol. 5, no. 5, pp. 44–46, 2021.
- [13] H. L. Bai, "Research on the challenges and countermeasures of college student management in the new media environment," *Journal of News Research*, vol. 13, no. 1, pp. 202–204, 2022.
- [14] X. Ye, "Research on effective countermeasures for college student management in the new media environment," *Journal of Liaoning Agricultural Technical College*, vol. 18, no. 1, pp. 48–49, 2016.
- [15] L. P. Tang, "Challenges and countermeasures of higher vocational student management in the new media environment," *Industrial & Science Tribune*, vol. 21, no. 1, pp. 281–282, 2022.
- [16] S. D. Adams, S. Hazelwood, and B. Hayden, "Student affairs case management: merging social work theory with student affairs practice," *Journal of Student Affairs Research and Practice*, vol. 51, no. 4, pp. 446–458, 2014.
- [17] A. M. Abdulazeez, S. R. M. Zeebaree, and M. A. M. Sadeeq, "Design and implementation of electronic student affairs system," *Academic Journal of Nawroz University*, vol. 7, no. 3, pp. 66–73, 2018.
- [18] B. Ji, Y. Li, D. Cao, C. Li, S. Mumtaz, and D. Wang, "Secrecy performance analysis of UAV assisted relay transmission for cognitive network with energy harvesting," *IEEE Transactions on Vehicular Technology*, vol. 69, no. 7, pp. 7404–7415, 2020.
- [19] X. Lin, J. Wu, S. Mumtaz, S. Garg, J. Li, and M. Guizani, "Blockchain-based on-demand computing resource trading in IoV-assisted smart city," *IEEE Transactions on Emerging Topics in Computing*, vol. 9, no. 3, pp. 1373–1385, 2021.
- [20] J. Pei, K. Zhong, M. A. Jan, and J. Li, "Personalized federated learning framework for network traffic anomaly detection," *Computer Networks*, vol. 209, article 108906, 2022.

## Research Article

# Immediate versus Delayed Implantation for Single-Tooth Restoration of Maxillary Anterior Teeth: A Comparative Analysis on Efficacy

Zhimin Chen , Shuhuai Zhang, Jun Zhou, and Hongling Liang

Department of Stomatology, Suzhou Kowloon Hospital, Shanghai Jiaotong University School of Medicine, Suzhou, 215028 Jiangsu Province, China

Correspondence should be addressed to Zhimin Chen; [chenzm1208@163.com](mailto:chenzm1208@163.com)

Received 6 April 2022; Revised 11 May 2022; Accepted 17 May 2022; Published 9 June 2022

Academic Editor: Naeem Jan

Copyright © 2022 Zhimin Chen et al. This is an open access article distributed under the Creative Commons Attribution License, which permits unrestricted use, distribution, and reproduction in any medium, provided the original work is properly cited.

**Objective.** The present research is aimed at determining the efficacy of immediate implantation (II) and delayed implantation (DI) for single-tooth restoration of maxillary anterior teeth. **Methods.** From February 2019 to June 2020, 80 patients who received single-tooth restoration of maxillary anterior teeth in Suzhou Kowloon Hospital, Shanghai Jiaotong University School of Medicine, were included, among which 38 cases with DI restoration were used as the control group (CG), and the remaining 42 cases with II were used as the research group (RG). The complications that occurred were recorded. Besides, subjective satisfaction (Visual Analogue Scale (VAS)), aesthetic effect after anterior teeth trauma restoration (Pink Esthetic Score (PES)), aesthetics of dental hard tissue (White Esthetic Score (WES)), pocket depth assessed by pure titanium periodontal probe, implant stability (Implant Stability Quotient (ISQ)), and oral health-related quality of life (Oral Health Impact Profile- (OHIP-14) were evaluated. Attachment height, general look, color, and chewing function were all much higher in RG than in CG, according to the evaluation results. Furthermore, at 3 months, 6 months, and 12 months after surgery, RG had greater PES, WES, ISQ, and OHIP-14 scores, while the periodontal depth was decreased. In both groups of patients, the incidence of complications was similar, with no discernible differences.

## 1. Introduction

Tooth loss not only affects patients' facial aesthetics but also their chewing function, digestive function, and normal vocalization, resulting in a sharp decline in patients' quality of life (QOL). As the dental implant technology and biomaterials constantly develop, implant-supported dental restoration has become the first choice to replace missing teeth [1]. In the past, delayed implantation (DI) was mostly used; that is, implantation was accomplished 3 to 6 months after tooth extraction when the tooth extraction site was completely healed and the bone reconstruction was basically stable, so that the implant could form bony union after implantation with favorable safety [2]. However, this implant procedure will result in a protracted period of tooth loss, as well as keratinization of the gums and insufficient bone mass in the edentulous area due to alveolar bone absorption follow-

ing tooth extraction, which will impact the aesthetic effect of implant repair [3, 4]. With the advances in stomatology, immediate implantation (II) technology has attracted the attention of stomatologists at home and abroad, as it not only shortens the number of surgical interventions and simplifies the treatment procedures but also preserves the soft tissue capsule to achieve the best soft tissue aesthetics [5, 6]. However, II is not omnipotent, and it will face challenges such as inadequate wound closure and insufficient soft tissue, which will greatly compromise the aesthetics of gingival formation of the implant in the aesthetic area [7]. In fact, the maxillary anterior teeth are very vulnerable to loss due to trauma or other causes given their special position. Once the maxillary anterior teeth are lost, it will not only affect patients' diet but also their appearance and image, seriously disturbing their normal life. At present, there are many comparative studies on II and DI restoration of single maxillary

anterior teeth loss, but the comparison of soft tissue stability and aesthetics between the two implant restoration methods is relatively lacking. So we conducted this research for verification.

The paper arrangements are as follows: Section 2 examines the data and methods. Section 3 analyzes the result. Section 4 discusses the discussion. Section 5 concludes the work.

## 2. Data and Methods

This section discusses the research participants and evaluates the various treatment methods. They analyze the endpoint and discuss the statistical processing.

**2.1. Research Participants.** From February 2019 to June 2020, 80 patients who received single dental implant restoration of maxillary anterior teeth in Suzhou Kowloon Hospital, Shanghai Jiaotong University School of Medicine, were included as the research participants, among which 38 patients who used DI were taken as the control group (CG) and the remaining 42 patients who used II as the research group (RG). Inclusion criteria are as follows: age  $\geq 18$ ; single implant in the maxillary anterior region; good treatment compliance, oral hygiene, and oral care habits; sufficient bone mass at the implant site; no smoking history; healthy gums and stable occlusal relationship; no obvious periodontal inflammation; no contraindications for dental implants; and available bone height in the apical region of the teeth  $\geq 3$  mm, with no obvious soft and hard tissue defect. Exclusion criteria are as follows: inflammatory lesions in planting areas; prior bone augmentation surgery such as flap implantation; osteoporosis, diabetes, or other serious systemic diseases; and habitual grinding of teeth with severe symptoms. All subjects were informed and signed the informed consent. This study conforms to the Helsinki Declaration and is ethically ratified by Suzhou Kowloon Hospital, Shanghai Jiaotong University School of Medicine.

**2.2. Treatment.** Periodontal tissue status, alveolar height, and alveolar bone width at the implant site were observed in both groups before surgery. Curved surface tomography and periapical film were taken and prepared before surgery, and the diameter and length of implants were determined. Antibiotics were prescribed half an hour prior to surgery.

**2.2.1. CG Was Treated with DI.** Three months after extraction and exfoliation of the damaged anterior teeth, the absorption level of alveolar ridge and alveolar fossa healing was observed, and the implant restoration treatment was carried out only when the above two conditions were determined satisfactorily. Patients were placed in the supine position after receiving articaine for local anesthetic and following normal cleaning and towel laying. To thoroughly expose the implant area, a tiny incision was made from the crest of the alveolar ridge slightly to the palatal side, and the mucous bone flap was opened with a stripper. Then, with a torque of 35-50 N · cm, implants were routinely put, bone meal was implanted, and the surface was covered with a biofilm. Postoperatively, patients gargled with mouthwash and

took antibiotics orally for 5-7 days. They were advised to return for a second-stage operation 5 months after the operation, and the full repair was carried out 2-3 months after the second-stage operation.

**2.2.2. RG Was Treated with II.** Similarly, local anesthesia with articaine and routine disinfection and towel laying were performed before operation. The patient was placed in the supine position, and the small incision was made angular. The decision to extract the affected tooth or not was made depending on the periodontal wall condition and alveolar bone height. When designing the flap range of the incision, the integrity of the gingival papilla was tried to preserve as much as possible. The trauma caused by increased alveolar fossa was minimized during minimally invasive tooth extraction, and the integrity of bone wall was maintained. Then, the implant socket was prepared, and the suitable implant was determined, which was planted with a torque of  $\geq 35$  N · cm, reaching at least 3.0-5.0 mm at the bottom of alveolar socket as the implant depth and reserving a tongue-labial bone wall with a thickness of more than 1.0 mm. The implant's crown square was about 0.5 mm smaller than the bottom of the alveolar socket, which was consistent with the long axis of the opposite side. The surface was then covered with biofilm, and bone meal was implanted in the space around the implant. According to the position of the missing teeth and the size of adjacent teeth, the specifications and models of the immediate implant abutment were determined, and nanoresin was used as temporary crown. After abutment implantation, attention was paid to tight suture, and the neck of abutment was highly polished to ensure no occlusal contact. Besides, the anterior, lateral, and median of the abutment were adjusted, after which central screws were used for fixation. After the operation, patients were gargled with mouthwash, and oral antibiotics were taken for 7 days. The full crown restoration was completed 6 months after surgery.

## 2.3. Endpoints

**2.3.1. Success Rate of Restoration.** Adequate periodontal tissue, no loosening of implants, and normal chewing function were all criteria for restoration success. Repair failure was defined as gingival periodontal redness and abscess, implant loosening, and no improvement or even deterioration of chewing ability following therapy. Besides, the common complications of dental implantation in both groups were recorded, including gingival margin recession, peri-implant inflammation, metal exposure, and infection.

Subjective satisfaction was assessed 1 year after surgery based on patients' subjective feelings using the Visual Analogue Scale (VAS). The indexes include attachment height, overall appearance, color, and chewing function. Satisfaction is positively correlated with the score (range: 0-10).

The Pink Esthetic Score (PES) [8] was used to evaluate the aesthetic effect of patients after the anterior tooth restoration, which was evaluated once at 3 months, 6 months, and 12 months after the operation, with a total of 7 items and 0-2 points for each item. The aesthetics of tooth hard

tissue was assessed using the White Esthetic Score (WES) [9] from five domains of color, surface texture, tooth form, tooth volume/outline, and translucency, and each item scored 0-2 points. For both scales, higher scores are associated with better aesthetic effects.

A pure titanium periodontal probe was used to detect the pocket depth (PD) at 3 months, 6 months, and 12 months postoperatively, and the detection position was the distance between the pocket bottom of the implant denture and the mesial, central, and distal gingival margins on the labial and lingual surfaces of the crowns. Implant stability was assessed using the Implant Stability Quotient (ISQ) [10] (score range: 0-100), with higher scores indicating better implant stability.

The evaluation of oral health-related QOL at 3, 6, and 12 months after surgery employed the Oral Health Impact Profile- (OHIP-) 14 scales [11]. The scale includes 7 dimensions with 2 items each, and the score of each item is 0-4 points, with a total score of 0-56 points. The higher the score, the lower the QOL related to oral health.

**2.4. Statistical Processing.** Data were statistically processed by SPSS 19.0 (Shanghai Yijun Information Technology) and visualized into figures via GraphPad Prism 6. Chi-square test and independent  $t$ -test were applied for comparison of counting data and measurement data in this paper, respectively, with the threshold of significance set as  $P < 0.05$ .

### 3. Results

Here, it examines the comparison of general data and occurrence of complications. We analyzed the comparison of attachment height, overall appearance, color, and masticatory function and define the PES and WES scores of patients in two groups at different time points. We also discussed the PD and ISQ scores at different time points in two groups and oral health-related QOL.

**3.1. Comparison of General Data.** General data like sex, age, BMI, educational level, and causes of tooth loss showed no distinct differences between RG and CG ( $P > 0.05$ ) (Table 1).

**3.2. Occurrence of Complications.** The common complications of dental implant in the two groups were recorded. In CG, gingival margin recession, peri-implant inflammation, metal exposure, and infection were observed in 2 (5.26%), 1 (2.63%), 2 (5.26%), and 0, respectively, with an overall incidence of 13.16%. While in RG, the data were 2 (4.76%), 1 (2.38%), 1 (2.38%), and 1 (2.38%), respectively, and the total incidence was 11.90%. Complications were similar between the two groups with no significant difference ( $P > 0.05$ ) nor was there any notable difference in the success rate of repair between RG and CG after statistical analysis (97.62% vs. 94.74%,  $P > 0.05$ ) (Table 2).

**3.3. Comparison of Attachment Height, Overall Appearance, Color, and Masticatory Function.** The results of patients' subjective satisfaction evaluated by VAS showed that the attachment height, overall appearance, color, and chewing

TABLE 1: Comparison of general data between two groups of patients.

Groups	Control group ( $n = 38$ )	Research group ( $n = 42$ )	$\chi^2/t$	$P$
Sex			0.637	0.425
Male	23 (60.53)	29 (69.05)		
Female	15 (39.47)	13 (30.95)		
Age (years old)	33.21 $\pm$ 9.56	33.98 $\pm$ 9.83	0.724	0.355
BMI (kg/m <sup>2</sup> )	22.93 $\pm$ 1.33	23.12 $\pm$ 1.56	0.583	0.562
Educational level			1.229	0.268
$\geq$ High school	17 (44.74)	24 (57.14)		
<High school	21 (55.26)	18 (42.86)		
Causes of tooth loss			2.036	0.361
Caries	13 (34.21)	11 (26.19)		
Trauma	13 (34.21)	21 (50.00)		
Others	12 (31.58)	10 (23.81)		

TABLE 2: Occurrence of complications.

Groups	Control group ( $n = 38$ )	Research group ( $n = 42$ )	$\chi^2$	$P$
Gingival margin recession	2 (5.26)	2 (4.76)		
Peri-implant inflammation	1 (2.63)	1 (2.38)		
Metal exposure	2 (5.26)	1 (2.38)		
Infection	0 (0.00)	1 (2.38)		
Total	5 (13.16)	5 (11.90)	0.03	0.87
Success rate of repair	36 (94.74)	41 (97.62)	0.46	0.49

TABLE 3: Comparison of attachment height, overall appearance, color, and masticatory function between the two groups.

Groups	Control group ( $n = 38$ )	Research group ( $n = 42$ )	$t$	$P$
Attachment height	7.26 $\pm$ 1.06	8.02 $\pm$ 1.42	2.690	0.009
Overall appearance	7.05 $\pm$ 1.11	7.79 $\pm$ 1.30	2.724	0.008
Color	7.42 $\pm$ 1.06	8.12 $\pm$ 1.38	2.524	0.014
Masticatory function	6.97 $\pm$ 1.08	7.55 $\pm$ 1.33	2.127	0.037

function were significantly higher in RG than in CG ( $P < 0.05$ ) (Table 3).

**3.4. PES and WES Scores of Patients in Two Groups at Different Time Points.** PES and WES were used to evaluate

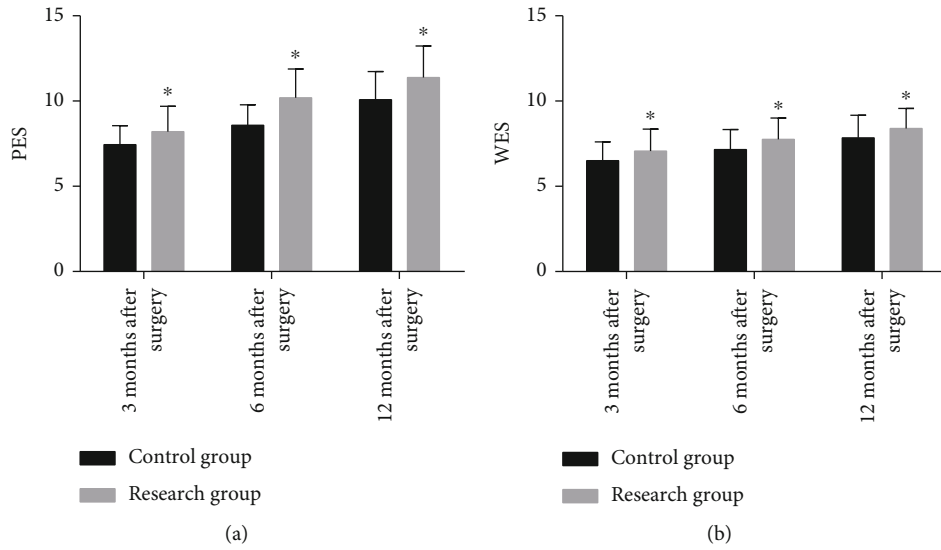


FIGURE 1: PES and WES scores of patients in two groups at different time points. (a) The PES scores of the research group at 3 months, 6 months, and 12 months after surgery were higher than those of the control group. (b) The WES scores of the research group at 3 months, 6 months, and 12 months after surgery were higher than those of the control group. \* represents  $P < 0.05$  compared with the control group at the same time point.

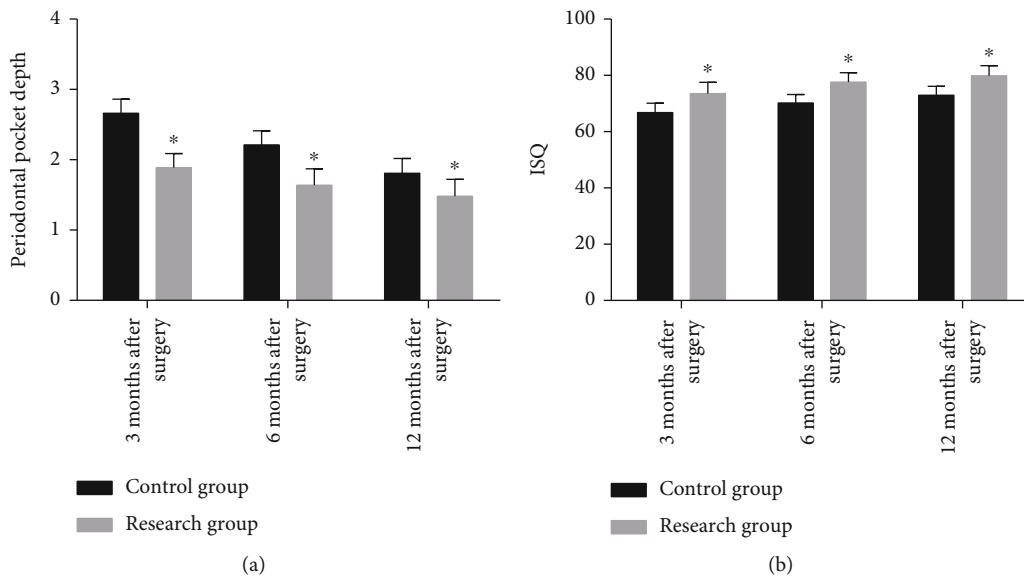


FIGURE 2: Pocket depth and ISQ score of two groups of patients at different time points. (a) The pocket depth of the research group was lower than that in the control group at 3 months, 6 months, and 12 months after surgery. (b) The ISQ score of the research group was higher than that of the control group at 3, 6, and 12 months after surgery. \* represents  $P < 0.05$  compared with the control group at the same time point.

the improvement of the aesthetic effect. The data revealed higher PES and WES scores in RG compared with CG at 3 months, 6 months, and 12 months after surgery ( $P < 0.05$ ) (Figure 1).

**3.5. PD and ISQ Scores at Different Time Points in Two Groups.** Compared with CG, the PD in RG decreased significantly at 3 months, 6 months, and 12 months after surgery, while the ISQ score increased significantly ( $P < 0.05$ ) as shown in Figure 2.

**3.6. Oral Health-Related QOL.** The oral health-related QOL assessed by OHIP-14 scale determined higher scores in RG compared with CG at 3 months, 6 months, and 12 months after surgery ( $P < 0.05$ ) (Figure 3).

#### 4. Discussion

The results of this study support the use of II as the preferred method of dental restoration for patients with single maxillary anterior teeth loss, as it provides better aesthetic support

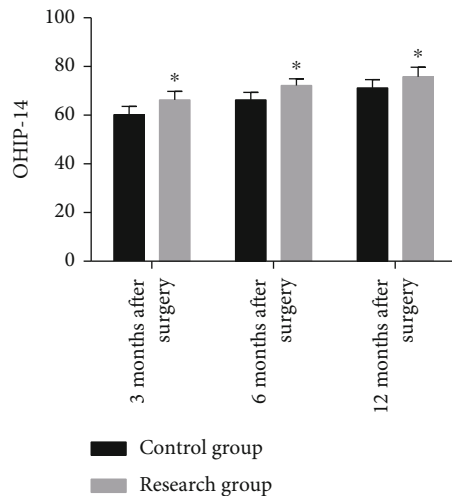


FIGURE 3: Oral health-related quality of life. The total score of OHIP-14 in the research group at 3 months, 6 months, and 12 months after surgery was significantly higher than that in the control group. \* represents  $P < 0.05$  compared with the control group at the same time point.

with higher treatment satisfaction, implant stability, and QOL compared to DI.

The teeth between the canines on both sides of the maxilla are known as maxillary anterior teeth. Losing anterior teeth will compromise the patient's physiological functions like as chewing and speech, as well as their overall looks, causing major negative effects on their physical and mental health and daily lives. At present, single-tooth implants have a good long-term survival rate, but implantation remains challenging due to the frequent presence of hard and soft tissue resorption defects and the high aesthetic requirements of the aesthetic area [12]. DI is a mature and reliable means of conventional plant restoration. Patients must, however, wait for the wound to heal following tooth extraction, and the resulting long period of time without teeth will damage their appearance and daily lives, putting a psychological and financial strain on the patients. Therefore, patients with anterior tooth loss will have certain concerns when choosing DI. II, on the other hand, can avoid the above shortcomings of DI [13, 14], but its influence on the aesthetic appearance of patients is controversial. Some studies suggest that II is not aesthetically friendly to patients [15, 16]. While some other evidence argues that II has similar effects and is even superior to DI on patients' aesthetic appearance [17–19]. In this study, RG showed better performance in the evaluation of attachment height, overall appearance, color, and chewing function, with higher PES and WES scores than CG at 3 months, 6 months, and 12 months after surgery, which shows that II is more esthetically pleasing. The reason may be that II can reduce and avoid alveolar bone absorption, better maintain soft tissue morphology, and effectively maintain the height and width as well as the physiological stimulation of the alveolar bone, thus achieving the aesthetic effect that DI cannot achieve [20].

It is shown that the success rate of II and DI is comparable, usually above 90% [21, 22]. The results of this study also

found that the success rate of the two plantation methods exceeded 90% with no significant difference. Following that, we discovered no statistically significant difference in the occurrence of problems between the two groups. However, when compared to CG, RG's PD fell dramatically at 3 months, 6 months, and 12 months following surgery, while the ISQ score climbed significantly. These findings show that both implantation procedures are feasible and safe for single-tooth maxillary anterior tooth repair. However, II better facilitates the formation of good periodontal attachment, provides favorable support conditions for the growth of attached gingiva, and protects the alveolar bone septum, playing a more significant role than DI in promoting the health of patients' periodontal tissue.

Due to the destruction of dental integrity, patients with tooth loss may suffer from alveolar bone atrophy, decreased masticatory function, food impaction, adjacent tooth displacement, and mandibular joint lesions, which may have adverse effects on patients' physiological function and psychological state, seriously affecting their QOL [23, 24]. Therefore, oral health-related QOL is one of the most important indicators to evaluate the success of implantation and restoration. In this study, the OHIP-14 scale was used to evaluate the influence of II and DI on patients' oral-related QOL. At 3, 6, and 12 months following surgery, RG had considerably higher OHIP-14 scores than CG, indicating that II could significantly enhance patients' oral-related QOL. This could be due to the fact that II minimizes the duration of missing teeth and the number of follow-up visits, eliminates aesthetic and pronunciation issues, and eliminates psychological and social barriers, all of which improve patients' QOL greatly.

## 5. Conclusions

Without causing major complications, II contributes to better aesthetic effects, higher subjective satisfaction, and superior postoperative quality of life for patients with single-tooth restoration of maxillary anterior teeth, which is worth for clinical use. For patients with single maxillary anterior tooth loss, II has higher prognostic value and is more conducive to improving implant stability, treatment satisfaction, and QOL with more significant aesthetic effects, which is worth promoting clinically.

## Data Availability

The labeled datasets used to support the findings of this study are available from the corresponding author upon request.

## Conflicts of Interest

The authors declare no competing interests.

## Authors' Contributions

Zhimin Chen and Shuhuai Zhang contributed equally to this work.



## References

- [1] D. Wu, L. Zhou, J. Lin, J. Chen, W. Huang, and Y. Chen, "Immediate implant placement in anterior teeth with grafting material of autogenous tooth bone vs xenogenic bone," *BMC Oral Health*, vol. 19, no. 1, p. 266, 2019.
- [2] W. Meng, Y. Chien, and H. Chien, "Immediate implant placement and provisionalization in the esthetic zone: a 6.5-year follow-up and literature review," *Case Reports in Dentistry*, vol. 2021, Article ID 4290193, 11 pages, 2021.
- [3] J. Cosyn, L. De, L. Seyssens, R. Doornewaard, E. Deschepper, and S. Vervaeke, "The effectiveness of immediate implant placement for single tooth replacement compared to delayed implant placement: a systematic review and meta-analysis," *Journal of Clinical Periodontology*, vol. 46, Suppl 21, pp. 224–241, 2019.
- [4] T. Aldhohrah, G. Qin, D. Liang et al., "Does simultaneous soft tissue augmentation around immediate or delayed dental implant placement using sub-epithelial connective tissue graft provide better outcomes compared to other treatment options? A systematic review and meta-analysis," *PLoS One*, vol. 17, no. 2, article e0261513, 2022.
- [5] A. Saijeva and G. Juodzbalys, "Immediate implant placement in non-infected sockets versus infected sockets: a systematic review and meta-analysis," *Journal of oral & maxillofacial research*, vol. 11, no. 2, article e1, 2020.
- [6] V. Amin, S. Kumar, S. Joshi, T. Hirani, and D. Shishoo, "A clinical and radiographical comparison of buccolingual crestal bone changes after immediate and delayed implant placement," *Medicine and Pharmacy Reports*, vol. 92, no. 4, pp. 401–407, 2019.
- [7] J. Fang, R. Xin, W. Li, C. Wang, X. Lv, and M. Zhou, "Immediate implant placement in combination with platelet rich-fibrin into extraction sites with periapical infection in the esthetic zone: a case report and review of literature," *World Journal of Clinical Cases*, vol. 9, no. 4, pp. 960–969, 2021.
- [8] R. Furhauser, D. Florescu, T. Benesch, R. Haas, G. Mailath, and G. Watzek, "Evaluation of soft tissue around single-tooth implant crowns: the pink esthetic score," *Clinical Oral Implants Research*, vol. 16, no. 6, pp. 639–644, 2005.
- [9] J. Chen, C. Chiang, and Y. Zhang, "Esthetic evaluation of natural teeth in anterior maxilla using the pink and white esthetic scores," *Clinical Implant Dentistry and Related Research*, vol. 20, no. 5, pp. 770–777, 2018.
- [10] P. Levin, "The correlation between immediate implant insertion torque and implant stability quotient," *The International Journal of Periodontics & Restorative Dentistry*, vol. 36, no. 6, pp. 833–840, 2016.
- [11] D. Slade, "Derivation and validation of a short-form oral health impact profile," *Community Dentistry and Oral Epidemiology*, vol. 25, no. 4, pp. 284–290, 1997.
- [12] I. Afrashtehfar, A. Assery, and R. Bryant, "Aesthetic parameters and patient-perspective assessment tools for maxillary anterior single implants," *International journal of dentistry*, vol. 2021, Article ID 6684028, 9 pages, 2021.
- [13] H. Bassir, K. Kholy, Y. Chen, H. Lee, and G. Intini, "Outcome of early dental implant placement versus other dental implant placement protocols: a systematic review and meta-analysis," *Journal of Periodontology*, vol. 90, no. 5, pp. 493–506, 2019.
- [14] H. Arora and S. Ivanovski, "Clinical and aesthetic outcomes of immediately placed single-tooth implants with immediate vs. delayed restoration in the anterior maxilla: a retrospective cohort study," *Clinical Oral Implants Research*, vol. 29, no. 3, pp. 346–352, 2018.
- [15] J. Cosyn, A. Eghbali, A. Hermans, S. Vervaeke, H. Bruyn, and R. Cleymaet, "A 5-year prospective study on single immediate implants in the aesthetic zone," *Journal of Clinical Periodontology*, vol. 43, no. 8, pp. 702–709, 2016.
- [16] S. Tonetti, P. Cortellini, F. Graziani et al., "Immediate versus delayed implant placement after anterior single tooth extraction: the timing randomized controlled clinical trial," *Journal of Clinical Periodontology*, vol. 44, no. 2, pp. 215–224, 2017.
- [17] D. Buser, V. Chappuis, M. Bornstein, G. Wittneben, M. Frei, and C. Belser, "Long-term stability of contour augmentation with early implant placement following single tooth extraction in the esthetic zone: a prospective, cross-sectional study in 41 patients with a 5- to 9-year follow-up," *Journal of Periodontology*, vol. 84, no. 11, pp. 1517–1527, 2013.
- [18] H. Arora and S. Ivanovski, "Evaluation of the influence of implant placement timing on the esthetic outcomes of single tooth implant treatment in the anterior maxilla: a retrospective study," *Journal of Esthetic and Restorative Dentistry*, vol. 30, no. 4, pp. 338–345, 2018.
- [19] J. Canellas, D. Medeiros, C. Figueredo, G. Fischer, and G. Ritto, "Which is the best choice after tooth extraction, immediate implant placement or delayed placement with alveolar ridge preservation? A systematic review and meta-analysis," *Journal of Cranio-Maxillo-Facial Surgery*, vol. 47, no. 11, pp. 1793–1802, 2019.
- [20] L. Mahesh, L. Calvo, S. Shukla, R. Kumar, and R. Kumar, "Clinical and radiographic findings without the use of bone substitute materials in extraction sockets and delayed implant placement- a case series," *Journal of Oral Biology and Craniofacial Research*, vol. 10, no. 2, pp. 141–145, 2020.
- [21] C. Thanissorn, J. Guo, D. Jing et al., "Success rates and complications associated with single immediate implants: a systematic review," *Dentistry Journal*, vol. 10, no. 2, p. 31, 2022.
- [22] B. Smith, P. Tarnow, and G. Sarnachiaro, "Immediate placement of dental implants in molar extraction sockets: an 11-year retrospective analysis," *The Compendium of Continuing Education in Dentistry*, vol. 40, pp. 166–170, 2019.
- [23] U. Khan, F. Ghani, and Z. Nazir, "The effect of some missing teeth on a subjects' oral health related quality of life," *Pakistan Journal of Medical Sciences*, vol. 34, no. 6, pp. 1457–1462, 2018.
- [24] O. Schierz, K. Baba, and K. Fueki, "Functional oral health-related quality of life impact: a systematic review in populations with tooth loss," *Journal of Oral Rehabilitation*, vol. 48, no. 3, pp. 256–270, 2021.

## Retraction

# Retracted: Research on Improving the Executive Ability of University Administrators Based on Deep Learning

### Computational and Mathematical Methods in Medicine

Received 17 October 2023; Accepted 17 October 2023; Published 18 October 2023

Copyright © 2023 Computational and Mathematical Methods in Medicine. This is an open access article distributed under the Creative Commons Attribution License, which permits unrestricted use, distribution, and reproduction in any medium, provided the original work is properly cited.

This article has been retracted by Hindawi following an investigation undertaken by the publisher [1]. This investigation has uncovered evidence of one or more of the following indicators of systematic manipulation of the publication process:

- (1) Discrepancies in scope
- (2) Discrepancies in the description of the research reported
- (3) Discrepancies between the availability of data and the research described
- (4) Inappropriate citations
- (5) Incoherent, meaningless and/or irrelevant content included in the article
- (6) Peer-review manipulation

The presence of these indicators undermines our confidence in the integrity of the article's content and we cannot, therefore, vouch for its reliability. Please note that this notice is intended solely to alert readers that the content of this article is unreliable. We have not investigated whether authors were aware of or involved in the systematic manipulation of the publication process.

Wiley and Hindawi regrets that the usual quality checks did not identify these issues before publication and have since put additional measures in place to safeguard research integrity.

We wish to credit our own Research Integrity and Research Publishing teams and anonymous and named external researchers and research integrity experts for contributing to this investigation.

The corresponding author, as the representative of all authors, has been given the opportunity to register their agreement or disagreement to this retraction. We have kept a record of any response received.

### References

- [1] C. Wei and S. Wang, "Research on Improving the Executive Ability of University Administrators Based on Deep Learning," *Computational and Mathematical Methods in Medicine*, vol. 2022, Article ID 6354801, 10 pages, 2022.

## Research Article

# Research on Improving the Executive Ability of University Administrators Based on Deep Learning

Chengyan Wei <sup>1</sup> and Shenxiang Wang<sup>2</sup>

<sup>1</sup>School Journal Editorial Department, Guangzhou College of Technology and Business, Guangzhou Guangdong 510850, China

<sup>2</sup>College of Intelligent Cold-Chain Industries, Guangzhou College of Technology and Business, Guangzhou Guangdong 510850, China

Correspondence should be addressed to Chengyan Wei; [gzgsxy@cumt.edu.cn](mailto:gzgsxy@cumt.edu.cn)

Received 15 April 2022; Revised 12 May 2022; Accepted 17 May 2022; Published 9 June 2022

Academic Editor: Naeem Jan

Copyright © 2022 Chengyan Wei and Shenxiang Wang. This is an open access article distributed under the Creative Commons Attribution License, which permits unrestricted use, distribution, and reproduction in any medium, provided the original work is properly cited.

Over the years, experts have focused their research on ways to increase the executive capacity of university administrators. This is because only by improving the quality of execution of college and university administrative personnel can they actively execute various policies and measures, fully exploit their subjective initiative, and ensure the educational reform of colleges and universities. Increasing the executive capacity of administrative staff can help colleges and universities manage more effectively. Therefore, in the development process of higher education institutions, it is necessary to strengthen the execution of administrative staff, especially the need to adhere to the problem as the basic orientation. Take scientific and practical steps to strengthen administrative personnel's executive ability in light of current issues with administrative management personnel's executive power, and establish the groundwork for ensuring the quality of management work. Combining deep learning, this paper proposes a path to improve the executive power of college administrators based on deep learning. To begin, familiarize yourself with the deep noise reduction autoencoder model and support vector regression (SVR) theory and build the DDAE-SVR deep neural network (DNN) model. Then, input a small-scale feature index sample data set and a large-scale short-term traffic flow data set for experiments; then, assess the model's parameters to achieve the optimal model. Finally, use performance indicators such as MSE and MAPE to compare with other shallow models to verify the effectiveness and advantages of the DDAE-SVR DNN model in the execution improvement path output of university administrators and large-scale data sets.

## 1. Introduction

In the process of Chinese higher education transition from elite to popular, comprehensive universities have generally achieved leapfrog development under the guidance of national education policies and relying on their own comprehensive advantages. However, as higher education develops, many colleges and universities face challenges in their development. For example, there is a lack of experience in management systems and operating mechanisms, a tendency to seek completeness in the setting of disciplines, a tendency to climb higher in the level of running a school, and a tendency to be greedy in the scale of running a school [1]. The magnificent blueprint can only be achieved by execution, and execution is an indispensable link between goals

and results. However, at the management level of many colleges and universities, usually because of the unscientific formulation of the school's own development plan, the executive power of the administrative staff is weakened, and the overall executive culture of the school is lacking, which ultimately leads to the lack of management, ineffective execution, and low efficiency. At present, in the context of the great development of higher education, how to continuously respond to challenges and opportunities, improve the executive ability of university administrators, and establish an executive organization that meets the characteristics of high-quality comprehensive university organizations and changes in the external environment are topics that need to be explored. Currently, universities generally have their own development plans. How to put these development

strategies into practice is inseparable from the super-high executive power of university administrators. Therefore, studying the executive ability of university administrators is very necessary for the university to maintain continuous, healthy, and leap-forward development.

- (1) The construction of executive power is the fundamental to achieve the school's strategic goals. Gao [2] analyzed the significance of executive power in school management in his book "School Strategic Management," from the point of view that executive power is a means to overcome various uncertain factors, and executive power is a touchstone to test the quality of school personnel and organization. Proceed from three aspects. Tang [3] believes that excellent execution is a weapon to eliminate loopholes in school management. Because execution is not only a powerful weapon for turning educational planning into reality, it is also a powerful weapon for filling management loopholes, and it is also a powerful weapon for optimizing educational planning programs. Therefore, while the school is scientifically formulating its own development plan, it should place a greater emphasis on enhancing plan execution and assuring the fulfillment of varied plans
- (2) The establishment of executive power is essential for the school's long-term success. The effective application of school policies by administrators, according to Wang [4], is a critical aspect in school development. Only proper implementation may enable strategic goals to be realized, and organizations rely on implementation to function effectively. When a school decides to implement an effective goal, the first consideration is whether the organization can accomplish this goal. The establishment of a dynamic execution organization is the prerequisite for accomplishing the university's goals
- (3) Execution building is a requirement to promote the establishment of a modern university system. Jiang Qingzhe pointed out that, to a certain extent, school execution is related to the survival and development of the school. It plays an important role in advancing the establishment of a modern university system, taking the road of high-level university construction with Chinese characteristics, and realizing the leap-forward development of the school [5]. Based on the above background, this article relies on the rapid development of deep learning technology, uses DNN to analyze the characteristics of administrative personnel, and outputs a personalized path to improve the executive power of university administrative personnel. Unlike traditional machine learning algorithms, deep learning is not a specific algorithm, but a collective term for a series of algorithms that adopt deep learning ideas

The structure of this article is organized as follows. The literary works related to this study are presented in Section 2. The proposed methods is explained in Section 3. The

experimentation and evaluation of the suggested method are presented in Section 4. Finally, section 5 summarizes the paper's main points.

## 2. Related Work

Raman et al. [6] called the gap between strategy and actual results the missing link and named it execution. Reference [7] also adopted this expression, defining execution as the missing link between the goal and the result, and gave a note that this statement comes from Darwin's theory of biological evolution. Reference [8] believes that execution means transforming a strategy into an action plan and measuring the results. From this perspective, execution can be understood as the link from strategy to result, and execution is the ability to transform strategic planning into actual performance. Discussions on the formulation and implementation of strategic planning have been uninterrupted in the past few decades. People's knowledge and understanding of strategy implementation is far less clear than strategy formulation, and the research results on strategy implementation are far less than those on strategy formulation [9]. The reason is that the premise of strategic research is that as long as the correct strategy is input to the enterprise, the expected result will naturally be produced. The enterprise's conduct calls this notion into question [10]. According to statistics, 87.5 percent of businesses that have not yet achieved their strategic goals have a clear strategic setting, but only 36.9% have developed a clear strategic execution path; for businesses that have fully achieved their strategic goals, these proportions are 96.5 percent and 81 percent, respectively. The results of a 1999 study by Fortune magazine are similar. The conclusion is that about 70.1% of CEOs fail not because of poor corporate strategy but because the corporate strategy is not effectively implemented [11]. According to Lazebnik et al., execution is the foundation of strategy, a critical organizational component of strategy, a collection of systematic procedures, and a systematic method of exposing reality and acting in accordance with reality [12, 13]. Strategy and execution are processes, not just events, but also continuous processes that are seamlessly intertwined [14]. After more than 20 years of research, according to Nutt, 50% of all decisions made in an organization fail. The main reason was that managers did not implement and implement it seriously [15]. The application of executive power theory to the field of university education management is a new attempt, but there is still a lack of research in this area at home and abroad, and there is no systematic and comprehensive work on the construction of university executive power. When collecting relevant materials, the author can only refer to and cite some related works and recent academic papers on the executive ability of university administrators. The construction of executive power in colleges and universities is a complex system engineering, which not only needs to be studied from the operational level but also needs the support of theoretical research. The current national competition is becoming increasingly fierce, and the competition between culture and education is the key to national competition, which is related to the future development of the country. Therefore, universities all over the world are comprehensively improving their

own school-running level and social influence, and our country is also constantly innovating teaching concepts. Under the new wave of education reform, my country's college education has entered a new stage, and it has become the consensus of many colleges and universities to cultivate all-round talents. The administrative personnel play a protective role in the training of talents and can provide favorable conditions for the development of education.

Deep learning is the general term for deep neural network, and it is the result of continuous in-depth research and development of artificial neural network (ANN) [16]. When researching the biological nervous system, ANN is created by simulating the biological process of neurons. The ANN is connected to each other through a number of nodes, and the output of each node is connected to the input of some other nodes to form a network system [17]. Over the past decades, through continuous experiments to sum up experience, people have gradually discovered that as the number of hidden layers (HL) increases, the expressive ability of neural network systems tends to improve, so that they can complete more complex classification tasks and approximate more complex mathematical function models. However, with the increase in the number of layers, the difficulty of network training has rapidly become larger. Gradient diffusion often affects the employment of standard BP algorithms for network training, resulting in very sluggish convergence. Since no effective method has been found to solve this problem, the development of ANNs has stagnated for a long time. Until 1981, "Early Research on the Visual Cortex" edited by Hubel and Wiesel won the Nobel Prize in Physiology & Medicine in recognition of their major contributions to information processing in the visual system [18].

Inspired by the above research results, in 2006, Professor Hinton and other scholars published papers entitled "Reducing the dimensionality of data with neural networks" and "Deep Belief Networks" in the "Science" magazine, which opened a wave of deep learning research [19]. These two articles mentioned the following points:

- (1) The bottleneck of the traditional neural network that cannot be effectively trained due to the increase of the number of layers can be overcome by the training method of layer-by-layer initialization
- (2) A multihidden-layer ANN outperforms a single-hidden-layer ANN. The network has stronger feature learning capabilities, and the features obtained through independent learning can more profoundly reflect the nature of the data, thereby achieving more effective classification and later summarized with the continuous development of deep learning
- (3) It is necessary to build a network model with multiple HLs
- (4) A large number of training samples need to be prepared in advance for training the network. These four points constitute the essential difference between deep learning and traditional pattern recognition methods. Since 2012, deep learning has once again made histor-

ical breakthroughs, mainly including deeper networks (ResNet), enhanced convolution module functions, from classification to detection (R-CNN and Fast R-CNN), generation of confrontation networks, and the addition of new function modules (FCN, STNet, and CNN+RNN/LSTM)

When it comes to processing small-scale evaluation data sets, the adaptive BP neural network (BPNN) model offers a number of advantages. However, because it only has one hidden layer, processing capacity, predictive ability, and modeling expression power will be limited when dealing with complicated and high-dimensional large-scale data sets. Therefore, The DDAE-SVR DNN model is proposed in this study to address the challenge of complicated high-dimensional large-scale data sets. There are many HLs in the DDAE-SVR DNN model. The Adam method is used throughout the unsupervised training phase to dynamically alter the learning step length of each parameter during training. After multiple hidden layers, the spatial characteristics of the original data are converted multiple times, with the purpose of obtaining the fundamental qualities of the reconstructed output data with the least amount of inaccuracy. SVR is used as a predictor for supervised prediction, which enables translating complicated nonlinear interactions to high-dimensional spaces (HDS) in order to create equivalent linear relationships in low-dimensional spaces in a similar way. Input the small-scale administrative staff characteristic data set and the large-scale data set for experiments, and compare them with other shallow models, validating the suggested model's efficacy and benefits in the output of the executive power development route for university administrators and the processing of large-scale data sets.

### 3. Method

#### 3.1. The Basic Model of Deep Neural Network

**3.1.1. Autoencoder Model.** There are a lot of DNN fundamental models. In this section, the autoencoder model is briefly discussed. An autoencoder was originally introduced in 1986. A feature extraction or dimensionality reduction technique is an unsupervised algorithm. Encoding and decoding networks are part of the autoencoder concept, which has three layers of networks. Errors are propagated backwards through the network using the BP method, and the network layers' weights and thresholds are continually adjusted to reduce error between original input data and the output data (OIDAOD). Transforming input data from a high-dimensional format into a low-dimensional format is one of the initial steps in the autoencoder processing process. Then, using the decoding network and the error function, compute the error between the OIDAOD and reduce the error to complete the decoding network reconstruction of the OID. The output of this encoder is used to approximate the identity function as closely as possible to the input; its construction is shown in Figure 1.

Suppose the input feature vector (IFV) is  $x = (x_1, x_2, \dots, x_n)$ , converted to feature vector  $h = (h_1, h_2, \dots, h_m)$  in the HL, and the output feature vector (OFV) is  $y = (y_1, y_2, \dots, y_n)$

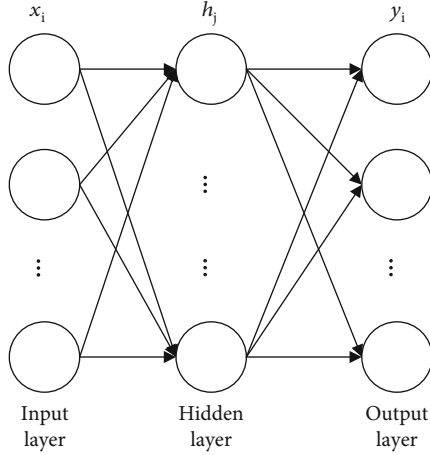


FIGURE 1: Autoencoder model structure.

); then, the mathematical expressions for mapping the autoencoder from the input layer (IL) to the intermediate HL and the decoder from the intermediate HL to the output layer (OL) are as follows:

$$\begin{aligned} h &= C(x_i) = A_C(W_C x_i + t_i), \\ y &= D(h_j) = A_D(W_D h_j + t_j), \end{aligned} \quad (1)$$

where  $C$  and  $D$  are the encoding function and the decoding function, respectively. And  $A_C$  and  $A_D$  are the activation functions of encoding and decoding, respectively, and they are generally nonlinear functions.  $W_C$  and  $W_D$  and  $t_i$  and  $t_j$  are the weight matrix and threshold matrix of the network, respectively.

The autoencoder generally adopts the gradient descent method to adjust the weights and thresholds between layers. The purpose is to minimize the error between the IFV  $x$  and the OFV  $y$  to reconstruct the OI. The cost function is generally the mean square error function or the cross-entropy loss function, and the expression is as follows:

$$l(x, y) = \frac{1}{n} \sum_{i=1}^n (y_i - x_i)^2, \quad (2)$$

$$l(x, y) = \frac{1}{n} \sum_{i=1}^n x_i \log(y_i) + (1 - x_i) \log(1 - y_i). \quad (3)$$

**3.1.2. Support Vector Regression.** In 1995, Vapnik introduced the support vector machine (SVM) to the world for the first time. To maximize the isolation edge between positive and negative samples, a classification hyperplane is used as a decision-making surface, with the isolation edge between positive and negative samples being maximized. This method is most commonly used to solve classification, pattern recognition, and regression problems. When it comes to dealing with difficult nonlinear issues and pattern recognition in vast dimensions, support vector machines provide

a number of advantages. It is a rough approximation of structural risk reduction with the goal of achieving good generalization for a small number of learning models in a short length of time. There are several characteristic indicators for the growth of executive power in university administrators, and a complex nonlinear relationship exists between the characteristic indicators and the development results, which makes it difficult to depict numerically. But because of its superior ability to fit nonlinear functions, SVR may be used to address this problem. SVR is used to anticipate the output outcomes of the deep neural network model's OL, as a result of which this chapter is structured as follows. It is possible to classify SVR as either linear or nonlinear depending on whether it is enclosed in a HDS or not. A significant portion of this section is devoted to nonlinear regression utilizing SVR because of the intricacy of the nonlinear problem of strengthening the executive capacity of higher education administrators. When used in SVR, the goal of nonlinear regression is to map a difficult nonlinear link to a HDS and then rebuild the linearized relationship in the HDS that has been defined. Assuming the data set is  $T = \{(x_1, y_1), (x_2, y_2), \dots, (x_n, y_n) | x_i \in S^n, y_i \in S\}$ , first define a nonlinear mapping function for the data set  $T$  that cannot be linearly separated in the original space  $S^n$ . Transform  $T$  to a HDS and ensure that  $\psi(T)$  exhibits favorable linear regression properties in the feature space  $F$ . As a result, to get a linearized representation of nonlinear issues, execute linear regression in the feature space  $F$  first and then in the original space  $S^n$ . The expression for creating a nonlinear function given a kernel function  $P(x_i, x) = (\psi(x_i), \psi(x))$  is as follows:

$$f(x) = \sum_{i=1}^T (\beta_i - \beta_i^*) P(x_i, x) + t. \quad (4)$$

The frequently used kernel functions are as follows, among which  $\tau$  is a parameter.

(1) Linear function

$$P(x_i, x) = x^Z x_i \quad (5)$$

(2) Polynomial function

$$P(x_i, x) = (1 + x^Z x_i)^\tau \quad (6)$$

(3) Radial basis function

$$P(x_i, x) = \exp\left(\frac{-\|x - x_i\|^2}{\tau^2}\right) \quad (\tau \text{ is the core width}) \quad (7)$$

(4) Sigmoid function

$$P(x_i, x) = \tanh(x_i, x) + \tau \quad (8)$$

### 3.2. DDAE-SVR Deep Neural Network

**3.2.1. Basic Model.** In this chapter, we introduce the DDAE-SVR DNN model, which can be used to handle challenging nonlinear problems or process large-scale data sets, which are difficult to solve with the current shallow neural network model because of its limited computation and modeling capabilities. SVR is utilized as the prediction OL, while deep denoising automatic encoding (DDAE) is used as the training OL in this study. When applying SVR, a linearized link in the set HDS equivalent to the low-dimensional space can be achieved. To denoise the original input data set before doing unsupervised layer-by-layer learning and training to reduce the error between the OI data set and training output data, an autoencoder is used to produce a feature vector from it. As a final OL prediction, SVR should be used, with the characteristics of your original data set being used as input for the SVR algorithm. The following two processes are the most significant in the DDAE-SVR DNN model.

#### (1) Unsupervised layer-by-layer training

Before the original input data is input to the DDAE-SVR DNN model training, because there will be some noise in the original input data that cannot be cleaned, the characteristics of the original input data will be set to 0 according to a certain ratio. To increase the model's durability and generalizability, noise reduction processing was used. The unsupervised training process is mainly to use the deep noise reduction autoencoder for training. The noise-reduction processed data enters the first DAE from the input layer for training, and the obtained output data is used as the IFV of the second DAE. After training all DAEs by analogy, each is equivalent to a hidden layer of DDAE. The error calculation between the last DAE decoded output data and the OI data is performed; then, the Adam method is used to optimize the error in order to reduce it until the desired accuracy is attained or the number of iterations is achieved.

#### (2) Supervised fine-tuning process

The feature vector of the last hidden layer of the deep noise reduction autoencoder is used as the IFV of the final OL of the DDAE-SVR DNN model, and the final OL is based on the supervised algorithm SVR as predictor. In this supervised prediction process, the relevant parameters of SVR are tuned to improve the prediction accuracy and efficiency of the entire model.

**3.2.2. Feature Index Samples and Data Sets.** The neural network model's deep structure has numerous hidden layers that can extract the properties of the original sample data with high computational capacity. Calculations and modeling may be performed successfully by neural network models that deal with complicated nonlinear issues or the deep structure of large-scale data sets. Therefore, the DDAE-SVR DNN model proposed in this chapter is used to solve the path to improve the executive power of university administrators. Given that traditional university administrators' personalized indicators

are mostly trained and improved from first-level indicators such as understanding, publicity, and implementation, the gender, age, and other aspects of their personalities are rarely improved in order to assess the effectiveness of the model proposed in this chapter. Taking into account the situation of transformation, the training improvement lacks comprehensiveness. In addition to the traditional evaluation indicators, this article adds two first-level indicators of gender and age to construct the evaluation indicator system of this article to comprehensively propose the promotion path of administrative personnel. The new two first-level indicators have a total of 5 second-level indicators, and all input characteristic indicators are shown in Table 1.

With a total of 17 assessment indexes, this article's evaluation index system combines the classic evaluation index with the newly introduced evaluation index. Obtain the relevant data set from 2015 to 2020 from the administrative staff management system of a university, the data set format  $(X_1, X_2, \dots, X_{17}, y)$ , a total of 1020 sample data. Among these, 17 secondary index data are employed as model input values. Due to the necessity of identifying the model's projected output value, a specific score segment corresponding to a path of execution power is utilized as the model's target expected output value, based on the many assessments and training records of the supervision group's teachers. The normalized preprocessing of the finally obtained data sample is to improve the computational efficiency of the deep neural network model. The sample data is normalized as shown in Table 2.

Using the normalized evaluation index sample data set in Table 1, the format is  $(X_1, X_2, \dots, X_{17}, y)$ , where  $X$  and  $y$  represent feature vector data and target label data, respectively, and set the total number of samples to  $n$ . Assuming that the weight matrix of each layer of the deep noise reduction autoencoder model is  $W$ , the threshold matrix is  $t$ , and  $\psi$  represents the deep noise reduction autoencoder model. When the input data set passes  $\psi$ , its expression is as follows:

When utilizing the normalized evaluation index sample data mentioned in Table 1, the format is  $(X_1, X_2, \dots, X_{17}, y)$ , where  $X$  and  $y$  represent feature vector data and target label data, respectively. The total number of samples is set to  $n$  using the normalized evaluation index sample data. If  $W$  indicates the weight matrix of each layer in the deep noise reduction autoencoder model,  $t$  denotes the threshold matrix, and  $\psi$  denotes the deep noise reduction autoencoder model, then the following is true. When the input data set satisfies the  $\psi$  test, the following equation is true:

$$\lambda = \psi(WX + t). \quad (9)$$

The  $\lambda$  in formulas ((3))--((5)) represents the deep noise reduction autoencoder model's OFV,  $\lambda$  is utilized as an input to the SVR model for evaluation and prediction, and  $f$  is used as the SVR model's function; the equation is as follows:

$$y_s = f(\lambda). \quad (10)$$

The evaluation sample data set is partitioned into training and test data sets, with the training data set being used to train the model discussed in this chapter. By modifying the

TABLE 1: Executive ability index of university administrative staff.

First-level index	Index number	Secondary index
Gender	X1	Man
	X2	Woman
	X3	≤35
Age	X4	35 < A ≤ 50
	X5	>50
	X6	Able to fully understand the superiors' instructions
Understanding	X7	Basic understanding of superiors' instructions
	X8	Unable to understand the superiors' instructions
	X9	Relevant plans or programs are understood by more than 90% of the execution targets
Publicity	X10	Relevant plans or programs are understood by more than 60% of the execution targets
	X11	Relevant plans or programs are understood by less than 60% of the execution targets
	X12	The plan or program can be perfectly implemented
Execution	X13	Occasionally flaws in plans or program
	X14	Frequent flaws in plans or program
	X15	Frequent creative proposals
Creativity	X16	Occasional creative proposals
	X17	No creative proposals

TABLE 2: Normalized feature index sample data set.

Index	X1	X2	X3	X4	X5	X6	X7	X8	X9
Score	0.8	0.7	0.6	0.7	0.8	0.8	0.7	0.6	0.8
Index	X10	X11	X12	X13	X14	X15	X16	X17	$\gamma$
Score	0.7	0.6	0.8	0.7	0.6	0.8	0.7	0.6	3.7-4.8

number of HLs in the model, the optimization technique, and other parameters, as well as the SVR parameters that affect prediction effectiveness, a stable and ideal model is created. Then, using the test data set, determine if the model is successful at increasing the executive authority of university administrators.

#### 4. Experiment and Analysis

In this chapter, we defined the model analysis and comparison, model parameter analysis, and comparison with shallow model briefly.

**4.1. Model Analysis and Comparison.** The small-scale feature data used in this article uses the data set in Section 3.2, while the large-scale data set uses the short-term traffic flow data set. Because large-scale feature data involves a large amount of privacy and is difficult to collect, large-scale short-term traffic flow data is used instead for verification, and the data structures of the two are similar and the dimensions are similar. If you use a deep noise reduction autoencoder, you should set the activation function of the Sigmoid function, the learning rate to 0.001, the accuracy goal to 0.001, the maximum number of training repetitions (5,000), and the

weight to be allocated at random, all with a threshold value of 0. The deep noise reduction autoencoder introduces the Adam algorithm and optimizes the number of HL and the number of neurons to minimize the error between the output data and the original data to obtain the essential characteristics of the original data. The important parameters of SVR are adjusted in the supervised OL to improve the prediction accuracy of the model. In order to verify that the DDAE-SVR deep neural network model proposed in this paper has more advantages than other models in terms of the promotion path of university administrators, in this section, the mean absolute percentage error (MAPE), mean square error (MSE), symmetric average absolute percentage error (SMAPE), and root mean square error (RMSE) are introduced as performance comparison indicators of model prediction accuracy. Their formulas are as follows, where  $n$  represents the sample size of the test data,  $R_i$  represents the actual true value of the test data, and  $P_i$  represents the predicted value of the test data by the model.

$$\begin{aligned}
 \text{MAPE} &= \frac{1}{n} \sum_{i=1}^n \left| \frac{R_i - P_i}{R_i} \right|, \\
 \text{MSE} &= \frac{1}{n} \sum_{i=1}^n (P_i - R_i)^2, \\
 \text{SMAPE} &= \frac{1}{n} \sum_{i=1}^n \frac{|P_i - R_i|}{(|R_i| + |P_i|)/2}, \\
 \text{RMPE} &= \sqrt{\frac{\sum_{i=1}^n (P_i - R_i)^2}{n}}.
 \end{aligned} \tag{11}$$



4.2. *Model Parameter Analysis.* Because a model’s output is the executive power route of university administrators, it is critical to optimize the model’s predictive performance by adjusting the proper parameters. I believe that is just the beginning. Experimentation is a continuous process of adjusting critical parameters in order to increase the model’s calculating abilities and forecast accuracy, and it is essential for this to happen. This section makes use of both unsupervised learning and training as well as supervised prediction output in order to increase the model’s ability to predict the executive power route of university administrators with more reliability.

- (1) There are various methods for optimizing the training process of neural network models, such as gradient descent algorithm, RMSProp algorithm, momentum algorithm, and Adam algorithm. While the current gradient descent technique is the most often used optimization strategy in neural network models, the convergence speed is sluggish and it is possible to slip into the local minimum and the gradient vanishes when training neural network models with several HLs. The Adam approach is provided as an optimization technique for the unsupervised learning training of the DDAE-SVR DNN model. First-order and second-order moment estimates are used to dynamically alter the learning step length for each parameter. Stabilizing parameters is a goal for each repeat of the learning process. When using the DDAE-SVR DNN model’s three HLs and 20 neurons in the HL, the mean square error function is employed to calculate the error between the unsupervised training output and the original input data. For training and error estimates, we use the gradient descent technique, RMSProp, the momentum algorithm, and the Adam algorithm. Their error curves are shown in Figure 2. Gradient descent and momentum algorithms have been dropping, but their decrease is gradual, and the number of iterations is increasing, resulting in a slow convergence rate, according to the chart. However, error convergence tends to flatten as the number of iterations grows. The first 500 iterations of RMSProp and Adam algorithms show a fast decrease in the OFV and original data errors. The graphic shows that the Adam algorithm is the best in recreating the original input data; hence, it has been selected as an ideal method for the process of unsupervised learning

The number of HLs in the DNN model is set to between two and five, with the number of neurons in each HL set to twenty, in order to determine the optimal number of HL for the DNN model while taking into consideration the size of the sample data set. Adam algorithm is a learning and training approach that is used to improve unsupervised learning and training processes. It is also known as Adam algorithm. Feed the properties of the sample data set into the DDAE-SVR DNN model during the training phase. After unsupervised training of the deep noise reduction autoencoder, the error curve between the output data feature vector and the

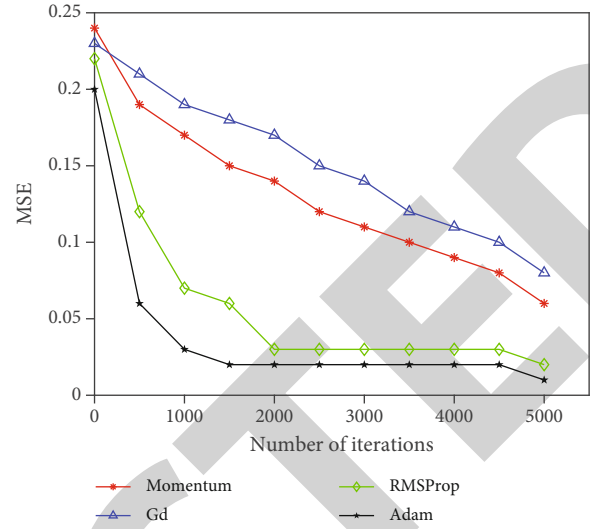


FIGURE 2: Error comparison of different optimization algorithms.

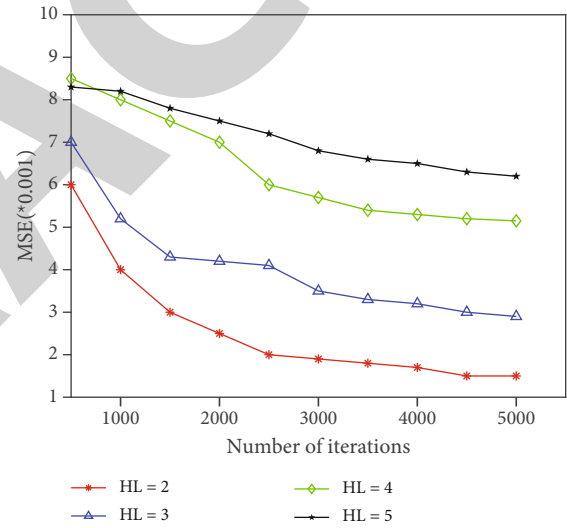


FIGURE 3: Error comparison of different hidden layers.

original input data set is displayed in Figure 3. Given a constant number of HL, the disparity between the reconstructed output data and the original input data shrinks rapidly as the number of recurrent training sessions grows. With a rise in HL, the error develops gradually as long as the number of repeated training sessions stays constant. Therefore, when the number of HL in the DDAE-SVR DNN model is reduced to two, the error between reconstructed output data and the original input data during unsupervised training is reduced to a bare minimum.

This component picks between 20 and 25 neurons for each HL in the DDAE-SVR DNN model. The Adam method is used to maximize the unsupervised learning and training process in the model, which has two HLs. The deep-noise autoencoder will automatically rebuild the error curve between the output data and the original input data after feeding the training data into the model and modifying the number of HL neurons, as shown in Figure 4. As the number

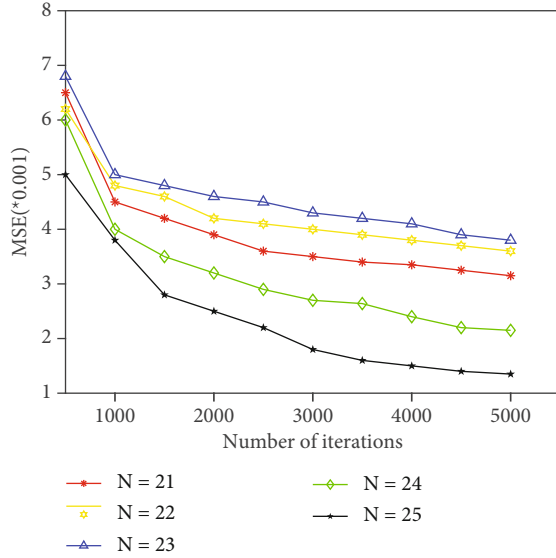


FIGURE 4: Selection of the number of different neurons in the hidden layer.

of iterations increases, the error between the reconstructed output data and the original input data decreases fast. This can be observed in the picture. Iterative training results in a progressive reduction in the error rate as the number of HL neurons increases. That is why 25 is chosen for each HL of the DDAE-SVR DNN. It is now at its best, in terms of inaccuracy, between reconstructed data and the original data used in the unsupervised training procedure.

## (2) Supervised prediction output process

Through the unsupervised learning training of the DDAE-SVR DNN model, the error between the reconstructed output data of the last HL and the original input data is minimized. Therefore, the feature vector of the last hidden layer neuron can be obtained as the IFV of the model prediction OL. The final prediction OL of the model uses SVR as the prediction period to predict the execution power improvement path. However, the main parameters that affect the performance of SVR are the error penalty coefficient,  $\nu$ , and the kernel function type. The error penalty coefficient is the key to adjust the model complexity and empirical risk,  $\nu$  is to control the number of support vectors and training errors, and its value range is (0.1). The kernel function type determines the distribution of sample data in HDS.

The kernel function types of SVR are mainly linear functions, polynomial functions, radial basis functions, and Sigmoid functions. In view of the size of the sample data set, the error penalty coefficient range is set to [1],  $\nu = 0.4$ . Obtain the eigenvector input of the last hidden layer in the unsupervised training process as the input eigenvector of the OL of the DDAE-SVR DNN model, and use SVR to predict and output, and then, obtain the error curve between the predicted result value and the true value. It can be seen from the Figure 5 that as the error penalty coefficient

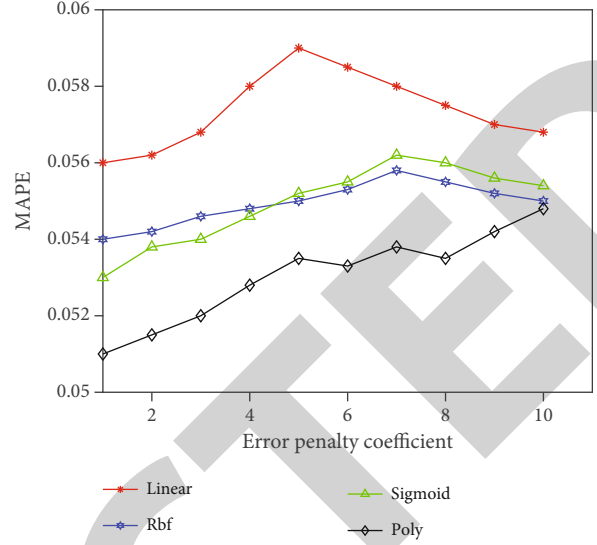
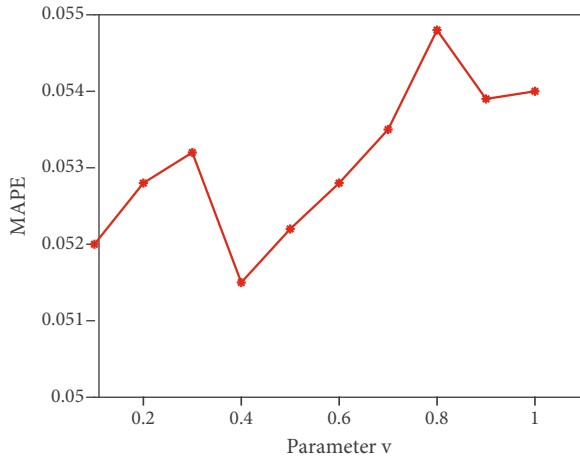
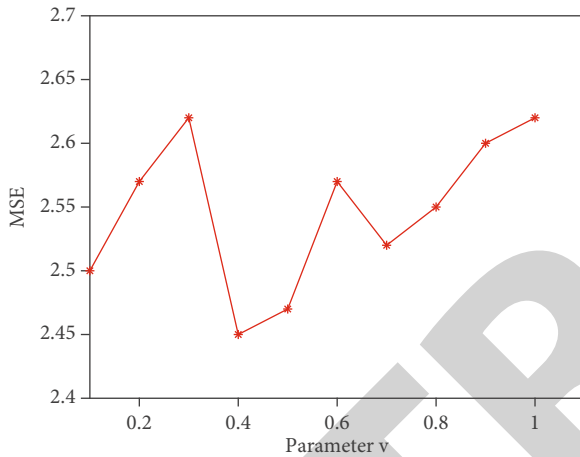


FIGURE 5: The selection of kernel function and error penalty coefficient.

increases, no matter which kernel function is used as the kernel function of SVR, the output prediction MAPE error will increase. Because the size of the sample data set is small, when the error penalty coefficient increases, it will cause excessive punishment and increase the MAPE. However, when the polynomial function is used as the kernel function of SVR, the prediction effect is better than the other three functions. Therefore, the error penalty coefficient of the SVR model is selected as 1, and the kernel function is selected as the polynomial function.

Verify that the DDAE-SVR DNN model's prediction output is accurate. The SVR of the prediction OL has an error penalty coefficient of 1, the kernel function is a polynomial function, and the value of the parameter  $\nu$ , which regulates the number of support vectors and the training error, is [0.1,1]. Then, the feature vector of the last hidden layer neuron after the unsupervised training of the model is used as the IFV of SVR. The graph of MAPE and MSE between the predicted result and the true value is shown in Figures 6 and 7. It can be seen from the figure that the curve change trends of the MAPE and MSE values are basically the same, which first decreases and then increases with the increase of  $\nu$ . When  $\nu = 0.4$ , the prediction error of the model in this chapter is the smallest and the prediction accuracy is the best.

**4.3. Comparison with Shallow Model.** DDAE-SVR DNN model is optimized to validate that the model provided in this chapter has more benefits than other shallow models in forecasting the execution power improvement route of university administrators. To minimize the error between the reconstructed output data and the original data, the Adam algorithm is used for optimization, with the number of HIs of the model and the number of neurons at 2 and 25, respectively. The essence of the original data is retrieved. The error penalty coefficient, the number of control support vectors, and the training error parameter  $\gamma$  are all adjusted in

FIGURE 6: Relationship between parameter  $\nu$  and MAPE.FIGURE 7: Relationship between parameter  $\nu$  and MSE.

the supervised prediction process, and the kernel function type is set to 1 and 0.4. The polynomial function optimization expenditure vector regression is the most efficient method for predicting model performance. To compare the DDAE-SVR DNN with three shallow models of standard BPNN, SVM, and adaptive BPNN, input the small-scale sample data set established in this article to train and verify the model, and predict the results using antinormalization processing. Table 3 shows the comparative findings for performance measures such as MAPE and MSE, which are utilized as comparison indicators. The table shows that all of the model's performance measures are optimum when compared to the typical BP neural network model. Although the model presented in this chapter requires more time to train than support vector machines, the other four performance characteristics are superior. However, when compared to the adaptive BPNN, this chapter's model performs better than it in other performance indicators, especially the two critical indicators of MAPE and MSE. Comparing these two models in this chapter shows that they each have their own benefits and weaknesses when dealing with small-scale data sets, which supports our claim that the neural network model in this chapter is successful.

TABLE 3: Comparison of results of different models.

Index Model	MAPE	MSE	SMAPE	RMSE	Time (s)
BPNN	0.085	48.250	2.12%	6.850	15.211
SVM	0.067	24.600	1.65%	4.960	0.256
Adaptive BPNN	0.065	20.520	1.58%	4.880	0.336
DDAE-SVR	0.06	18.860	1.59%	4.800	5.285

TABLE 4: Performance comparison of large-scale data sets.

Index Model	MAPE	MSE	SMAPE	RMSE	Time (s)
Adaptive BPNN	0.126	63.21	3.27%	7.24	34.63
DDAE-SVR	0.035	22.56	1.36%	3.52	91.57

Although the DDAE-SVR DNN model has advantages in dealing with small-scale and low-dimensional data on the issue of improving the executive ability of university administrators, it is difficult to reflect the application advantages of this model on large-scale high-dimensional data sets. Therefore, large-scale short-term traffic flow data is selected for experimental verification. Due to the increase in the size of the data set, the previously tuned parameters are all used for small-scale data sets. Therefore, the training process fine-tunes the parameters of the two models again and uses the training time of the model and performance indicators such as MAPE and MSE as comparison indicators. The comparison results of the two models are shown in Table 4.

When compared to an adaptive BPNN, which has a much shorter training period, the models discussed in this chapter are significantly more effective at correcting errors than the adaptive BPNN model. The number of HLs and the number of neurons in the model presented in this chapter is bigger than the adaptive BPNN model, resulting in a considerable amount of computation. There is a very little amount of error in this performance index, which shows that the model presented in this chapter has strong prediction accuracy and convergence to some degree, as well as its powerful computation and modeling abilities.

## 5. Conclusion

Under the new situation, the competition among the comprehensive education levels among universities is becoming increasingly fierce. It is not only necessary to continuously innovate teaching methods for the teaching staff, but also to improve the executive ability and master more political theories. The more the ability to assess and solve problems in complicated settings, the better the results in serving instructors and students and adopting higher-level policies will be. As a result, university administrators should understand and apply the spirit of university ideological and political work conferences, improve implementation, and contribute to the cause of higher education. A strategy for the promotion path of university administrators based on deep neural networks is provided in this research, which also

## Retraction

# Retracted: Value and Application of Traditional Culture of Embedded Network Teaching Platform in Moral Education in Colleges and Universities

### Computational and Mathematical Methods in Medicine

Received 25 July 2023; Accepted 25 July 2023; Published 26 July 2023

Copyright © 2023 Computational and Mathematical Methods in Medicine. This is an open access article distributed under the Creative Commons Attribution License, which permits unrestricted use, distribution, and reproduction in any medium, provided the original work is properly cited.

This article has been retracted by Hindawi following an investigation undertaken by the publisher [1]. This investigation has uncovered evidence of one or more of the following indicators of systematic manipulation of the publication process:

- (1) Discrepancies in scope
- (2) Discrepancies in the description of the research reported
- (3) Discrepancies between the availability of data and the research described
- (4) Inappropriate citations
- (5) Incoherent, meaningless and/or irrelevant content included in the article
- (6) Peer-review manipulation

The presence of these indicators undermines our confidence in the integrity of the article's content and we cannot, therefore, vouch for its reliability. Please note that this notice is intended solely to alert readers that the content of this article is unreliable. We have not investigated whether authors were aware of or involved in the systematic manipulation of the publication process.

Wiley and Hindawi regrets that the usual quality checks did not identify these issues before publication and have since put additional measures in place to safeguard research integrity.

We wish to credit our own Research Integrity and Research Publishing teams and anonymous and named

external researchers and research integrity experts for contributing to this investigation.

The corresponding author, as the representative of all authors, has been given the opportunity to register their agreement or disagreement to this retraction. We have kept a record of any response received.

### References

- [1] J. Yang, "Value and Application of Traditional Culture of Embedded Network Teaching Platform in Moral Education in Colleges and Universities," *Computational and Mathematical Methods in Medicine*, vol. 2022, Article ID 2096583, 13 pages, 2022.

## Research Article

# Value and Application of Traditional Culture of Embedded Network Teaching Platform in Moral Education in Colleges and Universities

Juanjuan Yang 

*School of Marxism, Haikou University of Economics, Haikou, 571000 Hainan, China*

Correspondence should be addressed to Juanjuan Yang; 201772513@yangtzeu.edu.cn

Received 11 April 2022; Revised 14 May 2022; Accepted 18 May 2022; Published 9 June 2022

Academic Editor: Naeem Jan

Copyright © 2022 Juanjuan Yang. This is an open access article distributed under the Creative Commons Attribution License, which permits unrestricted use, distribution, and reproduction in any medium, provided the original work is properly cited.

Higher education has always been the top priority of the country and society. With the gradual completion of the Chinese curriculum system, in addition to some subject knowledge, the education on ideology, morality, and quality has also become more and more perfect. Moral education in colleges and universities is an example of this. However, current moral education instruction in colleges and universities is still based on examination-oriented education, and students have not been exposed to the culture deeply. As a result, the goal of this study is to strengthen traditional culture's function in moral education instruction in colleges and universities, as well as conduct research on its application value. In response to this, this paper designs an embedded moral education network teaching platform, which focuses on increasing the importance of the role of administrators, and is responsible for collecting statistics of traditional culture resources and applying them to teaching. The education for traditional culture also traces its origins and provides suggestions for the new era with reference to historical moral education research. The results of this paper believe that, for the response time of the system, in the campus network environment, the response time is about 3 s, the minimum value is 2.8 s, and the maximum value is also 3.2 s. In an ordinary network environment, the response time is also within 3.8 s. This demonstrates that the approach proposed in this research is efficient and capable of meeting the needs of moral education instruction in colleges and universities.

## 1. Introduction

In a broad sense, college moral education workers are teachers and staff of universities, because they all have the responsibility of teaching and educating people. In a narrow sense, the moral education workers in colleges and universities are not only full-time party affairs personnel engaged in moral education and management but also professional teachers engaged in the teaching of Marxist theory. This research examines the moral development of college moral educators from a restricted perspective. Moral education workers in institutions of higher learning are responsible for the teaching, organization, coordination, decision-making,

and service of Marxism theory. Their work helps to adhere to the party's leadership over institutions of higher learning, so that colleges and universities always adhere to the socialist purpose of running schools and play an indispensable role in promoting the healthy growth of young students, while forming a positive inner belief. Most of the teachers engaged in ideological and political education are conscientious, honest and self-disciplined, and conscientiously perform the noble duties of an ideological and political educator. However, in the context of globalization, in the face of the increasingly open external environment, it is more necessary to strengthen their own ethics; apricot will lead to the decline of teachers' morality. Therefore, it is very

necessary to strengthen the self-cultivation of moral education workers in colleges and universities.

In the study of moral education in colleges and universities, there are mainly the following two innovations:

- (1) Based on the characteristics of traditional culture in moral education teaching, this paper designs an embedded moral education network teaching platform. The design of this platform can provide better help for teachers' teaching and students' learning
- (2) For moral education, this paper focuses on the role of Chinese traditional culture in teaching, and it believes that in moral education, the construction of teachers' ethics should pay more attention to the study of traditional culture

The focus of this paper's investigation is on the function of Confucianism in moral education. Of course, there are flaws in this paper's research. For example, in the design of embedded systems, numerous low-level frameworks are not attempted to improve the system's performance and functionality. More in-depth research will be carried out in the future.

The paper arrangements are as follows.

Section 2 examines the related work. Section 3 describes the university moral education and network platform application. Section 4 evaluates the embedded network teaching platform design. Section 5 concludes the article.

## 2. Related Work

The study of moral education in colleges and universities has always been a concern of many scholars, because it not only affects the teaching quality of colleges and universities but also affects the quality of college students. Liu believed that the moral quality of agricultural and forestry college students in the new era presents a positive mainstream trend, but there are also some unavoidable problems [1]. Song took Qingdao Library's proposed construction of Qingdao Memory Culture Center as the research object. He promoted the inheritance of intangible cultural heritage and preserves urban memory by mining and sorting cultural resources and building platforms and carriers, which is of great significance to innovative urban development [2]. Zhao-Fleming et al. have high insights into the study of moral education and even links it to medicine [3]. Teusch is interested in using semantics, nomenclature, and scientific description to investigate moral education languages. The results of the investigation revealed that moral education research has been integrated in dialect users' phonological actions [4]. Valentsova conducted research on an independent ethnocultural group. He believed that in various areas of spiritual culture in this mountainous region, many ancient elements of the common Slavic era are preserved, which are also known in different parts of the Slavic world. In traditional medicine, this common Slavic practice is a cure for the evil eye and witchcraft [5]. Nguyen et al. provided an analysis of changes in ritualism based on field data and earlier sources collected

from 2014-2019 and earlier in Karakalpak areas with contiguous or fragmented populations (Chinbesky, Karauzyaksky, Kegelski, Nukuski, Khodelsky, and Tahitashsky regions of the Republic of Uzbekistan, Karakalpakstan). His research found that the ritual innovations of the Karakalpaks, caused by sociocultural and economic changes, reflected the logic and content of traditional family festivals, and their complex symbolic meanings were related to status changes [6]. According to relevant research, it can be found that most scholars focus on the curriculum setting of moral education in colleges and the teaching level of teachers, and they do not really integrate traditional culture into the teaching of moral education in colleges and universities. At the same time, it lacks the application of science and technology and embedded network platform.

## 3. University Moral Education and Network Platform Application

This section discusses the current situation of moral education in colleges and universities. They examine the application of traditional culture in moral education in colleges and universities. They analyze the construction and application of university moral education network platform.

*3.1. Current Situation of Moral Education in Colleges and Universities.* The Chinese nation has been advocating culture and teaching since ancient times. The excellent traditional Chinese culture also contains profound educational ideas, in which special emphasis is placed on the importance of moral cultivation for personal growth. The moral cultivation of people in China has continued since ancient times [7]. Moral concepts in ancient China were not separated into distinct categories as they are today, but rather were woven throughout social conventions and culture. As a result, there was no distinct moral instruction in ancient China strictly speaking. However, researching ancient society's talent training system reveals that the content of moral education was dispersed throughout all elements of people's life, affecting people's lives all the time. In ancient China, the education system, imperial examination system, and management system formed the ancient feudal society's three-in-one talent system, which established the ancient feudal society's talent training system. The core contents of the system are all developed around "morality" and "talent," as shown in Figure 1.

From the Song Dynasty through the end of the Qing Dynasty, a specific type of academies formed, which were akin to private universities in today's culture. During the Qing Dynasty, schools of the type of private primary schools began to exist. In addition to official and private schools, family education as a supplement also promoted the formation of the ancient school education system to a certain extent. The establishment process of the ancient education system reflects the importance that ancient China attached to education. The core of ancient education is to teach people how to behave and attach importance to the cultivation of moral culture. Therefore, the social characteristics of

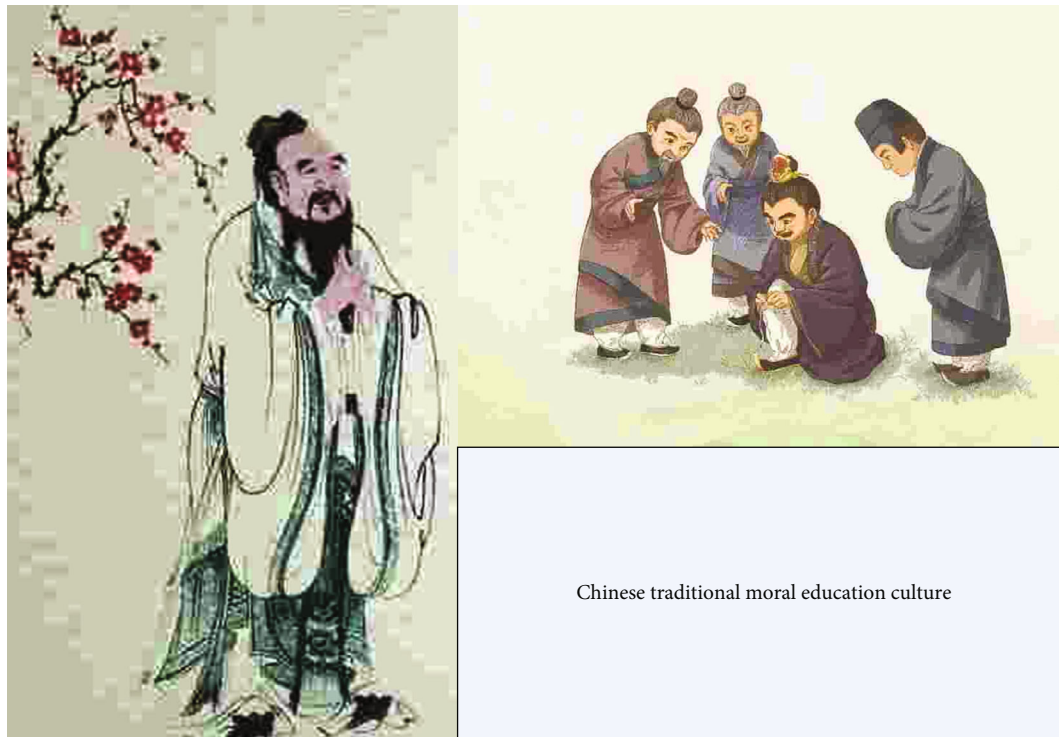


FIGURE 1: Chinese traditional moral education culture.

respecting teachers and teaching are formed in ancient times.

“Cultivating oneself, managing the family, controlling the country, and giving peace to the world” is how the ancient concept of moral education is summarized. The foundation is “self-cultivation,” and the purpose is “ordering the family, controlling the country, and bringing peace to the globe.” This puts forward requirements for the individual and the society. The individual’s own moral cultivation is the basis for helping the country and society progress, and the harmonious cultural atmosphere created by the country and society provides an environment for individual cultivation. Combining personal growth with the development of society and country is the core connotation of ancient moral education thought and has been deeply affecting the changes of Chinese moral education thought. After the struggle between the old and the new morality in modern times and the establishment and development of New China, whether it is the criticism of the dross of ancient feudal morality, the study of Western morality, or the establishment of socialist morality with Chinese characteristics, the development of Chinese moral education has not interrupted. Its unique historical continuity also provides experience that can be used for reference for the development of contemporary Chinese moral education theory [8].

Ancient moral education thought emphasized the moral quality of “people.” In modern times, although there is a debate between private morality and public morality, the focus of the debate is still on the moral development of “people.” Therefore, China’s moral education is, in the final anal-

ysis, an education that emphasizes cultivating and refining the ideological and moral qualities of “people.” What is ideological and moral literacy? Ideological and moral literacy takes “people” as the starting point and refers to people living in a certain social environment starting from certain moral standards, the basic stable behaviors and stable psychological characteristics shown when dealing with the relationship between individuals and others, and between individuals and society, as well as people’s moral cognition, cultural self-cultivation, and acceptance of moral standards.

From the perspective of history, Chinese moral education has always regarded the inner self-cultivation and development of “people” as the core of its essential development and paid attention to the importance of moral education to the country and society. This always links the moral quality of the individual with the development of the country. The improvement of the moral quality of the individual contributes to the progress of the country and society, which in turn affects the self-improvement of the moral quality of the individual. Under such conditions, as the fundamental goal of education, “cultivating morality and cultivating people” is the general trend and aspiration.

*3.2. Application of Traditional Culture in Moral Education in Colleges and Universities.* Traditional culture and modern and contemporary culture are divided based on the vertical development of history. But culture is fluid, not eternal. If we simply divide culture into two parts, “traditional” and “modern” according to time, it will inevitably fall into “cultural nihilism” and “cultural retroism.” The attitude of

cultural nihilism towards traditional Chinese culture is “cultural inferiority,” and the attitude of cultural retroism towards traditional Chinese culture is “cultural arrogance.” These two attitudes are a kind of separation of Chinese traditional culture and modern and contemporary culture. The “cultural self-confidence” insisted on does not simply refer to the culture at a certain stage in a certain historical period, but is a combination of traditional culture and modern and contemporary culture that is closely connected with the times through reform, innovation, and development [9].

The outstanding traditional Chinese culture is a one-of-a-kind national culture developed by the Chinese people. It is the culmination of thousands of years of Chinese civilization and has distinct value connotations. The realization of its value is of great significance to social progress and all-round development of human beings. The excellent traditional Chinese culture is produced in a certain social environment and formed in the public life of the people. The moral standards and values contained in it are based on the public and face the broad masses of the people. In the new era, students should inherit the dialectical method of the excellent traditional Chinese culture since the May 4th Movement. At the same time, they should also be based on the practice of reform and opening up and socialist modernization with Chinese characteristics in the new era and adapt to the characteristics of contemporary social development. Based on this understanding, traditional culture can be roughly divided into three parts. The first part is the class system and moral concept with distinct feudal society ruling class thought in traditional culture, which is negative and backward, and belongs to the bad part of traditional culture, which needs to be eliminated. The second part is the content of moral values in traditional culture that have far-reaching influence on the country and society, such as love of the motherland, honesty and trustworthiness, and hard work, which are still affecting the development of Chinese society and should continue to be preserved and inherited. The third part is the ideological and moral culture that is constantly changing with the development of history. This part of the culture is mainly the part that is constantly self-innovating with the development of social life, and it is also the part that needs to be creatively transformed. Like the understanding of “benevolence” and “li” in Confucianism, there is a deviation in understanding between ancient times and contemporary times, and it is necessary to continuously reform and adjust according to the social development situation [10].

A country cannot prosper without virtue, and a person cannot stand without virtue. To achieve the great rejuvenation of the Chinese nation and build a socialist cultural power with Chinese characteristics, it must be inherited the excellent traditional Chinese culture. The excellent traditional Chinese culture contains rich moral education ideas, which have been accumulated and passed down through the changes of the times and are essentially identical with the moral education in contemporary colleges and universities. The world today is undergoing profound changes unseen in a century. The incorporation of Chinese superb traditional culture into moral education in colleges and uni-

versities not only improves the philosophy of moral education in the current period but also aids the development of Chinese-style socialism. It is vital to China’s superb traditional culture as well as moral education in colleges and universities. It has three distinct meanings, as indicated in Figure 2.

- (1) *The Demands of the Times.* Chinese great traditional culture, which has influenced the Chinese people’s value system and spiritual power since ancient times, continues to do so in the modern period. In light of the changing development situation both at home and abroad, a thorough knowledge and excavation of China’s outstanding traditional culture is a key priority. Accelerate China’s superb traditional culture’s innovative transformation process and recognize its current value, which is favorable to fighting the detrimental impact of diverse ideological trends in the era of network big data. Through the contemporary transformation of the excellent traditional Chinese culture, the curriculum content of the talent training base in colleges and universities will be enriched, and the humanistic and moral cultivation of college students will be improved. This will help China show the world the spiritual outlook of the new generation of Chinese youth and the contemporary charm of China’s excellent traditional culture. In this way, it will further enhance cultural self-confidence, enhance the sense of national pride and identity, enhance the cultural literacy of the whole people, improve the country’s cultural soft power, and increase China’s international influence
- (2) *Social Needs.* Building a civilized and harmonious social environment has always been one of the goals of social governance. With the rapid development of society and economy, people’s material level has been greatly improved compared with before, and the quality of life has also been greatly improved, but what follows is a lack of spirituality. From the old man who has caused controversy in news reports and cannot help, to the frequent incidents of showing off his wealth, the pursuit of personal interests and material wealth has gradually led the social atmosphere to a deviated track
- (3) *Personal Needs.* In the context of world globalization, there are more and more cultural exchanges between countries around the world. The rapid development of new media such as the Internet has also accelerated the spread of various cultural ideas. In today’s fast-paced life, more young people use the Internet to learn about information. It is precisely because of this that various negative and negative thoughts such as “egoism” and “hedonism” spread rapidly through the Internet, which has formed a major impact on the values of young people. For a long time, colleges and universities have only paid attention to the quantitative indicators of academic



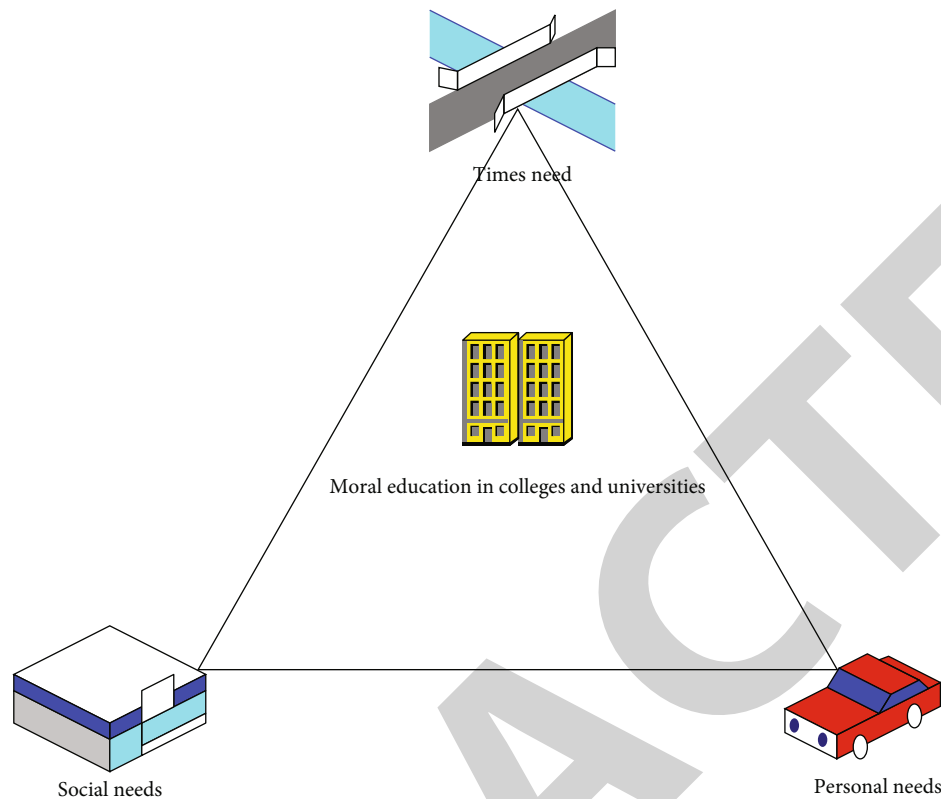


FIGURE 2: The significance of moral education in colleges and universities.

performance and ignored the impact of multiple thoughts on college students. They relax the cultivation of students' ideology and morality, which promotes the spread of many ideological and moral problems among college students. The individual's demand for moral ideals is likewise quite strong in this environment. Traditional Chinese culture is full of strong moral principles and values. Patriotism, taking responsibility, and daring to create are still valuable spiritual assets that have been impacted by superb traditional Chinese culture, and they have had a subtle impact on the Chinese people's way of life and behaviour. It plays an important role in the personal moral judgment and value orientation standards of the society. In the new era, inheriting and developing the excellent traditional Chinese culture will help improve personal cultural accomplishment and improve the ability to judge people or things. This requires consciously resisting negative and negative cultural thoughts and establishing a correct world outlook and outlook on life and values [11, 12].

**3.3. Construction and Application of University Moral Education Network Platform.** The original multimedia teaching system consists of projectors, electric screens, multimedia computers, physical display stands, DVD players, video recorders, recording decks, power amplifiers, and centralized control systems. The system greatly enriches the teacher's teaching content, the visual and intuitive audio/

video presentations make the classroom more attractive to the students, and the students are more interested in contacting new things, which greatly increases the teaching effect. At that time, the equipment in the classroom was more and more complicated, so a centralized control system (called the "local central control" stage) was adopted to assist teachers in using it.

Whether the types of courses are rich and whether the course system is comprehensive and perfect are important aspects for the development of the online teaching platform. Although the online Confucius Institute mentioned in the article has rich course types and a large number of free course resources, it has not formed a complete course system. Some types of courses may only have courseware resources for a certain lesson or unit, which makes it difficult for learners who take self-learning methods to learn Chinese to find a series of courses that meet their needs. In addition, the online Confucius Institute also has an online search function, which allows learners to search for courses through keywords, which is not yet available in online Beiyu. Therefore, the online teaching platform of Chinese as a foreign language should pay attention to two important types of curriculum type and curriculum system in the development process. It is not simply to set up many courses according to the classification of courses and pile these courses together in a mess, but to clarify the framework and context between courses, link them organically, and establish a complete course system. In addition, the search function of the website should be developed to facilitate Chinese learners to search for courses that meet their own learning needs [13, 14]. In

the process of cross-cultural communication, it is very likely that cultural conflicts will occur, which will lead to “culture shock.” The manifestations of this “cultural shock” vary from person to person. People who know less about the target language culture and have significant differences between their mother tongue culture and the target language culture are very prone to “cultural shock.” Conversely, people who know more about cultural differences are more likely to survive the “culture shock” stage. The two online teaching platforms for Chinese as a foreign language, the Online Confucius Institute and the Online Beiyu, have separate content on cultural teaching, and language teaching and cultural knowledge are separated.

#### 4. Embedded Network Teaching Platform Design

The system uses the most advanced high-performance embedded microprocessor ARM9 as the core control platform and uses its powerful and convenient communication function and storage function, and it uses sensor technology and signal processing technology to realize the real-time collection and detection of functioning status information and alarm report information of multimedia classroom teaching equipment, considerably improving the system’s performance and operational efficiency, so that managers can accurately grasp the real-time working status of multimedia classroom equipment through the network; through the dedicated audio processing chip and the storage function of ARM9, the system can realize the personalized setting of the sound effect for each teacher, so as to ensure the best teaching effect of each teacher. The multimedia classroom network group control management platform of this system also provides remote control of multimedia classroom equipment, real-time monitoring of the working status of multimedia classroom teaching equipment, automatic notification of failure and alarm of multimedia classroom teaching equipment, multimedia classroom teaching schedule management, multimedia classroom teaching schedule management, multimedia classroom podium access control card issuance management, multimedia classroom class attendance management, and other functions.

##### 4.1. System Design Principles

- (1) *Stability.* Through the optimized combination of software, hardware, and system design indicators, the system ensures that the system platform has better stability, so as to ensure that the system can continue to operate normally
- (2) *Security.* The core of this network teaching platform is content management. It bans unauthorized users from posting bad consultations using this teaching system to secure user data at all levels. The platform adopts a specific security mechanism to ensure the security of the system, such as only opening permissions to users with identities, and user information

and passwords need to be encrypted to ensure the security of data information

- (3) *Fault Tolerance.* In the system design process, the system requires a certain degree of fault tolerance to improve the user experience. For example, when users at all levels input illegal information or information that does not meet the requirements, it can log in the dialog box information incorrectly and give the system prompt information that meets the verification standard
- (4) *Response Speed.* When revamping the system database, data redundancy and page loading time should be reduced to increase the system’s response time and reduce user operations waiting time at all levels
- (5) *Interface.* In the design process of the front page, not only must consider the comprehensiveness of the system function implementation to make the user easy to operate but also consider the aesthetics of the interface at all levels of the system, so that the realization of each interface function can meet the advanced requirements of user-friendly interface

*4.2. Overall Structure Design of the System.* This system adopts B/S (Browser/Server) network structure, namely, browser and server network system design. The main application software of the client is a web browser, which enables the unified management and development of client applications. The main system functions are implemented on the server side. This B/S structure, on the basis of simplifying the user side, focuses on the development and maintenance of the WEB side, making system maintenance more targeted [15]. According to the B/S network structure mode, the system platform can be subdivided into three-layer framework structure of user application layer, program layer, and database layer. The specific workflow is as follows: input query conditions on the user’s foreground page, the application layer receives the data and calls the database layer; and then the database layer queries the database and returns the qualified information records to the database layer; finally, the information record obtained by the database is referenced by the program layer, and the data record obtained by the application layer is referenced by the user layer and displayed on the front page. The B/S three-tier architecture used in this system is shown in Figure 3.

The system platform is oriented to three user groups: system administrators, teachers, and students, and the permission levels of each category are different. It enters the main interface of users at all levels through the initial login interface, operates the user’s operable functions, and writes the data into the corresponding database. After the database is updated in real time, other users can continue to access the database to perform functions within their respective user rights and finally update the obtained data to the database. A schematic diagram of the overall structure of the system is shown in Figure 4.

The system login module contains three different types of operations, namely, system administrator, teacher user,

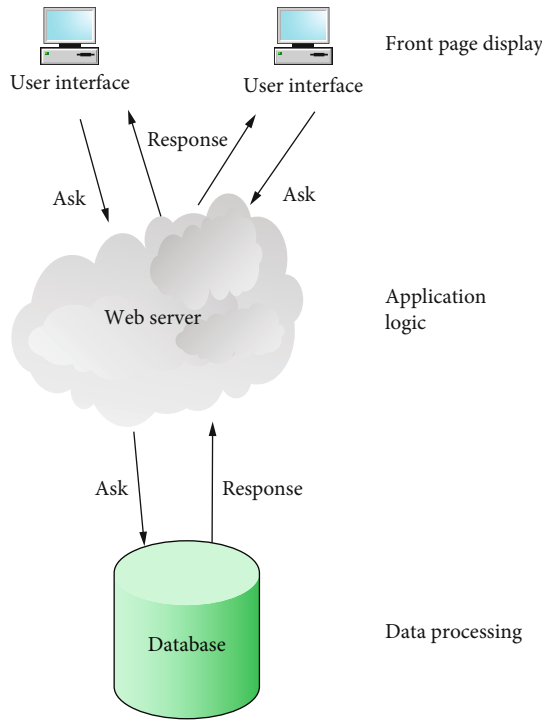


FIGURE 3: Three-layer B/S structure.

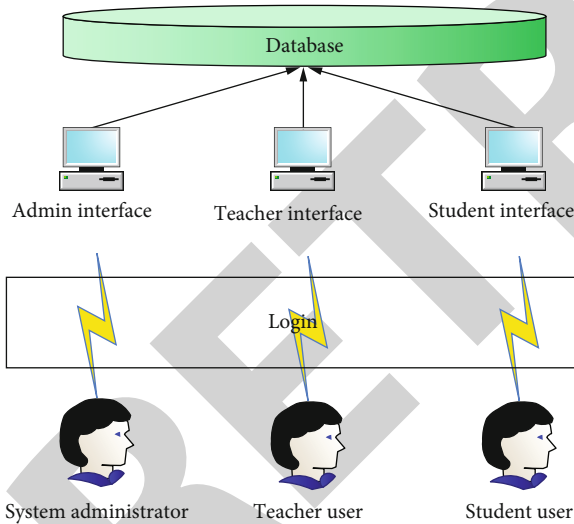


FIGURE 4: Overall system frame diagram.

and student user. Different users are required to enter a non-empty user name and password when logging in. The system retrieves the administrator table, teacher table, and student table in the database, determines the role type to which the user belongs, and then enters the respective welcome interface according to the specific role type, thereby obtaining different permissions and completing the corresponding specific operation tasks [16]. The flow chart of the main interface of the login function module of this system platform is shown in Figure 5.

In the course management module, the teacher first submits a new course application to the administrator and fills

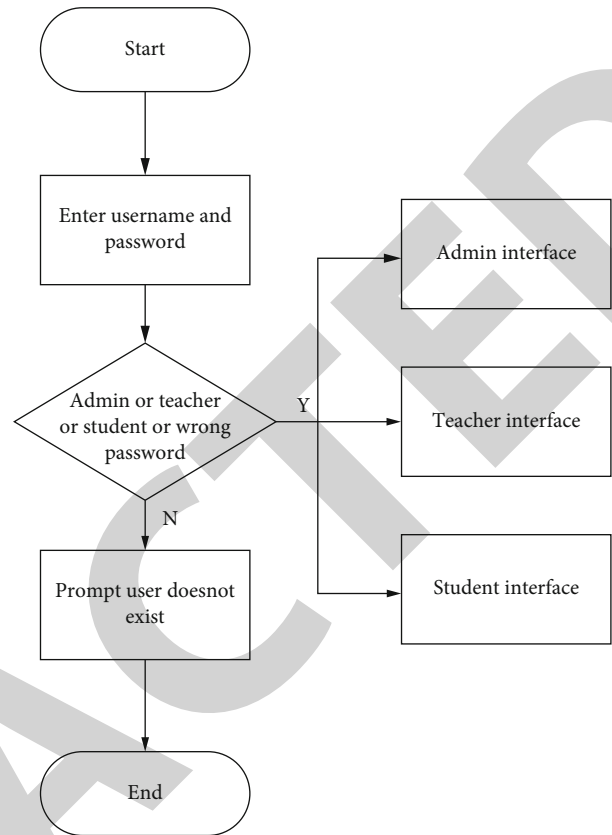


FIGURE 5: System module login function flowchart.

in the new course declaration form. After the system administrator approves and approves, teachers can reform ideas according to the new teaching. They use project-based teaching to organize courses according to project tasks, create a course catalog for the course, and complete the upload, modification, and deletion of course resources according to the subtasks of each course catalog. The types of course resources mainly include teaching text files, sound files, compressed package material files, and video files. Project task lesson plans, course electronic teaching materials, teaching electronic plans, course standards, task materials, electronic courseware, assignments, and exercises are all included in the classification of course teaching resources [17]. In the main interface of teacher user operation, users can view all course announcements, teacher information, and course content catalogs. And for the courses set up in this article, you can maintain and update operation permissions such as viewing, editing, adding, and deleting. Users can also view, add, edit, and modify the student information of the taught class. On the learner's main interface, users at this level can browse the teacher's profile, course content introduction, course announcements, and the catalog of specific project tasks, and then learn about the teacher's information and course information. After starting course study, users can have permission to browse and download course resources, submit homework and quizzes for each project and task of the course, and take course exams after course study. The flow chart of teacher course management is shown in Figure 6.

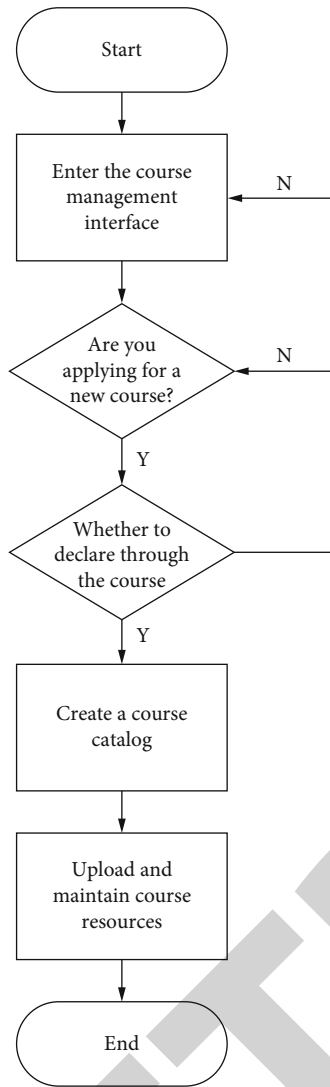


FIGURE 6: Flowchart of teacher course content management.

Candidates have the right to view the test paper scores in the score management function module, which can be found in “Student Main Interface - Course Exam - View Scores.” Teacher users can not only view test takers’ test scores but also re-edit test takers’ test paper scores. In addition to having the authority to view and modify student grades, the system administrator can also generate student grade sheets based on majors, classes, and other conditions. The operation flow chart of this module is shown in Figure 7.

**4.3. Database Design.** Through demand analysis, it is known that the entities included in this network teaching platform system mainly include system administrator, teacher, student, course, department, major, course catalog, question type, test question, test question answer, test paper, test information, score, announcement, problems, and many other entities. The following article describes the relationship between each entity and its attributes through E-R diagram, data logic structure, entity data table, and part of the module design, as well as the specific process of functional module implementation [18].

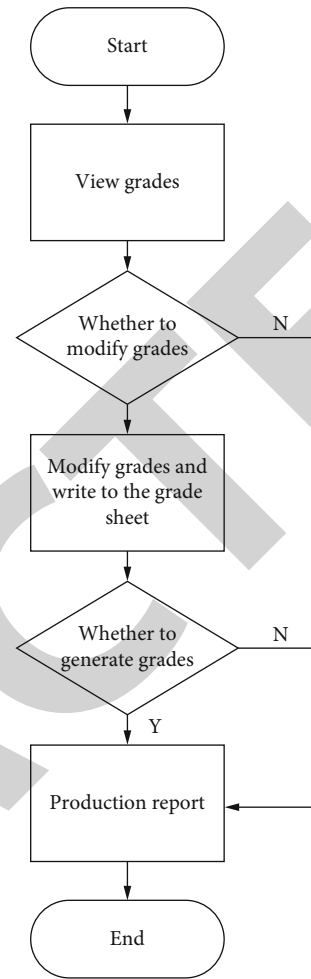


FIGURE 7: Grade management flowchart.

In the teacher type function module, the entities used include teacher profile, course announcement, students, course catalog, course content information, material resources, assignments, exam papers, and questions submitted by students. The relationship between each entity and the teacher is represented by the teacher-user E-R graph, as shown in Figure 8 [19].

In the student function module, the entities used include student profile, system announcement information, course announcement information, teacher information, course catalog, content resources, exam papers, assignments, grades, and questions submitted by the user. The relationship between each entity and student is represented by the student user E-R diagram, as shown in Figure 9 (some entities and attributes are omitted) [20].

The first two sections have completed the overall design of the system E-R diagram and the logical structure of the system database. Next, the MySQL database is used to establish the corresponding data forms. The administrator table is used to place the basic information of the system administrator user, and its detailed table structure is shown in Table 1.

The teacher table is a data table used to store the basic information of the teacher identity user, and its detailed table structure is shown in Table 2.

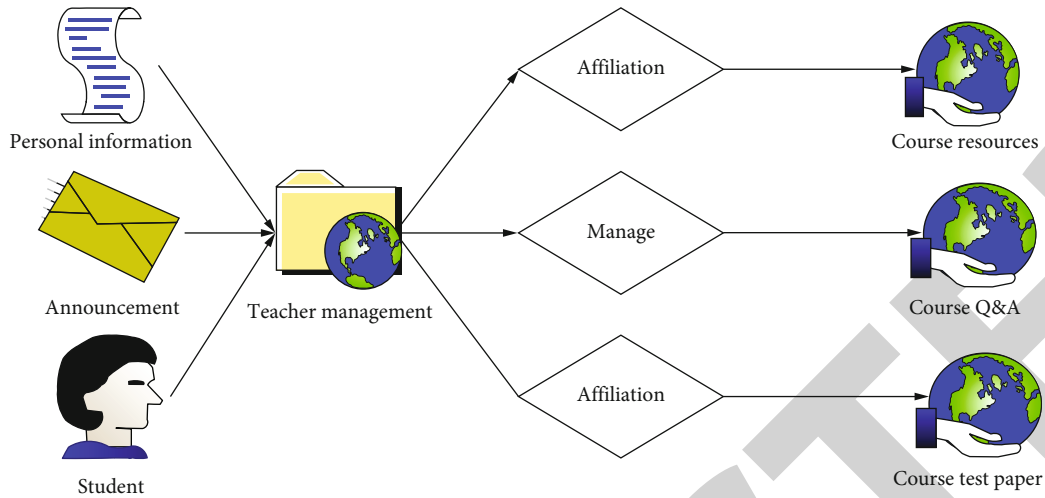


FIGURE 8: Teacher user E-R diagram.

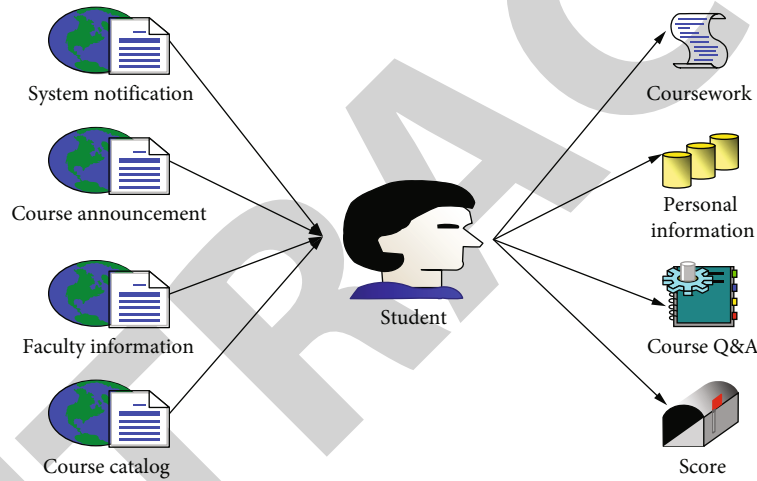


FIGURE 9: Student user E-R diagram.

TABLE 1: Administrator table.

Field name	Type of data	Describe
User ID	Int(10)	User ID, primary key
Name	Varchar(20)	User name
Password	Varchar(20)	Password
Admin number	Int	Employee number
Admin name	Varchar(20)	Actual name
Gender	Set("male," "female")	Gender
Email	Varchar(50)	Email information
Role	Enum("0," "1," "2")	Role information
Introduce	Varchar(2000)	Self-introduction
Remark	Varchar(200)	Remark

The student table is mainly used to store the data table of the basic information of the student identity user. The detailed table structure is shown in Table 3.

The curriculum table is a data table used to store all the courses offered. It can be associated not only with the user table but also with the related forms of the department table and the major. The detailed table is shown in Table 4.

A department table is a data table used to place information about the content of related colleges and departments. The department table can not only classify system users (such as teacher users and student users) but also can be used to divide departments and further divide courses. The detailed table is shown in Table 5.

**4.4. System Function Realization.** This chapter focuses on the realization of the major functions of the network teaching management platform and shows the interface realization effect of some functional modules and some important source codes. It includes system login module, announcement module, course module, student management module, student course selection module, question bank, and test question management module.

TABLE 2: Teacher table.

Field name	Type of data	Describe
User ID	Int(10)	User ID, primary key
Name	Varchar(20)	User name
Passwd	Varchar(20)	Password
t_number	Int(10)	Staff number
Zhsnaname	Varchar(20)	Actual name
Gender	Set("male," "female")	Gender
Dept_id	Varchar(50)	Department
Email	Varchar(50)	Email address
Role	Enum("0," "1," "2")	Role information
Introduce	Varchar(2000)	Self introduction
Remark	Varchar(200)	Remark
Regtime	Datetime	Registration time

TABLE 3: Student table.

Field name	Type of data	Describe
User ID	Int(10)	User ID, primary key
Name	Varechar(20)	User name
Passwd	Varchar(20)	Password
s_number	Int(10)	Student ID
Realname	Varchar(20)	Actual name
Gender	Set("male," "female")	Gender
Dept_id	Varchar(50)	Student's department
Class	Varchar(50)	Student's class

TABLE 4: Class schedule.

Field name	Type of data	Describe
Sub_id	Int(10)	Course number, primary key
Sub_name	Varchar(40)	Course title
User ID	Int(10)	User number, foreign key
Name	Varchar(20)	User name
Sub_text	Varchar(2000)	Course introduction

TABLE 5: Department table.

Field name	Type of data	Describe
Dept_id	Int(10)	Department number, primary key
Dept_name	Varchar(40)	School name
Dept_intro	Varchar(2000)	Introduction to the department

The design and implementation of the network teaching platform stems from the needs of the reform of the new teaching mode of the service college, changing the status quo of the traditional teaching mode and making college students more active and innovative in professional learning. The realization of the course management module is fully integrated with the new teaching mode. That is, on the basis

of the project-based teaching model, the creation of course catalogs and the reorganization of teaching resources will undoubtedly play a good role in promoting the ongoing course teaching reform. Furthermore, this online teaching platform is built using PHP development technology, adheres to software development best practices, rearranges relevant theories and technologies for learning, conducts a thorough and comprehensive demand analysis for the design of each functional module of the system, and finally completes the overall design of the system and the implementation of key functions. The system's primary function is summarized as follows:

- (1) The development status of the existing network teaching platforms at home and abroad is investigated and expounded, and the goal significance and feasibility of the construction of this network teaching platform are obtained
- (2) The system analyzes the development feasibility of the platform system from the perspectives of market, economy, technology, and operation. At the same time, through careful teaching research and student questionnaires, the functional requirements and nonfunctional requirements of the platform system are obtained
- (3) Based on the technical feasibility analysis of the system platform development, the overall structure frame of the system platform is designed, and the system development platform and main technical means are determined
- (4) The system platform's functions are meticulously created to make the system's function structure more intensive in order to suit the user's functional requirements. And it analyzes and designs the system database, creates data forms, creates user interfaces and functional main interfaces at all levels of the system, adds PHP dynamic code, and gradually realizes each functional module of the system
- (5) In the process of platform creation, each part of the function implementation has been tested, and problems can be found and corrected in time
- (6) The performance requirements of the system platform in the overall design process mainly include system practicability, system maintainability, system openness, system scalability, and system security

4.5. *System Performance Test.* The performance of the system is largely reflected in the ability of data analysis and processing. According to the above description, the mathematical description of the clustering problem is obtained:

Given data set

$$V\{v_i|i = 1, 2, \dots, n\}. \quad (1)$$

Among them,  $v_i$  represents the data object, and the data set is divided into  $k$  groups according to the similarity

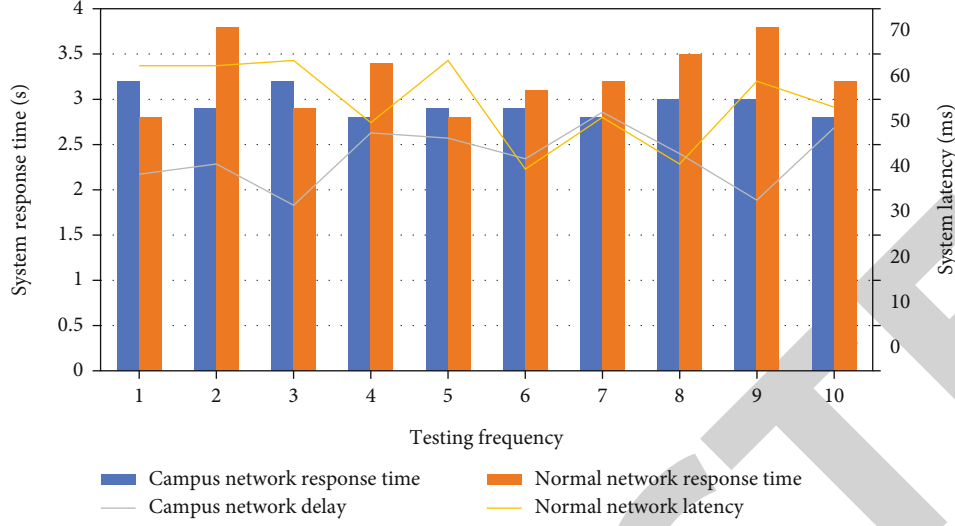


FIGURE 10: System test result graph.

between the data objects and satisfies

$$C_j | j = \{1, 2, \dots, k\}, \quad (2)$$

$$C_j \subseteq V, \quad (3)$$

$$C_i \cap C_j \neq \emptyset, \quad (4)$$

$$\bigcup_{i=1}^k C_i = V. \quad (5)$$

Then, the process is called clustering, and  $C_i (i = 1, 2, \dots, n)$  becomes a cluster (class).

It can also be described that the input to the cluster analysis is represented by a set of ordinal pairs  $(x, s)$  or  $(x, d)$ .  $x$  represents a set of samples,  $s$  and  $d$  are the similarity or dissimilarity criteria between clustered samples, respectively. The output of the cluster analysis is a partition:

$$x = (G_1, G_2, \dots, G_k), \quad (6)$$

where  $G_k (k = 1, 2, \dots, N)$  is a subset of  $x$  as follows:

$$G_i \cap G_j \neq \emptyset, i \neq j, \quad (7)$$

$$G_1 \cup G_2 \cup \dots \cup G_k = X. \quad (8)$$

The member  $G_1, G_2, \dots, G_k$  in  $x$  is the class, and each class is described by some characteristics. This is for example to represent a class of points in an  $n$ -dimensional space by their centroids or (boundary) points of relationships in the class, to represent a class graphically using nodes in a clustering tree, or to represent classes using logical expressions of sample attributes.

There are two main types of data structures in data analysis.

Data matrix:

$$\begin{bmatrix} x_{11} & \dots & x_{1p} \\ \vdots & \ddots & \vdots \\ x_{n1} & \dots & x_{np} \end{bmatrix}. \quad (9)$$

Dissimilarity matrix:

$$\begin{bmatrix} 0 & \dots & 0 \\ \vdots & \ddots & \vdots \\ d(n, 1) & \dots & 0 \end{bmatrix}. \quad (10)$$

Here,  $d(i, j)$  is a quantitative representation of the dissimilarity between objects  $i$  and  $j$ , usually it is a nonnegative number. When the objects  $i$  and  $j$  are more similar or "closer," the value is closer to 0; the more different the two objects are, the larger the value is. Since  $d(i, j) = d(j, i)$ , and  $d(i, i) = 0$ , a matrix of the form 10 can be obtained.

$$\forall x', x \in X \forall x', x \in X. \quad (11)$$

In general, a measure of similarity of clustering algorithms can be normalized as

$$0 \leq s(x, x') \leq 1 \forall x', x \in X. \quad (12)$$

However, a measure of dissimilarity rather than similarity is usually used as a criterion. The measure of dissimilarity is expressed as

$$d(x', x), \forall x', x \in X. \quad (13)$$

Generally speaking, the variable describing the object is a continuous interval, and the dissimilarity is usually called the distance. When  $x$  and  $x'$  are similar, the distance  $d(x,$

$x'$ ) is very small. If  $x$  and  $x'$  are not similar,  $d(x, x')$  is large. Here, this article only introduces the definition of the distance of the data object when the description attributes of the data object are all interval scale attributes. The commonly used distance definitions are as follows:

Manhattan distance:

$$d(i, j) = |x_{i1} - x_{j1}| + |x_{i2} - x_{j2}| + \dots + |x_{im} - x_{jm}|, \quad (14)$$

where  $d(i, j)$  is the distance from the data object  $i$  to the data object  $j$ ;

$$X_i(x_{i1}, x_{i2}, \dots, x_{im}), \quad (15)$$

$$X_j(x_{j1}, x_{j2}, \dots, x_{jm}). \quad (16)$$

Equations (15) and (16) are the  $m$  attributes of data object  $i$  and data object  $j$ , respectively.

Euclidean distance:

$$d(i, j) = \sqrt{|x_{i1} - x_{j1}|^2 + |x_{i2} - x_{j2}|^2 + \dots + |x_{im} - x_{jm}|^2}. \quad (17)$$

Minkowski distance:

$$d(i, j) = (|x_{i1} - x_{j1}|^q + |x_{i2} - x_{j2}|^q + \dots + |x_{im} - x_{jm}|^q)^{1/q}, \quad (18)$$

where  $q$  is a positive integer. When  $q = 1$ , the Minkowski distance is the Manhattan distance; when  $q = 2$ , the Minkowski distance is the Euclidean distance.

This paper uses virtual software to test the performance of the embedded network platform teaching system. In order to achieve the purpose of teaching, the simulation of the number of people online at the same time is 100, the response time of the test system and the delay of the interaction between teachers and students. The test is divided into campus network and ordinary 5G network environment, and 10 tests are carried out, respectively. The results are shown in Figure 10.

Figure 10 shows that the response time and delay of the embedded network teaching system are within the normal range, regardless of whether it is a campus network or a common network, demonstrating that the embedded moral education network teaching platform can meet the normal needs of teachers' teaching and students' learning. After observation, it can be found that for the response time of the system, in the campus network environment, the response time is about 3 s, the minimum value is 2.8 s, and the maximum value is also 3.2 s. Such a response time is relatively fast. In an ordinary network environment, the response time is also within 3.8 s. Normally, a response time of less than 5 s can be considered normal. The system interaction delay is between 30 and 50 milliseconds in the campus network environment and less than 60 milliseconds in the conventional network environment. The higher system performance in the campus network environment is because the system design of this paper considers the network proto-

col of the campus network, which has a higher priority for the campus network, so the performance will be better than that of the ordinary network.

## 5. Conclusions

"Taking history as a mirror, we can see prosperity and decline." The traditional Confucian idea of self-cultivation is like a mirror, which can reflect people's words and deeds. Traditional Confucian self-cultivation concept is also a ruler of civilization, allowing people's world views, beliefs, and outlook on life to be continuously corrected, as well as their ideological and moral consciousness. This research proposes a teaching platform for embedded moral education networks. This platform's design can assist professors in their teaching and students in their learning. The Confucian idea of self-cultivation is derived from the living educational practice, and it is a moral factor of universal significance. Although the conditions of the present age have changed, it can still guide the current moral practice. The research of this paper is more inclined to the role of Confucianism in the work of moral education. Of course, the research of this paper also has certain defects, for example, in the design of embedded systems, several low-level frameworks are not tried to improve the performance and functions of the system. In the later research, more in-depth research will be carried out.

## Data Availability

The datasets used during the current study are available from the corresponding author on reasonable request.

## Conflicts of Interest

The author declares that he has no conflict of interest.


## References

- [1] M. Liu, "Innovation of moral education mode in agricultural and forestry colleges and universities in the new period," *Asian Agricultural Research*, vol. 10, no. 5, pp. 96–98, 2018.
- [2] F. Song, "Inheriting traditional culture and building city memory –taking Qingdao City memory culture center as an example," *International Journal of Social Science and Education Research*, vol. 2, no. 5, pp. 57–61, 2019.
- [3] H. Zhao-Fleming, S. Barake, A. Hand et al., "Traditional culture methods fail to detect principle pathogens in necrotising soft tissue infection: a case report," *Journal of Wound Care*, vol. 27, no. Sup 4, pp. S24–S28, 2018.
- [4] A. Teusch, "Language of the forestry discursive community (based on the traditional culture of the Urals)," *Professional Discourse & Communication*, vol. 2, no. 1, pp. 88–95, 2020.
- [5] M. Valentsova, "Once again about archaic in the Gó ral traditional culture," *Slavic Almanac*, vol. 3-4, pp. 245–269, 2020.
- [6] H. Nguyen, K. Valcova, G. Zakirova, A. Larionova, and I. Lapidus, "Western science, religion and Vietnamese traditional culture: harmony or antagonism?," *XLinguae*, vol. 13, no. 3, pp. 94–113, 2020.



## Research Article

# Evaluation and Analysis of the Intervention Effect of Systematic Parent Training Based on Computational Intelligence on Child Autism

Xuejin He,<sup>1,2</sup> Yinzhen Yu,<sup>2</sup> and Yanqiong Ouyang<sup>1</sup> 

<sup>1</sup>The Wuhan University School of Nursing, Wuhan, Hubei 430000, China

<sup>2</sup>Tongji Hospital Affiliated to Tongji Medical College HUST, Wuhan, Hubei 430000, China

Correspondence should be addressed to Yanqiong Ouyang; 2016120232@jou.edu.cn

Received 15 April 2022; Revised 11 May 2022; Accepted 16 May 2022; Published 8 June 2022

Academic Editor: Naeem Jan

Copyright © 2022 Xuejin He et al. This is an open access article distributed under the Creative Commons Attribution License, which permits unrestricted use, distribution, and reproduction in any medium, provided the original work is properly cited.

Autism, also known as pervasive developmental disorder or autism spectrum disorder, is a group of clinical syndromes of developmental delay or impairment. Social impairment, verbal communication impairment, and behavioral impairment are the three conditions for the diagnosis of autism spectrum disorder, according to the American Psychiatric Association's Diagnostic and Statistical Manual. According to relevant statistics, about 1 in 100 children is now diagnosed with autism, and their rehabilitation treatment is also valued by people from all walks of life. In the rehabilitation training of autistic children, it is found that the rehabilitation training of autistic children should pay attention to the role of parents and family environment. It is crucial that parents receive systematic training and act as partners in the development of the intervention plan. Research shows that a specific structured education and skills training program for parents of children with autism can be beneficial in improving behavioral problems, functional communication, and symptoms of autism in children with autism. To this end, this paper has completed the following work: Secondly, a portion of the systematic training of CA parents is discussed, followed by an explanation of the structure and principles of BPNN. Finally, the BPNN is utilized to create a model for assessing the impact of systematic parent instruction on CA. The experimental findings suggest that the proposed BPNN outperforms the competition.

## 1. Introduction

CA is the most common developmental disorder among the extensive developmental disorders. Its main clinical manifestations are social interaction disorder, language communication disorder, and behavior disorder; often, the onset is before age 3, more boys than girls [1]. CA is a chronic functional disability that develops in childhood, and its long-term prognosis is related to ongoing community and family care [2]. Data released by the US Centers for Disease Control and Prevention in 2014 showed that the prevalence of autism spectrum disorder (ASD) was 1 in 68, with a male-to-female ratio of about 4.5:1. Among

the mentally disabled children in my country, CA ranks first. Due to the rising prevalence of autism, people's lives may be plagued by intense and ubiquitous lifelong illnesses, and families are greatly affected emotionally and financially. The etiology and pathological mechanism of CA are still unclear and may involve many factors, such as genetic factors, neurobiological factors, organic brain factors, maternal diseases, infections, and immune factors, but the exact cause and mechanism of the disease have not yet been determined [3]. Children with autism have poor verbal communication, social interaction, and self-care ability; stereotyped behaviors; and narrow interests, and most of them cannot integrate into the normal population. Mental

retardation, attention deficit hyperactivity disorder, learning difficulties, sleep issues, eating disorders, seizures, sensory abnormalities, and other comorbidities of children with autism place a severe strain on the family and society. Scholars in the United States and worldwide believe that there is presently no viable treatment to cure autism, and children with autism have a poor prognosis [4]. If children with autism can be detected early, diagnosed early, and carried out timely intervention and other effective rehabilitation education and training, about 5% of children with autism can return to society and live, study, and work independently [5]. The American National Standard Evidence-Based Practice Guidelines report concludes that there is currently no universally effective treatment for autism spectrum disorder and that a multimodal approach is more likely to promote child development, improve behavior, and reduce child and family stress [6]. At present, the internationally recognized rehabilitation measures for children with autism mainly include interpersonal relationship training, discrete unit teaching method, key skills training, language training, structured teaching, picture exchange communication system, music therapy, sensory integration ability training, functional communication training, and other comprehensive interventions. Reference [7] believes that accurate assessment of the problems of children with autism can play an important role in the early diagnosis and targeted intervention of children with autism. Children with autism may benefit from early discovery, diagnosis, and treatment, which can help alleviate their symptoms [8]. Due to the disadvantages of long-term drug treatment, domestic and foreign child psychologists have begun to focus on the application of nondrug interventions in the treatment of CA, and social psychological interventions are widely used in the treatment of CA, such as family intervention. Family interventions mainly include parental training and systematic family therapy [9]. Among them, parental training has been adopted by CA multimodal therapy research institute and has made great research progress. At present, domestic treatment is also changing to a comprehensive treatment method, but the current social and psychological intervention is relatively chaotic, and a complete comprehensive intervention system has not yet been established. There are also some studies on systematic parenting training in China, but there are still many deficiencies. For example, the eight-step method of parent training by Barkley is simply used, and it has not been properly revised according to the cultural environment of our country. It is easy to fall off; the evaluation of the effect of previous studies has mostly focused on the core symptoms and behavioral problems of children, and less attention has been paid to the psychological conditions of children and parents. In this context, this paper proposes a systematic parent training based on computational intelligence to evaluate and analyze the intervention effect of autistic children. Computational intelligence includes many methods. This paper uses the neural network method to evaluate the intervention effect.

The following is a description of the study: the introduction is in Section 1, and Section 2 goes over the related

studies. Methods of the proposed work are discussed in Section 3. Experimental results and evaluation are covered in Section 4; finally, in Section 5, the conclusion puts the paper to a close.

## 2. Related Work

Autism has received attention since it was first mentioned in 1943, and its definition has been constantly changing as research on such children progresses [10]. Autism is not a single disease, but a spectrum of developmental disorders consisting of several syndromes, and the spectrum of autism is constantly evolving with research. The first is the increase in the number of people covered, from the beginning of childhood autism to the definition of adult autism, making the concept of autism more comprehensive. The second is the continuous updating of connotation and extension, the increasingly clear diagnostic criteria in connotation, and the addition and removal of related syndromes in extension, all of which make the concept of autism more perfect [11]. But in this spectrum, the most important feature is the three core symptoms of autism: social interaction disorder, speech disorder, and behavior disorder. Reference [12] believes that the difference between autism and obsessive-compulsive disorder is that autistic people are immersed in stereotyped behaviors and ritualized behaviors, while obsessive-compulsive patients are accompanied by obsessive-compulsive behaviors in a depressed state; the difference between people with autism and people with language disabilities is that people with language disabilities can use nonverbal communication to compensate for verbal communication, while people with autism have impairments in both verbal and nonverbal communication; the difference between people with autism and people with mental retardation is that people with autism fluctuate greatly in their intellectual development, while people with mental retardation have been in a state of delayed intellectual development. CA, also known as classic autism, is characterized by significantly aberrant or hindered social interaction and communication development, as well as significantly stereotyped behaviors and interests [13]. So far, the treatment methods for children with autism are very diverse: there are play therapy, sensory integration therapy, behavioral therapy, music therapy, art therapy, TEACCH structured teaching, etc., each of which has its own characteristics. In my country, educational intervention and behavioral training have become the mainstream of rehabilitation for CA. Some approaches focus on emotional and interpersonal interactions in CA, while others focus on cognitive and communication development [14]. In the early 20th century, with society's emphasis on children's rights and legal status, experts in helping children with emotional disorders launched the child counseling movement. According to the interaction theory of family system, children with autism will not only have an impact on their families, but also, families will act on children with autism and affect the children's rehabilitation process. Reference [15] research suggests that family parenting style will affect the social ability of children with autism. These studies show that parental emotions,

behaviors, and stress can affect children's development, including social interaction and problem behaviors. Reference [16] conducted a comparative study on 151 families of children with autism and 113 families of ordinary children in a province. The findings suggest that families with autistic children, particularly moms, have higher psychological issues, marriage troubles, and family dysfunction. A study in reference [17] compared the personality traits of parents of autistic children to those of parents of typically developing children and found that the personality traits of parents of autistic children differed considerably from those of parents of typically developing children and they both showed emotional instability and psychotic personality characteristics. Reference [18] used "Parent-Child Interaction Therapy" for high-functioning autistic children aged 5-12 with behavioral problems. The adaptability of children with autism improved, and the positive interaction between children with autism and their parents increased. Reference [19] used the "Family-Implemented Treatment for Behavioral Inflexibility" on 5 autistic children with an average age of 48 months for a 12-week intervention. The results of the study showed that parental participation in the treatment of autistic children can significantly reduce self-esteem. Stereotyped behavior in children with autism was observed, 4 of whom were followed up at 2 or 4 weeks to show that the intervention continued to be effective. It can be seen that parental participation in the treatment of autistic children is conducive not only to the recovery of autistic children but also to the improvement of parents' mental health. Since the health level of both parents and children in the family system has improved, it can be speculated that involving parents in the rehabilitation training of autistic children can improve the function of the family system. Reference [20] conducted an intervention study on 5 autistic children aged 3-9 years in combination with family therapy. The results showed that family therapy can promote the psychological recovery of autistic children and improve the children's sensory ability, interpersonal skills, and physical motor skills. References [21-23] conducted an intervention study on 33 autistic children with assisted family therapy. The results showed that the children's abilities improved in various parts, but the progress was uneven, and communication and language were more significant. Family therapy is changing into a school of therapy based on empirical research, and family therapy is integrating techniques and theories from other schools. This integration trend is not only driven by its internal theoretical integration but also driven by external pressure and social responsibility. Thus, systematic parental training interventions for children with autism may have unexpected positive effects.

### 3. Method

*3.1. Systematic Training for Parents of Children with Autism.* The parent training system refers to New Forest's "Six-step Method of Parenting Plan" and Barkley's eight-step method of child behavior management, combined with the family characteristics of autistic children in my country to design a systematic parent training system, including two aspects:

child behavior and parent psychology. In each level of training guidance, the main training content is as follows.

#### (1) Basic knowledge training of CA

The trainer will explain the basic knowledge of CA's clinical manifestations, pathogenic factors, diagnosis, prognosis, epidemic status, etc., answer parents' questions about CA, help parents understand the reasons behind these behaviors of CA children, and understand and acceptance of children.

#### (2) Comprehensive intervention of CA

Parents express their own views, including the children's current medication, questions about medication, and desired intervention methods. The trainer introduces the current clinical treatment methods, the effects of treatment methods, and the treatment mechanism of drugs. Help parents understand how to deal with children with CA, and eliminate parents' confusion and concerns about drug treatment of CA.

#### (3) Learning management of CA children

Parents express their views and exchange experiences on the reasons for children's learning difficulties and how to better communicate with school teachers. The trainer explains the causes of CA children's learning difficulties, learning methods and strategies, behavioral skills for children to manage their own schoolwork, and how to develop a daily behavioral school report card to integrate home-based reward programs with school-based reward programs. On the basis of understanding the children in the first two steps, parents use the academic management skills they have learned to gradually help children solve their academic problems.

#### (4) Behavior modification of CA children

Parents express their opinions on the methods they have taken to manage children's bad behavior in the past and share their experiences with each other. The trainer explains the principles, common techniques and methods of behavioral therapy, the principles of establishing behavioral contracts, and how to choose reinforcers. Parents can flexibly apply the behavioral modification methods introduced by the trainer according to the different performances of their children.

#### (5) Help CA children deal with interpersonal relationships

CA parents talk to each other about their children's challenges with interpersonal interactions and social skills that have been covered with them. The trainer explained the types of social skills, how to help children learn to communicate with others, how to improve parent-child relationships, how to adjust the relationship between CA children and teachers and help parents understand the correct way to communicate with CA children, strategies for playing games with CA children, etc. Parents learn to teach their

children how to express their emotions and how to deal with their own emotions. Parents can use family reward systems, role-playing, and other methods to help children improve their social skills.

(6) Emotional and stress management of parents of CA children

Parents tell their parenting pressures and negative emotions and share their experiences according to their own adjustment methods. The trainer explained the causes of negative emotions and the management methods and skills of negative emotions and stress. Help parents understand the causes of negative emotions, how to deal with the negative emotions when facing children with CA, how to communicate with teachers reasonably and effectively, and with problem-solving strategies and skills.

**3.2. Artificial Neural Network Method.** Based on the structure and function of the biological brain, ANN is an information-processing system. Neural network theory is an information science that learns from the human brain. It is a field that developed rapidly in the mid- to late 1980s. Its development has had an important impact on computer science, AI, cognitive science, and other fields. A neural network is a network composed of many simple neurons connected to each other. Although the structure and function of each neuron are relatively simple, the behavior of the neural network is not a simple superposition of the behavior of each unit, and the overall dynamic behavior of the network is extremely complex, and it can form a highly nonlinear dynamic system, which can express many complex physical systems, showing the basic characteristics of general complex nonlinear systems and various properties as neural network systems. A wide range of neural network models are available, each of which may be used to explain and mimic distinct parts of the nervous system, such as perceptron, BP network, RBP network, two-way associative memory, Hopfield model, and others are good examples of network models. Approximation of functions, clustering of data, categorization of patterns, and optimization calculations are all possible with these network models. It is used mostly for function approximation, pattern recognition, classification, and data compression, among other things. The BP method or a variant on it is the basis for the majority of neural network models now being used in actual ANN applications.

**3.2.1. BP Neural Network.** The input, hidden, and output layers of a BPNN (a.k.a. multilayer feedforward neural network) are each separated by a layer of neurons. All neurons in each layer exclusively communicate with those in neighboring layers; there is no link across layers; and each layer does not have a feedback connection to other levels. To create an output response, data is sent from the input layer unit to the hidden layer unit, which processes it before sending it to the output layer unit, where it is further processed. Iteratively tracing the path of the output response and modifying the output response weights and thresholds one layer at a

time until it is within acceptable limits might reduce this mistake. The connection weights and thresholds for each layer are continuously computed and corrected until the error reaches the required level, at which point the estimated output response is compared to the anticipated output.

Figure 1 is the topology diagram of the BPNN. Among them, the input signal is represented by  $X_i$ , the output of the hidden layer node is represented by  $H_j$ , the output of the output node is represented by  $Y_k$ , the expected output is  $T_k$ , the connection weight of the input node  $i$  to the hidden layer node  $j$  is  $V_{ij}$ , the hidden layer node connection weight from  $j$  to the output node  $k$  is  $W_{jk}$ , and the given number of samples is  $N$ ;  $N_1$ ,  $N_2$ , and  $N_3$  are the number of input, hidden layer nodes, and output nodes, respectively. In practical application, BPNN can set up multiple hidden layers according to the needs of the problem.

The main characteristics of BPNN are as follows:

(1) Nonlinear mapping capability

Any nonlinear continuous function may be approximated with arbitrary accuracy using neural networks. The problems associated with data modeling are highly nonlinear.

(2) Parallel distributed processing method

Information is distributed and stored and processed in parallel, which makes it highly fault-tolerant and has a fast-processing speed.

(3) Self-adaptive ability

It can extract regular knowledge from input and output data, memorize it in the weights of the network, and have generalization ability, that is, the ability to apply this set of weights to general situations. Learning of neural networks can also be done online.

(4) The ability of data fusion

It can process quantitative information and qualitative information at the same time and can use traditional engineering technology and AI technology.

(5) Multivariable system

An unlimited number of input and output variables in a neural network may be used to describe both single-variable and multivariable systems without addressing the issue of decoupling between subsystems.

**3.2.2. Disadvantages of the BP Neural Network.** In the traditional BP approach, which is a gradient descent algorithm with weights and thresholds moving in the opposite direction as the gradient, which is the direction in which the operation processing function declines the fastest, the Widrow-Hoff learning rule is utilized. The error of BPNN is a function of the weights of each layer and the pair of input samples. Through the analysis of the error surface

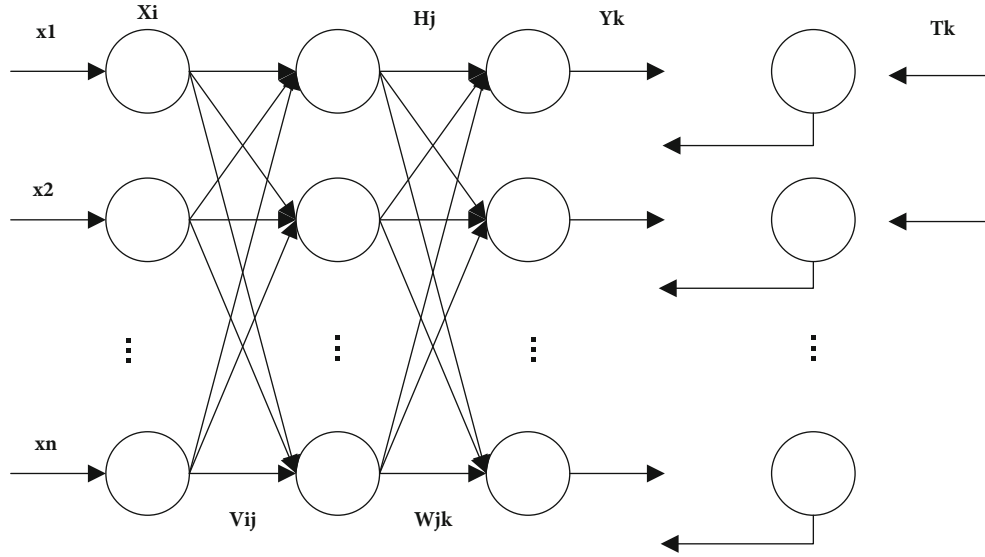


FIGURE 1: Topological structure diagram of the BP neural network.

distribution in its two-dimensional weight space, it can be seen that the BPNN has the following limitations.

(1) There are flat areas

Some areas on the error surface are relatively flat. In these areas, the gradient of the error changes very little. Even if the adjustment of the weights is large, the error still decreases slowly. Only when the adjustment direction is correct and the adjustment time is long enough it can exit the flat area and enter a certain valley, thus affecting the convergence speed.

(2) There are multiple minimum points

In the BP algorithm, which uses the gradient descent approach for nonlinear optimization, local minima are unavoidable. Because the solution space for real issues is generally a multidimensional surface with multiple local minima, the likelihood of trapping in local minima is considerably increased. Because random weights are often used in the BP method, it is difficult to train the network to its global optimum. As a result, the training cannot converge to the given error.

**3.2.3. Improved Algorithm Based on Gradient Descent.** When modifying weights, the standard BP technique just considers the error's gradient descent direction at time  $t$ , which can lead to training process oscillation and sluggish convergence. The improved algorithm based on gradient descent is based on the standard gradient descent method; that is, each time the network weights and thresholds are corrected, the correction amount of the previous learning is added according to a certain proportion, thereby accelerating the convergence of network learning. The specific method is

$$\Delta W(t+1) = c + \theta \Delta W(t), \quad (1)$$

TABLE 1: Childhood autism assessment index system.

Index	Score	Label
Interpersonal relationship	1-4	X1
Imitate	1-4	X2
Emotional response	1-4	X3
Physical ability	1-4	X4
Relationship with inanimate objects	1-4	X5
Adaptability to environmental changes	1-4	X6
Visual response	1-4	X7
Auditory response	1-4	X8
Proximity sensory response	1-4	X9
Anxiety response	1-4	X10
Language communication	1-4	X11
Nonverbal communication	1-4	X12
Activity level	1-4	X13
Intellectual function	1-4	X14
General impression	1-4	X15

where  $W(t+1)$  is the correction amount that should be obtained this time,  $W(t)$  is the previous correction amount,  $c$  is the correction amount calculated from the current error, and  $\theta$  is the learning rate.

It can be seen from the above formula that if the previous correction amount is overadjusted, the inertia term is opposite to the current error correction term, so that the actual correction amount this time is small, which has the effect of reducing oscillation, while the current correction amount is underadjusted. When the inertia term of this error calculation has the same sign as the correction term, the actual correction amount of this error increases, which helps to speed up the repair.

**3.3. Child Autism Evaluation Index System.** When constructing the evaluation index system of CA, this paper adopts the ‘‘Childhood Autism Rating Scale’’ (CARS), which is for professionals to evaluate, and it is composed of interpersonal relationship, imitation, emotional response, body movement ability, relationship with nonliving objects, adaptability to environmental changes, visual response, auditory response, near-sensory response, anxiety response, verbal communication, nonverbal communication, activity level, intellectual function, and general impression composition; each separate score is 1, 2, 3, and 4. The total score is greater or equal to 30 points as the cut-off point for diagnosing autism in children, that is, level I; the total score is 30-36 points, and less than 5 items are less than 3 points. When the overall score is greater than or equal to 36 points and more than 5 items are over 3 points, it is classified as severe autism, which is grade III. See Table 1 for details.

**3.4. Evaluation Design of Intervention Effect Based on Neural Network.** The algorithm flow of the BPNN is shown in Figure 2.

The formula involved in this training process is as follows:

$$H(s) = \sum_{i=1}^n V_{ij} x_i(s) - t_j, \quad (2)$$

where  $s$  refers to the number of samples in the  $s^{\text{th}}$ ,  $H$  refers to the number of hidden layers,  $V_{ij}$  is the connection weight between the  $i$ th input layer neuron and the  $j$ th hidden layer neuron, and  $t_j$  refers to the threshold of the  $j$ th neuron in the hidden layer of the network.

$$f(x) = \frac{1}{1 + e^{-x}}, \quad (3)$$

where  $x$  refers to the hidden layer input value and  $f(x)$  is the output function.

$$y_i(s) = \sum_{j=1}^m W_{jk} H_j(s) - t_k, \quad (4)$$

$$y_k(s) = f(y_i(s)), \quad (5)$$

where  $W_{jk}$  is the connection weight between the  $j$ th neuron cell in the innermost hidden layer and the  $k$ th output neuron cell,  $y_i(s)$  is the output function of the  $s$ th data sample,  $t_k$  is the output function of the output layer threshold of the  $k$ th neuron cell, and  $H_j$  is the value of

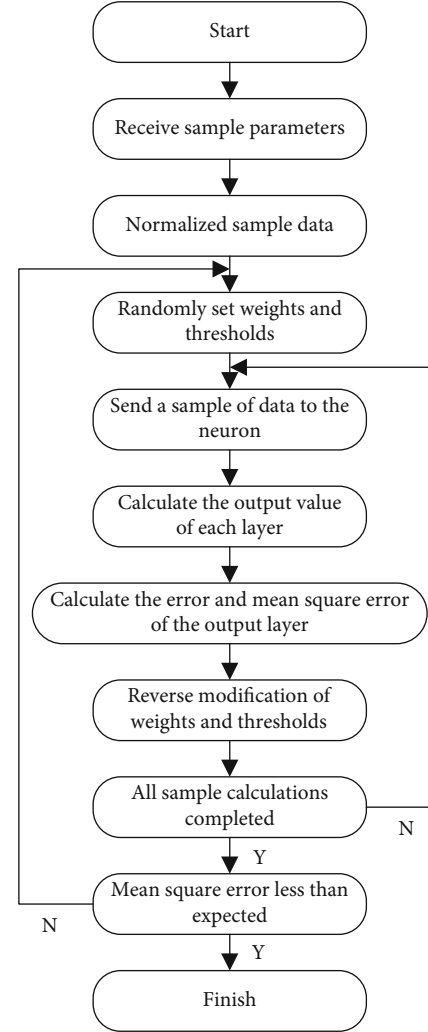


FIGURE 2: BP neural network algorithm flow chart.

the  $H$ th neuron cell.

$$\begin{aligned}
 E &= 0.5 * (T_j^i - yO_j^i), \\
 \delta_j^{(2)}(s) &= (T_j^s - yO_j^m) * yO_j^m * (1 - yO_j^m), \\
 \delta_j^{(1)}(s) &= \sum_{i=1}^n [V_{ij}^{(2)} * \delta_i^{(2)}(s)] * yI_j^s * (1 - yI_j^s), \\
 E &= \frac{\sum_{i=1}^s E_i}{s}, \\
 V_{ji}^{(2)} &= V_{ji}^{(2)} + \lambda * \sum_{l=1}^s [\delta_j^{(2)}(l) * yO_l^i], \\
 W_{ji}^{(1)} &= W_{ji}^{(1)} + \lambda * \sum_{l=1}^s [\delta_j^{(1)}(l) * x_l^i],
 \end{aligned} \quad (6)$$

where  $T_j^i$  is the expected output of the  $j$ th sample after the neural network training,  $E$  is the error value of the output, and  $yO_j^i$  is the actual output of the sample.

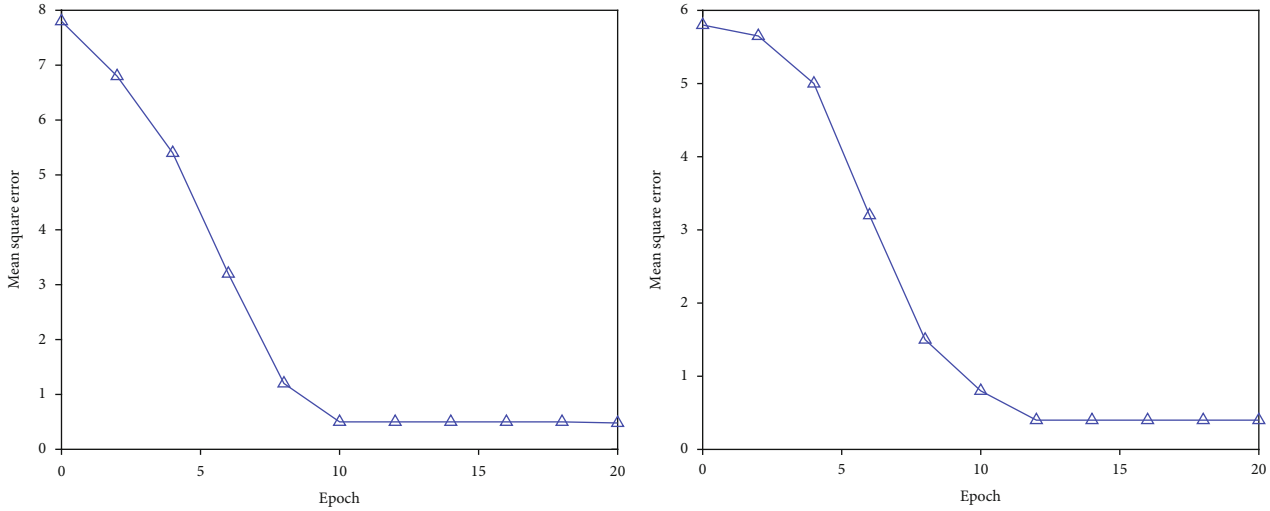


FIGURE 3: Training effect when  $N = 6$  and  $N = 8$ .

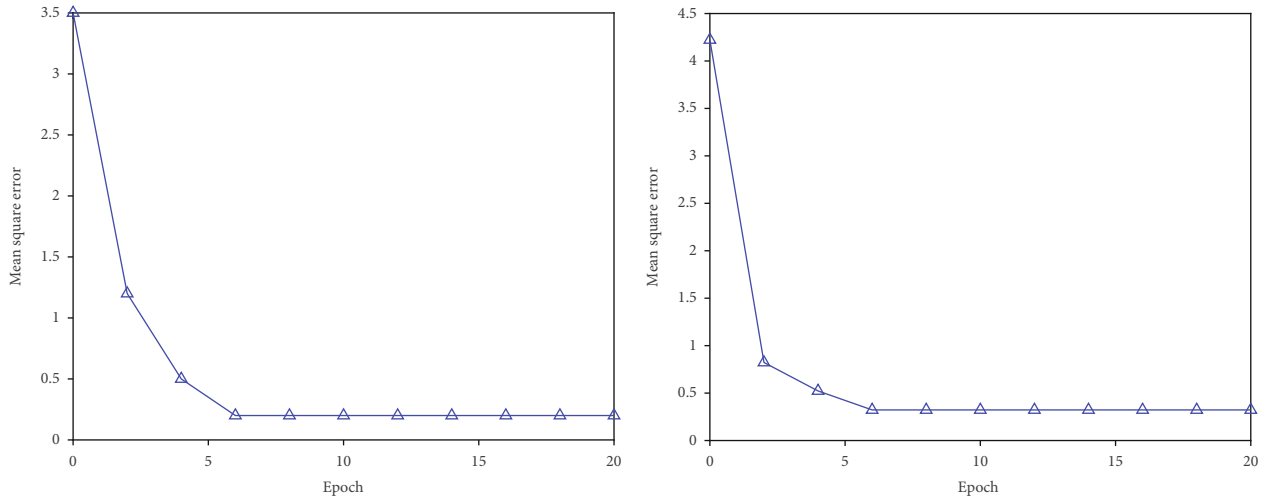


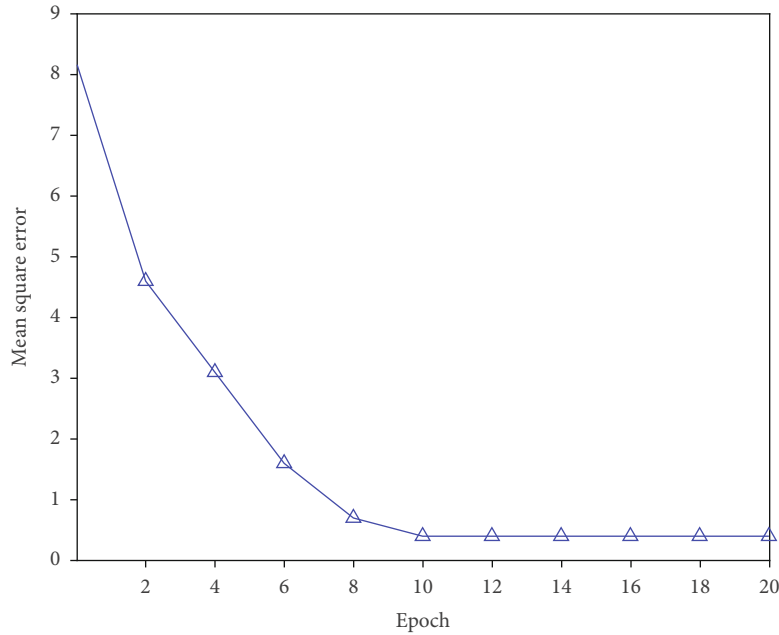
FIGURE 4: Training effect when  $N = 10$  and  $N = 12$ .

It will not be executed until  $E < \epsilon$ ; that is, the network training phase will not be executed until this requirement is met. The information is calculated and sorted according to the neural network model’s learning algorithm principle, and the preprocessed effective information can be utilized to enter the implementation process, with the BPNN model’s learning algorithm used for prediction and testing. The selection of a suitable network model structure plays a prominent role in the overall environment construction. An excellent network model structure can reduce the number of trainings, which is conducive to enhancing work efficiency and reducing engineering workload. The system is a nonlinear mapping from the input of the evaluation criteria to the output of the evaluation criteria. This paper uses a three-layer BPNN, and its advantages are mainly shown in the following: the three-layer BPNN uses a precision approx-

imation to any mapping relationship and can effectively solve some nonlinear problems by using input, implicit, and output. According to the characteristics of children’s autism evaluation indicators, in this topic, the evaluation criteria are divided into 15 secondary indicators, and the corresponding number of input nodes is established for the BP training network. The determination of the number of neurons in the hidden layer does not yet have an accepted standard. Here, a widely used empirical formula is used to calculate the number of hidden layers:

$$H = \sqrt{m + n} + a, \tag{7}$$

where  $m$  is the number of nodes in the input layer,  $n$  is the number of nodes in the output layer,  $H$  is the number of

FIGURE 5: Training effect when  $N = 14$ .

inputs in the hidden layer, and  $a$  is a constant from 1 to 10. It can be seen that the number of nodes in the hidden layer is in the range of 5 to 14, and the final number requires to be determined through experimentation.

#### 4. Experiment and Analysis

In this section, data set, parameter experiment, and evaluation accuracy of the BP network model are discussed in detail.

*4.1. Data Set and Parameter Experiment.* In order to facilitate the experiment, this paper designs a data set based on the evaluation index system of CA, with a total of 1200 sets of data, including 1000 training sets and 200 test sets. According to the formula of the hidden layer, it can be determined that the number of nodes in the hidden layer is in the range of 5 to 14. Therefore, this paper selects the number of nodes to be 6, 8, 10, 12, and 14 for experiments. The experimental results are shown in Figures 3–5.

The training impact is optimal when the number of hidden layer nodes is 12, according to the experimental results; hence, the number of hidden layer nodes picked is 12.

*4.2. Evaluation Accuracy of the BP Network Model.* The normalized data is used to conduct experiments, and the obtained results are compared with the evaluation results of experts, as shown in Table 2.

From the experimental results, the prediction results of the model are very close to the evaluation results of experts, and the error is small, which shows that the BP network model proposed in this paper has good performance.

TABLE 2: Comparison of network model output and expert evaluation results.

Number	1	2	3	4	5	6	7	8
Network output	0.71	0.68	0.85	0.89	0.68	0.74	0.81	0.79
Expert assessment	0.71	0.69	0.86	0.90	0.68	0.75	0.81	0.78

#### 5. Conclusion

It has been discovered that in the rehabilitation training of autistic children, the role of parents and family environment should be taken into consideration. Children's first teachers are their parents, and their primary living environment is their family. Family members spend a lot of time with children with autism. Parents are the persons who have the greatest interaction with their children, as well as the people who are closest to and most trusted by them. The cooperation of family members can significantly improve the effect of rehabilitation training for children with autism. Parents are also often involved in therapy and continue to look for other interventions, but a mixed approach or taking an eclectic approach can backfire and interfere with rehabilitation progression, especially if it is unsupported by evidence. Research has found that parents raising an autistic child are more likely to experience greater stress and mental health problems than those raising a child with other disabilities. It is crucial that parents receive systematic training and act as partners in the development of the intervention plan. According to some studies, providing parents of autistic children with an educational program that focuses on increasing their children's self-efficacy and educational approaches while also addressing their children's behavioral issues, functioning communication, and adaptive behavior can be beneficial. To this end, this paper has completed the



following work: firstly, the harm caused by CA and the current domestic and foreign researches on using different treatment methods to intervene in autistic children are introduced, focusing on the research on family therapy intervention in autistic children. Second, a portion of the systematic training for parents of autistic children is discussed, followed by an explanation of the structure and principles of BPNN. Finally, the BPNN is utilized to create a model for assessing the intervention effect of systematic parent training on autistic children. The experimental results show that the BPNN proposed in this paper has a high accuracy rate.

## Data Availability

The data sets used during the current study are available from the corresponding author on reasonable request.

## Conflicts of Interest

The authors declare that they have no conflict of interest.

## References

- [1] H. V. Ratajczak, "Theoretical aspects of autism: causes-a review," *Journal of Immunotoxicology*, vol. 8, no. 1, pp. 68–79, 2011.
- [2] A. M. Wetherby and B. M. Prizant, *Autism Spectrum Disorders: A Transactional Developmental Perspective*, Paul H Brookes Publishing, 2000.
- [3] J. L. Matson, M. Horovitz, A. M. Kozlowski, M. Sipes, J. A. Worley, and M. E. Shoemaker, "Person characteristics of individuals in functional assessment research," *Research in Developmental Disabilities*, vol. 32, no. 2, pp. 621–624, 2011.
- [4] M. Horovitz and J. L. Matson, "The baby and infant screen for children with autism traits-part 3: the development of age-based scoring procedures," *Research in Autism Spectrum Disorders*, vol. 7, no. 11, pp. 1291–1299, 2013.
- [5] A. Bailey, "Autism treatment research," *Autism Research*, vol. 7, no. 1, pp. 1–3, 2014.
- [6] G. T. Baranek, L. R. Watson, B. A. Boyd, M. D. Poe, F. J. David, and L. McGuire, "Hyporesponsiveness to social and nonsocial sensory stimuli in children with autism, children with developmental delays, and typically developing children," *Development and Psychopathology*, vol. 25, no. 2, pp. 307–320, 2013.
- [7] B. Rosenwasser and S. Axelrod, "More contributions of applied behavior analysis to the education of people with autism," *Behavior Modification*, vol. 26, no. 1, pp. 3–8, 2002.
- [8] W. J. Barbaresi, S. K. Katusic, and R. G. Voigt, "Autism," *Archives of Pediatrics & Adolescent Medicine*, vol. 160, no. 11, pp. 1167–1175, 2006.
- [9] L. Du, L. Shan, B. Wang et al., "A pilot study on the combination of applied behavior analysis and bumetanide treatment for children with autism," *Journal of Child and Adolescent Psychopharmacology*, vol. 25, no. 7, pp. 585–588, 2015.
- [10] M. B. Walsh, "The top 10 reasons children with autism deserve ABA," *Behavior Analysis in Practice*, vol. 4, no. 1, pp. 72–79, 2011.
- [11] J. Francke and E. A. Geist, "The effects of teaching play strategies on social interaction for a child with autism: a case study," *Journal of Research in Childhood Education*, vol. 18, no. 2, pp. 125–140, 2003.
- [12] S. Panerai, L. Ferrante, and V. Caputo, "The TEACCH strategy in mentally retarded children with autism: a multidimensional assessment. Pilot study. Treatment and Education of Autistic and Communication Handicapped children," *Journal of Autism and Developmental Disorders*, vol. 27, no. 3, pp. 345–347, 1997.
- [13] R. L. Lindsay, "Medical perspectives on autism spectrum disorders," *Seminars in Hearing*, vol. 26, no. 4, pp. 191–201, 2005.
- [14] D. V. M. Bishop, M. Maybery, A. Maley, D. Wong, W. Hill, and J. Hallmayer, "Using self-report to identify the broad phenotype in parents of children with autistic spectrum disorders: a study using the Autism-Spectrum Quotient," *Journal of Child Psychology and Psychiatry*, vol. 45, no. 8, pp. 1431–1436, 2004.
- [15] D. K. Anderson, R. S. Oti, C. Lord, and K. Welch, "Patterns of growth in adaptive social abilities among children with autism spectrum disorders," *Journal of Abnormal Child Psychology*, vol. 37, no. 7, pp. 1019–1034, 2009.
- [16] S. S. F. Gau, M. C. Chou, H. L. Chiang et al., "Parental adjustment, marital relationship, and family function in families of children with autism," *Research in Autism Spectrum Disorders*, vol. 6, no. 1, pp. 263–270, 2012.
- [17] A. Cox, M. Rutter, S. Newman, and L. Bartak, "A comparative study of infantile autism and specific developmental receptive language disorder: II. Parental characteristics," *The British Journal of Psychiatry*, vol. 126, no. 2, pp. 146–159, 1975.
- [18] M. Solomon, M. Ono, S. Timmer, and B. Goodlin-Jones, "The effectiveness of parent-child interaction therapy for families of children on the autism spectrum," *Journal of Autism and Developmental Disorders*, vol. 38, no. 9, pp. 1767–1776, 2008.
- [19] B. A. Boyd, S. G. McDonough, B. Rupp, F. Khan, and J. W. Bodfish, "Effects of a family-implemented treatment on the repetitive behaviors of children with autism," *Journal of Autism and Developmental Disorders*, vol. 41, no. 10, pp. 1330–1341, 2011.
- [20] P. Lu, "Family therapy of autistic children," *China Journal of Health Psychology*, vol. 12, p. 2, 2009.
- [21] J. Pei, K. Zhong, M. A. Jan, and J. Li, "Personalized federated learning framework for network traffic anomaly detection," *Computer Networks*, vol. 209, p. 108906, 2022.
- [22] B. Ji, Y. Li, D. Cao, C. Li, S. Mumtaz, and D. Wang, "Secrecy performance analysis of UAV assisted relay transmission for cognitive network with energy harvesting," *IEEE Transactions on Vehicular Technology*, vol. 69, no. 7, pp. 7404–7415, 2020.
- [23] X. Lin, J. Wu, S. Mumtaz, S. Garg, J. Li, and M. Guizani, "Blockchain-based on-demand computing resource trading in IoV-assisted smart city," *IEEE Transactions on Emerging Topics in Computing*, vol. 9, no. 3, pp. 1373–1385, 2021.

## Research Article

# Application of Neural Network Algorithm in Medical Artificial Intelligence Product Development

**Yineng Xiao** 

*School of Health Humanities, Peking University, Haidian District, Beijing, China 100191*

Correspondence should be addressed to Yineng Xiao; [xiaoyineng@pku.edu.cn](mailto:xiaoyineng@pku.edu.cn)

Received 27 April 2022; Revised 20 May 2022; Accepted 23 May 2022; Published 8 June 2022

Academic Editor: Naeem Jan

Copyright © 2022 Yineng Xiao. This is an open access article distributed under the Creative Commons Attribution License, which permits unrestricted use, distribution, and reproduction in any medium, provided the original work is properly cited.

With the continuous deepening of artificial intelligence (AI) in the medical field, the social risks brought by the development and application of medical AI products have become increasingly prominent, bringing hidden worries to the protection of civil rights, social stability, and healthy development. There are many new problems that need to be solved in our country's existing risk regulation theories when dealing with such risks. By introducing the theory of risk administrative law, it analyzes the social risks of medical AI, organically combines the principle of risk prevention with benefit measurement, and systematically and flexibly reconstructs the theoretical system of medical AI social risk assessment. This paper has completed the following work: (1) reviewed and sorted out the works and papers related to medical AI ethics, medical AI risk, etc., and sorted out the current situation of medical AI social risk regulation at home and abroad to provide help for follow-up research. (2) The related technologies of artificial neural network (ANN) are introduced, and the risk assessment index system of medical AI is constructed. (3) With the self-designed dataset, the trained neural network model is utilized to assess risk. The experimental results reveal that the created BPNN model's error is relatively tiny, indicating that the algorithm model developed in this research is worth popularizing and applying.

## 1. Introduction

Under the rapid development of science and technology, AI has been applied in various fields. Medicine, as a field closely related to human beings, has naturally also been impacted. While countries in the world are constantly refreshing their understanding of AI, they are also constantly changing seize the opportunity in this new field [1, 2]. Since the outbreak of the “new crown” epidemic in 2020, more and more people's values have been greatly changed, and more attention has been devoted to the medical field. With the gradual penetration of AI, its intersection with medical undertakings will definitely become the focus of society, and this intersection has also emerged. AI has shown broad application prospects in medical diagnosis, data statistics, health monitoring, etc., which greatly improves the efficiency of diagnosis and treatment activities and brings a lot of convenience to human beings, but related problems are also accompanied [3, 4]. Western countries have begun to take measures to solve this problem, such as the “Robot Civil Law Rules” passed by the

European Parliament and the “Restatement of Tort Law” passed by the United States, etc., which specifically introduced various measures to deal with AI. As a country that makes laws, due to the lag in legislation, the current legal system has not been perfected for new problems that may arise from AI, and the academic community also lacks a unified theoretical system. If the legal system in this area is not improved in time, it will inevitably hinder the advancement of artificial intelligence in the medical field [5]. Medical institutions, medical professionals, patients, designers and producers of medical AI, and other parties are all involved in the study, development, and implementation of medical AI products, making the ethical challenges raised by AI's use in medicine extremely complex. If we wish to improve human health, we must think about and act on the ethical challenges highlighted by medical AI. The ethical implications of medical technology can be viewed in two ways. The source of ethical worth is people. The ethical link between science and technology, people, and society is also what we research. The advancement of science and

technology and the spirit of humanism must thus be integrated. It is certain that the negative impacts of science and technology will arise if the progress of science and technology is not guided by literary values. As a result, the reasonable use of artificial intelligence in the medical area needs ethical guidelines. Ethical risk governance mechanisms for medical AI should be promoted in the second step. Ethical questions are typically raised late in the game, resulting in a paucity of future ethical study [6]. This study, conducted in the contemporary age, examines the issues and causes associated with the use of medical AI and makes some recommendations and solutions in an effort to address some of the ethical concerns raised by this technology. The Civil Code stipulates that medical personnel shall bear tort liability, and medical institutions shall bear vicarious liability in violation of industry regulations or legal norms. Producers and sellers bear product liability due to product defects, but it is difficult to have a unified conclusion on how to position AI. The reason why there are many disputes is that my country's current legal system is blank in this regard. This article will draw on the legislative experience of foreign AI in the medical field to put forward risk assessment suggestions for the development of medical AI products in my country.

Facing the focus of domestic controversy, this article will combine various viewpoints in the academic circles and classify them according to the degree of intelligence of artificial intelligence. Use the intelligent level to locate its position in the medical field to explore new legal regulation paths and provide important opinions on various issues of artificial intelligence medical care [7]. AI has a broad space for development in real-time health monitoring, diagnosis and treatment data statistics, drug development experiments, etc., and can even respond faster than medical staff. However, AI has the characteristics of unpredictability and complexity, coupled with its strong learning ability and replication ability, which makes it have a certain degree of autonomy. This also exacerbates the uncertainty of future accidents [8, 9]. At the same time, intelligent programs inevitably have technical loopholes in the design process, which will also increase the probability of security risks and cause social conflicts. Therefore, the practical significance of this paper is to use the neural network algorithm to conduct reasonable risk assessment in the development of medical AI products, in order to reduce the occurrence of medical AI infringement cases.

The paper structures are as follows: Section 2 discusses the related work. Section 3 defines the various methods of the proposed work. Section 4 analyzes the experiment and analysis. Section 5 concludes the article.

## 2. Related Work

Regarding the definition of artificial intelligence in the medical field, scholars have little controversy. Theoreticians generally believe that artificial intelligence is the intention of human beings to create intelligent machines that are close to humans, so that intelligent machines can replace medical personnel to complete various diagnosis and treatment activities, including health care, real-time monitoring, diag-

nosis and treatment data statistics, drug development trials, and intelligent surgical diagnosis. It is essentially a branch of computer science, and this science is then used in the medical field to provide medical services that are equivalent to or even greater than the responsibilities of medical personnel [10]. Reference [11], under the influence of foreign examples of "surgical robots," concretized AI as intelligent medical robots and provided medical services based on AI technical means. The "intelligent technology + medical service" model has become a reality, which also enables precision medicine to provide solutions to the medical problems of an aging society in the future while reducing operating costs. From the perspective of AI medical infringement and the legal and ethical issues involved, scholars divide AI social risks into three categories: ethics, polarization, and regulation [12]. Ethical risk mainly refers to the passive or active breaking of human ethical relationship in the process of AI development, so that people have to reexamine and plan the ethical relationship. Since developers develop AI based on their own ethical concepts, AI inevitably has the basic value orientation of human beings, so how to control the adverse effects of developers in advance in the research and development stage has become the focus of AI regulation. With the development of AI to superintelligence, AI has replaced humans in many fields such as simple repetitive work, high-risk work, and companion services. It has changed from the object of human behavior to the same subject as human beings. Whether artificial intelligence can obtain legal subject qualification has become the main point to regulate its social risks [13]. Polarization risk mainly refers to the high development of artificial intelligence, although it can solve the existing problems of resource shortage and uneven distribution and liberate part of the simple and repetitive or high-risk labor force. However, the data and information that provide the basis for artificial intelligence are controlled by a small number of people, which will lead to the possibility of polarization of resources and wealth. The big data that artificial intelligence relies on is the result of detailed monitoring and analysis of personal information, so that individuals are completely exposed to the computer. Once there is a problem with the storage and confidential components of the computer, personal information will be in a difficult situation to protect [14]. Regulatory risk mainly refers to the phenomenon of excessive attention to economic benefits and neglect of civil rights that may occur in the process of national regulation of AI. In the process of economic development, developers who formulate AI software standards and write codes have absolute control over AI. Due to the confidentiality of AI programming by developers, coupled with the inducement of excessive pursuit of commercial interests, and the deviation of their own ethical values, the country will involuntarily tilt towards the research and development side in the process of AI regulation, resulting in citizens unable to effectively maintain legitimate interests. For AI social risk regulation, scholars generally agree to regulate it on the basis of the principles of justice, fairness, science, and rationality [15]. Ethical and moral regulation and legal regulation have become two important means of AI social risk regulation.

Ethics and ethics regulation requires that the ethical and ethical norms that it needs to follow be incorporated into the programming at the beginning of AI research and development and solve problems from the source. Legal regulation necessitates that the entire process of AI research, development, and application, as well as all relevant individuals involved, be restrained on the basis of solid legislation and effective law enforcement, which is an effective measure to avoid social problems created by AI [16]. In general, foreign AI development strategies mainly include consolidating the theoretical foundation of AI, building an AI security system, accelerating supporting legislation, and promoting international cooperation in AI research and risk regulation [17]. The British National Medical Service System has the world's leading medical level and is the leader in the development of medical AI in the United Kingdom. Its medical AI development experience is of great significance to my country [18]. The mid- and long-term health service system development plan released by it outlines the future development direction of UK medical AI from six aspects: service model innovation, reducing health inequality, promoting quality of care, providing employee support, realizing digital transformation, and improving investment utilization efficiency, including medical AI empowerment and empowerment, promoting medical AI clinical diagnosis and treatment application, and using medical AI to improve the safety and efficiency of population health management [19]. The US government has a relatively deep understanding and cognition of the current situation and development prospects of AI. "Preparing the Report for the Future of AI" analyzes and predicts the development of AI in the country and the world, points out the future research direction of AI and its possible social risks, and puts forward constructive countermeasures with suggestions. At the same time, the U.S. Congress has also actively paved the way for the development of AI and has promulgated many AI-related bills, which reflects the high attention of the American legal community to the development of AI. Although these policies and bills do not directly involve medical AI, they delineate a framework for the development of AI, which indirectly guides the development of medical AI and lays a foundation for regulating the social risks it brings [20–23].

### 3. Method

In the "Method" section, we define the basic theory of artificial neural network, risk assessment system for medical AI product development, data normalization, and parameter settings of the model in detail.

#### 3.1. Basic Theory of Artificial Neural Network

**3.1.1. Artificial Neural Network Principle.** ANN, an information processing system that replicates the structure and operation of a human brain, was built using modern neurobiological research. It also has the mental faculties of thinking, absorbing new information, and remembering what it has learned. A process of information processing can be viewed as a nonlinear mapping from the input space to the

output space. Nonnormal distribution and nonlinear risk assessment issues may be solved efficiently by altering weights and thresholds to "learn" or discover the connection between variables. While each neuron in an ANN may be thought of as a fundamental operating unit, the method in which it processes information is not linear, and this is why ANNs are so complicated. The contact between these neurons also facilitates the processing of information across the whole neural network. The artificial neuron model is shown in Figure 1.

The  $j^{\text{th}}$  neuron in Figure 1 imitates the three most basic and important functions of biological neurons: weighting, summation, and transfer, where  $x_1, x_2, \dots, x_n$  represent the input from the neuron,  $w_{j1}, w_{j2}, \dots, w_{jn}$  represent the connection strength between the neuron and the  $j^{\text{th}}$  neuron, that is, the weight.  $\mu$  is the threshold, which mainly adjusts the input and output of neurons.  $f$  is the transfer function.  $y_j$  is the output of the  $j^{\text{th}}$  neuron. Among them, the net input value  $s_j$  of the  $j^{\text{th}}$  neuron is:

$$s_j = \sum_{i=1}^n w_{ij} * x_i + \mu = W_j X + \mu. \quad (1)$$

After the net input  $s_j$  passes through the transfer function  $f$ , the output of the  $j^{\text{th}}$  neuron is obtained:

$$y_j = f(s_j) = f\left(\sum_{i=1}^n w_{ij} * x_i + \mu\right) = F(W_j X). \quad (2)$$

Just as biological cells have the limit of information carrying, the signals transmitted by artificial neurons cannot increase indefinitely, and there must be a maximum value, where  $f$  should be a monotonically increasing bounded function.

ANN's learning and working phases are divided into two stages. To train a neural network, input and output data are fed into the network throughout this phase of development. Make the most of your network's settings. The network is given a new set of input samples as variables, and the learnt rules for processing yield new output results. In the working stage, a trained neural network looks like this. Self-learning and self-adaptation are other characteristics of the ANN, which may modify the weight values of neurons at each level as it learns to better suit the needs and requirements of its environment. In most cases, the neural network may be trained using two alternative ways. There are two types of algorithms: one utilizes a sample standard to modify the weight coefficients of each neuron to accomplish the goal of categorizing or mimicking the sample data; the other uses a neural network to learn. An algorithm with no tutor is another option, which merely describes how to learn. Depending on the input signal, the substance of the lesson changes. Environmental features and laws are discovered and stored by the system. The connection weights are also automatically adjusted. In order to group and aggregate

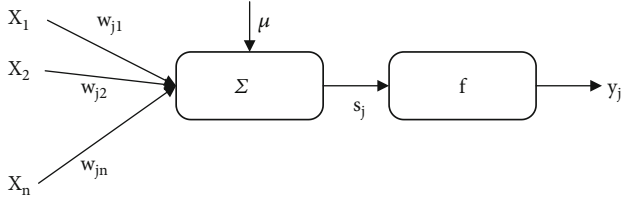


FIGURE 1: Artificial neuron model.

input samples, this learning method is closer to the function of the human brain.

**3.1.2. Characteristics of Artificial Neural Network.** Human brain neural networks may be modelled, simplified, and abstracted, and then used as a starting point for an ANN, which is built on this fundamental knowledge. In a similar way to the human brain, it can self-adapt, self-organize, and self-learn. It possesses strong intelligence qualities and has been effective in addressing numerous tough issues in the fields of pattern recognition, combinatorial optimization, and prediction. In general, ANN has the following characteristics:

- (1) It is quite good at nonlinear mapping

For a neural network to operate, it must be able to map data from the input layer to the output layer. Theoretically, any complicated nonlinear mapping may be realized by an ANN with three or more layers and sufficient hidden layer neurons, making it especially ideal for handling issues involving complex internal mechanics.

- (2) Strong mathematical skills

Strong mathematical skills, as well as the capacity to solve real-world situations, distributed parallel processing, associative memory extraction technique, and complete activation of relevant neurons are used to extract information from external stimuli and input data in this system. The rules of the learning samples are adaptively taught, and the memory rules are stored using the “tutored” learning approach. The model can employ the prestored rules from the partial information and noise interference when a fresh random sample is added. The sample information is associatively memorized to achieve complete original information recovery, with good fault tolerance and strong anti-interference ability. It is especially suitable for the recognition of complex patterns with complex content and inconspicuous features.

- (3) Strong sample identification and classification ability

The powerful nonlinear processing capability enables the neural network to handle the data classification of nonlinear samples well. As a nonlinear optimization algorithm, neural network has powerful optimization computing power; it can find a set of parameter combinations under known constraints, so that the objective function can quickly reach the minimum value.

- (4) Good generalization ability

The neural network adopts the learning algorithm of global approximation and has good generalization ability. The network is highly trained and can tackle similar challenges in real time.

**3.1.3. Artificial Neural Network Model.** Various ANN models, such as the BPNN model, the RBF neural network model, and the self-organizing mapping neural network model, have been established in the development of neural networks. This approach uses error back propagation, which is a hierarchical neural network made of an input layer, one or more hidden layers, and a final output layer. Layers of neurons are linked to each other like human nerve cells, and each layer has a certain number of neurons in it. Each layer of neurons is devoid of any connections. First, the input signal is sent from the input layer to the hidden node, where it is processed by the transformation function before being sent to the output node, where it is supplied as the final output result of the system. The number of network layers and the number of nodes in each layer are shown to have a positive correlation with the network’s fitting accuracy. Increased network layers may enhance fitting accuracy, but the network becomes more complex, and training time goes up. There is a three-layer neural network structure according to the Kolmogorov theory, which can approximate any continuous function or accurate data classification with the precision of the mean square error and handle most real-world issues under specific circumstances for  $\varepsilon > 0$ . Linear data processing is also the most prevalent challenge. The network structure of the three-layer back-propagation neural network (BPNN) is shown in Figure 2.

In this network structure, the input vector is  $X = (x_1, x_2, \dots, x_n)^T$ , and the output vector of the hidden layer is

$$O_k = f(\text{net}_k). \quad (3)$$

$Y = (y_1, y_2, \dots, y_m)^T$ , the output layer vector is  $k = 1, 2 \dots l$ , and the expected output vector is  $D = (d_1, d_2, \dots, d_l)^T$ .

$$\text{net}_k = \sum_{j=0}^m w_{jk} y_j. \quad (4)$$

The weight matrix between the input layer and the hidden layer is represented by  $V$ ,  $V = (v_{11}, v_{12}, \dots, v_{mn})^T$ , where  $v_{mn}$  represents the weight vector of the  $n$ th neuron in the hidden layer corresponding to the  $m$ th input layer neuron. The weight matrix between the hidden layer and the output layer is represented by  $W$ ,  $W = (w_{1l}, w_{2l}, \dots, w_{lm})^T$ , where  $w_{lm}$  represents the weight vector of the first output layer neuron corresponding to the  $m$ th hidden layer neuron. For the output layer:

$$O_k = f(\text{net}_k) (k = 1, 2, \dots, l); \text{net}_k = \sum_{j=0}^m w_{jk} y_j (k = 1, 2, \dots, l). \quad (5)$$

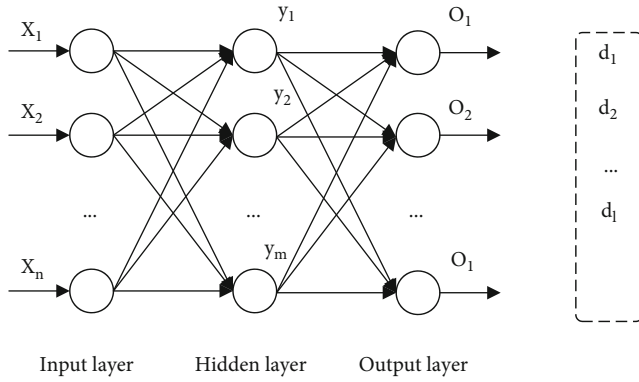


FIGURE 2: BP neural network structure diagram.

For the hidden layer:

$$y_j = f(\text{net}_j) (j = 1, 2, \dots, m), \text{net}_j = \sum_{i=0}^n v_{ij}x_i (j = 1, 2, \dots, m). \quad (6)$$

The transfer function  $f(x)$  of the hidden layer and the output layer is a unipolar or bipolar Sigmoid function with continuous derivable characteristics:

$$f(x) = \frac{1}{1 + e^{-x}}. \quad (7)$$

The algorithm learning steps of BPNN are as follows:

- (1) Select a part of the overall sample as a training sample, and input its information into the network
- (2) The sample information is output by the output layer after being processed by the hidden layer of the network
- (3) Calculate the error value between the actual output and the expected output of the network
- (4) Reverse calculation from the output layer to the first hidden layer, and adjust the weights of the entire network according to the principle of error reduction
- (5) Repeat the above steps until the total error of the network reaches the target error value. After the repeated training of the above steps, the connection weights between the nodes of the network are completely confirmed, that is, the BPNN is trained. At this time, it can be used to identify and predict unknown samples

**3.2. Risk Assessment System for Medical AI Product Development.** With the continuous development of medical artificial intelligence, the distortion of medical data collection and the leakage of medical data, the unemployment of simple labor force and the increased medical burden of patients, the influence of scientific diagnosis and treatment and the aggravation of unequal distribution of medical

resources, and other social risks will pose a huge threat to the benign development of society. At this point, all governments are working hard to create medical AI, as well as finding efficient strategies to manage the social hazards that come with it. However, in theory, the administrative laws and regulations governing medical AI social hazards are not very mature, and there are a number of issues. In practice, the merger of old administrative law leads to numerous loopholes. This paper analyzes the problems faced by the medical AI social administrative law regulation and combines the administrative process theory and the risk administrative law theory to build a basic theoretical framework for the social risk administrative law regulation of medical AI product development. The fundamental cognitive orientation of AI social risk administrative law regulation, the regulatory process monitoring, and the fundamental principles must be followed. And based on this, it analyzes and responds to the problems faced in the practice of medical AI social risk administrative law regulation.

**3.2.1. Risk Assessment.** Strengthening medical AI social risk regulation scientific and rational risk assessment is to use facts and assumptions to estimate the probability that a special management decision will cause harm to human society. When human beings face uncertain social risks, risk assessment provides decision-makers with an orderly and clear basis for social risk regulation through scientific monitoring and analysis methods, combined with the opinions of various stakeholders. Risk assessment is the scientific basis for administrative agencies to regulate medical AI social risks. The National Academy of Sciences of the United States has made a scientific division of risk assessment in the book “Federal Government Risk Assessment; Management of the Process”, which includes: hazard cognition, through scientific experiments to determine whether there is a real hazard in the assessment object; hazard degree confirmation, determination degree of damage to humans in subjects was assessed at different doses; exposure assessment, by calculating and simulating the hazard of exposing people to such risks by calculating the intensity and frequency of human exposure to dangerous substances; risk estimation, analyzing relevant information and making risk determinations. Risk assessment is mostly based on the conclusions reached through scientific study by professional and technical professionals. Problems have developed in risk assessment in terms of technology, standards, authority distribution, assessment candidates, and public disclosure in the social risk regulation of medical AI. The reason is that the science used as the assessment scale is unstable. The instability of science is first reflected in the uncertainty of science itself. Science is developing gradually, and it is difficult to draw conclusions about the science and technology of a certain period. Secondly, it is reflected in scientists. On the one hand, scientists are limited by scientific development, and on the other hand, because of their own risk perception differences and political and economic influences, it is difficult to draw definite, objective, and rational conclusions in the evaluation. The risk administration law provides ideas for solving the instability of science through research on science

and public participation, that is, introducing risk communication in the process of risk assessment.

**3.2.2. Risk Communication.** Strengthening medical AI social risk regulation rational public risk communication is not equal to simple information disclosure. It is a process of information sharing and opinion exchange between administrative agencies and the public around a social risk topic. Risk communication actually runs through the whole process of medical AI social risk regulation. In order to unblock risk communication channels and achieve effective risk communication, the following issues must be clarified. The first is to ensure the authority of the publisher of the communication information. The same information is released by different individuals to produce completely different effects. When the administrative organ publishes relevant information for the purpose of regulating social risks, it must not only consider the professionalism of the relevant information but also consider your own integrity. Once the relevant information released by the administrative agency is confirmed to be false, the public's trust in it will be reduced and the effect of subsequent risk communication will be affected. The second is to enrich risk considerations. Administrative agencies should get rid of their extreme reliance on professional knowledge and incorporate the most common fairness and justice factors of public concern into the scope of risk considerations. The third is to pay attention to communication skills and to share risk-related information to the public as easily as possible, so that the public can participate in discussions on the basis of understanding; grasp the start time of risk communication. Starting too early will bring unnecessary panic to the public, and starting too late will lead to the suspicion of concealment. The timely initiation of risk communication will help safeguard citizens' right to know and to participate; it will help to eliminate the public's distrust of administrative agencies and mutual suspicion of various stakeholders caused by the concealment of information; it helps to ensure the continuous advancement of democracy in the process of risk regulation.

**3.2.3. Risk Identification Standards.** Strengthening medical AI social risk regulation technology rational risk identification standards are the technical support for administrative agencies to regulate medical AI social risks and are also an important basis for risk assessment, communication, and management. Risk identification standards are authoritative, uncertain, professional, time-sensitive, and balanced. Legality means that the risk identification standards are formulated by the relevant institutions stipulated by law, and the risk identification standards have a legal basis. Uncertainty means that the risk identification standards are formulated under the uncertainty of scientific instability and social risks. As discussed above, it is extremely difficult to formulate risk identification standards under such circumstances. Professionalism means that although risk identification standards are formulated under the dual uncertainty of scientific and social risks, professional and technical personnel are still required to formulate them from a professional perspective. Timeliness means that the established criteria for identifying

a certain type of risk will lose its validity over time, which is caused by the constant changes in social risks. Trade-off means that in the process of formulating risk identification standards, the framers have to weigh their interests. Risk identification standards have a direct impact on people's perceptions of risk and play a key role in risk regulation decisions made by decision-makers. Therefore, when formulating standards, it is necessary to weigh the interests of all parties involved in regulatory risks, and consider factors such as political needs and economic development. In this process, the important role of risk communication to ensure the objective and rationality of risk identification standards has also emerged.

**3.2.4. Risk Management.** Strengthening medical AI social risk regulation to ensure rational risk management is the destination of medical AI social risk regulation. The purpose of administrative agencies to carry out risk management is to control the social risks of medical AI within an acceptable range and to minimize public losses and maximize public interests. The object of risk management of administrative organs is all risks that may threaten human society, mainly for those social risks that are identified as causing significant harm to human survival and development through risk assessment. With the continuous progress of society, the risk management of administrative agencies is bound to change from a power style to a communication style, and the risk management concept will also change from general management to refined management. Risk management is no longer an effort for the interests of some people, but to safeguard the legitimate rights and interests of all people. The administrative organ is no longer the only topic that must manage risk, and the latest development direction is for all stakeholders to work together.

According to the above evaluation of risk rules for medical AI product development, this paper designs an evaluation system that can be used for neural network experiments, such as Table 1. According to the evaluation results obtained by the input evaluation indicators, the risk of medical AI product development is divided into three levels.

**3.3. Data Normalization.** Since the hidden layer of the BPNN adopts a nonlinear and dimensional excitation function, it has the characteristics of saturated nonlinearity. If the difference between the input value of each neuron and the threshold is too large, the output of the neuron will fall in the saturation region, so that the actual output of the network is either the maximum value of the activation function or the minimum value of the activation function. The derivative value of the output tends to zero, resulting in a small change in the weights, which not only slows the learning speed but also makes the network difficult to converge. Therefore, in practical applications, in order to improve the training speed and sensitivity of the network and effectively avoid the saturation region of the excitation function, the value of the input data is generally required to be in the interval  $[0, 1]$ , and it is necessary to normalize the input data. Commonly used normalization methods include linear function transformation method, logarithmic function

TABLE 1: Medical AI product development risk assessment system.

Index	Label
Weakening of doctors' practical ability	R1
Weakening of the moral responsibility of doctors	R2
Patient privacy violated	R3
The humanity of the patient is challenged	R4
The rights of patients cannot be guaranteed	R5
Lack of doctor-patient trust	R6
Weakening of humanistic care	R7
Influencing the scientific nature of patient care research	R8
Exacerbating the unequal distribution of medical resources	R9
Simple labor unemployment risk	R10
Risk of increased medical burden on patients	R11
Medical data collection distortion	R12
Risk of medical data breach	R13
Generate ethical and moral hazard	R14

TABLE 2: Training results for different numbers of hidden layer nodes.

Number of hidden layer nodes	Mean squared error
5	0.0000977
6	0.0000869
7	0.0000619
8	0.0000602
9	0.0000788
10	0.0000872
11	0.0000948
12	0.0000982
13	0.0000965
14	0.0000990
15	0.0000974
25	0.0000893
35	0.0000989
45	0.0000948

transformation method, and arctangent function transformation method. This paper adopts the linear function conversion method:

$$x_i = \frac{x_c - x_{\min}}{x_{\max} - x_{\min}}, \quad (8)$$

where  $x_{\max}$  and  $x_{\min}$  are the maximum and minimum values of the sample data, respectively,  $x_i$  is the original sample data, and  $x_c$  is the transformed data. The normalized data not only prevents the input data from falling into the saturation region, but also maintains the original characteristics of the data.

**3.4. Parameter Settings of the Model.** When using the BPNN model for risk assessment and analysis of medical AI product development, we should first set the corresponding parameters of the neural network to ensure the effective

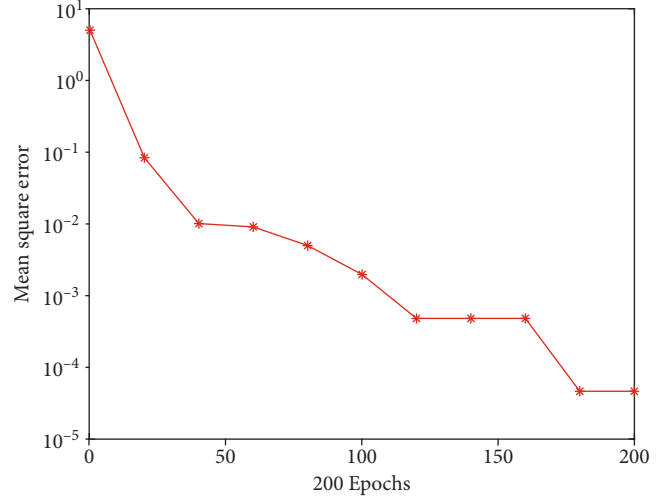


FIGURE 3: BP neural network training error curve.

operation of the assessment model. Then, using the risk assessment index value and the evaluation sample's target value, train the network to produce an output value that is close to the target value. After repeatedly adjusting the parameter settings of the network, the model meets the requirements of the operation, and the neural network obtains the sample "knowledge" and stores it in the network weights and thresholds. At this point, a suitable risk assessment model is obtained, which can be used in practical work. Specific steps are as follows:

#### (1) Setting of network nodes

After selecting a neural network, first set the network parameters, including the number of network layers and the number of nodes in each layer. The three-layer BPNN can solve most of the nonlinear data processing problems in reality, and it is the most common application. In this paper, the BPNN including the input layer, single hidden layer, and output layer is selected as the prediction model. In the simulation experiment, the number of nodes in the input layer is determined by the number of sample indicators, so the number of nodes in the input layer of the BP model in this paper is 14. The number of output layer nodes is 1. For the number of hidden layer nodes, there is still a lack of good theory as a guide, and different numbers of hidden layer nodes will form different neural network models. We need to perform constant and repeated debugging to obtain suitable network parameters, thus forming an effective risk assessment network model. The empirical formula used in this paper is as follows:

$$H = \sqrt{i + j} + a, \quad (9)$$

where  $H$  is the number of hidden layer nodes,  $i$  is the number of output layer nodes,  $j$  is the number of output layer nodes, and  $a$  is a constant in the range [1–10]. Subsequently, the number of hidden nodes corresponding to the minimum network error will be determined by trial and error, thereby forming an initial three-layer BPNN model.



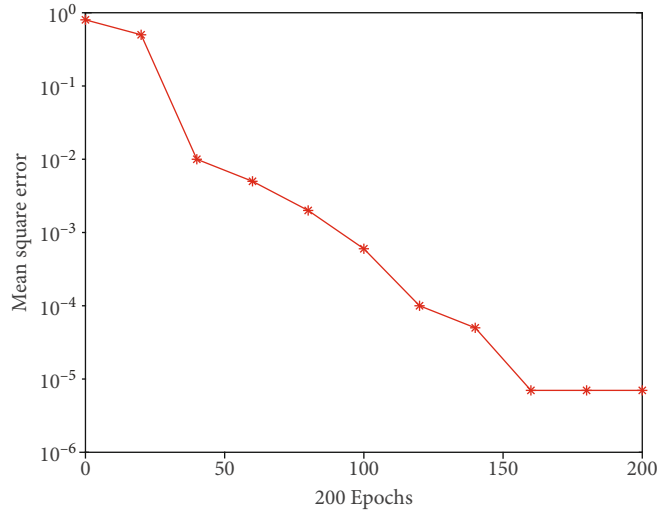


FIGURE 4: Variation curve of training simulation error of neural network.

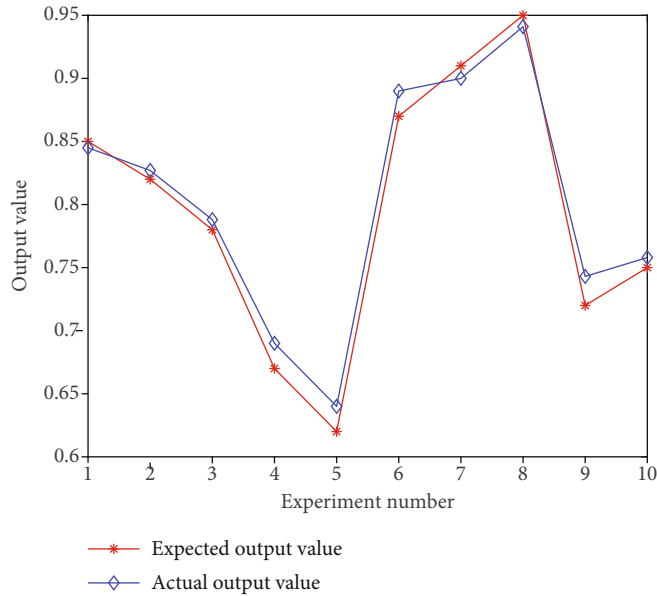


FIGURE 5: Training sample simulation results.

(2) Maximum training times

Set the maximum training times to 3000 times, that is, when the network training times reach 3000, stop training.

(3) Error accuracy

According to the software requirements and the needs of the model, the error precision set in this paper is  $10^{-5}$ . When the error of the two iteration results is less than this value, the system will end the iterative operation.

(4) Excitation function

The input data of the neural network has been normalized and is in the range of [0, 1]. The excitation function

of the hidden layer and the output layer of this paper is the logarithmic sigmoid function, that is, the Logsig function.

(5) Learning functions

Set to gradient descent momentum learning function (Learngdm).

(6) Training function

The gradient descent back-propagation algorithm function that adaptively adjusts the learning rate and adds a momentum factor is a combined optimization algorithm of the gradient descent method and the adaptive adjustment learning rate method. It has the characteristics of fast

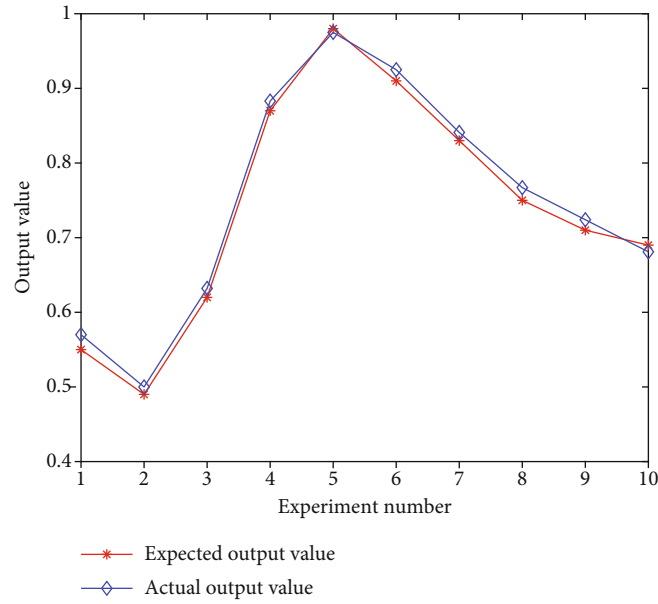


FIGURE 6: Test sample simulation results.

convergence speed, good learning effect, and high calculation accuracy, which improve the learning speed of the neural network and increase the reliability of the algorithm. The training function in this paper selects the traingdx algorithm.

#### (7) The error performance function

The error performance function of network convergence adopts the minimum mean square error value, and the target value is set as 0.0001.

## 4. Experiment and Analysis

In this chapter, we define the selection of evaluation samples, neural network model parameter selection and training, and test of neural network model in detail.

*4.1. Selection of Evaluation Samples.* My country's medical AI social risk legislation is still in the works, and the assessment of medical AI social hazards has flaws in terms of technology, norms, authority distribution, evaluation candidates, and public awareness. The current level of risk assessment technology development in my nation is insufficient to facilitate the effective development of assessment activities when compared to the actual needs of medical AI societal risk assessment. The cost-benefit analysis guides the standard risk assessment method. Due to the instability of the cost-benefit analysis itself, it is difficult to apply the traditional risk assessment method to the process of medical AI social risk assessment. Medical AI social risk assessment standards are an important part of medical AI social risk assessment, and an important basis for proving whether medical AI has social risks and whether it can be widely used in the medical field. Therefore, this standard cannot be limited to a single field, but should cover all areas where medical AI

may have social risks. The current medical technology evaluation standards obviously cannot meet this requirement. The social risk assessment of medical AI mainly relies on professionals in related fields and administrative staff to form an expert group for assessment. On the one hand, there are many administrative staff, which is easy to reduce the scientific nature of the assessment; because the majority of them are drawn from universities and scientific research institutions in related subjects, and specialists are constantly in contact with one another, ensuring the impartiality and scientificity of evaluation viewpoints is difficult. Administrative activities relating to the social risk assessment of medical AI are not included in the scope that can be reported to the public, making public oversight of the social risk of medical AI impossible. Therefore, there is no assessment data suitable for this paper. According to the evaluation index system constructed in chapter 3, this paper designs an experimental dataset that can be used for neural network evaluation, which contains 320 datasets, 280 training sets, and 40 test sets.

*4.2. Neural Network Model Parameter Selection and Training.* In this paper, 12 different hidden layer nodes are used to train the network to determine the optimal network structure. After several simulation tests, the results are shown in Table 2.

It can be seen from Table 2 that when the number of hidden layer nodes is 8, after 200 network iterations, the network performance is 0.0000602, which meets the set error limit of 0.0001, and the error of the neural network model is the smallest at this time. Stop the iterative operation, and the network training is completed. At this time, after repeated debugging, the final selected network learning rate is 0.05, and the momentum factor is 0.95. The training effect is shown in Figure 3.

Therefore, this paper uses 8 hidden layer nodes to train and test the network, and builds a 12-8-1 three-layer BPNN

model. To verify the application value of the constructed and trained neural network model, we must simulate the neural network constructed above using the training samples and compare the model's output results to the expected output results to see whether the simulation is right. If the correct rate is high, it means that the application of the neural network model constructed in this paper in judging the risk of medical AI development is scientific and effective and can be used in practice. To simulate the trained neural network, usually call the input variables of the sim function network in the neural network toolbox for simulation testing. After many simulation trainings, the error accuracy reaches the target value of 0.0001, and the network performance is 0.0000071526. It can be seen from Figure 4 that the constructed neural network model has a high-precision prediction and judgment ability.

The obtained training sample simulation results are shown in Figure 5.

**4.3. Test of Neural Network Model.** The neural network and simulation test constructed above are all derived from the training sample data, showing a good discriminative effect. The generalization effect of the model, that is, the discriminative effect of the nontraining sample data, needs to be tested to judge the promotion and application value of the model. This study simulates the neural network established above using the selected 40 sets of test sample data as input, then compares the model's output results to the expected output results to assess the simulation's accurate probability. For the simulation test, 40 groups of test sample data were entered into the trained neural network model, and its risk was assessed; 10 groups of data were chosen, and the results are presented in Figure 6. It can be seen from the experimental results that the error of the output results is very small, which shows that the application of the neural network model constructed in this paper in judging the development risk of medical AI is scientific and effective and has good promotion and application value.

## 5. Conclusion

AI technology in my country's medical field is still in the weak AI stage, and its research and development and application are still in the early stage, but AI has great potential in accelerating medical scientific discovery and transforming medical care. The era of "strong AI" may be close at hand. The application of technology in medicine is linked to human health and survival. Medical AI is difficult to implement. It is critical to comprehend the potential dangers and consequences of this new technology. Medical AI should be better regulated, and AI should be applied in the most efficient way feasible to ensure that the patient's experience and needs are prioritized. As a result, this article employs neural networks to assess risk in the development of medical AI and completes the following tasks: (1) reviewed and sorted out relevant works and papers on medical AI ethics, medical AI risks, etc. The current situation of regulation is sorted out to provide help for follow-up research. (2) The related technologies of ANN are introduced, and the risk

assessment index system of medical AI is constructed. (3) With the self-designed dataset, the trained neural network model is utilized to assess risk. The experimental results reveal that the created BPNN model's error is relatively tiny, indicating that the algorithm model developed in this research is worth popularizing and applying.

## Data Availability

The datasets used during the current study are available from the corresponding author on reasonable request.

## Conflicts of Interest

The author declares that he has no conflict of interest.

## References

- [1] Z. F. Jia and J. W. Zhang, "Approaches and system construction of infringement of intelligent medical robots," *Journal of Changchun University of Science and Technology: Social Science Edition*, vol. 31, no. 4, p. 7, 2018.
- [2] D. D. Miller and E. W. Brown, "Artificial intelligence in medical practice: the question to the answer?," *The American Journal of Medicine*, vol. 131, no. 2, pp. 129–133, 2018.
- [3] J. R. England and P. M. Cheng, "Artificial intelligence for medical image analysis: a guide for authors and reviewers," *American Journal of Roentgenology*, vol. 212, no. 3, pp. 513–519, 2019.
- [4] C. Longoni, A. Bonezzi, and C. K. Morewedge, "Resistance to medical artificial intelligence," *Journal of Consumer Research*, vol. 46, no. 4, pp. 629–650, 2019.
- [5] B. Watson, "A mind of its own—direct infringement by users of artificial intelligence systems," *IDEA*, vol. 58, p. 65, 2017.
- [6] J. R. Geis, A. P. Brady, C. C. Wu et al., "Ethics of artificial intelligence in radiology: summary of the joint European and North American multisociety statement," *Canadian Association of Radiologists Journal*, vol. 70, no. 4, pp. 329–334, 2019.
- [7] Z. I. Khisamova, I. R. Begishev, and R. R. Gaifutdinov, "On methods to legal regulation of artificial intelligence in the world," *International Journal of Innovative Technology and Exploring Engineering*, vol. 9, no. 1, pp. 5159–5162, 2019.
- [8] O. Yara, A. Brazheyev, L. Golovko, and V. Bashkatova, "Legal regulation of the use of artificial intelligence: problems and development prospects," *European Journal of Sustainable Development*, vol. 10, no. 1, pp. 281–281, 2021.
- [9] I. V. Ponkin and A. I. Redkina, "Artificial intelligence from the point of view of law," *RUDN Journal of Law*, vol. 22, no. 1, pp. 91–109, 2018.
- [10] K. H. Yu, A. L. Beam, and I. S. Kohane, "Artificial intelligence in healthcare," *Nature Biomedical Engineering*, vol. 2, no. 10, pp. 719–731, 2018.
- [11] T. M. Wang, Y. Tao, and H. Liu, "Current researches and future development trend of intelligent robot: a review," *International Journal of Automation and Computing*, vol. 15, no. 5, pp. 525–546, 2018.
- [12] T. Panch, J. Pearson-Stuttard, F. Greaves, and R. Atun, "Artificial intelligence: opportunities and risks for public health," *The Lancet Digital Health*, vol. 1, no. 1, pp. e13–e14, 2019.

- [13] B. Cheatham, K. Javanmardian, and H. Samandari, "Confronting the risks of artificial intelligence," *McKinsey Quarterly*, vol. 2, p. 38, 2019.
- [14] H. Neri and F. Cozman, "The role of experts in the public perception of risk of artificial intelligence," *AI & SOCIETY*, vol. 35, no. 3, pp. 663–673, 2020.
- [15] V. Galaz, M. A. Centeno, P. W. Callahan et al., "Artificial intelligence, systemic risks, and sustainability," *Technology in Society*, vol. 67, p. 101741, 2021.
- [16] K. Siau and W. Wang, "Artificial intelligence (AI) ethics," *Journal of Database Management (JDM)*, vol. 31, no. 2, pp. 74–87, 2020.
- [17] C. Cath, "Governing artificial intelligence: ethical, legal and technical opportunities and challenges," *Philosophical Transactions of the Royal Society A: Mathematical, Physical and Engineering Sciences*, vol. 376, no. 2133, p. 20180080, 2018.
- [18] C. L. Thompson and H. M. Morgan, "Ethical barriers to artificial intelligence in the national health service, United Kingdom of Great Britain and Northern Ireland," *Bulletin of the World Health Organization*, vol. 98, no. 4, pp. 293–295, 2020.
- [19] D. Y. Kang, K. J. Cho, O. Kwon et al., "Artificial intelligence algorithm to predict the need for critical care in prehospital emergency medical services," *Scandinavian Journal of Trauma, Resuscitation and Emergency Medicine*, vol. 28, no. 1, pp. 1–8, 2020.
- [20] F. Pesapane, C. Volonté, M. Codari, and F. Sardanelli, "Artificial intelligence as a medical device in radiology: ethical and regulatory issues in Europe and the United States," *Insights Into Imaging*, vol. 9, no. 5, pp. 745–753, 2018.
- [21] J. Pei, K. Zhong, M. A. Jan, and J. Li, "Personalized federated learning framework for network traffic anomaly detection," *Computer Networks*, vol. 209, p. 108906, 2022.
- [22] J. Li, Z. Zhou, J. Wu et al., "Decentralized on-demand energy supply for blockchain in Internet of Things: a microgrids approach," *IEEE transactions on computational social systems*, vol. 6, no. 6, pp. 1395–1406, 2019.
- [23] W. Duan, J. Gu, M. Wen, G. Zhang, Y. Ji, and S. Mumtaz, "Emerging technologies for 5G-IoV networks: applications, trends and opportunities," *IEEE Network*, vol. 34, no. 5, pp. 283–289, 2020.

## Research Article

# Design of Machine Learning Algorithm for Tourism Demand Prediction

Nan Yu <sup>1</sup> and Jiaping Chen<sup>2</sup>

<sup>1</sup>School of Tourism, Yellow River Conservancy Technical Institute, Kaifeng, Henan 475000, China

<sup>2</sup>School of Tourism, Henan Vocational & Technical College, Zhengzhou, Henan 450000, China

Correspondence should be addressed to Nan Yu; [yunan@yrcti.edu.cn](mailto:yunan@yrcti.edu.cn)

Received 21 April 2022; Revised 16 May 2022; Accepted 20 May 2022; Published 8 June 2022

Academic Editor: Naeem Jan

Copyright © 2022 Nan Yu and Jiaping Chen. This is an open access article distributed under the Creative Commons Attribution License, which permits unrestricted use, distribution, and reproduction in any medium, provided the original work is properly cited.

Unused hotel rooms, unused event tickets, and unsold items are all examples of wasted expenses and earnings. Governments require accurate tourism demand forecasting in order to make informed decisions on topics such as infrastructure development and lodging site planning; therefore, accurate tourism demand forecasting becomes vital. Artificial intelligence (AI) models such as neural networks and security violation report (SVR) have been used effectively in tourist demand forecasting as a result of the fast advancement of AI. This paper constructs a tourism demand forecasting model based on machine learning on the basis of the existing forecasting model research. The completed work is as follows: (1) It introduces a large number of domestic and foreign literatures on tourism volume forecasting and proposes the research content of this paper. (2) It is proposed to stack the long short-term memory- (LSTM-) based autoencoders deeply, by adopting a hierarchical greedy pretraining method to replace the random weight initialization method used in the deep network and combining this pretraining stage and fine-tuning network together to form the SAE-LSTM prediction model for improving the performance of deep learning models. (3) This paper uses the monthly search engine strength data of city A's monthly tourist volume and its related influencing factors as the data set; processes the data set to make the model adapt to the data input; uses mean absolute error (MAE), root mean square error (RMSE), MAPE, and other model evaluation indicators; and uses LSTM and the constructed SAE-LSTM model to conduct comparative experiments to predict the number of tourist arrivals in four years. The prediction results of the models proposed in this paper are better than those of the LSTM model. According to the experimental results, the superiority of the proposed LSTM-based unsupervised pretraining method is demonstrated.

## 1. Introduction

With the development of the times, tourism has become an important economic industry in today's world, and tourism has become an indispensable part of modern people's daily life. With the rapid development of the tourism industry, many other problems have arisen. Popular tourist attractions are overcrowded, causing damage to the environment and many safety incidents. The relevant management personnel lacked experience in emergency handling and could not handle it in a timely manner, and the scene was once chaotic. If the flow of people exceeds expectations and there is no effective management, it will bring about serious stampede incidents. For popular tourist attractions, people flow

restriction measures and emergency plans should be formulated to improve risk prevention awareness. Many studies have been carried out in the academic community. Nowadays, in the information age, various situations spread rapidly, and once a safety accident occurs, it will spread rapidly. Even if corresponding measures are formulated, it is difficult to reduce the social impact, causing losses to tourist attractions, which is not conducive to long-term development [1–3]. Therefore, relevant personnel of tourist attractions should pay attention to the occurrence of safety accidents, formulate effective management systems and countermeasures, and cultivate awareness of prevention among all employees. In the process, whether it is the scenic spot manager or the relevant departments, it is necessary to clarify the prevention

standards and build a perfect system to predict the tourist flow and prevent problems before they occur. While avoiding excessive tourist flow, it is also necessary to avoid the loss of tourism in the off-season, especially in hotels and transportation, which will cause waste of resources and affect the sustainable development of scenic spots [4, 5]. It can be seen that the development of the tourism industry is affected by many factors, which will cause seasonal and cyclical changes. It is necessary to pay attention to the timely and accurate judgment of the tourism volume, improve the utilization rate of resources, improve the management ability of scenic spots, and ensure that the tourism industry can form a sustainable development. In order to prevent various problems caused by excessive human flow, it is necessary to predict the passenger flow in advance, improve the carrying capacity of the scenic spot, and formulate effective preventive measures to avoid it, so as to improve the utilization rate of resources and evenly distribute the passenger flow. Therefore, research on the tourism industry must focus on the forecast of tourism volume, which can promote the simultaneous improvement of market value and academic value, and has attracted attention from all walks of life. Aiming at the problem of tourism demand forecasting, statistical methods are used for modeling, and good results have been achieved [6]. To begin, linear regression was employed to predict tourist demand. It was possible to develop a model for forecasting tourist demand by looking at the link between historical demand data and estimated model parameters. Because the cyclical variation in tourist demand is not taken into account, the inaccuracy in predicting tourism demand is rather substantial. Some researchers have proposed methods based on moving average, exponential smoothing, and other time series analysis techniques to address the shortcomings of the linear regression model; however, these techniques are still essentially linear modeling techniques, and as a result, their limitations are also obvious [7]. With the advancement of neural network research in recent years, some researchers have proposed a neural network-based tourism demand forecasting model, which is a nonlinear modelling method that can not only describe cyclical characteristics of tourism demand but also track time-varying travel demand and produce good travel demand forecast results.

It is suggested that the SVR model be employed in tourist forecasting. SVR is a small sample forecasting issue modeling that has the strong forecasting performance of a neural network and can overcome the disadvantages of overfitting. The neural network needs a large number of tourist demand samples, and tourism demand is a small sample prediction issue; thus, the neural network is prone to overfitting during the learning phase, although the fitting accuracy is rather good. The capacity of deep learning in tourism prediction is demonstrated by a tourism prediction model based on LSTM and attention mechanism [8–10]. As a result, the paper's main research goal is to present a tourism volume forecasting model that will improve forecasting accuracy. The proposed model will enable the tourist department comprehend the passenger flow distribution in advance so that scientific decisions can be made, and the strategy will also save a lot of tourism resources, which has far-reaching practical implications.

The paper structures are as follows: Section 2 discusses the related work. Section 3 defines the various methods. Section 4 analyzes the experiment and analysis. Section 5 concludes the article.

## 2. Related Work

Nowadays, the social economy is in a period of rapid development, and the proportion of tourism in the entire economic life is increasing. There is an urgent need to conduct more in-depth research on tourism volume forecasting. At present, after sorting out relevant literature, it is found that foreign research on tourism volume forecasting is mainly divided into three stages: traditional econometric model research, artificial intelligence model research, and hybrid model research, which have more accurate forecasting effects. The earliest traditional econometric model adopts the form of time series. Through long-term use, the model structure is relatively mature, focusing on the characteristics and variable parameters of the data associated with the model, which are determined by the changing trend and shape of the time series; then, through the analysis of the econometric model, the change of the target time series is determined. It can be seen that the observation object of the time series model is only the historical data of the predictor variable, so the data collection is simple, and the application cost is very low, but there is a certain deviation in the prediction result. For a long time in the past, time series models have been used in the forecast of tourism volume and have been popularized in many fields. The more famous one is the comprehensive autoregressive moving average model proposed by reference [11] in 1970. After that, the use of time series models made a breakthrough in 2000, and simple ARIMA models and SARIMA models were constructed, which were recognized and popularized by the academic community. Since the tourism measuring tool is greatly affected by the seasonality, the model can effectively grasp this feature and improve the prediction accuracy [6]. Many innovations were then carried out on this foundation. Reference [12] conducted extensive study on tourism volume forecasting, built a GARCH model using three multivariables, and examined the corresponding factors impacting tourism volume through real verification. Market demand is influenced by different types of markets. In addition, reference [13] analyzed and compared the forecast differences between the econometric models and analyzed the Indian tourism market through the forecast results obtained by the X-12-ARIMA model and the ARFIMA model. Also, typical is the traditional econometric model, which is also one of the more mature forecasting models. The core foundation of the traditional econometric model is statistics, which integrates the knowledge of various disciplines. Based on the mathematical model, the actual parameters are added to form a random setting form, and then, the relationship between variables and influencing factors is analyzed through the application of the model. At present, there are many forms of econometric methods in tourism volume forecasting, mainly including vector autoregressive model (VAR), autoregressive distributed lag model (ADLM), error correction model (ECM), and time-varying parameter (TVP) model, and all of them have been effectively applied [14–16].

Reference [17] used the VAR method to successfully predict the number of tourists in popular scenic spots in a certain region of France in recent years. Then, taking the characteristics of different countries as the analysis point, we got the conclusion that the country is the largest market in the future and then compared the actual state for verification and summarized the results that the VAR model can effectively predict the medium and long-term tourism volume. In addition, through extensive practical analysis, VAR models can be constructed more simply because they are mainly based on theoretical analysis. After that, the research of reference [18] introduced a new method, which led to the development of inbound tourism forecasting. Reference [19] carried out error analysis on the existing basis and optimized the prediction model, so that the British outbound tourism volume was effectively analyzed. With the continuous development of research methods, the academic community has gradually realized that due to the problems of time series, the previous prediction models often fail to achieve the expected results. To this end, artificial intelligence models have been proposed through a large number of innovations, and AI-based technology has been greatly developed [20, 21]. At the end of the last century, the concept of artificial neural network (ANN) was introduced into the tourism volume prediction model, which made the research greatly developed. In this regard, reference [22] summarizes the ANN model for tourism volume prediction and puts forward a conclusion that is superior to the traditional model through analysis. Reference [23] believes that the ANN model has great advantages in tourism volume forecasting. Compared with the traditional Naivel model, ES method, multiple regression, and other models, it has many characteristics, and the prediction results are more effective. Reference [24] optimizes on the basis of ANN, compares multiple prediction models after summarization, and obtains many rules and summarizes the multilayer perception prediction model. With the continuous research on tourism volume forecasting, the accuracy of tourism volume forecasting based on various models has been continuously improved, but the transparency of the model is low, so that users cannot understand the mechanism of the model and thus cannot gain the trust of users. It is of great significance to study the interpretability of tourism forecasting models, but at this stage, there is no or very little work focused on interpretable tourism demand forecasting [25–27]. Many machine learning models are widely used in time series forecasting. If the traditional ANN with shallow structure becomes too complex, for example, the network contains many layers and parameters; it is difficult to train. Deep neural networks (DNNs) have shown better performance than traditional neural networks in many time series forecasting applications. Deep learning can train DNNs with many hidden layers, and it is easy to learn features from raw data, so it is very popular in the field of machine learning.

### 3. Method

This section discusses the AE-LSTM prediction model construction. They define the SAE-LSTM prediction model construction, and they evaluate the selection of model evaluation indicators.

**3.1. AE-LSTM Prediction Model Construction.** Here, LSTM network and autoencoders are examined. They analyze the LSTM-based autoencoder pretraining model construction.

**3.1.1. LSTM Network.** RNN has been used to solve problems such as tourism demand predictions because it can simulate dependencies between sequence data through loops. However, because the neural network is in the process of forward transmission, the influence of the later time on the previous time diminishes as the later time passes, so it is unable to recall the long-term memory. LSTM not only has a loop learning unit inside the network but also through the design gate to collect longer and shorter states from the start unit to the last unit; the recall of long-term memory is superior to RNN. The design of LSTM can effectively deal with long-term memory. Figure 1 shows the LSTM model used in this paper. LSTM can process time series data sequentially and use the output of the last time step to predict the output of a linear regression layer. The LSTM memory cell is controlled by three gates to sequence the messages passed, thereby accurately capturing long-term dependencies. The three gates are responsible for controlling the interaction between different memory cells. The function of the input gate is to control whether the input signal can modify the state of the memory cell, the forget gate controls whether to remember the previous state, and the output gate controls the output of the memory cell.

In each time step  $T$ , the hidden state  $h^t$  is updated by the input  $x^t$  at the same time, the previous state of the hidden layer is  $h^{t-1}$ , the input gate is  $i^t$ , the output gate is  $o^t$ , the forget gate is  $f^t$ , and the storage unit is  $s^t$ ; the relational equation is as follows:

$$i^t = \lambda(w^i x^t + v^i h^{t-1} + a^i), \quad (1)$$

$$f^t = \lambda(w^f x^t + v^f h^{t-1} + a^f), \quad (2)$$

$$o^t = \lambda(w^o x^t + v^o h^{t-1} + a^o), \quad (3)$$

$$s^t = f^t \times s^{t-1} + i^t \times \tanh(w^s x^t + v^s h^{t-1} + a^s), \quad (4)$$

$$h^t = o^t \times \tanh(s^t), \quad (5)$$

where  $w$ ,  $v$ , and  $a$  are model parameters, which are continuously learned during model training;  $\lambda$  and  $\tanh$  are excitation functions, which are responsible for mapping the input of the neuron to the output;  $\times$  represents the product of the corresponding position elements of the two matrices; and the linear regression layer is as follows:

$$\bar{y}_i = w^r h_i^t, \quad (6)$$

where  $w^r$  is the weight parameter of the linear regression layer, and formula (6) is used to predict the output of the linear regression layer.

**3.1.2. Autoencoders.** Autoencoder (AE) is divided into three parts, namely, input layer, hidden layer, and output layer, and is an unsupervised learning algorithm. The autoencoder

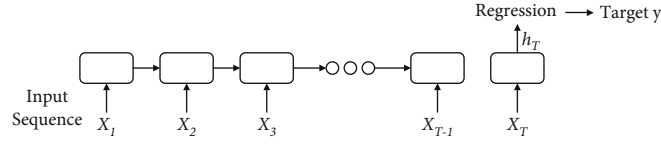


FIGURE 1: LSTM model.

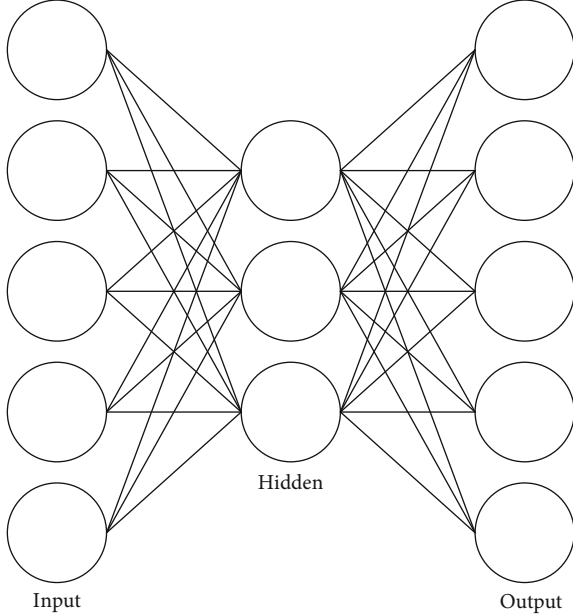


FIGURE 2: Autoencoder structure.

training process used in this paper is divided into two stages: the encoding stage compresses the input data, and the decoding stage reoutputs the compressed data. The autoencoder structure is shown in Figure 2.

Among them, given the unlabeled data set  $x_n, n = 1, 2, \dots, N$ , the two stages of the autoencoder used in this paper can be expressed as follows:

$$h_x = f(w_1 x + a_1), \quad (7)$$

$$x_o = g(w_2 h_x + a_2), \quad (8)$$

where  $w_1$  is the weight parameter from input to hidden neural layer,  $w_2$  is the weight parameter from hidden to output neural layer,  $a_1$  and  $a_2$  are the deviation vectors of input layer and hidden layer, respectively, encoding refers to from input to hidden neural layer conversion, decoding refers to the conversion from hidden to output neural layer,  $f$  is the encoding function,  $g$  is the decoding function, and  $h_x$  represents the hidden encoding layer vector calculated from the input vector  $x$ , where the relationship between the input vector  $x$  and the output vector  $x_o$  is shown as follows:

$$x_o \approx x. \quad (9)$$

Among them, the autoencoder is learned through training to ensure that  $x$  and  $x_o$  are equal to achieve a compressed

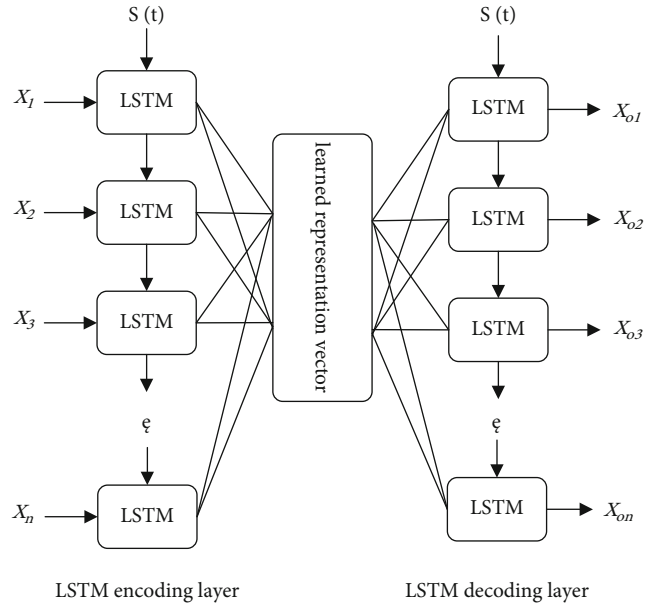


FIGURE 3: LSTM-based autoencoder pretrained model.

representation of  $x$ . Autoencoders are often used to extract nonlinear features.

**3.1.3. LSTM-Based Autoencoder Pretraining Model Construction.** The forecasting problem of tourism demand is a time series forecasting problem. Based on RNN, it is more suitable for modeling time series data. This paper proposes a new structure based on LSTM and autoencoder, which can extract features from time series problems, and is to replace the encoding layer and decoding layer of the autoencoder with the LSTM network layer, so as to propose an LSTM-based autoencoder pretraining model, as shown in Figure 3.

This paper proposes an LSTM-based autoencoder pretraining model, which consists of two LSTM layers, an LSTM encoding layer and an LSTM decoding layer, given an input sequence  $(x_1, x_2, \dots, x_n)$ ; the encoder accepts the input sequence and encodes it into the learned representation vector; then, the decoding layer takes this representation vector as input and tries to reconstruct the input sequence  $(x_{o1}, x_{o2}, \dots, x_{on})$ . This structure is an unsupervised learning algorithm.

**3.2. SAE-LSTM Prediction Model Construction.** This section examines the stacked autoencoders. They discuss the LSTM-based stacked autoencoder pretraining model construction. They analyze the SAE-LSTM prediction model construction.



**3.2.1. Stacked Autoencoders.** Deep learning is a machine learning method based on data learning. Data features are extracted through multilayered nonlinear processing units. Each layer uses the output of the preceding layer as input, and the data is translated from the bottom layer to the top layer. Deep networks can learn more representations and better identify correlations between data by stacking layers on top of each other. Stacked autoencoders (SAE) essentially use the output of the hidden layer of the previous autoencoder as the input of the next autoencoder, which is composed of multiple autoencoders. Each autoencoder is utilized as a hidden layer, and many hidden layers are piled successively from the bottom to produce the stacked autoencoder deep network. In this structure, multiple autoencoders are stacked, and each autoencoder layer is trained so that the input error is locally optimal, and the output of the hidden layer is used as the input layer of the next autoencoder layer. A single autoencoder can learn a feature representation through the three-layer network of equation (10), such as the following:

$$x \longrightarrow H_1 \longrightarrow x_o, \quad (10)$$

$$H_1 = f_\mu(x). \quad (11)$$

The stacked autoencoder obtains  $H_1$  through the training of the first autoencoder and then uses  $H_1$  as the input to train the next autoencoder to obtain  $H_2$  and then continues to train this deep learning structure. That is, first train equation (10) to obtain the transformation of equation (12), and then, train equation (13) to obtain the transformation of equation (14), and finally, stack the SAE layer by layer.

$$x \longrightarrow H_1, \quad (12)$$

$$H_1 \longrightarrow H_2 \longrightarrow H_1, \quad (13)$$

$$H_1 \longrightarrow H_2. \quad (14)$$

**3.2.2. LSTM-Based Stacked Autoencoder Pretraining Model Construction.** The progressive unsupervised pretrained stacked autoencoder can learn the features of the original data layer by layer, which is more suitable for complex features. Therefore, this paper proposes an LSTM-based stacked autoencoder pretraining model. The LSTM-based stacked autoencoder is also a greedy hierarchical pretraining, and its construction process is divided into the following three steps:

- (1) First train the first LSTM-based autoencoder; then, save its LSTM encoding layer and its learned network parameters, and use the first LSTM encoding layer as the input of the second LSTM-based autoencoder
- (2) In order to train an LSTM-based autoencoder, load and utilize the previously stored encoder layer to recreate the original input data, not the encoded input data. This allows the encoder to pick up on characteristics from the original data and improve its per-

formance. Save the learned network parameters and the second LSTM-based encoding layer using the second LSTM-based encoding layer as an input to the third LSTM-based self-encoder

- (3) Load the two saved encoder layers, use them to encode the input twice, then continue to train the third LSTM-based autoencoder with the saved encoded version, thereby reconstructing the original input and saving the third LSTM-based autoencoder encoding layer and its learned network parameters. And so on, this model can also be generalized to more than three layers

**3.2.3. SAE-LSTM Prediction Model Construction.** The SAE-LSTM tourism volume prediction model is constructed using a stacked autoencoder based on LSTM to replace the random initialization of weights used in the LSTM network. Taking the training of three LSTM-based autoencoder stacks as an example, the SAE-LSTM model is divided into a pre-training stage and a fine-tuning stage, in which the three encoding layers and the optimized network parameters are saved in the pretraining stage. The fine-tuning stage is divided into two steps:

- (1) Using the three LSTM encoding layers and their learned network parameters saved in the pretraining stage
- (2) Add an output layer on top of the three hidden layers, which have only one node and is utilized to solve the tourism volume forecast problem

**3.3. Selection of Model Evaluation Indicators.** In order to evaluate the performance of the prediction model, this paper uses three evaluation indicators to evaluate the prediction effect. They are mean absolute error (MAE), root mean square error (RMSE), and mean absolute percentage error (MAPE). Given the predicted value  $y_p$  and the actual value  $y$  as follows:

$$y_p = \{y_{p1}, y_{p2}, \dots, y_{pn}\}, \quad (15)$$

$$y = \{y_1, y_2, \dots, y_n\}. \quad (16)$$

The three index equations are as follows:

$$\text{MAE} = \frac{1}{n} \sum_{i=1}^n |y_{pi} - y_i|, \quad (17)$$

$$\text{RMSE} = \sqrt{\frac{1}{n} \sum_{i=1}^n (y_{pi} - y_i)^2}, \quad (18)$$

$$\text{MAPE} = \frac{1}{n} \sum_{i=1}^n \left| \frac{y_{pi} - y_i}{y_i} \right|, \quad (19)$$

where MAE is a measure of the average magnitude of a set of errors, and it is the sum of the absolute values of the differences between  $y$  and  $y_p$  and then divided by the number of

test samples; RMSE is a measure of the average magnitude of a set of errors, which is the square root of the average of the squared differences between  $y$  and  $y_p$ ; and MAPE is the mean of the absolute value of each error divided by  $y$ . The three indicator formulas are calculated by the predicted value and the actual value. The larger the three values, the larger the error.

#### 4. Experiment and Analysis

This section discusses the data preprocessing. They evaluate the experimental design and model parameter selection. They analyze the analysis of experimental results.

*4.1. Data Preprocessing.* Here, the data sources are defined. They examine the data preprocessing.

*4.1.1. Data Sources.* The data set used in this paper is the monthly search engine strength data of the number of monthly passenger arrivals and tourism-related influencing factors in a region from January 2014 to December 2019, and the region is represented by city A. Among them, the monthly tourist arrivals are provided by the tourism bureau of the city government. The tourist arrivals collected from the DSEC website in this article are the tourist arrivals from the global market. The experimental data of this paper adopts the search engine strength data of 168 influencing factors related to tourism in city A, of which 38 monthly search engine data are from Baidu and 130 monthly search engine data are from Google. The influencing factors of the seven tourism categories are extended, and Table 1 lists some of the influencing factors used in the experimental data.

To sum up, the experimental data in this paper consists of the monthly search intensity of 168 tourism keywords and the arrivals of tourists in city A. This time series data is a list with ordered values.

*4.1.2. Data Preprocessing*

*(1) Data Normalization.* Data normalization is the process of scaling data into a specific range. The data of city A is normalized using min-max normalization in this study, so that each characteristic is of the same order of magnitude. The conversion function used is shown as follows:

$$I^* = \frac{I - \min}{\max - \min}, \quad (20)$$

where min and max are the minimum and maximum values of the sample data; min-max normalization can make the sample data fall within the  $[0, 1]$  interval.

*(2) Data Conversion.* The sliding window is a fixed-length data movement, one unit at a time; for example, January 2014 to December 2019 is a fixed-length data, the length of this window is 12, and this window is from left to right glide; assuming the data collection is on a monthly basis, the next window is not January 2015 to December 2015 but February 2014 to January 2015. The window slide travels one unit to

TABLE 1: Influencing factors of tourism in city A.

Travel category	Influencing factors
Dining	Gourmet, snack, famous restaurant
Lodging	Hotels, homestay, city bus
Tour	Tourist volume, tourism index
Clothing	Weather, air quality
Shopping	Shopping mall, shopping street
Recreation	Bar, concert
Transportation	Yacht, motorboat

the right at a time, and each window is always 12 inches in length. In other words, the time series data employed in this study is cyclical. The impact of data periodicity on forecasting difficulties can be reduced by using a sliding window to provide a fixed length for data conversion. The time series is made up of sequences that are ordered in chronological order. The data for this study is collected on a monthly basis. This paper converts the original data into time series data based on sliding windows. Given a time series  $T$  and a window of length 12,  $T = (x_1, x_2, \dots, x_n)$ ,  $n$  is 72, representing 72 months of data collected from January 2014 to December 2019; each  $x$  is also a 168-dimensional vector, representing the monthly search intensity of 168 tourism-related features. In this paper, the data is moved by the shift function of pandas. First, the time window is placed at the starting position of  $T$ , and then, the time window is moved one month backward with time, and then, the second month of  $T$  is used as the starting position, get the second data of length 12, and so on; there are a total of 60 data of length 12  $c_1, c_2, \dots, c_{60}$ , where  $(c_1 = x_1, x_2, \dots, x_{12})$ ,  $(c_2 = x_2, x_3, \dots, x_{13})$ . The converted data is as follows:

$$W_{(c)} = \{c_i | i = 1, 2, \dots, 60\}. \quad (21)$$

The second step of data conversion is to convert the sliding window-based city A time series data into supervised learning data to facilitate subsequent training of the model. The supervised learning data format consists of input and output, that is, predicting the output from the input. This article adds the actual passenger arrivals to city A in the next month on the basis of each  $c_i$ .

*4.2. Experimental Design and Model Parameter Selection.* Here, the experiment design phase is discussed, and the model parameter selection is evaluated.

*4.2.1. Experiment Design Phase.* The specific experimental design phase is divided into three steps:

- (1) Process the city A data set, and then divide the processed data into training set, validation set, and test set. When predicting the 12-month tourism arrivals in 2016, the data sets of 2014 and 2015 are used as the training set, and the top 10% of the data are divided from the training set as the validation set,

and then, the test set of this paper is the 12-month 2016 data set. When predicting the 12-month tourism arrivals in 2017, the first three years of data are used as the training set, the first 10% of the data are divided from the training set as the validation set, and then, the 2017 12-month data set is used as the test set, and so on to forecast the tourism volume from 2016 to 2019

- (2) Use the training set to train each model separately and predict the total amount of tourism for each model. The corresponding real tourist volume will be collected from the test set to produce new training data once the prediction model predicts the tourism volume for a month. Then, do the next step of training and prediction and so on to predict the number of tourists in city A from 2016 to 2019. And the hyperparameter involved in this paper is set based on past experience, and grid search is performed to perform brute force search, so as to obtain the best experimental results
- (3) Save the experimental results of each model and analyze the experimental results

**4.2.2. Model Parameter Selection.** This paper uses the Keras deep learning framework to build the SAE-LSTM prediction model and builds the LSTM benchmark model for comparative experiments. This section describes the selection of model parameters during the experiment.

**(1) SAE-LSTM Prediction Model.** The construction process of the SAE-LSTM model used in this paper is the same as that in Section 3.2. For the SAE-LSTM model, it is divided into a pretraining stage and a fine-tuning stage. Regarding the preprocessing stage, the number of layers of the LSTM superimposed autoencoder is selected. In this paper, a trial and error method is used to predict the number of layers, and MAPE is used as the evaluation index. The specific experimental results are shown in Table 2.

It can be seen from Table 2 that the MAPE value of the SAE-LSTM model with more than three hidden layers is extremely high, which means that the error is very large; it shows that the high number of hidden layers will lead to overfitting. In order to avoid overfitting, the SAE-LSTM model with at most two hidden layers is used in the experiment. The SAE-LSTM of the two hidden layers is divided into a pretraining stage and a fine-tuning stage based on LSTM-based stacking autoencoders. The pretraining stage is the training of two LSTM-based autoencoders, thereby saving the two LSTM encoding layers and their trained parameters for the fine-tuning stage. The hyperparameters that need to be selected for the SAE-LSTM of the two hidden layers are the number of iterations epochs, the loss rate dropout, the number of units in the first coding layer `lstm_unit1` in the pretraining stage, and the number of units in the second coding layer `lstm_unit2`. In this paper, grid search is used to obtain the optimal hyperparameter set of the SAE-LSTM prediction model of two hidden layers.

TABLE 2: SAE-LSTM experimental results with different number of hidden layers.

Number of hidden layers	MAPE
1	3.158
2	3.125
3	3.388
4	6.753
5	6.923

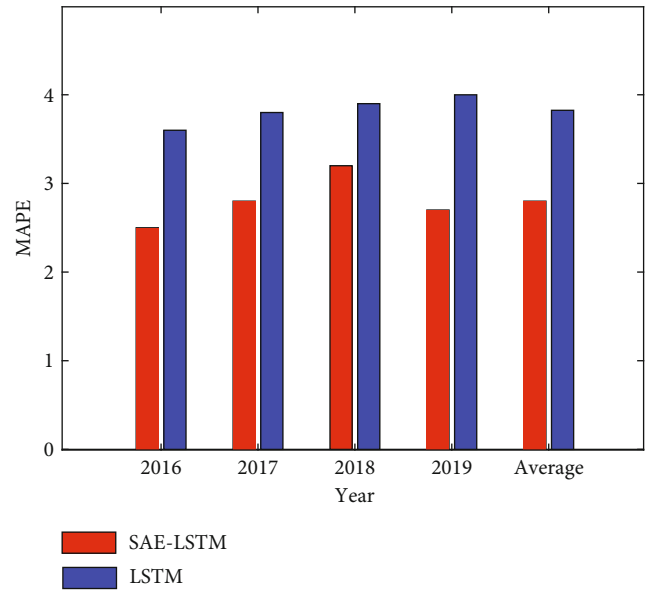


FIGURE 4: MAPE comparison of the two models.

Through grid search, the epochs are {200, 400, 500}, the dropout is {0.01, 0.2, 0.3}, `lstm_unit1` is {56, 64, 128}, and `lstm_unit2` is {32, 48, 64}.

**(2) LSTM Model.** In this paper, the LSTM model is selected as the benchmark model for the experiment. The LSTM model is introduced in Section 3.1.1. For the benchmark model, parameters are also selected from grid search.

**4.3. Analysis of Experimental Results.** In this paper, the SAE-LSTM model and the LSTM model are used to conduct experiments on the city A data set. In order to avoid overfitting, SAE-LSTM only selects the two optimal hidden layers in training. And three model evaluation indicators MAE, RMSE, and MAPE are used to predict the accuracy. The tourist arrivals of the data set are tourists from city A around the world, and the tourist arrivals of this type fluctuate periodically. This paper uses this data set for experiments, and the experimental results are shown in Figures 4–6.

It can be seen from Figures 4–6 that the evaluation index value of two-layer SAE-LSTM is smaller than that of LSTM for 4 consecutive years. So it can be concluded that the SAE-LSTM prediction accuracy proposed in this paper outperforms the LSTM model in all performance measures. The experimental results show that the pretraining method of superimposing LSTM in the way of autoencoder has better

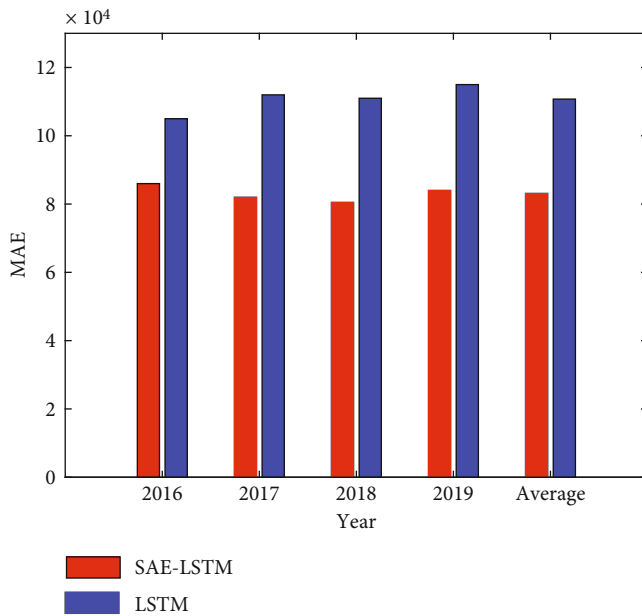


FIGURE 5: MAE comparison of the two models.

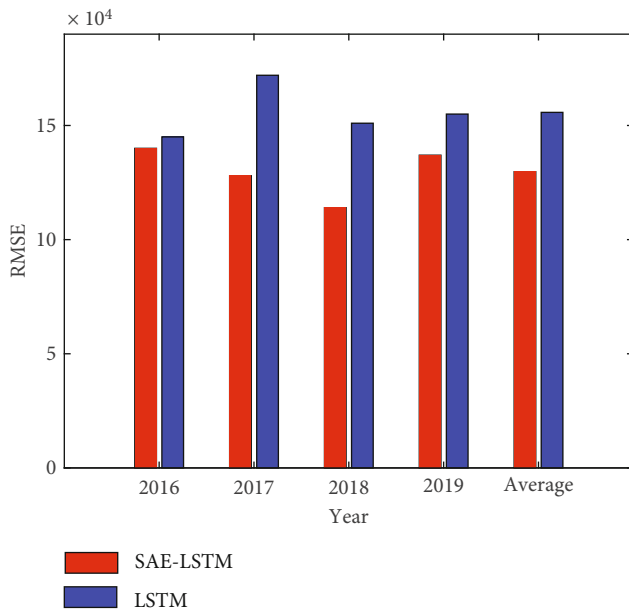


FIGURE 6: RMSE comparison of the two models.

performance than random initialization of LSTM weights, which proves that the proposed unsupervised pretraining method based on LSTM can replace the random weight initialization method used in deep networks. The feasibility of using this method to fine-tune the network improves the performance of the tourism volume prediction model.

## 5. Conclusion

With the increase in the number of tourists, the tourism industry has also tackled new challenges. The perishable nature of tourism products causes waste in the tourism industry, unsold rooms and air tickets cannot be stored,

and the number of tourists and the distribution of tourism resources in many tourist attractions are gradually uneven, and accurate forecast of tourism volume can enable the number of tourism practitioners to allocate appropriate tourism resources to meet the tourism demand and reduce the waste of resources, and government agencies and tourism enterprises can use the accurate tourism volume forecast results to invest in basic measures and formulate tourism-related policies. The accuracy of tourism demand forecasting is critical, and this research presents a deep learning approach to help with that. This paper's primary work is summarized as follows:

- (1) Since recurrent networks are more suitable for modeling time series data, this paper first proposes to stack LSTM-based autoencoders deeply and replace the deep network with a layered greedy pre-training method. The SAE-LSTM prediction model, which is based on the suggested random weight initialization method, combines this pretraining stage and fine-tuning network to improve the performance of the deep learning model and obtain superior prediction results
- (2) In order to prove the effectiveness of the proposed deep learning model, this paper uses the monthly search engine intensity data of city A's monthly visitor volume and its related influencing factors from January 2014 to December 2019 as a data set to process the data set; adapts the model to the data input; uses MAE, RMSE, and MAPE model assessment indicators; and performs comparison tests using LSTM and the developed SAE-LSTM model to forecast the number of tourists in four years. The prediction results of the model proposed in this paper are all better than the LSTM model. According to the experimental results, the superiority of the proposed LSTM-based unsupervised pretraining method is demonstrated

## Data Availability

The data sets used during the current study are available from the corresponding author on reasonable request.

## Conflicts of Interest

The authors declare that they have no conflict of interest.

## References

- [1] Y. C. Hu, "Developing grey prediction with Fourier series using genetic algorithms for tourism demand forecasting," *Quality & Quantity*, vol. 55, no. 1, pp. 315–331, 2021.
- [2] N. Sun and J. Ma, "Forecast on the tourist-generating market of Beijing Olympic Games in 2008 based on tourism background trend line," *Geographical Research*, vol. 27, no. 1, pp. 65–74, 2008.

- [3] P. Su, *Study on Scenic Area Tourism Passenger Flow Short-Term Forecast Method*, [Ph.D. thesis], Hefei University of Technology, 2013.
- [4] C. Vu, "Effect of demand volume on forecasting accuracy," *Tourism Economics*, vol. 12, no. 2, pp. 263–276, 2006.
- [5] W. Bi, Y. Liu, and H. Li, "Daily tourism volume forecasting for tourist attractions," *Annals of Tourism Research*, vol. 83, article 102923, 2020.
- [6] S. Sakhuja, V. Jain, S. Kumar, C. Chandra, and S. K. Ghildayal, "Genetic algorithm based fuzzy time series tourism demand forecast model," *Industrial Management & Data Systems*, vol. 116, no. 3, pp. 483–507, 2016.
- [7] L. Wu and J. Zhang, "The variance-covariance method using IOWGA operator for tourism forecast combination," *International Journal of Supply and Operations Management*, vol. 1, no. 2, pp. 152–166, 2014.
- [8] X. Yang, B. Pan, A. Evans, and B. Lv, "Forecasting Chinese tourist volume with search engine data," *Tourism Management*, vol. 46, pp. 386–397, 2015.
- [9] R. Kubicki and M. Kulbaczevska, "Modeling and forecasting of the volume of touristic flows in Poland," *Zeszyty Naukowe Uniwersytetu Szczecińskiego. Ekonomiczne Problemy Turystyki*, vol. 3, pp. 57–70, 2014.
- [10] R. Law, G. Li, C. Fong, and X. Han, "Tourism demand forecasting: a deep learning approach," *Annals of Tourism Research*, vol. 75, pp. 410–423, 2019.
- [11] H. Shen, Q. Wang, C. Ye, and J. S. Liu, "The evolution of holiday system in China and its influence on domestic tourism demand," *Journal of Tourism Futures*, vol. 4, no. 2, pp. 139–151, 2018.
- [12] W. Chang and Y. Liao, "A seasonal ARIMA model of tourism forecasting: the case of Taiwan," *Asia Pacific Journal of Tourism Research*, vol. 15, no. 2, pp. 215–221, 2010.
- [13] H. Aladag, E. Egrioglu, and C. Kadilar, "Improvement in forecasting accuracy using the hybrid model of ARFIMA and feed forward neural network," *American Journal of Intelligent Systems*, vol. 2, no. 2, pp. 12–17, 2012.
- [14] G. Li, H. Song, and S. F. Witt, "Recent developments in econometric modeling and forecasting," *Journal of Travel Research*, vol. 44, no. 1, pp. 82–99, 2005.
- [15] H. Song and G. Li, "Tourism demand modelling and forecasting—a review of recent research," *Tourism Management*, vol. 29, no. 2, pp. 203–220, 2008.
- [16] G. Li, F. Wong, H. Song, and S. F. Witt, "Tourism demand forecasting: a time varying parameter error correction model," *Journal of Travel Research*, vol. 45, no. 2, pp. 175–185, 2006.
- [17] U. Gunter and I. Önder, "Forecasting international city tourism demand for Paris: accuracy of uni- and multivariate models employing monthly data," *Tourism Management*, vol. 46, pp. 123–135, 2015.
- [18] M. Uysal and J. L. Crompton, "An overview of approaches used to forecast tourism demand," *Journal of Travel Research*, vol. 23, no. 4, pp. 7–15, 1985.
- [19] R. Rivera, "A dynamic linear model to forecast hotel registrations in Puerto Rico using Google Trends data," *Tourism Management*, vol. 57, pp. 12–20, 2016.
- [20] S. Collins and M. Moons, "Reporting of artificial intelligence prediction models," *The Lancet*, vol. 393, no. 10181, pp. 1577–1579, 2019.
- [21] Z. Wang and R. S. Srinivasan, "A review of artificial intelligence based building energy use prediction: contrasting the capabilities of single and ensemble prediction models," *Renewable and Sustainable Energy Reviews*, vol. 75, pp. 796–808, 2017.
- [22] A. Palmer, J. J. Montano, and A. Sesé, "Designing an artificial neural network for forecasting tourism time series," *Tourism Management*, vol. 27, no. 5, pp. 781–790, 2006.
- [23] R. Law, "Back-propagation learning in improving the accuracy of neural network-based tourism demand forecasting," *Tourism Management*, vol. 21, no. 4, pp. 331–340, 2000.
- [24] W. Höpken, T. Eberle, M. Fuchs, and M. Lexhagen, "Improving tourist arrival prediction: a big data and artificial neural network approach," *Journal of Travel Research*, vol. 60, no. 5, pp. 998–1017, 2021.
- [25] B. Ji, Y. Li, D. Cao, C. Li, S. Mumtaz, and D. Wang, "Security performance analysis of UAV assisted relay transmission for cognitive network with energy harvesting," *IEEE Transactions on Vehicular Technology*, vol. 69, no. 7, pp. 7404–7415, 2020.
- [26] X. Lin, J. Wu, S. Mumtaz, S. Garg, J. Li, and M. Guizani, "Blockchain-based on-demand computing resource trading in IoV-assisted smart city," *IEEE Transactions on Emerging Topics in Computing*, vol. 9, no. 3, pp. 1373–1385, 2021.
- [27] J. Pei, K. Zhong, M. A. Jan, and J. Li, "Personalized federated learning framework for network traffic anomaly detection," *Computer Networks*, vol. 209, p. 108906, 2022.

## Research Article

# A Study on Mobile Resources for Language Education of Preschool Children Based on Wireless Network Technology in Artificial Intelligence Context

QiuMing Li 

Guangzhou Huashang Vocational College, Guangzhou, 511300 Guangdong, China

Correspondence should be addressed to QiuMing Li; [liqiuming@stu.jnu.edu.cn](mailto:liqiuming@stu.jnu.edu.cn)

Received 9 April 2022; Revised 30 April 2022; Accepted 4 May 2022; Published 7 June 2022

Academic Editor: Naeem Jan

Copyright © 2022 QiuMing Li. This is an open access article distributed under the Creative Commons Attribution License, which permits unrestricted use, distribution, and reproduction in any medium, provided the original work is properly cited.

Preschool language education is a requirement of basic education reform as well as a requirement for children's growth in all aspects of body and mind. It is extremely important and valuable in encouraging the entire growth of preschool education as well as children's general harmonious development. The degree of informatization is changing day by day, and many information technology concepts and tools have entered the preschool education field. The Internet, electronic school bags, ECE whiteboards, terminal devices, and rich digital resources and tools have been introduced into kindergarten classrooms. The continuous advancement and application of information technology have provided the feasibility of building a smart learning environment for kindergartens. To this end, this paper starts from the core concepts and theoretical foundations of preschool education and sorts out the concepts of learning resources, smart learning, and smart learning environments. Learning theory, teaching theory, and activity theory provide the theoretical foundation for the creation of language learning tools in preschool education. The technologies of campus network, Internet of Things, artificial intelligence, and rich media are examined under the role and inspiration of smart learning environment to provide theoretical support for scientific design of smart language learning environment in preschool education.

## 1. Introduction

Today's society is developing rapidly, and in this era, the development and changes in the field of education have become a hot topic of concern [1]. To the dilemma faced by the reform of basic education at home and abroad, educational informatization has become an effective way out of the dilemma [2, 3]. The development of educational technology is a product of the combination of technological progress and educational development, and the concept of educational technology runs through the whole process of education, including, of course, preschool education [4–6]. The informatization of education has created more possibilities for learning [7]. The trend in modern preschool education is to build a wise learning environment in the early childhood learning environment, and this is one of the paths in the design of today's early childhood information-based learning environment [8]. Combining kindergarten curricu-

lum goals and the needs of early childhood development, building a smart learning environment, and integrating mobile educational resources are the changes to the early childhood learning environment [9]. Kindergarten, as a crucial component of basic education, is intimately linked to the quality of learning that continues later and has a foundational role in the development of young children throughout their lives [10].

Language, as a vehicle for the individual's development, is of great importance for all aspects of human development [11]. As far as the individual is concerned, language is an essential tool for thinking, a form of cognitive ability, and an important sign of individual socialization. The preschool years are a period of rapid language development for young children, and the improvement of their language skills is gradually developed through constant communication and use [12]. Therefore, in the early childhood stage, which has a key impact on individual development, it becomes an issue

that deserves our attention and in-depth research on how kindergartens can provide language education to children in a scientific and effective way during their natural growth process, so that children can acquire language skills and necessary communication skills in their life and learning [13].

Since the beginning of the twenty-first century, all walks of life around the world have proposed new-age goals and directions for the development of access to education [14]. As a result, smart learning environments have sprouted from the new era's requirements. Smart learning environments have become one of the core directions for the construction of learning environments. Since smart learning environments have been proposed, related research has sprung up, and the current stage is a critical period for exploration and construction. Most of the existing studies are on the application of smart learning environments in higher education, learning analytics in classrooms, and the application of Internet of Things technology in campuses [15–17]. Many modern information technologies have been developed to a more mature stage, but the application of modern information technologies in kindergartens and the study of smart learning environments in early childhood learning environments are sporadic [18]. Under the kindergarten wisdom learning environment, how to fully apply the existing technology to optimize the current kindergarten language learning environment, what level of kindergarten language education resources are actually available, and how to organically combine the information technology approach with the needs of the development of early childhood language education have become issues that need to be addressed urgently now.

To address this, we enhanced essential methodologies and characteristics of language education tools for young children based on their learning behavior characteristics, as well as their cognitive qualities and learning goals. We next examine and synthesize the data from the case studies in order to build an acceptable language learning programmer for early childhood preschool education. Explore the design of language education environments for young children based on the current state of their learning environments.

The paper's organization paragraph is as follows: The related work is presented in Section 2. Section 3 analyzes the key technologies and features of educational environment for preschool children in wireless network environment. Section 4 discusses the design of a kindergarten language education resource management system based on wireless network technology in an artificial intelligence environment. Finally, in Section 5, the research work is concluded.

## 2. Related Work

*2.1. Current Status of Research on Information-Based Learning Environments in Preschool Education.* The experimental study showed that teachers' use of whiteboards and electronic devices significantly improved children's literacy skills. Multimedia presentations create learning opportunities for children to interact tactilely with the whiteboard and also enrich the presentation of resources, giving children

the opportunity to engage in multimedia dialogue and interaction [19]. Through data collection, methods used included observations, interviews, and a review of children's related documents to explore how early childhood educators can enhance young children's motivation to read through manipulating the classroom environment [20]. The study concluded that thematic reading and shared reading would enhance young children's motivation to read. There is a growing body of research showing that high-quality preschool environments improve child-teacher interactions and that teacher-student communication and interaction are very important aspects of learning activities. The computerization of the learning environment provides more possibilities for interaction between children and teachers, with real-time communication and off-site interaction becoming the norm. Information and communication technologies have limitations for the development of young children, but when properly designed and utilized, they will contribute to the intellectual, linguistic, social, and creative development of children ages 3-6.

In order to promote the healthy and harmonious development of children, the use of information technology in kindergartens should follow the three principles of simplicity, gamification, and appropriateness, and teachers should be proficient in designing and implementing information-based teaching activities [21]. At the same time kindergartens and relevant management departments should strengthen the common sharing of kindergarten information-based education and learning resources. Creating a good environment for children's games is an important means to play the educational function of games and environment [22]. The environment plays an important role in promoting the learning and play life of young children. By creating different levels of play environments, the basic educational tools of kindergartens can be realized. The introduction of multitouch virtual learning gadgets has aided in the optimization and improvement of technical tools, as well as creating a new situation of hands-on learning for young children with technical assistance. Virtual learning devices for young children are more attractive than traditional learning devices in terms of perceptual dimension, extended reuse, diversity, and state preservation.

*2.2. Business Needs for Language Education Resources for Preschool Children.* With the popularity of smart phones, the size of the mobile education market is at a rapid growth stage. The conclusion reached through continuous practical tests is that educational resources for preschool children need to be short, interesting, and educational. The business demand characteristics of auxiliary early childhood language education are shown in Table 1.

### 2.3. Student-Centered Teaching Theory

*2.3.1. Generative Teaching.* Generative teaching emphasizes the subjectivity of students, and classroom ideas and teaching behaviors are adjusted according to the interactions and student responses in the classroom [23]. The characteristics of generative teaching are active student participation,

TABLE 1: Characteristics of business needs to support language instruction for young children.

1	Short and concise, able to tell a story, show a song, or complete a certain knowledge in a few minutes of scene presentation of a knowledge point
2	A combination of graphics, animation, and sound to enhance language learning for children
3	It takes up little space, is easy to transmit and store, and requires less hardware and equipment for teachers and institutions in weak clients.
4	You can find a wide variety of language works related to early childhood education materials or in line with teaching.

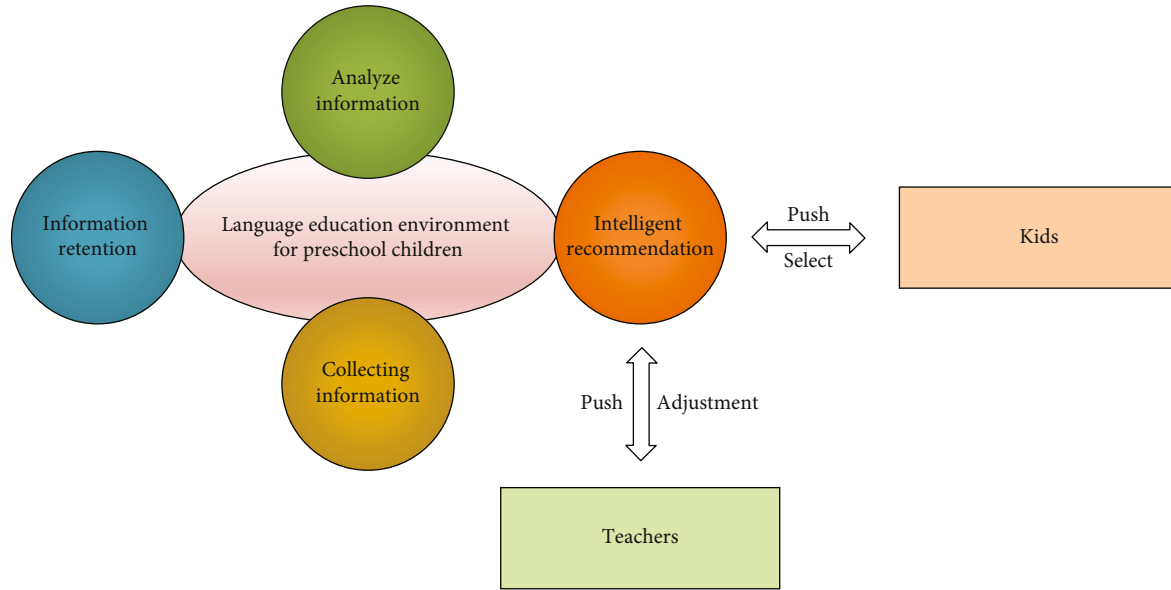


FIGURE 1: Generative teaching generation process.

nonpredetermined classroom, and interactivity. Generative teaching uses learning analytics to analyze and uncover dynamic learning paths and provide appropriate learning resources through data such as classroom learning records and online learning records of young children. Whether it is online learning, blended learning, or even traditional classrooms, as long as information technology exists, there is a need for learning analytics. The process of generative teaching and learning in a smart learning environment is shown in Figure 1.

2.3.2. *Effective Teaching.* Effective teaching and learning theory assign three typical characteristics to classrooms: student-centeredness, focus on internal management, and commitment to instructional improvement [24]. The optimization of the learning environment is a strong guarantee for teaching improvement, and effective teaching needs the environment as support. Effective teaching is concerned with the measurability and quantification of learning outcomes. Quantitative learning outcomes provide dynamic adjustments to learning objectives and information, allowing for multiple levels of learning objectives to be provided based on student variability. An effective classroom learning environment requires the integration of three elements: pedagogy, technology, and social interaction. These three pedagogical elements correspond to three types of interactions: learner-content interaction, learner-other interaction (social interaction), and learner-operator interface interaction, as shown in Figure 2.

### 3. Key Technologies and Features of Educational Environment for Preschool Children in Wireless Network Environment

#### 3.1. Key Technologies of Wireless Network Education Environment for Preschool Children

3.1.1. *Campus Network.* As the link between kindergartens and the outside world, the campus network is the basis for the construction of the environment. The convenience and rapid development of the Internet have impacted the traditional learning style and educational philosophy of kindergartens. Big data-based analysis of students' online behavior preferences, network-based learning resources sharing, and cloud-based campus network webcast platform construction are all inseparable from the network as a medium of information transmission. The unified management technology of wired network and wireless network is applied to the campus network to solve the shortcomings that the wired and wireless cannot be managed uniformly in the past. The solution is shown in Figure 3. The BRAS (broadband remote access server) is a new form of access gateway for broadband network applications that is positioned at the edge layer of the backbone network and can complete data access of IP/ATM networks of user bandwidth, as shown in Figure 3.

3.1.2. *Internet of Things.* IoT simply means connecting various objects through information and communication



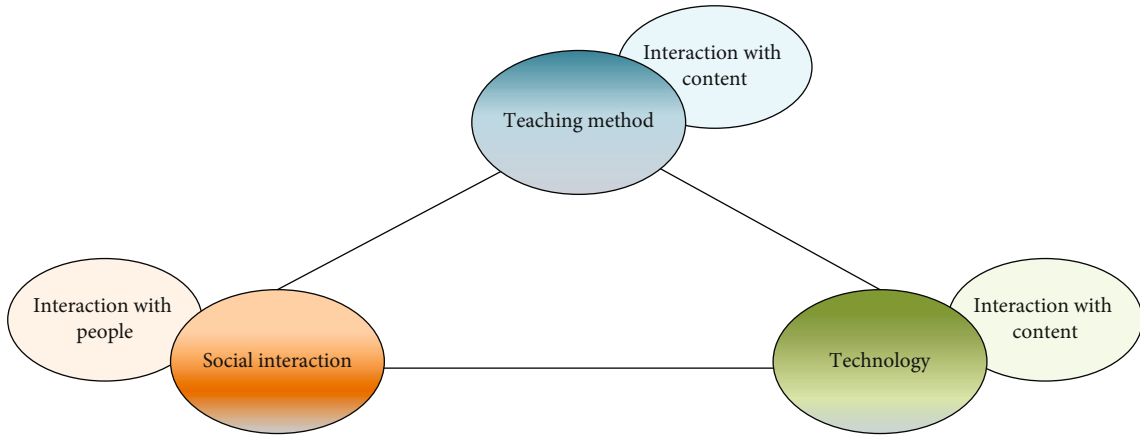


FIGURE 2: Interactive model of effective learning environments.

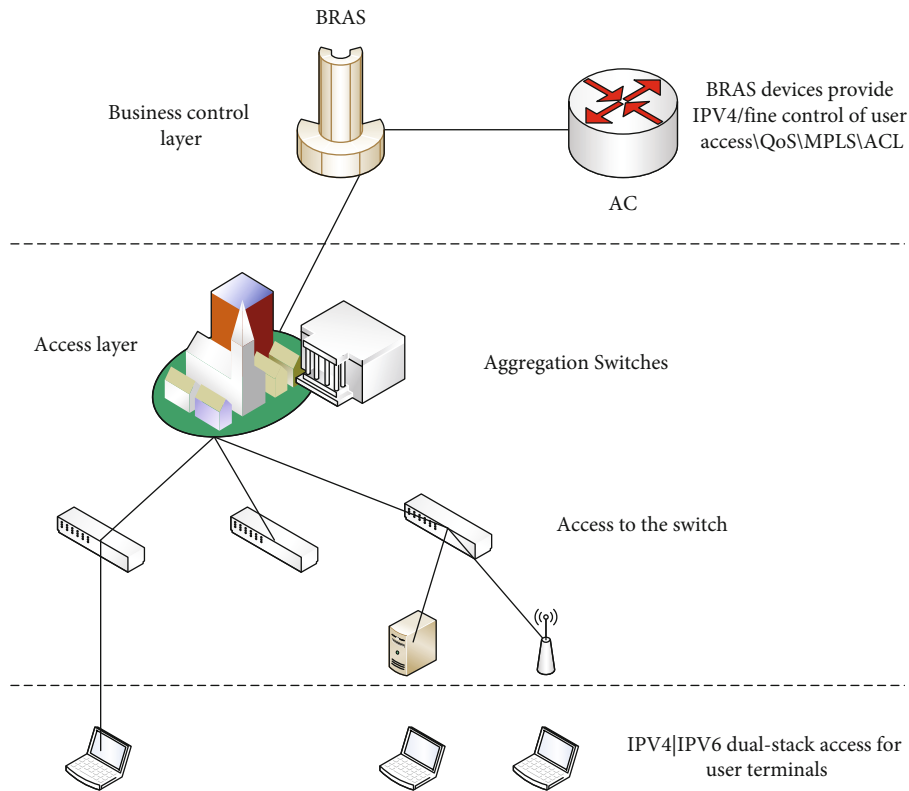


FIGURE 3: Integrated and flat campus network structure.

technology to form a connected and manipulee whole. With the characteristics of connectivity, human-object, and object-object union of wisdom, IoT plays a very important role in the smart learning environment. The purpose of IoT application in smart learning environment is sensing people and things and providing intelligent services. Intelligent sensing layer, information transfer layer, intelligent application support platform layer, and application layer are the four layers of the IoT structure. Figure 4 depicts the architectural architecture of an IoT application on campus.

3.1.3. *Cloud Computing.* The core idea of cloud computing is to manage and control a large number of network-connected computing resources to form a pool of computing resources that meet users' needs. Cloud computing is divided into three levels: cloud computing, cloud management, and cloud platform. The cloud computing platform is the key element to support the intelligent learning environment, and the intelligent learning environment based on cloud computing has three foundations. First, it supports the network infrastructure of the intelligent learning environment. The construction of the intelligent learning environment has a

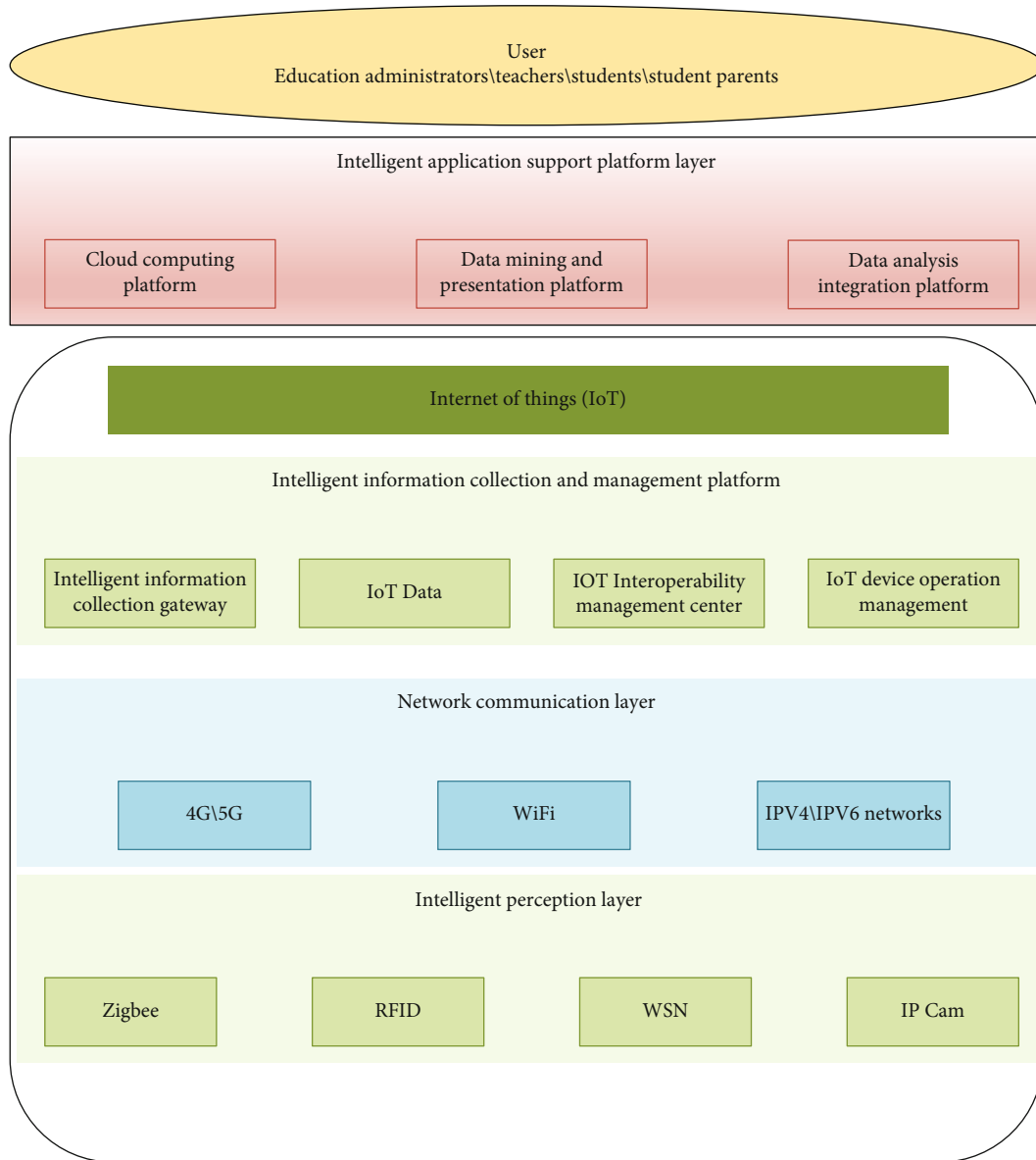


FIGURE 4: Structure diagram of IoT in smart kindergarten.

strong interconnection network, fiber optic network, remote backup storage network, centralized, secure, and high-speed network environment. At the same time, through the convergence of the three networks, the intelligent learning environment is provided with high-speed access to the cloud computing platform to ensure the safe and reliable operation of the intelligent learning environment network. Secondly, the cloud computing platform is the key element to support the intelligent learning environment. The cloud computing platform is the foundation to support the operation of the intelligent learning environment and provide huge services and resource management. It manages a large amount of highly virtualized computing, data, and resources generated by teachers and preschool children in the teaching process, forming a huge resource base and providing unified services. Third, the object-linked sensing system of the intelligent learning environment is the most common part of the over-

all intelligent learning environment operation and the most essential service level. Using FRID, sensors, collectors, QR codes, and ultrahigh definition camera monitoring devices and technologies, the intelligent management and safe, dynamic, real-time monitoring of the smart learning environment are realized.

**3.1.4. Augmented Reality.** Augmented reality (AR) is a computer application, and human-computer interaction technology is developed on the basis of virtual reality technology, which presents users with a new environment combining reality and reality by fusing virtual information into the real environment. The three basic features of augmented reality are the fusion of real and virtual worlds, real-time interaction, and the precise alignment of virtual and real objects in 3D space. The application of augmented reality in learning refers to the fusion of a real or near-real

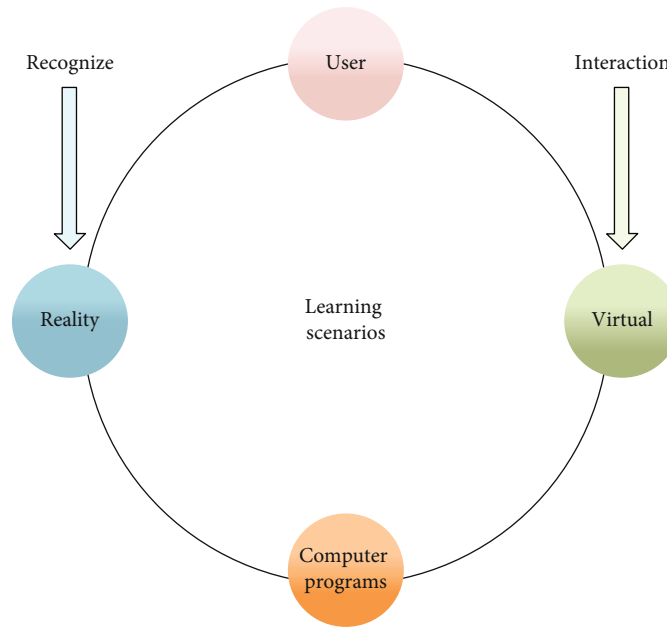


FIGURE 5: Augmented reality concept map.

3D virtual situation constructed by a computer into a real situation, and the student enters and interacts with the situation by some means, thus building a reasonable understanding of the virtual situation and presenting a real scene. Learning in an augmented reality scenario includes four dimensions, namely, computer program, user, real world, and virtual environment, and the concept diagram is shown in Figure 5. Augmented reality originates in reality and returns to reality, and students interact with virtual situations with the aim of better understanding the real world. In the construction of intelligent learning environments for young children, augmented reality technology is used to enhance the authenticity and live feeling of learning situations. The vivid learning scenes help children understand the learning content more accurately and quickly, increase their interest in learning, and maintain a stable and positive learning mindset.

**3.1.5. Artificial Intelligence.** Artificial intelligence technology has been widely applied in the sphere of education, thanks to the Internet's backing. Artificial intelligence has played a critical role in advancing smart education development. Providing the most effective intelligent learning support and services for learners is the goal of creating an intelligent learning environment. For example, in the development of intelligent question and answer system, intelligent learning system, and adaptive learning system, artificial intelligence technology needs to be combined with the Internet technology, multimedia technology, and big data technology. Through integration, they encourage each other to improve and expand one other's functions and application skills, so expanding and improving educational intelligence.

Currently, learning analytics technology analyzes the learning characteristics of learners using recorded data from the learning process in three forms: interactive text, video

and audio, and system logs. Artificial intelligence algorithms can analyze quantitative metrics such as the number and percentage of online materials read and written by each learner and the number and percentage of messages that are responded to. It can also use social network analysis to calculate the centrality of each learner and perform cluster analysis of learners based on the information about the communication relationship between learners attached to the interactive text. The main content, the information on the classroom activity behavior of students and teachers, such as statistics on the frequency and proportion of children actively answering questions in class, the overall activity of the classroom, the proportion of questions asked, and the proportion of student discussions, is extracted through video and audio analysis. Automatic recognition of learners based on eye dynamics and body posture, conversion of learners' voice content into text content for analysis, and dynamic recognition of facial expressions, such as happy, sad, and angry, have all become possible thanks to the advancement of intelligent video and audio analysis technology. The use of gesture motions in the learning field improves the human-computer interaction experience significantly. In addition, the data index information established based on these analyzed data can greatly improve the efficiency and accuracy of summative and formative evaluations in teaching, such as statistics on classroom participation of specific children over a period of time, changes in children's emotions in the learning environment, and comparison of classroom performance of different learning contents.

**3.2. Characteristics of Kindergarten Language Education Environment.** The most fundamental aspect of an early childhood language learning environment is to reflect the "wisdom" of the learning environment. Smart kindergartens are kindergartens where new technologies are applied, where

new technologies facilitate the kindergarten learning environment, and where the kindergarten learning environment is highly technologically oriented to achieve the integration of technology and the kindergarten. The design of smart learning environments for early childhood is a study of the application of technology, the development of kindergarten learning environments, and the design of smart kindergarten learning environments in the context of the use of new technologies. The integration of information technology with the characteristics of early childhood school environments has brought out more characteristics such as the playfulness and age-appropriateness of early childhood environments.

#### **4. Design of a Kindergarten Language Education Resource Management System Based on Wireless Network Technology in an Artificial Intelligence Environment**

After the previous analysis of the characteristics and technologies of the smart campus, we determined the architecture of the web-based preschool curriculum resource management information system with B/S mode, HTML+ASP technology in the foreground, and SQL SERVER 2019 in the background database.

*4.1. Language Knowledge Module Tree Mind Map Design Structure.* Examine the use of a tree route structure that resembles a mind map in the primary Chinese children's general knowledge modules. When compared to traditional structural system framework design ideas, it has numerous new advantages and features as part of the core framework architecture. This is particularly well suited to the dynamic embodiment of a user's thinking habits and the inner connection between knowledge points, which can realize the dynamic personality of the learning process for instant generation and is more in line with the constructivist concept of human-centered learning. Accordingly, the learning potential and learning needs also show obvious personalized characteristics. When using this module, there are several choice nodes on the learning path, and when reaching the nodes, different choices can form different learning paths, thus connecting the net-like learning resources through tree-like learning paths. Similar to the resource management structure of an interoperable highway network system, the learner is similar to a car driver driving on a highway network, whose choice of each turnoff determines the final route he or she will take.

This design structure is a cognitive structure for learning that best fits the natural attributes of children, changing the previous linear learning model in which learners passively receive learning content. Just like in the past, we could not choose the content of a movie; we could only decide to watch it or not; and once we bought a ticket, we had to enter on time. Later, we could choose the channel but not the content, and we could not jump back and forth. Later, with computers, you can select your own content, you can also play backwards and fast forward, and you can also have lim-

ited human-computer interaction, but there is no human-to-human communication. So there is the rapid development of the network, especially the popularity of instant messaging software such as WeChat, mobile portable chat software, and hardware represents the current trend of instant messaging interaction. The next step for wearable devices will eventually be to use wireless networks to connect people to people to form a true barrier-free interaction.

The nature of the thinking structure of the human brain's tree-like neuron mesh connection determines the technology's development in this direction, which means there is a logical isomorphism between the two, and the future will be towards the full depth of integration of the network management system and the human intelligent brain, i.e., embedded and wearable devices. Figure 6 shows a tree mind map of the broad language knowledge modules for toddlers.

*4.2. Literacy Module Design Structure for Preschoolers.* Take the early childhood literacy module part as an example to explain the design function and operation process of specific functional modules. Login and registration for ordinary users: The early childhood literacy learning system implements member registration and login; first of all, you have to register in the entrance of this module; register a new user; click the Register Member button on the left side of the page to enter the member registration page; and only after successful registration, can you become an official user. Be sure to enter the correct email address when registering, so that you can get in touch with members in a timely manner. After logging in on the login page with the username and password of the administrator or regular user, you will enter this module. After logging into the early childhood literacy module, regular users can do the following: (1) browse the information in this section, as well as the knowledge of children's education; (2) view lessons and videos and browse pictures and animations; and (3) leave voice messages. The structure schematic is shown in Figure 7.

*4.3. Learning Resources and Learning Activities in a Smart Learning Environment.* For learning and teaching, the smart learning environment provides a large library of learning resources. Learning resources for young children include text, voice, animation, and tools, which are kept in the cloud and on the student's side. The smart learning environment provides a rich media environment for young children. According to the current learning situation and learning interests of young children, the smart learning environment designed in this paper will push out relevant resources.

Student information in the classroom is collected through cameras, and student data are automatically updated in the student attendance system. The face recognition platform can complete face detection and face recognition functions and realize the creation, modification, and query of face database. The smart learning environment uses video face recognition to establish the face database of the class of young children and completes face detection and recognition through the video data collected in the

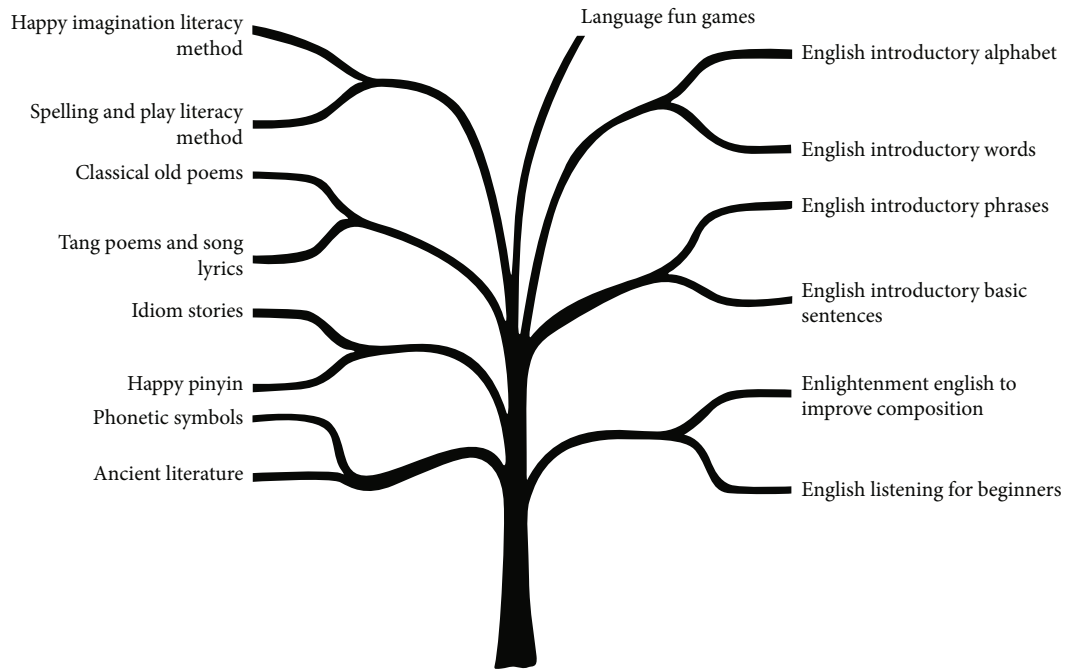


FIGURE 6: Tree mind map of language knowledge modules for preschoolers.

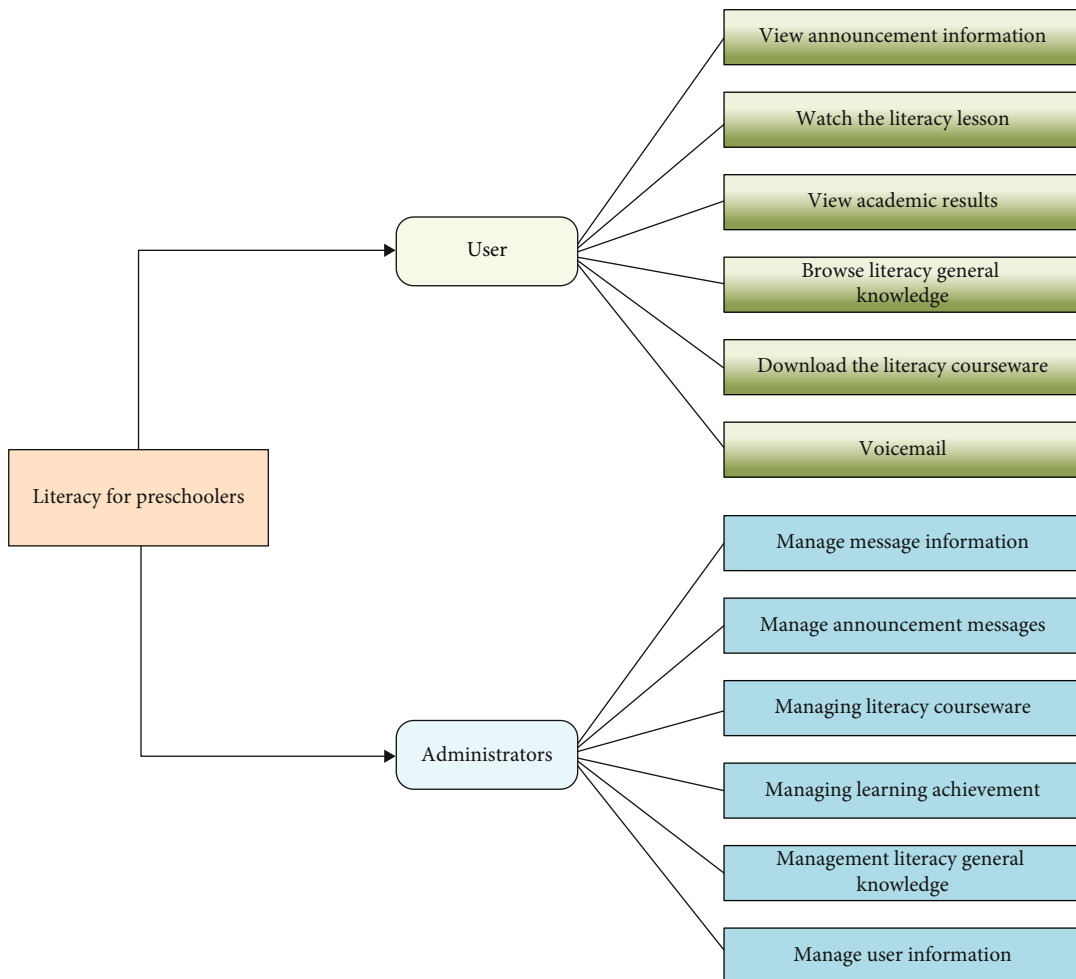


FIGURE 7: Diagram of the structure of the early childhood literacy module.

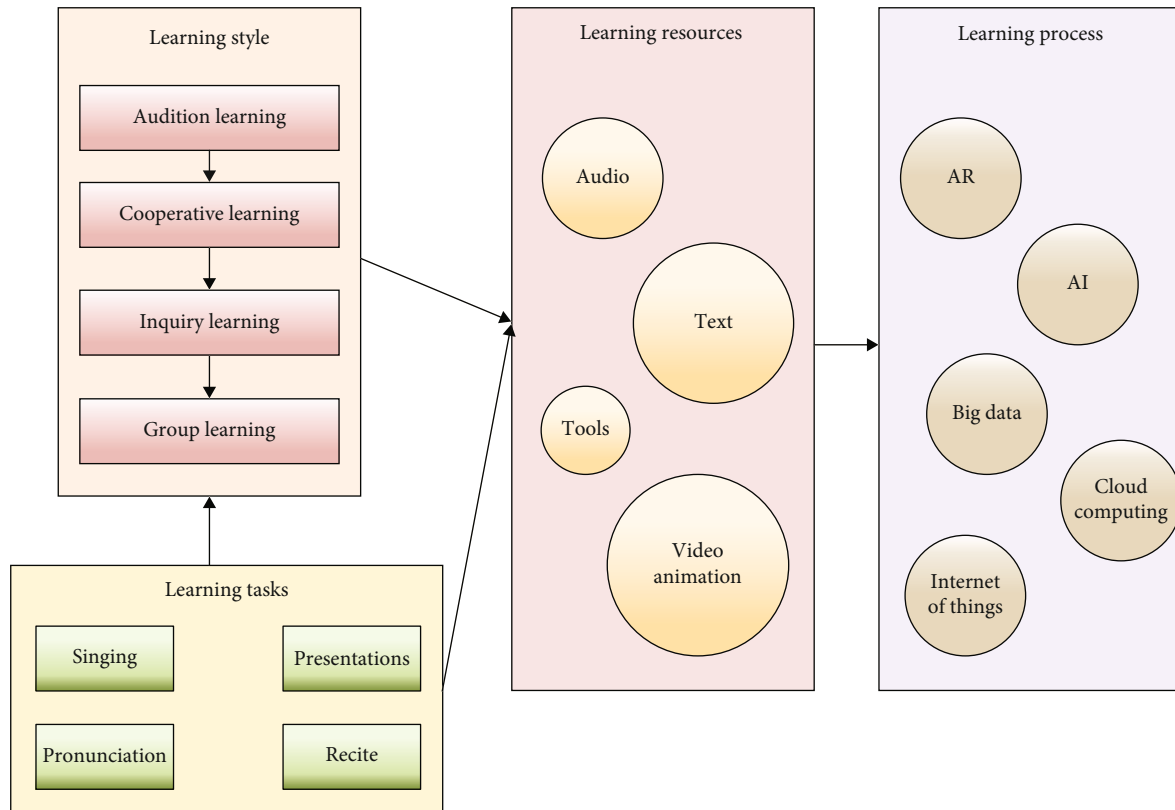


FIGURE 8: Language learning activities in an intelligent learning resource environment for preschool children.

classroom. This function allows dynamic monitoring of students' attendance and departure from the classroom.

Augmented reality technology decreases the environmental modeling link and effectively increases the speed, flexibility, and fidelity of virtual 3D modeling by leveraging the perceptible, locatable, and operable human-computer interaction qualities of virtual reality. This also results in some new key technologies, such as display technology, three-dimensional registration technology, virtual and real lighting consistency technology, tracking registration technology, and natural interaction technology. First, the creation of the learning environment for young children should be integrated into the process of learning activities. Second, the virtual and real environment should be easy to build and disassemble to facilitate the efficient use of space. Third, use a variety of ways to mobilize children's overall perception and participation. Fourth, attention should be paid to meeting the individual learning and growth needs of young children. It is worth pointing out that augmented reality systems are a supplement to learning methods and cannot completely replace physical objects.

The smart learning environment offers a variety of language learning activities for young children, including audio-visual learning, cooperative learning, inquiry learning, and group learning. The learning tasks in semester education are divided into five categories: science, arts, social studies, language, and health. Children's language learning activities in the smart learning environment are shown in Figure 8.

## 5. Conclusion

Many information technology concepts and technologies have entered the field of preschool education as education informatization improves, and smart learning environments and smart campuses are becoming more widely recognized. The maturity and continuing growth of technology promote the continual progress of educational technology, from traditional classroom environments to multimedia classroom environments, and from multimedia classroom environments to virtual learning environments and smart learning environments. Although the research is at the level of theoretical assumptions and environment design, its educational significance and research value are worthy of recognition.

The development of wireless network technology and artificial intelligence has advanced the digital and intelligent transformation of traditional campus scenes. Using large-scale digital data within the new campus scenes can effectively improve the accuracy and universality of research results, which is a research hotspot in the field of learner analysis in the future. The core of this research includes exploring the key technologies and environmental features of language learning for preschool children in a wireless network environment relying on various technological tools, including artificial intelligence. The principles governing learning and teaching ideas and activities are used to create language learning resources and learning environments for young children. However, building a language learning resource environment for young children from the

standpoint of a smart learning environment is insufficient; the research is locked at the level of design assumptions and lacks practical application consequences as support. Further validation of the environmental research design is needed in subsequent studies.

## Data Availability

The datasets used during the current study are available from the corresponding author on reasonable request.

## Conflicts of Interest

Declares that he has no conflict of interest.

## References

- [1] Y. Zhao, A. M. P. Llorente, and M. C. S. Gómez, "Digital competence in higher education research: a systematic literature review," *Computers & Education*, vol. 168, article 104212, 2021.
- [2] D. K. Cohen, J. P. Spillane, and D. J. Peurach, "The dilemmas of educational reform," *Educational Researcher*, vol. 47, no. 3, pp. 204–212, 2018.
- [3] R. O. Welsh and S. Little, "The school discipline dilemma: a comprehensive review of disparities and alternative approaches," *Review of Educational Research*, vol. 88, no. 5, pp. 752–794, 2018.
- [4] M. Coccia and J. Watts, "A theory of the evolution of technology: *technological parasitism* and the implications for innovation management," *Journal of Engineering and Technology Management*, vol. 55, article 101552, 2020.
- [5] X. Chen, D. Zou, G. Cheng, and H. Xie, "Detecting latent topics and trends in educational technologies over four decades using structural topic modeling: a retrospective of all volumes of *computers & education*," *Computers & Education*, vol. 151, article 103855, 2020.
- [6] A. Christopoulos, H. Kajasilta, T. Salakoski, and M. J. Laakso, "Limits and virtues of educational technology in elementary school mathematics," *Journal of Educational Technology Systems*, vol. 49, no. 1, pp. 59–81, 2020.
- [7] S. McGrew, J. Breakstone, T. Ortega, M. Smith, and S. Wineburg, "Can students evaluate online sources? Learning from assessments of civic online reasoning," *Theory & Research in Social Education*, vol. 46, no. 2, pp. 165–193, 2018.
- [8] A. Otterborn, K. J. Schönborn, and M. Hultén, "Investigating preschool educators' implementation of computer programming in their teaching practice," *Early Childhood Education Journal*, vol. 48, no. 3, pp. 253–262, 2020.
- [9] R. A. C. Vallberg, "What may characterise teaching in pre-school? The written descriptions of Swedish preschool teachers and managers in 2016," *Scandinavian Journal of Educational Research*, vol. 64, no. 1, pp. 1–21, 2020.
- [10] F. B. Senol, "Readiness for reading and writing in pre-school period: teachers' viewpoints on classroom environment and practices," *International Online Journal of Education and Teaching*, vol. 8, no. 1, pp. 432–453, 2021.
- [11] C. A. Lenkaitis, S. Calo, and E. S. Venegas, "Exploring the intersection of language and culture via telecollaboration: utilizing videoconferencing for intercultural competence development," *International Multilingual Research Journal*, vol. 13, no. 2, pp. 102–115, 2019.
- [12] W. G. Kronenberger, H. Xu, and D. B. Pisoni, "Longitudinal development of executive functioning and spoken language skills in preschool-aged children with cochlear implants," *Journal of Speech, Language, and Hearing Research*, vol. 63, no. 4, pp. 1128–1147, 2020.
- [13] S. R. Edmunds, S. T. Kover, and W. L. Stone, "The relation between parent verbal responsiveness and child communication in young children with or at risk for autism spectrum disorder: a systematic review and meta-analysis," *Autism Research*, vol. 12, no. 5, pp. 715–731, 2019.
- [14] A. Karpov, "Formation of the modern concept of research education: from new age to a knowledge society," *Procedia-Social and Behavioral Sciences*, vol. 214, pp. 439–447, 2015.
- [15] Z. Dai, C. Sun, L. Zhao, and Z. Li, "Assessment of smart learning environments in higher educational institutions: a study using ahp-fce and ga-bp methods," *IEEE Access*, vol. 9, pp. 35487–35500, 2021.
- [16] S. K. S. Cheung, K. Phusavat, and H. H. Yang, "Shaping the future learning environments with smart elements: challenges and opportunities," *International Journal of Educational Technology in Higher Education*, vol. 18, no. 1, pp. 1–9, 2021.
- [17] N. S. Chen, I. Cheng, and S. W. Chew, "Evolution is not enough: revolutionizing current learning environments to smart learning environments," *International Journal of Artificial Intelligence in Education*, vol. 26, no. 2, pp. 561–581, 2016.
- [18] S. Veličković and L. Stošić, "Preparedness of educators to implement modern information technologies in their work with preschool children," *International Journal of Cognitive Research in Science, Engineering and Education*, vol. 4, no. 1, pp. 23–30, 2016.
- [19] L. Yáñez and Y. Coyle, "Children's perceptions of learning with an interactive whiteboard," *ELT Journal*, vol. 65, no. 4, pp. 446–457, 2011.
- [20] M. J. Chou, J. C. Cheng, and Y. W. Cheng, "Operating classroom aesthetic reading environment to raise children's reading motivation," *Universal Journal of Educational Research*, vol. 4, no. 1, pp. 81–97, 2016.
- [21] V. Lamanuskas and D. Augienė, "Kindergarten teachers' health literacy: understanding, significance and improvement aspects," *Review of Science, Mathematics and ICT Education*, vol. 13, no. 2, pp. 39–60, 2019.
- [22] M. McCaslin and T. S. L. Good, "Compliant cognition: the misalliance of management and instructional goals in current school reform," *Educational Researcher*, vol. 21, no. 3, pp. 4–17, 1992.
- [23] M. C. Wittrock, "Generative teaching of comprehension," *The Elementary School Journal*, vol. 92, no. 2, pp. 169–184, 1991.
- [24] A. Harris, "Effective teaching: a review of the literature," *School Leadership & Management*, vol. 18, no. 2, pp. 169–183, 1998.

## Retraction

# Retracted: The Use of Deep Learning Model for Effect Analysis of Conventional Friction Power Confinement

### Computational and Mathematical Methods in Medicine

Received 19 September 2023; Accepted 19 September 2023; Published 20 September 2023

Copyright © 2023 Computational and Mathematical Methods in Medicine. This is an open access article distributed under the Creative Commons Attribution License, which permits unrestricted use, distribution, and reproduction in any medium, provided the original work is properly cited.

This article has been retracted by Hindawi following an investigation undertaken by the publisher [1]. This investigation has uncovered evidence of one or more of the following indicators of systematic manipulation of the publication process:

- (1) Discrepancies in scope
- (2) Discrepancies in the description of the research reported
- (3) Discrepancies between the availability of data and the research described
- (4) Inappropriate citations
- (5) Incoherent, meaningless and/or irrelevant content included in the article
- (6) Peer-review manipulation

The presence of these indicators undermines our confidence in the integrity of the article's content and we cannot, therefore, vouch for its reliability. Please note that this notice is intended solely to alert readers that the content of this article is unreliable. We have not investigated whether authors were aware of or involved in the systematic manipulation of the publication process.

Wiley and Hindawi regrets that the usual quality checks did not identify these issues before publication and have since put additional measures in place to safeguard research integrity.

We wish to credit our own Research Integrity and Research Publishing teams and anonymous and named external researchers and research integrity experts for contributing to this investigation.

The corresponding author, as the representative of all authors, has been given the opportunity to register their agreement or disagreement to this retraction. We have kept a record of any response received.

### References

- [1] C. Liu, X. Wang, and Z. He, "The Use of Deep Learning Model for Effect Analysis of Conventional Friction Power Confinement," *Computational and Mathematical Methods in Medicine*, vol. 2022, Article ID 8733919, 8 pages, 2022.



## Research Article

# The Use of Deep Learning Model for Effect Analysis of Conventional Friction Power Confinement

Chuntong Liu, Xin Wang, and Zhenxin He 

*Xi'an Research Institute of High Technology, Baqiao District, Tongxin Road, Xi'an City, Shaanxi 710025, China*

Correspondence should be addressed to Zhenxin He; 201701350129@lzpcc.edu.cn

Received 6 April 2022; Revised 24 April 2022; Accepted 28 April 2022; Published 7 June 2022

Academic Editor: Naeem Jan

Copyright © 2022 Chuntong Liu et al. This is an open access article distributed under the Creative Commons Attribution License, which permits unrestricted use, distribution, and reproduction in any medium, provided the original work is properly cited.

Nonlinear friction could affect the high-precision motion system, resulting in poor tracking accuracy in the end. This is due to the fact that the LuGre friction model's parameter identification process comprises both static and dynamic parameter identification. The convolutional neural network (CNN) model is used in this study to create the friction identification system. We suggest a hybrid methodology that combines the CNN method and the classic least-squares technique. The convolutional layer (CONV), which is defined by a convolutional kernel, analyzes and extracts features from an input image. In terms of accuracy and convergence, the results reveal that the upgraded CNN friction model outperforms the original CNN friction model. You may successfully reduce the influence of friction on your system while improving its performance by applying the feedforward correction.

## 1. Introduction

The industrial robot has become an indispensable automation tool in modern human society. Improving its control accuracy has always been a research hotspot at home and abroad. The traditional PID control has been unable to meet the accuracy requirements of the actual work, and the model-based control method has become the mainstream. The model-based controller needs to take the robot's dynamic parameters as a priori value [1], but the robot is a multivariable and strongly coupled nonlinear system [2]. It is difficult to obtain the dynamic model through a mathematical calculation, and the experimental identification method is generally used. In the process of moving, the machine will be disturbed by nonlinear friction [3]. This interference is local and has high frequency and huge amplitude, and it has a significant impact on the system's local performance. Due to the randomness of its position, the tracking accuracy of the whole travel range is reduced [4]. For this phenomenon, the corresponding friction model is used to identify the relevant parameters of the friction model through the parameter identification method, compensate for the nonlinear friction in the system, reduce the influence of the nonlinear friction in

the system on the high-precision motion of the system, and improve the local tracking accuracy [5, 6].

The LuGre friction model is a typical friction model for servo systems and can accurately describe the frictional characteristics of the system during motion [7]. As the parameter identification of the LuGre friction model involves both static and dynamic parameter identification [8], it is a harmonious combination of static and kinematic characteristics, and the improved genetic algorithm can effectively improve the accuracy of identification by taking into account both static characteristics and dynamic factors and prevent the problem of falling into local optimality instead of global optimality in the process of identification [9–12].

This study first defines and introduces the LuGre friction model, then moves on to the improved CNN model's implementation approach and the static parameter recognition procedures [13]. The method is confirmed by first collecting relevant position and drive force data in a loop system using a cylindrical linear motor based on dSPACE hardware using constant velocity trials, calculating the velocity and friction data values according to the basic physical equations, identifying the friction model using the basic and improved CNN models, and designing a feedforward compensation

controller based on the identified friction model to achieve the nonlinear friction compensation [14].

The paper's section-wise paragraph is as follows: The related work is presented in Section 2. Section 3 analyzes the LuGre friction model description and introduction. Section 4 describes the building convolutional neural network models. Section 5 discusses the experimental verifications. Finally, in Section 6, the research work is concluded.

## 2. Related Work

Many robot parameter identification methods have been proposed by researchers at home and abroad [15, 16]. A method for deriving the minimum set of parameters for tandem robots was proposed, which can reduce the number of operations for identification and improve the robustness of the algorithm. In [17], a recursive least-squares method was used to perform parameter operations, which improved the efficiency of the algorithm. [18] proposed a distribution identification method to reduce the complexity of the identification equations. The progress of robot dynamic parameter identification has been aided by intelligent control methods. [19] used an artificial bee colony algorithm, [20–22] used a particle swarm algorithm, and [23] used an improved genetic algorithm for identification, all of which achieved good identification results.

In order to improve the kinetic model recognition accuracy of industrial robots, this paper proposes a kinetic model recognition method based on an artificial neural network in combination with machine learning and deep learning algorithms that have emerged in recent years [24, 25].

## 3. LuGre Friction Model Description and Introduction

In 1995, scholars proposed the LuGre model [14], which is represented by the fact that the contact surfaces of two objects are in microscopic contact through elastic bristles, and when they are displaced by mutual tangential forces, the bristles of the contact surfaces will undergo elastic deformation, generating friction in the process, as shown in Figure 1.

The friction of the servo system can be expressed by the differential equation as

$$M \frac{d^2 x}{dt^2} = F - F_f, \quad (1)$$

where  $M$  represents the mass of the load,  $x$  represents the displacement of the mass of the load,  $F$  represents the driving force of the motor, and  $F_f$  represents the frictional force.

The frictional force  $F_f$  can be determined by the following mathematical formula:

$$\dot{z} = v - \frac{\sigma_0}{g(v)} z |v|, \quad (2)$$

$$g(v) = F_c + (F_s - F_c) e^{-(v/v_s)^2}, \quad (3)$$

$$F_f = \sigma_0 z + \sigma_1 \dot{z} + \sigma_2 v. \quad (4)$$

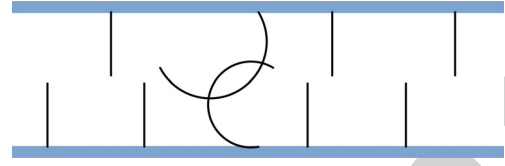


FIGURE 1: LuGre friction model object contact surface contact diagram.

When the system is in a steady state, at this time, the system  $dx/dt = a$ , where  $a$  is a constant, i.e., at this time  $z = 0$ , then from equation (5), we have

$$z = \frac{g(v)}{\sigma_0} \frac{v}{|v|} = \frac{g(v)}{\sigma_0} \operatorname{sgn}(v), \quad (5)$$

where the  $\operatorname{sgn}$  function is a symbolic function, substituting equations (5) and (3) into equation (4) is the frictional force when the system is in a steady state:

$$F_f = \left( F_c + (F_s - F_c) e^{-(v/v_s)^2} \right) \operatorname{sgn}(v) + \sigma_2 v. \quad (6)$$

## 4. Building Convolutional Neural Network Models

CNN is a type of neural network that may be used to classify images. CNN merely connects the nodes between two adjacent layers and shares the weights, unlike earlier fully connected neural networks. This optimizes the neural network, reduces the model's complexity, and enhances the operation's efficiency greatly.

The convolutional layer (CONV), which is defined by a convolutional kernel, performs feature extraction on the input image. The convolution is expressed as  $f(x) = wx + b$ . The convolution kernel is also known as a filter or "field of perception." The convolution kernel is weighted and processed by a weight matrix with the local data of the input image, and the kernel slides over the input data to extract features from the whole image. The convolutional feature map is calculated as

$$w_{\text{out}} = \frac{w_{\text{in}} - F + 2 * P}{S} + 1, \quad (7)$$

where  $w_{\text{out}}$  is the output feature map size,  $w_{\text{in}}$  is the input feature map size,  $F$  is the convolutional kernel size, and  $S$  is the convolutional step size.

The pooling layer (POOL), reduces the spatial dimension of the picture, keeps the depth constant, reduces the network connection parameters, optimizes computational efficiency, and prevents overfitting.

The fully connected layer (FC), where the previous layers have been completed with highly abstract information features, is used for classification through the fully connected layer. The last convolutional layer needs to be matrix flattened when connected to the fully connected layer.

TABLE 1: Structure of neural network for parameter identification based on CNN sassafras model.

Layered	Convolution layer (1 layer)	Convolution layer (2 layers)	Convolution layer (3 layers)	Convolution layer (4 layers)	Convolution layer (5 layers)	Convolution layer (6 layers)	Convolution layer (7 layers)	Convolution layer (8 layers)
Nuclear size	$5 \times 5 \times 3$	$2 \times 2 \times 3$	$5 \times 5 \times 32$	$2 \times 2 \times 32$	$3 \times 3 \times 64$	$2 \times 2 \times 64$	$3 \times 3 \times 128$	$2 \times 2 \times 128$
Step	1	2	1	2	1	2	1	2
Layered	Full connection layer (9 layers)	Full connection layer (10 layers)	Full connection layer (11 layers)	Output	Activation function		ReLU	
Size	$6 \times 6 \times 128$	$1024 \times 1$	$512 \times 1$	5	Classification function		Softmax	
Overfitting	Dropout	Dropout	L2	—	—		—	

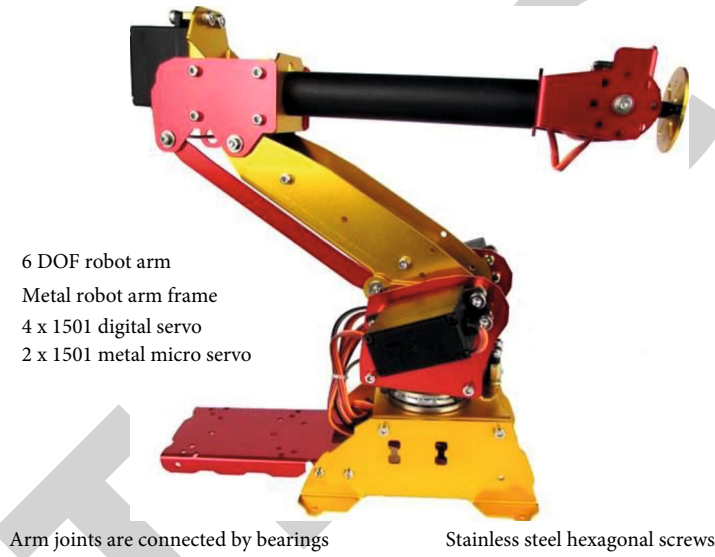


FIGURE 2: Six-degree-of-freedom robotic arm.

The Softmax layer uses Softmax to classify the linear output. Assuming the original array  $V$ ,  $V_i$  is the  $i^{\text{th}}$  element of the array, then  $V_i$  of  $\text{Softmax}(s)_i = e^i / \sum_{j=1}^n e^j$ .

The structural design of the CNN-based neural network for parameter identification of the sassafras model includes 11 hidden layers, 4 convolutional layers, 4 pooling layers, and 3 fully connected layers, and the specific parameters are shown in Table 1.

- (1) *Input Layer*. The input layer collects the image dataset of the quality inspection agency for the identification of the parameters of the sassafras model. The image dataset is preprocessed to remove noise and delete poor-quality data. The image preprocessing is in RGB ( $100 \times 100 \times 3$ ) format. The ratio = 0.8 was set to split the training and validation sets, with 80% of the data used for model training and 20% for model validation.
- (2) *Convolutional Layers*. The model is designed with 4 convolutional layers, the sizes of which are  $5 \times 5 \times 3$ ,

$5 \times 5 \times 32$ ,  $3 \times 3 \times 64$ , and  $3 \times 3 \times 128$ , all with a step size of 1. The first two layers are designed with larger sizes in order to expand the perceptual field in the first stage, extract more image features, and reduce the number of computation layers. The last two layers are smaller in order to increase the depth of the model, reduce the number of computational parameters, and reduce computational complexity.

- (3) *Pooling Layers*. Four pooling layers are designed to correspond to 4 convolutional layers, all of size  $2 \times 2$ , with depth corresponding to the previous convolutional layer. After pooling, the image data can be reduced in feature dimension and number of parameters to reduce overfitting.
- (4) *Fully Connected Layers*. Three fully connected layers are designed to flatten the convolutional pooled array matrix into a column vector. The final output is a parametric identification classification of the 5 levels of the sassafras model. The fully connected is chosen to reduce overfitting by dropout, L2 regular terms, etc.

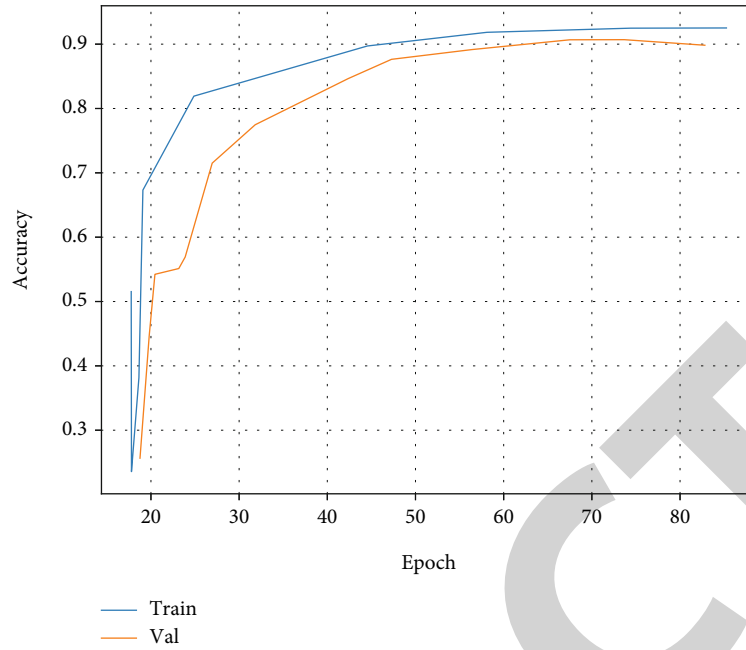


FIGURE 3: Neural network training accuracy.

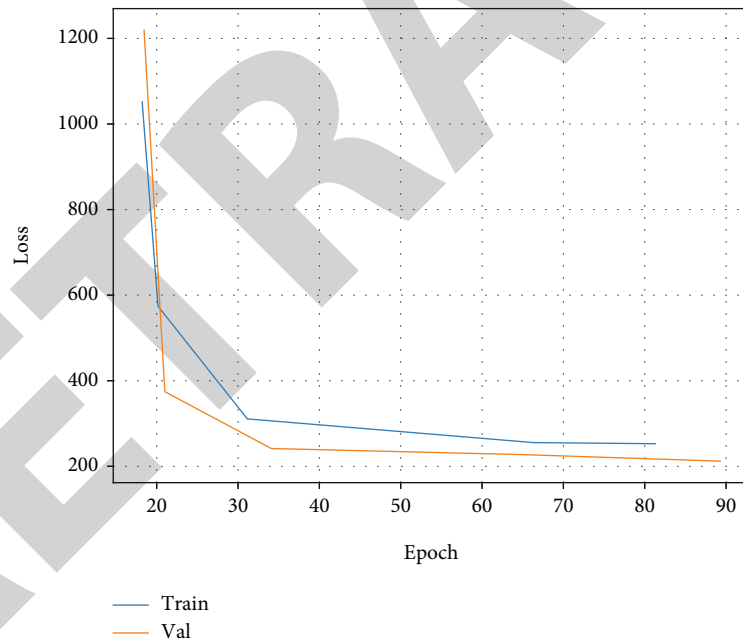


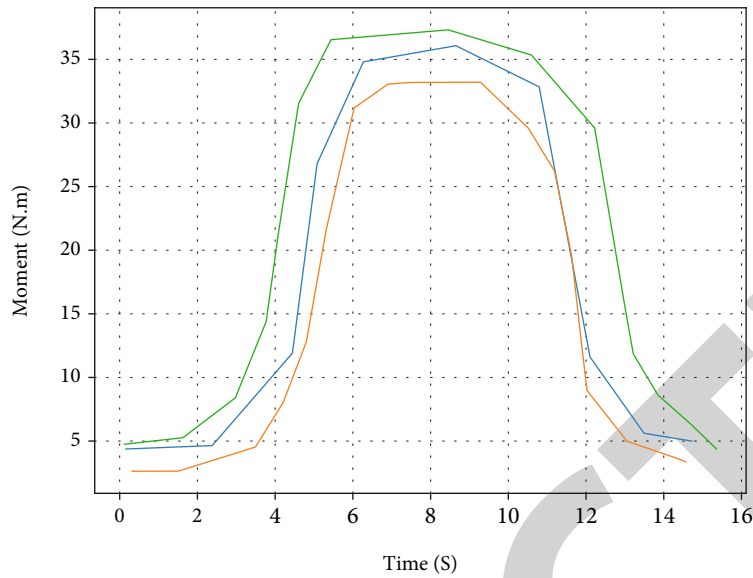
FIGURE 4: Neural network training loss.

- (5) *Activation Function.* Choose ReLU as the activation function; the function of the data processing has the characteristics of fast convergence and rapid gradient reduction.
- (6) *Classification Function.* Softmax is selected as the classification function, which will classify the input textile photos into five corresponding class categories, so as to achieve the goal of intelligent assessment of textile hairball.

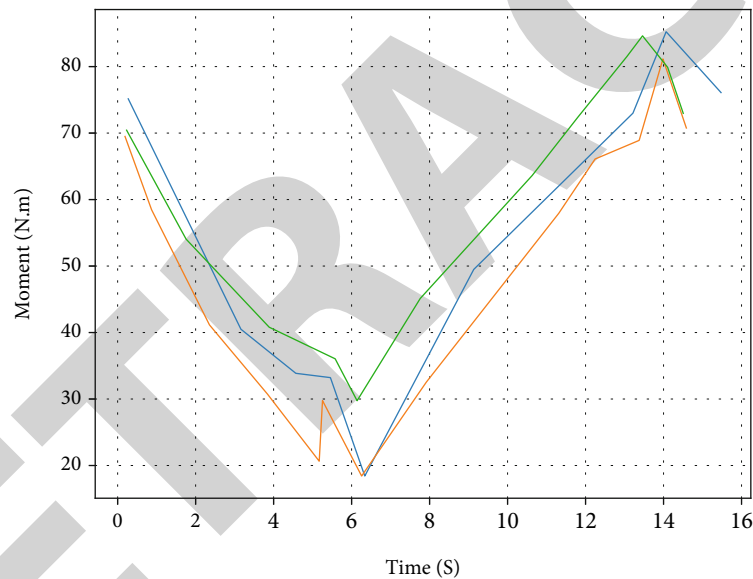
## 5. Experimental Verification

In this chapter, we defined the experimental design, identification results, and analysis of results in detail.

*5.1. Experimental Design.* A 6-degree-of-freedom robotic arm produced by a company is shown in Figure 2. The artificial neural network model presented in Sections 1 and 2 of this paper was built using the deep learning framework



(a)



(b)

FIGURE 5: Calculation of the joint moments.

Keras, with a dropout regularization layer added to avoid overfitting [26–30].

The more training data provided, the more features of the model are theoretically identified, and the greater generalization capacity the model will have while performing neural network identification. Using the stimulated trajectory design approach described in Section 2, we collected as much actual data from the robotic arm as possible and separated it into three parts: the training set (70%), the validation set (15%), and the test set (10%) (15 percent). Figures 3 and 4 demonstrate how the magnitude of the loss function and the training accuracy were assessed during the

training process. It can be seen that as the iterations progress, the loss function of the model gradually decreases close to zero and the accuracy gradually reaches its maximum value, reaching convergence at around the 100<sup>th</sup> round, and the accuracy no longer changes.

The use of machine learning and deep learning methods for solving similar nature problems has extensively been studied by the research community [31–33].

5.2. *Identification Results.* The traditional least-squares method paired with the Coulomb viscous friction model was used to identify the same experimental data and

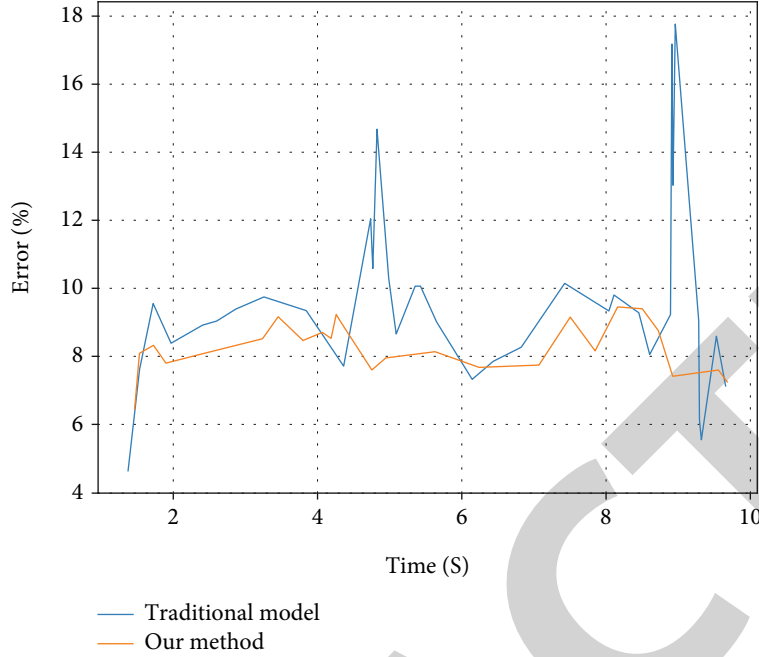


FIGURE 6: Joint 1 torque error curve.

TABLE 2: Matching of joints for identification.

	Joint 1	Joint 2	Joint 3	Joint 4	Joint 5	Joint 6	Average accuracy
Traditional model	85.53%	86.21%	92.14%	75.42%	75.24%	86.57%	84.71%
Neural network model	90.12%	94.10%	93.21%	86.35%	85.14%	86.24%	90.21%

validated on the same validation set in order to test the accuracy of the algorithm suggested in this paper. The moment curves obtained by the 2 algorithms were put together, and the results are shown in Figure 5.

From Figure 5, it can be seen that both algorithms have a good following effect on the actual torque. By looking at the local magnification, we can see that the neural network algorithm proposed in this paper has a better fit to the actual torque, especially around the peak, and has a smoother curve for the actual torque, which is more suitable for the controller design. The error curve of joint 1 is shown in Figure 6, which shows that the torque error calculated by the neural network recognition algorithm is smaller than that of the traditional algorithm, with a smaller peak error and a smoother curve. It is worth noting that there are some points in the curve with large jumps in error, mainly around the point where the joint speed of the robot arm is 0. The relative error is calculated with a small denominator, resulting in a larger relative error result, which has no impact on practical use.

As shown in equation (8), the matching degree  $\delta$  for kinetic discrimination can be calculated using the calculated moment  $\tau_i$  and the experimentally measured moment  $\tau$ :

$$\delta = \left(1 - \frac{\|\tau_i - \tau\|}{\|\tau_i\|}\right) \times 100\%. \quad (8)$$

The matching results of the 2 methods are shown in Table 2. As can be seen from Table 1, the matching degree of the neural network model can be improved by more than 5% on average compared to the traditional least-squares model.

In recent years, various optimization algorithms have been increasingly used in the field of robot identification; for example, the artificial bee colony algorithm combined with the nonlinear friction model has achieved good experimental results with an average accuracy of 89%. The average accuracy of the algorithm proposed in this paper is 90.70%, which is slightly better than the artificial swarm algorithm.

*5.3. Analysis of Results.* When compared to the traditional least-squares identification approach, the accuracy of the identification method described in this study is improved, and the torque fluctuations of the traditional identification model are successfully minimised and smoothed out. The method described in this paper is more suitable for controller design since frequent torque fluctuations can easily damage the controller. The combination of a neural network model and a traditional least-squares model can be used in a practical control system to obtain better results.

Frictional forces in robots are related to several external factors, and modeling and identification of frictional forces have been a major challenge. In recent years, many algorithms (e.g., artificial bee colony algorithms) have been

proposed whose recognition accuracy depends on the choice of the friction model, and the friction models of different robots in different working environments are not identical. The method proposed in this paper does not require special modeling of friction, is highly adaptable and portable for robots in different working environments, and ensures high accuracy. Therefore, the method proposed in this paper also has certain advantages over the more recent identification methods currently available.

## 6. Conclusions

To address the problem of low accuracy of classic kinetic parameter identification techniques, we present an artificial neural network-based identification method employing the ReLU activation function in combination with the RMSProp algorithm and the dropout method in this research. Experiments are being conducted to see how well they compare to the classic least-squares method. The results show that the proposed method can significantly improve the smoothness of the moment calculation, and the accuracy is improved by more than 5% compared to the traditional method. The algorithm does not require modeling of the system friction and has good adaptability.

## Data Availability

The datasets used during the current study are available from the corresponding author on reasonable request.

## Conflicts of Interest

The authors declare that they have no conflict of interest.

## References

- [1] J. Zhao and F. Wang, "Parameter identification by neural network for intelligent deep drawing of axisymmetric workpieces," *Journal of Materials Processing Technology*, vol. 166, no. 3, pp. 387–391, 2005.
- [2] J. Jia, M. Zhang, X. Zang, H. Zhang, and J. Zhao, "Dynamic parameter identification for a manipulator with joint torque sensors based on an improved experimental design," *Sensors*, vol. 19, no. 10, p. 2248, 2019.
- [3] N. Abas, A. Legowo, and R. Akmeliawati, "Parameter identification of an autonomous quadrotor," in *2011 4th international conference on mechatronics (ICOM)*, pp. 1–8, IEEE, 2011.
- [4] F. Alonge, M. Cirrincione, F. D'Ippolito, M. Pucci, and A. Sferlazza, "Parameter identification of linear induction motor model in extended range of operation by means of input-output data," *IEEE Transactions on Industry Applications*, vol. 50, no. 2, pp. 959–972, 2014.
- [5] F. Bu, Z. Ma, Y. Yuan, and Z. Wang, "WECC composite load model parameter identification using evolutionary deep reinforcement learning," *IEEE Transactions on Smart Grid*, vol. 11, no. 6, pp. 5407–5417, 2020.
- [6] M. Nolte, N. Kister, and M. Maurer, "Assessment of deep convolutional neural networks for road surface classification," in *2018 21st International Conference on Intelligent Transportation Systems (ITSC)*, pp. 381–386, IEEE, 2018.
- [7] C. Rechea, S. Levasseur, and R. Finno, "Inverse analysis techniques for parameter identification in simulation of excavation support systems," *Computers and Geotechnics*, vol. 35, no. 3, pp. 331–345, 2008.
- [8] E. Šabanovič, V. Žuraulis, O. Prentkovskis, and V. Skrickij, "Identification of road-surface type using deep neural networks for friction coefficient estimation," *Sensors*, vol. 20, no. 3, p. 612, 2020.
- [9] G. Yang, Q. J. Li, Y. Zhan, Y. Fei, and A. Zhang, "Convolutional neural network-based friction model using pavement texture data," *Journal of Computing in Civil Engineering*, vol. 32, no. 6, p. 04018052, 2018.
- [10] X. Tao, Z. Chunjiong, and X. Yongjian, "Collaborative parameter update based on average variance reduction of historical gradients [J]," *Journal of Electronics and Information Technology*, vol. 43, no. 4, pp. 956–964, 2021.
- [11] Z. H. A. N. G. Zhengwan, Z. H. A. N. G. Chunjiong, L. I. Hongbing, and X. I. E. Tao, "Multipath transmission selection algorithm based on immune connectivity model," *Journal of Computer Applications*, vol. 40, no. 12, p. 3571, 2020.
- [12] Z. Zhang, D. Wu, and C. J. Zhang, "Study of cellular traffic prediction based on multi-channel sparse LSTM [J]," *Computer Science*, vol. 48, no. 6, pp. 296–300, 2021.
- [13] J. Zhang and P. Xia, "An improved PSO algorithm for parameter identification of nonlinear dynamic hysteretic models," *Journal of Sound and Vibration*, vol. 389, pp. 153–167, 2017.
- [14] Z. H. Huang, L. L. Zhang, S. Y. Cheng, J. Zhang, and X. H. Xia, "Back-analysis and parameter identification for deep excavation based on Pareto multiobjective optimization," *Journal of Aerospace Engineering*, vol. 28, no. 6, p. A4014007, 2015.
- [15] R. Hasanpour, J. Rostami, J. Schmitt, Y. Ozcelik, and B. Sohrabian, "Prediction of TBM jamming risk in squeezing grounds using Bayesian and artificial neural networks," *Journal of Rock Mechanics and Geotechnical Engineering*, vol. 12, no. 1, pp. 21–31, 2020.
- [16] E. Heiden, D. Millard, E. Coumans, Y. Sheng, and G. S. Sukhatme, "NeuralSim: augmenting differentiable simulators with neural networks," in *2021 IEEE International Conference on Robotics and Automation (ICRA)*, pp. 9474–9481, IEEE, 2021.
- [17] A. Zirpoli, G. Maier, G. Novati, and T. Garbowski, "Dilatometric tests combined with computer simulations and parameter identification for in-depth diagnostic analysis of concrete dams," in *Life-Cycle Civil Engineering*, pp. 279–284, CRC press, 2008.
- [18] J. P. Ponthot and J. P. Kleinermann, "A cascade optimization methodology for automatic parameter identification and shape/process optimization in metal forming simulation," *Computer Methods in Applied Mechanics and Engineering*, vol. 195, no. 41–43, pp. 5472–5508, 2006.
- [19] S. Vardakos, M. Gutierrez, and C. Xia, "Parameter identification in numerical modeling of tunneling using the Differential Evolution Genetic Algorithm (DEGA)," *Tunnelling and Underground Space Technology*, vol. 28, pp. 109–123, 2012.
- [20] F. Aghazadeh, A. Tahan, and M. Thomas, "Tool condition monitoring using spectral subtraction and convolutional neural networks in milling process," *The International Journal of Advanced Manufacturing Technology*, vol. 98, no. 9–12, pp. 3217–3227, 2018.
- [21] M. Abendroth and M. Kuna, "Identification of ductile damage and fracture parameters from the small punch test using

## *Retraction*

# **Retracted: Effect of Sandplay Therapy on the Mental Health Level of College Students**

### **Computational and Mathematical Methods in Medicine**

Received 25 July 2023; Accepted 25 July 2023; Published 26 July 2023

Copyright © 2023 Computational and Mathematical Methods in Medicine. This is an open access article distributed under the Creative Commons Attribution License, which permits unrestricted use, distribution, and reproduction in any medium, provided the original work is properly cited.

This article has been retracted by Hindawi following an investigation undertaken by the publisher [1]. This investigation has uncovered evidence of one or more of the following indicators of systematic manipulation of the publication process:

- (1) Discrepancies in scope
- (2) Discrepancies in the description of the research reported
- (3) Discrepancies between the availability of data and the research described
- (4) Inappropriate citations
- (5) Incoherent, meaningless and/or irrelevant content included in the article
- (6) Peer-review manipulation

The presence of these indicators undermines our confidence in the integrity of the article's content and we cannot, therefore, vouch for its reliability. Please note that this notice is intended solely to alert readers that the content of this article is unreliable. We have not investigated whether authors were aware of or involved in the systematic manipulation of the publication process.

In addition, our investigation has also shown that one or more of the following human-subject reporting requirements has not been met in this article: ethical approval by an Institutional Review Board (IRB) committee or equivalent, patient/participant consent to participate, and/or agreement to publish patient/participant details (where relevant).

Wiley and Hindawi regrets that the usual quality checks did not identify these issues before publication and have since put additional measures in place to safeguard research integrity.

We wish to credit our own Research Integrity and Research Publishing teams and anonymous and named external researchers and research integrity experts for contributing to this investigation.

The corresponding author, as the representative of all authors, has been given the opportunity to register their agreement or disagreement to this retraction. We have kept a record of any response received.

### **References**

- [1] G. Li and X. Wu, "Effect of Sandplay Therapy on the Mental Health Level of College Students," *Computational and Mathematical Methods in Medicine*, vol. 2022, Article ID 3716849, 4 pages, 2022.



## Research Article

# Effect of Sandplay Therapy on the Mental Health Level of College Students

Gaoyong Li  and Xue Wu 

School of Economics Management, Kaili University, China

Correspondence should be addressed to Xue Wu; wuxuesisi@xs.ustb.edu.cn

Received 8 April 2022; Revised 10 May 2022; Accepted 17 May 2022; Published 3 June 2022

Academic Editor: Naeem Jan

Copyright © 2022 Gaoyong Li and Xue Wu. This is an open access article distributed under the Creative Commons Attribution License, which permits unrestricted use, distribution, and reproduction in any medium, provided the original work is properly cited.

To analyze the effect of sandplay (SP) therapy on the mental health level of college students. 500 college students were openly recruited, using the University Student Mental Health Questionnaire (UPI) to screen out 76 students in the UPI category. 34 college students were randomly selected and divided into two groups, 17 in the control group and 17 in the SP therapy group (experimental group); the control group received no treatment, and the experimental group was treated with SP therapy, to analyze the differences between groups before and after the intervention of SCL-90 and self-made group self-reflection questionnaire. (1) With a detection rate of 15.2 percent, 76 of the 500 college students solicited openly were identified as UPI students; (2) except for the terror factor, there were significant differences in other aspects and overall scores for the experimental group following SP therapy intervention, and the scores reduced. There were no significant differences in the total scores and scores of all factors in the control group ( $P > 0.05$ ). The overall score, somatization, interpersonal connection, depression, paranoia, and psychosis were all significantly different between the experimental and control groups in the independent sample  $t$ -test ( $P < 0.05$ ).

## 1. Introduction

SP therapy is an approach where the study subjects freely choose toys from the toy rack in the company of the therapist. It is a form of psychotherapy in which one performs self-expression in a box of fine sand, which is also called sand table play therapy [1]. The treatment process of the box court consists of two main parts: the creation of the group box court and the discussion after creation. SP therapy advocates that in a safe and free space, the healer takes the “motherly role” of a mother and child, faces the visitor with a silent, empathic, and understanding witness attitude, and emphasizes and believes in “self-healing power” [2, 3]. For a long time, intervention studies of SP therapy have focused on case studies [4]. The materials for SP therapy include a  $57 \times 72 \times 7$  (cm) sandboxes (painted blue on the inside), sand, and various types of toy models [5]. Its treatment hypothesis believes that everyone has a tendency to heal their psychological trauma in the depths of their souls, if there is a “free and protected” space; the self-healing ability

of research subjects can be brought into play [6]. In the mental health education of college students, the application of individual court and group court should be combined to make full use of its nonverbal advantages in the court therapy [7], to help students express their emotions well in the early stages of adult development, to provide a good solution for students who have problems in learning burnout, social anxiety, maladjustment, career decision-making, and so on, and to encourage them to constantly improve their ability of self-exploration, constantly explore the unknown self, and promote the improvement of self-healing ability and the growth of healthy psychology [8, 9]. Negative emotions can be channeled, psychological trauma can be cured, self-awareness can be enhanced, and self-potential can be stimulated when college students can freely express their ideas and therapists can make college students feel accepted, understood, and included through noncritical communication [10, 11]. 500 college students were openly recruited, using the University Student Mental Health Questionnaire (UPI) to screen out 76 students in the UPI category; 34 college

students were randomly selected and divided into two groups, 17 in the control group and 17 in the SP therapy group (experimental group), and the experimental group was treated with SP therapy.

SP therapy for college students is essentially an encouraging and reeducation procedure. Its main purpose is to foster college students' social interests. It has three primary functions: self-healing ability, way of life, and the spirit of mental health education for college students including diagnosis and assessment, expression, and communication.

The arrangements of the paper are as follows:

Section 2 discusses the materials and methods. Section 3 analyzes the results. Section 4 examines the discussion. Section 5 concludes the article.

## 2. Materials and Methods

Here, we discuss the general information and evaluate the various methods. We examine the observational index and analyze the statistical method.

**2.1. General Information.** 500 college students were openly recruited, using the University Student Mental Health Questionnaire (UPI) to screen out 76 students in the UPI category; 34 college students were randomly selected and divided into two groups, 17 in the control group and 17 in the SP therapy group (experimental group). There was no significant difference in general data between the two groups ( $P > 0.05$ ).

**2.2. Methods.** The control group received no treatment, the experimental group was treated with SP therapy, and the details were as follows.

- (1) The sandbox: a sandbox contained half a box of sand, measuring 57 cm in length, 72 cm in width, and 7 cm in height, painted blue on the inside and dark or woody on the outside
- (2) The sand tools: SP therapy requires a wide variety of toys
- (3) The implementation process: each group would make a group box court once a week, 5 to 6 rounds each time, and the time would be about 1.5 to 2 hours. Each time, the order of production was determined according to the drawing, punching, or custom form; intervention was given to the experimental group during each production—or according to the main research content of positive psychology, the theme (college life, class, and home) was designated before the production. Or in the production direction, sand movement and discussion and sharing in combination with Baker reconstruction of core belief technology and Ellis rational emotional therapy were conducted to give guidance [12]. For the recording of sand table works, different consultants also had different practices. Individual sand table records were utilized by some consultants to record which sand tools were placed by the research

subjects and in what sequence, as well as the first and last sand tool and the number of animals and plants, humans, and structures. Some consultants took photos; some consultants used sketches or scribbled notes; there were consultants who combined a variety of records

**2.3. Observational Index.** To analyze the differences between groups before and after the intervention of SCL-90 and self-made group self-reflection questionnaire.

- (1) University Student Mental Health Questionnaire (UPI) [13]: UPI was one of the most widely used mental health status tests at present. There were a total of 60 questions, of which 4 questions were false questions and the remaining 56 questions were scored, with the highest score of 56; the minimum score was 0. The higher the total score, the lower the mental health level
- (2) Symptom Checklist 90 (SCL-90) [14]: the scale had a total of 90 items and was divided into 10 factors. Each factor reflected one aspect of the subject, respectively. The 10 factors were somatization, obsessiveness, interpersonal relationship, depression, anxiety, hostility, fear, paranoia, psychosis, and others (mainly reflecting sleep and eating). A 1- to 5-point scoring system was used for each of the five grades. From 1 point for asymptomatic to 5 points for severe symptoms, the total score was the sum of the scores of 90 items. The lower the score, the better the psychological condition of the subject

**2.4. Statistical Method.** The statistical software SPSS 23.0 was used for analysis. The  $t$ -test was used for comparison data between groups, and the  $\chi^2$  test was used for counting data.  $P < 0.05$  was considered to be statistically significant.

## 3. Results

**3.1. Result of UPI.** Of the 500 college students recruited publicly, 76 were detected as UPI students, with a detection rate of 15.2%. 34 college students were randomly selected. Result of UPI is shown in Table 1.

**3.2. Result Symptom Self-Evaluation.** For the experimental group, after the intervention of SP therapy, there were significant differences in other factors and total scores except the terror factor, and the scores decreased. There were no significant differences in the total scores and scores of all factors in the control group ( $P > 0.05$ ). The independent sample  $t$ -test of the posttest data between the experimental group and the control group showed significant differences in total score, somatization, interpersonal relationship, depression, paranoia, and psychosis ( $P < 0.05$ ). Result symptom self-evaluation is shown in Table 2.

TABLE 1: Result of UPI.

Groups	Preintervention category	Postintervention category	Intervention efficiency
Control group ( $n = 17$ )	17	17	No intervention
Experimental group ( $n = 17$ )	17	2	88.24%
$\chi^2$			26.842
$P$			<0.05

TABLE 2: Result symptom self-evaluation.

Factors	Pretest		Posttest		t1①-②	t2②-④	t3④-③	t4①-③
	Experimental group	Control group	Experimental group	Control group				
Total scores	201.0 ± 34.2	190.1 ± 43.2	167.8 ± 36.6	182.0 ± 45.3	0.9	0.9	2.2*	4.1**
Somatization	19.8 ± 4.1	20.0 ± 6.3	16.6 ± 4.4	19.5 ± 6.8	-0.02	0.6	2.0*	3.4**
Obsessiveness	25.5 ± 7.0	25.1 ± 6.1	22.8 ± 6.0	25.0 ± 6.0	-0.05	0.3	1.1	2.3*
Interpersonal relationship	22.1 ± 4.6	20.8 ± 5.6	18.5 ± 4.4	20.5 ± 6.2	1.4	0.4	2.0*	2.8**
Depression	29.1 ± 7.6	26.4 ± 7.0	23.0 ± 6.0	25.5 ± 8.5	2.0	0.5	2.1*	3.8**
Anxiety	22.1 ± 5.2	21.4 ± 6.4	19.4 ± 4.6	20.8 ± 6.4	0.2	0.7	1.1	2.6*
Hostility	12.6 ± 3.5	11.3 ± 3.0	10.3 ± 3.1	10.6 ± 3.2	1.8	1.3	1.0	2.4*
Fear	15.8 ± 9.1	16.5 ± 5.2	12.7 ± 3.5	12.8 ± 8.4	0.3	1.6	1.3	1.3
Paranoia	13.7 ± 3.3	11.6 ± 3.5	10.9 ± 3.3	11.8 ± 4.3	5.2	-0.4	3.2**	4.6**
Psychosis	20.3 ± 5.6	19.6 ± 6.2	17.0 ± 4.3	18.0 ± 5.1	0.3	1.5	1.2	3.5**
Others	15.3 ± 3.1	13.2 ± 3.5	12.1 ± 6.4	12.3 ± 4.2	2.2	1.0	3.1	1.2

Note: \* $P < 0.05$ , \*\* $P < 0.01$ .

#### 4. Discussion

SP therapy is a therapy coming from Adler School that instructs group members to work together to produce a work that reflects a theme and to evaluate it effectively [15]; Adler style-guided chamber therapy from the perspective of Adler School attaches importance to the final fictional goal of the client and the activity towards that goal and believes that once the client undergoes changes in the experience, it is likely to transfer them to real life [16]. The nonverbal creation stage at the beginning of SP therapy avoids the pressure of direct face-to-face communication and effectively helps individuals with low psychological resilience to express themselves, which can maximize not being subject to the control of other people's words, the true expression of their own, figuring out other people's mind, and their own thoughts to match the thoughts of others [17, 18]. The essence of SP therapy for college students is a process of encouragement and reeducation. Its basic goal is to cultivate the social interests of college students. It has three key roles: sousing self-healing ability, life style diagnosis, and assessment; expression and communication are exactly in line with the spirit of college students' mental health education: promoting students' all-round development and preventing psychological development defects [19, 20]. The creation and discussion process of the box court makes the group members express themselves effectively as much as possible. The collision of each student's experience will produce new experience, which will be integrated into the group members' own experience, and the new construction will come into

being [21]. The whole intervention process of SP therapy is easy to trigger the inner experience of college students and imperceptibly learn interpersonal skills [22]. Due to various reasons, college students have a certain weariness, inferiority, not strong self-restraint ability, behavioral problems, and prominent problems; it is of great significance to strengthen and improve the construction of big heart curriculum for promoting students' overall and healthy development and enhancing the effect of mental health education [23]. In line with the "student-centered" education and teaching philosophy, with teachers as guides and organizers, let students as learners and experiencers learn in experience, feel in learning, and grow up healthy in perception [24].

This study showed that (1) of the 500 college students recruited publicly, 76 were detected as UPI students, with a detection rate of 15.2%; (2) except for the terror component, there were significant variations in other factors and overall scores for the experimental group following the intervention of SP therapy, and the scores reduced. In the control group, there were no significant differences in total scores or scores for all criteria ( $P > 0.05$ ). The overall score, somatization, interpersonal connection, depression, paranoia, and psychosis were all significantly different between the experimental and control groups in the independent sample  $t$ -test ( $P < 0.05$ ).

#### 5. Conclusion

SP therapy was an effective method to improve the mental health of college students.

## Research Article

# Ensemble Learning Framework with GLCM Texture Extraction for Early Detection of Lung Cancer on CT Images

Sara A. Althubiti <sup>1</sup>, Sanchita Paul <sup>2</sup>, Rajanikanta Mohanty <sup>3</sup>,  
Sachi Nandan Mohanty <sup>4</sup>, Fayadh Alenezi <sup>5</sup>, and Kemal Polat <sup>6</sup>

<sup>1</sup>Department of Computer Science, College of Computer and Information Sciences, Majmaah University, Al-Majmaah, Saudi Arabia

<sup>2</sup>Department of Computer Science & Engineering, Birla Institute of Technology, Mesra, Ranchi, India

<sup>3</sup>Department of Computer Science & Engineering, Specialisation Program, Faculty of Engineering and Technology, Jain University, Bangalore, India

<sup>4</sup>Department of Computer Science & Engineering, Vardhaman College of Engineering (Autonomous), Hyderabad, India

<sup>5</sup>Department of Electrical Engineering, College of Engineering, Jouf University, Saudi Arabia

<sup>6</sup>Department of Electrical and Electronics Engineering, Bolu Abant Izzet Baysal University, Faculty of Engineering, Bolu, Turkey

Correspondence should be addressed to Kemal Polat; [kpolat@ibu.edu.tr](mailto:kpolat@ibu.edu.tr)

Received 8 April 2022; Revised 29 April 2022; Accepted 10 May 2022; Published 2 June 2022

Academic Editor: Naeem Jan

Copyright © 2022 Sara A. Althubiti et al. This is an open access article distributed under the Creative Commons Attribution License, which permits unrestricted use, distribution, and reproduction in any medium, provided the original work is properly cited.

Lung cancer has emerged as a major cause of death among all demographics worldwide, largely caused by a proliferation of smoking habits. However, early detection and diagnosis of lung cancer through technological improvements can save the lives of millions of individuals affected globally. Computerized tomography (CT) scan imaging is a proven and popular technique in the medical field, but diagnosing cancer with only CT scans is a difficult task even for doctors and experts. This is why computer-assisted diagnosis has revolutionized disease diagnosis, especially cancer detection. This study looks at 20 CT scan images of lungs. In a preprocessing step, we chose the best filter to be applied to medical CT images between median, Gaussian, 2D convolution, and mean. From there, it was established that the median filter is the most appropriate. Next, we improved image contrast by applying adaptive histogram equalization. Finally, the preprocessed image with better quality is subjected to two optimization algorithms, fuzzy c-means and k-means clustering. The performance of these algorithms was then compared. Fuzzy c-means showed the highest accuracy of 98%. The feature was extracted using Gray Level Cooccurrence Matrix (GLCM). In classification, a comparison between three algorithms—bagging, gradient boosting, and ensemble (SVM, MLPNN, DT, logistic regression, and KNN)—was performed. Gradient boosting performed the best among these three, having an accuracy of 90.9%.

## 1. Introduction

Carcinoma is the leading cause of death in the world. Carcinomas are cancers that start in cells that make up the skin or the tissue lining organs, such as the lungs or kidneys. Lung cancer, also known as carcinoma of the lungs, is characterized by an unrestricted growth of cells in lung tissue and distinguished by a specific growth pattern. Lung cancer is dangerous to leave untreated, as it may propagate to other body parts. Small-cell lung carcinoma and nonsmall-cell

lung carcinoma are the two major categories, and the primary cause is smoking. Lung cancer has also been found in people with no smoking history but with exposure to air pollution, secondary smoking, and sometimes toxic gasses. Before the 12<sup>th</sup> century, occurrence of lung cancer was actually very rare. But nowadays, it is widespread. Many patients consult a doctor only when their disease and symptoms become extreme, thereby making these disease and symptoms very difficult to diagnose and cure. Thus, early-stage treatment of lung cancer is crucial in saving lives. One way

to detect the distinctive abnormal growth of cells is through X-ray. Another method of cancer detection is sputum cytology. If the lungs produce sputum, cancer can be seen by looking at the sputum through a microscope. Tissue sampling, also called biopsy, is another method for early detection of lung cancer. The conventional and most widespread method of detecting lung cancer is by using computer tomography (CT) and radiographs. CT scan uses X-ray and a computer to deliver a clear image of the lungs, giving better results than an X-ray alone. The CT scan image gives much more detail than a plain image, and the doctors can view a particular organ from different angles [1–33]. In this study, 20 lung image samples are taken for analysis. The image is denoised; then, the image is enhanced. Afterwards, features are extracted using GLCM. Lastly, classification is done. Integration of median filter, adaptive histogram equalization, and fuzzy *c*-means clustering for segmentation showed more accurate results. After applying feature extraction using GLCM (Haralick features), the accuracy of the ensemble classifier consisting of MLPNN, DT, SVM, and KNN classifiers was computed and confirmed to be highly effective. Thus, the study has great potential to advance the early detection of lung cancer.

## 2. Related Works

Senthil Kumar et al. [34] used a segmentation algorithm (*k*-means) on computer tomography (CT) scan images to detect lung cancer. Image segmentation was achieved by applying fuzzy *c*-means and *k*-means algorithms. Fuzzy *c*-means delivered enhanced performance in comparison to *k*-means. Using guaranteed convergence particle swarm optimization (GCPSO), an accuracy of 95.89% was achieved for the detection of lung cancer. Using a novel Multicrop Convolutional Neural Network (MC-CNN), an accuracy of 86.24% was achieved in identifying the lung module malignancy. In MC-CNN, features are extracted from the nodules by trimming distinct areas from convolution feature maps and applying max-pooling several times [35]. Sensitivity of 70%-90% was achieved using random forest and principal component analysis by extracting features using local shape analysis [36]. Using two successive *k*-nearest neighbor classifiers, a sensitivity of 80% was achieved using the curvedness and shape feature of the local image [37]. Accuracy of 95.91% was achieved using a probabilistic neural network (PNN) by extracting lung volume, and reduction was done using principal component analysis (PCA) [38]. Accuracy of 95.62% was achieved using texture, volumetric, intensity, and geometric features, and Fuzzy Particle Swarm Optimization (FPSO) was used for feature selection, with deep learning being applied for classification [39]. Sensitivity of 93.02% was achieved in detection detecting ground-glass opacity (GGO) using Support Vector Machine (SVM) twice and using four 2-dimensional features and 11 3-dimensional features [40]. Classification accuracy of 96% was achieved using speed up robust feature (SURF) along with genetic algorithms (GA) for optimization and a neural network (NN) for classification [41]. 97.61% accuracy was achieved using a genetic algorithm with wrapper approach (GAWA) using a multilevel

brightness-preserving approach and segmentation using a deep neural network. Features are derived from the segment and selected using a generalized rough set (hybrid spiral optimization intelligent) [42]. An accuracy of 89.29% was obtained using two 3D deep learning models [43]. Using 2D and 3D shape and texture features and histogram, *k*-means clustering (autocenter) provided a sensitivity of 88.88%. [44]. Using volumetric CT data, sensitivity reached more than 90% using a 3D convolution neural network. [45–52].

## 3. Materials and Methods

Firstly, a filtering technique is used to filter out the noise from the 20 images. In this study, 4 filters were used for the purpose of comparison. The filters used were mean, median, Gaussian, and 2D convolution. Afterwards, adaptive histogram equalization was applied so that images became clear. A segmentation algorithm was applied for the proper segmentation of images. This step used *k*-means clustering and fuzzy *c*-means clustering for segmentation. After segmentation, with the help of GLCM (Gray Level Cooccurrence Matrix), 8 features, i.e., contrast, energy, entropy, homogeneity, sum of entropy, sum of variance, dissimilarity, and sum of average, were extracted from the images to form the dataset of 41 CT scan images (20 were from [34] and 20 were from a different paper: Abnormalities Detection in CT Scan Lung Images Using GLCM [37]) where 28 are lung cancer patients and 13 are patients not affected by cancer. The use of two datasets makes the results more generalized. Ensemble learning was used for the classification of the dataset. Bagging and gradient boosting (a part of ensemble learning) were used for classification. Figure 1 shows the block diagram of framework for detection of lung cancer.

### 3.1. Filtering

**3.1.1. Mean Filter.** It blurs the image to reduce noise to a minimum. It involves calculating the mean values of pixels in the  $m \times m$  kernel. The mean will replace the intensity of the center element's pixel. This results in smoothing and removal of noise up to a certain extent. This can be implemented using the OpenCV library. For color images, it is necessary to convert the images from RGB to HSV, as the dimensions of RGB are interdependent, and the dimensions of HSV are independent separately.

**3.1.2. Gaussian Filter.** This filter is similar to the mean filter, but it calculates the weighted mean of the neighboring pixels having a parameter sigma with a discrete approximation. The kernel represents the value of the Gaussian distribution. Although it blurs edges like a standard filter, it is good at protecting edges compared to similar-sized filters. This can also be implemented using the OpenCV package. It allows us to specify the kernel's size.

**3.1.3. Median Filter.** This filter calculates the median of neighboring pixels to the center in the  $m \times m$  kernel. The median then changes the center pixel. It does an excellent job in removing slight noises compared to mean and Gaussian filters. It also preserves the edges of the image but fails to

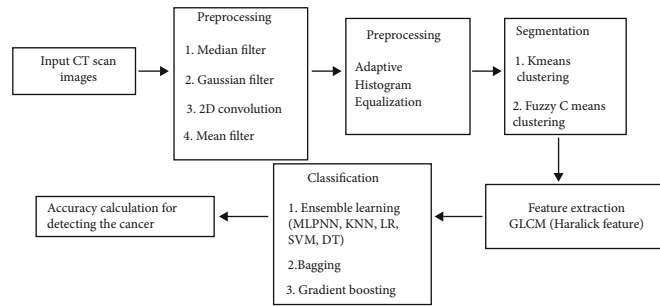


FIGURE 1: Block diagram of framework for detection of lung cancer.

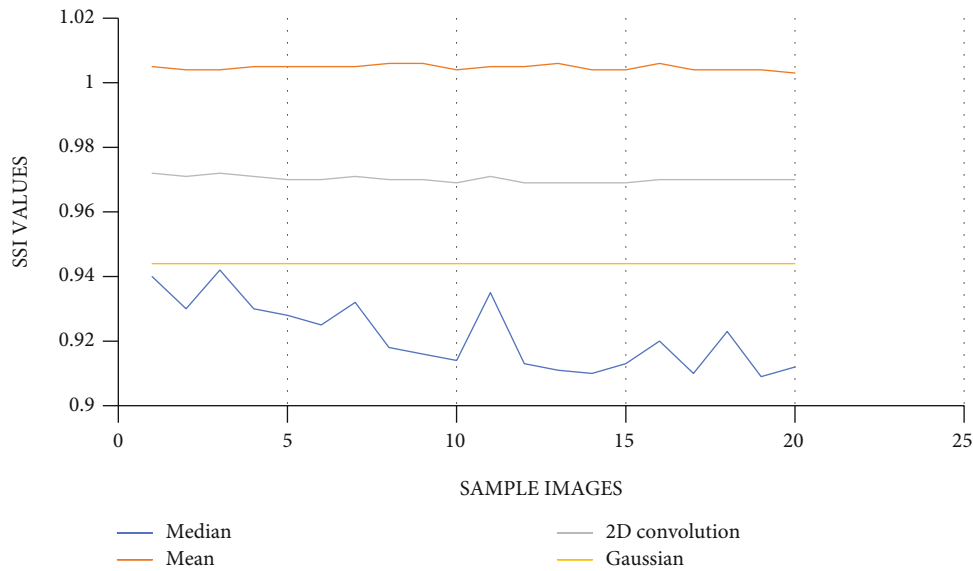


FIGURE 2: SSI comparison of filters using graph.

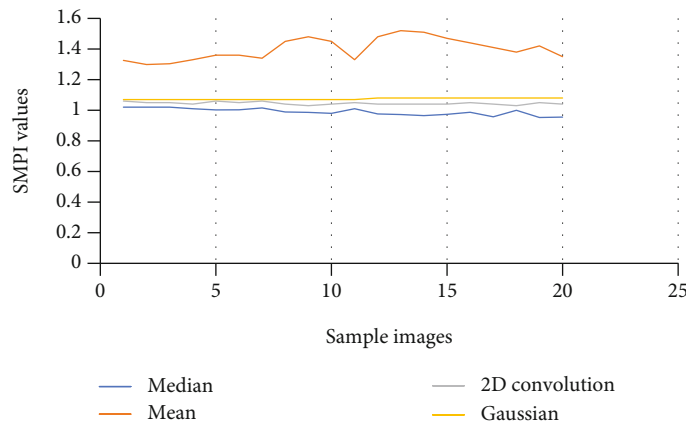


FIGURE 3: SMPI comparison of filters using graph.

deal with speckle noise. This can also be implemented using the OpenCV library.

**3.1.4. 2D Convolution Filter.** When applying a 2D Convolution filter, images are filtered utilizing Low Pass Filters (LPF) and High Pass Filters (HPF). Low Pass Filter blurs the image

and removes noise. High Pass filters detect edges. For each pixel, a  $3 \times 3$  window is centered on this pixel. All pixels falling within this frame are added, and then, the result is divided by 9. It is equivalent to computing the average pixel value inside that frame. This is performed for all image pixel values to give an output filtered image.

(1) *Performance Measure.* Performance measure of all the four filters, i.e., mean, median, Gaussian, and 2D convolution, is done by comparing SMPI (Speckle Suppression and Mean Preservation Index) and SSI (Speckle Suppression Index) metrics. Per these indices, a lower value represents better performance of filters for mean preservation and noise reduction. Figure 2 shows the SSI comparison of filters using graph. Figure 3 gives the SMPI comparison of filters using graph.

$$SSI = \frac{\sqrt{\text{Variance (final Image)}}}{\text{mean (final image)}} \times \frac{\text{mean (Initial Image)}}{\sqrt{\text{Variance (Initial Image)}}},$$

$$SMPI = Q \times \frac{\sqrt{\text{Variance (Final Image)}}}{\sqrt{\text{Variance (Initial Image)}}},$$

$$Q = 1 + |\text{mean (initial Image)} - \text{mean (final Image)}|. \quad (1)$$

In Table 1, the SSI value of the 4 filters (mean, median, Gaussian, and 2D convolution) is provided with their corresponding graphical comparisons in Figure 2. In Table 2, SMPI values of 4 filters are compared, with their graphical comparisons in Figure 3. The lower values of SSI and SMPI denote better preservation of the image after filtering. From the comparison of different filters, as shown in Figures 2 and 3 and Tables 1 and 2, it can be concluded that the median filter is the best and has more accurate characteristics than the remaining filters. Thus, we use median filtered images for image segmentation.

*3.2. Adaptive Histogram Equalization.* The color histogram in image processing addresses the number of pixels in each sort of colored part. Because the histogram equation causes a substantial change in the image's color balance, it cannot be applied independently for an image's red, green, and blue components. However, the algorithm can be applied to the luminance or value channel due to changes in the image's color and saturation if the image is first converted to another color space, such as the HSL/HSV color space. The primary difference between an adaptive histogram and ordinary histogram is that the adaptive approach generates numerous histograms for each image region and utilizes them to redistribute the image's lightness value. Therefore, it is appropriate for refining local contrast in each region of an image and increasing the definition of edges. This step enhances the image, and edges will become sharper and clearer which is necessary for medical image segmentation. Figure 4 shows the resultant image (1 to 20) after preprocessing.

*3.3. Image Segmentation.* Image segmentation is defined as the method by which a digital image is separated into several different regions, each a set of pixels with distinct objects or similar characteristics. Locating objects and boundaries in images is the main function of image segmentation. It can be divided into several methods. With this strategy, the distinct shapes of cancer cell clusters play an important role in determining how severe the cancer is. In our case, two clustering algorithms were used to perform segmentation of images—k-means clustering and fuzzy-c means clustering.

TABLE 1: SSI values of different filters.

Images	Median	Mean	2D convolution	Gaussian
1	0.94	1.005	0.972	0.944
2	0.93	1.004	0.971	0.944
3	0.942	1.004	0.972	0.944
4	0.93	1.005	0.971	0.944
5	0.928	1.005	0.97	0.944
6	0.925	1.005	0.97	0.944
7	0.932	1.005	0.971	0.944
8	0.918	1.006	0.97	0.944
9	0.916	1.006	0.97	0.944
10	0.914	1.004	0.969	0.944
11	0.935	1.005	0.971	0.944
12	0.913	1.005	0.969	0.944
13	0.911	1.006	0.969	0.944
14	0.91	1.004	0.969	0.944
15	0.913	1.004	0.969	0.944
16	0.92	1.006	0.97	0.944
17	0.91	1.004	0.97	0.944
18	0.923	1.004	0.97	0.944
19	0.909	1.004	0.97	0.944
20	0.912	1.003	0.97	0.944

TABLE 2: Comparison of SMPI values of 4 filters.

Images	Median	Mean	2D convolution	Gaussian
1	1.02	1.326	1.06	1.07
2	1.02	1.299	1.05	1.07
3	1.02	1.304	1.05	1.07
4	1.01	1.33	1.04	1.07
5	1.002	1.36	1.06	1.07
6	1.003	1.36	1.05	1.07
7	1.015	1.34	1.06	1.07
8	0.989	1.45	1.04	1.07
9	0.986	1.48	1.03	1.07
10	0.98	1.45	1.04	1.07
11	1.01	1.33	1.05	1.07
12	0.976	1.48	1.04	1.08
13	0.972	1.52	1.04	1.08
14	0.965	1.51	1.04	1.08
15	0.973	1.47	1.04	1.08
16	0.987	1.44	1.05	1.08
17	0.957	1.41	1.04	1.08
18	1	1.38	1.03	1.08
19	0.953	1.42	1.05	1.08
20	0.955	1.35	1.04	1.08

*3.3.1. K-Means Clustering Algorithm.* The k-means clustering algorithm is the most basic and classical form of cluster analysis. We apply k-means to separate the given dataset into two or more groups. The method's accuracy is measured by evaluating each cluster center produced by the

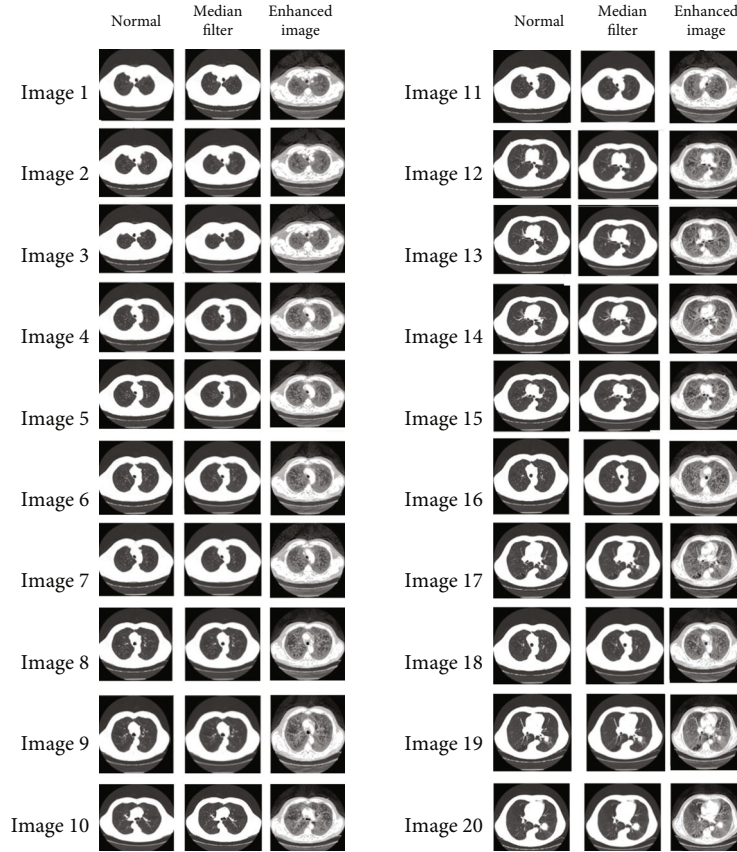


FIGURE 4: Resultant image (1 to 20) after preprocessing.

Step 1: Find cluster center - let it be “c”.  
 Step 2: Compute Euclidean distance.  
 Step 3: Assign every pixel to the appropriate pixel by checking the minimum Euclidean distance between pixel and cluster.  
 Step 4: If all pixel segregation is done, then again calculate the new cluster center using the k-means formula.  
 Step 5: Repeat steps 2 to 4 until the end condition is encountered.

ALGORITHM 1.

Step 1: Find the cluster center, let it be “c” randomly select the cluster center.  
 Step 2: Compute Fuzzy belonging using Equation (3).  
 Step 3: Compute new fuzzy cluster center using Equation (4).  
 Step 4: Repeat steps 2 to 3 until the end condition is encountered or the objective function is achieved.

ALGORITHM 2.

algorithm, as selecting the proper cluster center is essential for getting the best results. A very simple method to separate the dataset is by using Euclidean distance, which we use to assign pixels to an individual cluster. The following function is used in this algorithm:

$$J = \sum_{i=1}^m \sum_{k=1}^K W_{ik} \|x^i - \mu_k\|^2, \quad (2)$$

where  $x_i$  is the pixels,  $v_j$  is the cluster centers,  $|x_i - v_j|$  is the

Euclidean distance between  $x_i$  and  $v_j$ ,  $C_i$  is the number of data points for the  $i^{\text{th}}$  cluster, and  $C_j$  is the number of cluster centers. Approach k-m to solve the problem is called expectation-maximization. The expectation phase assigns data points to the nearest cluster. The maximization phase calculates the nucleus of each cluster. Below is how we solve it mathematically.

3.3.2. *Fuzzy C-Means Clustering Algorithm.* Fuzzy clustering (also known as soft clustering or soft k-means) is a clustering method by which each data point can be assigned to



multiple clusters. This clustering or cluster analysis includes grouping data points into clusters such that items in the same cluster are as similar as possible, while points in different clusters are as dissimilar as possible. Groups are distinguished through similarity metrics such as distance, connectivity, and intensity. Depending on the data or application, different similarity measures can be employed. The membership of each data point relating to each cluster center is determined by the distance between the cluster center and the data point. The more data in the cluster center, the more membership towards the special cluster center. The membership magnitude of each data point must sum to one, after updating each recursive membership and cluster center principle:

$$\mu_{ij} = \frac{1}{\sum_{k=1}^c (d_{ij}/d_{ik})^{(2/m-1)}}, \quad (3)$$

$$V_j = \frac{\left(\sum_{i=1}^n (\mu_{ij})^m x_i\right)}{\left(\sum_{i=1}^n (\mu_{ij})^m\right)}, \quad \forall j = 1, 2, 3..c, \quad (4)$$

where

“ $\mu_{ij}$ ” represents the membership of  $i^{\text{th}}$  data to  $j^{\text{th}}$  cluster center. “ $c$ ” represents the number of cluster centers. “ $d_{ij}$ ” represents the Euclidean distance between  $i^{\text{th}}$  data and  $j^{\text{th}}$  cluster center, and “ $n$ ” is the number of the data point. “ $m$ ” is the fuzziness index  $m \in [1, \infty]$ . “ $v_j$ ” represents the  $j^{\text{th}}$  cluster center.

Performance measure: Here, we do the accuracy measure of both clustering algorithms, i.e., k-means and Fuzzy c-means, with a median filter for the segmentation of the image

Accuracy: a performance measure that gives information about the correctness of any process

True positive (TP): foreground pixels are correctly segmented

True negative (TN): background pixels are correctly detected

False positive (FP): foreground pixels are incorrectly segmented

False negative (FN): background pixels are incorrectly detected

The above Tables 3 and 4 show the true positive rate, true negative rate, false positive rate, false negative rate, and accuracy of k-means clustering algorithm (Table 3) and fuzzy c-means clustering algorithm (Table 4). Figure 5 shows a graphical comparison of TPR between k-means and fuzzy c-means. Similarly, Figure 6 shows an FPR comparison. Figure 7 shows the TNR comparison. Figure 8 shows the FNR comparison. Figure 9 shows the accuracy comparison between k-means and fuzzy c-means using a graph.

Edge detection in an image is a crucial technique for determining the limits of various distinctive objects. It can be implemented by looking for discontinuities in the brightness. Masks can be used for edge detection. Some of them are Laplacian operators, Sobel, and Canny. They are calculated using dissimilarity between adjacent pixels of the image.

TABLE 3: Performance measure of fuzzy c-means clustering.

Images	TPR	FPR	TNR	FNR	Accuracy
1	96.4	0	100	3.5	98.71
2	96.4	0	100	3.5	98.74
3	96.6	0	100	3.3	98.78
4	95.9	0	100	4	98.63
5	95.7	0	100	4	98.61
6	95.5	0	100	4	98.57
7	96.1	0	100	3.8	98.68
8	95.1	0	100	4	98.51
9	94.6	0	100	5	98.37
10	94.4	0	100	5	98.28
11	96.3	0	100	3	98.74
12	94.4	0	100	5	98.9
13	94.4	0	100	5	98.29
14	93.9	0	100	6	98.15
15	94.6	0	100	5	98.34
16	95.3	0	100	4	98.53
17	91.6	0	100	8.3	97.39
18	95.5	0	100	4	98.56
19	91.1	0	100	8	97.2
20	94.3	0	100	5	98.27

TABLE 4: Performance measure of k-means clustering.

Images	TPR	FPR	TNR	FNR	Accuracy
1	84.5	1.2	98.7	15.4	93.07
2	82.2	1.1	98.8	17.7	92.11
3	85.8	1.1	98.8	14.1	93.65
4	75.1	1	98.9	24.8	89.04
5	74.3	1.2	98.7	25.6	88.71
6	75.3	1.1	98.8	24.6	89.39
7	76.4	1.1	98.8	23.5	89.49
8	68.7	1	98.9	31.2	86.19
9	68	1.1	98.8	31.9	86.02
10	67.4	1.3	98.6	32.5	85.54
11	79.8	1.1	98.8	20.1	91.08
12	70.6	1.4	98.5	29.3	87.35
13	66.9	1.2	98.7	33	85.25
14	67.3	1.2	98.7	32.6	85.65
15	70.7	1.3	98.6	29.2	87.40
16	67.7	1.1	98.8	32.2	85.35
17	68.9	1.4	98.5	31	86.27
18	74.6	1.15	98.8	25.3	89.17
19	69.8	1.5	98.4	30.1	86.71
20	69.7	1.4	98.5	30.2	86.96

3.4. *Feature Extraction.* Feature extractions from a segmented image yield several important properties that are utilized in defining the segmented image’s characteristics. The crucial information of the presence of nodules (or lack thereof), which is used to detect or distinguish between

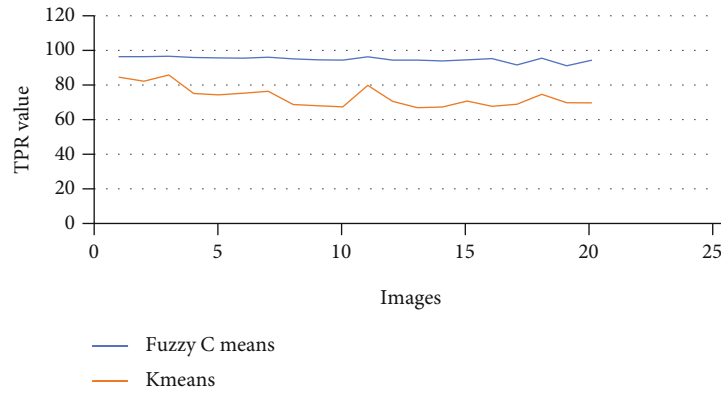


FIGURE 5: TPR comparison of k-means and fuzzy c-means.



FIGURE 6: FPR comparison of k-means and fuzzy c-means.

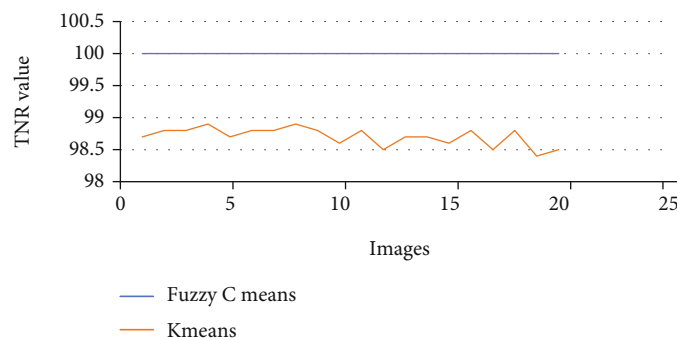


FIGURE 7: TNR comparison of k-means and fuzzy c-means.

malignant and nonmalignant images, can be diagnosed using the extracted features. 8 Haralick features, namely, contrast, energy, entropy, homogeneity, sum of entropy, sum of variance, dissimilarity, and sum, as shown in Table 5, were extracted by finding GLCM (Gray Level Cooccurrence Matrix). These 8 features of the images were used in the analysis in this study.

3.4.1. *Gray Level Cooccurrence Matrix (GLCM)*. GLCM is an image analysis technique. It is a statistical method for examining the shape of the pixels of an image as a gray-scale matrix, also known as the gray-scale spatial cooccurrence matrix. It is a classification technique, the final step of which is to train the classifier. Its main function is to extract the texture feature from the image. The GLCM function

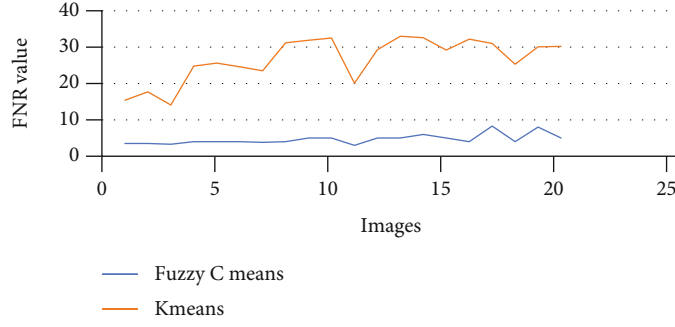


FIGURE 8: FNR comparison of k-means and fuzzy c-means.

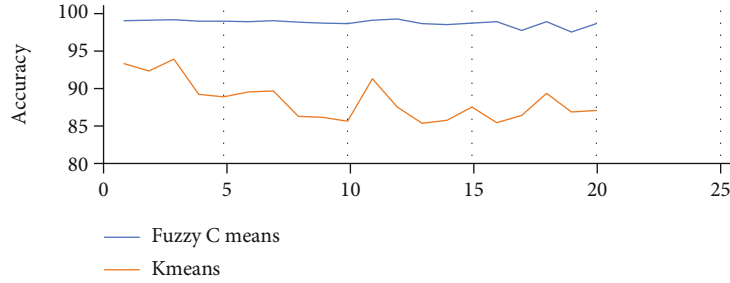


FIGURE 9: Accuracy comparison of k-means and fuzzy c-means.

TABLE 5: Haralick features extracted from GLCM.

1	Contrast	$\sum_i \sum_j (i-j)^2 p_d(i, j)$
2	Energy	$Energy = \sqrt{ASM}$ $ASM = \sum_i \sum_j p_d^2(i, j)$
3	Entropy	$-\sum_i \sum_j p_d(i, j) \ln p_d(i, j)$
4	Homogeneity	$\sum_i \sum_j \frac{1}{1 + (i-j)^2} p_d(i, j)$
5	Sum of entropy	$-\sum_{i=2}^{2N_g} p_{x+y}(i) \log \log \{p_{x+y}(i)\} = f_8$
6	Sum of variance	$\sum_{i=2}^{2N_g} (i - f_8)^2 p_{x+y}(i)$
7	Dissimilarity	$\sum_{j=1}^N  i-j  \cdot p(i, j)$
8	Sum of average	$\sum_{i=2}^{2N_g} i p_{x+y}(i)$

generates a GLCM and then extracts the statistical functions from this matrix with the specified values and spatial relationship of the shape of an image. The gray-coefficient matrix is derived from the gray-scale coefficient matrix. Gray-level cooccurring grids are also called gray-level spatial dependence grids. The gray-cum-matrix is used to generate

the GLCM by computation, but  $i$ , which usually represents gray-level (gray-level probability), is a valuable, horizontal neighbor to  $j$ . Each part of the GLCM  $(i, j)$  represents the sum of the image element. The figure below shows the gray-scale coherence grid-matrix (GLCM) of the gray-scale image ( $i$  and  $j$  = image element).

Haralick Features:

### 3.5. Classification

**3.5.1. Ensemble Learning.** Ensemble learning is a method for systematically building and combining a large number of machine learning models in tandem to solve a specific problem. By merging different models, machine learning outcomes can be dramatically improved. This method outperforms a single model in terms of prediction accuracy. Here, 5 models are considered for ensemble learning: decision tree classifier, multilayer perceptron classifier, Support Vector Machine, K-nearest neighbor classifier, and logistic regression classifier. For meta outcome evaluation, we use the maximum voting technique to find optimal accuracy among all 5 models.

**3.5.2. Bagging.** Bagging is a strategy used to boost the accuracy of a machine learning algorithm. The main goal is the creation of multiple different subsets of data from randomly chosen training samples, and then, substitution is done. The decision trees are trained by different subsets of data. This results in a collection of various models, which oftentimes multiplies the power of a model.

Bagging steps are as follows:

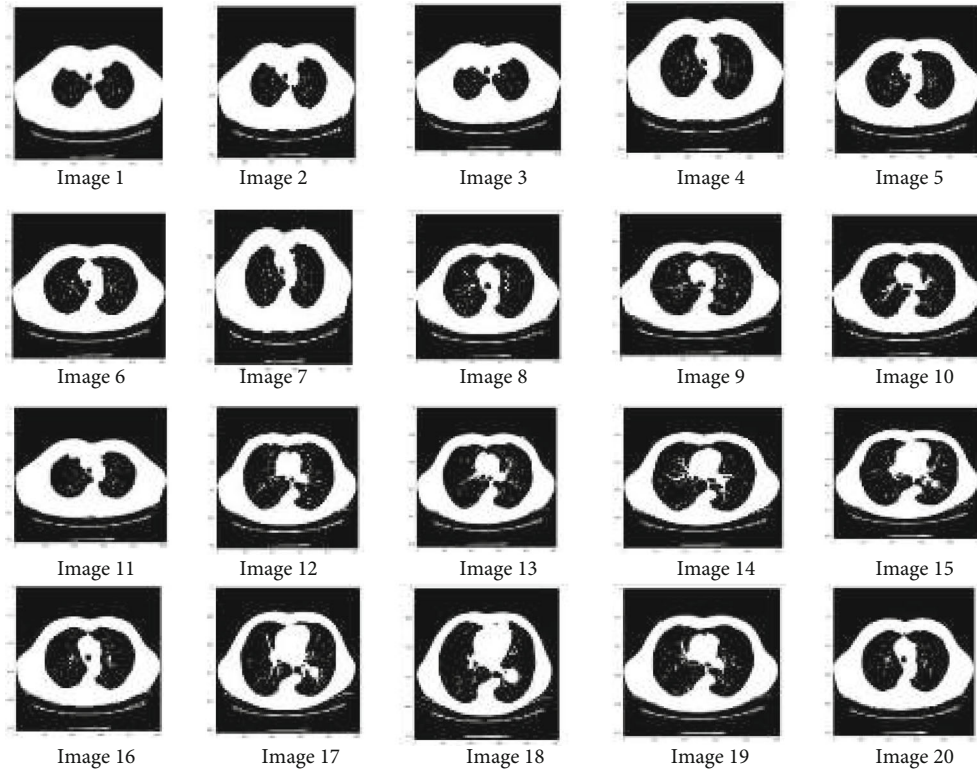


FIGURE 10: Resultant image (1 to 20) after segmentation.



FIGURE 11: Thresholding.

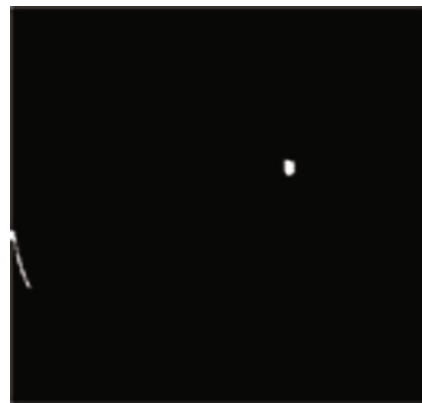


FIGURE 13: Extraction.



FIGURE 12: Masking.

- (i) Suppose that the training dataset has  $n$  observations and  $m$  characteristics. With substitution, one sample is randomly selected from the training dataset
- (ii) A subset of  $L$  features is chosen randomly, and the best features are used to iterate over the partition node
- (iii) The tree becomes the largest
- (iv) Repetition of the above steps is carried out  $n$  times, and the prediction is built on the sum of predictions by the number of  $n$  trees

3.5.3. *Boosting*. Boosting is used to convert weak learners to strong learners. It is one of the most used algorithms in data

TABLE 6: Confusion matrix of various classification algorithms.

	True positive	True negative	False positive	False negative
Ensemble	2	0	2	7
Bagging	1	1	2	7
Boosting	1	1	0	9

TABLE 7: Comparison of performance measure of various classification algorithms.

	Ensemble learning	Bagging	Boosting
	DT, logistic regression, MLPNN, SVM, KNN	Decision tree	Gradient boosting
Accuracy	81.81%	72.72%	90.90%
Error	18.18%	27.27%	9.09%
Sensitivity	50%	33.33%	100%
Prediction	100%	50%	50%

science. In this method, learners are sequentially trained with early learners to fit simple models to the data, after which, the data is analyzed to detect the errors. In order to achieve a progressively higher accuracy in each step from the preceding tree, successive trees are fitted. When a hypothesis implies an input, its weight is increased, making the next hypothesis more likely to be categorized correctly. This technique transforms low-performing learners into high-performing models.

Boosting steps are as follows:

- (i) Weak learner  $W$  is trained by drawing a random subset of training sample  $T$  without replacement from training set  $P$
- (ii) In order to train the weak learner  $W_2$ , a second random training subset  $P_2$  is drawn without replacement from the training set, then 50 percent of the earlier incorrect classified/miscall sample is added
- (iii) In order to train the third weak learner  $W_3$ , training samples  $P$  are found in training set  $P_3$ , on which there is a disagreement between  $W_1$  and  $W_2$
- (iv) All the weak learners are mixed through majority voting
- (v) In order to train the weak learner  $W_2$  again, a second random training subset  $T_2$  is drawn without replacement from the training set and 50 percent of the earlier incorrect classified/miscall sample is added
- (vi)  $W_3$ , the third weak learner, is trained by finding a training sample  $P$  in training set  $T_3$  where there is a disagreement between  $W_1$  and  $W_2$
- (vii) Weak learners are again mixed through majority voting

3.5.4. *Gradient boosting.* The gradient boosting machine (GBM) is a machine learning technique for boosting, regres-

sion, and classification problems that generates weak prediction models, usually a prediction model combined with a decision tree. It is an ensemble learning method where the weak models used are decision trees. It defines a loss function and minimizes it. It builds step-by-step models just like other boosting methods and simplifies them by allowing optimization of the arbitrary differential loss function. Gradient boosting can be understood more easily with the basic idea of AdaBoost. Gradient boosting is a proven powerful algorithm to build a predictive model, which is why we tested and selected it here.

## 4. Results and Discussions

A confusion matrix is a table that shows how well a classification model (or “classifier”) performs on a set of test data for which the true values are known. This enables the performance of an algorithm to be visualized.

In the preprocessing step, the performance of the median filter was the best among all the other tested filters—mean, Gaussian, and 2D convolution. From the SMPI and SSI values as shown in Tables 1 and 2 and Figures 2 and 3, it can be found that the image segmentation using a median filter has better performance than a mean filter—Gaussian and 2D convolution. True positive rate, true negative rate, false positive rate, and false negative rate were used to calculate the segmentation accuracy. For segmentation, the accuracy of fuzzy c-means clustering is higher than the k-means clustering algorithm. Fuzzy c-means achieves 97% accuracy. All the results are shown in Tables 3 and 4. All the comparisons of TPR, TNR, FNR, and FPR are shown in Figures 5–8. The accuracy comparison between k-means and fuzzy c-means was shown in Figure 9. The results show that the fuzzy c-means clustering algorithm outperforms k-means for lung cancer CT image segmentation. After that, the dataset was obtained by extracting Haralick features of 41 CT scan images (21 were from [34], and 20 were from abnormalities detection in CT scan lung images using GLCM [37]) and was classified using an ensemble learning algorithm. The resultant image of all 20 images after segmentation is shown in Figure 10. The output after

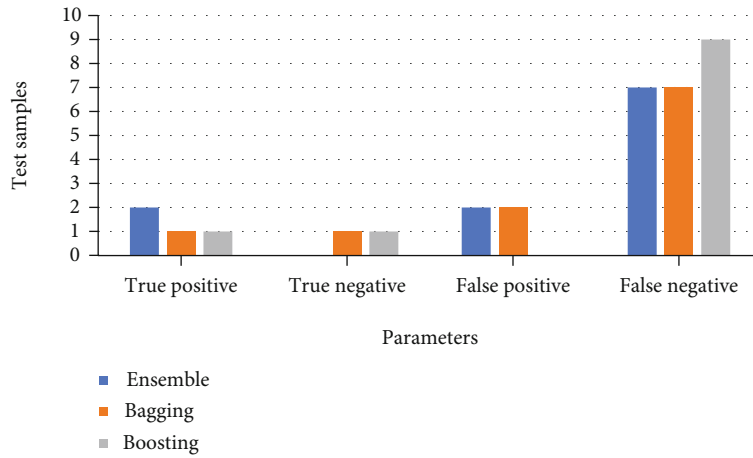


FIGURE 14: Confusion matrix of various classification algorithms.

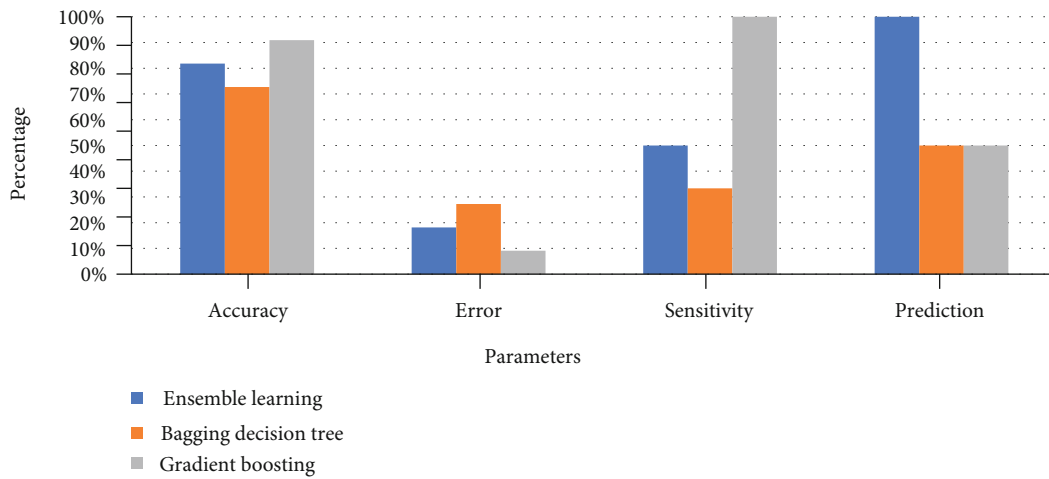


FIGURE 15: Performance measure of various classification algorithms.

TABLE 8

Paper name	Lung cancer detection using image segmentation by means of various evolutionary algorithms [34]	Lung cancer detection using image processing and classification techniques
Objective	To find a fast image segmentation algorithm for medical images to reduce the time it takes doctors to evaluate computer tomography (CT) scan images.	(i) Classification of lung cancer using extracted Haralick features (ii) Comparing the accuracy of various image segmentation algorithms
Features used	No features used.	Haralick features like contrast, energy, entropy, homogeneity, etc.
Segmentation also used	k-median, -means, particle swarm optimization, guaranteed convergence particle swarm optimization. Inertia-weighted particle swarm optimization, guaranteed convergence particle swarm optimization.	k-means, fuzzy c-means
Results	The highest accuracy is achieved in guaranteed convergence particle swarm optimization, i.e., 95.81%, and the average accuracy is above 90%.	The highest accuracy is achieved in fuzzy c-means, i.e., 98.78%, and the average accuracy is above 95%.

thresholding, masking, and extraction is shown in Figures 11–13.

The dataset was trained under 8 features and split into 75% for training the model and 25% for testing the model. The classifiers used in ensemble learning are DT, KNN, MLPNN, SVM, and logistic regression, with bagging using decision tree and gradient boosting. The performance measure of ensemble learning, bagging, and gradient boosting represented through a confusion matrix is shown in Table 6, and classification accuracy is compared in Table 7. The comparison of TP, TN, TP, and FP is shown in Figure 14, and a comparison of accuracy, sensitivity, and specificity is shown in Figure 15. Table 7 shows that the accuracy measure of gradient boosting was 90.9% which was found to be the highest.

A comparison between the proposed study and [34] was performed. The analysis was done using the same dataset. Table 8 shows that the proposed work achieved a higher accuracy of 98.78% using Fuzzy c-means.

A comparative study between existing and proposed methods is shown below in Table 8.

By combining two datasets [34, 37, 53, 54] into one, the study provided results that could be generalized. The limitation of this study is that the analysis and modeling are not powerful enough for even larger datasets.

## 5. Conclusions

In this paper, we performed image detection for lung cancer by combining the different strategies of GLCM texture extraction and ensemble learning for model-building. The first step, before undertaking any statistical analysis, was preprocessing the medical images. The median filter performed the best as shown by the result's superior SSI and SMPI metric values. Afterwards, clustering was implemented to achieve image segmentation for the cancer specimens. The fuzzy c-map clustering algorithm yielded the best results with a maximum accuracy of 98.78% and accuracy across all images of at least 95%. The classification of cancer was performed by implementing ensemble learning, which is the strategy of aggregating multiple models to reach a more generalized consensus. Developing the model also integrated the techniques of maximum voting, bagging, and gradient boosting. Gradient boosting helped improve the accuracy to 90.9%. Overall, the proposed framework achieved very high performance, with 98.78% accuracy in segmentation and 90.9% accuracy in classification. Thus, this proposed framework can assist medical practitioners and augment modern techniques in medical computer-aided diagnosis of lung cancer.

## Data Availability

We can send the datasets at the request of the authors.

## Ethical Approval

This article does not contain any studies with human participants. No animal studies were involved in this review.

## Conflicts of Interest

The authors declare no conflict of interest.

## Authors' Contributions

All authors contributed equally to this work. In addition, all authors have read and approved the final manuscript and given their consent to publish the article.

## References

- [1] A. El-Baz and J. S. Suri, *Lung Imaging and Computer Aided Diagnosis*, CRC Press, 2012.
- [2] V. Krishnan, A. Praisys, and M. Shalinie, "A customized particle swarm optimization for classification of multispectral imagery based on feature fusion," *International Arab Journal of Information Technology*, vol. 5, no. 4, pp. 71–78, 2008.
- [3] K. Venkatalakshmi, P. Praisys, R. Maragathavalli, and S. Shalinie, "Multispectral image clustering using enhanced genetic k-means algorithm," *Information Technology Journal*, vol. 6, no. 4, pp. 554–560, 2007.
- [4] G. Gupta, "Algorithm for image processing using improved median filter and comparison of mean, median and improved median filter," *International Journal of Soft Computing*, vol. 5, pp. 304–311, 2011, [http://ijscce.org/attachments/File/Vol-1\\_Issue-5/E0234101511.pdf](http://ijscce.org/attachments/File/Vol-1_Issue-5/E0234101511.pdf).
- [5] B. Rani, A. K. Goel, and R. Kaur, "A modified approach for lung cancer detection using bacterial forging optimization algorithm," *International Journal of Scientific Research Engineering and Technology*, vol. 5, no. 1, 2016.
- [6] K. Venkatalakshmi and S. S. Mercy, "Classification of multispectral images using support vector machines based on PSO and K-means clustering," in *Proceedings -2005 International Conference on Intelligent Sensing and Information Processing, ICISIP'05*, pp. 127–133, Chennai, India, 2005.
- [7] K. Venkatalakshmi and S. Shalinie, "Multispectral image classification using modified k-means clustering," *Neural Network World*, vol. 17, no. 2, pp. 113–120, 2007.
- [8] P. I. Dalatu, "Time complexity of K-means and K-medians clustering algorithms in outliers detection," *Global Journal of Pure and Applied Mathematics*, vol. 12, no. 5, pp. 4405–4418, 2016, <http://www.ripublication.com/gjppam.htm>.
- [9] P. Bhuvanawari and A. B. Therese, "Detection of cancer in lung with K-NN classification using genetic algorithm. Procedia," *Materials Science*, vol. 10, pp. 433–440, 2015.
- [10] X. Wang, L. Ge, and L. Xiaojing, "Evaluation of filters for ENVISAT ASAR speckle suppression in pasture area," *ISPRS Annals of the Photogrammetry, Remote Sensing and Spatial Information Sciences*, vol. 7, pp. 341–346, 2012.
- [11] M. S. Al-Tarawneh, "Lung cancer detection using image processing techniques," *Leonardo Electronic Journal of Practices and Technologies*, vol. 11, no. 20, pp. 147–158, 2012.
- [12] A. K. Mohanty, S. Beberta, and S. K. Lenka, "Classifying benign and malignant mass using GLCM and GLRLM based texture features from mammogram," *International Journal of Engineering Research and Applications (IJERA)*, vol. 1, no. 3, pp. 687–693, 2011.
- [13] J. C. Bezdek, R. Ehrlich, and W. Full, "FCM: the fuzzy c-means clustering algorithm," *Computers and Geosciences*, vol. 10, no. 2–3, pp. 191–203, 1984.

- [14] H. Rao, X. Shi, A. K. Rodrigue et al., "Feature selection based on artificial bee colony and gradient boosting decision tree," *Applied Soft Computing Journal*, vol. 74, pp. 634–642, 2019.
- [15] U. Pastorino, M. Bellomi, C. Landoni et al., "Early lung-cancer detection with spiral CT and positron emission tomography in heavy smokers: 2-year results," *Lancet*, vol. 362, no. 9384, pp. 593–597, 2003.
- [16] G. Bastarrika, M. J. García-Velloso, M. D. Lozano et al., "Early lung cancer detection using spiral computed tomography and positron emission tomography," *American Journal of Respiratory and Critical Care Medicine*, vol. 171, no. 12, pp. 1378–1383, 2005.
- [17] J. A. Howington, M. G. Blum, A. C. Chang, A. A. Balekian, and S. C. Murthy, "Treatment of stage I and II non-small cell lung cancer: diagnosis and management of lung cancer. 3rd American college of chest physicians evidence-based clinical practice guidelines," *Chest*, vol. 143, 5 Supplement, 2013.
- [18] L. Mao, R. H. Hruban, J. O. Boyle, M. Tockman, and D. Sidransky, "Detection of oncogene mutations in sputum precedes diagnosis of lung cancer," *Cancer Research*, vol. 11, no. 5-6, pp. 429–430, 1994.
- [19] A. Gajdhane and L. M. Deshpande, "Detection of lung cancer stages on CT scan images by using various image processing techniques," *IOSR Journal of Computer Engineering*, vol. 16, no. 5, pp. 28–35, 2014.
- [20] S. K. Anand, "Segmentation coupled textural feature classification for lung tumor prediction," in *International Conference On Communication Control And Computing Technologies*, pp. 518–524, Nagercoil, India, 2010.
- [21] M. S. Uzer, N. Yilmaz, and O. Inan, "Feature selection method based on artificial bee colony algorithm and support vector machines for medical datasets classification," *The Scientific World Journal*, vol. 2013, 10 pages, 2013.
- [22] W. Sun, X. Huang, T. L. B. Tseng, and W. Qian, "Automatic lung nodule graph cuts segmentation with deep learning false positive reduction," *Medical Imaging 2017: Computer-Aided Diagnosis International Society for Optics and Photonics*, vol. 10134, 2017.
- [23] K. Verma, S. B. Kumar, and A. S. Thokey, "An enhancement in adaptive median filter for edge preservation," *Procedia Computer Science*, vol. 48, pp. 29–36, 2015.
- [24] S. Makaju, P. W. C. Prasad, A. Alsadoon, A. K. Singh, and A. Elchouemi, "Lung cancer detection using CT scan images," *Procedia Computer Science*, vol. 125, no. 2009, pp. 107–114, 2018.
- [25] E. Magdy, N. Zayed, and M. Fakhr, "Automatic classification of normal and cancer lung CT images using multiscale AM-FM features," *International Journal of Biomedical Imaging*, vol. 2015, 7 pages, 2015.
- [26] J. Kuruvilla and K. Gunavathi, "Lung cancer classification using neural networks for CT images," *Computer Methods and Programs in Biomedicine*, vol. 113, no. 1, pp. 202–209, 2014.
- [27] M. A. Hussain, T. M. Ansari, P. S. Gawas, and N. N. Chowdhury, "Lung cancer detection using artificial neural network & fuzzy clustering," *Ijarccce*, vol. 4, no. 3, pp. 360–363, 2015.
- [28] D. P. Tian, "A review on image feature extraction and representation techniques," *International Journal of Multimedia and Ubiquitous Engineering*, vol. 8, no. 4, pp. 385–395, 2013.
- [29] Q. Z. Song, L. Zhao, X. K. Luo, and X. C. Dou, "Using deep learning for classification of lung nodules on computed tomography images," *Journal of Healthcare Engineering*, vol. 2017, 7 pages, 2017.
- [30] D. B. Larkins and W. Harvey, "Introductory computational science using MATLAB and image processing," *Procedia Computer Science*, vol. 1, no. 1, pp. 913–919, 2010.
- [31] O. Grove, A. E. Berglund, M. B. Schabath et al., "Data from: quantitative computed tomographic descriptors associate tumor shape complexity and intratumor heterogeneity with prognosis in lung adenocarcinoma," *PloS One*, vol. 10, no. 3, 2015.
- [32] <https://wiki.cancerimagingarchive.net/display/Public/LungCT-Diagnosis#19039728024ac253cffe4f7a9fb53e03368d83e3>.
- [33] Q. Dou, H. Chen, L. Yu, J. Qin, and P. A. Heng, "Multilevel contextual 3-D CNNs for false positive reduction in pulmonary nodule detection," *IEEE Transactions on Biomedical Engineering*, vol. 64, no. 7, pp. 1558–1567, 2017.
- [34] K. Senthil Kumar, K. Venkatalakshmi, and K. Karthikeyan, "Lung cancer detection using image segmentation by means of various evolutionary algorithms," *Computational and Mathematical Methods in Medicine*, vol. 2019, 16 pages, 2019.
- [35] W. Shen, M. Zhou, F. Yang et al., "Multi-crop convolutional neural networks for lung nodule malignancy suspiciousness classification," *Pattern Recognition*, vol. 61, pp. 663–673, 2017.
- [36] A. Chaudhary and S. S. Singh, "Lung cancer detection on CT images by using image processing," in *In 2012 International Conference on Computing Sciences*, pp. 142–146, Phagwara, India, 2012.
- [37] K. Murphy, B. van Ginneken, A. M. R. Schilham, B. J. de Hoop, H. A. Gietema, and M. Prokop, "A large-scale evaluation of automatic pulmonary nodule detection in chest CT using local image features and k-nearest-neighbour classification," *Medical Image Analysis. Elsevier BV*, vol. 13, no. 5, pp. 757–770, 2009.
- [38] E. Dandil, "A computer-aided pipeline for automatic lung cancer classification on computed tomography scans," *Journal of Healthcare Engineering*, vol. 2018, 12 pages, 2018.
- [39] N. Kalaivani, N. Manimaran, S. Sophia, and D. D. Devi, "Deep learning based lung cancer detection and classification," in *IOP Conference Series: Materials Science and Engineering. Multimedia Tools and Applications*, Tamil Nadu, India, 2020.
- [40] C. F. J. Kuo, C. C. Huang, J. J. Siao et al., "Automatic lung nodule detection system using image processing techniques in computed tomography," *Biomedical Signal Processing and Control*, vol. 56, p. 101659, 2020.
- [41] P. Nanglia, A. N. Mahajan, D. S. Rathee, and S. Kumar, "Lung cancer classification using feed forward back propagation neural network for CT images," *International Journal of Medical Engineering and Informatics*, vol. 12, no. 5, pp. 447–456, 2020.
- [42] P. M. Shakeel, M. A. Burhanuddin, and M. I. Desa, "Automatic lung cancer detection from CT image using improved deep neural network and ensemble classifier," *Neural Computing and Applications. Springer London*, vol. 6, 2022.
- [43] R. Gruetzemacher, A. Gupta, and D. Paradise, "3D deep learning for detecting pulmonary nodules in CT scans," *Journal of the American Medical Informatics Association*, vol. 25, no. 10, pp. 1301–1310, 2018.
- [44] S. Krishnamurthy, G. Narasimhan, and U. Rengasamy, "An automatic computerized model for cancerous lung nodule detection from computed tomography images with reduced false positives," *Communications in Computer and Information Science*, vol. 709, pp. 343–355, 2017.



- [45] “Optimal deep learning model for classification of lung cancer on CT images,” *Future Generation Computer Systems*, vol. 92, no. 1, pp. 374–382, 2019.
- [46] F. Alenezi, “Image dehazing based on pixel guided CNN with PAM via graph cut,” *CMC-Computers, Materials & Continua*, vol. 71, no. 2, pp. 3425–3443, 2022.
- [47] F. Alenezi, A. Armghan, S. N. Mohanty, R. H. Jhaveri, and P. Tiwari, “Block-greedy and CNN based underwater image dehazing for novel depth estimation and optimal ambient light,” *Water*, vol. 13, no. 23, p. 3470, 2021.
- [48] G. P. Joshi, F. Alenezi, G. Thirumoorthy, A. K. Dutta, and J. You, “Ensemble of deep learning-based multimodal remote sensing image classification model on unmanned aerial vehicle networks,” *Mathematics*, vol. 9, no. 22, p. 2984, 2021.
- [49] F. Alenezi and K. C. Santosh, “Geometric regularized hopfield neural network for medical image enhancement,” *International Journal of Biomedical Imaging*, vol. 2021, Article ID 6664569, 2021.
- [50] F. Alenezi and E. Salari, “A fuzzy-based medical image fusion using a combination of maximum selection and Gabor filters,” *International Journal of Engineering Science*, vol. 9, pp. 118–129, 2018.
- [51] F. S. Alenezi and S. Ganesan, “Geometric-pixel guided single-pass convolution neural network with graph cut for image dehazing,” *IEEE Access*, vol. 9, pp. 29380–29391, 2021.
- [52] S. Majid, F. Alenezi, S. Masood, M. Ahmad, E. S. Gündüz, and K. Polat, “Attention based CNN model for fire detection and localization in real-world images,” *Expert Systems with Applications*, vol. 189, article 116114, 2022.
- [53] A. Asuntha et al., “Lung cancer detection using SVM algorithm and optimization techniques,” *Journal of Chemical and Pharmaceutical Sciences*, vol. 9, no. 4, pp. 3198–3203, 2016.
- [54] S. K. Bandyopadhyay, “Edge detection from CT images of lung,” *International Journal of Engineering Science & Advanced Technology*, vol. 2, no. 1, pp. 34–37, 2012.

## Retraction

# Retracted: Music Art Teaching Quality Evaluation System Based on Convolutional Neural Network

### Computational and Mathematical Methods in Medicine

Received 25 July 2023; Accepted 25 July 2023; Published 26 July 2023

Copyright © 2023 Computational and Mathematical Methods in Medicine. This is an open access article distributed under the Creative Commons Attribution License, which permits unrestricted use, distribution, and reproduction in any medium, provided the original work is properly cited.

This article has been retracted by Hindawi following an investigation undertaken by the publisher [1]. This investigation has uncovered evidence of one or more of the following indicators of systematic manipulation of the publication process:

- (1) Discrepancies in scope
- (2) Discrepancies in the description of the research reported
- (3) Discrepancies between the availability of data and the research described
- (4) Inappropriate citations
- (5) Incoherent, meaningless and/or irrelevant content included in the article
- (6) Peer-review manipulation

The presence of these indicators undermines our confidence in the integrity of the article's content and we cannot, therefore, vouch for its reliability. Please note that this notice is intended solely to alert readers that the content of this article is unreliable. We have not investigated whether authors were aware of or involved in the systematic manipulation of the publication process.

Wiley and Hindawi regrets that the usual quality checks did not identify these issues before publication and have since put additional measures in place to safeguard research integrity.

We wish to credit our own Research Integrity and Research Publishing teams and anonymous and named external researchers and research integrity experts for contributing to this investigation.

The corresponding author, as the representative of all authors, has been given the opportunity to register their agreement or disagreement to this retraction. We have kept a record of any response received.

### References

- [1] F. Xu and Y. Xia, "Music Art Teaching Quality Evaluation System Based on Convolutional Neural Network," *Computational and Mathematical Methods in Medicine*, vol. 2022, Article ID 8479940, 9 pages, 2022.

## Research Article

# Music Art Teaching Quality Evaluation System Based on Convolutional Neural Network

Fumei Xu<sup>1</sup> and Yu Xia<sup>2</sup> 

<sup>1</sup>*School of Music, Jiangxi Normal University, Nanchang Jiangxi 330027, China*

<sup>2</sup>*School of Aviation Services and Music, Nanchang Hangkong University, Nanchang Jiangxi 330063, China*

Correspondence should be addressed to Yu Xia; 47056@nchu.edu.cn

Received 15 April 2022; Revised 14 May 2022; Accepted 18 May 2022; Published 2 June 2022

Academic Editor: Naeem Jan

Copyright © 2022 Fumei Xu and Yu Xia. This is an open access article distributed under the Creative Commons Attribution License, which permits unrestricted use, distribution, and reproduction in any medium, provided the original work is properly cited.

With the rapid growth of music and art education in colleges and universities today, the development of associated teaching quality assessment (TQE) is still in its infancy. In truth, most modern music and art education has yet to build a rigorous and appropriate evaluation system based on actual classroom teaching quality. Simply adopting classroom TQE indicators and approaches from other disciplines would unavoidably lead to formalization of music TQE findings in some schools and institutions. It has no bearing on evaluation, feedback, or advancement. Therefore, this paper uses the superior performance of neural network to solve nonlinear problems and constructs a music art TQE method based on convolutional neural network (CNN). The completed work is as follows: (1) The basic situation of domestic and foreign research on music art TQE is introduced. Several commonly used TQE methods at home and abroad are analyzed, and the CNN evaluation method is comprehensively introduced. (2) The principle and network structure of CNN are expounded, and a TQE system conforming to music art is constructed. (3) The final experimental results reveal that the CNN model has higher accuracy and better performance than the BP neural network when using the trained CNN, TQE model to conduct tests.

## 1. Introduction

My country's general higher music education started early, but in the 1960s and 1970s, due to the influence of many factors such as history, the development was relatively slow. The formulation and promulgation provided stronger theoretical support for the development of music education and pointed out the direction for the revitalization and development of music education [1, 2]. It emphasizes the status and role of art education in school education. According to the strategy, schools should emphasize art instruction as a key component of a broader effort to promote aesthetic sensibility among students. A powerful means of intellectual and physical health development, art education, as an important part of school education, has an irreplaceable role in other disciplines [3]. China's college music education is booming today, but some aspects of its construction are still immature. For example, music classroom teaching objectives, teaching content selection, teaching methods, and teaching

effect evaluation have different degrees of defects in classroom teaching performance and research. How to optimize the evaluation theory and practice of music classroom teaching is the top priority of current college music education. In fact, most of the current music teaching has not really established a scientific and reasonable evaluation system based on the actual teaching quality in the classroom [4]: for example, what kind of teaching configuration is required for music teaching in colleges and universities and what kind of TQE system is required, rather than just blindly copying the TQE indicators and models of other disciplines or any subject in the school, which will inevitably lead to some college music teaching. The results of evaluation are only a form and do not play a real role in evaluation, feedback, and promotion. Therefore, the research on the TQE system of music classroom teaching still needs to carry out research methods that are in-depth and systematic, combining theory and practice, so as to recognize the key elements of college music TQE in essence [5]. Music education is a music education

subject for ordinary college students who are not majoring in music, including classroom teaching, music art practice, campus music and cultural activities, and other educational forms. Because of its strong systematic teaching content, wide knowledge coverage, strong knowledge compatibility with related art and cultural fields, regular learning cycle, gradual knowledge difficulty, and ability to be carried out for many college students at different levels, music classroom teaching has become an important part of music classroom teaching. This is the most common method of music teaching in schools for ordinary college students [6]. The method of summative evaluation that formerly concentrated on results and overlooked the process has evolved to some extent in the evaluation of music classroom teaching. However, in view of the current situation of higher education, students can enter colleges basically through exam-oriented education. Such students have long been accustomed to the performance-based educational evaluation model. One of its consequences is that it is difficult to apply formative evaluation methods to classroom teaching evaluation. The TQE of music classroom should not only conform to the laws and characteristics of music art education and teaching but also combine the inherent characteristics of popular education and teaching. It should not only reflect the essential factors of classroom teaching work but also take into account the purpose and characteristics of popularization of teaching [7]. The activity of music education and instruction should be guided and promoted by evaluation indicators, and this may be considered a balance. Continuous development in the quality of education and instruction can only occur in this manner. TQE for music and art based on CNN is proposed in this study, following this backdrop, and uses the advantages of neural networks to solve nonlinear problems to find a more suitable teacher's TQE method and model for music and art education. The methodology eliminates the impact of human variables on the assessment outcomes, and the rational teaching evaluation offers a useful reference for the investigation of other areas of teaching evaluation.

The paper's section-by-section study paragraph is as follows: The related work is presented in Section 2. Section 3 analyzes the methods of the proposed work. Section 4 discusses the experiments and results. Finally, in Section 5, the research work is concluded.

## 2. Related Work

In the teaching thinking and exploration of music teaching method courses in colleges and universities, Reference [8] takes microteaching method and example teaching method as the breakthrough point and proposes how to train the basic skills of college students. On the one hand, it proposes to strengthen the basic knowledge of music. To study, we must also strengthen the training of basic teaching skills of college students. Only in this way can we solve the current situation of low teaching ability of graduates. In addition, the weak basic knowledge of music education theory and the lack of basic skills of music teaching are also the main problems that should be solved in music teaching in colleges and universities. Reference [9] focuses on research on theo-

retical music teaching. Calling on music education in normal schools not only introduces music pedagogy but also pointed out that there is a lack of teaching books for teachers and professional music teaching materials. Music teaching methods are generally the teaching experience of teachers themselves, lacking the theoretical guidance and scientific nature of pedagogy. It is suggested to incorporate teaching methods into the music pedagogy system in colleges and universities. Reference [10] explores how to optimize the classroom structure and how to improve the teaching effect of music class from the macro- and microlevels and analyzes its structure. Reference [11] advocates an eclectic and comprehensive teaching method in terms of teaching methods. It is thought that instructional materials should be methodical and scientific, adaptable and practical, ideological and national, and practical and fundamental. Since 2000, some key domestic universities and teachers have started to construct TQE systems, and the long-term application of the results has promoted other universities [12]. A normal university started to develop a TQE system in 2002. A public database platform was established. The establishment of the online evaluation system promoted teachers' and students' information feedback system and multiple management information aggregation systems based on public data platforms [13]. Our country has obtained the campus network TQE system of the majority. With the informatization of education, according to the latest information of the National Education Informatization Construction Work Conference, the introduction of new IT technology will apply positive and effective evaluation technology to modern education through the system and create favorable conditions for the leap-forward development of the information of the evaluation system of college teachers [14].

The current TQE system adopts different evaluation methods and index systems according to the specific implementation of different teacher evaluation systems. By strengthening the school's information technology, it realizes the management of the teaching and research environment with a high degree of resource sharing. Through reasonable allocation, the digitization and information networking of teaching management and scientific research service evaluation on campus can be realized, the safety, reliability and scientificity of the system can be ensured, and the reasonable planning of services and feedback information mechanism can be used to realize resource complementarity and further improve the school management process and quality on the management system, assuring efficiency and effectiveness [15]. Examine renowned universities from throughout the world, such as those in California. Every year, three exceptional teacher awards are given out by Berkeley's world-class research institution to teachers who have made noteworthy achievements based on teaching assessment reports. The Berkeley teacher assessment system [16] consists of teachers' self-evaluation, mutual evaluation, and student evaluation. Foreign countries completely broke the traditional learning management system before the 1990s, and the evaluation system has used computers to improve the management level and strive to improve the best TQE system possible, which will surpass the business

process to improve teaching and work efficiency [17]. As personal computers and local area networks became more common in the early 1990s, the TQE system began to use computers to change from mechanized business processes to scientific business processes, utilize the potential of modern information technology, and fully, more rationally, and effectively evaluate, which makes the school's teaching management more simplified. Subsequently, information technology has better penetrated into education and teacher evaluation, the rapid popularization of the Internet, and the wide application of the Internet, TQE has become the field of the Internet era [18, 19]. In the past two decades, in addition to the information resources provided by the Internet in classroom teaching, students and teachers have established a systematic interconnection system. Various services are implemented by students in computer networks. At the same time, using the Internet to surf the Internet also enhances the interaction between teachers and schools. Students, schools, and teachers establish strategic partnerships that provide new technological support in the information age, enhancing communication and interaction between them [20–22]. In today's Internet era, TQE also adopts a method that combines artificial intelligence technology to continuously develop and improve a better school evaluation mechanism. Neural network technology can upgrade the existing system structure to an advanced scientific evaluation system.

### 3. Method

In this chapter, we define the convolutional neural network structure, building a CNN prediction model and constructing a quality assessment system for music and art teaching in detail.

**3.1. Convolutional Neural Network Structure.** The layers of a basic CNN are often organized in a certain sequence. The data is transmitted from one layer to the next using a differentiable activation function at each node in the network. These layers include convolutional and activation layers as well as pooling and fully connected. It is possible to build a whole network by stacking these layers. Among them, the convolutional layer can affect the characteristics of the network, and the pooling layer affects the robustness of the network. The convolutional layer and the pooling layer together form a feature extraction layer for feature extraction.

**3.1.1. Convolutional Layers.** To build a CNN, you need a convolutional layer at the very bottom. Local connections and weight sharing enable it to be much larger than a standard neural network since it is responsible for the majority of the network's processing. The number of weights and the number of trainable parameters are reduced, the problem of overfitting caused by too many parameters is avoided, the local perception area is effectively used, and the memory required for operation is reduced. Different input characteristics are retrieved by the convolution process, which is mostly executed in the convolution layer. The convolution operation is that the convolution kernel travels upstream of the input data with a certain step size, the weight of the convolution kernel is multiplied by the corresponding ele-

ment of the traveled position, and the obtained results are added to obtain a new value as the output until the travel. Stop when all regions of the convolutional layer are finished. Its calculation formula is as follows:

$$y_i = f\left(\sum_{i=1}^n w_i x_i + p\right), \quad (1)$$

where  $y_i$  represents the result after convolution calculation,  $w_i$  represents the weight of the convolution kernel,  $x_i$  represents the locally convolved area, and  $p$  represents the bias. The convolution kernel multiplies the input data, adds the multiplied results, and utilizes the added result as the output during a convolution process. The end result of the convolution kernel traversing the full input data will output a feature matrix to the following layer.

**3.1.2. Activation Layer.** In the CNN structure, the activation function in the activation layer connects the convolutional, pooling, and fully connected layers in order. The activation function in the activation layer cannot be used to activate a neuron; rather, the function is used to maintain and transfer the active neuron characteristics to another space, with the goal of improving the features' linear separability. At present, the commonly used activation functions mainly include the following three functional forms: Sigmoid function, tanh function, and ReLU function. The specific formulas are as follows:

$$f(x) = \frac{1}{1 + e^{-x}}, \quad (2)$$

$$f(x) = \tanh(x) = \frac{e^x - e^{-x}}{e^x + e^{-x}} = 2\mu(2x) - 1, \quad (3)$$

$$f(x) = \max(0, x) = \begin{cases} 0, & x < 0, \\ x, & x \geq 0. \end{cases} \quad (4)$$

Therefore, it is hoped that the activation function must have nonlinear characteristics and be continuously differentiable to meet the requirements of gradient descent, while satisfying the condition that the gradient is not saturated in the range. Since the calculation speed of the sigmoid function is slow and the derivative value is small, the maximum value is only 1/4. When the input value is high or small, the derivative approaches zero, resulting in network back-propagation. The quick decay of the gradient reduces or even eliminates the gradient communicated to the previous layer, making network training extremely challenging. Gradient dispersion is another name for this phenomena. Similarly, the tanh function also has the problem of gradient saturation. Therefore, these two activation functions are less used at present. For the ReLU function, when  $x > 0$ , the gradient is always 1, which avoids the problem of gradient dispersion and at the same time converges faster; when  $x < 0$ , the output is 0 and the training result is 0. The more neurons, the sparseness of the network becomes larger, the stronger the extracted features, the stronger the robustness of the network, and the faster the operation rate.

Because of the above advantages, the ReLU function has now become the first choice for the CNN structure.

**3.1.3. Pooling Layer.** It is common practice to include a pooling layer between convolutional layers in order to minimize both the number of parameters and data size, hence enhancing resilience of features and successfully avoiding overfitting. In the pooling layer, the main operation is the pooling operation or the downsampling operation, so the pooling layer is also called the downsampling layer. The most commonly used downsampling methods mainly include max pooling and mean pooling, and the specific formulas are as follows:

$$P_m = \max_{d+1 \leq n \leq md} \{x_n\}, \quad (5)$$

$$P_a = \frac{1}{w} \sum_n^{md} x_n, \quad (6)$$

where  $P_m$  is the value after max pooling,  $P_a$  is the value after mean pooling,  $d$  is the width of the pooling filter, and  $x_n$  is the  $n$ th element in the pooling area.

During the pooling procedure, the filter is used to traverse the whole data set with a predetermined step size. When using a filter, it is best to utilize maximum and mean pooling, respectively, so that the pooled value of the area is equal to the sum of the area's values. As a result, the region's average is used as the pooled value. As of now, the vast majority of pooling in applications is maximum pooling, which provides location-independent characteristics.

**3.1.4. Fully Connected Layer.** Each node in the fully connected layer is linked to all nodes in the previous layer, and the front-end features are combined to connect all of the features. The specific formula is as follows:

$$f = p_j + \sum_{m=1}^j w_m z_m, \quad (7)$$

where  $p_j$  represents the bias matrix and  $w_m$  is the weight matrix, which describes the contribution of  $z_m$  to the output. The fully connected layer expands the output results obtained after pooling in turn into a one-dimensional feature vector and fully connects the feature vector with the output layer and finally outputs the result.

**3.2. Building a CNN Prediction Model.** Convolutional, pooling, and fully linked layers make up the bulk of the CNN. The number of convolutional layers, as well as the size, number, and stride of the convolution kernels in each convolutional layer, makes up the majority of the CNN structure. Other aspects, such as how many pooling layers there are and how they are sized, the activation function, the fully connected layer classifier, and other parameters are decided. In this section, for the planetary gear fault, the selected parameters are used to build the network structure, and the network model is trained at the same time, and finally,

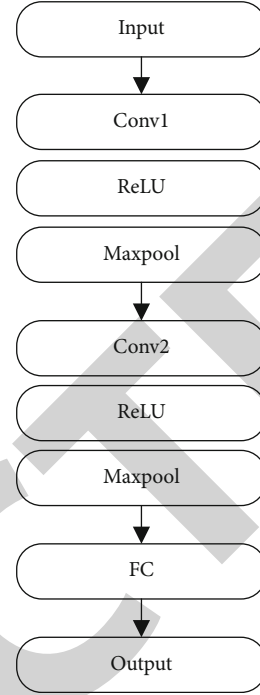


FIGURE 1: Network structure diagram.

the construction of the CNN network prediction model is completed.

**3.2.1. Determination of Input Sample Data Format.** In the field of TQE research, different from the two-dimensional input or time series data input generally used in CNNs, the data for TQE is a one-dimensional  $N \times 1$  data form. As a result, there are two types of input data: one-dimensional input, which involves directly entering the collected raw data, and two-dimensional input, which involves folding the one-dimensional data to maintain the overall quantity of data. In this case, the one-dimensional data is converted into a two-dimensional matrix input in the form of picture data, and the one-dimensional input form is selected in this paper.

**3.2.2. Build the Network Structure.** First, build the model network structure. This section intends to build a 3-layer deep network structure with 2 convolution layers, 2 pooling layers, and a fully connected layer. The schematic diagram of the network structure is shown in Figure 1. The input data first goes through the convolution operation of the first convolution layer CONV1 to extract features and then goes through the ReLU activation function layer to convert the features into a set of feature maps and then goes through the pooling layer for maximum pooling, and downsampling the features, after the second repetition, connect the second pooling result with the fully connected layer, and finally output the result. Because the input data is one-dimensional, the size of the convolution kernel and the structure of the convolutional neural network (CNN) are simplified, and the network's computational cost is reduced. If you do not want to complicate your model's structure and make it tough to train, you should keep the kernel size constant in the convolutional layer. Original input

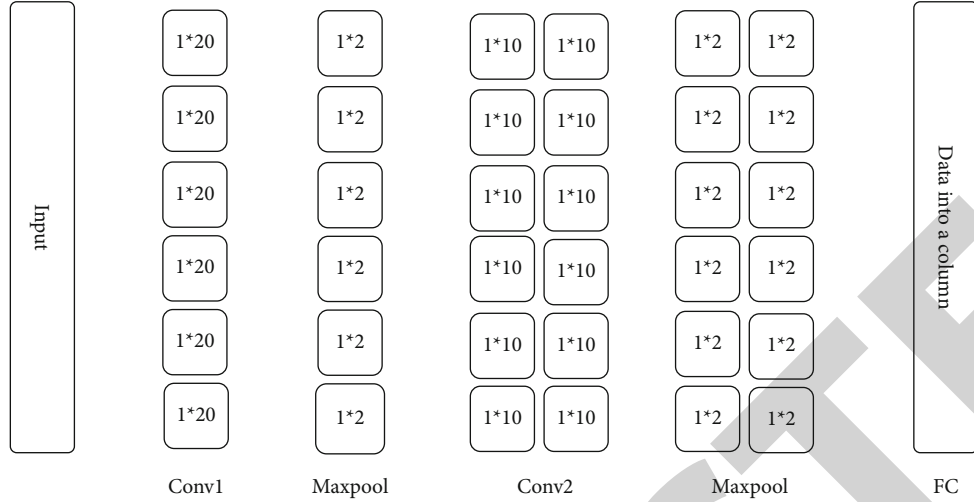


FIGURE 2: Network structure parameter diagram.

data is derived from the TQE data. There are two convolutional layers: the first has 6 convolution kernels with a stride of 4, and the second has 12 convolution kernels with a stride of 10, and the convolution kernel size is 1. Each layer's pooling area is set to the same size, and the step size is 2, for the pooling layer, as shown in Figure 2. The process of selecting parameters is in the experimental part.

After determining the size and step size of the convolution kernel and the pooling area, the size of the output data after the convolution layer and the pooling layer can be obtained based on the calculation formula according to the input data. In the convolutional layer, assuming that the size of the input data volume is  $W_1 \times H_1 \times D_1$ , the number of convolution kernels  $K$ , the size of the convolution kernel  $S$ , the step length  $L$ , and whether it has zero padding  $P$ , etc. parameters, the following formula calculates the output data  $W_2 \times H_2$  after the convolution layer; the specific formula is as follows:

$$W_2 = \frac{W_1 - S + 2P}{L} + 1, \quad (8)$$

$$H_2 = \frac{H_1 - S + 2P}{L} + 1, \quad (9)$$

$$D_2 = K. \quad (10)$$

In the same way, assuming that the size of the input data volume is  $W_1 \times H_1 \times D_1$  in the pooling layer, the maximum pooling downsampling operation of the pooling layer can be determined according to the size of the pooling area  $S$  and the step size  $L$ . The output data  $W_2 \times H_2 \times D_2$  were obtained later; the specific formula is as follows:

$$W_2 = \frac{W_1 - S}{L}, \quad (11)$$

$$H_2 = \frac{H_1 - S}{L}, \quad (12)$$

$$D_2 = D_1. \quad (13)$$

When the dimension of the input data is known to be one-dimensional and the size is known and according to the parameters set by each layer in the CNN structure, the final output data formed can be obtained by calculation.

**3.2.3. Model Training Process.** The CNN model's training method is divided into two parts: forward propagation and back propagation. Forward propagation is used to build the CNN structure, while back propagation is used to finish the CNN model's training. The chain rule is mostly used in backpropagation, also known as error backpropagation, to compute the derivative value of the objective function in relation to the ownership value layer by layer from the back to the front, and compare the output result with the target value already given in the training set to obtain the error value. A threshold is specified in the neural network model. When the error value exceeds this threshold, the weights of each layer will be modified until the weights converge, and the training of the model ends. Therefore, this paper will solve the problem layer by layer from the back to the front from the CNN structure.

**(1) Reverse Derivation of the Fully Connected Layer.** In the fully connected layer, first calculate the derivative of the objective function  $E$  based on the last logits value of the network  $t^{l+1}$ . The following formulas are shown:

$$\frac{\partial E}{\partial t^{l+1}} = \sum_{k=1}^m V_k R_k - V_k, \quad (14)$$

$$t^{l+1} = wx^l + p, \quad (15)$$

where  $V$  represents the one-hot vector,  $l$  represents the feature vector layer,  $l+1$  represents the output layer,  $x^l$  represents the output of the  $l$ th layer,  $w$  is the weight, and  $p$  is the bias.

TABLE 1: Music and art teaching quality evaluation system.

First-level indicator	Secondary indicators	Label
Teaching preparation	Scientific and reasonable teaching design	X1
	Reasonable progress	X2
	Teaching plan writing specification	X3
Basic literacy	Rigorous teaching attitude and clear thinking	X4
	Vivid and accurate language	X5
	Good manners and appearance	X6
Teaching content	Combining theory with practice	X7
	Rich in content and appropriate information	X8
	Reflect the frontiers of the discipline	X9
Teaching method	Flexible method, suitable for course characteristics	X10
	Teaching students according to their aptitude	X11
	Use advanced teaching methods	X12
Teaching effect	Student attendance rate	X13
	Active classroom atmosphere	X14
	Complete teaching tasks with quality and quantity	X15

During backpropagation, the error varies as the bias  $p$  of the neuron changes, so the error can be thought of as the sensitivity of  $p$ , the derivative of the error with respect to the basis. The derivative of the objective function  $E$  with respect to the fully connected layer weight  $w$  and the bias  $p$  can be expressed as

$$\frac{\partial E}{\partial w^l} = \frac{\partial E}{\partial t^{l+1}} \cdot \frac{\partial t^{l+1}}{\partial w^l} = \frac{\partial E}{\partial t^{l+1}} \cdot e^l, \quad (16)$$

$$\frac{\partial E}{\partial p^l} = \frac{\partial E}{\partial t^{l+1}} \cdot \frac{\partial t^{l+1}}{\partial p^l} = \frac{\partial E}{\partial t^{l+1}} \cdot e^l. \quad (17)$$

The activation function used in this paper is the ReLU function, so the derivative of the objective function  $E$  and ReLU is calculated as

$$\frac{\partial E}{\partial e^l} = \sum \frac{\partial E}{\partial t^{l+1}} \cdot \frac{\partial t^{l+1}}{\partial e^l} = \sum \frac{\partial E}{\partial t^{l+1}} \cdot w^l, \quad (18)$$

$$\frac{\partial E}{\partial t^l} = \frac{\partial E}{\partial e^l} \cdot \frac{\partial e^l}{\partial t^l} = \begin{cases} 0, & e^l \leq 0, \\ \frac{\partial E}{\partial e^l}, & e^l > 0. \end{cases} \quad (19)$$

The final objective function  $E$  is based on the derivative of the weight  $w$  in the fully connected hidden layer and the bias  $p$ , which can be obtained by substituting the result obtained from formula (19) into formulas (16) and (17).

(2) *Reverse Derivation of the Pooling Layer.* Since it is back propagation, after the derivative of the weight and bias of the objective function  $E$  is obtained in the fully connected layer, the derivative of the objective function with respect to each parameter in the pooling layer is then calculated. Unlike the fully connected layer, there are no weights in the pooling layer, so only the derivative of the neuron is cal-

culated. The pooling layer uses maximum pooling, and only the maximum value in the region is retained during forward propagation. Therefore, during back propagation, the derivative is only passed to the neuron with the maximum value  $N_{\max}$ , and the rest of the neurons are discarded due to the fact that the derivatives are all 0, and the specific formula is

$$\frac{\partial E}{\partial e^l} = \frac{\partial E}{\partial V^l} \cdot \frac{\partial V^l}{\partial e^l} = \begin{cases} 0, & N \neq N_{\max}, \\ \frac{\partial E}{\partial V^l}, & N = N_{\max}. \end{cases} \quad (20)$$

(3) *Reverse Derivation of the Convolutional Layer.* For the convolutional layer, the error is passed from the pooling layer, which is actually the reverse process of the downsampling operation. First, the derivative of the objective function with respect to each logits value is calculated. The specific formula as follows:

$$\frac{\partial E}{\partial y^l} = \frac{\partial E}{\partial e^l} \cdot \frac{\partial e^l}{\partial y^l} = \begin{cases} 0, & y^l \leq 0, \\ \frac{\partial E}{\partial e^l}, & y^l > 0. \end{cases} \quad (21)$$

(4) *Parameter Update.* During back-propagation, after the parameters in the fully connected layer, activation function layer, pooling layer, and convolutional layer are, respectively, derived, each parameter needs to be updated, and finally, the update of the network model is completed. For the fully connected layer, the update formula of its weight  $w$  and bias  $p$  can be expressed as

$$w = w - \lambda \frac{\partial E}{\partial w}, \quad (22)$$

$$p = p - \lambda \frac{\partial E}{\partial p}. \quad (23)$$



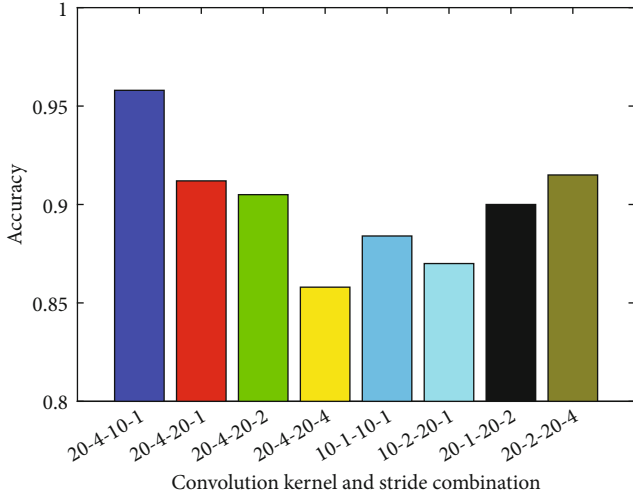


FIGURE 3: Convolution kernel number and step length experiment.

After the parameters are updated, the samples will be input into the updated CNN model again, and the cycle will repeat until the model reaches the iterative condition or when it converges, and the training is terminated to complete the training of the CNN model. The final model is the trained CNN model.

**3.3. Constructing a Quality Assessment System for Music and Art Teaching.** There are two main methods of classroom TQE that are often used in colleges and universities. One is for the purpose of reward and punishment. In this kind of evaluation, the purpose is to promote teaching reform. The results of the evaluation directly determine the dismissal, demotion, promotion, dismissal, salary, bonus, and other personnel decisions of teachers; the disadvantage of this kind of evaluation is that it is a top-down evaluation that will only cause reactions and attention to a few people. The second goal is to help instructors improve their skills via assessment and professional development. Teachers’ professional growth is the focus of this kind of review, which is also known as a developmental evaluation. There are no restrictions attached to rewards or penalties. The primary objective is to help college and university music instructors improve their skills and accomplish their ultimate goal of educating students in music. Under the developmental evaluation system, teachers can eliminate their concerns, because the results have little to do with rewards and punishments, they can evaluate more frankly, and teachers can accept the evaluation results more calmly. Teachers’ morality and style, students’ assessment and reflection of teachers’ teaching, school teaching reform and teaching management information management, and strategies to enhance teachers’ teaching quality are all included in the development evaluation of classroom teaching. The ultimate objective is to develop a scientific and fair framework for measuring teaching quality. In western countries, such as the US and the UK, more and more attention is paid to the use of development-oriented evaluation systems and methods. This is because develop-

TABLE 2: Parameter selection during training.

Network depth	Mini-batch	Learning rate	Epochs	Training set	Test set
3	100	0.005	50	80%	20%

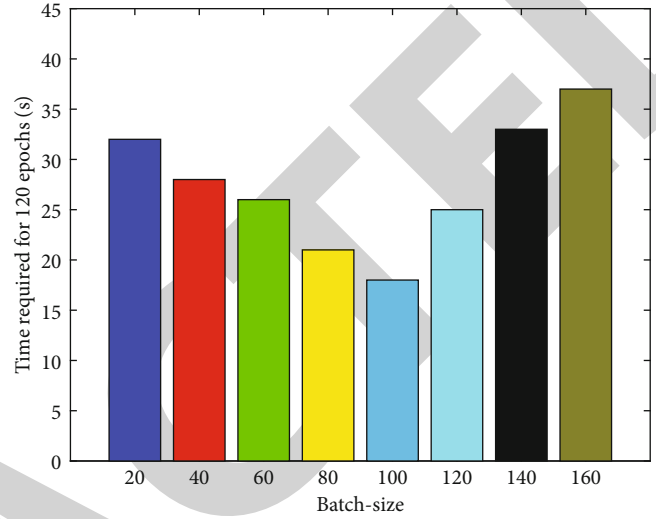


FIGURE 4: Minibatch parameters and their comparison.

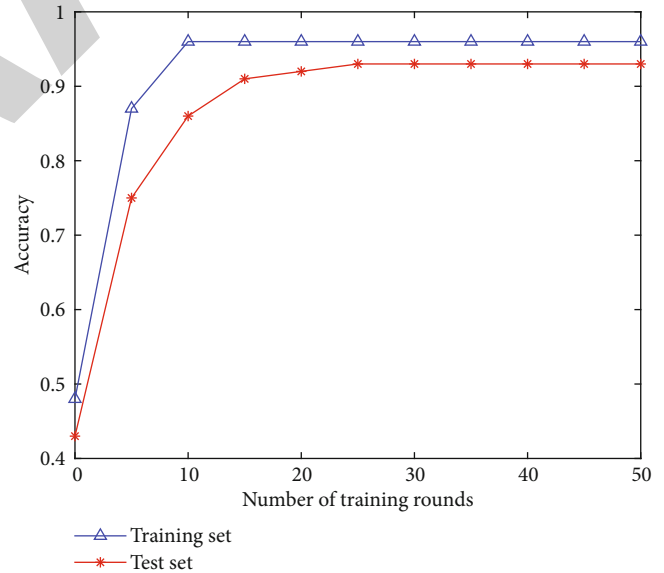


FIGURE 5: Accuracy on training and test sets.

mental evaluation can improve the motivation of teachers’ professional development, and evaluation can eliminate external rewards and punishments. Under such a mechanism, the progress of teachers’ work will bring teachers a certain sense of achievement, self-awareness, and self-evaluation, so that teachers will put the improvement of the TQE in the first place, rather than simply pursuing external rewards and punishments. This research combs the domestic and foreign related researches on TQE and music art

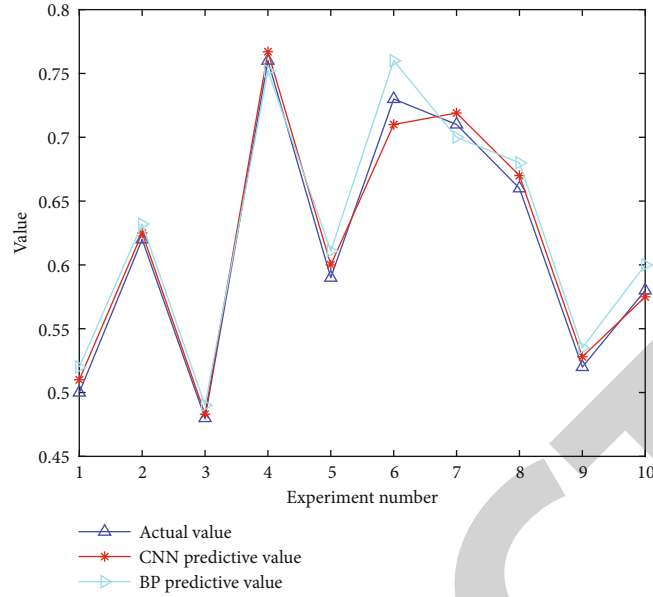


FIGURE 6: Comparison of predicted results of different models with actual results.

classroom TQE in colleges and universities by consulting relevant books, academic journals, network materials, etc. Based on the analysis of the current situation of TQE in the activity, a set of suitable teaching index evaluation system was designed, as shown in Table 1.

#### 4. Experiment and Analysis

**4.1. Data Source and Parameter Selection.** In order to meet the TQE model designed, this paper designs a teaching evaluation data set according to the evaluation index system in Chapter 3, which contains 1000 sets of data, of which 800 sets are used as training sets and 200 sets are used as test sets. At present, the parameter determination of CNN still lacks a clear guiding theory and still relies on manual experience. The parameters must be constantly adjusted and compared in order to get the best value for each one. There are two convolutional layers, two pooling layers, and one fully connected layer in this chapter's model, as shown in the figure. At present, the parameter adjustment of neural network still relies on experience and constant comparison and adjustment for setting. The following is the comparison and selection process of some main parameters of the model.

#### 5. Selection of Convolution Kernel and Step Size

In order to obtain the optimal number of convolution kernels and step size, this paper selects 8 combinations of convolution kernel and step size for experiments. The final result is shown in Figure 3. The results show that this paper chooses 20-4-10-1 parameter combination which is more advantageous.

#### 6. Minibatch Parameter

The application of minibatch technology can improve the convergence speed of the model. The batch-size option specifies the number of samples utilized in a single training. When the batch size is too high, it is essentially the same as not employing minibatch technology; if a value is too little, the model will struggle to converge, resulting in poor fitting accuracy. This section selects 8 cases of 20, 40, 60, 80, 100, 120, 140, and 160, and sets a fixed number of 120 epochs to compare the convergence process. The experimental results are shown in Figure 4.

#### 7. Model Parameter Verification Results

This paper uses Matlab to train the neural network, and the data training set and test set are divided according to 4:1. During the training process, each parameter selection is shown in Table 2. The number of training rounds is 50. During the training process, the accuracy of the training set and test set is shown in Figure 5:

**7.1. Comparative Analysis of Results.** This example takes the quality assessment of music and art teaching as an example and uses CNN model and back propagation (BP) neural network for prediction. The 15 evaluation indicators listed in Chapter 3 are the expected input. At the same time, the input data are normalised in order to make CNN training easier. The predicted values of 10 groups were selected to calculate the mean and plotted to observe. The results are shown in Figure 6.

The results show that the prediction accuracy of CNN is higher than that of BP network, and it is very close to the actual value. It can be shown that the network model proposed in this paper for the music and art TQE has very good performance.

## Research Article

# A Comparative Study of Text Genres in English-Chinese Translation Effects Based on Deep Learning LSTM

Xiaoda Zhao  and Xiaoyan Jin

Northeast Normal University, Changchun, 130024 Jilin, China

Correspondence should be addressed to Xiaoda Zhao; zhaoxd903@nenu.edu.cn

Received 8 April 2022; Revised 27 April 2022; Accepted 30 April 2022; Published 2 June 2022

Academic Editor: Naeem Jan

Copyright © 2022 Xiaoda Zhao and Xiaoyan Jin. This is an open access article distributed under the Creative Commons Attribution License, which permits unrestricted use, distribution, and reproduction in any medium, provided the original work is properly cited.

In recent years, neural network-based English-Chinese translation models have gradually supplanted traditional translation methods. The neural translation model primarily models the entire translation process using the “encoder-attention-decoder” structure. Simultaneously, grammar knowledge is essential for translation, as it aids in the grammatical representation of word sequences and reduces grammatical errors. The focus of this article is on two major studies on attention mechanisms and grammatical knowledge, which will be used to carry out the following two studies. Firstly, in view of the existing neural network structure to build translation model caused by long distance dependent on long-distance information lost in the delivery, leading to problems in terms of the translation effect which is not ideal, put forward a kind of embedded attention long short-term memory (LSTM) network translation model. Secondly, in view of the lack of grammatical prior knowledge in translation models, a method is proposed to integrate grammatical information into translation models as prior knowledge. Finally, the proposed model is simulated on the IWSLT2019 dataset. The results show that the proposed model has a better representation of source language context information than the existing translation model based on the standard LSTM model.

## 1. Introduction

It has been more than 60 years since the world’s first machine translation system came out in 1954. At the same time, machine translation has gone through the flourishing situation of flourishing flowers and thriving competition, as well as the depression and silence of all sorts. The development paradigm of the mainstream machine translation technology has evolved from a rule-based approach to a statistical approach and then to today’s neural network approach. Machine translation has also made its way out of the lab and into people’s daily lives, addressing cross-language communication needs such as reading, meeting, travelling, and shopping [1]. Since 2013, the nerve machine translation because of the complicated characteristics of the project does not need to design a model that is concise and effective to get the favor of the researchers and developers, and parallel computing, graphics processors, and the wide application of big data in academia and industry quickly raised a hot wave nerve of machine translation research

and development and advanced machine translation stride forward in the direction of practical application and commercialization.

Machine translation has both theoretical value and practical value and has experienced considerable development since its inception. Machine translation based on the neural network model has the following advantages:

- (1) End-to-end learning does not depend on too many prior assumptions. Phrase-based models, for example, assume that both source and target languages are sliced into sequences of phrases, with some alignment between them [2]. This hypothesis has both advantages and disadvantages. On the one hand, it draws lessons from the relevant concepts of linguistics and helps to integrate the model into human prior knowledge. On the other hand, the more assumptions there are the more constrained the model is. If the assumptions are correct, the model can describe the problem well. But if the assumptions are wrong, the model

can be biased. Deep learning does not rely on prior knowledge, nor does it require the manual design of features. The model learns directly from the mapping of input and output (end-to-end learning), which also avoids possible deviations caused by assumptions to a certain extent

- (2) The continuous space model of neural network has a stronger representation ability. A basic problem in machine translation is how to represent a sentence [3]. The discrete lexical representation is replaced with a distributed representation of the space of real numbers, and the complete sentence can be expressed as a vector of real numbers

One of the important ideas is to integrate linguistic knowledge into a neural network to improve system performance and translation quality. Throughout the history of machine translation, linguistic knowledge has been playing an irreplaceable role. In particular, in the early stage, when the rule-based approach is dominant, from semantic analysis to target language generation, including the design of translation rules, all are guided by the internal connection of languages. The development of morphology, syntax, and semantics has been providing fuel for rule-based machine translation technology [4]. In the golden decade of statistical machine translation, there is use of hierarchical phrases to solve the problem of long-distance-dependent word translation and the use of sentence theory to solve the problem of short intonation order of target language. The language has serialization features; the source language and target language are strings, making the model simple, no longer needing the segmentation of complex, alignment, and sequence, such as processing, but at the same time also makes many important information losses in the process of linguistics [5]. The integration of the neural machine translation model, with it, can ease the predicament of inherent in the nerve machine translation, improve the nerve machine translation model, and further enhance the quality of translation.

The paper's organization paragraph is as follows. The related work is presented in Section 2. Section 3 analyzes the algorithm design of the proposed work. Section 4 discusses the experiments and results. Finally, in Section 5, the research work is concluded.

## 2. Related Works

In this chapter, we define the traditional machine translation and neural machine translation in detail.

*2.1. Traditional Machine Translation.* As early as the 17th century, attempts were made to overcome the human language barrier by using robotic dictionaries, similar to the use of quick lexicography devices like Kuai to solve communication problems between speakers of different languages [6]. In the 1930s, French engineer Archovny and former Soviet inventor Troyansky, respectively, designed and implemented the machine translation model system, which can be regarded as the prototype of machine translation. In 1954, Georgetown University and IBM jointly developed the first

machine translation system in human history. Since then, with the joint efforts of colleges and universities, research institutes, enterprises, and even individuals, new technologies have emerged, new paradigms have emerged, and new systems have come into being. The level of machine translation has become higher and higher, and the quality of translation has become better and better, approaching or even surpassing the level of human beings in some specific fields [7]. In the development of machine translation, different machine translation technologies in different historical periods occupy the mainstream position.

Generally, rule-based machine translation can choose to transform at different levels, as shown in Figure 1. A complete rule-based machine translation process consists of the following steps:

- (1) Source language analysis: from shallow to deep, it can include morphological analysis, syntactic analysis, and semantic analysis, and ideally, it can become an intermediate language [8]. The segmentation and labeling rules for morphological analysis, the phrase structure rules for syntactic analysis, and the logical semantic rules for semantic analysis all need to be designed manually
- (2) Conversion from the source language to the target language: the bilingual dictionary is constructed, and the transformation mapping rules are designed on the basis of which, the transformation process is completed by replacing source language units with target language units and replacing source language structures with target language structures
- (3) Target language generation: according to the characteristics of the target language, the generation rules of the target language are designed

In the translation of low-resource languages and national languages with a short corpus, the rule-based method still provides unrivalled benefits. At present, some mature commercial machine translation systems on the market, especially those in certain limited fields, are based on rules. The advantage of the rule-based approach is that it is intuitive and can directly express linguistic knowledge. The degree of refinement of rules can be changed according to needs, and the rules with strong generalization ability can be used, and the rules with fine description ability can be used. It is easy to deal with complex structures and deep understanding; the system is highly adaptable and does not depend on a specific corpus [9]. However, the disadvantages are also obvious. The construction of rules relies too much on linguists, which is highly subjective and sometimes does not conform to the linguistic facts. The coverage of rules is poor, especially the knowledge of fine granularity is difficult to be summarized comprehensively, and the statements beyond the description of rules cannot be processed. As the number of rules increases, the conflicts between rules become more serious. The rule base is usually limited to a specific system, which is expensive to develop and difficult to maintain.

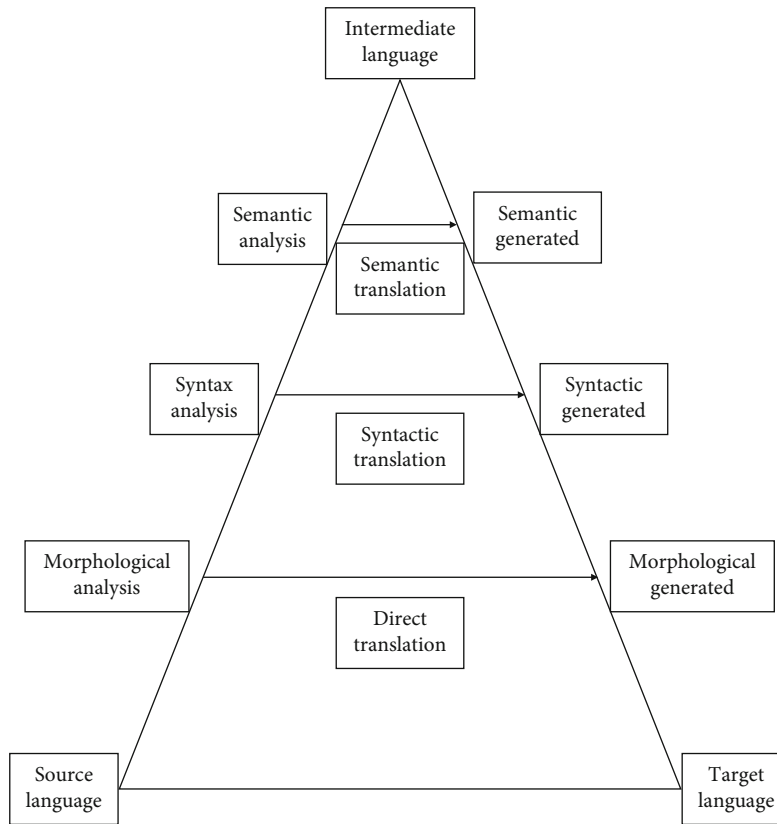


FIGURE 1: Machine translation at different levels of transformation.

Its basic idea is that it does not need to conduct deep linguistic analysis and does not need a large amount of artificial summarized linguistic knowledge, but uses the translated corpus in the past and carries out translation by analogy. It assumes that the same part of the source language corresponds to the same translation result and that, when the previously translated part appears again, the same translation result is most likely the correct result. The main knowledge source of the system is the bilingual-aligned translation instance library [10]. The three core problems of the case-based approach are the correct bilingual automatic alignment, the establishment of an effective instance matching mechanism, and the generation of translation corresponding to the source language sentence based on the retrieved instances. The key technique is similarity calculation. There are no manual rules, there is no deep language analysis, the system development cost is low, and the speed is fast. The knowledge learned from the corpus is objective and covered well. However, the system performance depends heavily on the corpus. With serious data sparsity problem, it is difficult to make use of coarse granularity, general knowledge, and other deficiencies.

Statistical machine translation studies the translation process, the word alignment, the phrase segmentation, short tone sequence, such as syntax tree as an implicit structure, with the help of the machine learning techniques, statistical analysis on massive parallel corpora, on the basis of learning from the characteristics of the translation rule, finally using the model

of the learning to translate. The basic idea of this model is as follows. Firstly, phrase-to-phrase translation rules are extracted from the parallel corpus of bilingual sentence alignment. During translation, the source language sentences are divided into phrase sequences, and the target language phrase sequences are obtained by translation rules. Then, the sequence of target language phrases is sorted by using the reordering model to obtain the best target translation [11]. While the research focus is on syntactic-based statistical translation models, how to improve the disambiguation ability of the models by introducing deeper linguistic analysis, while avoiding errors caused by analysis, has become the main problem faced by statistical translation models. In general, a statistical machine translation system has the following advantages: no need to write rules manually, translation model can be directly trained by corpus; system development cycle is short, labor cost is low, system robustness is good; high interpretability of hidden structure; exponential structural spaces are processed by local features and dynamic programming [12]. However, statistical machine translation systems also have the following shortcomings: discrete representation brings serious data sparsity problems; difficulty dealing with long-distance dependencies.

*2.2. Neural Machine Translation.* Neural network, especially deep learning technology, is the latest research achievement in the field of artificial intelligence. It enables people to use machine processing to process information in a new way

and method. In just three or four years, machine translation has surpassed statistical methods in most language translation, and since then, machine translation has entered a “new era.”

At the end of 2013, Kalchbrenner proposed an encoder-decoder structure that can be used for machine translation, which immediately attracted extensive attention in the academic world; Google neural machine translation uses the long and short memory model and attention mechanism of 8-layer encoder and 8-layer decoder, integrating the important achievements of deep learning research in recent years and advancing machine translation in engineering practice a big step forward [13]. In May 2017, Facebook announced neural machine translation that was nine times faster than Google’s accuracy. In September DeepL, based in Cologne, Germany, said its neuromachine translation product had beaten systems from Google, Microsoft, and Facebook in blind tests. On March 14, 2018, Microsoft announced that its Chinese-English system has achieved human-level performance on the news test set, a universal news corpus, and is “comparable to humans.” Other tech giants are also getting into the act, with Amazon, IBM, NVIDIA, and SYSTRAN all investing in neural machine translation systems. In this area, China is not to be outdone. Baidu, Youdao, Tencent, and Sougou have also joined the arms race, deploying their own neuromachine translation products. On May 20, 2015, Baidu Translation officially launched its neural machine translation system, becoming the first truly practical neural machine translation (NMT) system in the world [14]. On May 24, 2018, the Ali Machine Intelligence natural language processing (NLP) translation team won 5 titles in the workshop on machine translation (WMT), an internationally recognized top machine translation competition.

As early as 2003, Bengio, the father of deep learning, Turing Prize winner, and professor at the University of Montreal in Canada, proposed to improve the language model by using a neural network to represent each word as a continuous and dense vector of real numbers, effectively alleviating the problem of data sparsity. Jacob of BBN, an American company, further proposed a neural network combined model on this basis, which improved the quality of machine translation by about 6%. They adopted an “encoder-decoder” framework, and the translation process is shown in Figure 2. In this new framework, the linear model of statistical machine translation is replaced by the nonlinear model of the neural network, especially the circular neural network which is good at processing historical information, and variable-length string structure is added [15]. As soon as it comes into being, it attracts widespread attention from the academic circle and soon sets off a wave of research.

In addition to poor interpretability, neuromachine translation currently has the following problems. First, it is difficult to deal with rare words and unknown words. Second, there is the phenomenon of “overtranslation” and “omission.” Third, the translation is not faithful. The root cause of these problems is the neural machine translation architecture itself [16]. One of the important ideas is to integrate linguistic knowledge into a neural network to improve system

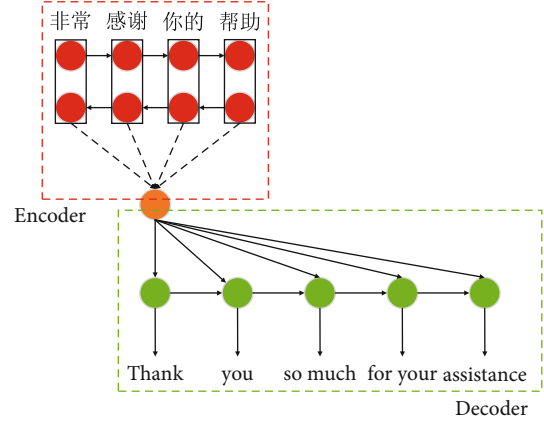


FIGURE 2: Encoder-decoder translation schematic diagram.

performance and translation quality. Throughout the history of machine translation, linguistic knowledge has been playing an irreplaceable role. The source language and target language have been serialized as a string, and this makes the model simple and does not need to go through complex segmentation, alignment, and sequence.

### 3. Algorithm Design

In this section, we studied the LSTM model, attention embedding model based on LSTM, and translation model combined with grammar dependence.

**3.1. LSTM Model.** LSTM solves the long order dependence problem in the recurrent neural network; its specific network structure is shown in Figure 3. In addition to input data  $X$  and hidden state  $H$ , the LSTM network structure also includes memory unit  $C$ , input gate  $I$ , output gate  $O$ , and forgetting gate  $F$  [17]. The core of the LSTM model is to delete or add information in the memory cell state through a threshold structure composed of a sigmoid network layer and point-by-point multiplier.

Assuming that there exists batch data  $X_t$  at time  $t$  with  $n$  sample numbers, vector  $x$ , hidden layer length  $H$ , hidden layer state  $H_t$  at time  $T$ , and hidden layer state  $H_{t-1}$  at the previous time, the forgetting gate at time  $T$  can be expressed as

$$f_t = \sigma(X_t W_{xf} + H_{t-1} W_{hf} + b_f), \quad (1)$$

where  $\sigma$  represents the sigmoid function;  $X_t$  represents the weight parameters that can be learned,  $H_t$  represents the bias vector parameters, and its addition process adopts the broadcast data operation method. Second, determine the information the memory unit needs to hold. The sigmoid network layer is adopted to determine the value of the update, as shown in equation (2). The hyperbolic tangent function  $\tanh$  layer is used to generate candidate values, as shown in equation (3).

$$i_t = \sigma(X_t W_{xi} + H_{t-1} W_{hi} + b_i), \quad (2)$$

$$\bar{C}_t = \tanh(X_t W_{xc} + H_{t-1} W_{hc} + b_c). \quad (3)$$

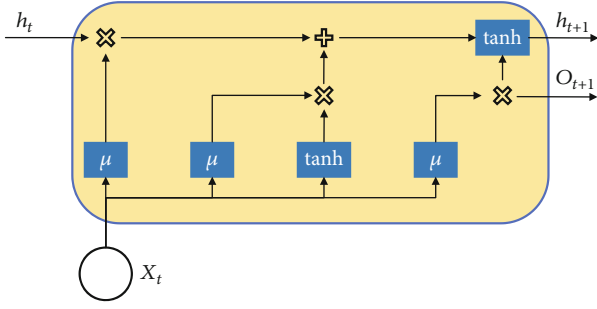


FIGURE 3: Schematic diagram of LSTM network structure.

Then, the memory state is updated. Dot product operation is adopted to update the state, and information flow is controlled by forgetting gate and input gate, so the updated state can be obtained, as shown in

$$C_t = f_t \odot C_{t-1} + i_t \tilde{C}_t. \quad (4)$$

When the input gate is constantly close to 0 and the forgetting gate is always close to 1, the memory unit in the old state is stored to the present moment [18], according to the preceding formula. Therefore, the LSTM network can solve the problem of gradient disappearance in the circulating nerve. Finally, the sigmoid layer is used to determine the state of memory unit output by the output gate, as shown in

$$O_t = \sigma(X_t W_{x_o} + H_{t-1} W_{h_o} + b_o), \quad (5)$$

$$H_t = O_t \odot \tanh(C_t). \quad (6)$$

According to the above formula, when the output gate is approximately 0, the memory unit retains the current information, and when the output gate outputs 1, the information will be transferred from the storage unit to the hidden layer.

**3.2. Attention Embedding Model Based on LSTM.** LSTM network model in the coding stage is fixed dimension, so it adopts the vector of the same dimension to encode the source language sequence of any length. However, in actual English machine translation, the English input sequence is an indefinite sequence, which leads to the problem that the model and the English input sequence cannot completely fit in the machine translation using the standard LSTM model, and thus, the translation effect is not ideal [19]. The LSTM translation model embedded with attentional mechanism is shown in Figure 4, including encoding source language, attentional mechanism assistance, and target language generation process.

The state calculation method of the next hidden layer at the target end of the model is the same as that of the LSTM decoder, as shown in

$$Z_i + 1 = \sigma(c_i, u_i, z_i), \quad (7)$$

where  $u_i$  represents the  $i^{\text{th}}$  word in the sequence of target language;  $c_i$  represents the background vector of the word  $i$  [20]. Assume that the hidden layer state at the moment  $j$

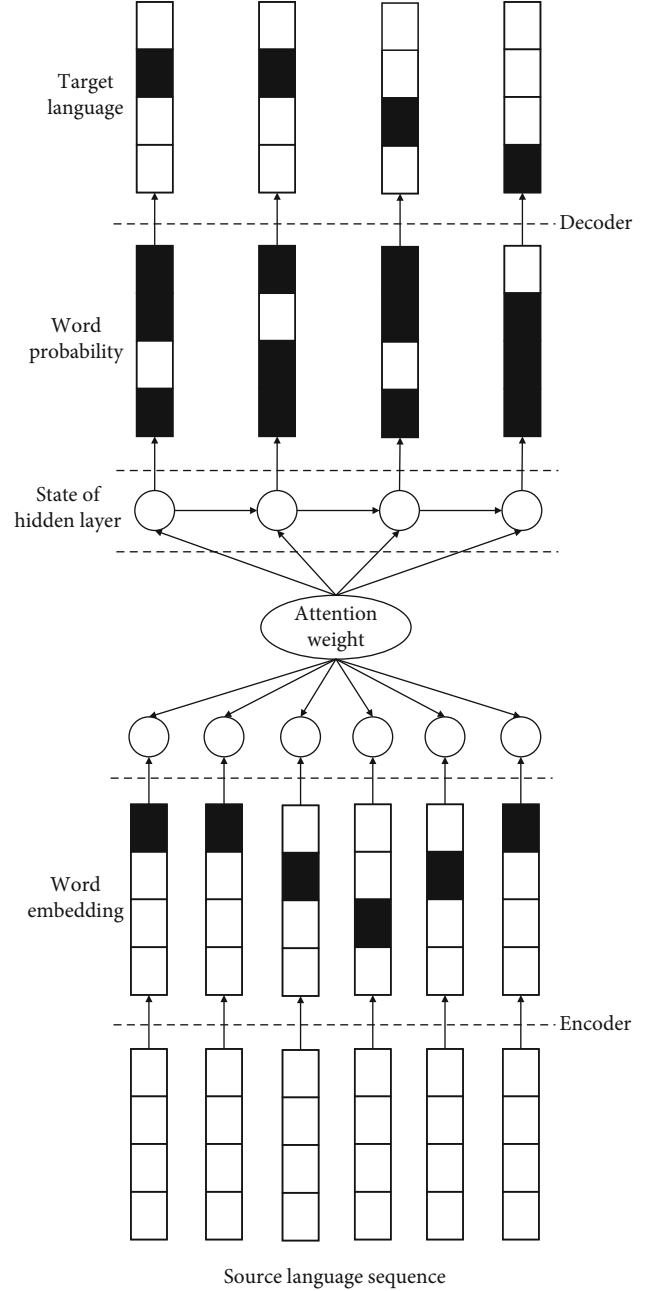


FIGURE 4: LSTM translation model embedded with attention mechanism.

of the encoder is  $H_j$ , and its corresponding background vector can be calculated by

$$C_i = \sum_{j=1}^T a_{ij} h_j, \quad (8)$$

where  $a_{ij}$  represents the weight, which can be calculated by

$$a_{ij} = \frac{\exp(e_{ij})}{\sum_{k=1}^T \exp(e_{ik})}, \quad (9)$$

$$e_{ij} = a(z_i, h_j), \quad (10)$$

where  $a$  is a function used to measure the matching degree between the current hidden state  $z_i$  of the target language sequence and the hidden state  $h_j$  of the source language sequence, which can be calculated by

$$e_{ij} = v^T \tanh(W_{z_i} z_i + W_h h_j), \quad (11)$$

where  $v$ ,  $W_z$ , and  $W_h$  represent the model parameters to be learned.

**3.3. Translation Model Combined with Grammar Dependence.** In neural machine translation, the degree of intimacy between each word in the sentence not only helps build a better earth beneath context, richer to express the meaning of the sentence, but it also allows the attention mechanism of dependencies between the source term to be passed to the decoder, better modelling source translation corresponding relationship between words and target words. This chapter will introduce how to obtain grammar dependence, introduce a distance mechanism based on grammar dependence, and combine grammar dependence with attention to improve the ability of attention to model words and grammar (machine translation generally considered rare between source language and target language, such as between Chinese and English grammar structure difference, is not suitable to handle this difference easily leading to loss of grammatical information, understanding sentences lack precision caused by translation system, failed to express the context of the sentence, a syntax, morphology, word order-disorder, such as error phenomenon) [21]. It makes the translation difficult to understand. It is the most direct and effective way to deal with the difference in grammatical structure to attach grammatical information to neural machine translation as prior knowledge. The common methods include, for example, taking dependent labels as input features of words, linearizing dependency tree to obtain source dependent representation sequence, learning source-side dependency graph representation by potential graph parsing, and using source and target-side dependency tree to improve neural machine translation. These methods are all based on the linear structure neural network to linearize the representation of grammatical information and grammatical structure. However, excessively long linearized sequences will affect the training efficiency, while using shorter sequences will lose the grammatical information, making it difficult to make a good compromise choice.

The article is the relative word between the head word of a noun phrase and its determinate word, according to the Stanford-type dependency manual [22]. The adjective modifier in a noun phrase is any word or phrase used to modify the meaning of a noun phrase, according to the Stanford-type dependency manual. To summarize, modifiers and articles alter and limit nouns, respectively, and it is clear that the former has a bigger impact on the word it operates on than the latter. “Excellent” describes the subject of the sentence “watchmaker,” whereas “this” characterises the subject of the sentence “watchmaker” who “produced many gorgeous

watches” for the following events. Through qualitative analysis, we can draw a preliminary conclusion: the degree of dependent grammatical intimacy between different parent-child or grandparent node pairs is different.

At the same time, though, grammatical distance can also describe how close dependent grammatical relationships are between words. However, at a higher level of granularity, notice that the grammatical distance between the contiguous words is defined as 1. In other words, the degree of dependence is defined as 1 by the two-word pairs that have a direct dependency relationship and then extends to any two-word pairs in the sentence [23]. However, it is difficult to accurately describe the degree of intimacy of dependence between different father-son pairs only by the grammatical distance, because their grammatical distance is 1. This shows two situations: one, we cannot get the contribution degree of different child nodes to the same parent node, as shown in the red and yellow boxes in Figure 5, and another, we cannot describe the syntactic dependence closeness degree of different parent-child pairs, as shown in the red and green boxes in Figure 5. In Figure 5, the basic grammatical distances between all contiguous word pairs are represented by blue numbers.

Although the transformation process of grammatical distance from qualitative to quantitative is easy to realize, quantification of all pairs of dependencies in the same degree will inevitably lead to inconsistency between the intimacy of the dependency relationship and the grammatical distance, and the corresponding noise information will be introduced. The concept of “grammar dependence degree” can accurately describe the degree of dependent grammar intimacy between different parent and child pairs and obtain the numerical dependent grammar relationship between parent and child pairs. In other words, it can obtain the contribution degree of different child nodes to the parent node in constructing a dependent grammar context.

## 4. Experiments

In this part, we study the dataset source and pretreatment, model experiment in detail.

**4.1. Dataset Source and Pretreatment.** In this study, data from the 2019 International Oral English and Translation Evaluation Competition with a relatively small scale were selected as the experimental dataset, including 220,000 Chinese-English parallel sentence pairs, 3 test sets, and 1 development pair. In this study, word segmentation was carried out for the data, and then, CBOW was used to vector the data.

Since the IWSLT2019 dataset contains Chinese and English parallel sentence pairs and the word segmentation methods in Chinese and English are different, the Chinese and English datasets are processed by word segmentation, respectively. For Chinese word segmentation, the word segmentation method based on statistics is adopted. Then, according to the credibility of the word, the threshold value is set to form the word-formation conditions and determine the word segmentation. For English word segmentation, because the basic constituent unit of English is a word, therefore, only according to the blank can be directly split.



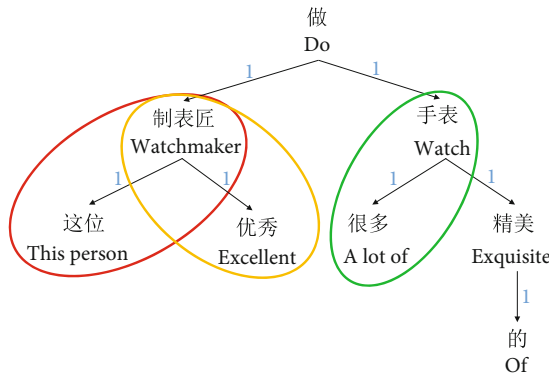


FIGURE 5: The basic grammatical distance between the connected word pairs in the dependency tree.

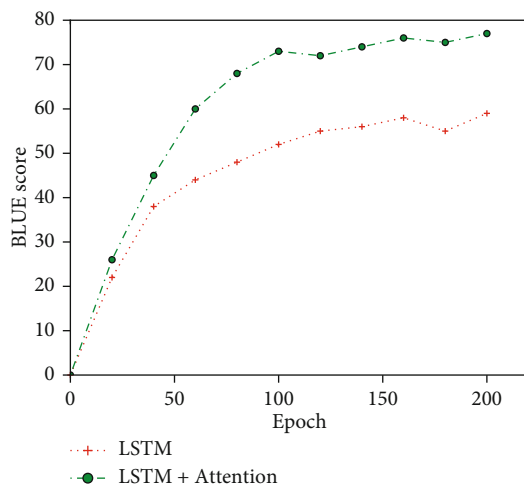


FIGURE 6: Epoch/BLEU variation diagram between LSTM and LSTM+Attention.

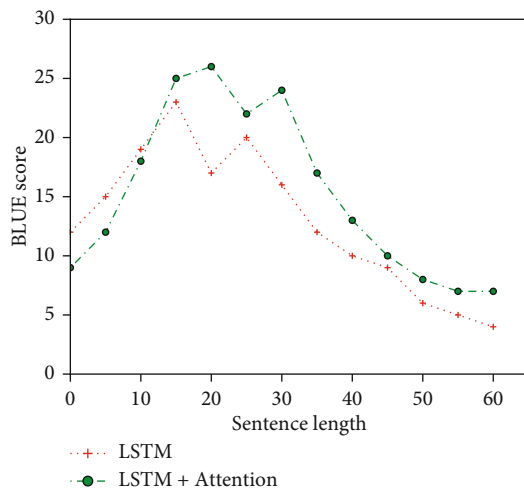


FIGURE 7: Sentence/BLEU variation diagram between LSTM and LSTM+Attention.

English stop words processing mainly include three steps, first in English uppercase to lowercase, and then the statement tail words and symbols on the blank space, finally, therefore,

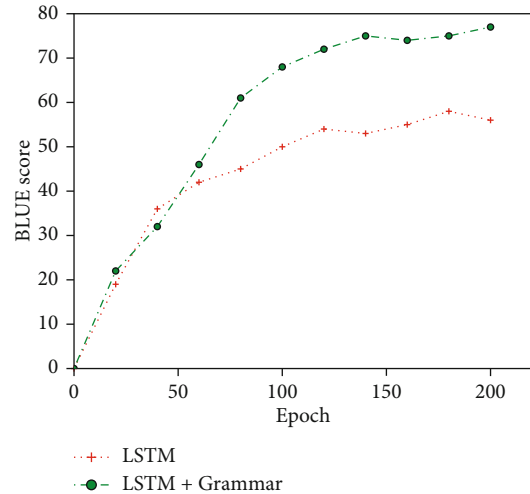


FIGURE 8: Epoch/BLEU variation diagram between LSTM and LSTM+Grammar.

adopt the method of proper nouns, with statements generalization processing, has completed the English word segmentation processing digitally to quantify the language symbols; language symbols can be input model to carry on the training study. In this study, CBOV was used to vectored words. In our study, the BLEU value is still used as an indicator to evaluate the performance of translation models. The higher the BLEU value, the better the translation quality.

4.2. Model Experiment. The regular LSTM model and the embedded LSTM model were initially trained on the experimental dataset to test the performance of the proposed translation model, and the results are collected in Figures 6 and 7. As can be seen from Figure 6, the LSTM model of attention embedded began to stabilize after 80 training rounds, which may be due to the strong learning ability of the attention mechanism, which enabled the LSTM model to learn the corresponding expression of text in a short time and thus tended to stabilize in a relatively short time.

However, it can also be seen from Figure 7 that due to the absence of term information input as prior knowledge in the source language, the translation model cannot fully learn the corresponding relationship between terms at the source end and terms at the target end during training and can only translate simple terms correctly, so the translation effect for long terms is not good.

Then, the standard LSTM model and the LSTM model combined with syntactical prior knowledge were used to train the experimental dataset. The results are shown in Figures 8 and 9. But because of using only a simple identifier for the target side terms are identified, therefore, the training time is longer than that without any identifiers and shorter than that with multiple complex identifiers.

Furthermore, as shown in Figure 9, simple identifiers used to identify target-end terms as a group can help the translation model better incorporate terminology knowledge during training, allowing the model to learn the semantic relationship between target-end terms and source statements.

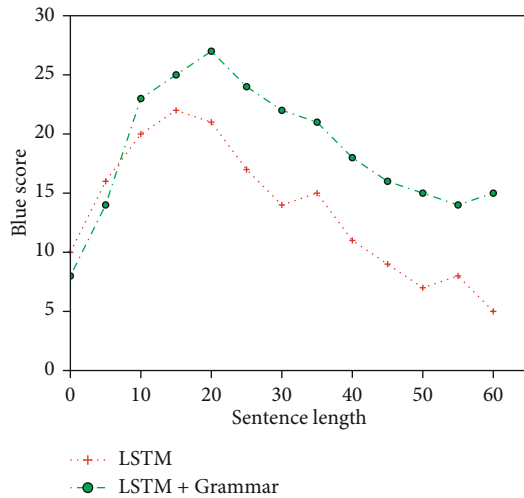


FIGURE 9: Sentence/BLUE variation diagram between LSTM and LSTM+Grammar.

TABLE 1: Experimental results of data enhancement method.

Method	Model	Validation set	Test set
Standard	LSTM	17.60	17.10
	LSTM+Attention	19.50	18.40
	LSTM+Grammar	21.30	20.20
Data enhance	LSTM	19.20	18.60
	LSTM+Attention	21.70	20.90
	LSTM+Grammar	23.10	22.50

TABLE 2: Experimental results of data pretreatment method.

Data format	Model	Validation set	Test set
Standard	LSTM	18.40	16.80
	LSTM+Attention	20.30	17.50
	LSTM+Grammar	20.70	19.40
Vector	LSTM	20.80	19.20
	LSTM+Attention	22.40	21.30
	LSTM+Grammar	24.30	22.70

The baseline model is based on standard LSTM, and the comparison method is attention-embedded LSTM model and grammatical prior knowledge LSTM model. The experimental results of each model are shown in Tables 1 and 2. As shown in Table 1, the BLEU value is still used as the evaluation standard when comparing the results of data enhancement methods of LSTM, LSTM+Attention, and LSTM+Grammar models during dataset verification. It can be seen that the bilingual corpus generated by using the translation model combining attention mechanism and prior grammar knowledge proposed in this paper achieves higher translation indicators than the standard LSTM translation model and is superior to the single data enhancement method as well as no data enhancement method.

Then, the experimental results of the standard LSTM model, the attention-embedded LSTM model, and the LSTM model with syntactic prior knowledge are compared on the processed dataset. As shown in Table 2, the LSTM model combining grammatical prior knowledge has the best translation effect. However, the attention-embedded LSTM model also has a good effect on the parallel corpus after grammar correction, which verifies the necessity of grammar correction for pseudocorpus. Experimental results show that the neural translation model is more sensitive to the quality of the corpus, and certain grammatical errors do not affect the translation performance but enhance the robustness of the model encoder.

## 5. Conclusion

To complete the translation process from source to destination language, the neural translation system employs the “encoder-attention-decoder” framework. The attention mechanism, on the other hand, has some flaws and unsolved issues, and syntactic prior information is not taken into account in the general neural machine translation system. As a result, how to improve the attention mechanism, lower computational costs, learn the internal relationships in the sequence better, and capture more accurate and rich context information; and how to integrate rich grammar knowledge, better model the semantic and syntactic representation of word sequence, improve sentence context understanding, and reduce grammatical errors in translation, among other things. Therefore, the English-Chinese translation model based on LSTM attention embedding and the LSTM model combined with grammatical prior knowledge is proposed. The innovation lies in the introduction of attention mechanism and grammatical prior knowledge into the standard LSTM translation model to enhance the representation of source language context information, thus improving the performance of the translation model and translation quality. Compared with the standard LSTM model, the proposed translation model has better performance, better translation effect, and better text genre.

## Data Availability

The datasets used during the current study are available from the corresponding author on reasonable request.

## Conflicts of Interest

The authors declare that they have no conflict of interest.

## References

- [1] P. F. Brown, J. Cocke, S. A. Della Pietra et al., “A statistical approach to machine translation,” *Computational Linguistics*, vol. 16, no. 2, pp. 79–85, 1990.
- [2] M. Johnson, M. Schuster, K. M. Le QV et al., “Google’s multilingual neural machine translation system: enabling zero-shot translation,” *Transactions of the Association for Computational Linguistics*, vol. 5, pp. 339–351, 2017.

- [3] H. Somers, "Example-based machine translation," *Machine Translation*, vol. 14, no. 2, pp. 113–157, 1999.
- [4] I. Dunder, "Machine translation system for the industry domain and Croatian language," *Journal of Information and Organizational Sciences*, vol. 44, no. 1, pp. 33–50, 2020.
- [5] V. Goyal and G. S. Lehal, "Web based Hindi to Punjabi machine translation system," *Journal of Emerging Technologies in Web Intelligence*, vol. 2, no. 2, pp. 148–151, 2010.
- [6] J. Hutchins, "Example-based machine translation: a review and commentary," *Machine Translation*, vol. 19, no. 3, pp. 197–211, 2007.
- [7] F. Stahlberg, "Neural machine translation: a review," *Journal of Artificial Intelligence Research*, vol. 69, pp. 343–418, 2020.
- [8] S. K. Mahata, D. Das, and S. Bandyopadhyay, "Mtil2017: machine translation using recurrent neural network on statistical machine translation," *Journal of Intelligent Systems*, vol. 28, no. 3, pp. 447–453, 2019.
- [9] Y. Xia, "Research on statistical machine translation model based on deep neural network," *Computing*, vol. 102, no. 3, pp. 643–661, 2020.
- [10] K. Chen, R. Wang, M. Utiyama, E. Sumita, and T. Zhao, "Neural machine translation with sentence-level topic context," *IEEE/ACM Transactions on Audio, Speech, and Language Processing*, vol. 27, no. 12, pp. 1970–1984, 2019.
- [11] J. Pei, K. Zhong, M. A. Jan, and J. Li, "Personalized federated learning framework for network traffic anomaly detection," *Computer Networks*, vol. 209, p. 108906, 2022.
- [12] J. Hutchins, "Machine translation and human translation: in competition or in complementation," *International Journal of Translation*, vol. 13, no. 1-2, pp. 5–20, 2001.
- [13] R. Dabre, C. Chu, and A. Kunchukuttan, "A survey of multilingual neural machine translation," *ACM Computing Surveys (CSUR)*, vol. 53, no. 5, pp. 1–38, 2020.
- [14] M. L. Forcada, "Making sense of neural machine translation," *Translation Spaces*, vol. 6, no. 2, pp. 291–309, 2017.
- [15] Á. Peris, M. Domingo, and F. Casacuberta, "Interactive neural machine translation," *Computer Speech & Language*, vol. 45, pp. 201–220, 2017.
- [16] J. Lee, K. Cho, and T. Hofmann, "Fully character-level neural machine translation without explicit segmentation," *Transactions of the Association for Computational Linguistics*, vol. 5, pp. 365–378, 2017.
- [17] J. Cao, Z. Li, and J. Li, "Financial time series forecasting model based on CEEMDAN and LSTM," *Physica A: Statistical Mechanics and its Applications*, vol. 519, pp. 127–139, 2019.
- [18] J. Zhang, Y. Zhu, X. Zhang, M. Ye, and J. Yang, "Developing a long short-term memory (LSTM) based model for predicting water table depth in agricultural areas," *Journal of Hydrology*, vol. 561, pp. 918–929, 2018.
- [19] L. Huang, Y. Ma, S. Wang, and Y. Liu, "An attention-based spatiotemporal lstm network for next poi recommendation," *IEEE Transactions on Services Computing*, vol. 14, no. 6, pp. 1585–1597, 2021.
- [20] Y. Chen, W. Shao, J. Liu, L. Yu, and Z. Qian, "Automatic modulation classification scheme based on LSTM with random erasing and attention mechanism," *IEEE Access*, vol. 8, pp. 154290–154300, 2020.
- [21] F. J. Och and H. Ney, "The alignment template approach to statistical machine translation," *Computational Linguistics*, vol. 30, no. 4, pp. 417–449, 2004.
- [22] S. Wu, D. Zhang, Z. Zhang, N. Yang, M. Li, and M. Zhou, "Dependency-to-dependency neural machine translation," *IEEE/ACM Transactions on Audio, Speech, and Language Processing*, vol. 26, no. 11, pp. 2132–2141, 2018.
- [23] W. Xu, C. Napoles, E. Pavlick, Q. Chen, and C. Callison-Burch, "Optimizing statistical machine translation for text simplification," *Transactions of the Association for Computational Linguistics*, vol. 4, pp. 401–415, 2016.

## Research Article

# Application of Graphic Design with Computer Graphics and Image Processing: Taking Packaging Design of Agricultural Products as an Example

Tianhe Xie, Rongyi Sun, Jiahao Zhang, Ruiqi Wang, and Jiashu Wang 

*College of Landscape Architecture and Art, Northwest A&F University, Xianyang 712100, China*

Correspondence should be addressed to Jiashu Wang; [jiashu.wang@nwfau.edu.cn](mailto:jiashu.wang@nwfau.edu.cn)

Received 10 April 2022; Revised 3 May 2022; Accepted 7 May 2022; Published 2 June 2022

Academic Editor: Naeem Jan

Copyright © 2022 Tianhe Xie et al. This is an open access article distributed under the Creative Commons Attribution License, which permits unrestricted use, distribution, and reproduction in any medium, provided the original work is properly cited.

With development of economy, all industries have undergone earthshaking changes. Various new technologies are starting to be employed in all aspects of life, and graphic design is no exception. The use of computer graphics and image processing technologies in graphic design can substantially improve design efficiency and make graphic design job more convenient to develop. The requirements for the quality of graphic design are higher. Quality inspection has become a necessary step in the production process, in which the detection of graphic design defects is an indispensable and important link. The traditional graphic design defect detection adopts the method of manual visual inspection, which has the disadvantages of poor stability, long consumption time, and high labor cost. As an efficient computer graphics and image processing technology, convolutional neural network has received extensive attention in graphic design defect detection because of its advantages of high speed, efficiency, and high degree of automation. Taking agricultural product packaging as an example, this paper studies application technology for graphic design defect detection with convolutional neural network (CNN). The main contents are as follows: construct the original YOLOv3 network model, input the graphic design images of agricultural product packaging into the network model in batches according to the computing power of the hardware equipment, train the YOLOv3 network, and deeply study and analyze the experimental results. The related improvement techniques are then given, based on the characteristics of agricultural product packaging design faults. The backbone network, multiscale feature map, a priori frame, and activation function of YOLOv3 are improved, and then performance of the improved model is verified by experiments.

## 1. Introduction

At this point, the development and applicability of computer graphics and image processing have made graphic design work much easier. Computer graphics and image processing technology have rapidly become an essential competence for designers in the work process in the graphic design business. Various picture information may be modified and optimized in terms of style, color, and theme using this technology, which can not only enhance the design effect but also improve job efficiency, effectively encouraging the design industry's development. The application of computer graphics and image processing technology in graphic design can solve the problems of diversity and aesthetics in graphic design to a certain extent and can also add more richness to

the content of graphic design. In the process of using computer graphics and image processing technology, it is necessary to fully exploit the role and value of computers. However, we must also realize that there are still many unreasonable problems, which cannot give full play to the role of computer graphics and image processing technology, which affects the sustainable and healthy development of graphic design. Among them, graphic design defects have become a long-standing problem, and most graphic design products have certain defects. How to detect the defects of graphic design products has become an important and practical topic [1–5].

Manual quality inspection is still widely used, especially in small and medium-sized businesses that use human detection methods, and it accounts for a significant portion

of the market. Manual quality inspection, on the other hand, must remain in a fixed position, which can lead to a variety of inspection issues when determining the presence of flaws by eye observation. Manual quality inspection cannot even ensure the stability and consistency of the detection of the same batch of graphic design products due to the influence of factors such as individual variances. In addition, missed detection and false detection are prone to occur during the detection process, the accuracy of the detection results is reduced, and the product quality is uneven. In addition, the upper limit of manual inspection efficiency is low, the cost is high, and a sampling inspection strategy is usually adopted to ensure production efficiency. The quality assessment of the entire product group by randomly selecting several products from the same group of products is far less rigorous than large-scale testing. Therefore, in the manual quality inspection process, quality control and production efficiency cannot always be achieved at the same time. In addition, defect detection requires not only qualitative inspection of the appearance of graphic design products but also statistics of defect size and other data. However, manual quality inspection can only rely on paper and pen to record, and the obtained data is not comprehensive and cannot be used as valuable information to guide production and production optimization and improvement [6–10].

Machine vision detection technology is a modern detection technology that integrates photoelectric sensing, computer science, image processing, pattern recognition, and other disciplines. It converts the captured target into an image signal, transmits it to a dedicated image processing system, and extracts the parameters to be detected, thereby realizing the defect detection of graphic design products. Machine vision inspection technology offers many advantages over hand visual inspection: noncontact measurement of the product to be inspected causes no damage to the product. The wider spectral response range and higher resolution extend the visual range and resolution of the naked eye. Stable, reliable, and fast work for a long time makes up for the shortcomings of poor visual stability and low work efficiency. The mechanized nature has greatly increased the degree of industrial automation. In recent years, due to the rapid development of machine vision and digital image processing, defect detection technology based on machine vision has received more and more attention in industrial quality inspection and has been widely used in various industries. Based on the above background, it is of great significance to study the defect detection technology of graphic design based on machine vision [11–15].

This work offers a computer graphics and image processing technology based on convolutional neural networks to detect faults in agricultural product packaging design, using the packaging design of agricultural products as an example. The characteristics of surface defects in agricultural product packaging design are studied in depth in this research, and then enhancements to the network model, feature maps, prior boxes, and activation functions are proposed. Finally, the revised network model is experimentally tested and compared to the original network model's experimental results. The results show that the improved network

model can improve the detection accuracy of agricultural product graphic design defects.

The paper's organization paragraph is as follows: the related work is presented in Section 2. Section 3 analyzes the methods of the proposed work. Section 4 discusses the experiments and results. Finally, in Section 5, the research work is concluded.

## 2. Related Work

Reference [16] proposed a real-time algorithm for weaving defect detection based on machine vision. The technique detects five types of fabric surface defects using image processing methods such as wavelet transform, double-threshold binarization, and morphological operations, with a 93.4 percent defect detection and 96.3 percent defect type identification accuracy. Reference [17] proposed a camshaft surface defect detection method based on neighborhood weighted segmentation. The method realizes the detection of typical defects such as trauma, trachoma, and poor grinding on the surface of the camshaft through defect segmentation and defect area marking. At a speed of 0.44 s per shaft, the method was able to detect defects larger than 1 mm in diameter on the camshaft surface. Reference [18] proposed a method for detection of bottle mouth defects based on threshold segmentation, which combines three-circle positioning method, residual analysis dynamic threshold, and global threshold segmentation to detect five kinds of bottle mouth defects. Reference [19] adopts NCC for defect detection and adopts the integral graph strategy to speed up the traditional NCC calculation, so that the calculation time does not change with the change of the template window size. Reference [20] proposed an engine block defect detection based on small area template matching. The method combines rough search and fine search strategy improvement algorithm to determine the exact position and similarity of the images to be matched, realizes defect detection, and has a faster operation speed and meets real-time requirements. Reference [21] proposed a method for detecting appearance defects of smart meters based on machine vision. The method uses image processing technologies such as median filtering, binarization, edge detection, template matching, and OCR to detect the defects of smart meter LCD screen, signage characters, barcodes, and LED indicators, and the detection takes 3 s. Reference [22] proposed a keyboard defect detection method based on template matching. The method utilizes local threshold segmentation and coordinate projection to locate keys and uses template matching to match key characters to realize keyboard defect detection. Reference [23] proposes a steel surface defect detection algorithm, which uses Hough transform, PCA, and self-organization map to detect three kinds of steel surface defects, and achieves an 87% accuracy on the Arcelor Mittal image set. Reference [24] proposed a TFT-LCD defect detection algorithm based on machine vision. The algorithm uses Gabor filtering, adaptive binarization, connected domain extraction, and blob algorithm to identify TFT-LCD point defects and line defects and achieves a high recognition rate. Reference [25] proposed a fabric defect

detection method based on SVM. The method extracts the geometric features of the fabric surface pattern and uses the SVM classifier to achieve defect detection, which can detect 5 kinds of fabric defects with an accuracy of 94.84%. Reference [26] proposed a defect detection and identification algorithm based on the PCA algorithm, which was applied to the surface of unshaded cover glass. Algorithms combine surface defect detection and identification processes into one. The missed detection rate and false alarm rate in the defect detection process reached 12% and 6%, and the recognition rate in the defect identification process reached more than 90%. Reference [27] proposed a defect detection algorithm based on CNN variant network Overfeat.

The algorithm uses Overfeat CNN combined with ASR for surface defect detection and achieves 98.7% and 60.3% accuracy on NEU and MO databases, respectively. Literature [28] developed a welding seam detection method based on multilayer perceptron and achieved good detection results on its data set. Literature [29] studied a variety of surface defect detection techniques based on texture feature extraction and summarized the progress of anomaly detection methods in the field of texture detection. Reference [30] used fractal dimension as feature quantity in hot-rolled strip surface defect identification and estimated an optimal scale to detect defects through fractal dimension curve graph to obtain better detection effect. Reference [31] proposes a method for detecting foreign matter in liquid medicine based on the idea of difference between frames, which achieves high detection accuracy and speed. Convolutional neural networks based on deep learning have demonstrated their powerful capabilities in feature extraction and pattern recognition; so, more and more defect detection methods incorporating deep learning have emerged. Reference [32] developed a visual inspection device for inspecting cigar pack labels at a speed of 500 packs per minute. Reference [33] used texture analysis to detect the seal quality of food packaging bags.

### 3. Method

This work uses convolutional neural network as a computer graphics image processing technology to detect the defects in the graphic design of agricultural product packaging. The convolutional network used is YOLOv3, and a series of improvement measures have been taken to effectively improve its performance.

**3.1. Convolutional Neural Network.** CNN is an artificial neural network designed to imitate the working mode of neurons in the human brain. The basic unit is artificial neurons. Artificial neurons also transmit signals hierarchically and perform extremely well when dealing with gridded data, especially for large image processing. Convolutional neural networks usually include the following structures: input layer, convolutional layer, pooling layer, fully connected layer, and output layer. The input layer is responsible for the input of the network, which is generally a matrix of numbers representing an image. The image input to the network will then go through a series of convolutional layers,

pooling layers, and fully connected layers, and finally, the output layer will input the result.

The convolutional layer is an important part of the convolutional neural network, and the layers are directly connected locally to map the underlying information into high-level features. Each convolutional layer has multiple convolution kernels, and the size and number of convolution kernels have an important impact on the recognition ability of the convolutional neural network. The essence of a convolution kernel is a set of trainable weight matrices. When convolution operation is performed on the input image, the convolution kernel covers part of the input image according to a certain rule, and the value of the convolution kernel is multiplied by the value of the corresponding position pixel in the image. Adding the products obtained in the previous step is the result of this convolution operation. Convolutional layers are often used to extract image features, and the result after a series of convolution operations is often referred to as a feature map. The mathematical expression of the convolution operation is as follows:

$$y_j^l = \sigma \left( \sum x_i^{l-1} * w_{ij}^l + b_j^l \right). \quad (1)$$

Weight sharing is an important feature of the convolution layer. Weight sharing means that when performing convolution operations, all positions of the image use convolution kernels with the same parameters. Weight sharing drastically decreases the network's parameters, allowing for much faster model training and inference. Another element of the convolution layer is multiconvolution operation, which refers to the employment of multiple separate convolution kernels to scan the input image. The scan result of each convolution kernel is a feature map, and finally, the multifeature map is used for prediction, and the accuracy can be greatly improved.

The pooling layer is generally located after the convolutional layer, and its main function is to compress the size of the feature map to reduce the amount of network parameters. The output of the pooling layer is the same as the convolutional layer, which is a feature map. These feature maps uniquely correspond to a feature map of the previous layer, and the size will be reduced to a certain extent. In theory, it is possible to directly input the feature map output by the convolutional layer into the classifier for result prediction. However, after the convolution operation of the image, the size of the image is not significantly reduced. Instead, due to the convolution operation of multiple convolution kernels, the feature map of the network increases. This increases the number of network parameters and the amount of computation, which seriously affects the training speed of the network. Therefore, it is necessary to perform a dimensionality reduction operation on the convolutional feature map, which is called a pooling operation. Pooling is the use of filters to filter out invalid information in the feature map after convolution operation, saving important information while reducing the amount of information and complexity. The pooling operation has strong advantages in reducing network parameters, reducing the amount of

computation, and enhancing the robustness of the network. The pooling operation is as follows:

$$y_j^l = \text{down}(y_j^{l-1}). \quad (2)$$

The pooling operation first divides the feature map into small matrices of equal size and does not overlap and then selects a value to replace the entire small matrix according to different criteria. There are two commonly used criteria, one is max pooling, which is to keep the one with the largest element in each small matrix. The second is average pooling, which is to average and retain all elements in each small matrix. After the feature map is pooled, the number will not change, but its scale will be significantly reduced, and only the most effective information in the feature map will be retained, thereby improving the robustness of the convolutional neural network model.

The fully connected layer is the most commonly used hidden layer of the network before the convolutional layer is proposed. Each artificial neuron in the layer establishes a connection relationship with all the neurons in the previous layer. The main feature is that there are many parameters and a large amount of calculation. In fact, it plays the role of integrating information through a large number of parameters and calculations. In a convolutional neural network, one or more fully connected layers are connected after multiple convolutional and pooling layers. Its main function is to fuse the extracted high-level features and then transform these fused features into a probability distribution. The classification result of the network is output according to the probability distribution through the output layer.

Activation functions are an important part of convolutional neural networks and are usually used in convolutional layers. The activation function is essentially a mathematical function, and its main task is to add nonlinear elements to the network model. The activation function is created by imitating the way the neurons in the human brain transmit information; that is, when the stimulation of the neuron reaches a certain threshold, the neuron will be activated to transmit the information of the neurons in the previous layer. Activation functions work in a similar way. Common activation functions are as follows:

$$\begin{aligned} \text{Sigmoid}(x) &= \frac{1}{1 + e^{-x}}, \\ \text{Tanh}(x) &= \frac{e^x - e^{-x}}{e^x + e^{-x}}, \\ \text{ReLU}(x) &= \max(0, x). \end{aligned} \quad (3)$$

*3.2. Defect Detection of Agricultural Product Packaging Design with YOLOv3.* The overall network structure of YOLOv3 is divided according to functions, which can be divided into backbone network and detection network. The backbone network is essentially a convolutional neural network, which is mainly responsible for the feature extraction of input images. The DarkNet-53 network is selected in the YOLOv3 model. The detection network takes the backbone

network's output as an input, does multiscale prediction using regression, and outputs the full network model's detection findings. Figure 1 shows a schematic diagram of YOLOv3's overall network topology. The backbone network DarkNet-53 is shown on the left, while the detection network on the right forecasts the outcomes based on DarkNet-53's output.

The process of performing target detection in the YOLOv3 network is as follows. The YOLOv3 network model first scales the image input to the network to a size of  $416 \times 416 \times 3$  and then inputs it into the backbone network to extract feature maps of three scales. The dimensions of the three feature maps are  $13 \times 13 \times 1024$ ,  $26 \times 26 \times 512$ , and  $52 \times 52 \times 256$ , respectively. Then, the feature maps of these three scales are input into the detection network module, the lower layer feature map performs upsampling operation, and the upper layer feature map performs feature fusion. Then, after a series of convolutional layers, three final feature maps are obtained. The dimensions of the three final feature maps are  $13 \times 13 \times 255$ ,  $26 \times 26 \times 255$ , and  $52 \times 52 \times 255$ , respectively, and these three feature maps are finally used to predict the results.

DarkNet-53 is mainly responsible for extracting feature maps of different scales. The network performs feature extraction through a series of  $1 \times 1$  convolutions and  $3 \times 3$  convolutions. A batch normalization layer is also included to standardize the data, speed up the network's convergence, and improve the network model's training efficiency. DarkNet-53 contains a total of 52 convolutional layers, which are composed of these 52 convolutional layers. The first is through a convolutional layer containing 32 convolutional kernels of size  $3 \times 3$  and then through 5 sets of repeated residual block structures. Each residual block structure consists of a single convolutional layer with a set of repeatedly executed convolutional modules. Before performing the convolution operation performed separately, the zero padding operation must be completed first; that is, the zero expansion of the upper border and the left border of the input image is first performed. Then, a convolution operation with a convolution kernel size of  $3 \times 3$  and a stride of 2 is performed. The number of specific convolution kernels is related to the depth of the network. After that, the convolution module operation is repeated, and it is repeated 1 time, 4 times, 8 times, 8 times, and 4 times, respectively. In each repeated convolution module, the convolution operation with the convolution kernel size of  $1 \times 1$  and the number of convolutions is halved first. Then, perform a normal number of convolution operations with a kernel size of  $3 \times 3$ . This cycle is repeated for many times; that is, the feature extraction work is completed. Subsequently, a fully connected layer completes the screening of feature maps. However, the fully connected layer is actually implemented by  $1 \times 1$  convolution; so, it can also be recorded as a convolution layer. So far, the entire network contains 53 convolutional layers, from which DarkNet-53 is named.

YOLOv3 outperforms YOLO and YOLOv2 in terms of backbone network performance. The backbone network, for starters, uses DarkNet-53 with deeper layers. DarkNet-53 employs a significant number of residual structures in

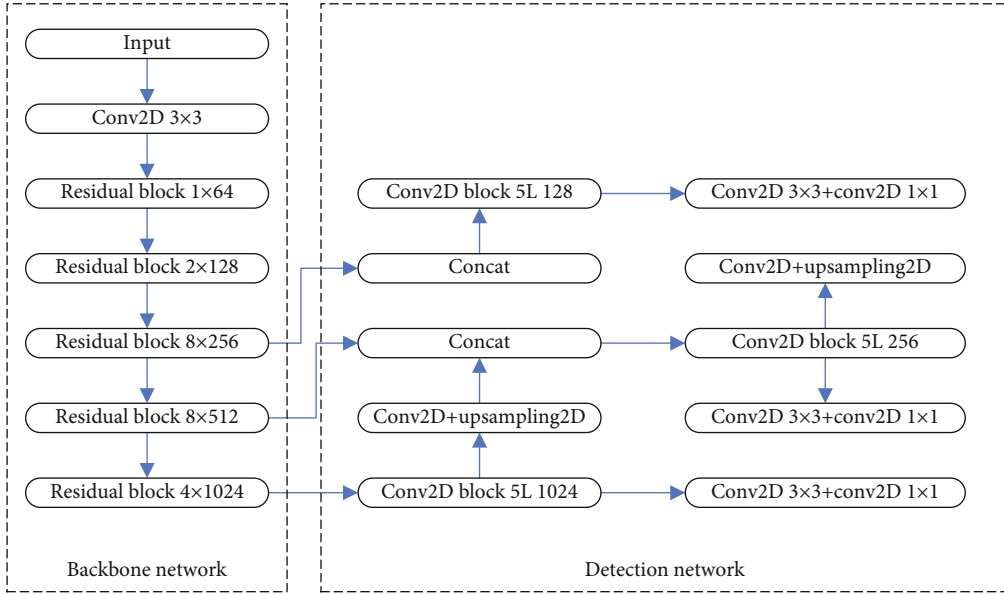


FIGURE 1: The structure of YOLOv3.

addition to layer deepening. A schematic diagram of the residual structure's operation flow is given in Figure 2. The second point is that before DarkNet-53 performs the convolution operation, it will first normalize the input data of the convolution layer and then send the processed data to the convolution layer. The advantage of using this execution process is that it can greatly speed up the convergence speed of the network training.

For the detection network, we mainly rely on the feature maps of different sizes output by DarkNet-53 for result prediction. YOLOv3 uses a total of 3 feature maps for object detection. These three feature maps are located after the residual convolution module repeated 8 times by the DarkNet-53 network, after the residual convolution module repeated 8 times, and after the residual convolution module repeated 4 times. Then, use a series of convolution operations to further extract features. First, a  $13 \times 13 \times 255$  output is obtained according to the feature map with the smallest size, denoted as  $y_1$ . A series of convolution operations and an upsampling operation are performed on the underlying feature map of DarkNet-53 to expand the size of the feature map. Then, perform a splicing operation with a feature map with a size of  $26 \times 26 \times 512$  and then go through a series of convolution operations to obtain a feature map with a size of  $26 \times 26 \times 255$ , denoted as  $y_2$ . Repeat this operation to get a new feature map, and the output size is  $52 \times 52 \times 255$ , denoted as  $y_3$ .

Finally, three different scales of  $y_1$ ,  $y_2$ , and  $y_3$  are simultaneously input into the subsequent network for the final result prediction. Among them, the feature map of  $y_1$  is small and contains high-level feature information, which is mainly responsible for the prediction of large targets. The feature map of  $y_2$  is of moderate size and is mainly responsible for the prediction of medium-sized objects. The feature map of  $y_3$  is the largest, which contains more detailed feature information, and is mainly responsible for the predic-

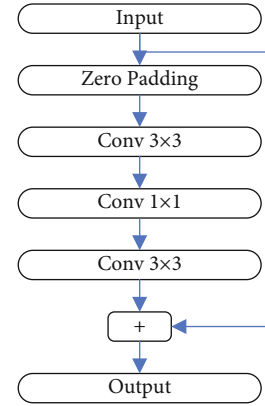


FIGURE 2: The structure of residual module.

tion of small targets. It is precisely because the feature maps of different scales are used in the YOLOv3 network model that the network can achieve better detection accuracy when detecting targets of different sizes.

**3.3. Backbone Network Improvement.** The original network model of YOLOv3 was designed to conduct target detection, with the aim of detection being everyday items, which is considerably different from the target job in this topic. This subject's goal is to find flaws in the graphic design of agricultural product packaging, and the features of numerous flaws differ significantly from those of the original target object. Continuing to use the original network model, although better detection results can be achieved, it is still not optimal. In view of this, this topic will carefully study and analyze the defect characteristics and make certain improvements to the original YOLOv3 detection algorithm accordingly.

To improve the detection algorithm of YOLOv3, we first need to improve the backbone network DarkNet-53. The final output feature map size of the DarkNet-53 feature extraction network is  $13 \times 13$ , and the feature map of this scale is



responsible for the detection of large objects. However, in this project, some defects have a size of more than 1000 pixels, and the detection effect of this feature map may be difficult to meet the project requirements. Therefore, this topic decided to add a residual convolution module on the basis of DarkNet-53, the internal convolution module is repeated 4 times, and the entire added module contains a total of 9 convolution operations. Aside from adding more convolutional layers, the number of repetitions of the residual convolution module of the feature extraction network must be adjusted, as well as the number of convolution kernels inside the residual convolution module. The new backbone network contains a total of 62 convolutional layers, which can be called DarkNet-62. The number of network layers is deepened, and the expressive ability of the network is enhanced. Figure 3 is a schematic diagram of the DarkNet-62 network model.

**3.4. Multiscale Improvement.** The original network model selected 3 feature maps for the final detection result prediction. And the small-scale feature map is responsible for the detection task of large objects, and the large-scale feature map is responsible for the detection task of small objects. Due to the unsatisfactory results of previous experiments, this project plans to improve the selection of feature maps, increasing from 3 feature maps to 5 feature maps. In the previous subsection, a residual convolution module has been added, taking the output of this part as one of the selected feature maps. Then, the output of the second residual convolution module of the network model is selected as one of the feature maps, where the size of the feature map is  $104 \times 104$ . And keep the original 3 feature maps and complete the screening of the improved YOLOv3 model feature maps. A total of 5 feature maps participate in subsequent detection.

In the subsequent feature fusion process, since the  $6 \times 6$  feature map has a size of  $12 \times 12$  after upsampling, it does not match the  $13 \times 13$  feature map; so, the upsampled feature map needs to be filled. Here, the method of zero padding is used to fill the upper and left sides of the  $12 \times 12$  feature map to ensure that the subsequent feature maps can be aligned.

**3.5. Priori Box Improvement.** The YOLOv3 target detection network follows the a priori frame design of the YOLOv2 network. In the original YOLOv3 algorithm model, there are 9 a priori boxes calculated on the dataset using the  $K$ -means algorithm. Most of the COCO datasets are common objects and animals in life, such as TV shows, chairs, cars, cats, and dogs. YOLOv3's initial a priori frame is capable of detecting these things. The flaws in this topic are some new YOLOv3 targets, and the original a priori frame is not up to the task of detecting them.

Therefore, this project plans to reset the prior frame suitable for the agricultural product packaging graphic design defect dataset. And on the basis of the original 3, it has been increased to 5. The reason is that the different types of defects in this subject are quite different, and the sizes of other types of defects are also different. As a result, additional a priori frames are required to improve flaw detection accuracy in this subject. Table 1 shows the distribution of the enhanced prior frame on the feature map.

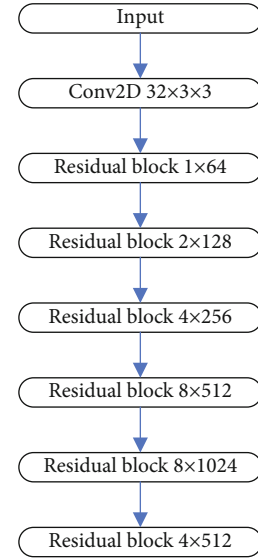


FIGURE 3: The structure of DarkNet-62.

TABLE 1: Improved priori box.

Priori box	Feature map size
$352 \times 1127, 465 \times 272, 725 \times 787$	$6 \times 6$
$189 \times 797, 228 \times 195, 296 \times 62$	$13 \times 13$
$104 \times 42, 122 \times 103, 147 \times 132$	$26 \times 26$
$57 \times 172, 76 \times 77, 87 \times 427$	$52 \times 52$
$27 \times 26, 42 \times 40, 52 \times 62$	$104 \times 104$

TABLE 2: Experimental environment information.

Name	Parameter
CPU	Intel i9-9900K
GPU	GeForce RTX 2080Ti(11GB)
Memory	32GB
Framework	PyTorch 1.6

**3.6. Activation Function Adjustment.** The Leaky ReLU activation function used in the original YOLOv3 network is an improved version of the ReLU activation function. But in the negative semiaxis region, Leaky ReLU presets a nonzero slope to ensure that the output of the function on the negative semiaxis is not equal to 0. This ensures that all neurons can participate in network training, and parameters can be updated in time. However, since the slope of the negative semiaxis region is preset and fixed, this makes it impossible to find the perfect parameter values that are exactly suitable for this topic, and there is no guarantee that the final result of the network is optimal.

In view of this, this project plans to use PReLU as the activation function of this defect detection network model. The advantage of PReLU is that the slope of the negative semiaxis region is a parameter that can be learned, not preset, but determined according to the data during the training of the network model. Moreover, the parameter values are

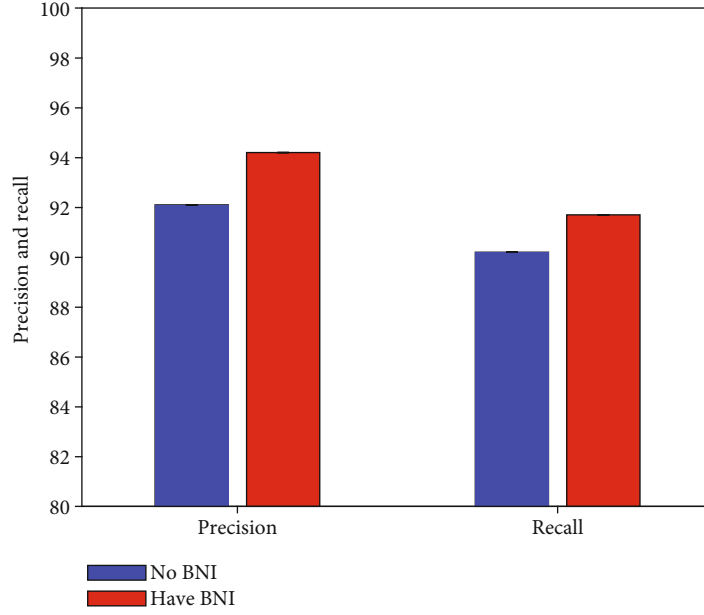


FIGURE 4: Result of backbone network improvement.

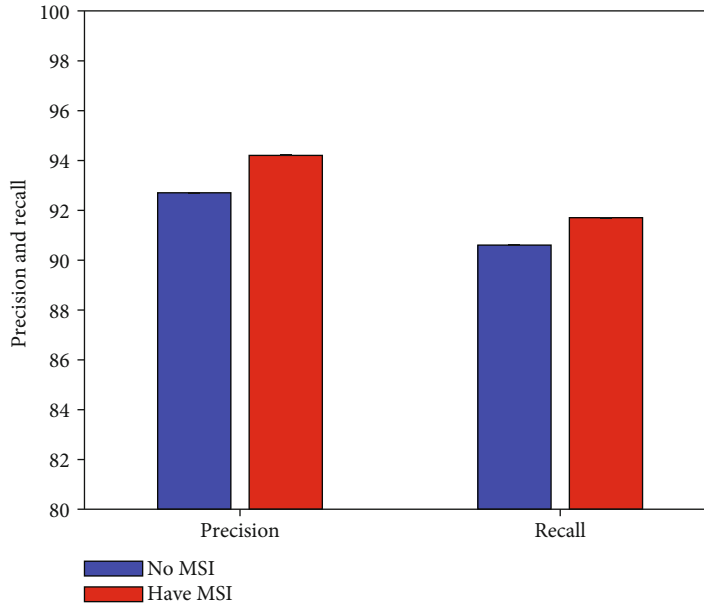


FIGURE 5: Result of multiscale improvement.

fixed when the model is trained and are also constant in the subsequent testing process. The expression of PReLU is as follows:

$$\text{PReLU}(x) = \begin{cases} x, & x > 0 \\ \frac{x}{a}, & \text{others} \end{cases} \quad (4)$$

#### 4. Experiments

In this section, we define the dataset and detail, result of backbone network improvement, result of multiscale

improvement, result of priori box improvement, and result of activation function improvement in detail.

*4.1. Dataset and Detail.* This work uses a self-made agricultural product packaging graphic design dataset. This dataset contains a total of 98,472 samples, of which 66,938 samples are training sets, and the remaining 31,534 samples are test sets. Precision and recall are used as evaluation metrics for this work. The experimental environment information is illustrated in Table 2.

*4.2. Result of Backbone Network Improvement.* As mentioned earlier, this work improves the backbone network.

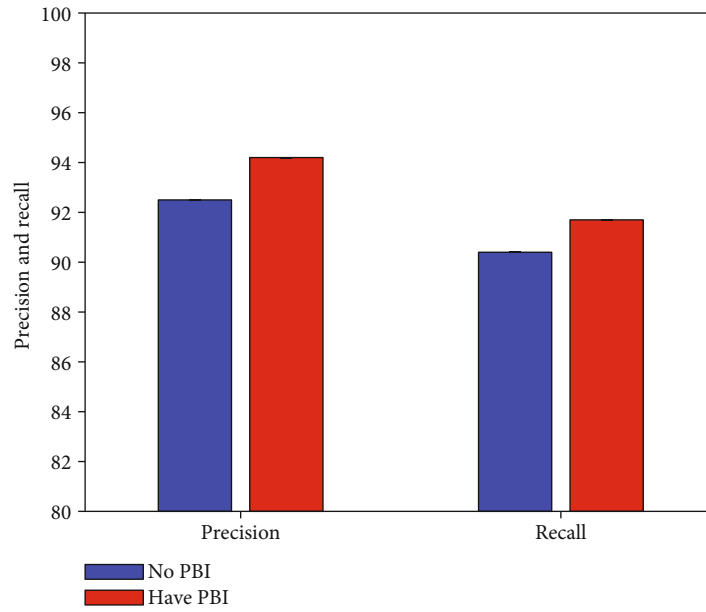


FIGURE 6: Result of priori box improvement.

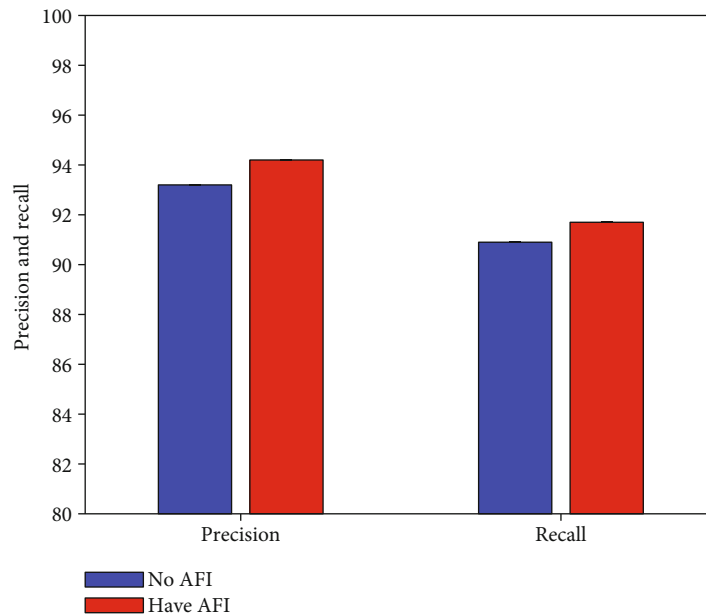


FIGURE 7: Result of activation function improvement.

To verify the effectiveness of this improvement strategy (BNI), this work conducts comparative experiments to compare the defect detection performance of agricultural packaging graphic design without and with BNI improvement, respectively. The experimental results are illustrated in Figure 4.

Compared with the non-BNI improvement strategy, after using the BNI strategy, the detection network can obtain 2.1% precision and 1.5% recall improvement. This can prove the effectiveness and correctness of this work using the BNI improvement strategy.

*4.3. Result of Multiscale Improvement.* As mentioned earlier, this work improves the multiscale prediction. To verify the effectiveness of this improvement strategy (MSI), this work conducts comparative experiments to compare the defect detection performance of agricultural packaging graphic design without and with MSI improvement, respectively. The experimental results are illustrated in Figure 5.

Compared with the non-MSI improvement strategy, after using the MSI strategy, the detection network can obtain 1.5% precision and 1.1% recall improvement. This

can prove the effectiveness and correctness of this work using the MSI improvement strategy.

**4.4. Result of Priori Box Improvement.** As previously stated, this effort enhances the priori box. This work performs comparison experiments to compare the defect detection performance of agricultural package graphic design without and with PBI improvement, respectively, to validate the usefulness of this improvement approach (PBI). The experimental results are illustrated in Figure 6.

Compared with the non-PBI improvement strategy, after using the PBI strategy, the detection network can obtain 1.7% precision and 1.3% recall improvement. This can prove the effectiveness and correctness of this work using the PBI improvement strategy.

**4.5. Result of Activation Function Improvement.** As mentioned earlier, this work improves the activation function. To verify the effectiveness of this improvement strategy (AFI), this work conducts comparative experiments to compare the defect detection performance of agricultural packaging graphic design without and with AFI improvement, respectively. The experimental results are illustrated in Figure 7.

Compared with the non-AFI improvement strategy, after using the AFI strategy, the detection network can obtain 1.0% precision and 0.8% recall improvement. This can prove the effectiveness and correctness of this work using the AFI improvement strategy.

## 5. Conclusion

Computer graphics and image processing technology are maturing in tandem with the rapid advancement of information technology. In graphic design, the use of computer graphics and image processing technology can help to simplify the process, enhance the design effect, and better the design expression. People's expectations for graphic design quality are rising in tandem with the manufacturing industry's rapid growth; although, flaws are unavoidable in the design process. Graphic design defects not only affect the appearance itself but also affect the use; so, enterprises pay special attention to product quality inspection to ensure the quality of products. At the same time, the quality inspection results are analyzed to further improve the graphic design process and reduce the occurrence of defects. As a result, this study examines the use of a convolutional neural network as a computer graphics and image processing technology in defect identification in graphic design, as well as the current position. To complete the enhancement of the YOLOv3 network model, this work uses the packaging design of agricultural products as an example. The network model is presented to improve the direction of this topic based on the experimental findings of the original YOLOv3 and an in-depth analysis of the characteristics of various agricultural product packaging graphic design faults. It includes the improvement of the backbone network, the improvement of the feature map, the improvement of the prior frame, and the improvement of the activation function. Finally, the validity and feasibility of the model improvement are proved by experiments.

## Data Availability

The datasets used during the current study are available from the corresponding author on reasonable request.

## Conflicts of Interest

The authors declare that they have no conflicts of interest.

## Funding

This paper is part of the provincial "University Student Innovation and Entrepreneurship Training Program" project of Northwest A&F University: the research results of "Mintian Agricultural Products Marketing Planning Studio".

## References

- [1] T. C. Bagiritima, J. M. Tesha, and M. Kimani, "Investigation on the poor computer graphic design skills among art and design students at university," *International Journal of Humanities Social Sciences and Education (IJHSSE)*, vol. 6, no. 10, pp. 61–71, 2019.
- [2] P. B. Siti, M. Mustaji, B. Bachri, and F. Patricia, "Building empathy: exploring digital native characteristic to create learning instruction for learning computer graphic design," *International Journal of Emerging Technologies in Learning (iJET)*, vol. 15, no. 20, pp. 145–159, 2020.
- [3] B. Ji, Y. Li, D. Cao, C. Li, S. Mumtaz, and D. Wang, "Secrecy performance analysis of UAV assisted relay transmission for cognitive network with energy harvesting," *IEEE Transactions on Vehicular Technology*, vol. 69, no. 7, pp. 7404–7415, 2020.
- [4] J. Li, Z. Zhou, J. Wu et al., "Decentralized on-demand energy supply for blockchain in internet of things: a microgrids approach," *IEEE transactions on Computational Social Systems*, vol. 6, no. 6, pp. 1395–1406, 2019.
- [5] Y. Chen, W. Zou, and A. Sharma, "Graphic design method based on 3D virtual vision technology," *Recent Advances in Electrical & Electronic Engineering (Formerly Recent Patents on Electrical & Electronic Engineering)*, vol. 14, no. 6, pp. 627–637, 2021.
- [6] J. F. I. Nturambirwe and U. L. Opara, "Machine learning applications to non-destructive defect detection in horticultural products," *Biosystems Engineering*, vol. 189, pp. 60–83, 2020.
- [7] Z. Ren, F. Fang, N. Yan, and Y. Wu, "State of the art in defect detection based on machine vision," *International Journal of Precision Engineering and Manufacturing-Green Technology*, vol. 9, pp. 661–691, 2021.
- [8] T. Wang, Y. Chen, M. Qiao, and H. Snoussi, "A fast and robust convolutional neural network-based defect detection model in product quality control," *The International Journal of Advanced Manufacturing Technology*, vol. 94, no. 9-12, pp. 3465–3471, 2018.
- [9] T. Bo, K. Jianyi, and W. Shiqian, "Review of surface defect detection based on machine vision," *Journal of Image and Graphics*, vol. 22, no. 12, pp. 1640–1663, 2017.
- [10] J. Yang, S. Li, Z. Wang, and G. Yang, "Real-time tiny part defect detection system in manufacturing using deep learning," *IEEE Access*, vol. 7, pp. 89278–89291, 2019.
- [11] S. Ghorai, A. Mukherjee, M. Gangadaran, and P. K. Dutta, "Automatic defect detection on hot-rolled flat steel products,"

- IEEE Transactions on Instrumentation and Measurement*, vol. 62, no. 3, pp. 612–621, 2013.
- [12] D. Guyer and X. Yang, “Use of genetic artificial neural networks and spectral imaging for defect detection on cherries,” *Computers and Electronics in Agriculture*, vol. 29, no. 3, pp. 179–194, 2000.
- [13] Q. Jin and L. Chen, “A survey of surface defect detection of industrial products based on a small number of labeled data,” 2022, <https://arxiv.org/abs/2203.05733>.
- [14] N. L. Maskuri, M. H. Abu Bakar, and A. K. Ismail, *Three-Dimensional Image Reconstruction for Automated Defect Detection at Artificial Metallic Surface Specimens, Progress in Engineering Technology III, [M.S. thesis]*, Springer, Cham, 2021.
- [15] X. Xu, J. Chen, H. Zhang, and W. W. Y. Ng, “D4Net: de-deformation defect detection network for non-rigid products with large patterns,” *Information Sciences*, vol. 547, pp. 763–776, 2021.
- [16] H. İ. Çelik, L. C. Dülger, and M. Topalbekiroğlu, “Development of a machine vision system: real-time fabric defect detection and classification with neural networks,” *The Journal of The Textile Institute*, vol. 105, no. 6, pp. 575–585, 2014.
- [17] X. Sun, X. Jiang, Y. Fu, C. Han, and M. Wen, “Surface defect detection system for camshaft based on computer vision,” *Infrared and Laser Engineering*, vol. 42, no. 6, pp. 1647–1653, 2013.
- [18] X. Zhou, Y. N. Wang, Q. Zhu, C. Z. Wu, and Y. Peng, “Research on defect detection method for bottle mouth based on machine vision,” *Journal of Electronic Measurement and Instrument*, vol. 30, no. 5, pp. 702–713, 2016.
- [19] D. M. Tsai and C. T. Lin, “Fast normalized cross correlation for defect detection,” *Pattern Recognition Letters*, vol. 24, no. 15, pp. 2625–2631, 2003.
- [20] S. Yin, H. Bao, B. Ji, J. Liu, and J. Zhang, “Defect detection of engine cylinder based on small region template matching,” *Transducer and Microsystem Technologies*, vol. 31, no. 6, pp. 143–145, 2012.
- [21] J. Liang, T. Hon, and D. Lin, “Design of smart meter visual inspection system based on machine vision,” *Electrical Measurement & Instrumentation*, vol. 10, pp. 64–68, 2013.
- [22] Y. Hong and Y. Yang, “Keyboard defects detection based on template matching method,” *DEStech Transactions on Engineering and Technology Research*, vol. 24, no. iect, pp. 317–320, 2016.
- [23] F. Y. Zhang and R. J. Liu, “Study on the parts surface defect detection method based on modified SVM algorithm,” *Applied Mechanics and Materials*, vol. 541-542, pp. 1447–1451, 2014.
- [24] X. X. Wang, W. J. Zhou, and J. W. Xu, “Research on detection system for TFT-LCD defects,” *Journal of E-lectronic Measurement and Instrument*, vol. 28, no. 3, pp. 278–284, 2014.
- [25] H. Abdellah, R. Ahmed, and O. Slimane, “Defect detection and identification in textile fabric by SVM method,” *IOSR Journal of Engineering*, vol. 4, no. 12, pp. 69–77, 2014.
- [26] T. Ojala, M. Pietikainen, and T. Maenpaa, “Multiresolution gray-scale and rotation invariant texture classification with local binary patterns,” *IEEE Transactions on Pattern Analysis and Machine Intelligence*, vol. 24, no. 7, pp. 971–987, 2002.
- [27] Y. Zhang, Y. Wang, and H. Jiang, “Edge detection of image based on Sobel and wavelet transformation,” *Computer Applications and Software*, vol. 24, no. 4, pp. 133-134, 2007.
- [28] T. W. Liao and K. Tang, “Automated extraction of welds from digitized radiographic images based on MLP neural networks,” *Applied Artificial Intelligence*, vol. 11, no. 3, pp. 197–218, 1997.
- [29] X. Xie, “A review of recent advances in surface defect detection using texture analysis techniques,” *ELCVIA: electronic letters on computer vision and image analysis*, vol. 7, no. 3, pp. 1–22, 2008.
- [30] D. Tabernik, S. Šela, J. Skvarč, and D. Skočaj, “Segmentation-based deep-learning approach for surface-defect detection,” *Journal of Intelligent Manufacturing*, vol. 31, no. 3, pp. 759–776, 2020.
- [31] P. Napolitano, F. Piccoli, and R. Schettini, “Anomaly detection in nanofibrous materials by CNN-based self-similarity,” *Sensors*, vol. 18, no. 2, p. 209, 2018.
- [32] T. S. Newman and A. K. Jain, “A survey of automated visual inspection,” *Computer Vision and Image Understanding*, vol. 61, no. 2, pp. 231–262, 1995.
- [33] K. D’huys, W. Saeys, and K. B. De, “Active infrared thermography for seal contamination detection in heat-sealed food packaging,” *Journal of Imaging*, vol. 2, no. 4, p. 33, 2016.

## Research Article

# Analysis of the Impact Mechanism of Occupational Identity on Occupational Well-Being Based on Big Data

Yuefen Wang  and Dianyi Yang

*School of Marxism, Northeast Forestry University, Harbin 150040, China*

Correspondence should be addressed to Yuefen Wang; [wytgyx@nefu.edu.cn](mailto:wytgyx@nefu.edu.cn)

Received 8 April 2022; Revised 30 April 2022; Accepted 5 May 2022; Published 29 May 2022

Academic Editor: Naeem Jan

Copyright © 2022 Yuefen Wang and Dianyi Yang. This is an open access article distributed under the Creative Commons Attribution License, which permits unrestricted use, distribution, and reproduction in any medium, provided the original work is properly cited.

Occupational identity is an individual's view, recognition, and approval of his long-term occupation, and its importance to every professional is self-evident. Only when a professional person agrees with the profession he is engaged in from the bottom of his heart can he devote himself wholeheartedly to it and unreservedly exert his greatest potential. On the basis of sorting out and analyzing the prevailing theoretical and empirical research results, this paper deliberates the empirical research on the influence mechanism between employees' occupational identity and occupational well-being. In this study, through big data analysis, literature search, questionnaire survey, and other methods, this paper obtained the professional identity data of employees in different companies and used a method of big data analysis, namely, BP neural network (BPNN) to design in this paper to verify the data, and finally obtain an effective theoretical model of the influence mechanism of occupational identity and occupational well-being. The main work of this paper is as follows: (1) it introduces the interpretation of the concept of "professional identity" by different scholars at home and abroad and makes a brief review of the researches on professional identity and professional well-being made by foreign scholars in recent years. (2) The basic knowledge and algorithm process of artificial neural network (ANN) are introduced, and the design of the evaluation model of the influence mechanism of occupational identity on occupational well-being based on BPNN is proposed. (3) The simulation software validates the neural network (NN) assessment system developed in this paper. Experiments reveal that the BPNN system is a reasonable and feasible evaluation approach for analyzing the impact of occupational identity on occupational well-being.

## 1. Introduction

Identity is generally believed to be derived from psychology. The famous psychologist Freud believed that identity is a process of human cognition and is the inner emotional connection between individuals and individuals, individuals and groups, and individuals and society. The individual's attitude towards the identification of the external world is embodied in the orientation of values [1–3]. An individual's sense of identity is a continuous process that will be precious by the surrounding environment. Once formed and transformed into a part of one's own cognition, it is difficult to change. Identity is the internal acceptance of the object by the subject, and it shows consistency in values and behaviors. Occupational identity is an individual's value orientation towards a certain occupation, with an attitude of approval, affirma-

tion, and yearning. This occupational role attracts the individual's attention and conforms to emotional experience, and the individual will strive to become a part of this type of occupation [4–6]. Occupational identity is a continuous dynamic process, and occupational identity has the same root and origin as "self-identity" in psychology. High occupational identity has a promoting consequence on individual work and can help individuals to do their job well. Occupational identity is embodied in many aspects and is an important criterion for measuring individual occupational mental health. Reference [7] believes that one of the internal factors affecting happiness is employees' professional identity. Nowadays, "happiness" is what employees of every enterprise want to pursue, and enterprise managers should also skillfully use the theory of happiness in the process of management according to the situation. Whether employees are

happy or not will have a great impact on an enterprise. If an employee feels that he is very happy in this enterprise, then, he will preserve a loyal attitude towards the enterprise, be full of energy at work, and there will be a respectable relationship between the employee and the enterprise. Labor relations and job performance are correspondingly higher, and vice versa [8]. If this condition continues for a long time, the enterprise will have such a condition: the market competitiveness will gain absolute advantage and will preserve the momentum of development. As a manager of an enterprise, you should clearly know that money is not what people really want, because even if you have money, it is for a good and happy life, and money serves life, so managers must understand that his employees ultimately what I want to pursue is "happiness" itself. This requires that enterprise managers should master the corresponding psychological knowledge, use the theory of happiness, and carry out scientific and reasonable management and decision-making under limited resources, so that employees can work and be happy. Based on the above analysis, it is necessary to study the influence mechanism of employees' occupational identity on their subjective well-being. Whether an employee of an enterprise agrees with his occupation and the degree of identity will directly affect his work progress and quality of life, and then, it is related to the organizational efficiency of the enterprise and the realization of the ultimate goal. Since NN is also an important method of data mining, it has excellent processing ability for nonlinear problems.

This paper focuses on using BPNN to study the influence mechanism of occupational identity on subjective well-being. The centripetal dimension refers to teachers' awareness of the importance of their professional identity in their work. Therefore, this study adopts the method of data mining to analyze the influence mechanism of employees' occupational identity on their subjective well-being.

## 2. Related Work

Identity is a concept closely related to the study of various academic circles, such as social identity, cultural identity, national identity, and political identity. Among them, social identity refers to the convergence of individual behaviors, values, and social norms, and one of its manifestations is occupational identity. Reference [9] first started from the perspective of identity theory and pointed out that occupational identity is the stability and clarity of an individual's understanding of the goals, values, and meanings of occupations, but they emphasize that occupational identity is a relatively stable state. Subsequently, reference [10] pointed out that occupational identity is a concept that is gradually constructed and matured in the process of psychological development and will change with continuous social learning and interaction. Reference [11] defines it from the perspective of the form adopted by professional identity. It believes that professional identity is an unconscious whole in the form of gestalt about needs, goals, emotions, values, prior knowledge, and behavioral inclinations. This will in turn affect professional beliefs and behavioral aspects. Reference [12] pointed out that occupational identity is the evaluation

of one's own ability and the thinking and clarification of occupational values in the process of engaging in occupation. To sum up, professional identity is not only an instrumental role played in the professional background nor is it a simple synthesis of a professional's achievements, values, and beliefs. We can think of occupational identity as an individual's cognition and construction of a specific occupation and self-role concept gradually developed from growth experience and social interaction. Reference [13] pointed out that teachers' professional identity is no single or absolute nor can it be static and immutable. It is a dynamic process that requires multifaceted, multiangle, and multilevel research and analysis. In the process of identification, teachers are constantly accumulating experience and constantly criticizing and correcting. Reference [14] proposes that the professional image of teachers reflects the professional role of employees to a large extent, which is relatively complex and a dynamic process. The formation process of employees' occupational roles is the formation process of occupational identity. Reference [15] introduced the individual's perception of occupation, such as entry motivation, working conditions, and life choices, into the category of teachers' occupational identity. Through the research on occupational identity, occupational identity is divided into four dimensions, namely, the level of centrality, the level of value, the level of solidarity, and the level of self-expression. The value dimension indicates that employees identify with their occupational value, and the occupation is more attractive. The solidarity dimension indicates that employees value the group and focus on good interpersonal relationships with colleagues. Employees can be appreciated, acknowledged, and loved by society, the company, colleagues, and others, and give greater attention to their own emotional attitudes, thanks to the dimension of self-expression. Reference [16] pointed out that in the research on the formation of employees' professional identity, the interaction between the individual and the collective is very important. Reference [17] conducted research on teachers' professional identity and came to a conclusion, starting from three aspects including emotion, persistence, and norm. Reference [18] believes that employees' professional identity has a great correlation with professional reality cognition. Reference [3] concluded through case studies that individual reflection helps professional identity development. Reference [19] found through research that occupational identity and turnover intention were significantly negatively correlated, occupational identity was closely related to turnover intention, and the level of occupational identity was poor, then turnover intention was relatively high. As domestic and foreign scholars gradually deepen their research on the internal aspects of the company's employees, they have made great progress in the professional identity of employees. My country mainly conducts quantitative research in this area, and the content of the research is mainly reflected in the analysis of the status quo of employees' occupational identity and the research on its relationship with other aspects. Because occupational identity and organizational identity are based on social identity theory, they are both developed on the basis of social identity theory. Therefore, as far as the current foreign

professional identification assessment tools are concerned, most of them are formed after the adaptation of the organizational identification assessment tools. This paper chooses a more representative scale, "Professional Identification Scale." The occupational identity scale developed by Brown et al. was initially composed of three dimensions: awareness of occupational membership, positive evaluation of occupational groups, and sense of belonging to occupational groups. After multiple structural validity tests, a single-dimensional scale was formed, consisting of 10 items, and scored on a Likert 5-point scale. The stronger the professional identification, the higher the score. The Cronbach's alpha coefficient of this scale is 0.71, which is a relatively widely used measurement tool at home and abroad. The Chinese version of the single-dimensional structure scale has a Cronbach's alpha coefficient of 0.82, and its reliability and validity are also relatively good.

Because most international researchers feel that work is a significant aspect of life, it should be included in studies of professional well-being [20]. Researchers disagree on the idea and structure of occupational well-being, according to a study of international literature. Reference [21], for example, suggested a two-dimensional model of emotion, health, and behavior based on the assumption that health is an important indication of well-being, in which behavior corresponds to work ability and ambition and placed job potential under the health dimension. The concept of health was integrated into one dimension, causing confusion. Reference [2] put forward a five-dimensional model of occupational well-being on the basis of synthesizing the results of previous researches, arguing that occupational well-being is an individual's evaluation of various aspects of their work, including cognitive, emotional factors, personal development, physical, and mental health and behavior. Therefore, to sum up, although the opinions of various researchers are inconsistent, they all emphasize that the measurement of occupational well-being should be based on the perspective of development, focusing on the background of well-being. In recent years, occupational well-being has gradually become the focus of domestic researchers. Some researchers believe that occupational well-being is the happiness experience of professionals in occupational activities, and it is the reflection of subjective well-being in the workplace, including emotional experience and recognition. There are two dimensions of knowledge evaluation, but there is no exact definition of the concept of occupational well-being [22]. Reference [23, 24] believes that occupational well-being is a relatively stable emotional experience dominated by positive emotions, which is accompanied by an individual's judgment of his or her occupational identity, occupational activity process, and occupational benefits and focuses on the satisfaction of spiritual needs and positive emotions, so professional well-being places more emphasis on the spiritual dimension of self-realization. We can know that occupational well-being is a multidimensional and flexible concept, and it is also a key indicator of an individual's comprehensive evaluation of occupation. Therefore, a broader concept of well-being can help recover the well-being of professional people and formulate relatively broad intervention strate-

gies. In this sense, a broad conceptualization enriches the theory and practice of occupational psychology.

### 3. Method

*3.1. Artificial Neural Networks.* In the evaluation of nonlinear problems, traditional common methods have many defects. ANNs can learn and train from a large amount of complex data with unknown patterns and find their regularity, especially, they can process any type of data. This is not possible with traditional methods. Therefore, applying the theory of ANN to analyze the influence mechanism of occupational identity on occupational well-being not only overcomes the problems of establishing complex mathematical analytical expressions and mathematical models in the traditional evaluation process but also avoids artificial subjective randomness. It is an effective way to evaluate the mechanism. NNs can be divided into biological NNs and ANNs. All of the NNs mentioned in this article are ANNs. NNs are a typical method to realize artificial intelligence through physiological structure simulation. It starts from the physiological structure of the human brain. Using the point of view of bionics to explore the mechanism of human intelligent activities, it is a method that combines the research on the microstructure of the human brain with the research on intelligent behavior. NN systems are highly nonlinear and self-adaptive and are often used to simulate intelligent behaviors such as cognition, decision-making, and control. The research of NN theory has laid the foundation for people to solve the parallel processing and parallel computing problems of large-scale information processing. Since the 1980s, NN theory has entered a period of rapid development, which has attracted the attention of scholars in many fields and penetrated into all engineering application fields. So far, NN has become a frontier research topic that has developed rapidly in the world.

Synaptic connections in the brain are used to process information in this mathematical model of ANN. Signals are routed across the system through processing units and channels. In addition to having local memory, these processing units may also perform local operations. There are multiple parallel connections for each processing unit, but the one-to-one output remains constant regardless of how many parallel connections are used; this means that even if the number of parallel connections is increased or decreased, each processing unit's signal and its magnitude remain constant. Any mathematical model may be used as the processing unit's output signal, and each processing unit performs local operations. The processing unit must only be constructed on the value stored in the local scope of the processing unit and the existing value of all input signals that influence the processing unit over the input. There are a vast number of nodes and interconnections between them in the NN, which is a model of functioning. The excitation function denotes the output function implied by each node. The memory of an ANN is represented by the weight of each link between two nodes, which is referred to as a weight. The output of the network is dependent on the weight of the network, the technique of connection, and the excitation



function. Each individual neuron in the brain is connected to the rest of the network through connections called neurons. There are various learning algorithms for NNs.

**3.1.1. Hebb Type Learning.** The idea of Hebb-type learning has a certain biological background, and its idea can be summarized into two points: if two neurons on both sides of a synapse are activated at the same time, the energy of the synapse will be selectively increased; conversely, if two neurons on either side of a synapse are activated asynchronously, the synapse's energy is selectively reduced. The mathematical description is as follows:

$$\Delta w_{ij}(n) = \varepsilon(x_j(n) - \bar{x}_j)(x_i(n) - \bar{x}_i). \quad (1)$$

**3.1.2. Error Correction Type Learning.** Error correction learning is a supervised learning process. The reference basis for adjusting the connection weights is the deviation between the expected output of the NN and the actual output and ultimately reduces this deviation.

**3.1.3. Random Learning.** The random learning algorithm introduces methods such as random process and probability into the algorithm, adjusts the variables of the network through these methods, and further maximizes the objective function of the network.

**3.1.4. Competitive Learning.** Competitive learning is to introduce a competitive mechanism into the learning algorithm. All units in a certain part of the NN compete to obtain who is the output. The unit connection weight that wins in the competition changes to a more favorable direction for the competition of this input stimulus pattern. Furthermore, the winning unit inhibits the response of the losing unit to the stimulus pattern, so that only one output neuron is active at any one time.

**3.1.5. Learning Based on Memory.** Memory-based learning is mainly used for pattern classification, such as nearest neighbor classifiers.

**3.1.6. Structural Revision Learning.** The modification of the NN structure, that is, the change of the network topology, also plays an important role in the learning process of animals. That is to say, the learning of the NN is not only reflected in the changes of the weights but also the changes of the network results will also affect the learning.

**3.2. BP Neural Network.** The multilayer feed-forward NN has greatly improved the classification ability of the network due to the introduction of the hidden layer. Since the error back-propagation method is often used in the training of the multilayer feed-forward network, the multilayer feed-forward network is often called BPNN.

**3.2.1. BP Algorithm Model.** Forward propagation and backward propagation of the mistake are two separate processes in BP's learning process. Forward propagation shows that input samples are first received from an external source, then managed by each hidden layer, and then sent to a final output layer. Errors will be propagated

backward if there is a significant difference between the actual output of the output layer and what was intended. Errors are propagated backwards in a layer-by-by-layer fashion from the output layer to the hidden layer and finally to the input layer via back-propagation error correction. Back-propagation distributes the mistake to each layer's units, and the apportionment results for each layer. As a foundation for the error signal, the weight of each unit and its error signal is rectified. The two sections of the BP algorithm cycle repeatedly to alter the weights of each layer in the learning process. The weights of each layer of the network are constantly being adjusted throughout the network's learning and training phase. Until the network output error is within an acceptable range or the number of loops hits the top limit, the two sections are looped back and forth.

**3.2.2. BP Learning Algorithm.** Figure 1 depicts the most generally used NN, as well as the most popular single hidden layer NN. The input layer, the hidden layer, and the output layer are the three layers of this single hidden layer feedforward network, which is also known as a three-layer perceptron or a three-layer feedforward network.

The fundamental of the BP algorithm is to iteratively obtain the minimum error value. The error  $E$  between the network output and the expected output is as follows.

$$E = \frac{1}{2(b - O)^2} = \frac{1}{2\sum_{k=1}^1 (b_k - O_k)^2}. \quad (2)$$

The formula of the error  $E$  in the hidden layer is as follows:

$$E = \frac{1}{2} \sum_{k=1}^1 \left[ b_k - g \left( \sum_{j=0}^m w_{jk} y_j \right) \right]^2. \quad (3)$$

The formula for the error  $E$  in the expansion to the output layer is as follows:

$$E = \frac{1}{2} \sum_{k=1}^1 \left\{ b_k - g \left[ \sum_{j=0}^m w_{jk} g \left( \sum_{i=0}^n V_{ij} x_i \right) \right] \right\}^2. \quad (4)$$

From formula (4), the input error of the BPNN is also the weight function of the overall layers, and the change of the error can be achieved by adjusting the weights. Using gradient descent, the weights are continuously adjusted as follows.

$$\Delta w_{jk} = -\frac{\lambda \partial E}{\partial w_{jk}}, j = 0, 1, \dots, m; k = 1, 2, \dots, l. \quad (5)$$

$$\Delta V_{ij} = -\frac{\lambda \partial E}{\partial V_{ij}}, i = 0, 1, \dots, n; j = 1, 2, \dots, m. \quad (6)$$

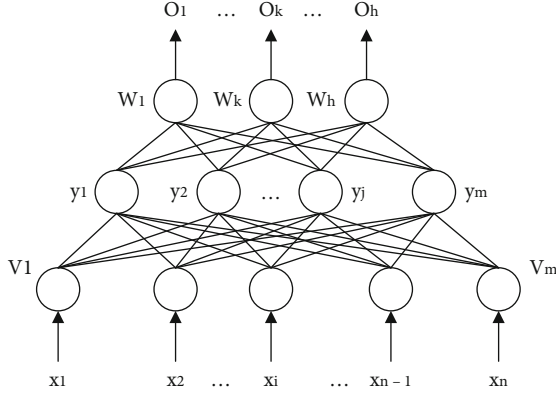


FIGURE 1: A single hidden layer NN structure.

After repeated cycles, the value adjustment function of the weight of the BP learning algorithm is

$$\Delta w_{jk} = \lambda \theta_k^O y_j = \lambda (b_k - O_k) O_k (1 - O_k) y_j, \quad (7)$$

$$\Delta V_{ij} = \lambda \theta_j^y x_i = \lambda \left( \sum_{k=1}^l \mu_k^O w_{jk} \right) y_j (1 - y_j) x_i. \quad (8)$$

In the BP learning algorithm, the weight adjustment formula of each layer of the network is the same in form, and the formula is determined by three factors, namely, the output error signal  $\theta$  of this layer, the learning rate  $\lambda$ , and the input signal  $X$  (or  $Y$ ). The error signal of the output layer comes from the transformation of the difference between the expected output and the actual output. The error signal of each hidden layer depends on the error signals of the layers before the layer. These error signals are all back-transmitted from the output layer by layer.

**3.2.3. Defects of BP Algorithm.** The BP algorithm can estimate any nonlinear function with any precision after being used in a three-layer feedforward network with a nonlinear transfer function, which is the reason why the BP network is more and more widely used. However, the standard BP algorithm has some inherent defects in its application:

- (1) It is easy to not obtain the global optimal solution and only obtain the local minimum solution
- (2) Too many training times will reduce the learning efficiency and slow down the speed of convergence
- (3) The selection of hidden nodes lacks theoretical guidance
- (4) During training, learn new samples but easily forget about old samples

**3.2.4. Improvement of BP Algorithm.** In order to overcome the shortcomings of the BP algorithm, a variety of new algorithms have been proposed to improve it in practice, and the network has been improved from different angles.

#### (1) Simulated annealing algorithm

It is a global optimization algorithm that simulates the metal annealing process. The adjustable weights of the network are equivalent to the particles in the metal, and the output error of the network is equivalent to the energy state of the metal. By adding “noise” to the variables, it is possible for the network to jump out of the minimum point of the cost function and converge to the global minimum point.

#### (2) Genetic algorithm

It is a probabilistic search method that mimics the genetic and evolutionary processes of animals in the wild. It is an adaptable global optimization algorithm. A number of beginning points are used to avoid the network from settling on a local solution instead of a global one; the algorithm employs the probability law to guide its search and conducts efficient heuristic search in the solution space. We would prefer thorough yet methodical research than haphazard or unfocused efforts. As a result, avoiding local minima is extremely probable. Apply the global search performance of a genetic algorithm first, and then use error back propagation to identify a solution that is best for your particular situation.

#### (3) Improve the normalization algorithm of training samples

Due to the large difference in the physical quantities of the input nodes of the network, the training samples of various indicators are not comparable, so the evaluation cannot be carried out smoothly. In order to prevent small values from being overwhelmed by large values, different normalization methods can be used to normalize the input samples to between  $[0, 1]$ .

#### (4) Reasonable selection of initial weights and thresholds

By selecting appropriate weights and thresholds, or making appropriate adjustments during the training process, the global optimal solution can be achieved to jump out of the local minimum area. In many literatures, a variety of initial values are set, and then, the one with the best training effect is selected as the weight and threshold after learning. This method is relatively simple and effective and is widely used.

#### (5) Improve the activation function

In the hidden layer of the network, the activation function of neurons generally uses the S function, but the S function has a defect. When the value is close to 0 or 1, the regions at both ends are defined as the saturated region, and the middle region is the unsaturated region. In the saturation region, the change of the independent variable has been unable to change the change of the function value well. If the output of the network neuron is different from the expected value at this time, and the adjustment amount of the connection weight is small, it is difficult to adjust the existing state of the neuron, and the convergence speed is

slowed down, which is the “platform” phenomenon. In order to solve this problem, the activation function of the neurons in the hidden layer can be in the form of formula (9). By adjusting the values of  $d$ ,  $g$ , and  $h$ , the saturation region of the function can be changed, so as to attain the determination of adjusting the output value of the neuron.

$$f(x) = \frac{1}{d} + ge^{-hx}. \quad (9)$$

#### (6) Adjust the network structure

The network structure is changed by increasing the number of nodes, layers, and connection methods according to certain rules, so as to solve the problem that the global optimal solution and the local minimum cannot be obtained.

#### (7) Determination of the number

Determination of the number of neurons in the hidden layer if the level of the network is certain, the increase in the number of hidden layers can effectively improve the training accuracy. The premise of ensuring that a nonlinear network has the ability to approximate any curve is to have enough hidden layer neurons, but if there are too many hidden layer neurons, the convergence speed will be slowed down. There is a theory in the literature that if there is a node in the input layer of a three-layer feedforward NN, then when the number of nodes in the hidden layer is  $2a + 1$ , the network can approximate any differentiable function with arbitrary precision.

**3.3. Evaluation Index System Based on BPNN.** The index system plays a critical role in the evaluation of nonlinear problems since it is scientific and fair. In the index system, the meaning and weight of each index are marked in detail, and the reasonable and scientific settings of the index system play a key role in the evaluation system. Regardless of the final result of the evaluation or the evaluation index of the evaluation index system, the correspondence between the rank and the output range is shown in Table 1. The evaluation system proposed in this paper for the impact of occupational identity on occupational well-being is designed with multiple evaluation indicators, as shown in Table 2.

**3.4. Evaluation Data Initialization Processing.** Since the input of indicators in this article is obtained by scoring or grades, the percentage system is used. However, the input data range of the BPNN is between  $[0, 1]$ , and the excitation function is the  $S$  function. Therefore, before the NN is trained, the input data should be normalized. Commonly used normalization functions are the maximum and minimum method, exponential function method, and so on. This paper uses the maximum and minimum method to normalize the input data. This method is a linear transformation of the data, which can better preserve the original meaning of

TABLE 1: NN output value and evaluation level corresponding table.

Evaluation level	NN output value
Totally suitable	0.900-1
Basically meet	0.800-0.890
Uncertain	0.700-0.790
Basically does not meet	0.600-0.690
Totally inconsistent	0-0.590

the data. The input data normalization formula is as follows:

$$X = I - \frac{I_{\min}}{I_{\max}} - I, \quad (10)$$

where  $X$  is the input value of the BPNN,  $I$  is the evaluation original data,  $I_{\min}$  is the minimum value of the BPNN input, and  $I_{\max}$  is the maximum value of the BPNN input.

## 4. Experiment and Analysis

**4.1. Determination of BP Network Results.** According to Kolmogorov’s theorem, a BPNN with a hidden layer can be used to approximate any continuous function mapping relationship. Any continuous rational function in a closed interval can be approximated by a BPNN with a sigmoid hidden layer and a linear output layer. Therefore, in the design of BPNN, the three-layer network can meet the basic requirements. If the number of layers is enlarged, the complexity of the network will be greatly enlarged, the training time will be increased, and the scope of reducing the error will be limited. This paper constructs the evaluation model using the three-layer BP network structure.

- (1) The number of neural units in the input layer is determined

The number of neural units in the input layer is determined as the number of indicators in the evaluation table, and the available indicators are 10, that is, the number of neural units in the input layer of the BPNN is 10.

- (2) The number of neural units in the output layer is determined

The number of neural units in the output layer is the evaluation result of the influence of occupational identity on occupational well-being, which is set to 1 in this paper. Through the qualitative and quantitative evaluation analysis of the course, a quantitative evaluation result output is finally obtained.

- (3) The number of neurons in the hidden layer is determined

In the BPNN, the number of neurons in the hidden layer has a great influence on the performance of the NN. If the number of neurons in the hidden layer is too small, the learning ability of the NN will be insufficient, and the network will easily fall into a local minimum point. Sometimes

TABLE 2: Occupational identity scale assessment indicators.

Index	Label
Work matches my expectations	X1
Work makes me proud	X2
Very satisfied with the work	X3
If you choose a job again, you will still choose the current one	X4
I want my children to do my current job	X5
I would like to do this job for the rest of my life	X6
Your current job is an important part of your self-image	X7
I really identify with my work	X8
The work I do will make me feel more fulfilled than others	X9
My career trajectory is important to realizing my self-worth	X10

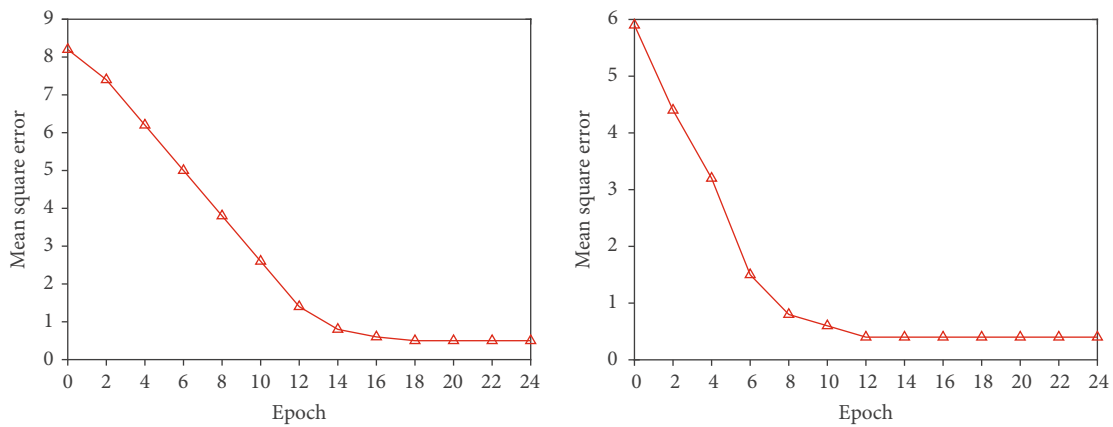


FIGURE 2: Train effect when  $N = 4$  and  $N = 6$ .

even unstable results may be obtained. On the contrary, if the number of NN elements in the hidden layer is too large, the network will fit the irregular information existing in the sample, resulting in the phenomenon of “overfitting” in the network, which will not only lead to prolonged training time but also errors are not necessarily minimal. Therefore, the appropriate selection of the number of neurons is a very important task. According to experience, for a three-layer NN, the following formula is used for the number of neural units in the hidden layer:

$$h = \sqrt{i + k} + c, \tag{11}$$

where  $i$  is the number of neurons in the input layer,  $k$  is the number of neurons in the output layer, and  $c$  is a constant in the range [1–10].

According to the above empirical formula, the number of neurons in the hidden layer of the network model in this paper ranges from [4–14], and the most suitable number of neurons needs to be verified through experiments. The experimental results obtained are shown in Figures 2–4. Finally, 8 is the number of neurons in the hidden layer.

(4) Determination of the training function

Different training functions have different convergence accuracy and number of training steps. From the experimental data, it is most appropriate to choose LM as the training function in this paper.

(5) Determination of the learning rate

In the BPNN, the learning rate remains unchanged. If the learning rate is too large, the network weights will be adjusted to a larger extent each time they are updated, which may cause the NN to jump back and forth around the minimum error value during the update iteration process. When it is true, the network diverges and cannot converge. On the contrary, if the learning rate is too small, the adjustment speed of the network weights will be small each time, and the convergence speed will be slow. Taken together, although the learning rate is small, the convergence rate will be slow, but it will eventually converge to the vicinity of the minimum error value. Therefore, this paper tends to choose a smaller learning plastic sheet to ensure the stability of the system, and the learning rate finally determined in this paper is 0.025.

(6) Determination of activation function

In this paper, the tagsig hyperbolic tangent function is used as the activation function on the hidden layer unit. As

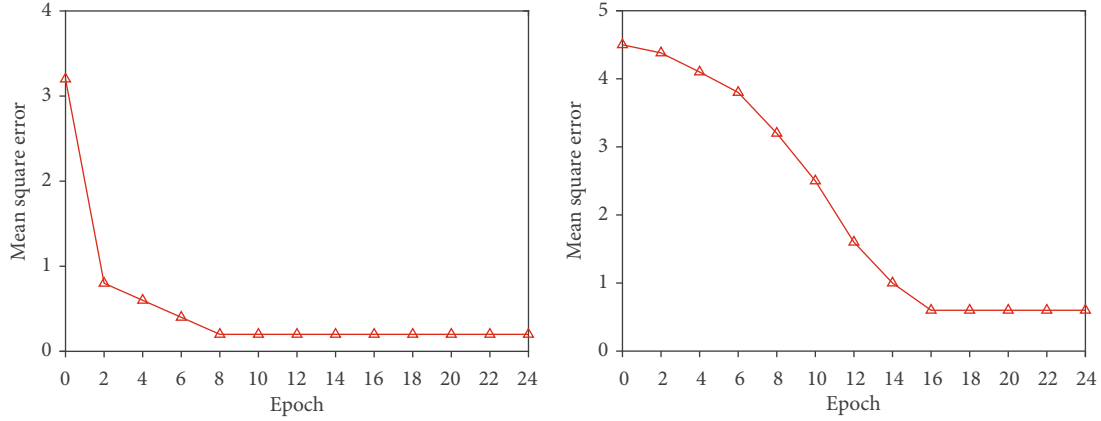


FIGURE 3: Train effect when  $N = 8$  and  $N = 10$ .

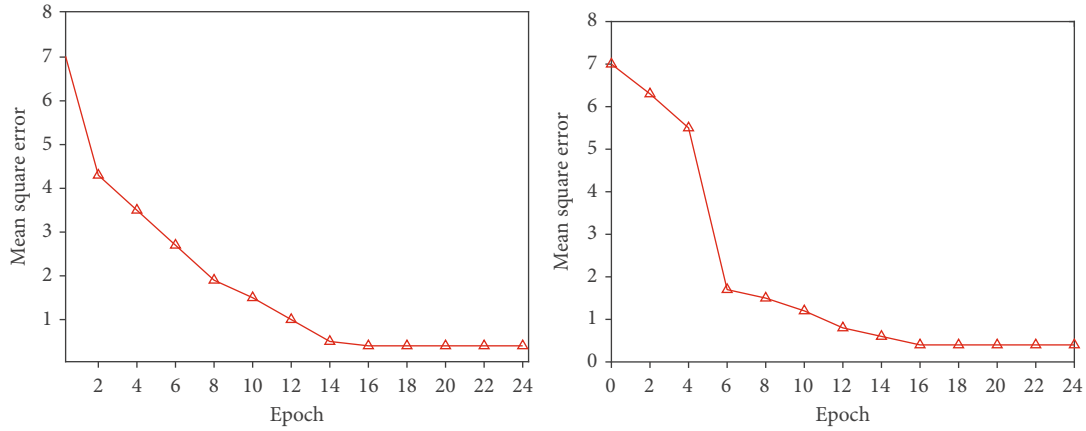


FIGURE 4: Train effect when  $N = 12$  and  $N = 14$ .

TABLE 3: Statistics of the final experimental results.

Result type	Num						
	1	2	3	4	5	6	7
Network evaluation results	0.829	0.815	0.728	0.925	0.682	0.871	0.966
Actual evaluation results	0.827	0.814	0.735	0.919	0.685	0.867	0.970
Error	0.020	0.010	0.070	0.060	0.030	0.040	0.040

mentioned above, the BPNN evaluation system in this paper performs data normalization processing in the first step, so the activation function of the output layer unit is selected as the sigmoid function.

4.2. Data Sources. The experiments in this paper are based on the MATLAB software package launched by MathWorks for modeling. This software package is not only a very practical and effective scientific research programming software environment but also an interactive program for scientific nuclear engineering calculation. MATLAB NN toolbox is the activation function of several typical NNs based on the theory of this algorithm designed by using scripting language and provides the function calling method, which is convenient for users to directly call the activation function

of the network without repeated construction. Users can also alter the weights according to the specific conditions of the network they developed, as well as the network’s training process, write design and training functions suitable for their own network using the scripting language, and learn the functions. At present, the MATLAB NN toolbox contains most of the NNs, including the perceptron model, the BPNN, and the self-organizing network model. In this paper, the results of 280 occupational identity scale B of employees in different types of companies are obtained through online questionnaire survey as experimental data. The screening of the survey data is to delete 5% of the lowest and highest scores to prevent “spam.” After that, the experimental data is initialized, and the following 240 data are randomly selected as training and simulation data.

4.3. *Experimental Results of BPNN Model.* Through model initialization, a network prediction model is created, and after training the NN, the obtained model is subjected to data-based simulation tests, and the final experimental results are shown in Table 3.

As shown in Table 3, the evaluation results after network training are compared with the actual evaluation results, in which the actual evaluation results are the evaluation data given by experts. From the experimental data, it can be concluded that the training accuracy of the evaluation model of the influence mechanism of occupational identity on occupational well-being based on BPNN is completely acceptable, and it is a scientific, reasonable, and feasible prediction model.

## 5. Conclusion

Wages, bonuses, benefits, and working circumstances, according to motivation theory, are external motivating factors for a person's work motivation, whereas belonging, respect, achievement, and challenge are internal motivational factors for a person's work motivation. Occupational identity is an individual's affirmative evaluation of the occupation he is engaged in. It not only overcomes the externality and sense of alienation of the occupation but also is a person who can internally unify his personal value and meaning with the value and meaning of the occupation he is engaged in. As a result, the occupational work motivation formed on the basis of occupational identity is more conscious, active, and active. Compared with various other external stimuli and inducements, occupational identity plays a more lasting and stable role. In addition, the final experimental results of this paper show that occupational identity has a positive effect on employees' occupational well-being, which can allow employees to bring greater benefits to the enterprise. Therefore, enterprise managers can take the cultivation of employees' professional identity as part of the enterprise culture. The work completed in this paper is as follows: (1) it introduces the interpretation of the concept of "professional identity" by different scholars at home and abroad and makes a brief review of the research on professional identity and professional well-being made by foreign scholars in recent years. (2) The basic knowledge and algorithm flow of ANN are introduced, and the evaluation model based on BPNN is proposed, including NN evaluation model, network structure, learning parameters, and learning algorithm. (3) The NN evaluation system constructed in this paper is verified by the simulation software. Experiments reveal that the BPNN system proposed in this study is a reasonable and feasible evaluation model for determining the process by which occupational identity influences occupational well-being.

## Data Availability

The datasets used during the current study are available from the corresponding author on reasonable request.

## Conflicts of Interest

The authors declare that they have no conflicts of interest.

## References

- [1] Y. Hong, "Pre-service and beginning teachers' professional identity and its relation to dropping out of the profession," *Teaching & Teacher Education*, vol. 26, no. 8, pp. 1530–1543, 2010.
- [2] J. Horn, D. Taris, B. Schaufeli, and P. J. G. Schreurs, "The structure of occupational well-being: a study among Dutch teachers," *Journal of Occupational and Organizational Psychology*, vol. 77, no. 3, pp. 365–375, 2004.
- [3] L. Antonek, E. McCormick, and R. Donato, "The student teacher portfolio as autobiography: developing a professional identity," *Modern Language Journal*, vol. 81, no. 1, pp. 15–27, 1997.
- [4] A. Julie and H. Fox, "Communication: improving RNs' organizational and professional identification in managed care hospitals," *Journal of Nursing Administration*, vol. 32, no. 2, pp. 106–114, 2002.
- [5] D. Bhanthumnavin, "Perceived social support from supervisor and group members' psychological and situational characteristics as predictors of subordinate performance in Thai work units," *Human Resource Development Quarterly*, vol. 14, no. 1, pp. 79–97, 2003.
- [6] D. Chan, "Interactive effects of situational judgment effectiveness and proactive personality on work perceptions and work outcomes," *The Journal of Applied Psychology*, vol. 91, no. 2, pp. 475–481, 2006.
- [7] E. Bess, *Learning to Teach Physics: Exploring Teacher Knowledge, Practice, and Identity*, Montclair State University, 2018.
- [8] L. Hong, E. While, and L. Barriball, "Job satisfaction and its related factors: a questionnaire survey of hospital nurses in Mainland China," *International Journal of Nursing Studies*, vol. 44, no. 4, pp. 574–588, 2007.
- [9] J. L. Holland, J. A. Johnston, and N. F. Asama, "The vocational identity scale: a diagnostic and treatment tool," *Journal of Career Assessment*, vol. 1, no. 1, pp. 1–12, 1993.
- [10] F. Meijers, "The development of a career identity," *International Journal for the Advancement of Counselling*, vol. 20, no. 3, pp. 191–207, 1998.
- [11] J. Craig, C. Meijer, and J. Broeckmans, *Chapter 12 in Search of the Essence of a Good Teacher: Toward a More Holistic Approach in Teacher Education*, vol. 20, no. 1, 2004 Emerald Group Publishing Limited, 2004.
- [12] G. Steyn and G. Kamper, "Understanding occupational stress among educators: an overview," *Africa Education Review*, vol. 3, no. 1-2, pp. 113–133, 2006.
- [13] K. Cooper and M. Olson, *The Multiple of Teacher Identity*, Falmer Press, London, 2020.
- [14] J. Coldron and R. Smith, "Active location in teachers' construction of their professional identities," *Journal of Curriculum Studies*, vol. 31, no. 6, pp. 711–726, 1999.
- [15] L. Kremer and E. Hofman, "Teachers' professional identity and burnout," *Research in Education*, vol. 34, no. 1, pp. 89–95, 1985.
- [16] D. Brickson, "The impact of identity orientation on individual and organizational outcomes in demographically diverse

- settings,” *Academy of Management Review*, vol. 25, no. 1, pp. 82–101, 2000.
- [17] P. Mayer, J. Allen, and A. Smith, “Commitment to organizations and occupations: extension and test of a three-component conceptualization,” *Journal of Applied Psychology*, vol. 78, no. 4, pp. 538–551, 1993.
- [18] F. Goodson and L. Cole, “Exploring the teachers' professional knowledge: constructing identity and community,” *Teacher Education Quarterly*, vol. 21, no. 1, pp. 85–105, 1994.
- [19] L. Kremer, H. Faraj, and T. Wubbels, “Burn-out among Israeli Arab school principals as a function of professional identity and interpersonal relationships with teachers,” *International Journal of Leadership in Education*, vol. 5, no. 2, pp. 149–162, 2002.
- [20] P. Warr, “Age and occupational well-being,” *Psychology and Aging*, vol. 7, no. 1, pp. 37–45, 1992.
- [21] U. Kinnunen, T. Parkatti, and A. Rasku, “Occupational well-being among aging teachers in Finland,” *Scandinavian Journal of Educational Research*, vol. 38, no. 3-4, pp. 315–332, 1994.
- [22] M. Shu and R. Yao, *Investigation and Reflection on the Reasons for Preschool Teachers to Obtain Occupational Happiness*, vol. 6, pp. 39–42, 2003.
- [23] B. Ji, Y. Li, D. Cao, C. Li, S. Mumtaz, and D. Wang, “Security performance analysis of UAV assisted relay transmission for cognitive network with energy harvesting,” *IEEE Transactions on Vehicular Technology*, vol. 69, no. 7, pp. 7404–7415, 2020.
- [24] X. Lin, J. Wu, S. Mumtaz, S. Garg, J. Li, and M. Guizani, “Blockchain-based on-demand computing resource trading in IoV-assisted smart n,” *IEEE Transactions on Emerging Topics in Computing*, vol. 9, no. 3, pp. 1373–1385, 2021.

## Research Article

# Effect of Midwives' Application of Intelligent Delivery Room Management System on Delivery Outcome

Xia Li, Ping Zhang, Yong Zhang, Gaiying Cui, and Hui Du 

Shijiazhuang Fourth Hospital, 16 Tanggu street, Chang'an District, Shijiazhuang City, Hebei Province, China

Correspondence should be addressed to Hui Du; xiaohui163111@163.com

Received 10 April 2022; Revised 10 May 2022; Accepted 13 May 2022; Published 27 May 2022

Academic Editor: Naeem Jan

Copyright © 2022 Xia Li et al. This is an open access article distributed under the Creative Commons Attribution License, which permits unrestricted use, distribution, and reproduction in any medium, provided the original work is properly cited.

**Objective.** To investigate the impact of midwives using an intelligent delivery room management system on the outcome of deliveries. **Method.** A total of 100 primiparas admitted to the department of obstetrics and gynecology of our hospital from January 2019 to June 2020 were selected as the research objects. They were randomly assigned to one of two groups: control or observation. The control group got standard obstetric care. On the basis of the control group, midwives in the observation group applied the intelligent delivery room management system for delivery management. The outcomes of childbirth, postpartum anxiety, and postpartum depression were recorded and compared between the two groups. **Results.** The observation group's first and second stages of labour were shorter than the control group's ( $P < 0.05$ ), postpartum NRS score was lower than the control group's ( $P < 0.05$ ), neonate Apgar score was higher than the control group's ( $P < 0.05$ ), and the rate of vaginal delivery to caesarean section was lower than the control group's ( $P < 0.05$ ). There was no statistical significance in prenatal S-AI scores between the observation group and the control group ( $P > 0.05$ ). After delivery, the S-AI score of the observation group was lower than that of the control group, and the comparison result was statistically significant ( $P < 0.05$ ). There was no significant difference in prenatal EPDS scores between the observation group and the control group ( $P > 0.05$ ). After delivery, the EPDS score of the observation group was lower than that of the control group, and the comparison result was statistically significant ( $P < 0.05$ ). **Conclusion.** Midwives may employ sophisticated delivery room management technologies to improve birth outcomes and reduce maternal anxiety and depression, and it is something that should be extensively promoted in clinic.

## 1. Introduction

Childbirth is a normal physiological process, and a constant and intense stressor, along with the delivery process, the maternal tension, anxiety, depression, and other adverse emotions increased sharply, and adverse emotions were correlated with the outcome of childbirth [1]. In obstetrics and gynecology, labor analgesia requires close observation. Turntable speed can also be slowed by prolonged work. Medical personnel are insufficient to address the demands of more women, resulting in the country's low natural birth rate [2, 3]. A clinic urgently needs a set of management system software to solve the problem of labor shortage in the delivery room. The system software can monitor the operation of the analgesic pump and physiological parameters of the pregnant women in

real time. Electronic delivery record sheet can be realized, doctors can view all maternal actual labor process on a computer and can meet the needs of information, mobile monitoring function, electronic files, and so on [4, 5]. Midwives use an intelligent delivery room management system to optimise medical staff work efficiency, improve childbirth quality, control childbirth risk, and collect delivery room data management information [4, 6]. The use of the intelligent delivery room management system by midwives in our hospital from January 2019 to June 2020 had a positive impact on the delivery outcome, according to this study. The following is the report:

The paper's organization paragraph is as follows: the materials and methods is presented in Section 1. Section 2 discusses the experiments and results. Finally, in Section 3, the research work is conclude with discussion.



## 2. Materials and Methods

**2.1. General Information.** A total of 100 primiparas admitted to the department of obstetrics and gynecology of our hospital from January 2019 to June 2020 were selected as the research objects. It had been approved by the Ethics Committee of our hospital. They were randomly divided into a control group and an observation group. Control group: the average age was  $24.68 \pm 4.21$  years from 20 to 34 years old; gestational weeks ranged from 35 to 41 weeks, with an average of  $39.64 \pm 0.78$  weeks. Observation group: the average age was  $25.10 \pm 4.22$  years from 21 to 35 years old; gestational weeks ranged from 36 to 41 weeks, with an average of  $39.88 \pm 0.72$  weeks. There was no significant difference in maternal age and gestational age between the two groups ( $P > 0.05$ ), which was comparable.

**2.1.1. Inclusion Criteria.** Inclusion criteria are as follows: ① 36 to 41 weeks of gestation; ② pseudonatural vaginal birth; ③ single live births; ④ age 20-35 years old; ⑤ the puerpera and her family members signed the informed consent.

**2.1.2. Exclusion Criteria.** Exclusion criteria are as follows: ① patients with pregnancy hypertension and diabetes mellitus; ② patients with insomnia, depression, and other serious mental disorders before pregnancy; ③ patients with communication difficulties; ④ other unsuitable candidates.

### 2.2. Methods

**2.2.1. Control Group.** Adopting routine obstetric management, that was, after entering the labor process, accompanied by the midwife, routine psychological support, breastfeeding guidance, and general guidance for the newborn.

**2.2.2. Observation Group.** On the basis of the control group, with the use of midwives and intelligent delivery room management system for delivery management, intelligent delivery room management system from the perspective of the actual needs of the delivery room, covering the whole delivery process in the delivery room; it was necessary to support the real-time monitoring of the operation status of the analgesia pump, the real-time monitoring of the maternal physiological parameters, and the real-time monitoring of the portable monitoring equipment data, supporting the mobile viewing of medical staff, meeting the interaction data with HIS and other hospital information systems, and avoiding the generation of information islands [7]. The intelligent delivery room management system setted the delivery and delivery and postpartum rehabilitation in the same delivery room. Prepare Dulla ball, Dulla instrument, bean bag, and other birthing auxiliary supplies while equipped with a multipurpose electric bed, foetal monitor, low-frequency pulse postpartum rehabilitation equipment, first aid medications, narcotics, and other essential equipment during labour [8]. According to the home conditions of the puerpera, the ward environment was arranged; wardrobe, sofa, TV, 24 h hot water, and other necessary items for family life were added, and speakers were introduced to create an intelligent environment. Obstetricians, midwives, operating room nurses,

neonatologists, nurses, and maternal family members collaborated during the delivery process to complete the perinatal management of the mother. Figure 1 depicts the intelligent delivery room management system.

**2.3. Observational Index.** The outcomes of childbirth, postpartum anxiety, and postpartum depression were recorded and compared between the two groups.

**2.3.1. Delivery Outcome.** The time of the first stage of labor, the time of the second stage of labor, the time of the third stage of labor, the number of cases of vaginal conversion to cesarean section, Apgar score of newborn, and labor pain were recorded in the two groups. Pain was assessed by numeral pain score (NRS) [9] at the first time after delivery; the pain intensity was expressed by 0~10 pain points, which were evaluated by the puerpera at the time of admission to the ward after delivery. The mean value was calculated by repeating twice.

**2.3.2. Postpartum Anxiety.** The State Anxiety Questionnaire (S-AI) [10] was used to measure the state of maternal anxiety before and after 3 days. A total of 20 items were filled in by the parturients according to their own actual feelings. Each item was divided into 4 levels, which counted as 1-4 points. The higher the score, the heavier the anxiety level.

**2.3.3. Postpartum Depression.** The Edinburgh Postpartum Depression Scale (EPDS) [11] was used to measure maternal depression at prenatal and postpartum 3 days. There were 10 items in total, and each item adopted a 4-level score of 0-3. The total score of each item was added into the total score, and the total score of  $>13$  was classified as postpartum depression. The higher the score, the more severe the depression.

**2.4. Statistical Methods.** SPSS22.0 statistical software was used. The statistical data were compared by  $\chi^2$  test of two independent samples. Two independent samples  $t$  or  $t'$  test were used to compare the measurement data of normal distribution. Rank sum test was used to compare the measurement data of nonnormal distribution, and the test level  $\alpha = 0.05$ .

## 3. Results

**3.1. Results of Delivery Outcome.** The time of the first stage of labor and the second stage of labor in the observation group were shorter than those in the control group ( $P < 0.05$ ), postpartum NRS score was lower than control group ( $P < 0.05$ ), Apgar score of neonates was higher than that of control group ( $P < 0.05$ ), and the rate of vaginal delivery to cesarean section was lower than that of control group ( $P < 0.05$ ). Results of delivery outcome are shown in Table 1.

**3.2. Results of Anxiety Score.** There was no statistical significance in prenatal S-AI scores between the observation group and the control group ( $P > 0.05$ ). After delivery, the S-AI score of the observation group was lower than that of the control group, and the comparison result was statistically

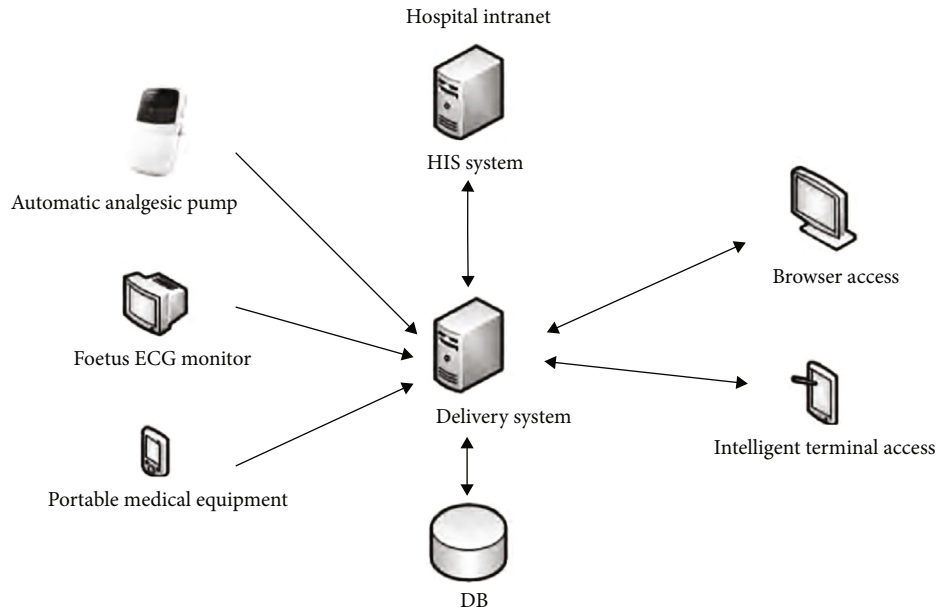


FIGURE 1: The intelligent delivery room management system.

TABLE 1: Results of delivery outcome.

Groups	Cases	Birth process time [M(Q <sub>n</sub> )•h]			Apgar score		NRS	Normal delivery to cesarean section
		First stage	Second stage	Third stage	8-10	<8		
Control group	50	11.04 (0.75)	0.65 (0.13)	0.12 (0.02)	37	13	8.860 ± 0.280	14
Observation group	50	9.05 (1.32)	0.40 (0.17)	0.11 (0.03)	44	6	6.41 ± 1.170	6
Statistics		7.531	5.201	1.254	4.506		11.571	7.303
P		<0.050	<0.050	>0.050	<0.050		<0.050	<0.050

significant ( $P < 0.05$ ). Results of anxiety score was shown in Table 2.

3.3. *Results of Depression Score.* There was no significant difference in prenatal EPDS scores between the observation group and the control group ( $P > 0.05$ ). After delivery, the EPDS score of the observation group was lower than that of the control group, and the comparison result was statistically significant ( $P < 0.05$ ). Results of depression score was shown in Table 3.

#### 4. Discussion

In a set of system software, the intelligent delivery room management system integrates maternal analgesia with maternal and foetal physiological data. Support access to data information from a range of devices to satisfy the practical demands of obstetricians, anesthesiologists, and midwives at the same time. The software can also be based on warehouse conditions [12], optimize the system warehouse management workflow, and realize drug expiration query, material use instructions, and so on. It is convenient for the trainees to use it efficiently. It creates an electronic combat team and provides the function of multiangle and multi-level statistical analysis data to assist the commander in

making decisions [13, 14]. Studies at home and abroad have reported that the incidence of anxiety and depression in pregnant women during pregnancy continues to increase. More than 50% of pregnant women show symptoms of anxiety or depression in the early and late stages of pregnancy, often showing extreme irritability, persistent fatigue and low mood, moodiness, and more tension, worry, and depression than before [15]. The physiological changes during pregnancy, social gestation pressure, postpartum fatigue, and complications that primipara face during pregnancy and delivery are likely to cause difficulty adapting to the role transition of novice mothers with no prior experience with pregnancy and delivery, an urgent demand for family support, and an easy to produce negative emotion [16]. Anxiety and depression during pregnancy not only directly damage the spirit and quality of life of pregnant women but also may develop into postpartum psychosis and bring long-term negative effects on the growth and development of infants [17]. The intelligent delivery room management system includes all living facilities and medical safety equipment, so that the parturient can feel warm during delivery and help the parturient to reduce the pain and stress reaction caused by negative emotions during delivery [18], prevent postpartum depression, and then reduce the risk of uterine weakness and prolonged labor, reduce the risk of

TABLE 2: Results of anxiety score.

Groups	Cases	S-AI	
		Before delivery	After delivery (3 d)
Control group	50	64.68 ± 1.650	60.31 ± 1.170
Observation group	50	65.03 ± 1.230	51.03 ± 1.610
Statistics		1.007	27.364
<i>P</i>		>0.050	<0.050

TABLE 3: Results of depression score.

Groups	Cases	EPDS	
		Before delivery	After delivery (3 d)
Control group	50	13.020 ± 2.340	9.020 ± 0.360
Observation group	50	13.140 ± 2.760	8.030 ± 0.760
Statistics		0.201	7.121
<i>P</i>		>0.050	<0.050

neonatal asphyxia, and increase the natural birth rate. Because the medical equipment in use has safety risks, risk identification, risk assessment, and risk control are required [19]; the application quality evaluation of the analgesia pump should be strengthened in order to ensure the accuracy and reliability of the data collection of the intelligent delivery room management system [19].

Research in this study showed that the time of the first stage of labor and the second stage of labor in the observation group was shorter than those in the control group ( $P < 0.05$ ), postpartum NRS score was lower than control group ( $P < 0.05$ ), Apgar score of neonates was higher than that of control group ( $P < 0.05$ ), and the rate of vaginal delivery to cesarean section was lower than that of control group ( $P < 0.05$ ). There was no statistical significance in prenatal S-AI scores between the observation group and the control group ( $P > 0.05$ ). After delivery, the S-AI score of the observation group was lower than that of the control group, and the comparison result was statistically significant ( $P < 0.05$ ). There was no significant difference in prenatal EPDS scores between the observation group and the control group ( $P > 0.05$ ). After delivery, the EPDS score of the observation group was lower than that of the control group, and the comparison result was statistically significant ( $P < 0.05$ ).

To summarize, midwives using an intelligent delivery room management system can improve the result of labor, minimize maternal anxiety and depression, and is deserving of widespread clinical promotion.

### Data Availability

The data used to support the findings of this study are included within the article.

### Conflicts of Interest

The authors declare that they have no conflicts of interest.

## References

- [1] K. Evans, H. Spiby, and J. C. Morrell, "Non-pharmacological interventions to reduce the symptoms of mild to moderate anxiety in pregnant women. A systematic review and narrative synthesis of women's views on the acceptability of and satisfaction with interventions," *Archives of Women's Mental Health*, vol. 23, no. 1, pp. 11–28, 2020.
- [2] A. Bittner, J. Peukert, C. Zimmermann et al., "Early intervention in pregnant women with elevated anxiety and depressive symptoms," *Journal of Perinatal & Neonatal Nursing*, vol. 28, no. 3, pp. 185–195, 2014.
- [3] M. Collins, "A case report on the anxiolytic properties of nitrous oxide during labor," *Journal of Obstetric, Gynecologic & Neonatal Nursing*, vol. 44, no. 1, pp. 87–92, 2015.
- [4] N. Donnelly, K. Butler-Henderson, M. Chapman, and E. Sullivan, "The development of a classification system for maternity models of care," *Him Journal*, vol. 45, no. 2, pp. 64–70, 2016.
- [5] N. Alharbe and A. S. Atkins, "Transforming to a smart hospital system: proposed application in the Medina Maternity and Children's Hospital," *IJPCC*, vol. 12, no. 4, pp. 503–522, 2016.
- [6] M. Forster, K. Dennison, J. Callen, A. Georgiou, and J. I. Westbrook, "Maternity patients' access to their electronic medical records: use and perspectives of a patient portal," *Health Information Management Journal*, vol. 44, no. 1, pp. 4–11, 2015.
- [7] J. Zhao, "The application effect of fine management in obstetrics and gynecology delivery room nursing safety management," *Wisdom Health*, vol. 6, no. 10, pp. 18–19, 2020.
- [8] X. Zhao, R. Ma, and W. Yang, "Analysis of the effect of humanized management on improving the quality of nursing care in delivery room," *Wisdom Health*, vol. 4, no. 34, pp. 17–18, 2018.
- [9] K. E. Göransson, U. Heilborn, J. Selberg, S. von Scheele, and T. Djärv, "Pain rating in the ED—a comparison between 2 scales in a Swedish hospital," *American Journal of Emergency Medicine*, vol. 33, no. 3, pp. 419–422, 2015.
- [10] Z. Jia, L. Geng, W. Wang et al., "The reliability of APAIS score in evaluating preoperative anxiety in Chinese," *Chinese Journal of Anesthesiology*, vol. 35, no. 9, pp. 1107–1109, 2015.
- [11] C. El-Hachem, J. Rohayem, R. Bou Khalil et al., "Early identification of women at risk of postpartum depression using the Edinburgh Postnatal Depression Scale (EPDS) in a sample of Lebanese women," *BMC Psychiatry*, vol. 14, no. 1, pp. 1–9, 2014.
- [12] J. Azaare and J. Gross, "The nature of leadership style in nursing management," *British Journal of Nursing*, vol. 20, no. 11, pp. 672–680, 2011.
- [13] C. Bowie and T. Mwase, "Assessing the use of an essential health package in a sector wide approach in Malawi," *HARPS*, vol. 9, no. 1, pp. ???–??4, 2011.
- [14] J. P. Kainu, E. Halmesmki, K. T. Korttila et al., "Persistent pain after cesarean delivery and vaginal delivery," *Anesthesia & Analgesia*, vol. 123, no. 6, pp. 1535–1545, 2016.
- [15] J. J. Wu, "Study on the application effect of midwife continuous nursing in delivery room," *Wisdom Health*, vol. 4, no. 6, pp. 153–154, 2018.
- [16] A. Cohen, Y. Cohen, I. Laskov, S. Maslovitz, J. B. Lessing, and A. Many, "Persistent abdominal pain over uterine scar during labor as a predictor of delivery complications," *International Journal of Gynecology & Obstetrics*, vol. 123, no. 3, pp. 200–202, 2013.

- [17] L. Wen, G. Hilton, and B. Carvalho, "The impact of breastfeeding on postpartum pain after vaginal and cesarean delivery," *Journal of Clinical Anesthesia*, vol. 27, no. 1, pp. 33–38, 2015.
- [18] B. M. H. Asl, A. Vatanchi, N. Golmakani, and A. Najafi, "Relationship between behavioral indices of pain during labor pain with pain intensity and duration of delivery," *Electronic Physician*, vol. 10, no. 1, pp. 6240–6248, 2018.
- [19] T. Hamer, S. Deverman, K. J. Nunes, J. Hofer, and B. M. Scavone, "Pain and analgesia during labor and delivery between 16 0/7 and 22 6/7 weeks of gestation," *Obstetrics & Gynecology*, vol. 127, no. 6, pp. 1161–1165, 2016.

## Research Article

# Analysis of the Effect of Exercise Combined with Diet Intervention on Postoperative Quality of Life of Breast Cancer Patients

Lihua Lu,<sup>1</sup> Xiaofeng Chen,<sup>1</sup> Ping Lu,<sup>1</sup> Jianli Wu,<sup>1</sup> Yunxia Chen,<sup>1</sup> Tiantian Ren,<sup>1</sup> Yiju Li <sup>1</sup> and Xiang Zhong<sup>2</sup>

<sup>1</sup>Thoracic and Breast Surgery, Affiliated Hospital of Nantong University, China

<sup>2</sup>School of Nursing, Medical College, Nantong University, China

Correspondence should be addressed to Yiju Li; 2013320193@stmail.ntu.edu.cn

Received 8 April 2022; Revised 10 May 2022; Accepted 13 May 2022; Published 27 May 2022

Academic Editor: Naeem Jan

Copyright © 2022 Lihua Lu et al. This is an open access article distributed under the Creative Commons Attribution License, which permits unrestricted use, distribution, and reproduction in any medium, provided the original work is properly cited.

To analyze the effect of exercise combined with diet intervention on postoperative quality of life of breast cancer patients, a total of 104 breast cancer patients randomly selected from October 2019 to September 2020 who received systemic adjuvant endocrine drug therapy in our hospital for the first time were divided into the observation group and control group as the research subjects. The control group was given exercise and exercise intervention on the basis of routine nursing, and the observation group was given exercise and exercise combined with diet intervention on the basis of basic nursing. Nutritional indexes, anxiety and depression, sleep quality, cancer-induced fatigue, and life quality were observed in both groups. The nutritional indicators of the observation group were slightly different from the control group after exercise and diet intervention, indicating that the observation group's data was higher than the control group ( $P > 0.05$ ). The HAMA (human anti-mouse antibody) and HAMD (Hamilton depression scale) ratings of the two groups did not differ significantly ( $P > 0.05$ ). Both groups' HAMA and HAMD ratings improved after intervention; although, the control group's increase was bigger than the observation group ( $P < 0.05$ ). Both groups' poor sleep quality assessment (PSQI) scores improved after intervention, with the observation group's increase rate being lower than the control group ( $P < 0.05$ ); the control group's sleep time fell more than the observation group ( $P < 0.05$ ).

## 1. Introduction

The World Health Organization (WHO) pointed out that breast cancer has become the highest incidence of malignant tumors in women worldwide [1]. Compared with other countries, the incidence of breast cancer in China is at a low level. However, the prevalence of breast cancer in China has been steadily increasing in recent years [2, 3]. The main treatment for breast cancer is surgical treatment, and in addition to radiotherapy and chemotherapy after surgery, the estrogen receptor and/or progesterone receptor positive patients need to receive at least 5 years of endocrine therapy [4]. Studies have shown that the 5-year survival rate of Chinese breast cancer patients can exceed 88%, which has

become a kind of malignant tumor with a relatively optimistic prognosis [5, 6]. But as patients live longer, other related problems emerge [7]. As a result of the adverse reactions caused by the disease and the treatment process, a variety of physical and psychological problems are exposed, such as the appearance of negative emotions, poor sleep quality, and cancer-related fatigue [8]. How to reduce the impact of these negative behaviors on patients and improve the quality of life of patients after surgery has become the focus of medical research [9, 10]. In this study, data of 104 cases of breast cancer patients treated in our hospital were analyzed to explore the influence of exercise combined with diet on postoperative quality of life of breast cancer patients, and the results are reported as follows.

TABLE 1: General information.

Projects		Observation group	Control group	$\chi^2$	$P$
Age		52.25 ± 12.30	54.12 ± 10.25	0.06	>0.05
Marriage	In marriage	41	39	0.04	>0.05
	Not in marriage	11	13		
Work	Yes	12	9	1.80	>0.05
	No	40	43		
Health care costs	Self-paying	3	4	0.02	>0.05
	Health care	49	48		
Mastectomy	Yes	38	37	0.12	>0.05
	No	14	15		
Lymph node metastasis	Yes	8	9	0.08	>0.05
	No	44	43		
Maximum tumor diameter		2.04 ± 1.14	1.85 ± 1.09	0.25	>0.05

The arrangements of the paper are as follows:

Section 2 discusses the materials and methods. Section 3 analyzes the result. Section 4 examines the various discussions. Section 5 concludes the article.

## 2. Materials and Methods

**2.1. General Information.** A total of 104 breast cancer patients who received the first systemic adjuvant endocrine drug therapy in our hospital from October 2019 to September 2020 were enrolled by convenience sampling. Patients signed informed consent before grouping, and this study had been approved by the ethics committee of our hospital.

**2.1.1. Inclusion Criteria.** The inclusion criteria were as follows: ① diagnosed by pathology as primary breast cancer with stage I~A and underwent surgical treatment in our hospital, ② after receiving chemotherapy in our hospital, the survival time was more than 6 months, ③ the body was free of serious comorbidities that could affect the results, and ④ sane and able to communicate normally.

**2.1.2. Exclusion Criteria.** The exclusion criteria were as follows: ① patients or their family members refused to accept the intervention in this study, ② patients who had been exercising regularly before, ③ accompanied by other diseases that affect the patient's activities, ④ had mental disorders and was unable to communicate, and ⑤ life expectancy was less than 1 year.

Patients were divided into the control group ( $n = 52$ ) and observation group ( $n = 52$ ) according to the random number table method. There was no significant difference in general clinical data between the two groups ( $P > 0.05$ ). General information was shown in Table 1.

### 2.2. Methods

**2.2.1. Conventional Nursing.** During their stay, all patients received normal treatment, which included exposing them to the hospital environment and staff following admission in order to help them transition into their roles as quickly as possible. Help patients to complete the examination, assist

them to complete the nursing operation, eliminate the patient's tension and fear of psychology, and ensure the treatment of cooperation.

**2.2.2. Nursing of the Control Group.** Exercise was administered as follows, based on traditional nursing: the nursing team will construct the appropriate exercise strategy based on the unique features of the patients. Exercise 3 times a week for the first three weeks for about 15 minutes and then gradually increase: maximum heart rate = 220 – patient age. During weeks 1 to 6, the intensity of exercise was 50% of the maximum heart rate. The intensity of exercise was 60% of maximal heart rate for weeks 7 to 10. All patients should choose an exercise that includes three parts: warm-up exercise, genuine exercise, and rest and relaxation, with a time control ratio of 1:3:1. Regular health education was taken for patients, to teach patients the benefits of physical exercise for breast cancer recovery.

**2.2.3. Nursing of the Experimental Group.** On the basis of exercise nursing in the control group, diet nursing intervention measures were given, as follows: ① diet nursing intervention on admission: to understand the eating habits and nutritional status of patients after admission and inform family members and patients of dietary taboo information, ② dietary intervention during chemotherapy: nursing staff should guide patients to eat high protein, high energy, high vitamin, and other diets and advice patients to eat a high-fiber diet, and ③ dietary care after discharge: develop a targeted diet plan, diet, and nutrition manual for patients upon discharge.

**2.3. Observational Index.** Observational index included the following:

- (1) Nutritional indicators: hemoglobin, serum albumin, lymphocyte count, and body mass index
- (2) Anxiety and depression: the Hamilton Anxiety Scale (HAMA) was used to score patients' anxiety [11]. The higher the anxiety level, the higher the score. The Hamilton Depression Scale (HAMD) was used

TABLE 2: Results of nutritional index.

Groups	Cases	Serum albumin (g/L)	Hemoglobin (g/L)	Body mass index (kg/m <sup>2</sup> )	Lymphocyte count ( $\times 10^9/L$ )
Observation group	52	36.45 $\pm$ 2.63	119.44 $\pm$ 3.55	20.24 $\pm$ 1.89	1.45 $\pm$ 0.65
Control group	52	25.01 $\pm$ 1.04	102.14 $\pm$ 1.57	15.87 $\pm$ 1.02	0.21 $\pm$ 0.27

TABLE 3: Results of anxiety and depression.

Groups	Cases	Time	HAMA	HAMD
Observation group	52	Before intervention	12.65 $\pm$ 2.01	14.78 $\pm$ 2.44
		After intervention	14.14 $\pm$ 3.02	17.34 $\pm$ 3.01
Control group	52	Before intervention	12.57 $\pm$ 2.08	15.14 $\pm$ 2.12
		After intervention	16.52 $\pm$ 3.21	20.58 $\pm$ 2.62

TABLE 4: Results of sleep quality.

Groups	Cases	Time	PSQI	Sleep time (h)
Observation group	52	Before intervention	10.55 $\pm$ 3.01	7.78 $\pm$ 2.04
		After intervention	12.13 $\pm$ 2.04	6.46 $\pm$ 0.84
Control group	52	Before intervention	10.14 $\pm$ 2.17	7.82 $\pm$ 1.64
		After intervention	14.64 $\pm$ 3.12	5.67 $\pm$ 0.41

to score the patients' depression [12]. The higher the score, the more depressed

- (3) Sleep quality: the Pittsburgh Sleep Quality Index (PSQI) was used to score patients' sleep quality. The scores were added up to a total score, which ranged from 0 to 21, with higher scores indicating poorer sleep quality
- (4) Cancer-related fatigue: the Piper fatigue scale was used to evaluate patients' cancer-induced fatigue [13]. Each item was scored on a scale of 0 to 6, with higher scores indicating more severe cancer-related fatigue
- (5) Quality of life: quality of life was assessed using the Concise Health Status Questionnaire (SF-36) and the Inventory Scale (QLQ-C30). The higher the score, better the quality of life

**2.4. Statistical Method.** SPSS 17.0 Chinese version was used for data input and data processing. Measurement data was expressed as ( $\bar{x} \pm s$ ). Independent sample  $t$ -test was used for analysis. Counting data is expressed as a percentage,  $\chi^2$  test was used for analysis, and  $P < 0.05$  was considered statistically significant.

### 3. Results

**3.1. Results of Nutritional Index.** After exercise and diet intervention, there was a slight difference in the nutritional indexes of the observation group compared with the control group, that was the data of the observation group was higher

than that of the control group ( $P < 0.05$ ). Results of nutritional index were shown in Table 2.

**3.2. Results of Anxiety and Depression.** The two groups' HAMA and HAMD scores were compared before and after intervention. Before intervention, there was no significant difference between the two groups' HAMA and HAMD scores ( $P > 0.05$ ). After intervention, HAMA and HAMD scores in both groups were increased, and the increase in the control group was greater than that in the observation group ( $P < 0.05$ ). Results of anxiety and depression were shown in Table 3.

**3.3. Results of Sleep Quality.** After intervention, the PSQI scores of both groups were improved, and the increase rate of observation group was less than that of the control group ( $P < 0.05$ ); the sleep time in the control group decreased more than that in the observation group ( $P < 0.05$ ). Results of sleep quality were shown in Table 4.

**3.4. Results of Cancer-Induced Fatigue.** Comparison of cancer-induced fatigue scores between the two groups before and after intervention showed that after the intervention, the scores of all dimensions of cancer-induced fatigue were increased in both groups, and the increase rate in the control group was higher than that in the observation group ( $P < 0.05$ ). Results of cancer-induced fatigue were shown in Table 5.

**3.5. Results of Quality of Life.** After treatment, the quality of life scores in both groups increased, and the increase rate in the control group was less than that in the observation group ( $P < 0.05$ ). Results of quality of life were shown in Table 6.

TABLE 5: Results of cancer-induced fatigue.

Groups		Observation group ( $n = 52$ )	Control group ( $n = 52$ )
Behavior	Before intervention	$4.160 \pm 0.712$	$4.133 \pm 0.855$
	After intervention	$4.753 \pm 0.271$	$5.611 \pm 0.170$
Feeling	Before intervention	$4.122 \pm 0.444$	$4.133 \pm 0.511$
	After intervention	$4.351 \pm 0.313$	$5.360 \pm 0.482$
Emotion	Before intervention	$4.052 \pm 0.343$	$4.061 \pm 0.522$
	After intervention	$4.341 \pm 0.255$	$5.255 \pm 0.655$
Cognition and mood	Before intervention	$4.042 \pm 0.383$	$4.022 \pm 0.444$
	After intervention	$4.521 \pm 0.272$	$5.133 \pm 0.344$
Overall assessment	Before intervention	$4.050 \pm 0.652$	$4.011 \pm 0.780$
	After intervention	$4.741 \pm 0.322$	$5.322 \pm 1.022$

TABLE 6: Results of quality of life.

Groups	Cases	Time	SF-36	QLQ-C30
Observation group	52	Before intervention	$58.455 \pm 4.061$	$59.460 \pm 6.744$
		After intervention	$69.580 \pm 3.662$	$74.522 \pm 7.455$
Control group	52	Before intervention	$57.721 \pm 4.062$	$58.044 \pm 7.133$
		After intervention	$63.581 \pm 4.070$	$70.311 \pm 2.544$

#### 4. Discussion

Breast cancer is a frequent disease in clinical practice, and its frequency is rising year after year, posing a major threat to patients' physical and mental health [14, 15]. Some researchers have discovered that eating patterns, radioactive chemicals, living routines, genetics, and other variables are all linked to disease [16]. Exercise can obviously improve the blood circulation of the body, promote the metabolism of the tissue, improve the body function, and provide sufficient guarantee for the operation of other systems of the body. Continued exercise can also stimulate the body's pituitary gland to secrete endorphins, improve the central nervous system response ability, and increase the body's tolerance to stimulation [17, 18]. The human body in the movement of the nervous system will appear weak electrical stimulation, and this stimulation can relieve muscle tension and mental depression and relax the cortex of the brain, so that the degree of psychological tension is weakened [19]. Due to the differences between the constitutions of patients, it is easy to cause different degrees of adverse reactions, such as loss of appetite, nausea, and vomiting, which will seriously affect the intake of nutrients, induce malnutrition, and other complications, and further reduce the resistance, thus affecting the effect of chemotherapy [14, 20].

This study showed that after exercise and diet intervention, there was a slight difference in the nutritional indexes of the observation group compared with the control group, that was the data of the observation group was higher than that of the control group ( $P < 0.05$ ). HAMA and HAMD scores of the two groups had no significant difference ( $P > 0.05$ ). After intervention, HAMA and HAMD scores

in both groups were increased, and the increase in the control group was greater than that in the observation group ( $P < 0.05$ ). Both groups' PSQI scores improved after intervention, but the observation group's increase rate was lower than the control group ( $P < 0.05$ ); the control group's sleep time fell more than the observation group ( $P < 0.05$ ). The scores of all dimensions of cancer-induced weariness increased in both groups after the intervention, with the increase rate in the control group being larger than the observation group ( $P < 0.05$ ).

#### 5. Conclusion

The human body in the movement of the nervous system will appear weak electrical stimulation, and this stimulation can relieve muscle tension and mental depression and relax the cortex of the brain. Exercise combined with diet intervention in breast cancer patients can alleviate the negative emotions of patients, reduce the degree of cancer-related fatigue, and improve sleep and quality of life, which is worthy of application and promotion.

#### Data Availability

The data used to support the findings of this study are included within the article.

#### Conflicts of Interest

The authors declare that they have no conflicts of interest.



## Authors' Contributions

All authors contributed equally to this work as first authors.

## References

- [1] H. Yip, B. Pathy, and H. Teo, "A review of breast cancer research in Malaysia," *The Medical Journal of Malaysia*, vol. 69 Suppl A, pp. 8–22, 2014.
- [2] M. Carayol, P. Bernard, J. Boiche et al., "Psychological effect of exercise in women with breast cancer receiving adjuvant therapy: what is the optimal dose needed?," *Annals of Oncology Official Journal of the European Society for Medical Oncology*, vol. 24, no. 2, pp. 291–300, 2013.
- [3] D. Rui, L. Zhou, and L. Jianjun, "Effects of aerobic exercise therapy combined with psychological intervention on quality of life of breast cancer patients," *Shanxi Medical Journal*, vol. 45, no. 6, pp. 689–691, 2016.
- [4] F. Abramo, U. Goerling, and C. Guastadisegni, "Targeted drugs and psycho-oncological intervention for breast cancer patients," *Journal of Negative Results in Biomedicine*, vol. 15, no. 1, pp. 1–10, 2016.
- [5] J. Moor, L. Moyé, M. Low et al., "Expressive writing as a pre-surgical stress management intervention for breast cancer patients," *Journal of the Society for Integrative Oncology*, vol. 6, no. 2, pp. 59–60, 2015.
- [6] V. Cerezo, M. Ortiz, V. Cardenal, and A. De La Torre-Luque, "Positive psychology group intervention for breast cancer patients: a randomised trial," *Psychological Reports*, vol. 115, no. 1, pp. 44–64, 2014.
- [7] L. Xinhua, Z. Lizhi, L. Jianjun, and Z. Shufang, "Effect of evidence-based nursing on postoperative functional exercise compliance and quality of life in patients with breast cancer," *Clinical and Rehabilitation of Oncology in China*, vol. 25, no. 2, pp. 194–197, 2018.
- [8] G. Halkett, M. Connor, S. Aranda et al., "Pilot randomised controlled trial of a radiation therapist-led educational intervention for breast cancer patients prior to commencing radiotherapy," *supportive care in cancer*, vol. 21, no. 6, pp. 1725–1733, 2013.
- [9] F. Munir, K. Kalawsky, C. Lawrence, J. Yarker, C. Haslam, and S. Ahmed, "Cognitive intervention for breast cancer patients undergoing adjuvant chemotherapy," *Cancer Nursing*, vol. 34, no. 5, pp. 385–392, 2011.
- [10] B. Yae and E. Hee, "The effect of diet intervention in breast cancer: a meta-analysis," *Asian Oncology Nursing*, vol. 17, no. 1, pp. 1–2, 2017.
- [11] H. Zhang, "Influence of psychological intervention on anxiety and depression and quality of life after radical breast cancer surgery," *Journal of Health Psychology*, vol. 27, no. 3, pp. 412–415, 2019.
- [12] T. Tan, Z. Lizhi, C. Changxiang, F. Li, and C. Zhichao, "Intervention effect of multisensory training on memory impairment in breast cancer patients during chemotherapy," *Chinese Journal of Physical Medicine and Rehabilitation*, vol. 42, no. 9, pp. 836–838, 2020.
- [13] L. Manne, D. Siegel, J. Heckman, and D. A. Kashy, "A randomized clinical trial of a supportive versus a skill-based couple-focused group intervention for breast cancer patients," *Journal of Consulting & Clinical Psychology*, vol. 84, no. 8, pp. 668–681, 2016.
- [14] H. Désiron, R. Crutzen, L. Godderis, E. van Hoof, and A. de Rijk, "Bridging health care and the workplace: formulation of a return-to-work intervention for breast cancer patients using an intervention mapping approach," *Journal of Occupational Rehabilitation*, vol. 26, no. 3, pp. 350–365, 2016.
- [15] H. Park, S. Jung, S. Kim, and S. H. Bae, "Effects of compensatory cognitive training intervention for breast cancer patients undergoing chemotherapy: a pilot study," *Supportive Care in Cancer*, vol. 25, no. 6, pp. 1887–1896, 2017.
- [16] K. Basen, L. Murray, A. Brewster et al., "Abstract B05: randomized pilot study of project BALANCE: a weight gain prevention intervention for breast cancer patients receiving neoadjuvant chemotherapy," *Cancer Prevention Research*, vol. 8, no. 10, pp. 5–6, 2015.
- [17] J. Lijun and Q. Shao, "Effect of follow-up path chart on self-care ability and compliance of breast cancer patients undergoing chemotherapy during chemotherapy," *Chinese Journal of Clinical Research*, vol. 30, no. 7, pp. 1003–1006, 2017.
- [18] T. Zimmermann, "A couples-based skills intervention for breast cancer patients: results of two RCTs," *International Journal of Behavioral Medicine*, vol. 21, pp. 75–76, 2014.
- [19] J. Vella and M. Budd, "Pilot study: Retreat intervention predicts improved quality of life and reduced psychological distress among breast cancer patients," *Complementary Therapies in Clinical Practice*, vol. 17, no. 4, pp. 209–214, 2011.
- [20] B. Guanjuan and M. Yuanyuan, "Pathway analysis of the effects of fear, discharge readiness and family function on quality of life in breast cancer patients during chemotherapy," *Chinese Journal of Practical Nursing*, vol. 37, no. 10, pp. 721–726, 2021.

## Research Article

# Efficacy and Safety Analysis of Phloroglucinol in Combination with Oxytocin for the Induction of Labor in Women with Term Premature Rupture of Membranes (PROM)

Jiazheng Yu,<sup>1</sup> Lili Chen,<sup>2</sup> Xia Wang,<sup>1</sup> and Xiangzhi Li <sup>1</sup>

<sup>1</sup>Department of Obstetrics, Taizhou Hospital of Zhejiang Province Affiliated to Wenzhou Medical University, Taizhou, 317000 Zhejiang, China

<sup>2</sup>Department of Gynecology, Taizhou Hospital of Zhejiang Province Affiliated to Wenzhou Medical University, Taizhou, 317000 Zhejiang, China

Correspondence should be addressed to Xiangzhi Li; [lixz@enzemed.com](mailto:lixz@enzemed.com)

Received 7 April 2022; Revised 30 April 2022; Accepted 6 May 2022; Published 27 May 2022

Academic Editor: Naeem Jan

Copyright © 2022 Jiazheng Yu et al. This is an open access article distributed under the Creative Commons Attribution License, which permits unrestricted use, distribution, and reproduction in any medium, provided the original work is properly cited.

**Objective.** The purpose of this study was to investigate the efficacy and safety of phloroglucinol in combination with oxytocin in the induction of labor in women who had experienced term premature rupture of membranes (PROM). **Methods.** Data from 100 women who experienced PROM between December 2020 and December 2021 were retrospectively evaluated in this study. The puerperae were categorized into observation and control groups based on their uterine contraction regimens. The observation group consisted of 53 participants that had been treated with phloroglucinol in combination with oxytocin, and the control group consisted of 47 participants that had been treated with oxytocin alone. It was observed and compared in terms of the Bishop score before and after the administration of the puerpera to see which group had the best index. A study was performed after the drug was administered to examine its effects on the duration of labor (including the first, second, and third stages of labor), the mode of delivery (including natural vaginal delivery and cesarean section), the incidence of adverse pregnancy outcomes (fetal distress and neonatal asphyxia), successful labor induction, and complication rates. **Results.** Patients in the observation group had a significantly higher Bishop score after administration than those in the control group ( $P < 0.05$ ), although there was no difference between the two groups before administration. In comparison to the control group, the observation group had a significantly higher efficacy rate for drug administration ( $P < 0.05$ ), as well as a significantly lower occurrence of the first stage of labor ( $P < 0.05$ ), a higher rate of vaginal natural delivery and successful induction of labor ( $P < 0.05$ ), and a significantly lower incidence of adverse pregnancy outcomes and complications ( $P < 0.05$ ). **Conclusion.** In conclusion, the use of phloroglucinol in combination with intravenous oxytocin in the process of promoting cervical ripening and induction of labor for women with PROM who are at term was investigated. This study could help women speed up cervical dilation, improve the cervical Bishop scores, shorten the total labour process, improve the effective rate of vaginal delivery, and be very safe, making it a good candidate for clinical promotion and application.

## 1. Introduction

Labor, also known as human parturition, is a physiological condition that results in the birth of a baby, the delivery of the placenta, and the signal for the initiation of lactation. It is a really difficult process [1]. If the labor is prolonged (more than 12 hours), the active laboring women become exhausted. Consequently, maternal issues like infection and excessive bleeding may develop, while fetal abnormalities

such as fetal distress and asphyxia may occur [2]. Most commonly, interventions in the laboring process to shorten the time are made by rupturing membranes, using drugs to speed up contractions, and providing constant care [3, 4].

The contraction of the uterus and the effacement of the cervical cavity are the two most important characteristics of labor. If the cervix remained rigid despite intense contractions, the labor will be unable to proceed. Throughout the history of childbirth, a variety of procedures have been

employed to expedite the laboring process [4]. Antispasmodic drugs are the most commonly used drugs to decrease the time of labor [5]. These drug works either by relaxing the muscles directly or by interfering with the signals sent by the nerves to the muscles that contract during labor.

The primary function of fetal membranes in pregnant women is to produce enough amniotic fluid to protect the fetus from the uterus throughout normal development. Premature rupture of membranes (PROM) refers to the rupture of fetal membranes before delivery, which causes an increase in intra-abdominal pressure in pregnant women, resulting in uneven pressure in the anterior amniotic sac and several undesirable consequences such as premature birth or dystocia [6]. PROM is closely associated with maternal gestational age, and it is more prevalent after 37 weeks of gestation. It can easily lead to infection, and if not treated in a timely and appropriate manner, it can endanger the life of the fetus [7, 8]. Therefore, if PROM occurs with an immature cervix during a maternal pregnancy of less than 37 weeks, appropriate measures should be performed to induce labor.

In clinical practice, oxytocin is frequently administered to PROM women to increase the frequency of uterine contractions. However, irregular uterine contractions may occur during the process of labor induction, resulting in a cervical spasm that prevents the expansion of the cervix during the birthing process [9]. Although the use of atropine, diazepam, and racemic anisodamine hydrochloride in obstetrics clinics was found to be effective in alleviating and promoting cervical ripening, edema, and cervical spasm to a certain extent, it was observed that these drugs are frequently associated with changes in the respiratory and circulatory systems of mothers and infants and that there are potential side effects to the use of these drugs [10, 11]. Therefore, the development of a safe and effective strategy for increasing cervical ripening is a clinical concern that must be addressed immediately in the clinical context.

Phloroglucinol is a myotropic antispasmodic drug that acts directly on the smooth muscle of the genitourinary tract and the gastrointestinal tract while having little impact on normal smooth muscle [12]. It has been extensively employed in recent years to enhance cervical ripening and softening, with promising outcomes [13, 14]. However, more studies are required to determine the efficacy and safety of its combined oxytocin in the induction of labor with the term PROM.

In this study, 100 women with PROM were chosen as the research subjects and the efficacy and safety of phloroglucinol combined with oxytocin in labor induction with term PROM were thoroughly analyzed, to provide additional evidence to support the clinical delivery plan for women with PROM.

## 2. Materials and Methods

The study population included a total of 100 women. A comparative study was conducted between patients comprising two groups (observation and control) based on their uterine contraction regimens. The observation group consisted of 53 participants that had been treated with phloro-

glucinol in combination with oxytocin, and the control group consisted of 47 participants that had been treated with oxytocin alone. The Bishop score was determined between two groups to see which group had the best index. Similarly, the duration of labor, the mode of delivery, the incidence of adverse pregnancy outcomes, successful labor induction, and rates of complications were all determined after the administration of combined medication in the observation group and treatment with oxytocin alone in the control group.

*2.1. Clinical Information.* The case data of 100 women with PROM who were diagnosed between December 2020 and December 2021 weeks were retrospectively analyzed. The puerperae were separated into two groups based on the different uterine contraction regimens used: the observation group, which included 53 cases (treated with phloroglucinol in combination with oxytocin), and the control group, which included 47 cases (treated with oxytocin alone). Parturients had to meet the following criteria: they must meet the clinical diagnostic criteria for term PROM, which were confirmed by B-ultrasound and laboratory tests; they must be between the ages of 20 and 35; they must have complete information and normal consciousness to participate in the study; they must be able to cooperate with the study. The following are the exclusion criteria for the investigation: parturients with mental illness, illiteracy, or communication disorder were excluded; parturients who were allergic to the medications employed in the present study were excluded; parturients with abnormal amniotic fluid, fetal heart rate, and placenta were excluded; parturients with a history of cervical surgery were excluded; parturients with liver and kidney disease, severe obstetric complications, and cardiovascular disease; parturients who do not cooperate with the research are excluded. Informed satisfaction letters were signed by all parturients indicating their consent to participate in the research. The present assessment has been confirmed by the ethics committee of Taizhou Hospital of Zhejiang Province, which is affiliated with the Wenzhou Medical University and complies with the Helsinki Declaration.

*2.2. Treatment Methods.* The control group was given an intravenous drip of 500 mL of sodium chloride injection (0.9%) and 2.5 U of oxytocin (Shanghai Harvest Pharmaceutical Co., Ltd., Shanghai, China, SFDA Approval No. H31020850). The observation group received 80 mg of phloroglucinol (Nanjing Hencor Pharmaceutical Co., Ltd., Nanjing, China, SFDA Approval No. H20046766) combined with 500 mL of sodium chloride injection (0.9%) and 2.5 U of oxytocin during labor. The infusion rate of both groups was adjusted to 8 drops/min at the beginning, and the fastest infusion rate was controlled at 40 drops/min. The concentration and rate of infusion were maintained in the presence of effective uterine contractions, for instance at an interval of 2-3 min, for a duration of 40-60s, and at a pressure of 50-60 mmHg. An examination of the vaginal cavity was performed regularly during the therapy period to assess cervical enlargement and the descent of the fetal head.

**2.3. Observation Indexes.** (1) The Bishop scores of the two groups were compared before and after treatment [15]. The higher the score, the more cervical ripeness there is (with a total score of 13). (2) The Bishop score was used to compare the effects of two groups of puerperae after medication, and specific evaluation criteria were as follows: the cervical Bishop score of the puerpera increased by  $\geq 3$  after 12 hours of medication was considered markedly effective, increased by 1-2 after 12 hours of medication was considered effective, and that did not change was considered invalid; total effective rate = (markedly effective + effective) number of cases/total number of cases  $\times 100\%$ . (3) We compared the time of labor in two groups, comprising the first, second, and third stages of labor. (4) Two groups were compared regarding their delivery methods, which included vaginal and cesarean sections (5) The incidence of adverse pregnancy outcomes was compared between two groups of puerperae, which included fetal distress and neonatal asphyxia. (6) The success rates of labor induction of two groups were compared, and the criteria for success and failure of labor induction were as follows [16]: a woman with PROM at term labor induced successfully within 24 hours means the success of the induction of labor; a woman who failed to deliver under the same circumstances within 24 hours means the failure of labor induction. (7) The incidence of complications, such as cervical edema, postpartum hemorrhage, and cervical laceration, was compared between the two groups in this study

**2.4. Statistical Analysis.** The statistical analysis of the data employed was carried out using SPSS19.0 (IBM) and Graph-Pad Prism 8 was used to generate the experimental images. The Chi-square test ( $\chi^2$ ) was used to analyze the number of cases as well as the percentage (%) of enumeration data. The mean  $\pm$  standard deviation was used to analyze measurement data. The Student *t*-test and the LSD/*t* test were used to analyze differences among groups and comparisons at different time points, followed by a post-hoc test. *P* values less than 0.05 were considered statistically significant.

### 3. Results

**3.1. Comparison of General Information.** There was no significant difference in age, BMI, or childbearing history between the two groups ( $P > 0.05$ ). The data is shown in Table 1 of the study.

**3.2. Comparison of Bishop Scores before and after Drug Administration between Two Groups.** The cervical bishop scores were evaluated before and after administration in both observation and control groups. The cervical Bishop score before administration in the observation group was  $3.14 \pm 0.34$ , while the cervical Bishop score in the control group was  $3.1 \pm 0.23$ , indicating that there was no significant difference in the cervical Bishop score between the two groups ( $P > 0.05$ ). While the cervical bishop scores after administration in the observation group were  $7.82 \pm 0.36$ , they were found to be  $6.06 \pm 0.28$  in the control groups, demonstrating that after administration, the scores in the

observation group were significantly higher compared to the control groups ( $P < 0.05$ ). The higher value of the bishop score indicates that the current finding is considered to be favorable for induction. The results of the study are illustrated in Table 2.

**3.3. Comparison of Therapeutic Efficacy between Two Groups.** Following administration, the number of parturients whose therapeutic efficacy was evaluated as significantly efficacious, effective, and ineffective in the group of observation was 32, 19, and 2, respectively, with an effective rate of 96.23%. As well as those of the control group, were 22, 12, and 13 correspondingly, and the effective rate was 72.34%, demonstrating that the effective rate of the observation group was significantly higher compared to the control group ( $P < 0.05$ ). Elaborated information was demonstrated in Table 3.

**3.4. Comparison of Labor Process between Two Groups.** We compared the time of labor in two groups, comprising the first, second, and third stages of labor. The time of the first stage of labor in the observation group was shorter compared to the control group ( $P < 0.05$ ), while no marked difference was presented for that between the second stage of labor and the third stage between the two groups ( $P > 0.05$ ). In the observation group, however, a slightly greater change was observed in the rate of the second and third stage of labor than in the control group, indicating that overall labor stages in the observation group were shorter than in the control group, with the first stage of labor being the most obvious and displaying the most significant differences between the two groups, as displayed in Table 4.

**3.5. Comparison of Delivery Mode between Two Groups.** The vaginal delivery and cesarean section modes were compared between the two groups. 35 participants had experienced a 74.47% vaginal delivery rate out of 47 in the control group (35/47), whereas the vaginal delivery rate of the observation group was determined to be 92.45% for the 49 participants out of 53 (49/53). The finding showed a markedly higher rate of vaginal delivery when treated with the combined medication in the observation group than in the control group ( $P < 0.05$ ), as illustrated in Figure 1.

**3.6. Comparison of the Incidence of Adverse Pregnancy Outcomes between Two Groups.** The number of neonates with fetal distress and neonatal asphyxia in the observation group was 2 and 3, respectively, and the overall incidence of adverse pregnancy outcomes was 9.43%; however, the number of neonates with fetal distress and neonatal asphyxia in the control group was 6 and 7, with a total incidence of adverse pregnancy outcomes of 27.66%, outranking the observation group in terms of incidence of adverse pregnancy outcomes ( $P < 0.05$ ), suggesting that the combined medication was safer. The findings of the investigation are presented in Table 5.

**3.7. Comparison of the Success Rate of Labor Induction between Two Groups.** Two groups were compared for the success rate of labor induction following the administration

TABLE 1: A comparative analysis of general data [ $n$  (%)].

Factors	Observation group $n = 53$	Control group $n = 47$	$t/X^2$	$P$
Age (years old)			0.107	0.744
$\geq 27$	31(58.49)	29(61.70)		
$< 27$	22(41.51)	18(38.30)		
BMI(kg/m <sup>2</sup> )	25.98 $\pm$ 1.23	25.88 $\pm$ 1.24	0.405	0.686
Average Gestational age			0.170	0.680
$\geq 41$	26(49.06)	25(53.19)		
$< 41$	27(50.94)	22(46.81)		
Times of pregnancy			0.076	0.783
$\geq 2$	20(37.74)	19(40.43)		
$< 2$	33(62.26)	28(59.57)		
Fetal position			0.058	0.810
Normal	43(81.13)	39(82.98)		
Abnormal	10(18.87)	8(17.02)		
Premature rupture of membrane time ( $h$ )			0.001	0.990
$\geq 12$	27(50.94)	24(51.06)		
$< 12$	26(49.06)	23(48.94)		

TABLE 2: Comparison of the Bishop scores between two groups prior to and following the drug administration.

Time	Observation group $n = 53$	Control group $n = 47$	$t$	$P$
Before administration	3.14 $\pm$ 0.34	3.1 $\pm$ 0.23	0.498	0.680
After administration	7.82 $\pm$ 0.36	6.06 $\pm$ 0.28	27.04	$< 0.001$

TABLE 3: Comparison of the therapeutic effects of two groups.

Therapeutic efficacy	Observation group $n = 53$	Control group $n = 47$	$X^2$	$P$
Markedly effective	32(60.38)	22(46.81)	—	—
Effective	19(35.85)	12(25.53)	—	—
Ineffective	2(3.77)	13(27.66)	—	—
Effective rate	51(96.23)	34(72.34)	11.15	$< 0.001$

of combination medicine. The success rate of labor induction was determined to be 94.34% in the observation group for 50 participants out of 53 (50/53), whereas the rate in the control group was determined to be 70.21% for 33 participants out of 47 (33/47). The findings indicate that the rate of labor induction was significantly higher in the observation group than in the control group following administration of the combined medication ( $P < 0.05$ ), implying that this result improves the success rate of labor induction, as illustrated in Figure 2.

3.8. *Comparison of the Incidence of Complications between the Two Groups of Puerperae.* The number of parturients who suffered from cervical laceration, postpartum hemorrhage, and cervical edema in the observation group was 2, 1, and 0, respectively, with a complication rate of 5.66%, which was drastically less than that in the control group with corresponding indexes of 5, 5, and 3 and a complication rate of 27.66% ( $P < 0.05$ ), as demonstrated in Table 6.

#### 4. Discussion

Clinically, PROM in the third trimester has greater negative effects on both the mother and the infant than in normal pregnancy [17]. Following membrane rupture, pathogenic bacteria in the vagina are susceptible to ascending infection, and the severity of infection is determined by the timing of membrane rupture [18]. Under normal conditions, if the membrane rupture is not treated appropriately and promptly, it is highly likely to induce fetal distress due to oligohydramnios, placental abruption, and umbilical cord prolapse and subsequently lead to neonatal aspiration pneumonia, which poses a serious threat to the fetus's life [19]. Consequently, in clinical practice, if there are no symptoms of labor or the cervix is not developed enough, appropriate therapies could be given to women with PROM at a term greater than 37 weeks to assist them in initiating labor [20].

Prostaglandin preparations and balloon dilation are forbidden when promoting cervical ripening and inducing labor in such women, and only low-dose oxytocin may be used to promote cervical ripening [21]. Oxytocin is a regularly used labor-inducing medication in clinical practice. It works by binding to the oxytocin receptor. While receiving an intravenous infusion of oxytocin to induce labor, the puerpera may suffer irregular uterine contractions, resulting

TABLE 4: Comparison of labor process between two groups (min).

Labor duration	Observation group $n = 53$	Control group $n = 47$	$T$	$P$
First stage of labor	420.78 $\pm$ 13.99	616.95 $\pm$ 12.01	74.75	<0.001
Second stage of labor	103.11 $\pm$ 10.8	104.06 $\pm$ 8.2	0.490	0.625
The third stage of labor	15.23 $\pm$ 1.09	15.47 $\pm$ 1.02	1.132	0.260

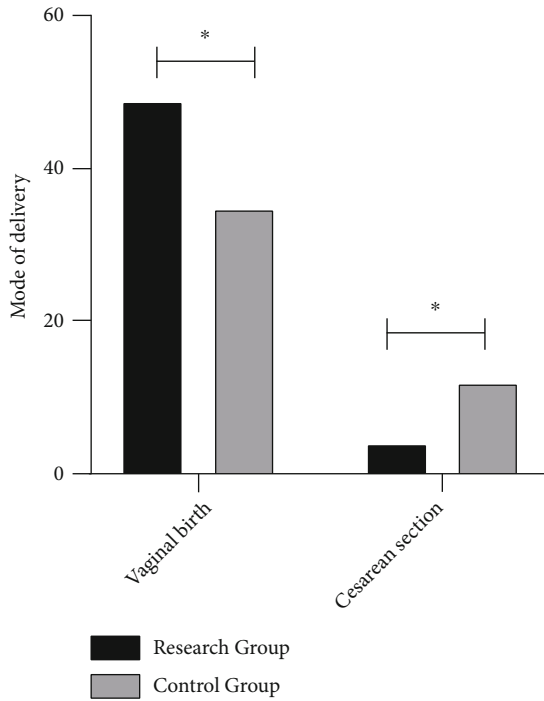


FIGURE 1: Comparison of the mode of delivery between two groups of women. Note: \* means  $P < 0.05$ .

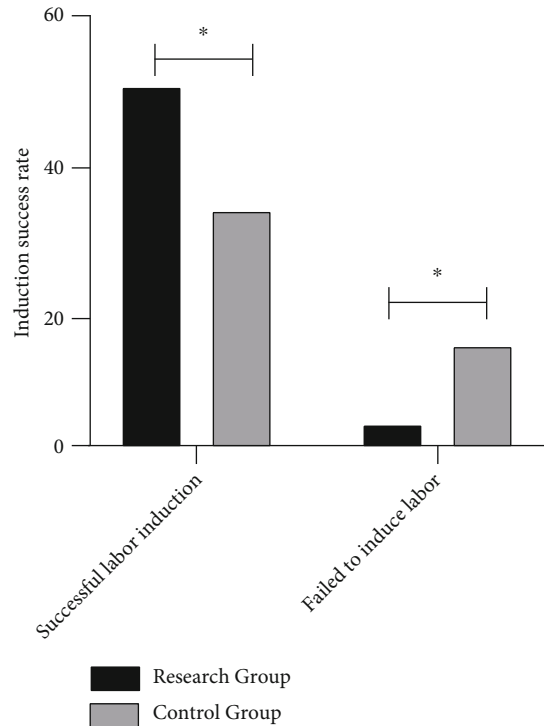


FIGURE 2: Comparison of success rate of labor induction between two groups of parturients. Note: \* means  $P < 0.05$ .

TABLE 5: Comparison of the incidence of adverse pregnancy outcomes between two groups.

Incidence of adverse pregnancy outcomes	Observation group $n = 53$	Control group $n = 47$	$t$	$P$
Fetal distress	2(3.77)	6(12.77)	—	—
Neonatal asphyxia	3(5.66)	7(14.89)	—	—
The overall incidence of adverse pregnancy outcomes	5(9.43)	13(27.66)	5.606	0.018

in cervical edema and impeding cervical dilation [22]. Numerous studies have also indicated that oxytocin alone is ineffective as a treatment since it takes a long time to induce labor. Furthermore, many women are unable to bear extended painful uterine contractions, lengthy labor, cervical edema, or cervical damage and thus abandon vaginal trial labor, increasing the rate of cesarean section [23]. As a result, to further test the effect of oxytocin and to find a more

appropriate labor induction strategy, we examined the effects of oxytocin alone and the effects of oxytocin and phloroglucinol in combination in women with PROM to discover which was more effective. The Bishop score is a scoring standard for determining cervical ripeness, which can predict whether or not a woman is ready to give birth and the anticipated timing of vaginal delivery [24]. We first evaluated the Bishop score and therapeutic efficacy of two groups, finding that the two indexes of the observation group were significantly higher after drug administration than those of the control group, indicating that the combined treatment may enhance cervical ripening in the first place. Then, we compared the labor process and the success rate of labor induction between the two groups, which revealed that the overall labor stages of the observation group were shorter compared to the control group, with the first stage of labor being the most evident and showing the most significant differences between the two groups. Furthermore, the success rate of labor induction was significantly higher in this group. Our findings suggested

TABLE 6: Comparison of the incidence of complications between the two groups of puerperae.

Adverse reactions	Observation group $n = 53$	Control group $n = 47$	$X^2$	$P$
Cervical laceration	2 (3.77)	5 (10.64)	—	—
Postpartum hemorrhage	1 (1.89)	5 (10.64)	—	—
Cervical edema	0	3 (6.38)	—	—
Incidence of complications	3 (5.66)	13 (27.66)	8.970	0.003

that the combination of medications used in our study could effectively relieve cervical spasm, minimize cervical edema, enhance cervical dilatation, shorten the labor phase, and increase the success rate of labor induction. The rationale for this is that phloroglucinol can effectively relieve irregular uterine contractions generated by intravenous oxytocin during labor induction, prevent cervical spasm and damage, and decrease maternal cervical edema [25]. Thus, it was concluded that phloroglucinol in combination with oxytocin could effectively promote regular uterine contractions and cervical canal flattening, stimulate cervix dilation, promote cervical dilation, accelerate cervical ripening, shorten labor, and improve the success rate of labor induction.

Following that, our findings on delivery methods revealed that the vaginal delivery rate of women in the observation group was significantly higher than that of women in the control group, indicating that a combination of medications may be beneficial in increasing the vaginal delivery rate of women. The explanation for this is that once phloroglucinol enters the body, it acts directly on the smooth muscle of the genitourinary tract without having an anticholinergic impact. Additionally, when smooth muscle spasms are relieved, anticholinergic adverse effects such as hypotension or an elevated heart rate are avoided. When taken with oxytocin, it has the potential to boost the therapeutic effect, promote quick cervix ripening, and raise the rate of natural childbirth [12]. The final neonatal result and the incidence of complications indicate that the overall incidence of adverse pregnancy outcomes and complications was significantly lower in the observation group than in the control group, indicating that combination treatment was more safe. This is mostly due to the fact that phloroglucinol has no effect on normal uterine smooth muscle contraction and will not result in a prolonging of the second stage of labor, postpartum uterine atony, or postpartum hemorrhage in most cases. The medicine will not produce unfavorable maternal effects such as high blood pressure, rapid heart rate, uterine rupture, or neonatal asphyxia [26]. On the other hand, phloroglucinol can effectively alleviate puerperium pain and lessen the probability of electing for a cesarean section due to fear of pain; additionally, due to the accelerated delivery process, it can help reduce the incidence of fetal distress, neonatal asphyxia, and puerperium infection with increased security [27].

To summarize, the use of phloroglucinol in combination with oxytocin intravenous infusion during the process of promoting cervical ripening and induction of labor in women with PROM at term can assist women in speeding up cervical dilation, improving the cervical Bishop score,

shortening the total labor process, and improving vaginal delivery. Its high success rate and safety profile make it an excellent candidate for clinical advancement and application. However, this study has certain shortcomings and limitations. For instance, certain restrictions apply to sample selection. While the screening was conducted following applicable criteria, it remains questionable whether the specimens chosen are reasonable. Additionally, because the number of samples is small and the research period is limited, clinical research can be expanded with additional time, hence increasing the accuracy of the research results.

### Data Availability

The labeled dataset employed for supporting the achievements of this research is accessible from the corresponding author upon request.

### Conflicts of Interest

The authors declare no competing interests.

### Authors' Contributions

Jiazheng Yu and Xia Wang contributed equally to this work.

### References

- [1] H. Bickerstaff and L. C. Kenny, *Gynaecology by Ten Teachers*, CRC Press, 2017.
- [2] M. S. Harrison, S. Ali, O. Pasha et al., "A prospective population-based study of maternal, fetal, and neonatal outcomes in the setting of prolonged labor, obstructed labor and failure to progress in low- and middle-income countries," *Reproductive Health*, vol. 12, no. S2, 2015.
- [3] S. Wood, S. Cooper, and S. Ross, "Does induction of labour increase the risk of caesarean section? A systematic review and meta-analysis of trials in women with intact membranes," *BJOG: An International Journal of Obstetrics & Gynaecology*, vol. 121, no. 6, pp. 674–685, 2014.
- [4] S. M. Khan, H. Khan, N. Khan, M. Qadir, H. Gul, and S. Jadoon, "Phloroglucinol and drotaverine in accelerating the first stage of labour; a comparative study," *Journal of The Society of Obstetricians and Gynaecologists of Pakistan*, vol. 9, no. 3, pp. 121–124, 2019.
- [5] K. Gupta, S. Dubey, S. Bhardwaj, and M. Parmar, "A programmed labour protocol for optimizing labour and delivery," *International Journal of Reproduction, Contraception, Obstetrics and Gynecology*, vol. 4, no. 2, pp. 457–460, 2015.

- [6] H. N. Simhan and T. P. Canavan, "Preterm premature rupture of membranes: diagnosis, evaluation and management strategies," *BJOG: An International Journal of Obstetrics & Gynaecology*, vol. 112, pp. 32–37, 2005.
- [7] K. J. Oh, R. Romero, J. Y. Park, J. S. Hong, and B. H. Yoon, "The earlier the gestational age, the greater the intensity of the intra-amniotic inflammatory response in women with preterm premature rupture of membranes and amniotic fluid infection by *Ureaplasma* species," *Journal of Perinatal Medicine*, vol. 47, no. 5, pp. 516–527, 2019.
- [8] M. Tchirikov, N. Schlabritz-Loutsevitch, J. Maher et al., "Mid-trimester preterm premature rupture of membranes (PPROM): etiology, diagnosis, classification, international recommendations of treatment options and outcome," *Journal of Perinatal Medicine*, vol. 46, no. 5, pp. 465–488, 2018.
- [9] D. Knapik, J. Świtała, and A. Olejek, "Premature rupture of membranes before 34 weeks of pregnancy as a medical problem," *Ginekologia Polska*, vol. 87, no. 3, pp. 211–216, 2016.
- [10] J. Zhu, C. Ma, X. Luan, J. Li, F. Peng, and L. Huang, "Inflammasome components and ADAMTS4 in premature rupture of membranes," *Molecular Medicine Reports*, vol. 23, no. 2, 2020.
- [11] A. El-Messidi and A. Cameron, "Diagnosis of premature rupture of membranes: inspiration from the past and insights for the future," *Journal of Obstetrics and Gynaecology Canada*, vol. 32, no. 6, pp. 561–569, 2010.
- [12] F. Wu, Y. Chen, and C. Zheng, "Efficacy of phloroglucinol for acceleration of labour: a systematic review and meta-analysis," *Archives of Gynecology and Obstetrics*, vol. 304, no. 2, pp. 421–428, 2021.
- [13] C. Li, L. Guo, M. Luo et al., "Risk factors of uterine contraction after ureteroscopy in pregnant women with renal colic," *International Urology and Nephrology*, vol. 53, no. 10, pp. 1987–1993, 2021.
- [14] C. M. Klier, B. Schmid-Siegel, M. R. Schäfer et al., "St. John's wort (*Hypericum perforatum*) and breastfeeding," *The Journal of Clinical Psychiatry*, vol. 67, no. 2, pp. 305–309, 2006.
- [15] N. G. Kulhan and M. Kulhan, "Labor induction in term nulliparous women with premature rupture of membranes: oxytocin versus dinoprostone," *Archives of Medical Science: AMS*, vol. 15, no. 4, pp. 896–901, 2019.
- [16] F. Bellussi, A. Livi, J. Diglio, J. Lenzi, L. Magnani, and G. Pilu, "Timing of induction for term prelabor rupture of membranes and intravenous antibiotics," *American Journal of Obstetrics & Gynecology MFM*, vol. 3, no. 1, article 100245, 2021.
- [17] S. Kenyon, D. Taylor, and W. Tarnow-Mordi, "Broad-spectrum antibiotics for preterm, prelabour rupture of fetal membranes: the ORACLE I randomised trial," *The Lancet*, vol. 357, no. 9261, pp. 979–988, 2001.
- [18] R. E. Packard and A. D. Mackeen, "Labor induction in the patient with preterm premature rupture of membranes," in *Seminars in Perinatology*, vol. 39, no. 6pp. 495–500, Elsevier, 2015.
- [19] Y. Athiel, S. Crequit, M. Bongiorno, S. Sanyan, and B. Renevier, "Term prelabor rupture of membranes: Foley catheter versus dinoprostone as ripening agent," *Journal of Gynecology Obstetrics and Human Reproduction*, vol. 49, no. 8, article 101834, 2020.
- [20] A. Puhl, C. Weiss, A. Schneid et al., "Erhöht die Geburtseinleitung wegen eines frühen vorzeitigen Blasensprungs ab 34+ 0 SSW das Risiko für einen Kaiserschnitt?," *Zeitschrift für Geburtshilfe und Neonatologie*, vol. 224, no. 5, pp. 269–274, 2020.
- [21] L. Pourali, N. Saghafi, S. Eslami Hasan Abadi, F. Tara, A. M. Vatanchi, and E. Motamedi, "Induction of labour in term premature rupture of membranes; oxytocin versus sublingual misoprostol; a randomised clinical trial," *Journal of Obstetrics and Gynaecology*, vol. 38, no. 2, pp. 167–171, 2018.
- [22] T. Schmitz, L. Sentilhes, E. Lorthe et al., "Preterm premature rupture of the membranes: guidelines for clinical practice from the French College of Gynaecologists and Obstetricians (CNGOF)," *European Journal of Obstetrics & Gynecology and Reproductive Biology*, vol. 236, pp. 1–6, 2019.
- [23] W. Grobman, J. Bailit, and Y. Lai, " Eunice Kennedy Shriver National Institute of Child Health and Human Development Maternal-Fetal Medicine Units Network. Defining failed induction of labor," *American Journal of Obstetrics and Gynecology*, vol. 218, no. 1, p. 122, 2018.
- [24] C. Huret, B. Pereira, V. Collange et al., "Premature rupture of membranes  $\geq$  37 weeks of gestation: predictive factors for labour onset within 24 hours," *Gynécologie Obstétrique Fertilité & Sénologie*, vol. 45, no. 6, pp. 348–352, 2017.
- [25] S. Yuan, F. Gao, Z. Xin et al., "Comparison of the efficacy and safety of phloroglucinol and magnesium sulfate in the treatment of threatened abortion: A meta-analysis of randomized controlled trials," *Medicine*, vol. 98, no. 24, 2019.
- [26] A. Schiattarella, G. Riemma, G. Sisti et al., "Efficacy of phloroglucinol in shortening the first stage of labor: systematic review and meta-analysis of randomized controlled trials," *The Journal of Maternal-Fetal & Neonatal Medicine*, pp. 1–7, 2021.
- [27] S. Tabassum, B. Afridi, and Z. Aman, "Phloroglucinol for acceleration of labour: double blind, randomized controlled trial," *Journal-Pakistan Medical Association*, vol. 55, no. 7, p. 270, 2005.



## *Retraction*

# **Retracted: Innovating Pedagogical Practices for Handmade Courses in Preschool Education Using Artificial Intelligence**

### **Computational and Mathematical Methods in Medicine**

Received 17 October 2023; Accepted 17 October 2023; Published 18 October 2023

Copyright © 2023 Computational and Mathematical Methods in Medicine. This is an open access article distributed under the Creative Commons Attribution License, which permits unrestricted use, distribution, and reproduction in any medium, provided the original work is properly cited.

This article has been retracted by Hindawi following an investigation undertaken by the publisher [1]. This investigation has uncovered evidence of one or more of the following indicators of systematic manipulation of the publication process:

- (1) Discrepancies in scope
- (2) Discrepancies in the description of the research reported
- (3) Discrepancies between the availability of data and the research described
- (4) Inappropriate citations
- (5) Incoherent, meaningless and/or irrelevant content included in the article
- (6) Peer-review manipulation

The presence of these indicators undermines our confidence in the integrity of the article's content and we cannot, therefore, vouch for its reliability. Please note that this notice is intended solely to alert readers that the content of this article is unreliable. We have not investigated whether authors were aware of or involved in the systematic manipulation of the publication process.

Wiley and Hindawi regrets that the usual quality checks did not identify these issues before publication and have since put additional measures in place to safeguard research integrity.

We wish to credit our own Research Integrity and Research Publishing teams and anonymous and named external researchers and research integrity experts for contributing to this investigation.

The corresponding author, as the representative of all authors, has been given the opportunity to register their agreement or disagreement to this retraction. We have kept a record of any response received.

### **References**

- [1] J. Zhao and N. Wang, "Innovating Pedagogical Practices for Handmade Courses in Preschool Education Using Artificial Intelligence," *Computational and Mathematical Methods in Medicine*, vol. 2022, Article ID 3585958, 8 pages, 2022.

## Research Article

# Innovating Pedagogical Practices for Handmade Courses in Preschool Education Using Artificial Intelligence

Jun Zhao<sup>1</sup> and Na Wang<sup>2</sup> 

<sup>1</sup>Department of Preschool and Special Education, Ganzhou Teachers College, 341000 Ganzhou, China

<sup>2</sup>College of Fine Arts, Gannan Normal University, 341000 Ganzhou, China

Correspondence should be addressed to Na Wang; 18402127@masu.edu.cn

Received 7 April 2022; Revised 24 April 2022; Accepted 28 April 2022; Published 26 May 2022

Academic Editor: Naeem Jan

Copyright © 2022 Jun Zhao and Na Wang. This is an open access article distributed under the Creative Commons Attribution License, which permits unrestricted use, distribution, and reproduction in any medium, provided the original work is properly cited.

Handmade is an important part of preschool education, which was aimed at improving children's ability to work with their hands. Preschool education is the most basic and important aspect of a country's educational system. As a result, individuals pursuing a degree in preschool education take on a lot of responsibility. The preschool education handmade course has become an important component of preschool education due to its practicality and creativity. Preschool education major offers classes in traditional crafts such as paper cutting, paper dyeing, origami, paper three-dimensional modeling, and ornamental painting. The teaching methods for custom-made preschool education courses are always evolving with the progress of society. The question of how to assess the efficacy of unique teaching methodologies for handmade courses has become crucial. This study employs artificial intelligence to create a neural network for assessing the creativity of teaching approaches for handmade courses in preschool education. The following is the specific work: Firstly, the idea, as well as the benefits and drawbacks of genetic algorithms, is investigated. To build an improved genetic algorithm (IGA), the chromosome encoding, fitness function, and three operation options are enhanced. Secondly, by improving the genetic algorithm, the selection of weights and thresholds in the BP neural network model is improved, and a combined model (IGA-BP) is created by integrating the improved genetic algorithm with the BP network. Finally, rigorous and systematic tests confirm the work's efficacy and viability.

## 1. Introduction

In preschool education, handmade education is very important. The primary goal of preschool education handcrafted classes is to develop pupils' capacity to work with their hands. Today's preschool education handmade courses mainly cultivate students' imitation ability, hands-on operation ability, and knowledge ability. Preschool education is the first step in cultivating students, it is the enlightenment education for many students, and has a very important impact on the overall education of the nation. Handmade in preschool education is very usable and innovative, and handmade has become an important course for education professionals. The education courses for students should carry out targeted education and training according to students' craft skills and learning ability and cultivate students' four abilities: first is the ability to express the aesthetic sense

of shape, second is the learning ability of craft skills, third is the ability to transfer skills widely, and fourth is the independent creativity. Handmade courses have inherent advantages. The main teaching content and learning content revolve around handmade ability, so the classroom atmosphere is more active and relaxed. Teachers should encourage students to cooperate and communicate with each other to solve problems. In addition, teachers should also encourage students in a timely manner. The perfection of handmade products not only gives students confidence in handcrafting but also cultivates students' conscientiousness in doing things and perfecting the fine quality of details [1–5].

When the handmade artwork is completed, it will bring the confidence of the students in handmade, improve the students' seriousness in doing things, and improve the details of the handicrafts and other good qualities. Different handicrafts also have different meanings. Teachers should

interact with students first before evaluating handicrafts and then base their judgments on the meaning and purpose of the students' completion of handicrafts. Teachers should not use the scoring mechanism, appearance, and perfection to evaluate the handicrafts made by students and should not ignore the thoughtful works only from the appearance of defects. On the premise that the students determine the situation that needs to be improved, the teacher should improve the students' crafts and recognize the students' ideological understanding of the crafts. Only by fully respecting the ideas and concepts of students can students make continuous progress and improvement, and the connotation and appearance of students' handicrafts can be perfected [1, 6–8].

The multitype teaching of handmade enables students to fully understand handmade art under the guidance of teachers, deepens art modeling, enables students to generate new concepts, enhances their interest in hand-making, enhances students' flexibility in thinking and creativity, and promotes students' comprehensive and efficient development. In the hands-on practice of manual learning, students can exercise their hands-on ability, improve their physical flexibility and coordination, and strengthen their abilities in all aspects, comprehensive application of technologies of various departments, which enrich the content of teaching in classrooms and attract students' attention. At this stage, students have an irresistible charm for new things and are easily attracted by new things. Therefore, handmade multitype teaching, deepening art modeling, and comprehensive application of technologies from various departments can effectively improve students' abilities, concentrate students' attention, and facilitate teachers' subsequent educational work. Handmade can improve students' hands-on ability in many ways and improve students' creative ability in practice. Practice is the only criterion for testing, and practice is also an important criterion for testing students' coordination abilities in education. Hands-on operation is the nature of students. In the process of hands-on practice, it can effectively improve the development of students' creative thinking. Innovation is an important source of inspiration in creation. Handmade can help cultivate students' innovative thinking awareness and promote the formation of students' comprehensive quality. In the development of students, innovative consciousness can motivate students to move forward [9–14].

Today's educational concept is child-centered, the master of the classroom is the child, and the teacher should cooperate with the auxiliary master and constantly reform and innovate teaching methods. Teachers should combine previous teaching experience and teaching plans to educate children's development needs. It should combine existing resources, upgrade and reform the teaching mode, and devote itself to research and innovative teaching. Therefore, it is very important to evaluate the innovative effect of the teaching method of handmade courses in preschool education. This paper designs a neural network based on artificial intelligence to complete this task.

The following is the paper's organization paragraph: The paper's related work is presented in Section 2. The method

of the proposed study is examined in Section 3. The experiments and results are discussed in Section 4. Finally, the research job is completed in Section 5.

## 2. Related Work

Literature [15] pointed out that the nature and functions of preschool education mainly include enlightenment, unity of education and conservation, public welfare and service, compensation, and connection. It emphasizes that preschool education prepares children for school and must promote the healthy growth of children. At the same time, through the development of rich educational activities and game activities, children are guided to accumulate social experiences and master the necessary emotions, attitudes, knowledge, skills, etc. before entering school, so as to make full preparations for children to enter primary school. Literature [16] has a great agreement on the nature, function, and orientation of preschool education. It pointed out that the nature of preschool education is basic and leading, welfare and public welfare. The function and main task of preschool education are to promote the all-around development of children and lay the foundation for children to enter the nine-year compulsory education, so as to solve the worries of parents, reduce the burden of parenting, and provide education compensation for children in disadvantaged positions. The positioning of preschool education is the first link of the school system and an important part of basic education. The academic aptitude of young children is restricted, according to literature [17], and the cornerstone of early childhood education is not in any type of learning region. It is to allow children to express their natural selves, to amass their experiences, and to explore and develop their interests. Literature [18] believes that early childhood education should provide an appropriate education for the development of each child so that it can develop as a whole. Early childhood education must adhere to the concept of children first and make it the center of education. Literature [19] analyzed the differences between early childhood education and primary education. It pointed out that, in nature, early childhood education is still noncompulsory education. From the perspective of educational tasks, early childhood education pays equal attention to protection and education. From the perspective of curriculum setting, early childhood education implements integrated courses or comprehensive theme courses. From the perspective of educational methods, early childhood education implements games as a basic activity. Therefore, there is a clear difference between early childhood education and primary education in the adjacent school stage and should not be confused with primary education.

The literature [20] elaborated the specific requirements of different fields according to the objectives, content requirements, and guiding points of the five fields of the kindergarten curriculum. Therefore, the content of preschool education courses must follow certain principles, not all knowledge. There is no unified national teaching book and specific curriculum format for preschool education. Therefore, the kindergarten-based curriculum is a common task and practical need of every kindergarten. Literature [21]

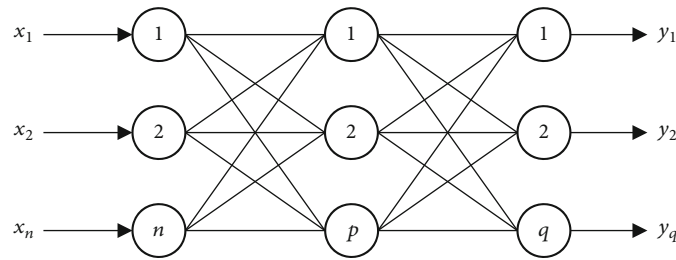


FIGURE 1: The structure of BP network.

pointed out that the three-level management system of the basic education curriculum is the diversification under the unified national requirements and standards, and the garden-based curriculum is the specification and diversification of the national curriculum. All localities and kindergartens should develop unique kindergarten-based courses under the guidance of the outline and closely integrate their actual needs. Therefore, the development of the garden-based curriculum is also carried out under the guidance of policy documents, and the selection is based on certain values. Literature [22] pointed out that in the content of the kindergarten curriculum, knowledge has the problem of how to choose and choose. The knowledge that can be recognized by young children and appropriate to their age must be carefully selected from human culture. And put forward the basis and standard of selection should be whether knowledge can improve and optimize the quality of children's learning and life. Literature [23] pointed out that the kindergarten curriculum organizes content around themes, and different curriculum designers may have different theme selection tendencies due to differences in values. Literature [24] pointed out that the kindergarten curriculum has the function of cultural dissemination, and it adjusts or integrates the mainstream culture and subculture in the society at the same time by criticizing and choosing the cultural content of the previous generation. Literatures [25, 26] compare the kindergarten textbook market to a vegetable market. Some textbooks are contaminated and some are fake and shoddy. But it is not easy to be identified, which makes a mixed curriculum entering kindergarten, which is really worrying. Literature [27] pointed out that the textbooks used in kindergartens in various places often coexist with multiple programs and focus on their own educational conditions, characteristics, or other specific circumstances. Some of these curriculum plans or teaching materials are created by relying on the professional strength of preschool education in colleges or kindergarten teachers. Some are developed with the help of local administrative departments or teaching and research units, while others are led by publishing and distribution units to invite professionals and lead preschool teachers from the front line with rich teaching experience to jointly compile.

### 3. Method

This work will combine the improved genetic algorithm with the back-propagation (BP) network and complete the evalu-

ation of the innovation effect of the teaching method of handmade courses in preschool education based on artificial intelligence technology.

*3.1. BP Network.* Three or more layers of feed-forward neural networks without feedback or connections are typical of BP networks. A typical three-layer BP network is shown in Figure 1. If a layer resides between the first and last layers of a stack, it is referred to as a hidden layer. Although there are no connections between neurons in the same layer in this neural network, all neurons between layers are connected.

A guided learning strategy is used to train and learn the BP network. Since the activation values of neurons propagate across each hidden layer, each neuron in the output layer is able to get the true output response of the network when a pair of learning patterns is presented to BP networks. Each neuron in the output layer is compared to its predicted output, and the error between the two is calculated. As a result, each connection weight is rectified one layer at a time from the output to each concealed level and finally back to the input layer. BP network's learning and training process will come to an end after the error has been decreased to an acceptable level, and the forward computation output-back propagating error loop will be repeated indefinitely. A neural network is constantly being repaired through the back-propagation of errors, which improves its ability to recognize input patterns. BP network's learning process is known as the error reverse algorithm, which is a learning algorithm in which the error function decreases as the gradient decreases.

In the context of BP neural network learning, supervised learning is the norm. There are four processes in the average 3-layer BP network. As soon as a network receives an input mode, it propagates it to the hidden layer units via mode forwarding. The output layer unit processes the hidden layers one at a time before sending them to the output layer unit, which then generates an output mode. This is a process known as forwarding propagation, which updates the state of the system layer-by-layer. An error back-propagation can be used if there is a discrepancy between an output response and an expected output pattern, layer by layer, along the course of the connection, pass the erroneous value, and correct the weight of each layer of the connection. Repetition and alternation are key components of memory training, and the connection settings between the layers must be tweaked to account for any differences between the actual and intended values. It is the goal of education

and training to reduce the discrepancy between what you expect and what you get. Learning convergence is the process by which the global error of the network decreases. There will be convergence when the actual output value is nearly identical to what was predicted.

Mode forward propagation and error back-propagation, memory training, and learning convergence are all part of the process. The forward- and error-back-propagation operations are continually repeated using a training pattern network for a given set of training patterns. The BP network has been learned if each training mode matches the requirements.

The input is propagated forward, and the value of hidden neurons is

$$b_j = \sigma \left( \sum_{i=1}^n W_{ji} x_i + \alpha_j \right). \quad (1)$$

The value of each neuron in the output layer is

$$y_k = \sigma \left( \sum_{i=1}^n W_{ki} x_i + \alpha_k \right). \quad (2)$$

Use the sum of squared errors as a measure of whether to stop training:

$$E = 0.5 \sum_{i=1}^N (o_i - y_i)^2. \quad (3)$$

If the incorrect sum of squares does not fulfill the requirements, the error signal must be back-propagated. The output layer gradually updates the input layer with new model parameters during this process. Calculate the gradient of the weights using the error function, and then move the weight vector from the output layer to the hidden layer to apply the changes:

$$\begin{aligned} w' &= w - \Delta w, \\ b' &= b - \Delta b. \end{aligned} \quad (4)$$

The pipeline of the BP network is illustrated in Figure 2.

A mapping is completed by the BP network. It is especially well suited to tackling nonlinear mathematical problems with complicated internal mechanisms and multiple variables influencing the final solution. With a high degree of self-learning capacity and great model generalization and promotion ability, the stable network structure established during the training phase can be directly applied to fresh data. When modeling, you only need to obtain input and output. The model integrates information storage and information processing and has a high degree of parallelism, which can quickly process complex tasks. The model has a certain fault-tolerant ability, and the trained network has strong generalizability, and can still maintain normal operation even if it is subject to local interference and damage. However, with the further development of research, BP neu-

ral network also began to expose some shortcomings and deficiencies, mainly the local search algorithm and gradient descent method used in it, which are easy to fall local minimum [28, 29].

**3.2. Improved Genetic Algorithm.** Genetic algorithms are drawn from the concept of biological evolution and are based on the principles of natural selection and genetics. It is a highly powerful global optimization search approach. Artificial evolution is used by the genetic algorithm to optimize the search for the target space in a manner similar to biological evolution. According to Darwinian criteria of survival of the fittest, a better group is constantly formed by evaluating each member against the predetermined target fitness function. A global parallel search is used to find the optimal solution for the optimization group at the same time as searching for the best individual.

Selection, crossover, and mutation are the only three basic genetic operators in the basic genetic algorithm. This approach is employed in one of the most basic and extensively used genetic algorithms. The basic genetic algorithm is broken down in the following sections.

**3.2.1. Chromosome Encoding Method.** Using a fixed-length binary string to represent individuals in the population and a binary symbol set for each allele, the basic genetic algorithm encodes chromosomes. Random integers with a uniform distribution can be used to create the gene values for each member of the starting population.

**3.2.2. Individual Fitness Evaluation.** Using a simple genetic algorithm, the possibility of each item being inherited into the next generation is determined by the probability proportional to their individual fitness. The fitness of all individuals must be positive or zero in order to calculate this probability accurately. Individual fitness can be calculated from objective function values by following a set of conversion rules, which must be specified in advance for each type of problem. This is especially true for cases in which the objective function value is negative.

**3.2.3. Genetic Operators.** There are three fundamental types of genetic operators in the genetic algorithm. Selective selection, crossover, and mutation operations all use the same fundamental bit mutation operator or uniform mutation operator for their respective operations.

Regardless of the problem domain or kind, genetic algorithms provide a general framework for solving complex system optimization challenges. The following stages can be used to build a genetic algorithm to address a real-world application problem that calls for optimization calculations: identify the decision factors and their restrictions, establish an optimization model, which means deciding on the type of objective function and the mathematical description or quantification approach for that objective function, identify the chromosomal encoding method that can be implemented, figure out how to decode the data, which means figuring out the relationship between each unique genotype and its matching phenotype. Individual fitness can be assessed quantitatively. It is also necessary to consider

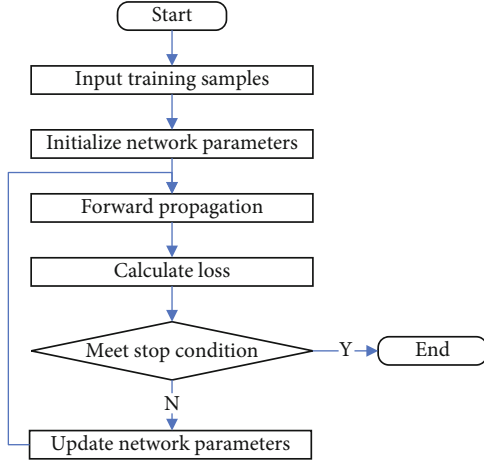


FIGURE 2: The pipeline of BP.

genetic operators in terms of their operating procedures, such as how crossovers and mutations are handled. The key working parameters of the genetic algorithm should be specified. As can be observed from the preceding construction processes, a genetic algorithm's coding method and genetic operator design are two important subjects to consider while building a genetic algorithm. They are also two vital steps in creating a genetic algorithm. For various optimization problems, multiple coding approaches and genetic operators with various operations are necessary. Figure 3 shows the fundamental genetic algorithm's operation flow.

The specific optimization of IGA mainly includes five parts. The chromosomes are encoded differently, the function is selected, and one that meets the fitness function is found. The third to fifth steps are three genetic operations, which can be divided into selection operations, crossover operations, and mutation operations.

The coding of chromosomes is an important part of the genetic algorithm, and it is also an important part of optimizing the BP neural network. This paper decides to use real numbers for encoding. The initial weights and initial thresholds determine the length of chromosome encoding, and the BP neural network determines which thresholds and weights.

The fitness level can basically determine the quality of the network prediction model, and fitness level is determined by absolute error. Only when the gap of absolute error is small can it prove prediction accuracy is better, and the value of fitness is equal to the gap between test value and actual value. Assuming that  $N$ th individual fitness is  $F$ , and its corresponding absolute error is  $E(x)$ , then the formula for the function value of the fitness value is

$$F_i = E(X_i). \quad (5)$$

From this formula, fitness can express the direct performance of the individual to varying degrees. The genetic algorithm will reduce the fitness value of the individual to be optimized as much as possible until the fitness value is 0.

The three genetic manipulations are crossover, selection, and mutation. Next, three different manipulations are ana-

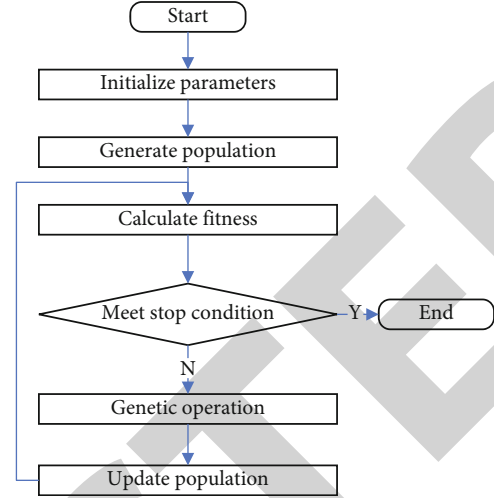


FIGURE 3: The pipeline of GA.

lyzed in detail. There are many methods for selecting operations, such as the well-known roulette method. The roulette method is mostly used in the traditional genetic algorithm BP network prediction model. However, the fitness used in this paper is the absolute error, whichever is closer to 0 and smaller, the better the prediction effect. However, the traditional selection operation method is not suitable for the experimental method. In this paper,  $i$  represents the individual,  $F$  represents the corresponding fitness,  $l$  represents the adjustment coefficient, and the probability is  $P$ . The formula for finding the probability is as follows:

$$P_i = \frac{l/F_i}{\sum_{i=1}^N l/F_i}. \quad (6)$$

Because the real numbers are used for chromosome encoding, the crossover operation is the crossover between real numbers:

$$\begin{aligned} a_{xj} &= (1 - \mu)a_{xj} + \partial a_{yj}, \\ a_{yj} &= (1 - \mu)a_{yj} + \partial a_{xj}. \end{aligned} \quad (7)$$

The mutation operation is

$$\begin{aligned} f(g) &= d \left( \frac{1-g}{g_{\max}} \right)^2, \\ c_{mn} &= c_{mn} + (c_{mn} - c_{\max})f(g), r > 0.5, \\ c_{mn} &= c_{mn} + (c_{\min} - c_{mn})f(g), r < 0.5. \end{aligned} \quad (8)$$

**3.3. IGA-BP Network.** Because the BP neural network must be given appropriate weights and thresholds when building the model, however, due to the characteristics of the BP network, the BP network is very sensitive to the selection of weights as well as thresholds. Once the weights or thresholds are improperly selected, the accuracy of the BP network will be greatly reduced. If it is heavy, it causes the network to fail

TABLE 1: The detailed feature indexes.

Index	Item
X1	Innovativeness of campaign goals
X2	Innovativeness of educational content
X3	Reasonableness of age characteristics
X4	Rationality of the observational evaluation
X5	Reflections on the effect of education
X6	Course safety
X7	Innovation in event design
X8	Innovation to ease convergence
X9	Innovativeness of educational strategies

for training. If it is light, it will make the whole prediction result show a large difference. The result may be that the training results of the BP network are not as good as those of some traditional linear prediction models.

On the premise of discarding the traditional roulette method in genetic algorithms, this paper adopts an operation method that improves fitness. An optimization model with the improvement of GA is proposed to optimize the content structure for the BP network, which is referred to as IGA-BP. The model is divided into three parts:

- (1) Determine various structures of the BP neural network, mainly to determine the number of layers in the BP network and required nodes
- (2) Optimizing the network with IGA, the main content is to adjust initial weights as well as thresholds in the network according to the selection in the genetic algorithm
- (3) Apply the optimized model to practice, and test whether the optimized model is better than the traditional network

## 4. Experiment and Discussion

**4.1. Dataset and Metric.** This work uses a self-made dataset to evaluate the innovativeness of teaching methods for hand-crafted curricula in preschool education. The dataset contains a total of 25,937 samples, of which 18,038 samples are training samples and the remaining 7,899 samples are test samples. The features of each sample are the corresponding evaluation indicators, as illustrated in Table 1, and the labels are the corresponding innovation levels. This work uses precision and recall to evaluate actual network performance.

**4.2. Training Loss.** In a neural network, the training loss is an important statistic for determining if the network can converge. This work undertakes tests to evaluate the loss at various phases of network training in order to verify the network's convergence. Figure 4 depicts the outcomes of the experiment.

At the beginning of training, as the training epoch increases, the loss of the network decreases significantly.

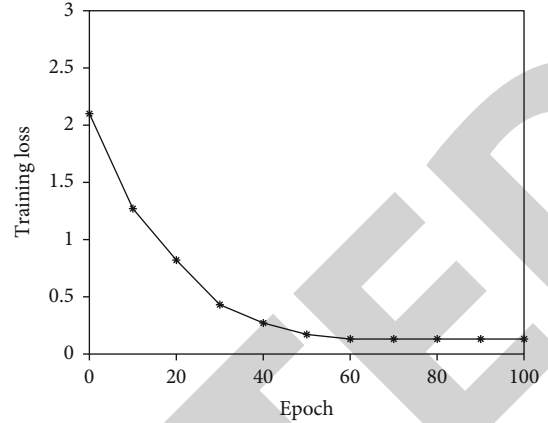


FIGURE 4: Training loss of IGA-BP.

TABLE 2: Result of method comparison.

Method	Precision	Recall
LG	86.30	83.60
RBF	90.20	87.70
SVM	92.80	91.20
IGA-BP	95.60	93.90

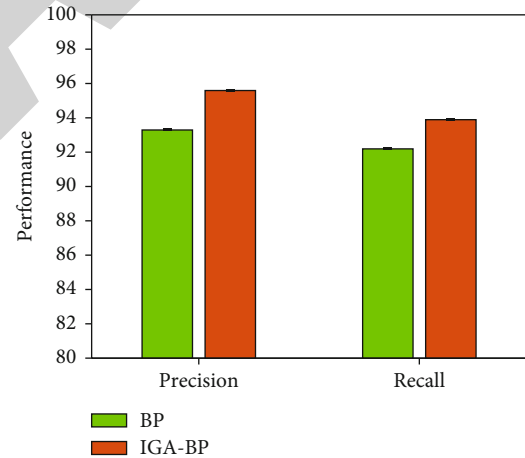


FIGURE 5: Comparison of BP and IGA-BP.

However, when the epoch reaches a certain value, the loss decreases very little, which means that the network has converged at this time. This proves the preliminary feasibility of the IGA-BP method designed in this paper.

**4.3. Method Comparison.** To verify the effectiveness of the IGA-BP method, this work compares it with other methods. The methods compared include LG, radial basis function kernel (RBF), and support vector machine (SVM). The experimental results are illustrated in Table 2.

It is obvious that the method proposed in this work can achieve the highest performance: 95.6% precision and 93.9% recall, compared with the best-listed method SVM, which can obtain 2.8% precision improvement and 2.7% recall

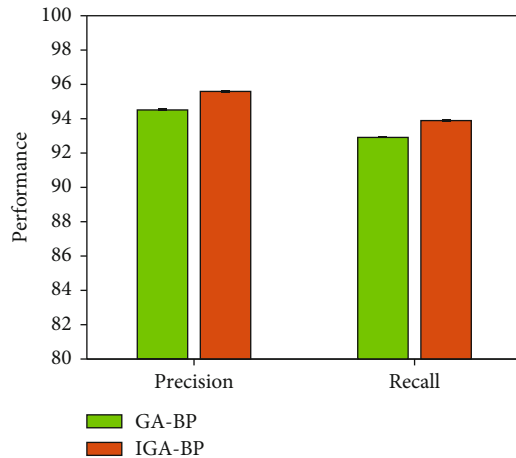


FIGURE 6: Comparison of GA-BP and IGA-BP.

improvement. This can verify the effectiveness of our proposed method.

**4.4. Effectiveness of IGA.** In this work, in order to alleviate the local optimal problem of BP, the IGA algorithm is introduced. To verify the effectiveness of this strategy, first, compare the network performance without using the IGA algorithm and using the IGA algorithm. The experimental results are shown in Figure 5.

Compared to not using IGA strategy, IGA-BP can obtain 2.3% precision improvement and 1.7% recall improvement. This proves the feasibility and correctness of this work using the IGA strategy to initialize the weights and thresholds of the neural network. To further verify the feasibility of improving the traditional GA algorithm, another comparative experiment was conducted in this work to compare the network performance when using GA and using IGA for optimization. The experimental results are shown in Figure 6.

Obviously, after improving the traditional GA algorithm, the IGA-BP algorithm can obtain better precision and recall. This proves the effectiveness of the improvement strategy proposed in this work.

## 5. Conclusion

With the emergence of the information society, there is a pressing need for individuals with a broad knowledge base who are adaptable to complex societal changes and capable of long-term development. Early childhood should be used to create the groundwork for this type of talent development. Preschool education must adapt to the needs of the times in terms of talent development and the implementation of specific knowledge education for young children. The study of preschool education knowledge supply is not only a reflection on preschool education knowledge but also an analysis of the complex relationship network of preschool education knowledge supply and the problems of interest competition and power distribution in the process of knowledge supply. Handmade education plays a very important role in preschool education. The main purpose of preschool education

handmade courses is to cultivate students' good hands-on ability. Today's preschool education handmade courses mainly cultivate students' imitation ability, hands-on operation ability, and knowledge-ability. With the change of society, the teaching methods of handmade courses in preschool education are constantly innovating. How to evaluate the effectiveness of the innovation of handmade course teaching methods has become a very important topic. This work builds a neural network to evaluate the innovative effectiveness of preschool handcrafted curriculum teaching methods. The specific content is that the genetic algorithm has been enhanced, a mode of the classic genetic algorithm roulette technique has been improved, and the moderation function has been adopted, allowing the BP neural network's starting weight and threshold to reach a higher standard. The revised genetic algorithm is substituted into the BP neural network model to optimize it, resulting in a new BP neural network. The data test and experiment were carried out, and it was found that in terms of training speed and prediction accuracy, the BP neural network optimized by the improved genetic algorithm has better accuracy and can better complete the prediction.

## Data Availability

The datasets used during the current study are available from the corresponding author on reasonable request.

## Conflicts of Interest

The authors declare that they have no conflict of interest.

## References

- [1] V. E. Lake and S. D. Adinolfi, "Preschool: young children take action: service learning with preschoolers," *YC Young Children*, vol. 72, no. 2, pp. 80–84, 2017.
- [2] S. Ikuta, R. Ishitobi, F. Nemoto, C. Urushihata, K. Yamaguchi, and H. Nakui, "Handmade content and school activities for autistic children with expressive language disabilities," in *Accessibility and Diversity in Education: Breakthroughs in Research and Practice*, pp. 464–493, IGI Global, 2020.
- [3] T. Basöz and D. T. Can, "The effectiveness of computers on vocabulary learning among preschool children: a semiotic approach," *Cypriot Journal of Educational Sciences*, vol. 11, no. 1, pp. 02–08, 2016.
- [4] X. Lin, J. Wu, S. Mumtaz, S. Garg, J. Li, and M. Guizani, "Blockchain-based on-demand computing resource trading in IoV-assisted smart city," *IEEE Transactions on Emerging Topics in Computing*, vol. 9, no. 3, pp. 1373–1385, 2021.
- [5] J. Li, Z. Zhou, J. Wu et al., "Decentralized on-demand energy supply for blockchain in Internet of Things: a microgrids approach," *IEEE Transactions on Computational Social Systems*, vol. 6, no. 6, pp. 1395–1406, 2019.
- [6] S. Kurbanova, "Toys-toys the role and importance of toys in preschool education," *International Journal of Innovative Analyses and Emerging Technology*, vol. 2, no. 1, pp. 46–48, 2022.
- [7] C. Weida, "Teaching artists and the craft of handmade books," *Teaching Artist Journal*, vol. 13, no. 1, pp. 5–13, 2015.



## Retraction

# Retracted: Evaluation and Stratification for Chinese International Education Quality with Deep Learning Model

### Computational and Mathematical Methods in Medicine

Received 25 July 2023; Accepted 25 July 2023; Published 26 July 2023

Copyright © 2023 Computational and Mathematical Methods in Medicine. This is an open access article distributed under the Creative Commons Attribution License, which permits unrestricted use, distribution, and reproduction in any medium, provided the original work is properly cited.

This article has been retracted by Hindawi following an investigation undertaken by the publisher [1]. This investigation has uncovered evidence of one or more of the following indicators of systematic manipulation of the publication process:

- (1) Discrepancies in scope
- (2) Discrepancies in the description of the research reported
- (3) Discrepancies between the availability of data and the research described
- (4) Inappropriate citations
- (5) Incoherent, meaningless and/or irrelevant content included in the article
- (6) Peer-review manipulation

The presence of these indicators undermines our confidence in the integrity of the article's content and we cannot, therefore, vouch for its reliability. Please note that this notice is intended solely to alert readers that the content of this article is unreliable. We have not investigated whether authors were aware of or involved in the systematic manipulation of the publication process.

Wiley and Hindawi regrets that the usual quality checks did not identify these issues before publication and have since put additional measures in place to safeguard research integrity.

We wish to credit our own Research Integrity and Research Publishing teams and anonymous and named external researchers and research integrity experts for contributing to this investigation.

The corresponding author, as the representative of all authors, has been given the opportunity to register their agreement or disagreement to this retraction. We have kept a record of any response received.

### References

- [1] M. He, "Evaluation and Stratification for Chinese International Education Quality with Deep Learning Model," *Computational and Mathematical Methods in Medicine*, vol. 2022, Article ID 9627116, 10 pages, 2022.

## Research Article

# Evaluation and Stratification for Chinese International Education Quality with Deep Learning Model

**Min He** 

*Department of Basic Education and Research, Shaanxi Police Vocational College, Xi'an 710021, China*

Correspondence should be addressed to Min He; 171847302@masu.edu.cn

Received 8 April 2022; Revised 30 April 2022; Accepted 6 May 2022; Published 23 May 2022

Academic Editor: Naeem Jan

Copyright © 2022 Min He. This is an open access article distributed under the Creative Commons Attribution License, which permits unrestricted use, distribution, and reproduction in any medium, provided the original work is properly cited.

In the process of human communication, language learning and communication play a fundamental, leading, broad, and long-lasting role. It serves as a link and a bridge between countries and peoples, allowing for greater understanding and camaraderie. The significance of Chinese in international commercial and cultural exchanges has been more obvious in the current era, as China's comprehensive strength continues to improve. Its cultural value and practical value have been continuously improved, the international community has an increasing demand for learning Chinese, and the cause of international Chinese language education has developed rapidly. China must strengthen the international dissemination of Chinese, so that the world can better understand and accept China, so that China can better integrate into the world. In this context, how to evaluate and stratify the quality of Chinese international education has become an important research topic. Relying on the hot deep learning technology in recent years, this work designs a neural network for evaluating the quality of international Chinese education. The content of this work is as follows: aiming at the serious defect of the current mainstream feature classification network that only uses the top-level features extracted by a single convolution layer to classify, which leads to the loss of classification accuracy. A multiscale feature pyramid fusion network is built in this paper, starting with the working mechanism of a convolutional neural network. It is capable of fully extracting and combining the representations of the network's shallow and deep outputs, based on first- and second-order characteristics of global and local discriminative region information. Second, the network structure has the bottleneck layer module and the batch normalization layer module, both of which are made up of varying numbers of  $1 \times 1$  convolution kernels.

## 1. Introduction

Language learning and communication play a fundamental, leading, extensive, and lasting role in human communication and are bridges and bonds for deepening understanding and friendship between different countries and peoples. In the new era, with the continuous enhancement of China's comprehensive strength, the role of Chinese in international trade and cultural exchanges has become increasingly apparent. Its cultural value and practical value have been continuously improved, and the international community has an increasing demand for learning Chinese. Teaching Chinese to Speakers of Other Languages (TCSOL) is an emerging discipline that emerged in response to the rapid development of China's national strength to meet the needs of international communication of Chinese language. It was

established in 2008. Teaching Chinese as a foreign language is based on coming in, while teaching Chinese as a foreign language is based on going out [1–5].

In the past ten years, China's international Chinese language education has achieved amazing results. Teaching Chinese as a foreign language has gone further and further in the field of going global, and it is also closely aligned with many major national strategies. The main way for international Chinese language education to cooperate with the national strategy is to support countries around the world to cultivate local talents who are proficient in Chinese and understand Chinese culture, actively carry out Chinese cultural teaching and exchange activities, and help create a good environment for public diplomacy and cultural diplomacy. Through the subtle international education of Chinese and Chinese culture, it cultivates a large number of

international friendly people who know and are friendly to China in a subtle and silent way and contributes to the promotion of China's international soft power. Therefore, the study of Chinese language education has become an indispensable research topic, which has very important theoretical and practical significance [6–10].

Teaching Chinese to Speakers of Other Languages is developing rapidly in both talent training and teaching research and is in a period of vigorous development. It can be seen that a scientific and systematic summary and analysis of the quality of education is a very important part of the field of Chinese language education research. Through the evaluation of education quality, stratified education can also be carried out. Dynamic stratified education teaches students according to their aptitude. It teaches on the premise of different personality characteristics. It can not only fully mobilize enthusiasm and initiative but also promote personality development, which has great advantages. At the same time, the dynamic layered teaching technique and the requirements of excellent education tend to be consistent; so, it is in line with the current teaching method reform and development. One of the foundations for the topic selection of this study [11–15] is the introduction of dynamic stratified teaching methods in teaching, organically merging with individual differences.

Neural network and deep learning is a very popular research method, and it has a solid theoretical foundation and powerful practical tools. Therefore, using deep learning as a means to analyze the quality of international Chinese language education is of great significance in detecting the hotspots and frontiers of the subject and choosing the direction of scientific research. On the one hand, it can make up for the inadequacy of the current deep learning analysis and research on Chinese international education in China. Through in-depth learning analysis, a new way of understanding Chinese international education research is formed. On the other hand, it can also summarize the achievements of the development and research of Chinese international education over the years, summarize the development law of the discipline, and provide information reference for Chinese experts and scholars in the research of the discipline theory. In this context, this work relies on the hot deep learning technology in recent years to design a neural network for evaluating the quality of Chinese international education. Its essence is a classification and identification network, and it is used for hierarchical research.

The paper's organization paragraph is as follows: the related work is presented in Section 2. Section 3 analyzes the design of application model. Section 4 discusses the experiments and results. Finally, in Section 5, the research work is concluded.

## 2. Related Work

Reference [16] looked assessed the Chinese pronunciation of native English-speaking students from Europe and the United States, as well as their acquisition of Chinese phonetic changes. It also evaluates the influence of mother tongue, learning environment, and other aspects on its Chinese

pronunciation based on its pronunciation. Reference [17] compares the initials, finals, and tones with the students' target language in the form of a survey report, finds out the reasons for the errors, and puts forward teaching suggestions. Reference [18] took foreign high school Chinese learners as the survey object and investigated the Chinese learning needs of these students. Reference [19] studies the needs of Chinese language learning at the Confucius Institute in Phuket, Thailand, and summarizes the completion of the work of the Confucius Institute. It includes the construction of Confucius Institutes/Classrooms, the construction of teaching staff, the compilation of local textbooks, the organization of international cultural activities, and the construction of online Confucius Institutes, as well as work plans and priorities. Literature [20] believes that the current scale of Confucius Institutes in China is developing steadily, the quality of running schools is constantly improving, the functions of running schools are constantly expanding, and the operating mechanism is gradually improving. At the same time, some suggestions and requirements are put forward for the future development of Confucius Institutes. Literature [21] emphasized the practical application value of Chinese language and the critical role of Confucius Institutes as incubators, predicting that Confucius Institutes' future development prospects would be broader. The literature [22] outlines the unique condition of studying in China, as well as the significant impact of the Belt and Road national policy on studying there. Literature [23] takes students whose immediate family members can speak Chinese in foreign schools as the research object, analyzes their different learning motivations, and puts forward different learning suggestions for different motivations. Reference [24] takes Confucius Institutes as the object of investigation and analyzes the current situation of Chinese language learning. It made a general exposition and analysis of the development status, existing problems, and future trends of Confucius Institutes based on the exchange materials of the 2nd Confucius Institute Conference, the relevant content of the Hanban website, and related articles. Literature [25] proposes that in the entire construction process of Confucius Institutes, innovative means must be used to continuously solve problems arising in the development and to continuously improve the effect of running schools. The Confucius Institute has become the brightest brand that reflects China's soft power. It is necessary to truly understand the soft power connotation of the Confucius Institute.

According to Literature [26], focus should be devoted to the development of a comprehensive applied linguistics curriculum in the undergraduate course of Chinese international education. The viewpoints of undergraduate students majoring in Teaching Chinese to Speakers of Other Languages on the evolution of the major, future careers, and their comprehension of Chinese language teachers were explored in reference [27]. Literature [28] proposed a set of policies to encourage undergraduates studying in Chinese to work for Speakers of Other Languages. Taking the graduation thesis of the Master of Teaching Chinese to Speakers of Other Languages as the survey object, the subject selection of the thesis was poor in the examination. Literature [29]

comprehensively investigates the current situation of Chinese talent courses in the majors of TESOL majors in four colleges and universities. Through the combination of questionnaire survey method, interview method, and other survey methods, this paper deeply analyzes the shortcomings and deficiencies in the curriculum setting of Chinese talent class. And trace back to the root of the problem and put forward reasonable suggestions for the improvement of Chinese talent courses from the aspects of colleges' attention, course offering, teachers' teaching, and students' learning. Literature [30] proposes that we should establish and enhance the subject awareness of teaching Chinese as a foreign language, strengthen the theoretical construction of teaching Chinese as a foreign language, and improve the quality of Chinese teaching that requires high-quality teachers, high-quality Chinese textbooks, and efficient teaching methods. Literature [31] proposed to strengthen the study of language acquisition laws and teaching methods to improve Chinese teaching. For the cultivation of the Master of Teaching Chinese to Speakers of Other Languages, not only skilled teaching skills are required but also good research quality. Literature [32] proposed that the principles of combining theory and practice and paying equal attention to knowledge transfer and skill training should be adopted in the process of master's degree training in Teaching Chinese to Speakers of Other Languages. We should emphasize the teaching of Chinese characters and knowledge of Chinese culture in specific courses, as well as the teaching of fundamental concepts and methods of foreign language teaching and the promotion of crosscultural teaching ability.

### 3. Method

This chapter will deeply study and analyze the key factors that affect the classification performance of the existing mainstream classification evaluation models. Combined with the idea of multiscale feature pyramid, the classical algorithm is improved. Three high-performance and end-to-end Chinese international education quality evaluation models are constructed.

**3.1. CNN.** Compared with artificial neural network, convolutional neural network (CNN) simulates the biological mechanism of animal visual cortex. It adopts operations such as local connection, weight sharing, and downsampling, so that the network has certain invariance to the translation, distortion, and distortion of the image and easy to train and optimize. CNN is a multilayer feed-forward neural network, generally including input layer, convolution layer, pooling layer, fully connected layer, and output layer. The feature map of each layer is composed of a two-dimensional plane composed of multiple independent neurons. By setting multiple different convolution kernels to perform convolution operations, more new and different two-dimensional feature map information is extracted. After the convolution operation, through the activation function processing, the extracted feature information is pooled to retain the most significant features and enhance the robustness of the network. After multiple convolution and pooling operations,

the extracted features are sent to the fully connected layer, and the mathematical statistics method is applied to construct a classifier to complete the classification and obtain the final output result.

The role of the convolutional layer in the deep convolutional neural network is to extract new feature information from the input feature map and provide the next layer as input, which plays the role of layer advancement and feature extraction. The convolution kernel is a weight matrix. The setting of the parameters of the convolution kernel is very critical, involving the size, number, and step size of the convolution kernel. The settings of these parameters will affect the recognition accuracy of the model. The working principle of the convolution layer is to perform an inner product operation on the input feature map and the convolution kernel, and the convolution kernel performs a sliding window calculation on the input feature map. It maps the feature information in the kernel range into a new information and forms a new feature map as the input of the next layer. The size of the convolution kernel is the size of the receptive field sliding window. The larger the convolution kernel, the richer the extracted features, but at the same time, the number of parameters will increase sharply. The step size is the magnitude of the sliding window movement. The larger the step size, the smaller the size of the output feature map and the less information it contains. The smaller the step size, the more swipes, and the slower the network training. The convolution kernel can be regarded as a feature extractor, and different convolution kernels can extract different feature information in the input feature map. Therefore, the network can obtain a variety of different features at the same position in the image by increasing the number of convolution kernels, enrich the features learned by the model, and improve the cognitive ability of the model. The convolution operation is as follows:

$$x_j^l = f \left( \sum_j x_i^{l-1} * w_{ij}^{l-1} + b_i^l \right). \quad (1)$$

After the convolution operation, the nonlinear output of the feature information is obtained through the activation function  $f$ , and the nonlinear transformation of the feature information is realized. This is a good way to solve classification problems that are tough to solve using linear classification [27]. The following are some of the most widely used activation functions:

$$\begin{aligned} \text{Sigmoid}(z) &= \frac{1}{1 + \exp(-z)}, \\ \text{Tanh}(z) &= \frac{\exp(z) - \exp(-z)}{\exp(z) + \exp(-z)}, \\ \text{ReLU}(z) &= \max(0, z). \end{aligned} \quad (2)$$

The pooling layer obtains the representative features in the local area image patch by downsampling. It further abstracts and reduces the dimension of the input feature map, reducing the computational cost. It can play the role

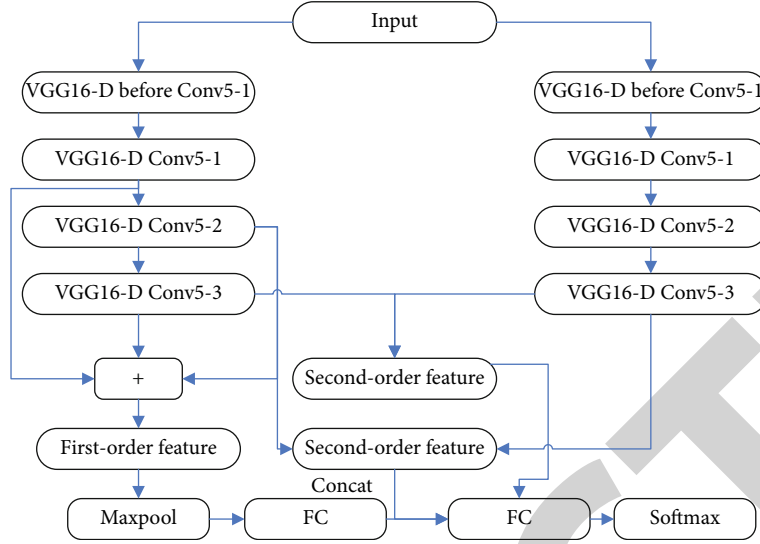


FIGURE 1: The structure of MSFPFN.

TABLE 1: The detailed parameters of MSFPFN.

Layer	Kernel size	Kernel number	Input size
Conv1-1	$3 \times 3$	64	$448 \times 448 \times 3$
Conv1-2	$3 \times 3$	64	$448 \times 448 \times 64$
Maxpool1	$2 \times 2$	—	$448 \times 448 \times 64$
Conv2-1	$3 \times 3$	128	$224 \times 224 \times 128$
Conv2-2	$3 \times 3$	128	$224 \times 224 \times 128$
Maxpool2	$2 \times 2$	—	$112 \times 112 \times 128$
Conv3-1	$3 \times 3$	256	$112 \times 112 \times 128$
Conv3-2	$3 \times 3$	256	$112 \times 112 \times 256$
Conv3-3	$3 \times 3$	256	$112 \times 112 \times 256$
Maxpool3	$2 \times 2$	—	$56 \times 56 \times 256$
Conv4-1	$3 \times 3$	512	$56 \times 56 \times 256$
Conv4-2	$3 \times 3$	512	$56 \times 56 \times 512$
Conv4-3	$3 \times 3$	512	$56 \times 56 \times 512$
Maxpool4	$2 \times 2$	—	$56 \times 56 \times 512$
Conv5-1	$3 \times 3$	512	$28 \times 28 \times 512$
Conv5-2	$3 \times 3$	512	$28 \times 28 \times 512$
Conv5-3	$3 \times 3$	512	$28 \times 28 \times 512$
Maxpool4	$2 \times 2$	—	$28 \times 28 \times 512$
FC1	—	1	$28 \times 28 \times 512$
FC2	—	1	262244
Softmax	—	1	16484

of secondary feature extraction while reducing the dimension of the feature map. If the network does not change the size of the feature map during operation, it will increase the computational complexity of the convolutional layer and the parameter complexity of the fully connected layer. This will have a greater impact on the training of the network,

making it difficult for the network to converge or even overfitting. The pooling layer can reduce the redundancy of features to a certain extent while reducing the size of the feature map. The pooling operation is similar to the convolution operation, using a pooling function without weight parameters. It begins in the upper left corner of the input feature map, slides to the right or down with a set step size, and outputs after pooling the pixels of the associated window block. The following is the calculating formula:

$$x_j^l = f\left(\beta \times \text{down}\left(x_i^{l-1}\right) + b_j^l\right). \quad (3)$$

The most commonly used pooling methods are average pooling and max pooling. Average pooling is similar to the effect of the mean filter, which has a smoothing effect and can effectively avoid the influence of noise points, but it is easy to lose texture edge features. Since max pooling can reduce the mean deviation caused by the convolution operation, it can better adapt to texture features. The pooled features discard irrelevant details and only retain the main feature information that is effective for the task, which enables CNN to have a certain tolerance for changes in image translation, tilt, scale scaling, etc. The pooling layer only reduces the scale of a single feature map through the pooling kernel, retaining important feature details, and does not need to extract new features like the convolutional layer. Therefore, the number of feature maps remains unchanged after passing through the pooling layer.

The function of the fully connected layer is to map the feature information obtained by operations such as convolution and pooling in front of the layer into the label space of the sample. Because the feature expression obtained by multiple convolutions and pooling of the convolutional neural network is still 3-dimensional, at this time, in order to calculate the gradient, the 3-dimensional feature expression must be corresponding to the 1-dimensional label. Therefore, a fully connected layer is required to convert 3-dimensional

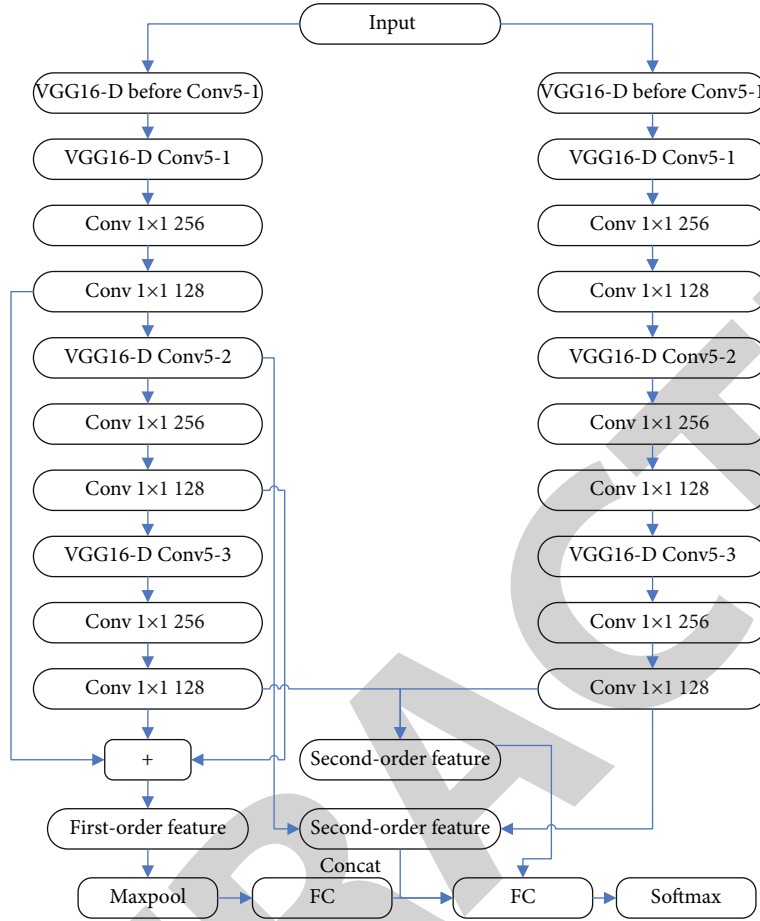


FIGURE 2: The structure of MSFPFN-DR.

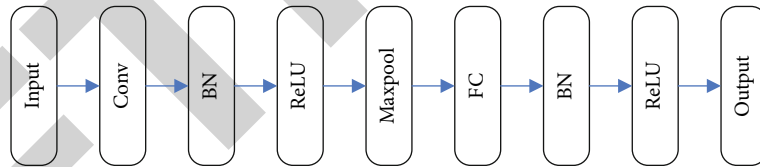


FIGURE 3: The network structure after adding the BN layer.

TABLE 2: Experimental environment.

Item	Parameter
Operating system	Ubuntu 18.04
CPU	Intel(R) Xeon(R) CPU E5-2620 v4 @ 2.10GHz
Memory	32G
Graphics card	NVIDIA GeForce GTX 1080Ti
Framework	PyTorch

features into 1-dimensional space. The neurons in the fully connected layer are fully connected, and the output of all neurons in the previous layer will be used as the input of each neuron in this layer, but the neurons in the same layer are not connected to each other. The calculation method is as follows:

$$x_j^l = f\left(\sum_i x_i^{l-1} * w_{ij}^{l-1} + b_i^l\right). \quad (4)$$

3.2. *Multiscale Feature Pyramid Fusion Network.* This section proposes an efficient multiscale feature pyramid fusion

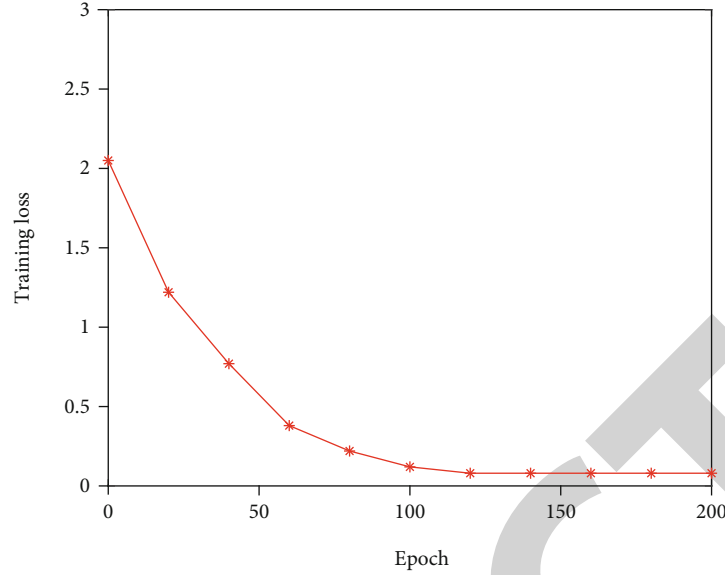


FIGURE 4: Training loss.

TABLE 3: Comparison of different methods.

Method	Precision	Recall
RBF	85.30	82.80
SVM	89.90	87.20
BP	92.70	91.60
MSFPFN-DR-BN	95.10	93.30

network (MSFPFN). Figure 1 shows the MFPP network structure. The network framework can fully extract the first-order and second-order features of the global and local discriminative regional information that characterize the characteristics of international Chinese education for the final evaluation process, so as to effectively enhance and improve the performance of the basic network. At the same time, part of the network layer of the dual-channel VGG16-D network is used as the basic feature extractor to build the B-CNN model and the CBP model based on the low-dimensional approximation method of the Tensor Sketch kernel function as the basic network to build the network framework.

The network first uses the first 14 layers of two symmetric VGG16-D networks to build a two-way feature extractor. Afterwards, the feature maps output by the last two convolutional layers of the two-way feature extractor are used to extract different forms of second-order features across layers in the form of symmetry and intersection. At the same time, the feature maps output by the last three convolutional layers of the single-channel VGG16-D network are fused in the form of adding corresponding position elements to obtain first-order features. This first-order feature is then downsampled by the pooling layer, and the dimensionality reduction is performed by the mapping operation of the fully connected layer. Finally, the obtained first-order dimensionality reduction features that can represent the global information of the data and

the second-order features with the characteristics of target discriminative region localization and identification are subjected to concat splicing and fusion operation and then sent to the Softmax classifier. At the same time, the MSFPFN network framework can also be extended to use other CNN networks with more advanced structure and better classification performance, such as ResNet and DenseNet, as the basic feature extractor to build. However, because the basic feature extractor chosen has a significant impact on the network model's final classification performance, it is necessary to avoid repeating related experiments and take into account the restricted computational resources. The goal of the related comparative experiments is to confirm that the proposed MSFPFN network framework's discriminative accuracy gain over the basic network comes from the first-order and second-order fusion features, which can effectively characterize the data's global and local discriminative region information, rather than merely using the improved classification performance of the underlying feature extractor. Therefore, in the research work of this paper, only part of the network layer of the VGG16-D network is used as the basic feature extractor to construct a high-performance Chinese international education quality assessment model. MSFPFN's specific parameters are listed in Table 1.

**3.3. Dimensionality Reduction Multiscale Feature Pyramid Fusion Network.** As the dimension of the extracted bilinear features is higher, the computational complexity of the dimensionality reduction operation increases. And the more GPU memory resources are consumed during the network training process. Therefore, it is urgent to build a high-performance network framework based on feature dimensionality reduction. The Inception module has an excellent local topology network structure by using dense component connections instead of local sparse connections. Many design ideas used in the Inception module have had a profound impact on the construction of subsequent CNN models.

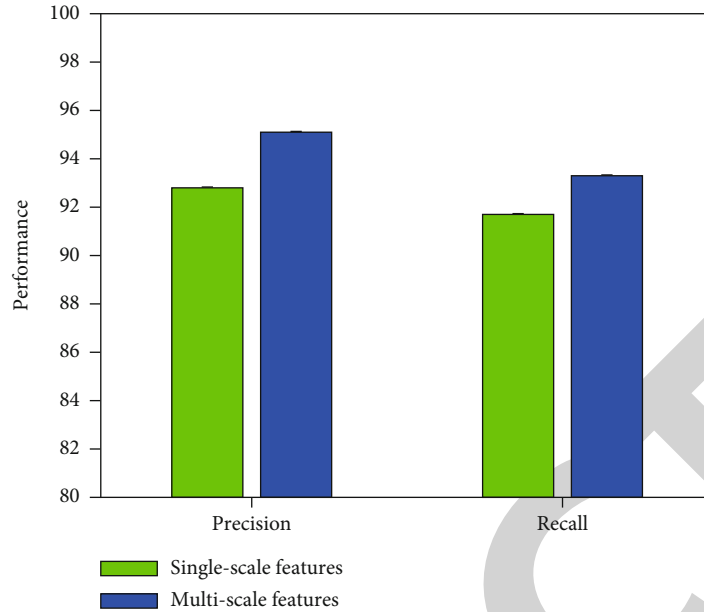


FIGURE 5: Multiscale feature fusion evaluation.

TABLE 4: Bottleneck module evaluation.

Method	Training time	Precision	Recall
MSFPFN	13.5 h	93.10	90.50
MSFPFN-DR	8.9 h	93.70	92.10

The Inception module adds several convolution and pooling bypass branches based on the convolutional sparse connection structure of the original direct connection. Feature maps representing different semantic information of the data are extracted by using parallel combination of convolution kernels of different sizes. Afterwards, these feature maps are subjected to concat splicing and fusion operation and then used as the input of subsequent network layers. In the Inception module, each bypass branch uses a  $1 \times 1$  convolution kernel. It can effectively realize the combination of spatial feature information in the dimension direction of the input feature map channel and can perform data dimension reduction in a way of reducing the number of feature map channels. At the same time, the ReLU activation unit will be followed closely to add more nonlinear transformations to the network to improve the generalization ability of the model. In addition, the network layer constructed by the  $1 \times 1$  convolution kernel is also called the bottleneck layer, which can be used to reduce the number of channels of the feature map first and then expand to the corresponding depth as needed.

Based on the advantages of the bottleneck layer, this section embeds different numbers of bottleneck layer modules in the two-way feature extraction network of the MSFPFN network to construct a more efficient dimensionality reduction multiscale feature pyramid fusion network (MSFPFN-DR). Figure 2 shows the network structure. The network structure of the two is similar, and the feature fusion method

is the same. The main difference is that the MSFPFN-DR network, respectively, adds two different numbers of bottleneck layer modules after the last three convolutional layers of the two-way feature extractor VGG16-D network. It is used to reduce the dimension of the extracted first-order and second-order features to reduce the computational complexity of the network model. The subsequent first-order feature extraction operations and second-order feature extraction operations are similar to those of the MSFPFN network, with the exception that the dimensionality reduction mapping operation of the bottleneck layer module is added to the input part, demonstrating the MSFPFN-DR network framework's scalability even further.

**3.4. DRMSFPFN with BN Layer.** The great nonlinear fitting ability of the deep CNN model is complemented with a large number of parameters. When utilizing stochastic gradient descent for network model training, there are a few apparent hazards to be aware of. The initial learning rate, learning decay rate, each network layer's initialization weight, and the dropout usage ratio, for example, are all parameters that must be manually specified. These parameters have a significant impact on the network model's ultimate training performance. These vast quantities of parameter tweaking effort, on the other hand, are time and labor-intensive. In response to this problem, researchers have proposed an efficient BN layer module to solve this problem. The BN layer module can be used to accelerate the training convergence speed of the network, prevent overfitting, and effectively avoid the gradient disappearance or explosion problem during deep network training. The calculation of BN is as follows:

$$x_i' = \frac{(x_i - \mu_B)}{\sqrt{\sigma^2 + \epsilon}}, \quad (5)$$

$$y = \alpha x_i' + \beta.$$



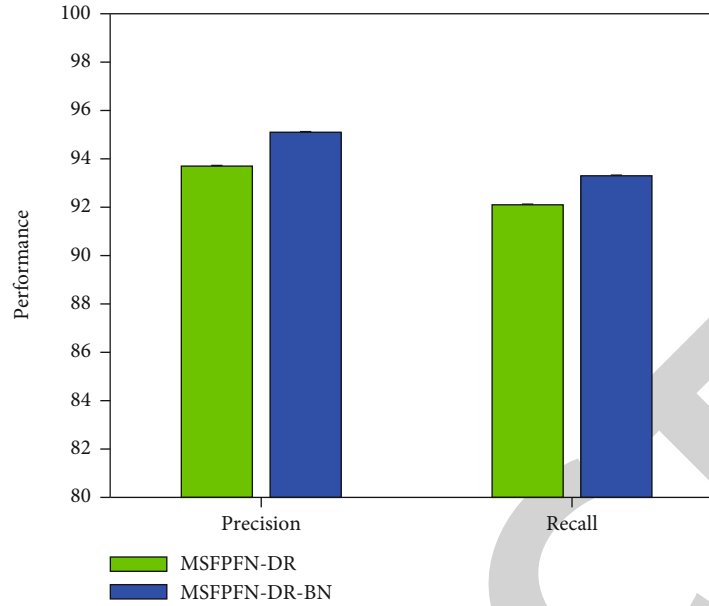


FIGURE 6: BN module evaluation.

At the same time, the BN layer module is usually added before the ReLU activation unit of each network layer when used in the CNN network. The feature maps extracted from each layer are first normalized and then nonlinearly mapped to smoothly accelerate the training convergence process of the network model. Figure 3 shows the network structure changes before and after adding the BN layer module.

Based on the benefits of the BN layer module, this part places the BN layer module before each MSFPFN-DR network layer ReLU activation unit to create the MSFPFN-DR-BN network, which improves the network's performance even more.

## 4. Experiment

**4.1. Implementation Details.** For experiments, this work uses a data collection that was created by the author. The data set contains a total of 87,314 samples, with 59,731 samples serving as the training set and 27,583 samples serving as the test set. Each sample's features are the appropriate evaluation indicators of Chinese international education quality, and the label is the quality level, which is then stratified according to the quality level. It should be emphasized that this work converts feature data into two-dimensional image data and views Chinese international education quality assessment as an image classification task. The experimental environment used in this work is shown in Table 2.

**4.2. Training Convergence Evaluation.** In deep learning, network training is a necessary and important process. The convergence of training directly affects the subsequent testing of the network. In order to evaluate the training process of the network, this work analyzes the losses in different stages of training. The experimental results are illustrated in Figure 4.

As the network training progresses, the loss gradually decreases. But when the epoch is 120, the loss value no longer decreases and tends to converge. This preliminarily shows the feasibility of the MSFPFN-DR-BN network designed in this paper.

**4.3. Comparison of Different Methods.** To further verify the effectiveness of MSFPFN-DR-BN, it is compared with other evaluation methods. The compared methods include RBF, SVM, and BP network, and the experimental results are illustrated in Table 3.

Compared with other methods in the table, MSFPFN-DR-BN can obtain 95.1% precision and 93.3% recall. It corresponds to the highest performance, which demonstrates the effectiveness and correctness of the method.

**4.4. Multiscale Feature Fusion Evaluation.** In this work, features of different scales are fused in order to extract more discriminative features. To verify the effectiveness of this strategy, this work conducts comparative experiments to compare the evaluation performance without feature fusion and when feature fusion is used. The experimental results are illustrated in Figure 5.

Compared with single-scale features, using multiscale feature fusion can achieve 2.3% precision and 1.6% recall improvement. It can thus prove the effectiveness of this work using this feature fusion strategy.

**4.5. Bottleneck Module Evaluation.** This work adopts the bottleneck module to reduce the dimension of the network to speed up network training. In order to verify the effectiveness of this dimensionality reduction strategy, this work conducts comparative experiments to compare the evaluation performance without using the bottleneck module and using the bottleneck module, respectively. The experimental results are illustrated in Table 4.

It can be seen that after using the dimensionality reduction module, the training time of the network is greatly reduced, and the precision and recall are improved to varying degrees. This proves the correctness and feasibility of using this strategy in this work.

**4.6. BN Module Evaluation.** This work uses the BN module to optimize the network structure and extract more effective features. To verify the effectiveness of this strategy, the evaluation performance without and with BN is compared. The experimental results are illustrated in Figure 6.

Compared with not using the BN module, after using this strategy, the network can obtain 1.4% precision improvement and 1.2% recall improvement. This proves that the use of BN structure can effectively improve the evaluation performance.

## 5. Conclusion

After more than ten years of unrelenting work, Chinese foreign communication has reached its pinnacle. The international Chinese language education market is now in good shape and has a bright future ahead of it. The number of students has also increased, and cultural exchange programmers have become more varied and colorful. At the same time, the development of the Chinese domestic foreign education market is excellent. A growing number of colleges and institutions are offering undergraduate and master's degrees in Teaching Chinese to Speakers of Other Languages, and the number of international students in China is at an all-time high. Domestic and foreign Chinese language training institutions have already entered the initial stage, the market scale has continued to expand, and the brand concentration has gradually increased. The good development status of the Chinese international education market in China will lay a solid foundation for the international dissemination of Chinese in the future. In this context, how to evaluate and stratify the quality of Chinese international education has become an important research topic. This work designs a neural network for evaluating the quality of Chinese international education and conducts a hierarchical research based on this. Aiming at the common defects of existing mainstream network models, this paper improves the model by combining the idea of multiscale feature pyramid. To begin, we offer a network framework with high evaluation performance that can fully extract the first-order and second-order features of global and local discriminative area information to effectively enhance and improve the baseline model's classification performance. Second, due to the high dimension of the second-order features retrieved by the network and the computational cost, a bottleneck layer module made up of numerous  $1 \times 1$  convolution kernels is integrated in the network structure to improve performance. In order to achieve effective dimensionality reduction of multilayer features, reduce the number of parameters of the model and improve the inference speed of the model. Finally, in order to effectively avoid and prevent the overfitting problem that is easy to occur in the deep network training process, BN layer modules are embedded before the ReLU activation units of each network layer to smoothly accelerate the training

convergence process of the network model. Comprehensive and systematic experiments verify the effectiveness of this work.

## Data Availability

The datasets used during the current study are available from the corresponding author on reasonable request.

## Conflicts of Interest

The author declares that he has no conflict of interest.

## Acknowledgments

The project supported by the Shaanxi Society of Technical and Vocational Education (Grant No. 2022SZX245), project task: research and practice of college Chinese teaching reform at Higher Vocational College based on OBE theory.

## References

- [1] T. T. Heng, "Examining the role of theory in qualitative research," *Journal of International Students*, vol. 10, no. 4, pp. 798–816, 2020.
- [2] T. T. Heng, "Understanding the heterogeneity of international students' experiences: a case study of Chinese international students in U.S. universities," *Journal of Studies in International Education*, vol. 23, no. 5, pp. 607–623, 2019.
- [3] X. Lin, J. Wu, S. Mumtaz, S. Garg, J. Li, and M. Guizani, "Blockchain-based on-demand computing resource trading in IoV-assisted smart city," *IEEE Transactions on Emerging Topics in Computing*, vol. 9, no. 3, pp. 1373–1385, 2021.
- [4] J. Chen and G. Zhou, "Chinese international students' sense of belonging in North American postsecondary institutions: a critical literature review," *Brock Education Journal*, vol. 28, no. 2, pp. 48–63, 2019.
- [5] X. Xu, H. Sit, and S. Chen, "International education through a bioecological development lens – a case study of Chinese doctoral students in Australia," *Higher Education Research & Development*, vol. 40, no. 6, pp. 1342–1357, 2021.
- [6] Y. Yu and M. Moskal, "Missing intercultural engagements in the university experiences of Chinese international students in the UK," *Compare: A Journal of Comparative and International Education*, vol. 49, no. 4, pp. 654–671, 2019.
- [7] R. Huang and R. Turner, "International experience, universities support and graduate employability – perceptions of Chinese international students studying in UK universities," *Journal of Education and Work*, vol. 31, no. 2, pp. 175–189, 2018.
- [8] J. Li, Z. Zhou, J. Wu et al., "Decentralized on-demand energy supply for blockchain in Internet of Things: a microgrids approach," *IEEE transactions on computational social systems*, vol. 6, no. 6, pp. 1395–1406, 2019.
- [9] Z. Lian, B. C. Wallace, and R. E. Fullilove, "Mental health help-seeking intentions among Chinese international students in the U.S. higher education system: the role of coping self-efficacy, social support, and stigma for seeking psychological help," *Asian American Journal of Psychology*, vol. 11, no. 3, pp. 147–157, 2020.